frontiers | Research Topics

Tumor microenvironment in cancer hallmarks and therapeutics

Edited by
Na Luo, Shengtao Zhou, Hongming Miao and José Alexandre Ferreira

Published in
Frontiers in Molecular Biosciences
Frontiers in Cell and Developmental Biology

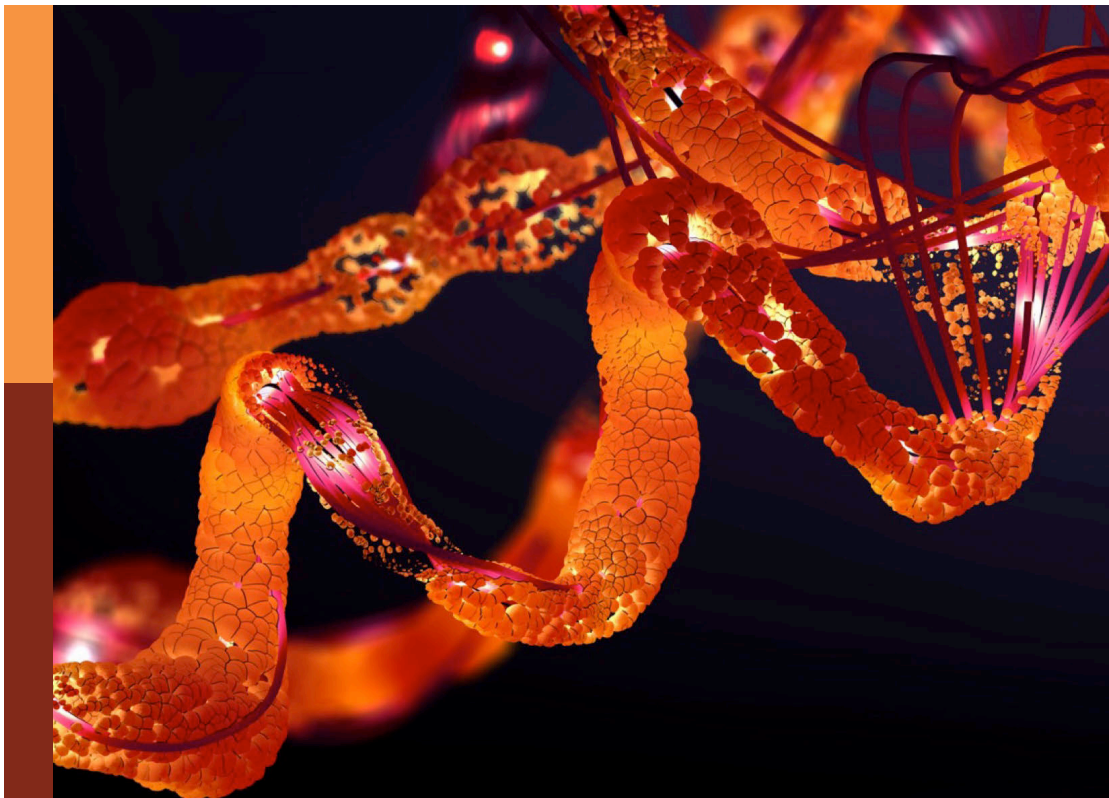

ISSN 1664-8714
ISBN 978-2-8325-2281-3
DOI 10.3389/978-2-8325-2281-3

About Frontiers

Frontiers is more than just an open access publisher of scholarly articles: it is a pioneering approach to the world of academia, radically improving the way scholarly research is managed. The grand vision of Frontiers is a world where all people have an equal opportunity to seek, share and generate knowledge. Frontiers provides immediate and permanent online open access to all its publications, but this alone is not enough to realize our grand goals.

Frontiers journal series

The Frontiers journal series is a multi-tier and interdisciplinary set of open-access, online journals, promising a paradigm shift from the current review, selection and dissemination processes in academic publishing. All Frontiers journals are driven by researchers for researchers; therefore, they constitute a service to the scholarly community. At the same time, the *Frontiers journal series* operates on a revolutionary invention, the tiered publishing system, initially addressing specific communities of scholars, and gradually climbing up to broader public understanding, thus serving the interests of the lay society, too.

Dedication to quality

Each Frontiers article is a landmark of the highest quality, thanks to genuinely collaborative interactions between authors and review editors, who include some of the world's best academicians. Research must be certified by peers before entering a stream of knowledge that may eventually reach the public - and shape society; therefore, Frontiers only applies the most rigorous and unbiased reviews. Frontiers revolutionizes research publishing by freely delivering the most outstanding research, evaluated with no bias from both the academic and social point of view. By applying the most advanced information technologies, Frontiers is catapulting scholarly publishing into a new generation.

What are Frontiers Research Topics?

Frontiers Research Topics are very popular trademarks of the *Frontiers journals series*: they are collections of at least ten articles, all centered on a particular subject. With their unique mix of varied contributions from Original Research to Review Articles, Frontiers Research Topics unify the most influential researchers, the latest key findings and historical advances in a hot research area.

Find out more on how to host your own Frontiers Research Topic or contribute to one as an author by contacting the Frontiers editorial office: frontiersin.org/about/contact

Tumor microenvironment in cancer hallmarks and therapeutics

Topic editors

Na Luo — Nankai University, China
Shengtao Zhou — Sichuan University, China
Hongming Miao — Army Medical University, China
José Alexandre Ferreira — Portuguese Oncology Institute, Portugal

Citation

Luo, N., Zhou, S., Miao, H., Ferreira, J. A., eds. (2023). *Tumor microenvironment in cancer hallmarks and therapeutics*. Lausanne: Frontiers Media SA. doi: 10.3389/978-2-8325-2281-3

Table of contents

09 Editorial: Tumor microenvironment in cancer hallmarks and therapeutics
Na Luo

14 The Prognostic Significance of Anisomycin-Activated Phospho-c-Jun NH2-Terminal Kinase (p-JNK) in Predicting Breast Cancer Patients' Survival Time
Li Chen, Xuantong Zhou, Xiangyi Kong, Zhaohui Su, Xiangyu Wang, Sen Li, Aiping Luo, Zhihua Liu, Yi Fang and Jing Wang

31 Cell Division Cycle Associated Genes as Diagnostic and Prognostic Biomarkers in Hepatocellular Carcinoma
Shan-Shan Jiang, Sheng-Jie Ke, Zun-Li Ke, Juan Li, Xiang Li and Xing-Wei Xie

42 Prognostic Nutritional Index (PNI) in Patients With Breast Cancer Treated With Neoadjuvant Chemotherapy as a Useful Prognostic Indicator
Li Chen, Ping Bai, Xiangyi Kong, Shaolong Huang, Zhongzhao Wang, Xiangyu Wang, Yi Fang and Jing Wang

61 Targeting the Complement Pathway in Malignant Glioma Microenvironments
Hongtao Zhu, Xingjiang Yu, Suojun Zhang and Kai Shu

77 Reconstruction and Analysis of the Immune-Related LINC00987/A2M Axis in Lung Adenocarcinoma
Jiakang Ma, Xiaoyan Lin, Xueting Wang, Qingqing Min, Tonglian Wang and Chaozhi Tang

93 Weighted Gene Co-expression Network Analysis Identifies CALD1 as a Biomarker Related to M2 Macrophages Infiltration in Stage III and IV Mismatch Repair-Proficient Colorectal Carcinoma
Hang Zheng, Yuge Bai, Jingui Wang, Shanwen Chen, Junling Zhang, Jing Zhu, Yucun Liu and Xin Wang

108 LINC02257, an Enhancer RNA of Prognostic Value in Colon Adenocarcinoma, Correlates With Multi-Omics Immunotherapy-Related Analysis in 33 Cancers
Junbo Xiao, Yajun Liu, Jun Yi and Xiaowei Liu

123 Circular RNA Circ0021205 Promotes Cholangiocarcinoma Progression Through MiR-204-5p/RAB22A Axis
Jianfei Tu, Weiqian Chen, Liyun Zheng, Shiji Fang, Dengke Zhang, Chunli Kong, Yang Yang, Rongfang Qiu, Zhongwei Zhao, Chenying Lu, Xiaojie Lu and Jiansong Ji

132 The Role of PI3K Inhibition in the Treatment of Breast Cancer, Alone or Combined With Immune Checkpoint Inhibitors
Zhizhu Zhang and Ann Richmond

142 Function of Non-coding RNA in *Helicobacter pylori*-Infected Gastric Cancer
Chao Wang, Yiyang Hu, Huan Yang, Sumin Wang, Bo Zhou, Yulu Bao, Yu Huang, Qiang Luo, Chuan Yang, Xia Xie and Shiming Yang

154 Development and Validation of a 7-Gene Prognostic Signature to Improve Survival Prediction in Pancreatic Ductal Adenocarcinoma
Zengyu Feng, Hao Qian, Kexian Li, Jianyao Lou, Yulian Wu and Chenghong Peng

167 Antitumor and Radiosensitization Effects of a CXCR2 Inhibitor in Nasopharyngeal Carcinoma
Xiaobei Liu, Tianxia Lan, Fei Mo, Jingyun Yang, Yuquan Wei and Xiawei Wei

181 The Biological Function, Mechanism, and Clinical Significance of m6A RNA Modifications in Head and Neck Carcinoma: A Systematic Review
Feng-Yang Jing, Li-Ming Zhou, Yu-Jie Ning, Xiao-Juan Wang and You-Ming Zhu

195 Overexpression of Interferon-Inducible Protein 16 Promotes Progression of Human Pancreatic Adenocarcinoma Through Interleukin-1β-Induced Tumor-Associated Macrophage Infiltration in the Tumor Microenvironment
Jing-Xian Chen, Chien-Shan Cheng, Hong-Fang Gao, Zi-Jie Chen, Ling-Ling Lv, Jia-Yue Xu, Xiao-Heng Shen, Jing Xie and Lan Zheng

209 Metabolic Remodeling in Glioma Immune Microenvironment: Intercellular Interactions Distinct From Peripheral Tumors
Runze Qiu, Yue Zhong, Qingquan Li, Yingbin Li and Hongwei Fan

230 Immunity-Related Gene Signature Identifies Subtypes Benefitting From Adjuvant Chemotherapy or Potentially Responding to PD1/PD-L1 Blockage in Pancreatic Cancer
Hao Qian, Hongzhe Li, Junjie Xie, Xiongxiong Lu, Fanlu Li, Weishen Wang, Xiaomei Tang, Minmin Shi, Linxi Jiang, Hongwei Li, Hao Chen, Chenghong Peng, Zhiwei Xu, Xiaxing Deng and Baiyong Shen

244 Comprehensive Analysis of the Immune Infiltrates and PD-L1 of m^6A RNA Methylation Regulators in Hepatocellular Carcinoma
Yangtao Xu, Xiaoqin He, Junjian Deng, Lin Xiong, Yue Li, Xiaoyu Zhang, Wenliang Chen, Xin Liu and Ximing Xu

255 Cancer-Associated Fibroblast-Derived Interleukin-8 Promotes Ovarian Cancer Cell Stemness and Malignancy Through the Notch3-Mediated Signaling
Zhaodong Ji, Wenjuan Tian, Wen Gao, Rongyu Zang, Huaying Wang and Gong Yang

266 Expression Characteristics and Significant Prognostic Values of PGK1 in Breast Cancer
Yanping Li, Shanshan Wang, Xiaoyuan Zhang, Rui Yang, Xiaonan Wei, Ruirong Yan, Yaru Jiang and Wenzhi Shen

281 Combination Foretinib and Anti-PD-1 Antibody Immunotherapy for Colorectal Carcinoma
Yuyin Fu, Yujia Peng, Shengyan Zhao, Jun Mou, Lishi Zeng, Xiaohua Jiang, Chengli Yang, Cheng Huang, Yuyan Li, Yin Lu, Mengdan Wu, Yanfang Yang, Ting Kong, Qinhuai Lai, Yangping Wu, Yuqin Yao, Yuxi Wang, Lantu Gou and Jinliang Yang

297 Identification of CDK2-Related Immune Forecast Model and ceRNA in Lung Adenocarcinoma, a Pan-Cancer Analysis
Ting-Ting Liu, Rui Li, Chen Huo, Jian-Ping Li, Jie Yao, Xiu-li Ji and Yi-Qing Qu

320 Molecular Subtypes of Oral Squamous Cell Carcinoma Based on Immunosuppression Genes Using a Deep Learning Approach
Simin Li, Zhaoyi Mai, Wenli Gu, Anthony Chukwunonso Ogbuehi, Aneesha Acharya, George Pelekos, Wanchen Ning, Xiangqiong Liu, Yupei Deng, Hanluo Li, Bernd Lethaus, Vuk Savkovic, Rüdiger Zimmerer, Dirk Ziebolz, Gerhard Schmalz, Hao Wang, Hui Xiao and Jianjiang Zhao

339 Fucoidan-Supplemented Diet Potentiates Immune Checkpoint Blockage by Enhancing Antitumor Immunity
Juan Yang, Xianzhi Yang, Wenfeng Pan, Mingshuo Wang, Yuxiong Lu, Jianeng Zhang, Ziqian Fang, Xiaomin Zhang, Yin Ji, Jin-Xin Bei, Jiajun Dong, Yi Wu, Chaoyun Pan, Guangli Yu, Penghui Zhou and Bo Li

355 The Identification of the Metabolism Subtypes of Skin Cutaneous Melanoma Associated With the Tumor Microenvironment and the Immunotherapy
Ronghua Yang, Zhengguang Wang, Jiehua Li, Xiaobing Pi, Runxing Gao, Jun Ma, Yi Qing and Sitong Zhou

373 miRNA-7062-5p Promoting Bone Resorption After Bone Metastasis of Colorectal Cancer Through Inhibiting GPR65
Liang Chen, Yu Wang, Xingchen Lu, Lili Zhang and Ziming Wang

384 Identification of the Immune-Related Genes in Tumor Microenvironment That Associated With the Recurrence of Head and Neck Squamous Cell Carcinoma
Liu Chengcheng, Qi Wenwen, Gong Ningyue, Zhu Fangyuan, Xu Runtong, Teng Zhenxiao, Xu Fenglei, Qin Yiming, Zhao Miaoqing, Li Xiaoming and Xia Ming

397 Differentiation Between Glioblastoma Multiforme and Metastasis From the Lungs and Other Sites Using Combined Clinical/Routine MRI Radiomics
Yuqi Han, Lingling Zhang, Shuzi Niu, Shuguang Chen, Bo Yang, Hongyan Chen, Fei Zheng, Yuying Zang, Hongbo Zhang, Yu Xin and Xuzhu Chen

408 Novel Characterization of Myeloid-Derived Suppressor Cells in Tumor Microenvironment
Yanan Li, Hongdan He, Ribu Jihu, Junfu Zhou, Rui Zeng and Hengxiu Yan

423 Prognostic Immunity and Therapeutic Sensitivity Analyses Based on Differential Genomic Instability-Associated LncRNAs in Left- and Right-Sided Colon Adenocarcinoma
Jun-Nan Guo, Tian-Yi Xia, Shen-Hui Deng, Wei-Nan Xue, Bin-Bin Cui and Yan-Long Liu

437 PPA1 Promotes Breast Cancer Proliferation and Metastasis Through PI3K/AKT/GSK3β Signaling Pathway
Chunlei Guo, Shuang Li, Ang Liang, Mengchao Cui, Yunwei Lou and Hui Wang

450 Cross-Talk of Focal Adhesion-Related Gene Defines Prognosis and the Immune Microenvironment in Gastric Cancer
Deli Mao, Rui Xu, Hengxing Chen, Xiancong Chen, Dongsheng Li, Shenglei Song, Yulong He, Zhewei Wei and Changhua Zhang

465 The Versatile Roles of Cancer-Associated Fibroblasts in Colorectal Cancer and Therapeutic Implications
Longfei Deng, Nianfen Jiang, Jun Zeng, Yi Wang and Hongjuan Cui

481 The Landscape of the Tumor Microenvironment in Skin Cutaneous Melanoma Reveals a Prognostic and Immunotherapeutically Relevant Gene Signature
Sitong Zhou, Yidan Sun, Tianqi Chen, Jingru Wang, Jia He, Jin Lyu, Yanna Shen, Xiaodong Chen and Ronghua Yang

498 The Role of Androgen Receptor in Cross Talk Between Stromal Cells and Prostate Cancer Epithelial Cells
Qianyao Tang, Bo Cheng, Rongyang Dai and Ronghao Wang

510 Crosstalk Between the Tumor Microenvironment and Cancer Cells: A Promising Predictive Biomarker for Immune Checkpoint Inhibitors
Xiaoying Li, Yueyao Yang, Qian Huang, Yu Deng, Fukun Guo, Gang Wang and Ming Liu

525 Comprehensive Analysis of Hexokinase 2 Immune Infiltrates and m6A Related Genes in Human Esophageal Carcinoma
Xu-Sheng Liu, Jia-Min Liu, Yi-Jia Chen, Fu-Yan Li, Rui-Min Wu, Fan Tan, Dao-Bing Zeng, Wei Li, Hong Zhou, Yan Gao and Zhi-Jun Pei

541 Weighted Gene Co-expression Network Analysis Identifies a Cancer-Associated Fibroblast Signature for Predicting Prognosis and Therapeutic Responses in Gastric Cancer
Hang Zheng, Heshu Liu, Huayu Li, Weidong Dou and Xin Wang

558 Clinical Value and Potential Mechanisms of Oxysterol-Binding Protein Like 3 (OSBPL3) in Human Tumors
Na Hao, Yudong Zhou, Yijun Li, Huimin Zhang, Bin Wang, Xiaona Liu, Yu Ren, Jianjun He, Can Zhou and Xiaojiang Tang

579 Genome Instability and Long Noncoding RNA Reveal Biomarkers for Immunotherapy and Prognosis and Novel Competing Endogenous RNA Mechanism in Colon Adenocarcinoma
Ziyuan Ren, Zhonglin Wang, Donghong Gu, Hanchen Ma, Yan Zhu, Menghua Cai and Jianmin Zhang

595 TR35 Exerts Anti-tumor Effects by Modulating Mitogen-Activated Protein Kinase and STAT3 Signaling in Lung Cancer Cells
Zhiyong Shi, Yang Gao, Lifeng Feng, Wencong Tian, Zhihua Dou, Chen Liu, Jie Liu, Yang Xu, Yachen Wang, Jie Yan, Qiang Wu, Jing Li, Liang Yang, Zhaocai Zhang, Jie Yang and Zhi Qi

605 Characterization of the Immune Cell Infiltration Landscape of Thyroid Cancer for Improved Immunotherapy
Jing Gong, Bo Jin, Liang Shang and Ning Liu

617 Ferroptosis-mediated Crosstalk in the Tumor Microenvironment Implicated in Cancer Progression and Therapy
Yini Liu, Chunyan Duan, Rongyang Dai and Yi Zeng

635 Identification of Key Genes Driving Tumor Associated Macrophage Migration and Polarization Based on Immune Fingerprints of Lung Adenocarcinoma
Jing Wu, Jiawei Zhou, Qian Xu, Ruth Foley, Jianqiang Guo, Xin Zhang, Chang Tian, Min Mu, Yingru Xing, Yafeng Liu, Xueqin Wang and Dong Hu

651 Prognostic Potential of Secreted Modular Calcium-Binding Protein 1 in Low-Grade Glioma
Jing Wang, Shu Xia, Jing Zhao, Chen Gong, Qingsong Xi and Wei Sun

664 Development of an Oxidative Phosphorylation-Related and Immune Microenvironment Prognostic Signature in Uterine Corpus Endometrial Carcinoma
Jinhui Liu, Tian Chen, Min Yang, Zihang Zhong, Senmiao Ni, Sheng Yang, Fang Shao, Lixin Cai, Jianling Bai and Hao Yu

682 Integrative Analysis of MALT1 as a Potential Therapeutic Target for Prostate Cancer and its Immunological Role in Pan-Cancer
Haotian Tan, Yaqi Xie, Xuebao Zhang, Shuang Wu, Hongwei Zhao, Jitao Wu, Wenting Wang and Chunhua Lin

697 CREM Is Correlated With Immune-Suppressive Microenvironment and Predicts Poor Prognosis in Gastric Adenocarcinoma
Kuai Yu, Linju Kuang, Tianmei Fu, Congkai Zhang, Yuru Zhou, Chao Zhu, Qian Zhang, Zhanglin Zhang and Aiping Le

705 Ikaros Proteins in Tumor: Current Perspectives and New Developments
Ruolan Xia, Yuan Cheng, Xuejiao Han, Yuquan Wei and Xiawei Wei

735 Current Research Progress of the Role of LncRNA LEF1-AS1 in a Variety of Tumors
Qingyuan Zheng, Xiao Yu, Menggang Zhang, Shuijun Zhang, Wenzhi Guo and Yuting He

744 Identification of Novel Tumor Microenvironment-Related Long Noncoding RNAs to Determine the Prognosis and Response to Immunotherapy of Hepatocellular Carcinoma Patients
Shenglan Huang, Jian Zhang, Xiaolan Lai, Lingling Zhuang and Jianbing Wu

762 Immune Signature-Based Risk Stratification and Prediction of Immunotherapy Efficacy for Bladder Urothelial Carcinoma
Fangfang Liang, Yansong Xu, Yi Chen, Huage Zhong, Zhen Wang, Tianwen Nong and Jincai Zhong

777 Comprehensive Characterization of Tumor Purity and Its Clinical Implications in Gastric Cancer
Shenghan Lou, Jian Zhang, Xin Yin, Yao Zhang, Tianyi Fang, Yimin Wang and Yingwei Xue

794 Lung Adenocarcinoma Cells Promote Self-Migration and Self-Invasion by Activating Neutrophils to Upregulate Notch3 Expression of Cancer Cells
Weidong Peng, Youjing Sheng, Han Xiao, Yuanzi Ye, Louis Boafo Kwantwi, Lanqing Cheng, Yuanchong Wang, Jiegou Xu and Qiang Wu

802 Immune Response on Optimal Timing and Fractionation Dose for Hypofractionated Radiotherapy in Non–Small-Cell Lung Cancer
Xianlan Zhao, Jixi Li, Linpeng Zheng, Qiao Yang, Xu Chen, Xiewan Chen, Yongxin Yu, Feng Li, Jianxiong Cui and Jianguo Sun

814 Metformin Combining PD-1 Inhibitor Enhanced Anti-Tumor Efficacy in *STK11* Mutant Lung Cancer Through AXIN-1-Dependent Inhibition of STING Ubiquitination
Zhiguo Wang, Conghua Lu, Kejun Zhang, Caiyu Lin, Fang Wu, Xiaolin Tang, Di Wu, Yuanyao Dou, Rui Han, Yubo Wang, Chao Hou, Qin Ouyang, Mingxia Feng, Yong He and Li Li

828 CXCL8 in Tumor Biology and Its Implications for Clinical Translation
Xingyu Xiong, Xinyang Liao, Shi Qiu, Hang Xu, Shiyu Zhang, Sheng Wang, Jianzhong Ai and Lu Yang

frontiers | Frontiers in Molecular Biosciences

TYPE Editorial
PUBLISHED 12 September 2022
DOI 10.3389/fmolb.2022.1019830

OPEN ACCESS

EDITED AND REVIEWED BY
William C. Cho,
QEH, Hong Kong SAR, China

*CORRESPONDENCE
Na Luo,
luon11@nankai.edu.cn

SPECIALTY SECTION
This article was submitted to Molecular Diagnostics and Therapeutics, a section of the journal Frontiers in Molecular Biosciences

RECEIVED 15 August 2022
ACCEPTED 22 August 2022
PUBLISHED 12 September 2022

CITATION
Luo N (2022), Editorial: Tumor microenvironment in cancer hallmarks and therapeutics.
Front. Mol. Biosci. 9:1019830.
doi: 10.3389/fmolb.2022.1019830

Editorial: Tumor microenvironment in cancer hallmarks and therapeutics

Na Luo*

Department of Anatomy and Histology, School of Medicine, Nankai University, Tianjin, China

KEYWORDS

tumor microenvironment, non-coding RNA, tumor immune microenvioronment, cancer biomarkers, cancer signature

Editorial on the Research Topic
Tumor microenvironment in cancer hallmarks and therapeutics

Introduction

Tumor cells reside in an acidic, hypoxic, immunosuppressive, and nutrition-deficient environment called the tumor microenvironment (TME) which reprograms both metabolism and signaling pathways to support the uncontrolled proliferation of tumor cells. The TME features blood and lymphatic vessels, stromal cells, immune cells, and an extracellular matrix (e.g., cytokines, chemokines, collagen, proteoglycans, etc.). The dynamic and reciprocal communication between the TME and tumor cells contributes to survival, proliferation, invasion, metastasis, angiogenesis, drug resistance, and immune evasion of the tumor. This manuscript focuses on the TME contributions to cancer progression and TME targets with the potential for pharmaceutical intervention in cancer treatment.

Non-coding RNA and cancer development

Many studies have focused on the connection between non-coding RNAs and cancer development. Non-coding RNAs are multifunctional molecules that interact with RNA, DNA, or proteins to either promote or prevent the expression of protein-coding genes (Anastasiadou et al., 2018). Non-coding RNAs are dysregulated in tumor cells as well as stromal cells which provides a novel perspective for the regulation of TME components (Di Agostino et al., 2022). Moreover, studies have shown that RNA N6-methyladenosine (m6A) modification plays a substantial role in TME diversity and complexity (Li et al., 2021; Si et al., 2021).

Zheng et al. reviewed the function, mechanism, and clinical significance of lymph enhancer-binding factor 1-antisense RNA1 (LEF1-AS1) which plays a dual-edged role in cancer development. In this regard, LEF1-AS1 functions either as a tumor suppressor in myeloid malignancy or a tumor promoter in other malignant tumors. Wang et al. reviewed the relationship of non-coding RNA expression and the influence of *H. pylori* on gastric cancer which provided a new perspective for gastric cancer treatment.

Furthermore, Tu et al. demonstrated that circ_0021205 promotes proliferation, migration, and invasion of cholangiocarcinomas (CCA) cells in addition to tumorigenesis in mice via sponging miR-204-5p which regulates RAB22A expression. This suggests that circ_0021205 may be a diagnostic biomarker or therapeutic target for CCA. Furthermore, Chen et al. showed that upregulation of miRNA-7062-5p promotes osteoclast genesis during bone metastasis via GPR65 inhibition. Consequently, we can postulate that the miRNA-7062-5p/GPR65 axis may serve as a therapeutic target for colorectal cancer (CRC) metastasis to the bone.

In addition, many studies have used comprehensive bioinformatics analysis to investigate the association of non-coding RNA and the TME, especially the immune environment of TME. Huang et al. analyzed the influence of the stromal, immune, and estimate scores on the prognosis of hepatocellular carcinoma (HCC) patients. They established a novel TME-related lncRNA risk model which may serve as an independent prognostic biomarker and predictor of immune checkpoint inhibitors (ICIs) for HCC patients. Xiao et al. showed that LINC02257 is the most significantly survival-associated enhancer RNA (eRNA) whose expression correlates with a multi-omics analysis of 33 cancer types, such as survival analysis and immunotherapy-related analysis. These findings suggest that LINC02257 is a multifaceted and important immunotherapy-related eRNA in different cancers. Ma et al. showed that the LINC00987/A2M axis is a functional and effective tumor suppressor of lung adenocarcinoma (LUAD). The LINC00987/A2M axis functions as a biomarker either for assessing the immune microenvironment or evaluating the prognostic and therapeutic potential of LUAD. In addition, Ren et al. proposed that a novel competing endogenous RNA (ceRNA) network modulates genomic integrity and demonstrated that a genome instability-related lncRNA serves as a novel prognosis biomarker for immunotherapy outcomes of colon adenocarcinoma (COAD). Moreover, Guo et al. analyzed the differential genomic instability-associated lncRNAs between left-sided and right-sided colon cancers (LCCs and RCCs) and identified six key DGIA lncRNAs. These six key DGIA lncRNAs not only predict the prognostic risk of patients but also serve as biomarkers for evaluating differences of genetic instability, immune infiltration, and therapeutic sensitivity.

m6A RNA modifications are reversible epigenetic RNA modifications that modulate splicing, degradation, and other biological processes of RNAs. m6A RNA modifications of non-coding RNA are associated with tumorigenesis, metastasis, and other tumor characteristics (Li et al., 2021; Si et al., 2021). Specifically, Jing et al. summarized the biological function, mechanism, and clinical significance of m6A RNA modifications in head and neck squamous cell carcinoma (HNSCC) from a systematic perspective. The authors thoroughly discussed the regulatory roles and potential molecular mechanisms of m6A in immune cells in the TME and the development of potential targets for treating HNSCC. Xu et al. comprehensively analyzed m6A RNA methylation regulators in HCC and revealed that m6A regulators were significantly associated with the tumor immune microenvironment in HCC. This finding may provide a new prognostic biomarker and therapeutic target for improving the efficacy of immunotherapy in HCC patients.

Tumor immune microenvironment and cancer development

Immune checkpoint inhibitor (ICI) therapy has revolutionized the field of cancer treatment. Despite the remarkable and substantial effects of ICIs on cancer patients, only a small percentage of patients achieve clinical benefits (Jacob et al., 2021). In this regard, the ability to increase the response rates and overcome ICI resistance is the key to improve clinical efficacy.

A prevalent strategy to increase the response rate of ICIs involves combination therapy with potential pharmaceutical targets and ICIs. For example, Fu et al. employed a novel combination therapy utilizing foretinib (a multiple receptor tyrosine kinase inhibitor) and anti-PD-1 antibody for CRC treatment. The combination therapy significantly inhibited tumor growth in mice by increasing PD-L1 expression via JAK2/STAT1 pathway. Simultaneously, combination therapy remodeled the tumor microenvironment by: 1) increasing the infiltration and function of T cells, 2) decreasing the percentage of tumor-associated macrophages (TAMs), and 3) inhibiting M2 polarization. Moreover, combination therapy inhibited metastasis to the lung and remodeled the tumor microenvironment in the lung. Wang et al. discovered that combination therapy with metformin and PD-1 inhibitor enhanced anti-tumor efficacy in STK11 mutant lung cancer. The metformin and PD-1 inhibitor combination therapy involved the inhibition of RNF5-mediated K48-linked ubiquitination of STING and showed AXIN-1 dependence.

The tumor immune microenvironment (TIME) consists of cancer cells, immune cells, cytokines, chemokines, etc. And potentially influences cancer development. Remodeling the TIME is a popular strategy to impede cancer development.

Li et al. reviewed the role of immune cells in the crosstalk between the TME and cancer cells and the effects of ICIs therapy on these cell populations. The authors also discuss the potential of the functional interaction between TME and cancer cells as a predictive biomarker for ICIs, and outline the potential personalized strategies to improve the effectiveness of ICIs. Peng et al. found that lung adenocarcinoma cells promote self-invasion and self-migration by activating neutrophils to upregulate the Notch3 expression of cancer cells. In this regard, the density of infiltrating tumor-associated neutrophils (TANs) may serve as a novel prognosis biomarker and a potential therapeutic target for lung adenocarcinoma. In addition, Li et al. reviewed the favorable TME conditions that promote recruitment, expansion, activation, and immunosuppression of myeloid-derived suppressor cells (MDSCs) and also discussed the precision targeting MDSCs for therapeutic intervention.

Xiong et al. reviewed the role of chemokine CXCL8 in directly promoting or indirectly facilitating tumor progression and also role of CXCL8 in ICI therapy. The preclinical studies suggest combinational therapy with CXCL8 blockade and ICIs therapy can enhance the anti-tumor efficacy, and the findings promote conduction of several clinical trials. Moreover, Liu et al. showed that SB225002 (a CXCR2 inhibitor) promotes antitumor and radio-sensitization effects in nasopharyngeal carcinoma (NPC). The authors proposed that the CXCL8/CCR2 axis functions as a prognosis biomarker for NPC patients and serves as a promising therapeutic target for NPC treatment. Chen et al. demonstrated that interferon-inducible protein 16 (IFI16) adversely correlates with the overall survival of pancreatic adenocarcinoma (PAAD) patients and promotes PAAD progression via IL-1β-induced TAMs infiltration. These findings suggest that IFI16 may function as a potential therapeutic target for PAAD.

Finally, Liu et al. compiled a list of immune genes and immune infiltrating cells that play a role in the prognosis of HNSCC. This list provides a valuable roadmap to assess HNSCC evolution and treatment selection. Gong et al. investigated the immune cell infiltration (ICI) landscape of thyroid cancer (THCA) and showed that the ICI score is an effective prognostic indicator and predictor of immunotherapy response in THCA.

Metabolism and TME

Metabolic factors are not only crucial for tumor growth, but also for remodeling the TME to produce a favorable environment for tumor invasion and metastasis. This metabolic adaptation requires the re-adjustment of metabolic pathways and signaling pathways that permits the import/consumption of organic compounds and subsequent energy and biomass production (Serpa, 2020).

Qiu et al. clarified the metabolic properties of cancer cells in glioma and the interactions with TME immunity. The authors also discuss the therapy strategies targeting metabolic remodeling to improve glioma immunity.

Li et al. found that the expression of phosphoglycerate kinase 1(PGK1) [a glycolytic enzyme that catalyzes the conversion of 1,3-diphosphoglycerate to 3-phosphoglycerate] was upregulated in various types of breast cancer. In this regard, PGK1 expression significantly associates with survival signature and correlates with TP53 and CDH1 mutations. These results indicate that PGK1 may serve as a potential biomarker for breast cancer.

Moreover, Hao et al. demonstrated that oxysterol binding protein like 3 (OSBPL3) which belongs to a group of intracellular lipid receptors plays an important role in tumorigenesis via comprehensive analyzation of publicly available databases of various cancers. These results provide insights into the biological functions of OSBPL3. Furthermore, Liu et al. performed comprehensive analysis and reported that hexokinase 2 (HK2) [an enzyme that phosphorylates glucose to produce glucose-6-phosphate in the first step of glucose metabolism] is associated with tumor infiltration and m6A modification in esophageal carcinoma (ESCA). This suggests that HK2 may serve as a potential biological target for diagnosis and treatment in ESCA.

Nutrition and TME

Nutritional stimuli modulate the homeostasis of tumor cells and TME which then leads to a consequent alteration of tumorigenesis and tumor progression (Thakkar et al., 2022).

Li et al. performed a retrospective study to investigate the prognostic nutritional index (PNI) calculated as serum albumin (ALB) (g/L) + 5x total lymphocyte count (109/L). They found that PNI before neoadjuvant chemotherapy (NACT) served as a useful prognostic indicator and as a promising biomarker for treatment decisions in breast cancer patients.

Yang et al. discovered that a fucoidan-supplemented diet improves the anti-tumor activities of PD-1 antibodies *in vivo*. The mechanism involves cooperation with the JAK/STAT pathway and interaction with the T-cell receptor (TCR)/CD3 complex in order to stimulate T cell activation and augment TCR-mediated signaling. Moreover, Shi et al. showed that TR35 (an active camel whey fraction) plays a role in NSCLC progression via MAPK and JAK/STAT pathway. This finding indicates that TR35 may serve as a potential therapeutic agent in lung cancer.

Cancer-associated fibroblasts or tumor-associated fibroblasts

CAFs or TAFs are hallmark features of the TME and promote cancer/tumor progression. In this regard, Deng et al. summarized the origins, biomarkers, prognostic significance, functional roles,

and underlying mechanisms of CAFs in the colorectal cancer (CRC) and discussed harnessing CAFs as promising therapeutic targets for CRC treatment. Moreover, Ji et al. found that IL-8 secretion from CAFs stimulated malignant growth and induced the stemness of ovarian cancer via the Notch3 signaling pathway which may provide a novel strategy for ovarian cancer treatment. In addition, Zheng et al. constructed a 4-gene prognostic CAF model which predicts prognosis and estimates the immunotherapy response in gastric cancer (GC) patients.

Pathways related to cancer development

It is well-established that cancer is caused by the dysregulation of pathways involved in cell survival, proliferation, migration, differentiation, and apoptosis (Yip and Papa, 2021). Zhang et al. describe the role of PI3K in breast cancer progression and resistance in currently used treatments. This minireview also addressed the clinical application of PI3K inhibitors and the potential synergistic benefit of combined PI3K/immunotherapy in breast cancer treatment. Zhu et al. extensively reviewed the expression and function of complement pathway components in multiple tumor types which may serve as prognostic factors or therapeutic targets in malignant glioma treatment.

Tang et al. reviewed the role of the androgen receptor (AR) in cross-talk between stromal cells and prostate cancer cells and discussed the development of novel therapeutic strategies targeting the AR pathway. Liu et al. reviewed the role of ferroptosis within the TME and its influence on cancer development and progression. The authors also discuss the novel therapeutic strategies targeting ferroptosis-related pathways and metabolism for cancer treatment. Furthermore, Guo et al. verified that PPA1 activates PI3K/AKT signaling and promotes breast cancer progression via the downstream GSK3β/Slug signaling. This verification suggests that PPA1 may serve as a potential therapeutic target to inhibit breast cancer progression.

Large-scale data mining and bioinformatics analysis with cancer signature

A gradually emerging phenomenon with the development of large-scale data mining and bioinformatics analysis is the establishment of immune, survival, or prognosis signatures which boost the development of precision medicine or individualized therapies.

Qian et al. constructed an immune-related 18 gene signature that predicts which PDAC subtype may benefit from gemcitabine-based adjuvant chemotherapy or may respond to PD1/PD-L1 blockade therapy. Zhou et al. constructed an immune-related gene signature of the TME landscape which may serve as a prognostic biomarker or as a predictor of an immunotherapy effect in skin cutaneous melanoma (SKCM). Wu et al. developed a TAM migration/transformation-related three gene signature which may serve as a prognostic biomarker and as a guide to individualized treatments in LUAD. Mao et al. constructed an adhesion-related 18 gene signature leading to the formation of the focal adhesion index (FAI) which may serve as a prognostic biomarker of the immune microenvironment in GC. Liang et al. constructed two immune-related genes (IRG)-relate prognostic signatures based on gene-immune interaction for predicting risk stratification and immunotherapeutic responses, which may be helpful to screen the people who will benefit from immunotherapy and guide the clinical decision-making of patients with bladder urothelial carcinoma (BLCA).

In addition to the above-mentioned immune-signature models, Feng et al. developed a 7-gene prognostic signature to improve survival prediction, individualized therapy, and appropriate management in PDAC patients. Li et al. established two survival subtypes of oral squamous cell carcinoma (OSCC) using a deep learning approach that provides novel precision-medicine treatment options and improves survival times in OSCC patients. Yang et al. established a novel skin cutaneous melanoma (SKCM) classification based on metabolic gene expression profiles to understand the metabolic diversity of SKCM and to provide guidance on precision targeted therapy. Liu et al. identified an oxidative phosphorylation (OXPHOS)-related signature which classifies uterine corpus endometrial carcinoma (UCEC) patients into different risk subsets and predicts prognosis.

Cancer biomarkers

Bioinformatics analysis of "omics" data provides a route to identify reliable cancer biomarkers for cancer diagnosis and prognosis and to discover molecular targets for therapeutic intervention (Feltes et al., 2020; Li et al., 2020). Jiang et al. found that the expression levels of cell division cycle associated (CDCA) 1/3/5/8 correlate with poor prognosis and may serve as a diagnostic gene in hepatocarcinogenesis and as a prognostic biomarker in hepatocellular carcinoma (LIHC) patients. Li et al. revealed that p-JNK effectively predicts the survival in breast cancer patients receiving NACT. Moreover, they found that anisomycin (a JNK agonist) increases p-JNK expression and may benefit breast cancer patients receiving NACT. In addition, Zheng et al. showed that CALD1 upregulation occurs in the CMS4 CRC subtype which is associated with angiogenesis and TGF-β signaling gene sets in stage III/IV mismatch repair-proficient (pMMR) CRC samples using multiple bioinformatic analyses and cell-level assays. CALD1 also associates with immune and stromal components in the TME (e.g., antigen processing and presentation,

chemokine/cytokine signaling). This suggests that CALD1 may serve as a prognostic biomarker and a therapeutic target for stage III/IV pMMR CRCs. Liu et al. identified a CDK2-related immune forecast model, a Nomogram model, a forest map, and a ceRNA network that may predict the prognosis and guide targeted therapy in LUAD patients utilizing a pan-cancer analysis. Yu et al. found that cAMP response element modulator (CREM) may serve as a prognostic biomarker in gastric adenocarcinoma (GAC) using integrated bioinformatics methods. Wang et al. showed that secreted modular calcium-binding protein 1 (SMOC1) influences the progression on glioma and may serve as a prognosis biomarker for glioma using multiple databases.

Besides bioinformatics analysis, Tan et al. showed that higher MALT1 expression levels occur in cancer samples versus normal tissues. MALT1 promotes proliferation, colony formation, and cancer establishment. Moreover, MALT1 expression is closely related to the occurrence and development of multiple cancers which suggest that MALT1 may serve as therapeutic target for a variety of cancers. Furthermore, Xia et al. reviewed the roles of Ikaros (a zinc finger transcription factor) in tumorigenesis and drug resistance, and discussed targeting Ikaros as a treatment either in single or combination use.

Clinical consideration and cancer development

Zhao et al. explored the dynamic changes in the TME after hypo-fractionated radiotherapy (HFRT) in NSCLC and established the timing and fractionation dose for achieving the optimal immune response. Han et al. revealed that the combination of radiomic (such as MRI scanning) and non-radiomic practices are helpful to differentiate among gliobastoma multiforme (GBM), metastasis (MET)-lung, and MET-other. Interestingly, Lou et al. found that tumor purity might be a patient-specific intrinsic characteristic of GC which associates with survival time and recurrence. Tumor purity is also associated with an invasive, metastatic phenotype along with immune and stromal cell functions. These findings highlight that tumor purity confers important clinical, biological, micro-environmental, and treatment implications for patients with GC.

Author contributions

NL contributes to design and writing the editorial.

Conflict of interest

The author declares that the research was conducted in the absence of any commercial or financial relationships that could be construed as a potential conflict of interest.

Publisher's note

References

Anastasiadou, E., Jacob, L. S., and Slack, F. J. (2018). Non-coding RNA networks in cancer. *Nat. Rev. Cancer* 18, 5–18. doi:10.1038/nrc.2017.99

Di Agostino, S. A.-O., Vahabi, M., Turco, C., and Fontemaggi, G. A.-O. (2022). Secreted non-coding RNAs: Functional impact on the tumor microenvironment and clinical relevance in triple-negative breast cancer. *Noncoding. RNA* 8, 5. doi:10.3390/ncrna8010005

Feltes, B. C., Poloni, J. F., Nunes, I. J. G., Faria, S. S., and Dorn, M. (2020). Multi-approach bioinformatics analysis of curated omics data provides a gene expression panorama for multiple cancer types. *Front. Genet.* 11, 586602. doi:10.3389/fgene.2020.586602

Jacob, J. B., Jacob, M. K., and Parajuli, P. (2021). Review of immune checkpoint inhibitors in immuno-oncology. *Adv. Pharmacol.* 91, 111–139. doi:10.1016/bs.apha.2021.01.002

Li, K., Du, Y., Li, L., and Wei, D. Q. (2020). Bioinformatics approaches for anti-cancer drug discovery. *Curr. Drug Targets* 21, 3–17. doi:10.2174/1389450120666190923162203

Li, M., Zha, X., and Wang, S. (2021). The role of N6-methyladenosine mRNA in the tumor microenvironment. *Biochim. Biophys. Acta. Rev. Cancer* 1875, 188522. doi:10.1016/j.bbcan.2021.188522

Serpa, J. (2020). Metabolic remodeling as a way of adapting to tumor microenvironment (TME), a job of several holders. *Adv. Exp. Med. Biol.* 1219, 1–34. doi:10.1007/978-3-030-34025-4_1

Si, C., Chen, C., Guo, Y., Kang, Q., and Sun, Z. (2021). Effect, mechanism, and applications of coding/non-coding RNA m6A modification in tumor microenvironment. *Front. Cell Dev. Biol.* 9, 711815. doi:10.3389/fcell.2021.711815

Thakkar, N., Shin, Y. B., and Sung, H. K. (2022). Nutritional regulation of mammary tumor microenvironment. *Front. Cell Dev. Biol.* 10, 803280. doi:10.3389/fcell.2022.803280

Yip, H. Y. K., and Papa, A. (2021). Signaling pathways in cancer: Therapeutic targets, combinatorial treatments, and new developments. *Cells* 10, 659. doi:10.3390/cells10030659

frontiers in Cell and Developmental Biology

ORIGINAL RESEARCH
published: 09 March 2021
doi: 10.3389/fcell.2021.656693

The Prognostic Significance of Anisomycin-Activated Phospho-c-Jun NH2-Terminal Kinase (p-JNK) in Predicting Breast Cancer Patients' Survival Time

Li Chen[1†], Xuantong Zhou[2†], Xiangyi Kong[1†], Zhaohui Su[3], Xiangyu Wang[1], Sen Li[4], Aiping Luo[2], Zhihua Liu[2], Yi Fang[1*] and Jing Wang[1*]*

[1] Department of Breast Surgical Oncology, National Cancer Center/National Clinical Research Center for Cancer/Cancer Hospital, Chinese Academy of Medical Sciences and Peking Union Medical College, Beijing, China, [2] State Key Lab of Molecular Oncology, National Cancer Center/National Clinical Research Center for Cancer/Cancer Hospital, Chinese Academy of Medical Sciences and Peking Union Medical College, Beijing, China, [3] Center on Smart and Connected Health Technologies, Mays Cancer Center, School of Nursing, UT Health San Antonio, San Antonio, TX, United States, [4] Department of General Surgery, The Affiliated Cancer Hospital of Zhengzhou University, Zhengzhou, China

This study aims to investigate the prognostic significance of p-JNK in breast cancer patients receiving neoadjuvant chemotherapy (NACT) and analyze the relationship between anisomycin, p-JNK. A total of 104 breast cancer patients had NACT were enrolled in this study. The western blot and immunohistochemistry assays were used to determine the protein expressions of p-JNK in human breast cancer cell lines and patients' cancer tissues. The chi-square test and Fisher's exact test were adopted to gauge the associations between breast cancer and clinicopathological variables by p-JNK expression, whereas the univariate and multivariate Cox proportional hazards regression models were used to analyze the prognostic value of p-JNK expression. The Kaplan-Meier plots and the log-rank test were adopted to determine patients' disease-free survival (DFS) and overall survival (OS). Findings indicated that the p-JNK expression had prognostic significance in univariate and multivariate Cox regression survival analyses. Results of log-rank methods showed that: (1) the mean DFS and OS times in patients with high p-JNK expression were significantly longer than those in patients with low p-JNK expression (χ^2 = 5.908, P = 0.015 and χ^2 = 6.593, P = 0.010, respectively). p-JNK expression is a significant prognostic factor that can effectively predict the survival in breast cancer patients receiving NACT. Treatment with the JNK agonist anisomycin can induce apoptosis, lead to increased p-JNK expression and decreased p-STAT3 expression. Moreover, the p-JNK expression was inversely correlated with p-STAT3 expression.

Keywords: p-JNK, anisomycin, p-STAT3, neoadjuvant chemotherapy, breast cancer

OPEN ACCESS

Edited by:
Na Luo,
Nankai University, China

Reviewed by:
Qingyu Luo,
Dana–Farber Cancer Institute, United States
Wenyue Liu,
Plastic Surgery Hospital, China

***Correspondence:**
Aiping Luo
luocjun@126.com
Yi Fang
fangyi@cicams.ac.cn
Jing Wang
wangjing@cicams.ac.cn

† These authors have contributed equally to this work

Specialty section:
This article was submitted to Molecular Medicine, a section of the journal Frontiers in Cell and Developmental Biology

Received: *21 January 2021*
Accepted: *15 February 2021*
Published: *09 March 2021*

Citation:
Chen L, Zhou X, Kong X, Su Z, Wang X, Li S, Luo A, Liu Z, Fang Y and Wang J (2021) The Prognostic Significance of Anisomycin-Activated Phospho-c-Jun NH2-Terminal Kinase (p-JNK) in Predicting Breast Cancer Patients' Survival Time. Front. Cell Dev. Biol. 9:656693. doi: 10.3389/fcell.2021.656693

INTRODUCTION

Breast cancer is the most common malignancy for females all over the world (Santucci et al., 2020; Siegel et al., 2020). Accounting for approximately 30% of all new cancer cases, breast cancer is the leading cause of cancer-related morbidity and mortality worldwide among women from 20 to 59 years old (Santucci et al., 2020; Siegel et al., 2020). Situations in China are even worse. It is estimated that around 9.6% breast cancer deaths occurred in China (Fan et al., 2014; Dibden et al., 2020). Since the 1990s, the incidence of breast cancer in China has been doubling the global rates (11.6%) (Linos et al., 2008; Bray et al., 2018). Researchers further estimate that, by 2021, for women aged 55–69 years old, breast cancer case numbers in China are expected to jump from less than 60 cases to more than 100 cases per 100,000, resulting in an unprecedented total of 2,500,000 cases (Linos et al., 2008; Bray et al., 2018). These daunting numbers, undoubtedly, call for timely research and innovations that can effectively address potential needs and wants of Chinese breast cancer patients.

With the help of screening tests, such as mammography and magnetic resonance imaging, an increasing number of breast cancer patients have benefited from an early stage diagnosis. These diagnoses, in turn, can often be effectively addressed by advanced diagnosis treatments (e.g., fine needle aspiration and core needle biopsy). However, it is important to note that approximately 20–25% of patients are diagnosed with advanced breast cancer (e.g., metastatic breast cancer) that requires more sophisticated cancer care and management (Harbeck and Gnant, 2017). In the last several decades, surgery, often combined with adjuvant chemoradiotherapy, has been used to treat patients with advanced breast cancer, distant metastasis, or local recurrence (Harbeck et al., 2019). However, to date, no treatment is available that has the potential to cure advanced breast cancer, or significantly prolongs long-term patient survival. This, in turn, calls for more effective treatment strategies that can improve breast cancer patients' quality of life and prolong their survival time.

Neoadjuvant chemotherapy (NACT) is regarded as one of most effective before-operation therapies in treating cancer, ranging from esophageal carcinoma, breast cancer, to colorectal cancer (Das, 2017; Derks and van de Velde, 2018; Montemurro et al., 2020). For early breast cancer, NACT can help patients avoid mastectomy by shrinking tumor volume (Mieog et al., 2007). For patients who need mastectomy, NACT can help increase breast-conserving surgery's success rates as well as the likelihood of eradicating micro metastatic disease (Asselain et al., 2018; Caldana et al., 2018). Moreover, NACT can provide useful information about local tumor's chemosensitivity to different chemotherapy regimens *in vivo*, helping clinicians and oncologists to make evidence-based decisions of subsequent drug selection (Adamson et al., 2019; Pathak et al., 2019).

Although a plethora of NACT regimens have been applied in the treatment of breast cancer, there has yet to be an internationally recognized NACT regimen for treating advanced breast carcinoma (Klein et al., 2019; Shien and Iwata, 2020). Some histologic and immunologic indicators, such as hormone receptor (HR), human epidermal growth factor receptor-2 (HER-2), and Ki-67 of breast cancer, have significant implications in the prognosis and choice of treatment for breast cancer (Ge et al., 2015). However, some cases received NACT failed to achieve tumor regression, furthermore, the prognosis of NACT-refractory patients would become worse due to the delay in the curative treatment (Kunnuru et al., 2020). Hence, there is an urgent need to identify novel and sensitive indicators, such as mitogen-activated protein kinase (MAPK), to improve therapeutic options for breast cancer patients and provide better treatment measures.

A growing body of research indicates that MAPK plays an important role in regulating inflammatory responses, cell proliferation and differentiation, stress responses, apoptosis, and immune response (Chen and Ávila, 2019; Wu et al., 2020). MAPK is often discussed in light of its major subfamilies, which include the extracellular signal-regulated kinases (ERKs), c-Jun NH2-terminal kinases (JNKs), and p38 MAPK isoforms as well as its activated expressions (p-ERK, p-JNK, and p-p38) (Davidson et al., 2006). Activation of MAPK is often followed by a cascade of sequential phosphorylation events, such as the phosphorylation of MAPKs on threonine and tyrosine residues by specific upstream MAPK kinases (MEKs or MKKs) (Oh et al., 2020).

Among MARK subfamilies, ERKs are largely activated by growth factor signals, while JNKs and p38 are largely activated by a spectrum of stress related stimuli (Haque et al., 2019; Farkhondeh et al., 2020). It is universally acknowledged that ERKs promote cell growth, proliferation, differentiation, while JNKs and p38 mediate apoptotic signals. The JNKs are the major protein kinases that regulate a variety of physiological processes, including cell proliferation, differentiation, and survival, inflammatory responses, as well as morphogenesis. Subsequently, the JNK pathway is associated with a number of disease states, including inflammatory, diabetes, neurodegenerative disorders, and cancer. It is becoming increasingly clear that the persistent activation of JNKs is closely related to cancer development, progression, and metastasis (Izadi et al., 2020; Xu and Hu, 2020). This realization, in turn, has made JNKs attractive as potential drug targets for therapeutic interventions with small molecule kinase inhibitors, such as ATP-competitive and ATP-non-competitive JNK inhibitors (Oh et al., 2019; Li et al., 2020).

Some studies have indicated that anisomycin is a potent protein synthesis inhibitor, and have the potential to interfere with protein and DNA synthesis by inhibiting peptidyl transferase or the 80S ribosome system (Li et al., 2012). Anisomycin is a key JNK activator that is known for its ability to increase levels of phospho-JNK (p-JNK) (Li et al., 2012). Anisomycin was widely used as an agonist for p38 mitogen-activated protein kinase (p38 MAPK) and Jun-NH2 terminal kinase (JNK), as it can induce apoptosis through the activation of the p38 MAPK and JNK signaling pathways (Nie et al., 2020). Several reports suggest that JNK can be used to study the formation of primary tumors as a tumor suppressor, where JNK serves an inhibitory role by mediating the activation of apoptosis (Reno et al., 2009).

The activated JNK phosphorylates various substrates, such as p53, nuclear factor-activated T cells (NFAT) and signal transducer and activator of transcription 3 (STAT3), could result in the stimulation of a series of apoptotic signaling cascades (Cellurale et al., 2012). JNK can also activate the phosphorylation of the STAT-3 at tyr-705 (Yacobi and Levy, 1975). However, activation of c-Jun NH_2-terminal kinase (JNK) and p-JNK has not been studied in breast cancer undergoing NACT, and the expression and clinical role of p-JNK in breast cancer are unknown at present. Hence, we aim to use anisomycin, a potent activator of JNK, to (1) examine the role played by JNK in breast cancer cells and (2) analyze the expression of p-JNK in breast malignant transformation and in breast cancer patients with clinical follow-up.

MATERIALS AND METHODS

Patients and Samples

In this study, 104 archived formalin fixed paraffin embedded (FFPE) breast cancer samples and 65 FFPE adjacent normal breast tissues were obtained from the Cancer Hospital Chinese Academy of Medical Sciences in China. All enrolled cases were diagnosed with the histology by core needle biopsy, and had received NACT between June of 2009 to December of 2015. Treatment details (i.e., clinical and demographic data) for all patients were extracted from the patients' medical records. Patients' clinical and pathological stages were defined in accordance with the eighth edition of the American Joint Committee Cancer Staging Manual (AJCC) (Abdel-Rahman, 2018).

Ethical Approval and Informed Consent

This study was approved by the ethics committee of the Cancer Hospital Chinese Academy of Medical Sciences and was performed within the standards of the Declaration of Helsinki as well as its later amendments for medical research involving human subjects. Written informed consent was obtained from all patients before the study.

Classification Standard and Response Evaluation

The eighth edition of the AJCC and the Union for International Cancer Control (UICC) were used to evaluate the Tumor Node Metastasis (TNM) stage groupings (Abdel-Rahman, 2018; Kandori et al., 2019). Molecular subtypes of breast cancer were divided into Luminal A, Luminal B HER2-positive, Luminal B HER2-negative, HER2-enriched and Triple negative (Zhao et al., 2020). The Miller and Payne grade (MPG) was used to estimate the histological response, and categorized into five grades that are in line with the number of tumor cells in excision/mastectomy specimens compared with the pretreatment core biopsy. Histologic tumor grades were accessed by the Elston-Ellis modification of Scarff-Bloom-Richardson grading system, and based on three factors (Phukan et al., 2015): (1) gland formation, (2) nuclear features, and (3) mitotic activity. The response rate was defined based on the Response Evaluation Criteria in Solid Tumors (RECIST) guidelines, and were stratified into four groups: (1) complete response (CR) was defined as the complete remission of the tumor; (2) partial response (PR) was defined as least a 50% decrease in the tumor volume; (3) stable disease (SD) was defined as a steady state or a response less than 50%; and (4) progression of disease (PD) was defined as an unequivocal increase of at least 25% in the tumor volume (Freites-Martinez et al., 2020). The sum of CR and PR forms the clinical objective response rate, the sum of SD and PD defines the non-clinical response rate, whereas and the sum of CR, PR and SD constitutes the clinical benefit rate.

Reagents and Materials

Anisomycin was purchased from TargetMol (Shanghai, China). Dulbecco's modified Eagle's medium (DMEM) and fetal bovine serum (FBS) for cell culture were purchased from Gibco-BRL (Grand Island, NY, United States). DMEM: F12 (1:1 Mix) and horse serum for cell culture were purchased from Beijing fine workmanship industry Biotechnology Co., Ltd (Beijing, China) and Gibco BRL (Grand Island, NY, United States), respectively. Cell Counting Kit-8 (CCK-8) reagents were purchased from Dojindo (Tokyo, Japan). The anti-PARP antibody (9542), anti-caspase3 antibody (9662), anti-cleaved caspase-3 antibody (9664), anti-STAT3 antibody (9132) and anti-p-STAT3 antibody (9131) were purchased from Cell Signaling Technology (CST, Danvers, MA, United States). The anti-p-JNK1/2/3 antibody (AP0631) was purchased from ABclonal Technology (Wuhan, China). The anti-β-actin antibody (A5316) were purchased from Sigma (St. Louis, MO, United States).

Cell Culture

Human breast cancer cell lines (MDA-MB-231, MDA-MB-436, BT549, Hs578T) were obtained from the Beijing Institute of Genomics in the Chinese Academy of Sciences (Beijing, China). MDA-MB-231 cells were cultured in Leibovitz's L-15 medium supplemented with 10% fetal bovine serum and L-glutamine. MDA-MB-231 cells were maintained at 37℃ in a humidified cell incubator without CO_2. BT549 was cultured in RPMI 1640 medium supplemented with 10% fetal bovine serum, penicillin (100 U/ml) and streptomycin (100 μg/ml). MDA-MB-436 and Hs578T cells were conventionally preserved in DMEM, which contained 10% FBS, 100 U/mL penicillin, 100 μg/mL streptomycin, 4.5 g/L D-Glucose, 5 ml L-Glutamine, and 110mg/L Sodium Pyruvate.

Human mammary epithelial cell line (184B5) was obtained from the Beijing Institute of Genomics in the Chinese Academy of Sciences (Beijing, China). And this cell line conventionally preserved in DMEM: F12 (1:1 Mix), which contained 5% horse serum, with 15 mM HEPES, 2mM L-glutamine, 100 U/mL penicillin and 100 μg/mL streptomycin, 20 ng/ml EGF, 100 ng/ml cholera toxin, 0.01 mg/ml insulin, 500 ng/ml hydrocortisone. Most of the cells were stored in a humidified cell incubator (at 37℃ with 5% CO_2), except MDA-MB-231.

IC50 of Anisomycin in Human Breast Cancer Cell Lines

In our study, in comparison with the controls, drug concentration required to inhibit exactly 50% of the cell viability is considered as the median inhibitory concentration (IC50). The relative cell viability (%) was calculated using the equation ODT/ODC × 100% (where ODT represents the absorbance of the treatment group, and ODC represents the absorbance of the control group). IC50 values were estimated from the concentration-response curve. Briefly, the appropriate number of cells was plated in each well of a 96-well plate and exposed to different concentrations of anisomycin for 48 h. Subsequently, the Cell Counting Kit-8 (CCK-8) reagents were added, and the cells were incubated for 1 h at a dilution of 1:10. At the end of the incubation, using a microplate reader (BioTek, Winooski, VT, United States), the absorbance in each well was measured at 450 nm.

Apoptosis and Western Blot

Apoptosis was analyzed with the FITC Annexin V Apoptosis Detection Kit (BD biosciences, CA, United States). Western blot was performed according to the standard protocol. β-actin was used as an endogenous control. The antibodies used for western blot in this study were listed with dilutions: PARP, caspase3, cleaved caspase3, p-JNK STAT3, and STAT3 (1:1000) as well as β-actin (1:5000).

Immunohistochemistry (IHC)

Breast tumors and normal samples used for immunohistochemical analyses were collected from breast cancer patients treated at the Cancer Hospital Chinese Academy of Medical Sciences between June of 2009 to December of 2015. Solutions made of 10% formaldehyde were used to treat fresh tissue specimens; formalin-fixed (pH 7.0) and paraffin-embedded archival tumor tissue of each patient were adopted in this study. 5-μm sections were cut from paraffin-embedded blocks for H&E staining and immunohistochemistry. Then they were dewaxed in xylene and dehydrated in an alcohol gradient of 100, 95, 85, and 70%. To deparaffinize, the slides were washed three times for a duration of 5 min. The endogenous peroxidase activity was blocked by incubating it in 0.3% hydrogen peroxide following methanol for 30 min at 37°C. To provide stable pH, we used phosphate buffered saline (PBS) to wash the slides three times for 5 min. Antigen retrieval was achieved by soaking the slices into citrate buffer at 95°C for 15 min, and then blocked with 10% goat serum albumin and incubated with primary antibodies overnight in a chamber with desired levels of moisture. After washing by PBS, the slides were incubated with a secondary antibody at room temperature for an hour before it was washed by PBS once again. Diaminobenzidine (DAB) was used as a chromogen, and the sections were counterstained with hematoxylin. The arrays were scanned by the Aperio Image Scope system (Leica Biosystems, United States), The antibody used for immunohistochemistry assay (IHC) in this study were listed with dilution: p-JNK (1:100). The immunoreactivity of the p-JNK protein were scored on the basis of the intensity of the predominant cytoplasmic staining area using the following classification system: 0, negative; 1, weakly-positive; 2, median-positive; 3, strongly-positive. All specimens were evaluated by two investigators blinded to the clinical information of the patients.

Follow-Up

All patients included in this study had postoperative follow-ups in the hospital inpatients or outpatients every 3 months for the first to second year, every 6 months for the third to fifth year after surgery, and then every 12 months from fifth year forward. Disease-free survival (DFS) was calculated from the date of the surgery operation to the time when either local recurrence, distant metastases, relapse, or death (from any reason) occurred. Overall survival (OS) was defined as the time from the date of operation to the date of death from any reason or final follow-up. Survival duration was measured from the date of the operation to death or at the final follow-up.

Statistical Analysis

Statistical analysis was performed using GraphPad Prism 8.0 and SPSS software version 17.0 (SPSS, Inc., Chicago, IL, United States). The clinicopathologic categorical variables were performed as frequencies and percentages (%). Based on the context, either chi-square test or Fisher's exact test was adopted to evaluate the associations between clinicopathological and cancer-related variables. Patients' survival rates were calculated with the help of the Kaplan-Meier method, where the log-rank test was used to examine the significance of the differences in the survival rate. The Cox proportional hazards regression model was used to examine the independent prognostic factors. The ImageJ software[1] was used to analyze cell activity and protein expression. We evaluated it by using unpaired Student's *t*-test for the comparison of two samples and using a one-way ANOVA test for the comparison of more than two samples. Each experiment was repeated at least three times, and the quantitative data were presented as mean ± standard deviations (SD). α was set at 0.05, and for all statistical analyzes, *P* values less than 0.05 were considered statistically significant.

RESULTS

p-JNK Expression in Human Breast Cancer and Survival in Breast Cancer Patients

p-JNK Expression in Human Breast Cancer and Adjacent Normal Breast Tissues

We stained 104 human breast cancer specimens and 65 human adjacent normal breast tissue for p-JNK expression by immunohistochemistry. In 104 human breast cancer specimens, 36 patient samples (34.6%, 36/104) were observed to negative or weakly-positive, and 68 patient samples (65.4%, 68/104) were observed to median-positive or strongly-positive. In 65 human adjacent normal breast tissues, 34 patient samples (52.3%, 34/65)

[1] http://rsb.info.nih.gov/ij/

were observed to negative or weakly-positive, and 31 patient samples (47.7%, 31/104) were observed to median-positive or strongly-positive (see **Figure 1**).

Demographic and Clinicopathologic Characteristics of Patients

Table 1 shows the clinicopathological characteristics of breast cancer patients included in the current study. Though both males and females are susceptible to breast cancer, all patients in our study were females (median age = 46 years, 27 to 73 years old). Among all patients, 98 of them were married (94.2%). A majority of the patients did not have a family history of cancer (n = 80; 76.9%). Patients' body mass index (BMI) ranged from 18.08 to 33.73 (median = 23.77). Overall, 64 patients (61.5%) were diagnosed with premenopausal breast cancer, whereas the rest of the patients had a postmenopausal breast cancer diagnosis (n = 40; 38.5%). Moreover, 88 patients (84.6%) had mastectomy surgery, while 16 (15.4%) patients received breast conserving surgery. The clinicopathological characteristics were similar between the two groups (see **Table 1**). Preliminary analyses showed that patients with low p-JNK expression were significantly associated with marital status ($\chi^2 = 3.973$, $P = 0.046$).

Univariate and Multivariate Cox Regression Survival Analyses

To analyze the independent prognostic factors, we adopted both the univariate and multivariate Cox proportional-hazards analyses, modeled on time-varying p-JNK expression. Univariate analysis and multivariate analysis were adopted to assess independent prognostic factors (US-LNM, US-BIRADS, clinical T stage, clinical N stage, clinical TNM stage, pre-chemotherapy times, response, tumor size, pathological response, pathological T stage, pathological N stage, pathological TNM stage, positive axillary lymph nodes, postoperative chemotherapy, postoperative endocrine therapy, postoperative targeted therapy, lymph vessel invasion, p-JNK expression). Results of univariate and multivariate Cox regression analyses showed that OS was significantly associated with US-LNM, US-BIRADS, clinical T stage, clinical N stage, clinical TNM stage, pre-chemotherapy times, tumor size, pathological response, pathological T stage, pathological N stage, pathological TNM stage, postoperative chemotherapy, postoperative endocrine therapy, postoperative targeted therapy, lymph vessel invasion, p-JNK expression (see **Supplementary Table 1**).

DFS and OS for the p-JNK Expression of Patients

Patients with high p-JNK expression had prolonged DFS and OS, as indicated by results of univariate analyses (P = 0.031, hazard ratio (HR): 0.276, 95% confidence interval (CI): 0.086–0.890 and P = 0.004, HR: 0.176, 95% CI: 0.053–0.581, respectively). Furthermore, patients with high p-JNK expression were also related to prolonged DFS and OS by multivariate analysis (P = 0.003, HR: 0.214, 95% CI: 0.077–0.597 and P = 0.007, HR: 0.194, 95% CI: 0.059–0.633, respectively; **Supplementary Table 1**). The mean DFS and OS for all enrolled cases with low p-JNK expression were 35.97 months (range from 4.67 to 85.07 months) and 58.40 months (range from 6.43 to 119.03 months), respectively; and the mean DFS and OS for all patients with high p-JNK expression were 38.66 months (range from 6.23 to 101.30 months) and 61.88 months (range from 14.47 to 133.50 months), respectively. The mean DFS and OS times in patients with high p-JNK expression were significantly longer than those in patients with low p-JNK expression by using log-rank methods ($\chi^2 = 5.908$, $P = 0.015$ and $\chi^2 = 6.593$, $P = 0.010$, respectively; see **Figures 2A,B**).

Association of Chemotherapy and p-JNK Expression in Patients

All patients had anthracyclines-based and taxanes-based neoadjuvant chemotherapy regimens. Among them, 4 patients

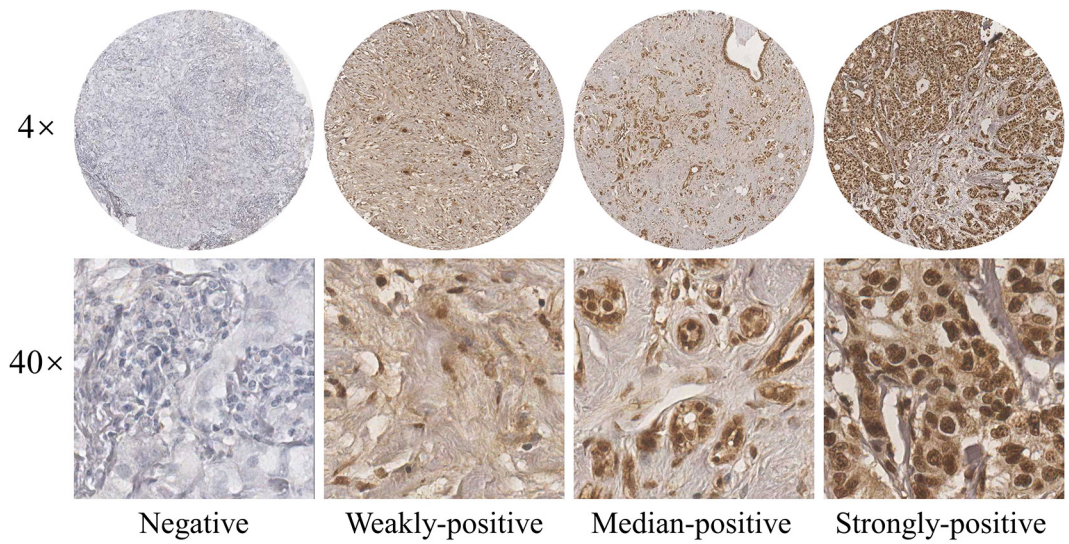

FIGURE 1 | Expression of p-JNK in human breast cancer tissues.

TABLE 1 | Patients' demographic and clinicopathologic characteristics.

Parameters	Low p-JNK	High p-JNK	χ^2	*P* value
Cases (*n*)	36	68		
Age (years)			0.446	0.504
<46	15 (41.67%)	33 (48.53%)		
≥46	21 (58.33%)	35 (51.47%)		
Marital status			3.973	0.046
Married	36 (100.00%)	62 (91.18%)		
Unmarried	0 (0.00%)	6 (8.82%)		
Family history			0.023	0.880
No	28 (77.78%)	52 (76.47%)		
Yes	8 (22.22%)	16 (23.53%)		
BMI			0.042	0.837
<23.77	18 (50.00%)	34 (50.00%)		
≥23.77	18 (50.00%)	34 (50.00%)		
Menopause			0.239	0.625
No	21 (58.33%)	43 (63.24%)		
Yes	15 (41.67%)	25 (36.76%)		
ABO blood type			0.105	0.999
A	10 (27.78%)	18 (26.47%)		
B	12 (33.33%)	22 (32.35%)		
O	9 (25.00%)	19 (27.94%)		
AB	5 (13.89%)	9 (13.24%)		
Tumor site			0.350	0.554
Right	17 (47.22%)	28 (41.18%)		
Left	19 (52.78%)	40 (58.82%)		
US-Primary tumor site			1.327	0.857
Upper outer quadrant	24 (66.67%)	46 (67.65%)		
Lower outer quadrant	4 (11.11%)	4 (5.88%)		
Lower inner quadrant	1 (2.78%)	2 (2.94%)		
Upper inner quadrant	6 (16.67%)	12 (17.65%)		
Central	1 (2.78%)	4 (5.88%)		
US-Tumor size			0.698	0.705
≤2 cm	9 (25.00%)	14 (20.59%)		
>2 and <5 cm	24 (66.67%)	45 (66.18%)		
≥5 cm	3 (8.33%)	9 (13.24%)		
US-LNM			0.003	0.960
No	24 (66.67%)	45 (66.18%)		
Yes	12 (33.33%)	23 (33.82%)		
US-BIRADS			3.654	0.161
4	4 (11.11%)	6 (8.82%)		
5	10 (27.78%)	32 (47.06%)		
6	22 (61.11%)	30 (44.12%)		
Clinical stage				
Clinical T stage			0.218	0.994
T1	5 (13.89%)	8 (11.76%)		
T2	19 (52.78%)	37 (54.41%)		
T3	7 (19.44%)	12 (17.65%)		
T4	5 (13.89%)	11 (16.18%)		
Clinical N stage			2.582	0.630
N0	6 (16.67%)	14 (20.59%)		
N1	15 (41.67%)	18 (26.47%)		
N2	11 (30.56%)	25 (36.76%)		
N3	4 (11.11%)	11 (16.18%)		
Clinical TNM stage			0.262	0.877
I	1 (2.78%)	3 (4.41%)		
II	14 (38.89%)	24 (35.29%)		
III	21 (58.33%)	41 (60.29%)		
Operative time			0.001	0.987
<90	17 (47.22%)	32 (47.06%)		
≥90	19 (52.78%)	36 (52.94%)		
Type of surgery			0.095	0.758
Mastectomy	31 (86.11%)	57 (83.82%)		
Breast-conserving surgery	5 (13.89%)	11 (16.18%)		
Tumor size			0.231	0.891
≤ 2 cm	15 (41.67%)	30 (44.12%)		
>2 and <5 cm	19 (52.78%)	33 (48.53%)		
≥ 5 cm	2 (5.56%)	5 (7.35%)		
Histologic type			0.535	0.465
Ductal	36 (100.00%)	67 (98.53%)		
Lobular	0 (0.00%)	1 (1.47%)		
Histologic grade			4.445	0.108
I	4 (11.11%)	2 (2.94%)		
II	24 (66.67%)	41 (60.29%)		
III	8 (22.22%)	25 (36.76%)		
Pathological TNM classification				
Pathological T stage			0.264	0.992
Tis/T0	1 (2.78%)	3 (4.41%)		
T1	14 (38.89%)	24 (35.29%)		
T2	17 (47.22%)	33 (48.53%)		
T3	2 (5.56%)	4 (5.88%)		
T4	2 (5.56%)	4 (5.88%)		
Pathological N stage			3.468	0.483
N0	12 (33.33%)	18 (26.47%)		
N1	12 (33.33%)	15 (22.06%)		
N2	4 (11.11%)	9 (13.24%)		
N3	8 (22.22%)	26 (38.24%)		
Pathological TNM stage			2.230	0.681
Tis/T0	1 (2.78%)	1 (1.47%)		
I	5 (13.89%)	11 (16.18%)		
II	16 (44.44%)	21 (30.88%)		
III	14 (38.89%)	35 (51.47%)		
Total lymph nodes			0.058	0.810
<23	15 (41.67%)	30 (44.12%)		
≥23	21 (58.33%)	38 (55.88%)		
Positive lymph nodes			1.700	0.192
<2	18 (50.00%)	25 (36.76%)		
≥2	18 (50.00%)	43 (63.24%)		
Total axillary lymph nodes			0.170	0.680
<23	17 (47.22%)	35 (51.47%)		
≥23	19 (52.78%)	33 (48.53%)		
Positive axillary lymph nodes			1.700	0.192
<2	18 (50.00%)	25 (36.76%)		
≥2	18 (50.00%)	43 (63.24%)		
Postoperative chemotherapy			0.421	0.517
No	4 (11.11%)	5 (7.35%)		
Yes	32 (88.89%)	63 (92.65%)		
Postoperative radiotherapy			0.422	0.516

(Cntinued)

TABLE 1 | Continued

Parameters	Low p-JNK	High p-JNK	χ^2	*P* value
No	10 (27.78%)	15 (22.06%)		
Yes	26 (72.22%)	53 (77.94%)		
Postoperative endocrine therapy			0.514	0.474
No	18 (50.00%)	29 (42.65%)		
Yes	18 (50.00%)	39 (57.35%)		
Postoperative targeted therapy			1.704	0.192
No	22 (61.11%)	50 (73.53%)		
Yes	14 (38.89%)	18 (26.47%)		

received the AC/ACF regimen, 10 patients received the CT/ACT regimen, 53 patients received the AT regimen, 25 patients received TP/ATP regimen, 10 patients received T regimen, whereas 2 patients had other regimens (e.g., ACTP, X regimen). The clinical objective response rate (CR + PR) was 57.7% (60/104), the clinical benefit rate (CR + PR + SD) was 99.0% (103/104), while the non-clinical response rate (SD + PD) was 42.3% (44/104). The Miller-Payne grading (MPG) system was used to evaluate patients' pathological response, and the grade 1 rate was 8.7% (9/104), the grade 2 rate was 40.4% (42/104), the grade 3 rate was 46.2% (48/104), the grade 4 rate was 1.0% (1/104), and the grade 5 rate was 3.8% (4/104). The pathological response of pCR rate was 5.8% (6/104), and the pathological response of non-pCR rate was 94.2% (98/104). Overall, most patients had postoperative chemotherapy (n = 95; 91.3%), only 9 patients (8.7%) did not receive postoperative chemotherapy. And there was no significance difference among these chemotherapy parameters (see **Table 2**).

Association of Pathology Parameters and p-JNK Expression in Patients

Prior to chemotherapy, patients' molecular subtypes were diagnosed by core needle biopsy. Analyses showed that 35 patients had Luminal B HER2 negative subtype, 32 patients were triple-negative subtype, 15 patients categorized with HER2-enriched subtype, 14 patients were Luminal B HER2 positive subtype, and 8 patients had Luminal A subtype. Furthermore, 57 patients were Luminal type and 47 patients were non-Luminal type, 32 patients were triple-negative type and 72 patients were non-triple-negative type, 15 patients were HER2 enriched type and 89 patients were non-HER2 enriched type. Among these different molecular subtypes, the results indicated that molecular by HER2 status were significantly different by p-JNK expression (χ^2 = 4.990, P = 0.025, see **Table 3**).

After operation, we also detected different molecular subtypes in patients by postoperative pathology (IHC). The molecular subtypes were shown in **Table 3**. We divided these molecular subtypes were into four categories: Luminal A, Luminal B, HER2-enriched, and triple-negative. Results of the log-rank test showed that the mean DFS and OS times for patients in molecular subtypes were not significant (χ^2 = 2.812, P = 0.422, see **Figure 3A**, and χ^2 = 2.757, P = 0.431, see **Figure 3B**, respectively). We found that mean DFS and OS times in patients with high p-JNK expression were longer than those in patients with low p-JNK expression in Luminal A (49.50 months vs 36.75 months, 68.35 months vs 51.57 months, respectively) and Luminal B molecular subtypes(37.24 months vs 35.48 months, 62.70 months vs 52.90 months, respectively). Whereas mean DFS and OS time in patients with high p-JNK expression was similar to patients with triple-negative molecular subtype (36.98 months vs 37.90 months, 65.44 months vs 65.42 months). However, the mean DFS and OS times in patients with high p-JNK expression were shorter than those in patients with low p-JNK expression in HER2-enriched molecular subtype (32.28 months vs 33.26 months, 41.67 months vs 57.56 months, respectively). Findings showed that the mean OS time in patients with high p-JNK expression was significantly longer than that in patients with low p-JNK expression in the Luminal B molecular subtype (χ^2 = 3.950, P = 0.047) (see **Figures 3C–J**).

Correlation Between Lymph Vessel Invasion and p-JNK Expression in Patients

According to univariate and multivariate analyses, the lymph vessel invasion was a significant prognostic factor (see **Supplementary Table 1**). To further investigate the prognostic efficiency of p-JNK expression, we analyzed the lymph vessel invasion by p-JNK expression. The lymph vessel invasion status was divided into two categories: without lymph vessel invasion and with lymph vessel invasion. The mean DFS and OS in patients without lymph vessel invasion were 43.13 months and 65.61 months with high p-JNK expression; 39.42 months and 64.76 months with low p-JNK expression, respectively. The results indicated that the mean DFS and OS times in patients with high p-JNK expression by the log-rank test were longer than those in patients with low p-JNK expression without lymph vessel invasion (χ^2 = 2.715, P = 0.099 and χ^2 = 3.477, P = 0.062, respectively; **Figures 4A,B**). The mean DFS and OS times in patients with lymph vessel invasion were 25.96 months and 48.31 months with low p-JNK expression; 37.57 months and 57.77 months with high p-JNK expression, respectively. The results indicated that the mean DFS and OS times in patients with high p-JNK expression by the log-rank test were longer than those in patients with low p-JNK expression with lymph vessel invasion (χ^2 = 4.302, P = 0.038 and χ^2 = 14.020, P<0.001, respectively; **Figures 4C,D**). The results also indicated that patients with lymph vessel invasion and low p-JNK expression survived shorter, and had worse prognose (see **Figure 4**).

Correlation Between p-JNK Expression and Side Effects of Chemotherapy

In this study, hematologic and gastrointestinal reactions were found to be common toxicities after NACT. The National Cancer Institute-Common Toxicity Criteria (NCI-CTC) was adopted to evaluate and analyze any potential side effects of NACT (Eisenhauer et al., 2009). To further evaluate side effects of NACT, p-JNKs were utilized in our study. Findings indicated that before-NACT p-JNK expressions were not significantly related to toxicities

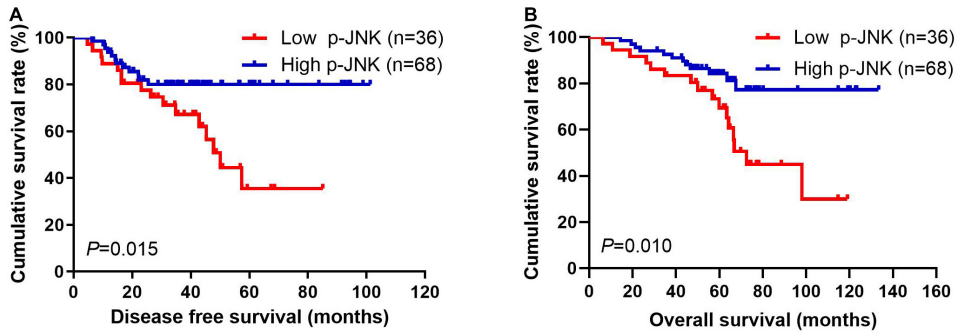

FIGURE 2 | Breast cancer patients' DFS and OS. **(A)** Patients' DFS for the p-JNK expression, assessed by the Kaplan-Meier analysis. **(B)** Patients' of OS for the p-JNK expression, assessed by the Kaplan-Meier analysis.

of enrolled patients, except mouth ulcers (see **Table 4**). None of the patients enrolled in the study suffered from chemotherapy-related deaths.

TABLE 2 | The relationship between patients' chemotherapy and p-JNK expression.

Parameters	Low p-JNK	High p-JNK	χ^2	*P* value
Cases (*n*)	36	68		
Neoadjuvant Chemotherapy			4.669	0.323
AC/ACF	2 (5.56%)	2 (2.94%)		
CT/ACT	3 (8.33%)	7 (10.29%)		
AT	21 (58.33%)	32 (47.06%)		
TP	8 (22.22%)	13 (19.12%)		
Others	2 (5.56%)	14 (20.59%)		
Pre-chemotherapy times			0.010	0.919
<6	12 (33.33%)	22 (32.35%)		
≥6	24 (66.67%)	46 (67.65%)		
Response			0.701	0.704
PR	20 (55.56%)	40 (58.82%)		
SD	16 (44.44%)	27 (39.71%)		
PD	0 (0.00%)	1 (1.47%)		
Miller and Payne grade			1.542	0.819
1	4 (11.11%)	5 (7.35%)		
2	16 (44.44%)	26 (38.24%)		
3	15 (41.67%)	33 (48.53%)		
4	0 (0.00%)	1 (1.47%)		
5	1 (2.78%)	3 (4.41%)		
Pathological response			1.080	0.299
pCR	0 (0.00%)	2 (2.94%)		
non-pCR	36 (100.00%)	66 (97.06%)		
Postoperative chemotherapy regimen			3.899	0.564
0	4 (11.11%)	5 (7.35%)		
AC/ACF	2 (5.56%)	4 (5.88%)		
CT/ACT	2 (5.56%)	7 (10.29%)		
AT	7 (19.44%)	10 (14.71%)		
TP	14 (38.89%)	19 (27.94%)		
Others	7 (19.44%)	23 (33.82%)		
Postoperative chemotherapy times			1.495	0.221
<4	14 (38.89%)	35 (51.47%)		
≥4	22 (61.11%)	33 (48.53%)		

Anisomycin Activates JNK and Induces Apoptosis

Anisomycin Induces Apoptosis in Breast Cancer

To assess the cytotoxicity of anisomycin on breast cancer cells, cells were treated with anisomycin at the following concentrations: 100, 50, 10, 5, 1, 0.8, 0.4, 0.2, 0.1, 0.05, 0.01, 0 μM for 48h. Cell viability was analyzed by CCK-8 assay. The data demonstrated that the IC50 value of human mammary epithelial cell line (184B5) was 0.3403μM. The IC50 value of human breast cancer cell lines (MDA-MB-231, MDA-MB-436, BT549, Hs578T) were 0.1316, 0.1080, 0.0582, 0.1063 μM, respectively (see **Figure 5A**). And 0.2 μM was chosen as the suitable concentration in the subsequent experiments.

We next investigate the effect of anisomycin on apoptosis. The breast cancer cells were treated with 0 or 0.2 μM anisomycin for 48h, and then detected by flow cytometry. As expected, anisomycin can induce apoptosis in breast cancer cell lines. Moreover, human mammary epithelial cell line (184B5) treated with anisomycin showed reduced apoptosis compared with human breast cancer cell lines (**Figures 5B,C**). And we also detected the expression of PARP and caspase-3 by western blot after adding different concentrations of anisomycin, and found that breast cancer cells with higher concentration anisomycin showed significantly increased expression of both cleaved caspase-3 and cleaved PARP than those with lower concentration anisomycin (see **Figures 6A–E**).

Anisomycin Activates JNK and Inhibits the Activation of STAT3

Anisomycin was known to induce cell death and JNK activation was required for Anisomycin induced apoptosis (Zhou et al., 2019; Zhang et al., 2020). We examined the p-JNK expression by western blot after the treatment of anisomycin in human breast cancer cell lines (MDA-MB-231, MDA-MB-436, BT549, Hs578T). The results indicated that anisomycin was a potent activator of JNK in human breast cancer cell lines. And anisomycin would present a better option for delineating the effects of p-JNK expression (**Figure 6**). Previous studies showed that STAT3 activation is mediated by the combined action of JAK, SRC, c-ABL, and JNKs (Chakraborty et al., 2017). To further investigate the mechanism of anisomycin inducing apoptosis,

TABLE 3 | The relationship between patients' pathology parameters and p-JNK expression.

Parameters	Low p-JNK	High p-JNK	χ^2	*P* value
Cases (*n*)	36	68		
Core needle biopsy (Before chemotherapy)				
Molecular subtype (common)			7.156	0.128
Luminal A	2 (5.56%)	6 (8.82%)		
Luminal B HER2 +	2 (5.56%)	12 (17.65%)		
Luminal B HER2-	12 (33.33%)	23 (33.82%)		
HER2 enriched	9 (25.00%)	6 (8.82%)		
Triple negative	11 (30.56%)	21 (30.88%)		
Molecular subtype (by Luminal)			2.387	0.122
Luminal type	16 (44.44%)	41 (60.29%)		
non-Luminal type	20 (55.56%)	27 (39.71%)		
Molecular subtype (by Triple)			0.001	0.973
Triple negative	11 (30.56%)	21 (30.88%)		
non-Triple negative	25 (69.44%)	47 (69.12%)		
Molecular subtype (by HER2)			4.990	0.025
HER2 enriched	9 (25.00%)	6 (8.82%)		
non-HER2 enriched	27 (75.00%)	62 (91.18%)		
ER status			0.784	0.376
Negative	17 (47.22%)	26 (38.24%)		
Positive	19 (52.78%)	42 (61.76%)		
PR status			0.377	0.539
Negative	16 (44.44%)	26 (38.24%)		
Positive	20 (55.56%)	42 (61.76%)		
HER2 status			0.369	0.543
Negative (0– + +)	25 (69.44%)	51 (75.00%)		
Positive (+ + +)	11 (30.56%)	17 (25.00%)		
Ki-67 status			0.317	0.573
Negative (≤ 14%)	8 (22.22%)	12 (17.65%)		
Positive (>14%)	28 (77.78%)	56 (82.35%)		
Postoperative pathology (IHC)				
Molecular subtype (common)			4.287	0.369
Luminal A	5 (13.89%)	12 (17.65%)		
Luminal B HER2 +	1 (2.78%)	8 (11.76%)		
Luminal B HER2-	8 (22.22%)	15 (22.06%)		
HER2 enriched	9 (25.00%)	9 (13.24%)		
Triple negative	13 (36.11%)	24 (35.29%)		
Molecular subtype (by Luminal)			1.495	0.221
Luminal type	14 (38.89%)	35 (51.47%)		
non-Luminal type	22 (61.11%)	33 (48.53%)		
Molecular subtype (by Triple)			0.007	0.934
Triple negative	13 (36.11%)	24 (35.29%)		
non-Triple negative	23 (63.89%)	44 (64.71%)		
Molecular subtype (by HER2)			2.276	0.131
HER2 enriched	9 (25.00%)	9 (13.24%)		
non-HER2 enriched	27 (75.00%)	59 (86.76%)		
ER status			3.286	0.070
Negative	21 (58.33%)	27 (39.71%)		
Positive	15 (41.67%)	41 (60.29%)		
PR status			0.487	0.485
Negative	19 (52.78%)	31 (45.59%)		
Positive	17 (47.22%)	37 (54.41%)		
HER2 status			0.685	0.408
Negative (0– + +)	26 (72.22%)	54 (79.41%)		
Positive (+ + +)	10 (27.78%)	14 (20.59%)		

(Cntinued)

TABLE 3 | Continued

Parameters	Low p-JNK	High p-JNK	χ^2	*P* value
Ki-67 status			2.350	0.125
Negative (≤ 14%)	16 (44.44%)	20 (29.41%)		
Positive (>14%)	20 (55.56%)	48 (70.59%)		
AR status			0.097	0.755
Negative	32 (88.89%)	59 (86.76%)		
Positive	4 (11.11%)	9 (13.24%)		
CK5/6 status			0.878	0.349
Negative	28 (77.78%)	47 (69.12%)		
Positive	8 (22.22%)	21 (30.88%)		
E-cad status			0.685	0.408
Negative	10 (27.78%)	14 (20.59%)		
Positive	26 (72.22%)	54 (79.41%)		
EGFR status			1.279	0.258
Negative	17 (47.22%)	40 (58.82%)		
Positive	19 (52.78%)	28 (41.18%)		
P53 status			0.009	0.923
Negative	15 (41.67%)	29 (42.65%)		
Positive	21 (58.33%)	39 (57.35%)		
TOP2A status			0.266	0.606
Negative	9 (25.00%)	14 (20.59%)		
Positive	27 (75.00%)	54 (79.41%)		
Lymph vessel invasion			0.002	0.961
Negative	21 (58.33%)	40 (58.82%)		
Positive	15 (41.67%)	28 (41.18%)		
Neural invasion			0.001	0.985
Negative	28 (77.78%)	53 (77.94%)		
Positive	8 (22.22%)	15 (22.06%)		

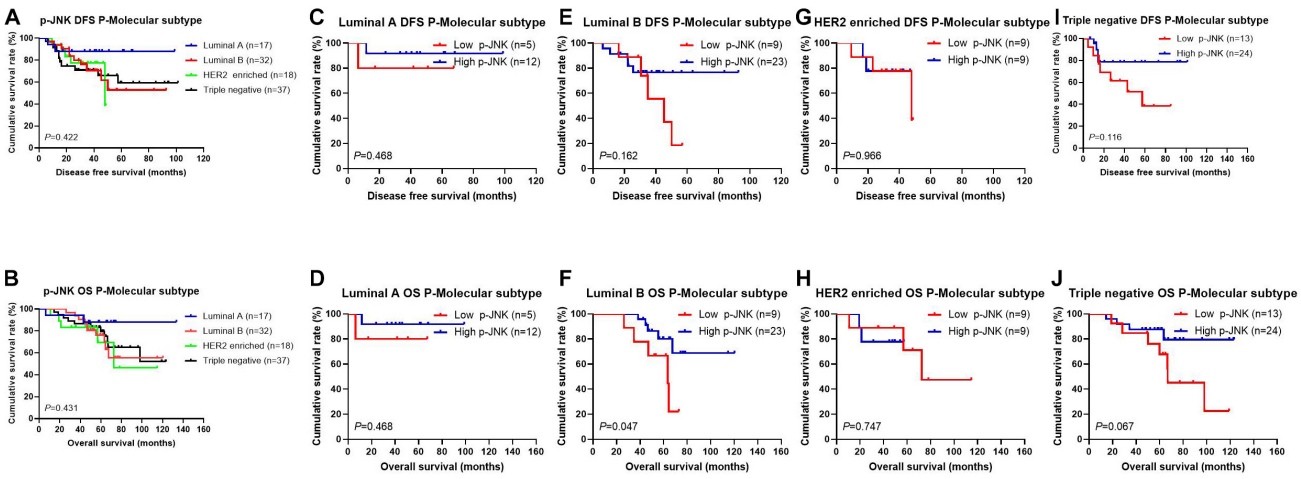

FIGURE 3 | Patients' DFS and OS for the p-JNK expression, by molecular subtypes. **(A)** Patients' DFS by molecular subtypes, assessed by the Kaplan-Meier analysis. **(B)** Patients' OS by molecular subtypes, assessed by the Kaplan-Meier analysis. **(C)** Patients' DFS by Luminal A subtype, assessed by the Kaplan-Meier analysis. **(D)** Patients' OS by Luminal A subtype, assessed by the Kaplan-Meier analysis. **(E)** Patients' DFS by Luminal B subtype, assessed by the Kaplan-Meier analysis. **(F)** Patients' OS by Luminal B subtype, assessed by the Kaplan-Meier analysis. **(G)** Patients' DFS by HER2-enriched subtype, assessed by the Kaplan-Meier analysis. **(H)** Patients' OS by HER2-enriched subtype, assessed by the Kaplan-Meier analysis. **(I)** Patients' DFS by triple-negative subtype, assessed by the Kaplan-Meier analysis. **(J)** Patients' OS by triple-negative subtype, assessed by the Kaplan-Meier analysis.

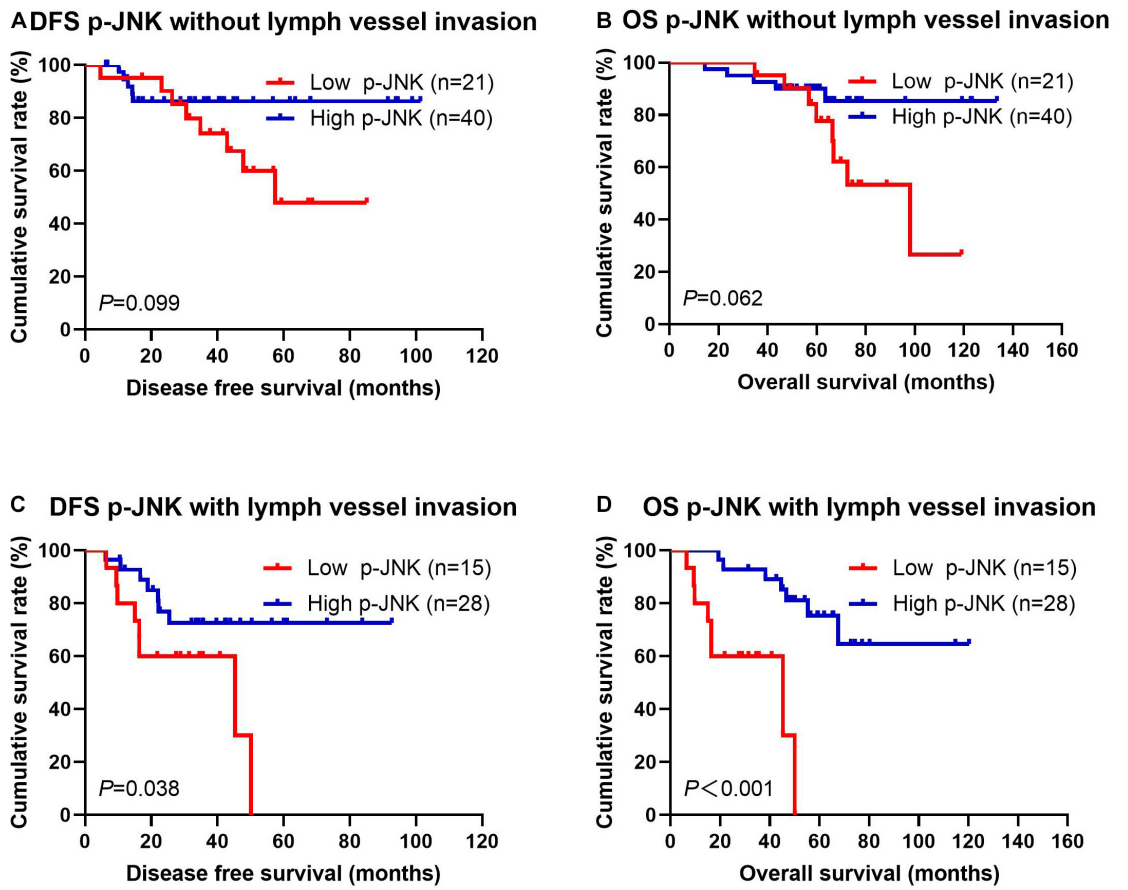

FIGURE 4 | Patients' DFS and OS by lymph vessel invasion status. **(A)** Patients' DFS without lymph vessel invasion by p-JNK expression, assessed by the Kaplan-Meier analysis. **(B)** Patients' OS without lymph vessel invasion by p-JNK expression, assessed by the Kaplan-Meier analysis. **(C)** Patients' DFS with lymph vessel invasion by p-JNK expression, assessed by the Kaplan-Meier analysis. **(D)** Patients' OS with lymph vessel invasion by p-JNK expression, assessed by the Kaplan-Meier analysis.

we used western blot to detect the STAT3/p-STAT3 expression after the treatment of anisomycin in human breast cancer cell lines (i.e., MDA-MB-231, MDA-MB-436, BT549, and Hs578T). The results indicated that anisomycin was a potent inhibitor of STAT3 in human breast cancer cell lines. In other words, findings showed that anisomycin induced apoptosis by activating JNKs and restraining the activation of STAT3 (see **Figure 7**).

DISCUSSION

Approximately 2.1 million people will be diagnosed with breast cancer in 2018, effectively making the ever-growing breast cancer population even larger (Ferlay et al., 2018). Breast cancer is a heterogeneous disease that can be caused by many signaling pathways that are responsible for cell proliferation and cell apoptosis, such as PI3K/AKT/mTOR, JAK/STAT, PTEN/AKT/MDM2/p53, and AKT/NF-κB signaling pathway (Wan et al., 2019; Lee et al., 2020; Martínez-Rodríguez et al., 2020; Narayanankutty, 2020; Nunnery and Mayer, 2020). Subsequently, due to genetic variability, different breast patients often exhibit varied susceptibility to different signaling pathways. Hence, providing patients with individualized treatments is of critical importance in helping patients better cope with cancer care and management. However, although many of potential targets of treatments exist in breast cancer cells, the mechanism of these anti-cancer targets is still not clear.

MAPKs can be activated via a kinase signaling cascade in which a MAP3K activates a MAP2K, and in turn activates a MAPK. JNKs are subfamilies of MAPKs (Aikin et al., 2020). There are three proteins of JNKs in mammals: JNK1, JNK2 and JNK3, and they are encoded by three distinctive genes jnk1 (Mapk8), jnk2 (Mapk9), and jnk3 (Mapk10), respectively. Although JNK1 and JNK2 are expressed in most tissues, JNK3 expression is mainly limited in brain, heart and testis (Kumar et al., 2015). Upon activation by the upstream MAP2Ks, JNKs phosphorylate can activate a considerable number of nuclear and non-nuclear proteins, such as the transcription factor activator protein-1 (AP-1) (Lee et al., 2020). And these proteins control a diversity of cellular responses, such as cell growth, cell proliferation, cell differentiation, cell survival and cell death. The aberrant expression and activation of JNKs are found in

TABLE 4 | Correlation between p-JNK expression and patients' chemotherapy side effects.

Parameters	Low p-JNK	High p-JNK	χ^2	*P* value
Cases (*n*)	36	68		
Decreased appetite			0.004	0.949
No	6 (16.67%)	11 (16.18%)		
Yes	30 (83.33%)	57 (83.82%)		
Nausea			0.017	0.897
No	4 (11.11%)	7 (10.29%)		
Yes	32 (88.89%)	61 (89.71%)		
Vomiting			0.487	0.485
No	19 (52.78%)	31 (45.59%)		
Yes	17 (47.22%)	37 (54.41%)		
Diarrhea			0.225	0.635
No	33 (91.67%)	64 (94.12%)		
Yes	3 (8.33%)	4 (5.88%)		
Mouth ulcers			3.851	0.049
No	34 (94.44%)	68 (100.00%)		
Yes	2 (5.56%)	0 (0.00%)		
Alopecia			0.446	0.504
No	15 (41.67%)	33 (48.53%)		
Yes	21 (58.33%)	35 (51.47%)		
Peripheral neurotoxicity			0.004	0.949
No	30 (83.33%)	57 (83.82%)		
Yes	6 (16.67%)	11 (16.18%)		
Anemia			2.781	0.095
Grade 0	15 (41.67%)	40 (58.82%)		
Grade 1-2	21 (58.33%)	28 (41.18%)		
Grade 3-4	0 (0.00%)	0 (0.00%)		
Leukopenia			4.347	0.113
Grade 0	11 (30.56%)	13 (19.12%)		
Grade 1-2	14 (38.89%)	41 (60.29%)		
Grade 3-4	11 (30.56%)	14 (20.59%)		
Neutropenia			0.979	0.613
Grade 0	7 (19.44%)	13 (19.12%)		
Grade 1-2	12 (33.33%)	29 (42.65%)		
Grade 3-4	17 (47.22%)	26 (38.24%)		
Thrombocytopenia			0.099	0.752
Grade 0	28 (77.78%)	51 (75.00%)		
Grade 1-2	8 (22.22%)	17 (25.00%)		
Grade 3-4	0 (0.00%)	0 (0.00%)		
Gastrointestinal reaction			1.910	0.385
Grade 0	4 (11.11%)	8 (11.76%)		
Grade 1-2	31 (86.11%)	60 (88.24%)		
Grade 3-4	1 (2.78%)	0 (0.00%)		
Myelosuppression			0.152	0.927
Grade 0	5 (13.89%)	10 (14.71%)		
Grade 1-2	10 (27.78%)	21 (30.88%)		
Grade 3-4	21 (58.33%)	37 (54.41%)		
Hepatic dysfunction			0.131	0.717
Grade 0	22 (61.11%)	44 (64.71%)		
Grade 1-2	14 (38.89%)	24 (35.29%)		
Grade 3-4	0 (0.00%)	0 (0.00%)		

many cancer cell lines and tissue samples (Mohebali et al., 2020; Qu et al., 2020). In primary hepatocellular carcinoma (HCC), compared with the non-neoplastic lesions, the activation of JNK1 in tumor size was significantly increased, and absence of JNK1 impaired hepatocyte proliferation and tumor formation (Chang et al., 2009; Gao et al., 2019). In mice with DEN induced liver cancer, the levels of activated JNK (p-JNK) were decreased by D-JNKI-1 injection for inhibited three months in the treatment group, whereas the levels of p-JNK was continuously expressed high (Davoli et al., 2014). However, the p-JNK was rarely studied, especially in breast cancer patients who had NACT.

In order to study the p-JNK expression in breast cancer patients' tissues, we stained 104 human breast cancer specimens and 65 human adjacent normal breast tissue for p-JNK expression by immunohistochemistry. The results indicated that 65.4% of reviewed cases were observed to be strongly-positive in human breast cancer specimens, however, 47.7% of the cases were observed to be strongly-positive in human adjacent normal breast tissues. To further analyze the relationship between the expression of p-JNK and the prognosis of breast cancer patients, we used the univariate and multivariate Cox proportional-hazards models to evaluate relevant independent prognostic factors. The results proved that p-JNK expression was an independent prognostic factor of DFS and OS. Patients with high p-JNK expression related to prolonged DFS and OS than those patients with low p-JNK expression by log-rank methods.

Anisomycin was a potent protein synthesis inhibitor, and was widely used as an agonist for p38 MAPK and JNK. It is generally known that anisomycin induced apoptosis in a variety of cell types through the activation of the p38 MAPK and the JNK pathway (Li et al., 2018; Yang et al., 2020). In our study, we found that anisomycin could significantly inhibit cell proliferation and promote cell apoptosis. The IC50 of human breast cancer cell lines were higher than human mammary epithelial cell lines. We also used western blot to detect the expression of cleaved caspase-3 and cleaved PARP, and found that the expression of cleaved caspase-3 and cleaved PARP were significantly higher by high concentration anisomycin. Some studies have proved that anisomycin was a JNK activator, and also increased phospho-JNK (Guan et al., 2020; Yoon et al., 2020). Hence, we used western blot to detect the p-JNK expression by anisomycin, and the results indicated that anisomycin was a potent activator of JNK in human breast cancer cell lines. Combined with cleaved caspase-3 and cleaved PARP, we found that the p-JNK expression is positively associated with the cleaved caspase-3 and cleaved PARP by anisomycin.

JNKs, as subtypes of MAPKs, mediate the stress-dependent serine phosphorylation of STAT3 (Chen et al., 2013). JNKs were activated by UV or anisomycin or by their upstream kinase MEKK1 phosphorylation STAT3 *in vitro* (Nikaido et al., 2018). STAT3 was also phosphorylated by cotransfection of JNKs with MEKK1 *in vivo* (Ni et al., 2003). And the experiments confirmed that the major phosphorylation site of STAT3 by JNKs was identified to be Ser-727 *in vitro* (Lim and Cao, 1999; Schuringa et al., 2000; Miyazaki et al., 2008). The STAT family of transcription factors integrated cytokine and growth factor signaling to transcriptionally regulate a diverse array of cellular processes (Corry et al., 2020). STAT3 had become one of the common investigated oncogenic transcription factors and was associated with cell

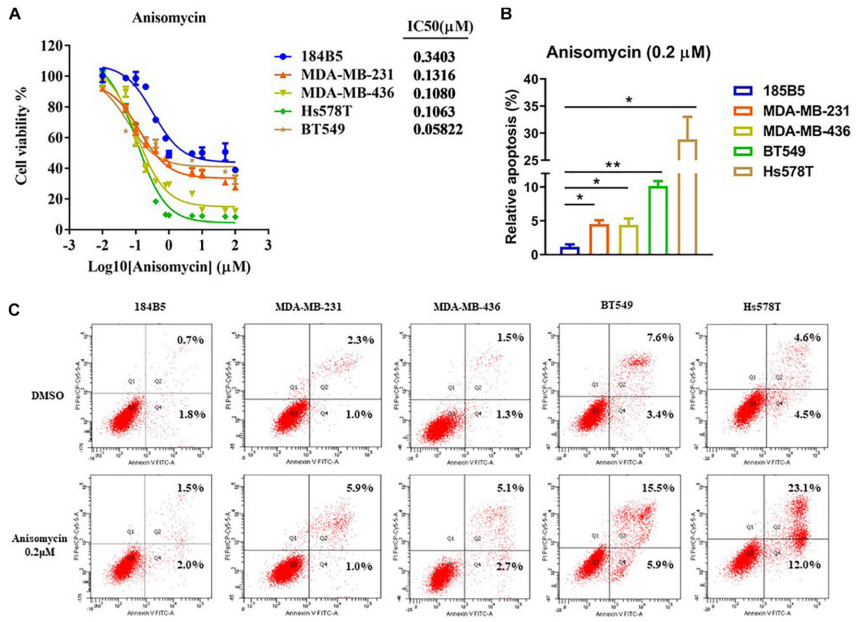

FIGURE 5 | Apoptosis induced by anisomycin in human breast cancer. **(A)** CCK-8 detected IC50 of human mammary epithelial cell line (184B5) and human breast cancer cell lines (MDA-MB-231, MDA-MB-436, BT549, and Hs578T). **(B)** Prior to flow cytometry, human mammary epithelial cell and breast cancer cells were conditioned with 0 μM or 0.2 μM anisomycin for 48 h. **(C)** Flow cytometry analyzed apoptosis of 184B5, MDA-MB-231, MDA-MB-436, BT549, and Hs578T.

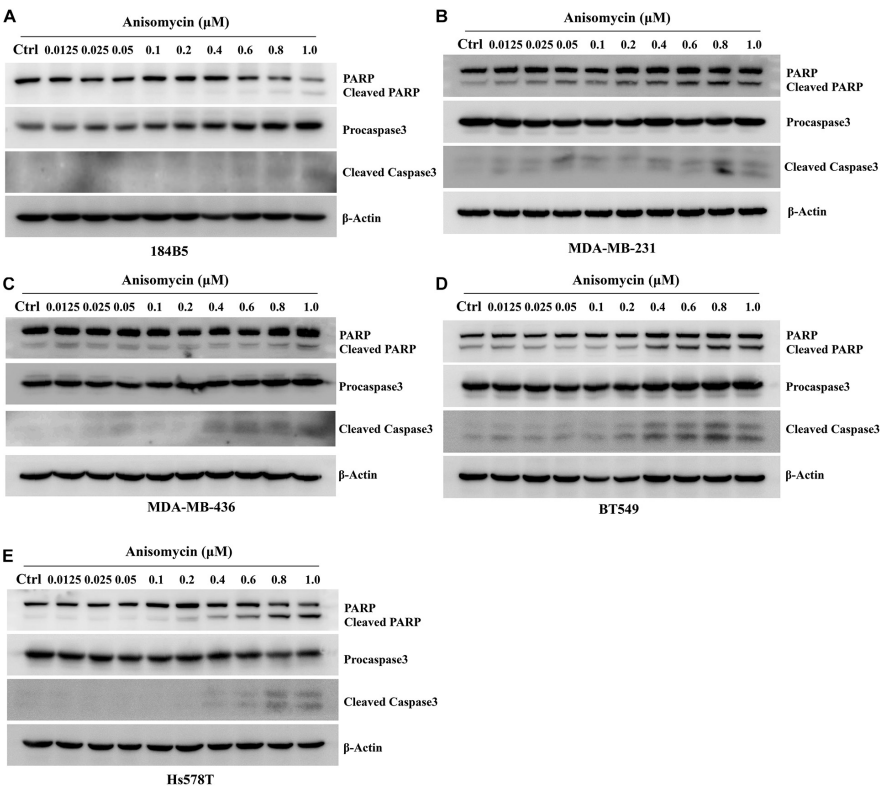

FIGURE 6 | Apoptosis induced by anisomycin in human mammary epithelial cell line and human breast cancer cell lines. **(A–E)** 184B5 **(A)**, MDA-MB-231 **(B)**, MDA-MB-436 **(C)**, BT549 **(D)**, and Hs578T **(E)** cells were treated with indicated concentration of anisomycin. After being treated with anixomycin for 48 h, western blot was adopted to examine PARP, procaspase3, cleaved caspase-3, and β-actin expressions.

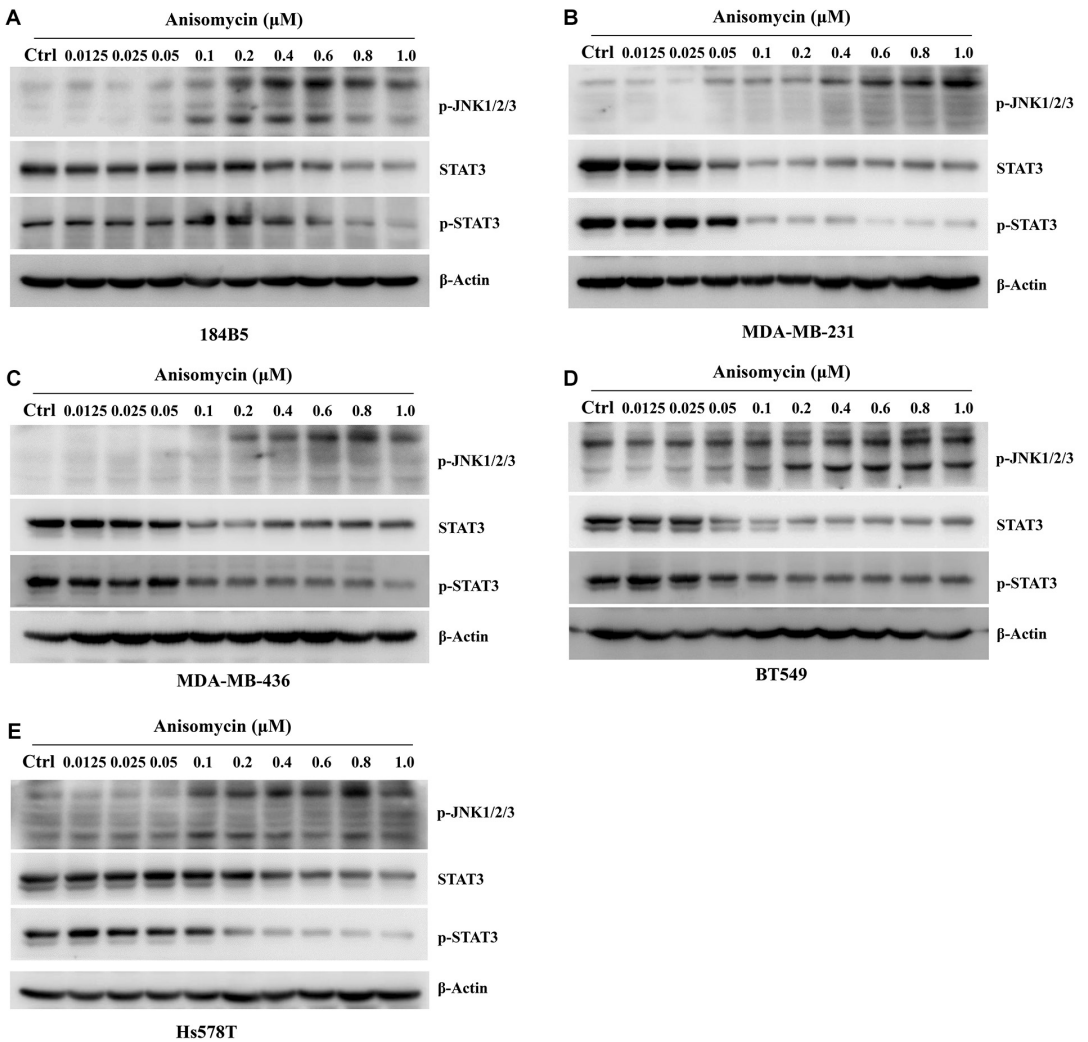

FIGURE 7 | Anisomycin activated JNK and inhibited the activation of STAT3. **(A–E)** 184B5 **(A)**, MDA-MB-231 **(B)**, MDA-MB-436 **(C)**, BT549 **(D)**, and Hs578T **(E)** cells were conditioned with anisomycin, concentration as indicated. After being treated with anixomycin for 48 h, western blot was adopted to examine STAT3, p-STAT3, p-JNK1/2/3, and -actin expression.

proliferation, differentiation, progression, metastasis and chemoresistance (Qin et al., 2019). STAT3 was activated via the phosphorylation of Y705 by cytoplasmic non-receptor tyrosine kinases (Johnson et al., 2018).

One study showed that NSC-743380 modulates functions of multipathways, including activating MAP kinase JNK and inhibiting JAK/STAT3 pathway, had potential *in vitro* and *in vivo* antitumor activities (Guo et al., 2011). In our study, we used western blot to detect the expression of p-JNK and p-STAT3 by anisomycin, and the results indicated that the protein expression of p-JNK increased with anisomycin concentration, whereas the protein expression of p-STAT3 decreased with anisomycin concentration, and they had the inverse correlation relations.

Meanwhile, as results of univariate and multivariate Cox regression analyses suggested, occupation, US-LNM, US-BIRADS, clinical T stage, clinical N stage, clinical TNM stage, tumor size, pathological T stage, postoperative endocrine therapy, postoperative targeted therapy, and lymph vessel invasion were significant prognostic factors in predicting patients' improved DFS and OS. Lymph vessel invasion is thought to play an important role in tumor metastasis, and acts as the modulation of antitumor immune responses (David Nathanson et al., 2020; Testa et al., 2020; Wang et al., 2020). The tumor angiogenesis and its indicative vascular density are closely related to the prognosis of breast cancer (Huang et al., 2020; Koch et al., 2020). In our research, the results also indicated that lymph vessel invasion was the significant prognostic factor, and the patients with lymph vessel invasion and low JNK expression survived shorter. Although the molecular subtypes were not significant prognostic factors by univariate and multivariate analyses, the mean DFS and OS times in patients with high JNK expression were longer than those in patients with low JNK expression in molecular subtypes, especially in Luminal B molecular subtype.

Limitations

There are several limitations in this study. Firstly, we only examined the anisomycin in breast cancer cells, but not in patients with breast cancer. Future prospective and randomized controlled trials can further extend our research on anisomycin in breast cancer patients. Secondly, this study was a retrospective single-center study and the number of enrolled patients was not large. Future study can benefit from having more patients enrolled, and adopting a multicenter study design. Furthermore, having a large sample size can also help improve rigor in subgroup analyses.

CONCLUSION

In summary, anisomycin was a potent activator of JNK in human breast cancer cell lines, and can present a better option for delineating the effects of p-JNK expression. p-JNK expression, on the other hand, is a significant and effective prognostic predictor of survival time in breast cancer patients receiving NACT. Taken together, we demonstrated that p-JNKs are independent prognostic markers for breast cancer patients. Further research should pour more attention into understanding the functions of p-JNKs and p-STAT3 in breast cancer formation and treatment, to help clinicians and scholars better understand breast cancer development and progression, and in turn, offer new insights and novel solutions that could guide future breast cancer research.

DATA AVAILABILITY STATEMENT

The raw data supporting the conclusions of this article will be made available by the authors, without undue reservation.

ETHICS STATEMENT

This study was approved by the Ethics Committee of the Cancer Hospital Chinese Academy of Medical Sciences. The patients/participants provided their written informed consent to participate in this study.

AUTHOR CONTRIBUTIONS

YF and JW: conceptualization and funding acquisition. AL and ZL: project administration and supervision. SL: validation. XK and XW: visualization. LC and XZ: writing-original draft. LC, XZ, and ZS: writing-review editing. The authors read and approved the final manuscript. All authors contributed to the article and approved the submitted version.

FUNDING

The work is partly supported by research grants from the National Nature Science Foundation of China (no. 81872160) and Beijing Nature Science Foundation of China (no. 7191009).

SUPPLEMENTARY MATERIAL

The Supplementary Material for this article can be found online at: https://www.frontiersin.org/articles/10.3389/fcell.2021.656693/full#supplementary-material

REFERENCES

Abdel-Rahman, O. (2018). Validation of the 8th AJCC prognostic staging system for breast cancer in a population-based setting. *Breast Cancer Res. Treat.* 168, 269–275. doi: 10.1007/s10549-017-4577-x

Adamson, K., Chavez-MacGregor, M., Caudle, A., Smith, B., Baumann, D., Liu, J., et al. (2019). Neoadjuvant chemotherapy does not increase complications in oncoplastic breast-conserving surgery. *Ann. Surg. Oncol.* 26, 2730–2737. doi: 10.1245/s10434-019-07408-6

Aikin, T. J., Peterson, A. F., Pokrass, M. J., Clark, H. R., and Regot, S. (2020). MAPK activity dynamics regulate non-cell autonomous effects of oncogene expression. *eLife* 9:e60541. doi: 10.7554/eLife.60541.sa2

Asselain, B., Barlow, W., Bartlett, J., Bergh, J., Bergsten-Nordström, E., Bliss, J., et al. (2018). Long-term outcomes for neoadjuvant versus adjuvant chemotherapy in early breast cancer: meta-analysis of individual patient data from ten randomised trials. *Lancet Oncol.* 19, 27–39. doi: 10.1016/S1470-2045(17)30777-5

Bray, F., Ferlay, J., Soerjomataram, I., Siegel, R. L., Torre, L. A., and Jemal, A. (2018). Global cancer statistics 2018: GLOBOCAN estimates of incidence and mortality worldwide for 36 cancers in 185 countries. *CA Cancer J. Clin.* 68, 394–424. doi: 10.3322/caac.21492

Caldana, M., Pellini, F., Lombardi, D., Mirandola, S., Invento, A., and Pollini, G. P. (2018). Breast cancer and neoadjuvant chemotherapy: indications for and limits of breast-conserving surgery. *Ann. Ital. Chir.* 89, 392–397.

Cellurale, C., Girnius, N., Jiang, F., Cavanagh-Kyros, J., Lu, S., Garlick, D. S., et al. (2012). Role of JNK in mammary gland development and breast cancer. *Cancer Res.* 72, 472–481. doi: 10.1158/0008-5472.CAN-11-1628

Chakraborty, D., Sumova, B., Mallano, T., Chen, C. W., Distler, A., Bergmann, C., et al. (2017). Activation of STAT3 integrates common profibrotic pathways to promote fibroblast activation and tissue fibrosis. *Nat. Commun.* 8:1130. doi: 10.1038/s41467-017-01236-6

Chang, Q., Zhang, Y., Beezhold, K. J., Bhatia, D., Zhao, H., Chen, J., et al. (2009). Sustained JNK1 activation is associated with altered histone H3 methylations in human liver cancer. *J. Hepatol.* 50, 323–333. doi: 10.1016/j.jhep.2008.07.037

Chen, B., Liu, J., Chang, Q., Beezhold, K., Lu, Y., and Chen, F. (2013). JNK and STAT3 signaling pathways converge on Akt-mediated phosphorylation of EZH2 in bronchial epithelial cells induced by arsenic. *Cell Cycle* 12, 112–121. doi: 10.4161/cc.23030

Chen, N., and Ávila, C. (2019). Mitogen-Activated Protein Kinases (MAPKs) and cholangiocarcinoma: the missing link. *Cells* 8:1172. doi: 10.3390/cells8101172

Corry, J., Mott, H. R., and Owen, D. (2020). Activation of STAT transcription factors by the Rho-family GTPases. *Biochem. Soc. Trans.* 48, 2213–2227. doi: 10.1042/BST20200468

Das, M. (2017). Neoadjuvant chemotherapy: survival benefit in gastric cancer. *Lancet Oncol.* 18:e307. doi: 10.1016/S1470-2045(17)30321-2

David Nathanson, S., Leonard-Murali, S., Burmeister, C., Susick, L., and Baker, P. (2020). Clinicopathological evaluation of the potential anatomic pathways of systemic metastasis from primary breast cancer suggests an orderly spread through the regional lymph nodes. *Ann. Surg. Oncol.* 27, 4810–4818. doi: 10.1245/s10434-020-08904-w

Davidson, B., Konstantinovsky, S., Kleinberg, L., Nguyen, M. T. P., Bassarova, A., Kvalheim, G., et al. (2006). The mitogen-activated protein kinases (MAPK) p38 and JNK are markers of tumor progression in breast carcinoma. *Gynecol. Oncol.* 102, 453–461. doi: 10.1016/j.ygyno.2006.01.034

Davoli, E., Sclip, A., Cecchi, M., Cimini, S., Carrà, A., Salmona, M., et al. (2014). Determination of tissue levels of a neuroprotectant drug: the cell permeable JNK inhibitor peptide. *J. Pharmacol. Toxicol. Methods* 70, 55–61. doi: 10.1016/j.vascn.2014.04.001

Derks, M. G. M., and van de Velde, C. J. H. (2018). Neoadjuvant chemotherapy in breast cancer: more than just downsizing. *Lancet Oncol.* 19, 2–3. doi: 10.1016/S1470-2045(17)30914-2

Dibden, A., Offman, J., Duffy, S. W., and Gabe, R. (2020). Worldwide review and meta-analysis of cohort studies measuring the effect of mammography screening programmes on incidence-based breast cancer mortality. *Cancers* 12:976. doi: 10.3390/cancers12040976

Eisenhauer, E. A., Therasse, P., Bogaerts, J., Schwartz, L. H., Sargent, D., Ford, R., et al. (2009). New response evaluation criteria in solid tumours: revised RECIST guideline (version 1.1). *Eur. J. Cancer* 45, 228–247. doi: 10.1016/j.ejca.2008.10.026

Fan, L., Strasser-Weippl, K., Li, J.-J., St Louis, J., Finkelstein, D. M., Yu, K.-D., et al. (2014). Breast cancer in China. *Lancet Oncol.* 15, e279–e289. doi: 10.1016/S1470-2045(13)70567-9

Farkhondeh, T., Mehrpour, O., Buhrmann, C., Pourbagher-Shahri, A. M., Shakibaei, M., and Samarghandian, S. (2020). Organophosphorus compounds and MAPK signaling pathways. *Int. J. Mol. Sci.* 21:4258. doi: 10.3390/ijms21124258

Ferlay, J., Colombet, M., Soerjomataram, I., Mathers, C., Parkin, D. M., Piñeros, M., et al. (2018). Estimating the global cancer incidence and mortality in 2018: GLOBOCAN sources and methods. *Int. J. Cancer* 144, 1941–1953. doi: 10.1002/ijc.31937

Freites-Martinez, A., Santana, N., Arias-Santiago, S., and Viera, A. (2020). Using the common terminology criteria for adverse events (CTCAE - Version 5.0) to evaluate the severity of adverse events of anticancer therapies. *Actas Dermosifiliogr.* 7310:30286. doi: 10.1016/j.adengl.2019.05.021

Gao, X., Wei, M., Shan, W., Liu, Q., Gao, J., Liu, Y., et al. (2019). An oral 2-hydroxypropyl-β-cyclodextrin-loaded spirooxindole-pyrrolizidine derivative restores p53 activity via targeting MDM2 and JNK1/2 in hepatocellular carcinoma. *Pharmacol. Res.* 148:104400. doi: 10.1016/j.phrs.2019.104400

Ge, W. K., Yang, B., Zuo, W. S., Zheng, G., Dai, Y. Q., Han, C., et al. (2015). Evaluation of hormone receptor, human epidermal growth factor receptor-2 and Ki-67 with core needle biopsy and neoadjuvant chemotherapy effects in breast cancer patients. *Thorac. Cancer* 6, 64–69. doi: 10.1111/1759-7714.12133

Guan, W. Y., Zhao, S., and Luo, Y. A.-O. (2020). Analysis of the expression and association of retinoblastoma binding protein 6 with the JNK signaling pathway in prostate cancers. *Cell. Biol. Int.* 44, 2107–2119. doi: 10.1002/cbin.11419

Guo, W., Wu, S., Wang, L., Wei, X., Liu, X., Wang, J., et al. (2011). Antitumor activity of a novel oncrasin analogue is mediated by JNK activation and STAT3 inhibition. *PLoS One* 6:e28487. doi: 10.1371/journal.pone.0028487

Haque, M. A., Jantan, I., Harikrishnan, H., and Ghazalee, S. (2019). Standardized extract of Zingiber zerumbet suppresses LPS-induced pro-inflammatory responses through NF-κB, MAPK and PI3K-Akt signaling pathways in U937 macrophages. *Phytomedicine* 54, 195–205. doi: 10.1016/j.phymed.2018.09.183

Harbeck, N., and Gnant, M. (2017). Breast cancer. *Lancet* 389, 1134–1150. doi: 10.1016/S0140-6736(16)31891-8

Harbeck, N., Penault-Llorca, F., Cortes, J., Gnant, M., Houssami, N., Poortmans, P., et al. (2019). Breast cancer. *Nat. Rev. Dis. Primers* 5:66. doi: 10.1038/s41572-019-0111-2

Huang, W., Liang, Y., Chung, H. Y., Wang, G., Huang, J. J., and Li, Y. (2020). Cyperenoic acid, a sesquiterpene derivative from Croton crassifolius, inhibits tumor growth through anti-angiogenesis by attenuating VEGFR2 signal pathway in breast cancer. *Phytomedicine* 76:153253. doi: 10.1016/j.phymed.2020.153253

Izadi, S., Moslehi, A., Kheiry, H., Karoon Kiani, F., Ahmadi, A., Masjedi, A., et al. (2020). Codelivery of HIF-1α siRNA and dinaciclib by carboxylated graphene oxide-trimethyl chitosan-hyaluronate nanoparticles significantly suppresses cancer cell progression. *Pharm. Res.* 37:196. doi: 10.1007/s11095-020-02892-y

Johnson, D. E., O'Keefe, R. A., and Grandis, J. R. (2018). Targeting the IL-6/JAK/STAT3 signalling axis in cancer. *Nat. Rev. Clin. Oncol.* 15, 234–248. doi: 10.1038/nrclinonc.2018.8

Kandori, S., Kojima, T., and Nishiyama, H. (2019). The updated points of TNM classification of urological cancers in the 8th edition of AJCC and UICC. *Jpn. J. Clin. Oncol.* 49, 421–425. doi: 10.1093/jjco/hyz017

Klein, J., Tran, W., Watkins, E., Vesprini, D., Wright, F. C., Look Hong, N. J., et al. (2019). Locally advanced breast cancer treated with neoadjuvant chemotherapy and adjuvant radiotherapy: a retrospective cohort analysis. *BMC Cancer* 19:306. doi: 10.1186/s12885-019-5499-2

Koch, M. K., Jaeschke, A., Murekatete, B., Ravichandran, A., Tsurkan, M., Werner, C., et al. (2020). Stromal fibroblasts regulate microvascular-like network architecture in a bioengineered breast tumour angiogenesis model. *Acta Biomater.* 114, 256–269. doi: 10.1016/j.actbio.2020.07.036

Kumar, A., Singh, U. K., Kini, S. G., Garg, V., Agrawal, S., Tomar, P. K., et al. (2015). JNK pathway signaling: a novel and smarter therapeutic targets for various biological diseases. *Future Med. Chem.* 7, 2065–2086. doi: 10.4155/fmc.15.132

Kunnuru, S. K. R., Thiyagarajan, M., Martin Daniel, J., and Singh, K. B. A. (2020). Study on clinical and pathological responses to neoadjuvant chemotherapy in breast carcinoma. *Breast Cancer* 12, 259–266. doi: 10.2147/BCTT.S277588

Lee, M. G., Lee, K. S., and Nam, K. S. (2020). Anti-metastatic effects of arctigenin are regulated by MAPK/AP-1 signaling in 4T-1 mouse breast cancer cells. *Mol. Med. Rep.* 21, 1374–1382. doi: 10.3892/mmr.2020.10937

Lee, M. M., Chan, B. D., Wong, W. Y., Qu, Z., Chan, M. S., Leung, T. W., et al. (2020). Anti-cancer activity of centipeda minima extract in triple negative breast cancer via inhibition of AKT, NF-kappaB, and STAT3 signaling pathways. *Front. Oncol.* 10:491. doi: 10.3389/fonc.2020.00491

Li, G., Qi, W., Li, X., Zhao, J., Luo, M., and Chen, J. (2020). Recent Advances in c-Jun N-terminal kinase (JNK) inhibitors. *Curr. Med. Chem.* [Epub ahead of print]. doi: 10.2174/0929867327666200210144114

Li, J., Xu, B., Chen, Z., Zhou, C., Liao, L., Qin, Y., et al. (2018). PI3K/AKT/JNK/p38 signalling pathway-mediated neural apoptosis in the prefrontal cortex of mice is involved in the antidepressant-like effect of pioglitazone. *Clin. Exp. Pharmacol. Physiol.* 45, 525–535. doi: 10.1111/1440-1681.12918

Li, J.-Y., Huang, J.-Y., Li, M., Zhang, H., Xing, B., Chen, G., et al. (2012). Anisomycin induces glioma cell death via down-regulation of PP2A catalytic subunit in vitro. *Acta Pharmacol. Sin.* 33, 935–940. doi: 10.1038/aps.2012.46

Lim, C. P., and Cao, X. (1999). Serine phosphorylation and negative regulation of Stat3 by JNK. *J. Biol. Chem.* 274, 31055–31061. doi: 10.1074/jbc.274.43.31055

Linos, E., Spanos, D., Rosner, B. A., Linos, K., Hesketh, T., Qu, J. D., et al. (2008). Effects of reproductive and demographic changes on breast cancer incidence in China: a modeling analysis. *J. Natl. Cancer Inst.* 100, 1352–1360. doi: 10.1093/jnci/djn305

Martínez-Rodríguez, O. A.-O., Thompson-Bonilla, M. A.-O., and Jaramillo-Flores, M. A.-O. (2020). Association between obesity and breast cancer: molecular bases and the effect of flavonoids in signaling pathways. *Crit. Rev. Food Sci. Nutr.* 60, 3770–3792. doi: 10.1080/10408398.2019.1708262

Mieog, J. S., van der Hage Ja, F. A. U., van de Velde, C. J. H., and van de Velde, C. J. (2007). Neoadjuvant chemotherapy for operable breast cancer. *Br. J. Surg.* 94, 1189–1200. doi: 10.1002/bjs.5894

Miyazaki, T., Bub, J. D., and Iwamoto, Y. (2008). c-Jun NH(2)-terminal kinase mediates leptin-stimulated androgen-independent prostate cancer cell proliferation via signal transducer and activator of transcription 3 and Akt. *Biochim. Biophys. Acta* 1782, 593–604. doi: 10.1016/j.bbadis.2008.07.005

Mohebali, N., Pandurangan, A. K., Mustafa, M. R., Anandasadagopan, S. K., and Alagumuthu, T. (2020). Vernodalin induces apoptosis through the activation of ROS/JNK pathway in human colon cancer cells. *J. Biochem. Mol. Toxicol.* 34:e22587. doi: 10.1002/jbt.22587

Montemurro, F., Nuzzolese, I., and Ponzone, R. (2020). Neoadjuvant or adjuvant chemotherapy in early breast cancer? *Expert Opin. Pharmacother.* 21, 1071–1082. doi: 10.1080/14656566.2020.1746273

Narayanankutty, A. (2020). Phytochemicals as PI3K/ Akt/ mTOR inhibitors and their role in breast cancer treatment. *Recent Pat. Anticancer Drug Discov.* 15, 188–199. doi: 10.2174/1574892815666200910164641

Ni, C.-W., Hsieh, H.-J., Chao, Y.-J., and Wang, D. L. (2003). Shear flow attenuates serum-induced STAT3 activation in endothelial cells. *J. Biol. Chem.* 278, 19702–19708. doi: 10.1074/jbc.M300893200

Nie, D., Liu, X., Wang, Y., He, W., Li, M., Peng, Y., et al. (2020). Involvement of the JNK signaling in granular corneal dystrophy by modulating TGF-β-induced TGFBI expression and corneal fibroblast apoptosis. *In Vitro Cell Dev. Biol. Anim.* 56, 234–242. doi: 10.1007/s11626-019-00424-6

Nikaido, M., Otani, T., Kitagawa, N., Ogata, K., Iida, H., Anan, H., et al. (2018). Anisomycin, a JNK and p38 activator, suppresses cell–cell junction formation in 2D cultures of K38 mouse keratinocyte cells and reduces claudin-7 expression, with an increase of paracellular permeability in 3D cultures. *Histochem. Cell Biol.* 151, 369–384. doi: 10.1007/s00418-018-1736-z

Nunnery, S. E., and Mayer, I. A. (2020). Targeting the PI3K/AKT/mTOR pathway in hormone-positive breast cancer. *Drugs* 80, 1685–1697. doi: 10.1007/s40265-020-01394-w

Oh, J. H., Joo, Y. H., Karadeniz, F., Ko, J., and Kong, C.-S. (2020). Syringaresinol inhibits UVA-induced MMP-1 expression by suppression of MAPK/AP-1 signaling in HaCaT keratinocytes and human dermal fibroblasts. *Int. J. Mol. Sci.* 21:3981. doi: 10.3390/ijms21113981

Oh, Y., Jang, M., Cho, H., Yang, S., Im, D., Moon, H., et al. (2019). Discovery of 3-alkyl-5-aryl-1-pyrimidyl-1H-pyrazole derivatives as a novel selective inhibitor scaffold of JNK3. *J. Enzyme Inhibit. Med. Chem.* 35, 372–376. doi: 10.1080/14756366.2019.1705294

Pathak, M., Dwivedi, S. N., Deo, S. V. S., Thakur, B., Sreenivas, V., and Rath, G. K. (2019). Effectiveness of added targeted therapies to neoadjuvant chemotherapy for breast cancer: a systematic review and meta-analysis. *Clin. Breast Cancer* 19, e690–e700. doi: 10.1016/j.clbc.2019.06.001

Phukan, J. P., Sinha, A., and Deka, J. P. (2015). Cytological grading of breast carcinoma on fine needle aspirates and its relation with histological grading. *S. Asian J. Cancer* 4, 32–34. doi: 10.4103/2278-330X.149948

Qin, J. A.-O. X., Yan, L., Zhang, J., and Zhang, W. D. (2019). STAT3 as a potential therapeutic target in triple negative breast cancer: a systematic review. *J. Exp. Clin. Cancer Res.* 38:195. doi: 10.1186/s13046-019-1206-z

Qu, J., Lu, W., Chen, M., Gao, W., Zhang, C., Guo, B., et al. (2020). Combined effect of recombinant human adenovirus p53 and curcumin in the treatment of liver cancer. *Exp. Ther. Med.* 20:18. doi: 10.3892/etm.2020.9145

Reno, E. M., Haughian, J. M., Jackson, T. A., Thorne, A. M., and Bradford, A. P. (2009). c-Jun N-terminal kinase regulates apoptosis in endometrial cancer cells. *Apoptosis* 14, 809–820. doi: 10.1007/s10495-009-0354-6

Santucci, C., Carioli, G., Bertuccio, P., Malvezzi, M., Pastorino, U., Boffetta, P., et al. (2020). Progress in cancer mortality, incidence, and survival: a global overview. *Eur. J. Cancer Prev.* 29, 367–381. doi: 10.1097/CEJ.0000000000000594

Schuringa, J. J., Jonk, L. J., Dokter, W. H., Vellenga, E., and Kruijer, W. (2000). Interleukin-6-induced STAT3 transactivation and Ser727 phosphorylation involves Vav, Rac-1 and the kinase SEK-1/MKK-4 as signal transduction components. *Biochem. J.* 1(Pt 1), 89–96. doi: 10.1042/bj3470089

Shien, T., and Iwata, H. (2020). Adjuvant and neoadjuvant therapy for breast cancer. *Jpn. J. Clin. Oncol.* 50, 225–229. doi: 10.1093/jjco/hyz213

Siegel, R. L., Miller, K. D., and Jemal, A. (2020). Cancer statistics, 2020. *CA Cancer J. Clin.* 70, 7–30. doi: 10.3322/caac.21590

Testa, U., Pelosi, E., and Castelli, G. (2020). Endothelial progenitors in the tumor microenvironment. *Adv. Exp. Med. Biol.* 1263, 85–115. doi: 10.1007/978-3-030-44518-8_7

Wan, W., Hou, Y., Wang, K., Cheng, Y., Pu, X., and Ye, X. (2019). The LXR-623-induced long non-coding RNA LINC01125 suppresses the proliferation of breast cancer cells via PTEN/AKT/p53 signaling pathway. *Cell Death Dis.* 10:248. doi: 10.1038/s41419-019-1440-5

Wang, L. A.-O., Hirano, Y. M., Ishii, T. M., Kondo, H. K., Hara, K. K., Obara, N., et al. (2020). The role of apical lymph node metastasis in right colon cancer. *Int. J. Colorectal. Dis.* 35, 1887–1894. doi: 10.1007/s00384-020-03661-4

Wu, Q., Wu, W., Jacevic, V., Franca, T. C. C., Wang, X., and Kuca, K. (2020). Selective inhibitors for JNK signalling: a potential targeted therapy in cancer. *J. Enzyme Inhib. Med. Chem.* 35, 574–583. doi: 10.1080/14756366.2020.1720013

Xu, R., and Hu, J. (2020). The role of JNK in prostate cancer progression and therapeutic strategies. *Biomed. Pharmacother.* 121:109679. doi: 10.1016/j.biopha.2019.109679

Yacobi, A., and Levy, G. (1975). Importance of assay specificity for plasma protein binding determinations. *J. Pharmacokinet. Biopharm.* 3, 439–441. doi: 10.1007/BF01059475

Yang, X., Li, Y., Chen, L., Xu, M., Wu, J., Zhang, P., et al. (2020). Protective effect of hydroxysafflor yellow A on dopaminergic neurons against 6-hydroxydopamine, activating anti-apoptotic and anti-neuroinflammatory pathways. *Pharm. Biol.* 58, 686–694. doi: 10.1080/13880209.2020.1784237

Yoon, J., Cho, Y., Kim, K. Y., Yoon, M. J., Lee, H. S., Jeon, S. D., et al. (2020). A JUN N-terminal kinase inhibitor induces ectodomain shedding of the cancer-associated membrane protease Prss14/epithin via protein kinase CβII. *J. Biol. Chem.* 295, 7168–7177. doi: 10.1074/jbc.RA119.011206

Zhang, Y. H., Zhang, Y. Q., Guo, C. C., Wang, L. K., Cui, Y. J., Dong, J. J., et al. (2020). Prostaglandin E1 attenuates high glucose-induced apoptosis in proximal renal tubular cells by inhibiting the JNK/Bim pathway. *Acta Pharmacol. Sin.* 41, 561–571. doi: 10.1038/s41401-019-0314-9

Zhao, X., Tang, Y., Wang, S., Yang, Y., Fang, H., Wang, J., et al. (2020). Locoregional recurrence patterns in women with breast cancer who have not undergone post-mastectomy radiotherapy. *Radiat. Oncol.* 15:212. doi: 10.1186/s13014-020-01637-w

Zhou, Y. A.-O., Ming, J., Li, Y., Deng, M., Chen, Q., Ma, Y., et al. (2019). Ligustilide attenuates nitric oxide-induced apoptosis in rat chondrocytes and cartilage degradation via inhibiting JNK and p38 MAPK pathways. *J. Cell. Mol. Med.* 23, 3357–3358. doi: 10.1111/jcmm.14226

Conflict of Interest: The authors declare that the research was conducted in the absence of any commercial or financial relationships that could be construed as a potential conflict of interest.

frontiers in Molecular Biosciences

ORIGINAL RESEARCH
published: 11 March 2021
doi: 10.3389/fmolb.2021.657161

Cell Division Cycle Associated Genes as Diagnostic and Prognostic Biomarkers in Hepatocellular Carcinoma

Shan-Shan Jiang[1†], *Sheng-Jie Ke*[2†], *Zun-Li Ke*[1], *Juan Li*[1], *Xiang Li*[3*] and *Xing-Wei Xie*[1*]

[1]Key Laboratory of Forensic Toxicology of Herbal Medicines, Guizhou Education Department, School of Basic Medicine, Guizhou University of Traditional Chinese Medicine, Guiyang, China, [2]Faculty of Basic Medicine, Zhengzhou Shuqing Medical College, Henan, China, [3]College of Plant Protection, Henan Agricultural University, Zhengzhou, China

With high mortality and poor prognosis, hepatocellular carcinoma (LIHC) has become the fourth leading cause of cancer-related deaths worldwide. Most of the LIHC patients missed the best treatment period because of the untimely diagnosis. For others, even if they are temporarily cured, they have to face a very low prognostic survival rate and a very high risk of recurrence. Based on the characteristics of abnormal proliferation and uncontrolled growth of tumor cells. Cell Division Cycle Associated (*CDCA*) family genes, which are responsible for regulating the cell cycle and proliferation, were selected as our research object to explore the mechanism of hepatocarcinogenesis. To this end, we investigated the expression profiles of *CDCA* family genes in LIHC and corresponding normal tissues, and the effect of *CDCAs* expression on the survival of prognosis and immune cell infiltration through bioinformatics analysis methods and the publicly accessible online databases. In addition, we also analyzed the expression correlation of *CDCAs* and screened the neighboring genes related to functional *CDCAs*. The results revealed that the expression levels of *CDCA1/3/5/8* were significantly increased in LIHC, regardless of stage, sex, race, drinking behavior, and other clinical factors. *CDCAs* expression was significantly correlated with poor prognosis and was positively correlated with the infiltration of dendritic cells, B cells, and macrophages. We also found that the most relevant neighboring genes to *CDCAs* in LIHC were *SGO2*, *NDC80*, *BIRC5*, *INCENP*, and *PLOD1*. In general, our work suggests that *CDCA1/3/5/8* has the potential to be a diagnostic gene in hepatocarcinogenesis and prognostic biomarkers for LIHC patients.

Keywords: CDCA, hepatocellular carcinoma, biomarkers, prognosis, tumor immunity

OPEN ACCESS

Edited by:
Hongming Miao,
Army Medical University, China

Reviewed by:
Huai-Qiang Ju,
Sun Yat-Sen University, China
Xiawei Wei,
West China Hospital, Sichuan University, China

***Correspondence:**
Xiang Li
lixiang0217@126.com
Xing-Wei Xie
xiexingwei123@163.com

†These authors have contributed equally to this work

Specialty section:
This article was submitted to Molecular Diagnostics and Therapeutics, a section of the journal Frontiers in Molecular Biosciences

Received: *22 January 2021*
Accepted: *08 February 2021*
Published: *11 March 2021*

Citation:
Jiang S-S, Ke S-J, Ke Z-L, Li J, Li X and Xie X-W (2021) Cell Division Cycle Associated Genes as Diagnostic and Prognostic Biomarkers in Hepatocellular Carcinoma. Front. Mol. Biosci. 8:657161. doi: 10.3389/fmolb.2021.657161

INTRODUCTION

Liver cancer is the fourth leading cause of cancer-related deaths worldwide, with an estimated incidence rate of over one million cases per year, which seriously endangers human health (Bray et al., 2018; Llovet et al., 2018). Hepatocellular carcinoma (LIHC), accounting for 75–85% of cases, is the main pathological type of primary liver cancer (Bray et al., 2018). The majority of LIHC cases

arise from hepatitis B and hepatitis C in hepatocytes (Zhang et al., 2004; Makarova et al., 2016). Additionally, the rising incidence of LIHC is due to a high rate of alcohol consumption and the occurrence of non-alcoholic fatty liver disease (Schütte et al., 2009; Gish et al., 2016). Although the development of various treatment technologies, including surgical resection, liver transplantation surgery, interventional therapy, chemotherapy, and radiotherapy, may reduce mortality to some extent, LIHC patients still bear a poor five-year survival rate of only 20–30% (Pang et al., 2008; Yang et al., 2009). Thus, there is an urgent need to deepen the understanding of LIHC tumorigenesis and develop new treatment and monitoring methods for early detection and prolong the survival of LIHC patients.

Dysregulation in any process of cell division may lead to malignancy (Collins and Garrett, 2005). Cell Division Cycle Associated (*CDCA*) family proteins, including eight respective members of *CDCA1-8*, function to regulate the cell cycle and proliferation, which play an important role in biological process. Previous studies have shown that the expression levels of all or part of *CDCA* family genes are significantly upregulated in lung cancer, breast cancer, renal cell cancer, etc. This high expression is usually associated with a poor prognosis. For example, *CDCA* genes are highly expressed in ovarian cancer tissues and act on the PLK pathway to promote tumor invasion and metastasis (Chen et al., 2020a; Chen et al., 2020b). *CDCA7* can accelerate the proliferation of lung adenocarcinoma and non-small cell lung cancer by regulating the cell cycle (Wang et al., 2019). High mRNA expression of *CDCA3/5/7/8* in breast cancer significantly reduced the survival rate of patients (Phan et al., 2018). These findings strongly suggest the potential role of *CDCAs* in the tumorigenesis and prognosis of patients. It is necessary and meaningful to understand the mechanism of action of *CDCAs* in LIHC. To date, however, there is no systematic and comprehensive analysis of *CDCAs* in LIHC.

To reveal the mechanism of LIHC tumorigenesis and to identify diagnostic and prognostic markers or therapeutic targets for LIHC patients, in the current study, the transcriptional levels of *CDCA* genes were investigated by Oncomine and GEPIA, and we found that *CDCA1/3/5/8* expression levels were significantly increased in LIHC. We also evaluated the impact of *CDCA1/3/5/8* on the prognosis of LIHC patients. Specifically, we analyzed the effect of *CDCAs* expression on the prognostic survival rate of LIHC patients, the correlation between *CDCAs* transcription and various clinical factors by Kaplan-Meier plotter, and the effect of genetic alterations of *CDCAs* on prognosis by cBioPortal. The relationship between *CDCA1/3/5/8* and immune cell infiltration was analyzed using TIMER 2.0. In addition, the interaction network between *CDCAs* and neighboring genes was mapped using GeneMANIA.

MATERIALS AND METHODS

Oncomine Analysis

The Oncomine platform (https://www.oncomine.org/) is a publicly accessible online tumor-related gene microarray database that collects related gene expression profiles and relevant clinical information. The transcriptional levels of *CDCA* family genes (*CDCA1–8*) in different tumors and corresponding normal tissues were analyzed by Oncomine with approximately 200 samples. The expression levels were considered significantly different when fold change > 2.0 and p-value < 0.0001. We set the threshold value of gene rank to "top 10%" and the data type to "mRNA" (Rhodes et al., 2007).

GEPIA Analysis

GEPIA (http://gepia.cancer-pku.cn/index.html) was used to analyze the expression of *CDCAs* sequencing in liver cancer tissue based on the GTEx and TCGA databases (Tang et al., 2017). GEPIA was used to compare the *CDCAs* expression levels in HCC with the thresholds of |Log2 (Fold Change)| Cut-off: 1 and p-value Cut-off: 0.01. *CDCAs* expression in different HCC stages was analyzed using the default parameters.

Kaplan-Meier Plotter Analysis

Kaplan-Meier plotter (http://kmplot.com/analysis/) was used to evaluate the influence of different expression levels of *CDCA* family genes on prognostic value, including overall survival (OS), disease-specific survival (DSS), relapse-free survival (RFS), progression-free survival (PFS), and OS of liver cancer patients with different clinical factors. We analyzed all samples in the database with the parameters of Group Cut-off: Median; Hazards Ratio: Yes; 95% Confidence Interval: Yes; Follow-up threshold: All.

cBioPortal Analysis

cBioPortal (http://www.cbioportal.org/) was used to perform the interactive analysis of biomolecules in tumor tissues in the TCGA database (Gao et al., 2016). Here, we used it to analyze the alterations in the frequency of *CDCAs* genes change. Putative copy-number calls on 370 cases determined using GISTIC 2.0. In module Comparison/Survival, we analyzed the influence of alterations on prognostic survival in HCC patients by default parameters.

GeneMANIA Analysis

GeneMANIA (http://genemania.org/), based on many large, publicly available biological datasets, is used to identify intra-genomic associations and find co-expressing biomolecules. Here, GeneMANIA was used to identify the physical interactions and co-expression of *CDCAs* with 20 related genes in Homo sapiens datasets by default parameters.

TIMER 2.0 Analysis

Using TIMER 2.0 (http://timer.comp-genomics.org/), we analyzed the relationship between the expression of *CDCAs* and infiltration levels of immune cells in liver cancer tissue. The TIMER database was used to determine the abundance of tumor infiltrates based on biomarker gene expression analysis (Li et al., 2017). Here, we chose *CDCA1/3/5/8* as input and, in turn, detected cancer cells under the Immune

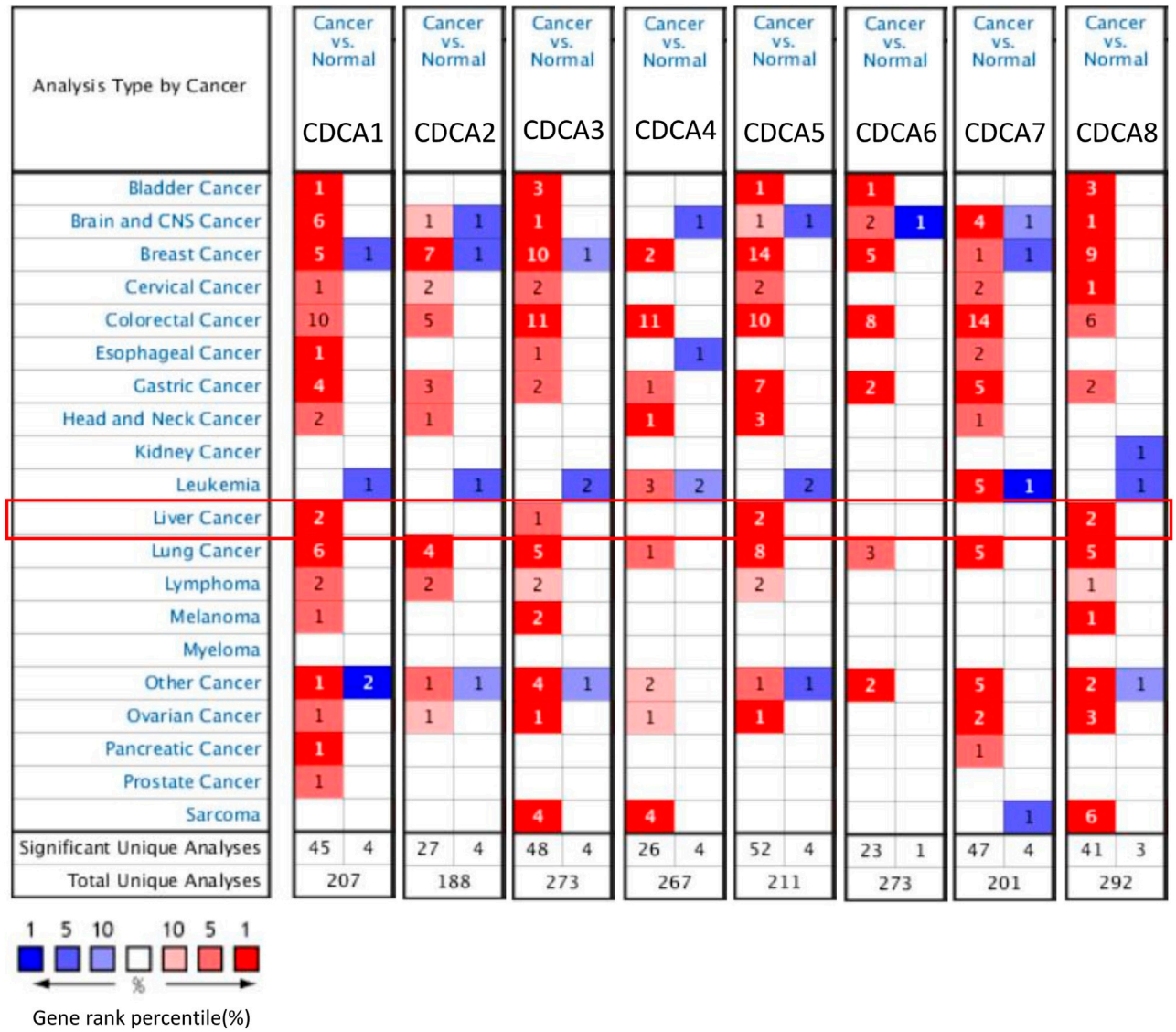

FIGURE 1 | Expression levels of *CDCAs* in various normal or cancer tissues via Oncomine analysis.

Association module. B cells, CD8+ T cells, CD4+ T cells, neutrophils, macrophages, and dendritic cells were selected as the test types according to Li et al. (Li et al., 2016; Danaher et al., 2017). Gene expression values were transformed to Log2 RSEM values.

RESULTS

Expression of Cell Division Cycle Associateds in Hepatocellular Carcinoma and Other Cancers

Dysregulation in any process of cell division may lead to malignancy. It has been reported that there are eight respective members in the *CDCA* family genes, among which members may play an independent role or function cooperatively. Oncomine analysis revealed that most *CDCA* gene members were significantly upregulated in 15 cancer types (**Figure 1**). For LIHC, in particular, we found consistent results in both the Oncomine and GEPIA databases, i.e., the expression of *CDCA1*, *CDCA3*, *CDCA5*, and *CDCA8* in LIHC was significantly higher than those in normal tissues (**Figures 1**, **2A**). Therefore, these genes were selected for follow-up analysis and research objects.

Tumor development is usually subdivided into four stages to assess the extent of cancer cell proliferation and to determine the prognostic potential of patients. In this study, significant differences were observed in the above four members of *CDCA* genes in different stages of liver cancer, suggesting that these four genes may function in the whole course of LIHC tumorigenesis (**Figure 2B**).

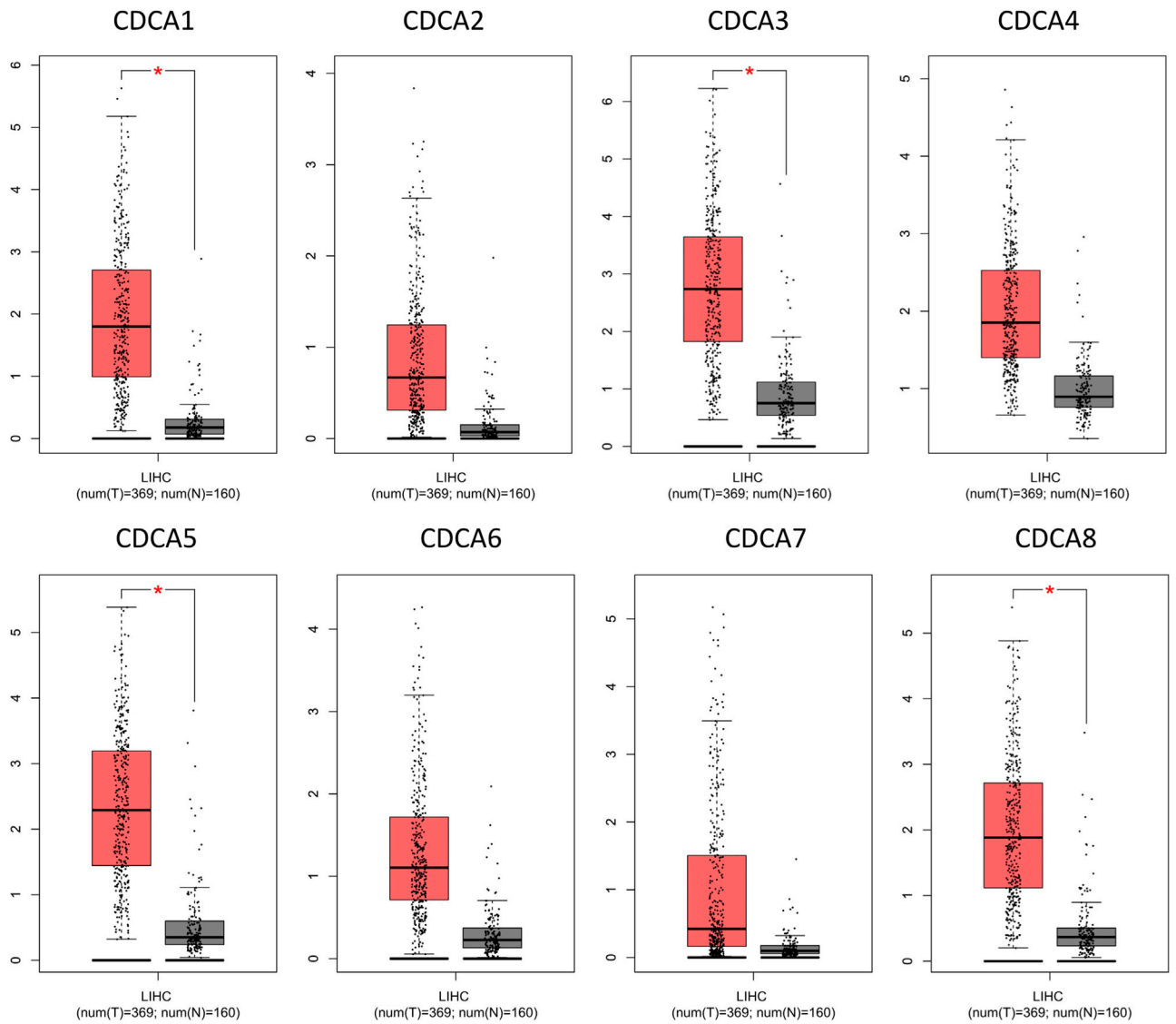

FIGURE 2 | Expression levels of *CDCAs* in LIHC via GEPIA analysis.

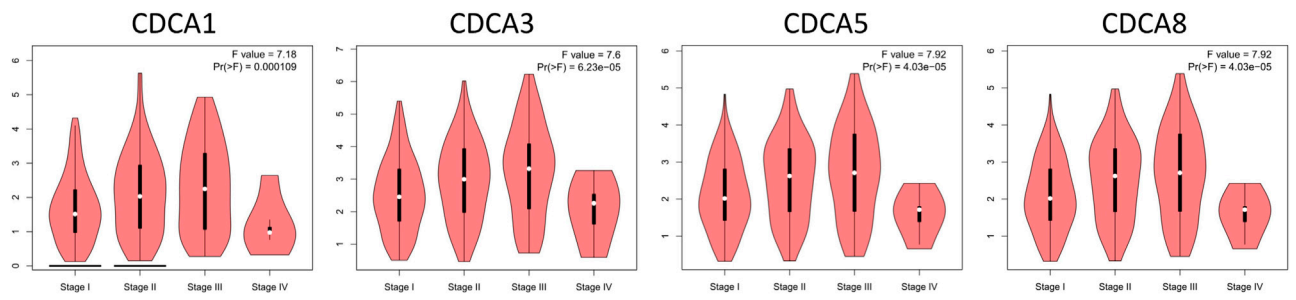

FIGURE 3 | Correlation of *CDCAs* expression with tumor stage among LIHC cases via GEPIA analysis.

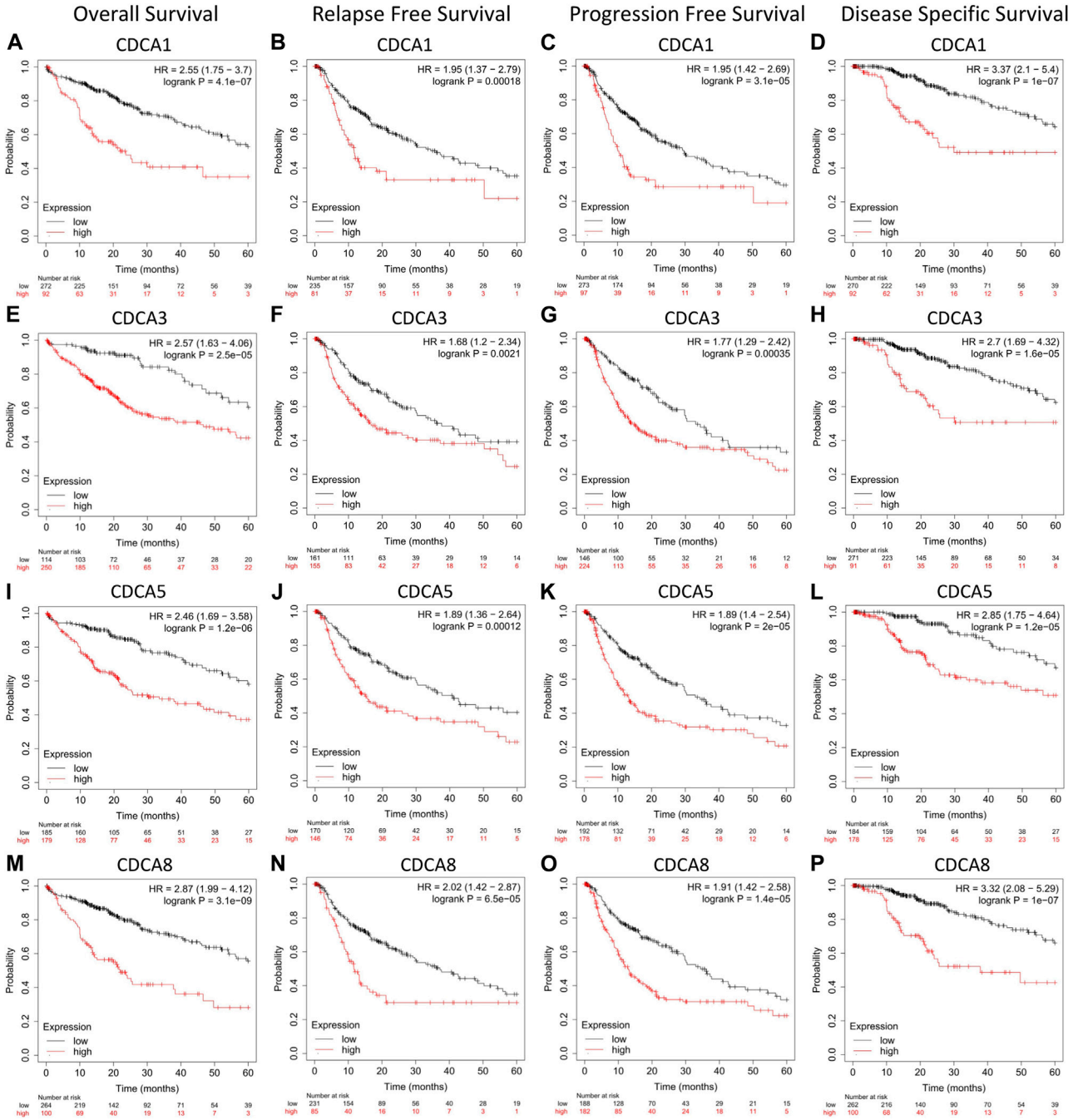

FIGURE 4 | Correlation analysis between *CDCAs* expression and prognostic survival in LIHC patients via Kaplan-Meier plotter analysis. **(A-D)** Correlation between expression of *CDCA1* and survival curves. **(E-H)** Correlation between expression of *CDCA3* and survival curves. **(I-L)** Correlation between expression of *CDCA5* and survival curves. **(M-P)** Correlation between expression of *CDCA8* and survival curves.

Prognostic Potential of Cell Division Cycle Associateds Expression in Hepatocellular Carcinoma

Using the Kaplan-Meier plotter, we found that the transcription level of the four test *CDCA* genes was significantly correlated with the prognostic survival rate of liver cancer patients (**Figure 3**). Specifically, high expression of *CDCAs* in OS, DSS, RFS, and PFS represented poor prognosis, indicating that active transcription of *CDCA1/3/5/8* might cause health risks, and these genes could be potential prognostic biomarkers for LIHC patients (**Figure 4**).

For different types of clinical factors, we further analyzed the relationship between the expression levels of *CDCA1/3/5/8*

TABLE 1 | Correlation analysis between *CDCAs* expression and prognostic overall survival in LIHC patients with different clinicopathological factors via Kaplan-Meier plotter analysis.

Clinical factors			CDCA1	CDCA3	CDCA5	CDCA8
Gender	male	HR (95% CI)	3.90	2.91	2.67	2.72
		p-value	**1.60E-05**	**1.60E-04**	**2.30E-05**	**9.50E-06**
	female	HR (95% CI)	2.37	2.73	2.16	3.16
		p-value	**5.30E-03**	**6.30E-04**	**0.012**	**7.50E-05**
Race	White	HR (95% CI)	2.42	3.30	1.70	2.31
		p-value	**1.90E-03**	**1.60E-03**	**0.029**	**5.30E-03**
	Asian	HR (95% CI)	5.63	4.14	6.26	6.19
		p-value	**2.40E-09**	**5.70E-07**	**8.80E-08**	**1.20E-10**
Alcohol consumption	yes	HR (95% CI)	5.26	3.03	3.39	4.12
		p-value	**1.80E-04**	**6.60E-03**	**4.10E-03**	**7.60E-04**
	none	HR (95% CI)	2.70	2.21	2.45	3.42
		p-value	**3.70E-05**	**8.90E-04**	**3.30E-04**	**1.10E-07**
Hepatitis virus	Yes	HR (95% CI)	1.94	1.68	1.93	2.26
		p-value	**0.04**	0.13	0.05	**0.02**
	None	HR (95% CI)	3.05	3.76	3.39	4.09
		p-value	**4.50E-06**	**5.20E-06**	**4.40E-06**	**4.80E-06**
Vascular invasion	yes	HR (95% CI)	2.65	2.63	2.37	4.54
		p-value	0.11	0.09	0.09	**0.04**
	none	HR (95% CI)	3.66	6.13	5.64	0.06
		p-value	**0.01**	**5.70E-03**	**0.0098**	**5.70E-03**

Bold values indicate p < *0.05.*

genes and prognostic OS (**Table 1**). Here, we concluded that the high expression levels of *CDCAs* led to poor prognosis regardless of sex, race, or alcohol consumption. Notably, when there was no hepatitis virus or vascular infection in LIHC patients, the expression of *CDCA1/3/5/8* was significantly correlated with the survival rate. Interestingly, only *CDCA8* was significantly associated with survival in patients with hepatitis virus or vascular infection (**Table 1**).

Alteration Analysis of Cell Division Cycle Associateds in Hepatocellular Carcinoma

We extracted *CDCA1/3/5/8* genes and investigated the percentages of genetic alterations in the TCGA dataset. In a total of 360 samples, the alteration frequency of *CDCAs* was as high as 29.44% in LIHC (106/360) (**Figure 5A**), with 27% of *CDCA1*, 0.8% of *CDCA3*, 7% of *CDCA5*, and 6% of *CDCA8* (**Figure 5B**). Next, we performed a correlation analysis between cases with (or without) *CDCAs* genetic alterations and prognostic survival. There was a significant correlation between *CDCA* alterations and survival of both OS (4.348e-3) (**Figure 5C**) and DFS (7.932e-3) (**Figure 5D**), implying that these alterations will aggravate the hepatocarcinogenesis mediated by high expression of *CDCAs*, which is not conducive to the survival of patients.

Correlation Analysis Between Cell Division Cycle Associateds Expression Levels and Immune Cell Infiltration in Hepatocellular Carcinoma

TIMER 2.0 was used to investigate the correlation between the expression of *CDCA1/3/5/8* and infiltration levels of immune cells (CD8+ T cells, CD4+ T cells, B cells, neutrophils, macrophages, and dendritic cells). Overall, there was a statistically significant positive correlation between *CDCAs* gene expression and most immune cell infiltration in LIHC. In detail, *CDCAs* showed a poor correlation with CD8+ T cells and neutrophils, but a stronger correlation with dendritic cells, B cells, and macrophages (**Figure 6**).

To provide a basis for exploring the immune mechanisms mediated by *CDCAs* and screening potential therapeutic targets, we further investigated the correlation of expression levels between *CDCA1/3/5/8* and biomarker genes of immune cells and their subsets in LIHC. We found that the *CDCA* gene was positively correlated with all test biomarker genes of dendritic cells and B cells (**Table 2**). Although *CDCAs* showed a significant positive correlation with most of the biomarker genes of M1 macrophage and M2 macrophage, there was no correlation between *CDCA1/3/5/8* and *iNOS* (macrophage biomarker). In addition, there was no association between *CDCA3* and *COX2* or *CD163* (**Table 2**).

Co-Expression and Interaction of Cell Division Cycle Associateds in Hepatocellular Carcinoma

At the genetic level, the expression correlation of the four member genes of *CDCA1/3/5/8* in liver cancer patients was analyzed using cBioPortal. According to our results, the Pearson correlation coefficients ranged from 0.85–0.90, indicating a strong correlation between the expression patterns of these four *CDCAs* in LIHC (**Figure 7A**). The GeneMANIA dataset was used to explore the co-expression of *CDCAs* with other biomolecules. Here, we found that there are physical interactions between *CDCA1*, *CDCA3*, *CDCA5*, and *CDCA8*. The interaction network of CDCAs and the 20 most frequently neighboring genes are shown in **Figure 7B**. The top five *CDCAs* neighboring genes in LIHC were *SGO2*, *NDC80*, *BIRC5*, *INCENP*, and *PLOD1*.

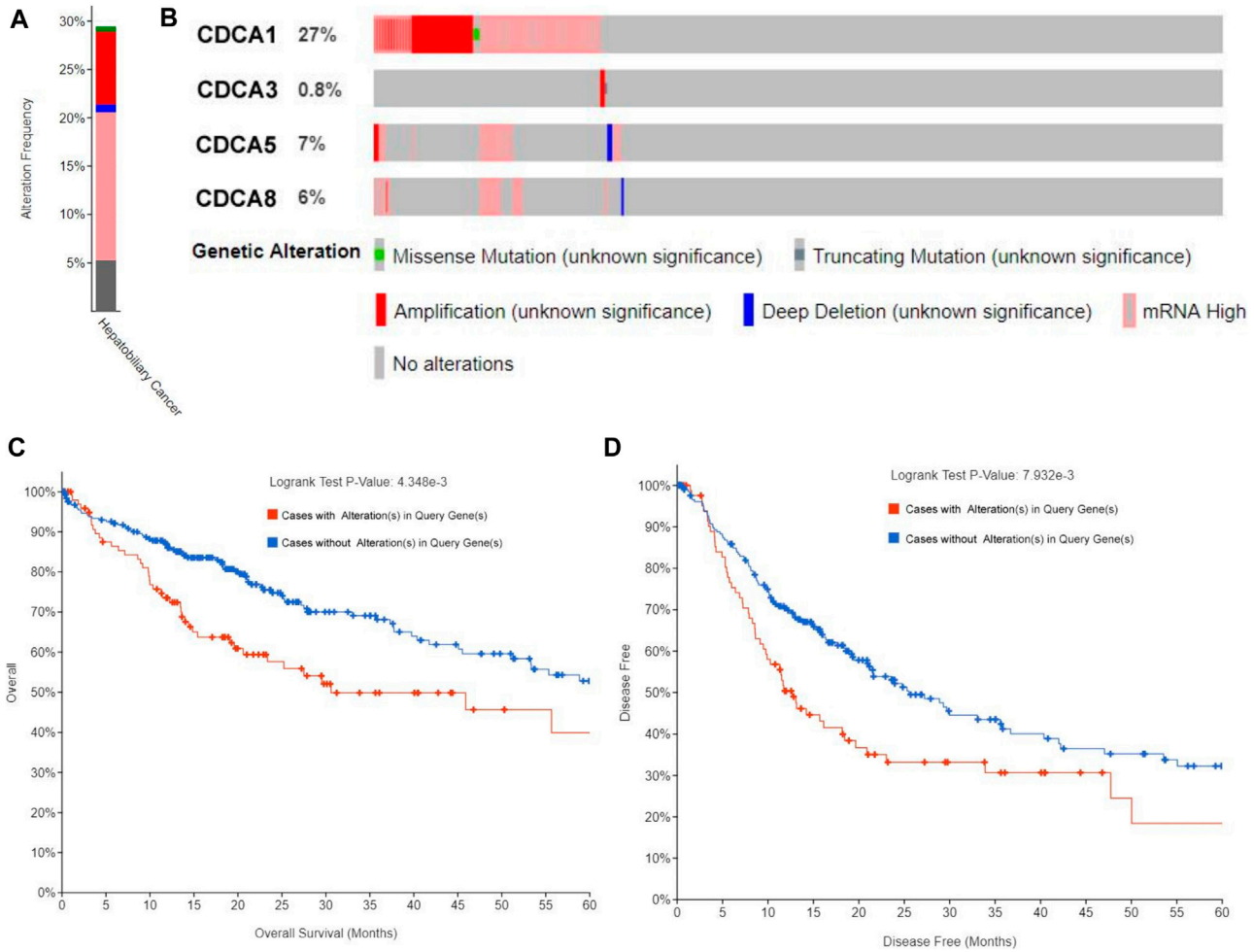

FIGURE 5 | Alteration frequency analysis of *CDCAs* and its influence on prognosis in LIHC patients via cBioPortal analysis. **(A,B)** Alteration frequency of *CDCAs* based on the TCGA provisional dataset. **(C,D)** Kaplan-Meier plots comparing OS **(C)** and DFS **(D)** in cases with/without *CDCAs* genetic alterations.

DISCUSSION

With high mortality and poor prognosis, LIHC has become the fourth leading cause of cancer-related deaths worldwide (Bray et al., 2018). Most of the LIHC patients missed the best treatment period because of the untimely diagnosis. For others, even if they are temporarily cured, they have to face a very low prognostic survival rate and a very high risk of recurrence. Based on the characteristics of abnormal proliferation and uncontrolled growth of tumor cells. *CDCA* genes, which are responsible for regulating the cell cycle and proliferation, were selected as our research object to explore the mechanism of hepatocarcinogenesis. Through a series of bioinformatics analysis methods and the use of publicly accessible online databases, including Oncomine, Kaplan-Meier plotter, GEPIA, GeneMANIA, cBioPortal, and TIMER 2.0, we investigated the expression profiles of *CDCA* family genes in LIHC and corresponding normal tissues, and the effect of *CDCAs* expression on the survival of prognosis and immune cell infiltration. In addition, we also analyzed the expression correlation of *CDCAs* and screened the neighboring genes related to functional *CDCAs*.

We found that the expression levels of *CDCA1/3/5/8* were significantly increased in LIHC, regardless of stage, sex, race, drinking behavior, and other clinical factors. *CDCAs* expression was significantly correlated with poor prognosis of OS, DSS, RFS, and PFS and was positively correlated with the infiltration of dendritic cells, B cells, and macrophages. We also found that the most relevant neighboring genes to *CDCAs* in LIHC were *SGO2*, *NDC80*, *BIRC5*, *INCENP*, and *PLOD1*. In general, our work suggests that *CDCA1/3/5/8* has the potential to be a diagnostic gene in hepatocarcinogenesis and prognostic biomarkers for LIHC patients.

The *CDCA* family consists of eight independent individuals named *CDCA1–8*. To clarify the role of *CDCAs* in LIHC, multiple database analysis was performed, and *CDCA1/3/5/8* was found to

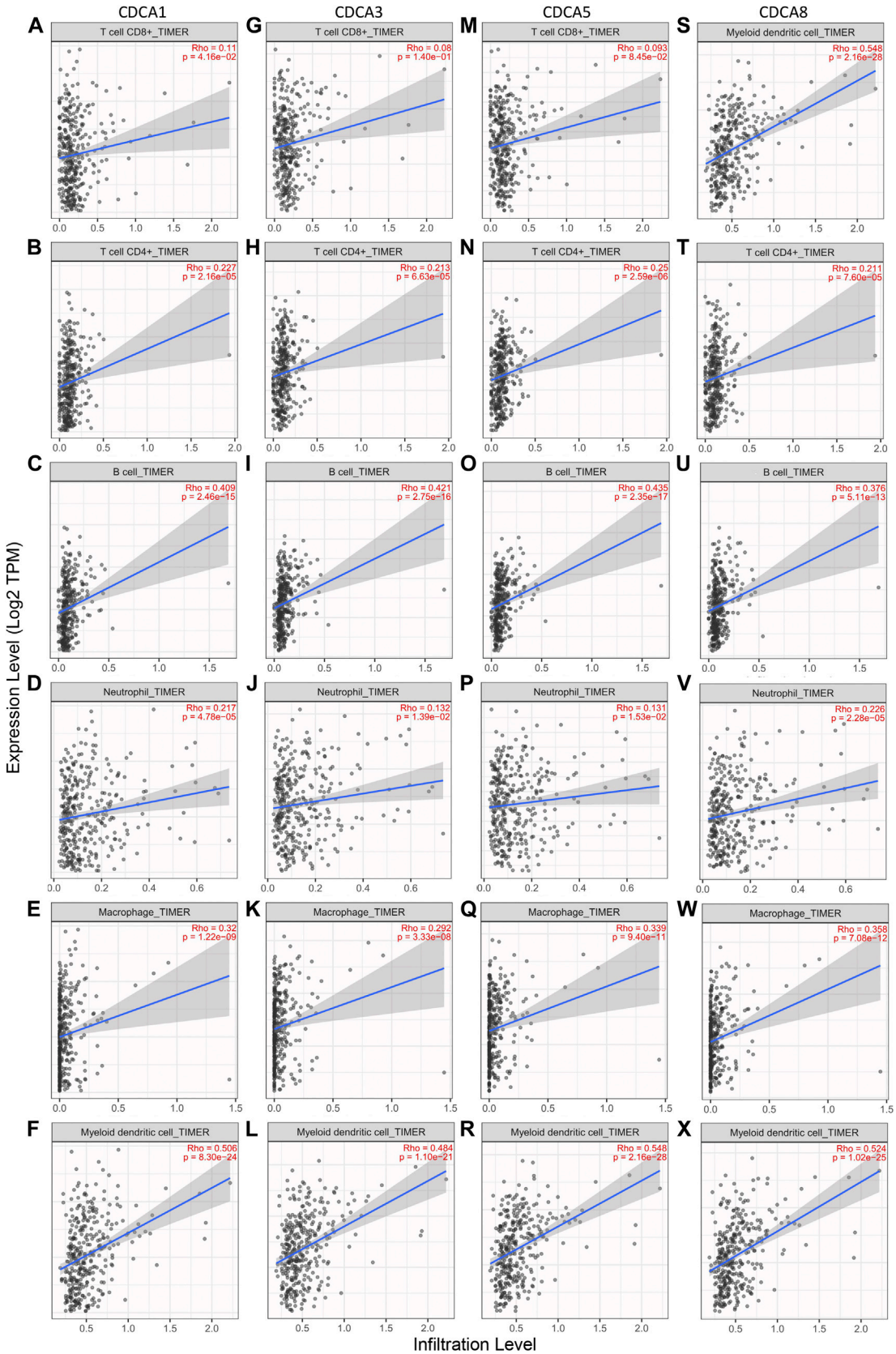

FIGURE 6 | Correlation analysis between *CDCAs* expression and immune cell infiltration levels in LIHC patients via TIMER 2.0 analysis. **(A-F)** Correlation analysis

(*Continued*)

TABLE 2 | Correlation analysis between the expression of *CDCAs* and immune cell biomarker genes in LIHC patients via TIMER 2.0 analysis.

Description	Gene markers	CDCA1		CDCA3		CDCA5		CDCA8	
		Rho	*p* -value	Rho	*p* -value	Rho	*p* -value	Rho	*p* -value
B Cell	CD19	0.372	**8.8E-13**	0.319	**1.38E-09**	0.315	**2.13E-09**	0.320	**1.19E-09**
	CD79A	0.291	**3.54E-08**	0.266	**5.19E-07**	0.260	**9.59E-07**	0.233	**1.19E-05**
M1 Macrophage	NOS2	0.028	6.09E-02	-0.061	2.26E-01	-0.018	7.34E-01	0.052	3.33E-01
	IRF5	0.437	**1.64E-17**	0.372	**9.36E-13**	0.379	**3.15E-13**	0.425	**1.33E-16**
	PTGS2	0.207	**1.09E-04**	0.089	1.00E-01	0.167	**1.83E-03**	0.218	**4.39E-05**
M2 Macrophage	CD163	0.136	**1.14E-02**	0.077	1.54E-01	0.159	**3.13E-03**	0.194	**2.99E-04**
	VSIG4	0.17	**1.58E-03**	0.117	**3.03E-02**	0.196	**2.40E-04**	0.230	**1.65E-05**
	MS4A4A	0.194	**2.82E-04**	0.236	**9.04E-06**	0.207	**1.04E-04**	0.234	**1.16E-05**
Dendritic cell	HLA-DPB1	0.258	**1.22E-06**	0.25	**2.61E-06**	0.297	**1.77E-08**	0.277	**1.78E-07**
	HLA-DQB1	0.231	**1.53E-05**	0.245	**3.96E-06**	0.28	**1.29E-07**	0.253	**1.92E-06**
	HLA-DRA	0.295	**2.47E-08**	0.236	**9.26E-06**	0.287	**5.95E-08**	0.309	**4.35E-09**
	HLA-DPA1	0.256	**1.41E-06**	0.203	**1.47E-04**	0.264	**6.75E-07**	0.290	**4.35E-08**
	CD1C	0.202	**1.59E-04**	0.159	**3.00E-02**	0.187	**4.88E-04**	0.171	**1.46E-03**
	NRP1	0.224	**2.73E-05**	0.141	**8.74E-03**	0.177	**9.40E-04**	0.274	**2.45E-07**
	ITGAX	0.442	**6.51E-18**	0.408	**2.98E-15**	0.445	**3.51E-18**	0.467	**4.50E-20**

Bold values indicate p < *0.05.*

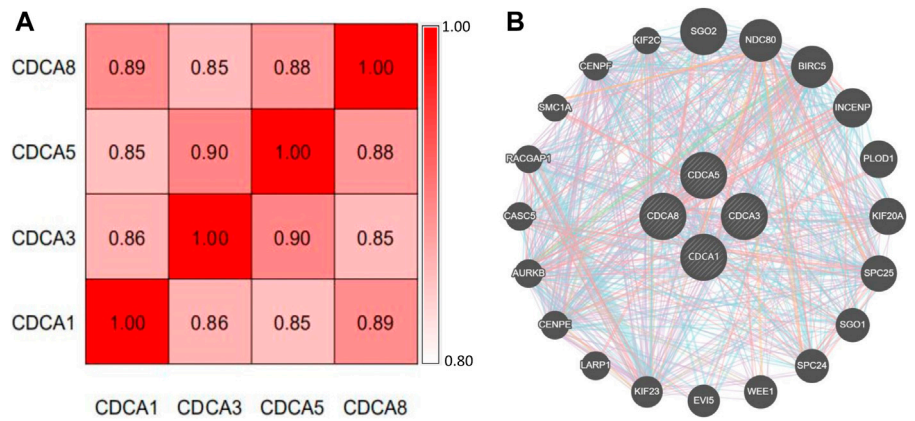

FIGURE 7 | Co-expression and interaction of *CDCAs* at the gene and protein levels in LIHC patients. **(A)** Spearman's correlation analysis of *CDCAs*. **(B)** Gene–gene interaction network among *CDCAs* in the GeneMANIA dataset.

be highly expressed in LIHC tissue. Moreover, this active expression of *CDCAs* was observed in all stages of LIHC, indicating that *CDCA1/3/5/8* has potential as a diagnostic gene for the occurrence and development of LIHC. Similarly, *CDCA* has been shown to be highly expressed in many other cancer types, such as breast cancer and lung cancer, indicating its wide applicability and functional conservation. However, there was no significant upregulation of *CDCAs* in leukemia, suggesting that it is necessary to distinguish the types of cancer when they were used as diagnostic genes.

According to previous reports, *CDCA1*, also known as *Nuf2*, is mainly responsible for regulating cell mitosis (Zhang et al., 2015). Downregulation of *CDCA1* expression can inhibit the proliferation of tumor cells, while overexpression of *CDCA1* is associated with poor prognosis (Hu et al., 2015). *CDCA3* has been shown to promote cell proliferation and invasion through activation of the Ras signaling pathway or hypomethylation in gastric cancer cells (Zhang et al., 2019). *CDCA5* plays important roles in migration, proliferation, apoptosis, and invasion of tumor cells by regulating sister chromatid segregation and cohesion (Xu et al., 2019). *CDCA8* is an integral part of the chromosomal passenger complex, which is involved in mitosis and contributes to distant metastasis of cancer cells (Jeon et al., 2017). It is worth noting that the high expression of these four genes has been

FIGURE 6 | between *CDCA1* expression and immune cell infiltration levels. **(G-L)** Correlation analysis between *CDCA3* expression and immune cell infiltration levels. **(M-R)** Correlation analysis between *CDCA5* expression and immune cell infiltration levels. **(S-X)** Correlation analysis between *CDCA8* expression and immune cell infiltration levels.

proven to reduce the prognostic survival rate of many cancer patients. This is consistent with the results of our study. In particular, there is a significant negative correlation between *CDCAs* and four common prognostic indices of OS, DSS, RFS, and PFS, and this correlation is applicable to different clinical factors, suggesting that high expression of *CDCAs* may be one of the causes of poor prognosis. These biomolecules have the potential to be prognostic biomarkers for LIHC patients.

However, in the presence of pathological conditions, such as hepatitis virus or vascular invasion, there was no correlation between *CDCAs* and OS, except for *CDCA8*, suggesting that we should consider the patient's clinical condition when selecting the diagnostic gene. In addition, we found that the alteration frequency of *CDCAs* is extremely high, and the genetic alteration will reduce the prognosis survival of LIHC patients. The factors causing gene alteration should be avoided in the process of treatment, and the degree of an alteration should be properly considered when detecting expression and evaluating prognosis.

Dendritic cells are special antigen-presenting cells that play a major role in activating T lymphocytes with anti-tumor effects (Wculek et al., 2020). B cells can produce a kind of IgG antibody to recognize a certain antigen in tumor tissue, which can inhibit tumor growth (Li et al., 2009). Macrophages were divided into M1 macrophages and M2 macrophages. M1 macrophages are mainly related to the recognition and attack of tumor cells, while M2 macrophages are related to tumor progression and immunosuppression (Yang and Zhang, 2017; Shapouri et al., 2018). *CDCAs* showed a significant positive correlation with dendritic cells, B cells, and macrophages, indicating that *CDCA*-mediated hepatocarcinogenesis might mobilize the activity of these immune cells and make them play an anti-tumor role. When we further analyzed the relationship between *CDCA1/3/5/8* expression and the biomarker genes of immune cells, we found a significant positive correlation between *CDCAs* expression and all test biomarkers of B cells and dendritic cells. However, for M1 macrophages and M2 macrophages, *CDCAs* were only related to some of macrophages biomarker genes, indicating that there is a certain specificity and selectivity in this interaction, which also provides some basis for immunotherapy in the future.

Although these four genes have some differences in function and target genes (pathways), they jointly regulate the cell division cycle to promote the proliferation and invasion of tumor cells. The Pearson correlation coefficients of these four genes were all greater than 0.85. GeneMANIA analysis showed twenty neighboring genes to *CDCAs*, and the functions of these genes are also related to cell cycle regulation. For example, *SGO1* is considered to play a major role in recruiting the chromosomal passenger complex to chromosomes (Bonner et al., 2020); *SGO2* is a pericentromeric protein that associates with cohesin at centromeres and regulates chromosomal segregation during meiosis (El et al., 2017). *SGO1/2* functions as an essential protector for centromeric cohesion and is required for accurate chromosome segregation during mitosis and meiosis (Dudas et al., 2011). *PLOD1* has been reported to function in extracellular matrix formation and is involved in various diseases, including cancer (Wang et al., 2018). The *NDC80* complex, including the main elements of *NDC80*, *SPC24*, and *SPC25*, is highly expressed in various tumors and cooperatively promotes the invasion and metastasis of tumor cells (Alushin et al., 2012; Umbreit et al., 2012). *BIRC5* is a negative regulatory protein that inhibits tumor cell apoptosis and promotes cell proliferation (Cho et al., 2020; Shi et al., 2020).

These proteins are more or less involved in the development of tumors, which explains the mechanism of *CDCA*-mediated hepatocarcinogenesis to a certain extent. This also screened out some targets for future research on new therapeutic methods. However, the specific roles of *CDCAs* in tumorigenesis and development, as well as their interaction with target proteins need to be further verified. The same shortcomings run through our research because the results were based on big data mining and analysis, which inevitably led to some false-positive results. An important purpose was to provide researchers with a more instructive research idea and tried to make our findings point out a direction for future research. Although we mined the data as comprehensively as possible and had obtained some meaningful conclusions, the relevant results still require further experimental and clinical verification.

DATA AVAILABILITY STATEMENT

The original contributions presented in the study are included in the article/Supplementary Material, further inquiries can be directed to the corresponding authors.

ETHICS STATEMENT

Ethical review and approval was not required for the study on human participants in accordance with the local legislation and institutional requirements. The patients/participants provided their written informed consent to participate in this study.

AUTHOR CONTRIBUTIONS

XL and X-WX contributed to the concept and wrote the manuscript. S-SJ, S-JK, Z-LK, and JL designed experiments, performed experiments, and analyzed data. S-SJ and S-JK contributed equally to this study.

FUNDING

This work was supported by 2019 Doctor Initiation Fund of Guizhou University of Chinese Medicine (3043-043190019) and Research Initiation Foundation for Doctor of Henan Agricultural University (30602107).

REFERENCES

Alushin, G. M., Musinipally, V., Matson, D., Tooley, J., Stukenberg, P. T., and Nogales, E. (2012). Multimodal microtubule binding by the Ndc80 kinetochore complex. *Nat. Struct. Mol. Biol.* 19, 1161–1180. doi:10.1038/nsmb.2411

Bonner, M. K., Haase, J., Saunders, H., Gupta, H., Li, B., and Kelly, A. E. (2020). The borealin dimerization domain interacts with Sgo1 to drive aurora B-mediated spindle assembly. *Mol. Biol. Cell.* 31, 2207–2218. doi:10.1091/mbc.E20-05-0341

Bray, F., Ferlay, J., Soerjomataram, I., Siegel, R. L., Torre, L. A., and Jemal, A. (2018). Global cancer statistics 2018: GLOBOCAN estimates of incidence and mortality worldwide for 36 cancers in 185 countries. *CA Cancer J. Clin.* 68, 394–424. doi:10.3322/caac.21492

Chen, C., Chen, S., Luo, M., Yan, H., Pang, L., Zhu, C., et al. (2020a). The role of the CDCA gene family in ovarian cancer. *Ann. Transl. Med.* 8, 190. doi:10.21037/atm.2020.01.99

Chen, C., Chen, S., Pang, L., Yan, H., Luo, M., Zhao, Q., et al. (2020b). Analysis of the expression of cell division cycle-associated genes and its prognostic significance in human lung carcinoma: a review of the literature databases. *Biomed. Res. Int.* 2020, 1–14. doi:10.1155/2020/6412593

Cho, M., Lee, O.-H., Chang, E. M., Lee, S., Moon, S., Lee, J., et al. (2020). BIRC5 expression is regulated in uterine epithelium during the estrous cycle. *Genes* 11, 282–295. doi:10.3390/genes11030282

Collins, I., and Garrett, M. D. (2005). Targeting the cell division cycle in cancer: CDK and cell cycle checkpoint kinase inhibitors. *Curr. Opin. Pharmacol.* 5, 366–373. doi:10.1016/j.coph.2005.04.009

Danaher, P., Warren, S., Dennis, L., D'Amico, L., White, A., Disis, M. L., et al. (2017). Gene expression markers of tumor infiltrating leukocytes. *J. Immunother. Cancer* 5, 18–32. doi:10.1186/s40425-017-0215-8

Dudas, A., Ahmad, S., and Gregan, J. (2011). Sgo1 is required for co-segregation of sister chromatids during achiasmate meiosis I. *Cell cycle* 10, 951–955. doi:10.4161/cc.10.6.15032

El, Y. W., Buffin, E., Cladière, D., Gryaznova, Y., Berenguer, I., Touati, S. A., et al. (2017). Mps1 kinase-dependent Sgo2 centromere localisation mediates cohesin protection in mouse oocyte meiosis I. *Nat. Commun.* 8, 1–15. doi:10.1038/s41467-017-00774-3

Gao, J., Lindsay, J., Watt, S., Bahceci, I., Lukasse, P., Abeshouse, A., et al. (2016). Abstract 5277: The cBioPortal for cancer genomics and its application in precision oncology. *Cancer Res.* 76, 5277. doi:10.1158/1538-7445.AM2016-5277

Gish, R. G., Lencioni, R., Di Bisceglie, A. M., Raoul, J. L., and Mazzaferro, V. (2016). Role of the multidisciplinary team in the diagnosis and treatment of hepatocellular carcinoma. *Expert Rev. Gastroenterol. Hepatol.* 6, 173–185. doi:10.1586/egh.11.105

Hu, P., Shangguan, J., and Zhang, L. (2015). Downregulation of NUF2 inhibits tumor growth and induces apoptosis by regulating lncRNA AF339813. *Int. J. Clin. Exp. Pathol.* 8, 2638–2648. doi:10.1287/orsc.12.5.599.10094

Jeon, T.-W., Ko, M. J., Seo, Y.-R., Baik, I. H., Hwang, I., Ryoo, H.-M., et al. (2017). Abstract 3113: Knockdown of cell division cycle-associated 8 (CDCA8) suppresses hepatocellular carcinoma growth via the upregulation of tumor suppressor ATF3. *Cancer Res.* 77, 3113. doi:10.1158/1538-7445.AM2017-3113

Li, Q., Song, H., Teitz-Tennenbaum, S., Donald, E. J., Li, M., and Chang, A. E. (2009). *In vivo* sensitized and *in vitro* activated B cells mediate tumor regression in cancer adoptive immunotherapy. *J. Immunol.* 183, 3195–3203. doi:10.4049/jimmunol.0803773

Li, B., Severson, E., Pignon, J. C., Zhao, H., Li, T., Novak, J., et al. (2016). Comprehensive analyses of tumor immunity: implications for cancer immunotherapy. *Genome Biol.* 17, 174–189. doi:10.1186/s13059-016-1028-7

Li, T., Fan, J., Wang, B., Traugh, N., Chen, Q., Liu, J. S., et al. (2017). TIMER: A web server for comprehensive analysis of tumor-infiltrating immune cells. *Cancer Res.* 77, 108–110. doi:10.1158/0008-5472.CAN-17-0307

Llovet, J. M., Montal, R., Sia, D., and Finn, R. S. (2018). Molecular therapies and precision medicine for hepatocellular carcinoma. *Nat. Rev. Clin. Oncol.* 15, 599–616. doi:10.1038/s41571-018-0073-4

Makarova, R. O. V., Altekruse, S. F., McNeel, T. S., Ulahannan, S., Duffy, A. G., Graubard, B. I., et al. (2016). Population attributable fractions of risk factors for hepatocellular carcinoma in the United States. *Cancer* 122, 1757–1765. doi:10.1002/cncr.29971

Pang, R. W. C., Joh, J. W., Johnson, P. J., Monden, M., Pawlik, T. M., Poon, R. T. P., et al. (2008). Biology of hepatocellular carcinoma. *Ann. Surg. Oncol.* 15, 962–971. doi:10.1245/s10434-007-9730-z

Phan, N. N., Wang, C. Y., Li, K. L., Chen, C. F., Chiao, C. C., Yu, H. G., et al. (2018). Distinct expression of CDCA3, CDCA5, and CDCA8 leads to shorter relapse free survival in breast cancer patient. *Oncotarget* 9, 6977–6992. doi:10.18632/oncotarget.24059

Rhodes, D. R., Kalyana-Sundaram, S., Mahavisno, V., Varambally, R., Yu, J., Briggs, B. B., et al. (2007). Oncomine 3.0: genes, pathways, and networks in a collection of 18,000 cancer gene expression profiles. *Neoplasia* 9, 166–180. doi:10.1593/neo.07112

Schütte, K., Bornschein, J., and Malfertheiner, P. (2009). Hepatocellular carcinoma-epidemiological trends and risk factors. *Dig. Dis.* 27, 80–92. doi:10.1159/000218339

Shapouri, M. A., Mohammadian, S., Vazini, H., Taghadosi, M., Esmaeili, S. A., Mardani, F., et al. (2018). Macrophage plasticity, polarization, and function in health and disease. *J. Cell.* Physiol. 233, 6425–6440. doi:10.1002/jcp.26429

Shi, J., Tan, S. Y., Lee, A., Zhang, S., Sasidharan, S. L., Wong, B., et al. (2020). Restoring apoptosis dysregulation using survivin inhibitor in nasopharyngeal cancer. *Head Neck* 42, 913–923. doi:10.1002/hed.26068

Tang, Z., Li, C., Kang, B., Gao, G., Li, C., and Zhang, Z. (2017). GEPIA: a web server for cancer and normal gene expression profiling and interactive analyses. *Nucleic Acids Res.* 45, 98–102. doi:10.1093/nar/gkx247

Umbreit, N. T., Gestaut, D. R., Tien, J. F., Vollmar, B. S., Gonen, T., Asbury, C. L., et al. (2012). From the Cover: The Ndc80 kinetochore complex directly modulates microtubule dynamics. *Proc. Natl. Acad. Sci. U.S.A.* 109, 16113–16118. doi:10.1073/pnas.1209615109

Wang, D., Zhang, S., and Chen, F. (2018). High expression of PLOD1 drives tumorigenesis and affects clinical outcome in gastrointestinal carcinoma. *Genet. Test. Mol. Biomarkers* 22, 366–373. doi:10.1089/gtmb.2018.0009

Wang, H. Y., Ye, L., Xing, Z., Li, H. Q., Lv, T. F., Liu, H. B., et al. (2019). CDCA7 promotes lung adenocarcinoma proliferation via regulating the cell cycle. *Pathol. Res. Pract.* 215, 152559. doi:10.1016/j.prp.2019.152559

Wculek, S. K., Cueto, F. J., Mujal, A. M., Melero, I., Krummel, M. F., and Sancho, D. (2020). Dendritic cells in cancer immunology and immunotherapy. *Nat. Rev. Immunol.* 20, 7–24. doi:10.1038/s41577-019-0210-z

Xu, J., Zhu, C., Yu, Y., Wu, W., Cao, J., Li, Z., et al. (2019). Systematic cancer-testis gene expression analysis identified CDCA5 as a potential therapeutic target in esophageal squamous cell carcinoma. *EBioMedicine* 46, 54–65. doi:10.1016/j.ebiom.07.03010.1016/j.ebiom.2019.07.030

Yang, L. Y., Fang, F., Ou, D. P., Wu, W., Zeng, Z. J., and Wu, F. (2009). Solitary large hepatocellular carcinoma: a specific subtype of hepatocellular carcinoma with good outcome after hepatic resection. *Ann. Surg.* 249, 118–123. doi:10.1097/SLA.0b013e3181904988

Yang, L., and Zhang, Y. (2017). Tumor-associated macrophages: from basic research to clinical application. *J. Hematol. Oncol.* 10, 1–12. doi:10.1186/s13045-017-0430-2

Zhang, B. H., Yang, B. H., and Tang, Z. Y. (2004). Randomized controlled trial of screening for hepatocellular carcinoma. *J. Cancer Res. Clin. Oncol.* 130, 417–422. doi:10.1007/s00432-004-0552-0

Zhang, T., Zhou, Y., Qi, S. T., Wang, Z. B., Qian, W. P., Ouyang, Y. C., et al. (2015). Nuf2 is required for chromosome segregation during mouse oocyte meiotic maturation. *Cell cycle* 14, 2701–2710. doi:10.1080/15384101.2015.1058677

Zhang, Y., Yin, W., Cao, W., Chen, P. S., Bian, L. J., and Ni, Q. F. (2019). CDCA3 is a potential prognostic marker that promotes cell proliferation in gastric cancer. *Oncol. Rep.* 41, 2471–2481. doi:10.3892/or.2019.7008

Conflict of Interest: The authors declare that the research was conducted in the absence of any commercial or financial relationships that could be construed as a potential conflict of interest.

frontiers in Cell and Developmental Biology

ORIGINAL RESEARCH
published: 30 March 2021
doi: 10.3389/fcell.2021.656741

Prognostic Nutritional Index (PNI) in Patients With Breast Cancer Treated With Neoadjuvant Chemotherapy as a Useful Prognostic Indicator

Li Chen[1†], Ping Bai[2†], Xiangyi Kong[1†], Shaolong Huang[3], Zhongzhao Wang[1], Xiangyu Wang[1], Yi Fang[1] and Jing Wang[1*]*

[1] Department of Breast Surgical Oncology, National Cancer Center/National Clinical Research Center for Cancer/Cancer Hospital, Chinese Academy of Medical Sciences and Peking Union Medical College, Beijing, China, [2] Department of Operation Room, National Cancer Center/National Clinical Research Center for Cancer/Cancer Hospital, Chinese Academy of Medical Sciences and Peking Union Medical College, Beijing, China, [3] Department of Breast and Thyroid, Traumatic and Plastic Surgery, Tongren Municipal People's Hospital, Guizhou, China

OPEN ACCESS

Edited by:
Na Luo,
Nankai University, China

Reviewed by:
Hongjiang Song,
Harbin Medical University, China
Lihua Zhu,
North China University of Science and Technology, China

****Correspondence:***
Yi Fang
fangyi@cicams.ac.cn
Jing Wang
wangjing@cicams.ac.cn

[†] These authors have contributed equally to this work

Specialty section:
This article was submitted to Molecular Medicine, a section of the journal Frontiers in Cell and Developmental Biology

Received: *21 January 2021*
Accepted: *08 February 2021*
Published: *30 March 2021*

Citation:
Chen L, Bai P, Kong X, Huang S, Wang Z, Wang X, Fang Y and Wang J (2021) Prognostic Nutritional Index (PNI) in Patients With Breast Cancer Treated With Neoadjuvant Chemotherapy as a Useful Prognostic Indicator. Front. Cell Dev. Biol. 9:656741. doi: 10.3389/fcell.2021.656741

Objective: Prognostic nutritional index (PNI), calculated as serum albumin (ALB) (g/L) + 5 × total lymphocyte count (10^9/L), is initially used to evaluate nutritional status in patients undergoing surgery and may evaluate the therapeutic effects and predict the survival of various solid tumors. The present study aimed to evaluate the potential prognostic significance of PNI in breast cancer patients receiving neoadjuvant chemotherapy (NACT).

Methods: A total of 785 breast cancer patients treated with neoadjuvant chemotherapy were enrolled in this retrospective study. The optimal cutoff value of PNI by receiver operating characteristic curve stratified patients into a low-PNI group (<51) and a high PNI group (≥51). The associations between breast cancer and clinicopathological variables by PNI were determined by chi-square test or Fisher's exact test. Kaplan–Meier plots and log-rank test were used to evaluate the clinical outcomes of disease-free survival (DFS) and overall survival (OS). The prognostic value of PNI was analyzed by univariate and multivariate Cox proportional hazards regression models. The toxicity of NACT was accessed by the National Cancer Institute Common Toxicity Criteria (NCI-CTC).

Results: The results indicated that PNI had prognostic significance by an optimal cutoff value of 51 on DFS and OS in univariate and multivariate Cox regression survival analyses. Breast cancer patients with a high PNI value had longer DFS and OS than those with a low PNI value [47.64 *vs*. 36.60 months, $P < 0.0001$, hazard ratio (HR) = 0.264, 95%CI = 0.160–0.435; 73.61 *vs*. 64.97 months, $P < 0.0001$, HR = 0.319, 95%CI = 0.207–0.491, respectively]. Furthermore, the results indicated that patients with high PNI had longer DFS and OS than those with low PNI in early stage and advanced breast cancer, especially in advanced breast cancer. The mean DFS and OS times for breast cancer patients with high PNI by the log-rank test were longer than in those with low PNI in different molecular subtypes. Moreover, the mean DFS

and OS times in patients with high PNI by the log-rank test were longer than in those patients with low PNI without or with lymph vessel invasion. The common toxicities after neoadjuvant chemotherapy were hematologic and gastrointestinal reaction, and the PNI had no significance on the toxicities of all enrolled patients, except in anemia, leukopenia, and myelosuppression.

Conclusion: Pretreatment PNI with the advantages of being convenient, noninvasive, and reproducible was a useful prognostic indicator for breast cancer patients receiving neoadjuvant chemotherapy and is a promising biomarker for breast cancer on treatment strategy decisions.

Keywords: prognostic nutritional index, breast cancer, neoadjuvant chemotherapy, survival, biomarker

INTRODUCTION

Breast cancer is the most common cancer in women and is the most frequent cause of cancer-related morbidity and mortality for women throughout the world (Siegel et al., 2019). The incidence of breast cancer is increasing year after year, and the survivors with this diagnosis account for almost one fourth of the over 14 million cancer survivors in the United States (Ganz and Goodwin, 2015). As many basic and clinical trial research have been conducted in breast cancer for several decades, we have learned much about the mechanisms of breast cancer and have evolved a complex and multidisciplinary treatment approach, such as surgery, chemotherapy, radiation therapy, targeted therapy, immunotherapy, and so forth (Nagini, 2017; Emens, 2018). However, the prolonged survival trajectory of breast cancer survivors remains complicated and unpredictable by breast cancer recurrence or treatment-related physical effects (Lucas et al., 2017). As a result of these posttreatment late effects, about 30% of breast cancer survivors have reported social difficulties, poorer mental health, physical function decline, and poorer quality of life (Falisi et al., 2017).

Around one third of cancer deaths are caused by the following lifestyle choices: low levels of physical activity, low fruit and vegetable intake, high body mass index (BMI), smoking, and alcohol consumption (Lacombe et al., 2019). Malnutrition is a common finding in cancer patients, and their nutritional status is an important factor influencing their prognosis depending on the clinical type, pathological stage, curative treatment, and the individual patient (Bumrungpert et al., 2018; Clemente et al., 2018). Nutritional immune status is closely related to many aspects of tumors. In Li's study, it was found that high levels of globulin (GLB) were correlated with poor survival in patients with rectal cancer (Li et al., 2015). The albumin-to-globulin ratio (AGR) was an independent prognostic factor for both overall survival (OS) and cancer-specific survival (CSS) for patients with localized or locally advanced clear cell renal cell carcinoma (CCRCC), and patients with low AGR had poorer OS and CSS (Chen et al., 2017). Moreover, BMI has been proven as an independent prognostic factor for breast cancer, and patients with very high or low BMI have poorer survival compared with normal-weight patients (Bhaskaran et al., 2014; Cespedes Feliciano et al., 2017). Malnutrition and poor immune status may increase the risk of postoperative complications, decrease the response to antitumor therapy, and be associated with poor survival (Liu et al., 2015; Okadome et al., 2020).

Neoadjuvant chemotherapy (NACT) is the standard of care for breast cancer with aggressive biological features (Li et al., 2017). NACT can improve the resectability of locally advanced breast cancer and inflammatory breast cancer, decrease the pathology stage and improve the feasibility and cosmetic effect of breast-conserving surgery, and decrease morbidity and the extent of axillary surgery in women with significant nodal disease (Echeverria et al., 2019). Despite the vast amount of NACT regimens having been conducted in the treatment of breast cancer, there is no internationally generally accepted NACT regimen for patients with advanced breast carcinoma (Wu et al., 2019). Some biomarkers that have been proven are applied to evaluate the treatment efficacy and prognosis of patients with locally advanced breast cancer who are receiving neoadjuvant therapy. In molecular subtypes of breast cancer, the estrogen receptor (ER) status, progesterone receptor (PR) status, Ki-67 status, and human epidermal growth factor receptor-2 (HER-2) status are also critical for the prognosis of breast cancer. Nevertheless, these indicators are usually expensive and time-consuming and achieved from the primary tumor sample (Zheng et al., 2017). Therefore, it is of importance to search easily accessible and reliable markers of breast cancer to evaluate treatment efficacy and provide a better prognosis factor.

Prognostic nutritional index (PNI), which is calculated as serum albumin (ALB) (g/L) + total lymphocyte count (10^9/L), is initially used to evaluate the nutritional status in patients undergoing surgery (Buzby et al., 1980). The PNI has been reported to be related to the therapeutic effects and predict the survival of various solid tumors (Sun et al., 2014, 2017; Nakatani et al., 2017). In colorectal cancer, a low PNI is an independent poor prognostic factor and is related to poor clinical outcomes (Mohri et al., 2013). In hepatocellular carcinoma, PNI is associated with the prognosis (Pinato et al., 2012). Although a low PNI is found to be related to poor survival in breast cancer, the PNI has been rarely studied in breast cancer patients with NACT treatment. Hence, our study aimed to analyze the prognostic significance of PNI in patients with breast cancer receiving NACT and the relationship between PNI and treatment efficacy.

MATERIALS AND METHODS

Study Population

The retrospective analysis included data from 477 patients with breast cancer who received NACT from January 1998 and December 2016; they form the neoadjuvant chemotherapy group (NACT group). As controls, we also enrolled 308 patients with pathology-proven breast cancer who were diagnosed from January 1998 and December 2016; they form the non-neoadjuvant chemotherapy group (non-NACT group). All enrolled patients were undergoing primary tumor resection at the Cancer Hospital Chinese Academy of Medical Sciences. The clinicopathological features, detailed treatment, and follow-up information were extracted from the medical records of the patients. This study was approved by the ethics committee of the Cancer Hospital Chinese Academy of Medical Sciences. It complied with the standards of the Declaration of Helsinki and its subsequent amendments or similar ethical standards. All patients provided written informed consent before the study.

Patients were included on the basis of the following criteria: (1) with breast cancer based on core needle biopsy before NACT treatment; (2) Karnofsky Performance Score (KPS) $\geq$ 80 and Performance Status (Zubrod-ECOG-WHO, ZPS) ranging from 0 to 2; (3) had operation after NACT; (4) had complete medical record and follow-up information; (5) survived more than 3 months; and (6) blood samples were obtained within 1 week before NACT treatment.

Patients were excluded on the basis of the following criteria: (1) had received anti-inflammatory medications, such as chemotherapy, radiotherapy, endocrine therapy, targeted therapy, immunotherapy, and so forth; (2) with synchronous and metachronous tumors or distant metastases; (3) with serious complications or any form of acute and chronic inflammatory disease; and (4) who had blood product transfusion within 1 month before NACT treatment.

Chemotherapy Protocols

Anthracycline-based and/or taxane-based NACT regimens were used for these patients, and every cycle was for 3 weeks: anthracyclines (A) (Zhejiang Hisun Pharmaceutical Co., Ltd., Taizhou, China), cyclophosphamide (C) (Baxter Oncology GmbH, Halle, Germany), 5-fluorouracil (F) (Tianjin Jinyao Pharmaceutical Co., Ltd., China), taxol (T) (Jiangsu Hengrui Medicine Co., Ltd., Lianyungang, China), and platinum compounds (P) (Bristol-Myers Squibb Biopharmaceutical Company, S.r.l., Italy). The following regimens (and doses) were used: AC regimen: 90 mg/m^2 A and 600 mg/m^2 C; ACF regimen: 90 mg/m^2 A, 600 mg/m^2 C, and 500 mg/m^2 F; CT regimen: 600 mg/m^2 C and 175 mg/m^2 T; ACT regimen: 90 mg/m^2 A, 600 mg/m^2 C, and 175 mg/m^2 A; AT regimen: 90 mg/m^2 A and 175 mg/m^2 T; and TP regimen: 175 mg/m^2 T and AUC 4–6 for P.

Pretreatment Evaluation, TNM Classification, and Response Evaluation

Pretreatment evaluation included medical history, clinical examination, and routine blood tests. Staging was performed according to the eighth edition of American Joint Committee on Cancer (AJCC) and the Union for International Cancer Control (UICC) TNM stage classification (Fouad et al., 2017; Abdel-Rahman, 2018). Response rates were determined using the Response Evaluation Criteria in Solid Tumors (RECIST) guidelines (Eisenhauer et al., 2009). Histological response was determined with the Miller and Payne grade (MPG) (Del Prete et al., 2019). The toxicity of NACT was evaluated according to the National Cancer Institute Common Toxicity Criteria (NCI-CTC) (Huynh-Le et al., 2014). The lymph vessel invasion and neural invasion of breast cancer were diagnosed by hematoxylin and eosin (HE) staining. Breast cancer molecular subtypes were classified as luminal A, luminal B HER2-positive, luminal B HER2-negative, HER2-enriched, and triple negative (Howlader et al., 2018).

Peripheral Venous Blood Parameters

Peripheral venous blood samples were collected within 7 days before the first round of NACT. PNI is calculated as serum ALB (g/L) + 5 $\times$ total lymphocyte count (10^9/L). Hematologic parameters were analyzed by an XE-2100 hematology analyzer (Sysmex, Kobe, Japan).

Follow-Up

All enrolled patients were treated as inpatients and outpatients every 3 months for the first to the second year after operation, every 6 months for the third to the fifth year after operation, then yearly thereafter and until death. Follow-up modalities included clinical examination with laboratory tests (routine blood and blood biochemical tests), ultrasonography of the breast, mammography, and some other examinations, as deemed fit. Disease-free survival (DFS) was defined as the time from the date of surgery to the date of local recurrence or distant metastases, death from any cause, or last follow-up. Overall survival (OS) was defined as the time from the date of surgery to the date of death from any cause or last follow-up.

Statistical Analysis

The clinicopathologic categorical variables were presented as absolute values and percentages and were compared *via* the chi-square test or Fisher's exact test. The receiver operating characteristic (ROC) curve was used to determine the optimal cutoff value, and the area under the curve was evaluated by the predictive value. The ratio closest to the point with maximum sensitivity and specificity was defined as the optimal cutoff value. The survival rates, including DFS and OS, were analyzed using Kaplan–Meier plots and compared using the log-rank test. A univariate and multivariate Cox proportional hazards regression model was accessed for the independent prognostic factors, and hazard ratios (HRs) and 95% confidence intervals (CIs) were used to evaluate the association between PNI and breast cancer prognosis. All statistical analyses were performed using the SPSS software (version 17.0, SPSS Inc., Chicago, IL, United States) and GraphPad prism software (version 8.0; GraphPad Inc., La Jolla, CA, United States). Alpha was set at 0.05, and a two-tailed $P < 0.05$ was considered statistically significant.

RESULTS

Demographic and Clinicopathologic Characteristics of All Breast Cancer Patients

The clinical and demographic attributes of the patients are shown in **Supplementary Table 1**. A total of 785 breast cancer patients were enrolled in this study: 477 breast cancer patients were assigned to the NACT group and 308 breast cancer patients were assigned to the non-NACT group. The ROC curve was used to determine the optimal cutoff value of PNI. The optimum cutoff value was 51, and this value was used for all analyses. Then, the patients were stratified into two groups by the optimal cutoff value of PNI: the low PNI group (PNI < 51) and the high PNI group (PNI ≥ 51). All enrolled patients were females. The median age of all breast cancer patients was 47 years, with range from 22 to 82 years. There were 253 breast cancer patients (32.23%) in the low PNI group and 532 breast cancer patients (67.77%) in the high PNI group. Furthermore, there were 167 breast cancer patients (35.01%) with a low PNI and 310 breast cancer patients (64.99%) with a high PNI in the NACT group and 86 breast cancer patients (27.92%) with a low PNI and 222 breast cancer patients (72.08%) with a high PNI in the non-NACT group. With respect to the clinical stage at diagnosis, 92 (11.72%), 382 (48.66%), and 311 (39.62%) breast cancer patients had stage I, II, and III disease, respectively. There were 493 premenopausal breast cancer patients and 292 postmenopausal breast cancer patients. The pathological stage was Tis/T0 in 74 (9.43%) patients, I in 157 (20.00%) patients, II in 262 (33.38%) patients, and III in 292 (37.20%) patients. Of all enrolled patients, statistically significant differences were found between the patients with low PNI and those with high PNI in marital status ($\chi^2 = 6.603$, $P = 0.010$), post-chemotherapy regimen ($\chi^2 = 11.260$, $P = 0.047$), type of surgery ($\chi^2 = 7.150$, $P = 0.008$), pathological T stage ($\chi^2 = 13.330$, $P = 0.010$), and pathological TNM stage ($\chi^2 = 9.303$, $P = 0.026$). No statistically significant differences were observed in the clinicopathological characteristics of the other parameters in all enrolled patients ($P > 0.05$). In the NACT group, statistically significant differences were found between the patients with low PNI and those with high PNI in marital status ($\chi^2 = 5.739$, $P = 0.017$) and MPG ($\chi^2 = 14.930$, $P = 0.005$). These findings are shown in **Supplementary Table 1**.

Nutritional Parameters and Blood Parameters

We chose alanine transaminase (ALT), aspartate transaminase (AST), lactate dehydrogenase (LDH), gamma-glutamyltransferase (GGT), alkaline phosphatase (ALP), glucose (GLU), immunoglobulin A (IgA), IgG, IgM, and ALB as parameters to evaluate the nutritional status of breast cancer patients. The median ALT, AST, LDH, GGT, ALP, GLU, IgA, IgG, IgM, and ALB values were 15.00, 18.00, 167.00, 17.00, and 64.00 U/L, 5.33 mmol/L, and 2.30, 11.70, 1.10, and 45.2 g/L, respectively. We have also chosen C-reactive protein (CRP), cancer antigen (CA)125, CA153, carcinoembryonic antigen (CEA), D-dimer (D-D), fibrinogen (FIB), international normalized ratio (INR), fibrin degradation product (FDP), white blood cell (W), red blood cell (R), hemoglobin (Hb), neutrophil (N), lymphocyte (L), monocyte (M), eosinophils (E), basophils (B), and platelet (P) counts as parameters to evaluate the inflammatory status of breast cancer patients. The median CRP, CA125, CA153, CEA, D-D, FIB, INR, FDP, W, R, Hb, N, L, M, E, B, and P counts were 0.20 mg/dl, 13.35 U/ml, 11.63 U/ml, 1.66 ng/ml, 0.29 mg/L, 2.85 g/L, 0.93, 1.40 μg/ml, 6.01×10^9/L, 4.40×10^{12}/L, 132 g/L, and 3.68×10^9, 1.76×10^9, 0.35×10^9, 0.06×10^9, 0.02×10^9, and 243×10^9/L, respectively. All of these peripheral venous blood parameters were collected before treatment. In the NACT group, there were significant differences in ALB ($\chi^2 = 184.400$, $P < 0.0001$), CRP ($\chi^2 = 9.251$, $P = 0.002$), W ($\chi^2 = 25.540$, $P < 0.0001$), R ($\chi^2 = 19.040$, $P < 0.0001$), Hb ($\chi^2 = 21.100$, $P < 0.0001$), N ($\chi^2 = 184.400$, $P = 0.008$), L ($\chi^2 = 17.430$, $P < 0.0001$), B ($\chi^2 = 8.100$, $P = 0.004$), and P ($\chi^2 = 8.975$, $P = 0.003$). In the non-NACT group, there were significant differences in GGT ($\chi^2 = 8.544$, $P = 0.004$), IgM ($\chi^2 = 5.171$, $P = 0.023$), ALB ($\chi^2 = 62.690$, $P < 0.0001$), CRP ($\chi^2 = 4.472$, $P = 0.035$), W ($\chi^2 = 6.609$, $P = 0.010$), R ($\chi^2 = 7.808$, $P = 0.005$), Hb ($\chi^2 = 15.030$, $P = 0.0001$), and M ($\chi^2 = 6.248$, $P = 0.012$). No other significant correlation was found. The correlations between the nutritional parameters/blood parameters and PNI are shown in **Supplementary Table 2**.

Univariate and Multivariate Cox Regression Survival Analyses

In univariate analysis, ALB, CA153, lymphocyte, PNI, type of surgery, histologic grade, pathological T stage, pathological N stage, pathological TNM stage, molecular subtype, HER2 status, Ki-67 status, CK5/6 status, TOP2A status, lymph vessel invasion, postoperative endocrine therapy, and postoperative targeted therapy were the significant prognostic factors for DFS and OS. In multivariate Cox regression analysis, ALB, CA153, lymphocyte, PNI, type of surgery, histologic grade, pathological T stage, pathological N stage, pathological TNM stage, molecular subtype, HER2 status, Ki-67 status, TOP2A status, lymph vessel invasion, postoperative endocrine therapy, and postoperative targeted therapy were the significant prognostic factors for DFS and OS. These results are shown in **Supplementary Table 3**.

DFS and OS by PNI

According to the univariate and multivariate Cox regression analyses, the results indicated that PNI had prognostic significance for DFS and OS using the cutoff value of 51. In univariate analysis, a high PNI was associated with prolonged DFS and OS ($P < 0.0001$, HR = 0.310, 95%CI = 0.194–0.494 and $P < 0.0001$, HR = 0.366, 95%CI = 0.243–0.550, respectively). In multivariate Cox regression analysis, a high PNI was associated with prolonged DFS and OS ($P < 0.0001$, HR = 0.264, 95%CI = 0.160–0.435 and $P < 0.0001$, HR = 0.319, 95%CI = 0.207–0.491, respectively). Of all enrolled breast patients, the mean DFS and OS for patients with low PNI were 36.60 months (range = 3.47–208.57 months) and 64.97 months (range = 9.13–247.33 months), and the mean DFS and OS

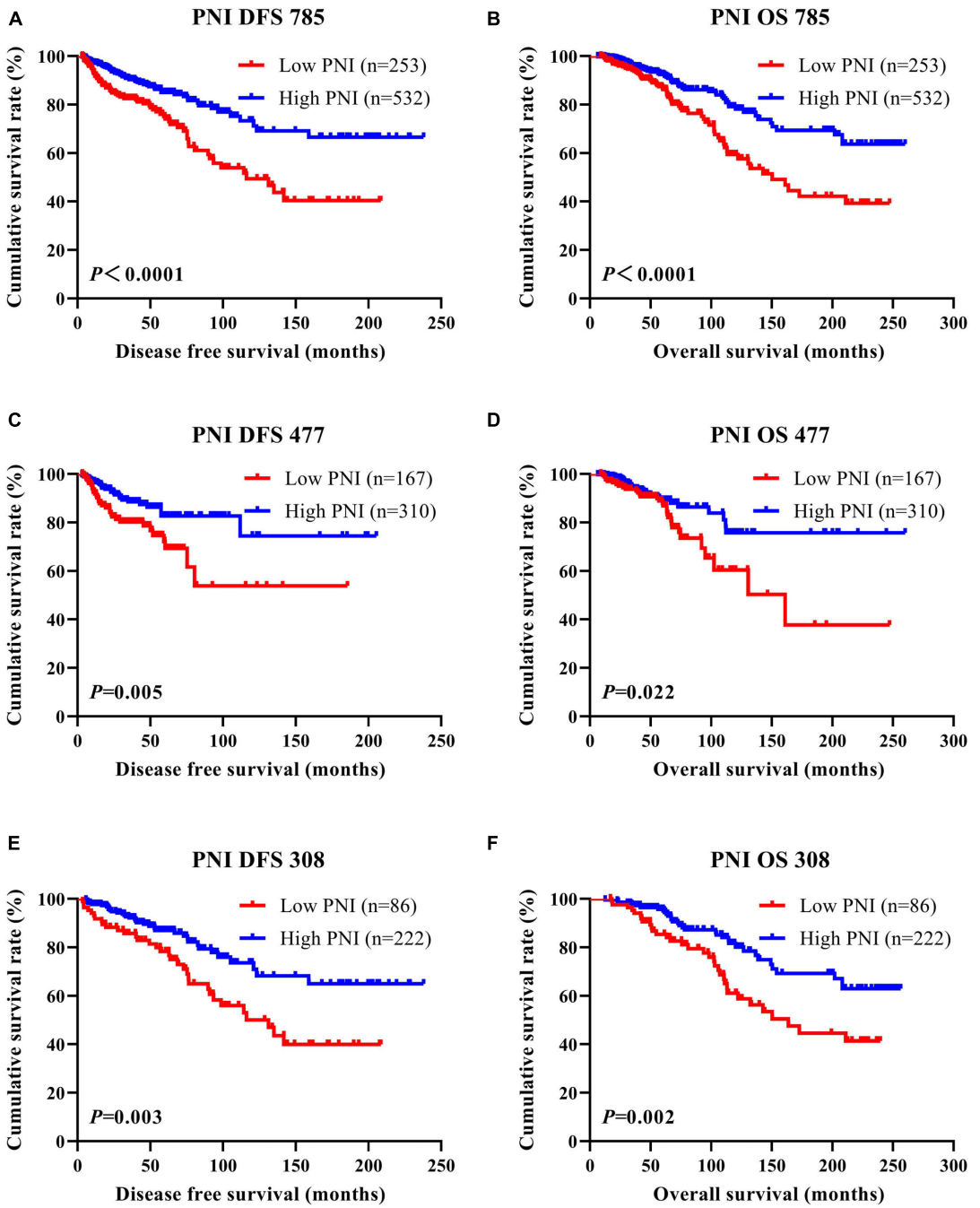

FIGURE 1 | Disease-free survival (DFS) and overall survival (OS) of patients with breast cancer. **(A,B)** Kaplan–Meier analyses of DFS **(A)** and OS **(B)** for the prognostic nutritional index (PNI) of all patients with breast cancer. **(C,D)** Kaplan–Meier analyses of DFS **(C)** and OS **(D)** for the PNI of patients with breast cancer in the neoadjuvant chemotherapy (NACT) group. **(E,F)** Kaplan–Meier analyses of DFS **(E)** and OS **(F)** for the PNI of patients with breast cancer in the non-NACT group.

for patients with high PNI were 47.64 months (range = 3.10–238.00 months) and 73.61 months (range = 6.43–260.03 months), respectively. Furthermore, the mean DFS and OS times for patients with high PNI were longer than for those with low PNI by the log-rank test ($\chi^2 = 18.540$, $P < 0.0001$ and $\chi^2 = 16.060$, $P < 0.0001$, respectively; **Figures 1A,B**). In the NACT group, the mean DFS and OS for patients with low PNI were 44.34 months (range = 3.47–185.63 months) and 65.27 months (range = 9.13–247.33 months), and the mean DFS and OS for patients with high PNI were 49.70 months (range = 3.10–205.47 months) and 79.85 months (range = 6.43–260.03 months), respectively. By the log-rank test, the mean DFS and OS times for patients with high PNI were longer than for those with low PNI ($\chi^2 = 8.044$, $P = 0.005$ and $\chi^2 = 5.285$, $P = 0.022$, respectively; **Figures 1C,D**).

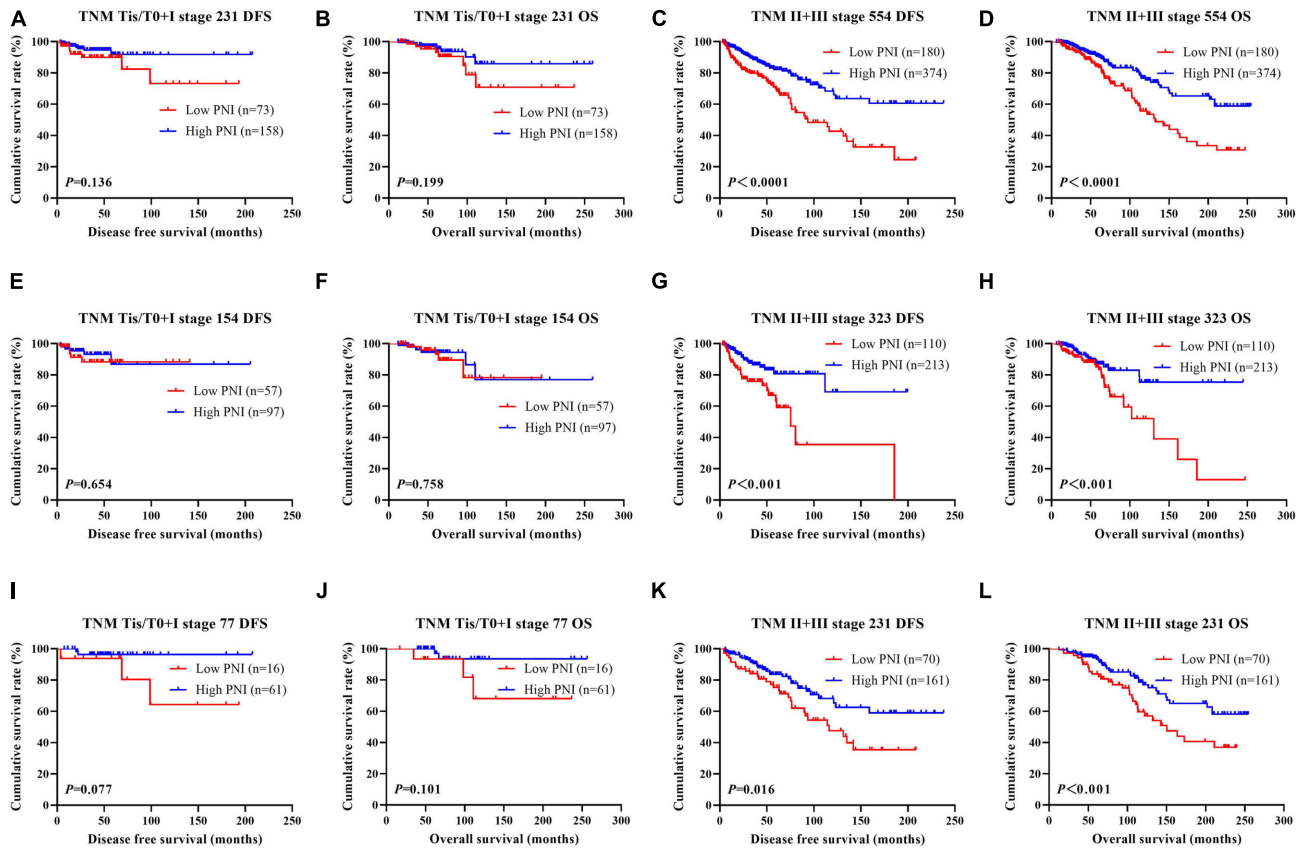

FIGURE 2 | Disease-free survival (DFS) and overall survival (OS) for the prognostic nutritional index (PNI) of patients with breast cancer in different pathologic stages. **(A,B)** Kaplan–Meier analysis of DFS **(A)** and OS **(B)** for the PNI of patients with early stage breast cancer (Tis/T0 + I stage) in all enrolled patients. **(C,D)** Kaplan–Meier analysis of DFS **(C)** and OS **(D)** for the PNI of patients with advanced stage breast cancer (II + III stage) in all enrolled patients. **(E,F)** Kaplan–Meier analysis of DFS **(E)** and OS **(F)** for the PNI of patients with early stage breast cancer (Tis/T0 + I stage) in the neoadjuvant chemotherapy (NACT) group. **(G,H)** Kaplan–Meier analysis of DFS **(G)** and OS **(H)** for the PNI of patients with advanced stage breast cancer (II + III stage) in the NACT group. **(I,J)** Kaplan–Meier analysis of DFS **(I)** and OS **(J)** for the PNI of patients with early stage breast cancer (Tis/T0 + I stage) in the non-NACT group. **(K,L)** Kaplan–Meier analysis of DFS **(K)** and OS **(L)** for the PNI of patients with advanced stage breast cancer (II + III stage) in the non-NACT group.

In the non-NACT group, the mean DFS and OS for patients with low PNI were 33.83 months (range = 3.53–208.57 months) and 59.75 months (range = 16.90–239.53 months), and the mean DFS and OS for patients with high PNI were 37.00 months (range = 5.73–238.00 months) and 71.20 months (range = 12.57–256.37 months), respectively. By the log-rank test, the mean DFS and OS times for patients with high PNI were longer than for those with low PNI (χ^2 = 8.960, P = 0.003 and χ^2 = 9.672, P = 0.002, respectively; **Figures 1E,F**).

Association of Pathologic Stage and PNI in Patients With Breast Cancer

According to the univariate and multivariate analyses, we found that pathologic T stage, pathologic N stage, and pathologic TNM stage were the significant prognostic factors (**Supplementary Table 3**). In order to further investigate the prognostic efficiency of PNI, the PNI was analyzed by the pathologic TNM stage. We defined the patients with pathologic Tis/T0 + I stage as early stage breast cancer and the patients with pathologic II + III stage as advanced stage breast cancer, and we used the log-rank test to analyze the PNI with the different pathologic stages. Of all enrolled breast patients, the results indicated that patients with high PNI had longer DFS and OS than those with low PNI in early stage breast cancer (χ^2 = 2.223, P = 0.136 and χ^2 = 1.650, P = 0.199, respectively; **Figures 2A,B**). Meanwhile, patients with high PNI had longer DFS and OS than those with low PNI in advanced stage breast cancer (χ^2 = 17.820, P < 0.0001 and χ^2 = 15.390, P < 0.0001, respectively; **Figures 2C,D**). In the NACT group, the results indicated that patients with high PNI had longer DFS and OS than those with low PNI in early stage breast cancer (χ^2 = 0.201, P = 0.654 and χ^2 = 0.095, P = 0.758, respectively; **Figures 2E,F**). Meanwhile, patients with high PNI had longer DFS and OS than those with low PNI in advanced stage breast cancer (χ^2 = 11.790, P < 0.001 and χ^2 = 7.119, P < 0.001, respectively; **Figures 2G,H**). In the non-NACT group, the results indicated that patients with high PNI had longer DFS and OS than those with low PNI in early stage breast cancer (χ^2 = 3.126, P = 0.077 and χ^2 = 2.697, P = 0.101, respectively; **Figures 2I,J**). Meanwhile, patients with high PNI had longer DFS

TABLE 1 | Association of molecular subtypes and prognostic nutritional index (PNI) in patients with breast cancer.

Parameters	PNI (*N* = 785)					PNI (*n* = 477)					PNI (*n* = 308)				
	N	Low PNI (*n* = 253)	High PNI (*n* = 532)	χ^2	*P* value	*N*	Low PNI (*n* = 167)	High PNI (*n* = 310)	χ^2	*P* value	*N*	Low PNI (*n* = 86)	High PNI (*n* = 222)	χ^2	*P* value
Core needle biopsy (*N* = 477)															
Molecular subtypes									2.454	0.653					
Luminal A						25 (5.24%)	12 (7.19%)	13 (4.19%)							
Luminal B HER2+						67 (14.05%)	22 (13.17%)	45 (14.52%)							
Luminal B HER2−						186 (38.99%)	62 (37.13%)	124 (40.00%)							
HER2 enriched						91 (19.08%)	31 (18.56%)	60 (19.35%)							
Triple negative						108 (22.64%)	40 (23.95%)	68 (21.94%)							
ER status									0.049	0.825					
Negative						191 (40.04%)	68 (40.72%)	123 (39.68%)							
Positive						286 (59.96%)	99 (59.28%)	187 (60.32%)							
ER status									1.179	0.758					
0–25%						228 (47.80%)	82 (49.10%)	146 (47.10%)							
26–50%						42 (8.80%)	17 (10.18%)	25 (8.06%)							
51–75%						33 (6.92%)	10 (5.99%)	23 (7.42%)							
76–100%						174 (36.48%)	58 (34.73%)	116 (37.42%)							
PR status									0.309	0.579					
Negative						189 (39.62%)	69 (41.32%)	120 (38.71%)							
Positive						288 (60.38%)	98 (58.68%)	190 (61.29%)							
PR status									0.082	0.994					
0–25%						286 (59.96%)	100 (59.88%)	186 (60.00%)							
26–50%						67 (14.05%)	24 (14.37%)	43 (13.87%)							
51–75%						45 (9.43%)	15 (8.98%)	30 (9.68%)							
76–100%						79 (16.56%)	28 (16.77%)	51 (16.45%)							
HER2 status									0.007	0.934					
Negative (0– + +)						313 (65.62%)	110 (65.87%)	203 (65.48%)							
Positive (+ + +)						164 (34.38%)	57 (34.13%)	107 (34.52%)							
Ki-67 status									0.426	0.514					
Negative (≤14%)						84 (17.61%)	32 (19.16%)	52 (16.77%)							
Positive (>14%)						393 (82.39%)	135 (80.84%)	258 (83.23%)							
Ki-67 status									1.477	0.688					
0–25%						161 (33.75%)	55 (32.93%)	106 (34.19%)							
26–50%						189 (39.62%)	66 (39.52%)	123 (39.68%)							
51–75%						88 (18.45%)	29 (17.37%)	59 (19.03%)							
76–100%						39 (8.18%)	17 (10.18%)	22 (7.10%)							
Postoperative pathology (IHC)															
Molecular subtype				2.118	0.714				1.093	0.895				2.149	0.708
Luminal A	62 (7.90%)	17 (6.72%)	45 (8.46%)			41 (8.60%)	13 (7.78%)	28 (9.02%)			21 (6.82%)	4 (4.65%)	17 (7.66%)		
Luminal B HER2+	98 (12.48%)	36 (14.23%)	62 (11.65%)			61 (12.79%)	24 (14.37%)	37 (11.94%)			37 (12.01%)	12 (13.95%)	25 (11.26%)		
Luminal B HER2-	325 (41.40%)	105 (41.50%)	220 (41.35%)			166 (34.80%)	58 (34.74%)	108 (34.84%)			159 (51.63%)	47 (54.66%)	112 (50.45%)		
HER2 enriched	129 (16.44%)	38 (15.02%)	91 (17.11%)			96 (20.12%)	31 (18.56%)	65 (20.97%)			33 (10.71%)	7 (8.14%)	26 (11.71%)		
Triple negative	171 (21.78%)	57 (22.53%)	114 (21.43%)			113 (23.69%)	41 (24.55%)	72 (23.23%)			58 (18.83%)	16 (18.60%)	42 (18.92%)		
ER status				0.049	0.826				0.003	0.958				0.355	0.552
Negative	296 (37.71%)	94 (37.15%)	202 (37.97%)			195 (40.88%)	68 (40.72%)	127 (40.97%)			101 (32.79%)	26 (30.23%)	75 (33.78%)		
Positive	489 (62.29%)	159 (62.85%)	330 (62.03%)			282 (59.12%)	99 (59.28%)	183 (59.03%)			207 (67.21%)	60 (69.77%)	147 (66.22%)		
ER status				3.722	0.293				0.841	0.840				5.508	0.138

(Continued)

TABLE 1 | Continued

Parameters	PNI (*N* = 785)					PNI (*n* = 477)					PNI (*n* = 308)				
	N	Low PNI (*n* = 253)	High PNI (*n* = 532)	χ^2	*P* value	*N*	Low PNI (*n* = 167)	High PNI (*n* = 310)	χ^2	*P* value	*N*	Low PNI (*n* = 86)	High PNI (*n* = 222)	χ^2	*P* value
0–25%	375 (47.77%)	129 (50.99%)	246 (46.24%)			235 (49.27%)	85 (50.90%)	150 (48.39%)			140 (45.46%)	44 (51.16%)	96 (43.24%)		
26–50%	66 (8.41%)	25 (9.88%)	41 (7.71%)			31 (6.50%)	12 (7.19%)	19 (6.13%)			35 (11.36%)	13 (15.12%)	22 (9.91%)		
51–75%	48 (6.11%)	13 (5.14%)	35 (6.58%)			27 (5.66%)	10 (5.99%)	17 (5.48%)			21 (6.82%)	3 (3.49%)	18 (8.11%)		
76–100%	296 (37.71%)	86 (33.99%)	210 (39.47%)			184 (38.57%)	60 (35.92%)	124 (40.00%)			112 (36.36%)	26 (30.23%)	86 (38.74%)		
PR status				0.154	0.694				0.009	0.926				1.339	0.247
Negative	315 (40.13%)	99 (39.13%)	216 (40.60%)			210 (44.03%)	74 (44.31%)	136 (43.87%)			105 (34.09%)	25 (29.07%)	80 (36.04%)		
Positive	470 (59.87%)	154 (60.87%)	316 (59.40%)			267 (55.97%)	93 (55.69%)	174 (56.13%)			203 (65.91%)	61 (70.93%)	142 (63.96%)		
PR status				0.546	0.909				0.426	0.935				1.558	0.669
0–25%	502 (63.95%)	161 (63.64%)	341 (64.10%)			335 (70.23%)	116 (69.46%)	219 (70.65%)			167 (54.22%)	45 (52.33%)	122 (54.95%)		
26–50%	90 (11.46%)	31 (12.25%)	59 (11.09%)			48 (10.06%)	16 (9.58%)	32 (10.32%)			42 (13.64%)	15 (17.44%)	27 (12.16%)		
51–75%	55 (7.01%)	19 (7.51%)	36 (6.76%)			38 (7.97%)	15 (8.98%)	23 (7.42%)			17 (5.52%)	4 (4.65%)	13 (5.86%)		
76–100%	138 (17.58%)	42 (16.60%)	96 (18.05%)			56 (11.74%)	20 (11.98%)	36 (11.61%)			82 (26.62%)	22 (25.58%)	60 (27.03%)		
HER2 status				0.065	0.799				0.045	0.833				0.062	0.804
Negative (0– + +)	557 (70.96%)	178 (70.36%)	379 (71.24%)			320 (67.09%)	111 (66.47%)	209 (67.42%)			237 (76.95%)	67 (77.91%)	170 (76.58%)		
Positive (+ + +)	228 (29.04%)	75 (29.64%)	153 (28.76%)			157 (32.91%)	56 (33.53%)	101 (32.58%)			71 (23.05%)	19 (22.09%)	52 (23.42%)		
Ki-67 status				0.566	0.452				0.538	0.463				4.138	0.042
Negative (≤14%)	219 (27.90%)	75 (29.64%)	144 (27.07%)			153 (32.08%)	50 (29.94%)	103 (33.23%)			66 (21.43%)	25 (29.07%)	41 (18.47%)		
Positive (>14%)	566 (72.10%)	178 (70.36%)	388 (72.93%)			324 (67.92%)	117 (70.06%)	207 (66.77%)			242 (78.57%)	61 (70.93%)	181 (81.53%)		
Ki-67 status				2.780	0.427				2.920	0.404				0.689	0.876
0–25%	342 (43.57%)	114 (45.06%)	228 (42.86%)			233 (48.84%)	82 (49.10%)	151 (48.71%)			109 (35.39%)	32 (37.21%)	77 (34.68%)		
26–50%	257 (32.74%)	74 (29.25%)	183 (34.40%)			139 (29.14%)	43 (25.75%)	96 (30.97%)			118 (38.31%)	31 (36.05%)	87 (39.19%)		
51–75%	137 (17.45%)	50 (19.76%)	87 (16.35%)			70 (14.68%)	30 (17.96%)	40 (12.90%)			67 (21.75%)	20 (23.25%)	47 (21.17%)		
76–100%	49 (6.24%)	15 (5.93%)	34 (6.39%)			35 (7.34%)	12 (7.19%)	23 (7.42%)			14 (4.55%)	3 (3.49%)	11 (4.96%)		
AR status				6.920	0.009				11.730	<0.001				0.017	0.896
Negative	666 (84.84%)	227 (89.72%)	439 (82.52%)			362 (75.89%)	142 (85.03%)	220 (70.97%)			304 (98.70%)	85 (98.84%)	219 (98.65%)		
Positive	119 (15.16%)	26 (10.28%)	93 (17.48%)			115 (24.11%)	25 (14.97%)	90 (29.03%)			4 (1.30%)	1 (1.16%)	3 (1.35%)		
AR status				6.354	0.096				10.260	0.017				0.044	0.834
0–25%	688 (87.65%)	232 (91.70%)	456 (85.71%)			383 (80.29%)	147 (88.02%)	236 (76.13%)			305 (99.03%)	85 (98.84%)	220 (99.10%)		
26–50%	25 (3.18%)	4 (1.58%)	21 (3.95%)			25 (5.24%)	4 (2.40%)	21 (6.77%)			0 (0.00%)	0 (0.00%)	0 (0.00%)		
51–75%	29 (3.69%)	6 (2.37%)	23 (4.32%)			29 (6.08%)	6 (3.59%)	23 (7.42%)			0 (0.00%)	0 (0.00%)	0 (0.00%)		
76–100%	43 (5.48%)	11 (4.35%)	32 (6.02%)			40 (8.39%)	10 (5.99%)	30 (9.68%)			3 (0.97%)	1 (1.16%)	2 (0.90%)		
CK5/6 status				0.109	0.741				1.248	0.264				2.092	0.148
Negative	684 (87.13%)	219 (86.56%)	465 (87.41%)			406 (85.12%)	138 (82.63%)	268 (86.45%)			278 (90.26%)	81 (94.19%)	197 (88.74%)		
Positive	101 (12.87%)	34 (13.44%)	67 (12.59%)			71 (14.88%)	29 (17.37%)	42 (13.55%)			30 (9.74%)	5 (5.81%)	25 (11.26%)		
E-cad status				8.716	0.003				3.612	0.057				11.140	<0.001
Negative	353 (44.97%)	133 (52.57%)	220 (41.35%)			170 (35.64%)	69 (41.32%)	101 (32.58%)			183 (59.42%)	64 (74.42%)	119 (53.60%)		
Positive	432 (55.03%)	120 (47.43%)	312 (58.65%)			307 (64.36%)	98 (58.68%)	209 (67.42%)			125 (40.58%)	22 (25.58%)	103 (46.40%)		
EGFR status				2.078	0.150				0.130	0.719				7.281	0.007
Negative	589 (75.03%)	198 (78.26%)	391 (73.50%)			335 (70.23%)	119 (71.26%)	216 (69.68%)			254 (82.47%)	79 (91.86%)	175 (78.83%)		
Positive	196 (24.97%)	55 (21.74%)	141 (26.50%)			142 (29.77%)	48 (28.74%)	94 (30.32%)			54 (17.53%)	7 (8.14%)	47 (21.17%)		
P53 status				1.381	0.240				0.137	0.712				1.994	0.158
Negative	395 (50.32%)	135 (53.36%)	260 (48.87%)			243 (50.94%)	87 (52.10%)	156 (50.32%)			152 (49.35%)	48 (55.81%)	104 (46.85%)		
Positive	390 (49.68%)	118 (46.64%)	272 (51.13%)			234 (49.06%)	80 (47.90%)	154 (49.68%)			156 (50.65%)	38 (44.19%)	118 (53.15%)		
P53 status				1.575	0.665				4.173	0.243				0.634	0.729
0–25%	576 (73.38%)	183 (72.33%)	393 (73.87%)			353 (74.00%)	118 (70.66%)	235 (75.81%)			223 (72.41%)	65 (75.58%)	158 (71.17%)		

(Continued)

TABLE 1 | Continued

Parameters	PNI (*N* = 785)					PNI (*n* = 477)					PNI (*n* = 308)				
	N	Low PNI (*n* = 253)	High PNI (*n* = 532)	χ^2	*P* value	*N*	Low PNI (*n* = 167)	High PNI (*n* = 310)	χ^2	*P* value	*N*	Low PNI (*n* = 86)	High PNI (*n* = 222)	χ^2	*P* value
26–50%	80 (10.19%)	23 (9.09%)	57 (10.72%)			45 (9.44%)	14 (8.38%)	31 (10.00%)			35 (11.36%)	9 (10.47%)	26 (11.71%)		
51–75%	108 (13.75%)	39 (15.42%)	69 (12.97%)			58 (12.16%)	27 (16.17%)	31 (10.00%)			50 (16.23%)	12 (13.95%)	38 (17.12%)		
76–100%	21 (2.68%)	8 (3.16%)	13 (2.44%)			21 (4.40%)	8 (4.79%)	13 (4.19%)			0 (0.00%)	0 (0.00%)	0 (0.00%)		
TOP2A status				4.598	0.032				0.024	0.877				15.940	<0.0001
Negative	299 (38.09%)	110 (43.48%)	189 (35.53%)			165 (34.59%)	57 (34.13%)	108 (34.84%)			134 (43.51%)	53 (61.63%)	81 (36.49%)		
Positive	486 (61.91%)	143 (56.52%)	343 (64.47%)			312 (65.41%)	110 (65.87%)	202 (65.16%)			174 (56.49%)	33 (38.37%)	141 (63.51%)		
TOP2A status				0.408	0.939				1.974	0.578				3.368	0.338
0–25%	575 (73.25%)	187 (73.91%)	388 (72.92%)			354 (74.21%)	120 (71.86%)	234 (75.48%)			221 (71.76%)	67 (77.90%)	154 (69.37%)		
26–50%	158 (20.13%)	48 (18.97%)	110 (20.68%)			88 (18.45%)	31 (18.56%)	57 (18.39%)			70 (22.73%)	17 (19.77%)	53 (23.87%)		
51–75%	49 (6.24%)	17 (6.72%)	32 (6.02%)			33 (6.92%)	15 (8.98%)	18 (5.81%)			16 (5.19%)	2 (2.33%)	14 (6.31%)		
76–100%	3 (0.38%)	1 (0.40%)	2 (0.38%)			2 (0.42%)	1 (0.60%)	1 (0.32%)			1 (0.32%)	0 (0.00%)	1 (0.45%)		
Lymph vessel invasion				0.756	0.385				0.001	0.995				3.936	0.047
Negative	558 (71.08%)	185 (73.12%)	373 (70.11%)			320 (67.09%)	112 (67.07%)	208 (67.10%)			238 (77.27%)	73 (84.88%)	165 (74.32%)		
Positive	227 (28.92%)	68 (26.88%)	159 (29.89%)			157 (32.91%)	55 (32.93%)	102 (32.90%)			70 (22.73%)	13 (15.12%)	57 (25.68%)		
Neural invasion				0.041	0.840				0.018	0.892				0.005	0.944
Negative	670 (85.35%)	215 (84.98%)	455 (85.53%)			384 (80.50%)	135 (80.84%)	249 (80.32%)			286 (92.86%)	80 (93.02%)	206 (92.79%)		
Positive	115 (14.65%)	38 (15.02%)	77 (14.47%)			93 (19.50%)	32 (19.16%)	61 (19.68%)			22 (7.14%)	6 (6.98%)	16 (7.21%)		

ER, estrogen receptor; PR, progesterone receptor; AR, androgen receptor; EFGR, epidermal growth factor receptor; IHC, immunohistochemistry.

and OS than those with low PNI in advanced stage breast cancer (χ^2 = 5.801, *P* = 0.016 and χ^2 = 7.078, *P* = 0.008, respectively; **Figures 2K,L**).

Association of Molecular Subtype and PNI in Patients With Breast Cancer

The results indicated that molecular subtype was the significant prognostic factor by univariate and multivariate analyses (**Supplementary Table 3**). Of all enrolled patients, 62 cases were luminal A subtype, 98 cases were luminal B HER2-positive subtype, 325 cases were luminal B HER2-negative subtype, 129 cases were HER2-enriched subtype, and 171 cases were triple-negative subtype (**Table 1**). In order to further evaluate the prognostic value of PNI, the PNI was accessed by the molecular subtypes. The PNI with different molecular subtypes was analyzed by the log-rank test. The mean DFS and OS times for patients with luminal A subtype were 47.31 and 69.72 months, respectively. Moreover, the mean DFS and OS times for patients with high PNI by the log-rank test were longer than for those with low PNI in luminal A subtype (χ^2 = 0.031, *P* = 0.861 and χ^2 = 0.026, *P* = 0.871, respectively; **Figures 3A,B**). The mean DFS and OS times for patients with luminal B HER2-positive subtype were 44.46 and 69.32 months, respectively. Moreover, the mean DFS and OS times for patients with high PNI by the log-rank test were longer than for those with low PNI in luminal B HER2-positive subtype (χ^2 = 0.979, *P* = 0.322 and χ^2 = 2.002, *P* = 0.157, respectively; **Figures 3C,D**). The mean DFS and OS times for patients with luminal B HER2-negative subtype were 42.13 and 63.13 months, respectively. Moreover, the mean DFS and OS times for patients with high PNI by the log-rank test were longer than for those with low PNI in luminal B HER2-negative subtype (χ^2 = 6.268, *P* = 0.012 and χ^2 = 6.457, *P* = 0.011, respectively; **Figures 3E,F**). The mean DFS and OS times for patients with HER2-enriched subtype were 24.30 and 49.40 months, respectively. Moreover, the mean DFS and OS times for patients with high PNI by the log-rank test were longer than for those with low PNI in HER2-enriched subtype (χ^2 = 5.291, *P* = 0.021 and χ^2 = 4.488, *P* = 0.034, respectively; **Figures 3G,H**). The mean DFS and OS times for patients with triple-negative subtype were 37.07 and 60.73 months, respectively. Moreover, the mean DFS and OS times for patients with high PNI by the log-rank test were longer than for those with low PNI in triple-negative subtype (χ^2 = 13.690, *P* < 0.001 and χ^2 = 12.980, *P* < 0.001, respectively; **Figures 3I,J**). The DFS and OS for the PNI of breast cancer patients with different molecular subtypes in the NACT and non-NACT groups are shown in **Figures 4**, **5**.

Association of Lymph Vessel Invasion (LVI) and PNI in Patients With Breast Cancer

According to the univariate and multivariate analyses, lymph vessel invasion was a significant prognostic factor (**Supplementary Table 3**). For the sake of further studying the prognostic efficiency of PNI, we analyzed the lymph vessel invasion by PNI. The lymph vessel invasion status

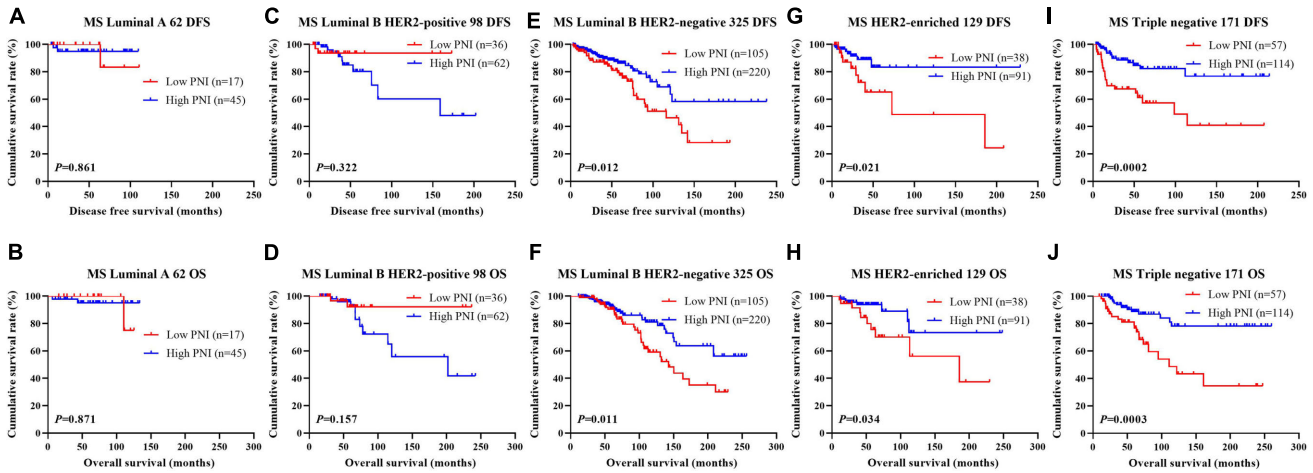

FIGURE 3 | Disease-free survival (DFS) and overall survival (OS) for the prognostic nutritional index (PNI) of patients with breast cancer in different molecular subtypes. **(A,B)** Kaplan–Meier analysis of DFS **(A)** and OS **(B)** for the PNI of patients with luminal A breast cancer in all enrolled patients. **(C,D)** Kaplan–Meier analysis of DFS **(C)** and OS **(D)** for the PNI of patients with luminal B HER2-positive breast cancer in all enrolled patients. **(E,F)** Kaplan–Meier analysis of DFS **(E)** and OS **(F)** for the PNI of patients with luminal B HER2-negative breast cancer in all enrolled patients. **(G,H)** Kaplan–Meier analysis of DFS **(G)** and OS **(H)** for the PNI of patients with HER2-enriched breast cancer in all enrolled patients. **(I,J)** Kaplan–Meier analysis of DFS **(I)** and OS **(J)** for the PNI of patients with triple-negative breast cancer in all enrolled patients.

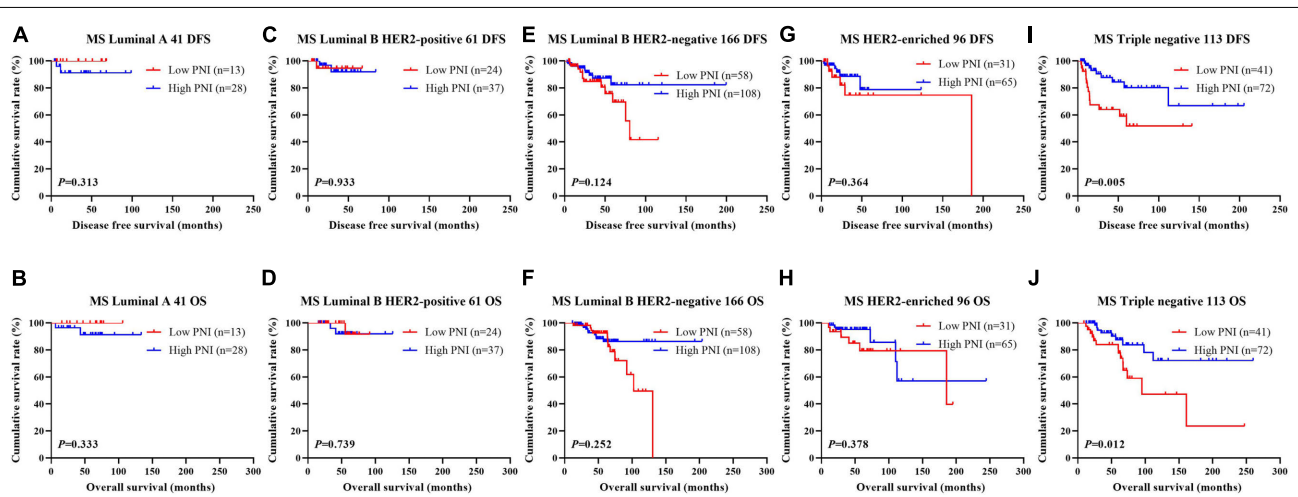

FIGURE 4 | Disease-free survival (DFS) and overall survival (OS) for the prognostic nutritional index (PNI) of patients with breast cancer in different molecular subtypes in the neoadjuvant chemotherapy (NACT) group. **(A,B)** Kaplan-Meier analysis of DFS **(A)** and OS **(B)** for the PNI of patients with luminal A breast cancer in NACT group. **(C,D)** Kaplan-Meier analysis of DFS **(C)** and OS **(D)** for the PNI of patients with luminal B HER2-positive breast cancer in NACT group. **(E,F)** Kaplan-Meier analysis of DFS **(E)** and OS **(F)** for the PNI of patients with luminal B HER2-negative breast cancer in NACT group. **(G,H)** Kaplan-Meier analysis of DFS **(G)** and OS **(H)** for the PNI of patients with HER2-enriched breast cancer in NACT group. **(I,J)** Kaplan-Meier analysis of DFS **(I)** and OS **(J)** for the PNI of patients with triple-negative breast cancer in NACT group.

was divided into without lymph vessel invasion and with lymph vessel invasion. The mean DFS and OS times of all enrolled patients without lymph vessel invasion were 50.96 and 79.65 months, respectively, and those with lymph vessel invasion were 28.97 and 53.37 months, respectively. The mean DFS and OS times of patients without lymph vessel invasion were longer than of those patients with lymph vessel invasion by the log-rank test (χ^2 = 20.940, P < 0.0001 and χ^2 = 26.540, P < 0.0001, respectively; **Figures 6A,B**). The mean DFS and OS times of patients without lymph vessel invasion were 41.47 and 66.60 months with low PNI and 64.75 and 108.00 months with high PNI, respectively. The results indicated that the mean DFS and OS times of patients with high PNI by the log-rank test were longer than of those patients with low PNI without lymph vessel invasion (χ^2 = 14.520, P < 0.001 and χ^2 = 14.120, P < 0.001, respectively; **Figures 6C,D**). The mean DFS and OS times of patients with lymph vessel invasion were 26.75 and 34.82 months

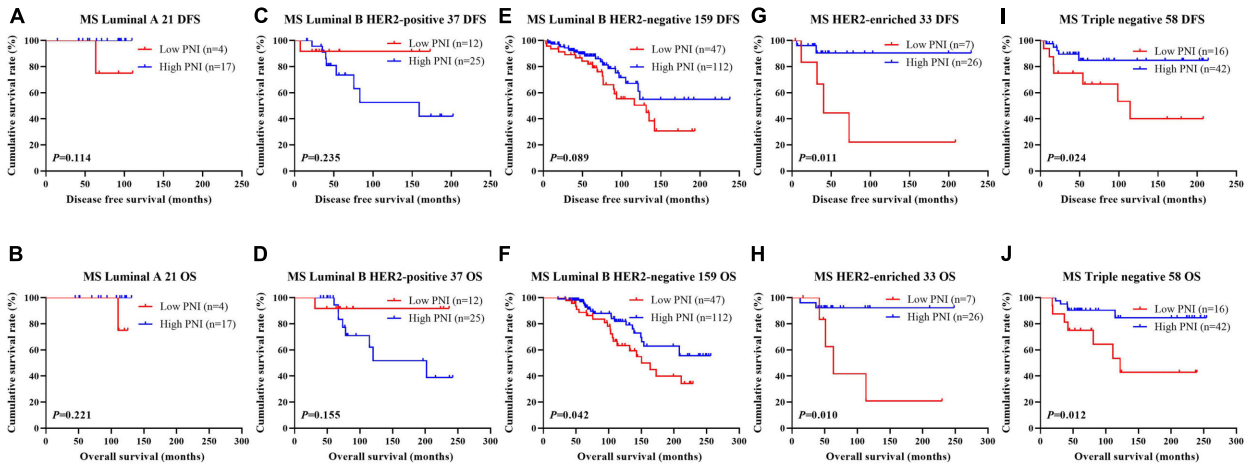

FIGURE 5 | Disease-free survival (DFS) and overall survival (OS) for the prognostic nutritional index (PNI) of patients with breast cancer in different molecular subtypes in the non-neoadjuvant chemotherapy (NACT) group. **(A,B)** Kaplan-Meier analysis of DFS **(A)** and OS **(B)** for the PNI of patients with luminal A breast cancer in non-NACT group. **(C,D)** Kaplan-Meier analysis of DFS **(C)** and OS **(D)** for the PNI of patients with luminal B HER2-positive breast cancer in non-NACT group. **(E,F)** Kaplan-Meier analysis of DFS **(E)** and OS **(F)** for the PNI of patients with luminal B HER2-negative breast cancer in non-NACT group. **(G,H)** Kaplan-Meier analysis of DFS **(G)** and OS **(H)** for the PNI of patients with HER2-enriched breast cancer in non-NACT group. **(I,J)** Kaplan-Meier analysis of DFS **(I)** and OS **(J)** for the PNI of patients with triple-negative breast cancer in non-NACT group.

with low PNI and 29.50 and 61.15 months with high PNI, respectively. The results indicated that the mean DFS and OS times of patients with high PNI by the log-rank test were longer than of those patients with low PNI with lymph vessel invasion (χ^2 = 6.266, P = 0.012 and χ^2 = 4.270, P = 0.039, respectively; **Figures 6E,F**). The DFS and OS for the PNI of breast cancer patients without or with lymph vessel invasion in the NACT and non-NACT groups are shown in **Figures 7**, **8**.

Association of PNI and Neoadjuvant Chemotherapy or Postoperative Chemotherapy

In the NACT group, 28 patients received the AC/ACF regimen, 27 patients received the CT/ACT regimen, 223 patients received the AT regimen, 141 patients received the TP regimen, and 58 patients received other regimens. After operation, there were 230 patients undergoing postoperative chemotherapy, and 247 patients did not receive postoperative chemotherapy. Forty-three patients received the AC/ACF regimen, 30 patients received the CT/ACT regimen, 37 patients received the AT regimen, 39 patients received the TP regimen, and 81 patients received other regimens. The clinical objective response rate [complete response (CR) + partial response (PR)] was 66.88% (319/477) and the clinical benefit rate [CR + PR + stable disease (SD)] was 98.53% (470/477); the non-clinical response rate [SD + partial disease (PD)] was 33.12% (158/477). We also used the MPG system to evaluate the pathological response. The grade 1 rate was 4.61% (22/477), the grade 2 rate was 26.42% (126/477), the grade 3 rate was 37.11% (177/477), the grade 4 rate was 13.00% (62/477), and the grade 5 rate was 18.87% (90/477). The pathologic complete response (pCR) rate was 15.09% (72/477) and the non-pCR rate was 84.91% (405/477).

In order to further evaluate the prognostic efficiency of PNI, we analyzed the PNI by MPG. The PNI with different MPG grades was analyzed by the log-rank test. There were significant differences in the different MPG grades on the mean DFS and OS times by using the log-rank test (χ^2 = 18.290, $P < 0.0001$ and χ^2 = 18.020, $P < 0.0001$, respectively). Moreover, the results indicated that the mean DFS and OS times of patients with high PNI were longer than of those with low PNI in the MPG 2 group (χ^2 = 13.980, P = 0.0002 and χ^2 = 11.800, P = 0.0006, respectively; **Figure 9**). We also analyzed the response by PNI, and there were significant differences in the response on the mean DFS and OS times by using the log-rank test (χ^2 = 12.540, P = 0.006 and χ^2 = 10.820, P = 0.013, respectively). Furthermore, the results indicated that the mean DFS and OS times of patients with high PNI were longer than of those with low PNI in the SD response status (χ^2 = 14.390, P = 0.0001 and χ^2 = 11.250, P = 0.0008, respectively; **Figure 10**).

Correlation Between PNI and Toxicity Assessment

In the NACT group, we evaluated and analyzed the toxicities after receiving NACT for two cycles. The common toxicities included decreased appetite, nausea, vomiting, diarrhea, mouth ulcers, alopecia, peripheral neurotoxicity, anemia, leukopenia, neutropenia, thrombocytopenia, gastrointestinal reaction, myelosuppression, and hepatic dysfunction (**Table 2**). There were no chemotherapy-related deaths in this study. The results indicated that there were significant differences using the PNI cutoff value of 51 in anemia (χ^2 = 7.064, P = 0.029), leukopenia (χ^2 = 13.570, P = 0.001), and myelosuppression (χ^2 = 7.066, P = 0.029).

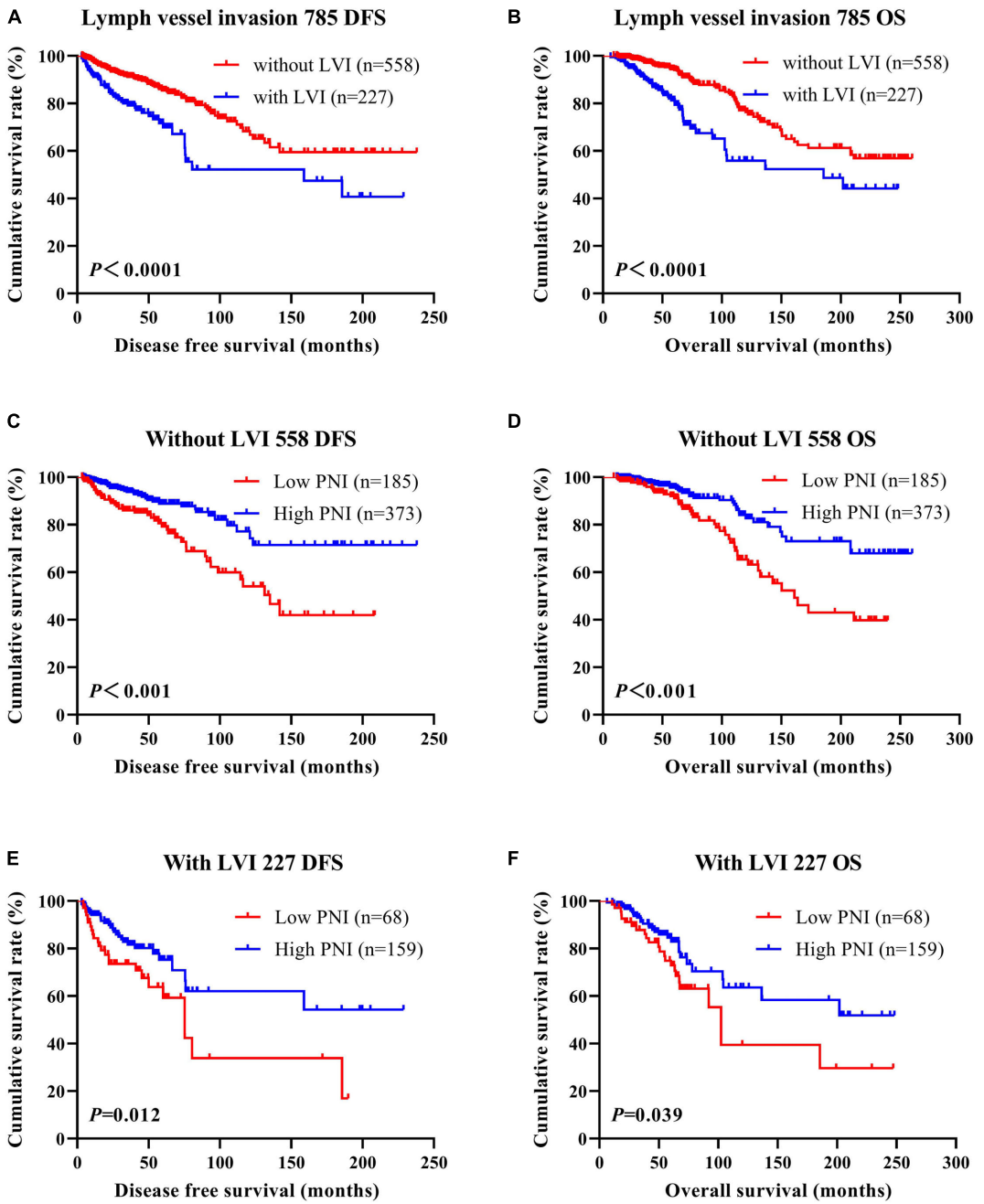

FIGURE 6 | Disease-free survival (DFS) and overall survival (OS) of patients with breast cancer by lymph vessel invasion status. **(A,B)** Kaplan–Meier analysis of the DFS **(A)** and OS **(B)** of breast cancer patients by lymph vessel invasion status. **(C,D)** Kaplan–Meier analysis of the DFS **(C)** and OS **(D)** of patients without lymph vessel invasion by prognostic nutritional index (PNI). **(E,F)** Kaplan–Meier analysis of the DFS **(E)** and OS **(F)** of patients with lymph vessel invasion by PNI.

DISCUSSION

Breast cancer is the most commonly diagnosed cancer among women all over the world and is a major public health problem worldwide (Siegel et al., 2020). Despite newer therapies in the recent years, recurrence and metastasis remain the main challenges of cancer management. In China, as a result of late diagnosis, about 30–40% of invasive breast cancer patients will eventually develop into metastatic breast cancer, and patients have a low 5-year survival rate of less than 30% (Early Breast Cancer Trialists' Collaborative Group et al., 2012; Noguchi et al., 2020). Although there were recent improvements in early detection and progress in surgical techniques and multimodal therapy, and the clinical outcomes and quality of life have improved, breast cancer remains the leading cause of cancer death for women (Waks and Winer,

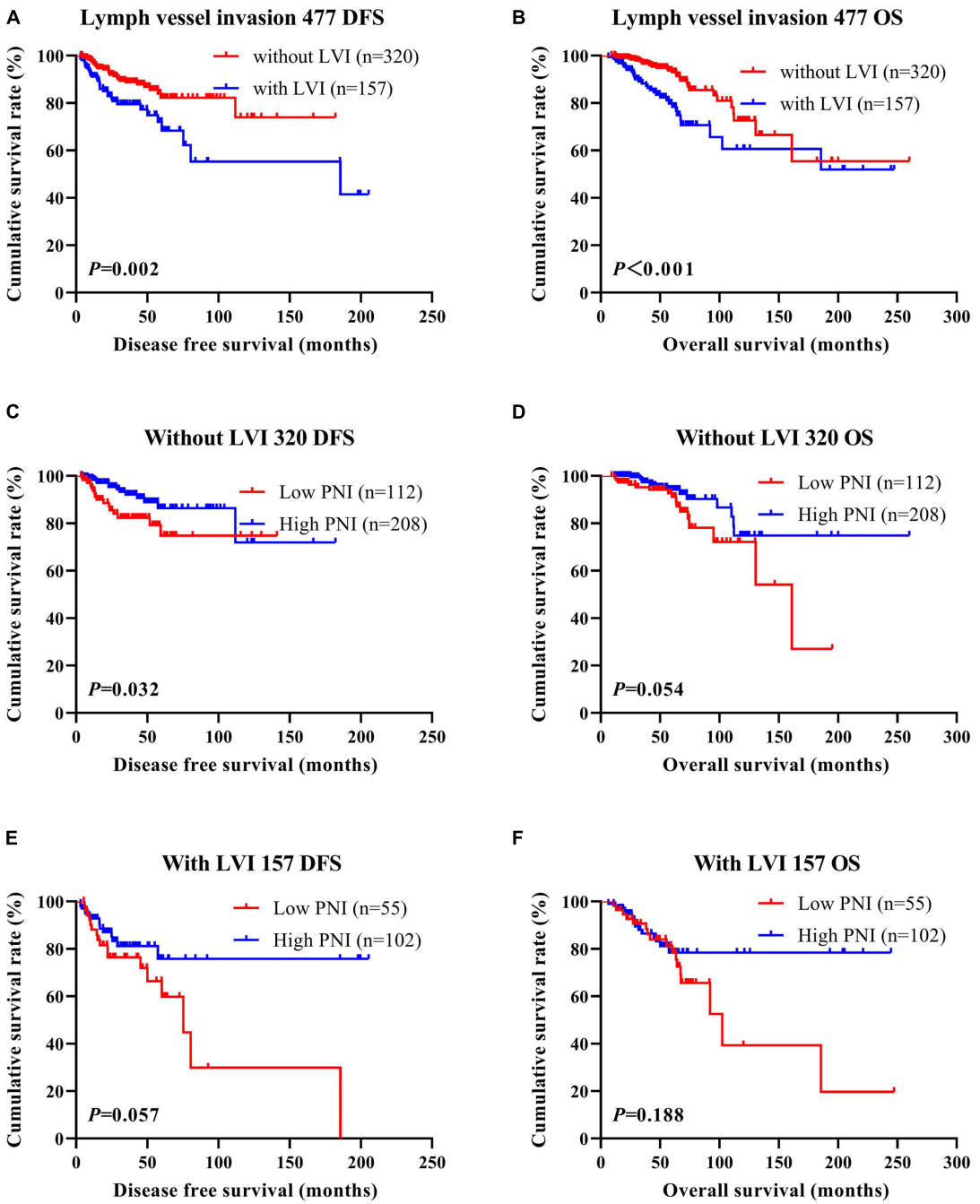

FIGURE 7 | Disease-free survival (DFS) and overall survival (OS) of patients with breast cancer by lymph vessel invasion status in the neoadjuvant chemotherapy (NACT) group. **(A,B)** Kaplan-Meier analysis of the DFS **(A)** and OS **(B)** of breast cancer patients by lymph vessel invasion status in NACT group. **(C,D)** Kaplan-Meier analysis of the DFS **(C)** and OS **(D)** of patients without lymph vessel invasion by prognostic nutritional index (PNI) in NACT group. **(E,F)** Kaplan-Meier analysis of the DFS **(E)** and OS **(F)** of patients with lymph vessel invasion by PNI in NACT group.

2019). Moreover, some breast cancer patients still develop recurrence and metastasis even after curative resection and neoadjuvant/adjuvant therapy (Tabor et al., 2020). Therefore, accurate prediction of prognosis is needed to improve patient survival and identify those patients who are more likely to benefit from neoadjuvant chemotherapy.

In this study, the clinical and demographic attributes of the 785 breast cancer patients enrolled were analyzed. The results indicated that a high PNI was significantly associated with marital status, post-chemotherapy regimen, type of surgery, pathological T stage, pathological TNM stage, AR status, E-cad status, and the TOP2A status of all enrolled patients. We also found that

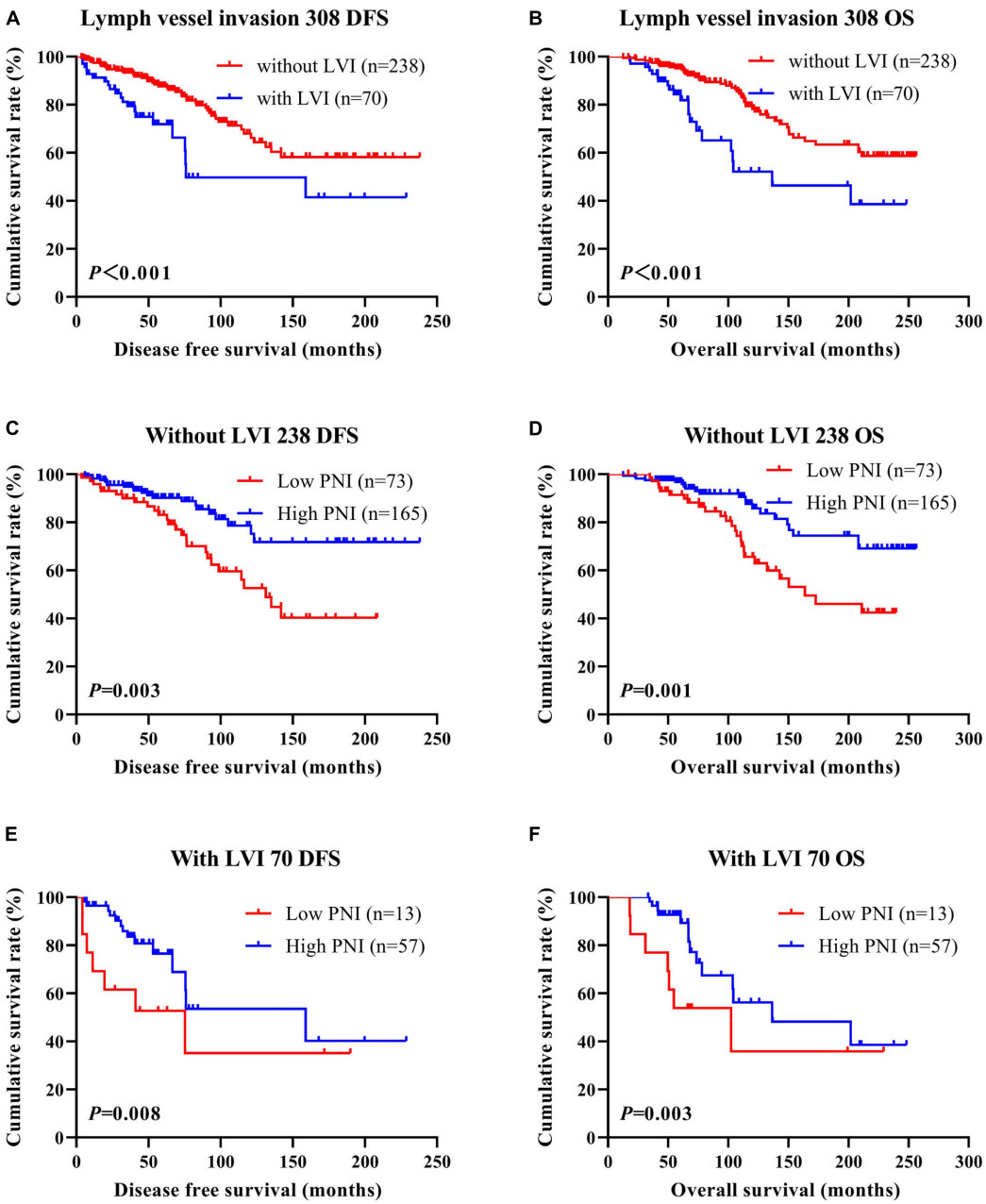

FIGURE 8 | Disease-free survival (DFS) and overall survival (OS) of patients with breast cancer by lymph vessel invasion status in the non-neoadjuvant chemotherapy (NACT) group. **(A,B)** Kaplan-Meier analysis of the DFS **(A)** and OS **(B)** of breast cancer patients by lymph vessel invasion status in non-NACT group. **(C,D)** Kaplan-Meier analysis of the DFS **(C)** and OS **(D)** of patients without lymph vessel invasion by prognostic nutritional index (PNI) in non-NACT group. **(E,F)** Kaplan-Meier analysis of the DFS **(E)** and OS **(F)** of patients with lymph vessel invasion by PNI in non-NACT group.

a high PNI was significantly associated with marital status and MPG in the NACT group and with tumor site, United States primary tumor site, operative time, type of surgery, tumor size, and pathological T stage in the non-NACT group. Moreover, we also analyzed the nutritional parameters and blood parameters. The results indicated that a high PNI was significantly associated with IgG, ALB, W, R, Hb, N, L, M, B, and P of all enrolled patients. Moreover, a high PNI was significantly associated with ALB, CRP, W, R, Hb, N, L, B, and P in the NACT group and with GGT, IgM, ALB, CRP, W, R, Hb, and M in the non-NACT group.

Several studies have investigated the prognostic value of the PNI in breast cancer patients (Yang et al., 2014; Wang et al., 2019; Hua et al., 2020). However, these studies did not determine the PNI among patients who had received neoadjuvant therapy. In the present study, we evaluated the prognostic impact of the PNI in breast cancer patients who received neoadjuvant

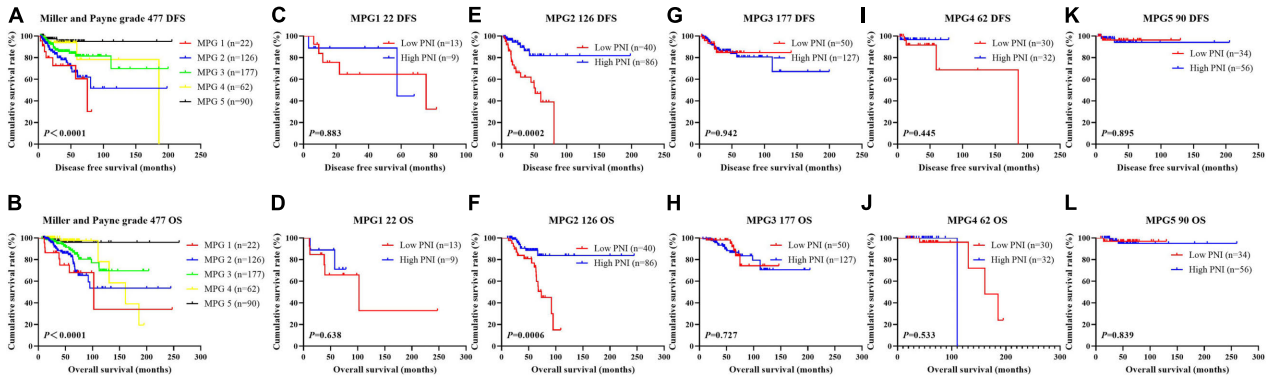

FIGURE 9 | Disease-free survival (DFS) and overall survival (OS) for the prognostic nutritional index (PNI) of patients with breast cancer in Miller and Payne grade (MPG) in the neoadjuvant chemotherapy (NACT) group. **(A,B)** Kaplan-Meier analysis of DFS **(A)** and OS **(B)** for the PNI of patients with different MPG in NACT group. **(C,D)** Kaplan-Meier analysis of DFS **(C)** and OS **(D)** for the PNI of patients with MPG 1 in NACT group. **(E,F)** Kaplan-Meier analysis of DFS **(E)** and OS **(F)** for the PNI of patients with MPG 2 in NACT group. **(G,H)** Kaplan-Meier analysis of DFS **(G)** and OS **(H)** for the PNI of patients with MPG 3 in NACT group. **(I,J)** Kaplan-Meier analysis of DFS **(I)** and OS **(J)** for the PNI of patients with MPG 4 in NACT group. **(K,L)** Kaplan-Meier analysis of DFS **(I)** and OS **(J)** for the PNI of patients with MPG 5 in NACT group.

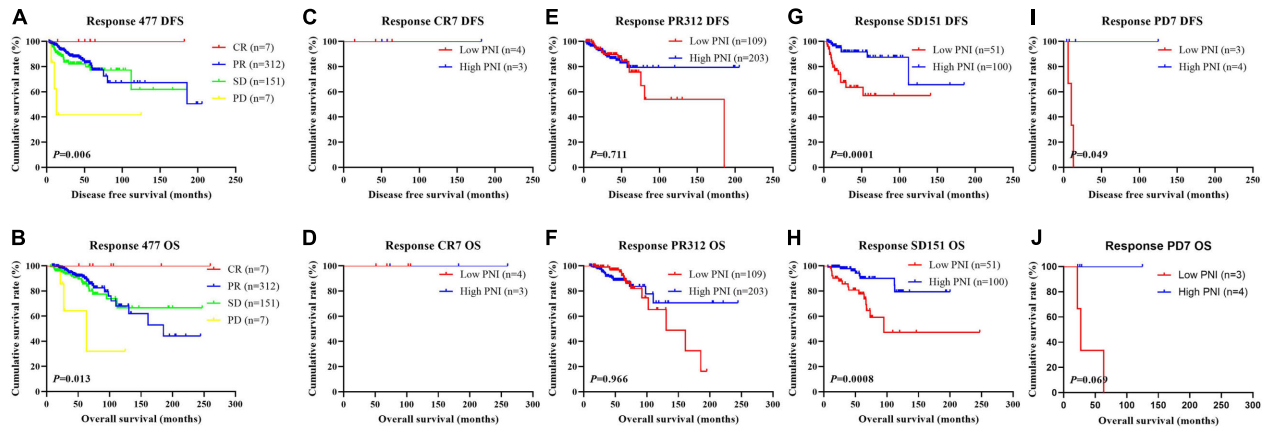

FIGURE 10 | Disease-free survival (DFS) and overall survival (OS) for the prognostic nutritional index (PNI) of patients with breast cancer in response status in the neoadjuvant chemotherapy (NACT) group. **(A,B)** Kaplan-Meier analysis of DFS **(A)** and OS **(B)** for the PNI of patients with different Response in NACT group. **(C,D)** Kaplan-Meier analysis of DFS **(C)** and OS **(D)** for the PNI of patients with Response CR in NACT group. **(E,F)** Kaplan-Meier analysis of DFS **(E)** and OS **(F)** for the PNI of patients with Response PR in NACT group. **(G,H)** Kaplan-Meier analysis of DFS **(G)** and OS **(H)** for the PNI of patients with Response SD in NACT group. **(I,J)** Kaplan-Meier analysis of DFS **(I)** and OS **(J)** for the PNI of patients with Response PD in NACT group.

chemotherapy followed by operation. The preoperative PNI was an independent prognostic factor of DFS and OS by univariate and multivariate Cox regression survival analyses. The results also indicated that the mean DFS and OS times of patients with high PNI were longer than of those with low PNI by the log-rank test in the NACT and non-NACT groups. The mechanism by which a low nutritional status decreases the survival time of breast cancer patients is still not sufficiently understood. The PNI, as a systemic immune–nutrition index based on the peripheral lymphocyte count and serum albumin levels, represents the immune and nutritional status and is also a significant biomarker for many tumors (Dai et al., 2020; Hao et al., 2020; Zhang et al., 2020). The PNI was initially developed to evaluate the postoperative complications in patients who received gastrointestinal surgery (Onodera et al., 1984). Lymphocytes and serum albumin are significantly closely related to the prognosis of cancer patients (Otagiri et al., 2020; Powell et al., 2020). Lymphocytes play an active role in the adaptive immune system to clear tumors from the body and to prevent their development and spread (Hanahan and Weinberg, 2011). Serum albumin has been reported to reflect an individual's nutrition and inflammatory status (Fuhrman et al., 2004; Yoshida et al., 2020). It is generally known that low levels of serum albumin and lymphocytes promote inflammatory tumor development and the spread and metastasis of cancer (Saroha et al., 2013; Mendez et al., 2016).

We also analyzed the association of pathologic stage and PNI in patients with breast cancer and observed that those with high PNI had longer DFS and OS than those with low PNI in early stage and advanced stage breast cancer in all enrolled breast

TABLE 2 | Correlations between PNI and toxicity assessment.

Parameters	PNI (*n* = 477)				
	N	**Low PNI (*n* = 167)**	**High PNI (*n* = 310)**	χ^2	***P* value**
Decreased appetite				0.898	0.343
No	70 (14.68%)	28 (16.77%)	42 (13.55%)		
Yes	407 (85.32%)	139 (83.23%)	268 (86.45%)		
Nausea				1.136	0.286
No	59 (12.37%)	17 (10.18%)	42 (13.55%)		
Yes	418 (87.63%)	150 (89.82%)	268 (86.45%)		
Vomiting				2.315	0.128
No	234 (49.06%)	74 (44.31%)	160 (51.61%)		
Yes	243 (50.94%)	93 (55.69%)	150 (48.39%)		
Diarrhea				0.299	0.584
No	444 (93.08%)	154 (92.22%)	290 (93.55%)		
Yes	33 (6.92%)	13 (7.78%)	20 (6.45%)		
Mouth ulcers				1.424	0.233
No	463 (97.07%)	160 (95.81%)	303 (97.74%)		
Yes	14 (2.93%)	7 (4.19%)	7 (2.26%)		
Alopecia				0.003	0.958
No	222 (46.54%)	78 (46.71%)	144 (46.45%)		
Yes	255 (53.46%)	89 (53.29%)	166 (53.55%)		
Peripheral neurotoxicity				0.132	0.717
No	390 (81.76%)	138 (82.63%)	252 (81.29%)		
Yes	87 (18.24%)	29 (17.37%)	58 (18.71%)		
Anemia				7.064	0.029
Grade 0	257 (53.88%)	77 (46.10%)	180 (58.06%)		
Grades 1–2	215 (45.07%)	87 (52.10%)	128 (41.29%)		
Grades 3–4	5 (1.05%)	3 (1.80%)	2 (0.65%)		
Leukopenia				13.570	0.001
Grade 0	138 (28.93%)	31 (18.56%)	107 (34.52%)		
Grades 1–2	233 (48.85%)	95 (56.89%)	138 (44.52%)		
Grades 3–4	106 (22.22%)	41 (24.55%)	65 (20.96%)		
Neutropenia				5.679	0.059
Grade 0	143 (29.98%)	39 (23.35%)	104 (33.55%)		
Grades 1–2	179 (37.53%)	71 (42.51%)	108 (34.84%)		
Grades 3–4	155 (32.49%)	57 (34.13%)	98 (31.61%)		
Thrombocytopenia				0.511	0.774
Grade 0	372 (77.99%)	128 (76.65%)	244 (78.71%)		
Grades 1–2	98 (20.55%)	37 (22.15%)	61 (19.68%)		
Grades 3–4	7 (1.46%)	2 (1.20%)	5 (1.61%)		
Gastrointestinal reaction				2.347	0.309
Grade 0	38 (7.97%)	9 (5.39%)	29 (9.35%)		
Grades 1–2	433 (90.78%)	156 (93.41%)	277 (89.35%)		
Grades 3–4	6 (1.25%)	2 (1.20%)	4 (1.30%)		
Myelosuppression				7.066	0.029
Grade 0	90 (18.87%)	21 (12.57%)	69 (22.26%)		
Grades 1–2	175 (36.69%)	63 (37.72%)	112 (36.13%)		
Grades 3–4	212 (44.44%)	83 (49.71%)	129 (41.61%)		
Hepatic dysfunction				0.612	0.736
Grade 0	371 (77.78%)	129 (77.25%)	242 (78.07%)		
Grades 1–2	105 (22.01%)	38 (22.75%)	67 (21.61%)		
Grades 3–4	1 (2.10%)	0 (0.00%)	1 (0.32%)		

cancer patients. Furthermore, patients with high PNI had longer DFS and OS than those with low PNI in early stage and advanced stage breast cancer, especially in those with advanced stage breast cancer in the NACT and non-NACT groups. Apart from these analyses, we also observed that patients with high PNI had longer DFS and OS than those with low PNI in different molecular

subtypes, except for luminal B HER2-positive subtype. Lymph vessel invasion (LVI) was the significant prognostic factor by univariate and multivariate analyses. The results indicated that patients without lymph vessel invasion survive longer than those patients with lymph vessel invasion, and the mean DFS and OS times of patients with high PNI were longer than of those patients with low PNI with lymph vessel invasion status. Moreover, patients with lymph vessel invasion and low PNI value had worse survival times. In Sahoo's study, the results indicated that poor overall as well as disease-free survival and overall survival pattern were observed for LVI-positive patients as compared with LVI-negative patients; LVI and PNI constitute potential targets for the treatment of breast cancer patients (Sahoo et al., 2014). In He's study, it was indicated that LVI was an independent poor prognostic factor for the development of recurrence in lymph node-negative breast cancer and was also promising in determining prognosis and treatment strategies (He et al., 2017). Another study indicated that both positive lymphatic invasion (LI) and positive vascular invasion (VI) showed inferior OS and DFS compared with negative LI and negative VI; moreover, both positive LI and positive VI showed worse survival rates in the luminal A and triple-negative subtypes (Hwang et al., 2017).

In the NACT group, all breast cancer patients could tolerate the neoadjuvant chemotherapy toxicities, and the regimens were safe and effective. The common toxicities after neoadjuvant chemotherapy were hematologic and gastrointestinal reaction, and the results indicated that, in toxicity assessment, there was no difference in these toxicities using the cutoff value of 51 for PNI, except in anemia, leukopenia, and myelosuppression.

However, there are several limitations that cannot be neglected in this study. Firstly, this is a retrospective design and was conducted in a single center with a limited number of patients. A multicenter study and more patients should be enrolled. Secondly, selection bias cannot be excluded, even if consecutive patients are included and eligibility criteria are implemented to minimize the bias. Thirdly, the PNI is a nonspecific tumor marker because other non-cancer diseases can be confused with a tumor. Further validation in a large prospective study is needed to further assess the prognostic and predictive value of PNI for patients with breast cancer in the future.

CONCLUSION

Prognostic nutritional index is a significant prognostic factor for patients with breast cancer and can effectively predict the survival and prognosis of breast cancer. It is of importance to take into consideration the unbalanced distribution of medical conditions in China, and noninvasive, reproducible, and convenient biomarkers should be used for the prevention and treatment of breast cancer.

DATA AVAILABILITY STATEMENT

The raw data supporting the conclusions of this article will be made available by the authors, without undue reservation.

ETHICS STATEMENT

The studies involving human participants were reviewed and approved by This study was approved by the Ethics Committee of Cancer Hospital Chinese Academy of Medical Sciences. The patients/participants provided their written informed consent to participate in this study.

AUTHOR CONTRIBUTIONS

LC and PB wrote the original draft and did the review and editing. XK and SH did the formal analysis. ZW did the data curation. XW contributed to the investigation. YF contributed to the methodology and supervision. JW helped with the resources, funding acquisition, and project administration. All authors contributed to the article and approved the submitted version.

FUNDING

The work is partly supported by research grants from The National Nature Science Foundation of China (No. 81872160) and Beijing Nature Science Foundation of China (No. 7191009).

SUPPLEMENTARY MATERIAL

The Supplementary Material for this article can be found online at: https://www.frontiersin.org/articles/10.3389/fcell.2021.656741/full#supplementary-material

REFERENCES

Abdel-Rahman, O. (2018). Validation of the 8th AJCC prognostic staging system for breast cancer in a population-based setting. *Breast Cancer Res. Treat.* 168, 269–275. doi: 10.1007/s10549-017-4577-x

Bhaskaran, K., Douglas, I., Forbes, H., dos-Santos-Silva, I., Leon, D. A., and Smeeth, L. (2014). Body-mass index and risk of 22 specific cancers: a population-based cohort study of 5·24 million UK adults. *Lancet* 384, 755–765. doi: 10.1016/S0140-6736(14)60892-8

Bumrungpert, A., Pavadhgul, P., Nunthanawanich, P., Sirikanchanarod, A., and Adulbhan, A. (2018). Whey protein supplementation improves nutritional status, glutathione levels, and immune function in cancer patients: a randomized, double-blind controlled trial. *J. Med. Food.* 21, 612–616. doi: 10.1089/jmf.2017.4080

Buzby, G. P., Mullen, J. L., Matthews, D. C., Hobbs, C. L., and Rosato, E. F. (1980). Prognostic nutritional index in gastrointestinal surgery. *Am. J. Surg.* 139, 160–167. doi: 10.1016/0002-9610(80)90246-9

Cespedes Feliciano, E. M., Kwan, M. L., Kushi, L. H., Chen, W. Y., Weltzien, E. K., Castillo, A. L., et al. (2017). Body mass index, PAM50 subtype, recurrence, and survival among patients with nonmetastatic breast cancer. *Cancer* 123, 2535–2542. doi: 10.1002/cncr.30637

Chen, Z., Shao, Y., Yao, H., Zhuang, Q., Wang, K., Xing, Z., et al. (2017). Preoperative albumin to globulin ratio predicts survival in clear cell renal

cell carcinoma patients. *Oncotarget* 8, 48291–48302. doi: 10.18632/oncotarget.15162

Clemente, G., Gallo, M., and Giorgini, M. (2018). AMD-associazione medici diabetologi "Diabetes and Cancer" working group. Modalities for assessing the nutritional status in patients with diabetes and cancer. *Diabetes Res. Clin. Pract.* 142, 162–172. doi: 10.1016/j.diabres.2018.05.039

Dai, Y., Liu, M., Lei, L., and Lu, S. (2020). Prognostic significance of preoperative prognostic nutritional index in ovarian cancer: a systematic review and meta-analysis. *Medicine (Baltimore).* 99:e21840. doi: 10.1097/MD.0000000000021840

Del Prete, S., Caraglia, M., Luce, A., Montella, L., Galizia, G., Sperlongano, P., et al. (2019). Clinical and pathological factors predictive of response to neoadjuvant chemotherapy in breast cancer: a single center experience. *Oncol Lett.* 18, 3873–3879. doi: 10.3892/ol.2019.10729

Early Breast Cancer Trialists' Collaborative Group, (E. B. C. T. C. G.), Peto, R., Davies, C., Godwin, J., Gray, R., Pan, H. C., et al. (2012). Comparisons between different polychemotherapy regimens for early breast cancer: meta-analyses of long-term outcome among 100,000 women in 123 randomised trials. *Lancet* 379, 432–444. doi: 10.1016/S0140-6736(11)61625-5

Echeverria, G. V., Ge, Z., Seth, S., Zhang, X., Jeter-Jones, S., Zhou, X., et al. (2019). Resistance to neoadjuvant chemotherapy in triple-negative breast cancer mediated by a reversible drug-tolerant state. *Sci. Transl. Med.* 11:eaav0936. doi: 10.1126/scitranslmed.aav0936

Eisenhauer, E. A., Therasse, P., Bogaerts, J., Schwartz, L. H., Sargent, D., Ford, R., et al. (2009). New response evaluation criteria in solid tumours: revised RECIST guideline (version 1.1). *Eur. J. Cancer* 45, 228–247. doi: 10.1016/j.ejca.2008.10.026

Emens, L. A. (2018). Breast cancer immunotherapy: facts and hopes. *Clin. Cancer Res.* 24, 511–520. doi: 10.1158/1078-0432.CCR-16-3001

Falisi, A. L., Wiseman, K. P., Gaysynsky, A., Scheideler, J. K., Ramin, D. A., and Chou, W. S. (2017). Social media for breast cancer survivors: a literature review. *J. Cancer Surviv.* 11, 808–821. doi: 10.1007/s11764-017-0620-5

Fouad, T. M., Barrera, A. M. G., Reuben, J. M., Lucci, A., Woodward, W. A., Stauder, M. C., et al. (2017). Inflammatory breast cancer: a proposed conceptual shift in the UICC-AJCC TNM staging system. *Lancet Oncol.* 18, e228–e232. doi: 10.1016/S1470-2045(17)30192-4

Fuhrman, M. P., Charney, P., and Mueller, C. M. (2004). Hepatic proteins and nutrition assessment. *J Am Diet Assoc.* 104, 1258–1264. doi: 10.1016/j.jada.2004.05.213

Ganz, P. A., and Goodwin, P. J. (2015). Breast cancer survivorship: where are we today? *Adv. Exp. Med. Biol.* 862, 1–8. doi: 10.1007/978-3-319-16366-6_1

Hanahan, D., and Weinberg, R. A. (2011). Hallmarks of cancer: the next generation. *Cell.* 144, 646–674. doi: 10.1016/j.cell.2011.02.013

Hao, J., Chen, C., Wan, F., Zhu, Y., Jin, H., Zhou, J., et al. (2020). Prognostic value of pre-treatment prognostic nutritional index in esophageal cancer: a systematic review and meta-analysis. *Front. Oncol.* 10:797. doi: 10.3389/fonc.2020.00797

He, K. W., Sun, J. J., Liu, Z. B., Zhuo, P. Y., Ma, Q. H., Liu, Z. Y., et al. (2017). Prognostic significance of lymphatic vessel invasion diagnosed by D2-40 in Chinese invasive breast cancers. *Medicine (Baltimore).* 96:e8490. doi: 10.1097/MD.0000000000008490

Howlader, N., Cronin, K. A., Kurian, A. W., and Andridge, R. (2018). Differences in breast cancer survival by molecular subtypes in the united states. *Cancer Epidemiol. Biomarkers Prev.* 27, 619–626. doi: 10.1158/1055-9965.EPI-17-0627

Hua, X., Long, Z. Q., Huang, X., Deng, J. P., He, Z. Y., Guo, L., et al. (2020). The value of prognostic nutritional index (PNI) in predicting survival and guiding radiotherapy of patients with T1-2N1 Breast Cancer. *Front. Oncol.* 9:1562. doi: 10.3389/fonc.2019.01562

Huynh-Le, M. P., Zhang, Z., Tran, P. T., DeWeese, T. L., and Song, D. Y. (2014). Low interrater reliability in grading of rectal bleeding using National cancer institute common toxicity criteria and radiation therapy oncology group toxicity scales: a survey of radiation oncologists. *Int. J. Radiat. Oncol. Biol. Phys.* 90, 1076–1082. doi: 10.1016/j.ijrobp.2014.08.014

Hwang, K. T., Kim, Y. A., Kim, J., Chu, A. J., Chang, J. H., Oh, S. W., et al. (2017). The influences of peritumoral lymphatic invasion and vascular invasion on the survival and recurrence according to the molecular subtypes of breast cancer. *Breast Cancer Res. Treat* 163, 71–82. doi: 10.1007/s10549-017-4153-4

Lacombe, J., Armstrong, M. E. G., Wright, F. L., and Foster, C. (2019). The impact of physical activity and an additional behavioural risk factor on cardiovascular disease, cancer and all-cause mortality: a systematic review. *BMC Public Health* 19:900. doi: 10.1186/s12889-019-7030-8

Li, Q., Meng, X., Liang, L., Xu, Y., Cai, G., and Cai, S. (2015). High preoperative serum globulin in rectal cancer treated with neoadjunctive chemoradiation therapy is a risk factor for poor outcome. *Am. J. Cancer Res.* 5, 2856–2864.

Li, X., Dai, D., Chen, B., Tang, H., and Wei, W. (2017). Oncological outcome of complete response after neoadjuvant chemotherapy for breast conserving surgery: a systematic review and meta-analysis. *World J. Surg. Oncol.* 15:210. doi: 10.1186/s12957-017-1273-6

Liu, X., Sun, X., Liu, J., Kong, P., Chen, S., Zhan, Y., et al. (2015). Preoperative C-reactive protein/albumin ratio predicts prognosis of patients after curative resection for gastric cancer. *Transl. Oncol.* 8, 339–345. doi: 10.1016/j.tranon.2015.06.006

Lucas, A. R., Levine, B. J., and Avis, N. E. (2017). Posttreatment trajectories of physical activity in breast cancer survivors. *Cancer* 123, 2773–2780. doi: 10.1002/cncr.30641

Mendez, J. S., Govindan, A., Leong, J., Gao, F., Huang, J., and Campian, J. L. (2016). Association between treatment-related lymphopenia and overall survival in elderly patients with newly diagnosed glioblastoma. *J. Neurooncol.* 127, 329–335. doi: 10.1007/s11060-015-2037-1

Mohri, Y., Inoue, Y., Tanaka, K., Hiro, J., Uchida, K., and Kusunoki, M. (2013). Prognostic nutritional index predicts postoperative outcome in colorectal cancer. *World J. Surg.* 37, 2688–2692. doi: 10.1007/s00268-013-2156-9

Nagini, S. (2017). Breast cancer: current molecular therapeutic targets and new players. *Anticancer Agents Med. Chem.* 17, 152–163. doi: 10.2174/1871520616666160502122724

Nakatani, M., Migita, K., Matsumoto, S., Wakatsuki, K., Ito, M., Nakade, H., et al. (2017). Prognostic significance of the prognostic nutritional index in esophageal cancer patients undergoing neoadjuvant chemotherapy. *Dis. Esophagus* 30, 1–7. doi: 10.1093/dote/dox020

Noguchi, M., Inokuchi, M., Noguchi, M., Morioka, E., Ohno, Y., and Kurita, T. (2020). Axillary surgery for breast cancer: past, present, and future. . *Breast Cancer* 28, 9–15. doi: 10.1007/s12282-020-01120-0

Okadome, K., Baba, Y., Yagi, T., Kiyozumi, Y., Ishimoto, T., Iwatsuki, M., et al. (2020). Prognostic nutritional index, tumor-infiltrating lymphocytes, and prognosis in patients with esophageal cancer. *Ann. Surg.* 271, 693–700. doi: 10.1097/SLA.0000000000002985

Onodera, T., Goseki, N., and Kosaki, G. (1984). Prognostic nutritional index in gastrointestinal surgery of malnourished cancer patients. *Nihon Geka Gakkai Zasshi.* 85, 1001–1005.

Otagiri, H., Yamadav, S., Hashidume, M., Sakurai, A., Morioka, M., Kondo, E., et al. (2020). Clinical investigation of the association between perioperative oral management and prognostic nutritional index in patients with digestive and urinary cancers. *Curr. Oncol.* 27, 257–262. doi: 10.3747/co.27.5963

Pinato, D. J., North, B. V., and Sharma, R. A. (2012). Novel, externally validated inflammation-based prognostic algorithm in hepatocellular carcinoma: the prognostic nutritional index (PNI). *Br. J. Cancer* 106, 1439–1445. doi: 10.1038/bjc.2012.92

Powell, A. G. M. T., Eley, C., Chin, C., Coxon, A. H., Christian, A., Lewis, W. G., et al. (2020). . Prognostic significance of serum inflammatory markers in esophageal cancer. *Esophagus* doi: 10.1007/s10388-020-00772-3 Epub ahead of print.,

Sahoo, P. K., Jana, D., Mandal, P. K., and Basak, S. (2014). Effect of lymphangiogenesis and lymphovascular invasion on the survival pattern of breast cancer patients. *Asian Pac. J. Cancer Prev.* 15, 6287–6293. doi: 10.7314/APJCP.2014.15.15.6287

Saroha, S., Uzzo, R. G., Plimack, E. R., Ruth, K., and Al-Saleem, T. (2013). Lymphopenia is an independent predictor of inferior outcome in clear cell renal carcinoma. *J. Urol.* 189, 454–461. doi: 10.1016/j.juro.2012.09.166

Siegel, R. L., Miller, K. D., and Jemal, A. (2019). Cancer statistics, 2019. *CA. Cancer J. Clin.* 69, 7–34. doi: 10.3322/caac.21551

Siegel, R. L., Miller, K. D., and Jemal, A. (2020). Cancer statistics, 2020. *CA. Cancer J. Clin.* 70, 7–30. doi: 10.3322/caac.21590

Sun, J., Wang, D., Mei, Y., Jin, H., Zhu, K., Liu, X., et al. (2017). Value of the prognostic nutritional index in advanced gastric cancer treated with preoperative chemotherapy. *J. Surg. Res.* 209, 37–44. doi: 10.1016/j.jss.2016.09.050

Sun, K., Chen, S., Xu, J., Li, G., and He, Y. (2014). The prognostic significance of the prognostic nutritional index in cancer: a systematic review and meta-analysis. *J. Cancer Res. Clin. Oncol.* 140, 1537–1549. doi: 10.1007/s00432-014-1714-3

Tabor, S., Szostakowska-Rodzos, M., Fabisiewicz, A., and Grzybowska, E. A. (2020). How to predict metastasis in luminal breast cancer? current solutions and future prospects. *Int. J. Mol. Sci.* 21:E8415. doi: 10.3390/ijms21218415

Waks, A. G., and Winer, E. P. (2019). Breast cancer treatment: a review. *JAMA* 321, 288–300. doi: 10.1001/jama.2018.19323

Wang, Y., Battseren, B., Yin, W., Lin, Y., Zhou, L., Yang, F., et al. (2019). Predictive and prognostic value of prognostic nutritional index for locally advanced breast cancer. *Gland Surg.* 8, 618–626. doi: 10.21037/gs.2019.10.08

Wu, D., Chen, T., Jiang, H., Duan, C., Zhang, X., Lin, Y., et al. (2019). Comparative efficacy and tolerability of neoadjuvant immunotherapy regimens for patients with HER2-positive breast cancer: a network meta-analysis. *J. Oncol.* 2019:3406972. doi: 10.1155/2019/3406972

Yang, Z., Zhang, B., Hou, L., Xie, Y., and Cao, X. (2014). Pre-operative prognostic nutritional index predicts the outcomes for triple-negative breast cancer. *Tumour Biol.* 35, 12165–12171. doi: 10.1007/s13277-014-2524-6

Yoshida, R., Gohara, S., Sakata, J., Matsuoka, Y., Hirosue, A., Kawahara, K., et al. (2020). Onodera's prognostic nutritional index correlates with tumor immune environment and survival in patients with oral squamous cell carcinoma undergoing chemoradiotherapy. *Transl. Oncol.* 13:100850. doi: 10.1016/j.tranon.2020.100850

Zhang, Z., Chen, A., Xie, F., Li, X., Hu, G., and Lin, G. (2020). Low prognostic nutrition index predicts poorer quality of life in late-stage lung cancer. *Ann. Palliat. Med.* 9, 3976–3984. doi: 10.21037/apm-20-1892

Zheng, T., Wang, A., Hu, D., and Wang, Y. (2017). Molecular mechanisms of breast cancer metastasis by gene expression profile analysis. *Mol. Med. Rep.* 16, 4671–4677. doi: 10.3892/mmr.2017.7157

Conflict of Interest: The authors declare that the research was conducted in the absence of any commercial or financial relationships that could be construed as a potential conflict of interest.

frontiers in Cell and Developmental Biology

REVIEW
published: 01 April 2021
doi: 10.3389/fcell.2021.657472

Targeting the Complement Pathway in Malignant Glioma Microenvironments

Hongtao Zhu[1,2], Xingjiang Yu[2], Suojun Zhang[1] and Kai Shu[1]**

[1] Department of Neurosurgery, Tongji Hospital, Tongji Medical College, Huazhong University of Science and Technology, Wuhan, China, [2] Department of Histology and Embryology, School of Basic Medicine, Tongji Medical College, Huazhong University of Science and Technology, Wuhan, China

Malignant glioma is a highly fatal type of brain tumor, and its reoccurrence is largely due to the ordered interactions among the components present in the complex microenvironment. Besides its role in immune surveillance and clearance under physiological conditions, the complement system is expressed in a variety of tumor types and mediates the interactions within the tumor microenvironments. Recent studies have uncovered the broad expression spectrum of complement signaling molecules in the tumor microenvironment and various tumor cells, in particular, malignant glioma cells. Involvement of the complement system in tumor growth, immunosuppression and phenotype transition have also been elucidated. In this review, we enumerate the expression and function of complement molecules in multiple tumor types reported. Moreover, we elaborate the complement pathways in glioma cells and various components of malignant glioma microenvironments. Finally, we summarize the possibility of the complement molecules as prognostic factors and therapeutic targets in the treatment of malignant glioma. Specific targeting of the complement system maybe of great significance and value in the future treatment of multi-type tumors including malignant glioma.

Keywords: glioblastoma microenvironments, malignant glioma, complement pathway, immunotherapy, tumor immunity

OPEN ACCESS

Edited by:
Na Luo,
Nankai University, China

Reviewed by:
Aleksandra Ellert-Miklaszewska,
Nencki Institute of Experimental Biology (PAS), Poland
Jianbo Wang,
Shandong University, China

***Correspondence:**
Suojun Zhang
zhangsuojun@163.com
Kai Shu
kshu@tjh.tjmu.edu.cn

Specialty section:
This article was submitted to Molecular Medicine, a section of the journal Frontiers in Cell and Developmental Biology

Received: *23 January 2021*
Accepted: *12 March 2021*
Published: *01 April 2021*

Citation:
Zhu H, Yu X, Zhang S and Shu K (2021) Targeting the Complement Pathway in Malignant Glioma Microenvironments. Front. Cell Dev. Biol. 9:657472. doi: 10.3389/fcell.2021.657472

INTRODUCTION

Glioblastoma treatments have been largely unsuccessful due to its rapid growth, multidimensional heterogeneity, and stubborn resistance to chemoradiotherapy (Lim et al., 2018). For decades, the main treatment for malignant glioma has been surgical resection combined with postoperative radiotherapy and chemotherapy. Unfortunately, even with the maximal treatment, the median survival time of patients with glioblastoma is still less than 15 months (McGranahan et al., 2019). Hence, new treatment strategies need to be developed.

Unlike early oncology research that focused on the proliferation and invasion of tumor cells, recent studies have shown that almost all solid tumors have a complex but highly ordered tumor microenvironment. For example, the glioma microenvironment contains glioma cells, glioma stem cells (GSCs), tumor-associated macrophages (TAMs), vascular endothelial cells, neurons, astrocytes, T cells, neutrophils, and extracellular matrix molecules. These components organically

interact with each other and work together to promote tumor progression (Broekman et al., 2018). It is well known that simultaneously targeting the interaction between the components in the tumor microenvironment when inhibiting the growth of tumor cells can inhibits tumor growth and prolongs the survival of tumor-bearing mice more effectively.

As an important part of the immune system, the complement system plays an irreplaceable role in a series of pathophysiological processes, such as immune surveillance, immune clearance, and inflammatory response (Ricklin et al., 2010; Ehrnthaller et al., 2011). Recent studies have found that complement-related molecules, including C1q, C3a/C3aR, and C5a/C5aR, are expressed in the tumor microenvironment (Roumenina et al., 2019b). These molecules are widely involved in a series of tumor biological processes, such as tumor cell proliferation and invasion, resistance to radiotherapy and chemotherapy, monocyte recruitment, phenotype polarization of TAMs, and tumor neovascularization (Zhang et al., 2019). In gliomas, other reports demonstrate that the expression of complement molecules and complement signals can promote tumor progression (van der Vlis et al., 2018).

In this review, we summarized the composition and function of the complement system, the expression and related roles of complement molecules in various types of tumors, and the effects of complement molecules in the malignant glioma microenvironment. Moreover, we discussed the potential of using complement signals in the diagnosis and treatments of malignant glioma. Complement signaling could promote the growth of malignant glioma cells and the proneural to mesenchymal transition; both of these factors promote tumor progression. We believe that the complement system participates in the recruitment of peripheral blood monocytes, polarization of TAMs, neovascularization, and maintenance of GSCs. The complement system may also play a significant role in hypoxia signaling. Targeting the complement signaling pathway will become important for the comprehensive treatment of malignant gliomas in the future.

THE COMPLEMENT SYSTEM

The complement system, which was first discovered and named by J. Bordet in 1890, is one of the most indispensable components of the human immune system (Morgan, 2000; Kolev et al., 2014). This system contains a series of membrane receptors and soluble proteins mainly synthesized in the liver and released into the circulatory system. Complement proteins are widely distributed in various parts of the human body, such as the blood and tissue fluids. When pathogenic microorganisms invade the body, the complement system is activated and works in conjunction with other immune components to remove foreign microorganisms via immune regulation and the direct killing of target cells (Morgan, 2000). In addition to the classical immune clearance function, several recent studies have shown that the complement system is also widely involved in a series of pathophysiological processes, such as hemolysis, intracellular homeostasis maintenance, recognition and clearance of apoptotic cells, and recruitment of inflammatory cells (Kolev et al., 2014). Three different pathways can activate the complement system, which are described in detail below (**Figure 1**).

Classical Pathway

When foreign pathogenic microorganisms invade the body, the immune system produces corresponding antibodies to help eliminate the pathogen. When IgG or IgM antibodies bind to foreign microorganisms or other non-self antigens, the complement system is activated through the classical pathway. The Fc segment of the antibody recognizes and binds to C1q and changes its configuration to activate C1r and C1s. The activated C1s cleaves C4 and C2 to C4a, C4b, C2a, and C2b. Then C4b combines with C2a to form C4b2a as C3 convertase; C3 convertase cleaves C3 and combines with the cleaved C3b to form C4b2a3b as C5 convertase. C5 convertase further hydrolyzes C5 into C5a and C5b; C5a and C3a, which are formed by the previous cleavage of C3, are secreted to the extracellular matrix and function as anaphylatoxins. C5b forms a membrane attack complex (MAC) with C6, C7, C8, and multiple C9 units. The MAC perforates the host cell membranes invaded by pathogens, thereby lysing the target cells and achieving immune clearance.

Alternative Pathway

Unlike the classical pathway that is activated in an antibody-dependent manner, the alternative pathway is activated by the microorganism components, including bacteria, endotoxins, yeast polysaccharides, and dextran. Under physiological conditions, C3 is spontaneously divided into a small amount of C3b, which combines with factor B to constitute C3bB. The alternative form of C3 convertase, C3bBb, is created when C3Bb combines with factor D and factor P; however, the whole process is suppressed by factor I and factor H. When the above pathogenic components are invading, the inhibitory effect of factor I and factor H is blocked, leading to the accumulation of C3bBb. C3bBb cleaves C3 into C3a and C3b, forming a positive feedback loop for C3 cleavage. And C3bBb combines with C3b to form C3bBb3b as C5 convertase. C5 convertase splits C5 to C5a and C5b. Eventually, the MAC is formed through the same mechanism as the classical pathway.

Lectin Pathway

The lectin pathway is well known as the mannose-binding lectin (MBL) pathway. When pathogens containing mannose or mannosamine residues invade the body, they can be recognized and combine with MBL to activate mannose-associated serine protease (MASP). MASP is similar to C1s in the classical pathway in which it can cleave C4 and C2 to C4a, C4b, C2a, and 2b. C4b combines with C2a to form C4b2a as C3 convertase. Then C4b2a cleaves C3 and C5 in the same way as the classical pathway, and the C5b6789n MAC is formed.

The Complement Pathway in Cancer Research

In recent years, cancer researchers have increasingly focused on the immune microenvironment of tumors. Immune

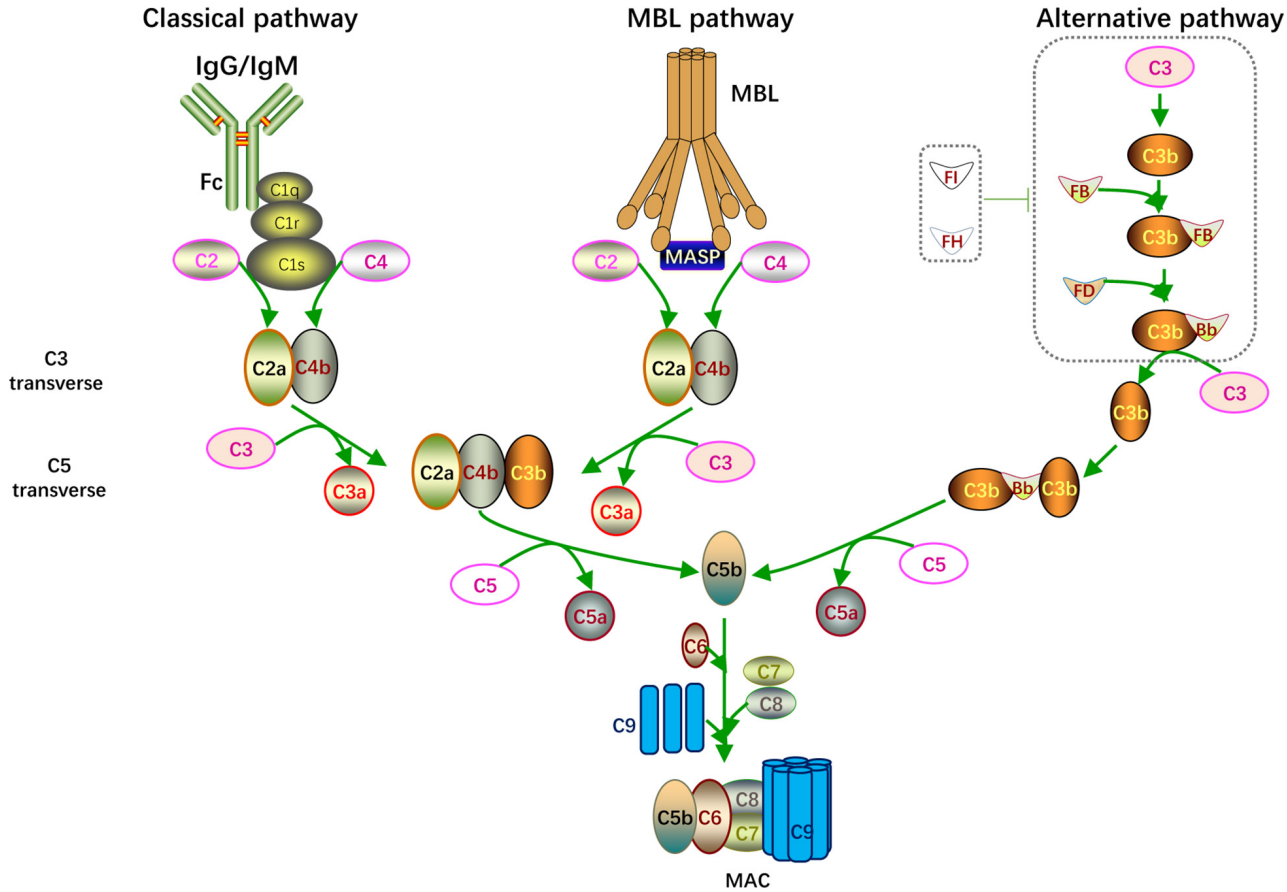

FIGURE 1 | Complement activation. Overview of the complement activation. There are three different pathways including classical pathway (initiated by IgG/IgM), MBL pathway (activated when MBL binding to MASP) and alternative pathway (microorganism components enhanced C3 autohydrolyzation and accumulation of C3 transverse). The catalytic activity of C3, C5 transverse and formation of C5b-9 complex (MAC) are common feature of these pathways.

microenvironment has been found in almost all types of tumors. Immune checkpoints and immunotherapy have become hot topics in cancer research. Tumors can hijack multiple components of the immune system, thereby achieving a widespread state of tumor immunosuppression. Researchers no longer focus solely on the mechanisms of malignant cell behaviors, such as tumor cell growth and invasion; rather, they have turned their attention to the interaction between tumor cells and their microenvironmental components. As mentioned earlier, the complement system is an important part of the classical immune system, and its expression in the tumor and effect on the tumor microenvironment and tumor progression has received a lot of attention. In the following sections, we will elaborate and discuss the research progress of several classical components of the complement system and the role of complement signaling pathways in tumors (**Table 1**).

C1q

As the starting molecule of the classical activation pathway, Clq can bind to the Fc segment of antibodies and initiate the complement system activation cascade. A variety of human cells, including monocytes/macrophages, epithelial cells, mesenchymal cells, dendritic cells, trophoblast cells, endothelial cells, and microglia, express C1q. C1q is also involved in various pathophysiological processes, such as trophoblast infiltration, placental development, eclampsia, and some autoimmune diseases. In the development of tumors, C1q can function as a tumor promoter or tumor suppressor (Mangogna et al., 2019a). C1q is highly expressed in Melanoma, breast cancer, clear-cell renal-cell carcinoma, and glioma (Bulla et al., 2016; Mangogna et al., 2019b; Roumenina et al., 2019a). It can promote malignant behaviors, such as tumor cell proliferation and invasion, and its expression level is negatively correlated with patient survival (Mangogna et al., 2019b; Roumenina et al., 2019a). However, the expression of C1q in lung adenocarcinoma and lung squamous cell carcinoma is lower than that in the corresponding normal tissue (Mangogna et al., 2019a). In ovarian cancer cell lines, C1q can induce apoptosis through the tumor necrosis factor (TNF) pathway (Kaur et al., 2016).

C3/C3a/C3aR

C3 is a key component of all three complement activation pathways. When the complement system is activated, C3 can be cleaved into C3a by C3 convertase. C3a is a small molecule

TABLE 1 | Complement components in tumors.

Molecules		Cancer type	Expression	Functions	References
C1q		Breast cancer, clear cell carcinoma, Glioma	high	Promotes proliferation and invasion; correlated with patient survival	Bulla et al., 2016; Mangogna et al., 2019b; Roumenina et al., 2019a
		Lung adenocarcinoma, lung squamous cell carcinoma, ovarian cancer	low	Induces apoptosis	Kaur et al., 2016; Mangogna et al., 2019a
C3/C3a/C3aR		melanoma, lung cancer, gastric cancer, colon cancer, breast cancer, pancreatic cancer	up	promotes tumor growth, metastasis, EMT, angiogenesis; regulates the microenvironment of TAMs, MDSCs, DCs, Tregs Function; prognosis biomarker	Zhang et al., 2019
C3d		lymphoma	high	marker for tumor staging and patient prognosis	Elvington et al., 2014
		Lymphoma, melanoma	low	enhance anti-tumor immunity, inhibit tumor growth in animal models	Platt et al., 2017
C4d		follicular lymphoma, astrocytoma, malignant pleural mesothelioma, esophageal squamous cell carcinoma, lung cancer, oral and oropharyngeal squamous cell carcinoma	high	promotes tumor cells growth, invasive and resistance to chemotherapy, markers for disease diagnosis and prognosis	Zhiyong et al., 2007; Makela et al., 2012; Ajona et al., 2015a,b; Klikovits et al., 2017
C5/C5a/C5aR		cervical cancer, lymphoma, lung cancer, melanoma, breast cancer, ovarian cancer, cholangiocarcinoma, gastric cancer, renal cancer, lymphoma, liver cancer, colon cancer, pancreas cancer and glioma	high	Promotes tumor cell growth, migration, invasion, EMT, angiogenesis and treatment resistance	Ajona et al., 2018; Mastellos et al., 2018; Medler et al., 2018; Wang et al., 2019
C5b-9		lymphoma, oral squamous cell carcinoma, prostate cancer	high	Promotes tumor cell growth, inhibits tumor cell apoptosis	Niculescu et al., 1997; Pilzer and Fishelson, 2005; Liu et al., 2012; Gallenkamp et al., 2018
C7		hepatocellular carcinoma	high	enhances stemness, promote tumor growth	Seol et al., 2016; de Lima et al., 2018
		prostate and esophageal cancer	low	prognosis biomarker	Oka et al., 2001; Loveridge et al., 2020
mCRPs	CD35	follicular dendritic cell sarcoma, malignant endometrioma, leukemia, bladder cancer, and nasopharyngeal carcinoma	high	prognosis biomarker	Murray et al., 2000; Srivastava and Mittal, 2009; He et al., 2012
	CD46	breast cancer, hepatocellular carcinoma, colon cancer, and multiple myeloma	high	prognosis biomarker	Simpson et al., 1997
	CD55	colon cancer, breast cancer, prostate cancer, ovarian cancer, cervical cancer, gastric cancer, hematological malignancies, and esophageal cancer	high	Promotes tumor progression	Bjorge et al., 1997; Guc et al., 2000; Loberg et al., 2006; Ikeda et al., 2008
	CD59	diffuse large B-cell lymphoma, colorectal cancer, and prostate cancer	High	prognosis biomarker	Chen et al., 2017; Zhou et al., 2018
		breast cancer	low	prognosis biomarker	Wang Y. et al., 2017
MBL-MASP		non-Hodgkin's lymphoma, central nervous system tumors, children with acute lymphoblastic leukemia, colon cancer, glioma	high	marker for prognosis and recurrence	Kuraya et al., 2003; Ytting et al., 2005; Fisch et al., 2011
		ovarian cancer	low	prognosis biomarker	Swierzko et al., 2007
Factor B		lung cancer, astrocytoma, pancreatic ductal adenocarcinoma and squamous cell carcinoma of the skin	high	promotes tumor growth, prognosis biomarker	Zhao et al., 2006; Lee et al., 2014; Riihila et al., 2017; Kim et al., 2019
Factor D		astrocytoma cells and gastric cancer cells	NA	NA	Barnum et al., 1992; Kitano and Kitamura, 2002
Factor H		ovarian cancer, lung cancer and breast cancer	high	promotes tumor growth and immunosuppression	Honda et al., 2017; Yoon et al., 2019; Smolag et al., 2020
RGC32		colon cancer, breast cancer, ovarian cancer, gastric cancer, pancreatic cancer, esophageal cancer, prostate cancer and lymphoma	high	promotes the proliferation, invasion, epithelial-mesenchymal transition (EMT) of tumor cells and prompts a poor prognosis	Fosbrink et al., 2005; Zhu et al., 2012; Wang X.Y. et al., 2017
		glioblastoma, astrocytoma, multiple myeloma, and adrenocortical tumors	low	Inhibits tumor growth	Vlaicu et al., 2019
		non-small cell lung cancer	high or low	undetermined	Kim D.S. et al., 2011; Sun et al., 2013; Xu et al., 2014; Zhang et al., 2020

composed of 77 amino acids, and work as anaphylatoxin. C3a can be secreted to the outside of the cell and bind to the C3aR receptor (C3aR) on the membrane of the target cell. C3aR is a G protein-coupled receptor that regulates various downstream signaling pathways and affects cellular activities (Ajona et al., 2019). At present, the upregulation of C3a/C3aR has been observed in melanoma, lung cancer, gastric cancer, colon cancer, breast cancer, and pancreatic cancer. Its upregulation can promote tumor growth, metastasis, epithelial-to-mesenchymal transition (EMT), and angiogenesis and regulate the microenvironment of TAMs, Myeloid-derived suppressor cells (MDSCs), dendritic cells (DCs), as well as the function of regulatory T cells (Tregs). C3a/C3aR can also be used to predict the prognosis of various tumor patients (Zhang et al., 2019).

C3d

When C3 convertase cleaves C3 into C3a and C3b, C3b binds to the immune complex and is further cleaved to form IC3b and C3f. Then iC3b is processed into C3c and C3dg, and C3dg decomposes into C3d and C3g (Dempsey et al., 1996). Some scholars found that C3d enhances antitumor immunity independently of B cells, natural killer cells (NK cells), or antibodies, but it does so by increasing tumor infiltrating $CD8^+$ lymphocytes, by depleting Tregs, and by suppressing expression of programmed cell death protein 1 (PD-1) by T cells, which hint the potential of C3d to be used as a marker for tumor staging and patient prognosis in lymphoma (Elvington et al., 2014). Also, other scholars have confirmed that C3d can enhance antitumor immunity and significantly inhibit tumor growth in animal models of lymphoma and melanoma (Platt et al., 2017).

C4d

C4d is the product of C4 cleavage when the complement system is activated via the classical pathway. C4b contains a highly unstable thioester bond, which can be covalently combined with the surrounding hydroxyl or amino acid-containing molecules to form an ester bond or an amide bond. The covalently bonded C4b is hydrolyzed into C4c and C4d; C4d, which retains the thioester site, can interact with type IV collagen in the basement membranes of capillaries and form stable covalent combinations with endothelial cells (Sapir-Pichhadze et al., 2015). C4d, which has been widely reported in the immune rejection of organ transplantation and related immune diseases, can be used as a specific marker for humoral immune rejection (Nickeleit and Mihatsch, 2003; Miranda Correa et al., 2013). C4d is highly expressed in follicular lymphoma, astrocytoma, malignant pleural mesothelioma, esophageal squamous cell carcinoma, lung cancer, and oral and oropharyngeal squamous cell carcinoma. Its expression is linked with the rapid growth and invasiveness of tumor cells, their resistance to chemotherapy, and poor patient prognosis (Zhiyong et al., 2007; Makela et al., 2012; Klikovits et al., 2017). In lung cancer patients, the concentration of C4d in bronchoalveolar lavage fluid and plasma may be used as a diagnostic and prognostic marker (Ajona et al., 2015b). In patients with oral and oropharyngeal squamous cell carcinoma, salivary C4d levels can also be used to indicate patient prognosis (Ajona et al., 2015a).

C5/C5a/C5aR

Like C3, C5 is an indispensable component of the complement system. Under the action of C5 convertase, C5 can be hydrolyzed into a 74-amino-acid peptide (C5a) that also has an anaphylatoxin effect. It can be secreted to the outside of the cell to bind to the corresponding G protein-coupled receptor (C5aR1) of the target cell (Cain and Monk, 2002). C5a also binds to another receptor named C5aR2 (C5L2). Although C5aR2 is a seven-transmembrane protein, it is not a G protein-coupled receptor. At present, the downstream effects of C5a binding are still unclear. Researchers found that C5aR2 competitively inhibits the binding between C5a and C5aR1 based on current reports (Cain and Monk, 2002; Ward, 2009). C5a and C5aR1 are also highly expressed in a variety of tumors, such as cervical cancer, lymphoma, lung cancer, melanoma, breast cancer, ovarian cancer, cholangiocarcinoma, gastric cancer, renal cancer, lymphoma, liver cancer, colon cancer, pancreatic cancer, and glioma. It also promotes malignant behaviors including tumor cell growth, migration, invasion, EMT, angiogenesis, and treatment resistance through mechanisms like C-X-C Motif Chemokine Ligand 16 (CXCL16) and T cell response regulation (Ajona et al., 2018; Mastellos et al., 2018; Medler et al., 2018; Wang et al., 2019).

C5b-9

C5b-9, also known as MAC, is the final product of the complement system activation which directly perforates the target cell membrane to lyse the target cell. The traditional view is that C5b-9 can lyse target cell, inhibiting the occurrence and development of tumors (Tegla et al., 2011). However, multiple membrane-bound complement regulatory proteins (mCRPs) are expressed in tumor cells. Under the action of these proteins, the MAC cannot form a complete permeable pore across the cell membrane and becomes a partially dissolved form, sublytic C5b-9(sC5b-9), which is embedded in the membrane. sC5b-9 can activate multiple signaling pathways, including PI3K-Akt, ERK, JAK1-STAT3, and NF-κB, and regulates tumor cell growth in a G protein-dependent manner (Vlaicu et al., 2019). sC5b-9 is highly expressed in lymphomas and oral squamous cell carcinoma cells (Niculescu et al., 1997; Pilzer and Fishelson, 2005; Gallenkamp et al., 2018). In prostate cancer, sC5b-9 also inhibits TNFα-induced apoptosis (Liu et al., 2012).

C7

C7 combines with C6, C8, C9, and C5b to form MAC, which is indispensable for complement-mediated cell lysis. The main function of C7 is to rivet the complex on the target cell membrane. Approximately 50% of serum C7 is synthesized by the liver, and it can also be synthesized by monocytes, macrophages, lymphocytes, fibroblasts, and certain cells in the central nervous system (Gonzalez et al., 2003). The low expression of C7 in prostate and esophageal cancer corresponds to poor prognosis (Oka et al., 2001; Loveridge et al., 2020). Interestingly, in hepatocellular carcinoma, C7 enhances the stemness of hepatocellular carcinoma cells and promotes tumor growth (Seol et al., 2016; de Lima et al., 2018).

mCRPs

mCRPs, which include CD35, CD46, CD55, and CD59, prevent the excessive activation of complement under physiological conditions and ensure that the complement system plays a role in clearing target cells when the activation is required (Zipfel and Skerka, 2009). Recent studies have shown that the abnormal expression of mCRPs in various tumors makes them promising diagnostic markers and therapeutic targets for various tumors (Yan et al., 2008; Geller and Yan, 2019). The research findings regarding the role of each mCRP in tumors are described below.

CD35

CD35, or its synonyms CR1 (complement receptor 1), is a transmembrane protein widely expressed on the surface of hematopoietic cells. CD35 participates in the cleavage of C3b into iC3b *in vivo* and combines with C4b to promote its degradation and accelerate the inactivation of C3 and C5 convertases (Morgan, 2000). These steps prevent the excessive activation of the complement system. CD35 is highly expressed in follicular dendritic cell sarcoma, malignant endometrioma, leukemia, bladder cancer, and nasopharyngeal carcinoma; its high expression in nasopharyngeal carcinoma patients indicates a poor prognosis (Murray et al., 2000; Srivastava and Mittal, 2009; He et al., 2012).

CD46

CD46, also called membrane cofactor protein, is a transmembrane glycoprotein expressed on the surface of all nucleated cells. It is indispensable for the protection of normal tissues during complement activation. CD46 can assist complement factor I in cleaving C3b and C4b *in vivo* to avoid overactivation of the complement system (Morgan, 2000). CD46 is also involved in sperm–egg binding during fertilization and T cell activation (Kemper et al., 2003). Abnormally high expression of CD46 is observed in breast cancer, hepatocellular carcinoma, colon cancer, and multiple myeloma and is negatively correlated with patient prognosis (Simpson et al., 1997).

CD55

CD55, also known as decay acceleration factor, can combines with C4b and C3b to inhibit the catalysis of C2 and factor B to form C3a and Bb, thus blocking the activation of the complement system (Ward et al., 1994). Studies have shown that CD55 is abnormally expressed in colon cancer, breast cancer, prostate cancer, ovarian cancer, cervical cancer, gastric cancer, hematological malignancies, and esophageal cancer and participates in the malignant progression of these tumors (Ward et al., 1994; Bjorge et al., 1997; Simpson et al., 1997; Guc et al., 2000; Loberg et al., 2006; Ikeda et al., 2008).

CD59

CD59 inhibits the polymerization of multiple C9 and competitively bind C5b with C8, ultimately inhibiting the formation of MAC and lysis of target cells *in vivo*. It is vital to the body's self-protection under physiological conditions. CD59 expression is abnormally high in diffuse large B-cell lymphoma, colorectal cancer, and prostate cancer, and its high expression suggests a poor patient prognosis (Chen et al., 2017; Zhou et al., 2018). However, Wang Y. et al. (2017) found that the high expression of CD59 in breast cancer correlates with better patient prognosis.

MBL–MASP

Mannose-binding lectin and mannose-associated serine protease constitute the most important starting components of the lectin pathway for complement activation. MBL and MASP2 are highly expressed in non-Hodgkin's lymphoma, central nervous system tumors, and pediatric cases of acute lymphoblastic leukemia (Fisch et al., 2011). The blood levels of MASP2 can be used as prognostic markers for colon cancer. High MASP2 levels in the blood suggest a poor prognosis and high risk of recurrence (Ytting et al., 2005). Notably, MASP1 and MASP3 are highly expressed in the C6 and T98G glioma cell lines (Kuraya et al., 2003; Pagliara et al., 2018), but their expression is low in some ovarian cancer patients and the MASP1 and MASP3 expression levels are positively correlated with patient prognosis (Swierzko et al., 2007).

Factors B and D

Both factors B and D are important for the alternative pathway of complement activation. Factor B, which is mainly synthesized by the liver and macrophages, plays a significant role in tissue damage and inflammation (Campbell et al., 1984). Factor B is highly expressed in lung cancer, astrocytoma, pancreatic ductal adenocarcinoma, and squamous cell carcinomas of the skin. It also promotes the growth of squamous cell carcinoma of the skin and may be used as a predictor for the prognosis of pancreatic ductal adenocarcinoma (Zhao et al., 2006; Lee et al., 2014; Riihila et al., 2017; Kim et al., 2019). Factor D, which is also known as a lipid-lowering hormone, is a lipid-derived protein that participates in the alternative pathway of complement activation. Factor D regulates energy balance and fat metabolism via acylation-stimulating protein, which is a complement protein closely related to energy balance and fat metabolism (Song et al., 2016). Factor D is expressed in astrocytoma cells and gastric cancer cells, but its involvement in tumorigenesis and development still needs further investigation (Barnum et al., 1992; Kitano and Kitamura, 2002).

Factor H

The key enzymes for C3b synthesis can be hydrolyzed by Factor H, a soluble inhibitor of the complement system. Under physiological conditions, it is combined with its own components and exerts inhibitory effect during complement activation. By exerting inhibitory effects, it prevents excessive activation that damages the normal tissues. When the gene encoding factor H is mutated, it cannot recognize "self" components, thus causing the abnormal activation of complement. Tumors may also hijack the function of factor H to achieve immune evasion (Parente et al., 2017). Studies have shown that factor H can form a complex with fibrin γ to promote disease progression in the blood of ovarian cancer patients (Honda et al., 2017). Factor H is also highly

expressed in lung cancer and breast cancer and promotes tumor growth via immunosuppression (Yoon et al., 2019; Smolag et al., 2020).

RGC32

Response gene to complement 32 (RGC32) was identified after sublytic complement activation, and it is widely expressed in the liver, kidney, skeletal muscle, and other tissues (Badea et al., 1998). RGC32 is involved in cell differentiation, cell cycle regulation, and immune regulation under physiological conditions (Badea et al., 1998; Vlaicu et al., 2008). In tumors, the expression and function of RGC32 are disease-dependent (Vlaicu et al., 2019). RGC32 is highly expressed in colon cancer, breast cancer, ovarian cancer, gastric cancer, pancreatic cancer, esophageal cancer, prostate cancer, and lymphoma. Moreover, it promotes the proliferation, invasion, and EMT of tumor cells and is associated with poor prognosis (Fosbrink et al., 2005; Zhu et al., 2012; Wang X.Y. et al., 2017). However, RGC32 is downregulated in glioblastoma, astrocytoma, multiple myeloma, and adrenocortical tumors and acts as a tumor suppressor instead (Vlaicu et al., 2019). Interestingly, RGC32 can be both upregulated and downregulated in non-small-cell lung cancer, and its specific expression and function still need more in-depth revelation in the context of this disease (Kim D.S. et al., 2011; Sun et al., 2013; Xu et al., 2014; Zhang et al., 2020).

THE COMPLEMENT PATHWAYS IN GLIOMA MICROENVIRONMENTS

Gliomas are the most prevalent and highly refractory tumors in the adult central nervous system. Glioblastoma multiform (GBM) representing approximately 57% of all gliomas, which have a high degree of malignancy (Tan et al., 2020). Even after receiving the maximum surgical resection within the safety range supplemented with standard postoperative radiotherapy and chemotherapy, the median survival time of patients with GBM is still less than 15 months (McGranahan et al., 2019). The poor prognosis of GBM patients is attributed to highly aggressive tumor cells and their resistance to radiochemotherapy. Solid glioblastoma tumors contain stromal cells, such as monocytes/macrophages, microglia, T cells, neurons, astrocytes, oligodendrocytes, vascular endothelial cells, and mast cells (Broekman et al., 2018). These cells and the extracellular matrix components together form a microenvironment that interacts organically with the tumor (**Figure 2A**). Current studies on the glioblastoma microenvironment mainly focus on the hypoxic microenvironment, perivascular microenvironment, and immune microenvironment that, composed of tumor-associated macrophages/microglias. As mentioned above, the complement system plays a significant role in the promotion or inhibition of tumor growth, and this is also true for gliomas. In the following sections, we will elaborate on research findings focusing on the complement system and its role in glioma cells and the glioma microenvironment (**Table 2**).

Research on the Complement Pathway in Glioma Cells

C1q

As the initial recognition component, C1q plays a significant role in the classical activation pathway of complement. Several studies show that C1q is expressed in various tumor microenvironments and widely involved in tumor progression. Bouwens et al. (2015) found the concentration of C1q increased in the blood of glioma patients. Next, Mangogna et al. searched the Oncomine, UALCAN, and CGGA databases and found that the *C1QA, C1QB*, and *C1QC* genes, which encode the three chains of C1q, were all highly expressed in gliomas. Furthermore, the high levels of expression for these three genes were associated with poor prognosis. These conclusions were verified by immunohistochemistry and immunofluorescence (Mangogna et al., 2019b).

C3a/C3aR

C3a is a small protein secreted originally from C3 cleavage, which can exert its biological functions when combined with its receptor on the surface of target cells through autocrine or paracrine signaling in various tumors (Morgan, 2000). At present, the mechanism of the C3a/C3aR signaling pathway and the expression of its components have not been elucidated in the context of gliomas. However, several studies have shown that human astrocytoma cell lines can express and secrete C3a, and the expression is regulated by IL-1β, TNFα, and IFN-γ (Barnum et al., 1993; Barnum and Jones, 1995). Nevertheless, its detailed function still needs further study.

C5a/C5aR1

C5a is the most active anaphylatoxin involved in multiple pathophysiological processes. C5a usually binds with its receptor (C5aR1) to mediate downstream signaling pathways and biological effects. As described, the C5a/C5aR1 axis is widely expressed in tumors, such as cervical cancer, lymphoma, lung cancer, and glioma, and participates in disease occurrence and development. Gasque et al. (1995) have identified C5aR1 on the surface of astrocytoma cells as early as 1995. C5L2, another C5a receptor, was also identified on the surface of astrocytes by Gavrilyuk et al. (2005). However, the detailed function of C5a and the conditions required for it to bind to each receptor have not been elucidated. Lim et al. confirmed that C5a is highly expressed in the Mesenchymal stem-like cells (MSLCs) of glioma microenvironment and promotes a series of malignant behaviors, such as invasion and migration of glioma cells and GSCs through its receptor C5aR1 *in vitro* and *in vivo*. MSLC-secreted C5a increases ZEB1 expression via activation of p38 MAPK in GBM cells, thereby enhancing the invasion of GBM cells into parenchymal brain tissue (Lim et al., 2020). This significantly promotes the growth of tumors and shortens the survival time of tumor-bearing mice. These findings suggest that the C5a/C5aR1 axis plays a significant role in the development of gliomas and the interaction of glioma cells with their microenvironmental components (Lim et al., 2020).

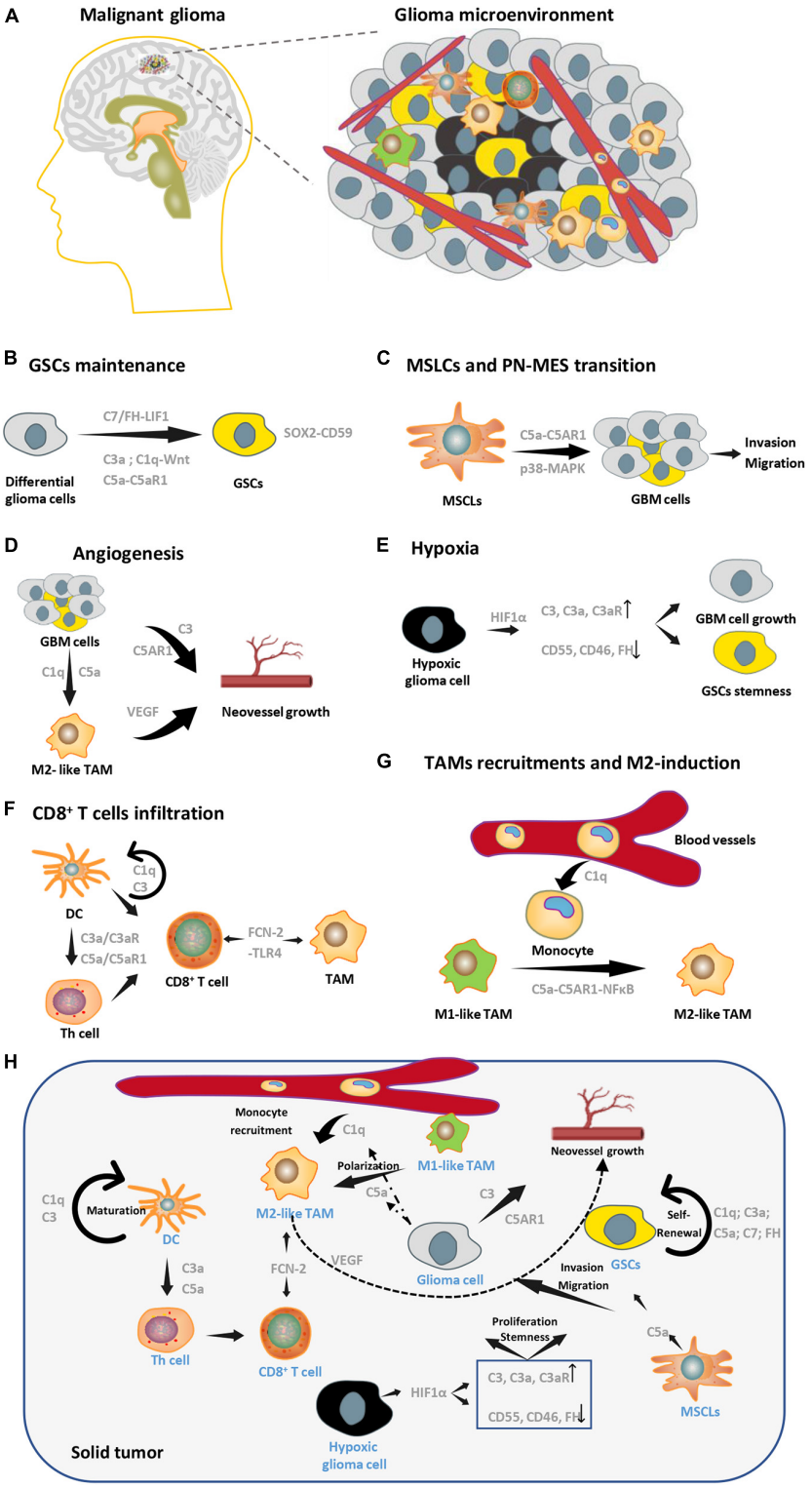

FIGURE 2 | Complement pathways in glioma microenvironment. **(A)** A brief schematic diagram of glioma microenvironments. **(B)** Complement molecules (C3a, C1q, C5a, and C7) can promote GSCs stemness maintenance. **(C)** C5a secreted by MSLCs enhances invasion and migration of GBM cells. **(D)** Complement pathways can enhance angiogenesis by targeting both tumor cells and M2-TAMs in GBM. **(E)** Expression patterns of complement molecules change in hypoxia, which facilitates GSCs stemness and GBM growth. **(F)** C3 and C1q are essential for DC's maturation, maturated DC can regulate the function of Th cell by C3a-C3aR and C5a-C5aR1 axis, which affect the infiltration of $CD8^+$ T cells. FCN2 can direct target TAM and $CD8^+$ T cell through its receptor, TLR4. **(G)** C1q and C5a are essential in recruitment of peripheral monocytes and M2 polarization of macrophages, respectively. **(H)** A conclusion of multicellular interactions in glioma microenvironments via complement signaling.

TABLE 2 | Complement components in Glioma.

Molecules	Expression	Functions	Evidence	References
C1q (three chain, C1qA C1qB C1qC)	up-regulated (tumor tissue)	unfavorable prognostic marker	Database (Oncomine UALCAN CGGA) IHC	Mangogna et al., 2019b
C1q	up-regulated (Patient Serum and tumor tissue)	N/A	ELISA IHC IF	Bouwens et al., 2015
Factor B	down-regulated (Patient Serum)	N/A	ELISA	Bouwens et al., 2015
MBL	up-regulated (Patient Serum)	N/A	ELISA	Bouwens et al., 2015
C3	up-regulated (tumor tissue)	N/A	IHC IF	Bouwens et al., 2015
	up-regulated (Cell line)	Promotes tumor cell proliferation and invasion	EdU Transwell	Li et al., 2014
RGC32	Down-regulated (Cell line)	Inhibits tumor cell mitosis and proliferation	WB qRT-PCR Colony-forming assay	Saigusa et al., 2007
C5aR1	up-regulated (Patient specimen and cell line)	unfavorable prognosis Promotes tumor cell invasion and migration	Database (TCGA) Transwell 3D invasion assay	Lim et al., 2020
C4d	up-regulated (Patient specimen)	unfavorable prognosis	IHC(Tissue- microarray)	Makela et al., 2012
Factor H	up-regulated (Patient CSF)	N/A	proteomic analysis	Gahoi et al., 2018

RGC32

RGC32 is a complement response gene induced by the MAC. It interacts with Akt and cyclin B1-CDC2 complex and is involved in cell cycle activation (Tegla et al., 2011). When the RGC32 protein was identified, the researchers revealed that its overexpression promotes DNA synthesis in the oligodendrocyte-C6 glioma hybrid cell (Badea et al., 1998). Other groups showed that compared with normal brain tissue, the protein and mRNA levels of RGC32 are low in several glioma cell lines, including T98G, U251, U373, and U87 (Fernandez-Aroca et al., 2019). They also found that mRNA expression of RGC32 is inversely correlated with the tumor grade of the cell line origin; this phenomenon is especially notable in p53 mutant tumors (Saigusa et al., 2007). RGC32 overexpression can significantly inhibit the growth of glioma cells. Also, RGC32 aggregates in the centrosomes of glioma cells during mitosis and can be phosphorylated *in vitro* by forming a protein complex with PLK1. This suggests that p53-induced RGC32 expression in gliomas inhibits mitosis and thereby inhibits tumor cell growth (Imoto et al., 2007). However, some researchers reached the opposite conclusion. Li et al. (2014) found that RGC32 is highly expressed in the U251 glioma cell line. Its overexpression can promotes proliferation and invasion of U251 cells but has no impact on apoptosis, however, its silencing enhances cell apoptosis and attenuates proliferation and invasion of U251 cells (Li et al., 2014). Since the above two studies were limited to cell lines, more in-depth investigation in patient specimens, primary cell lines, and animal experiments is required to determine the expression of RGC32 in gliomas and its mechanism in tumorigenesis and disease development.

Complement Pathways in the Glioma Microenvironment

Glioma Stem Cells (GSCs)

Glioma stem cells, a small subpopulation of tumor cells endowed with sustained clonogenic potential and high tumorigenic capability, are among the root causes of refractory tumors and recurrence (Lathia et al., 2015). GSCs was firstly identified by Singh, SK, and Houman in 2003 (Hemmati et al., 2003; Singh et al., 2003, 2004) and interacts with differential glioma cells, TAMs and hypoxic conditions of glioma microenvironments (Zhou et al., 2015; Shi et al., 2017; Man et al., 2018; Wang et al., 2018). Multiple studies have shown that complement signaling plays a significant role in maintaining the stemness of cancer stem cells. For example, C7 and factor H are highly expressed in hepatocellular carcinoma stem cells and stimulate LSF-1 expression, which is localized in the nucleus and binds to the promoters of the Nanog, Oct4, Sox2, and c-Myc genes. This leads to the upregulation of the stemness factors, which finally increases cancer stemness (Seol et al., 2016). The stem cell-specific transcription factor SOX2 upregulates the expression of the complement regulatory protein CD59 in epithelial tumor stem cells to help them avoid immune surveillance of the complement system (Chen et al., 2017). C5a promotes hematopoietic stem cell activation through C5aR1 signaling (Bujko et al., 2017). Although there is no direct evidence that the complement signaling pathway affects the stemness of GSCs, it has been confirmed that the differentiation and migration of neural stem cells under physiological conditions are regulated by C3a (Shinjyo et al., 2009). Furthermore, complement C1q activates canonical Wnt signaling and promotes aging-associated decline in tissue regeneration, which is important for the maintenance of the stemness of various tumor stem cells, including gliomas (Naito et al., 2012; Sadahiro et al., 2018; **Figure 2B**).

Mesenchymal Stem-Like Cells (MSLCs)

Mesenchymal stem cells (MSCs) refer to pluripotent stem cells derived from bone marrow that do not have a hematopoietic function. Under physiological conditions, MSCs exhibit tropism to tissue injury and participate in the renovation of damaged tissue (Bianco et al., 2008). The expression of molecular markers similar to MSCs and MSLCs occurs in several tumor stromata, including that of GBM (Kim S.M. et al., 2011; Ho et al., 2012). After being recruited to the glioma microenvironment,

MSCs are remodeled into MSLCs, which are important tumor-related stromal cells. Lim et al. (2020) found that MSLCs in the glioma microenvironment express and secrete high levels of C5a, which increases the expression of ZEB1 through C5aR1 and the activation of the p38-MAPK pathway in a paracrine manner. This signaling pathway promotes the invasion and migration of GBM cells, which relates to the prognosis of GBM patients (Lim et al., 2020; **Figure 2C**).

Endothelial Cells

Gliomas undergo extremely rapid growth, which is accompanied by vigorous neovascularization and the formation of incompletely functioning microvessels. In addition to providing nutrients for tumor growth, these vascular endothelial cells also facilitate organic interactions with other components of the tumor microenvironment in order to promote tumor growth. In ovarian cancer, inhibition of C3 or C5aR reduces the expression of vascular endothelial growth factor (VEGF) and neovascularization (Nunez-Cruz et al., 2012). C1q and C5a are involved in the recruitment of monocytes and the M2 polarization of TAMs which indirectly promote neovascularization through VEGF secretion (Benoit et al., 2012; Piao et al., 2018). Contrarily, C3a and C5a do not promote neovascularization in lung cancer and cervical cancer, which may be due to the different microenvironments and activation of various signaling pathways in different types of tumors (Markiewski et al., 2008; Corrales et al., 2012). Whether complement systems participate in glioma neovascularization needs further study. In addition to angiogenesis, complement signals also mediate the interaction between vascular endothelial cells and other microenvironmental components. Several studies have shown that endothelial cells promote the maintenance of GSC stemness through transforming growth factor-beta (TGFβ), NO, and other signaling pathways (Sharma and Shiras, 2016). The C5a/C5aR1 axis activates the TGFβ/Smad pathway in epithelial injury of pulmonary fibrosis, and the activation of NO is blocked after silencing the expression of C3 and C5 (Montalto et al., 2003; Gu et al., 2014). Therefore, complement signals are likely to play a significant role in the interaction between vascular endothelial cells and surrounding GSCs (**Figure 2D**).

Hypoxia

A highly hypoxic environment and necrosis are two of the most prominent features of glioma, especially glioblastomas, which are characterized by "pseudopalisading" necrosis (Colwell et al., 2017). Due to the rapid growth of the tumor, the blood vessels in the tumor are mostly incompletely functioning deformed blood vessels. Therefore, the inside of the tumor is always in a state of hypoxia. However, unlike normal cells that slowly grow under long-term hypoxic conditions and eventually die, many tumors, including gliomas, adapt to hypoxia by changing their main metabolic mode to glycolysis. Tumors can further use a series of signaling pathways that are activated during hypoxia, which are represented by hypoxia-inducible factor 1-alpha (HIF1α), to promote tumor growth (Broekman et al., 2018). Studies have shown that various complement signaling molecules interact with the hypoxic microenvironment. Under hypoxia, the expressions of CD55, CD46, and factor H are downregulated by HIF1α. Meanwhile, C3, C3a, and C3aR are upregulated during hypoxia, which leads to an increase in C3a/C3aR signaling (Greijer et al., 2005; Pedersen et al., 2007). The expression of signal transducer and activator of transcription 3 (STAT3), which is upstream of HIF1α, can also regulates complement signaling expression during hypoxia (Mantovani, 2010). STAT3 plays a significant role in a series of biological processes, such as the maintenance of GSC stemness under hypoxic conditions in gliomas (Qiang et al., 2012; **Figure 2E**).

Tumor-Associated Macrophages (TAMs)

Tumor-associated macrophages that account for about 30–40% of the total cells in solid gliomas are the most abundant immune cells in the glioma microenvironment (Broekman et al., 2018). TAMs in gliomas are composed of *in situ* microglial cells and monocytes/macrophages recruited from peripheral blood under the action of multiple chemokines. TAMs can be divided into two phenotypes: the M1 like phenotype promotes immunity and inhibits tumor growth, whereas the M2 like phenotype is immunosuppressive and promotes tumor progression. In the glioma microenvironment, TAMs are mostly dominated by the M2 like phenotype, and the conversion of M1 like TAMs to the M2 like phenotype occurs constantly. M2 like TAMs secrete a variety of anti-inflammatory cytokines that inhibit the immune response and interact with tumor cells and other microenvironmental components to promote tumor progression in multiple dimensions, which is also an important reason for glioma refractory (Hambardzumyan et al., 2016). Studies clear that C1q can participate in the recruitment of peripheral blood monocytes, suppress macrophage inflammation and inflammasome activation (Benoit et al., 2012), and C5a can activate the NF-κB pathway through the C5aR1 receptor and promote the M2 like polarization of TAMs, thereby inhibiting the tumor immune response and promoting tumor progression (Piao et al., 2018). Conversely, TAMs in tumors can also regulate the expression of the complement components of the surrounding cells by secreting a series of cytokines. Although currently the role of complement signaling in glioma TAMs is largely unclear, we believe that there is an organic interaction between TAMs and the complement system to jointly promote tumor progression in gliomas (**Figure 2G**).

$CD8^+$ T Cell

$CD8^+$ T cells are included in the group of cells known as effector T cells. They are cytotoxic and can lyse target cells, including tumor cells. $CD8^+$ T cells need to undergo maturation and activation to exert their cytotoxicity. First, CD3-T cell receptor on the surface of T cells recognizes the endogenous antigens (tumor antigens), which are bound by MHCI and presented by antigen-presenting cells (APCs) (Seder and Ahmed, 2003). With the help of helper T (Th) cells, a double-activated signal is formed, and the naïve T cell proliferates and differentiates into cytotoxic $CD8^+$ T cells. These $CD8^+$ T cells are responsible for lysing tumor cells under the action of IL-2 and other cytokines (Boyman and Sprent, 2012). Studies have shown that the activation of T cells is widely affected by complement signals. First, the maturation of

DCs, which plays a major role in antigen presentation, depends on complement molecules C1q and C3 (Peng et al., 2006; Baruah et al., 2009). Second, the binding of C3a and C5a to C3aR and C5aR1, respectively, promotes DC cell and Th cell function through monocytes, which finally facilitate $CD8^+$ T cell activation (Lalli et al., 2008). Furthermore, Treg cells also express C3aR and C5aR1 that, can inhibit their function after activation and indirectly promote T cell activation (van der Touw et al., 2013). However, studies have also shown that the complement system inhibits T cell activation and induces immune tolerance (Pio et al., 2019). C1q can inhibit the proliferation of Th cells in a DC-dependent manner (Benoit et al., 2012). When iC3b binds to its receptor CR3 on the surface of APCs, immunosuppressive cytokines, such as TGF-β2 and IL-10, are secreted, thus inhibiting the antigen presentation process (Sohn et al., 2003). CD46 also promotes the binding of endogenous C5a to the receptor C5aR2 to negatively regulate Th cell activity (Kemper et al., 2003). The effect of complement signaling on the regulation of $CD8^+$ T cell infiltration also differs between tumors. The inhibition of C5AR1 expression in squamous cell carcinoma can promote intratumoral $CD8^+$ T cell infiltration (Medler et al., 2018). Fatty Acid Binding Protein 5 (FABP5) is highly correlated with complement signaling in uveal melanoma, and it promotes $CD8^+$ T cell infiltration (Xu et al., 2020). C3 knockout mice-bearing lung cancer exhibited increased numbers of $CD8^+$ T cells and decreased tumor growth (Kwak et al., 2018). Ding et al. (2017) believe the serum complement component Ficolin-2 (FCN-2) in various cell lines, including colon cancer and lung cancer. FCN-2 combines with Toll-like receptor 4 (TLR4) on the surface of macrophages and DC cells to inhibit tumor growth by promoting M1 like phenotypic polarization and infiltration of $CD8^+$ T cells (Ding et al., 2017). In malignant gliomas, Zhang et al. clarified that the suppression of the complement system inhibited $CD8^+$ T cell infiltration in IDH-mutated gliomas. They also found that the tumor metabolite D2-HG significantly inhibits the classical and alternative pathways of complement activation while inhibiting T cell activation (Zhang et al., 2018). These data suggest a correlation between complement signal and $CD8^+$ T cell infiltration in malignant gliomas; however, its specific mechanism still needs further study (**Figure 2F**).

Complement Signals Function in Glioma Immune Evasion

For a long time, the body's central nervous system was considered to be "immune escapable" compared with peripheral organs. As the most commonly diagnosed central nervous system tumor in adult patients, gliomas are mainly composed of *in situ* microglial cells. However, more recent studies have subverted this point (Lim et al., 2018). Besides *in situ* microglia, there are multiple immune components in the brain under physiological conditions that exhibit persistent immune responses (Broekman et al., 2018). Louveau et al. (2015) demonstrate that the dural venous sinuses can function as lymphatic egress, and deep cervical lymph nodes can function as "transit stations" for a series of immune cells, including B cells and T cells, involved in the immune function of the brain. Due to the abnormally rapid growth of glioma cells and the existence of abundant microvessels with immature functions and structures, the blood–brain barrier is no longer intact. Therefore, peripheral blood mononuclear cells can be recruited into tumors via chemotaxis (Zhou et al., 2015). It has been reported that the components of immune cells in glioblastomas include microglia, monocytes/macrophages derived from peripheral blood, T cells, DCs, and neutrophils (Broekman et al., 2018). Microglia/macrophages are the predominant immune cell type; they account for approximately 30% of all the cellular components of solid tumors (Broekman et al., 2018). Importantly, the above immune cells are no longer able to effectively lyse tumor cells; instead, they promote tumor progression and immunosuppression in glioblastoma under the induction of various factors from the microenvironment. The complement signaling pathway plays a role in the immune surveillance of the central nervous system under physiological conditions and during glioblastoma-induced immunosuppression. As mentioned above, several complement components, including C1q, C3a/C3aR, C5a/C5aR1, CD46, and CD55, affect the functional status of DCs, Th cells, and T cells. C1q and C5a/C5aR1 signals promote the recruitment of monocyte/macrophages from the peripheral blood and M2 phenotypic polarization (Markiewski et al., 2008; Ajona et al., 2019; Roumenina et al., 2019a). We believe that complement signals that are widely involved in the physiological immune state of the central nervous system and malignant gliomas will be assignable targets in elucidating immune signaling in malignant gliomas.

Complement Signaling Mediates Multicellular Interactions in Glioma Microenvironments

As described above, a number of complement molecules like C1q, C5, and C3 are highly expressed in glioma cells, and are secreted into the microenvironment to participate in polarization of TAM, recruitment of peripheral monocyte and neoangiogenesis. In addition, C1q, C3a, C5a, C7, and FH are related to self-renewal of cancer stem cells (CSC). C5a secreted by MSLCs promotes the invasion and migration of glioma cells via p38-MAPK-ZEB1 axis. C1q, C3, and C5a are essential for DC maturation and Th cell function which combine with FCN2 to regulate $CD8^+$ T cell activity. Complement components expression of glioma cells in hypoxic microenvironment also altered due to transcriptional regulation of HIF1α. Hypoxic tumor cells have upregulated expression of C3-C3a-C3aR axis and downregulated CD55, CD46, and FH, which play important roles in tumor cell proliferation and CSCs stemness maintenance. To sum up, molecules of the complement pathway are mostly upregulated in glioma compared to normal brain tissue, and activated complement signaling participates in various interactions between glioma cells and its microenvironments, promoting the glioma growth (**Figure 2H**).

THERAPEUTIC OPPORTUNITIES

Diagnosis

As shown above, the complement signaling pathway plays a significant role in the interaction between the various

components of the malignant glioma microenvironment and promotes tumor progression. Complement signaling molecules can be used as targets for the early diagnosis of gliomas. Studies have shown that the C1q and MBL concentrations in the blood of glioma patients are higher and the concentration of factor B is lower compared with those of healthy volunteers (Bouwens et al., 2015). These suggest that early screening of the above factors in the patients' blood contributes to the diagnosis and prognostic judgment of glioma patients. And, the brain tumors represented by malignant gliomas are accompanied by specific changes in the properties of cerebrospinal fluid. Recently, Gahoi et al. (2018) found higher levels of factor H in the cerebrospinal fluid of glioma patients compared with those of healthy volunteers through proteomics analyses. The concentration of factor H is directly proportional to the tumor grade (Gahoi et al., 2018), thus indicating that changes in the levels of complement molecules in the cerebrospinal fluid may be used for disease diagnosis.

Treatment Strategy

Since complement signals participate in a variety of biological processes related to tumor progression, they are potentially excellent drug targets for comprehensive tumor therapy. Inhibiting complement signals can synergistically block multiple biological processes. Wang et al. (2020) found that inhibiting C3b/C4b while performing anti-vascular therapy can inhibit neovascularization, cell proliferation, MDSC infiltration and promote tumor cell apoptosis in the tumor microenvironment. It is also worth mentioning that the inhibitors of complement signals act in a relatively systematic manner to the in-depth investigation of complement signaling in non-tumor immune-related diseases, such as organ transplantation. There are at least 30 inhibitors or neutralizing antibodies targeting 14 complement signaling molecules that are currently undergoing clinical trials (Riihila et al., 2019), as represented by eculizumab, an inhibitor of C5, recently has been reported to effectively re-establishes regulation of the innate immune complement system to substantially reduce the pathophysiological manifestations of human CHAPLE disease (Ozen et al., 2021) and IPH5401, a C5aR neutralizing antibody was combined with Durvalumab to treat Patients with advanced solid tumors (STELLAR-001) (Clinical trail, NCT number: 03665129). All of the above descripted suggest that in numerous tumors, including malignant gliomas, targeting complement signaling pathways may become a new, effective, and easy treatment strategy in the future.

CONCLUSION

Although a lot of studies have revealed the role of complement signaling pathways in the development of a variety of tumors, complement components, and complement-related proteins are a large family of proteins, and their detailed mechanisms in tumor pathogenesis and applications in treatment strategies still need to be further elucidated. As mentioned above, complement signals widely impact tumor cells and several microenvironmental components in gliomas. Further revealing its detailed mechanism of action will certainly help the future comprehensive treatment of gliomas and improve patient prognosis.

AUTHOR CONTRIBUTIONS

KS and SZ designed the study. HZ and XY wrote and finished the manuscript. All authors contributed to the article and approved the submitted version.

FUNDING

This work was supported by the National Natural Science Foundation of China (82072805, 81974452, and 81402058) and start-up funding of Huazhong University of Science and Technology (2019 kfyXJJS187).

REFERENCES

Ajona, D., Ortiz-Espinosa, S., and Pio, R. (2019). Complement anaphylatoxins C3a and C5a: emerging roles in cancer progression and treatment. *Semin. Cell Dev. Biol.* 85, 153–163. doi: 10.1016/j.semcdb.2017.11.023

Ajona, D., Pajares, M. J., Chiara, M. D., Rodrigo, J. P., Jantus-Lewintre, E., Camps, C., et al. (2015a). Complement activation product C4d in oral and oropharyngeal squamous cell carcinoma. *Oral Dis.* 21, 899–904. doi: 10.1111/odi.12363

Ajona, D., Razquin, C., Pastor, M. D., Pajares, M. J., Garcia, J., Cardenal, F., et al. (2015b). Elevated levels of the complement activation product C4d in bronchial fluids for the diagnosis of lung cancer. *PLoS One* 10:e0119878. doi: 10.1371/journal.pone.0119878

Ajona, D., Zandueta, C., Corrales, L., Moreno, H., Pajares, M. J., Ortiz-Espinosa, S., et al. (2018). Blockade of the complement C5a/C5aR1 axis impairs lung cancer bone metastasis by CXCL16-mediated effects. *Am. J. Respir. Crit. Care Med.* 197, 1164–1176. doi: 10.1164/rccm.201703-0660oc

Badea, T. C., Niculescu, F. I., Soane, L., Shin, M. L., and Rus, H. (1998). Molecular cloning and characterization of RGC-32, a novel gene induced by complement activation in oligodendrocytes. *J. Biol. Chem.* 273, 26977–26981. doi: 10.1074/jbc.273.41.26977

Barnum, S. R., and Jones, J. L. (1995). Differential regulation of C3 gene-expression in human astroglioma cells by interferon-gamma and interleukin-1-beta. *Neurosci. Lett.* 197, 121–124. doi: 10.1016/0304-3940(95)11923-k

Barnum, S. R., Ishii, Y., Agrawal, A., and Volanakis, J. E. (1992). Production and interferon-gamma-mediated regulation of complement component C2 and factors B and D by the astroglioma cell line U105-MG. *Biochem. J.* 287, 595–601. doi: 10.1042/bj2870595

Barnum, S. R., Jones, J. L., and Benveniste, E. N. (1993). Interleukin-1 and tumor necrosis factor-mediated regulation of C3 gene-expression in human astroglioma cells. *Glia* 7, 225–236. doi: 10.1002/glia.440070306

Baruah, P., Dumitriu, I. E., Malik, T. H., Cook, H. T., Dyson, J., Scott, D., et al. (2009). C1q enhances IFN-gamma production by antigen-specific T cells via the CD40 costimulatory pathway on dendritic cells. *Blood* 113, 3485–3493. doi: 10.1182/blood-2008-06-164392

Benoit, M. E., Clarke, E. V., Morgado, P., Fraser, D. A., and Tenner, A. J. (2012). Complement protein C1q directs macrophage polarization and limits inflammasome activity during the uptake of apoptotic cells. *J. Immunol.* 188, 5682–5693. doi: 10.4049/jimmunol.1103760

Bianco, P., Robey, P. G., and Simmons, P. J. (2008). Mesenchymal stem cells: revisiting history, concepts, and assays. *Cell Stem Cell* 2, 313–319. doi: 10.1016/j.stem.2008.03.002

Bjorge, L., Hakulinen, J., Wahlstrom, T., Matre, R., and Meri, S. (1997). Complement-regulatory proteins in ovarian malignancies. *Int. J. Cancer* 70, 14–25. doi: 10.1002/(sici)1097-0215(19970106)70:1<14::aid-ijc3>3.0.co;2-9

Bouwens, T. A., Trouw, L. A., Veerhuis, R., Dirven, C. M., Lamfers, M. L., and Al-Khawaja, H. (2015). Complement activation in Glioblastoma multiforme pathophysiology: evidence from serum levels and presence of complement activation products in tumor tissue. *J. Neuroimmunol.* 278, 271–276. doi: 10.1016/j.jneuroim.2014.11.016

Boyman, O., and Sprent, J. (2012). The role of interleukin-2 during homeostasis and activation of the immune system. *Nat. Rev. Immunol.* 12, 180–190. doi: 10.1038/nri3156

Broekman, M. L., Maas, S. L. N., Abels, E. R., Mempel, T. R., Krichevsky, A. M., and Breakefield, X. O. (2018). Multidimensional communication in the microenvirons of glioblastoma. *Nat. Rev. Neurol.* 14, 482–495. doi: 10.1038/s41582-018-0025-8

Bujko, K., Rzeszotek, S., Hoehlig, K., Yan, J., Vater, A., and Ratajczak, M. Z. (2017). Signaling of the complement cleavage product anaphylatoxin C5a through C5aR (CD88) contributes to pharmacological hematopoietic stem cell mobilization. *Stem Cell Rev. Rep.* 13, 793–800. doi: 10.1007/s12015-017-9769-6

Bulla, R., Tripodo, C., Rami, D., Ling, G. S., Agostinis, C., Guarnotta, C., et al. (2016). C1q acts in the tumour microenvironment as a cancer-promoting factor independently of complement activation. *Nat. Commun.* 7:10346.

Cain, S. A., and Monk, P. N. (2002). The orphan receptor C5L2 has high affinity binding sites for complement fragments C5a and C5a des-Arg(74). *J. Biol. Chem.* 277, 7165–7169. doi: 10.1074/jbc.c100714200

Campbell, R. D., Bentley, D. R., and Morley, B. J. (1984). The factor B and C2 genes. *Philos. Trans. R. Soc. Lond. Ser. B Biol. Sci.* 306, 367–378. doi: 10.1098/rstb.1984.0097

Chen, J., Ding, P., Li, L., Gu, H., Zhang, X., Zhang, L., et al. (2017). CD59 regulation by SOX2 is required for epithelial cancer stem cells to evade complement surveillance. *Stem Cell Rep.* 8, 140–151. doi: 10.1016/j.stemcr.2016.11.008

Colwell, N., Larion, M., Giles, A. J., Seldomridge, A. N., Sizdahkhani, S., Gilbert, M. R., et al. (2017). Hypoxia in the glioblastoma microenvironment: shaping the phenotype of cancer stem-like cells. *Neuro Oncol.* 19, 887–896. doi: 10.1093/neuonc/now258

Corrales, L., Ajona, D., Rafail, S., Lasarte, J. J., Riezu-Boj, J. I., Lambris, J. D., et al. (2012). Anaphylatoxin C5a creates a favorable microenvironment for lung cancer progression. *J. Immunol.* 189, 4674–4683. doi: 10.4049/jimmunol.1201654

de Lima, R. E., de Holanda Martins, C. M., do Carmo, R. F., Barbosa Lins, Aroucha, D. C., Moreira Beltrao Pereira, L. M., et al. (2018). Two sides of a coin: GG genotype of C7 provides protection against fibrosis severity while showing a higher risk for hepatocellular carcinoma in patients with hepatitis C. *Hum. Immunol.* 79, 702–707. doi: 10.1016/j.humimm.2018.06.009

Dempsey, P. W., Allison, M. E. D., Akkaraju, S., Goodnow, C. C., and Fearon, D. T. (1996). C3d of complement as a molecular adjuvant: bridging innate and acquired immunity. *Science* 271, 348–350. doi: 10.1126/science.271.5247.348

Ding, Q. Q., Shen, Y. Y., Li, D. Q., Yang, J., Yu, J., Yin, Z. N., et al. (2017). Ficolin-2 triggers antitumor effect by activating macrophages and CD8(+) T cells. *Clin. Immunol.* 183, 145–157. doi: 10.1016/j.clim.2017.08.012

Ehrnthaller, C., Ignatius, A., Gebhard, F., and Huber-Lang, M. (2011). New insights of an old defense system: structure, function, and clinical relevance of the complement system. *Mol. Med.* 17, 317–329. doi: 10.2119/molmed.2010.00149

Elvington, M., Scheiber, M., Yang, X., Lyons, K., Jacqmin, D., Wadsworth, C., et al. (2014). Complement-dependent modulation of antitumor immunity following radiation therapy. *Cell Rep.* 8, 818–830. doi: 10.1016/j.celrep.2014.06.051

Fernandez-Aroca, D. M., Roche, O., Sabater, S., Pascual-Serra, R., Ortega-Muelas, M., Sanchez Perez, I., et al. (2019). P53 pathway is a major determinant in the radiosensitizing effect of Palbociclib: implication in cancer therapy. *Cancer Lett.* 451, 23–33. doi: 10.1016/j.canlet.2019.02.049

Fisch, U., Zehnder, A., Hirt, A., Niggli, F., Simon, A., Ozsahin, H., et al. (2011). Mannan-binding lectin (MBL) and MBL-associated serine protease-2 in children with cancer. *Swiss Med. Wkly.* 141:w13191.

Fosbrink, M., Cudrici, C., Niculescu, F., Badea, T. C., David, S., Shamsuddin, A., et al. (2005). Overexpression of RGC-32 in colon cancer and other tumors. *Exp. Mol. Pathol.* 78, 116–122. doi: 10.1016/j.yexmp.2004.11.001

Gahoi, N., Malhotra, D., Moiyadi, A., Varma, S. G., Gandhi, M. N., and Srivastava, S. (2018). Multi-pronged proteomic analysis to study the glioma pathobiology using cerebrospinal fluid samples. *Proteomics Clin. Appl.* 12:1870013. doi: 10.1002/prca.201870013

Gallenkamp, J., Spanier, G., Woerle, E., Englbrecht, M., Kirschfink, M., Greslechner, R., et al. (2018). A novel multiplex detection array revealed systemic complement activation in oral squamous cell carcinoma. *Oncotarget* 9, 3001–3013. doi: 10.18632/oncotarget.22963

Gasque, P., Chan, P., Fontaine, M., Ischenko, A., Lamacz, M., Gotze, O., et al. (1995). Identification and characterization of the complement C5A anaphylatoxin receptor on human astrocytes. *J. Immunol.* 155, 4882–4889.

Gavrilyuk, V., Kalinin, S., Hilbush, B. S., Middlecamp, A., McGuire, S., Pelligrino, D., et al. (2005). Identification of complement 5a-like receptor (C5L2) from astrocytes: characterization of anti-inflammatory properties. *J. Neurochem.* 92, 1140–1149. doi: 10.1111/j.1471-4159.2004.02942.x

Geller, A., and Yan, J. (2019). The role of membrane bound complement regulatory proteins in tumor development and cancer immunotherapy. *Front. Immunol.* 10:1074. doi: 10.3389/fimmu.2019.01074

Gonzalez, S., Martinez-Borra, J., and Lopez-Larrea, C. (2003). Cloning and characterization of human complement component C7 promoter. *Genes Immun.* 4, 54–59. doi: 10.1038/sj.gene.6363902

Greijer, A. E., van der Groep, P., Kemming, D., Shvarts, A., Semenza, G. L., Meijer, G. A., et al. (2005). Up-regulation of gene expression by hypoxia is mediated predominantly by hypoxia-inducible factor 1 (HIF-1). *J. Pathol.* 206, 291–304. doi: 10.1002/path.1778

Gu, H., Mickler, E. A., Cummings, O. W., Sandusky, G. E., Weber, D. J., Gracon, A., et al. (2014). Crosstalk between TGF-beta1 and complement activation augments epithelial injury in pulmonary fibrosis. *FASEB J.* 28, 4223–4234. doi: 10.1096/fj.13-247650

Guc, D., Canpinar, H., Kucukaksu, C., and Kansu, E. (2000). Expression of complement regulatory proteins CR1, DAF, MCP and CD59 in haematological malignancies. *Eur. J. Haematol.* 64, 3–9. doi: 10.1034/j.1600-0609.2000.80097.x

Hambardzumyan, D., Gutmann, D. H., and Kettenmann, H. (2016). The role of microglia and macrophages in glioma maintenance and progression. *Nat. Neurosci.* 19, 20–27. doi: 10.1038/nn.4185

He, J. R., Xi, J., Ren, Z. F., Qin, H., Zhang, Y., Zeng, Y. X., et al. (2012). Complement receptor 1 expression in peripheral blood mononuclear cells and the association with clinicopathological features and prognosis of nasopharyngeal carcinoma. *Asian Pac. J. Cancer Prev.* 13, 6527–6531. doi: 10.7314/apjcp.2012.13.12.6527

Hemmati, H. D., Nakano, I., Lazareff, J. A., Masterman-Smith, M., Geschwind, D. H., Bronner-Fraser, M., et al. (2003). Cancerous stem cells can arise from pediatric brain tumors. *Proc. Natl. Acad. Sci. U.S.A.* 100, 15178–15183. doi: 10.1073/pnas.2036535100

Ho, C. M., Chang, S. F., Hsiao, C. C., Chien, T. Y., and Shih, D. T. B. (2012). Isolation and characterization of stromal progenitor cells from ascites of patients with epithelial ovarian adenocarcinoma. *J. Biomed. Sci.* 19, 23. doi: 10.1186/1423-0127-19-23

Honda, K.-I., Asada, R., Kageyama, K., Fukuda, T., Terada, H., Yasui, T., et al. (2017). Protein complex of fibrinogen gamma chain and complement factor H in Ovarian cancer patient plasma. *Anticancer Res.* 37, 2861–2866.

Ikeda, J., Morii, E., Liu, Y., Qiu, Y., Nakamichi, N., Jokoji, R., et al. (2008). Prognostic significance of CD55 expression in breast cancer. *Clin. Cancer Res.* 14, 4780–4786. doi: 10.1158/1078-0432.ccr-07-1844

Imoto, I., Saigusa, K., Tanikawa, C., Aoyagi, M., Ohno, K., Nakamura, Y., et al. (2007). "RGC32, a novel p53-inducible tumor-suppressor gene, is located on centrosomes during mitosis and results in G2/M arrest," in *Proceedings of the 98th AACR Annual Meeting*, Los Angeles, CA.

Kaur, A., Sultan, S. H. A., Murugaiah, V., Pathan, A. A., Alhamlan, F. S., Karteris, E., et al. (2016). Human C1q induces apoptosis in an ovarian cancer cell line via tumor necrosis factor pathway. *Front. Immunol.* 7:599. doi: 10.3389/fimmu.2016.00599

Kemper, C., Chan, A. C., Green, J. M., Brett, K. A., Murphy, K. M., and Atkinson, J. P. (2003). Activation of human CD4+ cells with CD3 and CD46 induces a T-regulatory cell 1 phenotype. *Nature* 421, 388–392. doi: 10.1038/nature01315

Kim, D. S., Lee, J. Y., Lee, S. M., Choi, J. E., Cho, S., and Park, J. Y. (2011). Promoter methylation of the RGC32 gene in nonsmall cell lung cancer. *Cancer* 117, 590–596. doi: 10.1002/cncr.25451

Kim, S. H., Lee, M. J., Hwang, H. K., Lee, S. H., Kim, H., Paik, Y.-K., et al. (2019). Prognostic potential of the preoperative plasma complement factor

B in resected pancreatic cancer: a pilot study. *Cancer Biomark.* 24, 335–342. doi: 10.3233/cbm-181847

Kim, S. M., Kang, S. G., Park, N. R., Mok, H. S., Huh, Y. M., Lee, S. J., et al. (2011). Presence of glioma stroma mesenchymal stem cells in a murine orthotopic glioma model. *Childs Nerv. Syst.* 27, 911–922. doi: 10.1007/s00381-011-1396-y

Kitano, E., and Kitamura, H. (2002). Synthesis of factor D by gastric cancer-derived cell lines. *Int. Immunopharmacol.* 2, 843–848. doi: 10.1016/s1567-5769(02)00028-0

Klikovits, T., Stockhammer, P., Laszlo, V., Dong, Y. W., Hoda, M. A., Ghanim, B., et al. (2017). Circulating complement component 4d (C4d) correlates with tumor volume, chemotherapeutic response and survival in patients with malignant pleural mesothelioma. *Sci. Rep.* 7:16456.

Kolev, M., Le Friec, G., and Kemper, C. (2014). Complement - tapping into new sites and effector systems. *Nat. Rev. Immunol.* 14, 811–820. doi: 10.1038/nri3761

Kuraya, M., Matsushita, M., Endo, Y., Thiel, S., and Fujita, T. (2003). Expression of H-ficolin/Hakata antigen, mannose-binding lectin-associated serine protease (MASP)-1 and MASP-3 by human glioma cell line T98G. *Int. Immunol.* 15, 109–117. doi: 10.1093/intimm/dxg008

Kwak, J. W., Laskowski, J., Li, H. Y., McSharry, M. V., Sippel, T. R., Bullock, B. L., et al. (2018). Complement activation via a C3a Receptor pathway alters CD4(+) T lymphocytes and mediates lung cancer progression. *Cancer Res.* 78, 143–156. doi: 10.1158/0008-5472.can-17-0240

Lalli, P. N., Strainic, M. G., Yang, M., Lin, F., Medof, M. E., and Heeger, P. S. (2008). Locally produced C5a binds to T cell-expressed C5aR to enhance effector T-cell expansion by limiting antigen-induced apoptosis. *Blood* 112, 1759–1766. doi: 10.1182/blood-2008-04-151068

Lathia, J. D., Mack, S. C., Mulkearns-Hubert, E. E., Valentim, C. L. L., and Rich, J. N. (2015). Cancer stem cells in glioblastoma. *Genes Dev.* 29, 1203–1217.

Lee, M. J., Na, K., Jeong, S.-K., Lim, J.-S., Kim, S. A., Lee, M.-J., et al. (2014). Identification of human complement factor B as a novel biomarker candidate for pancreatic Ductal Adenocarcinoma. *J. Proteome Res.* 13, 4878–4888. doi: 10.1021/pr5002719

Li, W., Hui, C., and Zhang, G. (2014). The effect of response gene to complement 32 on the glioma cells proliferation, apoptosis and invasion. *Chin. J. Exp. Surg.* 31, 1866–1867.

Lim, E.-J., Kim, S., Oh, Y., Suh, Y., Kaushik, N., Lee, J.-H., et al. (2020). Crosstalk between GBM cells and mesenchymal stem-like cells promotes the invasiveness of GBM through the C5a/p38/ZEB1 axis. *Neuro Oncol.* 22, 1452–1462. doi: 10.1093/neuonc/noaa064

Lim, M., Xia, Y., Bettegowda, C., and Weller, M. (2018). Current state of immunotherapy for glioblastoma. *Nat. Rev. Clin. Oncol.* 15, 422–442. doi: 10.1038/s41571-018-0003-5

Liu, L., Li, W., Li, Z., and Kirschfink, M. (2012). Sublytic complement protects prostate cancer cells from tumour necrosis factor-alpha-induced cell death. *Clin. Exp. Immunol.* 169, 100–108. doi: 10.1111/j.1365-2249.2012.04596.x

Loberg, R. D., Day, L. L., Dunn, R., Kalikin, L. M., and Pienta, K. J. (2006). Inhibition of decay-accelerating factor (CD55) attenuates prostate cancer growth and survival *in vivo*. *Neoplasia* 8, 69–78. doi: 10.1593/neo.05679

Louveau, A., Smirnov, I., Keyes, T. J., Eccles, J. D., Rouhani, S. J., Peske, J. D., et al. (2015). Structural and functional features of central nervous system lymphatic vessels. *Nature* 523, 337–341. doi: 10.1038/nature14432

Loveridge, C. J., Slater, S., Campbell, K. J., Nam, N. A., Knight, J., Ahmad, I., et al. (2020). BRF1 accelerates prostate tumourigenesis and perturbs immune infiltration. *Oncogene* 39, 1797–1806. doi: 10.1038/s41388-019-1106-x

Makela, K., Helen, P., Haapasalo, H., and Paavonen, T. (2012). Complement activation in astrocytomas: deposition of C4d and patient outcome. *BMC Cancer* 12:565. doi: 10.1186/1471-2407-12-565

Man, J., Yu, X., Huang, H., Zhou, W., Xiang, C., Huang, H., et al. (2018). Hypoxic induction of vasorin regulates notch1 turnover to maintain glioma stem-like cells. *Cell Stem Cell* 22, 104–118.e6.

Mangogna, A., Agostinis, C., Bonazza, D., Belmonte, B., Zacchi, P., Zito, G., et al. (2019a). Is the complement protein C1q a pro- or Anti-tumorigenic Factor? Bioinformatics analysis involving human carcinomas. *Front. Immunol.* 10:865. doi: 10.3389/fimmu.2019.00865

Mangogna, A., Belmonte, B., Agostinis, C., Zacchi, P., Iacopino, D. G., Martorana, A., et al. (2019b). Prognostic implications of the complement protein C1q in gliomas. *Front. Immunol.* 10:2366. doi: 10.3389/fimmu.2019.02366

Mantovani, A. (2010). Molecular pathways linking inflammation and cancer. *Curr. Mol. Med.* 10, 369–373. doi: 10.2174/156652410791316968

Markiewski, M. M., DeAngelis, R. A., Benencia, F., Ricklin-Lichtsteiner, S. K., Koutoulaki, A., Gerard, C., et al. (2008). Modulation of the antitumor immune response by complement. *Nat. Immunol.* 9, 1225–1235. doi: 10.1038/ni.1655

Mastellos, D. C., Reis, E. S., and Lambris, J. D. (2018). Complement C5a-mediated TAM-ing of antitumor immunity drives squamous carcinogenesis. *Cancer Cell* 34, 531–533. doi: 10.1016/j.ccell.2018.09.005

McGranahan, T., Therkelsen, K. E., Ahmad, S., and Nagpal, S. (2019). Current state of immunotherapy for treatment of glioblastoma. *Curr. Treat. Options Oncol.* 20:24.

Medler, T. R., Murugan, D., Horton, W., Kumar, S., Cotechini, T., Forsyth, A. M., et al. (2018). Complement C5a fosters squamous carcinogenesis and limits T cell response to chemotherapy. *Cancer Cell* 34, 561–578.e6.

Miranda Correa, R. R., Machado, J. R., da Silva, M. V., Helmo, F. R., Oliveira Guimaraes, C. S., Rocha, L. P., et al. (2013). The importance of C4d in biopsies of kidney transplant recipients. *Clin. Dev. Immunol.* 2013, 678180.

Montalto, M. C., Hart, M. L., Jordan, J. E., Wada, K., and Stahl, G. L. (2003). Role for complement in mediating intestinal nitric oxide synthase-2 and superoxide dismutase expression. *Am. J. Physiol. Gastrointest. Liver Physiol.* 285, G197–G206.

Morgan, B. P. (2000). The complement system: an overview. *Methods Mol. Biol.* 150, 1–13. doi: 10.1385/1-59259-056-x:1

Murray, K. P., Mathure, S., Kaul, R., Khan, S., Carson, L. F., Twiggs, L. B., et al. (2000). Expression of complement regulatory proteins-CD 35, CD 46, CD 55, and CD 59-in benign and malignant endometrial tissue. *Gynecol. Oncol.* 76, 176–182. doi: 10.1006/gyno.1999.5614

Naito, A. T., Sumida, T., Nomura, S., Liu, M. L., Higo, T., Nakagawa, A., et al. (2012). Complement C1q activates canonical Wnt signaling and promotes aging-related phenotypes. *Cell* 149, 1298–1313. doi: 10.1016/j.cell.2012.03.047

Nickeleit, V., and Mihatsch, M. J. (2003). Kidney transplants, antibodies and rejection: is C4d a magic marker? *Nephrol. Dial. Transplant.* 18, 2232–2239. doi: 10.1093/ndt/gfg304

Niculescu, F., Rus, H., van Biesen, T., and Shin, M. L. (1997). Activation of Ras and mitogen-activated protein kinase pathway by terminal complement complexes is G protein dependent. *J. Immunol.* 158, 4405–4412.

Nunez-Cruz, S., Gimotty, P. A., Guerra, M. W., Connolly, D. C., Wu, Y. Q., DeAngelis, R. A., et al. (2012). Genetic and pharmacologic inhibition of complement impairs endothelial cell function and ablates ovarian cancer neovascularization. *Neoplasia* 14, 994–1004. doi: 10.1593/neo.121262

Oka, R., Sasagawa, T., Ninomiya, I., Miwa, K., Tanii, H., and Saijoh, K. (2001). Reduction in the local expression of complement component 6 (Cd) and 7 (C7) mRNAs in oesophageal carcinoma. *Eur. J. Cancer* 37, 1158–1165. doi: 10.1016/s0959-8049(01)00089-2

Ozen, A., Kasap, N., Vujkovic-Cvijin, I., Apps, R., Cheung, F., Karakoc-Aydiner, E., et al. (2021). Broadly effective metabolic and immune recovery with C5 inhibition in CHAPLE disease. *Nat. Immunol.* 22, 128–139. doi: 10.1038/s41590-020-00830-z

Pagliara, V., Parafati, M., Adornetto, A., White, M. C., Masullo, M., Grimaldi, M., et al. (2018). Dibutyryl cAMP- or Interleukin-6-induced astrocytic differentiation enhances mannose binding lectin (MBL)-associated serine protease (MASP)-1/3 expression in C6 glioma cells. *Arch. Biochem. Biophys.* 653, 39–49. doi: 10.1016/j.abb.2018.06.016

Parente, R., Clark, S. J., Inforzato, A., and Day, A. J. (2017). Complement factor H in host defense and immune evasion. *Cell. Mol. Life Sci.* 74, 1605–1624. doi: 10.1007/s00018-016-2418-4

Pedersen, E. D., Froyland, E., Kvissel, A. K., Pharo, A. M., Skalhegg, B. S., Rootwelt, T., et al. (2007). Expression of complement regulators and receptors on human NT2-N neurons - Effect of hypoxia and reoxygenation. *Mol. Immunol.* 44, 2459–2468. doi: 10.1016/j.molimm.2006.10.022

Peng, Q., Li, K., Patel, H., Sacks, S. H., and Zhou, W. D. (2006). Dendritic cell synthesis of C3 is required for full T cell activation and development of a Th1 phenotype. *J. Immunol.* 176, 3330–3341. doi: 10.4049/jimmunol.176.6.3330

Piao, C. M., Zhang, W. M., Li, T. T., Zhang, C. C., Qiu, S. L., Liu, Y., et al. (2018). Complement 5a stimulates macrophage polarization and contributes to tumor metastases of colon cancer. *Exp. Cell Res.* 366, 127–138. doi: 10.1016/j.yexcr.2018.03.009

Pilzer, D., and Fishelson, Z. (2005). Mortalin/GRP75 promotes release of membrane vesicles from immune attacked cells and protection from complement-mediated lysis. *Int. Immunol.* 17, 1239–1248. doi: 10.1093/intimm/dxh300

Pio, R., Ajona, D., Ortiz-Espinosa, S., Mantovani, A., and Lambris, J. D. (2019). Complementing the cancer-immunity cycle. *Front. Immunol.* 10:774. doi: 10.3389/fimmu.2019.00774

Platt, J. L., Silva, I., Balin, S. J., Lefferts, A. R., Farkash, E., Ross, T. M., et al. (2017). C3d regulates immune checkpoint blockade and enhances antitumor immunity. *JCI Insight* 2:e90201.

Qiang, L., Wu, T., Zhang, H. W., Lu, N., Hu, R., Wang, Y. J., et al. (2012). HIF-1alpha is critical for hypoxia-mediated maintenance of glioblastoma stem cells by activating Notch signaling pathway. *Cell Death Differ.* 19, 284–294. doi: 10.1038/cdd.2011.95

Ricklin, D., Hajishengallis, G., Yang, K., and Lambris, J. D. (2010). Complement: a key system for immune surveillance and homeostasis. *Nat. Immunol.* 11, 785–797. doi: 10.1038/ni.1923

Riihila, P., Nissinen, L., Farshchian, M., Kallajoki, M., Kivisaari, A., Meri, S., et al. (2017). Complement components C3 and complement factor B promote growth of cutaneous squamous cell carcinoma. *J. Invest. Dermatol.* 137, S20–S20.

Riihila, P., Nissinen, L., Knuutila, J., Nezhad, P. R., Viiklepp, K., and Kahari, V.-M. (2019). Complement system in cutaneous squamous cell carcinoma. *Int. J. Mol. Sci.* 20:3550. doi: 10.3390/ijms20143550

Roumenina, L. T., Daugan, M. V., Noe, R., Petitprez, F., Vano, Y. A., Sanchez-Salas, R., et al. (2019a). Tumor cells hijack macrophage-produced complement C1q to promote tumor growth. *Cancer Immunol. Res.* 7, 1091–1105.

Roumenina, L. T., Daugan, M. V., Petitprez, F., Sautes-Fridman, C., and Fridman, W. H. (2019b). Context-dependent roles of complement in cancer. *Nat. Rev. Cancer* 19, 698–715. doi: 10.1038/s41568-019-0210-0

Sadahiro, H., Kang, K. D., Gibson, J. T., Minata, M., Yu, H., Shi, J. F., et al. (2018). Activation of the receptor tyrosine kinase AXL regulates the immune microenvironment in Glioblastoma. *Cancer Res.* 78, 3002–3013.

Saigusa, K., Imoto, I., Tanikawa, C., Aoyagi, M., Ohno, K., Nakamura, Y., et al. (2007). RGC32, a novel p53-inducible gene, is located on centrosomes during mitosis and results in G2/M arrest. *Oncogene* 26, 1110–1121. doi: 10.1038/sj.onc.1210148

Sapir-Pichhadze, R., Curran, S. P., John, R., Tricco, A. C., Uleryk, E., Laupacis, A., et al. (2015). A systematic review of the role of C4d in the diagnosis of acute antibody-mediated rejection. *Kidney Int.* 87, 182–194. doi: 10.1038/ki.2014.166

Seder, R. A., and Ahmed, R. (2003). Similarities and differences in CD4(+) and CD8(+) effector and memory T cell generation. *Nat. Immunol.* 4, 835–842. doi: 10.1038/ni969

Seol, H. S., Lee, S. E., Song, J. S., Rhee, J.-K., Singh, S. R., Chang, S., et al. (2016). Complement proteins C7 and CFH control the stemness of liver cancer cells via LSF-1. *Cancer Lett.* 372, 24–35. doi: 10.1016/j.canlet.2015.12.005

Sharma, A., and Shiras, A. (2016). Cancer stem cell-vascular endothelial cell interactions in glioblastoma. *Biochem. Biophys. Res. Commun.* 473, 688–692. doi: 10.1016/j.bbrc.2015.12.022

Shi, Y., Ping, Y. F., Zhou, W. C., He, Z. C., Chen, C., Bian, B. S. J., et al. (2017). Tumour-associated macrophages secrete pleiotrophin to promote PTPRZ1 signalling in glioblastoma stem cells for tumour growth. *Nat. Commun.* 8:15080.

Shinjyo, N., Stahlberg, A., Dragunow, M., Pekny, M., and Pekna, M. (2009). Complement-derived anaphylatoxin C3a regulates in vitro differentiation and migration of neural progenitor cells. *Stem Cells* 27, 2824–2832. doi: 10.1002/stem.225

Simpson, K. L., Jones, A., Norman, S., and Holmes, C. H. (1997). Expression of the complement regulatory proteins decay accelerating factor (DAF, CD55), membrane cofactor protein (MCP, CD46) and CD59 in the normal human uterine cervix and in premalignant and malignant cervical disease. *Am. J. Pathol.* 151, 1455–1467.

Singh, S. K., Clarke, I. D., Terasaki, M., Bonn, V. E., Hawkins, C., Squire, J., et al. (2003). Identification of a cancer stem cell in human brain tumors. *Cancer Res.* 63, 5821–5828.

Singh, S. K., Hawkins, C., Clarke, I. D., Squire, J. A., Bayani, J., Hide, T., et al. (2004). Identification of human brain tumour initiating cells. *Nature* 432, 396–401.

Smolag, K. I., Mueni, C. M., Leandersson, K., Jirstrom, K., Hagerling, C., Morgelin, M., et al. (2020). Complement inhibitor factor H expressed by breast cancer cells differentiates CD14(+) human monocytes into immunosuppressive macrophages. *Oncoimmunology* 9:1731135. doi: 10.1080/2162402x.2020.1731135

Sohn, J. H., Bora, P. S., Suk, H. J., Molina, H., Kaplan, H. J., and Bora, N. S. (2003). Tolerance is dependent on complement C3 fragment iC3b binding to antigen-presenting cells. *Nat. Med.* 9, 206–212. doi: 10.1038/nm814

Song, N. J., Kim, S., Jang, B. H., Chang, S. H., Yun, U. J., Park, K. M., et al. (2016). Small molecule-induced complement factor D (Adipsin) promotes lipid accumulation and adipocyte differentiation. *PLoS One* 11:e0162228. doi: 10.1371/journal.pone.0162228

Srivastava, A., and Mittal, B. (2009). Complement receptor 1 (A3650G RsaI and intron 27 HindIII) polymorphisms and risk of gallbladder cancer in north Indian population. *Scand. J. Immunol.* 70, 614–620. doi: 10.1111/j.1365-3083.2009.02329.x

Sun, Q., Yao, X., Ning, Y., Zhang, W., Zhou, G., and Dong, Y. (2013). Overexpression of response gene to complement 32 (RGC32) promotes cell invasion and induces epithelial-mesenchymal transition in lung cancer cells via the NF-kappaB signaling pathway. *Tumour Biol.* 34, 2995–3002. doi: 10.1007/s13277-013-0864-2

Swierzko, A. S., Florczak, K., Cedzynski, M., Szemraj, J., Wydra, D., Bak-Romaniszyn, L., et al. (2007). Mannan-binding lectin (MBL) in women with tumours of the reproductive system. *Cancer Immunol. Immunother.* 56, 959–971. doi: 10.1007/s00262-006-0250-7

Tan, A. C., Ashley, D. M., Lopez, G. Y., Malinzak, M., Friedman, H. S., and Khasraw, M. (2020). Management of glioblastoma: state of the art and future directions. *CA Cancer J. Clin.* 70, 299–312.

Tegla, C. A., Cudrici, C., Patel, S., Trippe, R. III, Rus, V., Niculescu, F., et al. (2011). Membrane attack by complement: the assembly and biology of terminal complement complexes. *Immunol. Res.* 51, 45–60.

van der Touw, W., Cravedi, P., Kwan, W. H., Paz-Artal, E., Merad, M., and Heeger, P. S. (2013). Cutting edge: receptors for C3a and C5a modulate stability of alloantigen-reactive induced regulatory T cells. *J. Immunol.* 190, 5921–5925. doi: 10.4049/jimmunol.1300847

van der Vlis, T., Kros, J. M., Mustafa, D. A. M., van Wijck, R. T. A., Ackermans, L., van Hagen, P. M., et al. (2018). The complement system in glioblastoma multiforme. *Acta Neuropathol. Commun.* 6:91.

Vlaicu, S. I., Cudrici, C., Ito, T., Fosbrink, M., Tegla, C. A., Rus, V., et al. (2008). Role of response gene to complement 32 in diseases. *Arch. Immunol. Ther. Exp.* 56, 115–122.

Vlaicu, S. I., Tatomir, A., Rus, V., and Rus, H. (2019). Role of C5b-9 and RGC-32 in cancer. *Front. Immunol.* 10:1054. doi: 10.3389/fimmu.2019.01054

Wang, H., Li, Y., Shi, G., Wang, Y., Lin, Y., Wang, Q., et al. (2020). A novel antitumor strategy: simultaneously inhibiting angiogenesis and complement by targeting VEGFA/PIGF and C3b/C4b. *Mol. Ther. Oncolytics* 16, 20–29. doi: 10.1016/j.omto.2019.12.004

Wang, X. X., Prager, B. C., Wu, Q. L., Kim, L. J. Y., Gimple, R. C., Shi, Y., et al. (2018). Reciprocal signaling between glioblastoma stem cells and differentiated tumor cells promotes malignant progression. *Cell Stem Cell* 22, 514–528.e5.

Wang, X. Y., Li, S. N., Zhu, H. F., Hu, Z. Y., Zhong, Y., Gu, C. S., et al. (2017). RGC32 induces epithelial-mesenchymal transition by activating the Smad/Sip1 signaling pathway in CRC. *Sci. Rep.* 7:46078.

Wang, Y., Yang, Y.-J., Wang, Z., Liao, J., Liu, M., Zhong, X.-R., et al. (2017). CD55 and CD59 expression protects HER2-overexpressing breast cancer cells from trastuzumab-induced complement-dependent cytotoxicity. *Oncol. Lett.* 14, 2961–2969. doi: 10.3892/ol.2017.6555

Wang, Y., Zhang, H., and He, Y.-W. (2019). The complement receptors C3aR and C5aR Are a new class of immune checkpoint receptor in cancer immunotherapy. *Front. Immunol.* 10:1574. doi: 10.3389/fimmu.2019.01574

Ward, P. A. (2009). Functions of C5a receptors. *J. Mol. Med.* 87, 375–378. doi: 10.1007/s00109-009-0442-7

Ward, T., Pipkin, P. A., Clarkson, N. A., Stone, D. M., Minor, P. D., and Almond, J. W. (1994). Decay-accelerating factor CD55 is identified as the receptor for echovirus-7 using CELICS, a rapid immune-focal cloning method. *EMBO J.* 13, 5070–5074. doi: 10.1002/j.1460-2075.1994.tb06836.x

Xu, R., Shang, C., Zhao, J., Han, Y., Liu, J., Chen, K., et al. (2014). Knockdown of response gene to complement 32 (RGC32) induces apoptosis and inhibits cell

growth, migration, and invasion in human lung cancer cells. *Mol. Cell. Biochem.* 394, 109–118. doi: 10.1007/s11010-014-2086-3

Xu, Y., Xu, W. H., Yang, X. L., Zhang, H. L., and Zhang, X. F. (2020). Fatty acid-binding protein 5 predicts poor prognosis in patients with uveal melanoma. *Oncol. Lett.* 19, 1771–1780.

Yan, J., Allendorf, D. J., Li, B., Yan, R., Hansen, R., and Donev, R. (2008). The role of membrane complement regulatory proteins in cancer immunotherapy. *Adv. Exp. Med. Biol.* 632, 159–174.

Yoon, Y.-H., Hwang, H.-J., Sung, H.-J., Heo, S.-H., Kim, D.-S., Hong, S.-H., et al. (2019). Upregulation of complement factor H by SOCS-1/3-STAT4 in lung cancer. *Cancers* 11:471. doi: 10.3390/cancers11040471

Ytting, H., Christensen, I. J., Thiel, S., Jensenius, J. C., and Nielsen, H. J. (2005). Serum mannan-binding lectin-associated serine protease 2 levels in colorectal cancer: relation to recurrence and mortality. *Clin. Cancer Res.* 11, 1441–1446. doi: 10.1158/1078-0432.ccr-04-1272

Zhang, J., Lei, J.-R., Yuan, L.-L., Wen, R., and Yang, J. (2020). Response gene to complement-32 promotes cell survival via the NF-kappa B pathway in non-small-cell lung cancer. *Exp. Ther. Med.* 19, 107–114.

Zhang, L., Sorensen, M. D., Kristensen, B. W., Reifenberger, G., McIntyre, T. M., and Lin, F. (2018). D-2-hydroxyglutarate is an intercellular mediator in IDH-mutant gliomas inhibiting complement and T cells. *Clin. Cancer Res.* 24, 5381–5391. doi: 10.1158/1078-0432.ccr-17-3855

Zhang, R., Liu, Q., Li, T., Liao, Q., and Zhao, Y. (2019). Role of the complement system in the tumor microenvironment. *Cancer Cell Int.* 19:300.

Zhao, Y.-X., Wang, Z.-Y., Li, G., and Yu, R.-J. (2006). Effect of interleukin-4 on the secretion of complement 3 and factor B induced by tumor necrosis factor-alpha or interleukin-1 beta in lung cancer cell line A549. *J. China Med. Univ.* 35, 61–62.

Zhiyong, Z., Xianmin, B. U., Chen, W., Xisheng, X., Zaizeng, W. U., and Yinghao, Y. U. (2007). Significance of C4d deposition in the fomcular iymphoma. *Chin. J. Hematol.* 28, 227–229.

Zhou, W. C., Ke, S. Q., Huang, Z., Flavahan, W., Fang, X. G., Paul, J., et al. (2015). Periostin secreted by glioblastoma stem cells recruits M2 tumour-associated macrophages and promotes malignant growth. *Nat. Cell Biol.* 17, 170–182. doi: 10.1038/ncb3090

Zhou, Y., Chu, L., Wang, Q., Dai, W., Zhang, X., Chen, J., et al. (2018). CD59 is a potential biomarker of esophageal squamous cell carcinoma radioresistance by affecting DNA repair. *Cell Death Dis.* 9:887.

Zhu, L., Qin, H., Li, P. Y., Xu, S. N., Pang, H. F., Zhao, H. Z., et al. (2012). Response gene to complement-32 enhances metastatic phenotype by mediating transforming growth factor beta-induced epithelial-mesenchymal transition in human pancreatic cancer cell line BxPC-3. *J. Exp. Clin. Cancer Res.* 31:29. doi: 10.1186/1756-9966-31-29

Zipfel, P. F., and Skerka, C. (2009). Complement regulators and inhibitory proteins. *Nat. Rev. Immunol.* 9, 729–740. doi: 10.1038/nri2620

Conflict of Interest: The authors declare that the research was conducted in the absence of any commercial or financial relationships that could be construed as a potential conflict of interest.

frontiers in Molecular Biosciences

ORIGINAL RESEARCH
published: 27 April 2021
doi: 10.3389/fmolb.2021.644557

Reconstruction and Analysis of the Immune-Related LINC00987/A2M Axis in Lung Adenocarcinoma

Jiakang Ma[1†], Xiaoyan Lin[1†], Xueting Wang[2], Qingqing Min[3], Tonglian Wang[4] and Chaozhi Tang[5]*

[1] Department of Oncology, The Second Affiliated Hospital of Zhengzhou University, Zhengzhou, China, [2] Department of Ophthalmology, The First Affiliated Hospital and College of Clinical Medicine of Henan University of Science and Technology, Luoyang, China, [3] Department of Endodontics, Stomatological Hospital of China Medical University, Shenyang, China, [4] Research Center of Molecular Medicine of Yunnan Province, Faculty of Life Science and Technology, Kunming University of Science and Technology, Kunming, China, [5] Department of Urology, The First Affiliated Hospital of China Medical University, Shenyang, China

Enhancer RNAs (eRNAs) participate in tumor growth and immune regulation through complex signaling pathways. However, the immune-related function of the eRNA-mRNA axis in lung adenocarcinoma (LUAD) is unclear. Data on the expression of eRNAs and mRNAs were downloaded from The Cancer Genome Atlas, GEO, and UCSC Xena, including LUAD, and pan-cancer clinical data and mutational information. Immune gene files were obtained from ImmLnc and ImmPort databases. Survival indices, including relapse-free and overall survival, were analyzed using the Kaplan–Meier and log-rank methods. The level of immune cell infiltration, degree of tumor hypoxia, and tumor cell stemness characteristics were quantified using the single-sample gene set enrichment analysis algorithm. The immune infiltration score and infiltration degree were evaluated using the ESTIMATE and CIBERSORT algorithms. The tumor mutation burden and microsatellite instability were examined using the Spearman test. The LUAD-associated immune-related LINC00987/A2M axis was down-regulated in most cancer types, indicating poor survival and cancer progression. Immune cell infiltration was closely related to abnormal expression of the LINC00987/A2M axis, linking its expression to a possible evaluation of sensitivity to checkpoint inhibitors and response to chemotherapy. Abnormal expression of the LINC00987/A2M axis was characterized by heterogeneity in the degree of tumor hypoxia and stemness characteristics. The abnormal distribution of immune cells in LUAD was also verified through pan-cancer analysis. Comprehensive bioinformatic analysis showed that the LINC00987/A2M axis is a functional and effective tumor suppressor and biomarker for assessing the immune microenvironment and prognostic and therapeutic evaluations of LUAD.

Keywords: eRNA, LUAD, LINC00987/A2M axis, immune cell infiltration, tumor hypoxia, tumor cell stemness

OPEN ACCESS

Edited by:
Na Luo,
Nankai University, China

Reviewed by:
Yuanyong Wang,
People 's Liberation Army General Hospital, China
Wenzhi Shen,
Jining Medical University, China

****Correspondence:***
Chaozhi Tang
tangchaozhi123456@163.com

† These authors have contributed equally to this work

Specialty section:
This article was submitted to Molecular Diagnostics and Therapeutics, a section of the journal Frontiers in Molecular Biosciences

Received: *21 December 2020*
Accepted: *07 April 2021*
Published: *27 April 2021*

Citation:
Ma J, Lin X, Wang X, Min Q, Wang T and Tang C (2021) Reconstruction and Analysis of the Immune-Related LINC00987/A2M Axis in Lung Adenocarcinoma. Front. Mol. Biosci. 8:644557. doi: 10.3389/fmolb.2021.644557

INTRODUCTION

Non-small-cell lung carcinoma (NSCLC) is the main histological type accounting for approximately 85% of lung cancer (LC) patients (van Meerbeeck et al., 2011; Domingues et al., 2014). Of the 70% of NSCLC patients diagnosed with advanced or metastatic progression, only 30% of cases are operable (Travis et al., 2013). The most common type of NSCLC is lung

adenocarcinoma (LUAD), which reportedly comprises 40% of all LC and 60% of NSCLC (Meza et al., 2015; Torre et al., 2016).

Emerging evidence has emphasized the critical enhancer roles, a key non-coding DNA sequence in promoter-distal *cis*-regulatory DNA regions, in cancer genomic studies (Pennacchio et al., 2013). Enhancer RNAs (eRNAs) are a type of bidirectional RNA transcript originating during enhancer activation and transcription. In the process, enhancers attract, and bind transcription factors (TFs) by exposing DNA motifs of local chromatin, and TFs further enlist RNA Pol II to induce eRNA transcription (Kim et al., 2010; Heinz et al., 2015; Murakawa et al., 2016). eRNA is categorized as a type of long non-coding RNA (lncRNA) based on its length (Li et al., 2016). As many eRNAs have shown to be too unstable and low in abundance, they are rarely observed via steady-state RNA assays such as RNA-seq and thus cannot be completely captured in lncRNA databases (Derrien et al., 2012). Therefore, it is of great research significance to find an eRNA that exhibits overlap with lncRNAs. In particular, transcription of eRNA is known to be initiated from TF binding sites and has been reported to act as a robust readout predicting the activity of TFs (Azofeifa et al., 2018). Some studies have offered strong evidence that eRNAs could be induced to participate in regulating the activation of oncogenes or oncogenic signaling pathways, such as ESR1 (Li et al., 2015), and that of repressors such as TP53 (Melo et al., 2013) and Rev-Erbs (Lam et al., 2013). Besides, eRNA has shown to be functional in stimulating transcription of target mRNAs (Kim et al., 2010; Zhang et al., 2019). eRNAs have been found to promote transcription by establishing chromatin remodeling and Pol II assembly at defined loci, thereby suggesting higher expression of genes near eRNA + sites as compared to that at other sites (Mousavi et al., 2013). However, the functions and mechanisms of eRNAs with target mRNAs remain incompletely understood in LUAD.

Effective immunotherapies that induce or enhance antitumor responses have prospective clinical applications in the treatment of cancer. For example, combination therapy with immune checkpoint inhibitors of cytotoxic T lymphocyte-associated protein 4 (CTLA) and programmed cell death 1 (PDCD1, also known as PD1) has shown effective clinical application potential in the treatment of cancer (Liu J.-N. et al., 2020). Although the study of the molecular identification of tumor antigens for therapeutic anticancer vaccines is more urgent, the underlying active immunoregulatory processes in the tumor microenvironment are not negligible. Further, eRNAs correlated with six immune checkpoint proteins (CD200, PLEC, PDL2, HAVCR1, PDL1, and BTLA) in at least five cancer types (Zhang et al., 2019). They were suggested to play vital roles in evading immune destruction and maintaining the balance between activation of adaptive immunity and self-tolerance of autoimmunopathy. The associated transcript 1-long isoform (CCAT1-L) is a super-enhancer RNA known to positively regulate the expression of MYC in *cis*, which is a key regulator of the immune checkpoint (CD47 and PDCD1L1), immune surveillance, and antitumor immune response (Casey et al., 2016; Kim et al., 2017; Wu and Shen, 2019). In addition, eRNAs have been closely related to the development and release of inflammatory mediators in immune cells. For instance, IL1b-eRNA was found to decrease the lipopolysaccharide (LPS)-induced release of interleukin 1 beta (IL1b) and C-X-C motif chemokine ligand 8 (CXCL8) in human monocytes, which are suggested to be important regulators of the human innate immune response (Iiott et al., 2014). Likewise, LNCGme02323 was demonstrated to drastically alter the expression of marginal zone B cells. Briefly, LNCGme00432, LNCGme00344, and LNCGme00345 are known to be regulated by PAX5- and PAX5-dependent pathways, which might contribute to the differentiation of acute B lymphoblastic leukemia (B-ALL) cells and leukemia regression (Brazão et al., 2016). Therefore, continued detailed analysis of immune cell infiltration in the tumor microenvironment could help identify potential biomarkers and develop new immunotherapeutic strategies.

The therapeutic trait of atezolizumab, the PDL-1 blocking antibody used for the treatment of NSCLC, is currently under investigation (Ryu and Ward, 2018) and is thus still unavailable for clinical application. We aimed to explore more functional immunomodulators that can provide a powerful basis for immunotherapy of LUAD in the future. This study identified the immune-related eRNA-mRNA axis using data obtained from The Cancer Genome Atlas (TCGA), ImmLnc, and ImmPort databases and found that this axis plays a vital role in clinical cancer progression. We further explored the relationship between the eRNA-mRNA axis and the level of immune cell infiltration, degree of tumor hypoxia, tumor cell stemness, somatic mutations, and prognostic values for patients in LUAD TCGA and 3 GEO datasets. To verify the significance of the eRNA-mRNA axis in immunotherapy, a pan-cancer evaluation was conducted for tumor mutation burden (TMB), microsatellite instability (MSI), and immune cell populations. These results provided strong evidence for the role of eRNAs in regulating immune status and immunotherapy.

MATERIALS AND METHODS

Data Collection and Processing

Sequencing data (FPKM) and clinical data of LUAD included the datasets of 491 cases obtained from the TCGA data portal[1]. Pan-cancer and somatic mutation data in LUAD were downloaded from the UCSC Xena[2] (**Table 1**). Three GEO datasets, GSE31210, GSE37745, and GSE50081, containing the microarray-based expression data of patients with LUAD and associated clinical information, were downloaded from the GEO website[3]. GSE31230 (N = 226) was annotated using the data file for Agilent-021169 Arabidopsis 4 Oligo Microarray (V4; Feature Number version). The GSE37745 and GSE50081 datasets were filtered, and only LUAD cases were retained, following which both were annotated using the data files from the [HG-U133_Plus_2] Affymetrix Human Genome U133 Plus 2.0 Array platform. They were merged into a new dataset named

[1]https://gdc-portal.nci.nih.gov/

[2]http://xena.ucsc.edu/

[3]https://www.ncbi.nlm.nih.gov/geo/

TABLE 1 | TCGA pan-cancer description.

Abbreviation	Number	Full name
ACC	79	Adrenocortical carcinoma
BLCA	396	Bladder urothelial carcinoma
BRCA	1092	Breast invasive carcinoma
CESC	301	Cervical squamous cell carcinoma and endocervical adenocarcinoma
CHOL	36	Cholangiocarcinoma
COAD	280	Colon adenocarcinoma
DLBC	47	Lymphoid neoplasm diffuse large B-cell lymphoma
ESCA	183	Esophageal carcinoma
GBM	167	Glioblastoma multiforme
HNSC	516	Head and neck squamous cell carcinoma
KICH	65	Kidney chromophobe
KIRC	530	Kidney renal clear cell carcinoma
KIRP	270	Kidney renal papillary cell carcinoma
LAML	163	Acute myeloid leukemia
LGG	506	Brain lower-grade glioma
LIHC	361	Liver hepatocellular carcinoma
LUAD	497	Lung adenocarcinoma
LUSC	483	Lung squamous cell carcinoma
MESO	87	Mesothelioma
OV	264	Ovarian serous cystadenocarcinoma
PAAD	179	Pancreatic adenocarcinoma
PCPG	184	Pheochromocytoma and paraganglioma
PRAD	493	Prostate adenocarcinoma
READ	95	Rectum adenocarcinoma
SARC	249	Sarcoma
SKCM	463	Skin cutaneous melanoma
STAD	409	Stomach adenocarcinoma
TGCT	139	Testicular germ cell tumors
THCA	504	Thyroid carcinoma
THYM	118	Thymoma
UCEC	548	Uterine corpus endometrial carcinoma
UCS	57	Uterine carcinosarcoma
UVM	80	Uveal melanoma

GSEnew (N = 233), with batch effects eliminated, using the "sva" R package.

Identification of the Immune-Related eRNA-mRNA Axis

The eRNA-mRNA axis file was obtained from the work of Vucicevic et al. (2015). The gene set of LUAD-related immune lncRNA was downloaded from ImmLnc[4], whereas that of immune-related mRNA was obtained from the ImmPort database[5]. Using Venn diagram analysis, coexpression analysis (cor > 0.4 and $p < 0.001$), differential analysis ($|\log_2 FC| > 1$ and $p < 0.05$), and survival analysis ($p < 0.05$), we finally identified only a single immune-related eRNA-mRNA axis associated with LUAD (**Figure 1**).

[4]http://bio-bigdata.hrbmu.edu.cn/ImmLnc/

[5]https://www.immport.org/

Implementation of Single-Sample Gene Set Enrichment Analysis

Briefly, 29 immune-related gene sets containing immune cell types, immune-related pathways, and immune-related functions were derived from our previous study (Tang et al., 2020b). In addition, 26 stem cell gene sets were also obtained from our previous study (Tang et al., 2020a), whereas five mRNA-based hypoxia signatures were collected from the study of Winter et al. (2007), Buffa et al. (2010), Ragnum et al. (2015), Eustace et al. (2013), and Sorensen et al. (2010). Based on TCGA and GEO datasets, we applied the single-sample gene set enrichment analysis (ssGSEA) algorithm to quantify each signature's enrichment scores using the "GSVA" package. The enrichment scores reflected the level of immune cell infiltration, degree of tumor hypoxia, and tumor cell stemness characteristics. Based on these enrichment scores, the relationships between the LINC00987-A2M axis and immunity, stem cell characteristics, and hypoxia were identified.

Heatmap and Analysis of Significant Differences

The heatmaps of the ssGSEA score were visualized using the "heatmap" R package. The Wilcoxon test was used to calculate the significance of each signature score for eRNA and its target gene between the high- and low expression groups. Finally, we marked the significance of the heatmap values to show the difference between groups.

Survival Analysis

Kaplan-Meier survival curves were constructed for relapse-free survival (RFS) and overall survival (OS) by using the "survminer" R package. Differences between groups were determined using the log-rank test. A p-value < 0.05 was considered statistically significant.

Relationship Between LINC00987-A2M and Tumor Immunity

Based on the ESTIMATE algorithm (Yoshihara et al., 2013) and using gene expression profiles, we calculated the stromal score, immune score, ESTIMATE score, and tumor purity to verify the correlation between the proportion of immune cells and systemic content and LINC00987-A2M. We further evaluated the relationship between the infiltration degree of 22 immune cells and LINC00987-A2M based on analysis with the CIBERSORT algorithm (Newman et al., 2015), and only data with a CIBERSORT p-value < 0.05 were selected for consecutive analysis. Both the TMB and MSI have been associated with an increased response rate to immunotherapy (Narayanan et al., 2019; Liu J. et al., 2020), so we calculated the correlation between LINC0097-A2M and these indicators to evaluate the effectiveness of immunotherapy.

Gene Set Enrichment Analysis

Hallmark gene sets are coherently expressed signatures that represent well-defined biological states or processes. We identified the biological effects caused by the change in the

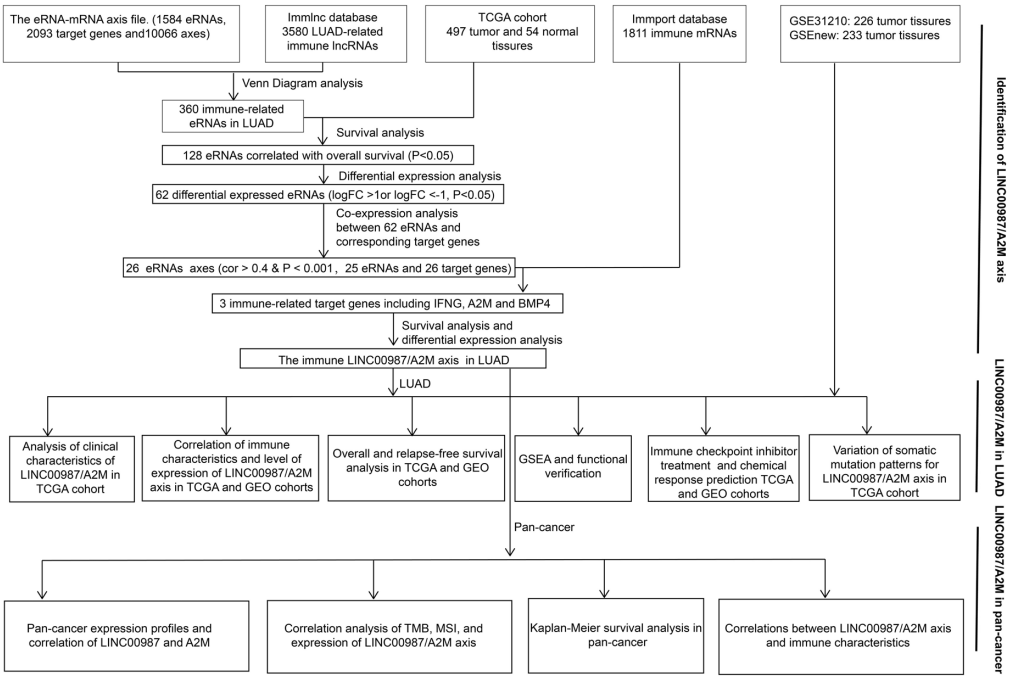

FIGURE 1 | Workflow. Workflow for the identification and verification of the immune-related LINC00987/A2M axis in LUAD and pan-cancer.

expression of LINC00987-A2M using h.all.v7.1.symbols.gmt [Hallmarks] (GSEA version 4.0.1). The analysis was performed using 1000 permutations, and a false discovery rate < 0.05 was set as the screening threshold.

Prediction of Immunotherapeutic and Chemotherapeutic Response

Based on the subclass mapping method, we used the TCGA LUAD FPKM RNA-seq expression profile to predict the drug response of the LINC00987-A2M axis to immune checkpoint blockade. Predictive analysis of the chemotherapeutic response of LINC00987-A2M was performed based on the Genomics of Drug Sensitivity in Cancer (GDSC)[6] using the "pRRophetic" package in R, where the half-maximum inhibitory concentration (IC50) of the sample was estimated using ridge regression, and the accuracy of the prediction was evaluated using 10-fold cross-validation, according to the GDSC training set. All parameters were set at default values, and the repeated gene expression was averaged. Three commonly used chemotherapeutic agents of LUAD were selected (Lu et al., 2019).

Statistical Analyses

Wilcoxon test was used to assess changes in LINC00987 and A2M expression between cancer tissues and adjacent normal tissues and to compare the immune characteristics and estimated IC50 of the high- and low-expression groups for these two genes. Spearman's and Pearson's correlation tests were used for the analyses. All statistical analyses were performed using R 3.5.3, and $p < 0.05$ was considered statistically significant.

RESULTS

Screening of Immune-Related eRNA-mRNA Axis Associated With LUAD

Using Venn diagram analysis, we obtained 360 immune **eRNA**s from the LUAD-related immune RNA and the eRNA-mRNA axis file, with 128 eRNAs associated with survival rate. The coexpression analysis results showed that out of 128 pairs of eRNA-mRNA axes, 53 pairs had a significant correlation between eRNAs and target genes. After differential analysis and survival analysis screening, we further obtained 16 differentially expressed and survival-related mRNAs. Besides, we found that when 16 mRNAs were again intersected with 1811 immune genes in the ImmPort database, only A2M was identified screened as an immune gene. Finally, we screened A2M and the upstream LINC00987 for subsequent immunological studies (**Figure 1**).

Downregulation of LINC00987/A2M Axis Portended Adverse LUAD Pathological Progression and Worse Survival

We employed the "ggpubr" package to investigate the impact of the LINC00987/A2M axis on clinical characteristics in the TCGA cohort. We accordingly observed that the expression levels of LINC00987 and A2M were both inversely correlated with T (tumor), N (node), and stage; however, M (metastasis) was not affected by either (**Figures 2A–H**).

[6]https://www.cancerrxgene.org/

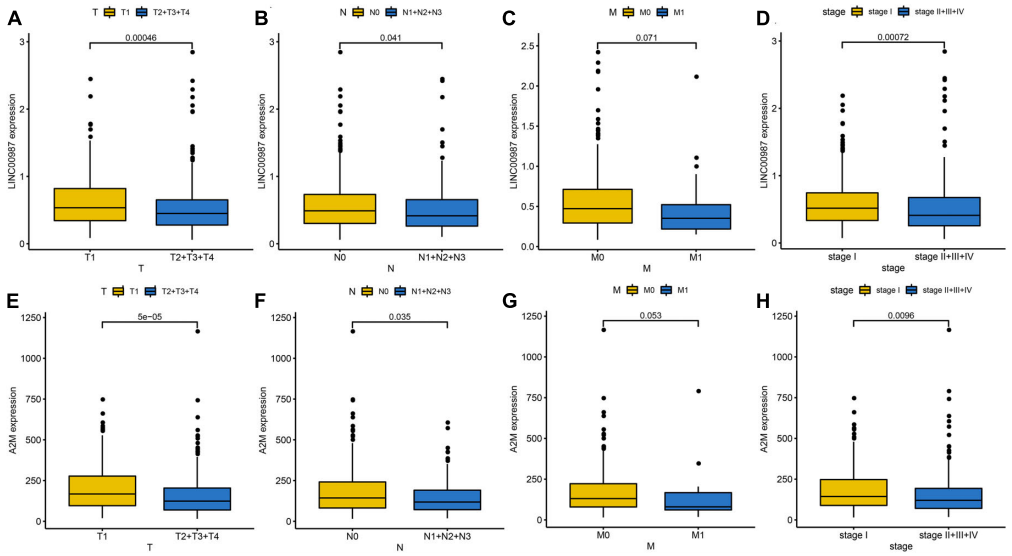

FIGURE 2 | Identification of clinical characteristics of the two immune-related genes in the LUAD TCGA cohort. Differential expression of LINC00987 **(A–D)** and A2M **(E–H)** among the T (tumor), N (node), M (metastasis), and stage, evaluated using the Wilcoxon test.

We speculated that patients with low expression of LINC00987 or A2M were more likely to have malignant pathology than patients with high expression. Kaplan–Meier analysis also showed that LINC00987 and A2M were protective predictors of OS (LINC00987: HR = 0.68, 95% CI [0.5–0.93], and p = 0.018; A2M: HR = 0.6, 95% CI [0.45–0.81], and p = 0.002) and RFS (LINC00987: HR = 0.62, 95% CI [0.39–0.99], and p = 0.037; A2M: HR = 0.59, 95% CI [0.36–0.98], and p = 0.025; **Figures 3A–D**). To further identify their impact on the survival prognostic values in patients with LUAD, we downloaded and integrated 3 GEO datasets (GSE31210, GSE37745, and GSE50081). We found that patients with high expression of A2M had longer OS (GSE31210: HR = 0.38, 95% CI [0.18–0.78], and p = 0.037; GSEnew: HR = 0.63, 95% CI [0.44–0.89], and p = 0.01) and RFS (GSE31210: HR = 0.48, 95% CI [0.29–0.81], and p = 0.003; GSEnew: HR = 0.58, 95% CI [0.35–0.94], and p = 0.033) than patients in the low expression group (**Figures 3E–H**). Combination group analysis revealed that patients with high expression of both genes had better OS ($p < 0.05$) and RFS ($p < 0.05$) among all four groups (**Figures 3I,J**).

Correlation of Immune Characteristics and Level of Expression of LINC00987/A2M Axis

The LINC00987/A2M axis was shown to be involved in LUAD immunity, but its relation to specific processes and the extent of participation remained unknown. We, therefore, focused on deciphering these aspects. We used the ssGSEA scores of 29 immune gene sets to evaluate the relationship between immune infiltration and LINC00987 or A2M expression in the low- and high- LINC00987 or A2M expression groups (**Figures 4A–D**).

Among these 3 cohorts, we found that most immune cell infiltration degree was significantly different in the TCGA cohort but only partially significant in the GEO datasets. This might have resulted from the small sample size and large error in the GEO datasets. Our ESTIMATE analysis demonstrated a high proportion of immune cells and systemic response in high LINC00987 and A2M expression groups among the three cohorts, reflected by higher stromal score, immune score, ESTIMATE score, and lower tumor purity (**Figures 4E–H**).

We further evaluated the relationship between the differential distribution of 22 human immune cell subgroups and the LINC00987/A2M axis based on the CIBERSORT algorithm. We observed that the populations of 22 immune cells in different active states, including CD4 memory T cells, M0 macrophages, and mast cells, showed significant differences in both the high LINC00987 and A2M expression groups compared with the low expression groups (**Figures 5A–D**). This finding suggested that the LINC00987/A2M axis might mainly regulate immune cell infiltration. In general, the above results consistently indicated that when the LINC00987/A2M axis is highly expressed, immune cells in the tumor microenvironment tend to be more abundant and characterized by increased immune cell components, which might contribute to the better prognosis of patients.

GSEA and Functional Verification

We performed Gene set enrichment analysis (GSEA) to assess the biological effects of the changes in LINC00987/A2M expression in LUAD. The hallmarks of the expression of LINC00987 and A2M are illustrated in **Figures 6A,B**. We observed that these hallmarks, including allograft rejection, DNA repair, E2F targets, G2M checkpoint, IL2-STAT5 signaling, Kras signaling, Mtorc1 signaling, and MYC targets, were consistent for the expression of both LINC00987 and A2M. However, LINC00987 and A2M were also shown to be related to epithelial-mesenchymal transition and hypoxia, respectively (**Figures 6A,B**). To further explore whether

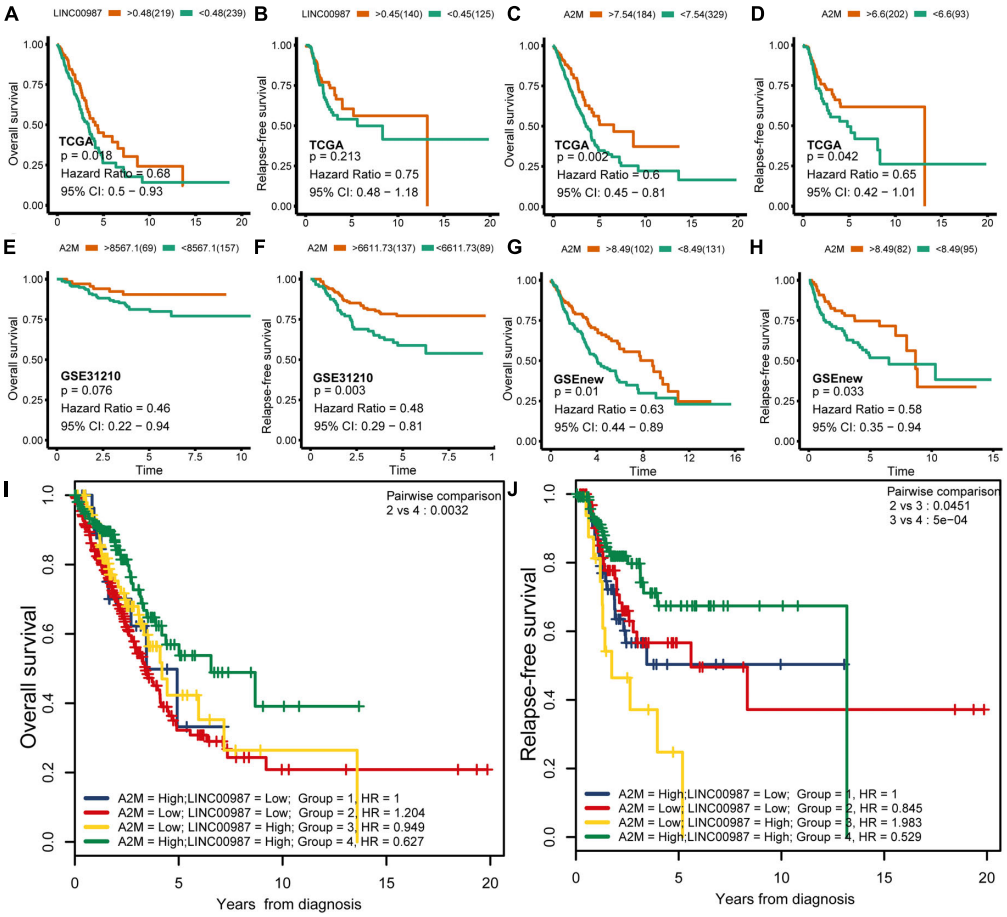

FIGURE 3 | Correlation of overall (OS) and relapse-free survival (RFS) with LINC00987 and A2M in datasets. **(A–D)** OS and RFS curves for LINC00987 and A2M in the TCGA cohort. **(E–H)** OS and RFS curves for A2M in the GSEnew and GSE31210 cohorts. **(I,J)** OS and RFS curves for combinations of LINC00987 and A2M in the TCGA cohort.

the immune-related LINC00987/A2M axis also affected tumor epithelial-mesenchymal transition and hypoxia, we analyzed the relationship between the five hypoxia-associated gene sets and the LINC00987/A2M axis in TCGA, GSE31210, and GSEnew cohorts. The ssGSEA scores of all five hypoxia-associated gene sets indicated that they were up-regulated in the low LINC00987 or A2M expression group, implying that the LINC00987/A2M axis facilitated tumor cell growth and proliferation under hypoxia (**Figures 6C,D** and **Supplementary Figures 1A,B**). Based on the 26 stem cell gene sets, we found that the distribution of the ssGSEA score related to various stemness characteristics was significantly different between high and low LINC00987 or A2M expression groups (**Figures 6E,F** and **Supplementary Figures 1C,D**).

Differences in Sensitivity of the LINC00987/A2M Axis to Checkpoint Inhibitors and Chemotherapy

With the approval of immune checkpoint inhibitors in cancer therapy, it is vital to understand the immune checkpoint regulation mechanism to improve their efficacy. We observed that the high LINC00987 and A2M expression groups were more sensitive to anti-PD-1 treatment in TCGA and GSE31210 cohorts ($p < 0.05$; **Figure 7A**), suggesting that the LINC00987/A2M axis is an effective sensitizer for the curative effect. In addition, compared to the conventional chemotherapy of LUAD, we found that variations in the LINC00987/A2M axis heralded different responses to immunotherapy. We evaluated the sensitivity of commonly used chemotherapeutic drugs in treating LUAD in each sample in TCGA and GEO cohorts by estimating the IC50. We accordingly observed that the low LINC00987 and A2M expression groups were more sensitive to treatment with paclitaxel than the high expression groups in TCGA and GSEnew cohorts ($p < 0.05$; **Figure 7B**).

Variation of Somatic Mutation Patterns for LINC00987/A2M Axis in LUAD

To gain further insights into the mutational processes in high and low expression of LINC00987 or A2M, we delineated the mutation patterns from the data on somatic mutations in

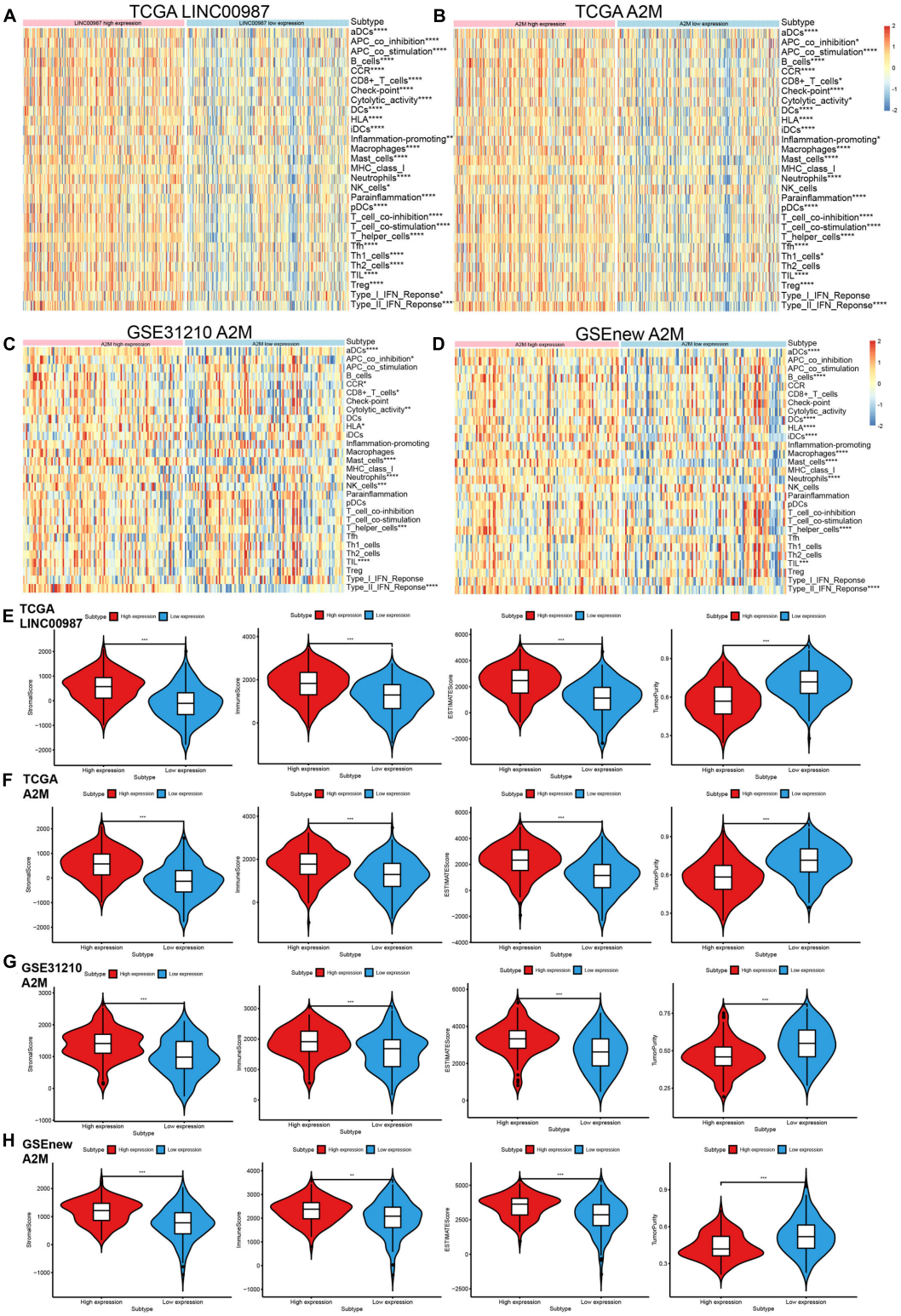

FIGURE 4 | Distribution of immune-related characteristics in different subgroups related to LINC00987 and A2M in the TCGA and GEO datasets. **(A,B)** Heatmap of the expression of LINC00987 and A2M and 29 immune-related gene sets generated by ssGSEA in TCGA cohort. **(C,D)** Heatmap of the expression of A2M and 29 immune-related gene sets generated by ssGSEA in two GEO cohorts. Violin-plot showing the difference in ImmuneScore, StromalScore, ESTIMATEScore, and TumorPurity in **(E)** LINC00987 and **(F–H)** A2M subgroups in TCGA and GEO cohorts. $^{*}p < 0.05$, $^{**}p < 0.01$, $^{***}p < 0.001$, and $^{****}p < 0.0001$.

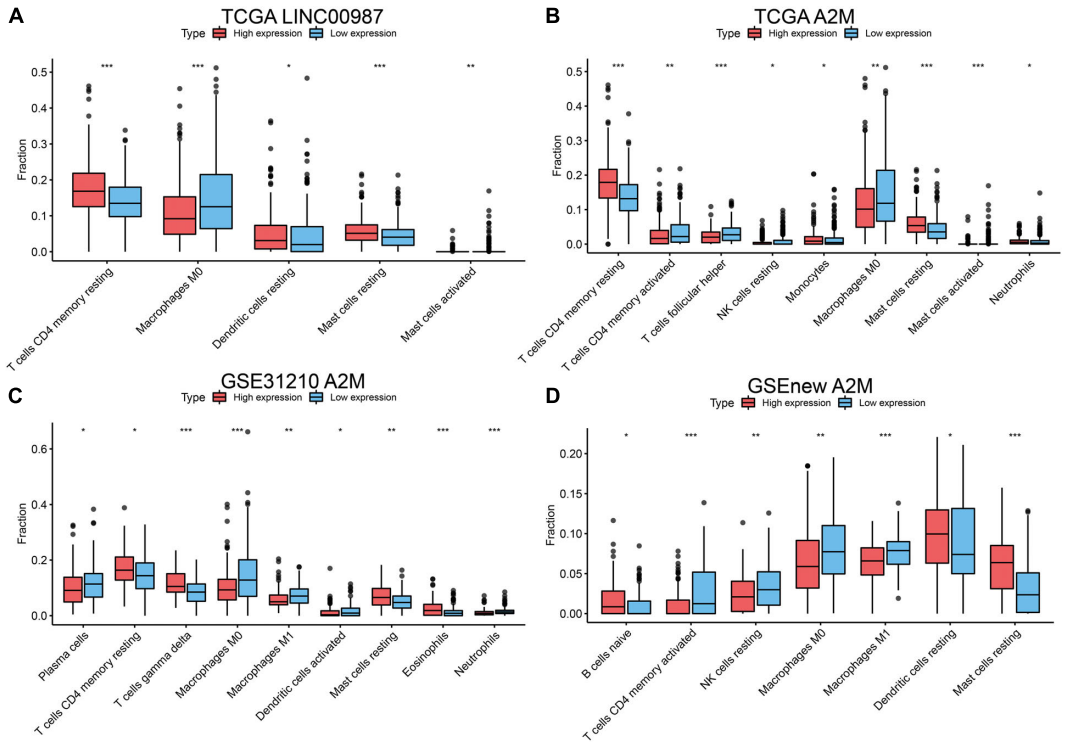

FIGURE 5 | Differences in the distribution of 22 human immune cells in LINC00987 and A2M expression groups estimated using the CIBERSORT algorithm. Boxplots for **(A)** LINC00987 and **(B)** A2M in the TCGA cohort. Boxplots for A2M in the **(C)** GSE31210 and **(D)** GSEnew cohorts. $^{*}p < 0.05$, $^{**}p < 0.01$, and $^{***}p < 0.001$.

LUAD. We noted that the overall mutational pattern was mainly dominated by C > T and C > A mutations. In particular, C > A mutations were shown to be increased, whereas C > T, and C > G mutations were decreased in the high LINC00987 expression group. However, these alterations were not observed in the high A2M expression group (**Figure 8** and **Supplementary Figure 2**).

Pan-Cancer Expression Profiles and Correlation of LINC00987 and A2M

Multiple lines of evidence are required to confirm the role of the LINC00987/A2M axis in tumor immunity. Therefore, we used the UCSC Xena datasets to investigate the pan-cancer expression profiles of LINC00987 and A2M and their prognostic significance. Cancer tissues lacking paired normal tissues were not included. We accordingly found that the levels of LINC00987 and A2M were consistently down-regulated in most tumor tissues in comparison with non-carcinoma tissues, both in overall and paired comparison of 22 cancer types, including LUAD, lung squamous cell carcinoma (LUSC), kidney renal papillary cell carcinoma (KIRP), colon adenocarcinoma (COAD), breast invasive carcinoma (BRCA), uterine corpus endometrial carcinoma (UCEC), urothelial bladder carcinoma (BLCA), cholangiocarcinoma (CHOL), and kidney chromophobe. However, we noted that both were up-regulated in prostate adenocarcinoma (PAAD). These two genes were shown not to be differentially expressed or unrelated in individual cancers (**Figures 9A–D**).

We further analyzed the association between the expression levels of LINC00987 and A2M and survival by using Kaplan–Meier survival analysis. We demonstrated that LINC00987 and A2M could be consistently regarded as protective factors in BRCA, kidney renal clear cell carcinoma, LUAD, sarcoma (SARC), cutaneous skin melanoma (SKCM), and UCEC; however, both were revealed to be risk factors for mesothelioma (MESO; **Figures 9E,F**). Combined with the above verification results, we assumed that the LINC00987/A2M axis might play key roles in cancer progression for LUAD, BRCA, and UCEC. In addition, the expression of LINC00987 and A2M was demonstrated to have an obvious correlation in almost all tumors (**Supplementary Table 1**).

Correlation Analysis of TMB, Microsatellite Instability, and Expression of LINC00987/A2M Axis

We next examined the associations between the expression of LINC00987/A2M and the levels of TMB and MSI (**Figure 10**). We found that TMB showed differences related to the expression of LINC00987 in BRCA, BLCA, cervical squamous cell carcinoma and endocervical adenocarcinoma (CESC), UCEC, uveal melanoma (UVM), thyroid carcinoma (THCA), stomach adenocarcinoma (STAD), SKCM, prostate adenocarcinoma

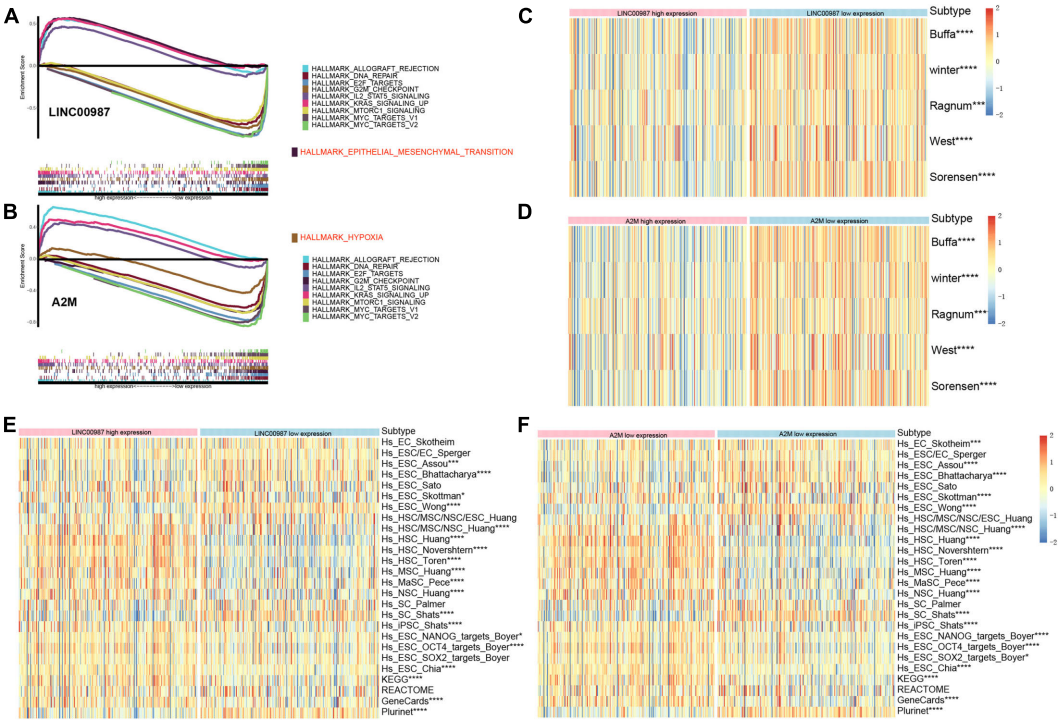

FIGURE 6 | Gene sets functional enrichment analysis. **(A)** GSEA of high vs. low expression of LINC00987. **(B)** GSEA of high vs. low expression of A2M in the TCGA cohort. Correlation of the expression of **(C)** LINC00987 and **(D)** A2M with hypoxia gene sets. Correlation of the expression of **(E)** LINC00987 and **(F)** A2M with tumor stem cell characteristics. *$p < 0.05$, ***$p < 0.001$, and ****$p < 0.0001$.

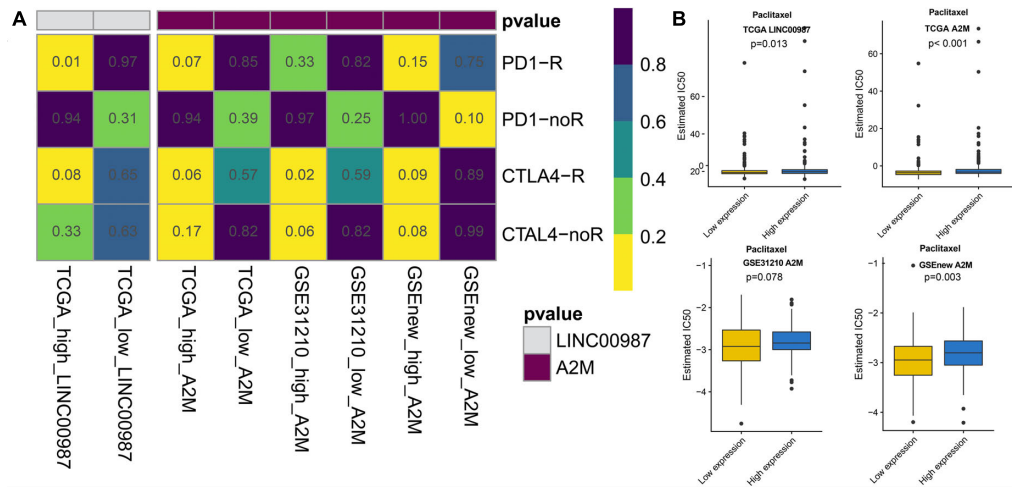

FIGURE 7 | Response to immunotherapy and sensitivity to chemotherapy in relation to the expression of LINC00987 and A2M in TCGA, GSE31210, and GSEnew cohorts. **(A)** Sensitivity response of high vs. low expression of LINC00987 to PD1 and CTLA-4 inhibitors ($p = 0.01$). **(B)** Boxplots of the estimated IC50 for paclitaxel in high vs. low expression of LINC00987/A2M.

(PRAD), pancreatic adenocarcinoma (PAAD), LUSC, LUAD, liver hepatocellular carcinoma (LIHC), brain lower-grade glioma (LGG), acute myeloid leukemia (LAML), KIRP, HNSC, esophageal carcinoma (ESCA), and lymphoid neoplasm diffuse large B-cell lymphoma (DLBC; **Figure 10A**). The expression of A2M was shown to be correlated with TMB in BRCA, BLCA, COAD, CESC, HNSC, UCEC, UVM, THCA, thymoma (THYM), TGCT, STAD, pheochromocytoma, and paraganglioma, PAAD, LUSC, LUAD, LIHC, LGG, and LAML (**Figure 10B**). The expression of LINC00987 was found to be correlated with MSI in UVM, COAD, DLBC, HNSC, KIRP, ovarian serous cystadenocarcinoma (OV), PAAD, rectum adenocarcinoma,

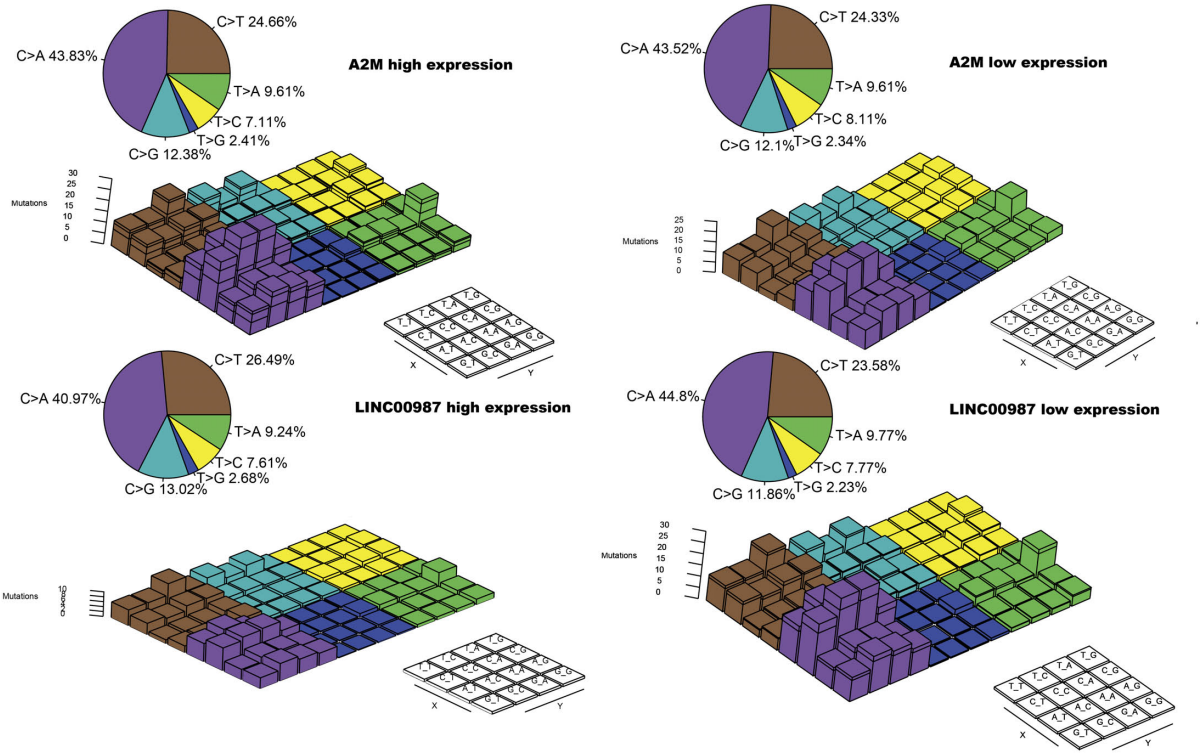

FIGURE 8 | Lego plot representation of mutation patterns in LUAD samples in relation to the LINC00987/A2M axis. Single-nucleotide substitutions are divided into six categories with 16 surrounding flanking bases. The pie chart in the upper left shows the proportion of six categories of mutation patterns.

STAD, and UCEC (**Figure 10C**), whereas the expression of A2M was correlated with MSI in BLCA, CHOL, HNSC, LGG, LUSC, SARC, STAD, THCA, and UCEC (**Figure 10D**).

Correlations Between LINC00987/A2M Axis and Immune Cell Infiltration via Pan-Cancer Analysis

Subsequently, we conducted a pan-cancer analysis to examine the association between the proportion of immune cells and their systemic content with LINC00987/A2M expression. We observed that nearly all of the tumors studied had a high degree of immune infiltration with a high stromal score, immune score, ESTIMATE score, and low tumor purity (**Figure 11A**). Furthermore, most immune cell distribution and activity in the immune microenvironment showed a similar trend (**Figure 11B**). Similar to the results analyzed in LUAD, resting mast cells and CD4 resting memory T cells were demonstrated to be up-regulated in most tumors, whereas the activation of memory M0 macrophages was inhibited.

DISCUSSION

Our results revealed the abnormal expression and mutual regulation of the LINC00987/A2M axis. We showed a correlation between the LINC00987/A2M axis expression and disease progression in LUAD. More specifically, patients with low LINC00987/A2M axis expression showed more aggressive malignancy and faster progression, as well as reduced OS and shorter RFS. Wang et al. reported that LINC00987 expression was down-regulated in COPD tissues and LPS-induced BEAS-2B cells. LINC00987 was transfected into LPS-induced 16HBE and BEAS-2B cells with a control group. LINC00987 protected 16HBE and BEAS-2B cells from LPS-induced apoptosis, oxidative stress, inflammation, and autophagy (Wang et al., 2020). In our research, LINC00987 upregulation was found to be deeply involved in immune system events. In terms of cellular components, LINC00987 upregulation involves the composition of immune receptors (IMMUNOLOGICAL_SYNAPSE, and T_CELL_RECEPTOR_COMPLEX, etc.); while regarding biological functions, LINC00987 upregulation is involved with a combination of chemokines, cytokines, immune receptors, and immunoglobulins. In terms of biological function, LINC00987 upregulation positively correlated with the proliferation and differentiation of B and T cells, as well as T cell activation. Therefore, in general, the upregulation of LINC00987 not only involves the recruitment of immune cells, antigen recognition, and presentation but also participates in the effect of immune cells on target cells (antitumor effects). Simultaneously, LINC00987 downregulation significantly affects mitochondrial translation, cell respiration, and other energy metabolism processes. The functional enrichment analysis of A2M was highly similar to that of LINC00987, as shown in **Supplementary Figure 3**. The A2M protein is known as an

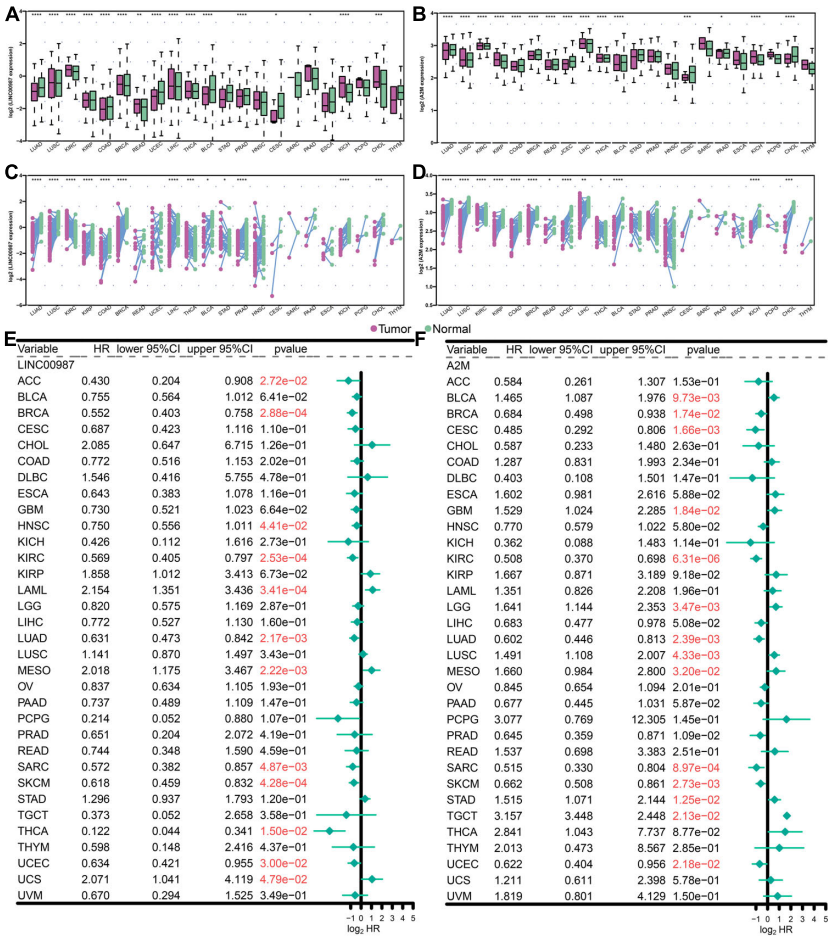

FIGURE 9 | Levels of expression and Kaplan-Meier survival analysis of LINC00987 and A2M in pan-cancer analysis. **(A,B)** Population differences in the expression of LINC00987 and A2M. **(C,D)** Pairing differences in the expression of LINC00987 and A2M. **(E,F)** Red values indicate statistical significance of the *p* value ($p < 0.05$). HR hazard ratio, 95% CI 95% confidence interval, $^{*}p < 0.05$, $^{**}p < 0.01$, $^{***}p < 0.001$, and $^{****}p < 0.0001$.

acute-phase protein of the innate immune system, acting as a protector in withstanding stress and inflammation in early age (Birkenmeier et al., 2003; Mocchegiani et al., 2007; Xue et al., 2017). α2-macroglobulin (α2M) and related proteins share the function of binding to the host or foreign peptides and particles, thereby becoming a humoral defense barrier against pathogens in vertebrate plasma and tissues (Borth, 1992). At present, the beneficial impact of a transformation-associated isoform of A2M on tumors and other diseases has been mainly discussed in terms of clearing growth factors, especially TGF-β1, which strongly promotes the malignancy of glioma (Lauer et al., 2001; Wick et al., 2001; Sinnreich et al., 2004). Lindner et al. (2010) discovered that the isoform of α2-macroglobulin A2M and its interaction with low-density lipoprotein receptor-related protein 1 (LRP1) inhibit tumor cell proliferation through the Wnt/β-catenin signaling pathway, migration, invasion, spheroid formation, and anchoring mechanisms for uncontrolled growth. Nevertheless, Alpha-2 macroglobulin (A2M) acts as a general protease inhibitor in serum and can bind various cytokines and growth factors. Taking advantage of the immunoaffinity of the A2M protein complex in human serum, more and more studies are using A2M protein complex as a new serum biomarker for cancer (Zhang et al., 2000; Kanoh et al., 2001; Burgess et al., 2008).

The high expression of LINC00987 and A2M was associated with the infiltration of numerous immune cells, high immune score signatures, and low tumor purity in multiple analyses of immune cell infiltration and scoring. For instance, CD4 resting memory T-cells and resting mast cells were shown to be increased in the high LINC00987 and A2M expression groups, whereas M0 macrophages were decreased. We found that both LINC00987 and A2M significantly affected the distribution of immune cells in the immune microenvironment of patients with LUAD. Mast cells play a key role in the infiltration of the tumor microenvironment by immune cells, during which they have been reported to release proangiogenic factors to promote angiogenesis and tumor development (Sammarco et al., 2019). Tumors lacking central memory CD4 T-cells were associated with better prognosis, consistent with our research (Wu et al., 2019). Tumor-associated macrophages (TAMs) are categorized

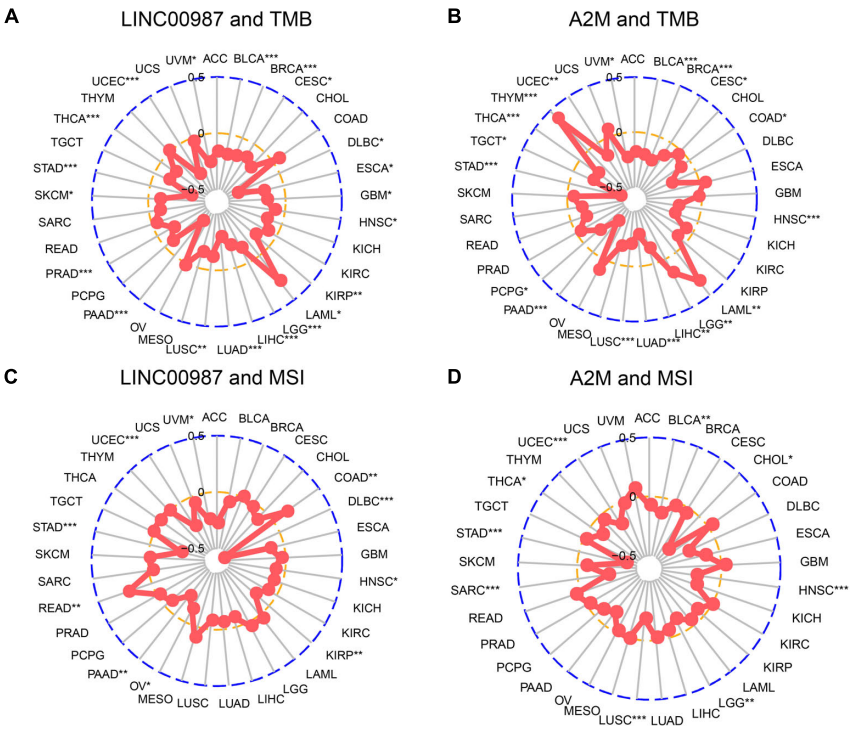

FIGURE 10 | Correlation of alterations in TMB and MSI with the level of expression of LINC00987 and A2M in various tumors. **(A,C)** Radar chart showing the correlation between LINC00987 and TMB **(A)** and MSI **(C)** in 33 cancer types. **(B,D)** Relationship between A2M and TMB **(B)** and MSI **(D)**. $^{*}p < 0.05$, $^{**}p < 0.01$, and $^{***}p < 0.001$.

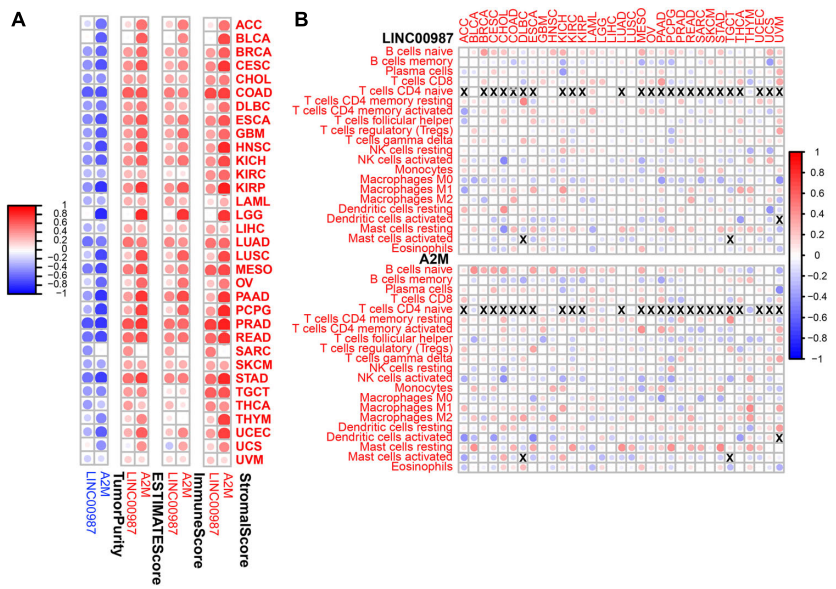

FIGURE 11 | Immune regulation according to the expression of LINC00987 and A2M in the pan-cancer analysis. **(A)** Correlation between the level of expression of LINC00987 and A2M and the immune score in multiple tumors determined by ESTIMATE. **(B)** Correlation between the expression of LINC00987/A2M and infiltration by 22 types of immune cells in pan-cancer analysis. Red indicates a correlation coefficient > 0, whereas blue indicates a correlation coefficient < 0. $p < 0.05$.

into two subtypes: M1 macrophages that are known to exhibit an antitumor effect, and M2 macrophages that have been reported to play a role in tumor promotion. Moreover, M1 and M2 macrophages can transform each other with the appropriate stimuli (Kim and Bae, 2018; Zhihua et al., 2019). Our results showed that the number of M0 macrophages decreased when

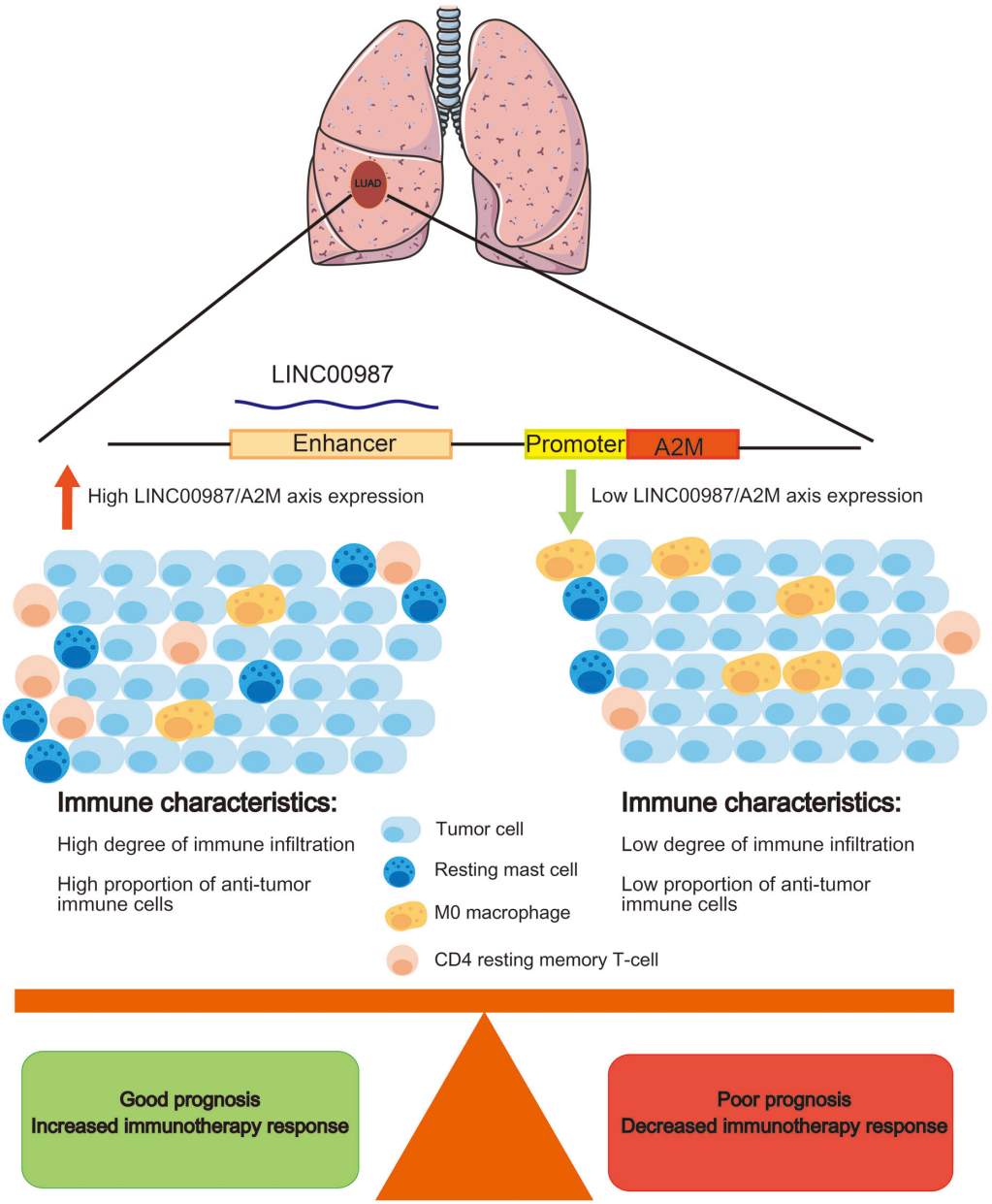

FIGURE 12 | Schematic diagram. LUAD patients with a high LINC00987/A2M axis expression have a better prognosis, with an increased proportion of antitumor immune cell infiltration. Immunotherapy may improve the prognosis of LUAD patients with a high LINC00987/A2M axis expression.

LINC00987 and A2M were highly expressed, which might have been the result of the transformation of M0 to M1 or M2 cells. According to our results, LINC00987 and A2M might inhibit tumor growth by suppressing mast cells and memory CD4 T-cells and promoting the conversion of M0 macrophages to M1 and M2 (**Figure 12**). However, the specific mechanism requires further study.

In GSEA, both LINC00987 and A2M were demonstrated to be enriched in immunoreaction, immune checkpoint, and STAT5/Kras cancer signaling pathways. This finding suggested that putatively eRNA-regulated target genes consisting of clinically actionable genes and immune checkpoints can also affect immunotherapy and drug response (Chen et al., 2016). We also found that patients with high LINC00987 and A2M expression had increased sensitivity to treatment with inhibitors of the PD1 and CTLA-4 immune checkpoints. This discovery characterized the therapeutic potential of the eRNA-mRNA axis against cancer in the clinical setting. Our GSEA analysis showed that LINC00987 might regulate the epithelial-mesenchymal transition process of tumors; however, due to the lack of relevant EMT gene sets for verification and the close relationship between epithelial-mesenchymal transition and

tumor stemness (Mani et al., 2008), we used stem gene sets for verification. We thus found that the LINC00987/A2M axis might play an important role in regulating tumor stemness and tumor hypoxia. Besides, we noted that the degree of tumor hypoxia and stemness characteristics were greatly influenced by LINC00987 and A2M. In particular, tumor cells in a hypoxic state were shown to continue to differentiate, with increases in neovascularization and abnormal activation of most TF, promoting cancer occurrence and metastasis. Moreover, it has been shown that hypoxic areas of solid tumors were infiltrated by a large number of immunosuppressive cells during hypoxia, influencing the antitumor immune response by promoting local immunosuppression (Noman et al., 2011). Therefore, we hypothesized that although LINC00987 and A2M are immune-related genes, they potentially promote an immune cell infiltration and antitumor immune response by suppressing the degree of hypoxia. Tumor cells have been reported to transmit inhibitory signals through immune checkpoints, inhibit the function of T cells, induce the apoptosis of T cells, and cause immune escape. However, the overexpression of LINC00987 and A2M might have caused resistance to paclitaxel. Our GSEA results showed that both LINC00987 and A2M had a regulatory effect on the G2M checkpoint. Paclitaxel-induced tumor cell death occurs without a prior G2/M-phase arrest, and thus LINC00987/A2M reduces the sensitivity to paclitaxel treatment by regulating the cell cycle (Dziadyk et al., 2004). This finding might help determine patients' response with LUAD to immunotherapy and their sensitivity to chemotherapy drugs (**Figure 12**).

Mutations can be the beginning of tumorigenesis, but they may also initiate self-destruction (Weinberg, 2011). We have known that tumors with increased numbers of somatic mutations, known as TMB, are characterized by the production of more neoantigens than could be recognized by T cells and have been reported to be sensitive to PD-1/PD-L1 inhibitors (Rooney et al., 2015; Yarchoan et al., 2017). The neoantigen load positively correlated to cytolytic activity among multiple tumor types, with the cytolytic immune response being beneficial to effective natural antitumor immunity (Rooney et al., 2015). Previous research has identified that in KRAS-mutant LUAD, STK11/LKB1 mutations were major drivers of resistance to PD-1 blockade (Koulidis et al., 2018). In this study, we detected somatic mutations, in which the distribution of the C > A modality was increased in the high LINC00987 expression group, and TMB was highly correlated with the LINC00987/A2M axis. It could be speculated that the generation of somatic mutations when the LINC00987/A2M axis was highly expressed was conducive to increasing the production of neoantigens and promoting the therapeutic sensitivity of immune checkpoint inhibitors, thus constituting a breakthrough in the treatment of LUAD. Microsatellites are regions of short tandem repeats of 10 to 60 base pairs, including both coding and non-coding areas (Ross et al., 2003), regularly maintained by the mismatch repair (MMR) system in normal cells (Bonneville et al., 2017). Owing to disorders in the MMR system, replication errors such as insertion or loss of base pairs might occur, resulting in MSI, which is the inability to guarantee the stable length of the microsatellite (Bonneville et al., 2017). Microsatellites influence the expression of genes and directly or indirectly regulate the genome by being located and linked to several important gene sites that are markers of human disease and etiology. Therefore, MSI has become an important feature in many diseases, especially in tumors. This has been reflected in the discovery that patients with colorectal cancer with high MSI had a better prognosis than patients with microsatellite stable (MSS) and low MSI (Benatti et al., 2005; Buckowitz et al., 2005). In addition, mutations in the CASP8 and MHC Class I cytolysis effector molecules were the most enriched mutations in MSI-high tumors, highlighting MSI-high as a contributor to promoting antigen presentation and extrinsic apoptosis and in promoting natural antitumor immunity (Rooney et al., 2015). Although LINC00987 and A2 M expression did not correlate with MSI in LUAD, other cancers have been reported to exhibit varying MSI degrees. As such, LINC00987 and A2M might be key factors in treatment strategies against these cancers. The pan-cancer validation results showed that the LINC00987/A2M axis was widely down-regulated in most cancer tissues compared with that in corresponding normal tissues, and this abnormally low expression might be a risk factor for the worse OS of patients with these cancer types, except for MESO and PAAD. In our correlation analysis, the expression of the LINC00987/A2M axis was related to immune cell infiltration in 33 tumors, with A2M, in particular, exhibiting a higher and more obvious correlation. Among the 22 immune cell types, resting mast cells and CD4 resting memory T cells were positively correlated, whereas M0 macrophages negatively correlated with the expression of LINC00987/A2M. These results were consistent with LUAD and confirmed the LINC00987/A2M axis's key role in immune regulation.

CONCLUSION

In conclusion, the LINC00987/A2M axis was down-regulated in LUAD, indicating poor survival and malignant progression. The heterogeneity in immune cell infiltration, sensitivity to checkpoint inhibitors and chemotherapy, degree of tumor hypoxia, stemness characteristics, and somatic mutations were demonstrated to differ after abnormal expression of the LINC00987/A2M axis. Validation of different methods of estimation of the immune status in four datasets indicated that the LINC00987/A2M axis could offer valuable new biomarkers for the prognosis and immunotherapy of LUAD and most human cancers.

DATA AVAILABILITY STATEMENT

The original contributions presented in the study are included in the article/**Supplementary Material**, further inquiries can be directed to the corresponding author/s.

AUTHOR CONTRIBUTIONS

JM: conceptualization, methodology, software, visualization, writing, review, and editing. XL: conceptualization, writing, review, and editing. XW: conceptualization and supervision.

QM: review and editing. TW: software and visualization. CT: conceptualization, methodology, and supervision. All authors contributed to the article and approved the submitted version.

ACKNOWLEDGMENTS

We would like to thank Editage for English language editing.

SUPPLEMENTARY MATERIAL

The Supplementary Material for this article can be found online at: https://www.frontiersin.org/articles/10.3389/fmolb.2021.644557/full#supplementary-material

Supplementary Figure 1 | Analysis of the functional characteristics of LINC00987/A2M. Correlation of the expression of **(A)** LINC00987 and **(B)** A2M with hypoxia gene sets. Correlation of the expression of **(C)** LINC00987 and **(D)** A2M with tumor stem cell characteristics. $^{*}p < 0.05$, $^{***}p < 0.01$, $^{***}p < 0.001$, and $^{****}p < 0.0001$.

Supplementary Figure 2 | Landscape of somatic mutation of LINC00987/A2M axis in TCGA. Top 20 genes in LINC00987 **(A)** high and **(B)** low expression group, A2M **(C)** high and **(D)** low expression group, respectively.

Supplementary Figure 3 | Function enrichment analysis of LINC00987/A2M axis in GSEA. Kyoto Encyclopedia of Genes and Genomes (KEGG) for high and low expression groups of **(A)** LINC00987 and **(B)** A2M; Gene Ontology (GO) term of Biological Process (BP) for high and low expression groups of **(C)** LINC00987 and **(D)** A2M; cellular component (CC) for high and low expression groups of **(E)** LINC00987 and **(F)** A2M; molecular function (MF) for high and low expression groups of **(G)** LINC00987 and **(H)** A2M.

REFERENCES

Azofeifa, J. G., Allen, M. A., Hendrix, J. R., Read, T., Rubin, J. D., and Dowell, R. D. (2018). Enhancer RNA profiling predicts transcription factor activity. *Genome Res.* 28, 334–344. doi: 10.1101/gr.225755.117

Benatti, P., Gafà, R., Barana, D., Marino, M., Scarselli, A., Pedroni, M., et al. (2005). Microsatellite instability and colorectal cancer prognosis. *Clin. Cancer Res.* 11, 8332–8340. doi: 10.1158/1078-0432.CCR-05-1030

Birkenmeier, G., Müller, R., Huse, K., Forberg, J., and Reichenbach, A. (2003). Human alpha2-macroglobulin: genotype-phenotype relation. *Exp. Neurol.* 184, 153–161. doi: 10.1016/s0014-4886(03)00110-9

Bonneville, R., Krook, M. A., Kautto, E. A., Miya, J., Wing, M. R., Chen, H. Z., et al. (2017). Landscape of microsatellite instability across 39 cancer types. *JCO Precis. Oncol.* 2017:17.00073. doi: 10.1200/PO.17.00073

Borth, W. (1992). Alpha 2-macroglobulin, a multifunctional binding protein with targeting characteristics. *FASEB J.* 6, 3345–3353. doi: 10.1096/fasebj.6.15.1281457

Brazão, T. F., Johnson, J. S., Müller, J., Heger, A., Ponting, C. P., and Tybulewicz, V. L. J. (2016). Long noncoding RNAs in B-cell development and activation. *Blood* 128, e10–e19. doi: 10.1182/blood-2015-11-680843

Buckowitz, A., Knaebel, H. P., Benner, A., Blker, H., Gebert, J., Kienle, P., et al. (2005). Microsatellite instability in colorectal cancer is associated with local lymphocyte infiltration and low frequency of distant metastases. *Br. J. Cancer* 92, 1746–1753. doi: 10.1038/sj.bjc.6602534

Buffa, F. M., Harris, A. L., West, C. M., and Miller, C. J. (2010). Large meta-analysis of multiple cancers reveals a common, compact and highly prognostic hypoxia metagene. *Br. J. Cancer* 102, 428–435. doi: 10.1038/sj.bjc.6605450

Burgess, E. F., Ham, A. J., Tabb, D. L., Billheimer, D., Roth, B. J., Chang, S. S., et al. (2008). Prostate cancer serum biomarker discovery through proteomic analysis of alpha-2 macroglobulin protein complexes. *Proteomics Clin. Appl.* 2:1223. doi: 10.1002/prca.200780073

Casey, S. C., Tong, L., Li, Y., Do, R., Walz, S., Fitzgerald, K. N., et al. (2016). MYC regulates the antitumor immune response through CD47 and PD-L1. *Science* 352, 227–231. doi: 10.1126/science.aac9935

Chen, W., Zheng, R., Baade, P. D., Zhang, S., Zeng, H., Bray, F., et al. (2016). Cancer statistics in China, 2015. *CA Cancer J. Clin.* 66, 115–132. doi: 10.3322/caac.21338

Derrien, T., Johnson, R., Bussotti, G., Tanzer, A., Djebali, S., Tilgner, H., et al. (2012). The GENCODE v7 catalog of human long noncoding RNAs: analysis of their gene structure, evolution, and expression. *Genome Res.* 22, 1775–1789. doi: 10.1101/gr.132159.111

Domingues, D., Turner, A., Silva, M. D., Marques, D. S., Mellidez, J. C., Wannesson, L., et al. (2014). Immunotherapy and lung cancer: current developments and novel targeted therapies. *Immunotherapy* 6, 1221–1235. doi: 10.2217/imt.14.82

Dziadyk, J. M., Sui, M., Zhu, X., and Fan, W. (2004). Paclitaxel-induced apoptosis may occur without a prior G2/M-phase arrest. *Anticancer Res.* 24, 27–36.

Eustace, A., Mani, N., Span, P. N., Irlam, J. J., Taylor, J., Betts, G. N. J., et al. (2013). A 26-gene hypoxia signature predicts benefit from hypoxia-modifying therapy in laryngeal cancer but not bladder cancer. *Clin. Cancer Res.* 19, 4879–4888. doi: 10.1158/1078-0432.CCR-13-0542

Heinz, S., Romanoski, C. E., Benner, C., and Glass, C. K. (2015). The selection and function of cell type-specific enhancers. *Nat. Rev. Mol. Cell Biol.* 16, 144–154. doi: 10.1038/nrm3949

Iiott, N. E., Heward, J. A., Roux, B., Tsitsiou, E., Fenwick, P. S., Lenzi, L., et al. (2014). Long non-coding RNAs and enhancer RNAs regulate the lipopolysaccharide-induced inflammatory response in human monocytes. *Nat. Commun.* 5:3979. doi: 10.1038/ncomms4979

Kanoh, Y., Ohtani, N., Ohara, T., Mashiko, T., Ohtani, S., Egawa, S., et al. (2001). Progression of prostate cancer: diagnostic and prognostic utility of prostate-specific antigen, alpha2-macroglobulin, and their complexes. *Oncol. Rep.* 8, 515–519. doi: 10.3892/or.8.3.515

Kim, E. Y., Kim, A., Kim, S. K., and Chang, Y. S. (2017). MYC expression correlates with PD-L1 expression in non-small cell lung cancer. *Lung Cancer* 110, 63–67. doi: 10.1016/j.lungcan.2017.06.006

Kim, J., and Bae, J. S. (2018). Metabolic regulation of macrophages in tumor microenvironment. *Curr. Opin. Hematol.* 25, 52–59. doi: 10.1097/MOH.0000000000000390

Kim, T.-K., Hemberg, M., Gray, J. M., Costa, A. M., Bear, D. M., Wu, J., et al. (2010). Widespread transcription at neuronal activity-regulated enhancers. *Nature* 465, 182–187. doi: 10.1038/nature09033

Koulidis, F., Goldberg, M. E., Greenawalt, D. M., Hellmann, M. D., Awad, M. M., Gainor, J. F., et al. (2018). STK11/LKB1 mutations and PD-1 inhibitor resistance in KRAS-mutant lung adenocarcinoma. *Cancer Discov.* 8, 822–835. doi: 10.1158/2159-8290

Lam, M. T. Y., Cho, H., Lesch, H. P., Gosselin, D., Heinz, S., Tanaka-Oishi, Y., et al. (2013). Rev-Erbs repress macrophage gene expression by inhibiting enhancer-directed transcription. *Nature* 498, 511–515. doi: 10.1038/nature12209

Lauer, D., Muller, R., Cott, C., Otto, A., Naumann, M., and Birkenmeier, G. (2001). Modulation of growth factor binding properties of alpha2-macroglobulin by enzyme therapy. *Cancer Chemother. Pharmacol.* 47(Suppl.), S4–S9. doi: 10.1007/s002800170002

Li, W., Hu, Y., Oh, S., Ma, Q., Merkurjev, D., Song, X., et al. (2015). Condensin I and II Complexes license full estrogen receptor α-dependent enhancer activation. *Mol. Cell* 59, 188–202. doi: 10.1016/j.molcel.2015.06.002

Li, W., Notani, D., and Rosenfeld, M. G. (2016). Enhancers as non-coding RNA transcription units: recent insights and future perspectives. *Nat. Rev. Genet.* 17, 207–223. doi: 10.1038/nrg.2016.4

Lindner, I., Hemdan, N. Y., Buchold, M., Huse, K., Bigl, M., Oerlecke, I., et al. (2010). Alpha2-macroglobulin inhibits the malignant properties of astrocytoma cells by impeding beta-catenin signaling. *Cancer Res.* 70, 277–287. doi: 10.1158/0008-5472.CAN-09-1462

Liu, J., Chen, Z., Zhao, P., and Li, W. (2020). Prognostic and immune regulating roles of YIF1B in Pan-Cancer: a potential target for both survival and therapy response evaluation. *Biosci. Rep.* 40:BSR20201384. doi: 10.1042/BSR20201384

Liu, J.-N., Kong, X.-S., Huang, T., Wang, R., Li, W., and Chen, Q.-F. (2020). Clinical implications of aberrant PD-1 and CTLA4 expression for cancer immunity and

prognosis: a pan-cancer study. *Front. Immunol.* 11:2048. doi: 10.3389/fimmu.2020.02048

Lu, X., Jiang, L., Zhang, L., Zhu, Y., Hu, W., Wang, J., et al. (2019). Immune signature-based subtypes of cervical squamous cell carcinoma tightly associated with human papillomavirus type 16 expression, molecular features, and clinical outcome. *Neoplasia* 21, 591–601. doi: 10.1016/j.neo.2019.04.003

Mani, S. A., Guo, W., Liao, M. J., Eaton, E. N., Ayyanan, A., Zhou, A. Y., et al. (2008). The epithelial-mesenchymal transition generates cells with properties of stem cells. *Cell* 133, 704–715. doi: 10.1016/j.cell.2008.03.027

Melo, C. A., Drost, J., Wijchers, P. J., van de Werken, H., de Wit, E., Oude Vrielink, J. A. F., et al. (2013). eRNAs are required for p53-dependent enhancer activity and gene transcription. *Mol. Cell* 49, 524–535. doi: 10.1016/j.molcel.2012.11.021

Meza, R., Meernik, C., Jeon, J., and Cote, M. L. (2015). Lung cancer incidence trends by gender, race and histology in the United States, 1973-2010. *PloS One* 10:e0121323. doi: 10.1371/journal.pone.0121323

Mocchegiani, E., Malavolta, M., and Mecocci, P. (2007). Zinc dyshomeostasis, ageing and neurodegeneration: implications of A2M and inflammatory gene polymorphisms. *J. Alzheimers Dis.* 12, 101–109. doi: 10.3233/jad-2007-12110

Mousavi, K., Zare, H., Dell'orso, S., Grontved, L., Gutierrez-Cruz, G., Derfoul, A., et al. (2013). eRNAs promote transcription by establishing chromatin accessibility at defined genomic loci. *Mol. Cell* 51, 606–617. doi: 10.1016/j.molcel.2013.07.022

Murakawa, Y., Yoshihara, M., Kawaji, H., Nishikawa, M., Zayed, H., Suzuki, H., et al. (2016). Enhanced identification of transcriptional enhancers provides mechanistic insights into diseases. *Trends Genet.* 32, 76–88. doi: 10.1016/j.tig.2015.11.004

Narayanan, S., Kawaguchi, T., Peng, X., Qi, Q., and Takabe, K. (2019). Tumor infiltrating lymphocytes and macrophages improve survival in microsatellite unstable colorectal cancer. *Sci. Rep.* 9:13455.

Newman, A. M., Liu, C. L., Green, M. R., Gentles, A. J., Feng, W., Xu, Y., et al. (2015). Robust enumeration of cell subsets from tissue expression profiles. *Nat. Methods* 12, 453–457. doi: 10.1038/nmeth.3337

Noman, M. Z., Messai, Y., Carré, T., Akalay, I., and Chouaib, S. (2011). Microenvironmental hypoxia orchestrating the cell stroma cross talk, tumor progression and antitumor response. *Crit. Rev. Immunol.* 31, 357–377. doi: 10.1615/critrevimmunol.v31.i5.10

Pennacchio, L. A., Bickmore, W., Dean, A., Nobrega, M. A., and Bejerano, G. (2013). Enhancers: five essential questions. *Nat. Rev. Genet.* 14, 288–295. doi: 10.1038/nrg3458

Ragnum, H. B., Vlatkovic, L., Lie, A. K., Axcrona, K., Julin, C. H., Frikstad, K. M., et al. (2015). The tumour hypoxia marker pimonidazole reflects a transcriptional programme associated with aggressive prostate cancer. *Br. J. Cancer* 112, 382–390. doi: 10.1038/bjc.2014.604

Rooney, M. S., Shukla, S. A., Wu, C. J., Getz, G., and Hacohen, N. (2015). Molecular and genetic properties of tumors associated with local immune cytolytic activity. *Cell* 160, 48–61.

Ross, C. L., Dyer, K. A., Tamar, E., Miller, S. J., John, J., and Markow, T. A. (2003). Rapid divergence of microsatellite abundance among species of Drosophila. *Mol. Biol. Evol.* 20, 1143–1157. doi: 10.1016/j.cell.2014.12.033

Ryu, R., and Ward, K. E. (2018). Atezolizumab for the first-line treatment of Non-small Cell Lung Cancer (NSCLC): current status and future prospects. *Front. Oncol.* 8:277. doi: 10.3389/fonc.2018.00277

Sammarco, G., Varricchi, G., Ferraro, V., Ammendola, M., Fazio, M. D., Altomare, D. F., et al. (2019). Mast cells, angiogenesis and lymphangiogenesis in human gastric cancer. *Int. J. Mol. Sci.* 20:2106. doi: 10.3390/ijms20092106

Sinnreich, O., Kratzsch, J., Reichenbach, A., Glaser, C., Huse, K., and Birkenmeier, G. (2004). Plasma levels of transforming growth factor-1beta and alpha2-macroglobulin before and after radical prostatectomy: association to clinicopathological parameters. *Prostate* 61, 201–208. doi: 10.1002/pros.20062

Sorensen, B. S., Toustrup, K., Horsman, M. R., Overgaard, J., and Alsner, J. (2010). Identifying pH independent hypoxia induced genes in human squamous cell carcinomas in vitro. *Acta Oncol.* 49, 895–905. doi: 10.3109/02841861003614343

Tang, C., Ma, J., Liu, X., and Liu, Z. (2020a). Development and validation of a novel stem cell subtype for bladder cancer based on stem genomic profiling. *Stem Cell Res. Ther.* 11:457. doi: 10.1186/s13287-020-01973-4

Tang, C., Ma, J., Liu, X., and Liu, Z. (2020b). Identification of four immune subtypes in bladder cancer based on immune gene sets. *Front. Oncol.* 10:544610. doi: 10.3389/fonc.2020.544610

Torre, L. A., Siegel, R. L., and Jemal, A. (2016). Lung cancer statistics. *Adv. Exp. Med. Biol.* 893, 1–19. doi: 10.1007/978-3-319-24223-1_1

Travis, W. D., Brambilla, E., and Riely, G. J. (2013). New pathologic classification of lung cancer: relevance for clinical practice and clinical trials. *J. Clin. Oncol.* 31, 992–1001. doi: 10.1200/JCO.2012.46.9270

van Meerbeeck, J. P., Fennell, D. A., and De Ruysscher, D. K. M. (2011). Small-cell lung cancer. *Lancet* 378, 1741–1755. doi: 10.1016/S0140-6736(11)60165-7

Vucicevic, D., Corradin, O., Ntini, E., Scacheri, P. C., and Orom, U. A. (2015). Long ncRNA expression associates with tissue-specific enhancers. *Cell Cycle* 14, 253–260. doi: 10.4161/15384101.2014.977641

Wang, Y., Chen, J., Chen, W., Liu, L., Dong, M., Ji, J., et al. (2020). LINC00987 ameliorates COPD by regulating LPS-induced cell apoptosis, oxidative stress, inflammation and autophagy through let-7b-5p/SIRT1 Axis. *Int. J. Chron. Obstruct. Pulmon. Dis.* 15, 3213–3225. doi: 10.2147/COPD.S276429

Weinberg, H. R. A. (2011). Hallmarks of cancer: the next generation. *Cell* 144, 646–674. doi: 10.1016/j.cell.2011.02.013

Wick, W., Platten, M., and Weller, M. (2001). Glioma cell invasion: regulation of metalloproteinase activity by TGF-beta. *J. Neurooncol.* 53, 177–185. doi: 10.1023/a:1012209518843

Winter, S. C., Buffa, F. M., Silva, P., Miller, C., Valentine, H. R., Turley, H., et al. (2007). Relation of a hypoxia metagene derived from head and neck cancer to prognosis of multiple cancers. *Cancer Res.* 67, 3441–3449. doi: 10.1158/0008-5472.CAN-06-3322

Wu, M., and Shen, J. (2019). From super-enhancer non-coding RNA to immune checkpoint: frameworks to functions. *Front. Oncol.* 9:1307. doi: 10.3389/fonc.2019.01307

Wu, S., Yang, W., Zhang, H., Ren, Y., Fang, Z., Yuan, C., et al. (2019). The prognostic landscape of tumor-infiltrating immune cells and immune checkpoints in glioblastoma. *Technol. Cancer Res. Treat* 18:1533033819869949. doi: 10.1177/1533033819869949

Xue, Z., Wang, L., Liu, Z., Wang, W., Liu, C., Song, X., et al. (2017). The fragmentation mechanism and immune-protective effect of CfTEP in the scallop Chlamys farreri. *Dev. Comp. Immunol.* 76, 220–228. doi: 10.1016/j.dci.2017.06.005

Yarchoan, M., Iii, B. A. J., Lutz, E. R., Laheru, D. A., and Jaffee, E. M. (2017). Targeting neoantigens to augment antitumour immunity. *Nat. Rev. Cancer* 17:569. doi: 10.1016/s0006-2952(99)00006-4

Yoshihara, K., Shahmoradgoli, M., Martinez, E., Vegesna, R., Kim, H., Torres-Garcia, W., et al. (2013). Inferring tumour purity and stromal and immune cell admixture from expression data. *Nat. Commun.* 4:2612. doi: 10.1038/ncomms3612

Zhang, W. M., Finne, P., Leinonen, J., Salo, J., and Stenman, U. H. (2000). Determination of prostate-specific antigen complexed to alpha(2)-macroglobulin in serum increases the specificity of free to total PSA for prostate cancer. *Urology* 56, 267–272. doi: 10.1016/s0090-4295(00)00609-9

Zhang, Z., Lee, J.-H., Ruan, H., Ye, Y., Krakowiak, J., Hu, Q., et al. (2019). Transcriptional landscape and clinical utility of enhancer RNAs for eRNA-targeted therapy in cancer. *Nat. Commun.* 10:4562. doi: 10.1038/s41467-019-12543-5

Zhihua, Y., Yulin, T., Yibo, W., Wei, D., Yin, C., Jiahao, X., et al. (2019). Hypoxia decreases macrophage glycolysis and M1 percentage by targeting microRNA-30c and mTOR in human gastric cancer. *Cancer Sci.* 110, 2368–2377. doi: 10.1111/cas.14110

Conflict of Interest: The authors declare that the research was conducted in the absence of any commercial or financial relationships that could be construed as a potential conflict of interest.

frontiers in Molecular Biosciences

ORIGINAL RESEARCH
published: 29 April 2021
doi: 10.3389/fmolb.2021.649363

Weighted Gene Co-expression Network Analysis Identifies CALD1 as a Biomarker Related to M2 Macrophages Infiltration in Stage III and IV Mismatch Repair-Proficient Colorectal Carcinoma

*Hang Zheng, Yuge Bai, Jingui Wang, Shanwen Chen, Junling Zhang, Jing Zhu, Yucun Liu and Xin Wang**

Department of General Surgery, Peking University First Hospital, Beijing, China

OPEN ACCESS

Edited by:
Na Luo,
Nankai University, China

Reviewed by:
Shalini Dimri,
The Ruth and Bruce Rappaport Faculty of Medicine, Technion Israel Institute of Technology, Israel
Pedro José Carlos Rondot Radío, University of Buenos Aires, Argentina

***Correspondence:**
Xin Wang
wangxin_guo@126.com

Specialty section:
This article was submitted to Molecular Diagnostics and Therapeutics, a section of the journal Frontiers in Molecular Biosciences

Received: *04 January 2021*
Accepted: *23 February 2021*
Published: *29 April 2021*

Citation:
Zheng H, Bai Y, Wang J, Chen S, Zhang J, Zhu J, Liu Y and Wang X (2021) Weighted Gene Co-expression Network Analysis Identifies CALD1 as a Biomarker Related to M2 Macrophages Infiltration in Stage III and IV Mismatch Repair-Proficient Colorectal Carcinoma. Front. Mol. Biosci. 8:649363. doi: 10.3389/fmolb.2021.649363

Immunotherapy has achieved efficacy for advanced colorectal cancer (CRC) patients with a mismatch-repair-deficient (dMMR) subtype. However, little immunotherapy efficacy was observed in patients with the mismatch repair-proficient (pMMR) subtype, and hence, identifying new immune therapeutic targets is imperative for those patients. In this study, transcriptome data of stage III/IV CRC patients were retrieved from the Gene Expression Omnibus database. The CIBERSORT algorithm was used to quantify immune cellular compositions, and the results revealed that M2 macrophage fractions were higher in pMMR patients as compared with those with the dMMR subtype; moreover, pMMR patients with higher M2 macrophage fractions experienced shorter overall survival (OS). Subsequently, weighted gene co-expression network analysis and protein–protein interaction network analysis identified six hub genes related to M2 macrophage infiltrations in pMMR CRC patients: *CALD1*, *COL6A1*, *COL1A2*, *TIMP3*, *DCN*, and *SPARC*. Univariate and multivariate Cox regression analyses then determined *CALD1* as the independent prognostic biomarker for OS. *CALD1* was upregulated specifically the in CMS4 CRC subtype, and single-sample Gene Set Enrichment Analysis (ssGSEA) revealed that *CALD1* was significantly correlated with angiogenesis and TGF-β signaling gene sets enrichment scores in stage III/IV pMMR CRC samples. The Estimation of STromal and Immune cells in MAlignant Tumor tissues using Expression data (ESTIMATE) algorithm and correlation analysis revealed that *CALD1* was significantly associated with multiple immune and stromal components in a tumor microenvironment. In addition, GSEA demonstrated that high expression of *CALD1* was significantly correlated with antigen processing and presentation, chemokine signaling, leukocyte transendothelial migration, vascular smooth muscle contraction, cytokine–cytokine

receptor interaction, cell adhesion molecules, focal adhesion, MAPK, and TGF-beta signaling pathways. Furthermore, the proliferation, invasion, and migration abilities of cancer cells were suppressed after reducing *CALD1* expression in CRC cell lines. Taken together, multiple bioinformatics analyses and cell-level assays demonstrated that *CALD1* could serve as a prognostic biomarker and a prospective therapeutic target for stage III/IV pMMR CRCs.

Keywords: colorectal cancer, microsatellite instability, M2 macrophages, tumor microenvironment, bioinformatics, prognosis

INTRODUCTION

Colorectal cancer (CRC) is expected to rank as the third leading incidence of new malignancy and the second for cancer-specific mortality (Bray et al., 2018). While CRC is relatively curable if detected and treated early, approximately 58% of CRCs are diagnosed at progressive and metastatic stages, which pose a grave threat to human health (Siegel et al., 2017). In the past decade, immunotherapy in first-line has achieved robust disease control and durable response for patients with advanced or metastatic mismatch repair-deficient (dMMR) CRCs (Couzin-Frankel, 2013; Diaz et al., 2017; Le et al., 2017; Overman et al., 2017; Morse et al., 2019); this is because dMMR cancers harbor higher numbers of somatic mutations, which result in the increasing generation of aberrant neopeptides, thus facilitating antitumor cytotoxic cell recruitments and immunotherapy responses (Dolcetti et al., 1999; Smyrk et al., 2001; Prall et al., 2004). However, little immunotherapy efficacy was observed in patients with the mismatch repair-proficient (pMMR) subtype (Le et al., 2015), who constitute a substantial proportion (approximately 80 to 85%) of CRCs (Boland et al., 1998; Peltomäki, 2003) and exhibit more unfavorable prognostic outcomes than those with the dMMR subtype (Gryfe et al., 2000; Popat et al., 2005; Malesci et al., 2007). Low mutational burden and lack of capability to recruit antitumor immune cells have been considered as the essential obstacles for pMMR tumors to benefit from immunotherapy (Ganesh et al., 2019). Therefore, alternative immune modulation approaches are eagerly awaited for the majority of CRC patients with the pMMR subtype.

Interactions in the tumor microenvironment (TME) between cancer cells and their surroundings are intricate (Hanahan and Coussens Lisa, 2012). Tumor-associated macrophages (TAMs) are the most abundant immune cells in the TME (up to 50%) and are generally categorized into M1 and M2 subtypes (Najafi et al., 2019). M1 plays a tumoricidal effect through secreting pro-inflammatory cytokines like CXCL9 and CXCL10 and initiating inflammatory response to enhance adaptive immune response at the preliminary oncogenesis stage, while the M2 subtype often releases anti-inflammatory cytokines and contributes to angiogenesis, tumor progression, and immunosuppression at the advanced tumor stage (Tan et al., 2018; Ubil et al., 2018; Xiang et al., 2018). Although fractions of M1 macrophages were higher in dMMR CRCs (Narayanan et al., 2019), no significant difference in M2 macrophages infiltration density was found between the pMMR and dMMR subgroups (Bernal et al., 2011; Zhao Y. et al., 2019). Collectively, these data raise constructive guidance regarding the identification of biomarkers related to M2 macrophage infiltrations to weaken the tumorigenic immunoediting activity in pMMR CRC patients.

Nowadays, widespread analysis of high-throughput technologies via advanced computational techniques facilitates the identification of disease-related biomarkers (Fernandes et al., 2020). Weighted gene co-expression network analysis (WGCNA) is a well-documented systematic bioinformatics tool to extract co-related gene modules and then identify hub genes that correlated with clinical traits of interest (Horvath and Dong, 2008; Kakati et al., 2019), and has been widely applied for potential therapeutic target detections in various cancers (Zeng et al., 2020; Zhang et al., 2020; Zhu and Hou, 2020). In this study, based on RNA-seq data acquired from public database, M2 macrophage fractions in stage III/IV pMMR CRC patients were calculated by the CIBERSORT algorithm, and WGCNA was then performed to identify the associated hub genes. By applying Cox regression analyses, CALD1 was identified as an independent prognostic biomarker. We further validated CALD1 for its roles in TME components and tumor progression at both the gene expression and cellular level. We propose CALD1 as a potential target for pMMR CRC for further study.

MATERIALS AND METHODS

Data Pre-processing

The RNA-Seq and corresponding clinical data were acquired from the Gene Expression Omnibus (GEO)[1] database, including GSE39582 (Marisa et al., 2013) and GSE41258 (Sheffer et al., 2009). GSE39582 was based on the GPL570 platform (Affymetrix Human Genome U133 Plus 2.0 Array), and 200 pMMR stage III/IV CRC samples were utilized as the training group for M2 macrophages-correlated genes selection. The GSE41258 dataset, which was based on GPL96 (Affymetrix Human Genome U133A Array) and contained 82 stage III/IV pMMR CRC samples, was used for external validation. The raw CEL microarray data were downloaded and preprocessed using the RMA method by the "affy" R package (Gautier et al., 2004). If more probes mapped one gene symbol, the maximum value was chosen. The function

[1]http://www.ncbinlm.nih.gov/geo/

normalizeBetweenArrays of the "limma" R package was used to achieve consistency between arrays (Ritchie et al., 2015).

Tumor-Infiltrating Immune Cell (TIIC) Assessment

The CIBERSORT algorithm could accurately quantify the relative infiltration fractions of 22 kinds of immune cells from normalized gene expression profiles by implementing the support vector regression (SVR) machine learning method (Scholkopf et al., 2000; Newman et al., 2015). The TIIC fractions in GSE39582 samples were calculated by "CIBERSORT" R script with the leukocyte gene signature matrix LM22; the significant CIBERSORT *P*-value was set as less than 0.05. The distribution differences of TIICs between dMMR and pMMR tumors were compared by Wilcoxon test, and the associations between M2 macrophage infiltrations and survival status in pMMR patients were investigated.

Co-expression Network Construction

Stage III/IV pMMR CRC samples with CIBERSORT $p < 0.05$ were screened for WGCNA analysis through the "WGCNA" R package (Langfelder and Horvath, 2008). Generally, the co-expression similarity s_{ij} was computed as the absolute value of Pearson's correlation between nodes i and j:

$$s_{ij} = |\mathrm{cor}(x_i, x_j)|$$

Following this, a weighted adjacency matrix could be calculated by raising s_{ij} to a soft thresholding power β, which could intensify strong correlations and reduce weak correlations:

$$a_{ij} = s_{ij}^{\beta}$$

Next, the adjacency matrix was transformed to a topological overlap matrix (TOM), and highly interconnected genes were clustered into different modules by calculating TOM dissimilarity (1-TOM) with a minimum cluster size of 30 (Yip and Horvath, 2007). Significant module and trait with the highest coefficient was identified for the following analysis. Module eigengene (ME) was defined as the first principal component of the specific module that could represent the module genes. Module membership (MM) was used to determine the correlation between ME and each module, and gene significance (GS) was the Pearson's correlation between each gene expression and the representative trait. Genes with high intramodular connectivity were regarded as hub genes; the parameters of candidate hub genes were set as MM > 0.8 and GS > 0.2 (Horvath and Dong, 2008).

Functional and Pathway Enrichment Analysis

Gene Ontology (GO) and Kyoto Encyclopedia of Genes and Genomes (KEGG) pathway enrichment analyses of candidate hub genes were conducted via the "clusterProfiler" R package; an adjusted *p*-value of less than 0.05 was regarded as statistically significant (Yu et al., 2012).

Protein–Protein Interaction (PPI) Network Integration and Analysis

The PPI network was built by the online STRING database[2] (Szklarczyk et al., 2019) and mapped in the Cytoscape software (version 3.7.2)[3] (Shannon et al., 2003). Hub genes were ranked by six methods provided from the cytoHubba plugin (Chin et al., 2014). Then we calculated and visualized Spearman's correlations between hub gene expressions and M2 macrophage fractions.

Prognostic Hub Gene Identification and Validation

The prognostic values of the hub genes were assessed by log-rank test on the total of 200 stage III/IV pMMR CRC patients of the GSE39582 dataset. Hub genes as well as clinicopathological factors such as sex, chemotherapy, and the TNM stage were subjected to univariate and multivariate Cox regression analyses to explore independent prognostic factors.

Tumor Microenvironment Analysis

Firstly, we conducted Spearman correlation analysis for CALD1 expression with 22 types of TIICs based on CIBERSORT results. Then, the consensus molecular subtype (CMS) categorizations of CRC patients were performed via the "CMSCaller" R package (Eide et al., 2017), and the differences in the CALD1 expression between CMS subgroups were analyzed using the Kruskal–Wallis test followed by Dunn *post hoc* tests for multiple comparisons via the "FSA" R package. Next, the Estimation of STromal and Immune cells in MAlignant Tumor tissues using Expression data (ESTIMATE) algorithm was applied via the "estimate" R package to presume the immune and stromal cellular heterogeneity in the TME (Yoshihara et al., 2013). In addition, based on "HALLMARK_ANGIOGENESIS" and "HALLMARK_TGF_BETA_SIGNALING" gene sets extracted from the Molecular Signature Database (MSigDB)[4], the single sample gene set enrichment analysis (ssGSEA) algorithm was employed via the "GSVA" R package to quantify each sample's enrichment score, which represents the cumulative enrichment degree of the genes in the assigned gene set in the individual sample (Hänzelmann et al., 2013). Finally, correlations of *CALD1* expression with ssGSEA enrichment scores, immune and stromal scores, as well as immune cell markers were analyzed and visualized via the "ggcorrplot" R package.

Gene Set Enrichment Analysis (GSEA) of Diverse Pathway Enrichments

Two hundred cases of GSE39582 were separated into CALD1-high and CALD1-low expression groups according to the median *CALD1* expression value. GSEA (Subramanian et al., 2005) was then performed to explore different enriched KEGG pathways between two groups via the "clusterProfiler" R package (Yu et al., 2012), and gene sets with an adjusted $P < 0.05$ was considered as significantly enriched.

[2]https://string-db.org/

[3]http://www.cytoscape.org/

[4]https://www.gsea-msigdb.org

Cell Culture and Transfection

Human pMMR CRC cell lines SW480, SW620, and Caco-2 and dMMR cell line HCT116 (Berg et al., 2017) were obtained from the Cancer Institute of the Chinese Academy of Medical Sciences. SW480, SW620, and Caco-2 cells were cultured in Dulbecco's modified Eagle's medium (DMEM, Biological Industries, Israel), and HCT116 was cultured in McCoy's 5A Medium (Biological Industries, Israel) supplemented with 10% fetal bovine serum (FBS, Biological Industries, Israel) and 1% penicillin–streptomycin (Biological Industries, Israel) at 5% CO_2 and 37°C.

Western Blotting (WB)

Total protein lysates of cells were extracted with a RIPA lysis buffer supplemented with 1 mM phenylmethylsulfonyl fluoride (PMSF) and 1 mM protease inhibitor cocktail (Beyotime, Shanghai, China). A BCA assay kit (Beyotime, Shanghai, China) was utilized to measure total protein concentration, and 30 μg of denatured proteins was subjected to 10% SDS-PAGE and electroblotted onto PVDF membranes (Millipore, Burlington, MA, United States). After that, the membranes were blocked with 5% milk in TBST for 1 h at room temperature and then incubated with primary antibodies containing rabbit monoclonal anti-Caldesmon (1:1000, Abcam, Cambridge, MA, United States) and GAPDH (1:1000, Cell Signaling Technology, Danvers, MA, United States) overnight at 4 °C. Finally, the membranes were incubated with corresponding secondary antibodies (1:8000, ZSGB-BIO, Beijing, China) for 1 h at room temperature and then treated with a chemiluminescent HRP substrate (Millipore, Burlington, MA, United States) and exposed to the Bio-Rad imaging system.

siRNA Transfection

Transient knockdown of *CALD1* in SW480 and SW620 cells was achieved by siRNA transfection. The siRNA sequences for *CALD1* (sense 5′–3′, GGAGGAGAUGCGACUCGAATT) and normal control (NC, sense 5′–3′, UUCUCCGAACGUGUCACGUTT) were synthesized by GenePharma (Jiangsu, China). Cells with confluences of 70–80% were transfected with 100 nM *CALD1* or NC siRNA using GP-siRNA-Mate (GenePharma, Jiangsu, China). After transfection for 48 h, cells were harvested and *CALD1* knockdown was confirmed by WB.

Cell Migration and Invasion Assay

The metastasis abilities of SW480 and SW620 cells were routinely measured in Transwell chambers (8-μm pore size, Corning, NY, United States). The cells (100,000 cells) were inoculated in a serum-free DMEM on the top chamber, while the bottom chamber contained a 600 μl complete medium. After incubation for an appropriate time, cells on the bottom of the membrane were fixed and stained with 0.1% crystal violet solution. For cell invasion assay, the upper compartment of the chamber was precoated with matrix gel.

Cell Proliferation Assay

After transfection for 24h, cells were plated into 96-well plates (2,000 cells/well). At the appointed time points (6, 24, 48, and 72 h), the cells were incubated with a 10 μL cell counting kit 8 (CCK8) solution (Bimake, Houston, TX, United States) for additional 2 h. Then, cell viability was determined by recording a 450 nm absorbance value, and comparisons between normal cancer cells, si-NC, and si-CALD1 transfected cells were conducted by Kruskal–Wallis one-way analysis of variance (ANOVA).

Statistical Analyses

All statistical analyses were performed via R software 3.6.3. Cox regression analysis and Kaplan–Meier log-rank test was performed for survival analysis, and the optimal cut-off value was produced by the "surv_cutpoint" function of the "survminer" R package. All experiments were repeated at least three times, and a *P*-value of <0.05 was deemed statistically significant.

RESULTS

TIIC Landscape in Stage III/IV pMMR and dMMR CRC Patients

The schematic diagram of this research is manifested in **Figure 1**. Firstly, CIBERSORT identified 85 pMMR and 20 dMMR significant samples (CIBERSORT *P*-value < 0.05), M2 macrophage fractions were higher in pMMR patients (**Figure 2A**), and pMMR patients with higher M2 macrophage fractions experienced shorter overall survival (OS) (**Figure 2B**). Subsequently, the M2 macrophage fractions in 85 stage III/IV pMMR CRC patients were chosen as clinical traits for WGCNA construction.

Co-expression Network Construction and M2 Macrophage Related Gene Identification

The top 5,000 genes with the highest median absolute deviation (MAD) expression values were incorporated for co-expression network construction. To ensure a scale-free network, a soft thresholding power β of 6 was chosen to plant a hierarchical clustering tree (**Figure 2C**), and 13 gene modules were identified by average linkage clustering (**Figure 2D**). Then, we calculated the correlations between MEs and M2 macrophage infiltration levels and noticed that the red module exhibited the highest correlation (cor = 0.28, $P = 0.009$) (**Figure 2E**). Next, we found that the GS for M2 macrophage infiltrations was significantly and positively correlated with MM in the red module (cor = 0.5, $P = 2.6e\text{-}95$, **Figure 2F**). Therefore, the red module was chosen for subsequent analysis.

GO and KEGG Enrichment Analysis

Taking GS > 0.2 and MM > 0.8 as the hub gene thresholds, 144 genes in the red module were screened for GO and KEGG analyses. In the GO analysis, extracellular matrix organization

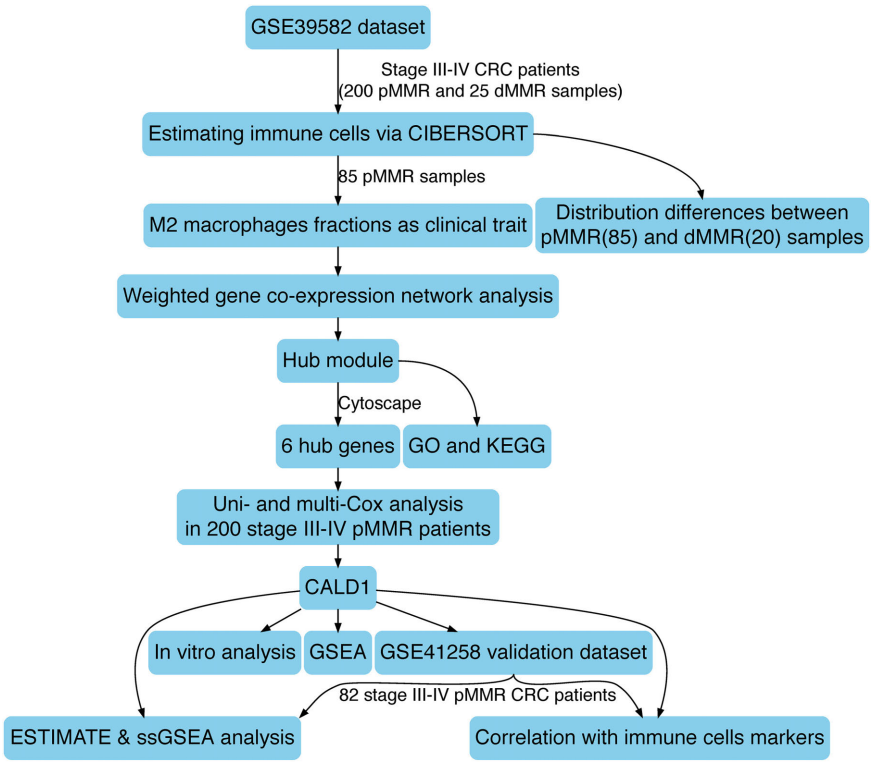

FIGURE 1 | The schematic diagram of this study.

(P = 2.60e-13) and extracellular structure organization (P = 2.82e-12) were the main enriched biological processes, collagen-containing extracellular matrix (P = 2.75e-18) was the major enriched cellular component, and extracellular matrix structural constituent (P = 1.01e-12) was the principal enriched molecular function term (**Figure 3A**). Focal adhesion (P = 0.0015), protein digestion and absorption (P = 0.0061), ECM–receptor interaction (P = 0.019), and tight junction (P = 0.0441) were the significantly enriched KEGG pathways (**Figure 3B**).

PPI Network Construction and Analysis

Based on the STRING database, a PPI network was built with the minimum interaction score (median confidence) of 0.4 and was then visualized in the Cytoscape software (**Figure 3C**). By overlapping the top 15 genes ranked by six methods in cytoHubba, six hub genes were identified for subsequent analysis (**Table 1**), and Spearman's correlation analyses revealed that *TIMP3* and *CALD1* expressions were the top two markers positively associated with M2 macrophage fractions (cor = 0.35 and 0.33, respectively) (**Figures 4A–F**).

Identification of *CALD1* as an Independent Prognostic Biomarker in Stage III/IV pMMR CRC

Two hundred CRC patients in the GSE39582 cohort were categorized into high/low-expression groups according to the median expression values of each hub gene, then the correlations between the six hub gene expressions and OS were assessed by log-rank test; the results revealed that higher expressions of *CALD1* and *COL1A2* were associated with poorer OS (log-rank P = 0.012 and 0.044, respectively) (**Figure 5**). Subsequently, univariate and multivariate Cox regression analyses were implemented to evaluate the association between hub gene expressions as well as clinicopathological variables and prognosis. As shown in **Table 2**, age, chemotherapy, tumor stage, *COL1A2*, and *CALD1* were significantly associated with worse prognosis (P < 0.05). In multivariate Cox analysis, *CALD1* (HR = 1.868, 95% CI: 1.165–2.995, P = 0.009), chemotherapy (HR = 1.869, 95% CI: 1.124–3.109, P = 0.016), and tumor stage (HR = 2.658, 95% CI: 1.414–4.996, P = 0.002) remained to be significantly correlated with OS. Furthermore, similar analyses were performed in the GSE41258 validation dataset, and multivariate Cox analysis identified that both *CALD1* (HR = 1.859, 95% CI: 1.095–3.158, P = 0.022) and tumor stage (HR = 4.951, 95% CI: 2.755–8.929, P < 0.001) were independent prognostic predictors (**Supplementary Figure 1** and **Supplementary Table 1**).

CALD1 Was Correlated With Diverse Tumor Immune Cell Subtypes

After identifying the prognostic value of *CALD1* in stage III/IV pMMR CRC patients, we examined the correlations between *CALD1* and TIICs as well as the biomarkers of various immune cells. **Figure 6A** revealed that *CALD1* was significantly

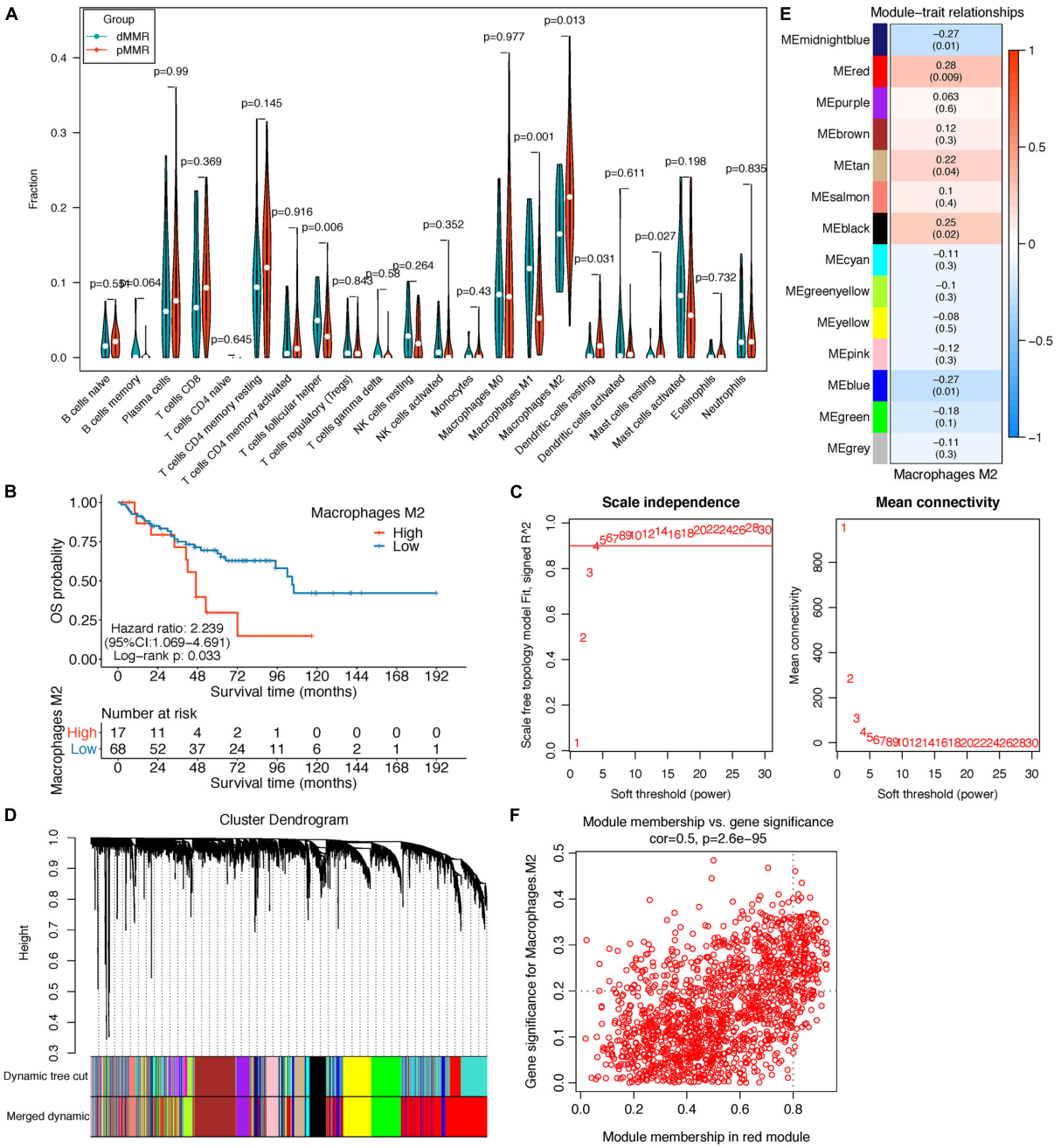

FIGURE 2 | (A) Violin plot displayed the CIBERSORT TIIC fraction difference between pMMR (85) and dMMR (20) stage III/IV CRC samples; only samples with a CIBERSORT *P*-value < 0.05 were screened for this analysis. **(B)** Survival curve of the high- and low-M2 macrophage groups in stage III/IV pMMR CRC patients. **(C–F)** Co-expression network analysis by WGCNA. **(C)** Analysis of network topology for optimal soft-threshold power. **(D)** Dendrogram of genes clustered with dissimilarity based on topological overlap; each color below represented an expression module of highly interconnected groups of genes in the constructed gene co-expression network. Gray indicated that genes were not incorporated into any module. **(E)** Heatmap of the correlation between each module's module eigengene and M2 macrophage fractions; each cell contains the Pearson's correlation coefficient and the corresponding *P*-value. The red module was the most significant module with the strongest correlation. **(F)** Scatterplot of gene significance (GS) for M2 macrophage fractions vs. module membership (MM) in the red modules. TIICs, tumor-infiltrating immune cells; pMMR, mismatch-repair-proficient; dMMR, mismatch-repair-deficient; CRC, colorectal cancer; WGCNA, weighted gene co-expression network analysis.

and positively correlated with fractions of M2 macrophages (cor = 0.33, P = 0.001) and M0 macrophages (cor = 0.35, P = 0.010), whereas it was negatively correlated with fractions of plasma cells (cor = −0.2, P = 0.021), CD8 T cells (cor = −0.25, P = 0.003), T cell CD4 memory activated (cor = −0.27, P = 0.042), NK cells resting (cor = −0.2, P = 0.018), and dendritic cells

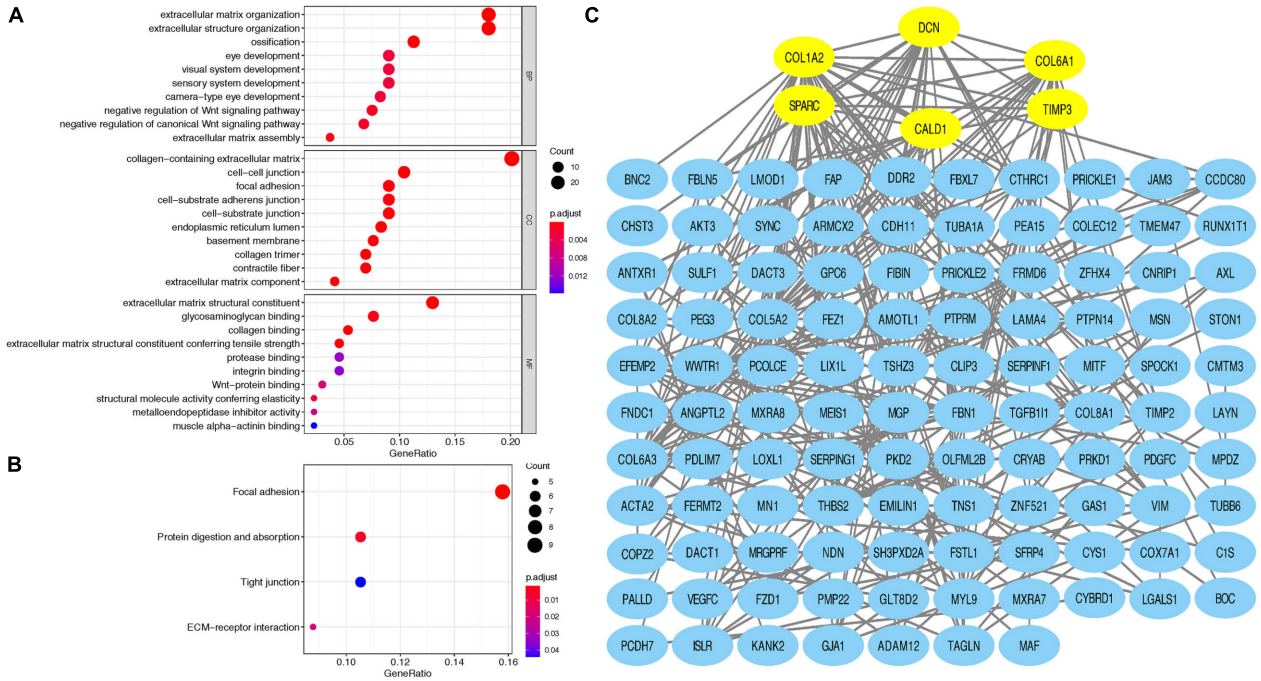

FIGURE 3 | (A) Top 10 GO terms, including BP, CC, and MF, respectively, enriched according to the hub genes in the red module; **(B)** KEGG terms enriched according to the hub genes in the red module; **(C)** Cytoscape software was used to establish the PPI network of hub genes in the red module based on the STRING website; yellow signifies the hub nodes. GO, Gene Ontology; BP, biological process; CC, cellular component; MF, molecular function; KEGG, Kyoto Encyclopedia of Genes and Genomes; PPI, protein–protein interaction.

activated (cor = −0.27, $P = 0.028$). As shown in **Table 3**, *CALD1* expression was significantly correlated with the biomarkers of monocyte, TAM, M2 macrophages, neutrophils, Treg, and T cell exhaustion in both GSE39582 and GSE41258 datasets ($P < 0.05$).

TABLE 1 | Top 15 genes identified by cytoHubba.

Rank	CytoHubba ranking methods					
	MNC	**Degree**	**EPC**	**Closeness**	**Radiality**	**Betweenness**
1	**COL1A2**	**COL1A2**	COL5A2	**COL1A2**	**COL1A2**	**DCN**
2	COL5A2	COL5A2	**COL1A2**	COL5A2	**SPARC**	WWTR1
3	**SPARC**	**DCN**	**SPARC**	**SPARC**	COL5A2	**COL1A2**
4	FBN1	**SPARC**	**COL6A1**	**DCN**	**COL6A1**	TNS1
5	**DCN**	FBN1	COL6A3	FBN1	**DCN**	**SPARC**
6	**COL6A1**	**COL6A1**	**DCN**	**COL6A1**	FBN1	**CALD1**
7	COL6A3	THBS2	FBN1	THBS2	**CALD1**	AXL
8	THBS2	COL6A3	THBS2	COL6A3	TAGLN	GJA1
9	EFEMP2	**CALD1**	CDH11	**CALD1**	**TIMP3**	CRYAB
10	PCOLCE	EFEMP2	ACTA2	ACTA2	ACTA2	MYL9
11	ACTA2	PCOLCE	EFEMP2	**TIMP3**	THBS2	ISLR
12	FSTL1	ACTA2	**CALD1**	TAGLN	COL6A3	TIMP3
13	CDH11	**TIMP3**	PCOLCE	PCOLCE	FSTL1	TAGLN
14	**TIMP3**	FSTL1	**TIMP3**	FSTL1	VIM	VIM
15	**CALD1**	CDH11	FSTL1	CDH11	CDH11	**COL6A1**

Symbols in bold type were the genes overlapped by six ranking methods in cytoHubba. MNC, maximum neighborhood component; degree, node connect degree; EPC: edge percolated component.

CALD1 Was Upregulated in CMS4 Subtype and Positively Correlated With Stromal and Immune Scores and Angiogenesis and TGF-β Signaling Enrichment Scores

We incorporated dMMR stage III/IV CRC patients and applied comparative analysis of *CALD1* expression in different CRC subgroups. As shown in **Figure 6B**, the *CALD1* expression between dMMR and pMMR CRC samples had no significant difference in the two datasets (Wilcoxon test, $P = 0.57$ and 0.74, respectively). Subsequently, we performed CMS analysis via the "CMSCaller" R package to divide CRCs of GSE39582 and GSE41258 into four biologically distinct classifications: CMS1 (dMMR-like immune), CMS2 (canonical), CMS3 (metabolic), and CMS4 (mesenchymal) (Guinney et al., 2015). The majority of dMMR samples were categorized as CMS1 (**Figure 6C**), and *CALD1* expression was significantly and specifically upregulated in the CMS4 subtype, which is characterized by TGF-β signaling activation, angiogenesis, and stromal invasion (Guinney et al., 2015).

Those results implied the potential regulation mechanisms of *CALD1* in CRC prognosis and TAM recruitments as well as polarizations, and as both intrinsic tumor features

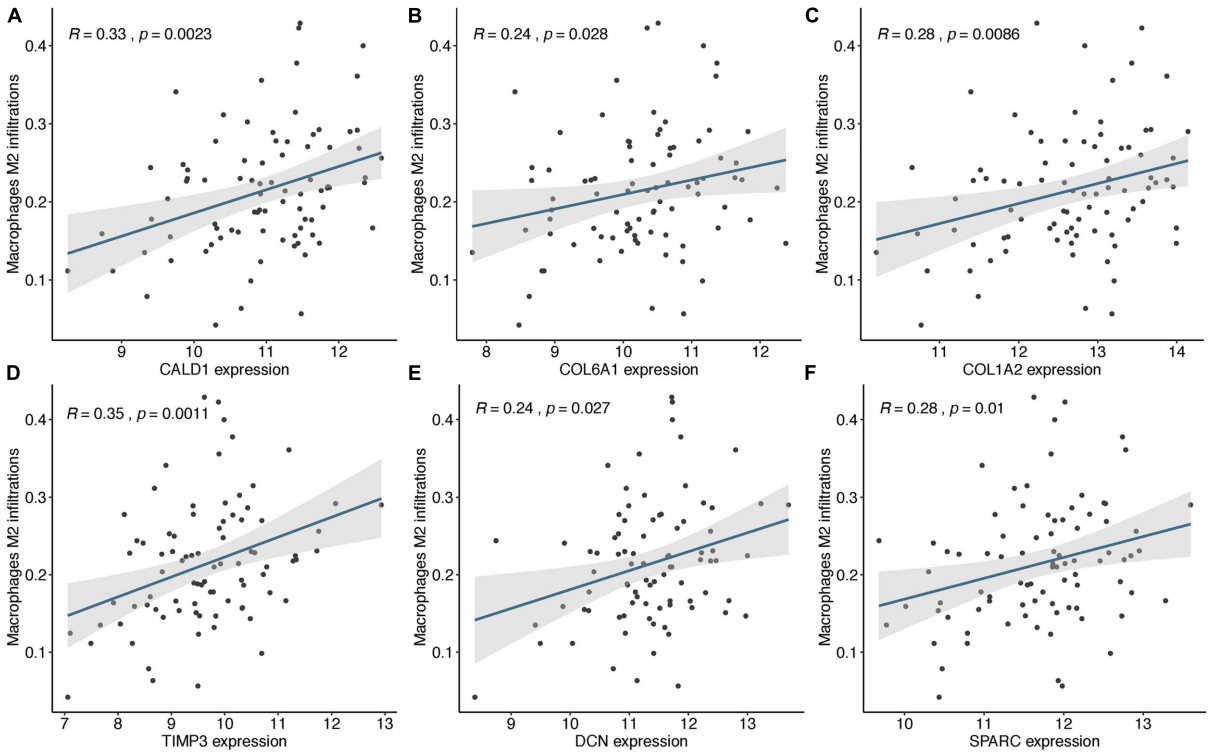

FIGURE 4 | The expressions of CALD1 **(A)**, COL6A1 **(B)**, COL1A2 **(C)**, TIMP3 **(D)**, DCN **(E)**, and SPARC **(F)** were significantly and positively correlated with M2 macrophage infiltrations.

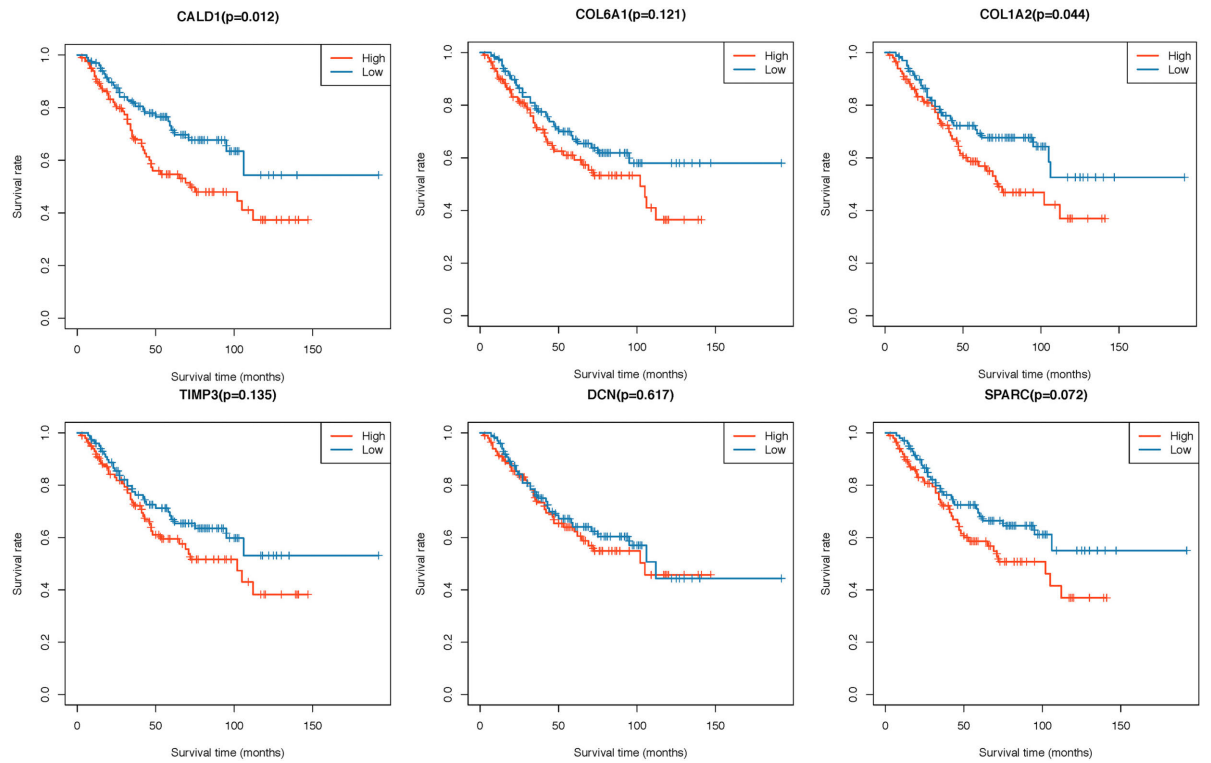

FIGURE 5 | Kaplan–Meier survival curves of six hub genes grouped by their median expression values in the GSE39582 dataset.

TABLE 2 | Univariate and multivariate Cox proportional hazard regression analysis on OS in GSE39582.

	Univariate analysis			Multivariate analysis		
	HR	**95% CI**	***P***	**HR**	**95% CI**	***P***
Age (>65 vs. ≤65)	1.035	1.015–1.055	<0.001	N/A	N/A	0.081
Gender (male vs. female)	1.328	0.838–2.104	0.228			
Location (proximal vs. distal)	1.534	0.969–2.43	0.068	N/A	N/A	0.097
Chemotherapy (no vs. yes)	2.265	1.415–3.625	0.001	1.869	1.124–3.109	0.016
TNM (IV vs. III)	3.559	1.989–6.367	<0.001	2.658	1.414–4.996	0.002
SPARC (high vs. low)	1.52	0.959–2.408	0.075	N/A	N/A	0.609
COL1A2 (high vs. low)	1.601	1.008–2.543	0.046	N/A	N/A	0.975
CALD1 (high vs. low)	1.811	1.131–2.901	0.013	1.868	1.165–2.995	0.009
DCN (high vs. low)	1.123	0.711–1.771	0.619			
COL6A1 (high vs. low)	1.434	0.906–2.27	0.124			
TIMP3 (high vs. low)	1.416	0.895–2.241	0.138			

OS, overall survival; HR, hazard ratio; CI, confidence interval; N/A, not applicable.

and extrinsic tumor microenvironment engage in tumor progression and macrophage polarization (Chen et al., 2019), we subsequently calculated the stromal and immune scores as well as the angiogenesis and TGF-β signaling gene sets enrichment scores of each stage III/IV pMMR CRC sample via the ESTIMATE and ssGSEA algorithms. Consistent with previous researches, higher stromal scores were associated with worse overall survival (GSE39582, log-rank $P = 0.004$; GSE41258, log-rank $P = 0.138$; **Supplementary Figures 2A,C**), while immune scores had non-significant impact on survival status (GSE39582, log-rank $P = 0.108$; GSE41258, log-rank $P = 0.578$; **Supplementary Figures 2B,D**) (Liu et al., 2020). The expression of *CALD1* exhibited strong positive correlations with stromal and immune scores in both GSE39582 (cor = 0.85, $P < 0.001$ and cor = 0.5, $P < 0.001$, respectively) (**Figure 6E**) and GSE41258 (cor = 0.83, $P < 0.001$ and cor = 0.56, $P < 0.001$, respectively) (**Figure 6F**). The angiogenesis and TGF-β signaling ssGSEA enrichment scores exhibited consistently significant and strong positive correlations with *CALD1* and macrophage marker expressions as well as stromal and immune scores in both GSE39582 and GSE41258 datasets (**Figures 6E,F**). The complicated interactions between CALD1, macrophage markers, as well as stromal and immune scores indicated that *CALD1* might engage in the complex modulation of macrophage activations across TME alternations, possibly through promoting angiogenesis and activating TGF-β signaling pathways.

GSEA of *CALD1* Related Signaling Pathways

Gene Set Enrichment Analysis identified several immune-related and oncogenic KEGG pathways that were enriched in the high-*CALD1* expression group (**Figures 7A,B**), including antigen processing and presentation, chemokine signaling, cytokine–cytokine receptor interaction, leukocyte transendothelial migration, vascular smooth muscle contraction, cell adhesion molecules, focal adhesion, MAPK signaling pathway, pathways in cancer, and TGF-beta signaling pathway.

Downregulation of *CALD1* Weakened the Proliferation, Migration, and Invasion in CRC Cells

To gain a better insight into the value of *CALD1* as a prognostic marker, si-CALD1 transfection was performed to transiently decrease *CALD1* expression in high-*CALD1* expressed SW620 and SW480 cells (**Figure 8A**), and its efficiency was verified by Western blotting (**Figures 8B,C**). CCK8 assay revealed that the viability of CRC cells was markedly restrained when *CALD1* was downregulated (**Figures 8E,G**). Furthermore, silencing *CALD1* conspicuously inhibited the invasion and migration capacities in CRC cells (**Figures 8D,F**). These findings suggested that *CALD1* could facilitate tumor progression of CRC.

DISCUSSION

Microsatellite stability accounts for the majority of CRC patients and indicates unfavorable outcomes (Popat et al., 2005). Although immunotherapy has achieved responsiveness in many intractable tumors, no effective immune therapy has demonstrated any benefit for those patients (Le et al., 2015), which inspired us to prioritize the exploration of immune biomarkers to guide immunotherapy applications. As the principal immune subset in the TME, M2 macrophages induce angiogenesis, remodel the matrix, restrain the therapeutic response, and facilitate malignance (Najafi et al., 2019). Hence, approaches that restrain the activity of M2 macrophages would be a compelling area for oncologic research.

In this study, we firstly found significant differences in M2 macrophage distributions between pMMR and dMMR stage III/IV CRC patients, and increased M2 macrophage levels were associated with poorer prognosis for pMMR patients. Then, by applying integrated bioinformatics analysis, we successfully identified *CALD1* as an independent prognostic biomarker closely correlated to M2 macrophage infiltrations. After that, we explored its relationship with diverse TME patterns and signaling pathway functions. In addition, by siRNA-mediated *CALD1*

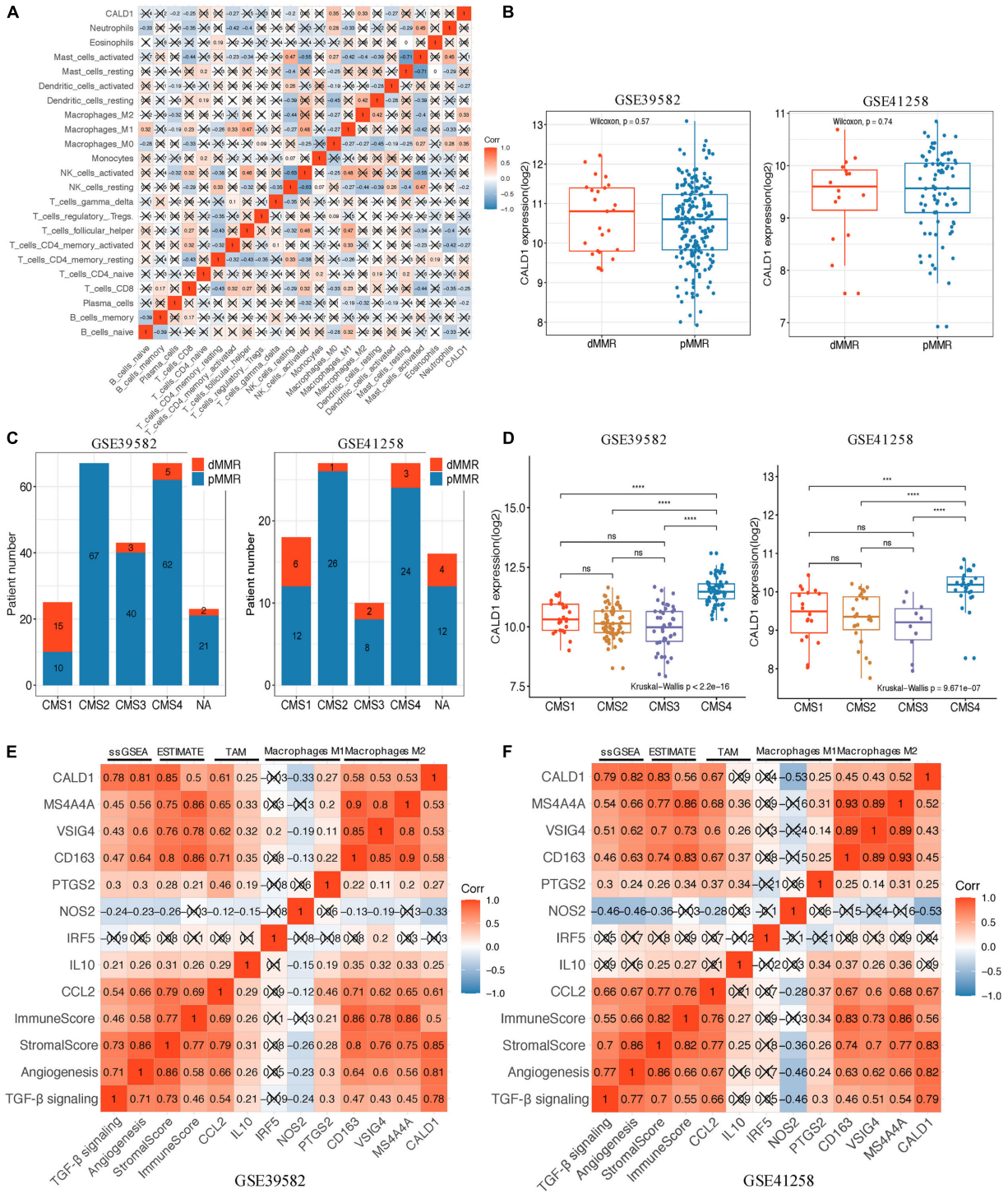

FIGURE 6 | (A) Spearman correlation matrix of CALD1 expression with the 22 tumor-infiltrating immune cell proportions in 85 stage III/IV pMMR CRC samples of GSE39582. **(B)** Boxplots of CALD1 expression between dMMR and pMMR stage III/IV CRC samples in both GSE39582 (left) and GSE41258 (right) datasets. **(C)** Histograms of the distribution characteristics of stage III/IV dMMR and pMMR CRC patients in each CMS subgroup. NA, not assigned. **(D)** Boxplots exhibiting CALD1 expression was significantly and specifically upregulated in the CMS4 subtype in both GSE39582 (left) and GSE41258 (right) datasets. Significant differences between CMS subgroups were indicated as follows: ns, not significant; ***$P < 0.001$, ****$P < 0.0001$ (Kruskal–Wallis test followed by Dunn's tests). **(E,F)** Correlation heatmap revealed that CALD1 expression was significantly and positively correlated with angiogenesis and TGF-β signaling ssGSEA enrichment scores, immune and stromal scores, gene markers of TAMs (CCL2 and IL10), and M2 macrophages (CD163, VSIG4, and MS4A4A) but was not clear with gene markers of macrophage M1 (IRF5, NOS2, and PTGS2) in the GSE39582 **(E)** and GSE41258 **(F)** datasets. pMMR, mismatch-repair-proficient; dMMR, mismatch-repair-deficient; CRC, colorectal cancer; CMS, consensus molecular subtypes; TAMs, tumor-associated macrophages.

TABLE 3 | Correlations between CALD1 and immune cells markers.

Description	Gene marker	GSE39582		GSE41258	
		Cor	*P*	Cor	*P*
CD8+ T cell	CD8A	0.072	0.313	0.143	0.199
	CD8B	−0.104	0.143	NA	NA
T cell (general)	CD3D	−0.017	0.816	0.134	0.231
	CD3E	−0.058	0.413	−0.036	0.745
	CD2	0.162	*	0.207	0.063
B cell	CD19	−0.025	0.727	0.053	0.634
	CD79A	−0.081	0.253	0.185	0.097
Monocyte	CD86	0.537	***	−0.132	0.236
	CD115	0.586	***	0.585	***
TAM	CCL2	0.630	***	0.681	***
	IL10	0.272	**	0.087	0.436
M1 Macrophage	NOS2	−0.338	***	−0.499	***
	IRF5	−0.033	0.645	−0.051	0.646
	PTGS2	0.246	**	0.252	*
M2 Macrophage	CD163	0.564	***	0.474	***
	VSIG4	0.521	***	0.459	***
	MS4A4A	0.529	***	0.573	***
Neutrophils	CEACAM8	−0.145	*	−0.364	**
	ITGAM	0.640	***	0.577	***
	CCR7	−0.035	0.618	0.115	0.305
Natural killer cell	KIR2DL1	−0.266	**	−0.037	0.740
	KIR2DL3	−0.254	**	−0.270	*
	KIR2DL4	−0.199	**	−0.038	0.737
	KIR3DL1	0.066	0.355	0.371	**
	KIR3DL3	−0.279	***	−0.040	0.721
Dendritic cell	HLA-DPB1	0.486	***	NA	NA
	HLA-DQB1	0.352	***	NA	NA
	HLA-DRA	0.422	***	NA	NA
	HLA-DPA1	0.385	***	NA	NA
	CD1C	0.094	0.187	−0.236	*
	NRP1	0.754	***	0.742	***
	ITGAX	0.421	***	0.312	**
Th1	TBX21	−0.032	0.654	−0.086	0.444
	STAT4	0.297	***	−0.279	*
	STAT1	0.406	***	0.281	*
	IFNG	0.047	0.511	−0.308	**
	TNF	0.073	0.301	−0.307	**
Th2	GATA3	0.315	***	−0.031	0.784
	STAT6	−0.210	**	0.070	0.534
	STAT5A	0.042	0.558	0.124	0.265
	IL13	−0.215	**	−0.219	*
Tfh	BCL6	0.585	***	0.705	***
	IL21	0.074	0.295	−0.272	*
Th17	STAT3	0.034	0.633	−0.002	0.984
	IL17A	−0.067	0.349	−0.370	**
Treg	FOXP3	−0.094	0.185	−0.400	**
	CCR8	−0.076	0.282	−0.132	0.236
	STAT5B	0.264	**	0.268	*
	TGFB1	0.598	***	0.502	***
T cell exhaustion	PDCD1	−0.270	**	−0.303	**
	CTLA4	−0.319	***	−0.135	0.226
	HAVCR2	0.390	***	NA	NA
	GZMB	−0.016	0.826	0.033	0.766

$^*p < 0.05$; $^{**}p < 0.01$; $^{***}p < 0.0001$. Cor, Pearson's correlation value; TAM, tumor-associated macrophage; Th, T helper cell; Tfh, follicular helper T cell; Treg, regulatory T cell; NA, not available.

depletion in CRC cell lines, we found that the proliferation and metastasis ability of tumor cells were repressed, which indicated that *CALD1* played a dual role in immunosuppression and tumor metastasis.

Caldesmon (CaD), encoded by *CALD1*, is an actomyosin-binding and cytoskeleton-related protein. There are two major CaD isoforms that evolved through alternative splicing, including high-molecular weight CaD (h-CaD) and low-molecular weight CaD (l-CaD) (Hayashi et al., 1992; Huber, 1997). H-CaD exists uniquely in vascular and visceral smooth muscle cells (SMC) and acts as a cellular contraction regulator and biomarker for SMC-associated neoplasms (Watanabe et al., 1999). L-CaD is widely distributed in non-muscle cells (Sobue and Sellers, 1991; Dabrowska et al., 2004), and studies have shown that l-CaD promoted malignancy in several cancers (Kim et al., 2012; Chang et al., 2013; Lee et al., 2015; Lian et al., 2020). Lee et al. (2015) identified that overexpression of l-CaD in primary non-muscle-invasive bladder cancer is significantly correlated with large tumor size, lymphovascular invasion, advanced stage, higher grade, and adverse prognosis and elucidated that l-CaD-derived morphological changes of tumor cells were the underlying mechanism responsible for enhancing tumor cell motility. Chang et al. (2013) demonstrated that in oral cavity squamous cell carcinoma, the expression of l-CaD was higher in metastatic lymph nodes than in primary tumor cells, and higher l-CaD was associated with tumor metastasis. In CRC, Lian et al. (2020) proved that l-CaD was the isoform derived from alternative splicing of *CALD1* and played a role in tumor metastasis. Kim et al. (2012) reported that the expression of l-CaD was higher in colon cancer than in normal colon mucosa and proposed that l-CaD could be a biomarker to predict neoadjuvant chemoradiotherapy susceptibility. In addition, Zhao et al. performed bioinformatics analysis and identified *CALD1* as candidate genes for the early onset of CRC (Zhao B. et al., 2019). However, until now, the effect of *CALD1* in CRC tumor microenvironment has rarely been addressed.

In the present study, we investigated the association between *CALD1* and M2 macrophage infiltrations at the genomic level by using GEO datasets. As shown in **Figure 6A**, based on the CIBERSORT results, *CALD1* was positively correlated with M0 and M2 macrophage fractions, whereas it was negatively correlated with CD8 T cell fractions, which were the principal components in antitumor immunity. **Figures 6E,F** revealed that the expression of *CALD1* was positively correlated with TAM marker *CCL2* and M2 macrophage markers (*CD163*, *VSIG4*, and *MS4A4A*). As for *CCL2*, studies have identified that *CCL2* played a vital role in activating and recruiting TAMs, thereby deriving immunosuppressive effects (Mu et al., 2019; Xue et al., 2019). The blockage of *CCL2* resulted in significantly elevated levels of M1 polarization-associated markers and cytokines, whereas M2-associated markers were diminished (Sierra-Filardi et al., 2014). The positive expression of *CALD1* and *CCL2* hinted that *CALD1* might stimulate and polarize TAMs by upregulating *CCL2* expression; however, further research is needed for confirmation.

Although CALD1 expression revealed no significant difference between dMMR and pMMR samples (**Figure 6B**), we observed that *CALD1* was specifically upregulated in the CMS4

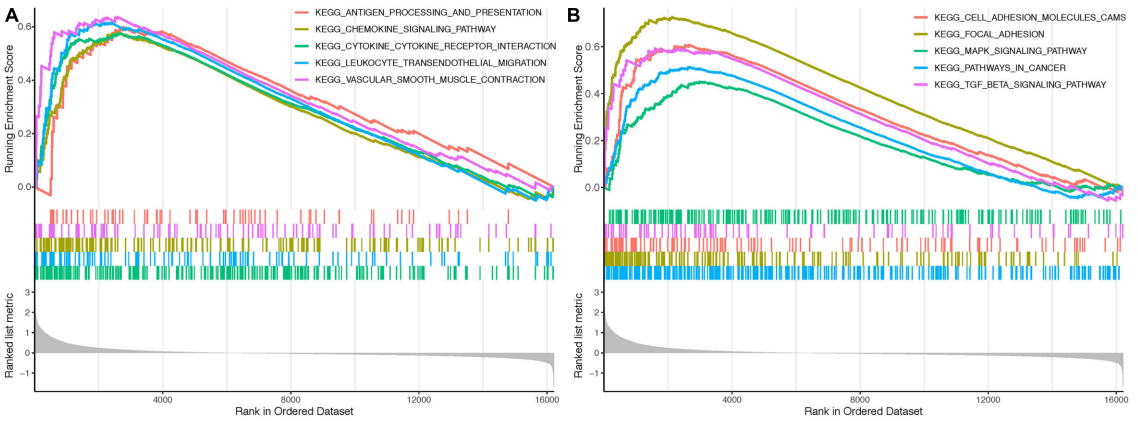

FIGURE 7 | Gene Sets Enrichment Analysis (GSEA) revealed that several immune-related **(A)** and tumor-related **(B)** pathways were highly enriched in the high CALD1 expression group.

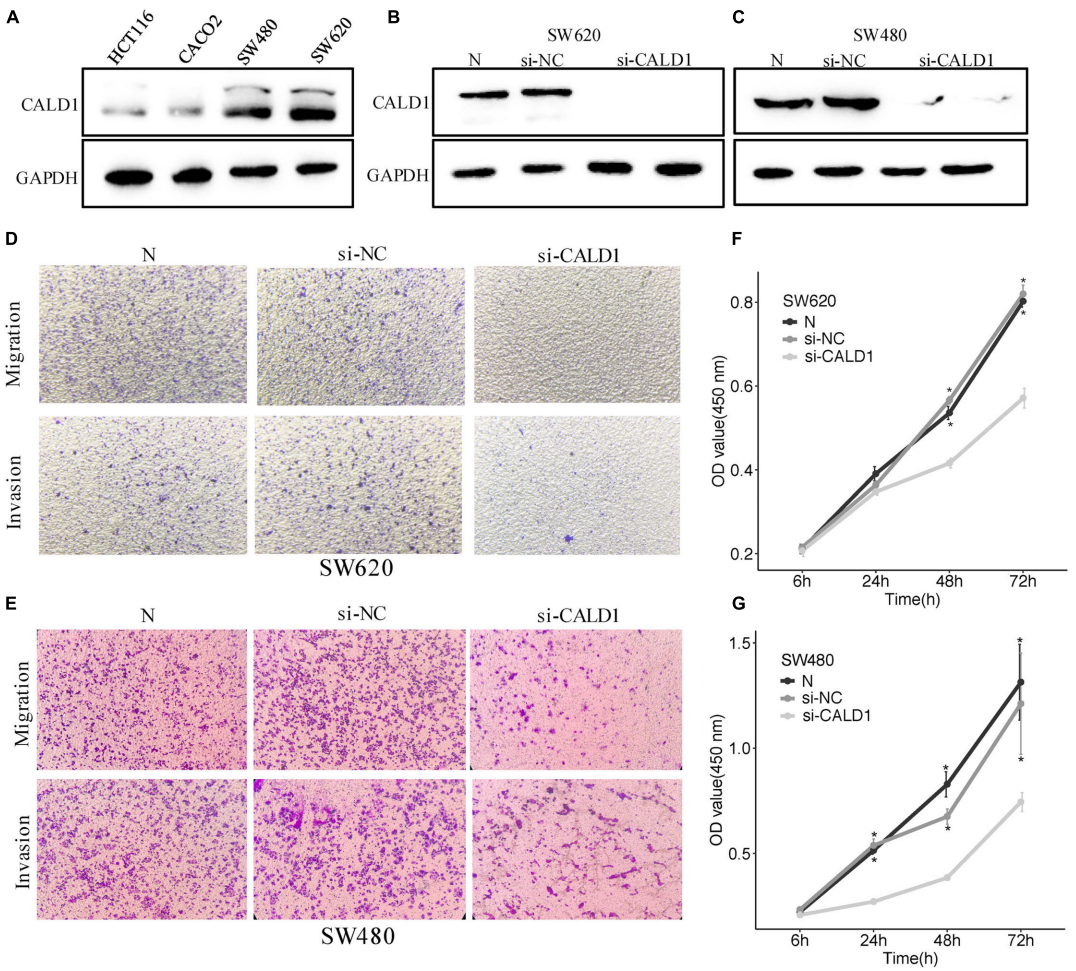

FIGURE 8 | CALD1 promotes cell proliferation, migration, and invasion in CRC cells. **(A)** The protein levels of CALD1 in four kinds of CRC cell lines were measured by Western blot. **(B,C)** The protein levels of normal, si-NC, and si-CALD1 transfected SW620 **(B)** and SW480 **(C)** cells by Western blot; si-CALD1 transfections were performed in duplicate. **(D,E)** Transwell assays revealed that *CALD1* knockdown attenuated SW620 **(D)** and SW480 **(E)** cell migration and invasion. **(F,G)** CCK8 assays were performed to assess cell viability in normal, si-NC, and si-CALD1 transfected SW620 **(F)** and SW480 **(G)** cells. *$p < 0.05$ in comparison with the si-CALD1 group using Kruskal–Wallis one-way analysis of variance (ANOVA). All assays were repeated at least three times.

subtype compared with that in CMS1-3 (**Figure 6D**). CMS4 has been characterized by the notable upregulation of genes correlated with angiogenesis, TGF-β signaling activation, stromal infiltration, and worse prognosis (Guinney et al., 2015). Given the previous literature on the crosstalk between angiogenesis and TGF-β in macrophage recruitments and M2 polarizations (Allavena et al., 2008; Erreni et al., 2011; Najafi et al., 2019; Rahma and Hodi, 2019), we investigated if *CALD1* correlated with the enrichments for the two gene sets in stage III/IV pMMR CRC samples. Indeed, *CALD1* expression significantly correlated with ssGSEA scores for angiogenesis and TGF-β signaling gene lists (**Figures 6E,F**), suggesting the prospective synergistic roles of *CALD1* in macrophage recruitments and polarizations as well as driving CRC progression and metastasis. In addition, accumulated evidence has revealed that the complex stromal medium is the core component of TME, and virtually every property of cancer-associated stroma plays a demonstrable role in sustaining hyperproliferation of tumor cells (Tsujino et al., 2007; Ueno et al., 2017; Liu et al., 2020) as well as therapy resistance in one condition or another (Gonçalves-Ribeiro et al., 2017). Our results revealed that stromal score was strongly and positively correlated with *CALD1* (cor = 0.85 and 0.82, $P < 0.001$) and *CCL2* (cor = 0.81 and 0.79, $P < 0.001$) expressions in the two datasets, indicating that signals from intricate *CALD1*, *CCL2*, and stromal interactions might drive M2 macrophage activation and polarization. Furthermore, GSEA disclosed that high expression of *CALD1* was correlated with several immunoregulation pathways associated with M2 macrophage activation and recruitment, such as cytokine–cytokine receptor interaction, leukocyte transendothelial migration, vascular smooth muscle contraction, TGF-beta signaling pathway, and MAPK signaling pathway (Jiang et al., 2017; Wongchana et al., 2018).

Several limitations still exist in our study. Firstly, although functional and enrichment analyses were performed, the specific mechanisms of how *CALD1* activated and recruited M2 macrophages require further clarification. In addition, the intratumoral immune and stromal compositions were estimated only through bioinformatics algorithms at molecular levels. The actual relationship between *CALD1* and M2 macrophage infiltrations was not histologically verified in this study. If possible, we will perform additional biochemical and histological analyses to reevaluate the robustness of our findings in the future. Moreover, although our in vitro validation revealed that *CALD1* was highly expressed in pMMR cell lines (SW480 and SW620), comparison between more CRC cell lines proficient and deficient in the MMR pathway will be necessary to clarify the specificity of *CALD1* for pMMR CRC cells. Finally, as our study was based on public transcriptomic datasets, the application of *CALD1* as a prognostic biomarker and potential target must be researched in prospective real-world pMMR CRC patients receiving immunotherapy.

CONCLUSION

In conclusion, this study is the first to reveal pMMR CRC patients possessed higher composition of M2 macrophages than dMMR tumors. We then identified *CALD1* as an independent prognostic marker positively correlated with M2 macrophage infiltrations in stage III/IV pMMR CRC via WGCNA and Cox regression analyses. *CALD1* was upregulated specifically in the CMS4 CRC subtype and was significantly correlated with angiogenesis and TGF-β signaling gene sets ssGSEA enrichment scores as well as immune and stromal ESTIMATE scores. In addition, *CALD1* promoted proliferation, invasion, and migration of CRC cells. *CALD1* could serve as an independent prognostic biomarker and a candidate M2 macrophage target for pMMR CRC patients. However, validation in large-scale genomics and functional and prospective clinical trials are still required.

DATA AVAILABILITY STATEMENT

The original contributions presented in the study are included in the article/**Supplementary Material**, further inquiries can be directed to the corresponding author/s.

AUTHOR CONTRIBUTIONS

HZ, SC, and XW contributed to the conception and design. YB, JW, and JLZ extracted the data from the databases. HZ, JZ, and SC contributed to the data analysis and interpretation. HZ drafted the manuscript. YL and XW revised the manuscript and supervised the entire study. All authors read and approved the final manuscript.

ACKNOWLEDGMENTS

We would like to thank the GEO database for the availability of the data.

SUPPLEMENTARY MATERIAL

The Supplementary Material for this article can be found online at: https://www.frontiersin.org/articles/10.3389/fmolb.2021.649363/full#supplementary-material

REFERENCES

Allavena, P., Sica, A., Solinas, G., Porta, C., and Mantovani, A. (2008). The inflammatory micro-environment in tumor progression: the role of tumor-associated macrophages. *Crit. Rev. Oncol. Hematol.* 66, 1–9. doi: 10.1016/j.critrevonc.2007.07.004

Berg, K. C. G., Eide, P. W., Eilertsen, I. A., Johannessen, B., Bruun, J., Danielsen, S. A., et al. (2017). Multi-omics of 34 colorectal cancer cell lines - a resource for biomedical studies. *Mol. Cancer* 16:116. doi: 10.1186/s12943-017-0691-y

Bernal, M., Concha, A., Sáenz-López, P., Rodríguez, A. I., Cabrera, T., Garrido, F., et al. (2011). Leukocyte infiltrate in gastrointestinal adenocarcinomas is strongly associated with tumor microsatellite instability but not with tumor

immunogenicity. *Cancer Immunol. Immunother.* 60, 869–882. doi: 10.1007/s00262-011-0999-1

Boland, C. R., Thibodeau, S. N., Hamilton, S. R., Sidransky, D., Eshleman, J. R., Burt, R. W., et al. (1998). A National Cancer Institute Workshop on microsatellite instability for cancer detection and familial predisposition: development of international criteria for the determination of microsatellite instability in colorectal cancer. *Cancer Res.* 58, 5248–5257.

Bray, F., Ferlay, J., Soerjomataram, I., Siegel, R. L., Torre, L. A., and Jemal, A. (2018). Global cancer statistics 2018: GLOBOCAN estimates of incidence and mortality worldwide for 36 cancers in 185 countries. *CA Cancer J. Clin.* 68, 394–424. doi: 10.3322/caac.21492

Chang, K.-P., Wang, C.-L. A., Kao, H.-K., Liang, Y., Liu, S.-C., Huang, L.-L., et al. (2013). Overexpression of caldesmon is associated with lymph node metastasis and poorer prognosis in patients with oral cavity squamous cell carcinoma. *Cancer* 119, 4003–4011. doi: 10.1002/cncr.28300

Chen, Y., Song, Y., Du, W., Gong, L., Chang, H., and Zou, Z. (2019). Tumor-associated macrophages: an accomplice in solid tumor progression. *J. Biomed. Sci.* 26:78. doi: 10.1186/s12929-019-0568-z

Chin, C.-H., Chen, S.-H., Wu, H.-H., Ho, C.-W., Ko, M.-T., and Lin, C.-Y. (2014). cytoHubba: identifying hub objects and sub-networks from complex interactome. *BMC Syst. Biol.* 8(Suppl. 4):S11. doi: 10.1186/1752-0509-8-S4-S11

Couzin-Frankel, J. (2013). Breakthrough of the year 2013. Cancer immunotherapy. *Science* 342, 1432–1433. doi: 10.1126/science.342.6165.1432

Dabrowska, R., Kulikova, N., and Gagola, M. (2004). Nonmuscle caldesmon: its distribution and involvement in various cellular processes. Review article. *Protoplasma* 224, 1–13. doi: 10.1007/s00709-004-0057-3

Diaz, L., Marabelle, A., Delord, J.-P., Shapira-Frommer, R., Geva, R., Peled, N., et al. (2017). Pembrolizumab therapy for microsatellite instability high (MSI-H) colorectal cancer (CRC) and non-CRC. *J. Clin. Oncol.* 35:3071. doi: 10.1200/JCO.2017.35.15_suppl.3071

Dolcetti, R., Viel, A., Doglioni, C., Russo, A., Guidoboni, M., Capozzi, E., et al. (1999). High prevalence of activated intraepithelial cytotoxic T lymphocytes and increased neoplastic cell apoptosis in colorectal carcinomas with microsatellite instability. *Am. J. Pathol.* 154, 1805–1813. doi: 10.1016/s0002-9440(10)65436-3

Eide, P. W., Bruun, J., Lothe, R. A., and Sveen, A. (2017). CMScaller: an R package for consensus molecular subtyping of colorectal cancer pre-clinical models. *Sci. Rep.* 7:16618. doi: 10.1038/s41598-017-16747-x

Erreni, M., Mantovani, A., and Allavena, P. (2011). Tumor-associated macrophages (TAM) and inflammation in colorectal cancer. *Cancer Microenviron.* 4, 141–154. doi: 10.1007/s12307-010-0052-5

Fernandes, E., Sores, J., Cotton, S., Peixoto, A., Ferreira, D., Freitas, R., et al. (2020). Esophageal, gastric and colorectal cancers: looking beyond classical serological biomarkers towards glycoproteomics-assisted precision oncology. *Theranostics* 10, 4903–4928. doi: 10.7150/thno.42480

Ganesh, K., Stadler, Z. K., Cercek, A., Mendelsohn, R. B., Shia, J., Segal, N. H., et al. (2019). Immunotherapy in colorectal cancer: rationale, challenges and potential. *Nat. Rev. Gastroenterol. Hepatol.* 16, 361–375. doi: 10.1038/s41575-019-0126-x

Gautier, L., Cope, L., Bolstad, B. M., and Irizarry, R. A. (2004). affy–analysis of Affymetrix GeneChip data at the probe level. *Bioinformatics* 20, 307–315.

Gonçalves-Ribeiro, S., Sanz-Pamplona, R., Vidal, A., Sanjuan, X., Guillen Díaz-Maroto, N., Soriano, A., et al. (2017). Prediction of pathological response to neoadjuvant treatment in rectal cancer with a two-protein immunohistochemical score derived from stromal gene-profiling. *Ann. Oncol.* 28, 2160–2168. doi: 10.1093/annonc/mdx293

Gryfe, R., Kim, H., Hsieh, E. T. K., Aronson, M. D., Holowaty, E. J., Bull, S. B., et al. (2000). Tumor microsatellite instability and clinical outcome in young patients with colorectal cancer. *N. Engl. J. Med.* 342, 69–77. doi: 10.1056/NEJM200001133420201

Guinney, J., Dienstmann, R., Wang, X., de Reyniès, A., Schlicker, A., Soneson, C., et al. (2015). The consensus molecular subtypes of colorectal cancer. *Nat. Med.* 21, 1350–1356. doi: 10.1038/nm.3967

Hanahan, D., and Coussens Lisa, M. (2012). Accessories to the crime: functions of cells recruited to the tumor microenvironment. *Cancer Cell* 21, 309–322. doi: 10.1016/j.ccr.2012.02.022

Hänzelmann, S., Castelo, R., and Guinney, J. (2013). GSVA: gene set variation analysis for microarray and RNA-Seq data. *BMC Bioinformatics* 14:7. doi: 10.1186/1471-2105-14-7

Hayashi, K., Yano, H., Hashida, T., Takeuchi, R., Takeda, O., Asada, K., et al. (1992). Genomic structure of the human caldesmon gene. *Proc. Natl. Acad. Sci. U.S.A.* 89, 12122–12126. doi: 10.1073/pnas.89.24.12122

Horvath, S., and Dong, J. (2008). Geometric interpretation of gene coexpression network analysis. *PLoS Comput. Biol.* 4:e1000117. doi: 10.1371/journal.pcbi.1000117

Huber, P. A. J. (1997). Caldesmon. *Int. J. Biochem. Cell Biol.* 29, 1047–1051. doi: 10.1016/S1357-2725(97)00004-6

Jiang, L., Li, X., Zhang, Y., Zhang, M., Tang, Z., and Lv, K. (2017). Microarray and bioinformatics analyses of gene expression profiles in BALB/c murine macrophage polarization. *Mol. Med. Rep.* 16, 7382–7390. doi: 10.3892/mmr.2017.7511

Kakati, T., Bhattacharyya, D. K., Barah, P., and Kalita, J. K. (2019). Comparison of methods for differential co-expression analysis for disease biomarker prediction. *Comput. Biol. Med.* 113:103380. doi: 10.1016/j.compbiomed.2019.103380

Kim, K.-H., Yeo, S.-G., Kim, W. K., Kim, D. Y., Yeo, H. Y., Hong, J. P., et al. (2012). Up-regulated expression of l-caldesmon associated with malignancy of colorectal cancer. *BMC Cancer* 12:601. doi: 10.1186/1471-2407-12-601

Langfelder, P., and Horvath, S. (2008). WGCNA: an R package for weighted correlation network analysis. *BMC Bioinformatics* 9:559. doi: 10.1186/1471-2105-9-559

Le, D. T., Durham, J. N., Smith, K. N., Wang, H., Bartlett, B. R., Aulakh, L. K., et al. (2017). Mismatch repair deficiency predicts response of solid tumors to PD-1 blockade. *Science* 357, 409–413. doi: 10.1126/science.aan6733

Le, D. T., Uram, J. N., Wang, H., Bartlett, B. R., Kemberling, H., Eyring, A. D., et al. (2015). PD-1 blockade in tumors with mismatch-repair deficiency. *N. Engl. J. Med.* 372, 2509–2520. doi: 10.1056/NEJMoa1500596

Lee, M.-S., Lee, J., Kim, J. H., Kim, W. T., Kim, W.-J., Ahn, H., et al. (2015). Overexpression of caldesmon is associated with tumor progression in patients with primary non-muscle-invasive bladder cancer. *Oncotarget* 6, 40370–40384. doi: 10.18632/oncotarget.5458

Lian, H., Wang, A., Shen, Y., Wang, Q., Zhou, Z., Zhang, R., et al. (2020). Identification of novel alternative splicing isoform biomarkers and their association with overall survival in colorectal cancer. *BMC Gastroenterol.* 20:171. doi: 10.1186/s12876-020-01288-x

Liu, J.-W., Yu, F., Tan, Y.-F., Huo, J.-P., Liu, Z., Wang, X.-J., et al. (2020). Profiling of tumor microenvironment components identifies five stroma-related genes with prognostic implications in colorectal cancer. *Cancer Biother. Radiopharm.* [Epub ahead of print]. doi: 10.1089/cbr.2020.4118

Malesci, A., Laghi, L., Bianchi, P., Delconte, G., Randolph, A., Torri, V., et al. (2007). Reduced likelihood of metastases in patients with microsatellite-unstable colorectal cancer. *Clin. Cancer Res.* 13, 3831–3839. doi: 10.1158/1078-0432.ccr-07-0366

Marisa, L., de Reyniès, A., Duval, A., Selves, J., Gaub, M. P., Vescovo, L., et al. (2013). Gene expression classification of colon cancer into molecular subtypes: characterization, validation, and prognostic value. *PLoS Med.* 10:e1001453. doi: 10.1371/journal.pmed.1001453

Morse, M. A., Overman, M. J., Hartman, L., Khoukaz, T., Brutcher, E., Lenz, H.-J., et al. (2019). Safety of nivolumab plus low-dose ipilimumab in previously treated microsatellite instability-high/mismatch repair-deficient metastatic colorectal cancer. *Oncologist* 24, 1453–1461. doi: 10.1634/theoncologist.2019-0129

Mu, J., Sun, P., Ma, Z., and Sun, P. (2019). BRD4 promotes tumor progression and NF-κB/CCL2-dependent tumor-associated macrophage recruitment in GIST. *Cell Death Dis.* 10:935. doi: 10.1038/s41419-019-2170-4

Najafi, M., Hashemi Goradel, N., Farhood, B., Salehi, E., Nashtaei, M. S., Khanlarkhani, N., et al. (2019). Macrophage polarity in cancer: a review. *J. Cell. Biochem.* 120, 2756–2765. doi: 10.1002/jcb.27646

Narayanan, S., Kawaguchi, T., Peng, X., Qi, Q., Liu, S., Yan, L., et al. (2019). Tumor infiltrating lymphocytes and macrophages improve survival in microsatellite unstable colorectal cancer. *Sci. Rep.* 9:13455. doi: 10.1038/s41598-019-49878-4

Newman, A. M., Liu, C. L., Green, M. R., Gentles, A. J., Feng, W., Xu, Y., et al. (2015). Robust enumeration of cell subsets from tissue expression profiles. *Nat. Methods* 12, 453–457. doi: 10.1038/nmeth.3337

Overman, M. J., McDermott, R., Leach, J. L., Lonardi, S., Lenz, H. J., Morse, M. A., et al. (2017). Nivolumab in patients with metastatic DNA mismatch repair-deficient or microsatellite instability-high colorectal cancer (CheckMate 142): an open-label, multicentre, phase 2 study. *Lancet Oncol.* 18, 1182–1191. doi: 10.1016/s1470-2045(17)30422-9

Peltomäki, P. (2003). Role of DNA mismatch repair defects in the pathogenesis of human cancer. *J. Clin. Oncol.* 21, 1174–1179. doi: 10.1200/JCO.2003.04.060

Popat, S., Hubner, R., and Houlston, R. S. (2005). Systematic review of microsatellite instability and colorectal cancer prognosis. *J. Clin. Oncol.* 23, 609–618. doi: 10.1200/JCO.2005.01.086

Prall, F., Dührkop, T., Weirich, V., Ostwald, C., Lenz, P., Nizze, H., et al. (2004). Prognostic role of CD8+ tumor-infiltrating lymphocytes in stage III colorectal cancer with and without microsatellite instability. *Hum. Pathol.* 35, 808–816. doi: 10.1016/j.humpath.2004.01.022

Rahma, O. E., and Hodi, F. S. (2019). The intersection between tumor angiogenesis and immune suppression. *Clin. Cancer Res.* 25, 5449–5457. doi: 10.1158/1078-0432.CCR-18-1543

Ritchie, M. E., Phipson, B., Wu, D., Hu, Y., Law, C. W., Shi, W., et al. (2015). limma powers differential expression analyses for RNA-sequencing and microarray studies. *Nucleic Acids Res.* 43:e47. doi: 10.1093/nar/gkv007

Scholkopf, B., Smola, A. J., Williamson, R. C., and Bartlett, P. L. (2000). New support vector algorithms. *Neural Comput.* 12, 1207–1245.

Shannon, P., Markiel, A., Ozier, O., Baliga, N. S., Wang, J. T., Ramage, D., et al. (2003). Cytoscape: a software environment for integrated models of biomolecular interaction networks. *Genome Res.* 13, 2498–2504.

Sheffer, M., Bacolod, M. D., Zuk, O., Giardina, S. F., Pincas, H., Barany, F., et al. (2009). Association of survival and disease progression with chromosomal instability: a genomic exploration of colorectal cancer. *Proc. Natl. Acad. Sci. U.S.A.* 106, 7131–7136. doi: 10.1073/pnas.0902232106

Siegel, R. L., Miller, K. D., Fedewa, S. A., Ahnen, D. J., Meester, R. G. S., Barzi, A., et al. (2017). Colorectal cancer statistics, 2017. *CA Cancer J. Clin.* 67, 177–193. doi: 10.3322/caac.21395

Sierra-Filardi, E., Nieto, C., Domínguez-Soto, Á, Barroso, R., Sánchez-Mateos, P., Puig-Kroger, A., et al. (2014). CCL2 shapes macrophage polarization by GM-CSF and M-CSF: identification of CCL2/CCR2-dependent gene expression profile. *J. Immunol.* 192, 3858–3867. doi: 10.4049/jimmunol.1302821

Smyrk, T. C., Watson, P., Kaul, K., and Lynch, H. T. (2001). Tumor-infiltrating lymphocytes are a marker for microsatellite instability in colorectal carcinoma. *Cancer* 91, 2417–2422.

Sobue, K., and Sellers, J. R. (1991). Caldesmon, a novel regulatory protein in smooth muscle and nonmuscle actomyosin systems. *J. Biol. Chem.* 266, 12115–12118.

Subramanian, A., Tamayo, P., Mootha, V. K., Mukherjee, S., Ebert, B. L., Gillette, M. A., et al. (2005). Gene set enrichment analysis: a knowledge-based approach for interpreting genome-wide expression profiles. *Proc. Natl. Acad. Sci. U.S.A.* 102, 15545–15550. doi: 10.1073/pnas.0506580102

Szklarczyk, D., Gable, A. L., Lyon, D., Junge, A., Wyder, S., Huerta-Cepas, J., et al. (2019). STRING v11: protein-protein association networks with increased coverage, supporting functional discovery in genome-wide experimental datasets. *Nucleic Acids Res.* 47, D607–D613. doi: 10.1093/nar/gky1131

Tan, B., Shi, X., Zhang, J., Qin, J., Zhang, N., Ren, H., et al. (2018). Inhibition of Rspo-Lgr4 facilitates checkpoint blockade therapy by switching macrophage polarization. *Cancer Res.* 78, 4929–4942. doi: 10.1158/0008-5472.can-18-0152

Tsujino, T., Seshimo, I., Yamamoto, H., Ngan, C. Y., Ezumi, K., Takemasa, I., et al. (2007). Stromal myofibroblasts predict disease recurrence for colorectal cancer. *Clin. Cancer Res.* 13, 2082–2090. doi: 10.1158/1078-0432.CCR-06-2191

Ubil, E., Caskey, L., Holtzhausen, A., Hunter, D., Story, C., and Earp, H. S. (2018). Tumor-secreted Pros1 inhibits macrophage M1 polarization to reduce antitumor immune response. *J. Clin. Invest.* 128, 2356–2369. doi: 10.1172/jci97354

Ueno, H., Kanemitsu, Y., Sekine, S., Ishiguro, M., Ito, E., Hashiguchi, Y., et al. (2017). Desmoplastic pattern at the tumor front defines poor-prognosis subtypes of colorectal cancer. *Am. J. Surg. Pathol.* 41, 1506–1512. doi: 10.1097/pas.0000000000000946

Watanabe, K., Kusakabe, T., Hoshi, N., Saito, A., and Suzuki, T. (1999). h-Caldesmon in leiomyosarcoma and tumors with smooth muscle cell-like differentiation: its specific expression in the smooth muscle cell tumor. *Hum. Pathol.* 30, 392–396. doi: 10.1016/S0046-8177(99)90113-2

Wongchana, W., Kongkavitoon, P., Tangtanatakul, P., Sittplangkoon, C., Butta, P., Chawalitpong, S., et al. (2018). Notch signaling regulates the responses of lipopolysaccharide-stimulated macrophages in the presence of immune complexes. *PLoS One* 13:e0198609. doi: 10.1371/journal.pone.0198609

Xiang, W., Shi, R., Kang, X., Zhang, X., Chen, P., Zhang, L., et al. (2018). Monoacylglycerol lipase regulates cannabinoid receptor 2-dependent macrophage activation and cancer progression. *Nat. Commun.* 9:2574. doi: 10.1038/s41467-018-04999-8

Xue, J., Ge, X., Zhao, W., Xue, L., Dai, C., Lin, F., et al. (2019). PIPKIγ regulates CCL2 expression in colorectal cancer by activating AKT-STAT3 signaling. *J. Immunol. Res.* 2019:3690561. doi: 10.1155/2019/3690561

Yip, A. M., and Horvath, S. (2007). Gene network interconnectedness and the generalized topological overlap measure. *BMC Bioinformatics* 8:22. doi: 10.1186/1471-2105-8-22

Yoshihara, K., Shahmoradgoli, M., Martínez, E., Vegesna, R., Kim, H., Torres-Garcia, W., et al. (2013). Inferring tumour purity and stromal and immune cell admixture from expression data. *Nat. Commun.* 4:2612. doi: 10.1038/ncomms3612

Yu, G., Wang, L.-G., Han, Y., and He, Q.-Y. (2012). clusterProfiler: an R package for comparing biological themes among gene clusters. *OMICS* 16, 284–287. doi: 10.1089/omi.2011.0118

Zeng, H., Ji, J., Song, X., Huang, Y., Li, H., Huang, J., et al. (2020). Stemness related genes revealed by network analysis associated with tumor immune microenvironment and the clinical outcome in lung adenocarcinoma. *Front. Genet.* 11:549213. doi: 10.3389/fgene.2020.549213

Zhang, J., Wang, L., Xu, X., Li, X., Guan, W., Meng, T., et al. (2020). Transcriptome-based network analysis unveils eight immune-related genes as molecular signatures in the immunomodulatory subtype of triple-negative breast cancer. *Front. Oncol.* 10:1787. doi: 10.3389/fonc.2020.01787

Zhao, B., Baloch, Z., Ma, Y., Wan, Z., Huo, Y., Li, F., et al. (2019). Identification of potential key genes and pathways in early-onset colorectal cancer through bioinformatics analysis. *Cancer Control* 26:1073274819831260. doi: 10.1177/1073274819831260

Zhao, Y., Ge, X., Xu, X., Yu, S., Wang, J., and Sun, L. (2019). Prognostic value and clinicopathological roles of phenotypes of tumour-associated macrophages in colorectal cancer. *J. Cancer Res. Clin. Oncol.* 145, 3005–3019. doi: 10.1007/s00432-019-03041-8

Zhu, N., and Hou, J. (2020). Assessing immune infiltration and the tumor microenvironment for the diagnosis and prognosis of sarcoma. *Cancer Cell Int.* 20:577. doi: 10.1186/s12935-020-01672-3

Conflict of Interest: The authors declare that the research was conducted in the absence of any commercial or financial relationships that could be construed as a potential conflict of interest.

frontiers in Molecular Biosciences

ORIGINAL RESEARCH
published: 30 April 2021
doi: 10.3389/fmolb.2021.646786

LINC02257, an Enhancer RNA of Prognostic Value in Colon Adenocarcinoma, Correlates With Multi-Omics Immunotherapy-Related Analysis in 33 Cancers

*Junbo Xiao, Yajun Liu, Jun Yi and Xiaowei Liu**

Department of Gastroenterology, Xiangya Hospital, Central South University, Changsha, China

Accumulated evidence supports that long non-coding RNAs (lncRNAs) are involved significantly in the development of human cancers. Enhancer RNAs (eRNAs), a subtype of lncRNAs, have recently attracted much attention about their roles in carcinogenesis. Colon adenocarcinoma is one of the most commonly diagnosed tumors with unfavorable prognosis. It highlights the great significance of screening and identifying novel biomarkers. More importantly, it remains to be elucidated with respect to the function of eRNAs in colon adenocarcinoma, as is in pan-cancers. The expression of LINC02257 was determined based on the data obtained from The Cancer Genome Atlas (TCGA). Further evaluation was performed on the basis of the following analyses: clinicopathology and survival analysis, gene ontology (GO) terms, and Kyoto Encyclopedia of Genes and Genomes (KEGG) pathway analysis, as well as multi-omics immunotherapy-related analysis and co-expression analysis. The statistical analysis was conducted in R software, and immune cell infiltration of LINC02257 expression in cancers was investigated by using the CIBERSORT algorithm. By large-scale data mining, our study highlighted that a total of 39 eRNA genes were associated with colon adenocarcinoma prognosis, among which 25 eRNAs showed significant associations with their predicted target genes. LINC02257 was identified as the most significant survival-associated eRNA, with DUSP10 as its target gene. Besides, the high expression of LINC02257 in colon adenocarcinoma was more vulnerable to unfavorable prognosis and correlated with various clinical characteristics. GO and KEGG analyses revealed that LINC02257 was closely correlated with extracellular matrix organization via the PI3K-Akt signaling pathway. Besides, LINC02257 expression correlated with a multi-omics analysis of 33 cancer types, such as survival analysis [overall survival (OS), disease-specific survival (DSS), disease-free interval (DFI), and progression-free interval (PFI)] and immunotherapy-related analysis [tumor microenvironment (TME), tumor mutational burden (TMB), and microsatellite instability (MSI)]. Finally, we investigated the co-expression genes of LINC02257 and its

OPEN ACCESS

Edited by:
Hongming Miao,
Army Medical University, China

Reviewed by:
Lian Xiang Luo,
Macau University of Science and Technology, Macau
Meng Sun,
Stanford University, United States

***Correspondence:**
Xiaowei Liu
liuxw@csu.edu.cn

Specialty section:
This article was submitted to Molecular Diagnostics and Therapeutics, a section of the journal Frontiers in Molecular Biosciences

Received: *28 December 2020*
Accepted: *01 March 2021*
Published: *30 April 2021*

Citation:
Xiao J, Liu Y, Yi J and Liu X (2021) LINC02257, an Enhancer RNA of Prognostic Value in Colon Adenocarcinoma, Correlates With Multi-Omics Immunotherapy-Related Analysis in 33 Cancers. Front. Mol. Biosci. 8:646786. doi: 10.3389/fmolb.2021.646786

potential signaling pathways across different cancer types. LINC02257 is screened and can function as an independent prognostic biomarker through the PI3K-Akt signaling pathway for colon adenocarcinoma. Simultaneously, LINC02257 may be a multifaceted and significant immunotherapy-related eRNA in different cancers.

Keywords: LINC02257, enhancer, pan-cancers, immune-related multi-omics analysis, bioinformatic analysis

INTRODUCTION

Colorectal cancer (CRC) encompasses cancers of the colon and the rectum, which has been recognized to be one of the most commonly diagnosed gastroenterological malignancies. It accounts for the second and third leading cause of cancer-related mortality among males and females worldwide, respectively (Esmaeili et al., 2020; Harada and Morlote, 2020). Colon adenocarcinoma is a malignancy that originates from the intestinal epithelium and has a rapid increase in its incidence. Despite remarkable advances in its diagnosis and treatment during the past decades, the prognosis is still not satisfying, with a 5-year survival rate of less than 60% (Zhou et al., 2020). Besides, accumulated evidence supports that frequent postoperative sporadic relapse and/or metastatic recurrence exerts crucial effects on the prognosis of colon adenocarcinoma patients. Accordingly, it is essential to clarify the molecular mechanisms concerning colon carcinogenesis and to explore promising diagnostic and therapeutic biomarkers to improve patients' prognosis (Vasaikar et al., 2019).

Enhancers are typically considered as regulatory DNA elements that enhance target genes' transcription, which is bound by RNA polymerase II (RNAP II), transcription factors, and co-regulators. Recently, enhancers have been reported to transcribe non-coding RNAs (ncRNAs), known as enhancer RNAs (eRNAs) (Zhang et al., 2019), large numbers of which have been identified to play pivotal roles in mediating the activation of target genes at the transcription level. Meanwhile, the activation and generation of eRNAs are indispensable in human cancers, specifically in the activation of oncogenes or oncogenic signaling pathways (Kim et al., 2010; Li et al., 2016; Zhang et al., 2019). Previous studies have demonstrated a possible dual effect of eRNAs in the tumorigenesis of cancers. For example, in prostate cancer, Kallikrein-related peptidase 3 eRNA (KLK3e), an eRNA produced by KLK3's upstream enhancers, can selectively enhance the androgen receptor (AR)-dependent gene expression, resulting in a positive effect on prostate cancer cell proliferation (Hsieh et al., 2014). However, p53-induced eRNAs are required for p53 transcription enhancement and p53-dependent cell-cycle arrest (Melo et al., 2013). Taken together, eRNAs may play crucial roles in tumorigenesis and show the promising clinical prospect of eRNA-targeted therapy (Leveille et al., 2015).

In addition to the development of chemotherapy and radiotherapy, immune-related mechanisms and immunotherapeutic strategies are currently under extensive investigation. Immunotherapy has undergone a tremendous transformation from mechanistically complicated protocols to the forefront of armamentarium for some malignant tumors (Gravitz, 2013), which targets components of tumor microenvironment (TME) or immunotherapy biomarkers of microsatellite instability (MSI) and tumor mutational burden (TMB), specifically in colon adenocarcinoma (Frankel et al., 2017; Chang et al., 2018; Locy et al., 2018; Chan et al., 2019). To the best of our knowledge, there are so far no reports on immunotherapy-associated eRNAs, as well as their underlying functions and mechanisms.

Here, the present study was carried out to identify potential prognostic eRNA, LINC02257, and its target gene in colon adenocarcinoma. Further comprehensive analysis was conducted focusing on LINC02257 expression and association with survival in colon adenocarcinoma patients (Gu et al., 2019; Sun and Ling, 2019). Meanwhile, gene ontology (GO) and Kyoto Encyclopedia of Genes and Genomes (KEGG) analyses were also performed in our subsequent investigation. Moreover, the connection between LINC02257 and 33 cancer types was analyzed by using immunotherapy-related analysis, including TMB, MSI, and TME. It is expected to shed light on the understanding of eRNAs in immune-related treatment among various cancers.

Abbreviations: ACC, adrenocortical carcinoma; AR, androgen receptor; BLCA, bladder urothelial carcinoma; BRCA, breast invasive carcinoma; CESC, cervical squamous cell carcinoma and endocervical adenocarcinoma; CHOL, cholangiocarcinoma; COAD, Colon adenocarcinoma; CRC, colorectal cancer; DFI, disease-free interval; DLBC, lymphoid neoplasm diffuse large B-cell lymphoma; DSS, disease-specific survival; eRNA, enhancer RNA; ESCA, esophageal carcinoma; ESTIMATE, Estimation of stromal and Immune cells in Malignant Tumors using Expression data; FDR, false discovery rate; GBM, glioblastoma multiforme; HNSC, head and neck squamous cell carcinoma; KICH, kidney chromophobe; KIRC, kidney renal clear cell carcinoma; KIRP, kidney renal papillary cell carcinoma; KLK3e, Kallikrein-related peptidase 3 eRNA; LAML, acute myeloid leukemia; LGG, brain lower-grade glioma; LIHC, liver hepatocellular carcinoma; LUAD, lung adenocarcinoma; LUSC, lung squamous cell carcinoma; MESO, mesothelioma; MSI, microsatellite instability; ncRNA, non-coding RNA; OS, overall survival; OV, ovarian serous cystadenocarcinoma; PAAD, pancreatic adenocarcinoma; PCPG, pheochromocytoma and paraganglioma; PFI, progression-free interval; PRAD, prostate adenocarcinoma; READ, rectum adenocarcinoma; RNAP II, RNA polymerase II; SARC, sarcoma; SKCM, skin cutaneous melanoma; STAD, stomach adenocarcinoma; TCGA, The Cancer Genome Atlas; TGCT, testicular germ cell tumors; THCA, thyroid carcinoma; THYM, thymoma; TMB, tumor mutational burden; TME, tumor microenvironment; UCEC, uterine corpus endometrial carcinoma; UCS, uterine carcinosarcoma; UVM, uveal melanoma.

MATERIALS AND METHODS

The Cancer Genome Atlas Data Analysis

The expression of eRNAs in a variety of cancer (Workflow Type: HTSeq-FPKM) was obtained from The Cancer Genome Atlas (TCGA) database [1], together with related clinical and survival information (Subramanian et al., 2005; Wang et al., 2016). Many

[1] https://portal.gdc.cancer.gov/

collected samples were screened, with data showing insufficient information (age, tumor stage, survival, etc.) excluded. Our study was conducted in line with TCGA publication guidelines[2]. Potential eRNAs with significant correlations with both overall survival (OS) ($p < 0.05$, a false discovery rate (FDR)-adjusted p-value < 0.05) and levels of their target genes ($R > 0.4$, $p < 0.001$, FDR-adjusted p-value < 0.05) were considered as key eRNAs in colon adenocarcinoma (Gu et al., 2019).

Gene Set Enrichment Analysis

Gene set enrichment analysis (GSEA) was performed by using normalized RNA-Seq data from TCGA database (Subramanian et al., 2005). GO terms and KEGG pathways were further analyzed to investigate possible biological functions of LINC02257. Specifically, the GO analysis revealed the LINC02257 function in the biology process, cell component, and molecular function, while the KEGG analysis showed the pathway enrichment of LINC02257. To be identified as statistically significant, enrichment results shall meet the following two criteria: a false discovery rate (FDR) < 0.050 and a nominal p-value < 0.050.

Analysis of Immune Cell Infiltrates

Calculation of the stromal and immune scores by using the Estimation of stromal and Immune cells in Malignant Tumors using Expression data (ESTIMATE) algorithm regarding the downloaded RNA expression data and cancer samples was categorized by the median of immune/stromal scores into high- and low-score groups. ESTIMATE output stromal and immune scores performed a single-sample GSEA (Verhaak et al., 2010; Yoshihara et al., 2013; Aran et al., 2015). Furthermore, an algorithm called CIBERSORT[3] was used for assessing the gene expression among sets in the samples (Newman et al., 2015), with the aim to measure the immune response of 22 tumor-infiltrating immune cells (TIICs), so as to evaluate their association with LINC02257 expression in different types of cancer and to uncover their relationships with TIICs.

[2]http://cancergenome.nih.gov/abouttcga/policies/publicationguidelines

[3]http://cibersort.stanford.edu/

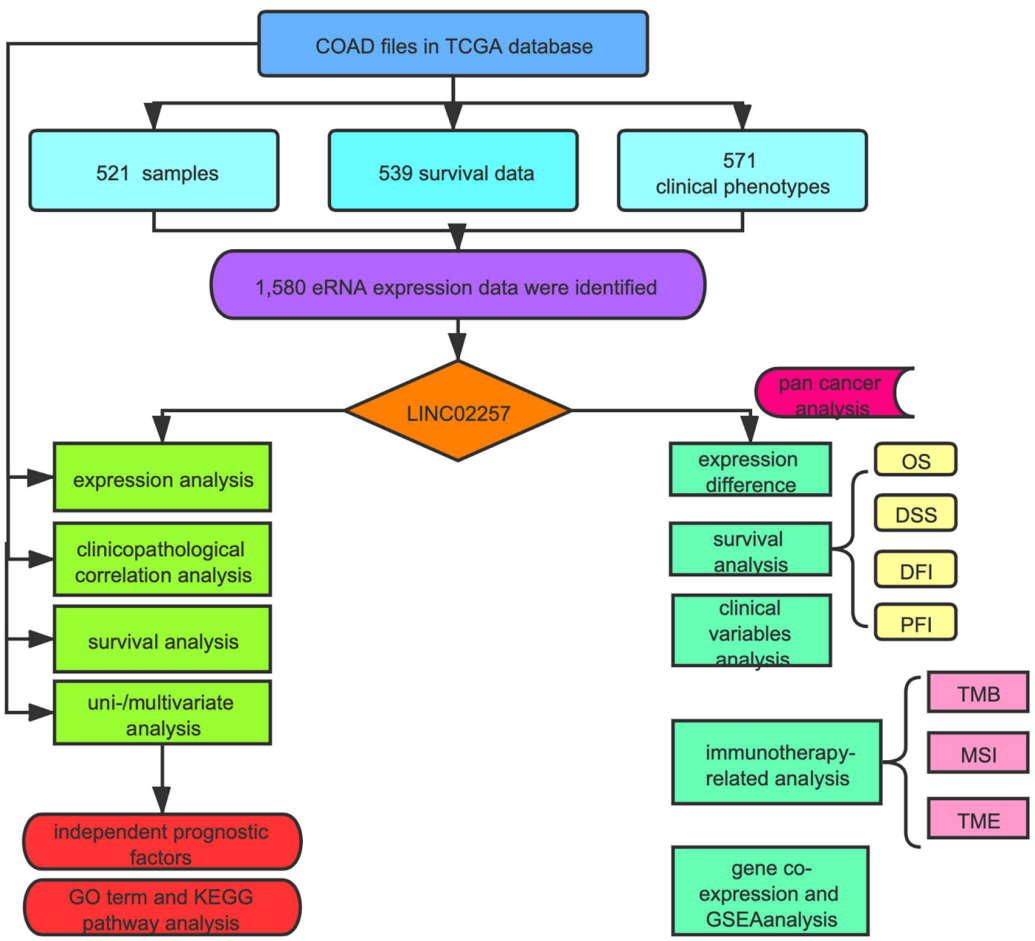

FIGURE 1 | Flowchart of the study.

Comprehensive Analysis

Samples from TCGA database were used to analyze the correlation between LINC02257 expression and clinicopathological features of patients with colon adenocarcinoma. Meanwhile, a swarmplot using cancer types as a variable was utilized to illustrate the differential expression of LINC02257. In addition, the OS, disease-specific survival (DSS), disease-free interval (DFI), and progression-free interval (PFI) analysis were performed to analyze the relationship between LINC02257 expression and patients' prognosis (Uhlen et al., 2015).

Statistical Analysis

All statistical analyses were conducted using R software (version 3.5.3). The comparison between tumor and normal tissues was evaluated by the non-parametric Wilcoxon signed-rank test. The correlation was assessed by using Spearman's rank correlation coefficient. Furthermore, both the univariate and multivariate models of the Cox analysis were applied to calculate the 95% confidence interval (CI) and hazard ratio (HR). Univariate survival analysis was used to compare several clinical characteristics with survival rate. Multivariate Cox analysis was further performed to evaluate the effect of LINC02257 expression, along with other pathological and clinical factors (age, gender, tumor size, distant metastasis, and tumor stage) on the OS of patients. R package "mediation" (version 3.5.3) was performed for mediation analysis for age as mediation between LINC02257 and survival. A p-value < 0.05 and FDR-adjusted p-value < 0.05 was considered to predict the presence of statistically significant difference.

TABLE 1 | List of overall survival associated genes derived from enhancers.

eRNA	KM	Target	cor	corPval	FDR-adjusted *p*-value
AC012368.1	0.04831255	PELI1	0.32603608	3.98E−13	4.01E−13
AC022784.1	0.00500228	PPP1R3B	0.13996317	0.00233081	0.00117483
AC046134.2	0.03415434	RBP1	0.10316519	0.02519561	0.01147073
AC053527.2	0.00236009	ALB	0.16513588	0.00031934	0.00017334
AC092944.1	0.01159129	CCNL1	0.33978972	3.42E−14	3.71E−14
AC108751.4	0.02061273	TM4SF1	0.35391784	2.41E−15	3.09E−15
AC108751.4	0.02061273	TM4SF18	0.07701974	0.09500592	0.03943662
AC139149.1	0.04345036	BAHCC1	0.25244199	2.79E−08	2.07E−08
AL139246.2	0.04486095	TNFRSF14	0.2854273	2.79E−10	2.32E−10
AL353747.3	0.03940883	UNC93A	0.57486828	8.86E−43	4.17E−42
AL683813.2	0.01629478	ARHGEF6	0.14910866	0.00117204	0.00061264
AP003555.1	0.00550634	ANO1	0.58781578	4.19E−45	2.95E−44
AP003555.2	0.00450645	ANO1	0.50814036	2.75E−32	9.69E−32
APELA	0.04674045	TRIM61	0.30716899	9.49E−12	8.37E−12
C2orf92	0.02682689	COX5B	−0.1376607	0.00277498	0.00135048
ELFN1	0.00517534	MAFK	0.34260487	2.74E−14	3.22E−14
ELFN1	0.00517534	TMEM184A	0.18242344	7.02E−05	4.31E−05
ELFN1	0.00517534	PSMG3	0.1089876	0.01801643	0.00847569
ELFN1-AS1	0.00372687	TMEM184A	0.31592828	2.94E−12	2.76E−12
LINC00174	0.03760549	TPST1	−0.0886271	0.05461454	0.02408719
LINC00649	0.00900198	SLC5A3	0.21018374	4.21E−06	2.83E−06
LINC00649	0.00900198	MRPS6	0.08409923	0.06822039	0.02917616
LINC02257	0.00012532	DUSP10	0.43606423	2.78E−23	5.60E−23
LINC02381	0.04837723	HOXC4	0.61105361	1.50E−49	2.11E−48
LINC02381	0.04837723	HOXC8	0.47911944	2.11E−28	5.94E−28
LINC02381	0.04837723	HOXC6	0.45614791	1.40E−25	3.29E−25
LINC02381	0.04837723	HOTAIR	0.20178279	1.02E−05	6.54E−06
LINC02381	0.04837723	HOXC11	0.17679999	0.00011467	6.74E−05
LINC02381	0.04837723	HOXC13	0.16609247	0.00029435	0.00016617
MIR4435-2HG	0.04207077	BCL2L11	0.2362846	2.31E−07	1.63E−07
MYOSLID	0.01159681	KLF7	0.27154907	2.09E−09	1.64E−09
STEAP1B	0.01517609	IL6	0.40453792	5.68E−20	8.91E−20
TMEM184A	0.02072743	MICALL2	0.37560806	2.69E−18	3.80E−18
ZNRF2P2	0.03039512	PRR15	0.40759279	2.81E−20	4.96E−20

Spearman's rank correlation coefficient $r > 0.4$, $p < 0.001$. FDR-adjusted p-value < 0.05 was considered statistically significant. eRNA, enhancer RNA; FDR, false discovery rate.

RESULTS

Enhancer RNAs of Prognostic Value in Colon Cancer

As indicated in **Figure 1**, data mining using TCGA database was achieved from a total of 60,484 RNA-seq gene expression data of colon adenocarcinoma samples (n = 521), survival data (n = 539), and clinical phenotypes (n = 571). After that, a targeted number of 1,580 eRNA expression data were extracted from those samples. For an in-depth analysis, the intersection between the screened eRNA expression and survival data was performed with the collection of 1,570 eRNA expression data of 449 samples. Two subgroups of high and low expression groups were divided based on the median value of eRNA expression, and 39 eRNA gene expressions were associated with the prognosis of colon adenocarcinoma (**Supplementary Table 1**, Kaplan–Meier log-rank test, $p < 0.05$, FDR-adjusted p-value < 0.05). In addition, significant correlation levels of these 39 eRNAs with their predicted target genes were only in 25 eRNAs (Spearman's rank correlation coefficient $r > 0.4$, $p < 0.001$, FDR-adjusted p-value < 0.05; **Table 1**). Specifically, LINC02257 and its predicted target DUSP10 (Png et al., 2016) were identified as the most prognostic eRNA with the least p-value of Kaplan–Meier log-rank test regarding the previous 25 eRNAs.

High Expression of LINC02257 Correlates With Clinicopathological Variables and Predicts Unfavorable Prognosis in Colon Adenocarcinoma

Data extraction was performed concerning the expression of LINC02257 in tumor and normal tissue samples from colon adenocarcinoma in TCGA database. Wilcoxon test was used to identify the difference of LINC02257 expression in a total of 398 tumor files and 39 normal files plotted on a swarmplot ($p < 0.05$, **Figure 2A**). Additionally, there was significant difference in LINC02257 expression between the paired tumor tissues and the normal tissues in the same sample ($p < 0.05$, **Figure 2B**). Furthermore, according to the correlation analysis between LINC02257 and a variety of clinicopathological variables, the increased expression of LINC02257 was related to patient age (p-value = 0.02, **Figure 2C**), T stage (p-value = 0.008, **Figure 2E**), N stage (p-value = 0.027, **Figure 2F**), and stages I–IV (p-value = 0.004, **Figure 2H**). Besides gender (p-value =

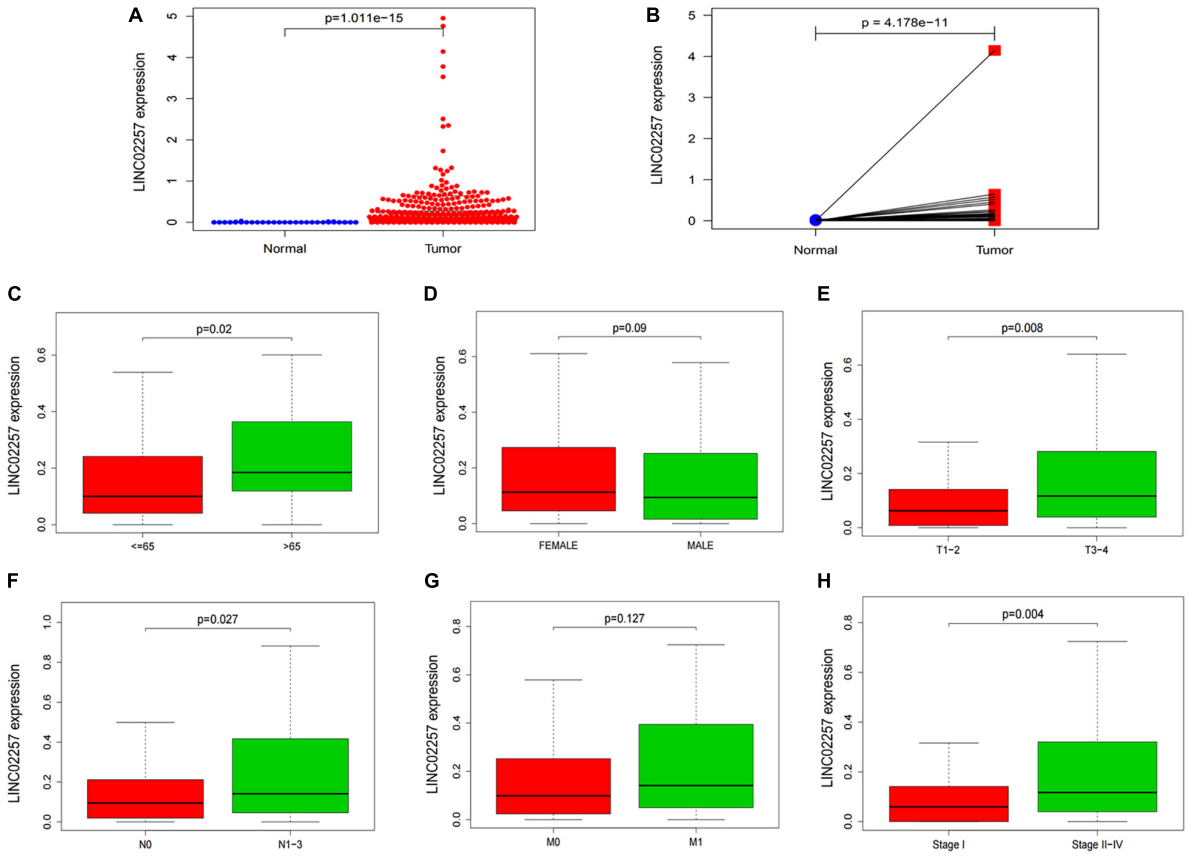

FIGURE 2 | LINC02257 is correlated with multiple Clinicopathological variables in COAD **(A)** LINC02257 expression in 39 normal tissues and 398 tumor tissues via Wilcox test in a swarm plot, **(B)** LINC02257 expression between the paired tumor tissues and the normal tissues in the same sample. **(C–H)** High expression of LINC02257 is related to the patients age, T, N and stages I–IV and shows no significant correlation with gender and M ($p < 0.05$ was considered significant).

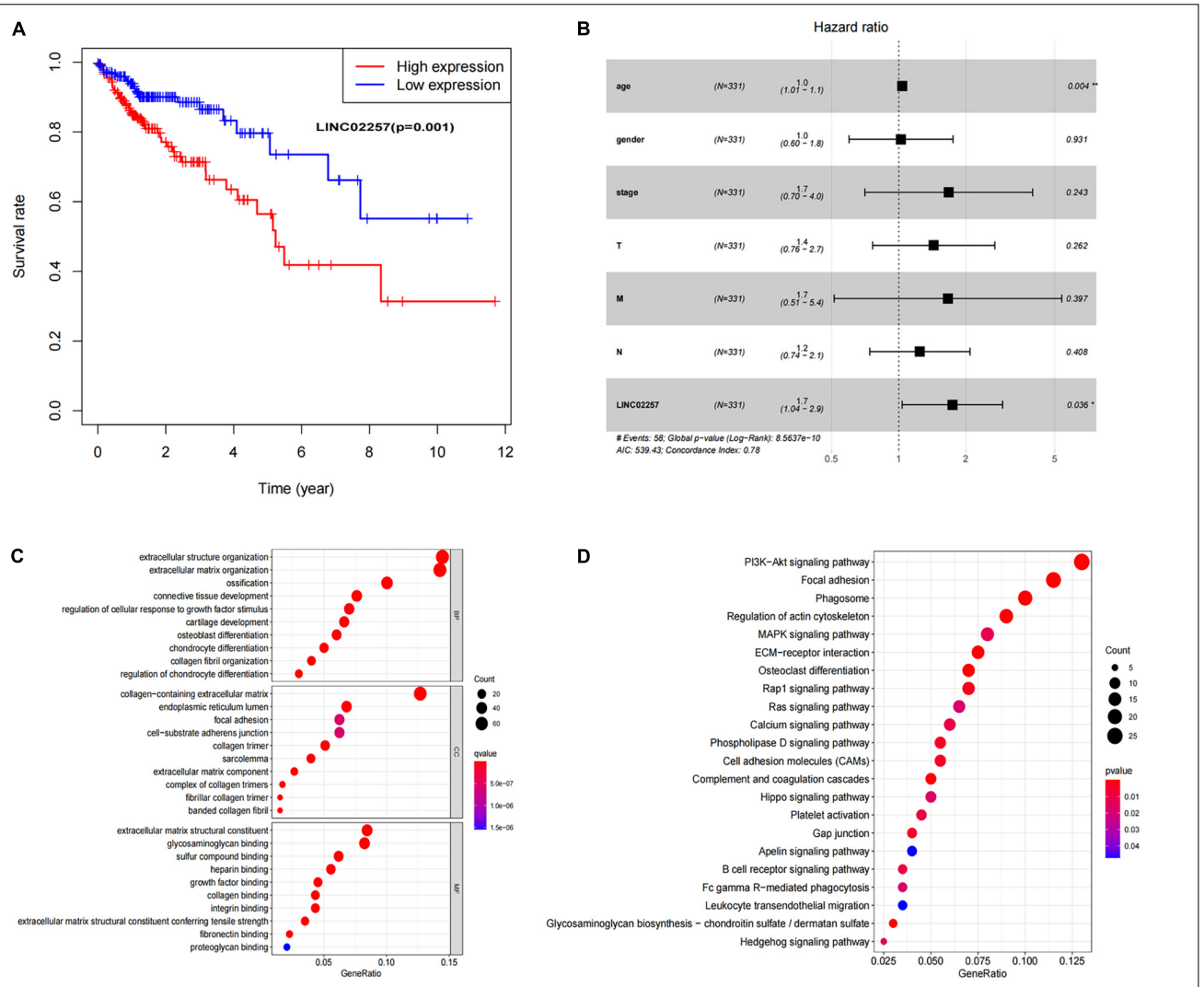

FIGURE 3 | Survival analysis of LINC02257 and GO term and KEGG pathway analysis in COAD **(A)** LINC02257 related to the survival time of patients, and with the increase of LINC02257 expression, the prognosis of colon cancer patients was worse. **(B)** Multivariate COX regression analysis suggests that age and expression of LINC02257 could be independent factors for the prognosis survival of colon cancer patients. **(C)** GO enrichment analysis shows that the biological processes and molecular functions are strongly associated with LINC02257 in extracellular structure organization, ossification, collagen fibril organization and connective tissue development. **(D)** KEGG pathway analysis shows five pathways of the significant correlation with LINC02257 expression: PI3K-Akt signaling pathway. Focal adhesion, Phagosome, Regulation of actin cytoskeleton and MAPK signaling pathway ($p < 0.05$ was considered significant).

TABLE 2 | Univariate analysis and multivariate analysis of the correlation of LINC02257 expression with OS among colon adenocarcinoma patients.

Parameter	Univariate analysis					Multivariate analysis			
	HR	HR.95L	HR.95H	*p*	FDR-adjusted *p*-value	HR	HR.95L	HR.95H	*p*-value
Age	1.030	1.005	1.055	**0.018**	**0.036**	1.037	1.012	1.063	**0.004**
Gender	1.126	0.668	1.899	0.655	0.655	1.024	0.599	1.751	0.930
Stage	2.502	1.851	3.382	**2.48E−09**	**1.49E−08**	1.675	0.705	3.980	0.243
T classification	2.927	1.742	4.917	**4.97E−05**	**1.99E−04**	1.434	0.764	2.695	0.262
N classification	5.226	3.065	8.911	**1.25E−09**	**2.20E−06**	1.661	0.513	5.375	0.397
M classification	2.175	1.609	2.941	**4.41E−07**	**8.78E−09**	1.243	0.742	2.086	0.408
LINC02257	1.911	1.245	2.932	**0.003**	**0.009**	1.738	1.036	2.918	**0.036**

Bold value indicates p < 0.005. FDR-adjusted p-value < 0.05 was considered statistically significant. OS, overall survival; HR, hazard ratio; FDR, false discovery rate.

0.19, **Figure 2D**) and M stage (p-value = 0.127, **Figure 2G**) show no significant correlation with LINC02257 expression. In accordance with the Cox analysis on the relationship between LINC02257 expression and OS, it was found that the expression of LINC02257 was related to the survival time of patients, and a worse prognosis was found along with the increase of LINC02257 expression (Kaplan–Meier log-rank test, p = 0.001, **Figure 3A**). As illustrated in **Table 2**, some

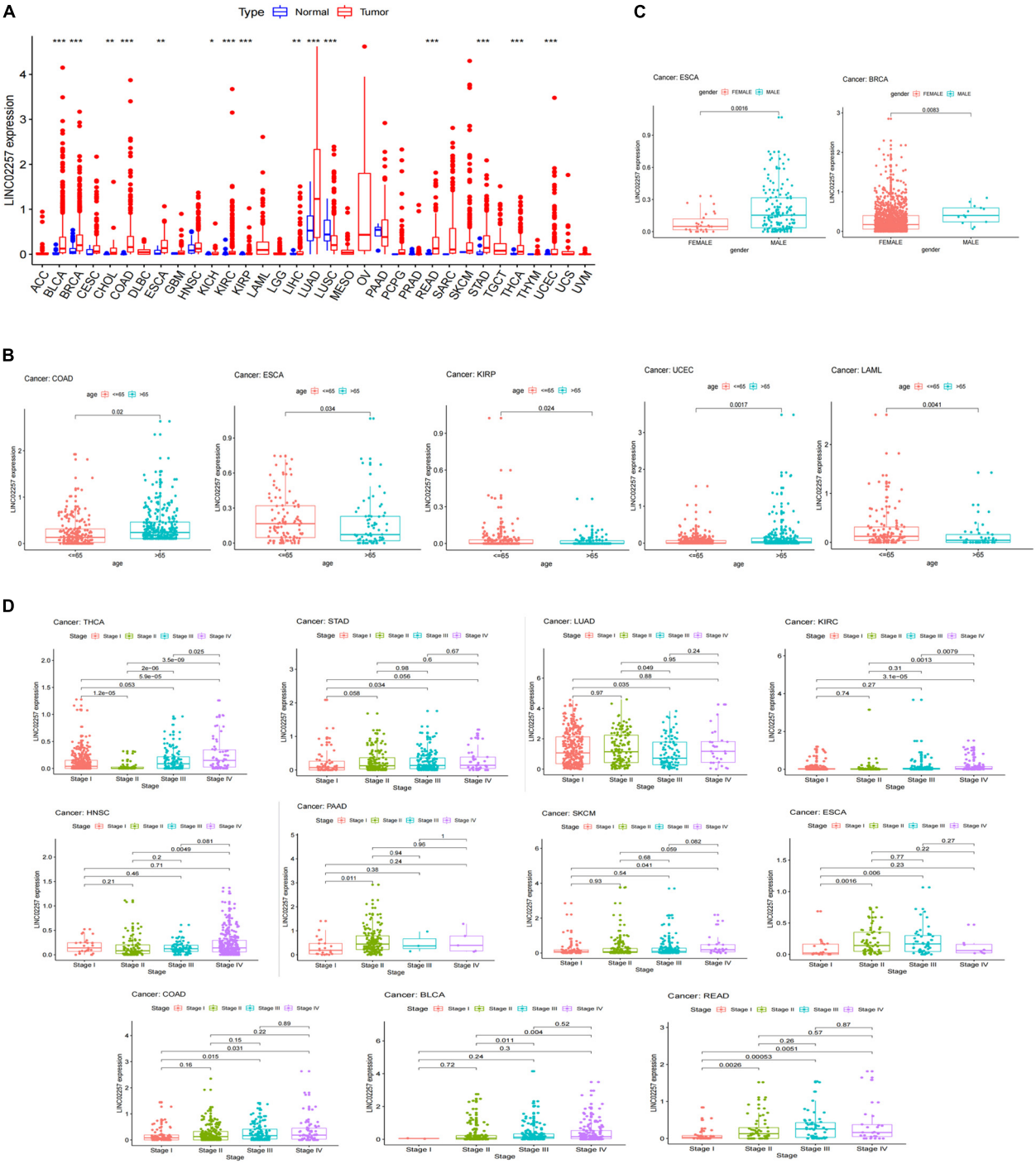

FIGURE 4 | LINC02257 expression in 33 cancer types and its correlation with various clinicopathology features **(A)** LINC02257 in 33 tumor tissues and normal tissues; (*P < 0.001, *P < 0.01, *P < 0.05, no *P > 0.05) **(B)** In terms of age, COAD, ESCA, KIRP, UCEC, LAML show significant differences with LINC02257 expression. **(C)** As for gender, LINC02257 expression significantly correlates with ESCA and BRCA. **(D)** The stage of THCA, STAD, SKCM, READ, PAAD, LUAD, KIRC, HNSC, ESCA, COAD, BLCAexerts significant correlations with LINC02257 expression (p < 0.05 was considered significant).

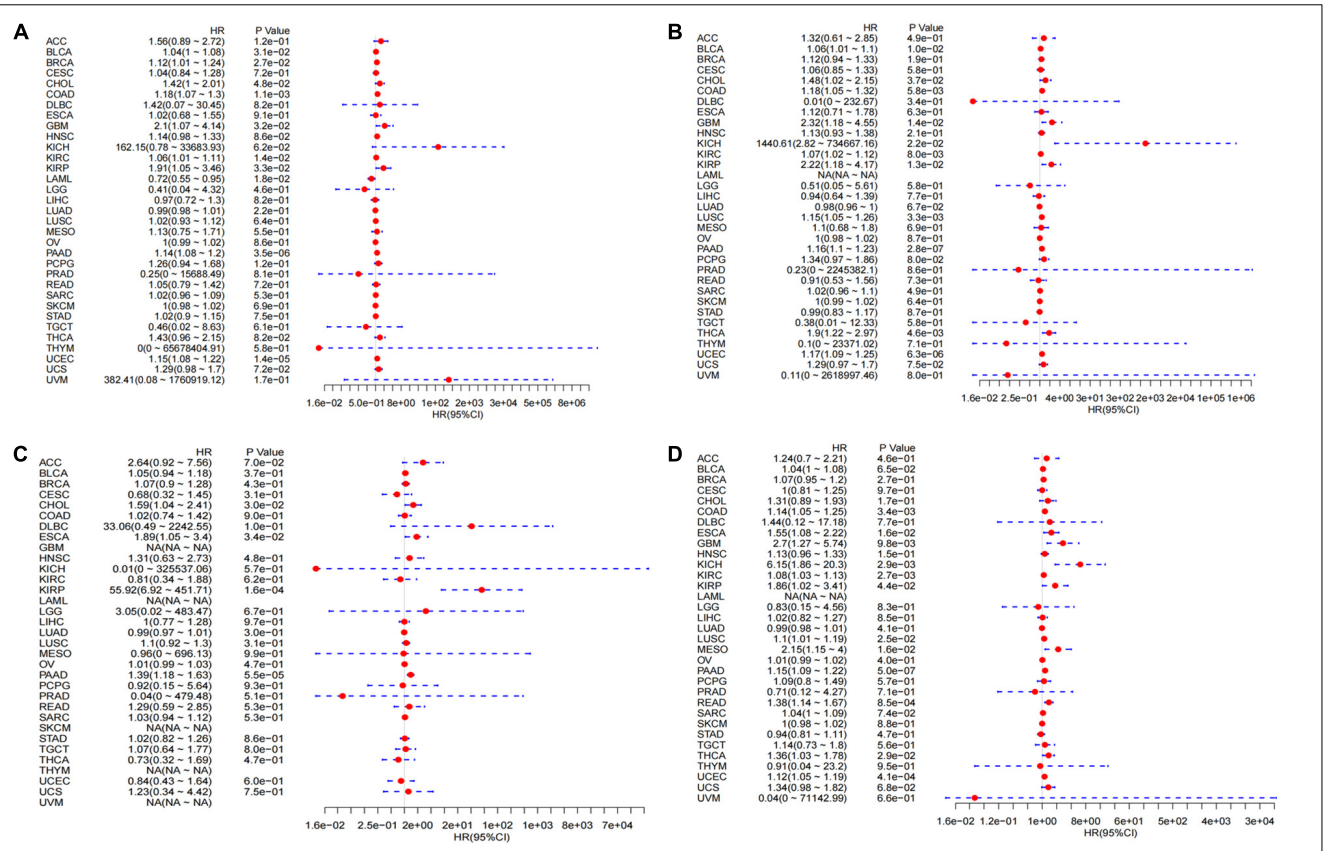

FIGURE 5 | Integrated survival analysis of LINC02257 expression in 33 cancer types **(A)** The expression of LINC02257 is significant related to OS in BLCA, BRCA, CHOL, COAD, GBM, KIRC, LAML, LUAD, PAAD, UCEC. **(B)** In respect to DSS, BLCA, CHOL, COAD, GBM, KICH, KIRC, KIRP, LUSC, PAAD, THCA, UCEC show significant correlation to LINC02257. **(C)** As for DFI, CHOL, ESCA, KIRP, PAAD is significantly related to LINC02257 expression. **(D)** PFI of COAD, GBM, KICH, KIRC, KIRP, LUSC, MESO, PAAD, READ, THCA, UCEC is significantly related to LINC02257 expression. $P < 0.05$ indicates that the expression of LINC02257 is significantly correlated with the prognosis and survival of the patients. HR > 1, with the increase of LINC02257 expression, the risk of poor prognosis is higher).

parameters, revealed by a univariate analysis of correlation, such as age (HR = 1.030, p-value < 0.018, FDR-adjusted p-value < 0.036), stage (HR = 2.502, p-value < 2.48E-09, FDR-adjusted p-value < 1.49E-08), T stage (HR = 2.927, p-value < 4.97E−05, FDR-adjusted p-value < 1.99E-04), N stage (HR = 5.226, p-value < 1.25E−09, FDR-adjusted p-value < 2.20E-06), M stage (HR = 2.175, p-value < 4.41E−07, FDR-adjusted p-value < 8.78E-09), and LINC02257 expression (HR = 1.911, p-value < 0.003, FDR-adjusted p-value < 0.009) were obviously associated with OS. Multivariate analysis, as shown in a forest boxplot in **Figure 3B**, revealed that age (HR = 1.037, p-value < 0.004) and LINC02257 expression (HR = 1.738, p-value < 0.036) were independent prognostic factors for colon adenocarcinoma patients.

Subsequently, in order to better understand the biological function of LINC02257 in colon adenocarcinoma, GO term and KEGG pathway analyses were performed after the normalization and preparation of transcriptome data from TCGA database (FDR < 0.050, p-value < 0.050, **Figures 3C,D**). As shown in **Figure 3C**, the biological processes and molecular functions strongly associated with LINC02257 expression were extracellular structure organization, ossification, collagen fibril organization, and connective tissue development. KEGG pathway analysis showed five pathways that had a significant correlation with LINC02257 expression: PI3K-Akt signaling pathway, Focal adhesion, Phagosome, Regulation of actin cytoskeleton, and MAPK signaling pathway (**Figure 3D**). Accordingly, these results suggest that LINC02257 expression may regulate extracellular structure organization through the PI3K-Akt signaling pathway, which is critically important in colon adenocarcinoma patients.

LINC02257 Gene Expression Correlates With a Multi-Omics Analysis of 33 Cancer Types

Clinical Characteristics and Survival Analysis

A swarmplot in **Figure 4A** shows the difference in LINC02257 expression across 33 cancer types and their corresponding normal tissues from TCGA project. Consequently, the expression differences could be found in BLCA, BRCA, CHOL, COAD, ESCA, KICH, KIRC, KIRP, LIHC, LUAD, LUSC, READ, STAD, THCA, and UCEC. Further analysis was performed concerning the correlation of LINC02257 expression and clinicopathological

TABLE 3 | Correlation analysis regarding the association of LINC02257 expression and TMB.

Cancer type	cor	*p*-value	Cancer type	cor	*p*-value
ACC	0.18	0.113	LUSC	−0.10	0.022*
BLCA	0.02	0.639	MESO	0.05	0.631
BRCA	0.03	0.354	OV	−0.07	0.226
CESC	0.03	0.577	PAAD	0.12	0.134
CHOL	0.18	0.300	PCPG	0.062	0.378
COAD	0.13	0.008**	PRAD	−0.03	0.536
DLBC	0.12	0.463	READ	0.073	0.409
ESCA	−0.04	0.620	SARC	0.25	8.81E-05***
GBM	−0.14	0.099	SKCM	0.08	0.069
HNSC	−0.09	0.045*	STAD	0.20	9.28E-05***
KICH	0.14	0.274	TGCT	0.24	0.004**
KIRC	0.09	0.117	THCA	0.14	0.001**
KIRP	−0.17	0.004**	THYM	0.25	0.007**
LAML	−0.46	0.0001***	UCEC	−0.02	0.608
LGG	0.031	0.487	UCS	0.04	0.770
LIHC	0.059	0.266	UVM	−0.10	0.388
LUAD	−0.04	0.318			

****p < 0.001, **p < 0.01, *p < 0.05, no *p > 0.05. TMB, tumor mutational burden.*

features in patients with different types of cancer. In respect to age, COAD, ESCA, KIRP, UCEC, and LAML showed significant differences with LINC02257 expression (**Figure 4B**). Regarding gender, LINC02257 expression significantly correlated with ESCA and BRCA in **Figure 4C**. In addition, the stage of THCA, STAD, SKCM, READ, PAAD, LUAD, KIRC, HNSC, ESCA, COAD, and BLCA exerted significant correlations with LINC02257 expression, as shown in **Figure 4D**. In terms of survival analysis, the relationship of LINC02257 expression with OS, DSS, DFI, and PFI in cancers clarified that LINC02257 expression, acting as a high hazardous factor, was associated with the prognosis of multiple cancer types (**Figure 5**).

Multi-Omics Immunotherapy-Related Analysis

Tumor mutational burden

Tumor mutational burden is considered as a hallmark of genomic alterations, the increase of which could induce new antigens to facilitate immune recognition, producing better immunotherapy responses or favorable prognosis (Sabari et al., 2018). However, it is still unclear with regard to the significance of LINC02257 expression in TMB. TMB data were obtained from 33 cancers, followed by Spearman correlation analysis to assess the association of LINC02257 expression and TMB (**Table 3**, as a radar legend in **Figure 6A**). The result showed that LINC02257 expressions in COAD, HNSC, KIRP, LAML, LUSC, SARC, STAD, TGCT, and THCA were of great significance with TMB, among which LAML, SARC, and STAD exhibited the strongest correlation with TMB ($p < 0.001$).

Microsatellite instability

MSI caused by hypermutability (gain or loss) of nucleotides from DNA elements, which was initially related to CRCs (Oki et al., 1999), is recently defined as a diagnostic hallmark of diverse cancer types and a promising marker for immune-checkpoint blockade therapy (Hause et al., 2016). However, there is no relevant research on MSI and LINC02257 expression. Accordingly, our subsequent experiment explored their relationship across multiple cancer types. To be more specific, after the MSI data were collected from TCGA database, Spearman analysis was performed between MSI and LINC02257 expression

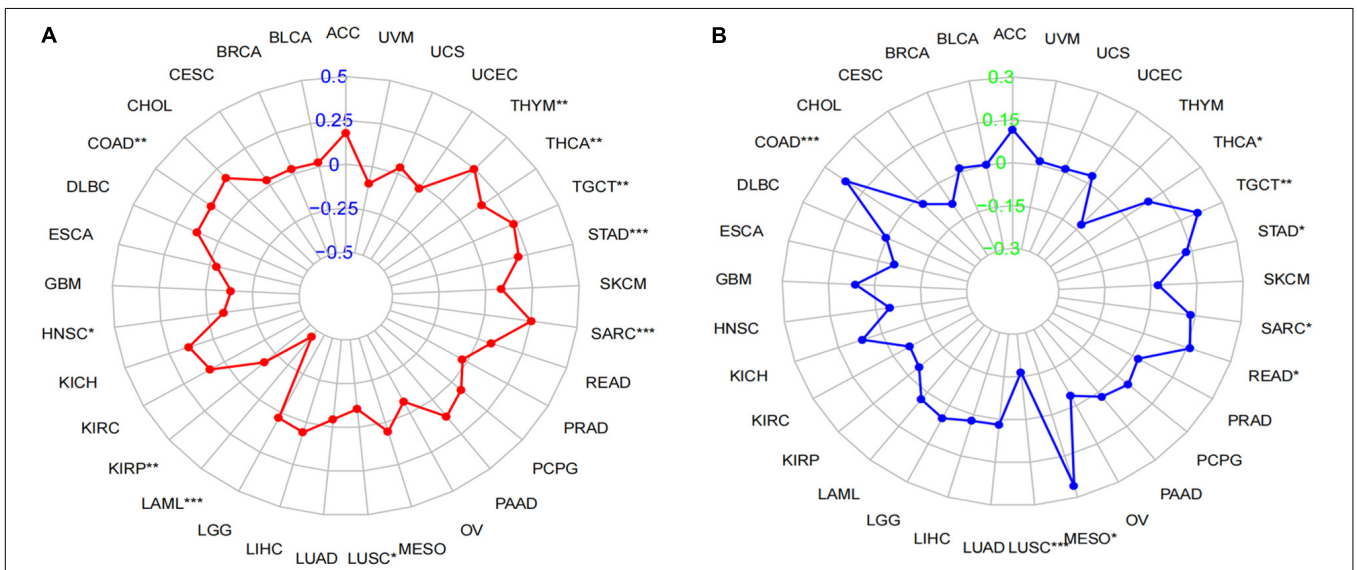

FIGURE 6 | Correlation of LINC02257 expression with TMB and MSI in multiple cancer. **(A)** Correlation between TMB and LINC02257 expression. **(B)** Correlation between MSI and LINC02257 expression. Spearman's correlation coefficients are shown above the bar graphs. (Spearman Correlation test, $p < 0.05$ was considered significant, $^*p < 0.05$, $^{**}p < 0.0l$, $^{***}p < 0.001$).

TABLE 4 | Correlation analysis regarding the association of LINC02257 expression and MSI.

Cancer type	cor	p-value	Cancer type	cor	p-value
ACC	0.12	0.308	LUSC	0.17	0.0002***
BLCA	0.001	0.976	MESO	0.26	0.019*
BRCA	0.01	0.642	OV	0.04	0.519
CESC	0.09	0.133	PAAD	0.02	0.806
CHOL	0.03	0.870	PCPG	0.05	0.535
COAD	0.21	7.175E-06***	PRAD	0.02	0.644
DLBC	0.002	0.989	READ	0.16	0.049*
ESCA	0.05	0.496	SARC	0.13	0.034*
GBM	0.062	0.452	SKCM	0.02	0.605
HNSC	0.05	0.306	STAD	0.13	0.011*
KICH	0.07	0.597	TGCT	0.21	0.009**
KIRC	0.06	0.245	THCA	0.09	0.042*
KIRP	0.05	0.431	THYM	0.13	0.172
LAML	0.03	0.805	UCEC	0.03	0.493
LGG	0.05	0.271	UCS	0.01	0.932
LIHC	0.02	0.676	UVM	0.01	0.908
LUAD	0.02	0.677			

$^{***}p < 0.001$, $^{**}p < 0.01$, $^{*}p < 0.05$, no $^{*}p > 0.05$. MSI, microsatellite instability.

(**Table 4**, as a radar legend in **Figure 6B**). Results indicate that LINC02257 expressions in COAD, LUSC, MESO, READ, SARC, STAD, TGCT, and THCA were significantly related to MSI. Furthermore, LINC02257 expressions in COAD and LUSC had the most connection with MSI ($p < 0.001$).

Tumor microenvironment

Tumor microenvironment consists of tumor cells and non-tumor components. Stromal and immune cells are two main types of the later ones, the evaluation of which has been identified to be beneficial for cancer-targeted immunotherapies. An algorithm, called ESTIMATE, can help infer the fraction of stromal and immune cells and predict tumor purity in tumor samples. Hence, our study further analyzed the relationship of LINC02257 expression in cancers with stromal and immune cell scores calculated by ESTIMATE (**Table 5** and **Figure 7**). A higher corresponding cell score might indicate a higher ratio of corresponding components in TME and lower corresponding tumor purity. Besides, the relationship between LINC02257 expression of LINC02257 and the infiltration of 22 immune cells was investigated in 33 different types of tumors, including CD8 + T cells, T cells (general), B cells, monocytes, TAMs, M1 and M2 macrophages, neutrophils, natural killer (NK) cells, and dendritic cells (DCs) (**Figure 8**). After the correlation adjustment by purity, the results revealed that LINC02257 expression was significantly correlated with the infiltration of various immune cells and different T cells. Furthermore, it was significantly related to macrophage infiltration in BLCA, BRCA, COAD, ESCA, HNSC, KIRC, LAML, LUAD, PAAD, READ, SARC, SKCM, STAD, TGCT, and THCA. Moreover, LINC02257 expression showed a significant association with T cell infiltration in BRCA, CESC, HNSC, LUSC, PAAD, SARC, SKCM, STAD, THCA, and UCEC.

Co-expression of LINC02257 and potential signaling pathways across different cancer types

Equally important, the co-expression of the target gene LINC02257 was analyzed in each of the 33 tumors and its correlation, gene correlation p-value uploaded in a supplementary material pdf file, named geneCor. pvalue.pdf, as illustrated in a heatmap (**Figure 9**). Finally, GSEA of potential function/pathway characteristics of target gene LINC02257 affecting the development of 33 tumors is elaborated in the **Supplementary Material**, which completes our integrated multi-omics study of LINC02257 expression in pan-cancers.

DISCUSSION

As a subclass of lncRNAs, eRNAs may regulate the expression of corresponding genes at the transcription level and hence be involved in the development of various types of cancer. Studies have revealed that there has been uncovered multiple information about colon cancer biomarkers and signatures, which are involved in a series of physio-pathological process (de la Chapelle and Hampel, 2010; Harada and Morlote, 2020). However, few studies have investigated the importance and mechanisms of eRNAs in colon cancer and other tumorigenesis. Meanwhile, current attention has been paid to a comprehensive analysis of immunotherapy-related studies regarding eRNA (Gu et al., 2019). Thus, our study provides insights into understanding the potential role of LINC02257 in tumor immunology and its use as a biomarker for cancer development.

In our study, eRNAs of prognostic value were identified for colon cancer. A total of 1,580 eRNAs were successfully obtained from 521 colon cancer samples, of which LINC02257 was found to have the most significant impact on patients' survival with its corresponding target gene DUSP10, making it our top key eRNA for colon cancer. It has been documented that DUSP10 had a higher expression in colon cancer tissue than normal tissues and was involved in regulating colorectal tumorigeneses (Png et al., 2016), which was in correspondence with our results. Data from TCGA were further utilized to assess the relationship of LINC02257 with clinicopathological variables of colon cancer and survival analysis, which suggested that age and unregulated expression of LINC02257 could act as an independent unfavorable prognostic factor. Further, high LINC02257 expression might be associated with a more advanced tumor status and stage. Taken together, colon adenocarcinoma patients with high expression of LINC02257 are more susceptible to unfavorable prognosis than those with low expression, with the discovery of correlation with various clinical characteristics as well. Importantly, GO term analysis revealed that high LINC02257 expression could be connected with extracellular structure organization, ossification, collagen fibril organization, and connective tissue development. Meanwhile, KEGG pathway analysis showed five pathways that had a significant correlation with LINC02257 expression: PI3K-Akt signaling pathway, Focal adhesion, Phagosome, Regulation of actin cytoskeleton, and MAPK signaling pathway in colon cancer. Our study may pave

TABLE 5 | The relationship of LINC02257 expression in cancers and stromal and immune cells scores by ESTIMATE.

Cancer type	Gene	Stromal score	Immune score	Cancer type	Gene	Stromal score	Immune score
ACC	LINC02257	0.684	0.602	LUSC	LINC02257	2.07E−41	4.365E−17
BLCA	LINC02257	1.12E−12	0.0003	MESO	LINC02257	0.589	0.213
BRCA	LINC02257	1.87E−46	0.419	OV	LINC02257	2.97E−05	4.982E−08
CESC	LINC02257	0.002	0.694	PAAD	LINC02257	0.015	0.700
CHOL	LINC02257	0.407	0.480	PCPG	LINC02257	0.631	0.019
COAD	LINC02257	2.68E−35	4.98E−13	PRAD	LINC02257	0.002	0.0001
DLBC	LINC02257	0.120	0.540	READ	LINC02257	2.94E−11	0.006
ESCA	LINC02257	1.14E−06	0.199	SARC	LINC02257	0.001	1.00E−05
GBM	LINC02257	0.0001	0.004	SKCM	LINC02257	0.503	0.858
HNSC	LINC02257	8.73E−26	0.521	STAD	LINC02257	2.649E−10	0.008
KICH	LINC02257	0.374	0.104	TGCT	LINC02257	0.599	0.0001
KIRC	LINC02257	0.0008	5.43E−08	THCA	LINC02257	2.84E−11	3.39E−16
KIRP	LINC02257	0.101	0.197	THYM	LINC02257	0.0006	0.898
LAML	LINC02257	0.0008	0.054	UCEC	LINC02257	0.961	0.716
LGG	LINC02257	0.369	0.061	UCS	LINC02257	0.907	0.247
LIHC	LINC02257	0.005	0.022	UVM	LINC02257	0.974	0.937
LUAD	LINC02257	0.101	0.689				

the way to understanding that overexpression of LINC02257 in colon adenocarcinoma patients may alter PI3K-Akt signaling pathway, with its cascade involved in extracellular structure organization and ossification, providing potential targets for further investigation. As it has been demonstrated in the past, the PI3K-Akt signaling pathway is implicated in various cancer types through regulating cell proliferation and survival, including colon cancer, which is also in accordance with our analysis (Pal and Mandal, 2012).

It is still an unanswered question whether LINC02257, a functionally unannotated transcript, plays any roles in other cancer development. In our study, a comprehensive pan-cancer analysis was performed to clarify its aberrant expression with patients' clinical characteristics and survival analysis (OS, DSS, DFI, and PFI) across 33 cancer types. The differential expression of LINC02257 between cancer and normal tissues was observed in many types of cancers, and LINC02257 is mainly more expressed in cancers, which means LINC02257 may function as an oncogene in tumorigenesis. It has been reported that age and gender may influence the prognosis of patients with colon adenocarcinoma, esophageal cancer, and other tumorigeneses (Jin et al., 2020; Badic et al., 2021; Chen et al., 2021). Based on this, we included these two factors in our study. Intriguingly, in addition to colon adenocarcinoma, expressions of LINC02257 in various tumor types, such as THCA and STAD, were linked with age, gender, and stage status. Concerning our survival analysis, LINC02257 expression could also play a detrimental role in several malignant tumors, especially in COAD and PAAD, which is consistent with the results of previous studies. Our analysis suggested a correlation between high LINC02257 and poor OS, DSS, and PFI. Besides, both age and LINC02257 expression are independent prognostic factors in colon adenocarcinoma. Then, we wanted to figure out the relationship concerning LINC02257, age, and survival. R package "mediation" (version 3.5.3) was performed for mediation analysis for age, as mediation between LINC02257 and survival showed non-significant average causal mediation effects (ACMEs; p-value = 0.79) and significant average direct effects (ADEs; p-value < 2E-16), which means that LINC02257 showed a direct and significant effect on survival and age, which was not a mediation value between LINC02257 and survival. The result pdf file, "mediation," was uploaded in the **Supplementary Material**. Still, it inspires us to extend our understanding of LINC02257 in pan-cancer analysis, in both diagnosis and prognosis evaluations. In a recent study, TMB, TME, and MSI were correlated with immunotherapy (Goodman et al., 2017). Considering that colon cancer strongly links with MSI, TME, and other immunotherapy-related elements, it requires further in-depth understanding of the correlation between LINC02257 expression and immunotherapy-related analysis in cancer. As for TMB, our study discovered that LINC02257 expression in LAML, SARC, and STAD exhibited the strongest correlation with TMB, suggesting that LINC02257 expression in these three cancers is much likely to induce mutation-driven tumorigenesis and may provide implications for guidance on related drug therapy. Theoretically, patients with a higher TMB are warranted to get an ideal immunotherapy efficacy. When it comes to the TME, it is the environment where the tumor cells live, in which immune cells, endothelial cells, fibroblasts, and extracellular matrix are also located (Bolouri, 2015; Kurebayashi et al., 2018). The interaction among non-tumor components in TME, such as stromal and immune cells, can crucially influence the gene expression and the consequent clinical outcomes. In our study, the stromal and immune scores were obtained by the ESTIMATE algorithm to delineate their association with LINC02257 expression (Turley et al., 2015). Corresponding analysis revealed that LINC02257 expression was significantly associated with immune scores of BLCA, COAD, KIRC, LUSC, OV, PRAD, SARC, TGCT, and THCA, while stromal scores of BLCA, BRCA, COAD, ESCA, GBM, HNSC, KIRC, LAML,

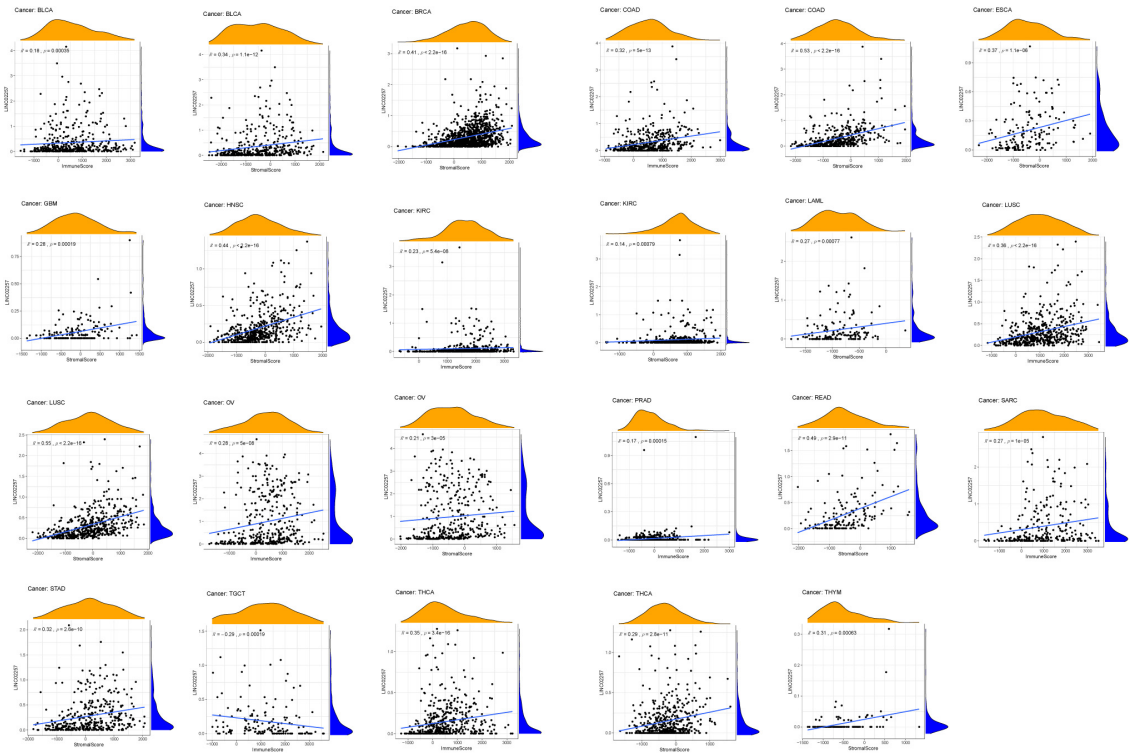

FIGURE 7 | The relationship of LINC02257 expression in cancers and stromal and immune cells scores.

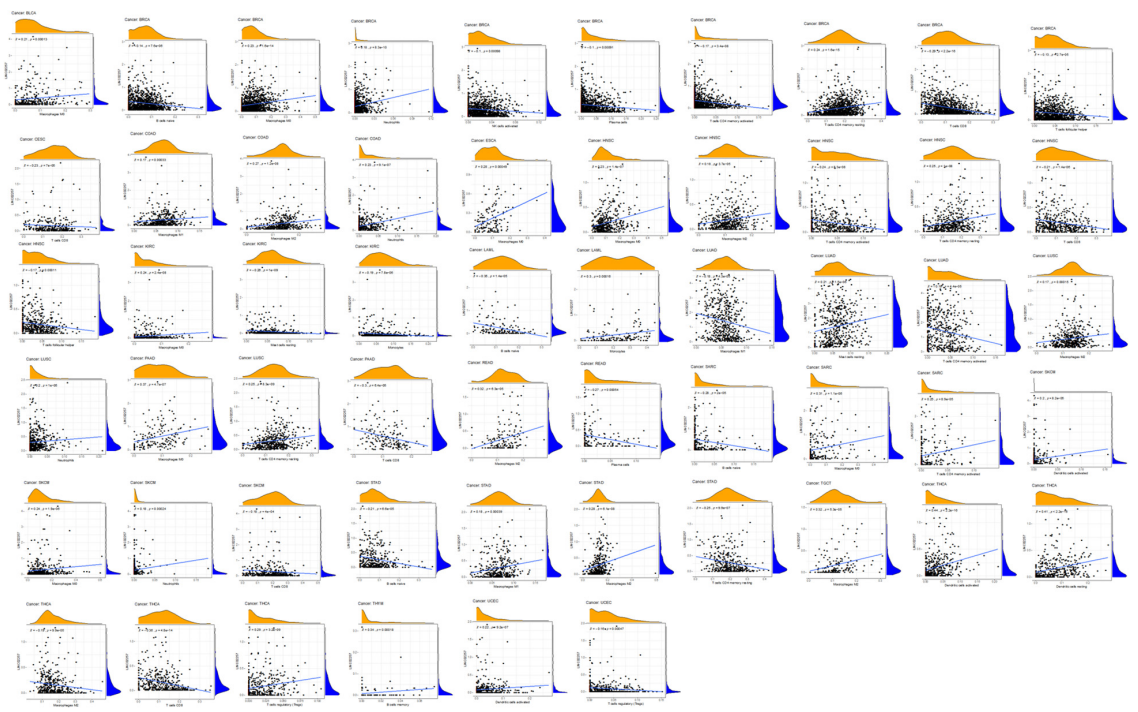

FIGURE 8 | The expression of LINC02257 and the infiltrations of 22 immune cells in 33 different types of tumors (the type and content of immune cells on the *X*-axis, the gene expression distribution on the *Y*-axis; *P*-value < 0.001 and $R > 0$, indicates positive correlation and the existence of statistically significance difference).

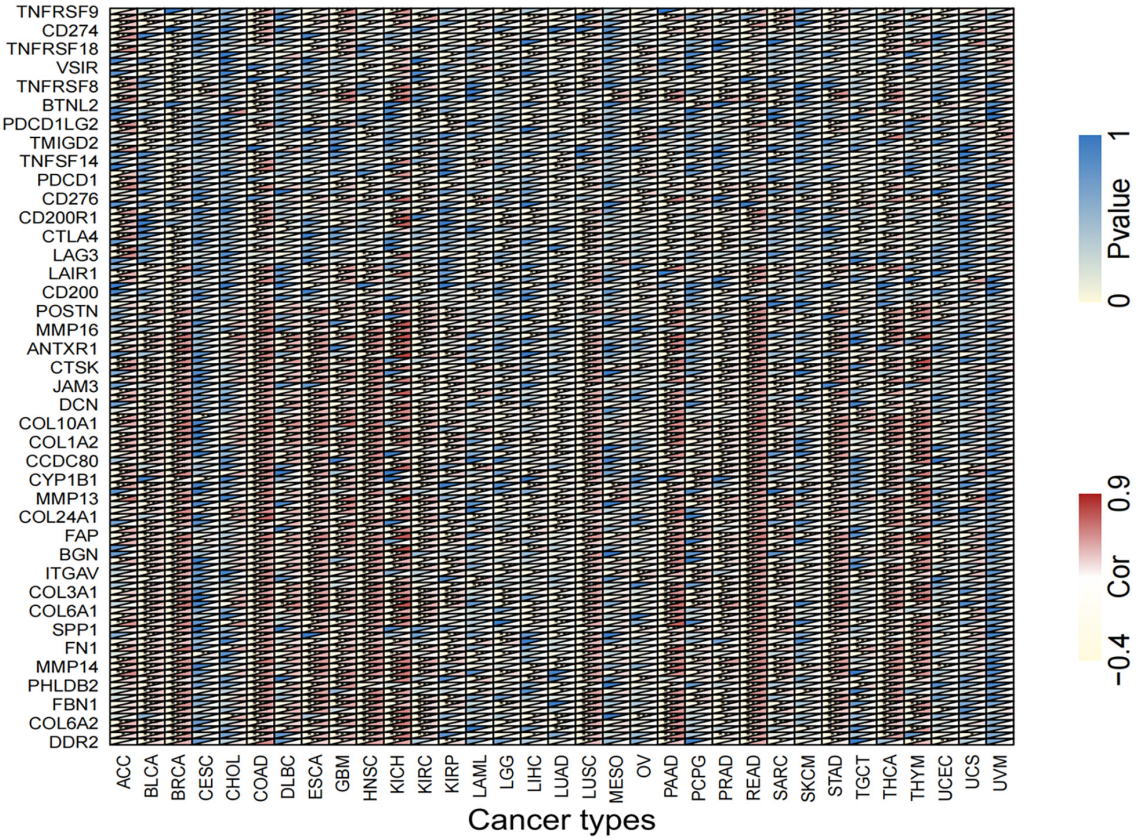

FIGURE 9 | Analysis of the co-expression of LINC02257 in 33 tumors and its correlation (The deeper the blue, the higher the P-value and the lower the correlation. Yellow represents a negative correlation and red represents a positive correlation. White indicates no correlation. ***$P < 0.001$, **$P < 0.01$, *$P < 0.05$, no *$P > 0.05$).

LUSC, OV, READ, STAD, THCA, and THYM were linked with the same gene expression. Accordingly, LINC02257 expression signature may be used to infer the ratio of the stromal and immune cells and thus predict the tumor purity in the TME. Besides, our study performed CIRBERSORT analysis to uncover the relationship between LINC02257 expression and immune cell infiltration in cancers. It was observed that LINC02257 expression was significantly associated with macrophages, B cells, neutrophils, NK cells, and T cells. Although we have yet to establish a cause–result relationship here, aberrant LINC02257 expression may alter tumor immune microenvironment across different cancer types. It in turn expands the pivotal role of eRNAs in the regulation of immune cell infiltration in various cancers. Apart from this, our study also elucidated the co-expression genes of LINC02257 and GSEA across different cancers. Concerning GSEA of LINC02257 expression across different cancer types, we uncovered that LINC02257 expression exerted shared mechanisms in that LINC02257 expression could regulate cell differentiation in BLCA, PRAD, SARC, TGCT, PADD, and LGG and hinder cell cycle (G1–S transition, sister chromatic segregation) in CESE, COAD, UCS, SKCM, and KICH, all of which are common carcinogenic patterns (Xiao et al., 2019; Garcia-Olivares et al., 2021; Tachiwana and Saitoh, 2021). Meanwhile, LINC02257 expression was also associated with NF-kappa B signaling pathway in LGG, providing us with various functional mechanisms of LINC02257 expression.

The notable strength of our study lies in the comprehensive omics analysis of eRNAs in 33 cancers, with the expectation to provide novel and robust evidence for potential cancer immunotherapy. And aberrant eRNAs expression may correlate with patient's prognosis, especially that LINC02257 is an independent prognostic factor in COAD patients, which suggests that our study has potential clinical use in cancer prognosis assessment and future follow-up investigation. While it is currently unclear that the precise mechanism is in regard to LINC02257 involved in COAD tumorigenesis, our study shows that the PI3K-Akt signaling pathway could possibly promote COAD occurrence and progression. However, several limitations existed in our study. Firstly, the newly identified LINC02257 we uncovered across cancers warrants basic experimental validation, including the potential regulatory mechanisms. Secondly, our study explored the prognostic value of LINC02257 in multiple cancers via different ways (OS, DSS, PFI, and DFI), which, however, is still insufficient for our understanding and mechanism explanation. Thirdly, although we evaluated TMB, MSI, TME, and other immunotherapy-related factors, we

did not analyze the association between LINC02257 expression and common immune checkpoint genes, such as CD276 and CD200, which could be potential indicators of patients' immunotherapy response. So the predictive value of LINC02257 regarding the immunotherapy response remains to be well-documented in the future.

To conclude, our study for the first time unveils key eRNA, LINC02257, as a new biomarker for colon and other cancers and attempts to elucidate its different roles in clinical parameters and prognosis. With a comprehensive analysis, LINC02257 may serve as a potential tool to enhance our understanding of the diagnosis and prognosis prediction of cancers and may be a promising immune-related therapeutic target for the precision treatment of malignant diseases in the future.

DATA AVAILABILITY STATEMENT

The original contributions presented in the study are included in the article/**Supplementary Material**, further inquiries can be directed to the corresponding author/s.

ETHICS STATEMENT

As this work benefited from the database of TCGA, informed consent was not applicable. This study was approved by the Xiangya Hospital, Central South University Ethics Committee, and the usage of the information and specimens collected has been handled and anonymized conformed to the ethical and legal standards.

AUTHOR CONTRIBUTIONS

JX wrote the article. YL and JY helped in the preparation of the manuscript, construction of tables and citation of references, and the critical revision of the literature. All authors contributed to the article and approved the submitted version.

FUNDING

This work was supported by the Xiangya Hospital Central South University.

SUPPLEMENTARY MATERIAL

The Supplementary Material for this article can be found online at: https://www.frontiersin.org/articles/10.3389/fmolb.2021.646786/full#supplementary-material

REFERENCES

Aran, D., Sirota, M., and Butte, A. J. (2015). Systematic pan-cancer analysis of tumour purity. *Nat. Commun.* 6:8971. doi: 10.1038/ncomms9971

Badic, B., Oguer, M., Cariou, M., Kermarrec, T., Bouzeloc, S., Nousbaum, J. B., et al. (2021). Prognostic factors for stage III colon cancer in patients 80 years of age and older. *Int. J. Colorectal. Dis.* 36, 811–819. doi: 10.1007/s00384-021-03861-3866

Bolouri, H. (2015). Network dynamics in the tumor microenvironment. *Semin. Cancer Biol.* 30, 52–59. doi: 10.1016/j.semcancer.2014.02.007

Chan, T. A., Yarchoan, M., Jaffee, E., Swanton, C., Quezada, S. A., Stenzinger, A., et al. (2019). Development of tumor mutation burden as an immunotherapy biomarker: utility for the oncology clinic. *Ann. Oncol.* 30, 44–56. doi: 10.1093/annonc/mdy495

Chang, L., Chang, M., Chang, H. M., and Chang, F. (2018). Microsatellite instability: a predictive biomarker for cancer immunotherapy. *Appl. Immunohistochem. Mol. Morphol.* 26, e15–e21. doi: 10.1097/PAI.0000000000000575

Chen, P., Zheng, Y., He, H., Wang, P. Y., Wang, F., and Liu, S. Y. (2021). The role of endoscopic tumor length in resected esophageal squamous cell carcinoma: a retrospective study. *J. Thorac Dis.* 13, 353–361. doi: 10.21037/jtd-21-108

de la Chapelle, A., and Hampel, H. (2010). Clinical relevance of microsatellite instability in colorectal cancer. *J. Clin. Oncol.* 28, 3380–3387. doi: 10.1200/JCO.2009.27.0652

Esmaeili, M., Keshani, M., Vakilian, M., Esmaeili, M., Peymani, M., Seyed Forootan, F., et al. (2020). Role of non-coding RNAs as novel biomarkers for detection of colorectal cancer progression through interaction with the cell signaling pathways. *Gene* 753:144796. doi: 10.1016/j.gene.2020.144796

Frankel, T., Lanfranca, M. P., and Zou, W. (2017). The role of tumor microenvironment in Cancer immunotherapy. *Adv. Exp. Med. Biol.* 1036, 51–64. doi: 10.1007/978-3-319-67577-0_4

Garcia-Olivares, M., Romero-Cordoba, S., Ortiz-Sanchez, E., Garcia-Becerra, R., Segovia-Mendoza, M., Rangel-Escareno, C., et al. (2021). Regulation of anti-tumorigenic pathways by the combinatory treatment of calcitriol and TGF-beta in PC-3 and DU145 cells. *J. Steroid Biochem. Mol. Biol.* 209:105831. doi: 10.1016/j.jsbmb.2021.105831

Goodman, A. M., Kato, S., Bazhenova, L., Patel, S. P., Frampton, G. M., Miller, V., et al. (2017). Tumor mutational burden as an independent predictor of response to immunotherapy in diverse Cancers. *Mol. Cancer Ther.* 16, 2598–2608. doi: 10.1158/1535-7163.MCT-17-0386

Gravitz, L. (2013). Cancer immunotherapy. *Nature* 504:S1. doi: 10.1038/504S1a

Gu, X., Wang, L., Boldrup, L., Coates, P. J., Fahraeus, R., Sgaramella, N., et al. (2019). AP001056.1, a prognosis-related enhancer RNA in squamous cell carcinoma of the head and neck. *Cancers (Basel)* 11:347. doi: 10.3390/cancers11030347

Harada, S., and Morlote, D. (2020). molecular pathology of colorectal Cancer. *Adv. Anat. Pathol.* 27, 20–26. doi: 10.1097/PAP.0000000000000247

Hause, R. J., Pritchard, C. C., Shendure, J., and Salipante, S. J. (2016). Classification and characterization of microsatellite instability across 18 cancer types. *Nat. Med.* 22, 1342–1350. doi: 10.1038/nm.4191

Hsieh, C. L., Fei, T., Chen, Y., Li, T., Gao, Y., Wang, X., et al. (2014). Enhancer RNAs participate in androgen receptor-driven looping that selectively enhances gene activation. *Proc. Natl. Acad. Sci. U S A.* 111, 7319–7324. doi: 10.1073/pnas.1324151111

Jin, H., Feng, Y., Guo, K., and Ruan, S. (2020). Prognostic nomograms for predicting overall survival and cancer-specific survival of patients with early onset colon adenocarcinoma. *Front. Oncol.* 10:595354. doi: 10.3389/fonc.2020.595354

Kim, T. K., Hemberg, M., Gray, J. M., Costa, A. M., Bear, D. M., Wu, J., et al. (2010). Widespread transcription at neuronal activity-regulated enhancers. *Nature* 465, 182–187. doi: 10.1038/nature09033

Kurebayashi, Y., Ojima, H., Tsujikawa, H., Kubota, N., Maehara, J., Abe, Y., et al. (2018). Landscape of immune microenvironment in hepatocellular carcinoma and its additional impact on histological and molecular classification. *Hepatology* 68, 1025–1041. doi: 10.1002/hep.29904

Leveille, N., Melo, C. A., and Agami, R. (2015). Enhancer-associated RNAs as therapeutic targets. *Expert Opin. Biol. Ther.* 15, 723–734. doi: 10.1517/14712598.2015.1029452

Li, W., Notani, D., and Rosenfeld, M. G. (2016). Enhancers as non-coding RNA transcription units: recent insights and future perspectives. *Nat. Rev. Genet.* 17, 207–223. doi: 10.1038/nrg.2016.4

Locy, H., de Mey, S., de Mey, W., De Ridder, M., Thielemans, K., and Maenhout, S. K. (2018). Immunomodulation of the tumor microenvironment: turn foe into friend. *Front. Immunol.* 9:2909. doi: 10.3389/fimmu.2018.02909

Melo, C. A., Drost, J., Wijchers, P. J., van de Werken, H., de Wit, E., Oude Vrielink, J. A., et al. (2013). eRNAs are required for p53-dependent enhancer activity and gene transcription. *Mol. Cell.* 49, 524–535. doi: 10.1016/j.molcel.2012.11.021

Newman, A. M., Liu, C. L., Green, M. R., Gentles, A. J., Feng, W., Xu, Y., et al. (2015). Robust enumeration of cell subsets from tissue expression profiles. *Nat. Methods* 12, 453–457. doi: 10.1038/nmeth.3337

Oki, E., Oda, S., Maehara, Y., and Sugimachi, K. (1999). Mutated gene-specific phenotypes of dinucleotide repeat instability in human colorectal carcinoma cell lines deficient in DNA mismatch repair. *Oncogene* 18, 2143–2147. doi: 10.1038/sj.onc.1202583

Pal, I., and Mandal, M. (2012). PI3K and Akt as molecular targets for cancer therapy: current clinical outcomes. *Acta Pharmacol. Sin.* 33, 1441–1458. doi: 10.1038/aps.2012.72

Png, C. W., Weerasooriya, M., Guo, J., James, S. J., Poh, H. M., Osato, M., et al. (2016). DUSP10 regulates intestinal epithelial cell growth and colorectal tumorigenesis. *Oncogene* 35, 206–217. doi: 10.1038/onc.2015.74

Sabari, J. K., Leonardi, G. C., Shu, C. A., Umeton, R., Montecalvo, J., Ni, A., et al. (2018). PD-L1 expression, tumor mutational burden, and response to immunotherapy in patients with MET exon 14 altered lung cancers. *Ann. Oncol.* 29, 2085–2091. doi: 10.1093/annonc/mdy334

Subramanian, A., Tamayo, P., Mootha, V. K., Mukherjee, S., Ebert, B. L., Gillette, M. A., et al. (2005). Gene set enrichment analysis: a knowledge-based approach for interpreting genome-wide expression profiles. *Proc. Natl. Acad. Sci. U S A.* 102, 15545–15550. doi: 10.1073/pnas.0506580102

Sun, Y., and Ling, C. (2019). Analysis of the long non-coding RNA LINC01614 in non-small cell lung cancer. *Medicine (Baltimore)* 98:e16437. doi: 10.1097/MD.0000000000016437

Tachiwana, H., and Saitoh, N. (2021). Nuclear long non-coding RNAs as epigenetic regulators in cancer. *Curr. Med. Chem.* doi: 10.2174/0929867328666210215114506 Online ahead of print.

Turley, S. J., Cremasco, V., and Astarita, J. L. (2015). Immunological hallmarks of stromal cells in the tumour microenvironment. *Nat. Rev. Immunol.* 15, 669–682. doi: 10.1038/nri3902

Uhlen, M., Fagerberg, L., Hallstrom, B. M., Lindskog, C., Oksvold, P., Mardinoglu, A., et al. (2015). Proteomics. tissue-based map of the human proteome. *Science* 347:1260419. doi: 10.1126/science.1260419

Vasaikar, S., Huang, C., Wang, X., Petyuk, V. A., Savage, S. R., Wen, B., et al. (2019). Proteogenomic analysis of human colon Cancer reveals new therapeutic opportunities. *Cell* 177, 1035–1049.e19. doi: 10.1016/j.cell.2019.03.030

Verhaak, R. G., Hoadley, K. A., Purdom, E., Wang, V., Qi, Y., Wilkerson, M. D., et al. (2010). Integrated genomic analysis identifies clinically relevant subtypes of glioblastoma characterized by abnormalities in PDGFRA, IDH1, EGFR, and NF1. *Cancer Cell* 17, 98–110. doi: 10.1016/j.ccr.2009.12.020

Wang, Z., Jensen, M. A., and Zenklusen, J. C. (2016). A practical guide to The Cancer Genome Atlas (TCGA). *Methods Mol. Biol.* 1418, 111–141. doi: 10.1007/978-1-4939-3578-9_6

Xiao, J. B., Leng, A. M., Zhang, Y. Q., Wen, Z., He, J., and Ye, G. N. (2019). CUEDC2: multifunctional roles in carcinogenesis. *Front. Biosci. (Landmark Ed)* 24:935–946. doi: 10.2741/4759

Yoshihara, K., Shahmoradgoli, M., Martinez, E., Vegesna, R., Kim, H., Torres-Garcia, W., et al. (2013). Inferring tumour purity and stromal and immune cell admixture from expression data. *Nat. Commun.* 4:2612. doi: 10.1038/ncomms3612

Zhang, Z., Lee, J. H., Ruan, H., Ye, Y., Krakowiak, J., Hu, Q., et al. (2019). Transcriptional landscape and clinical utility of enhancer RNAs for eRNA-targeted therapy in cancer. *Nat. Commun.* 10:4562. doi: 10.1038/s41467-019-12543-12545

Zhou, P., Xie, W., Huang, H. L., Huang, R. Q., Tian, C., Zhu, H. B., et al. (2020). circRNA_100859 functions as an oncogene in colon cancer by sponging the miR-217-HIF-1alpha pathway. *Aging (Albany NY)* 12, 13338–13353. doi: 10.18632/aging.103438

Conflict of Interest: The authors declare that the research was conducted in the absence of any commercial or financial relationships that could be construed as a potential conflict of interest.

frontiers in Cell and Developmental Biology

ORIGINAL RESEARCH
published: 03 May 2021
doi: 10.3389/fcell.2021.653207

Circular RNA Circ0021205 Promotes Cholangiocarcinoma Progression Through MiR-204-5p/RAB22A Axis

Jianfei Tu[1,2†], Weiqian Chen[1,2†], Liyun Zheng[1,2], Shiji Fang[1,2], Dengke Zhang[1,2], Chunli Kong[1,2], Yang Yang[1,2], Rongfang Qiu[1,2], Zhongwei Zhao[1,2], Chenying Lu[1,2], Xiaojie Lu[3,4] and Jiansong Ji[1,2*]*

[1] Key Laboratory of Imaging Diagnosis and Minimally Invasive Intervention Research, Lishui Hospital of Zhejiang University/Fifth Affiliated Hospital of Wenzhou Medical University, Lishui, China, [2] Clinical College of The Affiliated Central Hospital, Lishui University, Lishui, China, [3] Affiliated Hospital of Youjiang Medical University for Nationalities, Baise, China, [4] Department of General Surgery, The First Affiliated Hospital of Nanjing Medical University, Nanjing, China

Cholangiocarcinomas (CCA) are biliary tract tumors that are often challenging to diagnosis and treatment. Accumulated evidence reveals that circular RNAs (circRNAs) are involved in multiple cancer progression. However, the function of circRNAs in cholangiocarcinoma remains largely unclear. In this study, we found that circ_0021205 expression was up-regulated in CCA and positively correlated with tumor size and TNM stage. To further explore the role of circ_0021205 in CCA, cell functional assays were performed. The results showed that circ_0021205 promoted the proliferation, migration, and invasion of CCA cells. *In vivo* experiments showed that circ_0021205 inhibition reduced tumorigenesis in mice. In addition, mechanisms investigation demonstrated that circ_0021205 exerts its oncogenic function by sponging miR-204-5p to regulate the expression of RAB22A. Overall, this study revealed that circ_0021205 might serve as a potential diagnostic biomarker or therapeutic target for CCA.

Keywords: cholangiocarcinoma, circular RNAs, circ_0021205, miR-204-5p, RAB22A

OPEN ACCESS

Edited by:
Hongming Miao,
Army Medical University, China

Reviewed by:
Wei Zhai,
Shanghai Jiao Tong University, China
Xiong Yang,
Huazhong University of Science and Technology, China

****Correspondence:***
Xiaojie Lu
luzg88@163.com
Jiansong Ji
jijiansong@zju.edu.cn

† These authors have contributed equally to this work

Specialty section:
This article was submitted to Molecular Medicine, a section of the journal Frontiers in Cell and Developmental Biology

Received: *14 January 2021*
Accepted: *12 April 2021*
Published: *03 May 2021*

Citation:
Tu J, Chen W, Zheng L, Fang S, Zhang D, Kong C, Yang Y, Qiu R, Zhao Z, Lu C, Lu X and Ji J (2021) Circular RNA Circ0021205 Promotes Cholangiocarcinoma Progression Through MiR-204-5p/RAB22A Axis. Front. Cell Dev. Biol. 9:653207. doi: 10.3389/fcell.2021.653207

INTRODUCTION

Cholangiocarcinoma (CCA) is a highly malignant tumor found in the epithelial cells lining the bile duct, which is categorized according to anatomical location as intrahepatic, perihilar, and distal cholangiocarcinoma (Cunningham et al., 2007; Rizvi et al., 2018). In the past 30–40 years, the global incidence of cholangiocarcinoma has risen to 18% of all liver cancers (Erichsen et al., 2011). At present, the effective treatments of cholangiocarcinoma are surgical resection, liver transplantation, and drug therapy (Kinoshita et al., 2008; Wechagama et al., 2012). However, the therapeutic effects of radiotherapy and chemotherapy are relatively poor. The only effective treatment method is early surgical resection of cholangiocarcinoma (Fidelman et al., 2011; Patop et al., 2019). Therefore, it is urgently needed to further explore the pathogenesis of cholangiocarcinoma to develop new diagnostic and therapeutic methods for CCA.

Circular RNAs (circRNAs) are produced by reverse splicing, which is characterized by covalently closed continuous loops and canonical splicing sites (Jens et al., 2013; Li et al., 2018). Due to the lack of 5′ cap structure and 3′ poly(A) tails, circRNAs have a long half-life, which enables them to resist the conventional linear decay mechanism of RNA (Jeck and Sharpless, 2014; Chen et al., 2017). Previous studies have shown that some circRNAs can bind to specific miRNAs as miRNA

sponges (Hansen et al., 2013). In addition, recent studies have shown that circRNAs play a role in multiple cancer progression (Legnini et al., 2017; Yang et al., 2017). Because of the long half-life and resistance to common degradation pathways, circRNAs may serve as the potential biomarkers for cancer (Kulcheski et al., 2016). However, the reports about the mechanism and function of circRNAs in cholangiocarcinoma are limited.

MicroRNAs (miRNAs) are non-coding RNAs which play roles in the negative regulation of gene expression at the post-transcriptional level (Lee and Dutta, 2009; Lu and Rothenberg, 2018). In the past decade, it has been found that miRNAs are closely related to the development of cancer and can play the role of tumor suppressor or promoter (Rupaimoole and Slack, 2017). MiR-204-5p was identified as a tumor-suppressive miRNA, plays a role in cancer development and progression (Zhang et al., 2014). In addition, the deregulation of miRNAs is associated with the progression of many tumors, including cholangiocarcinoma (Wan et al., 2018). However, The regulatory mechanism of circRNA-miRNA network on cholangiocarcinoma is rarely reported.

MATERIALS AND METHODS

Tissues and Cell Lines

Cholangiocarcinomas tissues and adjacent tissues were obtained from Lishui Hospital of Zhejiang University. All patients gave written informed consent before this study start. This study was approved by the ethics committee of Lishui Hospital of Zhejiang University. The clinicopathological characteristics of 27 CCA patients were as shown below:

CCA patients	27
Sex	
Male	13
Female	15
Age	
≤50	17
>50	10
AFP (ng/ml)	
≤20	15
>20	12

All cell lines were purchased from China Center for Type Culture Collection (CCTCC). Normal biliary cell line HIBEC and CCA cell lines (HCCC-9810, Huh-28, and KMBC) were cultured in Roswell Park Memorial Institute (RPMI) 1640 Medium (Gibco, United States), CCA cell lines QBC939, RBE, and HuCCT1 were cultured in Dulbecco's Modified Eagle's Medium (DMEM, Gibco). All medium were supplemented with 10% fetal bovine serum (FBS, Gibco), 100 U/mL penicillin and 100 μg/mL streptomycin.

RNase R Treatment

Total RNA (10 μg) from HuCCT1 and KMBC cells were incubated with 5 U/μg RNase R (Epicenter Technologies, United States) for 15 min at 37 °C. Subsequently, the treated RNA was reverse transcribed and the level of circ_0021205 was examined by quantitative real time PCR (qRT-PCR) assay. Experiments were repeated for three times.

Cell Transfection

The si-circ_0021205-1 (GTCTAATTCCTGTGGTGAAGA), si-circ_0021205-2 (ATTGTCTAATTCCTGTGGTGA), miR-204-5p mimic (5′-UUCCCUUUGUCAUCCUAUGCCU-3′), and miR-204-5p inhibitor (5′-AGGCAUAGGAUGACAAAGGGAA-3′) were purchased from Thermo Fisher Scientific (United States). The oe-circ_0021205 pasmids were constructed using pLO5-ciR vectors (Geneseed, China). All cell transfection were performed using Lipofectamine 3000 (Thermo Fisher Scientific, United States).

RNA Extraction and Quantitative Real Time PCR (qRT-PCR)

Total RNA of CCA tissues and cell lines was extracted using TRIzol reagent (Invitrogen, United States), then the concentration and purity of RNA was measured by NanoDrop 2000 (Thermo Fisher Scientific, United States). The qRT-PCR was performed using SYBR Green qPCR Mix (Takara, Japan). For circRNA and mRNA, GAPDH was used as endogenous reference. For miRNA, U6 was used as endogenous reference. All qRT-PCR reactions were run on the ABI 7500 Fast Real-Time PCR System (Applied Biosystems, United States). The relative expression of RNAs was calculated with $2^{-\Delta\Delta CT}$ algorithm. All primers used in this study were listed in **Table 1**. Experiments were repeated for three times.

Luciferase Reporter Assay

The pGL3 Luciferase Reporter Vectors (Promega, United States) containing circ_0021205-WT, circ_0021205-MuT, *RAB22A*-WT, or *RAB22A*-MuT sequences were co-transfected with miR-204-5p mimics or NC-mimics into HuCCT1 and KMBC cells. After 24 h of incubation, cells were lysed by 1 × PLB, then the luciferase activities were measured using the Dual-Luciferase Reporter Assay System (Promega, United States). Experiments were repeated for three times.

Table 1 Primers used in qRT-PCR assay.

Gene	Sequences
circ_0021205	F: 5′-ACATGTTTGCACTTGTCTTTGACT-3′
	R: 5′-TGTCTTCACCACAGGAATTAGACA-3′
miR-204-5p	F: 5′-GGGAAACAGUAGGAUACGGA-3′
	R: 5′-CAGTGCGTGTCGTGGAGT-3′
GAPDH	F: 5′-CGCTCTCTGCTCCTCCTGTTC-3′
	R: 5′-ATCCGTTGACTCCGACCTTCAC-3′
U6	F: 5′-AGCCCGCACTCAGAACATC-3′
	R: 5′-GCCACCAAGACAATCATCC-3′

Cell Counting Kit-8 Proliferation Assay

3×10^3 HuCCT1 and KMBC cells were seeded into 96-well plates and cultured for 2–4 h. Then added 10 μL CCK-8 reagents (YEASEN, China) to each well. After 2 h of incubation, the optional density (OD) at 450 nm was measured by the Multiskan FC with Incubator (Thermo Fisher Scientific, United States). Experiments were repeated for three times.

Colony Formation Assay

2×10^2 HuCCT1 and KMBC cells in logarithmic growth phase were seeded into 12-well plates, and cultured for 2 weeks. Then cells were fixed using 4% paraformaldehyde for 15 min and stained by crystal violet staining solution for 15 min. Slowly washed the plates with running water and air-dried. Counted the number of colonies in the plates. Experiments were repeated for three times.

Transwell Migration and Invasion Assay

For migration assay, the transwell chambers (Millipore, United States) were paved without matrigel mix. For invasion assay, the upper transwell chambers were paved with matrigel mix. HuCCT1 and KMBC cells were suspended in medium without FBS and seeded into the upper transwell chambers. And medium supplemented with 10% FBS was infused into the bottom chambers as cell chemo attractant. After 24 h of incubation, the upper chamber was fixed with 4% paraformaldehyde and then stained by crystal violet staining solution for 15 min. The cell numbers were counted in five different fields under the microscope. Experiments were repeated for three times.

Western Blot and Immunohistochemistry Staining

Cells were lysed using RIPA buffer containing protease inhibitor (Sangon, China). 30 μg total protein extracted from CCA cells was separated by sodium dodecyl sulfate-polyacrylamide gel electrophoresis (SDS-PAGE), and transferred to polyvinylidene fluoride (PVDF) membranes (Millipore, United States). The membranes were blocked by 5% skimmed milk and incubated with the primary antibodies (anti-Ki-67, 1:1000, ab16667, Abcam, United States; anti-PCNA, 1:1000, ab265609, Abcam, United States; anti-GAPDH, 1:1000, ab9485, Abcam, United States; anti-RAB22A, 1:1000 ab137093, Abcam, United States) overnight at 4°C. And incubated with the HRP-conjugated secondary antibodies (1:10000; Abcam, United States) at room temperature for 1 h. Subsequently, the protein bands were visualized using the Clarity Western ECL Substrate (Bio-Rad, United States). The primary antibodies used in this study were as shown below: (anti-Ki-67, 1: 200, ab16667, Abcam, United States; anti-PCNA, 1:250, ab265609, Abcam, United States).

Xenografts in Mice

All male BALB/c nude mice were purchased from XX. 1×10^7 HuCCT1 cells stably transfected with si-circ_0021205 or si-NC were subcutaneously injected into the mice, respectively. After the injection, we measured the tumor and calculated the tumor volume every 4 days. 20 days after injection, the mice were euthanized, then tumors were excised and measured. We then used the tumor tissues for qOCR, WB, and IHC analysis.

Statistical Analysis

GraphPad Prism 8.0 (GraphPad Software, San Diego, CA, United States) and SPSS 22.0 (IBM, Chicago, IL, United States) were used in this study. Student's *t* test and One-way ANOVA followed by Dunnett's multiple comparisons test were used to analyze the difference between groups. $P < 0.05$ was considered statistically significant. Each experiment was triplicated.

RESULTS

Circ_0021205 Is Upregulated in CCA

To investigate the correlation between circ_0021205 expression and CCA development, we collected 27 pairs of CCA tissues and adjacent tissues, and detected the circ_0021205 expression using qRT-PCR. As shown in **Figure 1A**, the expression of circ_0021205 in CCA tissues was significantly upregulated compared with that in normal tissues. We also analyzed the circ_0021205 expression in CCA tissues with different size or TNM stage (**Figures 1B,C**). The results showed that the circ_0021205 expression in larger size or advanced stage tumor tissues was higher. In addition, the expression of circ_0021205 in CCA cell lines was also higher than in normal human intrahepatic biliary epithelial cells (**Figure 1D**). HuCCT1 and KMBC cell lines were selected for further study for the relative high or low expression level of circ_0021205 among 6 CCA cell lines. To verify the circular feature of circ_0021205, RNase R treatment was performed to examine the stability of circ_0021205 (**Figure 1E**). Random hexamer and oligo(dt) 18 were used to amplify circ_0021205 and liner mRNA (WEE1) respectively (**Figure 1F**), the results showed that circ_0021205 is a circular RNA.

Circ_0021205 Promotes the Proliferation, Migration, and Invasion of CCA Cells

To explore the role of circ_0021205 in CCA, the expression of circ_0021205 was down-regulated in HuCCT1 cells using si-circ_0021205-1 and si-circ_0021205-2 (**Figure 2A**) and up-regulated in KMBC cells using over-expression vectors (**Figure 2B**). si-circ_0021205-2 was selected for the subsequent experiments (**Figure 2A**). Results of CCK-8 assay showed that the down-regulation of circ_0021205 significantly inhibited CCA cell proliferation, whereas circ_0021205 up-regulation promoted the proliferation of CCA cells (**Figures 2C,D**). Colony formation assay indicated that circ_0021205 inhibition suppressed cell cloning capability of CCA cells, however, up-regulation of circ_0021205 exerted opposite effects (**Figure 2E**). We further confirmed the role of circ_0021205 in regulation of CCA cells proliferation using western blotting to detect the expression levels of proliferation makers, Ki-67 and PCNA (**Figure 2F**). In addition, transwell assay showed that the down-regulation of circ_0021205 inhibited the

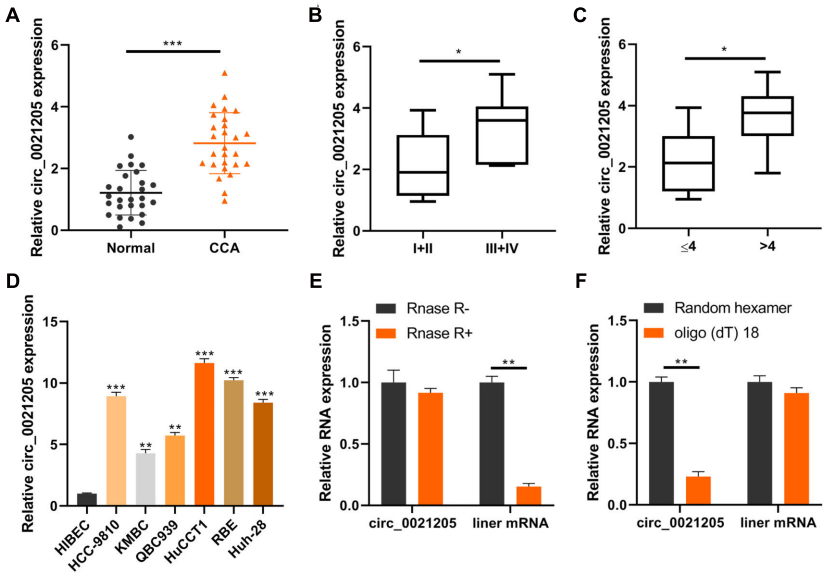

FIGURE 1 | Circ_0021205 is upregulated in CCA. **(A)** QRT-PCR data showed that circ_0021205 was significantly upregulated in CCA tissues than controls. **(B,C)** QRT-PCR data showed that circ_0021205 expression in ≥4 cm size or I + II stage tumor tissues was higher than in small size or III + IV stage tumors. **(D)** The relative expression of circ_0021205 in different cell lines was detected using qRT-PCR. **(E)** QRT-PCR data showed that circ_0021205 expression has not been decreased after RNase R treatment. **(F)** QRT-PCR data showed that circ_0021205 could not be amplified by oligo(dt) 18 primers. All experiments were repeated at least three time. *$P < 0.05$, **$P < 0.01$, ***$P < 0.001$.

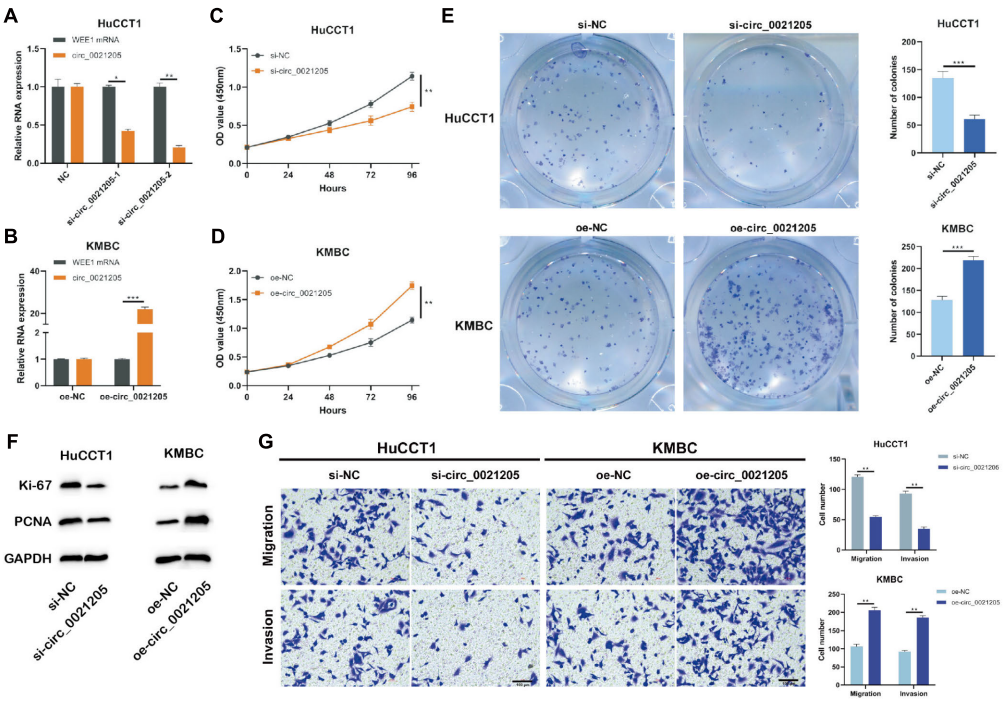

FIGURE 2 | Circ_0021205 promotes the proliferation, migration and invasion of CCA cell. **(A,B)** HuCCT1 cells were transfected with si-NC, si-circ_0021205-1, or si-circ_0021205-2. KMBC cells were transfected with oe-NC or oe-circ_0021205. The transfection efficiencies were analyzed by qRT-PCR. **(C,D)** The proliferation of transfected HuCCT1 and KMBC cells were determined by CCK-8 assay. **(E)** Colony formation assay were performed to detect the proliferation of HuCCT1 and KMBC cells transfected with si-circ_0021205 and oe-circ_0021205, respectively. **(F)** The levels of proliferation makers, Ki-67 and PCNA, were investigated using western blotting. **(G)** Cell migration and invasion were detected using transwell assay. All experiments were repeated at least three time. *$P < 0.05$, **$P < 0.01$, ***$P < 0.001$.

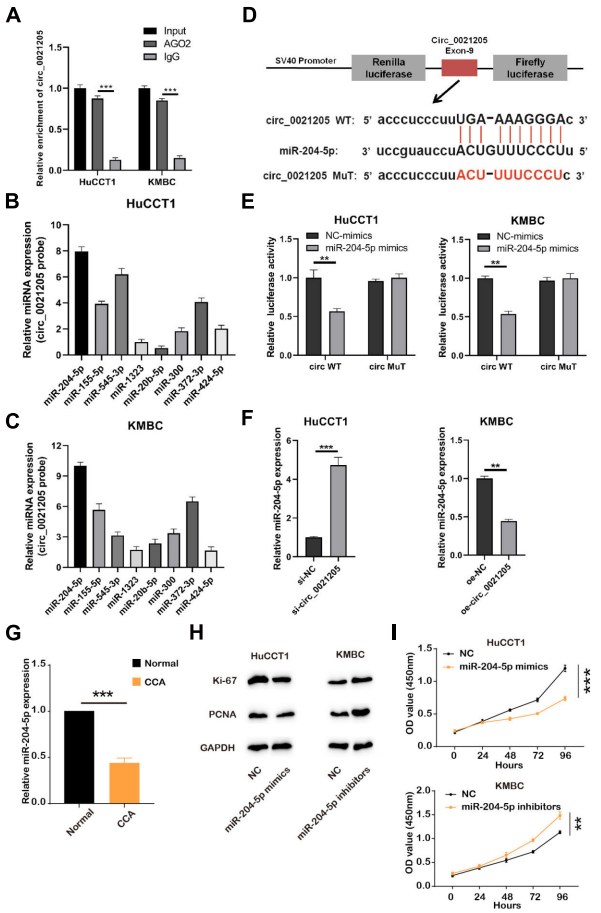

FIGURE 3 | Circ_0021205 serves as a miR-204-5p sponge. **(A)** RIP experiments with AGO2 antibody were conducted, the expression of circ_0021205 was detected using qRT-PCR. **(B,C)** The expression of miRNAs bind to circ_0021205 probes in HuCCT1 and KMBC cells was detected by qRT-PCR. **(D)** Schematic illustration of circ_0021205-WT and circ_0021205-MuT luciferase reporter vectors and the binding sites between circ_0021205 and miR-204-5p. **(E)** The relative luciferase activities were detected in HuCCT1 and KMBC cells after co-transfection with circ_0021205-WT/MuT and miR-204-5p mimics/NC-mimics, respectively. **(F)** The expression of miR-204-5p was detected in HuCCT1 and KMBC cells transfected with si-circ_0021205 and OE-circ_0021205 plasmids, respectively. **(G)** Relative expression of miR-204-5p was detected in CCA and normal tissues. **(H)** The levels of proliferation makers, Ki-67 and PCNA, were investigated using western blotting. **(I)** The proliferation of transfected CCA cells was determined by CCK-8 assay. All experiments were repeated at least three time. $^{**}P < 0.01$, $^{***}P < 0.001$.

migration and invasion of CCA cells, whereas circ_0021205 up-regulation promoted CCA cell migration and invasion (**Figure 2G**). These results demonstrated that circ_0021205 promoted the proliferation, migration and invasion of CCA cells *in vitro*.

Circ_0021205 Serves as a MiR-204-5p Sponge

To explore whether circ_0021205 sponging miRNAs, RIP experiments were performed. As shown in **Figure 3A**, the expression of circ_0021205 was enriched in AGO2 groups, indicating that circ_0021205 could bind to miRNAs through AGO2 protein. Then we predicted the potential target miRNAs through CircInteractome[1], and detected their levels bind to specific circ_0021205 probe in HuCCT1 (**Figure 3B**) and KMBC (**Figure 3C**) cells. Results showed that the levels of miR-204-5p binding to circ_0021205 probe were higher in both HuCCT1 and KMBC cells. Next, miR-204-5p was selected for subsequent experiments. To further verify the interaction between circ_0021205 and miR-204-5p, luciferase reporter vectors were constructed (**Figure 3D**). And miR-204-5p mimics significantly decreased the luciferase activity in circ_0021205 WT groups, whereas brought no changes in circ_0021205 MuT groups (**Figure 3E**). The results demonstrated that circ_0021205 could directly bind to miR-204-5p. In addition, the expression of miR-204-5p was significantly increased in HuCCT1 cells transfected with si-circ_0021205, and circ_0021205 over-expression inhibited miR-204-5p expression in KMBC cells (**Figure 3F**). We then further examined the expression level of miR-204-5p using CCA tissues, and found that miR-204-5p level was remarkably decreased (**Figure 3G**). Through *in vitro* assays, we also confirmed that miR-204-5p mimics inhibited the proliferation of CCA cells, and miR-204-5p inhibitors enhanced the proliferation ability of CCA cells with detection of proliferation markers and CCK-8 assay (**Figures 3H,I**). These data illustrated that circ_0021205 serve as a miR-204-5p sponge.

RAB22A Is a Direct Target of MiR-204-5p

We predicted target genes of miR-204-5p by Starbase 3.0, and RAB22A had been reported to involve in the progression of several cancers (Liao et al., 2020). The putative binding sites between miR-204-5p and RAB22A WT or MuT were shown in **Figure 4A**. Luciferase reporter vectors containing RAB22A WT/MuT sequences were co-transfected with miR-204-5p mimics/NC-mimics into HuCCT1 and KMBC cells. The results showed that miR-204-5p significantly reduced the luciferase activities in RAB22A WT groups, but no changes in RAB22A MuT groups (**Figures 4B,C**). In addition, the data from TGCA showed that the expression of miR-204-5p was negatively correlated with RAB22A levels in human CCA tissues (**Figure 4D**). We also confirmed that RAB22A level was increased in both CCA tissues abd CCA cell lines (**Figure 4G**). Furthermore, the expression of RAB22A was detected in HuCCT1 and KMBC cell transfected with miR-204-5p mimics and miR-204-5p inhibitors, respectively. The results showed that the up-regulation of miR-204-5p significantly inhibited RAB22A expression, whereas miR-204-5p down-regulation increased RAB22A expression (**Figures 4E,F**). Also, results collected using CCK-8 assay and proliferation makers measurement shown that si-RAB22A reduced the proliferation of CCA cells (**Figures 4H,I**). These data demonstrated that RAB22A is a target gene of miR-204-5p.

[1]https://circinteractome.nia.nih.gov

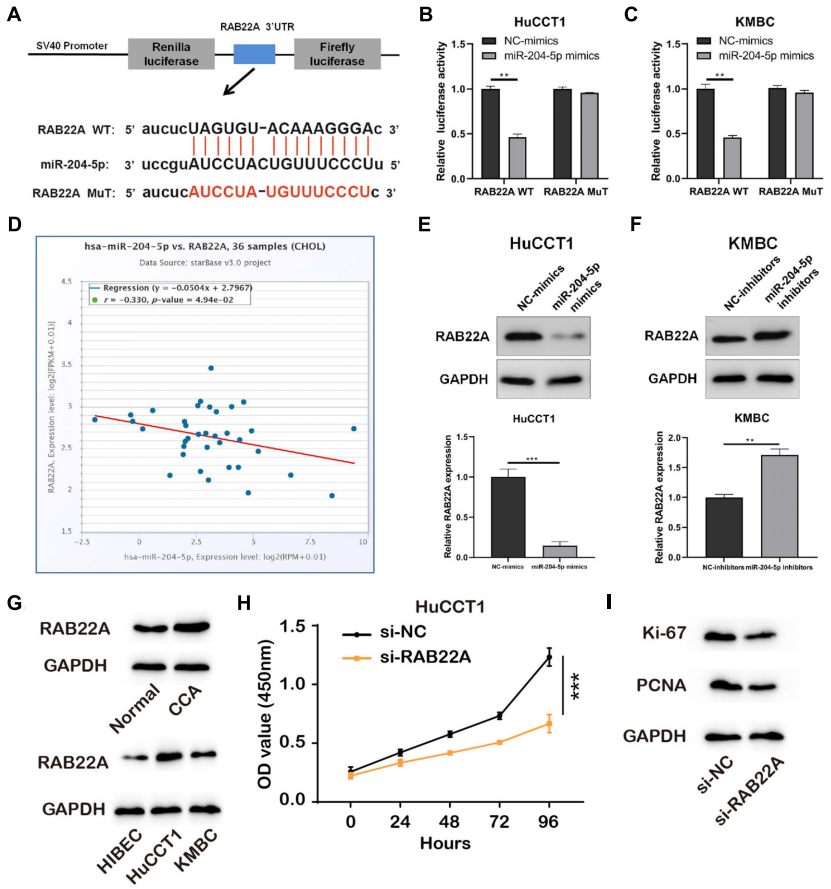

FIGURE 4 | RAB22A is a direct target of miR-204-5p. **(A)** Schematic illustration of RAB22A-WT and RAB22A-MuT luciferase reporter vectors and the binding sites between RAB22A and miR-204-5p. **(B,C)** The relative luciferase activities were detected in HuCCT1 and KMBC cells after co-transfection with RAB22A-WT/MuT and miR-204-5p mimics/NC-mimics, respectively. **(D)** The correlation between miR-204-5p and RAB22A in CCA tissues. **(E,F)** The western blot was used to detect the expression of RAB22A in HuCCT1 and KMBC cells transfected with miR-204-5p mimics and miR-204-5p inhibitors, respectively. **(G)** The levels of RAB22A in CCA and normal tissues and CCA cell lines were investigated using western blotting. **(H)** The proliferation of transfected CCA cells was determined by CCK-8 assay. **(I)** The levels of proliferation makers, Ki-67 and PCNA, were investigated using western blotting. All experiments were repeated at least three time. $^{**}P < 0.01$, $^{***}P < 0.001$.

Circ_0021205 Promotes CCA Cell Proliferation, Migration, and Invasion Through MiR-204-5p/RAB22A Axis

To further explore whether circ_0021205 served as a tumor promoter through miR-204-5p/RAB22A axis, rescue experiments were performed using miR-204-5p mimics and inhibitors. Western blot assay showed that knockdown of circ_0021205 decreased RAB22A expression in HuCCT1 cells, while circ_0021205 up-regulation enhanced RAB22A expression in KMBC cells. Simultaneously, these effects caused by knocking down or over-expressing circ_0021205 were reversed by miR-204-5p inhibitors or mimics, respectively (**Figures 5A,B**). Moreover, CCK-8 assay (**Figure 5C**), colony formation assay (**Figure 5D**), and transwell assay (**Figure 5E**) were also performed. The results indicated that miR-204-5p inhibitors reversed the suppressing effects of circ_0021205 down-regulation on proliferation, migration, and invasion in HuCCT1 cells, whereas miR-204-5p mimics blocked the promoting effects induced by circ_0021205 over-expression in KMBC cells. Collectively, these results revealed that circ_0021205 served as a miR-204-5p sponge to regulate RAB22A expression, thus promoting the progression of CCA.

Circ_0021205 Knockdown Inhibits the Tumorigenesis of CCA *in vivo*

To further explore the role of circ_0021205 *in vivo*, the HuCCT1 cells transfected with si-NC or si-circ_0021205 were subcutaneously injected into the mice, respectively ($n = 6$). Tumor volumes were recorded every 4 days (**Figure 6B**) and the tumors were excised at 20 days after injection (**Figure 6A**). Then the tumor weights were recorded (**Figure 6C**). We then detect the expression level of miR-204-5p and RAB22A with qPCR and WB, and confirmed that si-circ_0021205 increased the expression level of miR-204-5p and decreased RAB22A level in tumor tissues (**Figures 6D,E**). Next, we investigated the proliferation of the cells in the tumors with western

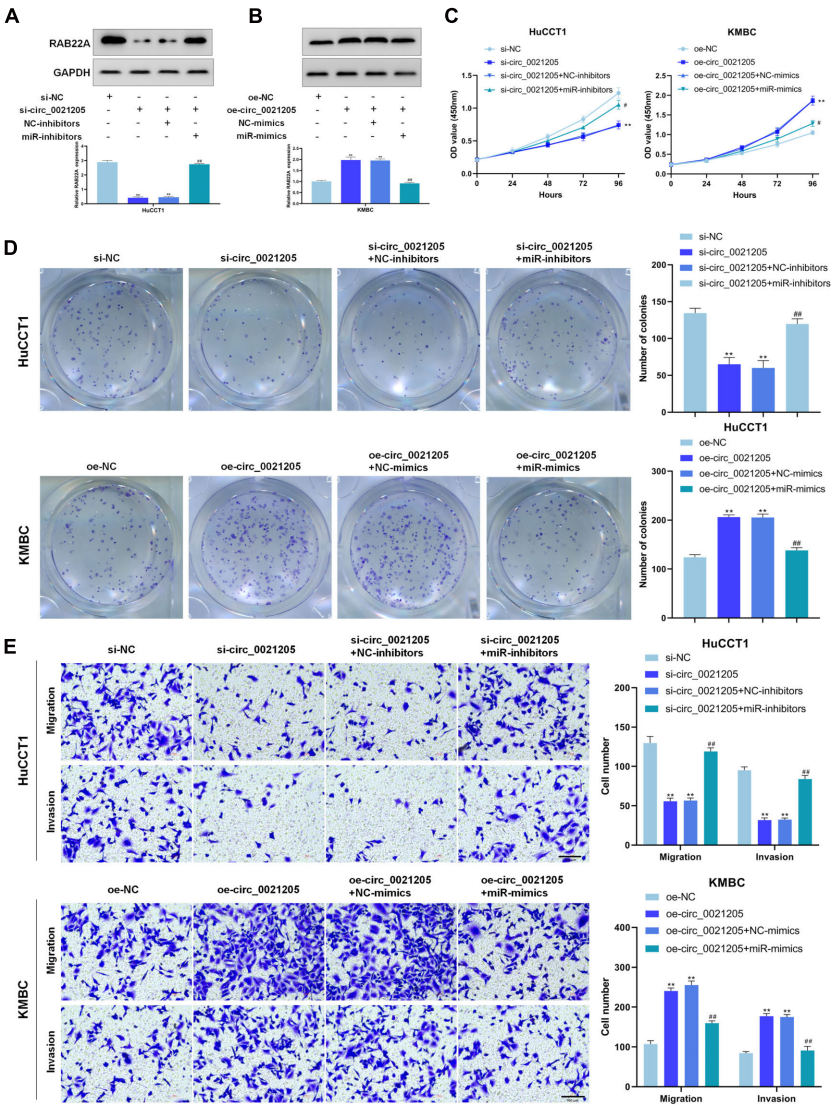

FIGURE 5 | Circ_0021205 suppresses CCA cell proliferation, migration and invasion through miR-204-5p/RAB22A axis. **(A,B)** Western blot results showed that circ_0021205 regulated RAB22A expression through sponging miR-204-5p. **(C,D)** The proliferation ability of treated HuCCT1 and KMBC cells were detected by CCK-8 assay and colony formation assay. **(E)** Transwell assay was performed to detect the migration and invasion of treated HuCCT1 and KMBC cells. All experiments were repeated at least three time. $^{**}P < 0.01$. # and ## mean the significant differences between oe-circ_0021205+miR-mimics and oe-circ_0021205+NC-mimics or si-circ_0021205+miR-inhibitors and si-circ_0021205+NC-inhibitors.

blotting and immunohistochemistry staining, and found the expression of Ki-67 and PCNA were significantly decreased after knocking down of circ_0021205 (**Figures 6F,G**). Six-month after the xenograft, we confirmed that si-circ_0021205 did not affect the mice survival. The results revealed that circ_0021205 knockdown could suppress the tumor growth of CCA *in vivo*.

DISCUSSION

In recent years, emerging evidence illustrates that many circRNAs function as tumor suppressors or promoters in several cancers, such as hepatocellular carcinoma, lung cancer, gastric cancer, and cholangiocarcinoma (Yang et al., 2019). So far, only a few CCA-related circRNAs have been recognized. In the present study, we first reveal that circ_0021205/miR-204-5p/RAB22A axis is involved in CCA progression.

In this study, we found that circ_0021205 was significantly up-regulated in CCA tissues and cells compare with the controls and associated with tumor size and TNM stage. Subsequently, the functional study demonstrated that circ_0021205 promoted the proliferation, metastasis, and invasion of CCA cells. Currently, accumulating studies reported that circRNAs could serve as miRNA sponges to regulate the expression of downstream genes. The "circRNA-miRNA-mRNA" axis has been reported to be involved in the development of multiple cancers. For example, circCCDC9 suppresses the progression of gastric

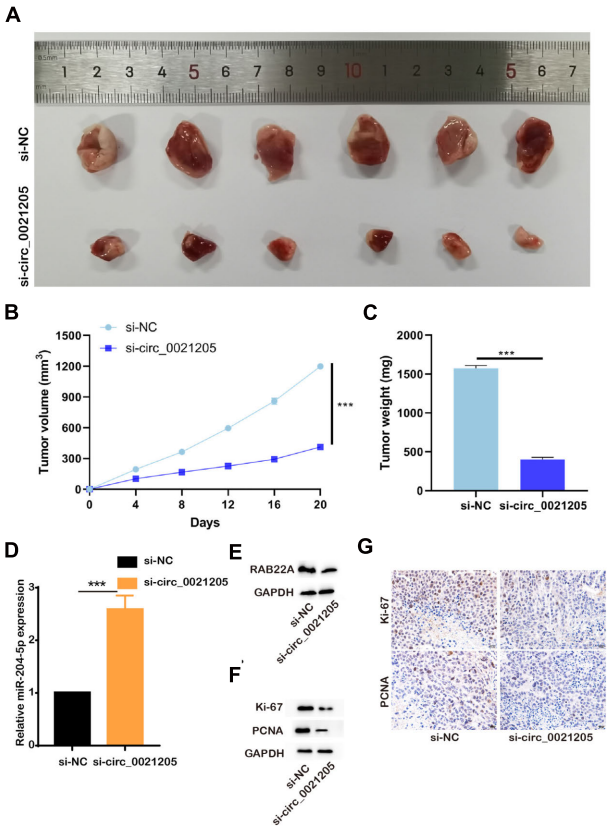

FIGURE 6 | Circ_0021205 knockdown inhibits the tumorigenesis of CCA *in vivo*. **(A)** The presentative image of xenograft tumors was showed. **(B)** Tumor volumes were recorded every 4 days. **(C)** Tumor weights were recorded. **(D)** Relative miR-204-5p expression after down-regulation of circ_0021205 was measured using qPCR. **(E)** The levels of RAB22A in si-NC and so-circ_0021205 tumor tissues were investigated using western blotting. **(F)** The levels of proliferation makers, Ki-67 and PCNA, were investigated using western blotting. **(G)** The proliferation properties of si-NC and so-circ_0021205 tumor tissues were detected using immunohistochemistry staining. ***$P < 0.001$.

cancer by regulating CAV1 via miR-6792-3p (Luo et al., 2020). Circ-ZKSCAN1 regulates FAM83A expression by sponging miR-330-5p to promote non-small lung cancer progression (Wang et al., 2019).

In our study, RIP experiment and liciferase report assay indicated that circ_0021205 could act as the sponge of miR-204-5p and RAB22A is the target gene of miR-204-5p. The rescue experiments demonstrated that circ_0021205 exerts carcinogenic effects in CCA by target RAB22A via miR-204-5p. RAB22A, a member of the RAB family of small GTPases, is known to be involved in several immune functions, and plays important roles in the endocytic recycling and the formation of T cell conjugates (Mayorga and Cebrian, 2019). Also, the expression of RAB22A determines the progression of multiple tumors, including liver cancer, ovarian cancer and malignant melanoma (Mayorga and Cebrian, 2019). In 2017, a study reported that Rab22a could enhance CD147 recycling and was required for the migration and invasion of lung cancer cells (Zhou et al., 2017). Given the above results, our results suggested the potential of circ_0021205 as a novel biomarker for the diagnosis of CCA. In CCA patients with elevated circ_0021205 level, circ_0021205, miR-204-5p and RAB22A could also be potential targets to be manipulated with the help of adeno-associated virus (AAV) to inhibit the progression of CCA. However, RAB22A plays important roles in multiple cancers containing liver cancer, ovarian cancer, malignant melanoma and CCA, and participates in multiple cell signaling pathways. So the manipulation of RAB22A may cause severe side effects in CCA patients. With the more specific manipulation of the upstream circ_0021205 and miR-204-5p, the side effects may be avoid. Nevertheless, there are some limitations in our study. Firstly, whether circ_0021205 can be stably detected in body fluids such as plasma still needs further study. Secondly, although the carcinogenic effects of circ_0021205 in CCA were revealed in this study, there also might be other critical circRNAs or mechanisms involved in the development of CCA. Therefore, the diagnostic potential of circ_0021205 in CCA is in need of further investigation.

In conclusion, this study demonstrates that circ_0021205 promotes CCA progression through miR-204-5p/RAB22A axis, which may provide a potential biomarker for CCA diagnosis.

DATA AVAILABILITY STATEMENT

The original contributions presented in the study are included in the article/supplementary material, further inquiries can be directed to the corresponding author/s.

ETHICS STATEMENT

The studies involving human participants were reviewed and approved by the Ethics Committee of Lishui Hospital of Zhejiang University. The patients/participants provided their written informed consent to participate in this study. The animal study was reviewed and approved by the Ethics Committee of Lishui Hospital of Zhejiang University.

AUTHOR CONTRIBUTIONS

JT and WC designed this study. LZ, SF, DZ, CK, and YY performed these experiments. RQ, ZZ, and CL analyzed the data. XL and JJ wrote the manuscript. All authors contributed to the article and approved the submitted version.

FUNDING

This study was supported by the National Key Research and Development projects intergovernmental cooperation in science and technology of China (2018YFE0126900), the National Natural Science Foundation of China (No. 82072025 and 82072026), the Key R&D Program of Lishui City (Nos. 2019ZDYF17 and 2019ZDYF09).

REFERENCES

Chen, Y. G., Kim, M. V., Chen, X., Batista, P. J., Aoyama, S., Wilusz, J. E., et al. (2017). Sensing Self and Foreign Circular RNAs by Intron Identity. *Mole. Cell* 67, 228–238. doi: 10.1016/j.molcel.2017.05.022

Cunningham, S. C., Cameron, J. L., Kamangar, F., Winter, J. M., Lillemoe, K. D., and Choti, M. A. (2007). Cholangiocarcinoma: thirty-one-year experience with 564 patients at a single institution. *Ann. Surg.* 245, 755–762. doi: 10.1097/01.sla.0000251366.62632.d3

Erichsen, R., Nørgaard, M., Høyer, M., Hansen, J. B., and Jacobsen, J. B. (2011). Survival of patients with primary liver cancer in central and northern Denmark, 1998-2009. *Clin. Epidemiol.* 3(Suppl. 1), 3–10. doi: 10.2147/clep.s20623

Fidelman, N., Roberts, J. P., and Yao, F. Y. (2011). Mixed hepatocellular cholangiocarcinoma and intrahepatic cholangiocarcinoma in patients undergoing transplantation for hepatocellular carcinoma. *Liver Transpl.* 17, 934–942. doi: 10.1002/lt.22307

Hansen, T. B., Jensen, T. I., Clausen, B. H., Bramsen, J. B., Finsen, B., Damgaard, C. K., et al. (2013). Natural RNA circles function as efficient microRNA sponges. *Nature* 495, 384–388. doi: 10.1038/nature11993

Jeck, W. R., and Sharpless, N. E. (2014). Detecting and characterizing circular RNAs. *Nat. Biotechnol.* 32, 453–461. doi: 10.1038/nbt.2890

Jens, M., Elefsinioti, A. L., Torti, F., Krueger, J., Rybak, A., and Maier, L. (2013). Circular RNAs are a large class of animal RNAs with regulatory potency. *Nature* 495, 333–338. doi: 10.1038/nature11928

Kinoshita, T., Konishi, M., Takahashi, S., and Gotohda, N. (2008). Surgical Outcome and Prognostic Factors in Intrahepatic Cholangiocarcinoma. *World J. Surg.* 32, 2675–2680. doi: 10.1007/s00268-008-9778-3

Kulcheski, F. R., Christoff, A. P., and Margis, R. (2016). Circular RNAs are miRNA sponges and can be used as a new class of biomarker. *J. Biotechnol.* 238, 42–51. doi: 10.1016/j.jbiotec.2016.09.011

Lee, Y. S., and Dutta, A. (2009). Micrornas in cancer. *Annu Rev. Pathol.* 4, 199–227.

Legnini, I., Di Timoteo, G., Rossi, F., Morlando, M., Briganti, F., Sthandier, O., et al. (2017). Circ-ZNF609 Is a Circular RNA that Can Be Translated and Functions in Myogenesis. *Mol. Cell* 66, 22–37. doi: 10.1016/j.molcel.2017.02.017

Li, X., Yang, L., and Chen, L. (2018). The Biogenesis, Functions, and Challenges of Circular RNAs. *Mole. Cell* 71, 428–442. doi: 10.1016/j.molcel.2018.06.034

Liao, D., Zhong, L., Yin, J., Zeng, C., Wang, X., Huang, X., et al. (2020). Chromosomal translocation-derived aberrant Rab22a drives metastasis of osteosarcoma. *Nat. Cell Biol.* 22, 868–881. doi: 10.1038/s41556-020-0522-z

Lu, T. X., and Rothenberg, M. E. (2018). MicroRNA. *J. Allergy Clin. Immunol.* 141, 1202–1207.

Luo, Z., Rong, Z., Zhang, J., Zhu, Z., Yu, Z., Li, T., et al. (2020). Circular RNA circCCDC9 acts as a miR-6792-3p sponge to suppress the progression of gastric cancer through regulating CAV1 expression. *Mol. Cancer* 19:86.

Mayorga, L. S., and Cebrian, I. (2019). Rab22a: A novel regulator of immune functions. *Mol. Immunol.* 113, 87–92. doi: 10.1016/j.molimm.2018.03.028

Patop, I. L., Wust, S., and Kadener, S. (2019). Past, present, and future of circRNAs. *EMBO J.* 38:e100836.

Rizvi, S., Khan, S. A., Hallemeier, C. L., Kelley, R. K., and Gores, G. J. (2018). Cholangiocarcinoma-evolving concepts and therapeutic strategies. *Nat. Rev. Clin. Oncol.* 15, 95–111. doi: 10.1038/nrclinonc.2017.157

Rupaimoole, R., and Slack, F. J. (2017). MicroRNA therapeutics: towards a new era for the management of cancer and other diseases. *Nat. Rev. Drug Discov.* 16, 203–222. doi: 10.1038/nrd.2016.246

Wan, P., Chi, X., Du, Q., Luo, J., Cui, X., Dong, K., et al. (2018). miR-383 promotes cholangiocarcinoma cell proliferation, migration, and invasion through targeting IRF1. *J. Cell Biochem.* 119, 9720–9729. doi: 10.1002/jcb.27286

Wang, Y., Xu, R., Zhang, D., Lu, T., Yu, W., Wo, Y., et al. (2019). Circ-ZKSCAN1 regulates FAM83A expression and inactivates MAPK signaling by targeting miR-330-5p to promote non-small cell lung cancer progression. *Transl. Lung Cancer Res.* 8, 862–875. doi: 10.21037/tlcr.2019.11.04

Wechagama, P., Namwat, N., Jusakul, A., Sripa, B., Miwa, M., Kuver, R., et al. (2012). Expression of oxysterol binding protein isoforms in opisthorchiasis-associated cholangiocarcinoma: a potential molecular marker for tumor metastasis. *Parasitol. Int.* 61, 136–139. doi: 10.1016/j.parint.2011.07.003

Yang, F., Hu, A., Li, D., Wang, J., Guo, Y., Liu, Y., et al. (2019). Circ-HuR suppresses HuR expression and gastric cancer progression by inhibiting CNBP transactivation. *Mol. Cancer* 18:158.

Yang, Q., Du, W. W., Wu, N., Yang, W., Awan, F. M., Fang, L., et al. (2017). A circular RNA promotes tumorigenesis by inducing c-myc nuclear translocation. *Cell Death Diff.* 24, 1609–1620. doi: 10.1038/cdd.2017.86

Zhang, B., Wang, W., Fei, B., Quan, C., Zhang, J., and Song, M. (2014). miR-204-5p Inhibits Proliferation and Invasion and Enhances Chemotherapeutic Sensitivity of Colorectal Cancer Cells by Downregulating RAB22A. *Clin. Cancer Res. Off. J. Am. Assoc. Cancer Res.* 20:6187. doi: 10.1158/1078-0432.ccr-14-1030

Zhou, Y., Wu, B., Li, J. H., Nan, G., Jiang, J. L., and Chen, Z. N. (2017). Rab22a enhances CD147 recycling and is required for lung cancer cell migration and invasion. *Exp. Cell Res.* 357, 9–16. doi: 10.1016/j.yexcr.2017.04.020

Conflict of Interest: The authors declare that the research was conducted in the absence of any commercial or financial relationships that could be construed as a potential conflict of interest.

frontiers in Molecular Biosciences

MINI REVIEW
published: 07 May 2021
doi: 10.3389/fmolb.2021.648663

The Role of PI3K Inhibition in the Treatment of Breast Cancer, Alone or Combined With Immune Checkpoint Inhibitors

Zhizhu Zhang[1] *and Ann Richmond*[2,3]*

[1] Department of Biological Sciences, Vanderbilt University, Nashville, TN, United States, [2] Department of Pharmacology, Vanderbilt University, Nashville, TN, United States, [3] Department of Veterans Affairs, Tennessee Valley Healthcare System, Nashville, TN, United States

Dysregulation of phosphoinositide 3-kinase (PI3K) signaling is highly implicated in tumorigenesis, disease progression, and the development of resistance to the current standard of care treatments in breast cancer patients. This review discusses the role of PI3K pathway in breast cancer and evaluates the clinical development of PI3K inhibitors in both early and metastatic breast cancer settings. Further, this review examines the evidence for the potential synergistic benefit for the combination treatment of PI3K inhibition and immunotherapy in breast cancer treatment.

Keywords: PI3K inhibition, breast cancer, immune checkpoint inhibitors, MDSC, tumor immune microenvironment

OPEN ACCESS

Edited by:
Shengtao Zhou,
Sichuan University, China

Reviewed by:
Snehal M. Gaikwad,
National Cancer Institute, United States
Maxim Sorokin,
I.M. Sechenov First Moscow State Medical University, Russia

***Correspondence:**
Ann Richmond
ann.richmond@vanderbilt.edu

Specialty section:
This article was submitted to Molecular Diagnostics and Therapeutics, a section of the journal Frontiers in Molecular Biosciences

Received: *01 January 2021*
Accepted: *06 April 2021*
Published: *07 May 2021*

Citation:
Zhang Z and Richmond A (2021) The Role of PI3K Inhibition in the Treatment of Breast Cancer, Alone or Combined With Immune Checkpoint Inhibitors. Front. Mol. Biosci. 8:648663. doi: 10.3389/fmolb.2021.648663

INTRODUCTION

Breast cancer is the most frequent cancer type in women worldwide (Bray et al., 2018). Breast cancer is generally divided into three subtypes, with targeted therapies determined by subtypes. Hormone receptor-positive (HR^+)/$HER2^-$ is the most common subtype and accounts for around 70% of breast cancer patients (Howlader et al., 2014). Treatment generally involves endocrine therapy (ET) (Waks and Winer, 2019). Recently, the approval of CDK4/6 inhibitors for use in combination with ET substantially improves survival outcomes (Shah et al., 2018). However, after resistance develops to hormone therapy, chemotherapy becomes the only standard treatment option (Cardoso et al., 2009); 15–20% of patients are diagnosed as $HER2^+$ (Howlader et al., 2014). The standard-of-care treatment for $HER2^+$ breast cancer incorporates $HER2^-$ targeted antibody with chemotherapy (Romond et al., 2005; Waks and Winer, 2019). However, even after disease progression on therapy, continued administration of anti-HER2 and chemotherapy remains as the subsequent treatment (Olson et al., 2012). Accounting for 10–20% of newly diagnosed breast cancer cases, triple-negative breast cancer (TNBC) is characterized by the lack of hormone receptor expression and lack of HER2/NEU gene overexpression (Dent et al., 2007). TNBC demonstrates high heterogeneity in the mutational profile and shows the highest relapse risks (Dent et al., 2007). Due to a lack of targets, chemotherapy is currently the primary treatment for TNBC, but the clinical benefits are usually not durable due to frequently acquired resistance (Liedtke et al., 2008).

Upregulation of the phosphoinositide 3-kinase (PI3K) signaling pathway is commonly observed in breast cancer patients. It has been associated with breast cancer tumorigenesis, progression, and the development of resistance to hormone therapy and chemotherapy (Guerrero-Zotano et al., 2016; Drullinsky and Hurvitz, 2020). Therefore, it is essential to elucidate the mechanism of the PI3K signaling pathway in breast cancer and explore the potential of PI3K inhibitors in the treatment of different subtypes of breast cancer, alone or combined

with other therapies in both early and metastatic settings. This review will provide an overview of the rationale for and development of PI3K inhibition and examine the potential of PI3K inhibitors to combine with immunotherapy in breast cancer treatment.

PHOSPHOINOSITIDE 3-KINASE SIGNALING PATHWAY AND ITS ABERRANT ACTIVATION IN BREAST CANCER

The PI3K signaling pathway is involved in many cellular processes, including glucose metabolism, cell growth, proliferation, and survival (Katso et al., 2001). PI3K is a family of lipid kinases. The Class I PI3Ks are the most commonly altered class in breast cancer and are composed of a heterodimer of a p85 regulatory subunit and a p110 catalytic subunit (Hiles et al., 1992). Upon receiving signals from receptor tyrosine kinases, PI3K catalyzes the conversion of phosphatidylinositol bisphosphate PI(4,5)P2 to phosphatidylinositol triphosphate PI(3,4,5)P3 (Schu et al., 1993). PIP3 recruits phosphoinositide-dependent kinase-1 (PDK1) and protein kinase B (AKT), thus promoting the activation of AKT by PDK1 phosphorylation (Alessi et al., 1997).

AKT activation results in multiple downstream signaling cascades, including mammalian target of rapamycin (mTOR), which upregulates processes such as transcription and translation, protein synthesis, and cell cycle progression, among others (Sarbassov et al., 2005). Negative regulators of the pathway include phosphate and tensin homolog (PTEN) and inositol polyphosphate 4-phosphatase (INPP4B), which dephosphorylate PIP3 and convert it back to PIP2 (Maehama and Dixon, 1998; Gewinner et al., 2009; **Figure 1**).

Several genetic aberrations associated with genes that encode for proteins in the PI3K signaling pathway have been identified in breast cancer. Mutations in the p110α subunit (PIK3CA) have been found in around 40% of $HR^+/HER2^-$ or $HER2^+$ advanced breast cancer tumors and around 9% of TNBC tumors (Cancer Genome Atlas Network, 2012; Guerrero-Zotano et al., 2016). Mutations in other subunits of p110 are much rarer. In TNBC tumors, inactivating mutations mutations, loss of PTEN, or heterozygous deletion of INPP4B are the more frequently observed PI3K pathway-related genetic alterations (Cancer Genome Atlas Network, 2012). Mice bearing TNBC tumors engineered with an INPP4B deficiency showed increased sensitivity to PI3K inhibition (Liu et al., 2020).

Therapy resistance across breast cancer subtypes can result from PI3K overactivation. For HR^+ breast cancer, ET serves as the first-line treatment. However, resistance to ET commonly arises. Evidence suggests that antiestrogen resistance might be conferred by the PI3K pathway (André et al., 2019). Increased PI3K pathway signaling is associated with the downregulation of endocrine receptor expression, which could lead to insensitivity to hormone therapies (Creighton et al., 2010). Treatment with the dual PI3K/mTOR inhibitor BEZ235 in the long-term estrogen-deprived, hormone-resistant cell line resulted in restored sensitivity to tamoxifen, induced apoptosis, and increased ER levels (Creighton et al., 2010). In $HER2^+$ cancers, resistance to the standard-of-care anti-HER2 antibody trastuzumab has also been associated with the constitutive activation of the PI3K pathway (Pohlmann et al., 2009). In trastuzumab-resistant breast cancer cell lines due to the PTEN deficiency, inhibition of PI3K pathway restores sensitivity to trastuzumab and significantly inhibits cell growth (Junttila et al., 2009). In TNBC, dysregulation in the PI3K pathway has been associated with chemotherapy resistance (Drullinsky and Hurvitz, 2020).

THE CLINICAL DEVELOPMENT OF PI3K INHIBITORS: EFFICACY, RESISTANCE, AND TOXICITY

Multiple PI3K inhibitors have been developed and evaluated in various stages of clinical trials. PI3K inhibitors can be divided into pan-PI3K inhibitors, isoform-specific PI3K inhibitors, and dual PI3K/mTOR inhibitors.

Pan-PI3K inhibitors target multiple isoforms of the Class I PI3K. Buparlisib targets all four isoforms (α, β, δ, γ) and, when combined with fulvestrant, showed only a moderate improvement in the median progression-free survival (PFS) for about 1.9 months compared with the placebo and fulvestrant group in $HR^+/HER2^-$ advanced breast cancer patients (Baselga et al., 2017). However, broad targeting of multiple forms of PI3K isozymes leads to a high rate of severe adverse events (AEs) that mandate dose reduction, interruptions, and discontinuation, thus discouraging further investigation (Baselga et al., 2017). Selective inhibitors for a combination of a few isoforms have been developed against solid tumor and hematological malignancies. Copanlisib targets PI3Kα and PI3Kδ isoforms and has been approved as a treatment for relapsed follicular lymphoma (FL) (Dreyling et al., 2017). Phase Ib/II studies are ongoing in evaluating the efficacy of Copanlisib in pretreated recurrent or metastatic $HER2^+$ BC in combination with trastuzumab (Keegan et al., 2018). Taselisib, a β-isoform-sparing pan-PI3K inhibitor, when combined with fulvestrant in the treatment of PIK3CA-mutated $ER^+/HER2^-$ locally advanced or metastatic BC, showed only a moderate 2-month improvement in median PFS (7.4 vs. 5.4) over the placebo arm (Baselga et al., 2018). Duvelisib targets PI3Kδ and PI3Kγ, which are isoforms highly expressed in lymphoid cells and implicated in malignant B- and T-cell proliferation and survival (Flinn et al., 2018). Duvelisib has been approved for the treatment of chronic lymphocytic leukemia (CLL) and FL (Flinn et al., 2018). However, PI3Kδ or PI3Kγ is not commonly mutated in breast cancer, and a direct stimulatory effect of PI3Kδ or PI3Kγ in breast cancer tumor growth is not obvious. The potential indirect benefit of targeting PI3Kδ or PI3Kγ in breast cancer for enhancing anti-tumor immunity will be discussed in the following section.

Isoform-specific PI3K inhibitors target only one or a few selected isoforms among the four. Alpelisib specifically inhibits p110α, the major mutated isoform in the PI3K pathway in breast

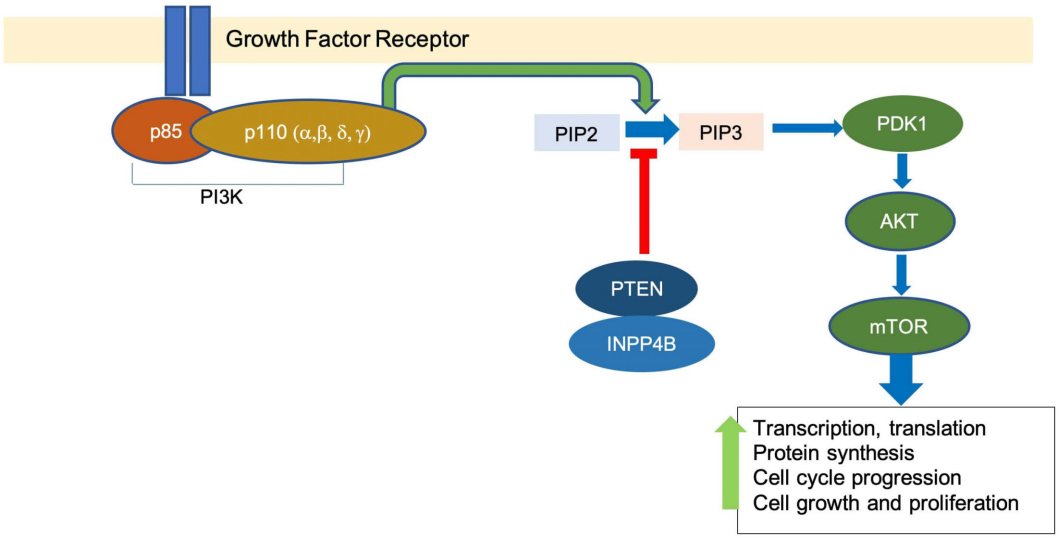

FIGURE 1 | The overview of PI3K pathway. Binding of growth factor activates the tyrosine kinase receptor, which promotes the transformation of PIP2 to PIP3 by PI3K. This leads to a downstream signaling cascade that upregulates events associated with cell growth and proliferation.

cancer, as discussed above. In the SOLAR-1 trial, a combination of alpelisib with fulvestrant showed a 5.3 month improvement in mPFS compared with the placebo-fulvestrant group in patients with PIK3CA mutation (André et al., 2019). The rates of AEs are also lower than pan-PI3K inhibitors, indicating a more tolerable toxicity profile that allows for more prolonged and uninterrupted dosing schedule and higher doses. The discontinuation rate is 25.0 vs. 4.2% in alpelisib vs. placebo, compared with 39 vs. 5% in the buparlisib study (Baselga et al., 2017; André et al., 2019). This result prompted alpelisib as the first approved PI3K inhibitor for $HR^+/HER2^-$ PIK3CA-mutated advanced/metastatic BC patients after progression on ET. However, alpelisib with letrozole for the neoadjuvant treatment of $HR^+/HER2^-$ early breast cancer patients reported no improvement in ORR regardless of whether the patients have PIK3CA mutation (Mayer et al., 2019). Further evaluation of alpelisib in TNBC and $HER2^+$ settings might provide encouraging results.

Although normal or PTEN-WT breast tumors do not depend on p110 β isoform activity in PI3K signaling, cancer cells with PTEN deficiency require p110β activity to sustain PI3K signaling and are sensitized to PI3Kβ-specific inhibition (Torbett et al., 2008). This suggests that while PI3Kα inhibition may be optimally tailored toward PIK3CA-mutated breast tumor types, PI3Kβ inhibition may be exploited for PTEN-deficient breast tumors, notably for TNBC. Research in the area of PI3Kβ inhibition for breast cancer is limited. A recent preclinical study evaluated the effect of AZD8186, a selective PI3Kβ/δ inhibitor, on mice injected with PTEN-deficient TNBC tumors, but demonstrated mediocre anti-tumor effect as a single agent or combined with paclitaxel (Owusu-Brackett et al., 2020). The lack of efficacy could be due to the feedback loop between PI3Kα and PI3Kβ, leading to a reactivation of the signaling that became inhibited with dual inhibition of the isoforms in prostate cancer (Schwartz et al., 2015). Other examples of isoform-specific PI3K inhibitors include idelalisib, an inhibitor specific for p110δ, approved for CHL treatment due to a significantly improved survival profile (Furman et al., 2014).

Dual PI3K/mTOR inhibitors compete for the ATP-binding cleft of PI3K and mTOR kinases (Guerrero-Zotano et al., 2016). However, phase I/II clinical trials for dual PI3K/mTOR inhibitors dactolisib (BEZ235), apitolisib (GDC-0980), and gedatolisib (PF-05212384) showed a relatively poor safety profile that results in low tolerable dosage and modest anti-tumor responses (Dolly et al., 2016; Wainberg et al., 2017; Wise-Draper et al., 2017). Several clinical studies are ongoing to explore their efficacy in breast cancer. Gedatolisib is being tested in treatment for metastatic TNBC and ER^+ patients (Forero-Torres et al., 2018; Radovich et al., 2018).

The limited efficacy of PI3K inhibitors could be attributed to the complex feedback loops in the PI3K/AKT/mTOR signaling network and its crosstalk with other signaling pathways. This results in subsequent reactivation of PI3K or parallel pathway that confers resistance and reduces the anti-tumor effects substantially. In PTEN-deficient tumor cells, resistance to a pan-PI3K inhibitor was conferred by over-activation of p110-beta (Nakanishi et al., 2016). The PI3K pathway engages in crosstalk with the RAS-RAF-MEK-ERK pathway at multiple nodes of interaction (Castellano and Downward, 2011). In HER2 amplified breast cancer cells, although PI3K inhibitors successfully suppress AKT activation downstream, there is enhanced activation of HER family receptors and a compensatory activation of the ERK signaling (Serra et al., 2011). Combined administration of anti-HER2 monoclonal antibodies and MEK inhibitors could antagonize the proliferative effect resulting from ERK dependency upon PI3K inhibition (Serra et al., 2011). A study using murine cancer models showed a combination of MEK and PI3K/mTOR inhibitor resulted in significant tumor regression and survival advantages in both basal-like and $HER2^+$

subtype models (Roberts et al., 2012). However, their data suggested that resistance to the triplet inhibition will still develop within months. Additionally, combined treatment could lead to a high toxicity profile, and the need for treatment breaks; as a result, significant weight loss in mice induces tumor regrowth (Roberts et al., 2012). Further research that elucidates the possible mechanism of PI3K inhibition, intrinsic and acquired resistance, is essential to enhance the durability of clinical benefit with targeted combination treatment tailored to specific subtypes of breast cancer and the mutational status of the patients.

Phosphoinositide 3-kinase inhibitors could lead to many AEs. Hyperglycemia is one of the most observed AEs across clinical trials (Drullinsky and Hurvitz, 2020). These AEs are related to the normal function of p110α in promoting insulin signaling, resulting in the breakdown of glycogen, minimal glucose uptake, and high glucose level in the circulatory system (Hopkins et al., 2018). Considered as an on-target result of PI3K inhibition, reduced insulin also impedes tumor cell proliferation by impairing their uptake of glucose (Hopkins et al., 2018). Gastrointestinal AEs are also commonly observed with PI3K inhibition. Severe diarrhea associated with PI3Kδ isoform inhibition is due to the impairment of colon macrophage functionality and pro-inflammatory response (Uno et al., 2010). This again justifies selective targeting of PI3K isoforms based on the observed mutational status of the patients to reduce AEs.

Overall, despite the importance of the PI3K pathway in breast cancer and therapy resistance, many PI3K inhibitors used as monotherapy reported limited efficacy and high toxicity profile in current clinical trials across breast cancer subtypes. This necessitates the examination of PI3K inhibition in combination with other types of therapies to potentially maximize anti-tumor effects.

IMMUNOTHERAPY IN BREAST CANCER

Immunotherapies based on the use of immune checkpoint inhibitors (ICI) target T-cell co-inhibitory signalings, namely, CTLA-4 and PD-1/PD-L1, and hence relieve their suppression of anti-tumor T-cell activity and prevent tumor immune evasion (Hargadon et al., 2018). ICI treatment exhibits significantly improved survival rate and inhibition of tumor growth across the treatment of various types of tumors, leading to FDA approval in many cancer indications (**Table 1**). However, single-agent treatment using monoclonal antibodies against PD-1 or PD-L1 generally reported mediocre efficacy in breast cancer patients since most breast cancer tumors have long been classified as immunologically "cold." "Cold" tumors are highly unresponsive to immunotherapy treatment (Szekely et al., 2018).

Triple-negative breast cancer is considered as the most immunogenic subtype of breast cancer, with a higher lymphocyte infiltration rate than $HER2^+$ or HR^+ tumors and thus regarded as a promising target for immunotherapies (Szekely et al., 2018). PD-L1 is a commonly overexpressed biomarker in TNBC (Mittendorf et al., 2014). TNBCs showed responsiveness to immunotherapies combined with chemotherapies in clinical trials, leading to the approval of both atezolizumab and pembrolizumab by the FDA to use in combination with chemotherapy for PD-L1 positive, unresectable, locally advanced, or metastatic TNBC (Cortes et al., 2020; Narayan et al., 2020). Pembrolizumab plus chemotherapy has demonstrated a 4.1 month improvement in median PFS over the placebo arm (9.7 vs. 5.6) (Cortes et al., 2020).

Based on tumor-infiltrating lymphocyte count and PD-L1 expression, primary breast cancer tumors show higher immunogenicity than the metastatic tumor samples (Szekely et al., 2018). Therefore, neoadjuvant and adjuvant immunotherapy targeting early stage breast cancer has been an area of increasing interest. In the phase 2 trial I-SPY2, pembrolizumab with neoadjuvant chemotherapy showed a 17% improvement (30 vs. 13%) in the estimated pathologic complete response (pCR) in $HR^+/HER2^-$ patients and a 38% improvement (60 vs. 22%) in the estimated pCR in TNBC patients as compared to the placebo (Nanda et al., 2020).

THE RATIONALE FOR PI3K INHIBITION COMBINATION APPROACH WITH IMMUNOTHERAPY

With the recent breakthroughs in both PI3K inhibitor alpelisib and immune checkpoint blockade (ICB) treatment in breast cancer, the potential for PI3K inhibition in combination with PD-1/PD-L1 blockade merits evaluation. Increasing evidence suggests that in addition to the direct proliferative effects on tumor cells, the PI3K-AKT-mTOR pathway is involved in creating an immunosuppressive tumor microenvironment. Okkenhaug et al. (2016) and O'Donnell et al. (2018) provided extensive reviews on the recent findings of the immunomodulatory roles of PI3K pathway on the tumor microenvironment, including the enhanced expression of PD-L1, recruitment, and differentiation of myeloid-derived suppressor cells (MDSCs) and Tregs into the tumor, and secretion of suppressive cytokines to impair stimulation of macrophages and dendritic cells and the migration, expansion, functionality, and memory development of T cells (Okkenhaug et al., 2016; O'Donnell et al., 2018). These authors hypothesized that inhibition of the PI3K pathway may further boost T-cell-mediated tumor killing when exploited for therapeutic combination with immunotherapy. However, whether the stimulatory effects of PI3K inhibition on anti-tumor immunity translate to breast cancer and sensitize breast tumors for immune checkpoint inhibition is not specifically discussed. This review will summarize the research results and clinical trials in the setting of breast cancer and will suggest a future direction to explore the synergy for combining PI3K inhibitors and ICI in breast cancer.

Phosphate and tensin (PTEN) homolog loss has been identified as one mechanism that induces PD-L1 expression in TNBC via transcriptional regulation, while inhibition of the PI3K pathway with the administration of an AKT inhibitor leads to decreased PD-L1 expression (Mittendorf et al., 2014). This establishes the connection between PTEN, the PI3K pathway, and the regulation of PD-L1 expression. The increased PD-L1

expression induced by PTEN loss leads to reduced proliferation and survival of T cells, inhibiting effective antitumor adaptive immunity (Mittendorf et al., 2014). Peng et al. showed that in the murine melanoma model, the immune resistance conferred by PTEN loss, including the reduction in T-cell infiltration and expansion, can be reversed by selective inhibition of PI3Kβ in combination with ICI treatment (anti-PD-1 and anti-CTLA-4). The combination treatment significantly reduces tumor progression, in contrast to the limited efficacy of treatment with every single agent (Peng et al., 2016). As suggested in Pascual and Turner (2019), the same synergistic potential could be exploited in PTEN-deficient TNBC.

p110δ and p110γ are mostly expressed in leukocytes and thus have been targeted for hematologic malignancies. Increasing evidence points to their role in immunosuppressive mechanisms on T cell and myeloid cell activity, suggesting the clinical potential for PI3Kδ and PI3Kγ inhibitors to enhance the anti-tumor sensitivity of the immune system across cancer types, including preclinical breast tumor models. The immunosuppressive effect of p110γ on the tumor microenvironment is demonstrated by its role in the recruitment of MDSCs into the tumor tissues. MDSCs are a heterogeneous population of immature myeloid cells that are known to induce suppression of the antitumor function, proliferation, and migration of immune cells, including T cell and NK cells, and promote tumor angiogenesis and metastases (Umansky et al., 2016). Selective inhibition or genetic knockout of p110γ significantly reduces α4β1 integrin-mediated trafficking and adhesion of MDSCs to the tumor, leading to the suppression of spontaneous breast carcinoma growth (Schmid et al., 2011). PI3Kγ-specific inhibition is also shown to polarize the myeloid cells to the more immune-stimulatory M1-like phenotype from the immunosuppressive M2-like phenotype in tumor models including 4T1 breast cancer, which correlates with higher CD8/Treg ratio from increased $CD8^+$ T-cell infiltration (De Henau et al., 2016; Kaneda et al., 2016). A similar observation of enhanced $CD8^+$ T-cell infiltration is observed in another study with PI3Kγ knockout mice injected with MMTV-PyMT tumor cells, which also correlates with slower growth of the tumor and reduced metastasis to lung (Sai et al., 2017).

The subversion of tumor-infiltrating myeloid recruitment by PI3Kγ inhibitor has the potential to enhance TNBC sensitivity to ICI. Kim et al. categorized TNBC models into neutrophil-enriched and macrophage-enriched subtypes. While the macrophage-enriched subtype (MES) exhibits increased $CD8^+$ T-cell infiltration and activity upon exposure to ICI, neutrophil-enriched subtypes (NES) of TNBC models respond minimally to ICI treatment due to the highly immunosuppressive microenvironment created by granulocytic MDSC accumulation (Kim et al., 2019). Acquired resistance to ICI treatment by the previously responsive MES tumor is also associated with increased accumulation of gMDSCs (Kim et al., 2019). Granulocytic MDSCs are similar to neutrophils in morphological and phenotypical ways and constituted the majority of the MDSC population in most types of cancer (Gabrilovich, 2017). The Gene Set Enrichment Analysis (GSEA) associates the high

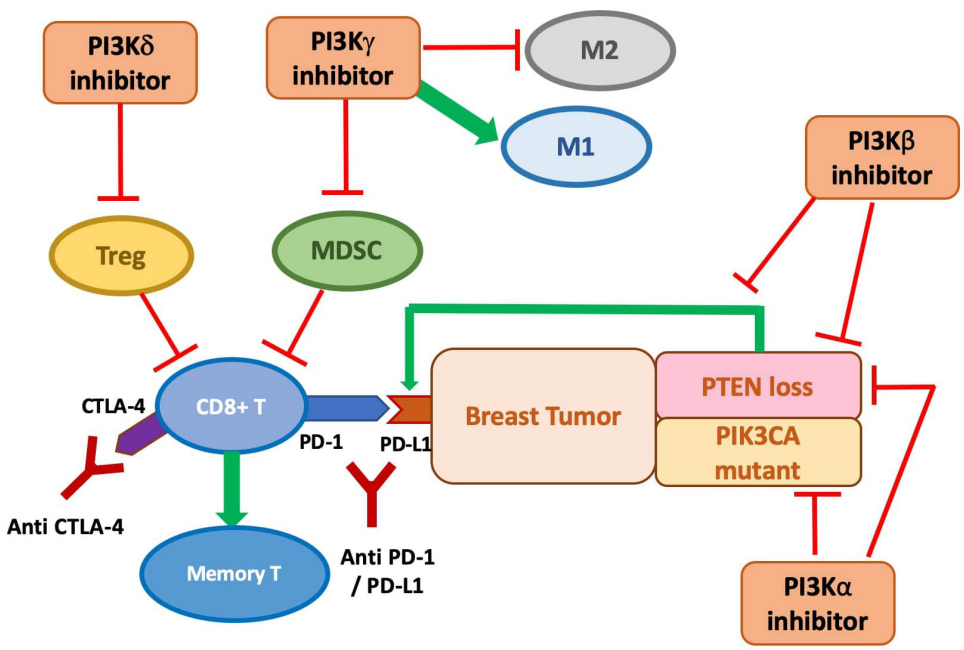

FIGURE 2 | The anti-tumor role of PI3K inhibitors on breast cancer with direct inhibition on cancer cell proliferation and indirect stimulation of the immune response, and potential synergy with immune checkpoint inhibition. PI3Kδ inhibitor is shown to suppress Treg function. PI3Kγ inhibitor may prevent MDSC infiltration and accumulation and polarize macrophages to the M1 phenotypes. PI3Kβ inhibition antagonizes the p110β activity required for PTEN-null tumor and targets the increased PD-L1 expression on PTEN-null tumor. PI3Kα inhibition is demonstrated to be effective at preventing tumor cell growth, especially in PIK3CA mutants, but might also be promising in PTEN-null tumor to prevent the PI3Kβ/α feedback loop.

tumor-associated neutrophil level to PI3K-AKT-mTOR pathway, which aligns with the previous finding of the group showing that mTOR signaling stimulates MDSC accumulation in the mammary tumor (Welte et al., 2016). The PI3K pathway has also been associated with immunosuppressive, neutrophil-recruiting cytokines and chemokines such as CXCL1 and CXCL-8, implicating the mechanism for MDSCs recruitment (Kim et al., 2019). Thus, targeting PI3K-mediated MDSC infiltration may sensitize intrinsic and acquired resistant breast tumors for ICI treatment. The preclinical combination of PI3Kγ inhibition and ICI showed promising outcomes: co-administration of PI3Kγ inhibitor with either anti-PD1 or anti-CTLA-4 significantly inhibits 4T1 tumor growth compared with ICI treatment alone (De Henau et al., 2016). Whether other components of the PI3K pathway besides PI3Kγ also modulate the ICI-resistance from MDSC infiltration in TNBC merits more investigation.

Inactivation of p110δ by genetic ablation or selective inhibition has been shown to reduce breast tumor growth and metastasis in mouse 4T1 model and other models of solid cancer by impairment of Treg function, including suppression in their secretion of interleukin (IL)-10 (Ali et al., 2014). Significantly, data from p110δ-inactivated mice suggest effective anti-tumor memory formation, with significant suppression of relapse from the surgical removal of breast tumor compared to wild type (Ali et al., 2014). This result is consistent with a study that revealed enhanced persistence of the $CD8^+$ memory T cells upon PI3Kδ inhibition in a melanoma model (Abu Eid et al., 2017).

The role and importance of each PI3K isoform in shaping the anti-tumor immune response in breast tumors still need further characterization to devise the optimal selective inhibition scheme for combination with ICI treatment. Given the complex direct and indirect anti-tumor role of different PI3K isoforms, the combination of a pan-PI3K inhibitor with ICI might also provide clinical advantages. Moreover, PTEN loss has been identified as one mechanism that induces PD-L1 expression in TNBC via transcriptional regulation. Simultaneously, inhibition of the PI3K pathway with the administration of an AKT inhibitor leads to decreased PD-L1 expression (Mittendorf et al., 2014). This establishes the connection between PTEN, the PI3K pathway, and the regulation of PD-L1 expression. The increased PD-L1 expression induced by PTEN loss leads to reduced proliferation and survival of T cells, inhibiting effective anti-tumor adaptive immunity (Mittendorf et al., 2014). Thus, there is a synergistic potential of anti-PD-L1 immunotherapy and targeted inhibition of the PI3K-AKT-mTOR pathway (**Figure 2**).

Preclinical studies with this combination scheme in breast cancer are still limited, but some show promising results. One study found that despite limited efficacy of anti-PD1 monotherapy in mice model bearing PyMT tumor, the co-treatment of a pan-PI3K inhibitor with anti-PD1 antibody leads to a significantly smaller mean tumor volume than with both agents used alone (Sai et al., 2017). Another preclinical study performed a quadruple combination using PI3Kα, CDK4/6, PD-1, and CTLA-4 inhibition. It showed highly durable tumor regression in the TNBC model, with a significant increase in granzyme B positive $CD8^+$ and $CD4^+$ T cells (Teo et al., 2017).

TABLE 1 | The FDA-approved immune checkpoint inhibitors and their approved indications.

Checkpoint target	FDA-approved drug	Approved indication(s)
Immune cytotoxic T-lymphocyte antigen-4 (CTLA-4)	Ipilimumab	Melanoma
		*Advanced renal cell carcinoma
		*MSI-H/dMMR metastatic colorectal cancer
		*Hepatocellular carcinoma
		*NSCLC
		*Malignant pleural mesothelioma
Programmed Death-1 (PD-1)	Pembrolizumab	NSCLC
		Squamous cell head and neck cancer
		Melanoma
		Merkel cell carcinoma
		Hepatocellular carcinoma
		MSI-H/dMMR cancer
		Cervical cancer
		Gastric carcinoma
		Classical Hodgkin's lymphoma
		PMBCL
		Urothelial bladder cancer
		Non-muscle invasive bladder cancer
		Advanced renal cell carcinoma
		Esophageal squamous cell carcinoma
		Cutaneous squamous cell carcinoma
	Nivolumab	Small cell lung cancer
		NSCLC
		Squamous cell head and neck cancer
		Melanoma
		Hepatocellular carcinoma
		Advanced renal cell carcinoma
		Urothelial cancer
		Esophageal squamous cell carcinoma
		Malignant pleural mesothelioma
		Classical Hodgkin lymphoma
		MSI-H/dMMR metastatic colorectal cancer
	Cemiplimab	Cutaneous squamous cell carcinoma
Programmed Death-Ligand 1 (PD-L1)	Atzolizumab	Small cell lung cancer
		NSCLC
		TNBC
		Urothelial cancer
		Hepatocellular carcinoma
		Melanoma
	Durvalumab	NSCLC
		Small cell lung cancer
		Urothelial carcinoma
	Avelumab	Merkel cell carcinoma
		Urothelial cancer
		Renal cell carcinoma

**The approved use of ipilimumab is in combination with nivolumab.*
NSCLC, non-small cell lung cancer; PMBCL, primary mediastinal large B-cell lymphoma; MSI-H/dMMR, microsatellite instability high/deficient mismatch repair.

TABLE 2 | Ongoing clinical trials combining immune checkpoint inhibitors with inhibitors of the PI3K/AKT/mTOR pathway.

Combination	Drug names	Indications	Phase	Clinical trial identifier
Anti-PD1 + PI3K inhibitor	Pembrolizumab + Copanlisib	Relapsed or refractory NK and T-cell non-Hodgkin lymphoma	I/II	NCT02535247
	Pembrolizumab + Duvelisib	Recurrent or metastatic (R/M) head and neck squamous cell carcinoma (HNSCC)	I/II	NCT04193293
	Pembrolizumab + Idealisib	NSCLC, relapsed or refractory chronic lymphocytic leukemia	Ib/II	NCT03257722, NCT02332980
	Pembrolizumab + PI3K-beta inhibitor GSK2636771	Metastatic melanoma and PTEN loss	I//II	NCT03131908
	Nivolumab + PI3K-gamma inhibitor IPI-549	Advanced urothelial carcinoma	II	NCT03980041
	Pembrolizumab + PI3K-delta inhibitor Umbralisib	Relapsed or refractory chronic lymphocytic leukemia	II	NCT03776864
	Nivolumab + Duvelisib	Richter syndrome or transformed follicular lymphoma	I	NCT03892044
	Nivolumab + Eganelisib (PI3Kγ)	Advanced solid tumors, NSCLC, melanoma, triple negative breast cancer, adrenocortical carcinoma, mesothelioma, high-circulating myeloid-derived suppressor cells	1/1b	NCT02637531
	Pembrolizumab + INCB050465 (PI3Kδ)	Colorectal cancer, endometrial cancer, melanoma, head and neck cancer, lung cancer, MMR-deficient tumors, breast cancer, pancreatic cancer, renal cell carcinoma, solid tumors, urothelial cancer	1	NCT02646748
Anti PD-L1 + AKT inhibitor	Durvalumab + Capivasertib + Paclitaxel	Metastatic triple-negative breast cancer	I/II	NCT03742102
Anti PD-L1 + PI3K inhibitor	Atezolizumab + PI3K-gamma inhibitor IPI-549	Triple-negative breast cancer, renal cell carcinoma	II	NCT03961698
Anti PD-L1 + mTOR inhibitor	Durvalumab + Sirolimus	Stage I-IIIA non-small cell lung cancer	I	NCT04348292
Anti-PD1 + mTOR inhibitor	PDR001 + Everolimus	Colorectal cancer, non-small cell lung carcinoma, triple negative breast cancer	Ib	NCT02890069

Clinical trial information from clinicaltrials.gov.

Several phase I/II clinical trials are ongoing to assess the combination of ICI with inhibitors of the PI3K/AKT/mTOR pathway, mostly in lymphoma and leukemia (**Table 2**). There are a few that look at this combination therapy in TNBC, including two trials that evaluate one PI3Kγ inhibitor: one with atezolizumab (NCT03961698) and one with nivolumab (NCT02637531). Another trial combines PI3Kδ inhibition with pembrolizumab (NCT02646748). Other clinical studies are in progress to investigate the potential synergistic benefit of AKT or mTOR inhibitors with ICIs (NCT03742102; NCT03961698; NCT02890069).

DISCUSSION

With the approval of the alpha selective PI3K inhibitor alpelisib in $HR^+/HER2^-$ PIK3CA-mutated advanced/metastatic breast cancer patients after progression on ET, several clinical trials evaluate its efficacy in advanced TNBC, and $HER2^+$ subtypes are ongoing (NCT04208178; NCT04216472). The success of SOLAR-1 demonstrates that stratification of patients by PIK3CA mutation is promising to identify the patient population that is more likely to respond maximally to PI3K alpha isoform inhibition. However, besides PIK3CA mutation, other potential biomarkers for predicting the efficacy of PI3K inhibition require further evaluation. PIK3CA mutation is not as common in the highly heterogenous TNBC patients and might exclude many patients from receiving PI3K inhibition treatment. Additionally, although activating PIK3CA mutation is generally associated with greater therapeutic response, some patients without this mutation benefited significantly from PI3K alpha isoform inhibition, while others with PIK3CA mutation exhibit minimal benefit (André et al., 2019). Thus, identifying more reliable biomarkers for patient selection would be critical for optimizing response to PI3K inhibition across breast cancer subtypes. Inevitably, this is dependent on the elucidation of the details of aberrant PI3K signaling in the different breast cancer subtypes and resistance mechanisms in response to PI3K inhibition and to previous or concurrent treatment.

PD-L1 expression has been the inclusion criteria for using anti-PD-1 or anti-PD-L1 immunotherapy drugs in TNBC patients. Another emerging biomarker for the prediction of patient response to ICIs independent of PD-L1 expression is the tumor mutation burden (TMB), which measures the total number of somatic mutations in a tumor genome (Chan et al., 2019). In melanoma and lung cancer, TMB has been suggested to associate with higher lymphocytic infiltration and enhanced immunogenicity with responsiveness to ICIs (Chan et al., 2019). However, the role of TMB and its relation to PD-L1 expression in BC has not yet been well elucidated

(Ravaioli et al., 2020). No study has yet explored the biomarkers that could predict maximized effectiveness and reduced AEs for the combination treatment of immunotherapy and PI3K inhibition. Considering the role of PI3K signaling in the recruitment of MDSCs, regulatory T cells, and expression of PD-L1, appropriate biomarkers might be mutations in the PI3K pathway that are specifically involved in creating an immunosuppressive tumor microenvironment.

Although breast cancer subtypes other than TNBC have been considered "cold tumor" unresponsive to immunotherapy, in light of the greater immunogenicity of the primary tumor and improved PCR in $HR^+/HER2^-$ early breast cancer patients with anti-PD-1 drugs in the I-SPY2 trial, this suggests the potential to extend immunotherapy beyond TNBC in early breast cancer treatment, and combination paradigm with PI3K inhibition could further transform the immunosuppressive environment and enhance T-cell infiltration. Given the toxicity of both PI3K inhibition and immunotherapy, the tolerability of dual combination or the addition of more types of therapies in the treatment regimens warrants careful investigation. With the potential mechanism of synergy, combination treatment might allow decreased toxicity by achieving greater efficacy with lower dosing needs.

Overall, the PI3K pathway is highly implicated in the tumorigenesis, progression, and intrinsic and acquired resistance to current anti-tumor treatment in breast cancers. Although several PI3K inhibitors have been tested, except for alpelisib, many currently demonstrated disappointing efficacy with intolerable toxicity in breast cancer patients. Also, only recently has immunotherapy been approved as an option for TNBC patients. With the possible synergistic benefit, there is considerable potential for a combination treatment for these two newly approved options for breast cancer: PI3K inhibition with immunotherapy. Further understanding of the PI3K signaling and crosstalk with related pathways, its role in activating or suppressing the tumor-infiltrating lymphocytes, and better patient stratification and selection strategies will be essential patient response in the clinical development of PI3K inhibitors and their possible combination approach with immunotherapies.

AUTHOR CONTRIBUTIONS

ZZ and AR wrote the manuscript. Both authors contributed to the article and approved the submitted version.

FUNDING

This work was supported by the VA Senior Career Scientist Award (to AR).

REFERENCES

Abu Eid, R., Ahmad, S., Lin, Y., Webb, M., Berrong, Z., Shrimali, R., et al. (2017). Enhanced therapeutic efficacy and memory of tumor-specific CD8 T Cells by ex vivo PI3K-δ inhibition. *Cancer Res.* 77, 4135–4145. doi: 10.1158/0008-5472.can-16-1925

Alessi, D. R., James, S. R., Downes, C. P., Holmes, A. B., Gaffney, P. R., Reese, C. B., et al. (1997). Characterization of a 3-phosphoinositide-dependent protein kinase which phosphorylates and activates protein kinase Alpha. *Curr. Biol.* 7, 261–269. doi: 10.1016/s0960-9822(06)00122-9

Ali, K., Soond, D. R., Pineiro, R., Hagemann, T., Pearce, W., Lim, E. L., et al. (2014). Inactivation of PI(3)K p110δ breaks regulatory T-cell-mediated immune tolerance to cancer. *Nature* 510, 407–411. doi: 10.1038/nature13444

André, F., Ciruelos, E., Rubovszky, G., Campone, M., Loibl, S., Rugo, H. S., et al. (2019). Alpelisib for *PIK3CA*-mutated, hormone receptor-positive advanced breast cancer. *N. Engl. J. Med.* 380, 1929–1940. doi: 10.1056/NEJMoa1813904

Baselga, J., Dent, S. F., Cortes, J., Im, Y. H., Dieras, V., Harbeck, N., et al. (2018). Phase III study of taselisib (GDC-0032) + fulvestrant (FULV) v FULV in patients (pts) with estrogen receptor (ER)-positive, *PIK3CA*-mutant (MUT), locally advanced or metastatic breast cancer (MBC): primary analysis from SANDPIPER. *J. Clin. Oncol.* 36 (suppl. 18):1006.

Baselga, J., Im, S. A., Iwata, H., Cortes, J., De Laurentiis, M., Jiang, Z., et al. (2017). Buparlisib plus fulvestrant versus placebo plus fulvestrant in postmenopausal, hormone receptor-positive, HER2-negative, advanced breast cancer (BELLE-2): a randomised, double-blind, placebo-controlled, phase 3 trial. *Lancet Oncol.* 18, 904–916. doi: 10.1016/s1470-2045(17)30376-5

Bray, F., Ferlay, J., Soerjomataram, I., Siegel, R. L., Torre, L. A., and Jemal, A. (2018). Global cancer statistics 2018: GLOBOCAN estimates of incidence and mortality worldwide for 36 cancers in 185 countries. *CA Cancer J. Clin.* 68, 394–424. doi: 10.3322/caac.21492

Cancer Genome Atlas Network (2012). Comprehensive molecular portraits of human breast tumours. *Nature* 490, 61–70. doi: 10.1038/nature11412

Cardoso, F., Bedard, P. L., Winer, E. P., Pagani, O., Senkus-Konefka, E., Fallowfield, L. J., et al. (2009). ESO-MBC task force. international guidelines for management of metastatic breast cancer: combination vs sequential single-agent chemotherapy. *J. Natl. Cancer Inst.* 101, 1174–1181. doi: 10.1093/jnci/djp235

Castellano, E., and Downward, J. (2011). RAS interaction with PI3K: more than just another effector pathway. *Genes Cancer* 2, 261–274. doi: 10.1177/1947601911408079

Chan, T. A., Yarchoan, M., Jaffee, E., Swanton, C., Quezada, S. A., Stenzinger, A., et al. (2019). Development of tumor mutation burden as an immunotherapy biomarker: utility for the oncology clinic. *Ann. Oncol.* 30, 44–56. doi: 10.1093/annonc/mdy495

Cortes, J., Cescon, D. W., Rugo, H. S., Nowecki, Z., Im, S., Yusof, M. M., et al. (2020). Pembrolizumab plus chemotherapy versus placebo plus chemotherapy for previously untreated locally recurrent inoperable or metastatic triple-negative breast cancer (KEYNOTE-355): a randomized, placebo-controlled, double-blind, phase 3 clinical trial. *Lancet* 396, 1817–1826.

Creighton, C. J., Fu, X., Hennessy, B. T., Casa, A. J., Zhang, Y., Gonzalez-Angulo, A. M., et al. (2010). Proteomic and transcriptomic profiling reveals a link between the PI3K pathway and lower estrogen-receptor (ER) levels and activity in ER + breast cancer. *Breast Cancer Res.* 12:R40.

De Henau, O., Rausch, M., Winkler, D., Campesato, L. F., Liu, C., Cymerman, D. H., et al. (2016). Overcoming resistance to checkpoint blockade therapy by targeting PI3Kγ in myeloid cells. *Nature* 539, 443–447. doi: 10.1038/nature20554

Dent, R., Trudeau, M., Pritchard, K. I., Hanna, W. M., Kahn, H. K., Sawka, C. A., et al. (2007). Triple-negative breast cancer: clinical features and patterns of recurrence. *Clin. Cancer Res.* 13, 4429–4434. doi: 10.1158/1078-0432.ccr-06-3045

Dolly, S. O., Wagner, A. J., Bendell, J. C., Kindler, H. L., Krug, L. M., Seiwert, T. Y., et al. (2016). Phase I study of apitolisib (GDC-0980), dual phosphatidylinositol-3-Kinase and mammalian target of rapamycin kinase inhibitor, in patients with advanced solid tumors. *Clin. Cancer Res.* 22, 2874–2884. doi: 10.1158/1078-0432.ccr-15-2225

Dreyling, M., Santoro, A., Mollica, L., Leppä, S., Follows, G. A., Lenz, G., et al. (2017). Phosphatidylinositol 3-kinase inhibition by copanlisib in relapsed or refractory indolent lymphoma. *J. Clin. Oncol.* 35, 3898–3905.

Drullinsky, P. R., and Hurvitz, S. A. (2020). Mechanistic basis for PI3K inhibitor anti-tumor activity and adverse reactions in advanced breast cancer. *Breast Cancer Res. Treatment* 181, 233–248. doi: 10.1007/s10549-020-05618-1

Flinn, I. W., Hillmen, P., Montillo, M., Nagy, Z., Illes, A., Etienne, G., et al. (2018). The phase 3 DUO trial: duvelisib vs ofatumumab in relapsed and refractory CLL/SLL. *Blood* 132, 2446–2455. doi: 10.1182/blood-2018-05-850461

Forero-Torres, A., Han, H., Dees, E. C., Wesolowski, R., Bardia, A., Kabos, P., et al. (2018). Phase Ib study of gedatolisib in combination with palbociclib and endocrine therapy (ET) in women with estrogen receptor (ER) positive (+) metastatic breast cancer (MBC) (B2151009). *J. Clin. Oncol.* 36(suppl. 15):1040. doi: 10.1200/jco.2018.36.15_suppl.1040

Furman, R. R., Sharman, J. P., Coutre, S. E., Cheson, B. D., Pagel, J. M., Hillmen, P., et al. (2014). Idelalisib and rituximab in relapsed chronic lymphocytic leukemia. *N. Engl. J. Med.* 370, 997–1007.

Gabrilovich, D. I. (2017). Myeloid-derived suppressor cells. *Cancer Immunol. Res.* 5, 3–8.

Gewinner, C., Wang, Z. C., Richardson, A., Teruya-Feldstein, J., Etemadmoghadam, D., Bowtell, D., et al. (2009). Evidence that inositol polyphosphate 4-phosphatase type II is a tumor suppressor that inhibits PI3K signaling. *Cancer Cell* 16, 115–125. doi: 10.1016/j.ccr.2009.06.006

Guerrero-Zotano, A., Mayer, I. A., and Arteaga, C. L. (2016). PI3K/AKT/mTOR: role in breast cancer progression, drug resistance, and treatment. *Cancer Metastasis Rev.* 35, 515–524. doi: 10.1007/s10555-016-9637-x

Hargadon, K. M., Johnson, C. E., and Williams, C. J. (2018). Immune checkpoint blockade therapy for cancer: an overview of FDA-approved immune checkpoint inhibitors. *Int. Immunopharmacol.* 62, 29–39. doi: 10.1016/j.intimp.2018.06.001

Hiles, I. D., Otsu, M., Volinia, S., Fry, J. M., Gout, I., Dhand, R., et al. (1992). Phosphatidylinositol 3-kinase: structure and expression of the 110 kd catalytic subunit. *Cell* 70, 419–429. doi: 10.1016/0092-8674(92)90166-a

Hopkins, B. D., Pauli, C., Du, X., Wang, D. G., Li, X., Wu, D., et al. (2018). Suppression of insulin feedback enhances the efficacy of PI3K inhibitors. *Nature* 560, 499–503. doi: 10.1038/s41586-018-0343-4

Howlader, N., Alterkruse, S. F., Li, C. I., Chen, V. W., Clarke, C. A., Ries, L. A. G., et al. (2014). US Incidence of breast cancer subtypes defined by joint hormone receptor and HER2 status. *J. Natl. Cancer Inst.* 106:dju055.

Junttila, T. T., Akita, R. W., Parsons, K., Fields, C., Lewis Phillips, G. D., Friedman, L. S., et al. (2009). Ligand-independent HER2/HER3/PI3K complex is disrupted by trastuzumab and is effectively inhibited by the PI3K inhibitor GDC-0941. *Cancer Cell* 15, 429–440. doi: 10.1016/j.ccr.2009.03.020

Kaneda, M. M., Messer, K. S., Ralainirina, N., Li, H., Leem, C. J., Gorjestani, S., et al. (2016). PI3Kgamma is a molecular switch that controls immune suppression. *Nature* 539, 437–442.

Katso, R., Okkenhaug, K., Ahmadi, K., White, S., Timms, J., and Waterfield, M. D. (2001). Cellular function of phosphoinositide 3-kinases: implications for development, homeostasis, and cancer. *Annu. Rev. Cell Dev. Biol.* 17, 615–675. doi: 10.1146/annurev.cellbio.17.1.615

Keegan, N. M., Walshe, J. M., Toomey, S., Gullo, G., Kennedy, M. J., Bulger, K. N., et al. (2018). A phase Ib trial of copanlisib and trastuzumab in pretreated recurrent or metastatic HER2-positive breast cancer "PantHER". *J. Clin. Oncol.* 36(suppl. 15):1036. doi: 10.1200/jco.2018.36.15_suppl.1036

Kim, I. S., Gao, Y., Welte, T., Wang, H., Liu, J., Janghorban, M., et al. (2019). Immuno-subtyping of breast cancer reveals distinct myeloid cell profiles and immunotherapy resistance mechanisms. *Nat. Cell Biol.* 21, 1113–1126. doi: 10.1038/s41556-019-0373-7

Liedtke, C., Mazouni, C., Hess, K. R., André, F., Tordai, A., Mejia, J. A., et al. (2008). Response to neoadjuvant therapy and long-term survival in patients with triple-negative breast cancer. *J. Clin. Oncol.* 26, 1275–1281. doi: 10.1200/jco.2007.14.4147

Liu, H., Paddock, M. N., Wang, H., Murphy, C. J., Geck, R. C., Navarro, A. J., et al. (2020). The INPP4B tumor suppressor modulates EGFR trafficking and promotes TNBC. *Cancer Discov.* 10, 1226–1239. doi: 10.1158/2159-8290.cd-19-1262

Maehama, T., and Dixon, J. E. (1998). The tumor suppressor, PTEN/MMAC1, dephosphorylates the lipid second messenger, phosphatidylinositol 3,4,5-trisphosphate. *J. Biol. Chem.* 273, 13375–13378. doi: 10.1074/jbc.273.22.13375

Mayer, I. A., Prat, A., Egle, D., Blau, S., Fidalgo, J. A. P., Gnant, M., et al. (2019). A phase II Randomized study of neoadjuvant letrozole plus alpelisib for hormone receptor-positive, human epidermal growth factor receptor 2-negative breast cancer (NEO-ORB). *Clin. Cancer Res.* 25, 2975–2987. doi: 10.1158/1078-0432.ccr-18-3160

Mittendorf, E. A., Philips, A. V., Meric-Bernstam, F., Qiao, N., Wu, Y., Harrington, S., et al. (2014). PD-L1 expression in triple-negative breast cancer. *Cancer Immunol. Res.* 2, 361–370.

Nakanishi, Y., Walter, K., Spoerke, J. M., O'Brien, C., Huw, L. Y., Hampton, G. M., et al. (2016). Activating mutations in PIK3CB confer resistance to PI3K inhibition and define a novel oncogenic role for p110beta. *Cancer Res.* 76, 1193–1203. doi: 10.1158/0008-5472.can-15-2201

Nanda, R., Liu, M. C., Yau, C., Shatsky, R., Pusztai, L., Wallace, A., et al. (2020). Effect of pembrolizumab plus neoadjuvant chemotherapy on pathologic complete response in women with early-stage breast cancer: an analysis of the ongoing phase 2 adaptively randomized I-SPY2 trial. *JAMA Oncol.* 6, 676–684. doi: 10.1001/jamaoncol.2019.6650

Narayan, P., Wahby, S., Gao, J. J., Amiri-Kordestani, L., Ibrahim, A., Bloomquist, E., et al. (2020). FDA approval summary: atezolizumab plus paclitaxel protein-bound for the treatment of patients with advanced or metastatic TNBC whose tumors express PD-L1. *Clin. Cancer Res.* 26, 2284–2289. doi: 10.1158/1078-0432.ccr-19-3545

O'Donnell, J. S., Massi, D., Teng, M. W. L., and Mandala, M. (2018). PI3K-AKT-mTOR inhibition in cancer immunotherapy, redux. *Semin. Cancer Biol.* 48, 91–103. doi: 10.1016/j.semcancer.2017.04.015

Okkenhaug, K., Graupera, M., and Vanhaesebroeck, B. (2016). Targeting PI3K in cancer: impact on tumor cells, their protective stroma, angiogenesis, and immunotherapy. *Cancer Discov.* 6, 1090–1105. doi: 10.1158/2159-8290.cd-16-0716

Olson, E. M., Lin, N. U., DiPiro, P. J., Najita, J. S., Krop, I. E., Winer, E. P., et al. (2012). Responses to subsequent anti-HER2 therapy after treatment with trastuzumab-DM1 in women with HER2-positive metastatic breast cancer. *Ann. Oncol.* 23, 93–97. doi: 10.1093/annonc/mdr061

Owusu-Brackett, N., Zhao, M., Akcakanat, A., Evans, K. W., Yuca, E., Dumbrava, E. I., et al. (2020). Targeting PI3Kβ alone and in combination with chemotherapy or immunotherapy in tumors with PTEN loss. *Oncotarget* 11, 969–981. doi: 10.18632/oncotarget.27503

Pascual, J., and Turner, N. C. (2019). Targeting the PI3-kinase pathway in triple-negative breast cancer. *Ann. Oncol.* 30, 1051–1060. doi: 10.1093/annonc/mdz133

Peng, W., Chen, J. Q., Liu, C., Malu, S., Creasy, C., Tetzlaff, M. T., et al. (2016). Loss of PTEN promotes resistance to T cell mediated immunotherapy. *Cancer Discov.* 6, 202–216. doi: 10.1158/2159-8290.CD-15-0283

Pohlmann, P. R., Mayer, I. A., and Mernaugh, R. (2009). Resistance to trastuzumab in breast cancer. *Clin. Cancer Res.* 15, 7479–7491. doi: 10.1158/1078-0432.CCR-09-0636

Radovich, M., Solzak, J. P., Hancock, B. A., Storniolo, A. M. V., Schneider, B. P., and Miller, K. D. (2018). "An initial safety study of gedatolisib plus PTK7-ADC for metastatic triple-negative breast cancer," in *Proceedings of the San Antonio Breast Cancer Symposium*, (San Antonio, TX).

Ravaioli, S., Limarzi, F., Tumedei, M. M., Palleschi, M., Maltoni, R., and Bravaccini, S. (2020). Are we ready to use TMB in breast cancer clinical practice? *Cancer Immunol. Immunother.* 69, 1943–1945. doi: 10.1007/s00262-020-02682-w

Roberts, P. J., Usary, J. E., Darr, D. B., Dillon, P. M., Pfefferle, A. D., Whittle, M. C., et al. (2012). Combined PI3K/mTOR and MEK inhibition provides broad antitumor activity in faithful murine cancer models. *Clin. Cancer Res.* 18, 5290–5303. doi: 10.1158/1078-0432.CCR-12-0563

Romond, E. H., Perez, E. A., Bryant, J., Suman, V. J., Geyer, C. E. Jr., Davidson, N. E., et al. (2005). Trastuzumab plus adjuvant chemotherapy for operable HER2-positive breast cancer. *N. Engl. J. Med.* 353, 1673–1684.

Sai, J., Owens, P., Novitskiy, S. V., Hawkins, O. E., Vilgelm, A. E., Yang, J., et al. (2017). PI3K inhibition reduces mammary tumor growth and facilitates anti-tumor immunity and anti-PD1 responses. *Clin. Cancer Res.* 23, 3371–3384. doi: 10.1158/1078-0432.CCR-16-2142

Sarbassov, D. D., Guertin, D. A., Ali, S. M., and Sabatini, D. M. (2005). Phosphorylation and regulation of Akt/PKB by the rictor-mTOR complex. *Science* 307, 1098–1101. doi: 10.1126/science.1106148

Schmid, M. C., Avraamides, C. J., Dippold, H. C., Franco, I., Foubert, P., Ellies, L. G., et al. (2011). Receptor tyrosine kinases and TLR/IL1Rs unexpectedly activate myeloid cell PI3kγ, a single convergent point promoting tumor inflammation and progression. *Cancer Cell* 19, 715–727. doi: 10.1016/j.ccr.2011.04.016

Schu, P. V., Takegawa, K., Fry, M. J., Stack, J. H., Waterfield, M. D., and Emr, S. D. (1993). Phosphatidylinositol 3-kinase encoded by yeast VPS34 gene essential for protein sorting. *Science* 260, 88–91. doi: 10.1126/science.8385367

Schwartz, S., Wongvipat, J., Trigwell, C. B., Hancox, U., Carver, B. S., Rodrik-Outmezguine, V., et al. (2015). Feedback suppression of PI3Kα signaling in PTEN-mutated tumors is relieved by selective inhibition of PI3Kβ. *Cancer Cell* 27, 109–122. doi: 10.1016/j.ccell.2014.11.008

Serra, V., Scaltriti, M., Prudkin, L., Eichhorn, P. J., Ibrahim, Y. H., Chandarlapaty, S., et al. (2011). PI3K inhibition results in enhanced HER signaling and acquired ERK dependency in HER2- overexpressing breast cancer. *Oncogene* 30, 2547–2557. doi: 10.1038/onc.2010.626

Shah, M., Nunes, M. R., and Stearns, V. (2018). CDK4/6 Inhibitors: game changers in the management of hormone receptor-positive advanced breast cancer? *Oncology* 32, 216–222.

Szekely, B., Bossuyt, V., Wali, V. B., Patwardhan, G. A., Frederick, C., Silber, A., et al. (2018). Immunological differences between primary and metastatic breast cancer. *Ann. Oncol.* 29, 2232–2239. doi: 10.1093/annonc/mdy399

Teo, Z. L., Versaci, S., Dushyanthen, S., Caramia, F., Savas, P., Mintoff, C. P., et al. (2017). Combined CDK4/6 and PI3Kα Inhibition Is Synergistic and Immunogenic in Triple-Negative Breast Cancer. *Cancer Res.* 77, 6340–6352. doi: 10.1158/0008-5472

Torbett, N. E., Luna-Moran, A., Knight, Z. A., Houk, A., Moasser, M., Weiss, W., et al. (2008). A chemical screen in diverse breast cancer cell lines reveals genetic enhancers and suppressors of sensitivity to PI3K isoform-selective inhibition. *Biochem. J.* 415, 97–110. doi: 10.1042/bj20080639

Umansky, V., Blattner, C., Gebhardt, C., and Utilkal, J. (2016). The role of Myeloid-Derived Suppressor Cells (MDSC) in cancer progression. *Vaccines* 4:36. doi: 10.3390/vaccines4040036

Uno, J. K., Rao, K. N., Matsuoka, K., Sheikh, S. Z., Kobayashi, T., Li, F., et al. (2010). Altered macrophage function contributes to colitis in mice defective in the phosphoinositide-3 kinase subunit p110delta. *Gastroenterology* 139, 1642-53, 1653.e1-6.

Wainberg, Z. A., Alsina, M., Soares, H. P., Braña, I., Britten, C. D., Del Conte, G., et al. (2017). A multi-arm phase I study of the PI3K/mTOR inhibitors PF-04691502 and Gedatolisib (PF-05212384) plus Irinotecan or the MEK Inhibitor PD-0325901 in advanced cancer. *Target. Oncol.* 12, 775–785. doi: 10.1007/s11523-017-0530-5

Waks, A. G., and Winer, E. P. (2019). Breast cancer treatment: a review. *JAMA* 321, 288–300.

Welte, T., Kim, I. S., Tian, L., Gao, X., Wang, H., Li, J., et al. (2016). Oncogenic mTOR signaling recruits myeloid-derived suppressor cells to promote tumour initiation. *Nat. Cell Biol.* 18, 632–644. doi: 10.1038/ncb3355

Wise-Draper, T. M., Moorthy, G., Salkeni, M. A., Karim, N. A., Thomas, H. E., Mercer, C. A., et al. (2017). A phase Ib study of the dual PI3K/mTOR Inhibitor Dactolisib (BEZ235) combined with everolimus in patients with advanced solid malignancies. *Target Oncol.* 12, 323–332. doi: 10.1007/s11523-017-0482-9

Conflict of Interest: The authors declare that the research was conducted in the absence of any commercial or financial relationships that could be construed as a potential conflict of interest.

frontiers in Molecular Biosciences

REVIEW
published: 11 May 2021
doi: 10.3389/fmolb.2021.649105

Function of Non-coding RNA in *Helicobacter pylori*-Infected Gastric Cancer

Chao Wang†, Yiyang Hu†, Huan Yang, Sumin Wang, Bo Zhou, Yulu Bao, Yu Huang, Qiang Luo, Chuan Yang, Xia Xie and Shiming Yang**

Department of Gastroenterology, Xinqiao Hospital, Third Military Medical University, Chongqing, China

Gastric cancer is a common malignant tumor of the digestive system. Its occurrence and development are the result of a combination of genetic, environmental, and microbial factors. *Helicobacter pylori* infection is a chronic infection that is closely related to the occurrence of gastric tumorigenesis. Non-coding RNA has been demonstrated to play a very important role in the organism, exerting a prominent role in the carcinogenesis, proliferation, apoptosis, invasion, metastasis, and chemoresistance of tumor progression. *H. pylori* infection affects the expression of non-coding RNA at multiple levels such as genetic polymorphisms and signaling pathways, thereby promoting or inhibiting tumor progression or chemoresistance. This paper mainly introduces the relationship between *H. pylori*-infected gastric cancer and non-coding RNA, providing a new perspective for gastric cancer treatment.

Keywords: non-coding RNA, *Helicobacter pylori* infection, gastric cancer, genetic polymorphisms, chemoresistance

OPEN ACCESS

Edited by:
José Alexandre Ferreira, Portuguese Oncology Institute, Portugal

Reviewed by:
Jiayin Tang, Shanghai Jiao Tong University, China
Enhao Zhao, Shanghai Jiao Tong University, China
Yuan Li, Southern Medical University, China

****Correspondence:***
Xia Xie
xiexia0128@163.com
Shiming Yang
shimingyang@yahoo.com

† These authors have contributed equally to this work

Specialty section:
This article was submitted to Molecular Diagnostics and Therapeutics, a section of the journal Frontiers in Molecular Biosciences

Received: *03 January 2021*
Accepted: *10 March 2021*
Published: *11 May 2021*

Citation:
Wang C, Hu Y, Yang H, Wang S, Zhou B, Bao Y, Huang Y, Luo Q, Yang C, Xie X and Yang S (2021) Function of Non-coding RNA in Helicobacter pylori-Infected Gastric Cancer. Front. Mol. Biosci. 8:649105. doi: 10.3389/fmolb.2021.649105

INTRODUCTION

As one of the most common digestive tumors worldwide, the morbidity and mortality of gastric cancer (GC) are increasing annually (Ferlay et al., 2019). The associated risk factors include smoking, overweight, salty food consumption, Epstein–Barr virus infection, and exposure to asbestos. Surgery, chemotherapy, and chemoradiation are the main treatments for GC, but the prognosis is not satisfactory. Numerous studies have shown that the pathogenesis and progression of GC are closely related to those of *Helicobacter pylori* infection (Helicobacter and Cancer Collaborative Group [HCCG], 2001). *H. pylori* is regarded as a gram-negative microaerophilic

Abbreviations: ABCG2, ATP-binding cassette, subfamily G, member 2; CagA, cytotoxin-related gene A; cag-PAI, cag pathogenicity island; ceRNA, competing endogenous RNA; CHRM2, cholinergic receptor, muscarinic 2; CIC, cancer-initiating cell; circRNAs, circular RNAs; EMT, epithelial–mesenchymal transition; FoxM1, Forkhead box protein M1; FZD7, Frizzled 7; GC, gastric cancer; GClnc1, GC-associated lncRNA 1; GKN1, Gastrokine 1; GML, gastric MALT lymphoma; *H. pylori*, *Helicopter pylori*; HIPK2, homeodomain-interacting protein kinase 2; IRAK1, IL-1 receptor-associated kinase 1; JAK2, Janus kinase 2; KLF4, Krüppel-like transcription factor; lncRNAs, long non-coding RNAs; LPS, lipopolysaccharide; miRNAs, microRNAs; MMR, mismatch repair; PBP1A, penicillin-binding protein 1A; piRNAs, PiWi-interacting RNAs; PRNCR1, prostate cancer non-coding RNA 1; RAGE, receptor for advanced glycation end product; RepG, regulator of polymeric G-repeats; siRNAs, small interfering RNAs; SMARCD1, SWI/SNF chromatin remodeling complex subunit; SMOX, spermine oxidase; snoRNAs, small nucleolar RNAs; SOX2OT, SOX2 overlapping transcript; SSRs, simple sequence repeats; SWI/SNF, SWItch/Sucrose Non-fermentable; TCS, two-component system; THAP9-AS1, THAP domain-containing 9 antisense RNA 1; TRAF6, tumor necrosis factor receptor-associated factor 6; tsRNAs, tRNA-derived small RNAs; ZEB1, zinc-finger E-box-binding homeobox 1; ZEB2, zinc finger E-box binding homeobox 2.

bacterium that is capable of entering the human body early and colonizing the mucosal area of the stomach for a long time (Blaser and Atherton, 2004). *H. pylori* infection is associated with inducing chronic gastritis, peptic ulcer, GC, and mucosa-associated lymphoid tissue (MALT) lymphoma (Petra et al., 2017). Various clinical analysis and basic biological research have revealed that patients with *H. pylori*-positive GC have more lymph node metastasis and a worse prognosis than have negative patients. Therapy for *H. pylori* eradication can effectively prevent GC (Choi et al., 2018; Mera et al., 2018; Suzuki and Matsuzaki, 2018). The Kyoto Global Consensus Report recommends that regardless of age or severity of gastric mucosal lesions, especially in areas with a high incidence of GC, all *H. pylori*-infected patients should be treated (Sugano et al., 2015; Malfertheiner et al., 2017; Sugano, 2019).

Non-coding RNA (ncRNA) refers to RNA that does not encode protein, which has been divided into long ncRNAs (lncRNAs) and short ncRNAs including microRNAs (miRNAs), PiWi-interacting RNAs (piRNAs), small nucleolar RNAs (snoRNAs), small interfering RNAs (siRNAs), tRNA-derived small RNAs (tsRNAs), circular RNAs (circRNAs), and heterochromatin-derived 24nt small RNA in plants according to their length. These RNAs are derived from genomic transcription, but they are not translated into proteins; and they play their respective biological roles at the RNA level. Among these RNAs, lncRNA, miRNA, and some special small ncRNAs (sncRNAs) are mainly involved in the progress of *H. pylori*-induced GC. LncRNA is an ncRNA that is greater than 200 nucleotides in length. It has many known functions, including transcriptional interference, regulation of alternative splicing, generation of endogenous siRNA, regulation of protein activity, and alteration of protein positioning (Wilusz et al., 2009). In addition, many studies have shown that lncRNA is more tissue-specific than mRNA, indicating that it is also closely related to the function of the tissue (Ransohoff et al., 2018). MiRNA is a non-coding 18- to 24-nucleotide RNA that regulates gene expression at the mRNA level. Mature miRNA can directly bind to the 3′UTR region of the target gene to rapidly degrade mRNA or inhibit protein expression (Bartel, 2004; Acunzo et al., 2015; Shomali et al., 2017).

This review mainly summarizes the mechanism of ncRNA in *H. pylori*-infected GC. *H. pylori* infection modulates expression of ncRNA and changes the expression of related target genes. Their impact on tumor progression and drug resistance treatment has been categorized and summarized, and a new perspective for clinical treatment is provided.

HELICOBACTER PYLORI PLAYS A VITAL ROLE IN GASTRIC CANCER

The prevalence of *Helicobacter pylori* presents large regional differences worldwide, which is related to factors such as geography and basic health conditions. *H. pylori* survival is facilitated in an acidic environment, and it colonizes in the gastric mucosa by virtue of its spiral shape, exercise ability, adhesion factors, and urease and ammonia production, subsequently producing a complex inflammatory response, damaging the gastric mucosa, and subsequently producing digestive diseases via the expression of various pathogenic markers such as cytotoxin-related gene A (CagA), BabA adhesin, and empty vesicular toxin (VacA) (Backert et al., 2017). Flagellar movement and various adhesion factors (AlpA/B, BabA, OipA, SabA, and HopQ) promote *H. pylori* adhesion to epithelial cells. Urease converts urea into ammonia, making the environment in which bacteria live weakly acidic and thereby reducing the level of intestinal bacteria. VacA produces proteins that are toxic to gastrointestinal epithelial cells (Morello, 1999; Amieva and El-Omar, 2008; Atherton and Blaser, 2009; Safaralizadeh et al., 2017; Su et al., 2019). The virulence factor CagA is involved in various signal transduction processes (Pachathundikandi et al., 2013). All these determine the importance of *H. pylori* in GC.

NON-CODING RNA INFLUENCES THE PROGRESSION AND TREATMENT OF *HELICOBACTER PYLORI*-INFECTED GASTRIC CANCER

Small RNA

Small ncRNAs produced by bacteria are classified as sRNAs, which exert their heterogeneity in a eubacterial environment. The length of sRNA ranges from 50 to 250 nucleotides, and its effect on biological process and its target genes have been identified by various methods *in vitro* and *in vivo* (Vogel and Wagner, 2007; Sharma and Vogel, 2009). The present mechanism displays a binding function to protein or an antisense RNA role on *trans*-encoded mRNAs, in which the latter usually shows translation inhibition or activation through imperfect complementarity between sRNA and its targets, modulating the stability and/or accessibility on the translational machinery (Majdalani et al., 2005; Livny and Waldor, 2007). The sRNAs have also been reported to participate in acid resistance in *Escherichia coli* (Opdyke et al., 2004; Tramonti et al., 2008), virulence of pathogens (Geissmann et al., 2006; Romby et al., 2006), and iron homeostasis (Chen and Crosa, 1996; Dühring et al., 2006). *Helicobacter pylori* also produced sRNAs that participate in the progression of GC. A large number of sRNAs were found in an analysis of *H. pylori* primary transcriptome study (Rieder et al., 2012). Reports show that bacterial Sm-like protein Hfq is necessary for effective function of sRNA (Valentin-Hansen et al., 2004). However, Hfq, an RNA molecular chaperone, is absent in *H. pylori*. By facilitating the pairing of small RNAs with their target mRNAs, Hfq can affect translation and turnover rates of specific transcripts and contribute to complex posttranscriptional networks (Vogel and Luisi, 2011). Thus, *H. pylori* was previously thought to lack ribosomal regulation (Mitarai et al., 2007). Because of the lack of Hfq in *H. pylori*, two methods were designed to identify other auxiliary proteins in sRNA-mediated regulation, and RNA–protein interactions were identified between ribosomal protein S1 and various mRNA and sRNA of *H. pylori*, which confirmed that *H. pylori* can control their gene expression via

ribosomal regulation (Rieder et al., 2012). The identification of *H. pylori* sRNA and the mechanism of ribose regulation have potential effects on the virulence mechanism and stress response (Pernitzsch and Sharma, 2012), which may be associated with the development of GC.

The HP0165–HP0166 two-component system (TCS) in *H. pylori* participates in the increased expression of urease genes, while whether the increased activity of urease is beneficial or harmful to organism is determined by the presence or absence of acid in the stomach (Clyne et al., 1995; Meyer-Rosberg et al., 1996; Pflock et al., 2004, 2005). HP0165 is the membrane sensor, while HP0166 is its response regulator. For survival and colonization on the gastric surface, *H. pylori* regulated TCS to change urease activity according to the different intragastric pH values (Wen et al., 2006). A novel *cis*-encoded antisense sRNA, identified as 5′ureB-sRNA, downregulates ureAB expression by enhancing transcription termination of 5′ region of ureB, which validates through an *in vitro* transcription assay (Wen et al., 2013). However, HP0165–HP0166 TCS negatively regulates expression of 5′ureB-sRNA to increase ureAB expression at low pH values and enhances 5′ureB-sRNA to decrease ureAB expression and to decrease urease activity at high pH values (Wen et al., 2011).

CncR1, a rich and conserved sRNA encoded by the virulence-associated cag pathogenicity island (cag-PAI) of *H. pylori*, interacts with the fliK mRNA and downregulates bacterial motility and adhesion ability, significantly impairing bacterial adhesion to host gastric cell lines (Vannini et al., 2016). The sRNA RepG (Regulator of polymeric G-repeats) in *H. pylori* was also found to directly target a variable homopolymeric G-repeat in the leader of the TlpB chemotaxis receptor mRNA, which contains simple sequence repeats (SSRs) (Pernitzsch et al., 2014). Phase variation in hypermutable SSRs contributes to host adaptation of bacterial pathogens. In this way, sRNA may ensure the survival of *H. pylori* in the human body, leading to severe disease. In fact, many features of the sRNA are unknown and worth exploring, as they may have important implications for *H. pylori*-induced GC.

Helicobacter pylori not only plays a role via its own nosotoxin but also participates in the homeostasis regulation of intestinal flora, and *H. pylori* eradication treatment has a significant effect on the change in intestinal flora (Zhang et al., 2016). For example, after the application of PPI for *H. pylori* eradication treatment, the abundance of streptococci, enterococci, staphylococci, and micrococci in the intestinal flora increased while clostridia decreased (Freedberg et al., 2015). A schematic diagram of the pathogenic mechanism of *H. pylori* is shown (**Figure 1**).

Long Non-coding RNA

The Mechanism of Long Non-coding RNAs in *Helicobacter pylori*-Infected Gastric Cancer

Polymorphisms in lncRNAs have been reported to influence the splicing and stability of mRNA (Burd et al., 2010; Chung et al., 2011), and the special region known as the "gene desert" was discovered to participate in prostate cancer, colorectal cancer,

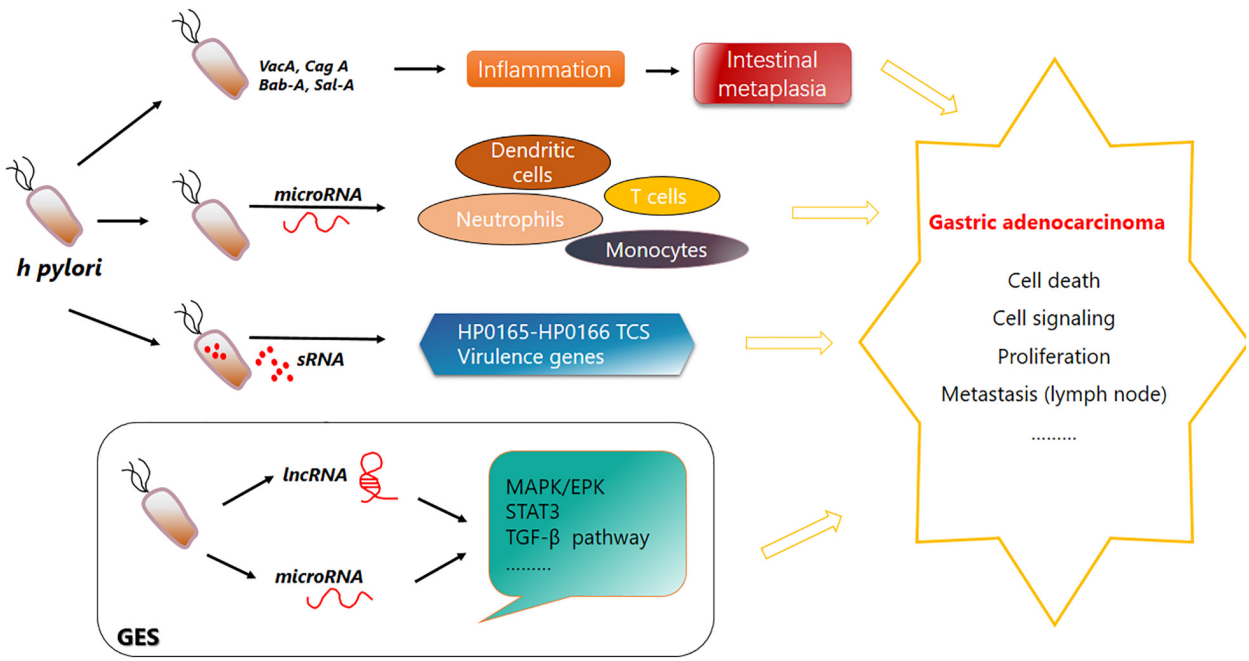

FIGURE 1 | Function of *Helicobacter pylori* in gastric carcinogenesis. *H. pylori* secretes Bab-A, Sab-A, VacA, CagA, and other substances to help invade and colonize in the human gastric mucosa and cause chronic inflammation and superficial gastritis. Its infection leads to a variety of signaling events. Immune cells such as dendritic cells, neutrophils, monocytes, and T cells can produce various microRNAs. Specific sRNA can combine with the HP0165–HP0166 two-component system to regulate the pH adaptability of *H. pylori* to help its inhabitation and colonization in stomach. *H. pylori* invasion also causes upregulation or downregulation of lncRNAs and microRNAs. Their complex regulatory network is disrupted, and pathways are affected. Bab-A, blood-group antigen binding adhesion; Sab-A, sialic acid binding protein A.

breast cancer, and *H. pylori*-infected GC (Tomlinson et al., 2007; Ghoussaini et al., 2008; Zhang et al., 2010; He et al., 2017). A case–control study revealed that rs16901946 of prostate cancer ncRNA 1 (PRNCR1) was associated with GC risk, which could be increased by *H. pylori* infection. Another case–control study showed that LINC00673 rs11655237 with GG genotype was more susceptible to *H. pylori* infection.

Based on the database analysis of The Cancer Genome Atlas (TCGA), a competing endogenous RNA (ceRNA) network was constructed, and four lncRNAs (LINC01254, LINC01287, LINC01524, and U95743.1) showed higher expression in *H. pylori* infection-positive GC patients, and the results were validated by real-time PCR. In contrast, microarray analysis showed different results, in which 23 lncRNAs were upregulated and 21 downregulated [such as lncRNA NR_026827 (Zhong et al., 2018)] in *H. pylori*-infected GES-1 gastric epithelial cell, and some of the results were also found by PCR (Yang et al., 2015; Polakovicova et al., 2018). Among them, a recent network analysis showed that RP11-169F17.1 and RP11-669N7.2 were related to *H. pylori* infection-induced gastritis, as their targets showed great overlap with *H. pylori*-infection associated genes (Yang and Song, 2019). Seven upregulated and 17 downregulated lncRNAs were found using GSE5081 and GSE66229 (Zhang et al., 2020). LINC00152 and H19 were previously shown to be significantly upregulated in GC patients' blood samples and cancer tissues, which was validated to be a risk factor in the diagnosis and prognosis of GC with *H. pylori* infection (Pang et al., 2014; Yang T. et al., 2016).

Regarding the underlying mechanism, the lncRNA–RNA network was constructed based on the profiling of *H. pylori*-infected GES-1 cells, for which a concrete example is the downregulation of MUC2 by lncRNA AF147447 to suppress cell proliferation and invasion in the *H. pylori*-infection background (Zhu et al., 2015; Zhou et al., 2016). According to the RNA-seq analysis of *H. pylori*-infected AGS cells, THAP domain-containing nine antisense RNA 1 (THAP9-AS1) was found to be induced by *H. pylori* infection and to promote the migration and proliferation of GC cells (Jia et al., 2019). The expression level of lnc-SGK1 was elevated as a consequence of *H. pylori* infection and a high-salt diet. Lnc-SGK1 increases the transcription of SGK1 in a *cis*-regulatory manner, which activates JunB and disrupts T helper cell differentiation (Yao et al., 2016).The results of lncRNA were mainly derived from database analysis, and there was a lack of clinical studies.

Long Non-coding RNAs Influence the Drug Resistance and Prognosis of *Helicobacter pylori*-Infected Gastric Cancer

Chemotherapy can achieve a certain effect on the treatment of GC, but the acquisition of drug resistance will lead to the failure of chemotherapy in GC patients. Although the mechanism of anticancer drug resistance has been extensively studied, its specific mechanism has not yet been elucidated. In recent years, more and more studies have shown that ncRNA plays a regulatory role in the generation and maintenance of drug resistance. Cisplatin is a commonly used drug in the treatment of GC (Zheng et al., 2017), but its resistance has been found to be closely related to ncRNA. It is reported that lncRNA BCAR4 expression was enhanced in cisplatin-resistant cell strain SGC7901/DDP. And the drug resistance of cell strains was positively correlated with the expression level of BCAR4 (Wang L. et al., 2017). And it was found that the removal of lncRNA ANRIL inhibited the development of multidrug resistance (MDR) in GC cells (Lan et al., 2016). At present, many ncRNAs have been found to play a regulatory role in chemotherapy resistance of GC, and even some ncRNAs play a relatively key role. Therefore, ncRNAs can be used to be a kind of candidate drugs to develop new molecular targeted therapy strategies or reverse the resistance of GC cells to chemotherapy.

Besides, lncRNA is also related to prognosis of GC. Researchers found that the knockdown of lncRNA CASC19 inhibited proliferation and migration of GC cells *in vitro*. And their multivariate Cox analysis confirmed that CASC19 overexpression was an independent prognostic factor for overall survival (Wang et al., 2019). A set of 24-lncRNAs significantly associated with disease-free survival (DFS) was even established and used to improve prognosis prediction of GC (Zhu et al., 2016). Actually, miRNAs have been studied for much longer than lncRNAs. And at the same time, there are more research results.

MicroRNA

The Mechanism of MicroRNAs in *Helicobacter pylori*-Infected Gastric Cancer

From the perspective of polymorphism, miR-27a rs895819 and *H. pylori* have shown an interaction effect in gastric carcinogenesis (Xu et al., 2017). In contrast, miR-124a, miR-34b, and miR-34c have been reported to be downregulated in *H. pylori*-infected gastric mucosa, and miR-124a downregulation is associated with CpG hypermethylation of the miR-124a3 locus and higher IL-8 expression (Tahara et al., 2019).Additionally, miR-124 downregulation leads to elevated expression of spermine oxidase (SMOX) as it directly binds directly to the 3′UTR of SMOX mRNA, and this process can be reversed by 5-azacytidine (Murray-Stewart et al., 2016). *H. pylori* eradication induces decreased methylation ($p < 0.01$) and increased expression ($p = 0.03$) of miR-133a (Hyun Lim et al., 2018). MiR-204 is upregulated in GC compared with *H. pylori*-positive gastritis ($p < 0.004$) (Kuo et al., 2019).Other examples about phenotype changes associated with miRNA in *H. pylori*-infected GC have been mentioned in **Table 1**.

Based on the mechanism, the change in miRNA expression is closely related to *H. pylori*-produced virulence factors. MiR-34a was found to be significantly reduced in the *H. pylori* + GC group by rTip-α (a toxin secreted by *H. pylori*), while its overexpression decreased the level of TLP4, TNF-α, and IL-6. Viability was enhanced by rTip-α but decreased by miR-34a, which induces cell proliferation (Wang et al., 2018). Lipopolysaccharide (LPS) from *H. pylori* activates sp1 to increase MDM2 expression, while MDM2 represses p63 to inhibit Dicer, leading to inhibition of miR-106b and miR-375. JAK1 and STAT3 are downstream target genes of miR-106b (Ye et al., 2015). MiR-134 targets FoxM1 (Forkhead box protein M1) to suppress the proliferation, invasion, and

TABLE 1 | Associated phenotype alteration in non-coding RNA.

MicroRNA	Phenotype change	References
MiR-27	rs895819	Xu et al., 2017
MiR-124a	CpG hypermethylation	Tahara et al., 2019
MiR-129-2	Methylation	Watari et al., 2019
MiR-133a	Methylation	Hyun Lim et al., 2018
MiR-149	Hypermethylation	Li et al., 2015
MiR-200a/b	Methylation	Choi et al., 2020
MiR-204(TRPM3)	Methylation	Chen et al., 2019
MiR-210	Methylation	Kiga et al., 2014
MiR-490-3p(CHRM2)	Methylation	Shen et al., 2015; Cho et al., 2016
MiR-4795	rs1002765	Wu et al., 2017
let-7b	rs8111742	Isomoto et al., 2012; Hayashi et al., 2013; Wu et al., 2017
lncPRNCR1	rs16901946	He et al., 2017
LINC00673	rs11655237	Zhao et al., 2019

epithelial–mesenchymal transition (EMT) of GC cell, while *H. pylori*$_{CagA+/P+}$ [CagA and penicillin-binding protein 1A (PBP1A) mutation-positive] infection suppresses miR-134 expression when compared with *H. pylori*$_{CagA+/P-}$ tissues (Huang et al., 2019). The miR-155 was found to be upregulated by CagA (cytotoxin-associated gene A) from *H. pylori*, and it can restrict KLF4 (Krüppel-like transcription factor) expression to promote EMT and tumor growth (Ou et al., 2019).

Many signaling pathways are involved in the regulation between *H. pylori* infection and miRNA. *H. pylori* infection causes activation of the NF-κB signaling pathway, which leads to miR-7 downregulation, while miR-7 targets the IκB kinase IKKε to repress RELA activation. In return IKKε and RELA repress miR-7. Thus, the repression of RELA and FOS is released, and cell proliferation and tumorigenesis are promoted (Zhao et al., 2015). *H. pylori* infection activates NF-κB, increases IL-6 secretion, and promotes AP-1 and STAT3, which induce transcription of miR-21; and it plays an oncogenic role in cancer development, including proliferation, migration, and apoptosis (Zhang et al., 2008; Belair et al., 2009; Ma and Tao, 2012). MiR-21 activates COX2, which participates in preneoplastic gastric lesions that are resistant to apoptosis (Shukla et al., 2016). MiR-3178 decreases the expression of TRAF3, TNF-α, and IL-6, accompanied by the inhibition of NF-κB signals, while *H. pylori* infection presents Tip-α to inhibit miR-3178 expression, thus activating the NF-κB signal and promoting inflammation and carcinogenesis (Zou et al., 2017). NF-κB is also involved in the upregulation of miR-223-3p by binding to the promoter of primary miR-223-3p. *H. pylori* infection promotes FZD7 (Frizzled 7) expression, which is an important coreceptor in the WNT signaling pathway, promoting cell proliferation, while miR-27b targets the 3′UTR of FZD7 to suppress FZD7 expression in GC (Geng et al., 2016). Double-stranded miR-30a is transformed to two single-stranded miRNAs, including miR-30a-3p and miR-30a-5p. The former regulates β-catenin nuclear translocation by inhibiting COX2, while the latter targets BCL9 to regulate TCF/LEF promoter activity. In *H. pylori*-infected GC, miR-30a plays a tumor suppressor role in cancer development (Liu et al., 2017). *H. pylori* infection in GC increases the level of miR-99b, which inhibits mTOR expression to upregulate autophagy, inducing intracellular *H. pylori* elimination and cell death (Yang L. et al., 2018).

However, there are also reports that miR-146 and miR-let-7 are significantly downregulated in *H. pylori*-infected GC (Ranjbar et al., 2018). MiR-146a acts as a tumor suppressor, as it reduces the expression of pro-metastatic genes like L1CAM and ROCK1 (Shomali et al., 2019). Some miRNAs have their own target genes and regulate the progression of GC at various time points. MiR-152 and miR-200b inhibit B7-H1 [a member of the B7 costimulatory family of molecules that bind to programmed death-1 (PD-1) and play a critical immunoregulatory role in the cell-mediated immune response] expression by binding to its 3′UTR, while *H. pylori* infection inhibits the ability of the miRNA to promote B7-H1 expression (Xie et al., 2017). *H. pylori* infection in GC tissue promotes miR-222-3p expression, decreasing the levels of its target HIPK2 (homeodomain-interacting protein kinase 2) and thus promoting proliferation and invasion and inhibiting apoptosis (Tan et al., 2018). Another analysis showed no significant difference in the expression of miR-222 between *H. pylori*-positive and *H. pylori*-negative GC tissues (Noormohammad et al., 2016). *H. pylori* infection leads to miR-328 downregulation and CD44v9 (CD44, variant 9) upregulation, and this upregulation can enhance reactive oxygen species resistance to prevent cell death (Ishimoto et al., 2015). Clinical statistical analysis showed that miR-375 downregulation and upregulation of its target JAK2 (Janus kinase 2) were associated with *H. pylori* infection in patients with GC ($p < 0.05$) (Chen B. et al., 2017). MiR-375 is regarded as an inhibitor of *H. pylori*-induced gastric carcinogenesis by inhibiting the expression of lncRNA SOX2OT (SOX2 overlapping transcript) and SOX2, a master regulator of the pluripotency of cancer stem cells (Shafiee et al., 2016). MiR-375 regulates the JAK2–STAT3 pathway, which affects BCL2 and TWIST1 expression to promote neoplastic transformation (Miao et al., 2014). A special miRNA requiring attention in *H. pylori* infection is the elevation of miR-30d expression, which enhances *H. pylori* intracellular survival via downregulation of the autophagy pathway (validated by several genes like ATG2B and BECN1) (Yang X. et al., 2016) (summarized in **Table 2**).

MicroRNAs Influence the Drug Resistance of *Helicobacter pylori*-Infected Gastric Cancer

Many miRNAs are also related to drug resistance and impact the treatment of GC. Early *H. pylori* eradication and aspirin use have been suggested to prevent development of the intestinal metaplasia in GC (Wang et al., 2019), while miR-21, 155, and 233 have been suggested to have a positive correlation with *H. pylori* infection to spasmolytic polypeptide-expressing metaplasia (SPEM) (Hyun Lim et al., 2018). *H. pylori* infection elevates miR-21 expression, while COE (*Celastrus orbiculatus*) inhibits this upregulation. COE upregulates PDCD4 expression by decreasing the methylation of its promoter and inhibits

TABLE 2 | Function of miRNA in Helicobacter pylori-infected gastric cancer.

MicroRNA (host gene)	Target gene of miRNA	Effector produced by H. pylori	Expression after H. pylori infection	Function to cancer after infection	References
MiR-34b			Down		Tahara et al., 2019
MiR-34c			Down		Tahara et al., 2019
MiR-124a	IL-8, SMOX		Down		Tahara et al., 2019
MiR-133a			Down		Hyun Lim et al., 2018
MiR-149	COX2, PGF2, IL-6		Down		Li et al., 2015
MiR-200a/b			Down		Choi et al., 2020
MiR-204(TRPM3)	BIRC2, NF-κB		Down	Metastasis, proliferation	Chen et al., 2019
MiR-210	STMN1, DIMT1	CagA	Down	Proliferation	Kiga et al., 2014
MiR-490-3p(CHRM2)	SMARCD1		Down	Viability, migration, invasion, colony formation, cell growth	Shen et al., 2015; Cho et al., 2016
let-7b	IL-1β, IL-8, Ras oncoprotein		Down	Immune response	Chen et al., 2015; Wu et al., 2017; Zhang et al., 2017
MiR-7	NF-κB, IKKε, RELA, FOS		Down	Proliferation	Zhao et al., 2015
MiR-22	NLRP3, IL-1β, CCND1		Down	Proliferation, inflammation	Li et al., 2018
MiR-24-3p			Down	Growth, migration, invasion, apoptosis	Li et al., 2016
MiR-30a-3p	β-Catenin, COX2		Down		Liu et al., 2017
MiR-30a-5p	BCL9, TCF/LEF		Down		Liu et al., 2017
MiR-34a	TLP4, TNF-α, IL-6	rTip-α	Down	Proliferation, viability	Wang et al., 2018
MiR-101/26	SOCS2, c-myc, CDK2, CDK4, CDK6, CCND2, CCND3, CCNE2; p14 p16, p21, p27		Down	Proliferation, colony formation	Zhou et al., 2015b
MiR-106b/375	JAK1, STAT3	LPS	Down		Ye et al., 2015
MiR-128/-148a	MMP-3/-7, E-cadherin		Down	Migration, invasion	Yang Y. et al., 2018
MiR-134	FoxM1	CagA, PBP1A	Down	Proliferation, invasion	Huang et al., 2019
MiR-145			Down		Demiryas et al., 2019
MiR-152, miR-200b	B7-H1(PDL1)		Down		Xie et al., 2017
MiR-204	SOX4		Down	Invasion, proliferation	Zhou et al., 2014a
MiR-320	Mcl-1	CagA	Down	Apoptosis	Noto et al., 2013
MiR-328	CD44v9		Down	Cell death	Ishimoto et al., 2015
MiR-375	SOX2OT, SOX2, JAK2–STAT3, BCL2, TWSIT1		Down	Cell proliferation, migration	Miao et al., 2014; Ye et al., 2015; Shafiee et al., 2016; Chen B. et al., 2017
MiR-490-3p			Down	Lymph node metastasis	Qu et al., 2017
MiR-1915	RAGE		Down	Proliferation, invasion, migration	Xu et al., 2019
MiR-3178	TRAF3, TNF-α and IL-6, NF-κB	Tip-α	Down	Inflammation	Zou et al., 2017
MiR-141	KEAP1		Down		Zhou et al., 2014b
MiR-143-3p	AKT2		Down		Wang F. et al., 2017
MiR-370	FoxM1	CagA	Down		Feng et al., 2013
MiR-21	RECK		Up		Zhang et al., 2008
MiR-30d	ATG2B, ATG5, ATG12, BECN1, BNIP3L		Up	Autophagy	Yang X. et al., 2016
MiR-99b	mTOR		Up	Autophagy, cell death	Yang L. et al., 2018
MiR-194			Up		Demiryas et al., 2019
MiR-146a	IRAK1, TRAF6, MyD88, TLRs, NF-κB, L1CAM, ROCK1		Up	Metastasis	Zabaglia et al., 2018; Li et al., 2019; Shomali et al., 2019
MiR-150-5p, miR-155-5p, and miR-3163	POLD3, MSH2, MSH3		Up	DNA damage, DNA repair	Santos et al., 2017
MiR-155	KLF4	CagA	Up	EMT, growth	Ou et al., 2019
MiR-221,222	RECK, PTEN		Up	Growth, invasion	Liu et al., 2015

(Continued)

TABLE 2 | Continued

MicroRNA (host gene)	Target gene of miRNA	Effector produced by H. pylori	Expression after H. pylori infection	Function to cancer after infection	References
MiR-223-3p	HIPK2, NF-κB, ARID1A, E-cadherin	CagA	Up	Proliferation, invasion, apoptosis	Ma et al., 2014; Tan et al., 2018; Yang F. et al., 2018- +
MiR-21			Up	EMT, inflammation	Zhu et al., 2019
MiR-135b-5p	NF-κB, KLF4		Up	Apoptosis	Shao et al., 2019
MiR-185	DNMT1, EZH2		Up		Yoon et al., 2013
MiR-223	FBXW7		Up		Zhou et al., 2015a
MiR-1289	HKα (H-K-ATPase α subunit)	CagA, SLT	Up	Transient hypochlorhydria	Zhang et al., 2014
MiR-223-3p			Up		Yang F. et al., 2018
MiR-29a-3p	A20		Up		Sun et al., 2018
MiR-320a, miR-4496	β-Catenin, ABCG2	CagA		Metastasis	Kang et al., 2016, 2017
MiR-490-3p	SMARCD1				Shen et al., 2015
MiR-155	Rheb			Autophagy, immune system response	Wu et al., 2016
MiR-29b-1-5p	PHLPP1, MMP2, MMP9				Datta et al., 2018

H. pylori-induced inflammation and EMT (Zhu et al., 2019). *H. pylori* infection enhances miR-135b-5p expression in a TNF-α-induced NF-κB-dependent manner and binds to KLF4 to attenuate its expression. The miRNA suppresses apoptosis and induces cisplatin resistance (Shao et al., 2019). *H. pylori* infection downregulates miR-141, thus reducing its target KEAP1, which enhances cisplatin resistance (Zhou et al., 2014b). GKN1 suppresses miR-185, which directly targets DNMT1 and EZH2 and exerts an anti-tumor effect together with 5-fluorouracil on tumor cell growth, while *H. pylori* infection causes GKN1 (Gastrokine 1) downregulation in GC cells (Yoon et al., 2013). *H. pylori*-infection elevates miR-223 expression, and it targets the 3′UTR of FBXW7 to modulate its expression and the G1/S transition of the cell cycle. Additionally, miR-223 shows cisplatin resistance, which can be reversed by overexpression of FBXW7 (Zhou et al., 2015a). Accompanied by *H. pylori* infection, CagA induces chemoresistance and CIC (cancer-initiating cell) properties like self-renewal and tumor-initiating capacity, while miR-320a and miR-4496 target β-catenin and ABCG2 (ATP-binding cassette, subfamily G, and member 2) at the transcriptional and posttranscriptional levels to attenuate CagA induction. Furthermore, the combination treatment of miR-320a/-4496 with 5-fluorouracil in an orthotopic mouse model has been shown to attenuate gastric tumorigenesis and metastatic potential (Kang et al., 2017). Rebamipide upregulates miR-320a/-4496 to suppress *H. pylori* CagA-induced β-catenin and CIC marker gene expression. This treatment could enhance sensitivity to chemotherapeutic drugs (Kang et al., 2016). It was found that the expression of miR-320a was downregulated in GC cells, and the sensitivity of GC cells to DDP was enhanced by directly regulating to ADAM10 (Ge et al., 2017). And miR-29b can enhance the sensitivity of GC cell by directly targeting PI3K/Akt pathway (Chen et al., 2015). In addition, the low expression of miR-125b (Zhang et al., 2017), miR-181a (Zhao et al., 2016), miR-22 (Qian et al., 2017), and so on was found to be associated with DDP resistance in GC. On the other hand, the development of MDR is also a key cause of treatment failure in GC, and it was found UCA could increase MDR of GC by directly downregulating miR-27b (Fang et al., 2016) (summarized in **Table 3**).

TABLE 3 | Drug resistance-associated miRNA in Helicobacter pylori-infected gastric cancer.

MicroRNA	Associated medicine	References
MiR-124a	5-Azacytidine	Tahara et al., 2019
MiR-21, 155, and 233	Spasmolytic polypeptide	Kuo et al., 2019
MiR-21	*Celastrus orbiculatus*	Zhu et al., 2019
MiR-135b-5p	Cisplatin	Shao et al., 2019
MiR-141	Cisplatin	Zhou et al., 2014b
MiR-185	5-Fluorouracil	Yoon et al., 2013
MiR-223	Cisplatin	Zhou et al., 2015a
MiR-320a, miR-4496	5-Fluorouracil	Kang et al., 2016, 2017

Several miRNAs have been found to be biomarkers for the prognosis of GC. MiR-490-3p is downregulated in *H. pylori*-positive GC and is significantly correlated with lymph node metastasis and clinical stage (Qu et al., 2017). According to microarrays and RT-PCR, miR-145 is downregulated and miR-194 is upregulated significantly in *H. pylori*-positive GC (Demiryas et al., 2019). Urinary miR-6807-5p and miR-6856-5p perform as biomarkers when combined with *H. pylori* infection (ACU = 0.885) in the detection of GC (Iwasaki et al., 2019). The mechanism remains unclear. It may provide doctors with another way to quickly detect GC in the future.

CONCLUSION

There are presently many reports on the mechanism of ncRNAs in relation to GC, but research on the mechanism related to *Helicobacter pylori* infection has not attracted sufficient attention. For instance, GClnc1 (GC-associated lncRNA 1) has been regarded as a modular scaffold of WDR45 and KAT2A

histone modifiers. It can regulate the localization and histone modification of SOD2. GClnc1 shows a strong correlation with the carcinogenesis, invasion, growth, and prognosis of GC. Another is clinical analysis showed that 78% of GC patients with higher GClnc1 expression are *H. pylori*-infected. The mechanism underlying the interaction between *H. pylori* and GClnc1 merits further exploration (Sun et al., 2016).

Most current research mainly shows the correlation and interaction (promotion or interference) of ncRNA in *H. pylori*-infected GC. *H. pylori* infection in GC causes expression changes in miRNAs or lncRNAs, while miRNAs and lncRNAs can interact with each other. Another miRNA in turn affects the efficiency of *H. pylori* infection. Data analysis has mainly been derived from clinical data, databases, or sequencing or array analyses of *H. pylori*-infected normal gastric epithelial cells. In this case, a large number of research targets are obtained, but there remains a lack of further clarification of the specific molecular mechanism, which needs to be further confirmed and evaluated in animal models or *in vitro* experiments to provide more reliable evidence for clinical treatment. Concurrently, in analyses of clinical data, focusing on the correlation and interaction between ncRNA and various *H. pylori* virulence factors also provides a good perspective. Array and database analyses have provided large amounts of data, but they need to be further confirmed and analyzed, a stage of research that is still in the preliminary phases. NcRNA plays a very important role in the progression of *H. pylori*-infected GC. It can not only affect the chemotherapy resistance of GC but also serve as a biomarker for the prognosis of GC. As a new type of ncRNA, circRNA has been found to have the potential as a prognostic biomarker for GC (Shan et al., 2019). For example, the expression of hsa_circ_0001649 in GC was significantly lower than that in paired non-tumor tissues. What is more, compared with preoperative plasma samples, the expression level of hsa_circ_0001649 was upregulated after surgery, suggesting that hsa_circ_0001649 may be a follow-up indicator for GC patients after surgery (Li et al., 2017). And CircPVT1 levels were observed to be independent prognostic indicators of overall survival and DFS in GC patients (Chen J. et al., 2017). At present, ncRNAs including circRNAs, miRNAs, and lncRNAs have the potential to be used as prognostic biomarkers for GC, and previous studies have shown that many ncRNAs can accurately predict the prognosis of patients, which is of great significance to both doctors and patients. However, more work and efforts are still needed to be done for clinical application. Actually, we can found that ncRNA has been studied much longer than lncRNAs, and its experimental technique is more mature. And at the same time, there are more research results. But it could not prove that miRNA plays a more important role than lncRNAs in *H. pylori*-infected GC. The mechanism about lncRNAs still needs to be explored. And there are many kinds of ncRNAs in which their function has not been discovered in *H. pylori*-infected GC, and it would be a very promising research direction in the field of biomedicine.

AUTHOR CONTRIBUTIONS

CW and YH wrote the manuscript. SW, BZ, and YB revised the manuscript. YH and QL was responsible for searching the references. CY projected and edited the manuscript. XX and SY reviewed the manuscript. All authors read and approved the final manuscript.

FUNDING

This work was supported by the National Natural Science Foundation of China (No. 81773037).

REFERENCES

Acunzo, M., Romano, G., Wernicke, D., and Croce, C. M. (2015). MicroRNA and cancer–a brief overview. *Adv. Biol. Regul.* 57, 1–9. doi: 10.1016/j.jbior.2014.09.013

Amieva, M. R., and El-Omar, E. M. (2008). Host-bacterial interactions in *Helicobacter* pylori infection. *Gastroenterology* 134, 306–323. doi: 10.1053/j.gastro.2007.11.009

Atherton, J. C., and Blaser, M. J. (2009). Coadaptation of *Helicobacter* pylori and humans: ancient history, modern implications. *J. Clin. Invest.* 119, 2475–2487. doi: 10.1172/JCI38605

Backert, S., Neddermann, M., Maubach, G., and Naumann, M. (2017). Pathogenesis of *Helicobacter* pylori infection. *Helicobacter* 21, 19–25. doi: 10.1111/hel.12335

Bartel, D. P. (2004). MicroRNAs: genomics, biogenesis, mechanism, and function. *Cell* 116, 281–297. doi: 10.1016/s0092-8674(04)00045-5

Belair, C., Darfeuille, F., and Staedel, C. (2009). *Helicobacter* pylori and gastric cancer: possible role of microRNAs in this intimate relationship. *Clin. Microbiol. Infect.* 15, 806–812. doi: 10.1111/j.1469-0691.2009.02960.x

Blaser, M. J., and Atherton, J. C. (2004). *Helicobacter* pylori persistence: biology and disease. *J. Clin. Invest.* 113, 321–333. doi: 10.1172/JCI20925

Burd, C. E., Jeck, W. R., Liu, Y., Sanoff, H. K., Wang, Z., and Sharpless, N. E. (2010). Expression of linear and novel circular forms of an INK4/ARF-associated non-coding RNA correlates with atherosclerosis risk. *PLoS Genet.* 6:e1001233. doi: 10.1371/journal.pgen.1001233

Chen, B., Guo, S., Yu, Z., Feng, Y., and Hui, L. (2017). Downregulation of microRNA-375, combined with upregulation of its target gene Janus kinase 2, predicts unfavorable prognosis in patients with gastric cancer. *Int. J. Clin. Exp. Pathol.* 10, 11106–11113.

Chen, D., Feng, L., Ye, R., He, Y., and Wang, Y. (2015). MiR-29b Reduces Cisplatin Resistance of Gastric Cancer Cell by Targeting PI3K/Akt Pathway. *Zhongguo Yi Xue Ke Xue Yuan Xue Bao* 37, 514–519. doi: 10.3881/j.issn.1000-503X.2015.05.005

Chen, J., Li, Y., Zheng, Q., Bao, C., He, J., Chen, B., et al. (2017). Circular RNA profile identifies circPVT1 as a proliferative factor and prognostic marker in gastric cancer. *Cancer Lett.* 388, 208–219. doi: 10.1016/j.canlet.2016.12.006

Chen, P., Guo, H., Wu, X., Li, J., Duan, X., Ba, Q., et al. (2019). Epigenetic silencing of microRNA-204 by *Helicobacter* pylori augments the NF-kappaB signaling pathway in gastric cancer development and progression. *Carcinogenesis* 41, 430–441. doi: 10.1093/carcin/bgz143

Chen, Q., and Crosa, J. H. (1996). Antisense RNA, fur, iron, and the regulation of iron transport genes in Vibrio anguillarum. *J. Biol. Chem.* 271, 18885–18891. doi: 10.1074/jbc.271.31.18885

Cho, C. H., Yu, J., and Wu, W. (2016). Identification of pathogenic microRNAs in *Helicobacter* pylori-associated gastric cancer using a combined approach of animal study and clinical sample analysis. *Hong Kong Med. J.* 6, 13–18.

Choi, I. J., Kook, M. C., Kim, Y. I., Cho, S. J., Lee, J. Y., Kim, C. G., et al. (2018). *Helicobacter* pylori Therapy for the Prevention of Metachronous Gastric Cancer. *N. Engl. J. Med.* 378, 1085–1095. doi: 10.1056/NEJMoa1708423

Choi, J. M., Kim, S. G., Yang, H., Lim, J. H., Cho, N., Kim, W., et al. (2020). *Helicobacter* pylori Eradication Can Reverse the Methylation-Associated Regulation of miR-200a/b in Gastric Carcinogenesis. *Gut Liver* 14, 571–580. doi: 10.5009/gnl19299

Chung, S., Nakagawa, H., Uemura, M., Piao, L., Ashikawa, K., and Hosono, N. (2011). Association of a novel long non-coding RNA in 8q24 with prostate cancer susceptibility. *Cancer Sci.* 102, 245–252. doi: 10.1111/j.1349-7006.2010.01737.x

Clyne, M., Labigne, A., and Drumm, B. (1995). *Helicobacter* pylori requires an acidic environment to survive in the presence of urea. *Infect. Immun.* 63, 1669–1673. doi: 10.1128/IAI.63.5.1669-1673.199

Datta, C., Subuddhi, A., Kumar, M., Lepcha, T. T., Chakraborty, S., Jana, K., et al. (2018). Genome-wide mRNA-miRNA profiling uncovers a role of the microRNA miR-29b-1-5p/PHLPP1 signalling pathway in *Helicobacter* pylori-driven matrix metalloproteinase production in gastric epithelial cells. *Cell Microbiol.* 20:e12859. doi: 10.1111/cmi.12859

Demiryas, S., Kocazeybek, B., Demirci, M., Caliskan, R., Kepil, N., Uysal, H., et al. (2019). *Helicobacter* pylori-miRNA interaction in gastric cancer tissues: first prospective study from Turkey. *New Microbiol.* 42, 210–220.

Dühring, U., Axmann, I. M., Hess, W. R., and Wilde, A. (2006). An internal antisense RNA regulates expression of the photosynthesis gene isiA. *Proc. Natl. Acad. Sci. U. S. A.* 103, 7054–7058. doi: 10.1073/pnas.0600927103

Fang, Q., Chen, X. Y., and Zhi, X. (2016). Long Non-Coding RNA (LncRNA) Urothelial Carcinoma Associated 1 (UCA1) Increases Multi-Drug Resistance of Gastric Cancer via Downregulating miR-27b. *Med. Sci. Monit.* 22, 3506–3513. doi: 10.12659/msm.900688

Feng, Y., Wang, L., Zeng, J., Shen, L., Liang, X., Yu, H., et al. (2013). FoxM1 is overexpressed in *Helicobacter* pylori-induced gastric carcinogenesis and is negatively regulated by miR-370. *Mol. Cancer Res.* 11, 834–844. doi: 10.1158/1541-7786.MCR-13-0007

Ferlay, J., Colombet, M., Soerjomataram, I., Mathers, C., Parkin, D. M., Piñeros, M., et al. (2019). Estimating the global cancer incidence and mortality in 2018: GLOBOCAN sources and methods. *Int. J. Cancer* 144, 1941–1953. doi: 10.1002/ijc.31937

Freedberg, D. E., Toussaint, N. C., Chen, S. P., Ratner, A. J., Whittier, S., and Wang, T. C. (2015). Proton Pump Inhibitors Alter Specific Taxa in the Human Gastrointestinal Microbiome: a Crossover Trial. *Gastroenterology* 149, 883–5.e9. doi: 10.1053/j.gastro.2015.06.043

Ge, X., Cui, H., Zhou, Y., Yin, D., Feng, Y., Xin, Q., et al. (2017). MiR-320a modulates cell growth and chemosensitivity via regulating ADAM10 in gastric cancer. *Mol. Med. Rep.* 16, 9664–9670. doi: 10.3892/mmr.2017.7819

Geissmann, T., Possedko, M., Huntzinger, E., Fechter, P., Ehresmann, C., and Romby, P. (2006). Regulatory RNAs as mediators of virulence gene expression in bacteria. *Handb. Exp. Pharmacol.* 173, 9–43. doi: 10.1007/3-540-27262-3_2

Geng, Y., Lu, X., Wu, X., Xue, L., Wang, X., Xu, J., et al. (2016). MicroRNA-27b suppresses *Helicobacter* pylori-induced gastric tumorigenesis through negatively regulating Frizzled7. *Oncol. Rep.* 35, 2441–2450. doi: 10.3892/or.2016.4572

Ghoussaini, M., Song, H., Koessler, T., Olama, A., Kote-Jarai, Z., and Driver, K. E. (2008). Multiple loci with different cancer specificities within the 8q24 gene desert. *J. Natl. Cancer Inst.* 100, 962–966. doi: 10.1093/jnci/djn190

Hayashi, Y., Tsujii, M., Wang, J., Kondo, J., Akasaka, T., Jin, Y., et al. (2013). CagA mediates epigenetic regulation to attenuate let-7 expression in *Helicobacter* pylori-related carcinogenesis. *Gut* 62, 1536–1546. doi: 10.1136/gutjnl-2011-301625

He, B., Sun, H., Xu, T., Pan, Y., Lin, K., and Gao, T. (2017). Association of Genetic Polymorphisms in the LncRNAs with Gastric Cancer Risk in a Chinese Population. *J. Cancer* 8, 531–536. doi: 10.7150/jca.17519

Helicobacter and Cancer Collaborative Group [HCCG] (2001). Collaborative G. Gastric cancer and *Helicobacter* pylori: a combined analysis of 12 case control studies nested within prospective cohorts. *Gut* 49, 347–353. doi: 10.1136/gut.49.3.347

Huang, L., Wang, Z., and Pan, D. (2019). Penicillinbinding protein 1A mutationpositive *Helicobacter* pylori promotes epithelialmesenchymal transition in gastric cancer via the suppression of microRNA134. *Int. J. Oncol.* 54, 916–928. doi: 10.3892/ijo.2018.4665

Hyun Lim, J., Kim, S. G., Choi, J. M., Yang, H., Kim, J. S., Jung, H. C., et al. (2018). *Helicobacter* pylori Is Associated with miR-133a Expression through Promoter Methylation in Gastric Carcinogenesis. *Gut Liver* 12, 58–66. doi: 10.5009/gnl17263

Ishimoto, T., Izumi, D., Watanabe, M., Yoshida, N., Hidaka, K., Miyake, K., et al. (2015). Chronic inflammation with *Helicobacter* pylori infection is implicated in CD44 overexpression through miR-328 suppression in the gastric mucosa. *J. Gastroenterol.* 50, 751–757. doi: 10.1007/s00535-014-1019-y

Isomoto, H., Matsushima, K., Inoue, N., Hayashi, T., Nakayama, T., Kunizaki, M., et al. (2012). Interweaving microRNAs and proinflammatory cytokines in gastric mucosa with reference to H. pylori infection. *J. Clin. Immunol.* 32, 290–299. doi: 10.1007/s10875-011-9626-3

Iwasaki, H., Shimura, T., Yamada, T., Okuda, Y., Natsume, M., Kitagawa, M., et al. (2019). A novel urinary microRNA biomarker panel for detecting gastric cancer. *J. Gastroenterol.* 54, 1061–1069. doi: 10.1007/s00535-019-01601-w

Jia, W., Zhang, J., Ma, F., Hao, S., Li, X., Guo, R., et al. (2019). Long noncoding RNA THAP9-AS1 is induced by *Helicobacter* pylori and promotes cell growth and migration of gastric cancer. *Onco Targets Ther.* 12, 6653–6663. doi: 10.2147/OTT.S201832

Kang, D. W., Noh, Y. N., Hwang, W. C., Choi, K., and Min, D. S. (2016). Rebamipide attenuates *Helicobacter* pylori CagA-induced self-renewal capacity via modulation of beta-catenin signaling axis in gastric cancer-initiating cells. *Biochem. Pharmacol.* 113, 36–44. doi: 10.1016/j.bcp.2016.06.003

Kang, D. W., Yang, E. S., Noh, Y. N., Hwang, W. C., Jo, S., Suh, Y., et al. (2017). MicroRNA-320a and microRNA-4496 attenuate *Helicobacter* pylori cytotoxin-associated gene A (CagA)-induced cancer-initiating potential and chemoresistance by targeting beta-catenin and ATP-binding cassette, subfamily G, member 2. *J. Pathol.* 241, 614–625. doi: 10.1002/path.4866

Kiga, K., Mimuro, H., Suzuki, M., Shinozaki-Ushiku, A., Kobayashi, T., Sanada, T., et al. (2014). Epigenetic silencing of miR-210 increases the proliferation of gastric epithelium during chronic *Helicobacter* pylori infection. *Nat. Commun.* 5:4497. doi: 10.1038/ncomms5497

Kuo, H., Chang, W., Yeh, Y., Cheng, H., Tsai, Y., Wu, C., et al. (2019). Spasmolytic polypeptide-expressing metaplasia associated with higher expressions of miR-21, 155, and 223 can be regressed by *Helicobacter* pylori eradication in the gastric cancer familial relatives. *Helicobacter* 24:e12578. doi: 10.1111/hel.12578

Lan, W. G., Xu, D., Xu, C., Ding, C., Ning, F. L., Zhou, Y., et al. (2016). Silencing of long non-coding RNA ANRIL inhibits the development of multidrug resistance in gastric cancer cells. *Oncol Rep.* 36, 263–270. doi: 10.3892/or.2016.4771

Li, N., Wang, J., Yu, W., Dong, K., You, F., Si, B., et al. (2019). MicroRNA146a inhibits the inflammatory responses induced by interleukin17A during the infection of *Helicobacter* pylori. *Mol. Med. Rep.* 19, 1388–1395. doi: 10.3892/mmr.2018.9725

Li, P., Shan, J., Chen, X., Zhang, D., Su, L., Huang, X., et al. (2015). Epigenetic silencing of microRNA-149 in cancer-associated fibroblasts mediates prostaglandin E2/interleukin-6 signaling in the tumor microenvironment. *Cell Res.* 25, 588–603. doi: 10.1038/cr.2015.51

Li, Q., Wang, N., Wei, H., Li, C., Wu, J., and Yang, G. (2016). MiR-24-3p Regulates Progression of Gastric Mucosal Lesions and Suppresses Proliferation and Invasiveness of N87 Via Peroxiredoxin 6. *Dig. Dis. Sci.* 61, 3486–3497. doi: 10.1007/s10620-016-4309-9

Li, S., Liang, X., Ma, L., Shen, L., Li, T., Zheng, L., et al. (2018). MiR-22 sustains NLRP3 expression and attenuates H. pylori-induced gastric carcinogenesis. *Oncogene* 37, 884–896. doi: 10.1038/onc.2017.381

Li, W., Song, Y., Zhang, H., Zhou, Z., Xie, X., Zeng, Q., et al. (2017). Decreased Expression of Hsa_circ_00001649 in Gastric Cancer and Its Clinical Significance. *Dis. Markers* 2017, 1–6.

Liu, W., Song, N., Yao, H., Zhao, L., Liu, H., and Li, G. (2015). MiR-221 and miR-222 Simultaneously Target RECK and Regulate Growth and Invasion of Gastric Cancer Cells. *Med. Sci. Monit.* 21, 2718–2725. doi: 10.12659/MSM.894324

Liu, X., Ji, Q., Zhang, C., Liu, X., Liu, Y., Liu, N., et al. (2017). MiR-30a acts as a tumor suppressor by double-targeting COX-2 and BCL9 in H. pylori gastric cancer models. *Sci. Rep.* 7:7113. doi: 10.1038/s41598-017-07193-w

Livny, J., and Waldor, M. K. (2007). Identification of small RNAs in diverse bacterial species. *Curr. Opin. Microbiol.* 10, 96–101. doi: 10.1016/j.mib.2007.03.005

Ma, L., Chen, Y., Zhang, B., and Liu, G. (2014). Increased microRNA-223 in *Helicobacter* pylori-associated gastric cancer contributed to cancer cell proliferation and migration. *Biosci. Biotechnol. Biochem.* 78, 602–608. doi: 10.1080/09168451.2014.895661

Ma, Y., and Tao, H. (2012). Microribonucleic acids and gastric cancer. *Cancer Sci.* 103, 620–625. doi: 10.1111/j.1349-7006.2011.02185.x

Majdalani, N., Vanderpool, C. K., and Gottesman, S. (2005). Bacterial small RNA regulators. *Crit. Rev. Biochem. Mol. Biol.* 40, 93–113. doi: 10.1080/10409230590918702

Malfertheiner, P., Megraud, F., O'Morain, C. A., Gisbert, J. P., Kuipers, E. J., Axon, A. T., et al. (2017). Management of *Helicobacter* pylori infection-the Maastricht V/Florence Consensus Report. *Gut* 66, 6–30. doi: 10.1136/gutjnl-2016-312288

Mera, R. M., Bravo, L. E., Camargo, M. C., Bravo, J. C., Delgado, A. G., Romero-Gallo, J., et al. (2018). Dynamics of *Helicobacter* pylori infection as a determinant of progression of gastric precancerous lesions: 16-year follow-up of an eradication trial. *Gut* 67, 1239–1246. doi: 10.1136/gutjnl-2016-311685

Meyer-Rosberg, K., Scott, D. R., Rex, D., Melchers, K., and Sachs, G. (1996). The effect of environmental pH on the proton motive force of *Helicobacter* pylori. *Gastroenterology* 111, 886–900. doi: 10.1016/s0016-5085(96)70056-2

Miao, L., Liu, K., Xie, M., Xing, Y., and Xi, T. (2014). MiR-375 inhibits *Helicobacter* pylori-induced gastric carcinogenesis by blocking JAK2-STAT3 signaling. *Cancer Immunol. Immunother.* 63, 699–711. doi: 10.1007/s00262-014-1550-y

Mitarai, N., Andersson, A., Krishna, S., Semsey, S., and Sneppen, K. (2007). Efficient degradation and expression prioritization with small RNAs. *Phys. Biol.* 4, 164–171. doi: 10.1088/1478-3975/4/3/003

Morello, J. A. (1999). Clinical Microbiology Reviews: genesis of a journal. *Clin. Microbiol. Rev.* 12, 183–186.

Murray-Stewart, T., Sierra, J. C., Piazuelo, M. B., Mera, R. M., Chaturvedi, R., Bravo, L. E., et al. (2016). Epigenetic silencing of miR-124 prevents spermine oxidase regulation: implications for *Helicobacter* pylori-induced gastric cancer. *Oncogene* 35, 5480–5488. doi: 10.1038/onc.2016.91

Noormohammad, M., Sadeghi, S., Tabatabaeian, H., Ghaedi, K., Talebi, A., Azadeh, M., et al. (2016). Upregulation of miR-222 in both *Helicobacter* pylori- infected and noninfected gastric cancer patients. *J. Genet* 95, 991–995. doi: 10.1007/s12041-016-0728-9

Noto, J. M., Piazuelo, M. B., Chaturvedi, R., Bartel, C. A., Thatcher, E. J., Delgado, A., et al. (2013). Strain-specific suppression of microRNA-320 by carcinogenic *Helicobacter* pylori promotes expression of the antiapoptotic protein Mcl-1. *Am. J. Physiol. Gastrointest. Liver Physiol.* 305, G786–G796. doi: 10.1152/ajpgi.00279.2013

Opdyke, J. A., Kang, J., and Storz, G. (2004). A small-RNA regulator of acid response genes in *Escherichia coli*. *J. Bacteriol.* 186, 6698–6705. doi: 10.1128/JB.186.20.6698-6705.2004

Ou, Y., Ren, H., Zhao, R., Song, L., Liu, Z., Xu, W., et al. (2019). *Helicobacter* pylori CagA promotes the malignant transformation of gastric mucosal epithelial cells through the dysregulation of the miR-155/KLF4 signaling pathway. *Mol. Carcinog.* 58, 1427–1437. doi: 10.1002/mc.23025

Pachathundikandi, S. K., Tegtmeyer, N., and Backert, S. (2013). Signal transduction of *Helicobacter* pylori during interaction with host cell protein receptors of epithelial and immune cells. *Gut Microbes* 4, 454–474. doi: 10.4161/gmic.27001

Pang, Q., Ge, J., Shao, Y., Sun, W., Song, H., Xia, T., et al. (2014). Increased expression of long intergenic non-coding RNA LINC00152 in gastric cancer and its clinical significance. *Tumour Biol.* 35, 5441–5447. doi: 10.1007/s13277-014-1709-3

Pernitzsch, S., and Sharma, C. M. (2012). Transcriptome complexity and riboregulation in the human pathogen *Helicobacter* pylori. *Front. Cell Infect. Microbiol.* 2:14. doi: 10.3389/fcimb.2012.00014

Pernitzsch, S. R., Tirier, S. M., Beier, D., and Sharma, C. M. (2014). A variable homopolymeric G-repeat defines small RNA-mediated posttranscriptional regulation of a chemotaxis receptor in *Helicobacter* pylori. *Proc. Natl. Acad. Sci. U. S. A.* 111, e501–e510. doi: 10.1073/pnas.1315152111

Petra, C. V., Rus, A., and Dumitraşcu, D. L. (2017). Gastric microbiota: tracing the culprit. *Clujul Med.* 90, 369–376. doi: 10.15386/cjmed-854

Pflock, M., Dietz, P., Schär, J., and Beier, D. (2004). Genetic evidence for histidine kinase HP165 being an acid sensor of *Helicobacter* pylori. *FEMS Microbiol. Lett.* 234, 51–61. doi: 10.1016/j.femsle.2004.03.023

Pflock, M., Kennard, S., Delany, I., Scarlato, V., and Beier, D. (2005). Acid-induced activation of the urease promoters is mediated directly by the ArsRS two-component system of *Helicobacter* pylori. *Infect. Immun.* 73, 6437–6445. doi: 10.1128/IAI.73.10.6437-6445.2005

Polakovicova, I., Jerez, S., Wichmann, I. A., Sandoval-Bórquez, A., Carrasco-Véliz, N., and Corvalán, A. H. (2018). Role of microRNAs and Exosomes in *Helicobacter* pylori and Epstein-Barr Virus Associated Gastric Cancers. *Front. Microbiol.* 9:636. doi: 10.3389/fmicb.2018.00636

Qian, X., Xu, W., Xu, J., Shi, Q., Li, J., Weng, Y., et al. (2017). Enolase 1 stimulates glycolysis to promote chemoresistance in gastric cancer. *Oncotarget* 8, 47691–47708. doi: 10.18632/oncotarget.17868

Qu, M., Li, L., and Zheng, W. (2017). Reduced miR-490-3p expression is associated with poor prognosis of *Helicobacter* pylori induced gastric cancer. *Eur. Rev. Med. Pharmacol. Sci.* 21, 3384–3388.

Ranjbar, R., Hesari, A. R., Ghasemi, F., and Sahebkar, A. (2018). Expression of microRNAs and IRAK1 pathway genes are altered in gastric cancer patients with *Helicobacter* pylori infection. *J. Cell Biochem.* 119, 7570–7576. doi: 10.1002/jcb.27067

Ransohoff, J., Wei, Y., and Khavari, P. A. (2018). The functions and unique features of long intergenic non-coding RNA. *Nat. Rev. Mol. Cell Biol.* 19, 143–157. doi: 10.1038/nrm.2017.104

Rieder, R., Reinhardt, R., Sharma, C., and Vogel, J. (2012). Experimental tools to identify RNA-protein interactions in *Helicobacter* pylori. *RNA Biol.* 9, 520–531. doi: 10.4161/rna.20331

Romby, P., Vandenesch, F., and Wagner, E. (2006). The role of RNAs in the regulation of virulence-gene expression. *Curr. Opin. Microbiol.* 9, 229–236. doi: 10.1016/j.mib.2006.02.005

Safaralizadeh, R., Dastmalchi, N., Hosseinpourfeizi, M., and Latifi-Navid, S. (2017). *Helicobacter* pylori virulence factors in relation to gastrointestinal diseases in Iran. *Microb. Pathog.* 105, 211–217. doi: 10.1016/j.micpath.2017.02.026

Santos, J. C., Brianti, M. T., Almeida, V. R., Ortega, M. M., Fischer, W., Haas, R., et al. (2017). *Helicobacter* pylori infection modulates the expression of miRNAs associated with DNA mismatch repair pathway. *Mol. Carcinog.* 56, 1372–1379. doi: 10.1002/mc.22590

Shafiee, S. M., Aleyasin, S. A., Mowla, S. J., Vasei, M., and Yazdanparast, S. A. (2016). The Effect of MicroRNA-375 Overexpression, an Inhibitor of *Helicobacter* pylori-Induced Carcinogenesis, on lncRNA SOX2OT. *Jundishapur J. Microbiol.* 9:e23464. doi: 10.5812/jjm.23464

Shan, C., Zhang, Y., Hao, X., Gao, J., Chen, X., and Wang, K. (2019). Biogenesis, functions and clinical significance of circRNAs in gastric cancer. *Mol. Cancer* 18:136. doi: 10.1186/s12943-019-1069-0

Shao, L., Chen, Z., Soutto, M., Zhu, S., Lu, H., Romero-Gallo, J., et al. (2019). *Helicobacter* pylori-induced miR-135b-5p promotes cisplatin resistance in gastric cancer. *FASEB J.* 33, 264–274. doi: 10.1096/fj.201701456RR

Sharma, C. M., and Vogel, J. (2009). Experimental approaches for the discovery and characterization of regulatory small RNA. *Curr. Opin. Microbiol.* 12, 536–546. doi: 10.1016/j.mib.2009.07.00

Shen, J., Xiao, Z., Wu, W., Wang, M. H., To, K. F., Chen, Y., et al. (2015). Epigenetic silencing of miR-490-3p reactivates the chromatin remodeler SMARCD1 to promote *Helicobacter* pylori-induced gastric carcinogenesis. *Cancer Res.* 75, 754–765. doi: 10.1158/0008-5472.CAN-14-1301

Shomali, N., Mansoori, B., Mohammadi, A., Shirafkan, N., Ghasabi, M., and Baradaran, B. (2017). MiR-146a functions as a small silent player in gastric cancer. *Biomed. Pharmacother.* 96, 238–245. doi: 10.1016/j.biopha.2017.09.138

Shomali, N., Shirafkan, N., Duijf, P., Ghasabi, M., Babaloo, Z., Yousefi, M., et al. (2019). Downregulation of miR-146a promotes cell migration in *Helicobacter* pylori-negative gastric cancer. *J. Cell Biochem.* 120, 9495–9505. doi: 10.1002/jcb.28225

Shukla, S., Khatoon, J., Prasad, K. N., Rai, R. P., Singh, A. K., Kumar, S., et al. (2016). Transforming growth factor beta 1 (TGF-beta1) modulates Epstein-Barr virus reactivation in absence of *Helicobacter* pylori infection in patients with gastric cancer. *Cytokine* 77, 176–179. doi: 10.1016/j.cyto.2015.07.023

Su, M., Erwin, A. L., Campbell, A. M., Pyburn, T. M., Salay, L. E., and Hanks, J. L. (2019). Cryo-EM Analysis Reveals Structural Basis of *Helicobacter* pylori VacA Toxin Oligomerization. *J. Mol. Biol.* 431, 1956–1965. doi: 10.1016/j.jmb.2019.03.029

Sugano, K. (2019). Effect of *Helicobacter* pylori eradication on the incidence of gastric cancer: a systematic review and meta-analysis. *Gastric Cancer* 22, 435–445. doi: 10.1007/s10120-018-0876-0

Sugano, K., Tack, J., Kuipers, E. J., Graham, D. Y., El-Omar, E. M., Miura, S., et al. (2015). Kyoto global consensus report on *Helicobacter* pylori gastritis. *Gut* 64, 1353–1367. doi: 10.1136/gutjnl-2015-309252

Sun, F., Ni, Y., Zhu, H., Fang, J., Wang, H., Xia, J., et al. (2018). MicroRNA-29a-3p, Up-Regulated in Human Gastric Cells and Tissues with H.Pylori Infection, Promotes the Migration of GES-1 Cells via A20-Mediated EMT Pathway. *Cell Physiol. Biochem*. 51, 1250–1263. doi: 10.1159/000495502

Sun, T., He, J., Liang, Q., Ren, L., Yan, T., Yu, T., et al. (2016). LncRNA GClnc1 Promotes Gastric Carcinogenesis and May Act as a Modular Scaffold of WDR5 and KAT2A Complexes to Specify the Histone Modification Pattern. *Cancer Discov*. 6, 784–801. doi: 10.1158/2159-8290.CD-15-0921

Suzuki, H., and Matsuzaki, J. (2018). Gastric cancer: evidence boosts *Helicobacter* pylori eradication. *Nat. Rev. Gastroenterol. Hepatol.* 15, 458–460. doi: 10.1038/s41575-018-0023-8

Tahara, T., Tahara, S., Horiguchi, N., Kawamura, N., Okubo, M., Nagasaka, M., et al. (2019). Gastric Mucosal Microarchitectures Associated with Irreversibility with *Helicobacter* pylori Eradication and Downregulation of Micro RNA (miR)-124a. *Cancer Invest*. 37, 417–426. doi: 10.1080/07357907.2019.1663207

Tan, X., Tang, H., Bi, J., Li, N., and Jia, Y. (2018). MicroRNA-222-3p associated with *Helicobacter* pylori targets HIPK2 to promote cell proliferation, invasion, and inhibits apoptosis in gastric cancer. *J. Cell Biochem.* 119, 5153–5162. doi: 10.1002/jcb.26542

Tomlinson, I., Webb, E., Carvajal-Carmona, L., Broderick, P., Kemp, Z., and Spain, S. (2007). A genome-wide association scan of tag SNPs identifies a susceptibility variant for colorectal cancer at 8q24.21. *Nat. Genet*. 39, 984–988. doi: 10.1038/ng2085

Tramonti, A., Canio, M. D., and Biase, D. D. (2008). GadX/GadW-dependent regulation of the *Escherichia coli* acid fitness island: transcriptional control at the gadY-gadW divergent promoters and identification of four novel 42 bp GadX/GadW-specific binding sites. *Mol. Microbiol.* 70, 965–982. doi: 10.1111/j.1365-2958.2008.06458.x

Valentin-Hansen, P., Eriksen, M., and Udesen, C. (2004). The bacterial Sm-like protein Hfq: a key player in RNA transactions. *Mol. Microbiol*. 51, 1525–1533. doi: 10.1111/j.1365-2958.2003.03935.x

Vannini, A., Roncarati, D., and Danielli, A. (2016). The cag-pathogenicity island encoded CncR1 sRNA oppositely modulates *Helicobacter* pylori motility and adhesion to host cells. *Cell Mol. Life Sci.* 73, 3151–3168. doi: 10.1007/s00018-016-2151-z

Vogel, J., and Luisi, B. F. (2011). Hfq and its constellation of RNA. *Nat. Rev. Microbiol*. 9, 578–589. doi: 10.1038/nrmicro2615

Vogel, J., and Wagner, E. (2007). Target identification of small noncoding RNAs in bacteria. *Curr. Opin. Microbiol*. 10, 262–270. doi: 10.1016/j.mib.2007.06.001

Wang, F., Liu, J., Zou, Y., Jiao, Y., Huang, Y., Fan, L., et al. (2017). MicroRNA-143-3p, up-regulated in H. pylori-positive gastric cancer, suppresses tumor growth, migration and invasion by directly targeting AKT2. *Oncotarget* 8, 28711–28724. doi: 10.18632/oncotarget.15646

Wang, L., Chunyan, Q., Zhou, Y., He, Q., Ma, Y., Ga, Y., et al. (2017). BCAR4 increase cisplatin resistance and predicted poor survival in gastric cancer patients. *Eur. Rev. Med. Pharmacol. Sci*. 21, 4064–4070.

Wang, W., Gu, C., Li, R., Xu, Z., Yu, J., Ye, Y., et al. (2019). Long non-coding RNA CASC19 is associated with the progression and prognosis of advanced gastric cancer. *Aging* 11, 5829–5847. doi: 10.18632/aging.102190

Wang, Y., Zhang, C., and He, X. (2018). Minor allele of rs1057317 polymorphism in TLR4 is associated with increased risk of *Helicobacter* pylori -induced gastric cancer. *J. Cell Biochem*. 120, 1969–1978. doi: 10.1002/jcb.27493

Watari, J., Ito, C., Shimoda, T., Tomita, T., Oshima, T., Fukui, H., et al. (2019). DNA methylation silencing of microRNA gene methylator in the precancerous background mucosa with and without gastric cancer: analysis of the effects of H. pylori eradication and long-term aspirin use. *Sci. Rep*. 9:12559. doi: 10.1038/s41598-019-49069-1

Wen, Y., Feng, J., and Sachs, G. (2013). *Helicobacter* pylori 5′ureB-sRNA, a cis-encoded antisense small RNA, negatively regulates ureAB expression by transcription termination. *J. Bacteriol*. 195, 444–452. doi: 10.1128/JB.01022-12

Wen, Y., Feng, J., Scott, D. R., Marcus, E. A., and Sachs, G. (2006). Involvement of the HP0165-HP0166 two-component system in expression of some acidic-pH-upregulated genes of *Helicobacter* pylori. *J. Bacteriol*. 188, 1750–1761. doi: 10.1128/JB.188.5.1750-1761.2006

Wen, Y., Feng, J., Scott, D. R., Marcus, E. A., and Sachs, G. (2011). A cis-encoded antisense small RNA regulated by the HP0165-HP0166 two-component system controls expression of ureB in *Helicobacter* pylori. *J. Bacteriol*. 193, 40–51. doi: 10.1128/JB.00800-10

Wilusz, J., Sunwoo, H., and Spector, D. (2009). Long noncoding RNAs: functional surprises from the RNA world. *Genes Dev.* 23, 1494–1504. doi: 10.1101/gad.1800909

Wu, K., Zhu, C., Yao, Y., Wang, X., Song, J., and Zhai, J. (2016). MicroRNA-155-enhanced autophagy in human gastric epithelial cell in response to *Helicobacter* pylori. *Saudi J. Gastroenterol.* 22, 30–36. doi: 10.4103/1319-3767.173756

Wu, Y., Xu, Q., He, C., Li, Y., Liu, J., Deng, N., et al. (2017). Association of Polymorphisms in three pri-miRNAs that Target Pepsinogen C with the Risk and Prognosis of Gastric Cancer. *Sci. Rep*. 7:39528. doi: 10.1038/srep39528

Xie, G., Li, W., Li, R., Wu, K., Zhao, E., Zhang, Y., et al. (2017). *Helicobacter* Pylori Promote B7-H1 Expression by Suppressing miR-152 and miR-200b in Gastric Cancer Cells. *PLoS One* 12:e0168822. doi: 10.1371/journal.pone.0168822

Xu, Q., Chen, T.-J., He, C.-Y., Sun, L. P., Liu, J.-W., Yuvan, Y., et al. (2017). MiR-27a rs895819 is involved in increased atrophic gastritis risk, improved gastric cancer prognosis and negative interaction with *Helicobacter* pylori. *Sci. Rep.* 7:41307. doi: 10.1038/srep41307

Xu, X., Zhang, W., Li, C. X., Gao, H., Pei, Q., Cao, B., et al. (2019). Up-Regulation of MiR-1915 Inhibits Proliferation, Invasion, and Migration of *Helicobacter* pylori-Infected Gastric Cancer Cells via Targeting RAGE. *Yonsei Med. J.* 60, 38–47. doi: 10.3349/ymj.2019.60.1.38

Yang, F., Xu, Y., Liu, C., Ma, C., Zou, S., Xu, X., et al. (2018). NF-kappaB/miR-223-3p/ARID1A axis is involved in *Helicobacter* pylori CagA-induced gastric carcinogenesis and progression. *Cell Death Dis*. 9:12. doi: 10.1038/s41419-017-0020-9

Yang, J., and Song, H. (2019). Identification of long noncoding RNA RP11-169F17.1 and RP11-669N7.2 as novel prognostic biomarkers of stomach adenocarcinoma based on integrated bioinformatics analysis. *Epigenomics* 11, 1307–1321. doi: 10.2217/epi-2019-0115

Yang, L., Li, C., and Jia, Y. (2018). MicroRNA-99b promotes *Helicobacter* pylori-induced autophagy and suppresses carcinogenesis by targeting mTOR. *Oncol. Lett*. 16, 5355–5360. doi: 10.3892/ol.2018.9269

Yang, L., Long, Y., Li, C., Cao, L., Gan, H., and Huang, K. (2015). Genome-wide analysis of long noncoding RNA profile in human gastric epithelial cell response to *Helicobacter* pylori. *Jpn. J. Infect. Dis*. 68, 63–66. doi: 10.7883/yoken.JJID.2014.149

Yang, T., Zeng, H., Chen, W., Zheng, R., Zhang, Y., Li, Z., et al. (2016). *Helicobacter* pylori infection, H19 and LINC00152 expression in serum and risk of gastric cancer in a Chinese population. *Cancer Epidemiol*. 44, 147–153. doi: 10.1016/j.canep.2016.08.015

Yang, X., Si, R., Liang, Y., Ma, B. Q., Jiang, Z., Wang, B., et al. (2016). Mir-30d increases intracellular survival of *Helicobacter* pylori through inhibition of autophagy pathway. *World J. Gastroenterol.* 22, 3978–3991. doi: 10.3748/wjg.v22.i15.3978

Yang, Y., Li, X., Du, J., Yin, Y., and Li, Y. (2018). Involvement of microRNAs-MMPs-E-cadherin in the migration and invasion of gastric cancer cells infected with *Helicobacter* pylori. *Exp. Cell. Res.* 367, 196–204. doi: 10.1016/j.yexcr.2018.03.036

Yao, Y., Jiang, Q., Jiang, L., Wu, J., Zhang, Q., Wang, J., et al. (2016). Lnc-SGK1 induced by *Helicobacter* pylori infection and highsalt diet promote Th2 and Th17 differentiation in human gastric cancer by SGK1/Jun B signaling. *Oncotarget* 7, 20549–20560. doi: 10.18632/oncotarget.7823

Ye, F., Tang, C., Shi, W., Qian, J., Xiao, S., Gu, M., et al. (2015). A MDM2-dependent positive-feedback loop is involved in inhibition of miR-375 and miR-106b induced by *Helicobacter* pylori lipopolysaccharide. *Int. J. Cancer* 136, 2120–2131. doi: 10.1002/ijc.29268

Yoon, J. H., Choi, J., Choi, W. S., Ashktorab, H., Smoot, D. T., Nam, S. W., et al. (2013). GKN1-miR-185-DNMT1 axis suppresses gastric carcinogenesis through regulation of epigenetic alteration and cell cycle. *Clin. Cancer Res.* 19, 4599–4610. doi: 10.1158/1078-0432.CCR-12-3675

Zabaglia, L. M., Sallas, M. L., Santos, M., Orcini, W. A., Peruquetti, R. L., Constantino, D. H., et al. (2018). Expression of miRNA-146a, miRNA-155, IL-2, and TNF-α in inflammatory response to *Helicobacter* pylori infection associated with cancer progression. *Ann. Hum. Genet*. 82, 135–142. doi: 10.1111/ahg.12234

Zhang, C., Zhi, W., Lu, H., Samanta, D., Chen, I., and Gabrielson, E. (2016). Hypoxia-inducible factors regulate pluripotency factor expression

by ZNF217- and ALKBH5-mediated modulation of RNA methylation in breast cancer cells. *Oncotarget* 7, 64527–64542. doi: 10.18632/oncotarget.11743

Zhang, H., Ahearn, T. U., Lecarpentier, J., Barnes, D., Beesley, J., and Qi, G. (2010). Genome-wide association study identifies five new breast cancer susceptibility loci. *Nat. Genet*. 42, 504–507. doi: 10.1038/s41588-020-0609-2

Zhang, J., Wei, J., Wang, Z., Feng, F., Wei, Z., Hou, X., et al. (2020). Transcriptome hallmarks in *Helicobacter* pylori infection influence gastric cancer and MALT lymphoma. *Epigenomics* 12, 661–671. doi: 10.2217/epi-2019-0152

Zhang, X., Yao, J., Guo, K., Huang, H., Huai, S., Ye, R., et al. (2017). The functional mechanism of miR-125b in gastric cancer and its effect on the chemosensitivity of cisplatin. *Oncotarget* 9, 2105–2119. doi: 10.18632/oncotarget.23249

Zhang, Y., Noto, J. M., Hammond, C. E., Barth, J. L., Argraves, W. S., Backert, S., et al. (2014). *Helicobacter* pylori-induced posttranscriptional regulation of H-K-ATPase alpha-subunit gene expression by miRNA. *Am. J. Physiol. Gastrointest. Liver Physio*l. 306, G606–G613. doi: 10.1152/ajpgi.00333.2013

Zhang, Z., Li, Z., Gao, C., Chen, P., Chen, J., Liu, W., et al. (2008). MiR-21 plays a pivotal role in gastric cancer pathogenesis and progression. *Lab. Invest.* 88, 1358–1366. doi: 10.1038/labinvest.2008.94

Zhao, J., Nie, Y., Wang, H., and Lin, Y. (2016). MiR-181a suppresses autophagy and sensitizes gastric cancer cells to cisplatin. *Gene* 576, 828–833. doi: 10.1016/j.gene.2015.11.013

Zhao, K., Zhang, R., Li, T., and Xiong, Z. (2019). Functional variants of lncRNA LINC00673 and gastric cancer susceptibility: a case-control study in a Chinese population. *Cancer Manag. Res*. 11, 3861–3868. doi: 10.2147/CMAR.S187011

Zhao, X., Lu, Y., Guo, H., Xie, H., He, J., Shen, G., et al. (2015). MicroRNA-7/NF-kappaB signaling regulatory feedback circuit regulates gastric carcinogenesis. *J. Cell Biol.* 210, 613–627. doi: 10.1083/jcb.201501073

Zheng, P., Chen, L., Yuan, X., Luo, Q., Liu, Y., Xie, G., et al. (2017). Exosomal transfer of tumor-associated macrophage-derived miR-21 confers cisplatin resistance in gastric cancer cells. *J. Exp. Clin. Cancer Res.* 1336:53. doi: 10.1186/s13046-017-0528-y

Zhong, F., Zhu, M., Gao, K., Xu, P., Yang, H., and Hu, D. (2018). Low expression of the long non-coding RNA NR_026827 in gastric cancer. *Am. J. Transl. Res.* 10, 2706–2711.

Zhou, X., Chen, H., Zhu, L., Hao, B., Zhang, W., Hua, J., et al. (2016). *Helicobacter* pylori infection related long noncoding RNA (lncRNA) AF147447 inhibits gastric cancer proliferation and invasion by targeting MUC2 and up-regulating miR-34c. *Oncotarget* 7, 82770–82782. doi: 10.18632/oncotarget.13165

Zhou, X., Jin, W., Jia, H., Yan, J., and Zhang, G. (2015a). MiR-223 promotes the cisplatin resistance of human gastric cancer cells via regulating cell cycle by targeting FBXW7. *J. Exp. Clin. Cancer Res*. 34:28. doi: 10.1186/s13046-015-0145-6

Zhou, X., Li, L., Su, J., and Zhang, G. (2014a). Decreased miR-204 in H. pylori-associated gastric cancer promotes cancer cell proliferation and invasion by targeting SOX4. *PLoS One* 9:e101457. doi: 10.1371/journal.pone.0101457

Zhou, X., Su, J., Zhu, L., and Zhang, G. (2014b). *Helicobacter* pylori modulates cisplatin sensitivity in gastric cancer by down-regulating miR-141 expression. *Helicobacter* 19, 174–181. doi: 10.1111/hel.12120

Zhou, X., Xia, Y., Li, L., and Zhang, G. (2015b). MiR-101 inhibits cell growth and tumorigenesis of *Helicobacter* pylori related gastric cancer by repression of SOCS2. *Cancer Biol. Ther*. 16, 160–169. doi: 10.4161/15384047.2014.987523

Zhu, H., Wang, Q., Yao, Y., Fang, J., Sun, F., Ni, Y., et al. (2015). Microarray analysis of Long non-coding RNA expression profiles in human gastric cells and tissues with *Helicobacter* pylori Infection. *BMC Med. Genomics* 8:84. doi: 10.1186/s12920-015-0159-0

Zhu, X., Tian, X., Yu, C., Shen, C., Yan, T., Hong, J., et al. (2016). A long non-coding RNA signature to improve prognosis prediction of gastric cancer. *Mol. Cancer* 15:60. doi: 10.1016/j.gastrohep.2020.01.016

Zhu, Y., Liu, L., Hu, L., Dong, W., Zhang, M., Liu, Y., et al. (2019). Effect of Celastrus orbiculatus in inhibiting *Helicobacter* pylori induced inflammatory response by regulating epithelial mesenchymal transition and targeting miR-21/PDCD4 signaling pathway in gastric epithelial cells. *BMC Complement. Altern. Med*. 19:91. doi: 10.1186/s12906-019-2504-x

Zou, M., Wang, F., Jiang, A., Xia, A., Kong, S., Gong, C., et al. (2017). MicroRNA-3178 ameliorates inflammation and gastric carcinogenesis promoted by *Helicobacter* pylori new toxin, Tip-alpha, by targeting TRAF3. *Helicobacter* 22:27493095.

Conflict of Interest: The authors declare that the research was conducted in the absence of any commercial or financial relationships that could be construed as a potential conflict of interest.

frontiers in Molecular Biosciences

ORIGINAL RESEARCH
published: 21 May 2021
doi: 10.3389/fmolb.2021.676291

Development and Validation of a 7-Gene Prognostic Signature to Improve Survival Prediction in Pancreatic Ductal Adenocarcinoma

Zengyu Feng[1,2,3†], *Hao Qian*[1,2†], *Kexian Li*[1,2], *Jianyao Lou*[3], *Yulian Wu*[3*] and *Chenghong Peng*[1,2*]

[1]Department of General Surgery, Pancreatic Disease Center, Ruijin Hospital, Shanghai Jiao Tong University School of Medicine, Shanghai, China, [2]Research Institute of Pancreatic Diseases, Shanghai Jiao Tong University School of Medicine, Shanghai, China, [3]Department of General Surgery, The Second Affiliated Hospital, School of Medicine, Zhejiang University, Hangzhou, China

OPEN ACCESS

Edited by:
Na Luo,
Nankai University, China

Reviewed by:
Xianxiu Qiu,
Guangdong Medical University, China
Wenzhi Shen,
Jining Medical University, China

***Correspondence:**
Yulian Wu
yulianwu@zju.edu.cn
Chenghong Peng
chhpeng@yeah.net

[†]These authors have contributed equally to this work

Specialty section:
This article was submitted to Molecular Diagnostics and Therapeutics, a section of the journal Frontiers in Molecular Biosciences

Received: 05 March 2021
Accepted: 06 May 2021
Published: 21 May 2021

Citation:
Feng Z, Qian H, Li K, Lou J, Wu Y and Peng C (2021) Development and Validation of a 7-Gene Prognostic Signature to Improve Survival Prediction in Pancreatic Ductal Adenocarcinoma. Front. Mol. Biosci. 8:676291. doi: 10.3389/fmolb.2021.676291

Background: Previous prognostic signatures of pancreatic ductal adenocarcinoma (PDAC) are mainly constructed to predict the overall survival (OS), and their predictive accuracy needs to be improved. Gene signatures that efficaciously predict both OS and disease-free survival (DFS) are of great clinical significance but are rarely reported.

Methods: Univariate Cox regression analysis was adopted to screen common genes that were significantly associated with both OS and DFS in three independent cohorts. Multivariate Cox regression analysis was subsequently performed on the identified genes to determine an optimal gene signature in the MTAB-6134 training cohort. The Kaplan–Meier (K-M), calibration, and receiver operating characteristic (ROC) curves were employed to assess the predictive accuracy. Biological process and pathway enrichment analyses were conducted to elucidate the biological role of this signature.

Results: Multivariate Cox regression analysis determined a 7-gene signature that contained ASPH, DDX10, NR0B2, BLOC1S3, FAM83A, SLAMF6, and PPM1H. The signature had the ability to stratify PDAC patients with different OS and DFS, both in the training and validation cohorts. ROC curves confirmed the moderate predictive accuracy of this signature. Mechanically, the signature was related to multiple cancer-related pathways.

Conclusion: A novel OS and DFS prediction model was constructed in PDAC with multi-cohort and cross-platform compatibility. This signature might foster individualized therapy and appropriate management of PDAC patients.

Keywords: pancreatic ductal adenocarcinoma, risk score, overall survival, disease-free survival, prognostic signature, immune cell infiltration

Abbreviations: AUC, area under the curve; BP, biological process; DFS, disease-free survival; GO, Gene Ontology; ICGC, International Cancer Genome Consortium; KEGG, Kyoto Encyclopedia of Genes and Genomes; K-M, Kaplan–Meier; OS, overall survival; PDAC, pancreatic ductal adenocarcinoma; ROC, receiver operating characteristic; TCGA, the Cancer Genome Atlas; TNM, tumor, node, and metastasis.

INTRODUCTION

Pancreatic ductal adenocarcinoma is an insidious and aggressive malignancy with a 5-year survival rate not exceeding 10% (Siegel et al., 2021; Garrido-Laguna and Hidalgo, 2015). Unfortunately, its incidence and mortality rates continue to increase, especially among women and people aged 50 years and over (Huang et al., 2021). Owing to the deep-seated location of the pancreas and the lack of available screening approaches of PDAC, most patients are diagnosed at an advanced, unresectable stage (Ducreux et al., 2015; Gillen et al., 2010), leading to a dismal prognosis (De La Cruz et al., 2014). Even after R0 resection, the most effective treatment for cure (Kamisawa et al., 2016), most patients will develop local recurrence or distant metastases despite adjuvant treatments, impairing a dramatic improvement of patient outcomes by surgical resection (Ghaneh et al., 2019; Strobel et al., 2017; Tummers et al., 2019). Therefore, novel identification of reliable biomarkers and predictive models is of significant need for PDAC patients, which will help to guide appropriate therapy and tailor postoperative surveillance in clinical management.

Accurate prediction of patient prognosis in PDAC has been the subject of many studies. Traditional clinicopathological features, including but not limited to tumor size (Ansari et al., 2017), resection margin status (Maeda et al., 2020), histological grade (Macías et al., 2018), and lymph node metastasis (Sho et al., 2015), have been investigated in previous studies. Recently, with the remarkable progress in bioinformatics and high-throughput sequencing technology, gene expression signatures considering the genetic and genomic differences of patients have emerged as a practical tool for survival assessment in human cancers (Yu et al., 2019; Supplitt et al., 2021; Doultsinos and Mills, 2021; Ahluwalia et al., 2021). In the context of PDAC, multiple prognostic gene models have been established with robust predictive performance (Luo et al., 2021; Gu et al., 2021; Xu et al., 2021a). However, most of these models are constructed to predict the overall survival (OS), and few predict disease-free survival (DFS). Given that postoperative recurrence is a feature of PDAC and it results in a poor prognosis, DFS prediction is of equivalent significance. Thus, development of a robust signature for both OS and DFS prediction is a laudable attempt.

To the best of our knowledge, only two previous gene signatures have the capability to predict both OS and DFS (Kim et al., 2019; Feng et al., 2020), and their predictive accuracy remains to be improved. In the current study, we identified a credible 7-gene signature for both OS and DFS prediction with moderate accuracy and cross-cohort compatibility. The area under the curve (AUC) values of this signature for survival prediction were no less than 0.7 in three independent cohorts. The relationship between gene signature, immune cell infiltration, and therapeutic effects was also investigated in this study.

MATERIALS AND METHODS

PDAC Cohorts

Three public PDAC cohorts with both clinical data and gene expression data including MTAB-6134 (N = 288), PACA-CA (N = 181), and TCGA (N = 141) were adopted in this study. Among them, the MTAB-6134 cohort was used as the training set, while PACA-CA and TCGA cohorts were used for external validation. Information about OS and DFS events and time was available from all of these three cohorts. Expression profiles and clinical data of MTAB-6134 cohort were downloaded from the ArrayExpress database (https://www.ebi.ac.uk/arrayexpress/). Normalized RNA-sequencing (RNA-seq) data and clinical data of the PACA-CA cohort were retrieved and downloaded from the International *Cancer* Genome Consortium (ICGC, https://icgc.org/) database. Processed RNA-seq data and clinical information of the TCGA cohort were obtained from the TCGA hub at UCSC Xena (https://tcga.xenahubs.net). Samples with an OS or DFS less than one month were excluded for survival analyses. Information regarding chemotherapy was provided in PACA-CA and TCGA cohorts. Patients whose response to chemotherapy is "clinical progressive disease" or "stable disease" were defined as chemotherapy-resistant, while patients whose response to chemotherapy is "complete response" or "partial response" were defined as chemotherapy-sensitive. In addition, MTAB-6690, a cohort that contained gene expression profiles of 108 PDAC samples and 70 normal samples, was downloaded from the ArrayExpress database.

Construction of the 7-Gene Signature

To identify candidate genes for model construction, we initially applied univariate Cox regression analysis to screen genes associated with both OS and DFS through the Venn diagram (https://bioinfogp.cnb.csic.es/tools/venny/) in each cohort. Consistently, survival-related genes in these three cohorts were identified and subsequently submitted to multivariate Cox regression analysis using OS events and time in order to determine an optimal signature in the training MTAB-6134 cohort. Based on the gene expression values and corresponding coefficients, the risk score of each sample was calculated as follows: risk score = (coefficient 1 * expression value of gene 1) + (coefficient 2 * expression value of gene 2) + ... + (coefficient N * expression value of gene N).

Prognostic Validation of the 7-Gene Signature

Patients in each cohort were divided into low- and high-risk groups based on the medium value of the risk score. The Kaplan–Meier (K-M) survival curves and calibration curves were used to evaluate the predictive performance of this signature. Receiver operating characteristic (ROC) curves were utilized to compare the predictive accuracy of the gene signature and clinical features.

Estimation of Tumor Immune Infiltrates

The deconvolution algorithm CIBERSORT (Chen et al., 2018) was used to estimate the relative proportions of 22 different immune cell infiltrates. The number of permutations was set to 1,000, and a p-value < 0.05 was considered as successful.

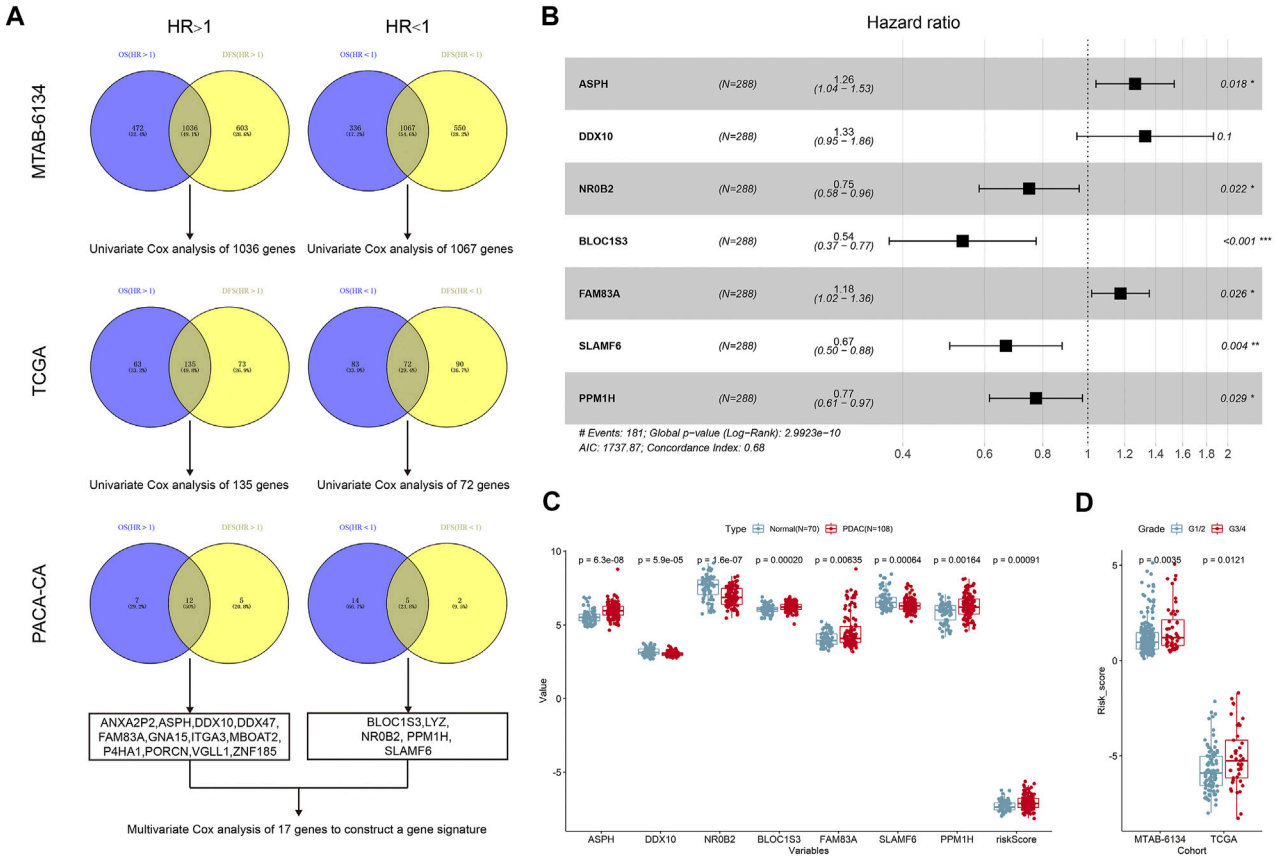

FIGURE 1 | Construction of the 7-gene signature. **(A)** The research workflow of model construction. **(B)** Forest plot of the seven genes. **(C)** Expression values of seven selected genes and risk scores in normal samples and PDAC samples based on the microarray data of MTAB-6690. **(D)** Distribution of risk scores in different histological grades in MTAB-6134 and TCGA samples.

Functional Annotation and Pathway Enrichment of the 7-Gene Signature

To shed light on high-risk score–resulted unfavorable prognosis, we performed the Pearson correlation analysis to identify correlated genes with risk scores in the MTAB-6134 training cohort. According to the correlation coefficients, the top 1,000 positively and negatively correlated genes were submitted to Gene Ontology-Biological Process (GO-BP) analysis and the Kyoto Encyclopedia of Genes and Genomes (KEGG) pathway enrichment analysis on the DAVID online Web site (Huang et al., 2007), respectively.

Statistical Analysis

Statistical analysis and graphical work were finished in the R environment (version 3.5.2). Cox regression analyses were performed by the "survival" package and visualized by the "forestplot" package. K-M survival curves with log-rank tests were plotted by the "survminer" package. The ROC curves were depicted by the "survivalROC" package. Boxplots were generated from the "ggpubr" package. Calibration curves were derived from the "rms" package. $p < 0.05$ was considered significant.

RESULTS

Construction of the 7-Gene Signature

The research workflow of model construction is illustrated in **Figure 1A**. Univariate Cox analysis and Venn diagram identified 1,036 risky genes (hazard ratio >1) and 1,067 protective genes (hazard ratio <1) that were associated with both OS and DFS in the MTAB-6134 training cohort. These genes were further screened in the PACA-CA cohort and TCGA cohort by the same method, respectively. Eventually, 12 credible risky indicators and five protective indicators were identified. These 17 genes were incorporated in the stepwise multivariate Cox hazard ratio regression to select the best model for predicting OS of PDAC patients in the MTAB-6134 cohort. Multivariate Cox analysis resulted in an optimal 7-gene signature containing ASPH, DDX10, NR0B2, BLOC1S3, FAM83A, SLAMF6, and PPM1H (**Figure 1B**). The PPI (protein–protein interaction) network was constructed using the STRING database (http://www.string-db.org/) to investigate the interactions of these seven genes. As illustrated in **Supplementary Figure S1**, there is no interaction between these proteins. According to the expression values and corresponding coefficients of the seven genes derived

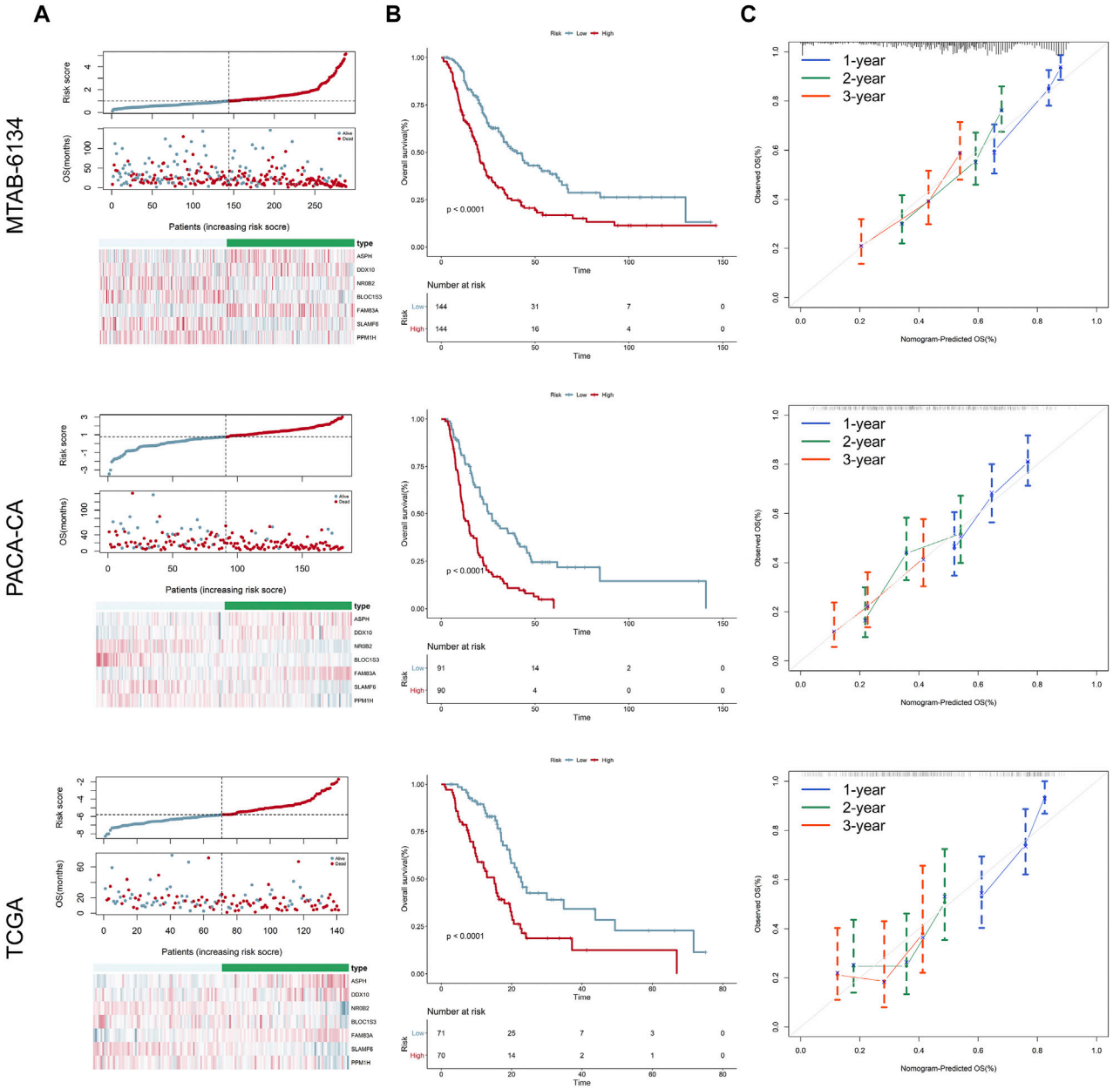

FIGURE 2 | Prognostic performance of the 7-gene signature for OS prediction. **(A)** From top to bottom are the risk score distribution, survival status distribution, and heatmap of seven genes in three independent cohorts, respectively. **(B)** K-M curves estimating the OS difference between low- and high-risk groups in three independent cohorts, respectively. **(C)** Calibration curves of the signature in three independent cohorts. Calibration curves represent the relationship between observed (the data markers represent the mean, and the error bars represent the 95% CI) and predicted (gray line) OS using the 7-gene risk score.

from multivariate Cox regression analysis, we constructed a risk-score formula: risk score = 0.234165*expression value of ASPH +0.284159*expression value of DDX10-0.29051*expression value of NR0B2-0.61974*expression value of BLOC1S3 + 0. The 161992*expression value of FAM83A-0.40561*expression value of SLAMF6-0.25676*expression value of PPM1H. The risk scores of PDAC patients were significantly higher than those of normal patients, indicating diagnostic potential of the signature (**Figure 1C**). Moreover, the risk scores were markedly elevated in patients with a high histological grade in MTAB-6134 and TCGA cohorts, suggesting that the 7-gene signature was associated with tumor malignancy (**Figure 1D**).

Prognostic Performance of the 7-Gene Signature for OS Prediction

Distribution of the risk scores, survival status, and expression level of the seven genes in three independent cohorts is

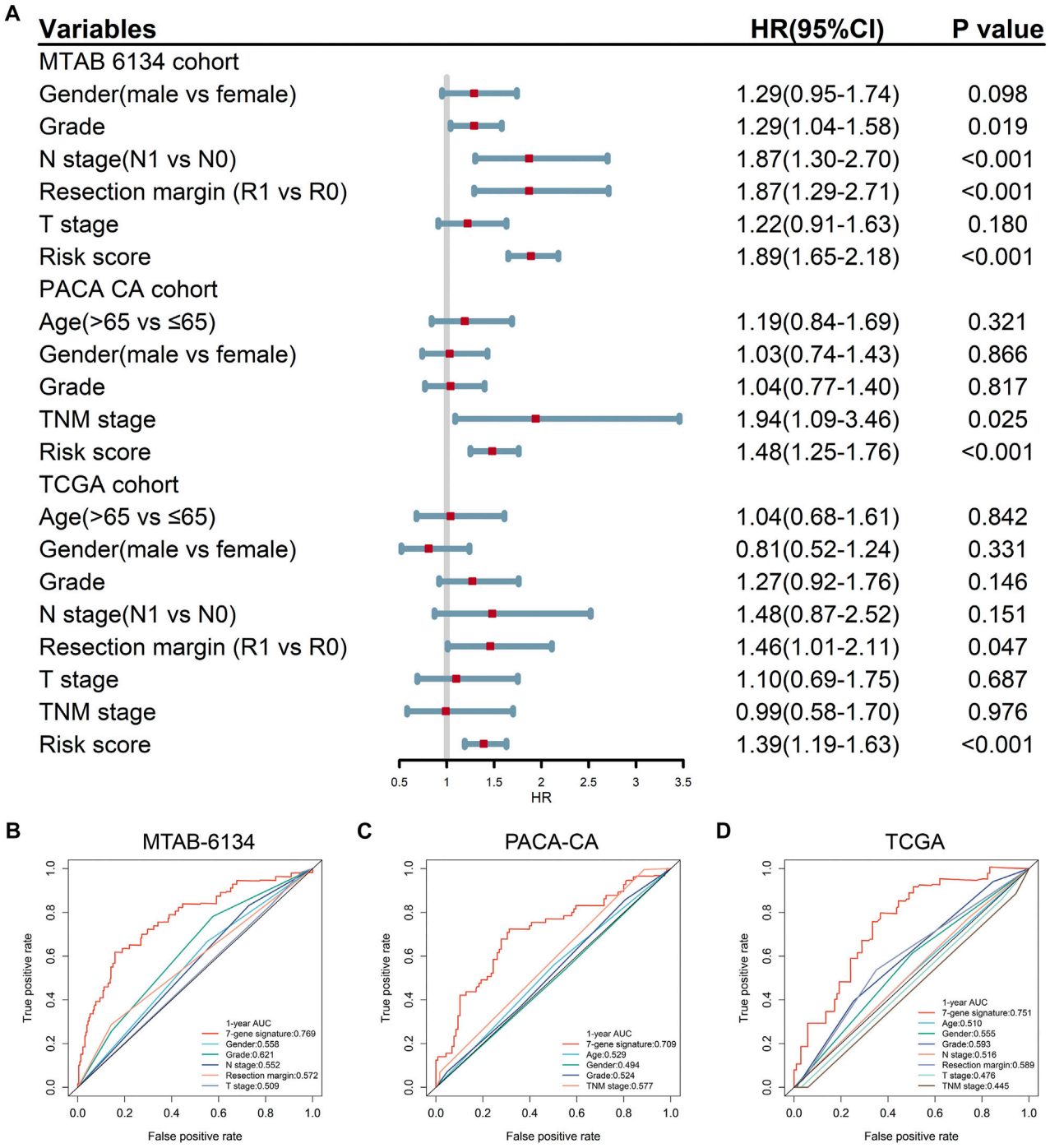

FIGURE 3 | Predictive accuracy of the 7-gene signature and clinical predictors for OS. **(A)** Univariate Cox regression analysis of the gene signature and clinical features for OS. **(B–D)** ROC curves of the risk signature and clinical features for the 1-year OS prediction in MTAB-6134 **(B)**, PACA-CA **(C)**, and TCGA **(D)** cohorts, respectively.

illustrated in **Figure 2A**. The results showed that patients in the high-risk group had higher mortality rates. K-M survival curves demonstrated that patients in the low-risk group had a significantly longer OS in three independent cohorts (**Figure 2B**). Calibration curves suggested that the predicted survival probabilities by the signature were in good agreement with the observed survival probabilities (**Figure 2C**).

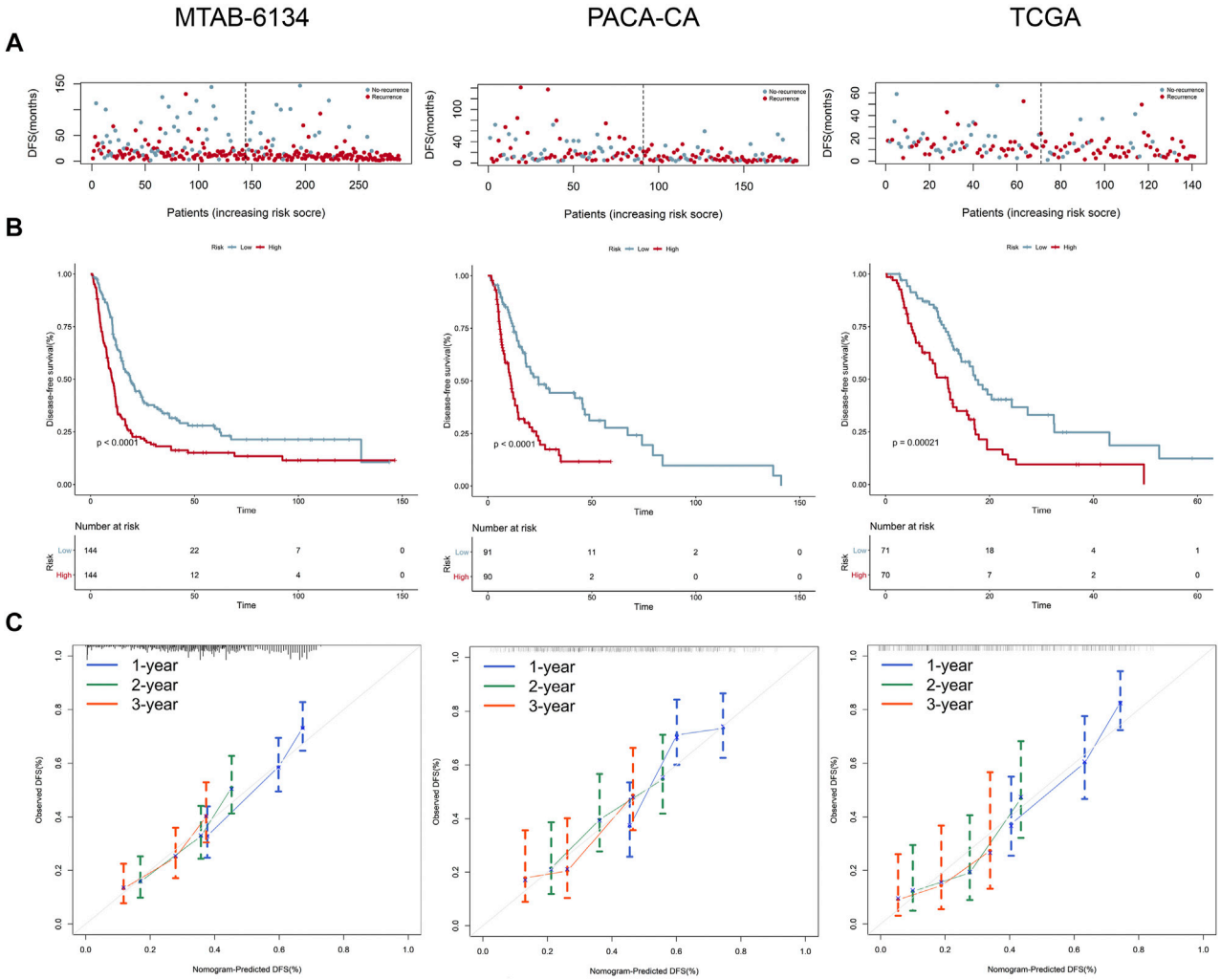

FIGURE 4 | Prognostic performance of the 7-gene signature for the DFS prediction. **(A–C)** From top to bottom are patients' survival overview, K-M survival curve, and calibration curve in MTAB-6134 **(A)**, PACA-CA **(B),** and TCGA **(C)** cohorts, respectively. Calibration curves represent the relationship between observed (the data markers represent the mean, and the error bars represent the 95% CI) and predicted (gray line) DFS using the 7-gene risk score.

Predictive Accuracy of the 7-Gene Signature and Clinical Predators for OS

Univariate Cox regression analysis proved that the proposed gene signature and several clinical features were independent risk factors for OS in three cohorts (**Figure 3A**). In order to clarify whether our signature could provide improved survival prediction, we conducted ROC analyses. As shown in **Figures 3B–D**, the AUC values of this signature were 0.769, 0.709, and 0.751 in MTAB-6134, PACA-CA, and TCGA cohorts, respectively, which were higher than those of clinical predictors. These findings demonstrated that the 7-gene signature outperformed clinical predictors in predicting OS.

Prognostic Performance of the 7-Gene Signature for DFS Prediction

Figure 4A shows the distribution of the DFS event and time in MTAB-6134, PACA-CA, and TCGA cohorts. The results illustrated that patients in the low-risk group had remarkably lower recurrence rates and a significantly longer DFS. K-M survival curves indicated that the high-risk group had a significantly shorter DFS than the low-risk group in all of the three cohorts ($p < 0.05$, **Figure 4B**). Calibration curves indicated that the predicted DFS was in good accordance with the observed DFS in three independent cohorts (**Figure 4C**).

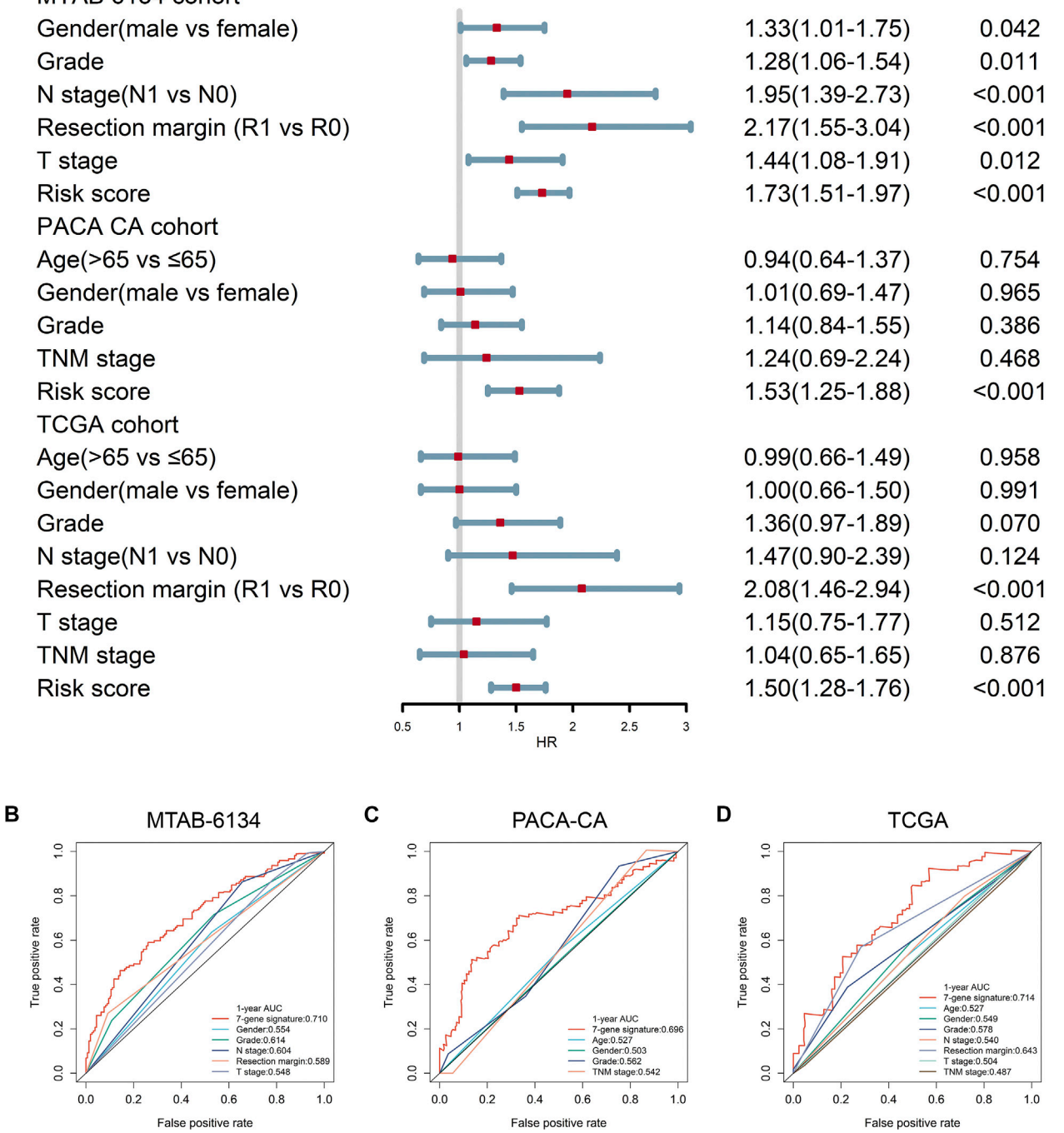

FIGURE 5 | Predictive accuracy of the 7-gene signature and clinical predictors for DFS. **(A)** Univariate Cox regression analysis of gene signature and clinical indicators for DFS. **(B–D)** ROC curves of the risk signature and clinical indicators for the 1-year DFS prediction in MTAB-6134 **(B)**, PACA-CA **(C)**, and TCGA **(D)** cohorts, respectively.

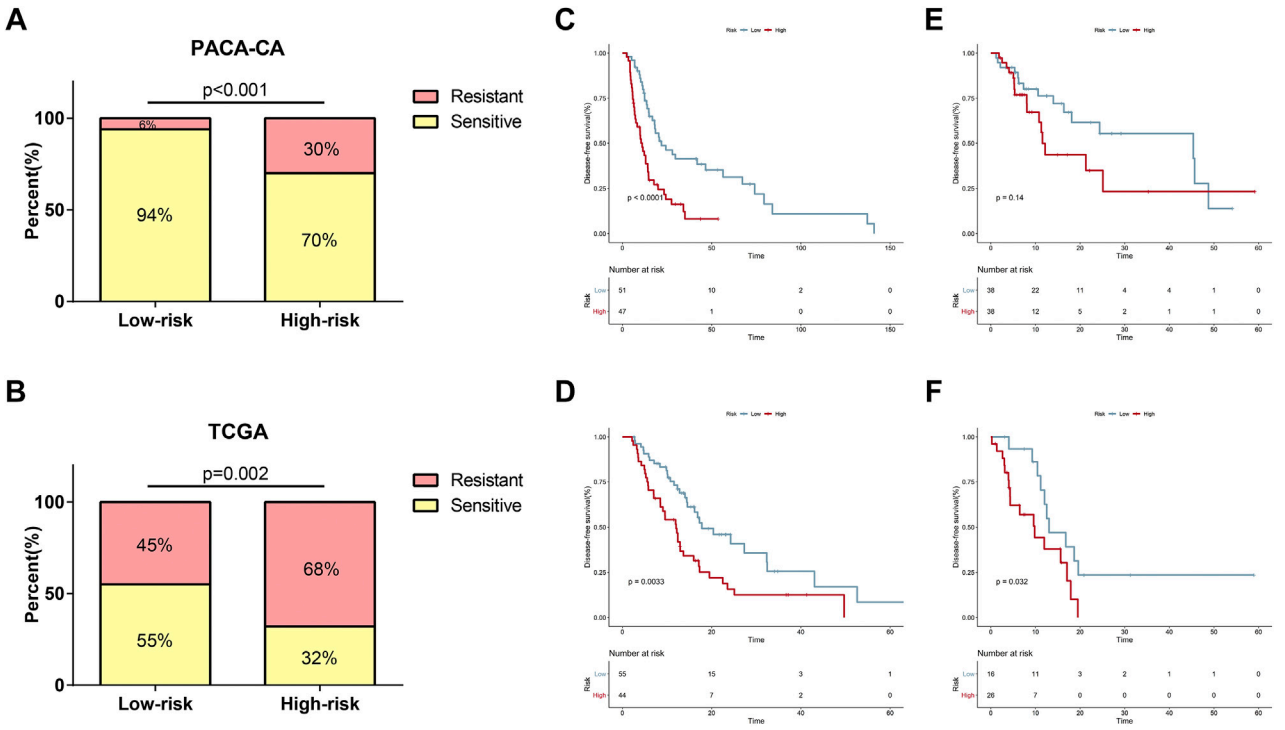

FIGURE 6 | Relationship between the risk signature and response to adjuvant chemotherapy. **(A,B)** Relationship of risk score and chemotherapy sensitivity in the PACA-CA cohort **(A)** and TCGA cohort **(B)**. **(C,D)** K-M curves for the risk signature in patients receiving adjuvant chemotherapy in the PACA-CA cohort **(C)** and TCGA cohort **(D)**. **(E,F)** K-M curves for the risk signature in patients not receiving adjuvant chemotherapy in the PACA-CA cohort **(E)** and TCGA cohort **(F)**.

Predictive Accuracy of the 7-Gene Signature and Clinical Predictors for DFS

Univariate Cox regression analysis confirmed that the 7-gene signature and multiple clinical indicators were closely related to DFS in three cohorts (**Figure 5A**). ROC curves showed that the AUC values of this signature for DFS prediction were 0.710, 0.696, and 0.714 in MTAB-6134, PACA-CA, and TCGA cohorts, respectively, which were superior to clinical predictors (**Figures 5B–D**).

Relationship Between the 7-Gene Signature and Response to Adjuvant Chemotherapy

Currently, adjuvant chemotherapy is administered empirically, and the individual survival benefit of this approach is still questionable in PDAC (Kleeff et al., 2016). Thus, we wondered whether the 7-gene signature could precisely predict chemotherapy sensitivity and provide references for clinical practice. As shown in **Figure 6A**, patients in the low-risk group had significantly higher response rates to adjuvant chemotherapy than patients in the high-risk group in the PACA-CA cohort (94 vs 70%, $p < 0.001$). A similar trend was seen in the TCGA cohort (55 vs 32%, $p = 0.001$, **Figure 6B**). In patients who received adjuvant chemotherapy, the proposed signature could efficaciously capture the DFS differences between low-risk and high-risk groups in both cohorts (**Figures 6C,D**). However, the predictive power of the model was weakened when applied to patients who had not received adjuvant chemotherapy. As shown in **Figure 6E**, DFS difference between high-risk and low-risk groups of this subset of patients was not significant in the PACA-CA cohort ($p = 0.14$). In the TCGA cohort, DFS difference was also not strongly trustworthy ($p = 0.034$, **Figure 6F**).

Relationship Between the 7-Gene Signature and Immune Cell Infiltration

The level of immune cell infiltration is closely related to the clinical efficiency of immunotherapy and the prognosis of PDAC patients (Zheng et al., 2013). Therefore, we explored the relationship between this signature and immune cell infiltration and inquired into the potential of our signature as a reliable predictor of immunotherapy response. In cases of the MTAB-6134 cohort, the abundance of macrophage M0, macrophage M2, and activated NK cells was significantly elevated in the high-risk patients, while $CD8^+$ T cell infiltration was remarkably decreased in the high-risk patients (**Figure 7A**). In the case of the TCGA cohort, the abundance of regulatory T cells, activated NK cells, and macrophage M0 was significantly elevated in the high-risk patients, while naïve B cells, $CD8^+$ T cell, naïve $CD4^+$ T cells, activated memory $CD4^+$ T cells, and monocyte infiltration were remarkably decreased in the high-risk patients (**Figure 7B**).

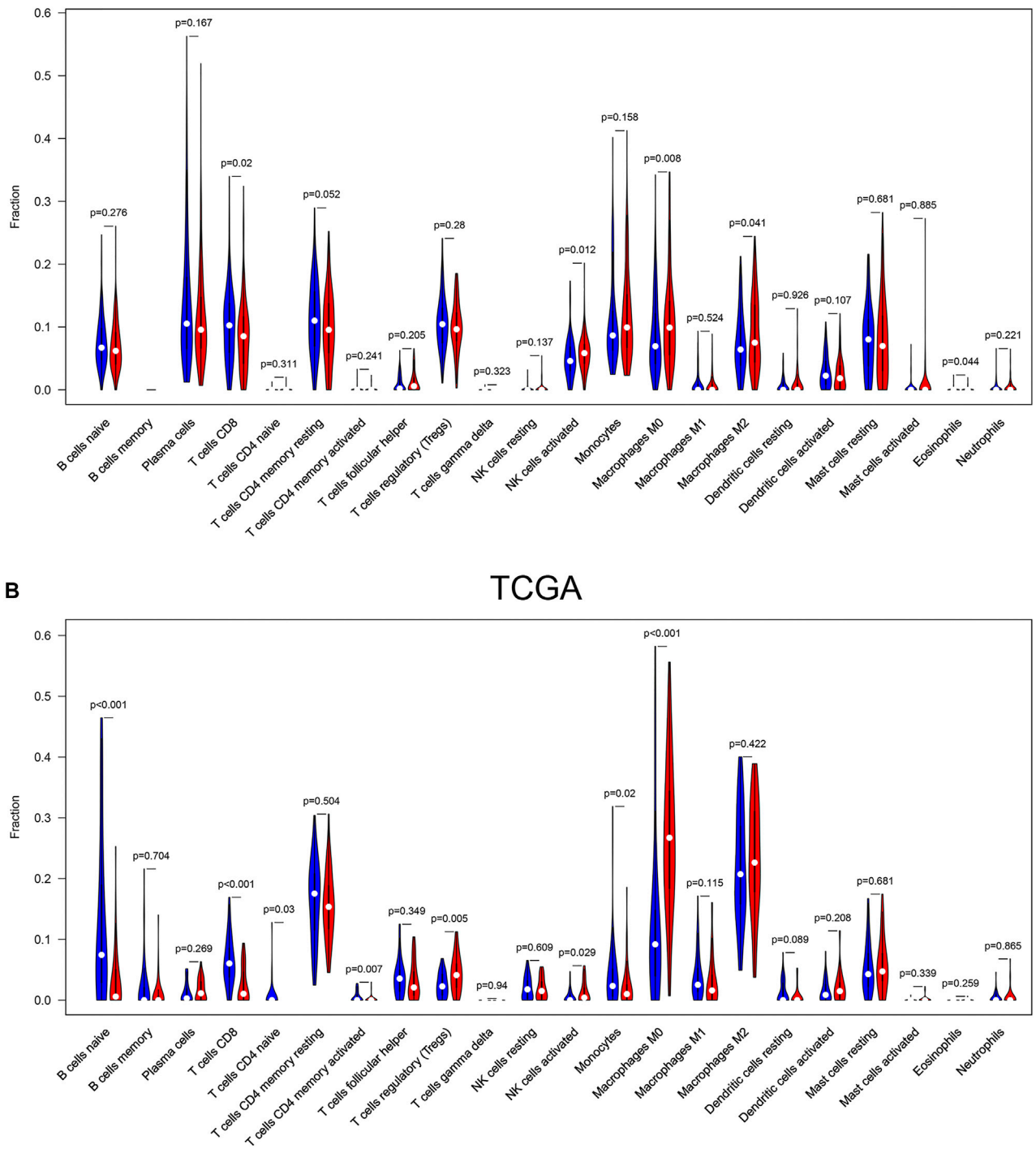

FIGURE 7 | Correlations between the risk signature and different immune cell infiltration in the MTAB-6134 cohort **(A)** and TCGA cohort **(B)**. The red color represented high-risk group, while the blue color represented low-risk group.

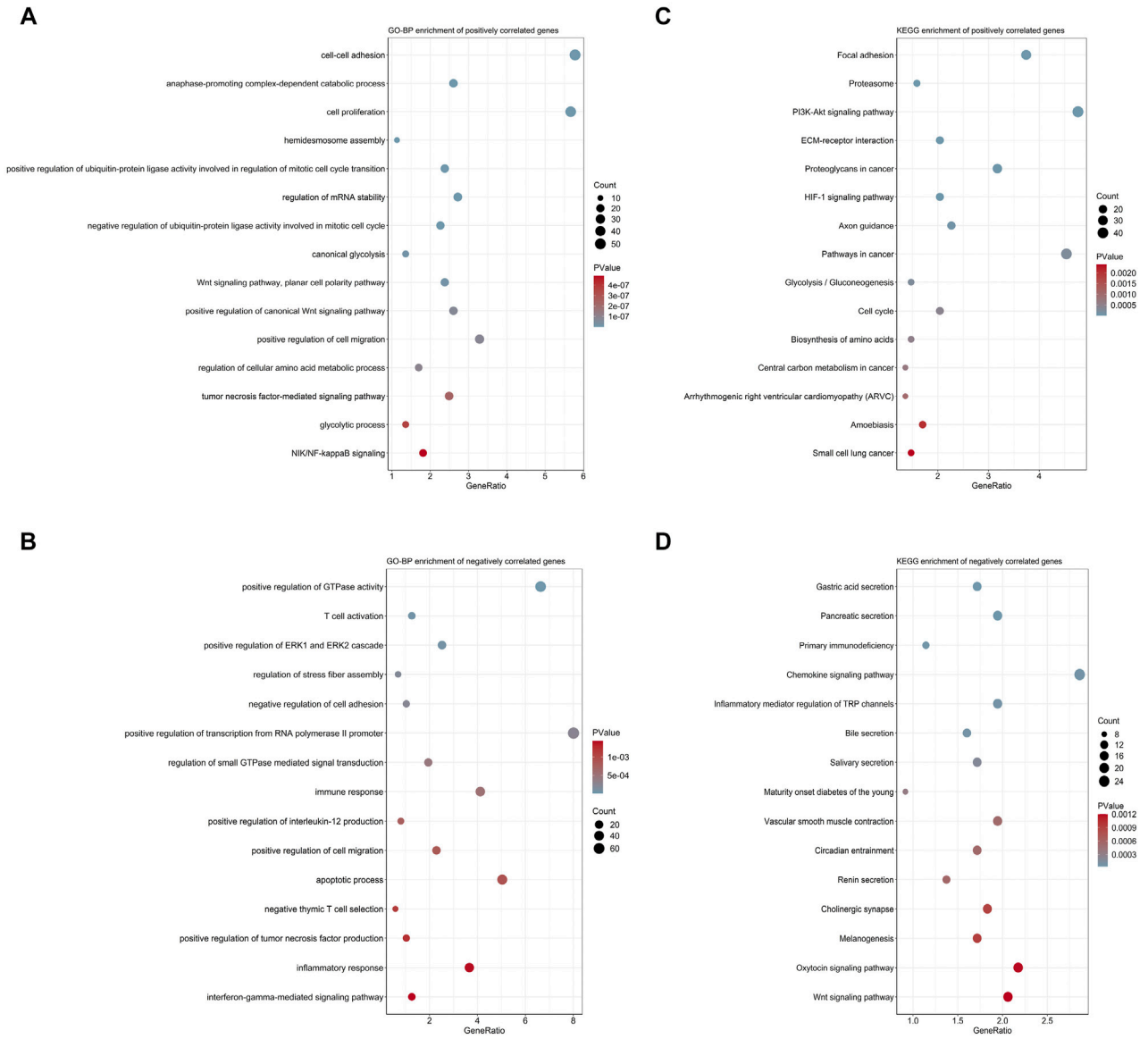

FIGURE 8 | Biological process and pathway analyses of the 7-gene signature. **(A)** Top 15 GO-BP terms of genes positively correlated with risk scores. **(B)** Top 15 GO-BP terms of genes negatively correlated with risk scores. **(C)** Top 15 KEGG terms of genes positively correlated with risk scores. **(D)** Top 15 KEGG terms of genes negatively correlated with risk scores.

Biological Process and Pathway Analyses of the 7-Gene Signature

With the purpose to preliminarily illuminate how the risk signature affected patient prognosis, chemotherapeutic response, and immune cell infiltration, we performed functional annotation and pathway enrichment analyses on genes correlated with risk scores in the MTAB-6134 training cohort. For biological processes, positively correlated genes were primarily involved in cell proliferation, cell migration, and glycolysis (**Figure 8A**), while negatively correlated genes were mainly related to T-cell activation, immune response, and apoptotic process (**Figure 8B**). For KEGG pathway enrichment, genes with positive correlation were chiefly associated with the PI3K-AKT signaling pathway, HIF-1 signaling pathway, glycolysis, and cell cycle (**Figure 8C**), while genes with negative correlation were principally enriched in primary immunodeficiency and the chemokine signaling pathway (**Figure 8D**).

DISCUSSION

PDAC is a fatal disease featured with high molecular heterogeneity. The current prognosis assessment of PDAC patients is mainly dependent on the TNM (tumor, node, and metastasis) staging system. However, it is not adequate for individual survival prediction, especially in patients at the same stage

(van Roessel et al., 2018). This intra-stage discrepancy is due to tumor heterogeneity (Juiz et al., 2019). As cancer treatment has entered into the area of precision medicine, overcoming molecular heterogeneity has become a hallmark in cancer research (McGranahan and Swanton, 2017). Hence, prognostic gene signatures that translate the increased understanding of tumor genetic and genomic alternations into clinical application are urgently needed. In this study, we developed and validated a 7-gene signature with powerful prognostic performance for both OS and DFS prediction in PDAC. These seven genes were not overlapped to other prognostic gene signatures for PDAC.

In the process of signature construction, we initially identified and overlapped genes associated with OS and DFS in three independent large cohorts. A total of 17 genes were screened, and multivariate Cox regression analysis determined an optimal 7-gene signature for OS prediction in the MTAB-6134 training cohort. In both training and external validation cohorts, its robustness was supported by the reproducibility of moderate predictive accuracy with the AUC values close to or exceeding 0.7. The superior accuracy of the 7-gene signature in both OS prediction and DFS prediction suggested that it could serve as a supplement to the existing staging system for prognosis evaluation and treatment decision. In addition to its prognostic value, the clinical implications of the 7-gene signature were also compelling.

Surgical resection combined with adjuvant chemotherapy has been the standard therapy for resectable PDAC patients (Von Hoff et al., 2013). Unfortunately, the clinical benefit response rates of chemotherapy are extremely low (Burris et al., 1997), and nonresponsive patients may experience a variety of adverse effects, including asthenia and nausea (Phua et al., 2018). Developing predictive biomarkers that can maximize survival benefits and minimize side effects is of significant importance for PDAC patients (Oshi et al., 2020). In this study, we found that the risk score was significantly related to chemotherapeutic sensitivity. In the cases who had received adjuvant chemotherapy, this signature could efficiently distinguish patients with different DFS time. We hypothesize that the 7-gene score may have a role in fostering personalized oncology to exempt PDAC patients from unnecessary cytotoxicity and heavy financial burden brought by overtreatment.

Recently, immunotherapy has drastically increased patient survival in multiple cancers, but it failed to elicit responses in the vast majority of patients with PDAC (Leinwand and Miller, 2020). The decreased number of tumor-infiltrating lymphocytes in a tumor microenvironment likely allows anticancer immunity to be overwhelmed in PDAC (Vonderheide and Bayne, 2013). In this study, $CD8^+$ T cells were less infiltrated in high-risk patients, while M2 macrophages were more infiltrated in high-risk patients. $CD8^+$ T cells recognize and kill the cancer cell (Farhood et al., 2019) and indicate a favorable prognosis in PDAC (Zhang et al., 2018; Carstens et al., 2017). M2 macrophages facilitate PDAC progression (Kurahara et al., 2011) and indicate an unfavorable prognosis in PDAC (McGuigan et al., 2021; Hu et al., 2016). These findings confirmed the hazardous role of this signature and suggested that it could be used to predict the immunotherapy response.

To preliminarily clarify the underlying mechanism of the risk signature–mediated poor prognosis, we investigated the biological function of this signature. Multiple oncogenic pathways that were strongly associated with tumor progression, chemotherapeutic resistance, and immune cell infiltration were enriched. Biological processes and pathways, including but not limited to the PI3K-AKT signaling pathway, HIF-1 signaling pathway, and glycolysis, were all implicated in the regulation of malignant behavior and anticancer immunity (Xu et al., 2021b; Kobayashi et al., 2020; Sun and Meng, 2020; You et al., 2020). These findings could partly explain how the risk score affected patient survival and immune cell infiltration.

Despite improved OS prediction and DFS prediction compared with previous models (Kim et al., 2019; Feng et al., 2020), this study is still based on retrospective data and presents several limitations. First, the clinical utility of the 7-gene signature in PDAC management should be reviewed and determined in more prospective studies. Second, all cohorts used in the current study were relatively small, probably because of the low surgical resection rates of PDAC. Thus, it needs to be validated in larger cohorts. Third, further *in vivo* and *in vitro* experiments are needed in order to clarify the biological roles of seven genes in PDAC tumorigenesis. Finally, due to the lack of significant data, we are unable to adequately assess the relationship between seven gene expression and clinical feature. With the development of follow-up studies, we hope to supplement them in future studies.

In conclusion, we proposed a 7-gene signature that provided improved OS prediction and DFS prediction. The clinical implications and biological relevance of this signature have been completed explored. However, the predictive efficacy of this signature needs to be tested in more larger cohorts and prospective studies.

DATA AVAILABILITY STATEMENT

Publicly available datasets were analyzed in this study. These data can be found here: Expression profiles and clinical data of the MTAB-6134 cohort and MTAB-6690 cohort were downloaded from the ArrayExpress database (https://www.ebi.ac.uk/arrayexpress/). Normalized RNA-sequencing (RNA-seq) data and clinical data of the PACA-CA cohort were retrieved and downloaded from the International Cancer Genome Consortium (ICGC, https://icgc.org/) database. Processed RNA-seq data, clinical information, and somatic mutation data of the TCGA cohort were obtained from the TCGA hub at UCSC Xena (https://tcga.xenahubs.net).

AUTHOR CONTRIBUTIONS

ZF and CP designed the study and wrote the manuscript. ZF, KL, HQ, and JL participated in data analysis, discussion, and language editing. HQ corrected grammatical errors of this manuscript. YW reviewed the manuscript. All authors contributed to the article and approved the submitted version.

FUNDING

This work was supported by grants from the National Natural Science Foundation of China (81672325 and 81802316).

ACKNOWLEDGMENTS

We thank the National Natural Science Foundation of China for the grant funding. We acknowledge the contributions from ArrayExpress, UCSC, TCGA, and ICGC databases.

SUPPLEMENTARY MATERIAL

The Supplementary Material for this article can be found online at: https://www.frontiersin.org/articles/10.3389/fmolb.2021.676291/full#supplementary-material

REFERENCES

Ahluwalia, P., Kolhe, R., and Gahlay, G. K. (2021). The clinical relevance of gene expression based prognostic signatures in colorectal cancer. *Biochimica et Biophysica Acta (BBA) - Reviews on Cancer* 1875, 188513. doi:10.1016/j.bbcan.2021.188513

Ansari, D., Bauden, M., Bergström, S., Rylance, R., Marko-Varga, G., and Andersson, R. (2017). Relationship between tumour size and outcome in pancreatic ductal adenocarcinoma. *Br J Surg* 104, 600–607. doi:10.1002/bjs.10471

Burris, H. A., 3rd., Moore, M. J., Andersen, J., Green, M. R., Rothenberg, M. L., Modiano, M. R., et al. (1997). Improvements in survival and clinical benefit with gemcitabine as first-line therapy for patients with advanced pancreas cancer: a randomized trial. *Jco* 15, 2403–2413. doi:10.1200/jco.1997.15.6.2403

Carstens, J. L., Correa de Sampaio, P., Yang, D., Barua, S., Wang, H., Rao, A., et al. (2017). Spatial computation of intratumoral T cells correlates with survival of patients with pancreatic cancer. *Nat Commun* 8, 15095. doi:10.1038/ncomms15095

Chen, B., Khodadoust, M. S., Liu, C. L., Newman, A. M., and Alizadeh, A. A. (2018). Profiling Tumor Infiltrating Immune Cells with CIBERSORT. *Methods Mol Biol* 1711, 243–259. doi:10.1007/978-1-4939-7493-1_12

De La Cruz, MS, Young, AP, and Ruffin, MT (2014). Diagnosis and management of pancreatic cancer. *Am Fam Physician* 89, 626–32.

Doultsinos, D., and Mills, I. G. (2021). Derivation and Application of Molecular Signatures to Prostate Cancer: Opportunities and Challenges. *Cancers* 13, 495. doi:10.3390/cancers13030495

Ducreux, M., Cuhna, A. S., Caramella, C., Hollebecque, A., Burtin, P., Goéré, D., et al. (2015). Cancer of the pancreas: ESMO Clinical Practice Guidelines for diagnosis, treatment and follow-up. *Annals of Oncology* 26 (Suppl 5), v56–v68. doi:10.1093/annonc/mdv295

Farhood, B., Najafi, M., and Mortezaee, K. (2019). CD8+cytotoxic T lymphocytes in cancer immunotherapy: A review. *J Cell Physiol* 234, 8509–8521. doi:10.1002/jcp.27782

Feng, Z., Shi, M., Li, K., Ma, Y., Jiang, L., Chen, H., et al. (2020). Development and validation of a cancer stem cell-related signature for prognostic prediction in pancreatic ductal adenocarcinoma. *J Transl Med* 18, 360. doi:10.1186/s12967-020-02527-1

Garrido-Laguna, I., and Hidalgo, M. (2015). Pancreatic cancer: from state-of-the-art treatments to promising novel therapies. *Nat Rev Clin Oncol* 12, 319–334. doi:10.1038/nrclinonc.2015.53

Ghaneh, P., Kleeff, J., Halloran, C. M., Raraty, M., Jackson, R., Melling, J., et al. (2019). The Impact of Positive Resection Margins on Survival and Recurrence Following Resection and Adjuvant Chemotherapy for Pancreatic Ductal Adenocarcinoma. *Ann Surg* 269, 520–529. doi:10.1097/sla.0000000000002557

Gillen, S., Schuster, T., Meyer zum Büschenfelde, C., Friess, H., and Kleeff, J. (2010). Preoperative/neoadjuvant therapy in pancreatic cancer: a systematic review and meta-analysis of response and resection percentages. *PLoS Med* 7, e1000267. doi:10.1371/journal.pmed.1000267

Gu, M., Sun, J., Zhang, S., Chen, J., Wang, G., Ju, S., et al. (2021). A novel methylation signature predicts inferior outcome of patients with PDAC. *Aging* 13, 2851–2863. doi:10.18632/aging.202347

Hu, H., Hang, J.-J., Han, T., Zhuo, M., Jiao, F., and Wang, L.-W. (2016). The M2 phenotype of tumor-associated macrophages in the stroma confers a poor prognosis in pancreatic cancer. *Tumor Biol.* 37, 8657–8664. doi:10.1007/s13277-015-4741-z

Huang, D. W., Sherman, B. T., Tan, Q., Kir, J., Liu, D., Bryant, D., et al. (2007). DAVID Bioinformatics Resources: expanded annotation database and novel algorithms to better extract biology from large gene lists. *Nucleic Acids Res* 35, W169–W175. doi:10.1093/nar/gkm415

Huang, J., Lok, V., Ngai, C. H., Zhang, L., Yuan, J., Lao, X. Q., et al. (2021). Worldwide Burden of, Risk Factors for, and Trends in Pancreatic Cancer. *Gastroenterology* 160, 744–754. doi:10.1053/j.gastro.2020.10.007

Juiz, N. A., Iovanna, J., and Dusetti, N. (2019). Pancreatic Cancer Heterogeneity Can Be Explained Beyond the Genome. *Front. Oncol.* 9, 246. doi:10.3389/fonc.2019.00246

Kamisawa, T., Wood, L. D., Itoi, T., and Takaori, K. (2016). Pancreatic cancer. *The Lancet* 388, 73–85. doi:10.1016/s0140-6736(16)00141-0

Kim, J., Jo, YH., Jang, M., Nguyen, NNY., Yun, HR., Ko, SH, et al. (2019). PAC-5 Gene Expression Signature for Predicting Prognosis of Patients with Pancreatic Adenocarcinoma. *Cancers* 11, 1749. doi:10.3390/cancers11111749

Kleeff, J., Korc, M., Apte, M., La Vecchia, C., Johnson, C. D., Biankin, A. V., et al. (2016). Pancreatic cancer. *Nat Rev Dis Primers* 2, 16022. doi:10.1038/nrdp.2016.22

Kobayashi, Y., Lim, S.-O., and Yamaguchi, H. (2020). Oncogenic signaling pathways associated with immune evasion and resistance to immune checkpoint inhibitors in cancer. *Seminars in Cancer Biology* 65, 51–64. doi:10.1016/j.semcancer.2019.11.011

Kurahara, H., Shinchi, H., Mataki, Y., Maemura, K., Noma, H., Kubo, F., et al. (2011). Significance of M2-polarized tumor-associated macrophage in pancreatic cancer. *Journal of Surgical Research* 167, e211–e219. doi:10.1016/j.jss.2009.05.026

Leinwand, J., and Miller, G. (2020). Regulation and modulation of antitumor immunity in pancreatic cancer. *Nat Immunol* 21, 1152–1159. doi:10.1038/s41590-020-0761-y

Luo, L, Li, Y, Huang, C, Lin, Y, Su, Y, Cen, H, et al. (2021). A new 7-gene survival score assay for pancreatic cancer patient prognosis prediction. *Am J Cancer Res* 11, 495–512.

Macías, N., Sayagués, J. M., Esteban, C., Iglesias, M., González, L. M., Quiñones-Sampedro, J., et al. (2018). Histologic Tumor Grade and Preoperative Bilary Drainage are the Unique Independent Prognostic Factors of Survival in Pancreatic Ductal Adenocarcinoma Patients After Pancreaticoduodenectomy. *J Clin Gastroenterol* 52, e11–e17. doi:10.1097/mcg.0000000000000793

Maeda, S., Moore, A. M., Yohanathan, L., Hata, T., Truty, M. J., Smoot, R. L., et al. (2020). Impact of resection margin status on survival in pancreatic cancer patients after neoadjuvant treatment and pancreatoduodenectomy. *Surgery* 167, 803–811. doi:10.1016/j.surg.2019.12.008

McGranahan, N., and Swanton, C. (2017). Clonal Heterogeneity and Tumor Evolution: Past, Present, and the Future. *Cell* 168, 613–628. doi:10.1016/j.cell.2017.01.018

McGuigan, A. J., Coleman, H. G., McCain, R. S., Kelly, P. J., Johnston, D. I., Taylor, M. A., et al. (2021). Immune cell infiltrates as prognostic biomarkers in pancreatic ductal adenocarcinoma: a systematic review and meta-analysis. *J Pathol Clin Res* 7, 99–112. doi:10.1002/cjp2.192

Oshi, M., Tokumaru, Y., Patel, A., Yan, L., Matsuyama, R., Endo, I., et al. (2020). A Novel Four-Gene Score to Predict Pathologically Complete (R0) Resection and Survival in Pancreatic Cancer. *Cancers* 12, 3635. doi:10.3390/cancers12123635

Phua, L. C., Goh, S., Tai, D. W. M., Leow, W. Q., Alkaff, S. M. F., Chan, C. Y., et al. (2018). Metabolomic prediction of treatment outcome in pancreatic ductal adenocarcinoma patients receiving gemcitabine. *Cancer Chemother Pharmacol* 81, 277–289. doi:10.1007/s00280-017-3475-6

Sho, M., Murakami, Y., Motoi, F., Satoi, S., Matsumoto, I., Kawai, M., et al. (2015). Postoperative prognosis of pancreatic cancer with para-aortic lymph node metastasis: a multicenter study on 822 patients. *J Gastroenterol* 50, 694–702. doi:10.1007/s00535-014-1005-4

Siegel, R. L., Miller, K. D., Fuchs, H. E., and Jemal, A. (2021). Cancer Statistics, 2021. *CA A Cancer J. Clin.* 71, 7–33. doi:10.3322/caac.21654

Strobel, O., Hank, T., Hinz, U., Bergmann, F., Schneider, L., Springfeld, C., et al. (2017). Pancreatic Cancer Surgery. *Ann Surg* 265, 565–573. doi:10.1097/sla.0000000000001731

Sun, P., and Meng, L.-h. (2020). Emerging roles of class I PI3K inhibitors in modulating tumor microenvironment and immunity. *Acta Pharmacol Sin* 41, 1395–1402. doi:10.1038/s41401-020-00500-8

Supplitt, S., Karpinski, P., Sasiadek, M., and Laczmanska, I. (2021). Current Achievements and Applications of Transcriptomics in Personalized Cancer Medicine. *Ijms* 22, 1422. doi:10.3390/ijms22031422

Tummers, W. S., Groen, J. V., Sibinga Mulder, B. G., Farina-Sarasqueta, A., Morreau, J., Putter, H., et al. (2019). Impact of resection margin status on recurrence and survival in pancreatic cancer surgery. *Br J Surg* 106, 1055–1065. doi:10.1002/bjs.11115

van Roessel, S., Kasumova, G. G., Verheij, J., Najarian, R. M., Maggino, L., de Pastena, M., et al. (2018). International Validation of the Eighth Edition of the American Joint Committee on Cancer (AJCC) TNM Staging System in Patients With Resected Pancreatic Cancer. *JAMA Surg* 153, e183617. doi:10.1001/jamasurg.2018.3617

Von Hoff, D. D., Ervin, T., Arena, F. P., Chiorean, E. G., Infante, J., Moore, M., et al. (2013). Increased survival in pancreatic cancer with nab-paclitaxel plus gemcitabine. *N Engl J Med* 369, 1691–1703. doi:10.1056/NEJMoa1304369

Vonderheide, R. H., and Bayne, L. J. (2013). Inflammatory networks and immune surveillance of pancreatic carcinoma. *Current Opinion in Immunology* 25, 200–205. doi:10.1016/j.coi.2013.01.006

Xu, D., Wang, Y., Liu, X., Zhou, K., Wu, J., Chen, J., et al. (2021a). Development and clinical validation of a novel 9-gene prognostic model based on multi-omics in pancreatic adenocarcinoma. *Pharmacological Research* 164, 105370. doi:10.1016/j.phrs.2020.105370

Xu, K., Yin, N., Peng, M., Stamatiades, E. G., Shyu, A., Li, P., et al. (2021b). Glycolysis fuels phosphoinositide 3-kinase signaling to bolster T cell immunity. *Science* 371, 405–410. doi:10.1126/science.abb2683

You, L., Wu, W., Wang, X., Fang, L., Adam, V., Nepovimova, E., et al. (2020). The role of hypoxia-inducible factor 1 in tumor immune evasion. *Med Res Rev* 41, 1622–1643. doi:10.1002/med.21771

Yu, F., Quan, F., Xu, J., Zhang, Y., Xie, Y., Zhang, J., et al. (2019). Breast cancer prognosis signature: linking risk stratification to disease subtypes. *Brief Bioinform* 20, 2130–2140. doi:10.1093/bib/bby073

Zhang, J., Wang, Y. F., Wu, B., Zhong, Z. X., Wang, K. X., Yang, L. Q., et al. (2018). Intraepithelial Attack Rather than Intratumorally Infiltration of CD8+T Lymphocytes is a Favorable Prognostic Indicator in Pancreatic Ductal Adenocarcinoma. *Cmm* 17, 689–698. doi:10.2174/1566524018666180308115705

Zheng, L., Xue, J., Jaffee, E. M., and Habtezion, A. (2013). Role of immune cells and immune-based therapies in pancreatitis and pancreatic ductal adenocarcinoma. *Gastroenterology* 144, 1230–1240. doi:10.1053/j.gastro.2012.12.042

Conflict of Interest: The authors declare that the research was conducted in the absence of any commercial or financial relationships that could be construed as a potential conflict of interest.

frontiers in Cell and Developmental Biology

ORIGINAL RESEARCH
published: 26 May 2021
doi: 10.3389/fcell.2021.689613

Antitumor and Radiosensitization Effects of a CXCR2 Inhibitor in Nasopharyngeal Carcinoma

*Xiaobei Liu†, Tianxia Lan†, Fei Mo, Jingyun Yang, Yuquan Wei and Xiawei Wei**

Laboratory of Aging Research and Cancer Drug Target, State Key Laboratory of Biotherapy and Cancer Center, National Clinical Research Center for Geriatrics, West China Hospital, Sichuan University, Chengdu, Sichuan, China

CXCR2, a member of the G-protein-coupled cell surface chemokine receptor family, is commonly found on leukocytes, endothelial cells and tumor cells including nasopharyngeal carcinoma cells. However, how the activity of CXCR2 and its ligand CXCL8 affects the development of nasopharyngeal carcinoma (NPC) remains unknown. Here, we found that CXCR2 and CXCL8 were both predicted poor prognosis in NPC patients. Furthermore, we identified that treatment with CXCR2 antagonist SB225002 of nasopharyngeal carcinoma cell lines resulted tumorigenesis inhibition *in vitro* and *in vivo*. In addition, we found that SB225002 could enhance NPC cells radiosensitivity through regulating cell circle distribution and interfering with cellular DNA damage repair. SB225002 also exhibited an efficient radiosensitization effect in C666-1 and HONE-1 bearing mice. Functionally, we showed that SB225002 reduced microvessel density and proliferation and induced tumor apoptosis. Furthermore, changes in the tumor microenvironment were also observed in this study. We observed that SB225002 reduced tumor-associated neutrophils (TANs) in the tumors tissue which were recruited especially after irradiation. Taken together, our results suggested that targeting the CXCL8-CXCR2 pathway is a promising therapeutic strategy for comprehensive NPC treatment.

Keywords: nasopharyngeal carcinoma, CXCR2, radiosensitization, angiogenesis, neutrophils

OPEN ACCESS

Edited by:
Hongming Miao,
Army Medical University, China

Reviewed by:
Yi Wang,
Zhejiang University, China
Guihua Wang,
Huazhong University of Science and Technology, China
Jingxuan Pan,
Sun Yat-sen University, China

***Correspondence:**
Xiawei Wei
xiaweiwei@scu.edu.cn

† These authors have contributed equally to this work

Specialty section:
This article was submitted to Molecular Medicine, a section of the journal Frontiers in Cell and Developmental Biology

Received: *01 April 2021*
Accepted: *29 April 2021*
Published: *26 May 2021*

Citation:
Liu X, Lan T, Mo F, Yang J, Wei Y and Wei X (2021) Antitumor and Radiosensitization Effects of a CXCR2 Inhibitor in Nasopharyngeal Carcinoma. Front. Cell Dev. Biol. 9:689613. doi: 10.3389/fcell.2021.689613

INTRODUCTION

Nasopharyngeal carcinoma (NPC), originating from the nasopharyngeal epithelium, is the most common head and neck malignancy (Kamran et al., 2015; Chua et al., 2016). Epidemiologically, NPC is highly prevalent in Southern China and Southeast Asia, particularly in the Cantonese region where the peak annual incidence rate reaches 30 per 1,00,000 individuals (Lee A.W.M. et al., 2012; Bei et al., 2016). Radiotherapy (RT) with or without chemotherapy is the standard treatment for patients with nasopharyngeal carcinoma. Despite dramatic improvements in the clinical outcomes achieved by modern radiotherapy technology, more than 20-30% of NPC patients still have local recurrence and distant metastasis (Lee et al., 2015). However, due to toxicity, side effects and radioresistance, existing standard chemoradiation strategies have reached the upper limit (Akervall et al., 2014). Therefore, there is an urgent need to develop novel small molecule inhibitors that can enhance the therapeutic effects of radiation against NPC with minimal toxicity to further improve the prognosis for NPC patients.

C-X-C motif chemokine receptor 2 (CXCR2), a member of the G-protein-coupled cell surface chemokine receptor family, is commonly found on leukocytes, endothelial cells and tumor cells (Cacalano et al., 1994; Rot and von Andrian, 2004). C-X-C motif chemokine ligand 8 (CXCL8) is a pleiotropic cytokine with high affinity for its receptor CXCR2. Accumulating evidence suggests that the CXCL8-CXCR2 pathway is crucial for the initiation and development of tumors. For instance, CXCR2 and CXCL8 are overexpressed in various human cancers, such as oesophageal cancer, pancreatic cancer and ovarian cancer, and this overexpression positively correlates with aggressive tumor behavior and poor prognosis (Wente et al., 2006; Waugh and Wilson, 2008; Nishi et al., 2015; Ignacio et al., 2018). Additionally, the CXCL8-CXCR2 pathway is associated with angiogenesis and tumor-stromal interactions, where it promotes tumor progression and metastasis (Wang et al., 2006; Waugh and Wilson, 2008; Singh et al., 2009; Ijichi et al., 2011; Lee Y.S. et al., 2012; Steele et al., 2016). More importantly, genetic or pharmaceutical blockade of CXCR2 reduces tumorigenesis and angiogenesis in mice with oesophageal cancer, lung cancer, breast cancer and pancreatic cancer (Keane et al., 2004; Wislez et al., 2006; Matsuo et al., 2009; Xu et al., 2018). A few studies have suggested that the CXCL8-CXCR2 pathway may also play a role in NPC tumor progression. Yoshizaki et al. (2001) observed that CXCR2 and CXCL8 are abundantly expressed in clinical samples of NPC (Horikawa et al., 2005). Lo et al. (2013) demonstrated that CXCR2 and CXCL8 are expressed in NPC cell lines and induce the growth of tumour spheroids. The above studies indicate that the CXCL8-CXCR2 pathway is a promising target for anticancer treatment.

SB225002 is a small-molecule inhibitor with selective affinity for CXCR2 that competes with ligands, including CXCL8, stopping them from binding to CXCR2. SB225002 has been applied to inhibit oncogenesis and metastasis in ovarian cancer and oesophageal cancer (Wang et al., 2006; Yung et al., 2018). Moreover, SB225002 has been indicated to be a negative regulator of the MAPK signaling pathway, and it has been reported that MAPK signalng is involved in the radioresistance (Eder et al., 2017; Pei et al., 2017). Thus, we hypothesized that SB225002 may increase the radiation sensitivity of NPC cells. In this study, we aimed to confirm the expression of CXCR2 in human nasopharyngeal carcinoma and attempted to study the antitumor and radiosensitization effects and mechanisms of SB225002 in NPC.

MATERIALS AND METHODS

Cell Lines and Cultures

Human NPC cell lines (C666-1, CNE-1, CNE-2, HNE-1, and HONE-1) were obtained from the American Type Culture Collection (ATCC). Cells were cultured in Dulbecco's modified Eagle's medium (DMEM, Gibco) supplemented with 10% foetal bovine serum (FBS; Gibco) and 1% antibiotics (penicillin and streptomycin). Human umbilical vein endothelial cells (HUVECs) were obtained from the State Key Laboratory of Biotherapy and were maintained in low-glucose DMEM. Cells were maintained at 37°C in a humidified atmosphere with 5% CO_2.

Prepare of SB225002

SB225002 was purchased from Selleck Chemicals. For *in vitro* studies, SB225002 was dissolved initially as a 10 mM stock solution in dimethyl sulfoxide (DMSO, Sigma-Aldrich), stored at −20°C and diluted in cell culture medium to achieve a final concentration. For *in vivo* studies, SB225002 was prepared in 25% (v/v) PEG 400 (Sigma-Aldrich) and 5% (v/v) Tween 80 (Sigma-Aldrich), containing 2% (v/v) DMSO.

Cell Proliferation Assay

Cell viability was measured using the Cell Counting Kit-8 (CCK8, MedChemExpress) assay. Briefly, tumor cells ($1–3 \times 10^3$ cells/well) were seeded in 96-well plates and cultured overnight. Then, the cells were treated with various concentrations of SB225002 for 24, 48, or 72 h. DMSO (0.1%) served as the vehicle control corresponding to the concentration present in the highest SB225002 dosage of 1 mM to exclude possible effects of the solvent. Thereafter, 10 μL of CCK8 reagent was added to each well, and the plates were incubated in a 5% CO_2 atmosphere at 37°C for an additional 0.5-2 h. The absorbance was measured at 450 nm using a Spectra MAX M5 microplate spectrophotometer (Molecular Devices). The percentage of the control samples of each cell line was calculated thereafter.

Clonogenic Survival Assays

Tumor cells (400 cells/well) were seeded in 6-well plates, incubated for 24 h and treated with various concentrations of SB225002. After 10-12 days of incubation, the cells were fixed with ethanol and stained with 0.5% crystal violet. Colonies comprising more than 50 cells were manually counted by microscope. For the radiosensitivity assay, tumor cells (200-1000 cells/well) were seeded in 6-well plates. After culturing for 24 h, the cells were treated with SB225002 (0, 0.5, and 1 μM) for 3-4 h and then irradiated with a single dose of 0 (control), 2, 4, 6, or 8 Gy. Following irradiation, the cells were incubated with SB225002 for an additional 20 h, and then the medium was replaced by fresh medium. The following steps are the same as described above. After correcting for initial plating efficiency, the colony survival data were used to plot clonogenic survival curves.

Cell Cycle Analysis

Cell cycle distribution was determined by flow cytometry with PI staining. Briefly, cells were treated with SB225002 at various concentrations or in combination with irradiation at a dose of 8 Gy. After culturing for 8 h, cells were fixed in 70% ice-cold ethanol at 4°C overnight. Then, the cells were stained with PI staining solution (Sigma Aldrich) containing RNase A for 30 min in the dark and analyzed by flow cytometry. Data were analyzed with Novo Express 1.1.2.

Endothelial Cell Migration and Tube Formation Assays

HUVEC cell mobility and migration was evaluated using a modified Boyden chamber (8-μm pore size; Merck Millipore).

A total of 1×10^5 HUVECs in 200 μl of serum-free medium were added to the top chamber, and 600 μl of serum-free medium, tumor culture medium supernatant or 50 ng/ml recombinant human IL-8 (Novoprotein) was added to the bottom chamber. Both chambers contained 0.5 μM SB225002 or 0.1% DMSO. After 24 h of migration, filters were rinsed with PBS, fixed with 4% paraformaldehyde and stained with 0.5% crystal violet. The migrated cells on the underside of the whole transwell inserts were quantified by manual counting and photographed under a light microscope. The ability of HUVECs to form capillary-like endothelial tubes was determined *in vitro*. Briefly, a total of 1×10^5 HUVECs were seeded on a Matrigel (Thermo Fisher Scientific) pre-coated 24-well plate and incubated in serum-free medium, tumor culture medium supernatant or 50 ng/ml recombinant human IL-8 with SB225002 (0.5 μM) or 0.1% DMSO for an additional 3-4 h. Photomicrographs from each well were captured and analyzed using ImageJ software, version 2.02 (National Institutes of Health, United States).

Western Blot Assay

NPC cells treated with SB225005 at various concentrations for 2 h were washed twice in ice-cold PBS and lysed in RIPA lysis buffer (Invitrogen) containing 1 mM phenylmethanesulfonylfluoride (PMSF, Sigma-Aldrich) and a protease inhibitor cocktail (Sigma-Aldrich). Protein extracts were quantified by the bicinchoninic acid (BCA) protein assay kit (Thermo Fisher Scientific), separated on 12.5% SDS-PAGE and transferred to 0.2 μm polyvinylidene fluoride (PVDF) membranes (Merck Millipore). After blocking with 5% bovine serum albumin (BSA, Sigma-Aldrich) in TBS/T for 2 h at room temperature, the membranes were incubated with specific primary antibodies overnight at 4°C, followed by incubation with appropriate horseradish-peroxidase (HRP)-conjugated secondary antibodies for 2 h at room temperature. The reactive bands were detected by an enhanced chemiluminescence kit (Millipore). The primary antibodies for Erk1/2, p-Erk1/2 (Thr202/Tyr204), P38, p-P38 (Thr180/Tyr182), JNK, p-JNK (Thr183/Tyr185) and β-actin were purchased from Cell Signaling Technology.

Immunofluorescence Staining

NPC cells (2×10^4 cells/well) were seeded on coverslips in 24-well plates for cell adherence. Then, the cells treated with or without SB225002 (0.5 μM) for 3-4 h before irradiation were exposed to 8 Gy radiation. Cells were harvested at the indicated time points after irradiation, fixed with 4% paraformaldehyde for 15 min and permeabilized with 0.5% Triton X-100 for 10 min. After blocking with 5% BSA at 37°C for 1 h, cells were stained with a γ-H2AX antibody (1:500; ab11174, Abcam) overnight at 4°C. After being washed with PBS twice, cells were incubated with an anti-rabbit FITC secondary antibody at 37°C for 2 h. Nuclei were counterstained with DAPI (Beyotime Biotechnology) in room tempreture for 5 min, and images were visualized and captured by an LSM 710 laser-scanning confocal microscope (Carl Zeiss Microscopy).

Mouse Models and Treatments

All animal experiments were approved by the Institutional Animal Care and Treatment Committee of Sichuan University, China. Nude mice (BALB/c, 4-5 weeks old) were purchased from Beijing Huafukang Bioscience and kept in a specific-pathogen-free (SPF) facility with consistent room temperature and humidity. A total of 5×10^6 C666-1 or 1×10^7 HONE-1 cells were injected subcutaneously into the right dorsal flank of BALB/c nude mice. After 5 days of tumor induction, the tumor-bearing mice were randomized into five groups (7 mice per group) and treated as follows: (Chua et al., 2016) blank, (Kamran et al., 2015) vehicle (25% PEG 400 and 5% Tween 80), (Lee A.W.M. et al., 2012) 10 mg/kg SB225002, (Bei et al., 2016) 8 Gy irradiation, and (Lee et al., 2015) a combination of 10 mg/kg SB225002 and 8 Gy irradiation. The administration of SB225002, by intraperitoneal injection once a day, began after the tumors reached approximately 0.6–0.7 cm in diameter. From the 3rd day of SB225002 administration, a single dose of 8 Gy radiation was administered. Tumor volumes were assessed by measurement of tumor diameters using a caliper every 3 days and calculated according to the formula: (long diameter) × (short diameter)^2 × 0.52. Body weight was measured every 3 days. On the 23rd day, the mice were sacrificed after final administration. The tumors and organs were harvested, weighed, dissected and fixed in 4% paraformaldehyde for histochemistry; another part of the tumor was stored in liquid nitrogen for further use. The inhibition ratio was calculated according to the following formula: inhibition ratio (%) = [(A-B)/A] × 100, where A represents the average tumor volume of the vehicle control, and B represents that of the treated group.

Tissue Microarray and Immunohistochemical (IHC) Staining

Commercially available tissue microarray slides (Outdo Biotech) of 99 NPC samples without adjacent normal nasopharyngeal tissues were obtained with detailed patient information, including age, gender, metastasis status, pathological pattern, tumor size, and TNM stage. The IHC analysis was carried out to assess the correlation between the protein expression of CXCR2 or CXCL8 and the prognosis of NPC patients based on the detailed survival data. In brief, the tissue sections were blocked with goat serum at 37°C for 40 min and then incubated overnight at 4°C with anti-human CXCR2 antibody (1:200; ab143935, Abcam) or anti-human CXCL8 antibody (1:500; ab18672, Abcam), followed by incubation with an HRP-conjugated secondary antibody. The tissue sections were then stained with a solution of 3,3-diaminobenzidine tetrahydrochloride and counterstained with haematoxylin. The expression of CXCR2 or CXCL8 was quantified based on the extent of staining (percentage of positive tumor cells) and the intensity of staining. The immunohistochemical score was independently assessed by 2 pathologists without knowledge of the patient characteristics. Additionally, the protein expression levels of Ki-67, CD31, VEGF, and Ly6G in xenograft mouse models were examined by IHC. The specific primary antibodies were anti-mouse Ki-67 antibody (1:200; ab16667, Abcam),

anti-mouse CD31 antibody (1:50; ab28364, Abcam), anti-mouse VEGF antibody (1:500; ab46154, Abcam) and anti-mouse Ly6G antibody (1:800; GB11229, Servicebio).

TUNEL Assay

To examine the apoptosis induction effect of SB225002 plus irradiation on tumor cells *in vivo*, paraffin sections of tumor tissue specimens were stained with terminal deoxynucleotidyl transferase (TdT)-mediated deoxyuridine triphosphate-biotin nick-end labeling (TUNEL) using a TUNEL kit (Promega) according to the manufacturer's instructions. Images were visualized and captured by a DM 2500 fluorescence microscope (Leica Microsystems CMS GmbH).

Flow Cytometry Analysis

Antibodies specific for mouse PerCP-cy5.5-CD45, FITC-CD11b, PE-Ly6C, BV510 or BV421-Ly6G, BV421-TGFβ, anti-IL-10 and anti-VEGF were purchased from Biolegend. Anti-human APC-CXCR2 antibodies and anti-rat FITC-secondary antibodies were purchased from BD Pharmingen. Anti-mouse CXCR2 antibodies were obtained from R&D Systems and LIVE/DEAD Fixable Blue Dead Cell Stain was obtained from Thermo Fisher Scientific.

To analyse the neutrophils and their functions in tumor tissues, tumors were minced into small pieces and dissociated using 1 mg/mL collagenase type IV (Sigma-Aldrich) in serum-free DMEM medium at 37°C for 1 h. After washing with PBS, cell suspensions were filtered with a 70-μm nylon cell strainer (BD Falcon) to remove clumps of cells and debris for subsequent flow cytometry. For cell surface staining, cells were stained with antibodies on ice for 30 min in the dark; for intracellular cytokine staining, cells were then fixed and permeabilized with paraformaldehyde and Triton-X100 and stained with intracellular antibodies overnight. Analyses were carried out on a NovoCyte flow cytometer (ACEA Biosciences) and data were analyzed using Novo Express 1.1.2.

Statistical Analysis

Data were presented as the mean ± SD of at least three independent experiments. Data were statistically evaluated using a 2-tailed Student's t test and a one-way analysis of variance (ANOVA) test. A Kaplan-Meier survival analysis (log-rank test) was used to illustrate the prognostic relevance of SB225002 in NPC patients. A P value < 0.05 was considered statistically significant. All statistical analyses were performed using GraphPad Prism 7.0 and the R Performance Analytics package.

RESULTS

Elevated CXCR2 and CXCL8 Co-expression Levels in Nasopharyngeal Carcinoma Correlate With Poor Prognosis

To explore the effect of CXCL8-CXCR2 signaling in nasopharyngeal carcinoma, we performed immunohistochemistry staining for CXCR2 and CXCL8 in an NPC tissue microarray and found CXCR2 localized in both tumor cells and stromal cells; CXCL8 was frequently observed in the cytosol of tumor cells (**Figure 1A** and **Supplementary Table**). Moreover, a significant positive correlation was detected between CXCR2 expression in stromal cells and CXCL8 expression in tumors in 99 NPC specimens ($P < 0.05$) but not between CXCR2 expression in tumor cells and CXCL8 expression in tumors ($P > 0.05$), which might indicate that tumor could regulate the behaviors of stromal cells in the tumor microenvironment via CXCL8-CXCR2 signaling (**Figure 1B**). Furthermore, the Kaplan-Meier analysis showed that the expression of CXCR2 and CXCL8 was significantly correlated with overall survival in NPC patients. As shown in **Figures 1C-E**, NPC patients with high CXCR2 expression levels in tumor cells or in stromal cells had shorter overall survival than patients with low CXCR2 levels ($P < 0.05$). Furthermore, NPC patients with high CXCL8 expression levels had shorter overall survival than patients with low CXCL8 levels ($P < 0.05$), suggesting that high CXCL8-CXCR2 signal levels correlate with poor prognosis. We then confirmed the expression of CXCR2 in nasopharyngeal carcinoma cell lines by flow cytometry (FCM) and Western blot (**Figures 1F,G**).

CXCR2 Inhibitor Treatment Suppresses Tumorigenesis in Nasopharyngeal Carcinoma *in vitro* and *in vivo*

To explore whether the CXCR2 inhibitor SB225002 has a direct effect on NPC cells, we treated a panel of 5 established NPC cell lines with various concentrations of SB2250002 for 24, 48, and 72 h and assayed cell viability by CCK8 assay. As shown in **Figure 2A** and **Supplementary Figure 1**, all these cell lines were sensitive to treatment with SB225002, and the cell proliferation was inhibited in a concentration- and time-dependent manner. In particular, the C666-1 cells and HONE-1 cells were most sensitive to SB225002, which corresponded with their CXCR2 expression levels. Thus, we chose C666-1 and HONE-1 cells for further study. Treatment of NPC cells with various concentrations of SB225002 also decreased the colony formation ability of NPC cells in a dose-dependent manner (**Figure 2B**). We also observed that SB225002 induced a sustained accumulation of NPC cells in the G2/M phase in the cell cycle analysis (**Figure 2C**). As shown in **Figure 2D**, SB225002 suppressed cell growth and proliferation through the inhibition of mitogen-activated protein kinase (MAPK) pathway activation in NPC cells. To further investigate the activity of SB225002 *in vivo*, C666-1-bearing mice were treated with 10 mg/kg SB225002. As shown in **Figures 2E-G**, both tumor size and tumor weight were substantially decreased in mice treated with SB225002 compared with those in mice treated with vehicle. Taken together, these results strongly indicate that SB225002 suppresses tumorigenesis in NPC *in vitro* and *in vivo*.

CXCR2 Inhibitor Treatment Sensitizes NPC Cells to Radiation Through the Suppression of DSB Repair *in vitro*

MAPK signaling activity has been reported to be involved in radioresistance (Eder et al., 2017; Pei et al., 2017). Since SB225002 has been indicated to be a negative regulator of the MAPK signaling pathway, we speculated that SB225002 may

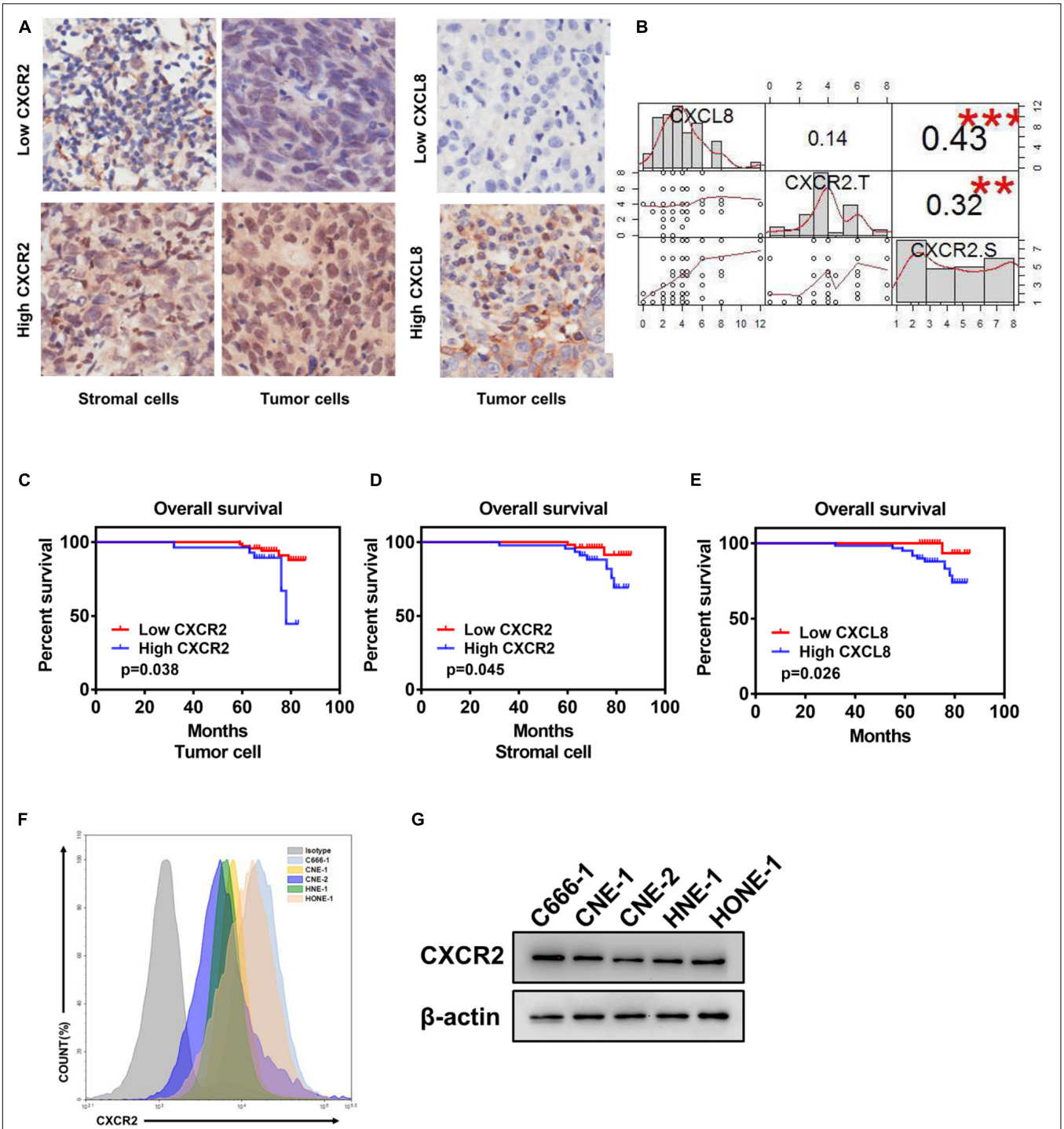

FIGURE 1 | Elevated CXCR2 and CXCL8 co-expression levels in NPC correlate with poor prognosis. **(A)** Representative immunohistochemistry images showing CXCR2 expression in stromal and tumor cells in different individual NPC tissue (left) and CXCL8 expression in other NPC tissues (right). Magnification, 20×. **(B)** Correlation analysis between CXCR2 and CXCL8. CXCL8 expression and CXCR2 expression in tumor cells was significantly positively associated with CXCR2 expression in stromal cells, R = 0.43, $p < 0.001$ and R = 0.32, $p < 0.01$, but no association was found between CXCR2 expression in tumor cells and CXCL8 expression in stromal cells, R = 0.14, $p > 0.05$. Statistical analysis was performed using the Pearson's correlation coefficient and linear regression. **(C–E)** According to IHC score, samples from NPC patients ($n = 99$) were divided into two groups based on low or high expression of the indicated markers, including CXCR2 in tumor and stromal cell and CXCL8. Overall survival was significantly negatively associated with the levels of CXCR2 in tumor cells, CXCR2 in stromal cells and CXCL8, as displayed in Kaplan–Meier survival curves of OS, **(C)** p = 0.038; **(D)** p = 0.045; and **(E)** p = 0.026. **(F–G)** CXCR2 expression analysis of six NPC cell lines using flow cytometry and western blot. (IHC score, immunohistochemical analysis score; R, Spearman's correlation).

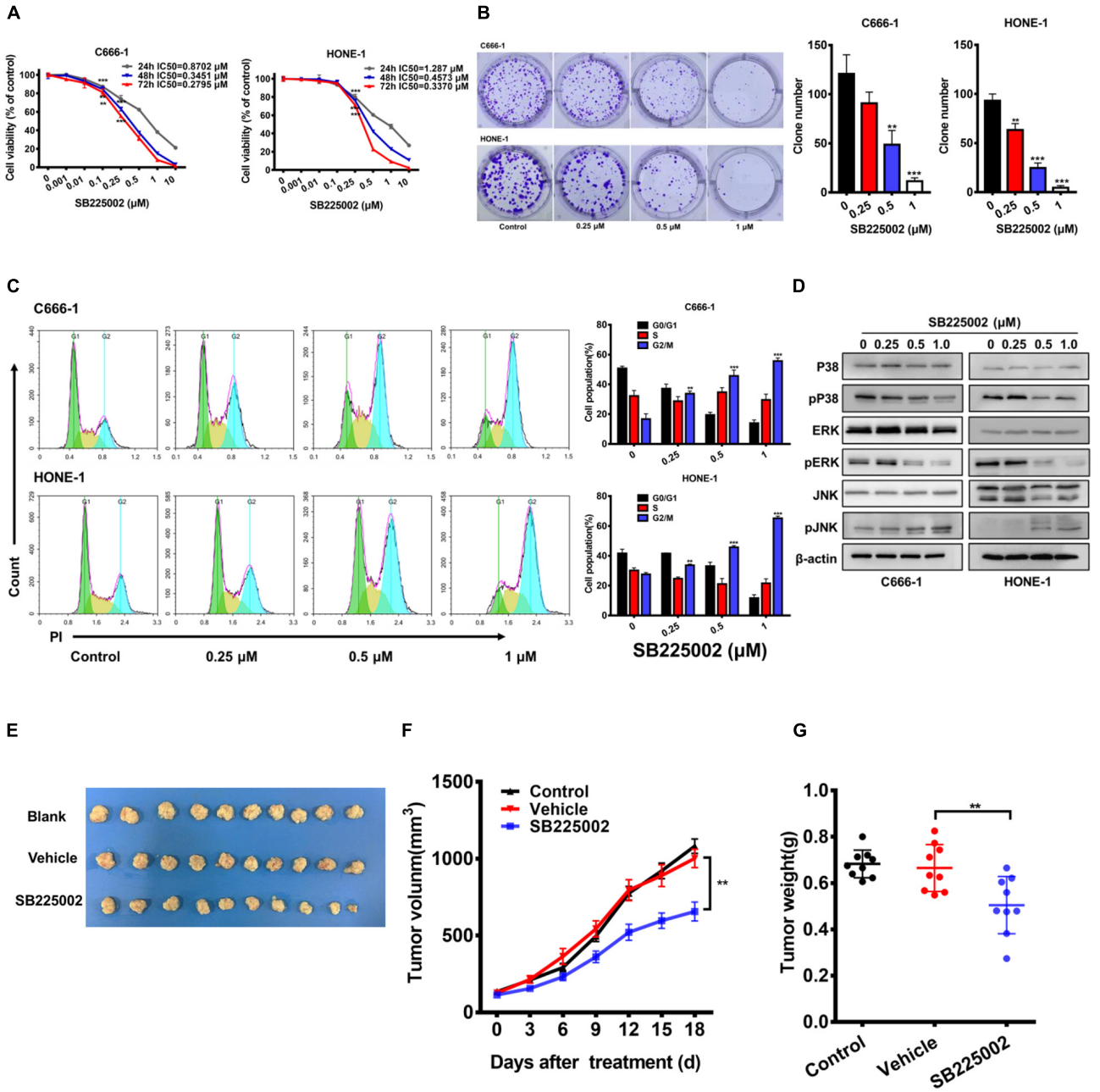

FIGURE 2 | SB225002 suppresses tumorigenesis in NPC cells *in vitro* and *in vivo*. **(A)** SB225002 inhibited cell proliferation. C666-1 and HONE-1 human NPC cells were treated with SB225002 for (24, 48, and 72 h), cell viability was evaluated by CCK8 assay (**$p < 0.01$; ***$p < 0.001$; Student's *t*-test). Values represent mean ± SD ($n = 5$). **(B)** The effects of SB225002 on colony formation in C666-1 and HONE-1 cells for 10-12 days. The colonies were counted and shown with histograms (**$p < 0.01$; ***$p < 0.001$; Student's t-test). Values represent mean ± SD (n = 3). **(C)** Cell cycle analysis of C666-1 and HONE-1 cells after SB225002 treatment for 8 h (**$p < 0.01$; ***$p < 0.001$; Student's *t*-test). Values represent mean ± SD (n = 3). **(D)** The expression of p38, p-p38, ERK, p-ERK, JNK and p-JNK in C666-1 and HONE-1 cells pre-treated with SB225002 for 2 h determined by western blot analyses and β-actin was employed as a standard. **(E–G)** C666-1 cells were established subcutaneous in female BALB/c mice and SB225002 at 10 mg/kg and vehicle administration once daily were started 5 days after inoculation. Tumor volumes and tumor weights were recorded every three days (seven mice per group). **(E)** Representative images of the xenograft tumors in three groups. **(F)** The growth curves of the tumors in groups were presented. Data are shown as the mean tumor volume ± SD ($n = 7$; **$p < 0.01$; two-way ANOVA). **(G)** The antitumor effects of SB225002 on the tumor weight in groups were shown as mean ± SD ($n = 7$; **$p < 0.01$; Student's *t*-test).

increase the radiation sensitivity of NPC cells. To investigate whether SB225002 directly regulates NPC cell radiosensitivity, we performed a clonogenic survival assay to assess the survival of C666-1 and HONE-1 cells exposed to radiation at graded doses (0, 2, 4, 6, and 8 Gy). As expected, SB225002 treatment sensitized the NPC cells to the effects of radiation *in vitro*

(**Figure 3A**). To further evaluate how SB225002 influence the cellular DNA damage repair, we investigated the levels of DNA double-strand breaks (DSBs) via immunofluorescence staining of γ-H2AX foci in NPC cells treated with SB225002 after exposure to X-rays. As shown in **Figures 3B,C**, compared to radiation alone, the combination of SB225002 treatment with irradiation (8 Gy) increased the expression of γ-H2AX nuclear foci at 1 h. Consistent with this result, the cell cycle analysis showed that SB225002 increased the sustained accumulation of cells in G2/M phase, which is a well-known occurrence in cells that are the most sensitive to radiotherapy. Notably, the treatment of irradiation significantly reduced the SB225002-induced accumulation of cells in the G2/M phase (**Figure 3D**). Collectively, these data suggest that SB225002 may interfere with cellular DNA damage repair, enhance radiation-induced cell killing and eventually contribute to the radiosensitization effect in NPC cells.

CXCR2 Inhibitor Treatment Sensitizes NPC Tumors to Radiation *in vivo*

To assess the antitumor and radiosensitization effects of SB225002, we used subcutaneous xenograft null mice models of nasopharyngeal carcinoma (C666-1 and HONE-1). We noticed that SB225002 treatment alone caused a modest but significant reduction in tumor volume and tumor weight in both NPC mouse models, with tumor inhibition rates of approximately 38 and 30% in the C666-1 and HONE-1 models, respectively. Moreover, the combination of SB225002 plus irradiation led to an approximately 55% more reduction in both tumor volume and tumor weight when compared with that of irradiation alone (**Figures 4A-C**). Ki67 immunohistochemistry staining and the TUNEL assay were conducted on tumor tissues to obtain additional insight into proliferation and apoptosis *in vivo*. The images clearly showed that compared with the single treatment, the combination treatment resulted in a significant reduction in proliferating cells with positive nuclear Ki-67 staining in the C666-1 tumor model (**Figure 4D**). Furthermore, TUNEL-positive cells were significantly increased in the cells in the combination group (**Figure 4E**). In addition, to examine the potential toxicity of the combination of irradiation and SB225002, histological examinations of vital organs by H&E staining and serum biochemical detection were performed. As shown in **Supplementary Figures 2A-C**, no body weight decrease, histological abnormalities or hepatorenal function changes were found, suggesting that the combined treatment was well tolerated. Taken together, these results show that SB225002 increases tumor radiosensitivity and is associated with proliferation inhibition and apoptosis induction.

CXCR2 Inhibitor Treatment Impairs the Recruitment of TANs Induced by Irradiation *in vivo*

In the tumor microenvironment, infiltrating myeloid cells, such as neutrophils and macrophages, contribute to tumor progression. In particular, CXCR2 is expressed in neutrophils, and tumor-associated neutrophils (TANs) have been shown to have antitumorigenic (N1) or pro-tumorigenic functions during tumor development. Thus, we evaluated the effect of SB225002 on TANs, and the functions of TANs in NPC to investigate whether the host immune system contributes to the antitumor and radiosensitization effects of CXCR2 inhibition. Flow cytometry and immunohistochemical staining of tumor tissue was performed to assess TANs in C666-1 tumor-bearing mice after 18 days of combined treatment. As shown in **Figure 5A**, the number of TANs ($CD45^{+}CD11b^{+}Ly6C^{mid}Ly6G^{high}$) significantly decreased in both SB225002 alone and combined treatment groups when compared with the vehicle and radiation alone groups. Immunostaining of Ly6G in tumor tissues also suggested a decrease in TAN infiltration after SB225002 treatment, while irradiation treatment induced TAN accumulation (**Figure 5B**). Furthermore, intracellular flow cytometry was conducted to determine the functions of TANs in NPC tumors. We found that the expression level of pro-tumor cytokines including TGF-β, IL-10 and VEGF were significantly higher in TANs comparing to those in neutrophils in the peripheral blood of both non-tumor-bearing mice and C666-1 tumor-bearing mice, which confirmed that TANs in NPC tumors have pro-tumorigenic properties (**Figures 5C,D**).

In order to verify our hypothesis that SB225002 impairs the sequential recruitment of TANs induced by irradiation *in vivo*, we utilized an air pouch model in which supernatants of irradiated NPC cells with or without SB225002 were injected (Krombach et al., 2019), and neutrophil recruitment was analyzed in the air pouch skin (**Figure 5E**). As shown in **Supplementary Figure 3**, culture supernatants of irradiated tumor cells were harvested 4 days after irradiation with 0 Gy and 8 Gy, while serum-free culture medium served as a control. The number of recruited neutrophils increased significantly when supernatants of 8 Gy-irradiated cells were injected compared to when supernatants of 0 Gy-irradiated cells were injected (**Figure 5F**). However, the supernatants of 8 Gy-irradiated cells recruited fewer neutrophils when 0.5 μM SB225002 was added (**Figure 5F**). In combination, these data suggest that SB225002 may contribute to the suppression of radioresistance by regulating the recruitment of TANs stimulated by radiation *in vivo*.

Regulation of Tumor Angiogenesis by CXCR2 Inhibitor Treatment

To further investigate the mechanisms through which SB225002 inhibits NPC tumour growth and increases radiosensitivity *in vivo*, we selected two well defined markers of angiogenesis, CD31 and VEGF, to evaluate angiogenesis in the tumor sections. As shown in **Figure 6A**, the densities of CD31-positive and VEGF-positive microvessels in tumor sections from vehicle and radiation alone groups were both significantly higher than those in the SB225002 alone and combined treatment groups. Moreover, to validate the antiangiogenic capacity of SB225002, we first measured the migration of HUVECs in a modified Boyden chamber. The culture supernatants of C666-1 cells or the medium containing the chemokine CXCL8 was added to the lower chamber, and HUVECs were added to the upper chamber. After 24 h of incubation, the number of migrated

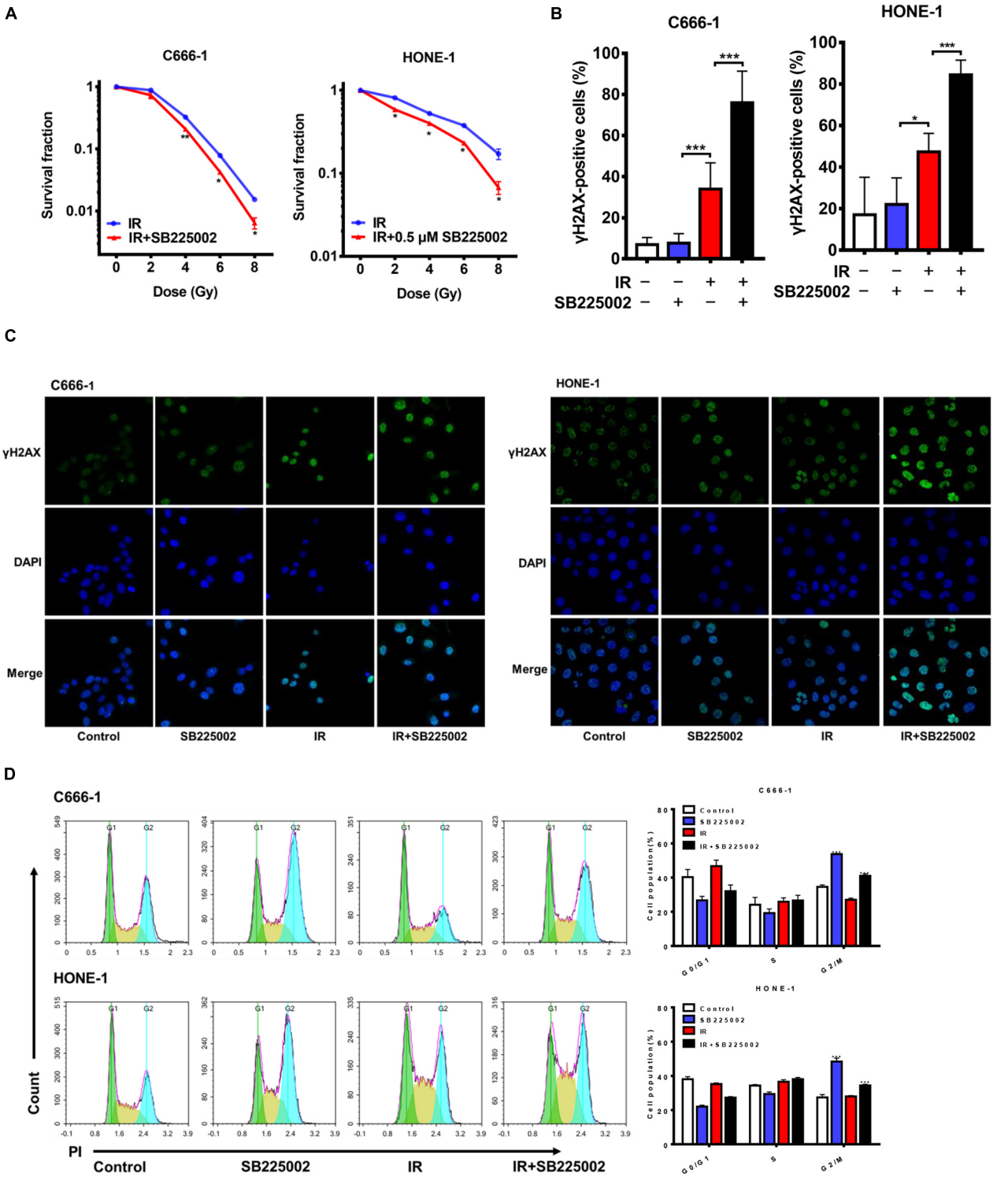

FIGURE 3 | SB225002 sensitizes NPC cells to radiation *in vitro*. **(A)** SB225002 sensitized C666-1 and HONE-1 cells to radiation. Cells were treated with 0.5 μM SB225002 and irradiated with doses as indicated. The colonies were counted 12 days later. Values represent mean ± SD ($n = 3$; $^{*}p < 0.05$; $^{**}p < 0.01$; Student's *t*-test). **(B,C)** DSB repair assay was performed by counting γ-H2AX foci. C666-1 and HONE-1 cells pre-treated with SB225002 for 3-4 h were irradiated with 8 Gy and harvested to immunofluorescence stain with DAPI and FITC for γ-H2AX at 1 h later. **(C)** Representative immunostaining images were shown, 20 × oil. **(B)** Cells with more than 10 foci were scored as positive and plotted with histograms. Data are shown with the mean ± SD of $n = 5$-8 fields obtained from three parallel experiments ($^{*}p < 0.05$; $^{***}p < 0.001$; Student's t-test). **(D)** Cell cycle distribution analyzed by flow cytometry of PI staining. C666-1 and HONE-1 cells pre-treated with SB225002 for 3-4 h were irradiated with 8 Gy and harvested to analyze by flow cytometry 4 h later ($n = 3$; $^{***}p < 0.001$; Student's *t*-test).

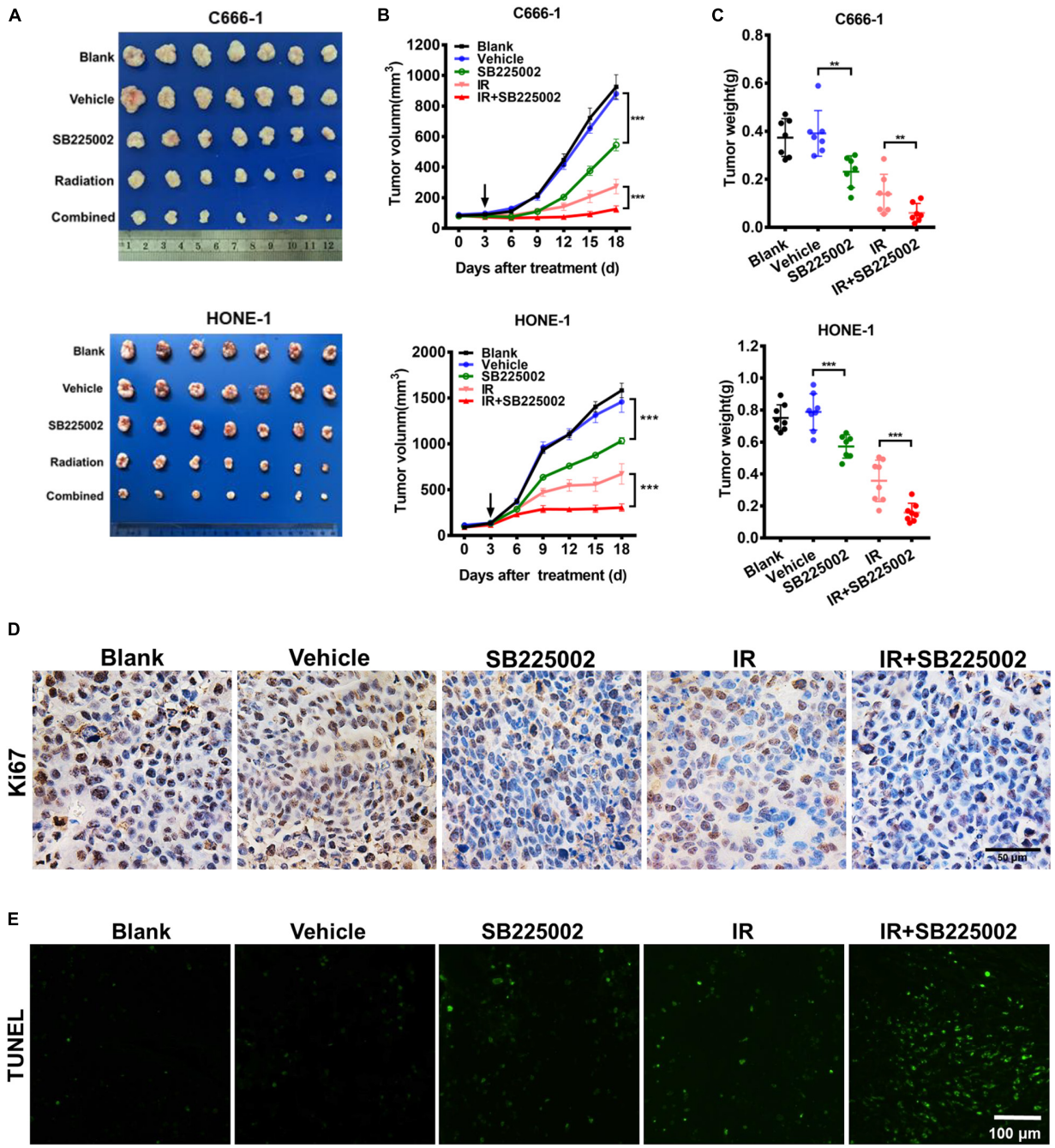

FIGURE 4 | SB225002 sensitizes tumor to radiation *in vivo*. C666-1 and HONE-1 cells were established subcutaneous in female BALB/c mice and SB225002 at 10 mg/kg and vehicle administration once daily were started 5 days after inoculation. A single dose of 8 Gy was administered at the 3th day of SB225002 administration. Tumor volumes and tumor weights were recorded every three days (seven mice per group). **(A)** Representative images of the xenograft tumors in five groups. Mice bearing C666-1 (Upper) and HONE-1-1 (Blow) tumors. **(B)** The growth curves of the tumors in five groups were presented. Data are shown as the mean tumor volume ± SD ($n = 7$; $^{***}p < 0.001$; two-way ANOVA). **(C)** The antitumor and radiosensitization effects of SB225002 on the tumor weight in five groups were shown as mean ± SD ($n = 7$; $^{**}p < 0.01$; $^{***}p < 0.001$; Student's *t*-test). **(D)** Tumor cell proliferation was assessed by Ki67 immunohistochemical staining of paraffin-embedded C666-1 tumor sections ($n = 3$; Scale bar, 50 μm). **(E)** Tumor cell apoptosis was measured on paraffin-embedded C666-1 tumor sections by TUNEL staining ($n = 3$; Scale bar, 100 μm).

HUVECs was significantly elevated following culture in tumor supernatants and medium containing CXCL8 relative to that of HUVECs cultured only in medium. In agreement with these observations, blockage of the binding between the CXCL8 receptor CXCR2 with SB225002 decreased the migration of HUVECs following exposure to tumor supernatants or CXCL8

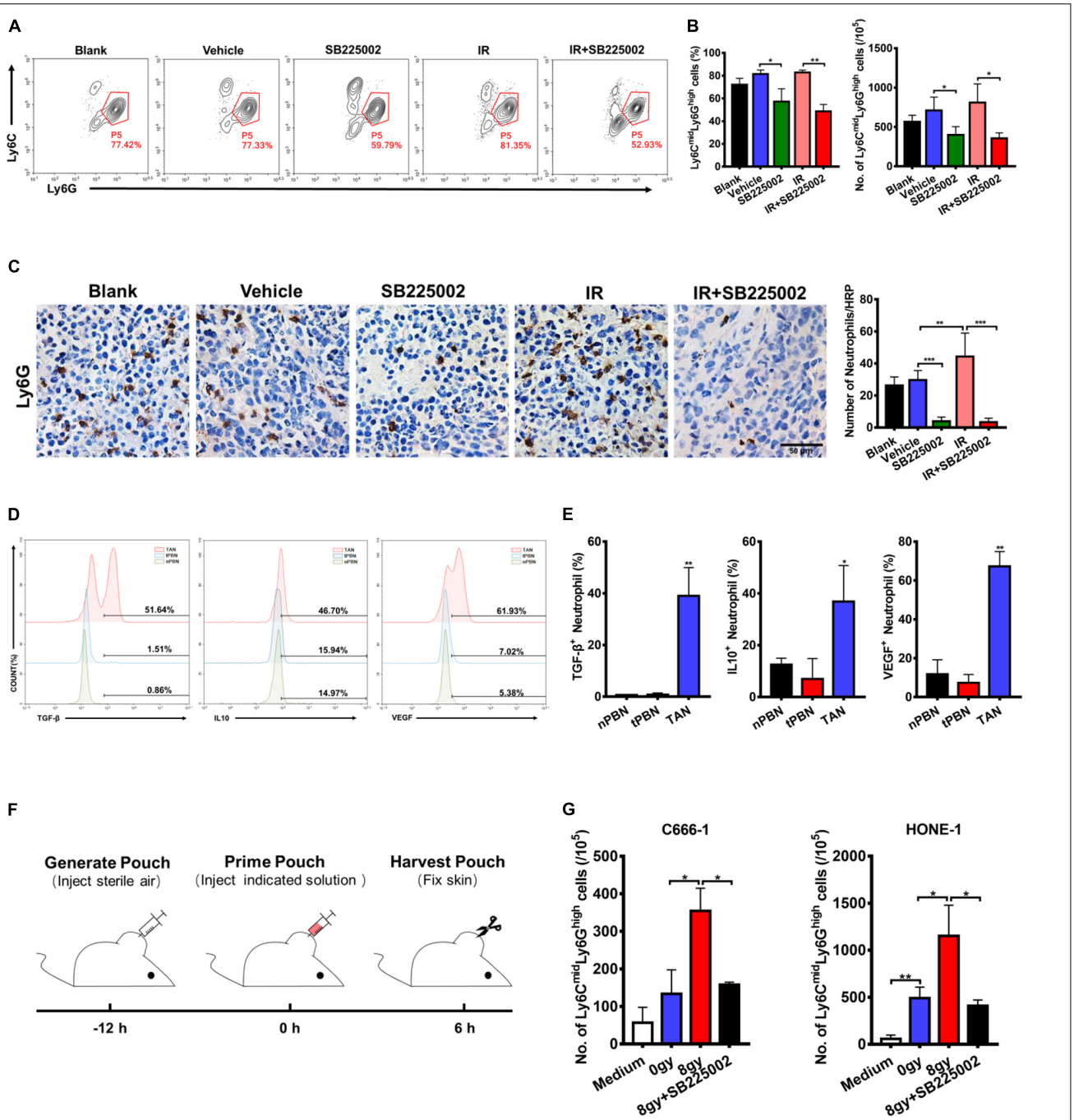

FIGURE 5 | Effects of SB225002 on recruitment of TANs *in vivo*. **(A)** SB225002 significantly reduced TANs in C666-1 tumor-bearing nude mice. Total numbers of 10,000 cells gated on CD45-positive cells were collected and $CD45^{+}CD11b^{+}Ly6C^{mid}Ly6G^{high}$ cells were gated as TANs. Numbers illustrated indicate the percentage of the cells. **(B)** Flow cytometry analysis quantified TANs in tumor at the end of treatment with SB225002 combined radiotherapy. The percentage of TANs and the absolute number of TANs were shown as mean ± SD ($n = 4$; $^{*}p < 0.05$; $^{**}p < 0.01$; Student's *t*-test). **(C)** TAN was assessed on paraffin-embedded C666-1 tumor sections by Ly6G immunohistochemical staining after SB225002 combined radiotherapy treatment. Representative immunohistochemistry images showing Ly6G-positive TANs in the xenograft tumors in five groups. Scale bar, 50 mm. Image analysis data for Ly6G-positive TANs were shown as mean ± SD ($n = 3$ animals each group, $^{**}p < 0.01$; $^{***}p < 0.001$; Student's *t*-test). **(D,E)** Intracellular flow cytometry detected the increased secretion of TGF-β, IL-10 and VEGF by Ly6G-positive neutrophils in C666-1 tumors (TAN) compared with the neutrophils in peripheral blood from both non-tumor bearing mice (nPBN) and C666-1 tumor-bearing mice (tPBN). Total numbers of 10,000 cells gated on CD45-positive cells were collected and the $CD45^{+}CD11b^{+}Ly6C^{mid}Ly6G^{high}$ cells in tumor were gated. Numbers illustrated indicate the percentage of the cells ($n = 3$; $^{*}p < 0.05$; $^{**}p < 0.01$; Student's t-test). **(F)** Schematic representation of the experiment sequence in air pouch experiments of recruitment of neutrophils stimulated by supernatants of irradiated tumor cells *in vivo*. **(G)** Flow cytometry analysis quantified neutrophils recruitment into the air pouch skin samples. Air pouch skin samples were collected at the indicated time point, and neutrophils were analyzed by flow cytometry. Total cell numbers per 10^5 cells are shown. Means ± SD are depicted ($n = 3$; $^{*}p < 0.05$; Student's *t*-test).

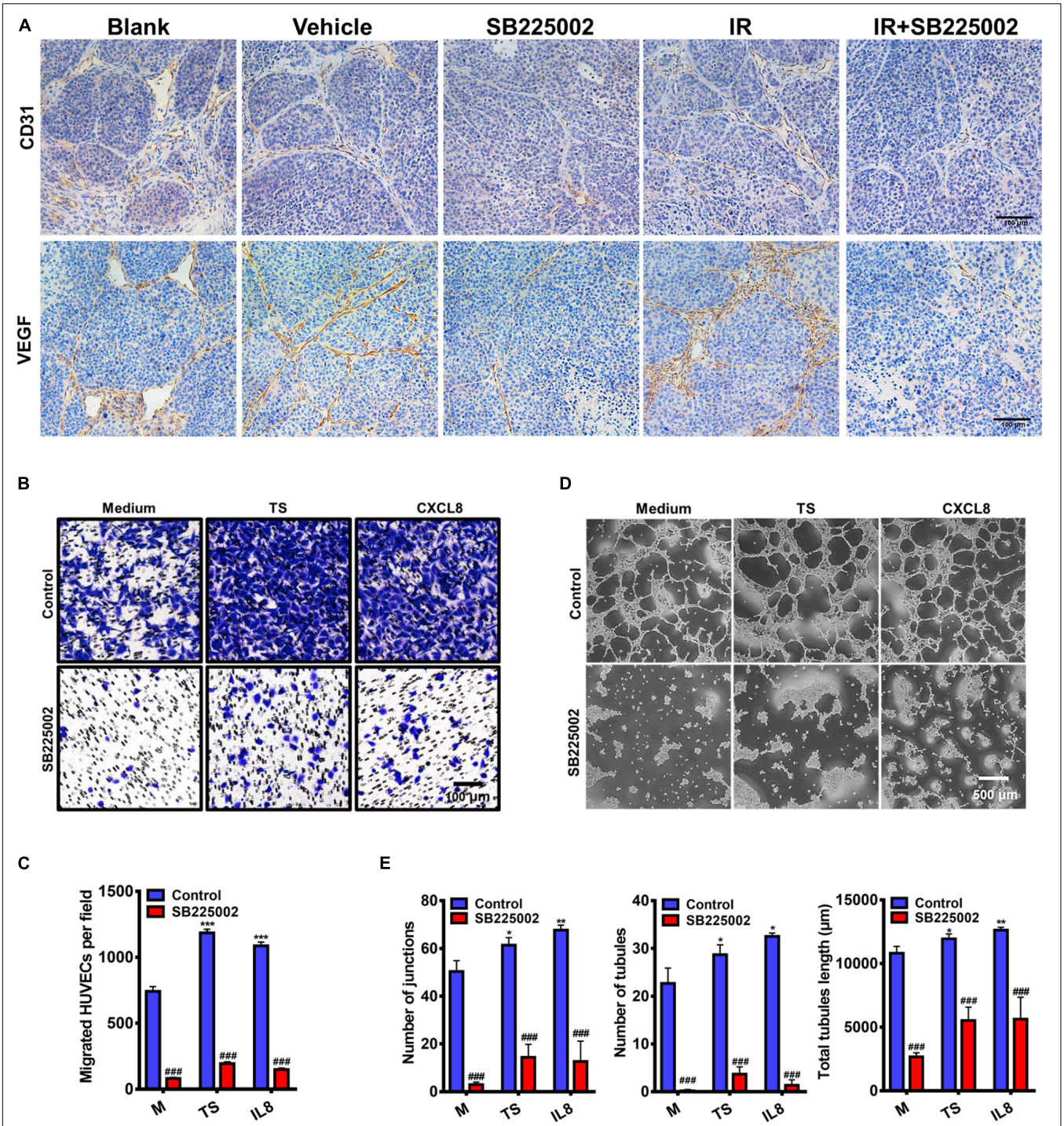

FIGURE 6 | Regulation of tumor angiogenesis by CXCR2 inhibitor. **(A)** Paraffin-embedded C666-1 tumor sections after SB225002 combined radiotherapy treatment were examined by immunohistochemical analysis with anti-CD31 and anti-VEGF antibody. Representative tumor vasculature from five groups was shown. **(B)** Representative photographs of HUVECs migration *in vitro*. HUVECs were seeded into the upper chamber of a transwell system, and tumor culture medium supernatant (TS) of nasopharyngeal carcinoma cell C666-1, human recombinant protein CXCL8 or SB225002 (0.5 μM), was added to the bottom chamber. Scale bar = 100 μm. **(C)** Statistical analysis of the number of migrated HUVECs. Data were assessed by ImageJ, showing as Mean ± SD ($n = 3$; ***$p < 0.001$; ###$p < 0.001$. * represent p value between tumor supernatant or CXCL8 group and serum free medium group, # represent p value between groups with or without SB225002. **(D)** Representative photographs of HUVEC tubule formation *in vitro* grown on the Matrigel after 3-4 h in the presence of tumor supernatant, human recombinant protein CXCL8 (50ng/ml) or SB225002(0.5 μM), compared to free serum medium. Scale bar = 500 μm. **(E)** Statistical analysis of junctions, tubules and total tubule length formed by HUVECs. Data were assessed by ImageJ showing as Mean ± SD ($n = 3$; *$p < 0.05$; **$p < 0.01$; ###$p < 0.001$. * represent p value between tumor supernatant or CXCL8 group and serum free medium group, # represent p value between groups with or without SB225002.

(**Figures 6B,C**). We next examined how SB225002 influences the tubule formation of endothelial cells when plated on Matrigel. As observed in **Figures 6D,E**, SB225002-mediated inhibition of CXCL8 prevented tumor supernatant-induced formation of tubules. Taken together, these results clearly indicate that the development of the microvascular network is inhibited by SB225002 treatment *in vitro* and *in vivo*.

DISCUSSION

Although modern radiotherapy technology has achieved considerable improvements in NPC, many NPC patients still have local recurrence and distant metastasis (Gupta et al., 2002; Yeh et al., 2005; Lee A.W.M. et al., 2012), owing to the upper limit of toxicity with associated side effects and complications (Akervall et al., 2014). Therefore, efforts are continuing to develop new strategies to enhance the antitumor effect of radiation therapy on NPC.

CXCR2, binding to its ligands, is important in tumorigenesis and tumor progression (Luan et al., 1997; Maxwell et al., 2007; Cataisson et al., 2009). There is clear evidence of the role played by CXCR2 and its associated ligands not only in promoting tumor proliferation but also in modulating blood vessel formation and neutrophil recruitment to the site of the tumor (Horton et al., 2007; Raman et al., 2011). Blockade of CXCR2 signaling pathways is a promising target for antitumor therapy.

Several observations have been made in this study concerning SB225002, the selective CXCR2 inhibitor, used in the treatment of NPC. In this study, we reveal that SB220552 suppresses tumorigenesis and radioresistance in NPC. By immunohistochemical staining of tissue microarray slides of NPC samples, we first found that an increased level of CXCR2 and CXCL8 predicts poor clinical outcomes which implies that CXCR2 is an attractive therapeutic target for NPC. We next demonstrated by CCK8 staining, clonogenicity and cell cycle assays, that SB225002 inhibits the viability and proliferation of NPC cells. Moreover, our data indicate that SB225002 sensitizes NPC cells to radiation *in vitro* by regulating the G2/M checkpoint and DNA damage repair. In our established NPC tumor model in nude BALB/c mice, the therapeutic effect of radiation against NPC was enhanced by SB225002 treatment. Furthermore, reduced recruitment of TANs and suppression of angiogenesis was observed using flow cytometry and immunohistochemical staining *in vivo*. Therefore, we may find out the possibility that the antitumor and radiosensitization activity of SB225002 results from improved sensitivity to radiation, suppression of angiogenesis as well as the disruption of immunosuppression induced by TANs.

Classically, CXCR2 is expressed on leukocytes, endothelial cells and tumor cells (Murphy et al., 2005; Vandercappellen et al., 2008; Yang et al., 2017). A number of studies have shown that blocking CXCR2 genetically or pharmacologically can inhibit angiogenesis and tumor growth (Hertzer, 2013; Wagner et al., 2015). For example, significant inhibition of human melanoma tumor growth and lung metastasis with a decrease in melanoma cell proliferation and angiogenesis has been shown in $Cxcr2^{-/-}$ mice compared to WT nude mice (Singh, 2014). Studies of colitis-associated tumorigenesis and pancreatic ductal adenocarcinoma show a clear role for CXCR2 in tumor growth associated with attenuated MDSC recruitment in $Cxcr2^{-/-}$ mice (Ijichi et al., 2011; Katoh et al., 2013). In addition, inhibition of CXCR2 reduces tumorigenesis and angiogenesis in the lung, oesophageal and ovarian cancer (Keane et al., 2004; Wang et al., 2006; Yung et al., 2018). Moreover, combining a CSF1R inhibitor with a CXCR2 inhibitor was shown to block granulocyte infiltration of tumors triggered by the inhibition of CSF1R and significantly reduce tumor growth (Kumar et al., 2017). A recently published study showed that dying tumor cell-derived DAMP release induced by radiotherapy triggers endothelial cell activation and the recruitment of myeloid cells (Krombach et al., 2019). These findings may help to explain the inhibitory and radiosensitization effects of SB225002 targeting CXCR2 in this study.

In this study, we found that SB225002 increases sensitivity to radiation in NPC cells by increasing the sustained accumulation of cells in G2/M phase, which is a well-known radiotherapy effect that increases sensitivity and suppresses DSB repair *in vitro*. In addition, the combination of radiotherapy with SB225002 suppressed angiogenesis and the recruitment of TANs triggered by irradiation *in vitro* and *in vivo* and showed strong antitumor effects. Moreover, in our study, the examinations of vital organs showed that there were no histological abnormalities or hepatorenal function changes, suggesting that the combined treatment was well tolerated.

Taken together, our results provide insights into the role of SB225002 used for NPC therapy both as an antitumor agent and radiosensitizer. SB225002 treatment dramatically enhanced the effect of radiotherapy with no toxicity to vital organs in treated mice. To the best of our knowledge, this is the first study to provide new perspectives on a CXCR2 inhibitor in combination with radiotherapy. Thus, we conclude that CXCR2 inhibition could be a potential therapeutic approach that might be further used in comprehensive NPC treatment.

DATA AVAILABILITY STATEMENT

The raw data supporting the conclusions of this article will be made available by the authors, without undue reservation.

ETHICS STATEMENT

The animal study was reviewed and approved by Ethics Committee of Sichuan Unicersity.

AUTHOR CONTRIBUTIONS

XW and YW have designed the study and revised the manuscript. XL, TL, and FM have conducted all the experiments. XL concluded the data and wrote the manuscript. TL and XW have

helped to revised it. All authors contributed to the article and approved the submitted version.

FUNDING

This work is supported by the National Natural Science Foundation Regional Innovation and Development (U19A2003), the Excellent Youth Foundation of Sichuan Scientific Committee Grant in China (No. 2019JDJQ008) and by the Development Program of China (No. 2016YFA0201402).

ACKNOWLEDGMENTS

We gratefully acknowledge Gaohua Zhang for helping with the tumor inoculation.

SUPPLEMENTARY MATERIAL

The Supplementary Material for this article can be found online at: https://www.frontiersin.org/articles/10.3389/fcell.2021.689613/full#supplementary-material

REFERENCES

Akervall, J., Nandalur, S., Zhang, J., Qian, C.-N., Goldstein, N., Gyllerup, P., et al. (2014). A novel panel of biomarkers predicts radioresistance in patients with squamous cell carcinoma of the head and neck. *Eur. J. Cancer* 50, 570–581. doi: 10.1016/j.ejca.2013.11.007

Bei, J.-X., Zuo, X.-Y., Liu, W.-S., Guo, Y.-M., and Zeng, Y.-X. (2016). Genetic susceptibility to the endemic form of NPC. *Chinese Clin. Oncol.* 5:15. doi: 10.21037/cco.2016.03.11

Cacalano, G., Lee, J., Kikly, K., Ryan, A. M., Pitts-Meek, S., Hultgren, B., et al. (1994). Neutrophil and B cell expansion in mice that lack the murine IL-8 receptor homolog. *Science* 265, 682–684. doi: 10.1126/science.8036519

Cataisson, C., Ohman, R., Patel, G., Pearson, A., Tsien, M., Jay, S., et al. (2009). Inducible cutaneous inflammation reveals a protumorigenic role for keratinocyte CXCR2 in skin carcinogenesis. *Cancer Res.* 69, 319–328. doi: 10.1158/0008-5472.can-08-2490

Chua, M. L. K., Wee, J. T. S., Hui, E. P., and Chan, A. T. C. (2016). Nasopharyngeal carcinoma. *Lancet (London, England)* 387, 1012–1024.

Eder, S., Arndt, A., Lamkowski, A., Daskalaki, W., Rump, A., Priller, M., et al. (2017). Baseline MAPK signaling activity confers intrinsic radioresistance to KRAS-mutant colorectal carcinoma cells by rapid upregulation of heterogeneous nuclear ribonucleoprotein K (hnRNP K). *Cancer Lett.* 385, 160–167. doi: 10.1016/j.canlet.2016.10.027

Gupta, A. K., McKenna, W. G., Weber, C. N., Feldman, M. D., Goldsmith, J. D., Mick, R., et al. (2002). Local recurrence in head and neck cancer: relationship to radiation resistance and signal transduction. *Clin. Cancer Res.* 8, 885–892.

Hertzer, K. M. (2013). CXCR2: a target for pancreatic cancer treatment? *Expert Opin. Ther. Targets* 17, 667–680. doi: 10.1517/14728222.2013.772137

Horikawa, T., Kaizaki, Y., Kato, H., Furukawa, M., and Yoshizaki, T. (2005). Expression of interleukin-8 receptor A predicts poor outcome in patients with nasopharyngeal carcinoma. *Laryngoscope* 115, 62–67. doi: 10.1097/01.mlg.0000150675.37860.f7

Horton, L. W., Yu, Y., Zaja-Milatovic, S., Strieter, R. M., and Richmond, A. (2007). Opposing roles of murine duffy antigen receptor for chemokine and murine CXC chemokine receptor-2 receptors in murine melanoma tumor growth. *Cancer Res.* 67, 9791–9799. doi: 10.1158/0008-5472.can-07-0246

Ignacio, R. M. C., Dong, Y.-L., Kabir, S. M., Choi, H., Lee, E.-S., Wilson, A. J., et al. (2018). CXCR2 is a negative regulator of p21 in p53-dependent and independent manner via Akt-mediated Mdm2 in ovarian cancer. *Oncotarget* 9, 9751–9765. doi: 10.18632/oncotarget.24231

Ijichi, H., Chytil, A., Gorska, A. E., Aakre, M. E., Bierie, B., Tada, M., et al. (2011). Inhibiting Cxcr2 disrupts tumor-stromal interactions and improves survival in a mouse model of pancreatic ductal adenocarcinoma. *J. Clin. Invest.* 121, 4106–4117. doi: 10.1172/jci42754

Kamran, S. C., Riaz, N., and Lee, N. (2015). Nasopharyngeal carcinoma. *Surg. Oncol. Clin. N. Am.* 24, 547–561.

Katoh, H., Wang, D., Daikoku, T., Sun, H., Dey, S. K., and Dubois, R. N. (2013). CXCR2-expressing myeloid-derived suppressor cells are essential to promote colitis-associated tumorigenesis. *Cancer Cell* 24, 631–644. doi: 10.1016/j.ccr.2013.10.009

Keane, M. P., Belperio, J. A., Xue, Y. Y., Burdick, M. D., and Strieter, R. M. (2004). Depletion of CXCR2 inhibits tumor growth and angiogenesis in a murine model of lung cancer. *J. Immunol.* 172, 2853–2860. doi: 10.4049/jimmunol.172.5.2853

Krombach, J., Hennel, R., Brix, N., Orth, M., Schoetz, U., Ernst, A., et al. (2019). Priming anti-tumor immunity by radiotherapy: dying tumor cell-derived DAMPs trigger endothelial cell activation and recruitment of myeloid cells. *Oncoimmunology* 8:e1523097. doi: 10.1080/2162402x.2018.1523097

Kumar, V., Donthireddy, L., Marvel, D., Condamine, T., Wang, F., Lavilla-Alonso, S., et al. (2017). Cancer-Associated fibroblasts neutralize the anti-tumor effect of CSF1 receptor blockade by inducing PMN-MDSC infiltration of tumors. *Cancer Cell* 32, 654–668.e5.

Lee, A. W. M., Lin, J. C., and Ng, W. T. (2012). Current management of nasopharyngeal cancer. *Semin. Radiat. Oncol.* 22, 233–244.

Lee, A. W. M., Ma, B. B. Y., Ng, W. T., and Chan, A. T. C. (2015). Management of nasopharyngeal carcinoma: current practice and future perspective. *J. Clin. Oncol.* 33, 3356–3364. doi: 10.1200/jco.2015.60.9347

Lee, Y. S., Choi, I., Ning, Y., Kim, N. Y., Khatchadourian, V., Yang, D., et al. (2012). Interleukin-8 and its receptor CXCR2 in the tumour microenvironment promote colon cancer growth, progression and metastasis. *Br. J. Cancer* 106, 1833–1841. doi: 10.1038/bjc.2012.177

Lo, M.-C., Yip, T.-C., Ngan, K.-C., Cheng, W.-W., Law, C.-K., Chan, P.-S., et al. (2013). Role of MIF/CXCL8/CXCR2 signaling in the growth of nasopharyngeal carcinoma tumor spheres. *Cancer Lett.* 335, 81–92. doi: 10.1016/j.canlet.2013.01.052

Luan, J., Shattuck-Brandt, R., Haghnegahdar, H., Owen, J. D., Strieter, R., Burdick, M., et al. (1997). Mechanism and biological significance of constitutive expression of MGSA/GRO chemokines in malignant melanoma tumor progression. *J. Leukoc. Biol.* 62, 588–597. doi: 10.1002/jlb.62.5.588

Matsuo, Y., Ochi, N., Sawai, H., Yasuda, A., Takahashi, H., Funahashi, H., et al. (2009). CXCL8/IL-8 and CXCL12/SDF-1alpha co-operatively promote invasiveness and angiogenesis in pancreatic cancer. *Int. J. Cancer* 124, 853–861. doi: 10.1002/ijc.24040

Maxwell, P. J., Gallagher, R., Seaton, A., Wilson, C., Scullin, P., Pettigrew, J., et al. (2007). HIF-1 and NF-kappaB-mediated upregulation of CXCR1 and CXCR2 expression promotes cell survival in hypoxic prostate cancer cells. *Oncogene* 26, 7333–7345. doi: 10.1038/sj.onc.1210536

Murphy, C., McGurk, M., Pettigrew, J., Santinelli, A., Mazzucchelli, R., Johnston, P. G., et al. (2005). Nonapical and cytoplasmic expression of interleukin-8, CXCR1, and CXCR2 correlates with cell proliferation and microvessel density in prostate cancer. *Clin. Cancer Res.* 11, 4117–4127. doi: 10.1158/1078-0432.ccr-04-1518

Nishi, T., Takeuchi, H., Matsuda, S., Ogura, M., Kawakubo, H., Fukuda, K., et al. (2015). CXCR2 expression and postoperative complications affect long-term survival in patients with esophageal cancer. *World J. Surg. Oncol.* 13:232.

Pei, H., Zhang, J., Nie, J., Ding, N., Hu, W., Hua, J., et al. (2017). RAC2-P38 MAPK-dependent NADPH oxidase activity is associated with the resistance of quiescent cells to ionizing radiation. *Cell Cycle* 16, 113–122. doi: 10.1080/15384101.2016.1259039

Raman, D., Sobolik-Delmaire, T., and Richmond, A. (2011). Chemokines in health and disease. *Exp. Cell Res.* 317, 575–589. doi: 10.1016/j.yexcr.2011.01.005

Rot, A., and von Andrian, U. H. (2004). Chemokines in innate and adaptive host defense: basic chemokinese grammar for immune cells. *Annu. Rev. Immunol.* 22, 891–928. doi: 10.1146/annurev.immunol.22.012703.104543

Singh, S. (2014). Host CXCR2-dependent regulation of melanoma growth, angiogenesis and experimental lung metastasis. *Cancer Res.* 71, 3831–3840.

Singh, S., Varney, M., and Singh, R. K. (2009). Host CXCR2-dependent regulation of melanoma growth, angiogenesis, and experimental lung metastasis. *Cancer Res.* 69, 411–415. doi: 10.1158/0008-5472.can-08-3378

Steele, C. W., Karim, S. A., Leach, J. D. G., Bailey, P., Upstill-Goddard, R., Rishi, L., et al. (2016). CXCR2 inhibition profoundly suppresses metastases and augments immunotherapy in pancreatic ductal adenocarcinoma. *Cancer Cell* 29, 832–845. doi: 10.1016/j.ccell.2016.04.014

Vandercappellen, J., Van Damme, J., and Struyf, S. (2008). The role of CXC chemokines and their receptors in cancer. *Cancer Lett.* 267, 226–244. doi: 10.1016/j.canlet.2008.04.050

Wagner, I. J., Damitz, L., Carey, E., Zolnoun, D., Surgery, R., and Pain, P. (2015). The CXCL8-CXCR1/2 pathways in cancer. *Cytokine Growth Factor Rev.* 70, 549–552.

Wang, B., Hendricks, D. T., Wamunyokoli, F., and Parker, M. I. (2006). A growth-related oncogene/CXC chemokine receptor 2 autocrine loop contributes to cellular proliferation in esophageal cancer. *Cancer Res.* 66, 3071–3077. doi: 10.1158/0008-5472.can-05-2871

Waugh, D. J. J., and Wilson, C. (2008). The interleukin-8 pathway in cancer. *Clin. Cancer Res.* 14, 6735–6741. doi: 10.1158/1078-0432.ccr-07-4843

Wente, M. N., Keane, M. P., Burdick, M. D., Friess, H., Buchler, M. W., Ceyhan, G. O., et al. (2006). Blockade of the chemokine receptor CXCR2 inhibits pancreatic cancer cell-induced angiogenesis. *Cancer Lett.* 241, 221–227. doi: 10.1016/j.canlet.2005.10.041

Wislez, M., Fujimoto, N., Izzo, J. G., Hanna, A. E., Cody, D. D., Langley, R. R., et al. (2006). High expression of ligands for chemokine receptor CXCR2 in alveolar epithelial neoplasia induced by oncogenic kras. *Cancer Res.* 66, 4198–4207. doi: 10.1158/0008-5472.can-05-3842

Xu, H., Lin, F., Wang, Z., Yang, L., Meng, J., Ou, Z., et al. (2018). CXCR2 promotes breast cancer metastasis and chemoresistance via suppression of AKT1 and activation of COX2. *Cancer Lett.* 412, 69–80. doi: 10.1016/j.canlet.2017.09.030

Yang, Y., Luo, B., Sun, H., An, Y., Sun, D., and Cai, H. (2017). Systematic review and meta-analysis of the prognostic value of CXCR2 in solid tumor patients. *Oncotarget* 8, 109740–109751. doi: 10.18632/oncotarget.22285

Yeh, S.-A., Tang, Y., Lui, C.-C., Huang, Y.-J., and Huang, E.-Y. (2005). Treatment outcomes and late complications of 849 patients with nasopharyngeal carcinoma treated with radiotherapy alone. *Int. J. Radiat. Oncol. Biol. Phys.* 62, 672–679. doi: 10.1016/j.ijrobp.2004.11.002

Yoshizaki, T., Horikawa, T., Qing-Chun, R., Wakisaka, N., Takeshita, H., Sheen, T. S., et al. (2001). Induction of interleukin-8 by Epstein-Barr virus latent membrane protein-1 and its correlation to angiogenesis in nasopharyngeal carcinoma. *Clin. Cancer Res.* 7, 1946–1951.

Yung, M. M.-H., Tang, H. W.-M., Cai, P. C.-H., Leung, T. H.-Y., Ngu, S.-F., Chan, K. K.-L., et al. (2018). GRO-α and IL-8 enhance ovarian cancer metastatic potential via the CXCR2-mediated TAK1/NFκB signaling cascade. *Theranostics* 8, 1270–1285. doi: 10.7150/thno.22536

Conflict of Interest: The authors declare that the research was conducted in the absence of any commercial or financial relationships that could be construed as a potential conflict of interest.

frontiers in Cell and Developmental Biology

REVIEW
published: 31 May 2021
doi: 10.3389/fcell.2021.683254

The Biological Function, Mechanism, and Clinical Significance of m6A RNA Modifications in Head and Neck Carcinoma: A Systematic Review

*Feng-Yang Jing, Li-Ming Zhou, Yu-Jie Ning, Xiao-Juan Wang and You-Ming Zhu**

Key Laboratory of Oral Diseases Research of Anhui Province, Department of Dental Implant Center, Stomatologic Hospital & College, Anhui Medical University, Hefei, China

Head and neck squamous cell carcinoma (HNSCC) is one of the most common cancers, yet the molecular mechanisms underlying its onset and development have not yet been fully elucidated. Indeed, an in-depth understanding of the potential molecular mechanisms underlying HNSCC oncogenesis may aid the development of better treatment strategies. Recent epigenetic studies have revealed that the m6A RNA modification plays important roles in HNSCC. In this review, we summarize the role of m6A modification in various types of HNSCC, including thyroid, nasopharyngeal, hypopharyngeal squamous cell, and oral carcinoma. In addition, we discuss the regulatory roles of m6A in immune cells within the tumor microenvironment, as well as the potential molecular mechanisms. Finally, we review the development of potential targets for treating cancer based on the regulatory functions of m6A, with an aim to improving targeted therapies for HNSCC. Together, this review highlights the important roles that m6A modification plays in RNA synthesis, transport, and translation, and demonstrates that the regulation of m6A-related proteins can indirectly affect mRNA and ncRNA function, thus providing a novel strategy for reengineering intrinsic cell activity and developing simpler interventions to treat HNSCC.

Keywords: head and neck squamous cell carcinoma, RNA methylation, N6-methyladenosine, epigenetics, tumor microenvironment, targeted therapy

OPEN ACCESS

Edited by:
Na Luo,
Nankai University, China

Reviewed by:
Sulen Sarioglu,
Dokuz Eylül University, Turkey
Dapeng Lei,
Shandong University, China

***Correspondence:**
You-Ming Zhu
95640021@qq.com

Specialty section:
This article was submitted to Molecular Medicine, a section of the journal Frontiers in Cell and Developmental Biology

Received: *20 March 2021*
Accepted: *10 May 2021*
Published: *31 May 2021*

Citation:
Jing F-Y, Zhou L-M, Ning Y-J, Wang X-J and Zhu Y-M (2021) The Biological Function, Mechanism, and Clinical Significance of m6A RNA Modifications in Head and Neck Carcinoma: A Systematic Review. Front. Cell Dev. Biol. 9:683254. doi: 10.3389/fcell.2021.683254

INTRODUCTION

Head and neck squamous cell carcinoma (HNSCC) is the sixth most common cancer worldwide, with an incidence of approximately 700,000 confirmed cases annually (Ferris et al., 2018). Head and neck tumors comprise neoplasms of the neck; ear, nose, and throat; and oral and maxillofacial regions. While thyroid carcinoma is the most common endocrine malignancy, nasopharyngeal

Abbreviations: AML, acute myeloid leukemia; ASF/SF2, alternative splicing factor/splicing factor 2; ALKBH5, alkB homolog 5; CCT/RT, chemoradiotherapy or radiation; CDKN1C, cyclin-dependent kinase inhibitor 1C; CDK, cyclin-dependent kinase; DDX3, DEAD-box helicase 3 X-linked; Dnmt3b, DNA methyltransferase 3 beta; eIF3, eukaryotic initiation factor 3; EBV, Epstein-Barr virus; FOXM1, fork head box protein M1; FTO, FTO alpha-ketoglutarate dependent dioxygenase; HPSCC, hypopharynx squamous cell carcinoma; HNRNP, heterogeneous nuclear ribonucleoprotein family protein; HNSCC, head and neck squamous cell carcinoma; ID4, inhibitor of DNA binding 4; m6A, N6-methyladenosine; MA, meclofenamic acid; NSUN2, NOP2/Sun RNA methyltransferase family member 2; OSCC, oral squamous cell carcinoma; RBM15, RNA binding motif protein 15; Sohlh2, spermatogenesis and oogenesis specific basic helix-loop-helix 2; SOCS, suppressor of cytokine signaling; YTH, YT521-B homolog; ZBTB16, zinc finger and BTB domain containing 16; ZFP217, zinc finger protein 217; 3'-UTR, 3'-untranslated region.

carcinoma and hypopharyngeal squamous cell carcinoma are common in otorhinolaryngological practice and oral carcinomas, such as tongue, gingival, and buccal cancer are the most common malignant neoplasms of the head and neck region. Although standard treatment strategies, such as surgery, chemotherapy, and radiotherapy have considerably improved the prognosis of patients with HNSCC, the rate of overall survival remains low (Wood et al., 2017). Recent advancements in molecular biology have allowed researchers to study the molecular mechanisms underlying tumorigenesis in greater detail. Consequently, targeted therapies based on the regulation of these molecular mechanisms have received increasing interest for treating cancer (Biktasova et al., 2017).

Over 100 types of post-transcriptional modification have been identified in eukaryotic cells (He, 2010; Cantara et al., 2011; Globisch et al., 2011), among which N6-methyladenosine (m6A), which was discovered in the 1970s, is the most common (Roundtree et al., 2017). m6A RNA methylation accounts for approximately 50% of all methylated nucleotides and occurs in 0.1–0.4% of RNA sequences in proximity to the stop codon in the 3'-untranslated region (3'-UTR) and in large exons (Desrosiers et al., 1974; Wei et al., 1975). Although the multi-component methyltransferase complex that catalyzes m6A formation was first reported in 1994 (Bokar et al., 1994), the biological function of m6A varies according to the environment and its precise mechanism of action remains poorly understood.

In this review, we briefly describe the mechanisms underlying m6A modification, as well as its important roles in RNA synthesis, transport, and translation. Next, we summarize the role of m6A modification in various types of HNSCC as well as its regulatory roles in immune cells within the tumor microenvironment. Finally, we review the development of potential therapeutic targets based on the regulatory functions of m6A that could improve the treatment of HNSCC.

m6A RNA MODIFICATION

Methyl groups are added, recognized, and removed by writer, reader, and eraser proteins, respectively, to generate m6A-modified RNA (**Figure 1**). To regulate RNA methylation, the methyltransferases METTL3, METTL14, and WTAP can form complexes with various binding proteins, such as YT521-B homologous (YTH) domain proteins and heterogeneous nuclear ribonucleoprotein (HNRNP) family proteins, which can identify and bind to methylated RNA. Conversely, m6A eraser proteins can catalyze RNA demethylation as part of the reversible dynamic process of m6A modification. Here, we briefly summarize our current understanding of the writer, reader, and eraser proteins that contribute toward m6A modification.

m6A Writers

Multiple cellular methyltransferases are known to mediate m6A modification, as listed in **Table 1**. In particular, METTL3 and METTL14 can form a stable complex with WTAP at the methylation site in mammalian cells (Liu et al., 2014). METTL14, a pseudo methyltransferase (Ondo et al., 2020) that lacks enzymatic activity, can stabilize METTL3 and recognize target RNA (Śledź and Jinek, 2016; Wang et al., 2016a,b), thereby acting as a connector between the RNA substrate and METTL3. However, the precise mechanism underlying the action of methyltransferases remains unclear and further studies are required to provide a more comprehensive understanding.

m6A Readers

The most important function of m6A is the recruitment of m6A-binding proteins to RNA. Recent studies have shown that m6A can be recognized by YT521B homology domain proteins and eukaryotic initiation factor 3 (eIF3) (Jiang et al., 2021). The mammalian genome contains five YTH domain proteins: YTHDC1 (DC1), YTHDC2 (DC2), YTHDF1 (DF1), YTHDF2 (DF2), and YTHDF3 (DF3). YTHDF2 is the most abundant DF family protein in almost all cell types and was the first m6A reader protein reported to facilitate the localization of mRNA to RNA decay sites (Wang et al., 2014a). Conversely, YTHDF1-mediated promoters are known to improve translation efficiency, whereas YTHDF3 plays an important role during the initial stages of translation; however, the detailed mechanism remains unclear (Li et al., 2017a). Various other binding proteins, such as hnRNPA2B1 and hnRNPC, have also been recently identified (**Table 1**) and their functions are described in detail throughout this review.

m6A Erasers

Currently, FTO (alpha-ketoglutarate dependent dioxygenase), and ALKBH5 (alkB homolog 5) are the only known m6A eraser proteins. FTO is an m6A demethylase that has previously been associated with obesity in humans (Jia et al., 2011). Indeed, this study demonstrated that the m6A modification is reversible and dynamic, not just formation-related, and thus greatly increased research on RNA methylation. The FTO homolog, ALKBH5 is also a m6A demethylase (Rubio et al., 2018; **Table 1**); however, limited evidence is available regarding its role in the direct demethylation of specific m6A loci in mRNA (Meyer and Jaffrey, 2017). Although m6A demethylases have been recognized to play an important role in regulating the extent of m6A RNA modification, our current understanding of their precise activity is limited and further studies are required to identify their other physiological roles.

Despite the limitations in our current understanding of the precise mechanisms underlying m6A RNA modification, various studies have examined the effects of m6A modification on the regulation of RNA transcripts.

ROLES OF m6A IN RNA REGULATION

m6A is thought to be the most abundant chemical modification of mammalian mRNA and non-coding RNA and is involved in the regulation of several physiological and disease processes (Perry et al., 1975; Fomenkov et al., 2020; Kontur et al., 2020; Wang and Lu, 2021). In particular, m6A can facilitate or be directly involved in RNA processing (**Figure 2**). Comprehensive methods to identify transcriptome-wide m6A profiles have improved

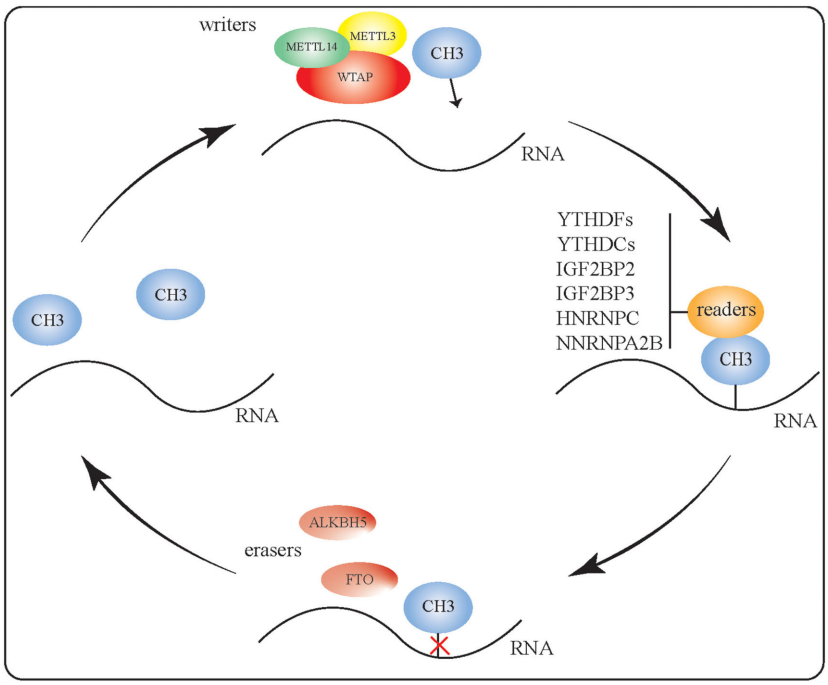

FIGURE 1 | RNA m6A modification. Methyl groups are added, recognized, and removed by writer, reader, and eraser proteins, respectively. The methyltransferases METTL3, METTL14, and WTAP can form complexes to regulate RNA methylation. Binding proteins such as YTH domain proteins and HNRNP proteins can identify and bind to methylated RNA. The two m6A eraser proteins—FTO and ALKBH5—perform RNA demethylation, making the m6A RNA modification a reversible and dynamic process.

TABLE 1 | Enzymes mediating N6-methyladenosine (m6A) deposition.

Symbol	Full name	HGHG ID	Function	Location
METTL3	Methyltransferase-like 3	17563	Writer	14q11.2
METTL14	Methyltransferase-like 14	29330	Writer	4q26
METTL16	Methyltransferase-like 16	29330	Writer	17p13.3
WTAP	WT1-associated protein	16846	Writer	6q25.3
ZC3H13	Zinc finger CCCH-type containing 13	20368	Writer	13q14.13
ZCCHC4	Zinc finger CCHC-type containing 4	22917	Writer	4p15.2
RBM15	RNA-binding motif protein 15	14959	Writer	1p13.3
RBM15B	RNA-binding motif protein 15B	24303	Writer	3p21.2
YTHDF1	YTH N6-methyladenosine RNA-binding protein 1	15867	Reader	20q13.33
YTHDF2	YTH N6-methyladenosine RNA-binding protein 2	31675	Reader	1p35.3
YTHDF3	YTH N6-methyladenosine RNA-binding protein 3	26465	Reader	8q12.3
YTHDC1	YTH domain-containing 1	30626	Reader	4q13.2
YTHDC2	YTH domain-containing 2	24721	Reader	5q22.2
IGF2BP2	Insulin-like growth factor 2 mRNA-binding protein 2	28867	Reader	3q27.2
IGF2BP3	Insulin-like growth factor 2 mRNA-binding protein 3	28868	Reader	7p15.3
HNRNPC	Heterogeneous nuclear ribonucleoprotein C	5035	Reader	14q11.2
HNRNPA2B1	Heterogeneous nuclear ribonucleoprotein A2/B1	5033	Reader	7p15.2
FTO	FTO alpha-ketoglutarate-dependent dioxygenase	24678	Eraser	16q12.2
ALKBH5	alkB homolog 5, RNA demethylase	25996	Eraser	17p11.2

HGHG, HUGO gene nomenclature committee.

our understanding of this modification and have shown that m6A can selectively regulate transcription. Proteins such as HnRNP, which can selectively bind to m6A-modified mRNAs in response to physiological factors (Liu et al., 2015; Jin et al., 2021), regulate mRNA function by modulating RNA splicing, export, translation, degradation, as well as miRNA maturation (Huang et al., 2018; Zhang et al., 2020; Chen et al., 2021a; Jin et al., 2021; Song et al., 2021). Here, we examine the effects of

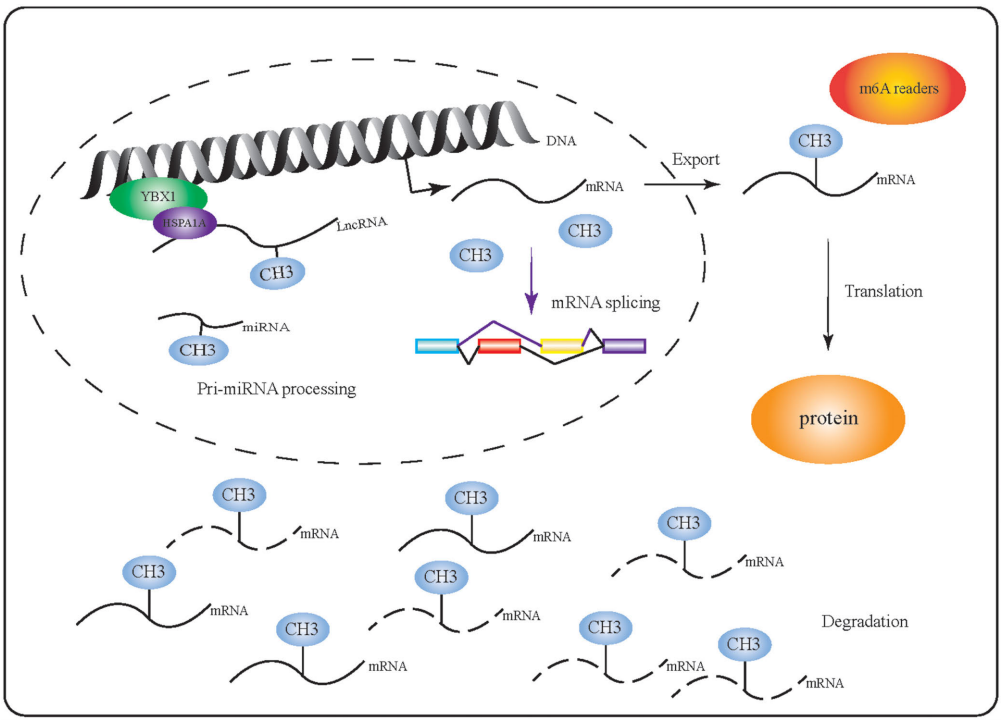

FIGURE 2 | m6A-modified RNA performs multiple functions. m6A-related proteins (including writers, readers, and erasers) affect mRNA function by regulating RNA synthesis, splicing, export, translation, degradation, and miRNA maturation.

m6A on the function of RNAs throughout different stages of their processing.

m6A in RNA Splicing

Previous studies have shown that m6A-modifications can spatially overlap with the splicing enhancer region and act as a pre-RNA splicing regulator to promote alternative mRNA splicing (Zhao et al., 2014). In addition, METTL16 was found to promote RNA splicing by targeting the downstream mRNAs and non-coding RNAs (Warda et al., 2017). During splicing, METTL16 can induce m6A modification in the 3′-UTR of mRNA and A43 modification in U6 nuclear RNA with 50 base pairs of pre-mRNA, indicating that METTL16 plays important roles in determining mRNA stability and splicing (Aoyama et al., 2020; Ovcharenko et al., 2021). The inhibition of other m6A methyltransferases was also shown to affect gene expression and alternative splicing patterns (Dominissini et al., 2012), while METTL3 downregulation alters RNA splicing in pancreatic cancer (Taketo et al., 2018). Furthermore, YTHDC1 has been shown to recruit the splicing factor SRSF3 to m6A-modified pre-RNAs to promote splicing (Kasowitz et al., 2018), suggesting that m6A binding proteins can also regulate RNA splicing.

In addition, demethylases have been reported to play important roles in regulating m6A-mediated RNA splicing. For instance, pre-mRNA in the preferential binding intron region of FTO is located close to the alternative splicing exon and polyA site (Hess et al., 2013), while the alternative splicing of nuclear pre-mRNA can be regulated by SRSF2 binding (Bartosovic et al., 2017). The removal of m6A by FTO inhibits SRSF2 recruitment and promotes exon 6 skipping, resulting in a short subtype of Runt-related transcription factor 1 (Ben-Haim et al., 2015). The downregulation of ALKBH5 can also enhance exon jumping and induce the rapid degradation of abnormally spliced transcripts (Tang et al., 2018). Furthermore, ALKBH5 can affect the phosphorylation of alternative splicing factor/splicing factor 2 (ASF/SF2) in the nucleus, whose hyperphosphorylated form is involved in pre-mRNA splicing (Zheng et al., 2013).

m6A in RNA Nuclear Export

Recent studies have shown that m6A writer, reader, and eraser proteins can promote RNA nuclear export. In particular, METTL3, METTL14, and WTAP-mediated m6A modification were found to promote the nuclear-to-cytoplasmic translocation of mRNA (Fustin et al., 2013). Meanwhile, the m6A reader protein YTHDC1 can promote the binding of RNA to SRSF3 and the mRNA export receptor Nxf1, thereby targeting m6A-modified mRNA for nuclear export (Wang et al., 2015). Similarly, ALKBH5 can promote mRNA export by reducing the phosphorylation of ASF/SF2, enabling it to bind to the TAP-p15 complex, a general mRNA nuclear export receptor that binds to and translocates mRNA (Li and Manley, 2005; Michlewski et al., 2008; Zheng et al., 2013).

m6A in mRNA Translation

m6A modification in the 5′- or 3′-UTR of mRNAs and non-coding RNAs has been found to regulate gene expression

(Selmi et al., 2021; Yao et al., 2021) and promote the translation of 5'-UTR-methylated mRNAs (Shen et al., 2020; Zhang et al., 2021). Moreover, translational regulation by m6A has been reported to play a key role in several cancers. In acute myeloid leukemia (AML), m6A upregulates the expression of the MYB proto-oncogene, MYC proto-oncogene, BCL2, phosphatase and tensin homolog, and SP1 transcription factor, which in turn enhance the binding ability and translation efficiency of the oncogenic RNA and ribosome to facilitate tumorigenesis (Li et al., 2017b; Wang et al., 2020a; Qing et al., 2021; Yankova et al., 2021). The upregulation of the m6A reader protein METTL3 has also been shown to enhance mRNA translation (Schumann et al., 2016; Coots et al., 2017), whereas its downregulation selectively inhibits mRNA translation (Coots et al., 2017), decreases AF4/FMR2 family member 4 and MYC proto-oncogene translation in bladder cancer (Cheng et al., 2019), and increases zinc finger protein 750 and fibroblast growth factor 14 translation in nasopharyngeal carcinoma (Zhang et al., 2018). Furthermore, METTL3 was found to increase m6A deposition in its target genes in the human AML cell line MOLM-13, as well as myelomatosis and B-cell lymphoma 2 (Vu et al., 2017), and has been reported to enhance the translation of its target mRNA, *tafazzin,* independently of its methyltransferase activity in lung cancer cells (Lin et al., 2016).

m6A-induced translational regulation also plays a key role in normal physiological function. For instance, m6A has been observed in the transcripts of key regulatory factors, such as ZBTB16, ID4, Dnmt3b, and Sohlh2, in spermatogonial stem cells/progenitor cells and regulates their transcription and translation to coordinate protein synthesis. Thus, the m6A modification is essential for spermatogenesis in mammals (Lin et al., 2017). Studies have shown that human YTHDF1 selectively recognizes m6A-modified mRNAs and enhances translation by interacting with initiation factors and ribosomes, indicating that YTHDF1 directly promotes translation initiation and transports cellular mRNAs to the translation machinery (Tassinari et al., 2021). During mRNA translation, the recognition and binding of m6A by YTHDFs also results in enhanced protein synthesis (Shi et al., 2017; Su et al., 2021). In particular, YTHDC2 selectively binds to m6A using its consensus motif to improve the translation efficiency and reduce the abundance of the target mRNA (Hsu et al., 2017; Wojtas et al., 2017).

Heat shock proteins are also involved in m6A-mediated translation regulation. Under heat shock conditions, m6A preferentially binds to the 5'-UTR of stress-induced transcripts, such as heat shock protein family H (Hsp110) member 1. Moreover, increased 5′-UTR m6A modification can further enhance the initiation of cap-independent translation (Zhou et al., 2015). m6A modification can also promote translational priming by interacting with the initiators eIF3, CBP80, and eIF4E in an RNA-independent manner. Cellular stress increases the 5′-UTR m6A modification of RNA transcripts, which in turn promotes mRNA translation by directly binding to eIF3 in a YTHDF1-independent manner (Liu et al., 2020a). Translation initiation typically requires the eIF4 protein complex, particularly the cap-binding protein eIF4e (Jackson et al., 2010). However, m6A-modified mRNA can recruit eIF3 in the absence of eIF4E and other components of the eIF4 complex, allowing the m6A-modified mRNAs to be translated in the presence of eIF3 and other priming factors (Orouji et al., 2020). Subsequent studies have also confirmed that m6A is required to recruit eIF3 to mRNA during protein translation (Hwang et al., 2021).

m6A in mRNA Degradation

The degree of m6A modification can determine the stability of cytoplasmic mRNA (Ke et al., 2017), with METTL3-, METTL14-, and WTAP-mediated m6A modification all reducing mRNA stability (Schwartz et al., 2014; Geula et al., 2015; Knuckles et al., 2017; Bertero et al., 2018). For instance, METTL3 or METTL14 downregulation in T cells inhibits the m6A mRNA modification and increases the expression of suppressor of cytokine signaling (SOCS) family mRNAs (Jiang et al., 2020).

YTHDF family proteins can also accelerate the decay of m6A-modified mRNA transcripts (Liu et al., 2020b) or target mRNAs (Wang and He, 2014b). For example, YTHDC1 recognizes the m6A-modified 3'-UTR of MAT2A to induce methyl donor S-adenosyl methionine-mediated MAT2A mRNA degradation (Shima et al., 2017). YTHDF2 can also recognize m6A-modified SOCS2 and accelerate its degradation to induce tumorigenesis (Chen et al., 2018); however, the downregulation of m6A methyltransferase weakens the interaction between YTHDF2 and the target mRNA, increasing SOCS2 mRNA stability (Mapperley et al., 2021). However, studies using YTHDF1-knockout cells have shown that YTHDF1 has minimal effect on mRNA stability (Wang et al., 2015). One study found that all YTHDF proteins can increase mRNA stability and protein expression (Kennedy et al., 2016), yet experiments conducted by other researchers showed that all three YTHDF proteins can initiate mRNA degradation and dealkylation (Du et al., 2016). These varying results have raised questions regarding the functions of YTHDF proteins. Meanwhile, a study on the m6A reader protein IGF2BP1/2/3 found that it recognized the common GG (m6A) C sequence via its K homologous domain and enhanced the stability and translation of its target mRNA in an m6A-dependent manner under normal and stress conditions (Huang et al., 2018).

The m6A eraser protein, FTO, was found to increase the stability of MYC mRNA by inhibiting YTHDF2-mediated RNA decay (Su et al., 2018; Weng et al., 2018), while ALKBH5 is also known to regulate mRNA stability. In particular, ALKBH5 has been found to localize at nuclear sites, regulate the assembly/modification of mRNA processing factors, demethylate m6A mRNA, and regulate mRNA export and stability (Zheng et al., 2013). In ALKBH5-deficient spermatocytes, increased nuclear RNA efflux significantly increases cytoplasmic RNA levels as well as the synthesis of newborn RNA, while decreasing overall RNA stability, leading to spermatocyte apoptosis (Zheng et al., 2017).

Functional proteins such as transcription factors can also affect mRNA stability by regulating the degree of m6A modification in mRNA transcripts. For example, zinc finger protein 217 (ZFP217) activates the transcription of key pluripotent genes and regulates the m6A modification of the corresponding transcripts. Thus, ZFP217 depletion enhances the m6A modification in *Nanog*, *Sox2*, *Klf4*, and *c-Myc* mRNAs

to accelerate their degradation, thereby disrupting the self-renewal of embryonic stem cells and somatic reprogramming (Aguilo et al., 2015).

METTL3 is also known to methylate pri-miRNAs, tag them for identification and processing, and promote global miRNA maturation in a cell type-independent manner (Bhat et al., 2020; Yi et al., 2020a). In breast cancer, METTL3 recognizes pri-miRNAs via the microprocessor protein DGCR8, increases mature miRNA levels, and decreases untreated pri-miRNA levels (Zhong et al., 2020). Other methylases are also involved in miRNA regulation. For instance, the activation of protease activated receptor 2 decreases miR-125b levels via NOP2/Sun RNA methyltransferase family member 2 (NSUN2), which methylates the miR-125b precursor, interferes with its processing, and reduces mature miR-125b levels (Yuan et al., 2014). m6A modification can also be performed by identifying DGCR8 and labeling the original RNA in a METTL3/m6A-dependent manner. In particular, the m6A binding protein hnRNPA2B1 can recruit DGCR8 to RNA by targeting the m6A site, thus playing an important role in promoting pri-miRNA processing (Alarcón et al., 2015; Chen et al., 2020); however, the precise mechanism remains poorly understood. Future studies are therefore required to determine whether m6A modification plays a key role in miRNA maturation and whether miRNA maturation could be regulated by targeting the m6A modification sites.

Other Functions of m6A in RNA Regulation

In addition to its roles in the processing of RNAs, the m6A modification of mRNAs and ncRNAs also plays key roles in the growth and development of various tumors. For instance, HBXIP upregulates METTL3 expression in breast cancer cells by inhibiting miRNA-let-7g, which downregulates METTL3 expression by targeting its 3'-UTR. METTL3 subsequently increases *HBXIP* expression by increasing m6A modification, thereby creating a positive feedback loop consisting of HBXIP/miR-let-7g/METLL3/HBXIP that accelerates breast cancer cell proliferation (Cai et al., 2018). FTO also interacts with METTL3 to regulate polyA site and 3'-UTR lengths (Begik et al., 2020), which can also be altered by YTHDC1 knockout (Chen et al., 2021b). Thus, all of these factors may contribute toward tumor development. Indeed, AML can be initiated by the chromosomal translocation of RNA binding motif protein 15 (RBM15), another component of the m6A writer complex (also known as OTT1), with myelin (Mercher et al., 2001). In hepatocellular carcinoma, reduced miRNA-126 m6A modification affects its function as a ceRNA (competing endogenous RNAs) and decreases its binding capacity, thus promoting tumor development (Ma et al., 2017).

Together, these studies demonstrate that m6A modification plays an important role in RNA synthesis, transport, and translation, and that the regulation of m6A-related proteins can indirectly affect mRNA and ncRNA function. Moreover, m6A modification also plays an important role in the occurrence and development of various tumors by regulating miRNA processing, mRNA translation, and RNA stability. These findings suggest a novel strategy for reengineering intrinsic cell activity and simplifying intervention measures that could provide novel strategies for the diagnosis and treatment of cancer. However, our understanding of the roles and mechanisms of m6A modification is currently very limited and further studies are required to elucidate these aspects in more detail.

ROLES OF m6A MODIFICATION IN HNSCC

Although current evidence suggests that m6A plays important roles in cancer, to our knowledge, no systematic reviews have yet described the role of m6A modification in HNSCC. Herein, we discuss the mechanism of m6A in several common HNSCCs and aim to provide novel ideas for future research regarding the pathogenesis and development of HNSCC (**Table 2**).

Thyroid Carcinoma

Thyroid cancer accounts for 1% of all malignant tumors; however, its incidence varies greatly according to region, ethnicity, and sex. For instance, females are more prone to thyroid cancer than males (Cabanillas et al., 2016; Roman et al., 2017), while papillary carcinoma is the most common malignant thyroid tumor, especially among young adults, and is characterized by a low malignancy and good prognosis (Carling and Udelsman, 2014; Araque et al., 2017). Therefore, the precise molecular mechanisms underlying the occurrence and development of thyroid cancer must be elucidated to develop targeted therapies.

In Xu et al. (2020) identified various m6A-related differentially expressed genes (*METTL3*, *YTHDC2*, *HNRNPC*, *WTAP*, *YTHDF1*, *ALKBH5*, *METTL14*, *YTHDC1*, *FTO*, *ZC3H13*, *KIAA1429*, *YTHDF2*, and *RBM15*) between patients with thyroid cancer and normal patients from TCGA datasets. After validating the gene signature using three GEO datasets (GSE33630, GSE35570, and GSE60542), the authors concluded that m6A modification affects the prognosis of thyroid cancer. Moreover, Wang et al. (2020b) found that the expression of *METTL3*, *YTHDC1*, *FTO*, *METTL14*, *RBM15*, *YTHDF3*, *WTAP*, *HNRNPA2B1*, *ALKBH5*, *METTL16*, *YTHDC2*, *KAA1429*, *IGF2BP3*, *RBM15B*, and *YTHDF1* was significantly lower in thyroid cancer tissues than that in normal thyroid tissues using bioinformatics analysis, consistent with the findings of Hou et al. (2020). However, studies have also shown that METTL3 can induce the m6A mRNA modification of TCF1, a downstream effector of the classical Wnt pathway encoded by *TCF7*, by activating the Wnt pathway, thereby accelerating the progression of thyroid cancer (Wang et al., 2020c). Although these results indicate that METTL3 exerts contradictory effects on thyroid cancer, the precise underlying mechanism remains unclear. This may be due to the fact that thyroid carcinoma has multiple subtypes that present with different clinical and pathological features. Therefore, the role of m6A-modification related proteins in different thyroid cancer subtypes should be validated in future studies.

TABLE 2 | Regulation of m6A modification in head and neck squamous cell carcinoma (HNSC).

Cancer	m6A regulators	Regulation	Mechanism	References
THCA	METTL3	Up	METTL3 can activate the Wnt pathway and mediate TCF1 methylation, which promotes THCA proliferation and migration.	Wang et al., 2020b
NPC	METTL3	Up	Via m6A modification, METTL3 can promote EZH2 expression and NPC progression. EZH2 can also inhibit CDKN1C and promote tumor cell proliferation.	Meng et al., 2020
	YTHDF1	Down	YTHDF1 inhibits BZLF1/BRLF1 to promote the recognition of EBV transcripts and inhibit NPC development.	Xia et al., 2021
HPSCC	YTHDF1	Up	YTHDF1 can promote the expression of TFRC, which promotes the entry of Fe3+ ions into cells and accelerates HPSCC formation.	Ye et al., 2020
OSCC	METTL3/ IGF2BP1	Up	By recognizing m6A on the 3′ UTR of BMI-1, METTL3 can interact with IGF2BP1, which promotes BMI-1 expression and accelerates OSCC proliferation and metastasis.	Liu et al., 2020c
	ALKBH5	Up	DDX3 can increase ALKBH5 expression and promote FOXM1/NANOG via m6A modification, thereby inducing OSCC chemotherapy resistance.	Shriwas et al., 2020
0 Others	METTL3/14	Up	METTL3/14 can stabilize lncAROD, which promotes YBX1 and HNSCC.	Ban et al., 2020
	YTHDC2	Down	YTHDC2 can interact with several immune cell types in cancer and improve HNSCC prognosis.	Li et al., 2020
	METTL3	Down	METTL3-mediated deposition of m6A can accelerate SOCS recognition and promote IL2-STAT5 signaling pathway activation, which can maintain the immunosuppressive function of Treg and inhibit tumor progression.	Zhao and Cui, 2019

THCA, thyroid carcinoma; NPC, nasopharyngeal carcinoma; HPSCC, hypopharynx squamous cell carcinoma; OSCC, oral squamous cell carcinoma.

Nasopharyngeal Carcinoma

Although chemotherapy and radiotherapy have improved the overall survival of patients with nasopharyngeal carcinoma, approximately 30% of treated patients develop metastasis or recurrence and their prognosis is often poor (Lee et al., 2017; Liu et al., 2018; Chen et al., 2019). Therefore, an improved understanding of the precise mechanisms underlying the occurrence and development of nasopharyngeal carcinoma is required to develop more effective treatment methods.

Epstein-Barr virus (EBV) is responsible for causing many types of malignant tumors and is widely associated with B-cell lymphoma, gastric cancer, and nasopharyngeal carcinoma (Shi et al., 2016; Young et al., 2016; Liu et al., 2019). Recently, the EBV transcriptome was studied in EBV-transformed lymphoblastoid and lymphoma cells, and the findings of this analysis revealed that m6A regulates EBV-associated tumorigenesis (Lang et al., 2019). Although the m6A modification was identified during the latent stage of EBV infection, the modification of EBV transcripts by the deposition of m6A was reduced during lytic infection. Increased EBNA3C levels have been shown to increase the expression and stability of METTL14, which can induce the proliferation and colony formation of EBV-positive cells (Zheng et al., 2021) and stabilize METTL3 via its interaction with RNAs (Klungland and Dahl, 2014; He and He, 2021). METTL3 is highly expressed in nasopharyngeal carcinoma tissues and affects the overall survival of patients with nasopharyngeal carcinoma. In addition, METTL3 can enhance the m6A modification of *EZH2* mRNA to increase the expression of EZH2 protein, an important component of the PRC2 complex that plays a role in gene silencing by depositing methyl groups on the lysine 27 residue of histone 3 (Zhong et al., 2013; Yamaguchi and Hung, 2014; Xu et al., 2019). Several studies have also shown that EZH2 can promote cell proliferation by inhibiting cyclin-dependent kinase (CDK) inhibitor 1C (CDKN1C) (Yang et al., 2009), which is inactivated by promoter DNA methylation in several human tumors (McGarvey et al., 2006; Fang et al., 2021), thereby promoting nasopharyngeal carcinoma development and increasing the malignancy of nasopharyngeal carcinoma cells (Meng et al., 2020).

In EBV-induced nasopharyngeal carcinoma, YTHDF1 has been shown to inhibit tumor development by downregulating BZLF1 and BRLF1, thereby reducing the stability of EBV transcripts, and interact with the RNA degradation complex to promote RNA degradation (Xia et al., 2021). The RNA degradation complex consists of two components, i.e., ZAP and DDX17. ZAP induces the degradation of target mRNAs, while DDX17 binds to ZAP-bound mRNAs to induce their degradation (Chen et al., 2008). However, a recent study demonstrated that the deletion of YTHDF2 and/or YTHDF3 can enhance the interaction between YTHDF1 and DDX17, suggesting that YTHDF1, YTHDF2, and YTHDF3 may compete for binding to DDX17 (Youn et al., 2018; Wu, 2020). These findings suggest that m6A-binding proteins have complex regulatory mechanisms in nasopharyngeal carcinoma; however, further experiments are required to determine their precise effects.

Hypopharynx Squamous Cell Carcinoma (HPSCC)

HPSCC has the worst prognosis among all types of head and neck tumors as it is generally detected at a late stage due to a lack of potent biomarkers for early diagnosis (Gatta et al., 2015; Arends et al., 2020). The unique clinical and biological characteristics of HPSCC are attributed to its distinct anatomical location as well as genetic and transcriptome alterations (Hajek et al., 2017; Morris et al., 2017). For example, the co-occurrence of CCND1 and CDKN2A mutations and chromosomal instability markers have been associated with radiotherapy and chemotherapy outcomes in patients with advanced HPSCC (Yamashita et al., 2019). Although various genomic alterations have been reported to be associated with sensitivity to chemotherapy, targeted therapy, and ionizing radiation (Jiang et al., 2019), only a few specific

biomarkers and therapeutic targets for HPSCC have been identified and validated. Therefore, a better understanding of the molecular mechanism underlying HPSCC progression is required to improve its treatment.

Several studies have reported the carcinogenic significance of transcription factor sets that regulate TFRC (Petronek et al., 2019), whose overexpression on the extracellular surface of the cell membrane of solid tumors results in increased iron uptake (Shen et al., 2018). Upon its release from the TF-TFRC complex into the cytoplasm, iron is reduced to its ferrous form by iron reductase *in vivo* (Ohgami et al., 2006; Gomes et al., 2012). YTHDF1 knockout was found to reduce TFRC protein expression in Detroit562 and FADU cells without affecting TFRC mRNA expression or protein stability, indicating that YTHDF1 upregulates TFRC translation via its methyltransferase domain. Moreover, high levels of YTHDF1 and TFRC have been associated with poor prognosis in patients receiving chemoradiotherapy or radiation (CCT/RT) adjuvant therapy and YTHDF1 has been shown to increase TFRC expression in HPSCC in an m6A-dependent manner (Ye et al., 2020). Although no other m6A modification-related molecules have yet been associated with HPSCC, m6A is thought to play an important role and future studies should be aimed at identifying the precise roles of various m6A-related proteins in HPSCC tumors.

Oral Squamous Cell Carcinoma (OSCC)

OSCC is the most common type of oral and maxillofacial cancer. Although surgery and CCT/RT are associated with prolonged patient survival, the rate of overall survival remains low (Ferlay et al., 2010; Leemans et al., 2011; Hedberg et al., 2016). Previous studies have shown that ncRNA-mediated epigenetic modifications play an important role in OSCC via multiple signaling pathways (González-Ramírez et al., 2014; Jithesh et al., 2013; Bavle et al., 2016). For instance, the m6A writer protein METTL3 can recognize m6A residues on the 3'-UTR of BMI1 and bind to the m6A reader protein IGF2BP1 to promote BMI1 translation, thereby inducing OSCC proliferation and metastasis (Liu et al., 2020c). However, the functional mechanism of m6A in OSCC requires further study.

m6A also plays an important role in mediating the development of drug resistance in OSCC. The chemotherapy regimen most commonly used to treat OSCC is cisplatin, either alone or in combination with 5-fluorouracil and docetaxel (Lorch et al., 2011). However, resistance to chemotherapy can reduce its ability to treat OSCC, ultimately resulting in continued tumor growth (Wang et al., 2016c). DEAD-box helicase 3 X-linked (DDX3) is a human dead-box RNA helicase that is involved in RNA metabolism and translation (Tanner and Linder, 2001; Geissler et al., 2012). DDX3 directly regulates m6A through the methylase ALKBH5 and reduces the transcription of cancer stem cell transcription factor FOXM1 (Fork head box protein M1) and Nanog homeobox, resulting in chemotherapy drug resistance (Shriwas et al., 2020). Interestingly, the DDX3 inhibitor ketorolac can restore cisplatin-mediated cell death and significantly reduce tumor burden (Shriwas et al., 2020), although it remains unclear whether this mechanism of drug resistance reversal directly involves the m6A modification. Thus, further experimental evidence and clinical studies are warranted.

Despite the fact that m6A has been implicated in the occurrence and progression of various cancers, m6A RNA modification has not been extensively studied in HNSCC. Indeed, there have been no reports of m6A modification in larynx, oropharynx, or nasal carcinoma. Furthermore, the precise mechanisms underlying m6A RNA modification in HNSCC are even less well understood. Although researchers have begun to study the effect of m6A in EBV, no studies have yet been conducted on the equally important Human Papilloma Virus (HPV). However, the findings discussed in this review suggest that m6A may play a key regulatory role in HNSCC (**Figure 3**) by promoting or inhibiting the occurrence and development of tumors, thus could help to predict tumor prognosis. Based on the discovered regulatory functions of non-coding RNA, we propose that future studies of m6A-modified RNA could help to elucidate the molecular events in HNSCC.

RELATIONSHIP BETWEEN m6A AND IMMUNE CELLS IN THE TUMOR MICROENVIRONMENT

Several studies have demonstrated that tumor immune cells can perform vastly different or even opposite functions under the influence of the tumor microenvironment (Jiménez-Sánchez et al., 2017; Wagner et al., 2019; Luoma et al., 2020; Kolb et al., 2021), with some studies suggesting that m6A modification plays an important regulatory role in these immune cells. Here, we discuss the relationship between immune cell infiltration and m6A modification in HNSCC, with a view to providing directions for future studies.

Members of the SOCS gene family, which consists of *Cish*, *Socs1*, *Socs2, Socs3*, and *Asb2*, play important roles in the signal transduction of negative regulatory factors. Studies have shown that SOCS mRNAs can be m6A-modified and that these mRNAs are m6A targets in $CD4^+$ T cells (Li et al., 2017c). In addition, the loss of METTL3 has been shown to reduce the overall levels of m6A-modified mRNA and cause the subsequent loss of specific SOCS gene transcription. Reduced m6A modification also enhances the stability of SOCS mRNA, increases the expression of SOCS proteins, and blocks cytokine signaling to inhibit tumor development and metastasis (Tong et al., 2018). Moreover, m6A can specifically regulate Tregs, which inhibit the tumor-killing function of $CD8^+$T cells in the tumor microenvironment (Li and Rudensky, 2016). Therefore, the selective removal of m6A from tumor-infiltrating Tregs might increase the efficacy of tumor immunotherapies.

YTHDC2 expression is significantly correlated with B cells, $CD4^+$T cells, neutrophils, and dendritic cells, but not with macrophage infiltration in HNSCC (Li et al., 2020), indicating that YTHDC2 may play an important role in immune cells in the tumor microenvironment, especially $CD4^+$T cells and dendritic cells. Further analysis revealed that changes in the somatic copy number of recognized m6A regulator-based signals significantly affect the infiltration of B cells, $CD4^+$T cells, $CD8^+$T

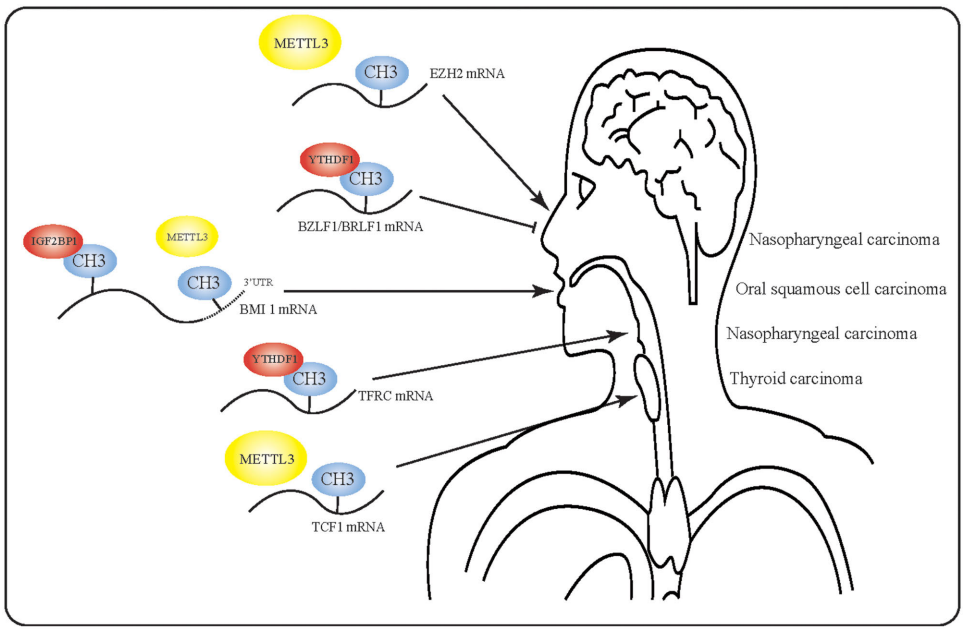

FIGURE 3 | Mechanism of action of m6A-modified mRNA in head and neck squamous cell carcinoma. m6A-modified RNA plays multiple roles in various tumors. In nasopharyngeal carcinoma, m6A-modified RNA may even exert opposite effects due to the presence of multiple m6A targets.

cells, neutrophils, macrophages, and dendritic cells in HNSCC (Yi et al., 2020b), consistent with the hypothesis that this m6A regulatory protein plays a key role in HNSCC development.

Prognostic survival curves obtained using the CIBERSORT-ABS and xCell algorithms showed that TFH or $CD4^+$T cells with increased YTHDC2 expression and high immune infiltration were associated with a better HNSCC prognosis than those with reduced YTHDC2 expression and low immune infiltration. However, the survival curves obtained using EPIC and CIBERSORT algorithms indicated that patients with low YTHDC2 expression and low $CD4^+$T or $CD4^+$ natural T cell infiltration had a better prognosis than those with high YTHDC2 expression and high $CD4^+$T or $CD4^+$ natural T cell infiltration. Moreover, when the effect of YTHDC2 expression on HNSCC prognosis was evaluated, tumors with high YTHDC2 expression displayed a better prognosis than those with low YTHDC2 expression (Li et al., 2020). Together, these findings suggest that different $CD4^+$T cell subsets may exert different effects on the prognosis of HNSCC.

POTENTIAL THERAPEUTIC TARGETS OF m6A

Low levels of METTL3 or METTL14, key components of the RNA methyltransferase complex, have been shown to reduce the expression of m6A-modified *ADAM19* RNA, whereas high *ADAM19* RNA expression in glioblastoma stem cells causes glioblastoma (Cui et al., 2017). Thus, m6A-modified ADAM19 could represent a potential drug target for treating glioblastoma ass its downregulation could prevent tumor development. Huang et al. (2016) showed for the first time that m6A RNA methylation in circulating tumor cells is significantly higher than that in whole blood cells, which may help to elucidate the mechanism underlying cancer metastasis and provide novel insights into the diagnosis of early tumors. Interestingly, meclofenamic acid (MA) and FTO competitively bind to m6A-containing nucleotides and increase the expression of m6A-modified mRNA (Huang et al., 2015); therefore, it may be possible to develop a therapeutic target for cancer that indirectly regulates m6A levels via MA. It has also been reported that the miR-33a-directed targeting of METTL3 inhibits NSCLC cell proliferation; therefore, miR-33a could represent a potential therapeutic molecule for treating NSCLC (Du et al., 2017) and this interaction should be studied in more detail to develop novel therapeutic targets.

The direct causal relationship between m6A RNA methylation and its role in inhibiting or promoting tumor growth requires further study, since it remains unclear whether tumor progression can be altered via the regulation of m6A modification alone or in combination with other regulatory factors. Therefore, future studies focusing on m6A-related targets should not only be limited to the few identified enzymes affecting m6A modification, but also target genes and ncRNAs that are closely related to m6A.

DISCUSSION

This review of current literature revealed that the role of m6A modification varies greatly in different tumors. For example, m6A modification mainly affects RNA stability and protein expression at the post-transcriptional and translational levels

in nasopharyngeal carcinoma, but affects post-translational protein modification in HPSCC rather than TFRC stability or mRNA expression. Interestingly, m6A modification plays a regulatory role in tumors via two main mechanisms: (1) the direct methylation of mRNA that encodes the regulated protein, which alters protein expression; and (2) the m6A modification of ncRNA, which affects tumor occurrence and development through ncRNA regulation. Although studies have shown that both of these mechanisms exist in HNSCC, the latter is seldom studied. At present, there are few studies on the regulatory mechanism involved in the m6A modifications in head and neck tumors. In the future, it is necessary to further clarify the key role of m6A in head and neck tumors, understand the mechanism of tumor occurrence and development comprehensively, and find more effective intervention measures and treatment approaches.

The role of m6A in various types of HNSCCs is being uncovered gradually and further studies could provide insights into this novel model of m6A-mediated epigenetic regulation and identify related diagnostic/therapeutic targets. Notably, the relationships between m6A modification, smoking, alcohol, and HPV, which are all closely related to head and neck tumors, require further study. In addition, the current bioinformatics results relating to thyroid cancer are inconsistent with those of molecular experiments, potentially due to a limited understanding of related molecular mechanisms and the broad classifications of thyroid cancer. Consequently, extensive studies are required to elucidate these molecular mechanisms and to develop more efficient methods for treating HNSCC.

AUTHOR CONTRIBUTIONS

F-YJ designed the study. F-YJ, L-MZ, and Y-JN collected data and aided in writing the manuscript. F-YJ, L-MZ, and X-JW edited the manuscript. Y-MZ provided direction and guidance through the preparation of this study and assisted in the revision of the manuscript. All authors read and approved the final manuscript.

FUNDING

This work was funded by the National Natural Science Foundation of China (31970677 and 31501103) and the Research Level Improvement Plan of Anhui Medical University (2019xkjT010).

REFERENCES

Aguilo, F., Zhang, F., Sancho, A., Fidalgo, M., Di Cecilia, S., Vashisht, A., et al. (2015). Coordination of m6A mRNA methylation and gene transcription by ZFP217 regulates pluripotency and reprogramming. *Cell Stem Cell* 17, 689–704. doi: 10.1016/j.stem.2015.09.005

Alarcón, C. R., Lee, H., Goodarzi, H., Halberg, N., and Tavazoie, S. F. (2015). N6-methyladenosine marks primary microRNAs for processing. *Nature* 519, 482–485. doi: 10.1038/nature14281

Aoyama, T., Yamashita, S., and Tomita, K. (2020). Mechanistic insights into m6A modification of U6 snRNA by human METTL16. *Nucleic Acids Res.* 48, 5157–5168. doi: 10.1093/nar/gkaa227

Araque, D. V. P., Bleyer, A., and Brito, J. P. (2017). Thyroid cancer in adolescents and young adults. *Future Oncol.* 13, 1253–1261.

Arends, C. R., Petersen, J. F., van der Noort, V., Timmermans, A. J., Leemans, C. R., de Bree, R., et al. (2020). Optimizing survival predictions of hypopharynx cancer: development of a clinical prediction model. *Laryngoscope* 130, 2166–2172. doi: 10.1002/lary.28345

Ban, Y., Tan, P., Cai, J., Li, J., Hu, M., Zhou, Y., et al. (2020). LNCAROD is stabilized by m6A methylation and promotes cancer progression via forming a ternary complex with HSPA1A and YBX1 in head and neck squamous cell carcinoma. *Mol. Oncol.* 14, 1282–1296. doi: 10.1002/1878-0261.12676

Bartosovic, M., Molares, H. C., Gregorova, P., Hrossova, D., Kudla, G., and Vanacova, S. (2017). N6-methyladenosine demethylase FTO targets pre-mRNAs and regulates alternative splicing and 3'-end processing. *Nucleic Acids Res.* 45, 11356–11370. doi: 10.1093/nar/gkx778

Bavle, R. M., Venugopal, R., Konda, P., Muniswamappa, S., and Makarla, S. (2016). Molecular classification of oral squamous cell carcinoma. *J. Clin. Diagn. Res.* 10, ZE18–ZE21. doi: 10.7860/JCDR/2016/19967.8565

Begik, O., Lucas, M. C., Liu, H., Ramirez, J. M., Mattick, J. S., and Novoa, E. M. (2020). Integrative analyses of the RNA modification machinery reveal tissue- and cancer-specific signatures. *Genome Biol.* 21:97. doi: 10.1186/s13059-020-02009-z

Ben-Haim, M. S., Moshitch-Moshkovitz, S., and Rechavi, G. (2015). FTO: Linking m6A demethylation to adipogenesis. *Cell Res.* 25, 3–4. doi: 10.1038/cr.2014.162

Bertero, A., Brown, S., Madrigal, P., Osnato, A., Ortmann, D., Yiangou, L., et al. (2018). The SMAD2/3 interactome reveals that TGFbeta controls m6A mRNA methylation in pluripotency. *Nature* 555, 256–259. doi: 10.1038/nature25784

Bhat, S. S., Bielewicz, D., Gulanicz, T., Bodi, Z., Yu, X., Anderson, S. J., et al. (2020). mRNA adenosine methylase (MTA) deposits m6A on pri-miRNAs to modulate miRNA biogenesis in Arabidopsis thaliana. *Proc. Natl. Acad. Sci. U.S.A.* 117, 21785–21795. doi: 10.1073/pnas.2003733117

Biktasova, A., Hajek, M., Sewell, A., Gary, C., Bellinger, G., Deshpande, H. A., et al. (2017). Demethylation therapy as a targeted treatment for human papillomavirus-associated head and neck cancer. *Clin. Cancer Res.* 23, 7276–7287. doi: 10.1158/1078-0432.ccr-17-1438

Bokar, J. A., Rath-Shambaugh, M. E., Ludwiczak, R., Narayan, P., and Rottman, F. (1994). Characterization and partial purification of mRNA N6-adenosine methyltransferase from HeLa cell nuclei. Internal mRNA methylation requires a multisubunit complex. *J. Biol. Chem.* 269, 17697–17704. doi: 10.1016/s0021-9258(17)32497-3

Cabanillas, M. E., McFadden, D. G., and Durante, C. (2016). Thyroid cancer. *Lancet* 388, 2783–2795.

Cai, X., Wang, X., Cao, C., Gao, Y., Zhang, S., Yang, Z., et al. (2018). HBXIP-elevated methyltransferase METTL3 promotes the progression of breast cancer via inhibiting tumor suppressor let-7g. *Cancer Lett.* 415, 11–19. doi: 10.1016/j.canlet.2017.11.018

Cantara, W. A., Crain, P. F., Rozenski, J., McCloskey, J. A., Harris, K. A., Zhang, X., et al. (2011). The RNA modification database, RNAMDB: 2011 update. *Nucleic Acids Res.* 39, D195–D201. doi: 10.1093/nar/gkq1028

Carling, T., and Udelsman, R. (2014). Thyroid cancer. *Ann. Rev. Med.* 65, 125–137.

Chen, G., Guo, X., Lv, F., Xu, Y., and Gao, G. (2008). p72 DEAD box RNA helicase is required for optimal function of the zinc-finger antiviral protein. *Proc. Natl. Acad. Sci. U.S.A.* 105, 4352–4357. doi: 10.1073/pnas.0712276105

Chen, H., Yao, J., Bao, R., Dong, Y., Zhang, T., Du, Y., et al. (2021a). Cross-talk of four types of RNA modification writers defines tumor microenvironment and pharmacogenomic landscape in colorectal cancer. *Mol. Cancer* 20:29. doi: 10.1186/s12943-021-01322-w

Chen, M., Wei, L., Law, C. T., Tsang, F. H., Shen, J., Cheng, C. L., et al. (2018). RNA N6-methyladenosine methyltransferase-like 3 promotes liver cancer progression through YTHDF2-dependent posttranscriptional silencing of SOCS2. *Hepatology* 67, 2254–2270. doi: 10.1002/hep.29683

Chen, P., Liu, X. Q., Lin, X., Gao, L. Y., Zhang, S., and Huang, X. (2021b). Targeting YTHDF1 effectively re-sensitizes cisplatin-resistant colon cancer cells by modulating GLS-mediated glutamine metabolism. *Mol. Ther. Oncolytics* 20, 228–239. doi: 10.1016/j.omto.2021.01.001

Chen, Y. P., Chan, A. T., Le, Q. T., Blanchard, P., Sun, Y., and Ma, J. (2019). Nasopharyngeal carcinoma. *Lancet* 394, 64–80.

Chen, Z., Chen, X., Lei, T., Gu, Y., Gu, J., Huang, J., et al. (2020). Integrative analysis of NSCLC identifies LINC01234 as an oncogenic lncRNA that interacts with HNRNPA2B1 and regulates miR-106b biogenesis. *Mol. Ther.* 28, 1479–1493. doi: 10.1016/j.ymthe.2020.03.010

Cheng, M., Sheng, L., Gao, Q., Xiong, Q., Zhang, H., Wu, M., et al. (2019). The m6A methyltransferase METTL3 promotes bladder cancer progression via AFF4/NF-κB/MYC signaling network. *Oncogene* 38, 3667–3680. doi: 10.1038/s41388-019-0683-z

Coots, R. A., Liu, X. M., Mao, Y., Dong, L., Zhou, J., Wan, J., et al. (2017). m6A facilitates eIF4F-independent mRNA translation. *Mol. Cell* 68, 504–514. doi: 10.1016/j.molcel.2017.10.002

Cui, Q., Shi, H., Ye, P., Li, L., Qu, Q., Sun, G., et al. (2017). m6A RNA methylation regulates the self-renewal and tumorigenesis of glioblastoma stem cells. *Cell Rep.* 18, 2622–2634. doi: 10.1016/j.celrep.2017.02.059

Desrosiers, R., Friderici, K., and Rottman, F. (1974). Identification of methylated nucleosides in messenger RNA from Novikoff hepatoma cells. *Proc. Natl. Acad. Sci. U.S.A.* 71, 3971–3975. doi: 10.1073/pnas.71.10.3971

Dominissini, D., Moshitch-Moshkovitz, S., Schwartz, S., Salmon-Divon, M., Ungar, L., Osenberg, S., et al. (2012). Topology of the human and mouse m6A RNA methylomes revealed by m6A-seq. *Nature* 485, 201–206. doi: 10.1038/nature11112

Du, H., Zhao, Y., He, J., Zhang, Y., Xi, H., Liu, M., et al. (2016). YTHDF2 destabilizes m6A-containing RNA through direct recruitment of the CCR4-NOT deadenylase complex. *Nat. Commun.* 7:12626. doi: 10.1038/ncomms12626

Du, M., Zhang, Y., Mao, Y., Mou, J., Zhao, J., Xue, Q., et al. (2017). MiR-33a suppresses proliferation of NSCLC cells via targeting METTL3 mRNA. *Biochem. Biophys. Res. Commun.* 482, 582–589. doi: 10.1016/j.bbrc.2016.11.077

Fang, R., Chen, X., Zhang, S., Shi, H., Ye, Y., Shi, H., et al. (2021). EGFR/SRC/ERK-stabilized YTHDF2 promotes cholesterol dysregulation and invasive growth of glioblastoma. *Nat. Commun.* 12:177. doi: 10.1038/s41467-020-20379-7

Ferlay, J., Shin, H. R., Bray, F., Forman, D., Mathers, C., and Parkin, D. M. (2010). Estimates of worldwide burden of cancer in 2008: GLOBOCAN 2008. *Int. J. Cancer* 127, 2893–2917. doi: 10.1002/ijc.25516

Ferris, R. L., Lenz, H. J., Trotta, A. M., García-Foncillas, J., Schulten, J., Audhuy, F., et al. (2018). Rationale for combination of therapeutic antibodies targeting tumor cells and immune checkpoint receptors: harnessing innate and adaptive immunity through IgG1 isotype immune effector stimulation. *Cancer Treat. Rev.* 63, 48–60. doi: 10.1016/j.ctrv.2017.11.008

Fomenkov, A., Sun, Z., Murray, I. A., Ruse, C., McClung, C., Yamaichi, Y., et al. (2020). Plasmid replication-associated single-strand-specific methyltransferases. *Nucleic Acids Res.* 48, 12858–12873. doi: 10.1093/nar/gkaa1163

Fustin, J. M., Doi, M., Yamaguchi, Y., Hida, H., Nishimura, S., Yoshida, M., et al. (2013). RNA-methylation-dependent RNA processing controls the speed of the circadian clock. *Cell* 155, 793–806. doi: 10.1016/j.cell.2013.10.026

Gatta, G., Botta, L., Sánchez, M. J., Anderson, L. A., Pierannunzio, D., Licitra, L., et al. (2015). Prognoses and improvement for head and neck cancers diagnosed in Europe in early 2000s: The EUROCARE-5 population-based study. *Eur. J. Cancer* 51, 2130–2143.

Geissler, R., Golbik, R. P., and Behrens, S. E. (2012). The DEAD-box helicase DDX3 supports the assembly of functional 80S ribosomes. *Nucleic Acids Res.* 40, 4998–5011. doi: 10.1093/nar/gks070

Geula, S., Moshitch-Moshkovitz, S., Dominissini, D., Mansour, A. A., Kol, N., Salmon-Divon, M., et al. (2015). Stem cells. m6A mRNA methylation facilitates resolution of naive pluripotency toward differentiation. *Science* 347, 1002–1006. doi: 10.1126/science.1261417

Globisch, D., Pearson, D., Hienzsch, A., Brückl, T., Wagner, M., Thoma, I., et al. (2011). Systems-based analysis of modified tRNA bases. *Angew Chem. Int. Ed. Engl.* 50, 9739–9742. doi: 10.1002/anie.201103229

Gomes, I. M., Maia, C. J., and Santos, C. R. (2012). STEAP proteins: from structure to applications in cancer therapy. *Mol. Cancer Res.* 10, 573–587. doi: 10.1158/1541-7786.mcr-11-0281

González-Ramírez, I., Soto-Reyes, E., Sánchez-Pérez, Y., Herrera, L. A., and García-Cuellar, C. (2014). Histones and long non-coding RNAs: The new insights of epigenetic deregulation involved in oral cancer. *Oral Oncol.* 50, 691–695. doi: 10.1016/j.oraloncology.2014.04.006

Hajek, M., Sewell, A., Kaech, S., Burtness, B., Yarbrough, W. G., and Issaeva, N. (2017). TRAF3/CYLD mutations identify a distinct subset of human papillomavirus-associated head and neck squamous cell carcinoma. *Cancer* 123, 1778–1790. doi: 10.1002/cncr.30570

He, C. (2010). Grand challenge commentary: RNA epigenetics nat. *Chem. Biol.* 6, 863–865. doi: 10.1038/nchembio.482

He, P. C., and He, C. (2021). m6A RNA methylation: from mechanisms to therapeutic potential. *EMBO J.* 40:e105977. doi: 10.15252/embj.2020105977

Hedberg, M. L., Goh, G., Chiosea, S. I., Bauman, J. E., Freilino, M. L., Zeng, Y., et al. (2016). Genetic landscape of metastatic and recurrent head and neck squamous cell carcinoma. *J. Clin. Invest.* 126, 169–180.

Hess, M. E., Hess, S., Meyer, K. D., Verhagen, L. A., Koch, L., Brönneke, H. S., et al. (2013). The fat mass and obesity associated gene (Fto) regulates activity of the dopaminergic midbrain circuitry. *Nat. Neurosci.* 16, 1042–1048. doi: 10.1038/nn.3449

Hou, J., Shan, H., Zhang, Y., Fan, Y., and Wu, B. (2020). m6A RNA methylation regulators have prognostic value in papillary thyroid carcinoma. *Am. J. Otolaryngol.* 41:102547. doi: 10.1016/j.amjoto.2020.102547

Hsu, P. J., Zhu, Y., Ma, H., Guo, Y., Shi, X., Liu, Y., et al. (2017). Ythdc2 is an N6-methyladenosine binding protein that regulates mammalian spermatogenesis. *Cell Res.* 27, 1115–1127. doi: 10.1038/cr.2017.99

Huang, H., Weng, H., Sun, W., Qin, X., Shi, H., Wu, H., et al. (2018). Recognition of RNA N6-methyladenosine by IGF2BP proteins enhances mRNA stability and translation. *Nat. Cell Biol.* 20, 285–295. doi: 10.1038/s41556-018-0045-z

Huang, W., Qi, C. B., Lv, S. W., Xie, M., Feng, Y. Q., Huang, W. H., et al. (2016). Determination of DNA and RNA methylation in circulating tumor cells by mass spectrometry. *Anal. Chem.* 88, 1378–1384. doi: 10.1021/acs.analchem.5b03962

Huang, Y., Yan, J., Li, Q., Li, J., Gong, S., Zhou, H., et al. (2015). Meclofenamic acid selectively inhibits FTO demethylation of m6A over ALKBH5. *Nucleic Acids Res.* 43, 373–384. doi: 10.1093/nar/gku1276

Hwang, S. Y., Jung, H., Mun, S., Lee, S., Park, K., Baek, S. C., et al. (2021). L1 retrotransposons exploit RNA m6A modification as an evolutionary driving force. *Nat. Commun.* 12:880. doi: 10.1038/s41467-021-21197-1

Jackson, R. J., Hellen, C. U., and Pestova, T. V. (2010). The mechanism of eukaryotic translation initiation and principles of its regulation. *Nat. Rev. Mol. Cell Biol.* 11, 113–127. doi: 10.1038/nrm2838

Jia, G., Fu, Y., Zhao, X., Dai, Q., Zheng, G., Yang, Y., et al. (2011). N6-methyladenosine in nuclear RNA is a major substrate of the obesity-associated FTO. *Nat. Chem. Biol.* 7, 885–887. doi: 10.1038/nchembio.687

Jiang, L., Chen, T., Xiong, L., Xu, J. H., Gong, A. Y., Dai, B., et al. (2020). Knockdown of m6A methyltransferase METTL3 in gastric cancer cells results in suppression of cell proliferation. *Oncol. Lett.* 20, 2191–2198. doi: 10.3892/ol.2020.11794

Jiang, X., Liu, B., Nie, Z., Duan, L., Xiong, Q., Jin, Z., et al. (2021). The role of m6A modification in the biological functions and diseases. *Signal. Transduct. Target. Ther.* 6:74. doi: 10.1038/s41392-020-00450-x

Jiang, X., Ye, J., Dong, Z., Hu, S., and Xiao, M. (2019). Novel genetic alterations and their impact on target therapy response in head and neck squamous cell carcinoma. *Cancer Manag. Res.* 11, 1321–1336. doi: 10.2147/cmar.s187780

Jiménez-Sánchez, A., Memon, D., Pourpe, S., Veeraraghavan, H., Li, Y., Vargas, H. A., et al. (2017). Heterogeneous tumor-immune microenvironments among differentially growing metastases in an ovarian cancer patient. *Cell* 170, 927–938. doi: 10.1016/j.cell.2017.07.025

Jin, D., Guo, J., Wu, Y., Du, J., Yang, L., Wang, X., et al. (2021). m6A mRNA methylation initiated by METTL3 directly promotes YAP translation and increases YAP activity by regulating the MALAT1-miR-1914-3p-YAP axis to induce NSCLC drug resistance and metastasis. *J. Hematol. Oncol.* 12:135. doi: 10.1186/s13045-019-0830-6

Jithesh, P. V., Risk, J. M., Schache, A. G., Dhanda, J., Lane, B., Liloglou, T., et al. (2013). The epigenetic landscape of oral squamous cell carcinoma. *Br. J. Cancer* 108, 370–379.

Kasowitz, S. D., Ma, J., Anderson, S. J., Leu, N. A., Xu, Y., Gregory, B. D., et al. (2018). Nuclear m6A reader YTHDC1 regulates alternative polyadenylation and splicing during mouse oocyte development. *PLoS Genet.* 14:e1007412. doi: 10.1371/journal.pgen.1007412

Ke, S., Pandya-Jones, A., Saito, Y., Fak, J. J., Vågbø, C. B., Geula, S., et al. (2017). m6A mRNA modifications are deposited in nascent pre-mRNA and are not required for splicing but do specify cytoplasmic turnover. *Genes Dev.* 31, 990–1006. doi: 10.1101/gad.301036.117

Kennedy, E. M., Bogerd, H. P., Kornepati, A. R., Kang, D., Ghoshal, D., Marshall, J., et al. (2016). Posttranscriptional m6A editing of HIV-1 mRNAs enhances viral gene expression. *Cell Host Microbe.* 19, 675–685. doi: 10.1016/j.chom.2016.04.002

Klungland, A., and Dahl, J. A. (2014). Dynamic RNA modifications in disease. *Curr. Opin. Genet. Dev.* 26, 47–52. doi: 10.1016/j.gde.2014.05.006

Knuckles, P., Carl, S. H., Musheev, M., Niehrs, C., Wenger, A., and Bühler, M. (2017). RNA fate determination through cotranscriptional adenosine methylation and microprocessor binding. *Nat. Struct. Mol. Biol.* 24, 561–569. doi: 10.1038/nsmb.3419

Kolb, R., De, U., Khan, S., Luo, Y., Kim, M. C., Yu, H., et al. (2021). Proteolysis-targeting chimera against BCL-XL destroys tumor-infiltrating regulatory T cells. *Nat. Commun.* 12:1281. doi: 10.1038/s41467-021-21573-x

Kontur, C., Jeong, M., Cifuentes, D., and Giraldez, A. J. (2020). Ythdf m6A readers function redundantly during zebrafish development. *Cell Rep.* 33:108598. doi: 10.1016/j.celrep.2020.108598

Lang, F., Singh, R. K., Pei, Y., Zhang, S., Sun, K., and Robertson, E. S. (2019). EBV epitranscriptome reprogramming by METTL14 is critical for viral-associated tumorigenesis. *PLoS Pathog.* 15:e1007796. doi: 10.1371/journal.ppat.1007796

Lee, V., Kwong, D., Leung, T. W., Lam, K. O., Tong, C. C., and Lee, A. (2017). Palliative systemic therapy for recurrent or metastatic nasopharyngeal carcinoma - how far have we achieved? *Crit. Rev. Oncol. Hematol.* 114, 13–23. doi: 10.1016/j.critrevonc.2017.03.030

Leemans, C. R., Braakhuis, B. J., and Brakenhoff, R. H. (2011). The molecular biology of head and neck cancer. *Nat. Rev. Cancer* 11, 9–22.

Li, A., Chen, Y. S., Ping, X. L., Yang, X., Xiao, W., Yang, Y., et al. (2017a). Cytoplasmic m6A reader YTHDF3 promotes mRNA translation. *Cell Res.* 27, 444–447. doi: 10.1038/cr.2017.10

Li, H. B., Tong, J., Zhu, S., Batista, P. J., Duffy, E. E., Zhao, J., et al. (2017c). m6A mRNA methylation controls T cell homeostasis by targeting the IL-7/STAT5/SOCS pathways. *Nature* 548, 338–342. doi: 10.1038/nature23450

Li, M. O., and Rudensky, A. Y. (2016). T cell receptor signalling in the control of regulatory T cell differentiation and function. *Nat. Rev. Immunol.* 16, 220–233. doi: 10.1038/nri.2016.26

Li, X., and Manley, J. L. (2005). Inactivation of the SR protein splicing factor ASF/SF2 results in genomic instability. *Cell* 122, 365–378. doi: 10.1016/j.cell.2005.06.008

Li, Y., Zheng, J. N., Wang, E. H., Gong, C. J., Lan, K. F., Ding, X., et al. (2020). The m6A reader protein YTHDC2 is a potential biomarker and associated with immune infiltration in head and neck squamous cell carcinoma. *PeerJ* 8:e10385. doi: 10.7717/peerj.10385

Li, Z., Weng, H., Su, R., Weng, X., Zuo, Z., Li, C., et al. (2017b). FTO plays an oncogenic role in acute myeloid leukemia as a N6-methyladenosine RNA demethylase. *Cancer Cell* 31, 127–141. doi: 10.1016/j.ccell.2016.11.017

Lin, S., Choe, J., Du, P., Triboulet, R., and Gregory, R. I. (2016). The m6A methyltransferase METTL3 promotes translation in human cancer cells. *Mol. Cell* 62, 335–345. doi: 10.1016/j.molcel.2016.03.021

Lin, Z., Hsu, P. J., Xing, X., Fang, J., Lu, Z., Zou, Q., et al. (2017). Mettl3-/Mettl14-mediated mRNA N6-methyladenosine modulates murine spermatogenesis. *Cell Res.* 27, 1216–1230. doi: 10.1038/cr.2017.117

Liu, B., Tan, Z., Jiang, Y., Chen, Y., Chen, Y., and Ling, K. (2018). Correlation between the expression of miR150 and FOXO4 and the local recurrence and metastasis of nasopharyngeal carcinoma after intensive radiotherapy. *J. BUON.* 23, 1671–1678.

Liu, J., Gao, M., Xu, S., Chen, Y., Wu, K., Liu, H., et al. (2020b). YTHDF2/3 are required for somatic reprogramming through different RNA deadenylation pathways. *Cell Rep.* 32:108120. doi: 10.1016/j.celrep.2020.108120

Liu, J., Yue, Y., Han, D., Wang, X., Fu, Y., Zhang, L., et al. (2014). A METTL3-METTL14 complex mediates mammalian nuclear RNA N6-adenosine methylation. *Nat. Chem. Biol.* 10, 93–95. doi: 10.1038/nchembio.1432

Liu, L., Wu, Y., Li, Q., Liang, J., He, Q., Zhao, L., et al. (2020c). METTL3 promotes tumorigenesis and metastasis through BMI1 m6A methylation in oral squamous cell carcinoma. *Mol. Ther.* 28, 2177–2190. doi: 10.1016/j.ymthe.2020.06.024

Liu, N., Dai, Q., Zheng, G., He, C., Parisien, M., and Pan, T. (2015). N 6-methyladenosine-dependent RNA structural switches regulate RNA-protein interactions. *Nature* 518, 560–564. doi: 10.1038/nature14234

Liu, S. L., Sun, X. S., Li, X. Y., Tang, L. Q., Chen, Q. Y., Lin, H. X., et al. (2019). The diagnostic and prognostic values of plasma Epstein–Barr virus DNA for residual cervical lymphadenopathy in nasopharyngeal carcinoma patients: a retrospective study. *Cancer Commun.* 39:14. doi: 10.1186/s40880-019-0357-9

Liu, T., Wei, Q., Jin, J., Luo, Q., Liu, Y., Yang, Y., et al. (2020a). The m6A reader YTHDF1 promotes ovarian cancer progression via augmenting EIF3C translation. *Nucleic Acids Res.* 48, 3816–3831. doi: 10.1093/nar/gkaa048

Lorch, J. H., Goloubeva, O., Haddad, R. I., Cullen, K., Sarlis, N., Tishler, R., et al. (2011). Induction chemotherapy with cisplatin and fluorouracil alone or in combination with docetaxel in locally advanced squamous-cell cancer of the head and neck: Long-term results of the TAX 324 randomised phase 3 trial. *Lancet Oncol.* 12, 153–159. doi: 10.1016/s1470-2045(10)70279-5

Luoma, A. M., Suo, S., Williams, H. L., Sharova, T., Sullivan, K., Manos, M., et al. (2020). Molecular pathways of colon inflammation induced by cancer immunotherapy. *Cell* 182, 655–671. doi: 10.1016/j.cell.2020.06.001

Ma, J. Z., Yang, F., Zhou, C. C., Liu, F., Yuan, J. H., Wang, F., et al. (2017). METTL14 suppresses the metastatic potential of hepatocellular carcinoma by modulating N6-methyladenosine-dependent primary microRNA processing. *Hepatology* 65, 529–543. doi: 10.1002/hep.28885

Mapperley, C., van de Lagemaat, L. N., Lawson, H., Tavosanis, A., Paris, J., Campos, J., et al. (2021). The mRNA m6A reader YTHDF2 suppresses proinflammatory pathways and sustains hematopoietic stem cell function. *J. Exp. Med.* 218:e20200829. doi: 10.1084/jem.20200829

McGarvey, K. M., Fahrner, J. A., Greene, E., Martens, J., Jenuwein, T., and Baylin, S. B. (2006). Silenced tumor suppressor genes reactivated by DNA demethylation do not return to a fully euchromatic chromatin state. *Cancer Res.* 66, 3541–3549. doi: 10.1158/0008-5472.can-05-2481

Meng, Q. Z., Cong, C. H., Li, X. J., Zhu, F., Zhao, X., and Chen, F. W. (2020). METTL3 promotes the progression of nasopharyngeal carcinoma through mediating M6A modification of EZH2. *Eur. Rev. Med. Pharmacol. Sci.* 24, 4328–4336.

Mercher, T., Coniat, M. B., Monni, R., Mauchauffe, M., Nguyen Khac, F., Gressin, L., et al. (2001). Involvement of a human gene related to the Drosophila spen gene in the recurrent t (1;22) translocation of acute megakaryocytic leukemia. *Proc. Natl. Acad. Sci. U.S.A.* 98, 5776–5779. doi: 10.1073/pnas.101001498

Meyer, K. D., and Jaffrey, S. R. (2017). Rethinking m6A readers, writers, and erasers. *Ann. Rev. Cell. Dev. Biol.* 33, 319–342. doi: 10.1146/annurev-cellbio-100616-060758

Michlewski, G., Sanford, J. R., and Cáceres, J. F. (2008). The splicing factor SF2/ASF regulates translation initiation by enhancing phosphorylation of 4E-BP1. *Mol. Cell* 30, 179–189. doi: 10.1016/j.molcel.2008.03.013

Morris, L. G. T., Chandramohan, R., West, L., Zehir, A., Chakravarty, D., Pfister, D. G., et al. (2017). The molecular landscape of recurrent and metastatic head and neck cancers: insights from a precision oncology sequencing platform. *JAMA Oncol.* 3, 244–255. doi: 10.1001/jamaoncol.2016.1790

Ohgami, R. S., Campagna, D. R., McDonald, A., and Fleming, M. D. (2006). The Steap proteins are metalloreductases. *Blood* 108, 1388–1394. doi: 10.1182/blood-2006-02-003681

Ondo, K., Isono, M., Nakano, M., Hashiba, S., Fukami, T., and Nakajima, M. (2020). The N6-methyladenosine modification posttranscriptionally regulates hepatic UGT2B7 expression. *Biochem. Pharmacol.* 182:114402. doi: 10.1016/j.bcp.2020.114402

Orouji, E., Peitsch, W. K., Orouji, A., Houben, R., and Utikal, J. (2020). Oncogenic role of an epigenetic reader of m6A RNA modification: YTHDF1 in Merkel cell carcinoma. *Cancers.* 12:202. doi: 10.3390/cancers12010202

Ovcharenko, A., Weissenboeck, F. P., and Rentmeister, A. (2021). Tag-free internal RNA labeling and photocaging based on mRNA methyltransferases. *Angew. Chem. Int. Ed. Engl.* 60, 4098–4103. doi: 10.1002/anie.202013936

Perry, R. P., Kelley, D. E., Friderici, K., and Rottman, F. (1975). The methylated constituents of L cell messenger RNA: evidence for an unusual cluster at the 5' terminus. *Cell* 4, 387–394. doi: 10.1016/0092-8674(75)90159-2

Petronek, M. S., Spitz, D. R., Buettner, G. R., and Allen, B. G. (2019). Linking cancer metabolic dysfunction and genetic instability through the lens of iron metabolism. *Cancers* 11:1077. doi: 10.3390/cancers11081077

Qing, Y., Dong, L., Gao, L., Li, C., Li, Y., Han, L., et al. (2021). R-2-hydroxyglutarate attenuates aerobic glycolysis in leukemia by targeting the FTO/m6A/PFKP/LDHB axis. *Mol. Cell* 81, 922–939. doi: 10.1016/j.molcel.2020.12.026

Roman, B. R., Morris, L. G., and Davies, L. (2017). The thyroid cancer epidemic, 2017 perspective. *Curr. Opin. Endocrinol. Diabetes Obes.* 24, 332–336. doi: 10.1097/med.0000000000000359

Roundtree, I. A., Evans, M. E., Pan, T., and He, C. (2017). Dynamic RNA modifications in gene expression regulation. *Cell* 169, 1187–1200. doi: 10.1016/j.cell.2017.05.045

Rubio, R. M., Depledge, D. P., Bianco, C., Thompson, L., and Mohr, I. (2018). RNA m6 A modification enzymes shape innate responses to DNA by regulating interferon β. *Genes Dev.* 32, 1472–1484. doi: 10.1101/gad.319475.118

Schumann, U., Shafik, A., and Preiss, T. (2016). METTL3 gains R/W access to the epitranscriptome. *Mol. Cell* 62, 323–324. doi: 10.1016/j.molcel.2016.04.024

Schwartz, S., Mumbach, M. R., Jovanovic, M., Wang, T., Maciag, K., Bushkin, G. G., et al. (2014). Perturbation of m6A writers reveals two distinct classes of mRNA methylation at internal and 5' sites. *Cell Rep.* 8, 284–296. doi: 10.1016/j.celrep.2014.05.048

Selmi, T., Hussain, S., Dietmann, S., Heiß, M., Borland, K., Flad, S., et al. (2021). Sequence- and structure-specific cytosine-5 mRNA methylation by NSUN6. *Nucleic Acids Res.* 49, 1006–1022. doi: 10.1093/nar/gkaa1193

Shen, C., Xuan, B., Yan, T., Ma, Y., Xu, P., Tian, X., et al. (2020). m6A-dependent glycolysis enhances colorectal cancer progression. *Mol. Cancer* 19:72. doi: 10.1186/s12943-020-01190-w

Shen, Y., Li, X., Dong, D., Zhang, B., Xue, Y., and Shang, P. (2018). Transferrin receptor 1 in cancer: A new sight for cancer therapy. *Am. J. Cancer Res.* 8, 916–931.

Shi, H., Wang, X., Lu, Z., Zhao, B. S., Ma, H., Hsu, P. J., et al. (2017). YTHDF3 facilitates translation and decay of N6 methyladenosine-modified RNA. *Cell Res.* 27, 315–328. doi: 10.1038/cr.2017.15

Shi, Y., Peng, S. L., Yang, L. F., Chen, X., Tao, Y. G., and Cao, Y. (2016). Co-infection of Epstein–Barr virus and human papillomavirus in human tumorigenesis. *Chin. J. Cancer* 35:16. doi: 10.1186/s40880-016-0079-1

Shima, H., Matsumoto, M., Ishigami, Y., Ebina, M., Muto, A., Sato, Y., et al. (2017). S-adenosylmethionine synthesis is regulated by selective N6-adenosine methylation and mRNA degradation involving METTL16 and YTHDC1. *Cell Rep.* 21, 3354–3363. doi: 10.1016/j.celrep.2017.11.092

Shriwas, O., Priyadarshini, M., Samal, S. K., Rath, R., Panda, S., Das Majumdar, S. K., et al. (2020). DDX3 modulates cisplatin resistance in OSCC through ALKBH5-mediated m6A-demethylation of FOXM1 and NANOG. *Apoptosis* 25, 233–246. doi: 10.1007/s10495-020-01591-8

Śledź, P., and Jinek, M. (2016). Structural insights into the molecular mechanism of the m6A writer complex. *ELife* 5:e18434. doi: 10.7554/eLife.18434.001

Song, P., Yang, F., Jin, H., and Wang, X. (2021). The regulation of protein translation and its implications for cancer. *Signal Transduct. Target. Ther.* 6:68. doi: 10.1038/s41392-020-00444-9

Su, R., Dong, L., Li, C., Nachtergaele, S., Wunderlich, M., Qing, Y., et al. (2018). R-2HG exhibits anti-tumor activity by targeting FTO/m6A/MYC/CEBPA signaling. *Cell* 172, 90–105. doi: 10.1016/j.cell.2017.11.031

Su, T., Huang, M., Liao, J., Lin, S., Yu, P., Yang, J., et al. (2021). Insufficient radiofrequency ablation promotes hepatocellular carcinoma metastasis through m6A mRNA methylation dependent mechanism. *Hepatology* doi: 10.1002/hep.31766 [Epub ahead of print].

Taketo, K., Konno, M., Asai, A., Koseki, J., Toratani, M., Satoh, T., et al. (2018). The epitranscriptome m6A writer METTL3 promotes chemo- and radioresistance in pancreatic cancer cells. *Int. J. Oncol.* 52, 621–629.

Tang, C., Klukovich, R., Peng, H., Wang, Z., Yu, T., Zhang, Y., et al. (2018). ALKBH5-dependent m6A demethylation controls splicing and stability of long 30 - UTR mRNAs in male germ cells. *Proc. Natl. Acad. Sci. U.S.A.* 115, E325–E333. doi: 10.1073/pnas.1717794115

Tanner, N. K., and Linder, P. (2001). DExD/H box RNA helicases: From generic motors to specific dissociation functions. *Mol. Cell* 8, 251–262. doi: 10.1016/s1097-2765(01)00329-x

Tassinari, V., Cesarini, V., Tomaselli, S., Ianniello, Z., Silvestris, D. A., Ginistrelli, L. C., et al. (2021). ADAR1 is a new target of METTL3 and plays a pro-oncogenic role in glioblastoma by an editing-independent mechanism. *Genome Biol.* 22:51. doi: 10.1186/s13059-021-02271-9

Tong, J., Cao, G., Zhang, T., Sefik, E., Amezcua Vesely, M. C., Broughton, J. P., et al. (2018). m6A mRNA methylation sustains Treg suppressive functions. *Cell Res.* 28, 253–256. doi: 10.1038/cr.2018.7

Vu, L. P., Pickering, B. F., Cheng, Y., Zaccara, S., Nguyen, D., Minuesa, G., et al. (2017). The N6-methyladenosine (m6A)-forming enzyme METTL3 controls myeloid differentiation of normal hematopoietic and leukemia cells. *Nat. Med.* 23, 1369–1376. doi: 10.1038/nm.4416

Wagner, J., Rapsomaniki, M. A., Chevrier, S., Anzeneder, T., Langwieder, C., Dykgers, A., et al. (2019). A single-cell atlas of the tumor and immune ecosystem of human breast cancer. *Cell* 177, 1330–1345. doi: 10.1016/j.cell.2019.03.005

Wang, C., Liu, X. Q., Hou, J. S., Wang, J. N., and Huang, H. Z. (2016c). Molecular mechanisms of chemoresistance in oral cancer. *Chin. J. Dent. Res.* 19, 25–33. doi: 10.1016/b978-0-12-819840-7.00011-x

Wang, J., Li, Y., Wang, P., Han, G., Zhang, T., Chang, J., et al. (2020a). Leukemogenic chromatin alterations promote AML leukemia stem cells via a KDM4C-ALKBH5-AXL signaling axis. *Cell Stem Cell* 27, 81–97. doi: 10.1016/j.stem.2020.04.001

Wang, J. Y., and Lu, A. Q. (2021). The biological function of m6A reader YTHDF2 and its role in human disease. *Cancer Cell Int.* 21:109. doi: 10.1186/s12935-021-01807-0

Wang, K., Jiang, L., Zhang, Y., and Chen, C. (2020c). Progression of thyroid carcinoma is promoted by the m6A methyltransferase METTL3 through regulating m6A methylation on TCF1. *Onco. Targets Ther.* 13, 1605–1612. doi: 10.2147/ott.s234751

Wang, P., Doxtader, K. A., and Nam, Y. (2016a). Structural basis for cooperative function of Mettl3 and Mettl14 methyltransferases. *Mol. Cell* 63, 306–317. doi: 10.1016/j.molcel.2016.05.041

Wang, X., Feng, J., Xue, Y., Guan, Z., Zhang, D., Liu, Z., et al. (2016b). Structural basis of N 6-adenosine methylation by the METTL3-METTL14 complex. *Nature* 534, 575–578. doi: 10.1038/nature18298

Wang, X., Fu, X., Zhang, J., Xiong, C., Zhang, S., and Lv, Y. (2020b). Identification and validation of m6A RNA methylation regulators with clinical prognostic value in Papillary thyroid cancer. *Cancer Cell Int.* 20:203. doi: 10.1186/s12935-020-01283-y

Wang, X., and He, C. (2014b). Dynamic RNA modifications in posttranscriptional regulation. *Mol. Cell* 56, 5–12. doi: 10.1016/j.molcel.2014.09.001

Wang, X., Lu, Z., Gomez, A., Hon, G. C., Yue, Y., Han, D., et al. (2014a). N6-methyladenosine-dependent regulation of messenger RNA stability. *Nature* 505, 117–120. doi: 10.1038/nature12730

Wang, X., Zhao, B. S., Roundtree, I. A., Lu, Z., Han, D., Ma, H., et al. (2015). N(6)-methyladenosine modulates messenger RNA translation efficiency. *Cell* 161, 1388–1399. doi: 10.1016/j.cell.2015.05.014

Warda, A. S., Kretschmer, J., Hackert, P., Lenz, C., Urlaub, H., Höbartner, C., et al. (2017). Human METTL16 is a N6-methyladenosine (m6A) methyltransferase that targets pre-mRNAs and various non-coding RNAs. *EMBO Rep.* 18, 2004–2014. doi: 10.15252/embr.201744940

Wei, C. M., Gershowitz, A., and Moss, B. (1975). Methylated nucleotides block 5' terminus of HeLa cell messenger RNA. *Cell* 4, 379–386. doi: 10.1016/0092-8674(75)90158-0

Weng, H., Huang, H., Wu, H., Qin, X., Zhao, B. S., Dong, L., et al. (2018). METTL14 inhibits hematopoietic stem/progenitor differentiation and promotes leukemogenesis via mRNA m6A modification. *Cell Stem Cell* 22, 191–205. doi: 10.1016/j.stem.2017.11.016

Wojtas, M. N., Pandey, R. R., Mendel, M., Homolka, D., Sachidanandam, R., and Pillai, R. S. (2017). Regulation of m6A transcripts by the 3′→5′ RNA helicase YTHDC2 is essential for a successful meiotic program in the mammalian germline. *Mol. Cell* 68, 374–387. doi: 10.1016/j.molcel.2017.09.021

Wood, O., Clarke, J., Woo, J., Mirza, A. H., Woelk, C. H., Thomas, G. J., et al. (2017). Head and neck squamous cell carcinomas are characterized by a stable immune signature within the primary tumor over time and space. *Clin. Cancer Res.* 23, 7641–7649. doi: 10.1158/1078-0432.ccr-17-0373

Wu, K. J. (2020). The role of miRNA biogenesis and DDX17 in tumorigenesis and cancer stemness. *Biomed. J.* 43, 107–114. doi: 10.1016/j.bj.2020.03.001

Xia, T. L., Li, X., Wang, X., Zhu, Y. J., Zhang, H., Cheng, W., et al. (2021). N(6)-methyladenosine-binding protein YTHDF1 suppresses EBV replication and promotes EBV RNA decay. *EMBO Rep.* 22:e50128. doi: 10.15252/embr.202050128

Xu, M., Chen, X., Lin, K., Zeng, K., Liu, X., Xu, X., et al. (2019). LncRNA SNHG6 regulates EZH2 expression by sponging miR-26a/b and miR-214 in colorectal cancer. *J. Hematol. Oncol.* 12:3. doi: 10.1186/s13045-018-0690-5

Xu, N., Chen, J., He, G., Gao, L., and Zhang, D. (2020). Prognostic values of m6A RNA methylation regulators in differentiated thyroid Carcinoma. *J. Cancer* 11, 5187–5197. doi: 10.7150/jca.41193

Yamaguchi, H., and Hung, M. C. (2014). Regulation and role of EZH2 in cancer. *Cancer Res. Treat.* 46, 209–222. doi: 10.4143/crt.2014.46.3.209

Yamashita, Y., Ikegami, T., Suzuki, M., Hirakawa, H., Maeda, H., Yamada, S., et al. (2019). Hypopharyngeal cancer risk in Japanese: genetic polymorphisms related to the metabolism of alcohol- and tobacco- associated carcinogens. *J. Cancer Res. Ther.* 15, 556–563. doi: 10.4103/jcrt.jcrt_980_17

Yang, X., Karuturi, R. M., Sun, F., Aau, M., Yu, K., Shao, R., et al. (2009). CDKN1C (p57 KIP2) is a direct target of EZH2 and suppressed by multiple epigenetic mechanisms in breast cancer cells. *PLoS One* 4:e5011. doi: 10.1371/journal.pone.0005011

Yankova, E., Aspris, D., and Tzelepis, K. (2021). The N6-methyladenosine RNA modification in acute myeloid leukemia. *Curr. Opin. Hematol.* 28, 80–85. doi: 10.1097/moh.0000000000000636

Yao, Y., Yang, Y., Guo, W., Xu, L., You, M., Zhang, Y. C., et al. (2021). METTL3-dependent m6A modification programs T follicular helper cell differentiation. *Nat. Commun.* 12:1333. doi: 10.1038/s41467-021-21594-6

Ye, J., Wang, Z., Chen, X., Jiang, X., Dong, Z., Hu, S., et al. (2020). YTHDF1-enhanced iron metabolism depends on TFRC m6A methylation. *Theranostics* 10, 12072–12089. doi: 10.7150/thno.51231

Yi, L., Wu, G., Guo, L., Zou, X., and Huang, P. (2020b). Comprehensive analysis of the PD-L1 and immune infiltrates of m6A RNA methylation regulators in head and neck squamous cell carcinoma. *Mol. Ther. Nucleic Acids* 21, 299–314. doi: 10.1016/j.omtn.2020.06.001

Yi, Y. C., Chen, X. Y., Zhang, J., and Zhu, J. S. (2020a). Novel insights into the interplay between m6A modification and noncoding RNAs in cancer. *Mol. Cancer* 19:121. doi: 10.1186/s12943-020-01233-2

Youn, J. Y., Dunham, W. H., Hong, S. J., Knight, J. D. R., Bashkurov, M., Chen, G. I., et al. (2018). High-density proximity mapping reveals the subcellular organization of mRNA-associated granules and bodies. *Mol. Cell* 69, 517–532. doi: 10.1016/j.molcel.2017.12.020

Young, L. S., Yap, L. F., and Murray, P. G. (2016). Epstein–Barr virus: More than 50 years old and still providing surprises. *Nat. Rev. Cancer* 16, 789–802. doi: 10.1038/nrc.2016.92

Yuan, S., Tang, H., Xing, J., Fan, X., Cai, X., Li, Q., et al. (2014). Methylation by NSun2 represses the levels and function of microRNA 125b. *Mol. Cell. Biol.* 34, 3630–3641. doi: 10.1128/mcb.00243-14

Zhang, H., Shi, X., Huang, T., Zhao, X., Chen, W., Gu, N., et al. (2020). Dynamic landscape and evolution of m6A methylation in human. *Nucleic Acids Res.* 48, 6251–6264. doi: 10.1093/nar/gkaa347

Zhang, L., Wan, Y., Zhang, Z., Jiang, Y., Gu, Z., Ma, X., et al. (2021). IGF2BP1 overexpression stabilizes PEG10 mRNA in an m6A-dependent manner and promotes endometrial cancer progression. *Theranostics* 11, 1100–1114. doi: 10.7150/thno.49345

Zhang, P., He, Q., Lei, Y., Li, Y., Wen, X., Hong, M., et al. (2018). m6A-mediated ZNF750 repression facilitates nasopharyngeal carcinoma progression. *Cell Death Dis.* 9:1169. doi: 10.1038/s41419-018-1224-3

Zhao, X., and Cui, L. (2019). Development and validation of a m6A RNA methylation regulators-based signature for predicting the prognosis of head and neck squamous cell carcinoma. *Am. J. Cancer Res.* 9, 2156–2169.

Zhao, X., Yang, Y., Sun, B. F., Shi, Y., Yang, X., Xiao, W., et al. (2014). FTO-dependent demethylation of N6-methyladenosine regulates mRNA splicing and is required for adipogenesis. *Cell Res.* 24, 1403–1419. doi: 10.1038/cr.2014.151

Zheng, G., Dahl, J. A., Niu, Y., Fedorcsak, P., Huang, C. M., Li, C. J., et al. (2013). ALKBH5 is a mammalian RNA demethylase that impacts RNA metabolism and mouse fertility. *Mol. Cell* 49, 18–29. doi: 10.1016/j.molcel.2012.10.015

Zheng, Q., Hou, J., Zhou, Y., Li, Z., and Cao, X. (2017). The RNA helicase DDX46 inhibits innate immunity by entrapping m6A-demethylated antiviral transcripts in the nucleus. *Nat. Immunol.* 18, 1094–1103. doi: 10.1038/ni.3830

Zheng, X., Wang, J., Zhang, X., Fu, Y., Peng, Q., Lu, J., et al. (2021). RNA m6A methylation regulates virus–host interaction and EBNA2 expression during Epstein–Barr virus infection. *Immun. Inflam. Dis.* doi: 10.1002/iid3.396 [Epub ahead of print].

Zhong, J., Min, L., Huang, H., Li, L., Li, D., Li, J., et al. (2013). EZH2 regulates the expression of p16 in the nasopharyngeal cancer cells. *Technol. Cancer Res. Treat.* 12, 269–274. doi: 10.7785/tcrt.2012.500315

Zhong, L., He, X., Song, H., Sun, Y., Chen, G., Si, X., et al. (2020). METTL3 induces AAA development and progression by modulating N6-methyladenosine-dependent primary miR34a processing. *Mol. Ther. Nucleic Acids* 21, 394–411. doi: 10.1016/j.omtn.2020.06.005

Zhou, J., Wan, J., Gao, X., Zhang, X., Jaffrey, S. R., and Qian, S. B. (2015). Dynamic m6A mRNA methylation directs translational control of heat shock response. *Nature* 526, 591–594. doi: 10.1038/nature15377

Conflict of Interest: The authors declare that the research was conducted in the absence of any commercial or financial relationships that could be construed as a potential conflict of interest.

frontiers in Cell and Developmental Biology

ORIGINAL RESEARCH
published: 04 June 2021
doi: 10.3389/fcell.2021.640786

Overexpression of Interferon-Inducible Protein 16 Promotes Progression of Human Pancreatic Adenocarcinoma Through Interleukin-1β-Induced Tumor-Associated Macrophage Infiltration in the Tumor Microenvironment

Jing-Xian Chen[1†], Chien-Shan Cheng[2,3†], Hong-Fang Gao[4], Zi-Jie Chen[5], Ling-Ling Lv[1], Jia-Yue Xu[1], Xiao-Heng Shen[1], Jing Xie[2,3] and Lan Zheng[1*]*

[1] Department of Traditional Chinese Medicine, Shanghai Jiao Tong University School of Medicine Affiliated Ruijin Hospital, Shanghai, China, [2] Department of Integrative Oncology, Fudan University Shanghai Cancer Center, Shanghai, China, [3] Department of Oncology, Shanghai Medical College, Fudan University, Shanghai, China, [4] Department of Oncology, Shanghai Yangpu Hospital of Traditional Chinese Medicine, Shanghai, China, [5] Department of Geriatrics, Shanghai Yangpu Hospital of Traditional Chinese Medicine, Shanghai, China

OPEN ACCESS

Edited by:
Na Luo,
Nankai University, China

Reviewed by:
Pan Pan,
Wuhan University, China
Song Yao,
Tongji University, China

***Correspondence:**
Jing Xie
isable624@163.com
Lan Zheng
zl10558@rjh.com

[†] These authors have contributed equally to this work

Specialty section:
This article was submitted to Molecular Medicine, a section of the journal Frontiers in Cell and Developmental Biology

Received: 12 December 2020
Accepted: 23 April 2021
Published: 04 June 2021

Citation:
Chen J-X, Cheng C-S, Gao H-F, Chen Z-J, Lv L-L, Xu J-Y, Shen X-H, Xie J and Zheng L (2021) Overexpression of Interferon-Inducible Protein 16 Promotes Progression of Human Pancreatic Adenocarcinoma Through Interleukin-1β-Induced Tumor-Associated Macrophage Infiltration in the Tumor Microenvironment. Front. Cell Dev. Biol. 9:640786. doi: 10.3389/fcell.2021.640786

Activation of inflammasomes has been reported in human pancreatic adenocarcinoma (PAAD); however, the expression pattern and functional role of inflammasome-related proteins in PAAD have yet to be identified. In this study, we systemically examined the expression and role of different inflammasome proteins by retrieving human expression data. Several genes were found to be differentially expressed; however, only interferon-inducible protein 16 (IFI16) expression was found to be adversely correlated with the overall survival of PAAD patients. Overexpression of IFI16 significantly promoted tumor growth, increased tumor size and weight in the experimental PAAD model of mice, and specifically increased the population of tumor-associated macrophages (TAMs) in the tumor microenvironment. Depletion of TAMs by injection of liposome clodronate attenuated the IFI16 overexpression-induced tumor growth in PAAD. *In vitro* treatment of conditioned medium from IFI16-overexpressing PAAD cells induced maturation, proliferation, and migration of bone marrow-derived monocytes, suggesting that IFI16 overexpression resulted in cytokine secretion that favored the TAM population. Further analysis suggested that IFI16 overexpression activated inflammasomes, thereby increasing the release of IL-1β. Neutralization of IL-1β attenuated TAM maturation, proliferation, and migration induced by the conditioned

medium from IFI16-overexpressing PAAD cells. Additionally, knockdown of IFI16 could significantly potentiate gemcitabine treatment in PAAD, which may be associated with the reduced infiltration of TAMs in the tumor microenvironment. The findings of our study shed light on the role of IFI16 as a potential therapeutic target for PAAD.

Keywords: IFI16, inflammasome, pancreatic adenocarcinoma, tumor-associated macrophages, IL-1β

INTRODUCTION

Pancreatic cancer, mainly in the form of pancreatic adenocarcinoma (PAAD), is one of the most malignant human cancers worldwide. PAAD is the fourth common cause of cancer-related death currently and has been projected to be the second one, after lung cancer, by 2030 (Rahib et al., 2014). Despite the rapid development in diagnostic technology and new treatments, PAAD is still very difficult to detect at an early stage, which results in a delayed intervention that largely causes poor prognosis in the patients (Oberstein and Olive, 2013). Surgical resection is the main optimal treatment; however, in patients with non-surgical PAAD, chemotherapeutic agents, such as gemcitabine, demonstrate a very poor response (Principe et al., 2020). The identification of novel diagnostic and therapeutic targets is necessary. Inflammation plays an important role in the pathogenesis of PAAD (Stone and Beatty, 2019). Patients with chronic pancreatitis are at a high risk of developing PAAD (Yadav and Lowenfels, 2013), and an experimental model of pancreatitis could reportedly accelerate PAAD progression (Carriere et al., 2009). At the cellular level, it was clinically observed that pro-inflammatory immune cells, such as macrophages, accumulate in PAAD (Deschenes-Simard et al., 2013). Release and infiltration of pro-inflammatory cytokines, as well as activation of pro-inflammatory signaling, including NF-κB, COX-2, and TLRs, also demonstrate the involvement of inflammation in PAAD (Pramanik et al., 2018). Thus, inflammation may be a potential target for the discovery of a new therapeutic strategy for PAAD.

The inflammasome is a cellular protein complex that mediates the inflammatory response toward various pathogenic microorganisms and sterile sensors (Guo et al., 2015). Particularly, the activation of inflammasomes in sterile inflammation was found to play an important role in the pathogenesis and progression of human cancers, including PAAD (Xu et al., 2019). Activation of the AIM2 inflammasome during the pathogenesis of PAAD caused HMGB1 release, which conferred an immunosuppressive tumor microenvironment and led to tumor cell immune evasion (Li et al., 2018). The product of inflammasome activation, IL-1β, was significantly increased in pancreatic cancer tissue. Inhibition of inflammasome activation prevents infiltration of IL-1β that retards pancreatic cancer cell proliferation (Mohammed et al., 2017). Inflammasome activation in PAAD tumor cells may also regulate stromal cells, such as cancer-associated fibroblasts, through IL-1β/IL-1R (Brunetto et al., 2019). Additionally, the activation of platelet inflammasomes in PAAD was found to positively regulate platelet aggregation and tumor growth in mice (Boone et al., 2019). These lines of reports indicate that targeting the inflammasome may be a potential therapeutic target for the treatment of PAAD. However, a systematic investigation of the expression profile of inflammasome-related molecules and their role in PAAD remains lacking.

Interferon-inducible protein 16 (IFI16) is a HIN-200 protein which contains a 200-amino-acid DNA binding domain at its C-terminus and a PYRIN domain at its N-terminus (Liao et al., 2011). As a DNA sensor of inflammation, IFI16 plays a critical role in the regulation of gene transcription and cellular response to stress (Choubey and Panchanathan, 2016). IFI16 regulates the inflammation response of cells in various mechanisms. In viral infection, IFI16 binds to viral double-stranded DNA (dsDNA) to activate STING-TBK1 for the production of IFN-β (Unterholzner et al., 2010). At the same time, the binding of IFI16 with ASC and procaspase-1 may form a DNA inflammasome complex that triggers IL-1β mutation and release (Zhao et al., 2015). In human cancers, the role of IFI16 may be far from conclusive. It was even found that IFI16 expression was reduced in liver cancer and may act as a tumor suppressor gene by triggering cell apoptosis and inhibiting cell proliferation (Lin et al., 2017). However, a controversial argument of the role of IFI16 in cancer was found in both oral cancer and renal clear cell carcinoma, in which IFI16 may serve as an oncogene to promote cell proliferation and tumor progression (Kondo et al., 2012; Yu et al., 2021). The role of IFI16 in mediating change in the tumor microenvironment remains unknown.

In this study, we profiled the expression pattern of inflammasome-related proteins in human PAAD by retrieving data from publicly available human cancer databases and identified its correlation with the survival of human cancer patients. Molecules that are differentially expressed and correlated with the survival of PAAD patients were studied to elucidate their functional role in tumor growth and immune response in the tumor microenvironment. Furthermore, we investigated the mechanism through which inflammasome-related proteins in the PAAD cells mediate the tumor microenvironment-driven development and progression of PAAD.

MATERIALS AND METHODS

Chemical, Plasmids, and Antibodies

Liposome PBS and liposome clodronate were obtained from Liposoma BV (Netherlands). Gemcitabine, bromodeoxyuridine (BrdU), and PKH26PCL were purchased from Sigma-Aldrich (United States). Calcein AM was purchased from Thermo Fisher (United States). Poly dA:dT and neutralizing antibody against IL-1β were obtained from InvivoGen (United States).

The CRISPR-cas activation plasmid and IFI16 shRNA were purchased from Santa Cruz (United States). Antibodies against IFI16, caspase-1, AIM2, IL-1β, ASC, and β-actin were purchased from Abcam (Cambridge, United Kingdom). FITC-conjugated antibodies against F4/80, APC-conjugated antibodies against CD11b, PE/Cy7-conjugated antibodies against CD11c, APC-conjugated antibodies against CD3, FITC-conjugated antibodies against CD4, and PE/Cy7-conjugated antibodies against CD8 were purchased from BioLegend (United Kingdom).

Cell and Cell Culture

The murine PAAD cell line, Panc-2, was obtained from the Frederick National Laboratory for Cancer Research (Frederick, MD, United States) and has been used in our previous study (Gao et al., 2019). Panc-1, BxPC3, and SW1990 cell lines were obtained from the American Type Culture Collection (ATCC, United States). All cells were cultured in DMEM, supplemented with 10% FBS and 1% penicillin/streptomycin (Thermo Fisher, United States), under humidified conditions of 37°C and 5% CO_2.

Orthotopic PAAD Murine Model

The orthotopic PAAD murine model was established according to the protocol described in our previous study (Gao et al., 2020). The animal study protocol was approved by the Animal Experimental Ethics Committee of Ruijin Hospital, Shanghai Jiao Tong University School of Medicine. Briefly, luciferase-tagged Panc-2 cells were mixed with the Matrigel matrix (BD Bioscience, United States). A 20-μl mixture containing 1×10^8 Panc-2 cells was injected into the pancreas of C57BL/J mice. Measurement of orthotopic tumor size was performed once per week, beginning 1 week post injection, using the IVIS Spectrum live animal imager (PerkinElmer, United States), with luciferin (30 mg/kg, i.p.) as the substrate. For the gemcitabine treatment, mice were orally administered gemcitabine at a dose of 100 mg/kg daily. At the end of the study, the mice were sacrificed, and the pancreas was dissected out.

Tumor-Associated Macrophage Depletion by Liposome Clodronate

Depletion of Tumor-Associated Macrophages (TAMs) was performed according to a published protocol, with minor modifications (Jordan et al., 2003). To minimize the early recruitment of TAMs, mice received a single injection of liposome PBS (as sham control) or liposome clodronate 3 days before orthotopic implantation of tumor cells and then subsequent injections twice per week after implantation at a dose of 15 mg/kg.

Isolation and Culture of Bone Marrow-Derived Macrophages

Bone Marrow-Derived Macrophages (BMDMs) were isolated using the Ficoll method, according to a published protocol (Pinton et al., 2019). Briefly, the femurs of C57BL/J mice were isolated, and monocytes were flushed out. Monocytes were enriched by gradient centrifugation using the Ficoll reagent. The enriched monocytes were then cultured in RPMI culture medium, supplemented with 10% FBS and 10 ng/ml recombinant murine M-CSF, for 7 days.

BrdU Incorporation Assay

For the *in vitro* BrdU incorporation assay, 10 μM BrdU was added to the culture medium 4 h before sample collection by trypsinization. For the *in vivo* BrdU incorporation assay, 10 mg/kg BrdU was intraperitoneally injected into the mice 24 h before sample collection, by enriching TAMs from the dissected tumor using the Ficoll method. The *in vitro* or *in vivo* collected cells were then processed according to the manufacturer's instructions (Promega, United States). Briefly, collected cells were stained with appropriate cell surface markers. The cells were then fixed and penetrated with fixatives for 2 h at room temperature, followed by incubation with 1 μg/mL FITC-conjugated anti-BrdU antibody for 30 min. The cells were then subjected to flow cytometry analysis.

Transwell Cell Migration Assay

Quantitative analysis of BMDM migration was performed using the Transwell cell migration assay. Briefly, 2×10^5 BMDMs cultured in conditioned medium from Panc-2 cells were seeded at the apical side of Transwell inserts with serum-free medium. Culture medium, supplemented with chemotaxis MCP-1 (10 ng/ml), was added to the receiving chambers and cultured for 3 h. Cells remaining on the apical side of the inserts were scraped away, and cells at the basal side of the membrane were collected by trypsinization. The cells were then collected and stained with 50 μM calcein AM and quantified using a fluorescence microplate reader (PerkinElmer, Germany).

Co-culture System

The Panc-2 cells were cultured on the apical side of the 0.8-μM-pore size Transwell, while BMDMs were seeded on the receiving chamber with the non-attached surface, supplemented with 10 ng/ml M-CSF. This co-culture was maintained for 7 days to allow all possible non-contact interactions between the Panc-2 cells and BMDMs. BMDMs were then collected for analysis of the TAM population with flow cytometry and quantitative real-time PCR (qPCR).

Blocking IL-1β With Neutralizing Antibody

Supplementation with IL-1β-neutralizing antibody mitigated the function of secreted IL-1β in the conditional medium from Panc-2 cells. This method was adopted from a published protocol, with minor modifications (Staudt et al., 2013). For the blocking experiments, the BMDMs were preincubated with 10 μg/ml of IL-1β-neutralizing antibody for 15 min before the functional studies.

Flow Cytometry

Cells were stained with various fluorescence-conjugated antibodies for 15 min in the dark at room temperature. Cells (1×10^6) were stained with 1 μg of antibody and washed with 300 μl of PBS. The cells were then resuspended in 300 μl of

PBS for analysis with flow cytometry (Canto II, BD Bioscience, United States). To sort TAMs, dissected tumors were digested with 0.8 mg/ml of collagenase IV for 30 min at 37°C with gentle shaking. TAMs were enriched using the Ficoll method and then stained with the cell surface markers F4/80 and CD11b. The F4/80 + CD11b + TAMs were then collected using a cell sorter (Aria I, BD Bioscience, United States).

Quantitative Reverse-Transcription PCR

Total RNA was extracted using the TRIzol method (Life Technologies, United States). First-strand cDNA was prepared using a reverse-transcription kit (Life Technologies, United States). SYBR Green qRT-PCR was performed to measure the gene expression on a qPCR platform (Bio-Rad, United States) with specific primer pairs as follows: HIF-1α (forward: 5′-TGATGTGGGTGCTGGTGTC-3′, reverse: 5′-TTGTGTTGG GGCAGTACTG-3′), CCL2 (forward: 5′-AGGTCCCTGTCAT GCTTCTGG-3′, reverse: 5′-CTGCTGCTGGTGATCCTCTTG-3′), PECAM1 (forward: 5′-CCAAAGCCAGTAGCATCATGG TC-3′, reverse: 5′-GGATGGTGAAGTTGGCTACAGG-3′), IF N-γ (forward: 5′-CAGCAACAGCAAGGCGAAAAAGG-3′, re verse: 5′-TTTCCGCTTCCTGAGGCTGGATα-3′), TGF-β (for ward: 5′-ACTGATACGCCTGAGTGGCT-3′, reverse: 5′-CCCT GTATTCCGTCTCCTTG-3′), and β-actin (forward: 5′-AAGG CCAACCGTGAAAAGAT-3′, reverse: 5′-GTGGTACGACCAG AGGCATAC-3′) as control.

Immunoblotting

Total protein was isolated by gel electrophoresis and transferred onto a polyvinylidene fluoride (PVDF) membrane (Millipore, United States). The membrane was then blocked using 10% BSA in TBST buffer at room temperature, for 2 h, and then incubated with primary antibodies overnight at 4°C. After washing, the membrane was incubated with the appropriate secondary antibodies at room temperature for 2 h. The bands were then read by ChemiDoc chemiluminescence using ECL Select as the substrate (Bio-Rad, United States).

Bioinformatic Analysis

Expression data of related genes in human pancreatic cancer were extracted from GEPIA[1] (Tang et al., 2017). GEPIA data were collected from the GCGA and GTEx projects using a standard processing pipeline. For the selection of inflammasome-related genes, we selected the key proteins shortlisted from GeneCards-listed inflammasome-related genes by including only those genes encoding intracellular proteins that are composed of inflammasome machinery. Data are presented as dot blots of transcripts per million in the sequencing. Gene expressions with a fold change of over 2 and a p-value lower than 0.05 were considered statistically significant in the difference between normal and tumor tissues. The Kaplan–Meier plot was automatically generated by GEPIA using the median expression of a particular gene as the group cutoff. For the correlation analysis, data of particular gene pairs were extracted from GEPIA and analyzed using Spearman's correlation coefficient. The results used a non-log scale for calculation and the log-scale axis for visualization. Two datasets, GDS4336 and GDS4103, were collected from the GEO[2] of NCBI and were analyzed by paired Student's t-test, with $p < 0.05$ considered statistically significant between groups.

Statistical Analysis

Experiments were performed in triplicate. Data are presented as mean ± SEM. Statistical analysis was performed using Student's t-test. Differences were considered statistically significant at $p < 0.05$.

RESULTS

Expression of IFI16 Was Increased in PAAD and Correlated to Poor Patient Prognosis

Several studies have observed inflammasome activation during tumorigenesis and progression of PAAD (Brunetto et al., 2019; Yaw et al., 2020); however, the expression pattern of inflammasome-related genes and their functional roles have yet to be systematically investigated. To profile the expression pattern, we extracted human expression profiles of inflammasome-associated genes in PAAD from the GEPIA database (**Figure 1A**). We selected the genes according to a literature review and GeneCards viewing of the machinery proteins involved in inflammasome priming. Both classic and non-classic pathways of inflammasome priming were searched, but only those proteins that directly compose the inflammasome complex were included, as we were not able to include all other proteins that indirectly regulate inflammasome pathways, owing to the size of the study. Only intracellular proteins were included; therefore, secreted proteins, such as IL-1β and IL-18, were ruled out. Seven of 12 inflammasome-related genes, namely, IFI16, NLRP1, PICARD, NLRP3, NLRC5, CASP1, and PSTPIP1, were found to be upregulated in PAAD compared to those in normal pancreatic tissues. To understand the clinical significance of the upregulation of genes, we extracted the data of patients' overall survival and plotted the survival curves of patients grouped by median expression of the individual gene (**Figure 1B**). A significant difference in overall survival was observed in patients grouped by median expression of NLRP1 and IFI16; however, a high expression of NLRP1 predicted better survival of PAAD patients. The two results are not in line with the function of NLRP1 in PAAD; therefore, we excluded this gene from further analysis. This contradiction may result from several different factors and may suggest that rather than an initiating factor in PAAD progression, NLRP1 overexpression may act as a response to restrict the growth and expansion of PAAD tumors at a particular stage to a certain level. Interestingly, only a lower expression of IFI16 predicted better patient survival (**Figure 1C**). IFI16 expression was not significantly correlated with the disease-free survival of PAAD patients (**Figure 1D**),

[1]http://gepia.cancer-pku.cn/

[2]https://www.ncbi.nlm.nih.gov/geo

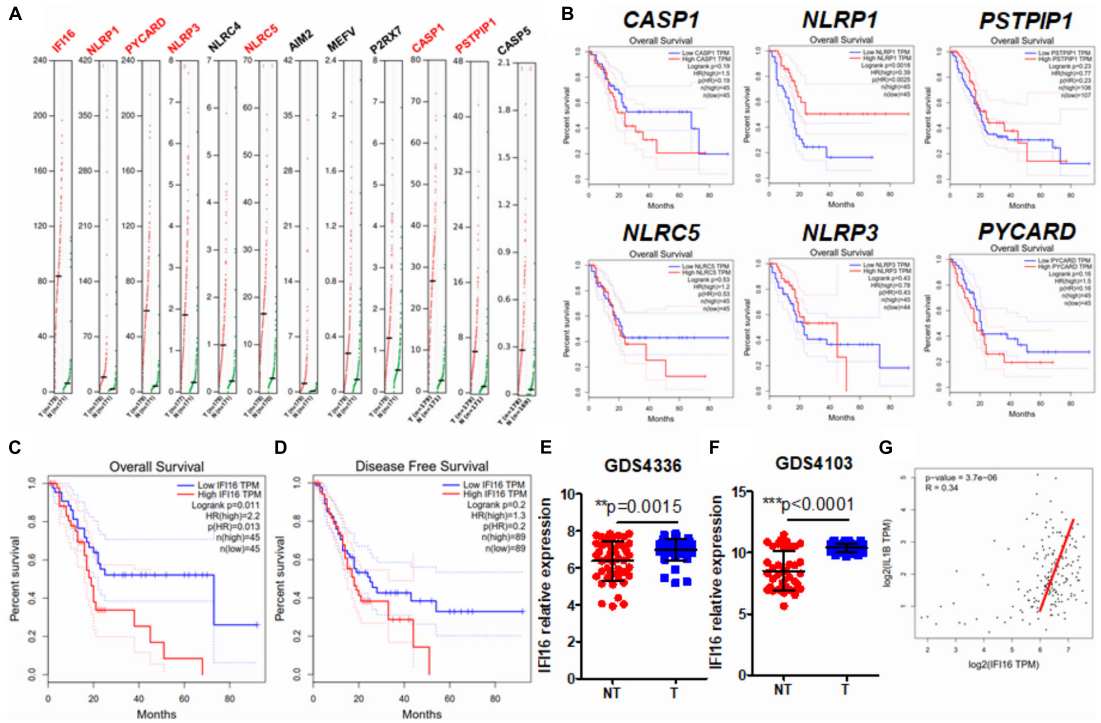

FIGURE 1 | IFI16 was overexpressed in human PAAD and correlated with poor survival of the patients. **(A)** Expression data of inflammasome-related proteins were retrieved from the human database GEPIA. A comparison of expression between normal pancreatic tissues and PAAD tissues was done. Genes with a significantly different expression between normal and tumor tissues are shown in red. **(B)** The data on overall survival and disease-free survival of PAAD patients were retrieved. Only NLRP1, among the genes with significantly different expression, showed a negative correlation with patients' overall survival. Overall survival **(C)** but not disease-free survival **(D)** was adversely correlated with the expression of IFI16 in PAAD. We further extracted expression data of IFI16 from the human GEO database, including GDS4336 **(E)** and GDS4103 **(F)**. IFI16 was significantly overexpressed in the tumor tissues of PAAD compared with that in the non-tumor adjacent normal pancreas. **(G)** Pearson correlation between the expression of IFI16 and IL-1β was analyzed, which showed a positive correlation in human PAAD. $^{*}p < 0.05$.

suggesting that IFI16 may not be related to the recurrence of the disease in patients who have received particular treatment such as surgical resection but may mainly be the factor of gross survival of the patients. This means that IFI16 overexpression may not be indicative in the short-term disease period once patients receive treatment but may suggest an unfavorable long-term outcome of survival of PAAD patients. The expression of IFI16 was further examined in two datasets of human PAAD samples, which revealed that IFI16 was significantly overexpressed in tumor tissues than in non-tumor adjacent tissues in both datasets (**Figures 1E,F**). Since IL-1β production is a common consequence of inflammasome activation, we extracted data on the expression of both IFI16 and IL-1β in PAAD. The analysis showed that the expression of IL-1β was positively correlated with the expression of IFI16, further suggesting the activation of inflammasomes in PAAD (**Figure 1G**). This observation indicates that IFI16 is overexpressed in PAAD, which correlates with the activation of the inflammasome and poor survival of patients.

Overexpression of IFI16 Accelerates Orthotopic Growth of PAAD in Mice

IFI16 is an intracellular protein that responds to DNA damage during the initiation of inflammasome activation (Choubey and Panchanathan, 2016). To identify the functional role of IFI16 in mediating PAAD progression, we stably overexpressed this protein in Panc-2 cells (**Figure 2A**). The wild-type and IFI16-overexpressing Panc-2 cells were orthotopically injected into the pancreas of mice, and the formation and growth of orthotopic tumors were observed by weekly measurement of the luciferase activity for 4 weeks. Overexpression of IFI16 in Panc-2 cells significantly accelerated tumor growth by a week (**Figure 2B**). At the end of the experiment, tumors were dissected out; representative tumors in each group are shown in **Figure 2C**. The weight of the tumor was then measured, which indicated that IFI16 overexpression remarkably increased the tumor weight (**Figure 2C**). Since IFI16 overexpression was reported to trigger innate immune cells (Unterholzner et al., 2010), we measured whether IFI16 overexpression in PAAD altered the immune cell profile in the tumor microenvironment. PAAD tissues with or without IFI16 overexpression were digested and were analyzed with flow cytometry using specific marker staining of different immune cells. Interestingly, IFI16 overexpression specifically increased the population of CD11b + F4/80 + macrophages in the tumor microenvironment but had minimal effect on the populations of CD11b + CD11c + dendritic cells, CD3 + CD4 + CD8- T helper cells, and CD3 + CD4- CD8 + cytotoxic T cells, suggesting that the effect of IFI16

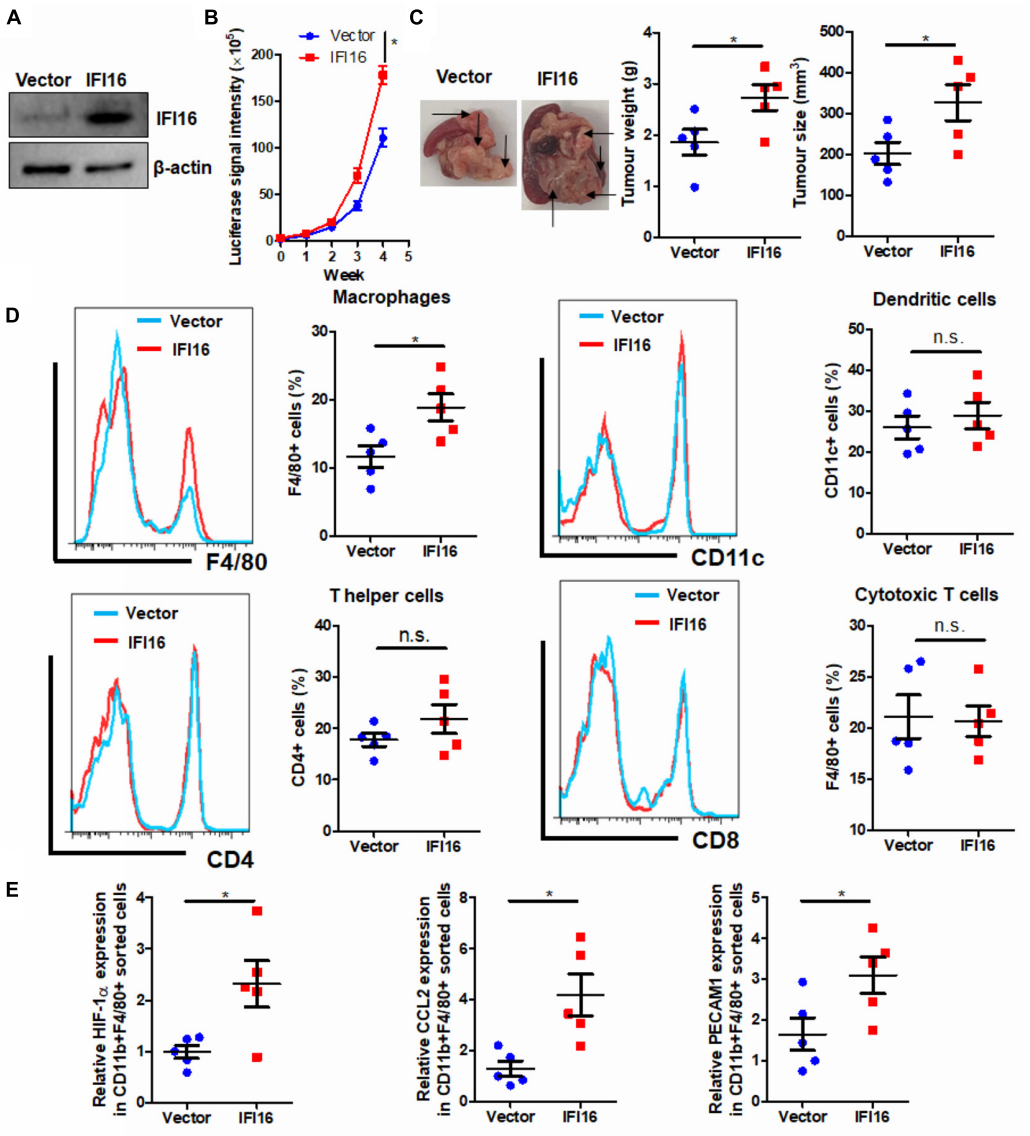

FIGURE 2 | Overexpression of IFI16 promoted tumor growth in an experimental model of PAAD. **(A)** The IFI16-overexpressing PAAD cell line was established by transfecting the CRISPR activation plasmid of IFI16 into the Panc-2 cells. Cells were selected with a culture medium containing 1 μg/ml of puromycin, until a stable IFI16-overexpressing clone was established. Overexpression of IFI16 was validated with immunoblotting. **(B)** Panc-2 of a stable clone expressing the luciferase reporter was established. Panc-2 cells were transfected with the PGL3 vector expressing firefly luciferase and selected by neomycin (50 μg/ml). Approximately 20 μg Matrigel matrix, containing 1×10^8 Panc-2 cells, was orthotopically injected into the pancreas of mice. The luciferase signal intensity was measured by intraperitoneal injection of luciferin (30 mg/kg) and quantification under a live animal imager once per week. Overexpression of IFI16 significantly accelerated the orthotopic growth of the pancreatic tumor. **(C)** At the end of the study, the mice were sacrificed, and the pancreas along with the spleen was dissected out. The tumor weight was measured, and tumor size was calibrated by the diameters of the tumor. Overexpression of IFI16 potently increased the tumor size and weight in the experimental PAAD model. The black arrow shows an obvious surface tumor nodule found in the pancreas. **(D)** The dissected tumor was then digested in 0.8 mg/ml of collagenase IV for 30 min at 37°C with gentle shaking. The immune cells were enriched with Ficoll methods. The profile of immune cells in the tumor microenvironment was measured with flow cytometry. Overexpression of IFI16 significantly increased the population of TAMs but not dendritic cells, T helper cells, or cytotoxic T cells. **(E)** The F4/80 + CD11b + TAMs were collected using a cell sorter, and expressions of HIF-1α, CCL2, and PECAM1 were measured with qRT-PCR. TAMs from IFI16-overexpressing tumors exhibited a significantly high expression of TAM markers, including HIF-1α, CCL2, and PECAM1. *$p < 0.05$.

overexpression in PAAD cells may specifically target TAMs in the tumor microenvironment (**Figure 2D**, gating shown in **Supplementary Figure 1**). To confirm the increased population as TAMs, we sorted the CD11b + F4/80 + cells from the pancreatic tumors using a FACS sorter and quantified the expression of some TAM markers, such as HIF-1α, CCL2, and PECAM1, with qRT-PCR. It was observed that the IFI16-overexpressing Panc-2 cells induced increased expression of HIF-1α, CCL2, and PECAM1 compared to vector-expressing Panc-2, which was consistent with our flow cytometric observation

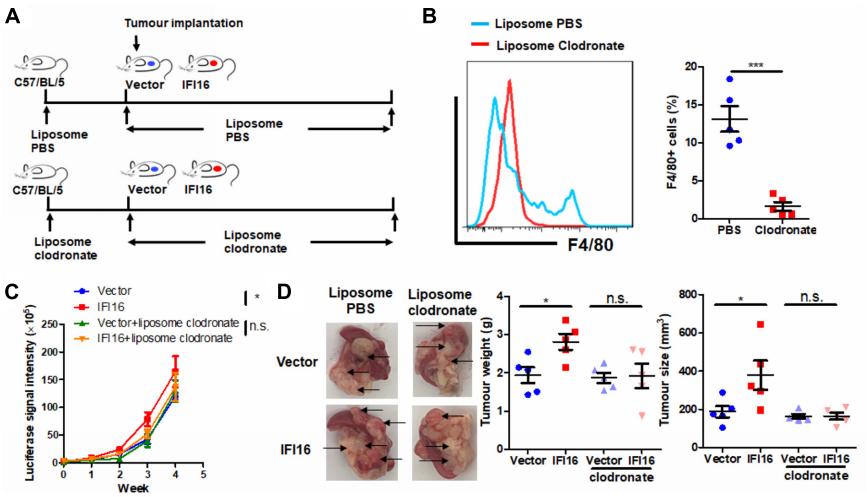

FIGURE 3 | Depletion of TAMs attenuated IFI16-induced tumor growth of PAAD. **(A)** Flowchart of TAM depletion treatment. To minimize early recruitment of TAMs, mice received a single injection of liposome PBS (as sham control) or liposome clodronate, 3 days before orthotopic implantation of tumor cells, and received subsequent injection twice per week after implantation at a dose of 15 mg/kg. **(B)** The tumor was dissected out, and TAMs were enriched with Ficoll methods. The enriched cells were stained with an antibody against F4/80 and subjected to flow cytometric analysis. Treatment with liposome clodronate could potently remove TAMs from mice with orthotopic PAAD tumors. **(C)** Panc-2 of a stable clone expressing the luciferase reporter was established. Panc-2 cells were transfected with the PGL3 vector expressing firefly luciferase and selected by neomycin (50 μg/ml). Approximately 20 μl Matrigel matrix, containing 1×10^8 Panc-2 cells, was orthotopically injected into the pancreas of mice. The luciferase signal intensity was measured by intraperitoneal injection of luciferin (30 mg/kg) and quantification under a live animal imager once per week. Depletion of TAMs attenuated the tumor growth of PAAD induced by IFI16 overexpression. **(D)** At the end of the study, the mice were sacrificed, and the pancreas along with the spleen was dissected out. The tumor weight was measured, and tumor size was calibrated by the diameters of the tumor. Depletion of TAMs abolished the IFI16 overexpression-induced increase in tumor size and weight in the experimental PAAD model. The black arrow shows an obvious surface tumor nodule found on the pancreas. $^*p < 0.05$ and $^{***}p < 0.001$.

(**Figure 2E**). Taken together, these observations suggest that IFI16 overexpression promotes tumor growth and progression of PAAD and may play a role in regulating TAMs in the tumor microenvironment.

TAMs Mediate the IFI16 Overexpression-Induced PAAD Tumor Growth and Progression

To further identify the role of TAMs in IFI16 overexpression-induced PAAD tumor growth and progression, we used liposome clodronate to deplete TAMs from mice bearing orthotopic PAAD (Jordan et al., 2003). To minimize the early recruitment of TAMs, mice received a single injection of liposome PBS (as control) or liposome clodronate 3 days before orthotopic implantation of tumor cells and then received subsequent injections twice per week after implantation (**Figure 3A**). It was observed that injection of liposome clodronate completely removed the TAMs from the tumor microenvironment, as evidenced by the rare appearance of F4/80 + cells in the tumor (**Figure 3B**, gating shown in **Supplementary Figure 2**). Injection of liposome PBS had minimal effect on the IFI16 overexpression-induced PAAD tumor growth and progression, suggesting that no vehicle effect was observed. In contrast, injection of liposomal clodronate to remove TAMs significantly abolished the promotion of PAAD growth and progression rate induced by IFI16 overexpression (**Figure 3C**). The size, as well as weight, of the representative tumor also suggested that IFI16 overexpression could be neutralized upon TAM clearance (**Figure 3D**). This observation indicates that TAMs are necessary for mediating the promoting effect of IFI16 overexpression on PAAD progression and growth.

IFI16 Overexpression in PAAD Cells Induces Maturation, Infiltration, and Proliferation of TAMs in the Tumor Microenvironment

Regulation of the TAM population in the tumor microenvironment may involve multiple processes, including the infiltration of circulating pro-inflammatory monocytes, maturation of infiltrated monocytes, and proliferation of local TAMs (Yang et al., 2018). To understand how IFI16 overexpression in PAAD cells regulates the TAM population in the tumor microenvironment, we collected the culture supernatant from PAAD cells with or without IFI16 overexpression. BMDMs treated with 30% culture supernatant from PAAD cells with IFI16 overexpression exhibited a higher level of CD11b + F4/80 + population after 7-day incubation, suggesting that IFI16 overexpression in PAAD cells can increase the maturation of TAMs from monocytic cells in the tumor microenvironment (**Figure 4A**). We further co-cultured the Panc-2 cells with BMDMs in a Transwell system. The Panc-2 cells with or without IFI16 overexpression were cultured on the apical side of the 0.8-μM-pore size Transwell, while BMDMs were seeded on the receiving chamber with the non-attached surface, supplemented with 10 ng/ml of

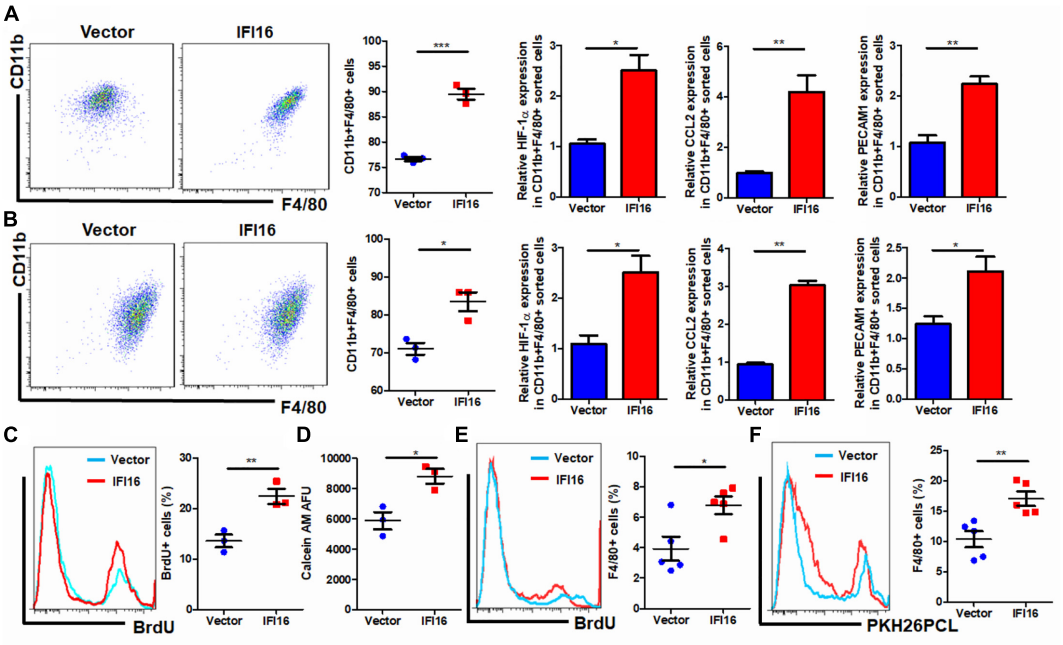

FIGURE 4 | Conditional medium from IFI16-overexpressing PAAD cells increased the TAM population. **(A)** The culture medium of wild-type and IFI16-overexpressing PAAD cells was collected. BMDMs were cultured with 30% of the aforementioned conditional medium for 7 days. Cells were then collected and stained with antibodies against CD11b and F4/80 and subjected to flow cytometric analysis. BMDMs cultured with IFI16-overexpressing PAAD cells showed a higher level of CD11b + F4/80 + cells. Total RNA was extracted, and the expressions of HIF-1α, CCL2, and PECAM1 were analyzed with qRT-PCR. BMDMs cultured with conditional medium from IFI16-overexpressing PAAD cells showed significantly higher expressions of HIF-1α, CCL2, and PECAM1. **(B)** The Panc-2 cells with or without IFI16 overexpression were cultured on the apical side of the 0.8-μM-pore size Transwell, while BMDMs were seeded on the receiving chamber with the non-attached surface, supplemented with 10 ng/ml of M-CSF. This co-culture was maintained for 7 days to allow all possible non-contact interaction between the Panc-2 cells and BMDMs. BMDMs were then collected for analysis of the TAM population with flow cytometry and qPCR. Co-culture of Panc-2 cells with IFI16 overexpression significantly increased the population of TAMs from the BMDM culture compared to the co-culture of vector-expressing Panc-2 cells. **(C)** Added to the culture medium was 10 μM of BrdU 4 h prior to sample collection by trypsinization. BrdU-incorporated CD11b + F4/80 + cells were stained with anti-BrdU antibody and detected with a flow cytometer. BMDMs cultured with the conditional medium from IFI16-overexpressing PAAD cells showed significantly higher incorporation of BrdU into the DNA. **(D)** Approximately 2×10^5 BMDMs cultured with the conditional medium from Panc-2 cells were seeded at the apical side of the Transwell insert with serum-free medium. A culture medium supplemented with chemotaxis MCP-1 (10 ng/ml) was added into the receiving chambers and cultured for 3 h. Cells remaining at the apical side of inserts were scraped away, and cells at the basal side of the membrane were collected by trypsinization. The cells were then collected and stained with 50 μM calcein AM and quantified with a fluorescence microplate reader. BMDMs cultured with the conditional medium from IFI16-overexpressing PAAD cells showed significantly higher motility. **(E)** Intraperitoneally injected into the mice was 10 mg/kg of BrdU 24 h prior to sample collection by enriching TAMs from the dissected tumor by Ficoll methods. BrdU-incorporated CD11b + F4/80 + cells were stained with an anti-BrdU antibody and detected with a flow cytometer. TAMs from tumors with IFI16 overexpression showed significantly high incorporation into the DNA. **(F)** BMDMs were isolated from the femurs and cultured into macrophages in a medium containing 10 μg/ml of M-CSF for 7 days. Cells were then stained with 100 μM PKH26PCL for labeling. Labeled cells were then intraperitoneally injected into the mice bearing PAAD tumors with or without IFI16 overexpression and allowed circulation for 24 h. The tumor was then dissected out, and the number of PKH26PCL-labeled cells infiltrated into the tumor was measured with a flow cytometer. IFI16-overexpressing tumors showed more cell infiltration into the tumor microenvironment. $^*p < 0.05$, $^{**}p < 0.01$ and $^{***}p < 0.001$.

M-CSF. This co-culture was maintained for 7 days to allow all possible non-contact interactions between the Panc-2 cells and BMDMs. BMDMs were then collected for the analysis of the TAM population by flow cytometry and qPCR. It was found that the co-culture of Panc-2 cells with IFI16 overexpression significantly increased the population of TAMs from BMDM cultures compared to the co-culture of vector-expressing Panc-2 cells (**Figure 4B**). qPCR analysis confirmed that TAM markers, including HIF-1α, CCL2, and PECAM1, were induced in the BMDMs receiving stimulus from Panc-2 cells with IFI16 overexpression. Simultaneously, the culture supernatant from PAAD cells with IFI16 overexpression accelerated the proliferation of TAMs, as evidenced by increased BrdU incorporation into the DNA of macrophages differentiated from BMDMs (**Figure 4C**, gating shown in **Supplementary Figure 3**). The culture supernatant from the PAAD cells overexpressing IFI16 could attract BMDMs from the upper chamber of the Transwell insert toward the receiving chambers (**Figure 4D**). To confirm that this action was comparable *in vivo*, we injected BrdU intraperitoneally into mice with orthotopic PAAD tumors with or without IFI16 overexpression. Mice with IFI16-overexpressing PAAD tumors showed increased BrdU incorporation into CD11b + F4/80 + TAMs in the tumor microenvironment (**Figure 4E**, gating shown in **Supplementary Figure 4**). Additionally, IFI16 overexpression in orthotopic tumors could significantly increase the infiltration of

PKH26PCL-stained BMDMs injected into the mice, suggesting that IFI16 overexpression could accelerate the migration of monocytic cells into the tumor microenvironment (**Figure 4F**, gating same as in **Figure 4E**). This observation suggests that IFI16 overexpression regulates TAMs in the tumor microenvironment by inducing their maturation, infiltration, and local proliferation.

IL-1β Production Is Responsible for the Induced Migration and Proliferation of TAMs in Tumor Microenvironments of IFI16-Overexpressing PAAD

IFI16 mediates DNA damage-induced inflammasome activation in cells (Xiao, 2015). To determine whether IFI16 overexpression in PAAD cells induces inflammasome activation, we probed the expression of major proteins related to inflammasomes. Cleavage of pro-caspase-1 and pro-IL-1β was observed in the presence and absence of poly dA:dT, suggesting the initiation of inflammasome machinery (**Figure 5A**), while other regulatory proteins, such as AIM2 and ASC, remained unchanged. Intracellular and extracellular cleaved forms of caspase-1 and IL-1β, as well as the secretion of mature IL-1β in the culture supernatant, were significantly induced (**Figures 5A,B**). To further understand how inflammasome activation and IL-1β production by IFI16-overexpressing PAAD cells regulate TAMs, we used neutralizing antibodies to block IL-1β in the culture supernatant from wild-type and IFI16-overexpressing PAAD cells, according to a published protocol with minor modifications (Staudt et al., 2013). The presence of a neutralizing antibody against IL-1β significantly attenuated the increase in the CD11b + F4/80 + population of BMDMs cultured with a supernatant from IFI16-overexpressing PAAD cells (**Figure 5C**). Similarly, the increased migration and proliferation of TAMs were potently attenuated by the presence of a neutralizing antibody against IL-1β (**Figures 5D,E**). This observation suggested that the IFI16-induced inflammasome activation in PAAD cells produces IL-1β, which mediates the maturation, migration, and local proliferation of TAMs in the tumor microenvironment.

Knockdown of IFI16 Suppresses Gemcitabine-Induced TAMs and Increases Its Antitumor Activity

To further examine the regulation of IFI16 in PAAD therapy, we introduced gemcitabine, the major chemotherapeutic agent clinically used for PAAD, to treat mice with orthotopic tumors (**Figure 6A**). PAAD cells were treated with gemcitabine to induce the expression of IFI16 (**Figure 6B**). To investigate whether IFI16 plays a role in mediating the sensitivity of PAAD cells in response to gemcitabine treatment, we established a stable IFI16-knockdown clone of PAAD cells (**Figure 6B**). Knockdown of IFI16 or treatment with gemcitabine moderately reduced the growth rate of orthotopic tumors of PAAD in mice, while the efficacy of gemcitabine in suppressing PAAD tumor was largely improved when IFI16 was knocked down (**Figure 6C**). Similarly, the size and weight of representative tumors suggested that IFI16-knockdown tumors responded better to gemcitabine treatment than the wild-type tumors (**Figure 6D**). Interestingly, we observed that gemcitabine treatment could induce TAM population in the tumor microenvironment of orthotopic PAAD and that knockdown of IFI16 could significantly abolish the increase in the TAM population (**Figure 6E**). To detect the sub-phenotype of the TAMs after gemcitabine treatment, we used qRT-PCR to detect the M1-like macrophage marker IFN-γ and M2-like macrophage marker TGF-β and calculated the ratio of M1/M2 by comparing their expressions. Interestingly, we found that in both mock and IFI16-knockdown tumors, gemcitabine treatment had no significant effect on the ratio of M1/M2 macrophages in the tumors (**Figure 6F**). This observation is consistent with a previous report stating that gemcitabine had no significant effect on the polarization of macrophages toward either phenotype (Cullis et al., 2017; Kleinerman et al., 2018). However, in our study, when we measured the markers of TAMs, including HIF-1α, CCL2, and PECAM1, we found that gemcitabine treatment potently activated the expression of TAM markers, while knockdown of IFI16 reversed the increase in TAMs in the tumor microenvironment (**Figure 6F**). To further prove that the effect of IFI16 is not only restricted in Panc-2 cells, we screened the PAAD cell lines in stock in our laboratory, including Panc-1, SW1990, BxPC3, and Panc-2. We found that expression of IFI16 was highest in BxPC3 cells, while lowest in Panc-1 cells, while expression of IFI16 in SW1990 was higher than that in Panc-2 cells (**Figure 6G**). We then knocked down and overexpressed the IFI16 expression in SW1990 cells (**Figure 6H**) and co-cultured the cells with BMDMs in the presence or absence of 100 nM of gemcitabine. BMDMs showed less activation into the CD11b + F4/80 + phenotype when co-cultured with SW1990 cells with IFI16 knockdown, and BMDM activation was completely blocked upon IFI16 knockdown (**Figure 6I**). Overexpression of IFI16 in SW1990 cells induced activation of co-cultured BMDMs in the absence of gemcitabine. Although induction of co-cultured BMDMs by IFI16-overexpressing SW1990 cells in the presence of gemcitabine may not be statistically significant (**Figure 6J**), which could be due to the high basic level, this observation in general consistently proved that IFI16 activation in PAAD cells could induce TAM activation in the tumor microenvironment.

DISCUSSION

Several studies have reported the role of TAMs in the tumorigenesis, development, and progression of PAAD (Krug et al., 2018; D'Errico et al., 2019; Zhang et al., 2019, 2020). TAMs promote PAAD growth by directly accelerating tumor cell expansion and spread (Ye et al., 2018) or indirectly generating the tumor-favoring immunosuppressive tumor microenvironment (Stromnes et al., 2019) or both (Mitchem et al., 2013). There are two subtypes of TAMs in the tumor microenvironment of PAAD: the pro-inflammatory M1 and immunosuppressive M2 phenotypes (Aras and Zaidi, 2017). It is far from conclusive which types of TAMs are predominant in mediating the tumor progression of PAAD, as studies have debated the pro-tumoral role of both TAMs (Partecke et al., 2013; Helm et al., 2014). Additionally, instead of the particular subtype

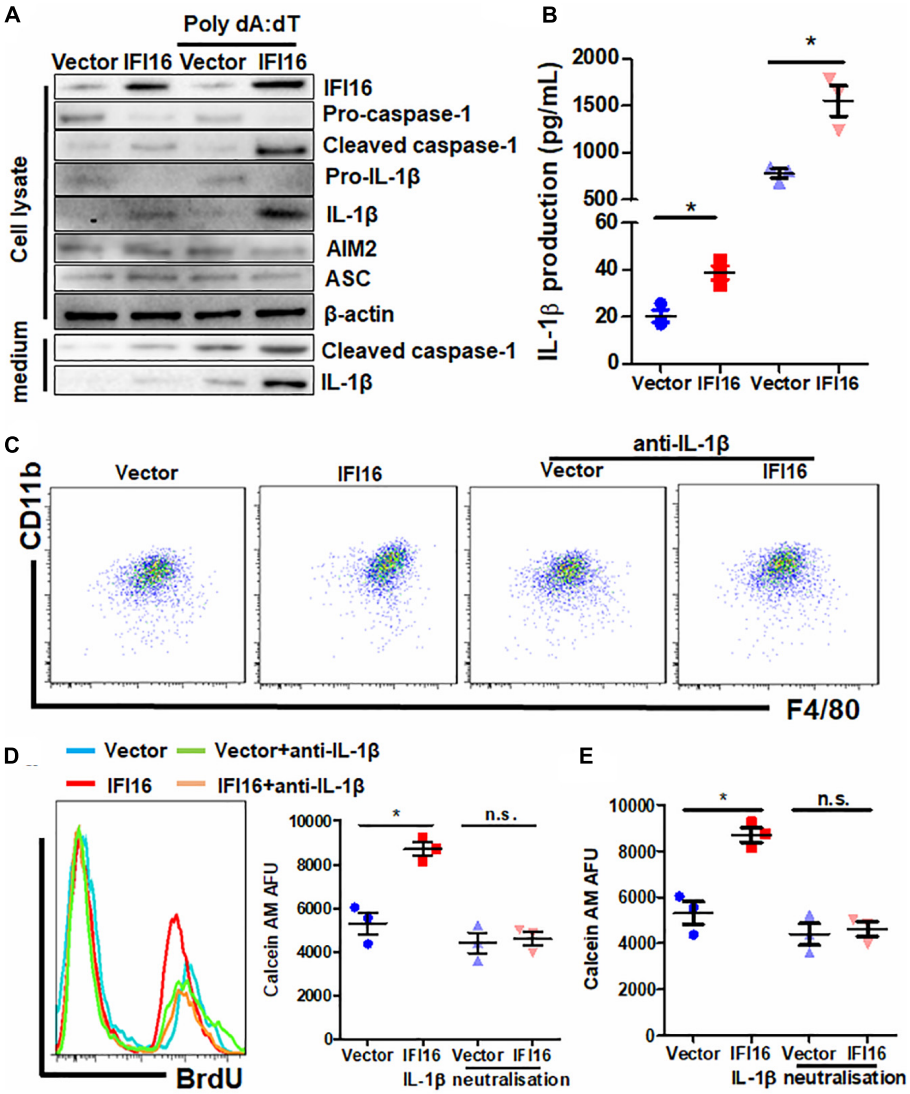

FIGURE 5 | IL-1β is responsible for the IFI16-induced TAM profile changes in PAAD. **(A)** Protein expression of Panc-2 cells at intracellular and extracellular levels was measured with immunoblotting. IFI16 overexpression induced further activation of the inflammasome, as evidenced by the cleavage of intracellular pro-caspase-1 and pro-IL-1β, as well as the extracellular expression of cleaved IL-1β and caspase-1 in the culture medium. **(B)** IL-1β levels were quantified with ELISA. IFI16 overexpression significantly increased IL-1β production and secretion in Panc-2 cells in the presence or absence of poly dA:dT. Supplementation with an IL-1β-neutralizing antibody mitigated the function of secreted IL-1β in the conditional medium from Panc-2 cells. This method was adopted from a published protocol, with minor modifications. For the blocking experiments, the BMDMs were preincubated with 10 μg/ml of the IL-1β-neutralizing antibody, for 15 min before the functional studies. **(C)** Cells were then collected and stained with antibodies against CD11b and F4/80 and subjected to flow cytometry analysis. Neutralization of IL-1β significantly blocked the increase in TAM population cultured in the conditioned medium from IFI16-overexpressing Panc-2 cells. **(D)** Added to the culture medium was 10 μM of BrdU 4 h prior to sample collection by trypsinization. BrdU-incorporated CD11b + F4/80 + cells were stained with anti-BrdU antibody and detected using a flow cytometer. Neutralization of IL-1β significantly blocked the increase in BrdU incorporation into the DNA of BMDMs cultured in conditioned medium from IFI16-overexpressing Panc-2 cells. **(E)** Approximately 2×10^5 BMDMs cultured with the conditioned medium from Panc-2 cells were seeded at the apical side of Transwell inserts with serum-free medium. Culture medium supplemented with chemotaxis MCP-1 (10 ng/ml) was added to the receiving chambers, followed by culture for 3 h. Cells remaining on the apical side of the inserts were scraped away, and cells at the basal side of the membrane were collected by trypsinization. The cells were then collected and stained with 50 μM calcein AM and quantified using a fluorescence microplate reader. Neutralization of IL-1β significantly blocked the increased motility of the BMDMs cultured in the conditioned medium from IFI16-overexpressing Panc-2 cells. *$p < 0.05$.

of TAMs, the gross TAM amount was positively correlated with the poor prognosis of PAAD patients (Yu et al., 2019). Therefore, in our study, we studied the effect of depletion of the whole TAM population on IFI16-mediated tumor growth because the specific removal of either subtype of TAMs is perceptually and technically difficult. Removal of TAMs using liposome clodronate attenuated IFI16 overexpression-induced tumor growth in PAAD. IFI16-induced IL-1β expression is responsible for the induction of TAMs. Although IL-1β is generally considered a pro-inflammatory cytokine, we cannot

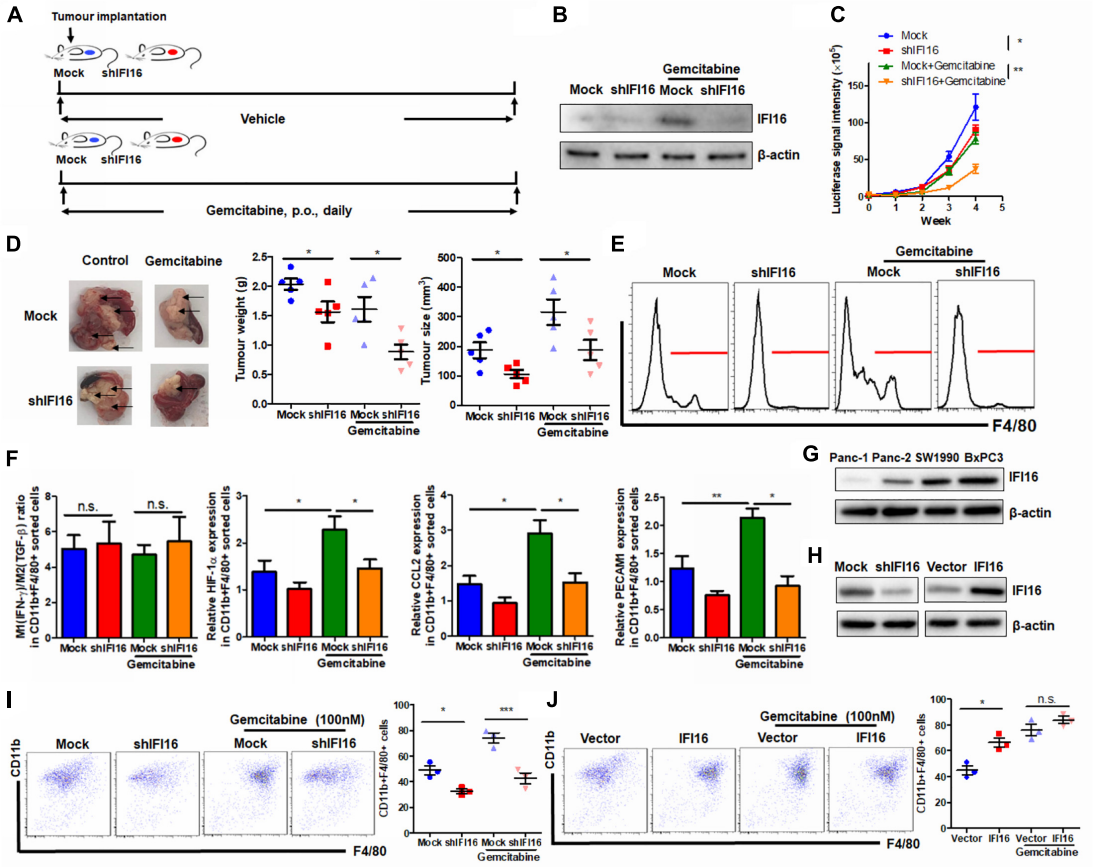

FIGURE 6 | Suppression of IFI16 improves gemcitabine sensitivity in PAAD tumors. **(A)** Flowchart of gemcitabine treatment. Approximately 20 μl Matrigel matrix, containing 1×10^8 Panc-2 cells, was orthotopically injected into the pancreas of mice. Mice were then orally administered gemcitabine at a dose of 100 mg/kg or vehicle every day. **(B)** The IFI16-knockdown PAAD cell line was established by transfecting the shRNA plasmid of IFI16 into the Panc-2 cells. Cells were selected with a culture medium containing 1 μg/ml of puromycin, until a stable IFI16-knockdown clone was established. Knockdown of IFI16 was validated with immunoblotting, which showed that RNA interference using shRNA against IFI16 can significantly attenuate gemcitabine-induced IFI16 upregulation. **(C)** The luciferase signal intensity was measured by intraperitoneal injection of luciferin (30 mg/kg) and quantification under a live animal imager once per week. Knockdown of IFI16 could significantly improve the suppression of tumor growth by gemcitabine. **(D)** At the end of the study, the mice were sacrificed, and the pancreas along with the spleen was dissected out. The tumor weight was measured, and tumor size was calibrated by the diameters of the tumor. Knockdown of IFI16 in gemcitabine-treated mice further reduced the size and weight of the tumor in the experimental PAAD model. The black arrow shows an obvious surface tumor nodule found on the pancreas. **(E)** The tumor was dissected out, and TAMs were enriched by Ficoll methods. The enriched cells were stained with an antibody against F4/80 and subjected to flow cytometry analysis. Knockdown of IFI16 could attenuate the infiltration of TAMs induced by gemcitabine in the tumor microenvironment of PAAD. **(F)** The major M1/M2/TAM markers were quantified using qPCR. The ratio of expression of IFN-γ and TGF-β was calculated to represent the M1/M2 ratio in the tumor microenvironment. Gemcitabine had no significant effect on the polarization of macrophages toward either phenotype but potently activated the expression of TAM markers HIF-1α, CCL2, and PECAM1. **(G)** Expression of IFI16 was measured by immunoblotting in different PAAD cell lines. Expression of IFI16 was highest in BxPC3 cells, then SW1990 cells, and then Panc-2 cells, while Panc-1 cells expressed the lowest level of IFI16. **(H)** Expression of IFI16 was forcefully activated and knocked down in SW1990 cells. **(I)** BMDMs were co-cultured with SW1990 cells with or without IFI16 knockdown in the presence or absence of 100 nM gemcitabine for 7 days. The activation of BMDMs was then examined by flow cytometry. Knockdown of IFI16 reduced co-cultured BMDM activation in the presence or absence of gemcitabine. **(J)** BMDMs were co-cultured with SW1990 cells with or without IFI16 overexpression in the presence or absence of 100 nM gemcitabine for 7 days. The activation of BMDMs was then examined by flow cytometry. Overexpression of IFI16 further increased co-cultured BMDM activation in the presence or absence of gemcitabine. $^*p < 0.05$, $^{**}p < 0.01$ and $^{***}p < 0.001$.

directly conclude that the IL-1β-induced TAMs in our study were prone to pro-inflammatory M1 phenotypes. Indeed, IL-1β could initiate M2 macrophage polarization, which also contributes to tumor growth in head and neck squamous cell carcinoma (Chen et al., 2018). It is possible that the IFI16-overexpressing TAM population is a heterogenic population that contains the M1 and M2 phenotypes of macrophages, which both contribute to the tumor growth of PAAD.

In our study, we found that IL-1β plays an important role in regulating the tumor microenvironment of PAAD. Use of neutralizing antibodies against IL-1β can modulate the maturation, proliferation, and migration abilities of TAMs, which may retard tumor growth. However, our study does not exclude the possibility that secretion of IL-1β from PAAD cells, as observed in our study, has no autonomous action on tumor cells itself, which means that we did not completely rule out the

possibility that IL-1β secretion can affect tumor cell expansion and spread. IL-1β secretion from TAMs was reported to promote the epithelial-to-mesenchymal transition of pancreatic tumor cells and therefore contribute to its distant metastasis (Chen et al., 2019). Additionally, IL-1β may also serve as a pro-tumoral factor by inducing cancer angiogenesis (Shchors et al., 2006) and cancer-associated fibroblasts (Brunetto et al., 2019). Further systematic investigation on the change in tumor and stromal cells upon IL-1β neutralization *in vivo* may be able to illustrate the overall effect of IL-1β on PAAD progression.

We also noticed that suppression of IFI16-induced inflammasome activation could significantly improve gemcitabine sensitivity. Gemcitabine remains the main treatment for patients with non-resectable PAAD; however, its efficacy in restricting tumor growth and prolonging patient survival is very limited, indicating the poor response of most PAAD to gemcitabine treatment. The reasons behind its poor responsiveness may be multiple, for instance, the primary resistance of PAAD cells due to the expression of multidrug resistance proteins and drug metabolism enzymes (Sarvepalli et al., 2019); however, we cannot rule out the possible involvement of the tumor microenvironment. Stromal cells, including TAMs, cancer-associated fibroblasts, myeloid-derived suppressor cells, and T lymphocytes, have been reported to be involved in gemcitabine resistance in PAAD (Thakur et al., 2013; Zhu et al., 2014; Wei et al., 2018; Halbrook et al., 2019). In our study, we found that gemcitabine treatment significantly induced the activation of the IFI16-related inflammasome and recruitment of TAMs. This further supports the role of TAMs in mediating gemcitabine sensitivity of PAAD tumors, although it is yet to be concluded that only TAMs play a dominant role. Gemcitabine could activate the tumor inflammasome, at least partially, by upregulating IFI16 expression. Gemcitabine is commonly reported as an inflammation inducer (Farr et al., 2017), which is considered an unfavorable factor when evaluating its treatment outcome in multiple types of cancers (Kim et al., 2020). Although we cannot fully conclude the mechanisms of IFI16 upregulation by gemcitabine treatment, it is postulated that gemcitabine, as a DNA damage agent, may cause the breakdown of dsDNA in both normal and cancer cells in the tumors (Jones et al., 2014). IFI16 was found to be a sensor of innate immunity in response to dsDNA (Morrone et al., 2014) and to mediate the activation of multiple cellular processes such as the inflammasome machinery. Further systemic investigation is required to determine whether dsDNA breakdown caused by gemcitabine majorly dominates the upregulation of IFI16 in cancer cells and reshapes the tumor microenvironment by increasing the TAM population in PAAD.

CONCLUSION

In this study, we systematically examined the expression patterns and functional roles of inflammasome-related proteins in PAAD. We found that several proteins were upregulated in the PAAD tissues compared with those in the normal adjacent pancreas; however, only the upregulation of IFI16 correlated with the poor survival of PAAD patients. Overexpression of IFI16 significantly promoted the orthotopic growth of PAAD tumors in a murine model and altered the immune cell profile in the tumor microenvironment by increasing the TAM population. Moreover, depletion of TAMs attenuated IFI16-induced PAAD tumor growth. Overexpression of IFI16 in tumor cells activated inflammasome machinery, thereby inducing the production of IL-1β and causing maturation, proliferation, and migration of TAMs in the tumor microenvironment. Neutralization of IL-1β abolished the effect of IFI16-overexpressing tumor cells on TAMs. Additionally, knockdown of IFI16 in gemcitabine-treated PAAD tumors reduced TAM infiltration in the tumor microenvironment, improving gemcitabine sensitivity. Our study sheds light on the role of IFI16 as a potential target for the development of a novel therapeutic strategy for PAAD.

DATA AVAILABILITY STATEMENT

The raw data supporting the conclusions of this article will be made available by the authors, without undue reservation.

ETHICS STATEMENT

The animal study was reviewed and approved by the Animal Experimental Ethics Committee of Ruijin Hospital, Shanghai Jiao Tong University School of Medicine.

AUTHOR CONTRIBUTIONS

JX and LZ conceived the idea, designed the experiments, analyzed the data, and wrote the manuscript. J-XC and C-SC conducted and wrote the experiments. H-FG and Z-JC conducted parts of the experiments. Z-JC, L-LL, J-YX, and X-HS revised the manuscript. All authors contributed to the article and approved the submitted version.

FUNDING

This study was financially supported by the Research Project of Traditional Chinese Medicine of Shanghai Health Committee (Project Code: 2020LZ007) and the National Natural Science Foundation of China (Project Code: 82074202).

SUPPLEMENTARY MATERIAL

The Supplementary Material for this article can be found online at: https://www.frontiersin.org/articles/10.3389/fcell.2021.640786/full#supplementary-material

REFERENCES

Aras, S., and Zaidi, M. R. (2017). TAMeless traitors: macrophages in cancer progression and metastasis. *Br. J. Cancer* 117, 1583–1591. doi: 10.1038/bjc.2017.356

Boone, B. A., Murthy, P., Miller-Ocuin, J. L., Liang, X., Russell, K. L., Loughran, P., et al. (2019). The platelet NLRP3 inflammasome is upregulated in a murine model of pancreatic cancer and promotes platelet aggregation and tumour growth. *Ann. Hematol.* 98, 1603–1610. doi: 10.1007/s00277-019-03692-0

Brunetto, E., De Monte, L., Balzano, G., Camisa, B., Laino, V., Riba, M., et al. (2019). The IL-1/IL-1 receptor axis and tumour cell released inflammasome adaptor ASC are key regulators of TSLP secretion by cancer associated fibroblasts in pancreatic cancer. *J. Immunother. Cancer* 7:45.

Carriere, C., Young, A. L., Gunn, J. R., Longnecker, D. S., and Korc, M. (2009). Acute pancreatitis markedly accelerates pancreatic cancer progression in mice expressing oncogenic Kras. *Biochem. Biophys. Res. Commun.* 382, 561–565. doi: 10.1016/j.bbrc.2009.03.068

Chen, L., Huang, C. F., Li, Y. C., Deng, W. W., Mao, L., Wu, L., et al. (2018). Blockage of the NLRP3 inflammasome by MCC950 improves anti-tumour immune responses in head and neck squamous cell carcinoma. *Cell Mol. Life. Sci.* 75, 2045–2058. doi: 10.1007/s00018-017-2720-9

Chen, Q., Wang, J., Zhang, Q., Zhang, J., Lou, Y., Yang, J., et al. (2019). Tumour cell-derived debris and IgG synergistically promote metastasis of pancreatic cancer by inducing inflammation via tumour-associated macrophages. *Br. J. Cancer* 121, 786–795. doi: 10.1038/s41416-019-0595-2

Choubey, D., and Panchanathan, R. (2016). IFI16, an amplifier of DNA-damage response: role in cellular senescence and aging-associated inflammatory diseases. *Ageing Res. Rev.* 28, 27–36. doi: 10.1016/j.arr.2016.04.002

Cullis, J., Siolas, D., Avanzi, A., Barui, S., Maitra, A., and Bar-Sagi, D. (2017). Macropinocytosis of nab-paclitaxel drives macrophage activation in pancreatic cancer. *Cancer Immunol. Res.* 5, 182–190. doi: 10.1158/2326-6066.cir-16-0125

D'Errico, G., Alonso-Nocelo, M., Vallespinos, M., Hermann, P. C., Alcala, S., Garcia, C. P., et al. (2019). Tumour-associated macrophage-secreted 14-3-3zeta signals via AXL to promote pancreatic cancer chemoresistance. *Oncogene* 38, 5469–5485. doi: 10.1038/s41388-019-0803-9

Deschenes-Simard, X., Mizukami, Y., and Bardeesy, N. (2013). Macrophages in pancreatic cancer: starting things off on the wrong track. *J. Cell Biol.* 202, 403–405. doi: 10.1083/jcb.201307066

Farr, S. E., Chess-Williams, R., and McDermott, C. M. (2017). Gemcitabine: selective cytotoxicity, induction of inflammation and effects on urothelial function. *Toxicol. Appl. Pharmacol.* 316, 1–9. doi: 10.1016/j.taap.2016.12.011

Gao, H. F., Chen, L. Y., Cheng, C. S., Chen, H., Meng, Z. Q., and Chen, Z. (2019). SLC5A1 promotes growth and proliferation of pancreatic carcinoma via glucose-dependent AMPK/mTOR signaling. *Cancer Manag. Res.* 11, 3171–3185. doi: 10.2147/cmar.s195424

Gao, H. F., Cheng, C. S., Tang, J., Li, Y., Chen, H., Meng, Z. Q., et al. (2020). CXCL9 chemokine promotes the progression of human pancreatic adenocarcinoma through STAT3-dependent cytotoxic T lymphocyte suppression. *Aging (Albany NY)* 12, 502–517. doi: 10.18632/aging.102638

Guo, H., Callaway, J. B., and Ting, J. P. (2015). Inflammasomes: mechanism of action, role in disease, and therapeutics. *Nat. Med.* 21, 677–687. doi: 10.1038/nm.3893

Halbrook, C. J., Pontious, C., Kovalenko, I., Lapienyte, L., Dreyer, S., Lee, H. J., et al. (2019). Macrophage-Released Pyrimidines Inhibit Gemcitabine Therapy in Pancreatic Cancer. *Cell Metab.* 29, 1390–1399. doi: 10.1016/j.cmet.2019.02.001

Helm, O., Held-Feindt, J., Grage-Griebenow, E., Reiling, N., Ungefroren, H., Vogel, I., et al. (2014). Tumour-associated macrophages exhibit pro- and anti-inflammatory properties by which they impact on pancreatic tumourigenesis. *Int. J. Cancer* 135, 843–861. doi: 10.1002/ijc.28736

Jones, R. M., Kotsantis, P., Stewart, G. S., Groth, P., and Petermann, E. (2014). BRCA2 and RAD51 promote double-strand break formation and cell death in response to gemcitabine. *Mol. Cancer Ther.* 13, 2412–2421. doi: 10.1158/1535-7163.mct-13-0862

Jordan, M. B., van Rooijen, N., Izui, S., Kappler, J., and Marrack, P. (2003). Liposomal clodronate as a novel agent for treating autoimmune hemolytic anemia in a mouse model. *Blood* 101, 594–601. doi: 10.1182/blood-2001-11-0061

Kim, H. J., Lee, S. Y., Kim, D. S., Kang, E. J., Kim, J. S., Choi, Y. J., et al. (2020). Inflammatory markers as prognostic indicators in pancreatic cancer patients who underwent gemcitabine-based palliative chemotherapy. *Korean J. Intern. Med.* 35, 171–184. doi: 10.3904/kjim.2018.076

Kleinerman, E. S., Yu, L., Dao, J., Hayes-Jordan, A. A., Lindsey, B., Kawedia, J. D., et al. (2018). Aerosol gemcitabine after amputation inhibits osteosarcoma lung metastases but not wound healing. *Sarcoma* 2018:3143096.

Kondo, Y., Nagai, K., Nakahata, S., Saito, Y., Ichikawa, T., Suekane, A., et al. (2012). Overexpression of the DNA sensor proteins, absent in melanoma 2 and interferon-inducible 16, contributes to tumourigenesis of oral squamous cell carcinoma with p53 inactivation. *Cancer Sci.* 103, 782–790. doi: 10.1111/j.1349-7006.2012.02211.x

Krug, S., Abbassi, R., Griesmann, H., Sipos, B., Wiese, D., Rexin, P., et al. (2018). Therapeutic targeting of tumour-associated macrophages in pancreatic neuroendocrine tumours. *Int. J. Cancer* 143, 1806–1816.

Li, C., Zhang, Y., Cheng, X., Yuan, H., Zhu, S., Liu, J., et al. (2018). PINK1 and PARK2 suppress pancreatic tumourigenesis through control of mitochondrial iron-mediated immunometabolism. *Dev. Cell* 46, 441–455. doi: 10.1016/j.devcel.2018.07.012

Liao, J. C., Lam, R., Brazda, V., Duan, S., Ravichandran, M., Ma, J., et al. (2011). Interferon-inducible protein 16: insight into the interaction with tumour suppressor p53. *Structure* 19, 418–429. doi: 10.1016/j.str.2010.12.015

Lin, W., Zhao, Z., Ni, Z., Zhao, Y., Du, W., and Chen, S. (2017). IFI16 restoration in hepatocellular carcinoma induces tumour inhibition via activation of p53 signals and inflammasome. *Cell Prolif.* 50:e12392. doi: 10.1111/cpr.12392

Mitchem, J. B., Brennan, D. J., Knolhoff, B. L., Belt, B. A., Zhu, Y., Sanford, D. E., et al. (2013). Targeting tumour-infiltrating macrophages decreases tumour-initiating cells, relieves immunosuppression, and improves chemotherapeutic responses. *Cancer Res.* 73, 1128–1141. doi: 10.1158/0008-5472.can-12-2731

Mohammed, A., Janakiram, N. B., Madka, V., Pathuri, G., Li, Q., Ritchie, R., et al. (2017). Lack of chemopreventive effects of P2X7R inhibitors against pancreatic cancer. *Oncotarget* 8, 97822–97834. doi: 10.18632/oncotarget.22085

Morrone, S. R., Wang, T., Constantoulakis, L. M., Hooy, R. M., Delannoy, M. J., and Sohn, J. (2014). Cooperative assembly of IFI16 filaments on dsDNA provides insights into host defense strategy. *Proc. Natl. Acad. Sci. U.S.A.* 111, E62–E71.

Oberstein, P. E., and Olive, K. P. (2013). Pancreatic cancer: why is it so hard to treat? *Therap. Adv. Gastroenterol.* 6, 321–337. doi: 10.1177/1756283x13478680

Partecke, L. I., Gunther, C., Hagemann, S., Jacobi, C., Merkel, M., Sendler, M., et al. (2013). Induction of M2-macrophages by tumour cells and tumour growth promotion by M2-macrophages: a quid pro quo in pancreatic cancer. *Pancreatology* 13, 508–516. doi: 10.1016/j.pan.2013.06.010

Pinton, L., Masetto, E., Vettore, M., Solito, S., Magri, S., D'Andolfi, M., et al. (2019). The immune suppressive microenvironment of human gliomas depends on the accumulation of bone marrow-derived macrophages in the center of the lesion. *J. Immunother. Cancer* 7:58.

Pramanik, K. C., Makena, M. R., Bhowmick, K., and Pandey, M. K. (2018). Advancement of NF-kappaB signaling pathway: a novel target in pancreatic cancer. *Int. J. Mol. Sci.* 19:3890. doi: 10.3390/ijms19123890

Principe, D. R., Narbutis, M., Kumar, S., Park, A., Viswakarma, N., Dorman, M. J., et al. (2020). Long-Term gemcitabine treatment reshapes the pancreatic tumour microenvironment and sensitizes murine carcinoma to combination immunotherapy. *Cancer Res.* 80, 3101–3115. doi: 10.1158/0008-5472.can-19-2959

Rahib, L., Smith, B. D., Aizenberg, R., Rosenzweig, A. B., Fleshman, J. M., and Matrisian, L. M. (2014). Projecting cancer incidence and deaths to 2030: the unexpected burden of thyroid, liver, and pancreas cancers in the United States. *Cancer Res.* 74, 2913–2921. doi: 10.1158/0008-5472.can-14-0155

Sarvepalli, D., Rashid, M. U., Rahman, A. U., Ullah, W., Hussain, I., Hasan, B., et al. (2019). Gemcitabine: a review of chemoresistance in pancreatic cancer. *Crit. Rev. Oncog.* 24, 199–212.

Shchors, K., Shchors, E., Rostker, F., Lawlor, E. R., Brown-Swigart, L., and Evan, G. I. (2006). The Myc-dependent angiogenic switch in tumours is mediated by interleukin 1beta. *Genes Dev.* 20, 2527–2538. doi: 10.1101/gad.1455706

Staudt, N. D., Jo, M., Hu, J., Bristow, J. M., Pizzo, D. P., Gaultier, A., et al. (2013). Myeloid cell receptor LRP1/CD91 regulates monocyte recruitment and

angiogenesis in tumours. *Cancer Res.* 73, 3902–3912. doi: 10.1158/0008-5472.can-12-4233

Stone, M. L., and Beatty, G. L. (2019). Cellular determinants and therapeutic implications of inflammation in pancreatic cancer. *Pharmacol. Ther.* 201, 202–213. doi: 10.1016/j.pharmthera.2019.05.012

Stromnes, I. M., Burrack, A. L., Hulbert, A., Bonson, P., Black, C., Brockenbrough, J. S., et al. (2019). Differential effects of depleting versus programming tumour-associated macrophages on engineered T cells in pancreatic ductal adenocarcinoma. *Cancer Immunol. Res.* 7, 977–989. doi: 10.1158/2326-6066.cir-18-0448

Tang, Z., Li, C., Kang, B., Gao, G., Li, C., and Zhang, Z. (2017). GEPIA: a web server for cancer and normal gene expression profiling and interactive analyses. *Nucleic Acids Res.* 45, W98–W102.

Thakur, A., Schalk, D., Tomaszewski, E., Kondadasula, S. V., Yano, H., Sarkar, F. H., et al. (2013). Microenvironment generated during EGFR targeted killing of pancreatic tumour cells by ATC inhibits myeloid-derived suppressor cells through COX2 and PGE2 dependent pathway. *J Transl Med* 11:35.

Unterholzner, L., Keating, S. E., Baran, M., Horan, K. A., Jensen, S. B., Sharma, S., et al. (2010). IFI16 is an innate immune sensor for intracellular DNA. *Nat. Immunol.* 11, 997–1004.

Wei, L., Ye, H., Li, G., Lu, Y., Zhou, Q., Zheng, S., et al. (2018). Cancer-associated fibroblasts promote progression and gemcitabine resistance via the SDF-1/SATB-1 pathway in pancreatic cancer. *Cell Death Dis.* 9:1065.

Xiao, T. S. (2015). The nucleic acid-sensing inflammasomes. *Immunol. Rev.* 265, 103–111. doi: 10.1111/imr.12281

Xu, S., Li, X., Liu, Y., Xia, Y., Chang, R., and Zhang, C. (2019). Inflammasome inhibitors: promising therapeutic approaches against cancer. *J. Hematol. Oncol.* 12:64.

Yadav, D., and Lowenfels, A. B. (2013). The epidemiology of pancreatitis and pancreatic cancer. *Gastroenterology* 144, 1252–1261. doi: 10.1053/j.gastro.2013.01.068

Yang, M., McKay, D., Pollard, J. W., and Lewis, C. E. (2018). Diverse functions of macrophages in different tumour microenvironments. *Cancer Res.* 78, 5492–5503. doi: 10.1158/0008-5472.can-18-1367

Yaw, A. C. K., Chan, E. W. L., Yap, J. K. Y., and Mai, C. W. (2020). The effects of NLRP3 inflammasome inhibition by MCC950 on LPS-induced pancreatic adenocarcinoma inflammation. *J. Cancer Res. Clin. Oncol.* 146, 2219–2229. doi: 10.1007/s00432-020-03274-y

Ye, H., Zhou, Q., Zheng, S., Li, G., Lin, Q., Wei, L., et al. (2018). Tumour-associated macrophages promote progression and the Warburg effect via CCL18/NF-kB/VCAM-1 pathway in pancreatic ductal adenocarcinoma. *Cell Death Dis.* 9:453.

Yu, B., Zheng, X., Sun, Z., Cao, P., Zhang, J., and Wang, W. (2021). IFI16 Can Be used as a biomarker for diagnosis of renal cell carcinoma and prediction of patient survival. *Front. Genet.* 12:599952. doi: 10.3389/fgene.2021.599952

Yu, M., Guan, R., Hong, W., Zhou, Y., Lin, Y., Jin, H., et al. (2019). Prognostic value of tumour-associated macrophages in pancreatic cancer: a meta-analysis. *Cancer Manag. Res.* 11, 4041–4058. doi: 10.2147/cmar.s196951

Zhang, J., Sun, H., Liu, S., Huang, W., Gu, J., Zhao, Z., et al. (2020). Alteration of tumour-associated macrophage subtypes mediated by KRT6A in pancreatic ductal adenocarcinoma. *Aging (Albany NY)* 12, 23217–23232.

Zhang, R., Liu, Q., Peng, J., Wang, M., Gao, X., Liao, Q., et al. (2019). Pancreatic cancer-educated macrophages protect cancer cells from complement-dependent cytotoxicity by up-regulation of CD59. *Cell Death Dis.* 10:836.

Zhao, H., Gonzalezgugel, E., Cheng, L., Richbourgh, B., Nie, L., and Liu, C. (2015). The roles of interferon-inducible p200 family members IFI16 and p204 in innate immune responses, cell differentiation and proliferation. *Genes Dis.* 2, 46–56. doi: 10.1016/j.gendis.2014.10.003

Zhu, Y., Knolhoff, B. L., Meyer, M. A., Nywening, T. M., West, B. L., Luo, J., et al. (2014). CSF1/CSF1R blockade reprograms tumour-infiltrating macrophages and improves response to T-cell checkpoint immunotherapy in pancreatic cancer models. *Cancer Res.* 74, 5057–5069. doi: 10.1158/0008-5472.can-13-3723

Conflict of Interest: The authors declare that the research was conducted in the absence of any commercial or financial relationships that could be construed as a potential conflict of interest.

frontiers in Cell and Developmental Biology

REVIEW
published: 11 June 2021
doi: 10.3389/fcell.2021.693215

Metabolic Remodeling in Glioma Immune Microenvironment: Intercellular Interactions Distinct From Peripheral Tumors

Runze Qiu[1†], Yue Zhong[2†], Qingquan Li[3], Yingbin Li[3] and Hongwei Fan[1]**

[1] Department of Clinical Pharmacology Lab, Nanjing First Hospital, Nanjing Medical University, Nanjing, China, [2] Center of Drug Discovery, State Key Laboratory of Natural Medicines, China Pharmaceutical University, Nanjing, China, [3] Department of Neurosurgery, The Second Affiliated Hospital of Nanjing Medical University, Nanjing, China

During metabolic reprogramming, glioma cells and their initiating cells efficiently utilized carbohydrates, lipids and amino acids in the hypoxic lesions, which not only ensured sufficient energy for rapid growth and improved the migration to normal brain tissues, but also altered the role of immune cells in tumor microenvironment. Glioma cells secreted interferential metabolites or depriving nutrients to injure the tumor recognition, phagocytosis and lysis of glioma-associated microglia/macrophages (GAMs), cytotoxic T lymphocytes, natural killer cells and dendritic cells, promoted the expansion and infiltration of immunosuppressive regulatory T cells and myeloid-derived suppressor cells, and conferred immune silencing phenotypes on GAMs and dendritic cells. The overexpressed metabolic enzymes also increased the secretion of chemokines to attract neutrophils, regulatory T cells, GAMs, and dendritic cells, while weakening the recruitment of cytotoxic T lymphocytes and natural killer cells, which activated anti-inflammatory and tolerant mechanisms and hindered anti-tumor responses. Therefore, brain-targeted metabolic therapy may improve glioma immunity. This review will clarify the metabolic properties of glioma cells and their interactions with tumor microenvironment immunity, and discuss the application strategies of metabolic therapy in glioma immune silence and escape.

Keywords: glioma, metabolic reprogramming, tumor microenvironment, immune escape, metabolic therapy

OPEN ACCESS

Edited by:
Hongming Miao,
Army Medical University, China

Reviewed by:
Jianmei Wu Leavenworth,
University of Alabama at Birmingham, United States
Hiroaki Shime,
Nagoya City University, Japan

****Correspondence:***
Hongwei Fan
fanhongwei178@njmu.edu.cn
Yingbin Li
yingbinli65@sina.com

† These authors have contributed equally to this work and share first authorship

Specialty section:
This article was submitted to Molecular Medicine, a section of the journal Frontiers in Cell and Developmental Biology

Received: *10 April 2021*
Accepted: *19 May 2021*
Published: *11 June 2021*

Citation:
Qiu R, Zhong Y, Li Q, Li Y and Fan H (2021) Metabolic Remodeling in Glioma Immune Microenvironment: Intercellular Interactions Distinct From Peripheral Tumors. Front. Cell Dev. Biol. 9:693215. doi: 10.3389/fcell.2021.693215

INTRODUCTION

Glioma is the most common primary intracranial cancer with a 5-year survival rate of less than 10% (Wang J. et al., 2019), occurring in glial cells such as astrocytes, oligodendrocytes and microglia. Glioblastoma multiforme (GBM) arose from astrocytes is the most frequent glioma with high malignancy and drug resistance, which was classified as grade IV in the WHO grade 2016, with

Abbreviations: 2-HG, 2-hydroxyglutarate; AA, arachidonic acid; ABCA, ATP-binding cassette sub-family A member; BCAA, branched-chain amino acid; BCKA, branched-chain ketoacid; B-FABP, brain fatty acid binding protein; EAAT, excitatory amino acids transporters; ELOVL2, elongation of very long chain fatty acids protein; FASN, fatty acid synthase; FPR, formylpeptide receptor 1; HK, hexokinase; HMGB, high mobility group protein B; MCT, monocarboxylate transporter; PFK, 6-phosphofructokinase; PGES, prostaglandin E synthase; PKM, pyruvate kinase M; R5P, ribose-5-phosphate; SHMT, serine hydroxymethyltransferase; SOAT, sterol *O*-acyltransferase; SREBP, sterol regulatory element-binding protein; α-KG, α-ketoglutarate.

a 5-year relative survival rate of only 5% because of rapid relapse after treatment (Gusyatiner and Hegi, 2018). According to gene transcription characteristics, GBM can be further classified into three subtypes: proneural [mutations on isocitrate dehydrogenase (IDH)-1 or tumor suppressor p53, and PDGFRA amplification], mesenchymal (mutation/deficiency of tumor suppressor NF1), and classical [EGFR amplification and CDKN2A (Ink4a/ARF) homozygous deletion] (Wang Q. et al., 2017). NF1 mutation-mediated proneural-mesenchymal transition is the key mechanism of relapse, causing resistance to treatment (Behnan et al., 2019).

Operative resection, although improving overall survival and prognosis in patients with low- and intermediate-grade gliomas (LGGs and IGGs) (Hervey-Jumper and Berger, 2016), shows limited effect on high-grade gliomas (HGGs) including anaplastic gliomas (WHO grade III) and GBM. Ironically, due to the changeable biological properties and the location of gliomas, non-specific interventions including radiation and brain-permeable cytotoxic drugs benefited patients even more than targeted therapies (Chen R. et al., 2017; Touat et al., 2017). Nevertheless, the tumor microenvironment (TME) makes gliomas resistant to chemotherapeutic drugs, and bring about inflammation to further reduce the prognosis of patients (Wu and Dai, 2017; Yang and Lin, 2017). In order to satisfactorily treat gliomas, one needs to be familiar with brain TME, which determine the evolution of tumors (Hirata and Sahai, 2017).

Since peripheral immune cells cannot enter the blood-brain barrier (BBB) and release inflammatory factors into brain under physiological conditions, brain tissues are protected from inflammation (Engelhardt et al., 2017; **Figure 1A**). Glial cells play an important role in the integrity and damage repair of BBB (Lou et al., 2016), so glioma cells originating from glial cells can impair BBB and allow peripheral immune cells to enter the brain (**Figure 1B**), forming a unique TME together with intracranial situ cells, tumor-associated vasculature, perivascular niche and lymphatic vessels (Quail and Joyce, 2017). Immune cells are major members of the glioma TME (Magana-Maldonado et al., 2016; Gieryng et al., 2017), which gradually lost tumor clearance duties or became associates when exposed to tumors. To support tumor growth, glioma cells and glioma stem-like cells (GSCs, also known as brain tumor initiating cells) interacted with adaptive immune cells and recruited immunotolerant innate immune cells to inhibit or evade anti-tumor responses (Broekman et al., 2018).

Although the BBB was damaged, glioma TME reconstructed the blood-brain tumor barrier (BBTB), whose structure is still dense and makes it difficult for antibodies to enter the lesion (van Tellingen et al., 2015). This may be the reason why immunotherapy such as PD-1/PD-L1 monoclonal antibody was less effective in glioma (Jackson et al., 2019). In contrast, metabolic therapies, such as ketogenic diet, significantly benefited patients (Winter et al., 2017). Metabolism is a medium of the communications between glioma and immune cells in TME (Thomas and Yu, 2017). Glioma cells interfere with immune cells through heterogeneous metabolism to mediate tumor growth, invasion, drug resistance and recurrence, which will be reviewed below.

METABOLIC PROPERTIES OF GLIOMA CELLS

Compared with normal tissues, tumors have specific anabolic and catabolic needs due to their rapid and uncontrolled growth. After metabolic reprogramming, tumors tend to gain energy through glycolysis rather than oxidative phosphorylation (OXPHOS) even under aerobic conditions (DeBerardinis and Chandel, 2016), which is called Warburg effect. Recent studies have found that glioma cells that initially grew in an ischemic environment relied on aerobic pentose phosphate pathway (PPP) instead of glycolysis after being exposed to adequate oxygen (Kathagen-Buhmann et al., 2016). When glucose was depleted, glioma cells re-converted the metabolic pattern to OXPHOS via the accumulation of lactate, which is the by-product of glycolysis (Duan et al., 2018). In addition to differentiated glioma cells, GSCs can also switch metabolism between glycolysis and OXPHOS catering to changing circumstances (Shibao et al., 2018), suggesting that the metabolism of glioma cells is environmentally plastic.

Mutations or changed levels of metabolic enzymes and accumulation of metabolites in TME were associated with the malignant progression and epigenetic modifications (Agnihotri and Zadeh, 2016; Masui et al., 2019). Isocitrate dehydrogenase (IDH), a key rate-limiting enzyme in tricarboxylic acid (TCA) cycle regulating carbohydrate, lipid and amino acid metabolism, was widely mutated in proneural GBM cells. Mutations in gliomas often occur in IDH1 and IDH2, both of which caused the conversion of α-ketoglutarate (α-KG) to 2-hydroxyglutarate (2-HG) in a NADPH-dependent manner (Waitkus et al., 2016). The overall survival of patients with proneural subtypes is longer than other subtypes, but the survival became the shortest after excluding IDH mutations, suggesting the positive significance of IDH mutations for prognosis (Behnan et al., 2019). However, IDH mutations may lead to the conversion of LGG to secondary HGG and the emergence of hypermutation phenotypes (Han et al., 2020). As another feature of proneural subtypes, mutations in p53 led to the loss of glycolysis inhibition and promoted tumor cells to adapt to hypoxic environments (Maurer et al., 2019). The expansion of PDGFRA also promoted glycolysis of proneural subtypes (Ran et al., 2013). In the classical GBM subtype, overexpression of EGFR activated PFK1 through PI3K-AKT signaling, leading to the upregulation of GLUT1 and the enhancement of glucose uptake (Lee et al., 2018). Although there is no direct evidence that the inactivation of tumor suppressor NF1 is associated with enhanced glycolysis, the glucose uptake and glycolysis of mesenchymal GBM cells are more active than other subtypes, which explains the increase in the malignancy of GBM caused by proneural-mesenchymal transition. The accumulation of ROS caused by hypoxic lesions can induce this transition, and PI3K-AKT was also stimulated under hypoxia, resulting in active glucose uptake and glycolysis (Talasila et al., 2017; Liu et al., 2020).

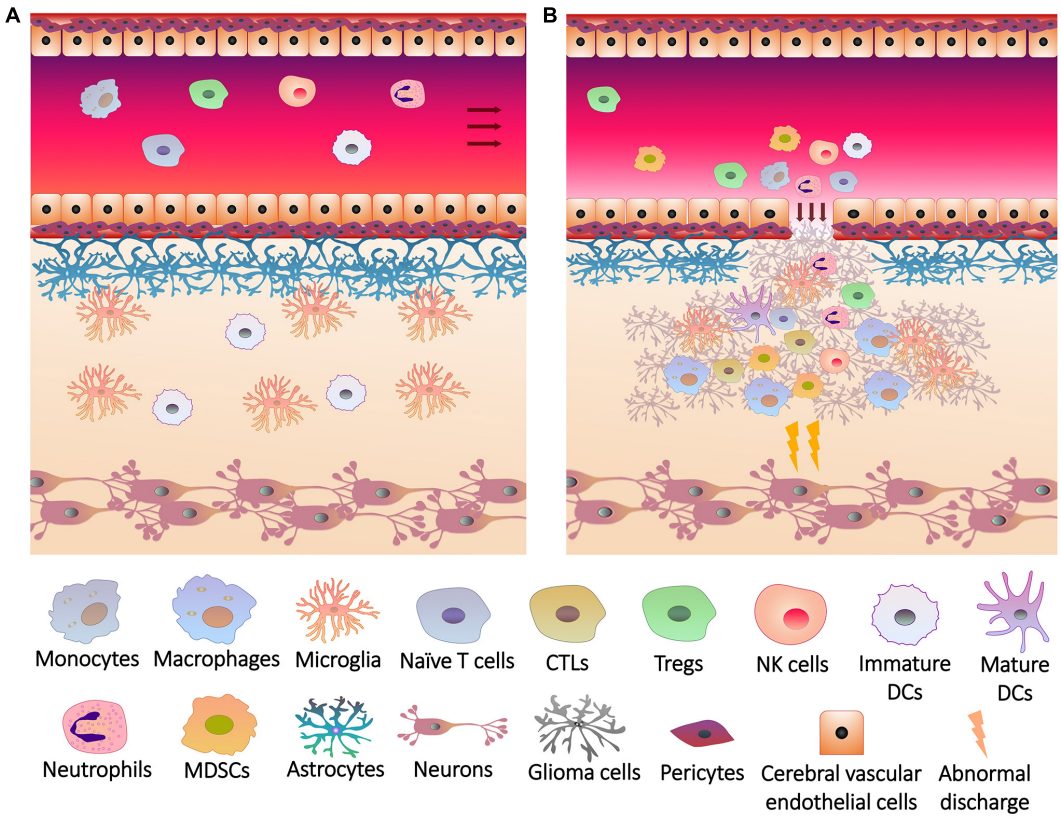

FIGURE 1 | The breakage of blood brain barrier and the infiltration of immune cells into glioma. **(A)** Under physiological conditions, the blood brain barrier consists of a firm multilayer barrier. Cerebral vascular endothelial cells form a tight junction structure, which is closely connected with pericytes, and is supported by basement membrane underneath. Astrocytes wrap the basement membrane through the end foot, and microglia maintain the integrity of the barrier. The immune cells originally present in the brain are mainly microglia and dendritic cells (DCs). Peripheral immune cells cannot penetrate the blood brain barrier, and brain tissues do not release recruitment signals to the cerebral blood vessels. **(B)** Rapid growth of glioma cells not only overexcites neurons to induce seizures, but also injures blood brain barrier. Glioma cells release chemokines and other cytokines through the cracks of blood brain barrier to induce the differentiation, expansion and recruitment of peripheral immune cells, including monocytes (in blood)/macrophages (differentiated from monocytes in brain tissue), cytotoxic T lymphocytes (CTLs), regulatory T cells (Tregs), natural killer (NK) cells, neutrophils, DCs and myeloid-derived suppressor cells (MDSCs), which infiltrate the lesions with immune cells *in situ*.

Dietary or pharmacological interventions on metabolism, such as ketogenic diet (Poff et al., 2019), dimethylbiguanide, statins and NSAIDs (Gerthofer et al., 2018; Seliger and Hau, 2018) inhibited the growth and invasion of HGGs and the malignant transformation of LGGs, and induced programmed tumor death. In view of the role of cell metabolism in the progression of gliomas, means of metabolomics based on high-throughput analysis has been developed currently (Pandey et al., 2017), whose application requires the familiarity with the metabolic characteristics of glioma cells and GSCs.

Carbohydrate Metabolism

The metabolic trend of glioma cells switches between glycolysis and PPP according to the concentration of oxygen. Under hypoxia, glioma cells overexpressed glycolytic enzymes to maintain energy supply and promote migration, while up-regulating PPP enzymes for rapid proliferation and division under oxygen-rich condition (Kathagen-Buhmann et al., 2016; Kathagen-Buhmann et al., 2018). Glycolysis was highly activated in HGG cells with invasiveness and resistance to conventional treatment (Corbin et al., 2017), but weaker glycolysis was detected in LGG cells with IDH1 mutations, which restricted their energy and made them less aggressive (Fack et al., 2017). Intracellular glucose was catalyzed to glucose-6-phosphate (G6P) by hexokinase (HK), followed by the transformation to 2 glyceraldehyde 3-phosphate (GA3P) via glucose-6-phosphate isomerase, 6-phosphofructokinase (PFK)-1, aldolase and triose phosphate isomerase sequentially, with the cost of 2 ATP. Then GA3P was converted to pyruvate catalyzed by glyceraldehyde 3-phosphate dehydrogenase, phosphaglycerate kinase (PGK), phosphoglycerate mutase 1, enolase and pyruvate kinase M (PKM), during which 4 ATP were generated. The product pyruvate was aerobically converted to acetyl-CoA to enter TCA cycle via pyruvate dehydrogenase (PDH), or became lactate by lactic dehydrogenase (LDH)-A without oxygen. The level of lactate was positively related to the speed of glycolysis, which was significantly higher in HGG cells than neuroblastoma cells and neurons (Kim J. et al., 2015). Apart from energy supply, abundant glycolytic enzymes in malignant glioma cells and GSCs promoted the shift of carbon to ribose-5-phosphate (R5P) for the

synthesis of nucleotide (Agnihotri and Zadeh, 2016), supporting tumor growth. To ensure enough raw materials for glycolysis, glioma cells and GSCs took up glucose efficiently via elevated glucose transporter (GLUT) (Libby et al., 2018), of which the level of GLUT3 is characteristic (Xu et al., 2015; Zheng et al., 2016), relating to the resistance to antiangiogenic drugs (Kuang et al., 2017). Glucose is not the only carbohydrate source for glioma cells. They also ingested fructose through GLUT5 and utilized by ketohexokinase for limited growth (Gao et al., 2018; Su et al., 2018).

Carbohydrate uptake and glycolysis of glioma cells were driven by the PI3K–AKT pathway activated by receptor tyrosine kinases including EGFR and c-Met, which up-regulated PFK1 and GLUT1/3 via the activation of PFK2 and glycoprotein synthase kinase (GSK)-3β (Kuang et al., 2017; Lee J.H. et al., 2017; Lee et al., 2018). The mTOR–c-Myc signaling also facilitated glycolysis by glutamine–fructose-6-phosphate aminotransferase 1 (Liu B. et al., 2019). In contrast, the AMP-activated protein kinase (AMPK) inhibited glycolysis and glucose uptake by inhibiting mTORC1 and attenuating transcription coactivator yes-associated protein-induced GLUT3 expression (Wang et al., 2015). As a downstream effector of mTORC2 and a regulator of the PI3K–AKT signaling (Oh et al., 2017; Wang G. et al., 2017), hypoxia-inducible factor (HIF)-1α induced the production of GLUT1/3 and glycolytic enzymes such as HK2 and PDH kinase 1 to drive glucose uptake and glycolysis, and reduced reactive oxygen species (ROS) to resist oxidative stress (Yang et al., 2014; Gabriely et al., 2017). Augmented levels of microRNAs that activate PI3K–AKT–mTOR and mTORC2–c-Myc axis and repress AMPK signaling have been observed in malignant glioma cells (Alfardus et al., 2017), reflecting the transcriptional activation of glycolysis and glucose transport.

As an important part of anabolism, PPP was activated by receptor tyrosine kinases–mTOR pathway by phosphorylated 6-phosphogluconate dehydrogenase (Liu R. et al., 2019), using G6P to produce substrates needed for glioma growth. The consumption of each G6P via 6-phosphogluconate dehydrogenase and 6-phosphate gluconate dehydrogenase produced 1 CO2, 3 H^+ and 2 NADPH, maintaining tumor growth by adjusting pH and producing NAPDH for the synthesis of GSH (reduced glutathione) and fatty acids, and the intermediate product R5P was converted into fructose-6-phosphate and GA3P for glycolysis or purine nucleotide synthesis (Payen et al., 2016). Over-activated PPP increased oxygen consumption and made glioma cells more sensitive to hypoxia-induced death (Thiepold et al., 2017). Therefore, irreversible activating mTORC1 to forcibly drive PPP, while obstructing the glycolysis may control gliomas by inducing hypoxic damage.

Lipid Metabolism

As building materials and energy sources, lipids are essential for glioma cells. Exogenous lipids were mainly obtained from intracranial glial cells in the form of lipoproteins through intercellular exchange, but rarely from the periphery (An and Weiss, 2016). The low-density lipoprotein (LDL) receptor-mediated cholesterol uptake supported the survival of glioma cells, which was counteracted by ATP-binding cassette sub-family A member (ABCA)-1-dependent cholesterol efflux promoted by liver X receptor agonists (Villa et al., 2016). Even without cholesterol intake, glioma cells and GSCs can synthesize cholesterol *de novo*. Cholesterol was synthesized from acetyl-CoA through sterol regulatory element-binding protein (SREBP)-2 and mobilized from endoplasmic reticulum via sterol *O*-acyltransferase (SOAT) and stored in lipid droplets in the form of cholesterol ester (Geng et al., 2016). Lipid droplets then activated SREBP-1, which was overexpressed in malignant glioma cells and can initiate angiogenesis and the synthesis of lipids on cell membrane and organelle via fatty acid synthase (FASN) (Zhou et al., 2016). Increased levels of polyunsaturated fatty acid synthetase ELOVL2 (elongation of very long chain fatty acids protein) and cholesterol synthase 3-hydroxy-3-methylglutaryl-CoA reductase (HMGCR) were also found in GSCs, involved in the elongation of fatty acids, synthesis of membrane lipids and facilitation of EGFR signaling to support cell growth (Wang X. et al., 2017; Gimple et al., 2019), and the impediment of fatty acid activator fatty acyl-CoA synthetase VL3 decreased the expression of stem-like phenotype CD133 and self-renewal functional molecules aldehyde dehydrogenase, musashi-1 and SOX2 on GSCs (Sun et al., 2014). The brain fatty acid binding protein (B-FABP, FABP7) participating in the utilization of unsaturated fatty acids also acted as a risk factor to drive the migration and infiltration of glioma cells and the growth of GSCs (Elsherbiny et al., 2013; Morihiro et al., 2013) dependent on the ratio of arachidonic acid (AA) to docosahexaenoic acid (DHA) (Elsherbiny et al., 2018). Prostaglandin E2 (PGE2) is another unsaturated fatty acid and known as an inducer of inflammation and pain, which was catalyzed from AA by cyclooxygenase (COX)-2 and prostaglandin E synthase (PGES) overexpressed in glioma cells, especially mesenchymal cells (Behnan et al., 2019). After binding to their receptors (EPs) in glioma tissues, PGE2 promoted tumor growth, invasion and immune escape (Jiang et al., 2017), and induced the angiogenesis with 20-hydroxyeicosatetraenoic acid (20-HETE), a transformation product of AA mediated by cytochrome P450 4A (CYP4A) (Feng et al., 2017; Wang C. et al., 2019). Inhibition of EPs or application of NSAIDs hindered the growth of gliomas (Seliger and Hau, 2018; Qiu et al., 2019). The synthesis and utilization of fatty acids and cholesterol participated in the malignant progression of gliomas, which were controllable under AMPK blockade (Guo et al., 2009; Kim et al., 2018).

Similar to carbohydrate, lipids were also catabolized by glioma cells to obtain energy. Ketone bodies are intermediate products of fatty acid oxidation, which were transported to brain tissues and converted to acetyl-CoA for vital activities. Considering that brain tumors cannot use ketone bodies and rely on glucose, the ketogenic diet was developed to limit the energy supply of gliomas rather than normal tissues (Poff et al., 2019). However, recent studies have proved that glioma cells can oxidize ketone bodies via up-regulated monocarboxylate transporter (MCT) during ketogenic diet (De Feyter et al., 2016), suggesting the ability of glioma cells to gain energy from lipids. In addition to fast-cycling glioma cells dependent on aerobic glycolysis, a subpopulation of slow-cycling cells with lipid transport and oxidation as the main metabolic mode has been confirmed, which

can obtain energy in the absence of glucose (Hoang-Minh et al., 2018). Under oxygen-rich conditions, fatty acid oxidation was an essential energy pathway for glioma cells expressing high levels of fatty acid oxidases such as carnitine palmitoyltransferase 1 to grow independently of glycolysis (Lin et al., 2017; Wu et al., 2019). Nevertheless, the energy-producing efficiency of fatty acid oxidation is far less than glycolysis. Conversion of glycolysis to fatty acid oxidation by activating PPARα eventually led to the depletion of ATP in glioma cells (Wilk et al., 2015).

Distinguishing from conventional lipid metabolism, lipid peroxidation is an over-oxidation of ROS and lipids in the cell membrane and cytoplasm, producing cytotoxic peroxides including malonaldehyde (MDA) and 4-hydroxy-2-nonenal (HNE). Although there is a potential correlation between lipid peroxidation and the grade of gliomas clinically (Atukeren et al., 2017), lipid peroxidation in differentiated glioma cells induced ferroptosis, a type of programmed death. To resist peroxidative damage, glioma cells initiate degradation of peroxidatively modified proteins through proteasome system (Nakayama et al., 2016), and abate ferroptosis by GSH, phospholipid hydroperoxidase glutathione peroxidase 4 (GPX4) and glutamate (Glu)/cystine (Cys) antiporter system Xc^-. Depleting GSH and Cys or inhibiting system Xc^- and GPX4 impeded the survival of glioma cells and increased their sensitivity to radiation-induced lipid peroxidation (Wang et al., 2018; Ye et al., 2020).

Controlling lipid metabolism resisted the invasion of gliomas, such as the application of phytol, retinol, and quercetin acting on FASN and SREBP1/2 (Facchini et al., 2018; Damiano et al., 2019), and the inhibition of acetyl-CoA carboxylase 1 and HMGCR by oleic acid and hydroxytyrosol (Priore et al., 2017). PPARα activator fenofibrate also inhibited glioma growth by inducing the dependence of tumor cells on fatty acid oxidation instead of glycolysis (Wilk et al., 2015). On this basis, using fatty acid oxidation inhibitors such as etomoxir may limit the leftover energy-producing pathways of glioma cells (Lin et al., 2017; Petovari et al., 2018), which is a potential treatment strategy.

Amino Acid and One-Carbon (C1) Metabolism

As synthesis materials or decomposition products of proteins, amino acids supported and regulated the growth of tumor cells and tumor stem-like cells (Mayers et al., 2016; Jones et al., 2018). The heterogeneous amino acid metabolism of glioma cells is formed during environmental adaptation. In order to eliminate ROS accumulation caused by vigorous glucose metabolism, the level of xCT, the light chain subunit of system Xc^- in glioma cells was up-regulated to promote the intake of Cys, providing raw material for the synthesis of GSH. This cytoprotective effect relied on glucose, whose deprivation rapidly depleted NADPH during ingestion of Cys, inducing cell death of GBM cells (Goji et al., 2017). Glu, another raw material of GSH, and its metabolite L-glutamine (Gln) are fuels for glioma growth, both of which can be autonomously synthesized by glioma cells or taken up from metabolites of astrocytes (Tardito et al., 2015). The bioenergy of conversion from Glu to Gln through Gln synthetase were provided by lactate produced during glycolysis of glioma cells and normal astrocytes. The glutaminase mediated the transformation from Gln to Glu, releasing amide nitrogen for the biosynthesis of purines and pyrimidines (Venneti and Thompson, 2017), which was accelerated by the generation of Gln via GSH (Tardito et al., 2015). The excessive secretion of Glu from glioma cells can trigger glioma-related seizures by binding to receptors on neurons around the tumor (Huberfeld and Vecht, 2016). Glu was also released from synaptic neurons as a neurotransmitter, initiating the cascade of AKT and MAPK signaling through the Glu receptor on the surface of glioma cells to promote invasion. Moreover, in a glucose-deficient condition, Glu were metabolized by Glu dehydrogenase (GLUD1)-1 into the intermediate product of TCA cycle, α-KG, which activated inhibitor of nuclear factor kappa-B kinase subunit β and nuclear factor κB (NF-κB) to promote glucose uptake by up-regulating GLUT1 (Wang X. et al., 2019). mTOR2 was activated by high levels of Gln (Liu B. et al., 2019) to regulate Glu/Gln metabolism, promoting Glu secretion, Cys uptake, GSH synthesis and Gln catabolism to obtain energy and transmit growth factor signaling for glioma cells by activating c-Myc (Gu et al., 2017).

As another critical part of amino acid metabolism, serine (Ser)/glycine (Gly) metabolism governs the synthesis of nucleotides, proteins and lipids, and is the hub of glycolysis and folate metabolism (Maddocks et al., 2017). Ser was synthesized from the glycolytic intermediate 3-phosphoglycerate via phosphoglycerate dehydrogenase (PHGDH), and was converted into Gly by mitochondrial serine hydroxymethyltransferase (SHMT2) (Kim D. et al., 2015; Venneti and Thompson, 2017). When Ser was sufficient, PKM2 was stimulated to promote glycolysis of glioma cells, while SHMT2 was activated to counteract augmented TCA cycle activity and save oxygen. Although Gly accumulation caused by SHMT2 was detrimental to cell growth, glioma cells expressed high levels of Gly decarboxylase (GLDC) to decompose Gly into innocuous metabolites, inhibition of which led to the loaded cytotoxic aminoacetone and methylglyoxal. Conversely, when Ser deficiency was sensed, glioma cells stopped cell cycle by activating cyclin-dependent kinase inhibitor p21 through p53 and promoted the synthesis of GSH to maintain survival (Venneti and Thompson, 2017).

Ser is the main source of C1 units during the conversion to Gly and the decomposition of Gly. Other amino acids including Glu, Gln, tryptophan (Trp), and methionine (Met) are also the source of C1 units. Glioma cells expressing high level of IDH3α up-regulated SHMT2 and facilitated the activation of cytosolic SHMT (SHMT1) to promote the release of C1 units (May et al., 2019). miR-940, which obstructs the folate cycle and C1 metabolism by inhibiting methylenetetrahydrofolate dehydrogenase, was also down-regulated in glioma cells (Xu et al., 2019). The abundant C1 units participate in the biosynthesis of nucleotide and produce CO2 and NADPH, enabling glioma cells to survive, proliferate and invade under hypoxic conditions (Wypych and Baranska, 2020). Furthermore, C1 units can be thoroughly utilized by GSCs with rich purine synthases (Wang Q. et al., 2017), promoting the onset and rapid recurrence of GBM.

For malignant invasion, glioma cells overexpressed amino acid metabolic enzymes to resist hypoxia and glucose deficiency.

Based on the distinct metabolic characteristics of tumors and normal brain tissues, intervention of amino acid metabolism was a selective means to improve gliomas (Panosyan et al., 2017). Moreover, considering efficient Gln uptake in glioma tissues, PET technology has been developed for imaging, which overcame the limitations of conventional nuclide ^{18}F-FDG in the context of normal brain tissues with similar strong capacity of glucose uptake (Venneti et al., 2015).

The metabolic reprogramming allowed glioma cells to proliferate regardless of the ischemic lesion (**Table 1**), and endowed them with strong migration capabilities for a better growth condition (Kathagen-Buhmann et al., 2018), enabling the rapid invasion into healthy brain tissues. Concurrently, to cope with changes in nutritional sources, the metabolic plasticity of glioma cells resulted in the resistance to anti-metabolic therapies, including diet and drugs (De Feyter et al., 2016; Shibao et al., 2018). It may be a forward therapeutic strategy to block the adaptively up-regulated metabolic enzymes and activating factors in glioma cells appropriately while limiting the intake of energy substrates.

GLIOMA CELL METABOLISM LINKS TO IMMUNE CELLS IN MICROENVIRONMENT

Metabolic plasticity not only promoted the energy supply and the synthesis of substrates required for growth and heredity of glioma cells, but also induced immune evasion (Ganapathy-Kanniappan, 2017). Immune cells accumulating and infiltrating in the glioma tissues include glioma-associated microglia/macrophages (GAMs), T lymphocytes, natural killer (NK) cells, neutrophils, dendritic cells (DCs) and myeloid-derived suppressor cells (MDSCs) (Magana-Maldonado et al., 2016; Gieryng et al., 2017; **Figures 2A,B**), supporting tumor growth instead of surveillance and annihilation and limiting the prognosis (Zhang et al., 2017; Boussiotis and Charest, 2018; **Figure 2C**). Metabolic remodeling increased the level of metabolites from glioma cells to induce immune tolerance in the TME (Kesarwani et al., 2017), and drove the production of immunosuppressive factors such as arginase (ARG)-1, IL-10, and TGF-β (Guo et al., 2018; **Figure 3A**). Moreover, the hypoxia caused by uncontrolled proliferation of metabolic reprogrammed glioma cells reduced the viability of tumor killer cells, further facilitating the survival of glioma cells (Colwell et al., 2017). The interactions between glioma cell metabolism and immune cells are a novel perspective for understanding the immune escape and refractoriness of gliomas.

GAMs

GAMs account for 30–50% of glioma-infiltrating immune cells, which is the highest proportion in tumor tissues (Hambardzumyan et al., 2016). Microglia were thought to be macrophages settled in the central nervous system (Sankowski et al., 2019), but their origins and phenotypes are different. Microglia originated from the neuroepithelial yolk sac progenitor cells (Gomez Perdiguero et al., 2015) with high level of CX3CR-1, but low level of CD45 and no CCR-2 expression (Hutter et al., 2019). In contrast, macrophages in glioma TME with CX3CR1 expression were differentiated from CX3CR1^{lo} peripheral monocytes entered the cranial cavity (Quail and Joyce, 2017), which highly express CD45 and CCR2 (Hambardzumyan et al., 2016; Chen Z. et al., 2017). Monocyte chemotactic protein 1 (MCP-1, CCL2) secreted by glioma cells mediated the recruitment of CCR2^{+} monocytes and macrophages (Chen Z. et al., 2017; Vakilian et al., 2017), and CX3CL1 induced the infiltration of CX3CR^{+} microglia (Hambardzumyan et al., 2016). Tumor recognition and phagocytosis functions of these innate immune cells were declined in glioma milieu (Poon et al., 2017), and cytokines such as TGF-β1 and IL-10 they secreted contributed to the formation of immunosuppressive TME (Roesch et al., 2018).

There is an interaction between GAMs and metabolites from glioma cells. Compared to homologous cells not exposed to the gliomas, up-regulated Glu receptors and GS and decreased xCT were detected in GAMs in response to Glu secreted by tumor cells (Choi et al., 2015). Meanwhile indoleamine 2,3-dioxygenase (IDO)-1/2 and tryptophan 2,3-dioxygenase (TDO)-2 were highly expressed in glioma cells and were proportional to tumor grade (Guastella et al., 2018), which catalyzed the decomposition of Trp into kynurenine (Kyn), a ligand of the aryl hydrocarbon receptor (AHR). The released Kyn induced the expression of CCR2 by activating AHR, and advanced the recruitment of macrophages to tumor sites by enhancing the response to MCP-1 secreted by glioma cells (Takenaka et al., 2019). In addition to the impact on recruitment, metabolism of glioma cells was involved in the regression of innate immune abilities. Branched-chain ketoacids (BCKAs) metabolized from branched-chain amino acids (BCAAs) and unsaturated fatty acid PGE2 released by glioma cells were taken up by GAMs, accompanied by decreased phagocytosis (Ghosh et al., 2010; Silva et al., 2017). On the other hand, Kyn secreted by glioma cells activated AHR in GAMs to inhibit the cytotoxicity of T lymphocytes by up-regulating the production of ectonucleotidase CD39 and adenosine (Takenaka et al., 2019). The polarization of GAMs to immunosuppressive M2 type is a representative tumorigenic process positively bound up with the grading and rapid recurrence of gliomas (Wang Q. et al., 2017; Sorensen et al., 2018), which was widely found in mesenchymal GBM cells and was related to NF1 loss (Wang Q. et al., 2017). M2 polarization was also induced by metabolites of glioma cells such as adenosine (Komohara et al., 2008; Kesarwani et al., 2019), along with the secretion of CSF-1 (Pyonteck et al., 2013), the expression of CCR5 (Laudati et al., 2017), and DNA damage repair (Meng et al., 2019) of glioma cells. However, GAMs polarized into immune-promoting M1 type were not facilely affected by metabolites (Guan et al., 2017). In addition to immunosuppressive functions, GAMs promoted the migration, angiogenesis, and invasion of gliomas via TGF-β2, IL-6, and VEGF (Roesch et al., 2018), which were affected by glioma cell metabolism as well. The secretion of VEGF and TGF-β from GAMs were reduced by blocking CYP4A to inhibit the synthesis of unsaturated fatty acid 20-HETE (Wang C. et al., 2017). The metabolism of glioma cells was also regulated by

TABLE 1 | Metabolism processes of glioma cells and GSCs.

Process	Reported cell lines	Condition	Substrate	Key media	Significance
Glucose uptake (Wang et al., 2015; Xu et al., 2015; Zheng et al., 2016; Kuang et al., 2017; Lee J.H. et al., 2017; Lee et al., 2018; Libby et al., 2018)	GBM (U87, U251, A172, LN229, U343, T98G), astrocytoma (U373); GSC isolated from GBM patients	Extracellular glucose	Glucose	GLUT1/3	Ensure enough raw materials for glucose metabolism
Fructose uptake (Su et al., 2018)	GBM (LN229, U87)	Extracellular fructose	Fructose	GLUT5	Provide supplemental energy sources other than glucose
Fructose decompose (Gao et al., 2018)	GBM (LN229, U87)	Abundant substrate	Fructose	Ketohexokinase	Provide fructose-1,6-diphosphate for glycolysis in glucose deficiency
Glycolysis (Wang et al., 2015; Agnihotri and Zadeh, 2016; Kathagen-Buhmann et al., 2016, 2018; Lee J.H. et al., 2017; Lee et al., 2018; Liu B. et al., 2019)	GBM (U87, U251, G55, U118, A172, LN229, U343, T98G), astrocytoma (U373), GSC (GS-11, GS-12, BT112)	Hypoxia	Glucose	HK, PFK1, PKM	Ensure energy source in hypoxic lesions; Promote migration to healthy brain tissues; Promote the shift of carbon from glucose into R5P for nucleotide generation
PPP (Kathagen-Buhmann et al., 2016; Payen et al., 2016; Liu R. et al., 2019)	GBM (G55, U87)	Oxygen, and sufficient substrate produced by HK	G6P	6-phosphogluconate dehydrogenase	Adjust pH; Produce R5P for glycolysis or purine nucleotide synthesis; Produce NAPDH for the synthesis of GSH and fatty acids
OXPHOS (Duan et al., 2018; Shibao et al., 2018)	GBM (U251), GSC derived from murine neural stem/progenitor cells	Glucose deficiency with sufficient oxygen	Lactate	Transport: MCT1/4; Reaction: TCA cycle	Switch metabolic mode from glycolysis to resist glucose-deficient environment
Cholesterol uptake (An and Weiss, 2016; Villa et al., 2016)	GBM (U87, U251, T98, A172), astrocytoma (U373)	Extracellular cholesterol from glial cells	LDL	LDL receptor	Provide material for organelle formation
Cholesterol efflux (An and Weiss, 2016; Villa et al., 2016)	GBM (U87, U251, T98, A172), astrocytoma (U373)	Intracellular cholesterol	Cholesterol ester	ABCA1	Induce cell death when over-activated
Cholesterol synthesis and mobilization (Geng et al., 2016)	GBM (U87, U251, T98), tumor cells isolated from GBM patients	Abundant substrate from glycolysis and fatty acid oxidation	Acetyl-CoA	Synthesis: SREBP-2, HMGCR; Mobilization: SOAT	Involve in the formation of cell membranes; Trigger SREBP-1-mediated lipid synthesis
Fatty acid synthesis and elongation (Geng et al., 2016; Zhou et al., 2016; Gimple et al., 2019)	GBM (U87, U251, T98), tumor cells and GSCs isolated from GBM patients	Intracellular glucose or cholesterol on ER membrane	Glucose, acetyl-CoA, cholesterol	SREBP-1, FASN, ELOVL2	Provide lipids on cell membrane and organelle
Unsaturated fatty acid utilization (Morihiro et al., 2013; Feng et al., 2017; Elsherbiny et al., 2018; Wang C. et al., 2019)	GBM (U87, U251, U373, M049, M103, M016), GSC (G144), astrocytoma (C6), GSC isolated from GBM patients	Abundant AA and less DHA	AA	B-FABP, COX-2, PGES	Provide eicosanoids and PGE2 for tumor growth, infiltration, immune escape and angiogenesis
Ketone body uptake and oxidation (De Feyter et al., 2016)	GBM (RG2); gliosarcoma (9L)	Ketogenic diet	Ketone bodies	Uptake: monocarboxylate transporter; Oxidation: hydroxybutyrate dehydrogenase	Resist the energy limitation of diet therapy
Fatty acid oxidation (Wilk et al., 2015; Lin et al., 2017)	GBM (U87, LN-229), tumor cells and GSCs isolated from GBM patients	Sufficient oxygen	Fatty acids	Carnitine palmitoyltransferase 1	Obtain energy in the absence of glucose (far less efficient than glycolysis)
Lipid peroxidation (Nakayama et al., 2016; Wang et al., 2018)	GBM (U87, U251, U373, SHG-44), astrocytoma (C6)	Depletion of GSH and Cys	Organelle lipids	ROS	Produce cytotoxic peroxide and induce cell death

(Continued)

TABLE 1 | Continued

Process	Reported cell lines	Condition	Substrate	Key media	Significance
Cys uptake (Goji et al., 2017)	GBM (U251, T98, A172, LN229)	Abundant glucose	Cys	System Xc^-	Provide synthetic raw materials for antioxidant GSH
Glu uptake and Glu/Gln generation (Tardito et al., 2015)	GBM (U87, U251, LN229, LN18, SF188, GUVW)	Gln starvation or abundant Gln	Glu (uptake); Glucose and alanine (*de novo* synthesis); Glu and Gln (mutual conversion)	Uptake: excitatory amino acids transporters; Synthesis: pentose phosphate pathway, glycolysis and TCA enzymes, ALT; Mutual conversion: glutaminase/Gln synthetase	Provide synthetic raw materials for antioxidant GSH; Trigger glioma-related seizures; Provide amide nitrogen for synthesis of purines and pyrimidines during transformation from Gln to Glu
Glu oxidative deamination (Wang X. et al., 2019)	GBM (U87, U251, LN18), GSC (GSC11)	Glucose deficiency	Glu	Glutamate dehydrogenase 1	Replenish α-ketoglutarate for TCA cycle; Up-regulate GLUT1 and promote glucose uptake
Ser synthesis (Kim D. et al., 2015)	GBM (U251, LN229, 0308, BT145)	Abundant substrate from glycolysis	3-phosphoglycerate	Phosphoglycerate dehydrogenase	Promote glycolysis, activation of TCA cycle and oxygen saving
Conversion of Ser to Gly (Kim D. et al., 2015)	GBM (U251, LN229, 0308, BT145)	Abundant substrate	Ser	SHMT2	Release C1 units; Produce cytotoxic aminoacetone and methylglyoxal
Gly decarboxylation (Kim D. et al., 2015)	GBM (U251, LN229, 0308, BT145)	Gly loading	Gly	Glycine decarboxylase	Convert Gly into non-cytotoxic metabolites
C1 unit release (May et al., 2019)	GBM (U87, LNZ308), GSC (GIC-20, GIC-387)	Functional IDH3α expression	Ser	SHMT2/SHMT1	Provide synthetic raw materials for nucleotide
Nucleotide synthesis (Wypych and Baranska, 2020)	Astrocytoma (C6)	Abundant substrate and carrier	C1 units, amino acids, R5P, CO2	*De novo* synthetase, remedial synthase, tetrahydrofolate (carrier)	Promote survival, proliferation and invasion

GAMs. IL-6 secreted by M2 macrophages promoted glycolysis of GBM cells by phosphorylating PGK1 via 3-phosphoinositide-dependent protein kinase 1 (PDPK1) (Zhang et al., 2018), and quinolinic acid secreted by microglia was taken up by glioma cells for the synthesis of NAD^+ to resist oxidative stress (Sahm et al., 2013).

Glioma-associated microglia/macrophages are body guards of gliomas from the host. The metabolism of glioma cells is closely related to the recruitment, infiltration, and polarization of GAMs (**Figure 3B**). Utilizing the communications between glioma cells and GAMs can create the possibility to kill gliomas at close range, such as proper interventions in metabolism.

T Lymphocytes

$CD8^+$ cytotoxic T lymphocytes (CTLs) and $CD4^+$ $CD25^+$ $FOXP3^+$ regulatory T cells (Tregs) are active lineages of glioma-infiltrating T lymphocytes. CTLs are the main contributors that infiltrate and kill tumor cells. In addition to the secretion of tumor-damaging cytokines such as IFN-γ, CTLs can recognize antigens such as HEAT repeat-containing protein 1 (HEATR1) expressed by glioma cells via human leukocyte antigen (HLA)-A2 [or major histocompatibility complex class 1 in animals] and trigger cell lysis (Wu et al., 2014; Shao et al., 2017). Due to less chance of the contact between ER and mitochondria, GSCs expressed low levels of sialylated glycans on cell surface and were more sensitive to CTLs than differentiated glioma cells (Bassoy et al., 2017). As part of TME, the cytotoxicity of CTLs cannot function properly. In response to the IFN-γ secreted by CTLs, glioma cells released PD-L1 through exosomes to interact with T cells for immune escape (Qian et al., 2018). IDH1/2 mutations reduced the release of CXCL10 that attract the accumulation of CTLs (Kohanbash et al., 2017), and increased the production of PD-L1 (Berghoff et al., 2017), hinting the involvement of glioma cell metabolism in the dysfunction of CTLs.

Glioma cells with heterogeneous carbohydrate and amino acid uptake capacity occupied the supply of glucose and amino acids in hypoxic niduses, leading to the exhaustion of CTLs (Mirzaei et al., 2017; Rashidi et al., 2020), and the accumulation of lactate during glycolysis destroyed the intracellular and extracellular concentration gradients, which hindered lactate efflux and reduced the viability of CTLs (Shao et al., 2017). As an immune checkpoint (Kesarwani et al., 2018), the Trp metabolism of glioma cells also limited the infiltration of CTLs through IDO1 (Zhai et al., 2018). In contrast, the histidine (His) metabolism promoted the activation of CTLs, and the decline of His decarboxylase (HDC) activated the inhibition of CTL infiltration by MDSCs (Ahn et al., 2015). The elevated levels of other metabolic enzymes including argininosuccinate lyase (ASL), ARG2, and COX-2 in glioma cells led to augmented synthesis of Trp, arginine

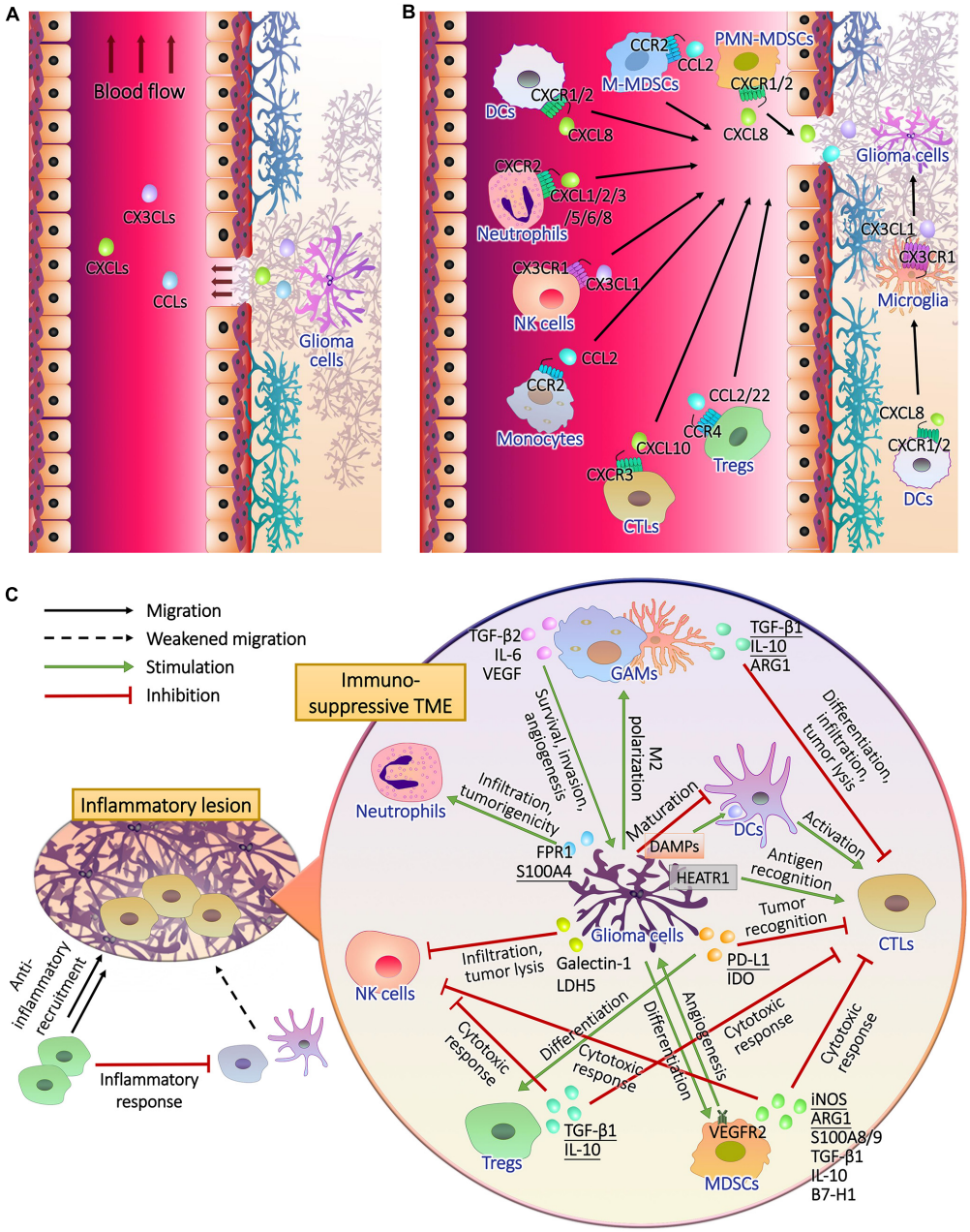

FIGURE 2 | The recruitment of immune cells and the formation of immunosuppressive glioma microenvironment. **(A)** Glioma cells release chemokines to lesion tissues, part of which entered peripheral blood through the pathological blood brain barrier. **(B)** After the chemokine receptors of peripheral and intracranial immune cells captured their ligands, they drive the cells to migrate upstream where chemokines are released. **(C)** During the infiltration of inflammatory T cells, anti-inflammatory cells, mainly regulatory T cells (Tregs), are recruited to inhibit the antigen presentation of dendritic cells (DCs) and T cell activation, resulting in impaired immune response. In addition to the activation of anti-inflammatory mechanisms, glioma cells perform complex intercellular interactions with immune cells in tumor microenvironment. Cytotoxic T lymphocytes (CTLs) should recognize tumor antigen HEAT repeat-containing protein 1 (HEATR1) and kill glioma cells with natural killer (NK) cells, and CTLs were activated by mature DCs during the presentation of damage associated molecular patterns (DAMPs) released by glioma cells. Glioma cells inhibited the maturation of DCs. Furthermore, glioma cells secreted cytokines to induce the generation and recruitment of tumorigenic Tregs, myeloid-derived suppressor cells (MDSCs), neutrophils and M2 polarized microglia and macrophages, and inhibit the infiltration and tumor lysis of CTLs and NK cells.

and PGE2, which induced the repression of CTLs as well (Eberstal et al., 2014; Authier et al., 2015; Kesarwani et al., 2019). CTLs also affect the metabolism of glioma cells through IFN-γ, which activated casein kinase (CK)-2 of tumor cells to hold up glycolysis, impeding the growth of gliomas (Ghildiyal and Sen, 2017).

Treg is a T cell subtype responsible for anti-inflammatory and immune tolerance, secreting high levels of inhibitory cytokines

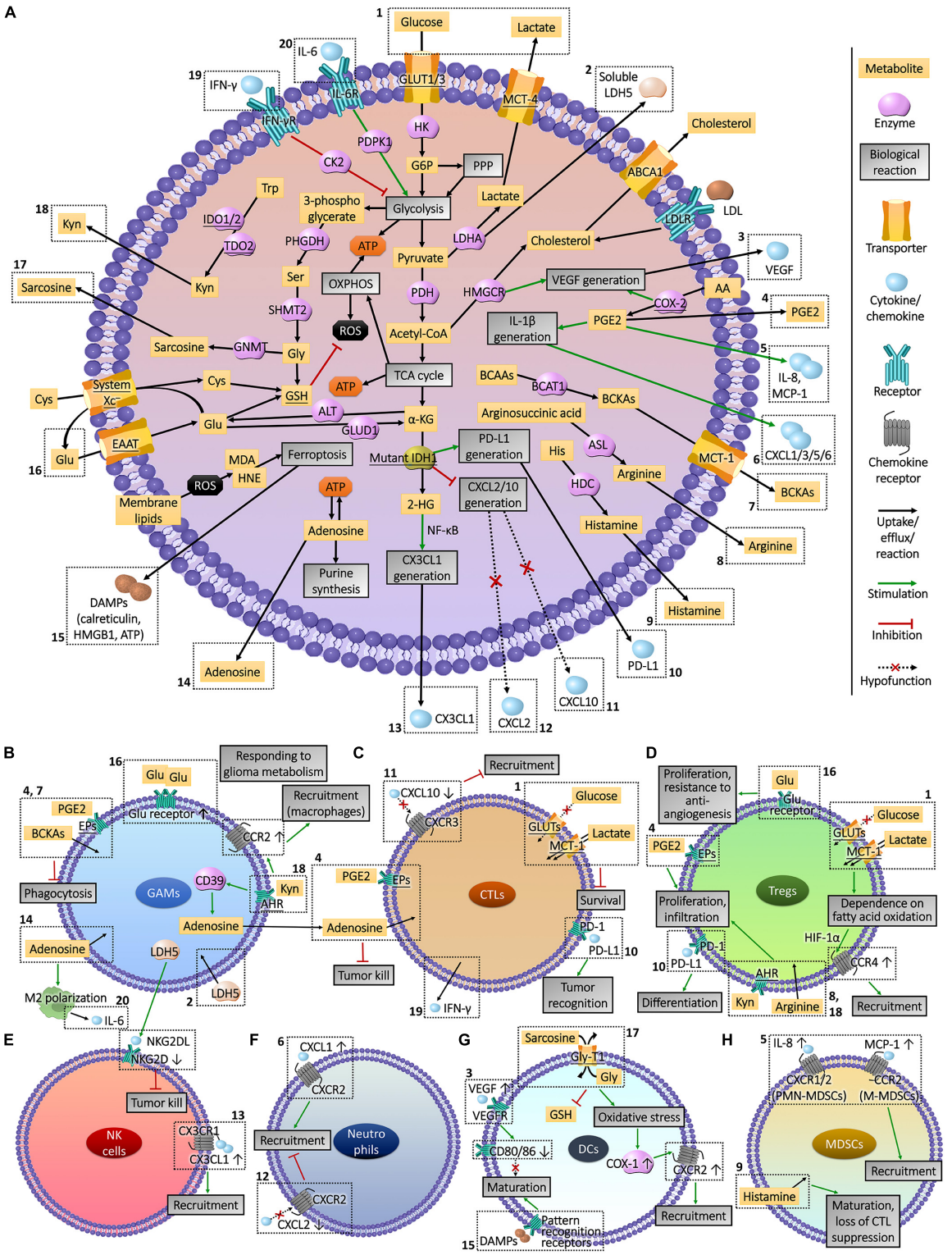

FIGURE 3 | Interactions between glioma cell metabolism and immunomicroenvironment. **(A)** Metabolic reprogramming enables glioma cells to express high levels of substrate transporters and metabolic enzymes to obtain sufficient energy in the harsh conditions of lesion, resulting in the deprivation of nutrient substrates and accumulation of immune-interfering metabolites in the extracellular fluid. Abnormally expressed or mutated metabolic enzymes also affected immune cells by regulating the production of chemokines and other cytokines. The actions of these molecules that enter the tumor microenvironment on immune cells and the influences of immune cells on glioma cells metabolism are presented in part **(B–H)**. The Arabic numerals in the figure link the metabolism of glioma cells **(A)** with immune cells **(B–H)**.

including TGF-β and IL-10 (Qiu et al., 2020), which allowed glioma cells to escape the cytotoxic damage of CTLs in TME (See et al., 2015). In malignant gliomas, Tregs were associated with the tumor recurrence, resistance to targeted drugs and decrease of survival period (Sayour et al., 2015; Du Four et al., 2016), whose depletion improved the condition of glioma mice by inducing spontaneous rejection of the tumor. Glioma cell metabolism also affects Tregs. Augmented production of Trp and arginine, and elevated expression of metabolic enzymes IDO1, ASL and ARG2 in glioma cells were accompanied by increased infiltration of Tregs (Kesarwani et al., 2019). Mutations in the metabolic enzyme IDH1/2 promoted the secretion of PD-L1 (Berghoff et al., 2017), which induce the differentiation of Tregs (DiDomenico et al., 2018). Differentiated Tregs recruited into tumor region were mediated by chemokines MCP-1 and CCL22 secreted by glioma cells (Jacobs et al., 2010; Chang et al., 2016). Due to the efficient glucose uptake and glycolysis, glucose was deprived in the hypoxic lesions by glioma cells, resulting in Tregs relying on fatty acids for mitochondrial metabolism and migrating to glioma tissues in response to CCL22 in a HIF-1α-dependent manner (Miska et al., 2019). Accumulated lactate further drove the infiltration of Tregs, and the depletion of lactate from glioma cells decreased tumor-infiltrating Tregs (Chirasani et al., 2013). PGE2 synthesis in glioma cells with up-regulated COX-2 were also related to the dilation and infiltration of Tregs (Rolle et al., 2012; Authier et al., 2015). In addition, glioma cells can activate Tregs by enhancing extracellular transport of Glu to survive anti-angiogenic therapy (Long et al., 2020).

CTLs and Tregs are T cell lineages with opposite effects in glioma TME, which were both influenced by the metabolic state of cancer cells (**Figures 3C,D**). The intervention of glioma cell metabolism can promote the infiltration of CTLs and restore their anti-tumor immunity, meanwhile hinder the recruitment of Treg, relieving the immune tolerance in TME.

NK Cells

$Ly6c^+$ NK cells in the glioma TME are a group of innate tumor killer cells derived from the bone marrow, which are part of glioma-infiltrating lymphocytes. Due to different metabolic properties, the grade of gliomas was inversely proportional to the infiltration and anti-tumor functions of NK cells. Attributing to the recruitment inhibitor galectin-1 secreted by HGG cells (Baker et al., 2016), low levels of infiltrating NK cells were observed (Domingues et al., 2016; Zhu et al., 2019), which possessed faint cytotoxicity and expressed high level of Tim-3 to prevent the tumor-killing helper T cells type 1, shortening the survival time of patients (Pereira et al., 2018). Conversely, mutations of metabolic enzyme IDH1 in LGG cells produced 2-HG and activated NF-κB to promote the secretion of CX3CL1, which attracted CX3CR1-expressing NK cells to infiltrate, making patients with a good prognosis (Ren et al., 2019). The decreased immune functions of NK cells were also related to the metabolism of glioma cells. Soluble lactate metabolic enzyme LDH5 secreted by glioma cells induced tumor infiltrating myeloid cells and circulating monocytes to release the ligand of NK group 2 member D (NKG2D), a surface receptor on NK cells in a long term, leading to the down-regulation of NKG2D and malfunction of tumor lysis (Crane et al., 2014; **Figure 3E**). According to the grade of gliomas, a suitable metabolic intervention scheme should be adjusted to effectively exert the tumor infiltration and cytotoxicity functions of NK cells.

Neutrophils

High proportion of neutrophils expressing CD11b and Ly6G in glioma tissues increased the tumor malignancy (Spiegel et al., 2016), becoming a powerful indicator of poor prognosis (Massara et al., 2017; Zhang et al., 2017). The S100A4 expressed in GSCs, which is a novel biomarker promoting the transcription of genes involving glycolysis and gluconeogenesis (Chow et al., 2017), induced tumorigenicity of neutrophils involving the promotion of tumor growth, metastasis, and resistance to anti-angiogenic drugs (Liang et al., 2014). Besides, metabolism of glioma cells interfered the recruitment and infiltration of neutrophils (**Figure 3F**). Neutrophils were recruited to the periphery of the glioma inflammatory region via chemokines including CXCL1/2/3/5/6 and IL-8 (CXCL8), which were secreted from glioma cells due to the expression of IL-1β (Lee S.Y. et al., 2017; Mostofa et al., 2017). Subsequently, neutrophils infiltrated the core area of tumor tissues through formylpeptide receptor 1 (FPR1) secreted by GBM cells to promote tumor growth, invasion and angiogenesis (Liu et al., 2012). The expression of COX-2 in glioma cells promoted the anabolic metabolism of PGE2, up-regulating the expression of IL-1β and CXCL1 (Jiang and Dingledine, 2013) to recruit neutrophils (Mostofa et al., 2017). The IDH1 mutation in glioma cells weakened the CXCL2-mediated recruitment of neutrophils (Amankulor et al., 2017), which may be one of the reasons for the low malignancy of LGGs. Despite the pro-glioma effects, utilizing the performance of directional migration and infiltration to the tumor area through BBB, the localized drug delivery and imaging tracer based on neutrophil carrier raised the treatment and staging diagnosis of glioma to a new height (Osuka and Van Meir, 2017; Xue et al., 2017; Wu et al., 2018), and can inspect the efficacy of metabolic interventions.

Dendritic Cells

As resident antigen presenting cells (APCs) in central nervous system, DCs possess the ability to activate glioma-killing CTLs (Malo et al., 2018a). The decrease of tumor-infiltrating DCs led to reduced survival of GBM mice (Mathios et al., 2016). DC vaccine-based immunotherapy has been widely investigated in the treatment of gliomas (Mitchell et al., 2015; Weller et al., 2017). However, the anti-tumor functions of DCs were covered by the glioma-induced immunosuppression, which limited the effectiveness of DC therapy (Garg et al., 2016; Li et al., 2018). Glioma cells recruited DCs through the CXC chemokine family (Dastmalchi et al., 2019). Under the exposure to glioma cells expressing VEGF, the maturation of DCs were suppressed and antigen presentation and T-cell activation capabilities were diminished (Sheng et al., 2020). What's more, DCs in the glioma TME exhibited tumor tolerable properties, expressing more IDO to induce Tregs to infiltrate glioma tissues for immune escape (Wainwright et al., 2014; He et al., 2015).

TABLE 2 | The impact of metabolic remodeling of glioma cells on immune cells.

Altered metabolic media	Metabolic characteristics after remodeling	Influence on immune cells in glioma TME	Significance	Treatment strategies
Upregulated GLUT1/3, amino acid transporters and glycolytic enzymes	Increased glucose and amino acid uptake and activation of glycolysis	Deprive nutrients and accumulate intracellular lactate in CTLs to deplete CTLs	Block tumor lysis (Mirzaei et al., 2017; Shao et al., 2017; Rashidi et al., 2020)	Glycolysis inhibitors (targeting HK, PFK-1, PKM), glucose and amino acid uptake inhibitors (targeting GLUT1/3 and MCT4), and ketogenic diet
		Induce Tregs to survive on fatty acid oxidation and promotes CCR4 expression by activating HIF-1α	Promote immunosuppressive recruitment (Miska et al., 2019)	
		Enhance lactate uptake of macrophages and DCs through MCT1 to induce the malignant transformation of macrophages and DCs	Induce the tumorigenicity of immune cells (Sheng et al., 2020)	
IDH1/2 mutations	Conversion of α-KG to 2-HG in TCA cycle	Inhibit the generation of CXCL10 to prevent the infiltration of CTLs	Block tumor lysis (Kohanbash et al., 2017)	Mutant IDH brain-targeted inhibitors (AG120, AG221, AG881) (Fujii et al., 2016)
		Induce glioma cells to secrete PD-L1 to inhibit the antigen recognition of CTLs and promote the differentiation of Tregs	Suppress anti-tumor response and promote immune suppression (Berghoff et al., 2017)	
		Activate NF-κB to promote the generation of CX3CL1 to promote the infiltration of NK cells	Promote anti-tumor infiltration in low-grade gliomas (Ren et al., 2019)	
		Inhibit the generation of CXCL2 to prevent the infiltration of neutrophils	Suppress the infiltration of tumorigenic cells (Amankulor et al., 2017)	
		Increase VEGF generation to reduce the expression of co-stimulatory molecule in DCs and hinder the maturation	Prevent antigen presentation to inhibit anti-tumor response (Wang et al., 2014; Malo et al., 2018b)	
Increased Trp synthesis and up-regulated IDO1	Increased synthesis of Kyn	Activate AHR of macrophages and increase CCR2 expression to promote the recruitment of macrophages	Promote the infiltration of tumorigenic cells (Takenaka et al., 2019)	IDO1/2 and TDO2 inhibitors
		Up-regulate CD39 to promote adenosine synthesis by GAMs to decrease the activity of CTLs	Suppress tumor lysis (Takenaka et al., 2019)	
		Activate AHR of Tregs to promote their proliferation and infiltration	Promote immunosuppressive infiltration (Kesarwani et al., 2019)	
Up-regulated COX-2 and PGES	Increased synthesis of PGE2	Impair the phagocytic activity of GAMs and the tumor lysis function of CTLs, and promote the proliferation and infiltration of Tregs by activating EPs	Suppress anti-tumor response and promote immunosuppressive infiltration (Ghosh et al., 2010; Kesarwani et al., 2019)	Drug uses NSAIDs as the lead compound
		Increase IL-1β transcription and CXCL1 generation to promote the recruitment of neutrophils	Promote the infiltration of tumorigenic cells (Jiang and Dingledine, 2013; Mostofa et al., 2017)	
		Increase IL-8 and MCP-1 generation to promote the recruitment of MDSCs	Promote immunosuppressive infiltration (Venza et al., 2011, 2012)	
		Increase VEGF generation to reduce the expression of costimulatory molecule in DCs and hinder the maturation	Prevent antigen presentation to inhibit anti-tumor response (Feng et al., 2017; Malo et al., 2018b)	

(Continued)

TABLE 2 | Continued

Altered metabolic media	Metabolic characteristics after remodeling	Influence on immune cells in glioma TME	Significance	Treatment strategies
Up-regulated MCT1	Excessive generation and efflux of BCKAs from the catabolism of BCAAs	Impair the phagocytic activity of GAMs during the uptake and re-aminate of BCKAs	Block tumor phagocytosis (Silva et al., 2017)	MCT1 inhibitors
Overexpressed Cys/Glu transporter (xCT)	Mass release of Glu to the outside of cell	Up-regulate Glu receptors and GSH, down-regulate xCT in GAMs	Reflect the response of immune cells to glioma cell metabolism (Choi et al., 2015)	xCT inhibitors
		Activate and expand Tregs	Promote the resistance to anti-VEGF therapy (Long et al., 2020)	
Activated adenosine metabolism	Increased synthesis and release of adenosine	Promote M2 polarization of GAMs	Induce the formation of immunosuppressive cells (Kesarwani et al., 2019)	inhibitors targeting adenosine or its receptors
Up-regulated ASL and downregulated iNOS	Increased synthesis and inhibited catabolism of arginine	Induce the proliferation of GAMs and Tregs	Enhance immune suppression (Kesarwani et al., 2019)	ASL inhibitors and agonists targeting iNOS and creatine kinase mitochondrial 1
Generation of LDH5	Secretion of extracellular soluble LDH5	Induce GAMs and circulating monocytes to release NKG2DL to inhibit the cytotoxicity of NK cells by down-regulating NKG2D	Block tumor lysis (Crane et al., 2014)	LDH5 inhibitors
Up-regulated HK2, PHGDH, and HMGCR	Increased synthesis of Ser and cholesterol, and stimulated glycolysis	Increase VEGF generation to reduce the expression of costimulatory molecule in DCs and hinder the maturation	Prevent antigen presentation to inhibit anti-tumor response (Wolf et al., 2011; Liu et al., 2013; Slawinska-Brych et al., 2014; Malo et al., 2018b)	HK2, PHGDH and HMGCR inhibitors
Up-regulated GPX4 and system Xc^-	Increased synthesis of GSH and inhibited lipid peroxidation	Block the release of DAMPs and prevent DCs from recognizing glioma cells	Inactivate CTL-mediated anti-tumor response (Li et al., 2018; Wang et al., 2018; Ye et al., 2020)	GPX4 and system Xc^- inhibitors

The decrease of immunosuppressive glioma-infiltrated DCs via immune checkpoint inhibitors improved T cell responses and survival of GBM mice (Hung et al., 2018).

The recruitment of DCs was affected by amino acid metabolism of glioma cells (**Figure 3G**). Glycine-*N*-methyl transferase mediates the conversion of Gly to sarcosine, which released from glioma cells and competed with DCs for Gly uptake through glycine transporter type-1 (Gly-T1) (Dastmalchi et al., 2019). Gly depletion led to decreased GSH and oxidative stress of DCs, leading to the up-regulation of COX-1 to promote CXCR2 expression and responding to IL-8 from glioma region. The immune tolerance and malignant transformation of DCs were also related to glioma cell metabolism. By inhibiting glycolysis or LDHA, the proliferation, migration and infiltration into glioma tissues of malignantly transformed DCs were repressed (Sheng et al., 2020), and these DCs secreted high levels of IL-12 to induce anti-tumor behavior of T cells (Chirasani et al., 2013). In addition, DCs stayed in immature state and co-stimulatory molecules CD80 and CD86 were down-regulated owing to elevated secretion of VEGF from glioma cells (Malo et al., 2018b) expressing elevated metabolic enzymes (He et al., 2015), involving HK2, PHGDH (Wolf et al., 2011; Liu et al., 2013), HMGCR (Slawinska-Brych et al., 2014), COX-2 (Feng et al., 2017), nitric oxide (NO) metabolic regulation enzyme dimethylarginine dimethylaminohydrolase (Boult et al., 2011) and mutated IDH1 (Wang et al., 2014).

The loss of immunogenicity of tumor cells is a cause of the failure of APCs. Inducing the release of damage associated molecular patterns (DAMPs) from glioma cells restored their immunogenicity, and triggered the activation of CTLs by DCs (Dastmalchi et al., 2019). Lipid peroxidation and ferroptosis induced by photodynamic therapy induced dying glioma cells to release DAMPs such as calreticulin, high mobility group protein B1 (HMGB1) and ATP that can be swallowed by DCs, stimulating DC maturation and activation (Turubanova et al., 2019). It can be inferred that the restoration of antigen recognition and presentation abilities of glioma-infiltrating DCs via the domination of glioma cell metabolism is critical to their anti-glioma functions, which could authentically exert the efficacy of DC vaccine on gliomas.

Myeloid-Derived Suppressor Cells

Myeloid-derived suppressor cells are a lineage of immature bone marrow-derived cells (BMDCs) activated under pathological conditions, including $CD11b^+$ $Ly6C^{hi}$ $Ly6G^-$ immature monocytes (M-MDSCs) and $CD11b^+$ $Ly6C^{lo}$ $Ly6G^+$ immature polymorphonuclear cells (PMN-MDSCs, also known as G-MDSCs, immature granulocytes) (Marvel and Gabrilovich,

2015). Regardless of their origins, the monocyte marker HLA-DR is hardly expressed in M-MDSCs, while PMN-MDSCs express lectin-type oxidized LDL receptor 1, which is hardly detected in neutrophils (Gabrilovich, 2017). MDSCs account for more than 40% of glioma-infiltrating immune cells (Kamran et al., 2017) and expressed IL-4Rα, inducible nitric oxide synthase (iNOS) and ARG1 to inhibit the responses of glioma-killer T lymphocytes and NK cells (Kohanbash et al., 2013; Gielen et al., 2016), causing patients poor prognosis (Alban et al., 2018). Among MDSCs, PMN-MDSCs induced $CD4^+$ glioma-infiltrating T lymphocytes to express PD-1, exhibiting more prominent T cell suppression (Dubinski et al., 2016). Furthermore, the expression of VEGFR2 in MDSCs promoted the malignant progression of gliomas by inducing angiogenesis (Huang et al., 2017).

The generation, infiltration, and acquisition of immunosuppressive capacity of MDSCs were regulated by the metabolism of unsaturated fatty acids and amino acids of glioma cells (**Figure 3H**). When exposed to the exosomes released by glioma cells, the expansion of BMDCs with MDSCs phenotype was induced in healthy BMDCs (Gielen et al., 2016; Guo et al., 2019), secreting IL-10, TGF-β, Fas-ligand and B7-H1 to inhibit the activation of T lymphocytes (Chae et al., 2015). The development of ARG1 phenotype in MDSCs was also induced by GSCs in a CXCR2-dependent manner, via the secretion of macrophage migration inhibitory factor (Otvos et al., 2016). Then, M-MDSCs and PMN-MDSCs migrated to TME in response to MCP-1 and IL-8 released from glioma cells separately, which can recruit monocytes and neutrophils expressing same chemokine receptors, CCR2 or CXCR1/2 (Chang et al., 2016; Ding et al., 2019). Anabolism of PGE2 in glioma cells was involved in the generation and recruitment of M-MDSCs and PMN-MDSCs. Depending on the level of COX-2 (Fujita et al., 2011; Kosaka et al., 2014), PGE2 promoted the secretion of IL-8 from glioma cells through autocrine (Venza et al., 2011, 2012), advanced the migratory response of M-MDSCs to MCP-1, and promoted the expression of ARG1 in PMN-MDSCs. However, histamine secreted from glioma cells mediated the maturation of MDSCs and the loss of immunosuppressive functions. The exhaustion of histamine via HDC knockout resulted in augmented infiltration of MDSCs into glioma tissues with suppressed CTLs (Ahn et al., 2015). Studying the relationship between the generation and recruitment of MDSCs and glioma cell metabolism is expected to improve the immune microenvironment of the lesions.

METABOLIC IMMUNOTHERAPY STRATEGIES FOR GLIOMA

Metabolic heterogeneity of tumor cells and their initiating cells promoted the rapid invasion and recurrence of gliomas (Kathagen-Buhmann et al., 2016; Shibao et al., 2018). In the hypoxic area of intracranial lesions, these malignant cells made thorough use of glucose, lipoproteins and amino acids to ingest energy, synthesize hereditary substance, and produce antioxidants to resist oxidative stress. Metabolic reprogramming also brought enhanced migratory ability for glioma cells to invade healthy brain tissues for more energy supply. In order to ensure the smoothness of these biological processes, glioma cells took advantage of their metabolic properties for immune tolerance and escape mainly through the following ways.

(1) Their powerful nutrient uptake depleted the energy supply of tumor killer cells, and enhanced the synthesis of immune checkpoints including PD-L1 and IDO, impairing the anti-tumor responses.
(2) The metabolites secreted into TME promoted the infiltration and expansion of inflammatory neutrophils and suppressive Tregs and MDSCs to activate

TABLE 3 | Differentials in cell metabolism and immune TME of gliomas compared with peripheral tumors.

What's special	Specific performance	Significance
Richer energy substrate	Compared with peripheral tissues, brain has higher energy substrate requirement, especially for glucose (Aldana, 2019). The vascular endothelial cells in BBB highly express GLUT1 to take up abundant glucose from the periphery blood into the brain (Jais et al., 2016).	Glioma cells possess more energy substrates than peripheral tumor cells.
Utilization of Glu/Gln metabolic coupling of brain cells	Glu released from synaptic ends is absorbed by astrocytes and metabolized into Gln, which can be absorbed and utilized by the glutamine transporters on glioma cells before being transported to neurons (Strickland and Stoll, 2017).	Provide a special source of amide nitrogen for glioma cells to synthesize purines and pyrimidines.
Special genetic mutations	Mutations or expression changes of IDH, p53, PDGFRA, EGFR, NF1 and other characteristic genes of glioma not only promote glucose uptake and glycolysis in glioma cells, but also induce the infiltration and M2 polarization of GAMs (Wang Q. et al., 2017).	Make glioma cells use the glucose-rich condition of brain TME more efficiently, and promote immune escape.
Participation of microglia	As a special member of glioma TME, microglia are recruited to lesions through CX3CL1/CX3CR1 chemokine channel (Hambardzumyan et al., 2016), while peripheral monocyte-macrophages through the MCP-1/CCR2 channel (Vakilian et al., 2017).	There is a certain difference in the immune recruitment between glioma cells and peripheral tumor cells.
Presence of a biological barrier	The chemokines released by glioma cells recruit most of the immune cells in the TME from the periphery after penetrating BBTB, and immune cells also need to penetrate this barrier to enter the lesion.	There is a barrier for glioma cells to recruit immune cells, which does not exist in peripheral tumors.

anti-inflammatory mechanisms and immunotolerant responses.

(3) The metabolites led to malignant transformation of tumor-infiltrating APCs and phagocytes and exerted immunosuppressive functions, indirectly resisting tumor killer cells.

(4) After metabolic remodeling, the ability to recruit immune-tolerant cells was enhanced, but anti-tumor cells were less recruited. On the contrary, peroxidation metabolism enhanced immunogenicity and attract the presentation of tumor antigens (Turubanova et al., 2019).

Energy production and antioxidant responses during metabolism of glioma cells can also be induced by GAMs (Sahm et al., 2013; Zhang et al., 2018), but inhibited by CTLs in TME (Ghildiyal and Sen, 2017), reflecting the bidirectional conversation between glioma cell metabolism and immune microenvironment.

Several strategies for improving glioma TME through metabolic therapy are recommended (**Table 2**). Glycolysis inhibitors, or drugs targeting GLUT3 and MCT4 can restore the supply of extracellular glucose and reduce the lactate stress, improving the growth of CTLs, and hindering the tendency of Tregs to fatty acid oxidation to inhibit the infiltration of Tregs. Inhibiting inflammation and the release of PGE2 by anti-COX drugs such as NSAIDs can hinder inflammatory infiltration and activate anti-inflammatory mechanisms, restore the phagocytosis of GAMs and tumor lysis of CTLs, and repress the recruitment of Tregs, neutrophils and MDSCs. Inhibiting key enzymes in Trp–Kyn pathway and adenosine synthesis to prevent the loaded Kyn from activating AHR of GAMs and Tregs, and reduce the concentration of adenosine to enhance the cytotoxicity of CTLs is also a good choice. Compounds designed to act on amino acid transporters, including MCT1 and system Xc^- can inhibit the release of BCKAs and the uptake of GSH synthetic materials, so as to restore GAMs phagocytosis, and induce the release of glioma-derived DAMPs recognized by DCs during ferroptosis. In addition, local injection of sarcosine and histamine can promote the migration of DCs to glioma region and promote the maturation of MDSCs. For glioma cells with IDH mutations, targeting mutant IDH can restore the release of CXCL10 and inhibit the production of PD-L1, promoting recruitment and tumor recognition of CTLs and inhibiting Tregs. It can be combined with imaging methods such as PET to analyze the metabolic characteristics of the lesions (Venneti et al., 2015) and formulate an individualized metabolic treatment plan.

DISCUSSION

The microenvironment where glioma cells regulate immune cells through metabolic reprogramming is in the brain. Therefore, a challenge for glioma metabolic immunotherapy is the BBTB. In order to selectively act drugs on the lesions and reduce the impact on peripheral tissues, a brain drug delivery system needs to be established. Osmotic BBB disruption based on intra-arterial infusion of hypertonic mannitol solution, intravenous bradykinin analogs that relax tight junctions, drugs coupling to a mediator targeting and shuttling insulin or transferrin receptors, nanoparticle drug delivery system, and direct delivery of drugs to the brain parenchyma or excision cavity are potential methods for metabolic immunotherapeutic drugs to cross BBTB (van Tellingen et al., 2015; Li et al., 2020). Targeting metabolic functional proteins selectively and highly expressed in glioma cells, such as GLUT3 (Xu et al., 2015; Zheng et al., 2016), or using targeted metabolic drug delivery systems based on neutrophils (Osuka and Van Meir, 2017; Xue et al., 2017) or other immune cells accumulating in glioma tissues is also a good solution.

To conclude, glioma cells show different metabolic pattern and immune microenvironment from peripheral tumors (**Table 3**). Interfering with cell metabolism could not only hinder the growth of glioma cells, but also improve the immune response in the focal area to systematically resist tumor progression, which is expected to become a new direction for clinical treatment of gliomas.

AUTHOR CONTRIBUTIONS

RQ and YZ contributed equally to this work and worked for the first draft of text writing and illustrations. QL participated in the literature search and revised the introduction part of the manuscript. YL and HF provided professional guidance on disease details and treatment status, and edited the manuscript. All of the authors approved the publication of this manuscript.

FUNDING

This work was supported by the Science and Technology Development Fund of Nanjing Medical University (Grant No. NMUB2019153) and Nanjing Health Youth Talent Fund (Grant No. QRX11032).

REFERENCES

Agnihotri, S., and Zadeh, G. (2016). Metabolic reprogramming in glioblastoma: the influence of cancer metabolism on epigenetics and unanswered questions. *Neuro Oncol.* 18, 160–172. doi: 10.1093/neuonc/nov125

Ahn, B., Kohanbash, G., Ohkuri, T., Kosaka, A., Chen, X., Ikeura, M., et al. (2015). Histamine deficiency promotes accumulation of immunosuppressive immature myeloid cells and growth of murine gliomas. *Oncoimmunology* 4:e1047581. doi: 10.1080/2162402X.2015.1047581

Alban, T. J., Alvarado, A. G., Sorensen, M. D., Bayik, D., Volovetz, J., Serbinowski, E., et al. (2018). Global immune fingerprinting in glioblastoma patient peripheral blood reveals immune-suppression signatures associated with prognosis. *JCI Insight* 3:e122264. doi: 10.1172/jci.insight.122264

Aldana, B. I. (2019). Microglia-specific metabolic changes in neurodegeneration. *J. Mol. Biol.* 431, 1830–1842. doi: 10.1016/j.jmb.2019.03.006

Alfardus, H., McIntyre, A., and Smith, S. (2017). MicroRNA regulation of glycolytic metabolism in glioblastoma. *Biomed. Res. Int.* 2017:9157370. doi: 10.1155/2017/9157370

Amankulor, N. M., Kim, Y., Arora, S., Kargl, J., Szulzewsky, F., Hanke, M., et al. (2017). Mutant IDH1 regulates the tumor-associated immune system in gliomas. *Genes Dev.* 31, 774–786. doi: 10.1101/gad.294991.116

An, Z., and Weiss, W. A. (2016). Cholesterol: an achilles'. Heel for Glioblastoma? *Cancer Cell* 30, 653–654. doi: 10.1016/j.ccell.2016.10.011

Atukeren, P., Oner, S., Baran, O., Kemerdere, R., Eren, B., Cakatay, U., et al. (2017). Oxidant and anti-oxidant status in common brain tumors: correlation to TP53 and human biliverdin reductase. *Clin. Neurol. Neurosurg.* 158, 72–76. doi: 10.1016/j.clineuro.2017.05.003

Authier, A., Farrand, K. J., Broadley, K. W., Ancelet, L. R., Hunn, M. K., Stone, S., et al. (2015). Enhanced immunosuppression by therapy-exposed glioblastoma multiforme tumor cells. *Int. J. Cancer* 136, 2566–2578. doi: 10.1002/ijc.29309

Baker, G. J., Chockley, P., Zamler, D., Castro, M. G., and Lowenstein, P. R. (2016). Natural killer cells require monocytic Gr-1(+)/CD11b(+) myeloid cells to eradicate orthotopically engrafted glioma cells. *Oncoimmunology* 5:e1163461. doi: 10.1080/2162402X.2016.1163461

Bassoy, E. Y., Kasahara, A., Chiusolo, V., Jacquemin, G., Boydell, E., Zamorano, S., et al. (2017). ER-mitochondria contacts control surface glycan expression and sensitivity to killer lymphocytes in glioma stem-like cells. *EMBO J.* 36, 1493–1512. doi: 10.15252/embj.201695429

Behnan, J., Finocchiaro, G., and Hanna, G. (2019). The landscape of the mesenchymal signature in brain tumours. *Brain* 142, 847–866. doi: 10.1093/brain/awz044

Berghoff, A. S., Kiesel, B., Widhalm, G., Wilhelm, D., Rajky, O., Kurscheid, S., et al. (2017). Correlation of immune phenotype with IDH mutation in diffuse glioma. *Neuro Oncol.* 19, 1460–1468. doi: 10.1093/neuonc/nox054

Boult, J. K., Walker-Samuel, S., Jamin, Y., Leiper, J. M., Whitley, G. S., and Robinson, S. P. (2011). Active site mutant dimethylarginine dimethylaminohydrolase 1 expression confers an intermediate tumour phenotype in C6 gliomas. *J. Pathol.* 225, 344–352. doi: 10.1002/path.2904

Boussiotis, V. A., and Charest, A. (2018). Immunotherapies for malignant glioma. *Oncogene* 37, 1121–1141. doi: 10.1038/s41388-017-0024-z

Broekman, M. L., Maas, S. L. N., Abels, E. R., Mempel, T. R., Krichevsky, A. M., and Breakefield, X. O. (2018). Multidimensional communication in the microenvirons of glioblastoma. *Nat. Rev. Neurol.* 14, 482–495. doi: 10.1038/s41582-018-0025-8

Chae, M., Peterson, T. E., Balgeman, A., Chen, S., Zhang, L., Renner, D. N., et al. (2015). Increasing glioma-associated monocytes leads to increased intratumoral and systemic myeloid-derived suppressor cells in a murine model. *Neuro Oncol.* 17, 978–991. doi: 10.1093/neuonc/nou343

Chang, A. L., Miska, J., Wainwright, D. A., Dey, M., Rivetta, C. V., Yu, D., et al. (2016). CCL2 Produced by the Glioma Microenvironment Is Essential for the Recruitment of Regulatory T Cells and Myeloid-Derived Suppressor Cells. *Cancer Res.* 76, 5671–5682. doi: 10.1158/0008-5472.CAN-16-0144

Chen, R., Smith-Cohn, M., Cohen, A. L., and Colman, H. (2017). Glioma subclassifications and their clinical significance. *Neurotherapeutics* 14, 284–297. doi: 10.1007/s13311-017-0519-x

Chen, Z., Feng, X., Herting, C. J., Garcia, V. A., Nie, K., Pong, W. W., et al. (2017). Cellular and molecular identity of tumor-associated macrophages in glioblastoma. *Cancer Res.* 77, 2266–2278. doi: 10.1158/0008-5472.CAN-16-2310

Chirasani, S. R., Leukel, P., Gottfried, E., Hochrein, J., Stadler, K., Neumann, B., et al. (2013). Diclofenac inhibits lactate formation and efficiently counteracts local immune suppression in a murine glioma model. *Int. J. Cancer* 132, 843–853. doi: 10.1002/ijc.27712

Choi, J., Stradmann-Bellinghausen, B., Yakubov, E., Savaskan, N. E., and Regnier-Vigouroux, A. (2015). Glioblastoma cells induce differential glutamatergic gene expressions in human tumor-associated microglia/macrophages and monocyte-derived macrophages. *Cancer Biol. Ther.* 16, 1205–1213. doi: 10.1080/15384047.2015.1056406

Chow, K. H., Park, H. J., George, J., Yamamoto, K., Gallup, A. D., Graber, J. H., et al. (2017). S100A4 is a biomarker and regulator of glioma stem cells that is critical for mesenchymal transition in glioblastoma. *Cancer Res.* 77, 5360–5373. doi: 10.1158/0008-5472.CAN-17-1294

Colwell, N., Larion, M., Giles, A. J., Seldomridge, A. N., Sizdahkhani, S., Gilbert, M. R., et al. (2017). Hypoxia in the glioblastoma microenvironment: shaping the phenotype of cancer stem-like cells. *Neuro Oncol.* 19, 887–896. doi: 10.1093/neuonc/now258

Corbin, Z., Spielman, D., and Recht, L. (2017). A metabolic therapy for malignant glioma requires a clinical measure. *Curr. Oncol. Rep.* 19:84. doi: 10.1007/s11912-017-0637-y

Crane, C. A., Austgen, K., Haberthur, K., Hofmann, C., Moyes, K. W., Avanesyan, L., et al. (2014). Immune evasion mediated by tumor-derived lactate dehydrogenase induction of NKG2D ligands on myeloid cells in glioblastoma patients. *Proc. Natl. Acad. Sci. U.S.A.* 111, 12823–12828. doi: 10.1073/pnas.1413933111

Damiano, F., Giannotti, L., Gnoni, G. V., Siculella, L., and Gnoni, A. (2019). Quercetin inhibition of SREBPs and ChREBP expression results in reduced cholesterol and fatty acid synthesis in C6 glioma cells. *Int. J. Biochem. Cell Biol.* 117:105618. doi: 10.1016/j.biocel.2019.105618

Dastmalchi, F., Karachi, A., Yang, C., Azari, H., Sayour, E. J., Dechkovskaia, A., et al. (2019). Sarcosine promotes trafficking of dendritic cells and improves efficacy of anti-tumor dendritic cell vaccines via CXC chemokine family signaling. *J. Immunother. Cancer* 7:321. doi: 10.1186/s40425-019-0809-4

De Feyter, H. M., Behar, K. L., Rao, J. U., Madden-Hennessey, K., Ip, K. L., Hyder, F., et al. (2016). A ketogenic diet increases transport and oxidation of ketone bodies in RG2 and 9L gliomas without affecting tumor growth. *Neuro Oncol.* 18, 1079–1087. doi: 10.1093/neuonc/now088

DeBerardinis, R. J., and Chandel, N. S. (2016). Fundamentals of cancer metabolism. *Sci. Adv.* 2:e1600200. doi: 10.1126/sciadv.1600200

DiDomenico, J., Lamano, J. B., Oyon, D., Li, Y., Veliceasa, D., Kaur, G., et al. (2018). The immune checkpoint protein PD-L1 induces and maintains regulatory T cells in glioblastoma. *Oncoimmunology* 7:e1448329. doi: 10.1080/2162402X.2018.1448329

Ding, A. S., Routkevitch, D., Jackson, C., and Lim, M. (2019). Targeting myeloid cells in combination treatments for glioma and other tumors. *Front. Immunol.* 10:1715. doi: 10.3389/fimmu.2019.01715

Domingues, P., Gonzalez-Tablas, M., Otero, A., Pascual, D., Miranda, D., Ruiz, L., et al. (2016). Tumor infiltrating immune cells in gliomas and meningiomas. *Brain Behav. Immun.* 53, 1–15. doi: 10.1016/j.bbi.2015.07.019

Du Four, S., Maenhout, S. K., Benteyn, D., De Keersmaecker, B., Duerinck, J., Thielemans, K., et al. (2016). Disease progression in recurrent glioblastoma patients treated with the VEGFR inhibitor axitinib is associated with increased regulatory T cell numbers and T cell exhaustion. *Cancer Immunol. Immunother.* 65, 727–740. doi: 10.1007/s00262-016-1836-3

Duan, K., Liu, Z. J., Hu, S. Q., Huo, H. Y., Xu, Z. R., Ruan, J. F., et al. (2018). Lactic acid induces lactate transport and glycolysis/OXPHOS interconversion in glioblastoma. *Biochem. Biophys. Res. Commun.* 503, 888–894. doi: 10.1016/j.bbrc.2018.06.092

Dubinski, D., Wolfer, J., Hasselblatt, M., Schneider-Hohendorf, T., Bogdahn, U., Stummer, W., et al. (2016). CD4+ T effector memory cell dysfunction is associated with the accumulation of granulocytic myeloid-derived suppressor cells in glioblastoma patients. *Neuro Oncol.* 18, 807–818. doi: 10.1093/neuonc/nov280

Eberstal, S., Fritzell, S., Sanden, E., Visse, E., Darabi, A., and Siesjo, P. (2014). Immunizations with unmodified tumor cells and simultaneous COX-2 inhibition eradicate malignant rat brain tumors and induce a long-lasting CD8(+) T cell memory. *J. Neuroimmunol.* 274, 161–167. doi: 10.1016/j.jneuroim.2014.06.019

Elsherbiny, M. E., Chen, H., Emara, M., and Godbout, R. (2018). omega-3 and omega-6 fatty acids modulate conventional and atypical protein kinase C activities in a brain fatty acid binding protein dependent manner in glioblastoma multiforme. *Nutrients* 10:454. doi: 10.3390/nu10040454

Elsherbiny, M. E., Emara, M., and Godbout, R. (2013). Interaction of brain fatty acid-binding protein with the polyunsaturated fatty acid environment as a potential determinant of poor prognosis in malignant glioma. *Prog. Lipid Res.* 52, 562–570. doi: 10.1016/j.plipres.2013.08.004

Engelhardt, B., Vajkoczy, P., and Weller, R. O. (2017). The movers and shapers in immune privilege of the CNS. *Nat. Immunol.* 18, 123–131. doi: 10.1038/ni.3666

Facchini, G., Ignarro, R. S., Rodrigues-Silva, E., Vieira, A. S., Lopes-Cendes, I., Castilho, R. F., et al. (2018). Toxic effects of phytol and retinol on human glioblastoma cells are associated with modulation of cholesterol and fatty acid biosynthetic pathways. *J. Neurooncol.* 136, 435–443. doi: 10.1007/s11060-017-2672-9

Fack, F., Tardito, S., Hochart, G., Oudin, A., Zheng, L., Fritah, S., et al. (2017). Altered metabolic landscape in IDH-mutant gliomas affects phospholipid, energy, and oxidative stress pathways. *EMBO Mol. Med.* 9, 1681–1695. doi: 10.15252/emmm.201707729

Feng, X., Yu, Y., He, S., Cheng, J., Gong, Y., Zhang, Z., et al. (2017). Dying glioma cells establish a proangiogenic microenvironment through a caspase 3 dependent mechanism. *Cancer Lett.* 385, 12–20. doi: 10.1016/j.canlet.2016.10.042

Fujii, T., Khawaja, M. R., DiNardo, C. D., Atkins, J. T., and Janku, F. (2016). Targeting isocitrate dehydrogenase (IDH) in cancer. *Discov. Med.* 21, 373–380.

Fujita, M., Kohanbash, G., Fellows-Mayle, W., Hamilton, R. L., Komohara, Y., Decker, S. A., et al. (2011). COX-2 blockade suppresses gliomagenesis by inhibiting myeloid-derived suppressor cells. *Cancer Res.* 71, 2664–2674. doi: 10.1158/0008-5472.CAN-10-3055

Gabriely, G., Wheeler, M. A., Takenaka, M. C., and Quintana, F. J. (2017). Role of AHR and HIF-1alpha in glioblastoma metabolism. *Trends Endocrinol. Metab.* 28, 428–436. doi: 10.1016/j.tem.2017.02.009

Gabrilovich, D. I. (2017). Myeloid-derived suppressor cells. *Cancer Immunol. Res.* 5, 3–8. doi: 10.1158/2326-6066.CIR-16-0297

Ganapathy-Kanniappan, S. (2017). Linking tumor glycolysis and immune evasion in cancer: emerging concepts and therapeutic opportunities. *Biochim. Biophys. Acta Rev. Cancer* 1868, 212–220. doi: 10.1016/j.bbcan.2017.04.002

Gao, W., Li, N., Li, Z., Xu, J., and Su, C. (2018). Ketohexokinase is involved in fructose utilization and promotes tumor progression in glioma. *Biochem. Biophys. Res. Commun.* 503, 1298–1306. doi: 10.1016/j.bbrc.2018.07.040

Garg, A. D., Vandenberk, L., Koks, C., Verschuere, T., Boon, L., Van Gool, S. W., et al. (2016). Dendritic cell vaccines based on immunogenic cell death elicit danger signals and T cell-driven rejection of high-grade glioma. *Sci. Transl. Med.* 8:328ra327. doi: 10.1126/scitranslmed.aae0105

Geng, F., Cheng, X., Wu, X., Yoo, J. Y., Cheng, C., Guo, J. Y., et al. (2016). Inhibition of SOAT1 suppresses glioblastoma growth via blocking SREBP-1-Mediated lipogenesis. *Clin. Cancer Res.* 22, 5337–5348. doi: 10.1158/1078-0432.CCR-15-2973

Gerthofer, V., Kreutz, M., Renner, K., Jachnik, B., Dettmer, K., Oefner, P., et al. (2018). Combined modulation of tumor metabolism by metformin and diclofenac in glioma. *Int. J. Mol. Sci.* 19:2586. doi: 10.3390/ijms19092586

Ghildiyal, R., and Sen, E. (2017). CK2 induced RIG-I drives metabolic adaptations in IFNgamma-treated glioma cells. *Cytokine* 89, 219–228. doi: 10.1016/j.cyto.2015.10.009

Ghosh, A., Bhattacharya, M., Sarkar, P., Acharya, S., and Chaudhuri, S. (2010). T11 target structure exerts effector function by activating immune cells in CNS against glioma where cytokine modulation provide favorable microenvironment. *Indian J. Exp. Biol.* 48, 879–888.

Gielen, P. R., Schulte, B. M., Kers-Rebel, E. D., Verrijp, K., Bossman, S. A., Ter Laan, M., et al. (2016). Elevated levels of polymorphonuclear myeloid-derived suppressor cells in patients with glioblastoma highly express S100A8/9 and arginase and suppress T cell function. *Neuro Oncol.* 18, 1253–1264. doi: 10.1093/neuonc/now034

Gieryng, A., Pszczolkowska, D., Walentynowicz, K. A., Rajan, W. D., and Kaminska, B. (2017). Immune microenvironment of gliomas. *Lab. Invest.* 97, 498–518. doi: 10.1038/labinvest.2017.19

Gimple, R. C., Kidwell, R. L., Kim, L. J. Y., Sun, T., Gromovsky, A. D., Wu, Q., et al. (2019). Glioma stem cell-specific superenhancer promotes polyunsaturated fatty-acid synthesis to support EGFR signaling. *Cancer Discov.* 9, 1248–1267. doi: 10.1158/2159-8290.CD-19-0061

Goji, T., Takahara, K., Negishi, M., and Katoh, H. (2017). Cystine uptake through the cystine/glutamate antiporter xCT triggers glioblastoma cell death under glucose deprivation. *J. Biol. Chem.* 292, 19721–19732. doi: 10.1074/jbc.M117.814392

Gomez Perdiguero, E., Klapproth, K., Schulz, C., Busch, K., Azzoni, E., Crozet, L., et al. (2015). Tissue-resident macrophages originate from yolk-sac-derived erythro-myeloid progenitors. *Nature* 518, 547–551. doi: 10.1038/nature13989

Gu, Y., Albuquerque, C. P., Braas, D., Zhang, W., Villa, G. R., Bi, J., et al. (2017). mTORC2 regulates amino acid metabolism in cancer by phosphorylation of the cystine-glutamate antiporter xCT. *Mol. Cell* 67, 128.e7–138.e7. doi: 10.1016/j.molcel.2017.05.030

Guan, J., Zhang, Z., Hu, X., Yang, Y., Chai, Z., Liu, X., et al. (2017). Cholera toxin subunit B enabled multifunctional glioma-targeted drug delivery. *Adv. Healthc Mater.* 6:1700709. doi: 10.1002/adhm.201700709

Guastella, A. R., Michelhaugh, S. K., Klinger, N. V., Fadel, H. A., Kiousis, S., Ali-Fehmi, R., et al. (2018). Investigation of the aryl hydrocarbon receptor and the intrinsic tumoral component of the kynurenine pathway of tryptophan metabolism in primary brain tumors. *J. Neurooncol.* 139, 239–249. doi: 10.1007/s11060-018-2869-6

Guo, D., Hildebrandt, I. J., Prins, R. M., Soto, H., Mazzotta, M. M., Dang, J., et al. (2009). The AMPK agonist AICAR inhibits the growth of EGFRvIII-expressing glioblastomas by inhibiting lipogenesis. *Proc. Natl. Acad. Sci. U.S.A.* 106, 12932–12937. doi: 10.1073/pnas.0906606106

Guo, X., Qiu, W., Liu, Q., Qian, M., Wang, S., Zhang, Z., et al. (2018). Immunosuppressive effects of hypoxia-induced glioma exosomes through myeloid-derived suppressor cells via the miR-10a/Rora and miR-21/Pten Pathways. *Oncogene* 37, 4239–4259. doi: 10.1038/s41388-018-0261-9

Guo, X., Qiu, W., Wang, J., Liu, Q., Qian, M., Wang, S., et al. (2019). Glioma exosomes mediate the expansion and function of myeloid-derived suppressor cells through microRNA-29a/Hbp1 and microRNA-92a/Prkar1a pathways. *Int. J. Cancer* 144, 3111–3126. doi: 10.1002/ijc.32052

Gusyatiner, O., and Hegi, M. E. (2018). Glioma epigenetics: from subclassification to novel treatment options. *Semin. Cancer Biol.* 51, 50–58. doi: 10.1016/j.semcancer.2017.11.010

Hambardzumyan, D., Gutmann, D. H., and Kettenmann, H. (2016). The role of microglia and macrophages in glioma maintenance and progression. *Nat. Neurosci.* 19, 20–27. doi: 10.1038/nn.4185

Han, S., Liu, Y., Cai, S. J., Qian, M., Ding, J., Larion, M., et al. (2020). IDH mutation in glioma: molecular mechanisms and potential therapeutic targets. *Br. J. Cancer* 122, 1580–1589. doi: 10.1038/s41416-020-0814-x

He, X. Z., Wang, Q. F., Han, S., Wang, H. Q., Ye, Y. Y., Zhu, Z. Y., et al. (2015). Cryo-ablation improves anti-tumor immunity through recovering tumor educated dendritic cells in tumor-draining lymph nodes. *Drug Des. Dev. Ther.* 9, 1449–1458. doi: 10.2147/DDDT.S76592

Hervey-Jumper, S. L., and Berger, M. S. (2016). Maximizing safe resection of low- and high-grade glioma. *J. Neurooncol.* 130, 269–282. doi: 10.1007/s11060-016-2110-4

Hirata, E., and Sahai, E. (2017). Tumor microenvironment and differential responses to therapy. *Cold Spring Harb. Perspect. Med.* 7:a026781. doi: 10.1101/cshperspect.a026781

Hoang-Minh, L. B., Siebzehnrubl, F. A., Yang, C., Suzuki-Hatano, S., Dajac, K., Loche, T., et al. (2018). Infiltrative and drug-resistant slow-cycling cells support metabolic heterogeneity in glioblastoma. *EMBO J.* 37:e98772. doi: 10.15252/embj.201798772

Huang, Y., Rajappa, P., Hu, W., Hoffman, C., Cisse, B., Kim, J. H., et al. (2017). A proangiogenic signaling axis in myeloid cells promotes malignant progression of glioma. *J. Clin. Invest.* 127, 1826–1838. doi: 10.1172/JCI86443

Huberfeld, G., and Vecht, C. J. (2016). Seizures and gliomas–towards a single therapeutic approach. *Nat. Rev. Neurol.* 12, 204–216. doi: 10.1038/nrneurol.2016.26

Hung, A. L., Maxwell, R., Theodros, D., Belcaid, Z., Mathios, D., Luksik, A. S., et al. (2018). TIGIT and PD-1 dual checkpoint blockade enhances antitumor immunity and survival in GBM. *Oncoimmunology* 7:e1466769. doi: 10.1080/2162402X.2018.1466769

Hutter, G., Theruvath, J., Graef, C. M., Zhang, M., Schoen, M. K., Manz, E. M., et al. (2019). Microglia are effector cells of CD47-SIRPalpha antiphagocytic axis disruption against glioblastoma. *Proc. Natl. Acad. Sci. U.S.A.* 116, 997–1006. doi: 10.1073/pnas.1721434116

Jackson, C. M., Choi, J., and Lim, M. (2019). Mechanisms of immunotherapy resistance: lessons from glioblastoma. *Nat. Immunol.* 20, 1100–1109. doi: 10.1038/s41590-019-0433-y

Jacobs, J. F., Idema, A. J., Bol, K. F., Grotenhuis, J. A., de Vries, I. J., Wesseling, P., et al. (2010). Prognostic significance and mechanism of Treg infiltration in human brain tumors. *J. Neuroimmunol.* 225, 195–199. doi: 10.1016/j.jneuroim.2010.05.020

Jais, A., Solas, M., Backes, H., Chaurasia, B., Kleinridders, A., Theurich, S., et al. (2016). Myeloid-cell-derived VEGF maintains brain glucose uptake and limits cognitive impairment in obesity. *Cell* 165, 882–895. doi: 10.1016/j.cell.2016.03.033

Jiang, J., and Dingledine, R. (2013). Role of prostaglandin receptor EP2 in the regulations of cancer cell proliferation, invasion, and inflammation. *J. Pharmacol. Exp. Ther.* 344, 360–367. doi: 10.1124/jpet.112.200444

Jiang, J., Qiu, J., Li, Q., and Shi, Z. (2017). Prostaglandin E2 signaling: alternative target for glioblastoma? *Trends Cancer* 3, 75–78. doi: 10.1016/j.trecan.2016.12.002

Jones, C. L., Stevens, B. M., D'Alessandro, A., Reisz, J. A., Culp-Hill, R., Nemkov, T., et al. (2018). Inhibition of amino acid metabolism selectively targets human leukemia stem cells. *Cancer Cell* 34, 724.e4–740.e4. doi: 10.1016/j.ccell.2018.10.005

Kamran, N., Kadiyala, P., Saxena, M., Candolfi, M., Li, Y., Moreno-Ayala, M. A., et al. (2017). Immunosuppressive myeloid cells' blockade in the glioma microenvironment enhances the efficacy of immune-stimulatory gene therapy. *Mol. Ther.* 25, 232–248. doi: 10.1016/j.ymthe.2016.10.003

Kathagen-Buhmann, A., Maire, C. L., Weller, J., Schulte, A., Matschke, J., Holz, M., et al. (2018). The secreted glycolytic enzyme GPI/AMF stimulates glioblastoma cell migration and invasion in an autocrine fashion but can have anti-proliferative effects. *Neuro Oncol.* 20, 1594–1605. doi: 10.1093/neuonc/noy117

Kathagen-Buhmann, A., Schulte, A., Weller, J., Holz, M., Herold-Mende, C., Glass, R., et al. (2016). Glycolysis and the pentose phosphate pathway are differentially associated with the dichotomous regulation of glioblastoma cell migration versus proliferation. *Neuro Oncol.* 18, 1219–1229. doi: 10.1093/neuonc/now024

Kesarwani, P., Kant, S., Prabhu, A., and Chinnaiyan, P. (2017). The interplay between metabolic remodeling and immune regulation in glioblastoma. *Neuro Oncol.* 19, 1308–1315. doi: 10.1093/neuonc/nox079

Kesarwani, P., Prabhu, A., Kant, S., and Chinnaiyan, P. (2019). Metabolic remodeling contributes towards an immune-suppressive phenotype in glioblastoma. *Cancer Immunol. Immunother.* 68, 1107–1120. doi: 10.1007/s00262-019-02347-3

Kesarwani, P., Prabhu, A., Kant, S., Kumar, P., Graham, S. F., Buelow, K. L., et al. (2018). Tryptophan metabolism contributes to radiation-induced immune checkpoint reactivation in glioblastoma. *Clin. Cancer Res.* 24, 3632–3643. doi: 10.1158/1078-0432.CCR-18-0041

Kim, D., Fiske, B. P., Birsoy, K., Freinkman, E., Kami, K., Possemato, R. L., et al. (2015). SHMT2 drives glioma cell survival in ischaemia but imposes a dependence on glycine clearance. *Nature* 520, 363–367. doi: 10.1038/nature14363

Kim, J., Han, J., Jang, Y., Kim, S. J., Lee, M. J., Ryu, M. J., et al. (2015). High-capacity glycolytic and mitochondrial oxidative metabolisms mediate the growth ability of glioblastoma. *Int. J. Oncol.* 47, 1009–1016. doi: 10.3892/ijo.2015.3101

Kim, S., Jing, K., Shin, S., Jeong, S., Han, S. H., Oh, H., et al. (2018). omega3-polyunsaturated fatty acids induce cell death through apoptosis and autophagy in glioblastoma cells: in vitro and in vivo. *Oncol. Rep.* 39, 239–246. doi: 10.3892/or.2017.6101

Kohanbash, G., Carrera, D. A., Shrivastav, S., Ahn, B. J., Jahan, N., Mazor, T., et al. (2017). Isocitrate dehydrogenase mutations suppress STAT1 and CD8+ T cell accumulation in gliomas. *J. Clin. Invest.* 127, 1425–1437. doi: 10.1172/JCI90644

Kohanbash, G., McKaveney, K., Sakaki, M., Ueda, R., Mintz, A. H., Amankulor, N., et al. (2013). GM-CSF promotes the immunosuppressive activity of glioma-infiltrating myeloid cells through interleukin-4 receptor-alpha. *Cancer Res.* 73, 6413–6423. doi: 10.1158/0008-5472.CAN-12-4124

Komohara, Y., Ohnishi, K., Kuratsu, J., and Takeya, M. (2008). Possible involvement of the M2 anti-inflammatory macrophage phenotype in growth of human gliomas. *J. Pathol.* 216, 15–24. doi: 10.1002/path.2370

Kosaka, A., Ohkuri, T., and Okada, H. (2014). Combination of an agonistic anti-CD40 monoclonal antibody and the COX-2 inhibitor celecoxib induces anti-glioma effects by promotion of type-1 immunity in myeloid cells and T-cells. *Cancer Immunol. Immunother.* 63, 847–857. doi: 10.1007/s00262-014-1561-8

Kuang, R., Jahangiri, A., Mascharak, S., Nguyen, A., Chandra, A., Flanigan, P. M., et al. (2017). GLUT3 upregulation promotes metabolic reprogramming associated with antiangiogenic therapy resistance. *JCI Insight* 2:e88815. doi: 10.1172/jci.insight.88815

Laudati, E., Curro, D., Navarra, P., and Lisi, L. (2017). Blockade of CCR5 receptor prevents M2 microglia phenotype in a microglia-glioma paradigm. *Neurochem. Int.* 108, 100–108. doi: 10.1016/j.neuint.2017.03.002

Lee, J. H., Liu, R., Li, J., Wang, Y., Tan, L., Li, X. J., et al. (2018). EGFR-phosphorylated platelet isoform of phosphofructokinase 1 promotes PI3K activation. *Mol. Cell* 70, 197.e7–210.e7. doi: 10.1016/j.molcel.2018.03.018

Lee, J. H., Liu, R., Li, J., Zhang, C., Wang, Y., Cai, Q., et al. (2017). Stabilization of phosphofructokinase 1 platelet isoform by AKT promotes tumorigenesis. *Nat. Commun.* 8:949. doi: 10.1038/s41467-017-00906-9

Lee, S. Y., Kim, J. K., Jeon, H. Y., Ham, S. W., and Kim, H. (2017). CD133 regulates IL-1beta signaling and neutrophil recruitment in glioblastoma. *Mol. Cells* 40, 515–522. doi: 10.14348/molcells.2017.0089

Li, J., Zhao, J., Tan, T., Liu, M., Zeng, Z., Zeng, Y., et al. (2020). Nanoparticle drug delivery system for glioma and its efficacy improvement strategies: a comprehensive review. *Int. J. Nanomed.* 15, 2563–2582. doi: 10.2147/IJN.S243223

Li, T. F., Li, K., Zhang, Q., Wang, C., Yue, Y., Chen, Z., et al. (2018). Dendritic cell-mediated delivery of doxorubicin-polyglycerol-nanodiamond composites elicits enhanced anti-cancer immune response in glioblastoma. *Biomaterials* 181, 35–52. doi: 10.1016/j.biomaterials.2018.07.035

Liang, J., Piao, Y., Holmes, L., Fuller, G. N., Henry, V., Tiao, N., et al. (2014). Neutrophils promote the malignant glioma phenotype through S100A4. *Clin. Cancer Res.* 20, 187–198. doi: 10.1158/1078-0432.CCR-13-1279

Libby, C. J., Zhang, S., Benavides, G. A., Scott, S. E., Li, Y., Redmann, M., et al. (2018). Identification of compounds that decrease glioblastoma growth and glucose uptake in vitro. *ACS Chem. Biol.* 13, 2048–2057. doi: 10.1021/acschembio.8b00251

Lin, H., Patel, S., Affleck, V. S., Wilson, I., Turnbull, D. M., Joshi, A. R., et al. (2017). Fatty acid oxidation is required for the respiration and proliferation of malignant glioma cells. *Neuro Oncol.* 19, 43–54. doi: 10.1093/neuonc/now128

Liu, B., Huang, Z. B., Chen, X., See, Y. X., Chen, Z. K., and Yao, H. K. (2019). Mammalian target of rapamycin 2 (MTOR2) and C-MYC Modulate Glucosamine-6-phosphate synthesis in glioblastoma (GBM) cells through glutamine: Fructose-6-phosphate aminotransferase 1 (GFAT1). *Cell Mol. Neurobiol.* 39, 415–434. doi: 10.1007/s10571-019-00659-7

Liu, J., Gao, L., Zhan, N., Xu, P., Yang, J. A., Yuan, F. E., et al. (2020). Hypoxia induced ferritin light chain (FTL) promoted epithelia mesenchymal transition and chemoresistance of glioma. *J. Exp. Clin. Cancer Res.* 39:137. doi: 10.1186/s13046-020-01641-8

Liu, J., Guo, S., Li, Q., Yang, L., Xia, Z., Zhang, L., et al. (2013). Phosphoglycerate dehydrogenase induces glioma cells proliferation and invasion by stabilizing forkhead box M1. *J. Neurooncol.* 111, 245–255. doi: 10.1007/s11060-012-1018-x

Liu, M., Zhao, J., Chen, K., Bian, X., Wang, C., Shi, Y., et al. (2012). G protein-coupled receptor FPR1 as a pharmacologic target in inflammation and human glioblastoma. *Int. Immunopharmacol.* 14, 283–288. doi: 10.1016/j.intimp.2012.07.015

Liu, R., Li, W., Tao, B., Wang, X., Yang, Z., Zhang, Y., et al. (2019). Tyrosine phosphorylation activates 6-phosphogluconate dehydrogenase and promotes tumor growth and radiation resistance. *Nat. Commun.* 10:991. doi: 10.1038/s41467-019-08921-8

Long, Y., Tao, H., Karachi, A., Grippin, A. J., Jin, L., Chang, Y. E., et al. (2020). Dysregulation of glutamate transport enhances treg function that promotes VEGF blockade resistance in glioblastoma. *Cancer Res.* 80, 499–509. doi: 10.1158/0008-5472.CAN-19-1577

Lou, N., Takano, T., Pei, Y., Xavier, A. L., Goldman, S. A., and Nedergaard, M. (2016). Purinergic receptor P2RY12-dependent microglial closure of the injured blood-brain barrier. *Proc. Natl. Acad. Sci. U.S.A.* 113, 1074–1079. doi: 10.1073/pnas.1520398113

Maddocks, O. D. K., Athineos, D., Cheung, E. C., Lee, P., Zhang, T., van den Broek, N. J. F., et al. (2017). Modulating the therapeutic response of tumours to dietary serine and glycine starvation. *Nature* 544, 372–376. doi: 10.1038/nature22056

Magana-Maldonado, R., Chavez-Cortez, E. G., Olascoaga-Arellano, N. K., Lopez-Mejia, M., Maldonado-Leal, F. M., Sotelo, J., et al. (2016). Immunological evasion in glioblastoma. *Biomed. Res. Int.* 2016:7487313. doi: 10.1155/2016/7487313

Malo, C. S., Huggins, M. A., Goddery, E. N., Tolcher, H. M. A., Renner, D. N., Jin, F., et al. (2018a). Non-equivalent antigen presenting capabilities of dendritic cells and macrophages in generating brain-infiltrating CD8 (+) T cell responses. *Nat. Commun.* 9:633. doi: 10.1038/s41467-018-03037-x

Malo, C. S., Khadka, R. H., Ayasoufi, K., Jin, F., AbouChehade, J. E., Hansen, M. J., et al. (2018b). Immunomodulation mediated by anti-angiogenic therapy improves CD8 T Cell immunity against experimental glioma. *Front. Oncol.* 8:320. doi: 10.3389/fonc.2018.00320

Marvel, D., and Gabrilovich, D. I. (2015). Myeloid-derived suppressor cells in the tumor microenvironment: expect the unexpected. *J. Clin. Invest.* 125, 3356–3364. doi: 10.1172/JCI80005

Massara, M., Persico, P., Bonavita, O., Mollica Poeta, V., Locati, M., Simonelli, M., et al. (2017). Neutrophils in gliomas. *Front. Immunol.* 8:1349. doi: 10.3389/fimmu.2017.01349

Masui, K., Onizuka, H., Cavenee, W. K., Mischel, P. S., and Shibata, N. (2019). Metabolic reprogramming in the pathogenesis of glioma: update. *Neuropathology* 39, 3–13. doi: 10.1111/neup.12535

Mathios, D., Kim, J. E., Mangraviti, A., Phallen, J., Park, C. K., Jackson, C. M., et al. (2016). Anti-PD-1 antitumor immunity is enhanced by local and abrogated by systemic chemotherapy in GBM. *Sci. Transl. Med.* 8:370ra180. doi: 10.1126/scitranslmed.aag2942

Maurer, G. D., Heller, S., Wanka, C., Rieger, J., and Steinbach, J. P. (2019). Knockdown of the TP53-Induced glycolysis and apoptosis regulator (TIGAR) Sensitizes glioma cells to hypoxia, irradiation and temozolomide. *Int. J. Mol. Sci.* 20:1061. doi: 10.3390/ijms20051061

May, J. L., Kouri, F. M., Hurley, L. A., Liu, J., Tommasini-Ghelfi, S., Ji, Y., et al. (2019). IDH3alpha regulates one-carbon metabolism in glioblastoma. *Sci. Adv.* 5:eaat0456. doi: 10.1126/sciadv.aat0456

Mayers, J. R., Torrence, M. E., Danai, L. V., Papagiannakopoulos, T., Davidson, S. M., Bauer, M. R., et al. (2016). Tissue of origin dictates branched-chain amino acid metabolism in mutant Kras-driven cancers. *Science* 353, 1161–1165. doi: 10.1126/science.aaf5171

Meng, X., Duan, C., Pang, H., Chen, Q., Han, B., Zha, C., et al. (2019). DNA damage repair alterations modulate M2 polarization of microglia to remodel the tumor microenvironment via the p53-mediated MDK expression in glioma. *EBioMedicine* 41, 185–199. doi: 10.1016/j.ebiom.2019.01.067

Mirzaei, R., Sarkar, S., and Yong, V. W. (2017). T cell exhaustion in glioblastoma: intricacies of immune checkpoints. *Trends Immunol.* 38, 104–115. doi: 10.1016/j.it.2016.11.005

Miska, J., Lee-Chang, C., Rashidi, A., Muroski, M. E., Chang, A. L., Lopez-Rosas, A., et al. (2019). HIF-1alpha is a metabolic switch between glycolytic-driven migration and oxidative phosphorylation-driven immunosuppression of tregs in glioblastoma. *Cell Rep.* 27, 226.e4–237.e4. doi: 10.1016/j.celrep.2019.03.029

Mitchell, D. A., Batich, K. A., Gunn, M. D., Huang, M. N., Sanchez-Perez, L., Nair, S. K., et al. (2015). Tetanus toxoid and CCL3 improve dendritic cell vaccines in mice and glioblastoma patients. *Nature* 519, 366–369. doi: 10.1038/nature14320

Morihiro, Y., Yasumoto, Y., Vaidyan, L. K., Sadahiro, H., Uchida, T., Inamura, A., et al. (2013). Fatty acid binding protein 7 as a marker of glioma stem cells. *Pathol. Int.* 63, 546–553. doi: 10.1111/pin.12109

Mostofa, A. G., Punganuru, S. R., Madala, H. R., Al-Obaide, M., and Srivenugopal, K. S. (2017). The process and regulatory components of inflammation in brain oncogenesis. *Biomolecules* 7:34. doi: 10.3390/biom7020034

Nakayama, N., Yamaguchi, S., Sasaki, Y., and Chikuma, T. (2016). Hydrogen peroxide-induced oxidative stress activates proteasomal trypsin-like activity in Human U373 glioma cells. *J. Mol. Neurosci.* 58, 297–305. doi: 10.1007/s12031-015-0680-9

Oh, E. T., Kim, C. W., Kim, H. G., Lee, J. S., and Park, H. J. (2017). Brusatol-mediated inhibition of c-Myc Increases HIF-1alpha degradation and causes cell death in colorectal cancer under hypoxia. *Theranostics* 7, 3415–3431. doi: 10.7150/thno.20861

Osuka, S., and Van Meir, E. G. (2017). Cancer therapy: neutrophils traffic in cancer nanodrugs. *Nat. Nanotechnol.* 12, 616–618. doi: 10.1038/nnano.2017.82

Otvos, B., Silver, D. J., Mulkearns-Hubert, E. E., Alvarado, A. G., Turaga, S. M., Sorensen, M. D., et al. (2016). Cancer stem cell-secreted macrophage migration inhibitory factor stimulates myeloid derived suppressor cell function and facilitates glioblastoma immune evasion. *Stem Cells* 34, 2026–2039. doi: 10.1002/stem.2393

Pandey, R., Caflisch, L., Lodi, A., Brenner, A. J., and Tiziani, S. (2017). Metabolomic signature of brain cancer. *Mol. Carcinog.* 56, 2355–2371. doi: 10.1002/mc.22694

Panosyan, E. H., Lin, H. J., Koster, J., and Lasky, J. L. III (2017). In search of druggable targets for GBM amino acid metabolism. *BMC Cancer* 17:162. doi: 10.1186/s12885-017-3148-1

Payen, V. L., Porporato, P. E., Baselet, B., and Sonveaux, P. (2016). Metabolic changes associated with tumor metastasis, part 1: tumor pH, glycolysis and the pentose phosphate pathway. *Cell Mol. Life Sci.* 73, 1333–1348. doi: 10.1007/s00018-015-2098-5

Pereira, M. B., Barros, L. R. C., Bracco, P. A., Vigo, A., Boroni, M., Bonamino, M. H., et al. (2018). Transcriptional characterization of immunological infiltrates and their relation with glioblastoma patients overall survival. *Oncoimmunology* 7:e1431083. doi: 10.1080/2162402X.2018.1431083

Petovari, G., Hujber, Z., Krencz, I., Danko, T., Nagy, N., Toth, F., et al. (2018). Targeting cellular metabolism using rapamycin and/or doxycycline enhances anti-tumour effects in human glioma cells. *Cancer Cell Int.* 18:211. doi: 10.1186/s12935-018-0710-0

Poff, A., Koutnik, A. P., Egan, K. M., Sahebjam, S., D'Agostino, D., and Kumar, N. B. (2019). Targeting the Warburg effect for cancer treatment: ketogenic diets for management of glioma. *Semin. Cancer Biol.* 56, 135–148. doi: 10.1016/j.semcancer.2017.12.011

Poon, C. C., Sarkar, S., Yong, V. W., and Kelly, J. J. P. (2017). Glioblastoma-associated microglia and macrophages: targets for therapies to improve prognosis. *Brain* 140, 1548–1560. doi: 10.1093/brain/aww355

Priore, P., Gnoni, A., Natali, F., Testini, M., Gnoni, G. V., Siculella, L., et al. (2017). Oleic acid and hydroxytyrosol inhibit cholesterol and fatty acid synthesis in C6 Glioma cells. *Oxid. Med. Cell Longev.* 2017:9076052. doi: 10.1155/2017/9076052

Pyonteck, S. M., Akkari, L., Schuhmacher, A. J., Bowman, R. L., Sevenich, L., Quail, D. F., et al. (2013). CSF-1R inhibition alters macrophage polarization and blocks glioma progression. *Nat. Med.* 19, 1264–1272. doi: 10.1038/nm.3337

Qian, J., Wang, C., Wang, B., Yang, J., Wang, Y., Luo, F., et al. (2018). The IFN-gamma/PD-L1 axis between T cells and tumor microenvironment: hints for glioma anti-PD-1/PD-L1 therapy. *J. Neuroinflammation* 15:290. doi: 10.1186/s12974-018-1330-2

Qiu, J., Li, Q., Bell, K. A., Yao, X., Du, Y., Zhang, E., et al. (2019). Small-molecule inhibition of prostaglandin E receptor 2 impairs cyclooxygenase-associated malignant glioma growth. *Br. J. Pharmacol.* 176, 1680–1699. doi: 10.1111/bph.14622

Qiu, R., Zhou, L., Ma, Y., Zhou, L., Liang, T., Shi, L., et al. (2020). Regulatory T Cell plasticity and stability and autoimmune diseases. *Clin. Rev. Allergy Immunol.* 58, 52–70. doi: 10.1007/s12016-018-8721-0

Quail, D. F., and Joyce, J. A. (2017). The microenvironmental landscape of brain tumors. *Cancer Cell* 31, 326–341. doi: 10.1016/j.ccell.2017.02.009

Ran, C., Liu, H., Hitoshi, Y., and Israel, M. A. (2013). Proliferation-independent control of tumor glycolysis by PDGFR-mediated AKT activation. *Cancer Res.* 73, 1831–1843. doi: 10.1158/0008-5472.CAN-12-2460

Rashidi, A., Miska, J., Lee-Chang, C., Kanojia, D., Panek, W. K., Lopez-Rosas, A., et al. (2020). GCN2 is essential for CD8(+) T cell survival and function in murine models of malignant glioma. *Cancer Immunol. Immunother.* 69, 81–94. doi: 10.1007/s00262-019-02441-6

Ren, F., Zhao, Q., Huang, L., Zheng, Y., Li, L., He, Q., et al. (2019). The R132H mutation in IDH1 promotes the recruitment of NK cells through CX3CL1/CX3CR1 chemotaxis and is correlated with a better prognosis in gliomas. *Immunol. Cell Biol.* 97, 457–469. doi: 10.1111/imcb.12225

Roesch, S., Rapp, C., Dettling, S., and Herold-Mende, C. (2018). When immune cells turn bad-tumor-associated microglia/macrophages in glioma. *Int. J. Mol. Sci.* 19:436. doi: 10.3390/ijms19020436

Rolle, C. E., Sengupta, S., and Lesniak, M. S. (2012). Mechanisms of immune evasion by gliomas. *Adv. Exp. Med. Biol.* 746, 53–76. doi: 10.1007/978-1-4614-3146-6_5

Sahm, F., Oezen, I., Opitz, C. A., Radlwimmer, B., von Deimling, A., Ahrendt, T., et al. (2013). The endogenous tryptophan metabolite and NAD+ precursor quinolinic acid confers resistance of gliomas to oxidative stress. *Cancer Res.* 73, 3225–3234. doi: 10.1158/0008-5472.CAN-12-3831

Sankowski, R., Bottcher, C., Masuda, T., Geirsdottir, L., Sagar, Sindram, E., et al. (2019). Mapping microglia states in the human brain through the integration of high-dimensional techniques. *Nat. Neurosci.* 22, 2098–2110. doi: 10.1038/s41593-019-0532-y

Sayour, E. J., McLendon, P., McLendon, R., De Leon, G., Reynolds, R., Kresak, J., et al. (2015). Increased proportion of FoxP3+ regulatory T cells in tumor infiltrating lymphocytes is associated with tumor recurrence and reduced survival in patients with glioblastoma. *Cancer Immunol. Immunother.* 64, 419–427. doi: 10.1007/s00262-014-1651-7

See, A. P., Parker, J. J., and Waziri, A. (2015). The role of regulatory T cells and microglia in glioblastoma-associated immunosuppression. *J. Neurooncol.* 123, 405–412. doi: 10.1007/s11060-015-1849-3

Seliger, C., and Hau, P. (2018). Drug repurposing of metabolic agents in malignant glioma. *Int. J. Mol. Sci.* 19:2768. doi: 10.3390/ijms19092768

Shao, S., Risch, E., Burner, D., Lu, L., Minev, B., and Ma, W. (2017). IFNgamma enhances cytotoxic efficiency of the cytotoxic T lymphocytes against human glioma cells. *Int. Immunopharmacol.* 47, 159–165. doi: 10.1016/j.intimp.2017.04.003

Sheng, Y., Jiang, Q., Dong, X., Liu, J., Liu, L., Wang, H., et al. (2020). 3-Bromopyruvate inhibits the malignant phenotype of malignantly transformed macrophages and dendritic cells induced by glioma stem cells in the glioma microenvironment via miR-449a/MCT1. *Biomed. Pharmacother.* 121:109610. doi: 10.1016/j.biopha.2019.109610

Shibao, S., Minami, N., Koike, N., Fukui, N., Yoshida, K., Saya, H., et al. (2018). Metabolic heterogeneity and plasticity of glioma stem cells in a mouse glioblastoma model. *Neuro Oncol.* 20, 343–354. doi: 10.1093/neuonc/nox170

Silva, L. S., Poschet, G., Nonnenmacher, Y., Becker, H. M., Sapcariu, S., Gaupel, A. C., et al. (2017). Branched-chain ketoacids secreted by glioblastoma cells via MCT1 modulate macrophage phenotype. *EMBO Rep.* 18, 2172–2185. doi: 10.15252/embr.201744154

Slawinska-Brych, A., Zdzisinska, B., and Kandefer-Szerszen, M. (2014). Fluvastatin inhibits growth and alters the malignant phenotype of the C6 glioma cell line. *Pharmacol. Rep.* 66, 121–129. doi: 10.1016/j.pharep.2014.01.002

Sorensen, M. D., Dahlrot, R. H., Boldt, H. B., Hansen, S., and Kristensen, B. W. (2018). Tumour-associated microglia/macrophages predict poor prognosis in high-grade gliomas and correlate with an aggressive tumour subtype. *Neuropathol. Appl. Neurobiol.* 44, 185–206. doi: 10.1111/nan.12428

Spiegel, A., Brooks, M. W., Houshyar, S., Reinhardt, F., Ardolino, M., Fessler, E., et al. (2016). Neutrophils suppress intraluminal NK cell-mediated tumor cell clearance and enhance extravasation of disseminated carcinoma cells. *Cancer Discov.* 6, 630–649. doi: 10.1158/2159-8290.CD-15-1157

Strickland, M., and Stoll, E. A. (2017). Metabolic reprogramming in glioma. *Front. Cell Dev. Biol.* 5:43. doi: 10.3389/fcell.2017.00043

Su, C., Li, H., and Gao, W. (2018). GLUT5 increases fructose utilization and promotes tumor progression in glioma. *Biochem. Biophys. Res. Commun.* 500, 462–469. doi: 10.1016/j.bbrc.2018.04.103

Sun, P., Xia, S., Lal, B., Shi, X., Yang, K. S., Watkins, P. A., et al. (2014). Lipid metabolism enzyme ACSVL3 supports glioblastoma stem cell maintenance and tumorigenicity. *BMC Cancer* 14:401. doi: 10.1186/1471-2407-14-401

Takenaka, M. C., Gabriely, G., Rothhammer, V., Mascanfroni, I. D., Wheeler, M. A., Chao, C. C., et al. (2019). Control of tumor-associated macrophages and T cells in glioblastoma via AHR and CD39. *Nat. Neurosci.* 22, 729–740. doi: 10.1038/s41593-019-0370-y

Talasila, K. M., Røsland, G. V., Hagland, H. R., Eskilsson, E., Flønes, I. H., Fritah, S., et al. (2017). The angiogenic switch leads to a metabolic shift in human glioblastoma. *Neuro Oncol.* 19, 383–393. doi: 10.1093/neuonc/now175

Tardito, S., Oudin, A., Ahmed, S. U., Fack, F., Keunen, O., Zheng, L., et al. (2015). Glutamine synthetase activity fuels nucleotide biosynthesis and supports growth of glutamine-restricted glioblastoma. *Nat. Cell Biol.* 17, 1556–1568. doi: 10.1038/ncb3272

Thiepold, A. L., Lorenz, N. I., Foltyn, M., Engel, A. L., Dive, I., Urban, H., et al. (2017). Mammalian target of rapamycin complex 1 activation sensitizes human glioma cells to hypoxia-induced cell death. *Brain* 140, 2623–2638. doi: 10.1093/brain/awx196

Thomas, T. M., and Yu, J. S. (2017). Metabolic regulation of glioma stem-like cells in the tumor micro-environment. *Cancer Lett.* 408, 174–181. doi: 10.1016/j.canlet.2017.07.014

Touat, M., Idbaih, A., Sanson, M., and Ligon, K. L. (2017). Glioblastoma targeted therapy: updated approaches from recent biological insights. *Ann. Oncol.* 28, 1457–1472. doi: 10.1093/annonc/mdx106

Turubanova, V. D., Balalaeva, I. V., Mishchenko, T. A., Catanzaro, E., Alzeibak, R., Peskova, N. N., et al. (2019). Immunogenic cell death induced by a new photodynamic therapy based on photosens and photodithazine. *J. Immunother. Cancer* 7:350. doi: 10.1186/s40425-019-0826-3

Vakilian, A., Khorramdelazad, H., Heidari, P., Sheikh Rezaei, Z., and Hassanshahi, G. (2017). CCL2/CCR2 signaling pathway in glioblastoma multiforme. *Neurochem. Int.* 103, 1–7. doi: 10.1016/j.neuint.2016.12.013

van Tellingen, O., Yetkin-Arik, B., de Gooijer, M. C., Wesseling, P., Wurdinger, T., and de Vries, H. E. (2015). Overcoming the blood-brain tumor barrier for effective glioblastoma treatment. *Drug Resist. Updates* 19, 1–12. doi: 10.1016/j.drup.2015.02.002

Venneti, S., Dunphy, M. P., Zhang, H., Pitter, K. L., Zanzonico, P., Campos, C., et al. (2015). Glutamine-based PET imaging facilitates enhanced metabolic evaluation of gliomas in vivo. *Sci. Transl. Med.* 7:274ra217. doi: 10.1126/scitranslmed.aaa1009

Venneti, S., and Thompson, C. B. (2017). Metabolic reprogramming in brain tumors. *Annu. Rev. Pathol.* 12, 515–545. doi: 10.1146/annurev-pathol-012615-044329

Venza, I., Visalli, M., Fortunato, C., Ruggeri, M., Ratone, S., Caffo, M., et al. (2012). PGE2 induces interleukin-8 derepression in human astrocytoma through coordinated DNA demethylation and histone hyperacetylation. *Epigenetics* 7, 1315–1330. doi: 10.4161/epi.22446

Venza, M., Visalli, M., Alafaci, C., Caffo, M., Caruso, G., Salpietro, F. M., et al. (2011). Interleukin-8 overexpression in astrocytomas is induced by prostaglandin E2 and is associated with the transcription factors CCAAT/enhancer-binding protein-beta and CCAAT/enhancer-binding homologous protein. *Neurosurgery* 69, 713–721. doi: 10.1227/NEU.0b013e31821954c6 discussion 721,

Villa, G. R., Hulce, J. J., Zanca, C., Bi, J., Ikegami, S., Cahill, G. L., et al. (2016). An LXR-Cholesterol axis creates a metabolic Co-Dependency for Brain Cancers. *Cancer Cell* 30, 683–693. doi: 10.1016/j.ccell.2016.09.008

Wainwright, D. A., Chang, A. L., Dey, M., Balyasnikova, I. V., Kim, C. K., Tobias, A., et al. (2014). Durable therapeutic efficacy utilizing combinatorial blockade against IDO, CTLA-4, and PD-L1 in mice with brain tumors. *Clin. Cancer Res.* 20, 5290–5301. doi: 10.1158/1078-0432.CCR-14-0514

Waitkus, M. S., Diplas, B. H., and Yan, H. (2016). Isocitrate dehydrogenase mutations in gliomas. *Neuro Oncol.* 18, 16–26. doi: 10.1093/neuonc/nov136

Wang, C., Chen, Y., Wang, Y., Liu, X., Liu, Y., Li, Y., et al. (2019). Inhibition of COX-2, mPGES-1 and CYP4A by isoliquiritigenin blocks the angiogenic Akt signaling in glioma through ceRNA effect of miR-194-5p and lncRNA NEAT1. *J. Exp. Clin. Cancer Res.* 38:371. doi: 10.1186/s13046-019-1361-2

Wang, C., Li, Y., Chen, H., Zhang, J., Zhang, J., Qin, T., et al. (2017). Inhibition of CYP4A by a novel flavonoid FLA-16 prolongs survival and normalizes tumor vasculature in glioma. *Cancer Lett.* 402, 131–141. doi: 10.1016/j.canlet.2017.05.030

Wang, G., Sai, K., Gong, F., Yang, Q., Chen, F., and Lin, J. (2014). Mutation of isocitrate dehydrogenase 1 induces glioma cell proliferation via nuclear factor-kappaB activation in a hypoxia-inducible factor 1-alpha dependent manner. *Mol. Med. Rep.* 9, 1799–1805. doi: 10.3892/mmr.2014.2052

Wang, G., Wang, J. J., Fu, X. L., Guang, R., and To, S. T. (2017). Advances in the targeting of HIF-1alpha and future therapeutic strategies for glioblastoma multiforme (Review). *Oncol. Rep.* 37, 657–670. doi: 10.3892/or.2016.5309

Wang, J., Xu, S. L., Duan, J. J., Yi, L., Guo, Y. F., Shi, Y., et al. (2019). Invasion of white matter tracts by glioma stem cells is regulated by a NOTCH1-SOX2 positive-feedback loop. *Nat. Neurosci.* 22, 91–105. doi: 10.1038/s41593-018-0285-z

Wang, Q., Hu, B., Hu, X., Kim, H., Squatrito, M., Scarpace, L., et al. (2017). Tumor evolution of glioma-intrinsic gene expression subtypes associates with immunological changes in the microenvironment. *Cancer Cell* 32, 42.e6–56.e6. doi: 10.1016/j.ccell.2017.06.003

Wang, W., Xiao, Z. D., Li, X., Aziz, K. E., Gan, B., Johnson, R. L., et al. (2015). AMPK modulates Hippo pathway activity to regulate energy homeostasis. *Nat. Cell Biol.* 17, 490–499. doi: 10.1038/ncb3113

Wang, X., Huang, Z., Wu, Q., Prager, B. C., Mack, S. C., Yang, K., et al. (2017). MYC-Regulated mevalonate metabolism maintains brain tumor-initiating cells. *Cancer Res.* 77, 4947–4960. doi: 10.1158/0008-5472.CAN-17-0114

Wang, X., Liu, R., Qu, X., Yu, H., Chu, H., Zhang, Y., et al. (2019). alpha-ketoglutarate-activated NF-kappaB signaling promotes compensatory glucose uptake and brain tumor development. *Mol. Cell* 76, 148.e7–162.e7. doi: 10.1016/j.molcel.2019.07.007

Wang, Z., Ding, Y., Wang, X., Lu, S., Wang, C., He, C., et al. (2018). Pseudolaric acid B triggers ferroptosis in glioma cells via activation of Nox4 and inhibition of xCT. *Cancer Lett.* 428, 21–33. doi: 10.1016/j.canlet.2018.04.021

Weller, M., Roth, P., Preusser, M., Wick, W., Reardon, D. A., Platten, M., et al. (2017). Vaccine-based immunotherapeutic approaches to gliomas and beyond. *Nat. Rev. Neurol.* 13, 363–374. doi: 10.1038/nrneurol.2017.64

Wilk, A., Wyczechowska, D., Zapata, A., Dean, M., Mullinax, J., Marrero, L., et al. (2015). Molecular mechanisms of fenofibrate-induced metabolic catastrophe and glioblastoma cell death. *Mol. Cell Biol.* 35, 182–198. doi: 10.1128/MCB.00562-14

Winter, S. F., Loebel, F., and Dietrich, J. (2017). Role of ketogenic metabolic therapy in malignant glioma: a systematic review. *Crit. Rev. Oncol. Hematol.* 112, 41–58. doi: 10.1016/j.critrevonc.2017.02.016

Wolf, A., Agnihotri, S., Micallef, J., Mukherjee, J., Sabha, N., Cairns, R., et al. (2011). Hexokinase 2 is a key mediator of aerobic glycolysis and promotes tumor growth in human glioblastoma multiforme. *J. Exp. Med.* 208, 313–326. doi: 10.1084/jem.20101470

Wu, F., Zhao, Z., Chai, R. C., Liu, Y. Q., Li, G. Z., Jiang, H. Y., et al. (2019). Prognostic power of a lipid metabolism gene panel for diffuse gliomas. *J. Cell Mol. Med.* 23, 7741–7748. doi: 10.1111/jcmm.14647

Wu, M., Zhang, H., Tie, C., Yan, C., Deng, Z., Wan, Q., et al. (2018). MR imaging tracking of inflammation-activatable engineered neutrophils for targeted therapy of surgically treated glioma. *Nat. Commun.* 9:4777. doi: 10.1038/s41467-018-07250-6

Wu, T., and Dai, Y. (2017). Tumor microenvironment and therapeutic response. *Cancer Lett.* 387, 61–68. doi: 10.1016/j.canlet.2016.01.043

Wu, Z. B., Qiu, C., Zhang, A. L., Cai, L., Lin, S. J., Yao, Y., et al. (2014). Glioma-associated antigen HEATR1 induces functional cytotoxic T lymphocytes in patients with glioma. *J. Immunol. Res.* 2014:131494. doi: 10.1155/2014/131494

Wypych, D., and Baranska, J. (2020). Cross-talk in nucleotide signaling in glioma C6 Cells. *Adv. Exp. Med. Biol.* 1202, 35–65. doi: 10.1007/978-3-030-30651-9_3

Xu, C. F., Liu, Y., Shen, S., Zhu, Y. H., and Wang, J. (2015). Targeting glucose uptake with siRNA-based nanomedicine for cancer therapy. *Biomaterials* 51, 1–11. doi: 10.1016/j.biomaterials.2015.01.068

Xu, T., Zhang, K., Shi, J., Huang, B., Wang, X., Qian, K., et al. (2019). MicroRNA-940 inhibits glioma progression by blocking mitochondrial folate metabolism through targeting of MTHFD2. *Am. J. Cancer Res.* 9, 250–269.

Xue, J., Zhao, Z., Zhang, L., Xue, L., Shen, S., Wen, Y., et al. (2017). Neutrophil-mediated anticancer drug delivery for suppression of postoperative malignant glioma recurrence. *Nat. Nanotechnol.* 12, 692–700. doi: 10.1038/nnano.2017.54

Yang, F., Zhang, H., Mei, Y., and Wu, M. (2014). Reciprocal regulation of HIF-1alpha and lincRNA-p21 modulates the Warburg effect. *Mol. Cell* 53, 88–100. doi: 10.1016/j.molcel.2013.11.004

Yang, L., and Lin, P. C. (2017). Mechanisms that drive inflammatory tumor microenvironment, tumor heterogeneity, and metastatic progression. *Semin. Cancer Biol.* 47, 185–195. doi: 10.1016/j.semcancer.2017.08.001

Ye, L. F., Chaudhary, K. R., Zandkarimi, F., Harken, A. D., Kinslow, C. J., Upadhyayula, P. S., et al. (2020). Radiation-induced lipid peroxidation triggers ferroptosis and synergizes with ferroptosis inducers. *ACS Chem. Biol.* 15, 469–484. doi: 10.1021/acschembio.9b00939

Zhai, L., Ladomersky, E., Lenzen, A., Nguyen, B., Patel, R., Lauing, K. L., et al. (2018). IDO1 in cancer: a gemini of immune checkpoints. *Cell Mol. Immunol.* 15, 447–457. doi: 10.1038/cmi.2017.143

Zhang, C., Cheng, W., Ren, X., Wang, Z., Liu, X., Li, G., et al. (2017). Tumor purity as an underlying key factor in glioma. *Clin. Cancer Res.* 23, 6279–6291. doi: 10.1158/1078-0432.CCR-16-2598

Zhang, Y., Yu, G., Chu, H., Wang, X., Xiong, L., Cai, G., et al. (2018). Macrophage-associated PGK1 phosphorylation promotes aerobic glycolysis and tumorigenesis. *Mol. Cell* 71, 201.e7–215.e7. doi: 10.1016/j.molcel.2018.06.023

Zheng, C., Yang, K., Zhang, M., Zou, M., Bai, E., Ma, Q., et al. (2016). Specific protein 1 depletion attenuates glucose uptake and proliferation of human glioma cells by regulating GLUT3 expression. *Oncol. Lett.* 12, 125–131. doi: 10.3892/ol.2016.4599

Zhou, Y., Jin, G., Mi, R., Zhang, J., Zhang, J., Xu, H., et al. (2016). Inhibition of fatty acid synthase suppresses neovascularization via regulating the expression of VEGF-A in glioma. *J. Cancer Res. Clin. Oncol.* 142, 2447–2459. doi: 10.1007/s00432-016-2249-6

Zhu, C., Zou, C., Guan, G., Guo, Q., Yan, Z., Liu, T., et al. (2019). Development and validation of an interferon signature predicting prognosis and treatment response for glioblastoma. *Oncoimmunology* 8:e1621677. doi: 10.1080/2162402X.2019.1621677

Conflict of Interest: The authors declare that the research was conducted in the absence of any commercial or financial relationships that could be construed as a potential conflict of interest.

frontiers in Cell and Developmental Biology

ORIGINAL RESEARCH
published: 23 June 2021
doi: 10.3389/fcell.2021.682261

Immunity-Related Gene Signature Identifies Subtypes Benefitting From Adjuvant Chemotherapy or Potentially Responding to PD1/PD-L1 Blockage in Pancreatic Cancer

Hao Qian[1,2†], Hongzhe Li[1,2†], Junjie Xie[1,2†], Xiongxiong Lu[1,2], Fanlu Li[1,2], Weishen Wang[1,2], Xiaomei Tang[1,2], Minmin Shi[1,2], Linxi Jiang[1,2], Hongwei Li[1,2], Hao Chen[1,2], Chenghong Peng[1,2], Zhiwei Xu[1,2], Xiaxing Deng[1,2]* and Baiyong Shen[1,2,3,4]**

[1] Department of General Surgery, Pancreatic Disease Center, Ruijin Hospital, Shanghai Jiao Tong University School of Medicine, Shanghai, China, [2] Research Institute of Pancreatic Diseases, Shanghai Jiao Tong University School of Medicine, Shanghai, China, [3] State Key Laboratory of Oncogenes and Related Genes, Shanghai, China, [4] Institute of Translational Medicine, Shanghai Jiao Tong University, Shanghai, China

Tumor microenvironment comprises of a variety of cell types, which is quite complex and involved in chemotherapy and immune checkpoint blockage resistance. In order to explore the mechanisms involved in tumor immune microenvironment in pancreatic ductal adenocarcinoma (PDAC), we first constructed an immunity-related 18-gene signature using The Cancer Genome Atlas (TCGA) PDAC project data. Then we applied the 18-gene signature to divide PDAC patients into low score and high score groups. Patients in high score group showed inferior prognosis, which was validated in another four independent cohorts, including Ruijin cohort. High score group showed significant enrichment of pathways involved in cell division and cell cycle especially in G1/S phase transition. In high score group, IHC analysis revealed higher levels of the proliferative indexes of Ki67 and PCNA than that in low score group. Prognostic analysis confirmed that patients in high score group could benefit from the gemcitabine-based adjuvant chemotherapy. In low score group, the programmed cell death 1 ligand 1(PD-L1) (+) cases showed worse prognosis but higher T cell infiltration than PD-L1(−) cases. Our immunity-related 18-gene signature could effectively predict PDAC prognosis, and it might be a practical predictive tool to identify PDAC subtype benefitting from gemcitabine-based adjuvant chemotherapy or potentially responding to PD1/PD-L1 blockade therapy.

Keywords: gene signature, immunity, pancreatic cancer, pancreatic ductal adenocarcinoma, prognosis

OPEN ACCESS

Edited by:
Na Luo,
Nankai University, China

Reviewed by:
Feng Gao,
The Sixth Affiliated Hospital of Sun Yat-sen University, China
Tao Peng,
Guangxi Medical University, China

***Correspondence:**
Baiyong Shen
shenby@shsmu.edu.cn
Xiaxing Deng
kejiadxx@hotmail.com
Zhiwei Xu
xzw10800@163.com

† These authors have contributed equally to this work

Specialty section:
This article was submitted to Molecular Medicine, a section of the journal Frontiers in Cell and Developmental Biology

Received: *18 March 2021*
Accepted: *26 May 2021*
Published: *23 June 2021*

Citation:
Qian H, Li H, Xie J, Lu X, Li F, Wang W, Tang X, Shi M, Jiang L, Li H, Chen H, Peng C, Xu Z, Deng X and Shen B (2021) Immunity-Related Gene Signature Identifies Subtypes Benefitting From Adjuvant Chemotherapy or Potentially Responding to PD1/PD-L1 Blockage in Pancreatic Cancer. Front. Cell Dev. Biol. 9:682261. doi: 10.3389/fcell.2021.682261

INTRODUCTION

Pancreatic cancer is a fatal malignancy with extremely poor prognosis (Sodir et al., 2020), accounting for an estimated 57,600 new cases and 47,050 deaths annually (Siegel et al., 2020). Owing to its anatomical and pathological features, pancreatic cancer occurs occultly and grows rapidly. Most patients have lost their chance of surgery when diagnosed (Strobel et al., 2019). Although significant improvement has been achieved in pancreatic cancer treatment, the 5-year survival rate of pancreatic ductal adenocarcinoma (PDAC) is still rather low (Zhu et al., 2018).

Immunity is the essential component of the tumor microenvironment, which plays a pivotal role in tumor initiation, progression, and metastasis (Qian and Pollard, 2010; Berraondo et al., 2016; Keren et al., 2018). Each immune subtype harbors different functions and can be used to predict the states of tumors (Mollaoglu et al., 2018). In the previous study, researchers showed that interfering with immune conditions by targeting specific molecules could suppress tumor progression and improve the effectiveness of chemotherapy (Galluzzi et al., 2015). Among the specific molecules, those mainly expressed on the cell membrane could maintain self-tolerance and modulate immune responses by triggering immunosuppressive signaling pathways, defining them as immune checkpoints (Wykes and Lewin, 2018). Novel therapy targeting immune checkpoints, such as programmed cell death 1 (PD1)/programmed cell death 1 ligand 1 (PD-L1), cytotoxic T-lymphocyte associated protein 4 (CTLA4) and T-cell membrane protein 3 (TIM3) have made breakthrough in many types of cancer treatment (Sharma and Allison, 2015; Topalian et al., 2016). However, only a fraction of patients could acquire significant effect from immune checkpoint blockade (Zappasodi et al., 2018). PDAC patients responding little to immune checkpoints blockade may be due to the insensitive immune microenvironment (Zhao et al., 2019). In a phase II trial, the advanced PDACs could not benefit from anti-CTLA4 (Ipilimumab) treatment (Royal et al., 2010). In addition, anti-PD-L1 immunotherapy also showed limited effects in PDAC in a phase I trial (Brahmer et al., 2012). Many studies have revealed some factors involved in the sensitivity of immune checkpoint blockade, such as the expression of targeted molecules, microsatellite instability, mutation load, and immune infiltration (Catalano et al., 2019; Mandal et al., 2019). For example, the tumors with CD3(+) and CD8(+) T cell infiltration were sensitive to anti-PD-L1 and anti-CTLA4 immunotherapy (Foy et al., 2017; Wu et al., 2018). Thus, exploring the tumor immune microenvironment could help us make the personalized treatment of immune checkpoint blockade in PDAC.

The method of combining immunity-related genes with clinical characteristics has been applied to predict prognosis, recurrence and response to therapy in multiple cancers (Wu et al., 2018). In a previous study, researchers constructed a stromal immunotype to predict patients' overall survival (OS) and diseases free survival (DFS) in bladder cancer (Foy et al., 2017). In gastric cancer, a least absolute shrinkage and selection operator (LASSO) Cox regression model was established to predict patients' prognosis and identify the subgroup suitable for adjuvant chemotherapy (Cheadle et al., 2003). These studies revealed the detailed mechanisms of the tumor immune microenvironment and provided significant indications for clinical therapy.

In the present study, we aimed to develop an immunity-related gene signature based on LASSO Cox regression to predict patients' outcomes using data from TCGA, which was further validated in another four independent cohorts from the International Cancer Genome Consortium (ICGC), the Gene Expression Omnibus (GEO), and Ruijin cohort. Furthermore, the signature could be used to identify PDAC subtype benefitting from gemcitabine-based adjuvant chemotherapy or possibly responding to anti-PD1/PD-L1 immunotherapy.

MATERIALS AND METHODS

PDAC Datasets Extraction and Data Processing

Raw count data and corresponding clinical characteristics of 173 patients with PDAC were downloaded from the TCGA database[1]. ICGC CA (Canada) raw RNA sequencing dataset and corresponding clinical characteristics of 115 patients, and the ICGC AU (Australia) gene expression microarray dataset and corresponding clinical characteristics of 68 patients were downloaded from the ICGC database[2]. The GEO dataset GSE57495 and corresponding clinical characteristics of 63 patients were downloaded from GEO database[3]. RNA-sequencing data was normalized by transcript per million (TPM), and gene expression was calculated as log2 (TPM + 1). For the gene expression microarray, if one gene was detected using multiple probes, the probe with the maximum average used. Then, gene expression values were normalized by log2 transformation. To remove the batch effects of different platform in this study, the expression values of each gene were z-score transformed.

Identification of Immunity-Associated Genes

By interrogating the ImmPort database[4], we obtained a total of 1,811 immunity-related genes. After matching with genes in the TCGA database, 1,308 immunity-related genes were used for further analysis.

Patients

A total of 101 fresh frozen primary PDAC samples were utilized as the validation cohort (Ruijin cohort), which were collected consecutively at Ruijin Hospital from April 2012 to November 2014. The inclusion and exclusion criteria were as follows: (1) Pathologically diagnosed as having pancreatic ductal adenocarcinoma (PDAC) without any other types of pancreatic cancer; (2) without other

[1]https://cancergenome.nih.gov/

[2]https://icgc.org/

[3]https://www.ncbi.nlm.nih.gov/geo/

[4]https://www.immport.org/home

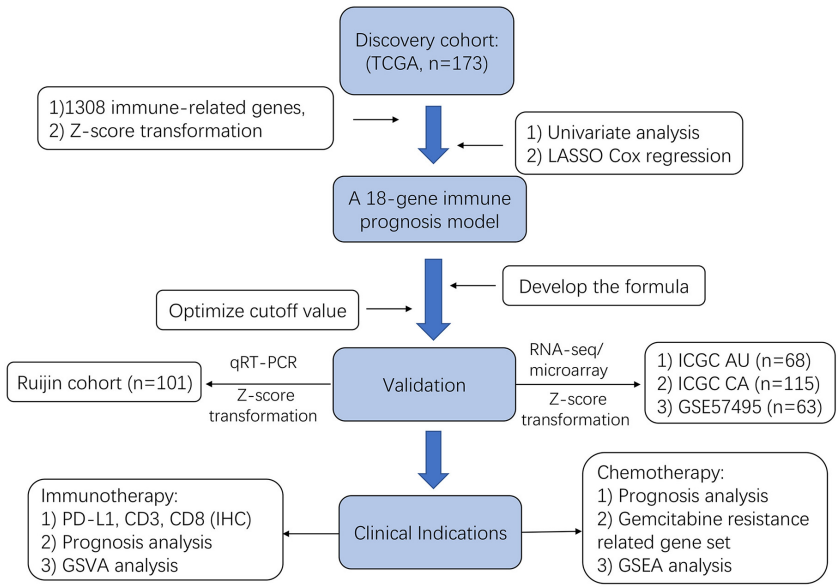

FIGURE 1 | Flowchart presenting the process of construction of immunity-related 18-gene signature, validation and clinical significance relevance in this study.

TABLE 1 | The association of the immune signature with clinicopathological characteristics in TCGA database.

Features	Total	Score level		*p-value*
		High	Low	
Gender				0.4997
Male	94	63	31	
Female	78	56	22	
Age				0.1493
≤60	58	36	22	
>60	114	83	31	
T				0.0078*
T1 + T2	30	15	15	
T3 + T4	141	105	36	
N				0.0121*
N0	48	27	21	
N1	120	91	29	
M				0.5745
M0	76	55	21	
M1	4	2	2	
TNM stage				0.0018*
I	20	8	12	
II + III + IV	150	111	39	
Histologic Grade				0.0469*
G1	29	14	15	
G2	93	67	26	
G3	48	36	12	
G4	2	2	0	

*$P < 0.05$.

malignant cancers; and (3) did not receive any preoperative adjuvant therapy. The clinicopathological variables are listed in **Supplementary Table 2**. All patients provide signed informed consent. The study was approved by the Ethical Committee of Ruijin Hospital, Shanghai Jiao Tong University School of Medicine, Shanghai, China.

RNA Extraction and Quantitative Real-Time Reverse Transcription PCR (qRT-PCR)

Total RNA from 101 PDAC samples (Ruijin cohort) was extracted using the TRIzol reagent (Invitrogen, Waltham, MA, United States) according to the manufacture's protocol. Reverse-transcription PCR was performed using a Reverse Transcription kit (TOYOBO, Osaka, Japan). Quantitative real-time PCR was carried out in 10 μl reaction mixtures with an HT 7900 machine (Applied Biosystems, Foster City, CA, United States) using SYBR™ Select Master Mix (Applied Biosystem). The gene primers were designed and synthesized by Sangon Biotech (Shanghai, China), and are listed in **Supplementary Table 3**. *GAPDH* (encoding glyceraldehyde-3-phosphate dehydrogenase) was applied as an internal control. Gene expression was normalized as $-\Delta CT = -$ (CT gene – CT GAPDH). Finally, expression values of each gene were z-score transformed (Cheadle et al., 2003).

Identification and Validation of the Immunity-Related Gene Signature

First, we used the TCGA PDAC dataset as the training cohort. Using univariate Cox analysis, immunity-related genes that were significantly associated with good or poor prognosis were identified using the "Survival" package in the R software[5]. The

[5]https://www.r-project.org/

TABLE 2 | The association of the immune signature with clinicopathological characteristics in Ruijin cohort.

Features	Total	Score level		*p-value*
		High	Low	
Gender				0.2518
Male	63	42	21	
Female	38	21	17	
Age				0.0757
≤60	46	33	13	
>60	55	30	25	
Tumor size				0.5461
≤4 cm	82	50	32	
>4 cm	19	13	6	
Vascular invasion				0.7750
Yes	55	35	20	
No	46	28	18	
Lymph node metastasis				0.3263
Yes	62	41	21	
No	39	22	17	
Differentiation				0.0145*
Well/moderate		15	18	
Poor		48	20	
TNM stage				0.1340
I	19	9	10	
II + III + IV	82	54	28	

*$P < 0.05$.

prognostic genes were displayed by a forest plot using "forestplot" in R. Then, LASSO Cox regression was performed to generate a prognostic signature with the immunity-related genes using the "glmnet" package in R (Liu et al., 2019). Finally, a nomogram based on 18 immunity-related genes was plotted using the "rms" package in R, and the corresponding formula was extracted using the "nomogramEx" package in R. According the risk score and survival status of every patient, optimal cutoff values were set and all patients could be assigned to a high score or low score group.

Gene Ontology (GO) and Kyoto Encyclopedia of Genes and Genomes (KEGG) Pathway Analyses

By comparing the differentially expressed genes (DEGs) between the high score or low score group using the "limma" package in R, we obtained the significantly changed genes between the two groups. The gene names were imported into the Metascape database, and GO and KEGG pathway analyses were performed. The significantly enriched pathways were displayed in a histogram ($p < 0.01$).

Gene Set Variation Analysis (GSVA) and Gene Set Enrichment Analysis (GSEA)

The GSVA analysis was performed using "GSVA" package in R. The gene sets using in GSVA analysis were downloaded from GSEA molecular database[6]. T cell immunoreaction and PD1-related immunosuppressive pathways were extracted and used for GSVA analysis. As for GSEA analysis (Mootha et al., 2003; Subramanian et al., 2005), we construct a gemcitabine resistance related gene set by comparing the DEGs between the gemcitabine resistance population and main tumor cell population in GSE 36563 dataset and using genes with p value < 0.05 and $|\text{Log2 fold change}| > 1$. The gemcitabine resistance related gene set was shown in **Supplementary Table 4**.

Immunohistochemistry (IHC)

Of the above 101 PDAC samples, 81 tissue specimens were fixed using 10% neutral buffered formaldehyde, and then embedded in paraffin. Tissue sections were cut into 5-μm thick slices, which were coated with 3-aminopropyltriethoxysilane. Expression of CD3 + T cell, CD8 + T cell, and PD-L1 in these paraffin-embedded tissue sections were examined by IHC using the streptavidin-peroxidase method. A rabbit anti-human Ki67 monoclonal antibody (dilution, 1:250; catalog no. ab16667; Abcam, Cambridge, United Kingdom), a rabbit anti-human PCNA monoclonal antibody (dilution, 1:250; catalog no. ab265609; Abcam, Cambridge, United Kingdom), a rabbit anti-human PD-L1 monoclonal antibody (dilution, 1:250; catalog no. ab 213524; Abcam, Cambridge, United Kingdom), a rabbit anti-human CD3 monoclonal antibody (dilution, 1:150; catalog no. ab135372; Abcam), a rabbit anti-human CD8 monoclonal antibody (dilution, 1:250; catalog no. ab93278; Abcam) were used. The experimental procedure was as follows: (1) Slides were baked at 65°C for 2 h, deparaffinized in xylene four times (8 min each time), and then rehydrated in 100, 95, 85, and 75% ethanol successively (5 min each time). For antigen retrieval, the sections were autoclaved at 121°C for 10 min in citrate buffer (10 mmol/l sodium citrate; pH 6.0). By incubating the slides in 0.3% H_2O_2 solution, the endogenous peroxidase activity was blocked. After blocking with normal goat serum, the sections were incubated with the primary antibodies overnight at 4°C. Secondary antibodies (goat anti-rabbit antibody; 1:100 dilution; cat no. CW2069A; CWBio, Beijing, China) was incubated with the tissue sections for 15 min at room temperature. Finally, the slides were stained with 3, 3-diaminobenzidine tetrahydrochloride (DAB) and the nuclei were counterstained with hematoxylin. To semi-quantify the expression of Ki67, PCNA, and PD-L1 in PDAC tissue, we referenced both the proportion and intensity of stained tumor cells. Proportion scores: <5%, 5–25%, 25–50%, 50–75%, and ≥75% were recorded as 0, 1, 2, 3, 4, respectively. Staining scores: negative, weak, moderate, and strong staining were recorded as 0, 1, 2, 3, respectively. Finally, IHC scores was calculated as "proportion score × intensity score." For each case, five high power fields (400×) were evaluated and averages were calculated.

Statistical Analysis

All statistical analyses were performed using GraphPad Prism 7.0 (GraphPad Software Inc., La Jolla, CA, United States). The Kaplan-Meier method was used to plot survival curves, and the

[6]https://www.gsea-msigdb.org/gsea/msigdb/index.jsp

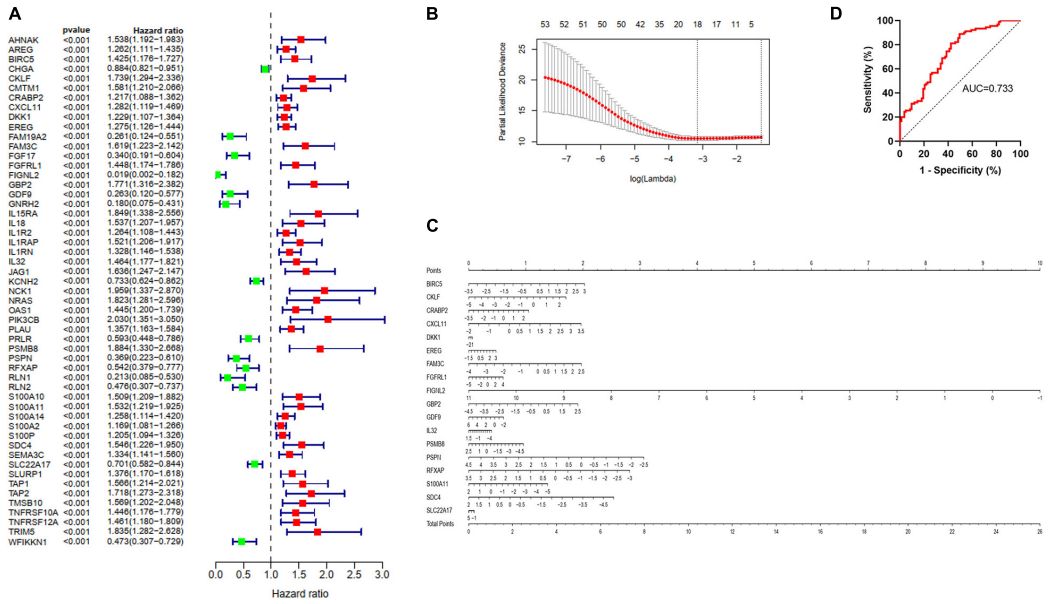

FIGURE 2 | Identification and validation of the immune predictive model. **(A)** A forest plot showing associations between the 53 proteins whose *p* value were less than 0.001 and overall survival in the training group. Unadjusted hazard ratios are shown with 95% confidence intervals. **(B)** The cross-test for selecting parameters in the LASSO model. Lambda represents the selected parameters, and partial likelihood deviance is plotted against log (lambda). **(C)** Nomogram predicting the probability overall survival. Eighteen genes were used to assign the points and draw a line depending on the corresponding values. "Total points," The sum of these 18 genes' points makes up the "Total points" and can predict overall survival. **(D)** The ROC curve of the TCGA (*n* = 173) training model for predicting patients' overall survival.

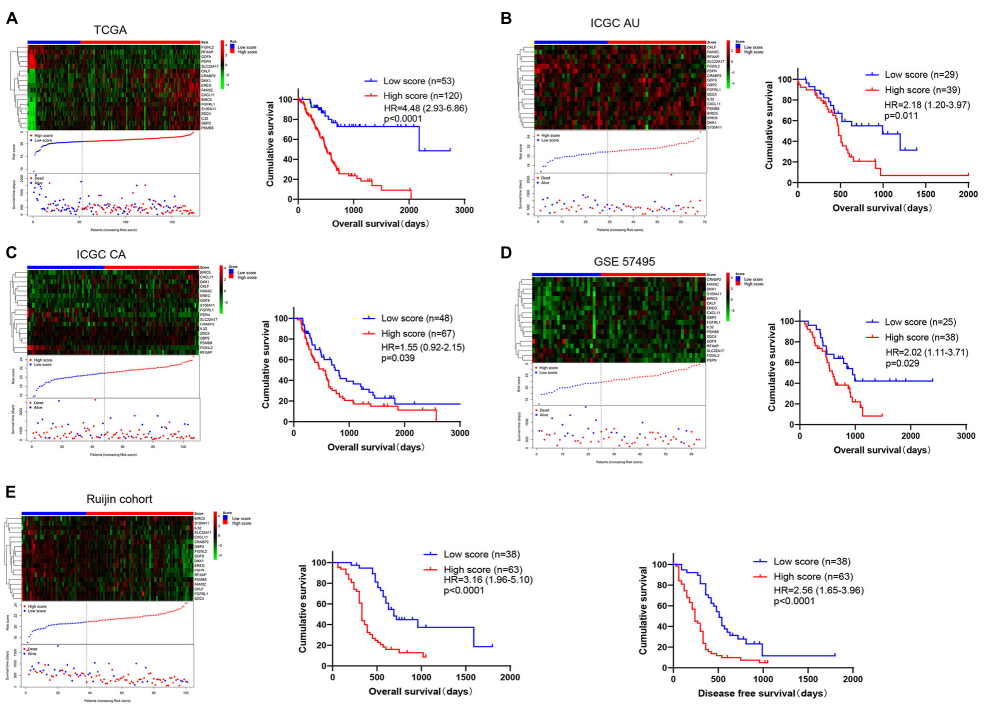

FIGURE 3 | The distribution and Kaplan-Meier survival curves of the immunity-related 18-gene signature depends on the patients' risk score. The risk score for all patients with PDAC were plotted in ascending order and marked as low score (blue) or high score (red). The survival status of the patients is marked as dead (red) and alive (blue). The proportion of patients who died in the high score group is obviously higher compared with that in the low score group. **(A)** TCGA (*n* = 173), **(B)** ICGC AU (*n* = 68), **(C)** ICGC CA (*n* = 115), **(D)** GSE57495 (*n* = 63), and **(E)** Ruijin cohort (*n* = 101) are shown, respectively, and the Ruijin cohort also exhibited the DFS.

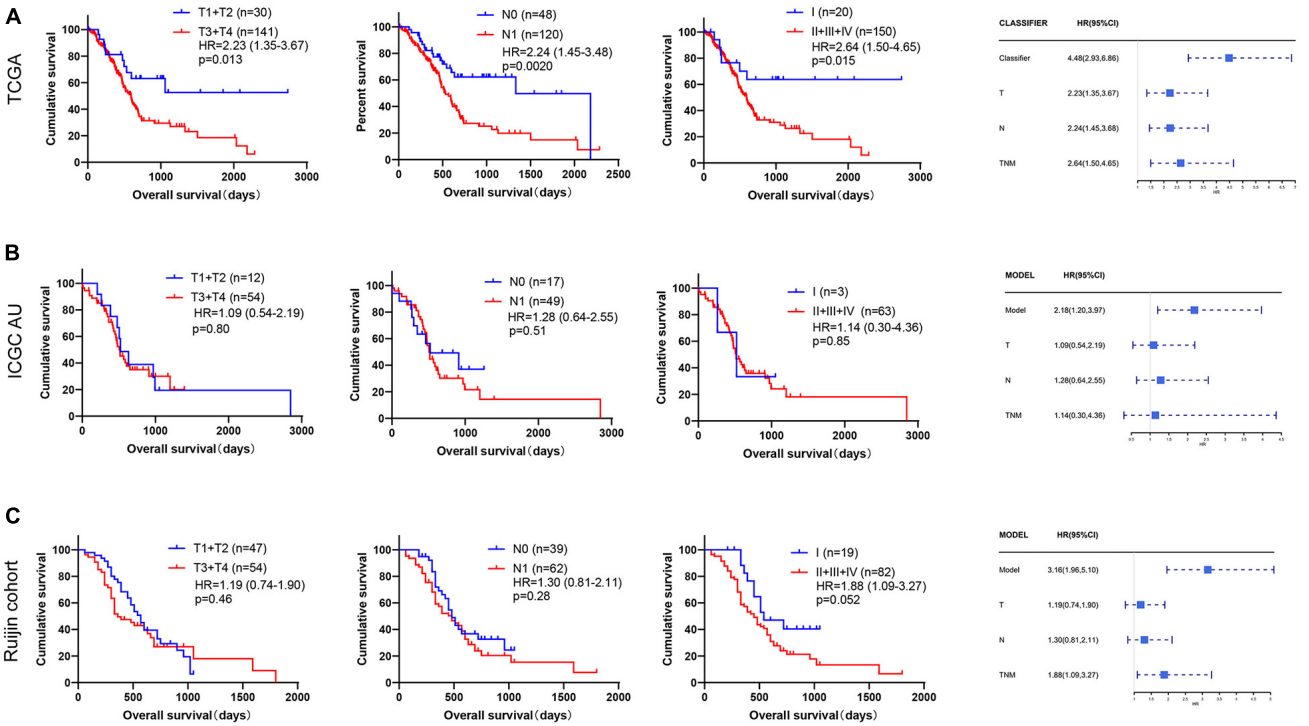

FIGURE 4 | Comparison of prognostic prediction ability between our immune signature and TNM stage. The Kaplan-Meier survival curves according to TNM stage, and forest plots show the HR value of our immune signature and TNM stage in **(A)** TCGA (n = 173), **(B)** ICGC AU (n = 68), and **(C)** Ruijin cohort (n = 101).

log-rank test was used to assess intergroup differences. Difference between two groups was assessed using Student's t-test. The χ^2 test was carried out to analyze the relationship between the 18-gene signature and clinical characteristics. $P < 0.05$ were considered statistically significant.

RESULTS

Characteristics of Patients With PDAC

The schematic flow chart of this study is shown in **Figure 1**. Our study totally enrolled 520 patients diagnosed with PDAC. Among them, the TCGA (n = 173) patients with PDAC were assigned as the training cohort, and the ICGC AU (n = 68), ICGC CA (n = 115) and GSE57495 (n = 63) PDAC patients were assigned as validation cohorts. Furthermore, patients (n = 101) with PDAC from Ruijin hospital, Shanghai Jiao Tong University School of Medicine were used as another independent validation cohort. The characteristics of the patients from the TCGA database and Ruijin cohort are shown in **Tables 1**, **2**, respectively.

Identification and Validation of Immunity-Associated Gene Signature in PDAC

We matched immunity-related genes from the ImmPort database with genes in the TCGA database and 1308 immunity-related genes (**Supplementary Table 1**) were obtained for further analysis. By performing univariate Cox regression analysis, 53 genes whose p values were less than 0.001 were chosen as candidates (**Figure 2A**). We then used the LASSO Cox regression algorithm and a total of 18 genes were identified to develop a risk score classifier (**Figure 2B**). A nomogram of the 18 genes predicting the probability of overall survival is shown in **Figure 2C**. The formula of risk score calculation was illustrated in **Supplementary Table 2**. We used a receiver operating characteristic (ROC) curve (**Figure 2D**) to test the effectiveness and determine the best cutoff value of the risk scores. The area under the curve (AUC) was 0.733, and 20.91 was identified as the optimal cutoff value. We divided patients into high score and low score group using the 18 immunity-related classifier and plotted the Kaplan-Meier survival curves. We found that patients in the low score group had more favorable prognosis than patients in the high score group, both in training and validation cohorts. In TCGA database (**Figure 3A**), patients in the low score group had significantly longer OS than patients in the high score group (HR = 4.48 (2.93–6.86), $p < 0.0001$). In the other four validation cohorts (**Figures 3B–E**), patients in the high score group also had inferior outcomes compared with those in the low score group (ICGC AU cohort: HR = 2.18 (1.20–3.97), $p = 0.011$; ICGC CA cohort: HR = 1.55 (0.92–2.15), $p = 0.039$; GSE57495 cohort: HR = 2.02 (1.11–3.71), $p = 0.029$; Ruijin cohort: HR = 3.16 (1.96–5.10), $p < 0.0001$). In Ruijin cohort, the phenomenon also applied to DFS, with an HR of 2.56 (1.65–3.96, $p < 0.0001$).

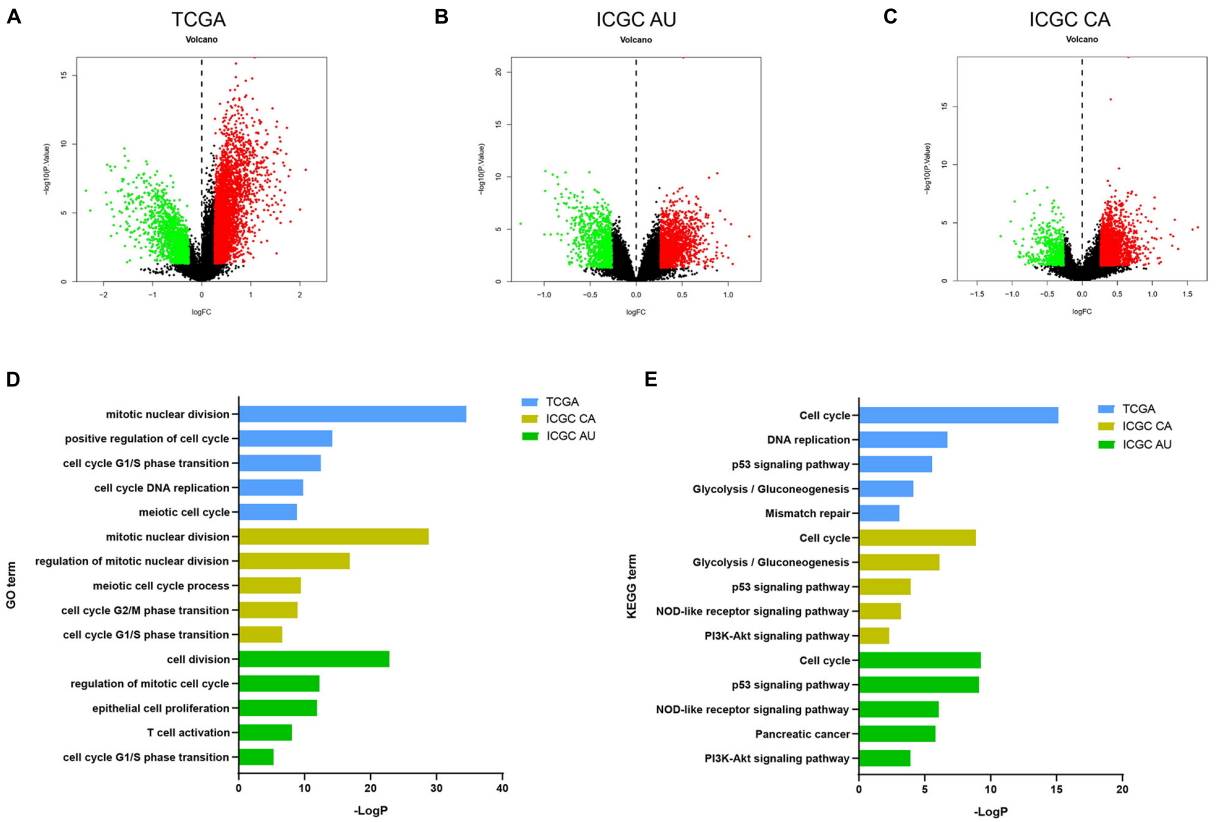

FIGURE 5 | Pathways involved in the immunity-related 18-gene signature. The volcano plot of DEGs in **(A)** TCGA, **(B)** ICGC AU, **(C)** ICGC CA databases. The volcano plots were constructed using fold-change and *p* values. Genes with fold-change > 1.2 and $p < 0.05$ were used to pathways analysis. **(D,E)** Similar GO and KEGG pathways enriched in high score group in TCGA, ICGC CA, and ICGC AU.

We also found that the immune signature was significantly related to TNM stage and histological grade in the TCGA database (**Table 1**), and similar results were observed in Ruijin cohort (**Table 2**).

Prognosis Prediction of Immunity-Related Gene Signature Is Superior to TMN Stage

After constructing the immunity-related 18-gene classifier, we performed univariate and multivariate Cox regression analysis involved in our immune signature and multiple clinicopathological features, such as TNM stage (II + III + IV vs. I), the CA19-9 level (>200 kU/L vs. ≤200 kU/L), the adjuvant chemotherapy status (yes or no), and PD-L1 expression. The CA 19-9 level was a moderate risk predictor in PDAC and we assigned 200 kU/L as boundary according to previous studies (Ballehaninna and Chamberlain, 2012; Aziz et al., 2019). In TCGA cohort, our immune signature ($p < 0.001$, HR = 5.09), TNM stage ($p = 0.026$, HR = 2.58), differentiation ($p = 0.042$, HR = 1.57), chemotherapy status ($p = 0.021$, HR = 0.61) and PD-L1 ($p = 0.035$, HR = 1.38) were found to be effective predictors of OS by univariate Cox regression analysis (**Supplementary Figure 1A**). Then we took these factors together to perform multivariate Cox regression analysis. Interestingly, our immune signature ($p < 0.001$, HR = 4.86) and chemotherapy status ($p < 0.001$, HR = 0.40) were independent prognosis factors (**Supplementary Figure 1B**). In Ruijin cohort, our immune signature ($p < 0.001$, HR = 3.65), CA 19-9 level ($p = 0.003$, HR = 2.05) and differentiation ($p = 0.002$, HR = 2.42) were significantly related to OS by univariate Cox regression analysis (**Supplementary Figure 1C**). Multivariate analysis revealed that our immune signature ($p < 0.001$, HR = 3.45), CA 19-9 level ($p = 0.002$, HR = 2.18) and differentiation ($p = 0.012$, HR = 2.05) could serve as independent predictors for OS in PDAC (**Supplementary Figure 1D**).

In order to compare the prognosis prediction ability between the immune signature and T stage, N stage, and TNM stage, we also plotted the Kaplan-Meier survival curves of these clinicopathological features, and the *p* value and HRs were obtained by log rank test. In the TCGA data (**Figures 3A**, **4A**), the HR value of our immune signature (HR = 4.48, 2.93–6.86) was superior to T stage (HR = 2.23, 1.35–3.67), N stage (HR = 2.24, 1.45–3.68) and TNM stage (HR = 2.64, 1.50–4.65). Similar results were observed in the ICGC AU and Ruijin cohorts (**Figures 3B,E**, **4B,C**).

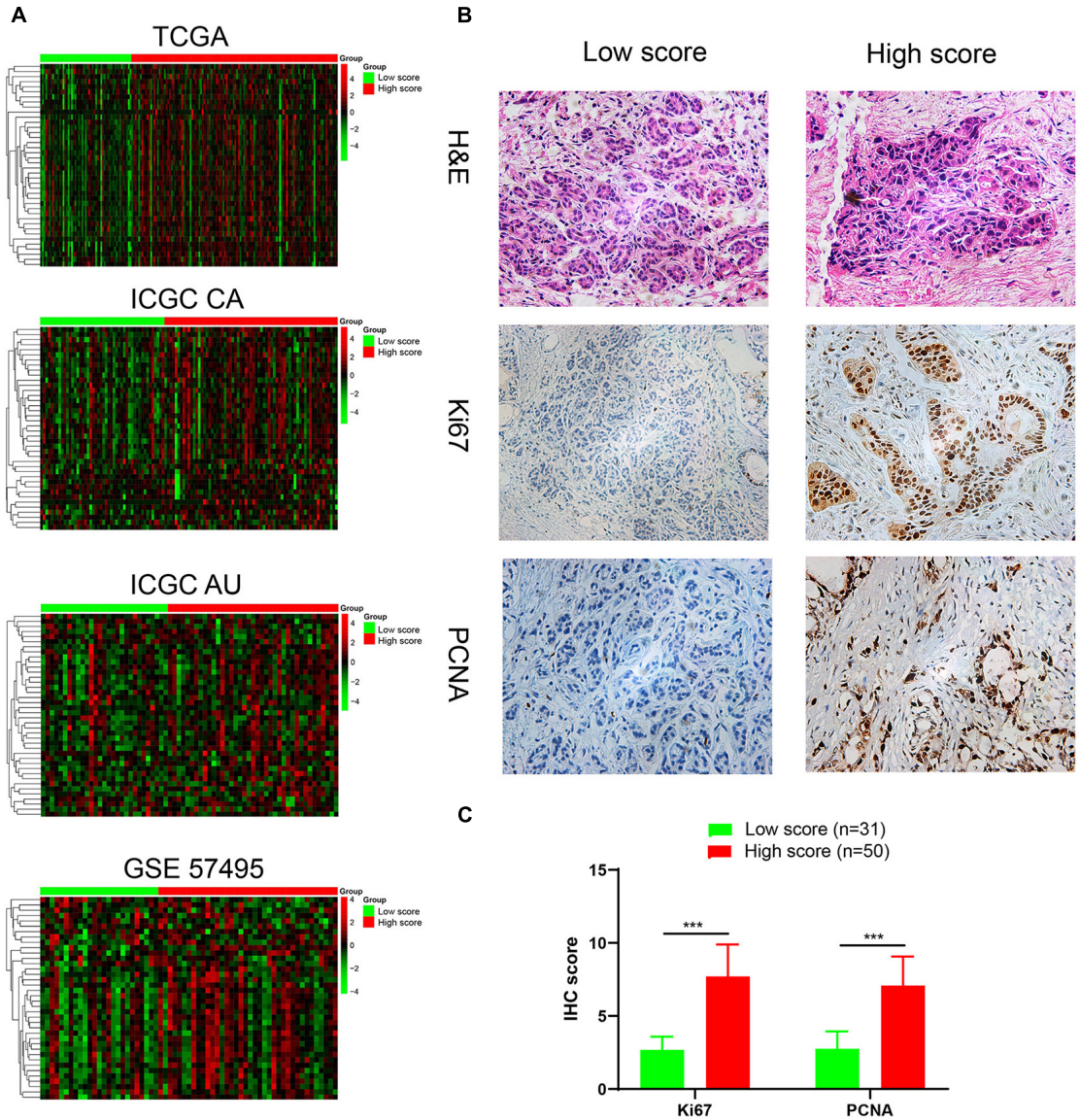

FIGURE 6 | Identification and validation of a highly proliferative subgroup of PDAC. **(A)** Heatmap showed that G1/S transition pathway was obviously enriched in high score group. We used kmeans clustering to draw heatmaps, and the lines left to heatmaps represent that the genes at ends of the lines had a high correlation. And the gene names in each row from top to bottom are ANXA1, AURKA, BCAT1, C10orf99, CCNA2, CCNB1, CCND1, CCNE1, CDC25C, CDC45, CDC6, CDK1, CDK2, CDK2AP2, CDK6, CDKN3, CDT1, E2F1, E2F7, E2F8, EGFR, EIF4EBP1, EZH2, GMNN, GTSE1, IQGAP3, KIF14, MCM10, MCM2, MCM4, MUC1, ORC1, ORC6, PML, PSME2, RCC1, RRM2, SFN, TNKS1BP1, TYMS. **(B)** H&E staining and immunohistochemical analyses of Ki-67, PCNA were performed on the tumor sections (low score group, $n = 31$; high score group, $n = 50$) **(C)** The IHC scores of Ki-67 and PCNA in low score ($n = 31$) and high score ($n = 50$) groups. ***$P < 0.001$.

The Immunity-Related 18-Gene Signature Predicts Patients' Response to Adjuvant Chemotherapy in PDAC

To interrogate potential signaling pathways involving in our immune signature in PDAC, we compared differentially expressed genes between high score group and low score group, and selected the genes with fold-change > 1.2 and p.adjust value < 0.05 to perform the GO and KEGG enrichment analyses (**Figures 5A–C** and **Supplementary Figures 2A–C**). Similar enriched pathways from the 3 datasets were displayed in **Figures 5D,E**. Cell cycle, cell division, p53 signaling pathways were significantly enriched in high score group, which indicated that it harbored higher proliferative potential. It is well known that gemcitabine exerts antitumor activity mainly by targeting G1/S phase. In GO term of G1/S phase transition, 40 genes were significantly enriched in high score group in TCGA cohort, and similar results were observed in another three independent cohorts (**Figure 6A**). Then H&E staining was used to detect the proliferation related markers (Ki67 and PCNA) in 81 PDAC patients (low score group, $n = 31$; high score group, $n = 50$) in

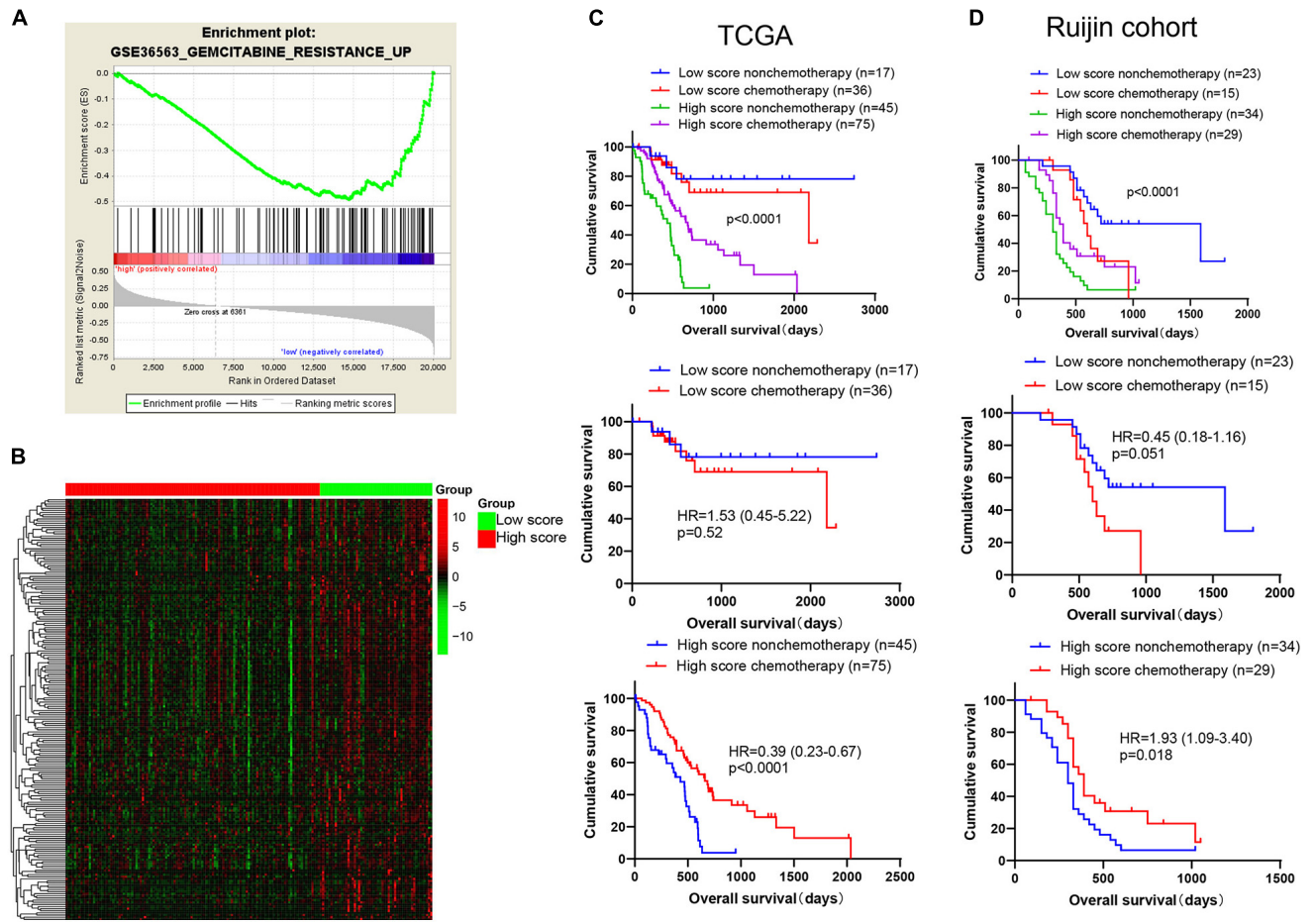

FIGURE 7 | Benefit of gemcitabine-based chemotherapy among patients in high and low score groups. **(A)** The gemcitabine resistance related gene set was significantly enriched in the low score group of TCGA cohort by GSEA analysis. The green curve represents enrichment score (ES). The highest point was used to represent ES value in gemcitabine resistance pathway. The ES value indicates the correlation between gene and gemcitabine resistance pathway. The black bar codes represent genes in gemcitabine resistance pathway and these genes were ordered according to their expression levels. The left end or right end genes are leading edge subset strongly contributed to ES value. The bottom numbers represent the order of expression levels in the genome from highest to lowest. **(B)** The 198 gemcitabine resistance-related genes were significantly attenuated in high score group of TCGA cohort ($p < 0.05$). Patients from the **(C)** TCGA database ($n = 173$) and **(D)** Ruijin cohort ($n = 101$) are divided into four groups (TCGA, Low score non-chemotherapy, $n = 17$, Low score chemotherapy, $n = 36$, high score non-chemotherapy, $n = 45$, high score chemotherapy, $n = 75$; Ruijin, Low score non-chemotherapy, $n = 23$, Low score chemotherapy, $n = 15$, high score non-chemotherapy, $n = 34$, high score chemotherapy, $n = 29$) and then Kaplan-Meier survival curves were plotted.

Ruijin cohort. The IHC analysis verified that higher levels of Ki67 and PCNA in high score group than that in low score group (**Figures 6B,C**). These results indicated that patients in high score group might be more responsive to chemotherapy targeting cell cycle (Venkatasubbarao et al., 2013).

As the first-line medicine for chemotherapy, gemcitabine has proven its effectiveness in PDAC (Fuchs et al., 2015). Cells possessing a vigorous proliferation ability are more sensitive to gemcitabine therapy (Zheng et al., 2015). Thus, we suspected that patients might be more sensitive to gemcitabine-based chemotherapy in high score group. We further constructed a gemcitabine resistance related gene set by using GSE36563 dataset (Van den Broeck et al., 2012), which contained 484 genes upregulated in gemcitabine resistance group, named as GEMCITABINE_RESISTANCE_UP. GSEA analysis showed that the gene set was significantly enriched in low score group in TCGA cohort (**Figure 7A**), and heatmap was further plotted to display 198 significantly attenuated genes of this gene set in high score group (**Figure 7B** and **Supplementary Table 5**). Prognosis analysis showed that the patients in high score group could benefit from chemotherapy in both the TCGA and Ruijin cohorts [**Figures 7C,D**, TCGA: chemotherapy vs. non-chemotherapy, $p < 0.0001$, HR = 0.39(0.23–0.67); Ruijin: chemotherapy vs. non-chemotherapy, $p = 0.0083$, HR = 0.46(0.25–0.82)]. However, the patients in low score group did not display this phenomenon [**Figure 7C**, TCGA: chemotherapy vs. non-chemotherapy, $p = 0.52$, HR = 1.53(0.45–5.22); Ruijin: chemotherapy vs. non-chemotherapy, $p = 0.21$, HR = 1.72(0.69–4.26)].

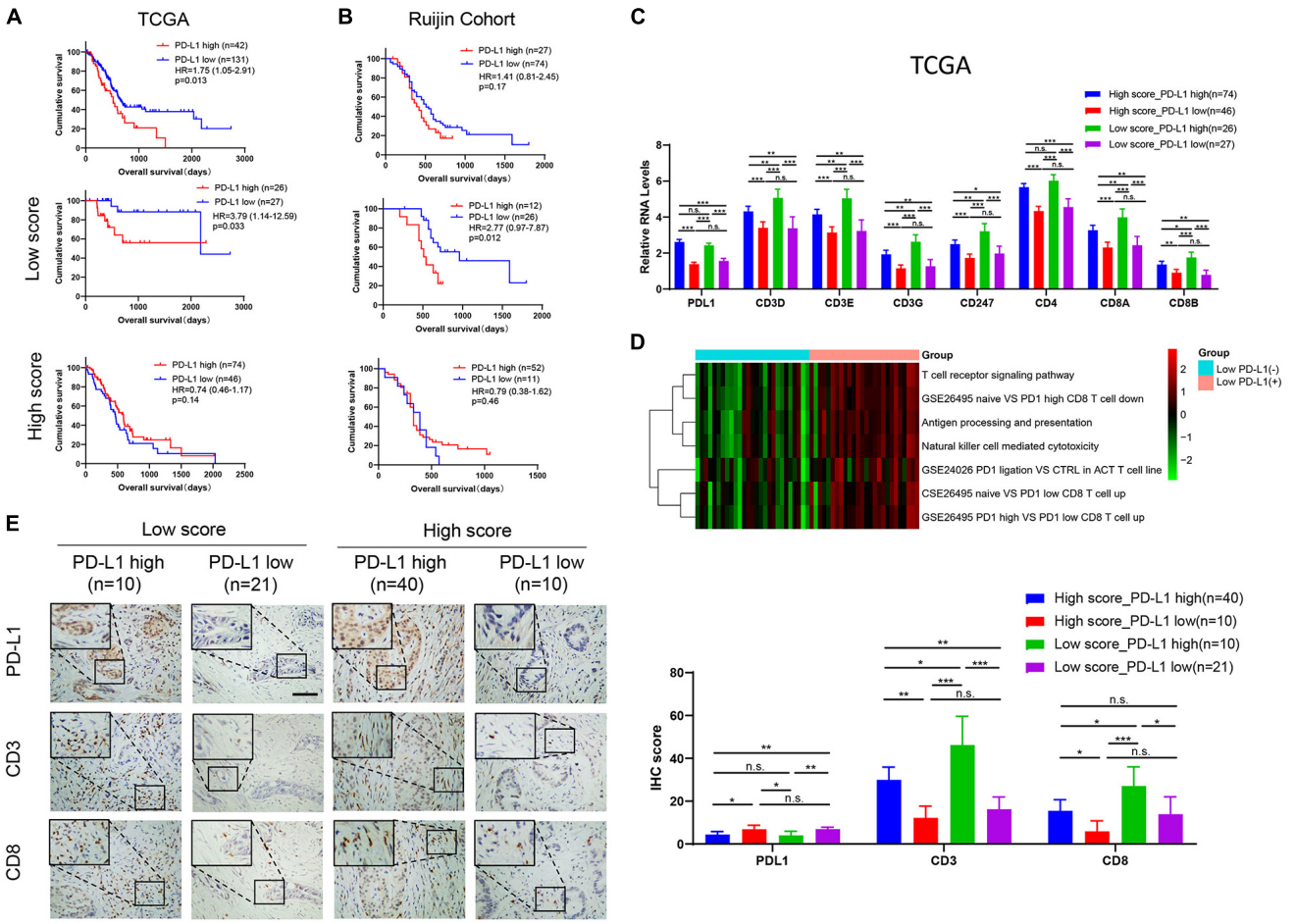

FIGURE 8 | PD-L1(+) cases in low score group show inferior prognosis and lymphocytes infiltration. Kaplan-Meier survival curves of PD-L1 expression in all patients, the low score group, and the high score group in **(A)** TCGA (High score: PD-L1 high, $n = 74$; PD-L1 low, $n = 46$. Low score: PD-L1 high, $n = 26$; PD-L1 low, $n = 27$) and **(B)** Ruijin cohort (High score: PD-L1 high, $n = 52$; PD-L1 low, $n = 11$. Low score: PD-L1 high, $n = 12$; PD-L1 low, $n = 26$). **(C)** The relative RNA level of immune infiltration markers in the TCGA database, including PD-L1, CD3D, CD3E, CD3G, CD247, CD4, CD8A, CD8B. **(D)** Heatmap showed that higher GSVA scores of T cell immunoreaction pathways and PD1-related immunosuppressive pathways in PD-L1(+) than in PD-L1(–) cases in low score group. **(E)** IHC profile and corresponding scores of PD-L1, CD3 and CD8 in four groups (High score_PD-L1 high, $n = 40$; High score_PD-L1 low, $n = 10$; Low score_PD-L1 high, $n = 10$; Low score_PD-L1 high, $n = 21$). $^*p < 0.05$; $^{**}p < 0.01$; $^{***}p < 0.001$; n.s., $p > 0.05$.

Identification of a Lymphocyte-Infiltrated PD-L1(+) PDAC Subgroup Associated With Poor Prognosis

The immunotherapy targeting PD-L1 showed impressive anti-tumor activity. In this study, PD-L1 expression could successfully predict the patients' outcome in PDAC in the TCGA data (**Figure 8A**), but not in the other four interdependent cohorts (**Figure 8B**, **Supplementary Figures 3A–C**). However, we found that low expression of PD-L1 was significantly related to longer OS in low score group in TCGA and Ruijin cohorts. In TCGA cohort (**Figure 8A**), patients with high PD-L1 expression had poorer OS than patients with low PD-L1 expression in low score group, with an HR of 3.79 (1.14–12.59, $p = 0.033$). In the Ruijin cohort (**Figure 8B**), patients with low PD-L1 expression had favorable outcomes compared with patients with high PD-L1in low score group, with an HR against low PD-L1 expression of 2.93 (1.01–8.45, $p = 0.0092$). Although the results did not show significant differences, we discovered the same trend in low score group of the ICGC AU cohort and GSE 57495 cohort (**Supplementary Figures 3B,C**). However, in high score group, PD-L1 expression showed the reverse function in the ICGC CA and ICGC AU cohorts [ICGC CA: PD-L1 high vs. PD-L1 low, $p = 0.035$, HR = 0.58(0.32–1.03); ICGC AU: PD-L1 high vs. PD-L1 low, $p = 0.032$, HR = 0.37(0.09–1.52)]. The mRNA level of PD-L1 expression did not show significant differences between low score and high score groups (**Supplementary Figure 3D**). In TCGA database, the CD3D, CD3E, CD3G, CD247, CD4, CD8A, and CD8B RNA levels were the highest in Low score_PD-L1 high group (**Figure 8C**). Moreover, we observed not only the activation of T cell immunoreaction pathways in low score group, but also the activation of PD1-related immunosuppressive pathways by GSVA analysis (**Figure 8D**).

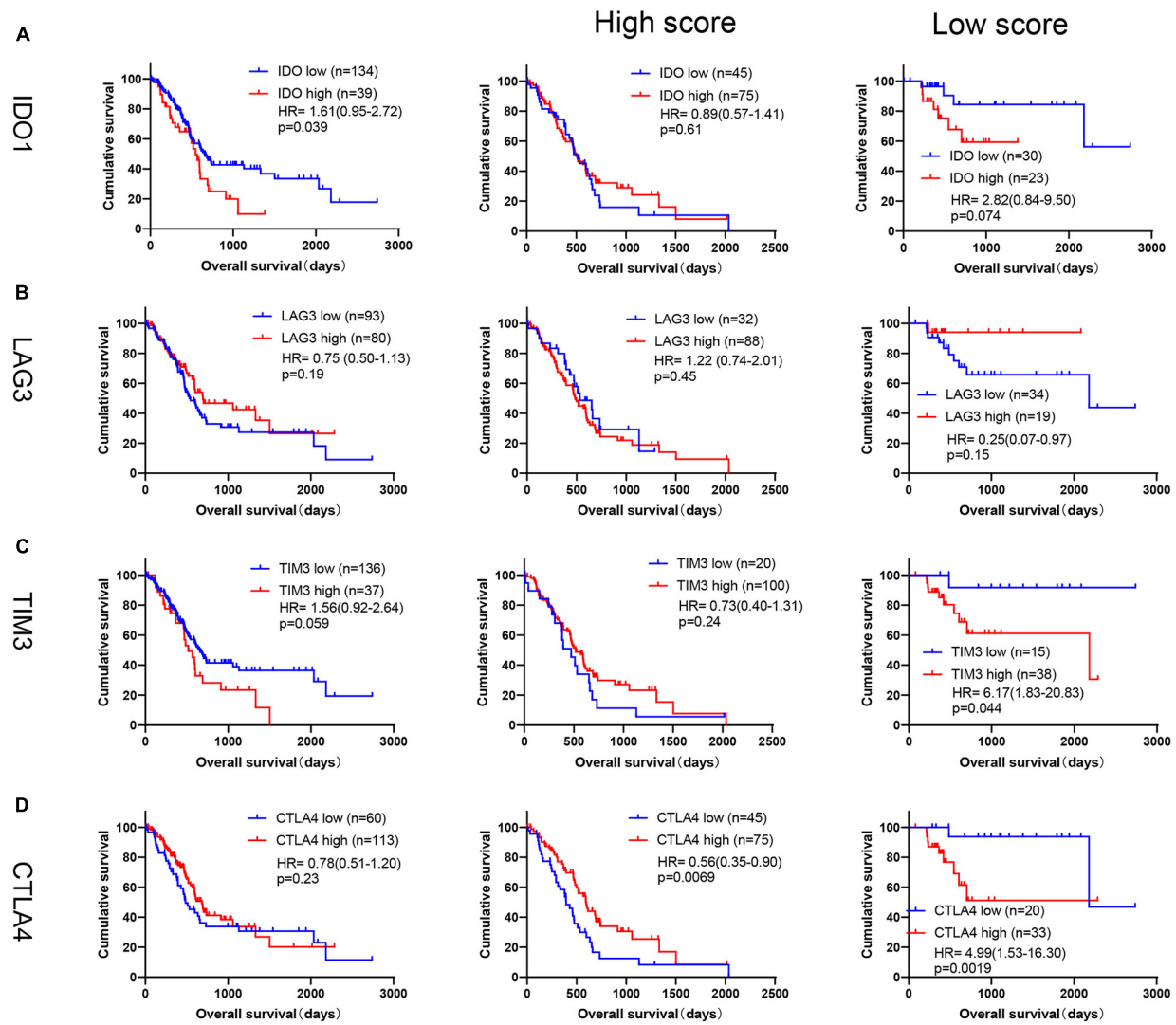

FIGURE 9 | Prognosis analysis of TIM3, CTLA4, IDO1 and LAG3 in TCGA database. Kaplan-Meier survival curves of **(A)** IDO1 (High score: PD-L1 high, $n = 75$; PD-L1 low, $n = 45$. Low score: PD-L1 high, $n = 23$; PD-L1 low, $n = 30$), **(B)** LAG3 (High score: PD-L1 high, $n = 88$; PD-L1 low, $n = 32$. Low score: PD-L1 high, $n = 19$; PD-L1 low, $n = 34$), **(C)** TIM3 (High score: PD-L1 high, $n = 100$; PD-L1 low, $n = 20$. Low score: PD-L1 high, $n = 38$; PD-L1 low, $n = 15$), **(D)** CTLA4 (High score: PD-L1 high, $n = 75$; PD-L1 low, $n = 45$. Low score: PD-L1 high, $n = 33$; PD-L1 low, $n = 20$) expression in all patients, or by subgroup analysis based on our immune signature in TCGA database.

In the Ruijin cohort, the IHC result showed higher numbers of CD3(+) T cells and CD8(+) T cells in PD-L1(+) cases in low score group (**Figure 8E**, all $p < 0.05$). The above results indicated that PD-L1(+) cases in low score group displayed stronger immune infiltration and may be suitable for PD1/PD-L1 blockade immunotherapy.

We also performed prognosis of other immune checkpoints in PDAC, such as IDO1, LAG3, TIM3, and CTLA4. As shown in **Figures 9A–D**, high expression of IDO1 was associated with poor outcome in PDAC in TCGA database [IDO1: $p = 0.039$, HR = 1.61(0.95–2.72)], but no significant difference for LAG3 [$p = 0.19$, HR = 0.75(0.50–1.13)], TIM3 [$p = 0.059$, HR = 1.56(0.92–2.64)] and CTLA4 [$p = 0.23$, HR = 0.78(0.51–1.20)]. However, by conducting subgroup analysis based on our immune signature, high levels of TIM3 and CTLA4 were significantly associated with poor OS in low score group [**Figures 9A–D**, TIM3: $p = 0.044$, 6.17 (1.83–20.83); CTLA4: $p = 0.0019$, HR = 4.99(1.53–16.30)], but not for LAG3 [**Figure 9B**, $p = 0.15$, HR = 0.25(0.07–0.97)]. High level of IDO1 also tended to be related to short OS in low score group [**Figure 9A**, IDO1: $p = 0.074$, HR = 2.82(0.84–9.50)], but did not show significant difference, which may be due to small sample size ($n = 53$). Because TIM3 and CTLA4 expression could significantly predict OS in low score group in TCGA database, we further performed the above analyses of TIM3 and CTLA4 in ICGC CA, ICGC AU and GSE57495 databases (**Supplementary Figure 4**). Although TIM3 and CTLA4 expression showed similar trends generally, but did not have the uniformity as PD-L1.

DISCUSSION

The immune microenvironment plays a pivotal role in tumor progression (Biswas, 2015; Chen and Mellman, 2017). Brooks used a 54-gene hypoxia-immune signature to identify subtype associated with prognosis and potentially responsive to targeted immunotherapies in head and neck cancer (Brooks et al., 2019). In breast cancer, Oshi et al. (2020) also generated a 4-gene score to determine the subtype which response to neoadjuvant chemotherapy and show with high expression of T cell exhaustion marker genes. The clinical significance of immune classification has been demonstrated in many diseases (Brooks et al., 2019; Li et al., 2019; Oshi et al., 2020); therefore, we attempted to explore the relationship between immunity-related genes and the clinical significance of PDAC in this study. Kandimalla et al. (2020) constructed an immune, stromal and proliferation (ISP) gene signature to predict patient outcome in PDAC. They obtained a 15-gene signature from a 170 ISP-related genes panel. However, we focused on the immune-related genes and acquired the 18 immunity-related gene signature from an 1,811 immunity-related genes panel. IL32 appeared both in ISP related signature and our immune signature, indicating that IL32 could be a pivotal molecule in PDAC progression. ISP signature and our 18 immunity-related gene signature could serve as independent predictors to predict OS of the PDAC patients, and our immune signature also showed stronger prediction capability than TNM stage. Furthermore, our results further indicated that patients in high score group PDACs could benefit from gemcitabine-based chemotherapy and patients in low score group may potentially response to PD1/PD-L1 blockade.

In this study, we firstly developed an 18 immunity-related gene classifier to predict patient outcome from TCGA data. PDAC patients with high immune score $\geq$20.91 were defined as high score group, and the others were defined as low score group. High score group showed shorter overall survival, which was validated in another four independent cohorts (a total of 347 patients). GO and KEGG pathway analysis revealed that the GO terms of cell cycle, cell and mitotic nuclear division were significantly enriched in high score group, such as G1/S phase transition. Besides, high score group also displayed higher levels of the proliferative indexes of Ki67 and PCNA and low expression of the gemcitabine resistance related genes. As is well known, gemcitabine mainly blocks cell cycle G1/S phase transition to exert anti-tumor activity (Fu et al., 2018). The above results indicated that high score group may be the candidate who benefited from gemcitabine-based chemotherapy. However, patients in low score group receiving chemotherapy showed no benefits and even worse prognosis.

Our signature construction was based on immunity; therefore, we explored the relationship between the subtypes and the response to immunotherapy. PD-L1 expressed on the surface of tumor cells could recognize and bind PD1 expressed on effector T cells, which transmit inhibitory immune signals to induce T cell apoptosis and inhibit T cell activation and proliferation (Gibney et al., 2016; Emens, 2018). However, the anti-PD1/PD-L1 agents in PDAC have limited efficacy (Lu et al., 2017; Mace et al., 2018). In addition to establishing effective combination therapy, it is also necessary to identify subtypes suitable for anti-PD1/PD-L1 immunotherapy (Topalian et al., 2015). In this study, patients with low PD-L1 expression suggested a favorable prognosis in low score group in two cohorts (TCGA and Ruijin). In the ICGC CA data, the result was different from other four datasets, perhaps because of microdissection which resulted in removal of immune component. In the ICGC AU and GSE 57495 cohorts, the lack of statistical differences might have been caused by the small sample size. However, in high score group, PD-L1 did not perform this function or even showed the reverse results. Furthermore, the RNA levels of CD3, CD4, and CD8 in low score group with high PD-L1 expression showed the highest level among the four subtypes in the TCGA database. GSVA analysis also indicated T cell immunoreaction activation and PD1-related immunosuppression in PD-L1(+) cases in low score group. These results were also supported by the IHC results in the Ruijin cohort, in which CD3(+), CD8(+) T cells displayed a distinct enrichment in PD-L1(+) low score group. The infiltration of CD3(+), CD8(+) T cells was evidence that could be used to predict a patient's response to anti-PD1/PD-L1 immunotherapy (Ribas et al., 2017; Danilova et al., 2019). In this study, the proportion of patients in low score group with high PD-L1 expression was approximately 20%. This finding was consistent with previous studies that only 10–30% of patients respond to anti-PD1/PD-L1 therapy (Page et al., 2014; Ott et al., 2019). Taken together, the patients with high PD-L1 expression in low score group might be a potential subtype suitable for anti-PD1/PD-L1 immunotherapy in PDAC.

In conclusion, by analyzing genomic data from the TCGA database, we constructed an immunity-related signature to divide PDACs into two subtypes: low score and high score groups. Patients in high score group showed inferior prognosis, but could benefit from gemcitabine-based chemotherapy. Furthermore, results also indicated that PD-L1(+) tumors in low score group might respond to PD1/PD-L1 blockade therapy.

DATA AVAILABILITY STATEMENT

Raw count data and corresponding clinical characteristics of 173 patients with PDAC were downloaded from the TCGA database (https://cancergenome.nih.gov/, Project ID: TCGA-PAAD). ICGC CA (Canada) raw RNA sequencing dataset and corresponding clinical characteristics of 115 patients, and the ICGC AU (Australia) gene expression microarray dataset and corresponding clinical characteristics of 68 patients were downloaded from the ICGC database (https://icgc.org/, Code: PACA-CA and PACA-AU). The GEO dataset GSE57495 and corresponding clinical characteristics of 63 patients were downloaded from GEO database (https://www.ncbi.nlm.nih.gov/geo/).

ETHICS STATEMENT

The studies involving human participants were reviewed and approved by the Ethical Committee of Ruijin Hospital, Shanghai

Jiao Tong University School of Medicine, Shanghai, China. The patients/participants provided their written informed consent to participate in this study.

AUTHOR CONTRIBUTIONS

HQ, HzL, and JX developed the concept and designed the experiments. HQ wrote the manuscript. HzL, JX, FL, XT, and MS performed the experiments. WW and XL collected the patients' information. HwL, HC, CP, ZX, XD, and BS performed the surgery. LJ, ZX, and XD helped to interpret results. BS coordinated the study and corrected the manuscript. All authors contributed to the article and approved the submitted version.

FUNDING

This study was supported by the National Natural Science Foundation of China (Grant No. 81871906), Natural Science Foundation of Shanghai (Grant No. 17ZR1417800), Shanghai Sailing Program (Grant No. 19YF1431100), National Natural Science Foundation of China (Grant No.81902387), and Ruijin Youth National Science Foundation Cultivation Fund (2019QNPY02022).

ACKNOWLEDGMENTS

We sincerely acknowledge the Cancer Genome Atlas (TCGA), the International Cancer Genome Consortium (ICGC), and the Gene Expression Omnibus (GEO) databases for the generous help.

SUPPLEMENTARY MATERIAL

The Supplementary Material for this article can be found online at: https://www.frontiersin.org/articles/10.3389/fcell.2021.682261/full#supplementary-material

Supplementary Figure 1 | Univariate and multivariate Cox regression analysis of our immune signature and clinicopathological features in TCGA and Ruijin cohorts. Forest plots show HR and *p* value in **(A,B)** TCGA and **(C,D)** Ruijin cohorts.

Supplementary Figure 2 | Pathways involved in the immunity-related 18-gene signature. The enrichment GO and KEGG pathway analyses of DEGs in **(A)** TCGA, **(B)** ICGC AU, **(C)** ICGC CA databases.

Supplementary Figure 3 | Low score/PD-L1(+) PDAC showed inferior prognosis. Kaplan-Meier survival curves of PD-L1 expression in all patients, the low score group, and the high score group in **(A)** ICGC CA (n = 115) and **(B)** ICGC AU (n = 68), and **(C)** GSE57495 (n = 63). **(D)** PD-L1 expression between the low score and the high score group in TCGA, ICGC CA, ICGC AU, GSE57495, and Ruijin cohorts (TCGA: p = 0.18; ICGC CA: p = 0.16; ICGC AU: p = 0.78; GSE57495: p = 0.24; Ruijin: p = 0.16).

Supplementary Figure 4 | Prognosis analysis of TIM3 and CTLA4 in ICGC CA, ICGC AU, and GSE57495 cohorts. Kaplan-Meier survival curves of TIM3 expression in all patients, or by subgroup analysis based on our immune signature in **(A)** ICGC CA (n = 115) and **(B)** ICGC AU (n = 68), and **(C)** GSE57495 (n = 63). Kaplan-Meier survival curves of CTLA4 expression in all patients, or by subgroup analysis based on our immune signature in **(D)** ICGC CA (n = 115) and **(E)** ICGC AU (n = 68), and **(F)** GSE57495 (n = 63).

Supplementary Table 1 | The 1308 immunity-related genes obtained by Cox univariate analysis.

Supplementary Table 2 | The risk score formula of immune-related 18-gene signature.

Supplementary Table 3 | Sequences of the qRT-PCR primers used in this study.

Supplementary Table 4 | The DEGs between the gemcitabine resistance population and main tumor cell population in GSE36563 dataset.

Supplementary Table 5 | The gene name of each row from the heatmap in **Figure 7B**.

REFERENCES

Aziz, M. H., Sideras, K., Aziz, N. A., Mauff, K., Haen, R., Roos, D., et al. (2019). The systemic-immune-inflammation index independently predicts survival and recurrence in resectable pancreatic cancer and its prognostic value depends on bilirubin levels: a retrospective multicenter cohort study. *Ann. Surg.* 270, 139–146. doi: 10.1097/sla.0000000000002660

Ballehaninna, U. K., and Chamberlain, R. S. (2012). The clinical utility of serum CA 19-9 in the diagnosis, prognosis and management of pancreatic adenocarcinoma: an evidence based appraisal. *J. Gastrointest. Oncol.* 3, 105–119.

Berraondo, P., Minute, L., Ajona, D., Corrales, L., Melero, I., and Pio, R. (2016). Innate immune mediators in cancer: between defense and resistance. *Immunol. Rev.* 274, 290–306. doi: 10.1111/imr.12464

Biswas, S. K. (2015). Metabolic reprogramming of immune cells in cancer progression. *Immunity* 43, 435–449. doi: 10.1016/j.immuni.2015.09.001

Brahmer, J. R., Tykodi, S. S., Chow, L. Q., Hwu, W. J., Topalian, S. L., Hwu, P., et al. (2012). Safety and activity of anti-PD-L1 antibody in patients with advanced cancer. *N. Engl. J. Med.* 366, 2455–2465.

Brooks, J. M., Menezes, A. N., Ibrahim, M., Archer, L., Lai, N., Bangnall, C. J., et al. (2019). Development and validation of a combined hypoxia and immune prognostic classifier for head and neck cancer. *Clin. Cancer Res.* 25, 5315–5328. doi: 10.1158/1078-0432.ccr-18-3314

Catalano, I., Grassi, E., Bertotti, A., and Trusolino, L. (2019). Immunogenomics of colorectal tumors: facts and hypotheses on an evolving saga. *Trends Cancer* 5, 779–788. doi: 10.1016/j.trecan.2019.10.006

Cheadle, C., Vawter, M. P., Freed, W. J., and Becker, K. G. (2003). Analysis of microarray data using Z score transformation. *J. Mol. Diagn.* 5, 73–81. doi: 10.1016/s1525-1578(10)60455-2

Chen, D. S., and Mellman, I. (2017). Elements of cancer immunity and the cancer-immune set point. *Nature* 541, 321–330. doi: 10.1038/nature21349

Danilova, L., Ho, W. J., Zhu, Q., Vithayathil, T., De Jesus-Acosta, A., Azad, N. S., et al. (2019). Programmed cell death ligand-1 (PD-L1) and CD8 expression profiling identify an immunologic subtype of pancreatic ductal adenocarcinomas with favorable survival. *Cancer Immunol. Res.* 7, 886–895. doi: 10.1158/2326-6066.cir-18-0822

Emens, L. A. (2018). Breast cancer immunotherapy: facts and hopes. *Clin. Cancer Res.* 24, 511–520. doi: 10.1158/1078-0432.ccr-16-3001

Foy, J. P., Bertolus, C., Michallet, M. C., Deneuve, S., Incitti, R., Bendriss-Vermare, N., et al. (2017). The immune microenvironment of HPV-negative oral squamous cell carcinoma from never-smokers and never-drinkers patients suggests higher clinical benefit of IDO1 and PD1/PD-L1 blockade. *Ann. Oncol.* 28, 1934–1941. doi: 10.1093/annonc/mdx210

Fu, H., Zhu, Y., Wang, Y., Liu, Z., Zhang, J., Xie, H., et al. (2018). Identification and validation of stromal immunotype predict survival and benefit from adjuvant chemotherapy in patients with muscle-invasive bladder cancer. *Clin. Cancer Res.* 24, 3069–3078. doi: 10.1158/1078-0432.ccr-17-2687

Fuchs, C. S., Azevedo, S., Okusaka, T., Van Laethem, J. L., Lipton, L. R., Riess, H., et al. (2015). A phase 3 randomized, double-blind, placebo-controlled trial of ganitumab or placebo in combination with gemcitabine as first-line therapy for metastatic adenocarcinoma of the pancreas: the GAMMA trial. *Ann. Oncol.* 26, 921–927. doi: 10.1093/annonc/mdv027

Galluzzi, L., Buque, A., Kepp, O., Zitvogel, L., and Kroemer, G. (2015). Immunological effects of conventional chemotherapy and targeted anticancer agents. *Cancer Cell* 28, 690–714. doi: 10.1016/j.ccell.2015.10.012

Gibney, G. T., Weiner, L. M., and Atkins, M. B. (2016). Predictive biomarkers for checkpoint inhibitor-based immunotherapy. *Lancet Oncol.* 17, e542–e551.

Kandimalla, R., Tomihara, H., Banwait, J. K., Yamamura, K., Singh, G., Baba, H., et al. (2020). A 15-gene immune, stromal and proliferation gene signature that significantly associates with poor survival in patients with pancreatic ductal adenocarcinoma. *Clin. Cancer Res.* 26, 3641–3648. doi: 10.1158/1078-0432.ccr-19-4044

Keren, L., Bosse, M., Marquez, D., Angoshtari, R., Jain, S., Varma, S., et al. (2018). A Structured tumor-immune microenvironment in triple negative breast cancer revealed by multiplexed ion beam imaging. *Cell* 174, 1373–1387 e19.

Li, B., Cui, Y., Nambiar, D. K., Sunwoo, J. B., and Li, R. (2019). The immune subtypes and landscape of squamous cell carcinoma. *Clin. Cancer Res.* 25, 3528–3537.

Liu, Y., Wu, L., Ao, H., Zhao, M., Leng, X., Liu, M., et al. (2019). Prognostic implications of autophagy-associated gene signatures in non-small cell lung cancer. *Aging* 11, 11440–11462. doi: 10.18632/aging.102544

Lu, C., Paschall, A. V., Shi, H., Savage, N., Waller, J. L., Sabbatini, M. E., et al. (2017). The MLL1-H3K4me3 axis-mediated PD-L1 expression and pancreatic cancer immune evasion. *J. Natl. Cancer Inst.* 109:djw283. doi: 10.1093/jnci/djw283

Mace, T. A., Shakya, R., Pitarresi, J. R., Swanson, B., McQuinn, C. W., Loftus, S., et al. (2018). IL-6 and PD-L1 antibody blockade combination therapy reduces tumour progression in murine models of pancreatic cancer. *Gut* 67, 320–332. doi: 10.1136/gutjnl-2016-311585

Mandal, R., Samstein, R. M., Lee, K. W., Havel, J. J., Wang, H., Krishna, C., et al. (2019). Genetic diversity of tumors with mismatch repair deficiency influences anti-PD-1 immunotherapy response. *Science* 364, 485–491.

Mollaoglu, G., Jones, A., Wait, S. J., Mukhopadhyay, A., Jeong, S., Arya, R., et al. (2018). The lineage-defining transcription factors SOX2 and NKX2-1 determine lung cancer cell fate and shape the tumor immune microenvironment. *Immunity* 49, 764–779 e9.

Mootha, V. K., Lindgren, C. M., Eriksson, K. F., Subramanian, A., Sihag, S., Lehar, J., et al. (2003). PGC-1alpha-responsive genes involved in oxidative phosphorylation are coordinately downregulated in human diabetes. *Nat. Genet.* 34, 267–273. doi: 10.1038/ng1180

Oshi, M., Katsuta, E., Yan, L., Ebos, J. M. L., Rashid, O. M., Matsuyama, R., et al. (2020). A Novel 4-Gene score to predict survival, distant metastasis and response to neoadjuvant therapy in breast cancer. *Cancers* 12:1148. doi: 10.3390/cancers12051148

Ott, P. A., Bang, Y. J., Piha-Paul, S. A., Razak, A. R. A., Bennouna, J., Soria, J. C., et al. (2019). T-Cell-Inflamed gene-expression profile, programmed death Ligand 1 expression, and tumor mutational burden predict efficacy in patients treated with pembrolizumab across 20 cancers: KEYNOTE-028. *J. Clin. Oncol.* 37, 318–327. doi: 10.1200/jco.2018.78.2276

Page, D. B., Postow, M. A., Callahan, M. K., Allison, J. P., and Wolchok, J. D. (2014). Immune modulation in cancer with antibodies. *Annu. Rev. Med.* 65, 185–202. doi: 10.1146/annurev-med-092012-112807

Qian, B. Z., and Pollard, J. W. (2010). Macrophage diversity enhances tumor progression and metastasis. *Cell* 141, 39–51. doi: 10.1016/j.cell.2010.03.014

Ribas, A., Dummer, R., Puzanov, I., VanderWalde, A., Andtbacka, R. H. I., Michielin, O., et al. (2017). Oncolytic virotherapy promotes intratumoral T Cell infiltration and improves Anti-PD-1 immunotherapy. *Cell* 170, 1109–1119 e10.

Royal, R. E., Levy, C., Turner, K., Mathur, A., Hughes, M., Kammula, U. S., et al. (2010). Phase 2 trial of single agent Ipilimumab (anti-CTLA-4) for locally advanced or metastatic pancreatic adenocarcinoma. *J. Immunother.* 33, 828–833. doi: 10.1097/cji.0b013e3181eec14c

Sharma, P., and Allison, J. P. (2015). The future of immune checkpoint therapy. *Science* 348, 56–61. doi: 10.1126/science.aaa8172

Siegel, R. L., Miller, K. D., and Jemal, A. (2020). Cancer statistics, 2020. *CA Cancer J. Clin.* 70, 7–30.

Sodir, N. M., Kortlever, R. M., Barthet, V. J. A., Campos, T., Pellegrinet, L., Kupczak, S., et al. (2020). Myc instructs and maintains pancreatic adenocarcinoma phenotype. *Cancer Discov.* 10, 588–607. doi: 10.1158/2159-8290.cd-19-0435

Strobel, O., Neoptolemos, J., Jager, D., and Buchler, M. W. (2019). Optimizing the outcomes of pancreatic cancer surgery. *Nat. Rev. Clin. Oncol.* 16, 11–26. doi: 10.1038/s41571-018-0112-1

Subramanian, A., Tamayo, P., Mootha, V. K., Mukherjee, S., Ebert, B. L., Gillette, M. A., et al. (2005). Gene set enrichment analysis: a knowledge-based approach for interpreting genome-wide expression profiles. *Proc. Natl. Acad. Sci. U. S. A.* 102, 15545–15550. doi: 10.1073/pnas.0506580102

Topalian, S. L., Drake, C. G., and Pardoll, D. M. (2015). Immune checkpoint blockade: a common denominator approach to cancer therapy. *Cancer Cell* 27, 450–461. doi: 10.1016/j.ccell.2015.03.001

Topalian, S. L., Taube, J. M., Anders, R. A., and Pardoll, D. M. (2016). Mechanism-driven biomarkers to guide immune checkpoint blockade in cancer therapy. *Nat. Rev. Cancer* 16, 275–287. doi: 10.1038/nrc.2016.36

Van den Broeck, A., Gremeaux, L., Topal, B., and Vankelecom, H. (2012). Human pancreatic adenocarcinoma contains a side population resistant to gemcitabine. *BMC Cancer* 12:354.

Venkatasubbarao, K., Peterson, L., Zhao, S., Hill, P., Cao, L., Zhou, Q., et al. (2013). Inhibiting signal transducer and activator of transcription-3 increases response to gemcitabine and delays progression of pancreatic cancer. *Mol. Cancer* 12:104. doi: 10.1186/1476-4598-12-104

Wu, S. P., Liao, R. Q., Tu, H. Y., Wang, W. J., Dong, Z. Y., Huang, S. M., et al. (2018). Stromal PD-L1-positive regulatory T cells and PD-1-positive CD8-positive t cells define the response of different subsets of non-small cell lung cancer to PD-1/PD-L1 blockade immunotherapy. *J. Thorac. Oncol.* 13, 521–532. doi: 10.1016/j.jtho.2017.11.132

Wykes, M. N., and Lewin, S. R. (2018). Immune checkpoint blockade in infectious diseases. *Nat. Rev. Immunol.* 18, 91–104. doi: 10.1038/nri.2017.112

Zappasodi, R., Merghoub, T., and Wolchok, J. D. (2018). Emerging concepts for immune checkpoint blockade-based combination therapies. *Cancer Cell* 33, 581–598. doi: 10.1016/j.ccell.2018.03.005

Zhao, J., Wen, X., Tian, L., Li, T., Xu, C., Wen, X., et al. (2019). Irreversible electroporation reverses resistance to immune checkpoint blockade in pancreatic cancer. *Nat. Commun.* 10:899.

Zheng, X., Carstens, J. L., Kim, J., Scheible, M., Kaye, J., Sugimoto, H., et al. (2015). Epithelial-to-mesenchymal transition is dispensable for metastasis but induces chemoresistance in pancreatic cancer. *Nature* 527, 525–530. doi: 10.1038/nature16064

Zhu, H., Li, T., Du, Y., and Li, M. (2018). Pancreatic cancer: challenges and opportunities. *BMC Med.* 16:214.

Conflict of Interest: The authors declare that the research was conducted in the absence of any commercial or financial relationships that could be construed as a potential conflict of interest.

frontiers in Cell and Developmental Biology

ORIGINAL RESEARCH
published: 30 June 2021
doi: 10.3389/fcell.2021.681745

Comprehensive Analysis of the Immune Infiltrates and PD-L1 of m^{6}A RNA Methylation Regulators in Hepatocellular Carcinoma

Yangtao Xu[1†], Xiaoqin He[1†], Junjian Deng[1†], Lin Xiong[2], Yue Li[1], Xiaoyu Zhang[1], Wenliang Chen[1], Xin Liu[1] and Ximing Xu[1]*

[1] Cancer Center, Renmin Hospital of Wuhan University, Wuhan, China, [2] Department of Pathology, Renmin Hospital of Wuhan University, Wuhan, China

Recently, N^6-methyladenosine (m^{6}A) RNA methylation in eukaryotic mRNA has become increasingly obvious in the pathogenesis and prognosis of cancer. Moreover, tumor microenvironment is involved in the regulation of tumorigenesis. In our research, the clinical data, including 374 tumor and 50 normal patients, were obtained from The Cancer Genome Atlas (TCGA). Then 19 m^{6}A regulators were selected from other studies. Hepatocellular carcinoma (HCC) patients were clustered in cluster1/2, according to the consensus clustering for the m^{6}A RNA regulators. We found that m^{6}A regulators were upregulated in cluster1. The cluster1 was associated with higher programmed death ligand 1 (PD-L1) expression level, higher immunoscore, worse prognosis, and distinct immune cell infiltration compared with cluster2. Five risk signatures were identified, including YTH N6-methyladenosine RNA-binding protein 1, YTHDF2, heterogeneous nuclear ribonucleoprotein C, WT1-associated protein, and methyltransferase-like 3, based on univariate Cox and least absolute shrinkage and selection operator regression analysis. High-risk group and low-risk group HCC patients were selected based on the risk score. Similarly, the high-risk group was extremely associated with higher PD-L1 expression level, higher grade, and worse overall survival (OS). Also, cluster1 was mainly enriched in high-risk group. Receiver operating characteristic (ROC) and a nomogram were used to predict the ability and the probability of 3- and 5-year OS of HCC patients. The time-dependent ROC curve (AUC) reached 0.77, 0.67, and 0.68 at 1, 3, and 5 years in the training dataset. Also, AUC areas of 1, 3, and 5 years were 0.7, 0.63, and 0.55 in the validation dataset. The gene set enrichment analysis showed that MTOR signaling pathway and WNT signaling pathway were correlated with cluster1 and high-risk group. Collectively, the research showed that the m^{6}A regulators were significantly associated with tumor immune microenvironment in HCC. Risk characteristics based on m^{6}A regulators may predict prognosis in patients with HCC and provide a new therapeutic target for improving the efficacy of immunotherapy.

Keywords: hepatocellular carcinoma, m^{6}A RNA methylation, PD-L1, tumor immune microenvironment, immune infiltrates, prognosis

OPEN ACCESS

Edited by:
Hongming Miao,
Army Medical University, China

Reviewed by:
Ming Liu,
Sichuan University, China
Fang Ma,
Central South University, China

****Correspondence:***
Ximing Xu
doctorxu120@aliyun.com

† These authors have contributed equally to this work

Specialty section:
This article was submitted to Molecular Medicine, a section of the journal Frontiers in Cell and Developmental Biology

Received: *17 March 2021*
Accepted: *28 May 2021*
Published: *30 June 2021*

Citation:
Xu Y, He X, Deng J, Xiong L, Li Y, Zhang X, Chen W, Liu X and Xu X (2021) Comprehensive Analysis of the Immune Infiltrates and PD-L1 of m^{6}A RNA Methylation Regulators in Hepatocellular Carcinoma. Front. Cell Dev. Biol. 9:681745. doi: 10.3389/fcell.2021.681745

INTRODUCTION

Hepatocellular carcinoma (HCC) is one of the most prevalent cancers in the world and the fourth most deadly cancer (Forner et al., 2012; Bray et al., 2018). In China alone, more than 466,100 people are diagnosed with HCC, and approximately 422,100 individuals succumb to HCC (Chen et al., 2016). Behind the high incidence of HCC, there are several modifiable factors, including hepatitis virus, alcohol abuse, smoking, and metabolic syndrome. Especially the hepatitis virus, in most of Africa and Asia, such as China, hepatitis B virus is the single leading risk factor for HCC, whereas in northern Europe and the United States, hepatitis C virus is the major risk factor (El-Serag, 2012). According to the location and clinical stage of HCC, the main treatment methods include surgery, chemotherapy, and radiotherapy, but the prognosis of advanced HCC is poor and treatment methods are limited. Interestingly, immunotherapy has developed rapidly in the past few years, improving survival of patients with HCC (Zhong et al., 2021). However, only a few patients with HCC could benefit from this treatment, and most patients still respond negatively to immune therapies. Immune system imbalance is involved in the development of immune-characterized HCC. For example, activation and ability of NK cells are reduced in HCC patients. Tumor-associated neutrophils are significantly associated with the development of HCC. Postoperative HCC patients with high-level lymphocyte infiltration, especially T cells, are closely related to better prognosis (Unitt et al., 2006; Margetts et al., 2018; Fu et al., 2019). Therefore, to identify more biomarkers for accurate prediction of prognosis and to optimize individualized immunotherapy management to a large extent, the mechanism of tumor immune microenvironment (TIME) needs to be further explored.

Post-transcriptional modification is also involved in the progression of various diseases and has attracted significant attention in the biomedicine (He et al., 2019). N^6-methyladenosine (m^6A) is the methylated modification of the sixth N atom of adenine and the most abundant mRNA modification among numerous RNA modifications. The average 1,000 nt contain one or two m^6A residues (Krug et al., 1976; Du et al., 2019). There are three types in the m^6A regulators, including writers, erasers, and readers. The m^6A is catalyzed by the methyltransferase complex (MTC), also known as the "writer," which included methyltransferase-like 3 (METTL3), METTL14, METTL16, WT1-associated protein (WTAP), zinc finger CCCH domain-containing protein 13 (ZC3H13), ZCCHC4, KIAA1429, zinc finger protein (ZFP217), RNA-binding motif protein 15 (RBM15), and RBM15B (Ping et al., 2014; Patil et al., 2016; Wang et al., 2016, 2017; Warda et al., 2017; Knuckles et al., 2018; Yue et al., 2018; Song et al., 2019; Pinto et al., 2020). Demethylase, also termed as "eraser," comprising fat mass- and obesity-associated protein (FTO) and α-ketoglutarate-dependent dioxygenase alkB homolog 5 (ALKBH5), removes m^6A methylation groups from RNA (Zhao et al., 2014; Zhang et al., 2017). The "readers" bind to the m^6A methylation site, which include YTH domain-containing 1 (YTHDC1), YTHDC2, heterogeneous nuclear ribonucleoprotein C (HNRNPC), HNRNPA2B1 YTH N6-methyladenosine RNA-binding protein 1 (YTHDF1), YTHDF2, and YTHDF3 (Wang et al., 2014, 2015; Alarcón et al., 2015; Liu et al., 2015; Hsu et al., 2017; Shi et al., 2017; Kasowitz et al., 2018). In HCC, patients with higher levels of YTHDF1 and METTL3 are associated with worse overall survival (OS). YTHDF1 can mediate the m^6A to enhance Snail expression. METTL3 deficiency leads to a decrease in m^6A, which blocks the EMT of cancer cells (Lin et al., 2019; Zhou et al., 2019). However, the mechanisms of other m^6A methylation regulators in liver cancer remain unclear. Moreover, the correlation between m^6A methylation modulator and programmed death ligand 1 (PD-L1) remains to be fully explored.

In this research, the relationship of m^6A RNA methylation regulators with PD-L1, prognosis, and TIME in HCC was analyzed. In addition, we established a cluster subtype and risk model for m^6A regulators to identify novel HCC markers and novel therapeutic strategies (**Supplementary Figure 1**).

MATERIALS AND METHODS

Dataset Source

The HCC clinical data and the mRNA expression data of patients were obtained from The Cancer Genome Atlas (TCGA) data portal.[1] The research included 374 tumor and 50 normal samples. The TCGA data were downloaded by using the R package "TCGAbiolinks" (Colaprico et al., 2016).

Identification of Consensus Clustering and Prognosis for m^6A RNA Methylation Regulators

In the research, 19 m^6A regulators were selected. HCC patients were clustered into cluster1 (n = 166) and cluster2 (n = 169) by using R package "ConsensusClusterPlus".[2] Furthermore, we used univariate Cox analysis and least absolute shrinkage and selection operator (LASSO) regression to identify five risk signatures, including YTHDF1, YTHDF2, HNRNPC, WTAP, and METTL3, and a risk score was generated for each HCC patient. Kaplan–Meier curves and receiver operating characteristic (ROC) curves were used to assess the prognostic capacity of the risk scores.

Identification of the Correction Between m^6A RNA Regulators and TIME in HCC

The R package "estimate" was used to calculate the immunoscore for each patient with the ESTIMATE algorithm. The fraction of 22 immune cell types between cluster1 and cluster2 and the gene set enrichment analysis (GSEA) were analyzed through Sangerbox website.[3] Also, the effect of somatic copy number

[1] https://portal.gdc.cancer.gov/
[2] http://www.bioconductor.org/
[3] http://sangerbox.com/

change (CNA) based on m^{6}A modulator signal on immune cell infiltration was explored based on CIBERSORT.[4]

A Predictive Nomogram

A nomogram was built to investigate the probability of prognosis in patients (Iasonos et al., 2008). Then the discrimination and accuracy of the nomogram were assessed by the concordance index (C-index) and a calibration.

Statistical Analysis

Statistical tests were carried out using GraphPad Prism 8.0 (GraphPad Software, San Diego, CA, United States) and R version 4.0.2 (version 4.0.2[5]). "limma," "ConsensusClusterPlus," "survival," "glmnet," "edgeR," and "timeROC" R package were used.

RESULTS

The m^{6}A RNA Methylation Regulators Expressed Differently in HCC

By comparing 50 normal and 374 tumor tissues, METTL14, YTHDC1, ZC3H13, ALKBH5, YTHDF2, and RBM15 had extremely lower expression in tumor tissues ($p < 0.001$, **Figure 1**). Also, the expression levels of YTHDC2, WTAP, and FTO were markedly lower in tumor tissues ($p < 0.05$). On the contrary, METTL3, KIAA1429, RBM15B, HNRNPA2B1, and HNRNPC had significantly higher expression in tumor tissues ($p < 0.001$). The results showed that m^{6}A regulators could be involved in biological development of HCC.

[4]https://cibersort.stanford.edu/

[5]https://www.r-project.org/

The Consensus Cluster of m^{6}A RNA Methylation Regulators Was Significantly Associated With Clinical Signatures of Patients With HCC

It is determined that $k = 2$ has the best clustering stability from $k = 2$ to 9, based on the similarity between the expression level of m^{6}A regulators and the proportion of fuzzy clustering measures (**Supplementary Figure 2**). According to the expression levels of the m^{6}A regulators, 335 HCC patients were clustered into cluster1 and cluster2 ($n1 = 166$, $n2 = 169$, **Figure 2A**). The findings indicated that the expression level of individual m^{6}A methylation regulators in cluster1 was higher than in cluster2 (**Figure 2B**). Moreover, the clinical futures were compared between cluster1 and cluster2. Female and low immunoscore HCC patients were significantly enriched in cluster1 ($p < 0.05$, **Figure 2B**). The OS (OS, $p = 0.0022$) and progression-free survival (PFS, $p = 0.0013$) were worse in cluster1 (**Figures 2C,D**).

Correction Between PD-L1 and m^{6}A RNA Methylation Regulators

It showed that the expression of PD-L1 was dramatically higher in cluster1 (**Figure 3A**). Furthermore, PD-L1 was positively correlated with ZCCHC4, WTAP, YTHDF2, RBM15, METTL3, YTHDF1, RBM15B, YTHDC1, HNRNPA2B1, HNRNPC, KIAA1429, ALKBH5, and METTL16 ($p < 0.001$, **Figure 3C**).

Association of Distinct Immune Cell Infiltration With m^{6}A RNA Methylation Regulators

To analyze the correction between m^{6}A regulators and TIME in HCC, we analyzed the immunoscore and immune infiltrate level

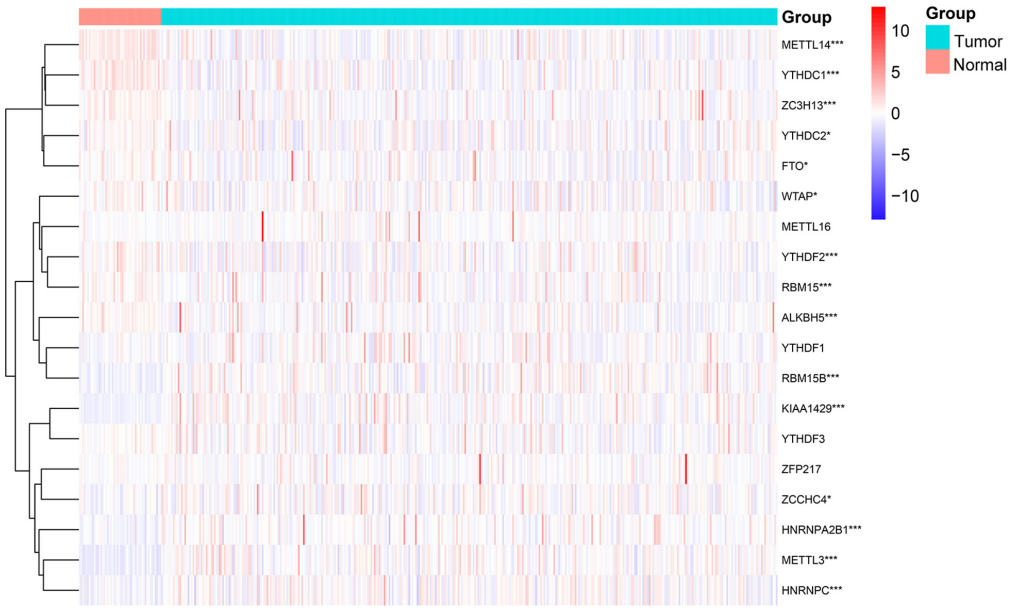

FIGURE 1 | Expression levels of m^{6}A RNA methylation regulators in normal and tumor samples. *$p < 0.05$ and ***$p < 0.001$.

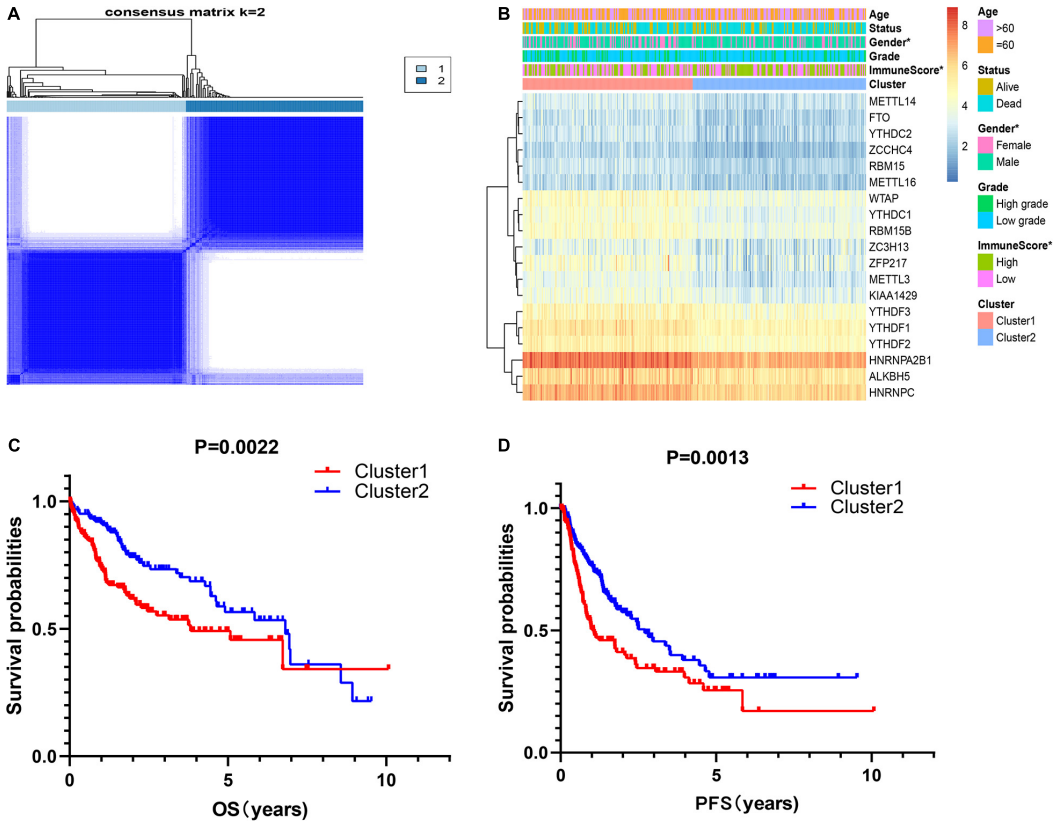

FIGURE 2 | Correlation of consensus clustering for m^{6}A RNA methylation regulators with the characteristics and survival of patients with HCC. **(A)** Consensus clustering matrix for $k = 2$. **(B)** Heatmap of correlation of m^{6}A RNA methylation regulators with characteristics of HCC patients. **(C,D)** OS and PFS of HCC patients in cluster1 and cluster2. $^*p < 0.05$.

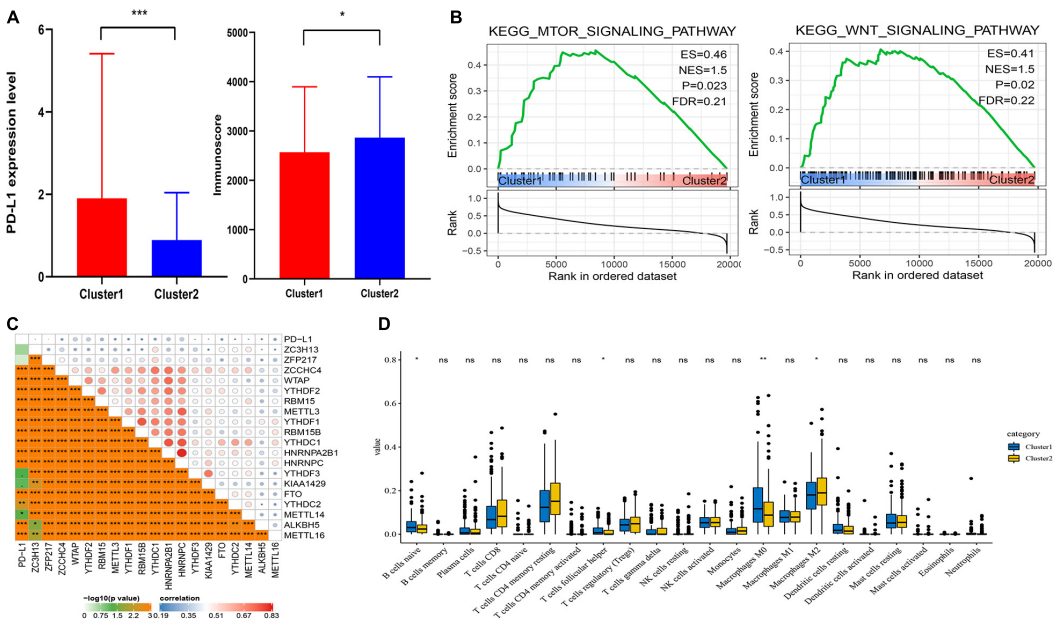

FIGURE 3 | Association of PD-L1 and immune cell infiltration with m^{6}A RNA methylation regulators. **(A)** Expression level of PD-L1 and immunoscore in cluster1 and cluster2. **(B)** GSEA showed that mTOR and Wnt signaling pathways were enriched in cluster1. **(C)** Correction between PD-L1 and m^{6}A RNA regulators. **(D)** Expression levels of 22 immune cell infiltration in cluster1 and cluster2. $^*p < 0.05$, $^{**}p < 0.01$, and $^{***}p < 0.001$.

of two subgroups (**Figure 3A**). The immunoscore was higher in cluster2 with a longer prognosis ($p = 0.0265$). Then we analyzed infiltration levels of 22 immune cell types between cluster1 and cluster2 (**Figure 3D**). The finding indicated that the infiltration levels of naïve B cells, T follicular helper cells, and macrophages M0 were higher in cluster1 ($p < 0.05$), whereas cluster2 showed higher infiltration levels of macrophages M2 ($p < 0.05$). To elucidate the underlying regulatory mechanisms that lead to temporal differences between cluster1 and cluster2, GSEA was used. Finally, the results indicated that mTOR and Wnt signaling pathways were correlated with cluster1 (**Figure 3B**).

Accurate Prognostic Prediction of Signatures for m^{6}A RNA Methylation Regulators

First, 340 HCC patients were randomly divided into validation dataset (170 patients) and training dataset (170 patients). Second, in the training dataset, 13 m^{6}A regulators were selected by using univariate regression analysis. Then five m^{6}A regulators were identified based on the LASSO regression analysis, including YTHDF1, YTHDF2, HNRNPC, WTAP, and METTL3 (**Figure 4**). Subsequently, these candidate m^{6}A regulators integrated into a predictive signature based on their risk coefficients. The formula went as follows: Risk Score = (0.4111 × YTHDF1 Expression) + (0.1969 × YTHDF2 Expression) + (0.0930 × HNRNPC Expression) + (0.2004 × WTAP Expression) + (0.3277 × METTL3 Expression). Afterward, according to the median risk score, patients were divided into high- and low-risk groups. The distributions of five m^{6}A regulators' expression profiles are shown in **Figure 5A**. The heatmap revealed higher expression levels of these m^{6}A regulators in the high-risk group compared with the low-risk group (**Figure 5A**). The high-risk group had worse prognosis, compared with the low-risk group, based on Kaplan–Meier curve analysis (**Figure 5C**). The results were validated in the validation dataset (**Supplementary Figure 3C**). Moreover, we constructed a time-dependent ROC curve (AUC). As shown in **Figure 5B**, the AUC of five risk signatures was 0.77, 0.67, and 0.68 at 1, 3, and 5 years. Regarding the validation dataset, the 1-, 3-, and 5-year AUC values were 0.7, 0.63, and 0.55 (**Supplementary Figure 3B**). The results revealed that five risk signatures had a strong predictive ability in the prognosis of HCC.

Risk Scores Was Associated With Clinical Features in HCC

Furthermore, we aimed to explore the correction between risk score and clinical characteristics in the training dataset (**Figure 6A**). The heatmap showed that the high-risk group mainly contained cluster1 ($p < 0.001$), alive status ($p < 0.001$), and high-grade patients ($p < 0.05$). Then we found that YTHDF1, YTHDF2, HNRNPC, WTAP, and METTL3 had higher expression in high-risk group. Also, PD-L1 was expressed higher in high-risk group with worse OS, which was validated in the validation dataset (**Figure 6C**). Similarly, mTOR and Wnt signaling pathways were enriched in the high-risk group (**Figure 6D**). Then we built a nomogram for HCC patients to investigate the probability of 3- and 5-year OS. The results demonstrated the risk score could be a prognostic biomarker for HCC patients (**Figure 6B**). Finally, we found that the C-index was 0.738 and the calibration curve was close to the ideal curve, which indicated that the nomogram has good predictive effects (**Supplementary Figure 4**).

Relationship Between Genetic Mutations of the m^{6}A Regulator Signatures and Immune Cell Infiltration

The correlation between risk score and immune cell infiltration was further analyzed (**Figure 7**). The risk score had a negative

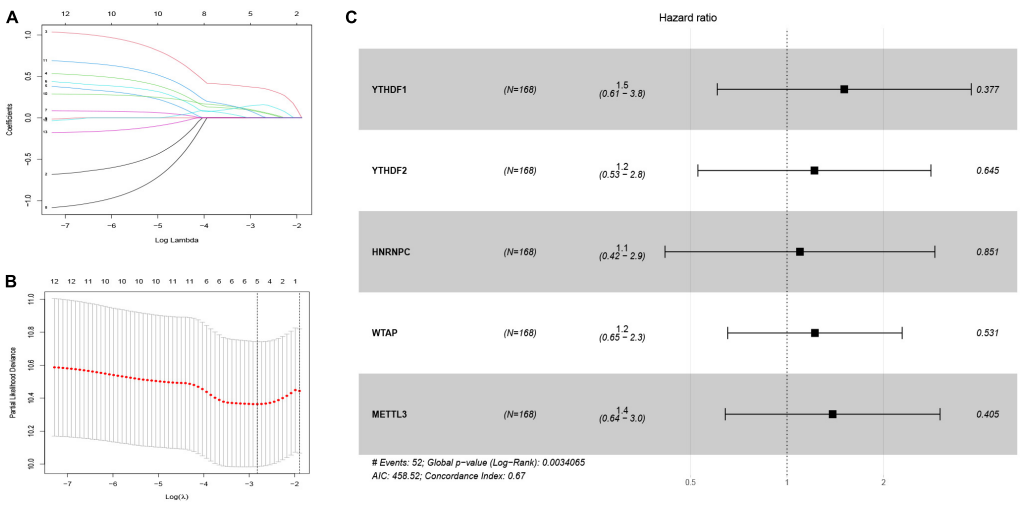

FIGURE 4 | Identification of five m^{6}A regulator-based risk signatures. **(A,B)** LASSO analysis of m^{6}A regulator-based risk signatures. **(C)** Multivariate Cox analysis of the five m^{6}A regulator-based risk signatures. #The five regulators have strong predictive ability and the results has statistical significance.

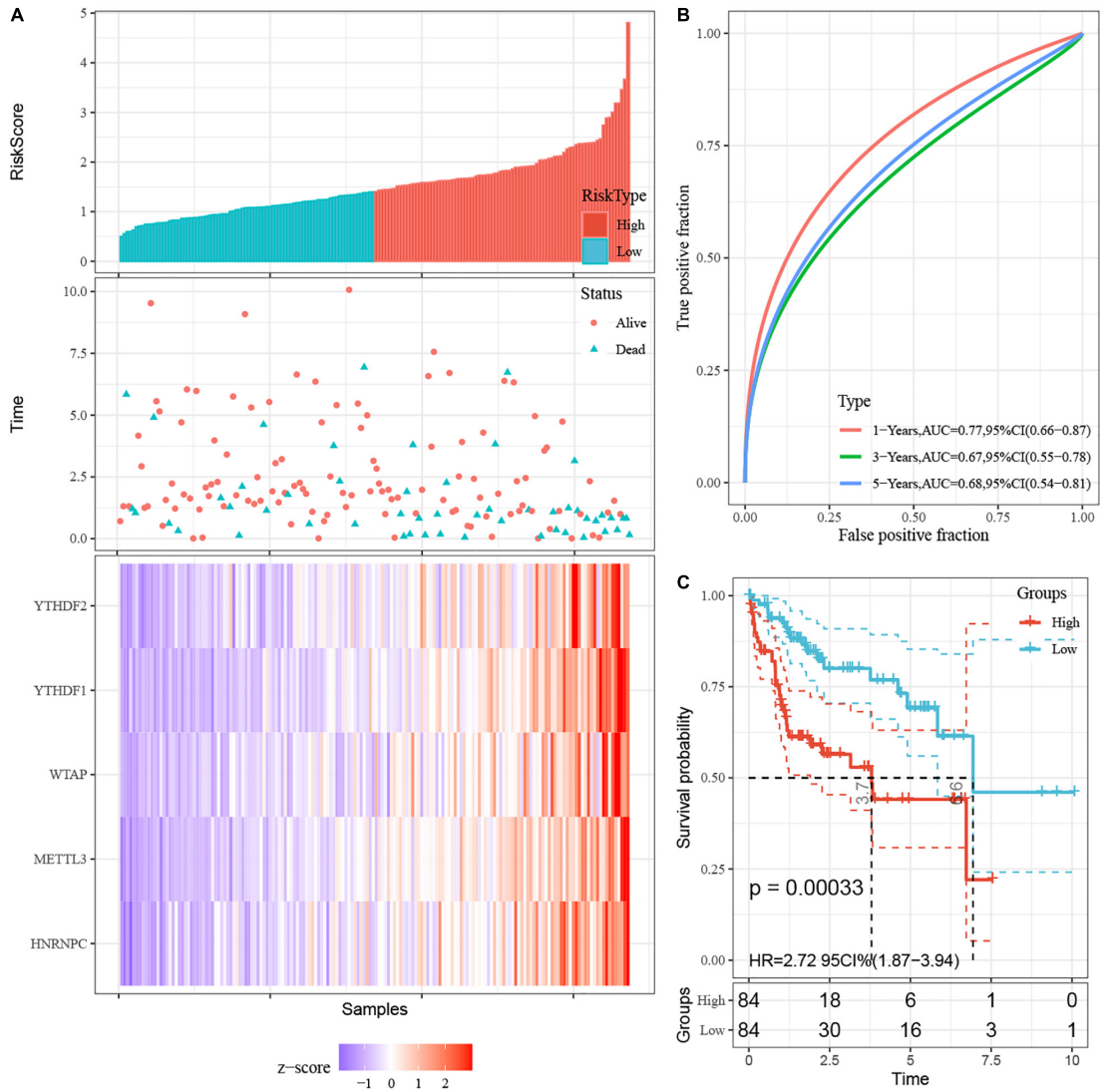

FIGURE 5 | Construction of prognostic signatures for m^{6}A regulator-based risk signatures. **(A)** Association of status and five m^{6}A RNA regulators with risk score. **(B)** The area under AUC of five risk signatures in training dataset. **(C)** OS of high-risk group and low-risk group in training dataset.

correction with infiltration levels of macrophages M2 and resting memory CD4 T cells ($p < 0.05$). Then the risk score was significantly corrected with B-cell memory, naïve B cells, T follicular helper cells, and eosinophils ($p < 0.05$). The results confirmed that the risk signatures based on m^{6}A regulators were related to the HCC immune microenvironment. Moreover, to clarify the potential mechanism of risk score and different immune cell infiltration, the effect of somatic CNA based on m^{6}A modulator signal on immune cell infiltration was analyzed (**Figure 8**). The CNAs of m^{6}A regulatory factor signaling, mainly including deep deletion and arm-level deletion, could affect the infiltration levels of B cells, CD8$^+$ T cells, CD4$^+$ T cells, neutrophils, dendritic cells, and especially macrophages ($p < 0.05$). It revealed that the five m^{6}A regulators play an important role in TIME of HCC patients.

DISCUSSION

The m^{6}A regulates gene expression, which regulates cellular processes such as cell self-proliferation, differentiation, invasion, and apoptosis (He et al., 2019). The m^{6}A is immobilized by m^{6}A methyltransferase, removed by m^{6}A demethylases, and recognized by the reader proteins to regulate RNA metabolism and progression of various tumors (Li et al., 2017; Ma et al., 2017; Roignant and Soller, 2017). However, the role of some m^{6}A regulators in tumor is unclear. For example, METTL14 plays different roles in different types of tumors. Yang et al. (2020) showed that METTL14 inhibits the proliferation and metastasis of colorectal cancer by downregulating the oncogenic long non-coding RNA XIST. Wang M. et al. (2020) reported that upregulation of METTL14 promotes the growth and metastasis of pancreatic cancer by mediating the increase of PERP mRNA

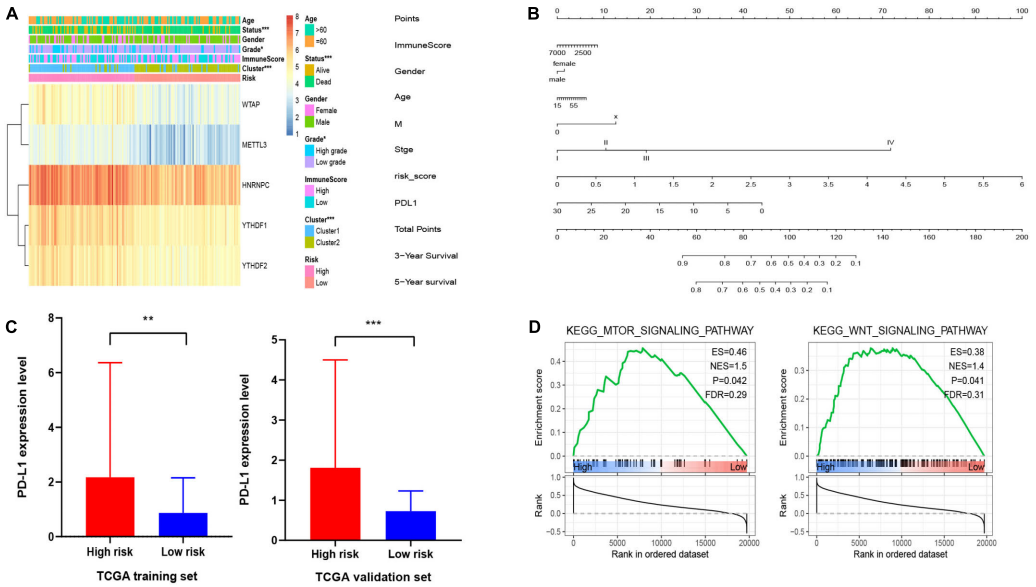

FIGURE 6 | Association of clinical features and functional features with m^{6}A regulator-based risk signatures. **(A)** Correction between clinical features and five m^{6}A regulator-based risk signatures. **(B)** A nomogram for HCC patients. **(C)** Expression level of PD-L1 in high-risk and low-risk groups. **(D)** GSEA showed that mTOR and Wnt signaling pathways were enriched in high-risk group. $^*p < 0.05$, $^{**}p < 0.01$, and $^{***}p < 0.001$.

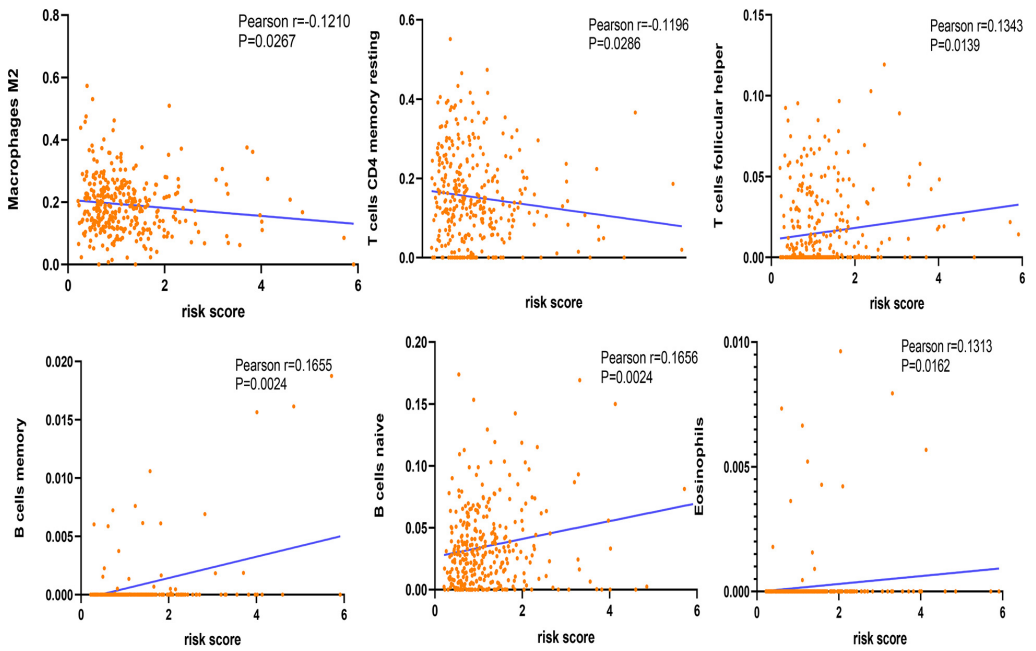

FIGURE 7 | Correction between immune cells and risk score.

N^6-adenosine methylation. Therefore, the expression levels and functions of m^{6}A regulators are complex in different tumors. The mechanism of RNA methylation in tumors needs to be further investigated. Currently, the effect of m^{6}A RNA methylation in the TIME of HCC needs to be analyzed further.

In the research, we demonstrated the expression of m^{6}A regulators in HCC, its prognostic value, and the effect of TIME, YTHDF1, YTHDF2, HNRNPC, WTAP, and METTL3. METTL3 and HNRNPC dramatically decreased in HCC compared with normal tissues ($p < 0.001$). YTHDF2 ($p < 0.001$) and WTAP ($p < 0.05$) were significantly upregulated in HCC tissues. However, the expression level of YTHDF1 was down-regulated in HCC tissues. Then, two subtypes of HCC, cluster1 and cluster2, were identified. We found that all m^{6}A regulators upregulated

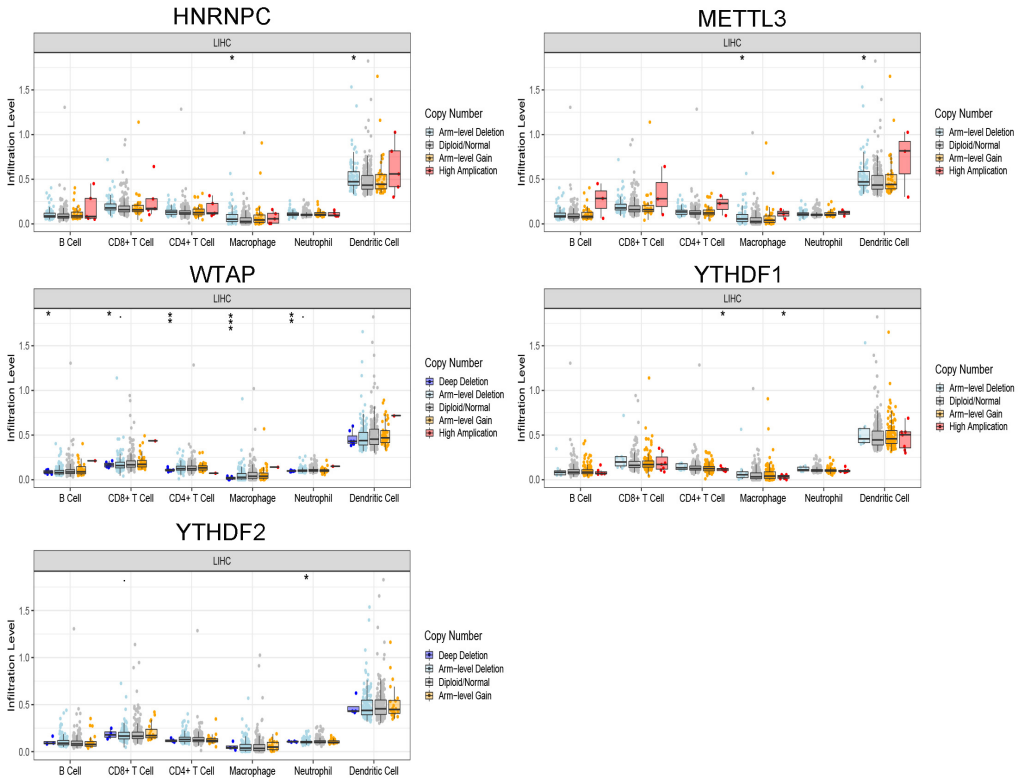

FIGURE 8 | The CNAs of m^{6}A regulatory factor signaling. *$p < 0.05$, **$p < 0.01$, and ***$p < 0.001$.

in cluster1. Also, OS and PFS of patients in cluster1 were worse compared with cluster2. Compared with cluster2, cluster1 was closely associated with lower immune score and higher PD-L1 expression level. The results were confirmed by a previous report, which showed that patients with high PD-L1 expression had a distinct poorer prognosis than those with low PD-L1 expression (Gao et al., 2009). Moreover, the expression levels of immune cells were significantly deferent in the two subtypes. The analysis showed that the infiltration levels of naïve B cells, T follicular helper cells, and macrophages M0 were higher in cluster1, whereas the level of macrophages M2 was lower. The results showed that the m^{6}A regulators were closely associated with prognosis and TIME in HCC patients. The GSEA reveled that the functional characteristics of HCC, especially Wnt and mTOR signaling pathways, were mainly enriched in cluster1. Tang et al. (2020) reported that m^{6}A demethylase inhibits tumor by mediating Wnt signaling. Zhao et al. (2020) reported that m^{6}A RNA modification regulates mTOR signal pathway in gastrointestinal cancer. Also, Zhang H. et al. (2020) found that the m^{6}A regulator METTL3 promotes the progression of retinoblastoma through mTOR signal pathway. The findings revealed that m^{6}A regulators could affect the progression of HCC by targeting Wnt and mTOR pathways, which could provide a new therapeutic strategy for the treatment of HCC.

Furthermore, high- and low-risk group patients were identified based on the five m^{6}A regulator-based risk signatures. Interestingly, we found that cluster1 was distinctly enriched in the high-risk group. Similarly, high-risk group with high PD-L1 expression level had worse prognosis than low-risk group with low PD-L1 expression level in the training dataset and the validation dataset. The nomogram indicated that the risk score could effectively predict the prognosis of patients with HCC. Regarding the five m^{6}A regulator-based risk signatures, four of five m^{6}A regulators, including YTHDF1, YTHDF2, WTAP, and METTL3, could facilitate the progression of HCC, and the results were confirmed by previous reports (Chen et al., 2018, 2019; Liu et al., 2020; Zhang C. et al., 2020). However, Zhong et al. (2019) showed that YTHDF2 suppresses cell proliferation and growth in HCC. Moreover, five m^{6}A regulators are also associated with different cancers. For example, YTHDF1, YTHDF2, and especially METTL3 are associated with gastric cancer. YTHDF1 and its m^{6}A-mediated regulation of Wnt/β-catenin signaling promote gastric cancer progression. METTL3-mediated m^{6}A modification facilitates gastric cancer progression and has poor prognosis (Pi et al., 2020; Shen et al., 2020; Wang Q. et al., 2020). Also, HNRNPC and YTHDF1 have an effect on prognosis in breast cancer patients (Wu et al., 2018; Anita et al., 2020). Also, the results were confirmed by the data obtained from Kaplan–Meier Plotter (**Supplementary Figure 5**). The results showed that the dysregulation of specific m^{6}A regulators plays a key role in the progression of various kinds of tumors.

Tumor microenvironment is involved in the regulation of patient prognosis and response to treatment

(Fridman et al., 2012; Galon et al., 2014; Hui and Chen, 2015). A previous study showed that tumor-infiltrating lymphocytes could serve as prognostic biomarkers and targets for immunotherapy in HCC (Ding et al., 2018). However, the mechanism of immune infiltration in response to HCC is largely unclear. In this study, we analyzed the correction between immune cell infiltration and risk score. We found that the risk score was positively associated with the infiltration levels of memory B cells, naïve B cells, T follicular helper cells, and eosinophils, and negatively associated with the infiltration levels of macrophages M2 and resting memory CD4 T cells. Zheng et al. (2020) reported that the RNA m^{6}A methylation and its reader proteins play a key regulatory role in early B-cell development. These findings reveled that the m^{6}A regulators are associated with TIME in HCC to some extent. Furthermore, we found that the CNAs of regulators were closely related to the immune infiltration levels, including B cells, CD8$^+$ T cells, CD4$^+$ T cells, neutrophils, dendritic cells, and especially macrophages. It is further confirmed that the m^{6}A regulators could affect TIME regulation in HCC.

However, there are some limitations in this research. First, the data of research are only obtained from the TCGA datasets. We lack our own independent clinical sample data to verify our findings. Then the results of our research need further experimental verification. In the future, we will further research the correction between m^{6}A regulators and TIME in HCC.

In summary, we systematically assessed the relationship of TIME, PD-L1, and m^{6}A regulators in HCC. According to the expression levels of the m^{6}A regulators, HCC patients were divided into cluster1 and cluster2. The two clusters were significantly different in PD-L1 expression level, immunoscore, prognosis, and TIME in HCC. HCC patients with higher PD-L1 expression or immunoscore were associated with worse prognosis. Then high-risk group and low-risk group patients were identified based on the five risk signatures. The high-risk group was significantly associated with higher PD-L1 expression levels, higher grades, and worse OS. The GSEA results revealed that the m^{6}A regulators were associated with the malignant functional features of HCC, including Wnt and mTOR signaling pathways. Therefore, the m^{6}A regulators are associated with TIME in HCC, which could provide a new treatment strategy for HCC patients.

DATA AVAILABILITY STATEMENT

The datasets presented in this study can be found in online repositories. The names of the repository/repositories and accession number(s) can be found in the article/ **Supplementary Material**.

AUTHOR CONTRIBUTIONS

XX: conceptualization, methodology, writing-review, and editing. YX: methodology, resources, software, formal analysis, and writing-original draft. XH: methodology, resources, formal analysis, and writing-original draft. JD: methodology, resources, software, and writing-original draft. LX: validation and data curation. YL and XZ: visualization and supervision. WC and XL: visualization. All authors contributed to the article and approved the submitted version.

FUNDING

This work was supported by funding from the National Natural Science Foundation of China (No. 31971166) and the Natural Science Foundation of Hubei Province (No. 2019CFB157).

SUPPLEMENTARY MATERIAL

The Supplementary Material for this article can be found online at: https://www.frontiersin.org/articles/10.3389/fcell.2021.681745/full#supplementary-material

Supplementary Figure 1 | Flowchart of the article.

Supplementary Figure 2 | Correlation of consensus clustering for m^{6}A RNA methylation regulators. Consensus clustering matrix from k = 2–9.

Supplementary Figure 3 | Construction of prognostic signatures for m^{6}A regulator-based risk signatures in the validation dataset. **(A)** Association of status and five m^{6}A RNA regulators with risk score. **(B)** The area under AUC of five risk signatures. **(C)** OS of high-risk group and low-risk group.

Supplementary Figure 4 | The calibration curve of 3 and 5 years.

Supplementary Figure 5 | OS of YTHTF1, METTL3, and HNRNPC in gastric carcinoma.

REFERENCES

Alarcón, C. R., Goodarzi, H., Lee, H., Liu, X., Tavazoie, S., and Tavazoie, S. F. (2015). HNRNPA2B1 is a mediator of m(6)A-dependent nuclear RNA processing events. *Cell* 162, 1299–1308. doi: 10.1016/j.cell.2015.08.011

Anita, R., Paramasivam, A., Priyadharsini, J. V., and Chitra, S. (2020). The m6A readers YTHDF1 and YTHDF3 aberrations associated with metastasis and predict poor prognosis in breast cancer patients. *Am. J. Cancer Res.* 10, 2546–2554.

Bray, F., Ferlay, J., Soerjomataram, I., Siegel, R., Torre, L. A., and Jemal, A. (2018). Global cancer statistics 2018: GLOBOCAN estimates of incidence and mortality worldwide for 36 cancers in 185 countries. *CA A Cancer J. Clin.* 68, 394–424. doi: 10.3322/caac.21492

Chen, M., Wei, L., Law, C. T., Tsang, F. H., Shen, J., Cheng, C., et al. (2018). RNA N6-methyladenosine methyltransferase-like 3 promotes liver cancer progression through YTHDF2-dependent posttranscriptional silencing of SOCS2. *Hepatology (Baltimore, MD)* 67, 2254–2270. doi: 10.1002/hep.29683

Chen, W., Zheng, R., Baade, P. D., Zhang, S., Zeng, H., Bray, F., et al. (2016). Cancer statistics in China, 2015. *CA A Cancer J. Clin.* 66, 115–132. doi: 10.3322/caac.21338

Chen, Y., Peng, C., Chen, J., Chen, D., Yang, B., He, B., et al. (2019). WTAP facilitates progression of hepatocellular carcinoma via m6A-HuR-dependent epigenetic silencing of ETS1. *Mol. Cancer* 18:127. doi: 10.1186/s12943-019-1053-8

Colaprico, A., Silva, T. C., Olsen, C., Garofano, L., Cava, C., Garolini, D., et al. (2016). TCGAbiolinks: an R/Bioconductor package for integrative analysis of TCGA data. *Nucleic Acids Res.* 44:e71. doi: 10.1093/nar/gkv1507

Ding, W., Xu, X., Qian, Y., Xue, W., Wang, Y., Du, J., et al. (2018). Prognostic value of tumor-infiltrating lymphocytes in hepatocellular carcinoma: a meta-analysis. *Medicine (Baltimore)* 97:e13301. doi: 10.1097/md.0000000000013301

Du, K., Zhang, L., Lee, T., and Sun, T. (2019). m(6)A RNA methylation controls neural development and is involved in human diseases. *Mol. Neurobiol.* 56, 1596–1606. doi: 10.1007/s12035-018-1138-1

El-Serag, H. B. (2012). Epidemiology of viral hepatitis and hepatocellular carcinoma. *Gastroenterology* 142, 1264–1273.e1261. doi: 10.1053/j.gastro.2011.12.061

Forner, A., Llovet, J. M., and Bruix, J. (2012). Hepatocellular carcinoma. *Lancet* 379, 1245–1255. doi: 10.1016/s0140-6736(11)61347-0

Fridman, W. H., Pagès, F., Sautès-Fridman, C., and Galon, J. (2012). The immune contexture in human tumours: impact on clinical outcome. *Nat. Rev. Cancer* 12, 298–306. doi: 10.1038/nrc3245

Fu, Y., Liu, S., Zeng, S., and Shen, H. (2019). From bench to bed: the tumor immune microenvironment and current immunotherapeutic strategies for hepatocellular carcinoma. *J. Exp. Clin. Cancer Res. CR* 38:396. doi: 10.1186/s13046-019-1396-4

Galon, J., Mlecnik, B., Bindea, G., Angell, H., Berger, A., Lagorce, C., et al. (2014). Towards the introduction of the 'Immunoscore' in the classification of malignant tumours. *J. Pathol.* 232, 199–209. doi: 10.1002/path.4287

Gao, Q., Wang, X. Y., Qiu, S. J., Yamato, I., Sho, M., Nakajima, Y., et al. (2009). Overexpression of PD-L1 significantly associates with tumor aggressiveness and postoperative recurrence in human hepatocellular carcinoma. *Clin. Cancer Res.* 15, 971–979. doi: 10.1158/1078-0432.Ccr-08-1608

He, L., Li, H., Wu, A., Peng, Y., Shu, G., and Yin, G. (2019). Functions of N6-methyladenosine and its role in cancer. *Mol. Cancer* 18:176. doi: 10.1186/s12943-019-1109-9

Hsu, P. J., Zhu, Y., Ma, H., Guo, Y., Shi, X., Liu, Y., et al. (2017). Ythdc2 is an N(6)-methyladenosine binding protein that regulates mammalian spermatogenesis. *Cell Res.* 27, 1115–1127. doi: 10.1038/cr.2017.99

Hui, L., and Chen, Y. (2015). Tumor microenvironment: sanctuary of the devil. *Cancer Lett.* 368, 7–13. doi: 10.1016/j.canlet.2015.07.039

Iasonos, A., Schrag, D., Raj, G. V., and Panageas, K. (2008). How to build and interpret a nomogram for cancer prognosis. *J. Clin. Oncol.* 26, 1364–1370. doi: 10.1200/jco.2007.12.9791

Kasowitz, S. D., Ma, J., Anderson, S. J., Leu, N. A., Xu, Y., Gregory, B., et al. (2018). Nuclear m6A reader YTHDC1 regulates alternative polyadenylation and splicing during mouse oocyte development. *PLoS Genet.* 14:e1007412. doi: 10.1371/journal.pgen.1007412

Knuckles, P., Lence, T., Haussmann, I. U., Jacob, D., Kreim, N., Carl, S., et al. (2018). Zc3h13/Flacc is required for adenosine methylation by bridging the mRNA-binding factor Rbm15/Spenito to the m(6)A machinery component Wtap/Fl(2)d. *Genes Dev.* 32, 415–429. doi: 10.1101/gad.309146.117

Krug, R. M., Morgan, M. A., and Shatkin, A. J. (1976). Influenza viral mRNA contains internal N6-methyladenosine and 5′-terminal 7-methylguanosine in cap structures. *J. Virol.* 20, 45–53. doi: 10.1128/jvi.20.1.45-53.1976

Li, Z., Weng, H., Su, R., Weng, X., Zuo, Z., Li, C., et al. (2017). FTO plays an oncogenic role in acute myeloid leukemia as a N(6)-Methyladenosine RNA demethylase. *Cancer Cell* 31, 127–141. doi: 10.1016/j.ccell.2016.11.017

Lin, X., Chai, G., Wu, Y., Li, J., Chen, F., Liu, J., et al. (2019). RNA m(6)A methylation regulates the epithelial mesenchymal transition of cancer cells and translation of Snail. *Nat. Commun.* 10:2065. doi: 10.1038/s41467-019-09865-9

Liu, N., Dai, Q., Zheng, G., He, C., Parisien, M., and Pan, T. (2015). N(6)-methyladenosine-dependent RNA structural switches regulate RNA-protein interactions. *Nature* 518, 560–564. doi: 10.1038/nature14234

Liu, X., Qin, J., Gao, T., Li, C., He, B., Pan, B., et al. (2020). YTHDF1 facilitates the progression of hepatocellular carcinoma by promoting FZD5 mRNA translation in an m6A-Dependent manner. *Mol. Ther. Nucleic Acids* 22, 750–765. doi: 10.1016/j.omtn.2020.09.036

Ma, J. Z., Yang, F., Zhou, C. C., Liu, F., Yuan, J., Wang, F., et al. (2017). METTL14 suppresses the metastatic potential of hepatocellular carcinoma by modulating N(6) -methyladenosine-dependent primary MicroRNA processing. *Hepatology (Baltimore, MD)* 65, 529–543. doi: 10.1002/hep.28885

Margetts, J., Ogle, L. F., Chan, S. L., Chan, A. W. H., Chan, K. C. A., Jamieson, D., et al. (2018). Neutrophils: driving progression and poor prognosis in hepatocellular carcinoma? *Br. J. Cancer* 118, 248–257. doi: 10.1038/bjc.2017.386

Patil, D. P., Chen, C. K., Pickering, B. F., Chow, A., Jackson, C., Guttman, M., et al. (2016). m(6)A RNA methylation promotes XIST-mediated transcriptional repression. *Nature* 537, 369–373. doi: 10.1038/nature19342

Pi, J., Wang, W., Ji, M., Wang, X., Wei, X., Jin, J., et al. (2020). YTHDF1 promotes gastric carcinogenesis by controlling translation of FZD7. *Cancer Res.* 81, 2651–2665. doi: 10.1158/0008-5472.Can-20-0066

Ping, X. L., Sun, B. F., Wang, L., Xiao, W., Yang, X., Wang, W., et al. (2014). Mammalian WTAP is a regulatory subunit of the RNA N6-methyladenosine methyltransferase. *Cell Res.* 24, 177–189. doi: 10.1038/cr.2014.3

Pinto, R., Vågbø, C. B., Jakobsson, M. E., Kim, Y., Baltissen, M., O'Donohue, M., et al. (2020). The human methyltransferase ZCCHC4 catalyses N6-methyladenosine modification of 28S ribosomal RNA. *Nucleic Acids Res.* 48, 830–846. doi: 10.1093/nar/gkz1147

Roignant, J. Y., and Soller, M. (2017). m(6)A in mRNA: an ancient mechanism for fine-tuning gene expression. *Trends Genet.* 33, 380–390. doi: 10.1016/j.tig.2017.04.003

Shen, X., Zhao, K., Xu, L., Cheng, G., Zhu, J., Gan, L., et al. (2020). YTHDF2 inhibits gastric cancer cell growth by regulating FOXC2 signaling pathway. *Front. Genet.* 11:592042. doi: 10.3389/fgene.2020.592042

Shi, H., Wang, X., Lu, Z., Zhao, B. S., Ma, H., Hsu, P. J., et al. (2017). YTHDF3 facilitates translation and decay of N(6)-methyladenosine-modified RNA. *Cell Res.* 27, 315–328. doi: 10.1038/cr.2017.15

Song, T., Yang, Y., Wei, H., Xie, X., Lu, J., Zeng, Q., et al. (2019). Zfp217 mediates m6A mRNA methylation to orchestrate transcriptional and post-transcriptional regulation to promote adipogenic differentiation. *Nucleic Acids Res.* 47, 6130–6144. doi: 10.1093/nar/gkz312

Tang, B., Yang, Y., Kang, M., Wang, Y., Wang, Y., Bi, Y., et al. (2020). m(6)A demethylase ALKBH5 inhibits pancreatic cancer tumorigenesis by decreasing WIF-1 RNA methylation and mediating Wnt signaling. *Mol. Cancer* 19:3. doi: 10.1186/s12943-019-1128-6

Unitt, E., Marshall, A., Gelson, W., Rushbrook, S., Davies, S., Vowler, S., et al. (2006). Tumour lymphocytic infiltrate and recurrence of hepatocellular carcinoma following liver transplantation. *J. Hepatol.* 45, 246–253. doi: 10.1016/j.jhep.2005.12.027

Wang, M., Liu, J., Zhao, Y., He, R., Xu, X., Guo, X., et al. (2020). Upregulation of METTL14 mediates the elevation of PERP mRNA N(6) adenosine methylation promoting the growth and metastasis of pancreatic cancer. *Mol. Cancer* 19:130. doi: 10.1186/s12943-020-01249-8

Wang, P., Doxtader, K. A., and Nam, Y. (2016). Structural basis for cooperative function of Mettl3 and Mettl14 methyltransferases. *Mol. Cell* 63, 306–317. doi: 10.1016/j.molcel.2016.05.041

Wang, Q., Chen, C., Ding, Q., Zhao, Y., Wang, Z., Chen, J., et al. (2020). METTL3-mediated m(6)A modification of HDGF mRNA promotes gastric cancer progression and has prognostic significance. *Gut* 69, 1193–1205. doi: 10.1136/gutjnl-2019-319639

Wang, X., Feng, J., Xue, Y., Guan, Z., Zhang, D., Liu, Z., et al. (2017). Corrigendum: structural basis of N(6)-adenosine methylation by the METTL3-METTL14 complex. *Nature* 542:260. doi: 10.1038/nature21073

Wang, X., Lu, Z., Gomez, A., Hon, G., Yue, Y., Han, D., et al. (2014). N6-methyladenosine-dependent regulation of messenger RNA stability. *Nature* 505, 117–120. doi: 10.1038/nature12730

Wang, X., Zhao, B. S., Roundtree, I. A., Lu, Z., Han, D., Ma, H., et al. (2015). N(6)-methyladenosine modulates messenger RNA translation efficiency. *Cell* 161, 1388–1399. doi: 10.1016/j.cell.2015.05.014

Warda, A. S., Kretschmer, J., Hackert, P., Lenz, C., Urlaub, H., Höbartner, C., et al. (2017). Human METTL16 is a N(6)-methyladenosine (m(6)A) methyltransferase that targets pre-mRNAs and various non-coding RNAs. *EMBO Rep.* 18, 2004–2014. doi: 10.15252/embr.201744940

Wu, Y., Zhao, W., Liu, Y., Tan, X., Li, X., Zou, Q., et al. (2018). Function of HNRNPC in breast cancer cells by controlling the dsRNA-induced interferon response. *EMBO J.* 37:e99017. doi: 10.15252/embj.201899017

Yang, X., Zhang, S., He, C., Xue, P., Zhang, L., He, Z., et al. (2020). METTL14 suppresses proliferation and metastasis of colorectal cancer by down-regulating oncogenic long non-coding RNA XIST. *Mol. Cancer* 19:46. doi: 10.1186/s12943-020-1146-4

Yue, Y., Liu, J., Cui, X., Cao, J., Luo, G., Zhang, Z., et al. (2018). VIRMA mediates preferential m(6)A mRNA methylation in 3′UTR and near stop codon and

associates with alternative polyadenylation. *Cell Discov.* 4:10. doi: 10.1038/s41421-018-0019-0

Zhang, C., Huang, S., Zhuang, H., Ruan, S., Zhou, Z., Huang, K., et al. (2020). YTHDF2 promotes the liver cancer stem cell phenotype and cancer metastasis by regulating OCT4 expression via m6A RNA methylation. *Oncogene* 39, 4507–4518. doi: 10.1038/s41388-020-1303-7

Zhang, H., Zhang, P., Long, C., Ma, X., Huang, H., Kuang, X., et al. (2020). m(6)A methyltransferase METTL3 promotes retinoblastoma progression via PI3K/AKT/mTOR pathway. *J. Cell. Mol. Med.* 24, 12368–12378. doi: 10.1111/jcmm.15736

Zhang, S., Zhao, B. S., Zhou, A., Lin, K., Zheng, S., Lu, Z., et al. (2017). m(6)A demethylase ALKBH5 maintains tumorigenicity of glioblastoma stem-like cells by sustaining FOXM1 expression and cell proliferation program. *Cancer Cell* 31, 591–606.e596. doi: 10.1016/j.ccell.2017.02.013

Zhao, Q., Zhao, Y., Hu, W., Zhang, Y., Wu, X., Lu, J., et al. (2020). m(6)A RNA modification modulates PI3K/Akt/mTOR signal pathway in Gastrointestinal Cancer. *Theranostics* 10, 9528–9543. doi: 10.7150/thno.42971

Zhao, X., Yang, Y., Sun, B. F., Shi, Y., Yang, X., Xiao, W., et al. (2014). FTO-dependent demethylation of N6-methyladenosine regulates mRNA splicing and is required for adipogenesis. *Cell Res.* 24, 1403–1419. doi: 10.1038/cr.2014.151

Zheng, Z., Zhang, L., Cui, X. L., Yu, X., Hsu, P. J., Lyu, R., et al. (2020). Control of early B cell development by the RNA N(6)-Methyladenosine methylation. *Cell Rep.* 31:107819. doi: 10.1016/j.celrep.2020.107819

Zhong, C., Li, Y., Yang, J., Jin, S., Chen, G., Li, D., et al. (2021). Immunotherapy for hepatocellular carcinoma: current limits and prospects. *Front. Oncol.* 11:589680. doi: 10.3389/fonc.2021.589680

Zhong, L., Liao, D., Zhang, M., Zeng, C., Li, X., Zhang, R., et al. (2019). YTHDF2 suppresses cell proliferation and growth via destabilizing the EGFR mRNA in hepatocellular carcinoma. *Cancer Lett.* 442, 252–261. doi: 10.1016/j.canlet.2018.11.006

Zhou, Y., Yin, Z., Hou, B., Yu, M., Chen, R., Jin, H., et al. (2019). Expression profiles and prognostic significance of RNA N6-methyladenosine-related genes in patients with hepatocellular carcinoma: evidence from independent datasets. *Cancer Manag. Res.* 11, 3921–3931. doi:10.2147/cmar.S191565

Conflict of Interest: The authors declare that the research was conducted in the absence of any commercial or financial relationships that could be construed as a potential conflict of interest.

frontiers in Cell and Developmental Biology

ORIGINAL RESEARCH
published: 01 July 2021
doi: 10.3389/fcell.2021.684505

Cancer-Associated Fibroblast-Derived Interleukin-8 Promotes Ovarian Cancer Cell Stemness and Malignancy Through the Notch3-Mediated Signaling

Zhaodong Ji[1,2†], Wenjuan Tian[1,2,3†], Wen Gao[4†], Rongyu Zang[5], Huaying Wang[2,3*] and Gong Yang[1,2,6*]*

[1] Cancer Institute, Fudan University Shanghai Cancer Center, Shanghai, China, [2] Department of Oncology, Shanghai Medical College, Fudan University, Shanghai, China, [3] Gynecological Oncology, Fudan University Shanghai Cancer Center, Shanghai, China, [4] The Cancer Hospital of the University of Chinese Academy of Sciences (Zhejiang Cancer Hospital), Institute of Basic Medicine and Cancer (IBMC), Chinese Academy of Sciences, Hangzhou, China, [5] Ovarian Cancer Program, Division of Gynecologic Oncology, Department of Obstetrics and Gynecology, Zhongshan Hospital, Fudan University, Shanghai, China, [6] Central Laboratory, The Fifth People's Hospital of Shanghai, Fudan University, Shanghai, China

OPEN ACCESS

Edited by:
Na Luo,
Nankai University, China

Reviewed by:
Do-Hee Kim,
Kyonggi University, South Korea
Toshiaki Ohara,
Okayama University, Japan

***Correspondence:**
Gong Yang
yanggong@fudan.edu.cn
Huaying Wang
huaying2004@shca.org.cn
Rongyu Zang
zang.rongyu@zs-hospital.sh.cn

† These authors have contributed equally to this work

Specialty section:
This article was submitted to Molecular Medicine, a section of the journal Frontiers in Cell and Developmental Biology

Received: 23 March 2021
Accepted: 01 June 2021
Published: 01 July 2021

Citation:
Ji Z, Tian W, Gao W, Zang R, Wang H and Yang G (2021) Cancer-Associated Fibroblast-Derived Interleukin-8 Promotes Ovarian Cancer Cell Stemness and Malignancy Through the Notch3-Mediated Signaling. Front. Cell Dev. Biol. 9:684505. doi: 10.3389/fcell.2021.684505

As a significant component in ovarian cancer microenvironment, cancer-associated fibroblasts (CAFs) contribute to cancer progression through interaction with cancer cells. Recent studies demonstrate that interleukin-8 (IL-8) is overexpressed in multiple cancer types and is essential for tumor development. Nonetheless, the underlying mechanism that the CAF-derived IL-8 promotes ovarian tumorigenesis is unknown. Here, we show that IL-8 secreted from CAFs could activate normal ovarian fibroblasts (NFs) through multiple signaling and that IL-8 stimulated malignant growth of ovarian cancer cells in animals and increased the IC_{50} of cisplatin (CDDP) in ovarian cancer cells. Further study showed that IL-8 induced cancer cell stemness via the activation of Notch3 and that the high level of IL-8 in ascites was positively correlated with the expression of Notch3 in ovarian cancer tissues. Collectively, IL-8 secreted from CAFs and cancer cells promotes stemness in human ovarian cancer via the activation of the Notch3-mediated signaling, which may provide a novel strategy for ovarian cancer treatment.

Keywords: IL-8, tumor stemness, epithelial ovarian cancer, cancer-associated ovarian fibroblasts, Notch3 signal pathway

INTRODUCTION

Ovarian cancer is the second most common cause of gynecologic malignancies around the world, with a high rate of metastatic recurrence and chemoresistance after first surgery (Eisenhauer, 2017). Over the past decades, most studies have been focused only on characteristics of cancer cells rather than the tumor stroma. A growing number of evidence suggests that the tumor microenvironment not only contributes to the initiation and development of malignancy but also promotes cancer metastasis and recurrence, while the secreted chemokines including interleukin (IL)-6 and IL-8 may play vital roles in ovarian tumorigenesis (Browning et al., 2018). In ovarian cancer microenvironment, IL-8, as an adipokine, can activate adipocytes along with the fatty acid-binding

protein 4 (FABP4) to provide fatty acids, which provides energy to promote cancer cell omental metastasis (Nieman et al., 2011). Cancer-associated fibroblasts (CAFs) also stimulate omental metastasis of cancer cell through TGF-β-activated of MMP-2 (Cai et al., 2012). However, the molecular mechanism that IL-8 mediates the stroma–cancer interaction to promote the growth and metastasis of ovarian cancer is still unclear.

Cellular senescence is an irreversible phenomenon that cells stop to divide due to shortened telomere. Senescent fibroblast is an important component of stromal cells in the tumor microenvironment with unique chracteristics (Wang et al., 2017). In the process of culture, they become morphologically flattened with the elevated activity of senescence-related acidic β-galactosidase. Many inflammatory cytokines including IL-8 can be secreted by senescent fibroblasts to promote tumorigenesis and metastasis (Krtolica et al., 2001; Orjalo et al., 2009; Lee et al., 2012). Our team previously found that the growth-regulated oncogene 1 (Gro-1) secreted from CAFs promoted epithelial ovarian tumorigenesis (Yang et al., 2006). However, the underlying mechanism that cytokines secreted from CAFs activate normal ovarian fibroblasts (NFs) and thereby promote epithelial malignancy remains unclear.

The Notch family genes were first identified in 1983 (Kidd et al., 1983) and reported to be involved in multiple functions including cancer stem cell (CSC) self-renewal, cancer angiogenesis, metastasis, recurrence, and chemoresistance (Miele et al., 2006; Purow, 2012). Activation of Notch signaling pathway in bone stroma enhances bone metastasis of breast cancer (Sethi et al., 2011). In ovarian cancer, Notch3 and Notch1 usually activate multiple signaling pathways to participate in cancer development (Park et al., 2006; Rose et al., 2010). Overexpression of Notch3 is associated with ovarian cancer recurrence and chemoresistance to carboplatin (Park et al., 2010), which predicts a poor prognosis in ovarian cancer (Jung et al., 2010). Overexpression of Notch3 also enriches ovarian cancer cells with stem-like cell properties, leading to chemoresistance to platinum-based therapy (McAuliffe et al., 2012). Jagged 1, as a Notch ligand, could promote angiogenesis in endothelial cells and lead to proliferation and chemoresistance in epithelial cancer cells (Steg et al., 2011). In addition, Notch/Delta-like ligand 4 (DII4) also functions in both tumor and endothelial cells, which could stimulate ovarian cancer growth (Hu et al., 2011). Blocking of the Notch1 activity by inhibiting gamma-secretase is unable to release Notch intracellular domain (NICD), which retards ovarian tumor growth and induces ovarian cancer cell apoptosis (Wang et al., 2010). Recent studies also revealed that the Notch signaling activity may regulate a network of inflammatory cytokines in ovarian tumor microenvironment (Kulbe et al., 2012; Wieland et al., 2017).

In the present study, we found that IL-8 derived from CAFs could promote angiogenesis and proliferation of NFs through the activation of the AKT and ERK pathways and could induce the stemness and malignant proliferation of ovarian cancer cells through the Notch3-mediated signaling.

MATERIALS AND METHODS

Cell Lines and Cell Culture

NFs (NF320 and NF325) and cancer-associated ovarian fibroblasts (CAF501 and CAF502) were isolated from ovarian tissues with informed consent of the donors according to a protocol approved by the Institutional Review Board and were cultured for this study at early population doublings according to the method described elsewhere (Rosen et al., 2006). Human epithelial ovarian cancer (EOC) cell line HEY-A8 was purchased from American Type Culture Collection (Manassas, VA, United States) and cultured in RPMI-1640 media containing 10% fetal calf serum, 2 mM of L-glutamine, penicillin (100 units/ml), and streptomycin (100 μg/ml). Ovarian cancer cell line HEY-A8 was infected with Notch3 report plasmid with green fluorescent protein (GFP). Ovarian cancer cell line HEY-A8 was infected with IL-8 cDNA and IL-8 shRNA viruses with anti-puro.

Measurement of Interleukin-8 Secretion

The levels of IL-8 in conditioned media (CM) from NFs and CAFs were measured by enzyme-linked immunosorbent assay (ELISA) Quantikine kits from R&D Systems (Minneapolis, MN, United States) (DGR00 and D8000C) according to the manufacturer's instructions. In brief, either 200 μl of CM collected after 48 h of cell culture or 200 μl of a diluted IL-8 standard (31.25–1,000 pg/ml; six dilutions) was added per well (each sample was tested in triplicate) in high-binding, flat-bottomed, 96-well polypropylene plates (NUNC) precoated with IL-8 antibody (supplied in kit). After incubation at room temperature and sufficient wash with phosphate-buffered saline (PBS) + 1% Tween 20, the plate was treated with 200 μl of conjugate (supplied in kit) for 1 h at 2°C to 8°C, followed by addition of substrate in a dark condition at room temperature. Last, a stop solution (1 mol/L of sulfuric acid) was added in a volume of 50 μl to each well to stop the reaction. The absorbance readings at 450 nm (subtracted from 579-nm readings) were determined using a SpectraMax 250 microplate reader (Molecular Devices, San Jose, CA, United States). The concentration (in pg/ml) of IL-8 was converted from absorbance readings by using a standard curve generated from absorbance readings of standard samples. This assay was repeated three times along with negative controls.

Treatment of HEY-A8 With Interleukin-8 and Cancer-Associated Fibroblast Conditioned Media

HEY-A8 was treated with IL-8 at the concentration of 200 ng/ml, or CAF CM alone, or CAF CM plus IL-8 antibody (10 ng/ml) over a time course of 24, 48, and 72 h. Cells were performed for Western blotting analysis.

Three-Dimensional Culture of Ovarian Cancer Cells

For three-dimensional (3-D) culture of ovarian cancer cells, Rat Tail Collagen Type 1 (RTCT1, from BD Biosciences, San Jose,

CA, United States) was used as matrigel and diluted to 50 μg/ml using 0.02 N of acetic acid; 24-well tissue culture plates were coated with matrigel at 5 $\mu g/cm^2$ and allowed to solidify for 1 h at room temperature. Ovarian cancer cells were trypsinized from monolayer cultures and pelleted at 1,000 rpm. Then the cells were washed twice with PBS to remove cell debris and counted under a microscope. A total of 250 cells were resuspended in 1 ml of fresh media mixed with RTCT1 and NaOH at the ratio of 10:1:0.0235 and plated into each well of precoated 24-well plates. Cells were kept at room temperature for 10 min and cultured for 5–10 days at 37° with 5% CO_2 in an incubator. 3-D spheroids were counted and recorded.

Measurement of Stem-Cell Like Properties in Notch-Activated Cells From 3-D Culture

Cells expressing GFP with activated Notch signaling were sorted with flow cytometery and replated for 3-D culture in 24 wells at 250 cells/well. The number and size of spheroids were counted and examined in comparison with Notch-inactivated cells without expression of GFP.

Analysis of Protein Expression by Immunoblotting

Total protein extract for each cell line was obtained by using a lysis buffer as described previously (Yang et al., 2010), and equal amounts (20 μg per load) were analyzed by immunoblotting. Antibody against β-actin was from Sigma-Aldrich (St. Louis, MO, United States) (A5441, 1:20,000); vascular endothelial growth factor (VEGF; sc-507, 1:1,000) was from Santa Cruz Biotechnology (Dallas, TX, United States). AKT (no. 9272, 1:1,000), extracellular signal-regulated kinase 1/2 (ERK1/2; mAb no. 4695, 1:1,000), and thrombospondin-1 (TSP-1) were from Lab Vision (MS-418, 1:500; Thermo Fisher Scientific, Waltham, MA, United States). Notch3 was from Cell Signaling Technology (Danvers, MA, United States) (cst-5276, 1:1,000). Western blotting reagents were from a chemiluminescence kit (Amersham Biosciences, Little Chalfont, United Kingdom).

Animal Experiments

Animal experiments were approved by the Institutional Animal Care and Use Committee of Fudan University Shanghai Cancer Center (FUSCC) and performed following the Institutional Guidelines and Protocols. The 6- to 7-week-old BALB/c athymic nude mice were purchased from Shanghai Slac Laboratory Animal Co., Ltd. (Shanghai, China) and housed in the Department of Laboratory Animals (Fudan University). To test whether the CAFs enhance EOC growth, 3×10^6 of tumor cells (HEY-A8) alone or mixed with 3×10^4 (100:1) of differently treated fibroblasts in 150 μl of PBS were injected into the dorsal flap of one mouse. The date at which the first grossly visible tumor appeared was recorded, and tumor size was measured every 3–7 days thereafter. Tumor volume was measured and recorded according to our previous method (Yang et al., 2010). Statistical analysis was done by Fisher's exact test at different time points for the mean tumor sizes of each group. When a tumor reached 1.5 cm in diameter, all mice in the same group were sacrificed by exposure to 5% carbon monoxide. The specific groups are as follows: each group including four to eight mice injected with 3×10^6 cells for ovarian cancer cell line HEY-A8 from subcutaneous was considered as the control group.

Immunohistochemical Staining

Ovarian normal and cancer tissues were obtained from FUSCC. Specimen collection was approved by the Clinical Research Ethics Committee of FUSCC and conducted with an informed consent signed by each participant before the use of tissues (No. 1711178-23). Tissue microarrays included core samples from 12 high-grade serous EOCs. Proteins including IL-8 and Notch3 were detected by immunostaining. Antibody was detected by using avidin–biotin–peroxidase method, as described elsewhere (Yang et al., 2010). Tissues with more than 5% of cells stained for the proteins were considered positive, and those with less than 5% staining were considered negative.

Immunocytochemistry

The spheroids cultured in 3-D were harvested and washed with PBS for four times, then fixed in 75% ethanol for 2 h, and embedded in paraffin. The paraffin was cut into 3- to 5-μm-thick slides, deparaffinized in xylene, soaked in alcohol with different concentrations (100, 95, and 75%), and rinsed with deionized water. The slides were placed in 3% hydrogen peroxide in methanol and rinsed in water. The slides were steamed in the pretreatment buffer for 50 min and then cooled for 30 min. The slides were stained with Notch3 (1:100 dilution) and incubated overnight, and the polymer was added and incubated for 40 min. 3,3-Diaminobenzidine tetrahydrochloride was added and incubated for 20 min. The slides were counterstained with hematoxylin for 1 min.

Measurement of Interleukin-8 in Ascites

The collection of ascetic fluid was performed in 12 EOC patients who were verified via histological analysis. The cell debris in ascitic fluid was removed by centrifugation at 2,500 rpm for 15 min. Each supernatant was collected, and then IL-8 was performed by the ELISA, as mentioned above.

Statistical Analysis

The data were calculated using GraphPad Prism IV software and expressed as the mean ± SD. The difference between two groups was evaluated by Student's *t*-test and chi-square test analyses. Values of $p < 0.05$ were considered statistically significant ($^*p < 0.05$; $^{**}p < 0.01$; $^{***}p < 0.001$). Center values are mean, and error bars are SD.

RESULTS

Interleukin-8 Activates Normal Ovarian Fibroblasts in Multiple Signal Pathways

As a predominant cell type in normal stroma, quiescent resident fibroblasts can be transformed into CAFs through interaction with CAFs and/or cancer cells to become a major component of the tumor stroma, but little is known how NFs are transformed

into CAFs (Mitra et al., 2012). In this study, we first isolated and successfully cultured the primary cultured CAFs and NFs from ovarian cancer and normal tissues, and then we measured the secretion of IL-8 in CAF CM and NF CM by ELISA. The results showed that the level of IL-8 was higher in CAF CM than NF CM (**Figure 1A**). It is generally known that the biological function of IL-8 is mediated through the binding of two cell-surface G protein-coupled receptors, CXCR1 and CXCR2, so their expression levels in NFs and CAFs were detected by Western blotting and qRT-PCR. We found that both receptors were highly expressed in CAFs compared with those in NFs (**Figures 1B,C**).

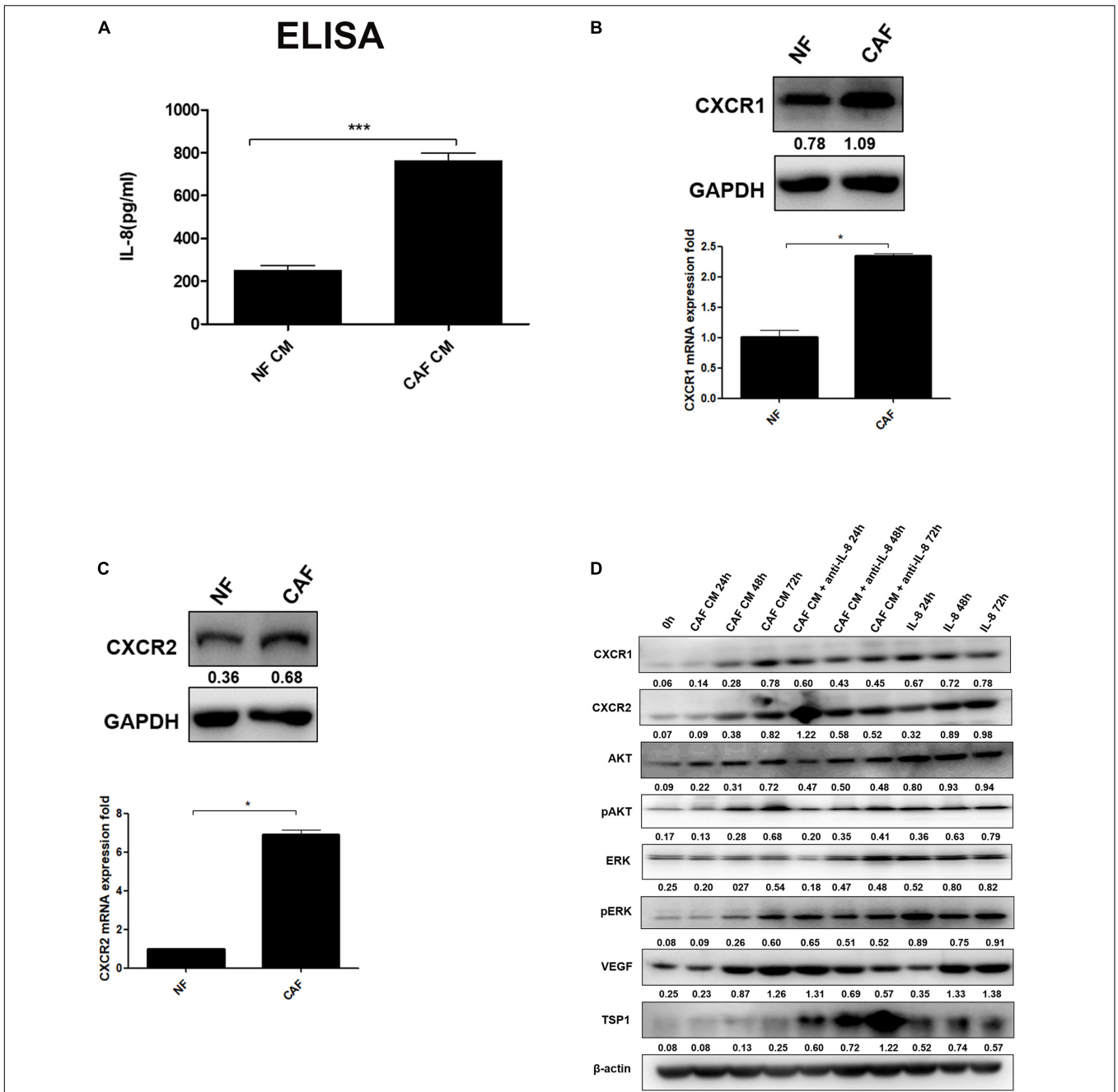

FIGURE 1 | IL-8 activates NFs in multiple signal pathways. **(A)** Measurement of IL-8 in CAF CM and NF CM by ELISA. **(B,C)** Detection of CXCR1 and CXCR2 in NFs and CAFs by Western blotting and qRT-PCR. Triple independent experiments were carried out, and representative results are shown. **(D)** Analysis of AKT/ERK-associated proteins including CXCR1/2, AKT, pAKT, ERK, pERK, and angiogenesis-related proteins (VEGF and TSP-1) by Western blotting in NFs treated with CAF CM, CAF CM + anti-IL-8, and IL-8 alone. β-Actin was used as a loading control. $^{*}p < 0.05$, $^{***}p < 0.001$. IL, interleukin; NFs, normal ovarian fibroblasts; CAFs, cancer-associated fibroblasts; CM, conditioned media; VEGF, vascular endothelial growth factor.

Furthermore, we treated NFs with CAF CM, CAF CM+IL-8 antibody (anti-IL-8), and IL-8 alone for 24, 48, and 72 h, respectively. As shown in **Figure 1D**, treatment of NFs with CAF CM increased the protein expression of CXCR1/2, AKT, pAKT, ERK, pERK, and VEGF in a time-dependent manner compared with control (0 h). Although treatment of NFs with IL-8 alone highly enhanced the expression of these molecules, the use of IL-8 antibody (anti-IL-8) to neutralize IL-8 in CAF CM only slightly reduced the expression of CXCR1/CXCR2, AKT, pAKT, ERK, pERK. The potential reasons are that more cytokines other than IL-8 from the CAF CM might also activate these signal molecules and that NFs also secreted IL-8 to rescue the neutralization

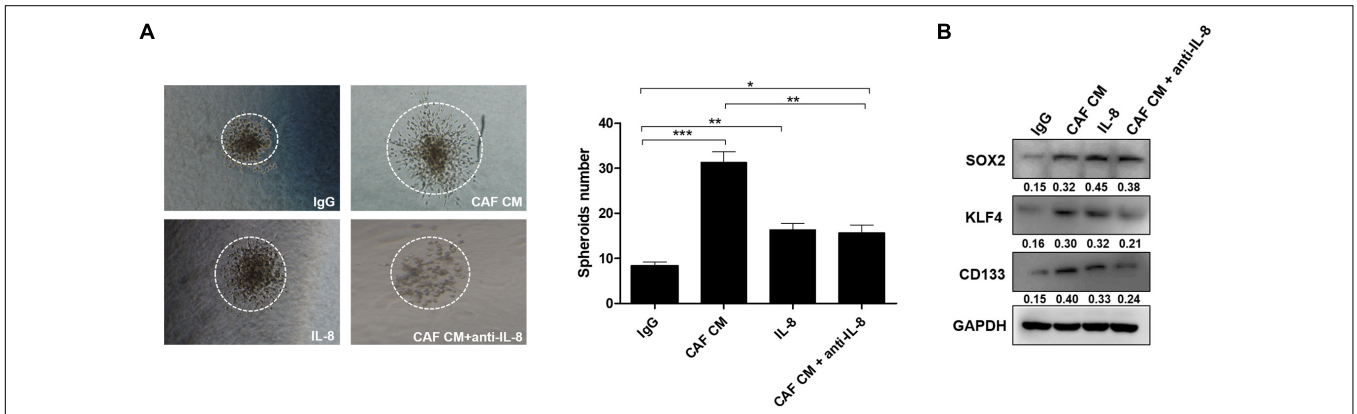

FIGURE 2 | IL-8 secreted from CAFs promotes cancer cell stemness. **(A)** Spheroids formed by HEY-A8 cells treated with IgG, CAF CM, CAF CM+anti-IL-8, or IL-8. **(B)** Analysis of KLF4, SOX2, and CD133 expression by Western blotting in HEY-A8 cells treated with IgG, CAF CM, CAF CM+anti-IL-8, or IL-8. GAPDH was used as a loading control. IL, interleukin; CAFs, cancer-associated fibroblasts. $^{*}p < 0.05$, $^{**}p < 0.01$, $^{***}p < 0.001$.

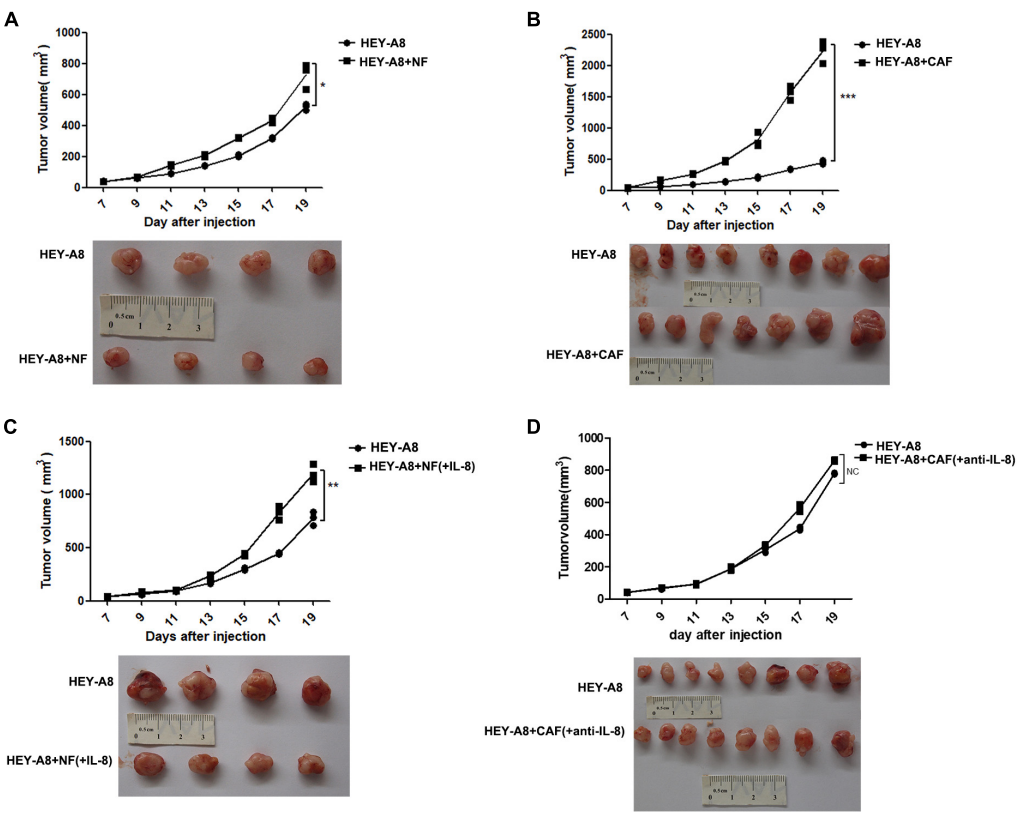

FIGURE 3 | IL-8 stimulates xenograft tumor growth in animals. Xenograft tumor growth by subcutaneous injection of HEY-A8 cells mixed with different fibroblast NFs **(A)**, CAFs **(B)**, NFs+IL-8 **(C)**, or CAFs neutralized by IL-8 antibody **(D)** as indicated. $^{*}p < 0.05$, $^{**}p < 0.01$, $^{***}p < 0.001$. IL, interleukin; NFs, normal ovarian fibroblasts; CAFs, cancer-associated fibroblasts.

during the treatment. However, neutralization of IL-8 with IL-8 antibody in NF treated with CAF CM apparently downregulated VEGF but upregulated thrombospondin 1 (TSP1), an anti-angiogenesis factor, in a time dependent manner. Therefore, it can be inferred that IL-8 activates NFs through PI3K/AKT and ERK pathways.

Interleukin-8 Secreted From Cancer-Associated Fibroblasts Promotes Cancer Cell Stemness

Since CSCs play a critical role in the formation of spheroids, we explored whether IL-8 could maintain tumor stemness through regulation of cancer cell growth and invasion. As the results shown in 3-D culture, the spheroids formed by cancer cells treated with CAF CM developed bigger than those formed by the control cells treated with IgG, or spheroids treated with IL-8 alone and CAF CM+anti-IL-8. Meanwhile, spheroids of cancer cells treated with IL-8 were much bigger than those of cells group treated with CAF CM+anti-IL-8, indicating that IL-8 derived from CAFs may promote proliferation and stemness of cancer cells. The number of spheroids formed by cells treated with CAF CM was significantly more than that formed by the cells treated with others (**Figure 2A**).

Further experiments showed that the stemness markers including KLF4, SOX2, and CD133 were increased by IL-8 stimulation, suggesting that IL-8 secreted from CAFs may promote ovarian cancer cell stemness (**Figure 2B**).

Interleukin-8 Stimulates Xenograft Tumor Growth in Animals

To investigate whether CAFs promote the growth of tumor *in vivo*, we injected ovarian cancer epithelial cells alone or with CAFs, and NFs treated with or without IL-8 into immunocompromised mice. The results showed that HEY-A8

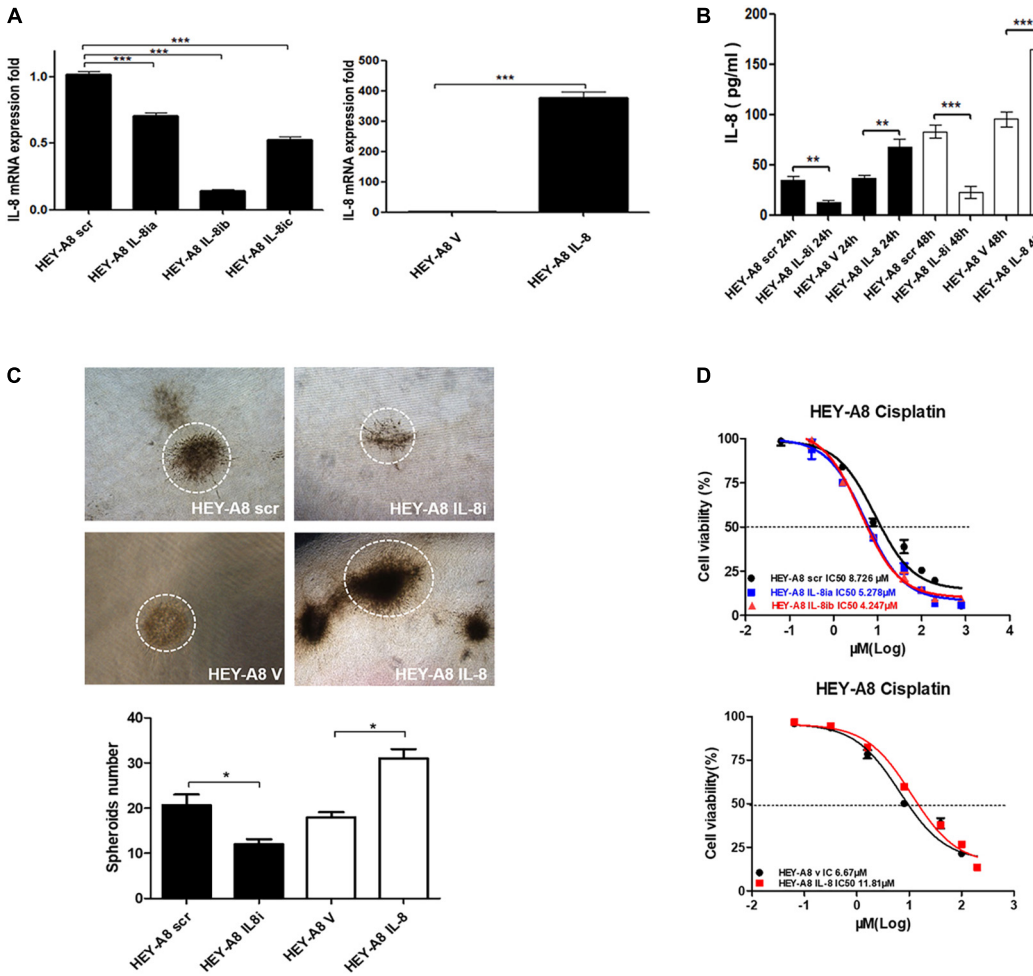

FIGURE 4 | IL-8 enhances ovarian cancer cell stemness and chemoresistance. **(A)** Examination of IL-8 expression in IL-8 overexpression and silencing ovarian cancer cells by qRT-PCR. **(B)** Measurement of IL-8 secreted from overexpression and silencing cells by ELISA. **(C)** Spheroids formed by IL-8 overexpression and silencing ovarian cancer cells in 3-D culture. **(D)** Survival rates of ovarian cancer cells expressing IL-8 shRNA or cDNA tested by CCK-8 following the treatment with cisplatin. OD values were measured after treatment with cisplatin at 48 h. $^{*}p < 0.05$, $^{**}p < 0.01$, $^{***}p < 0.001$. IL, interleukin; CCK-8, Cell Counting Kit-8; OD, optical density.

cells mixed with NFs enhanced cancer growth as compared with HEY-A8 cells alone (**Figure 3A**), whereas HEY-A8 cells mixed with CAFs stimulated tumor even much faster than cancer cells alone (**Figure 3B**). Although NFs+IL-8 induced the tumor growth of HEY-A8 cells faster than did HEY-A8 cells alone, cancer cells pretreated with CAF CM+IL-8 antibody to neutralize the function of IL-8, generated the similar tumor growth to that induced by HEY-A8 cells alone (**Figures 3C,D**).

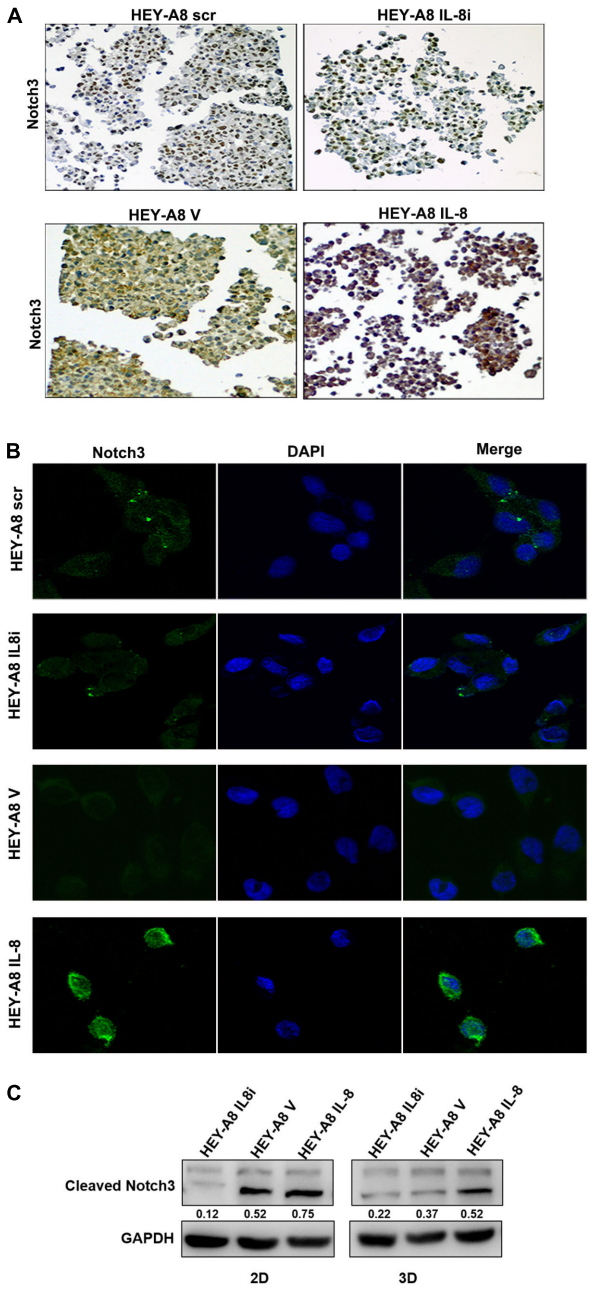

FIGURE 5 | IL-8 enhances ovarian cancer cell stemness through the Notch3-mediated signaling pathway. **(A)** Examination of Notch3 expression in spheroids by immunocytochemistry. **(B)** Notch3 activation in cells derived from spheroids. Notch3 was activated (green) in 3-D culture cells with IL-8 overexpression but was decreased in IL-8-silencing cells compared with control cells. DAPI (blue) was used as a nuclear dye. **(C)** Analysis of cleaved Notch3 by Western blotting in HEY-A8 cells cultured in 2-D and 3-D. IL, interleukin.

Interleukin-8 Enhances Ovarian Cancer Cell Stemness Through Notch3 Signaling Pathway

As a chemokine, IL-8 can be secreted into the tumor microenvironment by cancer cells in an autocrine manner to trigger a series of biological functions through the surface receptors in cancer cells. To understand the effect of IL-8 on cancer cells, IL-8 cDNA and shRNA were, respectively, introduced to HEY-A8 cells. qRT-PCR was used to verify that IL-8 was remarkably overexpressed or silenced in the resulting cells compared with control cells treated with empty vector (V) or scrambled shRNA (scr). From the data, we selected the cells expressing IL-8ib in the next experiment (**Figure 4A**). The secreted levels of IL-8 in both two cell lines were measured by ELISA. Compared with that of the control, the level of secreted IL-8 was significantly decreased in HEY-A8 IL-8i cells and increased in HEY-A8 IL-8 cells (**Figure 4B**).

The 3-D approach has been used in cancer research as an intermediate model between *in vitro* cancer cell line cultures and *in vivo* tumors, formation has gained popularity in CSC research (Weiswald et al., 2015). Thus, we confirmed proliferation and stemness of cell lines by 3-D culture. As shown in **Figure 4C**, the spheroids formed by HEY-A8 IL-8i cells were smaller than those formed by control cells. The spheroids formed by HEY-A8 IL-8 cells developed much bigger than those formed by control cells.

Chemotherapeutic resistance, whether intrinsic or acquired, is a multifactorial phenomenon that is associated with the tumor microenvironment (Sui et al., 2013). To explore the impact of IL-8 on chemoresistance, we evaluated the effects of IL-8 on response of cancer cells to cisplatin (CDDP). Cells treated with different concentrations of CDDP at 48 h were determined by Cell Counting Kit-8 (CCK-8) assay for their viabilities. Compared with that in control cells, the survival rate was increased in overexpressing cells, whereas that of cells expressing IL-8 shRNA was decreased. The IC_{50} values of CDDP were increased in cells overexpressing IL-8. In contrast, the IC_{50} values of IL-8 knockdown cells were reduced compared with those of control cells (**Figure 4D**). These data suggest that IL-8 confers CDDP resistance in ovarian cancer cells.

It has been reported that the Notch family is important for stem cell self-renewal through the enhanced cancer cell stemness in CSCs (Takebe et al., 2015). The Notch signaling can be activated by factors such as IL-6, which derived from CAFs (Guo et al., 2011). We then further explored the relationship between Notch3 and IL-8. 3-D spheroids were analyzed by immunochemical staining and immunofluorescence and showed that the expression of Notch3 was obviously higher in HEY-A8 IL-8 cells and lower in HEY-A8 IL-8i cells than in control cells (**Figures 5A,B**).

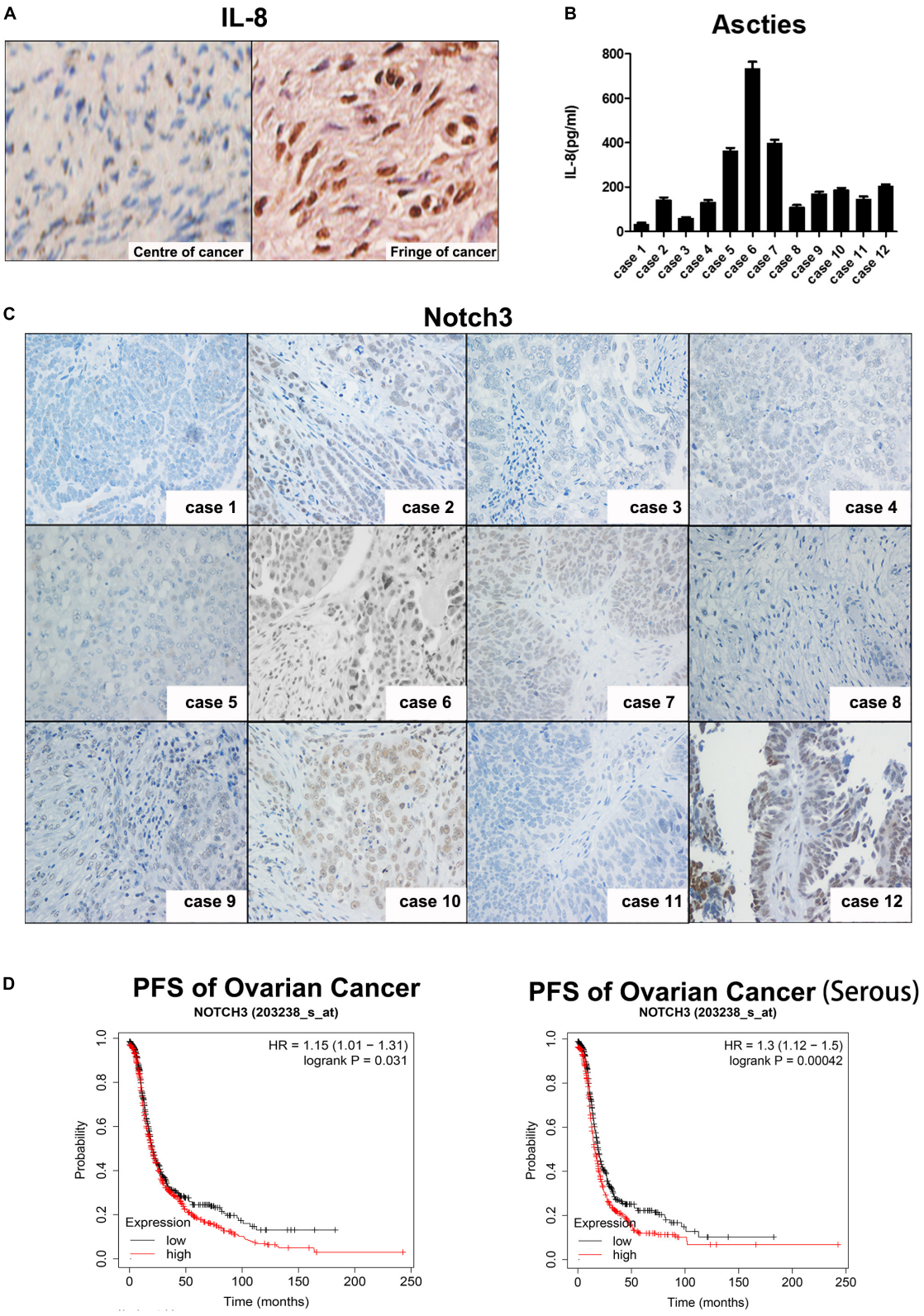

FIGURE 6 | Expression of IL-8 is associated with Notch3 in ovarian cancer tissues. **(A)** IHC staining of IL-8 expression in ovarian cancer tissues. Center (left) and fringe (right). Magnification, ×400. **(B)** IL-8 levels in ascitic fluid of 12 EOC patients were measured by ELISA. **(C)** Representative images showing Notch3 expression detected by IHC in ovarian cancer tissues. Magnification, ×200. **(D)** Prognostic analyses of ovarian cancer patients based on Notch3 mRNA levels calculated by the Kaplan–Meier survival curves (http://kmplot.com/analysis/index.php?p=service). IL, interleukin; IHC, immunohistochemistry; EOC, epithelial ovarian cancer.

To further investigate whether Notch3 is involved in pathway of IL-8-mediated tumor stemness, Western blotting was used to detect the expression of Notch3 in IL-8 knockdown and overexpression cells derived from 2-D and 3-D culture. The results showed that the cleaved Notch3 was decreased in IL-8 knockdown cells but was increased in IL-8 overexpression cells, indicating that IL-8 may promote ovarian cancer cell stemness through the activation of Notch3 signaling (**Figure 5C**). However, the expression of Nocth1 and Notch2 did not obviously change between cells derived from the 2-D and 3-D cultures (**Supplementary Figure 1**).

Expression of Interleukin-8 Is Associated With Notch3 in Ovarian Cancer Tissues

To determine whether IL-8 is expressed in tumor tissues in patients and which cells IL-8 is expressed in, we performed immunohistochemistry. As shown in **Figure 6A**, IL-8 was highly expressed in the stroma of ovarian tumor fringe tissues, where there were more CAFs (right), but little IL-8 was stained in the center of tissues with fewer fibroblasts (left).

We then investigated the relationship between Notch3 and IL-8 levels in patients diagnosed with ovarian cancer by examining the level of IL-8 in the ascites by ELISA and the expression of Nocth3 in tumor tissue samples from 12 ovarian cancer patients by immunohistochemical staining (**Figures 6B,C**). Interestingly, the expression of IL-8 in ascites was positively correlated with the nuclear expression of Notch3 in tissues.

Finally, we explored the critical role of Notch3 in the survival of patients with ovarian cancer. The Kaplan–Meier curve and log rank test analyses revealed that the high expression of Notch3 mRNA had a lower progression-free survival (PFS) rate in all pathological types of ovarian cancer, especially in serous ovarian cancer (**Figure 6D**).

DISCUSSION

In this study, we provide strong evidence that IL-8 plays a critical role in ovarian cancer microenvironment (**Figure 7**). CAFs have been reported to possess a prominent role in promoting tumor growth and predicting poor outcome in various cancers, which have gained many attentions as a promising target (Erdogan and Webb, 2017). CAF CM contains a bunch of growth factors, cytokines and chemokines, which may promote proliferation and survival of cancer cells (Nurmik et al., 2020). IL-8 is one of the critical chemokines in CAF CM. In the present study, we found that a higher level of IL-8 was present in CAF CM than in NF CM. Mechanistic studies revealed that IL-8 could activate NFs through PI3K/AKT and ERK signals. Furthermore, IL-8 also stimulated angiogenesis by increasing VEGF and decreasing TSP1 in NFs. The *in vivo* experiments showed that cancer cells mixed with

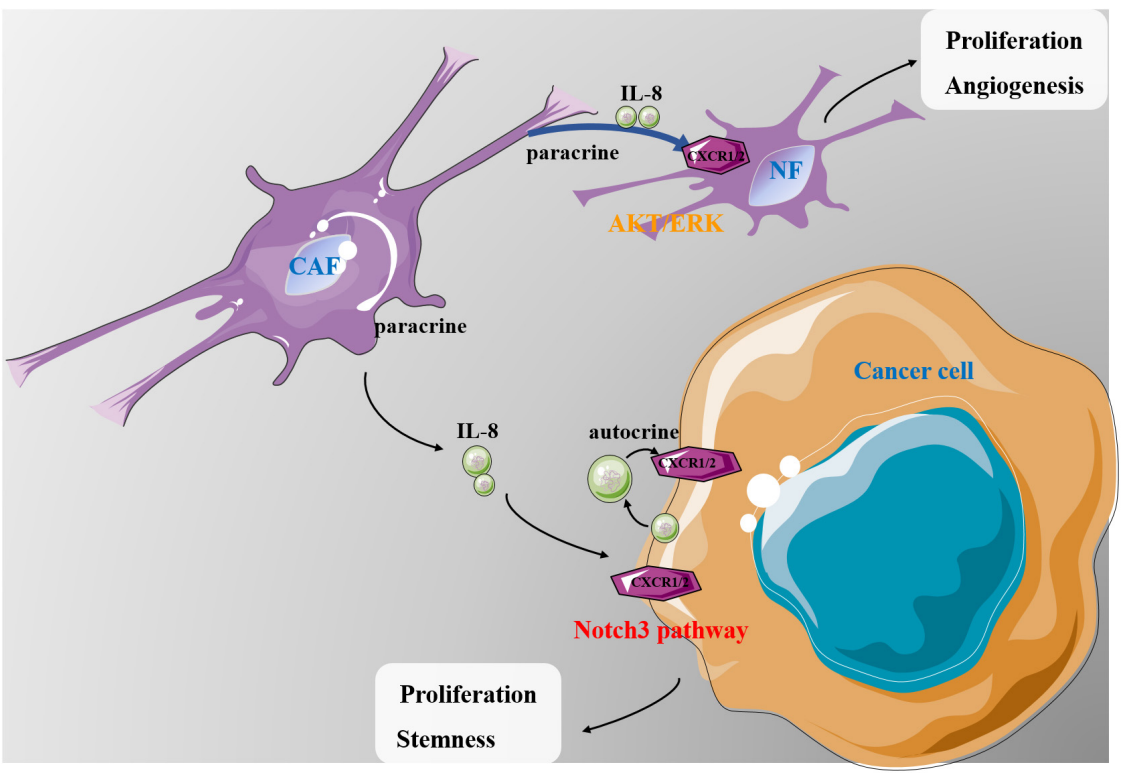

FIGURE 7 | A schematic diagram showing the possible mechanism of IL-8 in ovarian cancer microenvironment. CAF-derived IL-8 can activate the NFs in multiple signal pathways. IL-8 derived from both cancer cells and CAFs can promote proliferation and stemness of cancer cells through the Notch3-mediated signaling. IL, interleukin; CAFs, cancer-associated fibroblasts; NFs, normal ovarian fibroblasts.

NFs treated with IL-8 promoted ovarian xenograft tumor growth in mice. In 3-D culture, IL-8 induced the spheroid formation of ovarian cancer cells, whereas the IL-8-mediated cell stemness might be mediated through the Notch3 signaling. Analysis of clinical tissues further revealed that the levels of IL-8 in patient ascites were closely correlated with the activation of Notch3, suggesting a close link between IL-8 and Notch3, although the detailed mechanism requires further investigations.

Many cancers appear to contain a small population of pluripotent "CSCs" (Al-Hajj et al., 2004). The CSC hypothesis states that CSCs possess some of the biological properties of normal stem cells, including indefinite self-replication, asymmetric cell division, and resistance to toxic agents (De Francesco et al., 2018; Najafi et al., 2019). The CSC proliferation rate may depend on cancer microenvironment and also be associated with signal pathways (Eun et al., 2017). CSCs are responsible for chemotherapeutic resistance and finally cause disease recurrences and/or metastasis (Chang, 2016; Das et al., 2020). Ovarian cancer cell line HEY-A8 is reported to be enriched with CSCs. The Notch signaling members are critical in the regulation of CSCs, among which Notch3 overexpression in cancer cells can result in expansion of CSCs and increase platinum resistance (McAuliffe et al., 2012). In our study, we also found that overexpression of IL-8 in HEY-A8 can enhance CDDP resistance. However, whether IL-8 mediates chemoresistance via Notch3 remains unknown. Based on literature, the AKT pathway has been reported to stimulate the Notch activity in some experimental models, while VEGF is also found to regulate the expression of Notch genes through the phosphatidylinositol 3-kinase/AKT pathway (Liu et al., 2003). In the stromal microenvironment, many chemokines and cytokines may activate PI3K/AKT and Notch pathways, leading to tumor initiation and development, so we speculate that IL-8 may maintain the stemness of tumor cells through the PI3K/AKT/Notch3 pathway.

Certainly, there were still some limitations in our study. We only focused on the IL-8 derived from CAFs through which to activate NFs. However, in **Figure 1**, we also found that when NFs were treated with CAF CM and anti-IL-8, the expression of CXCR1/2, VEGF, and pERK was also increased, which prompted us to think whether other cytokines in CAF CM cooperated with IL-8 to promote the activation of NFs. CXCR1 and CXCR2 are reported to promote proliferation and invasion in many cancer cells. However, whether CAF-derived IL-8 mediates stemness via CXCR1/2 remains unknown.

Our data show that in ovarian tumor microenvironment, IL-8 derived from cancer cells and CAFs promotes the proliferation and stemness of cancer cells through the Notch3 signaling pathway, suggesting that the IL-8/Notch3 signaling may be a potential target for ovarian cancer treatment in the future.

DATA AVAILABILITY STATEMENT

The original contributions presented in the study are included in the article/**Supplementary Material**, further inquiries can be directed to the corresponding author/s.

ETHICS STATEMENT

The studies involving human participants were reviewed and approved by the Clinical Research Ethics Committee of Fudan University Shanghai Cancer Center. Written informed consent to participate in this study was provided by the participants' legal guardian/next of kin. The animal study was reviewed and approved by the Institutional Animal Care and Use Committee of Fudan University Shanghai Cancer Center.

AUTHOR CONTRIBUTIONS

ZJ, WT, and WG performed the experiments, collected all data, and drafted the manuscript. RZ and HW participated in the project design and manuscript discussion. GY designed the project and edited the manuscript. All authors contributed to the article and approved the submitted version.

FUNDING

This study was supported by grants from the National Natural Science Foundation of China (Nos. 81572553, 81372797, 81772789, and 81171911 to GY and No. 82002758 to WT).

SUPPLEMENTARY MATERIAL

The Supplementary Material for this article can be found online at: https://www.frontiersin.org/articles/10.3389/fcell.2021.684505/full#supplementary-material

REFERENCES

Al-Hajj, M., Becker, M. W., Wichal, M., Weissman, I., and Clarke, M. F. (2004). Therapeutic implications of cancer stem cells. *Curr. Opin. Genet. Dev.* 14, 43–47.

Browning, L., Patel, M. R., Horvath, E. B., Tawara, K., and Jorcyk, C. L. (2018). IL-6 and ovarian cancer: inflammatory cytokines in promotion of metastasis. *Cancer Manag. Res.* 10, 6685–6693. doi: 10.2147/cmar.s179189

Cai, J., Tang, H., Xu, L., Wang, X., Yang, C., Ruan, S., et al. (2012). Fibroblasts in omentum activated by tumor cells promote ovarian cancer growth, adhesion and invasiveness. *Carcinogenesis* 33, 20–29. doi: 10.1093/carcin/bgr230

Chang, J. C. (2016). Cancer stem cells: role in tumor growth, recurrence, metastasis, and treatment resistance. *Medicine (Baltimore)* 95(1 Suppl. 1), S20–S25.

Das, P. K., Islam, F., and Lam, A. K. (2020). The roles of cancer stem cells and therapy resistance in colorectal carcinoma. *Cells* 9:1392. doi: 10.3390/cells9061392

De Francesco, E. M., Sotgia, F., and Lisanti, M. P. (2018). Cancer stem cells (CSCs): metabolic strategies for their identification and eradication. *Biochem. J.* 475, 1611–1634. doi: 10.1042/bcj20170164

Eisenhauer, E. A. (2017). Real-world evidence in the treatment of ovarian cancer. *Ann. Oncol.* 28(suppl._8), viii61–viii65.

Erdogan, B., and Webb, D. J. (2017). Cancer-associated fibroblasts modulate growth factor signaling and extracellular matrix remodeling to regulate tumor metastasis. *Biochem. Soc. Trans.* 45, 229–236. doi: 10.1042/bst20160387

Eun, K., Ham, S. W., and Kim, H. (2017). Cancer stem cell heterogeneity: origin and new perspectives on CSC targeting. *BMB Rep.* 50, 117–125. doi: 10.5483/bmbrep.2017.50.3.222

Guo, S., Liu, M., and Gonzalez-Perez, R. R. (2011). Role of notch and its oncogenic signaling crosstalk in breast cancer. *Biochim. Biophys. Acta* 1815, 197–213. doi: 10.1016/j.bbcan.2010.12.002

Hu, W., Lu, C., Dong, H. H., Huang, J., Shen, D. Y., Stone, R. L., et al. (2011). Biological roles of the Delta family Notch ligand Dll4 in tumor and endothelial cells in ovarian cancer. *Cancer Res.* 71, 6030–6039. doi: 10.1158/0008-5472.can-10-2719

Jung, S. G., Kwon, Y. D., Song, J. A., Back, M. J., Lee, S. Y., Lee, C., et al. (2010). Prognostic significance of Notch 3 gene expression in ovarian serous carcinoma. *Cancer Sci.* 101, 1977–1983. doi: 10.1111/j.1349-7006.2010.01641.x

Kidd, S., Lockett, T. J., and Young, M. W. (1983). The Notch locus of Drosophila melanogaster. *Cell* 34, 421–433.

Krtolica, A., Parrinello, S., Lockett, S., Desprez, P. Y., and Campisi, J. (2001). Senescent fibroblasts promote epithelial cell growth and tumorigenesis: a link between cancer and aging. *Proc. Natl. Acad. Sci. U. S. A.* 98, 12072–12077. doi: 10.1073/pnas.211053698

Kulbe, H., Chakravarty, P., Leinster, D. A., Charles, K. A., Kwong, J., Thompson, R. G., et al. (2012). A dynamic inflammatory cytokine network in the human ovarian cancer microenvironment. *Cancer Res.* 72, 66–75. doi: 10.1158/0008-5472.can-11-2178

Lee, Y. S., Choi, I., Ning, Y., Kim, N. Y., Khatchadourian, V., Yang, D., et al. (2012). Interleukin-8 and its receptor CXCR2 in the tumour microenvironment promote colon cancer growth, progression and metastasis. *Br. J. Cancer* 106, 1833–1841. doi: 10.1038/bjc.2012.177

Liu, Z. J., Shirakawa, T., Li, Y., Soma, A., Oka, M., Dotto, G. P., et al. (2003). Regulation of Notch1 and Dll4 by vascular endothelial growth factor in arterial endothelial cells: implications for modulating arteriogenesis and angiogenesis. *Mol. Cell. Biol.* 23, 14–25. doi: 10.1128/mcb.23.1.14-25.2003

McAuliffe, S. M., Morgan, S. L., Wyant, G. A., Tran, L. T., Muto, K. W., Chen, Y. S., et al. (2012). Targeting Notch, a key pathway for ovarian cancer stem cells, sensitizes tumors to platinum therapy. *Proc. Natl. Acad. Sci. U. S. A.* 109, E2939–E2948.

Miele, L., Golde, T., and Osborne, B. (2006). Notch signaling in cancer. *Curr. Mol. Med.* 6, 905–918.

Mitra, A. K., Zillhardt, M., Hua, Y., Tiwari, P., Murmann, A. E., Peter, M. E., et al. (2012). MicroRNAs reprogram normal fibroblasts into cancer-associated fibroblasts in ovarian cancer. *Cancer Discov.* 2, 1100–1108. doi: 10.1158/2159-8290.cd-12-0206

Najafi, M., Farhood, B., and Mortezaee, K. (2019). Cancer stem cells (CSCs) in cancer progression and therapy. *J. Cell. Physiol.* 234, 8381–8395. doi: 10.1002/jcp.27740

Nieman, K. M., Kenny, H. A., Penicka, C. V., Ladanyi, A., Buell-Gutbrod, R., Zillhardt, M. R., et al. (2011). Adipocytes promote ovarian cancer metastasis and provide energy for rapid tumor growth. *Nat. Med.* 17, 1498–1503. doi: 10.1038/nm.2492

Nurmik, M., Ullmann, P., Rodriguez, F., Haan, S., and Letellier, E. (2020). In search of definitions: cancer-associated fibroblasts and their markers. *Int. J. Cancer* 146, 895–905. doi: 10.1002/ijc.32193

Orjalo, A. V., Bhaumik, D., Gengler, B. K., Scott, G. K., and Campisi, J. (2009). Cell surface-bound IL-1alpha is an upstream regulator of the senescence-associated IL-6/IL-8 cytokine network. *Proc. Natl. Acad. Sci. U. S. A.* 106, 17031–17036. doi: 10.1073/pnas.0905299106

Park, J. T., Chen, X., Trope, C. G., Davidson, B., Ie, M. Shih, and Wang, T. L. (2010). Notch3 overexpression is related to the recurrence of ovarian cancer and confers resistance to carboplatin. *Am. J. Pathol.* 177, 1087–1094. doi: 10.2353/ajpath.2010.100316

Park, J. T., Li, M., Nakayama, K., Mao, T. L., Davidson, B., Zhang, Z., et al. (2006). Notch3 gene amplification in ovarian cancer. *Cancer Res.* 66, 6312–6318. doi: 10.1158/0008-5472.can-05-3610

Purow, B. (2012). Notch inhibition as a promising new approach to cancer therapy. *Adv. Exp. Med. Biol.* 727, 305–319. doi: 10.1007/978-1-4614-0899-4_23

Rose, S. L., Kunnimalaiyaan, M., Drenzek, J., and Seiler, N. (2010). Notch 1 signaling is active in ovarian cancer. *Gynecol. Oncol.* 117, 130–133. doi: 10.1016/j.ygyno.2009.12.003

Rosen, D. G., Yang, G., Bast, R. C. Jr., and Liu, J. (2006). Use of Ras-transformed human ovarian surface epithelial cells as a model for studying ovarian cancer. *Methods Enzymol.* 407, 660–676. doi: 10.1016/s0076-6879(05)07052-7

Sethi, N., Dai, X., Winter, C. G., and Kang, Y. (2011). Tumor-derived JAGGED1 promotes osteolytic bone metastasis of breast cancer by engaging notch signaling in bone cells. *Cancer Cell* 19, 192–205. doi: 10.1016/j.ccr.2010.12.022

Steg, A. D., Katre, A. A., Goodman, B., Han, H. D., Nick, A. M., Stone, R. L., et al. (2011). Targeting the notch ligand JAGGED1 in both tumor cells and stroma in ovarian cancer. *Clin. Cancer Res.* 17, 5674–5685. doi: 10.1158/1078-0432.ccr-11-0432

Sui, X., Chen, R., Wang, Z., Huang, Z., Kong, N., Zhang, M., et al. (2013). Autophagy and chemotherapy resistance: a promising therapeutic target for cancer treatment. *Cell Death Dis.* 4:e838. doi: 10.1038/cddis.2013.350

Takebe, N., Miele, L., Harris, P. J., Jeong, W., Bando, H., Kahn, M., et al. (2015). Targeting Notch, Hedgehog, and Wnt pathways in cancer stem cells: clinical update. *Nat. Rev. Clin. Oncol.* 12, 445–464. doi: 10.1038/nrclinonc.2015.61

Wang, M., Wu, L., Wang, L., and Xin, X. (2010). Down-regulation of Notch1 by gamma-secretase inhibition contributes to cell growth inhibition and apoptosis in ovarian cancer cells A2780. *Biochem. Biophys. Res. Commun.* 393, 144–149. doi: 10.1016/j.bbrc.2010.01.103

Wang, T., Notta, F., Navab, R., Joseph, J., Ibrahimov, E., Xu, J., et al. (2017). Senescent carcinoma-associated fibroblasts upregulate IL8 to enhance prometastatic phenotypes. *Mol. Cancer Res.* 15, 3–14. doi: 10.1158/1541-7786.mcr-16-0192

Weiswald, L. B., Bellet, D., and Dangles-Marie, V. (2015). Spherical cancer models in tumor biology. *Neoplasia* 17, 1–15. doi: 10.1016/j.neo.2014.12.004

Wieland, E., Rodriguez-Vita, J., Liebler, S. S., Mogler, C., Moll, I., Herberich, S. E., et al. (2017). Endothelial Notch1 activity facilitates metastasis. *Cancer Cell* 31, 355–367. doi: 10.1016/j.ccell.2017.01.007

Yang, G., Chang, B., Yang, F., Guo, X., Cai, K. Q., Xiao, X. S., et al. (2010). Aurora kinase A promotes ovarian tumorigenesis through dysregulation of the cell cycle and suppression of BRCA2. *Clin. Cancer Res.* 16, 3171–3181. doi: 10.1158/1078-0432.ccr-09-3171

Yang, G., Rosen, D. G., Zhang, Z., Bast, R. C. Jr., Mills, G. B., Colacino, J. A., et al. (2006). The chemokine growth-regulated oncogene 1 (Gro-1) links RAS signaling to the senescence of stromal fibroblasts and ovarian tumorigenesis. *Proc. Natl. Acad. Sci. U. S. A.* 103, 16472–16477. doi: 10.1073/pnas.0605752103

Conflict of Interest: The authors declare that the research was conducted in the absence of any commercial or financial relationships that could be construed as a potential conflict of interest.

frontiers in Molecular Biosciences

ORIGINAL RESEARCH
published: 05 July 2021
doi: 10.3389/fmolb.2021.695420

Expression Characteristics and Significant Prognostic Values of PGK1 in Breast Cancer

*Yanping Li[1], Shanshan Wang[1], Xiaoyuan Zhang[1], Rui Yang[1], Xiaonan Wei[1], Ruirong Yan[1], Yaru Jiang[1] and Wenzhi Shen[1,2]**

[1]Department of Pathology and Institute of Precision Medicine, Jining Medical University, Jining, China, [2]Institute of Breast Research, Jining Medical University, Jining, China*

It was proven that PGK1 plays a vital role in the proliferation, migration, and invasion of human breast cancer. However, the correlation of PGK1 mRNA and protein expression with clinicopathologic characteristics and prognostic values according to various kinds of breast cancer patient classifications remains unsufficient. Here, we analyzed data from the Oncomine database, Breast cancer Gene-Expression Miner v4.5, TNMplot, MuTarget, PrognoScan database, and clinical bioinformatics to investigate PGK1 expression distribution and prognostic value in breast cancer patients. Our study revealed that the mRNA and protein expression levels of PGK1 were up-regulated in various clinicopathologic types of breast cancer. Moreover, the expression of PGK1 was correlated with mutations of common tumor suppressor genes TP53 and CDH1. In addition, we found that high mRNA level of PGK1 was significantly associated with poor OS, RFS, and DMFS. Notably, Cox regression analysis showed that PGK1 could be used as an independent prognostic marker. In summary, the aforementioned findings suggested that PGK1 might be not only explored as a potential biomarker, but also combined with TP53/CDH1 for chemotherapy in breast cancer.

Keywords: PGK1, breast cancer, prognostic, public databases, prognostic value, comprehensive analysis 3

OPEN ACCESS

Edited by:
José Alexandre Ferreira, Portuguese Oncology Institute, Portugal

Reviewed by:
Guangchao Cao, Jinan University, China
Ajay Dixit, University of Minnesota Twin Cities, United States

****Correspondence:***
Wenzhi Shen
shenwenzhi@mail.jnmc.edu.cn

Specialty section:
This article was submitted to Molecular Diagnostics and Therapeutics, a section of the journal Frontiers in Molecular Biosciences

Received: *15 April 2021*
Accepted: *21 June 2021*
Published: *05 July 2021*

Citation:
Li Y, Wang S, Zhang X, Yang R, Wei X, Yan R, Jiang Y and Shen W (2021) Expression Characteristics and Significant Prognostic Values of PGK1 in Breast Cancer. Front. Mol. Biosci. 8:695420. doi: 10.3389/fmolb.2021.695420

INTRODUCTION

Breast cancer is one of the leading diseases afflicting women worldwide. According to the data of International Agency for Research on Cancer (IARC) in 2020 (Siegel et al., 2021; Sung et al., 2021), the annual prevalence of breast cancer increased to 2.26 million cases and 0.68 million relevant death cases globally. Over the last few decades, with the development of the detection methods and treatment strategy, the survival rate of breast cancer has been improved. However, it remains an enormous health burden for woman globally (Qiu et al., 2018). In addition, breast cancer patients with metastases have an extremely poor prognosis (Nakhjavani et al., 2019). The classification and pathogenesis of BRCA is quite complex. It involves multiple processes such as cell cycle disorder and metabolic abnormalities, illustrating the interactions and functions of multiple genes at multiple processes (Saini et al., 2019). Thus, screening of effective biomarker networks is urgently needed for the diagnosis, treatment, and prognostic assessment of BRCA.

Notably, Warburg effect Warburg et al. (1927), Yang et al. (2018) as one of the prominent characteristics of cancer cell, was closely related with cancer progression. The most characteristic feature of tumor cells is that they are mainly powered by the glycolytic pathway even when they are well oxygenated (Warburg, 1956; Han et al., 2019). Phosphoglycerate kinase 1 (PGK1) works as an important rate-limiting enzyme in the metabolic glycolysis pathway which could catalyze the conversion

of 1,3-diphosphoglycerate to 3-phosphoglycerate and generate a molecule of ATP (Vas et al., 2010; He et al., 2019). In addition to the important role in glycolysis, PGK1 was also proved to have critical function in tumor progression. It was reported that PGK1 was high expressed and could be used as a diagnostic marker in many tumors including endometrial cancer, lung cancer, colon cancer, and gastric cancer (Ahmad et al., 2013; Tekade and Sun, 2017; Zhang et al., 2018). Other reports also show that PGK1 expression is associated with tumor progression and prognosis of patients with gallbladder cancer (Lay et al., 2000). However, the role and clinical significance of PGK1 in different pathology subtype of breast cancer remain unclear.

In this study, we analyzed data from various online databases and revealed that the mRNA and protein expression levels of PGK1 were up-regulated in various clinicopathologic types of breast cancer. Moreover, the expression of PGK1 was correlated with mutations of common tumor suppressor genes TP53 and CDH1. In addition, we also found that high mRNA level of PGK1 was significantly associated with poor OS, RFS, and DMFS. Notably, Cox regression analysis showed that PGK1 could be used as an independent prognostic marker. In summary, the aforementioned findings suggested that PGK1 might be not only explored as a potential biomarker, but also combined with TP53/CDH1 for chemotherapy in breast cancer.

MATERIALS AND METHODS

Oncomine Database Analysis

The Oncomine database (https: //www. oncomine.org/resource/login.html), was used to determine the transcription expression level of PGK1 gene in breast cancer (Toruner et al., 2004; Viala et al., 2017). The expression levels of PGK1 mRNA (log2-transformed) were assessed in BRCA tissue relative to its expression in normal tissue. To obtain the most significant PGK1 expression, thresholds were set as below: gene rank, 10%; fold change, 2; and *p*-value, 0.01.

UALCAN Database Analysis

To determine the reliability of the differential expression data, the UALCAN database was selected for further verification. UALCAN is a comprehensive, user-friendly, and interactive web resource for analyzing cancer OMICS data. It was designed to provide easy access to publicly available cancer OMICS data (TCGA and MET500), provide graphs and plots depicting pan-cancer gene expression and patient survival information based on gene expression, evaluate gene expression in molecular subtypes of breast cancer, and evaluate epigenetic regulation of gene expression by promoter methylation and correlate other clinicopathological features (Chandrashekar et al., 2017). UALCAN is publicly available at http://ualcan.path.uab.edu.

TNMplot Database Analysis

The TNMplot tool (https://www.tnmplot.com/) is suitable for differential gene expression analysis in tumor tissues, normal tissues, and metastatic tissues. TNMplot includes 56,938 unique multilevel quality-controlled samples including Genechip from GEO: 3,691 normal, 29,376 tumor, and 453 metastatic samples and RNA-seq from TCGA: 730 normal, 9,886 tumor, and 394 metastatic samples (Bartha and Győrffy, 2021). The expression of PGK1 in normal, cancerous, and metastatic tissues were compared and analyzed using this tool.

Differentially Expressed PGK1 at Protein Level

In addition to the Oncomine and UALCAN database, the protein expression analysis of PGK1 was studied using the data from the HPA (http://www.proteinatlas.org). HPA is a platform that contains representative immunohistochemistry-based protein expression data for 20 highly common kinds of cancers (Thul et al., 2017). In this study, immunohistochemistry images of protein expression of PGK1 between normal and BRCA samples were directly visualized by HPA.

Breast Cancer Gene-Expression Miner v4.5

The expression and prognostic value of PGK1 in breast cancer were assessed by using Breast Cancer Gene-Expression Miner v4.5 online data set (http://bcgenex.centregauducheau.fr). The online dataset is a statistical mining tool of published annotated breast cancer transcriptomic data including DNA microarrays, RNA-seq with large amount of published annotated genomic data and can perform statistical analysis of gene expression, correlation and prognosis. The data on this website were last updated in June 2020 (Jézéquel et al., 2021). The relationship between PGK1 and the clinic pathologic parameters of breast cancer were evaluated by using bc-GenExMiner v4.5.

PrognoScan Online Database

PrognoScan online database was used to explore the underlying tumor biomarkers or therapeutic targets (http://www.prognoscan.org/) (Mizuno et al., 2009). In this study, the PrognoScan database analysis was performed to validate the prognostic significance of PGK1 mRNA expression in breast cancer patients, and a corrected *p*-value was set to adjust the threshold. According to the median expression of the genes, the online tool could divide the expression of PGK1 into "high" group or "low" group. Blue curves correspond to low PGK1 expression, while red curves to high PGK1 expression.

MuTarget Analysis

The MuTarget includes two independent analyses platform which links target gene expression changes with common mutation status in human tumors. By using this, the changes of target gene expression associated to a gene mutation and mutations altering the expression of a selected gene could be identified. The R statistical tool was used in all data processing steps. RNA-sequencing and mutation data were acquired from TCGA database. In this established database, 7,876 solid tumor samples from 18 various tumor types with both RNA-seq data and somatic mutation (Nagy and Győrffy, 2021). The utility of this approach is presented *via* three analyses in breast cancer: gene expression changes related to CDH1 mutations, gene

expression changes related to TP53 mutations, and mutations mediated altered progesterone receptor (PGR) expression. The breast cancer database was split into equally sized training and test sets, and these data sets were analyzed independently. Based on the Mann-Whitney *p*-value and mean FC, significant genes were selected for the test, where we used the default thresh-olds of $p \leq 0.01$ and $0.714 > FC > 1.4$.

Construction of Related Gene Networks, GO, and KEGG Pathway Enrichment Analysis

GeneMANIA (http://www.genem ania.org) provides a flexible web interface for deriving hypotheses based on gene functions (Warde-Farley et al., 2010), which generates a list of genes with similar functions to the query gene and constructs an interactive functional-association network to illustrate relationships between genes and datasets. In the present study, PGK1 was submitted to the GeneMANIA to interpret the functional association network among PGK1 and their related genes. Next, we used Web Gestalt (http://www.webgestalt.org/), which is a functional enrichment analysis web tool with continuously updated and effectively reduced data redundancy (Liao et al., 2019). KEGG pathways and GO functions analysis of PGK1 and their 20 associated genes were enriched by the Web Gestalt. The method of interest is selected in Over-Representation Analysis (ORA). The GO functional enrichment was performed in the biological process no Redundant (BP), cellular component no Redundant (CC), and molecular function no Redundant (MF). The pathway analysis was processed in the KEGG pathway.

Assistant for Clinical Bioinformatics Analysis

Assistant for clinical bioinformatics database (www.aclbi.com) was used to study the influence of genes and clinical factors, such as age, sex, and TNM stages on prognosis. Univariate and multivariate cox regression analysis were performed to identify the proper terms to build the nomogram. Based on the multivariate Cox proportional hazards analysis results, a nomogram was developed to predict the X-year overall recurrence (Lin et al., 2020; Zhang et al., 2020). The nomogram provided a graphical representation of the factors, which can be used to calculate the risk of recurrence for an individual patient by the points associated with each risk factor. All analytical methods above and R packages were performed using R software version v4.0.3 (The R Foundation for Statistical Computing, 2020); $p < 0.05$ was considered as statistically significant.

RESULTS

High mRNA Expression of PGK1 was Found in Human Breast Cancer

Phosphoglycerate kinase (PGK) is the only kinase that plays an important role in glycolysis. It catalyzes the transfer of high-energy phosphate from the position 1 of 3-bisphosphoglycerate (1, 3-BPG) to ADP, which generates 3-phosphoglycerate (3-PG) and ATP. PGK includes two isoenzymes, phosphoglycerate kinase 1 (PGK1) and phosphoglycerate kinase 2 (PGK2), and the heterogeneity of their amino acid sequences is up to 88%. By using the TCGA and Oncomine database, the expression profile was examined. We determined the expression of PGK1 and PGK2 in various human cancer types and found that it was significantly elevated in breast cancer vs. the normal tissue (**Figures 1A,B**). We further compared the mRNA expression of PGK1 in tumor samples and normal tissues using the UALCAN database. Analysis of RNA sequence data based on the TCGA database, consistent with the Oncomine data, showed that PGK1 expression was obviously up-regulated in BRCA tissues vs. the normal controls ($p = 1.62 \times 10^{-12}$) (**Figure 1B**).

Moreover, the PGK1 expression level was apparently elevated in different subtypes of BRCA as well, which include invasive ductal breast carcinoma ($p = 1.20 \times 10^{-32}$) (**Table 1** and **Figure 2A**), intraductal cribriform breast adenocarcinoma($p = 8.98 \times 10^{-4}$) (**Table 1** and **Figure 2B**), invasive ductal and lobular carcinoma($p = 8.52 \times 10^{-4}$) (**Table 1** and **Figure 2C**), mixed ductal and lobular breast carcinoma ($p = 4.19 \times 10^{-4}$) (**Table 1** and **Figure 2D**), invasive breast carcinoma ($p = 1.66 \times 10^{-15}$) and invasive lobular breast carcinoma ($p = 9.32 \times 10^{-8}$) (**Table 1** and **Figure 2E,F**), compared with the normal tissue. Analysis PGK1 expression using the TNM plot analysis showed that PGK1 expression is higher in metastatic tissues than normal and tumor tissues from gene chip data and RNA-seq data (**Table 2** and **Figures 3A,B**) ($p = 3.78e{-}33$, $p = 6.84e{-}67$). The mRNA expressions of PGK1 are also remarkably correlated with the cancer stage, and patients with advanced cancer stages tended to express higher mRNA expression of PGK1 (**Figure 3C**). Together, these results indicated that PGK1 mRNA expression was up-regulated in human breast cancer.

PGK1 Protein was High-Expressed in BRCA Patients

After analyzing the mRNA expression of PGK1 in BRCA, we explored the protein expression of PGK1 using the Human Protein Atlas (HPA). PGK1 protein has high expressions in BRCA tissues (Ductal carcinoma and Lobular carcinoma), while it has low protein expression in normal breast tissues by HPA (**Figures 4A,B**). The above results showed that protein expression of PGK1 was high-expressed in patients with breast cancer.

The Correlation of PGK1 with the Breast Cancer Clinicopathologic Parameters

To evaluate the correlation of PGK1 expression with the clinicopathologic parameters of BRCA, we performed the analysis by bc-GenExMiner v4.5. The age criterion demonstrated there is no difference of PGK1 mRNA expression in patients tumors of aged over 51 (year) vs. the aged no more than 51 ($p > 0.5$) (**Figure 5A** and **Table 3**). Additionally, PGK1 mRNA expression was obviously

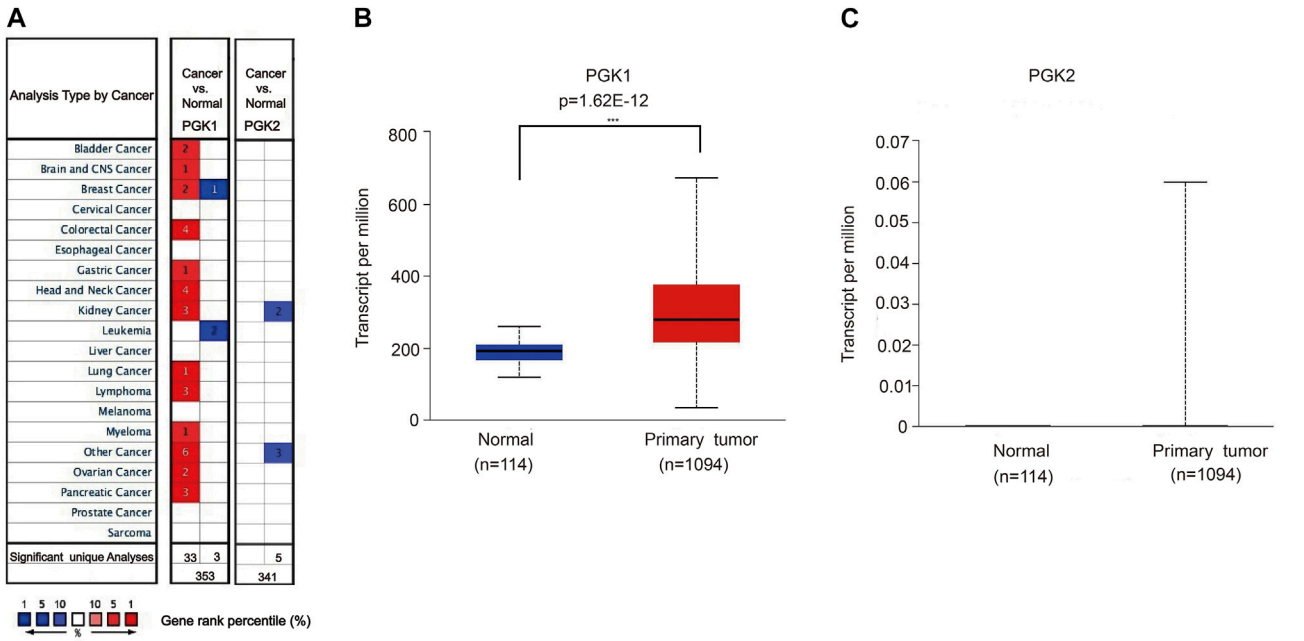

FIGURE 1 | (A) Transcriptional expressions of PGK1 and PGK2 in 20 types of cancers (cancer vs. corresponding normal tissue) were evaluated using the Oncomine database. Comparing the data by the *t*-test and cut-off *p*-value and fold change, following: *p*-value < 0.0001, fold change = 2, gene rank = 10%. Red represents significant overexpression, blue represents reduced expression. PGK1, phosphoglycerate kinase 1; PGK2, phosphoglycerate kinase 2. **(B,C)** High mRNA expressions of PGK1and PGK2 in patients with breast cancer and normal breast tissues by UALCAN (TCGA database), *** means $p < 0.001$.

up-regulated in estrogen receptor (HER2) (+) group vs. the corresponding HER2 (−) group ($p < 0.0001$) (**Figure 5B** and **Table 3**). Moreover, the PGK1 mRNA expression was apparently reduced in progesterone receptor (PR) (−) group vs. the PR (+) ($p < 0.0001$) (**Figure 5C** and **Table 3**). Similarly, PGK1 mRNA expression was also reduced estrogen receptor (ER) (−) group vs. the ER (+) group ($p < 0.0001$), compared with the corresponding negative group (**Figure 5D** and **Table 3**). Furthermore, the expression of PGK1 was determined in Triple-negative breast cancer (TNBC) and found that PGK1 mRNA expression was significantly up-regulated in TNBC patients ($p < 0.0001$) (**Figure 5E** and **Table 3**). Consistently, patients with basal-like characteristics also exhibited apparently increased PGK1 expression vs. patients with non-basal-like characteristics ($p < 0.0001$) (**Figure 5F**; **Table 3**). In the Nottingham Prognostic Index (NPI) criterion and Scarff Bloom and Richardson grade status (SBR), an increased NPI and SBR grade was correlated with PGK1 transcript level increase ($p < 0.0001$) vs. the SBR1 and NPI1 groups correspondingly (**Figures 5G,H**). However, there was no significant difference in terms of human nodal status (**Figure 5I** and **Table 3**). Taken together, the above results showed a prognostic value in breast cancer clinicopathologic parameters.

The Correlation of PGK1 Expression with Crucial Genes Mutations

In order to identify the correlation of mutations which could guide the therapy of breast cancer and PGK1 expression, the Mann-Whitney U analysis was performed to identify crucial gene mutations correlated with PGK1 expression. The condition of selected genes was FC > 1.4, $p < 0.01$. As shown in **Figure 6**, the six most strongly associated genes with PGK1 expression genes were described. PGK1

TABLE 1 | Significant changes in PGK1expression at the transcription level between different types of breast cancer and normal tissues (oncomine database).

Subtype of breast cancer	*p*-value	Fold-change	Rank (%)	Sample
Invasive ductal breast carcinoma	1.2×10^{-32}	2.003	3	450
Intraductal cribriform breast adenocarcinoma	8.89×10^{-4}	2.109	6	64
Invasive ductal and lobular carcinoma	8.52×10^{-4}	1.397	7	64
Mixed lobular and ductal breast carcinoma	4.19×10^{-4}	1.585	7	68
Invasive breast carcinoma	1.66×10^{-15}	1.621	6	137
Invasive lobular breast carcinoma	9.32×10^{-8}	1.507	11	97

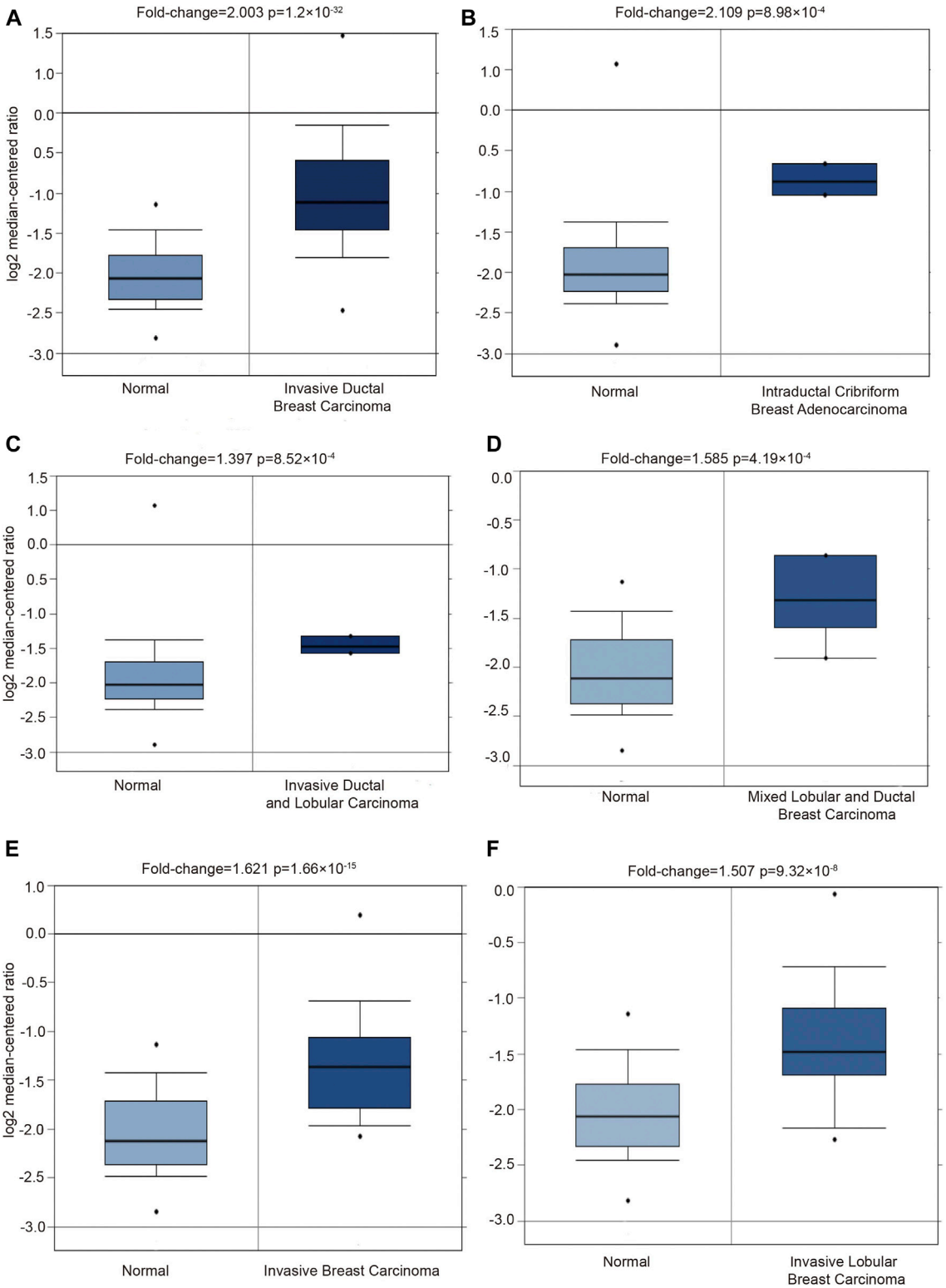

FIGURE 2 | Detecting the PGK1 gene expression in six types breast cancer by using Oncomine database. Six boxplots originated from gene expression data in the Oncomine, comparing the expression of PGK1 in normal tissues and six types of breast cancer tissues as follows: invasive ductal breast carcinoma **(A)**, intraductal cribriform breast adenocarcinoma **(B)**, invasive ductal and lobular carcinoma **(C)**, mixed ductal and lobular breast carcinoma **(D)**, invasive breast carcinoma **(E)** and invasive lobular breast carcinoma **(F)**.

TABLE 2 | Compare expression profiles of tumor, normal and metastatic tissues.

Data	n.Norm	n.Tumor	n.Meta	K.W.p	Fc.tumor.norm	Fc.tumor.norm
Gene chip data	242	7,659	82	3.78e–33	1.42	1.05
RNA-seq data	403	1,097	7	6.84e–67	1.84	0.89

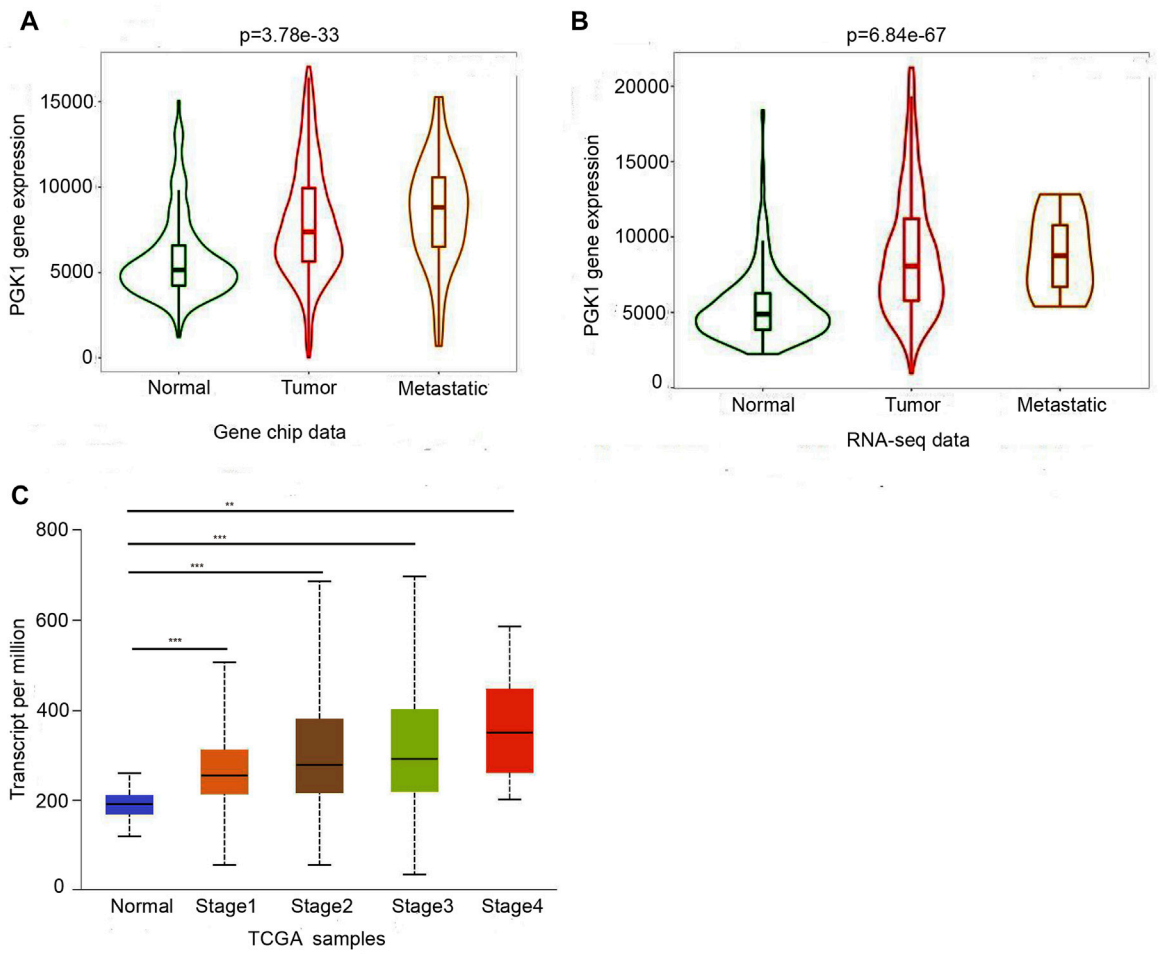

FIGURE 3 | Two boxplot graphs **(A,B)** of PGK1 gene expression in breast cancer by comparing paired normal, tumor, and metastatic tissues from gene chip data and RNA-seq data at TNMplot.com. Validation of differential expression using equally sized training and test sets confirmed the reliability of the database in breast cancer at an FDR below 10%.**(C)**Relationship between PGK1 expression and tumor stage in breast cancer patients. Boxplots displayed the PGK1 expression between normal and breast cance patients with stage 1, 2, 3, and 4, * means $p < 0.05$; ** means $p < 0.01$; ***means $p < 0.001$.

expression was higher in TP53-mutant (total mutation rate: 34%), PAPPA2-mutant (total mutation rate: 2%), RB1-mutant (total mutation rate: 2%), DYNC1H1-mutant (total mutation rate: 2%), and CMYA5-mutant (total mutation rate: 2.7%) breast cancer patients (**Figures 6A–C,E,F**). PGK1 expression was lower in tumor specimens containing somatic mutations of CDH1 (mutation prevalence 14.1%) (**Figure 6D**). The list of six genes with PGK1 expression change associated somatic mutations is presented in **Table 4**. Collectively, these results suggested that PGK1 expression has a closely correlation with gene mutations in breast cancer.

Construction Gene Interaction Network and Function Enrichment of PGK1 in Breast Cancer

In this study, we constructed a network for PGK1 and their 20 related genes and analyzed their functions using

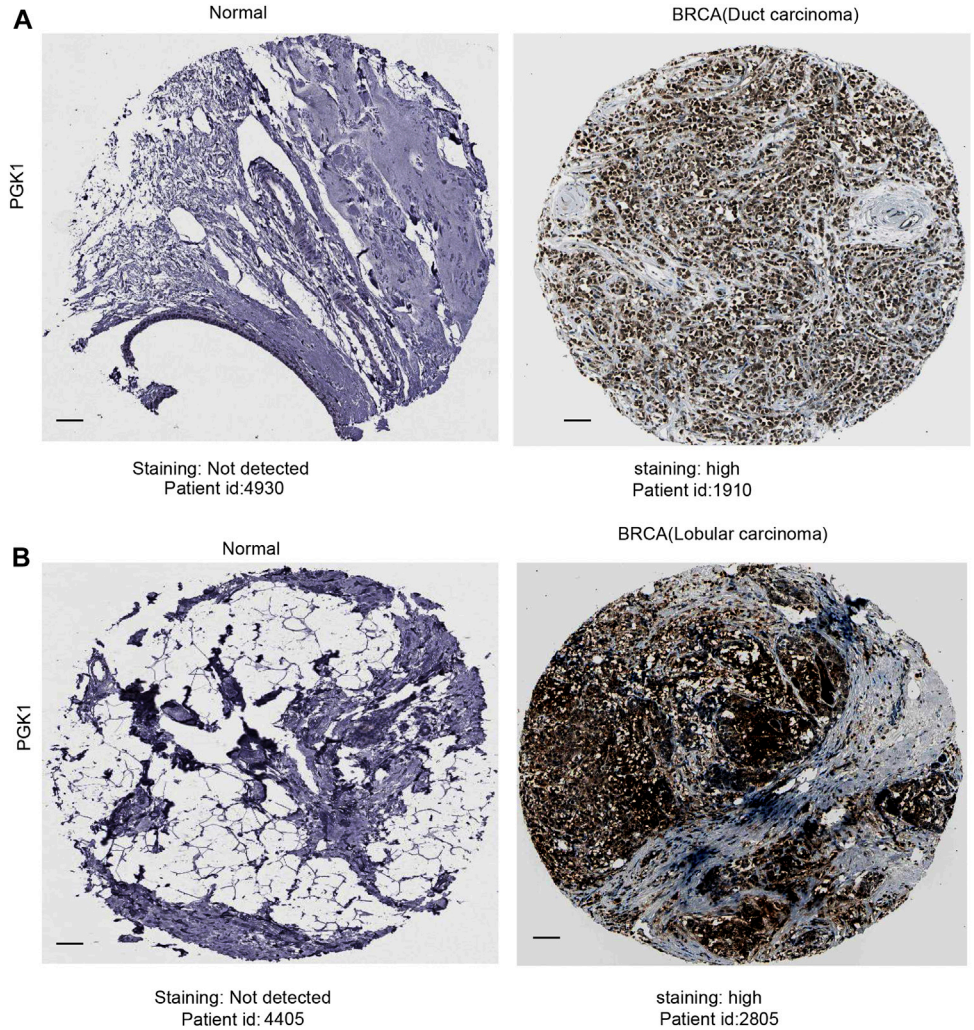

FIGURE 4 | Representative immunohistochemistry images of PGK1 in duct carcinoma **(A)** and lobular carcinoma (**B**) tissues and normal breast tissues (HPA database) were shown. Scale bar: 50 μM.

GeneMANIA. Proteins that interact with PGK1 are ATF1, GPI, TPI1, ATP13A1, EPAS1, TNC, NO1, LDHA, HSPH, EIF2AK4, ENO3, HIF1A, BOLA2B, U2AF2, NFIC, MMS19, PGK2, HARS, ALDOA, GAPDH (**Figure 7A**). Moreover, we performed the analysis of the physiological functions and biological processes of the 20 genes by using the Web Gestalt, the results showed that 20 genes were classified into the following categories: molecular function, cellular component, and biological process. Notably, most genes are enriched in the metabolic process, biological process, and protein binding et al. (**Figures 7B–D**). In addition, the Go and pathway functional analysis revealed that these proteins showed the greatest correlation with metabolic processes. These genes were significantly enriched in glycolysis/gluconeogenesis, biosynthesis of amino acids, HIF-signaling pathway, and carbon metabolism (**Figure 7E** and **Table 5**). The above results showed construction gene interaction network and function enrichment of PGK1 in breast cancer.

PGK1 Acts as an Independent Indicator for BRCA Prognosis

To determine the correlation of PGK1 expression with breast cancer patients survival, we performed the analysis and showed that increased expression of PGK1 mRNA is apparently correlated with reduced overall survival (OS) ($p < 0.05$), relapse free survival (RFS) ($p < 0.05$), and distant metastasis free survival (DMFS) in breast cancer ($p < 0.05$) (**Figure 8A**). Cox analysis was performed to assess the independent prognostic value of PGK1, and the results are shown in **Table 6** and **Table 7**. According to the results from univariate and multivariate

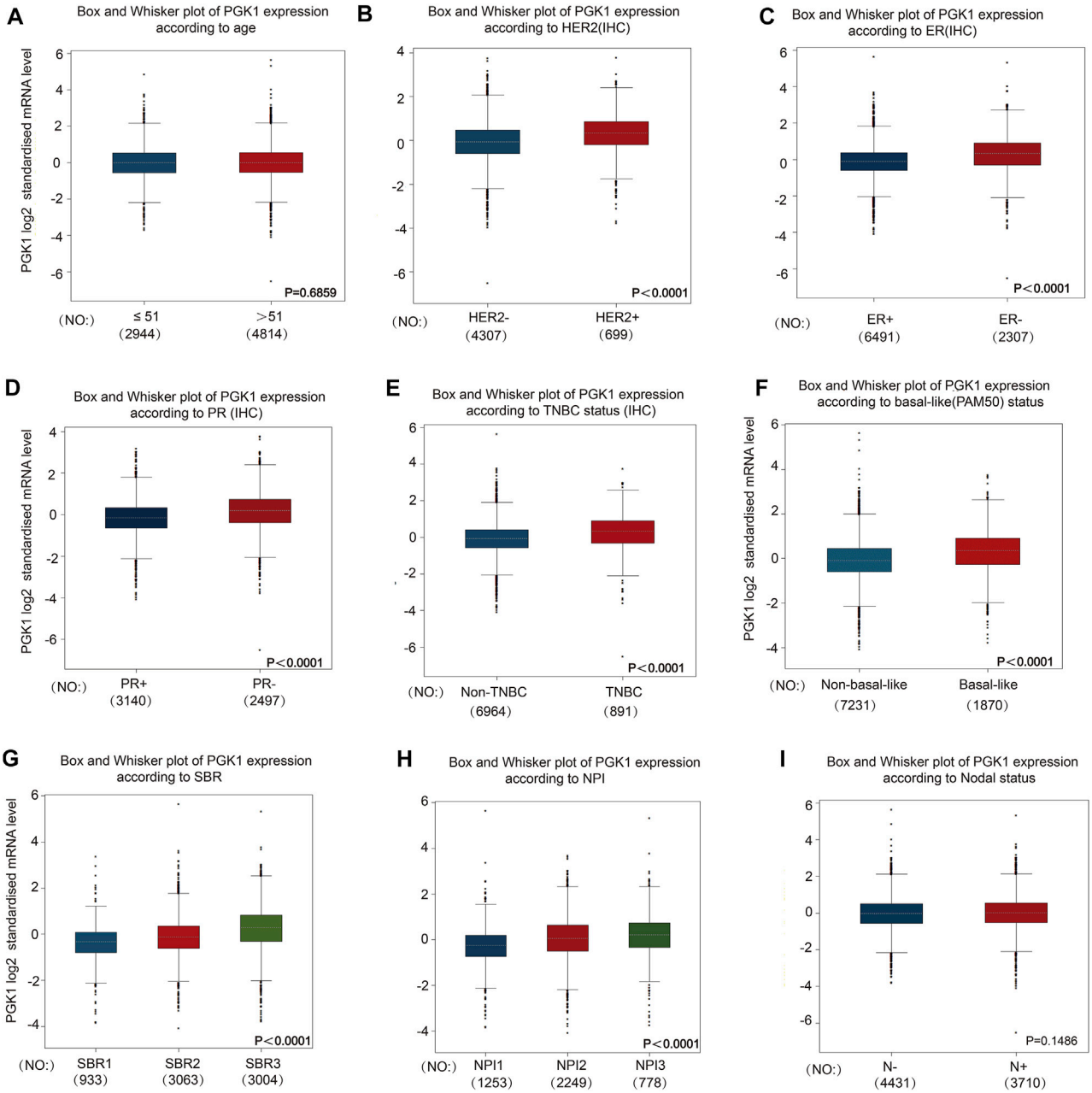

FIGURE 5 | To study the correlation of PGK1 expression with clinical pathological parameters including age **(A)**, HER2 **(B)**, ER **(C)**, PR **(D)**, TNBC status **(E)**, basal-like (PAM50) status **(F)**, SBR **(G)**, NPI **(H)** and Nodal status **(I)** in breast cancer patients. Notable differences between the groups were analyzed by Welch's *t*-test to generate the *p*-value. PGK1, phosphoglycerate kinase 1; ER, estrogen receptor; PR, progesterone receptor; HER2, human epidermal growth factor receptor 2; SBR, Scarff, Bloom and Richardson; TNBC, Triple-negative Breast Cancer; NPI, Nottingham Prognostic Index status; IHC, immunohistochemistry.

analysis, PGK1 gene, age, and pTNM stage were significantly associated with OS. The above results indicated that the PGK1 gene, age, and pTNM stage were independent prognostic factors in breast cancer. Based on multivariate Cox Regression analysis, variables with significant prognostic differences were automatically extracted using the tool (www.aclbi.com) to construct a prognostic nomogram for BRCA patients (**Figure 8B**). Moreover, as shown in **Figure 8C**, the calibration analysis results showed that the nomogram for 1-year survival rate (the red line) was highly approached to the ideal performance (the 45-degree gray line) vs. to the 3-years (the orange line) and 5-years (the blue line) survival rates, which suggested a remarkably accurate nomogram predicted by this model. The AUC can observe the efficacy of the gene as a prognostic biomarker, so AUC curves were obtained using R package. The result shows that AUC values at 1, 3, and 5 years are 0.716 (95% CI, 0.61–0.823), 0.

TABLE 3 | The correlation between PGK1 mRNA expression and the clinicopathological parameters of breast carcinoma.

Variables	PGK1		
	Number	mRNA	*p*-value
Age,years			0.6859
≤51	2,944	–	
>51	4,814	–	
HER2			< 0.0001
–	4,307	–	
+	699	↑	
ER			< 0.0001
–	2,307	↑	
+	6,491	–	
PR			< 0.0001
–	2,497	↑	
+	3,140	–	
Triple-negative status			< 0.0001
None	6,964	–	
TNBC	891	↑	
Basal-like status			< 0.0001
None	7,231	–	
Basal-like	1870	↑	
Nodal status			0.1486
–	4,431	–	
+	3,710	–	

682 (95% CI, 0.621–0.743), and 0.678 (95% CI, 0.622–0.734), respectively. The above results indicated the strong predictive ability of PGK1 for breast cancer (**Figure 8D**).

DISCUSSION

Along with the rapid development of precision medicine, accurate prognostic models are needed to guide clinical and to design a more personalized program for patients, especially those with a complex type of breast cancer. Moreover, breast cancer cells are easy to metastasize and are life-threatening (Yang et al., 2019). Aside from the role of PGK1 as a glycolytic enzyme in different cell cycle intervals, PGK1 also shows an indispensible role in tumor metabolism. The Aberrant expression of PGK1 in various tumor tissues, peripheral blood and saliva of patients, could promote rapid tumor growth and progression (Yu and Li, 2017). Abnormal expression level of PGK1 was detected not only in tumor tissues, but also in patients' peripheral blood and saliva. Therefore, PGK1 is a potential target of tumor therapy and an intensely studied molecule in tumor therapy research (Hwang et al., 2006). PGK1 promotes the breast cancer cell growth and the lactic acid generation, which is the end product of glycolysis (Li et al., 2016). In addition, PGK1 high expression was also representing higher tumor stage, which disclosed that PGK1 was correlated with tumor metastasis, progression and occurrence of breast cancer (Fu et al., 2018). However, the expression patterns of PGK1 in various types of breast cancer and the unique roles of PGK1 as a diagnostic marker of poor prognosis in breast cancer remain unknown.

In the previous studies, Sun et al. have proved that PGK1 expression was increased in breast cancer tissues vs. the normal breast tissues (Sun et al., 2015). Based on the existing research, we synthesized and analyzed multiple data sources including the Oncomine, UALCAN, TNMplot, and HPA database, the results showed that the PGK1 mRNA expression was also significantly upregulated in invasive ductal breast carcinoma, intraductal cribriform breast adenocarcinoma, invasive ductal and lobular carcinoma, mixed lobular and ductal breast carcinoma, invasive breast carcinoma, and invasive lobular breast carcinoma using the Oncomine database in-depth analysis. Following the TNMplot and UALCAN database data showed that the PGK1 transcriptional level was remarkably correlated with metastasis and cancer stages. Moreover, we found that the protein expression of PGK1 was higher in breast cancer tissues than in normal tissues by HPA. In addition, bc-GenExMiner 4.5 was used to investigate the expression profile of PGK1 across PAM50 breast cancer subtypes based on different clinicopathological parameters. High expression of PGK1 was associated with risk of HER (+), TNBC, basal-like characteristics, SBR grade status, and NPI grade status. However, the PGK1 mRNA expression was significantly downregulated in patients with ER (+) and PR (+) status.

HIF-1α serves as a transcriptional factor to promote cell glycolysis for Warburg effect. As an essential enzyme in the glycolytic pathway, it is proved that PGK1 is directly regulated by HIF-1α in many cancer types (Xie et al., 2017; Sun et al., 2019). Furthermore, PGK1 is relative with cancer cell metastatic ability because HIF-1α/PGK1 mediated epithelial-mesenchymal transition (EMT) process (Ai et al., 2011). In our analysis of PGK1 correlated signaling pathways in breast cancer, GeneMANIA and Web Gestalt analysis indicates PGK1 is involved in glycolysis/gluconeogenesis, biosynthesis of amino acids, HIF-signaling pathway, carbon metabolism and metabolic pathways. The results are consistent with previous studies and also indicate PGK1 acts energetically role in tumor cell metabolism. However, more details of PGK1 mediated tumor metabolism related signaling pathways need to be further investigated in future researches.

Accurate prognostic models can be used to guide the clinical decision-making process and design more personalized treatment plans for patients (Cao et al., 2019). Existing data analysis showed that elevated expression of PGK1 was related with short OS (Overall Survival) in diverse types of cancer (Shao et al., 2019) or PGK1 combined with other genes to predicting the survival of patients with breast cancer (Zhang et al., 2021). However, the performance of existing prognostic models is limited. Here, we in-depth analyzed the prognostic impact of PGK1 and clinical factors such as age, gender, race, and pTNM stage. First, the survival results revealed that high expression of PGK1 mRNA was associated with reduced OS, RFS, and DMFS via PrognoScan analysis. PGK1 was found to be an independent prognostic factor in determining breast cancer by univariate and multivariate cox regression. The PGK1-based model of breast cancer showed moderate predictive ability (AUC = 0.716, 0.682, and 0.678 for 1, 3, and 5-years survival). Thus, the PGK1 signature was an independent and the most important risk factor of the prognosis of breast cancer.

In addition to single gene indicators, multigene prognostic models have also gained acceptance in recent years (Győrffy et al.,

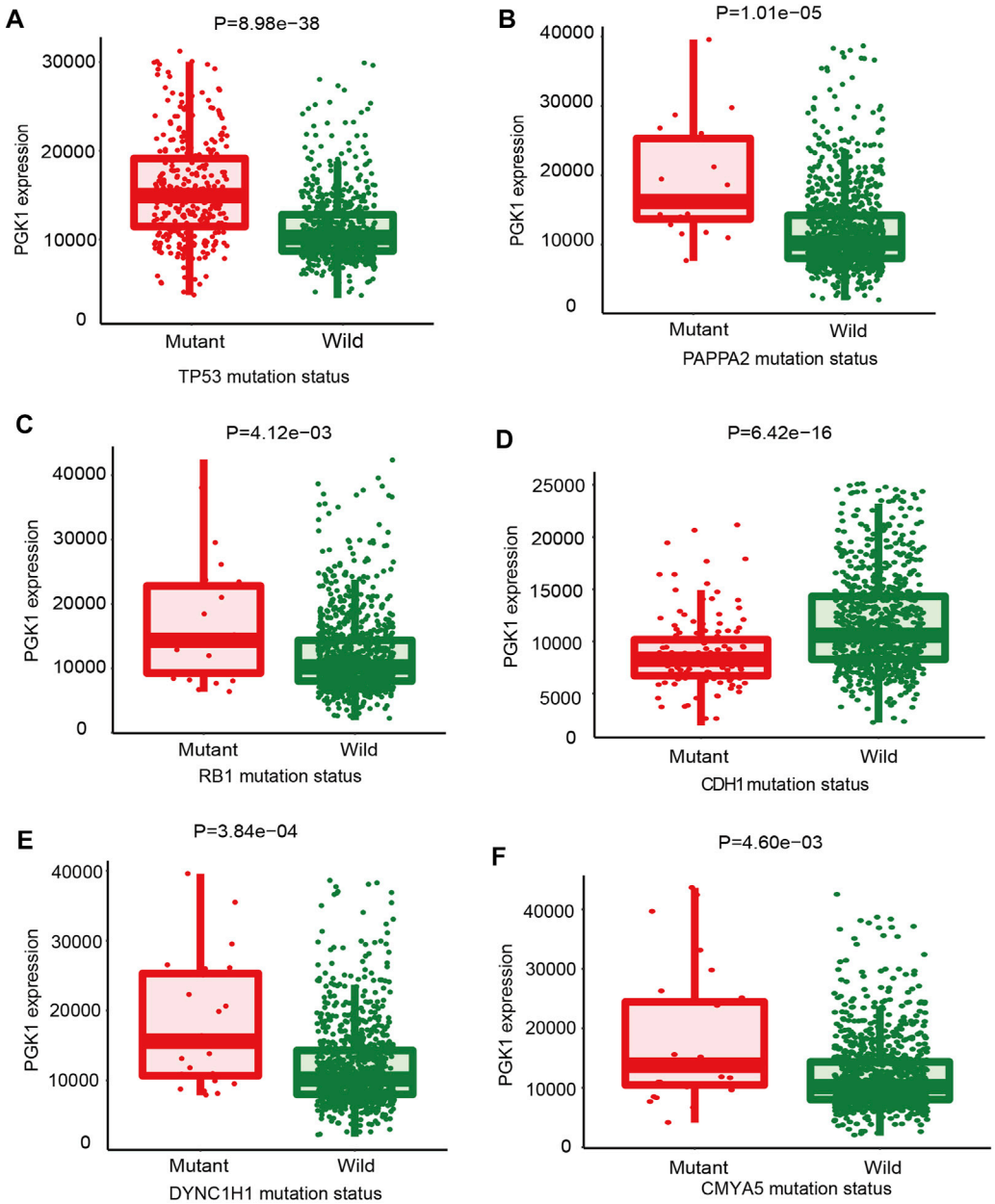

FIGURE 6 | The mutations that correlated with PGK1 gene expression in breast cancer were identified. The oncogenes or tumor suppressor genes mutations correlated with PGK1 expression was analyzed by TARGET from muTarget platform. The six genes whose mutations are most strongly correlated with PGK1 expression changes in breast cancer. TP53, tumor protein p53 **(A)**; PAPPA2, pappalysin 2 **(B)**; RB1, RB transcriptional co-repressor 1 **(C)**; CDH1, cadherin 1 **(D)**; dynein cytoplasmic 1 heavy chain 1 **(E)**; CMYA5, cardiomyopathy associated 5 **(F)**. Screening of significant genes were based on the Mann-Whitney *p* value and mean FC of the test, $p \leq 0.01$ and 0.714>FC>1.4 and a prevalence of at least 1%.

TABLE 4 | The six mutant genes most strongly associated with PGK1 expression.

Mutation of genes	Mean expression (mutant)	Mean expression (wild)	Number of mutant	Number of wild	FC (mutant/wild)	Direction	*p*-value
TP53	15,821.95	10,607.23	336	643	1.49	Up	8.98e−38
PAPPA2	19,023.6	12,258.76	20	959	1.55	Up	1.01e−05
RB1	18,605.74	12,247.59	23	956	1.52	Up	4.12e−03
CDH1	8,842.55	12,980.2	138	841	1.47	Down	6.42e−16
DYNC1H1	17,994.04	12,256.3 24	24	955	1.47	Up	3.84e−04
CMYA5	17,682.93	12,247.02	27	952	1.44	Up	4.60e−03

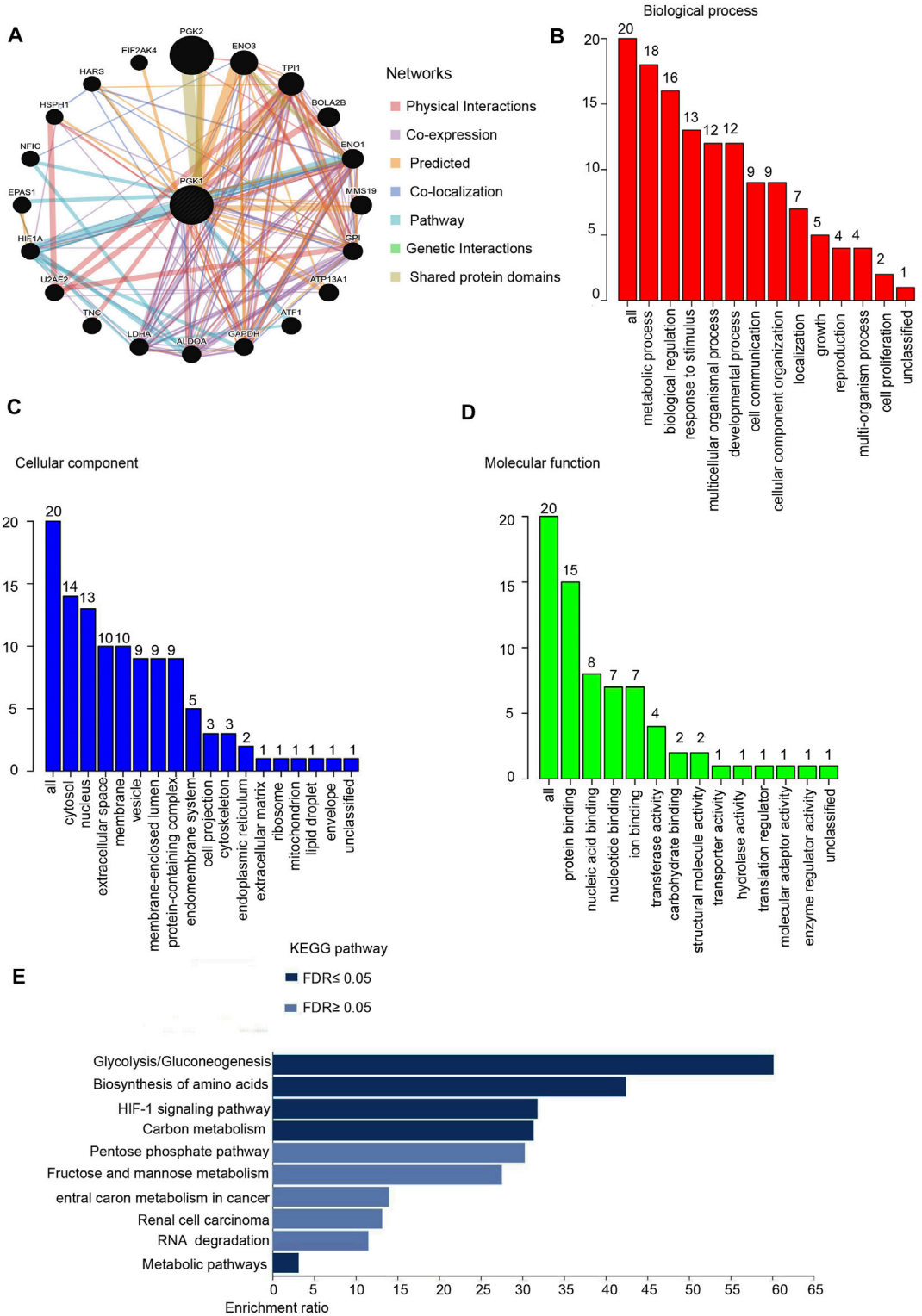

FIGURE 7 | Protein-protein interaction network and function enrichment analysis of PGK1 in breast cancer. **(A)** Protein-protein interaction network of PGK1 was analyzed by GeneMANIA and Screening for 20 genes interacting with PGK. Different colors of the network edge indicate the bioinformatics methods applied: Physical Interactions, Co-expression, Predicted, Co-localization, Pathway, Genetic Interactions, Shared protein domains. **(B)** Gene Ontology (GO) is analyzed and the screened 20 gene of BP (Biological Process) is shown. **(C)** CC (Cellular Component). **(D)** MF (Molecular Function). **(E)** KEGG pathways is analyzed the 20 genes co-expressed with PGK1 and the Top pathway is mapped according to the differential expression level of PGK1 ($p \leq 0.05$). *Y*-axis: name of the signaling pathway or function; *X*-axis: percentage of the number of genes assigned to a term among the total number of genes annotated in the network.

TABLE 5 | KEGG Pathway enrichment analysis of PGK1 gene–gene interaction network.

Gene set	FDR	*p*-value	Enrichment ratio	Overlap genes
hsa00010:Glycolysis/Gluconeogenesis	1.1220e–12	3.4417e–15	60.146	ALDOA,ENO1ENO3, TPI1 GAPDH,GPI,PGK1,PGK2,LDHA
hsa01230:Biosynthesis of amino acids	1.0780e–8	9.9204e–11	42.414	ALDOA,ENO1ENO3,TPI1, PGK2 GAPDH,PGK1
hsa04066:HIF-1signaling pathway	6.3447e–8	7.7849e–10	31.811	ALDOA,ENO1ENO3,HIF1A,GAPDH,PGK1,LDHA
hsa01200:Carbon metabolism	6.2082e–9	3.8087e–11	31.341	ALDOA,ENO1ENO3,TPI1, PGK2 GAPDH,PGK1,GPI
hsa00030:Pentose hosphate pathway	0.10352	0.0019053	30.296	ALDOA, GPI
hsa00051: Fructose and mannose metabolism	0.10729	0.0023037	27.542	ALDOA, TPI1
hsa05230:Central carbon metabolism in cancer	0.35406	0.0087108	13.983	HIF1A, LDHA
hsa05211:Renalcell carcinoma	0.35406	0.0097746	13.172	EPAS1, HIF1A
hsa03018:RNA degradation	0.41317	0.012674	11.505	ENO1ENO3
hsa01100:Metabolic pathways	0.041688	0.00063938	3.1341	ALDOA,ENO1ENO3, TPI1 GAPDH,GPI,PGK1,PGK2,LDHA

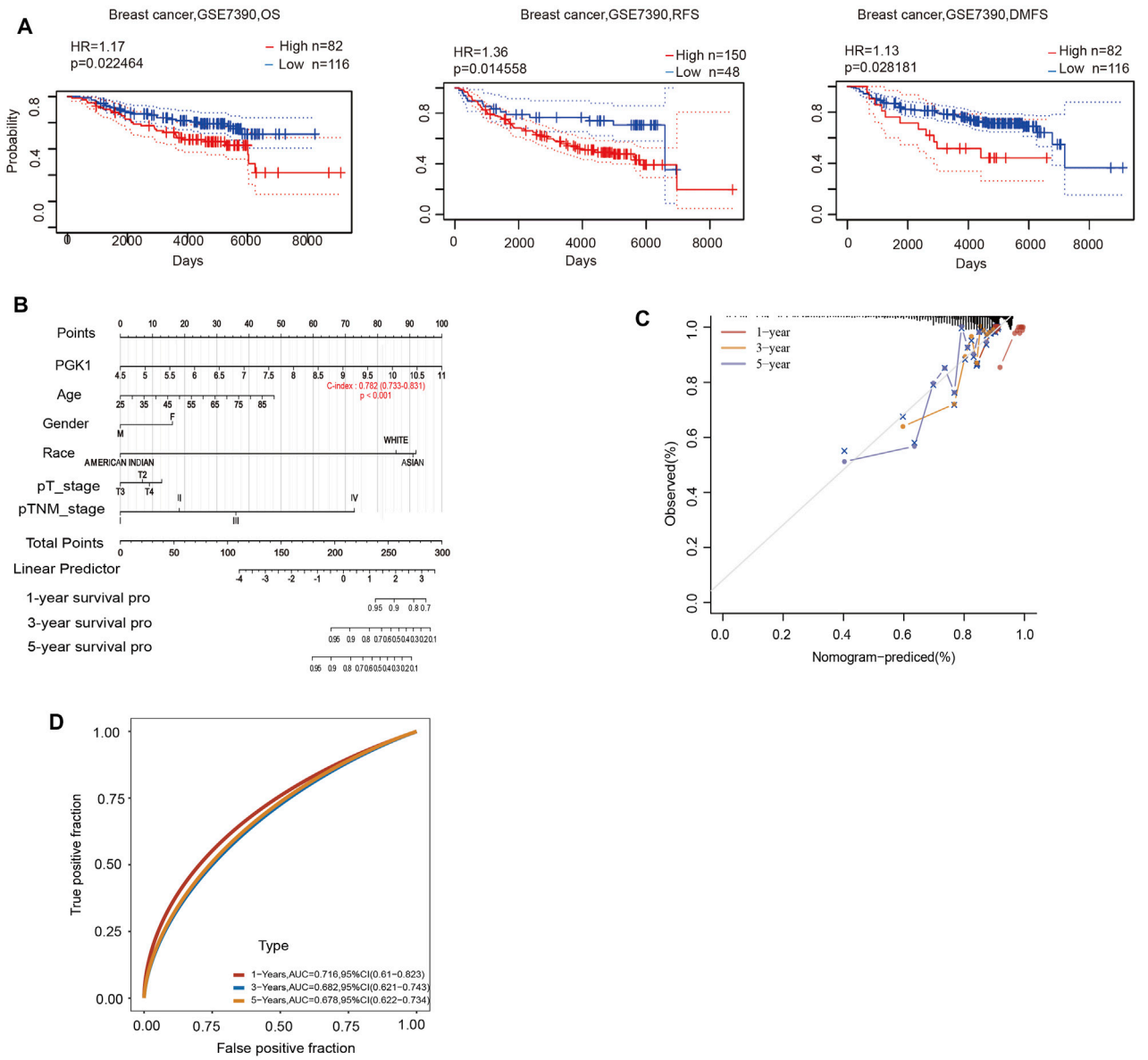

FIGURE 8 | (A) Prognostic significance of PGK1gene expression in patients with breast cancer (OS, RFS and DMFS time in the PrognoScan database). OS, overall survival; RFS, relapse-free survival; DMFS, distant metastasis free survival; HR, hazard ratio. **(B)** Nomogram to predict the 1-year, 3-years, and 5-years overall survival of breast cancer patients. **(C)** Calibration curve for the overall survival nomogram model in the breast cancer group.A dashed diagonal line represents the ideal nomogram, and the red line, orange line, and blue line represent the 1-year,3-years, and 5-years observed nomograms. **(D)** Time-dependent ROC analysis the of the five-gene signature. ROC, receiver operating characteristic.

TABLE 6 | Hazard ratio and *p*-value of constituents involved in univariate Cox regression and some parameters of the PGK1 gene.

Uni_cox	p.value	Hazard Ratio(95% CI)
PGK1	<0.0001	1.79792(1.43886,2.24657)
Age	<0.0001	1.03011(1.01768,1.04269)
Gender	0.85432	0.83157(0.11611,5.95553)
Race	0.76849	0.95227(0.68759,1.31884)
pT_stage	0.00017	1.45755(1.19757,1.77397)
pTNM_stage	<0.0001	1.96803(1.58396,2.44523)

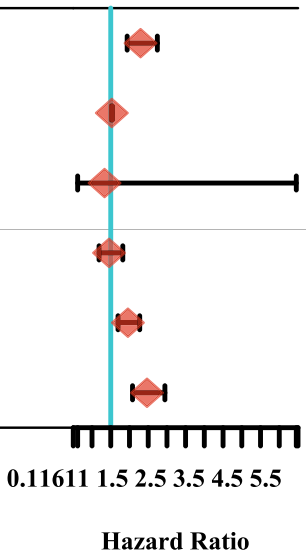

2015). However, large groups of breast cancer patients harboring different somatic mutations still do not have adequate targeted therapies. Thus, we used the muTarget software to identify mutations that alter the expression of the PGK1 gene. The TP53 gene encodes a tumor suppressor protein, and TP53 mutations influence the prognosis significantly in most cancer patients (Olivier et al., 2010; Li et al., 2020). Breast cancer accounts for over 50% of tumors in TP53 mutation carriers (Silwal-Pandit et al., 2017; Schon and Tischkowitz, 2018). Notably, we showed that PGK1 expression was higher in TP53-mutant than wild-type in breast cancer patients by muTarget analysis. CDH1 is another commonly mutated gene in breast cancer (Padmanaban et al., 2019). It encodes a tumor suppressor protein and its mutation contributes to the promotion of breast cancer invasion and metastasis (Lei et al., 2002). The current analysis showed that PGK1 expression was lower in CDH-mutant than wild-type in breast cancer patients. By linking TP53 and CDH1 mutations and PGK1 expression, it is possible to identify potential multi-gene therapeutic targets and develop novel personalized therapies in breast cancer.

TABLE 7 | Hazard ratio and *p*-value of constituents involved in multivariate Cox regression and some parameters of the PGK1 gene.

Mult_cox	p.value	Hazard Ratio(95% CI)
PGK1	<0.0001	1.86985(1.48133,2.36027)
Age	<0.0001	1.03392(1.02091,1.0471)
Gender	0.51772	0.51912(0.07121,3.78436)
Race	0.48843	0.88397(0.62359,1.25306)
pT_stage	0.66669	0.94336(0.72351,1.23002)
pTNM_stage	<0.0001	2.07511(1.5612,2.75819)

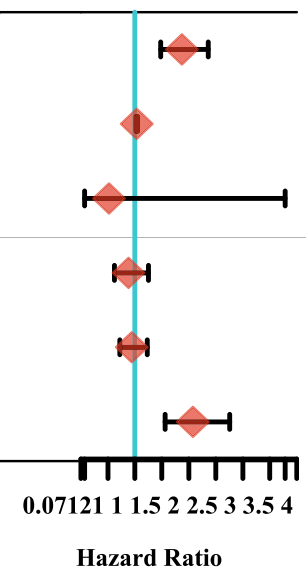

CONCLUSION

In conclusion, our results indicate the overexpression of PGK1 at the transcriptional and protein levels in breast cancer patients. Moreover, PGK1 was significantly associated with different molecular types, metastasis status, and patient's pTNM stage. Furthermore, high expressions of PGK1 were significantly related with shorter OS, RFS, and DMFS in breast cancer patients. Notably, PGK1 could be used as an independent prognostic marker in breast cancer patients. In summary, PGK1 could be a potential target in the development of anti-PGK1 therapeutics and an efficient marker for the prognosis of breast cancer. The present study was hypothetically driven and performed using experimental generated data available in public databases. Therefore, future experimental verification of the mechanism underlying PGK1 regulation of tumor metastasis and its multi-gene prognostic value for breast cancer patients is warranted.

DATA AVAILABILITY STATEMENT

The datasets presented in this study can be found in online repositories. The names of the repository/repositories and accession number(s) can be found in the article/ Supplementary Material.

AUTHOR CONTRIBUTIONS

YL: designed the methodology, prepared the software and the database data, writing, review, and editing the manuscript. SW, XZ, and RY: helped to prepare the software and the database data, perform the analysis. RrY and YJ: helped to prepare the software and the database data. WS: helped to prepare the software and the database data, writing, review, and revised the manuscript.

FUNDING

This work was supported by the National Natural Science Foundation of China (No. 82002961 to YL), National Natural Science Foundation Cultivation Project of Jining Medical University (No. JYP2019KJ07 to YL), Faculty Start-up Funds of Jining Medical University (No. 600825001 to YL), Supporting Funds for Teacher's Research of Jining Medical University (No. JYFC2018KJ011 to XZ), Shandong Medical Science and Technology Program (No. 2018WS460 to XZ) and Supporting Funds for Teacher's Research of Jining Medical University (No. JYFC2018KJ013 to SW).

ACKNOWLEDGMENTS

We would like to thank Editage for English language editing.

REFERENCES

Ahmad, S. S., Glatzle, J., Bajaeifer, K., Bühler, S., Lehmann, T., Königsrainer, I., et al. (2013). Phosphoglycerate Kinase 1 as a Promoter of Metastasis in colon Cancer. *Int. J. Oncol.* 43 (2), 586–590. doi:10.3892/ijo.2013.1971

Ai, J., Huang, H., Lv, X., Tang, Z., Chen, M., Chen, T., et al. (2011). FLNA and PGK1 Are Two Potential Markers for Progression in Hepatocellular Carcinoma. *Cell Physiol Biochem* 27 (3-4), 207–216. doi:10.1159/000327946

Bartha, Á., and Győrffy, B. (2021). TNMplot.com: A Web Tool for the Comparison of Gene Expression in Normal, Tumor and Metastatic Tissues. *Ijms* 22 (5), 2622. doi:10.3390/ijms22052622

Cao, R., Wu, Q., Li, Q., Yao, M., and Zhou, H. (2019). A 3-mRNA-Based Prognostic Signature of Survival in Oral Squamous Cell Carcinoma. *PeerJ* 7, e7360. doi:10.7717/peerj.7360

Chandrashekar, D. S., Bashel, B., Balasubramanya, S. A. H., Creighton, C. J., Ponce-Rodriguez, I., Chakravarthi, B. V. S. K., et al. (2017). UALCAN: A Portal for Facilitating Tumor Subgroup Gene Expression and Survival Analyses. *Neoplasia* 19 (8), 649–658. doi:10.1016/j.neo.2017.05.002

Fu, D., He, C., Wei, J., Zhang, Z., Luo, Y., Tan, H., et al. (2018). PGK1 Is a Potential Survival Biomarker and Invasion Promoter by Regulating the HIF-1α-Mediated Epithelial-Mesenchymal Transition Process in Breast Cancer. *Cel Physiol Biochem* 51 (5), 2434–2444. doi:10.1159/000495900

Győrffy, B., Hatzis, C., Sanft, T., Hofstatter, E., Aktas, B., and Pusztai, L. (2015). Multigene Prognostic Tests in Breast Cancer: Past, Present, Future. *Breast Cancer Res.* 17 (1), 11. doi:10.1186/s13058-015-0514-2

Han, X., Ren, C., Yang, T., Qiao, P., Wang, L., Jiang, A., et al. (2019). Negative Regulation of AMPKα1 by PIM2 Promotes Aerobic Glycolysis and Tumorigenesis in Endometrial Cancer. *Oncogene* 38 (38), 6537–6549. doi:10.1038/s41388-019-0898-z

He, Y., Luo, Y., Zhang, D., Wang, X., Zhang, P., Li, H., et al. (2019). PGK1-mediated Cancer Progression and Drug Resistance. *Am. J. Cancer Res.* 9 (11), 2280–2302.

Hwang, T.-L., Liang, Y., Chien, K.-Y., and Yu, J.-S. (2006). Overexpression and Elevated Serum Levels of Phosphoglycerate Kinase 1 in Pancreatic Ductal Adenocarcinoma. *Proteomics* 6 (7), 2259–2272. doi:10.1002/pmic.200500345

Jézéquel, P., Gouraud, W., Ben Azzouz, F., Guérin-Charbonnel, C., Juin, P. P., Lasla, H., et al. (2021). *Bc-GenExMiner 4.5: New Mining Module Computes Breast Cancer Differential Gene Expression Analyses*. Oxford: Database. doi:10.1093/database/baab007

Lay, A. J., Jiang, X.-M., Kisker, O., Flynn, E., Underwood, A., Condron, R., et al. (2000). Phosphoglycerate Kinase Acts in Tumour Angiogenesis as a Disulphide Reductase. *Nature* 408 (6814), 869–873. doi:10.1038/35048596

Lei, H., Sjöberg-Margolin, S., Salahshor, S., Werelius, B., Jandáková, E., Hemminki, K., et al. (2002). CDH1mutations Are Present in Both Ductal and Lobular Breast Cancer, but Promoter Allelic Variants Show No Detectable Breast Cancer Risk. *Int. J. Cancer* 98 (2), 199–204. doi:10.1002/ijc.10176

Li, L., Li, M., and Wang, X. (2020). Cancer Type-dependent Correlations between TP53 Mutations and Antitumor Immunity. *DNA Repair* 88, 102785. doi:10.1016/j.dnarep.2020.102785

Li, X., Jiang, Y., Meisenhelder, J., Yang, W., Hawke, D. H., Zheng, Y., et al. (2016). Mitochondria-Translocated PGK1 Functions as a Protein Kinase to Coordinate Glycolysis and the TCA Cycle in Tumorigenesis. *Mol. Cel* 61 (5), 705–719. doi:10.1016/j.molcel.2016.02.009

Liao, Y., Wang, J., Jaehnig, E. J., Shi, Z., and Zhang, B. (2019). WebGestalt 2019: Gene Set Analysis Toolkit with Revamped UIs and APIs. *Nucleic Acids Res.* 47 (W1), W199–w205. doi:10.1093/nar/gkz401

Lin, W., Wu, S., Chen, X., Ye, Y., Weng, Y., Pan, Y., et al. (2020). Characterization of Hypoxia Signature to Evaluate the Tumor Immune Microenvironment and Predict Prognosis in Glioma Groups. *Front. Oncol.* 10, 796. doi:10.3389/fonc.2020.00796

Mizuno, H., Kitada, K., Nakai, K., and Sarai, A. (2009). PrognoScan: a New Database for Meta-Analysis of the Prognostic Value of Genes. *BMC Med. Genomics* 2, 18. doi:10.1186/1755-8794-2-18

Nagy, Á., and Győrffy, B. (2021). muTarget : A Platform Linking Gene Expression Changes and Mutation Status in Solid Tumors. *Int. J. Cancer* 148 (2), 502–511. doi:10.1002/ijc.33283

Nakhjavani, M., Hardingham, J. E., Palethorpe, H. M., Tomita, Y., Smith, E., Price, T. J., et al. (2019). Ginsenoside Rg3: Potential Molecular Targets and

Therapeutic Indication in Metastatic Breast Cancer. *Medicines* 6 (1), 17. doi:10.3390/medicines6010017

Olivier, M., Hollstein, M., and Hainaut, P. (2010). TP53 Mutations in Human Cancers: Origins, Consequences, and Clinical Use. *Cold Spring Harbor Perspect. Biol.* 2 (1), a001008. doi:10.1101/cshperspect.a001008

Padmanaban, V., Krol, I., Suhail, Y., Szczerba, B. M., Aceto, N., Bader, J. S., et al. (2019). E-cadherin Is Required for Metastasis in Multiple Models of Breast Cancer. *Nature* 573 (7774), 439–444. doi:10.1038/s41586-019-1526-3

Qiu, N., He, Y., Zhang, S., Hu, X., Chen, M., and Li, H. (2018). Cullinï¿½7 Is a Predictor of Poor Prognosis in Breast Cancer Patients and Is Involved in the Proliferation and Invasion of Breast Cancer Cells by Regulating the Cell Cycle and Microtubule Stability. *Oncol. Rep.* 39 (2), 603–610. doi:10.3892/or.2017.6106

Saini, G., Ogden, A., McCullough, L. E., Torres, M., Rida, P., and Aneja, R. (2019). Disadvantaged Neighborhoods and Racial Disparity in Breast Cancer Outcomes: the Biological Link. *Cancer Causes Control* 30 (7), 677–686. doi:10.1007/s10552-019-01180-4

Schon, K., and Tischkowitz, M. (2018). Clinical Implications of Germline Mutations in Breast Cancer: TP53. *Breast Cancer Res. Treat.* 167 (2), 417–423. doi:10.1007/s10549-017-4531-y

Shao, F., Yang, X., Wang, W., Wang, J., Guo, W., Feng, X., et al. (2019). Associations of PGK1 Promoter Hypomethylation and PGK1-Mediated PDHK1 Phosphorylation with Cancer Stage and Prognosis: a TCGA Pan-Cancer Analysis. *Cancer Commun.* 39 (1), 54. doi:10.1186/s40880-019-0401-9

Siegel, R. L., Miller, K. D., Fuchs, H. E., and Jemal, A. (2021). Cancer Statistics, 2021. *CA A. Cancer J. Clin.* 71 (1), 7–33. doi:10.3322/caac.21654

Silwal-Pandit, L., Langerød, A., and Børresen-Dale, A.-L. (2017). TP53Mutations in Breast and Ovarian Cancer. *Cold Spring Harb Perspect. Med.* 7 (1), a026252. doi:10.1101/cshperspect.a026252

Sun, R., Meng, X., Pu, Y., Sun, F., Man, Z., Zhang, J., et al. (2019). Overexpression of HIF-1a Could Partially Protect K562 Cells from 1,4-benzoquinone Induced Toxicity by Inhibiting ROS, Apoptosis and Enhancing Glycolysis. *Toxicol. Vitro* 55, 18–23. doi:10.1016/j.tiv.2018.11.005

Sun, S., Liang, X., Zhang, X., Liu, T., Shi, Q., Song, Y., et al. (2015). Phosphoglycerate Kinase-1 Is a Predictor of Poor Survival and a Novel Prognostic Biomarker of Chemoresistance to Paclitaxel Treatment in Breast Cancer. *Br. J. Cancer* 112 (8), 1332–1339. doi:10.1038/bjc.2015.114

Sung, H., Ferlay, J., Siegel, R. L., Laversanne, M., Soerjomataram, I., Jemal, A., et al. (2021). Global Cancer Statistics 2020: GLOBOCAN Estimates of Incidence and Mortality Worldwide for 36 Cancers in 185 Countries. *CA A. Cancer J. Clin.* 71, 209–249. doi:10.3322/caac.21660

Tekade, R. K., and Sun, X. (2017). The Warburg Effect and Glucose-Derived Cancer Theranostics. *Drug Discov. Today* 22 (11), 1637–1653. doi:10.1016/j.drudis.2017.08.003

Thul, P. J., Åkesson, L., Wiking, M., Mahdessian, D., Geladaki, A., Ait Blal, H., et al. (2017). A Subcellular Map of the Human Proteome. *Science* 356 (6340), eaal3321. doi:10.1126/science.aal3321

Toruner, G. A., Ulger, C., Alkan, M., Galante, A. T., Rinaggio, J., Wilk, R., et al. (2004). Association between Gene Expression Profile and Tumor Invasion in Oral Squamous Cell Carcinoma. *Cancer Genet. Cytogenet.* 154 (1), 27–35. doi:10.1016/j.cancergencyto.2004.01.026

Vas, M., Varga, A., and Gráczer, E. (2010). Insight into the Mechanism of Domain Movements and Their Role in Enzyme Function: Example of 3-phosphoglycerate Kinase. *Cpps* 11 (2), 118–147. doi:10.2174/138920310790848403

Viala, M., Alexandre, M., Thezenas, S., Lamy, P.-J., Maran-Gonzalez, A., Gutowski, M., et al. (2017). Prognostic Impact of the Inclusion of uPA/PAI-1 for Adjuvant Treatment Decision-Making in ER+/Her2− pN0 Early Breast Cancers. *Breast Cancer Res. Treat.* 165 (3), 611–621. doi:10.1007/s10549-017-4373-7

Warburg, O. (1956). On the Origin of Cancer Cells. *Science* 123 (3191), 309–314. doi:10.1126/science.123.3191.309

Warburg, O., Wind, F., and Negelein, E. (1927). The Metabolism of Tumors in the Body. *J. Gen. Physiol.* 8 (6), 519–530. doi:10.1085/jgp.8.6.519

Warde-Farley, D., Donaldson, S. L., Comes, O., Zuberi, K., Badrawi, R., Chao, P., et al. (2010). The GeneMANIA Prediction Server: Biological Network Integration for Gene Prioritization and Predicting Gene Function. *Nucleic Acids Res.* 38, W214–W220. Web Server issue. doi:10.1093/nar/gkq537

Xie, H., Tong, G., Zhang, Y., Liang, S., Tang, K., and Yang, Q. (2017). PGK1 Drives Hepatocellular Carcinoma Metastasis by Enhancing Metabolic Process. *Ijms* 18 (8), 1630. doi:10.3390/ijms18081630

Yang, T., Ren, C., Lu, C., Qiao, P., Han, X., Wang, L., et al. (2019). Phosphorylation of HSF1 by PIM2 Induces PD-L1 Expression and Promotes Tumor Growth in Breast Cancer. *Cancer Res.* 79 (20), 5233–5244. doi:10.1158/0008-5472.can-19-0063

Yang, T., Ren, C., Qiao, P., Han, X., Wang, L., Lv, S., et al. (2018). PIM2-mediated Phosphorylation of Hexokinase 2 Is Critical for Tumor Growth and Paclitaxel Resistance in Breast Cancer. *Oncogene* 37 (45), 5997–6009. doi:10.1038/s41388-018-0386-x

Yu, X., and Li, S. (2017). Non-metabolic Functions of Glycolytic Enzymes in Tumorigenesis. *Oncogene* 36 (19), 2629–2636. doi:10.1038/onc.2016.410

Zhang, X., Wang, J., Zhuang, J., Liu, C., Gao, C., Li, H., et al. (2021). A Novel Glycolysis-Related Four-mRNA Signature for Predicting the Survival of Patients with Breast Cancer. *Front. Genet.* 12, 606937. doi:10.3389/fgene.2021.606937

Zhang, Y., Yu, G., Chu, H., Wang, X., Xiong, L., Cai, G., et al. (2018). Macrophage-Associated PGK1 Phosphorylation Promotes Aerobic Glycolysis and Tumorigenesis. *Mol. Cel* 71 (2), 201–215. doi:10.1016/j.molcel.2018.06.023

Zhang, Z., Lin, E., Zhuang, H., Xie, L., Feng, X., Liu, J., et al. (2020). Construction of a Novel Gene-Based Model for Prognosis Prediction of clear Cell Renal Cell Carcinoma. *Cancer Cel Int* 20, 27. doi:10.1186/s12935-020-1113-6

Conflict of Interest: The authors declare that the research was conducted in the absence of any commercial or financial relationships that could be construed as a potential conflict of interest.

frontiers in Cell and Developmental Biology

ORIGINAL RESEARCH
published: 08 July 2021
doi: 10.3389/fcell.2021.689727

Combination Foretinib and Anti-PD-1 Antibody Immunotherapy for Colorectal Carcinoma

Yuyin Fu[1†], Yujia Peng[1†], Shengyan Zhao[1], Jun Mou[2], Lishi Zeng[1], Xiaohua Jiang[1], Chengli Yang[1], Cheng Huang[1], Yuyan Li[1], Yin Lu[1], Mengdan Wu[1], Yanfang Yang[1], Ting Kong[1], Qinhuai Lai[1], Yangping Wu[3], Yuqin Yao[4], Yuxi Wang[5], Lantu Gou[1] and Jinliang Yang[1]**

[1] State Key Laboratory of Biotherapy and Cancer Center/Collaborative Innovation Center for Biotherapy, West China Hospital, Sichuan University, Chengdu, China, [2] Laboratory of Infectious Diseases and Vaccine, West China Hospital, Sichuan University, Chengdu, China, [3] Department of Clinical Research Management, West China Hospital, Sichuan University, Chengdu, China, [4] West China School of Public Health and Healthy Food Evaluation Research Center/No. 4 West China Teaching Hospital, Sichuan University, Chengdu, China, [5] Department of Respiratory and Critical Care Medicine, West China Hospital, Sichuan University, Chengdu, China

OPEN ACCESS

Edited by:
Hongming Miao,
Army Medical University, China

Reviewed by:
Bertrand Allard,
University of Montreal Hospital Centre (CRCHUM), Canada
Honglin Jin,
Huazhong University of Science and Technology, China
Chenggen Qian,
China Pharmaceutical University, China

***Correspondence:**
Jinliang Yang
jinliangyang@scu.edu.cn
Lantu Gou
goulantu@foxmail.com

† These authors have contributed equally to this work and share first authorship

Specialty section:
This article was submitted to Molecular Medicine, a section of the journal Frontiers in Cell and Developmental Biology

Received: 01 April 2021
Accepted: 11 June 2021
Published: 08 July 2021

Citation:
Fu Y, Peng Y, Zhao S, Mou J, Zeng L, Jiang X, Yang C, Huang C, Li Y, Lu Y, Wu M, Yang Y, Kong T, Lai Q, Wu Y, Yao Y, Wang Y, Gou L and Yang J (2021) Combination Foretinib and Anti-PD-1 Antibody Immunotherapy for Colorectal Carcinoma. Front. Cell Dev. Biol. 9:689727. doi: 10.3389/fcell.2021.689727

Immune checkpoint inhibitors have achieved unprecedented success in cancer immunotherapy. However, the overall response rate to immune checkpoint inhibitor therapy for many cancers is only between 20 and 40%, and even less for colorectal cancer (CRC) patients. Thus, there is an urgent need to develop an efficient immunotherapeutic strategy for CRC. Here, we developed a novel CRC combination therapy consisting of a multiple receptor tyrosine kinase inhibitor (Foretinib) and anti-PD-1 antibody. The combination therapy significantly inhibited tumor growth in mice, led to improved tumor regression without relapse (83% for CT26 tumors and 50% for MC38 tumors) and prolonged overall survival. Mechanistically, Foretinib caused increased levels of PD-L1 via activating the JAK2-STAT1 pathway, which could improve the effectiveness of the immune checkpoint inhibitor. Moreover, the combination therapy remodeled the tumor microenvironment and enhanced anti-tumor immunity by further increasing the infiltration and improving the function of T cells, decreasing the percentage of tumor-associated macrophages (TAMs) and inhibiting their polarization toward the M2 phenotype. Furthermore, the combination therapy inhibited the metastasis of CT26-Luc tumors to the lung in BALB/c mouse by reducing proportions of regulatory T-cells, TAMs and M2 phenotype TAMs in their lungs. This study suggests that a novel combination therapy utilizing both Foretinib and anti-PD-1 antibody could be an effective combination strategy for CRC immunotherapy.

Keywords: foretinib, anti-PD-1, combination therapy, immunotherapy, tumor microenvironment, colon cancer

INTRODUCTION

Colorectal cancer (CRC) is the third most commonly diagnosed cancer and the second leading cause of cancer-related deaths worldwide. Over 1.8 million new CRC cases and 881,000 deaths were estimated to occur in 2018 (Bray et al., 2018). Whilst there are many advanced diagnostic and therapeutic methods for CRC, it remains one of the major cancers with a relatively high mortality rate.

Immune checkpoint inhibitors (ICIs) that target PDCD1/CD274(PD-1/PD-L1) have been used to treat a variety of malignant tumors, including melanoma, lung cancer, renal cell cancer, head and neck cancer, Hodgkin's disease, urothelial cancer (Ribas and Wolchok, 2018; Xiao et al., 2020) and CRC with deficient mismatch repair (dMMR) or microsatellite instability-high (MSI-H). But CRC with dMMR/MSH-H only accounts for approximately 15% of all advanced CRC cases, therefore the majority of patients cannot benefit ICIs (Overman et al., 2017; Oliveira et al., 2019). The poor therapeutic effect for CRC patients is associated with the immunosuppressive tumor microenvironment (TME), which causes resistance to immune checkpoint blockade (ICB) (Pitt et al., 2016). Hence, there is an urgent need to overcome the CRC associated immunosuppression, which would enable the proportion of patients who benefit from PD-1/PD-L1 blockade to be expanded. Numerous preclinical studies have indicated that the combination of ICIs with other treatments such as chemotherapy, radiation therapy and targeted therapy could be a promising approach to overcome immunosuppression and improve therapeutic efficacy (O'Neill and Cao, 2019).

Low T cell infiltration, especially $CD8^+$ T cells or a high proportion of tumor-associated macrophages (TAMs) appear to be associated with reduced antitumor drug efficacy and seem to be associated with poor clinical outcomes in most carcinoma cases (Huang et al., 2017; Xu et al., 2018; Feng et al., 2019). Indeed, $CD8^+$ T cells are considered major drivers of antitumor immunity in tumors. These cells can specifically recognize and kill cancer cells via the release of cytotoxic molecules and cytokines (van der Leun et al., 2020). But, as the major tumor-infiltrating immune cell population, TAMs are commonly hijacked by tumor cells to inhibit the function of T cells and promote an immunosuppressive TME, ultimately leading to tumor growth, immunoevasion, metastasis and angiogenesis (De Palma and Lewis, 2013; Chen et al., 2018; Jeong et al., 2019). Previous studies have indicated that increased T cell or decreased TAM infiltration in tumors is correlated with a favorable prognosis and has a synergetic effect with anti-PD-1 immunotherapy.

Foretinib is an available inhibitor of multiple receptor tyrosine kinases (RTKs), including vascular endothelial growth factor receptor 2 (VEGFR2) and c-MET. It can be taken orally and has been demonstrated to have significant activity against a wide range of tumors *in vitro* and *in vivo* (Huynh et al., 2012; Choueiri et al., 2013; Faria et al., 2015; Yau et al., 2017). However, to date the impact of Foretinib on antitumor immunity has not been clarified. This study demonstrates that Foretinib increased PD-L1 expression via the activation of the JAK2-STAT1 pathway and improved the immune microenvironment by increased the infiltration of T cells. This provided the rationale for combining PD-1/PD-L1 inhibitors with Foretinib. The combination of Foretinib with anti-PD-1 antibody significantly inhibited the growth of MC38 and CT26 tumors by further enhancing the infiltration and function of T cells, decreasing the proportion of TAMs and inhibiting their polarization toward the M2 phenotype. Furthermore, the combination therapy significantly inhibited the CT26-Luc tumor metastasis to the lung in BALB/c mouse by reducing proportions of regulatory T cells (Tregs), TAMs and M2 phenotype TAMs in the lung. The results of this investigation have enabled proposition of a novel combination strategy to enhance the effects of immunotherapy for CRC.

RESULTS

Foretinib Increased the Expression of PD-L1 by Activating the JAK2-STAT1 Pathway

To investigate the effect of Foretinib on PD-L1 expression in colon cancer cells, different concentrations of Foretinib (0, 1, 2, 4 μM) were used to treat MC38 murine tumor cells for 24 h, after which the protein levels were analyzed by western blotting. These results demonstrated that the levels of PD-L1, JAK2, STAT1, phospho-STAT1(S727), phospho-STAT1(Y701) were elevated following Foretinib treatment (**Figures 1A,B**). The same changes were also observed in CT26 murine colon cancer cells and in HCT116, HT29 and SW480 human colon cancer cells (**Supplementary Figure 1**). Moreover, the expression of PD-L1, JAK2 phosphorylation and STAT1 phosphorylation (included S727 and Y701) were increased in MC38 tumor tissues from C57BL/6 mice after Foretinib treatment (**Figures 1J,K**).

Foretinib Enhanced T Cell Infiltration *in vivo*

Foretinib significantly inhibited MC38 tumor growth *in vivo* compared to the control (**Figures 1C,D**). To determine the immunomodulatory functions of Foretinib, the MC38 subcutaneous model was used. The infiltration of T cells, including $CD4^+$ and $CD8^+$ T cells (**Figures 1E–G**), were enhanced; whereas, the $CD11b^+$ cells (**Figure 1H**), which comprise abundant immunosuppressive cells such as TAMs and Myeloid-derived suppressor cells (MDSCs), were decreased in the tumors after Foretinib treatment. The PD-L1 expression on tumor cells ($CD45^-$) was also enhanced after Foretinib treatment (**Figure 1I**). Additionally, the number of T cells in the peripheral blood and spleen were increased after Foretinib treatment (**Supplementary Figure 2**). These results demonstrated that Foretinib could regulate the immune cells associated with colon cancer *in vivo*. It has previously been reported that inhibited the expression of VEGFR2 could ameliorate the TME and improve immunotherapy outcomes (Fukurnura et al., 2018; Khan and Kerbel, 2018). Consistent with previous reports, Foretinib significantly inhibited VEGFR2 expression in MC38 tumors (**Figures 1J,K**).

Combined Treatment of Foretinib and αPD-1 Significantly Inhibited the Growth of MC38 Tumors and Prolonged the Survival Rate

The results described above prompted an investigation into the *in vivo* antitumor effects of Foretinib when combined with anti-PD-1 (αPD-1) therapy. Tumor growth was inhibited by

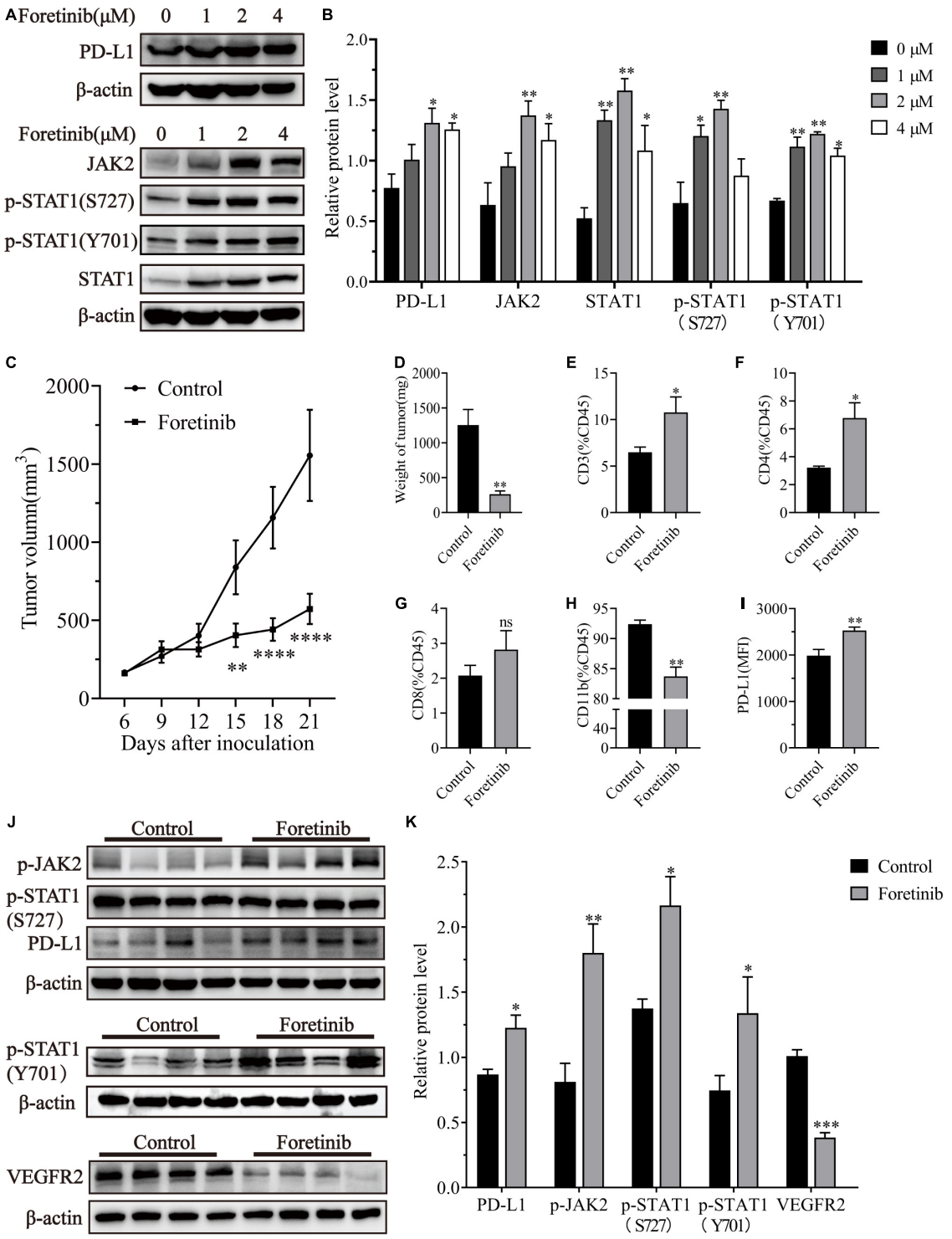

FIGURE 1 | Foretinib increased PD-L1 and enhanced the infiltration of T cells in MC38 tumors. The expression of PD-L1, JAK2, STAT1, phospho-STAT1(S727), phospho-STAT1(Y701) and β-actin was detected by Western-blotting in MC38 colon cancer cells, which were treated with different concentrations of Foretinib for 24 h. The relative protein levels were shown in figures **(A,B)**. MC38 cells (1×10^6) were transplanted subcutaneously into the right flank of C57BL/6 mice. Six days after transplantation (a tumor volume nearly of 100 mm^3), the mice were randomly allocated to either the control or treatment groups. Drugs were administered as described in the "Materials and Methods" section and the tumor volumes were measured every 3 days **(C)**, six mice were allocated per group ($n = 6$). After the treatment was completed, the tumors were harvested and weighed **(D)** and the infiltration of $CD3^+$ **(E)**, $CD4^+$ **(F)**, $CD8^+$ **(G)**, and $CD11b^+$ **(H)** cells was determined and the mean fluorescence intensity (MFI) of PD-L1 **(I)** in the tumors was determined by FCM. The relative protein levels in the tumor tissue for phospho-JAK2, STAT1, phospho-STAT1(S727), phospho-STAT1(Y701), PD-L1, VEGFR2, and β-actin were determined using Western-blotting **(J,K)** ($n = 4$ mice). The data was presented using the mean ± SEM where applicable, * ($P \leq 0.05$), ** ($P \leq 0.01$), *** ($P < 0.001$), **** ($P < 0.0001$) and ns (no statistical significance, $P \geq 0.05$).

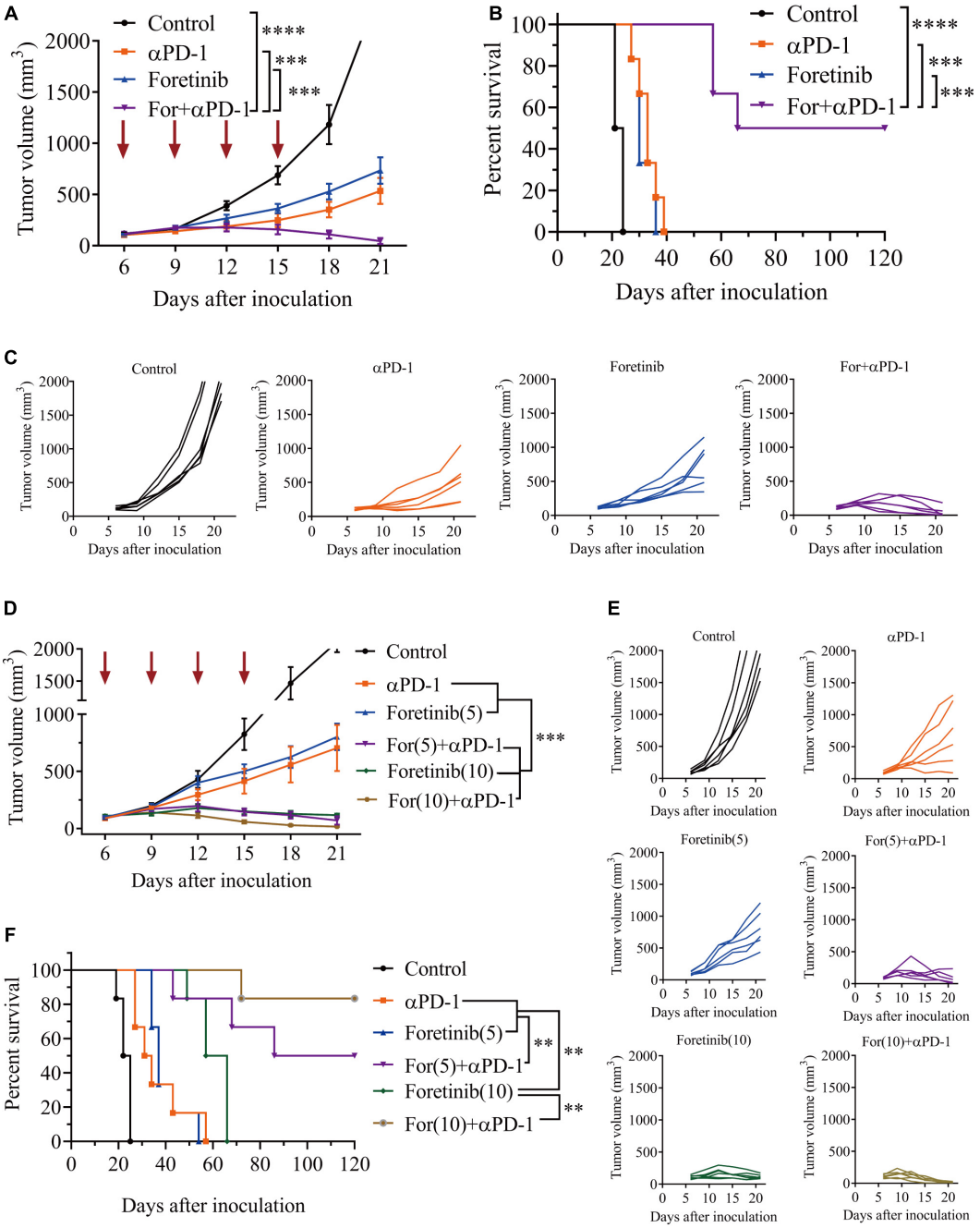

FIGURE 2 | Foretinib synergistically enhanced the anti-tumor function of the αPD-1 antibody *in vivo*. MC38 cells subcutaneously implanted into the mice and when the volume reached approximately 100 mm^3, the mice were randomly allocated to either the control or treatment groups ($n = 6$). The drugs were given as described in the "Materials and Methods" section. **(A)** The tumor volume was measured every 3 days. **(B)** The Kaplan–Meier survival distribution in the model is displayed for the mice following the treatment protocol. **(C)** Tumor growth curves for the mouse in each group are displayed. **(D–F)** The tumor volume and survival data were shown for mice with MC38 tumors that received the increased Foretinib dose (10 mg/kg). The data is presented using the mean ± SEM where applicable, * ($P \leq 0.05$), ** ($P \leq 0.01$), *** ($P < 0.001$), **** ($P < 0.0001$), and ns (no statistical significance, $P \geq 0.05$).

Foretinib (67.97% inhibition) and αPD-1 (76.69% inhibition), moreover the inhibitory effect was significantly enhanced after the combination treatment (For+αPD-1, 98.05% inhibition) (**Figures 2A,C**) in the murine MC38 colon cancer subcutaneous model. This combination led to complete tumor regression in 50% (three out of six mice), for which a recurrence-free survival pattern over 120 days was observed (**Figure 2B**). With an increased dose of 10 mg/kg, the inhibitory effect of Foretinib was enhanced (**Figures 2D,E**), with slow tumor regrowth observed after the Foretinib treatment. There was an 83% complete rate

of tumor regression without recurrence over 120 days after the combination treatment of the higher-dose (10 mg/kg) of Foretinib and αPD-1 (**Figure 2F**) in the murine MC38 colon cancer subcutaneous model. These results suggest that Foretinib has synergistic antitumor activity when combined with αPD-1, and that the synergistic antitumor efficacy was Foretinib dosage-dependent.

Combined Treatment Enhanced T Cell Infiltration and Induces $CD8^+$ T Cell-Dependent Anti-tumor Immune Response

T cells play a key role in antitumor immunity, therefore the T cell infiltration in tumor tissues after combined treatment was determined via immunohistochemistry (IHC). The IHC results showed the tumor in the combination therapy contained more $CD3^+$ and $CD8^+$ T cells than the αPD-1 and Foretinib monotherapy or the control group (**Figures 3A–C**). To validate this result, we detected T cell in TME by flow cytometry (FCM). Consistent with IHC results, the combination therapy exhibited increased T cell infiltration (**Figures 3D–F**) in the TME when compared to the control and those treated with Foretinib or αPD-1 alone. However, no statistically significant changes were identified for Tregs in tumors following combination therapy compared to the control (**Figure 3G**). Additionally, these results demonstrated that αPD-1 therapy decreased the portion of Tregs, while Foretinib enhanced Tregs infiltration in the TME, which is similar to some other multi-target kinase inhibitors (Kwilas et al., 2014; Chen et al., 2015). The conflicting roles of Foretinib and αPD-1 may explain why there were no obvious changes to the Tregs following the combination therapy. These results revealed that the combination therapy significantly enhanced the T cell infiltration in the tumor.

To determine the functionality of T cells after treatment, the secretion of IFN-γ in T cells and the expression of PD-1 on T cells that was a co-inhibitory molecule and linked to T cell dysfunction, were evaluated by FCM. The results demonstrated that the IFN-γ^+ cells in $CD4^+$ T cells (**Supplementary Figure 3A**) and $CD8^+$ T cells (**Supplementary Figure 3B**) were increased following each treatment, with combination therapy displaying the greatest change. And the PD-1^+ T cells were decreased after treatment, especially after combination therapy (**Supplementary Figures 3C–E**). At the same time, we detected the IFN-γ and TNF-α in plasma after treatments and the result demonstrated that the combination therapy increased both cytokines concentration in peripheral blood (**Supplementary Figures 3F,G**). This result suggested that the combination therapy enhanced the function of T cells *in vivo*, which when combined with the aforementioned results, suggests that the combination of Foretinib and αPD-1 significantly enhanced the infiltration and function of T cells and promoted antitumor immunity.

In order to validate $CD8^+$ T cells are responsible for tumor cell killing, the $CD8^+$ T cells were depleted. The result showed that the MC38 tumor bearing mice with depleted $CD8^+$ T cells showed complete abrogation of tumor rejection (**Figure 3H**). Hence, it is evident that the $CD8^+$ T cells are required to achieve therapeutic efficacy.

In summary, these results indicated that the combination treatment enhanced the infiltration and function of T cells in tumor microenvironment and elicited a $CD8^+$ T cell-dependent anti-tumor immune response.

Combined Treatment Reversed TAM Mediated Immunosuppression and Inhibited Angiogenesis

It has been widely reported that the infiltration of TAMs in tumors is associated with poor prognosis. To study the effects of the combined treatment on TAMs within the TME, the TAM population and functional tumor signaling molecules were assessed. 60% of the immune cells in the TME were observed to be TAMs for the control and all the treatments inhibited the recruitment of TAMs into the TME (**Figures 4A,B**). Moreover, the treatments inhibited TAM polarization toward the M2 phenotype and the proportion of $CD206^+$ cells was reduced, especially following the combination treatment (**Figure 4C**). Taken together, the combination therapy not only reduced the number of TAMs but also inhibited TAMs polarization toward the M2 phenotype.

Multi-target kinase inhibitors such as Apatinib and Regorafenib for angiogenesis inhibition have not only been shown inhibit TAM recruitment into tumors, but also enhanced antitumor immune functions (Tsai et al., 2017; Zhao et al., 2019; Wang et al., 2020). IHC was used to evaluate the effects of the combination treatment on angiogenesis. In accordance with previous studies, Foretinib significantly inhibited angiogenesis in tumor tissues, as evidenced by reduced vascular density ($CD31^+$) when compared to the αPD-1 treatment or control. The combination treatment yielded a further reduction in vascular density compared to Foretinib alone (**Figure 4D**). These results indicated that the combination therapy lessened the hypervascularization of the tumors and inhibited the recruitment of TAMs.

Additionally, the MDSC ($CD11b^+Gr\text{-}1^+$) population was assessed by FCM due to their immunosuppressive effects in tumors. However, the number of MDSCs in MC38 tumors were not significantly different despite a slight increase following treatment (**Supplementary Figure 4A**).

Combined Treatment Abrogates the Tumor Development in the CT26 Colon Cancer Model

To verify the effect of the combination treatment in another colon cancer allograft model, the combination strategies were employed in the murine CT26 subcutaneous colon cancer model. The combination therapy was demonstrated to be significantly more effective than either monotherapy and induced complete tumor clearance in 83% (five out of six mice) of the mice and prolonged overall survival (**Figures 5A,B**). An analysis of the immune cells in the TME following treatment demonstrated that the T cell population significantly increased, especially $CD3^+$ and $CD8^+$ T cells following combination treatment (**Figures 5C,D**).

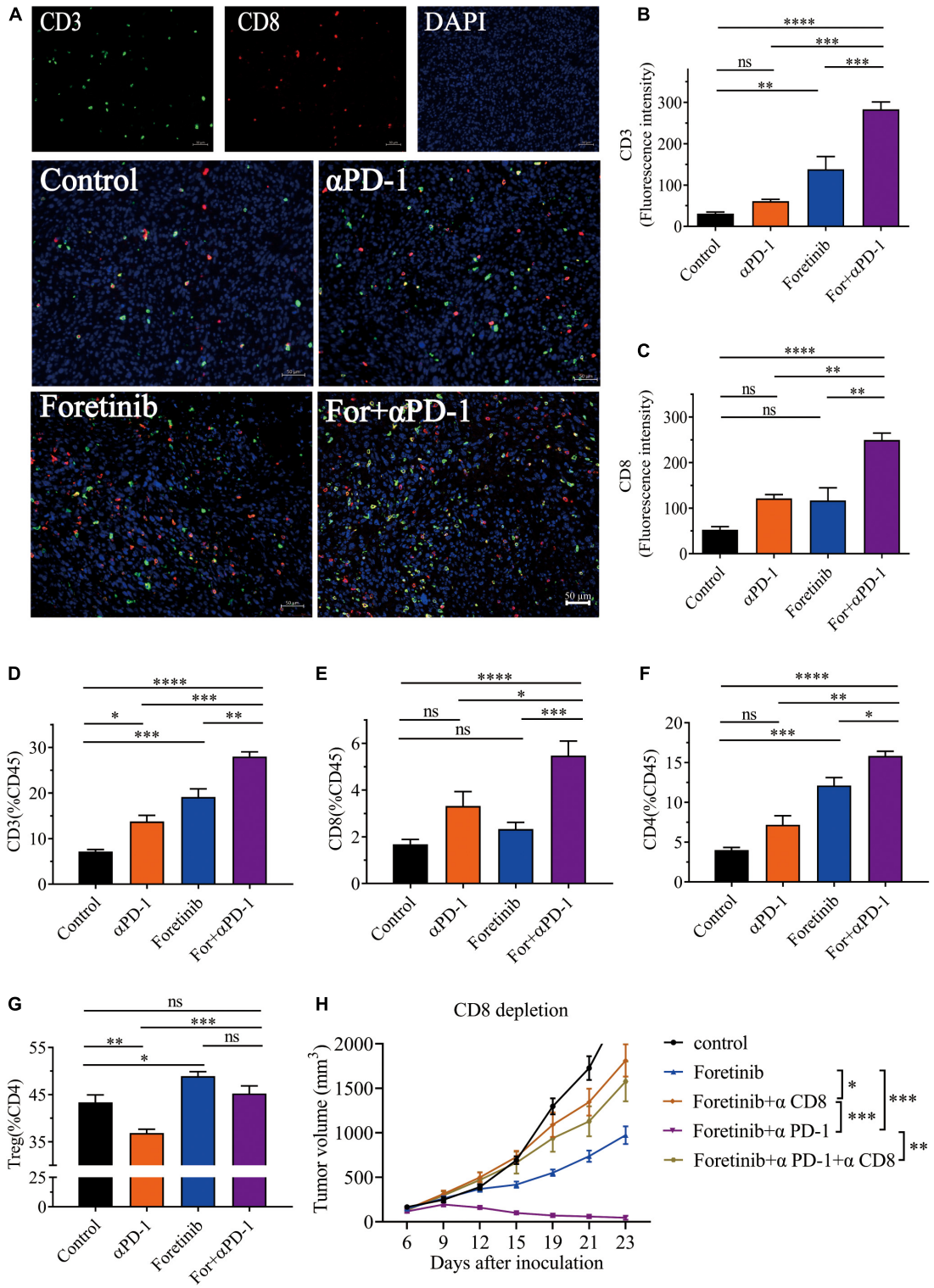

FIGURE 3 | Combination therapy enhanced T cell infiltration and induces $CD8^+$ T cell-dependent anti-tumor immune response. After the treatment was completed, T cell infiltration in MC38 tumor tissue was detected by immunohistochemistry. Representative immunofluorescent images of CD3, CD8, DAPI nuclear staining and the merge picture from each group **(A)**, and the fluorescence intensity of CD3 **(B)** and CD8 **(C)** were quantified in the tumor tissues. Scale bar, 50 μm (n = 5 mice per group). **(D–F)** Percentages of $CD3^+$ T cells, $CD8^+$ T cells and $CD4^+$ T cells in tumor. **(G)** The percentages of Tregs ($CD25^+FoxP3^+$), gated on $CD4^+$ T cells. **(H)** Tumor growth of $CD8^+$ T cell depletion assay (n = 6 mice per group). The data is presented using the mean ± SEM where applicable, * ($P \leq 0.05$), ** ($P \leq 0.01$), *** ($P < 0.001$), **** ($P < 0.0001$), and ns (no statistical significance, $P \geq 0.05$).

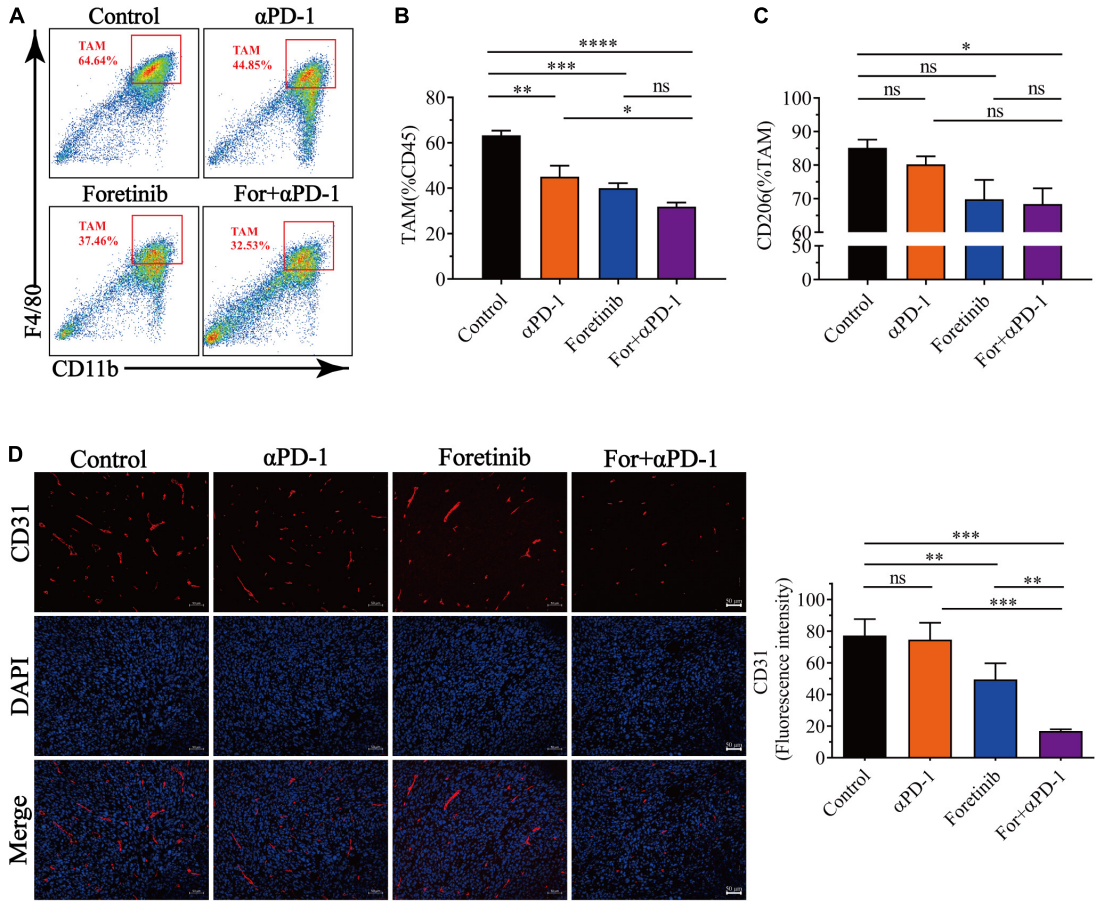

FIGURE 4 | Combination therapy decreased the number of TAM cells and inhibited angiogenesis. After finishing the treatment protocol, the tumor tissues were harvested and the TAMs and M2-type TAM infiltration was detected by FCM (n = 6), angiogenesis (CD31+ cells) were detected by immunofluorescent (n = 5). **(A)** Representative images of the gating strategy to defined TAMs. TAMs were characterized as being $CD11b^{+}F4/80^{+}$. **(B)** Percentage of TAMs from each group. **(C)** Percentage of CD206 expression in TAMs from each group. **(D)** Representative immunofluorescent images for the CD31 (Red) and DAPI nuclear staining (Blue) from each group (left) and fluorescence intensity of CD31 (right) was quantified in the tumor tissues. Scale bar, 50 μm. The data is presented using the mean ± SEM where applicable, * ($P \leq 0.05$), ** ($P \leq 0.01$), *** ($P < 0.001$), **** ($P < 0.0001$), and ns (no statistical significance, $P \geq 0.05$).

Moreover, the number of Tregs were significantly reduced following each treatment, particularly the combination treatment (**Figure 5E**). Interestingly, the Tregs in the CT26 tumor and MC38 tumor had opposite trends after Foretinib treatment (**Figures 3F**, **5E**). Moreover, the genes associated with T cell function (e.g., perforin and IFN-γ) and T cell recruitment (e.g., CCL5) (**Supplementary Figures 5A,B**) were enriched within the tumor and the level of IFN-γ and TNF-α (**Supplementary Figures 5C,D**) in plasma after treatments was elevated, especially following the combined treatment.

The expression levels of PD-1 on $CD3^{+}$ and $CD8^{+}$ T cells were decreased following αPD-1 and combination treatment (**Figure 5F**), whereas no noticeable changes occurred following the Foretinib monotherapy. This indicates that the decreased PD-1 levels on T cells following the combination therapy dependent upon αPD-1. This observation indicated that the antitumor immune response was enhanced by the combination treatment.

The infiltration of TAMs in the TME was also assessed after treatment. The combination treatment reduced the percentage of TAMs (**Figure 5G**) and promoted M2 phenotype polarization toward the M1 phenotype (**Figure 5H** and **Supplementary Figure 6**). Further study of functional genes via qPCR suggested that the combination therapy increased the expression of the proinflammatory genes such as NOS2 and TNF-α (**Figure 5I**), which represented the M1 phenotype TAMs and exert antitumor activity; whereas the expression of M2 phenotype TAM genes such as CD206 and Arg1 were decreased (**Figure 5J**). Following the combination therapy, the CT26 tumors displayed the same lack of MDSC changes as in the MC38 tumor (**Supplementary Figure 4B**).

Moreover, the levels of PD-L1 in the CT26 tumor tissues were determined by western blotting after Foretinib treatment, which demonstrated that PD-L1, p-JAK2 and p-STAT1 (included S727 and Y701) were significantly increased (**Supplementary Figure 7**), which was similar to the MC38 tumor (**Figures 1J,K**). This result means that it is likely that Foretinib caused increased PD-L1 levels via the activation of the JAK2-STAT1 pathway in the CT26 tumors.

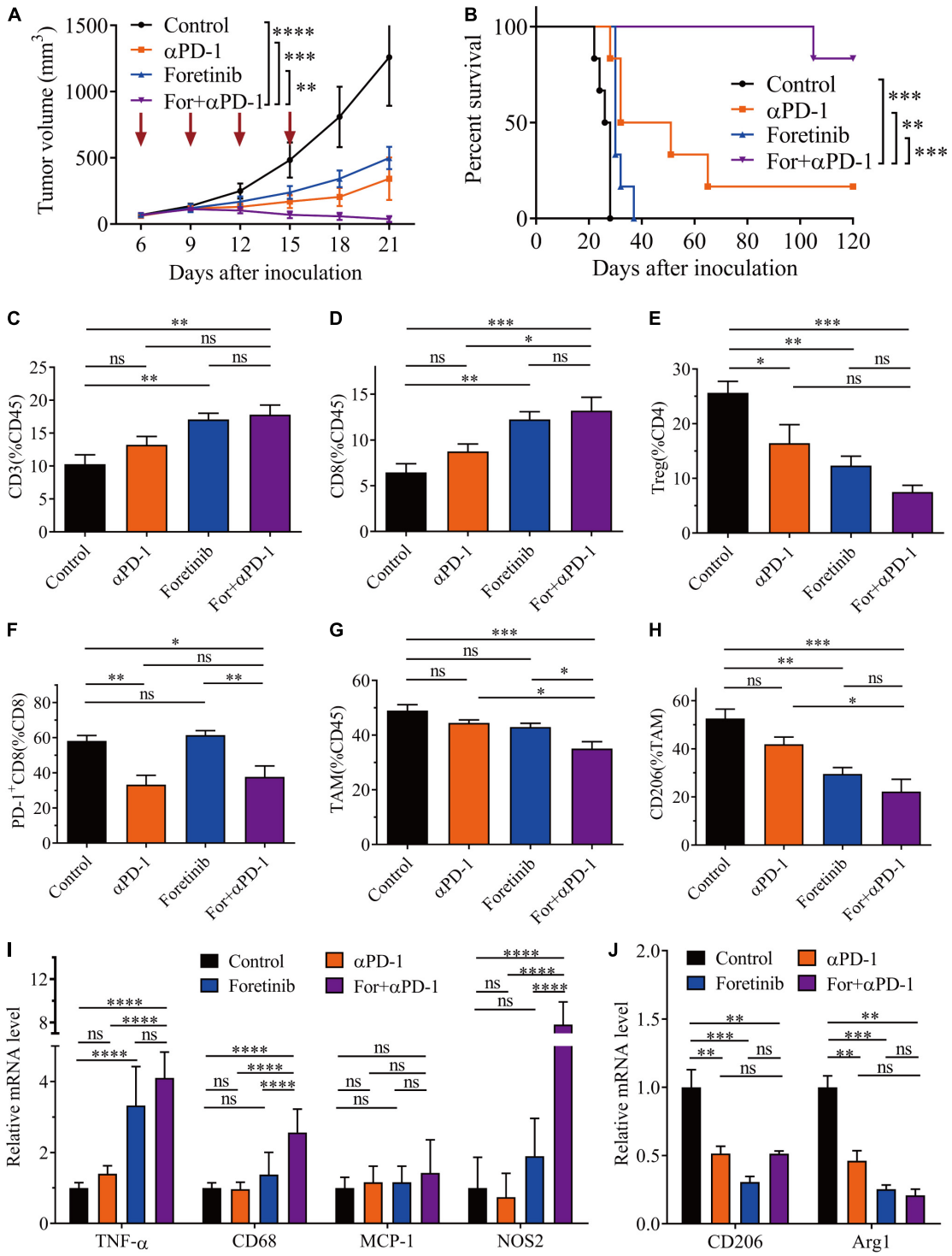

FIGURE 5 | Combination therapy ameliorated the TME in CT26 tumors. CT26 cells (5×10^5) were transplanted subcutaneously into the back of BALB/c mice. When the tumor volume reached 50–100 mm^3 (6 days after transplantation), the mice were randomly allocated to either the control or treatment groups. The drugs were given as described in "Materials and Methods" section. **(A)** Tumor volumes were monitored every 3 days and **(B)** the Kaplan–Meier survival distribution was plotting for the mice following the treatment protocol ($n = 6$). After treatment, the infiltration of $CD3^+$ T cells **(C)**, $CD8^+$ T cells **(D)**, and Tregs **(E)**, plus the expression of co-inhibitory molecules (PD-1) on $CD8^+$ T cells **(F)** was detected via FCM. The percentage of TAMs **(G)** and the expression of CD206 on TAMs **(H)** was detected by FCM ($n = 5$). **(I,J)** qRT-PCR analysis of TAM function-associated gene expression ($n = 4$). The data is presented using the mean ± SEM where applicable, * ($P \leq 0.05$), ** ($P \leq 0.01$), *** ($P < 0.001$), **** ($P < 0.0001$), and ns (no statistical significance, $P \geq 0.05$).

Combined Treatment Enhanced the Peripheral Immune Profile for Both Models

Since the peripheral immune plays a positive role in antitumor therapies, relevant immune cells in peripheral blood and spleen were detected by FCM. The results suggested that T cells were increased and MDSCs were decreased in the peripheral blood and spleen for both models (**Supplementary Figure 8**). Tregs were dramatically decreased in the spleen in the MC38 model after combination treatment (**Supplementary Figure 8B**). Additionally, macrophage was markedly decreased in the spleen for both models and in the peripheral blood of the CT26 model (while they remained unchanged in peripheral blood of the MC38 model) (**Supplementary Figure 8**). These results suggested that the combination therapy enhanced the peripheral immune profile *in vivo*.

Combined Treatment Inhibited Tumor Metastasis of CT26-Luc Colon Cancer to the Lung

In a similar manner to previous research (Qian et al., 2009), Foretinib inhibited the metastasis of CT26-Luc colon cancer cells (**Supplementary Figure 9**). To further determine the applicability of the combination therapy to advanced CRC, the effects upon colon cancer metastasis were assessed using a colon cancer lung metastasis model (CT26-Luc). The results demonstrated that both αPD-1 and Foretinib could inhibit cancer metastasis to the lung to some extent (**Figure 6A**) following injections of CT26-Luc colon cancer cells into mice. However, the inhibition was remarkably enhanced following the combination therapy, for which the bioluminescence was the lowest (**Figures 6A,B**). After treatment, the weight of lungs in each group were compared, the weight of lungs in the combination treatment was lower than other treatments and the control (**Figure 6C**). To study the effect of the combination therapy on the TME in the lungs, the T cells and TAMs were assessed after treatment. It was demonstrated that the T cells were increased slightly (**Figure 6D**), whereas the Tregs, TAMs and the M2 phenotype TAMs were decreased significantly after combination therapy (**Figures 6E,F**), that means the suppressive TME in lung was ameliorated, and the antitumor immune response was promoted.

Taken together, this data provided evidence that the combination treatment reduced Tregs, TAMs, inhibited TAM polarization toward M2 phenotype, and triggered a successful antitumor metastasis immune response.

DISCUSSION

Breakthroughs related to cancer immunotherapies have become a promising approach to cure cancer based upon the success of ICB (Couzin-Frankel, 2013; Baumeister et al., 2016; Kaiser and Couzin-Frankel, 2018). The response rates of this therapy are higher than the traditional therapy protocols, but not all types of cancer can benefit from ICB, only 20–40% of cancer patients have a favorable response, and CRC is at the lower end of the spectrum (Fritz and Lenardo, 2019). To enhance the antitumor effect, various trials have sought to establish combination treatments that utilize ICIs and other therapies, such as chemotherapy, targeted therapies, radiotherapy, and other immunotherapies (Postow et al., 2015; Hahn et al., 2017). In this study, Foretinib was combined with anti-PD-1 antibody, which significantly enhanced the antitumor effect.

Many studies have reported that RTKs inhibitors such as cabozantinib (Lu et al., 2017; Patnaik et al., 2017), lenvatinib (Kimura et al., 2018; Gunda et al., 2019), and sorafenib (Cabrera et al., 2013; Chen et al., 2014, 2015) not only inhibited angiogenesis via inhibiting the VEGF/VEGFR2 pathway and ameliorated the TME, but also improved the outcomes for ICI therapeutics. Likewise, the study contained herein identified that Foretinib inhibits the expression of VEGFR2 and inhibited angiogenesis in MC38 tumor tissues. Foretinib also ameliorated the suppressive TME and peripheral immune profile by increasing the infiltration of T cells and decreasing the number of CD11b positive myeloid cells. It is noteworthy that CD11b positive myeloid cells are previously been shown to be comprised of various cellular subtypes, most of them are immunosuppressive cells, such as TAMs and MDSCs (Engblom et al., 2016; Nguyen et al., 2018).

Herein, Foretinib was shown to increase the expression of PD-L1 via activating the JAK2-STAT1 pathway. However, Foretinib also activated other pathways in MC38 cells, such as the AKT/mTOR and MAPK pathways (data not shown), which have been associated with the expression of PD-L1, however, these pathways were inhibited in other tumor cells, such as human colon cancer cell line KM12SM, human esophageal adenocarcinoma cell line OE33, human gastric cancer cell line MKN45 and human lung carcinoma cell lines NCI-H1993 (Liu et al., 2011; Goltsov et al., 2018; Nishiyama et al., 2018; Sohn et al., 2020). Furthermore, Foretinib enhanced the phosphorylation of STAT3 in MC38 cells (data not shown), which contributes to and promotes immune suppression (Yu et al., 2009). These results suggested that Foretinib may regulate the state of cancer cells via several pathways in different cells and future research on the complex regulatory network might be warranted.

It has been proposed that increased expression of PD-L1 could enhance the antitumor effects of the anti-PD-1 antibody for many drugs (Chiang et al., 2019; Deng et al., 2019; Fournel et al., 2019; Huang et al., 2020). Additionally, JAK2-STAT1 pathway activation, especially increase STAT1 phosphorylation at Y701 has been proposed to be a potential biomarker for anticancer immunotherapy within the tumor (Koromilas and Sexl, 2013; Nakayama et al., 2019).

This study demonstrated that monotherapies utilizing Foretinib inhibited tumor growth, but following the cessation of treatment the tumors progressed rapidly. The combination of Foretinib with anti-PD-1 antibody significantly enhanced the antineoplastic function and prolonged the survival of mice bearing MC38 and CT26 tumors. This effect was more prominent for the CT26 tumors, for which nearly an 80% rate of tumor regression without recurrence was observed over 120 days; whereas a 50% rate was observed for the MC38

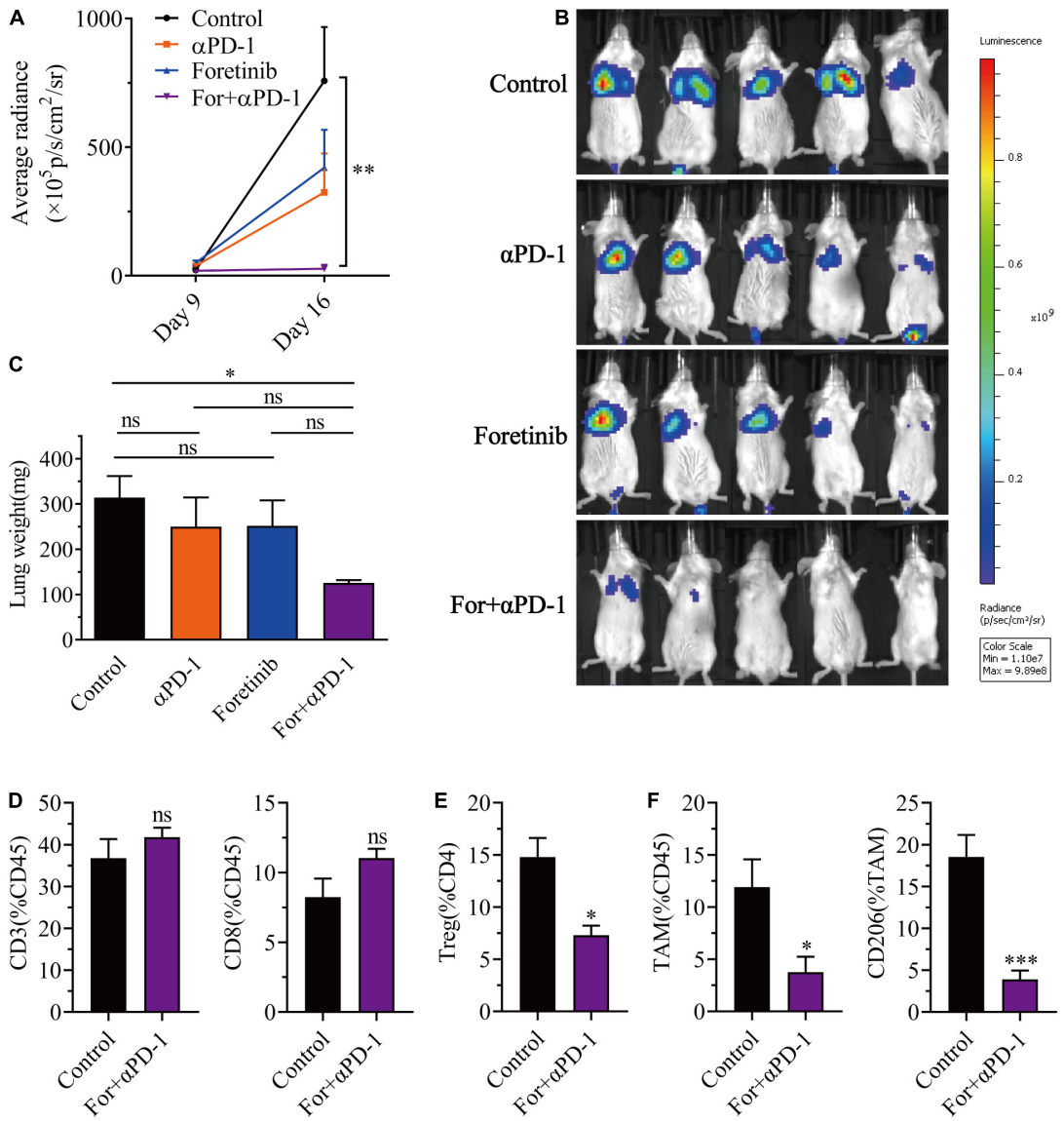

FIGURE 6 | Combination therapy inhibited CT26-Luc tumor metastasis to the lung. CT26-Luc cells (2×10^5) were intravenous injected into the BALB/c mice. On the third day after transplantation, the mice were randomly allocated to either the control or treatment groups. Drugs were given as described in "Materials and Methods" section. **(A,B)** The individual tumor load was evaluated via bioluminescence nine and 16 days after inoculation [**(A)**, the changes of bioluminescence in each group; **(B)**, bioluminescence images on day 16] ($n = 5$). **(C–F)** After treatment, the lungs from the mice in each group were weighed **(C)** and the $CD3^+$, $CD8^+$, and $CD4^+$ T cells **(D)**, Tregs **(E)**, TAMs were detected, plus the expression of CD206 in the TAMs **(F)** were identified using FCM ($n = 5$). The data is presented using the mean ± SEM where applicable, * ($P \leq 0.05$), ** ($P \leq 0.01$), *** ($P < 0.001$), **** ($P < 0.0001$), and ns (no statistical significance, $P \geq 0.05$).

tumor. This phenomenon may be because CT26 cells form highly immunogenic tumors, which have been shown to have a better response to ICB than MC38 tumors (Mosely et al., 2017; Kristensen et al., 2019).

It is widely recognized that high T cell infiltration into tumors has been associated with a high likelihood of a better prognosis and could be used as a biomarker to predict the effects of anti-PD-1 antibody therapies (Huang et al., 2017). Herein, T cell infiltration was rarely observed in both the tumor models, however, the infiltration was improved to the greatest extent after the administration of the combination treatment. It has been reported that Foretinib promote apoptosis, induce programmed cell death and inhibit angiogenesis by targeted multiple tyrosine kinases, these could release antigens and jumpstart the so-called cancer-immunity cycle, secrete chemoattractant to enhancing T cells infiltration (Huynh et al., 2012; Chen et al., 2017; Kogata et al., 2018; Liu et al., 2019; Hack et al., 2020; Petroni et al., 2021). And in our study, the genes associated with T cell recruitment were enriched within the tumor after the combination treatment, this implies there were more T cells infiltration in tumor. Furthermore, the combination treatment markedly inhibited the expression of PD-1 on T-cells and thereby reversed their

functional depletion in the CT26 tumor model. This inhibition was dependent upon the anti-PD-1 antibody, but not Foretinib.

Inhibition of the immunosuppressive functions of Tregs within tumor or a reduction of their numbers have been reported as a method enhance anti-tumor therapies (Zou, 2006). In this study, the combined treatment significantly decreased the infiltration of Tregs for the CT26 tumor, but there were no noticeable changes for MC38 tumor. This may explain why the efficacy of the combination treatment is higher in CT26 tumor than the MC38 tumor. Additionally, these results suggest that different tumor models have different active immune regulatory mechanisms. Indeed, this phenomenon is consistent with previous studies that experienced inconsistent change trends across different models for other RTKs, such as Sorafenib (Chen et al., 2014, 2015).

It is clear that TAMs play a pivotal role in tumor progression and resistance to the effects of PD-1 blockade (Biswas and Mantovani, 2010; Lewis et al., 2016; Mantovani and Locati, 2016), which is closely associated with a poor prognosis (Asgharzadeh et al., 2012; Koromilas and Sexl, 2013; Hambardzumyan et al., 2016). In this study, TAMs were the primary leukocyte infiltrates for both of the tumor models. More than 50% of the TAMs expressed CD206, which was identified as the marker of the M2 phenotype TAMs and were associated with immunosuppressive effects in tumors. Compared to the monotherapies, the Foretinib and anti-PD-1 antibody combination therapy exhibited a more effective rate of TAM reduction and a greater inhibition of the polarization of TAMs toward the M2 phenotype. Indicating that the TME was ameliorated in the tumors of mice receiving the combination treatment. Whilst the M2 phenotype TAMs were decreased for both of the models, the TAMs were decreased to a lesser extent in the CT26 tumor when compared to the significant decrease in the MC38 tumors after Foretinib treatment.

Since the peripheral immune profile can play a positive role in achieving greater antitumor effects, T-cells, Tregs, macrophages and MDSCs in the peripheral blood and spleen of both tumor models were analyzed using FCM following the different treatments. These results showed that the combination treatment increased the percentage of T-cells, especially $CD8^+$ T cells, and decreased the percentage of MDSCs in the peripheral blood and spleen for both tumor models. This indicates that the anti-tumor functions of the peripheral immune were enhanced. However, the number of Tregs were decreased in the spleens of the MC38 model and unchanged in the CT26 model after combination treatment, whereas the tumor tissues were observed to have the opposite trend. Macrophages were found to diminished in the blood of the CT26 model, but unchanged in the MC38 model. These results indicated that there are complex immune regulatory mechanisms occuring *in vivo*, many of which could impact this combination therapy and might need to be further explored in future studies.

The combination treatment also effectively reduced the metastasis of CT26-Luc cells to the lungs when compared with the monotherapies. Furthermore, the number of T cells were increased moderately and there was a decrease in the number of Tregs, TAMs and M2 phenotype TAMs in the lungs after the combination therapy, which indicates that there was an amelioration of the immune microenvironment in the lungs. The effect of Foretinib for the inhibition of CT26-Luc cell metastasis *in vitro* was pronounced in this study. However, the inhibitory effects of metastasis to the lung *in vivo* were poor. This indicates that there may be additional relevant immune regulatory mechanisms in TME in the lung, which could be worth further exploration.

CONCLUSION

In summary, this study describes that Foretinib (an RTKs inhibitor) therapy increases PD-L1 levels via the activation of the JAK2-STAT1 pathway. This in turn increased the therapeutic response to the anti-PD-1 antibody through the reprogramming of the immunosuppressive TME. This included enhanced T cell infiltration and function, inhibited TAMs and reversed TAM polarization toward the M2 phenotype. Moreover, Foretinib enhanced the peripheral immune profiles in the murine tumor models. This investigation forms a rational basis for the further exploration of a Foretinib/anti-PD-1 combination treatment strategy to enhance immunotherapy outcomes for CRC patients.

MATERIALS AND METHODS

Chemicals and Reagents

Foretinib was purchased from Lollane Biological Technology (Shanghai, China), and the anti-mouse PD-1 Ab (CD279) (clone RMP1-14) was purchased from BioXCell (West Lebanon, United States). DMSO was supplied by Solarbio Science and Technology (Beijing, China). Red Blood Cell Lysis Buffer (ACK Lysis Buffer, Beyotime, China) was used to lyse erythrocytes. Monoclonal antibodies against CD3 (11014), CD8 (11068), and CD31 (11063-2) were used for immunofluorescence, which were purchased from Servicebio (Wuhan, China). Monoclonal antibodies against CD16/32 (553142), CD45 (553079), CD3 (557596), CD8 (553079), CD4 (560782), IFN-γ (554412), CD25 (557192), Foxp3 (563101), Ly-6G/Ly-6C (Gr-1) (553128) and CD11b (557657), and Leukocyte Activation Cocktail with BD GolgiPlug (550583) for FCM were purchased from BD Biosciences (San Jose, United States). Monoclonal antibodies against CD4 (100559), PD-1 (135220), PD-L1 (124331), F4/80 (123110) and MHC class II (107625) for FCM were purchased from BioLegend (San Diego, United States). Monoclonal antibodies against CD206 (17-2061-82) for FCM was purchased from eBioscience (Worcester, MA, United States). A Transcription Factor Buffer Set (562725) kit for intracellular $Foxp3^+$ TReg staining was purchased from BD Biosciences (San Jose, United States). Mononuclear cells in mouse spleens were extracted using Histopaque-1083 (Sigma-Aldrich, United States). Fixation Buffer (420801) and Intracellular Staining Permeabilization Wash Buffer (10×) (421001) kit for intracellular IFN-γ staining were acquired from BioLegend (San Diego, United States). Antibodies against VEGFR2 (2479S) and phospho-STAT1 (Y701) (9167) for western-blot was purchased from Cell Signaling Technology (Danvers, MA, United States),

Abs of phospho-JAK2 (ET1607-34), JAK2 (ET1607-35), PD-L1 (ET1701-41), STAT1 (ET1606-39), phospho-STAT1 (S727) (ET1611-20) for western-blot were purchased from HUABIO (Hangzhou, China). A monoclonal antibody against β-actin (TA-09), Horseradish peroxidase (HRP)-conjugated goat anti-rabbit IgG (ZB-2301) and HRP-conjugated goat anti-mouse IgG (ZB-2305) for western-blotting were purchased from ZSGB-BIO (Beijing, China).

Mice and Cell Lines

Six to eight weeks-old C57BL/6 and BALB/c female mice were purchased from Beijing Vital River Laboratory Animal Technology Co., Ltd. (Beijing, China). The animals were housed and maintained under optimal conditions of light, temperature, and humidity with free access to food and water.

MC38, CT26 and CT26-Luc (a CT26 cell line that expresses luciferase) mouse colon carcinoma cell lines, and HT29, HCT116, SW480 human colon cancer cell lines were obtained from the Type Culture Collection of the Chinese Academy of Sciences (Shanghai, China). Cells were cultivated in DMEM or RPMI 1640 (Hyclone, United States) containing 10% fetal bovine serum (Bioind, IL), 100 U/ml penicillin (Thermo Scientific, United States), and 100 mg/ml streptomycin (Thermo Scientific, United States) and were cultured in a humidified 5% CO_2 atmosphere at 37°C in incubator.

Animal Experiments

For the subcutaneous tumor model, a total of 1×10^6 MC38 cells or 5×10^5 CT26 cells were resuspended in 100 μL serum-free medium and injected subcutaneously into the right flank of the C57BL/6 or BALB/c mice. Tumor sizes were measured with a digital caliper every 3 days. Tumor volume (mm^3) was estimated using the following formula: tumor volume = (long axis) × (short axis)^2 × 0.5. Mice were sacrificed when the tumor volume reached ∼2,000 mm^3 and the survival of the mice was recorded daily.

For the generation of the lung metastasis tumor model, 2×10^5 CT26-Luc cells in 100 μL serum-free medium were injected intravenously into BALB/c mice via the tail vein, and the development of tumors in the lungs was monitored using IVIS Lumina III (PerkinElmer) after intraperitoneal injection of D-luciferin potassium (meilunbio, China).

Foretinib (5 mg/kg) treatment was initiated via oral gavage every day on the sixth day after tumor cell inoculation for the subcutaneous tumor model and the second day for the lung metastasis tumor model. The αPD-1 monoclonal antibody was administered by intraperitoneal injection every 3 days for a total of four injections. The tumor-bearing mice were anesthetized on the indicated days and tissues were harvested for further analysis and measurement.

All the animal studies were approved by Sichuan University's Institutional Animal Care and Use Committee and were performed in accordance with the institutional guidelines.

$CD8^+$ T Cell Depletion

For in vivo depletion of CD8 T cells, neutralizing antibodies of αCD8 (YTS169.4 Clone, 250 μg/mouse) were intraperitoneally injected on day 2, 5, 8, 11, 14, 17 after MC38 cells inoculation and the tumor growth was evaluated.

FCM Analysis

Tumors and spleens from the subcutaneous models and lungs from the lung metastasis models were harvested after treatment and were digested at 37°C for 1 h in RIPM-1640 or DMEM medium containing 1 mg/mL collagenase type IV (Roche, CH) and 0.5 mg/ml DNase I (Roche, CH). Then passed through a 70-mm cell strainer and washed twice with PBS containing 1% BSA. After the erythrocytes were lysed, the single cells were blocked with a CD16/32 blocker and were stained for 30 min at 4°C using the following anti-mouse antibodies: CD45, CD3, CD4, CD8, CD25, PD-1, F4/80, CD11b, CD206, MHC-II, and Gr-1.

For the intracellular IFN-γ staining, spleens were harvested and the mononuclear cells were extracted and incubated in 24-well, flat-bottom plates with Leukocyte Activation Cocktail with BD GolgiPlug for 4 h at 37°C in a humidified 5% CO_2 incubator and subsequently stained with antibodies against CD45, CD3, CD4, and CD8 for 30 min at 4°C. The cells were then fixed and permeabilized with Fixation Buffer and Intracellular Staining Permeabilization Wash Buffer according to the kits' protocol and then stained with an anti-IFN-γ antibody.

For the $Foxp3^+$ Tregs staining, the surface markers were stained, fixed and permeabilized with a Transcription Factor Buffer Set according to the kit's protocol, then stained with the anti-Foxp3 antibody. To identify live cells, Fixable Viability Stain 450 (BD Biosciences, 562247) was used. Data was acquired on LSR Fortessa flow cytometer and analyzed using Flow Jo V10.0 software (BD Biosciences, United States).

Real-Time PCR

Total RNA was collected from tumor tissues using an Animal Total RNA Isolation Kit (Foregene Co., Ltd, China) following the manufacturer's protocol. cDNA was prepared using HiScript II Q RT SuperMix for qPCR (+gDNA Wiper) (Vazyme Biotech Co., Ltd., China). The qPCR was performed with AceQ SYBR qPCR Master Mix (Vazyme Biotech Co., Ltd., China) and the gene expression was normalized to the housekeeping gene ActB.

Western-Blot

Cells were treated with varying concentrations of Foretinib for 24 h and washed twice with PBS buffer and the tumor tissues were ground with liquid nitrogen following the drug treatment protocol, prior to lysis with RIPA buffer (Beyotime, China) containing protease inhibitor cocktail (MCE, United States) and phosphatase Inhibitor Cocktail I (MCE, HY-K0021), respectively. After sonication, the supernatant was obtained by centrifugation at 4°C and the protein concentrations were determined using a BCA protein assay kit (Thermo Scientific, United States). Total protein (50 or 100 μg) was separated by SDS-PAGE and then transferred onto a PVDF membrane (Millipore, IPVH00010). After blocking with 5% skimmed milk, the membranes were incubated with the appropriate antibody concentration (1:500-1:1000): JAK2, Phospho-JAK2, PD-L1, STAT1, phospho-STAT1

(including S727 and Y701), VEGFR2 and β-actin overnight at 4°C. HRP-conjugated goat anti-rabbit IgG and HRP-conjugated goat anti-mouse IgG were used as the secondary antibodies. The FUSION FX. EDGE System (VILBER LOURMAT) was used for the imaging and protein levels were based upon the signal intensity. The protein expression was normalized to β-actin.

Cytokine Assay

Peripheral blood was collected from the mice and the IFN-γ and TNF-α cytokine levels were evaluated in the plasma following separated by centrifugation at 4°C and then stored at −80°C. The concentration of IFN-γ and TNF-α in the plasma were assessed using a QuantiCyto Mouse IFN-γ ELISA kit (NeoBioscience, China) and a QuantiCyto Mouse TNF-α ELISA kit (NeoBioscience, China) according to the manufacturer's protocol.

Immunohistochemistry

For the immunohistochemistry (IHC) analysis, formalin-fixed paraffin-embedded tissue sections were deparaffinized and the slides were stained following antigen retrieval in EDTA buffer. After washing in PBS, the slides were incubated with 10% BSA for 30 min, Rat anti-CD3 (1:200) was added to the slides and incubated overnight at 4°C. After washing in PBS, goat-anti-rat FITC conjugated secondary antibodies were applied and incubated for 50 min at room temperature prior to being washed with PBS. This process was also used for the mouse anti-CD8 antibody or Rat anti-CD31 (1:200) antibody with the cy3-conjugated goat-anti-rat antibody. After PBS washes, DAPI was added and the slides were incubated for 10 min at room temperature. The slides were then rinsed with PBS and water before being imaged by confocal fluorescence microscopy (ZEISS, LSM 880, DE).

Statistical Analysis

The results were presented using the mean plus/minus the standard error of the mean (±SEM) where appropriate. All data analysis was performed using GraphPad Prism software (version 8.0). A One-way ANOVA and unpaired *t*-test was used for the statistical analyses of the data where appropriate. Animal survival was presented using Kaplan–Meier survival curves and analyzed via the log-rank test. A value of $P \leq 0.05$ was used as the threshold to reject the null hypothesis and determine the statistical significance of the data. The following standard form of abbreviation was used to indicate the significance of the data displayed in the figures: * ($P \leq 0.05$), ** ($P \leq 0.01$), *** ($P \leq 0.001$), **** ($P \leq 0.0001$) and ns (no statistical significance, $P \leq 0.05$).

DATA AVAILABILITY STATEMENT

The original contributions presented in the study are included in the article/**Supplementary Material**, further inquiries can be directed to the corresponding author/s.

ETHICS STATEMENT

The animal study was reviewed and approved by Ethics Committee of the State Key Laboratory of Biotherapy, Sichuan University, China.

AUTHOR CONTRIBUTIONS

YF and YP contributed equally to this work. YF, YP, and JY conceived and designed the experiments. YF, YP, and JM were involved in the acquisition and analysis of the data. YF, YP, and XJ performed the animal studies. YF, MW, and YiL were involved in the qPCR assay. YF, SZ, JM, LZ, CY, and CH conducted FCM and IHC assay. YaW, YuY, YuW, and LG provided advice. YF, YaY, TK, and YuL were involved in Western-Blot. YF wrote the manuscript. YF, YP, QL, and JY reviewed and/or revised of the manuscript. LG and JY supervised the study. All the authors contributed to the revision of the manuscript and approved the final version for publication.

FUNDING

This study was supported by grants from the National Natural Science Foundation of China (81572995, 82073318, 81860543, 81872907, 81602169, and 81703553), the National Major Scientific and Technological Special Projects (2017ZX09302010), and National Major Scientific and Technological Special Project for 'Significant New Drugs Development' (2018ZX09 201018-021).

SUPPLEMENTARY MATERIAL

The Supplementary Material for this article can be found online at: https://www.frontiersin.org/articles/10.3389/fcell.2021.689727/full#supplementary-material

Supplementary Figure 1 | Foretinib increased level of PD-L1 and activated the JAK2-STAT1 pathway in colon cancer cells. The expression of PD-L1, jak2, stat1, phosphor-stat1 and β-actin was detected by Western-blot in CT26, HCT116, HT29, and SW480 colon cancer cells that was treated with different concentrations of Foretinib for 24 h.

Supplementary Figure 2 | Foretinib regulated Peripheral immune microenvironment. The mice were successively gavage with Foretinib at the dose of 5 mg/kg for 15 days when the tumor volume was approximately reached to 100 mm^3. After the administration completed, the percentages of $CD3^+$, $CD4^+$ and $CD8^+$ T cells in the peripheral blood **(A)** and spleen **(B)** were detected by flow cytometry (n = 6 mice per group). The data is presented using the mean ± SEM where applicable, * ($P \leq 0.05$), ** ($P \leq 0.01$), *** ($P < 0.001$), **** ($P < 0.0001$), and ns (no statistical significance, $P \geq 0.05$).

Supplementary Figure 3 | Combination therapy enhanced the function of T cell in MC38 model. After treatment, the spleen cells were cultured 4 h with Leuko Act Cktl With GolgiPlug, and the IFN-γ^+ T cells were detected by flow cytometry (n = 5 mice per group). **(A)** Left, flow-cytometric analysis of IFN-γ^+ $CD4^+$ T cells. Right, the percentage of IFN-γ^+ T cells in $CD4^+$ T cells. **(B)** Left, flow-cytometric analysis of IFN-γ^+ $CD8^+$ T cells. Right, the percentage of IFN-γ^+ T cells in $CD8^+$ T cells. **(C–E)** The percentages of PD-1^+ cells in $CD3^+$, $CD4^+$, $CD8^+$ T cells were analysed by FCM (n = 5 mice per group). **(F,G)** The cytokines of IFN-γ and TNF-α

were detected in plasma by ELISA (n = 5 mice per group) when finished treatment in MC38 tumor. The data is presented using the mean ± SEM where applicable, * ($P \leq 0.05$), ** ($P \leq 0.01$), *** ($P < 0.001$), **** ($P < 0.0001$), and ns (no statistical significance, $P \geq 0.05$).

Supplementary Figure 4 | Combination therapy not effect MDSCs infiltration in both tumors. After the administration completed, the percentages of MDSC cells in MC38 tumor **(A)** and CT26 tumor **(B)** were detected by flow cytometry (n = 6 mice per group). The data is presented using the mean ± SEM where applicable, * ($P \leq 0.05$), ** ($P \leq 0.01$), *** ($P < 0.001$), **** ($P < 0.0001$), and ns (no statistical significance, $P \geq 0.05$).

Supplementary Figure 5 | Combination therapy enhanced the expression of T cell recruitment and function related genes and elevated the concentration of cytokines in CT26 model. The expression of T cell recruitment gene **(A)** and T cell function related genes **(B)** were analyzed by qRT-PCR (n = 4 mice per group) and the cytokines of IFN-γ **(C)** and TNF-α **(D)** were detected in plasma by ELISA (n = 5 mice per group) when finished treatment in CT26 tumor. The data is presented using the mean ± SEM where applicable, * ($P \leq 0.05$), ** ($P \leq 0.01$), *** ($P < 0.001$), **** ($P < 0.0001$), and ns (no statistical significance, $P \geq 0.05$).

Supplementary Figure 6 | Combination therapy inhibited TAMs polarization towards M2-type in CT26 model. The mean fluorescence intensity(MFI) of CD206 [**(A)**, left, the CD206 histogram of flow cytometry. right, percentages of CD206 positive cells] and MHCII **(B)** in TAMs in CT26 tumor were detected by flow cytometry after treatment (n = 6 mice per group). The data is presented using the mean ± SEM where applicable, * ($P \leq 0.05$), ** ($P \leq 0.01$), *** ($P < 0.001$), **** ($P < 0.0001$), and ns (no statistical significance, $P \geq 0.05$).

Supplementary Figure 7 | Foretinib enhanced the expression of PD-L1 in CT26 tumor. The level of proteins were detected by Western-blot in CT26 tumor tissue after treatment (left) and the relative protein expression was shown in (right), respectively (n = 3 mice per group). The data is presented using the mean ± SEM where applicable, * ($P \leq 0.05$), ** ($P \leq 0.01$), *** ($P < 0.001$), **** ($P < 0.0001$), and ns (no statistical significance, $P \geq 0.05$).

Supplementary Figure 8 | Combination therapy regulated Peripheral immune microenvironment. After the administration completed, the percentages of $CD3^+$, $CD4^+$, and $CD8^+$ T cells, MDSCs, TAMs and Tregs in the peripheral blood and spleen in MC38 tumor model **(A,B)** and CT26 tumor model **(C,D)** were detected by flow cytometry, respectively (n = 6 mice per group). The data is presented using the mean ± SEM where applicable, * ($P \leq 0.05$), ** ($P \leq 0.01$), *** ($P < 0.001$), **** ($P < 0.0001$), and ns (no statistical significance, $P \geq 0.05$).

Supplementary Figure 9 | Foretinib inhibited tumor cells invasion and metastasis. The invasion and metastasis of colon cancer cells was detected by Transwell assay after treatment by different concentration Foretinib. Briefly, cells were added into Transwell chamber that already covered matrix glue. Then, added the final concentration were 0.01% DMSO and 1, 2, and 4 μM Foretinib, and added 500 μL RPIM-1640 medium containing 5% FBS to the 24 well plate. Then place the chamber into the plate and cultivated for 24 h. Fixing by methanol, staining by crystal violet and washing two times by dd H_2O, and taking picture on microscope after drying the chamber. Scale bar, 50 μm.

REFERENCES

Asgharzadeh, S., Salo, J. A., Ji, L., Oberthuer, A., Fischer, M., Berthold, F., et al. (2012). Clinical significance of tumor-associated inflammatory cells in metastatic neuroblastoma. *J. Clin. Oncol.* 30, 3525–3532. doi: 10.1200/JCO.2011.40.9169

Baumeister, S. H., Freeman, G. J., Dranoff, G., and Sharpe, A. H. (2016). Coinhibitory pathways in immunotherapy for cancer. *Annu. Rev. Immunol.* 34, 539–573. doi: 10.1146/annurev-immunol-032414-112049

Biswas, S. K., and Mantovani, A. (2010). Macrophage plasticity and interaction with lymphocyte subsets: cancer as a paradigm. *Nat. Immunol.* 11, 889–896. doi: 10.1038/ni.1937

Bray, F., Ferlay, J., Soerjomataram, I., Siegel, R. L., Torre, L. A., and Jemal, A. (2018). Global cancer statistics 2018: GLOBOCAN estimates of incidence and mortality worldwide for 36 cancers in 185 countries. *CA Cancer J. Clin.* 68, 394–424. doi: 10.3322/caac.21492

Cabrera, R., Ararat, M., Xu, Y., Brusko, T., Wasserfall, C., Atkinson, M. A., et al. (2013). Immune modulation of effector CD4+ and regulatory T cell function by sorafenib in patients with hepatocellular carcinoma. *Cancer Immunol. Immunother.* 62, 737–746. doi: 10.1007/s00262-012-1380-8

Chen, D., Xie, J., Fiskesund, R., Dong, W., Liang, X., Lv, J., et al. (2018). Chloroquine modulates antitumor immune response by resetting tumor-associated macrophages toward M1 phenotype. *Nat. Commun.* 9:873. doi: 10.1038/s41467-018-03225-9

Chen, G. Z., Dai, W. S., Zhu, H. C., Song, H. M., Yang, X., Wang, Y. D., et al. (2017). Foretinib enhances the radiosensitivity in esophageal squamous cell carcinoma by inhibiting phosphorylation of c-Met. *J. Cancer* 8, 983–992. doi: 10.7150/jca.18135

Chen, M. L., Yan, B. S., Lu, W. C., Chen, M. H., Yu, S. L., Yang, P. C., et al. (2014). Sorafenib relieves cell-intrinsic and cell-extrinsic inhibitions of effector T cells in tumor microenvironment to augment antitumor immunity. *Int. J. Cancer* 134, 319–331. doi: 10.1002/ijc.28362

Chen, Y. C., Ramjiawan, R. R., Reiberger, T., Ng, M. R., Hato, T., Huang, Y. H., et al. (2015). CXCR4 inhibition in tumor microenvironment facilitates anti-programmed death receptor-1 immunotherapy in sorafenib-treated hepatocellular carcinoma in mice. *Hepatology* 61, 1591–1602. doi: 10.1002/hep.27665

Chiang, S. F., Huang, C. Y., Ke, T. W., Chen, T. W., Lan, Y. C., You, Y. S., et al. (2019). Upregulation of tumor PD-L1 by neoadjuvant chemoradiotherapy (neoCRT) confers improved survival in patients with lymph node metastasis of locally advanced rectal cancers. *Cancer Immunol. Immunother.* 68, 283–296. doi: 10.1007/s00262-018-2275-0

Choueiri, T. K., Vaishampayan, U., Rosenberg, J. E., Logan, T. F., Harzstark, A. L., Bukowski, R. M., et al. (2013). Phase II and biomarker study of the dual MET/VEGFR2 inhibitor foretinib in patients with papillary renal cell carcinoma. *J. Clin. Oncol.* 31, 181–186. doi: 10.1200/jco.2012.43.3383

Couzin-Frankel, J. (2013). Breakthrough of the year 2013. *Cancer Immunother. Sci.* 342, 1432–1433. doi: 10.1126/science.342.6165.1432

De Palma, M., and Lewis, C. E. (2013). Macrophage regulation of tumor responses to anticancer therapies. *Cancer Cell* 23, 277–286. doi: 10.1016/j.ccr.2013.02.013

Deng, S., Hu, Q., Zhang, H., Yang, F., Peng, C., and Huang, C. (2019). HDAC3 inhibition upregulates PD-L1 expression in B-Cell lymphomas and augments the efficacy of anti-PD-L1 therapy. *Mol. Cancer Ther.* 18, 900–908. doi: 10.1158/1535-7163.MCT-18-1068

Engblom, C., Pfirschke, C., and Pittet, M. J. (2016). The role of myeloid cells in cancer therapies. *Nat. Rev. Cancer* 16, 447–462. doi: 10.1038/nrc.2016.54

Faria, C. C., Golbourn, B. J., Dubuc, A. M., Remke, M., Diaz, R. J., Agnihotri, S., et al. (2015). Foretinib is effective therapy for metastatic sonic hedgehog medulloblastoma. *Cancer Res.* 75, 134–146. doi: 10.1158/0008-5472.can-13-3629

Feng, Q. Y., Chang, W. J., Mao, Y. H., He, G. D., Zheng, P., Tang, W. T., et al. (2019). Tumor-associated macrophages as prognostic and predictive biomarkers for postoperative adjuvant chemotherapy in patients with stage II colon cancer. *Clin. Cancer Res.* 25, 3896–3907. doi: 10.1158/1078-0432.ccr-18-2076

Fournel, L., Wu, Z., Stadler, N., Damotte, D., Lococo, F., Boulle, G., et al. (2019). Cisplatin increases PD-L1 expression and optimizes immune checkpoint blockade in non-small cell lung cancer. *Cancer Lett.* 464, 5–14. doi: 10.1016/j.canlet.2019.08.005

Fritz, J. M., and Lenardo, M. J. (2019). Development of immune checkpoint therapy for cancer. *J. Exp. Med.* 216, 1244–1254. doi: 10.1084/jem.20182395

Fukurnura, D., Kloepper, J., Amoozgar, Z., Duda, D. G., and Jain, R. K. (2018). Enhancing cancer immunotherapy using antiangiogenics: opportunities and challenges. *Nature Reviews Clinical Oncology* 15, 325–340. doi: 10.1038/nrclinonc.2018.29

Goltsov, A. A., Fang, B., Pandita, T. K., Maru, D. M., Swisher, S. G., and Hofstetter, W. L. (2018). HER2 confers resistance to foretinib inhibition of MET-amplified esophageal adenocarcinoma cells. *Ann. Thorac. Surg.* 105, 363–370. doi: 10.1016/j.athoracsur.2017.09.003

Gunda, V., Gigliotti, B., Ashry, T., Ndishabandi, D., McCarthy, M., Zhou, Z. H., et al. (2019). Anti-PD-1/PD-L1 therapy augments lenvatinib's efficacy by

favorably altering the immune microenvironment of murine anaplastic thyroid cancer. *Int. J. Cancer* 144, 2266–2278. doi: 10.1002/ijc.32041

Hack, S. P., Zhu, A. X., and Wang, Y. L. (2020). Augmenting anticancer immunity through combined targeting of angiogenic and PD-1/PD-L1 pathways: challenges and opportunities. *Front. Immunol.* 11:598877. doi: 10.3389/fimmu.2020.598877

Hahn, A. W., Gill, D. M., Pal, S. K., and Agarwal, N. (2017). The future of immune checkpoint cancer therapy after PD-1 and CTLA-4. *Immunotherapy* 9, 681–692. doi: 10.2217/imt-2017-0024

Hambardzumyan, D., Gutmann, D. H., and Kettenmann, H. (2016). The role of microglia and macrophages in glioma maintenance and progression. *Nat. Neurosci.* 19, 20–27. doi: 10.1038/nn.4185

Huang, A. C., Postow, M. A., Orlowski, R. J., Mick, R., Bengsch, B., Manne, S., et al. (2017). T-cell invigoration to tumour burden ratio associated with anti-PD-1 response. *Nature* 545, 60–65. doi: 10.1038/nature22079

Huang, K. C., Chiang, S. F., Chen, W. T., Chen, T. W., Hu, C. H., Yang, P. C., et al. (2020). Decitabine augments chemotherapy-induced PD-L1 upregulation for PD-L1 blockade in colorectal cancer. *Cancers (Basel)* 12:462. doi: 10.3390/cancers12020462

Huynh, H., Ong, R., and Soo, K. C. (2012). Foretinib demonstrates anti-tumor activity and improves overall survival in preclinical models of hepatocellular carcinoma. *Angiogenesis* 15, 59–70. doi: 10.1007/s10456-011-9243-z

Jeong, H., Kim, S., Hong, B. J., Lee, C. J., Kim, Y. E., Bok, S., et al. (2019). Tumor-associated macrophages enhance tumor hypoxia and aerobic glycolysis. *Cancer Res.* 79, 795–806. doi: 10.1158/0008-5472.CAN-18-2545

Kaiser, J., and Couzin-Frankel, J. (2018). Cancer immunotherapy sweeps nobel for medicine. *Science* 362:13. doi: 10.1126/science.362.6410.13

Khan, K. A., and Kerbel, R. S. (2018). Improving immunotherapy outcomes with anti-angiogenic treatments and vice versa. *Nat. Rev. Clin. Oncol.* 15, 310–324. doi: 10.1038/nrclinonc.2018.9

Kimura, T., Kato, Y., Ozawa, Y., Kodama, K., Ito, J., Ichikawa, K., et al. (2018). Immunomodulatory activity of lenvatinib contributes to antitumor activity in the Hepa1-6 hepatocellular carcinoma model. *Cancer Sci.* 109, 3993–4002. doi: 10.1111/cas.13806

Kogata, Y., Tanaka, T., Ono, Y. J., Hayashi, M., Terai, Y., and Ohmichi, M. (2018). Foretinib (GSK1363089) induces p53-dependent apoptosis in endometrial cancer. *Oncotarget* 9, 22769–22784. doi: 10.18632/oncotarget.25232

Koromilas, A. E., and Sexl, V. (2013). The tumor suppressor function of STAT1 in breast cancer. *JAKSTAT* 2:e23353. doi: 10.4161/jkst.23353

Kristensen, L. K., Frohlich, C., Christensen, C., Melander, M. C., Poulsen, T. T., Galler, G. R., et al. (2019). CD4(+) and CD8a(+) PET imaging predicts response to novel PD-1 checkpoint inhibitor: studies of Sym021 in syngeneic mouse cancer models. *Theranostics* 9, 8221–8238. doi: 10.7150/thno.37513

Kwilas, A. R., Ardiani, A., Donahue, R. N., Aftab, D. T., and Hodge, J. W. (2014). Dual effects of a targeted small-molecule inhibitor (cabozantinib) on immune-mediated killing of tumor cells and immune tumor microenvironment permissiveness when combined with a cancer vaccine. *J. Transl. Med.* 12:294.

Lewis, C. E., Harney, A. S., and Pollard, J. W. (2016). The Multifaceted Role of Perivascular Macrophages in Tumors. *Cancer Cell* 30:365. doi: 10.1016/j.ccell.2016.07.009

Liu, L., Shi, H., Liu, Y., Anderson, A., Peterson, J., Greger, J., et al. (2011). Synergistic effects of foretinib with HER-targeted agents in MET and HER1- or HER2-coactivated tumor cells. *Mol. Cancer Ther.* 10, 518–530. doi: 10.1158/1535-7163.MCT-10-0698

Liu, P., Zhao, L., Pol, J., Levesque, S., Petrazzuolo, A., Pfirschke, C., et al. (2019). Crizotinib-induced immunogenic cell death in non-small cell lung cancer. *Nat. Commun.* 10:1486. doi: 10.1038/s41467-019-09415-3

Lu, X., Horner, J. W., Paul, E., Shang, X., Troncoso, P., Deng, P., et al. (2017). Effective combinatorial immunotherapy for castration-resistant prostate cancer. *Nature* 543, 728–732. doi: 10.1038/nature21676

Mantovani, A., and Locati, M. (2016). Macrophage Metabolism Shapes Angiogenesis in Tumors. *Cell Metab.* 24, 887–888. doi: 10.1016/j.cmet.2016.11.007

Mosely, S. I., Prime, J. E., Sainson, R. C., Koopmann, J. O., Wang, D. Y., Greenawalt, D. M., et al. (2017). Rational selection of syngeneic preclinical tumor models for immunotherapeutic drug discovery. *Cancer Immunol. Res.* 5, 29–41. doi: 10.1158/2326-6066.CIR-16-0114

Nakayama, Y., Mimura, K., Tamaki, T., Shiraishi, K., Kua, L. F., Koh, V., et al. (2019). Phospho-STAT1 expression as a potential biomarker for anti-PD-1/anti-PD-L1 immunotherapy for breast cancer. *Int. J. Oncol.* 54, 2030–2038.

Nguyen, A., Ho, L., Workenhe, S. T., Chen, L., Samson, J., Walsh, S. R., et al. (2018). HDACi delivery reprograms tumor-infiltrating myeloid cells to eliminate antigen-loss variants. *Cell Rep.* 24, 642–654. doi: 10.1016/j.celrep.2018.06.040

Nishiyama, A., Yamada, T., Kita, K., Wang, R., Arai, S., Fukuda, K., et al. (2018). Foretinib overcomes entrectinib resistance associated with the NTRK1 G667C mutation in NTRK1 fusion-positive tumor cells in a brain metastasis model. *Clin. Cancer Res.* 24, 2357–2369. doi: 10.1158/1078-0432.CCR-17-1623

Oliveira, A. F., Bretes, L., and Furtado, I. (2019). Review of PD-1/PD-L1 inhibitors in metastatic dMMR/MSI-H colorectal cancer. *Front. Oncol.* 9:396. doi: 10.3389/fonc.2019.00396

O'Neill, R. E., and Cao, X. (2019). Co-stimulatory and co-inhibitory pathways in cancer immunotherapy. *Adv. Cancer Res.* 143, 145–194. doi: 10.1016/bs.acr.2019.03.003

Overman, M. J., McDermott, R., Leach, J. L., Lonardi, S., Lenz, H. J., Morse, M. A., et al. (2017). Nivolumab in patients with metastatic DNA mismatch repair-deficient or microsatellite instability-high colorectal cancer (CheckMate 142): an open-label, multicentre, phase 2 study. *Lancet Oncol.* 18, 1182–1191. doi: 10.1016/s1470-2045(17)30422-9

Patnaik, A., Swanson, K. D., Csizmadia, E., Solanki, A., Landon-Brace, N., Gehring, M. P., et al. (2017). Cabozantinib eradicates advanced murine prostate cancer by activating antitumor innate immunity. *Cancer Discov.* 7, 750–765. doi: 10.1158/2159-8290.CD-16-0778

Petroni, G., Buque, A., Zitvogel, L., Kroemer, G., and Galluzzi, L. (2021). Immunomodulation by targeted anticancer agents. *Cancer Cell* 39, 310–345. doi: 10.1016/j.ccell.2020.11.009

Pitt, J. M., Vetizou, M., Daillere, R., Roberti, M. P., Yamazaki, T., Routy, B., et al. (2016). Resistance mechanisms to immune-checkpoint blockade in cancer: tumor-intrinsic and -extrinsic factors. *Immunity* 44, 1255–1269. doi: 10.1016/j.immuni.2016.06.001

Postow, M. A., Callahan, M. K., and Wolchok, J. D. (2015). Immune checkpoint blockade in cancer therapy. *J. Clin. Oncol.* 33, 1974–1982. doi: 10.1200/JCO.2014.59.4358

Qian, F., Engst, S., Yamaguchi, K., Yu, P., Won, K. A., Mock, L., et al. (2009). Inhibition of tumor cell growth, invasion, and metastasis by EXEL-2880 (XL880, GSK1363089), a novel inhibitor of HGF and VEGF receptor tyrosine kinases. *Cancer Res.* 69, 8009–8016. doi: 10.1158/0008-5472.CAN-08-4889

Ribas, A., and Wolchok, J. D. (2018). Cancer immunotherapy using checkpoint blockade. *Science* 359, 1350–1355.

Sohn, S. H., Kim, B., Sul, H. J., Choi, B. Y., Kim, H. S., and Zang, D. Y. (2020). Foretinib inhibits cancer stemness and gastric cancer cell proliferation by decreasing CD44 and c-MET signaling. *Onco. Targets Ther.* 13, 1027–1035. doi: 10.2147/OTT.S226951

Tsai, A. K., Khan, A. Y., Worgo, C. E., Wang, L. L., Liang, Y., and Davila, E. (2017). A multikinase and DNA-PK inhibitor combination immunomodulates melanomas, suppresses tumor progression, and enhances immunotherapies. *Cancer Immunol. Res.* 5, 790–803. doi: 10.1158/2326-6066.CIR-17-0009

van der Leun, A. M., Thommen, D. S., and Schumacher, T. N. (2020). CD8(+) T cell states in human cancer: insights from single-cell analysis. *Nat. Rev. Cancer* 20, 218–232. doi: 10.1038/s41568-019-0235-4

Wang, Q., Gao, J., Di, W., and Wu, X. (2020). Anti-angiogenesis therapy overcomes the innate resistance to PD-1/PD-L1 blockade in VEGFA-overexpressed mouse tumor models. *Cancer Immunol. Immunother.* 69, 1781–1799. doi: 10.1007/s00262-020-02576-x

Xiao, Q. Y., Nobre, A., Pineiro, P., Berciano-Guerrero, M. A., Alba, E., Cobo, M., et al. (2020). Genetic and epigenetic biomarkers of immune checkpoint blockade response. *J. Clin. Med.* 9:286. doi: 10.3390/jcm9010286

Xu, J. M., Feng, Q. Y., Chang, W. J., Mao, Y. H., Tang, W. T., Wei, Y., et al. (2018). Ratio of M2 tumor-associated macrophages as a better prognostic and predictive biomarkers for postoperative adjuvant chemotherapy in patients with stage II colon cancer. *J. Clin. Oncol.* 36:e15582-e15582. doi: 10.1200/JCO.2018.36.15_suppl.e15582

Yau, T. C. C., Lencioni, R., Sukeepaisarnjaroen, W., Chao, Y., Yen, C. J., Lausoontornsiri, W., et al. (2017). A phase I/II multicenter study of single-agent foretinib as first-line therapy in patients with advanced hepatocellular

carcinoma. *Clin. Cancer Res.* 23, 2405–2413. doi: 10.1158/1078-0432.ccr-16-1789

Yu, H., Pardoll, D., and Jove, R. (2009). STATs in cancer inflammation and immunity: a leading role for STAT3. *Nat. Rev. Cancer* 9, 798–809. doi: 10.1038/nrc2734

Zhao, S., Ren, S., Jiang, T., Zhu, B., Li, X., Zhao, C., et al. (2019). Low-dose apatinib optimizes tumor microenvironment and potentiates antitumor effect of PD-1/PD-L1 blockade in lung cancer. *Cancer Immunol. Res.* 7, 630–643. doi: 10.1158/2326-6066.CIR-17-0640

Zou, W. (2006). Regulatory T cells, tumour immunity and immunotherapy. *Nat. Rev. Immunol.* 6, 295–307. doi: 10.1038/nri1806

Conflict of Interest: The authors declare that the research was conducted in the absence of any commercial or financial relationships that could be construed as a potential conflict of interest.

frontiers in Cell and Developmental Biology

ORIGINAL RESEARCH
published: 30 July 2021
doi: 10.3389/fcell.2021.682002

Identification of CDK2-Related Immune Forecast Model and ceRNA in Lung Adenocarcinoma, a Pan-Cancer Analysis

*Ting-Ting Liu[1,2], Rui Li[1,2], Chen Huo[1,2], Jian-Ping Li[1,2], Jie Yao[1,2], Xiu-li Ji[3] and Yi-Qing Qu[2,4]**

[1] Department of Pulmonary and Critical Care Medicine, Qilu Hospital, Cheeloo College of Medicine, Shandong University, Jinan, China, [2] Shandong Key Laboratory of Infectious Respiratory Diseases, Jinan, China, [3] Department of Pulmonary Disease, Jinan Traditional Chinese Medicine Hospital, Jinan, China, [4] Department of Respiratory and Critical Care Medicine, Qilu Hospital of Shandong University, Jinan, China

OPEN ACCESS

Edited by:
Na Luo,
Nankai University, China

Reviewed by:
Jingwu Xie,
Indiana University, United States
Min Zhou,
Shanghai Jiao Tong University, China

***Correspondence:**
Yi-Qing Qu
quyiqing@sdu.edu.cn

Specialty section:
This article was submitted to Molecular and Cellular Pathology, a section of the journal Frontiers in Cell and Developmental Biology

Received: *17 March 2021*
Accepted: *06 July 2021*
Published: *30 July 2021*

Citation:
Liu T-T, Li R, Huo C, Li J-P, Yao J, Ji X-l and Qu Y-Q (2021) Identification of CDK2-Related Immune Forecast Model and ceRNA in Lung Adenocarcinoma, a Pan-Cancer Analysis. Front. Cell Dev. Biol. 9:682002. doi: 10.3389/fcell.2021.682002

Background: Tumor microenvironment (TME) plays important roles in different cancers. Our study aimed to identify molecules with significant prognostic values and construct a relevant Nomogram, immune model, competing endogenous RNA (ceRNA) in lung adenocarcinoma (LUAD).

Methods: "GEO2R," "limma" R packages were used to identify all differentially expressed mRNAs from Gene Expression Omnibus (GEO) and The Cancer Genome Atlas (TCGA) databases. Genes with *P*-value <0.01, LogFC>2 or <-2 were included for further analyses. The function analysis of 250 overlapping mRNAs was shown by DAVID and Metascape software. By UALCAN, Oncomine and R packages, we explored the expression levels, survival analyses of CDK2 in 33 cancers. "Survival," "survminer," "rms" R packages were used to construct a Nomogram model of age, gender, stage, T, M, N. Univariate and multivariate Cox regression were used to establish prognosis-related immune forecast model in LUAD. CeRNA network was constructed by various online databases. The Genomics of Drug Sensitivity in Cancer (GDSC) database was used to explore correlations between CDK2 expression and IC50 of anti-tumor drugs.

Results: A total of 250 differentially expressed genes (DEGs) were identified to participate in many cancer-related pathways, such as activation of immune response, cell adhesion, migration, P13K-AKT signaling pathway. The target molecule CDK2 had prognostic value for the survival of patients in LUAD (*P* = 5.8e-15). Through Oncomine, TIMER, UALCAN, PrognoScan databases, the expression level of CDK2 in LUAD was higher than normal tissues. Pan-cancer analysis revealed that the expression, stage and survival of CDK2 in 33 cancers, which were statistically significant. Through TISIDB database, we selected 13 immunodepressants, 21 immunostimulants associated with CDK2 and explored 48 genes related to these 34 immunomodulators in cBioProtal database (*P* < 0.05). Gene Set Enrichment Analysis (GSEA) and Metascape indicated

that 49 mRNAs were involved in PUJANA ATM PCC NETWORK (ES = 0.557, P = 0, FDR = 0), SIGNAL TRANSDUCTION (ES = –0.459, P = 0, FDR = 0), immune system process, cell proliferation. Forest map and Nomogram model showed the prognosis of patients with LUAD (Log-Rank = 1.399e-08, Concordance Index = 0.7). Cox regression showed that four mRNAs (SIT1, SNAI3, ASB2, and CDK2) were used to construct the forecast model to predict the prognosis of patients ($P < 0.05$). LUAD patients were divided into two different risk groups (low and high) had a statistical significance (P = 6.223e-04). By "survival ROC" R package, the total risk score of this prognostic model was AUC = 0.729 (SIT1 = 0.484, SNAI3 = 0.485, ASB2 = 0.267, CDK2 = 0.579). CytoHubba selected ceRNA mechanism medicated by potential biomarkers, 6 lncRNAs-7miRNAs-CDK2. The expression of CDK2 was associated with IC50 of 89 antitumor drugs, and we showed the top 20 drugs with $P < 0.05$.

Conclusion: In conclusion, our study identified CDK2 related immune forecast model, Nomogram model, forest map, ceRNA network, IC50 of anti-tumor drugs, to predict the prognosis and guide targeted therapy for LUAD patients.

Keywords: tumor microenvironment, CDK2, pan-cancer analysis, nomogram model, prognostic model, ceRNA

INTRODUCTION

Lung cancer is the third leading cause of death in the world (Siegel et al., 2020; Kara et al., 2021), which is classified into small cell lung cancer (SCLC), lung squamous cell carcinoma (LUSC) and lung adenocarcinoma (LUAD) (Wu Y. et al., 2021). Non-small cell lung cancer (NSCLC) accounted for 85% of lung cancer and the 5-year survival rate of the patients is less than 20% (Bade and Dela Cruz, 2020). LUAD is the most important type of NSCLC (Chen and Zhou, 2021; Hou and Yao, 2021; Zhou C. et al., 2021). In recent years, although the treatment of lung cancer is diversified, such as chemotherapy, immunotherapy, targeted therapy, the prognosis of patients with advanced lung cancer is still poor (Noreldeen et al., 2020; Wang et al., 2020). More than 60% of LUAD patients missed the best targeted treatment time due to the difficulty of diagnosis, which can reduce the survival rate (Kris et al., 2014; Chen et al., 2016). In recent years, the resistance of the majority of LUAD patients to multiple antitumor drugs has led to a decrease in the cure rate of LUAD. Therefore, it is very necessary to explore the early gene markers and treatment targets for the prognosis of patients (He et al., 2021).

The immune system is currently recognized as a determinant of cancer (Janssen et al., 2017). With the development of modern technology, new immunotherapy drugs have made remarkable achievements and improved the prognosis of patients (Yang et al., 2021). Combined with various clinical studies, immunotherapy may replace the traditional treatment (Zhai et al., 2021). Understanding TME and recognizing genes related to TME can provide new ideas for immunotherapy. In the TME, many cancer cells and immune cells mediate signaling pathways (Marwitz et al., 2021), involving in tumor progression and drug resistance (Santaniello et al., 2019; Ling et al., 2020). In view of the low treatment rate of LUAD patients with high pathogenicity, it is imperative to find new gene markers (Zhou C. S. et al., 2021).

The mechanism of immune infiltration plays an irreplaceable role in the progress of various cancers (Esenboga et al., 2021; Huang H. et al., 2021; Jomrich et al., 2021; Mungan et al., 2021). The novel systemic immune-inflammation index (SII) is a new kind of marker, including peripheral lymphocytes, neutrophils, and platelets (Ju et al., 2021). SII features play important roles in various cancers, such as Esophageal Squamous Cell Carcinoma (Geng et al., 2016), hepatocellular carcinoma (Hu et al., 2014), and prostate cancer (Lolli et al., 2016).

As for a non-coding RNA, lncRNA was limited to code protein (Chen and Zhang, 2021). In recent years, there has been increasing evidence that the expression of lncRNA involves in cancer progression, such as cancer metastasis (Li et al., 2016; Kim et al., 2018), drug resistance (Han et al., 2017), and apoptosis (Zhao et al., 2017). ceRNA network was composed of mRNAs, lncRNAs, and miRNAs (Chen Y. et al., 2021). lncRNA MALAT1 modulates cell migration, proliferation by sponging miRNA146a to regulate CXCR4 in acute myeloid leukemia (Sheng X. F. et al., 2021). ceRNA network represents a novel layer of gene regulation that controls both physiological and pathological processes (Zhang et al., 2021).

Our study aims to explore immune-related genes and construct forecast model for clinical guidance and prognosis

Abbreviations: TME, tumor microenvironment; ceRNA, competing endogenous RNA; LUAD, lung adenocarcinoma; GEO, Gene Expression Omnibus; TCGA, The Cancer Genome Atlas; GDSC, Genomics of Drug Sensitivity in Cancer; DEG, differentially expressed genes; GSEA, Gene Set Enrichment Analysis; LUSC, lung squamous cell carcinoma; NSCLC, non-small cell lung cancer; SII, systemic immune-inflammation index; CDK, cell-dependent kinases; BP, biological process; CC, cellular component; MF, molecular function; OS, The Overall Survival; RFS, Relapse-Free Survival; FP, false positive; TP, true positive; KEGG, Kyoto Encyclopedia of Genes and Genomes; AML, acute myeloid leukemia; GO, Gene Ontology; HPA, Human Protein Atlas; PCR, polymerase chain reaction.

analysis in LUAD using TCGA and GEO common databases. The relationship between target genes and immune cells is studied through various authoritative databases. We built the lncRNAs-miRNAs-CDK2 ceRNA network innovatively, found potential prognostic markers with LUAD. Our study may provide new molecular and therapeutic strategies for the treatment and prognosis of LUAD patients.

MATERIALS AND METHODS

Gene Expression mRNA Seq, Clinical Data Collection

We downloaded the gene expression, clinical data, Pan-Cancer Atlas Hub from GEO database[1] (Chen C. et al., 2021), UCSC Xena[2] (Li F. et al., 2021), GDSC[3].

mRNA-Based Survival Prediction in LUAD

Four hundred and thirty three LUAD tissues and 19 normal tissues were selected from the GSE68465 (GPL96). By GEO2R (Liu et al., 2019), $P < 0.01$, Log FC > 2 or Log FC < -2 were defined as screening criteria. Next, Metascape[4] (Liu et al., 2020), KEGG[5] (Zheng et al., 2021), and DAVID[6] (Li J. et al., 2021) databases were used to analyze biological process (BP), cellular component (CC), molecular function (MF) and related pathways of differentially expressed mRNAs (DEmRNAs).

Validation of CDK2 in Different Databases

UALCAN[7] (Liu H. et al., 2021) is a comprehensive, user-friendly, and interactive web resource for analyzing cancer OMICS data. Combing with clinical data, we explored the correlation between CDK2 expression and clinical indicators, such as age, grade, sex, smoking habits, stage, TP-53 mutation, weight. Heat maps were showed the positive and negative related genes with CDK2. We analyzed the overall survival (OS) and Relapse-Free Survival (RFS) about CDK2 for LUAD patients by PrognoScan[8] (Liu X. et al., 2021).

Further Study About CDK2 Expression in 33-Cancers: Pan-Cancer Analysis

Compared with normal lung tissues, CDK2 expression was highly expressed ($P < 0.05$) in LUAD by Oncomine[9] (Dai et al., 2021) and TIMER[10] (Wu R. et al., 2021) databases. As for 33-cancers, we studied the relationships between the expression of CDK2 and clinical stage, survival conditions through different "R" packages.

Batch Related Genes, ROC Analysis, Functional Enrichment, GSEA Analysis in LUAD

To research the major molecule CDK2, we showed 50 positive and negative genes in LUAD by heat maps (Person test method). The 1, 3, 5, and 8 years' ROC curves were constructed by "ROC" R package. The abscissa of the prediction model was False Positive (FP) and the ordinate was True Positive (TP). Next, we screened out the top 300 genes with the most significant positive correlation with CDK2 for enrichment analysis. Bar and bubble charts showed the classical functions of 300 genes by "clusterprofiler" R package. We downloaded the GSEA4.1.0[11] (Cao et al., 2021a) to investigate Kyoto Encyclopedia of Genes and Genomes (KEGG) of CDK2-related 300 genes. The top of 50 terms were sorted by *P*-value in circle graph.

Immune Infiltration of CDK2 in LUAD

CIBERSORT[12] (Tan et al., 2021) is an analysis tool to provide an estimation of the abundances of member cell types in a mixed cell population using gene expression data. We selected immune cells associated with CDK2 (Pearson correlation coefficient $r > 0.15$). Four CDK2-related immune cells were shown in circle graph.

Correlation Analysis of Immune Cells and CDK2 Expression

R package was used to analyze the relation of CDK2 and immune cell infiltration score ($P \leq 0.05$). A total of 33-cancers, according to the median of CDK2 gene expression, the samples were divided into high expression groups and low expression groups. Then, we discussed the different expression of immune cells ($P < 0.05$). The above results were shown by scatter plots and box plots.

Exploring CDK2-Related Immune Genes and GSEA Analysis

TISIDB[13] (Huang X. Y. et al., 2021) is a web portal for tumor and immune system interaction, which integrates multiple heterogeneous data types. First, we found CDK2-related Immunomodulators with *P*-value < 0.05. Next, cBioPortal[14] (Lu et al., 2021) was used to explore the genes related to Immunomodulators. DAVID and STRING[15] (Zhuang et al., 2021) were used to analyze the Gene Ontology (GO), protein interaction of 49 genes. GSEA 4.1.0 further analyzed the NOM *p*-val and FDR *q*-val of these immune related genes.

[1]https://www.ncbi.nlm.nih.gov/gds/?term
[2]https://xena.ucsc.edu/
[3]https://www.cancerrxgene.org/
[4]https://metascape.org/gp/index.html#/main/step1
[5]https://www.kegg.jp/
[6]https://david.ncifcrf.gov/tools.jsp
[7]http://ualcan.path.uab.edu/index.html
[8]http://dna00.bio.kyutech.ac.jp/PrognoScan/index.html
[9]https://www.oncomine.org/resource/login.html
[10]https://cistrome.shinyapps.io/timer/
[11]https://www.gsea-msigdb.org/gsea/msigdb
[12]https://cibersort.stanford.edu/index.php
[13]http://cis.hku.hk/TISIDB/
[14]https://www.cbioportal.org/
[15]https://string-db.org/cgi/network

Combining Clinical Data and Constructing Nomogram Model

Through LUAD clinical data, "survival," "survminer" R packages were used to construct the COX regression model of age, gender, and stage. Forest plot (Xiang et al., 2021) was shown related Hazard ratio (HR), Log-Rank, Concordance index of LUAD. "rms" R package was used to structure the Nomogram model (Liu et al., 1976) of age, gender, stage, T, N, M.

Univariate, Multivariate Cox Regression and Time ROC Analysis

Using "Survival" R package, we explored the univariate Cox analysis of 49 genes ($P < 0.05$). Different *P*-value and HR of statistically significant genes were shown in forest map. According to the results of univariate regression analysis, the significant genes were further analyzed by multivariate analysis. According to the risk score of genes selected by multiple factors, the LUAD samples were divided into lower-risk and higher-risk groups. The risk score was as follows: Risk score = Expgene1 × Coefgene1+Expgene2 × Coefgene2+ Expgene3 × Coefgene3+ Expgene4 × Coefgene4. "survival," "survminer," "survival ROC" R packages were performed survival probability curve and ROC curve. Combining the patient's high and low risk situation and the state of life, death, we used "pheatmap" R package to show the heat map.

The CDK2 Expression Was Further Verified by Histochemistry

We use Human Protein Atlas (HPA) database to verify CDK2 expression in LUAD tissues and normal lung tissues.

Identification of CDK2 Related ceRNA Network

We explored CDK2 related miRNAs from Targetscan[16] (Barnett-Itzhaki et al., 2021), miRWalk[17] (Sheng L. P. et al., 2021), mirDB[18] (Ren et al., 2021), Starbase[19] (Li et al., 2014). All miRNAs from four databases were analyzed by Venn map[20]. Kaplan–Meier Plotter software was used to explore the prognostic value of miRNAs with LUAD. The lncRNAs that regulate common

[16]http:/www.targetscan.org
[17]http://mirwalk.umm.uni-heidelberg.de/
[18]http://mirdb.org/
[19]http://starbase.sysu.edu.cn/starbase2/index.php
[20]http://bioinformatics.psb.ugent.be/webtools/Venn/

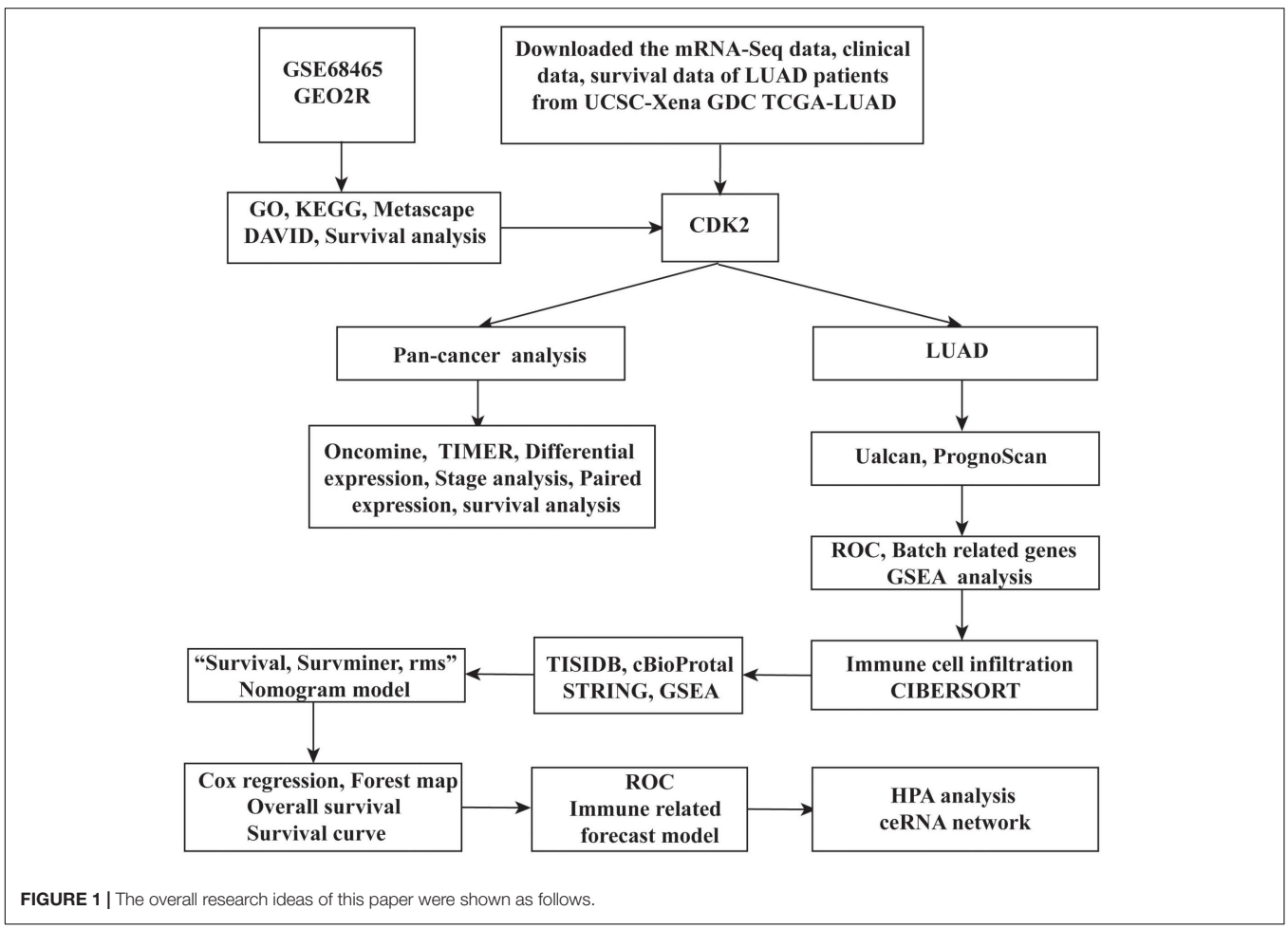

FIGURE 1 | The overall research ideas of this paper were shown as follows.

miRNAs were screened by Starbase database (Li et al., 2014). The Cytoscape (Han et al., 2021) was used to build ceRNA network and Cytohubba selected the key node genes according to the degree in the network.

The Expression of CDK2 Was Verified by Polymerase Chain Reaction (PCR)

We did the basic experimental verification of PCR about CDK2 in LUAD cell lines (A549, H1299, H1975) and normal bronchial epithelial cell line (BEAS-2B). GraphPad Prism7[21] software was used to count the differences between cancer cell lines and normal cell line.

[21]https://www.graphpad.com/

Correlation Between CDK2 and IC50 of Anti-tumor Drugs

We downloaded the response data of 192 anti-tumor drugs in more than 1000 cancer cell lines. "Ggplot2" R package was used to explore the correlation between the CDK2 expression and IC50 of 192 anti-tumor drugs by box diagrams and point diagrams.

RESULTS

Differentially Expressed mRNAs for GSE68465

A total of 250 genes were chosen by GEO2R according to the *P*-value and LogFC. 161 mRNAs were highly expressed and 78

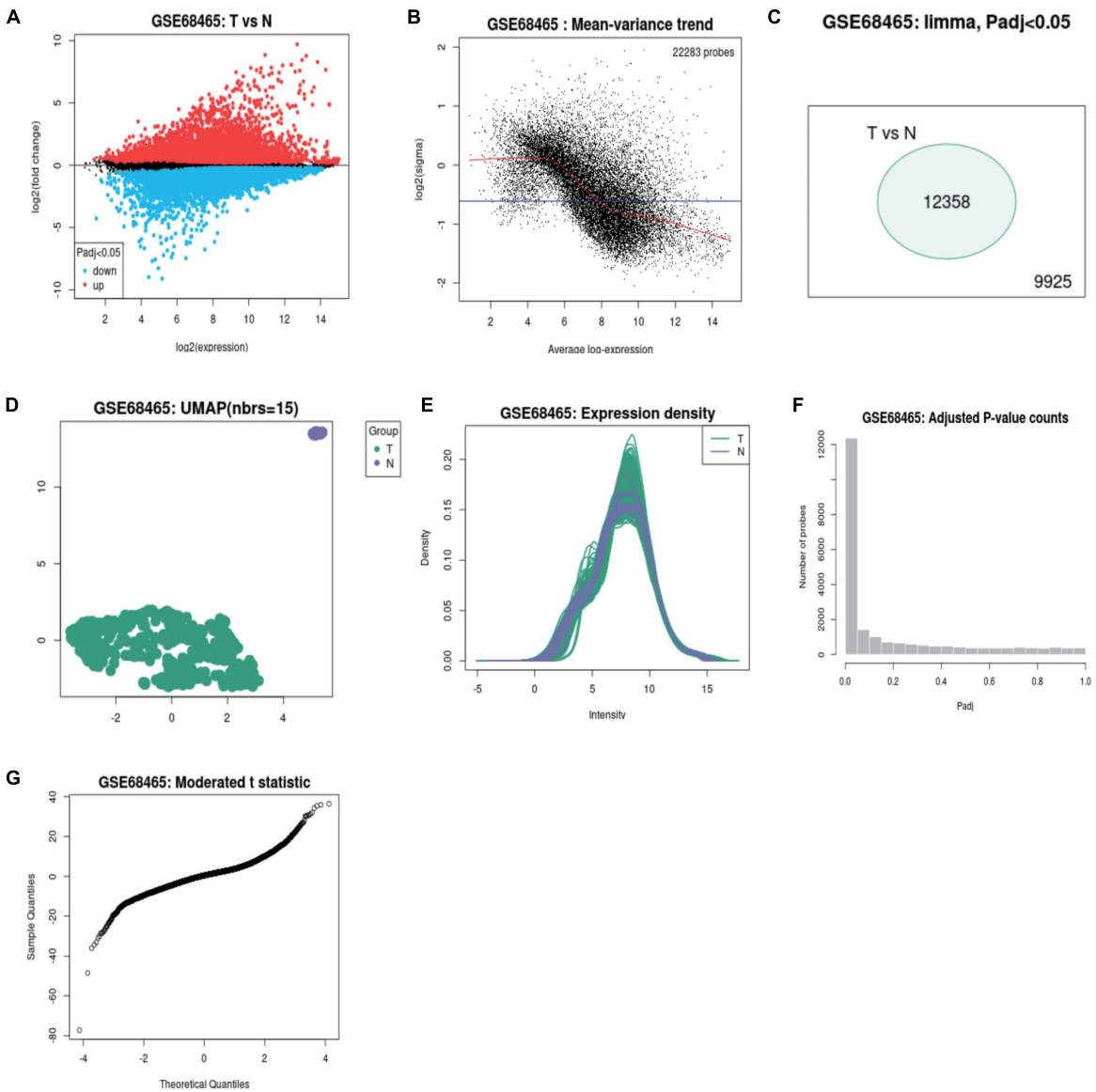

FIGURE 2 | The volcano map, scatter plot, peak plot of GSE68465 samples **(A–G)**.

mRNAs were expressed at lower levels in 19 adjacent non-LUAD tissues and 433 LUAD tissues. The study design of this project was shown in **Figure 1**. The volcano map, scatter plots, peak plot of GSE68465 samples were displayed in **Figure 2**. A total of 15 highly expressed genes and 15 low expressing genes were shown in **Table 1**.

GO, KEGG Analysis of 250 DEmRNAs

Through Metascape software, we identified a number of pathways significantly enriched, including activation of immune response, regulation of cell adhesion, T cell activation involved in immune response, regulation of cell adhesion, PID-HNF3B PATHWAY (**Figure 3A**). The interactions between different pathways were shown in **Figure 3B**. **Figures 3C,D** drew the *P*-value of different pathways. According to the relationship of DE mRNAs, several protein analyses were performed in the **Figure 3E**. CDK2, MYB, GATA3 related to each other in some tumor pathway and the results were listed in circle graph (**Figure 3F**). DAVID was used to analyze the KEGG results of genes and we found 9 mRNAs participated in the classic P13-AKT signaling pathway, such as MYB, COL3A1, COL4A1, CSF1R, CDK2, ITGB7, LAMA2, TLR2, and VWF. Combining with the Overall Survival (OS) of LUAD patients, we chose CDK2 as targeted molecule ($P < 0.05$). KEGG software further was used to identify the upstream molecules of CDK2 in P13-AKT signaling pathway. Finally, the CDKN1A might regulate downstream molecule CDK2 to influence cell cycle progression in LUAD. Through the scatter plot, there was a positive correlation between CDK2 and CDKN1A using GEPIA[22] ($P = 0$, $R = 0.59$) (**Figure 3G**).

TABLE 1 | The top of 15 higher expressed and 15 lower expressed genes.

Gene.symbol	logFC	adj.*P*.Val	*P*.Value
HLA-DRA	9.71	4.20E-134	5.65E-138
COL3A1	7.43	2.84E-132	6.37E-136
VWF	5.56	5.15E-130	1.39E-133
IGHG1	7.66	1.34E-125	4.79E-129
IGHA2	8.28	4.27E-116	1.92E-119
RGS1	8.84	1.47E-91	1.91E-94
IGK	4.9	4.78E-111	2.79E-114
COL3A1	6.72	2.56E-110	1.61E-113
HLA-DRB1	6.25	5.15E-109	3.46E-112
IGKC	4.86	1.02E-108	7.33E-112
CDH5	5.3	3.64E-108	2.78E-111
COL3A1	6.44	1.42E-98	1.40E-101
HLA-DRB5	5.9	1.88E-94	2.11E-97
C1QA	6.8	2.89E-94	3.37E-97
HLA-DPA1	5.79	6.27E-93	7.88E-96
HBZ	−9.92	1.40E-262	6.29E-267
DCT	−4.69	1.02E-179	9.14E-184
HBG2	−6.77	9.77E-133	1.75E-136
ALAS2	−4.84	8.02E-126	2.52E-129
HBG2	−9.11	1.26E-120	5.10E-124
HBG1	−6.15	3.06E-111	1.65E-114
HBE1	−7.47	4.18E-108	3.38E-111
AFP	−6.52	1.69E-101	1.44E-104
DCT	−4.83	1.76E-101	1.58E-104
AHSG	−8.98	5.18E-99	4.88E-102
SOX10	−4.59	6.18E-98	6.38E-101
DCT	−7.69	7.40E-95	7.97E-98
PMEL	−5.2	1.66E-93	2.01E-96
AHSG	−7.56	2.57E-89	3.58E-92
NANOG	−6.52	4.60E-86	6.81E-89

Further Study of CDK2 and Its Prognostic Values in LUAD

Through the Ualcan database, we studied the expression of CDK2 in LUAD tissues and normal tissues. CDK2 expression was high in 515 LUAD tissues in comparison with 59 normal tissues (P = 1.624E-12) (**Figure 4A**). Different ages had differential expression levels of CDK2 (Normal-vs.-Age 61–80, P = 1.044E-2) (**Figure 4B**). The expression of CDK2 was associated with various clinical features, such as Grade (Normal-vs.-Grade2, P = 5.088808E-03) (**Figure 4C**), the types of adenocarcinoma (Normal-vs.- Adenocarcinoma, P = 2.195E-02) (**Figure 4D**), gender (Male-vs.-Female, P = 1.338E-03) (**Figure 4E**), smoking habits (Normal-vs.-Smoker, P = 1.319E-11) (**Figure 4F**), stage (Normal-vs.-stage1, P = 3.458E-02) (**Figure 4G**), TP-53 mutation state (Normal-vs.-TP53 mutation, P = 1.624E-12) (**Figure 4H**), Weight (Normal-vs.-weight, P = 2.978E-2) (**Figure 4I**). The expression of CDK2 was related to the survival and prognosis of patients with LUAD (HR = 1.66, P = 5.8e-15) (**Figure 4J**). The higher the expression of CDK2, the shorter the survival time. Through this database, we discovered the CDK2-related genes and the heat maps were shown in **Figures 4K,L**. Many molecules involved in tumor classical signaling pathways were related to CDK2 expression. PrognoScan database: A new database for meta-analysis of the prognostic value of genes. We further found the expression of CDK2 influenced the OS and RFS of LUAD patients in different GSE datasets (GSE13213: COX *P*-value = 0.027245; GSE31210: COX *P*-value = 0.017966; GSE31210: COX *P*-value = 0.028818; GSE31210: COX *P*-value = 0.004197) (**Figures 4M–P**).

The Expression of CDK2 in Pan-Cancer Analysis

Through the Oncomine database, CDK2 expression was higher in 15 cancer tissues in comparison with normal tissues (**Figure 5A**). There was a great difference between cancer tissue and normal tissue. The statistical significance between normal and tumor tissues was further found in the TIMER database (the more "*" symbol, the greater the difference) (**Figure 5B**). Mata analysis of 15 published studies on LUAD showed that expression of CDK2 was higher in LUAD (Median Rank = 5384.0, P = 4.16E-6) (**Figure 5C**). By *t*-test, box plot and peak plot of CDK2 in LUAD were shown in **Figures 5D,E** (*t*-Test = 3.249, Fold Change = 1.332, P = 0.003). Using the R package, we ranked CDK2 by its expression in 33 cancers (**Figure 5F**). Through different R packages, the expression of CDK2 was relatively

[22]http://gepia.cancer-pku.cn/index.html

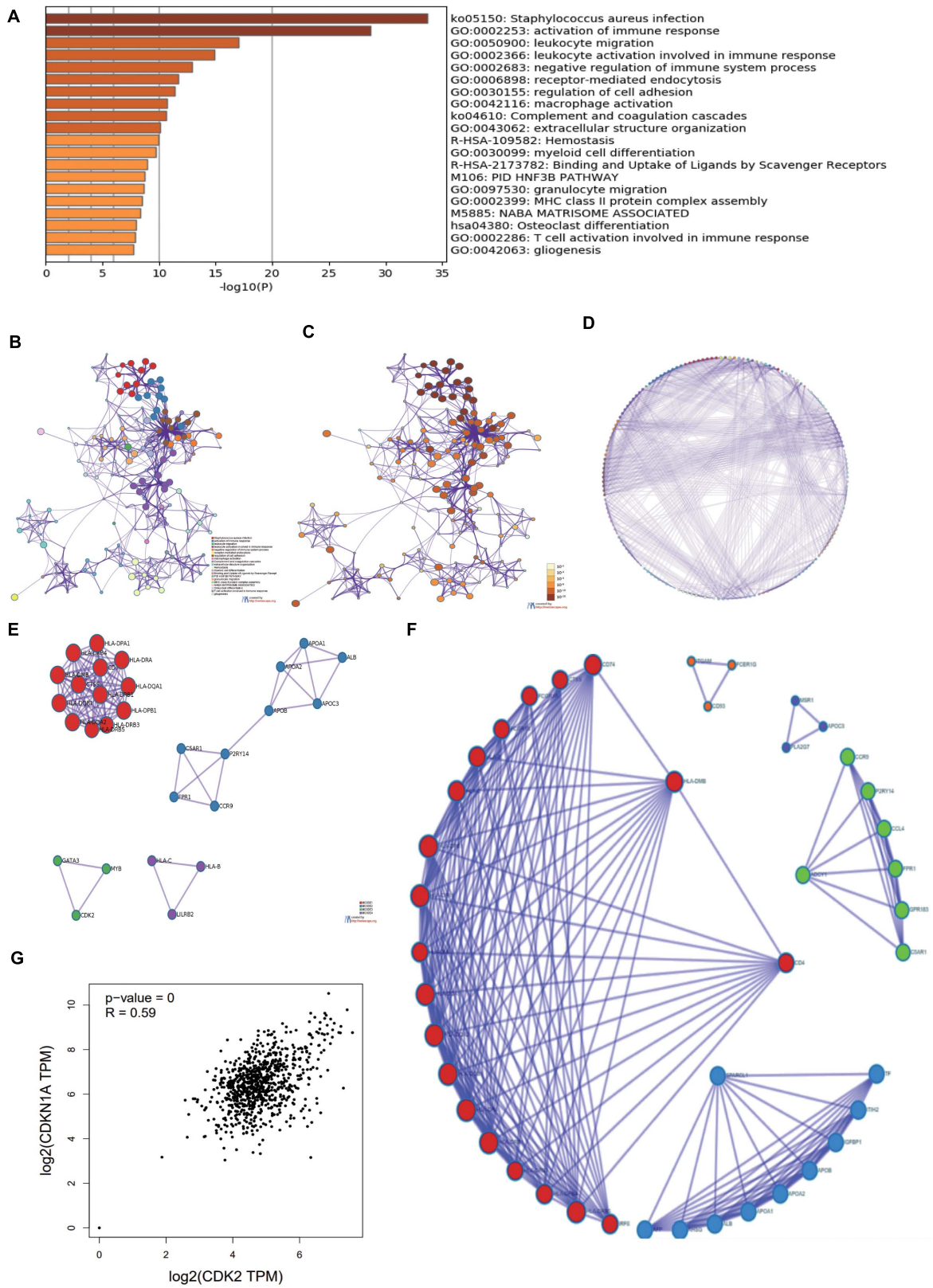

FIGURE 3 | The GO, KEGG analysis of 250 DEmRNAs. **(A)** Through Metascape software, we found most enriched items. **(B)** The related paths were shown in the network diagram. **(C,D)** the *P*-value of different pathways. **(E)** According to the relationship of DE mRNAs, several protein analyses were performed. **(F)** CDK2, MYB, GATA3 were connected each other in some tumor pathway from the circle graph. **(G)** There was a positive correlation between CDK2 and CDKN1A using GEPIA.

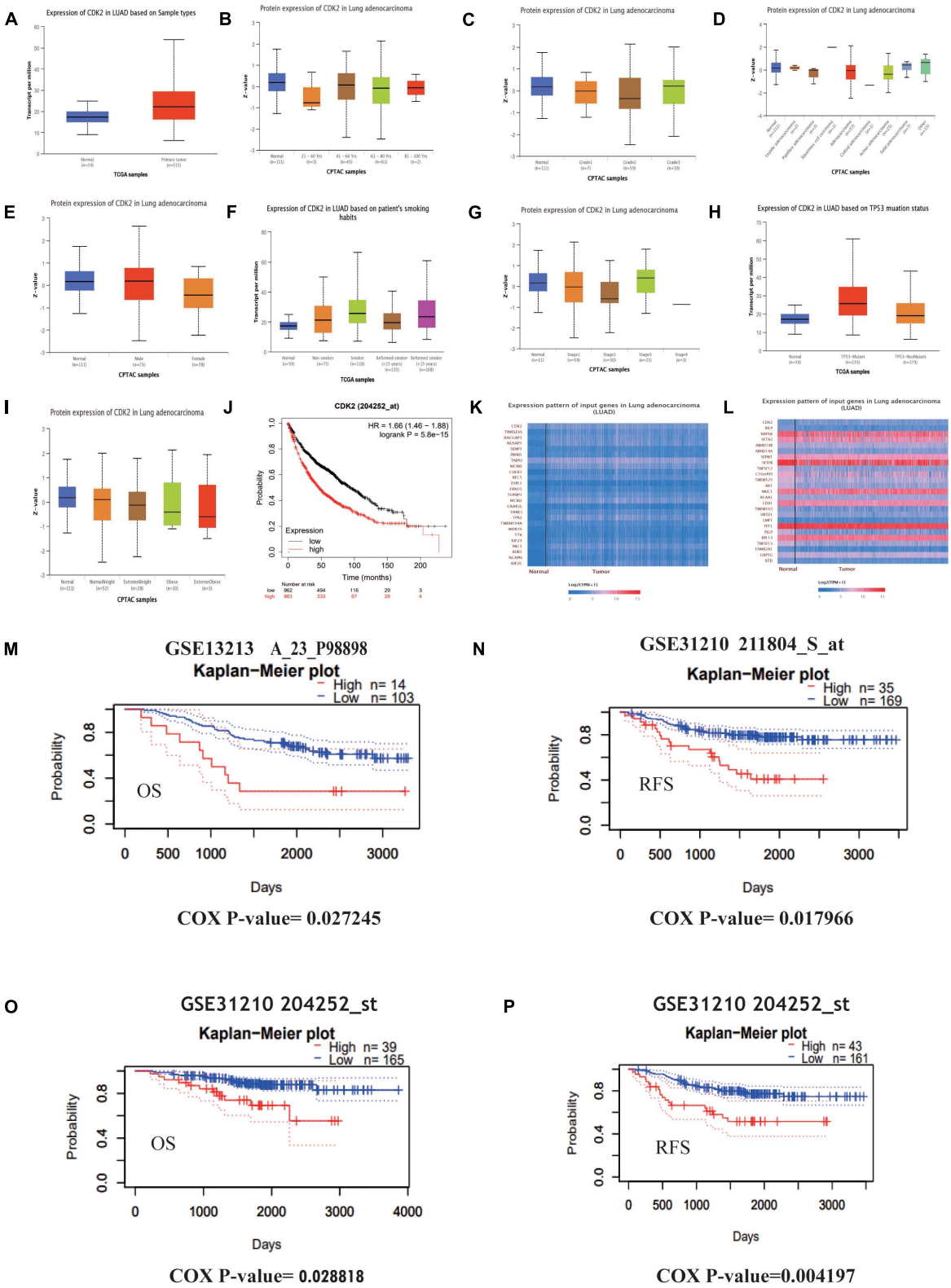

FIGURE 4 | Further study of CDK2 and prognosis analysis in LUAD. **(A)** The expression of CDK2 was highly in 515 LUAD tissues than 59 normal tissues. **(B)** Different ages might have differential expression levels of CDK2. **(C)** The expression of CDK2 was associated with Grade. **(D)** The types of adenocarcinoma. **(E)** Gender. **(F)** Smoking habits. **(G)** Stage. **(H)** TP-53 mutation state. **(I)** Weight. **(J)** The expression of CDK2 was related to the survival and prognosis of patients with LUAD. **(K,L)** CDK2-related genes and heat maps. **(M–P)** The expression of CDK2 influenced the OS and RFS of LUAD patients.

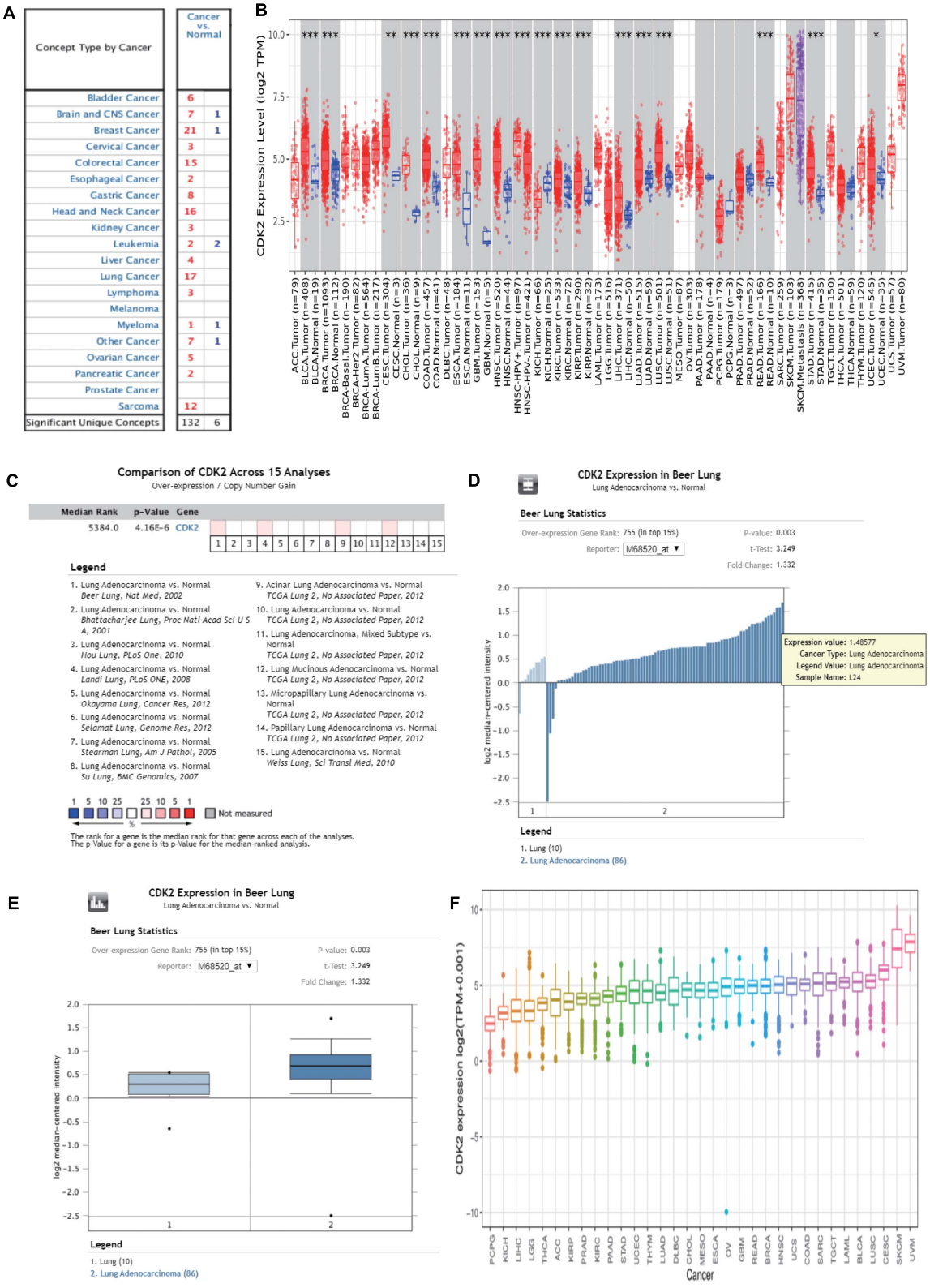

FIGURE 5 | The expression of CDK2 in pan-cancer analysis. **(A)** Through the Oncomine database, the expression of CDK2 was higher in 15 cancer tissues than normal tissues. **(B)** The expression of CDK2 in TIMER database. **(C)** Mata analysis of 15 published studies on LUAD showed that the expression of CDK2 was high in LUAD. **(D,E)** By *t*-test, Box plot and peak plot of CDK2 in LUAD. **(F)** The expression in 33 cancer, a pan-cancer analysis.

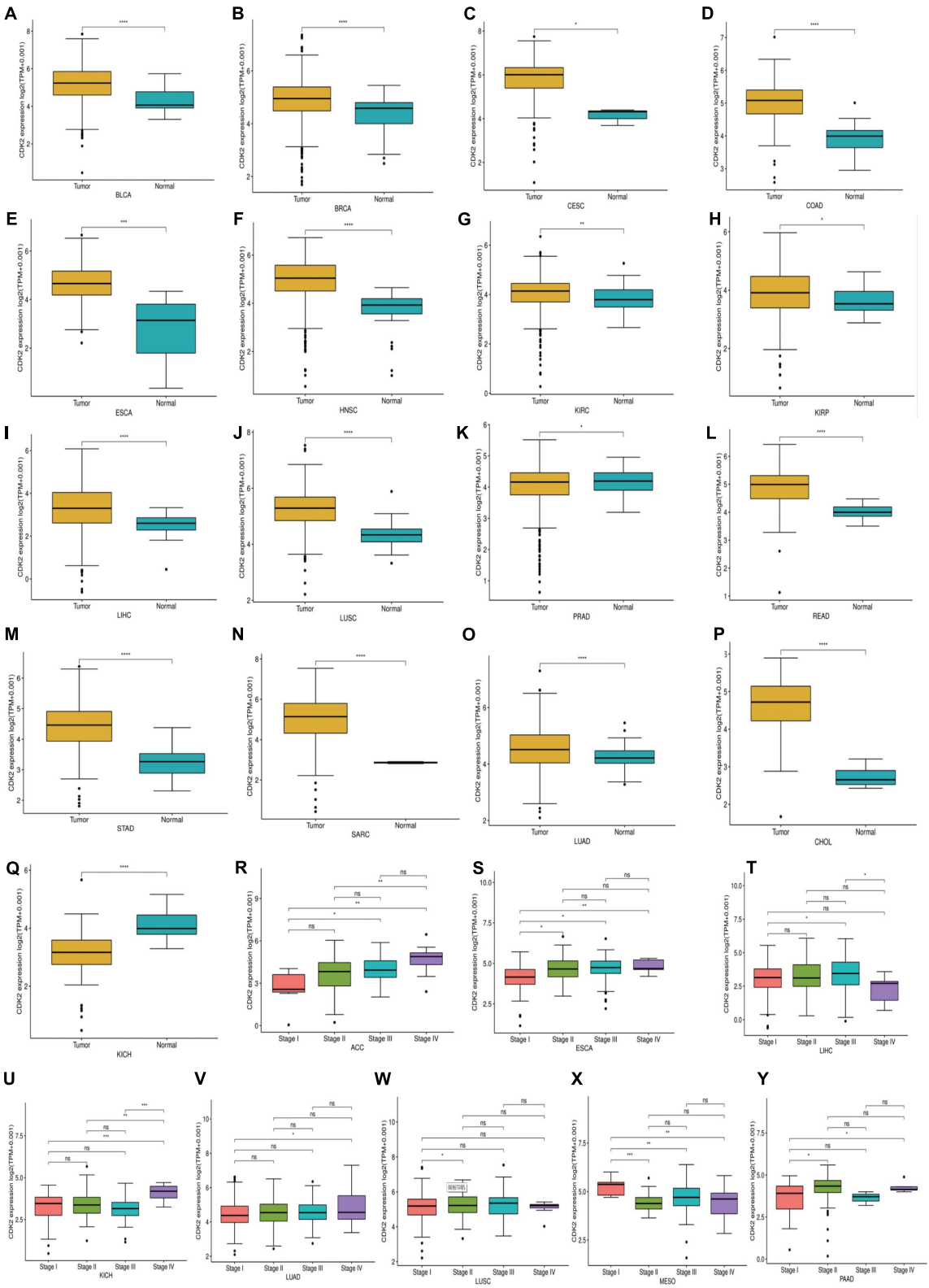

FIGURE 6 | The expression and stage of different cancer. **(A–Q)** The expression of CDK2 was relatively high in 17 cancers. **(R–Y)** The different expression levels of CDK2 had statistical significance on the stage of patients. (*$P < 0.05$, **$P < 0.01$, ***$P < 0.001$, ****$P < 0.0001$).

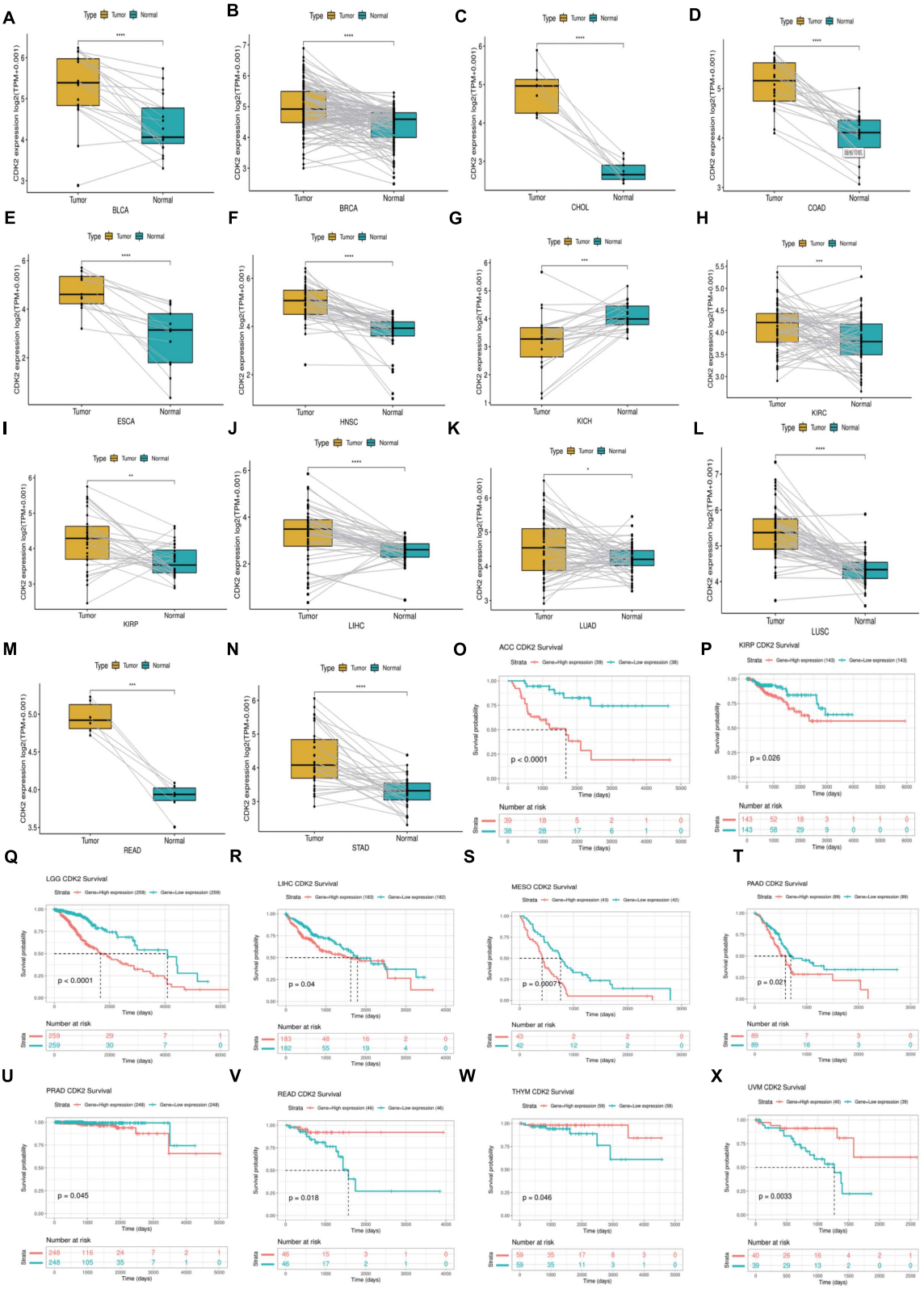

FIGURE 7 | The Paired expression and survival analysis of CDK2. **(A–N)** For different types of cancer, we carried out paired differential expression of CDK2. **(O–X)** In 10 kinds of cancers, the expression of CDK2 was related to the prognosis of patients. (*$P < 0.05$, **$P < 0.01$, ***$P < 0.001$, ****$P < 0.0001$).

higher in 17 cancers ($P < 0.05$) (**Figures 6A–Q**). The different expression levels of CDK2 had statistical significance on the stage of patients ($P < 0.05$) (**Figures 6R–Y**). There was significant difference in the expression of CDK2 between stage I and stage III, I and IV, II, and IV LUAD (*/**). For different types of cancer, we conducted paired differential expression of CDK2. Simultaneously, we found that there was statistical significance in 14 cancer types ($P < 0.05$) (**Figures 7A–N**). In 10 cancer types,

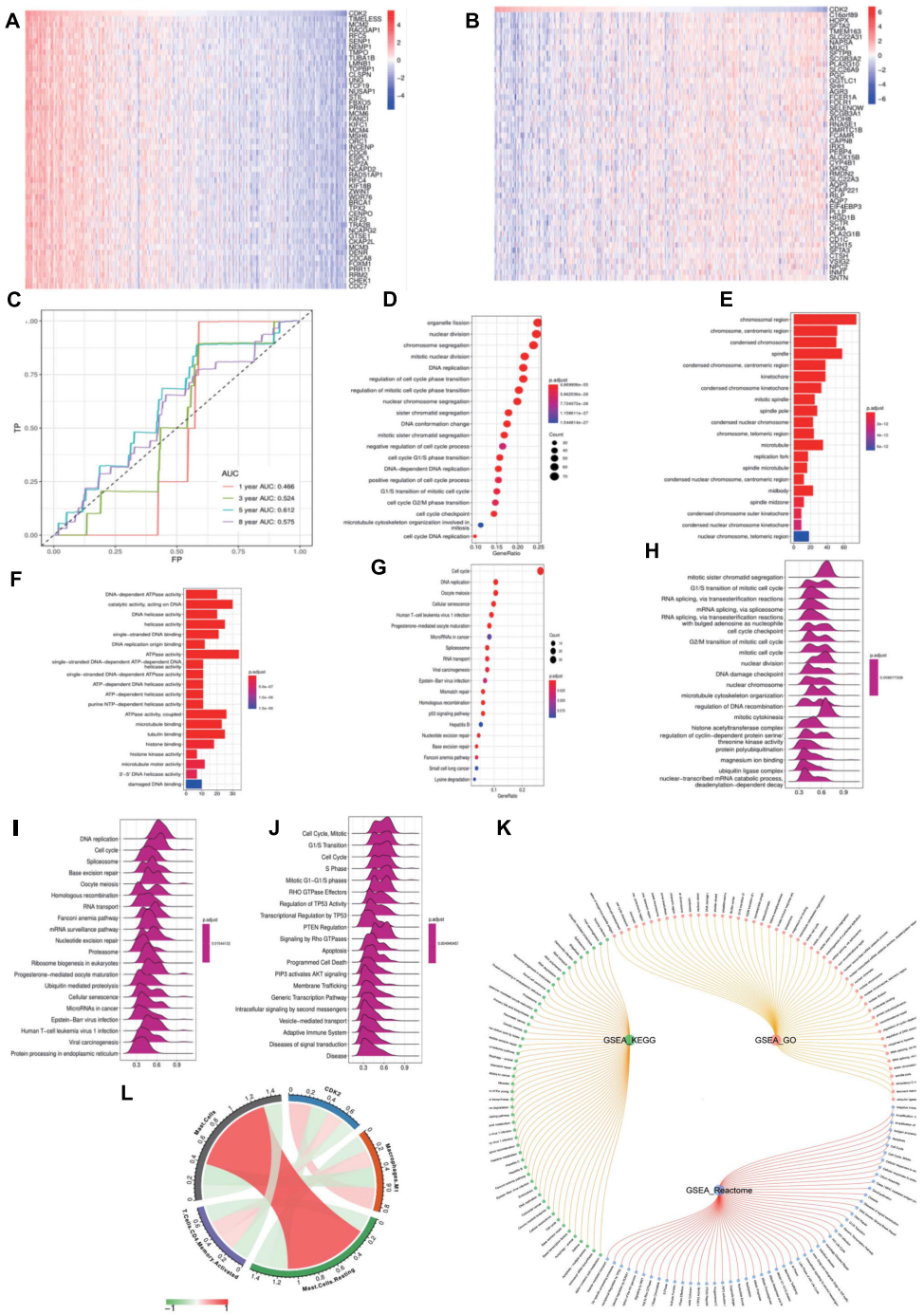

FIGURE 8 | Functional enrichment analysis of CDK2. **(A,B)** The top 50 heat maps of CDK2 positive and negative genes were shown. **(C)** The AUC curve of 1, 3, 5, and 8 years to forecast the survival of patients. **(D–G)** CDK2 was related to the DNA replication, regulation of cell cycle, cell cycle checkpoint, P53 signaling pathway. **(H–J)** Wave charts about GO, KEGG, Reactome showed that CDK2 involved in classic tumor signaling pathways, such as regulation of TP53 activity, PTEN regulation, apoptosis, P13K-AKT signaling pathway. **(K)** The circle graph of pathways. **(L)** CDK2 was positively correlated with CD4 T cells (Cor = 0.1679, $P = 0.0003$), macrophage M1 (Cor = 0.2437, $P = 1.40E-07$) and negatively correlated with Mast cells (Cor = –0.1545, $P = 0.0009$) by CIBERSOPT algorithm.

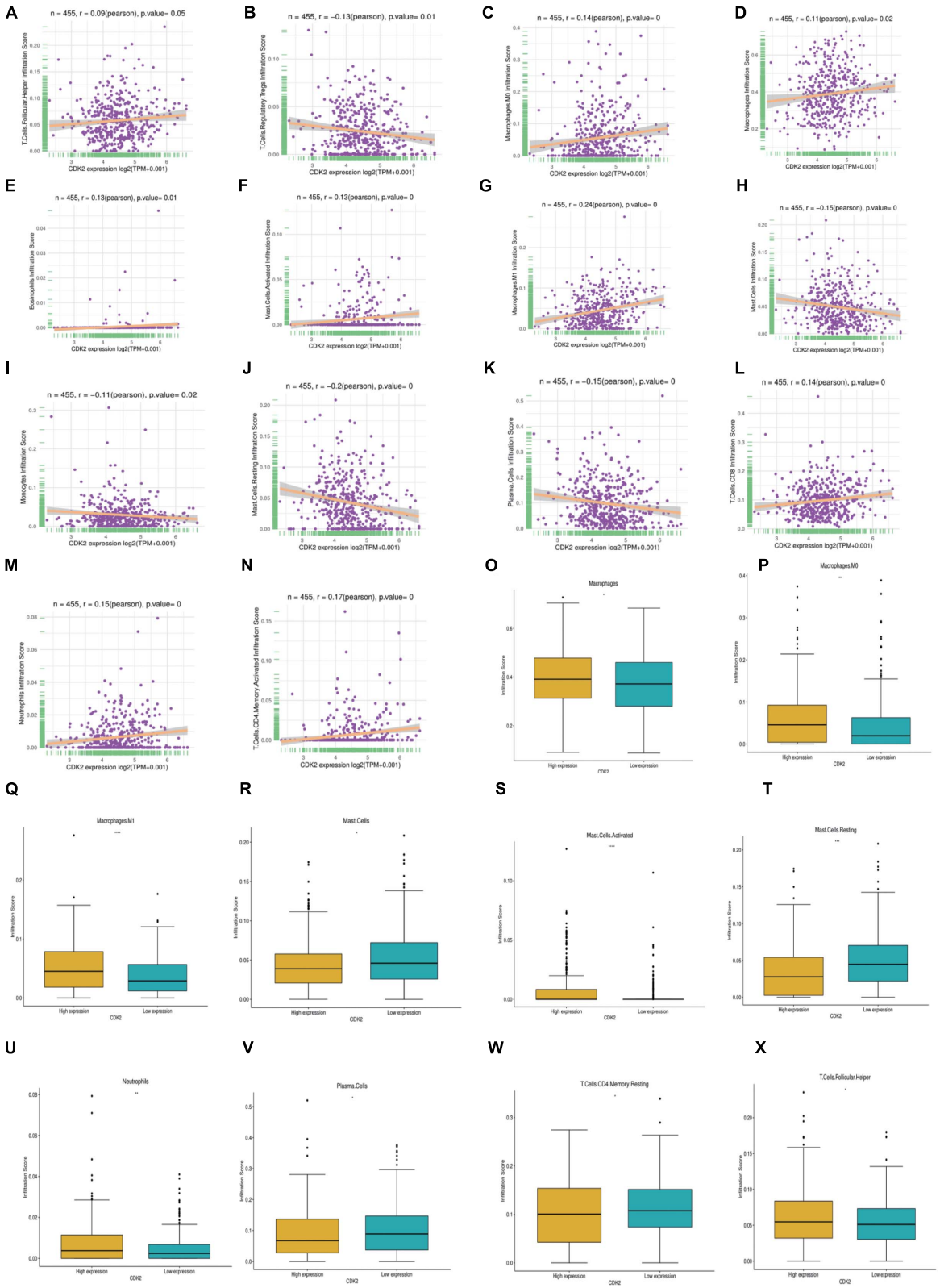

FIGURE 9 | Characteristics of CDK2 immune cells infiltration. **(A–N)** 14 immune cells (T cells Follicular, T cells Regulatory Tregs, Macrophages.M0, Macrophages, Eosinophils, Mast cells activated, Macrophages M1, Mast cells, Monocytes, Mast cells Resting, Plasma cells, T cells CD8, Neutrophils, T cells CD4) were closely related to the expression of CDK2 ($P \leq 0.05$). **(O–X)** In different CDK2 expression groups, the expression of immune cells had systematic differences ($P < 0.05$).

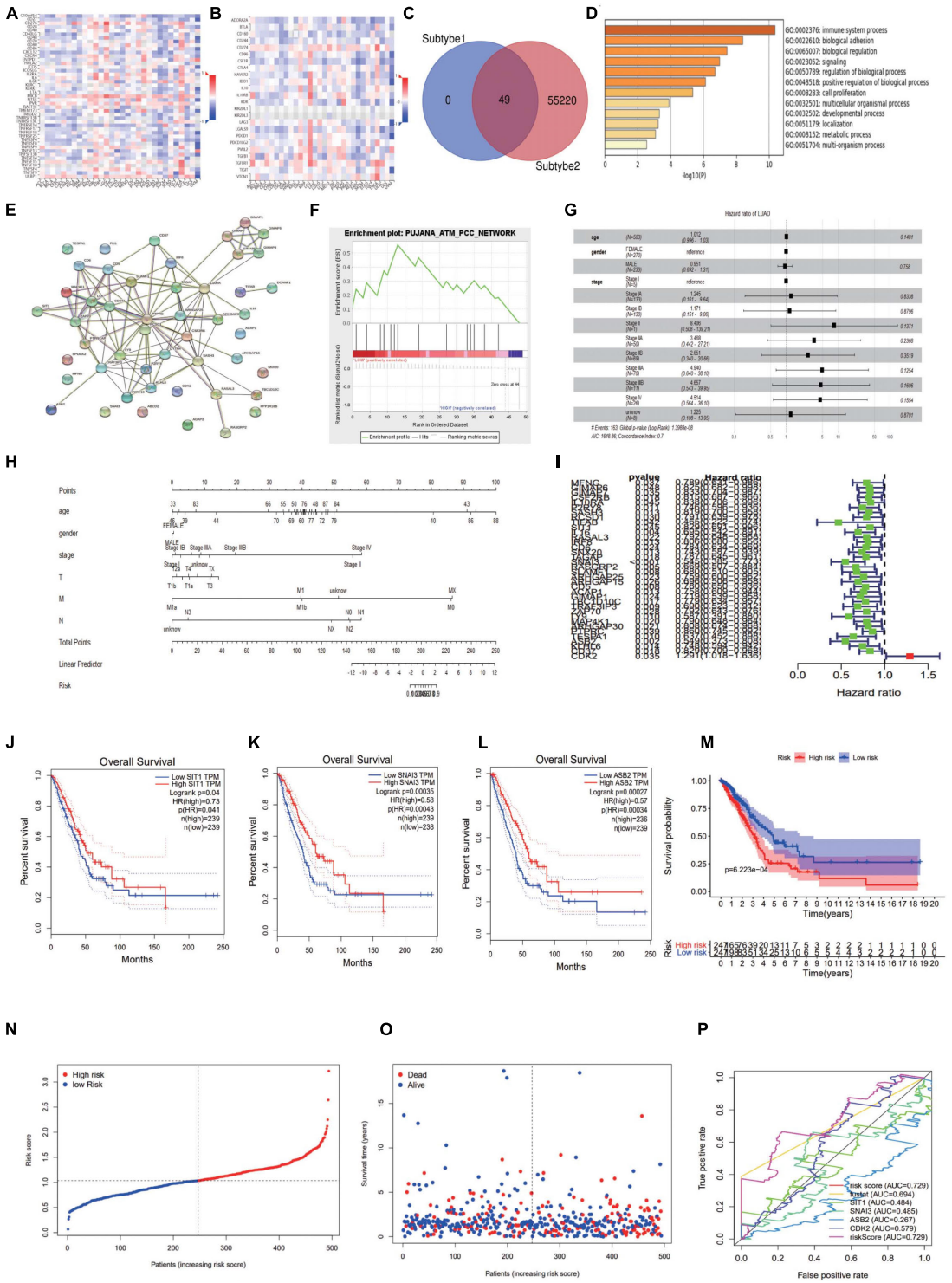

FIGURE 10 | Construction of immune related forecasting model. **(A,B)** The heat maps of immunopotentiators and immunosuppressants about CDK2. **(C)** 49 genes were mixed from the TCGA using "perl" and "R" package. **(D)** The most abundant pathway of 49 genes was immune system process. **(E)** The protein network interaction of these 49 immune related genes. **(F)** GSEA analyzed the function, ES, NES, NOM *p*-val, FDR *q*-val of 49 genes. **(G)** The forest map showed Hazard ratio and concordance index (0.7) of LUAD. **(H)** Nomogram model combined several clinical factors, such as age, gender, stage, T, N, M. **(I)** We showed the Hazard ratio (HR), HR95L, HR95H, p-value of these 36 significant genes. **(J–L)** Through the GEPIA database, SIT1, SNAI3, ASB2 were lower expressed in LUAD. **(M)** The risk curve showed that the high-risk group was more lethal to lung cancer patients. **(N,O)** The high and low risk maps. **(P)** The ROC curve showed the different AUC of four interesting genes.

TABLE 2 | The BP, CC, and MF were showed specifically of 49 immune related genes.

GO term	Subgroup	Enrichment score
Positive regulation of GTPase activity	BP	6.911710228
B cell receptor signaling pathway	BP	28.92678725
Signal transduction	BP	3.699937904
T cell differentiation	BP	39.05116279
Regulation of small GTPase mediated signal transduction	BP	11.65706352
T cell receptor signaling pathway	BP	10.55436832
Positive regulation of T cell proliferation	BP	19.5255814
T cell costimulation	BP	15.019678
Positive regulation of T cell receptor signaling pathway	BP	97.62790698
Innate immune response	BP	4.540832883
G-protein coupled purinergic nucleotide receptor signaling pathway	BP	55.78737542
Adaptive immune response	BP	7.915776241
Positive regulation of Rho protein signal transduction	BP	30.03935599
Response to lipopolysaccharide	BP	7.143505389
Positive regulation of cytosolic calcium ion concentration involved in phospholipase C-activating G-protein coupled signaling pathway	BP	27.89368771
Regulation of defense response to virus by virus	BP	27.89368771
Positive regulation of B cell proliferation	BP	20.02623733
Peptidyl-tyrosine autophosphorylation	BP	19.5255814
Release of sequestered calcium ion into cytosol	BP	19.0493477
Immunological synapse	CC	44.66666667
T cell receptor complex	CC	63.27777778
Membrane	CC	2.070909091
Plasma membrane	CC	1.658335355
Cytosol	CC	1.717948718
Integral component of plasma membrane	CC	2.146525324
Membrane raft	CC	5.529126214
GTPase activator activity	MF	10.75651135
GTP binding	MF	5.861458333
Receptor activity	MF	6.914900154
G-protein coupled purinergic nucleotide receptor activity	MF	53.59047619
Protein tyrosine kinase activity	MF	8.461654135
SH2 domain binding	MF	25.87126437

high CDK2 expression was associated with poor prognosis of the patients ($P < 0.05$) (**Figures 7O–X**).

Functional Enrichment Analysis of CDK2

We compared CDK2 high expression groups with low expression groups in LUAD, and **Figures 8A,B** showed the top differentially expressed genes in two groups of cancer specimens. We took FP as the abscissa and TP as the ordinate and showed the AUC curve of 1, 3, 5, and 8 years to forecast the survival of patients. The areas under the curve were 0.465, 0.524, 0.612, and 0.575 (**Figure 8C**). "Clusterprofiler" R package was used to show the function analysis. And CDK2 was related to the DNA replication, regulation of cell cycle, cell cycle checkpoint, P53 signaling pathway. The bubble and bar charts were shown in **Figures 8D–G**. Wave charts about GO, KEGG, Reactome showed that CDK2 involved in classic tumor signaling pathways, such as regulation of TP53 activity, PTEN regulation, apoptosis, P13K-AKT signaling pathway (**Figures 8H–J**). The circle graph was shown in **Figure 8K**. For different immune cells, CDK2 was positively correlated with CD4 T cells (Cor = 0.1679, $P = 0.0003$), macrophage M1 (Cor = 0.2437, P = 1.40E-07) and negatively correlated with Mast cells (Cor = –0.1545, $P = 0.0009$) by CIBERSOPT algorithm (**Figure 8L**).

Characteristics of CDK2 Immune Cells Infiltration

In LUAD, we further investigated different expression of CDK2 in different immune cell types. We found that 14 immune cells were closely related to CDK2 expression, such as T cells Follicular ($P = 0.05$, r = 0.09), T cells Regulatory Tregs ($P = 0.01$, $r = –0.13$), Macrophages.M0 ($P = 0$, $r = 0.14$), Macrophages ($P = 0.02$, $r = 0.11$), Eosinophils ($P = 0.01$, $r = 0.13$), Mast cells activated ($P = 0$, $r = 0.13$), Macrophages M1 ($P = 0$, $r = 0.24$), Mast cells ($P = 0$, $r = –0.15$), Monocytes ($P = 0.02$, $r = –0.11$), Mast cells Resting ($P = 0$, $r = –0.2$), Plasma cells ($P = 0$, $r = –0.15$), Tcells CD8 ($P = 0$, $r = 0.14$), Neutrophils ($P = 0$, $r = 0.15$), T cells CD4 ($P = 0$, $r = 0.17$) (**Figures 9A–N**). According to the median value of CDK2 expression, patients with LUAD were divided into the high expression groups and low expression groups. In different groups, the expression of 10 immune cells had systematic differences ($P < 0.05$) (**Figures 9O–X**).

Construction of Immune Related Forecasting Model

Through the TISIDB database, we found CDK2-related immunomodulators and the heat maps of immunopotentiators and immunosuppressants were shown in **Figures 10A,B**.

TABLE 3 | The GSEA analysis of 49 mRNAs.

Name	Size	ES	NES	NOM *p*-val	FDR *q*-val	FWER *p*-val	Rank at max	Leading edge
PUJANA_ATM_PCC_NETWORK	16	0.5574023	1.7549632	0	0	0	13	Tags = 50%, list = 27%, signal = 46%
LEE_DIFFERENTIATING_T_LYMPHOCYTE	16	0.5064702	1.1931181	0.33333334	0.6333333	0.8	22	Tags = 69%, list = 45%, signal = 84%
SMID_BREAST_CANCER_NORMAL_LIKE_UP	22	0.45970738	0.9803642	0.4	0.4888889	0.8	12	Tags = 36%, list = 24%, signal = 27%
SMID_BREAST_CANCER_LUMINAL_B_DN	15	0.344885	0.68991035	1	0.8833334	1	1	Tags = 13%, list = 2%, signal = 9%
GO_REGULATION_OF_INTRACELLULAR_SIGNAL_TRANSDUCTION	16	-0.45997676	-1.2494261	0	0	0	2	Tags = 6%, list = 4%, signal = 4%

By sorting the *P*-value ($P < 0.05$), we identified 13 immunosuppressants (ADORA2A, BTLA, CD274, CSF1R, IL10, KDR, LAG3, LGALS9, PDCD1, PDCD1LG2, TGFB1, TIGIT, VTCN1) and 21 immunopotentiators (CD27, CD276, CD28, CD40LG, CD48, CD70, CD80, CXCL12, CXCR4, ENTPD1, HHLA2, ICOSLG, IL2RA, IL6, IL6R, KLRC1, MICB, PVR, TMEM173, TNFRSF13B, ULBP1) with a high correlation of CDK2. In the cBioProtal, we explored forty-nine genes associated with 34 immunomodulators. Clinical data and gene expression data were downloaded from TCGA database. Forty-nine genes were mixed from the TCGA using "perl" and "R" package (**Figure 10C**). Through the Metascape database, the most abundant pathway of 49 genes was the immune system process, other function terms were biological adhesion, biological regulation, cell proliferation (**Figure 10D**). The BP, CC, MF was showed specifically in **Table 2**. The protein network interaction (PPI) of these 49 immune related genes were shown in the **Figure 10E** ($P < 1.0e-16$). GSEA analyzed the function, ES, NES, NOM p-val, FDR q-val of 49 genes. The statistically significant items were PUJANA_ATM_PCC_NETWORK and INTRACELLULAR_SIGNAL_TRANSDUCTION ($P < 0.01$) (**Figure 10F** and **Table 3**). Combing with clinical data and expression matrix, univariate and multivariate regression analyses were performed on age, gender and tumor stage (Total $P = 1.399e-08$) (**Table 4**). The forest map showed HR and concordance index (0.7) of LUAD. As predicted, the tumor stage was an independent risk factor for the prognosis of patients with LUAD (**Figure 10G**). Nomogram model combined several clinical factors, such as age, gender, stage, T, N, M to intuitively analyze the prognosis of LUAD (**Figure 10H**). Each patient can be assessed by nomogram model based on baseline clinical data. Univariate regression analysis showed that 36 genes were associated with the prognosis of LUAD ($P < 0.05$). We showed the HR, HR95L, HR95H, *P*-value of these 36 significant genes. CDK2 was an independent prognostic gene in LUAD (HR > 1) (**Table 5** and **Figure 10I**). Multivariate regression analysis was used to analyze the 36 genes and only four genes (SIT1, SNAI3, ASB2, and CDK2) were included in the prediction model (**Table 6**). Through the GEPIA database, SIT1 ($P = 0.04$), SNAI3 ($P = 0.00035$), ASB2 ($P = 0.00027$) were lower expressed in LUAD ($P < 0.05$) (**Figures 10J–L**). To verify the prognostic model, the risk curve showed that the high-risk group was more lethal to lung cancer patients ($P = 6.223E-04$) (**Figure 10M**). Based on different risk scores, patients were divided into high and low risk groups using "R" package (**Figures 10N,O**). The ROC curve showed the different AUC of 4 interesting genes and CDK2 had more predictive value in the prognostic model (AUC = 0.579) (**Figure 10P**).

TABLE 4 | Univariate and multivariate regression analysis of age, gender, and tumor stage.

	coef	exp(coef)	se(coef)	z	p
Age	0.011894	1.011965	0.008224	1.446	0.148
genderMALE	−0.050014	0.951216	0.162323	−0.308	0.758
stageStage IA	0.219186	1.245063	1.044445	0.21	0.834
stageStage IB	0.158106	1.17129	1.043788	0.151	0.88
stageStage II	2.128962	8.406135	1.432179	1.487	0.137
stageStage IIA	1.243594	3.468057	1.051101	1.183	0.237
stageStage IIB	0.9751	2.651431	1.047535	0.931	0.352
stageStage IIIA	1.597291	4.939634	1.042318	1.532	0.125
stageStage IIIB	1.538441	4.657324	1.096495	1.403	0.161
stageStage IV	1.50713	4.51376	1.060871	1.421	0.155
		$P = 1.399e-08$			

TABLE 5 | The analysis of Univariate regression about 36 genes.

Id	HR	HR.95L	HR.95H	*P*-value
MFNG	0.788791335	0.631264471	0.985627735	0.036858598
GIMAP6	0.825241244	0.68227954	0.998158484	0.04782116
GIMAP7	0.833265382	0.7035123	0.98694962	0.034680373
CSF2RB	0.814678719	0.687175564	0.965839662	0.018264635
IL10RA	0.838397617	0.705873794	0.995802041	0.044655471
P2RY8	0.746446286	0.595538414	0.935593818	0.011158897
SASH3	0.819264713	0.700490753	0.958177773	0.01261093
RCSD1	0.790672034	0.639423589	0.977696595	0.030144597
TIFAB	0.465083695	0.222080992	0.973981795	0.042370157
SIT1	0.829408759	0.690741005	0.995914365	0.045088923
IL16	0.694821369	0.541782159	0.89109013	0.004125937
RASAL3	0.791834804	0.648056113	0.967512448	0.022429427
IRF8	0.805982708	0.679749247	0.955658471	0.013071014
CD6	0.783523435	0.633680321	0.968799176	0.024280529
SNX20	0.742751039	0.587258851	0.939413865	0.013084672
TAGAP	0.786867105	0.644621205	0.960501822	0.018468635
SNAI3	0.545360728	0.384584195	0.773350355	0.000668422
RASGRP2	0.669309183	0.506911612	0.883733519	0.004630788
SLAMF1	0.679757859	0.510377564	0.905350821	0.008290951
ARHGAP25	0.759490747	0.599527918	0.962134	0.022615883
ARHGAP15	0.696431097	0.506489419	0.957603961	0.025975442
CD5	0.779912525	0.649789891	0.936092658	0.007605839
ACAP1	0.758479625	0.609407945	0.944016806	0.013287558
GIMAP1	0.718737917	0.539208263	0.958042056	0.024304367
TBC1D10C	0.778901559	0.634277612	0.956501738	0.01711004
TRAF3IP3	0.69040004	0.522777097	0.911769505	0.009030209
ZAP70	0.792228171	0.643311406	0.975616893	0.028356063
LY9	0.586557529	0.391159073	0.879564757	0.009858385
MAP4K1	0.790353869	0.64826384	0.963587971	0.019976631
ARHGAP30	0.808036247	0.674219373	0.968412661	0.021030946
PTPRC	0.859646397	0.744782085	0.992225703	0.038770457
TESPA1	0.637294984	0.452324142	0.897906742	0.010006127
ASB2	0.549252388	0.373292675	0.808154581	0.002358241
KLHL6	0.747994992	0.593856228	0.942141348	0.013656291
CD37	0.828826076	0.709387822	0.968373918	0.018042429
CDK2	1.290598521	1.017922999	1.636316836	0.035146972

TABLE 6 | The analysis of multivariate regression about four genes.

id	coef	HR	HR.95L	HR.95H	*P*-value
SIT1	0.255264409	1.290802876	0.925388716	1.800510461	0.132760088
SNAI3	−0.400450665	0.670018024	0.422135602	1.063459586	0.089332143
ASB2	−0.799324198	0.449632724	0.219800019	0.919788756	0.028601817
CDK2	0.203710988	1.22594379	0.967951804	1.552699391	0.09107145

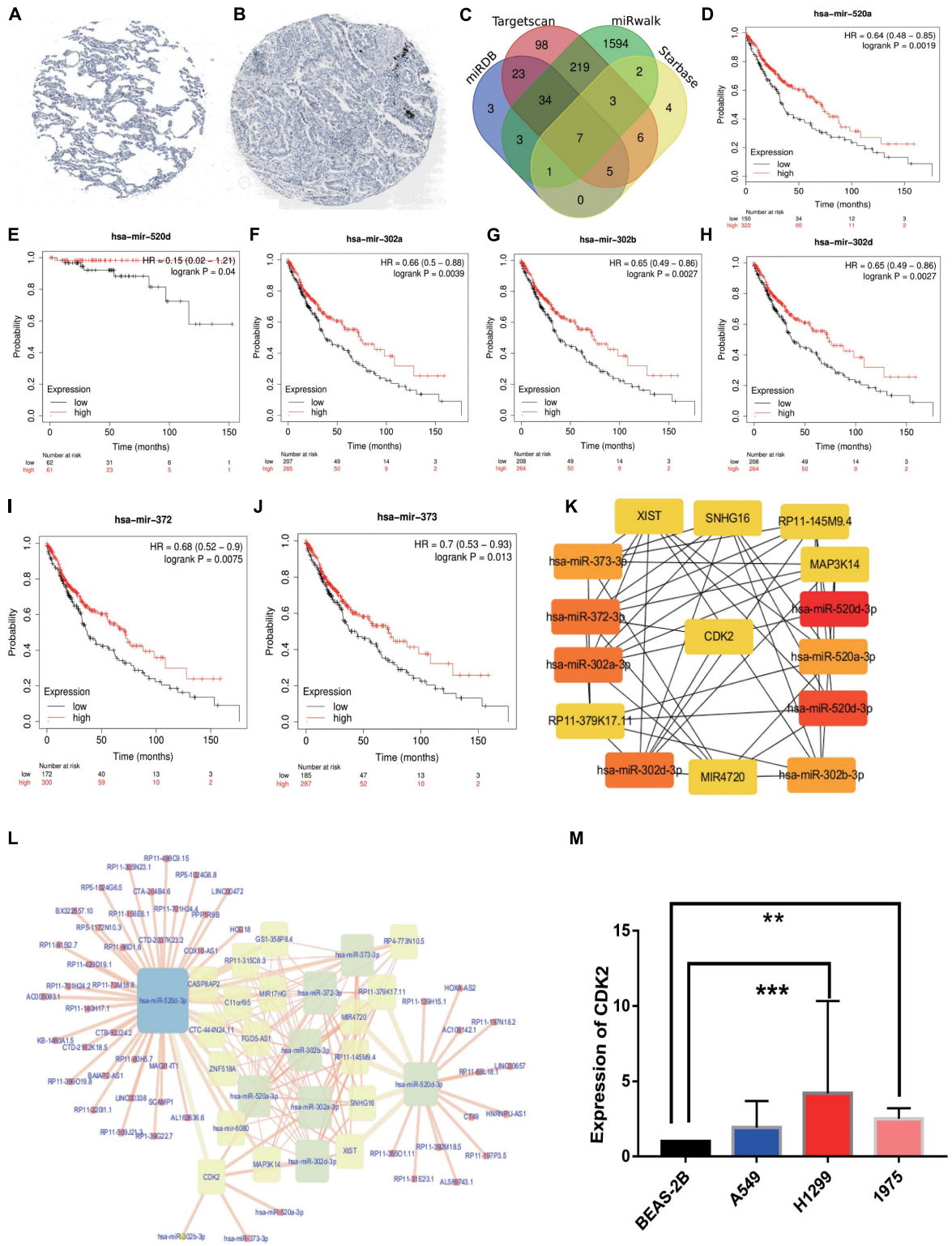

FIGURE 11 | HPA analysis and ceRNA network. **(A)** Immunohistochemical results in normal lung tissues. **(B)** Immunohistochemical results in LUAD tissues. **(C)** The intersection results of the four databases were shown by Venn diagram. **(D–J)** The survival analysis of seven miRNAs. **(K)** 6lncRNAs-7miRNAs-CDK2 were considered as top 15 genes by CytoHubba**. (L)** ceRNA network was constructed by Cytoscape. **(M)** The PCR results about CDK2 expression in BEAS-2B, A549 ($P = 0.0808$), H1299 ($P = 0.0006$), H1975 ($P = 0.0030$). (**$P < 0.01$, ***$P < 0.001$).

HPA Analysis and Construction of Predictive ceRNA Network in LUAD

Immunohistochemical result showed that the CDK2 expression in LUAD tissues was significantly higher than that in normal lung tissues (**Figures 11A,B**). We selected 455 miRNAs related to CDK2 from TargetScan database. 10,018 miRNAs were found in miRWalk database. And we explored 76 miRNAs from mirDB and 28 miRNAs from Starbase. Combining with differentially expressed miRNAs in LUAD, 7 miRNAs were joined in the network using Venn map, such as hsa-miR-302b-3p, hsa-miR-372-3p, hsa-miR-302a-3p, hsa-miR-373-3p, hsa-miR-520a-3p, hsa-miR-520d-3p, and hsa-miR-302d-3p (**Figure 11C**). These miRNAs had obvious influence on the prognosis of LUAD patients ($P < 0.05$) (**Figures 11D–J**). We used the Starbase database to find the potential lncRNAs that regulate seven miRNAs. These coding genes and non-coding genes were interacted with each other by using Cytoscape software (**Figure 11L**). According to the degree in the network, we screened out the top 15 genes using CytoHubba (six lncRNAs: XIST, SNHG16, RP11-145M9.4, MAP3K14, MIR4720, and RP11-379K17.11) (**Figure 11K**).

The PCR Results of CDK2 Expression

Compared with the expression of CDK2 in BEAS-2B cell line, the expression of CDK2 in A549 cell line was increased, but there was no statistical difference ($P = 0.0808$). There were significant differences between H1299 cell line ($P = 0.0006$) and H1975 cell line ($P = 0.0030$) (**Figure 11M**).

Correlation Analysis of Drug Resistance

A total of 192 anti-tumor drugs were included in the study. The IC50 level of 89 anti-tumor drugs were related to the expression of CDK2. According to the size of *P* value ($P < 0.05$), we screened out the top 20 anti-tumor drugs with positive or negative correlation, such as Camptothecin ($r = –0.074$, $P = 0.000018$), Vinblastine ($r = –0.085$, $P = 0.0000243$), Cisplatin ($r = –0.099$, $P = 0.0000843$), Cytarabine ($r = –0.0746$, $P = 0.0000975$), Navitoclax ($r = –0.106$, $P = 0.000158$), Vorinostat ($r = –0.113$, $P = 0.0002$), Nilotinib ($r = –0.127$, $P = 0.000258$), Olaparib ($r = –0.0966$, $P = 0.000302$), Axitinib ($r = 0.343$, $P = 0.000381$), AZD7762 ($r = –0.0902$, $P = 0.000382$), SB216763 ($r = 0.284$, $P = 0.000403$), KU-55933 ($r = 0.315$, $P = 0.000404$), PLX-4720 ($r = –0.0857$, $P = 0.000428$), Wee1 Inhibitor ($r = –0.141$, $P = 0.000780$), PD173074 ($r = –0.0963$, $P = 0.000794$), Obatoclax Mesylate ($r = –0.08009$, $P = 0.000872$), Sorafenib ($r = –0.076$, $P = 0.0009$), Irinotecan ($r = –0.0801$, $P = 0.00120$), BMS-536924 ($r = 0.0765$, $P = 0.0012$), and GSK1904529A ($r = –0.113$, $P = 0.0012$) (**Table 7** and **Figures 12A–T**).

TABLE 7 | Here are the top 20 anti-tumor drug resistance studies related to CDK2.

Correlation	*p* value	Type	Label
–0.073624414	1.88E-05	Camptothecin	Negative
–0.085496637	2.44E-05	Vinblastine	Negative
–0.099132332	8.43E-05	Cisplatin	Negative
–0.074684535	9.76E-05	Cytarabine	Negative
–0.106844461	0.000158572	Navitoclax	Negative
–0.11367658	0.000200639	Vorinostat	Negative
–0.127941152	0.000258313	Nilotinib	Negative
–0.096615555	0.000302571	Olaparib	Negative
0.343877551	0.000381858	Axitinib	Positive
–0.090294733	0.000382049	AZD7762	Negative
0.284802005	0.000403878	SB216763	Positive
0.315892314	0.00040404	KU-55933	Positive
–0.085796235	0.00042863	PLX-4720	Negative
–0.141613081	0.000780249	Wee1 Inhibitor	Negative
–0.09631745	0.000794901	PD173074	Negative
–0.080096541	0.000872875	Obatoclax Mesylate	Negative
–0.076063235	0.000903871	Sorafenib	Negative
–0.080170909	0.001206821	Irinotecan	Negative
0.076522222	0.00126849	BMS-536924	Positive
–0.113717172	0.001291814	GSK1904529A	Negative

DISCUSSION

In recent years, the role of immune invasion in the progression of LUAD has been improved. Immunotherapy can resist tumor cells by activating the activity of immune molecules. It is necessary to find effective immune related-markers to predict prognosis and apply the individual therapy. And the study of TME is the key to overcome drug resistance (Li et al., 2020).

Our study first explored the prognostic molecule CDK2, which was differently expressed in LUAD tissues and adjacent non-LUAD tissues ($P = 1.624E-12$). High expression of CDK2 in LUAD has poor prognosis. In order to verify CDK2 in all kinds of cancers, we carried out a pan-cancer study. We further showed the expression, stage analysis, paired expression, survival condition in 33-cancer. The expression, stage and prognosis of CDK2 were obviously different in many cancers. According to published articles, a gene marker is no longer limited to one cancer, but is extended to various cancers, so the credibility has been improved than before. Based on CDK2, we searched for relevant immunomodulators and combined with the clinical expression data of LUAD to conduct univariate and multivariate regression models. Then the Nomogram forecast model of age, gender, stage, T, N, M provided the clinical significance and prognosis. The patient's condition will be assessed according to the total risk score. Nomogram has a great effect on the prognosis of patients with LUAD. Finally, multivariate regression analysis showed that four mRNAs (SIT1, SNAI3, ASB2, and CDK2) were important for this immune model and significant for the prognosis of patients ($P < 0.05$). CDK2 was a risk molecule with independent prognosis (HR = 1.291, $P = 0.035$). This provides potential markers for targeted therapy with LUAD.

Cell-dependent kinases (CDKs) are involved in proliferation, DNA damage repair (Lim and Kaldis, 2013) and treatment of various tumors (Lin et al., 2021; Majumdar et al., 2021). A variety of mechanisms, including chaperone, positive phosphorylation and negative phosphorylation (Lee et al., 2021) regulate the activity of CDK family. Recently, CDK family molecules have

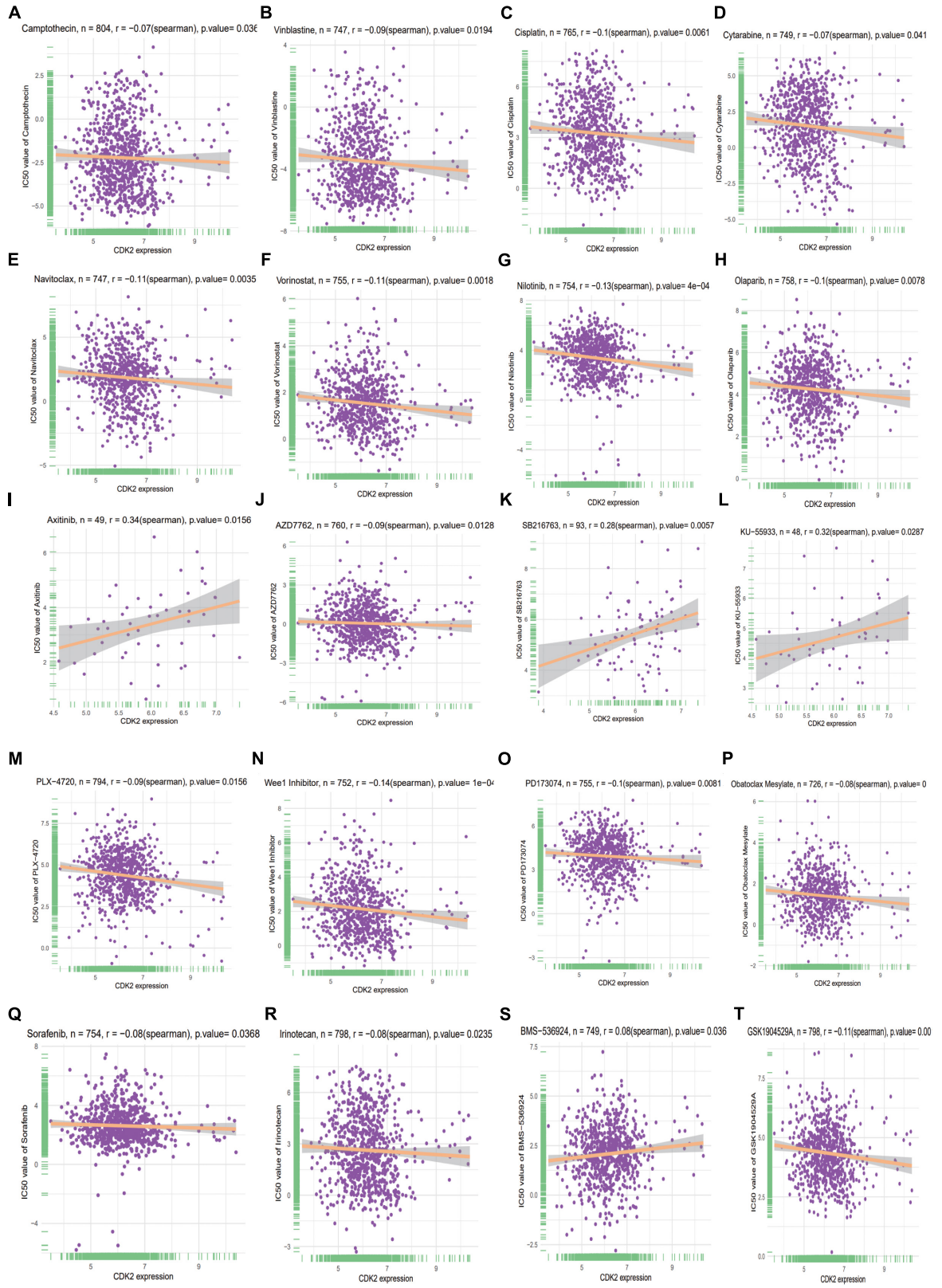

FIGURE 12 | The top 20 anti-tumor drug resistance studies related to CDK2 **(A–T)**.

been used as novel molecular markers for tumor-targeted therapy. As a star molecule, CDK2 (Kawakami et al., 2020) participates in classic pathways in various cancers, such as colorectal cancer (Somarelli et al., 2020), neuroblastoma (Poon et al., 2020), breast cancer (Hur et al., 2020), hepatocellular carcinoma (Hou et al., 2019), and prostate cancer (Washino et al., 2019). However, there are few studies on the mechanism of CDK2 in lung cancer. We studied the relationship between CDK2 and tumor immunity, providing a new idea for immunotherapy about LUAD.

In this study, we found that the expression of CDK2 was related to various immune cells including T cells ($P = 0.05$), Macrophages ($P = 0$), Eosinophils ($P = 0.01$), Mast cells ($P = 0$). Therefore, CDK2 can affect the tumorigenesis and proliferation by regulating the mechanism of immune inflammation. Combined with results of COX regression, target molecule CDK2 provides prognosis analysis and treatment strategy.

Cell cycle imbalance is common in different tumors (Chen T. et al., 2021). Cell-dependent kinase (CDK) is involved in many tumors related biological processes, such as cell cycle, immune checkpoint (Hume et al., 2020), RNA transcription (Al-Sanea et al., 2021), cell proliferation (Liu J. et al., 2021). Recently, there have been studies on CDK4 (Pandey et al., 2021) and CDK6 (Pandey et al., 2021), but the mechanism of CDK2 (El-Sattar et al., 2021) in cancer is relatively lacking. In our study, we deeply studied CDK2 and constructed the related immune prediction model. And CDK2 was associated in the P13K-AKT (Li Z. et al., 2021) signaling pathway in LUAD, inducing cell proliferation (Wu et al., 2020). Combing with clinical data, we constructed the forest map and Nomogram model (Cao et al., 2021b; Jang et al., 2021; Wang R. R. et al., 2021; Wang K. et al., 2021) of clinical characteristics. Through the features of patients, we can calculate the total score to evaluate the prognosis of patients. The prognosis of patients can be evaluated by a simple calculation method.

Compared with the current studies, the advantage is that we first established CDK2 related immune forecast model through the univariate, multivariate regression analysis and different "R" packages. This forecast was significant for LUAD patients. And the molecule CDK2 was related to various immune cells and may regulate mechanism in some way. The correlation between CDK2 and immune cells was listed by box diagram and point diagram. Compared with previous studies, they may research some markers in only signal cancer. But we explored detailed information of CDK2 in 33-cancer, a pan-cancer analysis was shown in our study. In various cancers, CDK2 has corresponding systematic significance with several clinical aspects ($P < 0.05$). CDK2 was associated with clinical stage, age, pathological type, TP-53 mutation, smoking with LUAD. According to the risk score, LUAD patients were divided into the high-risk group and low-risk group. There was a great difference between different risk curves (Yu et al., 2021). The survival time of the higher risk group was shorter than that of the lower risk group ($P = 6.223E-04$). This indicates that the immune related model is of great significance for the prognosis of patients with LUAD. All data were collected from reliable GEO database, TCGA, UCSC Xena and this increases the reliability of the data. In recent years, ceRNA network has certain significance in various cancers. The functions of many non-coding genes have been gradually explored (Yuan et al., 2014). Seven miRNAs (hsa-miR-302b-3p, hsa-miR-372-3p, hsa-miR-302a-3p, hsa-miR-373-3p, hsa-miR-520a-3p, hsa-miR-520d-3p, and hsa-miR-302d-3p), six lncRNAs (XIST, SNHG16, RP11-145M9.4, MAP3K14, MIR4720, and RP11-379K17.11) were considered as potential biomarkers in LUAD. Combined with the current literature, these non-coding genes have been studied in other cancers, but less in LUAD. This study provides potential therapeutic targets for LUAD and contributes to immunotherapy.

In recent years, nomogram model has been considered as a tool to predict tumor prognosis (Balachandran et al., 2015; Huang et al., 2016), such as colorectal cancer (Huang et al., 2016) and cervical cancer (Rose et al., 2015). Nomogram model meets our desire for biologically and clinically integrated models. It is not limited to one factor, but combines with various influencing factors to evaluate the prognosis of patients. We constructed nomogram model of age, gender, stage, T, N, M. According to the corresponding score of each influencing factor, the risk index of LUAD patients is estimated to evaluate the survival time.

According to our anti-tumor drug resistance research findings, the IC50 of four drugs (Axitinib, SB216763, KU-55933, BMS-536924) were positive with expression of CDK2. This indicates that cancer patients with high expression of CDK2 are prone to resistance to the above four drugs. Other 16 drugs were negative with the expression of CDK2. The patients with high expression of CDK2 had good response to the above 16 drugs and low resistance rate. Three drugs Cisplatin, Cytarabine, Nilotinib are considered as classic anti-cancer drugs. They are effective for patients with high expression of CDK2 cancer and it is not easy to cause drug resistance. Of course, the mechanism between CDK2 and drug resistance still needs to further be studied.

There are disadvantages in our study compared with the current articles. The target molecules lack of experimental verification and big data support. The regulatory mechanism of target genes is unclear.

In summary, immune-related forecast model was constructed by univariate regression and multivariate regression analysis to guide prognosis of LUAD. K–M curve verified the high-risk group had a poor prognosis ($P < 0.01$). Because of the correlation of CDK2 and various immune cells, CDK2 may be involved in tumor regulation of immune infiltration. CDK2 provides a new immunotherapy target for LUAD, which can improve the prognosis. The construction of ceRNA network provides a new way for exploring potential gene markers with LUAD. Drug resistance research can help patients choose a reasonable treatment plan, not blindly targeted therapy or immunosuppressive therapy.

CONCLUSION

In conclusion, we discovered a set of four genes, including expression of CDK2, has a significant prognostic value in LUAD. CDK2 expression is highly associated with immune responses in the cancer. We made some prediction to link CDK2 expression with drug responses and miRNA expression.

DATA AVAILABILITY STATEMENT

The datasets presented in this study can be found in online repositories. The names of the repository/repositories and accession number(s) can be found in the article/supplementary material.

AUTHOR CONTRIBUTIONS

T-TL and RL conceived and designed the study. CH, J-PL, JY, and X-LJ collected the literature. T-TL drafted the manuscript. Y-QQ revised the manuscript. All the authors read and approved the final manuscript.

FUNDING

This work was supported by grants from the Major Scientific and Technological Innovation Project of Shandong Province (Grant No. 2018CXGC1212), the CSCO-Qilu Cancer Research Fund (Grant No. Y-Q201802-014), the Medical and Health Technology Innovation Plan of Jinan City (Grant No. 201805002), and Special fund for clinical research of Jinan City (201912011).

REFERENCES

Al-Sanea, M. M., Obaidullah, A. J., Shaker, M. E., Chilingaryan, G., Alanazi, M. M., Alsaif, N. A., et al. (2021). CDK2 Inhibitor with 3-hydrazonoindolin-2-one scaffold endowed with anti-breast cancer activity: design, synthesis, biological evaluation, and in silico insights. *Molecules* 26:412. doi: 10.3390/molecules26020412

Bade, B. C., and Dela Cruz, C. S. (2020). Lung Cancer 2020: epidemiology, etiology, and prevention. *Clin. Chest. Med.* 41, 1–24. doi: 10.1016/j.ccm.2019.10.001

Balachandran, V. P., Gonen, M., Smith, J. J., and DeMatteo, R. P. (2015). Nomograms in oncology: more than meets the eye. *Lancet Oncol.* 16, e173–e180. doi: 10.1016/S1470-2045(14)71116-7

Barnett-Itzhaki, Z., Knapp, S., Avraham, C., Racowsky, C., Hauser, R., Bollati, V., et al. (2021). Association between follicular fluid phthalate concentrations and extracellular vesicle microRNAs expression. *Hum. Reprod.* 36, 1590–1599. doi: 10.1093/humrep/deab063

Cao, J., Wu, L., Lei, X., Shi, K., and Shi, L. (2021a). A signature of 13 autophagyrelated gene pairs predicts prognosis in hepatocellular carcinoma. *Bioengineered* 12, 697–707. doi: 10.1080/21655979.2021.1880084

Cao, J., Wu, L., Lei, X., Shi, K., Shi, L., and Shi, Y. (2021b). Long non-coding RNA-based signature for predicting prognosis of hepatocellular carcinoma. *Bioengineered* 12, 673–681. doi: 10.1080/21655979.2021.1878763

Chen, C., Chio, C. L., Zeng, H., and Li, Y. (2021). High expression of CD56 may be associated with favorable overall survival in intermediate-risk acute myeloid leukemia. *Hematology* 26, 210–214. doi: 10.1080/16078454.2021.1880734

Chen, J., and Zhou, R. (2021). Tumor microenvironment related novel signature predict lung adenocarcinoma survival. *PeerJ* 9:e10628. doi: 10.7717/peerj.10628

Chen, T., Liu, L., Zou, Y., Hu, X., Zhang, W., Zhou, T., et al. (2021). Nobiletin downregulates the SKP2-p21/p27-CDK2 axis to inhibit tumor progression and shows synergistic effects with palbociclib on renal cell carcinoma. *Cancer Biol. Med.* 18, 227–244. doi: 10.20892/j.issn.2095-3941.2020.0186

Chen, W., Zheng, R., Baade, P. D., Zhang, S., Zeng, H., Bray, F., et al. (2016). Cancer statistics in China, 2015. *CA Cancer J Clin* 66, 115–132. doi: 10.3322/caac.21338

Chen, Y., and Zhang, R. (2021). Long non-coding RNA AL139002.1 promotes gastric cancer development by sponging microRNA-490-3p to regulate hepatitis a virus cellular receptor 1 expression. *Bioengineered* 12, 1927–1938. doi: 10.1080/21655979.2021.1922329

Chen, Y., Zhou, H., Wang, Z., Huang, Z., Wang, J., Zheng, M., et al. (2021). Integrated analysis of ceRNA network and tumor-infiltrating immune cells in esophageal cancer. *Biosci. Rep.* 41:BSR20203804. doi: 10.1042/BSR20203804

Dai, W., Feng, J., Hu, X., Chen, Y., Gu, Q., Gong, W., et al. (2021). SLC7A7 is a prognostic biomarker correlated with immune infiltrates in non-small cell lung cancer. *Cancer Cell Int.* 21:106. doi: 10.1186/s12935-021-01781-7

El-Sattar, N., Badawy, E. H. K., AbdEl-Hady, W. H., Abo-Alkasem, M. I., Mandour, A. A., and Ismail, N. S. M. (2021). Design and synthesis of new CDK2 inhibitors containing thiazolone and thiazolthione scafold with apoptotic activity. *Chem. Pharm. Bull. (Tokyo)* 69, 106–117. doi: 10.1248/cpb.c20-00714

Esenboga, K., Kurtul, A., Yamanturk, Y. Y., Tan, T. S., and Tutar, D. E. (2021). Systemic immune-inflammation index predicts no-reflow phenomenon after primary percutaneous coronary intervention. *Acta. Cardiol.* 1–8. doi: 10.1080/00015385.2021.1884786 [Epub ahead of print].

Geng, Y., Shao, Y., Zhu, D., Zheng, X., Zhou, Q., Zhou, W., et al. (2016). Systemic immune-inflammation index predicts prognosis of patients with esophageal squamous cell carcinoma: a propensity score-matched analysis. *Sci Rep* 6, 39482. doi: 10.1038/srep39482

Han, P., Li, J. W., Zhang, B. M., Lv, J. C., Li, Y. M., Gu, X. Y., et al. (2017). The lncRNA CRNDE promotes colorectal cancer cell proliferation and chemoresistance via miR-181a-5p-mediated regulation of Wnt/beta-catenin signaling. *Mol. Cancer* 16:9. doi: 10.1186/s12943-017-0583-1

Han, T., Zhou, Y., and Li, D. (2021). Relationship between hepatocellular carcinoma and depression via online database analysis. *Bioengineered* 12, 1689–1697. doi: 10.1080/21655979.2021.1921552

He, M., Han, Y., Cai, C., Liu, P., Chen, Y., Shen, H., et al. (2021). CLEC10A is a prognostic biomarker and correlated with clinical pathologic features and immune infiltrates in lung adenocarcinoma. *J. Cell Mol. Med.* 25, 3391–3399. doi: 10.1111/jcmm.16416

Hou, J., and Yao, C. (2021). Potential prognostic biomarkers of lung adenocarcinoma based on bioinformatic analysis. *Biomed. Res. Int.* 2021:8859996. doi: 10.1155/2021/8859996

Hou, Y., Wang, Z., Huang, S., Sun, C., Zhao, J., Shi, J., et al. (2019). SKA3 Promotes tumor growth by regulating CDK2/P53 phosphorylation in hepatocellular carcinoma. *Cell Death Dis.* 10:929. doi: 10.1038/s41419-019-2163-3

Hu, B., Yang, X. R., Xu, Y., Sun, Y. F., Sun, C., Guo, W., et al. (2014). Systemic immune-inflammation index predicts prognosis of patients after curative resection for hepatocellular carcinoma. *Clin. Cancer Res.* 20, 6212–6222. doi: 10.1158/1078-0432.CCR-14-0442

Huang, H., Kong, L., Luan, S., Qi, C., and Wu, F. (2021). Ligustrazine suppresses platelet-derived growth factor-bb-induced pulmonary artery smooth muscle cell proliferation and inflammation by regulating the PI3K/AKT signaling pathway. *Am. J. Chin. Med.* 49, 437–459. doi: 10.1142/S0192415X21500208

Huang, X. Y., Liu, J. J., Liu, X., Wang, Y. H., and Xiang, W. (2021). Bioinformatics analysis of the prognosis and biological significance of VCAN in gastric cancer. *Immun. Inflamm. Dis.* 9, 547–559. doi: 10.1002/iid3.414

Huang, Y. Q., Liang, C. H., He, L., Tian, J., Liang, C. S., Chen, X., et al. (2016). Development and validation of a radiomics nomogram for preoperative prediction of lymph node metastasis in colorectal cancer. *J. Clin. Oncol.* 34, 2157–2164. doi: 10.1200/JCO.2015.65.9128

Hume, S., Dianov, G. L., and Ramadan, K. (2020). A unified model for the G1/S cell cycle transition. *Nucleic Acids Res.* 48, 12483–12501. doi: 10.1093/nar/gkaa1002

Hur, S., Kim, J. H., Yun, J., Ju, Y. W., Han, J. M., and Heo, W. (2020). Protein Phosphatase 1H, cyclin-dependent kinase inhibitor p27, and cyclin-dependent kinase 2 in paclitaxel resistance for triple negative breast cancers. *J. Breast Cancer* 23, 162–170. doi: 10.4048/jbc.2020.23.e20

Jang, S. Y., Kim, J. S., Baek, S. Y., Lee, H. A., and Lee, J. K. (2021). Proposed nomogram predicting neoplastic ampullary obstruction in patients with a suspected ampulla of Vater lesion on CT. *Abdom. Radiol. (NY)* 46, 3128–3138. doi: 10.1007/s00261-021-02975-3

Janssen, L. M. E., Ramsay, E. E., Logsdon, C. D., and Overwijk, W. W. (2017). The immune system in cancer metastasis: friend or foe? *J. Immunother. Cancer* 5:79. doi: 10.1186/s40425-017-0283-9

Jomrich, G., Paireder, M., Kristo, I., Baierl, A., Ilhan-Mutlu, A., Preusser, M., et al. (2021). High systemic immune-inflammation index is an adverse prognostic

factor for patients with gastroesophageal adenocarcinoma. *Ann. Surg.* 273, 532–541. doi: 10.1097/SLA.0000000000003370

Ju, Q., Huang, T., Zhang, Y., Wu, L., Geng, J., Mu, X., et al. (2021). Systemic immune-inflammation index predicts prognosis in patients with different EGFR-mutant lung adenocarcinoma. *Medicine (Baltimore)* 100:e24640. doi: 10.1097/MD.0000000000024640

Kara, A., Ozgur, A., Tekin, S., and Tutar, Y. (2021). Computational analysis of drug resistance network in lung adenocarcinoma. *Anticancer Agents Med. Chem* doi: 10.2174/1871520621666210218175439 [Epub ahead of print].

Kawakami, M., Mustachio, L. M., Chen, Y., Chen, Z., Liu, X., Wei, C. H., et al. (2020). CDK2/9 Inhibitor CYC065 causes anaphase catastrophe and represses proliferation, tumorigenesis, and metastasis in aneuploid cancers. *Mol. Cancer Ther.* 20, 477–489. doi: 10.1158/1535-7163.MCT-19-0987

Kim, J., Piao, H. L., Kim, B. J., Yao, F., Han, Z., Wang, Y., et al. (2018). Long noncoding RNA MALAT1 suppresses breast cancer metastasis. *Nat. Genet.* 50, 1705–1715. doi: 10.1038/s41588-018-0252-3

Kris, M. G., Johnson, B. E., Berry, L. D., Kwiatkowski, D. J., Iafrate, A. J., Wistuba, I. I., et al. (2014). Using multiplexed assays of oncogenic drivers in lung cancers to select targeted drugs. *JAMA* 311, 1998–2006. doi: 10.1001/jama.2014.3741

Lee, J. C., Hong, K. H., Becker, A., Tash, J. S., Schonbrunn, E., and Georg, G. I. (2021). Tetrahydroindazole inhibitors of CDK2/cyclin complexes. *Eur. J. Med. Chem.* 214:113232. doi: 10.1016/j.ejmech.2021.113232

Li, F., Jin, Y., Pei, X., Guo, P., Dong, K., Wang, H., et al. (2021). Bioinformatics analysis and verification of gene targets for renal clear cell carcinoma. *Comput. Biol. Chem.* 92:107453. doi: 10.1016/j.compbiolchem.2021.107453

Li, J. H., Liu, S., Zhou, H., Qu, L. H., and Yang, J. H. (2014). starBase v2.0: decoding miRNA-ceRNA, miRNA-ncRNA and protein-RNA interaction networks from large-scale CLIP-Seq data. *Nucleic Acids Res.* 42, D92–D97. doi: 10.1093/nar/gkt1248

Li, J., Huang, Y., Zhang, Y., Wen, J., Chen, Y., Wang, L., et al. (2021). Identification BCL6 and miR-30 family associating with Ibrutinib resistance in activated B-cell-like diffuse large B-cell lymphoma. *Med. Oncol.* 38:33. doi: 10.1007/s12032-021-01470-5

Li, J., Meng, H., Bai, Y., and Wang, K. (2016). Regulation of lncRNA and its role in cancer metastasis. *Oncol. Res.* 23, 205–217. doi: 10.3727/096504016X14549667334007

Li, Y., Tao, L., and Cai, W. (2020). Profiles of immune infiltration and prognostic immunoscore in lung adenocarcinoma. *Biomed. Res. Int.* 2020:5858092. doi: 10.1155/2020/5858092

Li, Z., Chen, C., Wang, J., Wei, M., Liu, G., Qin, Y., et al. (2021). Overexpressed PLAU and its potential prognostic value in head and neck squamous cell carcinoma. *PeerJ* 9:e10746. doi: 10.7717/peerj.10746

Lim, S., and Kaldis, P. (2013). Cdks, cyclins and CKIs: roles beyond cell cycle regulation. *Development* 140, 3079–3093. doi: 10.1242/dev.091744

Lin, T., Li, J., Liu, L., Li, Y., Jiang, H., Chen, K., et al. (2021). Design, synthesis, and biological evaluation of 4-benzoylamino-1H-pyrazole-3-carboxamide derivatives as potent CDK2 inhibitors. *Eur. J. Med. Chem.* 215:113281. doi: 10.1016/j.ejmech.2021.113281

Ling, B., Huang, Z., Huang, S., Qian, L., Li, G., and Tang, Q. (2020). Microenvironment analysis of prognosis and molecular signature of immune-related genes in lung adenocarcinoma. *Oncol. Res.* 28, 561–578. doi: 10.3727/096504020X15907428281601

Liu, H., Song, M., Sun, X., Zhang, X., Miao, H., and Wang, Y. (2021). T-box transcription factor TBX1, targeted by microRNA-6727-5p, inhibits cell growth and enhances cisplatin chemosensitivity of cervical cancer cells through AKT and MAPK pathways. *Bioengineered* 12, 565–577. doi: 10.1080/21655979.2021.1880732

Liu, J., Zeng, X., Han, K., Jia, X., Zhou, M., Zhang, Z., et al. (2021). The expression regulation of Cyclins and CDKs in ovary via miR-9c and miR-263a of scylla paramamosain. *Comp. Biochem. Physiol. B Biochem. Mol. Biol.* 254:110567. doi: 10.1016/j.cbpb.2021.110567

Liu, X. S., Gao, Y., Liu, C., Chen, X. Q., Zhou, L. M., Yang, J. W., et al. (2020). Comprehensive analysis of prognostic and immune infiltrates for E2F transcription factors in human pancreatic adenocarcinoma. *Front Oncol 10* 10:606735. doi: 10.3389/fonc.2020.606735

Liu, X., Zhan, Y., Xu, W., Liu, X., Geng, Y., Liu, L., et al. (2021). Prognostic and immunological role of Fam20C in pan-cancer. *Biosci. Rep.* 41:BSR20201920. doi: 10.1042/BSR20201920

Liu, Y., Chen, G., Liu, H., Li, Z., Yang, Q., Gu, X., et al. (2019). Integrated bioinformatics analysis of miRNA expression in ewing sarcoma and potential regulatory effects of miR-21 via targeting ALCAM/CD166. *Artif. Cells Nanomed. Biotechnol.* 47, 2114–2122. doi: 10.1080/21691401.2019.1620760

Liu, Y., Li, L., Jiang, D., Yang, M., Gao, X., Lv, K., et al. (1976). For survival prediction of patients with spinal metastasis from prostate cancer. *Spine (Phila Pa* 46, E364–E373. doi: 10.1097/BRS.0000000000003888

Lolli, C., Caffo, O., Scarpi, E., Aieta, M., Conteduca, V., Maines, F., et al. (2016). Systemic immune-inflammation index predicts the clinical outcome in patients with mCRPC treated with abiraterone. *Front. Pharmacol.* 7:376. doi: 10.3389/fphar.2016.00376

Lu, H. P., Du, X. F., Li, J. D., Huang, S. N., He, R. Q., Wu, H. Y., et al. (2021). Expression of cell division cycle protein 45 in tissue microarrays and the CDC45 gene by bioinformatics analysis in human hepatocellular carcinoma and patient outcomes. *Med. Sci. Monit.* 27:e928800. doi: 10.12659/MSM.928800

Majumdar, A., Burban, D. J., Muretta, J. M., Thompson, A. R., Engel, T. A., and Rasmussen, D. M. (2021). Allostery governs Cdk2 activation and differential recognition of CDK inhibitors. *Nat. Chem. Biol.* 17, 456–464. doi: 10.1038/s41589-020-00725-y

Marwitz, S., Ballesteros-Merino, C., Jensen, S. M., Reck, M., Kugler, C., and Perner, S. (2021). Phosphorylation of SMAD3 in immune cells predicts survival of patients with early stage non-small cell lung cancer. *J. Immunother. Cancer* 9:e001469. doi: 10.1136/jitc-2020-001469

Mungan, I., Bostanci, E. B., Turksal, E., Tezcan, B., Aktas, M. N., Can, M., et al. (2021). The predictive power of C-reactive protein- lymphocyte ratio for in-hospital mortality after colorectal cancer surgery. *Cancer Rep. (Hoboken)* 4:e1330. doi: 10.1002/cnr2.1330

Noreldeen, H. A. A., Liu, X., and Xu, G. (2020). Metabolomics of lung cancer: Analytical platforms and their applications. *J. Sep. Sci.* 43, 120–133. doi: 10.1002/jssc.201900736

Pandey, K., Lee, E., Park, N., Hur, J., Cho, Y. B., Katuwal, N. B., et al. (2021). Deregulated immune pathway associated with palbociclib resistance in preclinical breast cancer models: integrative genomics and transcriptomics. *Genes (Basel)* 12:159. doi: 10.3390/genes12020159

Poon, E., Liang, T., Jamin, Y., Walz, S., Kwok, C., and Hakkert, A. (2020). Orally bioavailable CDK9/2 inhibitor shows mechanism-based therapeutic potential in MYCN-driven neuroblastoma. *J. Clin. Invest.* 130, 5875–5892. doi: 10.1172/JCI134132

Ren, C., Li, M., Zheng, Y., Wu, F., Du, W., and Quan, R. (2021). , Identification of diagnostic genes and vital microRNAs involved in rheumatoid arthritis: based on data mining and experimental verification. *PeerJ* 9:e11427. doi: 10.7717/peerj.11427

Rose, P. G., Java, J., Whitney, C. W., Stehman, F. B., Lanciano, R., and Thomas, G. M. (2015). . Nomograms predicting progression-free survival, overall survival, and pelvic recurrence in locally advanced cervical cancer developed from an analysis of identifiable prognostic factors in patients from nrg oncology/gynecologic oncology group randomized trials of chemoradiotherapy. *J. Clin. Oncol.* 33, 2136–2142. doi: 10.1200/JCO.2014.57.7122

Santaniello, A., Napolitano, F., Servetto, A., De Placido, P., Silvestris, N., Bianco, C., et al. (2019). Tumour microenvironment and immune evasion in EGFR addicted NSCLC: hurdles and possibilities. *Cancers (Basel)* 11:1419. doi: 10.3390/cancers11101419

Sheng, L. P., Han, C. Q., Nie, C., Xu, T., Zhang, K., Li, X. J., et al. (2021). Identification of potential serum exosomal microRNAs involved in acinar-ductal metaplasia that is a precursor of pancreatic cancer associated with chronic pancreatitis. *Medicine (Baltimore)* 100:e25753. doi: 10.1097/MD.0000000000025753

Sheng, X. F., Hong, L. L., Li, H., Huang, F. Y., Wen, Q., and Zhuang, H. F. (2021). Long non-coding RNA MALAT1 modulate cell migration, proliferation and apoptosis by sponging microRNA-146a to regulate CXCR4 expression in acute myeloid leukemia. *Hematology* 26, 43–52. doi: 10.1080/16078454.2020.1867781

Siegel, R. L., Miller, K. D., and Jemal, A. (2020). Cancer statistics, 2020. *CA Cancer J. Clin.* 70, 7–30. doi: 10.3322/caac.21590

Somarelli, J. A., Roghani, R. S., Moghaddam, A. S., Thomas, B. C., Rupprecht, G., Ware, K. E., et al. (2020). A Precision medicine drug discovery pipeline identifies combined CDK2 and 9 inhibition as a novel therapeutic strategy in

colorectal cancer. *Mol. Cancer Ther* .19, 2516–2527. doi: 10.1158/1535-7163.MCT-20-0454

Tan, L., Xu, Q., Shi, R., and Zhang, G. (2021). Bioinformatics analysis reveals the landscape of immune cell infiltration and immune-related pathways participating in the progression of carotid atherosclerotic plaques. *Artif. Cells Nanomed. Biotechnol.* 49, 96–107. doi: 10.1080/21691401.2021.1873798

Wang, C., Qiao, W., Jiang, Y., Zhu, M., Shao, J., Wang, T., et al. (2020). The landscape of immune checkpoint inhibitor plus chemotherapy versus immunotherapy for advanced non-small-cell lung cancer: a systematic review and meta-analysis. *J. Cell Physiol.* 235, 4913–4927. doi: 10.1002/jcp.29371

Wang, K., Wu, Z., Wang, G., Shi, H., Xie, J., Yin, L., et al. (2021). Survival nomogram for patients with bone metastatic renal cell carcinoma: a population-based study. *Int. Braz. J. Urol.* 47, 333–349. doi: 10.1590/S1677-5538.IBJU.2020.0195

Wang, R. R., He, M., Gui, X., and Kang, Y. (2021). A nomogram based on serum cystatin C for predicting acute kidney injury in patients with traumatic brain injury. *Ren Fail* 43, 206–215. doi: 10.1080/0886022X.2021.1871919

Washino, S., Rider, L. C., Romero, L., Jillson, L. K., Affandi, T., and Ohm, A. M. (2019). Loss of MAP3K7 sensitizes prostate cancer cells to cdk1/2 inhibition and DNA damage by disrupting homologous recombination. *Mol. Cancer Res.* 17, 1985–1998. doi: 10.1158/1541-7786.MCR-18-1335

Wu, J., Gao, H., Ge, W., and He, J. (2020). Over expression of PTEN induces apoptosis and prevents cell proliferation in breast cancer cells. *Acta Biochim. Pol.* 67, 515–519. doi: 10.18388/abp.2020_5371

Wu, R., Zhuang, H., Mei, Y. K., Sun, J. Y., Dong, T., Zhao, L. L., et al. (2021). Systematic identification of key functional modules and genes in esophageal cancer. *Cancer Cell Int.* 21:134. doi: 10.1186/s12935-021-01826-x

Wu, Y., Liu, L., Shen, X., Liu, W., and Ma, R. (2021). Plakophilin-2 promotes lung adenocarcinoma development via enhancing focal adhesion and epithelial-mesenchymal transition. *Cancer Manag. Res.* 13, 559–570. doi: 10.2147/CMAR.S281663

Xiang, M., Feng, Y., Wang, Y., Wang, J., Zhang, Z., Liang, J., et al. (2021). Correlation between circulating interleukin-18 level and systemic lupus erythematosus: a meta-analysis. *Sci. Rep.* 11:4707. doi: 10.1038/s41598-021-84170-4

Yang, Y., Yang, L., and Wang, Y. (2021). [Immunotherapy for lung cancer: mechanisms of resistance and response strategy]. *Zhongguo Fei Ai Za Zhi* 24, 112–123. doi: 10.3779/j.issn.1009-3419.2021.101.02

Yu, J., Chen, X., Li, Y., Wang, Y., Cao, X., Liu, Z., et al. (2021). Pro-inflammatory cytokines as potential predictors for intradialytic hypotension. *Ren Fail* 43, 198–205. doi: 10.1080/0886022X.2021.1871921

Yuan, J. H., Yang, F., Wang, F., Ma, J. Z., Guo, Y. J., Tao, Q. F., et al. (2014). A long noncoding RNA activated by TGF-beta promotes the invasion-metastasis cascade in hepatocellular carcinoma. *Cancer Cell* 25, 666–681. doi: 10.1016/j.ccr.2014.03.010

Zhai, Y., Zhao, B., Wang, Y., Li, L., Li, J., Li, X., et al. (2021). Construction of the optimization prognostic model based on differentially expressed immune genes of lung adenocarcinoma. *BMC Cancer* 21:213. doi: 10.1186/s12885-021-07911-8

Zhang, M., Jin, X., Li, J., Tian, Y., Wang, Q., Li, X., et al. (2021). CeRNASeek: an R package for identification and analysis of ceRNA regulation. *Brief Bioinform.* 22:bbaa048. doi: 10.1093/bib/bbaa048

Zhao, C., Wang, Y., Jin, H., and Yu, T. (2017). Knockdown of microRNA-203 alleviates LPS-induced injury by targeting MCL-1 in C28/I2 chondrocytes. *Exp. Cell Res.* 359, 171–178. doi: 10.1016/j.yexcr.2017.07.034

Zheng, S., Wang, X., Fu, Y., Li, B., Xu, J., Wang, H., et al. (2021). Targeted next-generation sequencing for cancer-associated gene mutation and copy number detection in 206 patients with non-small-cell lung cancer. *Bioengineered* 12, 791–802. doi: 10.1080/21655979.2021.1890382

Zhou, C. S., Feng, M. T., Chen, X., Gao, Y., Chen, L., Li, L. D., et al. (2021). Exonuclease 1 (EXO1) is a potential prognostic biomarker and correlates with immune infiltrates in lung adenocarcinoma. *Onco. Targets Ther.* 14, 1033–1048. doi: 10.2147/OTT.S286274

Zhou, C., Wang, Y., Wang, Y., Lei, L., Ji, M. H., Zhou, G., et al. (2021). Predicting lung adenocarcinoma prognosis with a novel risk scoring based on platelet-related gene expression. *Aging (Albany NY)* 13, 8706–8719. doi: 10.18632/aging.202682

Zhuang, Z., Lin, T., Luo, L., Zhou, W., Wen, J., Huang, H., et al. (2021). Exploring the mechanism of aidi injection for lung cancer by network pharmacology approach and molecular docking validation. *Biosci. Rep.* 41:BSR20204062. doi: 10.1042/BSR20204062

Conflict of Interest: The authors declare that the research was conducted in the absence of any commercial or financial relationships that could be construed as a potential conflict of interest.

Publisher's Note: All claims expressed in this article are solely those of the authors and do not necessarily represent those of their affiliated organizations, or those of the publisher, the editors and the reviewers. Any product that may be evaluated in this article, or claim that may be made by its manufacturer, is not guaranteed or endorsed by the publisher.

frontiers in Cell and Developmental Biology

ORIGINAL RESEARCH
published: 05 August 2021
doi: 10.3389/fcell.2021.687245

Molecular Subtypes of Oral Squamous Cell Carcinoma Based on Immunosuppression Genes Using a Deep Learning Approach

Simin Li[1†], Zhaoyi Mai[1†], Wenli Gu[1†], Anthony Chukwunonso Ogbuehi[2], Aneesha Acharya[3], George Pelekos[4], Wanchen Ning[1], Xiangqiong Liu[5], Yupei Deng[5], Hanluo Li[6], Bernd Lethaus[6], Vuk Savkovic[6], Rüdiger Zimmerer[6], Dirk Ziebolz[7‡], Gerhard Schmalz[7‡], Hao Wang[8], Hui Xiao[1*] and Jianjiang Zhao[9*]*

[1] Stomatological Hospital, Southern Medical University, Guangzhou, China, [2] Faculty of Physics, University of Münster (Westfälische Wilhelms-Universität Münster), Münster, Germany, [3] Dr. D. Y. Patil Dental College and Hospital, Dr. D. Y. Patil Vidyapeeth, Pune, India, [4] Faculty of Dentistry, University of Hong Kong, Hong Kong, China, [5] Laboratory of Molecular Cell Biology, Beijing Tibetan Hospital, China Tibetology Research Center, Beijing, China, [6] Department of Cranio Maxillofacial Surgery, University Clinic Leipzig, Leipzig, Germany, [7] Department of Cariology, Endodontology and Periodontology, University of Leipzig, Leipzig, Germany, [8] Shanghai Tenth People's Hospital, Tongji University, Shanghai, China, [9] Shenzhen Stomatological Hospital, Southern Medical University, Shenzhen, China

OPEN ACCESS

Edited by:
José Alexandre Ferreira, Portuguese Oncology Institute, Portugal

Reviewed by:
Rafael Costa, New University of Lisbon, Portugal
Dongjun Lee, Pusan National University, South Korea

***Correspondence:**
Jianjiang Zhao
zjj2521@sina.com
Hao Wang
083836@tongji.edu.cn
Hui Xiao
zzmmxh@126.com

[†] These authors have contributed equally to this work and share first authorship

[‡] These authors have contributed equally to this work and share senior authorship

Specialty section:
This article was submitted to Molecular and Cellular Pathology, a section of the journal Frontiers in Cell and Developmental Biology

Received: *29 March 2021*
Accepted: *04 June 2021*
Published: *05 August 2021*

Citation:
Li S, Mai Z, Gu W, Ogbuehi AC, Acharya A, Pelekos G, Ning W, Liu X, Deng Y, Li H, Lethaus B, Savkovic V, Zimmerer R, Ziebolz D, Schmalz G, Wang H, Xiao H and Zhao J (2021) Molecular Subtypes of Oral Squamous Cell Carcinoma Based on Immunosuppression Genes Using a Deep Learning Approach. Front. Cell Dev. Biol. 9:687245. doi: 10.3389/fcell.2021.687245

Background: The mechanisms through which immunosuppressed patients bear increased risk and worse survival in oral squamous cell carcinoma (OSCC) are unclear. Here, we used deep learning to investigate the genetic mechanisms underlying immunosuppression in the survival of OSCC patients, especially from the aspect of various survival-related subtypes.

Materials and methods: OSCC samples data were obtained from The Cancer Genome Atlas (TCGA), International Cancer Genome Consortium (ICGC), and OSCC-related genetic datasets with survival data in the National Center for Biotechnology Information (NCBI). Immunosuppression genes (ISGs) were obtained from the HisgAtlas and DisGeNET databases. Survival analyses were performed to identify the ISGs with significant prognostic values in OSCC. A deep learning (DL)-based model was established for robustly differentiating the survival subpopulations of OSCC samples. In order to understand the characteristics of the different survival-risk subtypes of OSCC samples, differential expression analysis and functional enrichment analysis were performed.

Results: A total of 317 OSCC samples were divided into one inferring cohort (TCGA) and four confirmation cohorts (ICGC set, GSE41613, GSE42743, and GSE75538). Eleven ISGs (i.e., BGLAP, CALCA, CTLA4, CXCL8, FGFR3, HPRT1, IL22, ORMDL3, TLR3, SPHK1, and INHBB) showed prognostic value in OSCC. The DL-based model provided two optimal subgroups of TCGA-OSCC samples with significant differences (p = 4.91E-22) and good model fitness [concordance index (C-index) = 0.77]. The DL model was validated by using four external confirmation cohorts: ICGC cohort (n = 40, C-index = 0.39), GSE41613 dataset (n = 97, C-index = 0.86), GSE42743 dataset (n = 71, C-index = 0.87), and GSE75538 dataset (n = 14, C-index = 0.48). Importantly, subtype Sub1 demonstrated a lower probability of survival and thus a more aggressive

nature compared with subtype Sub2. ISGs in subtype Sub1 were enriched in the tumor-infiltrating immune cells-related pathways and cancer progression-related pathways, while those in subtype Sub2 were enriched in the metabolism-related pathways.

Conclusion: The two survival subtypes of OSCC identified by deep learning can benefit clinical practitioners to divide immunocompromised patients with oral cancer into two subpopulations and give them target drugs and thus might be helpful for improving the survival of these patients and providing novel therapeutic strategies in the precision medicine area.

Keywords: immunosuppression, oral squamous cell carcinoma, survival, deep learning, bioinformatics

INTRODUCTION

Tumor cells can produce a variety of immunosuppressive factors that can inhibit the normal antitumor functions of immune cells, such as tumor-associated macrophages (TAMs), tumor-associated neutrophils (TANs), cancer-associated fibroblasts (CAFs), and regulatory T cells (Tregs; Liu and Cao, 2016). By the immunosuppression mechanisms mediated by the interaction between tumor cells and immune cells, tumor cells can escape elimination from immune surveillance and tumor immunity, thereby further contributing to cancer progression (Kim et al., 2007). Immunosuppression is involved in oral squamous cell carcinoma (OSCC) pathogenesis and contributes to its increased incidence and poor cancer-specific outcomes (Chang et al., 2020). Patients with a history of immunosuppression (e.g., organ transplant, autoimmune disease, pulmonary disorder, hematological malignancy, myeloproliferative disorder, and HIV infection) have been shown to have an increased risk of a second malignancy in OSCC (Tota et al., 2018). In addition, immunosuppression is significantly associated with poor outcomes of OSCC, and immunosuppressed patients have been shown to have an approximately twofold increase in the cancer-specific outcomes (e.g., recurrence and overall survival) compared with non-immunosuppressed individuals (Margalit et al., 2016).

The application of immunosuppressive drug agents (e.g., calcineurin inhibitors, antiproliferative agents, mTOR inhibitor, and steroids) can inhibit the strength and activity of the immune system by affecting the expression of many immunosuppression genes (ISGs) {e.g., cytokines [interleukin (IL)-2, IL-4, IL-6, IL-15, IL-18, IL-23, interferon gamma (IFN-γ), and tumor necrosis factor alpha (TNF-α)] and chemoattractant chemokines (e.g., CCL-2, CXCL-9, and CXCL-10)} (Misra et al., 2020). Although the dysregulation of ISGs has been shown to contribute to the carcinogenesis of oral cancers (Jewett et al., 2006), the specific ISGs and their mediated signaling pathways involved in the pathogenesis of OSCC have not yet been identified from a comprehensive and systematic aspect. The identification of ISGs as biomarkers in OSCC might have significant value for the clinical practice: on the one hand, selected ISGs could be used for evaluating the incidence risk and prognosis of OSCC; on the other hand, these could be regarded as therapeutic targets for improved OSCC management.

In order to address this research gap, bioinformatic analyses were performed based on the human ISGs obtained from HisgAtlas (Liu et al., 2017) and DisGeNET (Piñero et al., 2017), and the immunosuppressive drug agents were downloaded from the DrugBank (Wishart et al., 2018). Gene expression data regarding OSCC was collected from the TCGA databases (Tomczak et al., 2015). Deep learning (DL), a machine learning method harvesting Artificial Intelligence, has shown high impact in cancer research for classifying the subtypes of cancer samples in liver cancer (Chaudhary et al., 2018), breast cancer (Rohani and Eslahchi, 2020), lung cancer (Asuntha and Srinivasan, 2020), and head and neck cancer (Zhao Z. et al., 2020). Since genetic heterogeneity is a common feature of different tumors, molecular subtyping of cancers could be very helpful in devising precision medicine approaches for treating each subtype of cancer patients (Koo et al., 2016). Therefore, a DL-based model was applied in this research for classifying OSCC patients into molecular subtypes based on their significant feature ISGs' biological functions.

Thus, this study aimed to investigate the genetic mechanisms of immunosuppression in the pathogenesis of OSCC using bioinformatics analyses to identify the ISGs with significant prognostic value in OSCC, and the ISGs-involving pathways enriched in the aggressive subtype of OSCC, as differentiated by a deep learning model.

MATERIALS AND METHODS

The Study Design

An overview of the workflow of this study is depicted in **Figure 1**. In brief, the TCGA set as inferring set and four confirmation cohorts were downloaded, and the data information in these datasets is shown in **Table 1**. The ISGs were obtained from three databases [DisGeNET (Piñero et al., 2017), HisgAtlas (Liu et al., 2017), and DrugBank (Wishart et al., 2018)]. First, the proportion and expression profiling of 22 TIICs were analyzed by using CIBERSORT. Second, the survival analysis was performed to screen out the ISGs that were most significantly related to prognosis. Afterward, the deep learning-based model was constructed to achieve the compression and transformation of gene features. These reduced new gene features were used for clustering the samples by the K-means clustering algorithm.

Then, a supervised classification model was constructed by using the support vector machine (SVM) algorithm. In order to investigate the difference between the subtypes identified by the deep learning-based model, the functional enrichment analysis was performed to identify the functional difference of the ISGs enriched in varying subtypes.

Data Procurement

Inferring Cohort

Head and neck squamous cell carcinoma (HNSCC) data were obtained from the TCGA portal[1] (Tomczak et al., 2015). Based on the TCGA-Assembler 2 (Version 2.0.6[2]) (Wei et al., 2018), the HNSCC samples with the RNA sequencing (RNA-Seq) data (UNC IlluminaHiSeq_RNASeqV2; Level 3) and the clinical information were obtained. Among the HNSCC data, a total of 317 OSCC samples were selected by choosing the specific anatomic sites, including buccal mucosa, alveolar ridge, floor of mouth, hard palate, oral cavity, and the anterior two-thirds of the tongue (Krishna et al., 2014). In order to normalize and preprocess the data, three steps introduced by Wang et al. were performed to deal with the missing values (Wang et al., 2014). First, the biological features [e.g., genes/microRNAs (miRNAs)] were removed if they have zero value in more than 20% of patients. The samples were removed if they have missing values across more than 20% features. Second, we used the impute function from the R impute package (Xiang et al., 2008) to fill out the missing values. Third, we removed input features with zero values across all samples.

Confirmation Cohorts

Confirmation cohort 1 (ICGC cohort and RNA-Seq)

A total of 178 OSCC samples with RNA-Seq data were obtained from the International Cancer Genome Consortium (ICGC) portal[3] (Zhang et al., 2011). Among these 178 OSCC samples, 40 samples with the survival information were selected. This cohort was used for validating the analyzing results.

Confirmation cohort 2 (NCI cohort, microarray gene expression, and GSE41613)

A total of 97 samples with survival information were chosen from the GSE41613 microarray dataset[4](, which was from a study of patients with OSCC (Lohavanichbutr et al., 2013). The experimental platform of this dataset is based on GPL570 [HG-U133_Plus_2] Affymetrix Human Genome U133 Plus 2.0 Array.

Confirmation cohort 3 (NCI cohort, microarray gene expression, and GSE42743)

A total of 97 samples with survival information were chosen from the GSE42743 microarray dataset[5](, which was from a study of patients with OSCC (Lohavanichbutr et al., 2013). The experimental platform of this dataset is based on GPL570 [HG-U133_Plus_2] Affymetrix Human Genome U133 Plus 2.0 Array.

Confirmation cohort 4 (NCI cohort, microarray gene expression, and GSE75538)

A total of 14 samples with survival information were chosen from the GSE75538 microarray dataset[6](, which was from a study of patients with OSCC (Krishnan et al., 2016). The experimental platform of this dataset is based on GPL18281 Illumina Human HT-12 WG-DASL V4.0 R2 expression beadchip.

Procurement of ISGs

The immunosuppression-related genes were downloaded from DisGeNET database[7] (Piñero et al., 2017), HisgAtlas database[8] (Liu et al., 2017), and Drugbank database[9] (Wishart et al., 2018). After combining ISGs obtained from the above three databases, a total of 1,181 immunosuppressant genes were obtained. Afterward, the expression profiling of these 1,181 immunosuppressant genes was extracted from the OSCC datasets. Among these 1,181 ISGs, the expression level of the only one gene TNFRSF6B in the OSCC samples was zero and thus removed, and finally, 1,180 ISGs were used for the subsequent analysis.

Analysis of Tumor-Infiltrating Immune Cells in OSCC Samples

Twenty-two tumor-infiltrating immune cells (TIICs) were obtained based on the CIBERSORT webtool[10] (Chen et al., 2018). First, the expression profiles of ISGs in the OSCC samples were normalized, and the proportion of tumor-infiltrating immune cells (TIICs) in OSCC and healthy control samples were predicted by the CIBERSORT webtool. Second, the expression levels of varying ISGs in each type of cell were obtained. The average value of all ISGs in a certain type of cell was regarded as the expression levels of this type of cell in samples. The heatmap was plotted to show the expression levels of 22 TIICs in 151 samples (3 healthy samples and 148 OSCC samples). Third, the correlation plot was drawn based on the expression levels of TIICs in 151 samples in order to analyze the correlation between TIICs in the pathogenesis of OSCC. The Pearson correlation coefficient was used for calculating the correlation between any two types of TIICs. In addition, the Wilcox test was used for examining the differential expression status of each TIIC in OSCC samples compared with the healthy samples. Afterward, Kaplan–Meier analysis was utilized to investigate the prognostic value of 22 tumors infiltrating immune cells in OSCC tissues.

The Survival Analysis of ISGs

The OSCC patients were divided into two groups (i.e., high expression group and low expression group) according to the median value of gene expression levels of ISGs. The R package survival (Lin and Zelterman, 2002) was employed to mine ISGs that were significant prognostic indicators using Cox proportional hazards model. The ISGs with a

[1]https://tcga-data.nci.nih.gov/tcga/

[2]http://www.compgenome.org/TCGA-Assembler/

[3]https://dcc.icgc.org/projects/ORCA-IN

[4]https://www.ncbi.nlm.nih.gov/geo/query/acc.cgi?acc=GSE41613

[5]https://www.ncbi.nlm.nih.gov/geo/query/acc.cgi?acc=GSE42743

[6]https://www.ncbi.nlm.nih.gov/geo/query/acc.cgi?acc=GSE75538

[7]http://www.disgenet.org

[8]http://biokb.nb.org/HisgAtlas/

[9]https://www.drugbank.ca/

[10]https://cibersort.stanford.edu/

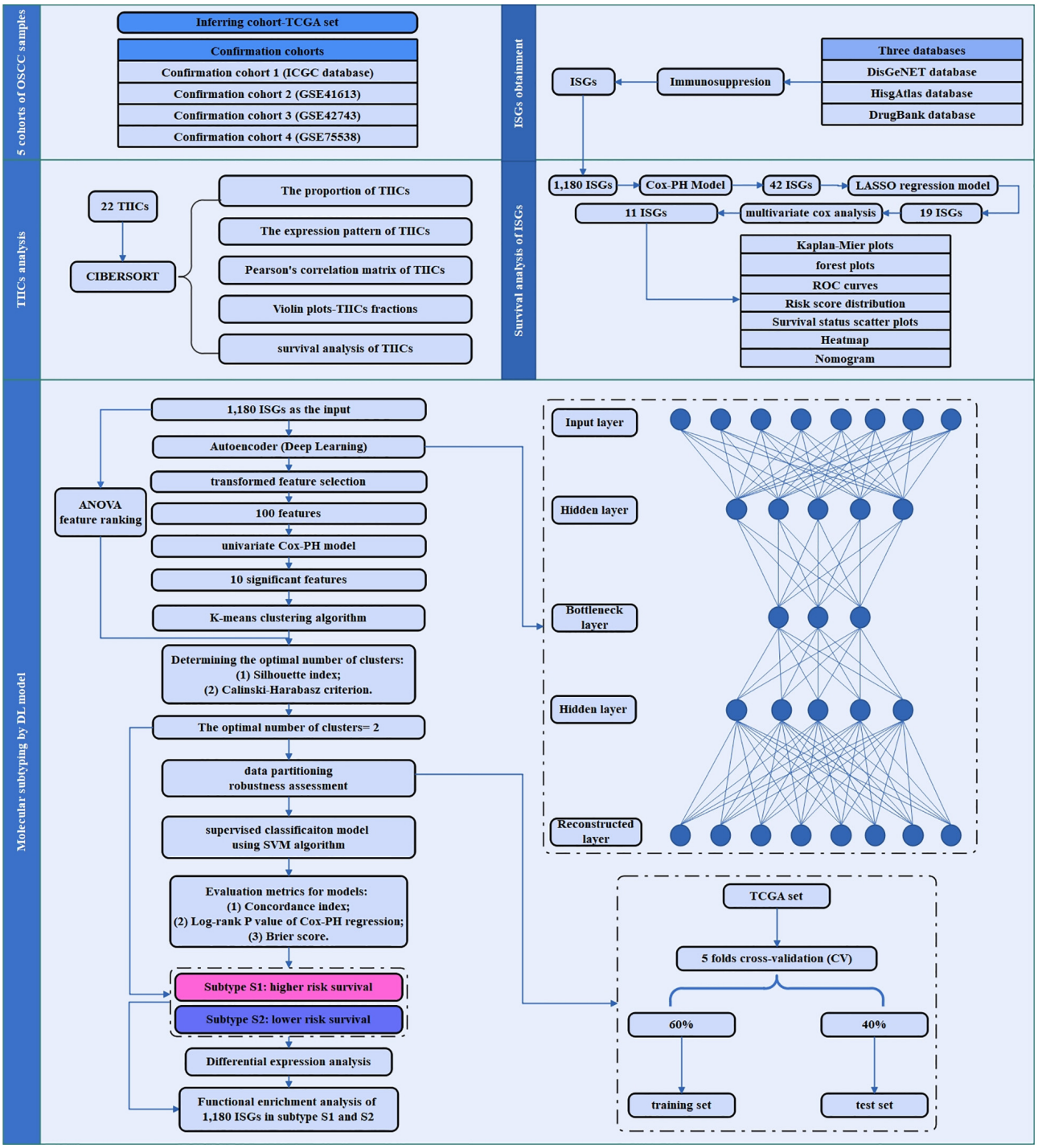

FIGURE 1 | The study flowchart of the current research. This flowchart consisted of five sections: sample data collection of five cohorts of OSCC sample; ISGs obtainment, TIICs analysis, survival analysis of ISGs, and molecular subtyping by DL-based model.

significance level < 0.01 were selected to be survival-associated ISGs. Regarding these survival-related ISGs, least absolute shrinkage and selection operator (LASSO) regression analysis was performed to further screen the genes that were more representative of prognosis. As for the ISGs obtained by LASSO regression analysis, multivariate Cox regression analysis was performed, and Akaike information criterion (AIC) was used for optimizing the statistical model, and the ISGs that were the most representative of prognosis were finally identified and defined as "risk ISGs." Afterward, a series of analyses were

TABLE 1 | The detailed data information (i.e., genes number, sample size in the expression profile, sample size with the clinical information, and events of dead and alive, respectively) of the inferring (TCGA dataset) and cohort datasets (i.e., GSE41613, GSE42743, GSE75538, and ICGC dataset) analyzed in the current research.

Dataset	Genes number	Samples from the expression profile	Samples with clinical information	Events (alive)	Events (dead)
TCGA	19754	335	317	203	114
GSE41613	23516	97	97	46	51
GSE42743	23516	103	71	31	40
GSE75538	20818	28	14	11	3
ICGC	24003	40	40	32	8

performed on the risk ISGs. First, the hazard ratio (HR) and 95% confidence interval (CI) were calculated from the univariate Cox proportional hazards regression model. Cox regression coefficients are directly related to hazard rates, where positive coefficients represent unfavorable prognosis (HR > 0.1) and negative coefficients exert protective effects (HR < 0.1). Based on the HR and CI values, the forest plot for the risk ISGs of the multivariable model was plotted.

Afterward, Kaplan–Meier survival analysis was performed to investigate the prognostic value of the risk ISGs in OSCC; Receiver operating characteristic (ROC) curve analysis by "survivalROC" package in R program was performed to assess the predictive accuracy of these risk ISGs' prognostic value for time-dependent cancer death. In the next step, risk curves analyses were performed to show the relationship between the survival status of patients and the risk score of genes. Multivariate Cox proportional hazards regression model was used to calculate the risk score based on the risk ISGs and the impact of OS information. The risk score of each sample was calculated using the formula of risk score = $\beta 1Exp1 + \beta 2Exp2 + \ldots + \beta xExpx$ (βi, the coefficient value; Expx, the gene expression level). The OSCC patients were classified into low- and high-risk groups according to the median RS survival analysis, and log-rank test was performed to evaluate the differences between the two groups. Furthermore, the nomogram was plotted to show the relationship between the expression levels of risk ISGs and survival time of OSCC patients. Afterward, the four clinical features (i.e., age, gender, risk score, and pathological stage) of OSCC samples were extracted from the TCGA database, ICGC database, and three datasets (i.e., GSE41613, GSE42743, and GSE75538), and thus, the nomogram related to the clinical features was plotted.

The Molecular Subtyping of OSCC Samples

The methods of this section for molecular subtyping of cancer samples mainly followed the methods described in detail by Chaudhary et al. (2017; 12). Briefly, an autoencoder with three hidden layers (500, 100, and 500 nodes, respectively) was implemented, and DL framework was constructed. The initial number (1,180) of ISGs gene features was compressed to 100 new gene features. For each of these transformed new gene features generated by the autoencoder, we built a univariate Cox proportional hazards (Cox-PH) model and selected features from which a significant Cox-PH model was obtained (log-rank $p < 0.05$). These 100 new gene features were used to cluster OSCC samples using the K-means clustering algorithm. The two metrics (Silhouette index and Calinski–Harabasz criterion) were used for determining the optimal number of clusters. The cross-validation (CV)-like procedure was used for data partition of TCGA data: 60% (training set) and 40% (test set). The supervised classification model using SVM algorithm was constructed. Afterward, three sets of evaluation metrics (i.e., Concordance index, log-rank p-value of Cox-PH regression, and Brier score) were used for evaluating the accuracy of survival prediction in the subgroups identified by the above-described methods. In addition, the performances of the DL framework were compared with an alternative approach—principal component analysis (PCA).

The Difference Between Subtypes of OSCC Samples

Based on the subtypes obtained by deep learning algorithm and K-means clustering, the differential expression analysis was performed by using the DESeq2 package (version 1.36.0) (Love et al., 2014) to identify the differentially expressed genes (DEGs) between the varying subtypes ($p < 0.05$, and llogFCl > 1). The heatmap was plotted to show the expression profiling of DEGs expressed in varying subtypes of OSCC. Most importantly, the Gene Set Enrichment Analysis (GSEA) was performed to identify the Kyoto Encyclopedia of Genes and Genomes (KEGG) signaling pathways of 1,180 ISGs in the varying subtypes, respectively. By performing the functional enrichment analysis, the difference between the function of varying subtypes can be identified. The significantly enriched signaling pathways with $p < 0.05$ were selected for the varying subtypes, respectively, and thus, the ISGs pathways for the varying subtypes were constructed by using Cytoscape (version 3.6.1) (Shannon et al., 2003).

Afterward, the protein–protein interaction pairs of 1,180 ISGs were obtained from the Human Protein Reference Database (HPRD; Keshava Prasad et al., 2009), and thus, an ISGs-related PPI network was constructed by using Cytoscape software (version 3.6.1) (Shannon et al., 2003). The DEGs dysregulated between these two subtypes were mapped to this PPI network. The topological characteristics of nodes in this PPI network were analyzed. In addition, the drugs targeting the ISGs were downloaded from the DrugBank database, and thus, an ISGs–target drug interaction network was constructed by using Cytoscape software (version 3.6.1) (Shannon et al., 2003). The DEGs dysregulated between subtypes were mapped to this network.

RESULTS

Tumor-Infiltrating Immune Cells in OSCC Samples

A total of 151 samples, including 148 OSCC samples and 3 healthy control samples, were obtained by selecting samples with a $p < 0.05$ from the CIBERSORT webtool. The proportion of 22 TIICs in each sample is shown in **Figure 2A**. The distribution proportion of macrophages M0, M1, and M2 was obviously shown to be the greatest in most of all samples, indicating that macrophages are playing more critical roles in the development of OSCC than the other types of TIICs.

The heatmap shows the expression levels of 22 TIICs in 151 samples (**Figure 2B**). As clearly observed from **Figure 2B**, macrophages M0 were highly expressed in the OSCC samples, and the other types of cells were downregulated or nearly non-expressed in the OSCC samples. The differential expression of 22 TIICs in 151 samples is shown in **Figure 2C**. In terms of macrophages (i.e., M0, M1, and M2), macrophages M0 occupying the highest fraction (approximately 90%) were significantly highly expressed in OSCC samples compared to the healthy control samples ($p = 0.012$), and macrophages M1 occupying approximately 20% among all immune cells were significantly lowly expressed in OSCC samples compared to the healthy control samples ($p = 0.016$), while macrophage M2 occupying approximately 40% among all immune cells did not show significant expression changes between OSCC samples and healthy control samples ($p = 0.164 > 0.05$). As for the other TIICs except macrophages, naive B cells and regulatory T cells (Treg) were found to be lowly expressed in OSCC samples compared to the healthy control samples [$p = 0.007$ (naive B cells) and p (0.048 (Treg)]. In addition, there were no statistical differences in expression levels between OSCC and healthy control samples and as for memory B cells (p = 0.924), plasma cells ($p = 0.549$), CD8 T cells ($p = 0.479$), naive CD4 T cells ($p = 0.792$), resting memory CD4 T cells ($p = 0.084$), activated memory CD4 T cells ($p = 0.925$), follicular helper T cells ($p = 0.738$), gammadelta T cells ($p = 0.521$), resting natural killer (NK) cells ($p = 0.441$), activated NK cells (p (0.714), resting dendritic cells ($p = 0.049$), activated dendritic cells ($p = 0.0636$), resting mast cells ($p = 0.958$), activated mast cells ($p = 0.978$), eosinophils ($p = 0.924$), and neutrophils ($p = 0.4$).

Figure 2D shows the correlation among TIICs in the pathogenesis of OSCC. The most interesting findings from **Figure 2D** are the negative correlations between macrophage M0 and M2 and between macrophage M0 and M1; however, a positive correlation between macrophage M1 and M2 was observed. Apart from such important finding regarding the three subsets of macrophages, the combination of TIICs with the most obvious correlation was also found and summarized herein: for example, resting NK cells were significantly positively correlated with resting memory CD4 T cells (Pearson correlation value = 0.62); follicular helper T cells were significantly positively correlated with monocytes (Pearson correlation value = 0.55); macrophage M1 was significantly negatively correlated with macrophage M0 (Pearson correlation value = −0.74); and resting

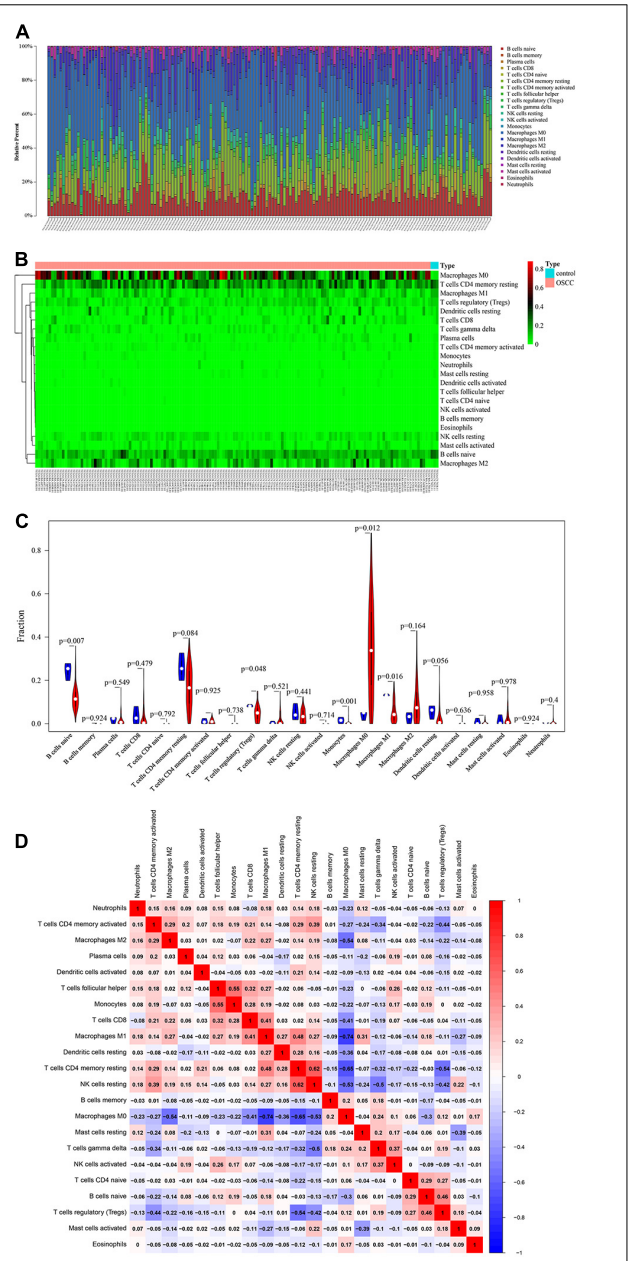

FIGURE 2 | Performance of CIBERORT across TIICs in OSCC. **(A)** The distribution of 22 tumor-infiltrating immune cells (TIICs) in OSCC samples. The abscissa represents the name of 151 samples, and the ordinate represents the composition ratio of the cells in each sample. Different color represents different types of cells. The longer column of each cell in a certain sample indicates that the proportion of this type of cell is higher in this sample. **(B)** Heat map of the 22 TIICs proportions in 148 OSCC and 3 healthy control samples. Each column represents a sample, and each row represents one type of immune cell population. The levels of the immune cell populations are shown in different colors, which transition from green to red with increasing proportions. The abscissa represents the 151 samples: The pink represents the 148 OSCC samples, and the sky blue represents the 3 healthy samples. The ordinate represents the expression levels of TIICs in each sample. In the color bar, green represents the low expression of TIICs in samples, red represents the high expression of TIICs in samples, and black represents that the TIICs were not expressed in the samples, meaning the expression level

(Continued)

FIGURE 2 | Continued
was zero. **(C)** The differential expression status of TIICs in 151 samples. Violin plot of OSCC samples and adjacent healthy samples groups for the target cohort. Red means the OSCC samples group, and blue represents the adjacent healthy samples group; white dots indicate the average expression level of TIICs in all samples. The *p*-value represents the differential expression status of TIICs in OSCC samples compared with healthy samples. The abscissa represents the TIICs, and the ordinate represents the overall expression status of each TIIC in all the 151 samples. **(D)** Correlation matrix of 22 immune cell proportions and immune/stromal score in OSCC. Variables have been ordered by average linkage clustering. For comparison, immune/stromal score has been rescaled to range between zero and one separately in each study. The correlation between TIICs in the pathogenesis of OSCC. Both the abscissa and ordinate represent the 22 types of TIICs. The color bar shows the correlation value of TIICs. Blue means the TIICs were negatively correlated, and red means the TIICs were positively correlated. The darker color means the correlation was more significant. The diagonal line drawn from coordinate (0,22) to coordinate (22,0) has a correlation of 1.

memory CD4 T cells were significantly negatively correlated with macrophage M0 (Pearson correlation value = −0.65). **Supplementary Figure 1** used the Kaplan–Meier curves to show the prognostic values of 22 TIICs for the overall survival of OSCC. Among the 22 TIICs, only one type of TIICs (neutrophils) was significantly related to overall survival ($p = 0.031$), while the other TIICs were not significantly related to the prognosis of OSCC.

Identification of Risk ISGs With Prognostic Values

By performing the univariate analysis, 42 ISGs with $p < 0.01$ were identified (**Supplementary Table 1**). These 42 gene features were reduced to 19 genes (**Figure 3A**) by performing the LASSO regression analysis. As shown in **Figure 3A** (b), when the log (Lambda) = 19, the partial likelihood deviance reached the lowest value. Regarding the 19 genes, multivariate survival analysis was performed, and thus, 11 risk ISGs were identified: CXCL8, TLR3, IL22, ORMDL3, FGFR3, CTLA4, HPRT1, BGLAP, CALCA, SPHK1, and INHBB (**Supplementary Table 2**). The forest plot of these 11 risk ISGs is shown in **Figure 3B**. In addition, Kaplan–Meier curves shown in **Figure 3C** shows that six ISGs (e.g., BGLAP, CTLA4, HPRT1, ORMDL3, SPHK1, and TLR3) were found to be significantly associated with the survival rate of OSCC, showing that the low expression of all these six ISGs has higher survival rate compared with the high expression group. **Figure 3D** uses the time-dependent receiver operating characteristic (ROC) curves to assess the prediction accuracy of the 11 risk ISGs signature. **Supplementary Table 3** shows the C-index values and time-dependent area under the curve (AUC) values of 11 risk ISGs in the ROC curves. In general, the ROC curve showed good performance in survival prediction as for the almost all 11 ISGs' 10-year overall survival (AUC > 0.5 and C-index > 0.5). Specifically, taking ORMDL3 as an example, the AUC values of ORMDL3 gene were shown to be 0.621, 0.68, and 0.71, respectively, for 3, 5, and 10 years. Taking CTLA4 as another example, the AUC values of CTLA4 gene were shown to be 0.571, 0.508, and 0.629, respectively, for 3, 5, and 10 years.

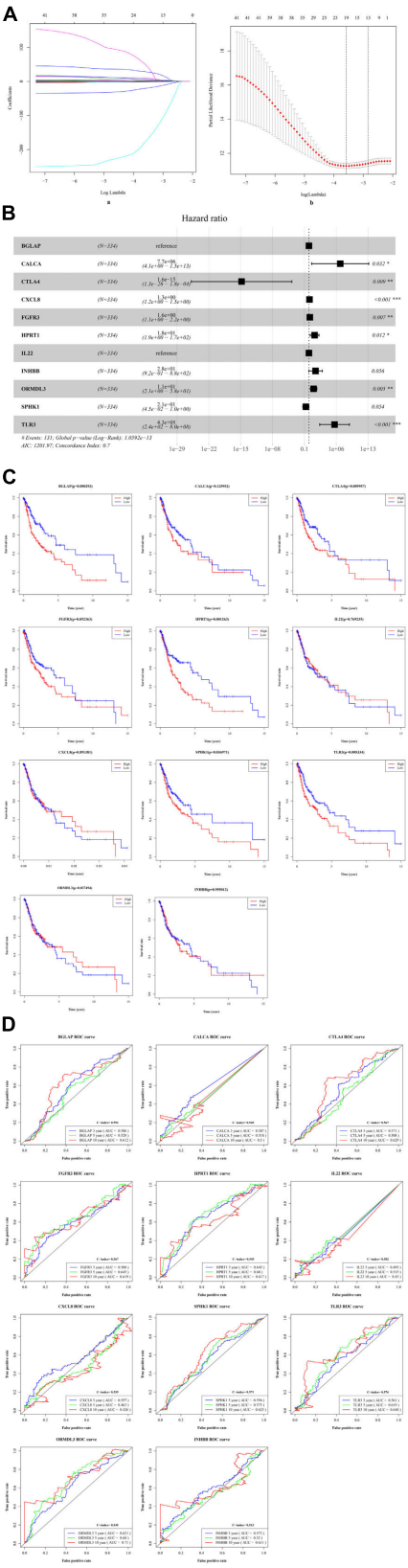

FIGURE 3 | Continued

FIGURE 3 | The identification of ISGs with significant prognostic values in OSCC. **(A)** Demographic and clinical feature selection using the LASSO binary logistic regression model. (a) LASSO coefficient profiles of the 42 gene features. A coefficient profile plot was produced against the log(lambda) sequence. All weights converge toward zero as the penalty parameter increases. Vertical line was drawn at the value selected using fivefold cross-validation, where optimal lambda resulted in five features with non-zero coefficients. (b) Optimal parameter (lambda) selection in the LASSO model used fivefold cross-validation via minimum criteria. The partial likelihood deviance (binomial deviance) curve was plotted versus log(lambda). Dotted vertical lines were drawn at the optimal values by using the minimum criteria and the 1 standard error (SE) of the minimum criteria (the 1-SE criteria). **(B)** The forest plot with hazard ratio (HR) for the 11 risk ISGs. HRs above one indicates that a gene is positively associated with the event probability and thus negatively with survival time. The box size is based on precision, and the x-axis has a logarithmic scale. A bigger box size represents a more precise confidence interval (95% CI). **(C)** The Kaplan–Meier curves of the 11 risk ISGs. Red lines represent high expression group, while blue lines represent low expression group. The upper line indicates the higher survival rate, while the lower line indicates the lower survival rate. **(D)** The time-dependent receiver operating curve (ROC) is generated for the survival prediction of 11 risk ISGs. The time-dependent (3-, 5-, and 10-year) area under curve (AUC) and C-index for each risk ISG are respectively labeled in the lower right corner of each gene's ROC curve.

Figure 4A (a) shows the risk score of all OSCC samples, and **Figure 4A** (b) shows the survival status of each OSCC sample during the follow-up time. Thereby, two genes (i.e., FGFR3 and CXCL8) were found to be highly expressed in the high-risk group. Furthermore, **Figure 4B** uses a nomogram to predict the probability of 1-, 2-, and 3-year overall survival according to the expression pattern of 11 risk ISGs. By adding up the points identified on the point scale for each variable, the total score on the bottom scale shows the probability of survival. **Supplementary Tables 4–8** respectively show the clinical characteristics of the OSCC samples collected from the TCGA database, ICGC database, and three datasets (i.e., GSE41613, GSE42743, and GSE75538). Based on the information obtained from **Supplementary Tables 4–8**, the clinical features-related nomogram was plotted and shown in **Figure 4C**.

Identification of Two Molecular Subtypes of OSCC by Using Deep Learning Framework

The univariate Cox-PH regression model revealed 10 features, which were subjective to K-means clustering with cluster number K ranging from 2 to 10. **Figure 5A** (a) and (b) show the clustering evaluation plots by using the silhouette index and Calinski–Harabasz criterion, respectively. **Figure 5A** indicates that $K = 2$ was the optimal number of clusters with the best evaluation scores for both metrics. Afterward, the two subtypes identified in the above analysis were used as labels to construct an SVM classification model. The parameter settings used in the SVM algorithm and the subsequent autoencoder algorithm are shown in **Supplementary Tables 9**, **10**, respectively. The classification effects of the SVM model were evaluated by assessing C-index to assess the accuracy of the survival subtype predictions and Brier score to calculate the error of the model fitting on survival data. The evaluation effects of the model in TCGA (e.g., training data,

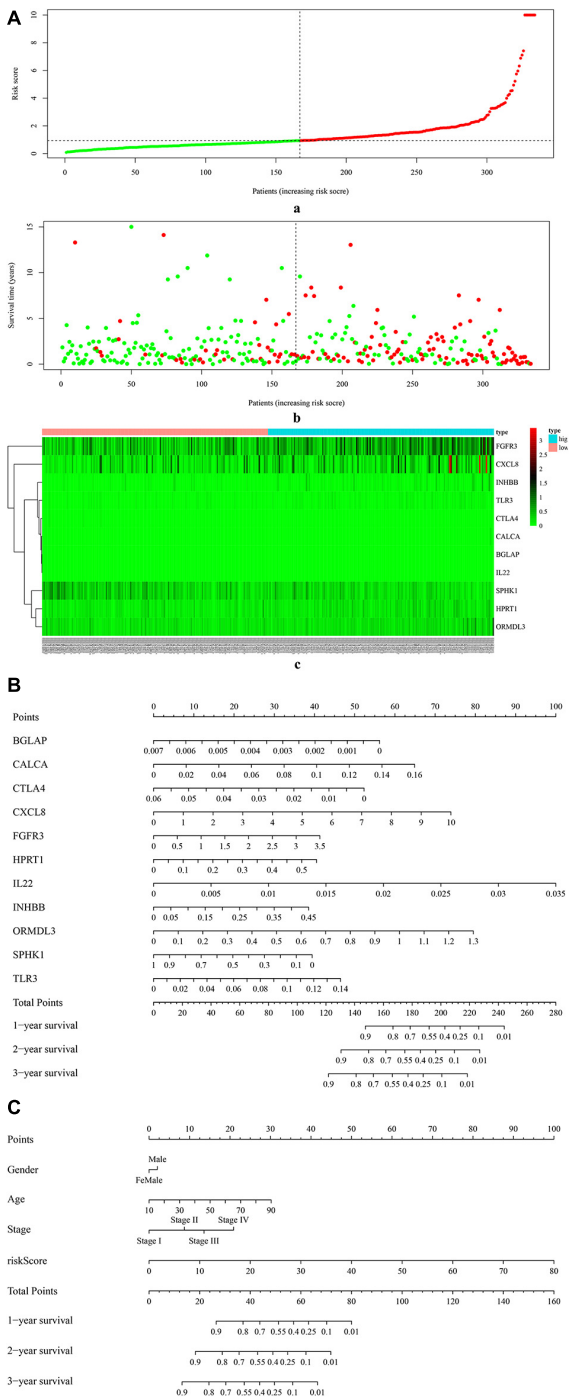

FIGURE 4 | The correlation between 11 risk ISGs and survival of OSCC. **(A)** Prognostic risk score model analysis of 11 risk ISGs in OSCC patients. (a) The distribution of the risk scores in the OSCC sample. The x-axis represents the sample number of OSCC samples; the y-axis represents the risk score corresponding to the sample number. The green part of the curve that is lower than the median value represents the comparatively lower risk of survival, and the red part of the curve that is higher than the median value represents the higher risk of survival. (b) The distribution of patients' survival status in the OSCC sample. The graph is drawn based on whether the final state of each OSCC patient during the follow-up period is alive or dead. The abscissa

(Continued)

FIGURE 4 | Continued
represents the risk score of OSCC patients, and the ordinate represents survival time. Each dot represents an OSCC patient: the red dot represents that the OSCC patient is dead at the final day of follow-up period, whereas the green dot represents that the OSCC patients is still alive at the final day of follow-up period. (c) The 11 risk ISGs expression profiles of patients in the low- and high-risk groups of OSCC samples. Each column represents a OSCC sample, and each row represents the expression profile of each gene within the 11 risk ISGs. The expression levels of the 11 risk ISGs in OSCC samples are shown in different colors, which transition from green to red. The abscissa represents the 148 OSCC samples: pink represents the OSCC samples with low risk of survival, and sky blue represents the OSCC samples with the high risk of survival. The ordinate represents the expression levels of TIICs in each OSCC sample. In the color bar, green represents the low expression of 11 ISGs in samples, red represents the high expression of 11 ISGs in samples, and black represents that the ISGs were not expressed in the OSCC samples, meaning the expression level was zero. **(B)** Nomogram for predicting 1-, 2-, and 3-year probabilities of overall survival in OSCC patients according to the expression level of 11 risk ISGs. The total score was 0–280. Total score of an individual patient is calculated and merged based on each variable. A high score indicates a high risk of survival. A line is drawn upward to determine the score received for each variable value. The sum of these scores is located on the total points axis; then, a line is drawn downward to the survival axes to determine the likelihood of 1-, 2-, or 3-year overall survival. **(C)** Nomogram for predicting 1-, 2-, and 3-year probabilities of overall survival in OSCC patients according to the risk score as well as clinical characteristics of samples (e.g., gender, age, and pathological stage). Total score was 0–160. Total score of an individual patient is calculated and merged based on each variable. A high score indicates a high risk of survival. A line is drawn upward to determine the score received for each variable value. The sum of these scores is located on the total points axis; then, a line is drawn downward to the survival axes to determine the likelihood of 1-, 2-, or 3-year overall survival.

test data, and all data), and four independent confirmation sets (i.e., GSE41613 dataset, GSE42743 dataset, GSE75538 dataset, and ICGC data) are shown in **Supplementary Table 8**.

Figure 5B shows the significant survival differences for the TCGA (a) and the two external confirmation cohorts [GSE41613 (b) and GSE42743 (c)]. For the TCGA set, subtype Sub1 received a lower survival rate compared with the subtype Sub2, showing that subtype Sub1 is more aggressive and represents the higher survival risk. Regarding the two confirmation sets (GSE41613 and GSE42743), the same trend was observed within the beginning years of the observed time (GSE4163, 0–3 years; GSE42743, 0–2 years), and the opposite trend was observed for the later years of observed time. In addition, the performance of the model was compared by using an alternative approach—PCA. **Figure 5C** shows the scatter plots of DL-based model (a) and PCA-based model (b). Obviously shown in **Figure 5C**, the two subtypes of OSCC can be clearly divided by using the DL model [**Figure 5C** (a)]; by contrast, the two subtypes of OSCC cannot be clearly divided by using the PCA model [**Figure 5C** (b)]. By checking the C-index and *p*-value data shown in **Supplementary Table 11**, it can be found that the PCA model produced a lower C-index (0.69) as compared with the DL model (0.77); although the PCA approach can also yield a significant log-rank *p*-value (5.36E-18) in detecting the survival subgroups, the *p*-value produced by the PCA model is still much less significant than that by the DL model (4.91E-22).

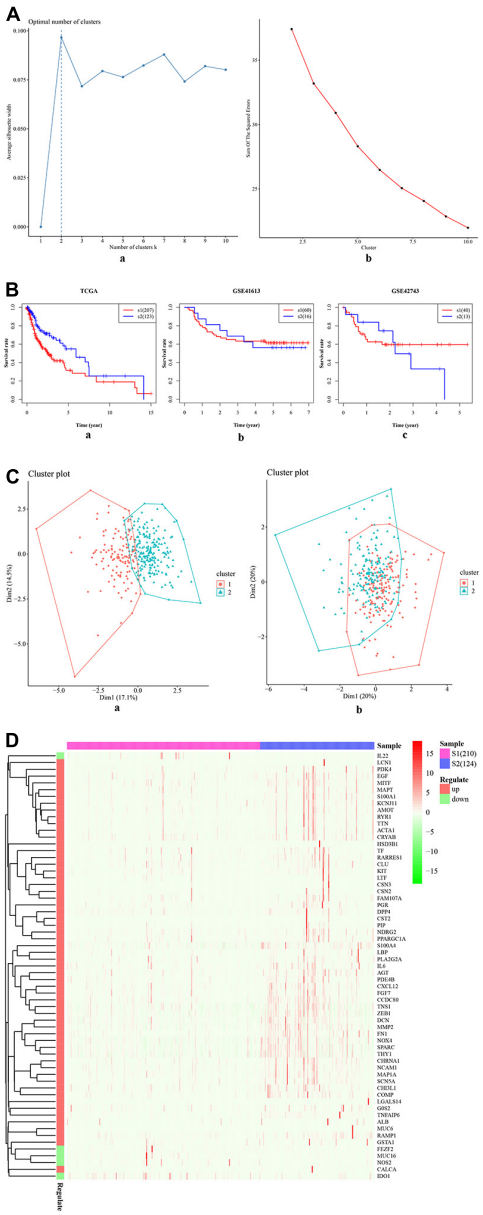

Subtype S1 samples			Subtype S2 samples		
Name of pathway	Genes_(N)	p-val	Name of pathway	Genes_(N)	p-val
Proteasome	8	0	Complement and coagulation cascades	21	0
Pyrimidine metabolism	19	0	Steroid hormone biosynthesis	9	9.80E-04
Neurotrophin signaling pathway	41	0	Neuroactive ligand receptor interaction	40	9.80E-04
Cell cycle	27	0	Cytokine cytokine receptor interaction	129	0.005097
Erbb signaling pathway	36	0	Metabolism of xenobiotics by cytochrome p450	12	0.005964
Nod like receptor signaling pathway	32	0	Arachidonic acid metabolism	18	0.030333
Pathways in cancer	129	0	Cell adhesion molecules cams	39	0.031377
Tight junction	13	0.000985	Tyrosine metabolism	10	0.036327
Apoptosis	32	0.002944	Drug metabolism cytochrome p450	12	0.036437
Adherens junction	20	0.003064			
P53 signaling pathway	19	0.005181			
B cell receptor signaling pathway	36	0.005731			
Base excision repair	13	0.005814			
Mapk signaling pathway	77	0.00675			
Cytosolic dna sensing pathway	19	0.006979			
Insulin signaling pathway	25	0.011011			
Ubiquitin mediated proteolysis	10	0.01506			
T cell receptor signaling pathway	61	0.01626			
Rig i like receptor signaling pathway	24	0.016346			
Purine metabolism	31	0.019569			
Inositol phosphate metabolism	6	0.023329			
Notch signaling pathway	9	0.025432			
Chemokine signaling pathway	74	0.03252			
Adipocytokine signaling pathway	25	0.035176			
Toll like receptor signaling pathway	55	0.04012			
Jak stat signaling pathway	65	0.043216			
Gnrh signaling pathway	25	0.048563			

FIGURE 5 | The two survival subtypes of OSCC differentiated by deep learning-based model. **(A)** The clustering evaluation plots drawn by using the silhouette index (a) and Calinski–Harabasz criterion (b), respectively. (a) The silhouette index values for each number of clusters. The abscissa represents the number of clusters, and the ordinate represents the value of average silhouette width. The plot shows that the highest value of average silhouette
(Continued)

FIGURE 5 | Continued
width occurs at two clusters, suggesting that the optimal number of clusters is two. (b) The Calinski–Harabasz criterion values for each number of clusters. The abscissa represents the number of clusters, and the ordinate represents the value of sum of squared errors. The plot shows that when the clusters = 2, the sum of squared errors arrived at the highest values, indicating that the optimal number of clusters is two. **(B)** The survival differences between two subtypes, respectively, for the TCGA (a) and the two external confirmation cohorts [GSE41613 (b) and GSE42743 (b)]. The red curve represents the subtype Sub1, and the blue curve represents the subtype Sub2. The abscissa represents the follow-up time that was calculated in the number of year, and the ordinate represents the survival rate. The upper line indicates the higher survival rate, while the lower line indicates the lower survival rate. **(C)** The two-dimensional (2D) scatter plots showing the comparisons between deep-learning based method (a) and PCA-based method (b). The abscissa represents the dimension 1 (Dim1), while the ordinate represents the dimension 2 (Dim2). (a) The scatterplot by using top 100 principal components as supposed to 100 hidden nodes in deep learning, followed by the subsequent Cox-PH and K-means clustering. (b) The scatterplot by using deep learning based method. **(D)** The heatmap shows the expression patterns of ISGs–DEGs in two types of samples, i.e., samples of subtype Sub1 and Sub2. The abscissa represents OSCC samples: the rose-red samples represent 210 subtype Sub1 samples, and blue samples represent 124 subtype Sub2 samples. The ordinate represents the ISGs that were also DEGs dysregulated between the two subtypes. Pink represents the upregulated DEGs, and emerald green represents the downregulated DEGs. **(E)** The top list of signaling pathways shows the significantly enriched cancer-related signaling pathways that were enriched by 1,180 ISGs in the samples of subtype Sub1 and Sub2, respectively.

Identification of the Difference Between Varying Subtypes

The DEGs dysregulated between two subtypes are shown in **Supplementary Table 12**, ranked by the ascending order of *p*-value. **Figure 5D** used a heatmap to show the expression pattern of DEGs in the samples of two subtypes. By performing the functional enrichment of 1,180 ISGs in two subtypes, the significantly enriched pathways were selected. Among the enriched pathways, the pathway that was obviously not related to oral cancer were deleted, and the pathways potentially related to OSCC were retained and shown as **Figure 5E**. As seen from **Figure 5E**, the ISGs in subtype Sub1 were mainly enriched in tumor-infiltrating immune cells-related pathways [e.g., B cell receptor (BCR) signaling and T cell receptor (TCR) signaling] and tumor progression-related pathways (e.g., cell cycle, apoptosis, p53, MAPK, Notch, chemokine, Toll-like receptor, and JAK-STAT), whereas the ISGs enriched in subtype 2 were mainly enriched in the metabolism-related pathways (e.g., metabolism of xenobiotics by cytochrome p450, arachidonic acid metabolism, and tyrosine metabolism). Based on the significant pathways listed in **Figure 5E**, the ISGs-pathways interaction network for subtype Sub1 and S2 are shown in **Figures 6A,B**, respectively.

Supplementary Table 13 lists the fold change, $\log_2$(fold change), *p*-values, and adjusted *p*-values of DEGs, which were differentiated between the two subtypes of OSCC samples. In addition, **Figure 7A** shows the ISGs–DEGs-related PPI network, and the topological characteristics of the top 20 DEGs in this network are shown in **Supplementary Table 14**. The PPI network identified several hub genes that play critical roles by targeting the greatest number of other genes, for example, the ISGs-upregulated DEGs (e.g., FN1, ALB, ACTA1, TTN, MAPT, MMP2), the ISGs-downregulated DEGs (e.g., NOS2, MUC16, IDO1, IL22, and FEZF2), and ISGs–non-DEGs (e.g., NTRK1, JUN, TP53, MYC, EGFR, HSP90AA1, and ESR1). Furthermore, the ISGs–target drugs interaction network shown in **Figure 7B** shows that NOS2—the only ISG-downregulated DEGs mapped in this network—was targeted by the drug dexamethasone. In addition, the drug Tretinoin was found to target three ISGs (i.e., LCN1, PDK4, and RARRES1), which were upregulated in subtype Sub1; the ISG-HSD3B1, which was upregulated in subtype Sub1, was found to be targeted by several drugs including hydrocortisone, hydrocortisone valerate, hydrocortisone aceponate, hydrocortisone butyrate, hydrocortisone probutate, hydrocortisone acetate, and trilostane; and the ISG-PGR, which was upregulated in subtype Sub1 was found to be targeted by several drugs including fluticasone, fluticasone furoate, mometasone, mometasone furoate, and fluticasone propionate.

DISCUSSION

The main findings of the present study include several key aspects, such as the correlation between tumor-infiltrating immune cells, identification of 11 ISGs that were significantly related to the overall survival of immunocompromised OSCC patients, signaling pathways differentiating the two key molecular subtypes of OSCC, and the identification of drugs that were targeted by ISGs.

The interaction between immune cells has been explored by many previous studies; however, the synergistic or antagonistic impact of specific immune cells on tumor immunology varies among different cancer types and therefore remains ill defined. Existing evidence strongly supports the findings of the present work; however, contradictory findings have also been reported. Heterogeneity in tumor-intrinsic type, tumor microenvironment (TME), and the tissue specificity in various cancer types may be plausible causes. For instance, considering macrophage M2 phenotype that displays immunosuppressive functions and interplays with other immune cells (e.g., NK cells, Treg, CD8 T cells, and neutrophils) showed a negative correlation with activated NK cells ($p = -0.04$) in our study. A study by Nuñez noted that M2 macrophages can restrain NK cell activation and effector functions, thereby resulting in suppression of IFN-γ production by NK cells with impaired cytotoxic capacity and degranulation ability (Nuñez et al., 2018). Here, a negative correlation between macrophage M2 and Treg in OSCC ($p = -0.22$) was noted, which is contradictory to previous findings shown in other cancer types. A recent study regarding renal cell carcinoma reported synergistic effects between macrophage M2 and Tregs, showing that macrophage M2 played its protumor and immunosuppressive role by releasing cytokines, thereby activating and recruiting Tregs (Davidsson et al., 2020). Another study investigating laryngeal cancer also showed that the combination of a high number of M2 macrophage and Tregs indicated worse prognosis (Sun et al., 2017). Furthermore, the

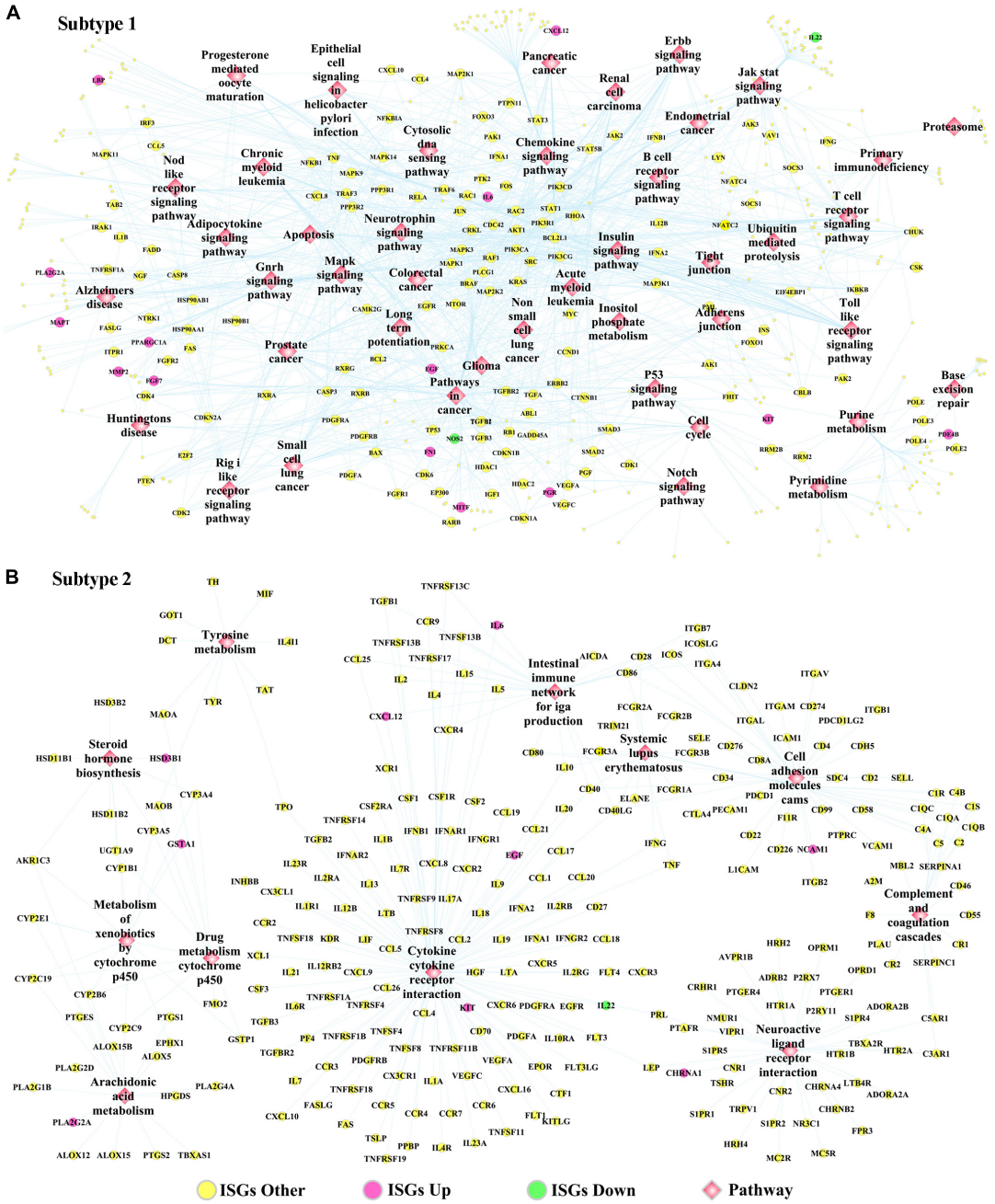

FIGURE 6 | The ISGs-pathways interaction network in OSCC samples of panel **(A)** subtype Sub1 and panel **(B)** subtype Sub2. The rose-red round nodes represent ISGs that were DEGs upregulated between two subtypes of OSCC, the emerald round nodes represent ISGs that were also DEGs downregulated between two subtypes of OSCC, the yellow round nodes represent ISGs that were not DEGs dysregulated between two subtypes of OSCC, and the diamond nodes represent the signaling pathways targeted by ISGs.

present study showed a positive correlation between macrophage M2 and CD8 T cells (p = 0.22), which is contradictory with previous evidence showing that macrophage M2-like TAMs can suppress the recruitment and function of CD8 + T cell, thereby favoring tumor immune escape and driving tumor progression (Dannenmann et al., 2013; Peranzoni et al., 2018; Quaranta and Schmid, 2019). Moreover, the present study showed a positive correlation between macrophage M2 and neutrophils (p = 0.16), similar to earlier reported findings showing both M2-like TAMs and TANs can exert immunosuppressive and protumoral functions and also share overlapping pathways to crosstalk with T cells (Kim and Bae, 2016). Both types of cells can work in a partnership to modulate tumor immunity, thus have been regarded as "partners in crime" (Kumar et al., 2018). Taken

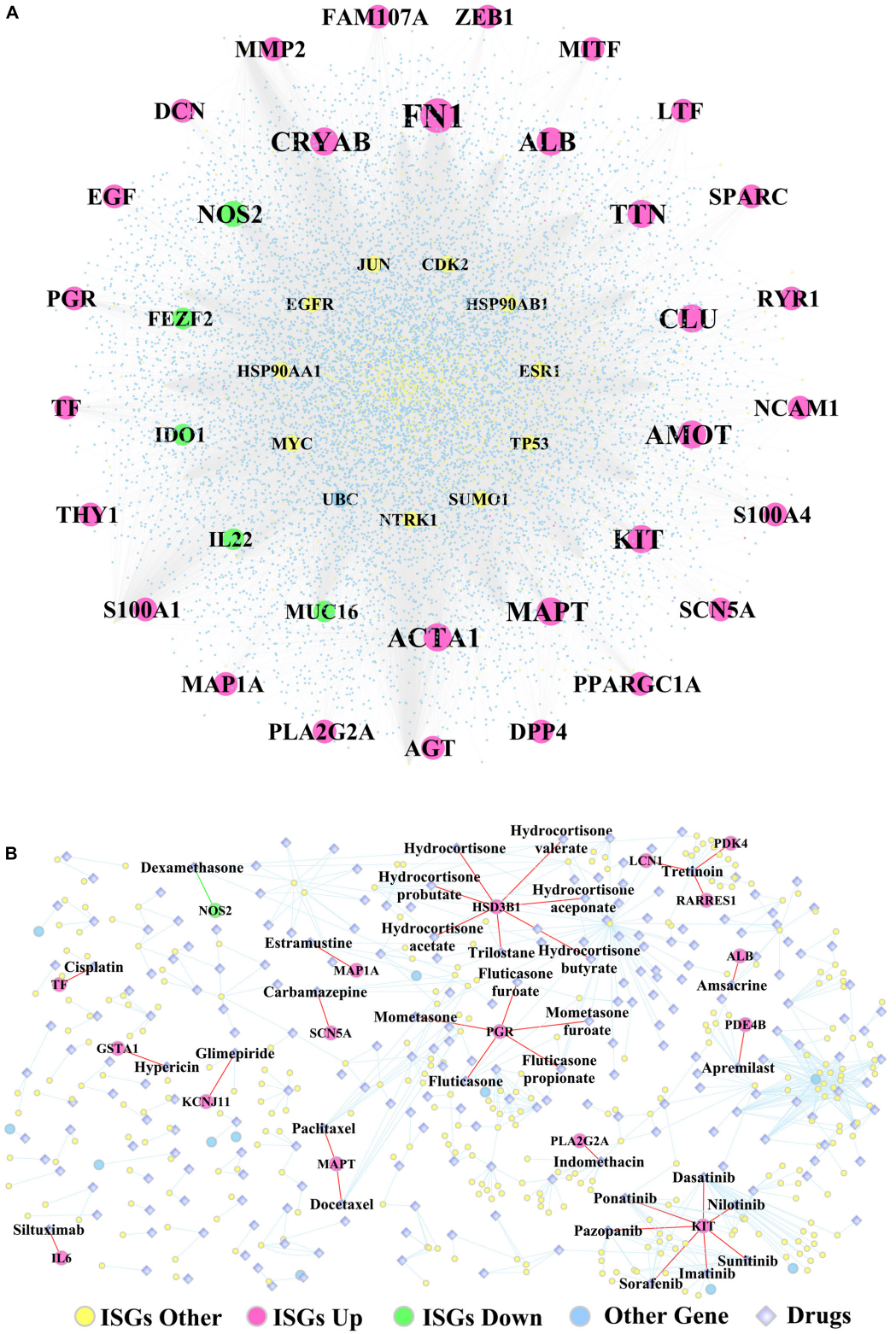

FIGURE 7 | (A) The PPI network constructed by ISGs and **(B)** the ISGs-target drugs regulatory network. The rose-red round nodes represent the ISGs that were DEGs upregulated between two subtypes of OSCC, the emerald round nodes represent the ISGs that were DEGs downregulated between two subtypes of OSCC, the yellow round nodes represent the ISGs that were not DEGs, the sky blue round nodes represent the genes that were not ISGs, and the diamond nodes represent the drugs targeted by ISGs.

together, the research regarding the crosstalk between immune cells in oral cancer immunology is still in progress and needs further investigation.

Another important finding regarding TIICs analysis is the correlation between three phenotypes of macrophages. The current research showed a positive correlation between M1 and M2 and negative correlations between macrophage M0 and M2 and between M0 and M1. Activated macrophages are classified as two subsets with the entirely different functions: M1 macrophages, which are proinflammatory and antitumoral, and M2 macrophages, which are anti-inflammatory and protumoral (Jayasingam et al., 2020). The current research found a positive correlation between M1 and M2, which is contradictory to some previous literature, which is quite variable. Some studies found negative correlation between M1 and M2 by showing that the promotion of M2 macrophage polarization could suppress the M1 macrophage polarization, and vice versa, the inhibition of M2 macrophage polarization could promote the M1 macrophage polarization (Abdelaziz et al., 2020; Peng et al., 2020). However, a previous study regarding breast cancer found a weak correlation between M1 and M2 macrophage densities in central tumor tissue of breast cancer (Schnellhardt et al., 2020). One reason for such contradictory results might be because of the different cancer types studied. Notably, research investigating the correlation between M1 and M2 is limited; however, much of the current cancer research has focused on investigating the M1/M2 ratio and its relationship with prognosis. It has been well concluded that the high infiltration of M1 macrophages and the low infiltration of tumor-infiltrating M2 macrophages are associated with better prognosis (Jayasingam et al., 2020). Another study based on TCGA database of oral cancer data also obtained the same conclusion by showing that a high M2/M1 ratio indicated poor overall survival in human primary oral cancers (Dan et al., 2020). In addition, the current research also found a negative correlation between the non-activated M0 macrophage and activated macrophages (M1 and M2); however, up until now, there is no research evidence showing the correlation between naive non-activated M0 and polarized macrophages M1/M2 phenotype. We speculate that high infiltration of M0 might inhibit the polarization of M0 to M1/2, and vice versa, the high infiltration of M1/M2 might promote the polarization of M0 to M1/2, which warrants validation by future work. Another observation showed a high expression of naive M0 in cancer samples compared with healthy control samples and significantly low expression of M1 macrophage in cancer samples compared to healthy control samples, which in turn confirmed a negative correlation between M0 and M1.

The role of the identified key genes and signaling pathways in regulating immunosuppression of OSCC has been largely validated in previous experimental studies. The survival analysis showed the 11 ISGs (i.e., CXCL8, TLR3, IL22, ORMDL3, FGFR3, CTLA4, HPRT1, BGLAP, CALCA, SPHK1, and INHBB) to be significantly correlated with overall survival in OSCC. Existing evidence has shown that almost all these genes are linked to inhibition of the immune response during the oncopathogenesis in OSCC and are also related to survival in oral cancer. The overexpression of C-X-C motif chemokine ligand 8 (CXCL8, also called IL-8) in OSCC has been related to poor prognostic outcome due to its promoting effect on the generation and infiltration of CD163-positive M2 type tumor-associated macrophages, which can support and exacerbate the immunosuppression by tumor-infiltrating T cells (Hosono et al., 2017). Toll-like receptor 3 (TLR3) stimulation of oral cancer cells can cause tumor progression (Urban-Wojciuk et al., 2019), which is evidenced by the fact that the stimulation of TLR3-expressing oral cancer cells lines (buccal OC2 cancer cells) was found to lead to tumor progression via the production of immunosuppressive factors (Chuang et al., 2012). IL-22 is a cytokine with tumor-promoting properties, which can mediate the attraction of immunosuppressive immune cells and regulate the release of pro- and anti-inflammatory cytokines (Voigt et al., 2017). ORMDL sphingolipid biosynthesis regulator 3 (ORMDL3) can encode a protein that belongs to a family of transmembrane proteins of the endoplasmic reticulum and is found to be involved in the activation of the immune system by regulating calcium signaling (Carreras Sureda, 2014). Fibroblast growth factor receptor 3 (FGFR3), a member of the fibroblast growth factor receptor (FGFR) family (FGFR 1–4), has been found to be frequently overexpressed in OSCC (Koole et al., 2016). Using an FGFR inhibitor to block the binding between FGFR and its ligand FGF was found to remodel the immune microenvironment of tumors by inducing new T-cell responses and in turn work synergistically with PD1 inhibitor in promoting antitumor immunity (Palakurthi et al., 2019). However, a previous study obtained conflicting results showing that the overexpression of FGFR3 protein was not related to overall survival or disease-free survival in OSCC (Koole et al., 2016).

In addition, ISGs with prognostic values also included CTLA4, HPRT1, BGLAP, CALCA, SPHK1, and INHBB. The blockade of cytotoxic T lymphocyte-associated antigen 4 (CTLA4) was demonstrated to decrease the number of immunosuppressed cells [e.g., myeloid-derived suppressor cells (MDSCs) and M2 macrophages] and further enhance the activation of T cells, thereby suggesting a novel therapeutic target for treating OSCC (Yu et al., 2016). The overexpression of hypoxanthine phosphoribosyltransferase 1 (HPRT1) can contribute to the formation of an immunosuppressive tumor microenvironment by significantly reducing the activation of immune cells (B cells, CD8 + T cells, CD4 + T cells, macrophages, and neutrophils) (Townsend et al., 2019). There is still no research reporting the involvement of bone gamma-carboxyglutamate protein (BGLAP, also named osteocalcin) in oral cancer. The uncarboxylated form of osteocalcin (GluOC) was found to suppress tumor growth of melanoma through immunostimulatory effects via increasing T-cell proliferation and promoting the interferon-γ production (Hayashi et al., 2017). Calcitonin-related polypeptide alpha (CALCA, also named as CGRP) was shown to suppress the immune reactions by inhibiting the production of tumor necrosis factor-α and interferon-γ by T helper type 1 cells via elevating intracellular cAMP levels (Kawamura et al., 1998) and impairing the capacity of Langerhans cells in stimulating the T cells proliferation (Hosoi et al., 1993). Sphingosine kinase 1 (SPHK1)-involved SphK–S1P–S1PR signaling axis was found to mediate immunosuppressive effects by affecting lymphocyte trafficking,

activating innate immune cells and inflammation, and directing T-cell differentiation (Chi, 2011). The inhibin subunit beta B (INHBB) gene encodes a member of the transforming growth factor-beta (TGF-β) superfamily. TGF-β has been well accepted as an immunosuppressive cytokine in cancer progression, which can suppress the expression of chemokine receptor CXC motif 3 (CXCR3) in CD8 + T cells and thus limit the tumor trafficking (Gunderson et al., 2020).

Apart from the prognosis-related ISGs described above, the tumor-infiltrating immune cells-related pathways and tumor progression-related pathways (TCR, BCR, p53, JAK-STAT, MAPK, and Notch) enriched in subtype Sub1 cancer samples were identified to predict worse survival in OSCC. Past work has highlighted the potential functions of these worse prognosis-related pathways in the immunosuppression in OSCC. The prognostic values of tumor-infiltrating T cells and B cells in OSCC have been widely accepted by cancer immunology researchers (O'Higgins et al., 2018; Taghavi et al., 2018). TCRs complex (e.g., costimulatory and coinhibitory receptors)-initiated TCR signaling has been demonstrated to play significant roles in regulating immune response, particularly in terms of the activation, differentiation, proliferation, and survival of T cells; thus, it might be a therapeutic target for immune suppression (Hwang et al., 2020). B cell receptor (BCR)-mediated calcium flux was found to play a crucial role in immunosuppression by promoting the secretion of an immunosuppressive cytokine—IL-10 in B cells (Klinker and Lundy, 2012). The mutant p53 was found to promote the development of tumorigenesis by interfering with the function of the cytoplasmic DNA sensing machinery pathway cGAS-STING-TBK1-IRF3 and further suppressing the innate immune response (Cooks et al., 2018). The transduction of Janus kinase-signal transducer and activator of transcription (JAK-STAT) signaling can lead to the production of the protumor cytokines [e.g., IL-1, IL-17, IL-10, TGF-β, vascular endothelial growth factor (VEGF)], which can promote tumor immunogenicity and inhibit the antitumor immune response (Owen et al., 2019). Mitogen-activated protein kinase (MAPK) signaling has been shown to inhibit the expression of negative immune checkpoints [e.g., programmed death-ligand 1 (PD-L1) and cytotoxic T-lymphocyte-associated protein 4 (CTLA-4)] and T-cell costimulatory molecules [e.g., tumor necrosis factor receptor superfamily member 4, and 9 (TNFRSF4, TNFRSF9)]; therefore, the inhibition of MAPK signaling is promising for combined use with T-cell-dependent immunotherapy for antitumor treatment (Kumar et al., 2020). The Notch pathway was found to be a multifaceted regulator of immune-suppressive cells—myeloid-derived suppressor cells (MDSCs); thus, inhibiting MDSCs by targeting the Notch pathway might be a novel immunotherapeutic strategy of cancer treatment (Hossain et al., 2018). In addition, the Notch pathway was shown to play a pivotal role in maintaining the stemness of cancer stem cells in tongue cancers and has prognostic value in OSCC (Upadhyay et al., 2016).

It is worthwhile to note that the signaling pathways enriched in subtype Sub1 and Sub2 were quite different, and metabolic pathways were mainly enriched in subtype Sub2. It has been well demonstrated that the dysregulated metabolic pathways of cancer cells could result in enhanced nutrient uptake, decreased oxygen (hypoxia), and increased acidity of extracellular milieu, and a shortage of nutrition, and the upregulation of protumor metabolite production (Jiang et al., 2020). All these alterations contribute greatly to an immunosuppressive TME, thereby impairing the antitumor immune response and further promoting the tumor progression (Biswas, 2015). Targeting metabolic pathways is therefore an immunotherapeutic approach to inhibit the tumor progression via restoring the TME environment (Shi et al., 2020). In the present study, several signaling pathways related to metabolism were mainly enriched in subtype Sub2, for example, tyrosine metabolism, cytochrome p450 metabolism, and arachidonic acid metabolism. The downregulation of tyrosine metabolism pathway-related genes (HPD, HGD, GSTZ1, and FAH) was observed in hepatocellular carcinoma and indicated poor prognosis (Nguyen et al., 2020); however, investigation of dysregulation of tyrosine metabolism pathways in OSCC is lacking. In addition, the inhibitor of tyrosine kinase, Imatinib, was shown to play both immunostimulatory and immunosuppressive role in the tumor immunology, an immunostimulatory role by stimulating the ability of dendritic cells and NK cells, and an immunosuppressive role by inhibiting the proliferation of T cells (Nishioka et al., 2011). In terms of the cytochrome p450 (CYP) metabolism pathway, the polymorphisms of CYP-involved genes (e.g., CYP26B1, CYP1A1, CYP2A6, and CYP2E1) have been found to activate areca nut (AN)-derived nitrosamines, thereby significantly increasing the susceptibility to tobacco-induced oral cancer (Lin et al., 2013). Considering the arachidonic acid metabolism (AAM) pathway, its mutation was shown to suppress the progression of oral cancer by downregulating it downstream PI3K-Akt pathway and was also predicted to indicate a better disease-free survival (Biswas et al., 2014). Together, these reports lend support to our findings.

Considering targeting drugs, the present study found that dysregulated ISGs that were differentially expressed between subtypes Sub1 and Sub2 were mapped to some target drugs, e.g., downregulated ISG-NOS2 targeting dexamethasone and target drug Tretinoin targeting three upregulated ISGs (e.g., PDK4, LCN1, and RARRES1). The overexpression of the inducible NO synthase including INOS and NOS2 has been documented to predict poor survival outcome in multiple cancers, based on the its involvement in immunosuppression by altering the tumor microenvironment and resulting in the resistance to the inhibitor of immune-checkpoint genes (Ekmekcioglu et al., 2017). However, the expression level and regulating function of NOS2 varies a lot depending on the cancer type; for example, the downregulation of NOS2 in the subtype 1 of OSCC was associated with the worse survival in the present study. The target drug dexamethasone has been found to mediate T cells-mediated immunosuppression by inhibiting the expression of inducible NOS2 and upregulating the expression of the immune-checkpoint gene CTLA-4 (Korhonen et al., 2002; Giles et al., 2018); therefore, using an antagonist of dexamethasone might be an immunotherapy approach for improving the survival outcome in immunocompromised patients with OSCC. For another example, the drug tretinoin (also named as all trans

retinoic acid) targeting three ISGs (PDK4, ICN1, RARRES1) was shown to dramatically reduce the presenter of immature myeloid cells, which promoted immunosuppression by increasing the production of reactive oxygen species, and thus contributed greatly to tumor progression (Kusmartsev et al., 2003; Wu et al., 2019). As one of the genes targeting tretinoin, the overexpression of pyruvate dehydrogenase kinase 4 (PDK4) was found to promote tumor cells proliferation and invasion by negatively regulating the IL-10 expression in macrophages and thus indicated poor prognosis (Atas et al., 2020; Na et al., 2020), which was in accordance with results obtained in the present study. As another gene targeting tretinoin, the Lipocalin 1 (LCN1) was found highly expressed in cholangiocarcinoma and its overexpression indicated poor survival outcome (Tian et al., 2018); however, its involvement in tumor immunosuppression has not yet been explored. Another gene targeting tretinoin, the retinoic acid receptor responder 1 (RARRES 1) gene, was found to play tumor suppressive function by negatively regulating metastasis (Huebner et al., 2017); however, its immunological function in oral cancer has not yet been researched. The target drugs highlighted through deep learning merit further experimental research.

Additionally, the potential applications of the present research findings in precision medicine need to be highlighted. In the past decade, much cancer research has been largely focused on identifying certain critical genetic/epigenetic biomarkers involved in cancers (Tao et al., 2017; Brenner, 2019); however, stratifying cancer patients according to the genetic biomarkers-defined subgroups can be of high clinical value. Cancer patients' response to the same therapeutic treatment is notably variable. Some show worse survival, while others show better outcomes. There is therefore a strong necessity to define the molecular subtypes of cancer patients and their association with prognosis (Téllez-Gabriel et al., 2013; Kim et al., 2019). Cancer precision treatment paradigm should be shifted from a biomarkers-based paradigm to a subtyping-based paradigm, and tandem research has also shifted from identification of certain critical genetic targets to detection of subtype-specific genetic targets (Dienstmann et al., 2017; Torres and Grippo, 2018; Zhao S. et al., 2020). Based on such shift in the precision medicine paradigm, increasing number of studies apply molecular subtyping to establish treatment paradigms incorporating a precision medicine approach in cancer treatment (Zhao et al., 2018; Jiang et al., 2019; Lin et al., 2019). The present research aimed to provide OSCC subtypes that can enable treatment regimes targeting specific molecules and also refine prognosis. Here, we devised a deep learning-based model and provided a simplified approach to successfully stratify compromised OSCC patients into two different treatment arms according to their molecular subtypes with different prognosis. This subclassification approach provided in the present research has potential clinical transfer value by enabling drug selection guidance. In the context of the current research, treatment approach for the two subtypes can be varied: subtype 1 could be treated with drugs targeting the tumor-infiltrating immune cells-related pathways (TCR and BCR) and tumor progression-related pathways (p53, JAK-STAT, MAPK, and Notch); subtype 2 could be treated with metabolism-related pathways, particularly tyrosine metabolism, cytochrome p450 metabolism, and arachidonic acid metabolism. The development of such treatment strategy has the potential to improve OSCC outcomes.

It is essential to state the strengths and limitations of the present research clearly. The greatest strength is that deep machine learning, an artificial intelligence approach, was used in combination with bioinformatics for subtype discovery of oral cancer. The discovery of oral cancer subtypes can benefit targeted therapy for different subtypes of cancer patients and guide the precision medicine in oral cancer. Another strength is that this research was focused on investigating the involvement of immune suppression in OSCC from different aspects, such as immune cells, ISGs related to overall survival, target drugs of ISGs involved in OSCC, and the ISGs-involved signaling pathways used for differentiating two subtypes of OSCC. The present study has two main limitations. First, the findings shown in this study were obtained by computational analysis and not yet verified by performing molecular biology experiments. Second, the synergistic relationship between the ISGs-targeting drugs and commonly used chemotherapeutic drugs used for treating OSCC was not investigated by designing a drug synergy prediction model. However, the investigation of this topic could be regarded as another separate study and comprises our subsequent research plan.

The current findings have several future implications and potential clinical transfer value. First, the genetic mechanisms of ISGs OSCC identified in this study provide a theoretical basis and research direction for future studies. Future research can select the most critical ISGs for experimental studies aimed at investigating the regulating role of these ISGs in influencing oral cancer cell lines and immune cells (e.g., macrophages, neutrophils, and T cells) in cancer cells—immune cells coculture systems—and also investigating the effects of ISGs-targeting drugs on promoting the functions of immune cells and their antitumor effects. Studying the synergistic/antagonistic relationship between ISGs-targeting drugs and common chemotherapeutic drugs will help identify novel treatment strategies for immune–chemotherapy combination drugs. Second, the two subtypes of OSCC discovered by using deep machine learning could be beneficial for designing precision treatment plans for OSCC patients. OSCC patients with molecular subtype 1 could be specially treated with drugs with the role of targeting tumor immunology and progression, whereas the patients with subtype 2 could be particularly treated with drugs targeting metabolism. Such findings could guide the oral and maxillofacial clinicians to select the right target chemotherapeutic drugs and further increase the survival time of OSCC patients.

CONCLUSION

Eleven immunosuppression genes (CXCL8, TLR3, IL22, ORMDL3, FGFR3, CTLA4, HPRT1, BGLAP, CALCA, SPHK1, and INHBB) were identified as significantly related to the

prognosis of OSCC in immunosuppressed patients. A deep learning-based model was able to differentiate OSCC patients into two survival subtypes: a subtype with a lower probability of survival and a subtype with a higher probability of survival. Several immunosuppression-involved signaling pathways (e.g., T cell and B cell receptor signaling, p53, Notch, JAK-STAT, and MAPK) enriched in the aggressive subtype of OSCC suggested therapeutic targets, which could be valuable for treating OSCC in immunosuppressed patients and improving the overall survival in specific groups of patients.

DATA AVAILABILITY STATEMENT

Publicly available datasets were analyzed in this study. This data can be found here: GSE41613 (https://www.ncbi.nlm.nih.gov/geo/query/acc.cgi?acc=GSE41613), GSE42743 (https://www.ncbi.nlm.nih.gov/geo/query/acc.cgi?acc=GSE42743), and GSE75538 (https://www.ncbi.nlm.nih.gov/geo/query/acc.cgi?acc=GSE75538).

AUTHOR CONTRIBUTIONS

SL: conceptualization, funding acquisition, methodology, formal analysis, and writing—original draft. ZM and WG: methodology, formal analysis, and writing—original draft. AO, AA, GP, and WN: methodology, formal analysis, and writing—review and editing. XL and YD: data curation, formal analysis, methodology, resources, software, and visualization. HL: formal analysis and methodology. BL: formal analysis and methodology. VS: formal analysis and methodology. RZ: methodology and writing—review and editing. DZ, GS, HW, HX, and JZ: project administration, supervision, and writing—review and editing. All authors contributed to the article and approved the submitted version.

FUNDING

We appreciate the funding by the Science Research Cultivation Program of Stomatological Hospital, Southern Medical University (No. PY2020004), which was provided to support the postdoc research of SL.

SUPPLEMENTARY MATERIAL

The Supplementary Material for this article can be found online at: https://www.frontiersin.org/articles/10.3389/fcell.2021.687245/full#supplementary-material

Supplementary Figure 1 | The Kaplan-Meier curves of the 22 TIICs. Red lines represent high expression group, while blue lines represent low expression group. The upper line indicates the higher survival rate, while the lower line indicates the lower survival rate. Among these 22 TIICs, only neutrophils have significant prognostic values in OSCC ($p = 0.031$), while the other 21 TIICs doesn't have significant prognostic values ($p > 0.05$).

Supplementary Table 1 | The 42 prognosis-related ISGs with *p*-value less than 0.01, ranked in the ascending order of *p*-value.

Supplementary Table 2 | The 11 risk ISGs with the prognostic values in OSCC, ranked in the ascending order of *p*-value.

Supplementary Table 3 | The C-index values and time-dependent AUC values of 11 prognosis-related ISGs shown in the ROC curves.

Supplementary Table 4 | The clinical characteristics of OSCC samples ($n = 317$) from TCGA database.

Supplementary Table 5 | The clinical characteristics of OSCC samples ($n = 40$) from ICGC database.

Supplementary Table 6 | The clinical characteristics of OSCC samples ($n = 97$) from GSE41613 dataset.

Supplementary Table 7 | The clinical characteristics of OSCC samples ($n = 71$) from GSE42743 dataset.

Supplementary Table 8 | The clinical characteristics of OSCC samples ($n = 14$) from GSE75538 dataset.

Supplementary Table 9 | The parameter settings of the SVM algorithm.

Supplementary Table 10 | The parameter settings of the autoencoder algorithm.

Supplementary Table 11 | The performance of the SVM classifier on training and test set in TCGA cohort, as well as the four external confirmation cohorts.

Supplementary Table 12 | The model performance comparison between Deep learning-based model with the PCA-based model.

Supplementary Table 13 | The all DEGs dysregulated between the two subtypes of OSCC samples, ranked by the ascending order of *p*-value.

Supplementary Table 14 | The topological characteristics of the nodes in the ISGs-DEGs related PPI network. The listed nodes in this table include the top 20 ISGs-upregulated DEGs, top 20 ISGs-downregulated DEGs, and top 20 ISGs-non-DEGs.

REFERENCES

Abdelaziz, M. H., Abdelwahab, S. F., Wan, J., Cai, W., Huixuan, W., Jianjun, C., et al. (2020). Alternatively activated macrophages; a double-edged sword in allergic asthma. *J. Transl. Med.* 18:58.

Asuntha, A., and Srinivasan, A. (2020). Deep learning for lung Cancer detection and classification. *Multimed. Tools Appl.* 79, 7731–7762. doi: 10.1007/s11042-019-08394-3

Atas, E., Oberhuber, M., and Kenner, L. (2020). The Implications of PDK1–4 on Tumor Energy Metabolism, Aggressiveness and Therapy Resistance. *Front. Oncol.* 10:583217. doi: 10.3389/fonc.2020.583217

Biswas, N. K., Das, S., Maitra, A., Sarin, R., and Majumder, P. P. (2014). Somatic mutations in arachidonic acid metabolism pathway genes enhance oral cancer post-treatment disease-free survival. *Nat. Commun.* 5: 5835.

Biswas, S. K. (2015). Metabolic reprogramming of immune cells in cancer progression. *Immunity* 43, 435–449. doi: 10.1016/j.immuni.2015.09.001

Brenner, C. (2019). Applications of Bioinformatics in Cancer. *Cancers* 11:1630. doi: 10.3390/cancers11111630

Carreras Sureda, A. (2014). *Modulation of T Lymphocite Activation by ORMDL3*. Ph.D. thesis Spain: Universitat Pompeu Fabra.

Chang, J., Sunwoo, J. B., Shah, J. L., Hara, W., Hong, J., Colevas, A. D., et al. (2020). Association Between Immunosuppression and Outcomes in Oral Cavity Squamous Cell Carcinoma. *Otolaryngol. Head Neck Surg.* 164, 1044–1051. doi: 10.1177/0194599820960146

Chaudhary, K., Poirion, O. B., Lu, L., and Garmire, L. X. (2018). Deep Learning-Based Multi-Omics Integration Robustly Predicts Survival in Liver Cancer. *Clin. Cancer Res.* 24, 1248–1259. doi: 10.1158/1078-0432.CCR-17-0853

Chen, B., Khodadoust, M. S., Liu, C. L., Newman, A. M., and Alizadeh, A. A. (2018). Profiling Tumor Infiltrating Immune Cells with CIBERSORT. *Methods Mol. Biol.* 1711, 243–259. doi: 10.1007/978-1-4939-7493-1_12

Chi, H. (2011). Sphingosine-1-phosphate and immune regulation: trafficking and beyond. *Trends Pharmacol. Sci.* 32, 16–24. doi: 10.1016/j.tips.2010.11.002

Chuang, H. C., Huang, C. C., Chien, C. Y., and Chuang, J. H. (2012). Toll-like receptor 3-mediated tumor invasion in head and neck cancer. *Oral Oncol.* 48, 226–232. doi: 10.1016/j.oraloncology.2011.10.008

Cooks, T., Pateras, I. S., Jenkins, L. M., Patel, K. M., Robles, A. I., Morris, J., et al. (2018). Mutant p53 cancers reprogram macrophages to tumor supporting macrophages via exosomal miR-1246. *Nat. Commun.* 9:771.

Dan, H., Liu, S., Liu, J., Liu, D., Yin, F., Wei, Z., et al. (2020). RACK1 promotes cancer progression by increasing the M2/M1 macrophage ratio via the NF−κB pathway in oral squamous cell carcinoma. *Mol. Oncol.* 14, 795–807. doi: 10.1002/1878-0261.12644

Dannenmann, S. R., Thielicke, J., Stöckli, M., Matter, C., Von Boehmer, L., Cecconi, V., et al. (2013). Tumor-associated macrophages subvert T-cell function and correlate with reduced survival in clear cell renal cell carcinoma. *Oncoimmunology* 2:e23562. doi: 10.4161/onci.23562

Davidsson, S., Fiorentino, M., Giunchi, F., Eriksson, M., Erlandsson, A., Sundqvist, P., et al. (2020). Infiltration of M2 Macrophages and Regulatory T Cells Plays a Role in Recurrence of Renal Cell Carcinoma. *Eur. Urol. Open Sci.* 20, 62–71. doi: 10.1016/j.euros.2020.06.003

Dienstmann, R., Vermeulen, L., Guinney, J., Kopetz, S., Tejpar, S., and Tabernero, J. (2017). Consensus molecular subtypes and the evolution of precision medicine in colorectal cancer. *Nat. Rev. Cancer* 17, 79–92. doi: 10.1038/nrc.2016.126

Ekmekcioglu, S., Grimm, E. A., and Roszik, J. (2017). Targeting iNOS to increase efficacy of immunotherapies. *Hum. Vaccin. Immunother.* 13, 1105–1108. doi: 10.1080/21645515.2016.1276682

Giles, A. J., Hutchinson, M.-K. N., Sonnemann, H. M., Jung, J., Fecci, P. E., Ratnam, N. M., et al. (2018). Dexamethasone-induced immunosuppression: mechanisms and implications for immunotherapy. *J. Immunother. Cancer* 6, 1–13.

Gunderson, A. J., Yamazaki, T., McCarty, K., Fox, N., Phillips, M., Alice, A., et al. (2020). TGFβ suppresses CD8+ T cell expression of CXCR3 and tumor trafficking. *Nat. Commun.* 11:1749. doi: 10.1038/s41467-020-15404-8

Hayashi, Y., Kawakubo-Yasukochi, T., Mizokami, A., Hazekawa, M., Yakura, T., Naito, M., et al. (2017). Uncarboxylated Osteocalcin Induces Antitumor Immunity against Mouse Melanoma Cell Growth. *J. Cancer* 8, 2478–2486. doi: 10.7150/jca.18648

Hosoi, J., Murphy, G., Egan, C., Lerner, E., Grabbe, S., Asahina, A., et al. (1993). Regulation of Langerhans cell function by nerves containing calcitonin gene-related peptide. *Nature* 363, 159–163. doi: 10.1038/363159a0

Hosono, M., Koma, Y.-I., Takase, N., Urakawa, N., Higashino, N., Suemune, K., et al. (2017). CXCL8 derived from tumor-associated macrophages and esophageal squamous cell carcinomas contributes to tumor progression by promoting migration and invasion of cancer cells. *Oncotarget* 8, 106071–106088. doi: 10.18632/oncotarget.22526

Hossain, F., Majumder, S., Ucar, D. A., Rodriguez, P. C., Golde, T. E., Minter, L. M., et al. (2018). Notch signaling in myeloid cells as a regulator of tumor immune responses. *Front. Immunol.* 9:1288. doi: 10.3389/fimmu.2018.01288

Huebner, H., Strick, R., Wachter, D., Kehl, S., Strissel, P., Schneider-Stock, R., et al. (2017). Hypermethylation and loss of retinoic acid receptor responder 1 expression in human choriocarcinoma. *J. Exp. Clin. Cancer Res.* 36, 1–12.

Hwang, J.-R., Byeon, Y., Kim, D., and Park, S.-G. (2020). Recent insights of T cell receptor-mediated signaling pathways for T cell activation and development. *Exp. Mol. Med.* 52, 750–761. doi: 10.1038/s12276-020-0435-8

Jayasingam, S. D., Citartan, M., Thang, T. H., Mat Zin, A. A., Ang, K. C., and Ch'ng, E. S. (2020). Evaluating the polarization of tumor-associated macrophages into M1 and M2 phenotypes in human cancer tissue: technicalities and challenges in routine clinical practice. *Front. Oncol.* 9:1512. doi: 10.3389/fonc.2019.01512

Jewett, A., Head, C., and Cacalano, N. A. (2006). Emerging mechanisms of immunosuppression in oral cancers. *J. Dent. Res.* 85, 1061–1073. doi: 10.1177/154405910608501201

Jiang, L., Xiao, Y., Ding, Y., Tang, J., and Guo, F. (2019). Discovering Cancer Subtypes via an Accurate Fusion Strategy on Multiple Profile Data. *Front. Genet.* 10:20. doi: 10.3389/fgene.2019.00020

Jiang, Z., Hsu, J. L., Li, Y., Hortobagyi, G. N., and Hung, M.-C. (2020). Cancer cell metabolism bolsters immunotherapy resistance by promoting an immunosuppressive tumor microenvironment. *Front. Oncol.* 10:1197. doi: 10.3389/fonc.2020.01197

Kawamura, N., Tamura, H., Obana, S., Wenner, M., Ishikawa, T., Nakata, A., et al. (1998). Differential effects of neuropeptides on cytokine production by mouse helper T cell subsets. *Neuroimmunomodulation* 5, 9–15. doi: 10.1159/000026321

Keshava Prasad, T. S., Goel, R., Kandasamy, K., Keerthikumar, S., Kumar, S., Mathivanan, S., et al. (2009). Human Protein Reference Database–2009 update. *Nucleic Acids Res.* 37, D767–D772. doi: 10.1093/nar/gkn892

Kim, D. W., Lee, S., Kwon, S., Nam, W., Cha, I.-H., and Kim, H. J. (2019). Deep learning-based survival prediction of oral cancer patients. *Sci. Rep.* 9:6994. doi: 10.1038/s41598-019-43372-7

Kim, J., and Bae, J.-S. (2016). Tumor-associated macrophages and neutrophils in tumor microenvironment. *Mediators Inflamm.* 2016:6058147.

Kim, R., Emi, M., and Tanabe, K. (2007). Cancer immunoediting from immune surveillance to immune escape. *Immunology* 121, 1–14. doi: 10.1111/j.1365-2567.2007.02587.x

Klinker, M. W., and Lundy, S. K. (2012). Multiple mechanisms of immune suppression by B lymphocytes. *Mol. Med.* 18, 123–137. doi: 10.2119/molmed.2011.00333

Koo, K. M., Wee, E. J., Mainwaring, P. N., Wang, Y., and Trau, M. (2016). Toward precision medicine: a cancer molecular subtyping nano-strategy for RNA biomarkers in tumor and urine. *Small* 12, 6233–6242. doi: 10.1002/smll.201602161

Koole, K., van Kempen, P. M. W., Swartz, J. E., Peeters, T., van Diest, P. J., Koole, R., et al. (2016). Fibroblast growth factor receptor 3 protein is overexpressed in oral and oropharyngeal squamous cell carcinoma. *Cancer Med.* 5, 275–284. doi: 10.1002/cam4.595

Korhonen, R., Lahti, A., Hämäläinen, M., Kankaanranta, H., and Moilanen, E. (2002). Dexamethasone inhibits inducible nitric-oxide synthase expression and nitric oxide production by destabilizing mRNA in lipopolysaccharide-treated macrophages. *Mol. Pharmacol.* 62, 698–704. doi: 10.1124/mol.62.3.698

Krishna, A., Singh, R. K., Singh, S., Verma, P., Pal, U. S., and Tiwari, S. (2014). Demographic risk factors, affected anatomical sites and clinicopathological profile for oral squamous cell carcinoma in a north Indian population. *Asian Pac. J. Cancer Prev.* 15, 6755–6760. doi: 10.7314/apjcp.2014.15.16.6755

Krishnan, N. M., Dhas, K., Nair, J., Palve, V., Bagwan, J., Siddappa, G., et al. (2016). A Minimal DNA Methylation Signature in Oral Tongue Squamous Cell Carcinoma Links Altered Methylation with Tumor Attributes. *Mol. Cancer Res.* 14, 805–819. doi: 10.1158/1541-7786.Mcr-15-0395

Kumar, K. P., Nicholls, A. J., and Wong, C. H. (2018). Partners in crime: neutrophils and monocytes/macrophages in inflammation and disease. *Cell Tissue Res.* 371, 551–565. doi: 10.1007/s00441-017-2753-2

Kumar, S., Principe, D. R., Singh, S. K., Viswakarma, N., Sondarva, G., Rana, B., et al. (2020). Mitogen-Activated Protein Kinase Inhibitors and T-Cell-Dependent Immunotherapy in Cancer. *Pharmaceuticals* 13:9. doi: 10.3390/ph13010009

Kusmartsev, S., Cheng, F., Yu, B., Nefedova, Y., Sotomayor, E., Lush, R., et al. (2003). All-trans-retinoic acid eliminates immature myeloid cells from tumor-bearing mice and improves the effect of vaccination. *Cancer Res.* 63, 4441–4449.

Lin, C.-Y., Pan, T.-S., Ting, C.-C., Liang, S.-S., Huang, S.-H., Liu, H.-Y., et al. (2013). Cytochrome p450 metabolism of betel quid-derived compounds: implications for the development of prevention strategies for oral and pharyngeal cancers. *Sci. World J.* 2013:618032.

Lin, C.-Y., Ruan, P., Li, R., Yang, J.-M., See, S., Song, J., et al. (2019). Deep learning with evolutionary and genomic profiles for identifying cancer subtypes. *J. Bioinform. Comput. Biol.* 17:1940005. doi: 10.1142/s0219720019400055

Lin, H., and Zelterman, D. (2002). Modeling survival data: extending the cox model. *Technometrics* 44, 85–86. doi: 10.1198/tech.2002.s656

Liu, Y., and Cao, X. (2016). Immunosuppressive cells in tumor immune escape and metastasis. *J. Mol. Med.* 94, 509–522. doi: 10.1007/s00109-015-1376-x

Liu, Y., He, M., Wang, D., Diao, L., Liu, J., Tang, L., et al. (2017). HisgAtlas 1.0: a human immunosuppression gene database. *Database* 2017:bax094. doi: 10.1093/database/bax094

Lohavanichbutr, P., Méndez, E., Holsinger, F. C., Rue, T. C., Zhang, Y., Houck, J., et al. (2013). A 13-gene signature prognostic of HPV-negative OSCC: discovery and external validation. *Clin. Cancer Res.* 19, 1197–1203. doi: 10.1158/1078-0432.Ccr-12-2647

Love, M. I., Huber, W., and Anders, S. (2014). Moderated estimation of fold change and dispersion for RNA-seq data with DESeq2. *Genome Biol.* 15:550. doi: 10.1186/s13059-014-0550-8

Margalit, D., Schoenfeld, J., Rawal, B., Puzanov, M., Haddad, R., Rabinowits, G., et al. (2016). Patient immunosuppression and the association with cancer-specific outcomes after treatment of squamous cell carcinoma of the oropharynx. *Int. J. Radiat. Oncol. Biol. Phys.* 94:913. doi: 10.1016/j.ijrobp.2015.12.145

Misra, A. K., Levy, M. M., and Ward, N. S. (2020). Biomarkers of Immunosuppression. *Crit. Care Clin.* 36, 167–176. doi: 10.1016/j.ccc.2019.08.013

Na, Y. R., Jung, D., Song, J., Park, J.-W., Hong, J. J., and Seok, S. H. (2020). Pyruvate dehydrogenase kinase is a negative regulator of interleukin-10 production in macrophages. *J. Mol. Cell Biol.* 12, 543–555. doi: 10.1093/jmcb/mjz113

Nguyen, T. N., Nguyen, H. Q., and Le, D.-H. (2020). Unveiling prognostics biomarkers of tyrosine metabolism reprogramming in liver cancer by cross-platform gene expression analyses. *PLoS One* 15:e0229276. doi: 10.1371/journal.pone.0229276

Nishioka, Y., Aono, Y., and Sone, S. (2011). Role of tyrosine kinase inhibitors in tumor immunology. *Immunotherapy* 3, 107–116. doi: 10.2217/imt.10.79

Nuñez, S. Y., Ziblat, A., Secchiari, F., Torres, N. I., Sierra, J. M., Iraolagoitia, X. L. R., et al. (2018). Human M2 macrophages limit NK cell effector functions through secretion of TGF-β and engagement of CD85j. *J. Immunol.* 200, 1008–1015. doi: 10.4049/jimmunol.1700737

O'Higgins, C., Ward, F. J., and Abu Eid, R. (2018). Deciphering the Role of Regulatory CD4 T Cells in Oral and Oropharyngeal Cancer: a Systematic Review. *Front. Oncol.* 8:442. doi: 10.3389/fonc.2018.00442

Owen, K. L., Brockwell, N. K., and Parker, B. S. (2019). JAK-STAT Signaling: a Double-Edged Sword of Immune Regulation and Cancer Progression. *Cancers* 11:2002. doi: 10.3390/cancers11122002

Palakurthi, S., Kuraguchi, M., Zacharek, S. J., Zudaire, E., Huang, W., Bonal, D. M., et al. (2019). The combined effect of FGFR inhibition and PD-1 blockade promotes tumor-intrinsic induction of antitumor immunity. *Cancer Immunol. Res.* 7, 1457–1471. doi: 10.1158/2326-6066.cir-18-0595

Peng, H., Xian, D., Liu, J., Pan, S., Tang, R., and Zhong, J. (2020). Regulating the Polarization of Macrophages: a Promising Approach to Vascular Dermatosis. *J. Immunol. Res.* 2020, 1–13. doi: 10.1155/2020/8148272

Peranzoni, E., Lemoine, J., Vimeux, L., Feuillet, V., Barrin, S., Kantari-Mimoun, C., et al. (2018). Macrophages impede CD8 T cells from reaching tumor cells and limit the efficacy of anti–PD-1 treatment. *Proc. Natl. Acad. Sci.U. S. A.* 115, E4041–E4050.

Piñero, J., Bravo, À, Queralt-Rosinach, N., Gutiérrez-Sacristán, A., Deu-Pons, J., Centeno, E., et al. (2017). DisGeNET: a comprehensive platform integrating information on human disease-associated genes and variants. *Nucleic Acids Res.* 45, D833–D839. doi: 10.1093/nar/gkw943

Quaranta, V., and Schmid, M. C. (2019). Macrophage-mediated subversion of anti-tumour immunity. *Cells* 8:747. doi: 10.3390/cells8070747

Rohani, N., and Eslahchi, C. (2020). Classifying Breast Cancer Molecular Subtypes by Using Deep Clustering Approach. *Front. Genet.* 11:553587. doi: 10.3389/fgene.2020.553587

Schnellhardt, S., Erber, R., Büttner-Herold, M., Rosahl, M.-C., Ott, O. J., Strnad, V., et al. (2020). Accelerated partial breast irradiation: macrophage polarisation shift classification identifies high-risk tumours in early hormone receptor-positive breast cancer. *Cancers* 12:446. doi: 10.3390/cancers12020446

Shannon, P., Markiel, A., Ozier, O., Baliga, N. S., Wang, J. T., Ramage, D., et al. (2003). Cytoscape: a software environment for integrated models of biomolecular interaction networks. *Genome Res.* 13, 2498–2504. doi: 10.1101/gr.1239303

Shi, R., Tang, Y. Q., and Miao, H. (2020). Metabolism in tumor microenvironment: implications for cancer immunotherapy. *MedComm* 1, 47–68. doi: 10.1002/mco2.6

Sun, W., Wei, F.-Q., Li, W.-J., Wei, J.-W., Zhong, H., Wen, Y.-H., et al. (2017). A positive-feedback loop between tumour infiltrating activated Treg cells and type 2-skewed macrophages is essential for progression of laryngeal squamous cell carcinoma. *Br. J. Cancer* 117, 1631–1643. doi: 10.1038/bjc.2017.329

Taghavi, N., Mohsenifar, Z., Baghban, A. A., and Arjomandkhah, A. (2018). CD20+ tumor infiltrating b lymphocyte in oral squamous cell carcinoma: correlation with clinicopathologic characteristics and heat shock protein 70 expression. *Pathol. Res. Int.* 2018:4810751.

Tao, Z., Shi, A., Li, R., Wang, Y., Wang, X., and Zhao, J. (2017). Microarray bioinformatics in cancer- a review. *J. Buon* 22, 838–843.

Téllez-Gabriel, M., Arroyo-Solera, I., León, X., Gallardo, A., López, M., Céspedes, M. V., et al. (2013). High RAB25 expression is associated with good clinical outcome in patients with locally advanced head and neck squamous cell carcinoma. *Cancer Med.* 2, 950–963. doi: 10.1002/cam4.153

Tian, Y., Han, Z., Dong, B., Ma, K., Wang, L., and Qin, H. (2018). LCN1 is highly expressed in cholangiocarcinoma patients and indicates poor prognosis. *Int. J. Clin. Exp. Med.* 11, 10917–10922.

Tomczak, K., Czerwińska, P., and Wiznerowicz, M. (2015). The Cancer Genome Atlas (TCGA): an immeasurable source of knowledge. *Contemp. Oncol.* 19, A68–A77. doi: 10.5114/wo.2014.47136

Torres, C., and Grippo, P. J. (2018). Pancreatic cancer subtypes: a roadmap for precision medicine. *Ann. Med.* 50, 277–287. doi: 10.1080/07853890.2018.1453168

Tota, J. E., Engels, E. A., Madeleine, M. M., Clarke, C. A., Lynch, C. F., Ortiz, A. P., et al. (2018). Risk of oral tongue cancer among immunocompromised transplant recipients and human immunodeficiency virus-infected individuals in the United States. *Cancer* 124, 2515–2522. doi: 10.1002/cncr.31359

Townsend, M. H., Ewell, Z. D., Freitas, C. M. T., Larsen, D. J., Bitter, E. L., Bennion, K. B., et al. (2019). "HPRT overexpression may contribute to the immunosuppressive tumor microenvironment," in *Proceedings of the American Association for Cancer Research Annual Meeting 2019*, (Atlanta, GA. Philadelphia (PA): AACR).

Upadhyay, P., Nair, S., Kaur, E., Aich, J., Dani, P., Sethunath, V., et al. (2016). Notch pathway activation is essential for maintenance of stem-like cells in early tongue cancer. *Oncotarget* 7, 50437–50449. doi: 10.18632/oncotarget.10419

Urban-Wojciuk, Z., Khan, M. M., Oyler, B. L., Fåhraeus, R., Marek-Trzonkowska, N., Nita-Lazar, A., et al. (2019). The Role of TLRs in Anti-cancer Immunity and Tumor Rejection. *Front. Immunol.* 10:2388. doi: 10.3389/fimmu.2019.02388

Voigt, C., May, P., Gottschlich, A., Markota, A., Wenk, D., Gerlach, I., et al. (2017). Cancer cells induce interleukin-22 production from memory CD4(+) T cells via interleukin-1 to promote tumor growth. *Proc. Natl. Acad. Sci. U. S. A.* 114, 12994–12999. doi: 10.1073/pnas.1705165114

Wang, B., Mezlini, A. M., Demir, F., Fiume, M., Tu, Z., Brudno, M., et al. (2014). Similarity network fusion for aggregating data types on a genomic scale. *Nat. Methods* 11, 333–7. doi: 10.1038/nmeth.2810

Wei, L., Jin, Z., Yang, S., Xu, Y., Zhu, Y., and Ji, Y. (2018). TCGA-assembler 2: software pipeline for retrieval and processing of TCGA/CPTAC data. *Bioinformatics* 34, 1615–1617. doi: 10.1093/bioinformatics/btx812

Wishart, D. S., Feunang, Y. D., Guo, A. C., Lo, E. J., Marcu, A., Grant, J. R., et al. (2018). DrugBank 5.0: a major update to the DrugBank database for 2018. *Nucleic Acids Res.* 46, D1074–D1082. doi: 10.1093/nar/gkx1037

Wu, W.-C., Sun, H.-W., Chen, J., OuYang, H.-Y., Yu, X.-J., Chen, H.-T., et al. (2019). Immunosuppressive immature myeloid cell generation is controlled by glutamine metabolism in human cancer. *Cancer Immunol. Res.* 7, 1605–1618. doi: 10.1158/2326-6066.cir-18-0902

Xiang, Q., Dai, X., Deng, Y., He, C., Wang, J., Feng, J., et al. (2008). Missing value imputation for microarray gene expression data using histone acetylation information. *BMC Bioinformatics* 9:252. doi: 10.1186/1471-2105-9-252

Yu, G.-T., Bu, L.-L., Zhao, Y.-Y., Mao, L., Deng, W.-W., Wu, T.-F., et al. (2016). CTLA4 blockade reduces immature myeloid cells in head and neck squamous cell carcinoma. *Oncoimmunology* 5:e1151594. doi: 10.1080/2162402X.2016.1151594

Zhang, J., Baran, J., Cros, A., Guberman, J. M., Haider, S., Hsu, J., et al. (2011). International Cancer Genome Consortium Data Portal–a one-stop shop for cancer genomics data. *Database* 2011:bar026. doi: 10.1093/database/bar026

Zhao, L., Lee, V. H. F., Ng, M. K., Yan, H., and Bijlsma, M. F. (2018). Molecular subtyping of cancer: current status and moving toward clinical applications. *Brief. Bioinform.* 20, 572–584. doi: 10.1093/bib/bby026

Zhao, S., Zuo, W.-J., Shao, Z.-M., and Jiang, Y.-Z. (2020). Molecular subtypes and precision treatment of triple-negative breast cancer. *Ann. Transl. Med.* 8:499. doi: 10.21037/atm.2020.03.194

Zhao, Z., Li, Y., Wu, Y., and Chen, R. (2020). Deep learning-based model for predicting progression in patients with head and neck squamous cell carcinoma. *Cancer Biomark.* 27, 19–28. doi: 10.3233/cbm-190380

Conflict of Interest: The authors declare that the research was conducted in the absence of any commercial or financial relationships that could be construed as a potential conflict of interest.

Publisher's Note: All claims expressed in this article are solely those of the authors and do not necessarily represent those of their affiliated organizations, or those of the publisher, the editors and the reviewers. Any product that may be evaluated in this article, or claim that may be made by its manufacturer, is not guaranteed or endorsed by the publisher.

frontiers in Cell and Developmental Biology

ORIGINAL RESEARCH
published: 09 August 2021
doi: 10.3389/fcell.2021.733246

Fucoidan-Supplemented Diet Potentiates Immune Checkpoint Blockage by Enhancing Antitumor Immunity

Juan Yang[1,2†], Xianzhi Yang[1†], Wenfeng Pan[1], Mingshuo Wang[1], Yuxiong Lu[2,3], Jianeng Zhang[2], Ziqian Fang[2], Xiaomin Zhang[2], Yin Ji[4], Jin-Xin Bei[2,5], Jiajun Dong[1], Yi Wu[1], Chaoyun Pan[1], Guangli Yu[6,7], Penghui Zhou[2]* and Bo Li[1,2,5]**

[1] Jiangmen Central Hospital, Affiliated Jiangmen Hospital, Zhongshan School of Medicine, Sun Yat-sen University, Guangdong, China, [2] State Key Laboratory of Oncology in South China, Collaborative Innovation Center for Cancer Medicine, Sun Yat-sen University Cancer Center, Guangdong, China, [3] Clinical Biological Resource Bank, Guangzhou Institute of Pediatrics, Guangzhou Women and Children's Hospital, Zhongshan School of Medicine, Sun Yat-sen University, Guangzhou, China, [4] State Key Laboratory of Translational Medicine and Innovative Drug Development, Simcere Diagnostics Co., Ltd., Jiangsu, China, [5] Center for Precision Medicine, Sun Yat-sen University, Guangdong, China, [6] Key Laboratory of Marine Drugs of Ministry of Education, Shandong Provincial Key Laboratory of Glycoscience and Glycotechnology, School of Medicine and Pharmacy, Ocean University of China, Shandong, China, [7] Laboratory for Marine Drugs and Bioproducts, Pilot National Laboratory for Marine Science and Technology (Qingdao), Shandong, China

OPEN ACCESS

Edited by:
Hongming Miao,
Army Medical University, China

Reviewed by:
Changliang Shan,
Nankai University, China
Wei Yang,
Southern Medical University, China

***Correspondence:**
Bo Li
liboqd@hotmail.com

[†]These authors share first authorship

Specialty section:
This article was submitted to Molecular and Cellular Pathology, a section of the journal Frontiers in Cell and Developmental Biology

Received: 30 June 2021
Accepted: 20 July 2021
Published: 09 August 2021

Citation:
Yang J, Yang X, Pan W, Wang M, Lu Y, Zhang J, Fang Z, Zhang X, Ji Y, Bei J-X, Dong J, Wu Y, Pan C, Yu G, Zhou P and Li B (2021) Fucoidan-Supplemented Diet Potentiates Immune Checkpoint Blockage by Enhancing Antitumor Immunity. Front. Cell Dev. Biol. 9:733246. doi: 10.3389/fcell.2021.733246

Immune checkpoint blockade (ICB) therapies such as PD-1 antibodies have produced significant clinical responses in treating a variety of human malignancies, yet only a subset of cancer patients benefit from such therapy. To improve the ICB efficacy, combinations with additional therapeutics were under intensive investigation. Recently, special dietary compositions that can lower the cancer risk or inhibit cancer progression have drawn significant attention, although few were reported to show synergistic effects with ICB therapies. Interestingly, Fucoidan is naturally derived from edible brown algae and exhibits antitumor and immunomodulatory activities. Here we discover that fucoidan-supplemented diet significantly improves the antitumor activities of PD-1 antibodies *in vivo*. Specifically, fucoidan as a dietary ingredient strongly inhibits tumor growth when co-administrated with PD-1 antibodies, which effects can be further strengthened when fucoidan is applied before PD-1 treatments. Immune analysis revealed that fucoidan consistently promotes the activation of tumor-infiltrating $CD8^+$ T cells, which support the evident synergies with ICB therapies. RNAseq analysis suggested that the JAK-STAT pathway is critical for fucoidan to enhance the effector function of $CD8^+$ T cells, which could be otherwise attenuated by disruption of the T-cell receptor (TCR)/CD3 complex on the cell surface. Mechanistically, fucoidan interacts with this complex and augments TCR-mediated signaling that cooperate with the JAK-STAT pathway to stimulate T cell activation. Taken together, we demonstrated that fucoidan is a promising dietary supplement combined with ICB therapies to treat malignancies, and dissected an underappreciated mechanism for fucoidan-elicited immunomodulatory effects in cancer.

Keywords: natural product, fucoidan, immunotherapy, cancer, T cells

INTRODUCTION

Immune checkpoint blockade (ICB) therapies have yielded appreciable clinical benefits in treating a variety of tumor types including melanoma (Pardoll, 2012; Li et al., 2016; Gong et al., 2018). Nivolumab and Pembrolizumab, two programmed death 1 (PD-1) antibodies approved by FDA, have been reported to significantly prolong progression-free and/or overall survival in patients with advanced melanoma (Eggermont et al., 2018; Eroglu et al., 2018), non-small cell lung cancer (Herbst et al., 2019), esophageal squamous-cell carcinoma (Kato et al., 2019), etc. Despite these impressive clinical effects, a great number of patients exhibit resistance or relapse after treatments (Minn and Wherry, 2016; Seidel et al., 2018). Therefore, there is an urgent need to improve the therapeutic efficacy by combining PD-1 antibodies with other therapeutics, such as tumor vaccines, oncolytic viruses, CTLA-4 antibodies, targeted therapies, radio- and chemo-therapies (Ott et al., 2017). In particular, the combination of two immunotherapies, CTLA-4 and PD-1 antibodies, exhibit enhanced efficacy against metastatic melanoma. However, the clinical incidence of immune-related adverse events (irAEs) is significantly higher with this combined approach (Kennedy and Salama, 2020). As such, alternative combination strategies with low side effects are under great demand to improve the therapeutic application of ICB.

Fucoidan, a fucose-enriched and sulfated polysaccharide molecule, is naturally derived from cell walls of edible brown algae and can be safely applied as a dietary supplement (Fitton, 2011; Citkowska et al., 2019). As a heterogeneous polysaccharide, the composition and structure of fucoidan vary widely in terms of seaweed species, growth environments, harvest seasons, and extraction methods (Kwak, 2014; Hsu and Hwang, 2019). Nevertheless, most fucoidan share common bioactivities including anti-cancer, anti-inflammatory, anti-bacterial, anti-viral, and anti-HIV activities. Among these functions, the anti-cancer properties of fucoidan attracted considerable attentions (Han et al., 2015; Atashrazm et al., 2016; Xue et al., 2020). Fucoidan has been observed to function as an antitumor agent in combination with conventional therapeutics in multiple models (Jin et al., 2014; Hsu and Hwang, 2019). However, the synergetic effects of fucoidan with immunotherapies have not been studied.

Using the murine melanoma model, we discovered that fucoidan-supplemented diet greatly improved the antitumor activities of PD-1 antibodies. If solely applied, however, fucoidan had no effect on melanoma cell proliferation and apoptosis *in vitro*, and failed to inhibit melanoma tumor growth *in vivo*. These results suggested that fucoidan synergizes with PD-1 antibodies to restrain tumor growth likely through immune modulation. Inspired by the increased T cell infiltration into tumor tissues upon fucoidan administration, we performed flow cytometry and RNA sequencing analysis on fucoidan-treated $CD8^+$ T cells, and found that fucoidan stimulated the activation and propagation of $CD8^+$ T cells. Mechanistically, fucoidan interacts with the T-cell receptor (TCR)/CD3 complex and potentiates its downstream JAK-STAT signaling, which is essential for T cell activation. Our findings provide new insight into the mechanism whereby dietary fucoidan strengthens the antitumor activity of PD-1 antibodies, and suggest a new combination approach that may potentiate the clinical effects of immunotherapies.

MATERIALS AND METHODS

Cell Culture

B16 and 293T cells were cultured in DMEM supplemented with 10% fetal bovine serum and 100 μg/ml penicillin/streptomycin. Jurkat cells were cultured in RPIM-1640 supplemented with 10% fetal bovine serum and 100 μg/ml penicillin/streptomycin. Primary T cells isolated by negative selection were cultured in complete RPMI media (RPMI 1640, 10% FBS, 100 μg/ml penicillin/streptomycin, 1% MEM Non-Essential Amino Acids Solution, 0.05 mM 2-mercaptoethanol, 2 mM L-glutamine). All cells were maintained in an incubator with a humidified atmosphere of 5% CO_2 at 37°C. Cells used in this study have been confirmed negative for Mycoplasma.

Fucoidan Extraction and Component Analysis

Fucoidan A and F were respectively extracted from the brown algae *Ascophyllum nodosum* and *Fucus vesiculosus*. *Ascophyllum nodosum* was sourced from Chile. *Fucus vesiculosus* was purchased from QingDao Gather Great Ocean Algae Industry Group Co., Ltd (Qingdao, China). Fucoidan was extracted by acid extraction with heat in aqueous media. In brief, dried seaweeds were grounded and delipidated using 95% ethanol at 80°C for 4 h. After extraction with water at 80°C for 3 cycles of 3h, supernatant harvested by centrifugation were precipitated with 80% ethanol at 4°C overnight. After that, crude fucoidan precipitate was vacuum-dried and dissolved in distilled water, then further purified by removing alginate at pH 1.0. The resultant solution was centrifuged at 8000 rpm for 10 min, and supernatant containing fucoidan was adjusted to pH 7.5 and lyophilized after dialysis.

The sulfate content and monosaccharide composition were further analyzed. Briefly, fucoidan was degraded in 1M HCl at 110°C for 6 h, and mixed with isopycnic $BaCl_2$-gelatin. Absorbance was then measured at 400 nm. The sulfate content was calculated according to the standard curve of Na_2SO_4. Monosaccharide composition was determined by a 1-phenyl-3-methyl-5-pyrazolone precolumn derivatization HPLC using an Eclipse XDB-C18 column (Agilent, Santa Clara, CA, USA). The fucoidan compositions are summarized in **Table 1**.

Allograft Mouse Model

C57BL/6 mice were purchased from Beijing Vital River Laboratory Animal Technology (Beijing, China) and maintained under the specific-pathogen-free condition. C57BL/6 mice

TABLE 1 | Chemical composition of Fucoidan A and F.

Fucoidan	Source	Sulfate content (%)	Molecular weight	Monosaccharide composition (%)					
				Man	GlcA	Glc	Gal	Xyl	Fuc
Fucoidan A	*Ascophyllum nodosum*	22.7	210kDa	7.5	5.3	8.1	3.8	17.8	58.5
Fucoidan F	*Fucus vesiculosus*	26.3	610kDa	5.7	5.5	9.9	5.3	8.3	65.8

(6-8 weeks old) were subcutaneously inoculated with B16 cells (2×10^5 cells per mouse) in the right lower abdomen area. After inoculation, mice were randomly divided into the following groups: PD-1 antibody treated only, fucoidan A-supplemented diet only, fucoidan F-supplemented diet only, PD-1 antibody combined with fucoidan A-supplemented diet, and PD-1 antibody combined with fucoidan F-supplemented diet. PD-1 antibody was administered intraperitoneally (i.p.) with 200 μg per mouse at day 7, 10, and 13 after tumor inoculation. Fucoidan supplementation were conducted by orally feeding the mice with 40 mg/ml fucoidan in sterile H_2O, 200 μl per day from the inoculation day until the experiment endpoint. In fucoidan pretreatment model, mice were fed with fucoidan containing diet 24 days before tumor inoculation. The anti-mouse PD-1 antibody was purified from culture supernatants of corresponding hybridoma cells (clone G4), provided by Dr. Lieping Chen at Yale University. Tumors were measured every 3 days by an electronic caliper from roughly day 7 when tumors were established, and tumor volumes calculated using the equation (length $\times$ width^2)/2. At the end point, tumors were surgically removed and weighed. Blood, tumor, spleen, and tumor-draining lymph node tissues were harvested for further analysis.

Xenograft Mouse Model

BALB/C nude mice were purchased from GemPharmatech (Nanjing, China) and maintained under the specific-pathogen-free condition. B16 cells (2×10^5 per mouse) were subcutaneously injected into BALB/C nude mice (aged 6-8 weeks). After tumor inoculation, mice were randomly divided into 2 groups: PD-1 antibody treated only and PD-1 antibody combined with fucoidan A-supplemented diet. Treatments were performed as previously described. Tumors were measured by an electronic caliper at day 8, 10, 12, and 14 after tumor inoculation. Mice were euthanized and tumors harvested at day 14.

Analysis of Bone Marrow-Derived Dendritic Cells (BMDCs)

Bone marrow was isolated from C57BL/6 mice and treated with ACK lysis buffer to remove the erythrocytes, then washed with PBS. Cells were cultured in complete RPMI media (RPMI 1640, 10% FBS, 100 μg/ml penicillin/streptomycin, 1% MEM Non-Essential Amino Acids Solution, 0.05 mM 2-mercaptoethanol, 2 mM L-glutamine) supplemented with 20 ng/ml IL-4 and 20 ng/ml granulocyte-macrophage colony stimulating factor (GM-CSF) for 6 days. After that, cells were treated with different concentrations of fucoidan A or F for 24 h, and the expression of CD40, CD80, CD86, and MHC II were analyzed by flow cytometry.

Isolation of Tumor-Infiltrating Lymphocytes

B16 melanomas were cut into small pieces in petri dishes containing 10 ml PBS supplemented with 2% FBS, and washed with PBS. Tumors were resuspended in 15 ml RPMI supplemented with 2% FBS, 50 U/ml collagenase type IV (Invitrogen), 20 U/ml DNase (Roche) and incubated at 37°C for 2 h. Processed tissues were further dissociated using a MACS Dissociator (Miltenyi Biotech). Suspensions were washed three times with PBS and passed through a 70 μm strainer. Lymphocytes were isolated by Ficoll density gradient centrifugation for further analysis.

Flow Cytometry

Spleens and tumor-draining lymph nodes were harvested from mice and rubbed with the rough surface of a glass slide to obtain single cell suspension. Spleens were treated with ACK lysis buffer to lyse the erythrocytes. Suspensions of spleens and lymph nodes were passed through a 70 μm strainer, incubated with specific antibodies for 30 minutes at room temperature, washed with PBS, and then analyzed using a FACSAria (BD Biosciences) flow cytometer. Peripheral blood was directly incubated with specific antibodies after processed with ACK lysis buffer. Fluorescence-conjugated anti-CD3, anti-CD19, anti-CD4, anti-CD8, anti-NK1.1, anti-CD11C, anti-CD40, anti-CD80, anti-CD86, and anti-MHC II were purchased from Biolegend.

Apoptosis Assay

Cells exposed to 100 μg/ml fucoidan for 48 h were harvested, incubated with Annexin V for 20 min at room temperature, subsequently with propidium iodide (PI) (Invitrogen) for another 20 min, and then analyzed by a flow cytometer.

Cell Cycle and Proliferation Assay

Cells were seeded in 6 well-plates and treated with 100 μg/ml fucoidan for 48 h. Then cells were collected, washed with cold PBS, and fixed with pre-cold 70% ethanol overnight at 4°C, followed by incubation with propidium iodide (PI) (Invitrogen) for 30 min shielded from light and analyzed by flow cytometry. Cell proliferation was determined using the CCK8 assay (Roche). Briefly, cells were seeded at 2×10^3 cells/well in 96-well plates. Cells were cultured overnight to adhere,

then incubated in 100 μl fresh medium containing various concentrations of fucoidan. At day 3, 10 μl CCK8 solution was added to each well, and incubated for 4 hours. Absorbance was measured at 450 nm.

T Cell Activation Assay

Primary $CD8^+$ T cells isolated by negative selection (Biolegend) from lymph nodes and spleens of C57BL/6 mouse were stimulated by immobilized anti-mouse CD3 and CD28 antibodies (3 μg/ml) in 96-well plate for 48 h. T cell activation and proliferation was indicated by CFSE staining.

Cytokine Analysis

Intracellular cytokine staining was performed according to the manufacturer's instructions (BD Bioscience). In brief, primary T and Jurkat cells were collected after stimulation for 48 h with anti-CD3 and anti-CD8. Cells were fixed, permeabilized and stained with antibodies specific for IFNγ, TNFα, or Granzyme B (Biolegend).

RNAseq Analysis

$CD8^+$ T cells activated by CD3/28 antibodies were divided into three groups: control group treated with PBS, fucoidan A group incubated with 10 μg/ml fucoidan A, and fucoidan F group incubated with 10 μg/ml fucoidan F. Total RNA was extracted with the TRIzol reagent (Invitrogen) according to the manufacturer's instructions. The quality of total RNA was tested (RNA integrity number ≥9.5) for construction of sequencing libraries. After mRNA capture, fragmentation, reverse transcription, terminal repair, linker ligation and PCR amplification, second-generation sequencing was performed according to Illumina's standard protocol. The sequencing results were further analyzed by gene set enrichment analysis (GSEA4.1). Genes with a ratio equal or greater than 2 were considered different. The R programming language was used to obtain the gene ontology category after running with Metascape[1].

ShRNA Interference

The shRNA oligoes of human CD3E were synthesized by BGI Tech (Guangzhou, China). ShRNA oligoes were cloned into a lentiviral vector with the miR30 backbone containing a U6 promotor. Lentiviral particles were produced from 293T cells transfected with the shRNA vector together with packaging plasmids. The shRNA sequences used in this study were designed as follows:

Human shCD3E-1

Forward: 5′-CCCCTGGTATTACACAGACACCATATAACTGTGACATGTCAAAAATTATATGGTGTCTGTGTAATACCT-3′

Reverse: 5′-CACCAGGTATTACACAGACACCATATAATTTTTTGACATGCACAGTTATATGGTGTCTGTGTAATACCA-3′

Human shCD3E-2

Forward: 5′-CCCCTCATCTCTGGAACCACAGTAATATCTGTGACATGTCAAAAAATATTACTGTGGTTCCAGAGATGT-3′

Reverse: 5′-CACCACATCTCTGGAACCACAGTAATATTTTTTTGACATGTCACAGATATTACTGTGGTTCCAGAGATGA-3′

Quantitative Reverse Transcription PCR

Total RNA was obtained from cells using TRIzol (Invitrogen) and reverse transcribed with the EasyScript One-Step gDNA Removal and cDNA Synthesis SuperMix (TransGen Biotech, AE311). The cDNA product was amplified with the SYBR Green qPCR MIX (TransGen Biotech) and a Biorad CFX96 Real-Time system according to the manufacturer's instructions. Relative gene expression was normalized to glyceraldehyde-3-phosphate (GAPDH)/actin beta (ACTB) and calculated by $2^{-\Delta\Delta CT}$.The sequence of specific primers used in this study were designed as follows:

Human CD3E Forward: 5′-GTAGTAAGTCTGCTGGCCTCC-3′

Reverse: 5′-CCCCAAACGCCAACTGATAA-3′

Human GAPDH Forward: 5′-GTCTCCTCTGACTTCAACAGCG-3′

Reverse: 5′-ACCACCCTGTTGCTGTAGCCAA-3′

Human GMZB Forward: 5′-CGACAGTACCATTGAGTTGTGCG-3′

Reverse: 5′-TTCGTCCATAGGAGACAATGCCC-3′

Human IL2 Forward: 5′-AGAACTCAAACCTCTGGAGGAAG-3′

Reverse: 5′-GCTGTCTCATCAGCATATTCACAC-3′

Mouse ACTB Forward: 5′-CATTGCTGACAGGATGCAGAAGG-3′

Reverse: 5′-TGCTGGAAGGTGGACAGTGAGG-3′

Mouse CD70 Forward: 5′-GCGGACTACTCAGTAAGCAGCA-3′

Reverse: 5′-TGTGAAGGACCTTCCCAAGGCT-3′

Mouse IL6 Forward: 5′-TACCACTTCACAAGTCGGAGGC-3′

Reverse: 5′-CTGCAAGTGCATCATCGTTGTTC-3′

Mouse CSF2 Forward: 5′-AACCTCCTGGATGACATGCCTG-3′

Reverse: 5′-AAATTGCCCCGTAGACCCTGCT-3′

Mouse IL3 Forward: 5′-CCTGCCTACATCTGCGAATGAC-3′

Reverse: 5′-GAGGTTAGCACTGTCTCCAGATC-3′

Mouse IL23A Forward: 5′-CATGCTAGCCTGGAACGCACAT-3′

Reverse: 5′-ACTGGCTGTTGTCCTTGAGTCC-3′

Mouse IL13 Forward: 5′-AACGGCAGCATGGTATGGAGTG-3′

Reverse: 5′-TGGGTCCTGTAGATGGCATTGC-3′

Mouse IL24 Forward: 5′-CGGCTTCACTTTAGGACCCTAG-3′

Reverse: 5′-CCCAAATCGGAACTCTTGACCC-3′

[1]http://metascape.org/

Western Blot

Cells were lysed with RIPA lysis buffer supplemented with 1x protease and phosphatase inhibitor. After quantified by the Pierce^{TM} BCA Protein Assay Kit (Thermo Scientific), proteins were separated by electrophoresis in a 12% sodium dodecyl sulfate-polyacrylamide gel (SDS-PAGE) (Bio-Rad, Hercules, CA) and electrophoretically transferred onto a PVDF membrane (Amersham Pharmacia Biotech, Piscataway, NJ). CD3E was detected with CD3E (CD3-12) rat mAb (CST Signaling, cat. #4443) at 1:1000 dilution and goat anti-rat IgG (H + L) HRP conjugates (Proteintech, cat. #SA00001) at 1:2000 dilution. The protein bands were visualized by chemiluminescent HRP substrates (Millipore).

FITC-UEA-I Staining

$CD8^+$ T cells isolated by negative selection were cultured in anti-CD3/CD28-coating 24-well plates with fucoidan A or F incubation at 100 μg/ml for 24 h. Cells were then collected, washed with PBS, and stained with FITC Ulex Europaeus Agglutinin I (FITC-UEA-I) (1:100 dilution) for 1.5 h at room temperature.

Confocal Microscopy

The overexpression of RFP-conjugated human CD3E (CD3E-RFP) in Jurkat cells were obtained by lentivirus infection. The human CD3E full-length sequence was amplified by PCR using Jurkat cDNA as template, and cloned into a lentiviral vector with the P2A-RFP cassette. The sequence of cloning primers were designed as follows:

CD3E-F: 5′-AAAAAGGATCCATGCAGTCGGGCA CTCA CTG-3′

CD3E-R: 5′-AAAAAGCTAGCGATGCGTCTCTGATTCA GGCC-3′

After overexpression, cells were cultured with fucoidan A or F at 100 μg/ml overnight, washed with PBS, and stained with FITC-UEA-I (1:100 dilution) for 1.5 h at room temperature. Nuclear counterstaining was performed with Hoechst 33342(1:5000) for 15 min at room temperature. Cells were then transferred into confocal dishes and analyzed by a Fast Airyscan LSM880 Confocal microscope (Zeiss) with 60x oil objective.

Pull-Down Assay

Jurkat or isolated $CD8^+$ T cells were collected and lysed with the Pierce IP lysis buffer (Thermo scientific) on ice for 30 min. Proteins lysates were then incubated with fucoidan for 8 h, and Ulex Europaeus Agglutinin I (UEA-I) conjugated agarose (Fisher scientific) overnight at 4°C under agitation, and then analyzed by immunoblot analysis.

Statistical Analysis

Statistical analysis was performed with two-tailed unpaired *t*-tests. All error bars displayed within figures indicate the mean of distribution and represent the standard error of the mean (SEM) unless otherwise stated. $P < 0.05$ was considered statistically significant and P values were indicated by asterisks as followed: $^*P < 0.05$, $^{**}P < 0.01$, $^{***}P < 0.001$, and n.s., non-significant.

RESULTS

Fucoidan Diet Enhances the Antitumor Efficacy of PD-1 Antibodies

To examine whether fucoidan-supplemented diet has a potentially synergistic effect with PD-1 immunotherapy, we subcutaneously inoculated B16 melanoma cells into C57BL/6 mice. Mice were treated with PD-1 antibodies in the presence or absence of fucoidan-supplemented diet (**Figure 1A**). Two unfractionated fucoidan species, namely fucoidan A and fucoidan F, were used throughout this study. They were respectively extracted from the brown algae *Ascophyllum nodosum* and *Fucus vesiculosus*, and subjected to composition analysis as previously described (Shang et al., 2016; Wang et al., 2019a; **Table 1**). We measured the growth of subcutaneous tumors and found that the combination of fucoidan diet and anti-PD-1 therapy resulted in synergistic antitumor responses. Compared with the anti-PD-1 treatment group, the tumor growth of mice was significantly slower in the combined treatment group (**Figure 1B**). Moreover, the tumor volumes and weights of combined treatment group were also markedly decreased (**Figures 1C,D**). To further investigate the potential immune changes, we performed flow cytometry analysis and found that mice receiving combined treatment exhibited increased population of $CD8^+$ T cells in their spleen, especially in the case of fucoidan A (**Figure 1E**, upper part). In addition, fucoidan co-treated mice displayed an increased percentage of natural killer (NK) cells in their spleen (**Figure 1E**, middle part), and a concomitant increase of tumor infiltrating T cells (**Figure 1E**, bottom part). The percentage of NK and T cells in blood and lymph node have no obvious variation. These results indicate that fucoidan-supplemented diet is capable of reducing the growth of melanoma tumors when combined with PD-1 antibodies, demonstrating that fucoidan is a promising dietary ingredient to enhance the therapeutic efficacy of immunotherapy.

Fucoidan Alone Is Insufficient to Inhibit Melanoma Cell Growth

To explore whether fucoidan induces intrinsic antitumor responses in melanoma cells, we first investigated the effects of fucoidan on melanoma cell growth *in vitro*. B16 cells were incubated with different doses of fucoidan A or F for 48 h. CCK8 assays indicated that fucoidan had no measurable effects on the growth of B16 cells (**Figure 2A**). According to previous studies, 100 μg/ml is the half maximal inhibitory concentration of fucoidan against a variety of cancer cells (Yang et al., 2015; Atashrazm et al., 2016). With such dosage, B16 cell proliferation remained unaffected by fucoidan even increasing the incubation time to 72 h (**Figure 2B**). Since fucoidan have been reported to induce cell cycle arrest and interact with selective components of apoptotic pathway (Hyun et al., 2009; Kim et al., 2010; Park et al., 2017), we next examined the apoptotic index and cell cycle status of B16 cells after fucoidan treatments. Annexin-V/PI staining indicated that fucoidan failed to induce B16 cell apoptosis (**Figure 2C**). Similarly, B16 cell cycle was unaffected by fucoidan

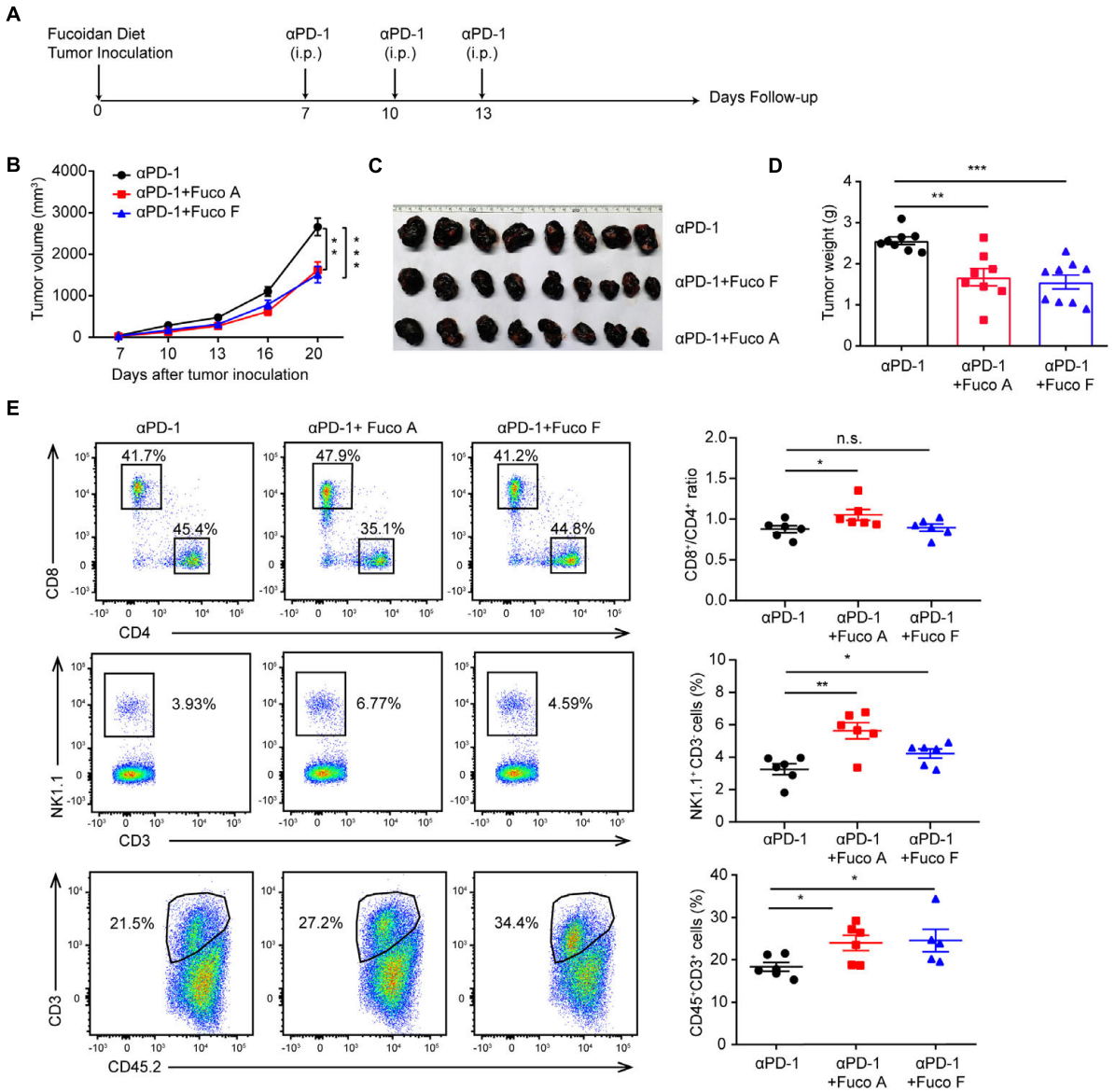

FIGURE 1 | Fucoidan diet enhances the antitumor efficacy of PD-1 antibodies. **(A)** Experimental scheme for fucoidan-supplemented diet combined with PD-1 immunotherapy in the B16 melanoma model. C57BL/6 mice were subcutaneously inoculated with B16 cells, fed with fucoidan A or F from the inoculation day (day 0) to the end point (day 20). Each mouse was administered with 200 μg PD-1 antibody at day 7, 10, and 13. i.p., intraperitoneally. **(B)** Tumor volumes recorded at indicated times are shown. **(C)** Tumor images and **(D)** weights of harvested tumors at day 20 are shown. **(E)** Flow cytometry analysis of spleen resident and tumor infiltrating lymphocytes (TILs). Spleens, tumor-draining lymph nodes, and tumor tissues were collected respectively for flow cytometry analysis. Top: Representative FCM plots (left) and analysis (right) of $CD8^+$ and $CD4^+$ T cells in spleen. Middle: Representative FCM plots (left) and analysis (right) of NK cells in spleen. Bottom: FCM plots (left) and analysis (right) of $CD45^+CD3^+$ TILs. A, B, C, D (n = 8 mice per group) and E (n = 6 mice per group) are representative of two independent experiments. Fuco, fucoidan. Error bars, mean ± SEM. $^*P < 0.05$, $^{**}P < 0.01$, $^{***}P < 0.001$. n.s., non-significant.

incubation (**Figure 2D**). These data suggested that fucoidan did not directly affect the growth or apoptosis of melanoma cells.

The next question is whether fucoidan alone is sufficient to confer immune remodelings that suppress tumor growth. To test this, we subcutaneously inoculated C57BL/6 mice with B16 cells and administrated dietary fucoidan in the absence of PD-1 antibodies. We followed the growth of subcutaneous tumors and found that tumor growth was comparable between fucoidan treated group and control group (**Figure 2E**), and at the end point fucoidan failed to reduce tumor weight (**Figure 2F**). Notably, a trend with lower tumor weight was associated with the fucoidan A group, suggesting that fucoidan A may be a bit more effective that fucoidan F in this setting. However, even with fucoidan A, we detected no significant difference between the experimental groups regarding the population of $CD4^+/CD8^+$ T cells in spleen (**Figure 2G**), as well as the number of tumor

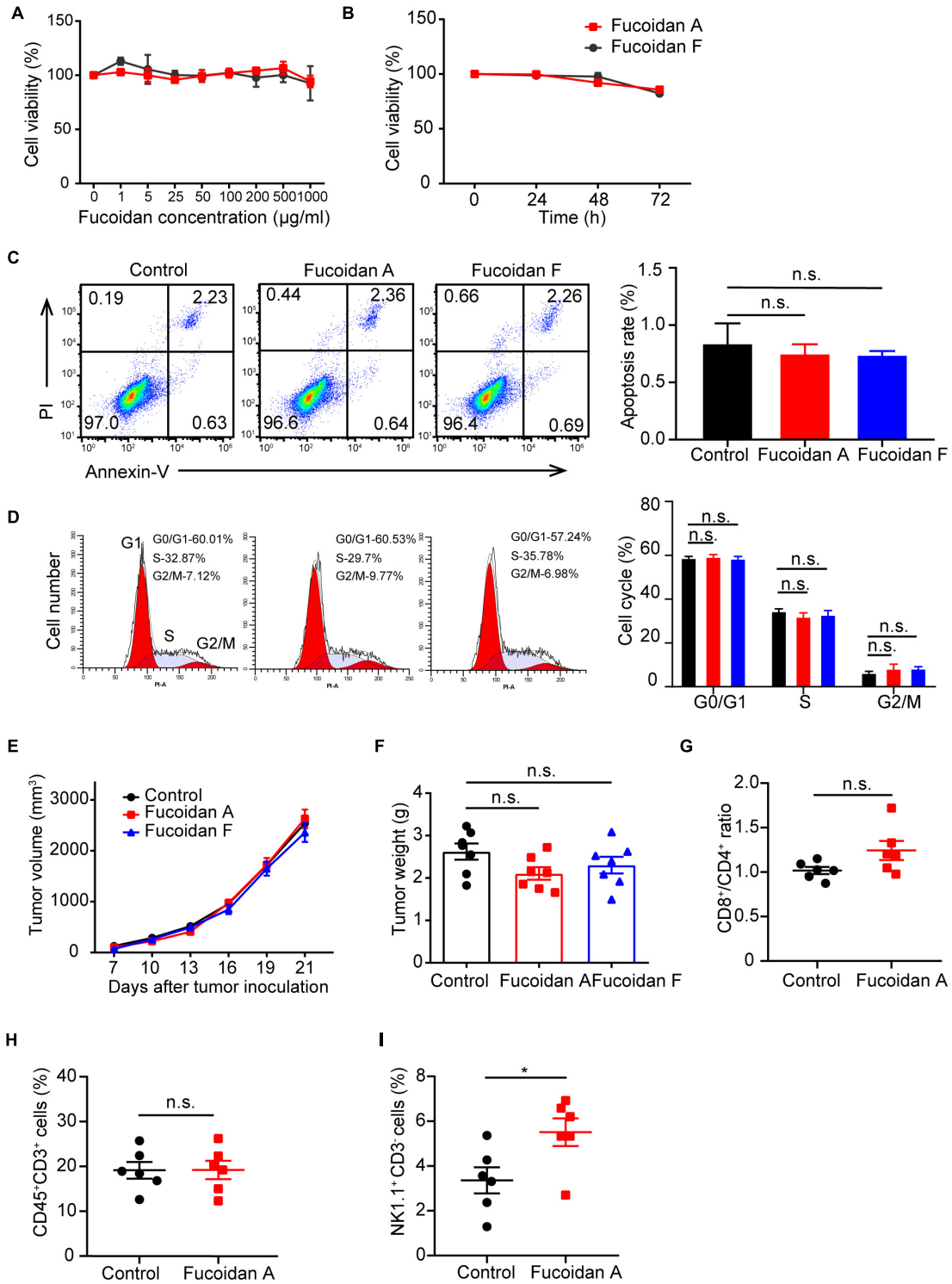

FIGURE 2 | Fucoidan alone is insufficient to inhibit melanoma cell growth. **(A)** B16 cells were cultured with fucoidan A or F with indicated concentration for 48 h in 96-well plates. CCK8 assay was used to monitor cell proliferation. **(B)** B16 cells were cultured with 100 μg/ml fucoidan A or F for different durations. Cell apoptosis **(C)** was assessed by Annexin V/PI staining and cell cycle **(D)** was measured using PI staining. B16 cells were incubated with 100 μg/ml fucoidan A or F for 48 hours. Growth **(E)** and weights **(F)** of B16 tumors harvested from control mice, or mice with dietary fucoidan A or F treatments. The flow cytometry analysis of splenic $CD8^+/CD4^+$ T cells **(G)**, $CD3^+$ TILs **(H)**, or splenic NK cells **(I)**, in fucoidan A treated or untreated B16-bearing mice. *In vitro* experiments were repeated at least three times. For *in vivo* experiments, data in E-F (n = 7 mice per group) and G-I (n = 6 mice per group) are representative of two independent replicates. Error bars, mean ± SEM. *$P < 0.05$, non-significant.

infiltrating T lymphocytes (**Figure 2H**). Similar to the results of combination therapy, we observed substantial increases in splenic NK population after fucoidan A treatments (**Figure 2I**). This finding is consistent with previous studies that fucoidan itself can elicit immune responses of NK cells (Ale et al., 2011; Atashrazm et al., 2016). Together, these results indicated that dietary fucoidan used in this study was insufficient to inhibit melanoma growth as a monotherapy, and its synergistic effects with PD-1 antibodies may not attributed to its ability to activate NK cells.

Fucoidan Differentially Activates Bone Marrow-Derived Dendritic Cells

In addition to inducing NK activation, ample studies have established that fucoidan treatments alone promote the maturation of dendritic cells (DCs) through binding to toll-like receptors (TLR) and scavenger receptors-A (SR-A) on the surface of DCs (Jin et al., 2009; Makarenkova et al., 2012). To evaluate the possible effects of fucoidan A and F on DC maturation, we isolated monocytes from mouse bone marrows and incubated them with IL4 and GM-CSF to induce their differentiation to DCs, followed by fucoidan treatments. The expression levels of CD40, CD80, CD86, and MHC II, four conventional DC maturation markers, were all strongly upregulated in DCs upon fucoidan F treatments (**Figures 3A-D**). This is consistent with a plethora of studies demonstrating fucoidan-mediated DC activation. Interestingly, fucoidan F exhibited much stronger effects on DC maturation compared with fucoidan A, which are in sharp contrast with our previous observations that fucoidan A and F were equally effective in combination therapy with PD-1 antibodies (**Figure 1B-D**). These data suggested that fucoidan may contribute to synergistic tumor suppression by modulating immune populations other than NK and DC. Accordingly, the increased number of infiltrating T cells in co-treated tumors revealed possible functions of T cells in this context.

Fucoidan Diet Enhances Antitumor Responses via Regulating T Cell Activities

To determine whether T cells are essential for the synergistic efficacy of fucoidan combined with PD-1 therapy, we utilized the BALB/C nude mouse model which is T-cell deficient. Briefly, we inoculated B16 cells into these mice and performed treatments according to the scheme as illustrated in **Figure 1A**. As expected, B16 melanoma growth remained unchanged irrespective of combination therapy (**Figure 4A**). The volumes (**Figure 4B**) and weights (**Figure 4C**) of formed tumors were comparable in mice receiving the fucoidan diet combined with PD-1 treatment and PD-1 treatment alone. This data suggested that the combination therapy could not achieve therapeutic synergy in T-cell deficient immunocompromised mice, and therefore T lymphocytes were critical for the antitumor effects of dietary fucoidan.

Next we examined whether the fucoidan pre-treatment would further enhance the therapeutic efficacy of PD-1 blockade. We fed mice with fucoidan containing diet 24 days before tumor inoculation (**Figure 4D**). We measured the growth of subcutaneous tumors and found that the efficacy of combination therapy was more pronounced. The tumor growth of fucoidan pre-treated mice in the combination therapy group were dramatically slower than the PD-1 monotherapy group (**Figure 4E**). The sizes and weights (**Figures 4F,G**) of co-treated tumors were also significantly decreased. Accordingly, FACS demonstrated that combination therapy increased the ratio of $CD8^+/CD4^+$ T cells and percentage of NK cells in spleen (**Figure 4H**). It is worth noting that compared with the conventional combination therapy, both tumor growth inhibition and T cell activation were more dramatic when mice were pre-treated with the fucoidan diet (**Figures 4H** vs. 1E). These results suggested that this enhanced anticancer activity may attribute to the activation of whole-body immune responses even before tumor growth. The higher ratio of $CD8^+/CD4^+$ caused by fucoidan pre-treatments suggests that such pre-treatments may intensify the function of PD-1 antibodies by inducing direct changes in T cells.

Fucoidan Activates the JAK-STAT Pathway and Promotes T Cell Proliferation and Activation

Next, we evaluated whether fucoidan directly stimulates T cell activity. On top of anti-CD3/28 co-stimulatory signals, fucoidan further augmented the effector function of primary $CD8^+$ T cells manifested by increased production of cytokines including IFNγ and TNFα (**Figure 5A**). The amounts of IFNγ were elevated in a dose-dependent manner (**Figure 5B**). Moreover, fucoidan-treated $CD8^+$ T cells underwent cell division more rapidly than PBS-treated control cells, as reflected by the CFSE (carboxyfluorescein succinimidyl amino ester) assay (**Figure 5C**). Collectively, these data demonstrated that fucoidan directly promotes the expansion and effector function of $CD8^+$ T lymphocytes.

To elucidate the molecular mechanisms by which fucoidan stimulates T cells, we performed RNAseq analysis of fucoidan-treated and control $CD8^+$ T cells. Gene set enrichment analysis (GSEA) demonstrated that genes within the JAK-STAT pathway were significantly upregulated by fucoidan treatments (**Figure 5D**). Core genes of this pathway were highlighted in the heatmap and volcano plots shown in **Figures 5E,F**, and the expression changes of several representative genes, including IL-3, IL-6, IL-13, IL-14, IL-24a, CSF2, and CD70, were further confirmed by qRT-PCR analysis (**Figure 5G**).

The JAK-STAT pathway is an essential signaling link between cell surface receptors and nuclear transcriptional events. Once activated by extracellular signals, phosphorylated STATs translocate into the nucleus and modulate the expression of multiple target genes, which are critical for T cell activation (Poehlmann et al., 2005; Bousoik and Montazeri Aliabadi, 2018). We next investigated whether fucoidan enhances T cell activity and proliferation through the JAK-STAT pathway. As expected, the JAK1/2 inhibitor AZD1480 impeded the basal activation of $CD8^+$ T cells by anti-CD3/28 beads, and fucoidan-mediated stimulatory effects on these T cells were strongly attenuated by AZD1480 administration (**Figures 5H,I**). These results suggested

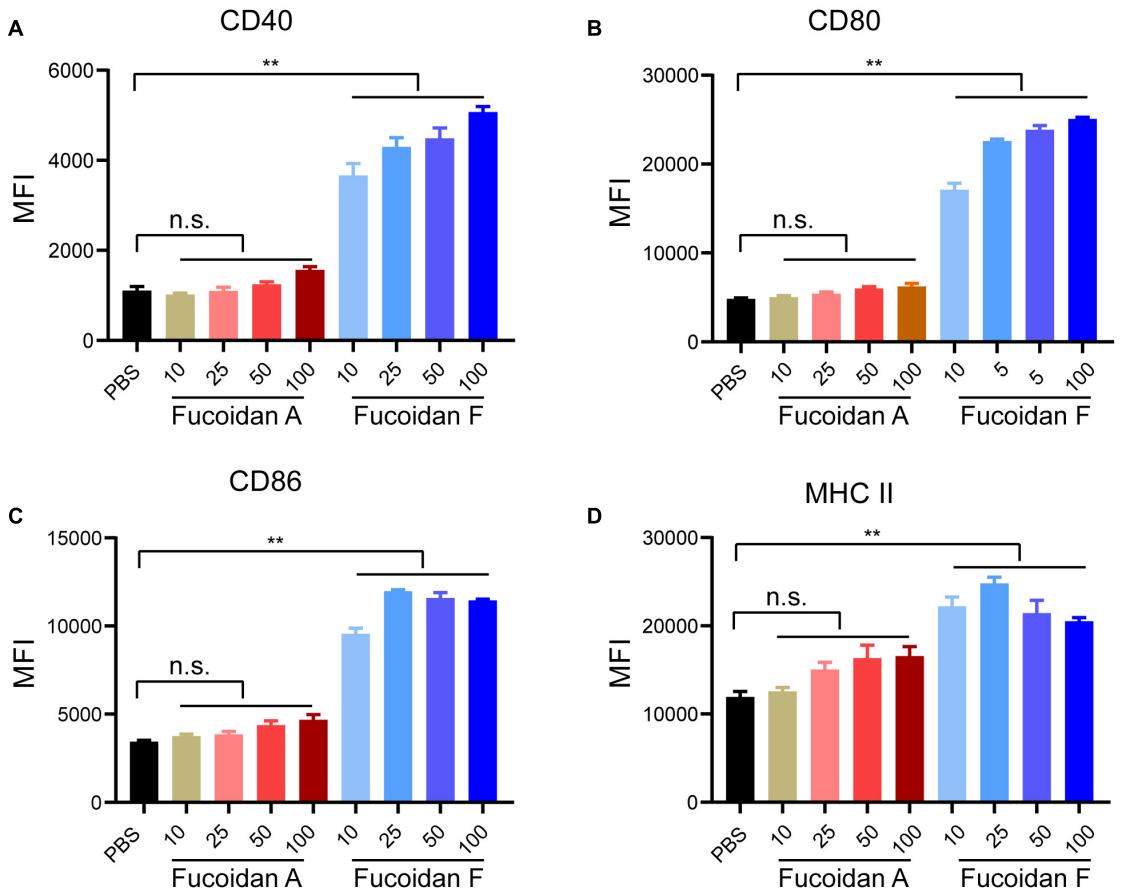

FIGURE 3 | Fucoidan differentially activates bone marrow-derived dendritic cells. Bone marrow-derived monocytes from C57BL/6 mice were differentiated into DCs after incubation with IL4 and GM-CSF for 6 days. Immature DCs were then treated with indicated concentrations of fucoidan A or F for 24 h. Relative expression levels of CD40 **(A)**, CD80 **(B)**, CD86 **(C)**, and MHC II **(D)** quantified by mean fluorescence intensity (MFI) using flow cytometry, in DCs treated with fucoidan A or F with indicated concentrations (μg/ml). Error bars, mean ± SD. $^{**}P < 0.01$. Data are representative of two independent experiments.

that fucoidan promotes the proliferation and effector function of $CD8^+$ T cells likely via activation of the JAK-STAT pathway.

Fucoidan Interacts With the T Cell Receptor Complex to Enhance T Cell Activity

Although fucoidan belongs to natural polysaccharide like starch or glycogen, dietary fucoidan can be absorbed by the human digestive system, which lacks fucoidanase for fucoidan hydrolysis (Silchenko et al., 2013; Atashrazm et al., 2015). Therefore, we reasoned that fucoidan exerts its function by engaging cell membrane receptors. To investigate this, we conducted gene ontology (GO) analysis to explore the potential signaling pathways regulated by fucoidan in $CD8^+$ T lymphocytes. GO results unraveled by sentence-based text mining (TRRUST) suggested that the top 5 enriched pathways stimulated by fucoidan are those regulated by transcription factors including *Nfkb*, *Jun*, *Rela*, and *Nfatc2* (**Figure 6A**). Importantly, the T cell receptor (TCR) signal transduction is triggered by forming a TCR/CD3 complex on the cell surface upon T cell activation, which leads to signal propagations via three major pathways: the Ca^{2+}-calcineurin pathway resulting in nuclear translocation of nuclear factor of activated T cells (NFAT), the NFκB signaling pathway resulting in nuclear translocation of REL/NFKB, and the MAPK pathway resulting in actin polymerization and activation of FOS, JUN, activator protein 1 (AP-1) (Gaud et al., 2018). Moreover, the JAK/STAT pathway intertwines with the TCR signaling cascade and potentiates the expression of multiple common target genes, which are essential for the effector function of cytotoxic T cells (Verdeil et al., 2006). Therefore, fucoidan activates all major pathways governed by the TCR signaling, and we speculated that fucoidan may interact with the TCR/CD3 complex in the extracellular space to augment T cell activation. To test this hypothesis, we first explored whether fucoidan associates with T cell membranes, by using a FITC-labeled Ulex Europaeus Agglutinin I (FITC-UEA-I) that specifically recognizes the fucose backbone of fucoidan. Indeed, flow cytometry analysis revealed that FITC-UEA-I fluorescently labeled T cells upon fucoidan treatments (**Figure 6B**). To confirm that fucoidan binds TCR/CD3 on the T cell surface, we stably overexpressed RFP (red fluorescent protein) labeled

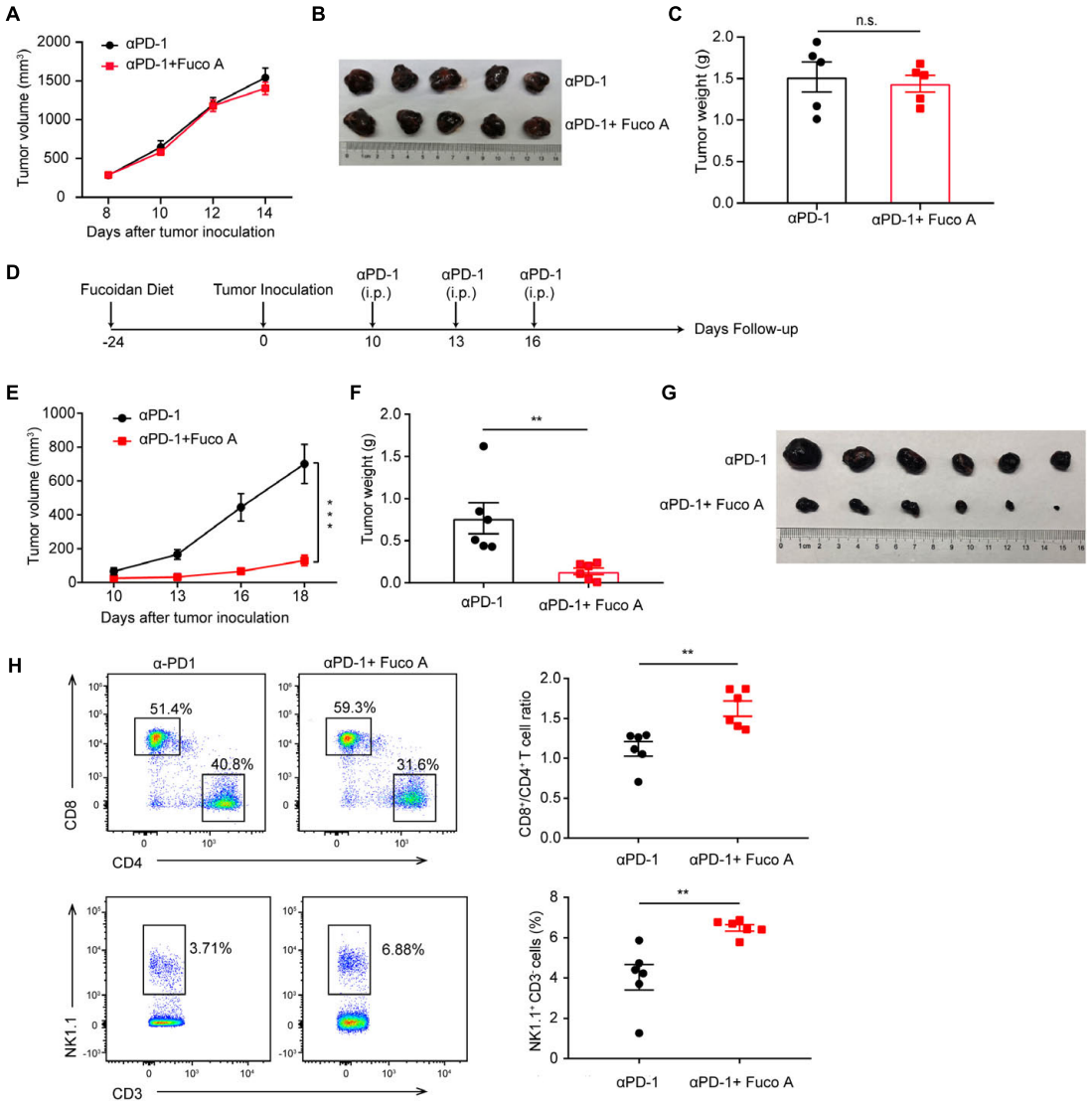

FIGURE 4 | Fucoidan diet enhances antitumor responses via regulating T cell activities. **(A)** Tumor volumes of B16 melanoma from BALB/C nude mice. BALB/C nude mice were subcutaneously inoculated with B16 cells, fed with fucoidan A from the inoculation day (day 0) to the end point (day 14). Each mouse were administered with 200 μg PD-1 antibody at day 8, 10, and 12 (n = 5 mice per group). **(B)** Tumor pictures and **(C)** weights at day 14 were shown. **(D)** Experimental scheme for fucoidan pre-treatments combined with PD-1 immunotherapy in the B16 tumor model. C57BL/6 mice were fed with fucoidan A for 24 days prior to B16 inoculation. **(E)** Tumor volumes recorded at indicated times are shown. **(F)** Weights and **(G)** images of harvested tumors are shown (n = 6 mice per group). **(H)** Flow cytometry analysis of splenic $CD8^+$, $CD4^+$ T cells, and NK cells. FCM plots (left) and analysis (right) are representative of two independent experiments. Error bars, mean ± SEM. $^*P < 0.05$, $^{**}P < 0.01$, and n.s., non-significant.

human CD3E, a major component of the TCR/CD3 complex (Gil et al., 2002), in Jurkat T cell leukemia cells exhibiting higher transfection efficiencies than primary T cells. Confocal microscopic imaging revealed that supplemented fucoidan, which can be labeled and visualized by FITC-UEA-I, partially colocalized with TCR/CD3 on the cell surface (**Figure 6C**). Subsequently, we confirmed the interaction between fucoidan and TCR/CD3 with pull-down assays (**Figure 6D**). Together, these results demonstrated the physical association between fucoidan and the TCR/CD3 complex, which may play important roles in T cell biology.

We next investigated whether the TCR/CD3 complex is required for fucoidan to promote T cell activation. Unlike primary $CD8^+$ T cells, Jurkat cells secrete little TNFα and INFγ, yet high amounts of granzyme B in response to TCR/CD3 (Huang et al., 2006; Rasooly et al., 2017) and JAK/STAT signalings upon activation. Indeed, fucoidan supplementation significantly upregulated the expression of granzyme B in Jurkat cells, which were suppressed by AZD1480 co-treatments (**Figures 6E,F**). Furthermore, we transfected Jurkat cells with shRNAs targeting CD3E or a scramble sequence. Two CD3E shRNAs were effective at the mRNA level, yet only the

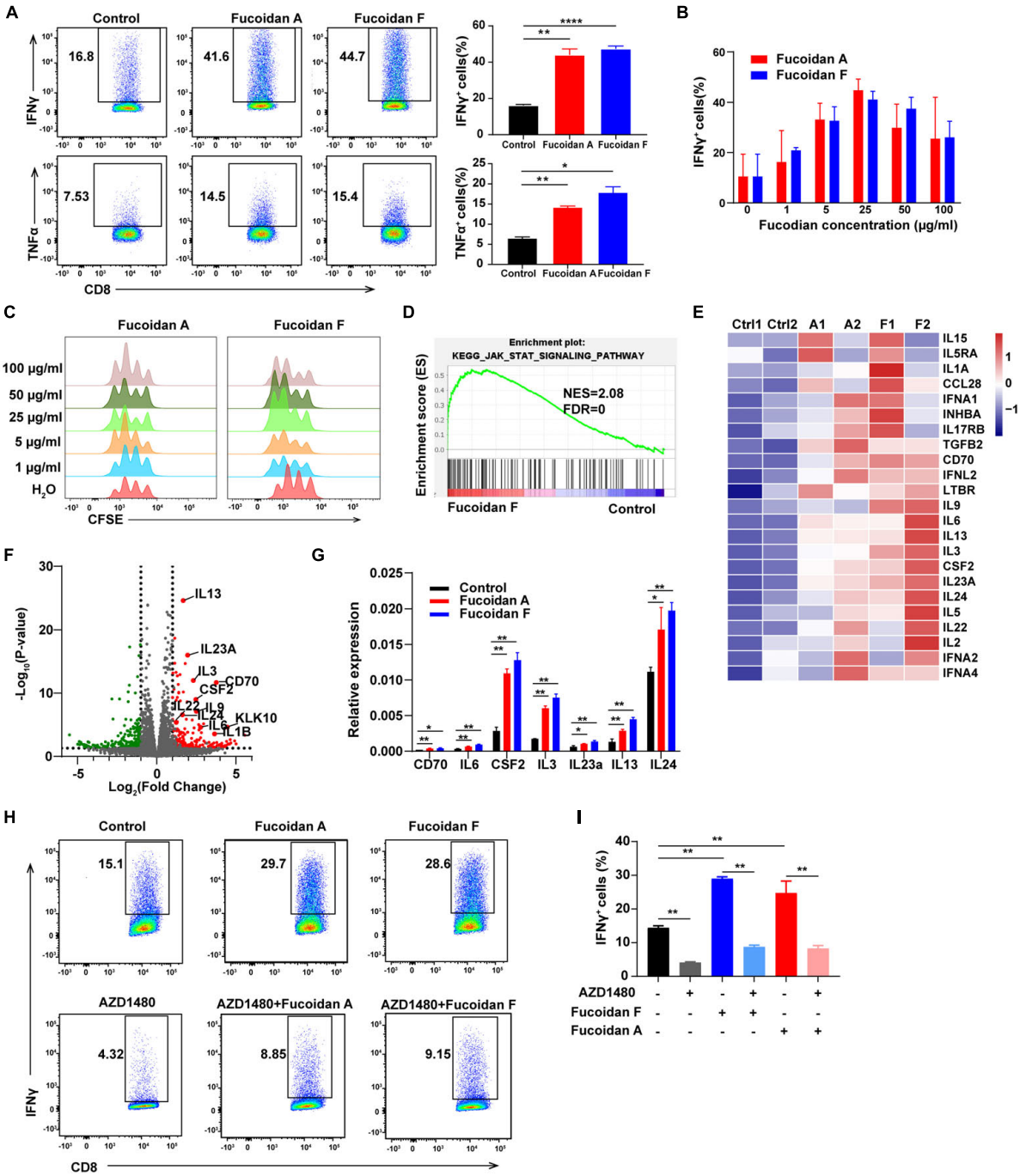

FIGURE 5 | Fucoidan activates the JAK-STAT pathway and promotes T cell proliferation and activation. **(A)** IFNγ and TNFα expression in primary $CD8^+$ T cells cultured with anti-CD3/CD28 beads, with or without fucoidan (25 μg/ml) treatments. Numbers adjacent to the outlined areas indicate the frequency of cells expressing IFNγ and TNFα. All data are quantified on the right. **(B)** IFNγ expression levels in $CD8^+$ T cells treated by indicated concentrations of fucoidan. **(C)** CFSE assays quantifying the proliferation of $CD8^+$ T cells stimulated by indicated concentrations of fucoidan. **(D)** Gene set enrichment analysis (GSEA) of the RNAseq data of fucoidan-treated (10 μg/ml) and control $CD8^+$ T cells. **(E)** Heatmap of fucoidan-regulated genes involved in the JAK-STAT pathway. Ctrl, control. A1, A2, two biological replicates of fucoidan A-treated samples. F1, F2, two biological replicates of fucoidan F-treated samples. **(F)** Volcano plots of differentially expressed genes from RNAseq data of fucoidan-treated and control $CD8^+$ T cells. The x axis represents log2 of fold changes (FC) of gene expression levels in fucoidan-treated cells relative to control cells, and the y axis represents log10 of corresponding P values. Genes within the JAK-STAT pathway were highlighted. **(G)** qRT-PCR analysis of the mRNA expression of indicated genes in fucoidan-treated and control $CD8^+$ T cells. **(H,I)** IFNγ expression in $CD8^+$ T cells activated by anti-CD3/CD28 beads, treated with fucoidan (10 μg/ml) and/or AZD1480 (50 nM). Data are representative of three independent experiments. Error bars, mean ± SD. $^*P < 0.05$, $^{**}P < 0.01$, $^{***}P < 0.001$, $^{****}P < 0.0001$.

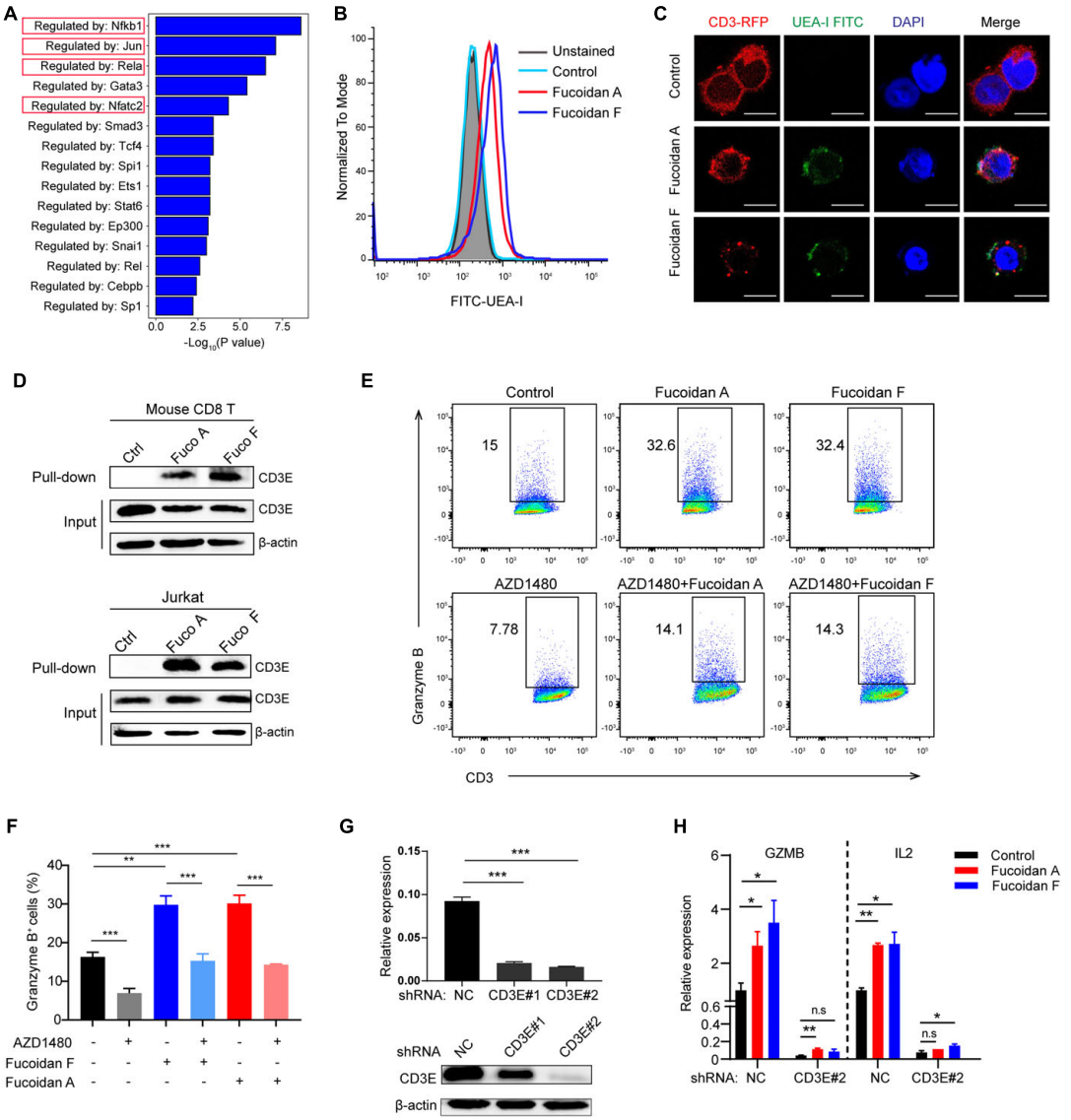

FIGURE 6 | Fucoidan interacts with the T cell receptor complex to enhance T cell activity. **(A)** Genes Ontology (GO) analysis showing the enrichment of specific pathways regulated by indicated transcription factors, based on upregulated hallmark genes in fucoidan-treated $CD8^+$ T cells. **(B)** Flow cytometry analysis of $CD8^+$ T cells unstained or stained with FITC-labeled Ulex Europaeus Agglutinin I (FITC-UEA-I), supplemented with or without 100 μg/ml fucoidan. **(C)** Representative fluorescent images of Jurkat cells overexpressing RFP-CD3E (red) stained with FITC-UEA-I (green), supplemented with or without 100 μg/ml fucoidan. Nuclei were stained with DAPI (blue). Scale bar, 10 μm. **(D)** Lysates from primary $CD8^+$ T and Jurkat cells treated with or without fucoidan were subjected to pull-down assays with Ulex Europaeus Agglutinin I (UEA I) conjugated agarose, followed by immunoblotting analysis with CD3E antibodies. **(E,F)** Granzyme B expression levels in Jurkat cells activated by anti-human CD3/CD28 supplemented with fucoidan (10 μg/ml) and/or AZD1480 (40 μM). **(G)** Knockdown efficiencies of CD3E mRNA and protein using indicated shRNAs in Jurkat cells. **(H)** qRT-PCR analysis of GZMB and IL2 mRNA expression in Jurkat cells transfected with CD3E shRNA#2 or shNC. GZMB, Granzyme B. NC, non-targeted control. Data are representative of two independent experiments. Error bars, mean ± SD. $^*P < 0.05$, $^{**}P < 0.01$, $^{***}P < 0.001$, and n.s., non-significant.

CD3E shRNA#2 significantly reduced the CD3E protein level (**Figure 6G**). Therefore, the qRT-PCR assay was applied to evaluate Jurkat T cells with CD3E depletion conferred by shRNA#2. As shown in **Figure 6H**, CD3E knockdown dramatically suppressed fucoidan-mediated activation of Jurkat cells, as reflected by blunted expression of granzyme B and IL2 upon CD3E depletion. These results suggested that fucoidan binds and functions through the TCR/CD3 complex to enhance TCR-mediated signal transduction and T cell activation (**Figure 7**).

DISCUSSION

Diet is the principal method to obtain nutrition for complex systems like human being, and it is well noted that diet

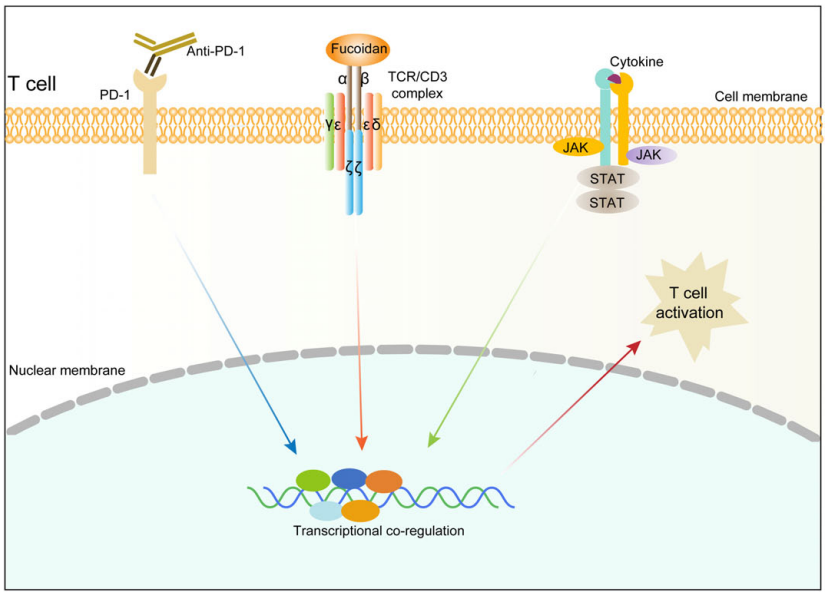

FIGURE 7 | Schematic diagram illustrating the molecular mechanism underlying fucoidan-promoted antitumor immunity.

intervention for human diseases exhibits characteristics of safety and feasibility. Although the underlying mechanisms remain elusive, an array of dietary approaches have shown powerful antitumor effects (Nencioni et al., 2018). For instance, fasting-mimicking and ketogenic diets have been reported to induce a T-cell dependent tumor growth delay (Lee et al., 2012; Lussier et al., 2016). Furthermore, protein restriction diet can synergize with immunotherapies through reprogramming the tumor associated macrophages (Orillion et al., 2018). Oral supplementation with *Akkermansia muciniphila* and ketone bodies were reported to enhance the efficacy of PD-1 blockade (Routy et al., 2018; Ferrere et al., 2021). Fucoidan in particular is a soluble dietary component that is considered functional food with health benefits (Di Daniele et al., 2017). Oral administration of fucoidan can regulate gut microbiome as a prebiotic (Chen et al., 2019). In addition to be absorbed in the small intestine, fucoidan can also pass through the stomach and small intestine, and produce short-chain fatty acids (SCFAs) when fermented by gut microbiota in the large intestine (Nagamine et al., 2014; Tao et al., 2020). SCFAs are the key energy source of colonocytes, and modulate the function of innate immune cells (Routy et al., 2018; Yao et al., 2020). In this study, we observed moderate increases of splenic NK cells after fucoidan treatments, which may attribute to augmented serum SCFAs.

The immune modulating effects of fucoidan were widely studied. It has been shown that fucoidan enhances the immune responses of NK cells, T cells, macrophages, and DCs (Fitton et al., 2015; Hsu and Hwang, 2019). Our data demonstrated that fucoidan treatments increased the number of NK cells *in vivo*, and promoted DC maturation *in vitro*. However, fucoidan A is more effective than F for inducing NK stimulation, whereas fucoidan F is more effective than A for inducing DC maturation. Unlike NK cells and DCs, mice receiving the fucoidan diet combined with PD-1 therapy exhibit consistent activation of tumor infiltrating $CD8^+$ T lymphocytes, which is the only immune cell subset paralleled with tumor shrinkage for two fucoidan species. Nevertheless, T cell activation and tumor inhibition cannot be achieved by fucoidan treatments alone, possibly due to the dampened activity of T cells residing in the immunosuppressive tumor microenvironment (Rabinovich et al., 2007; Thommen and Schumacher, 2018). These suppressed T cells can be partially reinvigorated by PD-1 blockade, explaining the efficacy of combination therapy.

Natural polysaccharides have been reported to play an immunomodulatory role by binding TCR/CD3 or TLR receptors on the T cell surface (Miao et al., 2005; Kabelitz, 2007), and regulate intracellular calcium signals and cytokine production (Zheng et al., 2002; Shuai et al., 2010). However, TLRs are mainly present in the innate immune system and expressed in $CD3^+$ T cells at extremely low or non-detectable levels (Applequist et al., 2002). By contrast, T cells in adaptive immunity prefer to receive activation signals through antigen-presenting cells under most circumstances. Although fucoidan was linked to T cells in several studies (Shimizu, 2005; Wang et al., 2019b), its specific role in regulating T cell responses remains unclear. Our RNAseq analysis indicated that fucoidan activates three major pathways downstream of the TCR/CD3 complex, and it is worth noting that TCR/CD3 relies on secondary signaling waves from the JAK/STAT axis to fully sustain its activation capacity. Moreover, we discovered that fucoidan physically interacts with TCR/CD3 on the cell surface and potentiates its activation. The TCR/CD3 complex is consist of multiple building blocks including TCRαβ, CD3ζζ, CD3δε, and CD3γε. The TCRαβ heterodimer is an antigen-binding subunit and lacks inherent signal-transducing domain, whereas CD3 subunits contain the immunoreceptor tyrosine-based activation motif

(ITAM) which could be phosphorylated and responsible for the signal transduction from TCR to intracellular pathways (Pitcher and van Oers, 2003; Kuhns et al., 2006; Xu et al., 2020). To test whether the TCR/CD3 complex is required for fucoidan to stimulate T cells, we suppressed CD3E expression using targeted shRNAs, as the encoded CD3ε is critical for T cell activation (Gil et al., 2002). CD3ε depletion significantly inhibits fucoidan-mediated T cell activation, combined with the fact that fucoidan physically associates with TCR/CD3, demonstrating that fucoidan exerts it antitumor function by engaging the TCR/CD3 complex and promoting cytotoxic T cell activities.

In conclusion, we discovered that fucoidan as a dietary integradent can coordinate with PD-1 therapy and strongly potentiate its antitumor effects. Mechanistically, fucidin enhances the proliferation and cytokine production of tumor infiltrating $CD8^+$ T cells through binding to the TCR/CD3 complex. Our study provides tangible evidence to underscoring orally-delivered fucoidan as a synergistic anti-cancer agent with immunotherapy.

DATA AVAILABILITY STATEMENT

The RNA-seq data generated in this study have been deposited in the Sequence Read Archive with the accession number PRJNA743936.

ETHICS STATEMENT

The animal study was reviewed and approved by Sun Yat-sen University laboratory animal center.

AUTHOR CONTRIBUTIONS

J-XB, CP, GY, PZ, and BL conceived the study and analyzed the data. JY, XY, WP, MW, JZ, ZF, XZ, YL, JD, YW, and YJ designed and performed the experiments. JY and BL wrote the manuscript. All authors contributed to the article and approved the submitted version.

FUNDING

This study was supported by National Key Research and Development Program of China (2016YFA0502600 and 2016YFA0500304), National Natural Science Foundation of China (82073074, 82003194, 81991522, 31670811, 81802853, 81773052, and 81572806), National Science and Technology Major Project for Significant New Drugs Development (2018ZX09735004), Guangdong Innovative and Entrepreneurial Research Team Program (2016ZT06S638), the Postdoctoral Science Foundation in China (2018M633237), Post-doctoral funding from Guangzhou Service Center for Scholarly Exchange (011302026), Guangzhou Science Technology and Innovation Commission (201607020038), the Science and Technology Projects of Guangdong Province (2016A020215086), the Science and Technology Planning Project of Jiangmen, China (2018630100110019805), the leading talents program of Guangdong Province (to PZ), Shandong Provincial Major Science and Technology Innovation Project (2018SDKJ0404 and 2018SDKJ0401), the National Program for Support of Top-Notch Young Professionals (to J-XB), Chang Jiang Scholars Program (to J-XB), Special Support Program of Guangdong (to J-XB), and Sun Yat-sen University Young Teacher Key Cultivate Project (17ykjc24).

REFERENCES

Ale, M. T., Maruyama, H., Tamauchi, H., Mikkelsen, J. D., Meyer, A. S., et al. (2011). Fucoidan from *Sargassum sp*. and *Fucus vesiculosus* reduces cell viability of lung carcinoma and melanoma cells in vitro and activates natural killer cells in mice in vivo. *Int. J. Biol. Macromol.* 49, 331–336. doi: 10.1016/j.ijbiomac.2011.05.009

Applequist, S. E., Wallin, R. P. A., and Ljunggren, H.-G. (2002). Variable expression of toll-like receptor in murine innate and adaptive immune cell lines. *Int. Immunol.* 14, 1065–1074.

Atashrazm, F., Lowenthal, R. M., Woods, G. M., Holloway, A. F., Dickinson, J. L., et al. (2015). Fucoidan and cancer: a multifunctional molecule with anti-tumor potential. *Mar. Drugs* 13, 2327–2346. doi: 10.3390/md13042327

Atashrazm, F., Lowenthal, R. M., Woods, G. M., Holloway, A. F., Karpiniec, S. S., Dickinson, J. L., et al. (2016). Fucoidan suppresses the growth of human acute promyelocytic leukemia cells in vitro and in vivo. *J. Cell Physiol.* 231, 688–697. doi: 10.1002/jcp.25119

Bousoik, E., and Montazeri Aliabadi, H. (2018). Do we know jack" about JAK? a closer look at JAK/STAT signaling pathway. *Front. Oncol.* 8:287. doi: 10.3389/fonc.2018.00287

Chen, Q., Liu, M., Zhang, P., Fan, S., Huang, J., Yu, S., et al. (2019). Fucoidan and galactooligosaccharides ameliorate high-fat diet-induced dyslipidemia in rats by modulating the gut microbiota and bile acid metabolism. *Nutrition* 65, 50–59. doi: 10.1016/j.nut.2019.03.001

Citkowska, A., Szekalska, M., and Winnicka, K. (2019). Possibilities of fucoidan utilization in the development of pharmaceutical dosage forms. *Mar. Drugs* 17:458. doi: 10.3390/md17080458

Di Daniele, N., Noce, A., Vidiri, M. F., Moriconi, E., Marrone, G., Annicchiarico-Petruzzelli, M., et al. (2017). Impact of mediterranean diet on metabolic syndrome, cancer and longevity. *Oncotarget* 8, 8947–8979. doi: 10.18632/oncotarget.13553

Eggermont, A. M. M., Blank, C. U., Mandala, M., Long, G. V., Atkinson, V., Dalle, S., et al. (2018). Adjuvant *Pembrolizumab versus* placebo in resected stage III melanoma. *N. Engl. J. Med.* 378, 1789–1801. doi: 10.1056/NEJMoa1802357

Eroglu, Z., Zaretsky, J. M., Hu-Lieskovan, S., Kim, D. W., Algazi, A., Johnson, D. B., et al. (2018). High response rate to PD-1 blockade in desmoplastic melanomas. *Nature* 553, 347–350. doi: 10.1038/nature25187

Ferrere, G., Tidjani Alou, M., Liu, P., Goubet, A. G., Fidelle, M., Kepp, O., et al. (2021). Ketogenic diet and ketone bodies enhance the anticancer effects of PD-1 blockade. *JCI Insight* 6:e145207. doi: 10.1172/jci.insight.145207

Fitton, J. H. (2011). Therapies from fucoidan; multifunctional marine polymers. *Mar, Drugs* 9, 1731–1760. doi: 10.3390/md9101731

Fitton, J. H., Stringer, D. N., and Karpiniec, S. S. (2015). Therapies from fucoidan: an update. *Mar. Drugs* 13, 5920–5946. doi: 10.3390/md13095920

Gaud, G., Lesourne, R., and Love, P. E. (2018). Regulatory mechanisms in T cell receptor signalling. *Nat. Rev. Immunol.* 18, 485–497. doi: 10.1038/s41577-018-0020-28

Gil, D., Montoya, M. A., Montoya, M., Sánchez-Madrid, F., and Alarcón, B. (2002). Recruitment of Nck by CD3e reveals a ligand-induced conformational change essential for T cell receptor signaling and synapse formation. *Cell* 109, 901–912.

Gong, J., Chehrazi-Raffle, A., Reddi, S., and Salgia, R. (2018). Development of PD-1 and PD-L1 inhibitors as a form of cancer immunotherapy: a comprehensive

review of registration trials and future considerations. *J. Immunother. Cancer* 6:8. doi: 10.1186/s40425-018-0316-z

Han, Y. S., Lee, J. H., and Lee, S. H. (2015). Antitumor effects of fucoidan on human colon cancer cells via activation of Akt signaling. *Biomol. Ther. (Seoul)* 23, 225–232. doi: 10.4062/biomolther.2014.136

Herbst, R. S., Arkenau, H. T., Santana-Davila, R., Calvo, E., Paz-Ares, L., Cassier, P. A., et al. (2019). Ramucirumab plus pembrolizumab in patients with previously treated advanced non-small-cell lung cancer, gastro-oesophageal cancer, or urothelial carcinomas (JVDF): a multicohort, non-randomised, open-label, phase 1a/b trial. *Lancet Oncol.* 20, 1109–1123. doi: 10.1016/S1470-2045(19)30458-30459

Hsu, H. Y., and Hwang, P. A. (2019). Clinical applications of fucoidan in translational medicine for adjuvant cancer therapy. *Clin. Transl. Med.* 8:15. doi: 10.1186/s40169-019-0234-239

Huang, C., Bi, E., Hu, Y., Deng, W., Tian, Z., Dong, C., et al. (2006). A novel NF-KB binding site controls human granzyme B gene transcription. *J. Immunol.* 176, 4173–4181.

Hyun, J. H., Kim, S. C., Kang, J. I., Kim, M. K., Boo, H. J., Kwon, J. M., et al. (2009). Apoptosis inducing activity of fucoidan in HCT-15 colon carcinoma cells. *Biol. Pharm. Bull.* 32, 1760–1764. doi: 10.1248/bpb.32.1760

Jin, J. O., Park, H. Y., Xu, Q., Park, J. I., Zvyagintseva, T., Stonik, V. A., et al. (2009). Ligand of scavenger receptor class a indirectly induces maturation of human blood dendritic cells via production of tumor necrosis factor-alpha. *Blood* 113, 5839–5847. doi: 10.1182/blood-2008-10-184796

Jin, J. O., Zhang, W., Du, J. Y., Wong, K. W., Oda, T., and Yu, Q. (2014). Fucoidan can function as an adjuvant in vivo to enhance dendritic cell maturation and function and promote antigen-specific T cell immune responses. *PLoS One* 9:e99396. doi: 10.1371/journal.pone.0099396

Kabelitz, D. (2007). Expression and function of Toll-like receptors in T lymphocytes. *Curr. Opin. Immunol.* 19, 39–45. doi: 10.1016/j.coi.2006.11.007

Kato, K., Cho, B. C., Takahashi, M., Okada, M., Lin, C. Y., Chin, K., et al. (2019). *Nivolumab versus* chemotherapy in patients with advanced oesophageal squamous cell carcinoma refractory or intolerant to previous chemotherapy (ATTRACTION-3): a multicentre, randomised, open-label, phase 3 trial. *Lancet Oncol.* 20, 1506–1517.

Kennedy, L. B., and Salama, A. K. S. (2020). A review of cancer immunotherapy toxicity. *CA Cancer J. Clin.* 70, 86–104. doi: 10.3322/caac.21596

Kim, E. J., Park, S. Y., Lee, J. Y., and Park, J. H. (2010). Fucoidan present in brown algae induces apoptosis of human colon cancer cells. *BMC Gastroenterol.* 10:96. doi: 10.1186/1471-230X-10-96

Kuhns, M. S., Davis, M. M., and Garcia, K. C. (2006). Deconstructing the form and function of the TCR/CD3 complex. *Immunity* 24, 133–139. doi: 10.1016/j.immuni.2006.01.006

Kwak, J. Y. (2014). Fucoidan as a marine anticancer agent in preclinical development. *Mar. Drugs* 12, 851–870. doi: 10.3390/md12020851

Lee, C., Raffaghello, L., Brandhorst, S., Safdie, F. M., Bianchi, G., Martin-Montalvo, A., et al. (2012). Fasting cycles retard growth of tumors and sensitize a range of cancer cell types to chemotherapy. *Sci. Transl. Med.* 4:124ra27. doi: 10.1126/scitranslmed.3003293

Li, Y., Li, F., Jiang, F., Lv, X., Zhang, R., Lu, A., et al. (2016). A mini-review for cancer immunotherapy: molecular understanding of PD-1/PD-L1 pathway & translational blockade of immune checkpoints. *Int. J. Mol. Sci.* 17:1151. doi: 10.3390/ijms17071151

Lussier, D. M., Woolf, E. C., Johnson, J. L., Brooks, K. S., Blattman, J. N., Scheck, A. C., et al. (2016). Enhanced immunity in a mouse model of malignant glioma is mediated by a therapeutic ketogenic diet. *BMC Cancer* 16:310. doi: 10.1186/s12885-016-2337-2337

Makarenkova, I. D., Logunov, D., Tukhvatulin, A. I., Semenova, I. B., Zviagintheva, T. N., Gorbach, V. I., et al. (2012). [Sulfated polysaccharides of brown seaweeds–ligands of toll-like receptors]. *Biomed. Khim* 58, 318–325. doi: 10.18097/pbmc20125803318

Miao, B., Li, J., Fu, X., Ding, J., and Geng, M. (2005). T-cell receptor (TCR)/CD3 is involved in sulfated polymannuroguluronate (SPMG)-induced T lymphocyte activation. *Int. Immunopharmacol.* 5, 1171–1182. doi: 10.1016/j.intimp.2005.02.011

Minn, A. J., and Wherry, E. J. (2016). Combination Cancer therapies with immune checkpoint blockade: convergence on interferon signaling. *Cell* 165, 272–275. doi: 10.1016/j.cell.2016.03.031

Nagamine, T., Nakazato, K., Tomioka, S., Iha, M., and Nakajima, K. (2014). Intestinal absorption of fucoidan extracted from the brown seaweed, *Cladosiphon okamuranus*. *Mar. Drugs* 13, 48–64. doi: 10.3390/md13010048

Nencioni, A., Caffa, I., Cortellino, S., and Longo, V. D. (2018). Fasting and cancer: molecular mechanisms and clinical application. *Nat. Rev. Cancer* 18, 707–719. doi: 10.1038/s41568-018-0061-60

Orillion, A., Damayanti, N. P., Shen, L., Adelaiye-Ogala, R., Affronti, H., Elbanna, M., et al. (2018). Dietary protein restriction reprograms tumor-associated macrophages and enhances immunotherapy. *Clin. Cancer Res.* 24, 6383–6395. doi: 10.1158/1078-0432.CCR-18-0980

Ott, P. A., Hodi, F. S., Kaufman, H. L., Wigginton, J. M., and Wolchok, J. D. (2017). Combination immunotherapy: a road map. *J. Immunother. Cancer* 5:16. doi: 10.1186/s40425-017-0218-215

Pardoll, D. M. (2012). The blockade of immune checkpoints in cancer immunotherapy. *Nat. Rev. Cancer* 12, 252–264. doi: 10.1038/nrc3239

Park, H. Y., Park, S. H., Jeong, J. W., Yoon, D., Han, M. H., Lee, D. S., et al. (2017). Induction of p53-Independent apoptosis and G1 cell cycle arrest by fucoidan in HCT116 human colorectal carcinoma Cells. *Mar. Drugs* 15:154. doi: 10.3390/md15060154

Pitcher, L. A., and van Oers, N. S. (2003). T-cell receptor signal transmission: who gives an ITAM? *Trends Immunol.* 24, 554–560. doi: 10.1016/j.it.2003.08.003

Poehlmann, T. G., Busch, S., Mussil, B., Winzer, H., Weinert, J., Mebes, I., et al. (2005). The possible role of the JAK/STAT pathway in lymphocytes at the fetomaternal interface. *Chem. Immunol. Allergy* 89, 26–35.

Rabinovich, G. A., Gabrilovich, D., and Sotomayor, E. M. (2007). Immunosuppressive strategies that are mediated by tumor cells. *Annu. Rev. Immunol.* 25, 267–296. doi: 10.1146/annurev.immunol.25.022106.141609

Rasooly, R., Do, P., and Hernlem, B. J. (2017). Interleukin 2 secretion by T cells for detection of biologically active staphylococcal enterotoxin Type E. *J. Food Prot.* 80, 1857–1862. doi: 10.4315/0362-028X.JFP-17-196

Routy, B., Le Chatelier, E., Derosa, L., Duong, C. P. M., Alou, M. T., Daillère, R., et al. (2018). Gut microbiome influences efficacy of PD-1–based immunotherapy against epithelial tumors. *Science* 359, 91–97.

Seidel, J. A., Otsuka, A., and Kabashima, K. (2018). Anti-PD-1 and Anti-CTLA-4 therapies in Cancer: mechanisms of action, efficacy, and limitations. *Front. Oncol.* 8:86. doi: 10.3389/fonc.2018.00086

Shang, Q., Shan, X., Cai, C., Hao, J., Li, G., Yu, G., et al. (2016). Dietary fucoidan modulates the gut microbiota in mice by increasing the abundance of *Lactobacillus* and *Ruminococcaceae*. *Food Funct.* 7, 3224–3232. doi: 10.1039/c6fo00309e

Shimizu, J. (2005). Proportion of murine cytotoxic T Cells is increased by high molecular-weight fucoidan extracted from *Okinawa mozuku* (*Cladosiphon okamuranus*). *J. Health Sci.* 51, 394–397.

Shuai, X. H., Hu, T. J., Liu, H. L., Su, Z. J., Zeng, Y., Li, Y. H., et al. (2010). Immunomodulatory effect of a *Sophora subprosrate* polysaccharide in mice. *Int. J. Biol. Macromol.* 46, 79–84. doi: 10.1016/j.ijbiomac.2009.10.016

Silchenko, A. S., Kusaykin, M. I., Kurilenko, V. V., Zakharenko, A. M., Isakov, V. V., Zaporozhets, T. S., et al. (2013). Hydrolysis of fucoidan by fucoidanase isolated from the marine bacterium, *Formosa algae*. *Mar. Drugs* 11, 2413–2430. doi: 10.3390/md11072413

Tao, J., Li, S., Gan, R. Y., Zhao, C. N., Meng, X., Li, H. B., et al. (2020). Targeting gut microbiota with dietary components on cancer: effects and potential mechanisms of action. *Crit. Rev. Food Sci. Nutr.* 60, 1025–1037. doi: 10.1080/10408398.2018.1555789

Thommen, D. S., and Schumacher, T. N. (2018). T Cell dysfunction in Cancer. *Cancer Cell* 33, 547–562. doi: 10.1016/j.ccell.2018.03.012

Verdeil, G., Chaix, J., Schmitt-Verhulst, A. M., and Auphan-Anezin, N. (2006). Temporal cross-talk between TCR and STAT signals for CD8 T cell effector differentiation. *Eur. J. Immunol.* 36, 3090–3100. doi: 10.1002/eji.200636347

Wang, X., Shan, X., Dun, Y., Cai, C., Hao, J., Li, G., et al. (2019a). Anti-Metabolic syndrome effects of fucoidan from *Fucus vesiculosus* via reactive oxygen species-mediated regulation of JNK, Akt, and AMPK signaling. *Molecules* 24:3319. doi: 10.3390/molecules24183319

Wang, Y., Xing, M., Cao, Q., Ji, A., Liang, H., and Song, S. (2019b). Biological activities of fucoidan and the factors mediating its therapeutic

effects: a review of recent studies. *Mar. Drugs* 17:183. doi: 10.3390/md17030183

Xu, X., Li, H., and Xu, C. (2020). Structural understanding of T cell receptor triggering. *Cell Mol. Immunol.* 17, 193–202. doi: 10.1038/s41423-020-0367-361

Xue, M., Liang, H., Ji, X., Zhou, Z., Liu, Y., Sun, T., et al. (2020). Effects of fucoidan on gut flora and tumor prevention in 1,2-dimethylhydrazine-induced colorectal carcinogenesis. *J Nutr. Biochem.* 82:108396. doi: 10.1016/j.jnutbio.2020.108396

Yang, G., Zhang, Q., Kong, Y., Xie, B., Gao, M., Tao, Y., et al. (2015). Antitumor activity of fucoidan against diffuse large B cell lymphoma in vitro and in vivo. *Acta Biochim. Biophys. Sin (Shanghai)* 47, 925–931. doi: 10.1093/abbs/gmv094

Yao, Y., Cai, X., Fei, W., Ye, Y., Zhao, M., and Zheng, C. (2020). The role of short-chain fatty acids in immunity, inflammation and metabolism. *Crit. Rev. Food Sci. Nutr.* doi: 10.1080/10408398.2020.1854675 Online ahead of print.

Zheng, Q. L., Zheng, Y. F., and Lu, Z. L. (2002). Immunomodulatory effects of polysaccharide of cistanche deserticola Y C Ma. *Zhejiang Da Xue Xue Bao Yi Xue Ban* 31, 284–287.

Conflict of Interest: The authors declare that the research was conducted in the absence of any commercial or financial relationships that could be construed as a potential conflict of interest.

Publisher's Note: All claims expressed in this article are solely those of the authors and do not necessarily represent those of their affiliated organizations, or those of the publisher, the editors and the reviewers. Any product that may be evaluated in this article, or claim that may be made by its manufacturer, is not guaranteed or endorsed by the publisher.

frontiers in Cell and Developmental Biology

ORIGINAL RESEARCH
published: 12 August 2021
doi: 10.3389/fcell.2021.707677

The Identification of the Metabolism Subtypes of Skin Cutaneous Melanoma Associated With the Tumor Microenvironment and the Immunotherapy

Ronghua Yang[1†], Zhengguang Wang[2†], Jiehua Li[3], Xiaobing Pi[3], Runxing Gao[4], Jun Ma[5], Yi Qing[6] and Sitong Zhou[3*]*

[1] Department of Burn Surgery and Skin Regeneration, The First People's Hospital of Foshan, Foshan, China, [2] Department of Orthopedics, The First Affiliated Hospital of China Medical University, Shenyang, China, [3] Department of Dermatology, The First People's Hospital of Foshan, Foshan, China, [4] Department of Anesthesiology, The First People's Hospital of Foshan, Foshan, China, [5] Department of Burns, Nanfang Hospital, Southern Medical University, Guangzhou, China, [6] Department of Oncology, Affiliated Hospital of Chengdu University, Chengdu, China

OPEN ACCESS

Edited by:
Na Luo,
Nankai University, China

Reviewed by:
Bingjie Li,
First Affiliated Hospital of Zhengzhou University, China
Yan Li,
Nanjing Medical University, China

***Correspondence:**
Yi Qing
qywxbb@hotmail.com
Sitong Zhou
sitongzhou@hotmail.com

[†] These authors have contributed equally to this work

Specialty section:
This article was submitted to Molecular and Cellular Pathology, a section of the journal Frontiers in Cell and Developmental Biology

Received: 10 May 2021
Accepted: 06 July 2021
Published: 12 August 2021

Citation:
Yang R, Wang Z, Li J, Pi X, Gao R, Ma J, Qing Y and Zhou S (2021) The Identification of the Metabolism Subtypes of Skin Cutaneous Melanoma Associated With the Tumor Microenvironment and the Immunotherapy. Front. Cell Dev. Biol. 9:707677. doi: 10.3389/fcell.2021.707677

Skin cutaneous melanoma (SKCM) is a highly aggressive and resistant cancer with immense metabolic heterogeneity. Here, we performed a comprehensive examination of the diverse metabolic signatures of SKCM based on non-negative matrix factorization (NMF) categorization, clustering SKCM into three distinct metabolic subtypes (C1, C2, and C3). Next, we evaluated the metadata sets of the metabolic signatures, prognostic values, transcriptomic features, tumor microenvironment signatures, immune infiltration, clinical features, drug sensitivity, and immunotherapy response of the subtypes and compared them with those of prior publications for classification. Subtype C1 was associated with high metabolic activity, low immune scores, and poor prognosis. Subtype C2 displayed low metabolic activity, high immune infiltration, high stromal score, and high expression of immune checkpoints, demonstrating the drug sensitivity to PD-1 inhibitors. The C3 subtype manifested moderate metabolic activity, high enrichment in carcinogenesis-relevant pathways, high levels of CpG island methylator phenotype (CIMP), and poor prognosis. Eventually, a 90-gene classifier was produced to implement the SKCM taxonomy and execute a consistency test in different cohorts to validate its reliability. Preliminary validation was performed to ascertain the role of SLC7A4 in SKCM. These results indicated that the 90-gene signature can be replicated to stably identify the metabolic classification of SKCM. In this study, a novel SKCM classification approach based on metabolic gene expression profiles was established to further understand the metabolic diversity of SKCM and provide guidance on precisely targeted therapy to patients with the disease.

Keywords: metabolism subtypes, tumor microenvironment, skin cutaneous melanoma, immune signature, mutation landscape, immunotherapy response

Abbreviations: SKCM, skin cutaneous melanoma; ICI, immune checkpoint inhibitors; CTLA-4, cytotoxic T-lymphocyte-associated protein-4; GDSC, genomics of drug sensitivity in cancer; GEO, Gene Expression Omnibus; TCGA, The Cancer Genome Atlas; Tem, effective memory T cell; GSVA, gene set variation analysis; GSEA, gene set enrichment analysis; SLC7A4, solute carrier family 7 member 4; NMF, non-negative matrix factorization; CIMP, CpG island methylator phenotype; OS, overall survival.

INTRODUCTION

Skin cutaneous melanoma (SKCM) is the deadliest type of skin cancer due to its high metabolic and metastatic rates, accounting for more than 80% of skin cancer-related deaths (Guy et al., 2015; Bolick and Geller, 2021). In the past few years, the advancement of immune checkpoint blockade agents has become a pillar of SKCM therapy, remarkably boosting the therapeutic outcomes. However, the response of patients with SKCM to immunotherapy is heterogeneous, with approximately 50% of them experiencing unfavorable responses (Robert et al., 2011; Schadendorf et al., 2015). Therefore, it is imperative to uncover the latent molecular mechanisms of SKCM heterogeneity to develop precise immunotherapies and determine the populations that would benefit the most from them.

Skin cutaneous melanoma is characterized by prominent metabolic plasticity, a feature that results from the activation of oncogenic pathways due to a high frequency of somatic mutations (Alexandrov et al., 2020). SKCM has been classified into four genomic subtypes, BRAF subtype, RAS subtype, NF1 subtype, and triple wild type based on the somatic mutations in these genes and their ratios (2015). These intrinsic oncogenes contribute to the metabolic conversion of SKCM, which leads to a high degree of plasticity and adaptation of melanoma to unfavorable conditions (Ratnikov et al., 2017). Moreover, the transformed metabolic microenvironment can reprogram the function of immune cell subpopulations, allowing melanoma to evade the immune system (Bristot et al., 2020).

A recent proteogenomic research divided patients with SKCM into two subgroups according to whether they responded to immunotherapy against PD-1 or TIL (Harel et al., 2019), namely, the responder and the non-responder subgroups. Differential protein expression analysis found that differences in mitochondrial metabolism were responsible for the response of patients to immunotherapy rather than the treatment protocol. In summary, the heterogeneity of melanoma metabolism is an important reason for the poor efficacy of immunotherapy. Therefore, this study was conducted to categorize SKCM from a metabolic viewpoint to reveal its heterogeneity.

In the present study, we performed a systematic examination of the diverse metabolic signatures of SKCM using a screened metabolic gene based on a non-negative matrix factorization (NMF) clustering algorithm and identified three distinct metabolic subtypes. In this process, The Cancer Genome Atlas (TCGA)-SKCM cohorts were merged into a metadata set for clustering based on the expression of metabolism genes. Additional processed microarray profiles of Gene Expression Omnibus (GEO) SKCM samples were used for external validation. Unsupervised transcriptomic analysis identified three subtypes of SKCM, namely, C1, C2, and C3. In addition, by comparing transcriptomic data from patients with different metabolic subtypes, differentially expressed genes (DEGs) were retrieved. We estimated the prognostic difference, transcriptome features, relationships with metabolic signatures, tumor microenvironment features, immune infiltration, clinical traits, somatic mutation signatures, immunotherapy, and drug sensitivity of the SKCM subtypes, and a comparison was made with previously established classifications. Finally, a 90-gene classifier was used to determine SKCM classification. This research may also provide in-depth insights into tumor–immune cell interactions, showing considerable promise for the clinical therapeutic interventions of patients with SKCM.

MATERIALS AND METHODS

Patients and Samples

Gene expression profiles of SKCM, including TCGA-SKCM (Cancer Genome Atlas Network, 2015), GSE54467, and GSE65904, were obtained from three independent cohorts of patients. In addition, only SKCM samples were retained for further analysis. TCGA-SKCM project was downloaded using the TCGAbiolinks package (Colaprico et al., 2016) and converted to the TPM format for subsequent analysis. The annotation of Ensembl ID for protein-coding mRNAs was transformed to the gene symbol based on the GENCODE gene model (GENCOED27). Then the batch effect from the different datasets was corrected using the ComBat package (Zhang et al., 2020) in the SKCM cohorts. Clinical data regarding the disease, including age, sex, tumor stage, and survival information, were retrieved from TCGA Pan-Cancer Clinical Data Resource (TCGA-CDR), and the clinical characteristics of the TCGA-SKCM patients are shown in **Supplementary Table 1**, of which only the overall survival (OS) information was obtained for further data processing. In addition, the copy number mutation data of TCGA-SKCM cohorts were downloaded from the GDAC-Firebrowse website[1].

Identification of Skin Cutaneous Melanoma Molecular Subtypes by Non-negative Matrix Factorization Clustering

The NMF clustering (Possemato et al., 2011) algorithm was used to cluster the SKCM samples. The 2,752 metabolism-related genes that encode all the well-known human metabolic enzymes and transporters were selected for follow-up screening. First, the metabolism-related genes that were significantly correlated with OS time were subjected to Cox survival regression using the survival R package. Then unsupervised NMF clustering (Gaujoux and Seoighe, 2010) was performed based on the TCGA-SKCM cohort, and validation was performed from the integrated cohorts from GSE54467 and GSE65904 using the same selected candidate genes. K values were chosen where the magnitude of the cophenetic correlation coefficient started to decrease with the optimum number of clusters (Brunet et al., 2004). Next, we evaluated the similarity of subtype classification between independent cohorts based on the expression profiles of mRNAs by employing the class mapping analysis (SubMap) (Gene pattern) method to assess whether the subtypes were analyzed in the training, and validation sets were significantly correlated. Simultaneously, the mRNA expression data of the

[1]http://firebrowse.org/

abovementioned candidate genes were analyzed to verify the subtype distributions using the T-distributed stochastic neighbor embedding (t-SNE) method.

Gene Set Variation Analysis

Gene set variation analysis (GSVA) (Hänzelmann et al., 2013) is a gene set enrichment method that computes an estimated fraction of certain pathways or signatures of different clusters based on expression profiles. The relevant metabolism (Rosario et al., 2018) and carcinogenesis- (Sanchez-Vega et al., 2018)-relevant pathway gene sets were obtained from previous studies, and the GSVA R package was used to investigate the gene set differences between samples. Subsequently, metabolism gene scores were obtained for differential analysis using the Limma package (Ritchie et al., 2015) in R software, and differentially expressed signatures were screened out with the following threshold ($|\log_2 FC| > 0.2$, adjusted $p < 0.05$).

Estimation of the Tumor Microenvironment Signatures

The microenvironment cell population counter (MCPcounter) (Becht et al., 2016) was used to estimate the number of infiltrated immune cell populations and two non-immune stromal cell populations (immune cell types: T cells, CD8 + T cells, natural killer cells, cytotoxic lymphocytes, B-cell lineage, monocytic lineage, myeloid dendritic cells, and neutrophils; stromal cell types: endothelial cells and fibroblasts). Furthermore, another approach applied to quantify tumor immune components was the single-sample gene set enrichment analysis (ssGSEA) method (Barbie et al., 2009), which calculates enrichment scores representing the degree to which genes in a particular gene set are coordinately upregulated or downregulated within a single sample. In particular, six immune cell populations, including regulatory T cells (Treg), helper T cells 1 (Th1), helper T cells 2 (Th2), helper T cells 17 (Th17), central memory T cells, and effective memory T cells (Tem), were analyzed using the GSVA R package. In addition, the ESTIMATE algorithm (Yoshihara et al., 2013) was applied to computer immune and stromal scores in different subtypes, thereby, reflecting the features of the tumor microenvironment.

Characterization of Skin Cutaneous Melanoma Subtypes

After data normalization, differentially expressed genes (DEGs) between different SKCM subtypes were identified using the Limma package ($|\log_2 FC| > 1$ and $p < 0.01$). The gene signature set files "c2.cp.kegg.v6.2. symbols.gmt" and "h,all,v60.2.symbols" were downloaded from the Molecular Signature Database (MSigDB)[2]. GSEA was then applied to investigate the pathway and functional enrichment using the Clusterprofiler R package (Yu et al., 2012) with the significance threshold set to an adjusted $p < 0.05$. Furthermore, previously published molecular classifications of SKCM were predicted using the nearest template prediction (NTP) analysis from gene pattern modules, and then the prediction outcome was compared with our classification.

[2]http://software.broadinstitute.org/gsea/msigdb/index.jsp

Construction and Validation of the Skin Cutaneous Melanoma Gene Classifier

To identify specific genes in the SKCM subtypes, we screened genes with statistically significant differences in the different subclasses according to the following criteria: for adjusted $p < 0.01$ and absolute $\log_2$ FC > 2. Only the genes with a significantly different expression in all three possible parameters were considered as subclass-specific genes. The top 30 genes with the largest $\log_2$FC values in each subtype (only genes with $\log_2 FC > 0$ were selected) were further used to generate the prediction models such that a 90-gene subtype classifier was created. Next, we used the NTP algorithm to predict the subclasses of the 90-gene signature in GSE14520 and compared them with the previous classification results derived from the NMF algorithm.

Prediction of the Efficacy of Each Subtype of Immunotherapy and Targeted Therapy

We used data from patients with melanoma treated with immunotherapy to indirectly predict the efficacy of immunotherapy in melanoma subclasses by measuring the similarity of gene expression profiles between the subclasses determined in this study and those in patients with melanoma based on SubMap analysis (gene pattern). Furthermore, we downloaded and performed SubMap analysis from the genomics of drug sensitivity in cancer (GDSC) database (Yang et al., 2013) to investigate its drug sensitivity.

Gene Ontology and KEGG Analyses

We performed Gene Ontology (GO) and KEGG enrichment analysis for the different subclasses of differentially expressed genes, where the GO includes biological process (BP), molecular function (MF), and cellular component (CC). GO analysis of differentially expressed genes was conducted using DAVID (Huang et al., 2007; Huang da et al., 2009) (FDR < 0.1) and visualized using the ggplot2[3] R package and Goplot package (Walter et al., 2015).

We performed the KEGG pathway enrichment analysis using the KOBAS 3.0 database[4] (Wu et al., 2006) for the integration of DEGs with Ensemble ID in the differential gene list and then obtained pathway enrichment lists where pathways with $p < 0.05$ were considered significantly enriched.

Mutation Analysis Using a 90-Gene Classifier

The gene mutation and gene copy number data of the 90-gene classifier in 32 TCGA pan-cancer databases were retrieved from the cBioportal (Gao et al., 2013) web portal. The mutation status of these genes in these databases were analyzed, and a bar chart showing the distribution ratio of the 90 genes in TCGA pan-cancer databases by mutation type, fusion, amplification, deep deletion, and multiple alterations were constructed.

[3]https://cran.r-project.org/web/packages/ggplot2/index.html

[4]http://kobas.cbi.pku.edu.cn

Transcription Factor Prediction

Transcription factors often modulate several metabolic genes that are closely functionally associated. Therefore, we utilized the NetworkAnalyst network platform (Zhou et al., 2019) to analyze and predict the transcription factors that are most likely to regulate the 90 genes included in the classifier and construct a molecular interaction network. The targeted gene–transcription factor interaction network also contains the TF–mRNA–miRNA molecular regulatory network data obtained from the RegNetwork information library.

Expression of Solute Carrier Family 7 Member 4 in Skin Cutaneous Melanoma and Kaplan–Meier Analysis

RNA-seq data were downloaded from UCSC XENA in TPM format, and GTEx was downloaded from UCSC XENA[5] and processed by the Toil project (Vivian et al., 2017). The Wilcoxon rank-sum test was used to compare solute carrier family 7 member 4 (SLC7A4) expression in normal TCGA and GTEx skin tissues and tumor samples from SKCM in TCGA. We categorized patients into high and low SLC7A4 expression groups according to the median value of their SLC7A4 expression (TPM format), following which Kaplan–Meier analysis of OS was performed for each group and visualized using the R package "survminer."

Patient Tissue Specimen Collection and Immunohistochemistry Validation

Melanoma tissues were collected from 25 melanoma patients of Han Chinese ethnicity from 2015 to 2020. Informed consent was obtained from each patient, and the study was approved by The Foshan Subject Review Board of the First People's Hospital. Paraffin-embedded tissues were sectioned at 4-mm thickness for immunohistochemistry (IHC) analysis. Antigen retrieval was performed by incubating the samples in citrate buffer (pH 6.0) for 15 min. After blocking with a mixture of methanol and 0.75% hydrogen peroxide, sections were incubated overnight with a primary antibody (SLC7A4, Proteintech, 1:200) followed by incubation with a secondary antibody conjugated with horseradish peroxidase (HRP; goat anti-rabbit IgG, 1:500, Cell Signaling Technology). The sections were washed three times with PBS and incubated with AEC (ZSGB-BIO). Staining was performed as described previously (Zhou et al., 2021). Tissues were examined through the cross-product (H score) of the percentage of tumor cell staining at each of the three staining intensities, and the staining score was graded through the H score as follows: low, H score = 0–100; moderate, H score = 101–200; and high, H score = 201–300.

Statistical Analysis

All data processing and analyses were performed using Excel (Microsoft) and R software (version 4.0.2). Unpaired Student's *t*-test was employed for the comparison of two groups with non-normal distribution, and the Mann–Whitney *U*-test was used for the comparison of two groups with non-normal distribution. One-way analysis of variance (ANOVA) and Kruskal–Wallis tests were performed for comparisons among three groups. Contingency table (χ^2) variables used the χ^2 test for statistical significance. Survival analysis was performed using the Kaplan–Meier method, and the log-rank test was used for comparison. Univariate Cox proportional risk regression models were used to evaluate risk ratios for univariate analyses. Two-tailed $p < 0.05$ was considered statistically significant.

[5]https://xenabrowser.net/datapages/

RESULTS

Non-negative Matrix Factorization Determined Three Subtypes of Skin Cutaneous Melanoma

Before conducting the NMF algorithm analysis of SKCM, we first utilized the ComBat algorithm to remove the batch effect for different SKCM cohorts and chart the PCA after batch effect removal (**Figure 1A**). A total of 2,752 previously reported metabolism-related genes were selected as the basis for NMF analysis. We then adopted univariate Cox regression for metabolism-related genes in the metadata set to identify prognostic genes associated with OS ($p < 0.1$), and a total of 517 candidate genes were obtained. We then extracted TCGA data expression profiles of SKCM, clustering the 517 candidate genes using the NMF clustering algorithm, and the non-negative matrix decomposition (NMF) with two to six clusters was plotted (**Figure 1B**). The best clustering number k value was established by computing the clustering correlation coefficient, and $k = 3$ was regarded as the optimal clustering number. The consensus NMF was performed again with several decompositions of 3, defining three subtypes C1 ($n = 113$), C2 ($n = 103$), and C3 ($n = 234$). To validate the clustering subtypes, we performed t-SNE dimension reduction to reduce the feature dimensionality for all samples of metabolic genes in the expression profile of the test TCGA dataset and showed the different two-dimensional distribution pattern plots for the three types of samples (**Figure 1C**), and the clinical characteristics of TCGA-SKCM are shown in **Supplementary Table 1**. We also found that our subtypes were largely consistent with the two-dimensional t-SNE distribution pattern. The same consensus NMF for the same set of metabolic genes was performed for the consolidated validation set (GSE54467 and GSE65904), and three classes C1 ($n = 93$), C2 ($n = 98$), and C3 ($n = 98$) were obtained. Finally, the subclass algorithm was used to identify the subtype matching model of TCGA and validation sets, and it was decided that TCGA-C1 = GEO-C1, TCGA-C2 = GEO-C3, and TCGA-C3 = GEO-C2. We also utilized survival information from the three cohorts to conduct a subtype survival analysis of the SKCM subset. In TCGA-SKCM cohort, the results showed a significantly higher OS in C2 than in C1 and C3 (log-rank test $p < 0.0001$, **Figure 1D**), and the same survival differences were also verified in the GEO validation dataset (GSE65904 and GSE54467). Similar survival outcomes

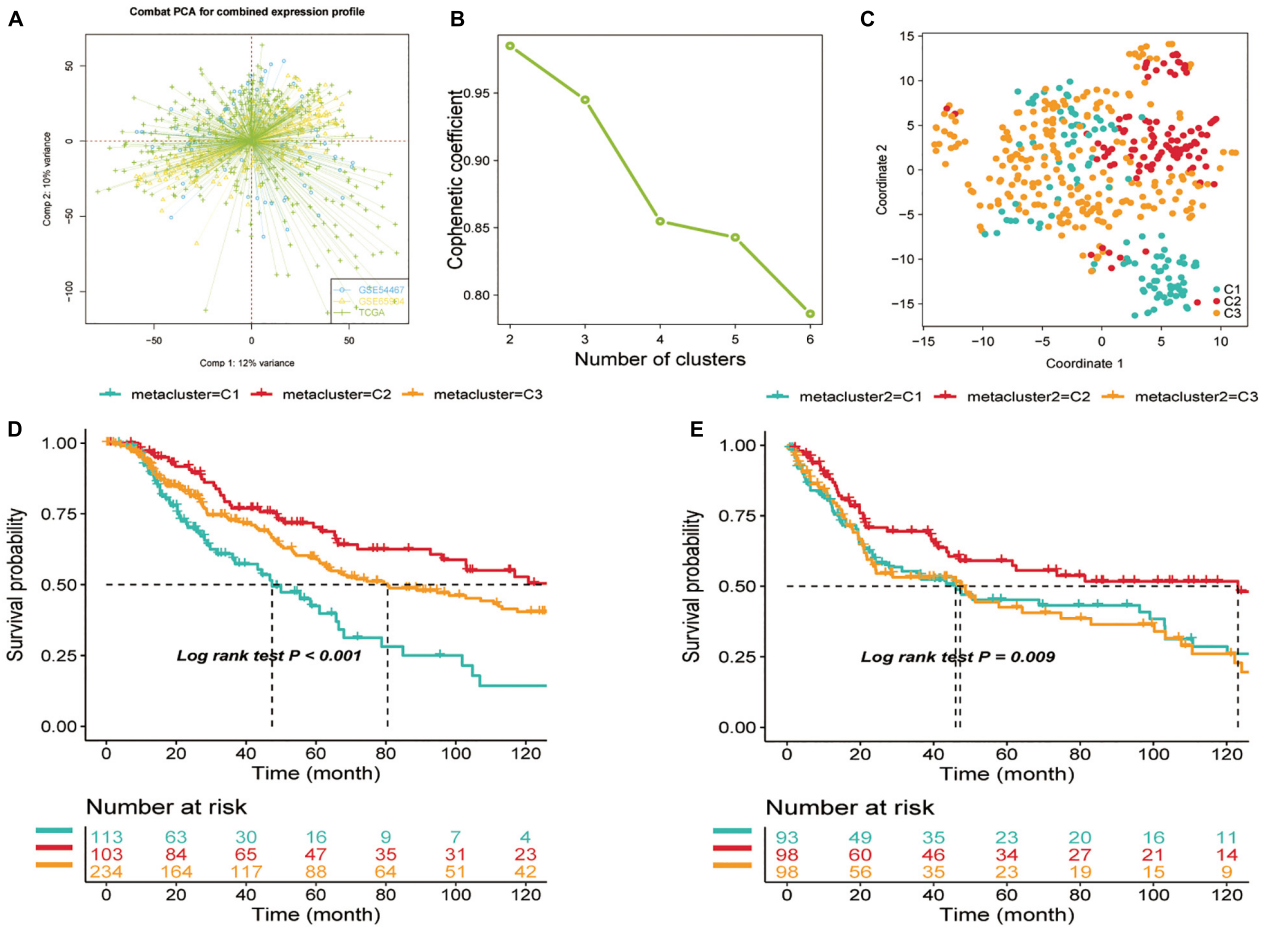

FIGURE 1 | Identification of skin cutaneous melanoma (SKCM) subtypes using non-negative matrix factorization (NMF) consensus clustering in the metadata set. **(A)** Visualization of principal component analysis of combined expression profiles of three cohort data sets. **(B)** Phenotype correlation coefficients for NMF clustering of 816 metabolism-related genes at k = 2–5. **(C)** t-SNE analysis rendered in support of classification into three SKCM subtypes. **(D)** Overall survival analysis of three subtypes (C1, C2, and C3) in two independent cohorts—test set (TCGA-SKCM) and **(E)** Validation set (GSE65904, GSE54467). Statistical significance of differences was determined using the log-rank test.

were observed; however, the prognosis of C2 in the validation set worsened, and the median survival time was more similar to that of C1 (**Figure 1E**).

Association of Skin Cutaneous Melanoma Subtypes With Metabolism-Related Signatures

Considering that the SKCM subclass classification was based on metabolism-related genes, we further investigated whether different metabolic signatures are present in the different subclasses. First, we scored the metabolic pathways (gene sets were acquired from the reported paper) using the GSVA R package in the subtype cohorts. In TCGA-SKCM cohort, GSVA enrichment scores of the metabolic pathways were estimated, and a cross-group Limma difference test was performed using two groups of "subtype n vs. other subtypes" to confirm subtype-specific differential metabolic pathways; the screening standard for GSVA enrichment was $|\log FC| > 0.2$, adjusted $p < 0.05$, and heat maps were constructed for visualization (**Figure 2A**).

The heat map showed that C1, C2, and C3 had 21, 3, and specific metabolic signatures, respectively. Among them, C1 demonstrated a distinct metabolic signature, with 21 metabolic pathways significantly upregulated. Both C2 and C3 were significantly downregulated in these pathways. These results demonstrated that each subtype was enriched in unique metabolic pathways and had dissimilar metabolic levels.

We also counted the GSVA enrichment points of carcinogenesis-related pathways and plotted a box line among groups. To further investigate their subtype characteristics, we selected a collection of 11 carcinogenesis-related pathways and quantified them using the GSVA algorithm. The results showed significant between-group differences among the three subgroups in cell cycle, HIPPO, MYC, NRF2, PI3K, TGF-β, TP53, WNT, and angiogenesis, which are carcinogenic signaling pathways (**Figure 3A**), indicating a close connection between

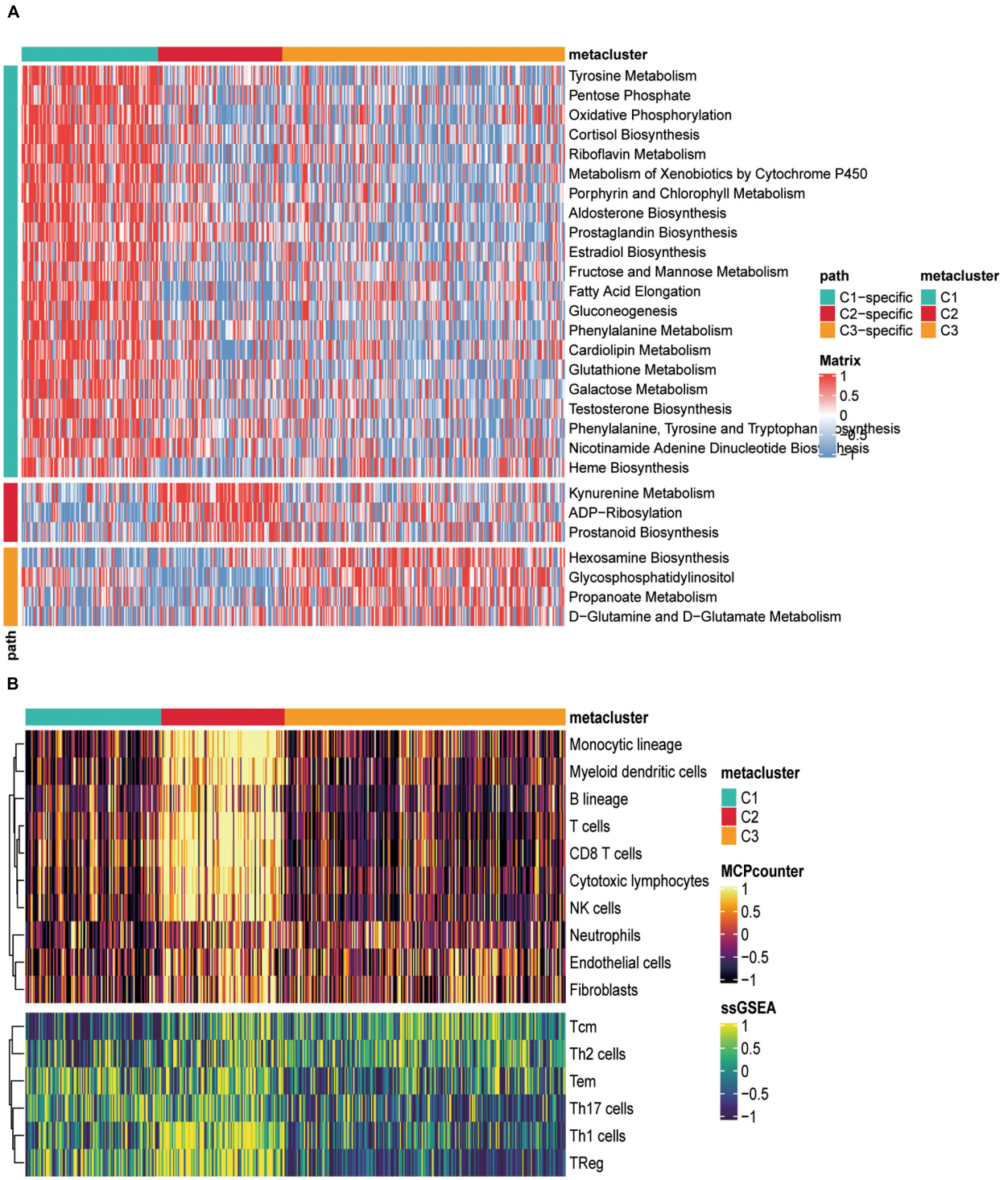

FIGURE 2 | Correlation between metabolically relevant features and immune infiltration in SKCM subtypes. **(A)** Heat map of specific metabolism-related signatures in three subtypes. **(B)** The heat map depicted the richness of immune and stromal cell populations in C1, C2, and C3 by MCPcounter and ssGSEA.

our subtypes and carcinogenesis. The results revealed that C1 had a significantly strong cell cycle and WNT signature than C2 and C3, C2 displayed increased expression of components of the angiogenesis pathway, and C3 was particularly enriched in the HIPPO, NRF2, PI3K, TGF-β, and TP53 pathways.

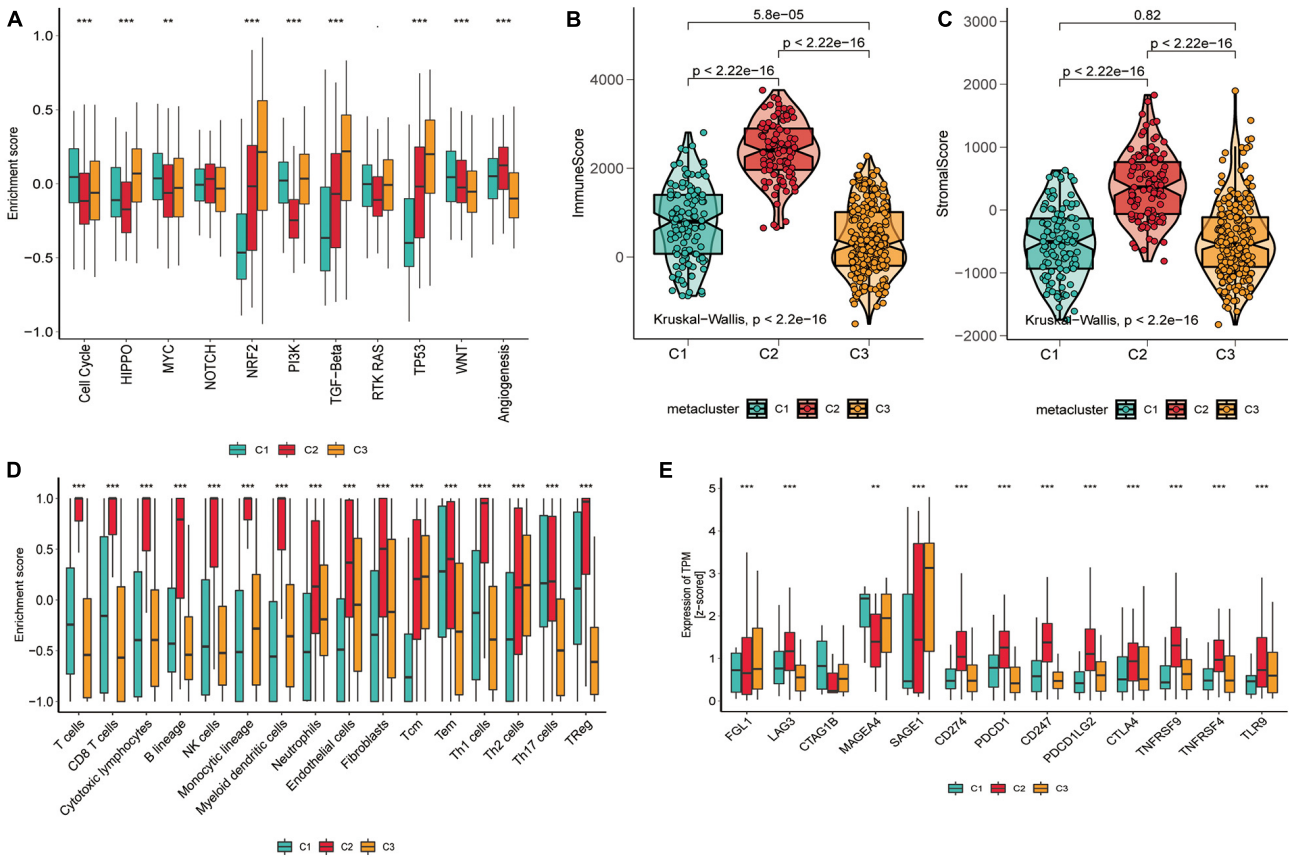

FIGURE 3 | Tumor microenvironment signatures of three subtypes in the TCGA-SKCM. **(A)** Box plots of characteristic marks discriminating different subtypes of SKCM progression-related features. Box-line plots of the immune score **(B)** and stromal score **(C)** estimate three subtypes. For the box-line plot, the lines in the box represent the median, the bottom, and top of the box, which are the 25th and 75th percentiles (interquartile range), and the vertical lines represent 1.5 times the interquartile range. Statistical differences were compared by the Kruskal–Wallis test, and *p*-values are marked with an asterisk above each box line plot (ns indicates no significance, $^{**}p < 0.01$, $^{****}p < 0.0001$). **(D)** The boxplot showed the accumulation of immune and stromal cell populations discriminated by different subtypes. **(E)** Expression level (normalized transcripts per million) of 14 immune checkpoint genes in three SKCM subtypes. The difference was verified statistically through the Kruskal–Wallis test, and the p-values are noted with asterisks at the top of each boxplot (ns stands for no significance, $^{*}p < 0.05$, $^{***}p < 0.001$).

Correlation Between Skin Cutaneous Melanoma Subtypes and Immune Infiltration

As significant differences in immune scores were detected between SKCM subtypes, we surveyed immune cell infiltration in SKCM subtypes to assess their immunological landscape. We utilized the MCP-counter and ssGSEA algorithms to compute the abundance of 16 immune infiltration cells and presented them in an immune heat map (**Figure 2B**). We also plotted box plots of inter-group differences in immune cells, and the results displayed significant inter-group differences in all types of immune cell populations among the three subtypes (**Figure 3D**). Notably, the box plots revealed that C2 showed a significantly higher enrichment immune score than C1 and C3 in almost all immune cells, except for Th17 cells, in which both C1 and C2 had significantly higher Th17 cell enrichment scores than C3. Of these results, C2 was enriched with more immune cells, which is consistent with the finding that C2 had the highest immune score among the three subtypes. With the current widespread use of immune checkpoint inhibitors (ICIs) in clinical trials and for the treatment of advanced melanoma (Woods et al., 2016), we explored the correlation between the expression of 13 classically targeted immune checkpoint genes in these subtypes, which are currently based on immunotherapy inhibitors in clinical trials or licensed for certain cancer types. The results showed significant differences between groups, while C2 displayed a higher expression of nine immune checkpoint genes than C1 and C3, except for FGL1, CTAG1B, and MAGEA4 (**Figure 3E**).

Relevance of Skin Cutaneous Melanoma Subtypes to the Clinical Characteristics of Patients and in TCGA and GEO Datasets

To investigate the associations between subtypes and clinical characteristics, we analyzed the clinical tumor pathology variables associated with subtypes based on TCGA-SKCM (**Figure 4A**) and GEO validation set (**Figure 4B**) cohorts to construct the clinical information heat map of subtypes. The

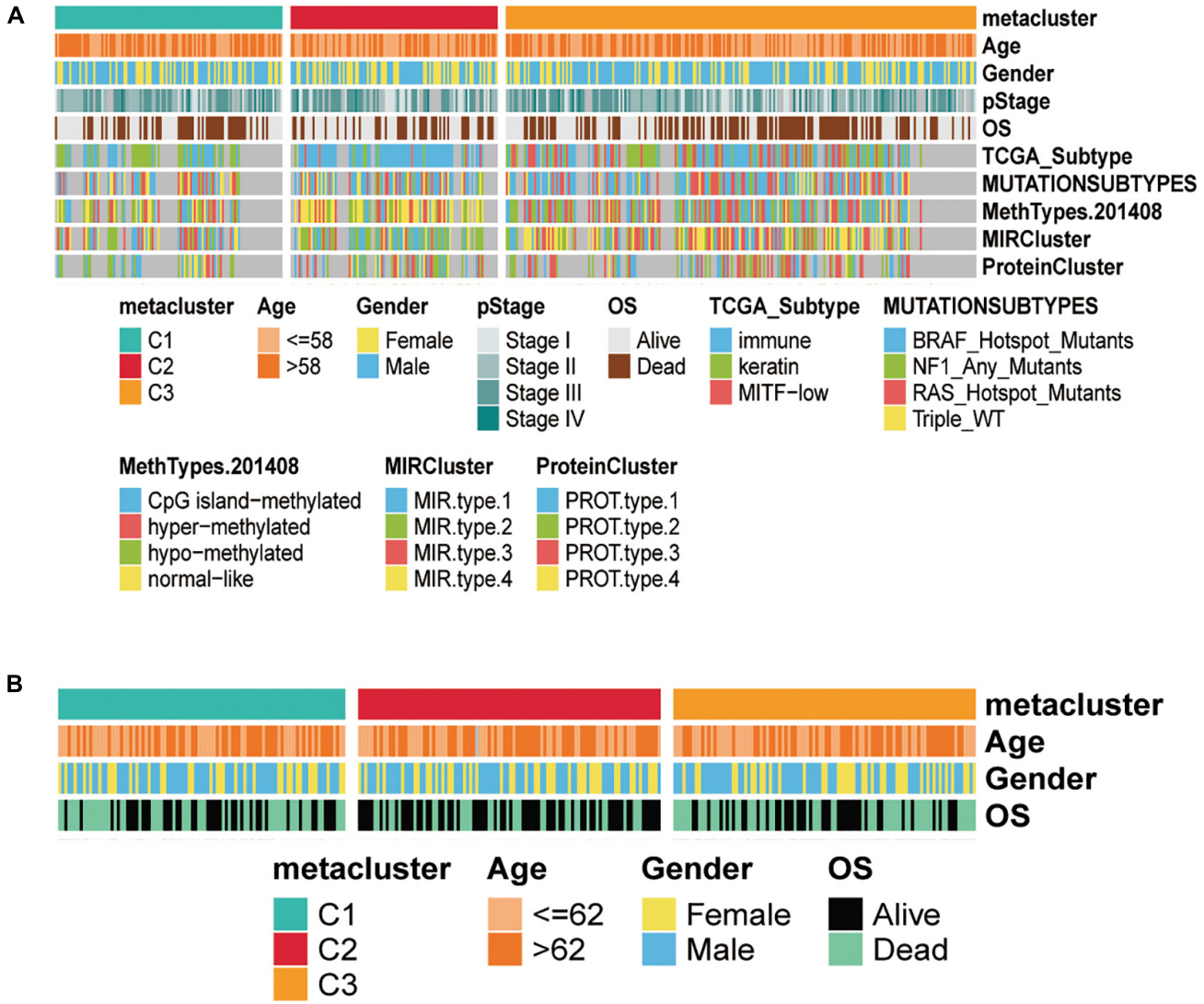

FIGURE 4 | Clinical characteristics of three subtypes in the TCGA-SKCM and GSE14520 cohorts. **(A)** Correlation of C1, C2, and C3 subtypes with clinical features and previous SKCM subtypes in the TCGA cohort. **(B)** Correlation of our classification with clinical features in the validation GSE14520 set cohorts.

results showed an independence test for discrepancies between clinicopathological characteristics and metabolic subtypes. Furthermore, we matched this metabolic classification with the previously reported subtypes of SKCM in the literature, including mutation subtypes (BRAF, NF1, RAS, and Triple-WT), MethTypes (CpG island-methylated, Hyper-methylated, Hypo-methylated, and Normal-like), the MIR cluster (four types), the Protein Cluster (four classes), and the classification of TCGA (Immune, Keratin, and MITF-low) (**Figure 4A** and **Supplementary Tables 2, 3**). In TCGA-SKCM, the C1 subtype was significantly correlated with protein cluster 2 ($p = 0.006$), MIR type 3 ($p < 0.001$), hypomethylated type ($p < 0.001$), and keratin type ($p < 0.001$). The C2 subtypes associated with protein cluster 1 ($p = 0.006$), MIR type 2 ($p < 0.001$), normal-like methylated type ($p < 0.001$), and immune type ($p < 0.001$). The C3 subtype was related to protein cluster 3 ($p = 0.006$), MIR type 3 ($p < 0.001$), hyper-methylated type ($p < 0.001$), and immune type ($p < 0.001$).

Association of Skin Cutaneous Melanoma Subtypes With the Tumor Microenvironment

To further evaluate whether the subtypes were associated with the tumor microenvironment, we estimated the immune and stromal scores using the ESTIMATE algorithm for each group and constructed box-violin plots (**Figures 3B,C**). The results showed statistically significant differences in immune scores between the three groups, while the stromal scores were not statistically significant among the three groups. C2 had the highest immune score among the three groups.

The melanoma mutation landscape has been demonstrated to lead to alterations in the tumor microenvironment (Nassar and Tan, 2020) and immunotherapeutic response (Havel et al., 2019). Next, we investigated whether somatic mutation frequencies varied across SKCM subtypes and examined the mutation patterns in these subtypes. We applied the maftools package (Mayakonda et al., 2018) to estimate TCGA-SKCM-driven gene mutations and mapped waterfall plots of clusters within each group. High frequencies of mutations were observed for BRAF, COL5A1, NRAS, MECOM, NF1, ARID2, TP53, and CDKN2A in SKCM subtypes (**Figure 5A** and **Supplementary Table 4**). We then classified the total number of mutations and the predicted neoantigens (**Figure 5B**). The tumor mutation burden (TMB) was calculated for each metabolic subtype (**Figure 5C**), and box-line violin plots were constructed separately. Subsequently, we determined the frequency of amplification (**Figure 5D**) and deletion (**Figure 5E**) for the three subtypes using online GISTIC 2.0 analysis (Mermel et al., 2011) to construct box-line violin plots of amplifications vs. deletions for each subtype.

Finally, we further reviewed the chromosomal segment values of the three subtypes to ascertain whether there were significant copy number alterations by performing online GISTIC2.0 analysis on genePattern[6] to map the copy number change cytoband of each subtype. Cytoband revealed an overall description of the copy number variation in each subgroup (red representing gains and blue representing losses) (**Figures 6A–C**). As expected, our profiling demonstrated that significant copy number alterations emerged in the three subtypes, including those observed in the chromosomal region of 9p21.3 (CDKN2A) (Ghiorzo et al., 2006); amplification at 11q13.3 (CCND1) (Gibcus et al., 2007) in C1 and C2; amplification at 22q13.2 (TOB2) (Thanasai et al., 2006) in G1 and G3, in which TOB2 was significantly amplified in C1; and a major amplification at 5p13.3 (TERT) (Peifer et al., 2015) in the C1 subtype. While the cytobands for C1 and C3 displayed more regional amplifications and deletions than C2, this could also be an essential explanation for the superior prognosis of C2 over the C1 and C3 subtypes. Thus, the alteration of copy number may be a dominant mechanism responsible for the differences in metabolism and prognosis among the three subtypes.

Ninety-Gene Classifier and Performance Validation

To build a subtype classifier for clinical application, we further selected subtype-related signature genes. The results of the Limma differential expression analysis were based on the whole expression map "subtype n vs. other subtypes." Using MOVICS (Lu et al., 2020) package analysis, we retrieved the top 30 genes specifically upregulated for each metabolic subtype as biomarkers and then constituted clinical models and plotted correlation heat maps (**Figure 7A** and **Supplementary Table 4**). Consequently, we derived a 90-gene classifier and executed a consistency test by operating the NTP algorithm to predict the metabolic subtype attribution of each sample in the TCGA cohort as well as the GEO test set cohort, and plotted the heat map of the true subtype if it matched the predicted subtype (**Figures 7B,C**). The results were largely consistent between NMF and NTP in the three different subtypes of the test and validation sets ($\kappa = 0.631$ $p < 0.001$, $\kappa = 0.714$ $p < 0.001$), indicating that this 90-gene signature could be replicated to identify the metabolic classification of SKCM.

Specific Sensitivity of Skin Cutaneous Melanoma Subtypes to Immunotherapy and Potentially Targeted Therapies

On the one hand, the different patterns of immune infiltration and expression levels of immune checkpoint genes in different SKCM subtypes suggest the need to further investigate the possibility of an immunotherapeutic response. Therefore, we matched the expression profiles of the three subtypes using a subclass algorithm to ascertain the degree of similarity of TCGA metabolic subtypes to the response profiles of 47 patients with melanoma receiving immunotherapy (Hoshida et al., 2007; Roh et al., 2017). The results indicate that the TCGA-C2 subtype was more likely to be responsive to immunotherapy with anti-PD1 treatment (**Figure 7E**) (Bonferroni correction, $p = 0.01$).

On the other hand, to identify potential anti-melanoma drugs that are associated with ICIs, we attempted to find potentially sensitive and selective chemotherapy drugs using the GDSC drug sensitivity database. We compared drug sensitivity for more than 100 drugs in the GDSC database, and the top 12 differential response drugs were plotted and listed according to the Kruskal-Wallis test (**Figure 7D**). We detected a significant difference in the estimated IC50 values between the three subtypes and found that C2 may be more sensitive to chemotherapeutic drugs.

Functional and Pathway Enrichment Analysis of the 90-Gene Classifier

Gene Ontology and KEGG enrichment analyses were conducted for the three group DEGs using the DAVID database, and GO enrichment analyses were performed for each of the three GO categories: BP, MF, and CC. The ggplot2 package was used for visualization, and the top 10 enrichment results are shown (**Supplementary Figure 1** and **Supplementary Table 6–8**). The GO enrichment results of the three groups of DEGs were mainly enriched in the metabolism process, immune-specific BP, protein binding, cell cycle, DNA damage and repair, and cancer-associated biological processes. By taking the intersection of the enrichment analysis results of the three groups of differential genes in the KOBAS database, we identified six KEGG pathways related to oncogenesis development and metabolism for presentation. The red dots represent the upregulated enriched genes, mainly enriched in apoptosis, cell cycle, HIF-1 signaling pathway, human T-cell leukemia virus 1, cancer infection pathway, PI3K–Akt signaling pathway, and carcinogenesis biological pathway (**Supplementary Figure 2** and **Supplementary Table 9**).

Mutation Analysis of the Gene Classifier in TCGA Pan-Cancer Database

Based on the gene mutation and gene copy number data of the 90-gene classifier in 32 TCGA pan-cancer databases retrieved

[6]http://www.genepattern.org/

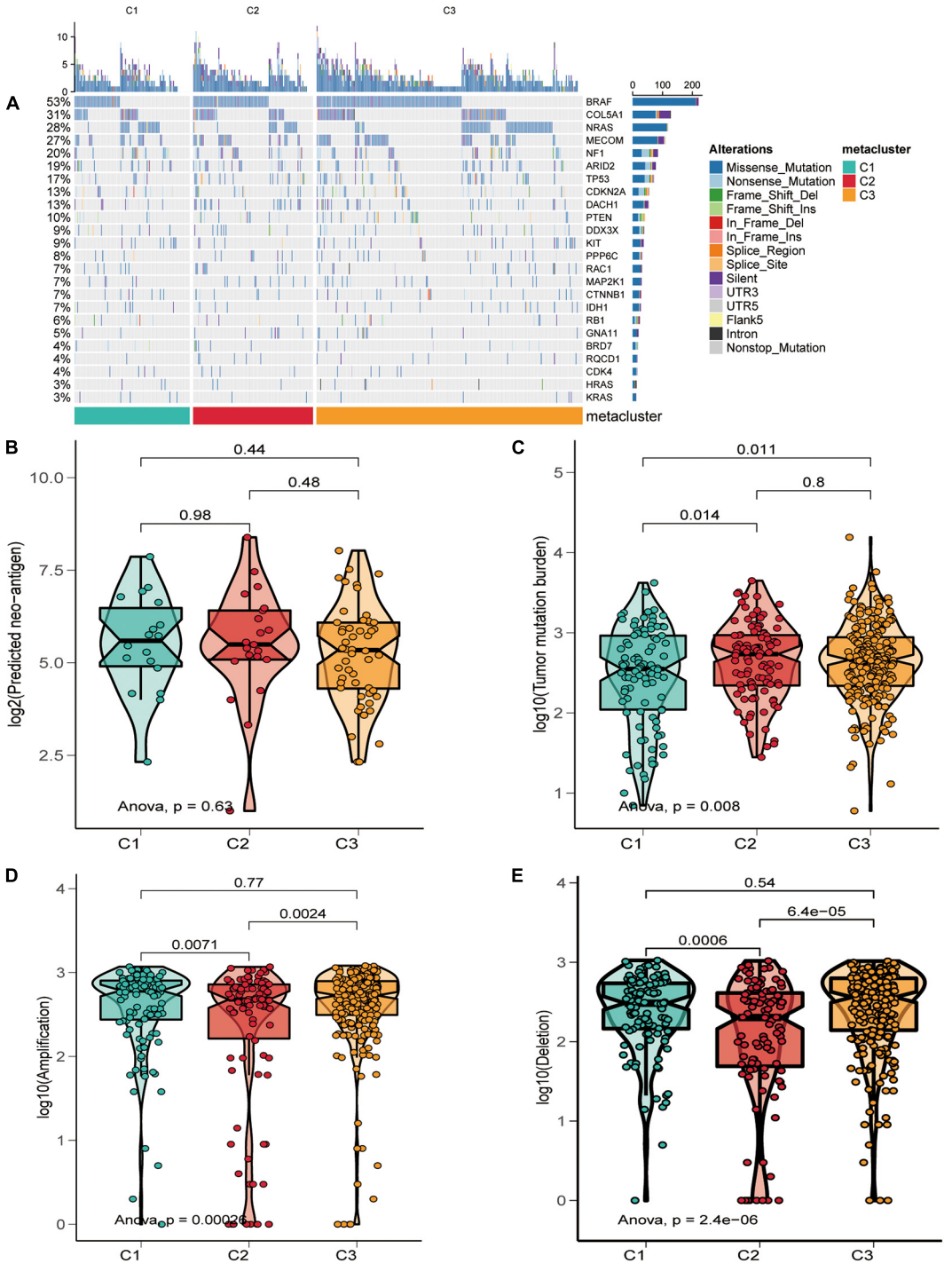

FIGURE 5 | Relationship of SKCM subtypes with tumor mutation burden characteristics. **(A)** Driver-type oncogenic mutations based on TCGA-SKCM typing with intra-group aggregation waterfall plots. **(B–E)** Violin plots of the number of mutation-predicted neoantigens **(B,C)** and copy number aberrations **(D,E)** box lines for SKCM subtypes. Wilcoxon rank-sum test was used to compare statistical differences (ns indicates not significant).

from the cBioportal web portal, the mutation rates of the genes in the classifier were analyzed, and the distribution ratio of each mutation type of the gene classifier in each pan-cancer tumor, including gene mutation, fusion, amplification, deep deletion, and multiple alterations, is shown in a bar chart (**Supplementary Figure 3A**). Among them, the mutation rate exceeded 50% in most tumor cancer types in TCGA, and the mutation rate was higher in lung squamous cell carcinoma,

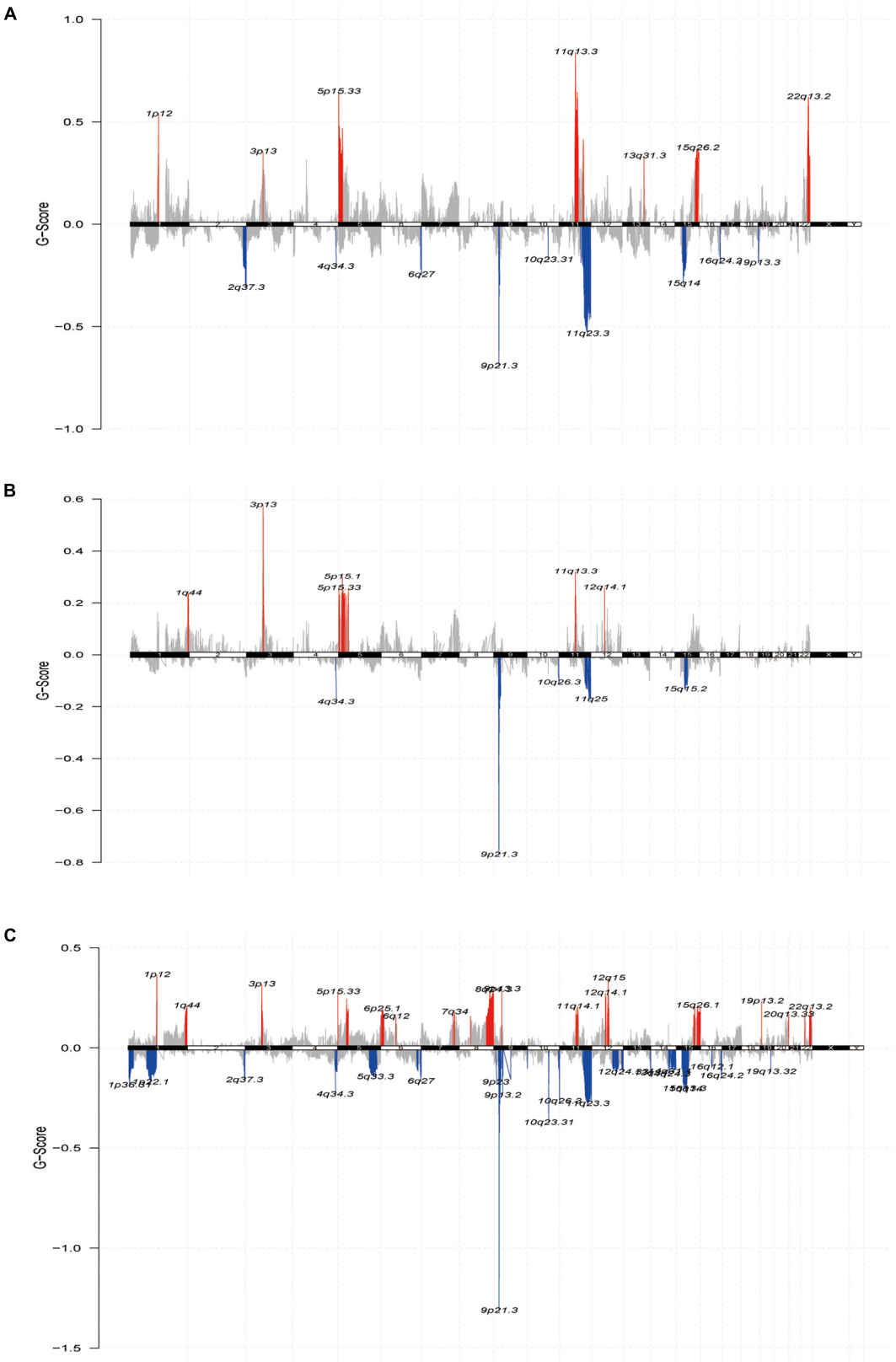

FIGURE 6 | The landscape of somatic copy-number alterations in the three subtypes. **(A–C)** Cytoband showed the genomic copy-number change from three subtypes. Amplification (red) and deletion (blue) of each regional peak are shown and highlighted.

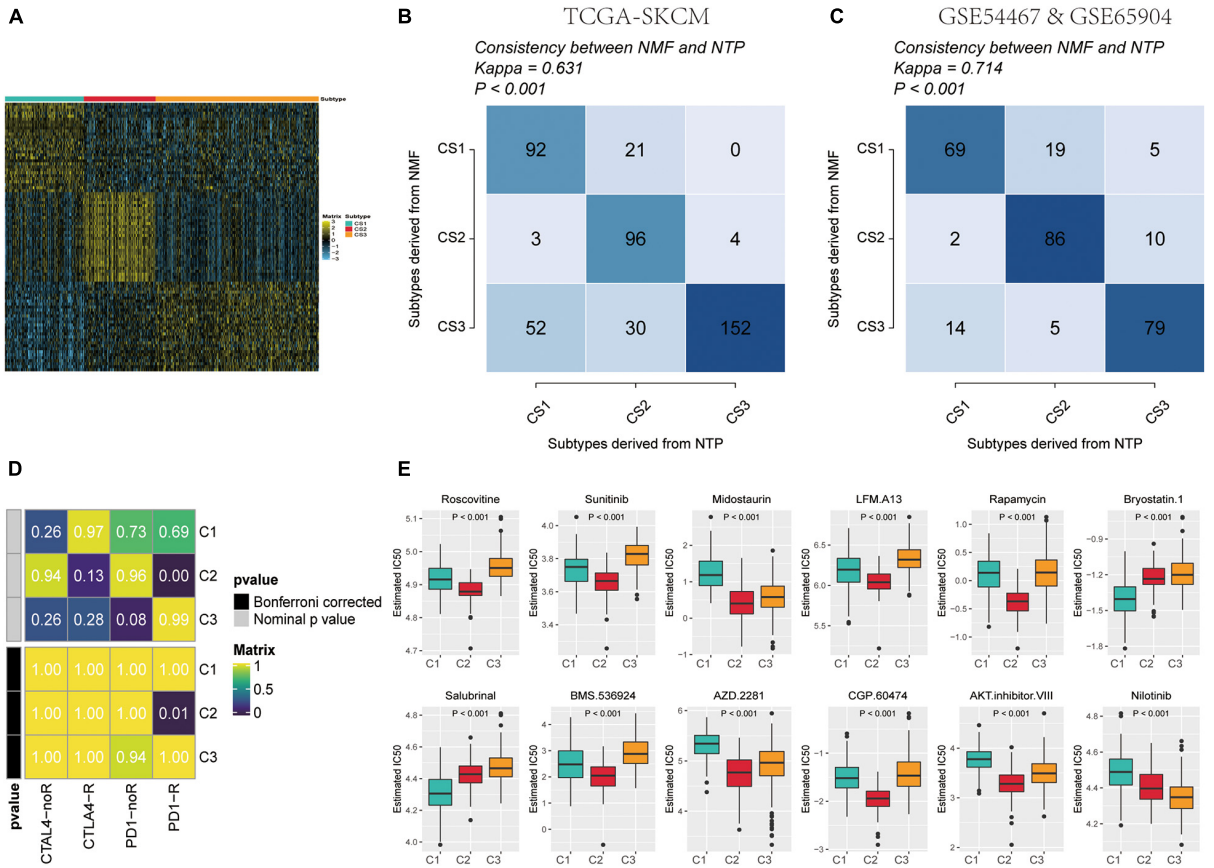

FIGURE 7 | Identification of predictive metabolism-gene classifier and prediction immunotherapeutic response. **(A)** The heat map exhibited the expression level of the 90-gene classifier in C1, C2, and C3. **(B)** Consistency of SKCM metabolism subtype predictions between the 90-gene classifier and the original NMF-based predictions in TCGA-SKCM. **(C)** Consistency of SKCM metabolism subtype predictions between the 90-gene classifier and the original NMF-based predictions in GSE54467 and GSE65904. **(D)** C2 is likely sensitive to the PD-1 receptor inhibitor (nominal $p = 0.01$) by SubMap analysis. **(E)** Top 12 box plots of predicted IC50 values based on GDSC database drugs in three subtypes of TCGA-SKCM dataset.

esophageal adenocarcinoma, stomach adenocarcinoma, SKCM, and bladder urothelial carcinoma, with an alteration frequency of more than 80%.

The TF–mRNA–miRNA Network Construction

Many closely related genes are often subject to simultaneous regulation by specific transcription factors; therefore, we utilized the NetworkAnalyst network platform to predict the transcription factors most likely to regulate the 90 genes in the classifier by analyzing them and constructing a TF–mRNA–miRNA molecular interaction regulatory network (**Supplementary Figure 3B**).

Expression Signature, Prognostic Value, and Preliminary Experimental Validation of Solute Carrier Family 7 Member 4

The 90-gene classifier distribution in the three subtypes and the fold changes are plotted in the heat map shown in **Figure 7A** and **Supplementary Table 5**. Of these, SLC7A4 was not reported to be associated with melanoma among the 90 genes. Therefore, we performed an analysis and preliminary experimental validation of the role of SLC7A4 in SKCM. SLC7A4 was overexpressed in SKCM than in the adjacent normal skin tissues (**Figure 8A**). The OS was poorer in patients with high SLC7A4 expression than in those with low SLC7A4 expression (hazard ratio [HR] = 1.34 [1.02–1.76], $p = 0.038$, **Figure 8B**). SLC7A4 expression was determined in tissue samples using IHC staining. The results showed that melanoma tissues presented the highest expression of SLC7A4, followed by benign nevi, whereas normal skin tissues showed the lowest expression (**Figures 8C,D**). Generally, the intensity of SLC7A4 staining increased with the progression of melanoma. These results demonstrated that SLC7A4 plays a hub role in SKCM progression and, to some extent, proved the accuracy of this gene classifier.

DISCUSSION

Metabolic reprogramming is a key hallmark of cancer (Pavlova and Thompson, 2016). On the one hand, SKCM is characterized

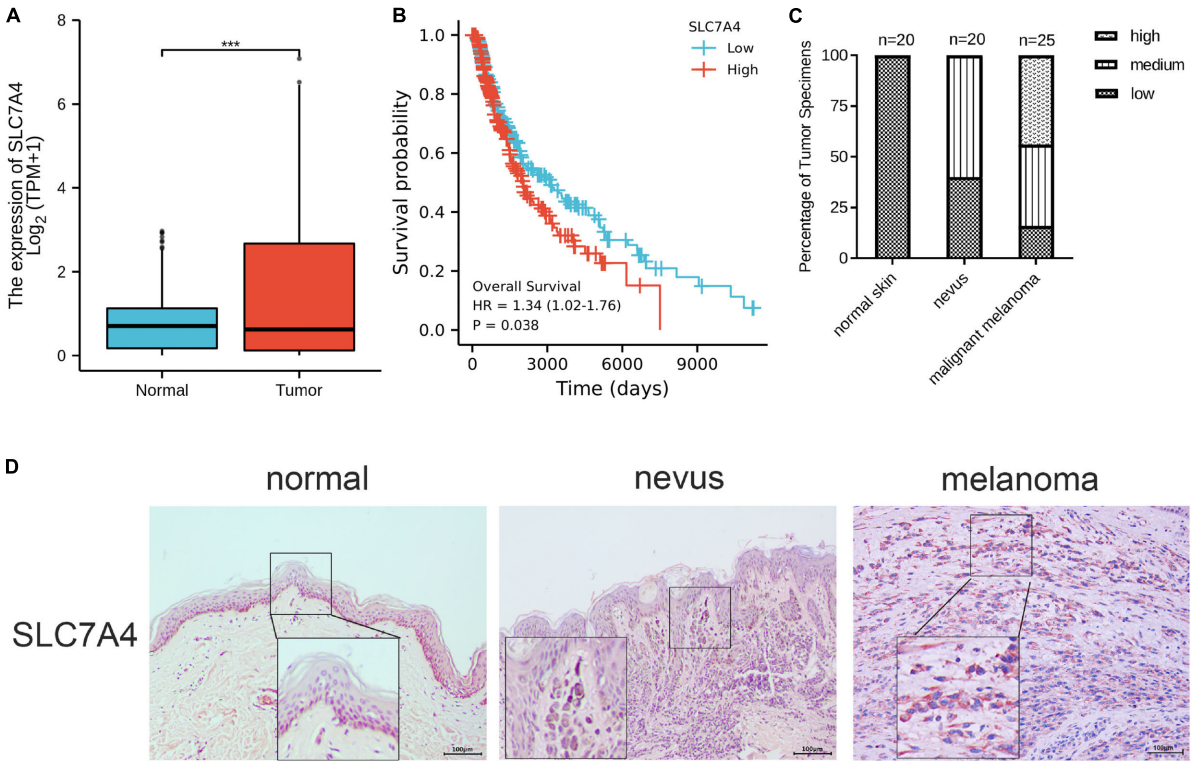

FIGURE 8 | The expression signature, prognostic value, and preliminary validation of solute carrier family 7 member 4 (SLC7A4). **(A)** The expression of SLC7A4 was higher in SKCM than in normal skin tissues. **(B)** The overall survival analysis of SLC7A4 in SKCM. **(C,D)** IHC staining demonstrated that the expressions of SLC7A4 staining increased with the progression of the disease. Normal skin tissues (n = 20) showed the lowest expression, followed by benign nevi (n = 20), and malignant melanoma tissues (n = 25) showing the highest expression. IHC, immunohistochemistry. IHC stain, AEC, original magnification × 100, scale bar = 0.1 mm (inset, IHC stain, AEC, original magnification ×400).

by its marked metabolic plasticity, and its development is associated with an important relationship between carcinogenesis and energy metabolism (Ruocco et al., 2019). On the other hand, metabolic reprogramming of melanoma alters the subset function of immune cells, enabling melanoma to evade the immune system. Thus, there is an urgent need to better understand the metabolic signatures of tumor heterogeneity in patients with melanoma to provide precise immunotherapy selection strategies and characterize the mechanisms of drug resistance. Herein, we performed a thorough classification of the metabolic profiles of SKCM specimens. Our findings revealed that SKCM could be categorized into three different metabolically relevant subtypes, and we verified the reproducibility of these subtypes in the GEO test set. Each subtype was characterized by different metabolic signatures, prognosis values, clinical parameters, tumor microenvironment features, immune cell infiltration, function and pathway enrichment, somatic copy number alterations, response to immunotherapy, and drug sensitivity. The C1 subtype displayed high metabolism levels, resembling the keratin subtype, with an advanced pathological stage and low immune infiltration. Furthermore, C1 had the worst prognosis and the shortest DFS among SKCM patients. In contrast, C2 was abundant in immune signatures with a relatively high expression of immune checkpoint genes and high immune and stromal scores, in line with the immune type and normal methylation type, demonstrating drug sensitivity to PD-1 inhibitors. This cluster was hardly engaged in metabolic signatures. The C3 subtype had the highest enrichment scores for carcinogenic pathways and the lowest enrichment scores for immune infiltration. It exhibited lower enrichment for metabolic signatures than C1 but greater enrichment than C2 for metabolic signatures. Overall, this research was undertaken to explore the metabolic landscape of SKCM and separately detect three clusters with different characteristics.

The results indicated that C1 had the most differential metabolic pathways, with 21 associated metabolic pathways all upregulated in this subtype. Therefore, we defined C1 as the metabolically active subtype. Several recent studies have focused on building a connection between endogenous tumor metabolism and immunotherapy. For example, recent studies have indicated that an increase in glycolytic metabolism in SKCM is linked to resistance to adoptive T-cell and immune checkpoint blockade therapies (Cascone et al., 2018). The hypermetabolic activation of C1 induces, on the one hand, nutrient depletion and hypoxia in the tumor microenvironment, thus, establishing metabolic competition between tumor cells and infiltrating immune cells. On the other hand, the active metabolism of SKCM in the tumor microenvironment leads to toxic concentrations

of certain metabolites, including elevated concentrations of adenosine, kynurenine, ornithine, and reactive oxygen species, all of which markedly inhibit the anti-tumor immune response (Leone and Powell, 2020). The taxonomic classification model of SKCM reported in 2015 identified three transcriptomic clusters based on mRNA transcriptional gene function, namely, "immune," "keratin," and "MITF-low" (2015). Of the three subtypes, the keratin subtype had the poorest prognosis among patients with localized melanoma metastases and featured high expression of keratin-coding genes and metabolic genes in organ development, which was consistent with C1 having the poorest prognosis and characterized by enrichment gene signatures of keratin-related metabolic procedures. In addition, the clinical signature analysis showed that most patients in C1 were in the advanced pathological stage, followed by C3.

Several metabolic processes were upregulated in subclass C1, including amino acid metabolism, carbohydrate metabolism, and lipid metabolism. Enrichment results of metabolic signatures indicate the possibility that C1 could benefit from targeted metabolism therapy. Metabolic therapies targeting certain metabolic processes provide alternatives for chemoresistant patients. For instance, metformin can exert an anti-melanoma effect (Li et al., 2018) and promote combination treatment efficacy with anti-PD-1 and anti-cytotoxic T-lymphocyte-associated protein-4 (CTLA4) agents (Afzal et al., 2018; Cha et al., 2018). Identifying the potential beneficiaries of metabolic therapies has always proven to be challenging (Goodpaster and Sparks, 2017). Meanwhile, some key processes, such as glycolytic metabolism, hexosamine biosynthesis pathway, and glutathione metabolic pathways, were enriched in C3, suggesting that patients with this (HBP) are a shunt pathway of glycolysis and a key metabolic juncture in cancer cells. Recent studies have demonstrated that treatment with small molecule drugs that target HBP lead to increased infiltration of CD8 + T cells, sensitizing pancreatic tumors to anti-PD1 therapy and causing tumor regression and prolonged survival (Sharma et al., 2020). This implies that we may achieve precise targeting of C3 subclasses by targeting HBP in SKCM. This subcategory survey provides new clues to forecast potential candidates for metabolic therapies, which needs further verification in a large clinical cohort.

Tumor immune infiltration results showed that C2 had elevated levels of all immune cell lineages, indicating that it was in a highly immune-activating state. We believe that it contributes to the best prognosis of C2 among the three subtypes. C2 matches the immune subtype and is accompanied by the highest associated immune score. The immune subtype exhibited high expression of immune cell subsets (T cells, B cells, and NK cells), immune signaling molecules, and immune checkpoint-related genes, and patients with regional metastatic SKCM in the immune subtype had a better prognosis than the other two subtypes due to their active host immune response (2015). Furthermore, tumor microenvironment-related assessments revealed that C2 had higher immune and stromal scores. Research on SKCM classification based on TMB found that those with high immune scores had a favorable prognosis, and those with low immune scores had a poor prognosis (Hu et al., 2020), and these findings were consistent with the favorable prognosis of the immune-high C2 subtype in our study. Immune checkpoint blocking antibodies, such as pembrolizumab, nivolumab, and ipilimumab, which target PD-1 or CTLA-4, have considerably transformed the therapeutic landscape of SKCM in recent years (Schvartsman et al., 2019). C2 exhibited a higher expression of immune checkpoint genes, especially LAG3, CD274 (also known as PD-L1), PDCD1, CD247, CTLA4, PDCD1LG2, TNFRSF9, TNFRSF4, and TLR9, demonstrating that it shows promising sensitivity against anti-PD-1 therapy and other checkpoint inhibitors. The high expression enrichment score of PD-1 (CD274) may contribute to the susceptibility of C2 to anti-PD-1 therapy. This aligns with the results of the TIDE algorithm, in which C2 was sensitive to PD-1 immunotherapy. In contrast, immune checkpoint expression of fibrinogen-like protein 1 (FGL1) was highest in the C3 subtype, and FGL1 is the major LAG-3 functional ligand that acts independently of MHC-II (Wang et al., 2019). FGL1 represses antigen-specific T-cell activation and exerts a tumor immunosuppressive effect, and it is associated with poor prognosis and resistance to anti-PD-1 therapy.

The C3 subtype paralleled the MITF-low subtype of SKCM. The "MITF-low" cluster is marked with a low expression of genes associated with immune regulation (2015) and pigmentation markers, which is consistent with the low immune cell infiltration in C3. Meanwhile, studies have consistently reported that low MITF expression is an early resistance to multiple targeted drugs (Müller et al., 2014). Furthermore, the enrichment scores of C3 were significantly higher than those of C1 and C2 in most carcinogenic pathways, such as NRF2, PI3K, TGF-β, TP53, and Hippo, which accounts for the poor prognosis of patients in the C3 subgroup. In particular, activation of NRF2 inhibits the activity of the melanocyte lineage marker MITF and blunts the induction of innate immune responses in SKCM (Jessen et al., 2020). This is in line with the similarity of C3 with the MITF-low cluster. These data suggested that the C3 subclass was of high heterogeneity and might be refractory. Notably, previous studies demonstrated that the MITF-low subpopulation can be reversed by combining NK-κB inhibitors with SKCM resistance to BRAF inhibitors (Konieczkowski et al., 2014; Su et al., 2020), implying that the C3 subclass would best respond to the combination of NFK-κB inhibitors and BRAF inhibitors. C3 was also similar to the CpG island methylator phenotype (CIMP) (2015), one of the reported molecular subtypes of SKCM. Studies have shown that the CIMP pattern is implicated in the progression of the clinical stage of malignant melanoma (Tanemura et al., 2009). This is due to the fact that patients with SKCM of the C3 subtype are mostly at a higher pathological grade. Therefore, the poor prognosis in C3 may be attributed to the combined effects of low infiltration of immune cells, high enrichment of carcinogenesis pathways, low MITF expression, CIMP, and advanced pathological stage.

Skin cutaneous melanoma has an extremely high TMB due to ultraviolet (UV) mutagenesis (Lo et al., 2021), and these neoantigen burdens may alter T-cell responses in the tumor microenvironment (Hollern et al., 2019). Therefore, we examined whether copy number aberrations (deletions and amplifications), TMB, and neoantigens could be associated with the subtypes

of SKCM. The results illustrated no statistically significant correlation between neoantigen burden and subtypes, with the TMB in C2 being the highest in the three types. Regarding copy number aberrations, C2 patients had fewer amplifications and deletions than C1 and C3. Our data revealed a high TMB in the C2 subclass, which is compatible with the result that the C2 subclass was sensitive to PD-1 treatment. Moreover, the number of somatic mutations was higher in C1 and C3 than in C2, which may lead to a poorer prognosis for C1 and C3. Notably, the high frequency of BRAF mutations in C2 and C3 implies that these two subtypes of patients may benefit from BRAF-targeted inhibitors (Menzer et al., 2019). In t-SNE analysis, C1 separated into two subpopulations, and some outliers of C1 were mixed with C3. We speculate that C1, which shows heterogeneity, is likely to be subdivided into two different subtypes, one of which is similar to C3 accompanied by similar stromal scores and mutation plots. In addition, C3 and C1 showed similar molecular patterns. Relatively higher metabolic signature level and worse prognosis, as well as lower abundance in immune signatures, distinguished C1 from C2. A more reasonable outcome will be attained if these C1 outliers are relabeled as C3.

Furthermore, we identified significant somatic mutation alteration sites in different subtypes according to GISTIC2.0. The number of loci and the degree of copy number variation of these genes were lower in C2 than in C1 and C3. In contrast, the number of amplification and deletion sites of the SKCM gene was higher in C3 than in C1 and C2. Furthermore, the magnitude of copy number variation showed the same trend. These results also showed a better prognosis of C2 than C1 and C3 and illustrated the association between the immune stromal infiltration of C1 and C3 and the occurrence of their tumor copy number variations. From the drug sensitivity analysis, we hypothesized that C2 may be more sensitive to chemotherapeutic agents than C1 and C3, suggesting that C2 may benefit from the combination of chemotherapy and immunotherapy. The GDSC drug sensitivity results indicated that two compounds, CGP-60474, a potent inhibitor of cyclin-dependent kinase (CDK), and bryostatin-1, a powerful protein kinase C (PKC) agonist, showed high drug sensitivity toward the three subtypes, representing promising chemotherapeutic drug candidates that target SKCM. The above discussion reveals that patients with the C2 subtype of SKCM may benefit from a combination of chemotherapy and immunotherapy. This study aimed to substantiate the need for personalized and precise treatment in clinical practice. The above discussion reveals that the three subtypes of SKCM may potentially benefit from the combination of chemotherapy and immunotherapy. This study aimed to provide supporting evidence for the availability of candidate target agents in clinical practice and achieve personalized precision therapy.

In the 90-gene classifier, many of the metabolic genes have been reported to play an important role in the inner metabolism and progression of SKCM, such as tyrosinase-related protein 1 (TYRP1) (Gilot et al., 2017) and OCA2 melanosomal transmembrane protein (OCN2) (Peterson et al., 2019), in particular, SLC7A4 of the solute carrier family of C1 to the transportation of cationic amino acids (Wolf et al., 2002). However, there have been no studies on SLC7A4 in SKCM. Therefore, we analyzed the expression signature of SLC7A4 and its prognostic value in TCGA-SKCM. We performed an IHC analysis of SLC7A4 from a clinical cohort to validate its role in SKCM. The results demonstrated that SLC7A4 was more highly expressed in melanoma tissues than in normal skin tissues, and the relatively higher expression of SLC7A4 presented a poor prognosis in SKCM patients, indicating that it could serve as a prognostic biomarker for SKCM. Moreover, the IHC results illustrated that the expression of SLC7A4 was proportional to the progression of melanoma. Therefore, SLC7A4 could be utilized as a therapeutic target for SKCM. These reports and experimental analyses reinforced the reliability of this gene classifier to a certain extent.

To the best of our knowledge, the present study is the first to generate a metabolic classification of SKCM that confirms the results of previous studies on SKCM subtypes while retaining their characteristics. Specifically, this classification matched the three subtypes from TCGA (keratin type, immune type, and MITF-low). C1 matched the keratin type and was highly metabolically active. C2 was the immune type, characterized by high immune infiltration, high expression of immune checkpoints, high immune and stromal scores, and favorable prognosis. We demonstrated for the first time that the C2 subtype corresponding to the immune type was prone to be a responder to PD-1 immunotherapy. C3 corresponded with MITF-low and was enriched in CpG island methylation. We also performed a preliminary experimental validation of the role of SLC7A4 in SKCM from the 90- gene classifier. Hence, the current study constitutes a novel demonstration of the presence of TCGA subtypes in TCGA-SKCM cohort and the GEO-SKCM cohort. Furthermore, this study not only validates the clinical significance of TCGA-SKCM classification but also reveals unexplored features, such as tumor microenvironment signatures and response to immunotherapy. This study provides new insights into the heterogeneity of SKCM in terms of the metabolic landscape by classifying SKCM into three clusters, active, intermediate, and depleted metabolic activity, which suggests possible therapeutic options for each subtype. However, we acknowledge several flaws in this study. First of all, more clinical data are needed to verify the reliability of this classification standard. Second, additional validation like cellular and molecular experiments of the classifier is required to prove the findings.

In conclusion, here, we proposed novel classifications of SKCM from a metabolic perspective with three subtypes, namely, metabolically active, intermediate, and depleted. C1 was closely associated with metabolic processes and had the worst prognosis, consistent with the keratin subtype. C2 exhibited higher immune infiltration, high immune and stromal scores, and sensitivity to PD-1 immune blockade agents, correlating with the immune type, and it had a favorable prognosis. C3 had an enriched carcinogenic pathway with a high degree of prognosis and relatively poor prognosis, and it was less metabolically active than C1 but more active than C2. Furthermore, the generated 90-gene classifier had a high predictive value for SKCM, and this classifier may help predict the prognosis of patients with SKCM more accurately and provide precise therapeutic approaches for these

patients. Thus, our study further enhanced the recognition of the metabolic hallmarks of SKCM and contributed valuable new information regarding SKCM subtypes such that patients with this disease can receive personalized immunotherapy and more accurate prognosis prediction.

DATA AVAILABILITY STATEMENT

The datasets presented in this study can be found in online repositories. The names of the repository/repositories and accession number(s) can be found in the article/ **Supplementary Material**.

ETHICS STATEMENT

The studies involving human participants were reviewed and approved by the Ethics Committee of Foshan First People's Hospital. The patients/participants provided their written informed consent to participate in this study.

AUTHOR CONTRIBUTIONS

RY and ZW conceived and designed the study. SZ, JL, ZW, RY, and YQ contributed to the data acquisition. JM, RG, and XP analyzed the data. ZW and SZ wrote the manuscript. All authors read and approved the final manuscript.

FUNDING

This study was supported by the National Natural Science Foundation of China (Nos. 82002913 and 81772136), the Foundation of Foshan City (Nos. FS0AA-KJ218-1301-0034 and 2018AB003411), the Special Fund of the Foshan Summit Plan (Nos. 2019C002, 2019D008, 2019A006, and 2020A015), the Foundation of Sichuan Science and Technology Department (2019YJ0652), Guang Dong Basic and Applied Basic Research Foundation (2021A1515011453), and the Medical Science Foundation of Cheng Du (2018003).

SUPPLEMENTARY MATERIAL

The Supplementary Material for this article can be found online at: https://www.frontiersin.org/articles/10.3389/fcell.2021.707677/full#supplementary-material

Supplementary Figure 1 | GO enrichment analysis of differential genes by Goplot package. GO enrichment of differential genes between C1 clusters and C2 and C3 clusters by the Goplot package, which is visualized as a taxonomic bubble plot **(A)** and a circle plot **(B)**. Venn diagram **(C)** of differential gene enrichment in "autophagy," "protein binding," "lysosome organization" three biological processes. Goplot package for GO enrichment of differential genes between C2 clusters and C1 and C3 clusters, and visualized as categorical bubble plots **(D)** and circle plots **(E)**. Venn diagram **(F)** of differential gene enrichment in the three biological processes "immune response," "regulation of immune response," "adaptive immune response." GO enrichment of differential genes between C3 clusters and C1 and C2 clusters was carried out by the Goplot package and visualized in the form of classification bubble plots **(G)** and circle plots **(H)**. Venn diagram **(I)** of differential genes enriched in three biological processes: "protein binding," "nucleotide-excision repair," "DNA damage recognition," and "poly(A) RNA binding."

Supplementary Figure 2 | KEGG pathway enrichment analysis was performed using KOBAS 3.0. The pathway figures depicted the common KEGG enrichment pathways for genes that are different between the three clustered subtypes and other subtypes. $p < 0.05$ pathways are considered significantly enriched. Apoptosis **(A)**, Cell cycle **(B)**, HIF-1 signaling pathway **(C)**, Human T-cell leukemia virus 1 **(D)**, Pathways in cancer infection **(E)**, PI3K-Akt signaling pathway **(F)**, red color stands for enriched genes with up-regulated expression.

Supplementary Figure 3 | Mutation profiling of 90-gene classifier in the pan-cancer analysis and the TF-mRNA-miRNA network construction. **(A)** The gene mutation and gene copy number of 90-gene classifier in 32 TCGA pan-cancer databases were obtained from the cBioportal online database, and the analysis of the mutation was performed to illustrate the distribution proportion of each mutation type of this gene classifier in pan-cancer types, including gene mutation, fusion, amplification, deep deletion and multiple alterations in a bar chart. **(B)** Construction of potential transcription factor and miRNA (TF-mRNA-miRNA) interaction network for 90-gene classifier using Cytoscape software, with red representing transcription factors, blue representing mRNA, and green representing miRNA.

Supplementary Table 1 | The information of clinical characteristics of TCGA-SKCM cohorts.

Supplementary Table 2 | Independency test between meta cluster and other clinical information and previous classification in TCGA-SKCM cohorts.

Supplementary Table 3 | Independency test between meta cluster and other clinical information in GEO-SKCM cohorts.

Supplementary Table 4 | The ratio of driver-type oncogenic mutations based on TCGA-SKCM in each subtype.

Supplementary Table 5 | The gene list of the 90 gene-classifier.

Supplementary Table 6 | Analysis of GO enrichment of differential genes between subtypes C1 and C2 and C3 by Goplot package.

Supplementary Table 7 | GO enrichment analysis of differential genes between subtypes C2 and subtypes C1 and C3 by Goplot package.

Supplementary Table 8 | The GO enrichment analysis of differential genes between subtypes C3 and C1 and C2 by the Goplot package.

Supplementary Table 9 | KEGG pathway enrichment analysis was performed using KOBAS 3.0 ($p < 0.05$), and the table showed the Top10 enriched KEGG pathways.

REFERENCES

Afzal, M. Z., Mercado, R. R., and Shirai, K. (2018). Efficacy of metformin in combination with immune checkpoint inhibitors (anti-PD-1/anti-CTLA-4) in metastatic malignant melanoma. *J. Immunother. Cancer* 6;64. doi: 10.1186/s40425-018-0375-1

Alexandrov, L. B., Kim, J., Haradhvala, N. J., Huang, M. N., Tian Ng, A. W., Wu, Y., et al. (2020). The repertoire of mutational signatures in human cancer. *Nature* 578, 94–101. doi: 10.1038/s41586-020-1943-3

Barbie, D. A., Tamayo, P., Boehm, J. S., Kim, S. Y., Moody, S. E., Dunn, I. F., et al. (2009). Systematic RNA interference reveals that oncogenic KRAS-driven cancers require TBK1. *Nature* 462, 108–112. doi: 10.1038/nature08460

Becht, E., Giraldo, N. A., Lacroix, L., Buttard, B., Elarouci, N., Petitprez, F., et al. (2016). Estimating the population abundance of tissue-infiltrating immune and

stromal cell populations using gene expression. *Genome Biol.* 17:218. doi: 10.1186/s13059-016-1070-5

Bolick, N. L., and Geller, A. C. (2021). Epidemiology of melanoma. *Hematol. Oncol. Clin. North Am.* 35, 57–72. doi: 10.1016/j.hoc.2020.08.011

Bristot, I. J., Kehl Dias, C., Chapola, H., Parsons, R. B., and Klamt, F. (2020). Metabolic rewiring in melanoma drug-resistant cells. *Crit. Rev. Oncol. Hematol.* 153:102995. doi: 10.1016/j.critrevonc.2020.102995

Brunet, J. P., Tamayo, P., Golub, T. R., and Mesirov, J. P. (2004). Metagenes and molecular pattern discovery using matrix factorization. *Proc. Natl. Acad. Sci. U.S.A.* 101, 4164–4169. doi: 10.1073/pnas.0308531101

Cancer Genome Atlas Network (2015). Genomic classification of cutaneous melanoma. *Cell* 161, 1681–1696. doi: 10.1016/j.cell.2015.05.044

Cascone, T., McKenzie, J. A., Mbofung, R. M., Punt, S., Wang, Z., Xu, C., et al. (2018). Increased tumor glycolysis characterizes immune resistance to adoptive T Cell therapy. *Cell Metab.* 27, 977–987.e4. doi: 10.1016/j.cmet.2018.02.024

Cha, J. H., Yang, W. H., Xia, W., Wei, Y., Chan, L. C., Lim, S. O., et al. (2018). Metformin promotes antitumor immunity via endoplasmic-reticulum-associated degradation of PD-L1. *Mol. Cell* 71, 606–620.e7. doi: 10.1016/j.molcel.2018.07.030

Colaprico, A., Silva, T. C., Olsen, C., Garofano, L., Cava, C., Garolini, D., et al. (2016). TCGAbiolinks: an R/Bioconductor package for integrative analysis of TCGA data. *Nucleic Acids Res.* 44:e71. doi: 10.1093/nar/gkv1507

Gao, J., Aksoy, B. A., Dogrusoz, U., Dresdner, G., Gross, B., Sumer, S. O., et al. (2013). Integrative analysis of complex cancer genomics and clinical profiles using the cBioPortal. *Sci. Signal.* 6:l1. doi: 10.1126/scisignal.2004088

Gaujoux, R., and Seoighe, C. (2010). A flexible R package for nonnegative matrix factorization. *BMC Bioinformatics* 11:367. doi: 10.1186/1471-2105-11-367

Ghiorzo, P., Gargiulo, S., Pastorino, L., Nasti, S., Cusano, R., Bruno, W., et al. (2006). Impact of E27X, a novel CDKN2A germ line mutation, on p16 and p14ARF expression in Italian melanoma families displaying pancreatic cancer and neuroblastoma. *Hum. Mol. Genet.* 15, 2682–2689. doi: 10.1093/hmg/ddl199

Gibcus, J. H., Kok, K., Menkema, L., Hermsen, M. A., Mastik, M., Kluin, P. M., et al. (2007). High-resolution mapping identifies a commonly amplified 11q13.3 region containing multiple genes flanked by segmental duplications. *Hum. Genet.* 121, 187–201. doi: 10.1007/s00439-006-0299-6

Gilot, D., Migault, M., Bachelot, L., Journé, F., Rogiers, A., Donnou-Fournet, E., et al. (2017). A non-coding function of TYRP1 mRNA promotes melanoma growth. *Nat. Cell Biol.* 19, 1348–1357. doi: 10.1038/ncb3623

Goodpaster, B. H., and Sparks, L. M. (2017). Metabolic flexibility in health and disease. *Cell Metab.* 25, 1027–1036. doi: 10.1016/j.cmet.2017.04.015

Guy, G. P. , Thomas, C. C., Thompson, T., Watson, M., Massetti, G. M., and Richardson, L. C. (2015). Vital signs: melanoma incidence and mortality trends and projections - United States, 1982-2030. *MMWR Morb. Mortal Wkly. Rep.* 64, 591–596.

Hänzelmann, S., Castelo, R., and Guinney, J. (2013). GSVA: gene set variation analysis for microarray and RNA-seq data. *BMC Bioinformatics* 14:7. doi: 10.1186/1471-2105-14-7

Harel, M., Ortenberg, R., Varanasi, S. K., Mangalhara, K. C., Mardamshina, M., Markovits, E., et al. (2019). Proteomics of melanoma response to immunotherapy reveals mitochondrial dependence. *Cell* 179, 236–250.e18. doi: 10.1016/j.cell.2019.08.012

Havel, J. J., Chowell, D., and Chan, T. A. (2019). The evolving landscape of biomarkers for checkpoint inhibitor immunotherapy. *Nat. Rev. Cancer* 19, 133–150. doi: 10.1038/s41568-019-0116-x

Hollern, D. P., Xu, N., Thennavan, A., Glodowski, C., Garcia-Recio, S., Mott, K. R., et al. (2019). B cells and T follicular helper cells mediate response to checkpoint inhibitors in high mutation burden mouse models of breast cancer. *Cell* 179, 1191–1206.e21. doi: 10.1016/j.cell.2019.10.028

Hoshida, Y., Brunet, J. P., Tamayo, P., Golub, T. R., and Mesirov, J. P. (2007). Subclass mapping: identifying common subtypes in independent disease data sets. *PLoS One* 2:e1195. doi: 10.1371/journal.pone.0001195

Hu, B., Wei, Q., Li, X., Ju, M., Wang, L., Zhou, C., et al. (2020). Development of an IFNγ response-related signature for predicting the survival of cutaneous melanoma. *Cancer Med.* 9, 8186–8201. doi: 10.1002/cam4.3438

Huang da, W., Sherman, B. T., and Lempicki, R. A. (2009). Bioinformatics enrichment tools: paths toward the comprehensive functional analysis of large gene lists. *Nucleic Acids Res.* 37, 1–13. doi: 10.1093/nar/gkn923

Huang, D. W., Sherman, B. T., Tan, Q., Kir, J., Liu, D., Bryant, D., et al. (2007). DAVID bioinformatics resources: expanded annotation database and novel algorithms to better extract biology from large gene lists. *Nucleic Acids Res.* 35, W169–W175. doi: 10.1093/nar/gkm415

Jessen, C., Kreß, J. K. C., Baluapuri, A., Hufnagel, A., Schmitz, W., Kneitz, S., et al. (2020). The transcription factor NRF2 enhances melanoma malignancy by blocking differentiation and inducing COX2 expression. *Oncogene* 39, 6841–6855. doi: 10.1038/s41388-020-01477-8

Konieczkowski, D. J., Johannessen, C. M., Abudayyeh, O., Kim, J. W., Cooper, Z. A., Piris, A., et al. (2014). A melanoma cell state distinction influences sensitivity to MAPK pathway inhibitors. *Cancer Discov.* 4, 816–827. doi: 10.1158/2159-8290.Cd-13-0424

Leone, R. D., and Powell, J. D. (2020). Metabolism of immune cells in cancer. *Nat. Rev. Cancer* 20, 516–531. doi: 10.1038/s41568-020-0273-y

Li, K., Zhang, T. T., Wang, F., Cui, B., Zhao, C. X., Yu, J. J., et al. (2018). Metformin suppresses melanoma progression by inhibiting KAT5-mediated SMAD3 acetylation, transcriptional activity and TRIB3 expression. *Oncogene* 37, 2967–2981. doi: 10.1038/s41388-018-0172-9

Lo, J. A., Kawakubo, M., Juneja, V. R., Su, M. Y., Erlich, T. H., LaFleur, M. W., et al. (2021). Epitope spreading toward wild-type melanocyte-lineage antigens rescues suboptimal immune checkpoint blockade responses. *Sci. Transl. Med.* 13:eabd8636. doi: 10.1126/scitranslmed.abd8636

Lu, X., Meng, J., Zhou, Y., Jiang, L., and Yan, F. (2020). MOVICS: an R package for multi-omics integration and visualization in cancer subtyping. *Bioinformatics* 36, 5539–5541. doi: 10.1093/bioinformatics/btaa1018

Mayakonda, A., Lin, D. C., Assenov, Y., Plass, C., and Koeffler, H. P. (2018). Maftools: efficient and comprehensive analysis of somatic variants in cancer. *Genome Res.* 28, 1747–1756. doi: 10.1101/gr.239244.118

Menzer, C., Menzies, A. M., Carlino, M. S., Reijers, I., Groen, E. J., Eigentler, T., et al. (2019). Targeted therapy in advanced melanoma with rare BRAF mutations. *J. Clin. Oncol.* 37, 3142–3151. doi: 10.1200/jco.19.00489

Mermel, C. H., Schumacher, S. E., Hill, B., Meyerson, M. L., Beroukhim, R., and Getz, G. (2011). GISTIC2.0 facilitates sensitive and confident localization of the targets of focal somatic copy-number alteration in human cancers. *Genome Biol.* 12:R41. doi: 10.1186/gb-2011-12-4-r41

Müller, J., Krijgsman, O., Tsoi, J., Robert, L., Hugo, W., Song, C., et al. (2014). Low MITF/AXL ratio predicts early resistance to multiple targeted drugs in melanoma. *Nat. Commun.* 5:5712. doi: 10.1038/ncomms6712

Nassar, K. W., and Tan, A. C. (2020). The mutational landscape of mucosal melanoma. *Semin. Cancer Biol.* 61, 139–148. doi: 10.1016/j.semcancer.2019.09.013

Pavlova, N. N., and Thompson, C. B. (2016). The emerging hallmarks of cancer metabolism. *Cell Metab.* 23, 27–47. doi: 10.1016/j.cmet.2015.12.006

Peifer, M., Hertwig, F., Roels, F., Dreidax, D., Gartlgruber, M., Menon, R., et al. (2015). Telomerase activation by genomic rearrangements in high-risk neuroblastoma. *Nature* 526, 700–704. doi: 10.1038/nature14980

Peterson, K. A., Neuffer, S., Bean, M. E., New, L., Coffin, A. B., and Cooper, C. D. (2019). Melanosome maturation proteins Oca2, Mitfa and Vps11 are differentially required for cisplatin resistance in zebrafish melanocytes. *Exp. Dermatol.* 28, 795–800. doi: 10.1111/exd.13937

Possemato, R., Marks, K. M., Shaul, Y. D., Pacold, M. E., Kim, D., Birsoy, K., et al. (2011). Functional genomics reveal that the serine synthesis pathway is essential in breast cancer. *Nature* 476, 346–350. doi: 10.1038/nature10350

Ratnikov, B. I., Scott, D. A., Osterman, A. L., Smith, J. W., and Ronai, Z. A. (2017). Metabolic rewiring in melanoma. *Oncogene* 36, 147–157. doi: 10.1038/onc.2016.198

Ritchie, M. E., Phipson, B., Wu, D., Hu, Y., Law, C. W., Shi, W., et al. (2015). limma powers differential expression analyses for RNA-sequencing and microarray studies. *Nucleic Acids Res.* 43:e47. doi: 10.1093/nar/gkv007

Robert, C., Thomas, L., Bondarenko, I., O'Day, S., Weber, J., Garbe, C., et al. (2011). Ipilimumab plus dacarbazine for previously untreated metastatic melanoma. *N. Engl. J. Med.* 364, 2517–2526. doi: 10.1056/NEJMoa1104621

Roh, W., Chen, P. L., Reuben, A., Spencer, C. N., Prieto, P. A., Miller, J. P., et al. (2017). Integrated molecular analysis of tumor biopsies on sequential CTLA-4 and PD-1 blockade reveals markers of response and resistance. *Sci. Transl. Med.* 9:eaah3560. doi: 10.1126/scitranslmed.aah3560

Rosario, S. R., Long, M. D., Affronti, H. C., Rowsam, A. M., Eng, K. H., and Smiraglia, D. J. (2018). Pan-cancer analysis of transcriptional metabolic

dysregulation using The Cancer Genome Atlas. *Nat. Commun.* 9:5330. doi: 10.1038/s41467-018-07232-8

Ruocco, M. R., Avagliano, A., Granato, G., Vigliar, E., Masone, S., Montagnani, S., et al. (2019). Metabolic flexibility in melanoma: a potential therapeutic target. *Semin. Cancer Biol.* 59, 187–207. doi: 10.1016/j.semcancer.2019.07.016

Sanchez-Vega, F., Mina, M., Armenia, J., Chatila, W. K., Luna, A., La, K. C., et al. (2018). Oncogenic signaling pathways in The Cancer Genome Atlas. *Cell* 173, 321–337.e10. doi: 10.1016/j.cell.2018.03.035

Schadendorf, D., Hodi, F. S., Robert, C., Weber, J. S., Margolin, K., Hamid, O., et al. (2015). Pooled analysis of long-term survival data from phase II and phase III trials of ipilimumab in unresectable or metastatic melanoma. *J. Clin. Oncol.* 33, 1889–1894. doi: 10.1200/jco.2014.56.2736

Schvartsman, G., Taranto, P., Glitza, I. C., Agarwala, S. S., Atkins, M. B., and Buzaid, A. C. (2019). Management of metastatic cutaneous melanoma: updates in clinical practice. *Ther. Adv. Med. Oncol.* 11:1758835919851663. doi: 10.1177/1758835919851663

Sharma, N. S., Gupta, V. K., Garrido, V. T., Hadad, R., Durden, B. C., Kesh, K., et al. (2020). Targeting tumor-intrinsic hexosamine biosynthesis sensitizes pancreatic cancer to anti-PD1 therapy. *J. Clin. Invest.* 130, 451–465. doi: 10.1172/jci127515

Su, Y., Ko, M. E., Cheng, H., Zhu, R., Xue, M., Wang, J., et al. (2020). Multi-omic single-cell snapshots reveal multiple independent trajectories to drug tolerance in a melanoma cell line. *Nat. Commun.* 11:2345. doi: 10.1038/s41467-020-15956-9

Tanemura, A., Terando, A. M., Sim, M. S., van Hoesel, A. Q., de Maat, M. F., Morton, D. L., et al. (2009). CpG island methylator phenotype predicts progression of malignant melanoma. *Clin. Cancer Res.* 15, 1801–1807. doi: 10.1158/1078-0432.Ccr-08-1361

Thanasai, J., Limpaiboon, T., Jearanaikoon, P., Bhudhisawasdi, V., Khuntikeo, N., Sripa, B., et al. (2006). Amplification of D22S283 as a favorable prognostic indicator in liver fluke related cholangiocarcinoma. *World J. Gastroenterol.* 12, 4338–4344. doi: 10.3748/wjg.v12.i27.4338

Vivian, J., Rao, A. A., Nothaft, F. A., Ketchum, C., Armstrong, J., Novak, A., et al. (2017). Toil enables reproducible, open source, big biomedical data analyses. *Nat. Biotechnol.* 35, 314–316. doi: 10.1038/nbt.3772

Walter, W., Sánchez-Cabo, F., and Ricote, M. (2015). GOplot: an R package for visually combining expression data with functional analysis. *Bioinformatics* 31, 2912–2914. doi: 10.1093/bioinformatics/btv300

Wang, J., Sanmamed, M. F., Datar, I., Su, T. T., Ji, L., Sun, J., et al. (2019). Fibrinogen-like protein 1 is a major immune inhibitory ligand of LAG-3. *Cell* 176, 334–347.e12. doi: 10.1016/j.cell.2018.11.010

Wolf, S., Janzen, A., Vékony, N., Martiné, U., Strand, D., and Closs, E. I. (2002). Expression of solute carrier 7A4 (SLC7A4) in the plasma membrane is not sufficient to mediate amino acid transport activity. *Biochem. J.* 364(Pt 3), 767–775. doi: 10.1042/bj20020084

Woods, K., Knights, A. J., Anaka, M., Schittenhelm, R. B., Purcell, A. W., Behren, A., et al. (2016). Mismatch in epitope specificities between IFNγ inflamed and uninflamed conditions leads to escape from T lymphocyte killing in melanoma. *J. Immunother. Cancer* 4:10. doi: 10.1186/s40425-016-0111-7

Wu, J., Mao, X., Cai, T., Luo, J., and Wei, L. (2006). KOBAS server: a web-based platform for automated annotation and pathway identification. *Nucleic Acids Res.* 34, W720–W724. doi: 10.1093/nar/gkl167

Yang, W., Soares, J., Greninger, P., Edelman, E. J., Lightfoot, H., Forbes, S., et al. (2013). Genomics of drug sensitivity in cancer (GDSC): a resource for therapeutic biomarker discovery in cancer cells. *Nucleic Acids Res.* 41, D955–D961. doi: 10.1093/nar/gks1111

Yoshihara, K., Shahmoradgoli, M., Martínez, E., Vegesna, R., Kim, H., Torres-Garcia, W., et al. (2013). Inferring tumour purity and stromal and immune cell admixture from expression data. *Nat. Commun.* 4:2612. doi: 10.1038/ncomms3612

Yu, G., Wang, L. G., Han, Y., and He, Q. Y. (2012). clusterProfiler: an R package for comparing biological themes among gene clusters. *Omics* 16, 284–287. doi: 10.1089/omi.2011.0118

Zhang, Y., Parmigiani, G., and Johnson, W. E. (2020). ComBat-seq: batch effect adjustment for RNA-seq count data. *NAR Genom. Bioinform.* 2:lqaa078. doi: 10.1093/nargab/lqaa078

Zhou, G., Soufan, O., Ewald, J., Hancock, R. E. W., Basu, N., and Xia, J. (2019). NetworkAnalyst 3.0: a visual analytics platform for comprehensive gene expression profiling and meta-analysis. *Nucleic Acids Res.* 47, W234–W241. doi: 10.1093/nar/gkz240

Zhou, S., Ouyang, W., Zhang, X., Liao, L., Pi, X., Yang, R., et al. (2021). UTRN inhibits melanoma growth by suppressing p38 and JNK/c-Jun signaling pathways. *Cancer Cell Int.* 21:88. doi: 10.1186/s12935-021-01768-4

Conflict of Interest: The authors declare that the research was conducted in the absence of any commercial or financial relationships that could be construed as a potential conflict of interest.

Publisher's Note: All claims expressed in this article are solely those of the authors and do not necessarily represent those of their affiliated organizations, or those of the publisher, the editors and the reviewers. Any product that may be evaluated in this article, or claim that may be made by its manufacturer, is not guaranteed or endorsed by the publisher.

frontiers in Cell and Developmental Biology

ORIGINAL RESEARCH
published: 17 August 2021
doi: 10.3389/fcell.2021.681968

miRNA-7062-5p Promoting Bone Resorption After Bone Metastasis of Colorectal Cancer Through Inhibiting GPR65

Liang Chen[1], Yu Wang[1], Xingchen Lu[1], Lili Zhang[2] and Ziming Wang[1]**

[1] Department of Orthopedics, Army Medical Center, Army Medical University, Chongqing, China, [2] Department of Military Psychology, College of Psychology, Army Medical University, Chongqing, China

Bone metastasis is positively associated with a poor prognosis in patients with colorectal cancer (CRC). CRC always leads to osteolytic change, which is regulated by aberrant activation of osteoclasts. MicroRNAs are remarkedly involved in metastasis of CRC; however, their role in bone metastasis of CRC is still unclear. The aim of this study is to find key microRNAs that are critical to bone resorption in bone metastasis of CRC. In this study, bone metastasis model was established through intratibially injecting CT-26 cells or MC-38 cells. Tartrate-resistant acid phosphatase (TRAP) staining was performed to explore the osteoclastogenesis of primary early osteoclast precursors (OCPs) after stimulation by CT-26 conditioned medium (CM). Then, microarray assay was performed to find differentially expressed miRNAs and mRNAs. The target gene of miRNA was confirmed by dual-luciferase analysis. The effect of miRNA, its target gene on osteoclastogenesis, and involved pathways were explored by Western blot, immunofluorescence analysis, and TRAP staining. Finally, the effect of miRNA on bone resorption *in vivo* was observed. miRNA-7062-5p was upregulated in early OCPs cultured in CT-26 CM or MC-38 CM. GPR65 was proven to be the target gene of miRNA-7062-5p. Overexpression of GPR65 can rescue the osteoclastogenesis caused by miRNA-7062-5p through activation of AMPK pathway. Local injection of miRNA-7062-5p inhibitors efficiently improved the bone resorption. Our study found the role of miRNA-7062-5p in regulating osteoclast formation, and our findings provided a potential therapeutic target in treatment of bone metastasis of CRC.

Keywords: miRNA-7062-5p, GPR65, colorectal cancer, bone metastasis, osteoclast

OPEN ACCESS

Edited by:
Na Luo,
Nankai University, China

Reviewed by:
Huai-Qiang Ju,
Sun Yat-sen University, China
Xiawei Wei,
Sichuan University, China

****Correspondence:***
Lili Zhang
lili_home20@163.com
Ziming Wang
zm_wang72@163.com

Specialty section:
This article was submitted to Molecular Medicine, a section of the journal Frontiers in Cell and Developmental Biology

Received: *17 March 2021*
Accepted: *06 May 2021*
Published: *17 August 2021*

Citation:
Chen L, Wang Y, Lu X, Zhang L and Wang Z (2021) miRNA-7062-5p Promoting Bone Resorption After Bone Metastasis of Colorectal Cancer Through Inhibiting GPR65. Front. Cell Dev. Biol. 9:681968. doi: 10.3389/fcell.2021.681968

INTRODUCTION

Although the incidence of bone metastasis from colorectal cancer (CRC) is relatively rare in clinic, the prognosis is pessimistic. Patients with CRC presenting with bone metastasis are often younger and have a poor prognosis; 5-year survival rate was only 5.7% (Kawamura et al., 2018). Moreover, the treatment is insufficient, partly because the underlying mechanism of bone metastasis of CRC is still clearly unexplored.

Abbreviations: CRC, colorectal cancer; TRAP, tartrate-resistant acid phosphatase; CM, conditioned medium; OCPs, osteoclast precursors; M-CSF, macrophage colony stimulating factor; RANKL, receptor activator of nuclear factor-κ B ligand; MMP, matrix metalloproteinase.

In bone microenvironment, the balance between osteoblasts and osteoclasts maintains the homeostasis of bone remodeling. CRC is a kind of osteolytic tumors. For these types of tumors, aberrant activation of osteoclasts promotes the bone resorption and pathologic fractures (Clohisy et al., 1996; Li et al., 2019b). Osteoclasts derive from monocytes/macrophage lineage. RANKL determines monocytes/macrophages to commit to osteoclast precursors (OCPs) (Liang et al., 2019). In tumor microenvironment, cancer cells can directly promote the osteoclastogenesis of OCPs through RANKL-dependent or independent ways (Liang et al., 2019). However, little is known on how the osteoclasts or its precursors change in CRC microenvironment.

MicroRNAs remarkedly participate in the progression and metastasis of CRC and are important regulators for osteoclastogenesis. Some microRNAs, such as miRNA-802, miRNA-875-3p, miRNA-574, miRNA-708, miRNA-206, and miRNA-27b, can attenuate the progression of CRC, whereas miRNA-503 facilitates the tumor growth (Ye et al., 2013; Park et al., 2018; Li et al., 2019a, 2020b; Sun et al., 2019; Zhang et al., 2020). In addition, miRNAs can also be used to predict the prognosis of CRC. It was also reported that miRNA-483, miRNA-218, miRNA-199a-5p, miRNA-133a, and miRNA-340 can regulate the osteoclast formation (Zhao et al., 2017; Guo et al., 2018, 2019; Li et al., 2018, 2020a). Considering the importance of miRNAs in both tumor progression and osteoclastogenesis, it is worthy to know the function of miRNAs in bone metastasis of CRC.

In this study, we identified that miRNA-7062-5p was treated by condional medium collected from CRC and promoted the osteoclastogenesis through targeting GPR65. Downregulating miRNA-7062-5p efficiently attenuated the progression of bone destruction caused by CRC.

MATERIALS AND METHODS

Animals

All procedures involving mice and experimental protocols were approved by the Institutional Animal Care and Use Committee of Daping Hospital at Army Medical University. C57BL/6 or BALB/c mice for all experiments were 6–8 weeks of age. CT-26 and MC-38 cells are two commonly used CRC cell lines. Thus, for bone metastasis studies, 500,000 CT-26 or MC-38 cells were resuspended in phosphate-buffered saline (PBS) and injected into tibias of mice after anesthetization. Antagomir-7062-5p or scrambled controls dissolved in PBS (10 μg/50 μL) were injected intravenously every 3 days for continuous 3 weeks. At specific timepoints, mice were killed, and the hindlimbs were removed and fixed in 4% paraformaldehyde for histochemical staining or tartrate-resistant acid phosphatase (TRAP) staining. Five to 10 mice were used per group.

Histological Analysis

Tibias were dissected and fixed for 48 h. Then, the samples were decalcified by daily change of 15% tetrasodium EDTA for 3 weeks and embedded in paraffin. For safranin O and fast green staining, samples were cleared twice in xylene and were rehydrated by passage through an ethanol series following by immersion in PBS. The samples were then stained in 0.1% safranin O solution for 3 min and washed in PBS three times. Next, the samples were immersed in 0.1% fast green solution for 10 s and separated in 1% acetum. The samples were then observed and captured. The TRAP staining was performed according to the manufacturers' instructions (BestBio Biotechnology, Beijing, China). For immunofluorescence analysis, early OCPs were seeded on coverslips and transfected by miRNAs. Then, the samples were fixed in 4% paraformaldehyde for 15 min in 4℃. After paraformaldehyde was discarded, the samples were washed in PBS and incubated in blocking buffer containing 10% donkey serum and 5% bovine serum albumin for 1 h in 37℃. Then, primary antibody was incubated overnight in 4℃. Secondary antibody was added after the samples were washed in PBS followed by staining with Hoechst 33342 (1:1,000) for 30 min. Primary antibody used was anti-GPR65 at 1:200 (Biorbyt, Cambridgeshire, United Kingdom). Secondary antibody was donkey anti-rabbit conjugated with Cy3 at 1:200 (Jackson ImmunoResearch Laboratories, Inc., West Grove, PA, United States).

Primary Early OCP Isolation and Culture

Bone marrows were rinsed out from marrow cavity of tibias and femurs by sterilized PBS. The cell suspension was collected and centrifuged at 500 *g* for 5 min. After discarding the supernatant, erythrocytes were removed. The cells were stained using CD115 antibody conjugated with APC and RANKL antibody conjugated with PE (Biolegend, San Diego, CA, United States) for 1 h in 4℃. Then, the primary early OCPs labeled as CD115-positive and RANKL-negative were sorted out by FACS.

Isolated early OCPs were cultured in Dulbecco modified eagle medium (DMEM) supplemented with 10% fetal bovine serum, 100 U/mL penicillin, and 100 U/mL streptomycin (Gibco, Thermo Fisher Scientific, Waltham, MA, United States) and macrophage colony-stimulating factor (M-CSF) (50 ng/mL) (Biolegend, San Diego, CA, United States). For osteoclastogenic induction, early OCPs were stimulated by M-CSF (50 ng/mL) and RANKL (50 ng/mL) for at least 4–6 days. In some experiments, early OCPs under osteoclastogenic induction were cultured with conditioned medium (CM) from CT-26 for 4 days.

Transient Transfection

Agomir-7062-5p, antagomir-7062-5p and their scrambled controls, siRNA pool, and pcDNA3.1 (+) plasmid containing GPR65 were synthesized by GenePharma, Co. (Shanghai, China). Transfection was performed using Lipofectamine RNAiMax Reagent (Invitrogen, Thermo Fisher Scientific). The siRNA sequence for AMPKα: 5′-CUAUGAAUGGAAGGUUGUA-3′, 5′-UACAACCUUCCAUUCAUA-3′.

Luciferase Reporter Assay

293T cells were seeded into 6-well plates. Cells were transfected with pGL3-GPR65 3′ UTR and pRL-TK (Promega, Madison, WI, United States) Renilla luciferase plasmid, as well as wild-type (wt) or mutant (mut) mir-7062-5p or controls using Lipofectamine

RNAiMax Reagent following the manufacturer's instructions. Luciferase assays were conducted using the dual-luciferase reporter assay system (Promega). The values of luminescent signals from firefly luciferase construct were normalized by Renilla luciferase assay.

Quantitative Real-Time Polymerase Chain Reaction

The total RNA was extracted from cells using TRIzol reagent (Invitrogen, Thermo Fisher Scientific). First-strand complementary DNA was reversed from 1 mg of total RNA using PrimeScript RT reagent Kit (TakaraBio, Tokyo, Japan) according to the manufacturer's instructions. The stem-loop reverse transcriptase–polymerase chain reaction (RT-PCR) was used for quantification of miRNA-7062-5p. Quantitative real-time PCR was performed using an SYBR Green Premix Ex TaqTMII Kit (TakaraBio, Tokyo, Japan). GAPDH and U6 were used as normalization controls for mRNA and miRNA, respectively. The sequences of the primers are shown as follows: GAPDH (forward: 5′-TGGATTTGGACGCATTGGTC-3′ and reverse: 5′-TTTGCACTGGTACGTGTTGAT-3′), cathepsin K (forward: 5′-CTGGCTGGGGTTATGTCTCAA-3′, and reverse: 5′-GGCTACGTCCTTACACACGAG-3′), MMP-2 (forward: 5′-TGACTTTCTTGGATCGGGTCG-3′, and reverse: 5′-AAGCACCACATCAGATGACTG-3′), MMP-9 (forward: 5′-TGTACCGCTATGGTTACACTCG-3′, and reverse: 5′-GGCAGGGACAGTTGCTTCT-3′).

Western Blot

The cells were lysed with RIPA buffer containing protease inhibitors (Beyotime, Shanghai, China). Total proteins were collected and subjected to sodium dodecyl sulfate–polyacrylamide gel electrophoresis and transferred to polyvinylidene difluoride membranes. The membranes were blocked and incubated with primary antibodies. After being washed, the membranes were then incubated with horseradish peroxidase–linked secondary antibodies. The antibodies used were as follows: GPR65 (1:1,000, Biorbyt), JNK (1:2,000; Santa Cruz, Dallas, TX, United States), phosphorylation JNK (1:2,000; Santa Cruz), AMPKα (Abcam, Cambridge, MA, United States), phosphorylation AMPKα(), GAPDH (Abcam), goat anti-rabbit immunoglobulin G (1:5,000; Abcam).

Microarray Assay

Total RNA was extracted from early OCPs. MiRNAs were isolated and labeled using biotin and detected with Ambion WT Expression Kit. MiRNA and mRNA microarray assays were completed by CNKINGBIO (Beijing, China). The miRNA 4.0 and Clariom D were used for microarray assay. The data sources of non-coding RNA were from Luo et al. (2013). The signal intensity of each spot was calculated by the program R (2.12.1). Spots that passed the criteria were normalized by the invariant set normalization method. Normalized spot intensities were transformed to gene expression log2 ratios between the control group and treatment group using the pairwise *t*-test. The spots with a $|\log2\ \text{ratio}| \geq 0.585$ and a $p < 0.05$ were selected for analysis.

Statistical Analysis

All data are representative of at least three experiments of similar results performed in triplicate unless otherwise indicated. Data are expressed as mean ± SD. One-way analysis of variance was used to determine the significance of difference between results, with $^{*}p < 0.05$ being regarded as significant.

RESULTS

Secreta Derived From CRC Cells Induce Osteoclastogenesis

Few studies focused on the bone metastasis of CRC and the onset of osteolysis. For establishing bone metastasis model in mice, we intratibially injected Balb/c mice with CT-26 CRC cell line. First, early OCPs labeled with CD115-positive and RANK-negative were isolated through FACS (so-called early OCPs). Approximately 4.5% of early OCPs can be sorted out from bone marrow in normal mice (**Figure 1A**). As expected, during osteoclastogenic induction treated with RANKL and M-CSF for 6 days, early OCPs formed TRAP-positive multinuclear giant cells. Notably, TRAP-staining results suggested higher TRAP activity and more osteoclast number were identified in OCPs after indirect coculture with CT-26 cells (**Figures 1B,C**). In addition, relative TRAP activity assay confirmed that TRAP activity increased after indirectly coculturing with CT-26 cells (**Figure 1D**). Consistently, the mRNA levels of osteoclastogenic markers, MMP-2, MMP-9, and cathepsin K, were significantly upregulated in OCPs stimulated with CT-26 CM (**Figures 1E–G**). These data suggested secreta from CRC cells induce osteoclastogenesis of OCPs.

miRNA-7062-5p Promotes Osteoclastogenesis of Early OCPs

To assess microRNAs involved in CRC cell–induced osteoclastogenesis, OCPs stimulated with CT-26 CM plus RANKL and M-CSF were collected. Microarray assays revealed that 60 miRNAs were differently expressed during differentiation. Among them, miRNA-7062-5p was the most obviously increased miRNA in CT-26 CM–treated OCPs (**Figure 2A**). To explore whether miRNA-7062-5p participates in CRC-induced osteoclastogenesis, CM was collected from two CRC cell lines, CT-26 and MC-38 cells, respectively. RT-PCR demonstrated the expression of miRNA-7062-5p upregulated in OCPs after stimulation with both CT-26 CM and MC-38 CM (**Figure 2B**). Notably, the level of miRNA-7062-5p in primary OCPs increased over time after injection of CT-26 or MC-38 cells intratibially (**Figure 2C**). These data indicated miRNA-7062-5p positively correlated with osteoclastogenesis and can be induced by secreta derived from CRC cells. To further assess whether miRNA-7062-5p plays a role in regulating osteoclastogenesis in tumor microenvironment, primary OCPs were treated with agomir-7062-5p or antagomir-7062-5p and then stimulated

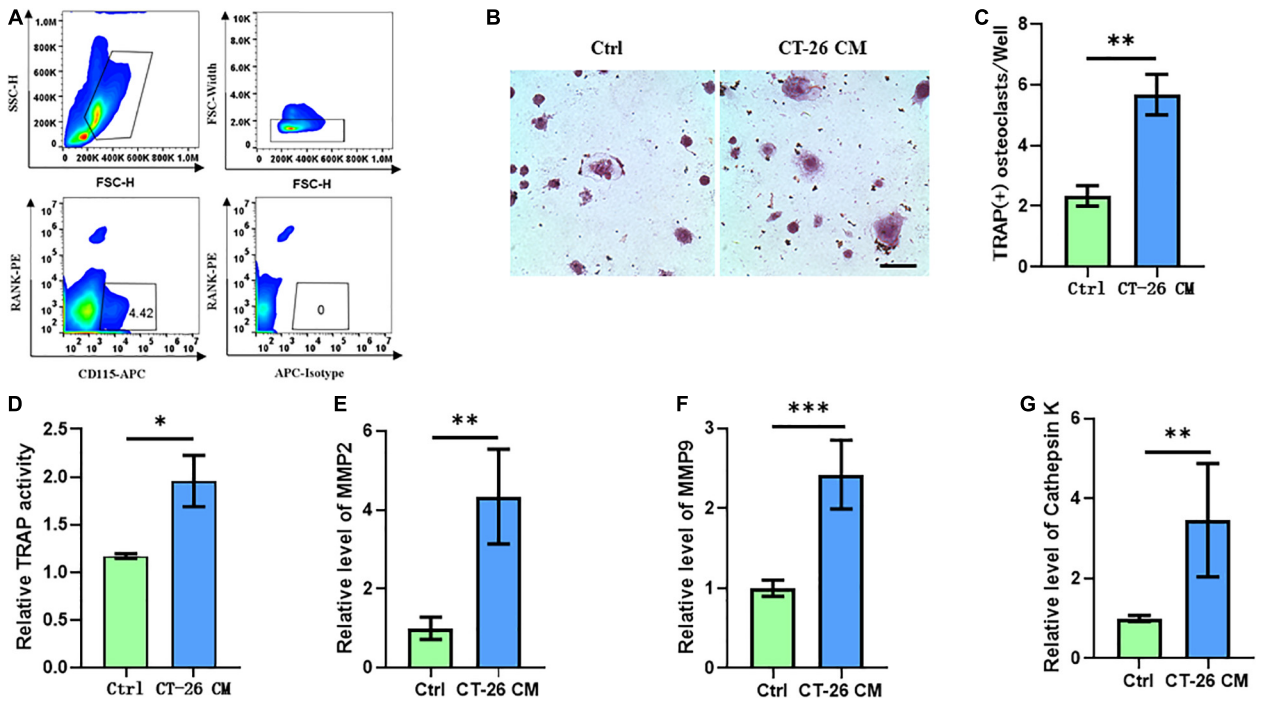

FIGURE 1 | Conditioned medium collected from CRC cell line, CT-26, promotes early osteoclast precursors to differentiate into osteoclasts. **(A)** Gating strategy for sorting out early osteoclast precursors. **(B)** Representative images of TRAP staining demonstrating osteoclast formation of early OCPs under stimulation of CT-26 CM or DMEM (scale bar = 250 μm). **(C)** Quantification of the number of TRAP-positive osteoclasts per well in **(B)**. **(D)** Quantification of relative TRAP activity per well in **(B)**. **(E–G)** The relative expression of osteoclastogenic biomarkers, MMP2, MMP9, and cathepsin K, was determined by real-time PCR. $^{*}p < 0.05$, $^{**}p < 0.01$, $^{***}p < 0.001$.

in CT-26 CM, as well as RANKL and M-CSF. TRAP staining and relative TRAP activity results indicated the number of osteoclasts, and TRAP activity significantly increased in the agomir-7062-5p–treated group and decreased in the antagomir-7062-5p–treated group (**Figures 2D–F**), demonstrating that miRNA-7062-5p directly promoted osteoclastogenesis of OCPs.

MiRNA-7062-5p Directly Targets GPR65

To understand the underlying mechanism in miRNA-7062-5p–activated osteoclastogenesis, transcriptomic profiling was analyzed in OCPs treated with CT-26 CM. We detected the differentially expressed genes related to osteoclastogenesis. Interestingly, our results showed the mRNA level of GPR65 downregulated approximately 25 folders (**Figure 3A**). As it was reported GPR65 negatively regulated osteoclastic activity in osteoporosis (Hikiji et al., 2014), it implied that GPR65 may play an important role in CRC-induced osteoclastogenesis. We next explored whether miRNA-7062-5p can target GPR65. Notably, online analysis tool (TargetScan[1]) predicted that GPR65 could be one potential target gene of miRNA-7062-5p (**Figure 3B**). Notably, the luciferase activity of 293T cells that were transfected wt 3′ UTR of GPR65 was remarkedly reduced by miRNA-7062-5p, whereas the luciferase activity in group transfection with the mutated-type (mut) 3′ UTR of GPR65 was not affected by miRNA-7062-5p (**Figure 3C**). In addition, up-regulation of miRNA-7062-5p significantly reduced the protein expression of GPR65 in OCPs; the immunofluorescence signals remarkedly reduced in the miRNA-7062-5p–treated group (**Figures 3D,E**). Together, these data indicated that GPR65 is the target gene of miRNA-7062-5p. Moreover, overexpression of miRNA-7062-5p can efficiently reduce the protein expression of GPR65 in OCPs.

miRNA-7062-5p Regulates Osteoclastogenesis of OCPs Dependent on GPR65

We demonstrated that GPR65 is the target gene of miRNA-7062-5p, and then we performed rescue experiments to further assess that GPR65 is essential to miRNA-7062-5p–mediated osteoclastogenesis of OCPs. As expected, the protein level of GPR65 downregulated in OCPs after transfection with agomir-7062-5p, whereas the expression of GPR65 was rescued after cotransfection with cDNA3.1(+) containing GPR65 in both normal and CT-26 CM–treated early OCPs (**Figures 4A,B**). Then, the differentiation of OCPs was investigated. TRAP staining showed that overexpression of GPR65 can decrease the increased number of osteoclasts that were promoted by miRNA-7062-5p transfection in the presence of CT-26 CM (**Figures 4C,D**). Meanwhile, relative TRAP activity supported the results in TRAP staining; the relative activity was enhanced in agomir-7062-5p–treated group and returned to the level in the control group after overexpression of GPR65 (**Figure 4E**).

[1]http://www.targetscan.org

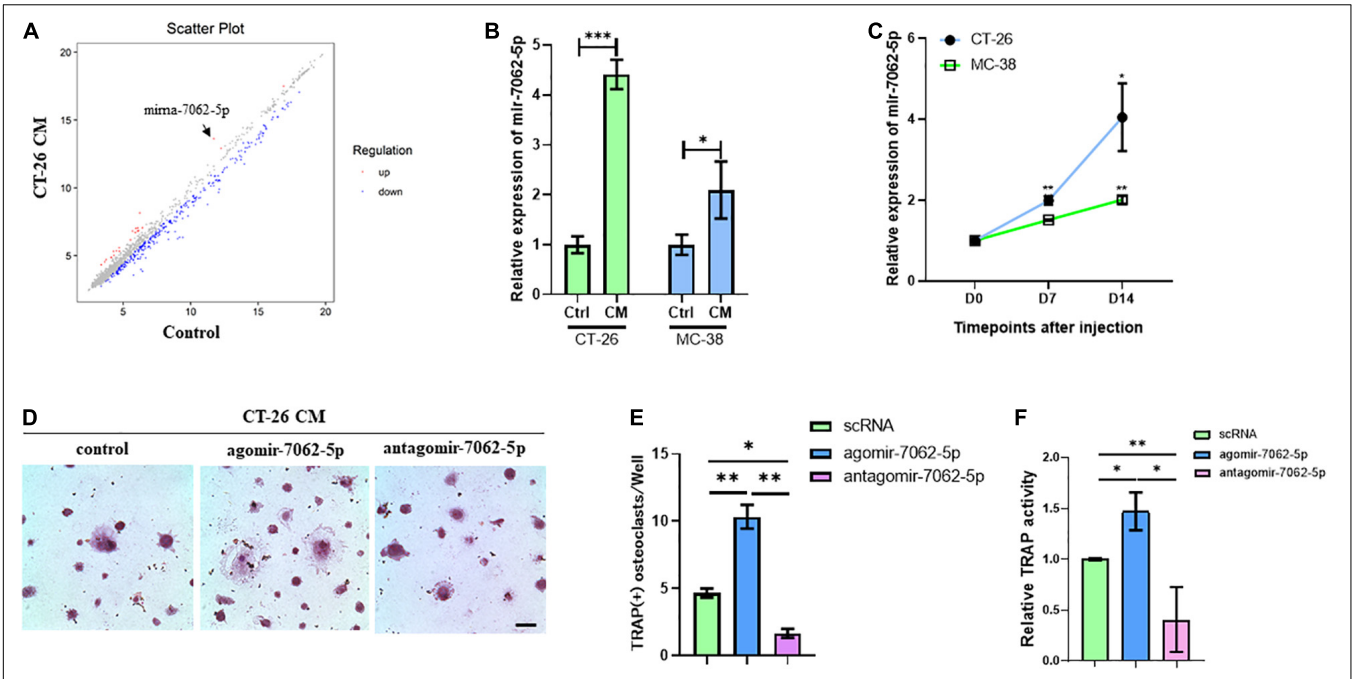

FIGURE 2 | The expression of miRNA-7062-5P upregulates during osteoclastogenesis induced by CT-26 CM and promotes osteoclast formation. **(A)** Scatter plots for microarray assay demonstrated differentially expressed miRNAs in early OCPs treated with CT-26 CM or DMEM. **(B)** The change folders of miRNA-7062-5p level in early OCPs after treatment by CT-26 CM or MC-38 CM compared with the control group. **(C)** The change of miRNA-7062-5p expression in sorted early OCPs at specific timepoints after injection of CT-26 cells or MC-38 cells into tibias. **(D)** Representative images of TRAP staining demonstrating osteoclastogenesis after early OCPs stimulated by RANKL and M-CSF in the presence of CT-26 CM after transfection with controls, agomir-7062-5p, or antagomir-7062-5p (scale bar = 250 μm). **(E)** Quantification of the number of TRAP positive osteoclasts per well in **(D)**. **(F)** Quantification of relative TRAP activity per well in **(D)**. $^{*}p < 0.05$, $^{**}p < 0.01$, $^{***}p < 0.001$.

Then, we further proved that miRNA-7062-5p inhibition attenuated osteoclast formation, and this process was dependent on regulating GPR65. OCPs were treated with antagomir-7062-5p or cotreated with siRNA targeting GPR65 in normal medium or CT-26 CM. Western blots showed the protein level of GPR65 in OCPs significantly upregulated after treatment with antagomir-7062-5p, whereas this upregulation can be prevented when cotransfected with siGPR65 (**Figures 5A,B**). TRAP staining showed miRNA-7062-5p inhibition can decrease the number of osteoclasts, whereas the number was rescued through inhibiting expression of GPR65 in the presence of CT-26 CM (**Figures 5C,D**). Furthermore, relative TRAP activity demonstrated that TRAP activity was downregulated in antagomir-7062-5p–treated group and recovered after cotransfection with siGPR65 (**Figure 5E**). These data proved that miRNA-7062-5p stimulated osteoclastogenesis of OCPs through targeting GPR65 in the presence of CT-26 CM.

GPR65/AMPKα Signaling Inhibited Osteoclastogenesis of OCPs Through Preventing Activation of the JNK Pathway

It has been demonstrated that GPR65 was associated with the increased level of cAMP, which can activate AMPK pathway. Interestingly, AMPK pathway may inhibit the activation of the JNK pathway, which is one of the most important pathways involved in osteoclastogenesis. We first detected the protein levels of the JNK pathway and AMPK pathway in CT-26 CM–treated early OCPs compared with normal early OCPs. As expected, the activated JNK protein was upregulated, and the level of activated AMPKα protein was significantly downregulated in early OCPs stimulated by CT-26 CM (**Figures 6A–C**). To test whether GPR65 regulates AMPK and JNK pathways in OCPs, plasmid containing GPR65 was transfected into OCPs. Interestingly, the activation of AMPKα was significantly enhanced after overexpression of GPR65, and the activation of JNK was prevented, and when cotransfected with AMPKα siRNA, the activation of JNK recovered in early OCPs treated with CT-26 CM (**Figures 6D–F**). These results showed that GPR65 inhibited activation of JNK through activating phosphorylation of AMPKα in OCPs in CRC microenvironment. To assess whether GPR65 can mediate activation of AMPKα-regulated osteoclastogenic induction in CRC microenvironment, OCPs were induced into osteoclastogenic fate by stimulating with RANKL and M-CSF in the presence of CT-26 CM; meanwhile, plasmid containing GPR65 was transfected or cotransfected with AMPKα siRNA. TRAP staining showed the number of OCs was decreased in GPR65 overexpression group comparing with control group while the number increased after co-transfected with AMPKα siRNA (**Figures 6G,H**). Consistently, TRAP activity assay revealed overexpression of GPR65 significantly decreased the TRAP activity, but it can be rescued when co-transfected with AMPKα siRNA (**Figure 6I**). These results demonstrated that

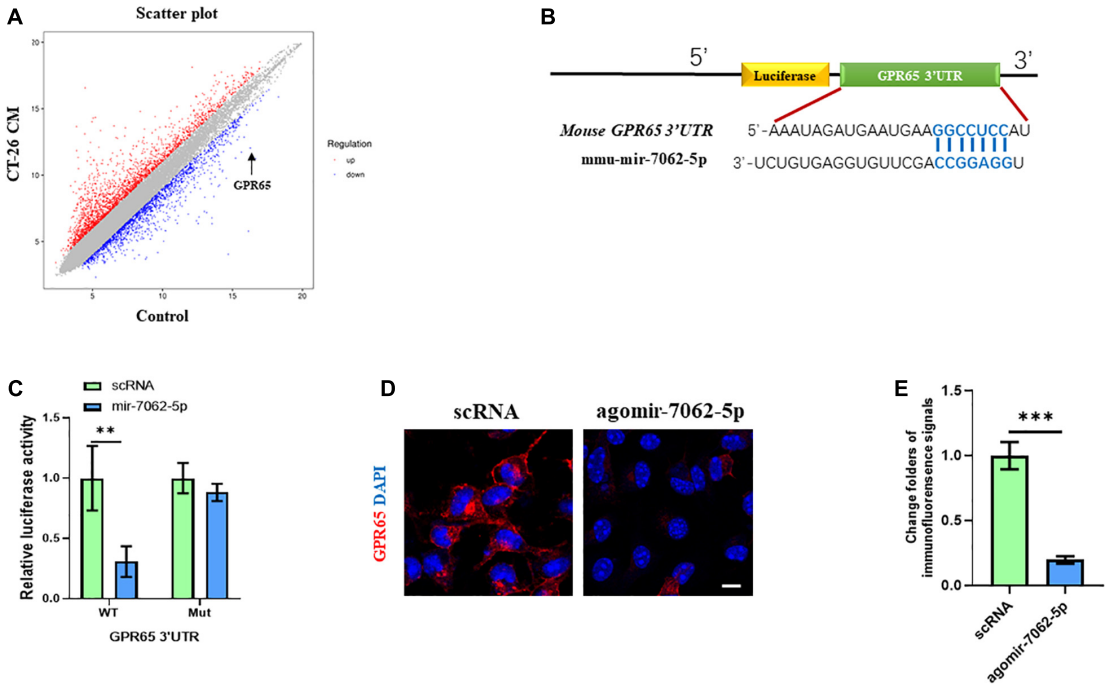

FIGURE 3 | GPR65 is the target gene of miRNA-7062-5p. **(A)** Scatter plots for microarray assay demonstrated differentially expressed mRNAs in early OCPs treated with CT-26 CM or DMEM. **(B)** The complementary sequences of miRNA-7062-5p were discovered in 3′ UTR of GPR65 mRNA using TargetScan. **(C)** Dual-luciferase analysis showed miRNA-70652-5p inversely regulated the luciferase activity of plasmids containing wild-type 3′ UTR of GPR65. **(D)** Immunofluorescence analysis revealed the protein expression of GPR65 in early OPCs after overexpression of miRNA-7062-5p (scale bar = 50 μm). **(E)** Quantification of immunofluorescence intensity in **(D)**. $^{**}p < 0.01$, $^{***}p < 0.001$.

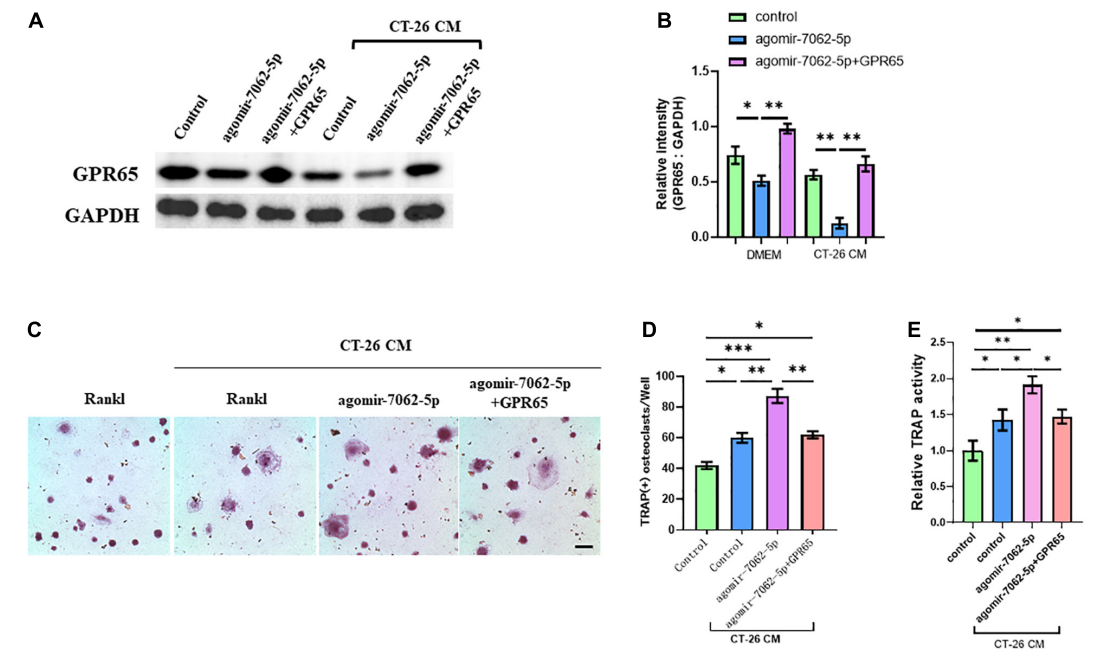

FIGURE 4 | Overexpression of GPR65 reverses the effect of miRNA-7062-5p in early OCPs. **(A)** Western blot analysis demonstrated the protein level of GPR65 in early OCPs after transfection with agomir-7062-5p alone or combination with plasmids containing GPR65 in the presence of CT-26 CM or in normal culture. **(B)** Quantification of relative intensity in **(A)**. **(C)** Representative images of TRAP staining demonstrating osteoclast formation of early OCPs induced by RANKL and M-CSF after transfection with agomir-7062-5p alone or combination with plasmids containing GPR65 in the presence of CT-26 CM (scale bar = 250 μm). **(D)** Quantification of the number of osteoclasts per well in **(C)**. **(E)** Quantification of relative TRAP activity per well in **(C)**. $^{*}p < 0.05$, $^{**}p < 0.01$, $^{***}p < 0.001$.

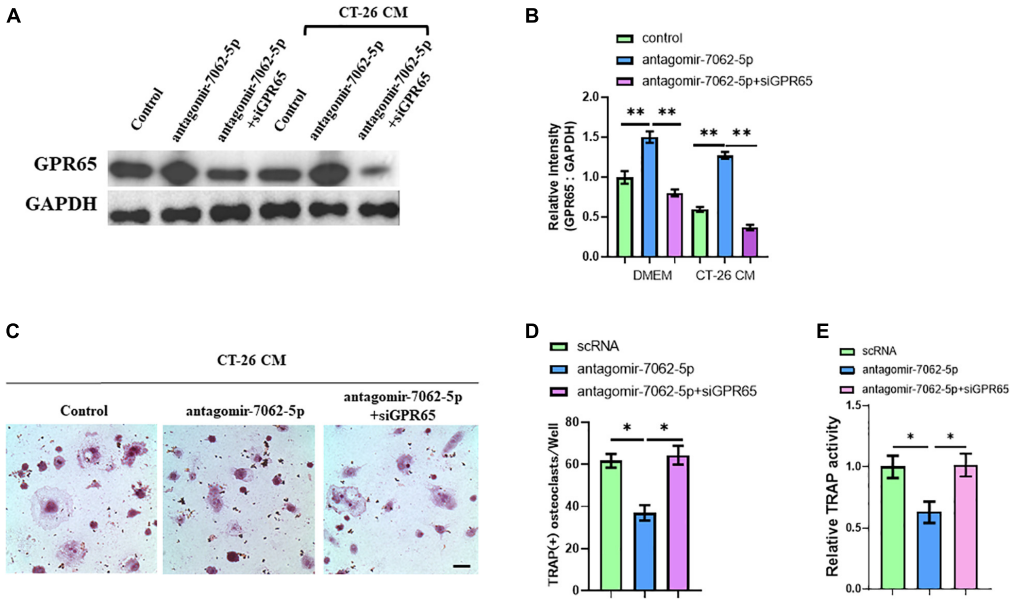

FIGURE 5 | Downregulation of GPR65 reverses the effect caused by inhibiting miRNA-7062-5p. **(A)** Western blot analysis demonstrated the protein level of GPR65 in early OCPs after transfection with antagomir-7062-5p alone or combination with GPR65 siRNA in the presence of CT-26 CM or in normal culture. **(B)** Quantification of relative intensity in **(A)**. **(C)** Representative images of TRAP staining demonstrating osteoclast formation of early OCPs induced by RANKL and M-CSF after transfection with antagomir-7062-5p alone or combination with GPR65 siRNA in the presence of CT-26 CM (scale bar = 250 μm). **(D)** Quantification of the number of osteoclasts per well in **(C)**. **(E)** Quantification of relative TRAP activity per well in **(C)**. $*p < 0.05$, $**p < 0.01$.

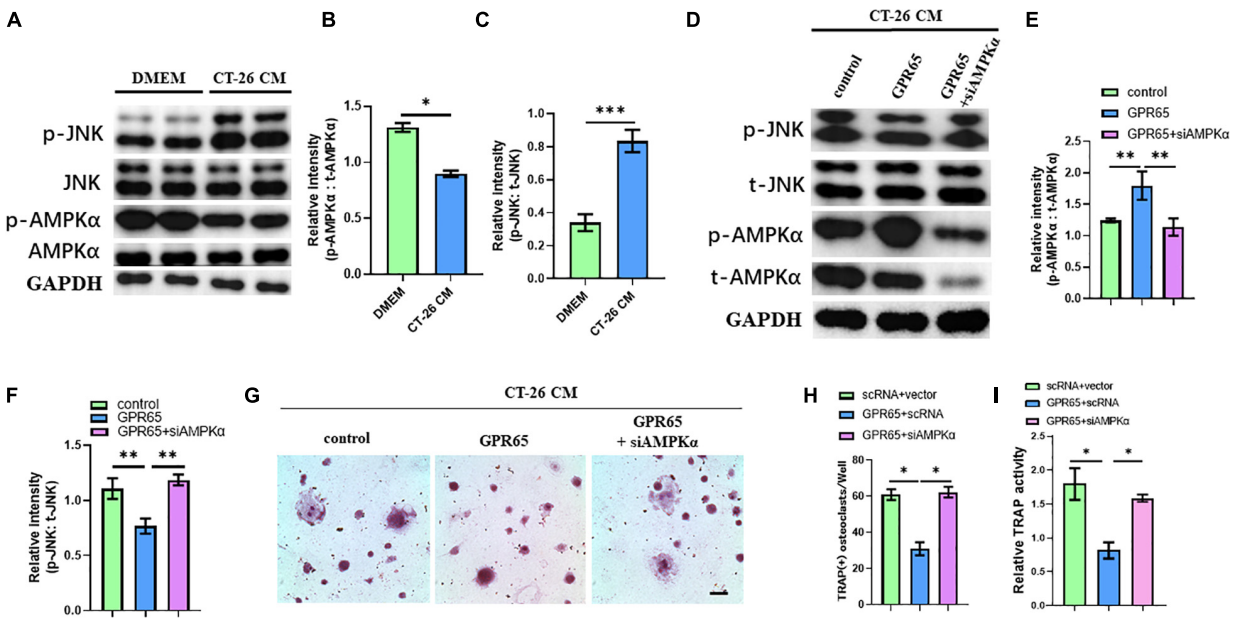

FIGURE 6 | Overexpression of GPR65 stimulates activation of AMPK pathway. **(A)** Western blot analysis showed protein level of activated AMPK and activated JNK compared with their own total proteins in early OCPs cultured in DMEM or CT-26 CM, respectively. **(B)** Quantification of relative intensity of phosphorylation of AMPKα compared with total AMPKαin **(A)**. **(C)** Quantification of relative intensity of phosphorylation of JNK compared with total JNK in **(A)**. **(D)** Western blot analysis showed protein level of activated AMPK and activated JNK compared with their own total proteins in early OCPs after transfection with plasmid containing GPR65 with/without AMPKα siRNA in the presence of CT-26 CM. **(E)** Quantification of relative intensity of phosphorylation of AMPKα compared with total AMPKαin **(D)**. **(F)** Quantification of relative intensity of phosphorylation of JNK compared with total JNK in **(D)**. **(G)** Representative images of TRAP staining demonstrating osteoclast formation of early OCPs induced by RANKL and M-CSF after transfection with plasmids containing GPR65 alone or combination with AMPKα siRNA in the presence of CT-26 CM (scale bar = 250 μm). **(H)** Quantification of relative TRAP activity per well in **(G)**. **(I)** Quantification of the number of osteoclasts per well in **(G)**. $*p < 0.05$, $**p < 0.01$, $***p < 0.001$.

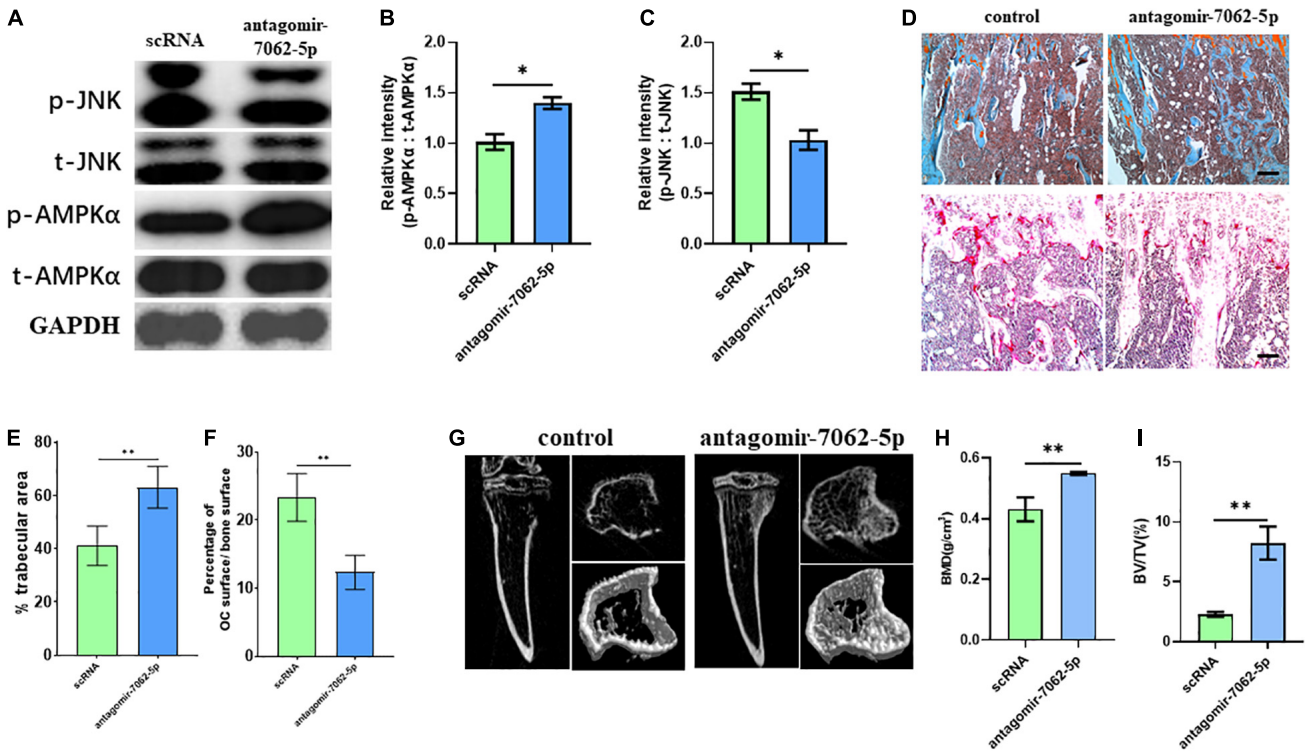

FIGURE 7 | Inhibition of miRNA-7062-5p attenuates bone resorption in bone metastatic model of CT-26 cell line *in vivo*. **(A)** Western blot analysis showed protein level of activated AMPK and JNK compared with its total protein in early OCPs sorted from antagomir-7062-5p–treated bone marrows after injection of CT-26 cells. **(B)** Quantification of relative intensity of phosphorylation of AMPKα compared with total AMPKαin **(A)**. **(C)** Quantification of relative intensity of phosphorylation of JNK compared with total JNK in **(A)**. **(D)** Upper: representative images of safranin O staining *in vivo* after injection with antagomir-7062-5p in bone metastatic model. Down: representative images of TRAP staining *in vivo* after injection with antagomir-7062-5p in bone metastatic model (scale bar = 100 μm). **(E)** Quantification of percentage of trabecular area in upper images in **(D)**. **(F)** Quantification of percentage of TRAP-positive osteoclast surface in total trabecular surface in down images in **(D)**. **(G)** Micro–computed tomography examined the bone destruction after injection with antagomir-7062-5p in bone metastatic model. **(H)** Quantification of bone mineral density in tibias after injection with antagomir-7062-5p in bone metastatic model. **(I)** Quantification of BV/TV in tibias after injection with antagomir-7062-5p in bone metastatic model. $*p < 0.05$, $**p < 0.01$.

GPR65-AMPK pathway regulated the osteoclastogenesis of OCPs in CRC microenvironment.

Inhibition of miRNA-7062-5p Attenuates Bone Resorption Through Regulating GPR65/AMPK Pathway

To detect whether anti–miRNA-7062-5p can inhibit osteoclastogenesis *in vivo*, antagomir-7062-5p was administered into tibias after injection of CT-26 cells, and the early OCPs were sorted out. Western blot revealed the activated JNK was inhibited, and the phosphorylated AMPKα was upregulated after treatment with antagomir-7062-5p (**Figures 7A–C**). Then, we tested whether inhibition of miRNA-7062-5p can prevent bone loss in the bone metastatic model of CRC *in vivo*. Notably, injection of antagomir-7062-5p significantly reduced number of OCs *in vivo* and restored trabecular area (**Figures 7D–F**). In addition, micro–computed tomography showed that the trabecular area was highly preserved after treatment with antagomir-7062-5p and the bone mineral density and trabecular bone volume fraction (BV/TV) were both improved (**Figures 7G–I**). These results demonstrated that antagmir-7062-5p can efficiently prevent bone resorption in bone metastasis of CRC.

DISCUSSION

In osteolytic tumors, bone destruction was positively associated with poor outcome (Powles et al., 1976; Kamalakar et al., 2014; Ma et al., 2018; Jie et al., 2019). It is well known that aberrant activation of osteoclasts contributes to bone resorption after tumor metastasis (Wilson et al., 2008; Das et al., 2011). Targeting osteoclastogenesis can prevent the progression of osteolysis and improve prognosis (Byrne et al., 2019).

Accumulating evidence has revealed that a large number of miRNAs play critical roles in regulating osteoclastogenesis; however, miRNAs involved in bone metastasis were elusive. Ell et al. identified that miR-16 and miR-378 promoted osteolytic bone metastasis in breast cancer and bladder cancer. These two miRNAs may be potential therapeutic targets and biomarkers, indicating that miRNAs could be critical to bone metastasis and tumor progression. As we described, although the incidence of bone metastasis in CRC is relatively less identified, the prognosis

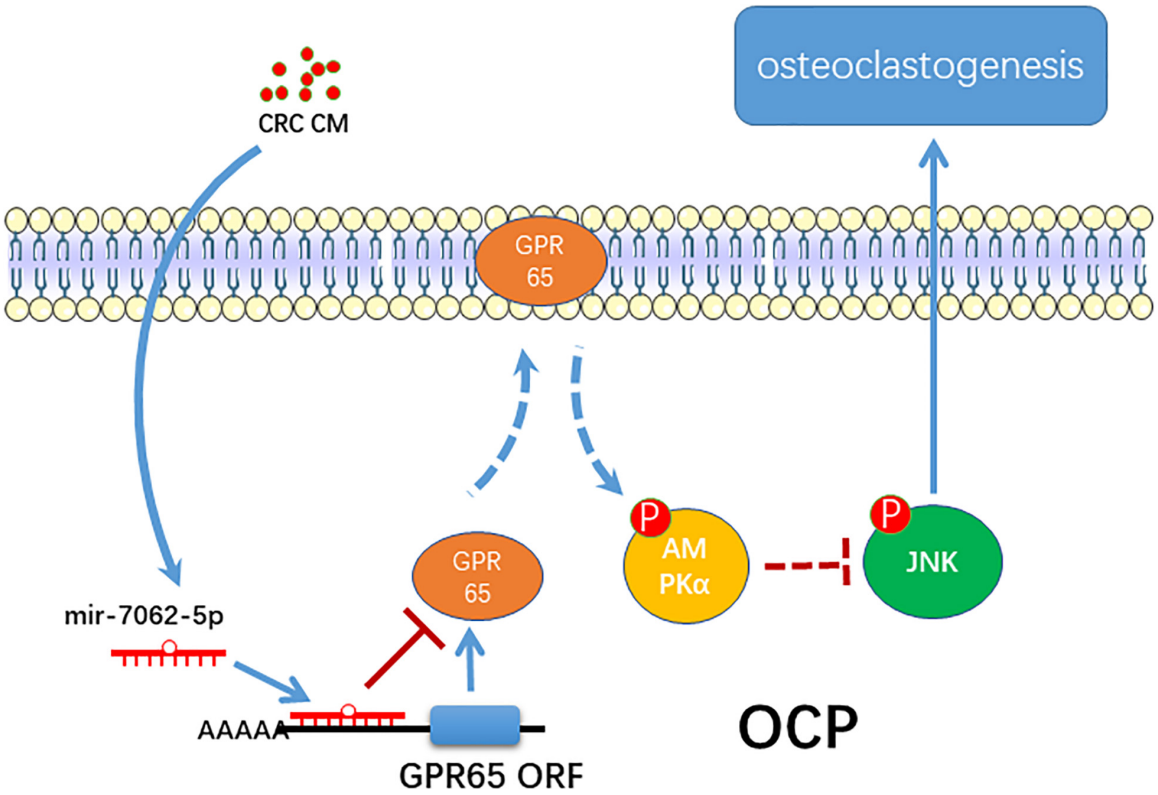

FIGURE 8 | The schematic of miR-7062-5p regulating osteoclastogenesis through targeting GPR65/AMPK pathway.

is worse. Numerous studies demonstrated that CRC is a kind of cancer that can be markedly regulated by miRNAs (Fang et al., 2012; Ma et al., 2013; Ye et al., 2013; Fu et al., 2014; Li et al., 2015; Xiao et al., 2015; Deng et al., 2016; Feiersinger et al., 2016; Noguchi et al., 2016; Fantini et al., 2017; Boriachek et al., 2018; Kandimalla et al., 2018; Lv et al., 2018). Typically, upregulated miRNAs in cancer promote the cancer, whereas downregulated miRNAs are likely to suppress tumor progression. MiR-155 and miR-503 were two reported miRNAs involved in invasion and metastasis of CRC (Noguchi et al., 2016; Liu et al., 2018). On the other hand, miR-320d, miR-203, miR-144, and miR-99b-5p prevented the proliferation, migration, or invasion in CRC cells (Xiao et al., 2015; Deng et al., 2016; Tang et al., 2019). Although correlation between miR-7062-5p and CRC was not identified in previous studies, we found that the expression of this miRNA can be upregulated in OCPs after stimulation by CRC cells and participate in osteoclast formation, indicating that a novel miRNA, miR-7062-5p, may specifically correlate with bone metastasis from CRC. Our findings together with previous studies revealed the diversity of miRNAs involved in different metastatic sites of CRC.

We here proved GPR65 is the target gene of miR-7062-5p. GPR65 is a member of G protein–coupled receptor family. Recently, the expression of GPR65 was found to be closely associated with intestinal diseases (Tcymbarevich et al., 2019a). Moreover, Tcymbarevich et al. revealed that deficiency in GRP65 in macrophages positively promoted the progression of inflammatory bowel diseases (Tcymbarevich et al., 2019b). As OCPs derive from monocyte/macrophage cell lines, these findings implied that GRP65 may play an important role in regulating physiological process in macrophages. In this study, we identified that overexpression of GPR65 can reverse the osteoclastogenesis induced by miR-7062-5p, indicating that GPR65 plays a role in anti–osteoclast differentiation in bone metastasis of CRC. One study ever reported that TDAG8, another name of GPR65, inhibited osteoclastic activity in osteoporosis (Hikiji et al., 2014), which supports our findings.

Several pathways were reported to be downstream of GPR65, including AP-1 and MEK/ERK (Ryder et al., 2012; Xu et al., 2013), notably, considering close association between GPR65 and MEK/ERK and cAMP, which is linked to the AMPK pathway. In this study, we tested the change of activation of AMPKα and indicated that the overexpression of GPR65 activated phosphorylation of AMPKα. Moreover, miR-7062-5p also downregulated activation of AMPKα, which can be rescued by overexpression of GPR65; thus, we demonstrated that AMPK is downstream of GPR65, and both of them can be regulated by miR-7062-5p. Numerous evidence demonstrated that activation of AMPK negatively regulated osteoclastogenesis (Dong et al., 2018; Tong et al., 2018; Mao et al., 2019). The AMPK pathway can inhibit the activation of the JNK pathway (Lin et al., 2016; Chen S. et al., 2018, Chen X. et al., 2018), which is a key way of

stimulating osteoclast formation. In our study, overexpression of GPR65 can inhibit phosphorylation of JNK through activation of AMPKα. Moreover, although overexpression of GPR65 inhibited osteoclast formation, this effect can be rescued by stimulating activation of JNK, indicating that the negative effect of GPR65 on osteoclastogenesis was regulated by activation of JNK.

MiRNAs have been reported to be a promising therapeutic target in tumors. Our results showed that inhibition of miRNA-7062-5p attenuated bone resorption after bone metastasis of CRC, which could be potentially used in the treatment of bone metastasis from CRC.

CONCLUSION

In summary, the present study proposes a novel role of miRNA-7062-5p in osteoclast formation in bone metastasis of CRC through targeting GPR65, as well as regulating its downstream, AMPK pathway (**Figure 8**).

DATA AVAILABILITY STATEMENT

The data presented in the study are deposited in the GEO repository, accession number GSE182097. The link is: https://www.ncbi.nlm.nih.gov/geo/query/acc.cgi?acc=GSE182097.

ETHICS STATEMENT

The animal study was reviewed and approved by the Institutional Animal Care and Use Committee of Daping Hospital at Army Medical University.

AUTHOR CONTRIBUTIONS

LC carried out the experiments, analyzed and interpreted the data, and wrote the manuscript. YW analyzed part of data and prepared the manuscript. YW and XL carried out animal experiments and collected samples. XL interpreted part of data and collected samples. LZ and ZW conceived the study, designed the experiments, and wrote the manuscript. All authors read and approved the final manuscript.

FUNDING

The research reported was supported by the Daping Hospital (2019CXLCC011).

ACKNOWLEDGMENTS

We would like to thank all members of our laboratory for their work.

REFERENCES

Boriachek, K., Umer, M., Islam, M. N., Gopalan, V., Lam, A. K., Nguyen, N. T., et al. (2018). An amplification-free electrochemical detection of exosomal miRNA-21 in serum samples. *Analyst* 143, 1662–1669. doi: 10.1039/c7an01843f

Byrne, N. M., Summers, M. A., and McDonald, M. M. (2019). Tumor cell dormancy and reactivation in bone: skeletal biology and therapeutic opportunities. *JBMR Plus* 3:e10125. doi: 10.1002/jbm4.10125

Chen, S., Zhao, L., Sherchan, P., Ding, Y., Yu, J., Nowrangi, D., et al. (2018). Activation of melanocortin receptor 4 with RO27-3225 attenuates neuroinflammation through AMPK/JNK/p38 MAPK pathway after intracerebral hemorrhage in mice. *J. Neuroinflammation* 15:106. doi: 10.1186/s12974-018-1140-6

Chen, X., Li, X., Zhang, W., He, J., Xu, B., Lei, B., et al. (2018). Activation of AMPK inhibits inflammatory response during hypoxia and reoxygenation through modulating JNK-mediated NF-kappaB pathway. *Metabolism* 83, 256–270. doi: 10.1016/j.metabol.2018.03.004

Clohisy, D. R., Palkert, D., Ramnaraine, M. L., Pekurovsky, I., and Oursler, M. J. (1996). Human breast cancer induces osteoclast activation and increases the number of osteoclasts at sites of tumor osteolysis. *J. Orthop. Res.* 14, 396–402. doi: 10.1002/jor.1100140309

Das, S., Samant, R. S., and Shevde, L. A. (2011). Hedgehog signaling induced by breast cancer cells promotes osteoclastogenesis and osteolysis. *J. Biol. Chem.* 286, 9612–9622. doi: 10.1074/jbc.M110.174920

Deng, B., Wang, B., Fang, J., Zhu, X., Cao, Z., Lin, Q., et al. (2016). MiRNA-203 suppresses cell proliferation, migration and invasion in colorectal cancer via targeting of EIF5A2. *Sci. Rep.* 6:28301. doi: 10.1038/srep28301

Dong, W., Qi, M., Wang, Y., Feng, X., and Liu, H. (2018). Zoledronate and high glucose levels influence osteoclast differentiation and bone absorption via the AMPK pathway. *Biochem. Biophys. Res. Commun.* 505, 1195–1202. doi: 10.1016/j.bbrc.2018.10.059

Fang, Y., Xiang, J., Chen, Z., Gu, X., Li, Z., Tang, F., et al. (2012). miRNA expression profile of colon cancer stem cells compared to non-stem cells using the SW1116 cell line. *Oncol. Rep.* 28, 2115–2124. doi: 10.3892/or.2012.2054

Fantini, S., Salsi, V., Reggiani, L., Maiorana, A., and Zappavigna, V. (2017). The miR-196b miRNA inhibits the GATA6 intestinal transcription factor and is upregulated in colon cancer patients. *Oncotarget* 8, 4747–4759. doi: 10.18632/oncotarget.13580

Feiersinger, F., Nolte, E., Wach, S., Rau, T. T., Vassos, N., Geppert, C., et al. (2016). MiRNA-21 expression decreases from primary tumors to liver metastases in colorectal carcinoma. *PLoS One* 11:e0148580. doi: 10.1371/journal.pone.0148580

Fu, X., Meng, Z., Liang, W., Tian, Y., Wang, X., Han, W., et al. (2014). miR-26a enhances miRNA biogenesis by targeting Lin28B and Zcchc11 to suppress tumor growth and metastasis. *Oncogene* 33, 4296–4306. doi: 10.1038/onc.2013.385

Guo, J., Zeng, X., Miao, J., Liu, C., Wei, F., Liu, D., et al. (2019). MiRNA-218 regulates osteoclast differentiation and inflammation response in periodontitis rats through Mmp9. *Cell Microbiol.* 21:e12979. doi: 10.1111/cmi.12979

Guo, K., Zhang, D., Wu, H., Zhu, Q., Yang, C., and Zhu, J. (2018). MiRNA-199a-5p positively regulated RANKL-induced osteoclast differentiation by target Mafb protein. *J. Cell. Biochem.* 120, 7024–7031. doi: 10.1002/jcb.27968

Hikiji, H., Endo, D., Horie, K., Harayama, T., Akahoshi, N., Igarashi, H., et al. (2014). TDAG8 activation inhibits osteoclastic bone resorption. *FASEB J.* 28, 871–879. doi: 10.1096/fj.13-233106

Jie, Z., Xie, Z., Xu, W., Zhao, X., Jin, G., Sun, X., et al. (2019). SREBP-2 aggravates breast cancer associated osteolysis by promoting osteoclastogenesis and breast cancer metastasis. *Biochim. Biophys. Acta Mol. Basis Dis.* 1865, 115–125. doi: 10.1016/j.bbadis.2018.10.026

Kamalakar, A., Bendre, M. S., Washam, C. L., Fowler, T. W., Carver, A., Dilley, J. D., et al. (2014). Circulating interleukin-8 levels explain breast cancer osteolysis in mice and humans. *Bone* 61, 176–185. doi: 10.1016/j.bone.2014.01.015

Kandimalla, R., Gao, F., Matsuyama, T., Ishikawa, T., Uetake, H., Takahashi, N., et al. (2018). Genome-wide Discovery and Identification of a Novel miRNA

Signature for Recurrence Prediction in Stage II and III Colorectal Cancer. *Clin. Cancer Res.* 24, 3867–3877. doi: 10.1158/1078-0432.CCR-17-3236

Kawamura, H., Yamaguchi, T., Yano, Y., Hozumi, T., Takaki, Y., Matsumoto, H., et al. (2018). Characteristics and prognostic factors of bone metastasis in patients with colorectal cancer. *Dis. Colon Rectum.* 61, 673–678. doi: 10.1097/DCR.0000000000001071

Li, K., Chen, S., Cai, P., Chen, K., Li, L., Yang, X., et al. (2020a). MiRNA-483-5p is involved in the pathogenesis of osteoporosis by promoting osteoclast differentiation. *Mol. Cell Probes.* 49:101479. doi: 10.1016/j.mcp.2019.101479

Li, S. S., Zhu, H. J., Li, J. Y., Tian, L. M., and Lv, D. M. (2020b). MiRNA-875-3p alleviates the progression of colorectal cancer via negatively regulating PLK1 level. *Eur. Rev. Med. Pharmacol. Sci.* 24, 1126–1133. doi: 10.26355/eurrev_202002_20163

Li, W. C., Wu, Y. Q., Gao, B., Wang, C. Y., and Zhang, J. J. (2019a). MiRNA-574-3p inhibits cell progression by directly targeting CCND2 in colorectal cancer. *Biosci. Rep.* 39:BSR20190976. doi: 10.1042/BSR20190976

Li, W., Chang, J., Wang, S., Liu, X., Peng, J., Huang, D., et al. (2015). miRNA-99b-5p suppresses liver metastasis of colorectal cancer by down-regulating mTOR. *Oncotarget* 6, 24448–24462. doi: 10.18632/oncotarget.4423

Li, X., Luo, W., Hu, J., Chen, Y., Yu, T., Yang, J., et al. (2019b). Interleukin-27 prevents LPS-induced inflammatory osteolysis by inhibiting osteoclast formation and function. *Am. J. Transl. Res.* 11, 1154–1169.

Li, Z., Zhang, W., and Huang, Y. (2018). MiRNA-133a is involved in the regulation of postmenopausal osteoporosis through promoting osteoclast differentiation. *Acta Biochim. Biophys. Sin. (Shanghai)* 50, 273–280. doi: 10.1093/abbs/gmy006

Liang, M., Ma, Q., Ding, N., Luo, F., Bai, Y., Kang, F., et al. (2019). IL-11 is essential in promoting osteolysis in breast cancer bone metastasis via RANKL-independent activation of osteoclastogenesis. *Cell Death Dis.* 10:353. doi: 10.1038/s41419-019-1594-1

Lin, K. C., Huang, D. Y., Huang, D. W., Tzeng, S. J., and Lin, W. W. (2016). Inhibition of AMPK through Lyn-Syk-Akt enhances FcepsilonRI signal pathways for allergic response. *J. Mol. Med. (Berl)* 94, 183–194. doi: 10.1007/s00109-015-1339-2

Liu, N., Jiang, F., Han, X. Y., Li, M., Chen, W. J., Liu, Q. C., et al. (2018). MiRNA-155 promotes the invasion of colorectal cancer SW-480 cells through regulating the Wnt/beta-catenin. *Eur. Rev. Med. Pharmacol. Sci.* 22, 101–109. doi: 10.26355/eurrev_201801_14106

Luo, H., Sun, S., Li, P., Bu, D., Cao, H., and Zhao, Y. (2013). Comprehensive characterization of 10,571 mouse large intergenic noncoding RNAs from whole transcriptome sequencing. *PLoS One* 8:e70835. doi: 10.1371/journal.pone.0070835

Lv, Q. L., Zhu, H. T., Li, H. M., Cheng, X. H., Zhou, H. H., and Chen, S. H. (2018). Down-regulation of miRNA-320c promotes tumor growth and metastasis and predicts poor prognosis in human glioma. *Brain Res. Bull.* 139, 125–132. doi: 10.1016/j.brainresbull.2018.02.009

Ma, G. T., Lee, S. K., Park, K. K., Park, J., Son, S. H., Jung, M., et al. (2018). Artemisinin-daumone hybrid inhibits cancer cell-mediated osteolysis by targeting cancer cells and osteoclasts. *Cell Physiol. Biochem.* 49, 1460–1475. doi: 10.1159/000493449

Ma, Y., Li, W., and Wang, H. (2013). Roles of miRNA in the initiation and development of colorectal carcinoma. *Curr. Pharm. Des.* 19, 1253–1261. doi: 10.2174/138161213804805784

Mao, Z., Zhu, Y., Hao, W., Chu, C., and Su, H. (2019). MicroRNA-155 inhibition up-regulates LEPR to inhibit osteoclast activation and bone resorption via activation of AMPK in alendronate-treated osteoporotic mice. *IUBMB Life* 71, 1916–1928. doi: 10.1002/iub.2131

Noguchi, T., Toiyama, Y., Kitajima, T., Imaoka, H., Hiro, J., Saigusa, S., et al. (2016). miRNA-503 promotes tumor progression and is associated with early recurrence and poor prognosis in human colorectal cancer. *Oncology* 90, 221–231. doi: 10.1159/000444493

Park, Y. R., Seo, S. Y., Kim, S. L., Zhu, S. M., Chun, S., Oh, J. M., et al. (2018). MiRNA-206 suppresses PGE2-induced colorectal cancer cell proliferation, migration, and invasion by targetting TM4SF1. *Biosci. Rep.* 38:BSR20180664. doi: 10.1042/BSR20180664

Powles, T. J., Dowsett, M., Easty, G. C., Easty, D. M., and Neville, A. M. (1976). Breast-cancer osteolysis, bone metastases, and anti-osteolytic effect of aspirin. *Lancet* 1, 608–610. doi: 10.1016/s0140-6736(76)90416-5

Ryder, C., McColl, K., Zhong, F., and Distelhorst, C. W. (2012). Acidosis promotes Bcl-2 family-mediated evasion of apoptosis: involvement of acid-sensing G protein-coupled receptor Gpr65 signaling to Mek/Erk. *J. Biol. Chem.* 287, 27863–27875. doi: 10.1074/jbc.M112.384685

Sun, S., Hang, T., Zhang, B., Zhu, L., Wu, Y., Lv, X., et al. (2019). miRNA-708 functions as a tumor suppressor in colorectal cancer by targeting ZEB1 through Akt/mTOR signaling pathway. *Am. J. Transl. Res.* 11, 5338–5356.

Tang, Y., Zhao, Y., Song, X., Song, X., Niu, L., and Xie, L. (2019). Tumor-derived exosomal miRNA-320d as a biomarker for metastatic colorectal cancer. *J. Clin. Lab. Anal.* 33:e23004. doi: 10.1002/jcla.23004

Tcymbarevich, I. V., Eloranta, J. J., Rossel, J. B., Obialo, N., Spalinger, M., Cosin-Roger, J., et al. (2019a). The impact of the rs8005161 polymorphism on G protein-coupled receptor GPR65 (TDAG8) pH-associated activation in intestinal inflammation. *BMC Gastroenterol* 19:2. doi: 10.1186/s12876-018-0922-8

Tcymbarevich, I., Richards, S. M., Russo, G., Kühn-Georgijevic, J., Cosin-Roger, J., Baebler, K., et al. (2019b). Lack of the pH-sensing Receptor TDAG8 [GPR65] in Macrophages Plays a Detrimental Role in Murine Models of Inflammatory Bowel Disease. *J. Crohns. Colitis.* 13, 245–258. doi: 10.1093/ecco-jcc/jjy152

Tong, X., Gu, J., Song, R., Wang, D., Sun, Z., Sui, C., et al. (2018). Osteoprotegerin inhibit osteoclast differentiation and bone resorption by enhancing autophagy via AMPK/mTOR/p70S6K signaling pathway in vitro. *J. Cell Biochem.* 120, 1630–1642. doi: 10.1002/jcb.27468

Wilson, T. J., Nannuru, K. C., Futakuchi, M., Sadanandam, A., and Singh, R. K. (2008). Cathepsin G enhances mammary tumor-induced osteolysis by generating soluble receptor activator of nuclear factor-kappaB ligand. *Cancer Res.* 68, 5803–5811. doi: 10.1158/0008-5472.CAN-07-5889

Xiao, R., Li, C., and Chai, B. (2015). miRNA-144 suppresses proliferation and migration of colorectal cancer cells through GSPT1. *Biomed. Pharmacother.* 74, 138–144. doi: 10.1016/j.biopha.2015.08.006

Xu, H., Chen, X., Huang, J., Deng, W., Zhong, Q., Yue, C., et al. (2013). Identification of GPR65, a novel regulator of matrix metalloproteinases using high through-put screening. *Biochem. Biophys. Res. Commun.* 436, 96–103. doi: 10.1016/j.bbrc.2013.05.065

Ye, J., Wu, X., Wu, D., Wu, P., Ni, C., Zhang, Z., et al. (2013). miRNA-27b targets vascular endothelial growth factor C to inhibit tumor progression and angiogenesis in colorectal cancer. *PLoS One* 8:e60687. doi: 10.1371/journal.pone.0060687

Zhang, Y., Ma, L. N., and Xie, Y. (2020). MiRNA-802 inhibits the metastasis of colorectal cancer by targeting FOXE1. *Eur. Rev. Med. Pharmacol. Sci.* 24, 1778–1785. doi: 10.26355/eurrev_202002_20355

Zhao, H., Zhang, J., Shao, H., Liu, J., Jin, M., Chen, J., et al. (2017). miRNA-340 inhibits osteoclast differentiation via repression of MITF. *Biosci. Rep.* 37:BSR20170302. doi: 10.1042/BSR20170302

Conflict of Interest: The authors declare that the research was conducted in the absence of any commercial or financial relationships that could be construed as a potential conflict of interest.

Publisher's Note: All claims expressed in this article are solely those of the authors and do not necessarily represent those of their affiliated organizations, or those of the publisher, the editors and the reviewers. Any product that may be evaluated in this article, or claim that may be made by its manufacturer, is not guaranteed or endorsed by the publisher.

frontiers in Cell and Developmental Biology

ORIGINAL RESEARCH
published: 20 August 2021
doi: 10.3389/fcell.2021.723721

Identification of the Immune-Related Genes in Tumor Microenvironment That Associated With the Recurrence of Head and Neck Squamous Cell Carcinoma

Liu Chengcheng[1], Qi Wenwen[2,3], Gong Ningyue[2], Zhu Fangyuan[2], Xu Runtong[2], Teng Zhenxiao[2], Xu Fenglei[2], Qin Yiming[4], Zhao Miaoqing[5†], Li Xiaoming[2*†] and Xia Ming[2*†]*

[1] Department of Central Laboratory, Shandong Provincial Hospital Affiliated to Shandong First Medical University, Jinan, China, [2] Department of Otolaryngology, Shandong Provincial Hospital Affiliated to Shandong First Medical University, Jinan, China, [3] Cheeloo College of Medicine, Shandong Provincial Hospital, Shandong University, Jinan, China, [4] College of Chemistry, Chemical Engineering and Materials Science, Shandong Normal University, Jinan, China, [5] Department of Pathology, Shandong Provincial Hospital Affiliated to Shandong First Medical University, Jinan, China

OPEN ACCESS

Edited by:
Na Luo,
Nankai University, China

Reviewed by:
Xingyi Li,
Affiliated Eye Hospital of Wenzhou Medical College, China
Lei Li,
Xi'an Jiaotong University, China

***Correspondence:**
Zhao Miaoqing
zhaomqsd@163.com
Li Xiaoming
lxmfmmu@sina.com
Xia Ming
xiamingsdu@sohu.com

[†] These authors have contributed equally to this work

Specialty section:
This article was submitted to Molecular and Cellular Pathology, a section of the journal Frontiers in Cell and Developmental Biology

Received: 11 June 2021
Accepted: 03 August 2021
Published: 20 August 2021

Citation:
Chengcheng L, Wenwen Q, Ningyue G, Fangyuan Z, Runtong X, Zhenxiao T, Fenglei X, Yiming Q, Miaoqing Z, Xiaoming L and Ming X (2021) Identification of the Immune-Related Genes in Tumor Microenvironment That Associated With the Recurrence of Head and Neck Squamous Cell Carcinoma. Front. Cell Dev. Biol. 9:723721. doi: 10.3389/fcell.2021.723721

Head and neck squamous cell carcinomas (HNSCC) are still one of the most common malignant tumors in China, with a high metastasis rate and poor prognosis. The tumor immune microenvironment can affect the occurrence, development and prognosis of tumors, but the underlying mechanism is still unclear. In this study, we tried to describe the correlation between the recurrence of HNSCC and the tumor microenvironment (TME). The expression data [estimate the level of tumor stromal and immune infiltration, expression data (ESTIMATE)] algorithm was used to identify and estimate highly correlated stromal cells, immune cells, and prognostic scores in 116 samples of head and neck cancer patients from The Cancer Genome Atlas (TCGA) dataset. The functional enrichment analysis and protein-protein interaction (PPI) networks of differential expressed genes (DEGs) were constructed. Subsequently, the abundance of various infiltrating immune cells was estimated with the tumor immune estimation resource (TIMER) and the infiltration pattern of immune cells were explored in HNSCC. A total of 407 immune-related genes were identified to involve in the TME. We found that CCR5, CD3E, CD4, and HLA -DRB1 were the most obvious DEGs and the dendritic cells (DCs) showed the highest abundance in the TME of HNSCC. In addition, the unsupervised cluster analysis determined 10 clusters of immune infiltration patterns, and indicated that immune infiltrated CD4 + T and B cells may be related to the prognosis of HNSCC. In conclusion, our research determined the list of immune genes and immune infiltrating cells related to the prognosis of HNSCC, and provided a perspective for HNSCC evolution, anti-tumor drugs selection, and drug resistance research.

Keywords: head and neck squamous cell carcinoma, recurrence, immune score, stromal score, immune infiltrating

INTRODUCTION

Head and neck squamous cell carcinomas (HNSCC), mainly including oral cavity, oropharyngeal, laryngopharyngeal, laryngeal cancers, and hypopharyngeal, are the sixth most common malignant tumors with a 5-year overall survival rate of less than 50% (Kanazawa et al., 2019; McDermott and Bowles, 2019). These dismal malignant tumors affect more than 6,00,000 patients worldwide annually, and nearly half of the newly diagnosed cases are found at an advanced stage (Brenner et al., 2014). Though significant development in multimodal therapeutic strategies, including surgery, radiotherapy, chemotherapy, immunotherapy, and combined treatment, the 5-year survival rate of HNSCC has improved slightly in the past decade due to the resistant nature of tumor cells to chemoradiotherapy (Paver et al., 2020). Recently, emerging genomic evidence indicates that significant immunosuppression and heterogeneous characteristics of HNSCC play vital roles in disease treatment and recurrence (Bhat et al., 2021). However, the detailed roles and underlying mechanisms of tumor heterogeneous on the relapse of HNSCC have not been fully understood.

Disturbance of the tumor microenvironment (TME) is one of the key causes of local immune dysfunction. It establishes a stable ecological environment and space for cancer cells, a variety of endothelial cells, immune cells, and extracellular components (Hanahan and Coussens, 2012; Quail and Joyce, 2013). More and more evidences show that TME is crucial in the occurrence and even recurrence of HNSCC. It has an adverse effect on the prognosis by promoting the evolution of aggressive HNSCC and resistance to chemo- or radio-treatment (Sharma et al., 2017). An in-depth understanding of the influencing factors of TME and the highly complex tumor-stromal interactions can promote the discovery of new therapeutic interventions for HNSCC. Therefore, identifying the immune genes and active types of immune cells related to TME can help to clarify the general mechanism of HNSCC immunosuppression.

Recent studies show that the regulation of the immune system played an important role in the prognosis of cancer patients, and tumor molecular profiling could help to predict clinical outcomes and determine the targets for treating tumors (Michot et al., 2016; Miyauchi et al., 2019; Bruni et al., 2020). It also revealed the prognostic characteristics of some genes in detail, which played an important role in the survival prediction of HNSCC (Zhou et al., 2019). Recently, researchers have identified some important immune checkpoint components that promote the tumor cells to evade from the immune surveillance, such as cytotoxic T lymphocyte-associated protein 4 (CTLA-4) and programmed cell death protein 1 (PD-1)/programmed cells Death ligand 1 (PD-L1) (Brunner-Weinzierl and Rudd, 2018; Lee et al., 2019). Subsequently, novel strategy for cancer therapy of the checkpoint immunosuppression was applied for multiple malignant tumors, including HNSCC. However, checkpoint blocking immunotherapy is not effective for all patients, and the observed effective rate is only in the range of 16–25% (Medina and Adams, 2016). Therefore, there is an urgent need for an immune-related prognostic feature that can predict not only the survival period, but also the immunotherapy response of different patient groups.

In this study, we constructed an immune-related prognostic feature with patient information from The Cancer Genome Atlas (TCGA) data set, and further verified its prognostic value. In addition, we also determined the relationship between the genetic characteristics, TME, and the prognosis of patients with recurrent HNSCC. We further obtained four new prognostic molecular biomarkers, which was closely related to the immune microenvironment of HNSCC. Finally, we verified the expression of these four genes in tumors in a cohort study. The purpose of this study is to provide a new immune-related molecular biomarker of HNSCC, which can more effectively predict the prognosis of HNSCC patients and is closely related to the immune microenvironment.

MATERIALS AND METHODS

Reagants

The rabbit polyclonal to CCR5 (Cat. No. ab7346), rabbit monoclonal to CD3 epsilon (Cat. No. ab237721), and CD4 (Cat. No. ab183685) were purchased from abcam (Cambridge, United Kingdom). The mouse monoclonal to GAPDH (Cat. No. ab8245) and HLA-DRB1 (Cat. No. ab215835) were also purchased from abcam (Cambridge, United Kingdom).

Gene Expression Data Extraction

The Cancer Genome Atlas dataset is downloaded from UCSC Xena.[1] RNA sequencing (RNA-seq) data is downloaded from the TCGA data portal. Then convert the FPKM value of the fragment to the value of TPM, including tumor grade and survival information. Our study included 116 tumor samples (Larynx HNSC) with complete prognostic information. We defined patients with new tumors new tumor events occurring after surgery to be recurrent HNSCC. **Supplementary Table 1** summarizes the characteristics of the patients in the training and validation cohort.

Calculation of Stromal and Immune Score

The expression data [estimate the level of tumor stromal and immune infiltration, expression data (ESTIMATE)] analysis by the "estimate" R software package was used to evaluate the stromal and immune scores in stromal cells and immune cells in recurrent HNSCC tissues (Van Landuyt et al., 2011). According to this algorithm, the tumor purity is calculated.

Differential Expression Analysis

According to the ESTIMATE analysis, we divided all patients into a high/low immune score group and a high/low stromal score group. Then, by using the "limma" package to analyze the differential expression between different immune groups, the selection criteria are log2|fold change| greater than 1 and adj.p

[1]https://xenabrowser.net/

less than 0.05. The corresponding heat maps and cluster maps were generated using the "pheatmap" package.

Survival Analysis

Kaplan–Meier analysis was performed to screen HNSCC with recurrent characteristics. The survival curves were also applied to illustrate the relationship between the expression levels of these genes and the recurrence of HNSCC.

Gene Ontology and Kyoto Encyclopedia of Genes and Genomes Analysis

Functional enrichment analysis was performed by the "clusterProfiler" package to determine the functions and pathways of the screened genes (Yu et al., 2012). Functional enhancements to gene ontology (GO) terms include cell component (CC), biological processes (BPs), molecular function categories (MF), and the Kyoto Encyclopedia of Genes and Genomes (KEGG) approach in the Kyoto Protocol. The cut-off value was false discovery rate <0.05.

Protein-Protein Interaction Network Construction

A total of 407 genes were obtained and mapped from the STRING database. The selected interaction score was greater than 0. The protein-protein interaction (PPI) network between the obtained genes was also analyzed. Search tool STRING[2] that retrieves interacting genes was used to predict the PPI network of immune-related genes (Ke et al., 2019). An interactive composite score greater than 0.4 is considered statistically significant. Use Cytoscape's Molecular Complex Detection (MCODE) plug-in to perform topological clustering of the network, where the recognition MCODE score is greater than 5, the degree cutoff is equal to 2, the node score cutoff is equal to 0.2, the maximum depth is equal to 100, and the *k* score is equal to 2 (Liu et al., 2019).

Immune Cell Infiltration Analysis

The abundance of the six infiltrating immune cells in recurrent HNSCC was calculated by the tumor immune estimation resource (TIMER) algorithm (a calculation method). The infiltrating cells mainly included dendritic cells (DCs), neutrophils, B cells, macrophages, CD4 + and CD8 + T cells. Then, the patients were divided into *k* clusters by unsupervised cluster analysis of these infiltrated immune cells based on *k*-means (Seo et al., 2018; Yang et al., 2019). In this analysis, we divide the patients into 10 Clusters, and investigated the association of different clusters with recurrence of HNSCC.

Quantitative Real Time-PCR

In this study, 30 HNSCC patients who underwent tumor resection but did not receive adjuvant therapy such as radio- or chemotherapy before surgery at Shandong Provincial Hospital Affiliated to Shandong First Medical University (Shandong, China) participated in this project in accordance with the Declaration of Helsinki. The tumor and control tissues are collected in RNase-free eppendorf tubes, and stored in −80°C. Then total RNA was isolated according to the manufacturer's protocol (RNeasy Mini Kit, Qiagen). The extracted RNA was then reverse transcribed using Superscript R reverse transcriptase. Quantitative real time-PCR (qRT-PCR) was performed using cDNA as a template with Platinum SYBR Green (Invitrogen). To obtain the best sensitivity and specificity of the primers, the cycle length of different PCR groups was adjusted to 40 cycles, and the annealing temperature was adjusted between 56 and 64°C. To analyze the qRT-PCR results, the 2-ΔΔCt method was used, and β-actin served as a housekeeping gene. All PCRs were performed in triplicate. Specific primer sequences are recorded below: CCR5-forward primer (AGGAATCATCTTTACCAGAT), reverse primer (ATGACAAGCAGCGGCA); CD3E-forward primer (TCCCAACCCAGACTATGAGC), reverse primer (CAAGACTAGCCCAGGAAACAG); CD4-forward primer (AGTCCAAGGGGTAAAAACAT), reverse primer (AAGGAG AACTCCACCTGTTC); HLA-DRB1-forward primer (AGAG CTTCACAGTGCAGCGG), reverse primer (GTCTTCTCTT CCTGGCCATT); and GAPDH-forward primer (GGGAAA CTGTGGCGTGAT), reverse primer (GAGTGGGTGTCG CTGTTGA).

Immunohistochemistry

All nasal biopsy specimens embedded in paraffin were cut into 4 um sections using a Leica microtome (Leica, Wetzlar, Germany). After dewaxing with xylene, a modified citrate buffer was used for thermally induced epitope repair. The samples were blocked with 10% goat serum and then incubated with the primary antibody overnight at 4°C. Modified horseradish peroxidase (HRP) technology was used to observe specific protein expression. High-resolution images were obtained on an Olympus digital electron microscope (Olympus, Tokyo, Japan).

Western Blot

The tumor and control tissues are lysed with cell lysis buffer with 1 mM phenylmethanesulfonyl fluoride (PMSF) and 1×protease inhibitor cocktail (Roche). For Western blot analysis, the protein sample concentration was adjusted to 40 μg/μl, separated by SDS-PAGE, then switched to a PVDF membrane, and incubated with the corresponding primary antibody at 4°C overnight. The next day, the corresponding secondary antibody was incubated for 1 h at room temperature. An ECL system (Cell Signaling Technology) was used to detect protein signals. The GAPDH protein in the whole protein was used as an internal control.

Statistical Analysis

The "ggplot2" R package was used for data visualization, and all statistical analysis was performed in R (version 3.6.1).[3] The Kaplan–Meier method was used to generate visual survival curves, and all survival curves were generated by the "survminer" R package. We performed the Benjamini–Hochberg method to convert the *P*-value of a gene into FDR for the analysis of differential expressed genes (DEGs). The "pheatmap" R package

[2]https://string-db.org/

[3]https://www.r-project.org/

was applied for heat map generation and visualization. For multiple groups, one-way analysis of variance (ANOVA) was selected as the parameter method for comparing means, and the Kruskal–Wallis test analysis was performed by the non-parametric method. The Wilcoxon test was used to compare non-normally distributed variables. The unpaired Student *t*-test was used to compare normally distributed variables. The Shapiro–Wilk normality test was used to test the normality of the variables. All tests are two-tailed tests, and a *P*-value of less than 0.05 was considered statistically significance.

RESULTS

Association of Immune and Stromal Scores With Pathological Characteristics of Recurrent HNSCC

A total of 116 eligible HNSCC data, including clinicopathological and prognostic informations, were extracted from the TCGA database. In general, 65.5% of the patients were over 60 years old, 43.1% were alive, and 75.9% were in stage III/IV at the time of diagnosis (**Supplementary Table 1**). Using ESTIMATE analysis, immune score and stroma score were performed according to age, tumor grade, and survival status and divided all patients into high- and low-score groups (**Supplementary Table 1**). Kaplan–Meier analysis was performed and the result indicated that the immune and stroma scores were obviously correlated with the prognosis of recurrent HNSCC patients (**Figures 1A,B**). In addition, we also tried to explore the relationship between immune and stromal scores and the age, tumor grade, and treatment methods of patients with recurrent HNSCC. The analysis showed that immunity and stromal scores have a certain relationship with age and tumor grade, but there is no significant correlation with treatment (**Supplementary Figure 1**).

Identification of Immune-Related Genes in Recurrent HNSCC

All patients were divided into a high or low immune score group and a high or low stroma score group according to the results of ESTIMATE analysis. Subsequently, gene differential expression analysis was performed to identify the DEGs between the high or low groups of immune score and stroma score. The heat map shows the gene expression pattern of DEGs between the high and low immune score or stroma score groups (**Figures 2A,B**). Then, gene expression levels in the high and low immune score groups were compared. There was 521 up-regulated genes and 3 down-regulated genes in the high immune score group (**Figure 2C**). Similarly, 648 genes were up-regulated and 18 genes were down-regulated in the high stroma score group (**Figure 2D**). As shown in the Venn diagram (**Figure 2E**), we selected the up-regulated overlapping genes as candidate immune-related genes (407 up-regulated genes), because there is no overlap of the down-regulated genes in the immune group and the stroma group. These crossover genes will be used for subsequent analysis.

Module-Related Central Gene Network

In order to further identify the DEGs related to TME in HNSCC, we constructed a modular-centric gene network. We also calculated a PPI network with 212 nodes and 2,016 edges to explore the interaction between the candidate immune-related genes of tumor prognosis (**Figure 3A**). It can be seen that the more a gene is associated with other genes in the network, the more relevant the module is. In addition, MCODE analysis identified 8 modules with at least 3 nodes (**Figure 3B**). Among the 8 modules, the red module had 29 nodes and 372 edges, which scored the highest among these modules, and the smallest brown and pink module had only 3 nodes and 3 edges. To some extent, there are fewer nodes with a large number and more nodes with

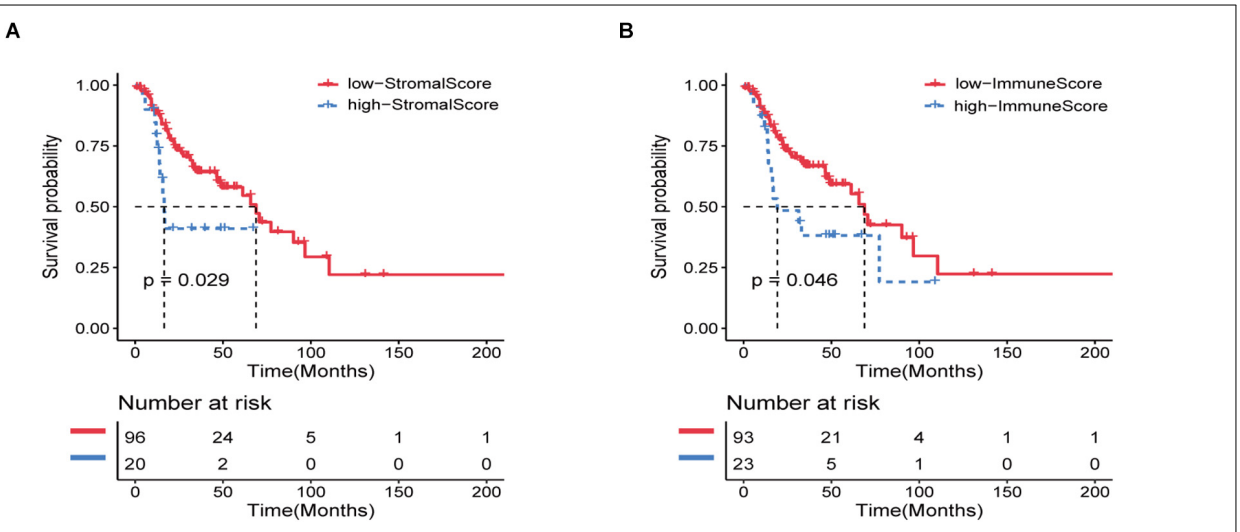

FIGURE 1 | Immune and stromal scores are significantly related to the prognosis of patients with recurrent HNSCC. Based on the immune/stromal scores, recurrent HNSCC patients were divided into high/low score groups. **(A)** Kaplan–Meier curve of the high and low immune score groups. **(B)** Kaplan–Meier curve of high and low stromal score groups.

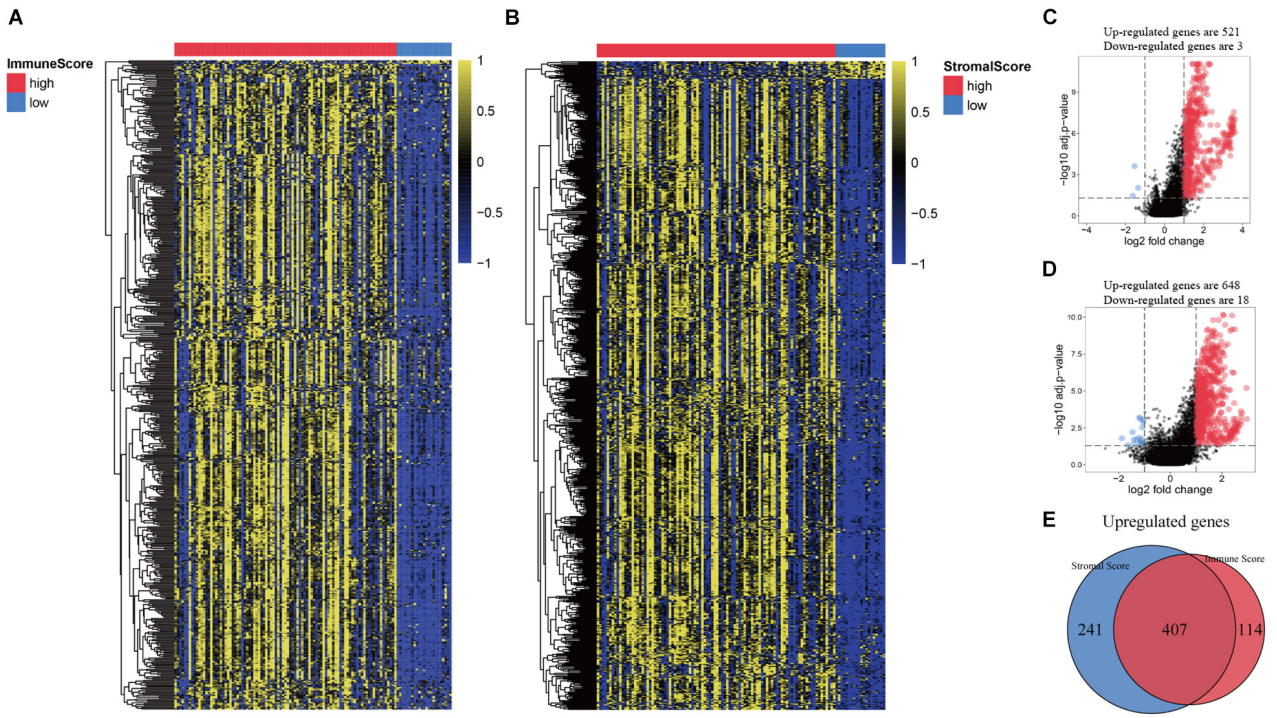

FIGURE 2 | Comparison of gene expression profiles based on immune score and stromal score in recurrent HNSCC. **(A)** Heat map of genes that are significantly expressed differently based on immune scores. **(B)** Heat map of genes that are significantly differently expressed based on stromal scores. **(C)** Volcano map of differential expressed genes (DEGs) according to the immune score. **(D)** Volcano map of DEGs according to the stromal scores. **(E)** Venn diagram analysis of abnormally expressed genes according to the immune and stromal scores.

a small number, which is consistent with the characteristics of biological networks.

Function Richness Analysis of Immune-Related Genes in Recurrent HNSCC

In order to explore the potential molecular mechanisms of 407 immune-related genes, we performed a functional enrichment analysis of these genes. As shown in **Figure 3** and **Supplementary Table 2**, the BP of GO analysis shows that immune-related genes are mainly enriched in the BP of leukocyte migration, immune response-regulating cell surface receptor signaling pathway and immune response-activating cell surface receptor signaling pathway (**Figure 4A**). In the CC group genes are mainly enriched in the extracellular matrix, side of membrane, and collagen-containing extracellular matrix (**Figure 4B**). MF enriches antigen binding, extracellular matrix structural constituent, peptide binding (**Figure 4C**). In addition, KEGG analysis showed that immune-related genes are related to staphylococcus aureus infection, hematopoietic cell lineage, cell adhesion molecules (CAMs), rheumatoid arthritis, viral protein interaction with cytokine and cytokine receptor, phagosome, and cytokine-cytokine receptor interaction (**Figure 4D** and **Supplementary Table 2**). The above results indicate that immune-related genes are related to the extracellular stroma, bacterial infections, and cell interactions of the TME.

Survival Analysis of Immune-Related Genes in Recurrent HNSCC

To further investigate the prognostic value of these immune-related genes, Kaplan–Meier analysis was performed and survival curves were illustrated to further investigate the relationship between the expression levels of these immune-related genes and the survival of recurrent HNSCC patients. The results indicated that a total of 206 genes were significantly associated with the survival of the recurrent HNSCC among which, OR2I1P, SPOCK2, CCR5, DPT, CD3E, C2, CD4, VCAM1, CD79A, HLA-DRB1, DOK3, TRBC1, RARRES2, AXL, and IGKV1-16 are the most significant prognostic factors in recurrent HNSCC patients (**Figure 5** and **Supplementary Table 3**). We therefore selected these prognostic immune-related genes for further analysis.

The Immune Landscape of Recurrent HNSCC TME

In order to evaluate the TME in recurrent HNSCC, we estimated the abundance of tumor infiltrating immune cells, and explored the impact of these infiltrating immune cells on the clinical outcome in recurrent HNSCC patients. Among the six types of immune cells, DCs have the highest abundance in the microenvironment of HNSCC (**Figure 6A**). **Figure 6B** summarizes the proportion of immune cells in each cluster. Subsequently, we analyzed the abundance matrix of different tumor infiltrating immune cells and found that the abundance

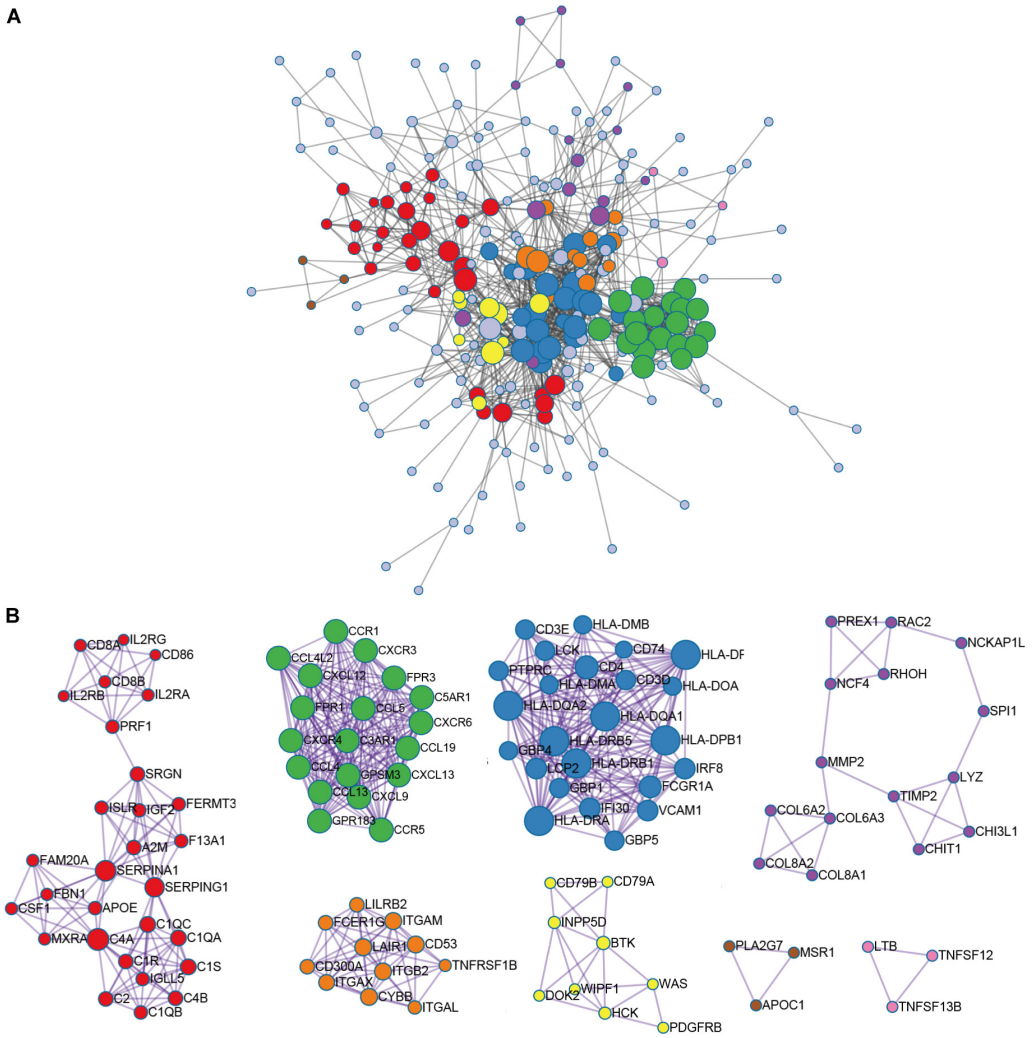

FIGURE 3 | Module-related central genes network in recurrent HNSCC. **(A)** STRING database and Cytoscape software were used to construct the protein-protein interaction (PPI) network module. In the PPI network, the color of the node reflects the logarithmic (FC) value, the size of the node indicates the number of interacting protein. **(B)** Through Molecular Complex Detection (MCODE) analysis, eight modules with at least three nodes are determined. The more a gene is associated with other genes in the network, the more relevant the module is.

of different infiltrating cells was weakly correlated (**Figure 6C** and **Supplementary Table 4**). Then, we further studied the relationship between different immune cell infiltration patterns and recurrence HNSCC survival. As shown in **Figure 6D**, cluster 3, defined by high levels of CD4 + T cells and low levels of B cells is associated with a better prognosis, while cluster 5 (defined by low levels of CD4 + T cells and low levels of B cells) is associated with better prognosis. Cell definition had the worst outcomes. The above results indicate that changes in the abundance of tumor infiltrating immune cells may be related to the prognosis of recurrent HNSCC.

Expression Verification of Four Screened Immune-Related Gene

In order to find the genes that are most critical to the TME in HNSCC, we combined the genes located in the middle node of the PPI network (**Figure 3A**) and the *p*-value less than 0.05 in the survival analysis to screen out four genes CCR5, CD3E, CD4, and HLA-DRB1. After grouping these four genes into high/low risk scores, the survival risk assessment was performed again, and it was found that CCR5, CD3E, CD4, and HLA-DRB1 genes significantly affected the survival risk of patients (**Figures 6E,F** and **Supplementary Table 5**). Considering the unique distribution of individual infiltrating immune cells, all patients were subjected to unsupervised clustering of *k*-means algorithm according to the proportion of immune cells, and the optimal number of clusters was ten (*k*-means = 10, **Figure 6G** and **Supplementary Table 6**).

To further verify the results, the relative mRNA expressions of CCR5, CD3E, CD4, and HLA-DRB1 in HNSCC tumor tissue and adjacent non-tumor tissues were tested. The results showed that the expression of CCR5, CD3E, CD4, and HLA-DRB1 mRNAs

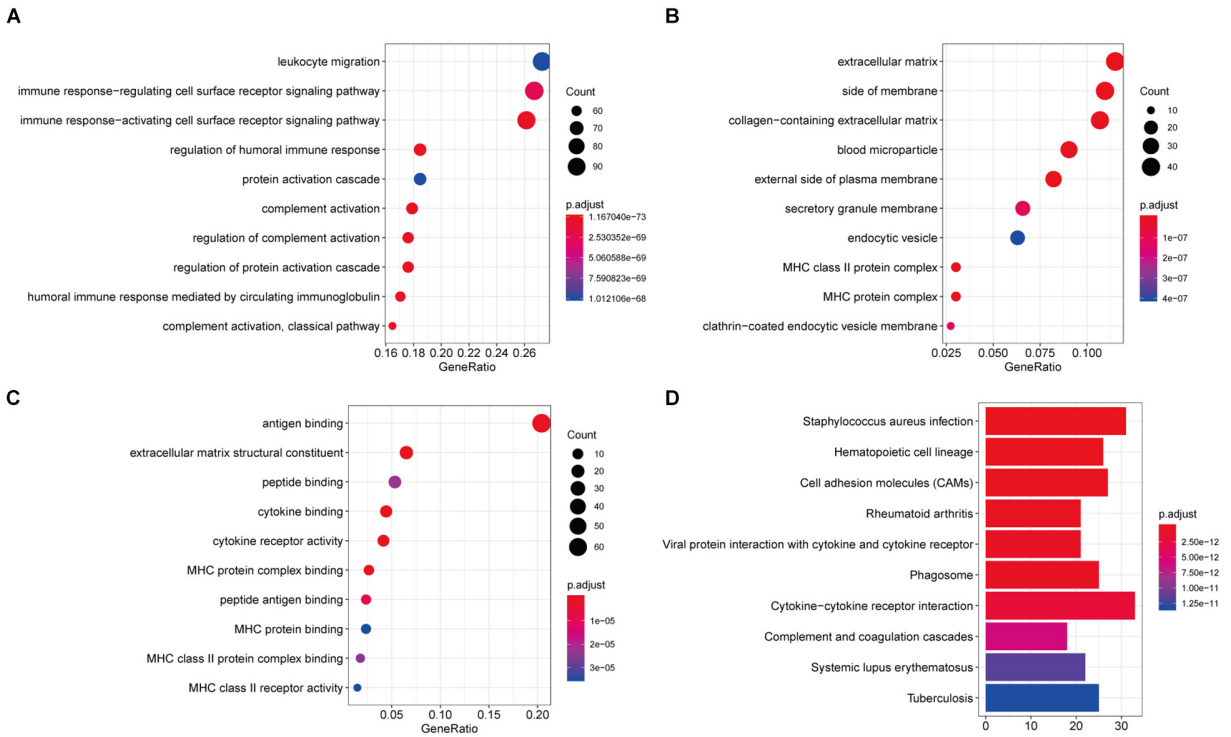

FIGURE 4 | Function richness analysis of immune-related genes in recurrent HNSCC. **(A)** The biological process (BP) of genetic ontology (GO) of prognostic immune-related genes. **(B)** Cellular components of the gene ontology (GO) of prognostic immune-related genes. **(C)** The molecular function (MF) of the GO of prognostic immune-related genes. **(D)** Kyoto Encyclopedia of Genes and Genomes (KEGG) pathway enrichment analysis of prognostic immune-related genes. The color of the bar indicates –log10 (*p*-value). The intersection of the KEGG pathway and GO Term is enriched by the number of genes.

in tumor tissues was significantly higher than that of normal tissues adjacent to the tumor (**Figures 7A–D**). Our western blot analysis showed that compared with normal tissues, HNSCC tissues showed relatively higher expression levels of CCR5, CD3E, CD4, and HLA-DRB1 proteins (**Figure 7E**). In addition, IHC analysis was performed to determine the protein expression levels of CCR5, CD3E, CD4, and HLA-DRB1 in HNSCC. From the immunostaining, we can observe that the expression of these four proteins is increased in tumor tissues compared with neighboring normal tissues (**Figure 7F**). The above results all indicate that CCR5, CD3E, CD4, and HLA-DRB1 are highly expressed in HNSCC tumor tissues.

DISCUSSION

Head and neck squamous cell carcinomas is one of the most common malignant tumors in the world, with a mortality rate of 40–50% (McDermott and Bowles, 2019). Considering the difficulty of early diagnosis, most HNSCC patients are already at an advanced stage at diagnosis. In these advanced HNSCC patients, local metastasis and recurrence of cancer cells are common and in need of improved treatment (Paver et al., 2020). The prognosis is even worse for relapsed HNSCC patients with progressive disease after platinum therapy (Burtness et al., 2019). In order to solve these difficulties faced by HNSCC treatment, new treatment methods have emerged. Cetuximab is a monoclonal antibody (mAb) that targets epidermal growth factor receptor (EGFR), which was introduced into platinum-based therapy for HNSCC (Cohen et al., 2019). Immunotherapy attracts people's attention due to it fights tumors by activating one's own immune cells (Poggio et al., 2019). Although immunotherapy provides HNSCC patients with a cancer treatment option, and HNSCC have a wide range of immune-related genomic features, the immune molecular mechanism of HNSCC is still little known. Therefore, we use TCGA databases to screen prognostic immune-related biomarkers through ESTIMATE and TIMER algorithms, and provide new insights for the treatment of HNSCC.

Increasing studies have shown that the regulation of TME is not only related to immunotherapy but also related to the prognosis of tumor patients (Chen et al., 2019; Liu G. et al., 2021). To ESTIMATE was used to model and test the estimation of stromal cells and immune cells in HNSCC tissue to calculate the purity of the tumor, stromal, and immune score through expression profiles, and give an overall view of the TME. We found that the immunity and stromal scores were significantly related to the prognosis of HNSCC patient. Then, we performed differential expression analysis between the high/low immune score groups and between the high/low stroma score groups, and identified 407 immune-related genes (**Figure 2**). In our results, almost all DEGs are up-regulated, we speculate that the possible reason is that tumor cells have faster energy metabolism

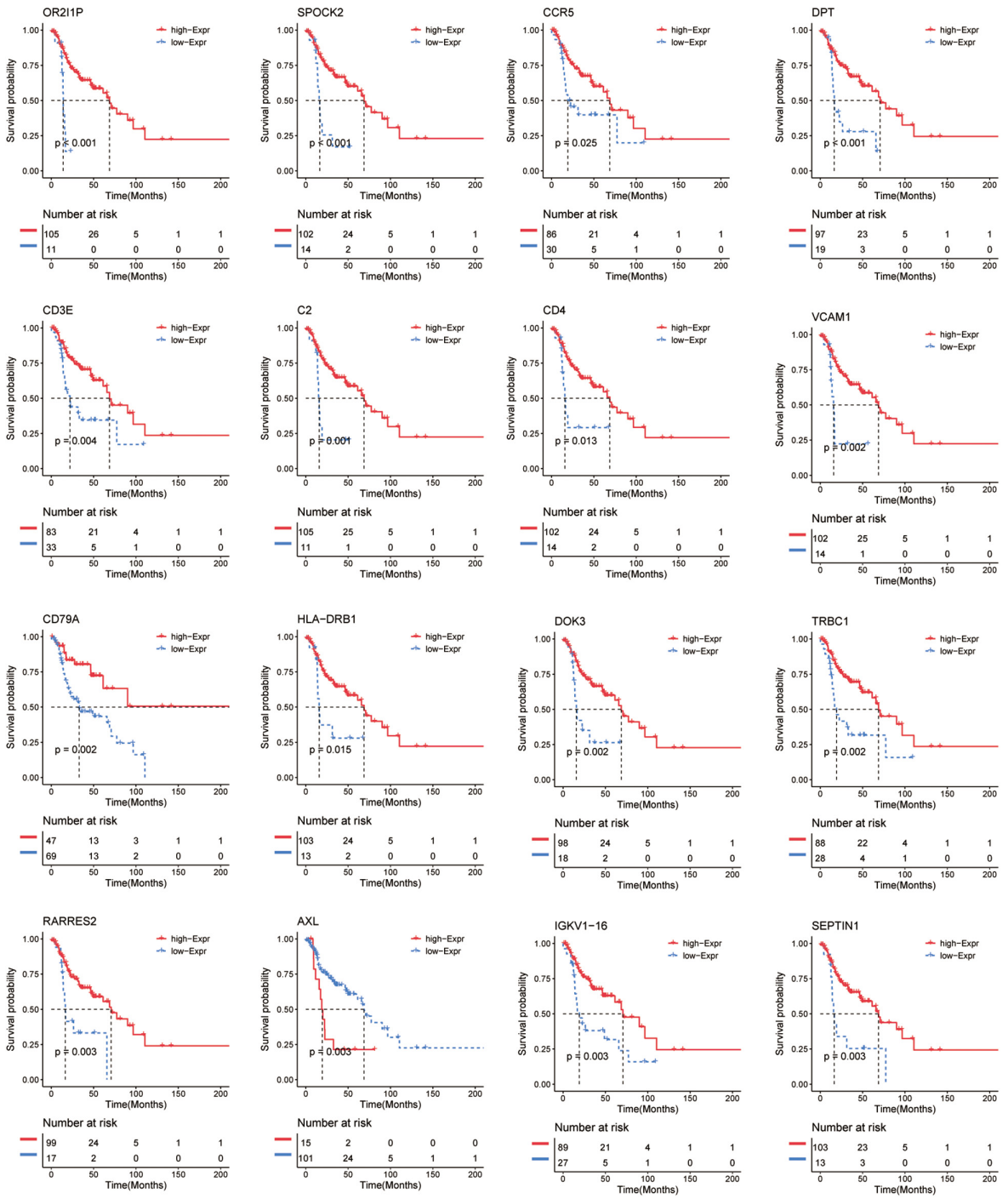

FIGURE 5 | Kaplan–Meier survival curve shows the survival analysis of immune-related genes in recurrent HNSCC. The expression level of 16 immune-related genes to affect the overall survival are selected randomly, and compare the overall survival of the high and low gene expression groups. The red and blue dashed lines represent the upper and lower limits of the 95% confidence interval for gene expression, respectively.

and proliferation, which leads to more active gene transcription. Subsequently, GO and KEGG were used to analyze these immune-related genes to reveal their functions. As expected, most of the immune-related genes are involved in immune processes (**Figure 3**). These results indicate that the extracellular matrix in the TME has a strong correlation with immune infiltrating cells. In addition, we constructed a PPI module, which is used to reveal the relationship and gene function between DEGs (**Figure 4**). The nodes with rich connectivity in the module are also related to immune/inflammatory response.

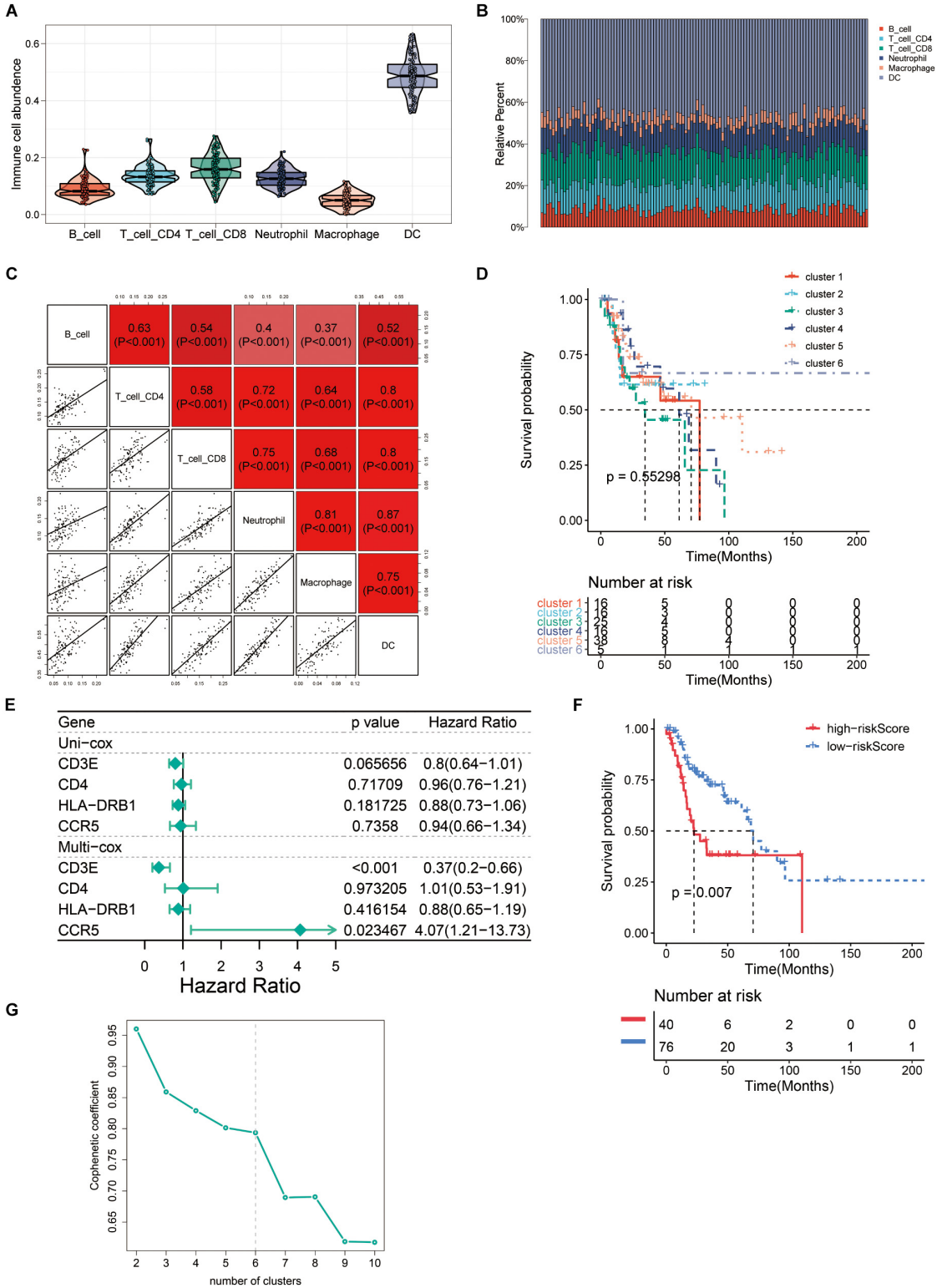

FIGURE 6 | The immune landscape of recurrent HNSCC tumor microenvironment (TME). **(A)** Abundance of immune infiltrating cells in recurrent HNSCC. **(B)** Stacked bar graph of samples arranged in the order of cluster assignment, and unsupervised clustering of all samples based on the proportion of immune cells. **(C)** Correlation stroma of the abundance of six immune cells. **(D)** Summary of survival analysis of patients in different groups. **(E)** Uni-Cox and Multi-Cox regression analysis of CCR5, CD3E, CD4, and HLA-DRB1 four genes. **(F)** Survival analysis of CCR5, CD3E, CD4, and HLA-DRB1 four genes in the high-risk group and the low-risk group. **(G)** Optimal number of clusters by unsupervised clustering analysis.

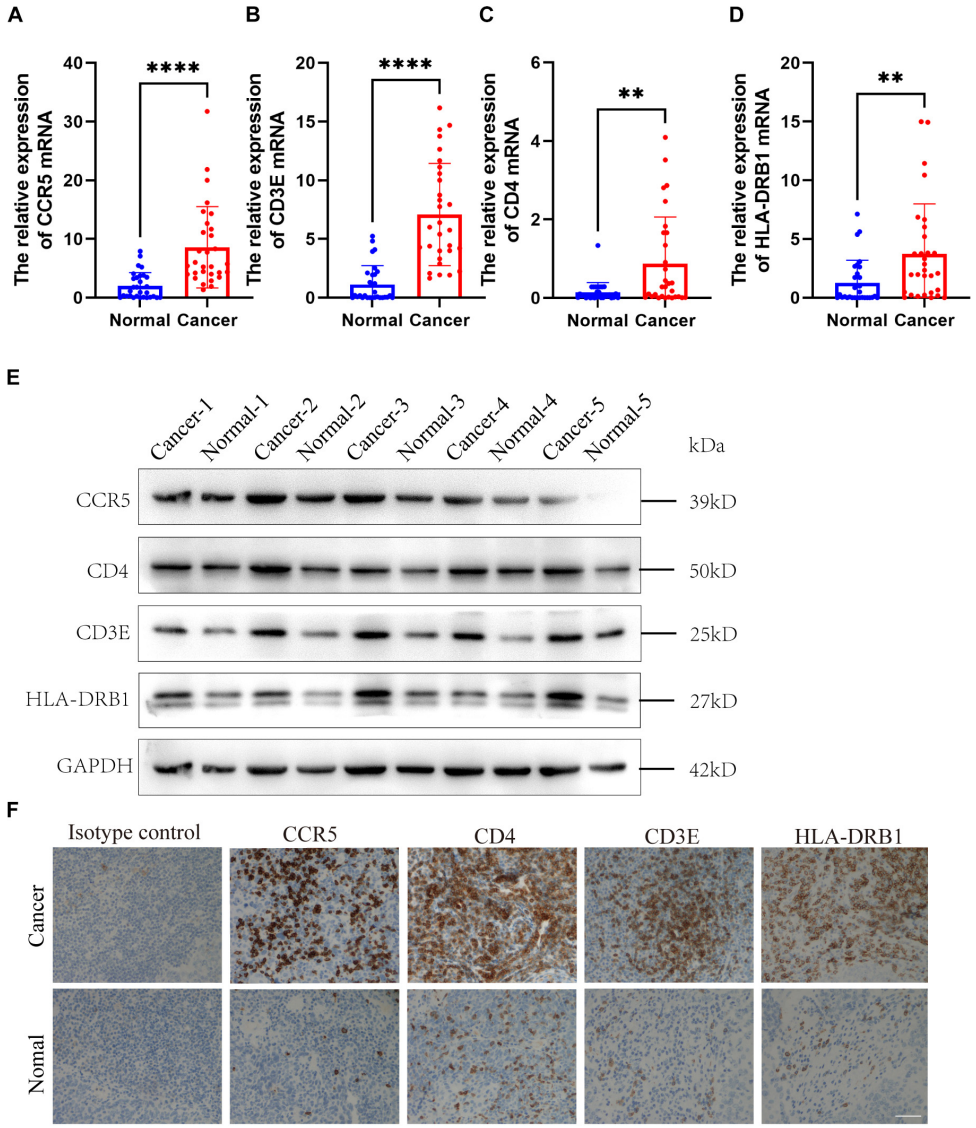

FIGURE 7 | Expression verification of four screened immune-related gene. **(A–D)** The mRNA levels of CCR5, CD3E, CD4, and HLA-DRB1 in HNSCC samples. **(E)** The protein levels of CCR5, CD3E, CD4, and HLA-DRB1 in HNSCC samples. **(F)** Representative immunohistochemical images of CCR5, CD3E, CD4, and HLA-DRB1. Original magnification: ×200. Bar = 50 um. $^{**}P < 0.01$, $^{****}P < 0.0001$.

To better explore the impact of immune infiltrating cells and extracellular matrix related genes on prognosis, we performed Kaplan–Meier analysis to explore potential regulatory mechanisms. Survival analysis was performed according to the 407 differential immune-related genes and 206 genes were closely correlated to the survival rate of the recurrent HNSCC patients (**Figure 5**). To further explore the relationship between these DEGs and immune cells, we performed the TIMER method to estimate the proportion of different immune infiltrating cells. Furthermore, unsupervised cluster analysis is also used to identify the immune infiltrating patterns in HNSCC. The results were consistent with other studies that monocyte immune cells such as B cells, CD4 + T cells, CD8 + T cells, macrophages, and natural killer (NK) cells played a key role in tumor immunity and were also related to tumor prognosis in HNSCC patients (Djaldetti and Bessler, 2014; Tamminga et al., 2020).

In order to investigate effects of the immune-related genes on HNSCC prognosis, we further screened these prognostic immune-related genes and explored the potential regulatory mechanisms. A total of four genes (CCR5, CD3E, CD4, and HLA-DRB1) were identified that related to the immune matrix and immune cells. We found that HNSCC patients with high expression of these four immune-related genes ($P > 0.05$) had a worse prognosis ($P < 0.05$). To further verify the accuracy, we conducted verification in HNSCC patient tissues, and found that the mRNA expression of CCR5, CD3E, CD4, and HLA-DRB1 were significantly upregulated in HNSCC tissues comparing with that of the controlled tissues. The protein levels of these

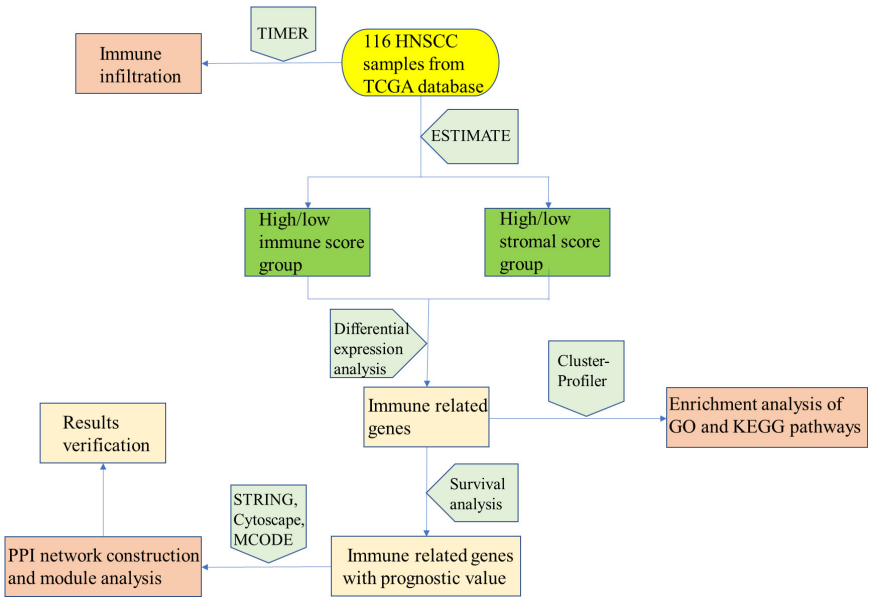

FIGURE 8 | Analysis process structure diagram.

genes were also identical to that (**Figure 7**). The immune microenvironment can reflect the immune status of tumor patients to a certain extent, which provides a reference for us to treat tumors more accurately. Many studies have shown that CCR5, CD3E, CD4, and HLA-DRB1 play an important role in the development of tumors. Anti-CCR5 therapy in cancer patients can effectively target tumor immune cells in colorectal cancer metastasis (Jiao et al., 2019). As an indicator of bladder cancer TME regulation, CD3E is closely related to immune infiltration (Liu Y. et al., 2021). The tumor antigen-specific CD4 + T cells in cancer immunity are a key strategy for tumor prognosis and treatment (Protti et al., 2014). HLA-DRB1 expression can predict the prognosis of patients with non-small cell lung cancer who receive PD-1/PD-L1 immune checkpoint blockade (Correale et al., 2020). In our study, a total of 10 clusters were formed, and further survival analysis showed that changes in the abundance of CD4 + T cells and B cells may be the main prognostic factors for HNSCC. In summary, these results indicate that the heterogeneity of immune infiltration in HNSCC can be used as a prognostic indicator and therapeutic target for immunotherapy.

In conclusion, as shown in **Figure 8**, our analysis process was mainly performed based on the ESTIMATE algorithm to calculate the immune as well as stromal scores and further detect the correlations between the immune/stromal scores and clinical parameters. According to the immune/stromal scores, we divided the HNSCC patient obtained in the TCGA database into high or low score immune group and matrix group to determine the DEGs. Subsequently, the results of functional enrichment analysis showed that these genes are mainly involved in the immune/inflammatory response, and the PPI network further demonstrated this discovery. Finally, we calculated the abundance of each type of immune cells in the TME to explore the relationship between immune scores and immune cells. The above analysis enables us to better understand the TEM and immune characteristics of HNSCC, and helps us to predict the prognosis of HNSCC patients through immune-related genes.

DATA AVAILABILITY STATEMENT

The datasets presented in this study can be found in online repositories. The names of the repository/repositories and accession number(s) can be found in the article/ **Supplementary Material**.

ETHICS STATEMENT

The studies involving human participants were reviewed and approved by the Biomedical Research Ethic Committee of Shandong Provincial Hospital. The patients/participants provided their written informed consent to participate in this study.

AUTHOR CONTRIBUTIONS

LC drafted the manuscript, performed the experiments, and analyzed the data. QW, GN, ZF, XR, TZ, XF, and QY designed the study and analyzed the data. XM, LX, and ZM revised the manuscript. All authors contributed to the article and approved the submitted version.

FUNDING

This present study was supported by funds from the National Natural Science Foundation of China (Grant Nos. 81900922 to

LC and 81770979 to XM) and the Natural Science Foundation of Shandong Province (Grant No. ZR2019BH019 to LC).

SUPPLEMENTARY MATERIAL

The Supplementary Material for this article can be found online at: https://www.frontiersin.org/articles/10.3389/fcell.2021.723721/full#supplementary-material

Supplementary Figure 1 | Correlation between immune and stromal scores and characteristics of patients with recurrent head and neck squamous cell carcinomas (HNSCC). **(A)** Immune scores' distribution for ages <60 and ≥60. **(B)** Immune scores' distribution of tumor grade. **(C)** Stromal scores' distribution for ages<60 and ≥ 60. **(D)** Stromal scores' distribution of tumor grade. **(E)** The associations of immune and stromal scores with the treatment of recurrent HNSCC patients.

Supplementary Table 1 | The characteristics of the patients in the training and validation cohort.

Supplementary Table 2 | Gene ontology (GO) and Kyoto Encyclopedia of Genes and Genomes (KEGG) analysis of 407 immune-related genes.

Supplementary Table 3 | Survival analysis of immune-related genes in recurrent head and neck squamous cell carcinomas (HNSCC).

Supplementary Table 4 | The abundance stroma of different tumor infiltrating immune cells in recurrent HNSCC.

Supplementary Table 5 | Survival analysis of CCR5, CD3E, CD4, and HLA-DRB1 genes in the high-risk group and the low-risk group.

Supplementary Table 6 | Optimal number of clusters by unsupervised clustering analysis.

REFERENCES

Bhat, A. A., Yousuf, P., Wani, N. A., Rizwan, A., Chauhan, S. S., Siddiqi, M. A., et al. (2021). Tumor microenvironment: an evil nexus promoting aggressive head and neck squamous cell carcinoma and avenue for targeted therapy. *Signal. Transduct. Target Ther.* 6:12.

Brenner, H., Kloor, M., and Pox, C. P. (2014). Colorectal cancer. *Lancet* 383, 1490–1502.

Bruni, D., Angell, H. K., and Galon, J. (2020). The immune contexture and Immunoscore in cancer prognosis and therapeutic efficacy. *Nat. Rev. Cancer* 20, 662–680. doi: 10.1038/s41568-020-0285-7

Brunner-Weinzierl, M. C., and Rudd, C. E. (2018). CTLA-4 and PD-1 control of T-cell motility and migration: implications for tumor immunotherapy. *Front. Immunol.* 9:2737.

Burtness, B., Harrington, K. J., Greil, R., Soulières, D., Tahara, M., de Castro, G., et al. (2019). Pembrolizumab alone or with chemotherapy versus cetuximab with chemotherapy for recurrent or metastatic squamous cell carcinoma of the head and neck (KEYNOTE-048): a randomised, open-label, phase 3 study. *Lancet* 394, 1915–1928.

Chen, Y. P., Wang, Y. Q., Lv, J. W., Li, Y. Q., Chua, M. L. K., Le, Q. T., et al. (2019). Identification and validation of novel microenvironment-based immune molecular subgroups of head and neck squamous cell carcinoma: implications for immunotherapy. *Ann. Oncol.* 30, 68–75.

Cohen, E. E. W., Soulières, D., Le Tourneau, C., Dinis, J., Licitra, L., Ahn, M. J., et al. (2019). Pembrolizumab versus methotrexate, docetaxel, or cetuximab for recurrent or metastatic head-and-neck squamous cell carcinoma (KEYNOTE-040): a randomised, open-label, phase 3 study. *Lancet* 393, 156–167.

Correale, P., Saladino, R. E., Giannarelli, D., Giannicola, R., Agostino, R., Staropoli, N., et al. (2020). Distinctive germline expression of class I human leukocyte antigen (HLA) alleles and DRB1 heterozygosis predict the outcome of patients with non-small cell lung cancer receiving PD-1/PD-L1 immune checkpoint blockade. *J. Immunother. Cancer* 8:e000733. doi: 10.1136/jitc-2020-000733

Djaldetti, M., and Bessler, H. (2014). Mononuclear cells phagocytic activity affects the crosstalk between immune and cancer cells. *Biomed. Pharmacother.* 68, 679–683. doi: 10.1016/j.biopha.2014.08.004

Hanahan, D., and Coussens, L. M. (2012). Accessories to the crime: functions of cells recruited to the tumor microenvironment. *Cancer Cell* 21, 309–322. doi: 10.1016/j.ccr.2012.02.022

Jiao, X., Nawab, O., Patel, T., Kossenkov, A. V., Halama, N., Jaeger, D., et al. (2019). Recent advances targeting CCR5 for cancer and its role in immuno-oncology. *Cancer Res.* 79, 4801–4807. doi: 10.1158/0008-5472.can-19-1167

Kanazawa, T., Misawa, K., Shinmura, K., Misawa, Y., Kusaka, G., Maruta, M., et al. (2019). Promoter methylation of galanin receptors as epigenetic biomarkers for head and neck squamous cell carcinomas. *Expert Rev. Mol. Diagn.* 19, 137–148. doi: 10.1080/14737159.2019.1567334

Ke, Z. B., Cai, H., Wu, Y. P., Lin, Y. Z., Li, X. D., Huang, J. B., et al. (2019). Identification of key genes and pathways in benign prostatic hyperplasia. *J. Cell Physiol.* 234, 19942–19950.

Lee, H. T., Lee, S. H., and Heo, Y. S. (2019). Molecular interactions of antibody drugs targeting PD-1, PD-L1, and CTLA-4 in immuno-oncology. *Molecules* 24:1190. doi: 10.3390/molecules24061190

Liu, F., Wu, Y., Mi, Y., Gu, L., Sang, M., and Geng, C. (2019). Identification of core genes and potential molecular mechanisms in breast cancer using bioinformatics analysis. *Pathol. Res. Pract.* 215:152436. doi: 10.1016/j.prp.2019.152436

Liu, G., Yuan, C., Ma, J., Pan, Y., and Xu, H. (2021). Influence of immune microenvironment on diagnosis and prognosis of head and neck squamous cell carcinoma. *Front. Oncol.* 11:604784.

Liu, Y., Wu, Y., Zhang, P., Xu, C., Liu, Z., He, C., et al. (2021). CXCL12 and CD3E as indicators for tumor microenvironment modulation in bladder cancer and their correlations with immune infiltration and molecular subtypes. *Front. Oncol.* 11:636870.

McDermott, J. D., and Bowles, D. W. (2019). Epidemiology of head and neck squamous cell carcinomas: impact on staging and prevention strategies. *Curr. Treat. Options Oncol.* 20:43.

Medina, P. J., and Adams, V. R. (2016). PD-1 pathway inhibitors: immuno-oncology agents for restoring antitumor immune responses. *Pharmacotherapy* 36, 317–334. doi: 10.1002/phar.1714

Michot, J. M., Bigenwald, C., Champiat, S., Collins, M., Carbonnel, F., Postel-Vinay, S., et al. (2016). Immune-related adverse events with immune checkpoint blockade: a comprehensive review. *Eur. J. Cancer* 54, 139–148.

Miyauchi, S., Kim, S. S., Pang, J., Gold, K. A., Gutkind, J. S., Califano, J. A., et al. (2019). Immune modulation of head and neck squamous cell carcinoma and the tumor microenvironment by conventional therapeutics. *Clin. Cancer Res.* 25, 4211–4223. doi: 10.1158/1078-0432.ccr-18-0871

Paver, E. C., Currie, A. M., Gupta, R., and Dahlstrom, J. E. (2020). Human papilloma virus related squamous cell carcinomas of the head and neck: diagnosis, clinical implications and detection of HPV. *Pathology* 52, 179–191. doi: 10.1016/j.pathol.2019.10.008

Poggio, M., Hu, T., Pai, C. C., Chu, B., Belair, C. D., Chang, A., et al. (2019). Suppression of exosomal PD-L1 induces systemic anti-tumor immunity and memory. *Cell* 177, 414–427.e13.

Protti, M. P., Monte, L De, and Lullo, G Di (2014). Tumor antigen-specific CD4+ T cells in cancer immunity: from antigen identification to tumor prognosis and development of therapeutic strategies. *Tissue Antigens* 83, 237–246. doi: 10.1111/tan.12329

Quail, D. F., and Joyce, J. A. (2013). Microenvironmental regulation of tumor progression and metastasis. *Nat. Med.* 19, 1423–1437. doi: 10.1038/nm.3394

Seo, J. S., Lee, J. W., Kim, A., Shin, J. Y., Jung, Y. J., Lee, S. B., et al. (2018). Whole exome and transcriptome analyses integrated with microenvironmental immune signatures of lung squamous cell carcinoma. *Cancer Immunol. Res.* 6, 848–859. doi: 10.1158/2326-6066.cir-17-0453

Sharma, P., Hu-Lieskovan, S., Wargo, J. A., and Ribas, A. (2017). Primary, adaptive, and acquired resistance to cancer immunotherapy. *Cell* 168, 707–723. doi: 10.1016/j.cell.2017.01.017

Tamminga, M., Hiltermann, T. J. N., Schuuring, E., Timens, W., Fehrmann, R. S. N., and Groen, H. J. M. (2020). Immune microenvironment composition in non-small cell lung cancer and its association with survival. *Clin. Transl. Immunol.* 9:e1142.

Van Landuyt, K. L., Nawrot, T., Geebelen, B., De Munck, J., Snauwaert, J., Yoshihara, K., et al. (2011). How much do resin-based dental materials release? A meta-analytical approach. *Dent. Mater.* 27, 723–747. doi: 10.1016/j.dental.2011.05.001

Yang, S., Liu, T., Cheng, Y., Bai, Y., and Liang, G. (2019). Immune cell infiltration as a biomarker for the diagnosis and prognosis of digestive system cancer. *Cancer Sci.* 110, 3639–3649. doi: 10.1111/cas.14216

Yu, G., Wang, L. G., Han, Y., and He, Q. Y. (2012). clusterProfiler: an R package for comparing biological themes among gene clusters. *OMICS* 16, 284–287. doi: 10.1089/omi.2011.0118

Zhou, R., Wu, J., Liu, B., Jiang, Y., Chen, W., Li, J., et al. (2019). The roles and mechanisms of Leydig cells and myoid cells in regulating spermatogenesis. *Cell Mol. Life Sci.* 76, 2681–2695. doi: 10.1007/s00018-019-03101-9

Conflict of Interest: The authors declare that the research was conducted in the absence of any commercial or financial relationships that could be construed as a potential conflict of interest.

Publisher's Note: All claims expressed in this article are solely those of the authors and do not necessarily represent those of their affiliated organizations, or those of the publisher, the editors and the reviewers. Any product that may be evaluated in this article, or claim that may be made by its manufacturer, is not guaranteed or endorsed by the publisher.

frontiers in Cell and Developmental Biology

ORIGINAL RESEARCH
published: 26 August 2021
doi: 10.3389/fcell.2021.710461

Differentiation Between Glioblastoma Multiforme and Metastasis From the Lungs and Other Sites Using Combined Clinical/Routine MRI Radiomics

Yuqi Han[1,2†], Lingling Zhang[3†], Shuzi Niu[4], Shuguang Chen[5], Bo Yang[6], Hongyan Chen[3], Fei Zheng[3], Yuying Zang[3], Hongbo Zhang[7], Yu Xin[8*] and Xuzhu Chen[3*]*

[1] School of Life Sciences and Technology, Xidian University, Xi'an, China, [2] Key Laboratory of Molecular Imaging, Institute of Automation, Chinese Academy of Sciences, Beijing, China, [3] Department of Radiology, Beijing Tiantan Hospital, Capital Medical University, Beijing, China, [4] Institute of Software, Chinese Academy of Sciences, Beijing, China, [5] School of Mathematical Sciences, Nankai University, Tianjin, China, [6] Department of Computing, The Hong Kong Polytechnic University, Hong Kong, China, [7] Department of Neurosurgery, Huizhou Third People's Hospital, Guangzhou Medical University, Huizhou, China, [8] Department of Neurosurgery, Beijing Tiantan Hospital, Capital Medical University, Beijing, China

OPEN ACCESS

Edited by:
José Alexandre Ferreira, Portuguese Oncology Institute, Portugal

Reviewed by:
Jinrong Qu, Henan Provincial Cancer Hospital, China
Ji Wenjun, Yulin No.2 People's Hospital, China

***Correspondence:**
Hongbo Zhang
hongbozhang99@163.com
Yu Xin
xinyu@mail.ccmu.edu.cn
Xuzhu Chen
radiology888@aliyun.com

[†] *These authors share first authorship*

Specialty section:
This article was submitted to Molecular and Cellular Pathology, a section of the journal Frontiers in Cell and Developmental Biology

Received: *16 May 2021*
Accepted: *09 August 2021*
Published: *26 August 2021*

Citation:
Han Y, Zhang L, Niu S, Chen S, Yang B, Chen H, Zheng F, Zang Y, Zhang H, Xin Y and Chen X (2021) Differentiation Between Glioblastoma Multiforme and Metastasis From the Lungs and Other Sites Using Combined Clinical/Routine MRI Radiomics. Front. Cell Dev. Biol. 9:710461. doi: 10.3389/fcell.2021.710461

Background: Differentiation between cerebral glioblastoma multiforme (GBM) and solitary brain metastasis (MET) is important. The existing radiomic differentiation method ignores the clinical and routine magnetic resonance imaging (MRI) features.

Purpose: To differentiate between GBM and MET and between METs from the lungs (MET-lung) and other sites (MET-other) through clinical and routine MRI, and radiomics analyses.

Methods and Materials: A total of 350 patients were collected from two institutions, including 182 patients with GBM and 168 patients with MET, which were all proven by pathology. The ROI of the tumor was obtained on axial postcontrast MRI which was performed before operation. Seven radiomic feature selection methods and four classification algorithms constituted 28 classifiers in two classification strategies, with the best classifier serving as the final radiomics model. The clinical and combination models were constructed using the nomograms developed. The performance of the nomograms was evaluated in terms of calibration, discrimination, and clinical usefulness. Student's *t*-test or the chi-square test was used to assess the differences in the clinical and radiological characteristics between the training and internal validation cohorts. Receiver operating characteristic curve analysis was performed to assess the performance of developed models with the area under the curve (AUC).

Results: The classifier fisher_decision tree (fisher_DT) showed the best performance (AUC: 0.696, 95% CI:0.608-0.783) for distinguishing between GBM and MET in internal validation cohorts; the classifier reliefF_random forest (reliefF_RF) showed the best performance (AUC: 0.759, 95% CI: 0.613-0.904) for distinguishing between MET-lung and MET-other in internal validation cohorts. The combination models incorporating the radiomics signature and clinical-radiological characteristics were superior to the clinical-radiological models in the two classification strategies (AUC: 0.764 for differentiation

between GBM in internal validation cohorts and MET and 0.759 or differentiation between MET-lung and MET-other in internal validation cohorts). The nomograms showed satisfactory performance and calibration and were considered clinically useful, as revealed in the decision curve analysis.

Data Conclusion: The combination of radiomic and non-radiomic features is helpful for the differentiation among GBM, MET-lung, and MET-other.

Keywords: glioblastoma multiforme, metastasis, magnetic resonance imaging, machine learning, radiomics

INTRODUCTION

Cerebral glioblastoma multiforme (GBM) and solitary brain metastasis (MET) are the most common brain tumors in adults (Ohgaki and Kleihues, 2005; Platta et al., 2010). Both GBM and MET show ring enhancement with peripheral edema on routine magnetic resonance imaging (MRI). Owing to the different treatment strategies available, a similar radiological appearance proposed a diagnostic dilemma for differentiation between the two lesions (Weller et al., 2014). Accurate differentiation between these two lesions is essential and has been one of the main focuses in radiological research for many years.

To date, studies aimed at the differentiation between GBM and MET have mainly shown two tendencies. The first tendency is to improve the performance of imaging modalities, and the second is to explore the differences among METs from different primary sites. For the first tendency, many imaging modalities have been proposed, including routine MRI and various advanced MRI modalities, such as magnetic resonance spectroscopy, diffusion-weighted imaging (DWI), diffusion tensor imaging, diffusion kurtosis imaging, perfusion-weighted imaging (PWI), arterial spin labeling, and amide proton transfer-weighted imaging (Chen et al., 2012; Tan et al., 2015; Salice et al., 2016; Durmo et al., 2018; Holly et al., 2018; Kamimura et al., 2019; Xi et al., 2019). For the second tendency, the relative cerebral blood volume showed no difference among METs from the lungs (MET-lung), breasts, gastrointestinal tract, and skin (Askaner et al., 2019). Another study showed that independent component analyses of dynamic susceptibility contrast PWI can show differences between breast MET and non-small-cell lung cancer (Chakhoyan et al., 2019). Moreover, breast METs were found to be less likely to be located in the posterior cerebral artery territory than MET-lung, kidneys, colon, and skin (Mampre et al., 2019).

Radiomics analysis has been proven to be useful in the diagnosis, prognosis assessment, and prediction of therapeutic responses in cancers by extracting exhaustive features from medical images (Aerts et al., 2014; Lambin et al., 2017). It has been used successfully in many studies of brain tumors, including those for tumor grading and genotype and overall survival assessment (Zacharaki et al., 2009; Grabowski et al., 2014; Li et al., 2018c; Chaddad et al., 2019). In particular, radiomics analysis was used to differentiate among METs from the breasts, lungs, and other sites in one study (Artzi et al., 2019). It was also used to differentiate METs among breast cancer, small-cell lung cancer, non-small-cell lung cancer, gastrointestinal cancer, and melanoma (Kniep et al., 2019). MET-lung, breasts, and skin also differed in texture features (Ortiz-Ramon et al., 2017; Ortiz-Ramón et al., 2018).

To date, the existing studies on the differentiation between GBM and MET have only focused on radiological data without consideration of clinical factors. Analyses of MET subtypes mainly considered the radiomic features without the routine MRI features. In addition, the subtypes of METs to be differentiated were not consistent in the existing studies. Of all METs, the top primary tumor is lung cancer (>50%) (Füreder et al., 2018; Rotta et al., 2018; Ascha et al., 2019). Therefore, we explored the differences between GBM and MET-lung and other sites (MET-other) with regard to the clinical and routine MRI and radiomic features in this study.

MATERIALS AND METHODS

This retrospective study was approved by the committees of two institutions; the need for obtaining informed consent from the patients was waived.

Patients

Cerebral GBM was searched in the pathological database of our institution between January 2014 and December 2015. The inclusion and exclusion criteria are shown in **Supplementary Material 1**. A total of 152 patients with GBM were included from the first institution, and 30 patients with GBM were included from the second institution. All patients showed a supratentorial enhanced lesion in the cerebral parenchyma.

Solitary supratentorial MET was searched in the pathological database of the two institutions between January 2010 and December 2017. The inclusion and exclusion criteria are shown in **Supplementary Material 1**. Finally, a total of 76 patients with MET-lung and 62 patients with MET-other were included from the first institution, and 15 patients with MET-lung and 15 patients with MET-other were included from the second institution. The detailed primary cancers are shown in **Supplementary Material 2**.

Image Acquisition and Analysis

All patients underwent MRI scanning within 2 weeks before cerebral operation. The tumor size was represented by the maximal diameter on the postcontrast axial image. Peritumoral edema was represented by the maximal diameter of the high signal around the tumor on the axial T2-weighted image (T2WI). The two parameters were manually measured using

the Neurosoft PACS software[1]. The edema ratio was calculated by dividing the peritumoral edema by the tumor size. The location (left side/right side) was also reviewed by an experienced radiologist. The detailed scanning protocol and parameters are shown in **Supplementary Material 3**.

Radiomics Analysis

Region of Interest (ROI) Segmentation

Using the ITK-SNAP software[2] version 3.x, we opened the postcontrast axial sequence for each case and manually drew the outline of the enhanced lesion on each slice showing the tumor, which was saved as the segmented region of interest (ROI). The segmentation was performed by a radiologist with 14 years of experience and reviewed by another radiologist with 28 years of experience. Any discrepancy was resolved through discussion. The details of the drawing are illustrated in **Supplementary Material 4**.

Radiomic Feature Extraction

The radiomic features were extracted using PyRadiomics, which is an open-source python package for the extraction of radiomic features from medical images (Van Griethuysen et al., 2017). For each ROI, we extracted three types of radiomic features, including non-textural, textural, and wavelet features. The non-textural features included 13 shape features and 18 first-order features, and 74 textural features were calculated on the basis of 5 texture matrices: the gray level co-occurrence matrix (GLCM), gray level dependence matrix (GLDM), gray level run-length matrix (GLRLM), gray level size zone matrix (GLSZM), and neighborhood gray-tone difference matrix (NGTDM). The three-dimensional wavelet transformation decomposed the original image set into eight filtered images set in three directions. Finally, a total of 841 radiomic features were extracted, consisting of shape features in the original image, first-order features, and textural features in all images. A detailed description is provided in **Supplementary Material 5**.

Feature Reduction

First, we randomly selected 50 patients and translated (three pixels in the up, down, left, and right directions) and rotated (3° in clockwise and anticlockwise directions) their ROIs to evaluate the stability of the features through the intraclass correlation coefficients (threshold = 0.8). After the prescreening, all features were standardized using the z-scores derived from the training cohort. Thereafter, seven feature selection methods were used, including information theoretical-based feature selection: conditional mutual information maximization (CMIM), minimal-redundancy and maximal-relevance (MRMR), and double input symmetrical relevance (DISR); similarity-based feature selection: Fisher score and reliefF; and sparse learning-based feature selection: multi-cluster feature selection (MCFS) and robust feature selection (RFS), to recognize the most discriminating features. For each feature selection method, we ranked the features by their relevance score, and the best features were selected for the later classifiers.

[1]http://www.neusoft.com

[2]http://www.itksnap.org/

Classifier Construction

Four algorithms were used to build the radiomics model: logistic regression (LR), support vector machine (SVM), decision tree (DT), and random forest (RF). These algorithms were implemented on the basis of the selected features and classification categories. The LR algorithm was used by tuning the regular term and penalty term. The SVM algorithm was used by tuning the penalty and gamma of the kernel function, where the kernel function is "rbf." The DT algorithm was used by tuning two parameters: the maximum sample of the leaf and the maximum node. The RF algorithm was used by tuning the number of DTs and the maximum sample of the leaf. Fivefold cross validation was used for all 28 classifiers. The optimal classifier served as the final radiomics model. These algorithms were implemented using the Python version 3.6.5 "scikit-learn" package.

Clinical-Radiological and Combination Models

The clinical characteristics (patient age and sex) and the routine radiological index (tumor size, edema ratio, and location) were used to construct the clinical-radiological model for differentiating between GBM and MET using an LR model (denoted as the clinical^{GBM} model). To distinguish MET-lung from MET-other, we used the same method to obtain the clinical-radiological model (denoted as the clinical^{MET} model). The clinical and routine radiological characteristics and radiomics signature were integrated to construct the combination models using the LR algorithm, and the optimal model was selected using AIC with a stepwise regression algorithm (denoted as the combination^{GBM} model and combination^{MET} model, respectively).

Model Assessment

Receiver operating characteristic (ROC) curve analysis of each model was performed, and the areas under the curve (AUCs) were calculated in both the training and validation cohorts. The optimal cutoff value in the training cohort was applied to obtain accuracy, sensitivity, and specificity. The DeLong test was used to evaluate the statistical differences between the models. All assessments were performed in both the training and validation cohorts.

Nomogram analysis was applied to assess the potential clinical utility of the combination models. Calibration curves were drawn to evaluate the degree of deviation between the predictions and actual outcomes obtained using the Hosmer–Lemeshow test. Additionally, to evaluate the clinical utility of the nomograms, we performed a decision curve analysis by calculating the net benefits at different threshold probabilities (Rios Velazquez et al., 2017).

Statistical Analysis

Patient age and sex, tumor size, and edema ratio were compared between the patients with GBM and MET and between those with MET-lung and MET-other using Student's *t*-test or the chi-square test between the training, internal and external validation cohorts. *P*- values of <0.05 were considered to indicate a

significant difference. The Spearman correlation coefficient was used to assess the relationship between the clinical and radiolocial characteristics and radiomic features. Statistical analysis was performed using IBM SPSS Statistics version 22.

RESULTS

Clinical-Radiological Characteristics

The first institution included 152 patients with GBM and 138 patients with MET, which were randomly divided into a training cohort (n = 193) and an internal validation cohort (n = 97) with a ratio of 2:1. In addition, the patients with MET were also randomly divided into the training (n = 92) and validation cohorts (n = 46) at a ratio of 2:1. The second institute included 30 patients with GBM and 30 patients with MET, which were used as the external validation cohort.

The baseline characteristics are summarized in **Table 1**. There was no significant difference between the training and internal validation cohort for the two classification strategies. And, no significant difference between the training and external validation cohort for the two classification strategies.

Radiomic Features

A total of 841 radiomic features were calculated for each patient. After prescreening using the intraclass correlation coefficients, 687 radiomic features with high stability were retained for subsequent analysis (**Figure 1**). Thereafter, the top 20 best features in each feature selection method were reserved to construct the radiomics models. Thus, seven feature subsets were formed for the two classification strategies. The detailed radiomic features are shown in **Supplementary Material 6**.

Performance of the Radiomics Models

The performance of each of the 28 classifiers in the training and internal validation cohorts was reserved and is listed in **Supplementary Material 7**. For distinguishing between GBM and MET, the classifier fisher_decision tree (fisher_DT) showed the best performance in the internal validation cohort (AUC: 0.696, 95% CI: 0.608-0.783 **Figure 2A** and **Supplementary Material 7**). For differentiating between MET-lung and MET-other, the classifier reliefF_random forest (reliefF_RF) showed the best performance in the internal validation cohort (0.759,95% CI: 0.613-0.904, **Figure 2B** and **Supplementary Material 7**). The classifiers fisher_DT and reliefF_RF were selected as the optimal radiomics models in the two classification strategies, which were denoted as the radiomics^{GBM} model and radiomics^{MET} model, respectively. These two models are shown in **Supplementary Material 8**.

Performance of the Clinical-Radiological and Combination Models

We summarized the performances of the clinical-radiological characteristics in the two classification strategies in **Table 2**.

TABLE 1 | Cohort demographics.

Cohort for differentiation of GBM and MET

Characteristics	Training cohort (n = 193)	Internal validation cohort (n = 97)	p-value	External validation cohort (n = 60)	p-value
Age [years, mean (SD)]	54.63 (11.63)	53.86 (13.39)	0.611	55.38 (11.45)	0.661
Sex [n (%)]			0.329		0.752
Male	117 (60.6)	53 (54.6)		35 (58.3)	
Female	76 (39.4)	44 (45.4)		25 (41.7)	
Diameter [mm, mean (SD)]	41.96 (14.88)	44.49 (16.10)	0.184	45.75 (14.80)	0.086
Location			0.902		—
Left	98 (50.8)	50 (51.5)		—	
Right	95 (49.2)	47 (48.5)		—	
Edema ratio [mean (SD)]	1.94 (0.79)	1.87 (0.82)	0.518	1.79 (0.66)	0.185

Cohort for differentiation of MET-lung and MET-other

Characteristics	Training cohort (n = 92)	Internal validation cohort (n = 46)	p-value	External validation cohort (n = 30)	p-value
Age [years, mean (SD)]	57.93 (9.11)	57.50 (10.92)	0.805	55.27 (11.69)	0.198
Sex			0.714		
Male	53 (57.6)	28 (60.9)		16 (53.3)	0.682
Female	39 (42.4)	18 (39.1)		14 (46.7)	
Diameter [mm, mean (SD)]	36.10 (14.82)	37.28 (16.31)	0.669	42.03 (17.25)	0.070
Edema ratio [mean (SD)]	2.30 (0.83)	2.19 (1.08)	0.543	2.01 (0.81)	0.114
Location			0.717		—
Left	49 (53.3)	26 (56.5)		—	
Right	43 (46.7)	20 (43.5)		—	

SD, standard deviation.

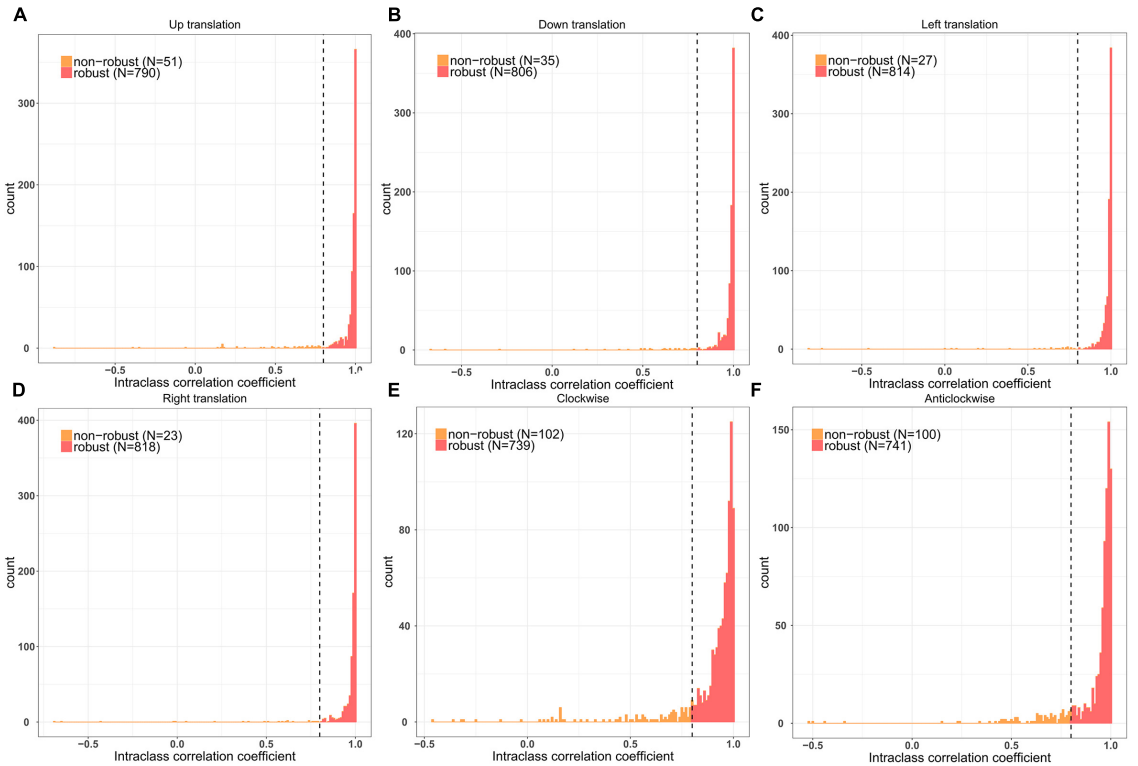

FIGURE 1 | Remaining feature numbers after stability analyses for each disturbance. **(A,B)** The ROI was translated 3 pixels in the up and down directions; **(C,D)** The ROI was translated 3 pixels in the left and right directions; **(E,F)** The ROI was rotated 3° in clockwise and anticlockwise directions.

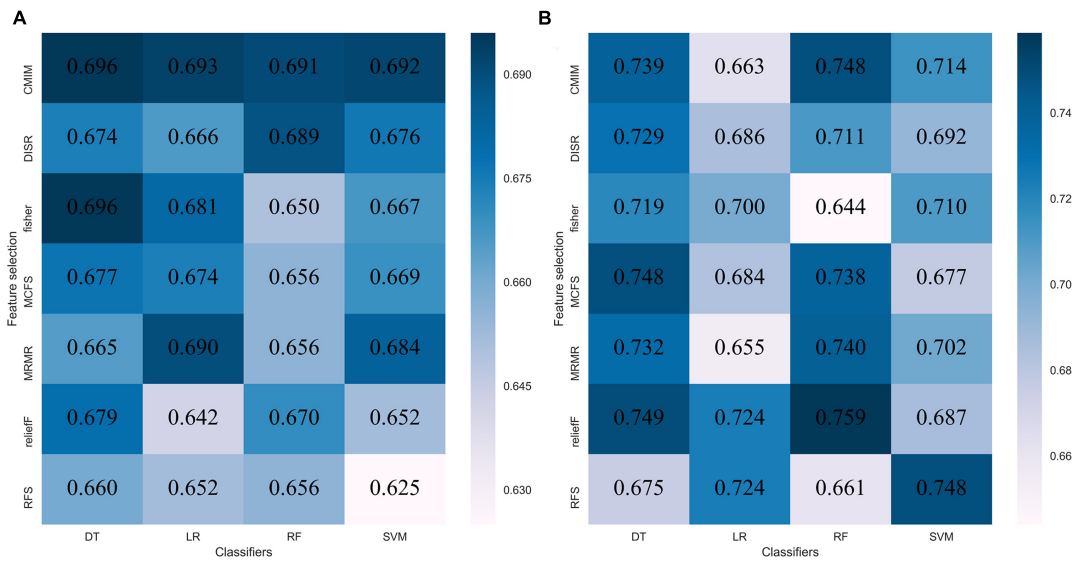

FIGURE 2 | Performance of 28 classifiers in two classification strategies. **(A)** AUC of distinguishing GBM and MET in the internal validation cohort; **(B)** AUC of distinguishing MET-lung and MET-other in the external validation cohort. AUC, area under the curve; GBM, glioblastoma multiforme; MET, metastasis.

For distinguishing between GBM and MET, the clinical^{GBM} model exhibited satisfactory performance in all cohorts (training: AUC: 0.803, 95% CI: 0.740-0.867; internal validation: AUC: 0.744 95% CI: 0.643-0.846; external validation: AUC:0.674, 95% CI: 0.528-0.821, **Figures 3A–C** and **Table 2**). For distinguishing between MET-lung and MET-other, the AUC of the clinical^{MET}

TABLE 2 | Predictive performance of each model.

Differentiation of GBM and MET

Model	Traning cohort				Internal validation cohort				External validation cohort			
	AUC	ACC	SEN	SPE	AUC	ACC	SEN	SPE	AUC	ACC	SEN	SPE
Clinical^{GBM} model	0.803 (0.740,0.867)	0.762	0.876	0.646	0.744 (0.643,0.846)	0.721	0.854	0.548	0.674 (0.528,0.821)	0.683	0.900	0.467
Radiomics^{GBM} model	0.772 (0.718,0.827)	0.757	0.938	0.573	0.696 (0.608,0.783)	0701	0.873	0.476	0.676 (0.572,0.779)	0.683	0.933	0.433
Combined^{GBM} model	0.859 (0.809,0.911)	0.783	0.794	0.771	0.764 (0.667,0.860)	0.691	0.655	0.738	0.708 (0.570,0.846)	0.617	0.567	0.667

Differentiation of MET-lung and MET-other

Model	Training cohort				Internal validation cohort				External validation cohort			
	AUC	ACC	SEN	SPE	AUC	ACC	SEN	SPE	AUC	ACC	SEN	SPE
Clinical^{MET} model	0.660 (0.547,0.772)	0.663	0.771	0.546	0.598 (0.430,0.767)	0.457	0.621	0.177	0.759 (0.548,0.971)	0.700	0.750	0.667
Radiomics^{MET} model	0.798 (0.708,0.888)	0.728	0.771	0.682	0.759 (0.613, 0.904)	0.630	0.552	0.765	0.704 (0.492,0.901)	0.733	0.750	0.722
Combined^{MET} model	0.770 (0.672,0.869)	0.750	0.875	0.614	0.759 (0.609,0.908)	0.761	0.793	0.706	0.741 (0.527,0.954)	0.667	0.667	0.667

ACC, accuracy; SEN, sensitivity; SPE, specificity.

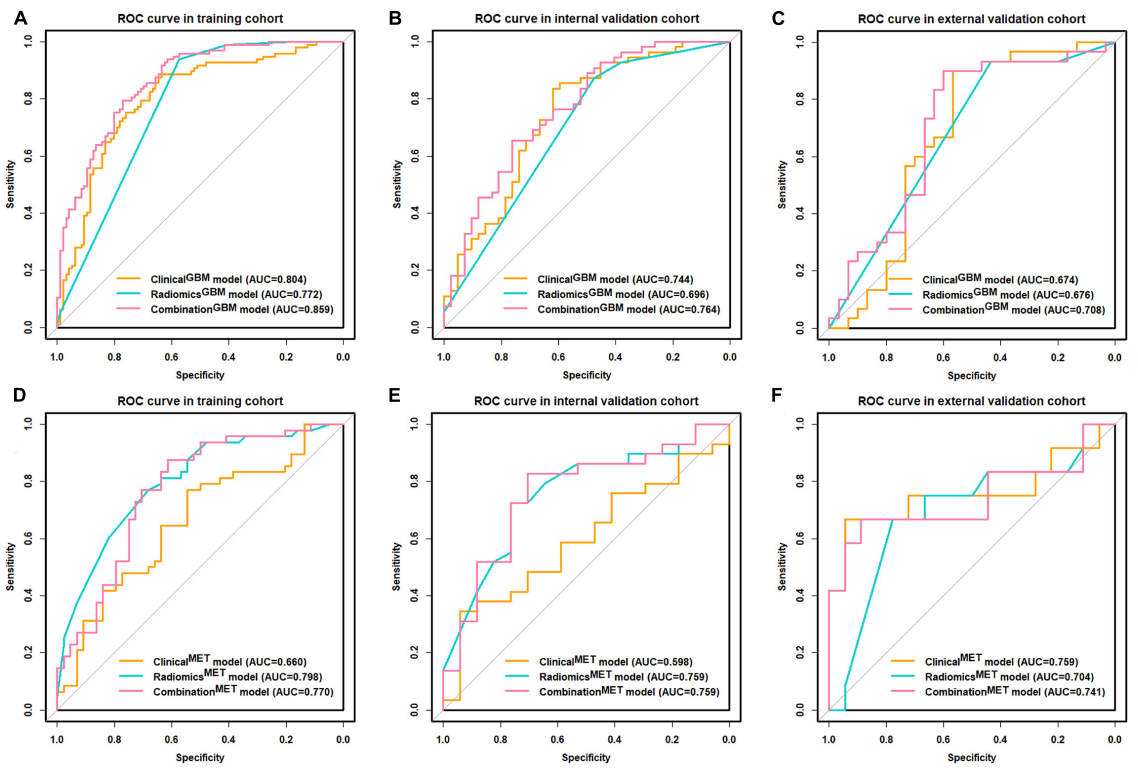

FIGURE 3 | ROC curve for clinical, radiomics, and combination models. **(A–C)** ROC curves of distinguishing GBM and MET; **(D–F)** ROC curves of distinguishing MET-lung and MET-other. ROC, receiver operating characteristic; GBM, glioblastoma multiforme; MET, metastasis.

model was 0.598 (95% CI: 0.430-0.767) and 0.759 (95% CI: 0.548-0.971) in the internal and external validation cohort, respectively (**Figures 3D–F** and **Table 2**). For distinguishing between GBM and MET, the patient age, tumor diameter, edema ratio, and radiomics^{GBM} signature were considered as the input variables of the combination^{GBM} model after a stepwise

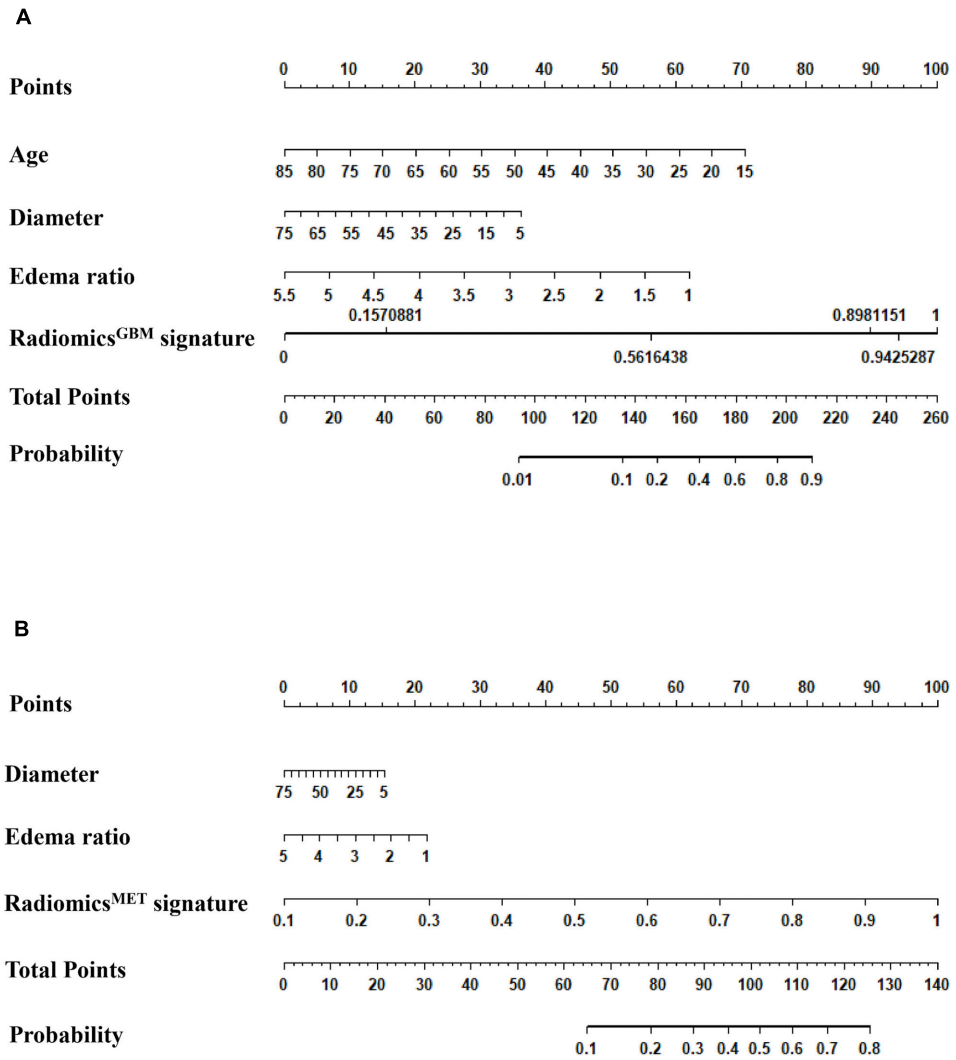

FIGURE 4 | Model assessment. **(A)** Nomogram for distinguishing GBM and MET; **(B)** Nomogram for distinguishing MET-lung and MET-other. GBM, glioblastoma multiforme; MET, metastasis.

search. For distinguishing between MET-lung and MET-other, the tumor diameter, edema ratio, and radiomics^{MET} signature were considered as the input variables of the combination^{MET} model. After the incorporation of the radiomics signatures, the performance of the combination models in the two classification strategies improved compared with that of the clinical models (**Table 2**). In particular, the performance of the combination^{MET} model was significantly better than that of the clinical^{MET} model (DeLong test: $P = 0.019$ in the internal validation cohort). The violin figures of all models in the training and validation cohorts are shown in **Supplementary Material 9**.

Nomogram Implementation

We used the nomograms to show the graphical representation of the combination models. The nomograms for the two classification strategies are illustrated in **Figure 4**. The calibration curves demonstrated good agreement between the predictive and observational probabilities for the two classification strategies ($P > 0.05$ for all cohorts, Hosmer–Lemeshow test, **Figure 5**). The AUCs for the nomogram were 0.859 (95% CI: 0.809-0.911) in the training cohort, 0.764 (95% CI:0.667-0.860) in the internal validation cohort and 0.708 (95% CI: 0.570-0.846) in the external validation cohort for the differentiation between GBM and MET. The AUCs for the nomogram were 0.770 (95% CI: 0.672-0.869) in the training cohort, 0.759 (95% CI:0.609-0.908 in the internal validation cohort and 0.741 (95%CI:0.527-0.954) in the external validation cohort for the differentiation between MET-lung and MET-other. The decision curves showed that the combination GBM nomogram added more benefit than did the clinical^{GBM} nomogram when the threshold probability was >6% (**Figure 6A**); for the differentiation between MET-lung and MET-other, the combination^{MET} nomogram added more benefit than did the clinical^{MET} nomogram when the threshold probability was > 16% (**Figure 6B**). The correlation between

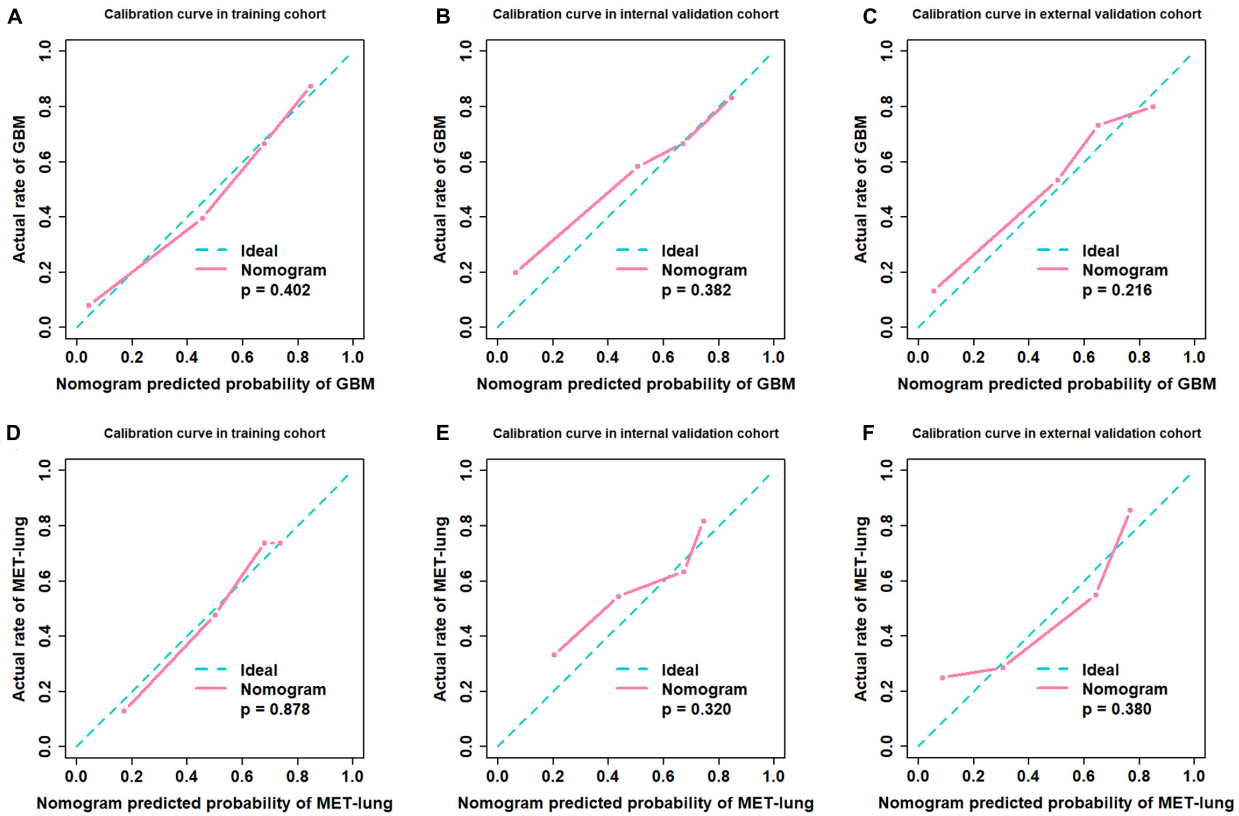

FIGURE 5 | Calibration curves. **(A–C)** Calibration curves of distinguishing GBM and MET; **(D–F)** Calibration curves of distinguishing MET-lung and MET-other. GBM, glioblastoma multiforme; MET, metastasis.

the clinical-radiological characteristics and radiomic features was demonstrated in the heat map with the absolute value of the Spearman correlation coefficients (**Supplementary Material 10**).

DISCUSSION

We utilized radiomics analysis to distinguish between GBM and MET and between MET-lung and MET-other. For both classification strategies, we applied seven methods to select features and four algorithms to construct the radiomics model. Of all 28 classifiers for distinguishing between GBM and MET, the classifier fisher_DT exhibited the best classification performance, with an AUC of 0.696 in the internal validation cohort. For distinguishing between MET-lung and MET-other, the classifier reliefF_RF exhibited the best classification performance, with an AUC of 0.759 in the validation cohort. The combination models exhibited an improved predictive performance compared with the clinical models when the radiomics signatures were added to the models, especially for identifying the primary tumor of MET.

Radiomics analysis has been used for the differentiation between GBM and MET. To determine the best classification model for differentiation, 12 feature selection methods and 7 classification methods were used; the highest AUC obtained was 0.90 in the study by Qian et al. (2019). Artzi et al. (2019) used four machine-learning algorithms to differentiate between the GBM and MET subtypes, and the accuracies were 0.85, 0.89, 0.82, and 0.89 for identifying GBM and METs from breast, lung, and other cancers, respectively. All these studies have high clinical applicability but have only focused on the comparison of imaging features and radiomics models and did not consider the clinical factors. The complementarity of radiomic features and clinical-radiological factors should also be explored.

Considering the importance of patient age and sex in medical diagnosis, these variables were included in this study. Moreover, the tumor size, perilesional edema, and location are important radiological signs for diagnosis, which are readily obtained by routine radiological scans. The radiomics^{GBM} model and clinical^{GBM} model yielded a comparable predictive performance (P = 0.361 in the internal validation cohort, DeLong test). In addition, the predictive performance of the combination^{GBM} model improved compared with that of the clinical^{GBM} model when the radiomics^{GBM} signature and clinical-radiological factors were combined. However, the DeLong test showed no significant improvement (P = 0.064 in the internal validation cohort). This indicates that the radiomics signature can be used as a signal predictor to obtain satisfactory results. For differentiation between MET-lung and MET-other, and the performance of radiomics^{MET} model significantly better than that of the clinical^{MET} model (P = 0.019 in the internal validation

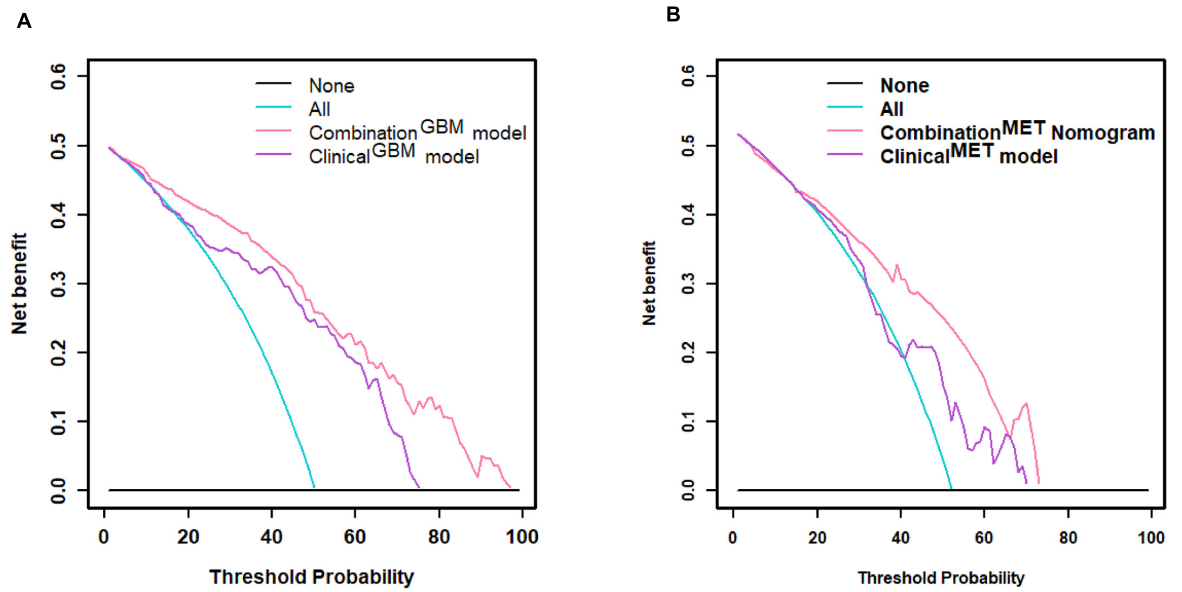

FIGURE 6 | Decision curve. **(A)** Decision curve of distinguishing GBM and MET; **(B)** decision curve of distinguishing MET-lung and MET-other. GBM, glioblastoma multiforme; MET, metastasis.

cohort, DeLong test). The combination^{MET} model also showed a better predictive performance than the clinical^{MET} model, and the DeLong test showed significant improvements in the internal validation cohorts ($P = 0.019$), which suggested that the radiomics signature can increase the predictive power of clinical factors. Based on the results of the two classification strategies, we observed that radiomics analysis has a superior classification ability in differentiating tumor types, which is consistent with previous study findings (Artzi et al., 2019; Qian et al., 2019).

Our study also showed that the tumor size was related to the type of tumor, which was consistent with a previous study finding (Baris et al., 2016). Compared with the other characteristics, the tumor size had a higher correlation with the radiomic features used in the radiomics^{GBM} model (**Supplementary Material 10**), as observed in the Spearman correlation analysis. This may explain why the clinical^{GBM} model and radiomics^{GBM} model yielded a comparable predictive performance; however, the performance of the combination GBM model did not improve significantly, which emphasizes the importance of the tumor size in distinguishing between GBM and MET. With regard to the features used in the radiomics^{MET} model, most radiomic features showed low correlations with the clinical-radiological characteristics (**Supplementary Material 10**); thus, the performance of the combination^{MET} model improved significantly. This indicated that the radiomic features could complement the clinical factors, and the difference between MET-lung and MET-other could not be accurately recognized using simple tumor phenotypes.

We segmented tumors on post-contrast axial T1-weighted image (T1WI) not on other images, such as T2WI, et al. This is due to the different findings on different MRI images. For low-grade gliomas, they usually show no or partial enhancement, without or with minimal peritumoral edema. They are low signal intensity on post-contrast T1WI. Therefore, it is difficult to outline the border of the tumor on post-contrast T1WI images. On T2WI, however, low-grade gliomas are high signal intensity and prone to the identification of the tumor border. That is why many research studies segmented low-grade gliomas on T2WI (Li et al., 2018a,b; Liu et al., 2018, 2019; Qian et al., 2018). GBM, however, often shows a mass with vivid peritumoral edema. On post-contrast images, the mass usually demonstrates strong enhancement with non-enhanced peritumoral edema. Hence, the tumor mass is high signal while the peritumoral edema is low signal intensity on post-contrast T1WI, which is prone to outline the border of the mass. On T2WI, both the tumor itself and peritumoral edema are hyperintensity. It is difficult to distinguish the tumor from the perilesional edema. If the area of high signal intensity on T2WI is considered as the ROI for segmentation, the ROI would be larger than the tumor itself because the peritumoral edema is also recruited in the ROI. Cerebral metastasis often demonstrates as a mass with obvious edema. On T2WI and post-contrast T1WI, both the metastatic mass and the peritumoral edema show the same findings as that of GBM. Therefore, the radiomic analysis of cerebral metastasis is also based on post-contrast T1WI in some researches (Artzi et al., 2019; Karami et al., 2019a,b).

There are several limitations of this study. First, the radiomic imaging data used were only T1 enhanced sequences. Other sequences, including T2WI, DWI, and PWI, may contain additional functional and biological information; therefore, more imaging modalities should be taken into account for future research. Second, although the number of cases in our study was relatively large, the MET-other cases involved many origins, with each origin having a small case number. More detailed subgroups

based on the primary origin of METs should be considered in future studies. Finally, this was a retrospective study. Although we used external validation to reduce the impact, the prospective multi-center study was still required.

CONCLUSION

Our study suggests that radiomics analysis has a superior classification ability in the differentiation among GBM, MET-lung, and MET-other. The combination of radiomic and non-radiomic features is helpful for the differentiation of these three types of tumors.

DATA AVAILABILITY STATEMENT

The raw data supporting the conclusions of this article will be made available by the authors, without undue reservation.

ETHICS STATEMENT

The studies involving human participants were reviewed and approved by Beijing Tiantan Hospital. Written informed consent for participation was not provided by the participants' legal guardians/next of kin because: As a retrospective study, it was approved by our institute committee without the informed consent of the patients.

AUTHOR CONTRIBUTIONS

YH and LZ performed the study design, information collection, statistical analysis, and manuscript editing. HZ, YX, and XC guided and study design, reviewed images, and revised the manuscript. SN, SC, and BY provided the technical support. HC, FZ, and YZ collected the images and clinical information. All authors contributed to the article and approved the submitted version.

FUNDING

This work was supported by the National Natural Science Foundation of China under grant number 81772005, the National Key Research and Development Program of China Grant under grant number 2018YFC0115604, and Collaborative innovative major special project supported by Beijing Municipal Science & Technology Commission under grant number Z191100006619088.

SUPPLEMENTARY MATERIAL

The Supplementary Material for this article can be found online at: https://www.frontiersin.org/articles/10.3389/fcell.2021.710461/full#supplementary-material

REFERENCES

Aerts, H. J., Velazquez, E. R., Leijenaar, R. T., Parmar, C., Grossmann, P., Carvalho, S., et al. (2014). Decoding tumour phenotype by noninvasive imaging using a quantitative radiomics approach. *Nat. Commun.* 5:4006. doi: 10.1038/ncomms5006

Artzi, M., Bressler, I., and Ben Bashat, D. (2019). Differentiation between glioblastoma, brain metastasis and subtypes using radiomics analysis. *J. Magn. Reson. Imaging* 50, 519–528. doi: 10.1002/jmri.26643

Ascha, M. S., Ostrom, Q. T., Wright, J., Kumthekar, P., Bordeaux, J. S., Sloan, A. E., et al. (2019). Lifetime occurrence of brain metastases arising from lung, breast, and skin cancers in the elderly: a SEER-medicare study. *Cancer Epidemiol. Biomarkers Prev.* 28, 917–925. doi: 10.1158/1055-9965.Epi-18-1116

Askaner, K., Rydelius, A., Engelholm, S., Knutsson, L., Lätt, J., Abul-Kasim, K., et al. (2019). Differentiation between glioblastomas and brain metastases and regarding their primary site of malignancy using dynamic susceptibility contrast MRI at 3T. *J. Neuroradiol.* 46, 367–372. doi: 10.1016/j.neurad.2018.09.006

Baris, M. M., Celik, A. O., Gezer, N. S., and Ada, E. (2016). Role of mass effect, tumor volume and peritumoral edema volume in the differential diagnosis of primary brain tumor and metastasis. *Clin. Neurol. Neurosurg* 148, 67–71. doi: 10.1016/j.clineuro.2016.07.008

Chaddad, A., Daniel, P., Desrosiers, C., Toews, M., and Abdulkarim, B. (2019). Novel radiomic features based on joint intensity matrices for predicting glioblastoma patient survival time. *IEEE J. Biomed. Health Inform.* 23, 795–804. doi: 10.1109/jbhi.2018.2825027

Chakhoyan, A., Raymond, C., Chen, J., Goldman, J., Yao, J., Kaprealian, T. B., et al. (2019). Probabilistic independent component analysis of dynamic susceptibility contrast perfusion MRI in metastatic brain tumors. *Cancer Imaging* 19:14. doi: 10.1186/s40644-019-0201-0

Chen, X. Z., Yin, X. M., Ai, L., Chen, Q., Li, S. W., and Dai, J. P. (2012). Differentiation between brain glioblastoma multiforme and solitary metastasis: qualitative and quantitative analysis based on routine MR imaging. *AJNR Am. J. Neuroradiol.* 33, 1907–1912. doi: 10.3174/ajnr.A3106

Durmo, F., Rydelius, A., Baena, S. C., Askaner, K., Lätt, J., Bengzon, J., et al. (2018). Multivoxel ^{1}H-MR spectroscopy biometrics for preoprerative differentiation between brain tumors. *Tomography* 4, 172–181. doi: 10.18383/j.tom.2018.00051

Füreder, L. M., Dieckmann, B., Hainfellner, K., Bartsch, J. A., Zielinski, R., Preusser, C. C., and Berghoff, A. S. (2018). Brain metastases as first manifestation of advanced cancer: exploratory analysis of 459 patients at a tertiary care center. *Clin. Exp. Metastas.* 35, 727–738. doi: 10.1007/s10585-018-9947-1

Grabowski, M. M., Recinos, P. F., Nowacki, A. S., Schroeder, J. L., Angelov, L., Barnett, G. H., et al. (2014). Residual tumor volume versus extent of resection: predictors of survival after surgery for glioblastoma. *J. Neurosurg.* 121, 1115–1123. doi: 10.3171/2014.7.Jns132449

Holly, K. S., Fitz-Gerald, J. S., Barker, B. J., Murcia, D., Daggett, R., Ledbetter, C., et al. (2018). Differentiation of high-grade glioma and intracranial metastasis using volumetric diffusion tensor imaging tractography. *World Neurosurg.* 120, e131–e141. doi: 10.1016/j.wneu.2018.07.230

Kamimura, K., Nakajo, M., Yoneyama, T., Fukukura, Y., Hirano, H., Goto, Y., et al. (2019). Histogram analysis of amide proton transfer-weighted imaging: comparison of glioblastoma and solitary brain metastasis in enhancing tumors and peritumoral regions. *Eur. Radiol.* 29, 4133–4140. doi: 10.1007/s00330-018-5832-1

Karami, E., Ruschin, M., Soliman, H., Sahgal, A., Stanisz, G. J., and Sadeghi-Naini, A. (2019a). An MR radiomics framework for predicting the outcome of stereotactic radiation therapy in brain metastasis. *Annu. Int. Conf. IEEE Eng. Med. Biol. Soc.* 2019, 1022–1025. doi: 10.1109/embc.2019.8856558

Karami, E., Soliman, H., Ruschin, M., Sahgal, A., Myrehaug, S., Tseng, C. L., et al. (2019b). Quantitative MRI biomarkers of stereotactic radiotherapy outcome in brain metastasis. *Sci. Rep.* 9:19830. doi: 10.1038/s41598-019-56185-5

Kniep, H. C., Madesta, F., Schneider, T., Hanning, U., Schg, S., Tseng, C. L., et al. (2019). Quantitative MRI biomarkers of ste. *Radiology* 290, 479–487. doi: 10.1148/radiol.2018180946

Lambin, P., Leijenaar, R. T. H., Deist, T. M., Peerlings, J., De Jong, E. E. C., Van Timmeren, J., et al. (2017). Radiomics: the bridge between medical imaging and personalized medicine. *Nat. Rev. Clin. Oncol.* 14, 749–762. doi: 10.1038/nrclinonc.2017.141

Li, Y., Liu, X., Xu, K., Qian, Z., Wang, K., Fan, X., et al. (2018a). MRI features can predict EGFR expression in lower grade gliomas: a voxel-based radiomic analysis. *Eur. Radiol.* 28, 356–362. doi: 10.1007/s00330-017-4964-z

Li, Y., Qian, Z., Xu, K., Wang, K., Fan, X., Li, S., et al. (2018b). MRI features predict p53 status in lower-grade gliomas via a machine-learning approach. *Neuroimage Clin.* 17, 306–311. doi: 10.1016/j.nicl.2017.10.030

Li, Z. C., Bai, H., Sun, Q., Li, Q., Liu, L., Zou, Y., et al. (2018c). Multiregional radiomics features from multiparametric MRI for prediction of MGMT methylation status in glioblastoma multiforme: a multicentre study. *Eur. Radiol.* 28, 3640–3650. doi: 10.1007/s00330-017-5302-1

Liu, X., Li, Y., Li, S., Fan, X., Sun, Z., Yang, Z., et al. (2019). IDH mutation-specific radiomic signature in lower-grade gliomas. *Aging (Albany N. Y.)* 11, 673–696. doi: 10.18632/aging.101769

Liu, X., Li, Y., Qian, Z., Sun, Z., Xu, K., Wang, K., et al. (2018). A radiomic signature as a non-invasive predictor of progression-free survival in patients with lower-grade gliomas. *Neuroimage Clin.* 20, 1070–1077. doi: 10.1016/j.nicl.2018.10.014

Mampre, D., Ehresman, J., Alvarado-Estrada, K., Wijesekera, O., Sarabia-Estrada, R., Quinones-Hinojosa, A., et al. (2019). Propensity for different vascular distributions and cerebral edema of intraparenchymal brain metastases from different primary cancers. *J. Neurooncol.* 143, 115–122. doi: 10.1007/s11060-019-03142-x

Ohgaki, H., and Kleihues, P. (2005). Epidemiology and etiology of gliomas. *Acta Neuropathol.* 109, 93–108. doi: 10.1007/s00401-005-0991-y

Ortiz-Ramon, R., Larroza, A., Arana, E., and Moratal, D. (2017). A radiomics evaluation of 2D and 3D MRI texture features to classify brain metastases from lung cancer and melanoma. *Annu. Int. Conf. IEEE Eng. Med. Biol. Soc.* 2017, 493–496. doi: 10.1109/embc.2017.8036869

Ortiz-Ramón, R., Larroza, A., España, S., Arana, E., and Moratal, D. (2018). Classifying brain metastases by their primary site of origin using a radiomics approach based on texture analysis: a feasibility study. *Eur. Radiol.* 28, 4514–4523. doi: 10.1007/s00330-018-5463-6

Platta, C. S., Khuntia, D., Mehta, M. P., and Suh, J. H. (2010). Current treatment strategies for brain metastasis and complications from therapeutic techniques: a review of current literature. *Am. J. Clin. Oncol.* 33, 398–407. doi: 10.1097/COC.0b013e318194f744

Qian, Z., Li, Y., Sun, Z., Fan, X., Xu, K., Wang, K., et al. (2018). Radiogenomics of lower-grade gliomas: a radiomic signature as a biological surrogate for survival prediction. *Aging (Albany N. Y.)* 10, 2884–2899. doi: 10.18632/aging.101594

Qian, Z., Li, Y., Wang, Y., Li, L., Li, R., Wang, K., et al. (2019). Differentiation of glioblastoma from solitary brain metastases using radiomic machine-learning classifiers. *Cancer Lett.* 451, 128–135. doi: 10.1016/j.canlet.2019.02.054

Rios Velazquez, E., Parmar, C., Liu, Y., Coroller, T. P., Cruz, G., Stringfield, O., et al. (2017). Somatic mutations drive distinct imaging phenotypes in lung cancer. *Cancer Res.* 77, 3922–3930. doi: 10.1158/0008-5472.Can-17-0122

Rotta, J. M., Rodrigues, D. B., Diniz, J. M., Abreu, B. M., Kamimura, F., Sousa, U. O., et al. (2018). Analysis of survival in patients with brain metastases treated surgically: impact of age, gender, oncologic status, chemotherapy, radiotherapy, number and localization of lesions, and primary cancer site. *Rev. Assoc. Med. Bras. (1992)* 64, 717–722. doi: 10.1590/1806-9282.64.08.717

Salice, S., Esposito, R., Ciavardelli, D., Delli Pizzi, S., Di Bastiano, R., and Tartaro, A. (2016). Combined 3 tesla MRI biomarkers improve the differentiation between benign vs. malignant single ring enhancing brain masses. *PLoS One* 11:e0159047. doi: 10.1371/journal.pone.0159047

Tan, Y., Wang, X. C., Zhang, H., Wang, J., Qin, J. B., Wu, X. F., et al. (2015). Differentiation of high-grade-astrocytomas from solitary-brain-metastases: comparing diffusion kurtosis imaging and diffusion tensor imaging. *Eur. J. Radiol.* 84, 2618–2624. doi: 10.1016/j.ejrad.2015.10.007

Van Griethuysen, J. J. M., Fedorov, A., Parmar, C., Hosny, A., Aucoin, N., Narayan, V., et al. (2017). Computational radiomics system to decode the radiographic phenotype. *Cancer Res.* 77, e104–e107. doi: 10.1158/0008-5472.Can-17-0339

Weller, M., Van Den Bent, M., Hopkins, K., Tonn, J. C., Stupp, R., Falini, A., et al. (2014). EANO guideline for the diagnosis and treatment of anaplastic gliomas and glioblastoma. *Lancet Oncol.* 15, e395–e403. doi: 10.1016/s1470-2045(14)70011-7

Xi, Y. B., Kang, X. W., Wang, N., Liu, T. T., Zhu, Y. Q., Cheng, G., et al. (2019). Differentiation of primary central nervous system lymphoma from high-grade glioma and brain metastasis using arterial spin labeling and dynamic contrast-enhanced magnetic resonance imaging. *Eur. J. Radiol.* 112, 59–64. doi: 10.1016/j.ejrad.2019.01.008

Zacharaki, E. I., Wang, S., Chawla, S., Soo Yoo, D., Wolf, R., Melhem, E. R., et al. (2009). Classification of brain tumor type and grade using MRI texture and shape in a machine learning scheme. *Magn. Reson. Med.* 62, 1609–1618. doi: 10.1002/mrm.22147

Conflict of Interest: The authors declare that the research was conducted in the absence of any commercial or financial relationships that could be construed as a potential conflict of interest.

Publisher's Note: All claims expressed in this article are solely those of the authors and do not necessarily represent those of their affiliated organizations, or those of the publisher, the editors and the reviewers. Any product that may be evaluated in this article, or claim that may be made by its manufacturer, is not guaranteed or endorsed by the publisher.

frontiers in Cell and Developmental Biology

REVIEW
published: 30 August 2021
doi: 10.3389/fcell.2021.698532

Novel Characterization of Myeloid-Derived Suppressor Cells in Tumor Microenvironment

*Yanan Li[1], Hongdan He[2], Ribu Jihu[1], Junfu Zhou[1], Rui Zeng[1] and Hengxiu Yan[1]**

[1] Immunotherapy Laboratory, College of Pharmacology, Southwest Minzu University, Chengdu, China, [2] Immunotherapy Laboratory, Qinghai Tibet Plateau Research Institute, Southwest Minzu University, Chengdu, China

Myeloid-derived suppressor cells (MDSCs) are a heterogeneous group of cells generated in various pathologic conditions, which have been known to be key components of the tumor microenvironment (TME) involving in tumor immune tolerance. So MDSCs have been extensively researched recently. As its name suggests, immunosuppression is the widely accepted function of MDSCs. Aside from suppressing antitumor immune responses, MDSCs in the TME also stimulate tumor angiogenesis and metastasis, thereby promoting tumor growth and development. Therefore, altering the recruitment, expansion, activation, and immunosuppression of MDSCs could partially restore antitumor immunity. So, this view focused on the favorable TME conditions that promote the immunosuppressive effects of MDSCs and contribute to targeted therapies with increased precision for MDSCs.

Keywords: tumor microenvironment, myeloid-derived suppressor cells, targeted therapy, multivariate effects, regulation

OPEN ACCESS

Edited by:
Shengtao Zhou,
Sichuan University, China

Reviewed by:
Alice Turdo,
University of Palermo, Italy
Dong-Joo (Ellen) Cheon,
Albany Medical College, United States

****Correspondence:***
Hengxiu Yan
719306512@qq.com

Specialty section:
This article was submitted to Molecular and Cellular Pathology, a section of the journal Frontiers in Cell and Developmental Biology

Received: *21 April 2021*
Accepted: *09 August 2021*
Published: *30 August 2021*

Citation:
Li Y, He H, Jihu R, Zhou J, Zeng R and Yan H (2021) Novel Characterization of Myeloid-Derived Suppressor Cells in Tumor Microenvironment. Front. Cell Dev. Biol. 9:698532. doi: 10.3389/fcell.2021.698532

INTRODUCTION

The tumor microenvironment (TME) is the direct environment in which tumor cells live, consists of lymphocytes, immune cells, stromal cells, and extracellular matrix (ECM), and it is closely associated with tumor growth, invasion, and metastasis (Chen et al., 2015). A series of tumor-promoting cells exist in the TME, including T regulatory cells (Tregs), T helper type 2 cells, tumor-associated macrophages (TAMs), and myeloid-derived suppressor cells (MDSCs). The cytokines and chemokines secreted by these cells create an immunosuppressive circumstance that prevents immune cells from functioning. Therefore, TME provides a permissive environment for the progression and metastatic dissemination of tumor cells (Ugel et al., 2015). And, MDSCs are currently considered to be major players in the development of tumor immune tolerance. At present, studies have shown that cytokines from tumor cells and activated immune cells in the TME promote the recruitment, activation, expansion, and suppressive activities of MDSCs in tumor progression (**Table 1**). These cytokines are divided into two groups in light of the different roles on MDSCs. The first class is in charge of the expansion of MDSCs, and it mainly includes vascular endothelial growth factor (VEGF), granulocyte-macrophage colony-stimulating factor (GM-CSF), macrophage colony-stimulating factor (M-CSF), and granulocyte colony-stimulating factor (G-CSF). The second class plays a remarkable part in the MDSC activation procedure and mainly includes interferon-γ (IFN-γ), high-mobility group box 1 (HMGB1), tumor necrosis factor (TNF), and interleukin-1β (IL-1β), IL-4, IL-6, and IL-13 (Umansky and Sevko, 2013; Condamine et al., 2015). In addition, there are some newly discovered factors, such as endoplasmic reticulum (ER)

stress and tumor-derived exosomes (TEXs), which are also implicated as key factors that regulate MDSCs to play a tumor-promoting aspect in the TME. Concurrently, MDSCs in the TME directly enhance tumor angiogenesis and migration in addition to facilitating immune response (**Table 1**). MDSCs have become one of the main impediments to effective cancer immunotherapy and have been considered as valuable markers of predicting cancer progression in numerous clinical studies. Therefore, extensive efforts in the development of targeting MDSC therapies are ongoing vigorously (Betsch et al., 2018; Li et al., 2018).

As mentioned above, there are many factors existed in the TME for MDSC recruitment, activation, and expansion, which may be targets to the cancer treatment by modifying MDSC function. This review highlighted the recruitment, expansion, and activation of MDSC in the TME and may provide more effective strategies for MDSC-based cancer therapy.

DEFINITION OF MDSCs

Myeloid-derived suppressor cells are derived from myeloid progenitors and immature myeloid cells (IMCs). Under physiological conditions, they rapidly differentiate into mature granulocytes, dendritic cells (DCs), and macrophages, then migrate the corresponding peripheral organs and tissues from the bone marrow to exert normal immune functions. Nevertheless, under pathological situations, such as cancer, infection, inflammation, sepsis, and surgical injury, the maturation of these myeloid-derived progenitors is blocked by cytokines, so they stay in various differentiation stages to become MDSCs with immunosuppressive function, which are also recruited, migrated and amplified under the action of cytokines, throughout the whole process of disease occurrence (Gabrilovich and Nagaraj, 2009). Of note, MDSC expansion does not exclusively result from myelopoiesis in the bone marrow, but also the differentiation of MDSC progenitors as well as reprogramming of monocytes and neutrophils in peripheral tissues (Bergenfelz et al., 2015; Heine et al., 2017; Yaseen et al., 2021). In 1995, $CD11b^+/Gr\text{-}1^+$ myeloid cells were found to be involved in tumor immune escape and development, and they were described as MDSCs in 2007 (Gabrilovich et al., 2007). Traditionally, two subpopulations of MDSCs are shown to exist, namely, granulocytic $CD11b^+Ly6G^+Ly6C^{lo}$ [G-MDSCs or polymorphonuclear (PMN)-MDSCs] and monocytic $CD11b^+Ly6G^-Ly6C^{hi}$ (M-MDSCs), in mouse (Bronte et al., 2016). In human, M-MDSCs are characterized as $CD11b^+CD33^+CD14^+HLA\text{-}DR^{lo/-}CD15^-$ and PMN-MDSCs as $CD11b^+CD33^+CD15^+CD66b^+HLA\text{-}DR^{lo/-}$ (Bronte et al., 2016; Elliott et al., 2017). Besides, a group of IMCs was found in human peripheral blood which was referred to as early stage MDSCs. Lin cocktail, including CD3, CD14, CD15, CD19, and CD56, could be used to differentiate early stage MDSCs from MDSCs, and early stage MDSCs are characterized as $Lin^-HLA\text{-}DR^-CD33^+$ in human (Almand et al., 2001; Bronte et al., 2016). Another novel subpopulation of tumor-induced MDSCs was identified in the peripheral blood of a patient with metastatic pediatric sarcoma, which shares the fibrocytes phenotypic and

TABLE 1 | Myeloid-derived suppressor cells in a variety of tumors.

Tumor	Contribution of MDSCs to tumor development	Regulatory effect of factors on MDSC	Reference
Prostate cancer	MDSCs promoted tumor survival	Tumor-derived G-CSF promoted the proliferation of MDSCs via a STAT3-dependent pathway	Yu et al., 2015
	MDSCs promoted tumor progression	Chemokines promoted the expansion of $CCR5^+$PMN-MDSCs at the BM, and potentiated their immunosuppression at the tumor site	Hawila et al., 2017
	MDSCs promoted tumor angiogenesis	CSF1R signaling promoted tumor recruitment of M-MDSC recruitment from peripheral blood	Priceman et al., 2010
Breast cancer	MDSCs promoted tumor growth	TEXs with abundant PGE2 and TGF-β enhanced the expansion and immunosuppression of MDSCs	Xiang et al., 2009
	MDSCs promoted tumor progression	Transmembrane Tm-TNF-α induced the immunosuppression of MDSCs	Hu et al., 2014
	MDSCs promoted tumor growth and metastasis	Mir-494 induced the expansion of MDSCs in tumor tissues by increasing the activity of the Akt pathway	Liu et al., 2012
	MDSCs stimulated tumor cell metastasis to distant sites	IL-6 secreted from breast cancer cells facilitated MDSC recruitment	Oh et al., 2013
Melanoma	MDSCs promoted tumor growth	Lnc-chop encouraged the activity of C/EBP β, improved the immunosuppression of MDSCs	Gao et al., 2018
	MDSCs promoted tumor progression	Tumor-derived chemokines CCL3, CCL4, and CCL5 recruited $CCR5^+$ MDSCs to the tumor site	Blattner et al., 2018
	PMN-MDSCs induced the proliferation and EMT of tumor cells	Tumor-derived chemokines CXCL1, CXCL2, and CXCL5 recruited $CXCR2^+$ MDSC to the tumor site	Toh et al., 2011
Colon cancer	MDSCs promoted tumor growth	HMGB1 promoted the differentiation of MDSCs from bone marrow progenitor cells, and activated the immunosuppression of MDSCs via the NF-κB pathway	Parker et al., 2014
	MDSCs promoted tumor growth	MiR-200c promoted immunosuppression of MDSCs by targeting PTEN/FOG2, which led to STAT3 and PI3K/Akt activation	Mei et al., 2015
	MDSCs formed PMN in the pre-metastatic liver	VEGFA secreted by colon cancer cells stimulated CXCL1 production by TAMs, which recruited $CXCR2^+$ MDSCs to promote liver metastasis.	Wang et al., 2017

functional characteristics (Zhang et al., 2013). And, Zoso et al. (2014) found this subpopulation simultaneously expressing surface markers of MDSCs, DCs as well as fibrocytes, which were defined as fibrocystic MDSCs ($CD11b^{low}CD11c^{low}CD33^{+}IL\text{-}4Ra^{+}$). Recently, a novel group of MDSCs with immature eosinophilic phenotype was found to accumulate at the site of infection to exacerbate the chronic Staphylococcus infection in mice, which defined as eosinophilic MDSCs (Eo-MDSCs) by Goldmann et al. (2017), characterizing as SSC^{high} $Ly6C^{low}$ $Ly6G^{-}CCR3^{low}$ $Siglec\text{-}F^{low}$ $IL\text{-}5R^{low}$. These new MDSCs subpopulations enrich the diversity of MDSCs, which attract researchers to study and classify MDSCs more carefully to promote the development of targeting MDSCs treatment.

With the ongoing advance in research on MDSCs, several other potential markers have been identified. For example, CD84 and CD36 have been used to identify MDSCs, while CD244, fatty acid transport protein 2 (FATP2) are thought to more effectively distinguish M-MDSCs from PMN MDSCs in mice (Al-Khami et al., 2017; Veglia et al., 2019, 2021; Alshetaiwi et al., 2020). And, in human, CD84 and S100A9 are also suggested to identify MDSCs, CD66b is used to distinguish PMN-MDSCs from M-MDSCs. Of note, lectin-type oxidized LDL receptor 1 (LOX-1), as a specific marker for human PMN-MDSCs, is used to distinguish PMN-MDSCs from M-MDSCs and normal neutrophils (Zhao F. et al., 2012; Condamine et al., 2016; Lin et al., 2018). In a recent study, by using single-cell RNA-seq (scRNA-seq), Alshetaiwi et al. (2020) found that there were 642 differentially expressed genes between PMN-MDSCs and normal neutrophils as well as 223 differentially expressed genes between M-MDSCs and normal monocytes in the MMTV-PyMT mouse breast cancer model, revealing that MDSCs were quite different from normal myeloid cells. At the same time, there was a large overlap between the genomes of PMN-MDSCs and M-MDSCs involved in immunosuppression, such as IL-1B, ARG-2, CD84, and WFDC17, and chemokine receptors, such as CCR2 and CXCR2, revealing that MDSCs could be migrated to the primary tumor by tumor-derived chemokines. Of note, CD84 could be identified as a specific surface marker of MDSCs in breast cancer, but whether it can be used to identify MDSCs in other cancers needs further test (Alshetaiwi et al., 2020; Veglia et al., 2021). In the future, bulk or single-cell genomics could be considered to accurately identify MDSCs cell surface markers and specific genomic features in different types of malignancies, which could help identify potential therapeutic targets and improve cancer treatment by targeting MDSCs.

CONTRIBUTION OF MDSCs To Tumor Development

MDSC Immunosuppression

As important immunosuppressive cells in the TME, MDSCs inhibit antitumor immunity by inhibiting T cells and natural killer cells proliferation and function and inducing Treg recruitment. Thus, the tumor cells escape the immune surveillance and in turn promote the development of tumors (**Figure 1**).

Myeloid-derived suppressor cells exert immunosuppressive effects by depleting the fundamental amino acids, including L-arginine and cysteine, that are cardinal for T cell function in the TME. MDSCs have a high expression of arginase-1 (ARG-1) and inducible NO synthase (iNOS) in the TME. Decomposition of L-arginine by iNOS produces large amounts of NO and L-citrulline, while ARG-1 converts L-arginine to L-ornithine (Consonni et al., 2019). Depletion of L-arginine and generation of large amounts of NO in the TME leads to downregulated expression of the TCR complex CD3 ζ chain and arrest of T-cell proliferation (Yang et al., 2020). T cells depend on macrophages and DCs to take up cysteine from the extracellular medium. Under normal circumstances, antigen presenting cells take up extracellular oxidized cysteine, which is converted into cysteines and then presented to T cells that provide conditions for the activation versus proliferation of T cells. By taking up cysteine, MDSCs reduce cysteine levels in the TME, leading to impaired T-cell activation (Srivastava et al., 2010). MDSCs drive reactive oxygen species (ROS) production by upregulating NADPH oxidase activity, particularly NOX2 subunit 47 (phox) and gp91 (phox). The immunosuppressive effect of ROS on T-cell function has been widely demonstrated, and studies have found that the administration of ROS inhibitors counteracted the suppressive effect of human MDSCs on T cells (Corzo et al., 2009; Wei et al., 2015). Besides, ROS by MDSCs relying on NOX2 supports MDSC expansion and recruitment in the TME by upregulating VEGF receptors on MDSCs to further promote tumor development (Kusmartsev et al., 2008; Corzo et al., 2009). By contrast, MDSCs prohibit the homing of naive $CD4^{+}$ and $CD8^{+}$ T cells to lymph nodes, which in turn interfere with T-cell activation. The underlying mechanism is that MDSCs express the adisintegrinandmetalloproteinase17 (ADAM17) to downregulate the L-selectin level on the membrane surface of $CD4^{+}$ and $CD8^{+}$ T cells (Hanson et al., 2009). MDSCs were found in multiple tumor models of mice and in patients with cancer to have been able to increase programmed cell death ligand 1 (PD-L1) expression, promote T-cell anergy by interacting with the programmed cell death protein 1 (PD-1) on T cells infiltrating tumor lesions, and in turn to drastically downregulate T cell-mediated antitumor reactivity (Weber et al., 2018). Fuse et al. (2016) reported that PD-L1 blockade decreased the immune suppression ability of MDSCs on T cells. Moreover, recent studies have found that MDSCs mediate their suppression on T cells through adenosine. MDSCs from tumor tissues of patients with cancer increased adenosine production through considerable upregulation of CD39 and CD73 *in vitro*, and adenosine signals mainly through A2A type and A3 type adenosine receptors to suppress T cell activation and immune response (Umansky et al., 2014; Li et al., 2018).

In addition to inhibiting T cells, MDSCs inhibit NK cell cytotoxicity as a tumor immune evasion mechanism. Overexpression of indoleamine 2,3-dioxygenase (IDO) by MDSCs reduces tryptophan levels in the TME, and this phenomenon not only stimulates the differentiation of Tregs from naive T cells but also induces NK cell apoptosis (Fleming et al., 2018). MDSCs suppress NK cell cytotoxicity by expressing the immunosuppressive cytokine TGF-β, including

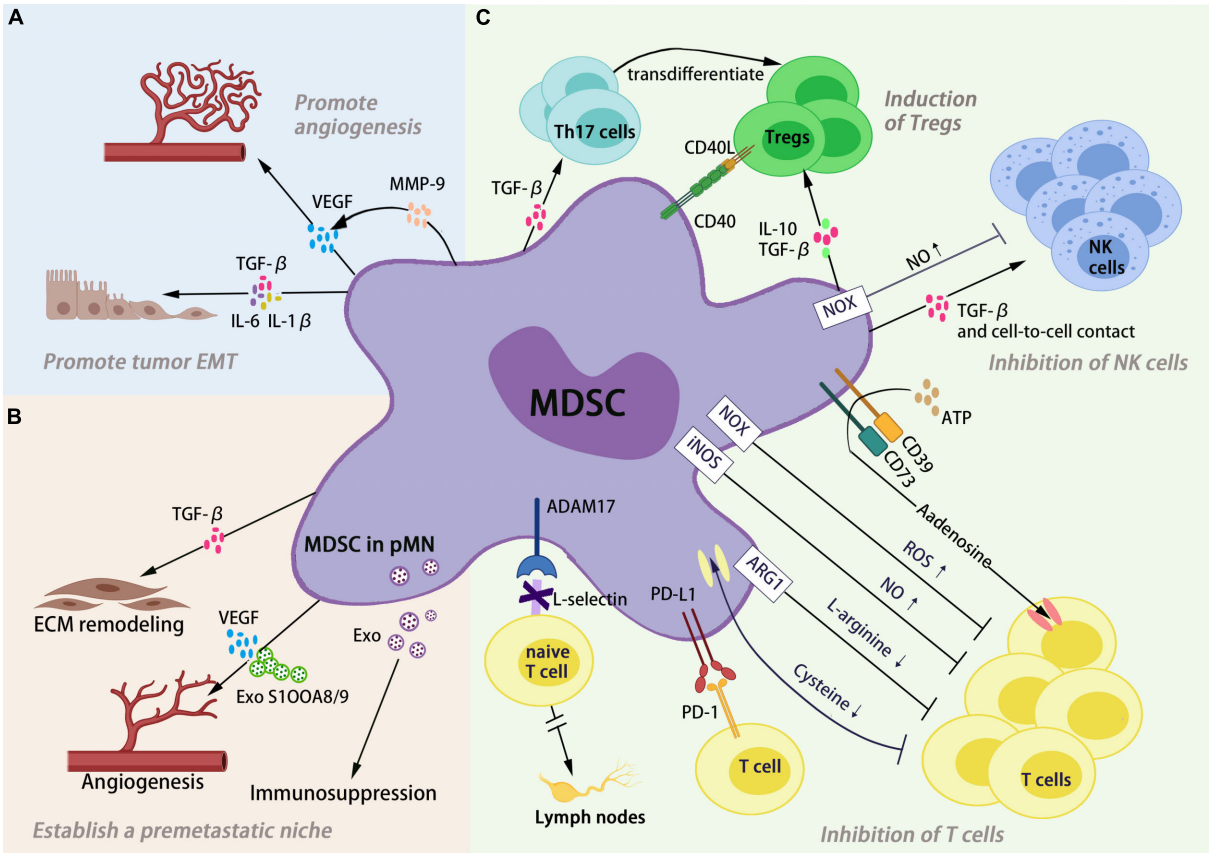

FIGURE 1 | Myeloid-derived suppressor cells (MDSCs) promote tumor development through different pathways. **(A)** MDSC non-immunologic functions. MDSCs in the TME promote tumor progression by promoting angiogenesis and EMT of tumors. **(B)** MDSC establish a pre-metastatic niche. MDSC-derived factors participate in the stepwise establishment of the PMN, resulting in a "soil" that supports the colonization of CTCs. **(C)** MDSC immunosuppression. MDSCs inhibit antitumor immunity by inhibiting T cells and natural killer cell proliferation and function and inducing Treg recruitment.

the suppression of NKG2D expression and IFN-γ secretion of NK cells (Trikha and Carson, 2014). MDSCs were recently found in the co-culture of autologous NK cells and MDSCs from patients with cancer to inhibit NK cell downstream effector functions, including cytokine production and antitumor activity, which was dependent on NO produced by MDSCs (Stiff et al., 2018).

T regulatory cells are a group of T-cell subsets downregulating immune responses; they promote the immune escape of tumors primarily by releasing inhibitory cytokines or by cell-to-cell contact. MDSCs produce the CCR5 ligands CCL4 and CCL5, which recruit Tregs to tumor tissues by CCR5 receptors highly expressed on Treg surface (Qu et al., 2016). Schlecker et al. (2012) have shown that the intratumoral injection of CCL4 or CCL5 increased the number of Tregs in the TME, whereas the lack of CCR5 resulted in a substantial reduction in Treg recruitment to the tumor. MDSCs in the TME overexpress IDO, an important enzyme-degrading tryptophan, which induces naive T cells to differentiate toward Treg phenotype by reducing tryptophan levels (Fallarino et al., 2006). Huang et al. (2006) demonstrated that IFN-γ secreted by T cells stimulated MDSCs in tumor to enhance their IL-10 and TGF-β secretion levels, which induce the activation of Tregs dependent on IL-10 and IFN-γ secreted by MDSCs. Besides, the interaction between CD40 and CD40L is critical for the induction of Tregs. Early studies have shown that MDSCs are recruited Tregs by expressing CD40 and the lack of CD40 results in significantly reduced Treg expansion (Pan et al., 2010). Apart from MDSCs inducing the development of Tregs, Th17 cells are induced by MDSCs to transdifferentiate into Tregs, which is dependent on human MDSC-derived TGF-β and retinoic acid (Hoechst et al., 2011).

MDSC Non-immunologic Functions

Besides modulating the immune system through immunosuppression, the MDSCs in the TME could contribute to the progression of the primary tumor through non-immunological functions, including promoting angiogenesis and metastasis of tumor (**Figure 1**). As shown in the mouse model, the co-injection of Gr-1^{+}CD11b^{+} cells and tumor cells stimulated tumor angiogenesis (Yang et al., 2004). VEGF is a potent angiogenic factor that promotes tumor angiogenesis. Kujawski et al. (2008) have found that MDSCs from mouse tumors increased VEGF production through the activation of signal transducer and the activator of transcription 3 (STAT3) (Li et al., 2019). In another study, MDSCs also increased VEGF

levels by expressing matrix metalloproteinase-9 (MMP-9), which further improves angiogenesis (Yang et al., 2004). In addition to promoting tumor angiogenesis, MDSCs also promote tumor cells to acquire a mesenchymal phenotype by secreting inflammatory factors Hepatocyte Growth Factor (HGF), TGF-β, IL-6, and IL1-β, which lead to the reduction or deletion of E-cadherin in tumor cells, and drive tumor cell epithelial mesenchymal transition (EMT) (Toh et al., 2011; Ouzounova et al., 2017; Pastaki Khoshbin et al., 2019). Additionally, MDSCs play an indispensable role in establishing the pre-metastatic niche (pMN). Primary tumors release signals before metastasis to regulate secondary organ resident cells or recruitment cells, including neutrophils, macrophages, and MDSCs. These cells respond to signals that transform healthy secondary organs and tissues into a "soil" that supports the colonization of circulating tumor cells (CTCs) (Peinado et al., 2017; Nasrollahzadeh et al., 2020; Wu et al., 2020). $VEGF^+$ MDSCs at tumor specific pre-metastatic sites provided a favorable microenvironment for the entry of CTCs, which was first identified by Kaplan et al. (2005). And, Yan et al. (2010) found MDSCs in the lungs of breast cancer model mice increased significantly 2 weeks before CTCs arrival and was associated with decreased lung immune function. The liver, like the lung, is a metastatic target organ for major malignancies. Infiltration of MDSCs in pre-metastatic liver tissue has been found in a variety of tumor models such as pancreatic and colorectal cancer (Kruger, 2015). Further studies revealed that MDSCs-derived exosomes, TGF-β, S100A8/A9, and VEGF induce angiogenesis, ECM remodeling, and immunosuppression to promote PMN formation and metastasis (Hsu et al., 2019; Wang et al., 2019). Metastasis has become a leading cause of cancer-related death. So, targeting MDSCs treatments hold promise to halt PMN formation and progression, prolonging the survival of tumor patients.

Taken together, the MDSCs in the TME contribute to the development of tumors and immune escape through multiple pathways, which are generally related to poor patient prognosis. MDSC-based cancer therapy has thus become a major research direction to reestablishing anticancer immunity, and it is thriving.

MDSC RECRUITMENT, EXPANSION, AND ACTIVATION IN TME

Factors Affecting MDSC Recruitment

Chemokines are a class of small secreted proteins that regulate the migration of immune cells, and more than 50 human chemokines have been currently discovered since they were first named chemokines in 1986 (Schulz et al., 2016). In accordance with the differences in the sequence of the first two conserved cysteines at the N-terminus of their molecules, chemokines are classified into four subfamilies: CXC, CC, C, and CX3C (Li et al., 2020). Several studies have demonstrated that chemokines expressed by cancer cells induce MDSC recruitment into the TME by binding to their specific receptors on MDSCs.

CCL2 is a necessary member of the CC family of chemokines, also described as monocyte chemotactic protein-1 (MCP-1), with a high affinity to the chemokine receptor CCR2 found on the MDSC cell membrane (Behfar et al., 2018). In a study of a mouse glioma model, M-MDSCs were found to be recruited to the tumor site by CCL2 that produced by microglia and macrophages in the TME, whereas MDSC infiltration into the tumor was significantly reduced in CCL2-deficient mice (Chang et al., 2016). Human breast, ovarian, and gastric tumor cells cultured *in vitro* secrete CCL2; the cognate MDSCs from these patients express CCR2; and the recruitment of MDSCs to the tumor site is mediated by CCL2-CCR2 signaling. Similarly, MDSC recruitment to tumor tissues via CCL2-CCR2 signaling has been found in hepatocellular carcinoma (HCC) (Huang et al., 2007; Lesokhin et al., 2012). In a mouse model of intraosseous prostate cancer, CCL2 signaling was blocked using neutralizing anti-CCL2 antibodies alone or in combination with the chemotherapeutic drug docetaxel; the results indicated that CCL2 blockade inhibits prostate cancer development and the effect is more profound when combined with docetaxel (Kirk et al., 2013). Thus, the critical role of CCL2-CCR2 signaling in MDSC recruitment and tumor progression makes it a promising target for anticancer therapy.

CCR5 is a cell membrane protein whose ligands include CCL3, CCL4, and CCL5. In a melanoma mouse model and patients with melanoma, the $CCR5^+$ MDSCs accumulated in tumor tissues were positively correlated with the upregulation of CCL3, CCL4, and CCL5. These $CCR5^+$ MDSCs exhibited stronger suppressive activity during the progression of tumors (Blattner et al., 2018). Similarly, in TRAMP-C1 prostate tumors, CCR5 ligands induced the expansion of MDSCs in the bone marrow, and CCR5 drove the migration of MDSCs from the bone marrow into the blood and finally their recruitment at the tumor site (Hawila et al., 2017). CCR5 blockade decreased the percentage of MDSCs and inhibited melanoma proliferation, mainly through upregulating suppressor of cytokine signaling 3 (SOCS3) expression, which in turn inhibited the IL-STAT3 pathway (Hawila et al., 2017). In addition, chemokine receptors are more effective targets than chemokines, and targeting chemokine receptors is a promising therapeutic means because multiple chemokines generally correspond to a single chemokine receptor, such as CCL2/CCL12-CCR2, CCL3/4/5-CCR5, and CXCL5/CXCL2/CXCL1-CXCR2 (Bronte et al., 2016).

CXCR2 was cloned from a human neutrophil cell line in 1991, and it is also known as interleukin-8 receptor B (IL8RB) because of its ability to bind non-specifically to IL-8 (Murphy and Tiffany, 1991). The CXCR2 expressed by MDSCs has three chemokine ligands in the TME, including CXCL5, CXCL2, and CXCL1. In bladder cancer, tumor cells secreted CXCL2-stimulating nuclear factor kappa B (NF-κB) pathways in MDSCs to induce MDSC accumulation in the TME via CXCL2-CXCR2 signaling (Zhang et al., 2017). A study by Wang et al. (2017) on liver metastasis of colorectal cancer in mice has suggested that CXCL1-CXCR2 promotes tumor liver metastasis. Mechanistically, colorectal cancer cells stimulate TAMs to produce CXCL1 by secreting VEGFA, and CXCL1 recruits $CXCR2^+$ MDSCs from the blood into the pre-metastatic liver. In a prostate adenocarcinoma model, heterotypic CXCL5-CXCR2 signaling upregulated and activated YAP1, consequently recruiting MDSCs into tumor

tissues. Further study found that blocking CCR2 inhibits tumor development (Wang et al., 2016).

Major Signaling Pathways Associated With MDSC Expansion and Activation in TME

The expansion and activation of MDSCs in the TME involve multiple signaling pathways, among which AMP-activated protein kinase (AMPK) is a potential regulator of MDSC functions. AMPK is mainly responsible for regulating energy metabolism as well as immune system regulation, and its expression is downregulated during the progression of tumor development (Pineda et al., 2015). AMPK activation regulates downstream immune signaling pathways, thereby affecting the function of immune cells. A study by Trikha et al. (2016) found that the use of AMPK activators was able to reduce the levels of MDSCs in the spleen and tumors. In addition, studies have shown that AMPK activation inhibits its downstream signaling pathways NF-κB and STAT signaling pathways, while NF-κB and STAT signal pathways are essential for the expansion and activation of MDSCs in the TME (Salminen et al., 2011; Rutherford et al., 2016).

The expansion and activation of MDSCs in the TME are mainly induced by cytokines secreted by tumor cells or activated immune cells, such as VEGF, GM-CSF, M-CSF, G-CSF, IL-1β, IL-4, IL-6, and IFN-γ. STAT1, -3, -5, and -6 play a distinct role in the MDSC immunosuppression induced by the above cytokines. STATs belong to a family of transcription factors with dual functions of signal transduction and transcription. Upon stimulation with M-CSF, IL-6, GM-CSF, and VEGF by tumor cells, STAT signaling regulates Tregs, TAMs, and MDSCs, consequently exerting a tumor-promoting effect (Ko and Kim, 2016).

Signal transducer and the activator of transcription 3 is implicated as a major driver promoting MDSC expansion, and multiple cytokines in the TME all promote MDSC proliferation and survival by activating STAT3 (Gabrilovich et al., 2012). Colony-stimulating factors are essential in the regulation of myeloid cell differentiation. STAT3 was described to improve the expansion of intratumoral MDSCs in conjunction with other factors, such as GM-CSF, M-CSF, and G-CSF. In addition, the G-CSF secreted by tumor cells induced MDSC recruitment and decreased their generation number by using STAT3 inhibitor. Further study by Yu et al. (2015) found that SOCS3 attenuated the effect of G-CSF on MDSC recruitment by blocking the induction of STAT3 activation. In another study, GM-CSF and G-CSF activated STAT3 to induce the downregulation of IFN-related factor-8 (IRF-8). As a transcription factor, IRF-8 not only induces monocyte and DC development but also restricts granulocyte development. Thus, inhibition of IRF-8 is associated with a block in MDSC differentiation and an increased number of MDSC (Waight et al., 2013). Furthermore, tumor releases GM-CSF and IL-6 promotes the conversion of myeloid cells to an MDSC phenotype, mainly through the activation of a CCAA T-enhancer-binding protein β(C/EBP β)-mediated program that implicates the downstream blockade of STAT3 for terminal differentiation (Marigo et al., 2010; Zhang et al., 2010). A high secretion level of GM-CSF, which is present in a range of tumor entities, such as pancreatic cancer, has been demonstrated to stimulate the accumulation of MDSCs in the TME. Blocking GM-CSF by using neutralizing antibodies or antagonists in in-vitro tumor models also inhibited the expansion of MDSCs and their suppressive activity on T cells (Gargett et al., 2016). Interestingly, pre-clinical and clinical evidence suggested that the role of GM-CSF on MDSCs is related to its concentration level. *In vitro*, the time to generate MDSCs from mouse bone marrow cells cultivated in GM-CSF was inversely correlated with GM-CSF concentration (Lutz et al., 2000). All of the above emphasized that the GM-CSF from the TME promoted the expansion of MDSCs. The VEGF in the TME not only promotes tumor angiogenesis but also induces the activation of MDSCs. As early as Gabrilovich et al. (1996) have shown that VEGF secreted by different cancer cells could affect the functional maturation of myeloid progenitor cells, especially inhibiting the maturation of DCs. In a recent study, a murine ovarian tumor cell line overexpressing VEGF stimulated the expansion of MDSCs in the TME while reducing the number of effector T cells (Horikawa et al., 2017). A further study has suggested that VEGF induced MDSC expansion through VEGFR-2/STAT 3 signaling, and the activation of STAT3 induced VEGF expression, which in turn formed a positive feedback loop (Bartoli et al., 2003; Zhao et al., 2015). IL-6 has also been reported to be one of the important cytokines that mediate MDSC expansion via STAT3. In mice, the overexpression of peroxisome proliferator-activated receptor γ (PPARγ), which is defined as an anti-inflammatory molecule, could upregulate the IL-6 level to activate STAT3 and expand MDSCs. Further study has demonstrated that in a mouse model of breast cancer, MDSCs secreted IL-6 at the tumor site, thus inducing PSTAT3 expression by tumor cells and promoting tumor progression and metastatic potential (Oh et al., 2013). In addition, STAT3 upregulates the expression of S100A8/9, which is considered as a pro-inflammatory protein, and leads to the inhibition of DC differentiation, consequently leading to MDSC expansion. NOX2 expression is required for S100A8/A9 upregulation mediated by STAT3, while NOX2 activation also inhibits the immune response of T cells (Cheng et al., 2008; Zheng et al., 2015).

Signal transducer and the activator of transcription 6 is a downstream transcription factor for IL-4R and IL-13R, while IL-4 and IL-13 bind to IL-4R α kinase subunit and induce the activation of MDSCs (Gallina et al., 2006). Another study proved that STAT6 activation associated with IL4-Rα induces TGF-β secretion and ARG-1 expression to mediate immunosuppression (Gabrilovich and Nagaraj, 2009). Furthermore, in the $STAT6^{-/-}$ mouse model, the MDSCs in the body exhibited diminished suppressive activity due to reduced ARG-1 expression (Munera et al., 2010).

Previous studies demonstrated that blocking the secretion of IFN-γ from T cells eliminated MDSC immunosuppression by blocking the upregulation of iNOS (Gallina et al., 2006). A further study found that MDSC activation by IFN-γ is dependent on STAT1 signaling. Mechanistically, IFN-γ activated the transcription of IRF1 by inducing STAT1 phosphorylation,

consequently inducing the upregulation of PD-L1 expression on MDSCs (Lu et al., 2016).

Besides STAT-related signaling pathways, the NF-κB pathway is a remarkable factor in stimulating the activation of MDSCs, and the cytokines associated with it include TNF-α and IL-1 β. TNF-α is an inflammatory cytokine enriched in the TME, and it is related to the accumulation and suppressive activity of MDSCs. Transmembrane TNF-α (Tm-TNF-α) is the main ligand of TNFR2, and the binding between Tm-TNF-α and TNFR2 activates MDSC immunosuppression, as evidenced by upregulating ARG-1 and iNOS to promote the secretion of NO. Further study proved that the induction of MDSC immunosuppression by Tm-TNF-α was dependent on the activation of the NF-κB signaling pathway by IκBα degradation and the translocation of NF-κB p65 (Hu et al., 2014). Another study has analogously demonstrated that TNFR-2 activated NF-κB signaling, which in turn promoted MDSC survival by upregulating cellular FLICE inhibitory protein (c-FLIP) and inhibiting caspase-8 activity (Zhao X. et al., 2012). Considering IL-1 is a key downstream mediator of inflammation, it plays a leading role in the progression of tumor development. An early study has shown that the transfection of murine 4T1 breast cancer cells with the proinflammatory cytokine IL-1 β created a chronic inflammatory microenvironment at the tumor site, resulting in elevated levels of MDSCs and shortened survival of mice (Bunt et al., 2006). Similarly, Tu et al. (2008) have shown that IL-1 β was associated with gastric cancer development and mainly activated MDSCs *in vitro* and *in vivo* through the IL-1RI/NF-κB pathway, thereby inducing immunosuppression and promoting tumor development.

Toll-like receptors (TLRs) are recognized as critical factors involved in tumor pathogenesis, with a high probability of activating various signaling pathways during cancer progression. The TLR family induces NF-κB activation mainly dependent MyD88, which in turn activates immunosuppression in MDSCs. MDSCs lacking MyD88 lost their immunosuppression and even gained immunostimulatory activity in the TME (Hong et al., 2013). HMGB1 is a highly conserved nuclear protein that is released by some necrotic cells as an inflammatory mediator in the TME, and is it also a factor contributing to MDSC immunosuppression. Parker et al. (2014) have shown that HMGB1 in the TME regulated the MDSC level and immunosuppression by activating the NF-κB pathway. HMGB1 also promoted the differentiation of MDSCs by contributing to its inhibition of $CD4^+$ and $CD8^+$ T-cell activation.

Effect and Mechanism of TEX on MDSCs

Tumor-derived exosomes are exosomes secreted by tumor cells, and they have attracted much attention in recent years. Exosomes are a sort of EVs that could be secreted from many different cells, such as erythrocytes, lymphocytes, and tumor cells (Whiteside, 2016). Exosomes contain nucleic acids, proteins, and lipids, and different content loadings into exosomes rely on different sorting mechanisms. As a kind of important vesicles in human body, exosomes can be associated with almost any disease. Since 2013, exosomes have gradually become a research hotspot of disease markers, disease mechanisms, and drug development. Multiple favorable conditions exist in the TME and promote TEX formation and release, including extracellular acidity, hypoxia, and genotoxic stress. TEXs have been reported to regulate the expansion and immunosuppression function of MDSCs in different tumors. For example, TEXs released by melanoma cells inhibit the ability of normal monocytes to differentiate into DCs, consequently supporting the accumulation of MDSC in the TME (Filipazzi et al., 2012). Therefore, investigating the mechanism of TEXs on MDSCs may provide a new direction to target MDSCs and control tumor development.

Prostaglandin E2 (PGE2) and TGF-β conveyed by TEXs are necessary for the amplification and activation of MDSC in tumors. This class of TEXs induces MDSC accumulation, which promotes tumor progression. Meanwhile, further study has found that blocking PGE2 and TGF-β inhibited the induction of the effect of these exosomes on MDSCs and then attenuate the tumor immune escape mediated by MDSCs (Xiang et al., 2009). Chalmin et al. (2010) found that TEXs promoted MDSC immunosuppression rather than their expansion by STAT3 activation, which was triggered by TEXs membrane-associated heat shock protein 72 in a TLR2/MyD88 dependent manner. This study also found that dimethyl amiloride promoted the antitumor effect of the chemotherapeutic drug cyclophosphamide by blocking the immunosuppression of MDSCs through depletion of TEXs in a mouse model. Dimethyl amiloride was proved to inhibit exosome release by several studies (Panigrahi et al., 2018; Liu et al., 2020; Peak et al., 2020). As an inhibitor of H^+/Na^+ and Na^+/Ca^{2+} channels, dimethyl amiloride was considered to prevent the establishment of the calcium gradient necessary for exosome release (Savina et al., 2003; Peak et al., 2020). Therefore, dimethyl amiloride is expected to be a modulator of MDSCs. Besides, recently exosomal miRNAs effects on MDSC expansion and immunosuppression have been focused, which will be discussed in detail in the next sections.

MiRNAs With Regulatory Effects on MDSCs

MiRNAs are a kind of endogenous non-coding small molecular RNAs that play a crucial role in the biological processes of cells, and the abnormality of their expression is a characteristic shared by many tumors (Peng and Croce, 2016). Recent studies have revealed that miRNA regulated the differentiation and expansion of MDSCs through different signaling pathways. MiR-155 and miR-21 are the two most highly expressed miRNAs in MDSC proliferation and differentiation. TGF-β promotes the expansion of MDSC by increasing miR-155 and miR-21 expression; meanwhile, miR-155 and miR-21 could exert synergistic effects on MDSC expansion, and the mechanism is STAT3 activation resulting from targeting SHIP-1 and PTEN (Li et al., 2014). The GM-CSF in the TME induces miR-200c expression, which in turn promotes the immunosuppressive effects of MDSCs. The induction of MDSCs by miR-200c is dependent on the activation of STAT3 and PI3K/Akt by targeting PTEN/friend of Gata 2 (FOG2) (Mei et al., 2015). In B lymphoma tumor-bearing mice, miR-30a promoted the expansion and immunosuppressive capacity of MDSCs through two pathways:

upregulated ARG-1 expression and downregulated SOCS3 to activate STAT3 signaling (Xu et al., 2017). The PEG2 from breast cancer cells improved miR-10a expression by activating PKA signaling, and miR-10a could stimulate the amplification and activation of MDSCs through the activation of AMPK signaling (Rong et al., 2016). MiR-494 induced by TGF-β 1 in the TME increases the activity of the Akt pathway by downregulating PTEN, that is, regulating the expansion of MDSCs in tumor tissue through PTEN/Akt (Liu et al., 2012). Interestingly, in addition to upregulation, downregulation of some miRNAs could promote the function of MDSCs. Tumor-related factors promote the immunosuppression of MDSCs *in vivo* by downregulating miR-17-5p and miR-20a expression, and MDSCs transfected with miR-17-5p or miR-20a have a decreased capacity to specifically inhibit $CD4^+$ and $CD8^+$ T cells (Zhang et al., 2011).

Additionally, miRNAs conveyed by TEXs have also been suggested to affect the cell biology of MDSCs. After analyzing the miRNA expression profiles in these TEXs from glioma, Guo et al. (2019) found that miR-10a and miR-21 played a major role on MDSCs immunosuppression by targeting RAR-related orphan receptor alpha (RORA) and phosphatase and tensin homolog (PTEN). Similarly, exosomal miR-29a and mir-92a were transferred by TEXs to MDSCs in a mouse glioma cell model, and their transfection promoted the expansion of MDSCs by targeting high-mobility group box transcription factor 1 (HBP1) and protein kinase cAMP-dependent type I regulatory subunit alpha (Prkar1a), respectively (Guo et al., 2019). An overexpression of miR-107 was also observed in gastric cancer cells, mainly accumulated in their discharged exosomes. By TEXs, miR-107was delivered into host cell MDSCs to inhibit DICER1 and PTEN gene expression, which in turn expanded MDSCs and elevated ARG-1 expression to promote tumor escape and development (Ren et al., 2019).

Expression and Function of LncRNAs in MDSCs

In addition to miRNAs, long non-coding (Lnc) RNAs are momentous cancer-related elements, and recent studies have shown that they were essential for the immunosuppressive function of MDSCs. A high expression of Hox antisense intergenic RNA (HOTAIR) was found in HCC, accompanied by differential expression of CCL2, and HOTAIR promoted the secretion of CCL2. Increased levels of MDSCs were also found in cell co-cultures *in vitro*, and HOTAIR was speculated to regulate CCL2 expression to induce the recruitment of MDSCs into the TME (Fujisaka et al., 2018). Tian et al. (2018) have found that the runt-related transcription factor-1 overlapping RNA (RUNXOR) was highly expressed in MDSCs isolated from tissues of patients with lung cancer. Further studies have shown that a decreased RUNXOR expression in MDSCs could lead to attenuation of their immunosuppression (Tian et al., 2018). Lnc-chop interacts with the inhibitory proteins of chop and C/EBP β to promote the activation of C/EBP β, and it promotes the immunosuppression of MDSCs in the TME by upregulating the level of ARG-1 and increasing NOX2 and COX2 expression (Gao et al., 2018). Pvt1 is an intergenic LncRNA with a high expression in multiple types of human cancers. The knockdown of LncRNA pvt1 inhibits the immunosuppression of PMN-MDSCs by decreasing ROS and ARG-1 activity *in vitro*. Further studies have found that hypoxic conditions and HIF-1α expression increased the production of Pvt1 in PMN MDSCs *in vitro* (Zheng et al., 2019). Interestingly, in addition to upregulation, downregulation of LncRNA promotes the immunosuppression of MDSCs. MALAT1 LncRNA is considered to play a significant role in tumor initiation and progression. Zhou et al. (2018) have found decreased MALAT1 expression levels in patients with lung cancer compared with healthy individuals, but MDSCs expanded and accompanied by ARG-1 level increased, demonstrating that MALAT1 negatively regulated MDSCs.

ER Stress

The ER maintains homeostasis under normal physiological conditions by handling the folding of the secretory or transmembrane proteins. The unfavorable circumstances such as hypoxia, oxidative stress, and increased extracellular acidity, in the TME could impair the normal function of the ER and disrupt the loading and distribution of newly synthesized proteins, consequently inducing ER stress. A recent study has shown that ER stress induced apoptosis in MDSCs by upregulating TRAIL-R. This stress response promoted the further expansion of MDSCs, although it shortened their lifespan (Condamine et al., 2014). Thapsigargin, a class of highly oxidized sesquiterpene lactones isolated from the Mediterranean plant *Thapsia garganica*, has been recognized as an ER stressor because of its irreversible inhibition of the sarcoplasmic/ER Ca^{2+}-ATPase pump which pump Ca^{2+} ions from the cytoplasm into ER (Jaskulska et al., 2020). Thapsigargin inhibited Ca^{2+} transport from the cytosol to ER, declining Ca^{2+} concentration in the ER to lead ER dysfunction and eventually trigger ER stress. Lee et al. (2014) have demonstrated that Thapsigargin induced persistent ER stress, which enhanced tumor-infiltrating MDSCs generation and their immunosuppression by upregulating ARG-1, iNOS, and NOX2. Further studies have found that blocking ER stress effect response by using 4-phenyl butyric acid alleviated the expansion of MDSCs in TME and tumor growth (Lee et al., 2014). Chop is a transcription factor that plays a momentous role in ER stress-induced MDSCs. Immunosuppression of tumor infiltrating chop-deficient MDSCs is attenuated, which not only failed to suppress T cells but instead induced the antitumor function of T cells. The decreased immunosuppressive function of chop-deficient MDSCs was mainly mediated by pSTAT3 downregulation, reduced IL-6 secretion, and inhibition of the C/EBP β signaling pathway (Thevenot et al., 2014). Unfolded protein response (UPR) is an adaptive response of cancer cells and tumor associated myeloid cells to cope with ER stress, restoring ER proteostasis. Recently, the regulation of UPR on MDSCs has also been paid attention by researchers. Mohamed et al. (2020) showed that tumor infiltrating MDSCs elevated pancreatic ER kinase-like ER kinase (PERK) activity, while PERK deletion converted MDSCs into cells activating $CD8^+$ T cell

antitumor immunity. This study suggests that relieving the UPR may reprogram the MDSCs function in TME.

Driving Effects of Energy Metabolism on MDSCs

In recent years, with the advancement of research in the field of immunometabolism, metabolic regulation has become a hot spot in the field of immunotherapy. The level of metabolism is tightly bound to the state of cells. Previous reports have indicated that different energy metabolism pathways could produce an effect on the differentiation and biological characteristics of MDSCs in the TME. Glucose and fatty acid (FA) metabolism play a crucial role in MDSC differentiation and its suppressive effects, underscoring the potential of MDSCs as targets for immune-metabolic regulation.

Cancer cells undergo metabolic reprogramming to adapt to the TME and provide energy for their rapid proliferation. Tumor cells still tend to produce energy in the glycolysis pathway under aerobic conditions, and approximately 95% of ATP is obtained through this pathway. This phenomenon is called aerobic glycolysis (also known as the Warburg effect), which penetrates the TME and produces an effect on immune cells (Sica and Strauss, 2017). The Warburg effect is present in MDSCs during their maturation, mainly related to a high rate of glucose and glutamine uptake (Goffaux et al., 2017). Cancer cell glycolysis preferentially converts accumulated pyruvate to lactate, which could induce HIF-1α and promote MDSC generation (Chiarugi et al., 2012). Husain et al. (2013) have demonstrated that this process was supported by lactate dehydrogenase isoform A, silencing of which reduced the levels of MDSCs in a pancreatic cancer mouse model. Moreover, as a part of overall metabolism, mTOR-mediated induction of HIF-1α is necessary for glycolysis activation (Liu et al., 2014). In addition to glycolysis, lipid metabolism pathways provide energy for ATP production. Tumor-infiltrating MDSCs have been found in different murine tumor models to have increased FA uptake and activation and activated FAO, and employing FAO inhibitors could block immunosuppressive pathways and functions in MDSCs. Therefore, targeting FAO may become an effective strategy to restrict MDSCs (Hossain et al., 2015).

MDSCs as a Therapeutic Target for Tumor Treatment

As discussed above, MDSCs are on the higher levels in various cancers compared with normal controls, such as colorectal cancer, pancreatic cancer, and so on (Markowitz et al., 2015; Limagne et al., 2016; Goldmann et al., 2017; Cha and Koo, 2020). MDSCs have been considered one of the major obstacles in cancer treatment because of their immunosuppression and non-immunologic functions. Therapeutic approaches targeting MDSCs are thriving and mainly include eliminating MDSCs, promoting MDSCs differentiation to a mature myeloid cell phenotype, attenuating the immunosuppressive function of MDSCs, as well as blocking MDSC recruitment to tumor sites (**Figure 2**).

Elimination of MDSCs is the most straightforward strategy for targeting MDSCs therapy. Earlier studies have shown that both gemcitabine and 5-fluorouracil specifically reduce MDSCs (Strauss et al., 2007; Vincent et al., 2010). However, a recent clinical study in pancreatic patients found that though gemcitabine in combination with omega 3 significantly reduced MDSC levels in patients, gemcitabine alone was not effective (Hou et al., 2020). Liver X receptor (LXR) induced MDSC apoptosis by activating the LXR/apolipoprotein E (APOE) axis (Tavazoie et al., 2018). Liang and Shen (2020) proved that LXR agonists GW3965 and RGX-104 enhanced antitumor immune responses and improved radiosensitive effects of non-small cell lung cancer (NSCLC) by reducing the level of tumor-infiltrating MDSCs induced by radiotherapy. CD33 is highly expressed on MDSCs in humans, Fultang et al. (2019) found that the combination of the anti-CD33 monoclonal antibody gemtuzumab and the immunotoxin ozogamicin nicely eliminated $CD33^+$ MDSC, providing a novel strategy in targeting MDSCs treatment.

Additionally, promoting the differentiation of MDSCs into mature myeloid cells is another effective targeting MDSCs therapy. All-trans retinoic acid (ATRA) produced via vitamin A metabolism was the first therapeutic compound used to target MDSCs. ATRA upregulated glutathione (GSH) expression, which suppressed ROS levels in MDSCs, thereby promoting their differentiation. In addition, ATRA decreased the expression of immunosuppressive genes mediated by MDSCs, including PD-L1, IL-10, and IDO, thereby downregulating their immunosuppressive effects (Tobin et al., 2018). Fleet et al. (2020) found that MDSCs in TME had higher vitamin D receptor levels, and active vitamin D3 may also promote the differentiation of MDSCs. In the mouse model of breast cancer, docetaxel administration polarized mouse spleen MDSCs to M1-like macrophages with anti-tumor activity (Kodumudi et al., 2010).

Reducing the immunosuppressive function of MDSCs can also reduce its tumor promoting effect. STAT3 signaling pathway is an indispensable loop in the tumor development promoted by MDSCs. Sunitinib, AG490, and Curcumin attenuated the immunosuppressive function of MDSCs mainly through negative regulation of STAT3 (Ko et al., 2010; Liu et al., 2018; Salminen et al., 2018). The IL-6 in the TME induces MDSCs to mediate tumor immune escape through different pathways. Liu et al. (2016) have demonstrated that curcumin downregulated the levels of IL-6 in tumor tissues to impair MDSC function, thus significantly inhibiting tumor growth in Lewis lung carcinoma tumor models.

Furthermore, there are studies focused on blocking MDSC migration to tumor sites. VEGF favors the accumulation of MDSCs into tumor tissue and contributes to tumor development by promoting tumor angiogenesis. Bevacizumab was used for anti-VEGF treatment in patients with NSCLC. Compared with that in the non-bevacizumab regimen, the level of PMN-MDSCs was significantly decreased (Koinis et al., 2016). CSF-1 recruits MDSCs with the ability to support tumor immune escape by binding to CSF-1R expressed by MDSCs, and studies demonstrated that selective inhibitors PLX3397 and GW2580 could block their signaling by targeting CSF-1R

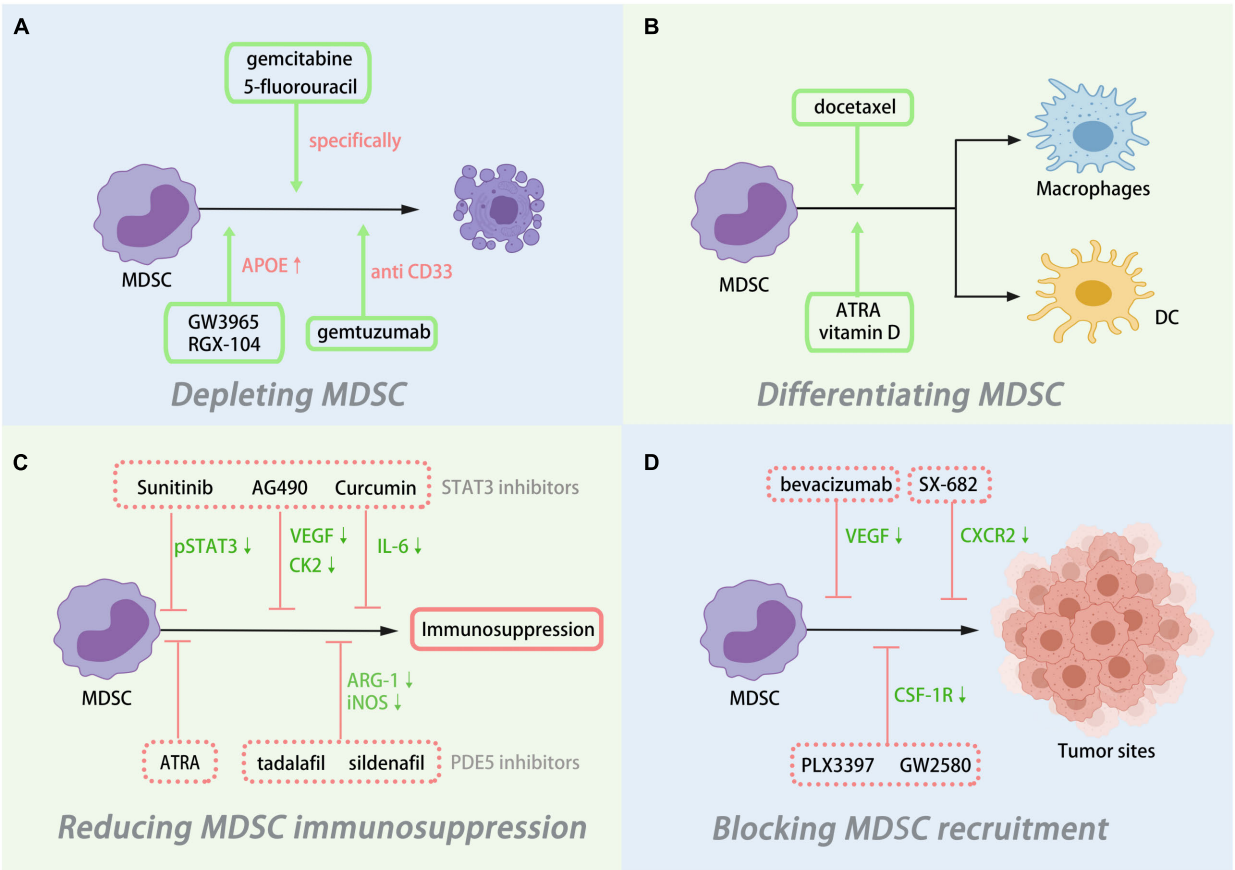

FIGURE 2 | Myeloid-derived suppressor cells (MDSCs) as therapeutic targets in tumor. MDSC modulation could be achieved by **(A)** depleting MDSC, **(B)** differentiating MDSC, **(C)** reducing MDSC immunosuppression, and **(D)** blocking MDSC recruitment.

(Priceman et al., 2010; Mok et al., 2014). Targeting the specific chemokine receptor CXCR2 on MDSCs also prevented MDSCs recruitment to tumor tissues, treatment with the CXCR2 inhibitor SX-682 reduced MDSCs migration to TME and improved the efficacy of anti-PD1 therapy (Highfill et al., 2014).

CONCLUSION

As research on MDSCs has progressed, the expansion and activation of MDSCs appear to be a universal feature in malignant tumors, highlighting the importance of understanding their biological functions in the TME. In this review, the facilitative roles of TME on MDSC recruitment expansion and immunosuppression were highlighted. The suppression of their pro-tumorigenic effects by changing the favorable conditions in the TME for MDSC development may provide a new direction for MDSC-targeted antitumor therapy. Given the multiple tumor-promoting effects of MDSCs, their targeting becomes an attractive option. But there are still many problems to be solved for the clinical application of MDSC-targeted therapy in cancer. MDSCs have multiple subpopulations and exhibit high heterogeneity in different tumors. Therefore, more in-depth studies are needed to find specific markers under different tumor contexts so as to understand MDSCs more accurately. Emerging bulk or single-cell genomics analyses are perhaps providing a direction for the identification of MDSCs, but more robust experimental validation is needed. Second, MDSCs have a short- lifespan in tissues, so it is difficult to alleviate the tumor by reversing the pathological activation of tissue MDSCs. Therefore, effective therapies could aim to block MDSCs differentiation in the bone marrow, inhibit their migration to the affected tissues, or by manipulating the tissue microenvironment. More importantly, the TME is so complex that multiple immune cells and cytokines derived from multiple pathways constitute a complex network. Treatments that targeting MDSCs alone are difficult to achieve perfect therapeutic outcomes. So, it is necessary to consider combining with other treatment schemes to achieve the best therapeutic effect. For instance, the combination of LXR agonists and radiotherapy has shown a positive therapeutic effect in NSCLC, which is a promising prospect (Liang and Shen, 2020). Future studies are required to further unravel the intricacies of MDSC tumor-promoting pathways and provide a more reliable basis for targeting MDSCs alone and in combination with immunotherapy regimens.

AUTHOR CONTRIBUTIONS

YL wrote the manuscript. YL, HH, RJ, and JZ participated in the manuscript content collation. HY and RZ contributed to revisions of the manuscript. All authors contributed to the article and approved the submitted version.

FUNDING

This work was supported by the Applied Basic Research Project of Sichuan Science Technology Department (2021YJ0256) and the innovative research project for graduate students of Southwest Minzu University in 2021(CX2021SZ88).

REFERENCES

Al-Khami, A. A., Zheng, L., Del Valle, L., Hossain, F., Wyczechowska, D., Zabaleta, J., et al. (2017). Exogenous lipid uptake induces metabolic and functional reprogramming of tumor-associated myeloid-derived suppressor cells. *Oncoimmunology* 6:e1344804. doi: 10.1080/2162402x.2017.1344804

Almand, B., Clark, J. I., Nikitina, E., van Beynen, J., English, N. R., Knight, S. C., et al. (2001). Increased production of immature myeloid cells in cancer patients: a mechanism of immunosuppression in cancer. *J. Immunol.* 166, 678–689. doi: 10.4049/jimmunol.166.1.678

Alshetaiwi, H., Pervolarakis, N., McIntyre, L. L., Ma, D., Nguyen, Q., Rath, J. A., et al. (2020). Defining the emergence of myeloid-derived suppressor cells in breast cancer using single-cell transcriptomics. *Sci. Immunol.* 5:eaay6017. doi: 10.1126/sciimmunol.aay6017

Bartoli, M., Platt, D., Lemtalsi, T., Gu, X., Brooks, S. E., Marrero, M. B., et al. (2003). VEGF differentially activates STAT3 in microvascular endothelial cells. *FASEB J.* 17, 1562–1564. doi: 10.1096/fj.02-1084fje

Behfar, S., Hassanshahi, G., Nazari, A., and Khorramdelazad, H. (2018). A brief look at the role of monocyte chemoattractant protein-1 (CCL2) in the pathophysiology of psoriasis. *Cytokine* 110, 226–231. doi: 10.1016/j.cyto.2017.12.010

Bergenfelz, C., Larsson, A. M., von Stedingk, K., Gruvberger-Saal, S., Aaltonen, K., Jansson, S., et al. (2015). Systemic Monocytic-MDSCs are generated from monocytes and correlate with disease progression in breast cancer patients. *PLoS One* 10:e0127028. doi: 10.1371/journal.pone.0127028

Betsch, A., Rutgeerts, O., Fevery, S., Sprangers, B., Verhoef, G., Dierickx, D., et al. (2018). Myeloid-derived suppressor cells in lymphoma: the good, the bad and the ugly. *Blood Rev.* 32, 490–498. doi: 10.1016/j.blre.2018.04.006

Blattner, C., Fleming, V., Weber, R., Himmelhan, B., Altevogt, P., Gebhardt, C., et al. (2018). CCR5(+) myeloid-derived suppressor cells are enriched and activated in melanoma lesions. *Cancer Res.* 78, 157–167. doi: 10.1158/0008-5472.Can-17-0348

Bronte, V., Brandau, S., Chen, S. H., Colombo, M. P., Frey, A. B., Greten, T. F., et al. (2016). Recommendations for myeloid-derived suppressor cell nomenclature and characterization standards. *Nat. Commun.* 7:12150. doi: 10.1038/ncomms12150

Bunt, S. K., Sinha, P., Clements, V. K., Leips, J., and Ostrand-Rosenberg, S. (2006). Inflammation induces myeloid-derived suppressor cells that facilitate tumor progression. *J. Immunol.* 176, 284–290. doi: 10.4049/jimmunol.176.1.284

Cha, Y. J., and Koo, J. S. (2020). Role of tumor-associated myeloid cells in breast cancer. *Cells* 9:1785. doi: 10.3390/cells9081785

Chalmin, F., Ladoire, S., Mignot, G., Vincent, J., Bruchard, M., Remy-Martin, J. P., et al. (2010). Membrane-associated Hsp72 from tumor-derived exosomes mediates STAT3-dependent immunosuppressive function of mouse and human myeloid-derived suppressor cells. *J. Clin. Invest.* 120, 457–471. doi: 10.1172/JCI40483

Chang, A. L., Miska, J., Wainwright, D. A., Dey, M., Rivetta, C. V., Yu, D., et al. (2016). CCL2 produced by the glioma microenvironment is essential for the recruitment of regulatory t cells and myeloid-derived suppressor cells. *Cancer Res.* 76, 5671–5682. doi: 10.1158/0008-5472.Can-16-0144

Chen, F., Zhuang, X., Lin, L., Yu, P., Wang, Y., Shi, Y., et al. (2015). New horizons in tumor microenvironment biology: challenges and opportunities. *BMC Med.* 13:45. doi: 10.1186/s12916-015-0278-7

Cheng, P., Corzo, C. A., Luetteke, N., Yu, B., Nagaraj, S., Bui, M. M., et al. (2008). Inhibition of dendritic cell differentiation and accumulation of myeloid-derived suppressor cells in cancer is regulated by S100A9 protein. *J. Exp. Med.* 205, 2235–2249. doi: 10.1084/jem.20080132

Chiarugi, A., Dölle, C., Felici, R., and Ziegler, M. (2012). The NAD metabolome–a key determinant of cancer cell biology. *Nat. Rev. Cancer* 12, 741–752. doi: 10.1038/nrc3340

Condamine, T., Dominguez, G. A., Youn, J. I., Kossenkov, A. V., Mony, S., Alicea-Torres, K., et al. (2016). Lectin-type oxidized LDL receptor-1 distinguishes population of human polymorphonuclear myeloid-derived suppressor cells in cancer patients. *Sci. Immunol.* 1:aaf8943. doi: 10.1126/sciimmunol.aaf8943

Condamine, T., Kumar, V., Ramachandran, I. R., Youn, J. I., Celis, E., Finnberg, N., et al. (2014). ER stress regulates myeloid-derived suppressor cell fate through TRAIL-R-mediated apoptosis. *J. Clin. Invest.* 124, 2626–2639. doi: 10.1172/jci74056

Condamine, T., Mastio, J., and Gabrilovich, D. I. (2015). Transcriptional regulation of myeloid-derived suppressor cells. *J. Leukoc. Biol.* 98, 913–922. doi: 10.1189/jlb.4RI0515-204R

Consonni, F. M., Porta, C., Marino, A., Pandolfo, C., Mola, S., Bleve, A., et al. (2019). Myeloid-derived suppressor cells: ductile targets in disease. *Front. Immunol.* 10:949. doi: 10.3389/fimmu.2019.00949

Corzo, C. A., Cotter, M. J., Cheng, P., Cheng, F., Kusmartsev, S., Sotomayor, E., et al. (2009). Mechanism regulating reactive oxygen species in tumor-induced myeloid-derived suppressor cells. *J. Immunol.* 182, 5693–5701. doi: 10.4049/jimmunol.0900092

Elliott, L. A., Doherty, G. A., Sheahan, K., and Ryan, E. J. (2017). Human tumor-infiltrating myeloid cells: phenotypic and functional diversity. *Front. Immunol.* 8:86. doi: 10.3389/fimmu.2017.00086

Fallarino, F., Grohmann, U., You, S., McGrath, B. C., Cavener, D. R., Vacca, C., et al. (2006). The combined effects of tryptophan starvation and tryptophan catabolites down-regulate T cell receptor zeta-chain and induce a regulatory phenotype in naive T cells. *J. Immunol.* 176, 6752–6761. doi: 10.4049/jimmunol.176.11.6752

Filipazzi, P., Bürdek, M., Villa, A., Rivoltini, L., and Huber, V. (2012). Recent advances on the role of *tumor exosomes* in immunosuppression and disease progression. *Semin. Cancer Biol.* 22, 342–349. doi: 10.1016/j.semcancer.2012.02.005

Fleet, J. C., Burcham, G. N., Calvert, R. D., Elzey, B. D., and Ratliff, T. L. (2020). 1α, 25 *Dihydroxyvitamin* D (1,25(OH)(2)D) inhibits the T cell suppressive function of myeloid derived suppressor cells (MDSC). *J. Steroid Biochem. Mol. Biol.* 198:105557. doi: 10.1016/j.jsbmb.2019.105557

Fleming, V., Hu, X., Weber, R., Nagibin, V., Groth, C., Altevogt, P., et al. (2018). Targeting myeloid-derived suppressor cells to bypass tumor-induced immunosuppression. *Front. Immunol.* 9:398. doi: 10.3389/fimmu.2018.00398

Fujisaka, Y., Iwata, T., Tamai, K., Nakamura, M., Mochizuki, M., Shibuya, R., et al. (2018). Long non-coding RNA HOTAIR up-regulates chemokine (C-C motif) ligand 2 and promotes proliferation of macrophages and myeloid-derived suppressor cells in hepatocellular carcinoma cell lines. *Oncol. Lett.* 15, 509–514. doi: 10.3892/ol.2017.7322

Fultang, L., Panetti, S., Ng, M., Collins, P., Graef, S., Rizkalla, N., et al. (2019). MDSC targeting with Gemtuzumab ozogamicin restores T cell immunity and immunotherapy against cancers. *EBioMedicine* 47, 235–246. doi: 10.1016/j.ebiom.2019.08.025

Fuse, H., Tomihara, K., Heshiki, W., Yamazaki, M., Akyu-Takei, R., Tachinami, H., et al. (2016). Enhanced expression of PD-L1 in oral squamous cell carcinoma-derived CD11b(+)Gr-1(+) cells and its contribution to immunosuppressive activity. *Oral Oncol.* 59, 20–29. doi: 10.1016/j.oraloncology.2016.05.012

Gabrilovich, D. I., Bronte, V., Chen, S. H., Colombo, M. P., Ochoa, A., Ostrand-Rosenberg, S., et al. (2007). The terminology issue for myeloid-derived suppressor cells. *Cancer Res.* 67:425. doi: 10.1158/0008-5472.Can-06-3037

Gabrilovich, D. I., Chen, H. L., Girgis, K. R., Cunningham, H. T., Meny, G. M., Nadaf, S., et al. (1996). Production of vascular endothelial growth factor by

human tumors inhibits the functional maturation of dendritic cells. *Nat. Med.* 2, 1096–1103. doi: 10.1038/nm1096-1096

Gabrilovich, D. I., and Nagaraj, S. (2009). Myeloid-derived suppressor cells as regulators of the immune system. *Nat. Rev. Immunol.* 9, 162–174. doi: 10.1038/nri2506

Gabrilovich, D. I., Ostrand-Rosenberg, S., and Bronte, V. (2012). Coordinated regulation of myeloid cells by tumours. *Nat. Rev. Immunol.* 12, 253–268. doi: 10.1038/nri3175

Gallina, G., Dolcetti, L., Serafini, P., De Santo, C., Marigo, I., Colombo, M. P., et al. (2006). Tumors induce a subset of inflammatory monocytes with immunosuppressive activity on CD8+ T cells. *J. Clin. Invest.* 116, 2777–2790. doi: 10.1172/jci28828

Gao, Y., Wang, T., Li, Y., Zhang, Y., and Yang, R. (2018). Lnc-chop promotes immunosuppressive function of myeloid-derived suppressor cells in tumor and inflammatory environments. *J. Immunol.* 200, 2603–2614. doi: 10.4049/jimmunol.1701721

Gargett, T., Christo, S. N., Hercus, T. R., Abbas, N., Singhal, N., Lopez, A. F., et al. (2016). GM-CSF signalling blockade and chemotherapeutic agents act in concert to inhibit the function of myeloid-derived suppressor cells in vitro. *Clin. Transl. Immunol.* 5:e119. doi: 10.1038/cti.2016.80

Goffaux, G., Hammami, I., and Jolicoeur, M. (2017). A dynamic metabolic flux analysis of myeloid-derived suppressor cells confirms immunosuppression-related metabolic plasticity. *Sci. Rep.* 7:9850. doi: 10.1038/s41598-017-10464-1

Goldmann, O., Beineke, A., and Medina, E. (2017). Identification of a novel subset of myeloid-derived suppressor cells during chronic staphylococcal infection that resembles immature *Eosinophils. J. Infect Dis.* 216, 1444–1451. doi: 10.1093/infdis/jix494

Guo, X., Qiu, W., Wang, J., Liu, Q., Qian, M., Wang, S., et al. (2019). Glioma exosomes mediate the expansion and function of myeloid-derived suppressor cells through microRNA-29a/Hbp1 and microRNA-92a/Prkar1a pathways. *Int. J. Cancer* 144, 3111–3126. doi: 10.1002/ijc.32052

Hanson, E. M., Clements, V. K., Sinha, P., Ilkovitch, D., and Ostrand-Rosenberg, S. (2009). Myeloid-derived suppressor cells down-regulate L-selectin expression on CD4+ and CD8+ T cells. *J. Immunol.* 183, 937–944. doi: 10.4049/jimmunol.0804253

Hawila, E., Razon, H., Wildbaum, G., Blattner, C., Sapir, Y., Shaked, Y., et al. (2017). CCR5 directs the mobilization of CD11b(+)Gr1(+)Ly6C(low) *Polymorphonuclear* myeloid cells from the bone marrow to the blood to support tumor development. *Cell Rep.* 21, 2212–2222. doi: 10.1016/j.celrep.2017.10.104

Heine, A., Held, S. A. E., Schulte-Schrepping, J., Wolff, J. F. A., Klee, K., Ulas, T., et al. (2017). Generation and functional characterization of MDSC-like cells. *Oncoimmunology* 6:e1295203. doi: 10.1080/2162402x.2017.1295203

Highfill, S. L., Cui, Y., Giles, A. J., Smith, J. P., Zhang, H., Morse, E., et al. (2014). Disruption of CXCR2-mediated MDSC tumor trafficking enhances anti-PD1 efficacy. *Sci. Transl. Med.* 6:237ra267. doi: 10.1126/scitranslmed.3007974

Hoechst, B., Gamrekelashvili, J., Manns, M. P., Greten, T. F., and Korangy, F. (2011). Plasticity of human Th17 cells and iTregs is orchestrated by different subsets of myeloid cells. *Blood* 117, 6532–6541. doi: 10.1182/blood-2010-11-317321

Hong, E. H., Chang, S. Y., Lee, B. R., Kim, Y. S., Lee, J. M., Kang, C. Y., et al. (2013). Blockade of Myd88 signaling induces antitumor effects by skewing the immunosuppressive function of myeloid-derived suppressor cells. *Int. J. Cancer* 132, 2839–2848. doi: 10.1002/ijc.27974

Horikawa, N., Abiko, K., Matsumura, N., Hamanishi, J., Baba, T., Yamaguchi, K., et al. (2017). Expression of vascular endothelial growth factor in ovarian cancer inhibits tumor immunity through the accumulation of myeloid-derived suppressor cells. *Clin. Cancer Res.* 23, 587–599. doi: 10.1158/1078-0432.Ccr-16-0387

Hossain, F., Al-Khami, A. A., Wyczechowska, D., Hernandez, C., Zheng, L., Reiss, K., et al. (2015). Inhibition of fatty acid oxidation modulates immunosuppressive functions of myeloid-derived suppressor cells and enhances cancer therapies. *Cancer Immunol. Res.* 3, 1236–1247. doi: 10.1158/2326-6066.Cir-15-0036

Hou, A., Hou, K., Huang, Q., Lei, Y., and Chen, W. (2020). Targeting myeloid-derived suppressor cell, a promising strategy to overcome resistance to immune checkpoint inhibitors. *Front. Immunol.* 11:783. doi: 10.3389/fimmu.2020.00783

Hsu, Y. L., Yen, M. C., Chang, W. A., Tsai, P. H., Pan, Y. C., Liao, S. H., et al. (2019). CXCL17-derived CD11b(+)Gr-1(+) myeloid-derived suppressor cells contribute to lung metastasis of breast cancer through platelet-derived growth factor-BB. *Breast Cancer Res.* 21:23. doi: 10.1186/s13058-019-1114-3

Hu, X., Li, B., Li, X., Zhao, X., Wan, L., Lin, G., et al. (2014). Transmembrane TNF-α promotes suppressive activities of myeloid-derived suppressor cells via TNFR2. *J .Immunol.* 192, 1320–1331. doi: 10.4049/jimmunol.1203195

Huang, B., Lei, Z., Zhao, J., Gong, W., Liu, J., Chen, Z., et al. (2007). CCL2/CCR2 pathway mediates recruitment of myeloid suppressor cells to cancers. *Cancer Lett.* 252, 86–92. doi: 10.1016/j.canlet.2006.12.012

Huang, B., Pan, P. Y., Li, Q., Sato, A. I., Levy, D. E., Bromberg, J., et al. (2006). Gr-1+CD115+ immature myeloid suppressor cells mediate the development of tumor-induced T regulatory cells and T-cell anergy in tumor-bearing host. *Cancer Res.* 66, 1123–1131. doi: 10.1158/0008-5472.Can-05-1299

Husain, Z., Huang, Y., Seth, P., and Sukhatme, V. P. (2013). Tumor-derived lactate modifies antitumor immune response: effect on myeloid-derived suppressor cells and NK cells. *J. Immunol.* 191, 1486–1495. doi: 10.4049/jimmunol.1202702

Jaskulska, A., Janecka, A. E., and Gach-Janczak, K. (2020). Thapsigargin-from traditional medicine to anticancer drug. *Int. J. Mol. Sci.* 22:4. doi: 10.3390/ijms22010004

Kaplan, R. N., Riba, R. D., Zacharoulis, S., Bramley, A. H., Vincent, L., Costa, C., et al. (2005). VEGFR1-positive haematopoietic bone marrow progenitors initiate the pre-metastatic niche. *Nature* 438, 820–827. doi: 10.1038/nature04186

Kirk, P. S., Koreckij, T., Nguyen, H. M., Brown, L. G., Snyder, L. A., Vessella, R. L., et al. (2013). Inhibition of CCL2 signaling in combination with docetaxel treatment has profound inhibitory effects on prostate cancer growth in bone. *Int. J. Mol. Sci.* 14, 10483–10496. doi: 10.3390/ijms140510483

Ko, H. J., and Kim, Y. J. (2016). Signal transducer and activator of transcription proteins: regulators of myeloid-derived suppressor cell-mediated immunosuppression in cancer. *Arch. Pharm. Res.* 39, 1597–1608. doi: 10.1007/s12272-016-0822-9

Ko, J. S., Rayman, P., Ireland, J., Swaidani, S., Li, G., Bunting, K. D., et al. (2010). Direct and differential suppression of myeloid-derived suppressor cell subsets by sunitinib is compartmentally constrained. *Cancer Res.* 70, 3526–3536. doi: 10.1158/0008-5472.Can-09-3278

Kodumudi, K. N., Woan, K., Gilvary, D. L., Sahakian, E., Wei, S., and Djeu, J. Y. (2010). A novel *chemoimmunomodulating* property of docetaxel: suppression of myeloid-derived suppressor cells in tumor bearers. *Clin. Cancer Res.* 16, 4583–4594. doi: 10.1158/1078-0432.Ccr-10-0733

Koinis, F., Vetsika, E. K., Aggouraki, D., Skalidaki, E., Koutoulaki, A., Gkioulmpasani, M., et al. (2016). Effect of first-line treatment on myeloid-derived suppressor cells' subpopulations in the peripheral blood of patients with non-small cell lung cancer. *J. Thorac. Oncol.* 11, 1263–1272. doi: 10.1016/j.jtho.2016.04.026

Kruger, A. (2015). Premetastatic niche formation in the liver: emerging mechanisms and mouse models. *J. Mol. Med. (Berl)* 93, 1193–1201. doi: 10.1007/s00109-015-1342-7

Kujawski, M., Kortylewski, M., Lee, H., Herrmann, A., Kay, H., and Yu, H. (2008). Stat3 mediates myeloid cell-dependent tumor angiogenesis in mice. *J. Clin. Invest.* 118, 3367–3377. doi: 10.1172/jci35213

Kusmartsev, S., Eruslanov, E., Kübler, H., Tseng, T., Sakai, Y., Su, Z., et al. (2008). Oxidative stress regulates expression of VEGFR1 in myeloid cells: link to tumor-induced immune suppression in renal cell carcinoma. *J. Immunol.* 181, 346–353. doi: 10.4049/jimmunol.181.1.346

Lee, B. R., Chang, S. Y., Hong, E. H., Kwon, B. E., Kim, H. M., Kim, Y. J., et al. (2014). Elevated endoplasmic reticulum stress reinforced immunosuppression in the tumor microenvironment via myeloid-derived suppressor cells. *Oncotarget* 5, 12331–12345. doi: 10.18632/oncotarget.2589

Lesokhin, A. M., Hohl, T. M., Kitano, S., Cortez, C., Hirschhorn-Cymerman, D., Avogadri, F., et al. (2012). Monocytic CCR2(+) myeloid-derived suppressor cells promote immune escape by limiting activated CD8 T-cell infiltration into the tumor microenvironment. *Cancer Res.* 72, 876–886. doi: 10.1158/0008-5472.Can-11-1792

Li, B. H., Garstka, M. A., and Li, Z. F. (2020). Chemokines and their receptors promoting the recruitment of myeloid-derived suppressor cells into the tumor. *Mol. Immunol.* 117, 201–215. doi: 10.1016/j.molimm.2019.11.014

Li, L., Wang, L., Li, J., Fan, Z., Yang, L., Zhang, Z., et al. (2018). Metformin-induced reduction of CD39 and CD73 blocks myeloid-derived suppressor cell activity in patients with ovarian cancer. *Cancer Res.* 78, 1779–1791. doi: 10.1158/0008-5472.Can-17-2460

Li, L., Zhang, J., Diao, W., Wang, D., Wei, Y., Zhang, C. Y., et al. (2014). MicroRNA-155 and MicroRNA-21 promote the expansion of functional myeloid-derived suppressor cells. *J. Immunol.* 192, 1034–1043. doi: 10.4049/jimmunol.1301309

Li, S., Xu, H. X., Wu, C. T., Wang, W. Q., Jin, W., Gao, H. L., et al. (2019). Angiogenesis in pancreatic cancer: current research status and clinical implications. *Angiogenesis* 22, 15–36. doi: 10.1007/s10456-018-9645-2

Liang, H., and Shen, X. (2020). LXR activation *radiosensitizes* non-small cell lung cancer by restricting myeloid-derived suppressor cells. *Biochem. Biophys. Res. Commun.* 528, 330–335. doi: 10.1016/j.bbrc.2020.04.137

Limagne, E., Euvrard, R., Thibaudin, M., Rébé, C., Derangère, V., Chevriaux, A., et al. (2016). Accumulation of MDSC and Th17 cells in patients with metastatic colorectal cancer predicts the efficacy of a FOLFOX-Bevacizumab Drug Treatment Regimen. *Cancer Res.* 76, 5241–5252. doi: 10.1158/0008-5472.Can-15-3164

Lin, A., Liang, F., Thompson, E. A., Vono, M., Ols, S., Lindgren, G., et al. (2018). Rhesus macaque myeloid-derived suppressor cells demonstrate T Cell inhibitory functions and are transiently increased after vaccination. *J. Immunol.* 200, 286–294. doi: 10.4049/jimmunol.1701005

Liu, D., You, M., Xu, Y., Li, F., Zhang, D., Li, X., et al. (2016). Inhibition of curcumin on myeloid-derived suppressor cells is requisite for controlling lung cancer. *Int. Immunopharmacol.* 39, 265–272. doi: 10.1016/j.intimp.2016.07.035

Liu, G., Bi, Y., Shen, B., Yang, H., Zhang, Y., Wang, X., et al. (2014). SIRT1 limits the function and fate of myeloid-derived suppressor cells in tumors by orchestrating HIF-1α-dependent glycolysis. *Cancer Res.* 74, 727–737. doi: 10.1158/0008-5472.Can-13-2584

Liu, J. F., Deng, W. W., Chen, L., Li, Y. C., Wu, L., Ma, S. R., et al. (2018). Inhibition of JAK2/STAT3 reduces tumor-induced angiogenesis and myeloid-derived suppressor cells in head and neck cancer. *Mol. Carcinog.* 57, 429–439. doi: 10.1002/mc.22767

Liu, X., Miao, J., Wang, C., Zhou, S., Chen, S., Ren, Q., et al. (2020). Tubule-derived exosomes play a central role in fibroblast activation and kidney fibrosis. *Kidney Int.* 97, 1181–1195. doi: 10.1016/j.kint.2019.11.026

Liu, Y., Lai, L., Chen, Q., Song, Y., Xu, S., Ma, F., et al. (2012). MicroRNA-494 is required for the accumulation and functions of tumor-expanded myeloid-derived suppressor cells via targeting of PTEN. *J. Immunol.* 188, 5500–5510. doi: 10.4049/jimmunol.1103505

Lu, C., Redd, P. S., Lee, J. R., Savage, N., and Liu, K. (2016). The expression profiles and regulation of PD-L1 in tumor-induced myeloid-derived suppressor cells. *Oncoimmunology* 5:e1247135. doi: 10.1080/2162402x.2016.1247135

Lutz, M. B., Suri, R. M., Niimi, M., Ogilvie, A. L., Kukutsch, N. A., Rössner, S., et al. (2000). Immature dendritic cells generated with low doses of GM-CSF in the absence of IL-4 are maturation resistant and prolong allograft survival in vivo. *Eur. J. Immunol.* 30, 1813–1822.

Marigo, I., Bosio, E., Solito, S., Mesa, C., Fernandez, A., Dolcetti, L., et al. (2010). Tumor-induced tolerance and immune suppression depend on the C/EBPbeta transcription factor. *Immunity* 32, 790–802. doi: 10.1016/j.immuni.2010.05.010

Markowitz, J., Brooks, T. R., Duggan, M. C., Paul, B. K., Pan, X., Wei, L., et al. (2015). Patients with pancreatic adenocarcinoma exhibit elevated levels of myeloid-derived suppressor cells upon progression of disease. *Cancer Immunol. Immunother.* 64, 149–159. doi: 10.1007/s00262-014-1618-8

Mei, S., Xin, J., Liu, Y., Zhang, Y., Liang, X., Su, X., et al. (2015). MicroRNA-200c promotes suppressive potential of myeloid-derived suppressor cells by modulating PTEN and FOG2 expression. *PLoS One* 10:e0135867. doi: 10.1371/journal.pone.0135867

Mohamed, E., Sierra, R. A., Trillo-Tinoco, J., Cao, Y., Innamarato, P., Payne, K. K., et al. (2020). The unfolded protein response mediator PERK governs myeloid cell-driven immunosuppression in tumors through inhibition of STING Signaling. *Immunity* 52, 668–682e667. doi: 10.1016/j.immuni.2020.03.004

Mok, S., Koya, R. C., Tsui, C., Xu, J., Robert, L., Wu, L., et al. (2014). Inhibition of CSF-1 receptor improves the antitumor efficacy of adoptive cell transfer immunotherapy. *Cancer Res.* 74, 153–161. doi: 10.1158/0008-5472.Can-13-1816

Munera, V., Popovic, P. J., Bryk, J., Pribis, J., Caba, D., Matta, B. M., et al. (2010). Stat 6-dependent induction of myeloid derived suppressor cells after physical injury regulates nitric oxide response to endotoxin. *Ann. Surg.* 251, 120–126. doi: 10.1097/SLA.0b013e3181bfda1c

Murphy, P. M., and Tiffany, H. L. (1991). Cloning of complementary DNA encoding a functional human interleukin-8 receptor. *Science* 253, 1280–1283. doi: 10.1126/science.1891716

Nasrollahzadeh, E., Razi, S., Keshavarz-Fathi, M., Mazzone, M., and Rezaei, N. (2020). Pro-tumorigenic functions of macrophages at the primary, invasive and metastatic tumor site. *Cancer Immunol. Immunother.* 69, 1673–1697. doi: 10.1007/s00262-020-02616-6

Oh, K., Lee, O. Y., Shon, S. Y., Nam, O., Ryu, P. M., Seo, M. W., et al. (2013). A mutual activation loop between breast cancer cells and myeloid-derived suppressor cells facilitates spontaneous metastasis through IL-6 trans-signaling in a murine model. *Breast Cancer Res.* 15:R79. doi: 10.1186/bcr3473

Ouzounova, M., Lee, E., Piranlioglu, R., El Andaloussi, A., Kolhe, R., Demirci, M. F., et al. (2017). Monocytic and granulocytic myeloid derived suppressor cells differentially regulate spatiotemporal tumour plasticity during metastatic cascade. *Nat. Commun.* 8:14979. doi: 10.1038/ncomms14979

Pan, P. Y., Ma, G., Weber, K. J., Ozao-Choy, J., Wang, G., Yin, B., et al. (2010). Immune stimulatory receptor CD40 is required for T-cell suppression and T regulatory cell activation mediated by myeloid-derived suppressor cells in cancer. *Cancer Res.* 70, 99–108. doi: 10.1158/0008-5472.Can-09-1882

Panigrahi, G. K., Praharaj, P. P., Peak, T. C., Long, J., Singh, R., Rhim, J. S., et al. (2018). Hypoxia-induced exosome secretion promotes survival of African-American and Caucasian prostate cancer cells. *Sci. Rep.* 8:3853. doi: 10.1038/s41598-018-22068-4

Parker, K. H., Sinha, P., Horn, L. A., Clements, V. K., Yang, H., Li, J., et al. (2014). HMGB1 enhances immune suppression by facilitating the differentiation and suppressive activity of myeloid-derived suppressor cells. *Cancer Res.* 74, 5723–5733. doi: 10.1158/0008-5472.Can-13-2347

Pastaki Khoshbin, A., Eskian, M., Keshavarz-Fathi, M., and Rezaei, N. (2019). Roles of myeloid-derived suppressor cells in cancer metastasis: immunosuppression and beyond. *Arch. Immunol. Ther. Exp. (Warsz)* 67, 89–102. doi: 10.1007/s00005-018-0531-9

Peak, T. C., Panigrahi, G. K., Praharaj, P. P., Su, Y., Shi, L., Chyr, J., et al. (2020). Syntaxin 6-mediated exosome secretion regulates enzalutamide resistance in prostate cancer. *Mol. Carcinog.* 59, 62–72. doi: 10.1002/mc.23129

Peinado, H., Zhang, H., Matei, I. R., Costa-Silva, B., Hoshino, A., Rodrigues, G., et al. (2017). Pre-metastatic niches: organ-specific homes for metastases. *Nat. Rev. Cancer* 17, 302–317. doi: 10.1038/nrc.2017.6

Peng, Y., and Croce, C. M. (2016). The role of MicroRNAs in human cancer. *Signal. Transduct. Target Ther.* 1:15004. doi: 10.1038/sigtrans.2015.4

Pineda, C. T., Ramanathan, S., Fon Tacer, K., Weon, J. L., Potts, M. B., Ou, Y. H., et al. (2015). Degradation of AMPK by a cancer-specific ubiquitin ligase. *Cell* 160, 715–728. doi: 10.1016/j.cell.2015.01.034

Priceman, S. J., Sung, J. L., Shaposhnik, Z., Burton, J. B., Torres-Collado, A. X., Moughon, D. L., et al. (2010). Targeting distinct tumor-infiltrating myeloid cells by inhibiting CSF-1 receptor: combating tumor evasion of antiangiogenic therapy. *Blood* 115, 1461–1471. doi: 10.1182/blood-2009-08-237412

Qu, P., Wang, L. Z., and Lin, P. C. (2016). Expansion and functions of myeloid-derived suppressor cells in the tumor microenvironment. *Cancer Lett.* 380, 253–256. doi: 10.1016/j.canlet.2015.10.022

Ren, W., Zhang, X., Li, W., Feng, Q., Feng, H., Tong, Y., et al. (2019). Exosomal miRNA-107 induces myeloid-derived suppressor cell expansion in gastric cancer. *Cancer Manag. Res.* 11, 4023–4040. doi: 10.2147/cmar.S198886

Rong, Y., Yuan, C. H., Qu, Z., Zhou, H., Guan, Q., Yang, N., et al. (2016). Doxorubicin resistant cancer cells activate myeloid-derived suppressor cells by releasing PGE2. *Sci. Rep.* 6:23824. doi: 10.1038/srep23824

Rutherford, C., Speirs, C., Williams, J. J., Ewart, M. A., Mancini, S. J., Hawley, S. A., et al. (2016). Phosphorylation of Janus kinase 1 (JAK1) by AMP-activated protein kinase (AMPK) links energy sensing to anti-inflammatory signaling. *Sci. Signal.* 9:ra109. doi: 10.1126/scisignal.aaf8566

Salminen, A., Hyttinen, J. M., and Kaarniranta, K. (2011). AMP-activated protein kinase inhibits NF-κB signaling and inflammation: impact on healthspan and lifespan. *J. Mol. Med. (Berl)* 89, 667–676. doi: 10.1007/s00109-011-0748-0

Salminen, A., Kaarniranta, K., and Kauppinen, A. (2018). Phytochemicals inhibit the immunosuppressive functions of myeloid-derived suppressor cells (MDSC):

impact on cancer and age-related chronic inflammatory disorders. *Int. Immunopharmacol.* 61, 231–240. doi: 10.1016/j.intimp.2018.06.005

Savina, A., Furlan, M., Vidal, M., and Colombo, M. I. (2003). Exosome release is regulated by a calcium-dependent mechanism in K562 cells. *J. Biol. Chem.* 278, 20083–20090. doi: 10.1074/jbc.M301642200

Schlecker, E., Stojanovic, A., Eisen, C., Quack, C., Falk, C. S., Umansky, V., et al. (2012). Tumor-infiltrating monocytic myeloid-derived suppressor cells mediate CCR5-dependent recruitment of regulatory T cells favoring tumor growth. *J. Immunol.* 189, 5602–5611. doi: 10.4049/jimmunol.1201018

Schulz, O., Hammerschmidt, S. I., Moschovakis, G. L., and Förster, R. (2016). Chemokines and chemokine receptors in lymphoid tissue dynamics. *Annu. Rev. Immunol.* 34, 203–242. doi: 10.1146/annurev-immunol-041015-055649

Sica, A., and Strauss, L. (2017). Energy metabolism drives myeloid-derived suppressor cell differentiation and functions in pathology. *J. Leukoc. Biol.* 102, 325–334. doi: 10.1189/jlb.4MR1116-476R

Srivastava, M. K., Sinha, P., Clements, V. K., Rodriguez, P., and Ostrand-Rosenberg, S. (2010). Myeloid-derived suppressor cells inhibit T-cell activation by depleting cystine and cysteine. *Cancer Res.* 70, 68–77. doi: 10.1158/0008-5472.Can-09-2587

Stiff, A., Trikha, P., Mundy-Bosse, B., McMichael, E., Mace, T. A., Benner, B., et al. (2018). Nitric oxide production by myeloid-derived suppressor cells plays a role in impairing Fc receptor-mediated natural killer cell function. *Clin. Cancer Res.* 24, 1891–1904. doi: 10.1158/1078-0432.Ccr-17-0691

Strauss, L., Bergmann, C., Szczepanski, M., Gooding, W., Johnson, J. T., and Whiteside, T. L. (2007). A unique subset of CD4+CD25highFoxp3+ T cells secreting interleukin-10 and transforming growth factor-beta1 mediates suppression in the tumor microenvironment. *Clin. Cancer Res.* 13(15 Pt 1), 4345–4354. doi: 10.1158/1078-0432.Ccr-07-0472

Tavazoie, M. F., Pollack, I., Tanqueco, R., Ostendorf, B. N., Reis, B. S., Gonsalves, F. C., et al. (2018). LXR/ApoE activation restricts innate immune suppression in cancer. *Cell* 172, 825–840.e18. doi: 10.1016/j.cell.2017.12.026

Thevenot, P. T., Sierra, R. A., Raber, P. L., Al-Khami, A. A., Trillo-Tinoco, J., Zarreii, P., et al. (2014). The stress-response sensor chop regulates the function and accumulation of myeloid-derived suppressor cells in tumors. *Immunity* 41, 389–401. doi: 10.1016/j.immuni.2014.08.015

Tian, X., Ma, J., Wang, T., Tian, J., Zheng, Y., Peng, R., et al. (2018). Long non-coding RNA RUNXOR accelerates MDSC-mediated immunosuppression in lung cancer. *BMC Cancer* 18:660. doi: 10.1186/s12885-018-4564-6

Tobin, R. P., Jordan, K. R., Robinson, W. A., Davis, D., Borges, V. F., Gonzalez, R., et al. (2018). Targeting myeloid-derived suppressor cells using all-trans retinoic acid in melanoma patients treated with Ipilimumab. *Int. Immunopharmacol.* 63, 282–291. doi: 10.1016/j.intimp.2018.08.007

Toh, B., Wang, X., Keeble, J., Sim, W. J., Khoo, K., Wong, W. C., et al. (2011). Mesenchymal transition and dissemination of cancer cells is driven by myeloid-derived suppressor cells infiltrating the primary tumor. *PLoS Biol.* 9:e1001162. doi: 10.1371/journal.pbio.1001162

Trikha, P., and Carson, W. E. III (2014). Signaling pathways involved in MDSC regulation. *Biochim. Biophys. Acta* 1846, 55–65. doi: 10.1016/j.bbcan.2014.04.003

Trikha, P., Plews, R. L., Stiff, A., Gautam, S., Hsu, V., Abood, D., et al. (2016). Targeting myeloid-derived suppressor cells using a novel adenosine monophosphate-activated protein kinase (AMPK) activator. *Oncoimmunology* 5:e1214787. doi: 10.1080/2162402x.2016.1214787

Tu, S., Bhagat, G., Cui, G., Takaishi, S., Kurt-Jones, E. A., Rickman, B., et al. (2008). Overexpression of interleukin-1beta induces gastric inflammation and cancer and mobilizes myeloid-derived suppressor cells in mice. *Cancer Cell* 14, 408–419. doi: 10.1016/j.ccr.2008.10.011

Ugel, S., De Sanctis, F., Mandruzzato, S., and Bronte, V. (2015). Tumor-induced myeloid deviation: when myeloid-derived suppressor cells meet tumor-associated macrophages. *J. Clin. Invest.* 125, 3365–3376. doi: 10.1172/jci80006

Umansky, V., and Sevko, A. (2013). Tumor microenvironment and myeloid-derived suppressor cells. *Cancer Microen.* 6, 169–177. doi: 10.1007/s12307-012-0126-7

Umansky, V., Shevchenko, I., Bazhin, A. V., and Utikal, J. (2014). Extracellular adenosine metabolism in immune cells in melanoma. *Cancer Immunol. Immunother.* 63, 1073–1080. doi: 10.1007/s00262-014-1553-8

Veglia, F., Sanseviero, E., and Gabrilovich, D. I. (2021). Myeloid-derived suppressor cells in the era of increasing myeloid cell diversity. *Nat. Rev. Immunol.* 21, 485–498. doi: 10.1038/s41577-020-00490-y

Veglia, F., Tyurin, V. A., Blasi, M., De Leo, A., Kossenkov, A. V., Donthireddy, L., et al. (2019). Fatty acid transport protein 2 reprograms neutrophils in cancer. *Nature* 569, 73–78. doi: 10.1038/s41586-019-1118-2

Vincent, J., Mignot, G., Chalmin, F., Ladoire, S., Bruchard, M., Chevriaux, A., et al. (2010). 5-Fluorouracil selectively kills tumor-associated myeloid-derived suppressor cells resulting in enhanced T cell-dependent antitumor immunity. *Cancer Res.* 70, 3052–3061. doi: 10.1158/0008-5472.Can-09-3690

Waight, J. D., Netherby, C., Hensen, M. L., Miller, A., Hu, Q., Liu, S., et al. (2013). Myeloid-derived suppressor cell development is regulated by a STAT/IRF-8 axis. *J. Clin. Invest.* 123, 4464–4478. doi: 10.1172/jci68189

Wang, D., Sun, H., Wei, J., Cen, B., and DuBois, R. N. (2017). CXCL1 is critical for premetastatic niche formation and metastasis in colorectal cancer. *Cancer Res.* 77, 3655–3665. doi: 10.1158/0008-5472.Can-16-3199

Wang, G., Lu, X., Dey, P., Deng, P., Wu, C. C., Jiang, S., et al. (2016). Targeting YAP-dependent MDSC infiltration impairs tumor progression. *Cancer Discov.* 6, 80–95. doi: 10.1158/2159-8290.Cd-15-0224

Wang, Y., Ding, Y., Guo, N., and Wang, S. (2019). MDSCs: key criminals of tumor pre-metastatic niche formation. *Front. Immunol.* 10:172. doi: 10.3389/fimmu.2019.00172

Weber, R., Fleming, V., Hu, X., Nagibin, V., Groth, C., Altevogt, P., et al. (2018). Myeloid-derived suppressor cells hinder the anti-cancer activity of immune checkpoint inhibitors. *Front. Immunol.* 9:1310. doi: 10.3389/fimmu.2018.01310

Wei, J., Zhang, M., and Zhou, J. (2015). Myeloid-derived suppressor cells in major depression patients suppress T-cell responses through the production of reactive oxygen species. *Psychiatry Res.* 228, 695–701. doi: 10.1016/j.psychres.2015.06.002

Whiteside, T. L. (2016). Exosomes and tumor-mediated immune suppression. *J. Clin. Invest.* 126, 1216–1223. doi: 10.1172/jci81136

Wu, M., Ma, M., Tan, Z., Zheng, H., and Liu, X. (2020). Neutrophil: a new player in metastatic cancers. *Front. Immunol.* 11:565165. doi: 10.3389/fimmu.2020.565165

Xiang, X., Poliakov, A., Liu, C., Liu, Y., Deng, Z. B., Wang, J., et al. (2009). Induction of myeloid-derived suppressor cells by *tumor exosomes*. *Int. J. Cancer* 124, 2621–2633. doi: 10.1002/ijc.24249

Xu, Z., Ji, J., Xu, J., Li, D., Shi, G., Liu, F., et al. (2017). MiR-30a increases MDSC differentiation and immunosuppressive function by targeting SOCS3 in mice with B-cell lymphoma. *Febs j* 284, 2410–2424. doi: 10.1111/febs.14133

Yan, H. H., Pickup, M., Pang, Y., Gorska, A. E., Li, Z., Chytil, A., et al. (2010). Gr-1+CD11b+ myeloid cells tip the balance of immune protection to tumor promotion in the premetastatic lung. *Cancer Res.* 70, 6139–6149. doi: 10.1158/0008-5472.Can-10-0706

Yang, L., DeBusk, L. M., Fukuda, K., Fingleton, B., Green-Jarvis, B., Shyr, Y., et al. (2004). Expansion of myeloid immune suppressor Gr+CD11b+ cells in tumor-bearing host directly promotes tumor angiogenesis. *Cancer Cell* 6, 409–421. doi: 10.1016/j.ccr.2004.08.031

Yang, Y., Li, C., Liu, T., Dai, X., and Bazhin, A. V. (2020). Myeloid-Derived suppressor cells in tumors: from mechanisms to antigen specificity and microenvironmental regulation. *Front. Immunol.* 11:1371. doi: 10.3389/fimmu.2020.01371

Yaseen, M. M., Abuharfeil, N. M., Darmani, H., and Daoud, A. (2021). Recent advances in myeloid-derived suppressor cell biology. *Front. Med.* 15:232–251. doi: 10.1007/s11684-020-0797-2

Yu, H., Liu, Y., McFarland, B. C., Deshane, J. S., Hurst, D. R., Ponnazhagan, S., et al. (2015). SOCS3 deficiency in myeloid cells promotes tumor development: involvement of STAT3 activation and myeloid-derived suppressor cells. *Cancer Immunol. Res.* 3, 727–740. doi: 10.1158/2326-6066.CIR-15-0004

Zhang, H., Maric, I., DiPrima, M. J., Khan, J., Orentas, R. J., Kaplan, R. N., et al. (2013). Fibrocytes represent a novel MDSC subset circulating in patients with metastatic cancer. *Blood* 122, 1105–1113. doi: 10.1182/blood-2012-08-449413

Zhang, H., Nguyen-Jackson, H., Panopoulos, A. D., Li, H. S., Murray, P. J., and Watowich, S. S. (2010). STAT3 controls myeloid progenitor growth during emergency *granulopoiesis*. *Blood* 116, 2462–2471. doi: 10.1182/blood-2009-12-259630

Zhang, H., Ye, Y. L., Li, M. X., Ye, S. B., Huang, W. R., Cai, T. T., et al. (2017). CXCL2/MIF-CXCR2 signaling promotes the recruitment of myeloid-derived

suppressor cells and is correlated with prognosis in bladder cancer. *Oncogene* 36, 2095–2104. doi: 10.1038/onc.2016.367

Zhang, M., Liu, Q., Mi, S., Liang, X., Zhang, Z., Su, X., et al. (2011). Both miR-17-5p and miR-20a alleviate suppressive potential of myeloid-derived suppressor cells by modulating STAT3 expression. *J. Immunol.* 186, 4716–4724. doi: 10.4049/jimmunol.1002989

Zhao, D., Pan, C., Sun, J., Gilbert, C., Drews-Elger, K., Azzam, D. J., et al. (2015). VEGF drives cancer-initiating stem cells through VEGFR-2/Stat3 signaling to upregulate Myc and Sox2. *Oncogene* 34, 3107–3119. doi: 10.1038/onc.2014.257

Zhao, F., Hoechst, B., Duffy, A., Gamrekelashvili, J., Fioravanti, S., Manns, M. P., et al. (2012). S100A9 a new marker for monocytic human myeloid-derived suppressor cells. *Immunology* 136, 176–183. doi: 10.1111/j.1365-2567.2012.03566.x

Zhao, X., Rong, L., Zhao, X., Li, X., Liu, X., Deng, J., et al. (2012). TNF signaling drives myeloid-derived suppressor cell accumulation. *J. Clin. Invest.* 122, 4094–4104. doi: 10.1172/jci64115

Zheng, R., Chen, S., and Chen, S. (2015). Correlation between myeloid-derived suppressor cells and S100A8/A9 in tumor and autoimmune diseases. *Int. Immunopharmacol.* 29, 919–925. doi: 10.1016/j.intimp.2015.10.014

Zheng, Y., Tian, X., Wang, T., Xia, X., Cao, F., Tian, J., et al. (2019). Long noncoding RNA Pvt1 regulates the immunosuppression activity of granulocytic myeloid-derived suppressor cells in tumor-bearing mice. *Mol. Cancer* 18:61. doi: 10.1186/s12943-019-0978-2

Zhou, Q., Tang, X., Tian, X., Tian, J., Zhang, Y., Ma, J., et al. (2018). LncRNA MALAT1 negatively regulates MDSCs in patients with lung cancer. *J. Cancer* 9, 2436–2442. doi: 10.7150/jca.24796

Zoso, A., Mazza, E. M., Bicciato, S., Mandruzzato, S., Bronte, V., Serafini, P., et al. (2014). Human fibrocytic myeloid-derived suppressor cells express IDO and promote tolerance via Treg-cell expansion. *Eur. J. Immunol.* 44, 3307–3319. doi: 10.1002/eji.201444522

Conflict of Interest: The authors declare that the research was conducted in the absence of any commercial or financial relationships that could be construed as a potential conflict of interest.

Publisher's Note: All claims expressed in this article are solely those of the authors and do not necessarily represent those of their affiliated organizations, or those of the publisher, the editors and the reviewers. Any product that may be evaluated in this article, or claim that may be made by its manufacturer, is not guaranteed or endorsed by the publisher.

frontiers in Molecular Biosciences

ORIGINAL RESEARCH
published: 31 August 2021
doi: 10.3389/fmolb.2021.668888

Prognostic Immunity and Therapeutic Sensitivity Analyses Based on Differential Genomic Instability-Associated LncRNAs in Left- and Right-Sided Colon Adenocarcinoma

Jun-Nan Guo[1†], *Tian-Yi Xia*[1†], *Shen-Hui Deng*[2], *Wei-Nan Xue*[1], *Bin-Bin Cui*[1*] and *Yan-Long Liu*[1*]

[1]*Department of Colorectal Surgery, Harbin Medical University Cancer Hospital, Harbin, China,* [2]*Department of Anesthesiology, The Fourth Affiliated Hospital of Harbin Medical University, Harbin, China*

OPEN ACCESS

Edited by:
William. C Cho, Hong Kong, SAR China

Reviewed by:
Anita Chopra, All India Institute of Medical Sciences, India
Liu Yahui, Jilin University, China

***Correspondence:**
Bin-Bin Cui
cbbhrb@163.com
Yan-Long Liu
2355@hrbmu.edu.cn

[†]*These authors have contributed equally to this work*

Specialty section:
This article was submitted to Molecular Diagnostics and Therapeutics, a section of the journal Frontiers in Molecular Biosciences

Received: *17 February 2021*
Accepted: *06 August 2021*
Published: *31 August 2021*

Citation:
Guo J-N, Xia T-Y, Deng S-H, Xue W-N, Cui B-B and Liu Y-L (2021) Prognostic Immunity and Therapeutic Sensitivity Analyses Based on Differential Genomic Instability-Associated LncRNAs in Left- and Right-Sided Colon Adenocarcinoma. Front. Mol. Biosci. 8:668888. doi: 10.3389/fmolb.2021.668888

Background: The purpose of our study was to develop a prognostic risk model based on differential genomic instability-associated (DGIA) long non-coding RNAs (lncRNAs) of left-sided and right-sided colon cancers (LCCs and RCCs); therefore, the prognostic key lncRNAs could be identified.

Methods: We adopted two independent gene datasets, corresponding somatic mutation and clinical information from The Cancer Genome Atlas (TCGA) and Gene Expression Omnibus (GEO) databases. Identification of differential DGIA lncRNAs from LCCs and RCCs was conducted with the appliance of "Limma" analysis. Then, we screened out key lncRNAs based on univariate and multivariate Cox proportional hazard regression analysis. Meanwhile, DGIA lncRNAs related prognostic model (DRPM) was established. We employed the DRPM in the model group and internal verification group from TCGA for the purpose of risk grouping and accuracy verification of DRPM. We also verified the accuracy of key lncRNAs with GEO data. Finally, the differences of immune infiltration, functional pathways, and therapeutic sensitivities were analyzed within different risk groups.

Results: A total of 123 DGIA lncRNAs were screened out by differential expression analysis. We obtained six DGIA lncRNAs by the construction of DRPM, including AC004009.1, AP003555.2, BOLA3-AS1, NKILA, LINC00543, and UCA1. After the risk grouping by these DGIA lncRNAs, we found the prognosis of the high-risk group (HRG) was significantly worse than that in the low-risk group (LRG) (all $p < 0.05$). In all TCGA samples and model group, the expression of $CD8^+$ T cells in HRG was lower than that in LRG (all $p < 0.05$). The functional analysis indicated that there was significant upregulation with regard to pathways related to both genetic instability and immunity in LRG, including cytosolic DNA sensing pathway, response to double-strand RNA, RIG-I like receptor signaling pathway, and Toll-like receptor signaling pathway. Finally, we analyzed the difference and significance of key DGIA lncRNAs and risk groups in multiple therapeutic sensitivities.

Conclusion: Through the analysis of the DGIA lncRNAs between LCCs and RCCs, we identified six key DGIA lncRNAs. They can not only predict the prognostic risk of patients but also serve as biomarkers for evaluating the differences of genetic instability, immune infiltration, and therapeutic sensitivity.

Keywords: colon adenocarcinoma, left-sided, right-sided, genomic instability, immunity, prognosis, therapeutic sensitivity

INTRODUCTION

Colon cancer (CC) is one of the most common cancers diagnosed in humans and, globally, there are more than 1.8 million new cases of this disease each year (Siegel et al., 2020; Verkuijl et al., 2021). Lately, immunotherapy has achieved breakthroughs and is considered a leading therapy against tumors. However, some CC patients show a low response and drug resistance (Wu, 2018). Traditional treatments such as surgery, radiotherapy, and chemotherapy are used to suppress cancers, but their long-term effects are difficult to predict. The differences of these phenomena are more obvious in the left-sided and right-sided CCs (LCCs and RCCs, respectively) (Grass et al., 2019). As mentioned in the literature review, LCC patients benefit more from chemotherapies and targeted therapies and have a better prognosis. RCC patients do not respond well to conventional chemotherapies but demonstrate more promising results with immunotherapies (Baran et al., 2018). It is well known that the differences in terms of molecular and clinical heterogeneity between LCCs and RCCs are complex, as are their occurrence, development, and response to treatment and prognosis (Blakely et al., 2020). Patients with RCC were found to have different molecular biological tumor patterns and a poorer prognosis than patients with LCC (Hansen and Jess, 2012). Thus, it is important to understand the underlying potential molecular mechanisms as they will influence the choice of treatments.

Recently, researchers have revealed that LCCs and RCCs are different in clinical and genomic characteristics (Mjelle et al., 2019). In addition to the microsatellite instability status, the identified differences include APC, TP53, RAS, and BRAF mutations (Guinney et al., 2015; Molina-Cerrillo et al., 2020; Requena and Garcia-Buitrago, 2020). The dissimilarities of gene expression patterns could be used to analyze LCCs and RCCs. It is mainly beneficial to doctors by selecting the most effective individualized treatment via the degree and nature of these molecular mutations. Therefore, while we are looking for novel and precise prognostic biomarkers, the utility is more vital for guiding targeted therapy.

Prior to cell division, the fidelity of our genome copies is remarkable in its consistency over time (Bebenek, 2008). However, these high fidelity processes can be compromised by a variety of genomic alterations that subsequently result in the development of cancer (Mardis, 2019). In CC, mutations in mismatch repair genes lead to functional defects, which can cause microsatellite instability (MSI). The distinction in MSI status is also one of the aspects that help to differentiate between LCCs and RCCs (Lichtenstern et al., 2020). In addition, a variety of biological processes are related to genome instability, such as abnormal transcription and post-transcriptional regulation and DNA damage regulation (Boulianne and Feldhahn, 2018). The latest findings disclosed that variations in the instability of genomes produce new antigens, which affect the immunophenotype and immunotherapy response (Mardis, 2019). Long non-coding RNAs (lncRNAs) are incapable of encoding proteins but they play an indispensable regulatory role in tumors. Currently, lncRNAs have been shown to be related to genome stability (Thapar, 2018). However, in LCCs and RCCs, the influence of differential genomic instability-associated (DGIA) lncRNAs on tumor-associated immune microenvironment has not been explored yet.

Therefore, in this research, we proposed to create a prognostic model and risk factor clustering containing key lncRNAs based on differentially expressed genes and genomic instability in the LCCs and RCCs in The Cancer Genome Atlas (TCGA) database; the leading goal of this study was to analyze the differences in immune infiltration between high- and low-risk groups (HRG and LRG, respectively) and to verify using the Gene Expression Omnibus (GEO) database. Moreover, we aimed to screen out new prognostic biomarkers related to genetic instability in LCCs and RCCs and to provide a molecular basis for identifying therapeutic sensitivities.

MATERIALS AND METHODS

The flowchart of the whole study is presented in **Supplementary figure S1**.

Data Collection

In this research, we selected two independent gene datasets from different high-throughput platforms, including 473 colon adenocarcinoma (COAD) samples from TCGA (https://portal.gdc.cancer.gov/) and 156 COAD samples from GEO (http://www.ncbi.nlm.nih.gov/geo/) (GSE103479). The downloaded data included paired lncRNA and mRNA expression profiles, somatic mutation information, and clinical information. The RCC tumors arise from ascending colon, and proximal two-thirds of the transverse colon and the LCC tumors arise from the descending and sigmoid colon and distal one-third of the transverse colon (Baran et al., 2018). After screening based on CCs location, there were a total of 411 samples with integrated information available for analysis, of which 322 were from TCGA and 89 from GEO. The TCGA samples were divided into two groups randomly—model group and internal verification group. To ensure the undifferentiated clustering, we performed an

analysis to determine the differences in stratification of various clinical factors. The GEO sample was used as the external validation group to verify the accuracy of prognostic lncRNAs. The analysis excluded RNA that was undetectable in more than 10% of the samples. Concerning each dataset, the gene ID was converted to the corresponding gene symbol according to the corresponding annotation package.

Identification of Differential Genomic Instability-Associated lncRNAs From LCCs and RCCs

Initially, we examined differentially expressed genes (DEGs) in LCCs and RCCs from TCGA by the R package "Limma" (|log2foldchange| >0.5, false discovery rate (FDR) <0.05) (Ritchie et al., 2015). These DEGs were distributed by the human genome annotation package into mRNAs and lncRNAs. In order to assess the genomic instability, we proposed a mutator hypothesis-derived calculation method: we determined the cumulative number of somatic mutations (CNSMs) on the basis of the number of changed sites in each gene of each sample and categorized the patients in descending order. The top 25% of patients were titled with genomic unstable like (GU) group and the last 25% as genomic stable like (GS) group. The differentially expressed lncRNAs of the two groups were evaluated and named as DGIA lncRNAs from LCCs and RCCs (| log2foldchange | >0.5, FDR <0.05).

Cluster and Analyze the TCGA Samples According to DGIA

Hierarchical cluster test (HCA) was performed to verify the grouping effect of DGIA lncRNAs and to batch all TCGA samples according to DGIA by the R package "sparcl" (Witten and Tibshirani, 2010). HCA is an approach commonly used to classify similar samples or variables using Euclidean distances and Ward's linkage method. The samples were classified into GU group and GS group by clustering. Subsequently, we explored the two groups on the CNSMs by univariate analysis.

Functional Enrichment Analysis

To investigate the potential functions of DGIA lncRNAs, two methods were applied to identify mRNAs that were more likely to be co-expressed with them. The first one was used to analyze the co-expressing relationship between lncRNAs and mRNAs by Pearson's correlation tests. Here, we designated that the top 10 mRNAs with the highest coefficients have a strong co-expressing relationship with each DGIA lncRNA.

The second one was used to analyze the DEGs between LCCs and RCCs through weighted gene co-expression network assessment by the R package "WGCNA" (Langfelder and Horvath, 2008). At first, the construction of an adjacency matrix (AM) of genes was done using the power function with an appropriate power index selected. Then, AM was converted into a topological overlap matrix. Finally, the gene consensus modules were collected and the correlation analysis was performed with CNSMs. The mRNAs in the modules with the highest absolute correlation coefficient with CNSMs were selected for further examination.

Overall, the intersection of the mRNAs was screened by two methods and we employed Gene Ontology (GO) functional annotations and Kyoto Encyclopedia of Genes and Genomes (KEGG) pathway enrichment analysis by R package "clusterProfiler" (Yu et al., 2012).

Construction of DGIA lncRNAs Related Prognostic Model

To check the effect of DGIA lncRNAs on the prognosis, DGIA lncRNAs were secluded by univariate Cox proportional hazard regression analysis (COX). LncRNAs with $p < 0.05$ in univariate COX were retained and multivariate COX was performed in the model group by the R package "glmnet" (Friedman et al., 2010). The risk scores (RS) of the model group and the internal validation group were estimated according to the coefficient of each lncRNAs within the model. The patients in TCGA were separated into HRG and LRG with poor prognosis.

Validation of the DGIA lncRNAs in DRPM

Log-rank test was used to disclose the difference in survival of HRG and LRG in the model group and internal validation group by R packages "survcomp" (Schröder et al., 2011). Simultaneously, the predictive effect of DRPM was figured out through the receiver operating characteristics curve (ROC) and the area under the ROC curve (AUC) by the R package "survivalROC" (Heagerty and Zheng, 2005). Additionally, univariate and multivariate COX was utilized to verify the independent predictive effect of the RS obtained by the model.

In the external verification group, DGIA lncRNAs were employed in DRPM to construct a prognostic model again by multivariate COX. The Log-rank test was also used for survival analysis, and time-dependent ROC (timeROC) of 1, 3, and 5 years was plotted. The purpose was to verify the accuracy of prognostic DGIA lncRNAs.

The survival curves of DGIA lncRNAs in DRPM were plotted and the differences were analyzed by log-rank test. The R package "maxstat" (Laska et al., 2012) was performed to obtain the best cut-off value.

Immune Infiltration and Gene Set Enrichment Analysis in HRG and LRG

The R package "CIBERSORT" (Newman et al., 2015) was employed in the TCGA samples to estimate the relative infiltration abundance of 22 immune cells and to assess the variations in the various immune cells' infiltration of HRG and LRG. The results with $p < 0.05$ were retained. "CIBERSORT" calculated the p value of the deconvolution for each sample by Monte Carlo simulation to provide the assessed confidence. The differences in the abundance of 22 immune cells in HRG and LRG were examined by the Wilcoxon rank-sum test.

Besides, to study the differences in biological functions of genes between HRG and LRG, we downloaded the biological process (BP), molecular function (MF) datasets related to GO, and the KEGG dataset. GSEA was performed using the

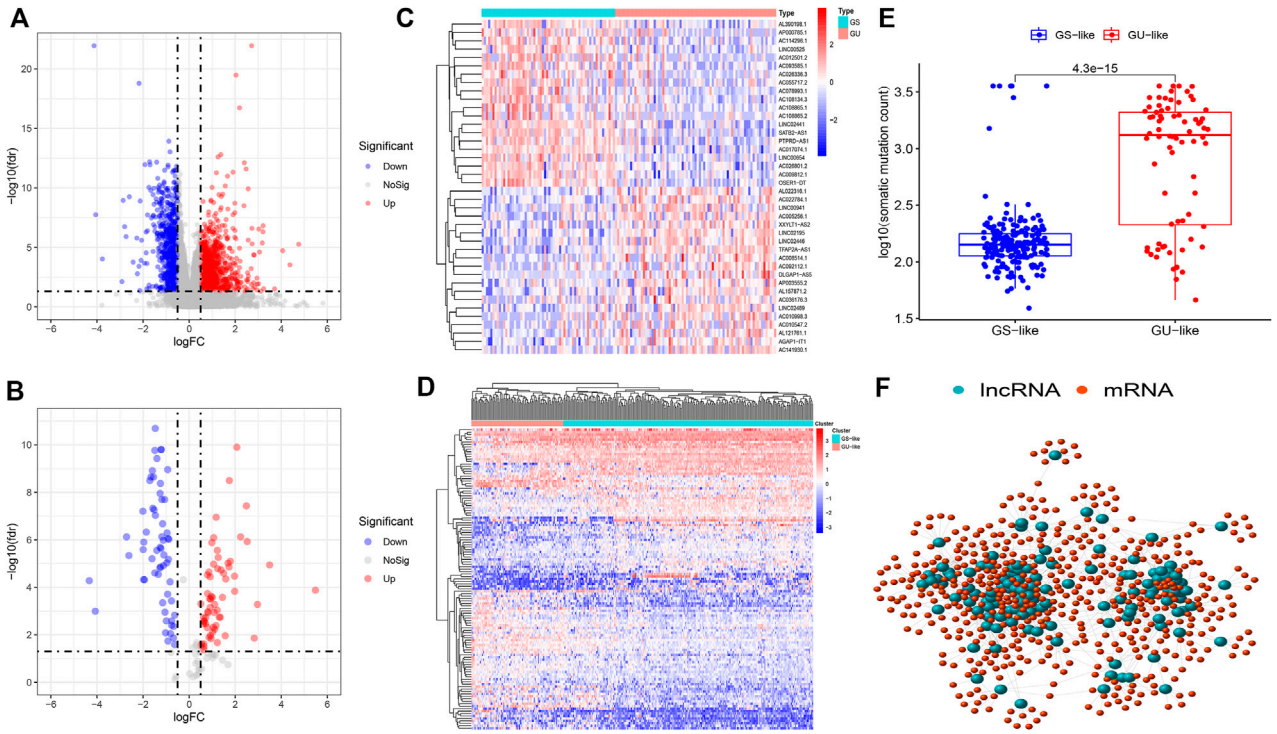

FIGURE 1 | (A) Differentially expressed genes between LCCs and RCCs. **(B)** Differentially expressed DGIA lncRNAs between GU group and GS group. Red and blue circles indicate high and low genes expression, respectively. **(C)** Heat map depicts the differentially expressed DGIA lncRNAs in TCGA patients. **(D)** Unsupervised clustering of TCGA patients based on the expression pattern of 128 candidate DGIA lncRNAs. **(E)** In boxplot, cumulative number of somatic mutations in the GU-like group is significantly higher than that in the GS-like group **(F)** Co-expression network of DGIA lncRNAs and intersection of mRNAs based on two methods. The red circles represent lncRNAs, and the blue circles represent mRNAs. LCCs and RCCs: left- and right-sided colon adenocarcinoma; DGIA lncRNAs: genomic instability-associated long non-coding RNAs; GU: genomic unstable; GS: genomic stable.

Bioconductor package "fgsea" (Subramanian et al., 2005) with 10,000 permutations between LRG and HRG. The threshold values were $p < 0.05$.

Related Analysis of Therapeutic Sensitivity

To evaluate the application of the DRPM and DGIA lncRNAs in clinical therapy of CC, we analyzed the therapeutic sensitivity from three aspects: chemotherapy, targeted inhibitors (TIs) therapy, and immunotherapy. Gene expression data and chemotherapeutic drug response data were downloaded from CellMiner™ (https://discover.nci.nih.gov/cellminer/); these data were from the same batch. We deleted drugs without FDA approval or clinical trials and selected chemotherapy drugs for CC. Then, we extracted the lncRNAs and co-expressed mRNA from the gene expression data and analyzed the correlation between their expression and drug sensitivity.

In addition, we calculated the concentration causing 50% reduction growth (IC50) of TIs by R package "pRRophetic" (Geeleher et al., 2014), including vascular endothelial growth factor receptor (VEGFR), Hedgehog (HH), and Wnt inhibitors. Wilcoxon rank-sum test was used to compare the IC50 difference between HRG and LRG. Finally, we analyzed the differences in gene expression of the six immunosuppressive checkpoints in HRG and LRG.

RESULT

DEGs and DGIA lncRNAs in LCCs and RCCs

Firstly, we selected, separated, and bundled TCGA samples in furtherance of segregating DGIA lncRNAs from DEGs of LCCs and RCCs. Soon after, the corresponding gene expression data were standardized and analyzed. We obtained 1724 DEGs (**Figure 1A**), including 1,325 mRNAs and 399 lncRNAs. According to the CNSMs, the top 25% (n = 75) and last 25% (n = 62) patients were labeled as GU group and GS group, respectively. By comparing the lncRNAs between these two groups, 123 DGIA lncRNAs were attained, of which 63 lncRNAs showed upregulation whereas 60 exhibited downregulation in the GU group (**Figures 1B,C**). Based on these DGIA lncRNAs, we carried out unsupervised HCA on TCGA specimens and distributed them into the GU group and GS group (**Figure 1D**). The CNSMs in both groups were significantly different with the median higher in the GU group compared to the GS group (**Figure 1E**). These findings

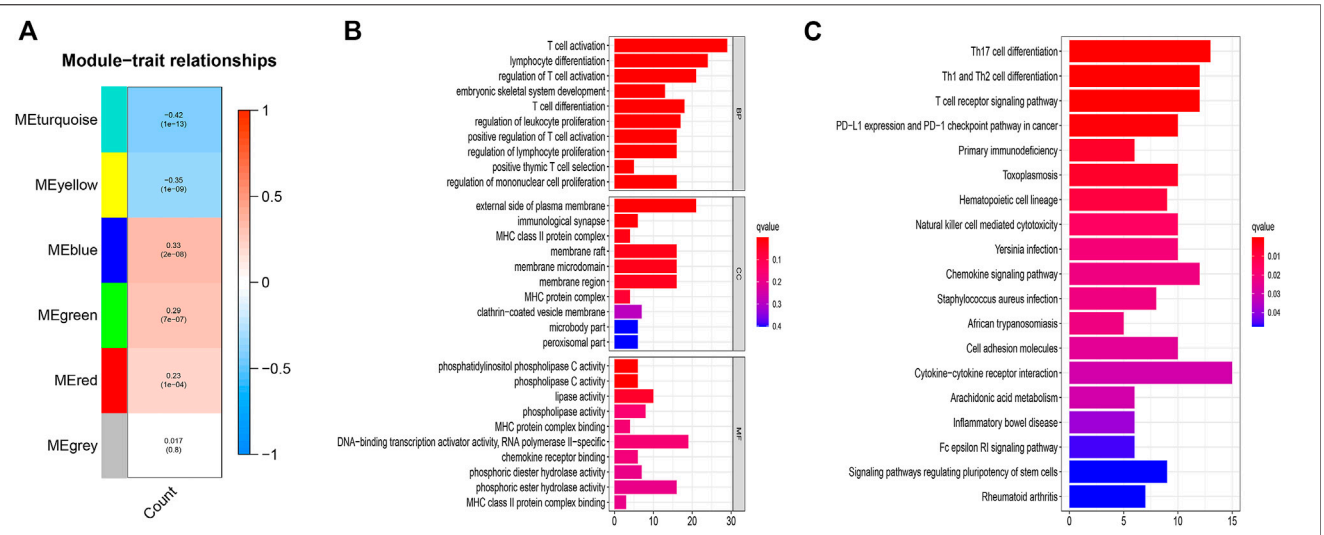

FIGURE 2 | (A) Correlation between the gene modules and CNSMs. Each cell contains a corresponding correlation coefficient and *p* value. The correlation coefficient decreased in size from red to blue. **(B)** GO functional annotations for mRNAs co-expressed with lncRNAs. **(C)** KEGG enrichment analysis for mRNAs co-expressed with lncRNAs. CNSMs: cumulative number of somatic mutations; GO: Gene Ontology; KEGG: Kyoto Encyclopedia of Genes and Genomes.

conclusively depicted that the selected DGIA lncRNAs had a valid classification effect.

Functional Enrichment Analysis for DGIA lncRNAs

To explore the functions and pathways concerned with 123 DGIA lncRNAs, we operated functional enrichment analysis on protein-coding genes (PCGs) co-expressed with DGIA lncRNAs. The first method's procedure included a correlation analysis between the selected DGIA lncRNAs and 1,325 differential mRNAs from LCCs and RCCs. The PCGs of DGIA lncRNAs, that is, the top 10 mRNAs with the strongest correlation with each lncRNAs, were achieved.

The second method disclosed, after constructing the co-expression network (**Supplementary Figure S2**), the blue module with the highest positive correlation, and the turquoise module with the highest negative correlation (**Figure 2A**). We intersected the selective mRNAs from the blue and turquoise modules with PCGs chosen by the first method. Thereby, these genes were used to construct a lncRNAs-mRNA co-expression network (**Figure 1F**).

The results of functional enrichment analysis with the intersection PCGs comprised DNA-binding transcription activator activity, RNA polymerase II-specific, and various phospholipase-related enzyme activities. These molecular functions are closely associated with the formation and development of genomic instability. More importantly, the enrichments of biological processes are mainly related to immune processes, such as T cell activation, lymphocyte differentiation, regulation of T cell activation. (**Figure 2B**). KEGG enrichment analysis displayed that regulatory pluripotency of both stem cells signaling pathways and immune-related pathways, including Th17 cell differentiation, Th1 and Th2 cell differentiation, PD−L1 expression, and PD−1 checkpoint pathway in cancer, were significantly enriched (**Figure 2C**). These results indicated that 123 DGIA lncRNAs not only cause genomic instability but also influence the regulation of the immune system. The variation in the expression of these 123 DGIA lncRNAs potentially disturbs the balance of co-expressed PCGs regulatory network and, consequently, causes instability in the cell genome. It also affects the killing of tumors by immune cells, mostly by proliferation, differentiation, activation, and receptor recognition of T cells. Thus, these DGIA lncRNAs play an essential role in immune regulation while affecting gene instability.

Construction of DRPM Using DGIA lncRNAs

The samples from TCGA were randomly and uniformly arranged into model group (n = 162) and validation group (n = 160). The clinical factors were not statistically significantly different between each group (all $p > 0.05$) (**Supplementary Table S1**). In the model group, we employed univariate and multivariate COX to assort and construct DRPM with 123 DGIA lncRNAs, and six prognostic-related DGIA lncRNAs with corresponding risk coefficients were determined (**Table 1**). All patients in TCGA were divided into HRG and LRG on the basis of the median of RS (0.851) measured by DRPM in the model group (**Supplementary Table S2**).

Validation of the DRPM

To confirm the anticipated effects of DRPM, we conducted the Kaplan–Meier test to plot a survival curve. The results demonstrated that the survival outcomes of HRG were worse than those in LRG (all $p < 0.05$) (**Figure 3A**). The ROC curves plotted for patients in different groups confirmed the consistency

TABLE 1 | DRPM information including six DGIA lncRNAs.

LncRNAs	Coefficients	HR	95% CI lower	95% CI upper	*p* value
NKILA	0.198	1.219	1.027	1.447	0.024
AC004009.1	0.316	1.371	1.128	1.668	0.002
AP003555.2	0.377	1.457	1.227	1.731	< 0.001
BOLA3-AS1	0.329	1.390	1.038	1.860	0.027
LINC00543	0.074	1.077	1.007	1.152	0.030
UCA1	0.013	1.014	1.004	1.023	0.004

CI: confidence interval; DGIA: differential genomic instability-associated; DRPM: DGIA lncRNAs related prognostic model; HR: hazard ratio; LncRNAs: long non-coding RNAs.

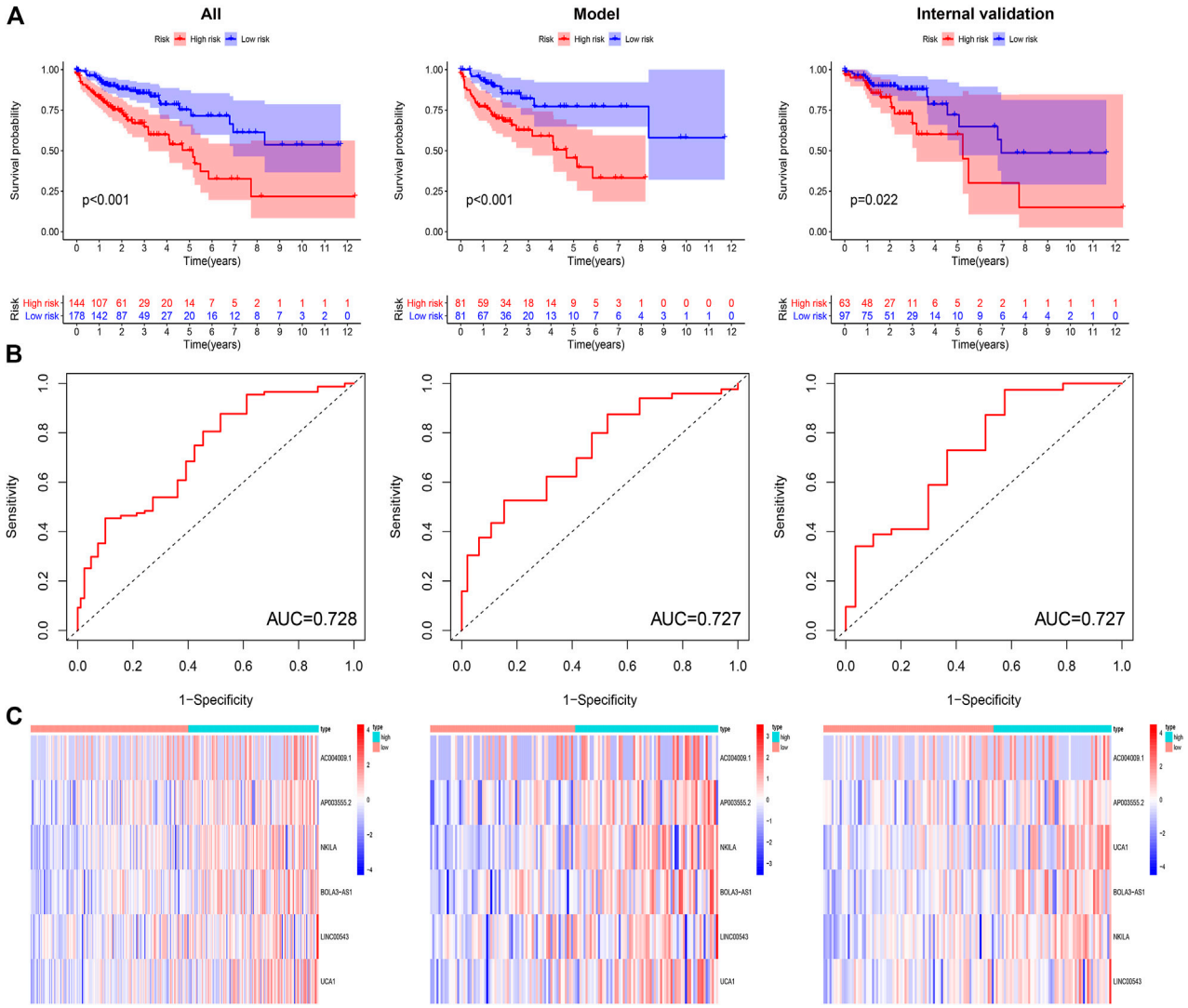

FIGURE 3 | (A) Kaplan–Meier curves of overall survival in different groups. **(B)** ROC curves in different groups. **(C)** The heat map of six key lncRNA expression patterns with increasing risk score. ROC: receiver operating characteristics.

and categorization effects of DRPM. The AUC were shown in the figures respectively (**Figure 3B**). Using RS, we organized the patients into different groups and detected changes in the expression level of the prognostic DGIA lncRNAs. The heat map presented the increment in the expression levels of six lncRNAs in HRG (**Figure 3C**).

To verify the independent predictive effects of RS, we combined RS with clinical factors for univariate and

TABLE 2 | Univariate and multivariate COX of prognostic factors in different groups.

Factors	Univariate COX				Multivariate COX			
	HR	95% CI lower	95% CI upper	*p* value	HR	95% CI lower	95% CI upper	*p* value
All patients in TCGA (n = 322)								
Age	1.031	1.010	1.053	0.004	1.043	1.021	1.066	< 0.001
Gender	1.330	0.828	2.134	0.238	1.149	0.698	1.891	0.584
T	3.555	2.155	5.864	< 0.001	2.897	1.601	5.240	< 0.001
N	1.898	1.438	2.506	< 0.001	1.132	0.804	1.595	0.477
M	4.484	2.740	7.337	< 0.001	2.985	1.603	5.559	0.001
Risk score	1.228	1.161	1.300	< 0.001	1.196	1.127	1.269	< 0.001
Model group (n = 162)								
Age	1.024	0.996	1.053	0.094	1.033	1.002	1.065	0.038
Gender	0.734	0.393	1.369	0.331	0.758	0.388	1.480	0.417
T	2.359	1.235	4.507	0.009	1.465	0.702	3.060	0.309
N	1.904	1.315	2.756	0.001	1.216	0.763	1.940	0.411
M	4.654	2.451	8.838	< 0.001	3.405	1.500	7.726	0.003
Risk score	1.235	1.158	1.317	< 0.001	1.160	1.078	1.249	< 0.001
Internal validation group (n = 160)								
Age	1.040	1.006	1.076	0.021	1.063	1.026	1.102	0.001
Gender	3.060	1.361	6.878	0.007	2.179	0.904	5.248	0.083
T	6.649	3.078	14.362	< 0.001	9.612	3.662	25.230	< 0.001
N	2.074	1.313	3.276	0.002	1.378	0.744	2.555	0.308
M	4.349	1.992	9.493	< 0.001	2.299	0.767	6.891	0.137
Risk score	1.178	1.033	1.343	0.015	1.250	1.088	1.436	0.002

COX: Cox proportional hazard regression analysis.

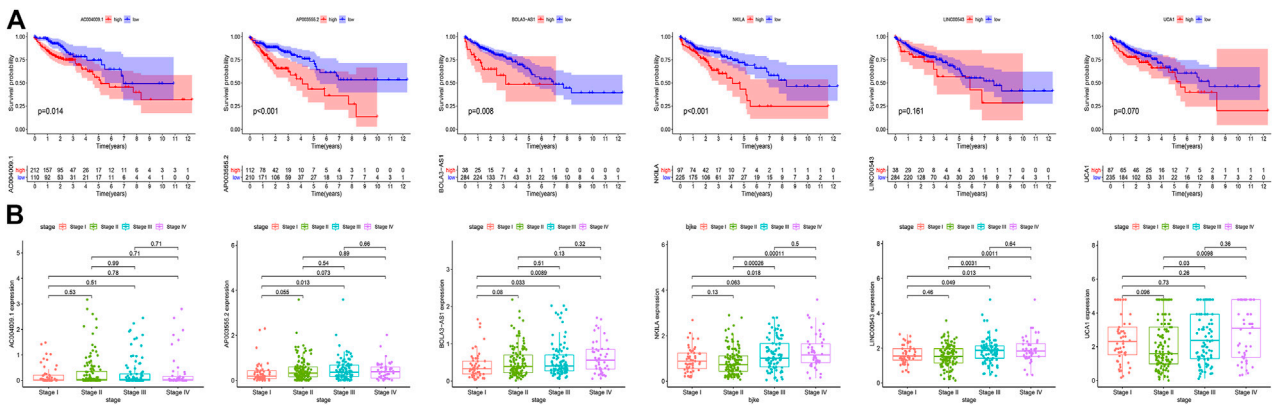

FIGURE 4 | (A) Kaplan–Meier curves of overall survival in six key DGIA lncRNAs. **(B)** The correlation between six key DGIA lncRNAs and pathologic stages.

multivariate COX analysis. These clinical factors were age, gender, and TNM stage. The results indicated that RS was an independent prognostic factor (**Table 2**). Besides, to assess the risk clustering ability of DRPM in different strata, we separately stratified age (<65 years and ≥65 years), gender (male and female), and clinical stage (stages I-II and stages III-IV). The survival curves of HRG and LRG were plotted through the stratification of different clinical factors. HRG and LRG exhibited a significant difference in overall the strata of age, gender, and stages I-II (all $p < 0.05$) (**Supplementary Figure S3**). In the strata of stages III-IV, the difference was very close but was not statistically significant ($p = 0.077$) (**Supplementary Figure S3**). In summary, the DRPM revealed a consistent and promising prognostic evaluation ability in different strata.

Validation of the Prognostic DGIA lncRNAs

To verify the accuracy of prognostic DGIA lncRNAs, we plotted survival curves for the lncRNAs in TCGA samples. In AC004009.1, AP003555.2, BOLA3-AS1, NKILA, LINC00543, and UCA1, the prognosis of the high expression group was worse compared to the low expression group (all $p < 0.05$) (**Figure 4A**). Also, we investigated the correlation between these lncRNAs at different stages, and the results indicated that the expression levels of AP003555.2, BOLA3-AS1, NKILA, LINC00543, and UCA1 were significantly different between the least two stages (**Figure 4B**).

Meanwhile, in the external validation group from GEO, we constructed a model and grouped patients with four prognostic DGIA lncRNAs, including BOLA3-AS1, NKILA, LINC00543,

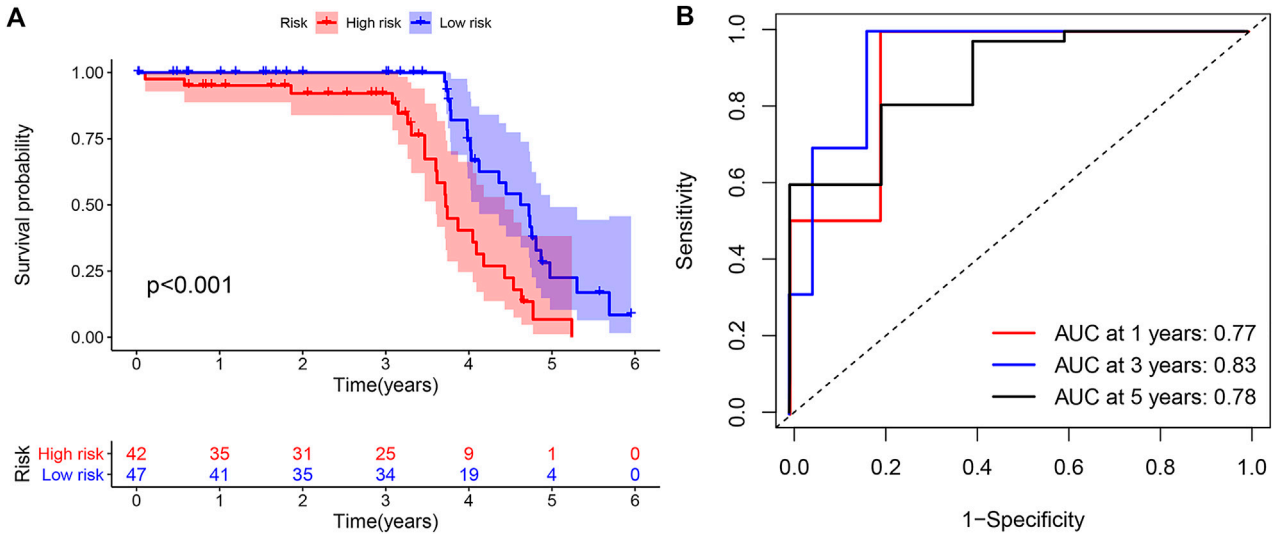

FIGURE 5 | (A) Kaplan–Meier curve of overall survival in external validation group. **(B)** TimeROC curves for 1, 3, 5 years in external validation group. TimeROC: time-dependent ROC.

and UCA1. The prognosis of HRG was also worse than that of LRG ($p < 0.001$) (**Figure 5A**). The timeROC of 1, 3, and 5 years proved that the model had a promising classification effect and that of 3 years displayed an optimum effect (AUC = 0.83) (**Figure 5B**).

Immune Infiltration and GSEA Within Different Risk Groups

The enrichment investigation mentioned above demonstrated that DGIA lncRNAs also influence immune regulation. Hence, we evaluated the differences in the infiltration of 22 immune cells in HRG and LRG according to the results of CIBERSORT. The expression of $CD8^+$ T cells in all TCGA samples and model group was lower in HRG than in LRG (**Figure 6**). $CD8^+$ T cells are cytotoxic immune cells that can kill tumor cells directly, and their abundance difference indicated the immune-related cause of the prognostic difference in HRG and LRG.

To explore the significantly altered MF, BP, and pathways in HRG and LRG, we performed GO- and KEGG-related GSEA. Mainly, immune and genomic instability-related pathways in LRG were significantly enriched. In GO enrichment terms, immune-related pathways encompassed response to type I interferon (IFN-I), natural killer cell activation, and T cell activation involved in the immune response. Simultaneously, some genomic instability-related pathways were also significantly enriched, including structural constituent of ribosome, transcription elongation from RNA polymerase II promoter, response to double-strand RNA (dsRNA), and some energy-related pathways in glucose metabolism (**Figures 7A,B**). In KEGG enrichment terms, apart from the regulation of autophagy and cytosolic DNA sensing pathway involved with genomic instability, there were also immune-related pathways, including antigen processing and presentation, and enriched cytokine receptor interaction (**Figure 7C**). Finally, we noticed that the CNSMs of LRG were significantly higher compared with HRG (all $p < 0.05$) (**Supplementary Figure S4**).

Sensitivity of Different Therapies Within Different Risk Groups

In the analysis of chemotherapy, we found that key DGIA lncRNAs and their co-expressed PCGs could reduce the sensitivity of most chemotherapy drugs, including oxaliplatin, fluorouracil, and irinotecan (new drug for CC) (**Figure 8**). As for TIs, different sensitivities were shown in HRG and LRG (**Figure 9**). In lapatinib (epidermal growth factor receptor inhibitor), AKT inhibitor VIII, and JNK Inhibitor VIII, the median IC50 of the LRG was significantly higher than that of HRG (all $p < 0.05$). In sunitinib (VEGFR inhibitor), cyclopamine (HH signaling inhibitor), and GDC.0449 (HH signaling inhibitor), the median IC50 of HRG was significantly higher than that of LRG. As for the immunosuppressive checkpoints, the expressions of PDCD1, CTLA4, TIGIT, and LAG3 were higher in LRG than those in HRG (**Figure 10**), which indicated that LRG patients could benefit potentially from immunotherapy. These results proved that the DRPM and key DGIA lncRNAs were useful in clinical therapy to some extent, and they provided predictive value for the sensitivity of multiple drugs.

DISCUSSION

The crucial role of the primary site in treatment decision-making has been progressively clarified. Around 2015, the "dispute between LCC and RCC" become one of the hotspots in CC. Tumor primary site is considered an independent prognostic factor for CC in stages III/IV. The prognosis of RCC is

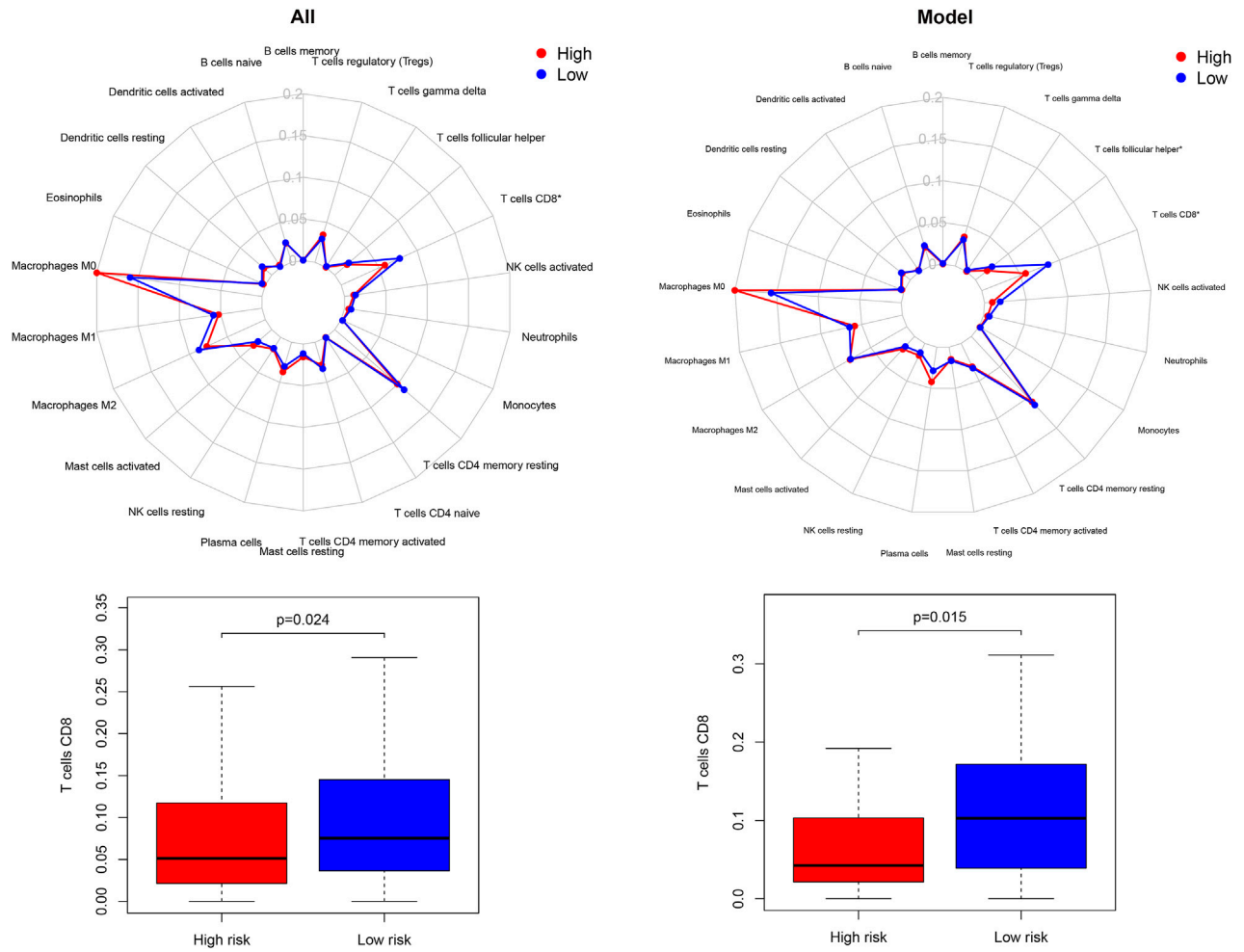

FIGURE 6 | The differences of 22 immune cell types abundance within different risk groups.

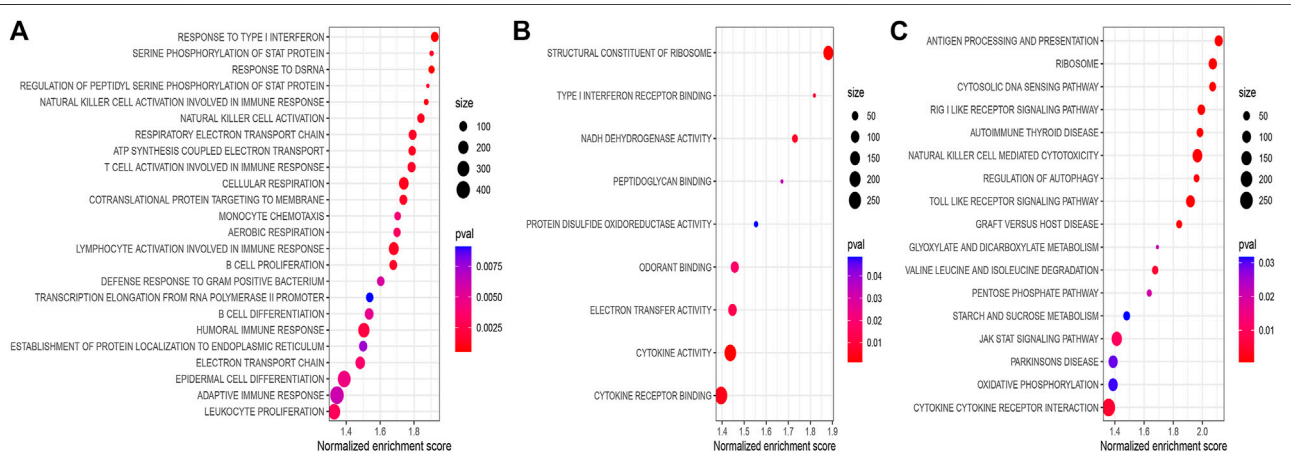

FIGURE 7 | (A) BP of GO-related GSEA between different risk groups. **(B)** MF of GO-related GSEA between different risk groups. **(C)** KEGG-related GSEA between different risk groups. BP: biological process; MF: molecular function.

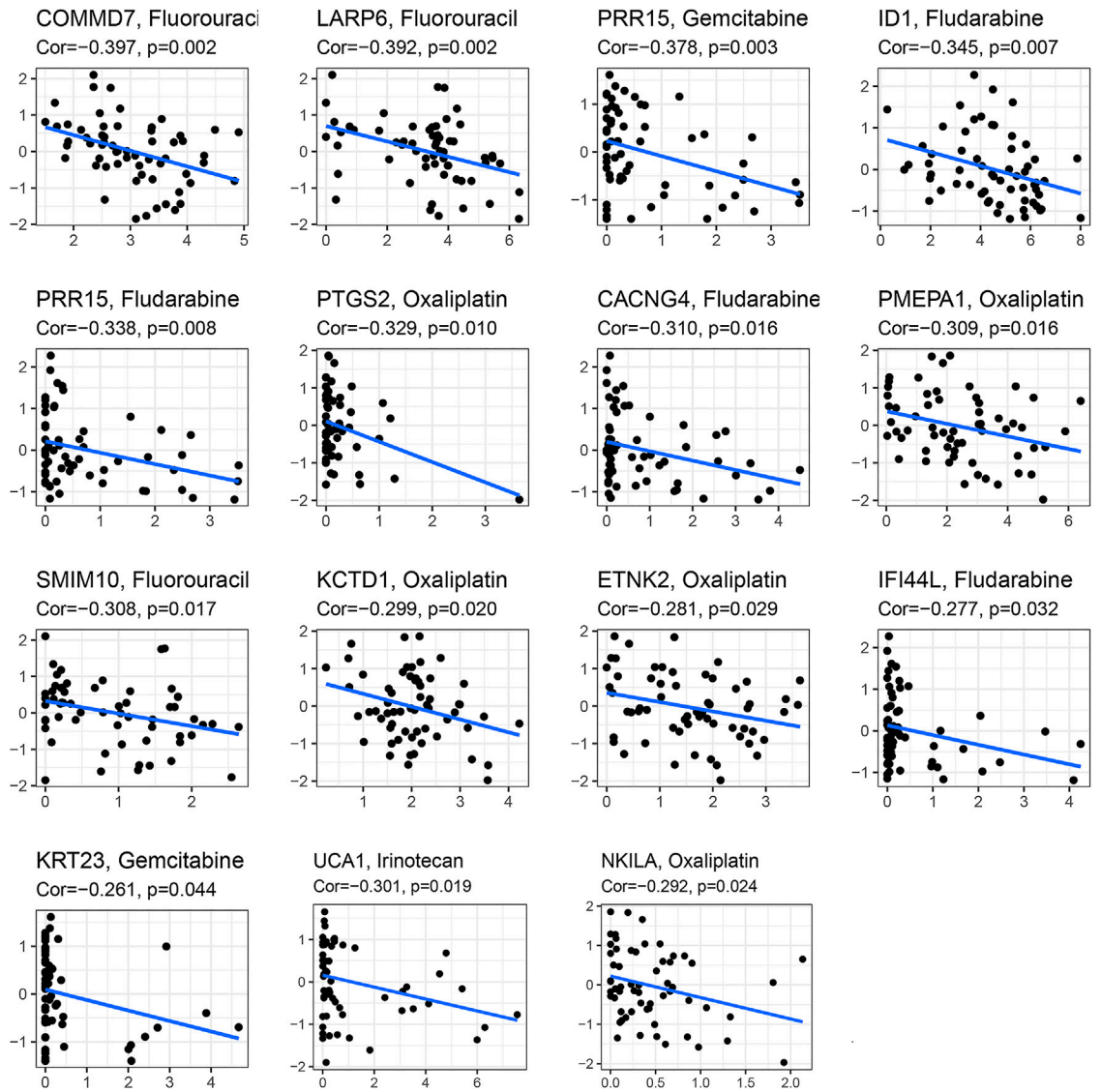

FIGURE 8 | The correlation analysis in the expression of DGIA lncRNAs and co-expressed mRNA with a sensitivity of chemotherapy drugs.

significantly worse than that of LCC, which is not related to treatment. Additionally, RCC acts as a negative predictor of EGFR-targeted therapy (Benson et al., 2017). As a matter of fact, LCC and RCC are inconsistent in many aspects (e.g., embryonic origin, anatomical blood supply, and clinical manifestations). However, the critical culprit could cause the difference in treatment response, and the prognosis is the molecular biological characteristics (Stintzing et al., 2017). Thus, drawing upon primary site alone is inadequate to formulate a treatment strategy and evaluate prognosis. Lately, it has been proclaimed that genomic instability is one of the key prognostic factors for most cancers (Andor et al., 2017). Various assays were used to assess the genomic instability by estimating the expression of certain characteristic proteins and gene mutations (Cortes-Ciriano et al., 2017; Davies et al., 2017). Moreover, with the development of gene sequencing technology, the detection of genomic instability has achieved an increased resolution (Stadler et al., 2016). In recent times, researchers have put a great effort to identify PCGs and microRNAs and to find biomarkers related to genomic instability and prognosis (Mettu et al., 2010; Habermann et al., 2011). Simultaneously, the increasing number of studies on lncRNAs also makes researchers aware of their role in genomic stability. Although many works have been done by scientists, identification of DGIA lncRNAs in LCCs and RCCs and their relationship in terms of immunity are still rarely mentioned. Therefore, we explored the influence of genomic instability in LCCs and RCCs, as well as the key prognostic DGIA lncRNAs.

We identified 123 DGIA lncRNAs from the DEGs of LCCs and RCCs. The functional analysis on their co-expressed PCGs surprisingly affirmed that these DGIA lncRNAs potentially

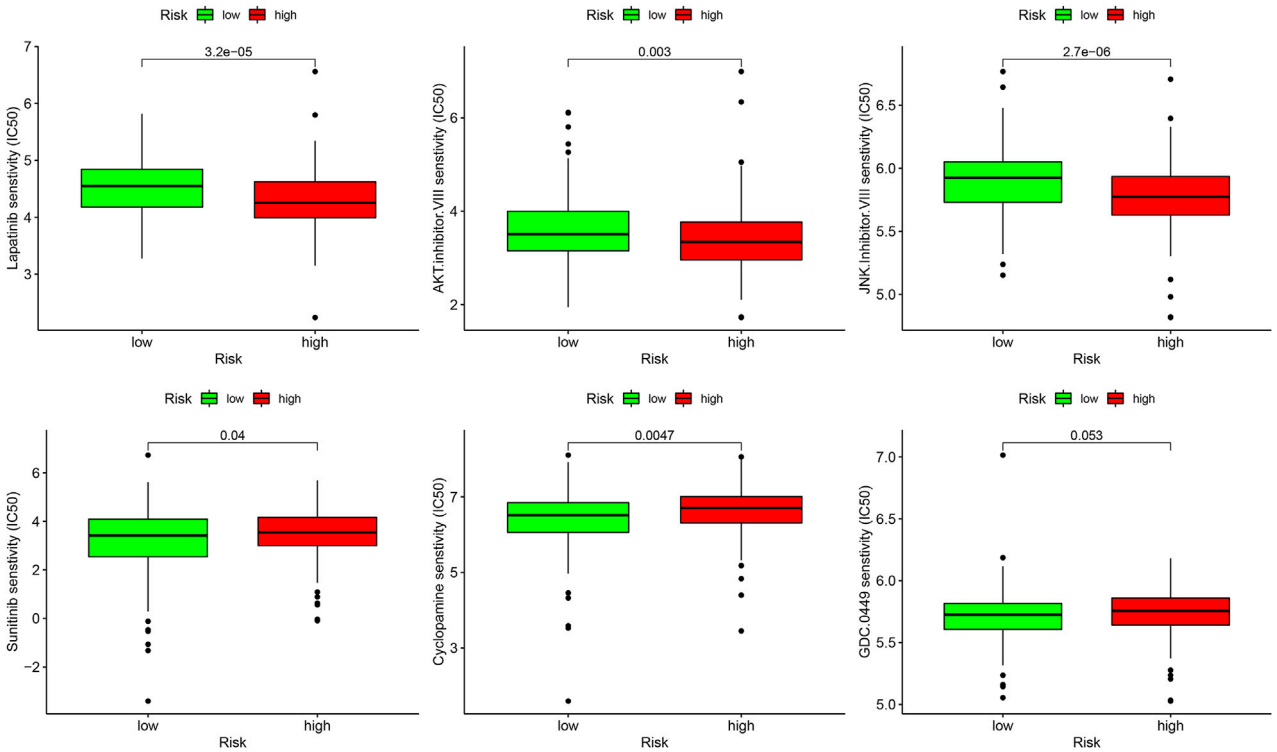

FIGURE 9 | The sensitivity difference of multiple targeted inhibitors within different risk groups.

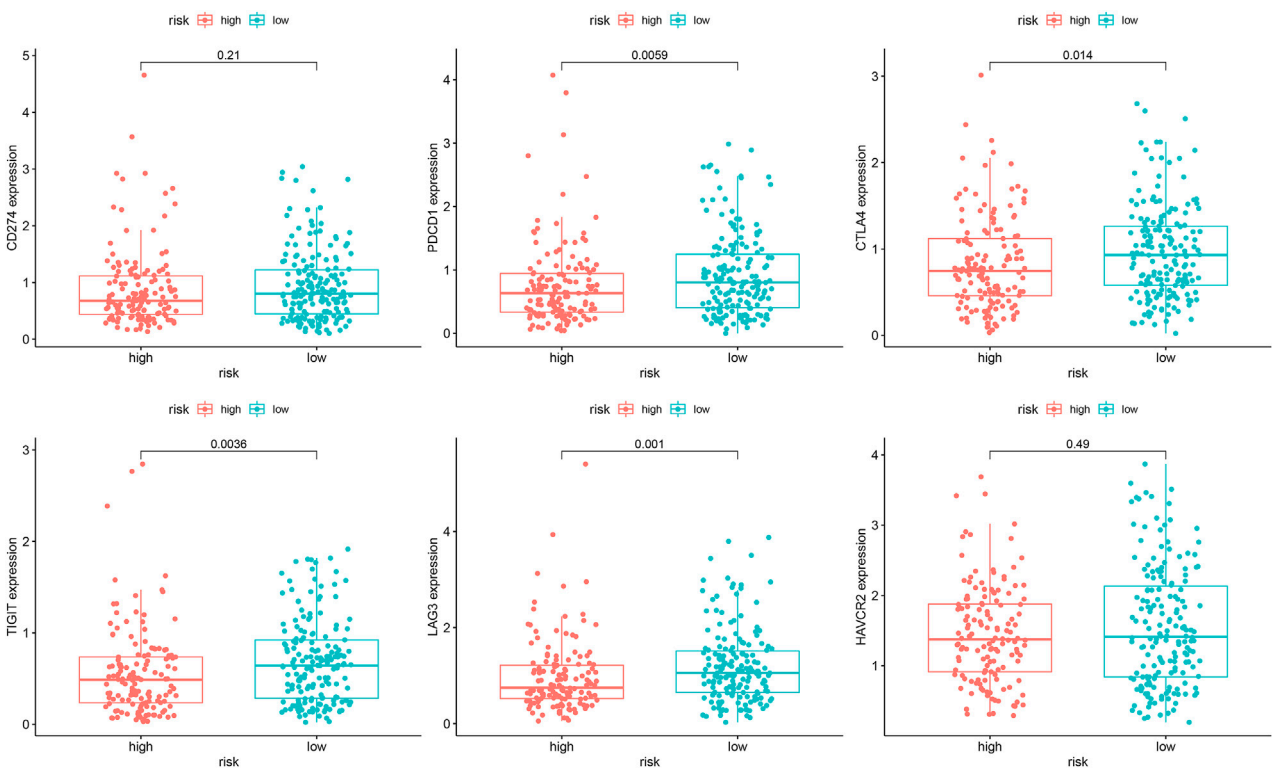

FIGURE 10 | The difference of the expression of immunosuppressive checkpoints within different risk groups.

influenced the genomic instability and immune functions through PCGs. In terms of molecular functions, the accumulation of errors during DNA transcription under the action of RNA polymerase is the source of genomic instability in all organisms (Khristich and Mirkin, 2020). Additionally, phospholipase C participates in numerous physiological processes within the cell, especially signal transduction pathways that regulate cell functions and proliferation (Jang et al., 2018; Owusu Obeng et al., 2020). These processes are also involved with genomic mutations and even lead to cancers (Koss et al., 2014). Other enriched pathways are mainly related to the positive activation and differentiation of T cells. Thus, we suspected that genomic instability could potentially cause differences in the prognosis and immunity of LCCs and RCCs.

Moreover, we investigated whether DGIA lncRNAs can identify differences in immunity while predicting clinical outcomes. Upon identification of DRPM containing six key lncRNAs, we successfully divided the patients into HRG and LRG with poor prognosis. From the study of differences in immune infiltration and the GSEA between HRG and LRG, it has been concluded that some pathways related to genetic instability in the LRG are significantly enriched, including regulation of autophagy and glucose metabolism-related pathways (**Figure 7C**). Genomic instability could induce the production of a large number of misfolded proteins, and autophagy may result in the degradation of ubiquitinated and misfolded proteins (Matsumoto et al., 2011). Autophagy has also been reported to be involved in regulating the number of centrosomes during cell division to maintain genomic instability (Watanabe et al., 2016). Besides, some pathways are associated with both genetic instability and immunity, such as the cytosolic DNA sensing pathway, response to dsRNA, RIG-I like receptor signaling pathway, and Toll-like receptor signaling pathway (**Figures 7A,C**). In somatic cells, cytoplasmic DNA sensors, after identifying the double-strand DNA (dsDNA), activate the cytosolic DNA sensing pathway and innate immune responses (Kwon and Bakhoum, 2020). These dsDNA may be endogenous and are the yields of inaccurate replication of mitochondrial DNA (mtDNA) or micronuclear DNA (Kawai and Akira, 2010; Dhir et al., 2018). dsDNA can be transformed into dsRNA by the action of RNA polymerase III for recognition by the RNA sensor RIG-I (Hur, 2019; Samuel, 2019). dsRNA can also be recognized by Toll-like receptors to induce inflammatory cytokines and IFN-I (Kawai and Akira, 2010; Miyake et al., 2018). Some pieces of research disclosed that dsRNA accumulates in the mitochondria as a result of gene deletion during transcription of mtDNA, which promotes the production of IFN-I (eliciting innate immune response) after being recognized (Dhir et al., 2018). The evidence and our enrichment results explain the potential mechanism of immune activation by genomic instability.

The immune-related pathways are also significantly enriched and $CD8^+$ T cell infiltration is higher in LRG. Antigen processing and presentation, response to IFN-I, and cytokine related pathways also provide the basis for the immune system activation processes (**Figure 7B**). CNSM in LRG is significantly higher than that in HRG (**Supplementary Figure S4**), which indicates that the degree of genetic instability is higher. Mardis suggested that genomic instability could predict immunotherapy response more accurately. Various forms of genomic instability in cancers produce new antigens and immune-responsive phenotypes eventually (Mardis, 2019). In the analysis of LCCs and RCCs, we have confirmed that genomic instability does affect the immune response and the prognosis through a series of potential mechanisms.

Finally, in terms of clinical applications, we could significantly distinguish the sensitivity of multiple drugs by using DRPM and risk grouping. Chemotherapy has been routinely used in CC therapy, but the therapeutic effects of TIs have not been confirmed effectively (Shen et al., 2015) and a little fraction of patients benefit from immunotherapy (Lichtenstern et al., 2020). It is important to identify the patients who benefit from these treatments. We found that a variety of TIs had significant differences in sensitivity between HRG and LRG, including VEGFR inhibitor and HH inhibitors. HH has been proved to be the stemness-related signals of cancer stem cells (CSCs) (Grazioli et al., 2017; Grund-Gröschke et al., 2019). CSCs are sparks for igniting tumor recurrence and the instigators of low response to immunotherapy and drug resistance. CSCs promote the development of cancer and immunosuppression through their stemness-related signals (Lytle et al., 2018). Therefore, it has great potential to develop TIs, and the results of our research provide references for their application in CC. Meanwhile, we found that the gene expression of immunosuppressive checkpoints, T cell infiltration, and immune-related pathways was significantly enriched in LRG. In cancers with overactive T cell regulatory pathways, immune checkpoint inhibitors have been shown to be an effective strategy to enhance the anti-tumor effect and clinical impact of T cell (Hargadon et al., 2018). Therefore, we speculate that patients in the low-risk group could benefit from immunotherapy. However, the effect of immunotherapy in patients with colon cancer still needs to be further investigated.

The main limitations are as follows: firstly, while using GEO data for the verification of key lncRNAs predictive effects, two key lncRNAs were missed. Although the classification effect was propitious, the verification was not sufficient. In this regard, we examined the prognosis and clinical characteristics of all key lncRNAs to support the evidence. Secondly, we defined a mutator hypothesis-derived calculation method to evaluate genomic instability. An in-depth study is required to corroborate the functionality and significance of this method.

CONCLUSION

We constructed DRPM based on the DGIA lncRNAs of LCCs and RCCs. Apart from using DRPM to predict the prognosis, we also deeply investigated the effect and mechanism of genetic instability on immunity. Meanwhile, six key DGIA lncRNAs were identified. They can not only predict the prognostic risk of patients but also serve as biomarkers for evaluating the differences of genetic instability and immune infiltration. The findings of our research can provide some basis for identifying the sensitivities of multiple treatments through genetic instability.

AUTHOR'S NOTE

This is the pre-peer-reviewed version of the article: Junnan Guo, Tianyi Xia, Shenhui Deng et al. Differential Genomic Instability-Associated LncRNAs Predict Differences of Clinical Outcome and Immunity in Left- And Right- Sided Colon Adenocarcinoma, February 04, 2021, PREPRINT (Version 1) available at Research Square [https://doi.org/10.21203/rs.3.rs-175488/v1] (Junnan et al., 2021), which has been published in final form at Research Square. We have confirmed the text is our deposition as pre-print of this manuscript at Research Square (https://www.researchsquare.com/article/rs-175488/v1). This article may be used for non-commercial purposes in accordance with Frontiers Terms and Conditions for Use of Self-Archived Versions.

DATA AVAILABILITY STATEMENT

Publicly available datasets were analyzed in this study. This data can be found here: https://portal.gdc.cancer.gov and https://www.ncbi.nlm.nih.gov/gds/.

AUTHOR CONTRIBUTIONS

B-BC and Y-LL designed the study. J-NG and T-YX drafted the manuscript. J-NG and S-HD collected, analyzed, and interpreted the data. J-NG, W-NX, and S-HD drew the figures and tables. B-BC and Y-LL helped with the final revision of the article. All authors have read and approved the final manuscript.

FUNDING

This work was supported by the Natural Science Foundation of Heilongjiang Province of China (ZD2017019), Nn10 Program of Harbin Medical University Cancer Hospital (Nn102017-02), Post-doctoral Scientific Research Developmental Fund of Heilongjiang (LBH-Q18085), and Harbin Medical University Cancer Hospital Preeminence Youth Fund (JCQN 2019-04).

SUPPLEMENTARY MATERIAL

The Supplementary Material for this article can be found online at: https://www.frontiersin.org/articles/10.3389/fmolb.2021.668888/full#supplementary-material

Supplementary Figure S1 | Overall flowchart of this study.

Supplementary Figure S2 | **(A)** In order to achieve a scale-free co-expression network, we chose power index = 3 as the appropriate soft threshold. **(B)** Identification of a co-expression module. The branches of the dendrogram correspond to 6 different gene modules.

Supplementary Figure S3 | Kaplan-Meier curves of HRG and LRG were plotted through stratification of different clinical factors. HRG and LRG, respectively.

Supplementary Figure S4 | The differences of CNSMs between HRG and LRG.

REFERENCES

Andor, N., Maley, C. C., and Ji, H. P. (2017). Genomic Instability in Cancer: Teetering on the Limit of Tolerance. *Cancer Res.* 77 (9), 2179–2185. doi:10.1158/0008-5472.CAN-16-1553

Baran, B., Mert Ozupek, N., Yerli Tetik, N., Acar, E., Bekcioglu, O., and Baskin, Y. (2018). Difference between Left-Sided and Right-Sided Colorectal Cancer: A Focused Review of Literature. *Gastroenterol. Res.* 11 (4), 264–273. doi:10.14740/gr1062w

Bebenek, A. (2008). DNA Replication Fidelity. *Postepy Biochem.* 54 (1), 43–56.

Benson, A. B., 3rd, Venook, A. P., Cederquist, L., Chan, E., Chen, Y. J., Cooper, H. S., et al. (2017). Colon Cancer, Version 1.2017, NCCN Clinical Practice Guidelines in Oncology. *J. Natl. Compr. Canc Netw.* 15 (3), 370–398. doi:10.6004/jnccn.2017.0036

Blakely, A. M., Lafaro, K. J., Eng, O. S., Ituarte, P. H. G., Fakih, M., Lee, B., et al. (2020). The Association of Tumor Laterality and Survival After Cytoreduction for Colorectal Carcinomatosis. *J. Surg. Res.* 248, 20–27. doi:10.1016/j.jss.2019.10.001

Boulianne, B., and Feldhahn, N. (2018). Transcribing Malignancy: Transcription-Associated Genomic Instability in Cancer. *Oncogene* 37 (8), 971–981. doi:10.1038/onc.2017.402

Cortes-Ciriano, I., Lee, S., Park, W.-Y., Kim, T.-M., and Park, P. J. (2017). A Molecular Portrait of Microsatellite Instability across Multiple Cancers. *Nat. Commun.* 8, 15180. doi:10.1038/ncomms15180

Davies, H., Glodzik, D., Morganella, S., Yates, L. R., Staaf, J., Zou, X., et al. (2017). HRDetect Is a Predictor of BRCA1 and BRCA2 Deficiency Based on Mutational Signatures. *Nat. Med.* 23 (4), 517–525. doi:10.1038/nm.4292

Dhir, A., Dhir, S., Borowski, L. S., Jimenez, L., Teitell, M., Rötig, A., et al. (2018). Mitochondrial Double-Stranded RNA Triggers Antiviral Signalling in Humans. *Nature* 560 (7717), 238–242. doi:10.1038/s41586-018-0363-0

Friedman, J., Hastie, T., and Tibshirani, R. (2010). Regularization Paths for Generalized Linear Models via Coordinate Descent. *J. Stat. Softw.* 33 (1), 1–22. doi:10.18637/jss.v033.i01

Geeleher, P., Cox, N., and Huang, R. S. (2014). pRRophetic: an R Package for Prediction of Clinical Chemotherapeutic Response from Tumor Gene Expression Levels. *PLoS One* 9 (9), e107468. doi:10.1371/journal.pone.0107468

Grass, F., Lovely, J. K., Crippa, J., Ansell, J., Hübner, M., Mathis, K. L., et al. (2019). Comparison of Recovery and Outcome after Left and Right Colectomy. *Colorectal Dis.* 21 (4), 481–486. doi:10.1111/codi.14543

Grazioli, P., Felli, M. P., Screpanti, I., and Campese, A. F. (2017). The Mazy Case of Notch and Immunoregulatory Cells. *J. Leukoc. Biol.* 102 (2), 361–368. doi:10.1189/jlb.1VMR1216-505R

Grund-Gröschke, S., Stockmaier, G., and Aberger, F. (2019). Hedgehog/GLI Signaling in Tumor Immunity - New Therapeutic Opportunities and Clinical Implications. *Cell Commun Signal* 17 (1), 172. doi:10.1186/s12964-019-0459-7

Guinney, J., Dienstmann, R., Wang, X., de Reyniès, A., Schlicker, A., Soneson, C., et al. (2015). The Consensus Molecular Subtypes of Colorectal Cancer. *Nat. Med.* 21 (11), 1350–1356. doi:10.1038/nm.3967

Habermann, J. K., Brucker, C. A., Freitag-Wolf, S., Heselmeyer-Haddad, K., Krüger, S., Barenboim, L., et al. (2011). Genomic Instability and Oncogene Amplifications in Colorectal Adenomas Predict Recurrence and Synchronous Carcinoma. *Mod. Pathol.* 24 (4), 542–555. doi:10.1038/modpathol.2010.217

Hansen, I. O., and Jess, P. (2012). Possible Better Long-Term Survival in Left versus Right-Sided colon Cancer - a Systematic Review. *Dan Med. J.* 59 (6), A4444.

Hargadon, K. M., Johnson, C. E., and Williams, C. J. (2018). Immune Checkpoint Blockade Therapy for Cancer: An Overview of FDA-Approved Immune Checkpoint Inhibitors. *Int. Immunopharmacol.* 62, 29–39. doi:10.1016/j.intimp.2018.06.001

Heagerty, P. J., and Zheng, Y. (2005). Survival Model Predictive Accuracy and ROC Curves. *Biometrics* 61 (1), 92–105. doi:10.1111/j.0006-341X.2005.030814.x

Hur, S. (2019). Double-Stranded RNA Sensors and Modulators in Innate Immunity. *Annu. Rev. Immunol.* 37, 349–375. doi:10.1146/annurev-immunol-042718-041356

Jang, H.-J., Suh, P.-G., Lee, Y. J., Shin, K. J., Cocco, L., and Chae, Y. C. (2018). PLCγ1: Potential Arbitrator of Cancer Progression. *Adv. Biol. Regul.* 67, 179–189. doi:10.1016/j.jbior.2017.11.003

Junnan, G., Tianyi, X., Shenhui, D., Binbin, C., and Yanlong, L. (2021). Differential Genomic Instability-Associated LncRNAs Predict Differences of Clinical Outcome and Immunity in Left- and Right- Sided Colon Adenocarcinoma. *Res. Square*. doi:10.21203/rs.3.rs-175488/v1

Kawai, T., and Akira, S. (2010). The Role of Pattern-Recognition Receptors in Innate Immunity: Update on Toll-like Receptors. *Nat. Immunol.* 11 (5), 373–384. doi:10.1038/ni.1863

Khristich, A. N., and Mirkin, S. M. (2020). On the Wrong DNA Track: Molecular Mechanisms of Repeat-Mediated Genome Instability. *J. Biol. Chem.* 295 (13), 4134–4170. doi:10.1074/jbc.REV119.007678

Koss, H., Bunney, T. D., Behjati, S., and Katan, M. (2014). Dysfunction of Phospholipase Cγ in Immune Disorders and Cancer. *Trends Biochem. Sci.* 39 (12), 603–611. doi:10.1016/j.tibs.2014.09.004

Kwon, J., and Bakhoum, S. F. (2020). The Cytosolic DNA-Sensing cGAS-STING Pathway in Cancer. *Cancer Discov.* 10 (1), 26–39. doi:10.1158/2159-8290.CD-19-0761

Langfelder, P., and Horvath, S. (2008). WGCNA: an R Package for Weighted Correlation Network Analysis. *BMC Bioinf.* 9, 559. doi:10.1186/1471-2105-9-559

Laska, E., Meisner, M., and Wanderling, J. (2012). A Maximally Selected Test of Symmetry about Zero. *Statist. Med.* 31 (26), 3178–3191. doi:10.1002/sim.5384

Lichtenstern, C. R., Ngu, R. K., Shalapour, S., and Karin, M. (2020). Immunotherapy, Inflammation and Colorectal Cancer. *Cells* 9 (3), 618. doi:10.3390/cells9030618

Lytle, N. K., Barber, A. G., and Reya, T. (2018). Stem Cell Fate in Cancer Growth, Progression and Therapy Resistance. *Nat. Rev. Cancer* 18 (11), 669–680. doi:10.1038/s41568-018-0056-x

Mardis, E. R. (2019). Neoantigens and Genome Instability: Impact on Immunogenomic Phenotypes and Immunotherapy Response. *Genome Med.* 11 (1), 71. doi:10.1186/s13073-019-0684-0

Matsumoto, G., Wada, K., Okuno, M., Kurosawa, M., and Nukina, N. (2011). Serine 403 Phosphorylation of p62/SQSTM1 Regulates Selective Autophagic Clearance of Ubiquitinated Proteins. *Mol. Cel* 44 (2), 279–289. doi:10.1016/j.molcel.2011.07.039

Mettu, R. K. R., Wan, Y.-W., Habermann, J. K., Ried, T., and Guo, N. L. (2010). A 12-Gene Genomic Instability Signature Predicts Clinical Outcomes in Multiple Cancer Types. *Int. J. Biol. Markers* 25 (4), 219–228. doi:10.5301/jbm.2010.6079

Miyake, K., Shibata, T., Ohto, U., Shimizu, T., Saitoh, S.-I., Fukui, R., et al. (2018). Mechanisms Controlling Nucleic Acid-Sensing Toll-like Receptors. *Int. Immunol.* 30 (2), 43–51. doi:10.1093/intimm/dxy016

Mjelle, R., Sjursen, W., Thommesen, L., Sætrom, P., and Hofsli, E. (2019). Small RNA Expression from Viruses, Bacteria and Human miRNAs in colon Cancer Tissue and its Association with Microsatellite Instability and Tumor Location. *BMC Cancer* 19 (1), 161. doi:10.1186/s12885-019-5330-0

Molina-Cerrillo, J., San Román, M., Pozas, J., Alonso-Gordoa, T., Pozas, M., Conde, E., et al. (2020). BRAF Mutated Colorectal Cancer: New Treatment Approaches. *Cancers* 12 (6), 1571. doi:10.3390/cancers12061571

Newman, A. M., Liu, C. L., Green, M. R., Gentles, A. J., Feng, W., Xu, Y., et al. (2015). Robust Enumeration of Cell Subsets from Tissue Expression Profiles. *Nat. Methods* 12 (5), 453–457. doi:10.1038/nmeth.3337

Owusu Obeng, E., Rusciano, I., Marvi, M. V., Fazio, A., Ratti, S., Follo, M. Y., et al. (2020). Phosphoinositide-Dependent Signaling in Cancer: A Focus on Phospholipase C Isozymes. *Ijms* 21 (7), 2581. doi:10.3390/ijms21072581

Requena, D. O., and Garcia-Buitrago, M. (2020). Molecular Insights into Colorectal Carcinoma. *Arch. Med. Res.* 51 (8), 839–844. doi:10.1016/j.arcmed.2020.09.014

Ritchie, M. E., Phipson, B., Wu, D., Hu, Y., Law, C. W., Shi, W., et al. (2015). Limma powers Differential Expression Analyses for RNA-Sequencing and Microarray Studies. *Nucleic Acids Res.* 43 (7), e47. doi:10.1093/nar/gkv007

Samuel, C. E. (2019). Adenosine Deaminase Acting on RNA (ADAR1), a Suppressor of Double-Stranded RNA-Triggered Innate Immune Responses. *J. Biol. Chem.* 294 (5), 1710–1720. doi:10.1074/jbc.TM118.004166

Schröder, M. S., Culhane, A. C., Quackenbush, J., and Haibe-Kains, B. (2011). Survcomp: an R/Bioconductor Package for Performance Assessment and Comparison of Survival Models. *Bioinformatics* 27 (22), 3206–3208. doi:10.1093/bioinformatics/btr511

Shen, H., Yang, J., Huang, Q., Jiang, M. J., Tan, Y. N., Fu, J. F., et al. (2015). Different Treatment Strategies and Molecular Features between Right-Sided and Left-Sided colon Cancers. *Wjg* 21 (21), 6470–6478. doi:10.3748/wjg.v21.i21.6470

Siegel, R. L., Miller, K. D., and Jemal, A. (2020). Cancer Statistics, 2020. *CA A. Cancer J. Clin.* 70 (1), 7–30. doi:10.3322/caac.21590

Stadler, Z. K., Battaglin, F., Middha, S., Hechtman, J. F., Tran, C., Cercek, A., et al. (2016). Reliable Detection of Mismatch Repair Deficiency in Colorectal Cancers Using Mutational Load in Next-Generation Sequencing Panels. *Jco* 34 (18), 2141–2147. doi:10.1200/JCO.2015.65.1067

Stintzing, S., Tejpar, S., Gibbs, P., Thiebach, L., and Lenz, H.-J. (2017). Understanding the Role of Primary Tumour Localisation in Colorectal Cancer Treatment and Outcomes. *Eur. J. Cancer* 84, 69–80. doi:10.1016/j.ejca.2017.07.016

Subramanian, A., Tamayo, P., Mootha, V. K., Mukherjee, S., Ebert, B. L., Gillette, M. A., et al. (2005). Gene Set Enrichment Analysis: a Knowledge-Based Approach for Interpreting Genome-wide Expression Profiles. *Proc. Natl. Acad. Sci.* 102 (43), 15545–15550. doi:10.1073/pnas.0506580102

Thapar, R. (2018). Regulation of DNA Double-Strand Break Repair by Non-coding RNAs. *Molecules* 23 (11), 2789. doi:10.3390/molecules23112789

Verkuijl, S. J., Jonker, J. E., Trzpis, M., Burgerhof, J. G. M., Broens, P. M. A., and Furnée, E. J. B. (2021). Functional Outcomes of Surgery for colon Cancer: A Systematic Review and Meta-Analysis. *Eur. J. Surg. Oncol.* 47, 960–969. doi:10.1016/j.ejso.2020.11.136

Watanabe, Y., Honda, S., Konishi, A., Arakawa, S., Murohashi, M., Yamaguchi, H., et al. (2016). Autophagy Controls Centrosome Number by Degrading Cep63. *Nat. Commun.* 7, 13508. doi:10.1038/ncomms13508

Witten, D. M., and Tibshirani, R. (2010). A Framework for Feature Selection in Clustering. *J. Am. Stat. Assoc.* 105 (490), 713–726. doi:10.1198/jasa.2010.tm09415

Wu, C. (2018). Systemic Therapy for Colon Cancer. *Surg. Oncol. Clin. North America* 27 (2), 235–242. doi:10.1016/j.soc.2017.11.001

Yu, G., Wang, L.-G., Han, Y., and He, Q.-Y. (2012). clusterProfiler: an R Package for Comparing Biological Themes Among Gene Clusters. *OMICS: A J. Integr. Biol.* 16 (5), 284–287. doi:10.1089/omi.2011.0118

Conflict of Interest: The authors declare that the research was conducted in the absence of any commercial or financial relationships that could be construed as a potential conflict of interest.

Publisher's Note: All claims expressed in this article are solely those of the authors and do not necessarily represent those of their affiliated organizations, or those of the publisher, the editors, and the reviewers. Any product that may be evaluated in this article, or claim that may be made by its manufacturer, is not guaranteed or endorsed by the publisher.

frontiers in Cell and Developmental Biology

ORIGINAL RESEARCH
published: 14 September 2021
doi: 10.3389/fcell.2021.730558

PPA1 Promotes Breast Cancer Proliferation and Metastasis Through PI3K/AKT/GSK3β Signaling Pathway

Chunlei Guo[1,2†], Shuang Li[1,2†], Ang Liang[3], Mengchao Cui[1,2], Yunwei Lou[1,2] and Hui Wang[1,2]*

[1] Henan Key Laboratory of Immunology and Targeted Drugs, School of Laboratory Medicine, Xinxiang Medical University, Xinxiang, China, [2] Henan Collaborative Innovation Center of Molecular Diagnosis and Laboratory Medicine, Xinxiang Medical University, Xinxiang, China, [3] School of Nursing, Xinxiang Medical University, Xinxiang, China

OPEN ACCESS

Edited by:
Na Luo,
Nankai University, China

Reviewed by:
Guang Yang,
Tianjin Medical University Cancer Institute and Hospital, China
Xiaolong Tang,
Shenzhen University Health Science Centre, China
Yizhou Jiang,
Shenzhen University, China

***Correspondence:**
Hui Wang
wanghui@xxmu.edu.cn

[†] These authors have contributed equally to this work and share first authorship

Specialty section:
This article was submitted to Molecular and Cellular Pathology, a section of the journal Frontiers in Cell and Developmental Biology

Received: 25 June 2021
Accepted: 25 August 2021
Published: 14 September 2021

Citation:
Guo C, Li S, Liang A, Cui M, Lou Y and Wang H (2021) PPA1 Promotes Breast Cancer Proliferation and Metastasis Through PI3K/AKT/GSK3β Signaling Pathway. Front. Cell Dev. Biol. 9:730558. doi: 10.3389/fcell.2021.730558

Breast cancer is the most common malignancy among women. Inorganic pyrophosphatase 1 (PPA1) is a multifunctional protein involved in the development of several tumors. However, the role of PPA1 in breast cancer progression remains unclear. In this study, we found that PPA1 was highly expressed in breast cancer compared to its levels in normal breast tissue and that it was correlated with breast cancer clinicopathological characteristics, as well as poor survival in breast cancer patients. Silencing PPA1 restrained breast cancer proliferation and metastasis by regulating Slug-mediated epithelial-mesenchymal transition (EMT). Opposite results were observed following PPA1 overexpression. In addition, investigation of the underlying mechanism demonstrated that PPA1 ablation led to decrease phosphatidylinositol 3 kinase (PI3K) phosphorylation levels and attenuate phosphorylated AKT and glycogen synthase kinase-3 β (GSK3β), while ectopic PPA1 expression had the opposite effects. Moreover, PI3K inhibitors suppress the signaling pathways mediating the effects of PPA1 on breast cancer, resulting in tumor growth and metastasis suppression *in vitro* and *in vivo*. In summary, our results verify that PPA1 can act as an activator of PI3K/AKT/GSK3β/Slug-mediated breast cancer progression and that it is a potential therapeutic target for the inhibition of tumor progression.

Keywords: PPA1, breast cancer, EMT, metastasis, proliferation

INTRODUCTION

Breast cancer is the most common female malignancy and a major cause of cancer-related mortality among women worldwide (Li et al., 2021; Siegel et al., 2021). Globally, although remarkable advancements have been achieved in the detection and treatment of breast cancer, the lethality is still severe (Cai et al., 2018; Fan et al., 2020).

The high mortality of breast cancer patients is mainly attributed to distal metastases, such as lung, bone, and lymph nodes metastases (Davis et al., 2020). Metastasis is a multistep process that includes tumor cells epithelial-mesenchymal transition (EMT), cytoskeleton reorganization, and microenvironment remodeling (Sleeman and Thiery, 2011; Cui et al., 2021). It is imperative to understand the detailed molecular mechanism involved in EMT for efficient identification of novel therapeutic targets and the development of effective treatment strategies for breast cancer.

The EMT is a complicated development process in which epithelial cells get deprived of polarity and transform into highly motile mesenchymal cells (Pastushenko et al., 2018; Xu et al., 2020). Profound changes in cell motility and morphology enable cells to travel long distances and integrate into surrounding tissues or remote organs (Chaffer et al., 2016). Furthermore, EMT contributes to tumor progression by granting aggressive traits to tumor cells, such as cell migration and other invasive properties that facilitate them departure from the epithelial cell community and arrival at the site of future migration (Popper, 2020). Therefore, EMT plays an important role in tumor metastasis.

Inorganic pyrophosphatase 1 (PPA1) catalyzes the hydrolysis of inorganic pyrophosphate (PPi) into inorganic phosphates (Pi). Therefore, it plays critical roles in multiple cellular metabolic processes, such as nucleic acid, proteins and carbohydrates synthesis, and neurite growth, owing to its highly catalytic property (Baykov et al., 1999). Meanwhile, it also provides extra energy source besides ATP (Li et al., 2018), which is indispensable for accelerating tumor growth and development (Yazdani et al., 2019).

Recently, proteomic studies have demonstrated that PPA1 was overexpressed in various types of malignancies, such as colorectal cancer (Tomonaga et al., 2004), ovarian cancer (Giri et al., 2014), lung adenocarcinoma (Chen et al., 2002), hepatocellular carcinoma (Megger et al., 2013), and prostate cancer (Lexander et al., 2005), compared to its levels in normal tissues. Notably, PPA1 was considered a negative prognostic marker of gastric cancer and participated in cancer-related metabolic alterations (Yang et al., 2015). Moreover, Bodnar et al. (2016) reported that PPA1 may be considered as biomarker of metastasis in laryngeal squamous cell carcinoma, and Luo et al. (2019) illustrated that ectopic PPA1 expression ameliorated cell proliferation properties in non-small cell lung cancer. Therefore, the association of PPA1 to cell proliferation and metastasis in cancer is undisputable. However, the significance of PPA1 expression and its role in breast cancer remains unclear. The mechanisms underlying these potential functions also require further investigation.

Our study demonstrated that PPA1 plays an important role in breast cancer progression for the first time and we extensively explored its functions *in vitro* and *in vivo*. We found that PPA1 was significantly upregulated in the tissues of patients with breast cancer, and its expression was correlated with clinicopathological characteristics. Meanwhile, cell-based and mouse models studies indicated that PPA1 promoted proliferation, migration, and invasion of breast cancer. Moreover, we provided evidence for its effect on EMT process. In particular, we found that overexpression of PPA1 enhanced EMT under Slug stimulation. Finally, we investigated the mechanism of action of PPA1 in breast cancer progression. Taken together, these findings provide novel insight into how PPA1 regulates tumor metastasis, suggesting its potential as a therapeutic target in breast cancer.

MATERIALS AND METHODS

Cell Culture

Human breast cancer cell line T47D and MDA-MB-231 were purchased from American Type Culture Collection (ATCC). T47D cells were cultured in high glucose Dulbecco's Modified Eagle's Medium (Gibco, Waltham, MA, United States) supplemented with 10% fetal bovine serum (FBS), 100 U/mL penicillin, 0.1 mg/mL streptomycin and 1% non-essential amino acid (NEAA) solution (Gibco). And the cells were maintained in the incubator at 37°C and in the presence of 5% CO_2. MDA-MB-231 cells were cultured in L-15 medium (Gibco, Waltham, MA, United States) supplemented with 10% FBS, 100 U/mL penicillin, 0.1 mg/mL streptomycin. The cells were maintained in the incubator at 37°C.

Vector Construction and Stable Cell Line Establishment

In order to better analyze the correlation between PPA1 and breast cancer progression, we hope to choose the cell line with relatively lower expression level at basal status for overexpression assays and with relatively higher expression level for knockdown assays. Meanwhile, we would like to select the cell line with high malignancy and aggressively metastatic characteristics for overexpression, and study the role of PPA1 in different molecular subtypes of breast cancer. For above considerations, we choose T47D for knockdown and MDA-MB-231 for overexpression assays.

To stably knockdown PPA1 in breast cancer cells, T47D cells were infected with lentivirus carrying pLV-H1-shPPA1-puro or pLV-H1-shRNA-scramble-puro plasmid, then treated with puromycin to obtain the stable cell line with PPA1 silencing (shPPA1) and the shRNA control. The sequences of shRNAs were: shPPA1#1: GCTACTGTGGACTGGTTTA; shPPA1#2: GGAATCAGTTGCATGAATA; shRNA control: GCTACACTATCGAGCAATT.

For the stable overexpression of PPA1 in mammalian cells, the cDNA of *PPA1* was inserted into the pLV-EF1α-MCS-IRES-Bsd plasmid. MDA-MB-231 cells were infected with lentivirus carrying the recombinant plasmid and empty plasmid which was used as the control. Cells were selected using blasticidin to generate stable cell lines with PPA1 overexpression and their control.

Western Blotting

Cell lysates were prepared from T47D and MDA-MB-231 with RIPA buffer containing protease inhibitor cocktail, phosphatase inhibitor cocktails 2 and 3 (Sigma-Aldrich, St Louis, MO, United States). Proteins (20–40 μg) were loaded onto 10–15% Tris-Acrylamide gels and blotted with primary antibodies that included: anti-PPA1 (Cat. # HPA019878, Sigma, St. Louis MO), anti-β-actin (sc-47778, Santa Cruz Biotechnology Inc., Santa Cruz, CA), anti-E-cadherin, N-cadherin, Vimentin, ZO-1, Claudin-1, Slug, PI3K, p-PI3K (Tyr458), AKT, p-AKT (Ser473), p-GSK3β (Ser9), P38, p-P38 (Thr180/Tyr182), JNK, p-JNK (Thr183/Tyr185), (Cat. # 3195, Cat. # 13116, Cat. # 5741, Cat. # 8193, Cat. # 13255, Cat. # 9585, Cat. # 4292, Cat. # 4228, Cat. # 4691, Cat. # 4060, Cat. # 5558, Cat. # 8690, Cat. # 9216, Cat. # 9252, Cat. # 4668, Cell Signal Technology Inc., Danvers, MA, United States), anti-Ki67 (Cat. # ab16667, Abcam Inc., Cambridge, United Kingdom), and followed by incubation with horseradish peroxidase-conjugated secondary antibodies

(Santa Cruz Biotechnology, Inc., Santa Cruz, CA). Images were acquired using the Amersham Imager 600RGB detection system (GE Healthcare).

Real-Time PCR

Total RNA was extracted from cells using the TRIZOL reagent and reverse transcription was performed using the M-MLV reverse transcriptase (Promega, Madison, MI). Real-time PCR was performed using the TransStart Green qPCR Super Mix Kit (TransGen Biotech, Beijing, China). The $2^{-\Delta\Delta Ct}$ method was used to obtain the relative fold changes. The primers for human *GAPDH* were CTCTGATTTGGTCGTATTGGG and TGGAAGATGGTGATGGGATT. The primers for human *PPA1* were CGCTATGTTGCGAATTTGTTC and CCAGTATGTTTATCATTGTGCC.

Transwell Assay

Transwell chambers were pre-coated with Matrigel. The bottom chamber was filled with culture medium containing 10% FBS. Equal amounts of cells were plated in the upper chamber in serum-free medium. After 12–24 h, the invasive cells were fixed and stained with 0.5% crystal violet. Then, we used microscope to observe the invasive cells.

Wound Healing Assay

For each test, T47D or MDA-MB-231 cells were seeded in plates. When the cells reached full confluence, a "wound" was created in the middle of the culture plate and the concentration of the serum in culture medium was changed from 10 to 1% to avoid the influence of cell growth rate on wound healing. The wound healing process was recorded at 0, 12, and 24 h after wound creation. The wound healing rate was quantified as the distance between the wound recovered compared to that of the original wound.

Cell Proliferation Assay

Cell proliferation was measured using the Cell Counting Kit-8 (CCK-8). Equal amounts of cells were seeded in 96-well plates. At designated time points (0, 24, 48, 72, and 96 h), the CCK-8 reagent was added to each well and then incubated for 2 h. Finally, the absorbance was measured at 450 nm.

Immunohistochemistry and Tissue Microarrays

The tissue microarray used for the analysis of PPA1 expression in breast cancer were purchased from Biomax Inc. (Cat. # BR2086, Rockville, United States). Immunohistochemistry (IHC) was performed on tissue microarray using antibodies against PPA1 at 1:200 dilution. The expression level of PPA1 was evaluated according to the percentage of positive cells and its staining intensity in each tumor tissue. The percentage of positive cells was separated into $< 10\%$, 10%–29%, 30%–49%, and $\geq 50\%$ subgroups, which were scored as 1, 2, 3, and 4, respectively. The staining intensities were evaluated as negative, weak, moderate, and strong, which were scored as 1, 2, 3, and 4, respectively. The cell percentage score and staining intensity score were multiplied to obtain the IHC score.

Immunofluorescence

Cells grown on glass slides were fixed in 4% paraformaldehyde and labeled with primary antibodies overnight at 4°C, followed by incubation with Alexa Fluor 488 goat anti-mouse IgG (Invitrogen) or Alexa Fluor 594 goat anti-rabbit IgG (Invitrogen) at RT for 1 h. The cells were then subjected to confocal imaging (Leica, Germany).

Animal Study

All *in vivo* mouse experiments were approved by the Ethics Committee of Xinxiang Medical University. Female nude mice at 5–6 weeks old were separated randomly into four groups ($n = 5$ for each group). Cells were subcutaneously inoculated into the fourth mammary fat pad of each mouse. Tumor volume was measured using calipers and calculated using the formula: length $\times$ width^2/2. Fifty days after inoculation, tumor and lung tissues were collected and subjected to IHC or hematoxylin and eosin (H&E) staining. For the inhibitor treatment assay, 10 days after tumor cells injection, mice were treated with PI3K inhibitor (LY294002, 70 mg/kg) every 2 days, while dimethyl sulfoxide (DMSO) was used as the control.

Patient Datasets

Survival analyses were conducted using an online tool.[1] Patients with breast cancer ($n = 1{,}070$) were selected for the overall survival assay. The log-rank test was computed automatically.

Statistical Analysis

Values were expressed as the mean ± SEM. Statistical significance was determined using the Student's *t*-test. A value of $p < 0.05$ was considered statistically significant. * indicates significant difference with $p < 0.05$, ** indicates significant difference with $p < 0.01$, *** indicates significant difference with $p < 0.001$.

RESULTS

PPA1 Is Highly Expressed in Human Breast Cancer and Correlates With TNM Stage and Histological Grade

In order to verify the clinical significance of PPA1 in breast cancer, we first examined PPA1 expression in tissue microarray containing human normal/para-carcinoma breast tissues and breast tumors with different TNM stage and histological grade by IHC. The results indicated that PPA1 was highly expressed in tumor tissues compared to normal/para-carcinoma tissues (**Figures 1A,B**). In addition, since the pathological grade and clinical stage of tumor were closely correlate with tumor malignancy and progression, we investigated the associations between PPA1 expression and clinicopathological characteristics. We found that PPA1 expression was positively correlated with TNM stage and histological grade of human breast cancer (**Figures 1C,D**). Moreover, the increased expression of PPA1 was also observed in breast cancer cell lines compared to that in the normal breast cell line (**Figures 1E,F**). Furthermore, we analyzed

[1] http://gepia2.cancer-pku.cn/#survival

the correlation between the expression of PPA1 and patient overall survival (OS), and found that high PPA1 expression was associated with poor clinical outcomes in patients with breast cancer (**Figure 1G**). Taken together, these results indicate that PPA1 may play a vital role in breast cancer development, and that it may be a diagnostic marker for tumor progression.

PPA1 Promotes Breast Cancer Cell Proliferation, Migration, and Invasion

To elucidate the function of PPA1 in breast cancer, we first silencing PPA1 in T47D cells by stable expression of control or two PPA1-targeting shRNAs. Meanwhile, we established stable MDA-MB-231 cell lines that overexpressed PPA1.

Wound healing assays were performed to detect the role of PPA1 in migration. As shown in **Figure 2A**, although gap-filling was significantly retarded in T47D-shPPA1 cells, the control cells migrated and almost filled the gap at 24 h after wounding (**Figures 2A,B**), indicating that silencing PPA1 suppressed the migration properties of T47D cells. Moreover, the transwell assay also demonstrated that PPA1 knockdown reduced the cell invasion properties of T47D-shPPA1 cells compared to that in the control group (**Figures 2C,D**). The CCK-8 results revealed that silencing PPA1 inhibited cell proliferation (**Figure 2E**).

To strengthen our conclusions, we examined the effect of PPA1 overexpression in MDA-MB-231 cells. Consistently, wound healing and transwell assay confirmed that ectopic PPA1 facilitated breast cancer cell migration and invasion (**Figures 2F–I**). Furthermore, PPA1 overexpression increased cell proliferation (**Figure 2J**). Taken together, these findings verified that PPA1 promoted proliferation, migration, and invasion of breast cancer cells.

PPA1 Triggers Breast Cancer EMT

To tested the regulatory effect of PPA1 on EMT, we first examined the expression of EMT-related proteins by western blot. We observed that PPA1 deficiency contributed to an epithelial phenotype as the expression levels of E-cadherin, ZO-1, and Claudin-1 were elevated, and those of the mesenchymal marker proteins Vimentin and N-cadherin were diminished in PPA1-deficient cells compared to those of the control group (**Figure 3A**), while ectopic PPA1 contribute to mesenchymal characteristic by attenuating expression levels of E-cadherin, ZO-1 and Claudin-1, and augmenting levels of Vimentin and N-cadherin (**Figure 3C**), indicating the EMT-promoting effects of PPA1. Consistently, this was further supported by the immunofluorescence results, which revealed an elevation in the intensity of the E-cadherin and ZO-1 signals in T47D-shPPA1 cells, and a decrease in the intensity of these signals in MDA-MB-231-PPA1 cells. Meanwhile, the expression of N-cadherin and Vimentin was attenuated in T47D-shPPA1 cells, and enhanced in MDA-MB-231-PPA1 cells (**Figures 3B,D**).

In addition, several transcriptional factors, including Slug, Twist, and ZEB1, function as molecular switches in the EMT program. Especially Slug, a major EMT inducer, is closely associated with tumor metastasis. To investigate which transcriptional factors mediate the regulatory effects of PPA1 on EMT, we used western blotting and found that the protein expression levels of Slug decreased in two T47D-shPPA1 cells, but increased in MDA-MB-231-PPA1 cells (**Figures 3A,C**). Meanwhile, PPA1 knockdown or overexpression elicited no change in ZEB1, Twist, and Snail expression. These results verified that PPA1 played a vital role in triggering EMT and revealed the crucial function of Slug in mediating EMT promotion effect of PPA1.

PPA1 Facilitates Breast Cancer Progression and EMT Through the PI3K/AKT/GSK3β Pathway

To further investigate the mechanism underlying the regulatory effects of PPA1 on breast cancer progression and EMT, we first performed western blot and the results demonstrated that silencing PPA1 restrained the phosphorylation levels of PI3K, AKT, and GSK3β. In contrast, ectopic PPA1 augmented the expression of p-PI3K (Tyr458), p-AKT (Ser473), and p-GSK3β (Ser9) (**Figures 4A,B**). PPA1 also could induce more phosphorylated GSK3β accumulation in the cytoplasm and less in the nucleus (**Supplementary Figures 1A,B**). However, significantly changes in JNK, p-JNK (Thr183/Tyr185), P38, and p-P38 (Thr180/Tyr182) were not as evident (**Figures 4A,B**). Consistently, this was further supported by immunofluorescence assay results (**Figures 4C,D**). Collectively, these findings indicated that PPA1 facilitated breast cancer progression and EMT via activating PI3K/AKT/GSK3β signaling pathway.

Inhibitors Targeted PPA1 Mediated Signaling Pathway Suppresses Breast Cancer Progression and EMT *in vitro*

To gain insights into the importance of PPA1 mediated signaling pathway in promoting the breast cancer progression and EMT, we investigated the effects of PI3K inhibitor (LY294002) in MDA-MB-231-PPA1 cells. We verified that the PI3K inhibitor reversed the proliferation, migration and invasion promoting effects of PPA1 in MDA-MB-231 cells (**Figures 5A–E**). Consistently, the treatment of the cells with PI3K inhibitor rescued expression levels of ZO-1, attenuated Slug activity, and blunted PPA1-induced PI3K/AKT/GSK3β signaling pathway activation (**Figure 5F**). Taken together, these results confirmed that inhibitors targeted PPA1 mediated signaling pathway suppressed breast cancer progression and EMT *in vitro*.

PPA1 Promotes Tumor Growth and Metastasis via the PI3K/AKT/GSK3β Signaling Pathway *in vivo*

To evaluate the function of PPA1 in breast cancer progression *in vivo*, we performed xenograft experiments using MDA-MB-231 cells. To this end, stable MDA-MB-231-control and MDA-MB-231-PPA1 cells were injected into the fourth mammary fat pad of mice. We verified that ectopic PPA1 significantly promoted tumor growth, which could be reversed by the PI3K inhibitor (**Figures 6A–C**). In addition, we observed that more PPA1-upregulated cells metastasized to the lung and initiated secondary tumor, which was also rescued by the PI3K inhibitor (**Figures 6D–F**). Furthermore, immunohistochemical

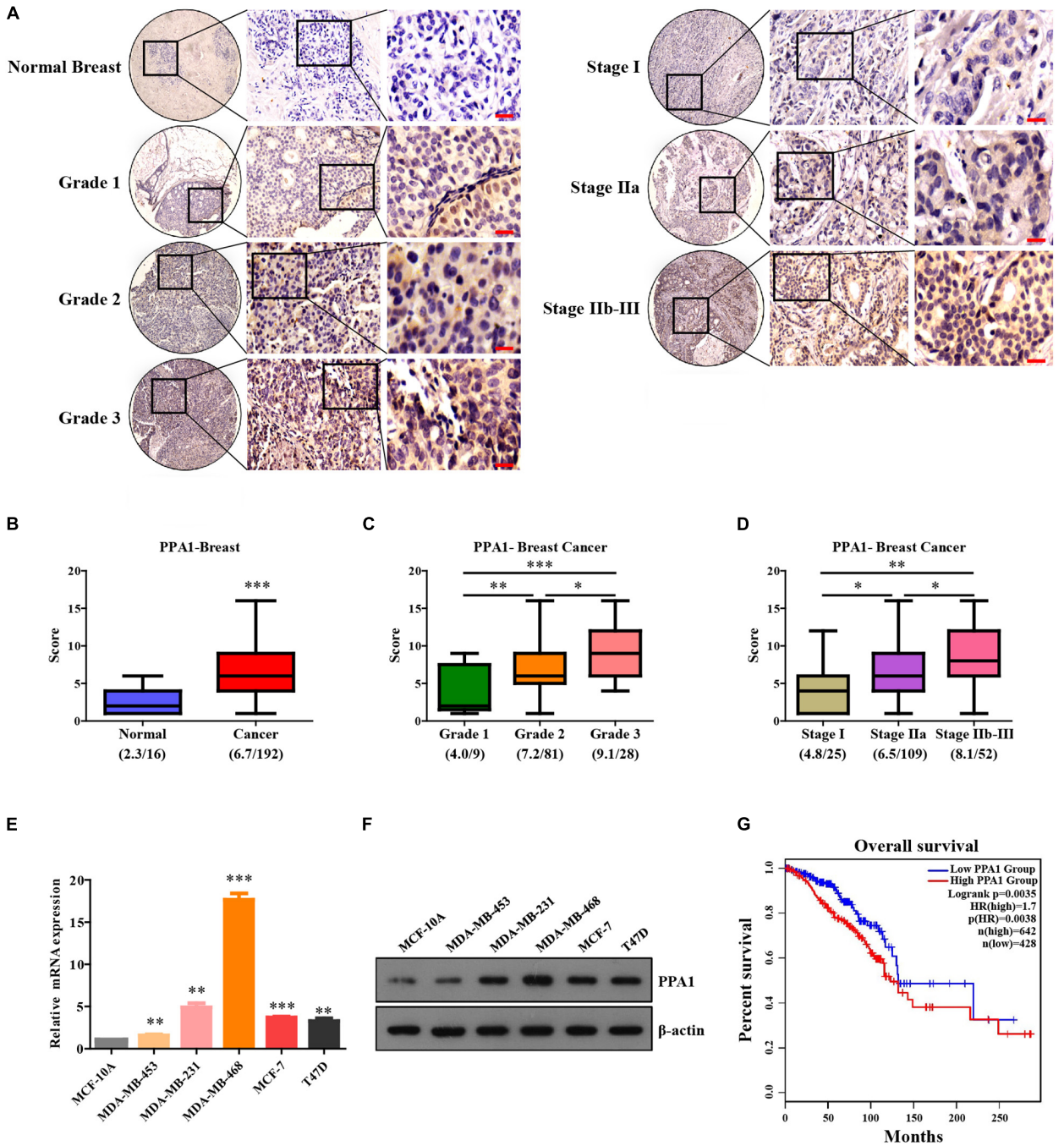

FIGURE 1 | PPA1 is highly expressed in breast cancer and correlates with TNM stage and histological grade. **(A)** Immunohistochemical analysis of PPA1 protein expression using human breast cancer tissue microarray. Scale bars: 20 μm. **(B)** Statistical analyses of the IHC scores of PPA1 in the breast cancer tissue microarray. **(C)** Quantification of PPA1 immunostaining and pathological grades. **(D)** Quantification of PPA1 immunostaining and clinical stages. **(E)** Real-time PCR showing the expression level of PPA1 in the normal breast cell line compared to that in breast cancer cell lines. **(F)** PPA1 protein expression examined using western blotting in the normal breast cell line compared to that in breast cancer cell lines. **(G)** Correlation of PPA1 expression in breast cancer patients with the overall survival rate. *$p < 0.05$, **$p < 0.01$, and ***$p < 0.001$.

staining demonstrated that PPA1 upregulated boosted the expression of mesenchymal effect (N-cadherin, Vimentin) and reduced epithelial protein expression (E-cadherin). Meanwhile, the levels of Ki-67, Slug, p-PI3K (Tyr458), p-AKT (Ser473) and p-GSK3β (Ser9) were elevated in tumor tissues (**Figures 6G,H**). However, the PI3K inhibitor reversed the expression levels of EMT markers and modulated the activation of PI3K/AKT/GSK3β pathway (**Figures 6G,H**),

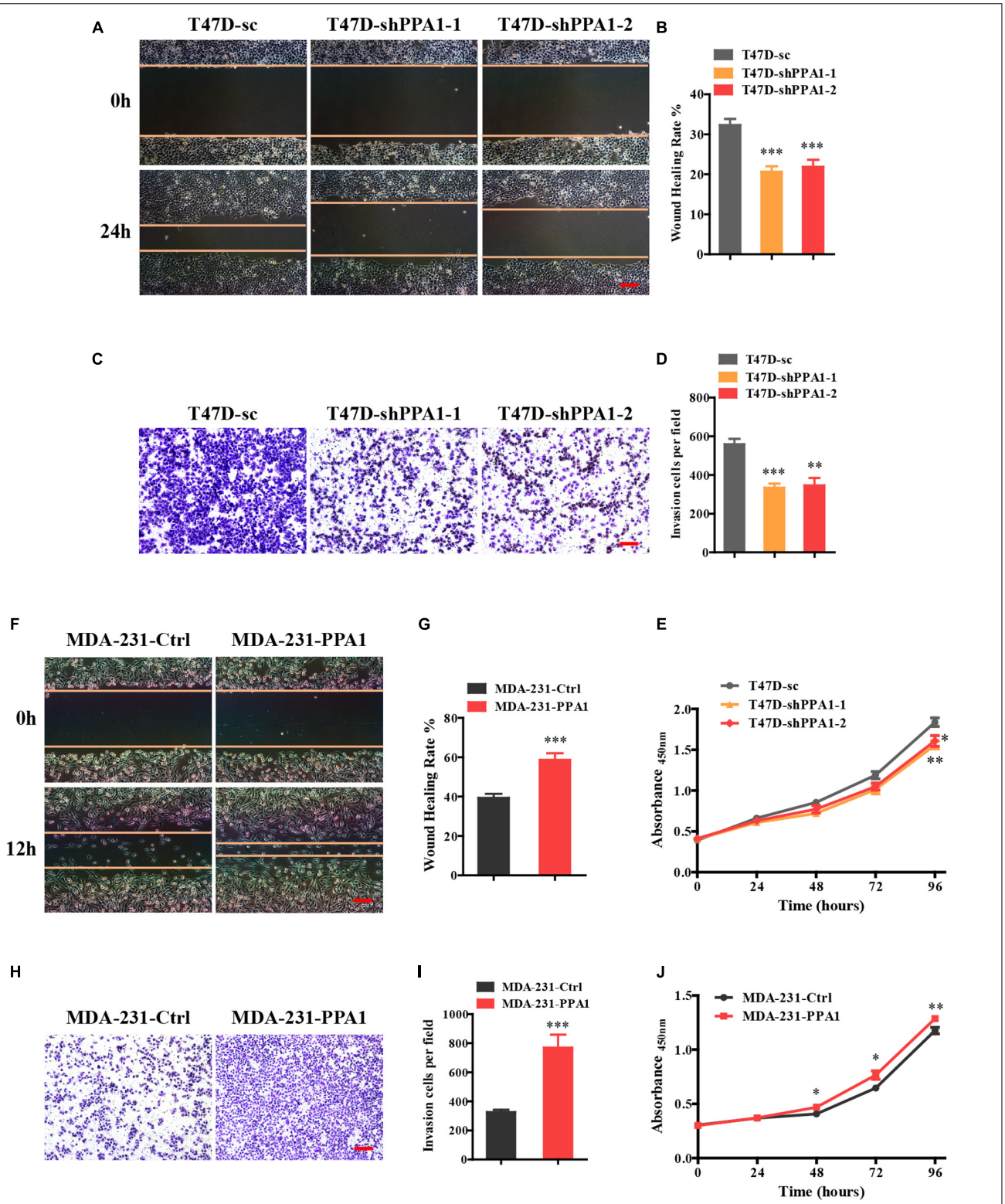

FIGURE 2 | PPA1 promotes proliferation, migration, and invasion of breast cancer cells. **(A)** Silencing PPA1 suppresses breast cancer cell migration as demonstrated in the wound healing assay. Scale bars: 100 μm. **(B)** Quantitative analysis of the wound healing rate. **(C)** Transwell assay showing that silencing PPA1 decreases cell invasion. Scale bars: 100 μm. **(D)** Quantitative analysis of invasion cells. **(E)** PPA1 knockdown inhibits breast cancer cell proliferation in T47D cells. **(F–I)** Ectopic PPA1 facilitates tumor migration and invasion in MDA-MB-231 cells. Scale bars: 100 μm. **(J)** PPA1 overexpression increases cell proliferation. $^{*}p < 0.05$, $^{**}p < 0.01$, and $^{***}p < 0.001$.

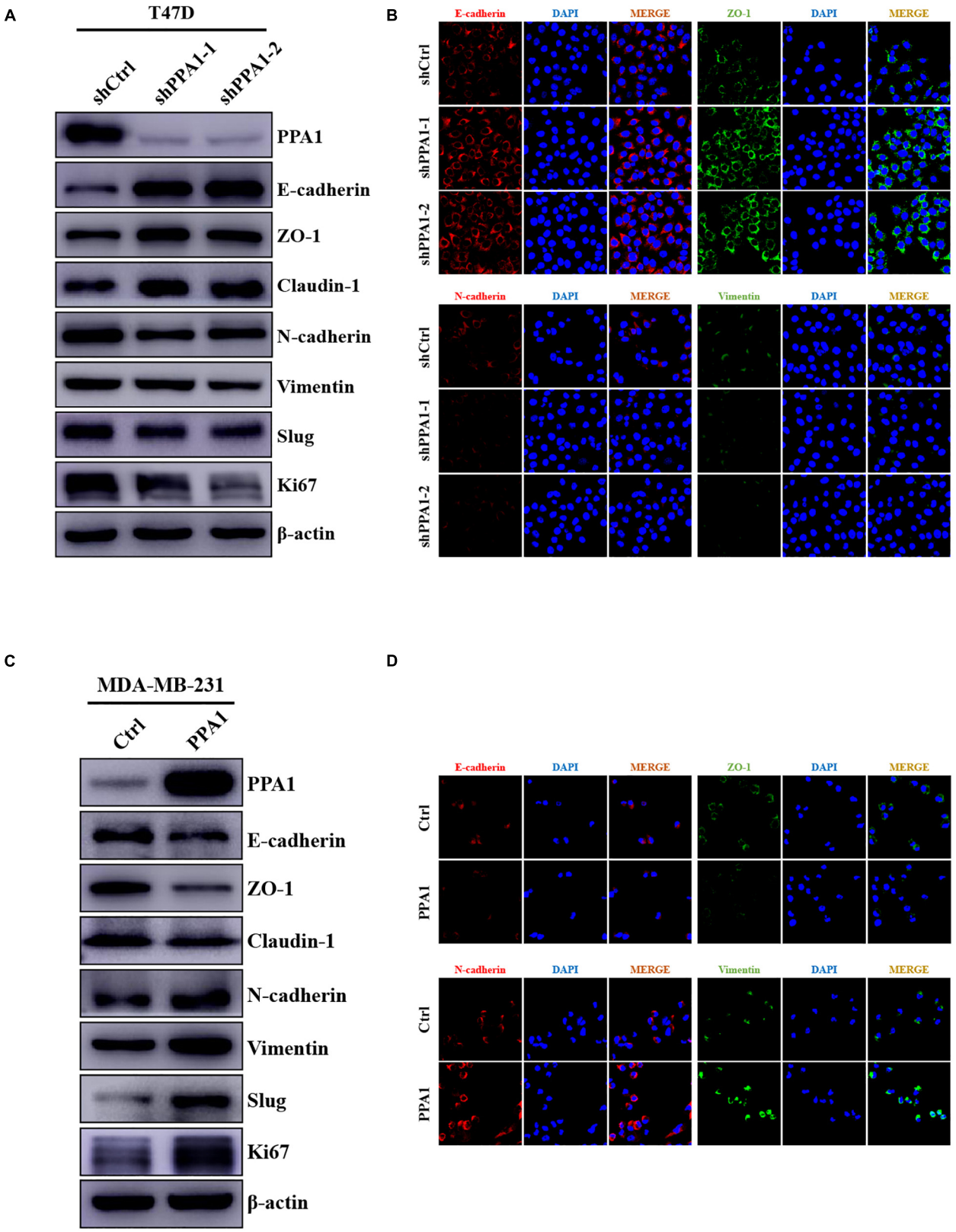

FIGURE 3 | PPA1 triggers EMT in breast cancer. **(A,C)** Western blot analysis showing the protein expression of EMT-related markers after PPA1 knockdown in T47D cells and overexpression PPA1 in MDA-MB-231 cells, respectively; **(B,D)** Representative immunofluorescence staining images of EMT-related markers in T47D and MDA-MB-231 cells.

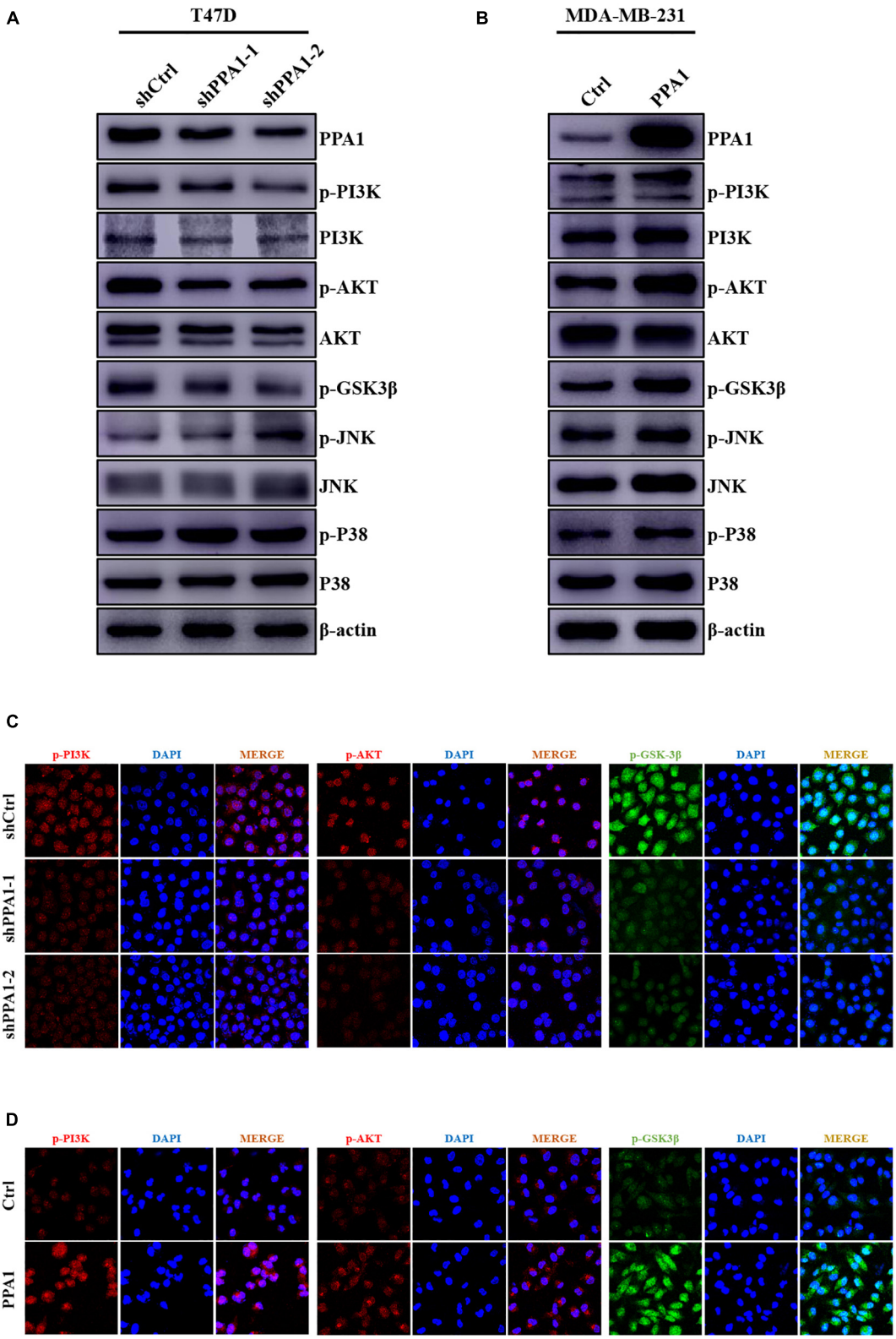

FIGURE 4 | PPA1 facilitates breast cancer progression and EMT through the PI3K/AKT/GSK3β signaling. **(A,B)** Western blot analysis showing the protein expression of JNK, p-JNK, P38, p-P38, and PI3K/AKT/GSK3β signaling molecules after PPA1 knockdown in T47D cells and overexpression PPA1 in MDA-MB-231 cells, respectively; **(C,D)** Representative immunofluorescence staining images of p-PI3K, p-AKT, and p-GSK3β in T47D and MDA-MB-231 cells.

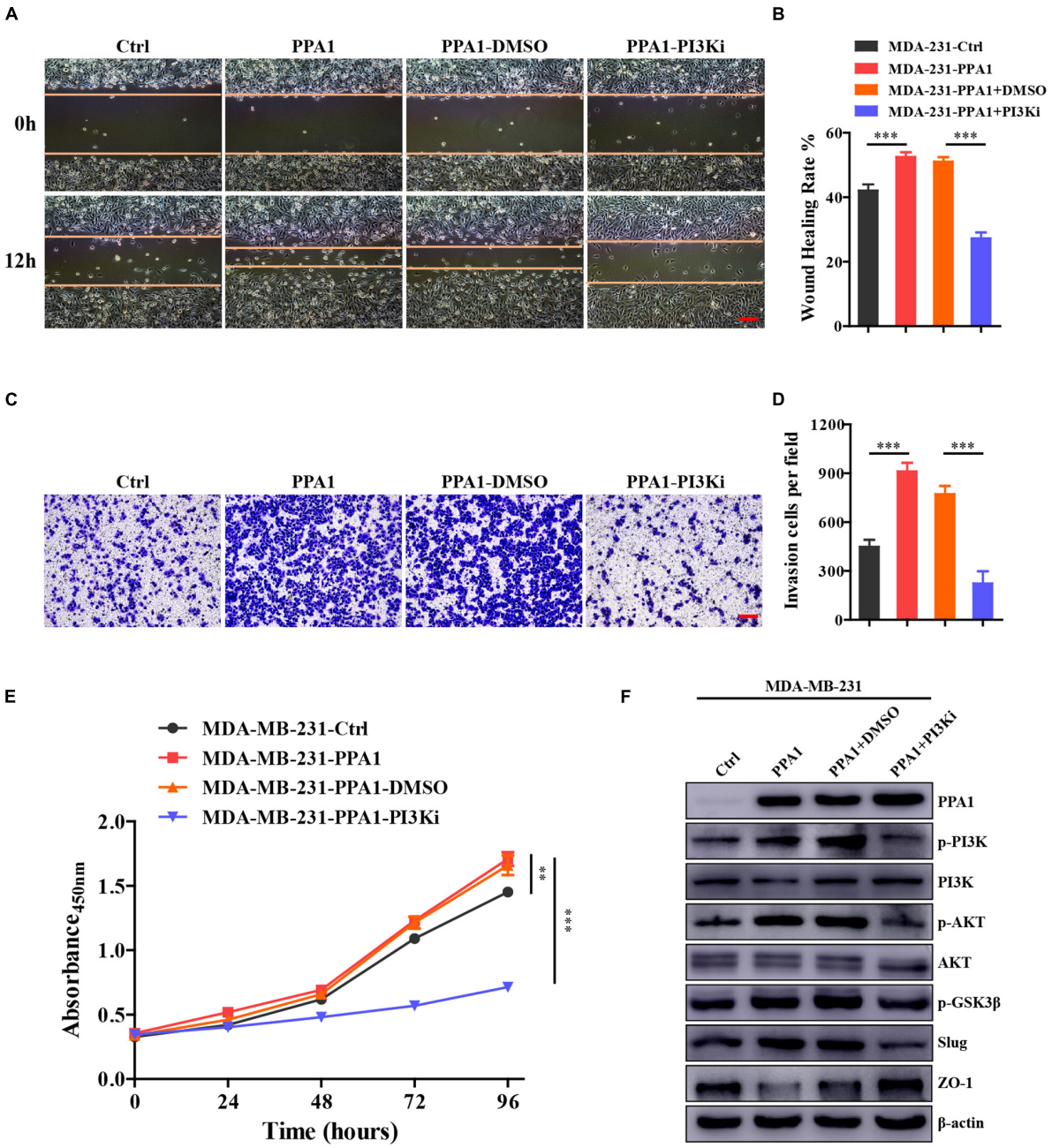

FIGURE 5 | Inhibitors of the PI3K/AKT/GSK3β signaling pathway can restore PPA1-induced breast cancer cell proliferation, invasion and migration. **(A,B)** Cell migration are detected by wound healing assay after cells are treated with PI3K inhibitor. Scale bars: 100 μm. **(C,D)** Cell invasion are detected by transwell assay after cells are treated. Scale bars: 100 μm. **(E)** Cell proliferation examined by CCK-8 assay. **(F)** Western blot analysis showing the protein expression of PPA1, p-PI3K, p-AKT, p-GSK3β and EMT markers in PPA1-expressing cells treated with the PI3K inhibitor. *$p < 0.05$, **$p < 0.01$, and ***$p < 0.001$.

demonstrating that inhibitors targeted PPA1 mediated signaling pathways suppressed breast cancer progression. Taken together, these results confirmed that PPA1 promoted tumor growth and metastasis via the PI3K/AKT/GSK3β signaling *in vivo*.

In summary, our study demonstrated a critical role of PPA1 in mediating PI3K/AKT/GSK3β signaling-induced tumor progression, which could be a useful target to prevent breast cancer.

Proposed Model of PPA1 in Breast Cancer Progression

Based on the totality of our findings, we propose the following model: PPA1 activates PI3K/AKT signaling, which enhances

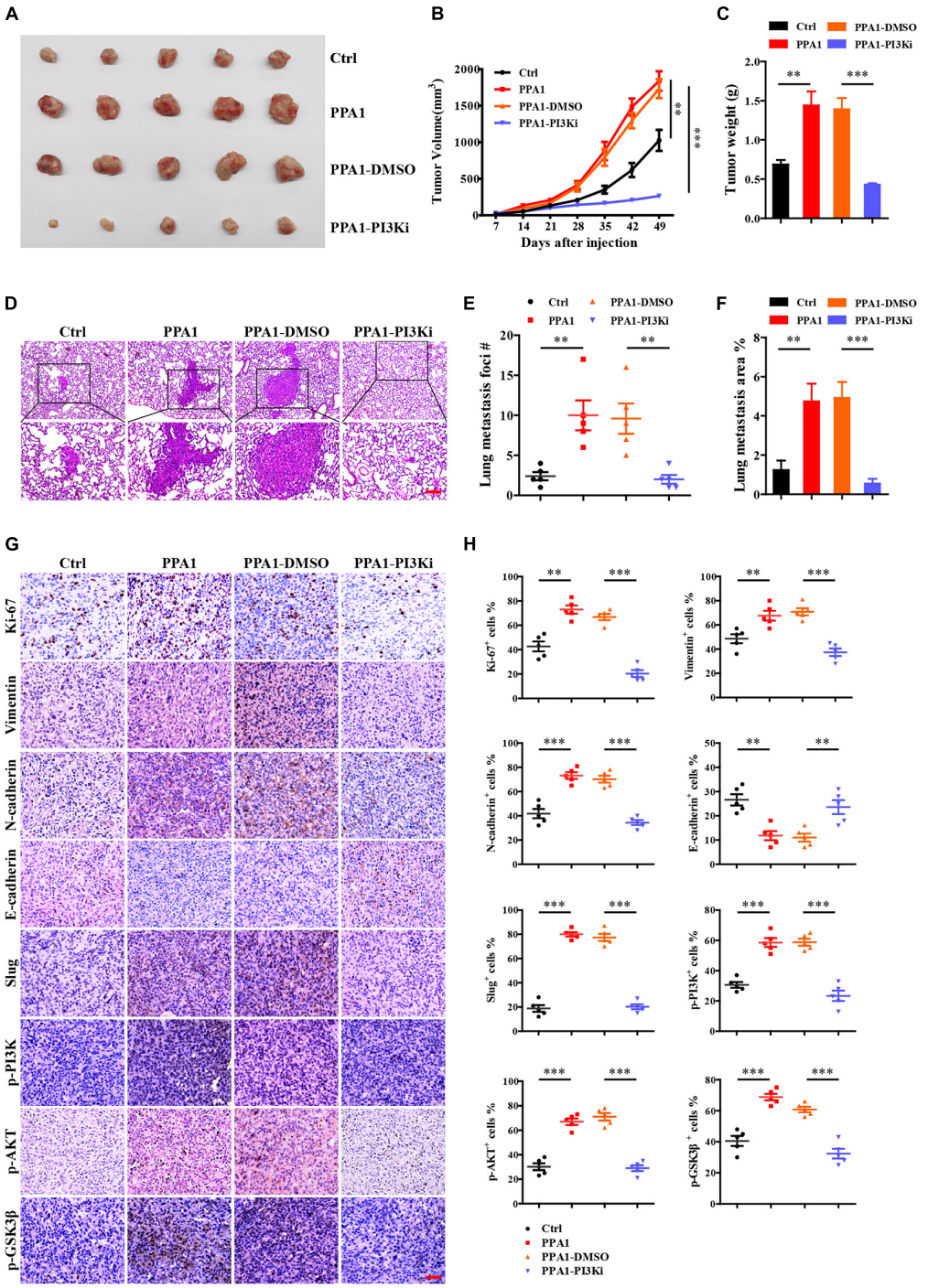

FIGURE 6 | PPA1 promotes tumor growth and metastasis via the PI3K/AKT/GSK3β signaling *in vivo*. **(A–C)** Ectopic PPA1 promotes tumor growth, which is reversed by the PI3K inhibitor. **(D)** H&E staining is used to analyze lung metastasis from the indicated mice. Scale bars: 100 μm. **(E,F)** Quantification of metastases ($n = 5$). **(G,H)** Immunohistochemistry staining of p-PI3K, p-AKT, p-GSK3β, and EMT markers in tumor tissue sections and quantification ($n = 5$). Scale bars: 50 μm. $^{*}p < 0.05$, $^{**}p < 0.01$, and $^{***}p < 0.001$.

GSK3β phosphorylation, thereby maintains Slug stability and promotes Slug nuclear translocation. Slug then leads to the repression of E-cadherin expression, which promotes the EMT process and tumor metastasis (**Figure 7**).

DISCUSSION

Breast cancer is a heterogeneous, malignant, and life-threatening tumor that affects women worldwide. The prognosis of breast

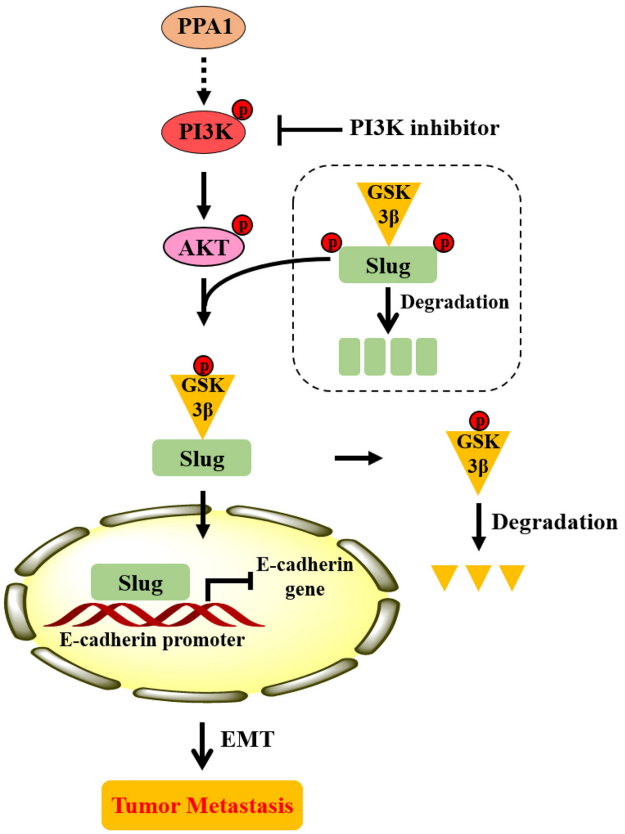

FIGURE 7 | Proposed model illustrating the role of PPA1 in promoting breast cancer proliferation and metastasis.

cancer patients has not markedly improved because of the high frequency of metastasis, relapse, and drug resistance. Hence, the identification of cancer progression targets may contribute to the development of more effective diagnostic and therapeutic strategies.

In this study, we determined the function of PPA1 in breast cancer and identified the potential molecular mechanism. Our results demonstrated that PPA1 was overexpressed in breast cancer and its expression was significantly correlates with clinical progression. Furthermore, we verified that PPA1 overexpression promoted proliferation, migration, invasion, and EMT *in vitro* and *in vivo*. The opposite effects were observed when PPA1 was silenced. Most importantly, we revealed the underlying mechanism that PPA1 regulated breast cancer progression and EMT through the PI3K/AKT/GSK3β pathway.

Metastasis is the major cause of high mortality rate in patients with breast cancer. There are multiple steps in the metastatic cascade, including cancer cells are divorced from primary tumor, invasion into stromal tissues, intravasation into lymphatic or blood vessels, survival within the circulation, extravasation, metastatic colonization and growth at secondary sites (Pantel and Brakenhoff, 2004). As a hallmark of metastasis, EMT is involved in the metastatic cascade of most carcinomas.

EMT is a highly conserved process that entails molecular reprogramming and is characterized by the phenotypic transformation of immobile epithelial cells to migratory mesenchymal cells. Previous studies have verified that activation of the EMT in primary breast cancer is indispensable for tumor cell dissemination to the distant sites, such as lung, bone, and lymph nodes (Ocana et al., 2012; Liu et al., 2019). Consequently, in order to develop effective therapeutic strategies for suppressing tumor metastasis and improve treatment outcomes, it is indispensable for us to investigate the mechanism of EMT. In our study, we identified that PPA1 promoted breast cancer metastasis via Slug-mediated EMT, proceeding through the PI3K/AKT/GSK3β signaling pathway.

Several transcriptional factors, such as Slug, Twist, and ZEB1, have been reported to play a vital function in EMT (Kurppa et al., 2020; Dufourt et al., 2021; Huang et al., 2021). Slug is one of the critical regulators which lead to EMT and is closely related to cancer metastasis. It induces EMT by repressing the expression of E-cadherin (Rao et al., 2021). Slug is also involved in various cellular processes, including neural crest cell migration and mesoderm formation (Reece-Hoyes et al., 2009; Ke et al., 2019; Flach et al., 2021). Additionally, Slug plays an important role in tumor metastasis and recurrence. It has been reported that Slug is essential in the metastatic process of melanoma cells (Furst et al., 2019). Increased levels of Slug were associated with cancer recurrence (Schinke et al., 2021). In this study, we identified a novel mechanism by which PPA1 selectively up-regulates the expression of the EMT master regulator Slug to drive EMT and enhance tumor metastasis.

Many signaling pathways, including PI3K/AKT/GSK3β, Wnt/β-catenin, and JAK/STAT signaling, play a pivotal role in EMT promotion (Pan et al., 2020; Wang et al., 2020; Yu et al., 2021). The activation of the PI3K/AKT/GSK3β axis is emerging as a central feature of EMT. PI3K/AKT constitutive activation results in the repression of epithelial characteristics and induction of the expression of mesenchymal protein, that increased tumor motility, invasiveness, and metastatic potential. GSK3β is highly inactivated in cancers, and GSK3β-mediated phosphorylation of Slug facilitates Slug protein ubiquitylation and degradation. In contrast, the p-GSK3β (Ser9) level is associated with Slug expression and maintains Slug protein stability (Kao et al., 2014). The accumulation of non-degradable Slug may further lead to restrain the expression of E-cadherin and accelerate the EMT process. In this study, we demonstrated that PPA1 activated the PI3K/AKT pathway, which then enhanced GSK3β phosphorylation, thereby preventing Slug destruction. Taken together, we confirmed that PPA1 promoted breast cancer proliferation, migration, and invasion through PI3K/AKT/GSK3β signaling.

Furthermore, recent evidence has revealed that a variety of small molecule inhibitors that targeting the PI3K/AKT/GSK3β axis attenuated tumor progression (Zhang et al., 2020; Crabb et al., 2021). We observed that PI3K inhibitor (LY294002)

reversed the metastasis-promotion effect of PPA1 and the EMT process by inhibiting PI3K/AKT/GSK3β signaling. In addition, Slug expression was also repressed, suggesting a role for this pathway in Slug induction.

However, how does PPA1 regulate PI3K and further activate PI3K/AKT/GSK3β phosphorylation cascades. In order to verify the relationship between PPA1 and PI3K, we performed immunoprecipitation assay and the result revealed that there was no interaction between PPA1 and PI3K. That indicates PI3K activation requires another protein. It was reported that FAM120A could recruit PI3K and functioned as a scaffold protein to enable phosphorylation and activation of PI3K by Src family kinases (Bartolomé et al., 2015). In addition, PI3K is composed of a catalytic subunit (p110) and a regulatory subunit (p85). As a key molecular target of PI3K, p85 plays an important role in the activation of the PI3K/AKT signaling pathway. The stem cell biomarker CD133 direct interaction with PI3K-p85, resulting in activation of PI3K/AKT pathway (Song et al., 2018). According to these results, we reckon that there will be one or more linking proteins between PPA1 and PI3K. Therefore, we will continue to identify the important interlinking protein and explore the molecular mechanism in the following research.

CONCLUSION

In conclusion, we verify that PPA1 is highly expressed in breast cancer and that it is correlated with clinicopathological characteristics. PPA1 promotes proliferation, migration, and invasion of breast cancer through the PI3K/AKT/GSK3β pathway. Thus, PPA1 may serve as a potential marker for evaluating breast cancer progression, and targeting PPA1 may be an attractive therapeutic strategy in breast cancer to prevent tumor metastasis.

DATA AVAILABILITY STATEMENT

The original contributions presented in the study are included in the article/**Supplementary Material**, further inquiries can be directed to the corresponding author/s.

ETHICS STATEMENT

The animal study was reviewed and approved by the Committee on the Ethics of Animal Experiments of Xinxiang Medical University.

AUTHOR CONTRIBUTIONS

HW designed the project and supervised the study. CG, SL, AL, and MC carried out the experiments. CG, SL, and AL analyzed the data. CG and AL drafted the manuscript. YL provided support with experimental techniques. All authors read and approved the final manuscript.

FUNDING

This work was supported by the National Natural Science Foundation of China (Grant No. 81802967), the Key Scientific Research Projects of Higher Education Institutions in Henan Province (Grant No. 19A320004), the Program for Ph.D. Starting Research Funding from Xinxiang Medical University (Grant No. 505247) and the 111 Project (No. D20036).

ACKNOWLEDGMENTS

We thank Bo Yang, Yuna Niu, and Liangwei Duan for reagents and/or valuable advice. We also would like to thank Editage for English language editing.

SUPPLEMENTARY MATERIAL

The Supplementary Material for this article can be found online at: https://www.frontiersin.org/articles/10.3389/fcell.2021.730558/full#supplementary-material

REFERENCES

Bartolomé, R. A., García-Palmero, I., Torres, S., López-Lucendo, M., Balyasnikova, I. V., and Casal, J. I. (2015). IL13 Receptor α2 signaling requires a scaffold protein, FAM120A, to Activate the FAK and PI3K pathways in colon cancer metastasis. *Cancer Res.* 75, 2434–2444. doi: 10.1158/0008-5472.Can-14-3650

Baykov, A. A., Cooperman, B. S., Goldman, A., and Lahti, R. (1999). Cytoplasmic inorganic pyrophosphatase. *Prog. Mol. Subcell Biol.* 23, 127–150. doi: 10.1007/978-3-642-58444-2_7

Bodnar, M., Luczak, M., Bednarek, K., Szylberg, L., Marszalek, A., Grenman, R., et al. (2016). Proteomic profiling identifies the inorganic pyrophosphatase (PPA1) protein as a potential biomarker of metastasis in laryngeal squamous cell carcinoma. *Amino Acids* 48, 1469–1476. doi: 10.1007/s00726-016-2201-8

Cai, X., Wang, X., Cao, C., Gao, Y., Zhang, S., Yang, Z., et al. (2018). HBXIP-elevated methyltransferase METTL3 promotes the progression of breast cancer via inhibiting tumor suppressor let-7g. *Cancer Lett.* 415, 11–19. doi: 10.1016/j.canlet.2017.11.018

Chaffer, C. L., San Juan, B. P., Lim, E., and Weinberg, R. A. (2016). EMT, cell plasticity and metastasis. *Cancer Metastasis. Rev.* 35, 645–654. doi: 10.1007/s10555-016-9648-7

Chen, G., Gharib, T. G., Huang, C. C., Thomas, D. G., Shedden, K. A., Taylor, J. M., et al. (2002). Proteomic analysis of lung adenocarcinoma: identification of a highly expressed set of proteins in tumors. *Clin. Cancer Res.* 8, 2298–2305.

Crabb, S. J., Griffiths, G., Marwood, E., Dunkley, D., Downs, N., Martin, K., et al. (2021). Pan-AKT inhibitor capivasertib with docetaxel and prednisolone in metastatic castration-resistant prostate cancer: a randomized, placebo-controlled phase II Trial (ProCAID). *J. Clin. Oncol.* 39, 190–201. doi: 10.1200/JCO.20.01576

Cui, Y., Yang, J., Bai, Y., Li, Q., Yao, Y., Liu, C., et al. (2021). ENC1 facilitates colorectal carcinoma tumorigenesis and metastasis via JAK2/STAT5/AKT axis-mediated epithelial mesenchymal transition and stemness. *Front. Cell Dev. Biol.* 9:616887. doi: 10.3389/fcell.2021.616887

Davis, R. T., Blake, K., Ma, D., Gabra, M. B. I., Hernandez, G. A., Phung, A. T., et al. (2020). Transcriptional diversity and bioenergetic shift in human breast cancer metastasis revealed by single-cell RNA sequencing. *Nat. Cell Biol.* 22, 310–320. doi: 10.1038/s41556-020-0477-0

Dufourt, J., Bellec, M., Trullo, A., Dejean, M., De Rossi, S., Favard, C., et al. (2021). Imaging translation dynamics in live embryos reveals spatial heterogeneities. *Science* 372, 840–844. doi: 10.1126/science.abc3483

Fan, H., Yuan, J., Li, X., Ma, Y., Wang, X., Xu, B., et al. (2020). LncRNA LINC00173 enhances triple-negative breast cancer progression by suppressing miR-490-3p expression. *Biomed. Pharmacother* 125:109987. doi: 10.1016/j.biopha.2020.109987

Flach, H., Basten, T., Schreiner, C., Dietmann, P., Greco, S., Nies, L., et al. (2021). Retinol binding protein 1 affects Xenopus anterior neural development via all-trans retinoic acid signaling. *Dev. Dyn.* 250:1096–1112. doi: 10.1002/dvdy.313

Furst, K., Steder, M., Logotheti, S., Angerilli, A., Spitschak, A., Marquardt, S., et al. (2019). DNp73-induced degradation of tyrosinase links depigmentation with EMT-driven melanoma progression. *Cancer Lett.* 442, 299–309. doi: 10.1016/j.canlet.2018.11.009

Giri, K., Shameer, K., Zimmermann, M. T., Saha, S., Chakraborty, P. K., Sharma, A., et al. (2014). Understanding protein-nanoparticle interaction: a new gateway to disease therapeutics. *Bioconjug. chem.* 25, 1078–1090. doi: 10.1021/bc500084f

Huang, W., Zhang, J., Huo, M., Gao, J., Yang, T., Yin, X., et al. (2021). CUL4B promotes breast carcinogenesis by coordinating with transcriptional repressor complexes in response to hypoxia signaling pathway. *Adv. Sci.* 8:2001515. doi: 10.1002/advs.202001515

Kao, S. H., Wang, W. L., Chen, C. Y., Chang, Y. L., Wu, Y. Y., Wang, Y. T., et al. (2014). GSK3β controls epithelial-mesenchymal transition and tumor metastasis by CHIP-mediated degradation of Slug. *Oncogene* 33, 3172–3182. doi: 10.1038/onc.2013.279

Ke, B., Zeng, Y., Zhao, Z., Han, F., Liu, T., Wang, J., et al. (2019). Uric acid: a potent molecular contributor to pluripotent stem cell cardiac differentiation via mesoderm specification. *Cell Death Differ.* 26, 826–842. doi: 10.1038/s41418-018-0157-9

Kurppa, K. J., Liu, Y., To, C., Zhang, T., Fan, M., Vajdi, A., et al. (2020). Treatment-induced tumor dormancy through YAP-mediated transcriptional reprogramming of the apoptotic pathway. *Cancer Cell* 37, 104–122. doi: 10.1016/j.ccell.2019.12.006

Lexander, H., Palmberg, C., Auer, G., Hellstrom, M., Franzen, B., Jornvall, H., et al. (2005). Proteomic analysis of protein expression in prostate cancer. *Anal. Quant. Cytol. Histol.* 27, 263–272.

Li, L., Aruna Luo, D., and Jin, A. (2018). Clinical significance and functional validation of inorganic pyrophosphatase in diffuse large B cell lymphoma in humans. *Cytotechnology* 70, 641–649. doi: 10.1007/s10616-017-0165-5

Li, Z., Li, C., Wu, Q., Tu, Y., Wang, C., Yu, X., et al. (2021). MEDAG enhances breast cancer progression and reduces epirubicin sensitivity through the AKT/AMPK/mTOR pathway. *Cell Death Dis.* 12:97. doi: 10.1038/s41419-020-03340-w

Liu, X., Li, J., Cadilha, B. L., Markota, A., Voigt, C., Huang, Z., et al. (2019). Epithelial-type systemic breast carcinoma cells with a restricted mesenchymal transition are a major source of metastasis. *Sci. Adv.* 5:eaav4275. doi: 10.1126/sciadv.aav4275

Luo, D., Liu, D., Shi, W., Jiang, H., Liu, W., Zhang, X., et al. (2019). PPA1 promotes NSCLC progression via a JNK- and TP53-dependent manner. *Oncogenesis* 8:53. doi: 10.1038/s41389-019-0162-y

Megger, D. A., Bracht, T., Kohl, M., Ahrens, M., Naboulsi, W., Weber, F., et al. (2013). Proteomic differences between hepatocellular carcinoma and nontumorous liver tissue investigated by a combined gel-based and label-free quantitative proteomics study. *Mol. Cell. Proteomics* 12, 2006–2020. doi: 10.1074/mcp.M113.028027

Ocana, O. H., Corcoles, R., Fabra, A., Moreno-Bueno, G., Acloque, H., Vega, S., et al. (2012). Metastatic colonization requires the repression of the epithelial-mesenchymal transition inducer Prrx1. *Cancer Cell* 22, 709–724. doi: 10.1016/j.ccr.2012.10.012

Pan, J., Fang, S., Tian, H., Zhou, C., Zhao, X., Tian, H., et al. (2020). lncRNA JPX/miR-33a-5p/Twist1 axis regulates tumorigenesis and metastasis of lung cancer by activating Wnt/β-catenin signaling. *Mol. Cancer* 19:9. doi: 10.1186/s12943-020-1133-9

Pantel, K., and Brakenhoff, R. H. (2004). Dissecting the metastatic cascade. *Nat. Rev. Cancer* 4, 448–456. doi: 10.1038/nrc1370

Pastushenko, I., Brisebarre, A., Sifrim, A., Fioramonti, M., Revenco, T., Boumahdi, S., et al. (2018). Identification of the tumour transition states occurring during EMT. *Nature* 556, 463–468. doi: 10.1038/s41586-018-0040-3

Popper, H. (2020). Primary tumor and metastasis-sectioning the different steps of the metastatic cascade. *Transl. Lung Cancer Res.* 9, 2277–2300. doi: 10.21037/tlcr-20-175

Rao, C., Frodyma, D. E., Southekal, S., Svoboda, R. A., Black, A. R., Guda, C., et al. (2021). KSR1- and ERK-dependent translational regulation of the epithelial-to-mesenchymal transition. *Elife* 10:66608. doi: 10.7554/eLife.66608

Reece-Hoyes, J. S., Deplancke, B., Barrasa, M. I., Hatzold, J., Smit, R. B., Arda, H. E., et al. (2009). The C. elegans Snail homolog CES-1 can activate gene expression in vivo and share targets with bHLH transcription factors. *Nucleic Acids Res.* 37, 3689–3698. doi: 10.1093/nar/gkp232

Schinke, H., Heider, T., Herkommer, T., Simon, F., Blancke Soares, A., Kranz, G., et al. (2021). Digital scoring of EpCAM and slug expression as prognostic markers in head and neck squamous cell carcinomas. *Mol. Oncol.* 15, 1040–1053. doi: 10.1002/1878-0261.12886

Siegel, R. L., Miller, K. D., Fuchs, H. E., and Jemal, A. (2021). Cancer Statistics, 2021. *CA: Cancer J. Clin.* 71, 7–33. doi: 10.3322/caac.21654

Sleeman, J. P., and Thiery, J. P. (2011). SnapShot: the epithelial-mesenchymal transition. *Cell* 145:e161. doi: 10.1016/j.cell.2011.03.029

Song, S., Pei, G., Du, Y., Wu, J., Ni, X., Wang, S., et al. (2018). Interaction between CD133 and PI3K-p85 promotes chemoresistance in gastric cancer cells. *Am. J. Transl. Res.* 10, 304–314.

Tomonaga, T., Matsushita, K., Yamaguchi, S., Oh-Ishi, M., Kodera, Y., Maeda, T., et al. (2004). Identification of altered protein expression and post-translational modifications in primary colorectal cancer by using agarose two-dimensional gel electrophoresis. *Clin. Cancer Res.* 10, 2007–2014. doi: 10.1158/1078-0432.ccr-03-0321

Wang, J., Jiang, C., Li, N., Wang, F., Xu, Y., Shen, Z., et al. (2020). The circEPSTI1/mir-942-5p/LTBP2 axis regulates the progression of OSCC in the background of OSF via EMT and the PI3K/Akt/mTOR pathway. *Cell Death Dis.* 11:682. doi: 10.1038/s41419-020-02851-w

Xu, Z., Gu, C., Yao, X., Guo, W., Wang, H., Lin, T., et al. (2020). CD73 promotes tumor metastasis by modulating RICS/RhoA signaling and EMT in gastric cancer. *Cell Death Dis.* 11:202. doi: 10.1038/s41419-020-2403-6

Yang, Y., Cai, J., Yin, J., Wang, D., Bai, Z., Zhang, J., et al. (2015). Inorganic pyrophosphatase (PPA1) is a negative prognostic marker for human gastric cancer. *Int. J. Clin. Exp. Pathol.* 8, 12482–12490.

Yazdani, H. O., Roy, E., Comerci, A. J., van der Windt, D. J., Zhang, H., Huang, H., et al. (2019). Neutrophil extracellular traps drive mitochondrial homeostasis in tumors to augment growth. *Cancer Res.* 79, 5626–5639. doi: 10.1158/0008-5472.CAN-19-0800

Yu, F., Liang, M., Huang, Y., Wu, W., Zheng, B., and Chen, C. (2021). Hypoxic tumor-derived exosomal miR-31-5p promotes lung adenocarcinoma metastasis by negatively regulating SATB2-reversed EMT and activating MEK/ERK signaling. *J. Exp. Clin. Cancer Res.* 40:179. doi: 10.1186/s13046-021-01979-7

Zhang, J., Ding, C., Zhang, S., and Xu, Y. (2020). Neuroprotective effects of astaxanthin against oxygen and glucose deprivation damage via the PI3K/Akt/GSK3β/Nrf2 signalling pathway in vitro. *J. Cell. Mol. Med.* 24, 8977–8985. doi: 10.1111/jcmm.15531

Conflict of Interest: The authors declare that the research was conducted in the absence of any commercial or financial relationships that could be construed as a potential conflict of interest.

Publisher's Note: All claims expressed in this article are solely those of the authors and do not necessarily represent those of their affiliated organizations, or those of the publisher, the editors and the reviewers. Any product that may be evaluated in this article, or claim that may be made by its manufacturer, is not guaranteed or endorsed by the publisher.

frontiers in Cell and Developmental Biology

ORIGINAL RESEARCH
published: 01 October 2021
doi: 10.3389/fcell.2021.716461

Cross-Talk of Focal Adhesion-Related Gene Defines Prognosis and the Immune Microenvironment in Gastric Cancer

Deli Mao[1,2,3†], Rui Xu[1,2,3†], Hengxing Chen[1,2], Xiancong Chen[1,2], Dongsheng Li[1,2], Shenglei Song[1,2], Yulong He[1,2], Zhewei Wei[3*] and Changhua Zhang[1,2*]*

[1] Digestive Diseases Center, The Seventh Affiliated Hospital of Sun Yat-sen University, Shenzhen, China, [2] Guangdong Provincial Key Laboratory of Digestive Cancer Research, The Seventh Affiliated Hospital of Sun Yat-sen University, Shenzhen, China, [3] Department of Gastrointestinal Surgery, The First Affiliated Hospital of Sun Yat-sen University, Guangzhou, China

OPEN ACCESS

Edited by:
Na Luo,
Nankai University, China

Reviewed by:
Yuming Jiang,
Stanford University, United States
Chuan Hu,
Qingdao University Medical College, China

***Correspondence:**
Yulong He
heyulong@mail.sysu.edu.cn
Zhewei Wei
weizhw5@mail.sysu.edu.cn
Changhua Zhang
zhchangh@mail.sysu.edu.cn

†These authors have contributed equally to this work

Specialty section:
This article was submitted to Molecular and Cellular Pathology, a section of the journal Frontiers in Cell and Developmental Biology

Received: 28 May 2021
Accepted: 14 September 2021
Published: 01 October 2021

Citation:
Mao D, Xu R, Chen H, Chen X, Li D, Song S, He Y, Wei Z and Zhang C (2021) Cross-Talk of Focal Adhesion-Related Gene Defines Prognosis and the Immune Microenvironment in Gastric Cancer. Front. Cell Dev. Biol. 9:716461. doi: 10.3389/fcell.2021.716461

Background: Focal adhesion, as the intermediary between tumor cells and extracellular matrix communication, plays a variety of roles in tumor invasion, migration, and drug resistance. However, the potential role of focal adhesion-related genes in the microenvironment, immune cell infiltration, and drug sensitivity of gastric cancer (GC) has not yet been revealed.

Methods: The genetic and transcriptional perspectives of focal adhesion-related genes were systematically analyzed. From a genetic perspective, the focal adhesion index (FAI) was constructed based on 18 prognosis-related focus adhesion-related genes to evaluate the immune microenvironment and drug sensitivity. Then three prognosis-related genes were used for consistent clustering to identify GC subtypes. Finally, use FLT1, EGF, COL5A2, and M2 macrophages to develop risk signatures, and establish a nomogram together with clinicopathological characteristics.

Results: Mutations in the focal adhesion-related gene affect the survival time and clinical characteristics of GC patients. FAI has been associated with a shorter survival time, immune signaling pathways, M2 macrophage infiltration, epithelial-mesenchymal transition (EMT) signaling, and diffuse type of GC. FAI recognizes ALK, cell cycle, and BMX signaling pathways inhibitors as sensitive agents for the treatment of GC. FLT1, EGF, and COL5A2 may distinguish GC subtypes. The established risk signature is of great significance to the prognostic evaluation of GC based on FLT1, EGF, and COL5A2 and M2 macrophage expression.

Conclusion: The focal adhesion-related gene is a potential biomarker for the evaluation of the immune microenvironment and prognosis. This work emphasizes the potential impact of the focal adhesion pathway in GC therapy and highlights its guiding role in prognostic evaluation.

Keywords: gastric cancer, focal adhesion, immune microenvironment, prognostic signature, biomarker

INTRODUCTION

Gastric cancer (GC) is a highly heterogeneous tumor. The death of GC patients every year brings a huge burden to the global economy. The 2019 survey showed that GC deaths accounted for 8% of all patients (Ferlay et al., 2019). The view that the interaction of multiple genes is an important promoter of tumor progression has been continuously accepted by the public. For this reason, many prognostic models have been established in recent years in an attempt to accurately evaluate prognosis and treatment. Zhang et al. (2020) revealed the potential role of N6-methyladenosine (m6A) modification in the microenvironment of GC from the perspective of epigenetics. Using transcriptomics of long non-coding RNA (lncRNA) to explore a new GC subtype with prognostic value (Chen et al., 2021). In addition, a proteomics signature has been developed to improve the diagnostic ability of GC (Song et al., 2021). Due to the individual differences and complexity of the pathogenesis of GC, the results of a single omics prognosis model are not satisfactory from the perspective of multiple omics, which forces people to explore new perspective models to accurately describe the prognosis of GC.

Previous studies have shown that GC is driven by a variety of key signaling pathways (Molaei et al., 2018). Focal adhesion kinase (FAK) is a kind of cytoplasmic non-receptor protein tyrosine kinase, which regulates tumor invasion, movement, and survival (Lee et al., 2015). FAK activates Ras (Fu et al., 2017), PI3K (Guo et al., 2020), ERK1/2 (Salgado-Lucio et al., 2020) by transmitting extracellular signaling from integrins, growth factors, and mechanical stimuli to cells, finally causing tumor adhesion and migration. The combination of extracellular matrix (ECM) and integrin will recruit FAK to the position where integrin gathers, which is called "focal adhesion". The focal adhesion signaling pathway has been proved to have a great influence on the regulation of ECM cell migration (Zhou et al., 2021) and tumor microenvironment (Murphy et al., 2020). Molecular crosstalk in the focal adhesion pathway is a key factor in mediating tumor-ECM interactions (Eke and Cordes, 2015). Cytokines secreted by cancer-related fibroblasts derived from ECM in GC activate the β1 integrin-FAK-YAP signaling axis to induce drug resistance of tumors (Uchihara et al., 2020). CXCL1 is secreted by lymphatic endothelial cells in the tumor microenvironment and promotes the invasion, migration and adhesion of GC cells by activating integrin β1-FAK-AKT signaling (Wang et al., 2017). Immune evasion is a complex problem in tumor immunotherapy. Interference of small molecule inhibitor VS-4718 with focal adhesion pathway induces tumor regression and enhances antitumor immunity (Serrels et al., 2015). FAK Improves expression of inflammatory factors IL33 and SST2 in rat squamous cell carcinoma and inhibits $CD8^{+}$T cell-mediated antitumor effect (Serrels et al., 2017). Adjuvant chemotherapy for breast cancer targeting FAK can reduce macrophage infiltration and tumor growth (Wendt and Schiemann, 2009). Focal adhesion pathway is the bridge between tumor and ECM. However, there is currently no focal adhesion-related gene signature to evaluate the prognosis of GC, and which is expected to become a new target for evaluating the immune microenvironment and prognosis of GC.

In this study, we explored genomic changes in 875 GC samples based on The Cancer Genome Atlas (TCGA) and gene expression omnibus (GEO) database. It is found that the mutation of genes related to the focal adhesion pathway significantly affects the prognosis of GC patients. Focal adhesion gene expression may identify GC prognostic subtypes. Based on the expression of the focal adhesion-related gene, we calculated the focal adhesion index (FAI), which is not only related to M2 macrophage cell infiltration, but also significantly related to microsatellite instability (MSI), tumor mutation burden (TMB), and epithelial-mesenchymal transition (EMT). Finally, we established a focal adhesion signature and verified its guiding significance in GC prognostic evaluation.

MATERIALS AND METHODS

Data Acquisition and Processing

The Cancer Genome Atlas-STAD somatic mutation data, RNA-seq profile (FPKM value), and corresponding GC patient clinical information were obtained from TCGA website[1]. Expression data and clinical information for both GEO cohorts including GSE66229 and GSE15459 were downloaded from the Gene-Expression Omnibus (GEO) Database[2]. The FPKM value of the TCGA dataset was converted into transcripts per kilobase million (TPM) values. The microarray data of the GEO datasets were background corrected and normalized by "simpleaffy" and "affy" packages. The "sva" package is used to correct batch effect based on the ComBat method (Leek et al., 2012). The mRNA expression-based stemness index (mRNAsi) of GC was reported by Malta et al. (2018). TMB of GC was extracted according to the method we reported before (Mao et al., 2021). The focal adhesion-related genes (**Supplementary Table 1**) were obtained from c2.cp.kegg.v7.2.symbols of the Molecular Signatures Database (Msigdb)[3]. In this study, TCGA data were divided into training datasets and GEO data were classified as validation datasets.

Functional Enrichment Analysis

The DAVID online functional annotation website[4] was adopted for prognostic-related somatic mutation gene KEGG enrichment analysis. The analysis results are visualized using the R package "ggplot2". To study the signaling difference of participation under different FAI subtypes, the "GSVA" R package (Hanzelmann et al., 2013) was applied to analyze Gene Set Variation Analysis (GSVA) based on h.all.v7.2 gene set. Difference analysis was performed using the "limma" package for analysis results, and the "pheatmap" package was used for visual heatmap drawing. Gene Set Enrichment Analysis (GSEA) was performed *via* GSEA software (Subramanian et al., 2007). FDR <0.25 was considered statistically significant.

[1]https://portal.gdc.cancer.gov/

[2]https://www.ncbi.nlm.nih.gov/GEO/

[3]http://www.gsea-MSIGDB.org/gsea/MSIGDB/index.jsp

[4]https://david.ncifcrf.gov/

Evaluation of Immune Cell Infiltration Abundance and Calculation of the Immune Score

The CIBERSORT algorithm was used to assess the abundance of infiltration of 22 immune cells based on gene expression microarray[5](Becht et al., 2016), which includes immune cells of different functional states and cell types. The immune score of the samples was calculated using the R-package "estimate" according to the mRNA expression matrix, which represents the total immune cell infiltration level in the tumor tissue (Yoshihara et al., 2013).

Construction of Focal Adhesion Index and Subtype Recognition

Single Sample Gene Set Enrichment Analysis (ssGSEA) was used to evaluate sample FAI based on the transcriptome data of 18 prognostic-related somatic mutation genes using the "GSVA" package. ssGSEA score was normalized to the range of 0–1. The "survminer" package was used to find the optimal cut-off value for FAI for the best prognostic subgroup. In order to reduce that dimension, the Univariant Cox regression analysis was performed to screen for prognosis-related focal adhesion genes from a transcriptional perspective. To evaluate the ability of prognosis-related genes to recognize GC subtypes, Consensus Clustering was applied to explore subtype classification based on gene transcription level through the "ConsensusClusterPlus" package. Relevant parameter settings refer to previous research reports (Gong et al., 2020).

Establishment of Prognostic Signature

The Least Absolute Shrinkage and Selection Operator (LASSO) cox regression algorithm is performed to construct the prognostic signature and calculate the factor weight coefficients through the R package "glmnet". The sample riskscore is calculated according to the following formula:

$$\text{riskscore} = \sum_{i=1}^{n} Coef_i \times X_i$$

$Coef_i$ represented the weight coefficient of each factor, and X_i represented the factor expression level. The median value of riskscore of all samples of the training set was defined as the cut-off value. According to the cut-off value, the samples of the training and validation cohorts were divided into a high-risk group (greater than cut-off) and a low-risk group (less than cut-off).

Drug Sensitivity Analysis

Genomics of Drug Sensitivity in Cancer (GDSC) (Yang et al., 2013) is a publicly available genomic database for tumor therapy, dedicated to finding potential therapeutic targets to improve tumor therapeutic efficacy. We downloaded GC cell line expression data and corresponding IC50 values[6] for 265 drugs from the GDSC database. Samples FAI were evaluated based on transcription levels. Spearman correlation analysis was used to calculate the correlation between FAI and drug IC50. $P < 0.05$ was considered statistically significant.

Statistical Analysis

Kaplan-Meier curve analysis is used for prognostic analysis. A Chi-square test is used to compare the clinical characteristics of mutation or non-mutation mode. The Wilcoxon test was performed to compare the differences between the two sets of data. The receiver operating characteristic (ROC) curve was tested to predict the efficiency of the overall survival rate of GC patients. Pearson's correlation analysis was used to compare the correlation of mRNA expression levels among 18 focal adhesion-related genes. Prism 8, SPSS19.0, and R software (version 3.6) were applied for statistical analysis and graphing. $P < 0.05$ was considered statistically significant.

RESULTS

Screening of Somatic Mutations Related to Prognosis

This study was conducted following the (**Figures 1A–D**) process. According to the published somatic mutation data of TCGA-STAD, genes with a mutation frequency of more than 10 were subjected to prognostic analysis, and the results showed that the mutations of 416 genes were related to the prognosis of GC (**Supplementary Table 2**). To identify the signaling pathways involved in these prognosis-related mutated genes, we performed KEGG enrichment analysis. The focal adhesion pathway was most significantly enriched (**Figure 2A**). In addition to ECM-receptor interaction, cell adhesion. Therefore, we seriously suspect that somatic mutations in genes related to the focal adhesion pathway have a profound impact on patients with GC. For this reason, we investigated 18 somatic mutations in the focal adhesion pathway that are related to prognosis. Kaplan-Meier curve analysis of these 18 genes showed that the survival time of patients in the mutation group was significantly longer than that in the non-mutation group (**Figure 2B**).

Focal Adhesion Mutation Type Is Closely Related to Prognosis and Clinicopathological Characteristics

Genetic alteration in the prognosis-related focal adhesion gene was explored in GC to assess the frequency of somatic mutations in 18 genes. In the TCGA-STAD cohort, each of the focal adhesion genes had a low mutation rate (**Figure 3A**), COL4A1 and CTNNB1 had the highest mutation rate (7%) followed by ACTN2 (6%), and ITGA1, ITGB6, ITGB7, PAK1, and IGF1 had the lowest mutation rate. To observe the overall mutation pattern of these genes, samples with focal adhesion mutations were considered to be mutation samples. Therefore, the samples were divided into mutation groups and non-mutation groups. We found that the survival time of GC patients in the mutation group was significantly longer than that in the non-mutation

[5]https://cibersort.stanford.edu/

[6]http://www.cancerrxgene.org

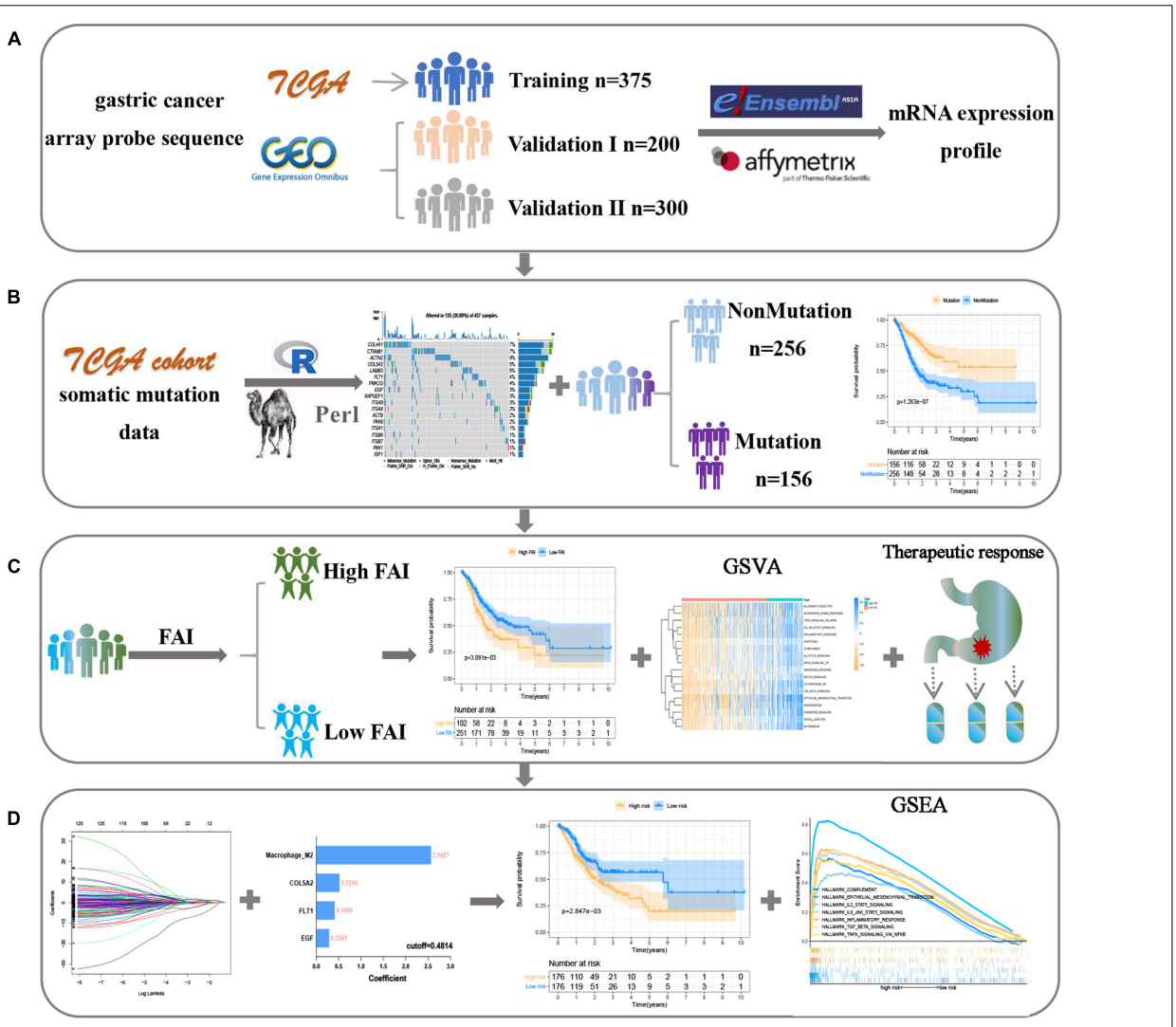

FIGURE 1 | The flow chart shows the process of this work. **(A)** Data acquisition and processing. **(B)** Explore focal adhesion mutation type. **(C)** The establishment of FAI is based on the expression of focal adhesion-related genes. **(D)** Development and verification of the prognostic signature.

group (P = 1.263E^{-7}) (**Figure 3B**). To more accurately reflect the relationship between mutation efficiency and prognosis, we divided GC patients into the non-mutation group, single gene mutation group, and multiple gene mutation groups. We found that the survival time of the multi-mutation group was longer than that of the single mutation group, and that of the single mutation group was longer than that of the non-mutation group ($P < 0.001$) (**Figure 3C**). This result suggested that focal adhesion acted as an oncogene pathway, and these genes mainly underwent missense mutation, which might cause structural changes of proteins and loss of functions, thus losing the main functions of focal adhesion. Subsequently, the association of the focal adhesion mutation with the clinicopathological characteristics of GC patients was analyzed (**Figure 3D**). We found that the mutations were the result of time accumulation, and the proportion of patients older than 60 years in the mutant group was significantly higher than that in the non-mutant group (P = 0.003). At the same time, the number of women in the mutant group was significantly higher than that of men ($P < 0.001$), while the number of men in the non-mutant group was higher than that of women. In addition, the N stage (P = 0.0235) and stage (P = 0.0388) were also closely related to the mutation state. In recent years, Gurzu et al. (2017) proposed a new Dukes-MAC-like staging system to classify GC subtypes, which was defined according to the T and N stage. Probably because T staging (P = 0.1541) was not significantly different from the mutant group, the Dukes-MAC-like stage system was not significantly different between the mutant and non-mutant groups (P = 0.3036) (**Supplementary Figure 1A**). Next, we explored and found that the mutation group was more likely to cause microsatellite instability and higher tumor mutation load. It has been reported in the previous study that the tumor stem cell index is an important indicator to drive tumor progress (Malta et al., 2018). Here, whether there is an association between the

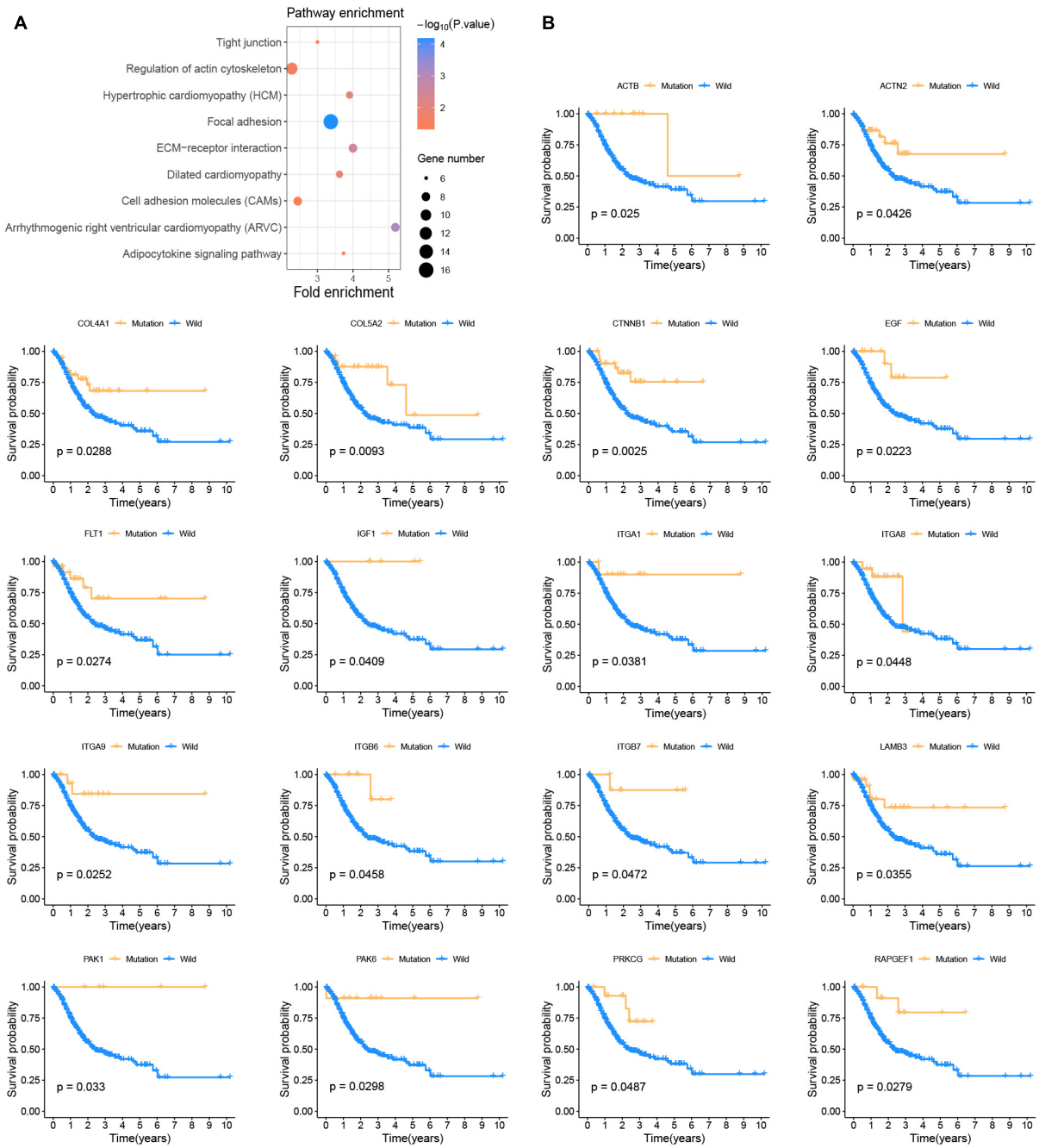

FIGURE 2 | Somatic mutations affect the prognosis of patients with GC **(A)** KEGG enrichment analysis of prognostic-related somatic mutation genes. **(B)** Kaplan-Meier survival curve of 18 focal adhesion pathway-related genes.

focal adhesion mutation and mRNAsi, our results show that the mRNAsi of patients with mutations is significantly higher than that of patients without mutations ($P < 0.0001$) (**Supplementary Figure 1B**). The previous study (Mao et al., 2021) has reported that patients with high mRNAsi have a better prognosis. In terms of prognosis, the results of this study are consistent with them. In summary, focal adhesion-related gene mutation in GC patients is closely related to the prognosis and clinical characteristics.

Genetic and Transcriptional Alteration of Focal Adhesion-Related Genes

Since genetic alterations are associated with the prognosis of patients with GC, does it affect gene expression? First, we compared the expression of these genes in normal and tumor tissues and found that most of the genes were up-regulated in the tumor (**Figure 4A**). Somatic copy number changes of focal adhesion-related genes were then examined (**Figure 4B**). ACTB,

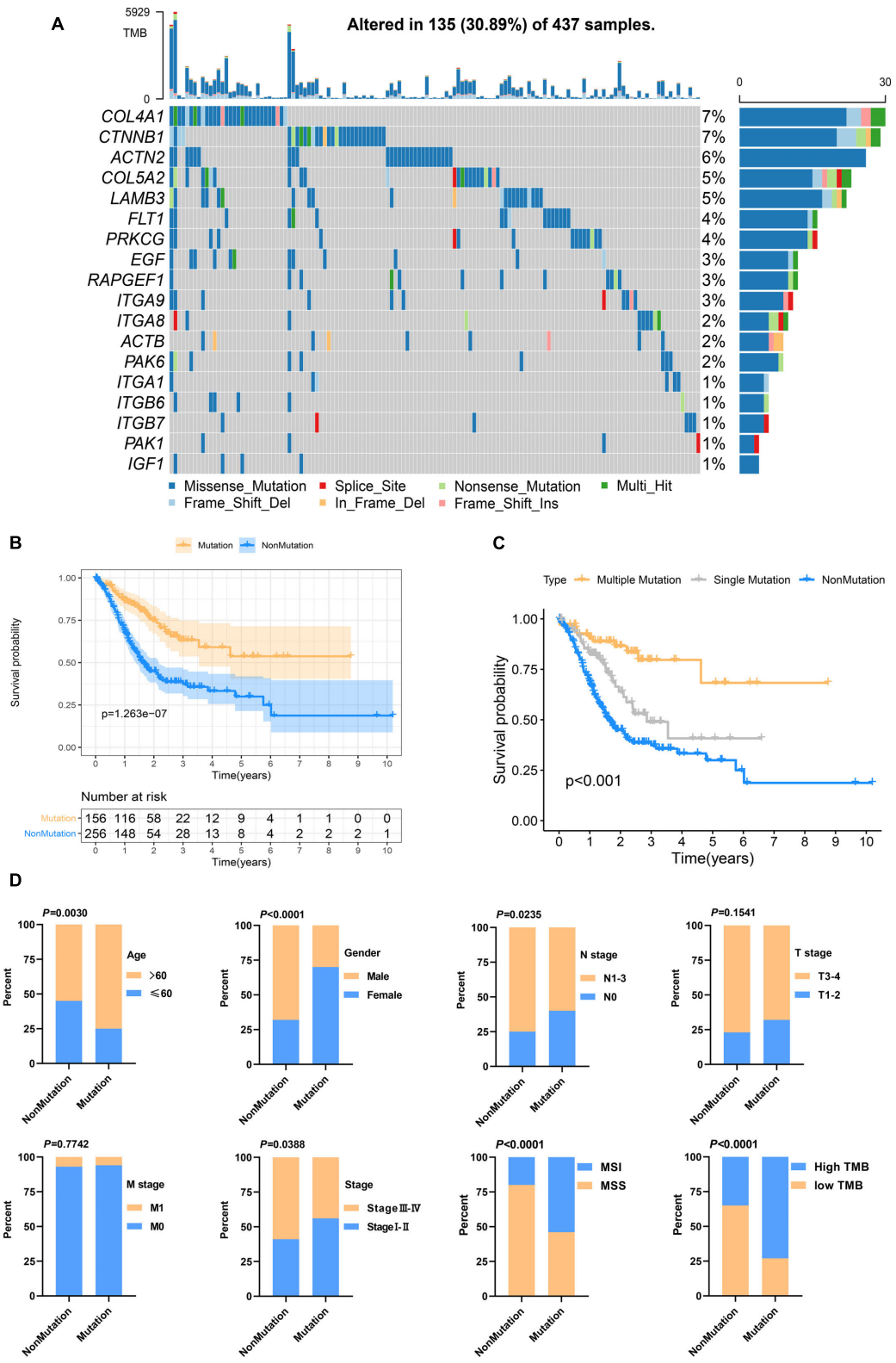

FIGURE 3 | Focal adhesion mutations are closely related to the prognosis and clinicopathological characteristics of GC patients **(A)** The mutation frequency of 18 focal adhesion-related genes in 437 GC patients in the TCGA cohort. **(B)** Kaplan-Meier curve shows that the survival time of the focal adhesion mutation group of GC patients in the TCGA cohort is significantly longer than that of the non-mutation group. **(C)** The overall survival of GC patients under different mutation types. **(D)** Chi-square test shows that the focal adhesion mutation is closely related to the clinicopathological characteristics.

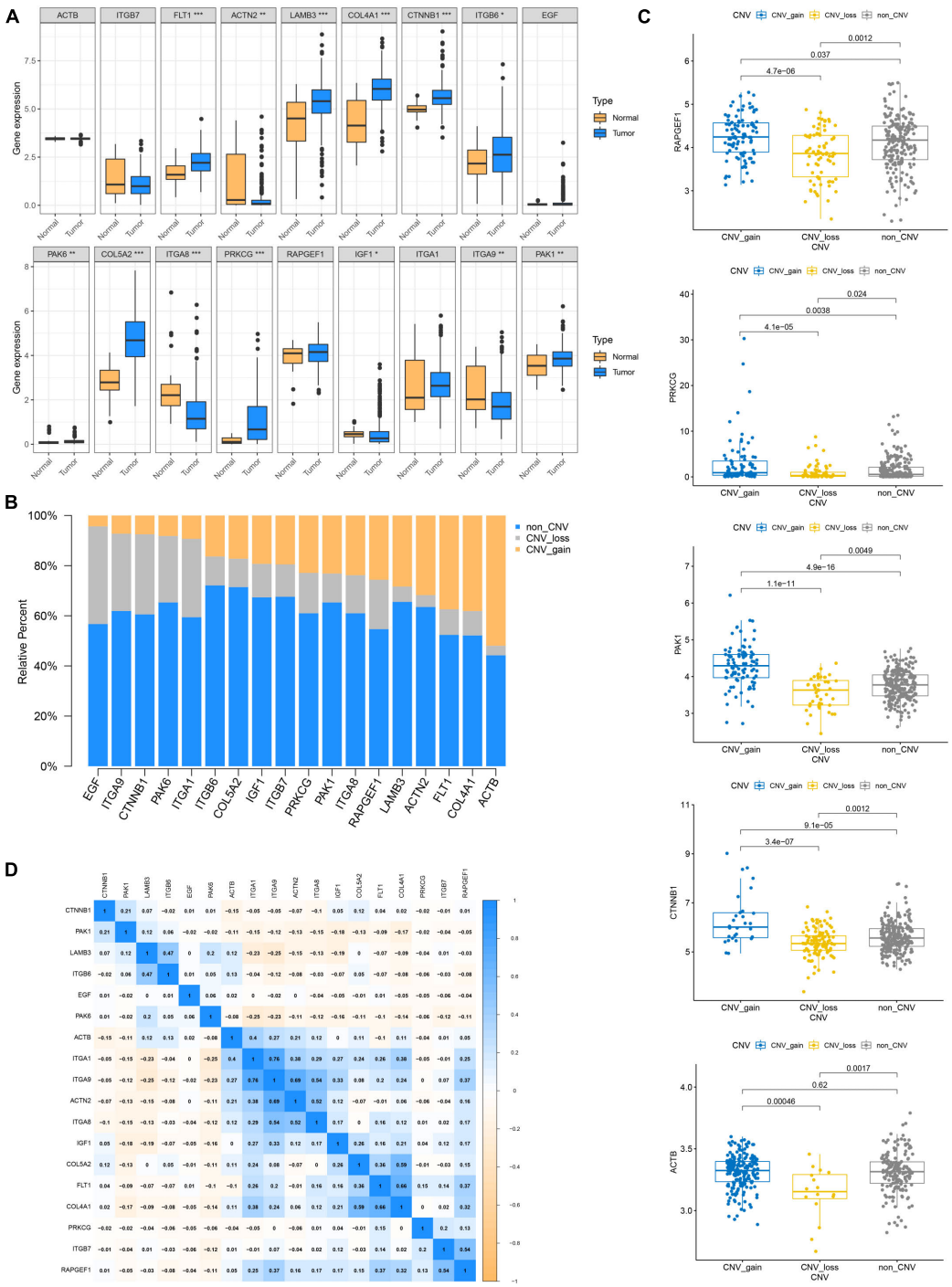

FIGURE 4 | Genetic and transcriptional alteration of focal adhesion-related genes. **(A)** The expression of genes related to focal adhesion is different between normal and tumor tissues, $^{*}P < 0.05$; $^{**}P < 0.01$; $^{***}P < 0.001$. **(B)** CNV again, CNV loss, and non-CNV frequency of focal adhesion-related genes in the TCGA cohort. **(C)** Correlation between CNV alteration of focal adhesion-related genes and gene expression. **(D)** Correlation between expression levels of focal adhesion-related genes.

COL4A1, FLT1, and ACTN2 were found to have abundant CNV gain. EGF, ITA9, CTnNB1, and PAK6 have extensive CNV loss. Next, the relationship between the expression level of 18 genes and CNV were analyzed. The expression levels of PAPGEF1, PRKCG, PAK1, and CTNNB1 were higher than that of non-CNV on CNV gain and lower than that of non-CNV on CNV loss. ACTB expression level was lower than that of non-CNV on CNV loss, but CNV gain was not higher than that of non-CNV

(**Figure 4C**). CNV gain drives the increase of gene expression in tumors, while CNV loss causes the decrease of gene expression. However, this complex mechanism cannot completely explain the change of expression level of all focal adhesion-related genes (**Supplementary Figure 2**). Finally, based on transcriptome level, we evaluated the expression correlations of 18 genes and found that most of them exhibited positive correlations (**Figure 4D**), especially the expressions of ITGA 1, ITG A9, ACT N2, ITG A8, IFG 1, Col 5A2, FLT 2, and Col 4A1, suggesting that there was crosstalk between focal adhesion-related genes, which was important for GC progression.

Focal Adhesion Index Construction

In order to enable focal adhesion-related genes to better evaluate the overall adhesion ability of the sample, we constructed FAI based on the expression levels of 18 genes in the TCGA cohort. The optimal cut-off value (cut-off = 0.6361) was calculated according to the steps described in the method to classify the samples as High FAI and Low FAI. The survival time of patients with high FAI in the TCGA cohort was significantly lower than that of patients with Low FAI ($P = 3.091E^{-3}$). The validation cohorts also came to a consistent conclusion (GSE66229, $P = 1.803E^{-2}$; GSE15459, $P = 1.085E^{-3}$) (**Figure 5A**). GSVA was used to explore the differences in signaling pathways between Low and High FAI. The results showed that there was significant enrichment of immune-related signaling, such as Interferon-gamma response, IL6 JAK STAT3 signaling, IL2 STAT5 signaling, and TGF-β signaling. Significant enrichment of epithelial-mesenchymal transition (EMT) signaling was also observed (**Figure 5B**). This result suggested that FAI was closely related to tumor immunity and tumor microenvironment. Next, we analyzed whether FAI was related to the immune score. It was found that the immune score of high FAI samples was correspondingly increased in both the training ($P < 0.0001$) and the validation groups (GSE66229, $P < 0.0001$; GSE15459, $P = 0.0005$) (**Supplementary Figure 3A**). Cumulative evidence indicates the relationship between focal adhesion and the immune microenvironment. Different immunocyte infiltration was specifically analyzed to assess the effect of FAI on the immune microenvironment. The levels of $CD8^+$T cells, M2 macrophage, and regulatory T cells (Tregs) at high FAI were significantly increased, while the levels of macrophage M0, T cell $CD4^+$ memory activated, and myeloid dendritic cell activated were significantly decreased (**Figure 5C**). M2 macrophage markers were then compared at low-high FAI. Consistent with previous results, these markers were significantly up-regulated in the High FAI group ($P < 0.01$) (**Figure 5D**). Subsequently, significant differences between low-high FAI were observed for MSI and TMB. The Low FAI group corresponded to MSI ($P = 0.0061$) and high TMB ($P = 0.0006$) (**Supplementary Figure 3B**). The previous GSVA enriched the EMT signaling among the low-high FAI groups. Epithelial markers were found to be significantly increased in the Low FAI group, while mesenchymal markers were significantly decreased in the Low FAI group (**Supplementary Figure 3C**). This result is consistent with GSVA. Lauren classification is currently a widely used GC classification method in clinical applications. According to histological characteristics, it is divided into the diffuse, intestine, and mixed types (Lauren, 1965). The diffuse type generally shows resistance to chemotherapy and has a worse prognosis (Gurzu et al., 2015; Pernot et al., 2015). We found that the diffuse type has a higher FAI than the Intestine and mixed type, and there is no statistical difference between the Intestine and mixed type (**Supplementary Figure 3D**). In addition, we also found a statistically significant difference in the transcription of focal adhesion-related genes between low-high FAI groups (**Supplementary Figure 4A**). Patients with high FAI groups correspond to higher stages and stages ($P < 0.05$) (**Supplementary Figure 4B**). Finally, in order to further reflect the effect of FAI on the drug, the correlation was evaluated between FAI and the response to the drug in GC cell lines. 12 pairs of compounds showed sensitivity related to FAI. Including ALK inhibitor TAE684 (Rs = $^-$0.557, $P = 0.0022$); cell cycle inhibitor CGP-60474 (Rs = −0.498, $P = 0.0052$); bone marrow tyrosine kinase on chromosome X(BMX) inhibitor WZ-1- 84 (Rs = −0.49, $P = 0.0059$). 3 pairs of drug-resistant compounds are related to FAI. Including BRAF inhibitor AZ628 (Rs = 0.713, $P = 0.0062$); MET inhibitor PHA-665752 (Rs = 0.683, $P = 0.0092$); MET inhibitor Crizotinib (Rs = 0.646, $P = 0.0151$) (**Figure 5E**). Taken together, these results suggest that FAI can assess GC immune cell infiltration and is associated with drug susceptibility. FAI may be used as a potential biomarker to guide the treatment and effect evaluation of GC.

Molecular Subtype Recognition of Gastric Cancer

To classify the focal adhesion status of GC samples in TCGA and GEO cohorts, the consensus clustering method was conducted to identify molecular subtypes based on the expression levels of three prognostic-related focal adhesion genes (FLT1, EGF, and COL5A2) (**Supplementary Figure 4C**). From the results of **Supplementary Figure 5** when $K = 2$ is displayed; the relative change in the area under the CDF curve is large. When $k = 2$, the higher the intra-group correlation, the lower the correlation between groups (**Figure 6A**), so we divided the GC patients into two groups in the TCGA cohort, respectively, cluster1 and cluster2. Kaplan-Meier curves were drawn to evaluate the prognostic differences between clusters. The survival time of GC patients in the cluster1 group was significantly higher than that in the cluster2 group ($P = 5.345E^{-3}$) and was also confirmed in the validation cohorts (GSE66229, $P = 3.478E^{-2}$; GSE15459, $P = 8.068E^{-3}$) (**Figure 6B**). The results confirmed that three prognosis-related focal adhesion genes could well distinguish the different subtypes of GC, and these molecular subtypes could significantly identify the prognosis stratification of GC.

Development and Verification of the Prognostic Signature

In the previous study, M2 macrophage was found to be closely related to the focal adhesion pathway (Ngabire et al., 2020; Li et al., 2021). In the past, it has been widely reported that M2 macrophage derived from immune microenvironment participate in the process of GC metastasis and EMT

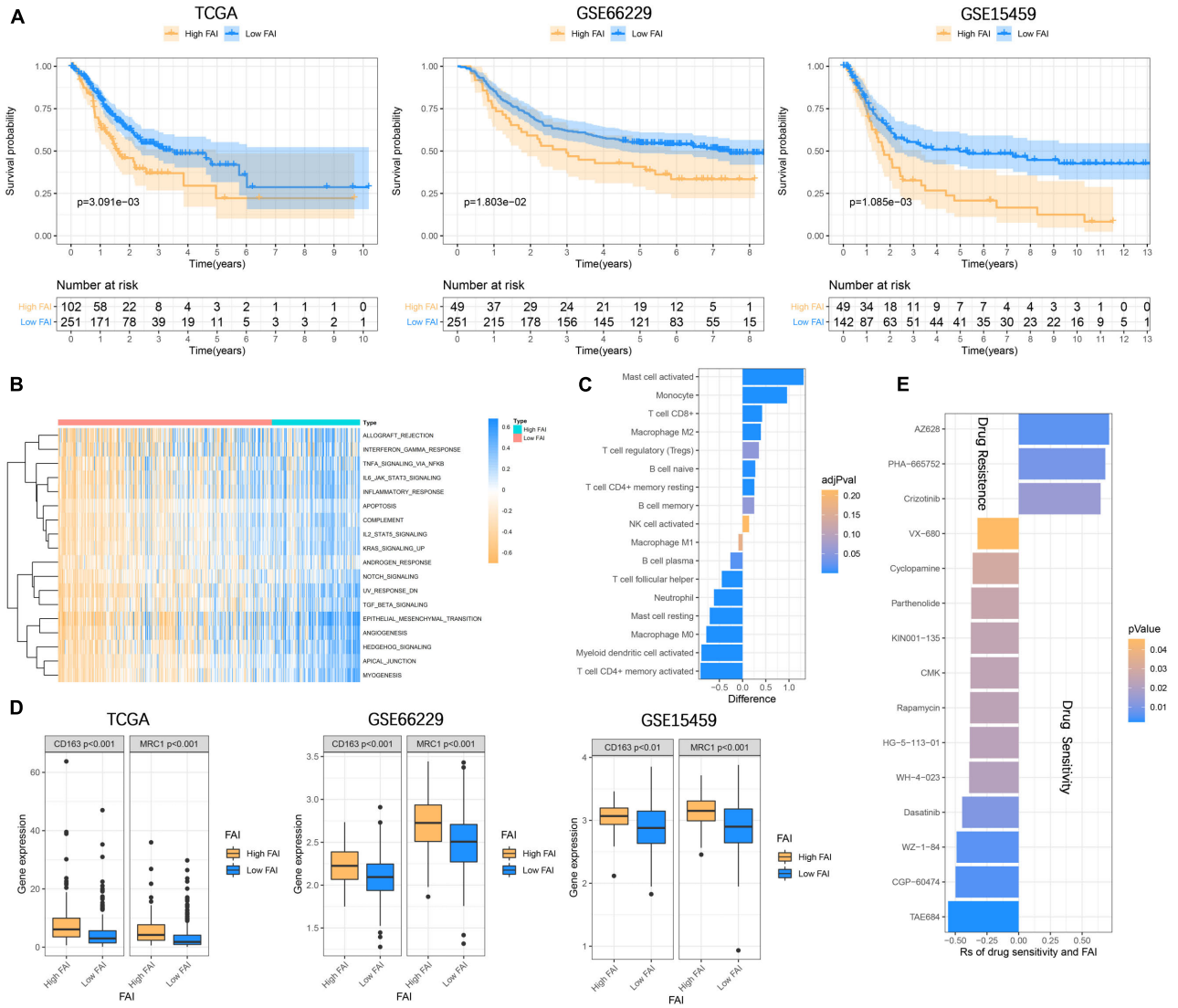

FIGURE 5 | Focal adhesion index assesses the prognosis and immune cell infiltration **(A)** FAI is closely related to the overall survival of GC patients, and the survival time of High FAI patients is significantly lower than that of Low FAI. **(B)** The heatmap shows that the immune signaling pathway is significantly enriched in the High FAI group. **(C)** The immune cells infiltrated in the high and low FAI groups. **(D)** M2 macrophage markers expression. **(E)** Major signaling pathway inhibitor explorations in the GDSC database.

(Chen et al., 2017; Li et al., 2019). Here we incorporate the M2 macrophage together with COL5A2, FLT1, and EGF into the LASSO Cox regression model (**Figure 7A**), and evaluate the riskscore according to the coefficient of each variable (**Figure 7B**). According to the cut-off = 0.4814 in the training group, the samples were divided into high-low risk groups. The Kaplan-Meier curve revealed that the overall survival of GC patients in the high-risk group was significantly lower than that in the low-risk group in the training (P = 2.847E^{-3}) and validation (GSE66229, P = 5.509E^{-4}; GSE15459, P = 1.491E^{-3}) datasets (**Figure 7C**). The area under the curves (AUC) for 1, 3, and 5-years overall survival were 0.701, 0.626, and 0.613, respectively, in the training set. 1, 3 and 5-years AUC in the GSE66229 dataset were 0.647, 0.617, and 0.609, respectively. 1, 3, and 5-years AUC in the GSE15459 dataset were 0.654, 0.640, and 0.613, respectively (**Supplementary Figure 6A**). Multivariate cox regression analysis also suggests that riskscore is a more important risk factor for GC than stage level (**Figure 7D**) (**Supplementary Figure 6B**). Finally, GSEA was carried out to explore the signaling pathways between the high-low risk groups. It was consistent with our previous GSVA results. IL6 JAK STAT3 signaling, IL2 STAT5 signaling, TGF-β signaling, and inflammatory response, and other immune signals were enriched in the high-risk group (**Figure 7E**).

To enhance the efficiency of traditional clinicopathological characteristics in predicting the 1-, 3-, and 5-year overall survival of GC. We introduce riskscore into the nomogram model to improve the accuracy of the prediction. When the total points

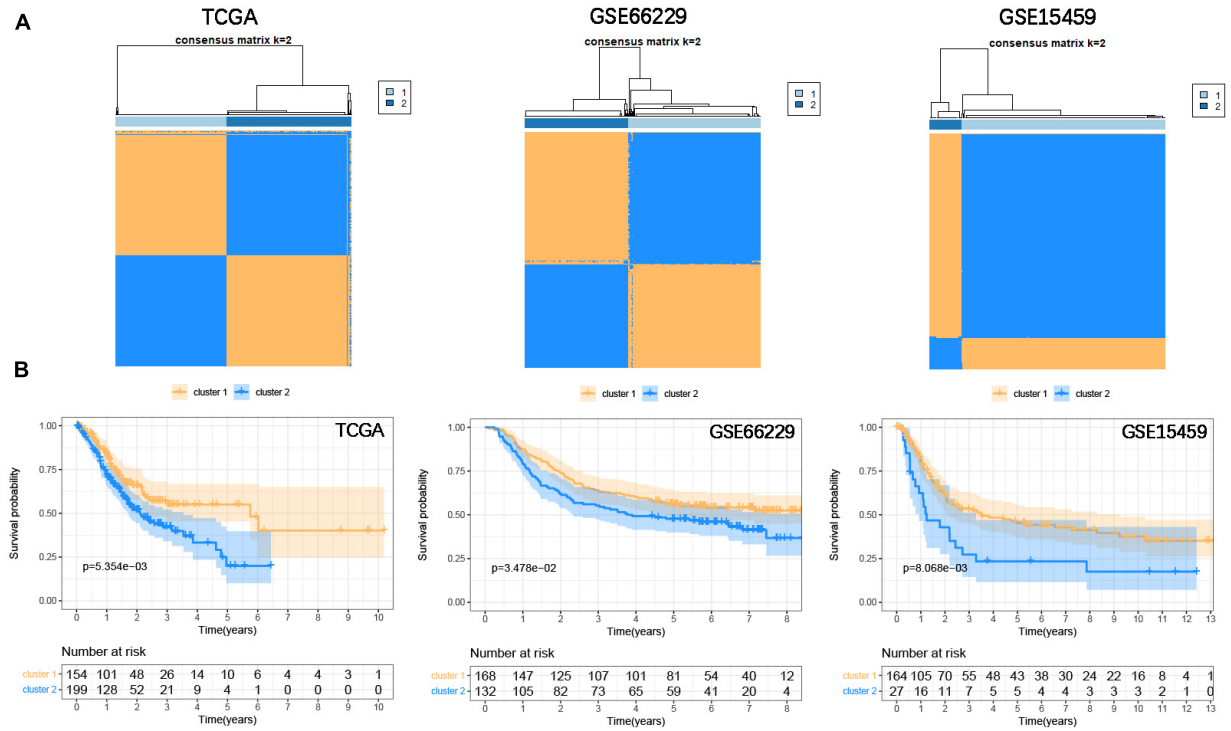

FIGURE 6 | Identify the molecular subtypes of GC based on the prognostic-related focal adhesion genes. **(A)** Identify two different GC molecular subtypes in the training and validation cohorts through the consensus clustering method. **(B)** Kaplan-Meier curve is depicted to observe the relationship between molecular subtypes and the overall survival of GC patients in the training and validation cohorts.

were 115, the 1-year survival rate for GC patients was 0.926, the 3-year survival rate was 0.796, and the 5-year survival rate was 0.705 (**Figure 8A**). The ROC curve showed that the nomograms were efficient in predicting the 1, 3, and 5-year overall survival of GC patients in the training (AUC = 0.673, 0.681 and 0.681, respectively) and validation (GSE66229, AUC = 0.891, 0.809 and 0.778, respectively; GSE15459, AUC = 0.743, 0.699 and 0.688, respectively) cohorts (**Figure 8B**). Finally, the difference between the prediction probability and the observation probability of the five-year overall survival of GC patients was compared by using the calibration curve, and the result showed that the difference was low (**Figure 8C**), suggesting that the nomogram was more accurate in predicting the five-year overall survival of GC patients. The above results have demonstrated that the focal adhesion-related gene can be used as an important molecule in GC risk stratification, and is a key marker for GC prognosis and immune microenvironment assessment.

DISCUSSION

The accumulated evidence indicates that the focal adhesion pathway plays an important role in regulating cell survival, mediating tumor-ECM interaction, and proliferation, migration, and invasion. Although many studies have focused on the mechanism of a molecule in the pathway based on omics. However, there is no study on the overall molecular interaction of the focal adhesion pathway from the perspective of multi-omics. In this study, we revealed the alterations and differences in the GC of focal adhesion pathway-related molecules from the Genetic and transcriptional perspectives. Somatic accumulation of the focal adhesion gene with a low mutation rate favors a better prognosis for patients with GC. The focal adhesion genes are oncogenes that drive tumor progression, and their mutations cause structural changes and functional defects of proteins, thereby inhibiting tumor growth (Chattopadhyay et al., 2010; Malfait et al., 2010). Therefore, they are low mutation and relatively conservative in tumors. In addition, the focal adhesion mutation has also been associated with pathological characteristics, MSI, and TMB. Then, we constructed FAI based on the transcription levels of 18 focal adhesion genes to describe the strength of the focal adhesion pathway. The High FAI subtype is closely related to the short survival time of GC patients. The FAI subtype can also be used as an important reference basis for clinical Lauren classification. Our study shows that high FAI corresponds to the diffuse type of GC. GSVA showed that immune signaling such as IL6, IL2, TNFA, and EMT was activated in the high FAI subtype. The infiltration abundance of M2 macrophages and Tregs cells was significantly increased in the high FAI subtype. The M2 macrophage marker was also significantly elevated in the high FAI subtype.

Previous studies have shown that M2 macrophage is a marker of peritoneal metastasis of GC, and the interaction between M2 macrophages and tumor cells in the immune microenvironment

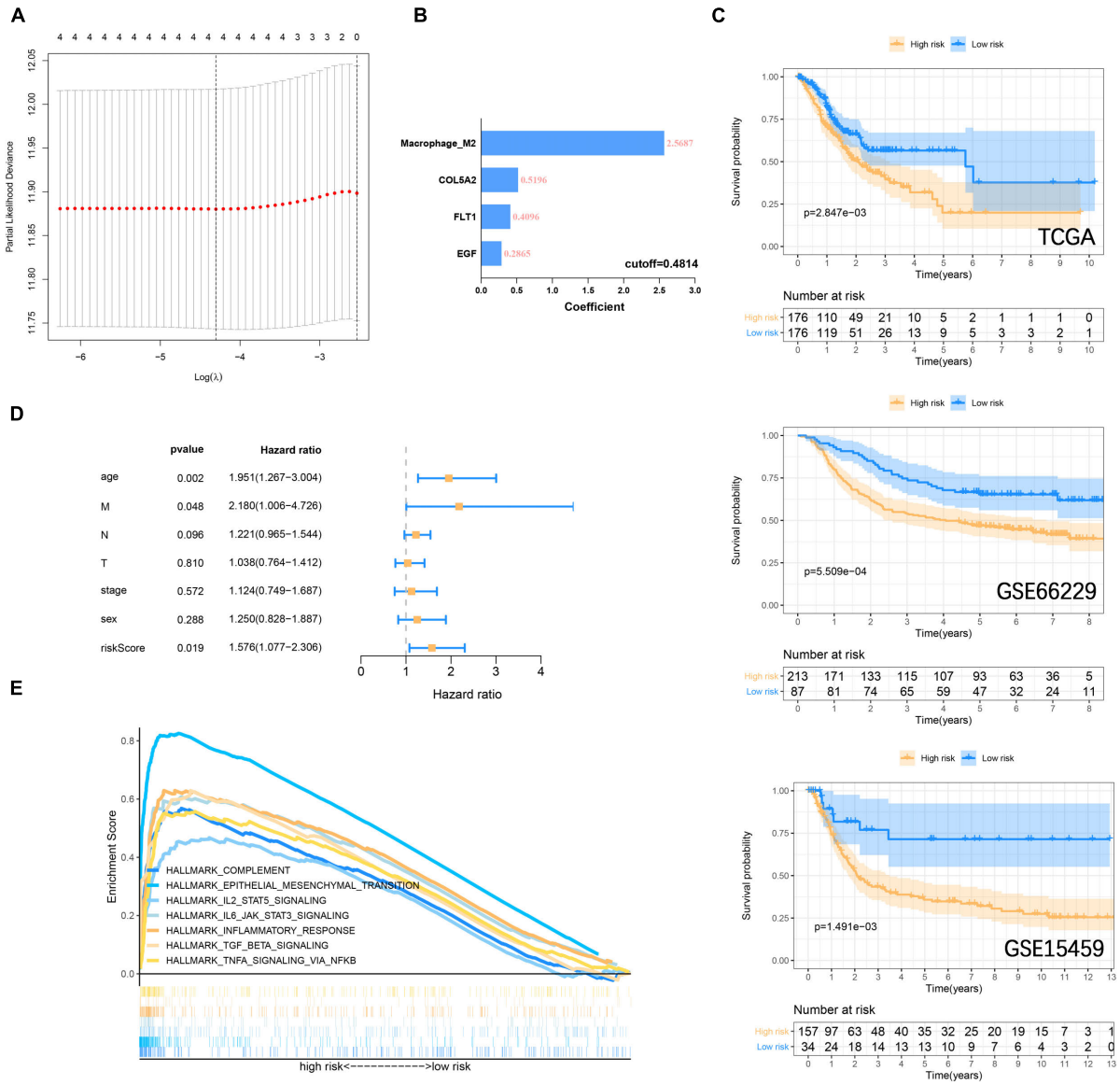

FIGURE 7 | Construction and verification of risk prognostic signature **(A)** LASSO Cox regression model shows that four risk factors are included in the risk signature. **(B)** Four risk factor coefficients and cut-off values. **(C)** Kaplan-Meier curve is drawn to evaluate the overall survival of GC patients in low-high risk groups. **(D)** Riskscore and clinicopathological characteristics Multivariate cox regression analysis in the TCGA cohort. **(E)** GSEA shows that immune-related signaling pathways are significantly enriched in the high-risk group.

is an important factor to promote tumor proliferation and metastasis (Yamaguchi et al., 2016). At the same time, M2 macrophage is also a marker of tumor immunotherapy and anti-angiogenesis treatment response (Gambardella et al., 2020). Inhibition of the focal adhesion pathway slows tumor infiltration by attenuating TGF-β signaling and macrophage infiltration (Wendt and Schiemann, 2009). In this study, we established FAI using the focal adhesion gene and found that it was closely related to M2 macrophage infiltration. M2 macrophage markers CD163 (Yamaguchi et al., 2016) and MRC1 (Xiao et al., 2021) were also observed to be significantly higher in the high FAI group than in the low FAI group. EMT signaling is a key factor for tumor resistance, regulation of angiogenesis, and promotion of growth (Sabbah et al., 2008; Banias et al., 2020). We observed a decrease in the epithelial marker in the high-FAI group and an increase in the mesenchymal markers. TGF-β signaling regulates tumor apoptosis, differentiation, proliferation, immune evasion, and other activities. It is also a key regulatory pathway for EMT signaling (Syed, 2016). TGF-β pathway facilitates the polarization of M2 macrophages, inactivates M1-macrophages, and inhibits T cell proliferation (Mia et al., 2014; Liu et al., 2019). Conversely, M2 macrophages also induce EMT processes through TGF-β signaling (Zhu et al., 2017). In this study, we found that TGF-β was significantly enriched in the high FAI

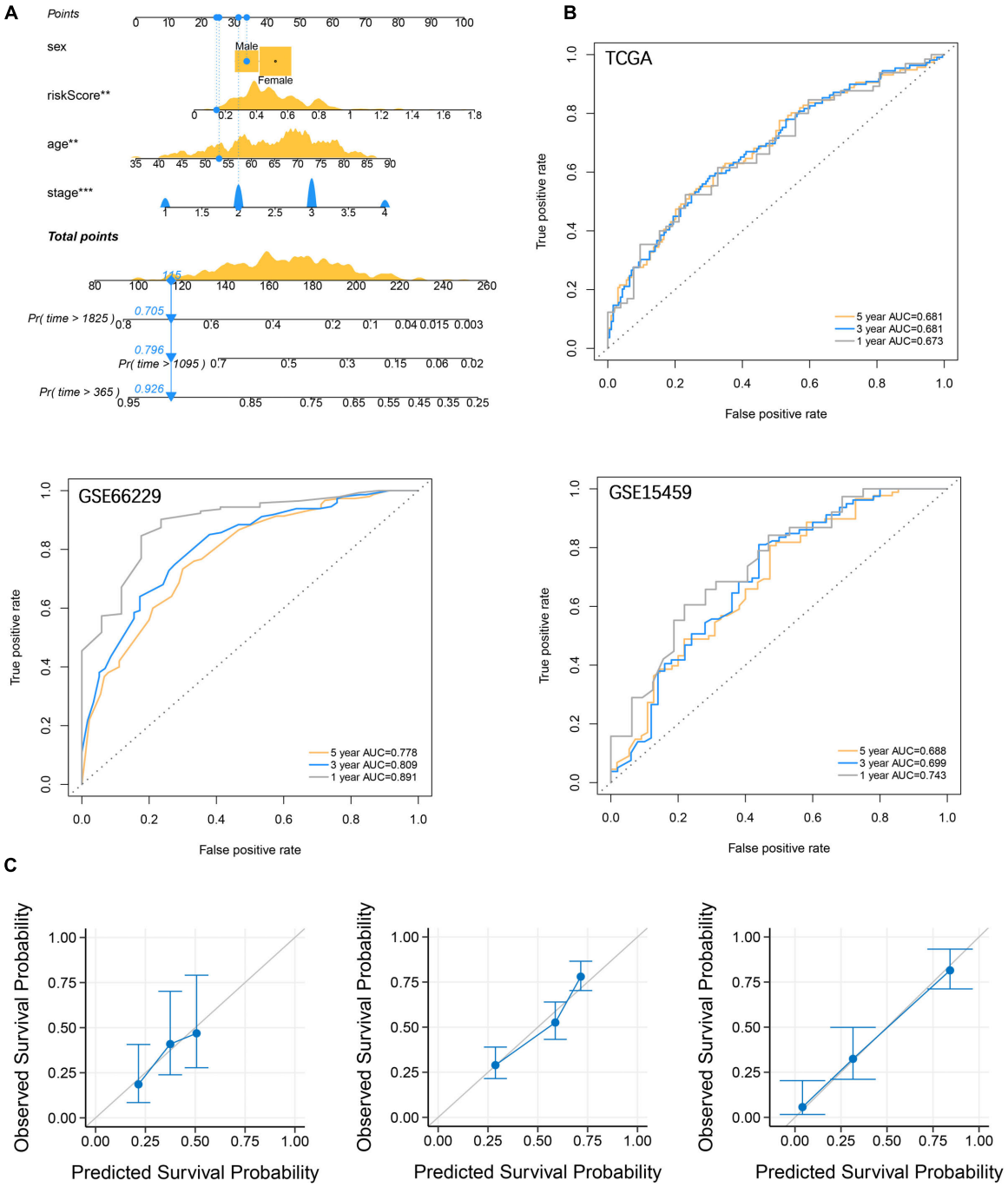

FIGURE 8 | Establishment and verification of nomograms. **(A)** Riskscore and clinicopathological characteristics were used to construct nomograms **(B)** The ROC curve describes the efficiency of the nomogram for predicting the overall survival of GC 1, 3, and 5 years. **(C)** Calibration curves were used to evaluate the accuracy of nomograms in predicting the 5-year overall survival of GC patients.

group. The interaction among M2 macrophages, TGF-β signals, and EMT is an important biological process to promote tumor progression. Finally, we use FAI to further explore sensitive drug molecules targeting key pathways. ALK, cell cycle, and BMX inhibitors were sensitive compounds in the high FAI group. This indicates that patients with high FAI may benefit from these signaling pathways rather than the BRAF and MET signaling pathways.

Next, we used the three focal adhesion genes FLT1, EGF, and COL5A2 related to prognosis to divide the samples into two subtypes in the TCGA cohort. And it was verified in the GEO cohorts. It suggested that the transcriptomics of these three genes

could be used as an important basis for prognosis stratification of GC. Wang et al. (2020) reported that FLT1 promoted GC peritoneal metastasis through the p-ERK/p-JNK pathway. EGF mediates the activation of Rab35 by DENND1A to regulate GC invasion and migration (Ye et al., 2018). A retrospective study found that COL5A2 was a potential risk factor for prognosis in GC patients ($P < 0.001$, HR = 18.834) (Ding et al., 2021). The above genes have been confirmed to be important participants in the development of GC, and we are also the first to find that they are important markers for GC stratification from a holistic perspective. We then included FLT1, EGF, and COL5A2 with M2 macrophages in the LASSO Cox regression model to establish a prognostic signature to evaluate overall survival. Numerous prognostic signatures have been reported in the past (Zhu et al., 2016; Jiang et al., 2019; Zhao et al., 2019), but these signatures are used to evaluate the prognosis from a certain perspective. It is the first time that we have combined transcriptomics with immune cells to predict the overall survival of GC. We believe that the signature established from a multi-omics perspective provides a new reference for clinical guidance of immunotherapy. However, our research results are mined and verified by bioinformatics methods, and more adequate molecular biological evidence and clinical sample needs to be adopted to prove our viewpoint.

CONCLUSION

The influence of Genetic and transcriptional alteration of focal adhesion-related genes on GC patients has been systematically revealed. FAI established based on transcriptomics is an important reference index for evaluating GC prognosis, immune microenvironment, microsatellite instability, TMB, Lauren classification, and sensitive drug molecular screening. FLT1, EGF, and COL5A2 are practicable markers for the identification of GC subtypes. The prognostic signature established together with M2 macrophages provides a new reference for guiding clinical immunotherapy. This study emphasizes the role of focal adhesion-related genes in promoting the progression of GC. Contribute to the development of individualized treatment for GC patients based on the perspective of immunity.

DATA AVAILABILITY STATEMENT

The datasets presented in this study can be found in online repositories. The names of the repository/repositories and accession number(s) can be found in the article/ **Supplementary Material**.

AUTHOR CONTRIBUTIONS

DM, RX, and HC: conceptualization. DM, RX, HC, and SS: data curation. DM, RX, and XC: formal analysis. DM, RX, XC, and DL: data analysis. YH and ZW: funding acquisition. YH, ZW, and CZ: investigation and Project administration. DM, RX, ZW, and CZ: methodology. DM, RX, DL, and SS: resources. DM and RX: original draft and writing—review and editing. All authors contributed to the article and approved the submitted version.

FUNDING

This study was supported by the National Natural Science Foundation of China (82073148), the Sanming Project of Medicine in Shenzhen (SZSM201911010), the Shenzhen Key Medical Discipline Construction Fund (SZXK016), the Guangdong Provincial Key Laboratory of Digestive Cancer Research (No. 2021B1212040006), the Shenzhen Sustainable Project (KCXFZ202002011010593), and the Research start-up fund of part-time PI, SAHSYSU (ZSQYJZPI202001).

SUPPLEMENTARY MATERIAL

The Supplementary Material for this article can be found online at: https://www.frontiersin.org/articles/10.3389/fcell.2021.716461/full#supplementary-material

REFERENCES

Banias, L., Jung, I., Bara, T., Fulop, Z., Simu, P., Simu, I., et al. (2020). Immunohistochemical-based molecular subtyping of colorectal carcinoma using maspin and markers of epithelial-mesenchymal transition. *Oncol. Lett.* 19, 1487–1495. doi: 10.3892/ol.2019.11228

Becht, E., Giraldo, N. A., Lacroix, L., Buttard, B., Elarouci, N., Petitprez, F., et al. (2016). Erratum to: estimating the population abundance of tissue-infiltrating immune and stromal cell populations using gene expression. *Genome Biol.* 17:249. doi: 10.1186/s13059-016-1113-y

Chattopadhyay, I., Singh, A., Phukan, R., Purkayastha, J., Kataki, A., Mahanta, J., et al. (2010). Genome-wide analysis of chromosomal alterations in patients with esophageal squamous cell carcinoma exposed to tobacco and betel quid from high-risk area in India. *Mutat. Res.* 696, 130–138. doi: 10.1016/j.mrgentox.2010.01.001

Chen, Y., Cheng, W. Y., Shi, H., Huang, S., Chen, H., Liu, D., et al. (2021). Classifying gastric cancer using FLORA reveals clinically relevant molecular subtypes and highlights LINC01614 as a biomarker for patient prognosis. *Oncogene* 40, 2898–2909. doi: 10.1038/s41388-021-01743-3

Chen, Y., Zhang, S., Wang, Q., and Zhang, X. (2017). Tumor-recruited M2 macrophages promote gastric and breast cancer metastasis via M2 macrophage-secreted CHI3L1 protein. *J. Hematol. Oncol.* 10:36. doi: 10.1186/s13045-017-0408-0

Ding, Y. L., Sun, S. F., and Zhao, G. L. (2021). COL5A2 as a potential clinical biomarker for gastric cancer and renal metastasis. *Medicine (Baltimore)* 100:e24561. doi: 10.1097/MD.0000000000024561

Eke, I., and Cordes, N. (2015). Focal adhesion signaling and therapy resistance in cancer. *Semin. Cancer Biol.* 31, 65–75. doi: 10.1016/j.semcancer.2014.07.009

Ferlay, J., Colombet, M., Soerjomataram, I., Mathers, C., Parkin, D. M., Pineros, M., et al. (2019). Estimating the global cancer incidence and mortality in 2018: GLOBOCAN sources and methods. *Int. J. Cancer* 144, 1941–1953. doi: 10.1002/ijc.31937

Fu, Q., Song, X., Liu, Z., Deng, X., Luo, R., Ge, C., et al. (2017). miRomics and proteomics reveal a miR-296-3p/PRKCA/FAK/Ras/c-Myc feedback loop

modulated by HDGF/DDX5/beta-catenin complex in lung adenocarcinoma. *Clin. Cancer Res.* 23, 6336–6350. doi: 10.1158/1078-0432.CCR-16-2813

Gambardella, V., Castillo, J., Tarazona, N., Gimeno-Valiente, F., Martinez-Ciarpaglini, C., Cabeza-Segura, M., et al. (2020). The role of tumor-associated macrophages in gastric cancer development and their potential as a therapeutic target. *Cancer Treat. Rev.* 86:102015. doi: 10.1016/j.ctrv.2020.102015

Gong, P. J., Shao, Y. C., Huang, S. R., Zeng, Y. F., Yuan, X. N., Xu, J. J., et al. (2020). Hypoxia-associated prognostic markers and competing endogenous RNA co-expression networks in breast cancer. *Front. Oncol.* 10:579868. doi: 10.3389/fonc.2020.579868

Guo, D., Zhang, D., Ren, M., Lu, G., Zhang, X., He, S., et al. (2020). THBS4 promotes HCC progression by regulating ITGB1 via FAK/PI3K/AKT pathway. *FASEB J.* 34, 10668–10681. doi: 10.1096/fj.202000043R

Gurzu, S., Jung, I., Orlowska, J., Sugimura, H., Kadar, Z., Turdean, S., et al. (2015). Hereditary diffuse gastric cancer–an overview. *Pathol. Res. Pract.* 211, 629–632. doi: 10.1016/j.prp.2015.06.003

Gurzu, S., Sugimura, H., Orlowska, J., Szederjesi, J., Szentirmay, Z., Bara, T., et al. (2017). Proposal of a Dukes-MAC-like staging system for gastric cancer. *J. Investig. Med.* 65, 316–322. doi: 10.1136/jim-2016-000270

Hanzelmann, S., Castelo, R., and Guinney, J. (2013). GSVA: gene set variation analysis for microarray and RNA-seq data. *BMC Bioinformatics* 14:7. doi: 10.1186/1471-2105-14-7

Jiang, Y., Xie, J., Huang, W., Chen, H., Xi, S., Han, Z., et al. (2019). Tumor immune microenvironment and chemosensitivity signature for predicting response to chemotherapy in gastric cancer. *Cancer Immunol. Res.* 7, 2065–2073. doi: 10.1158/2326-6066.CIR-19-0311

Lauren, P. (1965). The two histological main types of gastric carcinoma: diffuse and so-called intestinal-type carcinoma. An attempt at a histo-clinical classification. *Acta Pathol. Microbiol. Scand.* 64, 31–49. doi: 10.1111/apm.1965.64.1.31

Lee, B. Y., Timpson, P., Horvath, L. G., and Daly, R. J. (2015). FAK signaling in human cancer as a target for therapeutics. *Pharmacol. Ther.* 146, 132–149. doi: 10.1016/j.pharmthera.2014.10.001

Leek, J. T., Johnson, W. E., Parker, H. S., Jaffe, A. E., and Storey, J. D. (2012). The sva package for removing batch effects and other unwanted variation in high-throughput experiments. *Bioinformatics* 28, 882–883. doi: 10.1093/bioinformatics/bts034

Li, W., Zhang, X., Wu, F., Zhou, Y., Bao, Z., Li, H., et al. (2019). Gastric cancer-derived mesenchymal stromal cells trigger M2 macrophage polarization that promotes metastasis and EMT in gastric cancer. *Cell Death Dis.* 10:918. doi: 10.1038/s41419-019-2131-y

Li, X., Xu, H., Yi, J., Dong, C., Zhang, H., Wang, Z., et al. (2021). miR-365 secreted from M2 Macrophage-derived extracellular vesicles promotes pancreatic ductal adenocarcinoma progression through the BTG2/FAK/AKT axis. *J. Cell. Mol. Med.* 25, 4671–4683. doi: 10.1111/jcmm.16405

Liu, F., Qiu, H., Xue, M., Zhang, S., Zhang, X., Xu, J., et al. (2019). MSC-secreted TGF-beta regulates lipopolysaccharide-stimulated macrophage M2-like polarization via the Akt/FoxO1 pathway. *Stem Cell Res. Ther.* 10:345. doi: 10.1186/s13287-019-1447-y

Malfait, F., Wenstrup, R. J., and De Paepe, A. (2010). Clinical and genetic aspects of Ehlers-Danlos syndrome, classic type. *Genet. Med.* 12, 597–605. doi: 10.1097/GIM.0b013e3181eed412

Malta, T. M., Sokolov, A., Gentles, A. J., Burzykowski, T., Poisson, L., Weinstein, J. N., et al. (2018). Machine learning identifies stemness features associated with oncogenic dedifferentiation. *Cell* 173, 338–354.e15. doi: 10.1016/j.cell.2018.03.034

Mao, D., Zhou, Z., Song, S., Li, D., He, Y., Wei, Z., et al. (2021). Identification of stemness characteristics associated with the immune microenvironment and prognosis in gastric cancer. *Front. Oncol.* 11:626961. doi: 10.3389/fonc.2021.626961

Mia, S., Warnecke, A., Zhang, X. M., Malmstrom, V., and Harris, R. A. (2014). An optimized protocol for human M2 macrophages using M-CSF and IL-4/IL-10/TGF-beta yields a dominant immunosuppressive phenotype. *Scand. J. Immunol.* 79, 305–314. doi: 10.1111/sji.12162

Molaei, F., Forghanifard, M. M., Fahim, Y., and Abbaszadegan, M. R. (2018). Molecular signaling in tumorigenesis of gastric cancer. *Iran. Biomed. J.* 22, 217–230. doi: 10.22034/ibj.22.4.217

Murphy, J. M., Rodriguez, Y. A. R., Jeong, K., Ahn, E. E., and Lim, S. S. (2020). Targeting focal adhesion kinase in cancer cells and the tumor microenvironment. *Exp. Mol. Med.* 52, 877–886. doi: 10.1038/s12276-020-0447-4

Ngabire, D., Niyonizigiye, I., Patil, M. P., Seong, Y. A., Seo, Y. B., and Kim, G. D. (2020). M2 macrophages mediate the resistance of gastric adenocarcinoma cells to 5-fluorouracil through the expression of integrin beta3, focal adhesion kinase, and cofilin. *J. Immunol. Res.* 2020:1731457. doi: 10.1155/2020/1731457

Pernot, S., Voron, T., Perkins, G., Lagorce-Pages, C., Berger, A., and Taieb, J. (2015). Signet-ring cell carcinoma of the stomach: impact on prognosis and specific therapeutic challenge. *World J. Gastroenterol.* 21, 11428–11438. doi: 10.3748/wjg.v21.i40.11428

Sabbah, M., Emami, S., Redeuilh, G., Julien, S., Prevost, G., Zimber, A., et al. (2008). Molecular signature and therapeutic perspective of the epithelial-to-mesenchymal transitions in epithelial cancers. *Drug Resist. Updat.* 11, 123–151. doi: 10.1016/j.drup.2008.07.001

Salgado-Lucio, M. L., Ramirez-Ramirez, D., Jorge-Cruz, C. Y., Roa-Espitia, A. L., and Hernandez-Gonzalez, E. O. (2020). FAK regulates actin polymerization during sperm capacitation via the ERK2/GEF-H1/RhoA signaling pathway. *J. Cell Sci.* 133:jcs239186. doi: 10.1242/jcs.239186

Serrels, A., Lund, T., Serrels, B., Byron, A., McPherson, R. C., von Kriegsheim, A., et al. (2015). Nuclear FAK controls chemokine transcription, Tregs, and evasion of anti-tumor immunity. *Cell* 163, 160–173. doi: 10.1016/j.cell.2015.09.001

Serrels, B., McGivern, N., Canel, M., Byron, A., Johnson, S. C., McSorley, H. J., et al. (2017). IL-33 and ST2 mediate FAK-dependent antitumor immune evasion through transcriptional networks. *Sci. Signal.* 10:eaan8355. doi: 10.1126/scisignal.aan8355

Song, Y., Wang, J., Sun, J., Chen, X., Shi, J., Wu, Z., et al. (2021). Screening of potential biomarkers for gastric cancer with diagnostic value using label-free global proteome analysis. *Genomics Proteomics Bioinformatics* 18, 679–695. doi: 10.1016/j.gpb.2020.06.012

Subramanian, A., Kuehn, H., Gould, J., Tamayo, P., and Mesirov, J. P. (2007). GSEA-P: a desktop application for gene set enrichment analysis. *Bioinformatics* 23, 3251–3253. doi: 10.1093/bioinformatics/btm369

Syed, V. (2016). TGF-beta signaling in cancer. *J. Cell. Biochem.* 117, 1279–1287. doi: 10.1002/jcb.25496

Uchihara, T., Miyake, K., Yonemura, A., Komohara, Y., Itoyama, R., Koiwa, M., et al. (2020). Extracellular vesicles from cancer-associated fibroblasts containing annexin A6 induces FAK-YAP activation by stabilizing beta1 integrin, enhancing drug resistance. *Cancer Res.* 80, 3222–3235. doi: 10.1158/0008-5472.CAN-19-3803

Wang, X., Che, X., Yu, Y., Cheng, Y., Bai, M., Yang, Z., et al. (2020). Hypoxia-autophagy axis induces VEGFA by peritoneal mesothelial cells to promote gastric cancer peritoneal metastasis through an integrin alpha5-fibronectin pathway. *J. Exp. Clin. Cancer Res.* 39:221. doi: 10.1186/s13046-020-01703-x

Wang, Z., Wang, Z., Li, G., Wu, H., Sun, K., Chen, J., et al. (2017). CXCL1 from tumor-associated lymphatic endothelial cells drives gastric cancer cell into lymphatic system via activating integrin beta1/FAK/AKT signaling. *Cancer Lett.* 385, 28–38. doi: 10.1016/j.canlet.2016.10.043

Wendt, M. K., and Schiemann, W. P. (2009). Therapeutic targeting of the focal adhesion complex prevents oncogenic TGF-beta signaling and metastasis. *Breast Cancer Res.* 11:R68. doi: 10.1186/bcr2360

Xiao, M., Bian, Q., Lao, Y., Yi, J., Sun, X., Sun, X., et al. (2021). SENP3 loss promotes M2 macrophage polarization and breast cancer progression. *Mol. Oncol.* doi: 10.1002/1878-0261.12967 [Epub ahead of print].

Yamaguchi, T., Fushida, S., Yamamoto, Y., Tsukada, T., Kinoshita, J., Oyama, K., et al. (2016). Tumor-associated macrophages of the M2 phenotype contribute to progression in gastric cancer with peritoneal dissemination. *Gastric Cancer* 19, 1052–1065. doi: 10.1007/s10120-015-0579-8

Yang, W., Soares, J., Greninger, P., Edelman, E. J., Lightfoot, H., Forbes, S., et al. (2013). Genomics of Drug Sensitivity in Cancer (GDSC): a resource for therapeutic biomarker discovery in cancer cells. *Nucleic Acids Res.* 41, D955–D961. doi: 10.1093/nar/gks1111

Ye, B., Duan, B., Deng, W., Wang, Y., Chen, Y., Cui, J., et al. (2018). EGF stimulates Rab35 activation and gastric cancer cell migration by regulating DENND1A-Grb2 complex formation. *Front. Pharmacol.* 9:1343. doi: 10.3389/fphar.2018.01343

Yoshihara, K., Shahmoradgoli, M., Martinez, E., Vegesna, R., Kim, H., Torres-Garcia, W., et al. (2013). Inferring tumour purity and stromal and immune cell admixture from expression data. *Nat. Commun.* 4:2612. doi: 10.1038/ncomms3612

Zhang, B., Wu, Q., Li, B., Wang, D., Wang, L., and Zhou, Y. L. (2020). m(6)A regulator-mediated methylation modification patterns and tumor microenvironment infiltration characterization in gastric cancer. *Mol. Cancer* 19:53. doi: 10.1186/s12943-020-01170-0

Zhao, L., Jiang, L., He, L., Wei, Q., Bi, J., Wang, Y., et al. (2019). Identification of a novel cell cycle-related gene signature predicting survival in patients with gastric cancer. *J. Cell. Physiol.* 234, 6350–6360. doi: 10.1002/jcp.27365

Zhou, D. W., Fernandez-Yague, M. A., Holland, E. N., Garcia, A. F., Castro, N. S., O'Neill, E. B., et al. (2021). Force-FAK signaling coupling at individual focal adhesions coordinates mechanosensing and microtissue repair. *Nat. Commun.* 12:2359. doi: 10.1038/s41467-021-22602-5

Zhu, L., Fu, X., Chen, X., Han, X., and Dong, P. (2017). M2 macrophages induce EMT through the TGF-beta/Smad2 signaling pathway. *Cell Biol. Int.* 41, 960–968. doi: 10.1002/cbin.10788

Zhu, X., Tian, X., Yu, C., Shen, C., Yan, T., Hong, J., et al. (2016). A long non-coding RNA signature to improve prognosis prediction of gastric cancer. *Mol. Cancer* 15:60. doi: 10.1186/s12943-016-0544-0

Conflict of Interest: The authors declare that the research was conducted in the absence of any commercial or financial relationships that could be construed as a potential conflict of interest.

Publisher's Note: All claims expressed in this article are solely those of the authors and do not necessarily represent those of their affiliated organizations, or those of the publisher, the editors and the reviewers. Any product that may be evaluated in this article, or claim that may be made by its manufacturer, is not guaranteed or endorsed by the publisher.

frontiers in Cell and Developmental Biology

REVIEW
published: 01 October 2021
doi: 10.3389/fcell.2021.733270

The Versatile Roles of Cancer-Associated Fibroblasts in Colorectal Cancer and Therapeutic Implications

Longfei Deng[1†], Nianfen Jiang[2†], Jun Zeng[3], Yi Wang[4] and Hongjuan Cui[1,4,5*]*

[1] Cancer Center, Medical Research Institute, Southwest University, Chongqing, China, [2] Health Management Center, Southwest University Hospital, Chongqing, China, [3] Department of Genetics and Cell Biology, College of Life Sciences, Chongqing Normal University, Chongqing, China, [4] Department of General Surgery, The Ninth People's Hospital of Chongqing, Affiliated Hospital of Southwest University, Chongqing, China, [5] State Key Laboratory of Silkworm Genome Biology, Southwest University, Chongqing, China

OPEN ACCESS

Edited by:
Hongming Miao, Army Medical University, China

Reviewed by:
Cornelis F. M. Sier, Leiden University, Netherlands
Bingwen Zou, Sichuan University, China

***Correspondence:**
Hongjuan Cui
hcui@swu.edu.cn
Yi Wang
3048978619@qq.com

[†] These authors have contributed equally to this work

Specialty section:
This article was submitted to Molecular and Cellular Pathology, a section of the journal Frontiers in Cell and Developmental Biology

Received: *30 June 2021*
Accepted: *14 September 2021*
Published: *01 October 2021*

Citation:
Deng L, Jiang N, Zeng J, Wang Y and Cui H (2021) The Versatile Roles of Cancer-Associated Fibroblasts in Colorectal Cancer and Therapeutic Implications. Front. Cell Dev. Biol. 9:733270. doi: 10.3389/fcell.2021.733270

The tumor microenvironment (TME) is populated by abundant cancer-associated fibroblasts (CAFs) that radically influence the disease progression across many cancers, including the colorectal cancer (CRC). In theory, targeting CAFs holds great potential in optimizing CRC treatment. However, attempts to translate the therapeutic benefit of CAFs into clinic practice face many obstacles, largely due to our limited understanding of the heterogeneity in their origins, functions, and mechanisms. In recent years, accumulating evidence has uncovered some cellular precursors and molecular markers of CAFs and also revealed their versatility in impacting various hallmarks of CRC, together helping us to better define the population of CAFs and also paving the way toward their future therapeutic targeting for CRC treatment. In this review, we outline the emerging concept of CAFs in CRC, with an emphasis on their origins, biomarkers, prognostic significance, as well as their functional roles and underlying mechanisms in CRC biology. At last, we discuss the prospect of harnessing CAFs as promising therapeutic targets for the treatment of patients with CRC.

Keywords: cancer-associated fibroblast, colorectal cancer, hallmark, tumor microenvironment, therapeutics

INTRODUCTION

Colorectal cancer (CRC), a term referring to colonic cancer and rectal cancer synonymously, ranks the third most common malignant disease across the world and accounts for 9.2% cancer-related mortality (Bray et al., 2018). Despite achievements made in the innovative medicines and therapeutic methods, the success of effective treatment in CRC patients is hindered to some extent by only targeting tumor cells and ignoring the tumor microenvironment (TME) as an accomplice in nursing disease progression. Indeed, the TME significantly blunts the therapeutic responses, and thus, multitargeting tumor cells and co-opted cells simultaneously in the TME compartments is

thought to improve the efficacy of current therapeutics (Wu and Dai, 2017). As the predominant architects of the TME, cancer-associated fibroblasts (CAFs) play a tremendous role in cancer progression, including CRC (Sahai et al., 2020). In recent few years, increasing studies have yielded a mass of updated insights into the biology of CAFs which constitute the CRC. In this review, we aimed to summarize these advancements in this field, mainly including the identification of cellular precursors and molecular markers of CAFs, and verification of their prognostic significance in CRC patients, as well as numerous new discoveries in their versatile roles in key hallmarks of CRC pathogenesis and related novel mechanisms. According to these latest findings, we also analyzed the therapeutic potential and prospect of targeting CAFs in future CRC treatment.

CELLS OF ORIGIN OF CANCER-ASSOCIATED FIBROBLASTS IN COLORECTAL CANCER

It is now becoming increasingly clear that CAFs can originate from diverse potential cellular precursors through distinct mechanisms. As known, normal resident tissue fibroblasts upregulate the expression of smooth muscle α-actin (α-SMA), the most common marker of myofibroblasts, and acquire a myofibroblast-like phenotype upon de novo activation by numerous soluble factors, such as the transforming growth factor-β (TGF-β) and platelet-derived growth factor (PDGF) secreted from the neighboring tumor cells (Vonlaufen et al., 2008; Yin et al., 2013). While local fibroblasts are commonly deemed as the dominating origins of CAFs, additional sources also contribute to the pool of tumor stromal CAFs depending on tumor histological types. Among them, the best-studied CAF precursors are mesenchymal stem cells (MSCs), which are recruited from the adult human tissues including bone marrow and connective tissues, and constitute a large portion of CAFs in some cancers such as breast (Weber et al., 2015), prostate (Jung et al., 2013), gastric (Zhu et al., 2014), and pancreatic cancers (Kabashima-Niibe et al., 2013). In addition, circulating fibrocytes recruited from the bone marrow can migrate into the TME and also give origin to CAFs, as observed in the tumor stroma of breast cancer (Barth et al., 2002) and gastric cancer (Terai et al., 2015). Moreover, epithelial cells adjacent to cancer cells are able to differentiate into CAFs by undergoing epithelial-to-mesenchymal transition (EMT) (Iwano et al., 2002). Similar to this scenario, endothelial cells (ECs) represent other progenitors of CAFs by means of endothelial-to-mesenchymal transition (EndMT) (Zeisberg et al., 2007). The remaining CAF sources, though maybe less common, include adipocytes, pericytes, and smooth muscle cells (SMCs) that possess the capacity to convert into CAFs by transdifferentiation (Chen and Song, 2019). Collectively, these categories of cellular precursors diversify CAF population with overt original heterogeneity.

Cancer-associated fibroblasts are present in high abundance in CRC (Adegboyega et al., 2002; Powell et al., 2005). Although the precise origins of CAFs in CRC have not yet been elucidated explicitly, mounting evidence has suggested that fibroblasts remain the major sources (**Table 1**). TGF-β is a classic stimulus inducing the differentiation of quiescent fibroblasts into CAFs in the TME. It has been reported that upon induction by CRC cell-derived soluble factors, the TGF-β signaling is activated in CAFs, accompanied by increased expression of TGF-β itself, suggesting a cumulative production of TGF-β within the TME that promotes the transdifferentiation of resident fibroblasts into CAFs (Hawinkels et al., 2014). TGF-β is secreted in a form of latent complex. One study has shown that CRC cell-secreted latent TGF-β could be activated by integrin αvβ6, which is expressed on CRC cells, and subsequently activates fibroblasts to exhibit CAF phenotypes. The integrin αvβ6 appears indispensable for this process, since fibroblast activation is disrupted in the absence of integrin αvβ6 (Peng et al., 2018). These studies indicate that interacting with either tumor cells or secreted soluble factors enables TGF-β activation and favors the generation of CAFs in CRC.

Moreover, like TGF-β, another TGF superfamily member Nodal has recently been shown correlated positively with α-SMA expression in human CRC tissues. Through activating TGF-β/Smad/Snail pathway, tumor cell-derived Nodal facilitates the transition of normal fibroblasts into CAFs that function to support the tumor growth of CRC cells *in vitro* and *in vivo* (Li et al., 2019a). Some lines of evidence also show that Snail-positive fibroblasts display CAFs properties (Li et al., 2018), further supporting that Snail is an important regulator of CAF formation derived from fibroblasts. Snail is a TGF-β target gene that mediates some pro-tumorigenic roles of TGF-β signaling (David et al., 2016; Moon et al., 2017), and is also necessary for mediating the pro-tumorigenic effects of fibroblasts on CRC cells (Herrera et al., 2014). It is therefore reasonable to speculate that Nodal-mediated CAF formation via Snail signaling could promote aggressive phenotypes in CRC. Moreover, except Nodal, the interleukin (IL)-34, a cytokine overexpressed by CRC cells, can

TABLE 1 | The cellular origins of CAFs in CRC.

Type	Location	Differentiation mechanism	References
Fibroblasts	Local tissue	Stimuli: TGF-β, Nodal, IL-34; Regulators: αvβ6, Snail, TIMP-1, dickkopf-3, PKCζ	Gong et al., 2013; Hawinkels et al., 2014; Li et al., 2018, 2019a; Peng et al., 2018; Ferrari et al., 2019; Franze et al., 2020; Kasashima et al., 2021
MSCs	Bone marrow	Cell-cell contacts mediated by Notch-Jagged1 signaling	Peng et al., 2014
ECs	Endothelium	Tubulin-β3 activation and EndMT	Wawro et al., 2018
HSCs	Perisinusoidal	CXCR4/TGF-β1 axis activation	Tan et al., 2020
MCs	Mesothelium	MMT	Gordillo et al., 2020

MSCs, mesenchymal stem cells; ECs, endothelial cells; EndMT, endothelial-to-mesenchymal transition; HSCs, hepatic stellate cells; MCs, mesothelial cells; MMT, mesothelial-to-mesenchymal transition.

also stimulate normal fibroblasts to display a cellular phenotype resembling that of CAFs (Franze et al., 2020). Thus, the crosstalk between CRC and fibroblasts mediated by soluble factors, such as Nodal and IL-34, plays a significant role in enhancing CAF formation in the TME of CRC. Probably, other CRC cell-secreted factors may also participate in regulating the differentiation of fibroblasts into CAFs, which warrants further explorations.

Some up-to-date studies have also shown the pivotal roles of cancer stroma in the development of CAFs in CRC. For instance, the increased stromal expression of the tissue inhibitor matrix metalloproteinase-1 (TIMP-1) stimulates the accumulation of CAFs within CRC tissues partly through transdifferentiation of resident fibroblasts (Gong et al., 2013). Additionally, dickkopf-3 expressed in the stroma orchestrates a concomitant activation of Wnt signaling and YAP/TAZ signaling which are coordinated to generate CAFs in CRC (Ferrari et al., 2019). Moreover, stromal loss of protein kinase Cζ (PKCζ) promotes generation of a pro-tumorigenic CAF population in human CRC through a SOX2-dependent mechanism (Kasashima et al., 2021). Hence, cues for converting fibroblasts into CAFs in the TME could stem from both CRC cells and the stroma.

In addition to fibroblasts, recent studies have shown that CAFs in CRC also originate from other sources including MSCs, ECs, pericytes, and mesothelial cells (MCs). It is known that bone marrow-derived MSCs can travel to tumor stroma, where they differentiate into CAFs. In an in vitro co-culture model, CRC cells have been reported to induce differentiation of MSCs into CAFs by cell–cell contacts, which is mediated by Notch-Jagged1 signaling and downstream activation of TGF-β/Smad pathway (Peng et al., 2014). This study provides a molecular mechanism explaining the bone marrow-derived MSCs as sources of CAFs in CRC. Further, ECs undergo conversion into CAFs via the process of EndMT, which is associated with microtubule cytoskeleton reorganization. One study has shown a mechanistic perspective that invasive CRC cells induce the EndMT of ECs to generate CAFs via upregulation and phosphorylation of tubulin-β3, which is mainly dependent on TGF-β stimulation (Wawro et al., 2018). However, whether CRC cells induce transform of ECs *in vivo* needs more investigations. Analogous to activation process following liver damage, the quiescent hepatic stellate cells (HSCs), a subset of liver-specific pericytes, are activated and differentiated into myofibroblasts when tumor micrometastases are developed in liver lobules (Vidal-Vanaclocha, 2008). A recent discovery has represented data showing that CRC cells are able to interact with HSCs and promote SDF-1 secretion, which in turn binds to CXCR4 and induces TGF-β1 expression and secretion in CRC cells, eventually resulting in HSCs differentiation into CAFs. In contrast, blockade of this CXCR4/TGF-β1 axis inhibits hepatic CAFs differentiation and CRC metastases to the liver (Tan et al., 2020). These findings seemingly underscore a critical role of TGF-β in mediating the generation of CAFs derived from not only fibroblasts but also non-fibroblasts in CRC. Interestingly, some histological observations have described that the source of CAFs in CRC can also be ascribed to MCs achieved via a mesothelial-to-mesenchymal transition (MMT) (Gordillo et al., 2020). Nevertheless, how MCs undergo MMT and following conversion into CAFs remains largely unclear in CRC. An RNA-sequencing analysis has revealed that the TGF-β signaling is related to MMT (Rynne-Vidal et al., 2017). It would be intriguing to test the possibilities that TGF-β may also be involved in MMT-mediated differentiation of MCs into CAFs in CRC.

It has been established that the MSCs have the potential to differentiate into mesenchymal tissues like osteocytes, chondrocytes, and adipocytes. They also have a differentiation potential beyond the mesenchymal lineage, such as myogenic, cardiomyogenic, and neurogenic potentials (Jackson et al., 2007). Besides, the MSCs were found to be differentiated into ECs (Oswald et al., 2004) and deeply associated with HSCs (Kordes et al., 2013). Further, the fibroblasts share many similarities between MSCs, including differentiation potential (Haniffa et al., 2009; Soundararajan and Kannan, 2018). Hence, the tight relationships between these cells may possibly influence the pool of cellular precursors of CAFs, whereby affecting the generation of CAFs in CRC. Nevertheless, it should be noted that given the original heterogeneity of CAFs, the sources of CAFs in CRC may not be limited to the above-described precursor cells (**Table 1**). Techniques like the lineage tracing, a powerful tool of deciphering cell-fate decisions (Kretzschmar and Watt, 2012), are expected to be employed in future studies to identify other cellular origins of CAFs in CRC, which would be very helpful to understand the complex nature of CAFs in CRC in the TME.

MARKERS OF CANCER-ASSOCIATED FIBROBLASTS IN COLORECTAL CANCER

A number of markers that are highly expressed in CAFs, such as the α-SMA, fibroblast activation protein alpha (FAP), fibroblast-specific protein 1 (FSP-1), platelet-derived growth factor receptor-α (PDGFRα) and PDGFRβ, have already been widely used to identify or isolate CAFs from the pool of fibroblasts present in the whole body (Nurmik et al., 2020). However, a critical issue remains as CAFs are composed of heterogeneous population of cells, and accordingly, markers of CAFs are vastly heterogeneous in different CAF subpopulations and consequently show low specificity. To date, there are no specific or reliable markers for CAFs in various tumors. Despite this dismay, many progresses have been witnessed over the last decade in seeking potential markers of CAFs in CRC and elucidating their relations to disease progression (**Table 2**). For example, the cell-surface molecule CD10 (Zhu et al., 2016) and the interleukin (IL)-11 (Nishina et al., 2021) might serve as possible markers of CAFs in CRC, although more lines of evidence are required to consolidate this possibility. Theoretically, candidate biomarkers of CAFs may be those molecules displaying significantly different expression levels between CAFs and normal counterparts. It is well accepted that compared with normal fibroblasts, differences in genetic, epigenetic, morphology and secretions are evident in CAFs in CRC (Mrazek et al., 2014; Wen et al., 2015). A proteome profiling of CAFs and normal fibroblasts purified from colon tissues has identified LTBP2, CDH11, OLFML3, and FSTL1 as selective biomarkers of CAFs (Torres et al., 2013). Aside

TABLE 2 | Candidate markers of CAFs in CRC.

Name	Description	Confirmed material	References
IL-11	IL-6 family cytokine	Animal CRC model	Nishina et al., 2021
CD10	Cell surface zinc metalloendopeptidase	Human CRC specimen	Cui et al., 2010; Zhu et al., 2016
LTBP2 CDH11 OLFML3 FSTL1	ECM protein Adhesion molecule ECM-related protein Extracellular glycoprotein	Animal CRC model; Human and mouse CRC specimen	Torres et al., 2013
ADAMs	Proteases	Human CRC specimen	Mochizuki et al., 2020
Exosomal ncRNAs	RNA molecules	Human CRC specimen	Herrera et al., 2018
Tenascin C ED-A FN SDF1	ECM glycoprotein ECM protein Chemokine	Human CRC specimen	De Boeck et al., 2013

ECM, extracellular matrix; CDH11, cadherin-11; ADAMs, a disintegrin and metalloproteinases; ncRNAs, non-coding RNAs; ED-A FN, fibronectin ED-A domain; SDF1, stromal-derived factor-1.

from these proteins, CAFs from colon tissues of CRC patients show increased expression in several species of a disintegrin and metalloproteinases (ADAMs), including ADAM9, ADAM10, ADAM12, and ADAM17 (Mochizuki et al., 2020), as compared with normal fibroblasts. Moreover, normal fibroblasts and CAFs have significant differences in their protein expression profiles among 7 patient pairs, with 145 differentially expressed proteins revealed by the proteomic data, and 15 differentially expressed molecules shown by a secretomic analysis (Atanasova et al., 2020). Interestingly, by performing the next generation sequencing, a significant number of non-coding RNAs (ncRNAs) in exosomes were also found as potential biomarkers present in CAFs-derived exosomes (Herrera et al., 2018). Furthermore, a differential secretome approach of CAFs and bone marrow-derived precursors has identified in clinical CRC specimens a series of candidate biomarkers such as tenascin C, fibronectin ED-A domain and stromal-derived factor-1 (SDF1) that are associated with a CAF-specific phenotype (De Boeck et al., 2013). These comparative studies replenish the repository of candidate markers of CAFs in CRC, which need verifications by more investigations.

Along with the appearance of a growing body of potential markers of CAFs, accumulating evidence has also related some markers to the roles involved in CRC progression. Collagen I, PDGFR-β and α-SMA have been known as molecular markers of CAFs, and in advanced CRC, their expression varies in CAFs and is significantly associated with vessel markers CD31 and CD34, indicating that individual CAFs may have different expression patterns and effects on venous invasion of advanced CRC (Nishishita et al., 2018). In consistence, the expression of CAFs markers, like α-SMA, CD10, podoplanin and FSP1, is correlated with lymph node metastasis in the submucosal invasive CRC, therefore may allow for stratification of patients with high risk of lymph node metastasis (Sugai et al., 2018). Furthermore, a transcriptomic analysis has also shown that CAF markers, such as α-SMA, PDGFR-β, FAP, FSP-1, are expressed in a higher level in stroma-high compared to stroma-low CRC tissues, particularly with higher FAP expression in the invasive part of tumors (Sandberg et al., 2019), together suggesting that these molecular markers, as indicative of CAFs, could play a promotive role in CRC progression.

Although the research approaches mentioned above have yielded a cohort of promising candidate markers for CAFs, novel selection methods based on cellular functions such as lineage tracing and single-cell sequencing will be preferable for improving the identification and targeting of CAFs in CRC in a more specific manner.

CANCER-ASSOCIATED FIBROBLASTS IN COLORECTAL CANCER PROGNOSIS

Cancer-associated fibroblasts accumulated in large numbers in the TME are often associated with high-grade malignancies and poor prognosis across different human cancers. The prognostic impact of CAF-derived markers or gene signatures has also been demonstrated in CRC (Herrera et al., 2013b; Paulsson and Micke, 2014). For example, the expression of CAF markers, including α-SMA, FSP1, and FAP, is associated with the clinical outcome of a cohort of 289 CRC patients, and surprisingly, the combination of these CAF markers with M2 macrophage markers, CD163 and DCSIGN, identifies significant differences in the survival of advanced-stage patients, demonstrating a prognostic involvement of interrelationships between markers of CAFs and M2 macrophages in CRC patient survival (Herrera et al., 2013a). Specifically, the common and high intratumoral expression of FAP is associated with poorer prognosis of CRC patients, which emphasizes FAP as an independent negative prognostic factor (Wikberg et al., 2013). In general, CAFs serve as a useful prognostic biomarker in CRC, but it should be noticed that podoplanin, α-SMA or S100A4 expressing CAFs have been shown to be associated with different prognosis in CRC (Choi et al., 2013), which possibly indicate varying prognostic significances conferred by different populations of CAFs. On the other hand, a CAF-derived 5-gene classifier selected from 108 differentially expressed genes, including CCL11, PDLIM3, AMIGO2, SLC7A2, and ULBP2, is significantly associated with increased relapse risk and death from CRC across all validation series of stage II/III patients (Berdiel-Acer et al., 2014). In addition, a recent study has reported that the 1,25-dihydroxyvitamin D3 [1,25(OH)2D3]-associated gene signature in CAFs predicts a favorable clinical outcome in CRC (Ferrer-Mayorga et al., 2017). This association may be explained by a protective effect of the active vitamin D metabolite 1,25(OH)2D3 against CRC via regulation of CAFs. Besides, a CAF-related gene osteopontin (OPN) was also found to be a predictive biomarker for metastatic CRC patients treated with first-line FOLFIRI/bevacizumab in two independent randomized phase III trials (Puccini et al., 2018). Moreover, GREM1 and ISLR are newly identified CAF-specific genes, and their stromal high levels in CRC patients are associated with poor and favorable survival,

respectively, which is mechanistically attributed to their inverse regulation of the bone morphogenetic protein (BMP) signaling in the stroma (Kobayashi et al., 2021). This finding also suggests that the status of this pathway could be considered as a predictive factor for CRC survival.

Apart from CAF markers or gene signatures, accumulating studies also have revealed other prognostic markers that are expressed in CAFs of CRC. In an immunohistochemical evaluation of 110 CRC patient cases, the ubiquitin carboxyl-terminal hydrolase L1 (UCH-L1) in CAFs was shown to be an independent prognostic factor for predicting shorter survival and a higher incidence of recurrence and lymph node metastasis (Akishima-Fukasawa et al., 2010). Additionally, protein expression of the lysyl oxidase-like 2 (LOXL2) in CAFs of CRC was identified to be associated with poor outcome of CRC patients and as a prognostic biomarker particularly for stage II patients (Torres et al., 2015). Further, the expression of an immune checkpoint molecule CD70 was detected on the majority of CAFs in invasive CRC specimens and shown significantly correlated with clinicopathological parameters such as metastasis, differentiation and advanced stage, and consequently, CD70-positive CAFs were defined as poor prognostic markers for CRC (Jacobs et al., 2017). In concert, another immunohistochemical evaluation of 269 primary CRCs also uncovers that CAFs exhibit various CD70 expression, which predicts worse survival in CRC patients (Inoue et al., 2019). CAFs are known to secrete different cytokines. One study using a cytokine chip has found that CAFs in CRC secrete the c-type lectin domain family 3 member B (CLEC3B), and that CRC patients with combined expression of CLEC3B and α-SMA have worse survival than those with either CLEC3B or α-SMA expression alone (Zhu et al., 2019), offering CLEC3B as a potential valuable CAF-based biomarker for CRC prognosis. Furthermore, some proteins deregulated in the CAFs of CRC also show significant prognostic value. In distant metastases, PTEN expression in CAFs was detected lost in some CRC patients, which was linked closely to a worse prognosis (Kwak et al., 2014). On the contrary, another report has documented that STAT3 is activated in CAFs of human CRC, and pSTAT3 expression in CAFs is negatively correlated with the survival of CRC patients, illustrating it as a prognostic marker (Heichler et al., 2020). Together, these numerous studies as outlined above reinforce the concept that CAFs and CAF-derived factors have a prognostic significance in human CRC (**Table 3**).

TABLE 3 | Prognostic impact of CAFs in CRC patients.

Name	CRC prognosis	Clinical case	References
CAF marker			
α-SMA	Poorer DFS and OS	591	Choi et al., 2013; Herrera et al., 2013a
FSP1	Poorer DFS and OS	289	Herrera et al., 2013a
FAP	Poorer DFS and OS	738	Herrera et al., 2013a; Wikberg et al., 2013
Podoplanin, S100A4	Poorer DFS and OS	302	Choi et al., 2013
CAF gene signature			
CCL11, PDLIM3, AMIGO2, SLC7A2, ULBP2	Poorer DFS	108	Berdiel-Acer et al., 2014
Vitamin D receptor	Better PFS and OS	658	Ferrer-Mayorga et al., 2017
Osteopontin variant	Better DFS and OS	451	Puccini et al., 2018
GREM1	Poorer DFS and OS	556	Kobayashi et al., 2021
ISLR	Better DFS and OS	556	Kobayashi et al., 2021
CAF-derived protein			
UCH-L1	Poorer RFS and OS	110	Akishima-Fukasawa et al., 2010
LOXL2	Poorer DFS and OS	121	Torres et al., 2015
CD70	Poorer OS	269	Inoue et al., 2019
CLEC3B	Poorer OS	225	Zhu et al., 2019
PTEN	Better OS	181	Kwak et al., 2014
pSTAT3	Poorer OS	375	Heichler et al., 2020

DFS, disease-free survival; OS, overall survival; PFS, Progression-free survival; RFS, recurrence-free survival.

THE VERSATILE ROLES OF CANCER-ASSOCIATED FIBROBLASTS IN COLORECTAL CANCER

Cancer-associated fibroblasts are indispensable architects in the TME that play fundamental roles to radically influence multiple malignant behaviors. Over the recent decade, increasing lines of evidence have revealed the versatility of CAFs in CRC biology, including tumorigenesis, proliferation, angiogenesis, invasion and metastasis, stemness, therapy resistance, and tumor immunity (**Figure 1**). In this section, we will discuss these pivotal roles of CAFs in the regulation of pathogenic processes during CRC development and progression.

Tumorigenesis

It is well recognized that CAFs play a critical role in modulating tumorigenesis. However, the role and mechanism of CAFs in CRC tumorigenesis are still poorly understood. Emerging studies have unveiled several CAF-based regulators and signaling pathways that could control CRC development. For instance, the myofibroblast MyD88-deficient mice were found resistant to AOM/DSS-induced intestinal tumorigenesis, and the STAT3/PPARγ pathway activated by the MyD88 signaling in myofibroblasts was demonstrated to contribute to this phenotype (Yuan et al., 2021). Further, periostin, a multifunctional extracellular matrix protein, is induced in fibroblasts by STAT3 activation, which ultimately facilitates CRC development in AOM/DSS and genetically modified mice (Ma et al., 2020). It has also been recently shown that the constitutive activation of STAT3 in the CAFs of CRC promotes tumorigenesis, and in contrast, STAT3 inactivation reduces the development of CRC in a mouse model established with AOM/DSS (Heichler et al., 2020). Hence, these findings may identify a crucial role of CAFs' STAT3 signaling in facilitating CRC tumorigenesis. In addition, the selective loss of PKCζ in colonic fibroblasts induces

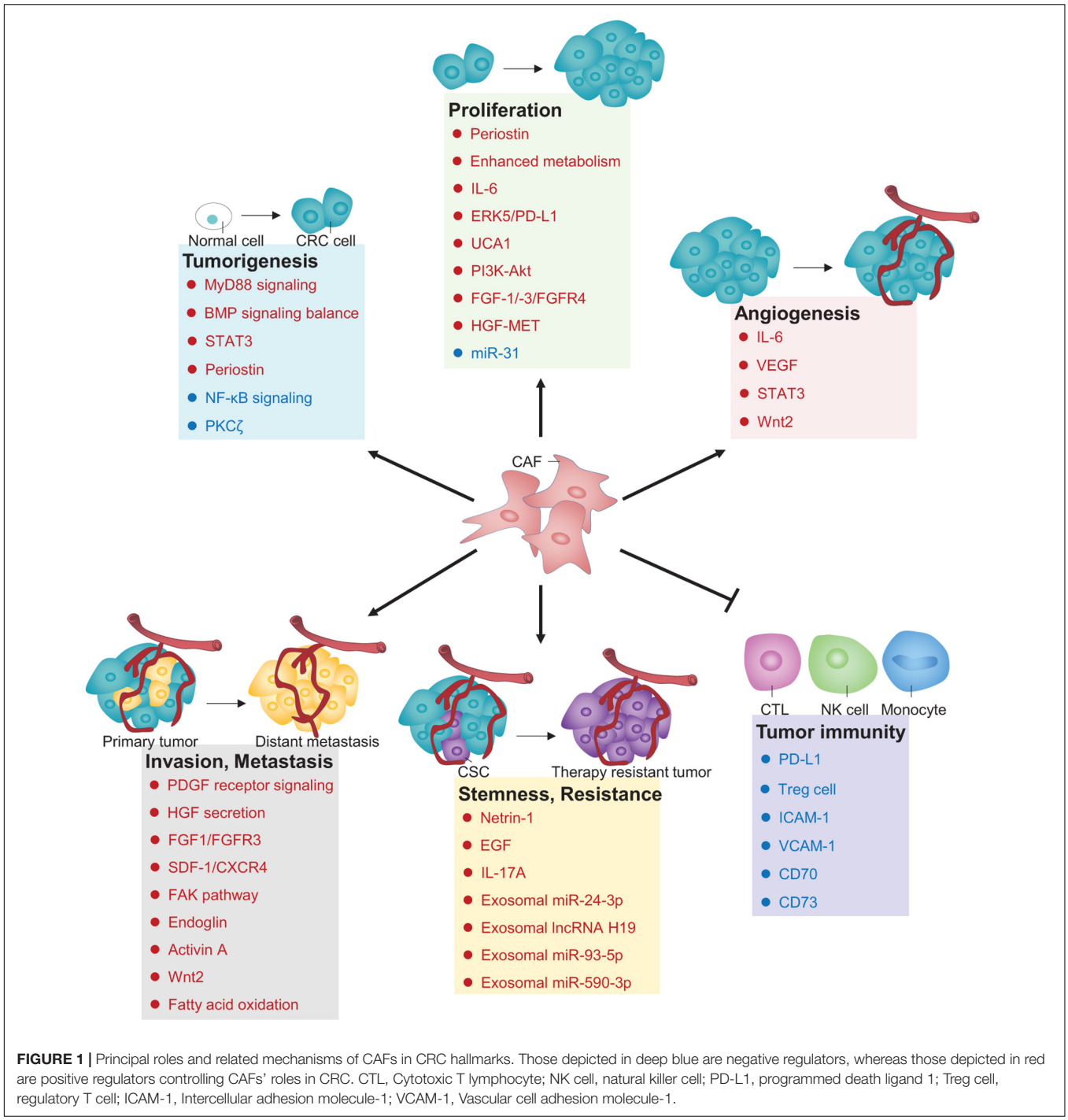

FIGURE 1 | Principal roles and related mechanisms of CAFs in CRC hallmarks. Those depicted in deep blue are negative regulators, whereas those depicted in red are positive regulators controlling CAFs' roles in CRC. CTL, Cytotoxic T lymphocyte; NK cell, natural killer cell; PD-L1, programmed death ligand 1; Treg cell, regulatory T cell; ICAM-1, Intercellular adhesion molecule-1; VCAM-1, Vascular cell adhesion molecule-1.

a CAF phenotype in vitro and promotes intestinal tumorigenesis *in vivo*, which depends on the activation of SOX2 that drives the generation of a CAF population (Kasashima et al., 2021). Moreover, the bone morphogenetic proteins (BMPs) are key growth factors secreted by CAFs. A recent study has discovered that the stromal BMP signaling balanced by GREM1 and ISLR functions to drive CRC carcinogenesis (Kobayashi et al., 2021). These findings provide further supportive evidence depicting CAFs as a positive regulators in assisting CRC development.

While CAFs have been generally perceived to be driving forces for tumorigenesis, they also retard tumorigenesis via largely unknown mechanisms (Gieniec et al., 2019). CAFs have been reported to support tumorigenesis through mediating tumor-enhancing inflammation in an NF-κB-dependent manner, and a proinflammatory NF-κB gene signature in CAFs promotes tumorigenesis in models of pancreatic and skin cancers (Erez et al., 2010). Nevertheless, using an animal model of colitis-associated cancer (CAC) and sporadic colon tumors initiated

by AOM, lines of direct genetic evidence have been obtained, which uncover an unexpected tumor-suppressive role of NF-κB signaling in CAFs that confers anti-tumorigenic effects and suppresses intestinal tumorigenesis *in vivo* (Pallangyo et al., 2015). Given the high plasticity in CAFs, this disparate finding may be attributed to distinct functions of NF-κB signaling depending on the activation status of CAF subpopulations. In any case, these results shed new light on the CAF regulation of CRC tumorigenesis.

Proliferation and Angiogenesis

Except cellular autonomous properties, the progression of malignant tumors also relies on the active involvements of CAFs. In a non-contact co-culture system, the conditioned media (CM) from CAF cultures was found to enhance the proliferation of CRC cells stronger than those from normal fibroblasts (Nakagawa et al., 2004). CAFs indeed promote proliferation of CRC in vitro and tumor-bearing mouse models *in vivo* (Li et al., 2019a). The proliferative advantage endowed by CAFs could be at least partially explained by the CAF-secreted periostin (Kikuchi et al., 2008), CAF-enhanced metabolism of CRC cells (Zhou W. et al., 2017), and CAF-derived IL-6 (Xu et al., 2021). The mechanistic insights into CAF-promoted CRC proliferation are provided by other non-negligible clues, which show that the microRNA-31 (Yang et al., 2016), the long non-coding RNA UCA1 (Jahangiri et al., 2019), and some signaling pathways, including PI3K-Akt (Yamamura et al., 2015), FGF-1/-3/FGFR4 (Bai et al., 2015), HGF-MET (Wen et al., 2020), and ERK5/PD-L1 signaling axes (Zhang M. et al., 2020), also act as important modifiers mediating the pro-proliferative effects of CAFs on CRC. These distinct molecular mechanisms support the notion that CAFs can form a favorable microenvironment for the proliferation of CRC cells. Instead, CRC cell-derived hydrogen sulfide was found to enhance CAF cell proliferation (Coletta et al., 2014), possibly postulating a reciprocal interaction between CAFs and CRC cells that may enhance the tumor cell proliferation more robust.

Tumor angiogenesis establishes new microvessels that support cancer cell proliferation by providing nutrients and oxygen. During this complex process, many angiogenic factors, especially the vascular endothelial growth factor (VEGF), play a vital role (Lugano et al., 2020). In CRC tissues, CAFs are important sources of IL-6, which enhances VEGF production, whereby inducing tumor angiogenesis (Nagasaki et al., 2014). In accordance with this, the eicosapentaenoic acid was proved to suppress CRC angiogenesis via reducing the secretion of IL-6 and VEGF from CAFs (Ando et al., 2019). Moreover, it has been shown that IL-6-activated STAT3 in fibroblast subpopulations regulates the transcriptional patterns associated with angiogenesis, and blockade of proangiogenic signaling impedes CRC growth in genetically modified mice with constitutive STAT3 activation in fibroblasts (Heichler et al., 2020). This study suggests that STAT3 might be a downstream target that mediates the proangiogenic effect of CAF-produced IL-6 on CRC. Except IL-6, CAFs-derived Wnt2 can also increase tumor angiogenesis in CRC, owing largely to Wnt2-upreglated expression of some proangiogenic proteins (Unterleuthner et al., 2020). Based on these discoveries, it is tempting to speculate that the transcriptional reprogramming initiated by CAF-secreted IL-6 or Wnt2 could shift the balance toward proangiogenic signals in favor of tumor angiogenesis and proliferation.

Epithelial-to-Mesenchymal Transition, Migration, Invasion, and Metastasis

The malignant progression of cancer is a dynamic process depending not solely on genetic alterations, but also on additional regulations by the TME (Brabletz et al., 2005). A molecular profiling analysis of CAFs isolated from human CRC has delineated them as major participators in promoting CRC metastasis (Potdar and Chaudhary, 2017). The maturity of CAFs was also associated significantly with cancer invasion for CRC patients (Shin et al., 2019). Moreover, an earlier study has reported that compared with the CM of normal colonic fibroblasts or CAFs from primary tumors, the CM of CAFs from liver metastasis leads to more aggressive phenotypes, including the epithelial-to-mesenchymal transition (EMT), migration and invasion (Berdiel-Acer et al., 2011). These reports suggest that CAFs serve to accelerate the malignant progression of CRC. Yet, the functional contributions to this process and the molecular mechanisms are not fully clear.

In recent years, increasing studies has indicated that an intense biochemical cross-talk between CRC cells and CAFs is forged by the CAF-secreted numerous factors, which is critical for tumor progression into a metastatic malignancy. For example, the secreted glycoprotein stanniocalcin-1 (STC1) was identified to mediate the function of the platelet-derived growth factor (PDGF) receptor signaling in increasing the migration, invasion and metastasis of CRC (Pena et al., 2013). Typically, the hepatocyte growth factor (HGF) can activate cancer cell invasion and metastasis. Consistently, it was reported that the migration of CRC cells could be promoted by the Ras-related protein Rab-31 (RAB31) through regulating HGF secretion in the tumor stroma (Yang et al., 2020). Human CRC-derived CAFs also enhance the adhesion of CRC cells to ECs by secretion of HGF (Zhang et al., 2019a). Additionally, HGF contributes to EMT induction in CRC cells by CAFs' secretomes (Wanandi et al., 2021). Moreover, studies have shown that CAFs secrete the fibroblast growth factor 1 (FGF1) to increase CRC cell invasion via FGFR3 signaling (Henriksson et al., 2011), as well as the stromal cell-derived factor-1 (SDF-1) to promote CRC metastasis to distant organs via the C-X-C chemokine receptor type 4 (CXCR4) axis (Peng et al., 2018). Combining another research which shows that by secreting the LOXL2, CAFs stimulate the focal adhesion kinase (FAK) pathway and consequently induce the EMT and metastasis of CRC cells (Xuefeng et al., 2020), those research progresses characterize these signaling as vital mediators in transducing CAFs' notorious effects on malignant behaviors of CRC. Other CAF-secreted factors that have recently been shown to promote the EMT, migration and invasion of CRC include the CLEC3B (Zhu et al., 2019), activin A (Bauer et al., 2020), and Wnt2 (Aizawa et al., 2019). However, how Wnt signaling regulates CRC progression is still in controversies, since a phenotypic switch of CAFs induced by Wnt was reported to inhibit EMT in CRC, implying that the Wnt signaling may induce

subtypes of CAFs with differential activities in CRC progression (Mosa et al., 2020). Furthermore, CAFs-derived exosomal miR-17-5p (Zhang Y. et al., 2020) and LINC00659 (Zhou et al., 2021) were found to promote CRC metastasis, and invasion and migration, respectively. These advancements also manifest that CAFs could promote CRC progression through secreting exosomes to influence adjacent cancer cells.

Recently, growing study efforts have been devoted to understanding how metabolic reprogramming is mechanistically involved in CAF-promoted CRC progression. In orthotopic CRC models, the activated CAFs have been discovered to promote a metabolic switch favoring glutamine consumption in CRC cells, which results in increased number of organ metastases (Tommelein et al., 2018). On the other side, CAFs were uncovered to undergo a lipidomic reprogramming in order to accumulate and accordingly secrete more fatty acids, and CRC cells were confirmed to take up these lipids metabolites, eventually leading to their potentiated migration (Gong et al., 2020). Keeping in line with this, CAFs were proved to promote the migration and invasion of CRC cells, and drive the peritoneal metastasis via activating fatty acid oxidation and modulating glycolysis (Peng et al., 2021). These results provide further insights into CRC progression regulated by CAFs.

Some divergent mechanisms also emerge to underlie the roles of CAFs in CRC progression. At the invasive borders of CRC, CAFs specifically express endoglin, with its levels correlated positively with disease stages and poor metastasis-free survival. Functionally, endoglin neutralization inhibits CRC cell invasion *in vitro* and decreases metastatic spread of CRC cells to the liver (Paauwe et al., 2018), suggesting a significant role of endoglin-expressing CAFs in promoting CRC progression. Moreover, the activation of RNA editing of the antizyme inhibitor 1 (AZIN1) in CAFs was revealed to enhance the invasive potential of CAFs in CRC (Takeda et al., 2019). It is also worth to note that CAFs can induce CRC cell migration and invasion by a contact-dependent manner (Knuchel et al., 2015). Actually, CRC cells are not bystanders upon encountering the interaction with CAFs. It has been shown that CRC cells express the structural maintenance of chromosomes 1A (SMC1A), a subunit of cohesion, which functions to recruit CAFs, whereby promoting CRC metastasis (Zhou P. et al., 2017). Additionally, when interacting with CAFs, the activation of the phospholipase D in CRC cells is required to mediate the pro-migration effects (Majdop et al., 2018). However, it remains unclarified how SMC1A and phospholipase D exert their functions during these processes. Another clue is that in the circulation system, the tumor cell clusters play a primary role in cancer metastasis, which can be enhanced by the interaction with clusters of CAFs (Hurtado et al., 2020). It would be therefore very tempting to test whether SMC1A and phospholipase D regulate cluster interactions between CRC cells and CAFs, whereby enhancing the effect of CAFs on CRC metastasis.

Stemness and Therapy Resistance

Cancer-associated fibroblasts stimulate an EMT-driven gain of cancer stemness through a paracrine interplay between CAFs and prostate cancer cells (Giannoni et al., 2010), and also constitute a supporting niche for cancer stemness in lung cancer through a paracrine IGF-II/IGF1R signaling (Chen et al., 2014). These studies indicate that CAFs can maintain cancer stemness in some cancer types. In truth, this function of CAFs can be applied to CRC as well, wherein CAFs can upregulate netrin-1 to increase its stemness in vitro and in mice (Sung et al., 2019). Being clinically relevant, the expression of CRC stemness markers are also upregulated by CAF secretomes from CRC patients (Wanandi et al., 2020). It has also been documented that CAFs promote CRC stemness by transferring exosomal lncRNA H19, which acts as a miR-141 sponge to suppress its inhibitory effect on stemness (Ren et al., 2018), therefore consolidating the role of CAFs in increasing stemness in CRC. Similarly, this mechanism is analog to that found in a variety of solid tumors, with their stemness regulated by CAF-secreted exosomes (Huang et al., 2019).

Functionally, cancer stem cells (CSCs) are believed to be a driving force behind tumorigenesis and also play major roles in tumor resistance and recurrence. In CRC patients, a significant increase in the number of CAFs was observed after cytotoxic treatment, and CSCs were shown to be promoted by CAFs via augmented secretion of specific cytokines, including IL-17A, which in turn lead to increased resistance to chemotherapy (Lotti et al., 2013). Coincidently, it is established that CAFs could promote chemoresistance by supporting a niche to sustain cancer stemness (Su et al., 2018). In regard to CRC resistance to chemotherapeutics, CAFs and CAF-derived exosomal miR-24-3p have been validated to accelerate resistance of CRC cells to oxaliplatin, 5-fluorouracil and methotrexate (Goncalves-Ribeiro et al., 2016; Yadav et al., 2020; Zhang et al., 2021). Also, in the presence of CAFs, tumor cells show reduced sensitivity to cetuximab, a monoclonal antibody therapy targeting the epidermal growth factor receptor (EGFR) (Garvey et al., 2017). A recent finding has discovered that cetuximab increases CAFs' EGF secretion, which is sufficient to render neighboring cancer cells resistant to cetuximab in combination with chemotherapy for metastatic CRC patients (Garvey et al., 2020). Moreover, CAF-derived exosomal miR-93-5p or miR-590-3p has been shown to rescue CRC cells from radiation-induced apoptosis (Chen et al., 2020, 2021), and the promoted CRC stemness was demonstrated to account for the radioresistance imposed by CAF-derived exosomes (Liu L. et al., 2020). Thus, these discoveries build a mechanistic connection between CAF-maintained cancer stemness and therapy resistance in CRC.

Tumor Immunity

The immunomodulatory effects of CAFs on CRC have been observed in a progressive rat model, in which T lymphocytes and monocytes were found outside the myofibroblast-surrounded tumors (Lieubeau et al., 1999). Recent findings have also shown that the levels of CAFs markers such as α-SMA, thrombin and fibronectin are significantly higher in CRC than in normal colonic mucosa, and α-SMA expression is negatively correlated with the number of tumor-infiltrating lymphocytes (TILs), while fibronectin displays positive coexpression (Zadka et al., 2021), and that CAF phenotypes are also correlated with $CD8^+$ T-cell infiltration (Johnson et al., 2020), hence underscoring the importance of CAFs in regulating CRC immunity. CAFs are also positively correlated with PD-L1 expression in CRC tissues,

and through secreting CXCL5, CAFs are able to promote PD-L1 expression in cancer cells (Li et al., 2019b). And moreover, a significant association has been validated between elevated Treg amounts and CD70-expressing CAFs (Jacobs et al., 2017). These observations illustrate CAFs as regulators of tumoral immunosuppression of the T cell response.

Monocytes affect the TME and induce immune tolerance (Ugel et al., 2021). CAFs have been shown to increase the recruitment of monocytes into the CRC TME via various mechanisms. Firstly, CRC CAFs exhibit upregulated ICAM-1 expression and affinity for monocytes, as such, increasing their interaction to elongate monocyte residence in CRC tissues (Schellerer et al., 2014). Secondly, CRC CAFs promote the adhesion of monocytes by upregulating VCAM-1 expression in CRC cells. Thirdly, CAFs can also attract monocytes by secreting IL-8 (Zhang et al., 2019b). Subsequently, CAFs promote M2 polarization of macrophages to suppress the activity of natural killer (NK) cells in CRC (Zhang et al., 2019b), favoring the escape from attack by the tumor immunity.

Notably, it has been reported that CAFs can regulate immune checkpoint in CRC. CAFs in human CRC tissues constitute the major population expressing CD73, a molecule acting as an immune checkpoint to suppress immune activation through the A2A receptor, and importantly, CD73 expression on CAFs is enhanced via A2B-mediated feedforward circuit triggered by tumor cell death, which enforces the CD73 immune checkpoint and consequently counteracts the antitumor immunity in CAF-rich CRC (Yu et al., 2020). Taken together, these immunosuppressive activities of CAFs on CRC have significant clinical impacts, rendering CAFs to be potential therapeutic biomarkers as well as targets for CRC.

CANCER-ASSOCIATED FIBROBLASTS AS THERAPEUTIC TARGETS IN COLORECTAL CANCER TREATMENT

As discussed above, the increasingly deep understanding into the CAFs' exquisite regulation of CRC pathogenesis achieved over recent years by pioneering studies has sparked vast inspirations to develop some potential mechanism-based targeted therapies, which can be classified according to their respective effects directed to each functional role of CAFs in impacting CRC, as illustrated in **Figure 2**.

A number of preclinical studies have described the tight control of CRC tumorigenesis by CAFs, implicating that there are some druggable targets in CAFs that possess the potentialities for CRC prevention or intervention. For example, MyD88 signaling in CAFs contributes crucially to colitis-associated CRC carcinogenesis via promoting macrophage M2 polarization (Yuan et al., 2021). Interestingly, interfering with this pathway by a novel synthetic inhibitor TJ-M2010-5 has been demonstrated to prevent colitis-associated CRC in mice (Xie et al., 2016). These clues suggest that inhibiting MyD88 signaling in CAFs with synthetic inhibitors may be used as a therapeutic modality for treating CRC. Moreover, CAF-secreted periostin is revealed to promote CRC tumorigenesis and proliferation (Kikuchi et al., 2008; Ma et al., 2020). Some clinical trials by inhibition of periostin function are ongoing to test its therapeutic effects on periostin-related diseases (Kudo, 2019). Encouragingly, an earlier study has shown that the benzyl-d(U)TP-modified DNA aptamers targeting human periostin inhibit breast cancer growth (Lee et al., 2013). Hence, these studies prompt that targeting periostin may inhibit CRC development. Moreover, through loss-of-function approaches, the constitutive activation of STAT3 in CAFs is also shown to accelerate CRC tumorigenesis in mice (Heichler et al., 2020). A series of STAT3 inhibitors and analogs have been identified and show considerable anti-CRC effects (Chalikonda et al., 2021). Hopefully, these agents could be exploited to suppress CRC tumorigenesis by inhibiting STAT3 in CAFs. Further, the enhanced CRC tumorigenesis *in vivo* by the deletion of CAFs' PKCζ supports a revised paradigm holding a view that the PKC family acts as a tumor suppressor (Newton and Brognard, 2017). As a result, restoring rather than inhibiting PKCζ activity in CAFs could be a strategy to restrict CRC. The disruption of stromal BMP signaling using small molecule agonists/activators, such as DMH1, a highly selective small-molecule inhibitor of BMP receptor (Owens et al., 2015), also represents a possible avenue to interfere CRC development, since its balance could drive CRC carcinogenesis (Kobayashi et al., 2021).

Cancer-associated fibroblasts-secreted IL-6 and ensuing STAT3 activation promote CRC proliferation and angiogenesis. Because targeting IL-6 are effective in some inflammatory diseases in clinical trials (Kang et al., 2019). It is very tempting to assess whether therapeutic agents blocking IL-6 also yield satisfactory outcomes for CRC patients. In addition, inhibitors of signaling axes, including PI3K-Akt, FGF-1/-3/FGFR4, HGF-MET, and ERK5/PD-L1, also hold promise to combat CRC, due to the fact that they can mediate the pro-proliferative effect of CAFs on CRC. In the process of tumor angiogenesis in CRC tissues, CAFs-derived Wnt2 and its elevated proangiogenic signals play an important role. Besides, autocrine Wnt2 signaling in CAFs also promotes CRC progression (Kramer et al., 2017). Noticeably, targeting CAF-secreted Wnt2 was recently reported to restore anti-tumor immunity (Kang et al., 2019). These findings classify Wnt2 as a promising stromal target to confine CRC progression. Future studies are needed to test the effect of Wnt2 neutralizing antibodies toward CRC. The result may be predictably satisfactory, because an earlier study has already shown a therapeutic effect of an anti-Wnt2 monoclonal antibody against malignant melanoma (You et al., 2004).

The PDGF receptor signaling functions to transduce the pro-metastatic signals from CAFs into CRC cells, and inhibition of this signaling has proven useful for treating patients with some tumors (Heldin, 2013). Whether PDGF/PDGF receptor antagonists will be beneficial for reducing metastasis and prolonging survival for CRC patients is an ongoing and future study direction for the management of patients with metastatic CRC (Advani and Kopetz, 2019). Moreover, signaling pathways induced by HGF, FGF1, SDF-1, and FAK are profoundly involved in CAFs' roles in enhancing the malignant behaviors of CRC, providing them as potential targets to obstruct disease progression. These topics have been intensively

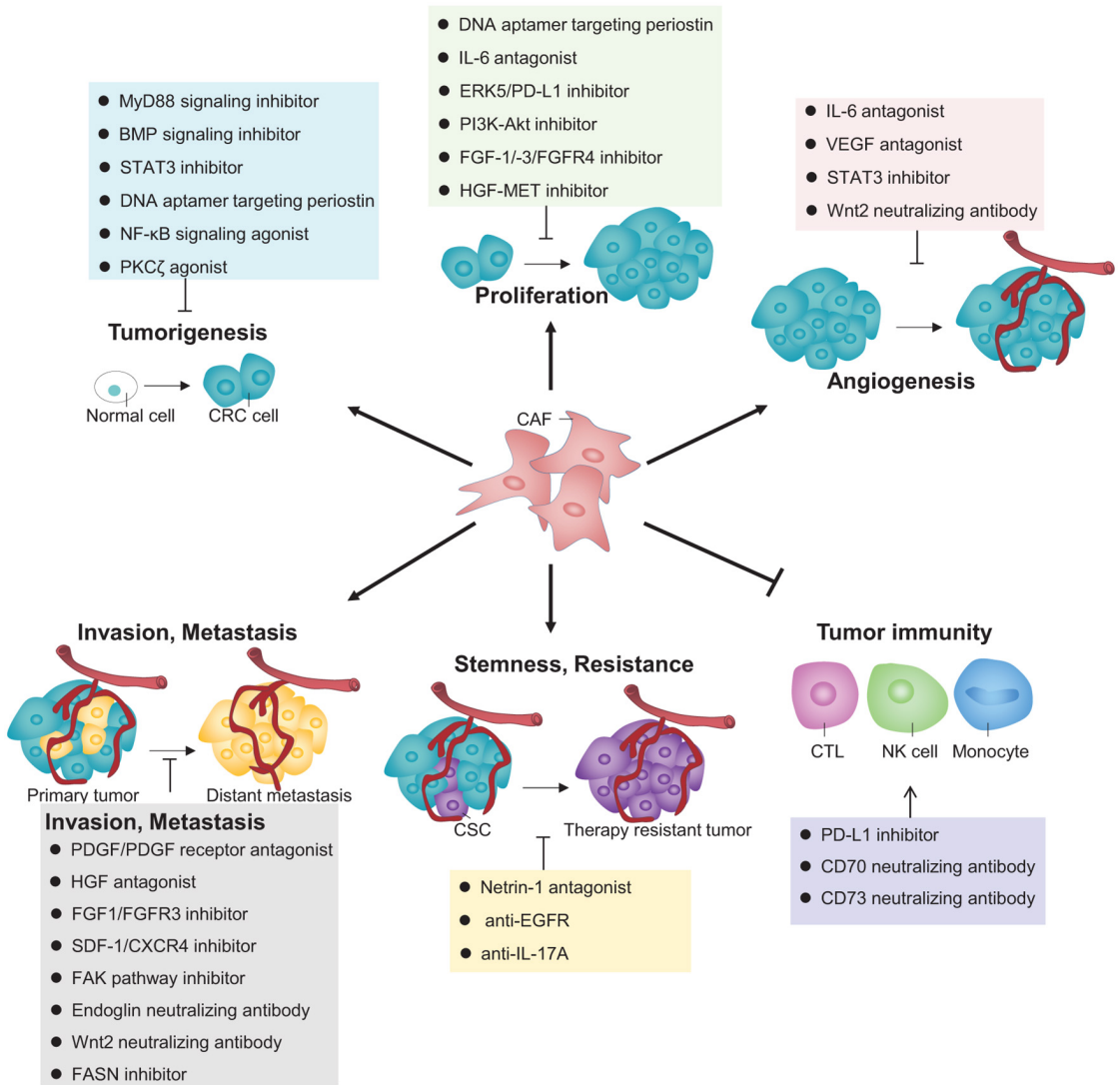

FIGURE 2 | Therapeutic strategies that target CAFs for CRC treatment. A variety of inhibitors, agonists, or neutralizing antibodies targeting different signaling pathways or molecules that contribute to CAFs' versatile roles are proposed to interfere some key processes during CRC pathogenesis for clinical treatment.

reviewed or discussed elsewhere (Tommelein et al., 2015; Jeong, 2018; Parizadeh et al., 2019). Additionally, the metabolic reprogramming in CAFs that aids to expedite CRC progression also offers attractive targets for therapeutic intervention. For instance, the fatty acids synthase (FASN) is crucial for fatty acids synthesis and is significantly increased in CAFs, which is responsible for CAF-induced CRC cell migration *in vitro* and *in vivo* (Gong et al., 2020). These results suggest that the FASN of CAFs may be a target for anti-metastasis in CRC treatment. Recently, the first FASN inhibitor (TVB-2640) has completed the phase 1 clinical trial for solid tumors (Angeles and Hudkins, 2016). This successful translation from bench to clinic may open new opportunities for expanding the utility of FASN inhibitors to inhibit CRC metastasis. Further, the selectively high expression of endoglin in CAFs and its correlation with metastasis and poor survival in CRC patients will lead to the exploration of testing it as a therapeutic target. The coincidence is that the endoglin neutralizing antibodies such as TRC105 are being tested in clinical studies in cancer patients as a monotherapy or incorporated into combinatory therapies (Liu Y. et al., 2020). These studies will enable us to learn the prospect of treating malignant CRC through targeting endoglin-expressing CAFs.

The CAF-increased chemoresistance in CRC can be achieved via CSC self-renewal that is promoted by CAF-derived IL-17A, and accordingly, targeting IL-17A signaling impairs CSC growth and overrides chemoresistance (Lotti et al., 2013). The anti-IL-17A was approved by FDA for the treatment of psoriasis in 2015, proving its effectiveness clinically (Chen and Kolls, 2017). It therefore would be of clinical significance to examine the impact of anti-IL-17A on improving the efficacy of chemotherapy for CRC. The exploitation of immunomodulatory activities of CAFs as promising targets for CRC treatment cannot be ignored either.

For example, by applying the therapeutic anti-EGFR humanized antibody cetuximab, the inhibition of NK cell function by the CAFs of CRC can be relieved (Costa et al., 2018), and neutralizing CD73 enhances antitumor immunity in CAF-rich CRC (Yu et al., 2020), therefore visualizing the therapeutic potential of the strategic targeting of CAF-mediated immune suppression.

Although the versatile pro-tumoral functions of CAFs performed during CRC development and progression make them to be attractive and promising therapeutic targets that can be harnessed for CRC treatment, the total depletion of CAFs unexpectedly results in more aggressive tumors (Ozdemir et al., 2014; McAndrews et al., 2021), demonstrating that different CAF subpopulations have opposite roles in cancer. Truly, CAFs in CRC tissues exhibit divergent phenotypes which can be differentiated at least by expression profiles and functions, as evidenced by transcriptional heterogeneity (Li et al., 2017) and functional heterogeneity (Herrera et al., 2013b). Since attempts to therapeutically target CAFs have been obstructed by our poor understanding of their heterogeneity (Kobayashi et al., 2021), future breakthroughs in translating basic sciences into CAF-based therapies will be witnessed with the better understanding of CAF heterogeneity, which can improve the therapeutic outcomes of cancer patients by targeting specific CAF subsets that promote cancer progression.

CONCLUSION

Cancer-associated fibroblasts are crucial components of the TME which interacts intensively with proliferating tumor cells, together creating a developing tumor, including CRC. Currently, the first-line treatment options for advanced CRC are chemotherapy combined with targeted therapy. Despite some achievements in improving patients' survival rates, the success of treatment is limited by targeting tumor cells alone. This dilemma has redirected more research attentions into investigating on the roles of the TME in the progression of CRC and their underlying mechanisms, in an effort to discover novel and more effective therapeutic strategies and targets for improving the available therapies. With the CAFs becoming the study focus, many advancements in our understanding of the CAF biology in CRC pathogenesis have been obtained in recent decade. We now know that the CAFs in CRC have heterogeneous precursors and markers, and also show a clinical significance in predicting patients' prognosis. Mounting analyses in preclinical models have unveiled versatile roles and distinct mechanisms of CAFs that profoundly promote many key malignant behaviors of CRC, including tumorigenesis, proliferation, angiogenesis, invasion and metastasis, stemness and therapy resistance, and simultaneously attenuate tumor immune responses. These findings indisputably support the notion that CAFs can be considered as a prominent therapeutic target of stroma-based therapy in CRC treatment. However, targeting specific CAF subpopulation that promote cancer progression encounters a huge challenge in clinic, as little is known about a myriad of functions of different CAF subsets originated from their high heterogenetic nature. To address this difficulty, novel techniques like the lineage tracing and single-cell sequencing should be applied in the future to distinguish targetable subpopulations from the whole pool of CAFs within tumors. As such, the selective eradication of the tumor-promoting CAF subsets will be realized and then implemented in combination with the current therapeutic rationales for the better treatment of CRC and even other cancers.

AUTHOR CONTRIBUTIONS

LD and NJ conceived and wrote the manuscript. JZ helped with the table drawing. YW and HC reviewed and revised the manuscript. All the authors have read and agreed to the published version of the manuscript.

FUNDING

This work was supported by the National Natural Science Foundation of China (81872071), the Natural Science Foundation of Chongqing (cstc2019jcyj-zdxmX0033), the Fundamental Research Funds for the Central Universities (SWU120054), and the Natural Science Foundation of Chongqing (cstc2018jcyjAX0573).

ACKNOWLEDGMENTS

We thank all members of the HC group for their helpful discussions. We apologize to those authors whose relevant work could not been included in this review due to space limitations.

REFERENCES

Adegboyega, P. A., Mifflin, R. C., DiMari, J. F., Saada, J. I., and Powell, D. W. (2002). Immunohistochemical study of myofibroblasts in normal colonic mucosa, hyperplastic polyps, and adenomatous colorectal polyps. *Arch. Pathol. Lab. Med.* 126, 829–836.

Advani, S., and Kopetz, S. (2019). Ongoing and future directions in the management of metastatic colorectal cancer: update on clinical trials. *J. Surg. Oncol.* 119, 642–652. doi: 10.1002/jso.25441

Aizawa, T., Karasawa, H., Funayama, R., Shirota, M., Suzuki, T., Maeda, S., et al. (2019). Cancer-associated fibroblasts secrete Wnt2 to promote cancer progression in colorectal cancer. *Cancer Med.* 8, 6370–6382. doi: 10.1002/cam4.2523

Akishima-Fukasawa, Y., Ino, Y., Nakanishi, Y., Miura, A., Moriya, Y., Kondo, T., et al. (2010). Significance of PGP9.5 expression in cancer-associated fibroblasts for prognosis of colorectal carcinoma. *Am. J. Clin. Pathol.* 134, 71–79. doi: 10.1309/AJCPRJP39MIDSGBH

Ando, N., Hara, M., Shiga, K., Yanagita, T., Takasu, K., Nakai, N., et al. (2019). Eicosapentaenoic acid suppresses angiogenesis via reducing secretion of IL6 and VEGF from colon cancerassociated fibroblasts. *Oncol. Rep.* 42, 339–349. doi: 10.3892/or.2019.7141

Angeles, T. S., and Hudkins, R. L. (2016). Recent advances in targeting the fatty acid biosynthetic pathway using fatty acid synthase inhibitors. *Expert. Opin. Drug Discov.* 11, 1187–1199. doi: 10.1080/17460441.2016.1245286

Atanasova, V. S., Tiefenbacher, A., Clement, J., Wöran, K., Bergmann, M., Dolznig, H., et al. (2020). Identification of proteome and secretome signatures in primary

colorectal cancer associated fibroblasts. *Annals of Oncology* 31, S445. doi: 10.1016/j.annonc.2020.08.593

Bai, Y. P., Shang, K., Chen, H., Ding, F., Wang, Z., Liang, C., et al. (2015). FGF-1/-3/FGFR4 signaling in cancer-associated fibroblasts promotes tumor progression in colon cancer through Erk and MMP-7. *Cancer Sci.* 106, 1278–1287. doi: 10.1111/cas.12745

Barth, P. J., Ebrahimsade, S., Ramaswamy, A., and Moll, R. (2002). CD34+ fibrocytes in invasive ductal carcinoma, ductal carcinoma in situ, and benign breast lesions. *Virchows. Arch.* 440, 298–303. doi: 10.1007/s00428100530

Bauer, J., Emon, M. A. B., Staudacher, J. J., Thomas, A. L., Zessner-Spitzenberg, J., Mancinelli, G., et al. (2020). Increased stiffness of the tumor microenvironment in colon cancer stimulates cancer associated fibroblast-mediated prometastatic activin A signaling. *Sci. Rep.* 10:50. doi: 10.1038/s41598-019-55687-6

Berdiel-Acer, M., Berenguer, A., Sanz-Pamplona, R., Cuadras, D., Sanjuan, X., Paules, M. J., et al. (2014). A 5-gene classifier from the carcinoma-associated fibroblast transcriptomic profile and clinical outcome in colorectal cancer. *Oncotarget* 5, 6437–6452. doi: 10.18632/oncotarget.2237

Berdiel-Acer, M., Bohem, M. E., Lopez-Doriga, A., Vidal, A., Salazar, R., Martinez-Iniesta, M., et al. (2011). Hepatic carcinoma-associated fibroblasts promote an adaptative response in colorectal cancer cells that inhibit proliferation and apoptosis: nonresistant cells die by nonapoptotic cell death. *Neoplasia* 13, 931–946. doi: 10.1593/neo.11706

Brabletz, T., Hlubek, F., Spaderna, S., Schmalhofer, O., Hiendlmeyer, E., Jung, A., et al. (2005). Invasion and metastasis in colorectal cancer: epithelial-mesenchymal transition, mesenchymal-epithelial transition, stem cells and beta-catenin. *Cells Tissues Organs* 179, 56–65. doi: 10.1159/000084509

Bray, F., Ferlay, J., Soerjomataram, I., Siegel, R. L., Torre, L. A., and Jemal, A. (2018). Global cancer statistics 2018: GLOBOCAN estimates of incidence and mortality worldwide for 36 cancers in 185 countries. *CA Cancer J. Clin.* 68, 394–424. doi: 10.3322/caac.21492

Chalikonda, G., Lee, H., Sheik, A., and Huh, Y. S. (2021). Targeting key transcriptional factor STAT3 in colorectal cancer. *Mol. Cell Biochem.* 476, 3219–3228. doi: 10.1007/s11010-021-04156-8

Chen, K., and Kolls, J. K. (2017). Interluekin-17A (IL17A). *Gene* 614, 8–14. doi: 10.1016/j.gene.2017.01.016

Chen, W. J., Ho, C. C., Chang, Y. L., Chen, H. Y., Lin, C. A., Ling, T. Y., et al. (2014). Cancer-associated fibroblasts regulate the plasticity of lung cancer stemness via paracrine signalling. *Nat. Commun.* 5:3472. doi: 10.1038/ncomms4472

Chen, X., and Song, E. (2019). Turning foes to friends: targeting cancer-associated fibroblasts. *Nat. Rev. Drug Discov.* 18, 99–115. doi: 10.1038/s41573-018-0004-1

Chen, X., Liu, J., Zhang, Q., Liu, B., Cheng, Y., Zhang, Y., et al. (2020). Exosome-mediated transfer of miR-93-5p from cancer-associated fibroblasts confer radioresistance in colorectal cancer cells by downregulating FOXA1 and upregulating TGFB3. *J. Exp. Clin. Cancer Res.* 39:65. doi: 10.1186/s13046-019-1507-2

Chen, X., Liu, Y., Zhang, Q., Liu, B., Cheng, Y., Zhang, Y., et al. (2021). Exosomal miR-590-3p derived from cancer-associated fibroblasts confers radioresistance in colorectal cancer. *Mol. Therapy Nucleic Acids* 24, 113–126. doi: 10.1016/j.omtn.2020.11.003

Choi, S. Y., Sung, R., Lee, S. J., Lee, T. G., Kim, N., Yoon, S. M., et al. (2013). Podoplanin, alpha-smooth muscle actin or S100A4 expressing cancer-associated fibroblasts are associated with different prognosis in colorectal cancers. *J. Korean Med. Sci.* 28, 1293–1301. doi: 10.3346/jkms.2013.28.9.1293

Coletta, C., Dikman, A., Szabo, C., Hellmich, M. R., and Chao, C. (2014). P16 Hydrogen sulfide stimulates colorectal cancer-associated fibroblast proliferation and migration. *Nitric. Oxide* 39, S20–S21.

Costa, D., Vene, R., Benelli, R., Romairone, E., Scabini, S., Catellani, S., et al. (2018). Targeting the epidermal growth factor receptor can counteract the inhibition of natural killer cell function exerted by colorectal tumor-associated fibroblasts. *Front. Immunol.* 9:1150. doi: 10.3389/fimmu.2018.01150

Cui, L., Ohuchida, K., Mizumoto, K., Moriyama, T., Onimaru, M., Nakata, K., et al. (2010). Prospectively isolated cancer-associated CD10(+) fibroblasts have stronger interactions with CD133(+) colon cancer cells than with CD133(−) cancer cells. *PLoS One* 5:e12121. doi: 10.1371/journal.pone.0012121

David, C. J., Huang, Y. H., Chen, M., Su, J., Zou, Y., Bardeesy, N., et al. (2016). TGF-beta tumor suppression through a lethal EMT. *Cell* 164, 1015–1030. doi: 10.1016/j.cell.2016.01.009

De Boeck, A., Hendrix, A., Maynard, D., Van Bockstal, M., Daniels, A., Pauwels, P., et al. (2013). Differential secretome analysis of cancer-associated fibroblasts and bone marrow-derived precursors to identify microenvironmental regulators of colon cancer progression. *Proteomics* 13, 379–388. doi: 10.1002/pmic.201200179

Erez, N., Truitt, M., Olson, P., Arron, S. T., and Hanahan, D. (2010). Cancer-associated fibroblasts are activated in incipient neoplasia to orchestrate tumor-promoting inflammation in an NF-kappaB-dependent manner. *Cancer Cell* 17, 135–147. doi: 10.1016/j.ccr.2009.12.041

Ferrari, N., Ranftl, R., Chicherova, I., Slaven, N. D., Moeendarbary, E., Farrugia, A. J., et al. (2019). Dickkopf-3 links HSF1 and YAP/TAZ signalling to control aggressive behaviours in cancer-associated fibroblasts. *Nat. Commun.* 10:130. doi: 10.1038/s41467-018-07987-0

Ferrer-Mayorga, G., Gomez-Lopez, G., Barbachano, A., Fernandez-Barral, A., Pena, C., Pisano, D. G., et al. (2017). Vitamin D receptor expression and associated gene signature in tumour stromal fibroblasts predict clinical outcome in colorectal cancer. *Gut* 66, 1449–1462. doi: 10.1136/gutjnl-2015-310977

Franze, E., Di Grazia, A., Sica, G. S., Biancone, L., Laudisi, F., and Monteleone, G. (2020). Interleukin-34 enhances the tumor promoting function of colorectal cancer-associated fibroblasts. *Cancers (Basel)* 12:3537. doi: 10.3390/cancers12123537

Garvey, C. M., Chen, O., and Mumenthaler, S. M. (2017). Abstract 5908: Cancer-associated fibroblast driven drug resistance in colorectal cancer. *Cancer Res.* 77(13 Suppl.):5908. doi: 10.1158/1538-7445.am2017-5908

Garvey, C. M., Lau, R., Sanchez, A., Sun, R. X., Fong, E. J., Doche, M. E., et al. (2020). Anti-EGFR therapy induces EGF secretion by cancer-associated fibroblasts to confer colorectal cancer chemoresistance. *Cancers (Basel)* 12:1393. doi: 10.3390/cancers12061393

Giannoni, E., Bianchini, F., Masieri, L., Serni, S., Torre, E., Calorini, L., et al. (2010). Reciprocal activation of prostate cancer cells and cancer-associated fibroblasts stimulates epithelial-mesenchymal transition and cancer stemness. *Cancer Res.* 70, 6945–6956. doi: 10.1158/0008-5472.CAN-10-0785

Gieniec, K. A., Butler, L. M., Worthley, D. L., and Woods, S. L. (2019). Cancer-associated fibroblasts-heroes or villains? *Br. J. Cancer* 121, 293–302. doi: 10.1038/s41416-019-0509-3

Goncalves-Ribeiro, S., Diaz-Maroto, N. G., Berdiel-Acer, M., Soriano, A., Guardiola, J., Martinez-Villacampa, M., et al. (2016). Carcinoma-associated fibroblasts affect sensitivity to oxaliplatin and 5FU in colorectal cancer cells. *Oncotarget* 7, 59766–59780. doi: 10.18632/oncotarget.11121

Gong, J., Lin, Y., Zhang, H., Liu, C., Cheng, Z., Yang, X., et al. (2020). Reprogramming of lipid metabolism in cancer-associated fibroblasts potentiates migration of colorectal cancer cells. *Cell Death Dis.* 11:267. doi: 10.1038/s41419-020-2434-z

Gong, Y., Scott, E., Lu, R., Xu, Y., Oh, W. K., and Yu, Q. (2013). TIMP-1 promotes accumulation of cancer associated fibroblasts and cancer progression. *PLoS One* 8:e77366. doi: 10.1371/journal.pone.0077366

Gordillo, C. H., Sandoval, P., Munoz-Hernandez, P., Pascual-Anton, L., Lopez-Cabrera, M., and Jimenez-Heffernan, J. A. (2020). Mesothelial-to-mesenchymal transition contributes to the generation of carcinoma-associated fibroblasts in locally advanced primary colorectal carcinomas. *Cancers (Basel)* 12:499. doi: 10.3390/cancers12020499

Haniffa, M. A., Collin, M. P., Buckley, C. D., and Dazzi, F. (2009). Mesenchymal stem cells: the fibroblasts' new clothes? *Haematologica* 94, 258–263. doi: 10.3324/haematol.13699

Hawinkels, L. J., Paauwe, M., Verspaget, H. W., Wiercinska, E., van der Zon, J. M., van der Ploeg, K., et al. (2014). Interaction with colon cancer cells hyperactivates TGF-beta signaling in cancer-associated fibroblasts. *Oncogene* 33, 97–107. doi: 10.1038/onc.2012.536

Heichler, C., Scheibe, K., Schmied, A., Geppert, C. I., Schmid, B., Wirtz, S., et al. (2020). STAT3 activation through IL-6/IL-11 in cancer-associated fibroblasts promotes colorectal tumour development and correlates with poor prognosis. *Gut* 69, 1269–1282. doi: 10.1136/gutjnl-2019-319200

Heldin, C. H. (2013). Targeting the PDGF signaling pathway in tumor treatment. *Cell Commun. Signal.* 11:97. doi: 10.1186/1478-811X-11-97

Henriksson, M. L., Edin, S., Dahlin, A. M., Oldenborg, P. A., Oberg, A., Van Guelpen, B., et al. (2011). Colorectal cancer cells activate adjacent fibroblasts resulting in FGF1/FGFR3 signaling and increased invasion. *Am. J. Pathol.* 178, 1387–1394. doi: 10.1016/j.ajpath.2010.12.008

Herrera, A., Herrera, M., Alba-Castellon, L., Silva, J., Garcia, V., Loubat-Casanovas, J., et al. (2014). Protumorigenic effects of Snail-expression fibroblasts on colon cancer cells. *Int. J. Cancer* 134, 2984–2990. doi: 10.1002/ijc.28613

Herrera, M., Islam, A. B., Herrera, A., Martin, P., Garcia, V., Silva, J., et al. (2013b). Functional heterogeneity of cancer-associated fibroblasts from human colon tumors shows specific prognostic gene expression signature. *Clin. Cancer Res.* 19, 5914–5926. doi: 10.1158/1078-0432.CCR-13-0694

Herrera, M., Herrera, A., Dominguez, G., Silva, J., Garcia, V., Garcia, J. M., et al. (2013a). Cancer-associated fibroblast and M2 macrophage markers together predict outcome in colorectal cancer patients. *Cancer Sci.* 104, 437–444. doi: 10.1111/cas.12096

Herrera, M., Llorens, C., Rodriguez, M., Herrera, A., Ramos, R., Gil, B., et al. (2018). Differential distribution and enrichment of non-coding RNAs in exosomes from normal and Cancer-associated fibroblasts in colorectal cancer. *Mol. Cancer* 17:114. doi: 10.1186/s12943-018-0863-4

Huang, T. X., Guan, X. Y., and Fu, L. (2019). Therapeutic targeting of the crosstalk between cancer-associated fibroblasts and cancer stem cells. *Am. J. Cancer Res.* 9, 1889–1904.

Hurtado, P., Martinez-Pena, I., and Pineiro, R. (2020). Dangerous liaisons: circulating tumor cells (CTCs) and cancer-associated fibroblasts (CAFs). *Cancers (Basel)* 12:2861. doi: 10.3390/cancers12102861

Inoue, S., Ito, H., Tsunoda, T., Murakami, H., Ebi, M., Ogasawara, N., et al. (2019). CD70 expression in tumor-associated fibroblasts predicts worse survival in colorectal cancer patients. *Virchows. Arch.* 475, 425–434. doi: 10.1007/s00428-019-02565-1

Iwano, M., Plieth, D., Danoff, T. M., Xue, C., Okada, H., and Neilson, E. G. (2002). Evidence that fibroblasts derive from epithelium during tissue fibrosis. *J. Clin. Invest.* 110, 341–350. doi: 10.1172/JCI15518

Jackson, L., Jones, D. R., Scotting, P., and Sottile, V. (2007). Adult mesenchymal stem cells: differentiation potential and therapeutic applications. *J. Postgrad. Med.* 53, 121–127. doi: 10.4103/0022-3859.32215

Jacobs, J., Deschoolmeester, V., Zwaenepoel, K., Hermans, C., Rolfo, C., Peeters, M., et al. (2017). Abstract 958: blocking CD70+ cancer associated fibroblasts: are we paving the way towards immunotherapy in colorectal cancer. *Cancer Res.* 77(13 Suppl.), 958. doi: 10.1158/1538-7445.am2017-958

Jahangiri, B., Khalaj-Kondori, M., Asadollahi, E., and Sadeghizadeh, M. (2019). Cancer-associated fibroblasts enhance cell proliferation and metastasis of colorectal cancer SW480 cells by provoking long noncoding RNA UCA1. *J. Cell Commun. Signal.* 13, 53–64. doi: 10.1007/s12079-018-0471-5

Jeong, K. Y. (2018). Inhibiting focal adhesion kinase: a potential target for enhancing therapeutic efficacy in colorectal cancer therapy. *World J. Gastrointest. Oncol.* 10, 290–292. doi: 10.4251/wjgo.v10.i10.290

Johnson, K. A., Emmerich, P. B., Pasch, C. A., Clipson, L., Matkowskyj, K. A., and Deming, D. A. (2020). Abstract 5110: cancer-associated fibroblast phenotypes vary across colorectal cancers and correlate with CD8+ T-cell infiltration. *Cancer Res.* 80(16 Suppl.):5110. doi: 10.1158/1538-7445.am2020-5110

Jung, Y., Kim, J. K., Shiozawa, Y., Wang, J., Mishra, A., Joseph, J., et al. (2013). Recruitment of mesenchymal stem cells into prostate tumours promotes metastasis. *Nat. Commun.* 4:1795. doi: 10.1038/ncomms2766

Kabashima-Niibe, A., Higuchi, H., Takaishi, H., Masugi, Y., Matsuzaki, Y., Mabuchi, Y., et al. (2013). Mesenchymal stem cells regulate epithelial-mesenchymal transition and tumor progression of pancreatic cancer cells. *Cancer Sci.* 104, 157–164. doi: 10.1111/cas.12059

Kang, S., Tanaka, T., Narazaki, M., and Kishimoto, T. (2019). Targeting interleukin-6 signaling in clinic. *Immunity* 50, 1007–1023. doi: 10.1016/j.immuni.2019.03.026

Kasashima, H., Duran, A., Martinez-Ordonez, A., Nakanishi, Y., Kinoshita, H., Linares, J. F., et al. (2021). Stromal SOX2 upregulation promotes tumorigenesis through the generation of a sfrp1/2-expressing cancer-associated fibroblast population. *Dev. Cell* 56, 95–110 e110. doi: 10.1016/j.devcel.2020.10.014

Kikuchi, Y., Kashima, T. G., Nishiyama, T., Shimazu, K., Morishita, Y., Shimazaki, M., et al. (2008). Periostin is expressed in pericryptal fibroblasts and cancer-associated fibroblasts in the colon. *J. Histochem. Cytochem.* 56, 753–764. doi: 10.1369/jhc.2008.951061

Knuchel, S., Anderle, P., Werfelli, P., Diamantis, E., and Ruegg, C. (2015). Fibroblast surface-associated FGF-2 promotes contact-dependent colorectal cancer cell migration and invasion through FGFR-SRC signaling and integrin alphavbeta5-mediated adhesion. *Oncotarget* 6, 14300–14317. doi: 10.18632/oncotarget.3883

Kobayashi, H., Gieniec, K. A., Wright, J. A., Wang, T., Asai, N., Mizutani, Y., et al. (2021). The balance of stromal BMP signaling mediated by GREM1 and ISLR drives colorectal carcinogenesis. *Gastroenterology* 160, 1224–1239 e1230. doi: 10.1053/j.gastro.2020.11.011

Kordes, C., Sawitza, I., Gotze, S., and Haussinger, D. (2013). Hepatic stellate cells support hematopoiesis and are liver-resident mesenchymal stem cells. *Cell Physiol. Biochem.* 31, 290–304. doi: 10.1159/000343368

Kramer, N., Schmollerl, J., Unger, C., Nivarthi, H., Rudisch, A., Unterleuthner, D., et al. (2017). Autocrine WNT2 signaling in fibroblasts promotes colorectal cancer progression. *Oncogene* 36, 5460–5472. doi: 10.1038/onc.2017.144

Kretzschmar, K., and Watt, F. M. (2012). Lineage tracing. *Cell* 148, 33–45. doi: 10.1016/j.cell.2012.01.002

Kudo, A. (2019). Clinical applications targeting periostin. *Adv. Exp. Med. Biol.* 1132, 207–210. doi: 10.1007/978-981-13-6657-4_19

Kwak, Y., Lee, H. E., Kim, W. H., Kim, D. W., Kang, S. B., and Lee, H. S. (2014). The clinical implication of cancer-associated microvasculature and fibroblast in advanced colorectal cancer patients with synchronous or metachronous metastases. *PLoS One* 9:e91811. doi: 10.1371/journal.pone.0091811

Lee, Y. J., Kim, I. S., Park, S. A., Kim, Y., Lee, J. E., Noh, D. Y., et al. (2013). Periostin-binding DNA aptamer inhibits breast cancer growth and metastasis. *Mol. Ther.* 21, 1004–1013. doi: 10.1038/mt.2013.30

Li, H., Courtois, E. T., Sengupta, D., Tan, Y., Chen, K. H., Goh, J. J. L., et al. (2017). Reference component analysis of single-cell transcriptomes elucidates cellular heterogeneity in human colorectal tumors. *Nat. Genet.* 49, 708–718. doi: 10.1038/ng.3818

Li, Z., Chan, K., Qi, Y., Lu, L., Ning, F., Wu, M., et al. (2018). Participation of CCL1 in snail-positive fibroblasts in colorectal cancer contribute to 5-fluorouracil/paclitaxel chemoresistance. *Cancer Res. Treat.* 50, 894–907. doi: 10.4143/crt.2017.356

Li, Z., Zhang, J., Zhou, J., Lu, L., Wang, H., Zhang, G., et al. (2019a). Nodal facilitates differentiation of fibroblasts to cancer-associated fibroblasts that support tumor growth in melanoma and colorectal cancer. *Cells* 8:538. doi: 10.3390/cells8060538

Li, Z., Zhou, J., Zhang, J., Li, S., Wang, H., and Du, J. (2019b). Cancer-associated fibroblasts promote PD-L1 expression in mice cancer cells via secreting CXCL5. *Int. J. Cancer* 145, 1946–1957. doi: 10.1002/ijc.32278

Lieubeau, B., Heymann, M. F., Henry, F., Barbieux, I., Meflah, K., and Gregoire, M. (1999). Immunomodulatory effects of tumor-associated fibroblasts in colorectal-tumor development. *Int. J. Cancer* 81, 629–636.

Liu, L., Zhang, Z., Zhou, L., Hu, L., Yin, C., Qing, D., et al. (2020). Cancer associated fibroblasts-derived exosomes contribute to radioresistance through promoting colorectal cancer stem cells phenotype. *Exp. Cell Res.* 391:111956. doi: 10.1016/j.yexcr.2020.111956

Liu, Y., Paauwe, M., Nixon, A. B., and Hawinkels, L. (2020). Endoglin targeting: lessons learned and questions that remain. *Int. J. Mol. Sci.* 22:147. doi: 10.3390/ijms22010147

Lotti, F., Jarrar, A. M., Pai, R. K., Hitomi, M., Lathia, J., Mace, A., et al. (2013). Chemotherapy activates cancer-associated fibroblasts to maintain colorectal cancer-initiating cells by IL-17A. *J. Exp. Med.* 210, 2851–2872. doi: 10.1084/jem.20131195

Lugano, R., Ramachandran, M., and Dimberg, A. (2020). Tumor angiogenesis: causes, consequences, challenges and opportunities. *Cell Mol. Life Sci.* 77, 1745–1770. doi: 10.1007/s00018-019-03351-7

Ma, H., Wang, J., Zhao, X., Wu, T., Huang, Z., Chen, D., et al. (2020). Periostin promotes colorectal tumorigenesis through integrin-FAK-Src pathway-mediated YAP/TAZ activation. *Cell Rep.* 30, 793–806 e796. doi: 10.1016/j.celrep.2019.12.075

Majdop, S., Skornick, Y., Avital, S., and Berkovich, L. (2018). Phospholipase D activation mediates growth and migration of colon cancer cells interacting with cancer-associated fibroblasts. *Cell Mol. Biol. (Noisy-le-grand)* 64, 84–88.

McAndrews, K. M., Vazquez-Arreguin, K., Kwak, C., Sugimoto, H., Zheng, X., Li, B., et al. (2021). alphaSMA(+) fibroblasts suppress Lgr5(+) cancer stem cells and restrain colorectal cancer progression. *Oncogene* 40, 4440–4452. doi: 10.1038/s41388-021-01866-7

Mochizuki, S., Ao, T., Sugiura, T., Yonemura, K., Shiraishi, T., Kajiwara, Y., et al. (2020). Expression and function of a Disintegrin and metalloproteinases in

cancer-associated fibroblasts of colorectal cancer. *Digestion* 101, 18–24. doi: 10.1159/000504087

Moon, H., Ju, H. L., Chung, S. I., Cho, K. J., Eun, J. W., Nam, S. W., et al. (2017). Transforming growth factor-beta promotes liver tumorigenesis in mice via up-regulation of snail. *Gastroenterology* 153, 1378–1391 e1376. doi: 10.1053/j.gastro.2017.07.014

Mosa, M. H., Michels, B. E., Menche, C., Nicolas, A. M., Darvishi, T., Greten, F. R., et al. (2020). A Wnt-induced phenotypic switch in cancer-associated fibroblasts inhibits EMT in colorectal cancer. *Cancer Res.* 80, 5569–5582. doi: 10.1158/0008-5472.CAN-20-0263

Mrazek, A. A., Carmical, J. R., Wood, T. G., Hellmich, M. R., Eltorky, M., Bohanon, F. J., et al. (2014). Colorectal cancer-associated fibroblasts are genotypically distinct. *Curr. Cancer Ther. Rev.* 10, 97–218. doi: 10.2174/1573394710021411241231O3

Nagasaki, T., Hara, M., Nakanishi, H., Takahashi, H., Sato, M., and Takeyama, H. (2014). Interleukin-6 released by colon cancer-associated fibroblasts is critical for tumour angiogenesis: anti-interleukin-6 receptor antibody suppressed angiogenesis and inhibited tumour-stroma interaction. *Br. J. Cancer* 110, 469–478. doi: 10.1038/bjc.2013.748

Nakagawa, H., Liyanarachchi, S., Davuluri, R. V., Auer, H., Martin, E. W. Jr., de la Chapelle, A., et al. (2004). Role of cancer-associated stromal fibroblasts in metastatic colon cancer to the liver and their expression profiles. *Oncogene* 23, 7366–7377. doi: 10.1038/sj.onc.1208013

Newton, A. C., and Brognard, J. (2017). Reversing the paradigm: protein kinase C as a tumor suppressor. *Trends Pharmacol. Sci.* 38, 438–447. doi: 10.1016/j.tips.2017.02.002

Nishina, T., Deguchi, Y., Ohshima, D., Takeda, W., Ohtsuka, M., Shichino, S., et al. (2021). Interleukin-11-expressing fibroblasts have a unique gene signature correlated with poor prognosis of colorectal cancer. *Nat. Commun.* 12:2281. doi: 10.1038/s41467-021-22450-3

Nishishita, R., Morohashi, S., Seino, H., Wu, Y., Yoshizawa, T., Haga, T., et al. (2018). Expression of cancer-associated fibroblast markers in advanced colorectal cancer. *Oncol. Lett.* 15, 6195–6202. doi: 10.3892/ol.2018.8097

Nurmik, M., Ullmann, P., Rodriguez, F., Haan, S., and Letellier, E. (2020). In search of definitions: cancer-associated fibroblasts and their markers. *Int. J. Cancer* 146, 895–905. doi: 10.1002/ijc.32193

Oswald, J., Boxberger, S., Jorgensen, B., Feldmann, S., Ehninger, G., Bornhauser, M., et al. (2004). Mesenchymal stem cells can be differentiated into endothelial cells in vitro. *Stem Cells* 22, 377–384. doi: 10.1634/stemcells.22-3-377

Owens, P., Pickup, M. W., Novitskiy, S. V., Giltnane, J. M., Gorska, A. E., Hopkins, C. R., et al. (2015). Inhibition of BMP signaling suppresses metastasis in mammary cancer. *Oncogene* 34, 2437–2449. doi: 10.1038/onc.2014.189

Ozdemir, B. C., Pentcheva-Hoang, T., Carstens, J. L., Zheng, X., Wu, C. C., Simpson, T. R., et al. (2014). Depletion of carcinoma-associated fibroblasts and fibrosis induces immunosuppression and accelerates pancreas cancer with reduced survival. *Cancer Cell* 25, 719–734. doi: 10.1016/j.ccr.2014.04.005

Paauwe, M., Schoonderwoerd, M. J. A., Helderman, R., Harryvan, T. J., Groenewoud, A., van Pelt, G. W., et al. (2018). Endoglin expression on cancer-associated fibroblasts regulates invasion and stimulates colorectal cancer metastasis. *Clin. Cancer Res.* 24, 6331–6344. doi: 10.1158/1078-0432.CCR-18-0329

Pallangyo, C. K., Ziegler, P. K., and Greten, F. R. (2015). IKKbeta acts as a tumor suppressor in cancer-associated fibroblasts during intestinal tumorigenesis. *J. Exp. Med.* 212, 2253–2266. doi: 10.1084/jem.20150576

Parizadeh, S. M., Jafarzadeh-Esfehani, R., Fazilat-Panah, D., Hassanian, S. M., Shahidsales, S., Khazaei, M., et al. (2019). The potential therapeutic and prognostic impacts of the c-MET/HGF signaling pathway in colorectal cancer. *IUBMB Life* 71, 802–811. doi: 10.1002/iub.2063

Paulsson, J., and Micke, P. (2014). Prognostic relevance of cancer-associated fibroblasts in human cancer. *Semin. Cancer Biol.* 25, 61–68. doi: 10.1016/j.semcancer.2014.02.006

Pena, C., Cespedes, M. V., Lindh, M. B., Kiflemariam, S., Mezheyeuski, A., Edqvist, P. H., et al. (2013). STC1 expression by cancer-associated fibroblasts drives metastasis of colorectal cancer. *Cancer Res.* 73, 1287–1297. doi: 10.1158/0008-5472.CAN-12-1875

Peng, C., Zou, X., Xia, W., Gao, H., Li, Z., Liu, N., et al. (2018). Integrin alphavbeta6 plays a bi-directional regulation role between colon cancer cells and cancer-associated fibroblasts. *Biosci. Rep.* 38:BSR20180243. doi: 10.1042/BSR20180243

Peng, S., Chen, D., Cai, J., Yuan, Z., Huang, B., Li, Y., et al. (2021). Enhancing cancer-associated fibroblast fatty acid catabolism within a metabolically challenging tumor microenvironment drives colon cancer peritoneal metastasis. *Mol. Oncol.* 15, 1391–1411. doi: 10.1002/1878-0261.12917

Peng, Y., Li, Z., Yang, P., Newton, I. P., Ren, H., Zhang, L., et al. (2014). Direct contacts with colon cancer cells regulate the differentiation of bone marrow mesenchymal stem cells into tumor associated fibroblasts. *Biochem. Biophys. Res. Commun.* 451, 68–73. doi: 10.1016/j.bbrc.2014.07.074

Potdar, P. D., and Chaudhary, S. (2017). Molecular characterization of cancer-associated fibroblasts isolated from human colorectal cancer as a major stromal cell component promoting metastasis. *J. Unexplored Med. Data* 2, 1–8. doi: 10.20517/2572-8180.2016.10

Powell, D. W., Adegboyega, P. A., Di Mari, J. F., and Mifflin, R. C. (2005). Epithelial cells and their neighbors I. Role of intestinal myofibroblasts in development, repair, and cancer. *Am. J. Physiol. Gastrointest. Liver Physiol.* 289, G2–G7. doi: 10.1152/ajpgi.00075.2005

Puccini, A., Berger, M. D., Tokunaga, R., Naseem, M., Battaglin, F., Cao, S., et al. (2018). Polymorphism in cancer-associated fibroblasts (CAFs) related genes and clinical outcome in metastatic colorectal cancer (mCRC) patients (pts) enrolled in two independent randomized phase III trials: TRIBE and FIRE-3. *J. Clin. Oncol.* 36(4_suppl):645. doi: 10.1200/JCO.2018.36.4_suppl.645

Ren, J., Ding, L., Zhang, D., Shi, G., Xu, Q., Shen, S., et al. (2018). Carcinoma-associated fibroblasts promote the stemness and chemoresistance of colorectal cancer by transferring exosomal lncRNA H19. *Theranostics* 8, 3932–3948. doi: 10.7150/thno.25541

Rynne-Vidal, A., Au-Yeung, C. L., Jimenez-Heffernan, J. A., Perez-Lozano, M. L., Cremades-Jimeno, L., Barcena, C., et al. (2017). Mesothelial-to-mesenchymal transition as a possible therapeutic target in peritoneal metastasis of ovarian cancer. *J. Pathol.* 242, 140–151. doi: 10.1002/path.4889

Sahai, E., Astsaturov, I., Cukierman, E., DeNardo, D. G., Egeblad, M., Evans, R. M., et al. (2020). A framework for advancing our understanding of cancer-associated fibroblasts. *Nat. Rev. Cancer* 20, 174–186. doi: 10.1038/s41568-019-0238-1

Sandberg, T. P., Stuart, M., Oosting, J., Tollenaar, R., Sier, C. F. M., and Mesker, W. E. (2019). Increased expression of cancer-associated fibroblast markers at the invasive front and its association with tumor-stroma ratio in colorectal cancer. *BMC Cancer* 19:284. doi: 10.1186/s12885-019-5462-2

Schellerer, V. S., Langheinrich, M., Hohenberger, W., Croner, R. S., Merkel, S., Rau, T. T., et al. (2014). Tumor-associated fibroblasts isolated from colorectal cancer tissues exhibit increased ICAM-1 expression and affinity for monocytes. *Oncol. Rep.* 31, 255–261. doi: 10.3892/or.2013.2860

Shin, N., Son, G. M., Shin, D. H., Kwon, M. S., Park, B. S., Kim, H. S., et al. (2019). Cancer-associated fibroblasts and desmoplastic reactions related to cancer invasiveness in patients with colorectal cancer. *Ann. Coloproctol.* 35, 36–46. doi: 10.3393/ac.2018.09.10

Soundararajan, M., and Kannan, S. (2018). Fibroblasts and mesenchymal stem cells: two sides of the same coin? *J. Cell Physiol.* 233, 9099–9109. doi: 10.1002/jcp.26860

Su, S., Chen, J., Yao, H., Liu, J., Yu, S., Lao, L., et al. (2018). CD10(+)GPR77(+) cancer-associated fibroblasts promote cancer formation and chemoresistance by sustaining cancer stemness. *Cell* 172, 841–856 e816. doi: 10.1016/j.cell.2018.01.009

Sugai, T., Uesugi, N., Kitada, Y., Yamada, N., Osakabe, M., Eizuka, M., et al. (2018). Analysis of the expression of cancer-associated fibroblast- and EMT-related proteins in submucosal invasive colorectal cancer. *J. Cancer* 9, 2702–2712. doi: 10.7150/jca.25646

Sung, P. J., Rama, N., Imbach, J., Fiore, S., Ducarouge, B., Neves, D., et al. (2019). Cancer-associated fibroblasts produce netrin-1 to control cancer cell plasticity. *Cancer Res.* 79, 3651–3661. doi: 10.1158/0008-5472.CAN-18-2952

Takeda, S., Shigeyasu, K., Okugawa, Y., Yoshida, K., Mori, Y., Yano, S., et al. (2019). Activation of AZIN1 RNA editing is a novel mechanism that promotes invasive potential of cancer-associated fibroblasts in colorectal cancer. *Cancer Lett.* 444, 127–135. doi: 10.1016/j.canlet.2018.12.009

Tan, H. X., Gong, W. Z., Zhou, K., Xiao, Z. G., Hou, F. T., Huang, T., et al. (2020). CXCR4/TGF-beta1 mediated hepatic stellate cells differentiation into carcinoma-associated fibroblasts and promoted liver metastasis of colon cancer. *Cancer Biol. Ther.* 21, 258–268. doi: 10.1080/15384047.2019.1685157

Terai, S., Fushida, S., Tsukada, T., Kinoshita, J., Oyama, K., Okamoto, K., et al. (2015). Bone marrow derived "fibrocytes" contribute to tumor proliferation and fibrosis in gastric cancer. *Gastric. Cancer* 18, 306–313. doi: 10.1007/s10120-014-0380-0

Tommelein, J., De Vlieghere, E., Verset, L., Melsens, E., Leenders, J., Descamps, B., et al. (2018). Radiotherapy-activated cancer-associated fibroblasts promote tumor progression through paracrine IGF1R activation. *Cancer Res.* 78, 659–670. doi: 10.1158/0008-5472.CAN-17-0524

Tommelein, J., Verset, L., Boterberg, T., Demetter, P., Bracke, M., and De Wever, O. (2015). Cancer-associated fibroblasts connect metastasis-promoting communication in colorectal cancer. *Front. Oncol.* 5:63. doi: 10.3389/fonc.2015.00063

Torres, S., Bartolome, R. A., Mendes, M., Barderas, R., Fernandez-Acenero, M. J., Pelaez-Garcia, A., et al. (2013). Proteome profiling of cancer-associated fibroblasts identifies novel proinflammatory signatures and prognostic markers for colorectal cancer. *Clin. Cancer Res.* 19, 6006–6019. doi: 10.1158/1078-0432.CCR-13-1130

Torres, S., Garcia-Palmero, I., Herrera, M., Bartolome, R. A., Pena, C., Fernandez-Acenero, M. J., et al. (2015). LOXL2 is highly expressed in cancer-associated fibroblasts and associates to poor colon cancer survival. *Clin. Cancer Res.* 21, 4892–4902. doi: 10.1158/1078-0432.CCR-14-3096

Ugel, S., Cane, S., De Sanctis, F., and Bronte, V. (2021). Monocytes in the tumor microenvironment. *Annu. Rev. Pathol.* 16, 93–122. doi: 10.1146/annurev-pathmechdis-012418-013058

Unterleuthner, D., Neuhold, P., Schwarz, K., Janker, L., Neuditschko, B., Nivarthi, H., et al. (2020). Cancer-associated fibroblast-derived WNT2 increases tumor angiogenesis in colon cancer. *Angiogenesis* 23, 159–177. doi: 10.1007/s10456-019-09688-8

Vidal-Vanaclocha, F. (2008). The prometastatic microenvironment of the liver. *Cancer Microenviron.* 1, 113–129. doi: 10.1007/s12307-008-0011-6

Vonlaufen, A., Joshi, S., Qu, C., Phillips, P. A., Xu, Z., Parker, N. R., et al. (2008). Pancreatic stellate cells: partners in crime with pancreatic cancer cells. *Cancer Res.* 68, 2085–2093. doi: 10.1158/0008-5472.CAN-07-2477

Wanandi, S. I., Hilbertina, N., Siregar, N. C., Abdullah, M., and Jeo, W. S. (2021). Cancer-associated fibroblast (CAF) secretomes-induced epithelial-mesenchymal transition on HT-29 colorectal carcinoma cells associated with hepatocyte growth factor (HGF) signalling. *J. Pak. Med. Assoc.* 71(Suppl 2), S18–S24.

Wanandi, S. I., Lestari, D. R., Hilbertina, N., Siregar, N. C., Jusman, S. W., and Abdullah, M. (2020). Secretomes of primary cancer-associated fibroblasts upregulate the expression of stemness markers in HT-29 human colorectal carcinoma cells. *Indones. Biomed. J.* 12, 333–339.

Wawro, M. E., Chojnacka, K., Wieczorek-Szukala, K., Sobierajska, K., and Niewiarowska, J. (2018). Invasive colon cancer cells induce transdifferentiation of endothelium to cancer-associated fibroblasts through microtubules enriched in tubulin-beta3. *Int. J. Mol. Sci.* 20:53. doi: 10.3390/ijms20010053

Weber, C. E., Kothari, A. N., Wai, P. Y., Li, N. Y., Driver, J., Zapf, M. A., et al. (2015). Osteopontin mediates an MZF1-TGF-beta1-dependent transformation of mesenchymal stem cells into cancer-associated fibroblasts in breast cancer. *Oncogene* 34, 4821–4833. doi: 10.1038/onc.2014.410

Wen, D., Wang, Y., Zhu, Z., Huang, Z., Cui, L., Wu, T., et al. (2020). Bromodomain and Extraterminal (BET) protein inhibition suppresses tumor progression and inhibits HGF-MET signaling through targeting cancer-associated fibroblasts in colorectal cancer. *Biochim. Biophys. Acta Mol. Basis Dis.* 1866:165923. doi: 10.1016/j.bbadis.2020.165923

Wen, H., Nie, Q., Jiang, Z., and Deng, H. (2015). [Primary culture and characteristics of colorectal cancer-associated fibroblasts]. *Zhonghua Bing Li Xue Za Zhi* 44, 719–724.

Wikberg, M. L., Edin, S., Lundberg, I. V., Van Guelpen, B., Dahlin, A. M., Rutegard, J., et al. (2013). High intratumoral expression of fibroblast activation protein (FAP) in colon cancer is associated with poorer patient prognosis. *Tumour. Biol.* 34, 1013–1020. doi: 10.1007/s13277-012-0638-2

Wu, T., and Dai, Y. (2017). Tumor microenvironment and therapeutic response. *Cancer Lett.* 387, 61–68. doi: 10.1016/j.canlet.2016.01.043

Xie, L., Jiang, F. C., Zhang, L. M., He, W. T., Liu, J. H., Li, M. Q., et al. (2016). Targeting of MyD88 homodimerization by novel synthetic inhibitor TJ-M2010-5 in preventing colitis-associated colorectal cancer. *J. Natl. Cancer Inst.* 108:djv364. doi: 10.1093/jnci/djv364

Xu, Y., Kuai, R., Chu, Y., Zhou, L., Zhang, H.-Q., and Li, J. (2021). Hypoxia facilitates the proliferation of colorectal cancer cells by inducing cancer-associated fibroblast-derived IL6. *Res. Sq.* doi: 10.4149/neo_2021_210308N296 [Epub ahead of print].

Xuefeng, X., Hou, M. X., Yang, Z. W., Agudamu, A., Wang, F., Su, X. L., et al. (2020). Epithelial-mesenchymal transition and metastasis of colon cancer cells induced by the FAK pathway in cancer-associated fibroblasts. *J. Int. Med. Res.* 48:300060520931242. doi: 10.1177/0300060520931242

Yadav, V. K., Huang, Y. J., George, T. A., Wei, P. L., Sumitra, M. R., Ho, C. L., et al. (2020). Preclinical evaluation of the novel small-molecule MSI-N1014 for treating drug-resistant colon cancer via the LGR5/beta-catenin/miR-142-3p network and reducing cancer-associated fibroblast transformation. *Cancers (Basel)* 12:1590. doi: 10.3390/cancers12061590

Yamamura, Y., Asai, N., Enomoto, A., Kato, T., Mii, S., Kondo, Y., et al. (2015). Akt-Girdin signaling in cancer-associated fibroblasts contributes to tumor progression. *Cancer Res.* 75, 813–823. doi: 10.1158/0008-5472.CAN-14-1317

Yang, T., Zhiheng, H., Zhanhuai, W., Qian, X., Yue, L., Xiaoxu, G., et al. (2020). Increased RAB31 expression in cancer-associated fibroblasts promotes colon cancer progression through HGF-MET signaling. *Front. Oncol.* 10:1747. doi: 10.3389/fonc.2020.01747

Yang, X., Xu, X., Zhu, J., Zhang, S., Wu, Y., Wu, Y., et al. (2016). miR-31 affects colorectal cancer cells by inhibiting autophagy in cancer-associated fibroblasts. *Oncotarget* 7, 79617–79628. doi: 10.18632/oncotarget.12873

Yin, C., Evason, K. J., Asahina, K., and Stainier, D. Y. (2013). Hepatic stellate cells in liver development, regeneration, and cancer. *J. Clin. Invest.* 123, 1902–1910. doi: 10.1172/JCI66369

You, L., He, B., Xu, Z., Uematsu, K., Mazieres, J., Fujii, N., et al. (2004). An anti-Wnt-2 monoclonal antibody induces apoptosis in malignant melanoma cells and inhibits tumor growth. *Cancer Res.* 64, 5385–5389. doi: 10.1158/0008-5472.CAN-04-1227

Yu, M., Guo, G., Huang, L., Deng, L., Chang, C. S., Achyut, B. R., et al. (2020). CD73 on cancer-associated fibroblasts enhanced by the A2B-mediated feedforward circuit enforces an immune checkpoint. *Nat. Commun.* 11:515. doi: 10.1038/s41467-019-14060-x

Yuan, Q., Gu, J., Zhang, J., Liu, S., Wang, Q., Tian, T., et al. (2021). MyD88 in myofibroblasts enhances colitis-associated tumorigenesis via promoting macrophage M2 polarization. *Cell Rep.* 34:108724. doi: 10.1016/j.celrep.2021.108724

Zadka, L., Chabowski, M., Grybowski, D., Piotrowska, A., and Dziegiel, P. (2021). Interplay of stromal tumor-infiltrating lymphocytes, normal colonic mucosa, cancer-associated fibroblasts, clinicopathological data and the immunoregulatory molecules of patients diagnosed with colorectal cancer. *Cancer Immunol. Immunother.* 70, 2681–2700. doi: 10.1007/s00262-021-02863-1

Zeisberg, E. M., Potenta, S., Xie, L., Zeisberg, M., and Kalluri, R. (2007). Discovery of endothelial to mesenchymal transition as a source for carcinoma-associated fibroblasts. *Cancer Res.* 67, 10123–10128. doi: 10.1158/0008-5472.CAN-07-3127

Zhang, H. W., Shi, Y., Liu, J. B., Wang, H. M., Wang, P. Y., Wu, Z. J., et al. (2021). Cancer-associated fibroblast-derived exosomal microRNA-24-3p enhances colon cancer cell resistance to MTX by down-regulating CDX2/HEPH axis. *J. Cell Mol. Med.* 25, 3699–3713. doi: 10.1111/jcmm.15765

Zhang, M., Shi, R., Guo, Z., and He, J. (2020). Cancer-associated fibroblasts promote cell growth by activating ERK5/PD-L1 signaling axis in colorectal cancer. *Pathol. Res. Pract.* 216:152884. doi: 10.1016/j.prp.2020.152884

Zhang, R., Qi, F., Shao, S., Li, G., and Feng, Y. (2019a). Human colorectal cancer-derived carcinoma associated fibroblasts promote CD44-mediated adhesion of colorectal cancer cells to endothelial cells by secretion of HGF. *Cancer Cell Int.* 19:192. doi: 10.1186/s12935-019-0914-y

Zhang, R., Qi, F., Zhao, F., Li, G., Shao, S., Zhang, X., et al. (2019b). Cancer-associated fibroblasts enhance tumor-associated macrophages enrichment and suppress NK cells function in colorectal cancer. *Cell Death Dis.* 10:273. doi: 10.1038/s41419-019-1435-2

Zhang, Y., Wang, S., Lai, Q., Fang, Y., Wu, C., Liu, Y., et al. (2020). Cancer-associated fibroblasts-derived exosomal miR-17-5p promotes colorectal cancer aggressive phenotype by initiating a RUNX3/MYC/TGF-beta1 positive feedback loop. *Cancer Lett.* 491, 22–35. doi: 10.1016/j.canlet.2020.07.023

Zhou, L., Li, J., Tang, Y., and Yang, M. (2021). Exosomal LncRNA LINC00659 transferred from cancer-associated fibroblasts promotes colorectal cancer cell progression via miR-342-3p/ANXA2 axis. *J. Transl. Med.* 19:8. doi: 10.1186/s12967-020-02648-7

Zhou, P., Xiao, N., Wang, J., Wang, Z., Zheng, S., Shan, S., et al. (2017). SMC1A recruits tumor-associated-fibroblasts (TAFs) and promotes colorectal cancer metastasis. *Cancer Lett.* 385, 39–45. doi: 10.1016/j.canlet.2016.10.041

Zhou, W., Xu, G., Wang, Y., Xu, Z., Liu, X., Xu, X., et al. (2017). Oxidative stress induced autophagy in cancer associated fibroblast enhances proliferation and metabolism of colorectal cancer cells. *Cell Cycle* 16, 73–81. doi: 10.1080/15384101.2016.1252882

Zhu, H. F., Zhang, X. H., Gu, C. S., Zhong, Y., Long, T., Ma, Y. D., et al. (2019). Cancer-associated fibroblasts promote colorectal cancer progression by secreting CLEC3B. *Cancer Biol. Ther.* 20, 967–978. doi: 10.1080/15384047.2019.1591122

Zhu, Q., Zhang, X., Zhang, L., Li, W., Wu, H., Yuan, X., et al. (2014). The IL-6-STAT3 axis mediates a reciprocal crosstalk between cancer-derived mesenchymal stem cells and neutrophils to synergistically prompt gastric cancer progression. *Cell Death Dis.* 5:e1295. doi: 10.1038/cddis.2014.263

Zhu, Y., Zheng, J. J., Yang, F., Nie, Q. Q., Zhu, Z. L., and Deng, H. (2016). Expression of CD10 in cancer-associated fibroblasts and its effect on initiation and progression of colorectal carcinoma. *Zhonghua Bing Li Xue Za Zhi* 45, 859–865. doi: 10.3760/cma.j.issn.0529-5807.2016.12.009

Conflict of Interest: The authors declare that the research was conducted in the absence of any commercial or financial relationships that could be construed as a potential conflict of interest.

Publisher's Note: All claims expressed in this article are solely those of the authors and do not necessarily represent those of their affiliated organizations, or those of the publisher, the editors and the reviewers. Any product that may be evaluated in this article, or claim that may be made by its manufacturer, is not guaranteed or endorsed by the publisher.

frontiers in Cell and Developmental Biology

ORIGINAL RESEARCH
published: 01 October 2021
doi: 10.3389/fcell.2021.739594

The Landscape of the Tumor Microenvironment in Skin Cutaneous Melanoma Reveals a Prognostic and Immunotherapeutically Relevant Gene Signature

Sitong Zhou[1†], Yidan Sun[2†], Tianqi Chen[2], Jingru Wang[3], Jia He[3], Jin Lyu[4], Yanna Shen[5], Xiaodong Chen[3*] and Ronghua Yang[3*]*

[1] Department of Dermatology, The First People's Hospital of Foshan, Foshan, China, [2] Department of Oncology, First Teaching Hospital of Tianjin University of Traditional Chinese Medicine, Tianjin, China, [3] Department of Burn Surgery and Skin Regeneration, The First People's Hospital of Foshan, Foshan, China, [4] Department of Pathology, The First People's Hospital of Foshan, Foshan, China, [5] School of Medical Laboratory, Tianjin Medical University, Tianjin, China

The tumorigenesis of skin cutaneous melanoma (SKCM) remains unclear. The tumor microenvironment (TME) is well known to play a vital role in the onset and progression of SKCM. However, the dynamic mechanisms of immune regulation are insufficient. We conducted a comprehensive analysis of immune cell infiltration in the TME. Based on the differentially expressed genes (DEGs) in clusters grouped by immune infiltration status, a set of hub genes related to the clinical prognosis of SKCM and tumor immune infiltration was explored.

Methods: We analyzed immune cell infiltration in two independent cohorts and assessed the relationship between the internal pattern of immune cell infiltration and SKCM characteristics, including clinicopathological features, potential biological pathways, and gene mutations. Genes related to the infiltration pattern of TME immune cells were determined. Furthermore, the unsupervised clustering method (k-means) was used to divide samples into three different categories according to TME, which were defined as TME cluster-A, -B, and -C. DEGs among three groups of samples were analyzed as signature genes. We further distinguished common DEGs between three groups of samples according to whether differences were significant and divided DEGs into the Signature gene-A group with significant differences and the Signature gene-B group with insignificant differences. The Signature gene-A gene set mainly had exon skipping in SKCM, while the Signature gene-B gene set had no obvious alternative splicing form. Subsequently, we analyzed genetic variations of the two signatures and constructed a competing endogenous RNA (ceRNA) regulatory network. LASSO Cox regression was used to determine the immune infiltration signature and risk score of SKCM. Finally, we obtained 13 hub genes and calculated the risk score based on the coefficient of each gene to explore the impact of the high- and low-risk scores on biologically related functions and prognosis of SKCM patients further.

OPEN ACCESS

Edited by:
Na Luo,
Nankai University, China

Reviewed by:
Weifeng Hong,
The First Affiliated Hospital of Guangdong Pharmaceutical University, China
Mingwei Zhang,
First Affiliated Hospital of Fujian Medical University, China

***Correspondence:**
Ronghua Yang
a_hwa991316@163.com
Xiaodong Chen
cxd234@163.com
Yanna Shen
shenyanna@tmu.edu.cn

† These authors have contributed equally to this work

Specialty section:
This article was submitted to Molecular and Cellular Pathology, a section of the journal Frontiers in Cell and Developmental Biology

Received: *11 July 2021*
Accepted: *23 August 2021*
Published: *01 October 2021*

Citation:
Zhou S, Sun Y, Chen T, Wang J, He J, Lyu J, Shen Y, Chen X and Yang R (2021) The Landscape of the Tumor Microenvironment in Skin Cutaneous Melanoma Reveals a Prognostic and Immunotherapeutically Relevant Gene Signature. Front. Cell Dev. Biol. 9:739594. doi: 10.3389/fcell.2021.739594

The correlation between the risk score and clinicopathological characteristics of SKCM patients indicated that a low-risk score was associated with TME cluster-A classification ($p < 0.001$) and metastatic SKCM ($p < 0.001$). Thirteen hub genes also showed different prognostic effects in pan-cancer. The results of univariate and multivariate Cox analyses revealed that risk score could be used as an independent risk factor for predicting the prognosis of SKCM patients. The nomogram that integrated clinicopathological characteristics and immune characteristics to predict survival probability was based on multivariate Cox regression. Finally, 13 hub genes that showed different prognostic effects in pan-cancers were obtained. According to immunohistochemistry staining results, *Ube2L6*, *SRPX2*, and *IFIT2* were expressed at higher levels, while *CLEC4E*, *END3*, and *KIR2DL4* were expressed at lower levels in 25 melanoma specimens.

Conclusion: We performed a comprehensive assessment of the immune-associated TME. To elucidate the potential development of immune-genomic features in SKCM, we constructed an unprecedented set of immune characteristic genes (*EDN3*, *CLEC4E*, *SRPX2*, *KIR2DL4*, *UBE2L6*, and *IFIT2*) related to the immune landscape of TME. These genes are related to different prognoses and drug responses of SKCM. The immune gene signature constructed can be used as a robust prognostic biomarker of SKCM and a predictor of an immunotherapy effect.

Keywords: skin cutaneous melanoma, prognostic biomarker, tumor microenvironment, gene signature, immuno-genomic landscape, clinicopathological characteristics

INTRODUCTION

Skin cutaneous melanoma (SKCM) is currently one of the most lethal human malignancies. As the deadliest form of skin cancer, it accounts for almost 75% of skin cancer lethality (Siegel et al., 2021). Although the 5-year survival of early stage SKCM patients exceeds 95% (Thompson et al., 2009), the reported survival time for advanced-stage melanoma barely exceeds 1 year (Fecher et al., 2007). Currently, patients with primary melanoma require surgical resection as a first-line therapy. However, advanced melanoma is highly aggressive, making it insensitive to radiotherapy and chemotherapy (Goodson and Grossman, 2009). The emergence of immune checkpoint inhibitors, such as ipilimumab (Jameson-Lee and Luke, 2021) and nivolumab (Zhao et al., 2020), for melanoma has revolutionized the treatment of SKCM and offers new hope for patients. However, approximately 50% of patients do not benefit from immune checkpoint inhibitors (Hodi et al., 2010; Topalian et al., 2012).

Recently, growing evidence has demonstrated that tumor microenvironment (TME) plays an important role in SKCM progression (Hanahan and Weinberg, 2011; Quezada et al., 2011). TME influences tumorigenesis and metastasis through various biological processes. In contrast to this, TME heterogeneity is also an important cause of alterations in prognosis and sensitivity to immunotherapy in various cancers (Koikawa et al., 2021). Notably, it may regulate the immune response through a variety of mechanisms, thereby affecting the inner metabolism process and immunosuppressive state. Among these, tumor-infiltrating immune cells (TIICs) exhibit tumor-promoting effects according to the tumor type. In most cancers, CD8+ T cells play crucial roles in TME, inhibiting the proliferation and invasion of malignant cells. T cell-mediated immune responses to melanoma antigens have been extensively documented (Marron et al., 2021). Furthermore, immunosuppression may act as an additional tumor burden that fosters tumor growth or immune escape in TME. Hence, a comprehensive understanding of TME is urgently needed to improve the efficacy of immunotherapies.

Considering the positive effect of immunotherapy in SKCM patients, understanding the molecular composition and function of TME is important to facilitate effective diagnosis, prognosis, mitigation, and immunotherapeutic responsiveness of SKCM patients.

We integrated The Cancer Genome Atlas (TCGA)-SKCM-independent cohort and validated the predictive model in four additional independent cohorts (GSE8401, GSE35640, GSE15605, and GSE46517) from Gene Expression Omnibus (GEO) datasets, to develop and verify a new set of personalized immune signature models. We also analyzed clinical and pathological characteristics of all existing SKCM patients, including somatic cell copy number variation (CNV), tumor mutation burden (TMB), and gene variable splicing. Several bioinformatics methods were employed to estimate the abundance of immune cell infiltration in SKCM patients, and the correlation between genomic characteristics of the immune landscape and pathological characteristics and prognosis of

Abbreviations: TME, tumor microenvironment; AUC, area under the curve; TMB, tumor mutation burden; SKCM, skin cutaneous melanoma; ICI, immune checkpoint inhibitors; GEO, gene expression omnibus; TCGA, the cancer genome atlas; GSVA, gene set variation analysis; GSEA, gene set enrichment analysis; OS, overall survival; PCA, principal component analysis.

SKCM was determined. Therefore, in the present study, we sought to develop and evaluate the risk-based model of six novel immune-related genes (*EDN3*, *CLEC4E*, *SRPX2*, *KIR2DL4*, *Ube2L6*, and *IFIT2*). In addition, immunohistochemistry (IHC) staining and qRT-PCR were used to verify the difference in the expression level of the novel 6-gene signature in 25 frozen SKCM tissue samples and normal tissues. Notably, gene signatures that affect the immune landscape may be closely related to different prognosis and treatment responses of SKCM. Accordingly, we established an unprecedented set of immune signatures that can be used as robust prognostic biomarkers and predictors of the immunotherapy effects in SKCM patients.

MATERIALS AND METHODS

Acquisition and Preprocessing of the SKCM Expression Datasets

Data from two publicly available datasets were included in the study. RNA-seq data were extracted for 471 patients, in addition to clinical features, from TCGA-SKCM cohort (Tomczak et al., 2015). Clinical data were downloaded from the University of California Santa Cruz Xena browser[1]. Somatic CNV data and TMB were downloaded from the Genomic Data Commons Data Portal (Grossman et al., 2016). Data on alternative splicing events were downloaded from TCGASpliceSeq database. "RCircos" (Zhang et al., 2013) package was used to generate a map for the genome-wide CNV analysis of SKCM patients using 23 pairs of chromosomes. Somatic mutation data were downloaded in mutation annotation format, and the maftools package (Mayakonda et al., 2018) was used for visualization. We obtained SKCM microarray data from two GeneChips (GPL570 [HG-U133_Plus_2] Affymetrix Human Genome U133 Plus 2.0 Array and GPL96-57554 [HG-U133A] Affymetrix Human Genome U133A Array) in GSE84014 (Xu et al., 2008), GSE356405 (Dreno et al., 2018), GSE156056 (Raskin et al., 2013), and GSE46517 (He et al., 2020) from GEO[1] as validation sets. The limma package (Ritchie et al., 2015) in R was used for gene expression normalization, while the sva (Leek et al., 2012) package (3.20) was used to correct for plate batch effects.

TIICs Analysis and Clustering of Samples

CIBERORT (Newman et al., 2015), an algorithm that quantifies the proportion of TIICs with 547 signature genes to infer the representation in bulk tumor transcriptomes, was used to evaluate the cell components of TIICs. The proportions of 22 types of TIICs in the cohort from TCGA were estimated. Cluster analysis was performed using an unsupervised hierarchical clustering method, an algorithmic approach that groups individuals with similar observations based on the Euclidean distance method. Three immune microenvironment subtypes were defined using the ConsensusClusterPlus package (Wilkerson and Hayes, 2010). The procedure was repeated 1,000 times to stabilize the stratification.

Differential Gene Expression Pattern Clustering Analysis

To determine genes associated with TME cell infiltration patterns, we divided patients into three different pattern types according to TME; these types were defined as TME cluster-A, -B, and -C. We further analyzed common differentially expressed genes (DEGs) between the three groups of samples and, based on the significance of the differential expression changes of the specific genes, divided the samples into two groups of signature genes: A and B. Signature gene-A was an immune-related specific gene with a significant difference, and Signature gene-B was an insignificantly different part of an immune-related specific gene. The limma package was used to analyze DEGs between these three groups of SKCM patients, and the significant DEGs were defined as genes with an absolute log value of fold-change >1 and FDR <0.05. The overlapping DEGs among the three groups were further analyzed as specific genes using the VennDiagram (Venn diagram) package (Chen and Boutros, 2011). The k-means clustering algorithm, which is an unsupervised clustering method, was used to cluster these specific genes into meaningful groups in the GEO datasets according to the expression of specific genes in TME cluster-A, -B, and -C. Meanwhile, based on changes in gene expression, specific genes were divided into two groups: Signature gene-A and -B. Among them, Signature gene-A and Signature gene-B were obtained by cluster analysis of the three subtypes, where Signature gene-A was highly expressed in cluster A and relatively less expressed in clusters B and C.

RNA Sequence Expression Analysis in Gene Expression Profiling Interactive Analysis

Gene Expression Profiling Interactive Analysis (GEPIA)[2] is an online data processing webpage containing RNA sequence expression information of 9,736 tumors and 8,587 normal tissue samples (Tang et al., 2019). The differential expression of hub genes between tumor and normal tissues, correlations, and survival prediction was determined using the GEPIA database. Student's *t*-test was used to analyze the correlation between the expression and clinicopathological features. Statistical significance was set at $p < 0.05$.

Gene Set Enrichment Analysis

Gene Ontology (GO) analysis was performed to illustrate the unique biological significance of gene expression of signature genes. Gene functions were categorized into three series: cellular components, molecular functions, and biological processes (BPs). Crucial pathways were identified using Kyoto Encyclopedia of Genes and Genomes pathway analysis. GO annotations were visualized using the R package clusterProfiler (Yu et al., 2012). Gene Set Enrichment Analysis (GSEA; Subramanian et al., 2005) is a calculation method for identifying the potential biological mechanisms between two biological states. GSEA was

[1]http://www.ncbi.nlm.nih.gov/geo

[2]http://gepia.cancer-pku.cn/index.html

conducted in the Molecular Signatures Database (MSigDB)[3], which provided hallmark gene sets to predict BPs between normal and SKCM samples.

Evaluation of Patient Biological Characteristics

We further analyzed correlations between different groups and some biologically related processes. Gene sets for storing genes related to certain BPs, including immune checkpoints, antigen processing, CD8+ T cells, and epithelial–mesenchymal transition (EMT) markers, such as EMT1, EMT2, and EMT3, angiogenesis characteristics, pan-fibroblast TGF-β response characteristics, WNT characteristics, DNA damage repair, mismatch repair, nucleotide excision repair, DNA replication, and antigen processing and presentation, were collected.

Establishment of the Immune Characteristic Model and Clinical Prediction Model

We adopted a two-step method to establish a signature-based risk score. First, univariate Cox regression was used to analyze the impact of signature genes on the prognosis of SKCM patients according to the cutoff, with $p < 0.05$. The most commonly used model to establish clinical prognosis and survival-related models is the Cox proportional hazards model owing to its flexibility and relative robustness. The Cox grade-scoring test was used for repeated prediction and prognostic analyses. The Cox grade-scoring test was robust to outliers. Accordingly, outliers were removed for the sensitivity analysis. The potential prognostic hub genes were validated to enhance risk profiling after surgery and to define new targets in the prediction models for SKCM patients. To prove the significance of risk score combined with clinicopathological characteristics for a personalized evaluation of patient prognosis, we first tested the expression correlation of hub genes in different tumors in TCGA database and the predictive ability of the risk score for the prognosis of patients with different tumors. Multiple regression was the main analysis method for building immune prediction models. Multiple regressions were performed using standard statistical methods. In addition, we fitted the multivariate Cox regression model using the least absolute contraction and selection operator (LASSO). LASSO regression is a regularized approach commonly used for high-dimensional predictor selection. A system of risk score was established using the LASSO Cox proportional hazards model to identify gene signatures for predicting the overall survival (OS) of SKCM. A predictive score was developed using the weighted sum of genes, with the coefficients of the LASSO regularization.

$$riskScore = \sum Coefficient\ (hub\ genei)\ * mRNA\ Expression\ (hub\ genei)$$

Factors related to OS and clinical pathological characteristics were evaluated using univariate and multivariate analyses with Cox and logistic regression, respectively. Variables with a value of $p < 0.05$ in the multivariate analysis were included in the prognostic model. The performance and discriminative ability were assessed using Harrell's concordance index. Nomograms were constructed to predict the 3-year, 5-year, and 10-year survival rates of SKCM patients based on predictive models with identified prognostic factors. Calibration is defined as a prediction from the nomogram compared with the observed outcomes.

IHC Validation

Tumor tissues were collected from 25 melanoma patients in the Han Chinese group from 2015 to 2020. Informed consent was obtained from patients, and the study was approved by the First People's Hospital of the Foshan Subject Review Board. Paraffin-embedded tissues were sectioned to be 4 μm thick for IHC analysis. Antigen retrieval was performed by incubating the samples in citrate buffer (pH 6.0) for 15 min at 100°C in a microwave oven. After blocking with a mixture of methanol and 0.75% hydrogen peroxide, sections were incubated overnight with appropriate dilutions of primary antibodies (CLEC4E, 1:500, Sigma; END3, 1:500, Sangon Biotech; IFIT2, 1:500, Proteintech; SRPX2, 1:600, Proteintech; Ube2L6, 1:500, Abcam; KIR2DL4, 1:500, Abcam), followed by incubation with a secondary antibody conjugated with HRP (goat anti-rabbit, 1:500, Cell Signaling Technology). The sections were washed three times with phosphate buffer saline and incubated with AEC (ZSGB-BIO). All specimens were examined by the cross-product (H score) of the percentage of tumor cell staining at each of three staining intensities. The intensity of immunopositivity was scored as follows: none, 0; weak, 1; moderate, 2; and strong, 3. For example, a particular tumor may have 50% cell staining at an intensity of 1 and 50% of cell staining at an intensity of 3, for a combined H score of 200 [(50 × 1) + (50 × 3) = 200], which yields a range from 0 to 300. The final score was graded by the H score as follows: low, H score 0–100; moderate, H score 101–200; and high, H score 201–300.

Statistical Analysis

All statistical analyses were performed using R version 3.6.2. Differences in continuous variables between the two groups were estimated by independent Student's *t*-test, and the differences between non-normally distributed variables were analyzed using the Mann–Whitney U rank-sum test. If the normality test failed, Kruskal–Wallis One Way ANOVA on Ranks was performed. Pearson's χ^2 test or Fisher's exact test was used to compare qualitative variables. *p*-Values and hazard ratios were obtained from univariate Cox proportional hazards regression models using the R package, *survival* (Zeng et al., 2019). The log-rank test was used to evaluate the significance of the difference in survival time between the two groups. Receiver operating characteristic curve analysis was conducted using the pROC package (Robin et al., 2011) to evaluate the prognostic capabilities of different risk models and the time-dependent AUC values. Univariate and multivariate Cox analyses were used to determine independent prognostic factors. All statistical

[3]http://software.broadinstitute.org/gsea/index.jsp

TABLE 1 | Baseline data of SKCM patients in TCGA database.

Variables	All (*n* = 422)	Low risk (*n* = 205)	High risk (*n* = 217)	*p*-value
Gender				0.02*
—Male	264 (62.6%)	117 (57.1%)	147 (67.7%)	
—Female	158 (37.4%)	88 (42.9%)	70 (32.3%)	
Age				0.68
—<60	220 (52.1%)	109 (53.2%)	111 (51.2%)	
—≥60	202 (47.9%)	96 (46.8%)	106 (48.8%)	
T stage				<0.001***
—T1 & T2	147 (34.8%)	91 (44.4%)	56 (25.8%)	
—T3 & T4	236 (55.9%)	93 (45.4%)	143 (65.9%)	
N stage				0.85
—N0	218 (51.7%)	108 (52.7%)	110 (50.7%)	
—N1	72 (17.1%)	37 (18.0%)	35 (16.1%)	
—N2	47 (11.1%)	24 (11.7%)	23 (10.6%)	
—N3	55 (13.0%)	32 (15.6%)	23 (10.6%)	
M stage				0.836
—M0	392 (92.9%)	192 (93.7%)	200 (92.2%)	
—M1	23 (5.5%)	10 (4.9%)	13 (6.0%)	
Pathologic stage				0.03*
—I	83 (19.7%)	54 (26.3%)	29 (13.4%)	
—II	146 (34.6%)	58 (28.3%)	88 (40.6%)	
—III	170 (40.3%)	83 (40.5%)	87 (40.1%)	
—IV	23 (5.5%)	10 (4.9%)	13 (6.0%)	
Type				<0.001***
—Primary	97 (23.0%)	28 (13.7%)	69 (31.8%)	
—Metastatic	325 (77.0%)	177 (86.3%)	148 (68.2%)	
Status				<0.001***
—Alive	232 (55.0%)	139 (67.8%)	93 (42.9%)	
—Dead	190 (45.0%)	66 (32.2%)	124 (57.1%)	

*$p < 0.05$; ***$p < 0.001$; ns, no significance.*

tests were two-sided, and statistical significance was set at $p < 0.05$.

RESULTS

Immune Infiltration Analysis Related to SKCM Patients

We obtained the gene expression data of SKCM patients from TCGA database(**Table 1**) and analyzed 22 different immune cell infiltrations in each sample using the CIBERSORT algorithm (Newman et al., 2015; **Figure 1A**). The TME cell network depicted interactions between tumor immune cells (**Supplementary Figure 1**). The comprehensive status of the cell lineage and its impact on the overall survival of patients with SKCM were also analyzed (**Figure 1B**). The TME cell network demonstrated that cell clusters B, C, and D were positively correlated with each other, including CD8+ T cells, naïve B cells, plasma cells, CD4 naïve T cells, activated NK cells, monocytes, resting dendritic cells, regulatory T cells, monocytes, and CD4 memory activated T cells. Moreover, there was a significant positive correlation among immune cells in cluster A, such as between gamma delta T cells, resting NK cells, neutrophils, activated mast cells, M0 macrophages, eosinophils, and activated dendritic cells. Meanwhile, M0 macrophages, activated CD4 memory T cells, and monocytes showed a significant negative correlation. NK cell resting and NK cell activation showed the same significant negative correlation. An exploratory analysis was also performed to measure survival benefits and potential risks. Results showed that CD4+ T cells, CD8+ T cells, activated NK cells, regulatory T cells, dendritic cells, and M1 macrophages were associated with shortened OS, while resting NK cells, neutrophils, M0 macrophages, and dendritic cells were activated and associated with prolonged OS. To construct the best clusters and classification, we used the ConsensusClusterPlus package to assess the stability of the clustering structure and divided SKCM patients into TME cluster-A, -B, and -C. Unsupervised hierarchical clustering was used to analyze the normalized immune cell fractions. The heatmap showed correlation between the infiltration abundance of 22 types of immune cells and immune scores in the three groups (**Figure 1C**). Results showed that patients with TME cluster-A had higher immune scores, whereas patients with TME cluster-B and -C mainly had tumor purity and stromal scores. In addition, the principal component analysis results showed that based on the expression data of SKCM patients, the three TME cluster groups could

be significantly distinguished (**Figure 1D**). Survival analysis related to the TME phenotype showed that TME cluster-C ($N = 92$) was associated with a better prognosis (log-rank test, $p < 0.001$) (**Figure 1E**).

We selected and analyzed the gene expression profile data and immune cell infiltration abundance of SKCM samples from the GEO database. The ConsensusClusterPlus package was used to evaluate the stability of the clustering (**Figure 2A**). Subsequently, the heatmap showed that patients with TME cluster-A had higher immune scores (**Figure 2B**), which was consistent with the results in TCGA database. This finding also aligned with that of previous studies that have reported melanoma being a highly immune-dependent malignant tumor.

Construction of the TME-Related Signature Gene in SKCM Patients

TME has a crucial impact on tumor epigenetics, metastasis, and immune escape. We used the limma package to analyze the 486 DEGs among the three groups of TME cluster in TCGA database to determine the potential biological characteristics of different TME phenotypes. Similarly, 330 DEGs were analyzed in the GEO datasets (**Figure 3A**). Unsupervised clustering using these DEGs provided three distinct clusters: TME cluster-A, -B, and -C (**Figure 3B**). Simultaneously, according to the differential expression of DEGs in different clusters, genes were further divided into Signature gene-A and -B. GO enrichment analysis showed that Signature gene-A and -B had different unique BPs. Signature gene-A was associated with the overexpression of immune-activated genes (**Figure 3C**), while Signature gene-B showed upregulation of genes related to stromal and transmembrane receptors (**Figure 3D**). There were significant differences in the infiltration of TME cells (**Figure 3E**) and the enrichment of related biological pathways (**Figure 3F**) between the three GeneClusters, which was consistent with our functional enrichment results.

CeRNA Regulatory Network Construction and Signature Gene Expression in SKAM Patients

To further analyze differences between Signature gene-A and -B gene sets and determine whether these differences have a profound impact on cancer genetics, we analyzed genetic levels of single nucleotide polymorphisms. CNV and SNP analyses showed that there were obvious mutations in both gene sets. Notably, somatic SPTA1 mutations were more frequent in TME cluster-A (**Figure 4A**). TNN was the most frequently observed somatic mutation in TME cluster-B (**Figure 4B**). Moreover, the examination of this frequency change in CNV revealed that CNV changes were common in both groups and most were concentrated on the amplification of copy numbers. We then elucidated positions of these CNV changes on the chromosome (**Figures 4C,D**). In the AS analysis, Signature gene-A mainly had exon skipping (ES) in SKCM patients (**Figure 4E**), while Signature gene-B had no obvious AS forms (**Figure 4F**). In addition, Signature gene-A and -B gene sets may have a certain significance for the prognosis of SKCM. Further research is necessary for the interaction between immune-related molecules. Based on the gene expression of Signature gene-A and -B, we screened out lncRNAs that may be related to immunity using correlation coefficients >0.4 and $p < 0.05$. The starBase database[4] was used to obtain targeted differentially expressed miRNAs to construct the regulatory ceRNA network of the mRNA–miRNA–LncRNA interaction (**Figure 4G**).

Construction of the Immune-Related Prognostic Gene Signature

To predict the impact of immune characteristics on the prognosis of patients better, we constructed a new prognostic-related risk scoring system. The Signature gene-A and-B were incorporated into univariate Cox analyses, and 233 genes related to prognosis were obtained ($p < 0.05$). The LASSO Cox analyses were further used for dimensionality reduction and model construction, and finally, a total of 16 hub genes were included in the risk scoring model (**Figure 5A**). A risk score (RS) formula was established by including individual normalized gene expression values weighted by their LASSO Cox coefficients. The risk score for each SKCM patient was calculated according to the locking of the coefficients in each gene signature. The high- and low-risk groups were divided according to the median risk score. Kaplan–Meier analysis showed that patients with high-risk scores had a relatively poor prognosis (**Figure 5B**). The time-dependent receiver operating characteristic curve analysis also showed that the risk score had a good predictive ability for OS (**Figure 5C**). The area under the curve (AUC) of 1-year, 3-year, and 5-year OS was 0.713, 0.694, and 0.734, respectively. The distribution of each patient's risk score, survival status, and gene expression map is shown in **Figure 5D**.

GSEA

We analyzed the impact of the high- and low-risk groups on the biologically relevant functions of SKCM patients. GSEA revealed that pathways related to metabolism and oxidative phosphorylation were mainly enriched in the high-risk group (**Figures 6A,C**), while pathways related to immune response, including cytokine signaling pathway, JAK–STAT signaling pathway, and natural killer cell-mediated cytotoxicity, were significantly enriched in low-risk patients (**Figures 6B,D**). At the same time, expression levels of TME cells (**Figure 6E**), as well as some other pathways, such as angiogenesis, mismatch-related features, and stromal-related features (**Figure 6F**), were significantly different between the high- and low-risk groups of SKCM patients ($p < 0.05$).

Correlation Analysis of the Risk Score and Clinicopathological Characteristics

We assessed the correlation between the risk score and the clinicopathological characteristics of SKCM. The analysis results showed that the low-risk score was correlated with TME cluster-A classification ($p < 0.001$; **Figure 7A**) and metastatic SKCM ($p < 0.001$; **Figure 7B**). In addition, the low-risk score was

[4]http://starbase.sysu.edu.cn/

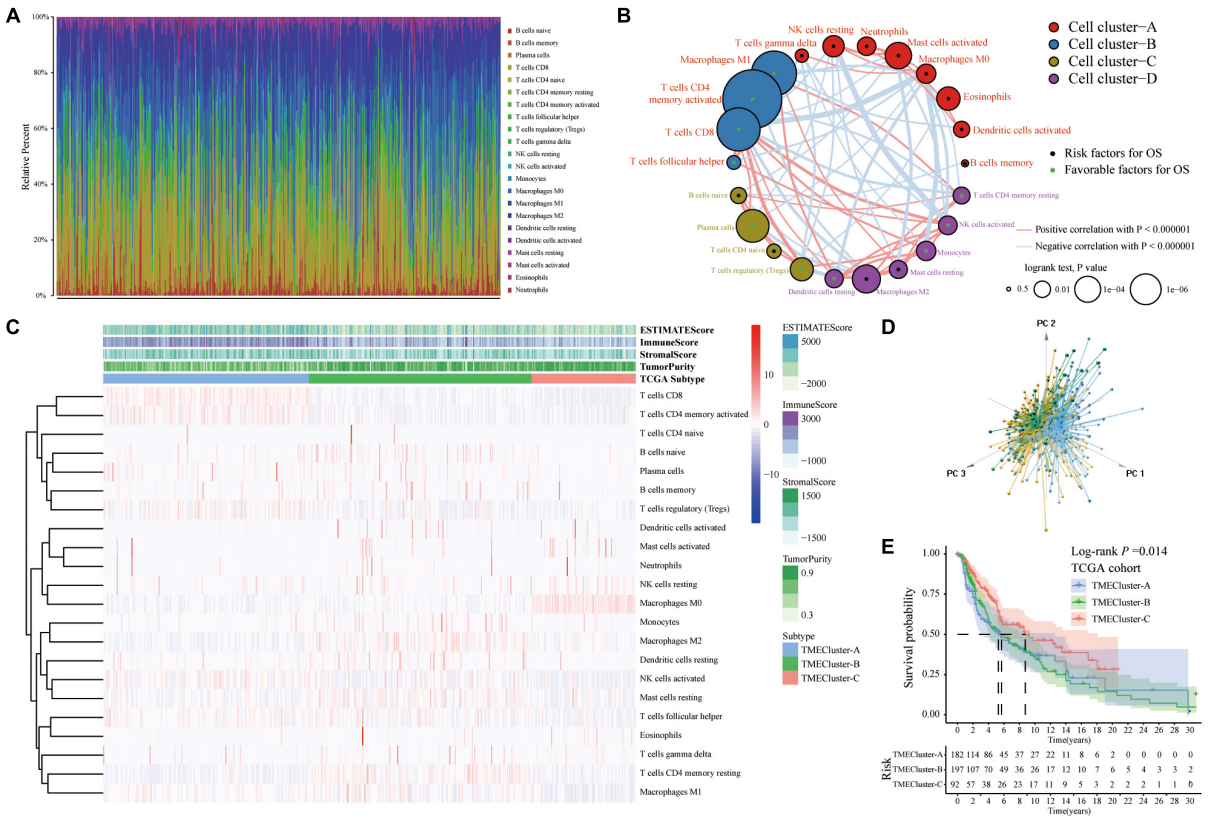

FIGURE 1 | Immune cellprotect infiltration in TCGA-SKCM database. **(A)** Histogram showing the infiltration of 22 different specific immune cells in each sample CIBERSORT. Different colors indicate different tumor-infiltrating immune cells. **(B)** The interaction between immune cells in TME in TCGA-SKCM. Cell cluster-A, red; Cell cluster-B, blue; Cell cluster-C, brown; Cell cluster-D, purple. The size of the circle represents the impact of each TME cell type on survival, and the log-rank test was used for analysis. The green part in the center of the circle indicates that the cell protects against overall survival, and the black indicates the risk to overall survival. The lines connecting TME cells represent cell interactions. The thickness of the line represents the correlation strength estimated by Spearman correlation analysis, in which positive correlation is represented by red and negative correlation is represented by blue. **(C)** Heatmap showing the infiltration of TIICs in 471 SKCM patients in TCGA database combined with the immune score. Unsupervised clustering grouping the samples into three major clusters. **(D)** The PCA of the gene expression profile distinguishes patients in the TME cluster-A, -B, and -C groups in TCGA-SKCM. The results can distinguish three different immune infiltration pattern samples (TME cluster-A: blue, TME cluster-B: yellow, TME cluster-C: green). **(E)** The Kaplan–Meier curve of the patient's overall survival (OS) shows that TME infiltration is significantly related to the overall survival (Log-rank test, $p = 0.014$).

correlated with gender ($p = 0.031$; **Figure 7E**), and significantly correlated with pathological stage ($p = 0.0027$; **Figure 7F**) and T stage ($p < 0.001$; **Figure 7G**). There was no significant correlation between the risk score and TMB, age, M stage, and N stage ($p > 0.05$; **Figures 7C,D,H,I** and **Table 2**).

Evaluation and Validation of the Prognostic Signature

Correlation analysis revealed that the expression of 13 hub genes in different tumors was significantly correlated (**Figure 8A**). The heterogeneity between tumors caused the risk score to have different prognostic effects on different cancers (**Figure 8B**). Univariate and multivariate Cox analyses showed that the risk score was an independent risk factor for predicting the prognosis of patients with SKCM (**Figure 8C**). We included the index of $p < 0.05$ in the multivariate Cox model to construct a nomogram to predict the 1-, 2-, and 3-year survival probability of SKCM patients. The C-indexes [0.732 (95% CI: 0.697–0.767)] of the nomogram were used to calculate the discriminative ability of the nomogram, showing a high degree of discrimination (**Figure 8D**). The calibration also showed a great agreement between the 1-year, 2-year, and 3-year OS estimates and the actual observed values of SKCM patients through a comparison to the nomogram (**Figure 8E**).

Prognostic Value of Hub Genes in SKCM Patients

We focused on the potential prognostic value of EDN3, CLEC4E, SRPX2, KIR2DL4, UBE2L6, and IFIT2 as immune scores for melanoma patients. In the group of novel hub genes, low expression levels of *UBE2L6*, *KIR2DL4*, *IFIT2*, and *CLEC4E* were observed in tumor cells, while high expression levels of *SRPX2* and *EDN3* were found in SKCM. However, only *UBE2L6* and *IFIT2* showed significant expression differences in TCGA-SKCM cohort. A larger sample size may be required to verify the differential expression of these molecules in SKCM. The open

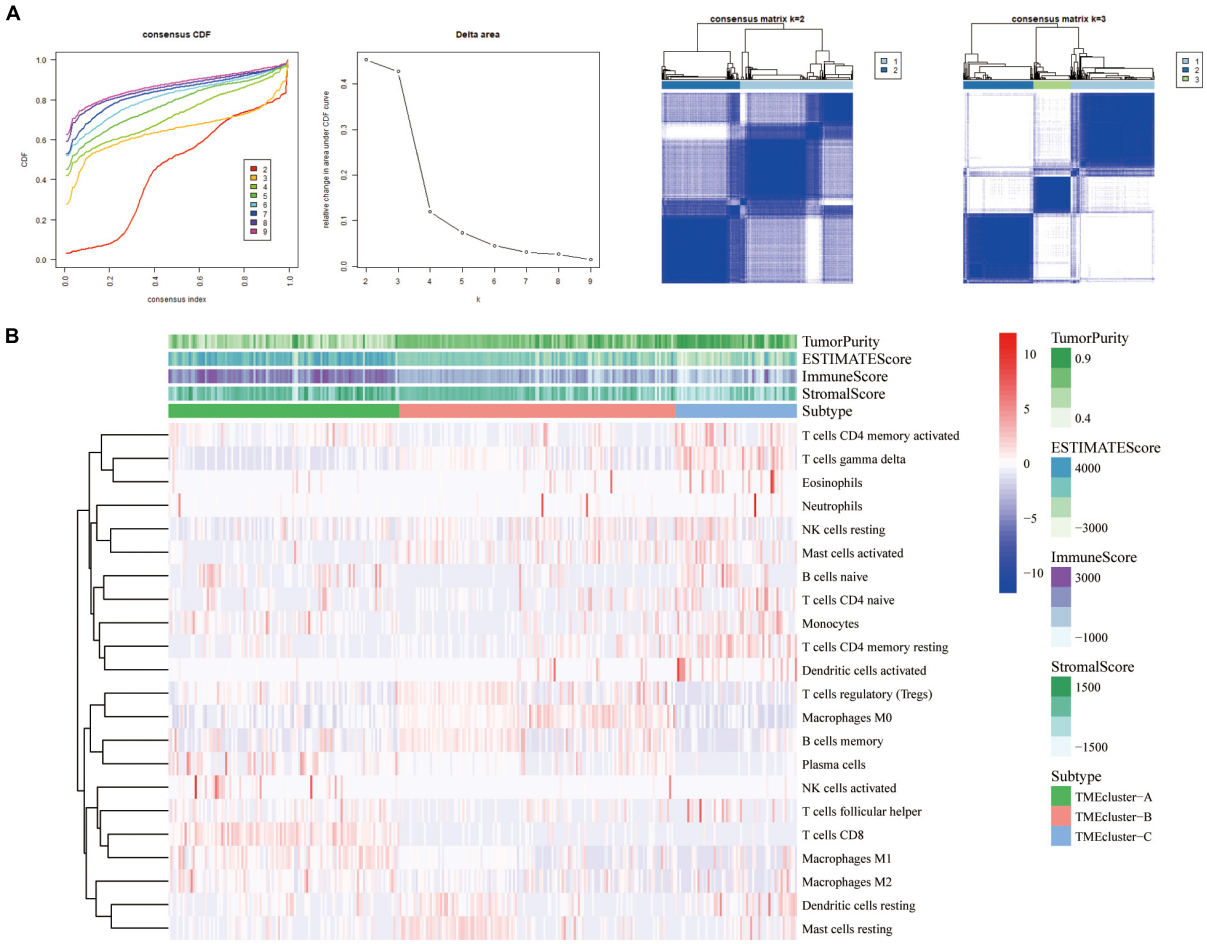

FIGURE 2 | Three types of SKCM patients in the GEO database based on TIICs infiltration. **(A)** Hierarchical clustering determined the number of clusters of the immune cell infiltration patterns of 310 SKCM patients in the GEO database (GSE8401, GSE35640, GSE15605, and GSE46517) and repeats 1,000 times to ensure the stability of the classification. **(B)** Heatmap displaying the expression of tumor-infiltrating immune cells in SKCM patients from GEO database was reviewed.

online tool, GEPIA, was used to analyze the prognostic value of these novel hub genes. We found that the low expressions of *UBE2L6*, *KIR2DL4*, *IFIT2*, and *CLEC4E* were significantly associated with poor prognosis in SKCM.

Preliminary IHC Validation in Melanoma Specimens

We evaluated the expression of six novel genes in melanoma tissues. The IHC staining results showed that *Ube2L6*, *SRPX2*, and *IFIT2* were expressed at higher levels, while *CLEC4E*, *END3*, and *KIR2DL4* were expressed at lower levels in 25 melanoma specimens (**Figure 9**).

DISCUSSION

The incidence of SKCM continues to increase annually. The recurrence and metastasis of SKCM caused by functional variations in TME markedly contribute to the extremely poor prognosis of SKCM. TME plays a key role in the response to immunotherapy. Several treatments have improved the survival rate of patients with advanced diseases, such as radiotherapy, chemotherapy, and immunotherapy (Wagner et al., 2019). In particular, the application of immunotherapy in SKCM has enabled remarkable breakthroughs (Mitchell et al., 2018). However, there are still many patients who exhibit resistance to cancer immunotherapy and adoptive cell therapy due to the immunosuppressive barriers that exist in TME (Hu et al., 2020). Therefore, there is an urgent need to determine more therapeutic targets and prognostic biomarkers based on TME. In this study, we conducted a comprehensive assessment of immune cell infiltration in TME, identified novel tumor immune subtypes, and assessed the prognostic value of immune cells in SKCM patients. The prognostic characteristics proposed herein are reliable for predicting the survival of patients with SKCM.

To verify the key role of immune cell-infiltrated TME in SKCM, we performed independent microarray data analysis on four datasets in the GEO database. Notably, cross-platform research increased the reliability of our novel prognosis model. We used the CIBERSORT algorithm to evaluate the immune

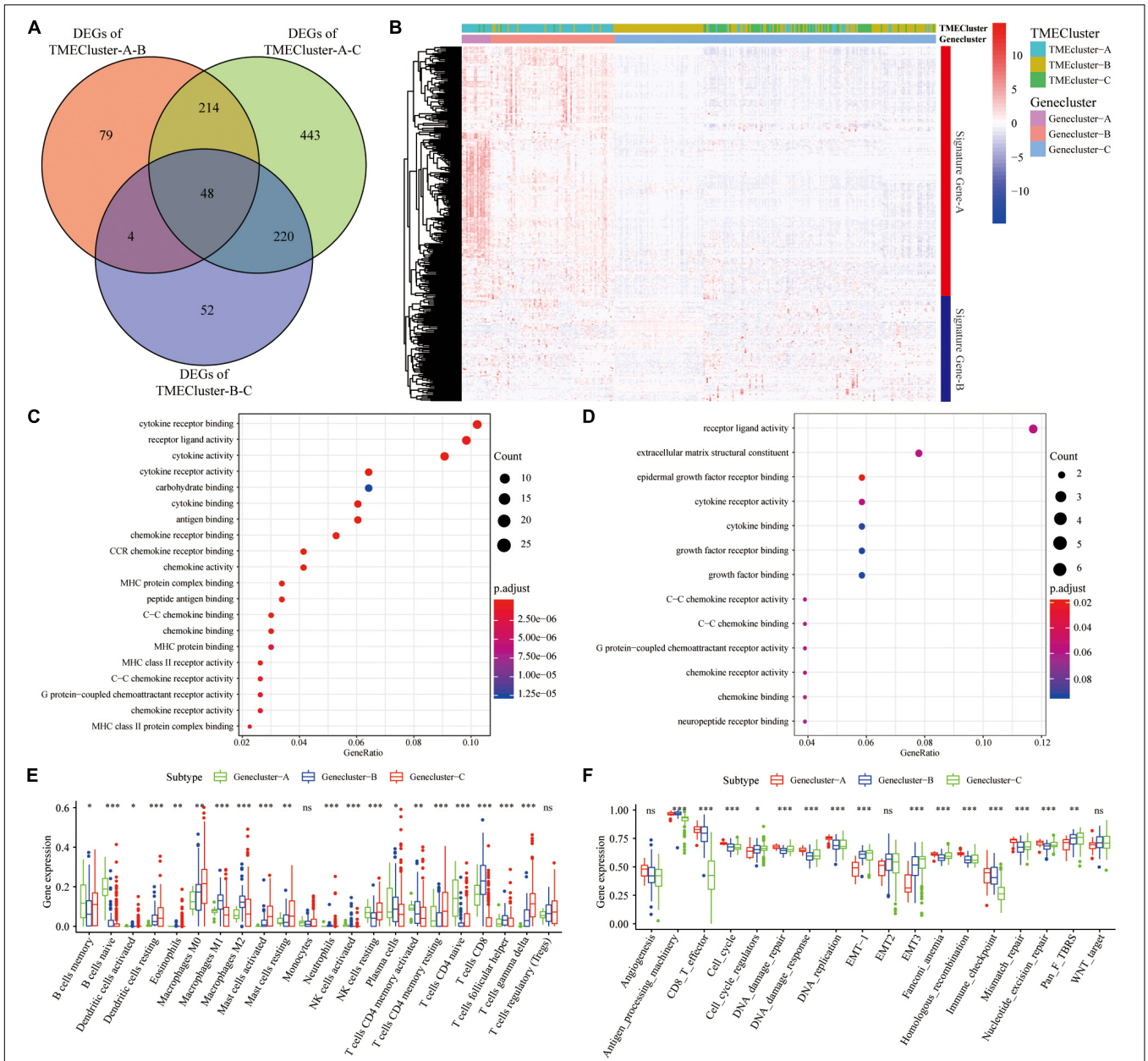

FIGURE 3 | Construction and functional annotation of TME-related characteristic genes. **(A)** The Venn diagram showing the DEGs between the three TME clusters in TCGA database. **(B)** Based on the gene expression profile of SKCM patients in the GEO database, unsupervised analysis and hierarchical clustering of DEGs were carried out, divided into GeneCluster-A, -B, and -C. According to their expression changes, DEGs were classified into Signature gene-A and -B. **(C,D)** Gene Ontology (GO) enrichment analysis of Signature gene-A **(C)** and -B **(D)** gene sets. **(E)** The expression of cells in the three GeneCluster groups. **(F)** The enrichment of different pathway characteristics (immune-related features, mismatch-related features, and matrix-related features) in three different GeneCluster groups (*$p < 0.05$, **$p < 0.01$, ***$p < 0.001$).

cell infiltration status of the SKCM cohort transcriptome data in TGCA database comprehensively and obtained 22 different immune cell infiltration abundances in each patient. We depicted the tumor immune cell interaction network, including the overall situation of the cell lineage and its impact on the overall survival of SKCM patients, which was reviewed and verified in the SKCM patient cohort from the GEO database. To evaluate the tumor heterogeneity and interaction with TME that can guide better and earlier targeted treatments better, we hierarchically clustered tumor samples based on essential differences in immune cell infiltration patterns. Principal component analysis (PCA) based on the expression profile data of SKCM patients could distinguish the three TME cluster groups well. Thus, we proceeded to analyze the immune-related scores of three groups, tumor purity, and matrix scores. Patients with TME cluster-A had higher immune scores, whereas patients with TME cluster-B and -C mainly

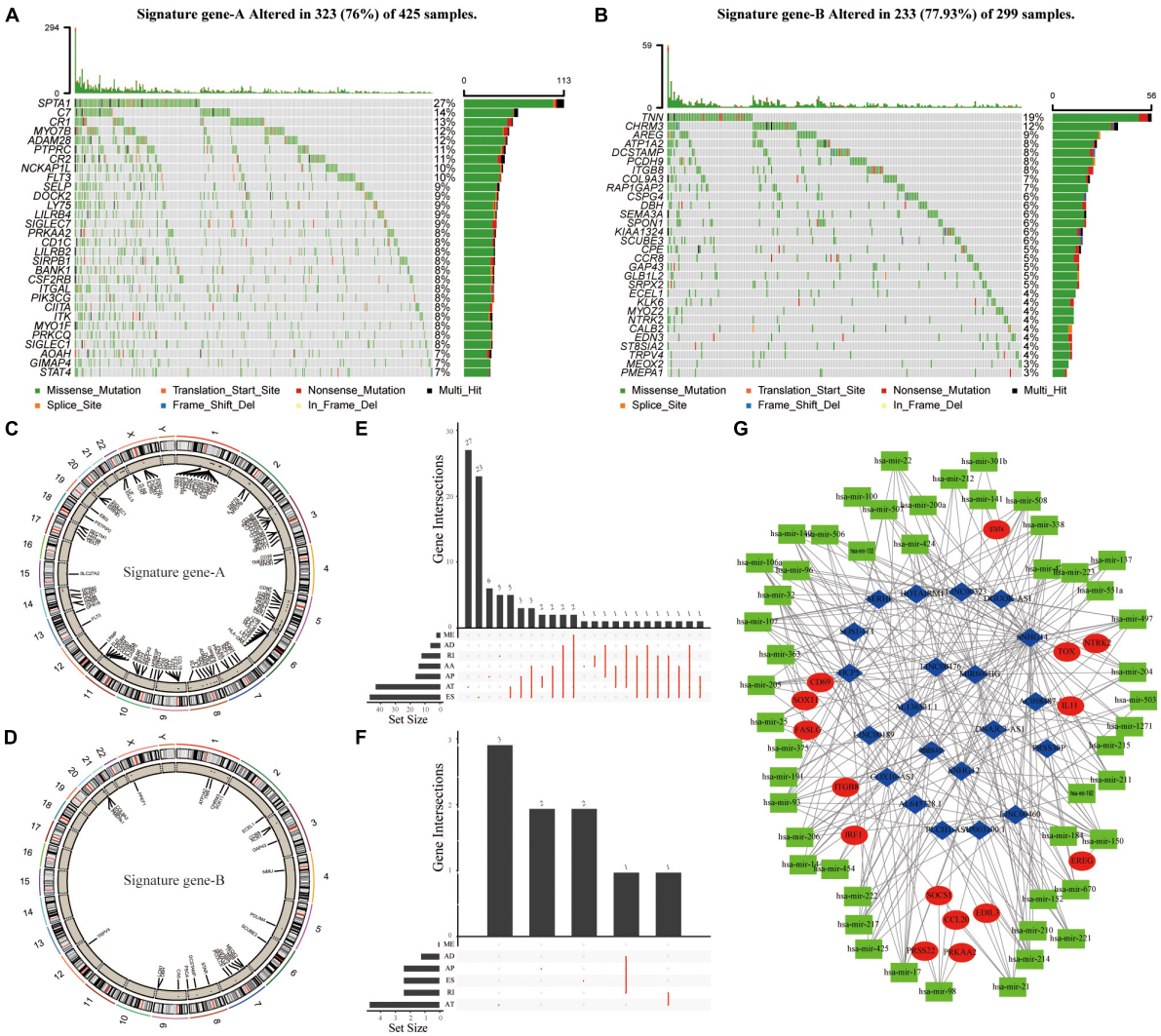

FIGURE 4 | The genetic variation and ceRNA network of Signature gene-A and -B in SKCM patients. **(A,B)** The mutation maps of Signature gene-A and -B, respectively, in SKCM patients. The mutation information of each gene was displayed in the waterfall chart, and various colors indicated different mutation types; the upper section of the legend showed the mutation load. **(C,D)** Signature gene-A and -B are, respectively, on 23 chromosomes of SKCM patients. The CNV difference and its position on the above. **(E,F)** UpSet diagram showing the variable splicing of Signature gene-A and -B in SKCM patients. **(G)** Based on the expression of Signature gene-A and -B in SKCM patients. To construct a ceRNA regulatory network of mRNA–miRNA–LncRNA and summarize the complex relationship between Signature gene-A and -B (red dots), immune-related LncRNA (blue dots), and miRNA targeting LncRNA (green dots).

had tumor purity and matrix scores. In the GEO database, the GSE8401, GSE35640, GSE15605, and GSE46517 datasets verified the gene expression profile data and immune cell infiltration of SKCM patients and revealed consistent clustering results. To gain a new understanding of the relationship between the above grouping and TME phenotype, we conducted a series of survival analyses and found that TME cluster-C (n = 92) was associated with a better prognosis among the three clusters.

We explored the potential biological characteristics of the different TME phenotypes and performed a different analysis on the three TME clusters and displayed the intersection of 486 DEGs using a Venn diagram. Based on the above differential genes, we finally obtained 330 repeated DEGs from the four datasets in the GEO database. We used unsupervised clustering to divide SKCM patients into three different subtypes based on the expression of DEGs, namely GeneCluster-A, -B, and -C. According to the expression of DEGs in the different groups, they were divided into Signature gene-A and -B. We confirmed that the expression of these genes was quite different between the two clusters due to various tumor heterogeneities. These clusters were also clearly associated with different mutational patterns. GO enrichment analysis showed that Signature genes-A and -B had different unique BPs. Immune-activating genes are associated with the activation of immune surveillance and immune activation during tumor immunization; Signature gene-A involves the overexpression

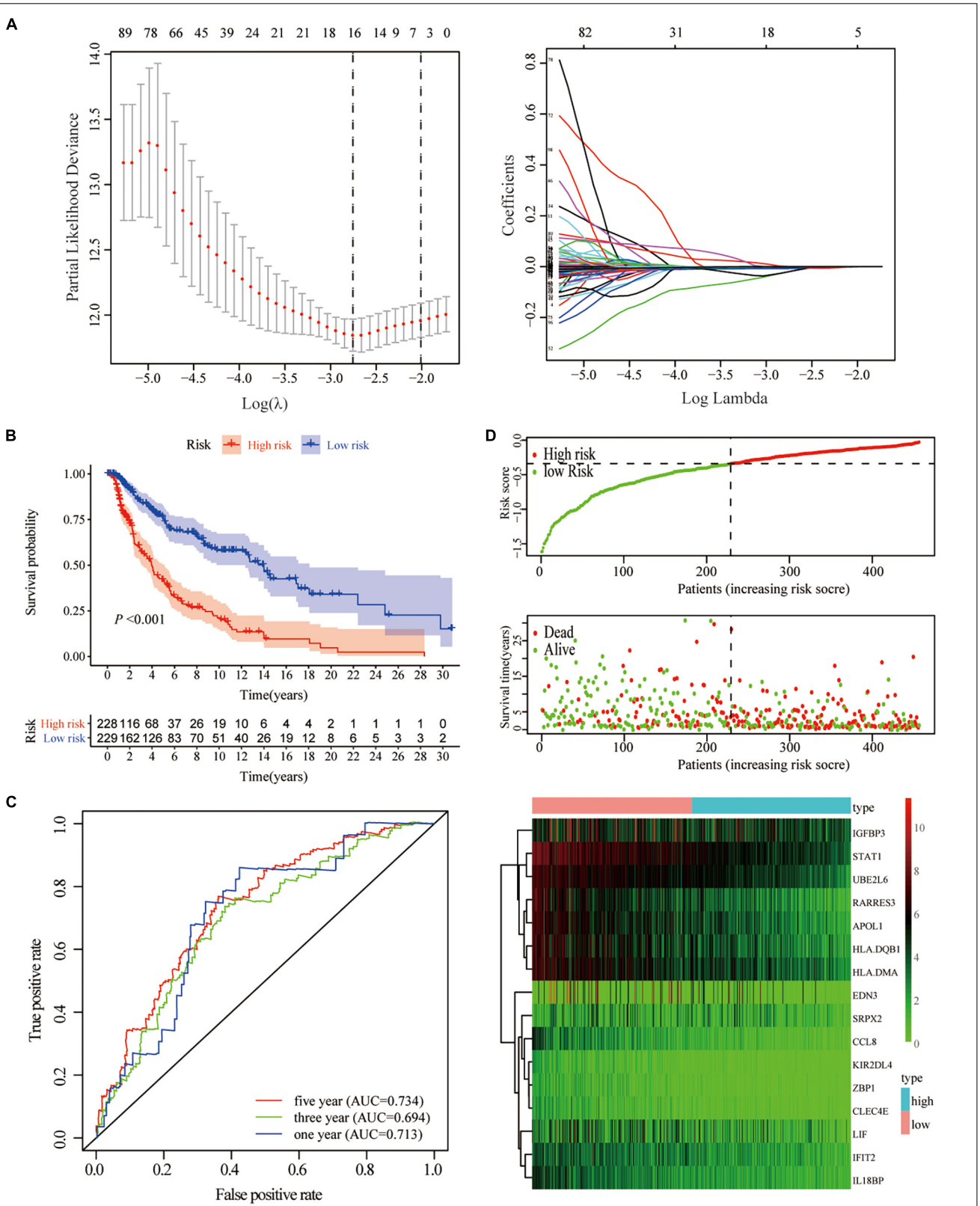

FIGURE 5 | Construction of gene-based risk prediction model. **(A)** LASSO Cox regression analysis identified 13 hub genes closely related to OS of TCGA-SKCM. **(B)** Kaplan–Meier plots assessed the impact of risk scores on the OS of SKCM patients in TCGA. **(C)** Time-dependent ROC curve analysis of the risk score. **(D)** The distribution of risk scores, the expression values of the 13 hub genes, and the survival status of SKCM patients ranked according to the risk scores.

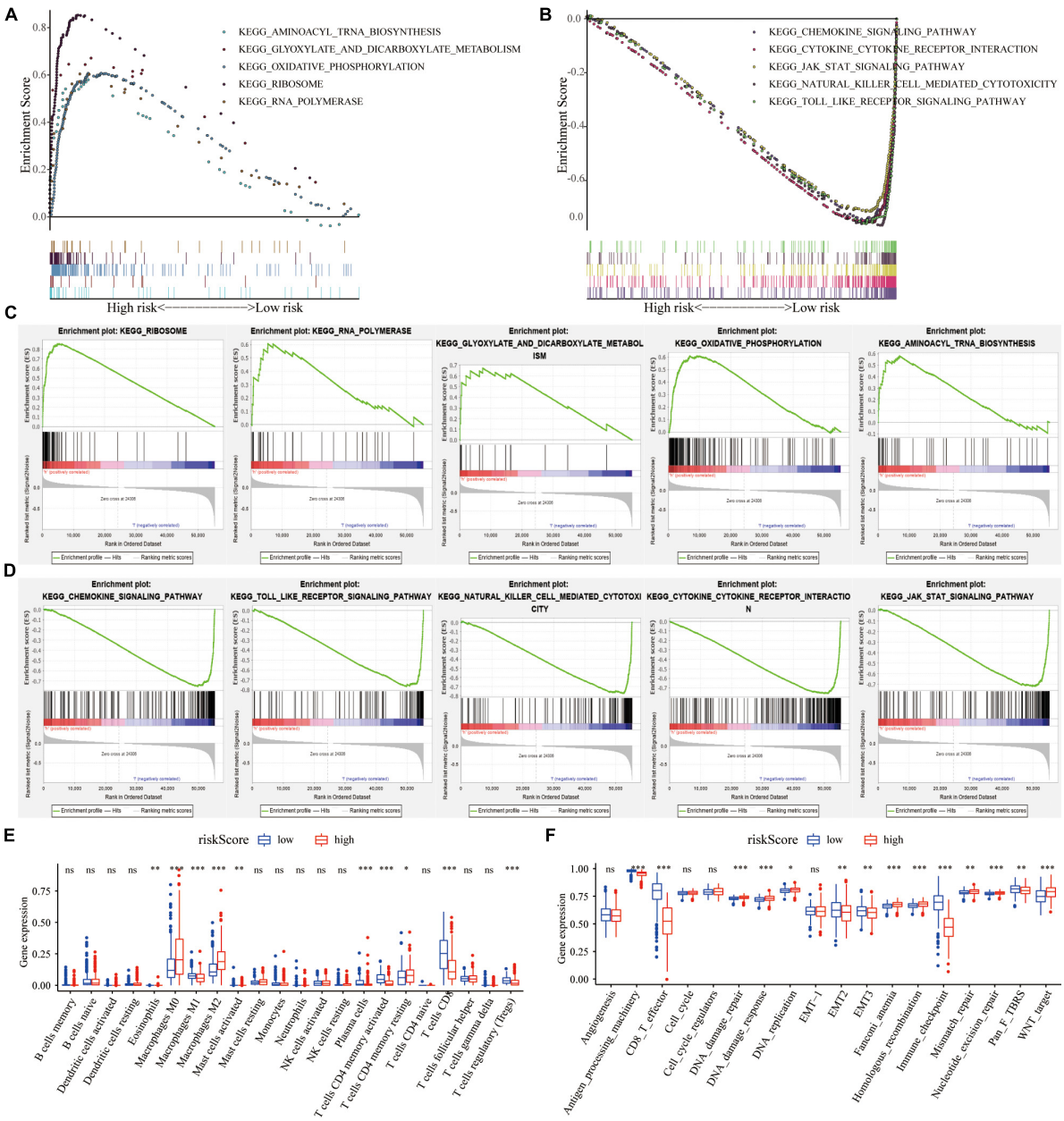

FIGURE 6 | The regulation of risk score on tumor gene expression and biological processes. **(A,B)** GSEA revealed the most significant hallmarks with high- and low-risk clusters. **(C,D)** Enrichment of representative pathways between high- and low-risk patients in GSEA analysis. **(E)** TIICs in the high- and low-risk groups. **(F)** The enrichment of different pathway characteristics (immune-related characteristics, mismatch-related characteristics, and matrix-related characteristics) in high- and low-risk patients (*$p < 0.05$, **$p < 0.01$, ***$p < 0.001$).

of immune-activated genes, and the gene set overexpressing Signature gene-B is mainly demonstrated by upregulation of genes related to the matrix and transmembrane receptors. Such finding suggests that the Signature gene-A gene set may have an impact on the immunophenotypic landscape of TME. In addition, the analysis results showed that there were significant differences in the expression of TME cells and the enrichment of some related biological pathways among the three GeneCluster groups.

To explore causes of tumor immune microenvironment heterogeneity more deeply, we analyzed the tumor mutation-related characteristics of patients. The CNV information of SKCM was downloaded in addition to the somatic mutation data and TMB of each patient in Signature gene-A and -B. We also explored SNPs and CNVs in SKCM patients. The gene variable splicing information of SKCM patients in TCGA was also obtained from TCGA Spliceseq website. The results of SNP analysis revealed that there were obvious mutations in both gene

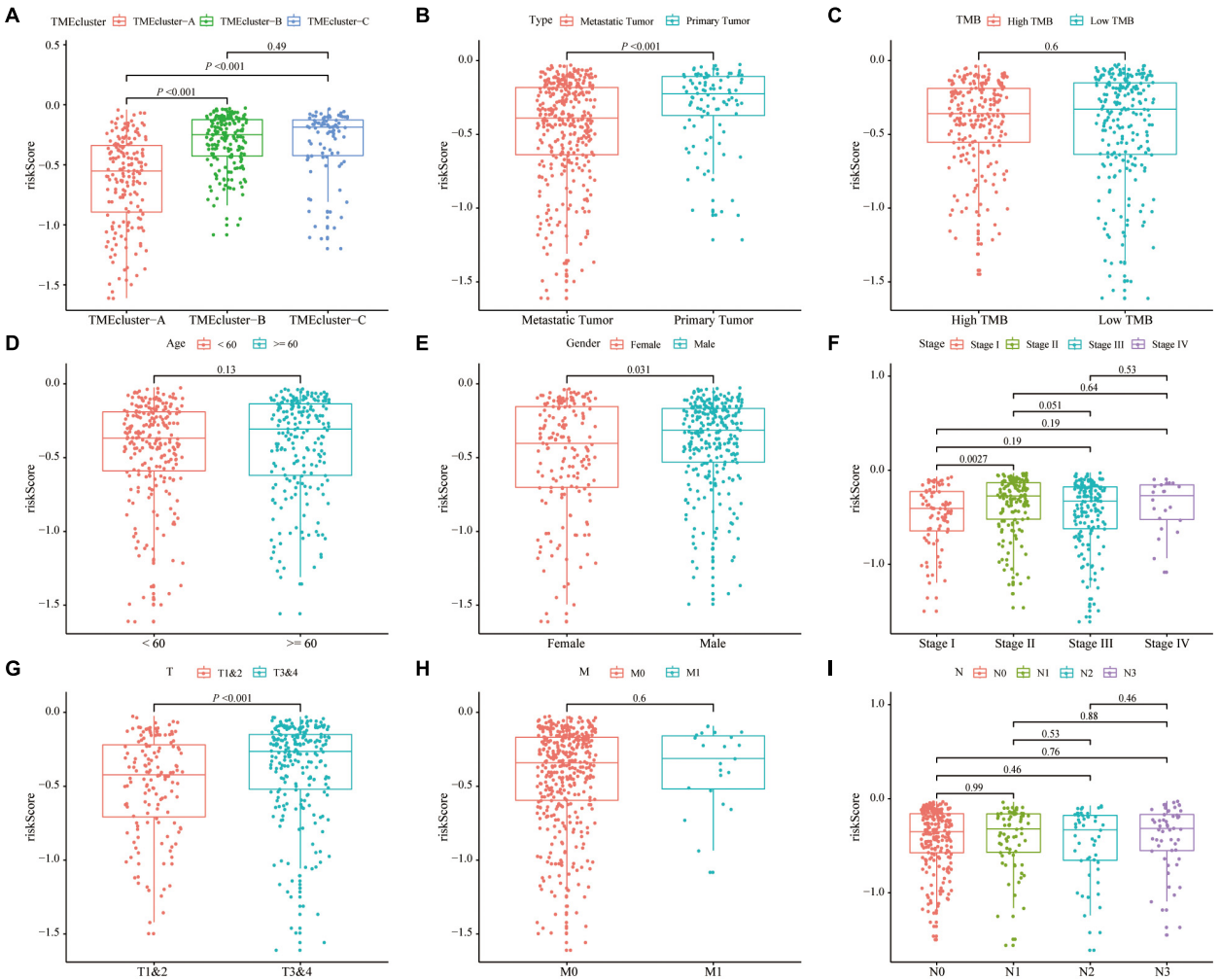

FIGURE 7 | Correlation analysis of risk score and clinicopathological characteristics of SKCM patients in TCGA. **(A–C)** Correlation analysis between risk score and different patient types showed that risk score was related to TME cluster grouping ($p < 0.001$) **(A)** and tumor type ($p < 0.001$) **(B)**. There was no significant correlation with the patient's tumor mutation burden (TMB) ($p = 0.6$). **(D–I)** The correlation analysis between the risk score and different clinicopathological characteristics of SKCM patients showed that the risk score and gender ($p = 0.01$) **(D)**, stage ($p = 0.0027$) **(E)**, and T stage ($p < 0.001$) **(F)** are related, but there is no significant correlation between the patient's age **(G)**, M stage **(H)**, and N stage **(I)**.

TABLE 2 | Univariate and multivariate Cox analyses of patients' OS prediction based on risk score in TCGA database.

Variables	Univariate Cox analysis		Multivariate Cox analysis	
	HR (95% CI)	*p*-Value	HR (95% CI)	*p*-value
Age (≥ 60 vs. <60)	1.47(1.09 – 1.98)	0.009**	1.44(1.07 – 1.94)	0.02*
Gender (male vs. female)	1.04(0.77 – 1.42)	0.78	0.97(0.71 – 1.32)	0.84
Stage (III + IV vs. I + II)	1.76(1.31 – 2.37)	<0.001***	1.96(1.45 – 2.64)	<0.001***
Type (Metastatic vs. primary)	0.36(0.22 – 0.59)	<0.001***	0.47(0.29 – 0.76)	0.002**
riskScore (high vs. low)	11.49(6.10 – 21.64)	<0.001***	11.10(5.89 – 20.92)	<0.001***

*$p < 0.05$; **$p < 0.01$; ***$p < 0.001$; ns, no significance.*

sets, and most of the changes in CNV were concentrated on the amplification of copy number. The variable splicing analysis showed that the Signature gene-A set mainly had ES in SKCM patients, while the Signature gene-B set had no obvious form of variable splicing. This result highlighted the influence of the Signature gene-A set on the immune landscape. According to the expression of Signature gene-A and -B sets, we screened out the more relevant lncRNAs as immune-related lncRNAs and constructed a ceRNA regulatory network of mRNA–miRNA–LncRNA interaction.

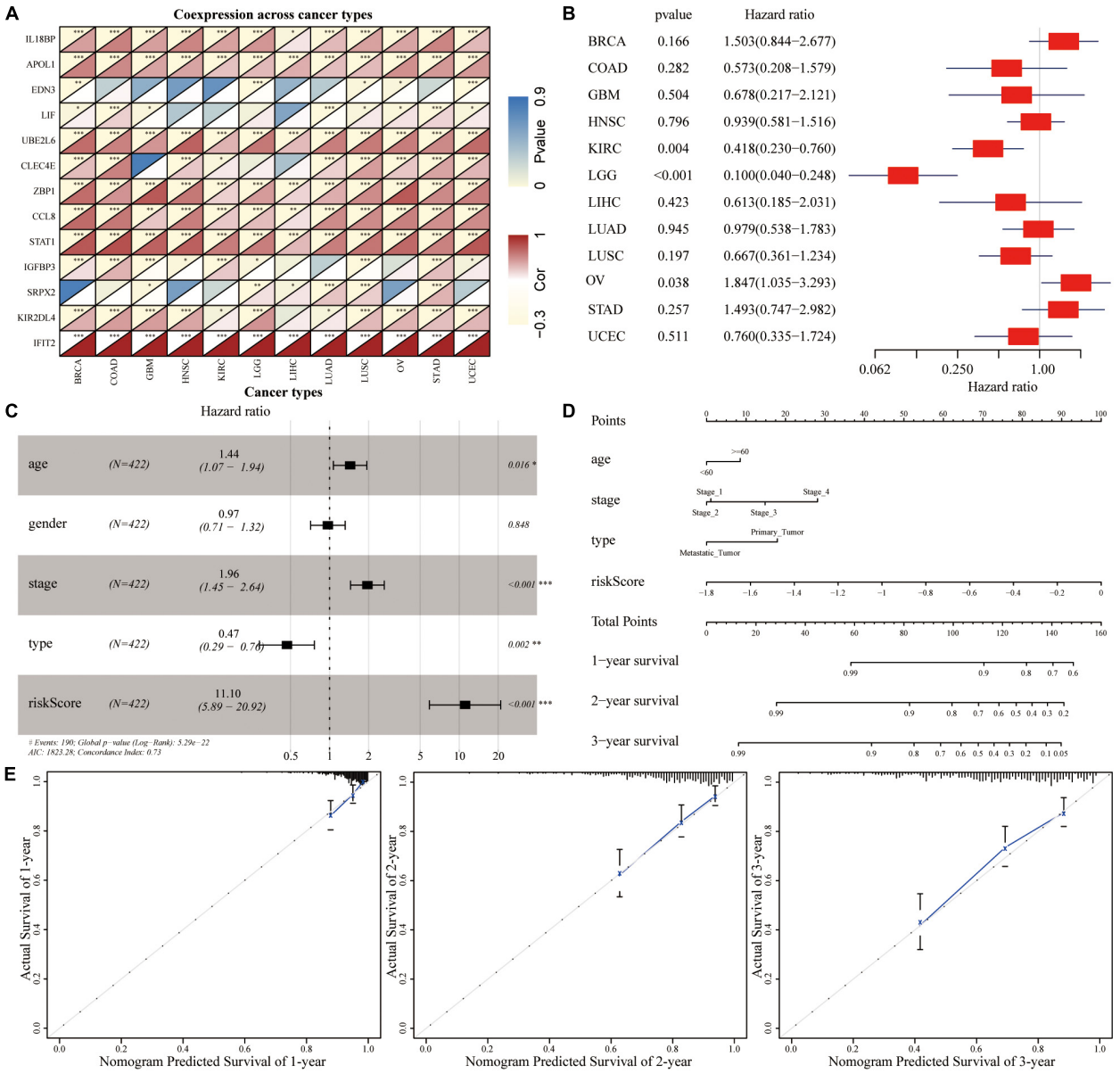

FIGURE 8 | The predictive power of genetic risk score on the prognosis of pan-cancer. **(A)** Correlation analysis between the expressions of 13 hub genes in pan-cancer. **(B)** Subgroup analysis of the prognostic value of the risk score in pan-cancer in TCGA dataset. **(C)** Multivariate Cox regression analysis of risk score combined with clinicopathological characteristics. **(D)** Nomogram prediction of the 1-, 2-, and 3-year survival probability. **(E)** The calibration curve of the nomogram showed that the prediction model had a good predictive value for the prognosis of SKCM patients at 1, 2, and 3 years.

To create a better clinical prediction model for different SKCM patients, a novel prognostic-related risk scoring system was developed. First, we incorporated Signature gene-A and -B sets into the univariate Cox model and obtained 233 prognostic-related genes. A subsequent LASSO Cox analysis was performed for dimensionality reduction and model construction, and finally, 13 hub genes were obtained. This novel scoring system had good predictive ability for OS. The AUC of 1-year, 3-year, and 5-year OS was 0.713, 0.694, and 0.734, respectively. Furthermore, GSEA was employed to evaluate the correlation between the high- and low-risk groups and biological characteristics. Pathways, such as metabolism-related pathways and oxidative phosphorylation, were mainly enriched in the high-risk group, while immune response-related pathways, including cytokine signaling pathway, JAK–STAT signaling pathway, and natural killer cell-mediated cytotoxicity, were significantly enriched in low-risk patients. This finding is consistent with a previous report (Hu et al., 2020). Moreover, the expression of TME cells, as well as some other pathways, such as angiogenesis, mismatch-related characteristics, and

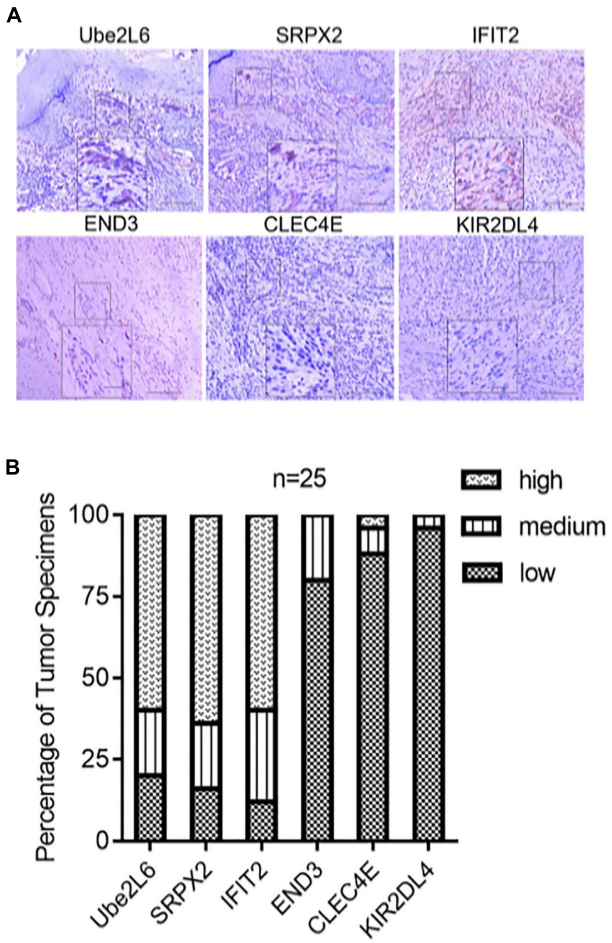

FIGURE 9 | (A) Pictures of inmunohistochemical staining of Ube2L6, SRPX2, IFIT2, END3, CLEC4E, and KIR2DL4. **(B)** Higher expressions of Ube2L6, SRPX2, and IFIT2 were presented, while lower expressions of CLEC4E, END3, and KIR2DL4 were shown in melanoma tissues (n = 25) by IHC staining.

matrix-related characteristics, was significantly different between the high- and low-risk groups. Finally, we assessed the correlation between the risk score and the clinical classification and pathological characteristics of SKCM patients and found that low-risk scores were often associated with patients' TME cluster-A classification and metastatic SKCM. In different tumors, 13 hub genes showed different prognostic effects. Furthermore, the results of univariate and multivariate Cox analyses showed that risk scores could be identified as independent risk factors for predicting the prognosis of patients with SKCM. We subsequently selected statistically significant clinical indicators in the multivariate Cox model to construct a nomogram to predict the OS of patients with SKCM. The C-index indicates that the model had a high degree of discrimination. Validation of the calibration curve also revealed good concordance between the estimated values and the actual probability. To our knowledge, this is the first study to explore factors that directly alter the TME in SKCM. Thus, our immune model is more predictable for facilitating treatment than TMB and other predictive factors.

Among the six prognostic signatures, Ubiquitin/ISG15-conjugating enzyme E2 L6 (Ube2L6) has been reported to promote insulin resistance and hepatic steatosis and is related to cisplatin resistance (Murakami et al., 2020; Wei et al., 2021). SRPX2 is invasive by upregulating the FAK/SRC/ERK pathway and can lead to pancreatic cancer drug resistance in PI3K/AKT in lung cancer. Additionally, the NFATc3/SRPX2 axis participates in human embryonic stem cell differentiation, indicating that SRPX2 plays a critical role in pan-cancers (Gao et al., 2020; Li et al., 2020; Chen et al., 2021). SRPX2 is a component of the extracellular matrix, which is important for regulating tumor formation, as demonstrated in diverse tumors, such as colorectal cancer (Øster et al., 2013), gastrointestinal cancer (Tanaka et al., 2012), prostate cancer (Zhang et al., 2018), and pancreatic cancer (Gao et al., 2015). Interferon-induced protein with tetratricopeptide repeats protein may be a new therapeutic target for cancer therapy and can be used as a prognostic marker for cancers, such as glioblastoma and pancreatic cancer (Pidugu et al., 2019). In previous studies, CLEC4E was found to be related to tuberculosis and could be used to constrain tuberculosis through autophagy against drug-resistant strains (Kabuye et al., 2019; Pahari et al., 2020). Killer cell immunoglobulin-like receptor 2DL4 (KIR2DL4) is expressed by NK cells. According to some reports, KIR2DL4 may be an intervention for cancer immunotherapy (Attia et al., 2020). In our IHC analysis, some of these relationships were verified in SKCM patients. Only few studies have examined the relationship between SKCM and these hub genes. Thus, our study revealed their underlying relationships and found a novel important signature.

Therefore, the novel six-gene signature, which was developed to evaluate the comprehensiveness of TME in SKCM, is a reliably developed gene classifier that can be used to predict prognosis and guide more accurate molecular therapy.

CONCLUSION

In conclusion, we have developed and verified an unprecedented set of effective prognostic markers based on immune infiltrating cells, which have certain potential application value in predicting the clinical prognosis of patients with SKCM and the benefit of immunotherapy. This study provides a systematic view of the immune-related characteristics in SKCM and suggests their good prognostic performance.

DATA AVAILABILITY STATEMENT

The datasets presented in this study can be found in online repositories. The names of the repository/repositories and accession number(s) can be found in the article/ **Supplementary Material**.

ETHICS STATEMENT

The studies involving human participants were reviewed and approved by The First People's Hospital of Foshan Subject Review Board. The patients/participants provided their written informed consent to participate in this study. Written informed consent was obtained from the individual(s) for the publication of any potentially identifiable images or data included in this manuscript.

AUTHOR CONTRIBUTIONS

SZ and YS conceived and designed the study and wrote the manuscript. TC, JW, JH, JL, and YS contributed to the data acquisition. RY and XC analyzed the data. All authors read and approved the final manuscript.

FUNDING

This study was supported by the National Natural Science Foundation of China (Nos. 82002913 and 81772136), Foundation of Foshan City (Nos. FS0AA-KJ218-1301-0034 and 2018AB003411), and the Special Fund of the Foshan Summit plan (Nos. 2019C002, 2019D008, 2019A006, and 2020A015).

SUPPLEMENTARY MATERIAL

The Supplementary Material for this article can be found online at: https://www.frontiersin.org/articles/10.3389/fcell.2021.739594/full#supplementary-material

Supplementary Figure 1 | The correlation between the expression of different immune cells in TCGA-SKCM cohorts.

REFERENCES

Attia, J. V. D., Dessens, C. E., van de Water, R., Houvast, R. D., Kuppen, P. J. K., and Krijgsman, D. (2020). The molecular and functional characteristics of HLA-G and the interaction with its receptors: where to intervene for cancer immunotherapy? *Int. J. Mol. Sci.* 21:8678. doi: 10.3390/ijms21228678

Chen, H., and Boutros, P. C. (2011). VennDiagram: a package for the generation of highly-customizable Venn and Euler diagrams in R. *BMC Bioinformatics* 12:35. doi: 10.1186/1471-2105-12-35

Chen, H., Zeng, Y., Shao, M., Zhao, H., Fang, Z., Gu, J., et al. (2021). Calcineurin A gamma and NFATc3/SRPX2 axis contribute to human embryonic stem cell differentiation. *J. Cell Physiol.* 236, 5698–5714. doi: 10.1002/jcp.30255

Dreno, B., Thompson, J. F., Smithers, B. M., Santinami, M., Jouary, T., Gutzmer, R., et al. (2018). MAGE-A3 immunotherapeutic as adjuvant therapy for patients with resected, MAGE-A3-positive, stage III melanoma (DERMA): a double-blind, randomised, placebo-controlled, phase 3 trial. *Lancet Oncol.* 19, 916–929. doi: 10.1016/s1470-2045(18)30254-7

Fecher, L. A., Cummings, S. D., Keefe, M. J., and Alani, R. M. (2007). Toward a molecular classification of melanoma. *J. Clin. Oncol.* 25, 1606–1620. doi: 10.1200/jco.2006.06.0442

Gao, Z., Wu, J., Wu, X., Zheng, J., and Ou, Y. (2020). SRPX2 boosts pancreatic cancer chemoresistance by activating PI3K/AKT axis. *Open Med. (Wars.)* 15, 1072–1082. doi: 10.1515/med-2020-0157

Gao, Z., Zhang, J., Bi, M., Han, X., Han, Z., Wang, H., et al. (2015). SRPX2 promotes cell migration and invasion via FAK dependent pathway in pancreatic cancer. *Int. J. Clin. Exp. Pathol.* 8, 4791–4798.

Goodson, A. G., and Grossman, D. (2009). Strategies for early melanoma detection: approaches to the patient with nevi. *J. Am. Acad. Dermatol.* 60, 719–735. doi: 10.1016/j.jaad.2008.10.065

Grossman, R. L., Heath, A. P., Ferretti, V., Varmus, H. E., Lowy, D. R., Kibbe, W. A., et al. (2016). Toward a shared vision for cancer genomic data. *N. Engl. J. Med.* 375, 1109–1112. doi: 10.1056/NEJMp1607591

Hanahan, D., and Weinberg, R. A. (2011). Hallmarks of cancer: the next generation. *Cell* 144, 646–674. doi: 10.1016/j.cell.2011.02.013

He, C., Zhang, Y., Jiang, H., Niu, X., Qi, R., and Gao, X. (2020). Identification of differentially expressed methylated genes in melanoma versus nevi using bioinformatics methods. *PeerJ* 8:e9273. doi: 10.7717/peerj.9273

Hodi, F. S., O'Day, S. J., McDermott, D. F., Weber, R. W., Sosman, J. A., Haanen, J. B., et al. (2010). Improved survival with ipilimumab in patients with metastatic melanoma. *N. Engl. J. Med.* 363, 711–723. doi: 10.1056/NEJMoa1003466

Hu, B., Wei, Q., Li, X., Ju, M., Wang, L., Zhou, C., et al. (2020). Development of an IFNγ response-related signature for predicting the survival of cutaneous melanoma. *Cancer Med.* 9, 8186–8201. doi: 10.1002/cam4.3438

Hu, X., Yuan, L., and Ma, T. (2020). Mechanisms of JAK-STAT signaling pathway mediated by CXCL8 gene silencing on epithelial-mesenchymal transition of human cutaneous melanoma cells. *Oncol. Lett.* 20, 1973–1981. doi: 10.3892/ol.2020.11706

Jameson-Lee, M., and Luke, J. J. (2021). Ipilimumab combination dosing: less is more. *Clin Cancer Res.* doi: 10.1158/1078-0432.Ccr-21-2406

Kabuye, D., Chu, Y., Lao, W., Jin, G., and Kang, H. (2019). Association between CLEC4E gene polymorphism of mincle and pulmonary tuberculosis infection in a northern Chinese population. *Gene* 710, 24–29. doi: 10.1016/j.gene.2019.05.011

Koikawa, K., Kibe, S., Suizu, F., Sekino, N., Kim, N., Manz, T. D., et al. (2021). Targeting Pin1 renders pancreatic cancer eradicable by synergizing with immunochemotherapy. *Cell* doi: 10.1016/j.cell.2021.07.020 [Epub ahead of print]

Leek, J. T., Johnson, W. E., Parker, H. S., Jaffe, A. E., and Storey, J. D. (2012). The sva package for removing batch effects and other unwanted variation in high-throughput experiments. *Bioinformatics* 28, 882–883. doi: 10.1093/bioinformatics/bts034

Li, X., Liu, J., Sun, H., Zou, Y., Chen, J., Chen, Y., et al. (2020). SRPX2 promotes cell proliferation and invasion via activating FAK/SRC/ERK pathway in non-small cell lung cancer. *Acta Biochim. Pol.* 67, 165–172. doi: 10.18388/abp.2020_5158

Marron, T. U., Ryan, A. E., Reddy, S. M., Kaczanowska, S., Younis, R. H., Thakkar, D., et al. (2021). Considerations for treatment duration in responders to immune checkpoint inhibitors. *J. Immunother. Cancer* 9:e001901. doi: 10.1136/jitc-2020-001901

Mayakonda, A., Lin, D. C., Assenov, Y., Plass, C., and Koeffler, H. P. (2018). Maftools: efficient and comprehensive analysis of somatic variants in cancer. *Genome Res.* 28, 1747–1756. doi: 10.1101/gr.239244.118

Mitchell, T. C., Hamid, O., Smith, D. C., Bauer, T. M., Wasser, J. S., Olszanski, A. J., et al. (2018). Epacadostat plus pembrolizumab in patients with advanced solid tumors: phase I results from a multicenter, open-label phase I/II trial (ECHO-202/KEYNOTE-037). *J. Clin. Oncol.* 36, 3223–3230. doi: 10.1200/jco.2018.78.9602

Murakami, M., Izumi, H., Kurita, T., Koi, C., Morimoto, Y., and Yoshino, K. (2020). UBE2L6 is involved in cisplatin resistance by regulating the transcription of ABCB6. *Anticancer Agents Med. Chem.* 20, 1487–1496. doi: 10.2174/1871520620666200424130934

Newman, A. M., Liu, C. L., Green, M. R., Gentles, A. J., Feng, W., Xu, Y., et al. (2015). Robust enumeration of cell subsets from tissue expression profiles. *Nat. Methods* 12, 453–457. doi: 10.1038/nmeth.3337

Øster, B., Linnet, L., Christensen, L. L., Thorsen, K., Ongen, H., Dermitzakis, E. T., et al. (2013). Non-CpG island promoter hypomethylation and miR-149 regulate the expression of SRPX2 in colorectal cancer. *Int. J. Cancer* 132, 2303–2315. doi: 10.1002/ijc.27921

Pahari, S., Negi, S., Aqdas, M., Arnett, E., Schlesinger, L. S., and Agrewala, J. N. (2020). Induction of autophagy through CLEC4E in combination with TLR4: an innovative strategy to restrict the survival of Mycobacterium tuberculosis. *Autophagy* 16, 1021–1043. doi: 10.1080/15548627.2019.1658436

Pidugu, V. K., Pidugu, H. B., Wu, M. M., Liu, C. J., and Lee, T. C. (2019). Emerging functions of human IFIT proteins in cancer. *Front. Mol. Biosci.* 6:148. doi: 10.3389/fmolb.2019.00148

Quezada, S. A., Peggs, K. S., Simpson, T. R., and Allison, J. P. (2011). Shifting the equilibrium in cancer immunoediting: from tumor tolerance to eradication. *Immunol. Rev.* 241, 104–118. doi: 10.1111/j.1600-065X.2011.01007.x

Raskin, L., Fullen, D. R., Giordano, T. J., Thomas, D. G., Frohm, M. L., Cha, K. B., et al. (2013). Transcriptome profiling identifies HMGA2 as a biomarker of melanoma progression and prognosis. *J. Invest. Dermatol.* 133, 2585–2592. doi: 10.1038/jid.2013.197

Ritchie, M. E., Phipson, B., Wu, D., Hu, Y., Law, C. W., Shi, W., et al. (2015). limma powers differential expression analyses for RNA-sequencing and microarray studies. *Nucleic Acids Res.* 43, e47. doi: 10.1093/nar/gkv007

Robin, X., Turck, N., Hainard, A., Tiberti, N., Lisacek, F., Sanchez, J. C., et al. (2011). pROC: an open-source package for R and S+ to analyze and compare ROC curves. *BMC Bioinformatics* 12:77. doi: 10.1186/1471-2105-12-77

Siegel, R. L., Miller, K. D., Fuchs, H. E., and Jemal, A. (2021). Cancer Statistics, 2021. *CA Cancer J. Clin.* 71, 7–33. doi: 10.3322/caac.21654

Subramanian, A., Tamayo, P., Mootha, V. K., Mukherjee, S., Ebert, B. L., Gillette, M. A., et al. (2005). Gene set enrichment analysis: a knowledge-based approach for interpreting genome-wide expression profiles. *Proc. Natl. Acad. Sci. U. S. A.* 102, 15545–15550. doi: 10.1073/pnas.0506580102

Tanaka, K., Arao, T., Tamura, D., Aomatsu, K., Furuta, K., Matsumoto, K., et al. (2012). SRPX2 is a novel chondroitin sulfate proteoglycan that is overexpressed in gastrointestinal cancer. *PLoS One* 7:e27922. doi: 10.1371/journal.pone.0027922

Tang, Z., Kang, B., Li, C., Chen, T., and Zhang, Z. (2019). GEPIA2: an enhanced web server for large-scale expression profiling and interactive analysis. *Nucleic Acids Res.* 47, W556–W560. doi: 10.1093/nar/gkz430

Thompson, J. F., Scolyer, R. A., and Kefford, R. F. (2009). Cutaneous melanoma in the era of molecular profiling. *Lancet* 374, 362–365. doi: 10.1016/s0140-6736(09)61397-0

Tomczak, K., Czerwińska, P., and Wiznerowicz, M. (2015). The Cancer Genome Atlas (TCGA): an immeasurable source of knowledge. *Contemp. Oncol. (Pozn.)* 19, A68–A77. doi: 10.5114/wo.2014.47136

Topalian, S. L., Hodi, F. S., Brahmer, J. R., Gettinger, S. N., Smith, D. C., McDermott, D. F., et al. (2012). Safety, activity, and immune correlates of anti-PD-1 antibody in cancer. *N. Engl. J. Med.* 366, 2443–2454. doi: 10.1056/NEJMoa1200690

Wagner, N. B., Weide, B., Gries, M., Reith, M., Tarnanidis, K., Schuermans, V., et al. (2019). Tumor microenvironment-derived S100A8/A9 is a novel prognostic biomarker for advanced melanoma patients and during immunotherapy with anti-PD-1 antibodies. *J. Immunother. Cancer* 7:343. doi: 10.1186/s40425-019-0828-1

Wei, W., Li, Y., Li, Y., and Li, D. (2021). Adipose-specific knockout of ubiquitin-conjugating enzyme E2L6 (Ube2l6) reduces diet-induced obesity, insulin resistance, and hepatic steatosis. *J. Pharmacol. Sci.* 145, 327–334. doi: 10.1016/j.jphs.2020.12.008

Wilkerson, M. D., and Hayes, D. N. (2010). ConsensusClusterPlus: a class discovery tool with confidence assessments and item tracking. *Bioinformatics* 26, 1572–1573. doi: 10.1093/bioinformatics/btq170

Xu, L., Shen, S. S., Hoshida, Y., Subramanian, A., Ross, K., Brunet, J. P., et al. (2008). Gene expression changes in an animal melanoma model correlate with aggressiveness of human melanoma metastases. *Mol. Cancer Res.* 6, 760–769. doi: 10.1158/1541-7786.Mcr-07-0344

Yu, G., Wang, L. G., Han, Y., and He, Q. Y. (2012). clusterProfiler: an R package for comparing biological themes among gene clusters. *OMICS* 16, 284–287. doi: 10.1089/omi.2011.0118

Zeng, L., Fan, X., Wang, X., Deng, H., Zhang, K., Zhang, X., et al. (2019). Bioinformatics analysis based on multiple databases identifies hub genes associated with hepatocellular carcinoma. *Curr. Genomics* 20, 349–361. doi: 10.2174/1389202920666191011092410

Zhang, H., Meltzer, P., and Davis, S. (2013). RCircos: an R package for Circos 2D track plots. *BMC Bioinformatics* 14:244. doi: 10.1186/1471-2105-14-244

Zhang, M., Li, X., Fan, Z., Zhao, J., Liu, S., Zhang, M., et al. (2018). High SRPX2 protein expression predicts unfavorable clinical outcome in patients with prostate cancer. *Onco. Targets Ther.* 11, 3149–3157. doi: 10.2147/ott.S158820

Zhao, X., Shen, J., Ivaturi, V., Gopalakrishnan, M., Feng, Y., Schmidt, B. J., et al. (2020). Model-based evaluation of the efficacy and safety of nivolumab once every 4 weeks across multiple tumor types. *Ann. Oncol.* 31, 302–309. doi: 10.1016/j.annonc.2019.10.015

Conflict of Interest: The authors declare that the research was conducted in the absence of any commercial or financial relationships that could be construed as a potential conflict of interest.

Publisher's Note: All claims expressed in this article are solely those of the authors and do not necessarily represent those of their affiliated organizations, or those of the publisher, the editors and the reviewers. Any product that may be evaluated in this article, or claim that may be made by its manufacturer, is not guaranteed or endorsed by the publisher.

frontiers in Cell and Developmental Biology

REVIEW
published: 06 October 2021
doi: 10.3389/fcell.2021.729498

The Role of Androgen Receptor in Cross Talk Between Stromal Cells and Prostate Cancer Epithelial Cells

Qianyao Tang[1†], Bo Cheng[2†], Rongyang Dai[1] and Ronghao Wang[1*]*

[1] Department of Biochemistry and Molecular Biology, School of Basic Medical Sciences, Southwest Medical University, Luzhou, China, [2] Department of Urology, The Affiliated Hospital of Southwest Medical University, Luzhou, China

Prostate cancer (PCa) lists as the second most lethal cancer for men in western countries, and androgen receptor (AR) plays a central role in its initiation and progression, which prompts the development of androgen deprivation therapy (ADT) as the standard treatment. Prostate tumor microenvironment, consisting of stromal cells and extracellular matrix (ECM), has dynamic interactions with PCa epithelial cells and affects their growth and invasiveness. Studies have shown that both genomic and non-genomic AR signaling pathways are involved in the biological regulation of PCa epithelial cells. In addition, AR signaling in prostate stroma is also involved in PCa carcinogenesis and progression. Loss of AR in PCa stroma is clinically observed as PCa progresses to advanced stage. Especially, downregulation of AR in stromal fibroblasts dysregulates the expression levels of ECM proteins, thus creating a suitable environment for PCa cells to metastasize. Importantly, ADT treatment enhances this reciprocal interaction and predisposes stromal cells to promote cell invasion of PCa cells. During this process, AR in PCa epithelium actively responds to various stimuli derived from the surrounding stromal cells and undergoes enhanced degradation while elevating the expression of certain genes such as MMP9 responsible for cell invasion. AR reduction in epithelial cells also accelerates these cells to differentiate into cancer stem-like cells and neuroendocrine cells, which are AR-negative PCa cells and inherently resistant to ADT treatments. Overall, understanding of the cross talk between tumor microenvironment and PCa at the molecular level may assist the development of novel therapeutic strategies against this disease. This review will provide a snapshot of AR's action when the interaction of stromal cells and PCa cells occurs.

Keywords: PCa, AR, microenvironment, stroma, androgen deprivation therapy (ADT)

OPEN ACCESS

Edited by:
Na Luo,
Nankai University, China

Reviewed by:
Gabriella Castoria,
Second University of Naples, Italy
Damien Leach,
Imperial College London, United Kingdom

****Correspondence:***
Ronghao Wang
ronghao_wang@swmu.edu.cn
Rongyang Dai
dryrun2502@163.com

† These authors have contributed equally to this work

Specialty section:
This article was submitted to Molecular and Cellular Pathology, a section of the journal Frontiers in Cell and Developmental Biology

Received: *23 June 2021*
Accepted: *06 September 2021*
Published: *06 October 2021*

Citation:
Tang Q, Cheng B, Dai R and Wang R (2021) The Role of Androgen Receptor in Cross Talk Between Stromal Cells and Prostate Cancer Epithelial Cells. Front. Cell Dev. Biol. 9:729498. doi: 10.3389/fcell.2021.729498

INTRODUCTION

Prostate cancer (PCa) is a malignant growth of prostate epithelial cells, and it continuously causes severe mortality among men. According to a survey in 2020, an estimated 190,000 new cases of PCa are diagnosed and 33,000 associated deaths are reported worldwide (Siegel et al., 2020), suggesting an urgent need to identify effective therapeutic strategies against this disease. Given the fact that

androgen receptor (AR) plays central roles in PCa carcinogenesis (Heinlein and Chang, 2004; Lonergan and Tindall, 2011), androgen deprivation therapy (ADT) is the mainstream treatment for PCa, which is effective for 2–3 years before PCa progresses to castration-resistant PCa (CRPC; Ruizeveld de Winter et al., 1994; Henshall et al., 2001; Scher et al., 2004). The reactivation of AR in CRPC, owing to gene amplification (Koivisto et al., 1997), gene mutation (Tilley et al., 1996), or the production of constitutively active AR variants (Nakazawa et al., 2014), makes it still a promising therapeutic target.

Androgen receptor, also called NR3C4 (nuclear receptor subfamily 3, group C, member 4), is one member of the steroid and nuclear receptor superfamily and is encoded by the AR gene located at Xq11-12 (Tan et al., 2015). AR mainly contains four functional domains, as indicated in **Figure 1**: the amino-terminal domain (NTD; exon 1), DNA-binding domain (DBD; exons 2–3), hinge region (exon 4), and ligand-binding domain (LBD; exons 4–8). As a hormone-inducible transcription factor, AR is ubiquitously expressed in multiple tissues and is involved in various physiological and pathological events by controlling gene expression (Waghray et al., 2001; DePrimo et al., 2002). Genomic AR signaling in PCa is well studied: AR disassociates from its cytoplasmic chaperones such as HSP70 and translocates to the nucleus upon androgenic hormone binding, working as either homodimer or heterodimer to regulate its downstream genes such as *PSA*, *FKBP5*, and *TMPRSS2*, in order to provide survival signals for PCa growth (**Figure 1**; Smith and Toft, 2008). Of note, activation of non-genomic AR signaling is also critical to PCa development. An early study demonstrated that AR in both prostatic smooth muscle cells and prostatic epithelial cells rapidly responded to androgen stimulation (Peterziel et al., 1999) and interacted with non-receptor tyrosine kinase Src (Migliaccio et al., 2000; Castoria et al., 2017). This interaction impaired the inhibitory intramolecular binding of Src and allowed it in its active form to activate PI3K and MAPK signaling pathways, which promoted cell proliferation and cell invasion of PCa (Cai H. et al., 2011; Castoria et al., 2017). Although castration leads to a remarkable decline of AR activity, AR utilizes various novel ways to escape androgen ablation and continues to support PCa growth in castration-resistant stage (**Figure 2**). For instance, upregulated EGF and IGF in CRPC could activate AR transactivation. Mechanistically, Src responded to EGF stimulation and phosphorylated AR at the residue of tyrosine 534, leading to AR activation (Migliaccio et al., 2005; Liu et al., 2010). IGF-stimulated AKT and ERK1/2 signaling pathways were directly responsible for AR activation (Wu et al., 2006). In addition, elevated cytokines in CRPC such as IL-6 or IL-8 also had the capacity to activate AR signaling *via* MAPK and JAK/STAT3 signaling pathways (Chen et al., 2000; Seaton et al., 2008). Studies also revealed that AR mutation including aberrant AR splicing and AR gene amplification were frequently (10–30%) observed in CRPC patients (Visakorpi et al., 1995; Tilley et al., 1996; Koivisto et al., 1997), which allowed it to be active even under castrated conditions, effectively conferring androgen independence to AR.

Prostate cancer is a malignant mass infiltrated with endothelial cells, bone marrow stem cells, fibroblasts, and immune cells (Sejda et al., 2020; Thienger and Rubin, 2021). Evidence suggested that the infiltration of these cells increased as PCa progressed to the CRPC stage. These stromal cells provide cytokines and growth factors to drive PCa progression. Clinical evidence indicated that stromal AR was a protective factor for PCa patients as its expression was inversely related to poor PCa outcomes including tumor stage, metastasis, cancer relapse, and cancer-related death (Olapade-Olaopa et al., 1999; Henshall et al., 2001; Ricciardelli et al., 2005; Li et al., 2008; Wikstrom et al., 2009; Leach et al., 2015). In contrast, AR in PCa epithelium acted as a tumor-promoting factor to control PCa development. Therefore, comprehensive knowledge of AR's role in the cross talk between PCa and its surrounding stromal component is necessary for scientists to better understand this disease.

ANDROGEN RECEPTOR INHIBITION AS A STANDARDIZED TREATMENT FOR PROSTATE CANCER

Androgen receptor inhibition is the major way to treat PCa, and AR-targeted therapies are listed in **Table 1**. ADT has been the mainstay treatment for PCa patients in past decades, which includes surgical and chemical castration. Surgical castration refers to one operation in which the entire testes is removed to ablate androgen synthesis, while chemical castration utilizes various types of compounds to antagonize AR signaling pathway in PCa. Leuprorelin and triptorelin are clinically used as LHRH agonists to fulfill androgen deprivation (Crawford and Hou, 2009; Lepor and Shore, 2012). Mechanistically, LHRH agonist treatment leads to LHRH downregulation and eventually inhibits pituitary production of follicle-stimulating hormone (FSH) and luteinizing hormone (LH), two important hormones responsible for androgen synthesis in testes, while LHRH antagonists such as degarelix and relugolix interact with LHRH receptor and impair the physiological binding of LHRH and its receptor, reducing androgen synthesis. However, LHRH agonists and antagonists only block testes from producing androgens. Evidence show that 5–10% of androgens are generated from adrenal glands and they are sufficient to drive AR signaling (Montgomery et al., 2008), which facilitates the development of other compounds in order to reduce the synthesis of adrenal androgens. CYP17 is a key enzyme required for the biosynthesis of adrenal androgens so that its specific inhibitors such as abiraterone, TAK-700, and TOK-001 have been developed to treat CRPC patients who are resistant to LHRH agonists and antagonists (Schweizer and Antonarakis, 2012).

Of note, the castration level of androgen still has the ability to activate AR signaling and to support CRPC growth. To reach a deep AR inhibition, anti-androgens are developed to treat metastatic CRPC patients. They directly inhibit the binding of androgen to AR and to prevent AR nuclear translocation and the subsequent transactivation. However, first-generation anti-androgens such as bicalutamide cannot completely block AR activity due to their relatively low

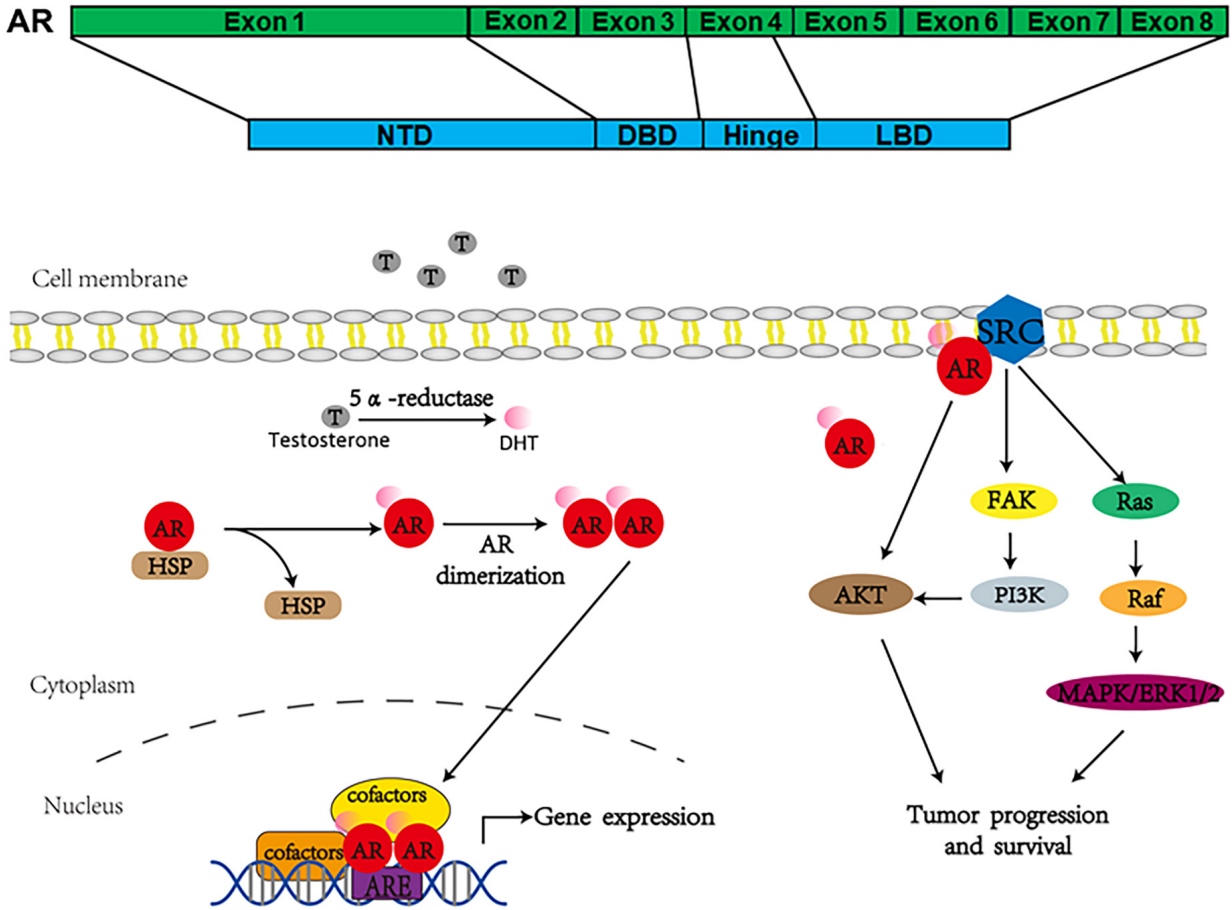

FIGURE 1 | Androgen receptor's structure and how it works to regulate gene expression.

affinity to AR. This leads to the emergence of second-generation anti-androgens in the standard treatment of metastatic CRPC patients. Enzalutamide is one of these second-generation anti-androgens and significantly improves patients' survival (Scher et al., 2010; Roumiguie et al., 2021). Overall, AR inhibition is the main strategy to prevent PCa development.

ANDROGEN RECEPTOR SIGNALING IN CROSS TALK BETWEEN ENDOTHELIAL CELLS AND PROSTATE CANCER

Endothelial cells are key builders of vascular structure, and their proliferation, migration, and remodeling are tightly associated with angiogenesis (Dudley, 2012). Early reports demonstrated that initial ADT treatment led to the apoptosis of endothelial cells and decreased the number of microvascules (Shabsigh et al., 1998). Very intriguingly, microvascules showed regrowth and the number of endothelial cells evidently increased as PCa progressed to the CRPC stage (Godoy et al., 2011; Tomic et al., 2012). This regrowth of microvascules was accompanied by PCa metastasis. Indeed, *in vitro* evidence supported the notion that endothelial cells could increase PCa cell migration and invasion. By coculturing HUVECs (human umbilical vein endothelial cells) with PCa cells, Chang et al. found that HUVECs had the capacity to enhance cell migration and cell invasion of CWR22Rv1 and C4-2 cells (Wang et al., 2013). According to their data, PCa cells exposed to HUVECs expressed lower levels of AR than non-exposed controls. AR seemingly regulated TGFβ and MMP9 in a negative manner, as evidenced by the enhanced expression levels of TGFβ and MMP9 when AR was depleted by siRNAs. They also identified that IL-6, a cytokine secreted by HUVECs, was sufficient to drive AR downregulation. Consistent with this report, HUVEC-enhanced cell invasion of PCa cells *via* downregulating the AR level was also observed by Jiang et al. AR reduction was promoted by the interaction of CCL5 on endothelial cells with its receptor CCR5 on PCa cells, triggering mitochondria-mediated autophagy, one mechanism responsible for cell invasion of PCa cells (Zhao et al., 2018). Interestingly, another study documented that MMP9, together with PIP5K1α, could interact with AR to promote its transcriptional activity on the downstream target cyclin A1, leading to enhanced growth of

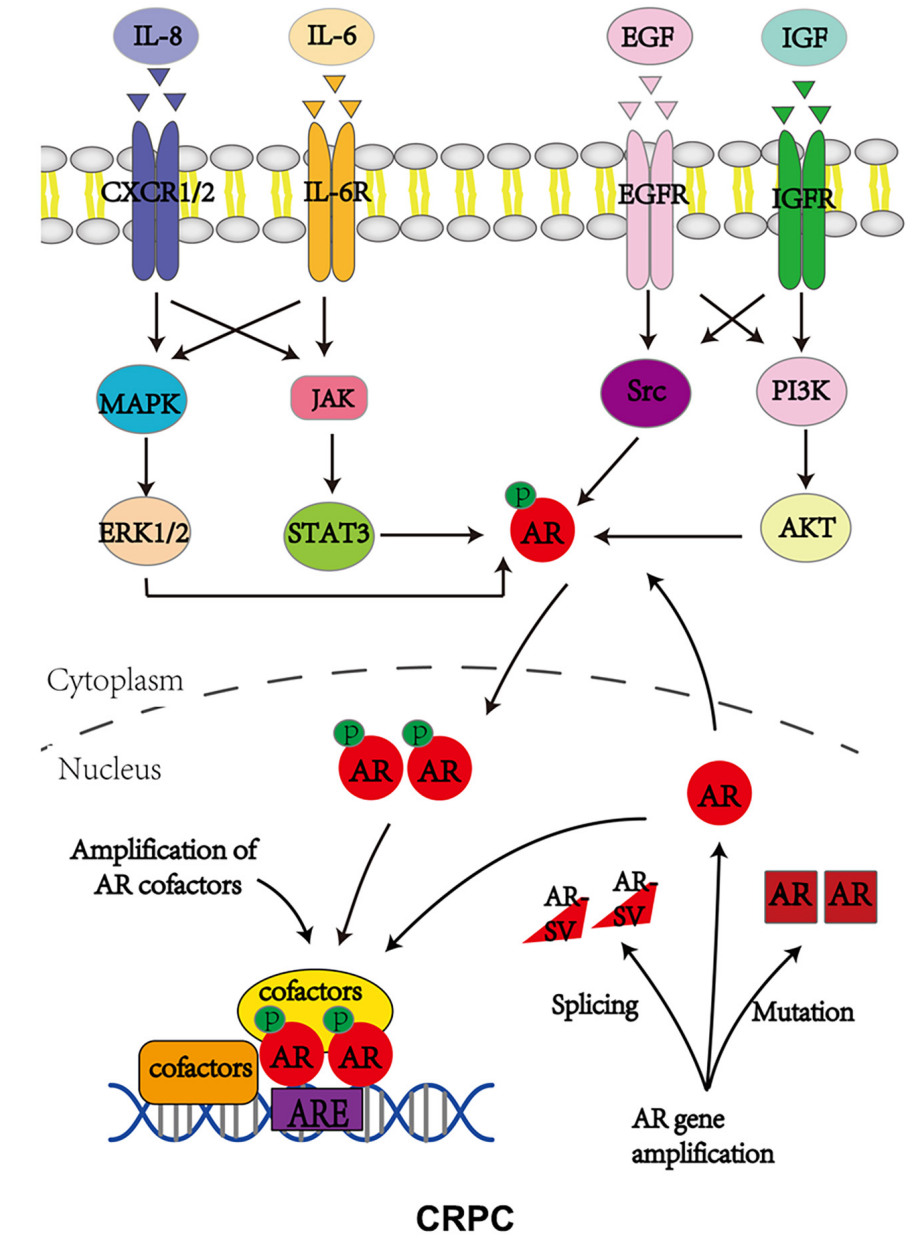

FIGURE 2 | Androgen receptor utilizes various ways to bypass AR inhibition to support CRPC growth. P stands for phosphorylation.

metastatic CRPC tumor (Larsson et al., 2020). However, as a transcription factor, how AR regulates TGFβ, MMP9, and autophagy in the presence of HUVECs is still largely unknown and requires further exploration. In addition, it remains to be clarified how IL-6 and CCL5/CCR5 signals at a molecular level reduce AR expression.

On the other hand, anti-androgen-resistant PCa tends to express a higher level of endothelial nitric oxide synthase (eNOS) compared to hormone naive PCa (Yu et al., 2013), suggesting that chronic inhibition of AR signaling causes an upregulation of eNOS, a critical molecule involved in supporting endothelial cell survival and proliferation. Together, all these data pinpoint a positive feedback loop between PCa cells and endothelial cells during PCa development.

How does AR function in endothelial cells? Literature revealed that androgen could promote cell proliferation of HUVECs by activating the AR/VEGF/Cyclin A signaling axis (Cai J. et al., 2011; Torres-Estay et al., 2017; Eisermann et al., 2013). However, another study contradictorily showed that AR activation triggered TNF-α-induced cell apoptosis of EA.hy926 endothelial cells (Ling et al., 2002). One possible explanation to this is that different endothelial cell lines have distinct

TABLE 1 | Androgen receptor targeted therapies in prostate cancer.

Established therapies	AR based drugs	Type of PCa	Mechanistic action
LHRH agonists	Leuprolide; Leuprolide mesylate; Triptorelin; Goserelin; Histrelin	Localized	Suppress LHRH expression and reduce the production of FSH and LH. Impair androgen synthesis in testes
LHRH antagonists	Degarelix; Relugolix	Localized; Advanced	Compete LHRH to bind its receptor and prevent its biological function
CYP17 inhibitors	Abiraterone; TAK-700 (Orteronel); Ketoconazole;	mCRPC	Inhibition of biosynthesis of adrenal androgens by suppressing CYP17 activity
	TOK-001 (Galeterone)	CRPC	
Antiandrogen	Bicalutamide; Nilutamide; Flutamide	Localized; Advanced	First generation antiandrogen, compete androgen to interact with AR
	Enzalutamide	mCRPC	Second generation antiandrogen, compete androgen to interact with AR, block AR nuclear translocation, inhibit AR DNA binding and the recruitment of AR cofactors
	Apalutamide (ARN-509)	mCSPC	
	Darolutamide	nmCRPC	

CRPC stands for castration resistant prostate cancer; mCRPC means metastatic castration resistant prostate cancer; nmCRPC means non-metastatic castration resistant prostate cancer; mCSPC stands for metastatic castration sensitive prostate cancer.

responses to androgen treatment. Therefore, the exact role of AR in endothelial cells during PCa progression is still open to investigation.

INTERACTION BETWEEN BONE MARROW MESENCHYMAL STEM CELLS AND ANDROGEN RECEPTOR SIGNALING IN PROSTATE CANCER

An observation of the migration of mesenchymal stem cells (BM-MSCs) into PCa stroma implies their possible participation in the regulation of PCa development (Placencio et al., 2010; Brennen et al., 2017). As multipotent stromal cells, BM-MSCs bear the ability to differentiate into various cell types (Pittenger et al., 1999; Mendez-Ferrer et al., 2010) including fibroblasts, adipocytes, and smooth muscle cells in PCa stroma. Moreover, the recruited BM-MSCs promoted cell invasion and stemness differentiation of PCa cells, ultimately allowing PCa cells to survive in an androgen-independent manner (Chang et al., 2014; Luo et al., 2014, 2015). Mechanistic dissection illustrated that BM-MSCs could secrete CCL5 and IL-1β, which independently acted to reduce the AR level. According to the literature, secreted CCL5 from BM-MSCs led to decreased levels of prolyl hydroxylase (PHD) 1 and 4, which prevented the hydroxylation of HIF2α and caused it to become more stable (Luo et al., 2015). Immunoprecipitation assay also confirmed that CCL5-induced HIF2α enhanced HSP70-AR interaction, which inhibited AR nuclear translocation and the subsequent transactivation. Another study also verified that conditioned medium from BM-MSCs could decrease the AR protein level, which was mediated by the cytokine IL-1β(Chang et al., 2014). However, the detailed mechanism by which IL-1βdecreased AR was not clearly explored. These studies also proved that the reduction of AR was a central driving force to promote PCa cell invasion. Further explorations revealed that AR downregulation by BM-MSCs increased the stemness of PCa, owing to the upregulation of several CSC (cancer stem cells) related markers such as CXCR4, ZEB1, and Snail1 (Luo et al., 2014). Given the fact that prostatic CSCs are more malignant than parental PCa cells, it is understandable that BM-MSCs promote PCa invasion and metastasis.

Of note, a lack of evidence showing that AR in BM-MSCs exerts its function to regulate PCa survival and invasion may prompt scientists to explore this direction.

INTERACTION BETWEEN ANDROGEN RECEPTOR SIGNALING IN CANCER-ASSOCIATED FIBROBLASTS AND PROSTATE CANCER

Cancer-associated fibroblasts (CAFs), one type of activated fibroblasts, typically express high levels of αSMA (α-smooth muscle actin) and fibroblast activation protein (FAP; Sahai et al., 2020). Studies indicate that CAFs have a malignant property by affecting their surrounding compartments including cancerous cells and other stromal cells (Taylor et al., 2012). Compared to normal fibroblasts, CAFs have distinct genome-wide DNA methylation signatures at enhancers and promoters, causing aberrant expression of cancer-related genes to impact cancer fate (Pidsley et al., 2018). Abundant studies show that CAFs exist in the primary site of localized or metastatic PCa microenvironment and promote its initiation and progression. By comparing immortalized CAFs and normal prostate fibroblasts, researchers noticed that CAFs had stronger ability to promote malignant transformation of BPH-1 cells *in vitro* and *in vivo* (Yu et al., 2017), suggesting that CAF was a central driving source for PCa initiation. In this process, AR in stromal fibroblasts but not in epithelium is necessary for prostatic epithelia malignant

transformation (Ricke et al., 2012). According to this study, loss of stromal AR did not impair prostate homeostasis but decreased the expression levels of several stroma fibroblast-derived growth factors such as FGF-2 and FGF-10, impeding PCa carcinogenesis (Ricke et al., 2012). Moreover, studies also indicated that CAFs had better capacity to increase cell proliferation and invasion of LNCaP cells *in vitro* (Yu et al., 2017), compared to normal prostate fibroblasts. The LNCaP xenografted mouse model also strengthened the tumor-promoting role of CAFs in PCa carcinogenesis (Yu et al., 2017). Consistent with this report, another study also found that CAFs significantly enhanced PCa growth and distant metastases when compared to normal prostate fibroblasts (Linxweiler et al., 2020). Why are CAFs so effective in promoting PCa development? Focus cytokine array showed that CAFs secreted more growth factors such as EGF, FGF, HGF, TGFβ and VEGF, than normal prostate fibroblasts, providing survival advantage to PCa cells (Yu et al., 2017).

How does AR contribute to fibroblast proliferation and migration? Results from mouse embryo fibroblasts NIH3T3 and fibrosarcoma HT1080 revealed that androgen stimulation (10 nM) could suppress proliferation while increasing migration of these two cell lines (Castoria et al., 2014). Mechanistic dissection unfolded that the androgen-stimulated AR/FlnA complex led to the activation of Rac1 as well as its downstream effector DYRK 1B, which phosphorylated p27 at Ser 10. The phosphorylated p27 at Ser 10 was stabilized and attributable to cell cycle arrest at G0/G1 of fibroblasts (Castoria et al., 2014). Meanwhile, the AR/FlnA complex also triggered the activation of focal adhesion kinase FAK, Rac1, and paxillin *via* recruiting integrin beta 1, promoting cell migration of NIH3T3, HT1080 cells, and PCa-derived fibroblasts (Castoria et al., 2011; Di Donato et al., 2021). These findings suggest the therapeutic value of targeting the AR/FlnA complex to suppress the malignant activity of CAFs. Indeed, knockdown of FlnA with siRNAs or inhibition of AR by enzalutamide could abolish the migration and invasiveness of CAFs induced by androgen treatment (Di Donato et al., 2021). Similarly, disruption of the AR/FlnA complex by drug-like compound Rh-2025u-stapled peptide, which was developed from the AR amino acid sequence required for the interaction with FlnA (Loy et al., 2003; Castoria et al., 2011), abolished the androgen-induced migration and invasiveness of CAFs, consequently leading to less recruitment of CAFs to PCa and suppressing PCa-CAF organoid growth (Di Donato et al., 2021). How does AR in CAFs function to influence PCa growth and invasion? Several studies have demonstrated that the reduced expression level of AR in CAFs was a prognostic indicator of PCa progression, suggesting that AR in CAFs serves as a negative regulator to determine PCa development. A study showed that AR regulated extracellular matrix (ECM) components and maintained its inhibition on PCa cell invasion. Loss of AR in fibroblasts led to the downregulation of adhesive proteins such as FBXO32 and FBN1 as well as the upregulation of ECM-degrading enzyme MMP1, establishing an environment permissive for PCa cells to invade (Leach et al., 2015). By using the *in vitro* coculture system, Smith and colleagues found that immortalized human prostate myofibroblast cell line PShTert with AR activation could retard the cell growth of various PCa cells including PC3, Du145, C4-2B, and LNCaP cells, highlighting the protective role of AR in CAFs during PCa development (Palethorpe et al., 2018). Additionally, another report further proved that loss of AR in CAFs promoted cell migration of PCa cells (Cioni et al., 2018). As described in this report, AR negatively regulated the expressions of CCL2 and CXCL8 at the transcriptional level. Therefore, loss of AR released its inhibitory regulation on these two cytokines, which were secreted and promoted PCa cell migration in a paracrine manner. Another document strengthened this conclusion by pinpointing that loss of AR in CAFs led to the enhanced expression levels of interferon gamma (IFN-γ) and macrophage colony-stimulating factor (M-CSF), which acted on PCa cells and educated them to differentiate into cancer stem-like cells (Liao et al., 2017) characterized with more invasive properties. Contradictorily, the group of Chang illustrated that myofibroblast stromal cell line WPMY-1 with AR siRNAs could suppress the cell invasion of PCa cells in the coculture system (Niu et al., 2008), and the group of Gross described that reduction of AR in CAFs with antisense oligonucleotide (ASO) dramatically suppressed CAF-promoted PCa growth *in vitro* and *in vivo* (Liao et al., 2017). It can be argued that the group of Chang reached the conclusion on the basis of an artificial coculture system. In the study by Gross, ASOs were utilized to reduce the AR protein level, while the previous study applied anti-androgen RD162 for AR inhibition. It is possible that the physiological effects of anti-androgen and ASO on CAFs are different so that opposite conclusions are generated. Besides, Gross et al. utilized mouse CAFs as a source to study their contribution to the cell growth of human PCa cells, which was not an optimal *in vitro* model.

Although AR signaling is very important for PCa growth and metastasis, few studies examined AR status in PCa epithelial cells that interprets the signal from CAFs to influence PCa epithelial cells when these two types of cells are communicating with each other, which should be explored with future efforts.

ANDROGEN RECEPTOR SIGNALING IN CROSS TALKS BETWEEN IMMUNE CELLS AND PROSTATE CANCER

Infiltration of immune cells into PCa is frequently observed, which is further increased upon ADT treatment, indicating that immune cells are actively involved in PCa progression. Macrophages, T lymphocytes, NK cells, and mast cells are the most important components of immune cells, and their cross talk with AR signaling in PCa will be summarized as follows.

ANDROGEN RECEPTOR SIGNALING IN CROSS TALK BETWEEN CD4+T CELLS AND PROSTATE CANCER

T cells consist of CD8 + cytotoxic T cells and CD4 + helper T cells, playing a central role in the adaptive immune response. Kwon et al. demonstrated that androgen ablative therapy (ADT) could increase the infiltration of CD4 + T cells but not

CD8 + T cells into the PCa (Mercader et al., 2001). In agreement with this observation, Underwood et al. also found that the infiltration of CD4 + T cells was strongly associated with poor outcome in PCa patients (McArdle et al., 2004). Collectively, all these findings suggest that CD4 + T cells may participate in PCa progression. Consistently, another study documented that androgen (testosterone) could inhibit the differentiation of CD4 + T cells (Kissick et al., 2014). CD4 + T cells isolated from castrated mice exhibited reduced STAT4 phosphorylation and IFN-γ production upon testosterone treatment. Testosterone activated AR to transcriptionally upregulate the expression level of Ptpn1 (protein tyrosine phosphatase non-receptor type 1), which in turn served as a negative regulator of STAT4 signaling (Kissick et al., 2014). Therefore, castration not only increased the infiltration of CD4 + T cells but also promoted their differentiation. Collectively, these data suggest that CD4 + T cells may play a tumor-promoting role in PCa development. Indeed, through an *in vitro* cell model, Chang et al. found that PCa cells had a better capacity to recruit CD4 + HH and Molt-3 T cells compared to normal prostate epithelial RWPE-1 cells (Hu et al., 2015). Mechanistically, FGF11 secreted from HH and Molt-3 T cells led to the reduction of AR in PCa cells by enhancing miR-541-mediated AR mRNA degradation (Hu et al., 2015). AR downregulation could elevate the MMP9 expression level, promoting PCa invasion and metastasis. Again, detailed mechanisms underlying AR regulation of MMP9 were not investigated in this study. In addition, it was unlikely that FGF11 directly increased the expression level of miR-541 to reduce the AR level. PCa cells must undergo multiple signaling events upon FGF11 treatment to complete miR-541 induction.

Although ADT with enzalutamide treatment initially increased the infiltration of CD4 + helper cells, it sensitized PCa cells to CD8 + T cell killing by downregulating the expression of antiapoptotic gene NAIP (neuronal apoptosis inhibitory protein) (Ardiani et al., 2014). NAIP played a critical role in conferring the killing ability of CD8 + cytotoxic cells toward PCa cells. In enzalutamide-resistant PCa, AR signaling was reactivated in various ways so that AR drove NAIP expression, decreasing the sensitivity of PCa cells to CD8 + cytotoxic cells (Ardiani et al., 2014). Therefore, a combined therapy using T cell immunotherapy with anti-androgen therapy becomes ideal for PCa management (Sanchez et al., 2013).

ANDROGEN RECEPTOR SIGNALING IN CROSS TALK BETWEEN MACROPHAGES AND PROSTATE CANCER

As the most predominant immune cells within the PCa microenvironment, macrophages play a central role in PCa development including cell survival, cell invasion, angiogenesis, lineage plasticity, and anti-androgen resistance. Macrophages can be classified into pro-inflammatory/anti-tumoral M1 type and anti-inflammatory/pro-tumoral M2 type. Typically, M2 macrophages, featured with high IL-10 production, increasingly infiltrate PCa, and this infiltration is strongly correlated with PCa aggressiveness (Comito et al., 2014). Studies demonstrated that PCa could promote differentiation and polarization of macrophages. PCa-derived IL-6, SDF1, and antimicrobial peptide LL-37 (leucin leucin 37) could promote M1–M2 differentiation/polarization (Comito et al., 2014; Cha et al., 2016), which in turn increased PCa invasiveness. Indeed, depletion of M2 macrophages remarkably inhibited tumor progression in various mouse tumor models (Sica et al., 2008), including PCa. Previous studies revealed that there was much more macrophage infiltration in PCa compared to matched normal tissues, monitored by the specific macrophage marker CD68 (Zhu et al., 2006; Fang et al., 2013), suggesting that macrophages may play a role in PCa tumorigenesis. In an experimental setting mimicking *in vivo* cell–cell interaction, Fang et al. (2013) applied the coculture system using immortalized prostate epithelial cells (RWPE-1) and macrophages (THP-1) to induce prostate tumorigenesis. The results demonstrated that RWPE-1 cells cocultured with THP-1 cells could well differentiate into prostate spheres and had better ability to develop tumor in xenografted mouse models, and strengthening macrophage infiltration can promote PCa tumorigenesis.

Castration further increased the infiltration of M2 macrophages into PCa (Lin et al., 2013; Yuri et al., 2020), and this recruitment of macrophages by ADT may be attributable to CCL2 production from PCa cells (Tsai et al., 2018). One publication illustrated that a transcriptional repressor of CCL2, SPDEF (SAM pointed domain-containing ETS transcription factor), was positively regulated by AR. ADT inactivated AR transcriptional activity to reduce the transcription of SPDEF, which in turn promoted the expression of CCL2. CCL2 bound its receptor CCR2 on macrophages in a paracrine manner and enhanced their recruitment to PCa cells (Tsai et al., 2018). Furthermore, the infiltrated macrophages would enhance PCa invasion/metastasis *via* downregulating AR and activating STAT3 signaling. Chang et al. found that coculture of THP-1 with PCa cells led to AR reduction in PCa cells (Izumi et al., 2013). They also identified that PIAS3 was an AR-inducible gene, which was transcriptionally decreased in the presence of THP-1 cells. Without the negative regulator PIAS3, STAT3 signaling was activated and drove PCa invasion/metastasis. Nevertheless, how AR is reduced when PCa cells receive the signals from macrophages remains unknown and requires additional investigation.

Androgen receptor seemingly acts as a tumor-suppressing factor in PCa-associated macrophages. According to Izumi et al. (2013), AR knockdown in THP-1 cells promoted the expression of CCL2, which bound its receptor CCR2 on PCa cells and activated STAT3-mediated EMT (epithelial mesenchymal transition) and cell invasion/metastasis. However, studies also showed that androgen had the capacity to promote M2 macrophage polarization (Becerra-Diaz et al., 2018; Larsson et al., 2020), supporting the tumor-promoting role of AR signaling in PCa-associated macrophages. Indeed, conditioned medium from PMA-activated THP-1 cells with R1881 stimulation could promote cell migration and cell invasion of CWR-R1 PCa cells without affecting their proliferating ability *in vitro*

(Cioni et al., 2020). By applying ChIP-seq and Ingenuity Pathway Analysis, they identified that TREM-1 signaling was remarkably enriched in R1881-treated THP-1 cells compared to vehicle-treated ones, and AR physically bound to the proximal or distal upstream region of various genes related to TREM-1 signaling, implying that AR transcriptionally regulates the expression levels of these genes to control TREM-1 signaling. Further explorations revealed that several chemokines such as CCL2, CCL7, CCL13, and CXCL8 secreted by R1881-stimulated THP-1 were responsible for PCa migration. Importantly, TREM-1 signaling inhibitory peptide LP17 could block the R1881-stimulated production of these chemokines in THP-1 cells and attenuate the associated PCa migration.

THE ROLE OF ANDROGEN RECEPTOR IN CROSS TALK BETWEEN NATURAL KILLER CELLS AND PROSTATE CANCER

Natural killer (NK) cells are cytotoxic lymphocytes which play an important role in the regulation of innate immune response (Vivier et al., 2011; Perera Molligoda Arachchige, 2021). Accumulating evidence suggests that the infiltration of NK cells is greater in PCa than that in normal prostate tissues (Lin et al., 2017; Wu et al., 2020) and castration amplifies this phenomenon. By using the coculture system, Galustian et al. confirmed that PCa cells had a stronger ability to enhance IL-15-mediated expansion and cytotoxicity of NK cells than non-cancerous cell lines (PNT2 and WPMY-1) (Sakellariou et al., 2020), suggesting that the human body applies a protective strategy against PCa by activating NK cells. Accordantly, another study showed that AR could transcriptionally regulate the expression of NK inhibitory ligand LLT1 (lectin-like transcript 1) in PCa cells (Tang et al., 2020). Castration led to a short decline of AR activity so that the LLT1 level was reduced, eventually contributing to the expansion and activation of NK cells.

Specifically, the recruited NK cells could suppress the progression of CRPC by selectively degrading ARv7 (Lin et al., 2017), the most important AR variant determining CRPC growth and drug resistance (Antonarakis et al., 2014; Scher et al., 2016; Wang et al., 2017). NK cells could not only sensitize CRPC cells to anti-androgen treatment but also inhibit cell invasion of CRPC cells. More importantly, the suppression effect of NK cells on CRPC progression could be attenuated by the introduction of ARv7 into PCa cells. NK cells allowed CRPC cells to express high levels of miR-34 and miR-449, which bound the 3′-UTR of ARv7 and caused its degradation (Lin et al., 2017). As the direct downstream effect of ARv7, EZH2 was reduced upon NK cell treatment and was the key causal factor controlling PCa invasion. All these data indicate that targeting ARv7 or EZH2 may overcome CRPC progression.

CROSS TALK BETWEEN MAST CELLS AND PROSTATE CANCER

Mast cells are immune cells originated from myeloid stem cells. The wide distribution of mast cells across various tissues suggests that they act as key players to regulate a variety of physiological and pathological functions (Halova et al., 2012; Krystel-Whittemore et al., 2015). Typically, mast cells can be classified into intra-tumoral and peri-tumoral mast cells based on their location in specific tissues. Intra-tumoral mast cells exert a protective role to prevent cancer development while peri-tumoral mast cells support tumor growth (Fleischmann et al., 2009). Evidence supports the tumor-promoting role of mast cells in PCa owing to their peri-tumoral addiction (Johansson et al., 2010). Castration with ADT stimulates mast cell recruitment. Chang et al. used the coculture system to identify several chemoattractants including IL8, adrenomedullin (AM), and CCL8 as key molecules indispensable for mast cell recruitment (Dang et al., 2015). Interestingly, the expression levels of these cytokines were tightly regulated by AR. Castration-mediated AR inhibition increased the expression levels of IL8, AM, and CCL8 in PCa cells so that more mast cells were attracted. Their results also revealed that the recruited mast cells

TABLE 2 | The role of AR in PCa stromal cells.

Cell type	The role of AR	Effect on PCa	References
Endothelial cells	Is involved in TNF-induced apoptosis	Inhibits progression	Ling et al., 2002
	Induces VEGF-A and VCAM-1 expression, promotes proliferation	Promotes progression	Cai J. et al., 2011; Eisermann et al., 2013; Torres-Estay et al., 2017
CD4 T cells	Decreases IFN-γ production and suppresses CD4 T cell proliferation	Inhibits progression	Kissick et al., 2014
Fibroblasts	Upregulates FGF-2 and FGF-10 levels	Promotes initiation	Ricke et al., 2012
	Decreases cell proliferation while increase cell migration of fibroblasts cells		Castoria et al., 2011, 2014
	Negatively regulates the expression levels of CCL2, CCL8, M-CSF and IFN-γ	Inhibits invasion	Cioni et al., 2018; Palethorpe et al., 2018
	Regulates cytokines secretion	Increases growth invasion	Niu et al., 2008; Liao et al., 2017
Macrophages	Negatively regulates the expression levels of CCL2	Inhibits invasion	Izumi et al., 2013
	Promotes M2 macrophages polarization and regulates TREM-1 signaling	Promotes invasion	Becerra-Diaz et al., 2018; Cioni et al., 2020

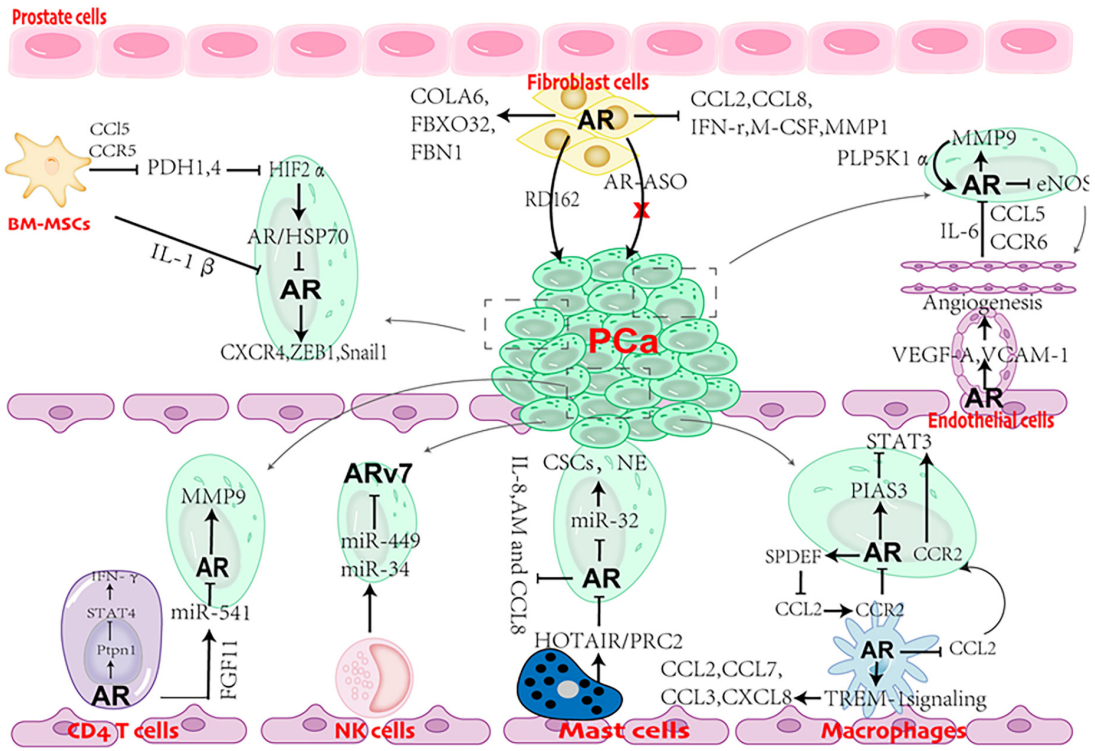

FIGURE 3 | Cartoon showing the role of AR in cross talks between stromal cells and prostate cancer (PCa) cells.

could drive neuroendocrine (NE) and stemness differentiation of PCa cells (Li et al., 2015), promoting cancer invasion and tumor metastasis. According to their data, miR-32 upregulation in PCa after AR inhibition was the causal factor determining NE differentiation. However, the targets of miR-32, potentially the direct downstream effectors regulating NE differentiation, are still not yet identified.

Evidence also revealed that infiltrating mast cells could enhance the occupation of the HOTAIR/PRC2-suppressing complex at the upstream promoter region of the AR gene locus, leading to the suppressive transcription of AR (Li et al., 2015). The exact role of AR in mast cells in regard to PCa growth and invasion/metastasis is another direction for further investigation.

CONCLUSION AND FUTURE PERSPECTIVE

Although clinical evidence suggests that stromal AR is gradually lost as PCa progresses to advanced stage, experimental results indicate that the role of AR in stromal cells is complicated (**Table 2**) and is still open for investigation. Stromal cells (CAFs, BM-MSCs, endothelial cells, CD4 + T cells, macrophages, NK cells, and mast cells) are clearly observed in PCa and castration with ADT or anti-androgen treatment further increasing the infiltration, leading to AR reduction (**Figure 3**). Although AR reduction retards PCa growth, it promotes PCa cell invasion and tumor metastasis. Further explorations support that AR inhibition increases the populations of cancer stem-like cells and neuroendocrine cells, which are widely viewed as AR negative and lethal type of PCa cells with little response to current treatments. Besides, AR inhibition also releases the transcriptional suppression on MMP9 and multiple cytokines (CCL5, CCL2 IL8, IL-1β and more). These cytokines serve as chemoattractants to recruit stromal cells into PCa. MMP9, as one of matrix metallopeptidases, can degrade the ECM and allow PCa cells to invade. From this point of view, although ADT can slow down PCa tumor growth, it predisposes PCa to undergo malignant transformation. Therefore, a simultaneous inhibition of AR signaling and the supporting stimuli from the surrounding microenvironment or signaling pathways involved in tumor metastasis is a promising therapeutic strategy to battle against PCa progression.

AUTHOR CONTRIBUTIONS

QT and BC drafted the manuscript. RD and RW oversaw this manuscript. All authors contributed to the article and approved the submitted version.

FUNDING

This work was supported by the China National Natural Science Foundation (81903113).

REFERENCES

Antonarakis, E. S., Lu, C., Wang, H., Luber, B., Nakazawa, M., Roeser, J. C., et al. (2014). AR-V7 and resistance to enzalutamide and abiraterone in prostate cancer. *N. Engl. J. Med.* 371, 1028–1038.

Ardiani, A., Gameiro, S. R., Kwilas, A. R., Donahue, R. N., and Hodge, J. W. (2014). Androgen deprivation therapy sensitizes prostate cancer cells to T-cell killing through androgen receptor dependent modulation of the apoptotic pathway. *Oncotarget* 5, 9335–9348. doi: 10.18632/oncotarget.2429

Becerra-Diaz, M., Strickland, A. B., Keselman, A., and Heller, N. M. (2018). Androgen and androgen receptor as enhancers of M2 macrophage polarization in allergic lung inflammation. *J. Immunol.* 201, 2923–2933. doi: 10.4049/jimmunol.1800352

Brennen, W. N., Zhang, B., Kulac, I., Kisteman, L. N., Antony, L., Wang, H., et al. (2017). Mesenchymal stem cell infiltration during neoplastic transformation of the human prostate. *Oncotarget* 8, 46710–46727. doi: 10.18632/oncotarget.17362

Cai, H., Babic, I., Wei, X., Huang, J., and Witte, O. N. (2011). , Invasive prostate carcinoma driven by c-Src and androgen receptor synergy. *Cancer Res.* 71, 862–872. doi: 10.1158/0008-5472.can-10-1605

Cai, J., Hong, Y., Weng, C., Tan, C., Imperato-McGinley, J., and Zhu, Y. S. (2011). Androgen stimulates endothelial cell proliferation via an androgen receptor/VEGF/cyclin A-mediated mechanism. *Am. J. Physiol. Heart Circ. Physiol.* 300, H1210–H1221.

Castoria, G., Auricchio, F., and Migliaccio, A. (2017). Extranuclear partners of androgen receptor: at the crossroads of proliferation, migration, and neuritogenesis. *FASEB J.* 31, 1289–1300. doi: 10.1096/fj.201601047r

Castoria, G., D'Amato, L., Ciociola, A., Giovannelli, P., Giraldi, T., Sepe, L., et al. (2011). Androgen-induced cell migration: role of androgen receptor/filamin A association. *PLoS One* 6:e17218. doi: 10.1371/journal.pone.0017218

Castoria, G., Giovannelli, P., Di Donato, M., Ciociola, A., Hayashi, R., Bernal, F., et al. (2014). Role of non-genomic androgen signalling in suppressing proliferation of fibroblasts and fibrosarcoma cells. *Cell Death Dis.* 5:e1548. doi: 10.1038/cddis.2014.497

Cha, H. R., Lee, J. H., Hensel, J. A., Sawant, A. B., Davis, B. H., Lee, C. M., et al. (2016). Prostate cancer-derived cathelicidin-related antimicrobial peptide facilitates macrophage differentiation and polarization of immature myeloid progenitors to protumorigenic macrophages. *Prostate* 76, 624–636. doi: 10.1002/pros.23155

Chang, M. A., Patel, V., Gwede, M., Morgado, M., Tomasevich, K., Fong, E. L., et al. (2014). IL-1beta induces p62/SQSTM1 and represses androgen receptor expression in prostate cancer cells. *J. Cell Biochem.* 115, 2188–2197.

Chen, T., Wang, L. H., and Farrar, W. L. (2000). Interleukin 6 activates androgen receptor-mediated gene expression through a signal transducer and activator of transcription 3-dependent pathway in LNCaP prostate cancer cells. *Cancer Res.* 60, 2132–2135.

Cioni, B., Nevedomskaya, E., Melis, M. H. M., van Burgsteden, J., Stelloo, S., Hodel, E., et al. (2018). Loss of androgen receptor signaling in prostate cancer-associated fibroblasts (CAFs) promotes CCL2- and CXCL8-mediated cancer cell migration. *Mol. Oncol.* 12, 1308–1323. doi: 10.1002/1878-0261.12327

Cioni, B., Zaalberg, A., van Beijnum, J. R., Melis, M. H. M., van Burgsteden, J., Muraro, M. J., et al. (2020). Androgen receptor signalling in macrophages promotes TREM-1-mediated prostate cancer cell line migration and invasion. *Nat. Commun.* 11:4498.

Comito, G., Giannoni, E., Segura, C. P., Barcellos-de-Souza, P., Raspollini, M. R., Baroni, G., et al. (2014). Cancer-associated fibroblasts and M2-polarized macrophages synergize during prostate carcinoma progression. *Oncogene* 33, 2423–2431. doi: 10.1038/onc.2013.191

Crawford, E. D., and Hou, A. H. (2009). The role of LHRH antagonists in the treatment of prostate cancer. *Oncology* 23, 626–630.

Dang, Q., Li, L., Xie, H., He, D., Chen, J., Song, W., et al. (2015). Anti-androgen enzalutamide enhances prostate cancer neuroendocrine (NE) differentiation via altering the infiltrated mast cells –> androgen receptor (AR) –> miRNA32 signals. *Mol. Oncol.* 9, 1241–1251. doi: 10.1016/j.molonc.2015.02.010

DePrimo, S. E., Diehn, M., Nelson, J. B., Reiter, R. E., Matese, J., Fero, M., et al. (2002). Transcriptional programs activated by exposure of human prostate cancer cells to androgen. *Genome Biol.* 3:RESEARCH0032.

Di Donato, M., Zamagni, A., Galasso, G., Di Zazzo, E., Giovannelli, P., Barone, M. V., et al. (2021). The androgen receptor/filamin A complex as a target in prostate cancer microenvironment. *Cell Death Dis.* 12:127.

Dudley, A. C. (2012). Tumor endothelial cells. *Cold Spring Harb. Perspect. Med.* 2:a006536.

Eisermann, K., Broderick, C. J., Bazarov, A., Moazam, M. M., and Fraizer, G. C. (2013). Androgen up-regulates vascular endothelial growth factor expression in prostate cancer cells via an Sp1 binding site. *Mol. Cancer* 12:7.

Fang, L. Y., Izumi, K., Lai, K. P., Liang, L., Li, L., Miyamoto, H., et al. (2013). Infiltrating macrophages promote prostate tumorigenesis via modulating androgen receptor-mediated CCL4-STAT3 signaling. *Cancer Res.* 73, 5633–5646. doi: 10.1158/0008-5472.can-12-3228

Fleischmann, A., Schlomm, T., Kollermann, J., Sekulic, N., Huland, H., Mirlacher, M., et al. (2009). Immunological microenvironment in prostate cancer: high mast cell densities are associated with favorable tumor characteristics and good prognosis. *Prostate* 69, 976–981. doi: 10.1002/pros.20948

Godoy, A., Montecinos, V. P., Gray, D. R., Sotomayor, P., Yau, J. M., Vethanayagam, R. R., et al. (2011). Androgen deprivation induces rapid involution and recovery of human prostate vasculature. *Am. J. Physiol. Endocrinol. Metab.* 300, E263–E275.

Halova, I., Draberova, L., and Draber, P. (2012). Mast cell chemotaxis - chemoattractants and signaling pathways. *Front. Immunol.* 3:119. doi: 10.3389/fimmu.2012.00119

Heinlein, C. A., and Chang, C. (2004). Androgen receptor in prostate cancer. *Endocr. Rev.* 25, 276–308.

Henshall, S. M., Quinn, D. I., Lee, C. S., Head, D. R., Golovsky, D., Brenner, P. C., et al. (2001). Altered expression of androgen receptor in the malignant epithelium and adjacent stroma is associated with early relapse in prostate cancer. *Cancer Res.* 61, 423–427.

Hu, S., Li, L., Yeh, S., Cui, Y., Li, X., Chang, H. C., et al. (2015). Infiltrating T cells promote prostate cancer metastasis via modulation of FGF11–>miRNA-541–>androgen receptor (AR)–>MMP9 signaling. *Mol. Oncol.* 9, 44–57. doi: 10.1016/j.molonc.2014.07.013

Izumi, K., Fang, L. Y., Mizokami, A., Namiki, M., Li, L., Lin, W. J., et al. (2013). Targeting the androgen receptor with siRNA promotes prostate cancer metastasis through enhanced macrophage recruitment via CCL2/CCR2-induced STAT3 activation. *EMBO Mol. Med.* 5, 1383–1401. doi: 10.1002/emmm.201202367

Johansson, A., Rudolfsson, S., Hammarsten, P., Halin, S., Pietras, K., Jones, J., et al. (2010). Mast cells are novel independent prognostic markers in prostate cancer and represent a target for therapy. *Am. J. Pathol.* 177, 1031–1041. doi: 10.2353/ajpath.2010.100070

Kissick, H. T., Sanda, M. G., Dunn, L. K., Pellegrini, K. L., On, S. T., Noel, J. K., et al. (2014). Androgens alter T-cell immunity by inhibiting T-helper 1 differentiation. *Proc. Natl. Acad. Sci. U.S.A.* 111, 9887–9892. doi: 10.1073/pnas.1402468111

Koivisto, P., Kononen, J., Palmberg, C., Tammela, T., Hyytinen, E., Isola, J., et al. (1997). Androgen receptor gene amplification: a possible molecular mechanism for androgen deprivation therapy failure in prostate cancer. *Cancer Res.* 57, 314–319.

Krystel-Whittemore, M., Dileepan, K. N., and Wood, J. G. (2015). Mast cell: a multi-functional master cell. *Front. Immunol.* 6:620. doi: 10.3389/fimmu.2015.00620

Larsson, P., Syed Khaja, A. S., Semenas, J., Wang, T., Sarwar, M., Dizeyi, N., et al. (2020). The functional interlink between AR and MMP9/VEGF signaling axis is mediated through PIP5K1alpha/pAKT in prostate cancer. *Int. J. Cancer* 146, 1686–1699. doi: 10.1002/ijc.32607

Leach, D. A., Need, E. F., Toivanen, R., Trotta, A. P., Palethorpe, H. M., Tamblyn, D. J., et al. (2015). Stromal androgen receptor regulates the composition of the microenvironment to influence prostate cancer outcome. *Oncotarget* 6, 16135–16150. doi: 10.18632/oncotarget.3873

Lepor, H., and Shore, N. D. (2012). LHRH agonists for the treatment of prostate cancer: 2012. *Rev. Urol.* 14, 1–12. doi: 10.1016/j.eursup.2005.04.002

Li, L., Dang, Q., Xie, H., Yang, Z., He, D., Liang, L., et al. (2015). Infiltrating mast cells enhance prostate cancer invasion via altering LncRNA-HOTAIR/PRC2-androgen receptor (AR)-MMP9 signals and increased stem/progenitor cell population. *Oncotarget* 6, 14179–14190. doi: 10.18632/oncotarget.3651

Li, Y., Li, C. X., Ye, H., Chen, F., Melamed, J., Peng, Y., et al. (2008). Decrease in stromal androgen receptor associates with androgen-independent disease and promotes prostate cancer cell proliferation and invasion. *J. Cell Mol. Med.* 12, 2790–2798. doi: 10.1111/j.1582-4934.2008.00279.x

Liao, C. P., Chen, L. Y., Luethy, A., Kim, Y., Kani, K., MacLeod, A. R., et al. (2017). Androgen receptor in cancer-associated fibroblasts influences stemness in cancer cells. *Endocr. Relat. Cancer* 24, 157–170. doi: 10.1530/erc-16-0138

Lin, S. J., Chou, F. J., Li, L., Lin, C. Y., Yeh, S., and Chang, C. (2017). Natural killer cells suppress enzalutamide resistance and cell invasion in the castration resistant prostate cancer via targeting the androgen receptor splicing variant 7 (ARv7). *Cancer Lett.* 398, 62–69. doi: 10.1016/j.canlet.2017.03.035

Lin, T. H., Izumi, K., Lee, S. O., Lin, W. J., Yeh, S., and Chang, C. (2013). Anti-androgen receptor ASC-J9 versus anti-androgens MDV3100 (Enzalutamide) or Casodex (Bicalutamide) leads to opposite effects on prostate cancer metastasis via differential modulation of macrophage infiltration and STAT3-CCL2 signaling. *Cell Death Dis.* 4:e764. doi: 10.1038/cddis.2013.270

Ling, S., Dai, A., Williams, M. R., Myles, K., Dilley, R. J., Komesaroff, P. A., et al. (2002). Testosterone (T) enhances apoptosis-related damage in human vascular endothelial cells. *Endocrinology* 143, 1119–1125. doi: 10.1210/endo.143.3.8679

Linxweiler, J., Hajili, T., Korbel, C., Berchem, C., Zeuschner, P., Muller, A., et al. (2020). Cancer-associated fibroblasts stimulate primary tumor growth and metastatic spread in an orthotopic prostate cancer xenograft model. *Sci. Rep.* 10:12575.

Liu, Y., Karaca, M., Zhang, Z., Gioeli, D., Earp, H. S., and Whang, Y. E. (2010). Dasatinib inhibits site-specific tyrosine phosphorylation of androgen receptor by Ack1 and Src kinases. *Oncogene* 29, 3208–3216. doi: 10.1038/onc.2010.103

Lonergan, P. E., and Tindall, D. J. (2011). Androgen receptor signaling in prostate cancer development and progression. *J. Carcinog.* 10:20. doi: 10.4103/1477-3163.83937

Loy, C. J., Sim, K. S., and Yong, E. L. (2003). Filamin-A fragment localizes to the nucleus to regulate androgen receptor and coactivator functions. *Proc. Natl. Acad. Sci. U.S.A.* 100, 4562–4567. doi: 10.1073/pnas.0736237100

Luo, J., Lee, S. O., Cui, Y., Yang, R., Li, L., and Chang, C. (2015). Infiltrating bone marrow mesenchymal stem cells (BM-MSCs) increase prostate cancer cell invasion via altering the CCL5/HIF2alpha/androgen receptor signals. *Oncotarget* 6, 27555–27565.

Luo, J., Ok Lee, S., Liang, L., Huang, C. K., Li, L., Wen, S., et al. (2014). Infiltrating bone marrow mesenchymal stem cells increase prostate cancer stem cell population and metastatic ability via secreting cytokines to suppress androgen receptor signaling. *Oncogene* 33, 2768–2778. doi: 10.1038/onc.2013.233

McArdle, P. A., Canna, K., McMillan, D. C., McNicol, A. M., Campbell, R., and Underwood, M. A. (2004). The relationship between T-lymphocyte subset infiltration and survival in patients with prostate cancer. *Br. J. Cancer* 91, 541–543. doi: 10.1038/sj.bjc.6601943

Mendez-Ferrer, S., Michurina, T. V., Ferraro, F., Mazloom, A. R., Macarthur, B. D., Lira, S. A., et al. (2010). Mesenchymal and haematopoietic stem cells form a unique bone marrow niche. *Nature* 466, 829–834. doi: 10.1038/nature09262

Mercader, M., Bodner, B. K., Moser, M. T., Kwon, P. S., Park, E. S., Manecke, R. G., et al. (2001). T cell infiltration of the prostate induced by androgen withdrawal in patients with prostate cancer. *Proc. Natl. Acad. Sci. U.S.A.* 98, 14565–14570.

Migliaccio, A., Castoria, G., Di Domenico, M., de Falco, A., Bilancio, A., Lombardi, M., et al. (2000). Steroid-induced androgen receptor-oestradiol receptor beta-Src complex triggers prostate cancer cell proliferation. *EMBO J.* 19, 5406–5417. doi: 10.1093/emboj/19.20.5406

Migliaccio, A., Di Domenico, M., Castoria, G., Nanayakkara, M., Lombardi, M., de Falco, A., et al. (2005). Steroid receptor regulation of epidermal growth factor signaling through Src in breast and prostate cancer cells: steroid antagonist action. *Cancer Res.* 65, 10585–10593. doi: 10.1158/0008-5472.can-05-0912

Montgomery, R. B., Mostaghel, E. A., Vessella, R., Hess, D. L., Kalhorn, T. F., Higano, C. S., et al. (2008). Maintenance of intratumoral androgens in metastatic prostate cancer: a mechanism for castration-resistant tumor growth. *Cancer Res.* 68, 4447–4454. doi: 10.1158/0008-5472.can-08-0249

Nakazawa, M., Antonarakis, E. S., and Luo, J. (2014). Androgen receptor splice variants in the era of enzalutamide and abiraterone. *Horm. Cancer* 5, 265–273. doi: 10.1007/s12672-014-0190-1

Niu, Y., Altuwaijri, S., Lai, K. P., Wu, C. T., Ricke, W. A., Messing, E. M., et al. (2008). Androgen receptor is a tumor suppressor and proliferator in prostate cancer. *Proc. Natl. Acad. Sci. U.S.A.* 105, 12182–12187.

Olapade-Olaopa, E. O., MacKay, E. H., Taub, N. A., Sandhu, D. P., Terry, T. R., and Habib, F. K. (1999). Malignant transformation of human prostatic epithelium is associated with the loss of androgen receptor immunoreactivity in the surrounding stroma. *Clin. Cancer Res.* 5, 569–576.

Palethorpe, H. M., Leach, D. A., Need, E. F., Drew, P. A., and Smith, E. (2018). Myofibroblast androgen receptor expression determines cell survival in co-cultures of myofibroblasts and prostate cancer cells in vitro. *Oncotarget* 9, 19100–19114. doi: 10.18632/oncotarget.24913

Perera Molligoda Arachchige, A. S. (2021). Human NK cells: from development to effector functions. *Innate Immun.* 27, 212–229. doi: 10.1177/17534259211001512

Peterziel, H., Mink, S., Schonert, A., Becker, M., Klocker, H., and Cato, A. C. (1999). Rapid signalling by androgen receptor in prostate cancer cells. *Oncogene* 18, 6322–6329. doi: 10.1038/sj.onc.1203032

Pidsley, R., Lawrence, M. G., Zotenko, E., Niranjan, B., Statham, A., Song, J., et al. (2018). Enduring epigenetic landmarks define the cancer microenvironment. *Genome Res.* 28, 625–638. doi: 10.1101/gr.229070.117

Pittenger, M. F., Mackay, A. M., Beck, S. C., Jaiswal, R. K., Douglas, R., Mosca, J. D., et al. (1999). Multilineage potential of adult human mesenchymal stem cells. *Science* 284, 143–147.

Placencio, V. R., Li, X., Sherrill, T. P., Fritz, G., and Bhowmick, N. A. (2010). Bone marrow derived mesenchymal stem cells incorporate into the prostate during regrowth. *PLoS One* 5:e12920. doi: 10.1371/journal.pone.0012920

Ricciardelli, C., Choong, C. S., Buchanan, G., Vivekanandan, S., Neufing, P., Stahl, J., et al. (2005). Androgen receptor levels in prostate cancer epithelial and peritumoral stromal cells identify non-organ confined disease. *Prostate* 63, 19–28. doi: 10.1002/pros.20154

Ricke, E. A., Williams, K., Lee, Y. F., Couto, S., Wang, Y., Hayward, S. W., et al. (2012). Androgen hormone action in prostatic carcinogenesis: stromal androgen receptors mediate prostate cancer progression, malignant transformation and metastasis. *Carcinogenesis* 33, 1391–1398. doi: 10.1093/carcin/bgs153

Roumiguie, M., Paoletti, X., Neuzillet, Y., Mathieu, R., Vincendeau, S., Kleinclauss, F., et al. (2021). Apalutamide, darolutamide and enzalutamide in nonmetastatic castration-resistant prostate cancer: a meta-analysis. *Future Oncol.* 17, 1811–1823. doi: 10.2217/fon-2020-1104

Ruizeveld de Winter, J. A., Janssen, P. J., Sleddens, H. M., Verleun-Mooijman, M. C., Trapman, J., Brinkmann, A. O., et al. (1994). Androgen receptor status in localized and locally progressive hormone refractory human prostate cancer. *Am. J. Pathol.* 144, 735–746.

Sahai, E., Astsaturov, I., Cukierman, E., DeNardo, D. G., Egeblad, M., Evans, R. M., et al. (2020). A framework for advancing our understanding of cancer-associated fibroblasts. *Nat. Rev. Cancer* 20, 174–186. doi: 10.1038/s41568-019-0238-1

Sakellariou, C., Elhage, O., Papaevangelou, E., Giustarini, G., Esteves, A. M., Smolarek, D., et al. (2020). Prostate cancer cells enhance interleukin-15-mediated expansion of NK cells. *BJU Int.* 125, 89–102. doi: 10.1111/bju.14893

Sanchez, C., Chan, R., Bajgain, P., Rambally, S., Palapattu, G., Mims, M., et al. (2013). Combining T-cell immunotherapy and anti-androgen therapy for prostate cancer. *Prostate Cancer Prostatic Dis.* 16, 123–31,S1.

Scher, H. I., Beer, T. M., Higano, C. S., Anand, A., Taplin, M. E., Efstathiou, E., et al. (2010). Antitumour activity of MDV3100 in castration-resistant prostate cancer: a phase 1-2 study. *Lancet* 375, 1437–1446.

Scher, H. I., Buchanan, G., Gerald, W., Butler, L. M., and Tilley, W. D. (2004). Targeting the androgen receptor: improving outcomes for castration-resistant prostate cancer. *Endocr. Relat. Cancer* 11, 459–476. doi: 10.1677/erc.1.00525

Scher, H. I., Lu, D., Schreiber, N. A., Louw, J., Graf, R. P., Vargas, H. A., et al. (2016). Association of AR-V7 on circulating tumor cells as a treatment-specific biomarker with outcomes and survival in castration-resistant prostate cancer. *JAMA Oncol.* 2, 1441–1449. doi: 10.1001/jamaoncol.2016.1828

Schweizer, M. T., and Antonarakis, E. S. (2012). Abiraterone and other novel androgen-directed strategies for the treatment of prostate cancer: a new era of hormonal therapies is born. *Ther. Adv. Urol.* 4, 167–178. doi: 10.1177/1756287212452196

Seaton, A., Scullin, P., Maxwell, P. J., Wilson, C., Pettigrew, J., Gallagher, R., et al. (2008). Interleukin-8 signaling promotes androgen-independent proliferation

of prostate cancer cells via induction of androgen receptor expression and activation. *Carcinogenesis* 29, 1148–1156. doi: 10.1093/carcin/bgn109

Sejda, A., Sigorski, D., Gulczynski, J., Wesolowski, W., Kitlinska, J., and Izycka-Swieszewska, E. (2020). Complexity of neural component of tumor microenvironment in prostate cancer. *Pathobiology* 87, 87–99. doi: 10.1159/000505437

Shabsigh, A., Chang, D. T., Heitjan, D. F., Kiss, A., Olsson, C. A., Puchner, P. J., et al. (1998). Rapid reduction in blood flow to the rat ventral prostate gland after castration: preliminary evidence that androgens influence prostate size by regulating blood flow to the prostate gland and prostatic endothelial cell survival. *Prostate* 36, 201–206. doi: 10.1002/(sici)1097-0045(19980801)36:3<201::aid-pros9>3.0.co;2-j

Sica, A., Larghi, P., Mancino, A., Rubino, L., Porta, C., Totaro, M. G., et al. (2008). Macrophage polarization in tumour progression. *Semin. Cancer Biol.* 18, 349–355.

Siegel, R. L., Miller, K. D., and Jemal, A. (2020). Cancer statistics, 2020. *CA Cancer J. Clin.* 70, 7–30.

Smith, D. F., and Toft, D. O. (2008). Minireview: the intersection of steroid receptors with molecular chaperones: observations and questions. *Mol. Endocrinol.* 22, 2229–2240. doi: 10.1210/me.2008-0089

Tan, M. H., Li, J., Xu, H. E., Melcher, K., and Yong, E. L. (2015). Androgen receptor: structure, role in prostate cancer and drug discovery. *Acta Pharmacol. Sin.* 36, 3–23. doi: 10.1038/aps.2014.18

Tang, M., Gao, S., Zhang, L., Liu, B., Li, J., Wang, Z., et al. (2020). Docetaxel suppresses immunotherapy efficacy of natural killer cells toward castration-resistant prostate cancer cells via altering androgen receptor-lectin-like transcript 1 signals. *Prostate* 80, 742–752. doi: 10.1002/pros.23988

Taylor, R. A., Toivanen, R., Frydenberg, M., Pedersen, J., Harewood, L., and Australian Prostate Cancer Bioresource. (2012). Human epithelial basal cells are cells of origin of prostate cancer, independent of CD133 status. *Stem Cells* 30, 1087–1096. doi: 10.1002/stem.1094

Thienger, P., and Rubin, M. A. (2021). Prostate cancer hijacks the microenvironment. *Nat. Cell Biol.* 23, 3–5. doi: 10.1038/s41556-020-00616-3

Tilley, W. D., Buchanan, G., Hickey, T. E., and Bentel, J. M. (1996). Mutations in the androgen receptor gene are associated with progression of human prostate cancer to androgen independence. *Clin. Cancer Res.* 2, 277–285.

Tomic, T. T., Gustavsson, H., Wang, W., Jennbacken, K., Welen, K., and Damber, J. E. (2012). Castration resistant prostate cancer is associated with increased blood vessel stabilization and elevated levels of VEGF and Ang-2. *Prostate* 72, 705–712. doi: 10.1002/pros.21472

Torres-Estay, V., Carreno, D. V., Fuenzalida, P., Watts, A., . San Francisco, I. F., Montecinos, V. P., et al. (2017). Androgens modulate male-derived endothelial cell homeostasis using androgen receptor-dependent and receptor-independent mechanisms. *Angiogenesis* 20, 25–38. doi: 10.1007/s10456-016-9525-6

Tsai, Y. C., Chen, W. Y., Abou-Kheir, W., Zeng, T., Yin, J. J., Bahmad, H., et al. (2018). Androgen deprivation therapy-induced epithelial-mesenchymal transition of prostate cancer through downregulating SPDEF and activating CCL2. *Biochim. Biophys. Acta Mol. Basis Dis.* 1864, 1717–1727. doi: 10.1016/j.bbadis.2018.02.016

Visakorpi, T., Hyytinen, E., Koivisto, P., Tanner, M., Keinanen, R., Palmberg, C., et al. (1995). In vivo amplification of the androgen receptor gene and progression of human prostate cancer. *Nat. Genet.* 9, 401–406. doi: 10.1038/ng0495-401

Vivier, E., Raulet, D. H., Moretta, A., Caligiuri, M. A., Zitvogel, L., Lanier, L. L., et al. (2011). Innate or adaptive immunity? The example of natural killer cells. *Science* 331, 44–49.

Waghray, A., Feroze, F., Schober, M. S., Yao, F., Wood, C., Puravs, E., et al. (2001). Identification of androgen-regulated genes in the prostate cancer cell line LNCaP by serial analysis of gene expression and proteomic analysis. *Proteomics* 1, 1327–1338. doi: 10.1002/1615-9861(200110)1:10<1327::aid-prot1327>3.0.co;2-b

Wang, R., Sun, Y., Li, L., Niu, Y., Lin, W., Lin, C., et al. (2017). Preclinical study using malat1 small interfering RNA or androgen receptor splicing variant 7 degradation enhancer ASC-J9((R)) to suppress enzalutamide-resistant prostate cancer progression. *Eur. Urol.* 72, 835–844. doi: 10.1016/j.eururo.2017.04.005

Wang, X., Lee, S. O., Xia, S., Jiang, Q., Luo, J., Li, L., et al. (2013). Endothelial cells enhance prostate cancer metastasis via IL-6–>androgen receptor–>TGF-beta–>MMP-9 signals. *Mol. Cancer Ther.* 12, 1026–1037. doi: 10.1158/1535-7163.mct-12-0895

Wikstrom, P., Marusic, J., Stattin, P., and Bergh, A. (2009). Low stroma androgen receptor level in normal and tumor prostate tissue is related to poor outcome in prostate cancer patients. *Prostate* 69, 799–809. doi: 10.1002/pros.20927

Wu, J. D., Haugk, K., Woodke, L., Nelson, P., Coleman, I., and Plymate, S. R. (2006). Interaction of IGF signaling and the androgen receptor in prostate cancer progression. *J. Cell Biochem.* 99, 392–401.

Wu, Z., Chen, H., Luo, W., Zhang, H., Li, G., Zeng, F., et al. (2020). The landscape of immune cells infiltrating in prostate Cancer. *Front. Oncol.* 10:517637. doi: 10.3389/fonc.2020.517637I

Yu, S., Jia, L., Zhang, Y., Wu, D., Xu, Z., Ng, C. F., et al. (2013). Increased expression of activated endothelial nitric oxide synthase contributes to antiandrogen resistance in prostate cancer cells by suppressing androgen receptor transactivation. *Cancer Lett.* 328, 83–94. doi: 10.1016/j.canlet.2012.09.006

Yu, S., Jiang, Y., Wan, F., Wu, J., Gao, Z., and Liu, D. (2017). Immortalized cancer-associated fibroblasts promote prostate cancer carcinogenesis. Proliferation and Invasion. *Anticancer Res.* 37, 4311–4318.

Yuri, P., Shigemura, K., Kitagawa, K., Hadibrata, E., Risan, M., Zulfiqqar, A., et al. (2020). Increased tumor-associated macrophages in the prostate cancer microenvironment predicted patients' survival and responses to androgen deprivation therapies in Indonesian patients cohort. *Prostate Int.* 8, 62–69. doi: 10.1016/j.prnil.2019.12.001

Zhao, R., Bei, X., Yang, B., Wang, X., Jiang, C., Shi, F., et al. (2018). Endothelial cells promote metastasis of prostate cancer by enhancing autophagy. *J. Exp. Clin. Cancer Res.* 37:221.

Zhu, P., Baek, S. H., Bourk, E. M., Ohgi, K. A., Garcia-Bassets, I., Sanjo, H., et al. (2006). Macrophage/cancer cell interactions mediate hormone resistance by a nuclear receptor derepression pathway. *Cell* 124, 615–629. doi: 10.1016/j.cell.2005.12.032

Conflict of Interest: The authors declare that the research was conducted in the absence of any commercial or financial relationships that could be construed as a potential conflict of interest.

Publisher's Note: All claims expressed in this article are solely those of the authors and do not necessarily represent those of their affiliated organizations, or those of the publisher, the editors and the reviewers. Any product that may be evaluated in this article, or claim that may be made by its manufacturer, is not guaranteed or endorsed by the publisher.

frontiers in Cell and Developmental Biology

REVIEW
published: 07 October 2021
doi: 10.3389/fcell.2021.738373

Crosstalk Between the Tumor Microenvironment and Cancer Cells: A Promising Predictive Biomarker for Immune Checkpoint Inhibitors

Xiaoying Li[1†], Yueyao Yang[2†], Qian Huang[1], Yu Deng[3], Fukun Guo[4], Gang Wang[2] and Ming Liu[1*]*

[1] Department of Abdominal Oncology, West China Hospital, Sichuan University, Chengdu, China, [2] National Engineering Research Center for Biomaterials, Sichuan University, Chengdu, China, [3] School of Basic Medical Science, Chengdu University, Chengdu, China, [4] Division of Experimental Hematology and Cancer Biology, Children's Hospital Medical Center, Cincinnati, OH, United States

OPEN ACCESS

Edited by:
Na Luo,
Nankai University, China

Reviewed by:
Shou Jiawei,
Zhejiang University, China
Guoku Hu,
University of Nebraska Medical Center, United States

****Correspondence:***
Ming Liu
mingliu721@aliyun.com
Gang Wang
wgang@scu.edu.cn

[†] These authors have contributed equally to this work

Specialty section:
This article was submitted to Molecular and Cellular Pathology, a section of the journal Frontiers in Cell and Developmental Biology

Received: *08 July 2021*
Accepted: *20 September 2021*
Published: *07 October 2021*

Citation:
Li X, Yang Y, Huang Q, Deng Y, Guo F, Wang G and Liu M (2021) Crosstalk Between the Tumor Microenvironment and Cancer Cells: A Promising Predictive Biomarker for Immune Checkpoint Inhibitors. Front. Cell Dev. Biol. 9:738373. doi: 10.3389/fcell.2021.738373

Immune checkpoint inhibitors (ICIs) have changed the landscape of cancer treatment and are emerging as promising curative treatments in different type of cancers. However, only a small proportion of patients have benefited from ICIs and there is an urgent need to find robust biomarkers for individualized immunotherapy and to explore the causes of immunotherapy resistance. In this article, we review the roles of immune cells in the tumor microenvironment (TME) and discuss the effects of ICIs on these cell populations. We discuss the potential of the functional interaction between the TME and cancer cells as a predictive biomarker for ICIs. Furthermore, we outline the potential personalized strategies to improve the effectiveness of ICIs with precision.

Keywords: tumor microenvironment, innate immunity, responsive or resistant biomarkers, immune checkpoint inhibitors, immune cells

INTRODUCTION

The tumor microenvironment (TME) is a key component of tumors that consists of various cell types including immune cells, endothelial cells, cancer-associated fibroblasts (CAFs) along with cytokines, chemokines and the extracellular matrix (ECM) (Hanahan and Weinberg, 2011). While certain cells in the TME have the potential to inhibit tumor development, other cells in the TME act synergistically with tumor cells to enhance tumor development (**Figure 1**). The tumor-promoting factors in the TME include immunosuppressive effector molecules and effector cells such as regulatory T cells (Tregs), myeloid-derived suppressor cells (MDSCs), and tumor-associated macrophages (TAMs) (Junttila and de Sauvage, 2013). The interaction between immunosuppressive TME and tumor cells regulates a range of cellular processes including tumor cell proliferation and metastasis. It also protects tumor cells from the clearance by immune effector cells. In addition, tumor cells can escape host immune reactions through immune checkpoints (Sharpe and Freeman, 2002; Francisco et al., 2010; Pardoll, 2012). Recently, immune checkpoint inhibitors (ICIs) targeting programmed cell death protein (PD-1), programmed death-ligand (PD-L1), and T-lymphocyte-associated protein 4 (CTLA-4) have shown efficacies in restoring antitumor immunity in multiple tumor types with tolerable adverse-event profiles (Zheng et al., 2017; Ren and Zhang, 2019; Yost et al., 2019). However, only a small proportion of patients showed strong responses to ICIs, as

many patients developed primary or acquired resistance (Zheng et al., 2017). Thus, there is a need to find biomarkers to inform patient-specific treatments and to better understand the molecular mechanisms underlying the drug resistance. At present, predictive biomarkers are limited to PD-L1, tumor mutation burden (TMB) and MSI-H/dMMR. As these biomarkers are often unreliable, better biomarkers are highly desired. Given that the TME is a major obstacle to the success of cancer immunotherapy (Yost et al., 2019), one could imagine that the TME may serve as a predictive biomarker for ICIs. In this context, it is desired to better understand the complexities of immune cells within the TME, which may be achieved by using cutting-edge techniques such as single-cell RNA sequencing and mass cytometry (Spitzer and Nolan, 2016; Zheng et al., 2017; Simoni et al., 2018; Kiselev et al., 2019; Ren and Zhang, 2019; Zhang and Zhang, 2019). In this paper, we review the molecular heterogeneity of the TME and relate it to the unique challenges and opportunities for ICIs (**Figure 1**).

THE BIOLOGICAL FUNCTIONS OF INNATE IMMUNITY WITHIN THE TME IN CANCER IMMUNOTHERAPY

Anti-tumor immunity depends on tumor immunogenicity and the immune function of the host and other factors. The tissue of origin and occurrence of tumor cells leads to significant variations in immunogenicity and anti-tumor immune responses. Tumor immune responses include innate and adaptive response. Innate immunity develops gradually with age and involves the evolution and adaptation of the immune system. Generally, innate immune response is the first line anti-tumor effectors whilst the adaptive immune response plays more specific roles in the immune responses. However, innate immune response [dendritic cells (DCs), natural killer (NK) cells, TAMs, and tumor-associated neutrophils (TANs)] and adaptive immune response [$CD8^+$ cytotoxic T cells (CTLs), $CD4^+$ T helper 1 (Th1), and B cells] are complementary and interdependent (Tanaka et al., 1999).

Dendritic Cells Within the TME Coordinate the Priming and Differentiation of T Cells

Dendritic cells are the central antigen-presenting cells (APCs) that can directly activate naïve T cells. DCs initiate the adaptive immune response and mediate interactions between innate and adaptive immune responses (von Andrian, 2002; Batista and Harwood, 2009). Following the activation of DCs, an inflammatory response is triggered and pro-inflammatory cytokines and chemokines are released to regulate immune function. The maturation and metastasis of DCs to the lymph nodes result in the activation of antigen-specific T cells that participate in adaptive immunity. DCs express high levels of adhesion molecules such as intracellular cell adhesion molecule 1 (ICAM-1) that allow strong binding to T cells and facilitate intercellular interactions (Segura et al., 2005). ICAM can participate in the innate immune response by recognizing and transporting antigens and can initiate an adaptive immune response, as well as enhancing antigen presentation and CTLs priming (von Andrian, 2002; Allan et al., 2006). Mature DCs express high levels of costimulatory molecules such as CD86, CD40, and CD80. CD40 and its ligand CD40L are also expressed on the surface of other APCs, such as B cells and macrophages, and act to significantly increase antigen presentation and co-stimulatory capacity (Schoenberger et al., 1998).

Dendritic cells present tumor-associated neoantigens through pattern recognition receptors (PRRs) in the early stages of tumorigenesis. Inter-tumoral stimulatory dendritic cells (SDCs) can stimulate CTLs and initiate immune responses against cancer. The activation of DCs is positively correlated with T-cell inflammatory status and response to PD-1/PD-L1 pathway inhibition (Barry et al., 2018).

A previous study investigated the TME in gastric cancer using single-cell RNA sequencing. The study reported that DCs infiltrating the TME (TIDCs) expressed chemokines such as CCL17, CCL19, CCL22, and IL-32 that helped recruit naïve T cells. These cells also displayed unique gene expression programs that differed from peripheral blood mononuclear cells (PBMCs) (Sathe et al., 2020). Although TIDCs have anti-tumor potential within the TME, the function of these cells is often impaired at the later stages of tumor development due to interactions among tumor cells and surrounding immune cells. In the early stage of tumorigenesis, PD-1 expression is low on TIDCs and cytokines such as IL-10, TGF-β, and arginase in the TME can upregulate the expression of immunosuppressive molecules, such as PD-1 and Tim-3, on TIDC cells. The overexpression of the molecules acts to convert DCs with anti-tumor potential into immunosuppressive DCs (Gardner et al., 2020).

Within the TME, cytokines produced by DCs may induce the activation and proliferation of Tregs (**Figure 1**). A novel subset of tolerogenic DCs can also promote the differentiation of T-regulatory cells (Tr1) through producing high levels of IL-10 (Gregori et al., 2010). DCs can secrete CCL22 that promotes interactions between DCs and Tregs *via* binding to its receptor CCR4. The recruitment of Tregs into the tumors cause immune suppression and downregulation of co-stimulatory molecules on DCs, causing CTLs dysfunction (Curiel et al., 2004; Bauer et al., 2014; Rapp et al., 2019). Ibrahim et al. (2012) showed that liver DCs with low lipid concentrations induced anergy in Tregs whilst DCs with high levels of lipids were immunogenic in many models and functioned to activate T and NK cells.

Function of NK Cells in the TME

$CD3^-CD56^+$ NK cells can be divided into $CD56^{bright}$ and $CD56^{dim}$ subtypes. The main function of $CD56^{bright}$ NK cells is to secrete cytokines whilst $CD56^{dim}$ NK cells mainly mediate cytotoxicity. NK cells can kill targeted cells through several specific pathways including antibody-dependent cellular cytotoxicity (ADCC), the Fas-FasL pathway, the perforin-granzyme pathway and the secretion of pro-inflammatory cytokines, such as TNF, IFN-γ, GM-CSF, IL-6, and CCL5 (Voskoboinik et al., 2006; Guillerey et al., 2016; Habif et al., 2019).

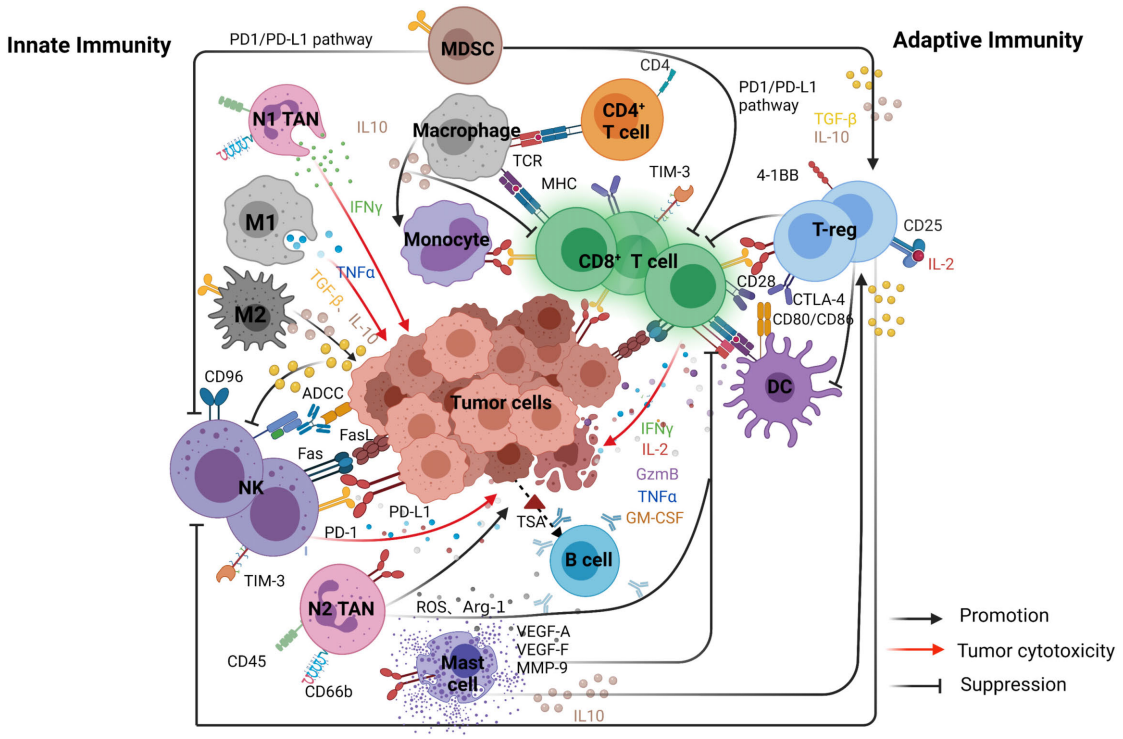

FIGURE 1 | The main interactions of immune cells and the relationships between tumor and immune cells in the TME. The figure is divided into two parts to show the complementary and interdependent relationship between innate and adaptive immunity. Left, represents innate immunity included natural killer (NK) cells, dendritic cells (DCs), tumor-associated macrophages (TAMs), and tumor-associated neutrophils (TANs). Right, represents adaptive immunity included CD8 + cytotoxic T cells (CTLs), CD4 + T helper 1 (Th1), and B cells.

In the early stages of tumor development, NK cells are the first line of defense against tumors. NK cells could migrate into tumors in response to chemokines secreted by DCs (Guillerey et al., 2016). The deletion or decreased expression of MHC molecules on the surface of tumor cells prevent the binding of NKs to the inhibitory receptor (killer inhibitory receptor, KIR) that inhibits the initiation of killing inhibitory signal. However, surface carbohydrate ligands can bind to the activated receptor (killer activation receptor, KAR) on the surface of NK cells to activate NK cells and exert a killing effect (Long, 2008; Thielens et al., 2012; Myers and Miller, 2021). Similar to TIDC, tumor-infiltrating NK cells have anti-tumor and anti-metastatic potential. In melanoma patients, it has been reported that NK cells positively regulated intratumoral SDCs through the production of cytokine FLT3L to enhance T cell responses (Veglia et al., 2018). In some tumors, tumor-infiltrating NK cells undergo phenotypic changes and dysfunctions compared to normal NK cells, which partially explains why NK cell-targeted therapies have low efficacy in some tumor types. The function of NK cells is suppressed by soluble regulatory factors (e.g., TGF-β) in the TME that can act directly on NK cells, leading to reduced cytotoxicity and cytokine secretion. Tumor-infiltrating NK cells' function can also be dampened by NK cell-autonomous inhibitory checkpoints such as PD-1, TIGIT, CD96, TIM-3, LAG-3, CTLA-4, KIR2DL-1/2/3 and NKG2A (Guillerey et al., 2016). Previous studies have indicated that PD-1 expression on tumor-associated NK cells requires glucocorticoids (Quatrini et al., 2021; **Figure 1**). While ICIs may restore NK cell-mediated anti-tumor immunity (Kamran et al., 2017; Holmgaard et al., 2018; Sivori et al., 2020). Furthermore, anti-CD96 has been shown to stimulate NK cell function and improve the efficacy of ICIs (Du Four et al., 2016; Davis et al., 2017).

Macrophages Within the TME Can Play a Tumor-Inhibitory or Tumor-Promoting Role

Tumor-associated macrophages are the main component of the TME where they can promote the formation of an immunosuppressive microenvironment or suppress tumorigenesis and metastasis, depending on the direct or indirect suppression of cytotoxic T-cell activity (Mantovani et al., 2017; Lin et al., 2019), accordingly divided into anti-tumor M1 and pro-tumor M2 types (Biswas and Mantovani, 2010; **Figure 1**). TAMs can suppress immune responses by producing immunosuppressive mediators/cytokines and also by expressing the inhibitory receptor, thus affect the infiltration of CTLs and suppress the function of CTLs by expressing the molecular triggers of checkpoint proteins (De Palma and Lewis, 2013; Ruffell and Coussens, 2015; Mantovani et al., 2017; Lin et al., 2019). As TAMs are the primary source of IL-10 in tumors and IL-10 can promote the expression of PD-L1 on monocytes,

PD-L1$^+$ monocytes can effectively inhibit tumor-specific T-cell immunity *via* the infiltration of Tregs and dysfunction of CD8 T-cells (Zhang et al., 2020; **Figure 1**). They can also promote tumor growth, indicating that PD-L1 expression on activated macrophages is a potential mechanism linking the pro-inflammatory response to the immune tolerance of the TME (Wynn et al., 2013; Romano et al., 2015; Zhang et al., 2020).

M1 macrophages, characterized with production of inflammatory cytokines and reactive oxygen/nitrogen species, showed anti-tumor effect and were valuable for host defense (Wynn et al., 2013). Moreover, it were reported to show high ratios in responder treated with ipilimumab (a fully human CTLA-4-specific mAb) in comparison with non-responder (Romano et al., 2015).The expression of PD-1 on TAMs and its interaction with PD-L1 on tumor cells may impair phagocytic capacity of macrophage. Interestingly, most of the PD-1 were found in M2 macrophages, and ICIs treatment could revert their function to M1 phenotype for killing tumor (Gordon et al., 2017; **Figure 1**). Tumor cells can cause macrophages to exhibit an immunosuppressive phenotype *via* releasing the autophagosome (TRAPs). The expression of PD-L1 and IL-10 can hinder the proliferation of CD4$^+$ and CD8$^+$ T cells, indicating that the TRAPs-PD-L1 axis is a promising option by simultaneously targeting autophagy and PD-L1 (Wen et al., 2018).

In contrast to M1 macrophages' antitumor role, M2 macrophages predominate within the TME and can promote vascular growth, invasion and metastasis, and enhance chemoresistance (Xia et al., 2020). It has been reported that M2 polarization increased the expression of PD-L2 in TAMs that could lead to immune escape and tumor promotion through the PD-1 signal pathway (Huber et al., 2010). These data indicated that TAMs-targeting *via* blocking the CCL2-CCR2 axis was potential strategy to overcome immune evasion, and inhibiting the recruitment of TAMs might enhance the antitumor effect of CTLs in the TME (Yang et al., 2020). Besides, the ratio of M1/M2 macrophages can be used to evaluate the effectiveness of immunotherapy. Sathe et al. found that the TME could be reprogrammed based on the state of macrophages. The phenomena that TAMs differentiated from monocytes and retained basic features of macrophages were also found in normal tissues (Sathe et al., 2020).

The interaction of PD-L1 on T-cells with PD-1 on macrophage impacts the tolerance of macrophage differentiation (Diskin et al., 2020). Although macrophages have immuno-suppressive roles, the pro-inflammatory F480$^+$MHCII$^+$Ly6Cc low macrophage can induce interferon by secreting CXCL9. In patients treated with avelumab (an anti-PL-L1), the baseline levels of CXCL9 are related to clinical outcome, indicating that this subgroup of macrophages improves response rates to ICIs (Qu et al., 2020). Class IIa HDAC inhibition (TMP195) was used to modulate the phenotype of macrophages by Guerriero et al. (2017), they showed that the anti-tumor effect of TMP195 was enhanced when combined with T-cell checkpoint blockade. Macrophages may result in complete inability of T-cells to initiate an immune response against their target cells, therefore the effect of blocking immune checkpoints on monocytes within the TME may offer improved responses to ICIs.

MDSCs Within the TME Are Associated With Resistance to Immunotherapy

Myeloid-derived suppressor cells originate from bone marrow progenitor cells that have not fully matured into granulocytes, monocytes and DCs (Weiskopf et al., 2016). MDSCs include groups of cells with different phenotypes that are biologically diverse in humans. In the TME, the proliferation of MDSCs is induced by various immune molecules produced by tumor, stromal and activated immune cells, such as GM-CSF and VEGF. In mice, MDSCs have been broadly identified as CD11b$^+$ GR1$^+$ cells, whilst in humans, they have been identified as LIN$^-$ HLA$^-$DR$^-$ CD33$^+$ cells (Veglia et al., 2018).

The primary function of MDSCs is to suppress CD8$^+$ T-cell immunity by enhancing the expression of ROS, NO, arginase-1 and PGE-2 through PD-L1/PD-1 interaction (Veglia et al., 2018; Adeshakin et al., 2021; **Figure 1**). Other mechanisms include the induction of some immunosuppressive cells, the depletion of metabolites critical for T-cell function, the blocking of lymphocyte homing and the expression of ectoenzymes, etc. (Groth et al., 2019). MDSCs were recruited into the TME, their potent suppressive activities against effector lymphocytes may limit the efficacy of ICIs. The depletion of MDSCs is associated with the activation of CTLs' responses. Several preclinical studies have shown that inhibition of MDSCs during immunotherapy could improve efficacy. MDSC-depleting chemotherapy increases the effects of anti-PD1 mAb whilst simultaneously improving CD8$^+$ T-cell infiltration and effector cytokine secretion, thereby delaying tumor progression. Targeting MDSCs can improve patient response rate to immunotherapy. For example, tumor MDSCs can make TME immunosuppress through cell-specific mechanisms like TGF-β or nitric oxide in head and neck squamous cell carcinoma. And inhibiting CXCR1 and CXCR2 can eliminate MDSC accumulation and improve NK-Cell immunotherapy therapeutic efficacy (Greene et al., 2020). Apoptosis of MDSCs is caused by the high expression of TNF-related apoptosis-induced ligand receptors (TRAIL-Rs), and TRAIL-Rs' expression is stronger at MDSCs in tumor sites. So that targeting TRAIL-Rs can lead to rapid and significant depletion of MDSCs, which can be used to improve the antitumor effect of various immunotherapy drugs (Condamine et al., 2014; von Karstedt et al., 2017). Thus, blocking the immunosuppressive environment mediated by MDSCs may be a potential area for the future development of effective treatments (Highfill et al., 2014; Du Four et al., 2016; Davis et al., 2017; Iida et al., 2017; Kamran et al., 2017; Veglia et al., 2018). Finally, high levels of circulating MDSCs in cancer patients often correlate with poor response rate to immunotherapy (Ai et al., 2018; Tavazoie et al., 2018), suggesting that MDSCs may serve as a predictive marker for ICIs.

Mast Cells Have an Immunosuppressive Role in the TME

Mast cells are a group of innate immune sentinels. Mast cells secrete a variety of cytokines and participate in the regulation of key immune cell types including T, B, and APC cells (Voehringer, 2013). While mast cells may play an anti-tumor role in the TME, they are more appreciated to promote tumor

progression. For example, mast cells have a pro-tumorigenic role in gastric cancer through the release of angiogenic (VEGF-A, CXCL8, and MMP-9) and lymphangiogenic factors (VEGF-C and VEGF-F) (Sammarco et al., 2019). Lv et al. found that mast cell infiltration into tumors through CXCL12-CXCR4-mediated chemotaxis resulted in immunosuppression (Lv et al., 2019). Mechanistically, mast cells secrete IL10, leading to increased numbers of Tregs in draining lymph nodes (Gan et al., 2012; **Figure 1**). Moreover, tumor-derived TNF-α activates NF-κB pathway in mast cells, causing mast cells to express PD-L1. In this context, inhibition of PD-L1 on mast cells may benefit cancer patients (Lv et al., 2019).

Neutrophils Plays a Double-Edged Role in the TME

As a critical component of innate immunity, neutrophils are recruited to sites of inflammation by chemokines, cytokines and complement fragments (CXCL1, CXCL2, CXCL5, IL-8, C5a, and C3a) to enable host defenses against invading pathogens (Basu et al., 2002; Pagano et al., 2009; Ueha et al., 2011; Coffelt et al., 2016; Zhang and Houghton, 2021). On the other hand, the accumulation of peripheral blood polymorphonuclear neutrophils (PMN) within the TME promotes tumor growth and invasiveness in humans. TANs are $CD45^{+}CD66b^{+}$ (Zhang and Houghton, 2021) and can be classified as N1 and N2 subtypes. While N1 TANs exert anti-tumor activity through ADCC and proinflammatory factors production, such as IFN-γand MMP-8, in the innate immune response (Mihaila et al., 2021), N2 TANs promote tumor growth. Blocking TGF-β and inducing IFN-γ can cause N2 to convert to N1 (Fridlender et al., 2009).

N2 TANs are viewed as immunosuppressive cells (Kargl et al., 2019). In line with this, increased levels of neutrophils in tumors are associated with worse prognosis and poor outcomes in patients. This may be partially due to that PMN in the tumor matrix prevents T-cell infiltration. Concomitantly, increased neutrophil infiltration into tumors is associated with decreased efficacy of ICIs (Heng et al., 2009; Kargl et al., 2019; Schalper et al., 2020; Yuen et al., 2020). Vice versa, Kargl et al. (2019) found that higher ratio of $CD8^{+}$ T cells to neutrophils was associated with more favorable responses. Mechanistically, tumor-derived GM-CSF induces PD-L1 expression in neutrophils through the Janus kinase (JAK) signal transduction and activator of transcription 3 (STAT3) signaling pathway (**Figure 1**). $PD\text{-}L1^{+}$ neutrophils in turn inhibit T-cell immunity and promote tumor growth (Wang et al., 2017). These findings form a basis for the ongoing clinical trials (ClinicalTrials.gov NCT03161431, NCT03184870, NCT04123379) of a combination therapy by targeting neutrophil recruitment and ICIs.

THE ROLE OF ADAPTIVE IMMUNE RESPONSE CELLS WITHIN THE TME IN TUMOR IMMUNOTHERAPY

In general, the adaptive immune response plays a more important role than innate immunity in a specific immune response. However, innate and adaptive immunity are complementary as the innate immune response acts to initiate the adaptive immune response. Tumor antigens can be classified as tumor-specific antigens (TSAs) and tumor-associated antigens (TAAs). TSAs are recognized by T cells and induce a cellular immune response whilst TAAs can be recognized by B cells and induce humoral immunity (Jhunjhunwala et al., 2021). It is believed that humoral immunity acts synergistically with cellular immunity to inhibit tumor growth with cellular immunity being the main force in anti-tumor immunity. CTLs and Th1 responses are the main mechanisms of cellular immunity (Vesely et al., 2011). On the other hand, tumor cells can evade the attack of the immune system through loss of tumor antigens, decreased expression of MHC class I molecules, downregulation of costimulatory signals, secretion of immune suppressants and induction of immunosuppressive cells such as Tregs. Enhancing and improving the adaptive immune response is a priority for the development of immunotherapies (Vesely et al., 2011).

T-Cell Infiltration and Activation Within the TME Are Key Drivers of Anti-tumor Immune Response

$CD8^{+}$ cytotoxic T cells are the main effector cells of anti-tumor immunity. The complete activation of T-cells depends on the activation of antigen and costimulatory signals as well as the action of cytokines. These processes form the basis of T-cell proliferation and differentiation. The first signal is the antigen stimulation signal that allows the initial activation of T-cells and upregulates the expression of activation-related molecules such as costimulatory molecules (Tanaka et al., 1999). T-cells and APCs have multiple pairs of costimulatory molecules expressed on their surfaces. Interactions between costimulatory molecules, such as CD80 (B7-1), CD86 (B7-2), and CD28, are essential for the specific activation of T-cells to promote IL-2 transcription and stabilize mRNA (Watts and DeBenedette, 1999). Other costimulatory molecules are 4-1BB and 4-1BBL, ICOS and ICOSL, CD40 and CD40L. Fully activated T-cells express co-inhibitory receptors such as PD-1 and Tim-3. The balance between positive costimulatory and negative costimulatory molecules affects the activation of T cells. ICIs can increase the ratio of costimulatory to co-inhibitory mediators (Im et al., 2016). Inhibitory checkpoints like PD-1 and CTLA-4 have been targeted to relieve the depletion of $CD8^{+}$ T-cells and have shown efficacy in the clinic (Croft, 2003; Farhood et al., 2019; Kallies et al., 2020; **Figure 1**). Other checkpoint receptor targets such as TIM-3, VISTA, LAG-3, TIGIT, and CD96 are currently being explored for clinical applications (Anderson et al., 2016; Dougall et al., 2017; Kakavand et al., 2017; Qin et al., 2019; Tu et al., 2020).

$CD8^{+}$ cytotoxic T cells will enter an exhausted state as antigens and inflammation persist in the TME leading to T-cell dysfunction (Zheng et al., 2017; Bengsch et al., 2018; Sathe et al., 2020). By blocking the PD-1 inhibitory pathway, exhausted CD8 T (Tex) characterized by loss of the effector functions can be reinvigorated, indicating the therapeutic potential of improving immune control (Im et al., 2016; McLane et al., 2019). The most critical aspect of anti-PD-1 therapy is the survival

of effector T-cells that are active in the TME (Beltra et al., 2020). In a study conducted in metastatic melanoma patients, patients who responded to pembrolizumab (anti-PD-1 therapy) showed proliferation of inter-tumoral $CD8^+$ T-cells that directly correlated with tumor regression (Tumeh et al., 2014). According to other reports, sufficient T-cell infiltration is also a prerequisite for tumor responses to PD-L1 blockade. These data indicate that targeting LIGHT might increase responses to checkpoint blockades by creating a T-cell inflamed microenvironment that can also overcome tumor resistance to checkpoint blockade in non-T-cell inflamed tumors (Tang et al., 2016). Furthermore, pre-existed tumor-specific T-cells may have limited reactivation ability, whilst T-cell clones that have just entered the tumor may account for the response of T-cells to checkpoint blockade (Yost et al., 2019).

The relationship between $CD8^+$ effector T-cells and PD-1 expression on Tregs in the TME could be used to predict the efficacy of anti-PD-1 immunotherapy. PD-1^+ Tregs in tumor-infiltrating lymphocytes (TILs) can be used as therapeutic targets to enhance the clinical efficacy of ICIs. In addition, PD-1 expression by Tregs in TILs may explain the resistance to PD-1 blockade therapies (Kumagai et al., 2020; **Figure 1**).

An in-depth analysis of PD-1-$CD8^+$ TIL found that these three subgroups shared common characteristics with naive, memory and effector $CD8^+$ T-cells. Also, the proportions of these cell types may change the response to different ICIs in different cancers. Increases in the number of memory precursor-like $CD8^+$ T-cells after treatment are related to a good prognosis and response to ICIs. Also, the transcription factor Tcf7/Tcf1 is a key regulator of this subgroup. If it is not expressed, checkpoint blockade and innate agonist immunotherapy can fail (Kurtulus et al., 2019).

Programmed death-ligand can be detected both on tumor cells and in the immune stroma. Higher $CD8^+$ T-cell densities are accompanied by higher PD-L1 expression, indicating a possible mechanism of adaptive immune resistance (Thompson et al., 2017). TGF-β1 derived from tumor cells promotes the Smad3-dependent expression of PD-1 and Smad2-dependent dysfunction of CTLs, whilst PD-1 blockade cannot reverse this immunosuppressive environment (Shen et al., 2020). Diskin et al. (2020) found that PD-$L1^+$ T-cells suppressed neighboring T-cells in the TME. The interaction between PD-L1 and PD-1 induces inhibitory signaling in T-cells and drives TH17 differentiation and signaling pathways related to T-cell immunogenicity such as STAT1, AKT, p38, and ERK. PD-$L1^+$ T-cell expression has multiple effects on the innate and adaptive immune tolerance, immune synaptic cell crosstalk and TME signal transduction in cancer patients. These interactions may play important roles in immunotherapy response and drug resistance in cancer patients.

Th Cells Are Indirectly Involved in Anti-tumor Immune Effects in Tumor Immunity

$CD4^+$ Th cells include T helper type 1 (Th1), Th2, and Th17 cells (Ruterbusch et al., 2020). Although $CD4^+$ Th cells are not the main effector cells of cellular immunity, $CD4^+$ Th cells assist in activating CTLs and producing cytokines and chemokines that are indirectly involved in anti-tumor immune effects (Borst et al., 2018). For example, Th1 can influence APC antigen processing and also secrete chemokines including IL-2 and IFN-γ to recruit CTLs and NK to exert a local anti-tumor effect and to stimulate DC cells (Knutson and Disis, 2005). Cytokines secreted by Th2 cells are important for DCs maturation, clonal proliferation and class switching of B-cells, therefore these changes also promote humoral immunity (Ruterbusch et al., 2020). Th17 was initially identified as a $CD4^+$ T-cell that secretes IL17 which is a separate lineage to Th1 and Th2 cells. It was found that Th17 mainly secretes IL-17A, IL-17F, and IL-22 which recruit and activate neutrophils. Th17 may also promote angiogenesis and participate in tumor formation, yet it remains unclear whether Th17 is predominantly tumor-suppressive or tumor-promoting (Weaver et al., 2007; Silva-Santos, 2010).

Regulatory T Cells Within the TME Limit the Efficacy of ICIs

T-cells that constitutively express CD4 and CD25 are essential for maintaining self-tolerance and are therefore termed regulatory T cells (Tregs). The function of Tregs is defined by the transcription factor Foxp3 (Samstein et al., 2012; Bin Dhuban et al., 2014). By single-cell sequencing, it was showed that Tregs were significantly enriched in the TME in gastric cancer compared to normal tissue and contributed to an immunosuppressive TME. Also, Tregs express several immune checkpoints such as CTLA-4 and costimulatory molecules such as 4-1BB that are potential targets for regulating their functions (Sathe et al., 2020; **Figure 1**). The number of Tregs expressing immunosuppressive receptors in tumors is correlated with the activation and proliferation of $CD4^+$ and $CD8^+$ effector T-cells. Along with increases in Tregs, the cytokines (such as IL10 and TGF-β) that inhibit the effects in tumors are also up-regulated.

In a preclinical model, anti-CTLA-4 mAb has been shown to effectively induced the depletion of Tregs *via* an Fc-dependent mechanism in the TME but not in the peripheral lymphoid organs (Tang et al., 2018). This may be because the expression of CTLA-4 by Tregs in the tumor may be significantly higher than in the peripheral lymphatic organs. In human tumors, anti-CTLA-4 immunotherapy increases infiltration of inter-tumoral $CD8^+$ and $CD4^+$ cells without depleting $FOXP3^+$ cells (Sharma et al., 2019).

The blocking of PD-1 and CTLA-4 can increase the ratio of effector T-cells to Tregs in tumors. However, the blocking of PD-1 is not entirely positive for T-cells. ICIs can also activate and stable Tregs. Comparison of GC tissue samples before and after anti-PD-1 mAb therapy found that the infiltration of Tregs was associated with rapid disease progression known as hyper progressive disease (HPD). Moreover, PD-1 blockade by enhancing the proliferation and immunosuppressive activity of PD-1^+ Tregs in humans and mice inhibits antitumor immunity and enhances the suppressive activity of Tregs. The presence of actively proliferating PD-1^+ Tregs in tumors may be a reliable biomarker for HPD and can be used to guide the use of PD-1 blockade (Kamada et al., 2019). When the number of effector cells

increases, their activity also increases and Tregs are eliminated to maximize the antitumor effect.

CD25 expression is largely restricted to tumor infiltrating Tregs in mice and humans. Anti-CD25 antibody enhances binding to activate Fc gamma receptor (FcγRs), depleting tumor-infiltrating Tregs and increasing effector cells to Tregs ratios. The changes synergize with anti-PD-1 to eradicate established tumors (Arce Vargas et al., 2017). Eliminating Tregs in the TME could be an effective cancer treatment and prevent HPD during anti-PD-1 therapy. Fc-mediated depletion of inter-tumoral regulatory T-cells may be effective in combination with immunotherapy.

B-Cells in the TME Play Controversial Roles in Tumor Immunity

The role of T-cells in tumor immune monitoring is well known, however, the role of B-cells in the TME has not been extensively studied. B-cells mediate humoral immunity mainly through the production of antibodies and exert immune-regulatory functions by producing cytokines. The role of B-cells in tumor immunity is multifaceted. Antibodies can mediate ADCC and cytokines (such as IL6, IL10) are involved in regulating the function of macrophages and dendritic, NK and T-cells (Fridman et al., 2021). For example, Bregs can secrete inhibitory cytokines, such as IL-10, TGF-β, and IL-35, that inhibit the physiological functions of effector $CD4^+$ T cells by direct or indirect means. They can kill macrophages, dendritic cells and other immune cells during tumor development (Dasgupta et al., 2020). However, in breast cancer, B-cells express activated markers and produce cytokines and immunoglobulins to activate the humoral immune responses to effective anti-tumor immunity (Garaud et al., 2019).

B-cells may also play a prominent role in tumor infiltration and negatively regulate tumor growth. Higher tumor-infiltrating B-cells in HPV-associated oropharyngeal squamous cell carcinoma were associated with high CXCL9 production and high levels of tumor-infiltrating CD8 T-cells. These data indicated CD8 T-cells might be recruited *via* CXCL9 (Inoue et al., 2006; Hladíková et al., 2019). In addition, B-cells play roles in the formation of tumor-associated tertiary lymphoid structures (TLS) that may promote the induction of T-cell phenotypes required for response to ICIs. However, specific B-cell subsets are associated with immune-related adverse events (irAEs) in ICIs treatments (Willsmore et al., 2020). Recently, by bulk RNA sequencing, it was shown that B-cells were different in the tumors of responders versus non-responders during ICIs treatment, implying that B-cells were predictive and potential therapeutic targets (Helmink et al., 2020).

THE COMPLEXITY OF IMMUNE EFFECTOR MOLECULES WITH THE TME

Immune molecules produced by immune cells and enzymes are involved in the anti-tumor effects of the immune response. Tumor cells can activate B-cells to secrete antibodies with an anti-tumor effect because of the expression of tumor antigens. These antibodies can exert their anti-tumor effect. In some cases, tumor-specific antibodies interfere with the specific killing effect of tumor cells. This growth-promoting antibody is called the enhancing antibody. Also, antibodies can change or lose the adhesion characteristics of tumor cells to promote tumor cell metastasis (Vesely et al., 2011). Other immune effector molecules in anti-tumor immunity, such as IFN and TNF, complement molecules and various enzymes have non-specific inhibitory or killing effects on tumor cells (Demaria et al., 2019). Prolonged exposure of tumor cells to a microenvironment in which IFN-γ is presented induces high expression of PD-L1 and IDO1. These tumor cells, in turn, inhibit the release of IFN-γ by effector T-cells, leading to T-cell depletion and tumor progression.

Chemokines are essential for immune cell recruitment and the therapeutic efficacy of ICIs. For example, CXCR3 and its ligand CXCL9 were critical for a productive $CD8^+$ T cell response in tumor-bearing mice treated with anti-PD-1, indicating that the CXCR3 chemokine system was an indicator of the clinical sensitivity to anti-PD-1 mAb. Mechanistically, inter-tumoral $CD103^+$ dendritic cells produce CXCL9, facilitating interactions between DCs and T-cells within the TME (Chow et al., 2019). Moreover, after dual PD-1/CTLA-4 blockade, the CXCR3 ligands, CXCL9, and CXCL10 were significantly up-regulated, indicating that macrophage-derived CXCR3 ligands were essential for the efficacy ICIs (House et al., 2020).

Interleukins are the most common and most diverse cytokines in the TME. Different interleukins have completely different effects on tumors, but the same interleukin can also have double-sided effects on tumors. For example, IL22 has been found to induce endothelial cell proliferation and promote the formation of blood vessels in tumors (Protopsaltis et al., 2019). While IL2 is a cytokine that has a positive role in immune activation by activating NK cells and CTLs to cause tumor regression. However, IL2 also can bind to the IL2Rα receptor on Tregs to stabilize and expand Tregs and play a negative role (Lim et al., 2020).

Intra-tumor expression or inhibition of cytokines or chemokines is a promising approach for tumor therapy. IL-12 is a cytokine that activates both innate and adaptive immunity, partially due to IFN-γ secretion from NK cells, $CD8^+$ and $CD4^+$ T cells. Although in a past clinical study, systemic administration of IL-12 caused severe adverse events, IL-12 remains an attractive candidate for cancer immunotherapy. Vaccinia virus encoding both IL-7 and IL-12 completely changed the tumor immune microenvironment by boosting the inflammatory immune status, which showed beneficial systemic antitumor efficacy and markedly improved the sensitivity of solid tumors to systemic anti-PD-1 and anti-CTLA4 (Nakao et al., 2020).

THE COMPLEX INTERACTIONS AMONG STROMA AND IMMUNE CELLS AS WELL AS TUMOR CELLS IN TME

The development of solid tumors is accompanied by excessive deposition of ECM, abnormal tissue pattern and activation and enrichment of CAFs. A large amount of evidence has shown that the key components of stroma in the TME not only were conducive to the growth and metastasis of

tumor cells but also hindered immune cell infiltration and affected the anti-tumor immune response (**Figure 2**). Cancer-associated fibroblasts are highly heterogeneous for their dynamic origins, by signals like TGF-β, PDGF, and YAP in tumors inducing fibroblasts into activation state (Kalluri, 2016; Biffi and Tuveson, 2021). CAF is closely related to the changing state of ECM. On the other hand, ECM affects the activation of CAFs and their functional exertion. Both CAFs and ECM play important pro-tumorigenic and antitumorigenic roles in the creation of TME, especially in solid tumors (Cox, 2021). CAFs and ECM dynamically interact with the tumor cell, which is not only important pathological features of solid tumors but also important driving forces for malignant tumor development (Najafi et al., 2019; Yoshida, 2020), such as changing the microenvironment, regulating paracrine signals through inflammatory cytokines, controlling tumor immune responses, depositing different extracellular matrix components, stimulating angiogenesis, providing scaffolds for tumor metastasis and invasion and regulating malignant cell metabolism (Levental et al., 2009; Erdogan and Webb, 2017; LeBleu and Kalluri, 2018; Demircioglu et al., 2020). With the secretion of cytokines like CXCL12 and IL-6, CAFs regulate the recruitment of macrophages and their contribution to tumor-promoting M2 type differentiation, thus affecting innate immunity (Ruffell and Coussens, 2015). Moreover, CAFs and ECM allow the TME to be maintained in a state of immunosuppression, thus greatly limiting the effect of cancer immunotherapy. For instance, FAP-positive CAFs suppress the anti-tumor efficacy by expressing CXCL12, which causes T-cells in tumors exclusion and regulates adaptive immunity. The removal of CAFs or CXCR4 antagonists causes tumors to internal T-cell immersion and enhanced PD-L1 antibody immunotherapy (Feig et al., 2013). As TGF-β, PDGF, and FGF2 are the main activating factors of CAFs, strategies targeting CAFs and ECM remodeling like re-educating of the tumor stroma have also made some progresses. For example, suppressing PDGF signal pathway can make CAFs reversed to normal tissue fibroblasts and inhibit tumor growth, thus better regulating therapeutic efficacy and sensitivity (Pietras et al., 2008; Kalluri, 2016). The normalization of CAFs and ECM is a promising direction in tumor therapy and potential stromal targeting cancer therapies are underway.

Vascular endothelial cells are a major component of non-immune stromal cells. However, during tumor angiogenesis, vascular endothelial cells do not form a dense structure, but

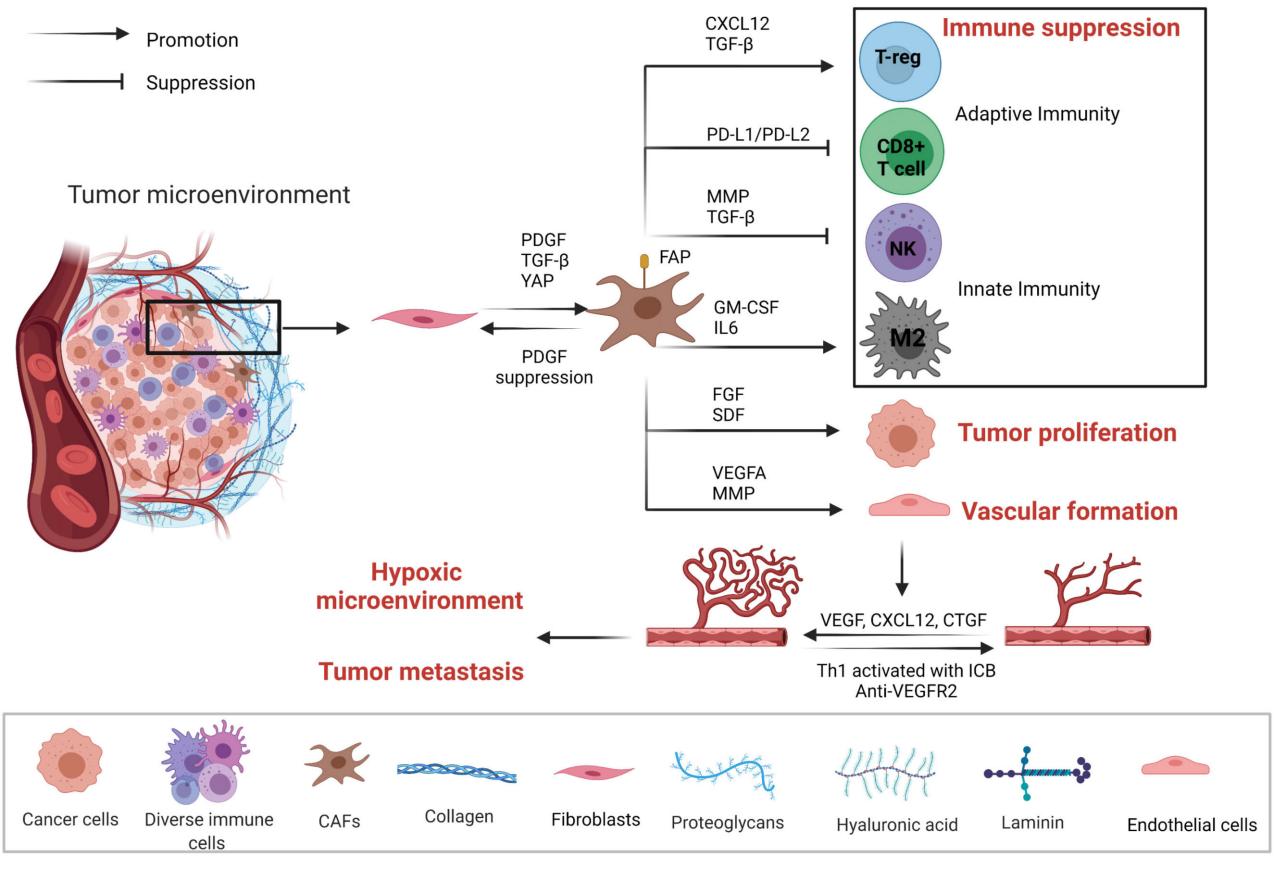

FIGURE 2 | Mechanisms of tumor-associated fibroblasts (CAFs) and vascular endothelial cells affecting the TME. CAFs, vascular endothelial cells, tumor cells, and immune cells are in a dynamic relationship. CAFs through the secretion of cytokines and PD1/PDL1, PDL-2 pathways form the immunosuppression microenvironment to promote tumor proliferation. Tumor microenvironment regulates vascular endothelial cell proliferation and the formation of blood vessels through the secretion of growth factors and cytokines. Eventually, TME becomes hypoxic, accelerating tumor metastasis.

form a loosely structured, highly permeable vessel, thus affecting the infiltration of lymphocytes. Moreover, the permeability of blood vessels is closely related to the hypoxic microenvironment inside the tumor, tumor metastasis and tumor response to drugs (**Figure 2**). By normalizing vasculature may mitigate hypoxia and facilitate infiltration of lymphocytes. For instance, Th1 activated with ICB plays a pivotal role in tumor vessel normalization, and ICIs-activated $CD4^+$ T lymphocytes increases vessel normalization. Moreover, subgroup TH1 cells that secrete interferon-γ play more critical roles in vessel normalization (Tian et al., 2017). CAFs can induce angiogenesis by secreting cytokines such as VEGF, CXCL12 and CTGF (Wu et al., 2021). VEGF/VEGFR-2 signaling induces the proliferation, migration, and angiogenesis of vascular endothelial cells, but also elevates the permeability of blood vessels. Anti-angiogenic treatment by blocking VEGF has shown anti-tumor effect by disturbing angiogenesis (Dvorak, 2002). In HCC murine models, dual PD-1/VEGFR-2 antibodies overcome anti-PD-1 treatment resistance *via* promoting $CD4^+$ cell-mediated vessel normalization and reducing negative regulatory components like Tregs and $CCR2^+$ monocytes, thus converting TAMs from M2 to M1 type,as well as facilitating infiltration and activation of CTL. Therefore, synergistic ICIs with anti-angiogenesis may improve sensitization of the tumors to ICIs (Shigeta et al., 2020; **Figure 2**).

TARGETING TME IN COMBINATION WITH IMMUNOTHERAPY

Cancer immunotherapy using ICIs and CAR-T cells has developed rapidly, and has revolutionized cancer therapy. Immunotherapies targeting TME are also emerging, for example, targeting CTLs by blockading inhibitory checkpoints or by activating stimulatory checkpoints. Since the approval of Ipilimumab by the FDA in 2011, anti-CTLA-4 and anti-PD-1/L1 have demonstrated efficacy in various tumor types (Hodi et al., 2010). Different cells within the TME have roles in promoting or inhibiting tumor growth. CTLA-4 can be expressed on the surface of CTLs, NK cells and Tregs. CTLA-4 monoclonal antibody can relieve the inhibitory effect of CTLA-4 on CTLs and NK cells (Krummel and Allison, 1995; Benson et al., 2010). Other emerging ICIs, such as anti-tim3, can also play critical roles in driving anti-tumor immune responses (Gleason et al., 2012; Anderson, 2014). These drugs are able to indirectly improve the anti-tumor activity of CTLs and NK cells by reducing the cell number of Tregs (Bulliard et al., 2013). Specific targeting on different cells with ICIs may have synergistic effects. Although only drugs that activate T-cells have been brought to market, the scope for other combinations will be rapidly developed in clinical trials to explore the impact of these drugs within the TME (**Table 1**).

Not all patients are responsive to ICIs and primary resistance may be due to low levels of lymphocytes within the TME (Ochoa de Olza et al., 2020). Additionally, patients who respond to ICIs also have the possibility to ultimately develop acquired resistance. This occurs through several mechanisms such as downregulation of the antigen presentation machinery, loss of IFN-γ sensitivity, neoantigen depletion, tumor-mediated immunosuppression, and the expression of other inhibitory checkpoints (Schoenfeld and Hellmann, 2020). Although the mechanisms of immune checkpoints are largely dependent on $CD8^+$ effector cells, an increasing number of studies have found that the response to ICIs is correlated with other components of the TME. The combination of ICIs with agents that target the TME components has major potential to optimize therapeutic efficacy and overcome challenges associated with drug resistance and tumor recurrence. TGF-β promote immune evasion in TME, thereby limiting the efficacy of ICIs. And it has been found that TGF-β inhibitor combined with PD-L1 antibody inhibits tumor metastasis of colorectal cancer in preclinical mouse models (Tauriello et al., 2018).

DISCUSSION

So far, predictive biomarkers, such as PD-L1, TMB, and microsatellite instability (MSI) et al., are often not reliable, and better sensitive biomarkers are highly desirable. Higher PD-L1 expression on tumor cells is likely to increase susceptibility to ICIs and achieve an objective response (Topalian et al., 2012). In addition to PD-L1 expression on the cell surface, metastatic melanoma with high level of exosomal PD-L1 (a circulating form of extracellular PD-L1) are positively responsive to ICIs therapy. Consumption of PD-L1 inhibitors by soluble PD-L1 may contribute to further understanding the mechanisms of tumor resistance to PD-L1 inhibitors. PD-L1 in tumor-derived exosomes can assist tumor cells in immune escape, therefore the combinations of small molecule drugs that inhibit the release of exosomes with ICIs may be used to improve therapeutic efficacy. It has been indicated that exosomal PD-L1 might be more predictive and facilitate the identification of responders and non-responders (Chen G. et al., 2018; Poggio et al., 2019; Orme et al., 2020). Tumor mutation burden (TMB-H) was supposed to be a predictive biomarker for the efficacy of response to ICIs in multiple cancer types (Samstein et al., 2019; Jardim et al., 2020), but a recent study indicated that TMB-H tumors indeed have higher objective response rates (ORRs) in melanoma, lung and bladder cancers, but failed to show the same predictive efficacy among breast cancer, prostate cancer and gliom. Moreover, the predictive power of TMB in dual anti-PD-1/CTLA-4 checkpoint blockade is less satisfactory than monotherapy (Klein et al., 2021; McGrail et al., 2021). Besides, the cutoffs of TMB-H are not universal. Generally, TMB of 10 or more mutations per megabase is more likely to have higher response rates after ICIs treatment (Valero et al., 2021). Other specific mutations may also provide insights into the effects of immunotherapy, such as MMR, PRKDC, HED and POLE (Le et al., 2015; Chowell et al., 2019).

Tumor cells are inextricably linked to their microenvironment from occurrence, development, growth, metastasis and invasion. They can be further divided into "hot tumor" and "cold tumor" according to the types of invading immune cells, as the suppressive immune microenvironment of tumors limits the infiltration of effector immune cells. Inhibitory changes and the heterogeneity in the TME are important factors

TABLE 1 | Landmark and ongoing trials of targeting tumor immune microenvironment synergize ICIs.

Treatment type	Treatment mechanism	Trial name (NCT number)	Current status
CTLs-based therapy with ICIs	Blockade of inhibitory checkpoints: Anti-PD-1/Anti-PD-L1/Anti-CTLA-4/Other ICIs, enabling tumor-reactive T cells to overcome regulatory inhibitory mechanisms.	NCT02453594/NCT00094653/NCT01927419 NCT01721746/NCT02108652/NCT02125461	Combination therapies to overcome tumor immune evasion, other ICIs have emerged as potential targets.
NK cells -based therapy with ICIs	1. Targeting NK inhibitory molecules 2. Targeting NK cell activating signals 3. Adoptive NK cells therapy	NCT02665650/NCT03586869/NCT04261439 NCT03387085/NCT04143711/NCT03841110	Natural killer (NK) cell-based therapies are emerging as safe and effective treatments for some cancers, auxiliary methods for enhancing the therapeutic activity of NK cells include immune- checkpoint inhibitors
TAMs-targeted therapy with ICIs	1. Anti-CSF-1 antibodies and CSF-1R inhibition to deplete macrophages 2. Agonistic anti-CD40 or inhibitory anti-CD47 antibodies to stimulate macrophages 3. Modulation of macrophage phenotype 4. Eliminating TAMs already present in the TME 5. Inhibition of monocyte recruitment 6. Reprogramming of TAMs	NCT04123379/NCT03767582/NCT03059147 NCT02826486/NCT02907099/NCT04058145 NCT02777710/NCT02323191/NCT03768531 NCT02554812/NCT03558139/NCT03869190 NCT02807844/NCT02890368/NCT02663518 NCT01103635/NCT03123783/NCT02304393 NCT04116320/NCT03435640/NCT04193293	To convert its immunosuppressive ability to its potential immunostimulatory function, which is beneficial to the current ICI-based immunotherapy
MDSC-targeted therapy with ICIs	1. Decrease MDSCs recruitment 2. Promote MDSC depletion 3. Reprogram MDSCs to enhance anti-tumor immunity	NCT03214666/NCT02403778	Combined treatment with ICIs along with small molecule inhibitors to precise target MDSC remains challenge.
Neutrophils-targeted therapy with ICIs	Inhibition of various chemokines(IL8, Arg1, CXCR2, IL1β)to retard PMN recruitment and function.	NCT03161431/NCT03184870/NCT03473925 /NCT04123379/NCT02903914/NCT03631199	Pre-clinical studies by targeting neutrophil recruitment and neutrophil immunosuppressive function are currently under to complement the ICIs monotherapy
Tregs-targeted therapy with ICIs	Depletion of Tregs synergizes with ICIs to eradicate established tumors, for example blocking CCR4 and Tregs chemotaxis; blocking various chemokines and chemokine receptor (TGF-β, IL-10 and IL-35)	NCT02476123/NCT02705105/NCT02444793 /NCT02301130/NCT02503774	Through depleting Tregs depletion combination with ICIs, eliminating Tregs mediated resistance
Stroma–targeted therapy/anti-angiogenesis with ICIs	Stroma–targeted therapy by reversing CAFs and ECM to antitumorigenic roles. By normalizing vessel formation, reducing negative regulatory components like Tregs, promoting of CTL infiltration and activation	NCT02681549/NCT02337491/NCT02348008 NCT03475004/NCT02443324/NCT03650764 NCT02210117/NCT02873962/NCT03452579 NCT02999295/NCT03502746/NCT02336165	Potential stromal targeting cancer therapies are underway. ICIs coupling with anti-angiogenesis have already shown efficacy in the clinic, but deeper understanding of the immunomodulatory capacity still unsatisfactory

that can promote tumor progression and affect responses to immunotherapy. TILs can exert an antitumor effect through the host cellular immune response. It was reported that TIL levels could predict tumor control in EBV-positive gastric cancers (Kang et al., 2016). PD-L1 positivity has been shown to correlate with the presence of high TIL infiltration, as a higher TIL density was also associated with a lower risk of progression in gastric cancer patients (Dai et al., 2016). The infiltration of multiple immune cell types, such as TAMs and Tregs, may explain the limited efficacy of ICIs based on subgroup analysis of immune cell infiltration. The TME is a complex integrated system. Genomic and transcriptomic analysis offer a multifaceted view on TME and provide approaches for precision medicine (Cieślik and Chinnaiyan, 2018; Beaubier et al., 2019; Rodon et al., 2019). For example, by transcriptomic analysis, over 10,000 cancer patients were classified into four distinct TME subtypes. Among them, the immune-favorable TME subtypes were more likely to be susceptible to ICIs than the suppressive subtypes. So it has been demonstrated that visual tools containing transcriptomic and genomic data could help us better understand the tumor framework, mutational load, immune composition, anti-tumor immunity and immunosuppressive escape mechanisms (Bagaev et al., 2021). Comprehensive analysis and visualization may also help us identify biomarkers and guide therapeutic decision.

Interventions have been applied to target different components of the TME, aiming to convert a tumor-promoting into a tumor-suppressive TME. That is also optimal for ICIs-based therapies. Strategies targeting the TME were used to overcome the tumor resistance to immunotherapy, for

example, through CD40-mediated immune cell activation (Diggs et al., 2020), tumor-penetrating peptide iRGD-mediated tumor-specific lymphocyte infiltration (Ding et al., 2019), combined inhibition of CD38 and PD-L1 (Chen L. et al., 2018) or radiotherapy combined with immunotherapy (Yu et al., 2021). TGF-β released from cancer cells, stromal fibroblasts and other cells can shape the architecture of the TME by suppressing the antitumor activities of immune cells to attenuate the anti-tumor efficacy of ICIs (Mariathasan et al., 2018; Derynck et al., 2020). The blockade of TGF-β signaling may alter the immune microenvironment, making it more amenable to immunotherapy and offering synergy with ICIs. These changes may augment intra-tumoral CD8 T-cell proliferation, reduce exhaustion and evoke pro-inflammatory cytokines that can promote antitumor immunity (Greco et al., 2020).

In this review, we focus on the TME and its interactions with ICIs. However, the immunosuppressive TME is a complex network regulated by a variety of immunosuppressive signals that are dynamic and continuously changing. Targeting single specific immunosuppressive signal may not be optimal to achieve long-term efficacy. Immunotherapy biomarkers are supposed to associate with advantages and shortcomings, such as positive biomarkers to assess the benefit of treatment while negative biomarkers predict the patient's immune resistance, hyper progression, severe toxicity, *etc*. As a combination of TMB, PD-L1 and neutrophil-lymphocyte, ratio (NLR)status has shown improved predictive power (Bruni et al., 2020; Kao et al., 2021). Screening of sensitive biomarkers like exosomal PD-L1, TMB, specific mutations and combined assessment of multiple biomarkers may be the future research directions. Designing multiple combined immunotherapy strategies and exploring new immunotherapy targets are the potential priority areas in scientific researches and clinical trials.

AUTHOR CONTRIBUTIONS

ML put forward the conception and design. GW completed the critical comments and revision. XL drafted the manuscript. YY, QH, YD, and FG collected, analyzed the data, and prepared the table. All authors contributed to the article and approved the submitted version.

FUNDING

This work was supported by the National Natural Science Foundation of China (Grant No.81572850) and 1.3.5 Project for Disciplines of Excellence, West China Hospital, Sichuan University (Grant No. ZYJC21043).

REFERENCES

Adeshakin, A. O., Liu, W., Adeshakin, F. O., Afolabi, L. O., Zhang, M., Zhang, G., et al. (2021). Regulation of ROS in myeloid-derived suppressor cells through targeting fatty acid transport protein 2 enhanced anti-PD-L1 tumor immunotherapy. *Cell Immunol.* 362:104286. doi: 10.1016/j.cellimm.2021.104286

Ai, L., Mu, S., Wang, Y., Wang, H., Cai, L., Li, W., et al. (2018). Prognostic role of myeloid-derived suppressor cells in cancers: a systematic review and meta-analysis. *BMC Cancer* 18:1220. doi: 10.1186/s12885-018-5086-y

Allan, R. S., Waithman, J., Bedoui, S., Jones, C. M., Villadangos, J. A., Zhan, Y., et al. (2006). Migratory dendritic cells transfer antigen to a lymph node-resident dendritic cell population for efficient CTL priming. *Immunity* 25, 153–162. doi: 10.1016/j.immuni.2006.04.017

Anderson, A. C. (2014). Tim-3: an emerging target in the cancer immunotherapy landscape. *Cancer Immunol. Res.* 2, 393–398. doi: 10.1158/2326-6066.cir-14-0039

Anderson, A. C., Joller, N., and Kuchroo, V. K. (2016). Lag-3, Tim-3, and TIGIT: co-inhibitory receptors with specialized functions in immune regulation. *Immunity* 44, 989–1004. doi: 10.1016/j.immuni.2016.05.001

Arce Vargas, F., Furness, A. J. S., Solomon, I., Joshi, K., Mekkaoui, L., Lesko, M. H., et al. (2017). Fc-optimized anti-cd25 depletes tumor-infiltrating regulatory T cells and synergizes with PD-1 blockade to eradicate established tumors. *Immunity* 46, 577–586.

Bagaev, A., Kotlov, N., Nomie, K., Svekolkin, V., Gafurov, A., Isaeva, O., et al. (2021). Conserved pan-cancer microenvironment subtypes predict response to immunotherapy. *Cancer cell* 39, 845–865.e847.

Barry, K., Hsu, J., Broz, M., Cueto, F., Binnewies, M., Combes, A., et al. (2018). A natural killer-dendritic cell axis defines checkpoint therapy-responsive tumor microenvironments. *Nat. Med.* 24, 1178–1191. doi: 10.1038/s41591-018-0085-8

Basu, S., Hodgson, G., Katz, M., and Dunn, A. (2002). Evaluation of role of G-CSF in the production, survival, and release of neutrophils from bone marrow into circulation. *Blood* 100, 854–861. doi: 10.1182/blood.v100.3.854

Batista, F. D., and Harwood, N. E. (2009). The who, how and where of antigen presentation to B cells. *Nat. Rev. Immunol.* 9, 15–27. doi: 10.1038/nri2454

Bauer, C. A., Kim, E. Y., Marangoni, F., Carrizosa, E., Claudio, N. M., and Mempel, T. R. (2014). Dynamic Treg interactions with intratumoral APCs promote local CTL dysfunction. *J. Clin. Invest.* 124, 2425–2440. doi: 10.1172/jci66375

Beaubier, N., Bontrager, M., Huether, R., Igartua, C., Lau, D., Tell, R., et al. (2019). Integrated genomic profiling expands clinical options for patients with cancer. *Nat. Biotechnol.* 37, 1351–1360. doi: 10.1038/s41587-019-0259-z

Beltra, J., Manne, S., Abdel-Hakeem, M., Kurachi, M., Giles, J., Chen, Z., et al. (2020). Developmental relationships of four exhausted CD8 T cell subsets reveals underlying transcriptional and epigenetic landscape control mechanisms. *Immunity* 52, 825–841.e828.

Bengsch, B., Ohtani, T., Khan, O., Setty, M., Manne, S., O'Brien, S., et al. (2018). Epigenomic-guided mass cytometry profiling reveals disease-specific features of exhausted CD8 T cells. *Immunity* 48, 1029–1045.e1025.

Benson, D. M. Jr., Bakan, C. E., Mishra, A., Hofmeister, C. C., Efebera, Y., Becknell, B., et al. (2010). The PD-1/PD-L1 axis modulates the natural killer cell versus multiple myeloma effect: a therapeutic target for CT-011, a novel monoclonal anti-PD-1 antibody. *Blood* 116, 2286–2294. doi: 10.1182/blood-2010-02-271874

Biffi, G., and Tuveson, D. A. (2021). Diversity and biology of cancer-associated fibroblasts. *Physiol. Rev.* 101, 147–176. doi: 10.1152/physrev.00048.2019

Bin Dhuban, K., Kornete, M., Sm, E., and Piccirillo, C. A. (2014). Functional dynamics of Foxp3$^+$ regulatory T cells in mice and humans. *Immunol. Rev.* 259, 140–158. doi: 10.1111/imr.12168

Biswas, S. K., and Mantovani, A. (2010). Macrophage plasticity and interaction with lymphocyte subsets: cancer as a paradigm. *Nat. Immunol.* 11, 889–896. doi: 10.1038/ni.1937

Borst, J., Ahrends, T., Bąbała, N., Melief, C. J. M., and Kastenmüller, W. (2018). CD4(+) T cell help in cancer immunology and immunotherapy. *Nat. Rev. Immunol.* 18, 635–647. doi: 10.1038/s41577-018-0044-0

Bruni, D., Angell, H. K., and Galon, J. (2020). The immune contexture and immunoscore in cancer prognosis and therapeutic efficacy. *Nat. Rev. Cancer* 20, 662–680. doi: 10.1038/s41568-020-0285-7

Bulliard, Y., Jolicoeur, R., Windman, M., Rue, S. M., Ettenberg, S., Knee, D. A., et al. (2013). Activating Fc γ receptors contribute to the antitumor activities of immunoregulatory receptor-targeting antibodies. *J. Exp. Med.* 210, 1685–1693. doi: 10.1084/jem.20130573

Chen, G., Huang, A. C., Zhang, W., Zhang, G., Wu, M., Xu, W., et al. (2018). Exosomal PD-L1 contributes to immunosuppression and is associated with anti-PD-1 response. *Nature* 560, 382–386.

Chen, L., Diao, L., Yang, Y., Yi, X., Rodriguez, B., Li, Y., et al. (2018). CD38-mediated immunosuppression as a mechanism of tumor cell escape from PD-1/PD-L1 blockade. *Cancer Discov.* 8, 1156–1175.

Chow, M., Ozga, A., Servis, R., Frederick, D., Lo, J., Fisher, D., et al. (2019). Intratumoral activity of the CXCR3 chemokine system is required for the efficacy of anti-PD-1 therapy. *Immunity* 50, 1498–1512.e1495.

Chowell, D., Krishna, C., Pierini, F., Makarov, V., Rizvi, N., Kuo, F., et al. (2019). Evolutionary divergence of HLA class I genotype impacts efficacy of cancer immunotherapy. *Nat. Med.* 25, 1715–1720. doi: 10.1038/s41591-019-0639-4

Cieślik, M., and Chinnaiyan, A. M. (2018). Cancer transcriptome profiling at the juncture of clinical translation. *Nat. Rev. Genet.* 19, 93–109. doi: 10.1038/nrg.2017.96

Coffelt, S. B., Wellenstein, M. D., and de Visser, K. E. (2016). Neutrophils in cancer: neutral no more. *Nat. Rev. Cancer* 16, 431–446. doi: 10.1038/nrc.2016.52

Condamine, T., Kumar, V., Ramachandran, I. R., Youn, J. I., Celis, E., Finnberg, N., et al. (2014). ER stress regulates myeloid-derived suppressor cell fate through TRAIL-R-mediated apoptosis. *J. Clin. Invest.* 124, 2626–2639. doi: 10.1172/jci74056

Cox, T. R. (2021). The matrix in cancer. *Nat. Rev. Cancer* 21, 217–238.

Croft, M. (2003). Costimulation of T cells by OX40, 4-1BB, and CD27. *Cytokine Growth Factor Rev.* 14, 265–273. doi: 10.1016/s1359-6101(03)00025-x

Curiel, T. J., Coukos, G., Zou, L., Alvarez, X., Cheng, P., Mottram, P., et al. (2004). Specific recruitment of regulatory T cells in ovarian carcinoma fosters immune privilege and predicts reduced survival. *Nat. Med.* 10, 942–949. doi: 10.1038/nm1093

Dai, C., Geng, R., Wang, C., Wong, A., Qing, M., Hu, J., et al. (2016). Concordance of immune checkpoints within tumor immune contexture and their prognostic significance in gastric cancer. *Mol. Oncol.* 10, 1551–1558. doi: 10.1016/j.molonc.2016.09.004

Dasgupta, S., Dasgupta, S., and Bandyopadhyay, M. (2020). Regulatory B cells in infection, inflammation, and autoimmunity. *Cell Immunol.* 352:104076. doi: 10.1016/j.cellimm.2020.104076

Davis, R. J., Moore, E. C., Clavijo, P. E., Friedman, J., Cash, H., Chen, Z., et al. (2017). Anti-PD-L1 efficacy can be enhanced by inhibition of myeloid-derived suppressor cells with a selective inhibitor of PI3Kδ/γ. *Cancer Res.* 77, 2607–2619.

De Palma, M., and Lewis, C. E. (2013). Macrophage regulation of tumor responses to anticancer therapies. *Cancer Cell* 23, 277–286. doi: 10.1016/j.ccr.2013.02.013

Demaria, O., Cornen, S., Daëron, M., Morel, Y., Medzhitov, R., and Vivier, E. (2019). Harnessing innate immunity in cancer therapy. *Nature* 574, 45–56. doi: 10.1038/s41586-019-1593-5

Demircioglu, F., Wang, J., Candido, J., Costa, A. S. H., Casado, P., de Luxan Delgado, B., et al. (2020). Cancer associated fibroblast FAK regulates malignant cell metabolism. *Nat. Commun.* 11:1290.

Derynck, R., Turley, S., and Akhurst, R. (2020). TGFβ biology in cancer progression and immunotherapy. *Nat. Rev. Clin. Oncol.* 18, 9–34.

Diggs, L., Ruf, B., Ma, C., Heinrich, B., Cui, L., Zhang, Q., et al. (2020). CD40-mediated immune cell activation enhances response to anti-PD1 in murine intrahepatic cholangiocarcinoma. *J. Hepatol.* 74, 1145–1154. doi: 10.1016/j.jhep.2020.11.037

Ding, N., Zou, Z., Sha, H., Su, S., Qian, H., Meng, F., et al. (2019). iRGD synergizes with PD-1 knockout immunotherapy by enhancing lymphocyte infiltration in gastric cancer. *Nat. Commun.* 10:1336.

Diskin, B., Adam, S., Cassini, M., Sanchez, G., Liria, M., Aykut, B., et al. (2020). PD-L1 engagement on T cells promotes self-tolerance and suppression of neighboring macrophages and effector T cells in cancer. *Nat. Immunol.* 21, 442–454. doi: 10.1038/s41590-020-0620-x

Dougall, W. C., Kurtulus, S., Smyth, M. J., and Anderson, A. C. (2017). TIGIT and CD96: new checkpoint receptor targets for cancer immunotherapy. *Immunol. Rev.* 276, 112–120. doi: 10.1111/imr.12518

Du Four, S., Maenhout, S. K., Niclou, S. P., Thielemans, K., Neyns, B., and Aerts, J. L. (2016). Combined VEGFR and CTLA-4 blockade increases the antigen-presenting function of intratumoral DCs and reduces the suppressive capacity of intratumoral MDSCs. *Am. J. Cancer Res.* 6, 2514–2531.

Dvorak, H. F. (2002). Vascular permeability factor/vascular endothelial growth factor: a critical cytokine in tumor angiogenesis and a potential target for diagnosis and therapy. *J. Clin. Oncol.* 20, 4368–4380. doi: 10.1200/jco.2002.10.088

Erdogan, B., and Webb, D. J. (2017). Cancer-associated fibroblasts modulate growth factor signaling and extracellular matrix remodeling to regulate tumor metastasis. *Biochem. Soc. Trans.* 45, 229–236. doi: 10.1042/bst20160387

Farhood, B., Najafi, M., and Mortezaee, K. (2019). CD8(+) cytotoxic T lymphocytes in cancer immunotherapy: a review. *J. Cell Physiol.* 234, 8509–8521. doi: 10.1002/jcp.27782

Feig, C., Jones, J. O., Kraman, M., Wells, R. J., Deonarine, A., Chan, D. S., et al. (2013). Targeting CXCL12 from FAP-expressing carcinoma-associated fibroblasts synergizes with anti-PD-L1 immunotherapy in pancreatic cancer. *Proc. Natl. Acad. Sci. U.S.A.* 110, 20212–20217. doi: 10.1073/pnas.1320318110

Francisco, L. M., Sage, P. T., and Sharpe, A. H. (2010). The PD-1 pathway in tolerance and autoimmunity. *Immunol. Rev.* 236, 219–242. doi: 10.1111/j.1600-065x.2010.00923.x

Fridlender, Z. G., Sun, J., Kim, S., Kapoor, V., Cheng, G., Ling, L., et al. (2009). Polarization of tumor-associated neutrophil phenotype by TGF-beta: "N1" versus "N2" TAN. *Cancer Cell* 16, 183–194. doi: 10.1016/j.ccr.2009.06.017

Fridman, W., Petitprez, F., Meylan, M., Chen, T., Sun, C., Roumenina, L., et al. (2021). B cells and cancer: to B or not to B? *J. Exp. Med.* 218:e20200851.

Gan, P. Y., Summers, S. A., Ooi, J. D., O'Sullivan, K. M., Tan, D. S., Muljadi, R. C., et al. (2012). Mast cells contribute to peripheral tolerance and attenuate autoimmune vasculitis. *J. Am. Soc. Nephrol.* 23, 1955–1966. doi: 10.1681/asn.2012060572

Garaud, S., Buisseret, L., Solinas, C., Gu-Trantien, C., de Wind, A., Van den Eynden, G., et al. (2019). Tumor infiltrating B-cells signal functional humoral immune responses in breast cancer. *JCI Insight* 5:e129641.

Gardner, A., de Mingo Pulido, Á, and Ruffell, B. (2020). Dendritic cells and their role in immunotherapy. *Front. Immunol.* 11:924. doi: 10.3389/fimmu.2020.00924

Gleason, M. K., Lenvik, T. R., McCullar, V., Felices, M., O'Brien, M. S., Cooley, S. A., et al. (2012). Tim-3 is an inducible human natural killer cell receptor that enhances interferon gamma production in response to galectin-9. *Blood* 119, 3064–3072.

Gordon, S., Maute, R., Dulken, B., Hutter, G., George, B., McCracken, M., et al. (2017). PD-1 expression by tumour-associated macrophages inhibits phagocytosis and tumour immunity. *Nature* 545, 495–499.

Greco, R., Qu, H., Qu, H., Theilhaber, J., Shapiro, G., Gregory, R., et al. (2020). Pan-TGFβ inhibition by SAR439459 relieves immunosuppression and improves antitumor efficacy of PD-1 blockade. *Oncoimmunology* 9:1811605.

Greene, S., Robbins, Y., Mydlarz, W. K., Huynh, A. P., Schmitt, N. C., Friedman, J., et al. (2020). Inhibition of MDSC trafficking with SX-682, a CXCR1/2 inhibitor, enhances NK-cell immunotherapy in head and neck cancer models. *Clin. Cancer Res.* 26, 1420–1431. doi: 10.1158/1078-0432.CCR-19-2625

Gregori, S., Tomasoni, D., Pacciani, V., Scirpoli, M., Battaglia, M., Magnani, C., et al. (2010). Differentiation of type 1 T regulatory cells (Tr1) by tolerogenic DC-10 requires the IL-10-dependent ILT4/HLA-G pathway. *Blood* 116, 935–944.

Groth, C., Hu, X., Weber, R., Fleming, V., Altevogt, P., Utikal, J., et al. (2019). Immunosuppression mediated by myeloid-derived suppressor cells (MDSCs) during tumour progression. *Br. J. Cancer* 120, 16–25. doi: 10.1038/s41416-018-0333-1

Guerriero, J. L., Sotayo, A., Ponichtera, H. E., Castrillon, J. A., Pourzia, A. L., Schad, S., et al. (2017). Class IIa HDAC inhibition reduces breast tumours and metastases through anti-tumour macrophages. *Nature* 543, 428–432. doi: 10.1038/nature21409

Guillerey, C., Huntington, N. D., and Smyth, M. J. (2016). Targeting natural killer cells in cancer immunotherapy. *Nat. Immunol.* 17, 1025–1036. doi: 10.1038/ni.3518

Habif, G., Crinier, A., André, P., Vivier, E., and Narni-Mancinelli, E. (2019). Targeting natural killer cells in solid tumors. *Cell Mol. Immunol.* 16, 415–422. doi: 10.1038/s41423-019-0224-2

Hanahan, D., and Weinberg, R. A. (2011). Hallmarks of cancer: the next generation. *Cell* 144, 646–674. doi: 10.1016/j.cell.2011.02.013

Helmink, B. A., Reddy, S. M., Gao, J., Zhang, S., Basar, R., Thakur, R., et al. (2020). B cells and tertiary lymphoid structures promote immunotherapy response. *Nature* 577, 549–555. doi: 10.1038/s41586-019-1922-8

Heng, D. Y., Xie, W., Regan, M. M., Warren, M. A., Golshayan, A. R., Sahi, C., et al. (2009). Prognostic factors for overall survival in patients with metastatic renal cell carcinoma treated with vascular endothelial growth factor-targeted agents: results from a large, multicenter study. *J. Clin. Oncol.* 27, 5794–5799. doi: 10.1200/JCO.2008.21.4809

Highfill, S. L., Cui, Y., Giles, A. J., Smith, J. P., Zhang, H., Morse, E., et al. (2014). Disruption of CXCR2-mediated MDSC tumor trafficking enhances anti-PD1 efficacy. *Sci. Transl. Med.* 6:237ra267. doi: 10.1126/scitranslmed.3007974

Hladíková, K., Koucký, V., Bouček, J., Laco, J., Grega, M., Hodek, M., et al. (2019). Tumor-infiltrating B cells affect the progression of oropharyngeal squamous cell carcinoma via cell-to-cell interactions with CD8 T cells. *J. Immunother. Cancer* 7:261. doi: 10.1186/s40425-019-0726-6

Hodi, F. S., O'Day, S. J., McDermott, D. F., Weber, R. W., Sosman, J. A., Haanen, J. B., et al. (2010). Improved survival with ipilimumab in patients with metastatic melanoma. *N. Engl. J. Med.* 363, 711–723. doi: 10.1056/NEJMoa1003466

Holmgaard, R. B., Schaer, D. A., Li, Y., Castaneda, S. P., Murphy, M. Y., Xu, X., et al. (2018). Targeting the TGFβ pathway with galunisertib, a TGFβRI small molecule inhibitor, promotes anti-tumor immunity leading to durable, complete responses, as monotherapy and in combination with checkpoint blockade. *J. Immunother. Cancer* 6:47. doi: 10.1186/s40425-018-0356-4

House, I., Savas, P., Lai, J., Chen, A., Oliver, A., Teo, Z., et al. (2020). Macrophage-derived CXCL9 and CXCL10 are required for antitumor immune responses following immune checkpoint blockade. *Clin. Cancer Res.* 26, 487–504. doi: 10.1158/1078-0432.CCR-19-1868

Huber, S., Hoffmann, R., Muskens, F., and Voehringer, D. (2010). Alternatively activated macrophages inhibit T-cell proliferation by Stat6-dependent expression of PD-L2. *Blood* 116, 3311–3320. doi: 10.1182/blood-2010-02-271981

Ibrahim, J., Nguyen, A., Rehman, A., Ochi, A., Jamal, M., Graffeo, C., et al. (2012). Dendritic cell populations with different concentrations of lipid regulate tolerance and immunity in mouse and human liver. *Gastroenterology* 143, 1061–1072. doi: 10.1053/j.gastro.2012.06.003

Iida, Y., Harashima, N., Motoshima, T., Komohara, Y., Eto, M., and Harada, M. (2017). Contrasting effects of cyclophosphamide on anti-CTL-associated protein 4 blockade therapy in two mouse tumor models. *Cancer Sci.* 108, 1974–1984. doi: 10.1111/cas.13337

Im, S. J., Hashimoto, M., Gerner, M. Y., Lee, J., Kissick, H. T., Burger, M. C., et al. (2016). Defining CD8+ T cells that provide the proliferative burst after PD-1 therapy. *Nature* 537, 417–421. doi: 10.1038/nature19330

Inoue, S., Leitner, W. W., Golding, B., and Scott, D. (2006). Inhibitory effects of B cells on antitumor immunity. *Cancer Res.* 66, 7741–7747. doi: 10.1158/0008-5472.CAN-05-3766

Jardim, D., Goodman, A., de Melo Gagliato, D., and Kurzrock, R. (2020). The challenges of tumor mutational burden as an immunotherapy biomarker. *Cancer Cell* 39, 154–173. doi: 10.1016/j.ccell.2020.10.001

Jhunjhunwala, S., Hammer, C., and Delamarre, L. (2021). Antigen presentation in cancer: insights into tumour immunogenicity and immune evasion. *Nat. Rev. Cancer* 21, 298–312. doi: 10.1038/s41568-021-00339-z

Junttila, M. R., and de Sauvage, F. J. (2013). Influence of tumour microenvironment heterogeneity on therapeutic response. *Nature* 501, 346–354. doi: 10.1038/nature12626

Kakavand, H., Jackett, L. A., Menzies, A. M., Gide, T. N., Carlino, M. S., Saw, R. P. M., et al. (2017). Negative immune checkpoint regulation by VISTA: a mechanism of acquired resistance to anti-PD-1 therapy in metastatic melanoma patients. *Mod. Pathol.* 30, 1666–1676. doi: 10.1038/modpathol.2017.89

Kallies, A., Zehn, D., and Utzschneider, D. T. (2020). Precursor exhausted T cells: key to successful immunotherapy? *Nat. Rev. Immunol.* 20, 128–136. doi: 10.1038/s41577-019-0223-7

Kalluri, R. (2016). The biology and function of fibroblasts in cancer. *Nat. Rev. Cancer* 16, 582–598. doi: 10.1038/nrc.2016.73

Kamada, T., Togashi, Y., Tay, C., Ha, D., Sasaki, A., Nakamura, Y., et al. (2019). PD-1 regulatory T cells amplified by PD-1 blockade promote hyperprogression of cancer. *Proc. Natl. Acad. Sci. U.S.A.* 116, 9999–10008. doi: 10.1073/pnas.1822001116

Kamran, N., Kadiyala, P., Saxena, M., Candolfi, M., Li, Y., Moreno-Ayala, M. A., et al. (2017). Immunosuppressive myeloid cells' blockade in the glioma microenvironment enhances the efficacy of immune-stimulatory gene therapy. *Mol. Ther.* 25, 232–248. doi: 10.1016/j.ymthe.2016.10.003

Kang, B., Seo, A., Yoon, S., Bae, H., Jeon, S., Kwon, O., et al. (2016). Prognostic value of tumor-infiltrating lymphocytes in Epstein-Barr virus-associated gastric cancer. *Ann. Oncol.* 27, 494–501. doi: 10.1093/annonc/mdv610

Kao, C., Powers, E., Wu, Y., Datto, M., Green, M., Strickler, J., et al. (2021). Predictive value of combining biomarkers for clinical outcomes in advanced non-small cell lung cancer patients receiving immune checkpoint inhibitors. *Clin. Lung Cancer* S1525-7304(21)00071-1. doi: 10.1016/j.cllc.2021.03.017

Kargl, J., Zhu, X., Zhang, H., Yang, G., Friesen, T., Shipley, M., et al. (2019). Neutrophil content predicts lymphocyte depletion and anti-PD1 treatment failure in NSCLC. *JCI Insight* 4:e130850. doi: 10.1172/jci.insight.130850

Kiselev, V. Y., Andrews, T. S., and Hemberg, M. (2019). Challenges in unsupervised clustering of single-cell RNA-seq data. *Nat. Rev. Genet.* 20, 273–282. doi: 10.1038/s41576-018-0088-9

Klein, O., Kee, D., Markman, B., Carlino, M. S., Underhill, C., Palmer, J., et al. (2021). Evaluation of TMB as a predictive biomarker in patients with solid cancers treated with anti-PD-1/CTLA-4 combination immunotherapy. *Cancer Cell* 39, 592–593. doi: 10.1016/j.ccell.2021.04.005

Knutson, K. L., and Disis, M. L. (2005). Tumor antigen-specific T helper cells in cancer immunity and immunotherapy. *Cancer Immunol. Immunother.* 54, 721–728. doi: 10.1007/s00262-004-0653-2

Krummel, M. F., and Allison, J. P. (1995). CD28 and CTLA-4 have opposing effects on the response of T cells to stimulation. *J. Exp. Med.* 182, 459–465. doi: 10.1084/jem.182.2.459

Kumagai, S., Togashi, Y., Kamada, T., Sugiyama, E., Nishinakamura, H., Takeuchi, Y., et al. (2020). The PD-1 expression balance between effector and regulatory T cells predicts the clinical efficacy of PD-1 blockade therapies. *Nat. Immunol.* 21, 1346–1358. doi: 10.1038/s41590-020-0769-3

Kurtulus, S., Madi, A., Escobar, G., Klapholz, M., Nyman, J., Christian, E., et al. (2019). Checkpoint blockade immunotherapy induces dynamic changes in PD-1CD8 tumor-infiltrating T cells. *Immunity* 50, 181–194.e186. doi: 10.1016/j.immuni.2018.11.014

Le, D. T., Uram, J. N., Wang, H., Bartlett, B. R., Kemberling, H., Eyring, A. D., et al. (2015). PD-1 blockade in tumors with mismatch-repair deficiency. *N. Engl. J. Med.* 372, 2509–2520. doi: 10.1056/NEJMoa1500596

LeBleu, V. S., and Kalluri, R. (2018). A peek into cancer-associated fibroblasts: origins, functions and translational impact. *Dis. Model Mech.* 11:dmm029447. doi: 10.1242/dmm.029447

Levental, K. R., Yu, H., Kass, L., Lakins, J. N., Egeblad, M., Erler, J. T., et al. (2009). Matrix crosslinking forces tumor progression by enhancing integrin signaling. *Cell* 139, 891–906. doi: 10.1016/j.cell.2009.10.027

Lim, S. P., Costantini, B., Mian, S. A., Perez Abellan, P., Gandhi, S., Martinez Llordella, M., et al. (2020). Treg sensitivity to FasL and relative IL-2 deprivation drive idiopathic aplastic anemia immune dysfunction. *Blood* 136, 885–897. doi: 10.1182/blood.2019001347

Lin, C., He, H., Liu, H., Li, R., Chen, Y., Qi, Y., et al. (2019). Tumour-associated macrophages-derived CXCL8 determines immune evasion through autonomous PD-L1 expression in gastric cancer. *Gut* 68, 1764–1773. doi: 10.1136/gutjnl-2018-316324

Long, E. O. (2008). Negative signaling by inhibitory receptors: the NK cell paradigm. *Immunol. Rev.* 224, 70–84. doi: 10.1111/j.1600-065X.2008.00660.x

Lv, Y., Zhao, Y., Wang, X., Chen, N., Mao, F., Teng, Y., et al. (2019). Increased intratumoral mast cells foster immune suppression and gastric cancer progression through TNF-α-PD-L1 pathway. *J. Immunother. Cancer* 7:54. doi: 10.1186/s40425-019-0530-3

Mantovani, A., Marchesi, F., Malesci, A., Laghi, L., and Allavena, P. (2017). Tumour-associated macrophages as treatment targets in oncology. *Nat. Rev. Clin. Oncol.* 14, 399–416. doi: 10.1038/nrclinonc.2016.217

Mariathasan, S., Turley, S. J., Nickles, D., Castiglioni, A., Yuen, K., Wang, Y., et al. (2018). TGFβ attenuates tumour response to PD-L1 blockade by contributing to exclusion of T cells. *Nature* 554, 544–548. doi: 10.1038/nature25501

McGrail, D., Pilié, P., Rashid, N., Voorwerk, L., Slagter, M., Kok, M., et al. (2021). High tumor mutation burden fails to predict immune checkpoint blockade response across all cancer types. *Ann. Oncol.* 32, 661–672. doi: 10.1016/j.annonc.2021.02.006

McLane, L. M., Abdel-Hakeem, M. S., and Wherry, E. J. (2019). CD8 T cell exhaustion during chronic viral infection and cancer. *Annu. Rev. Immunol.* 37, 457–495. doi: 10.1146/annurev-immunol-041015-055318

Mihaila, A. C., Ciortan, L., Macarie, R. D., Vadana, M., Cecoltan, S., Preda, M. B., et al. (2021). Transcriptional profiling and functional analysis of N1/N2 neutrophils reveal an immunomodulatory effect of S100A9-blockade on the pro-inflammatory N1 subpopulation. *Front. Immunol.* 12:708770. doi: 10.3389/fimmu.2021.708770

Myers, J. A., and Miller, J. S. (2021). Exploring the NK cell platform for cancer immunotherapy. *Nat. Rev. Clin. Oncol.* 18, 85–100. doi: 10.1038/s41571-020-0426-7

Najafi, M., Farhood, B., and Mortezaee, K. (2019). Extracellular matrix (ECM) stiffness and degradation as cancer drivers. *J. Cell Biochem.* 120, 2782–2790. doi: 10.1002/jcb.27681

Nakao, S., Arai, Y., Tasaki, M., Yamashita, M., Murakami, R., Kawase, T., et al. (2020). Intratumoral expression of IL-7 and IL-12 using an oncolytic virus increases systemic sensitivity to immune checkpoint blockade. *Sci. Transl. Med.* 12:eaax7992. doi: 10.1126/scitranslmed.aax7992

Ochoa de Olza, M., Navarro Rodrigo, B., Zimmermann, S., and Coukos, G. (2020). Turning up the heat on non-immunoreactive tumours: opportunities for clinical development. *Lancet Oncol.* 21, e419–e430. doi: 10.1016/S1470-2045(20)30234-5

Orme, J. J., Enninga, E. A. L., Lucien-Matteoni, F., Dale, H., Burgstaler, E., Harrington, S. M., et al. (2020). Therapeutic plasma exchange clears circulating soluble PD-L1 and PD-L1-positive extracellular vesicles. *J. Immunother. Cancer* 8:e001113. doi: 10.1136/jitc-2020-001113

Pagano, M. B., Zhou, H. F., Ennis, T. L., Wu, X., Lambris, J. D., Atkinson, J. P., et al. (2009). Complement-dependent neutrophil recruitment is critical for the development of elastase-induced abdominal aortic aneurysm. *Circulation* 119, 1805–1813. doi: 10.1161/CIRCULATIONAHA.108.832972

Pardoll, D. M. (2012). The blockade of immune checkpoints in cancer immunotherapy. *Nat. Rev. Cancer* 12, 252–264. doi: 10.1038/nrc3239

Pietras, K., Pahler, J., Bergers, G., and Hanahan, D. (2008). Functions of paracrine PDGF signaling in the proangiogenic tumor stroma revealed by pharmacological targeting. *PLoS Med.* 5:e19. doi: 10.1371/journal.pmed.0050019

Poggio, M., Hu, T., Pai, C. C., Chu, B., Belair, C. D., Chang, A., et al. (2019). Suppression of exosomal PD-L1 induces systemic anti-tumor immunity and memory. *Cell* 177, 414–427.e413. doi: 10.1016/j.cell.2019.02.016

Protopsaltis, N. J., Liang, W., Nudleman, E., and Ferrara, N. (2019). Interleukin-22 promotes tumor angiogenesis. *Angiogenesis* 22, 311–323. doi: 10.1007/s10456-018-9658-x

Qin, S., Xu, L., Yi, M., Yu, S., Wu, K., and Luo, S. (2019). Novel immune checkpoint targets: moving beyond PD-1 and CTLA-4. *Mol. Cancer* 18:155. doi: 10.1186/s12943-019-1091-2

Qu, Y., Wen, J., Thomas, G., Yang, W., Prior, W., He, W., et al. (2020). Baseline Frequency of Inflammatory Cxcl9-Expressing Tumor-Associated Macrophages Predicts Response to Avelumab Treatment. *Cell Rep.* 32:107873. doi: 10.1016/j.celrep.2020.108115

Quatrini, L., Vacca, P., Tumino, N., Besi, F., Di Pace, A. L., Scordamaglia, F., et al. (2021). Glucocorticoids and the cytokines IL-12, IL-15, and IL-18 present in the tumor microenvironment induce PD-1 expression on human natural killer cells. *J. Allergy Clin. Immunol.* 147, 349–360. doi: 10.1016/j.jaci.2020.04.044

Rapp, M., Wintergerst, M. W. M., Kunz, W. G., Vetter, V. K., Knott, M. M. L., Lisowski, D., et al. (2019). CCL22 controls immunity by promoting regulatory T cell communication with dendritic cells in lymph nodes. *J. Exp. Med.* 216, 1170–1181.

Ren, X., and Zhang, Z. (2019). Understanding tumor-infiltrating lymphocytes by single cell RNA sequencing. *Adv. Immunol.* 144, 217–245.

Rodon, J., Soria, J. C., Berger, R., Miller, W. H., Rubin, E., Kugel, A., et al. (2019). Genomic and transcriptomic profiling expands precision cancer medicine: the WINTHER trial. *Nat. Med.* 25, 751–758.

Romano, E., Kusio-Kobialka, M., Foukas, P., Baumgaertner, P., Meyer, C., Ballabeni, P., et al. (2015). Ipilimumab-dependent cell-mediated cytotoxicity of regulatory T cells ex vivo by nonclassical monocytes in melanoma patients. *Proc. Natl. Acad. Sci. U.S.A.* 112, 6140–6145.

Ruffell, B., and Coussens, L. M. (2015). Macrophages and therapeutic resistance in cancer. *Cancer Cell* 27, 462–472.

Ruterbusch, M., Pruner, K. B., Shehata, L., and Pepper, M. (2020). In vivo CD4(+) T cell differentiation and function: revisiting the Th1/Th2 paradigm. *Annu. Rev. Immunol.* 38, 705–725.

Sammarco, G., Varricchi, G., Ferraro, V., Ammendola, M., De Fazio, M., Altomare, D., et al. (2019). Mast cells, angiogenesis and lymphangiogenesis in human gastric cancer. *Int. J. Mol. Sci.* 20:2106.

Samstein, R. M., Arvey, A., Josefowicz, S. Z., Peng, X., Reynolds, A., Sandstrom, R., et al. (2012). Foxp3 exploits a pre-existent enhancer landscape for regulatory T cell lineage specification. *Cell* 151, 153–166.

Samstein, R. M., Lee, C. H., Shoushtari, A. N., Hellmann, M. D., Shen, R., Janjigian, Y. Y., et al. (2019). Tumor mutational load predicts survival after immunotherapy across multiple cancer types. *Nat. Genet.* 51, 202–206.

Sathe, A., Grimes, S., Lau, B., Chen, J., Suarez, C., Huang, R., et al. (2020). Single-cell genomic characterization reveals the cellular reprogramming of the gastric tumor microenvironment. *Clin. Cancer Res.* 26, 2640–2653.

Schalper, K. A., Carleton, M., Zhou, M., Chen, T., Feng, Y., Huang, S. P., et al. (2020). Elevated serum interleukin-8 is associated with enhanced intratumor neutrophils and reduced clinical benefit of immune-checkpoint inhibitors. *Nat. Med.* 26, 688–692.

Schoenberger, S. P., Toes, R. E., van der Voort, E. I., Offringa, R., and Melief, C. J. (1998). T-cell help for cytotoxic T lymphocytes is mediated by CD40-CD40L interactions. *Nature* 393, 480–483.

Schoenfeld, A. J., and Hellmann, M. D. (2020). Acquired resistance to immune checkpoint inhibitors. *Cancer Cell* 37, 443–455.

Segura, E., Nicco, C., Lombard, B., Véron, P., Raposo, G., Batteux, F., et al. (2005). ICAM-1 on exosomes from mature dendritic cells is critical for efficient naive T-cell priming. *Blood* 106, 216–223.

Sharma, A., Subudhi, S. K., Blando, J., Scutti, J., Vence, L., Wargo, J., et al. (2019). Anti-CTLA-4 immunotherapy does not deplete FOXP3(+) regulatory T cells (Tregs) in human cancers. *Clin. Cancer Res.* 25, 1233–1238.

Sharpe, A. H., and Freeman, G. J. (2002). The B7-CD28 superfamily. *Nat. Rev. Immunol.* 2, 116–126.

Shen, Y., Teng, Y., Lv, Y., Zhao, Y., Qiu, Y., Chen, W., et al. (2020). PD-1 does not mark tumor-infiltrating CD8+ T cell dysfunction in human gastric cancer. *J. Immunother. Cancer* 8:e000422.

Shigeta, K., Datta, M., Hato, T., Kitahara, S., Chen, I. X., Matsui, A., et al. (2020). Dual programmed death receptor-1 and vascular endothelial growth factor receptor-2 blockade promotes vascular normalization and enhances antitumor immune responses in hepatocellular carcinoma. *Hepatology* 71, 1247–1261.

Silva-Santos, B. (2010). Promoting angiogenesis within the tumor microenvironment: the secret life of murine lymphoid IL-17-producing gammadelta T cells. *Eur. J. Immunol.* 40, 1873–1876.

Simoni, Y., Chng, M. H. Y., Li, S., Fehlings, M., and Newell, E. W. (2018). Mass cytometry: a powerful tool for dissecting the immune landscape. *Curr. Opin. Immunol.* 51, 187–196.

Sivori, S., Pende, D., Quatrini, L., Pietra, G., Della Chiesa, M., Vacca, P., et al. (2020). NK cells and ILCs in tumor immunotherapy. *Mol. Aspects Med.* 80:100870.

Spitzer, M. H., and Nolan, G. P. (2016). Mass cytometry: single cells, many features. *Cell* 165, 780–791.

Tanaka, H., Yoshizawa, H., Yamaguchi, Y., Ito, K., Kagamu, H., Suzuki, E., et al. (1999). Successful adoptive immunotherapy of murine poorly immunogenic tumor with specific effector cells generated from gene-modified tumor-primed lymph node cells. *J. Immunol.* 162, 3574–3582.

Tang, F., Du, X., Liu, M., Zheng, P., and Liu, Y. (2018). Anti-CTLA-4 antibodies in cancer immunotherapy: selective depletion of intratumoral regulatory T cells or checkpoint blockade? *Cell Biosci.* 8:30.

Tang, H., Wang, Y., Chlewicki, L., Zhang, Y., Guo, J., Liang, W., et al. (2016). Facilitating T cell infiltration in tumor microenvironment overcomes resistance to PD-L1 blockade. *Cancer Cell* 29, 285–296.

Tauriello, D. V. F., Palomo-Ponce, S., Stork, D., Berenguer-Llergo, A., Badia-Ramentol, J., Iglesias, M., et al. (2018). TGFβ drives immune evasion in genetically reconstituted colon cancer metastasis. *Nature* 554, 538–543.

Tavazoie, M. F., Pollack, I., Tanqueco, R., Ostendorf, B. N., Reis, B. S., Gonsalves, F. C., et al. (2018). LXR/ApoE Activation Restricts Innate Immune Suppression in Cancer. *Cell* 172, 825–840.e818.

Thielens, A., Vivier, E., and Romagné, F. (2012). NK cell MHC class I specific receptors (KIR): from biology to clinical intervention. *Curr. Opin. Immunol.* 24, 239–245.

Thompson, E., Zahurak, M., Murphy, A., Cornish, T., Cuka, N., Abdelfatah, E., et al. (2017). Patterns of PD-L1 expression and CD8 T cell infiltration in gastric adenocarcinomas and associated immune stroma. *Gut* 66, 794–801.

Tian, L., Goldstein, A., Wang, H., Ching Lo, H., Sun Kim, I., Welte, T., et al. (2017). Mutual regulation of tumour vessel normalization and immunostimulatory reprogramming. *Nature* 544, 250–254.

Topalian, S. L., Hodi, F. S., Brahmer, J. R., Gettinger, S. N., Smith, D. C., McDermott, D. F., et al. (2012). Safety, activity, and immune correlates of anti-PD-1 antibody in cancer. *N. Engl. J. Med.* 366, 2443–2454.

Tu, L., Guan, R., Yang, H., Zhou, Y., Hong, W., Ma, L., et al. (2020). Assessment of the expression of the immune checkpoint molecules PD-1, CTLA4, TIM-3 and LAG-3 across different cancers in relation to treatment response, tumor-infiltrating immune cells and survival. *Int. J. Cancer* 147, 423–439.

Tumeh, P., Harview, C., Yearley, J., Shintaku, I., Taylor, E., Robert, L., et al. (2014). PD-1 blockade induces responses by inhibiting adaptive immune resistance. *Nature* 515, 568–571.

Ueha, S., Shand, F., and Matsushima, K. (2011). Myeloid cell population dynamics in healthy and tumor-bearing mice. *Int. Immunopharmacol.* 11, 783–788. doi: 10.1016/j.intimp.2011.03.003

Valero, C., Lee, M., Hoen, D., Zehir, A., Berger, M., Seshan, V., et al. (2021). Response rates to anti-PD-1 immunotherapy in microsatellite-stable solid tumors with 10 or more mutations per megabase. *JAMA Oncol.* 7, 739–743. doi: 10.1001/jamaoncol.2020.7684

Veglia, F., Perego, M., and Gabrilovich, D. (2018). Myeloid-derived suppressor cells coming of age. *Nat. Immunol.* 19, 108–119. doi: 10.1038/s41590-017-0022-x

Vesely, M. D., Kershaw, M. H., Schreiber, R. D., and Smyth, M. J. (2011). Natural innate and adaptive immunity to cancer. *Annu. Rev. Immunol.* 29, 235–271. doi: 10.1146/annurev-immunol-031210-101324

Voehringer, D. (2013). Protective and pathological roles of mast cells and basophils. *Nat. Rev. Immunol.* 13, 362–375. doi: 10.1038/nri3427

von Andrian, U. H. (2002). Immunology. T cell activation in six dimensions. *Science* 296, 1815–1817. doi: 10.1126/science.296.5574.1815

von Karstedt, S., Montinaro, A., and Walczak, H. (2017). Exploring the TRAILs less travelled: TRAIL in cancer biology and therapy. *Nat. Rev. Cancer* 17, 352–366. doi: 10.1038/nrc.2017.28

Voskoboinik, I., Smyth, M. J., and Trapani, J. A. (2006). Perforin-mediated target-cell death and immune homeostasis. *Nat. Rev. Immunol.* 6, 940–952. doi: 10.1038/nri1983

Wang, T. T., Zhao, Y. L., Peng, L. S., Chen, N., Chen, W., Lv, Y. P., et al. (2017). Tumour-activated neutrophils in gastric cancer foster immune suppression and disease progression through GM-CSF-PD-L1 pathway. *Gut* 66, 1900–1911. doi: 10.1136/gutjnl-2016-313075

Watts, T. H., and DeBenedette, M. A. (1999). T cell co-stimulatory molecules other than CD28. *Curr. Opin. Immunol.* 11, 286–293. doi: 10.1016/S0952-7915(99)80046-6

Weaver, C. T., Hatton, R. D., Mangan, P. R., and Harrington, L. E. (2007). IL-17 family cytokines and the expanding diversity of effector T cell lineages. *Annu. Rev. Immunol.* 25, 821–852. doi: 10.1146/annurev.immunol.25.022106.141557

Weiskopf, K., Schnorr, P. J., Pang, W. W., Chao, M. P., Chhabra, A., Seita, J., et al. (2016). Myeloid cell origins, differentiation, and clinical implications. *Microbiol. Spectr.* 4. doi: 10.1128/microbiolspec.MCHD-0031-2016

Wen, Z., Liu, H., Gao, R., Zhou, M., Ma, J., Zhang, Y., et al. (2018). Tumor cell-released autophagosomes (TRAPs) promote immunosuppression through induction of M2-like macrophages with increased expression of PD-L1. *J. Immunother. Cancer* 6:151. doi: 10.1186/s40425-018-0452-5

Willsmore, Z. N., Harris, R. J., Crescioli, S., Hussein, K., Kakkassery, H., Thapa, D., et al. (2020). B cells in patients with melanoma: implications for treatment with checkpoint inhibitor antibodies. *Front. Immunol.* 11:622442. doi: 10.3389/fimmu.2020.622442

Wu, F., Yang, J., Liu, J., Wang, Y., Mu, J., Zeng, Q., et al. (2021). Signaling pathways in cancer-associated fibroblasts and targeted therapy for cancer. *Signal Transduct. Target Ther.* 6:218. doi: 10.1038/s41392-021-00641-0

Wynn, T., Chawla, A., and Pollard, J. (2013). Macrophage biology in development, homeostasis and disease. *Nature* 496, 445–455. doi: 10.1038/nature12034

Xia, Y., Rao, L., Yao, H., Wang, Z., Ning, P., and Chen, X. (2020). Engineering macrophages for cancer immunotherapy and drug delivery. *Adv. Mater.* 32:e2002054. doi: 10.1002/adma.202002054

Yang, H., Zhang, Q., Xu, M., Wang, L., Chen, X., Feng, Y., et al. (2020). CCL2-CCR2 axis recruits tumor associated macrophages to induce immune evasion through PD-1 signaling in esophageal carcinogenesis. *Mol. Cancer* 19:41. doi: 10.1186/s12943-020-01165-x

Yoshida, G. J. (2020). Regulation of heterogeneous cancer-associated fibroblasts: the molecular pathology of activated signaling pathways. *J. Exp. Clin. Cancer Res.* 39:112. doi: 10.1186/s13046-020-01611-0

Yost, K. E., Satpathy, A. T., Wells, D. K., Qi, Y., Wang, C., Kageyama, R., et al. (2019). Clonal replacement of tumor-specific T cells following PD-1 blockade. *Nat. Med.* 25, 1251–1259. doi: 10.1038/s41591-019-0522-3

Yu, J., Green, M. D., Li, S., Sun, Y., Journey, S. N., Choi, J. E., et al. (2021). Liver metastasis restrains immunotherapy efficacy via macrophage-mediated T cell elimination. *Nat. Med.* 27, 152–164. doi: 10.1038/s41591-020-1131-x

Yuen, K. C., Liu, L. F., Gupta, V., Madireddi, S., Keerthivasan, S., Li, C., et al. (2020). High systemic and tumor-associated IL-8 correlates with reduced clinical benefit of PD-L1 blockade. *Nat. Med.* 26, 693–698. doi: 10.1038/s41591-020-0860-1

Zhang, H., and Houghton, A. M. (2021). Good cops turn bad: the contribution of neutrophils to immune-checkpoint inhibitor treatment failures in cancer. *Pharmacol. Ther.* 217:107662. doi: 10.1016/j.pharmthera.2020.107662

Zhang, H., Li, R., Cao, Y., Gu, Y., Lin, C., Liu, X., et al. (2020). Poor clinical outcomes and immunoevasive contexture in intratumoral IL-10-producing macrophages enriched gastric cancer patients. *Ann. Surg.* [Epub ahead of print]. doi: 10.1097/SLA.0000000000004037

Zhang, L., and Zhang, Z. (2019). Recharacterizing tumor-infiltrating lymphocytes by single-cell RNA sequencing. *Cancer Immunol. Res.* 7, 1040–1046. doi: 10.1158/2326-6066.CIR-18-0658

Zheng, C., Zheng, L., Yoo, J. K., Guo, H., Zhang, Y., Guo, X., et al. (2017). Landscape of infiltrating T Cells in liver cancer revealed by single-cell sequencing. *Cell* 169, 1342–1356.e1316. doi: 10.1016/j.cell.2017.05.035

Conflict of Interest: The authors declare that the research was conducted in the absence of any commercial or financial relationships that could be construed as a potential conflict of interest.

Publisher's Note: All claims expressed in this article are solely those of the authors and do not necessarily represent those of their affiliated organizations, or those of the publisher, the editors and the reviewers. Any product that may be evaluated in this article, or claim that may be made by its manufacturer, is not guaranteed or endorsed by the publisher.

frontiers in Cell and Developmental Biology

ORIGINAL RESEARCH
published: 07 October 2021
doi: 10.3389/fcell.2021.715883

Comprehensive Analysis of Hexokinase 2 Immune Infiltrates and m6A Related Genes in Human Esophageal Carcinoma

*Xu-Sheng Liu[1,2], Jia-Min Liu[3,4], Yi-Jia Chen[1], Fu-Yan Li[1], Rui-Min Wu[1], Fan Tan[1], Dao-Bing Zeng[1], Wei Li[1], Hong Zhou[1], Yan Gao[1] and Zhi-Jun Pei[1,2]**

[1] Department of Nuclear Medicine and Institute of Anesthesiology and Pain, Taihe Hospital, Hubei University of Medicine, Shiyan, China, [2] Hubei Clinical Research Center for Precise Diagnosis and Treatment of Liver Cancer, Taihe Hospital, Hubei University of Medicine, Shiyan, China, [3] Shiyan Emergency Medical Center, Shiyan, China, [4] School of Public Health, Hubei University of Medicine, Shiyan, China

Background: Hexokinase 2 not only plays a role in physiological function of human normal tissues and organs, but also plays a vital role in the process of glycolysis of tumor cells. However, there are few comprehensive studies on HK2 in esophageal carcinoma (ESCA) needs further study.

Methods: Oncomine, Tumor Immune Estimation Resource (TIMER), The Cancer Genome Atlas (TCGA) and Gene Expression Omnibus (GEO) database were used to analyze the expression differences of HK2 in Pan-cancer and ESCA cohort, and to analyze the correlation between HK2 expression level and clinicopathological features of TCGA ESCA samples. GO/KEGG, GGI, and PPI analysis of HK2 was performed using R software, LinkedOmics, GeneMANIA and STRING online tools. The correlation between HK2 and ESCA immune infiltration was analyzed TIMER and TCGA ESCA cohort. The correlation between HK2 expression level and m6A modification of ESCA was analyzed by utilizing TCGA ESCA cohort.

Results: HK2 is highly expressed in a variety of tumors, and its high expression level in ESCA is closely related to the weight, cancer stages, tumor histology and tumor grade of ESCA. The analysis results of GO/KEGG showed that HK2 was closely related to cell adhesion molecule binding, cell-cell junction, ameboidal-type cell migration, insulin signaling pathway, hif-1 signaling pathway, and insulin resistance. GGI showed that HK2 associated genes were mainly involved in the glycolytic pathway. PPI showed that HK2 was closely related to HK1, GPI, and HK3, all of which played an important role in tumor proliferation. The analysis results of TIMER and TCGA ESCA cohort indicated that the HK2 expression level was related to the infiltration of various immune cells. TCGA ESCA cohort analyze indicated that the HK2 expression level was correlated with m6A modification genes.

Conclusion: HK2 is associated with tumor immune infiltration and m6A modification of ESCA, and can be used as a potential biological target for diagnosis and therapy of ESCA.

Keywords: HK2, esophageal carcinoma, immune infiltration, m6A modification, tumor microenvironment

OPEN ACCESS

Edited by:
Shengtao Zhou,
Sichuan University, China

Reviewed by:
Yi Liao,
Affiliated Hospital of Southwest Medical University, China
Jiao Hu,
Central South University, China
Xiao Yang,
Shanghai Jiao Tong University, China

****Correspondence:***
Zhi-Jun Pei
pzjzml1980@taihehospital.com

Specialty section:
This article was submitted to Molecular and Cellular Pathology, a section of the journal Frontiers in Cell and Developmental Biology

Received: *27 May 2021*
Accepted: *17 September 2021*
Published: *07 October 2021*

Citation:
Liu X-S, Liu J-M, Chen Y-J, Li F-Y, Wu R-M, Tan F, Zeng D-B, Li W, Zhou H, Gao Y and Pei Z-J (2021) Comprehensive Analysis of Hexokinase 2 Immune Infiltrates and m6A Related Genes in Human Esophageal Carcinoma. Front. Cell Dev. Biol. 9:715883. doi: 10.3389/fcell.2021.715883

INTRODUCTION

Recent studies show that Esophageal carcinoma (ESCA) ranks seventh in terms of incidence and sixth in mortality overall (Sung et al., 2021). Despite substantial improvements in the diagnosis and treatment of esophageal diseases, the prognosis for patients with ESCA remains poor (Bray et al., 2018). The occurrence and development of ESCA is an extremely complex biological process, and the expression of many genes has changed. Therefore, further research on the molecular mechanism of ESCA can provide new theoretical value for the diagnosis and treatment of tumors.

Hexokinase (HK) is an enzyme capable of phosphorylating hexose and is a rate-limiting enzyme in the glycolytic pathway. Four subtypes of human HK have been discovered, which are encoded by the genes HK1, HK2, HK3, and HK4, respectively (Zhang et al., 2017). HK1 is widely expressed in mammalian tissues, HK2 is usually expressed in insulin-sensitive tissues such as fat, bone and heart muscle, and HK3 is expressed at a low level, while HK4 expression is limited to pancreas and liver (Smith, 2000; Zhang et al., 2017). HK2 not only plays a role in physiological function of human normal tissues and organs, but also plays an important role in the glycolysis of tumor cells (Yu et al., 2021). Currently, researchers have found that expression of HK2 is increased in a variety of tumors and promotes the development of tumors (Shen et al., 2020; Wang et al., 2020). Our previous study found that HK2 was highly expressed in ESCA, but no more studies were conducted on the biological function of HK2 (Liu et al., 2020b).

Tumor immunotherapy and N6-methyladenosine (m6A) modification are hot spots in tumor treatment, which are extensively used in the investigation and therapy of ESCA (Baba et al., 2020; Wu S. et al., 2020; Wu X. et al., 2020; Yang et al., 2020). However, there are less investigates on the overall understanding of HK2 in ESCA, particularly the correlation between HK2 and ESCA immune cell infiltration and m6A modification.

On this project, we processed The Cancer Genome Atlas (TCGA) ESCA cohort and performed bioinformatics analysis using the R software, online website and other databases. The differences of HK2 expression in different cancer tissues were studied, and the mRNA and protein expression of HK2 in ESCA were verified by cell assay and immunohistochemistry (IHC). The co-expression gene networks of HK2 in ESCA were analyzed, and the possible biological mechanisms and signal pathways involved in associated genes were analyzed. Eventually, the correlation between the expression difference of HK2 and the tumor immune cell infiltration and m6A modification of ESCA will be explored, which will help to study the potential pathogenesis of ESCA.

MATERIALS AND METHODS

Ethics Statement

The protocol of this study had been approved by the Ethics Committee of Taihe Hospital Affiliated of Hubei University of Medicine (Shiyan, China) (document NO.2021KS021) and conducted according to the principles stated in the Declaration of Helsinki, and the requirement to obtain informed consent was waived.

Expression of Hexokinase 2 in Pan-Cancer and Esophageal Carcinoma

Oncomine[1] (Rhodes et al., 2004, 2007) and TIMER[2] (Li et al., 2016, 2017) databases were used to analyze the expression level of HK2 in different tumors. Oncomine database used Student's *t*-test to compare the transcription level of HK2 in clinical cancer samples and normal control group, and selected data with multiple change > 2 and P-value < 0.01. We also downloaded the RNA sequencing data of ESCA from TCGA[3] (Tomczak et al., 2015) and GEO (GSE38129)[4] ($n = 60$; GSE23400, $n = 106$) cohort to analyze the difference of HK2 expression between ESCA and normal tissues. UALCAN database[5] (Chandrashekar et al., 2017) was used to analyze the relationship between the expression level of HK2 and the clinicopathological characteristics of ESCA patients. Eventually, we validated the mRNA and protein expression of HK2 in ESCA and control sample by qRT-PCR and IHC assay according to the method described previously (Liu et al., 2020a, 2021a), as detailed in **Supplementary Materials**.

Enrichment Analysis of Hexokinase 2 Gene Co-expression Network

The co-expression network of HK2 in TCGA ESCA cohort was analyzed using LinkedOmics[6] database. Pearson correlation coefficient was used for statistical analysis, and volcanic maps and heat maps were used for display. The rank criterion was an FDR < 0.05. The ClusterProfiler software package of R was used to analyze the Gene Ontology (GO) function and Kyoto Encyclopedia of Genes and Genomes (KEGG) pathway that co-expressed genes may participate in, and the ggplot2 software package was used to visually analyze the data.

Analysis of Gene-Gene Interaction and Protein-Protein Interaction of Hexokinase 2 Gene

We use GeneMANIA database[7] (Warde-Farley et al., 2010) to query and generate a list of genes that have similar functions with the HK2 gene and constructed an interactive network to illustrate the relationship between genes. The PPI of HK2 protein was calculated and predicted by using the STRING database[8] (Szklarczyk et al., 2019).

[1] www.oncomine.org
[2] https://cistrome.shinyapps.io/timer/
[3] https://portal.gdc.cancer.gov/
[4] www.ncbi.nlm.nih.gov/geo
[5] http://ualcan.path.uab.edu/index.html
[6] www.linkedomics.org/login.php
[7] www.genemania.org
[8] www.string-db.org

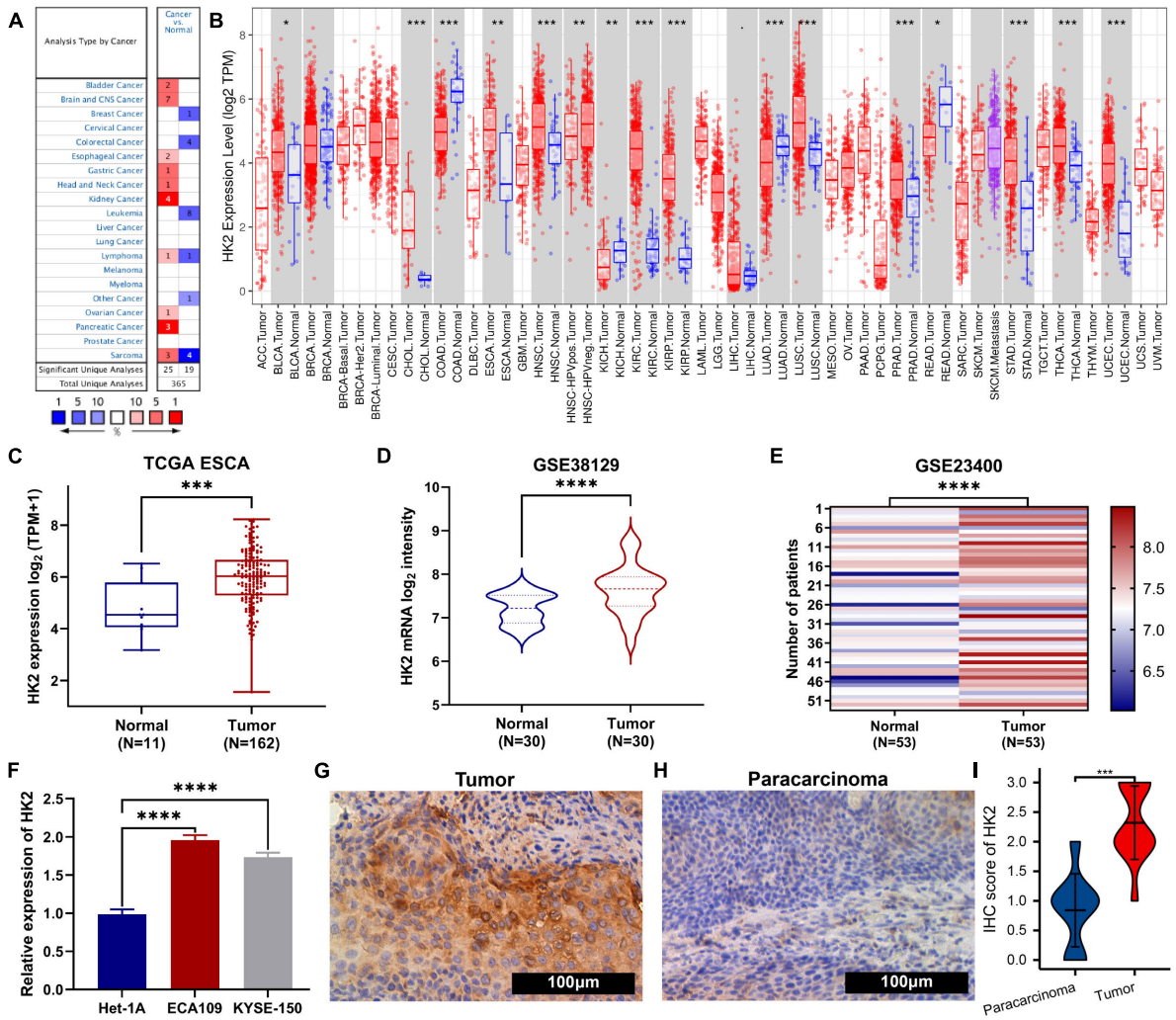

FIGURE 1 | The expression of HK2 in esophageal carcinoma (ESCA) and pan-carcinoma. **(A)** Oncomine analysis showed the expression level of HK2 mRNA in different tumor types. **(B)** The TIMER ESCA cohort shows that HK2 mRNA expression levels in different tumor types. **(C)** Differential expression of HK2 in ESCA and normal tissues was analyzed by TCGA ESCA cohort **(D)** Difference expression of HK2 in ESCA and normal tissues was analyzed by GSE38129 cohort. **(E)** Difference expression of HK2 between ESCA and matched normal tissues in GSE23400 cohort. **(F)** Difference expression of HK2 in different ESCA cell lines and human normal epithelial cell lines. Immunohistochemical staining showed the expression of HK2 in ESCA samples **(G)** and paracarcinoma samples **(H)**. **(I)** The mean HK2 IHC score in ESCA tissue (2.32 ± 0.621) was significantly higher than that of matched peritumoral tissue (0.84 ± 0.618). *$P < 0.05$; **$P < 0.01$; ***$P < 0.001$; ****$P < 0.0001$.

Correlation Analysis of Hexokinase 2 and Immune Infiltrating Cells

The correlation between HK2 and immune infiltrating cells in ESCA samples was evaluated using the TIMER database. Immune infiltrating cells include B cell, neutrophil, $CD4^+$ T cell, macrophage, $CD8^+$ T cell, and dendritic cell. The somatic copy number alteration (SCNA) module of the TIMER tool was used to associate the genetic copy number variation (CNV) of HK2 with the relative abundance of tumor infiltrating cells. The CIBERSORT (Newman et al., 2015) software package of R was utilized to analyze the differences of 22 immune cells between high and low HK2 expression groups in ESCA samples. In addition, we also analyzed the correlation between HK2 and immune cell markers in ESCA samples utilizing TIMER databases and TCGA ESCA cohort. Immunofiltration marker genes refer to the previous study (Liu et al., 2021b).

Correlations of Hexokinase 2 Expression With m6A Associated Genes in Esophageal Carcinoma

The R software package was utilized to evaluate the correlation between the expression of HK2 and the expression of m6A associated gene in the TCGA ESCA cohort, including ZC3H13, YTHDF3, HNRNPC, METTL14, HNRNPA2B1,

TABLE 1 | HK2 expression in cancerous vs. normal tissue in ONCOMINE.

Cancer Site	Cancer type	*P*-value	*t*-test	Fold change	References (PMID)
Bladder	Infiltrating bladder urothelial carcinoma	1.47E-12	8.112	3.119	16432078
	Superficial bladder cancer	1.51E-16	10.627	4.207	16432078
Brain and CNS	Anaplastic oligoastrocytoma	0.001	5.698	4.095	16357140
	Brain glioblastoma	1.85E-8	14.506	5.631	TCGA Brain
	Glioblastoma	0.006	3.978	5.856	TCGA Brain
	Glioblastoma	8.11E-5	6.873	3.455	16204036
	Oligodendroglioma	1.50E-6	5.268	2.460	16616334
	Anaplastic astrocytoma	8.43E-5	4.200	2.491	16616334
	Glioblastoma	1.41E-4	7.815	2.820	18565887
Breast	Breast phyllodes tumor	3.98E-4	− 6.710	− 2.365	22522925
Colorectal	Cecum adenocarcinoma	1.20E-6	− 6.579	− 2.080	17615082
	Rectal adenocarcinoma	4.02E-17	− 9.720	− 2.146	20725992
	Rectal mucinous adenocarcinoma	1.33E-4	− 4.615	− 2.337	TCGA Colorectal
	Colorectal carcinoma	1.05E-5	− 5.676	− 2.198	20143136
Esophageal	Barrett's esophagus	0.003	2.929	3.157	16952561
	Esophageal adenocarcinoma	9.76E-4	3.433	3.062	16952561
Gastric	Gastric mixed adenocarcinoma	3.09E-5	5.339	2.638	19081245
Head-Neck	Thyroid gland papillary carcinoma	2.29E-4	4.668	2.487	17296934
Kidney	Hereditary clear cell renal cell Carcinoma	7.96E-29	30.305	13.568	19470766
	Non-hereditary clear cell renal cell Carcinoma	4.45E-18	16.554	8.081	19470766
	Clear cell renal cell carcinoma	1.19E-7	10.778	14.045	17699851
	Clear cell renal cell carcinoma	5.80E-10	9.709	4.871	16115910
Leukemia	Acute myeloid leukemia	4.30E-5	− 5.734	− 3.633	14770183
	B-Cell acute lymphoblastic leukemia	1.74E-10	− 15.717	− 7.694	17410184
	Acute myeloid leukemia	5.30E-7	− 7.117	− 2.898	17410184
	T-Cell acute lymphoblastic leukemia	1.94E-6	− 7.774	− 9.190	17410184
	B-Cell acute lymphoblastic leukemia	2.46E-30	− 13.938	− 2.545	20406941
	Chronic Lymphocytic Leukemia	2.19E-38	− 20.361	− 3.118	20406941
	T-Cell acute lymphoblastic leukemia	1.77E-25	− 12.090	− 2.282	20406941
	B-Cell childhood acute lymphoblastic Leukemia	1.07E-26	− 13.463	− 2.221	20406941
Lymphoma	Unspecified peripheral T-cell Lymphoma	2.43E-10	7.895	2.280	17304354
	Cutaneous follicular lymphoma	1.68E-4	− 4.963	− 2.329	12713594
Ovarian	Ovarian serous adenocarcinoma	1.00E-4	5.492	9.472	19486012
Pancreas	Pancreatic carcinoma	9.31E-10	8.709	6.691	19732725
	Pancreatic ductal adenocarcinoma	1.92E-11	7.825	3.038	19260470
	Pancreatic adenocarcinoma	0.005	3.955	8.921	12651607
Sarcoma	Synovial sarcoma	2.43E-5	5.554	3.867	15994966
	Round cell liposarcoma	1.07E-4	5.031	3.686	15994966
	Pleomorphic liposarcoma	5.83E-4	4.806	5.595	15994966
	Leiomyosarcoma	2.03E-10	− 11.795	− 5.138	20601955
	Dedifferentiated liposarcoma	3.12E-9	− 10.393	− 4.032	20601955
	Myxofibrosarcoma	1.35E-7	− 6.913	− 2.914	20601955
	Myxoid/round cell liposarcoma	1.53E-5	− 5.634	− 2.140	20601955

IGF2BP1, METTL3, WTAP, RBM15, ALKBH5, IGF2BP2, RBMX, RBM15B, YTHDC1, VIRMA, IGF2BP3, YTHDC2, YTHDF1, FTO, and YTHDF2 (Li et al., 2019). The R software was utilized to analyze the differences of 20 m6A associated genes between high and low HK2 expression groups in ESCA samples. The data were analyzed visually by ggplot2 software package.

RESULTS

Transcriptional Levels of Hexokinase 2 in Pan-Cancer

We analyzed the difference of HK2 mRNA expression between ESCA samples and normal tissue samples using Oncomine and TIMER databases, respectively. Oncomine database analysis

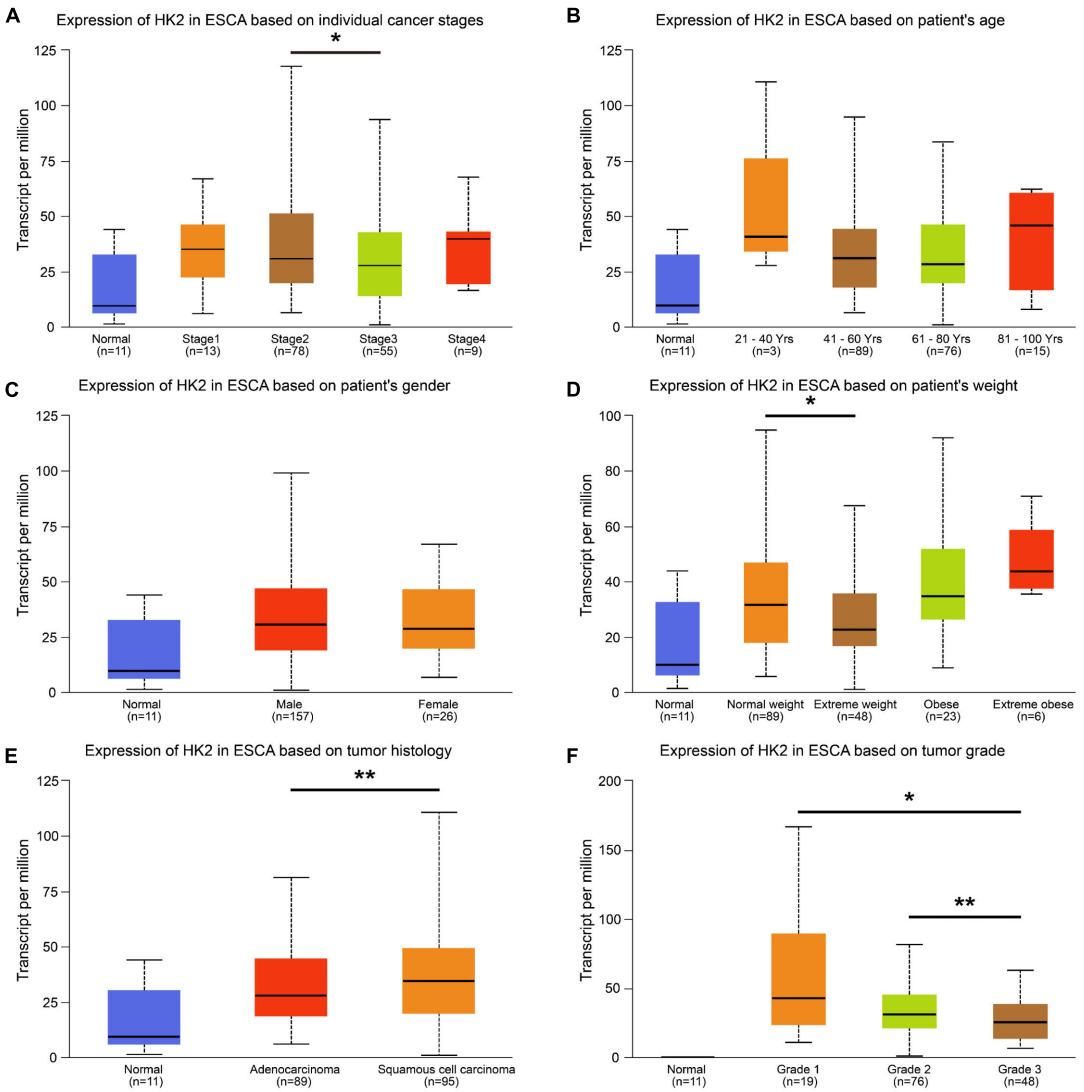

FIGURE 2 | Relationship between HK2 mRNA expression and clinicopathological parameters in esophageal carcinoma (ESCA) patients. The block diagram using the UALCAN network tool shows the correlation between hK2 mRNA expression level and clinicopathological features, including **(A)** individual cancer stages, **(B)** patient age, **(C)** patient gender, **(D)** patient weight, **(E)** tumor histology and **(F)** tumor grade. *$P < 0.05$; **$P < 0.01$.

showed that HK2 expression in bladder (Sanchez-Carbayo et al., 2006), brain and CNS (Bredel et al., 2005; French et al., 2005; Murat et al., 2008; Sun et al., 2006), esophageal (Hao et al., 2006), gastric (D'Errico et al., 2009), head and neck (Vasko et al., 2007), kidney (Jones et al., 2005; Gumz et al., 2007; Beroukhim et al., 2009), ovarian (Yoshihara et al., 2009), and pancreatic adenocarcinoma (Iacobuzio-Donahue et al., 2003; Badea et al., 2008; Pei et al., 2009) was higher than that in normal tissue samples. However, the expression of HK2 in breast cancer (Curtis et al., 2012), colorectal cancer (Kaiser et al., 2007; Gaedcke et al., 2010; Hong et al., 2010) and leukemia (Stegmaier et al., 2004; Andersson et al., 2007; Haferlach et al., 2010) was lower than that in normal tissues. Confusingly, there are different data suggesting that HK2 may be highly expressed in both lymphoma (Piccaluga et al., 2007) and normal tissue samples (Storz et al., 2003), and it is speculated that this may be due to different sample sizes (**Figure 1A**). HK2 may be highly expressed in both sarcomas (Detwiller et al., 2005) and normal tissue samples (Barretina et al., 2010), presumably due to the difference in tissue origin of the tissues designated as normal. **Table 1** provides the corresponding summary results in detail.

The expression of HK2 mRNA in human tumor samples was further analyzed by TIMER database. **Figure 1B** shows the differentially expression of HK2 in different tumor tissue samples and normal tissue samples. Compared with normal tissue samples, the expression level of HK2 was remarkable increased in BLCA (bladder urothelial carcinoma), CHOL (cholangiocarcinoma), ESCA (esophageal carcinoma), HNSC (head and neck squamous cell carcinoma), KIRC (kidney renal clear cell carcinoma), KIRP (kidney

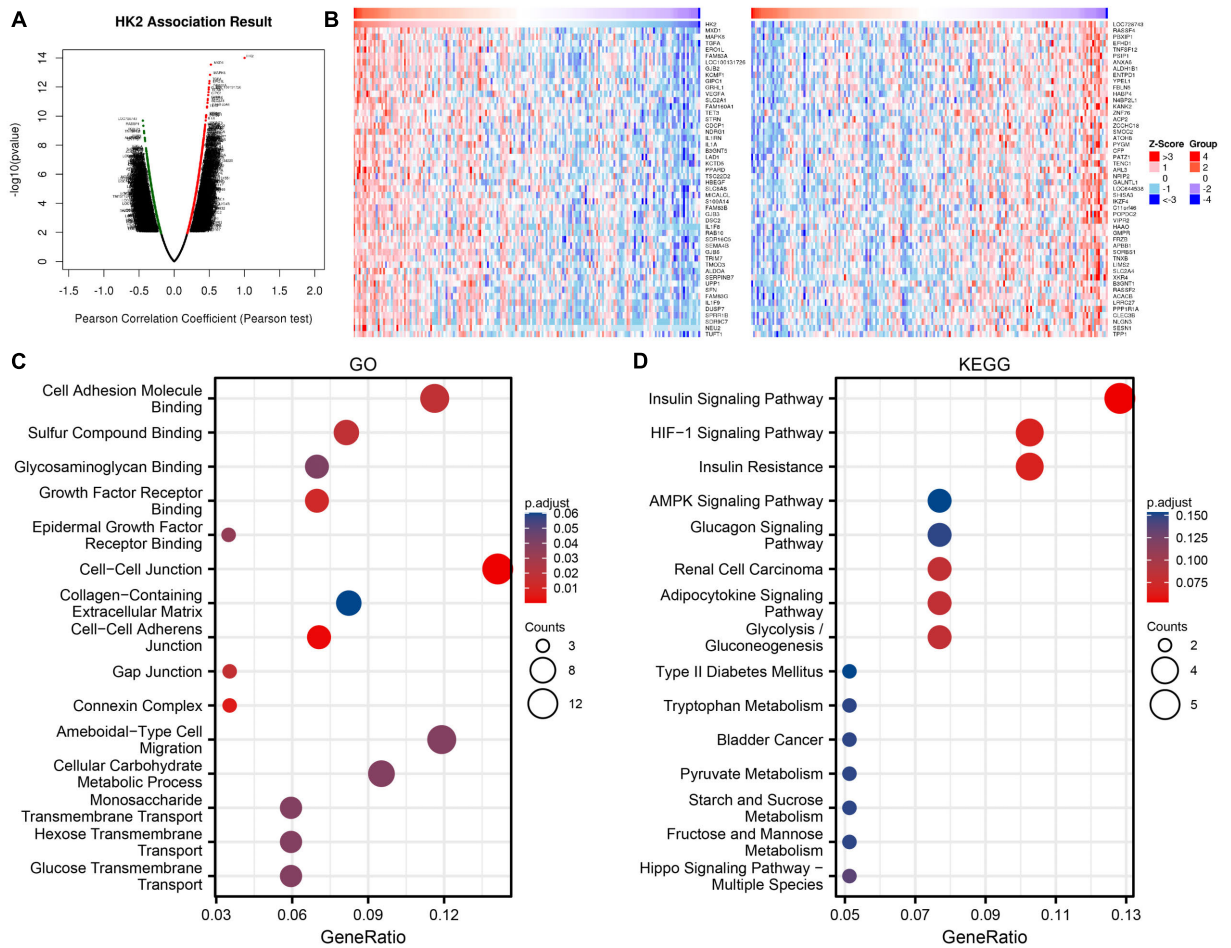

FIGURE 3 | Enrichment analysis of HK2 gene co-expression network in esophageal carcinoma (ESCA). **(A)** The co-expressed genes related to HK2 expression in TCGA ESCA cohort were shown by volcanic map. **(B)** The first 50 co-expressed genes positively and negatively correlated with HK2 expression were shown by heat map. **(C)** Enrichment of gene ontology (GO) terms for HK2 co-expression genes. **(D)** Enrichment of Kyoto Encyclopedia of Genes and Genomes (KEGG) terms for HK2 co-expression genes.

renal papillary cell carcinoma), LUSC (lung squamous cell carcinoma), PRAD (prostate adenocarcinoma), STAD (stomach adenocarcinoma), THCA (thyroid carcinoma) and UCEC (uterine corpus endometrial carcinoma), while it was remarkable decreased in COAD (colon adenocarcinoma), KICH (kidney chromophobe), LUAD (lung adenocarcinoma) and READ (rectum adenocarcinoma).

Transcriptional Levels of Hexokinase 2 in Esophageal Carcinoma Patients

The ESCA cohort of TCGA and GEO was utilized to analyze the differential expression of HK2 in ESCA tissue samples and normal tissue samples. Both TCGA and GEO cohort analysis indicated that the HK2 expression level in ESCA tissue samples was remarkable higher than that in normal tissue samples (**Figures 1C–E**). To further verified the accuracy of data investigation, we conducted qRT-PCR and IHC experiments, respectively. The qRT-PCR results indicated that the HK2 mRNA expression in the two ESCA cell lines (ECA109 and KYSE-150) was remarkable higher than that in the normal human esophageal epithelial cells (Het-1A) (**Figure 1F**). The results IHC staining revealed that HK2 was mainly expressed in the cytoplasm. The HK2 IHC score in tumor tissue samples was remarkable higher than that in paracarcinoma tissue samples (2.32 ± 0.621 vs. 0.84 ± 0.618) (**Figures 1G–I**, $P < 0.0001$). These results believe that HK2 plays a potential role in the occurrence and development of ESCA.

We analyzed clinical data from the ESCA cohort using the UALCAN database to better understand the clinical correlation between HK2 expression and ESCA. The results indicated that the expression of HK2 in cancer stage 2 was higher than that in cancer stage 3 ($P < 0.05$). The expression of HK2 in normal weight patients was higher than that in extreme weight patients ($P < 0.05$). The expression of HK2 in esophageal squamous cell carcinoma was higher than that in esophageal adenocarcinoma ($P < 0.05$). The expression of HK2 in tumor grade 3 was lower

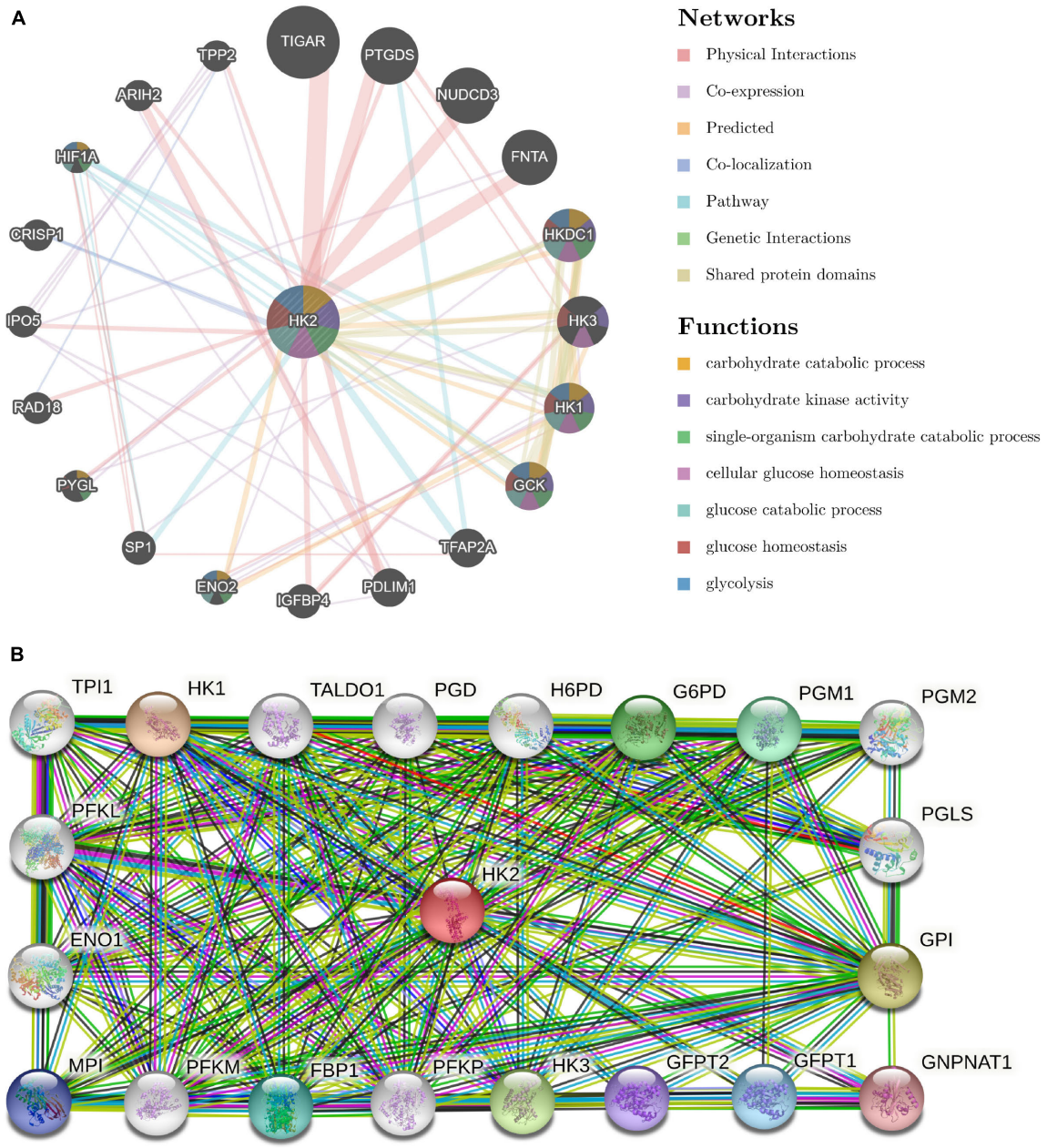

FIGURE 4 | Analysis of gene–gene interaction (GGI) and protein–protein interaction (PPI) of HK2 Gene. **(A)** GGI network of HK2. **(B)** PPI interaction network of HK2.

than that in tumor grade 2 ($P < 0.01$) and 1 ($P < 0.05$), respectively. However, the expression level of HK2 did not differ in different gender and age groups (**Figure 2**).

Enrichment Analysis of Hexokinase 2 Gene Co-expression Network

The co-expressed genes related to HK2 expression in TCGA ESCA cohort were analyzed using LinkedOmics database. The analysis results are shown in **Figure 3A**, 1682 genes were positively associated with the HK2 expression, and 2,855 genes were negatively associated with the HK2 expression (FDR < 0.05). The heat map indicated the top 50 important genes that are positively and negatively associated with HK2 expression, respectively (**Figure 3B**). **Supplementary Table 1** shows all co-expressed genes.

GO function and KEGG pathway research of HK2 co-expressed genes were carried by R language. Under the condition of p.adj < 0.1, HK2 co-expressed genes were participated in 25 biological processes (BP), 6 cell component (CC), 19 molecular function (MF) and 6 KEGG. The bubble graph shows the top 15 messages of GO and KEGG, including 5 messages of BP, CC, and

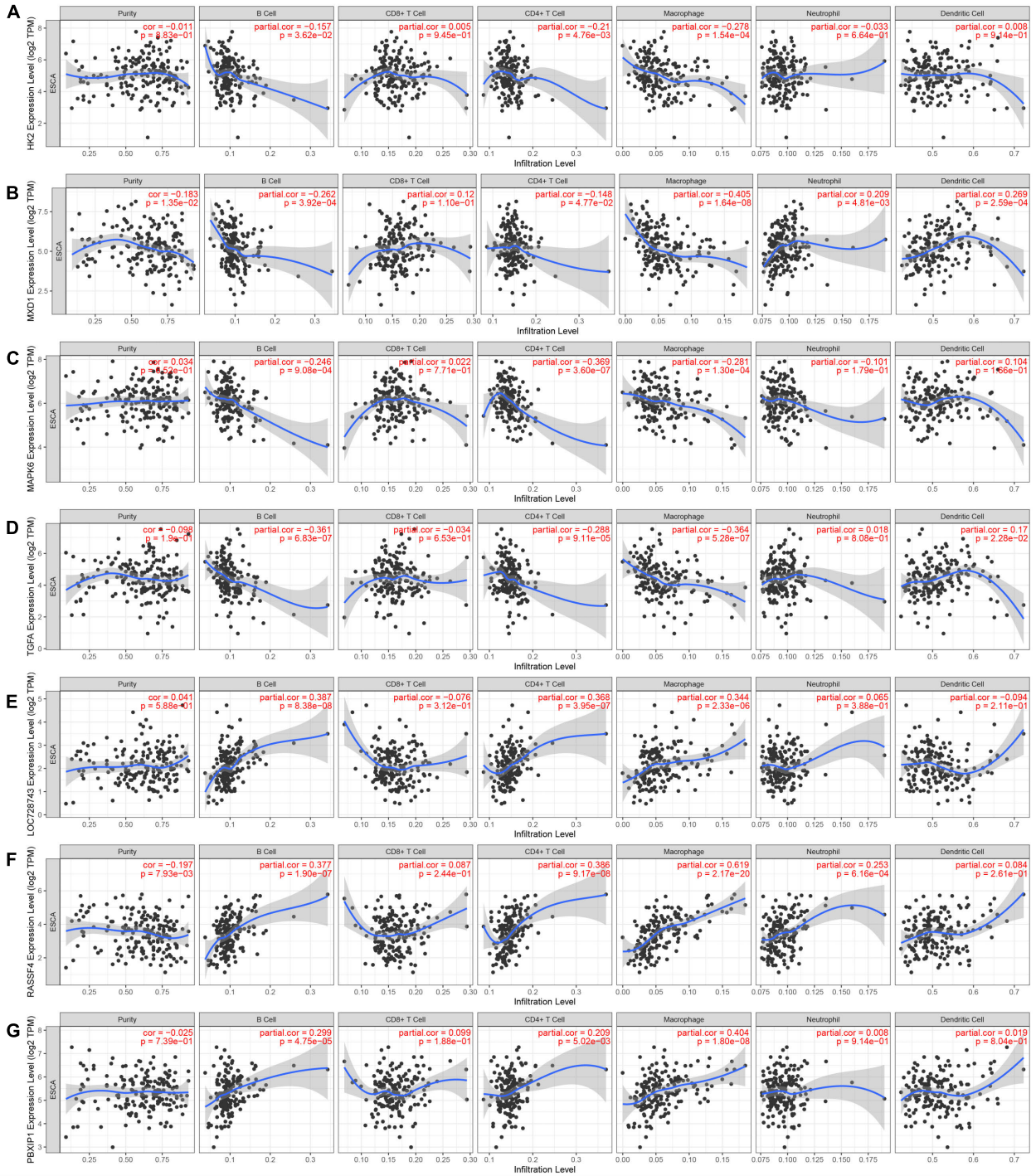

FIGURE 5 | Association between HK2 and tumor immune infiltrating cells. **(A)** Association between the expression of HK2 and the expression of immune infiltrating cell. Correlation between expression of HK2 co-expressed genes and expression in immune infiltrating cells, including MXD1 **(B)**, MAPK6 **(C)**, TGFA **(D)**, LOC728743 **(E)**, RASSF4 **(F)** and PBXIP1 **(G)**.

MF. The results of GO functional annotations showed that HK2 co-expressed genes were mainly participated in the cell adhesion molecule binding, cell-cell junction, and ameboidal-type cell migration (**Figure 3C**). KEGG pathway analysis showed that these genes were mainly related to the insulin signaling pathway, hif-1 signaling pathway, and insulin resistance (**Figure 3D**). **Supplementary Table 2** shows all GO function and KEGG pathway research.

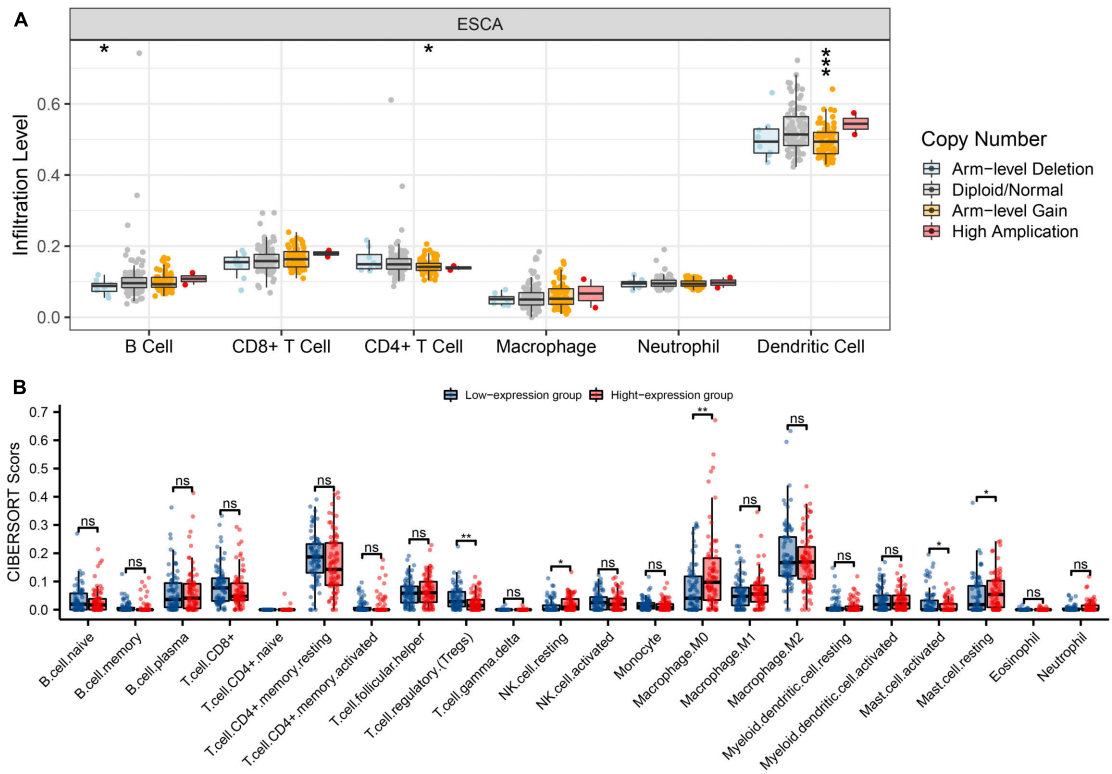

FIGURE 6 | Genetic copy number variations (CNV) of HK2 with the relative abundance of tumor infiltrating cells and CIBERSORT analysis. **(A)** HK2 CNV affects the infiltrating levels of $CD4^+$ T cells, neutrophils, and dendritic cells in ESCA. **(B)** The change ratio of 22 immune cell subtypes in the high and low HK2 expression groups in ESCA tumor sample. $^*P < 0.05$; $^{**}P < 0.01$; $^{***}P < 0.001$; ns, no significance.

Analysis of Gene-Gene Interaction and Protein-Protein Interaction of Hexokinase 2 Gene

A GGI network composed of 21 genes was constructed, and the HK2 gene was surrounded by 20 nodes. Their functionality was analyzed using the GeneMANIA database (**Figure 4A**). These nodes represent genes closely related to HK2 in terms of physical interactions, shared protein domains, predicted, co-localization, pathway, co-expression, and genetic interactions. Analysis showed that there were five genes most related to HK2, which were TIGAR (TP53 induced glycolysis regulatory phosphatase), PTGDS (prostaglandin D2 synthase), NUDCD3 (NudC domain containing 3), FNTA (farnesyltransferase) and HKDC1 (hexokinase domain containing 1). Among them, TIGAR, PTGDS, NUDCD3 and FNTA are related to the physical interaction with HK2, respectively. Both HKDC1 and HK2 have predicted function and shared protein domains. The results also showed that these genes were most strongly associated with glycolysis (FDR = 4.53E-08). In addition, these genes are associated with carbohydrate catabolic process, carbohydrate kinase activity, single-organism carbohydrate catabolic process, cellular glucose homeostasis, glucose catabolic process and glucose homeostasis.

Use STRING to further analyze PPI network of HK2. The results show that HK2 is related to HK1 (hexokinase 1), GPI (glucose-6-phosphate isomerase), HK3 (hexokinase 3), G6PD (glucose-6-phosphate 1-dehydrogenase), PGM1 (phosphoglucomutase-1), FBP1 (fructose-1,6-bisphosphatase 1), GFPT1 (glutamine–fructose-6-phosphate aminotransferase 1), MPI (mannose-6-phosphate isomerase), GFPT2 (glutamine–fructose-6-phosphate aminotransferase 2), GNPNAT1 (glucosamine-phosphate N-acetyltransferase 1), PGM2 (phosphoglucomutase-2), H6PD (hexose-6-phosphate dehydrogenase), PFKM (ATP-dependent 6-phosphofructokinase), TALDO1 (transaldolase), PFKL (ATP-dependent 6-phosphofructokinase), PFKP (ATP-dependent 6-phosphofructokinase), ENO1 (alpha-enolase), TPI1 (triosephosphate isomerase 1) and PGD (6-phosphogluconate dehydrogenase). The combined scores were 0.986, 0.97, 0.967, 0.955, 0.944, 0.941, 0.937, 0.935, 0.933, 0.931, 0.929, 0.925, 0.918, 0.905, 0.866, 0.864, 0.704, 0.66, and 0.495, respectively (**Figure 4B**).

Correlation Between Hexokinase 2 and Tumor Immune Infiltrating Cells

To explore the relationship between HK2 expression and immune infiltrating cells in ESCA by using TIMER database. Our results indicated that the expression of HK2 was negatively

associated with the expression levels of different immune infiltrating cells, including B cell (r = –0.157, P = 3.62E-2), $CD4^+$ T cell (r = –0.21, P = 4.76E-3) and macrophage (r = –0.278, P = 1.54E-4) (**Figure 5A**). In addition, the association between HK2 co-expressed genes and immune infiltrating cells was also analyzed. The first 3 genes positively and negatively correlated with HK2 were selected for correlation analysis of immune infiltrating. We found that HK2 co-expression genes MXD1, MAPK6, TGFA, LOC728743, RASSF4, and PBXIP1 were also significantly associated with the immune cell expression. The expression of MXD1 was associated with B cell (r = –0.262, P = 3.92E-4), $CD4^+$ T cell (r = –0.148, P = 4.77E-2), macrophage (r = –0.405, P = 1.64E-8), neutrophil (r = 0.209, P = 4.81E-3) and dendritic cell (r = 0.269, P = 2.59E-4) (**Figure 5B**). The expression of MAPK6 was negatively associated with B cell (r = –0.246, P = 9.08E-4), $CD4^+$ T cell (r = –0.369, P = 3.60E-7) and macrophage (r = –0.281, P = 1.30E-4) (**Figure 5C**). The expression of TGFA was associated with B cell (r = –0.361, P = 6.83E-7), $CD4^+$ T cell (r = –0.288, P = 9.11E-5), macrophage (r = –0.364, P = 5.28E-7) and dendritic cell (r = 0.17, P = 2.28E-2) (**Figure 5D**). LOC728743 expression was positively associated with B cell (r = 0.387, P = 8.38E-8), $CD4^+$ T cell (r = 0.368, P = 3.95E-7) and macrophage (r = 0.344, P = 2.33E-6) (**Figure 5E**). RASSF4 expression was positively associated with B cell (r = 0.377, P = 1.90E-7), $CD4^+$ T cell (r = 0.386, P = 9.17E-8), macrophage (r = 0.619, P = 2.17E-20) and neutrophil (r = 0.253, P = 6.16E-4) (**Figure 5F**). PBXIP1 expression was positively associated with B cell (r = 0.299, P = 4.75E-5), $CD4^+$ T cell (r = 0.209 P = 5.02E-3) and macrophage (r = 0.404, P = 1.80E-6) (**Figure 5G**). These results suggest that HK2 and its co-expressed genes may be participated in the immune response of ESCA tumor microenvironment, especially on B cell, $CD4^+$ T cell and macrophage. In addition, it was also found that HK2 CNV has a significant correlation with the infiltration level of B cell, $CD4^+$ T cell, and dendritic cell (**Figure 6A**).

CIBERSORT investigation indicated that HK2 expression had associated with tumor immune cell infiltration, including regulatory T cells (P = 0.004), resting NK cells (P = 0.018), M0 macrophages (P = 0.002), activated mast cells (P = 0.042) and resting mast cells (P = 0.025). Overall, HK2 and its co-expression genes have correlation with tumor immune cell infiltration in ESCA (**Figure 6B**).

Correlation Analysis Between Hexokinase 2 Expression and Immune Marker Sets

To explore the relationship between HK2 and various immune infiltrating cells of ESCA, we used TIMER databases and TCGA ESCA cohort to study the associated between HK2 and immune marker genes of various immune cells (**Table 2**). Both analyses indicated that the expression of HK2 was associated with the immune marker genes of $CD8^+$ T Cell, Th1, T cell exhaustion and dendritic cell. The scatter plots showed the correlation between HK2 expression level and these three immune marker genes, respectively (**Figure 7**).

Hexokinase 2 Expression Is Correlated With m6A RNA Methylation Regulators in Esophageal Carcinoma

The TCGA ESCA cohort was analyzed to study the association between the expression of HK2 and the expression of 20 m6A related genes in ESCA. Analysis indicated that the expression of HK2 was remarkable positively associated with 4 m6A associated genes in ESCA, including IGF2BP2 (r = 0.200, P = 0.010), HNRNPA2B1 (r = 0.170, P = 0.035), YTHDC2 (r = 0.220, P = 0.004) and YTHDF2 (r = 0.200, P = 0.010) (**Figure 8A**). The scatter plot indicates the correlation between HK2 and m6A associated genes (**Figure 8B**). In addition, 162 cases of ESCA were divided into high expression group (n = 81) and low expression group (n = 81) according to the expression level of HK2. We further evaluated the expression abundance of m6A associated genes between high and low HK2 expression groups to study whether m6A modification was different between the two groups (**Figure 8C**). Analysis indicated that compared with the low expression group, the expression of YTHDF3 and YTHDF2 were increased in the high expression group of HK2 ($P < 0.05$). These analyses suggest that HK2 is strongly associated to m6A modification in ESCA.

DISCUSSION

As one of the isozyme subtypes of HK, HK2 is the first rate-limiting enzyme in the catalytic glycolysis pathway and mainly distributed in the cytoplasmic region (Smith, 2000; Zhang et al., 2017). HK2 overexpression can promote the process of glycolysis of tumor cells and provide necessary energy for the proliferation and migration of tumor cells, thus promoting the occurrence and development of tumor cells (Shen et al., 2020; Wang et al., 2020; Yu et al., 2021). Chen et al. (2019) discovered that high expression of HK2 was remarkable associated with the degree of malignancy and poor prognosis of gallbladder tumors. Downregulation of HK2 expression could significantly inhibit the proliferation, migration and invasion of gallbladder cancer cells, and at the same time reduce glucose consumption and cellular lactic acid production. DeWaal et al. (2018) discovered that HK2 knockout inhibited the glycolytic effect of HCC cell, promoted the level of oxidative phosphorylation, and at the same time increased sensitivity of cancer cells to metformin. These results suggest that HK2 can be used as a potential target for cancer gene therapy.

Studies have shown that HK2 is highly expressed in a variety of tumors and plays an important role in the development and progression of tumors. Nevertheless, there are few researches on the comprehensive investigation of HK2 in ESCA. On the project, we predicted the expression differences of HK2 in cancers through bioinformatics investigation, and verified the HK2 expression in ESCA through *in vitro* experiments. Bioinformatics is widely used in tumor research (Chen et al., 2021; Hu et al., 2021; Liao et al., 2021). Investigation of the Oncomine database discovered that HK2 was highly expressed in 8 types of cancer, and investigation of the TIMER discovered that HK2 was highly expressed in 11 types of cancer. According to GEO and TCGA

TABLE 2 | Correlation analysis between HK2 and immune cell marker gene in TIMER and TCGA.

Description	Gene markers	TIMER		TCGA	
		Purity		Tumor	
		Rho	*P*	Rho	*P*
B cell	CD19	– 0.108	1.48E-01	– 0.144	6.85E-02
	MS4A1	– 0.130	8.19E-02	– 0.132	9.43E-02
	CD79A	– 0.145	5.14E-02	– 0.173	**2.73E-02**
$CD8^+$ T Cell	CD8A	– 0.241	**1.12E-03**	– 0.256	**1.03E-03**
	CD8B	– 0.258	**4.81E-04**	– 0.289	**1.93E-04**
	IL2RA	– 0.147	**4.97E-02**	– 0.183	**1.98E-02**
Tfh	CXCR3	– 0.289	**8.15E-05**	– 0.339	**1.03E-05**
	CXCR5	– 0.159	**3.26E-02**	– 0.145	6.50E-02
	ICOS	– 0.115	1.25E-01	– 0.149	5.85E-02
Th1	IL12RB1	– 0.226	**2.31E-03**	– 0.222	**4.48E-03**
	CCR1	– 0.152	**4.11E-02**	– 0.198	**1.14E-02**
	CCR5	– 0.167	**2.53E-02**	– 0.240	**2.13E-03**
Th2	CCR4	– 0.131	7.94E-02	– 0.247	**1.54E-03**
	CCR8	– 0.122	1.03E-01	– 0.217	**5.46E-03**
	HAVCR1	– 0.123	1.01E-01	– 0.182	**2.05E-02**
Th17	IL21R	– 0.174	**1.96E-02**	– 0.248	**1.49E-03**
	IL23R	– 0.035	6.42E-01	0.003	9.68E-01
	CCR6	– 0.214	**3.84E-03**	– 0.196	**1.27E-02**
Treg	FOXP3	– 0.147	**4.92E-02**	– 0.254	**1.13E-03**
	NT5E	– 0.008	9.19E-01	– 0.023	7.68E-01
	IL7R	0.029	7.01E-01	– 0.018	8.18E-01
T cell exhaustion	PDCD1	– 0.251	**6.84E-04**	– 0.235	**2.58E-03**
	CTLA4	– 0.153	**4.09E-02**	– 0.176	**2.49E-02**
	LAG3	– 0.155	**3.71E-02**	– 0.174	**2.66E-02**
M1 Macrophage	NOS2	– 0.022	7.72E-01	0.077	3.30E-01
	IRF5	0.134	7.27E-02	0.165	**3.60E-02**
	PTGS2	0.220	**3.06E-03**	0.229	**3.41E-03**
M2 Macrophage	CD163	– 0.143	5.59E-02	– 0.181	**2.09E-02**
	MRC1	0.029	7.00E-01	– 0.010	9.02E-01
	CD209	– 0.150	**4.47E-02**	– 0.190	**1.56E-02**
TAM	CCL2	– 0.198	**7.84E-03**	– 0.209	**7.68E-03**
	CD86	– 0.113	1.31E-01	– 0.093	2.39E-01
	CD68	0.078	2.97E-01	– 0.044	5.81E-01
Monocyte	CD14	– 0.167	**2.47E-02**	– 0.150	5.70E-02
	CD33	– 0.208	**5.11E-03**	– 0.207	**8.15E-03**
	ITGAX	0.006	9.40E-01	– 0.033	6.77E-01
Natural killer cell	B3GAT1	– 0.193	**9.50E-03**	– 0.128	1.04E-01
	KIR3DL1	– 0.098	1.92E-01	– 0.059	4.57E-01
	CD7	– 0.289	**8.45E-05**	– 0.281	**2.94E-04**
Neutrophil	FCGR3A	– 0.103	1.67E-01	– 0.166	**3.48E-02**
	CD55	0.028	7.13E-01	0.073	3.58E-01
	ITGAM	– 0.020	7.92E-01	– 0.104	1.88E-01
Dendritic cell	CD1C	– 0.167	**2.53E-02**	– 0.227	**3.71E-03**
	THBD	0.224	**2.53E-03**	0.245	**1.67E-03**
	NRP1	– 0.070	3.52E-01	– 0.171	**3.00E-02**

Bold values indicate P < 0.05.

ESCA cohort analysis, the expression level of HK2 in ESCA tissue samples was remarkable higher than that in normal tissue samples. We also detected the expression of HK2 in ESCA sample and normal sample by qRT-PCR and IHC. The investigation results were consistent with the above analysis. At present, we also found that the expression of HK2 was associated to weight, cancer

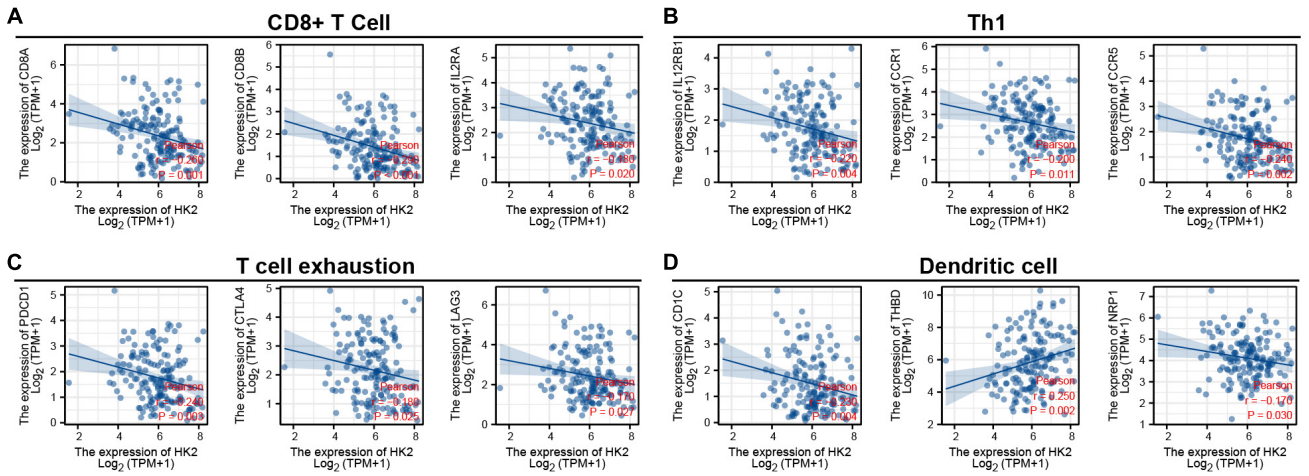

FIGURE 7 | HK2 expression correlated with CD8$^+$ T Cell, Th1, T cell exhaustion and dendritic cell in esophageal carcinoma (ESCA). Markers include CD8A, CD8B, and IL2RA of CD8$^+$ T Cell **(A)**; IL12RB1, CCR1 and CCR5 of Th1 **(B)**; PDCD1, CTLA4, and LAG3 of T cell exhaustion **(C)**; CD1C, THBD and NRP1 of dendritic cell **(D)**.

stages, tumor histology and tumor grade. In summary, HK2 may serve as a possible diagnostic and therapeutic biomarker of ESCA.

Nevertheless, previous researches on the role of HK2 in ESCA are limited to the energy metabolism of glycolytic pathway. Liu et al. (2019) found that the stem cell characteristics and abnormal metabolic reprogramming of esophageal cancer stem cells were dependent on the Hsp27-AKT-HK2 pathway, and ESCA patients with overexpression of Hsp27 and HK2 in tumor tissues had the worst prognosis. Mao et al. (2018) found that inhibiting the expression of HK2 could significantly inhibit the glycolytic effect of ESCA and affect the proliferation of cancer cell. Nevertheless, there are few reports on other biological functions of HK2 in ESCA. In this study, the co-expressed genes related to HK2 expression in TCGA ESCA cohort were analyzed using LinkedOmics database. The GO and KEGG function enrichment investigation of 100 co-expressed genes associated to the expression of HK2 indicated that the co-expression of HK2 was significantly correlated to the cell adhesion molecule binding, cell-cell junction, and ameboidal-type cell migration. KEGG pathway investigation indicated that HK2 co-expression was significantly correlated to the insulin signaling pathway, hif-1 signaling pathway, and insulin resistance. All these biological functions and pathways are associated to the occurrence and development of ESCA. GGI investigation discovered 20 genes related to HK2, and these genes were mainly closely related to glycolysis. The three genes most related to HK2 are TIGAR, PTGDS, and NUDCD3, respectively. Studies have shown that inhibition of TIGAR expression can reduce the proliferation of ESCA tumors, and patients who had high expression of TIGAR had poorer prognosis (Chu et al., 2020). PPI analysis showed that HK2 had the strongest correlation with the proteins of HK1, GPI and HK3, and inhibition of the expression of HK1 could significantly inhibit the proliferation of ESCA cells (Li et al., 2014). HK1, HK3, and GPI are all key genes in glycolysis, which can promote the proliferation and development of tumor cells by promoting the glycolysis effect of tumor cells. We discovered that the above three proteins had the highest association with HK2. These researches may suggest an association between HK2 and glycolysis and proliferative development of ESCA. These researches indicated that HK2 is not only involved in the glycolysis of ESCA, but also may play a variety of biological functions in the development and development of ESCA.

Tumor cell infiltration immunity has been shown to be associated with tumor progression and prognosis of ESCA (Baba et al., 2020; Wu X. et al., 2020). We used TIMER database and TCGA cohort to analyze the association between HK2 and ESCA immune infiltrating cells. TIMER database analysis showed that HK2 expression was correlated with B cell, CD4$^+$ T cell and macrophage. In addition, the relationship between six co-expressed genes of HK2 and immune infiltrating cells was also analyzed. The co-expressed genes were MXD1, MAPK6, TGFA, LOC728743, RASSF4, and PBXIP1. We found that the expression of these six genes was also closely related to the infiltration of ESCA immune cells, which were all related to the infiltration of B cell, CD4$^+$ T cell and macrophage. These results suggest that HK2 and its co-expressed genes may be participated in the immune response of ESCA tumor microenvironment, especially on B cell, CD4$^+$ T cell and macrophage. In addition, it was also discovered that HK2 CNV has a remarkable correlation with the infiltration level of B cell, CD4$^+$ T cell, and dendritic cell. According to the differential expression of HK2, the proportion of 22 tumor immune cells in ESCA was assessed by CIBERSORT research. We discovered five types of immune cells, including regulatory T cells, resting NK cells, M0 macrophages, activated mast cells and resting mast cell, whose proportions varied significantly according to the expression level of HK2. Furthermore, through the analysis of TIMER database and TCGA ESCA cohort, we discovered that the expression of HK2 was remarkable associated with the gene markers of CD8$^+$ T Cell, Th1, T cell exhaustion and dendritic cell. We believe that high expression of HK2 in ESCA

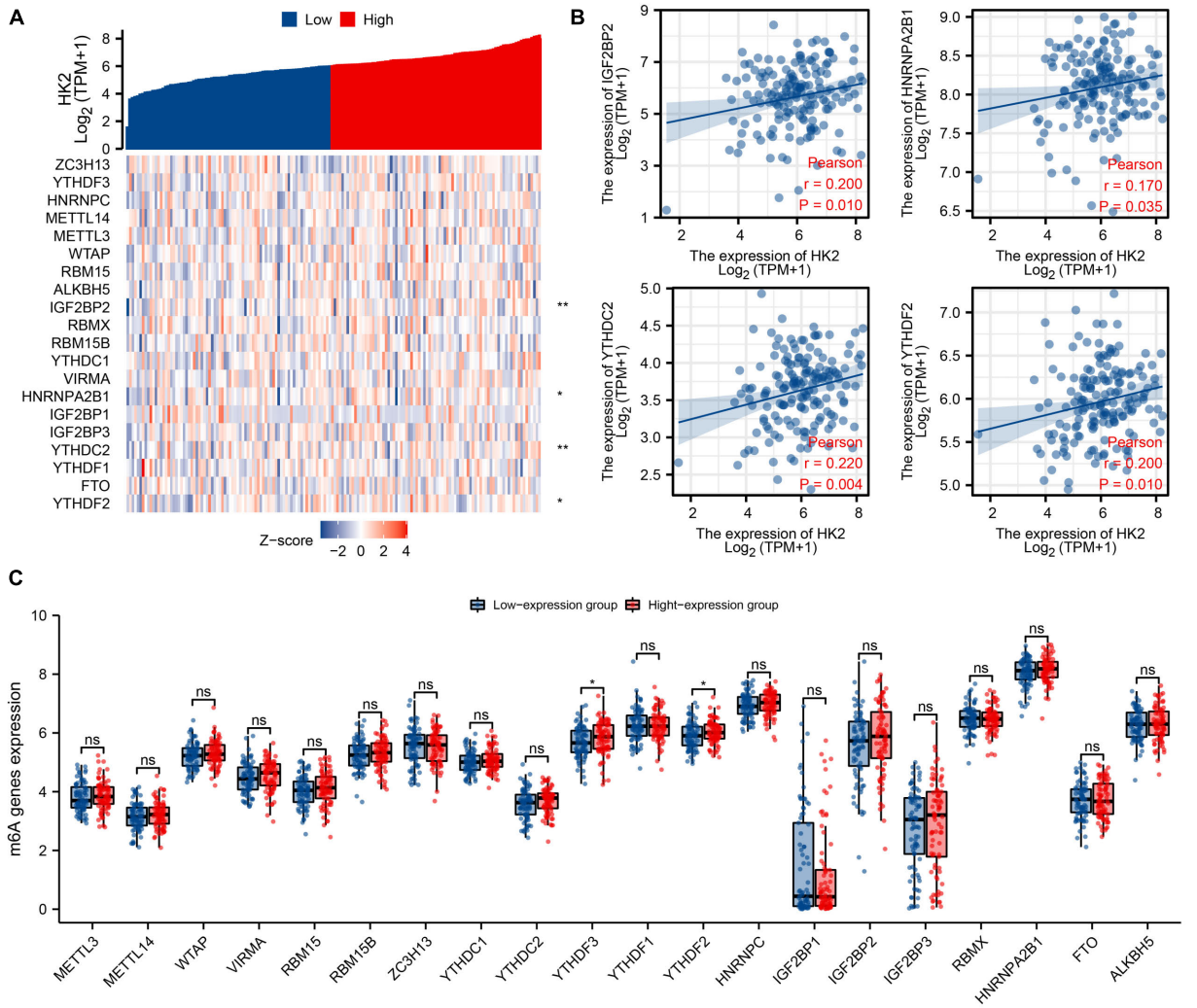

FIGURE 8 | Association of HK2 expression with m6A associated genes in esophageal carcinoma (ESCA). **(A)** The association between the expression level of HK2 and the expression of m6A associated genes in TCGA ESCA cohort was analyzed. **(B)** The association between HK2 and m6A associated genes was displayed by scatter plot, include IGF2BP2, HNRNPA2B1, YTHDC2, and YTHDF2. **(C)** The differential expression of m6A associated genes in the high and low HK2 expression groups was analyzed. $^{*}P < 0.05$; $^{**}P < 0.01$; ns, no significance.

patients may trigger an immune response. These results suggest that HK2 plays a remarkable role in the immune regulation of ESCA. Nevertheless, more studies are needed to further certify our speculation.

As part of epigenetics research, m6A is the most common and plentiful modification in post-transcriptional modification of RNA, which can affect the progress of tumor by regulating the biological functions associated with tumor. Shen et al. (2020) found that m6A associated gene METTL3 stabilizes the expression of HK2 and SLC2A1 in colorectal cancer through the m6A-IGF2BP2/3 dependent mechanism, and enhances the glycolysis ability of tumor cells, thus promoting the progress of colorectal cancer. Wang et al. (2020) discovered that METTL3 enhanced the stability of HK2 through YTHDF1-mediated m6A modification, thus promoting the Warburg effect of cervical cancer, and finally promoting the malignant proliferation of tumors. On the project, we attempted to analyze whether the expression level of HK2 is associated to the m6A modification in ESCA. We discovered that the expression of HK2 was remarkable associated with IGF2BP2, HNRNPA2B1, YTHDC2, and YTHDF2. We also discovered that the expression levels of YTHDF3 and YTHDF2 were remarkable increased in the group with high expression of HK2. We believe that HK2 gene may have a regulatory relationship with m6A modification, and this regulatory mechanism is involved in glycolysis and malignant proliferation of ESCA.

CONCLUSION

In conclusion, we verified that HK2 is overexpressed in ESCA, and its expression level is associated to clinical case

characteristics. The expression level of HK2 is strongly associated to the degree of immune cell infiltration. HK2 is associated with m6A modification, which may enhance the stability of HK2 through m6A modification, and thus promote the glycolytic effect and malignant proliferation of ESCA. HK2 can be used as a potential biological target for diagnosis and therapy of ESCA.

DATA AVAILABILITY STATEMENT

The datasets presented in this study can be found in online repositories. The names of the repository/repositories and accession number(s) can be found in the article/ **Supplementary Material**.

ETHICS STATEMENT

The studies involving human participants were reviewed and approved by the Ethics Committee of Taihe Hospital Affiliated of Hubei University of Medicine. Written informed consent for participation was not required for this study in accordance with the national legislation and the institutional requirements.

AUTHOR CONTRIBUTIONS

X-SL conceived the project and wrote the manuscript. X-SL, Y-JC, F-YL, and R-MW participated in data analysis. X-SL, J-ML, FT, D-BZ, WL, YG, and HZ participated in discussion and language editing. Z-JP reviewed the manuscript. All authors contributed to the article and approved the submitted version.

FUNDING

This work was supported by the Hubei province's Outstanding Medical Academic Leader program, the Foundation for Innovative Research Team of Hubei Provincial Department of Education (grant no. T2020025), the Hubei Provincial Department of Science and Technology Innovation Group Program (grant no. 2019CFA034), the Free-exploring Foundation of Hubei University of Medicine (grant no. FDFR201903), the Innovative Research Program for Graduates of Hubei University of Medicine (grant no. YC2020011), the Shiyan Taihe Hospital Hospital-Level Project (2021JJXM006), and the Key Discipline Project of Hubei University of Medicine.

SUPPLEMENTARY MATERIAL

The Supplementary Material for this article can be found online at: https://www.frontiersin.org/articles/10.3389/fcell.2021.715883/full#supplementary-material

REFERENCES

Andersson, A., Ritz, C., Lindgren, D., Edén, P., Lassen, C., Heldrup, J., et al. (2007). Microarray-based classification of a consecutive series of 121 childhood acute leukemias: prediction of leukemic and genetic subtype as well as of minimal residual disease status. *Leukemia* 21, 1198–1203. doi: 10.1038/sj.leu.2404688

Baba, Y., Nomoto, D., Okadome, K., Ishimoto, T., Iwatsuki, M., Miyamoto, Y., et al. (2020). Tumor immune microenvironment and immune checkpoint inhibitors in esophageal squamous cell carcinoma. *Cancer Sci.* 111, 3132–3141. doi: 10.1111/cas.14541

Badea, L., Herlea, V., Dima, S. O., Dumitrascu, T., and Popescu, I. (2008). Combined gene expression analysis of whole-tissue and microdissected pancreatic ductal adenocarcinoma identifies genes specifically overexpressed in tumor epithelia. *Hepato Gastroenterol.* 55:2016.

Barretina, J., Taylor, B. S., Banerji, S., Ramos, A. H., Lagos-Quintana, M., DeCarolis, P. L., et al. (2010). Subtype-specific genomic alterations define new targets for soft-tissue sarcoma therapy. *Nat. Genet.* 42, 715–721. doi: 10.1038/ng.619

Beroukhim, R., Brunet, J., Di Napoli, A., Mertz, K. D., Seeley, A., Pires, M. M., et al. (2009). Patterns of gene expression and copy-number alterations in von-hippel lindau disease-associated and sporadic clear cell carcinoma of the kidney. *Cancer Res.* 69, 4674–4681. doi: 10.1158/0008-5472.CAN-09-0146

Bray, F., Ferlay, J., Soerjomataram, I., Siegel, R. L., Torre, L. A., and Jemal, A. (2018). Global cancer statistics 2018: GLOBOCAN estimates of incidence and mortality worldwide for 36 cancers in 185 countries. *CA Cancer J. Clin.* 68, 394–424. doi: 10.3322/caac.21492

Bredel, M., Bredel, C., Juric, D., Harsh, G. R., Vogel, H., Recht, L. D., et al. (2005). Functional network analysis reveals extended gliomagenesis pathway maps and three novel MYC-interacting genes in human gliomas. *Cancer Res. (Chicago, Il.)* 65, 8679–8689. doi: 10.1158/0008-5472.CAN-05-1204

Chandrashekar, D. S., Bashel, B., Balasubramanya, S. A. H., Creighton, C. J., Ponce-Rodriguez, I., Chakravarthi, B. V. S. K., et al. (2017). UALCAN: a portal for facilitating tumor subgroup gene expression and survival analyses. *Neoplasia* 19, 649–658. doi: 10.1016/j.neo.2017.05.002

Chen, J., Liao, Y., and Fan, X. (2021). Prognostic and clinicopathological value of BUB1B expression in patients with lung adenocarcinoma: a meta-analysis. *Expert Rev. Anticanc.* 21, 795–803. doi: 10.1080/14737140.2021.1908132

Chen, J., Yu, Y., Li, H., Hu, Q., Chen, X., He, Y., et al. (2019). Long non-coding RNA PVT1 promotes tumor progression by regulating the miR-143/HK2 axis in gallbladder cancer. *Mol. Cancer* 18:33. doi: 10.1186/s12943-019-0947-9

Chu, J., Niu, X., Chang, J., Shao, M., Peng, L., Xi, Y., et al. (2020). Metabolic remodeling by TIGAR overexpression is a therapeutic target in esophageal squamous-cell carcinoma. *Theranostics* 10, 3488–3502. doi: 10.7150/thno.41427

Curtis, C., Shah, S. P., Chin, S., Turashvili, G., Rueda, O. M., Dunning, M. J., et al. (2012). The genomic and transcriptomic architecture of 2,000 breast tumours reveals novel subgroups. *Nature* 486, 346–352. doi: 10.1038/nature10983

D'Errico, M., Rinaldis, E. D., Blasi, M. F., Viti, V., Falchetti, M., Calcagnile, A., et al. (2009). Genome-wide expression profile of sporadic gastric cancers with microsatellite instability. *Eur. J. Cancer* 45, 461–469. doi: 10.1016/j.ejca.2008.10.032

Detwiller, K. Y., Fernando, N. T., Segal, N. H., Ryeom, S. W., D'Amore, P. A., and Yoon, S. S. (2005). Analysis of hypoxia-related gene expression in sarcomas and effect of hypoxia on RNA interference of vascular endothelial cell growth factor A. *Cancer Res.* 65, 5881–5889. doi: 10.1158/0008-5472.CAN-04-4078

DeWaal, D., Nogueira, V., Terry, A. R., Patra, K. C., Jeon, S., Guzman, G., et al. (2018). Hexokinase-2 depletion inhibits glycolysis and induces oxidative phosphorylation in hepatocellular carcinoma and sensitizes to metformin. *Nat. Commun.* 9:446. doi: 10.1038/s41467-017-02733-4

French, P. J., Swagemakers, S. M. A., Nagel, J. H. A., Kouwenhoven, M. C. M., Brouwer, E., van der Spek, P., et al. (2005). Gene expression profiles associated with treatment response in oligodendrogliomas. *Cancer Res. (Chicago, Il.)* 65, 11335–11344. doi: 10.1158/0008-5472.CAN-05-1886

Gaedcke, J., Grade, M., Jung, K., Camps, J., Jo, P., Emons, G., et al. (2010). Mutated KRAS results in overexpression of DUSP4, a MAP-kinase phosphatase, and SMYD3, a histone methyltransferase, in rectal carcinomas. *Genes Chromosomes Cancer* 49, 1024–1034. doi: 10.1002/gcc.20811

Gumz, M. L., Zou, H., Kreinest, P. A., Childs, A. C., Belmonte, L. S., LeGrand, S. N., et al. (2007). Secreted frizzled-related protein 1 loss contributes to tumor phenotype of clear cell renal cell carcinoma. *Clin. Cancer Res.* 13, 4740–4749. doi: 10.1158/1078-0432.ccr-07-0143

Haferlach, T., Kohlmann, A., Wieczorek, L., Basso, G., Kronnie, G. T., Béné, M., et al. (2010). Clinical utility of microarray-based gene expression profiling in the diagnosis and subclassification of leukemia: report from the international microarray innovations in leukemia study group. *J. Clin. Oncol.* 28, 2529–2537. doi: 10.1200/JCO.2009.23.4732

Hao, Y., Triadafilopoulos, G., Sahbaie, P., Young, H. S., Omary, M. B., and Lowe, A. W. (2006). Gene expression profiling reveals stromal genes expressed in common between Barrett's Esophagus and Adenocarcinoma. *Gastroenterology (New York, N.Y. 1943)* 131, 925–933. doi: 10.1053/j.gastro.2006.04.026

Hong, Y., Downey, T., Eu, K. W., Koh, P. K., and Cheah, P. Y. (2010). A 'metastasis-prone' signature for early-stage mismatch-repair proficient sporadic colorectal cancer patients and its implications for possible therapeutics. *Clin. Exp. Metastas* 27, 83–90. doi: 10.1007/s10585-010-9305-4

Hu, J., Yu, A., Othmane, B., Qiu, D., Li, H., Li, C., et al. (2021). Siglec15 shapes a non-inflamed tumor microenvironment and predicts the molecular subtype in bladder cancer. *Theranostics* 11, 3089–3108. doi: 10.7150/thno.53649

Iacobuzio-Donahue, C. A., Maitra, A., Olsen, M., Lowe, A. W., Van Heek, N. T., Rosty, C., et al. (2003). Exploration of global gene expression patterns in pancreatic adenocarcinoma using cDNA microarrays. *Am. J. Pathol.* 162, 1151–1162. doi: 10.1016/S0002-9440(10)63911-9

Jones, J., Otu, H., Spentzos, D., Kolia, S., Inan, M., Beecken, W. D., et al. (2005). Gene signatures of progression and metastasis in renal cell cancer. *Clin. Cancer Res.* 11, 5730–5739. doi: 10.1158/1078-0432.CCR-04-2225

Kaiser, S., Park, Y., Franklin, J. L., Halberg, R. B., Yu, M., Jessen, W. J., et al. (2007). Transcriptional recapitulation and subversion of embryonic colon development by mouse colon tumor models and human colon cancer. *Genome Biol.* 8:R131. doi: 10.1186/gb-2007-8-7-r131

Li, B., Severson, E., Pignon, J. C., Zhao, H., Li, T., Novak, J., et al. (2016). Comprehensive analyses of tumor immunity: implications for cancer immunotherapy. *Genome Biol.* 17:174. doi: 10.1186/s13059-016-1028-7

Li, T., Fan, J., Wang, B., Traugh, N., Chen, Q., Liu, J. S., et al. (2017). TIMER: a web server for comprehensive analysis of tumor-infiltrating immunecells. *Cancer Res.* 77, e108–e110. doi: 10.1158/0008-5472.CAN-17-0307

Li, W., Xu, Z., Hong, J., and Xu, Y. (2014). Expression patterns of three regulation enzymes in glycolysis in esophageal squamous cell carcinoma: association with survival. *Med. Oncol. (Northw. Lond. Engl.)* 31:118. doi: 10.1007/s12032-014-0118-1

Li, Y., Xiao, J., Bai, J., Tian, Y., Qu, Y., Chen, X., et al. (2019). Molecular characterization and clinical relevance of m(6)A regulators across 33 cancer types. *Mol. Cancer* 18:137. doi: 10.1186/s12943-019-1066-3

Liao, Y., He, D., and Wen, F. (2021). Analyzing the characteristics of immune cell infiltration in lung adenocarcinoma via bioinformatics to predict the effect of immunotherapy. *Immunogenetics* 73, 369–380. doi: 10.1007/s00251-021-01223-8

Liu, C., Chou, K., Hsu, J., Lin, J., Hsu, T., Yen, D. H., et al. (2019). High metabolic rate and stem cell characteristics of esophageal cancer stem-like cells depend on the Hsp27-AKT-HK2 pathway. *Int. J. Cancer* 145, 2144–2156. doi: 10.1002/ijc.32301

Liu, X., Yuan, L., Gao, Y., Zhou, L., Yang, J., and Pei, Z. (2020b). Overexpression of METTL3 associated with the metabolic status on ^{18}F-FDG PET/CT in patients with esophageal carcinoma. *J. Cancer* 11, 4851–4860. doi: 10.7150/jca.44754

Liu, X., Huang, H., Gao, Y., Zhou, L., Yang, J., Li, X., et al. (2020a). Visualization of gene therapy with a liver cancer-targeted adeno-associated virus 3 vector. *J. Cancer* 11, 2192–2200. doi: 10.7150/jca.39579

Liu, X., Gao, Y., Liu, C., Chen, X., Zhou, L., Yang, J., et al. (2021a). Comprehensive analysis of prognostic and immune infiltrates for E2F transcription factors in human pancreatic adenocarcinoma. *Front. Oncol.* 10:606735. doi: 10.3389/fonc.2020.606735

Liu, X., Zhou, L., Yuan, L., Gao, Y., Kui, X., Liu, X., et al. (2021b). NPM1 is a prognostic biomarker involved in immune infiltration of lung adenocarcinoma and associated with m6A modification and glycolysis. *Front. Immunol.* 12:724741. doi: 10.3389/fimmu.2021.724741

Mao, X., Zhu, H., Luo, D., Ye, L., Yin, H., Zhang, J., et al. (2018). Capsaicin inhibits glycolysis in esophageal squamous cell carcinoma by regulating hexokinase-2 expression. *Mol. Med. Rep.* 17, 6116–6121. doi: 10.3892/mmr.2018.8574

Murat, A., Migliavacca, E., Gorlia, T., Lambiv, W. L., Shay, T., Hamou, M., et al. (2008). Stem cell–related "Self-Renewal" signature and high epidermal growth factor receptor expression associated with resistance to concomitant chemoradiotherapy in glioblastoma. *J. Clin. Oncol.* 26, 3015–3024. doi: 10.1200/JCO.2007.15.7164

Newman, A. M., Liu, C. L., Green, M. R., Gentles, A. J., Feng, W., Xu, Y., et al. (2015). Robust enumeration of cell subsets from tissue expression profiles. *Nat. Methods* 12, 453–457. doi: 10.1038/nmeth.3337

Pei, H., Li, L., Fridley, B. L., Jenkins, G. D., Kalari, K. R., Lingle, W., et al. (2009). FKBP51 affects cancer cell response to chemotherapy by negatively regulating Akt. *Cancer Cell* 16, 259–266. doi: 10.1016/j.ccr.2009.07.016

Piccaluga, P. P., Agostinelli, C., Califano, A., Rossi, M., Basso, K., Zupo, S., et al. (2007). Gene expression analysis of peripheral T cell lymphoma, unspecified, reveals distinct profiles and new potential therapeutic targets. *J. Clin. Investig.* 117, 823–834. doi: 10.1172/JCI26833

Rhodes, D. R., Kalyana-Sundaram, S., Mahavisno, V., Varambally, R., Yu, J., Briggs, B. B., et al. (2007). Oncomine 3.0: genes, pathways, and networks in a collection of 18,000 cancer geneexpression profiles. *Neoplasia (New York, N.Y.)* 9, 166–180. doi: 10.1593/neo.07112

Rhodes, D. R., Yu, J., Shanker, K., Deshpande, N., Varambally, R., Ghosh, D., et al. (2004). ONCOMINE: a cancer microarray database and integrated data-mining platform. *Neoplasia* 6, 1–6. doi: 10.1016/S1476-5586(04)80047-2

Sanchez-Carbayo, M., Socci, N. D., Lozano, J., Saint, F., and Cordon-Cardo, C. (2006). Defining molecular profiles of poor outcome in patients with invasive bladder cancer using oligonucleotide microarrays. *J. Clin. Oncol.* 24, 778–789. doi: 10.1200/JCO.2005.03.2375

Shen, C., Xuan, B., Yan, T., Ma, Y., Xu, P., Tian, X., et al. (2020). m6A-dependent glycolysis enhances colorectal cancer progression. *Mol. Cancer* 19:72. doi: 10.1186/s12943-020-01190-w

Smith, T. A. (2000). Mammalian hexokinases and their abnormal expression in cancer. *Br. J. Biomed. Sci.* 57, 170–178.

Stegmaier, K., Ross, K. N., Colavito, S. A., O'Malley, S., Stockwell, B. R., and Golub, T. R. (2004). Gene expression-based high-throughput screening(GE-HTS) and application to leukemia differentiation. *Nat. Genet.* 36, 257–263.

Storz, M. N., van de Rijn, M., Kim, Y. H., Mraz-Gernhard, S., Hoppe, R. T., and Kohler, S. (2003). Gene expression profiles of cutaneous B cell lymphoma. *J. Invest. Dermatol.* 120, 865–870.

Sun, L., Hui, A., Su, Q., Vortmeyer, A., Kotliarov, Y., Pastorino, S., et al. (2006). Neuronal and glioma-derived stem cell factor induces angiogenesis within the brain. *Cancer Cell* 9, 287–300. doi: 10.1016/j.ccr.2006.03.003

Sung, H., Ferlay, J., Siegel, R. L., Laversanne, M., Soerjomataram, I., Jemal, A., et al. (2021). Global cancer statistics 2020: GLOBOCAN estimates of incidence and mortality worldwide for 36 cancers in 185 countries. *CA Cancer J. Clin.* 71, 209–249. doi: 10.3322/caac.21660

Szklarczyk, D., Gable, A. L., Lyon, D., Junge, A., Wyder, S., Huerta-Cepas, J., et al. (2019). STRING v11: protein-protein association networks with increased coverage,supporting functional discovery in genome-wide experimental datasets. *Nucleic Acids Res.* 47, D607–D613. doi: 10.1093/nar/gky1131

Tomczak, K., Czerwińska, P., and Wiznerowicz, M. (2015). Review the cancer genome atlas (TCGA): an immeasurable source of knowledge. *Współczesna Onkol.* 1A, 68–77. doi: 10.5114/wo.2014.47136

Vasko, V., Espinosa, A. V., Scouten, W., He, H., Auer, H., Liyanarachchi, S., et al. (2007). gene expression and functional evidence of epithelial-to-mesenchymal transition in papillary thyroid carcinoma invasion. *Proc. Natl. Acad. Sci. U.S.A.* 104, 2803–2808. doi: 10.1073/pnas.0610733104

Wang, Q., Guo, X., Li, L., Gao, Z., Su, X., Ji, M., et al. (2020). N(6)-methyladenosine METTL3 promotes cervical cancer tumorigenesis and Warburg effect through YTHDF1/HK2 modification. *Cell Death Dis.* 11:911. doi: 10.1038/s41419-020-03071-y

Warde-Farley, D., Donaldson, S. L., Comes, O., Zuberi, K., Badrawi, R., Chao, P., et al. (2010). The GeneMANIA prediction server: biological network integration for geneprioritization and predicting gene function. *Nucleic Acids Res.* 38, W214–W220. doi: 10.1093/nar/gkq537

Wu, S., Zhang, L., Deng, J., Guo, B., Li, F., Wang, Y., et al. (2020). A novel micropeptide encoded by Y-linked LINC00278 links cigarette smoking and AR signaling in male esophageal squamous cell carcinoma. *Cancer Res. (Chicago, Il.)* 80, 2790–2803. doi: 10.1158/0008-5472.CAN-19-3440

Wu, X., Ke, X., Ni, Y., Kuang, L., Zhang, F., Lin, Y., et al. (2020). Tumor-infiltrating immune cells and PD-L1 as prognostic biomarkers in primary esophageal small cell carcinoma. *J. Immunol. Res.* 2020:8884683. doi: 10.1155/2020/8884683

Yang, N., Ying, P., Tian, J., Wang, X., Mei, S., Zou, D., et al. (2020). Genetic variants in m6A modification genes are associated with esophageal squamous-cell carcinoma in the Chinese population. *Carcinogenesis (New York)* 41, 761–768. doi: 10.1093/carcin/bgaa012

Yoshihara, K., Tajima, A., Komata, D., Yamamoto, T., Kodama, S., Fujiwara, H., et al. (2009). Gene expression profiling of advanced-stage serous ovarian cancers distinguishes novel subclasses and implicates ZEB2 in tumor progression and prognosis. *Cancer Sci.* 100, 1421–1428. doi: 10.1111/j.1349-7006.2009.01204.x

Yu, H., Zhao, K., Zeng, H., Li, Z., Chen, K., Zhang, Z., et al. (2021). N(6)-methyladenosine (m(6)A) methyltransferase WTAP accelerates the Warburg effect of gastric cancer through regulating HK2 stability. *Biomed. Pharmacother.* 133:111075. doi: 10.1016/j.biopha.2020.111075

Zhang, J., Wang, S., Jiang, B., Huang, L., Ji, Z., Li, X., et al. (2017). c-Src phosphorylation and activation of hexokinase promotes tumorigenesis and metastasis. *Nat. Commun.* 8:13732. doi: 10.1038/ncomms13732

Conflict of Interest: The authors declare that the research was conducted in the absence of any commercial or financial relationships that could be construed as a potential conflict of interest.

Publisher's Note: All claims expressed in this article are solely those of the authors and do not necessarily represent those of their affiliated organizations, or those of the publisher, the editors and the reviewers. Any product that may be evaluated in this article, or claim that may be made by its manufacturer, is not guaranteed or endorsed by the publisher.

frontiers in Molecular Biosciences

ORIGINAL RESEARCH
published: 08 October 2021
doi: 10.3389/fmolb.2021.744677

Weighted Gene Co-expression Network Analysis Identifies a Cancer-Associated Fibroblast Signature for Predicting Prognosis and Therapeutic Responses in Gastric Cancer

Hang Zheng[1†], *Heshu Liu*[2†], *Huayu Li*[1], *Weidong Dou*[1] *and Xin Wang*[1*]

[1]*Department of General Surgery, Peking University First Hospital, Peking University, Beijing, China,* [2]*Department of Oncology, Beijing Chaoyang Hospital, Capital Medical University, Beijing, China*

OPEN ACCESS

Edited by:
José Alexandre Ferreira, Portuguese Oncology Institute, Portugal

Reviewed by:
Manish Charan, The Ohio State University, United States
Ila Pant, Icahn School of Medicine at Mount Sinai, United States

***Correspondence:**
Xin Wang
wangxin_guo@126.com

[†]*These authors have contributed equally to this work and share first authorship*

Specialty section:
This article was submitted to Molecular Diagnostics and Therapeutics, a section of the journal Frontiers in Molecular Biosciences

Received: *20 July 2021*
Accepted: *01 September 2021*
Published: *08 October 2021*

Citation:
Zheng H, Liu H, Li H, Dou W and Wang X (2021) Weighted Gene Co-expression Network Analysis Identifies a Cancer-Associated Fibroblast Signature for Predicting Prognosis and Therapeutic Responses in Gastric Cancer. Front. Mol. Biosci. 8:744677. doi: 10.3389/fmolb.2021.744677

Background: Cancer-associated fibroblasts (CAFs) are the most prominent cellular components in gastric cancer (GC) stroma that contribute to GC progression, treatment resistance, and immunosuppression. This study aimed at exploring stromal CAF-related factors and developing a CAF-related classifier for predicting prognosis and therapeutic effects in GC.

Methods: We downloaded mRNA expression and clinical information of 431 GC samples from Gene Expression Omnibus (GEO) and 330 GC samples from The Cancer Genome Atlas (TCGA) databases. CAF infiltrations were quantified by the estimate the proportion of immune and cancer cells (EPIC) method, and stromal scores were calculated via the Estimation of STromal and Immune cells in MAlignant Tumors using Expression data (ESTIMATE) algorithm. Stromal CAF-related genes were identified by weighted gene co-expression network analysis (WGCNA). A CAF risk signature was then developed using the univariate and least absolute shrinkage and selection operator method (LASSO) Cox regression model. We applied the Spearman test to determine the correlation among CAF risk score, CAF markers, and CAF infiltrations (estimated *via* EPIC, xCell, microenvironment cell populations-counter (MCP-counter), and Tumor Immune Dysfunction and Exclusion (TIDE) algorithms). The TIDE algorithm was further used to assess immunotherapy response. Gene set enrichment analysis (GSEA) was applied to clarify the molecular mechanisms.

Results: The 4-gene (COL8A1, SPOCK1, AEBP1, and TIMP2) prognostic CAF model was constructed. GC patients were classified into high– and low–CAF-risk groups in accordance with their median CAF risk score, and patients in the high–CAF-risk group had significant worse prognosis. Spearman correlation analyses revealed the CAF risk score was strongly and positively correlated with stromal and CAF infiltrations, and the four model genes also exhibited positive correlations with CAF markers. Furthermore, TIDE analysis revealed high–CAF-risk patients were less likely to respond to immunotherapy.

GSEA revealed that epithelial–mesenchymal transition (EMT), TGF-β signaling, hypoxia, and angiogenesis gene sets were significantly enriched in high–CAF-risk group patients.

Conclusion: The present four-gene prognostic CAF signature was not only reliable for predicting prognosis but also competent to estimate clinical immunotherapy response for GC patients, which might provide significant clinical implications for guiding tailored anti-CAF therapy in combination with immunotherapy for GC patients.

Keywords: gastric cancer, cancer-associated fibroblasts, weighted gene co-expression network analysis, biomarker, prognosis, immunotherapy

INTRODUCTION

Gastric cancer (GC) ranks fifth among the most common cancers and is the fourth leading cause of cancer-related mortality worldwide (Sung et al., 2021). Leaving aside improvements in gastroscopic screening and various treatment strategies, recurrence and metastasis remain the main causes of GC death, and the current therapeutic efficacy on recurrent and metastatic GC is still unsatisfactory (Lee et al., 2016; Thrift and El-Serag, 2020). GC tissues are composed of neoplastic cancer cells as well as the immune and stromal milieu where tumor cells are located, which is termed as tumor microenvironment (TME). Accumulating evidence indicated tumor stromal components in TME are critical for tumor growth and metastasis, immunosuppression, and drug resistance (Hanahan and Coussens, 2012; Quail and Joyce, 2013), which have embraced a spacious field of investigation.

As the most prominent cell type of tumor stroma, cancer-associated fibroblasts (CAFs) are crucial sources of growth factors and cytokines that promote tumor progression and migration (Kojima et al., 2010; Tommelein et al., 2015), stimulate epithelial–mesenchymal transition (EMT) (Wu et al., 2017; Fiori et al., 2019), and induce chemoresistance (Lotti et al., 2013; Li et al., 2016) and immunosuppression (Kraman et al., 2010; Monteran and Erez, 2019). CAFs are also capable of depositing and reorganizing the extracellular matrix (ECM), which serves as a thick physical barrier that supports tumor cell invasion and restrains the infiltrations of antitumor leukocytes, leading to tumor progression, immune evasion, and therapy resistance (Ma et al., 2016; Lakins et al., 2018; Kaur et al., 2019; Gamradt et al., 2021). Thus, targeting CAF-mediated immunosuppressive stromal microenvironment in combination with immunotherapy could promisingly ameliorate the response to immune checkpoint inhibitors. For instance, exhaustion of fibroblast activation protein (FAP)–positive CAFs in murine models led to increased $CD8^+$ T cell infiltrations and decreased macrophages proportions (Duperret et al., 2018), and therapeutic effects of anti-CTLA4 and anti-PD-1 were consequently enhanced (Feig et al., 2013). Unfortunately, FAP-based drugs against CAFs failed to pass Phase II trials owing to the unsatisfactory clinical response in metastatic colorectal cancer patients (Hofheinz et al., 2003; Narra et al., 2007), and such a CAF inhibitory strategy is currently lacking in GC treatment. In this regard, it is imperative to explore stromal CAF-related factors in GC.

Weighted gene co-expression network analysis (WGCNA) is a systematic bioinformatics algorithm that is competent to incorporate highly and coordinately expressed genes into several gene modules and investigate the module's relationships with the phenotype of interest (Langfelder and Horvath, 2008). WGCNA has been successfully applied for identifying CAF markers (Liu et al., 2021a; Liu et al., 2021b). So far, CAF and stromal infiltrations have not been subjected to WGCNA analysis in GC. In this study, for the first time, WGCNA was employed simultaneously on two transcriptome datasets collected from publicly available Gene Expression Omnibus (GEO) and The Cancer Genome Atlas (TCGA) databases. We detected hub modules that were most correlated with stromal CAF infiltrations. Then, by applying univariate and Least Absolute Shrinkage and Selection Operator (LASSO) Cox regression analyses, we identified COL8A1, SPOCK1, AEBP1, and TIMP2 as prognostic CAF markers and constructed the four-gene CAF signature capable of predicting prognosis and therapeutic responses in GC. Our results hint that the CAF model might be a novel anti-CAF therapeutic approach in GC.

MATERIALS AND METHODS

Data Acquisition and Preprocessing

The fragments per kilobase of transcript per million mapped reads (FPKM) format RNA-seq data and corresponding prognostic data (follow-up time more than 30 days) of 330 TCGA stomach adenocarcinoma (TCGA-STAD) samples were downloaded through UCSC Xena browser (GDC hub) (https://gdc.xenahubs.net) (Goldman et al., 2020). The normalized FPKM values were converted to transcripts per million (TPM) and log2(TPM+1) transformed (Wagner et al., 2012). We also obtained normalized expression data and clinical information of 431 GC samples in GSE84437 from the GEO database (Yoon et al., 2020). The highest value was reserved if one gene matched multiple probes.

CAF Infiltration Estimation and Stromal Score Calculation

CAF abundances were separately estimated *via* four methods: cell-type deconvolution (constrained least square optimization)–based Estimate the Proportion of Immune and Cancer cells (EPIC) algorithm (Racle et al., 2017), gene signature enrichment–based xCell algorithm (Aran et al., 2017), marker

genes expressions–based microenvironment cell populations-counter (MCP-counter) (Becht et al., 2016), and Tumor Immune Dysfunction and Exclusion (TIDE) algorithms (Jiang et al., 2018). The first three methods were achieved *via* a deconvolute() function of immunedeconv R package (version 2.0.3) (Sturm et al., 2020), and the TIDE method was implemented through http://tide.dfci.harvard.edu/. In addition, the Estimation of STromal and Immune cells in MAlignant Tumor tissues using Expression data (ESTIMATE) algorithm was applied to calculate the stromal score *via* estimate R package (version 1.0.13), which indicates the stromal infiltrating levels of each tumor sample (Yoshihara et al., 2013).

CAF and Stromal Co-expression Network Constructions

Co-expression networks and hub genes that targeted CAF infiltrations as well as stromal scores were constructed and detected *via* WGCNA R package (version 1.68) (Langfelder and Horvath, 2008). Genes with the top 5,000 of median absolute deviation (MAD) were first chosen as the input genes for network constructions in both TCGA-STAD and GSE84437 cohorts. Then, the Pearson's correlation similarity matrix between any gene pairs was calculated (s_{ij}, where ij represents pair-wise genes) and increased to soft-thresholding power β (s_{ij}^{β}) based on the scale-free topology network criterion. Subsequently, the adjacency matrix was clustered using topological overlap measure (TOM) and dissimilarity (1-TOM) between genes, and we conducted a dynamic tree cut algorithm on the dendrogram for gene module identifications with minimum gene numbers as 30 in each module. Each module expression's first principal component was summarized as module eigengenes (MEs), the Pearson's correlations between MEs and EPIC-quantified CAF infiltrations as well as the stromal score were evaluated, and the most correlated module was picked for further analysis. Then, we measured gene significance (GS) for the traits and module membership (MM indicates the correlation between ME and gene expression) of individual genes in the identified hub module, and hub genes were filtered out under the strict criteria of GS > 0.4 and MM > 0.8. Finally, the overlapping hub genes between TCGA-STAD and GSE84437 cohorts constituted the final hub genes.

Gene Ontology (GO) and the Kyoto Encyclopedia of Genes and Genomes (KEGG) Analyses

GO and KEGG pathway enrichment analyses were performed on the final hub genes to identify the biological functions (including biological processes (BPs), molecular functions (MFs), and cellular components (CCs)) and pathways through clusterProfiler R package (version 3.14.3) (Yu et al., 2012). $p < 0.05$ was considered statistically enriched.

Prognostic Model Construction and Validation

The GSE84437 cohort was selected for CAF risk model construction owing to its larger sample size, while 330 cases from TCGA-STAD were assigned to the validation cohort. The univariate Cox regression model was performed to identify prognostic stromal CAF hub genes on overall survival (OS); genes with $p < 0.05$ were subsequently put into LASSO Cox regression analysis with 1,000 iterations for gene reduction *via* glmnet R package (Simon et al., 2011). Then, the CAF risk model was constructed as follows: CAF risk score = Σ (β_i * Exp_i), where β_i refers to the LASSO coefficient of *i*th gene, and Exp_i represents the *i*th gene's expression value. GC patients were classified into high– and low–CAF-risk groups based on their median CAF risk scores, and the OS difference between two groups was estimated *via* Kaplan–Meier curves and the log-rank test. Similarly, the CAF risk model was validated in the TCGA-STAD cohort.

CAF Markers Collections and Correlation Analysis

CAF specific and nonspecific markers were collected from published literature (Gascard and Tlsty, 2016; Han et al., 2020). To ensure the reliability of our CAF model markers in GC, we analyzed the Spearman's correlations between the CAF risk score and stromal score as well as multi-estimated CAF infiltrations (EPIC, xCell, MCP-counter, and TIDE). Correlations between CAF model genes and published CAF markers were also analyzed on both TCGA-STAD and GSE84437 cohorts.

Chemotherapy and Immunotherapy Response Predictions

Based on the largest publicly attainable pharmacogenomics database, Genomics of Drug Sensitivity in Cancer (GDSC) (https://www.cancerrxgene.org/) (Yang et al., 2013), half-maximal inhibitory concentration (IC50) values of common drugs (bleomycin, lapatinib, paclitaxel, camptothecin, cisplatin, docetaxel, methotrexate, and sunitinib) in each GC sample were estimated based on the transcriptome data by ridge regression with ten-fold cross-validation in pRRophetic R package (version 0.5) (Geeleher et al., 2014a; Geeleher et al., 2014b). Subsequently, the TIDE (http://tide.dfci.harvard.edu/) online algorithm was adopted for immune checkpoint blockade therapy response predictions (Jiang et al., 2018). Differences in response rates between high– and low–CAF-risk groups were examined by the chi-squared test, and the predictive efficacy of the CAF risk signature was evaluated by ROC curves and area under the curve (AUC) values.

Somatic Alteration Data Collection and Analyses

The somatic mutation data of the TCGA-STAD cohort were downloaded *via* the GDCquery_Maf() function (pipelines = "mutect2" (Cibulskis et al., 2013)) of TCGAbiolinks R package (Colaprico et al., 2016). The top 20 highest mutational frequencies in both low– and high–CAF-risk groups were recognized and visualized *via* maftools R package (Mayakonda et al., 2018). Tumor mutation burden (TMB) has been proposed as an immunotherapy efficacy predictor (Yarchoan et al., 2017),

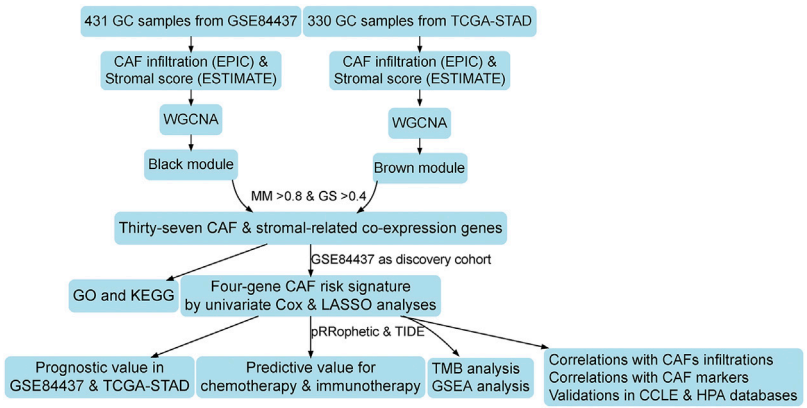

FIGURE 1 | Work flow of this study.

and the TMB value of each STAD sample was then calculated *via* the tmb() function of maftools package, and Spearman's correlation between TMB and CAF risk scores were analyzed.

Enrichment Analyses

Gene set enrichment analysis (GSEA) was performed to explore the enriched hallmark and KEGG pathway gene sets between high– and low–CAF-risk groups in GSE84437 *via* enrichplot and clusterProfiler R packages. The "c2. cp.kegg.v7.4. symbols" and "h.all.v7.4. symbols" gene sets were derived from the Molecular Signatures Database (MSigDB) (Liberzon et al., 2015). Furthermore, ssGSEA was applied to calculate the enrichment scores of EMT, TGF-β, and angiogenesis hallmark gene sets (Hänzelmann et al., 2013). Spearman's correlations analysis was performed to assess the correlation between the CAF risk score and gene set enrichment scores.

Validation *via* Cancer Cell Line Encyclopedia (CCLE) and Human Protein Atlas (HPA) Databases

For cellular level validation, the mRNA expressions of the identified markers in 38 fibroblasts and 39 GC cell lines were downloaded from the CCLE database (https://portals.broadinstitute.org/ccle) (Ghandi et al., 2019), and we examined their expression patterns in fibroblasts and CRC cell lines *via* heat map and Wilcoxon tests. In addition, with respect to protein level investigation, immunohistochemical (IHC) staining images of these markers in GC tissues were downloaded from the HPA online database (https://www.proteinatlas.org/) (Uhlén et al., 2015), and the target protein localization could be directly observed.

Statistical Analysis

All statistical analyses were performed using R software (version 3.6.3; https://www.r-project.org/). The median CAF risk score was the cutoff value for each cohort in dividing GC patients into high– and low–CAF-risk subgroups. The Wilcoxon test was applied for pairwise comparisons. The Kaplan–Meier curve with the log-rank test was adopted for overall survival comparisons *via* survival and survminer R packages. $p < 0.05$ was regarded as statistically significant.

RESULTS

Higher CAF Infiltrations and Stromal Scores Indicate Worse OS in GC Patients

The flowchart of this research is displayed in **Figure 1**. CAF infiltrations were multiply predicted by EPIC, xCell, MCP-counter, and TIDE methods, and the stromal score was calculated by the estimate algorithm. Their prognostic values on OS were evaluated *via* log-rank tests; Kaplan–Meier curves indicated that higher CAF infiltrations and stromal scores were notably correlated with poorer OS of GC patients in both GSE84437 (**Figure 2A**) and TCGA-STAD (**Figure 2B**) cohorts, which highlighted the importance of further exploration of CAF and stromal-related genes for GC. Herein, the EPIC-estimated CAF abundances and stromal scores were summarized as phenotype data for the subsequent analysis, and the other three estimated CAF infiltrations data were utilized for the identified CAF model external validations.

Co-Expression Network of CAF and Stromal Scores

WGCNA analysis was performed in both GSE84437 and TCGA-STAD. To construct a scale-free topology network, the soft threshold power (β) of 8 in GSE84437 (scale-free R^2 = 0.97) (**Figure 3A**) and 6 in TCGA-STAD (scale-free R^2 = 0.87) (**Figure 3B**) was estimated. For GSE84437, the hierarchical clustering tree revealed that 11 co-expression models were clustered (**Figure 3C**), and the black module had the strongest positive correlation with the CAF proportion (Cor = 0.91, P = 6e-161) and stromal score (Cor = 0.84, P = 3e-116) (**Figure 3E**). For TCGA-STAD, the dynamic hybrid cutting clustered 9 co-expression models (**Figure 3D**), with the brown module having the strongest positive correlation with the CAF proportion (Cor = 0.88, P = 4e-108) and stromal score (Cor = 0.88, P = 3e-104) (**Figure 3F**). Hence, the two modules were focused for in-depth

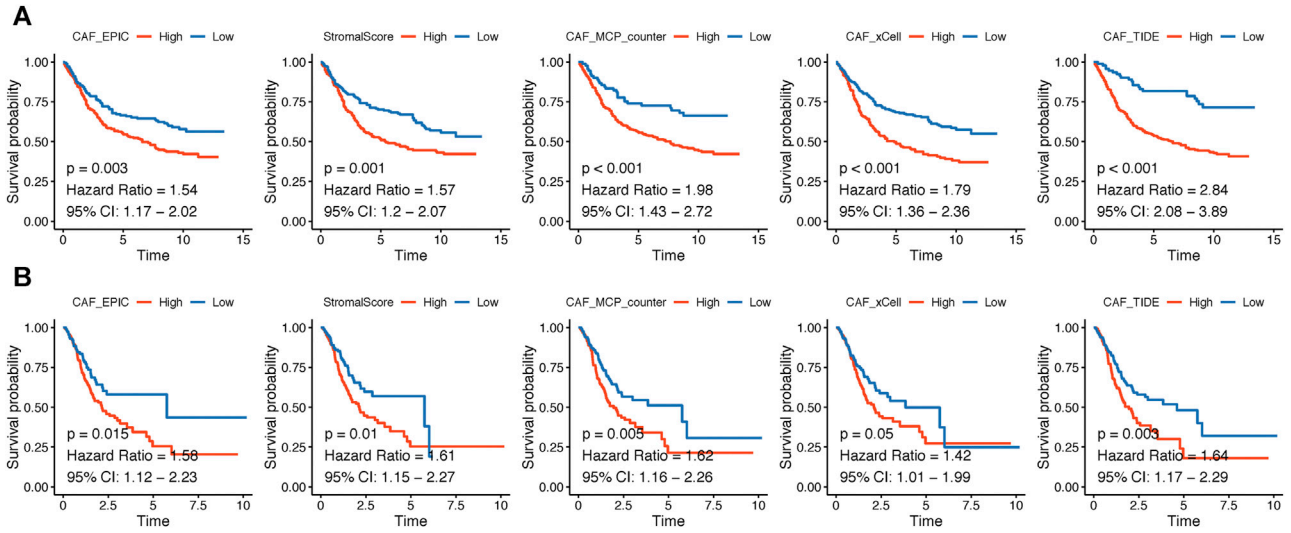

FIGURE 2 | (A–B). Kaplan–Meier analyses showing gastric cancer patients with higher CAF infiltrations as well as stromal scores had worse overall survival in GSE84437 **(A)** and TCGA-STAD **(B)**.

investigations. A total of 356 and 302 genes were incorporated in the black and brown modules, respectively. In the black module, the scatter plots illustrated the strong correlations between MM and GS for CAF (Cor = 0.94, p = 2.1e-167) and stromal scores (Cor = 0.85, p = 1.4e-100) (**Figure 3G**); in the brown module, the strong correlations were also observed between MM and GS for CAF (Cor = 0.93, P = 2e-132) and stromal scores (Cor = 0.95, p = 1.1e-153) (**Figure 3H**). Then, by taking MM > 0.8 and GS > 0.4 as the threshold criteria, a total of 48 genes in the black model of GSE84437 and 101 genes in the brown module of TCGA-STAD were, respectively, screened out as hub genes which are highly correlated with CAF and stromal scores.

Functional Analyses of Hub Genes

As shown in **Figure 4A**, by the intersection of two hub gene sets, 37 common genes were detected and visualized *via* a Venn diagram. Subsequently, we performed GO and KEGG analyses on these 37 genes. Extracellular matrix organization and extracellular structure organization were the major enriched BP terms; the collagen-containing extracellular matrix and extracellular matrix structural constituents were the major enriched CC and MF terms, respectively. Protein digestion and absorption, focal adhesion, and the PI3K-Akt signaling pathway were the main enriched KEGG pathways.

Construction of the Stromal CAF-Based Prognostic Risk Model

Four hundred and thirty-one GC samples from GSE84437 were used as the training cohort owing to the larger sample size, and 330 TCGA-STAD samples were used as the validation group. By performing univariate Cox regression analysis of the 37 common hub genes, 33 OS-related genes with $p < 0.05$ were screened out and subjected to the following LASSO Cox regression analysis (**Figures 4D,E**). Four genes were finally identified for the CAF risk model construction: CAF risk score = expression of COL8A1 * 0.1 + expression of SPOCK1 * 0.007 + expression of AEBP1 * 0.021 + expression of TIMP2 * 0.064 (**Figure 4F**). GC patients in each cohort were divided into high– and low–CAF-risk groups with the median risk score as the cutoff value. Kaplan–Meier curves revealed that GC patients in the high–CAF-risk group experienced worse OS than those in the low–CAF-risk group in both GSE84437 (HR = 1.768, 95%CI: 1.339–2.335, log-rank $p < 0.001$) (**Figure 4G**) and TCGA-STAD (HR = 1.522, 95%CI: 1.086–2.134, log-rank p = 0.015) (**Figure 4H**). These results indicated CAF and stromal-related signature genes were crucial prognostic markers in GC.

CAF Signature Genes Were Highly Correlated With CAF Infiltrations and CAF Markers

To further verify the robustness of the CAF model as an indicator in predicting CAF infiltrations, we performed Spearman's correlation analyses between the CAF risk score and stromal score as well as CAF abundances predicted by EPIC and other three methods: xCell, MCP-counter, and TIDE. Consistently, we observed the CAF risk score was strongly and positively correlated with multi-estimated CAF infiltrations and the stromal score in both GSE84437 (**Figure 5A**) and TCGA-STAD (**Figure 5B**) cohorts. Moreover, we observed the CAF risk score and the expression levels of the four genes were highly and positively correlated with a bunch of the collected CAF markers in both GSE84437 (**Figures 5C,E**) and TCGA-STAD (**Figures 5D,F**) cohorts.

Sensitivity of Chemotherapy and Immunotherapy Between CAF-Risk Groups

Adjuvant chemotherapy following radical surgery has been the standard approach regarding GC. IC50 values of several drugs mentioned in the methods section were estimated based on the

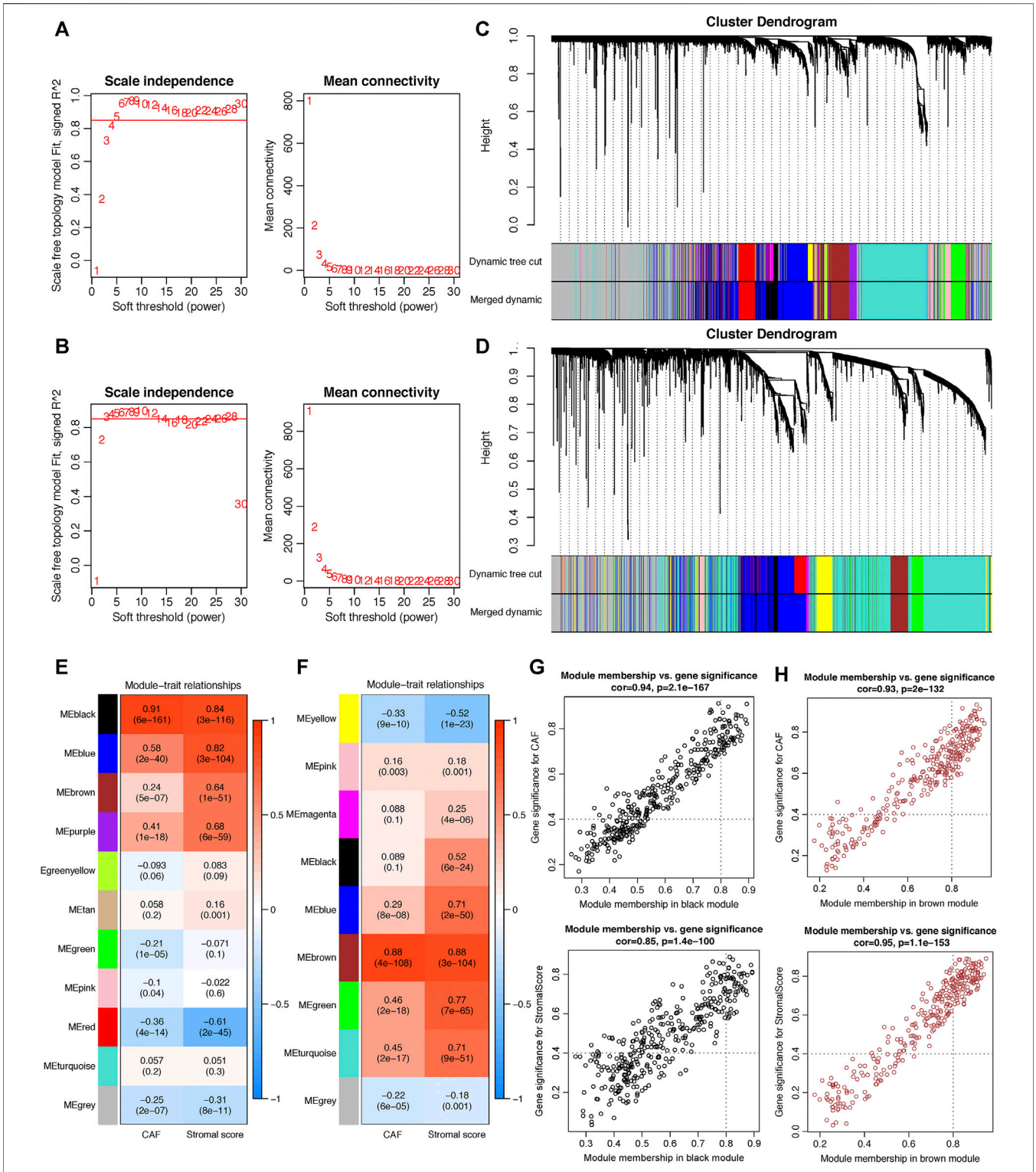

FIGURE 3 | Co-expression network constructed by WGCNA. **(A–B).** The soft-thresholding power (β) of 8 and 6 was, respectively, selected based on the scale-free topology criterion in GSE84437 **(A)** and TCGA-STAD **(B)**. **(C–D).** Clustering dendrograms showing genes with similar expression patterns were clustered into co-expression modules in GSE84437 **(C)** and TCGA-STAD **(D)**. The gray module indicates that genes were not assigned to any module. **(E–F)** Module-trait relationships revealing the correlations between each gene module eigengene and phenotype in GSE84437 **(E)** and TCGA-STAD **(F)**. **(G–H)** Scatter plots of the module membership (MM) and gene significance (GS) of each gene in the black module of GSE84437 **(G)** and the brown module of TCGA-STAD **(H)**. The horizontal axis is the correlation between the gene and co-expression module, and the vertical axis is the correlation between the gene and phenotype.

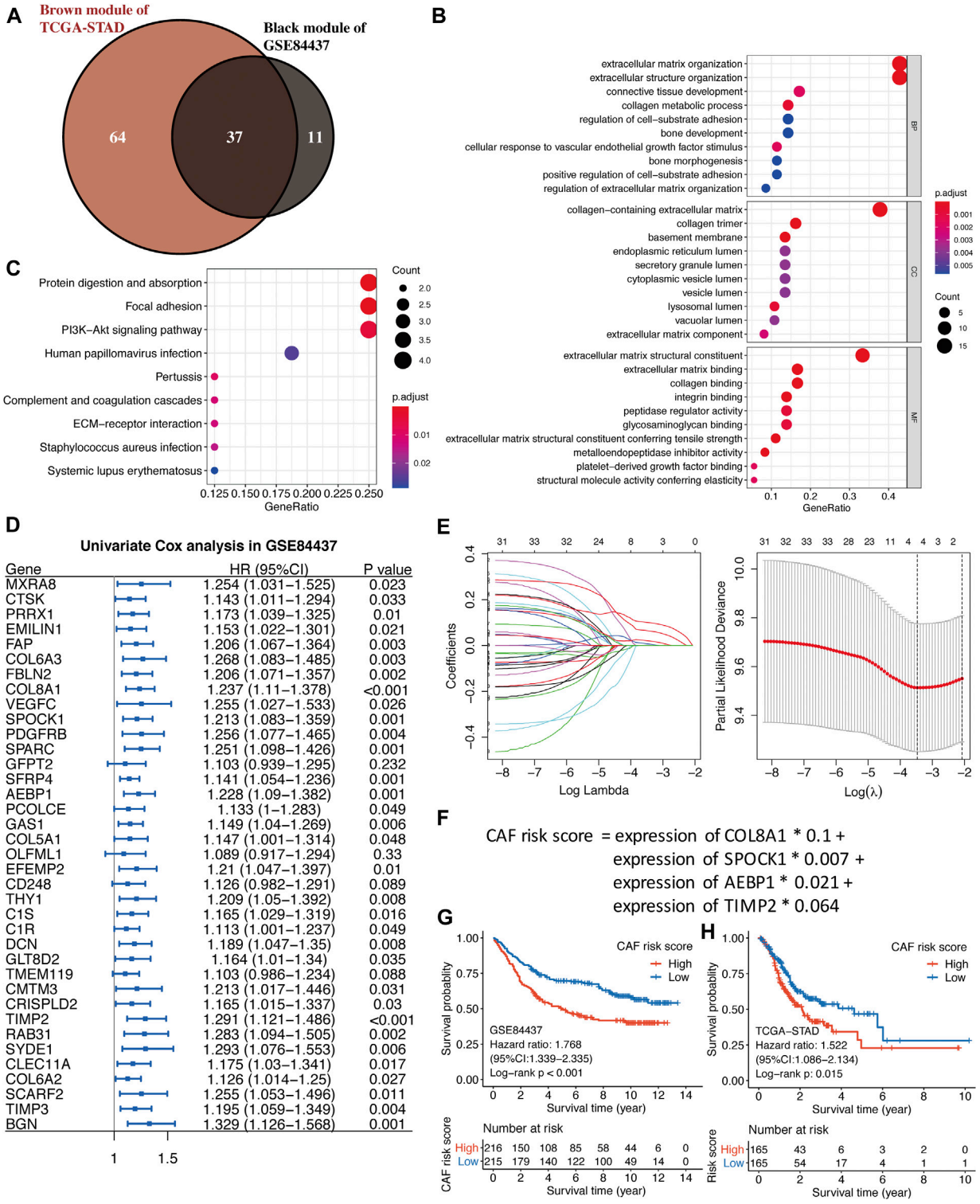

FIGURE 4 | (A) The intersection of GSE84437 black and TCGA-STAD brown module genes was presented in the Venn diagram. **(B–C)** GO analyses of the enriched biological process (BP), cellular component (CC), and molecular function (MF) terms **(B)** and KEGG pathway analysis **(C)** of the 37 genes. **(D)** Univariate Cox analysis for the screening of overall survival-associated genes in GSE84437. **(E)** Coefficient profiles of least absolute shrinkage and selection operator (LASSO) Cox regression analysis, and the adjustment parameter (lambda) was calculated based on the partial likelihood deviance with ten-fold cross validation. **(F)** Formulation of the CAF risk model. **(G,H)** Kaplan–Meier analyses identified gastric cancer patients in the high–CAF-risk group which exhibited worse overall survival in both GSE84437 **(G)** and TCGA-STAD **(H)** cohorts.

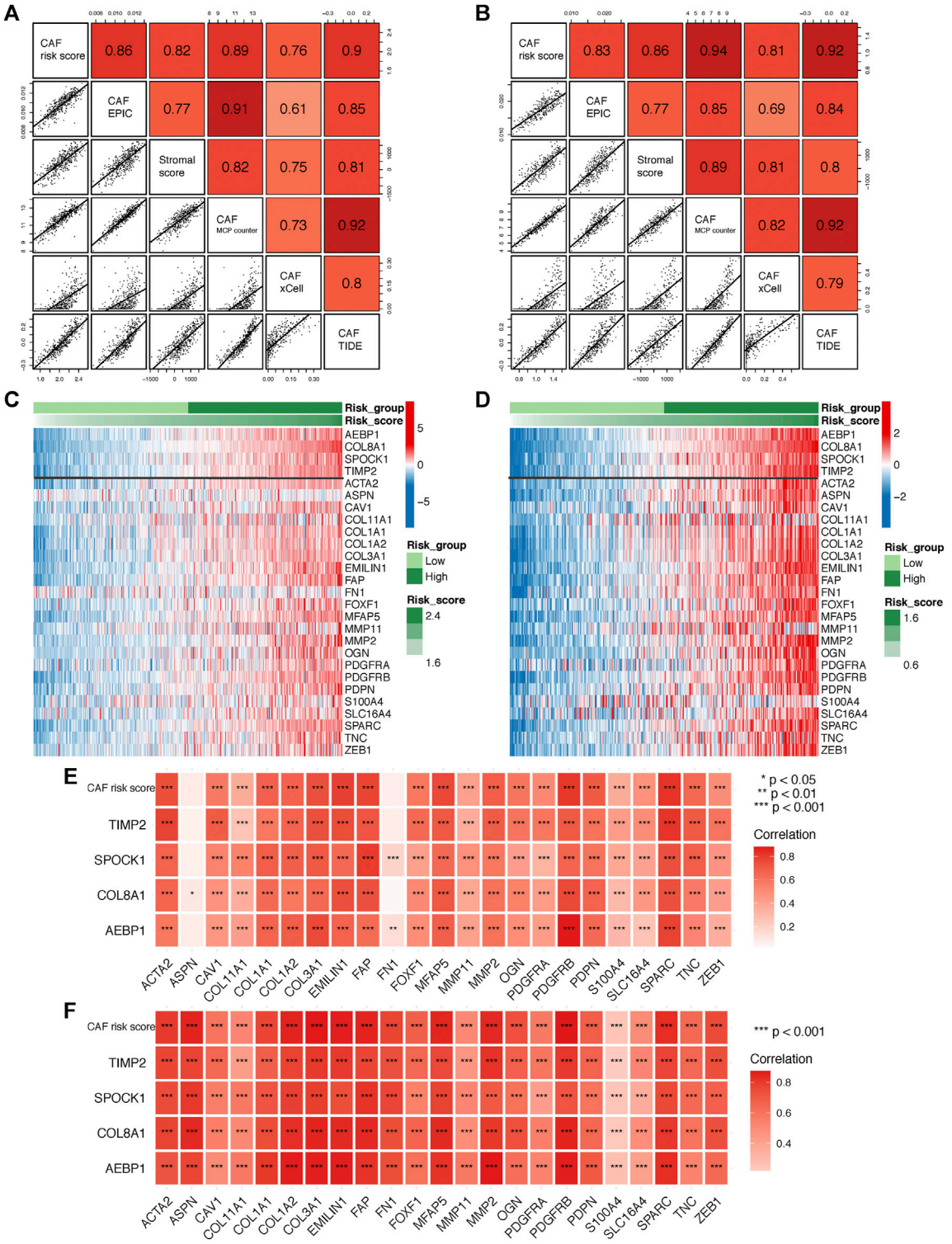

FIGURE 5 | (A–B) Spearman's correlation analyses revealing the CAF risk score was strongly and positively correlated with stromal scores and multi-estimated CAF infiltrations in GSE84437 **(A)** and TCGA-STAD **(B)** cohorts. **(C–D)** The heat map revealing the expression patterns of CAF markers identified four CAF genes with the CAF risk score in GSE84437 **(C)** and TCGA-STAD **(D)** cohorts. **(E–F)** The CAF risk score and four signature genes were positively correlated with literature that reported CAF markers in GSE84437 **(E)** and TCGA-STAD **(F)** cohorts.

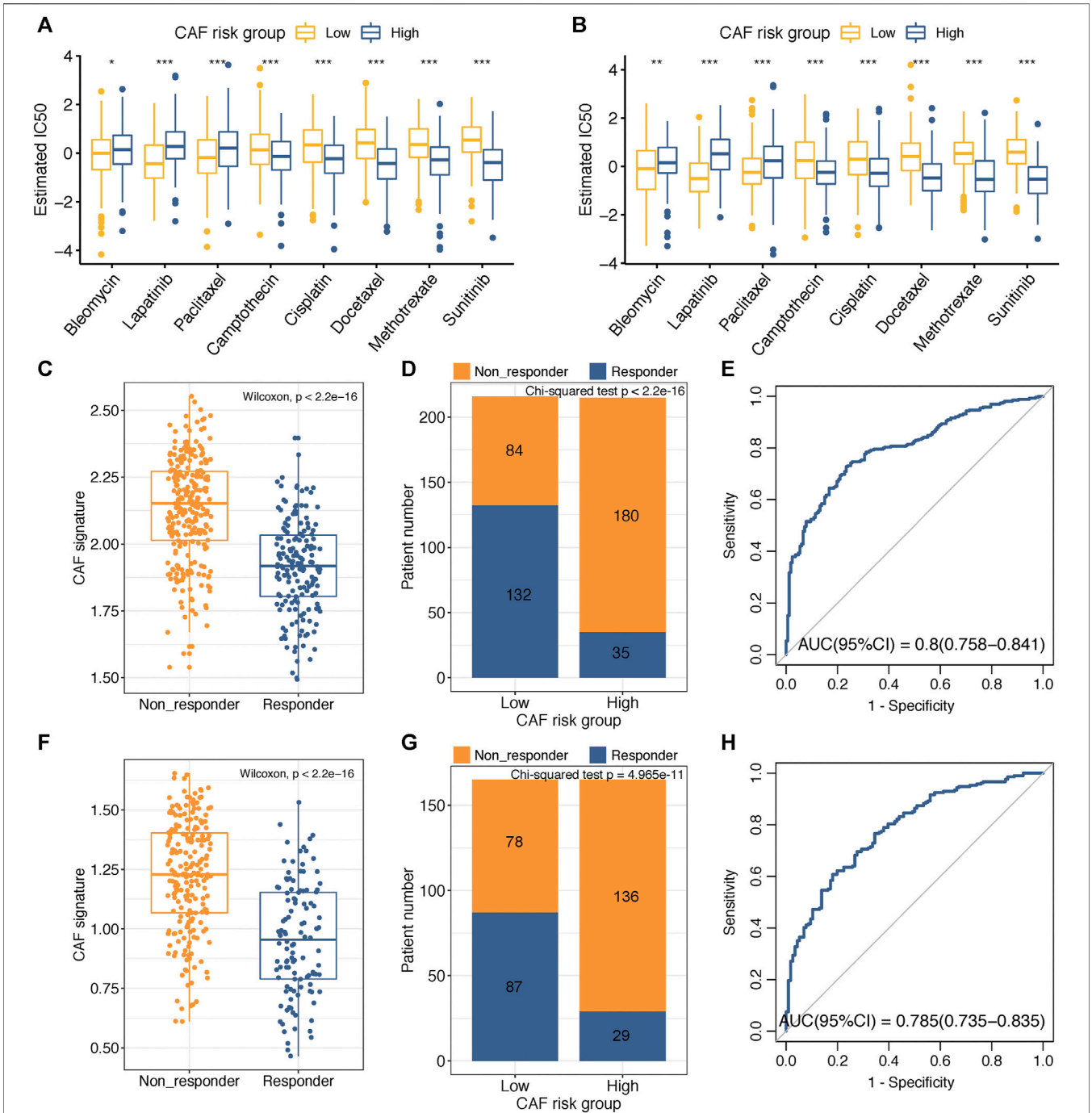

FIGURE 6 | (A–B) Box plots comparing IC50 values of several chemotherapy drugs between high– and low–CAF-risk groups in GSE84437 **(A)** and TCGA-STAD **(B)** cohorts. **(C–H)** TIDE immunotherapy prediction analyses. **(C,F)** The CAF risk score between TIDE-predicted immunotherapy-responders and non-responders in GSE84437 **(C)** and TCGA-STAD **(F)**; **(D,G)** Distributions of responders and non-responders in high– and low– CAF-risk groups in GSE84437 **(D)** and TCGA-STAD **(G)**; **(E,H)** ROC curves of the CAF risk score in predicting immunotherapy responses in GSE84437 **(E)** and TCGA-STAD **(H)**. $*p < 0.05$, $**p < 0.01$, $***p < 0.001$.

GDSC database. Wilcoxon analyses identified significant differences in IC50 values between GC patients in high– and low–CAF-risk groups, with high–CAF-risk GC patients revealing increased sensitivity to camptothecin, cisplatin, docetaxel, methotrexate, and sunitinib, while the low-CAF score subgroup was estimated to be more sensitive to bleomycin, lapatinib, and paclitaxel in both GSE84437 (**Figure 6A**) and TCGA-STAD (**Figure 6B**) cohorts.

Immunotherapy using immune checkpoint inhibitors has brought hope to GC patients. We applied the TIDE method to assess whether the CAF risk score could serve as an immunotherapy predictor for GC patients. For GSE84437, the

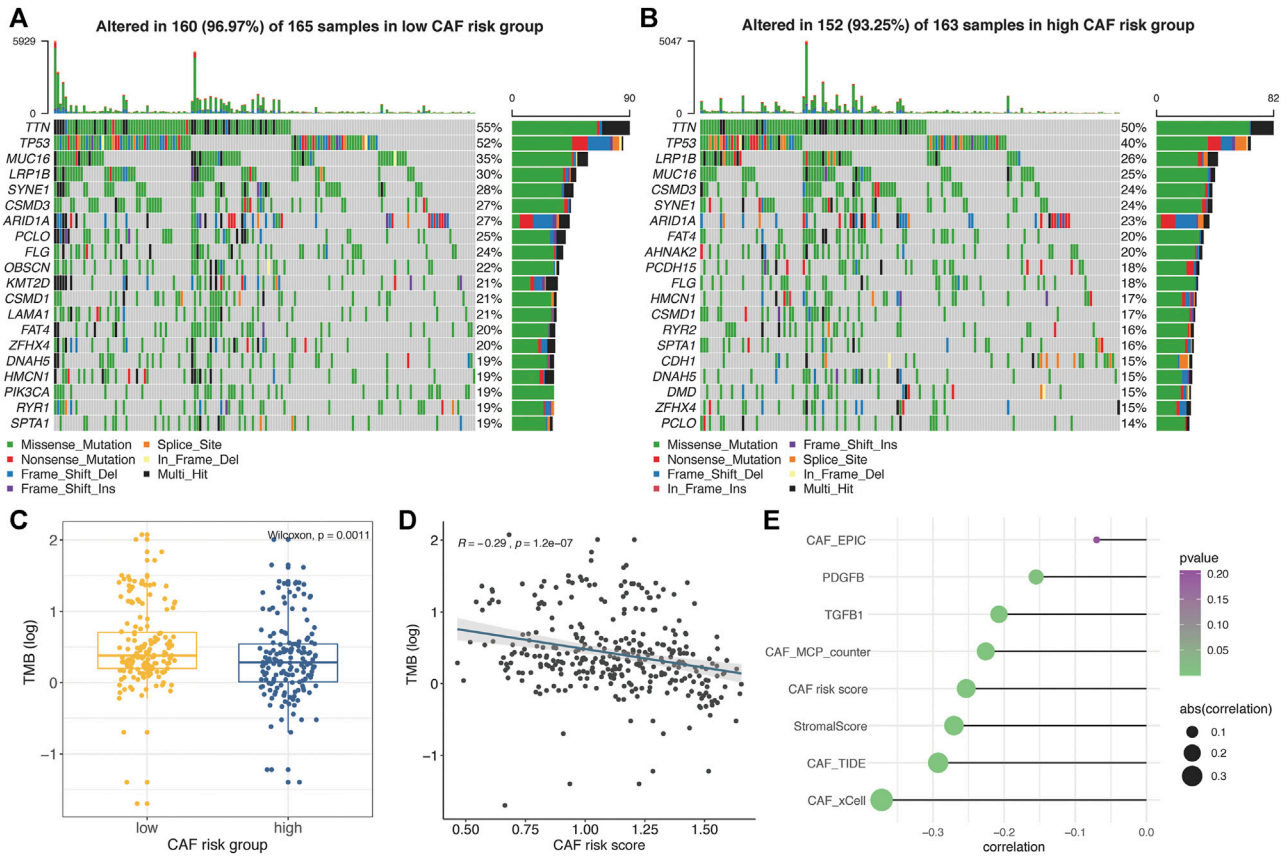

FIGURE 7 | (A–B) Oncoplots depicting the top 20 mutational genes in low– **(A)** and high– **(B)** CAF-risk groups of TCGA-STAD. **(C)** The boxplot revealing TMB values was higher in the low–CAF-risk group. **(D)** Spearman's correlation analyses revealed that the CAF risk score was significantly and negatively correlated with the TMB value. **(E)** Spearman's correlation analyses revealed the TMB value was negatively correlated with CAF activators as well as CAF infiltrations.

CAF score in the non-responder subgroup (n = 264) was significantly higher than that in the responder cohort (n = 167) (Wilcoxon test, p < 2.2e-16; **Figure 6C**); higher sensitivity to immunotherapy was observed for GC patients in the low–CAF-risk group (132/216) than that in the high–CAF-risk group (35/215) (Chi-square test, p < 2.2e-16; **Figure 6D**). For TCGA-STAD, the CAF score was also significantly higher in the non-responder subgroup (n = 214) than that in the responder cohort (n = 116) (Wilcoxon test, p < 2.2e-16; **Figure 6F**); GC patients in the low–CAF-risk group were much more sensitive to immunotherapy (87/165) than those in high-CAF risk group (29/165) (chi-square test, p < 2.2e-16; **Figure 6G**). Furthermore, the AUC values of 0.8 (95%CI: 0.758–0.841) in GSE84437 (**Figure 6E**) and 0.785 (95%CI: 0.735–0.835) in TCGA-STAD (**Figure 6H**) indicated the excellent performance of our CAF model for immunotherapy response predictions.

Correlation Between CAF-Related Signature and Somatic Variation

The top 20 genes with highest mutational frequencies in the low– (**Figure 7A**) and high– (**Figure 7B**) CAF-risk subgroups were, respectively, recognized and displayed as waterfall plots. Intriguingly, several frequent mutational genes were shared in both low– and high–CAF-risk groups, including TTN, TP53, MUC16, LRP1B, SYNE1, CSMD3, ARID1A, PCLO, FLG, CSMD1, FAT4, ZFHX4, DNAH5, HMCN1, and SPTA1. In addition, mutations of LAMA1, RYR1, OBSCN, KMT2D, and PIK3CA genes were more common in the low–CAF-risk group, while mutations of DMD, AHNAK2, PCDH15, RYR2, and CDH1 belonged specifically to the top 20 frequent mutational genes in the high–CAF-risk group. Subsequently, we observed that the TMB values were significantly higher in the low–CAF-score subgroup (Wilcoxon test, p = 0.0011, **Figure 7C**), and Spearman's correlation analysis revealed that the CAF-risk score was significantly and negatively correlated with the TMB value (Cor = -0.29, p = 1.2e-07, **Figure 7D**). Furthermore, Spearman correlation analyses also confirmed that the TMB values were negatively correlated with stromal CAF infiltrations as well as CAF-activating factors like TGF-β (Quante et al., 2011) and PDGF (Pietras et al., 2008) (**Figure 7E**), suggesting that higher TMB might be also able to intense tumor-killing effects *via* modulating a stromal fibroblast-weak local microenvironment.

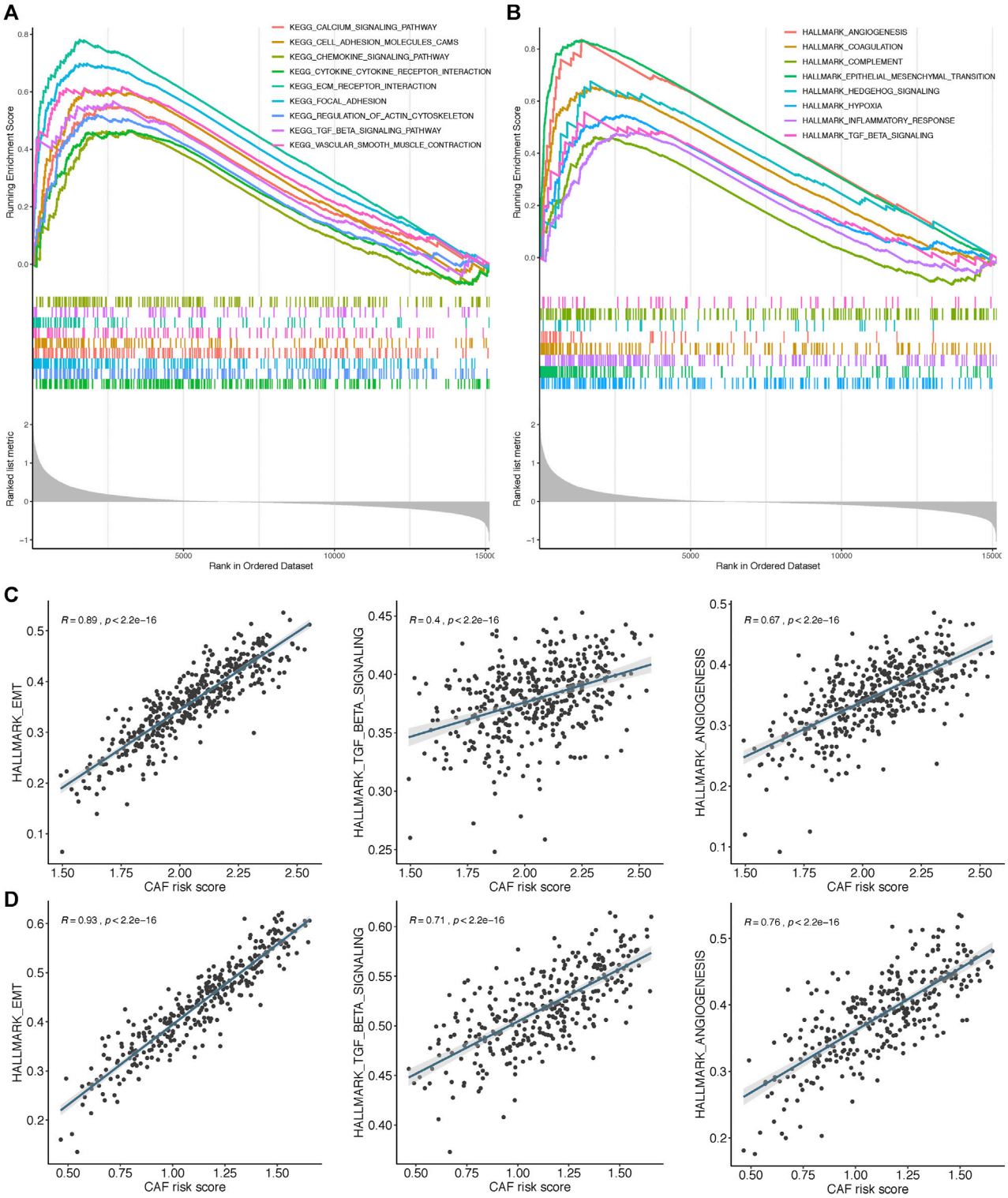

FIGURE 8 | Gene set enrichment analysis (GSEA) of KEGG **(A)** and hallmark **(B)** gene sets between high-and low-CAF risk groups. **(C,D)** ssGSEA results showed CAF risk score was positively correlated with EMT, TGF-β and angiogenesis enrichment scores in both GSE84437 **(C)** and TCGA-STAD **(D)**.

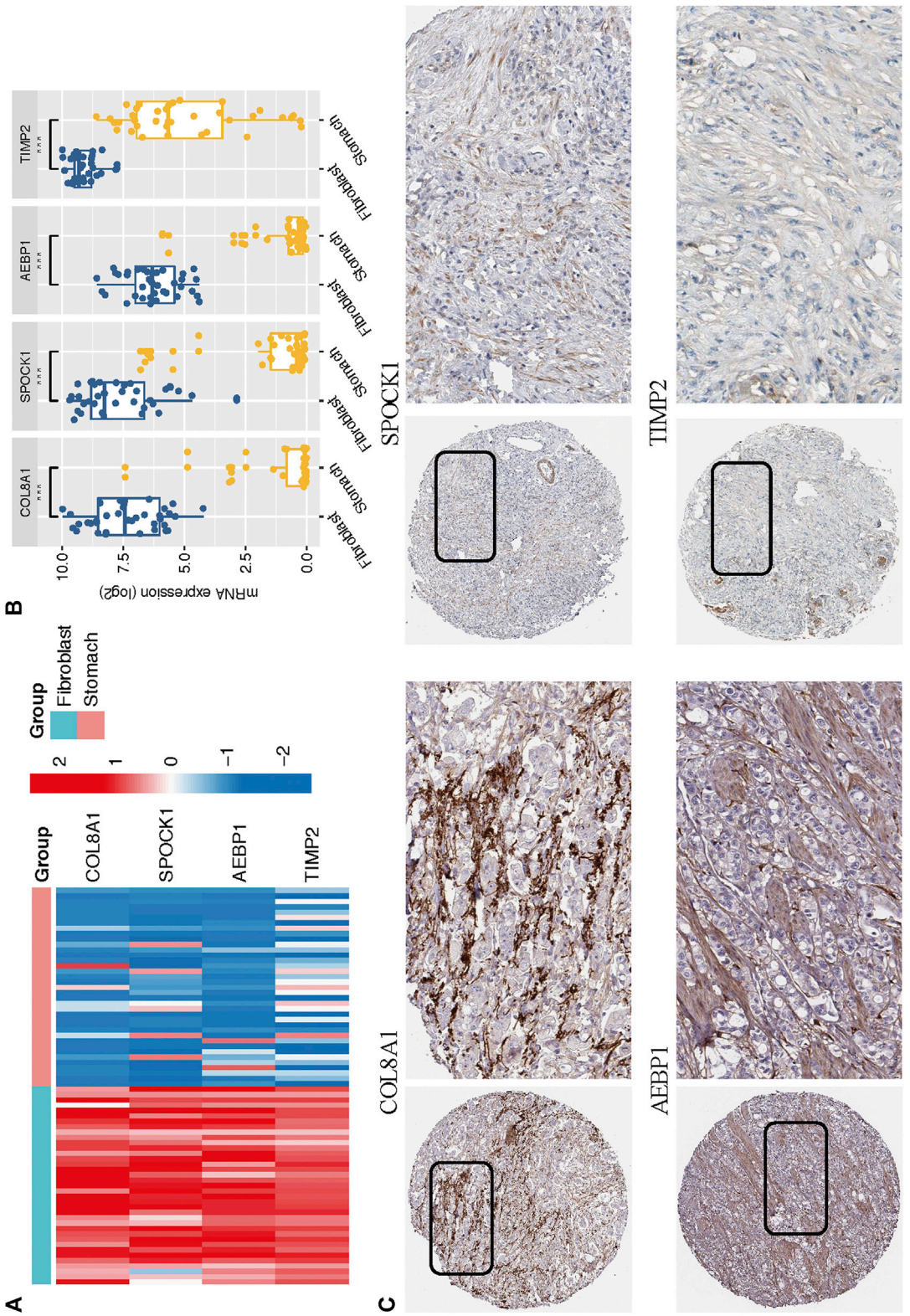

FIGURE 9 | (A–B) The mRNA expression levels of the four CAF genes in the fibroblasts and gastric cancer cell lines were illustrated in the heat map **(A)** and compared by Wilcoxon analysis **(B)**. **(C)** Protein expressions of COL8A1, SPOCK1, AEBP1, and TIMP2 in gastric cancer specimens from the Human Protein Atlas database.

GSEA of the Four-Gene CAF Signature

To further elucidate the functional enrichment of the CAF signature, GSEA was performed on the GSE84437 dataset between high– and low–CAF-risk groups. As displayed in **Figure 8A**, the major enriched KEGG signaling pathways were calcium signaling pathway, ECM receptor interaction, chemokine signaling, and transforming growth factor beta (TGF-β) signaling pathways. Additionally, genes in the high–CAF-risk group were mainly enriched in angiogenesis, epithelial–mesenchymal transition (EMT), inflammatory response, and TGF-β signaling hallmarker gene sets (**Figure 8B**). Extensively, ssGSEA results also showed the CAF risk score was positively correlated with EMT, TGF-β, and angiogenesis enrichment scores in both GSE84437 (**Figure 8C**) and TCGA-STAD (**Figure 8D**).

Multidimensional Validation of Key Genes in CCLE and HPA Databases

Based on the CCLE database, we verified that the mRNA expressions of the four hub genes (COL8A1, SPOCK1, AEBP1, and TIMP2) were higher in fibroblast cell lines than those in GC cell lines (Wilcoxon test, all $p < 0.001$; **Figures 9A,B**). In addition, to determine the protein expression characteristics of these CAF signature genes, we analyzed the IHC images from the HPA database. The data demonstrated that these proteins were deeply stained in GC stroma (**Figure 9C**). These verifications implied that these four genes might be CAF-specific markers.

DISCUSSION

Gastric cancers, especially poorly and undifferentiated gastric cancers, often exhibit massive fibrosis with abundant infiltration of CAFs, which shield TME from antitumor lymphocyte infiltrations and contribute to GC progression, treatment resistance, and immunosuppression (Abe et al., 2017; Ham et al., 2019). Consistently, we observed that higher CAF and stromal scores were associated with worse OS after initial treatment in GC. Therefore, investigation of novel molecular targets in GC is pivotal for the development of stromal CAF-targeting therapies. This is the first research based on WGCNA and multiple computational algorithms to mine the mutual CAF and stromal co-expressed networks in 2 GC cohorts: GSE84437 and TCGA-STAD. By applying univariate Cox and LASSO regression algorithms, a four-gene (COL8A1, SPOCK1, AEBP1, and TIMP2) prognostic CAF model was constructed and validated. By taking the median CAF risk score as the cutoff value, we observed high–CAF-risk GC patients were more sensitive to camptothecin, cisplatin, docetaxel, methotrexate, and sunitinib. In addition, based on the TIDE online algorithm, we observed the lower CAF risk score was highly correlated with improved immunotherapeutic effects in GC patients, and higher TMB levels were observed in low–CAF-risk group STAD patients, which indicated that the CAF model could potentially serve as an immunotherapeutic stratification biomarker for GC. However, interactions between TMB and CAF infiltrations have not been well studied to date. Our study first revealed that the TMB levels were also negatively associated with CAF activators as well as infiltrations in GC patients. It is widely acknowledged that cancer cells with a high level of mutations are easier to be recognized by the immune system, which can then strengthen the immune response and lead to improved immunotherapeutic efficacy (Miao et al., 2018). Based on our analyses, we propose another mechanism that higher TMB might also be able to intense tumor-killing effects *via* modulating a stromal fibroblast-weak local microenvironment. However, more experiments are needed to clarify the crosstalk between CAFs and TMB.

GSEA revealed that EMT, TGF-β signaling, hypoxia, and angiogenesis gene sets were highly and significantly enriched in the high–CAF-risk group; ssGSEA results also showed that the CAF risk score was positively correlated with EMT, TGF-β, and angiogenesis-enrichment scores in both two cohorts. Polarized epithelial cells gain invasive capacities through the EMT process (Huang et al., 2015), and TGF-β signaling has been reported to be responsible for the CAF activation (Yeung et al., 2013; Zheng et al., 2016; Ishimoto et al., 2017). Interactively, CAFs are capable of synergistically initiating and enhancing EMT (Bhowmick et al., 2004; Lee et al., 2006; Thiery and Sleeman, 2006; Ham et al., 2019); CAFs could also regulate and maintain the stemness of gastric cancer cells *via* TGFβ signaling (Hasegawa et al., 2014). Pathological angiogenesis has been widely described as a crucial process enabling the expansion of cancerous tissues, as well as the invasion and metastasis of GC cells (Chen et al., 2004; Hoff and Machado, 2012; Forma et al., 2021). CAFs contributed dominantly to the uncontrolled angiogenesis by inducing a hypoxia TME (Kugeratski et al., 2019) and producing pro-angiogenic factors like galectin-1 (Tang et al., 2016), vascular endothelial growth factor (VEGF) (De Francesco et al., 2013), and hepatocyte growth factor (HGF) (Ding et al., 2018).

To guarantee the model's robustness and avoid over-fitting, we adopted four bioinformatics methods to quantify CAF infiltrations in GC: the EPIC method for model construction and xCell, MCP-counter, and TIDE methods for correlation verifications, and we found that our model was strongly correlated with CAF infiltrations as well as CAF markers. Meanwhile, according to the CCLE database, we further confirmed that the expressions of four identified genes were significantly higher in fibroblast cell lines, and IHC images from the HPA database also revealed higher staining of these proteins in stromal parts of GC. These results implied these genes as CAF-specific markers for GC, and our model was capable of accurately assessing CAF infiltration levels.

With respect to the four identified markers in the model, elevated expression of COL8A1 has been found in CAFs and was significantly associated with a high risk of death in head and neck squamous cell carcinoma (Lai et al., 2019). Zhang et al. identified COL8A1 as the prognostic hub gene highly correlated with Wnt2, which is elevated selectively in CAFs, and high co-expression of COL8A1 and Wnt2 was an independent adverse prognostic factor for colon cancer patients (Katoh, 2001; Zhang et al., 2020). At an epithelial cellular level, Zhou et al. reported that the knockdown of COL8A1 significantly suppressed the

proliferation and promoted the apoptosis of GC cells (Zhou et al., 2020). As for SPOCK1, studies have proved SPOCK1 as an EMT-related marker that was closely correlated with tumorigenesis and invasiveness in gastric cancer (Yan et al., 2017; Chen et al., 2018), prostate cancer (Wang et al., 2016), pancreatic cancer (Li et al., 2020), gallbladder cancer (Shu et al., 2015), and lung cancer (Miao et al., 2013). We observed that high–CAF-risk group GC patients were less sensitive to several drugs like lapatinib, and this result fits well with the finding that SPOCK1-regulated EMT derived the acquiring of lapatinib resistance in HER2-positive GC (Kim et al., 2014). Veenstra et al. identified that SPOCK1 expressed restrictively in tumor stroma, and the stromal SPOCK1 would promote pancreatic ductal adenocarcinoma invasion by mediating extracellular matrix remodeling (Veenstra et al., 2017). Sasaki et al. identified AEBP1 as a novel CAF- and EMT-related protein responsible for tumor invasiveness and metastasis in basal cell carcinoma, squamous cell carcinoma, and malignant melanoma (Sasaki et al., 2018). AEBP1 has also been reported as a pivotal proinflammatory mediator (Majdalawieh et al., 2006; Majdalawieh et al., 2007; Majdalawieh and Ro, 2010), and the overexpression of stromal AEBP1 would induce mammary tumorigenesis *via* paracrine proinflammatory signaling (Holloway et al., 2012). In addition, AEBP1 is upregulated in vascular endothelial cells and promotes tumor angiogenesis in colorectal cancer by inducing angiogenesis-related genes like AQP1 (Yorozu et al., 2020). AEBP1 has also been demonstrated as an adverse prognostic marker in GC that facilitates invasion and migration, metastasis, and EMT of GC cells *via* activating NF-κB signaling (Liu et al., 2018). TIMP2 was previously found as a matrix metalloproteinase (MMP) inhibitor (Basu et al., 2012) that restrained cell proliferation and metastasis in GC (Johansson et al., 2010) and breast cancer (Mendes et al., 2007). However, literature on its functions in cancer is inconsistent. TIMP2 was correlated with higher pN and pM stages as well as unfavorable prognosis in GC (Alakus et al., 2010; Wang et al., 2018). Besides, TIMP2 expressed by CAFs was independently related to lower relapse-free and overall survival in breast cancer (Eiró et al., 2015; Cid et al., 2018). Nonetheless, not much of their functions are known in CAFs of GC, which necessitates further experiments of the four CAF marker's mechanisms that underline the invasiveness and metastasis, drug resistance, and immunosuppression of GC.

Some limitations should be noted in our research. First, this was a retrospective bioinformatic analysis based on two public gene expression data; the real prognostic and therapeutic values of the CAF model should be cross-validated in multicenter and perspective data. In addition, the specific biological roles of the CAF signature biomarkers in GC should be verified through molecular and animal experiments. Nevertheless, our instructive results could serve as a framework for the future mapping of CAFs in GC.

CONCLUSION

In summary, we confirmed higher infiltration of stromal CAFs in TME was correlated with worse prognosis in GC and identified COL8A1, SPOCK1, AEBP1, and TIMP2 as novel prognostic CAF biomarkers by constructing an integrated co-expression network of infiltrated CAF and stromal scores. A CAF model comprising of these four markers was constructed and validated, which could precisely predict prognosis, CAF infiltrations, chemotherapy, and immunotherapy responses in GC patients, which might provide novel insights for targeting CAF therapeutic strategies in GC.

DATA AVAILABILITY STATEMENT

Publicly available datasets were analyzed in this study. These data can be found here: GDC TCGA Hub of the UCSC XENA database (https://gdc.xenahubs.net); GEO datasets (https://www.ncbi.nlm.nih.gov/geo/): GSE84437.

AUTHOR CONTRIBUTIONS

HZ and HSL contributed to the conception and design. HZ and HYL extracted the data from the databases. HZ, HSL, and XW contributed to the data analysis and interpretation. HZ and WDD drafted the manuscript. HSL and XW revised the manuscript. XW supervised the entire study. All authors contributed to the article and approved the final manuscript.

ACKNOWLEDGMENTS

We would like to thank the TCGA and GEO databases for the availability of the data.

REFERENCES

Abe, A., Nagatsuma, A. K., Higuchi, Y., Nakamura, Y., Yanagihara, K., and Ochiai, A. (2017). Site-Specific Fibroblasts Regulate Site-Specific Inflammatory Niche Formation in Gastric Cancer. *Gastric Cancer* 20 (1), 92–103. doi:10.1007/s10120-015-0584-y

Alakus, H., Afriani, N., Warnecke-Eberz, U., Bollschweiler, E., Fetzner, U., Drebber, U., et al. (2010). Clinical Impact of MMP and TIMP Gene Polymorphisms in Gastric Cancer. *World J. Surg.* 34 (12), 2853–2859. doi:10.1007/s00268-010-0761-4

Aran, D., Hu, Z., and Butte, A. J. (2017). xCell: Digitally Portraying the Tissue Cellular Heterogeneity Landscape. *Genome Biol.* 18 (1), 220. doi:10.1186/s13059-017-1349-1

Basu, B., Correa de Sampaio, P., Mohammed, H., Fogarasi, M., Corrie, P., Watkins, N. A., et al. (2012). Inhibition of MT1-MMP Activity Using Functional Antibody Fragments Selected Against its Hemopexin Domain. *Int. J. Biochem. Cel Biol.* 44 (2), 393–403. doi:10.1016/j.biocel.2011.11.015

Becht, E., Giraldo, N. A., Lacroix, L., Buttard, B., Elarouci, N., Petitprez, F., et al. (2016). Estimating the Population Abundance of Tissue-Infiltrating Immune and Stromal Cell Populations Using Gene Expression. *Genome Biol.* 17 (1), 218. doi:10.1186/s13059-016-1070-5

Bhowmick, N. A., Chytil, A., Plieth, D., Gorska, A. E., Dumont, N., Shappell, S., et al. (2004). TGF- Signaling in Fibroblasts Modulates the Oncogenic Potential of Adjacent Epithelia. *Science.* 303 (5659), 848–851. doi:10.1126/science.1090922

Chen, C.-N., Hsieh, F.-J., Cheng, Y.-M., Cheng, W.-F., Su, Y.-N., Chang, K.-J., et al. (2004). The Significance of Placenta Growth Factor in Angiogenesis and Clinical Outcome of Human Gastric Cancer. *Cancer Lett.* 213 (1), 73–82. doi:10.1016/j.canlet.2004.05.020

Chen, D., Zhou, H., Liu, G., Zhao, Y., Cao, G., and Liu, Q. (2018). SPOCK1 Promotes the Invasion and Metastasis of Gastric Cancer Through Slug-Induced Epithelial-Mesenchymal Transition. *J. Cel. Mol. Med.* 22 (2), 797–807. doi:10.1111/jcmm.13357

Cibulskis, K., Lawrence, M. S., Carter, S. L., Sivachenko, A., Jaffe, D., Sougnez, C., et al. (2013). Sensitive Detection of Somatic Point Mutations in Impure and Heterogeneous Cancer Samples. *Nat. Biotechnol.* 31 (3), 213–219. doi:10.1038/nbt.2514

Cid, S., Eiro, N., Fernández, B., Sánchez, R., Andicoechea, A., Fernández-Muñiz, P. I., et al. (2018). Prognostic Influence of Tumor Stroma on Breast Cancer Subtypes. *Clin. Breast Cancer.* 18 (1), e123–e133. doi:10.1016/j.clbc.2017.08.008

Colaprico, A., Silva, T. C., Olsen, C., Garofano, L., Cava, C., Garolini, D., et al. (2016). TCGAbiolinks: an R/Bioconductor Package for Integrative Analysis of TCGA Data. *Nucleic Acids Res.* 44 (8), e71. doi:10.1093/nar/gkv1507

De Francesco, E. M., Lappano, R., Santolla, M. F., Marsico, S., Caruso, A., and Maggiolini, M. (2013). HIF-1α/GPER Signaling Mediates the Expression of VEGF Induced by Hypoxia in Breast Cancer Associated Fibroblasts (CAFs). *Breast Cancer Res.* 15 (4), R64. doi:10.1186/bcr3458

Ding, X., Xi, W., Ji, J., Cai, Q., Jiang, J., Shi, M., et al. (2018). HGF Derived from Cancer associated Fibroblasts Promotes Vascularization in Gastric Cancer via PI3K/AKT and ERK1/2 Signaling. *Oncol. Rep.* 40 (2), 1185–1195. doi:10.3892/or.2018.6500

Duperret, E. K., Trautz, A., Ammons, D., Perales-Puchalt, A., Wise, M. C., Yan, J., et al. (2018). Alteration of the Tumor Stroma Using a Consensus DNA Vaccine Targeting Fibroblast Activation Protein (FAP) Synergizes With Antitumor Vaccine Therapy in Mice. *Clin. Cancer Res.* 24 (5), 1190–1201. doi:10.1158/1078-0432.CCR-17-2033

Eiró, N., Fernandez-Garcia, B., Vázquez, J., Del Casar, J. M., González, L. O., and Vizoso, F. J. (2015). A Phenotype From Tumor Stroma Based on the Expression of Metalloproteases and Their Inhibitors, Associated with Prognosis in Breast Cancer. *Oncoimmunology.* 4 (7), e992222. doi:10.4161/2162402X.2014.992222

Feig, C., Jones, J. O., Kraman, M., Wells, R. J. B., Deonarine, A., Chan, D. S., et al. (2013). Targeting CXCL12 From FAP-Expressing Carcinoma-Associated Fibroblasts Synergizes With Anti-PD-L1 Immunotherapy in Pancreatic Cancer. *Proc. Natl. Acad. Sci.* 110 (50), 20212–20217. doi:10.1073/pnas.1320318110

Fiori, M. E., Di Franco, S., Villanova, L., Bianca, P., Stassi, G., and De Maria, R. (2019). Cancer-Associated Fibroblasts as Abettors of Tumor Progression at the Crossroads of EMT and Therapy Resistance. *Mol. Cancer.* 18 (1), 70. doi:10.1186/s12943-019-0994-2

Forma, A., Tyczyńska, M., Kędzierawski, P., Gietka, K., and Sitarz, M. (2021). Gastric Carcinogenesis: a Comprehensive Review of the Angiogenic Pathways. *Clin. J. Gastroenterol.* 14 (1), 14–25. doi:10.1007/s12328-020-01295-1

Gamradt, P., De La Fouchardière, C., and Hennino, A. (2021). Stromal Protein-Mediated Immune Regulation in Digestive Cancers. *Cancers.* 13 (1), 146. doi:10.3390/cancers13010146

Gascard, P., and Tlsty, T. D. (2016). Carcinoma-Associated Fibroblasts: Orchestrating the Composition of Malignancy. *Genes Dev.* 30 (9), 1002–1019. doi:10.1101/gad.279737.116

Geeleher, P., Cox, N., and Huang, R. S. (2014a). pRRophetic: an R Package for Prediction of Clinical Chemotherapeutic Response From Tumor Gene Expression Levels. *PLoS One.* 9, e107468. doi:10.1371/journal.pone.0107468

Geeleher, P., Cox, N. J., and Huang, R. (2014b). Clinical Drug Response Can Be Predicted Using Baseline Gene Expression Levels and *In Vitro* Drug Sensitivity in Cell Lines. *Genome Biol.* 15 (3), R47. doi:10.1186/gb-2014-15-3-r47

Ghandi, M., Huang, F. W., Jané-Valbuena, J., Kryukov, G. V., Lo, C. C., McDonald, E. R., et al. (2019). Next-Generation Characterization of the Cancer Cell Line Encyclopedia. *Nature.* 569 (7757), 503–508. doi:10.1038/s41586-019-1186-3

Goldman, M. J., Craft, B., Hastie, M., Repečka, K., McDade, F., Kamath, A., et al. (2020). Visualizing and Interpreting Cancer Genomics Data Via the Xena Platformn. *Nat. Biotechnol.* 38 (6), 675–678. doi:10.1038/s41587-020-0546-8

Ham, I.-H., Lee, D., and Hur, H. (2019). Role of Cancer-Associated Fibroblast in Gastric Cancer Progression and Resistance to Treatments. *J. Oncol.* 2019, 1–11. doi:10.1155/2019/6270784

Han, C., Liu, T., and Yin, R. (2020). Biomarkers for Cancer-Associated Fibroblasts. *Biomark Res.* 8 (1), 64. doi:10.1186/s40364-020-00245-w

Hanahan, D., and Coussens, L. M. (2012). Accessories to the Crime: Functions of Cells Recruited to the Tumor Microenvironment. *Cancer Cell.* 21 (3), 309–322. doi:10.1016/j.ccr.2012.02.022

Hänzelmann, S., Castelo, R., and Guinney, J. (2013). GSVA: Gene Set Variation Analysis for Microarray and RNA-Seq Data. *BMC Bioinformatics.* 14 (1), 7. doi:10.1186/1471-2105-14-7

Hasegawa, T., Yashiro, M., Nishii, T., Matsuoka, J., Fuyuhiro, Y., Morisaki, T., et al. (2014). Cancer-Associated Fibroblasts Might Sustain the Stemness of Scirrhous Gastric Cancer Cells via Transforming Growth Factor-β Signaling. *Int. J. Cancer.* 134 (8), 1785–1795. doi:10.1002/ijc.28520

Hoff, P. M., and Machado, K. K. (2012). Role of Angiogenesis in the Pathogenesis of Cancer. *Cancer Treat. Rev.* 38 (7), 825–833. doi:10.1016/j.ctrv.2012.04.006

Hofheinz, R.-D., al-Batran, S.-E., Hartmann, F., Hartung, G., Jäger, D., Renner, C., et al. (2003). Stromal Antigen Targeting by a Humanised Monoclonal Antibody: an Early Phase II Trial of Sibrotuzumab in Patients With Metastatic Colorectal Cancer. *Oncol. Res. Treat.* 26 (1), 44–48. doi:10.1159/000069863

Holloway, R. W., Bogachev, O., Bharadwaj, A. G., McCluskey, G. D., Majdalawieh, A. F., Zhang, L., et al. (2012). Stromal Adipocyte Enhancer-Binding Protein (AEBP1) Promotes Mammary Epithelial Cell Hyperplasia via Proinflammatory and Hedgehog Signaling. *J. Biol. Chem.* 287 (46), 39171–39181. doi:10.1074/jbc.M112.404293

Huang, L., Wu, R. L., and Xu, A. M. (2015). Epithelial-Mesenchymal Transition in Gastric Cancer. *Am. J. Transl Res.* 7 (11), 2141–2158.

Ishimoto, T., Miyake, K., Nandi, T., Yashiro, M., Onishi, N., Huang, K. K., et al. (2017). Activation of Transforming Growth Factor Beta 1 Signaling in Gastric Cancer-Associated Fibroblasts Increases Their Motility, via Expression of Rhomboid 5 Homolog 2, and Ability to Induce Invasiveness of Gastric Cancer Cells. *Gastroenterology.* 153 (1), 191–204. doi:10.1053/j.gastro.2017.03.046

Jiang, P., Gu, S., Pan, D., Fu, J., Sahu, A., Hu, X., et al. (2018). Signatures of T Cell Dysfunction and Exclusion Predict Cancer Immunotherapy Response. *Nat. Med.* 24 (10), 1550–1558. doi:10.1038/s41591-018-0136-1

Johansson, E., Komuro, A., Iwata, C., Hagiwara, A., Fuse, Y., Watanabe, A., et al. (2010). Exogenous Introduction of Tissue Inhibitor of Metalloproteinase 2 Reduces Accelerated Growth of TGF-β-Disrupted Diffuse-Type Gastric Carcinoma. *Cancer Sci.* 101 (11), 2398–2403. doi:10.1111/j.1349-7006.2010.01688.x

Katoh, M. (2001). Frequent Up-Regulation of WNT2 in Primary Gastric Cancer and Colorectal Cancer. *Int. J. Oncol.* 19 (5), 1003–1007. doi:10.3892/ijo.19.5.1003

Kaur, A., Ecker, B. L., Douglass, S. M., Kugel, C. H., Webster, M. R., Almeida, F. V., et al. (2019). Remodeling of the Collagen Matrix in Aging Skin Promotes Melanoma Metastasis and Affects Immune Cell Motility. *Cancer Discov.* 9 (1), 64–81. doi:10.1158/2159-8290.CD-18-0193

Kim, H.-P., Han, S.-W., Song, S.-H., Jeong, E.-G., Lee, M.-Y., Hwang, D., et al. (2014). Testican-1-Mediated Epithelial-Mesenchymal Transition Signaling Confers Acquired Resistance to Lapatinib in HER2-Positive Gastric Cancer. *Oncogene.* 33 (25), 3334–3341. doi:10.1038/onc.2013.285

Kojima, Y., Acar, A., Eaton, E. N., Mellody, K. T., Scheel, C., Ben-Porath, I., et al. (2010). Autocrine TGF- and Stromal Cell-Derived Factor-1 (SDF-1) Signaling Drives the Evolution of Tumor-Promoting Mammary Stromal Myofibroblasts. *Proc. Natl. Acad. Sci.* 107 (46), 20009–20014. doi:10.1073/pnas.1013805107

Kraman, M., Bambrough, P. J., Arnold, J. N., Roberts, E. W., Magiera, L., Jones, J. O., et al. (2010). Suppression of Antitumor Immunity by Stromal Cells Expressing Fibroblast Activation Protein-. *Science.* 330 (6005), 827–830. doi:10.1126/science.1195300

Kugeratski, F. G., Atkinson, S. J., Neilson, L. J., Lilla, S., Knight, J. R. P., Serneels, J., et al. (2019). Hypoxic Cancer-Associated Fibroblasts Increase NCBP2-AS2/

HIAR to Promote Endothelial Sprouting Through Enhanced VEGF Signaling. *Sci. Signal.* 12 (567), eaan8247. doi:10.1126/scisignal.aan8247

Lai, S. L., Tan, M. L., Hollows, R. J., Robinson, M., Ibrahim, M., Margielewska, S., et al. (2019). Collagen Induces a More Proliferative, Migratory and Chemoresistant Phenotype in Head and Neck Cancer via DDR1. *Cancers.* 11 (11), 1766. doi:10.3390/cancers11111766

Lakins, M. A., Ghorani, E., Munir, H., Martins, C. P., and Shields, J. D. (2018). Cancer-Associated Fibroblasts Induce Antigen-Specific Deletion of CD8 + T Cells to Protect Tumour Cells. *Nat. Commun.* 9 (1), 948. doi:10.1038/s41467-018-03347-0

Langfelder, P., and Horvath, S. (2008). WGCNA: an R Package for Weighted Correlation Network Analysis. *BMC bioinformatics.* 9, 559. doi:10.1186/1471-2105-9-559

Lee, J.-H., Kim, H.-I., Kim, M. G., Ha, T. K., Jung, M.-S., and Kwon, S. J. (2016). Recurrence of Gastric Cancer in Patients Who Are Disease-free for More Than 5 Years After Primary Resection. *Surgery.* 159 (4), 1090–1098. doi:10.1016/j.surg.2015.11.002

Lee, T. K., Poon, R. T. P., Yuen, A. P., Ling, M. T., Kwok, W. K., Wang, X. H., et al. (2006). Twist Overexpression Correlates With Hepatocellular Carcinoma Metastasis Through Induction of Epithelial-Mesenchymal Transition. *Clin. Cancer Res.* 12 (18), 5369–5376. doi:10.1158/1078-0432.ccr-05-2722

Li, J., Guan, J., Long, X., Wang, Y., and Xiang, X. (2016). Mir-1-Mediated Paracrine Effect of Cancer-Associated Fibroblasts on Lung Cancer Cell Proliferation and Chemoresistance. *Oncol. Rep.* 35 (6), 3523–3531. doi:10.3892/or.2016.4714

Li, J., Ke, J., Fang, J., and Chen, J. P. (2020). A Potential Prognostic Marker and Therapeutic Target: SPOCK1 Promotes the Proliferation, Metastasis, and Apoptosis of Pancreatic Ductal Adenocarcinoma Cells. *J. Cel Biochem.* 121 (1), 743–754. doi:10.1002/jcb.29320

Liberzon, A., Birger, C., Thorvaldsdóttir, H., Ghandi, M., Mesirov, J. P., and Tamayo, P. (2015). The Molecular Signatures Database Hallmark Gene Set Collection. *Cel Syst.* 1 (6), 417–425. doi:10.1016/j.cels.2015.12.004

Liu, B., Chen, X., Zhan, Y., Wu, B., and Pan, S. (2021a). Identification of a Gene Signature for Renal Cell Carcinoma-Associated Fibroblasts Mediating Cancer Progression and Affecting Prognosis. *Front. Cel Dev. Biol.* 8, 604627. doi:10.3389/fcell.2020.604627

Liu, B., Zhan, Y., Chen, X., Hu, X., Wu, B., and Pan, S. (2021b). Weighted Gene Co-Expression Network Analysis Can Sort Cancer-Associated Fibroblast-Specific Markers Promoting Bladder Cancer Progression. *J. Cel Physiol.* 236 (2), 1321–1331. doi:10.1002/jcp.29939

Liu, J.-Y., Jiang, L., Liu, J.-J., He, T., Cui, Y.-H., Qian, F., et al. (2018). AEBP1 Promotes Epithelial-Mesenchymal Transition of Gastric Cancer Cells by Activating the NF-Kb Pathway and Predicts Poor Outcome of the Patients. *Sci. Rep.* 8 (1), 11955. doi:10.1038/s41598-018-29878-6

Lotti, F., Jarrar, A. M., Pai, R. K., Hitomi, M., Lathia, J., Mace, A., et al. (2013). Chemotherapy Activates Cancer-Associated Fibroblasts to Maintain Colorectal Cancer-Initiating Cells by IL-17A. *J. Exp. Med.* 210 (13), 2851–2872. doi:10.1084/jem.20131195

Ma, H.-Y., Liu, X.-Z., and Liang, C.-M. (2016). Inflammatory Microenvironment Contributes to Epithelial-Mesenchymal Transition in Gastric Cancer. *World J. Gastroenterol.* 22 (29), 6619–6628. doi:10.3748/wjg.v22.i29.6619

Majdalawieh, A., and Ro, H.-S. (2010). PPARγ1 and LXRα Face a New Regulator of Macrophage Cholesterol Homeostasis and Inflammatory Responsiveness, AEBP1. *Nucl. Recept Signal.* 8, nrs.08004–e004. doi:10.1621/nrs.08004

Majdalawieh, A., Zhang, L., Fuki, I. V., Rader, D. J., and Ro, H.-S. (2006). Adipocyte Enhancer-Binding Protein 1 Is a Potential Novel Atherogenic Factor Involved in Macrophage Cholesterol Homeostasis and Inflammation. *Proc. Natl. Acad. Sci. U S A.* 103 (7), 2346–2351. doi:10.1073/pnas.0508139103

Majdalawieh, A., Zhang, L., and Ro, H.-S. (2007). Adipocyte Enhancer-Binding Protein-1 Promotes Macrophage Inflammatory Responsiveness by Up-Regulating NF-Kb via IκBα Negative Regulation. *MBoC.* 18 (3), 930–942. doi:10.1091/mbc.e06-03-0217

Mayakonda, A., Lin, D.-C., Assenov, Y., Plass, C., and Koeffler, H. P. (2018). Maftools: Efficient and Comprehensive Analysis of Somatic Variants in Cancer. *Genome Res.* 28 (11), 1747–1756. doi:10.1101/gr.239244.118

Mendes, O., Kim, H.-T., Lungu, G., and Stoica, G. (2007). MMP2 Role in Breast Cancer Brain Metastasis Development and its Regulation by TIMP2 and ERK1/2. *Clin. Exp. Metastasis.* 24 (5), 341–351. doi:10.1007/s10585-007-9071-0

Miao, D., Margolis, C. A., Vokes, N. I., Liu, D., Taylor-Weiner, A., Wankowicz, S. M., et al. (2018). Genomic Correlates of Response to Immune Checkpoint Blockade in Microsatellite-Stable Solid Tumors. *Nat. Genet.* 50 (9), 1271–1281. doi:10.1038/s41588-018-0200-2

Miao, L., Wang, Y., Xia, H., Yao, C., Cai, H., and Song, Y. (2013). SPOCK1 Is a Novel Transforming Growth Factor-β Target Gene That Regulates Lung Cancer Cell Epithelial-Mesenchymal Transition. *Biochem. Biophysical Res. Commun.* 440 (4), 792–797. doi:10.1016/j.bbrc.2013.10.024

Monteran, L., and Erez, N. (2019). The Dark Side of Fibroblasts: Cancer-Associated Fibroblasts as Mediators of Immunosuppression in the Tumor Microenvironment. *Front. Immunol.* 10, 1835. doi:10.3389/fimmu.2019.01835

Narra, K., Mullins, S. R., Lee, H.-O., Strzemkowski-Brun, B., Magalong, K., Christiansen, V. J., et al. (2007). Phase II Trial of Single Agent Val-boroPro (Talabostat) Inhibiting Fibroblast Activation Protein in Patients With Metastatic Colorectal Cancer. *Cancer Biol. Ther.* 6 (11), 1691–1699. doi:10.4161/cbt.6.11.4874

Pietras, K., Pahler, J., Bergers, G., and Hanahan, D. (2008). Functions of Paracrine PDGF Signaling in the Proangiogenic Tumor Stroma Revealed by Pharmacological Targeting. *Plos Med.* 5 (1), e19. doi:10.1371/journal.pmed.0050019

Quail, D. F., and Joyce, J. A. (2013). Microenvironmental Regulation of Tumor Progression and Metastasis. *Nat. Med.* 19 (11), 1423–1437. doi:10.1038/nm.3394

Quante, M., Tu, S. P., Tomita, H., Gonda, T., Wang, S. S. W., Takashi, S., et al. (2011). Bone Marrow-Derived Myofibroblasts Contribute to the Mesenchymal Stem Cell Niche and Promote Tumor Growth. *Cancer Cell.* 19 (2), 257–272. doi:10.1016/j.ccr.2011.01.020

Racle, J., de Jonge, K., Baumgaertner, P., Speiser, D. E., and Gfeller, D. (2017). Simultaneous Enumeration of Cancer and Immune Cell Types From Bulk Tumor Gene Expression Data. *eLife.* 6, e26476. doi:10.7554/eLife.26476

Sasaki, K., Sugai, T., Ishida, K., Osakabe, M., Amano, H., Kimura, H., et al. (2018). Analysis of Cancer-Associated Fibroblasts and the Epithelial-Mesenchymal Transition in Cutaneous Basal Cell Carcinoma, Squamous Cell Carcinoma, and Malignant Melanoma. *Hum. Pathol.* 79, 1–8. doi:10.1016/j.humpath.2018.03.006

Shu, Y.-J., Weng, H., Ye, Y.-Y., Hu, Y.-P., Bao, R.-F., Cao, Y., et al. (2015). SPOCK1 as a Potential Cancer Prognostic Marker Promotes the Proliferation and Metastasis of Gallbladder Cancer Cells by Activating the PI3K/AKT Pathway. *Mol. Cancer.* 14 (1), 12. doi:10.1186/s12943-014-0276-y

Simon, N., Friedman, J., Hastie, T., and Tibshirani, R. (2011). Regularization Paths for Cox's Proportional Hazards Model via Coordinate Descent. *J. Stat. Soft.* 39 (5), 1–13. doi:10.18637/jss.v039.i05

Sturm, G., Finotello, F., and List, M. (2020). "Immunedeconv: An R Package for Unified Access to Computational Methods for Estimating Immune Cell Fractions From Bulk RNA-Sequencing Data," in *Bioinformatics for Cancer Immunotherapy: Methods and Protocols*. Editor S. Boegel (New York, NY: Springer US), 223–232. doi:10.1007/978-1-0716-0327-7_16

Sung, H., Ferlay, J., Siegel, R. L., Laversanne, M., Soerjomataram, I., Jemal, A., et al. (2021). Global Cancer Statistics 2020: GLOBOCAN Estimates of Incidence and Mortality Worldwide for 36 Cancers in 185 Countries. *CA A. Cancer J. Clin.* 71 (3), 209–249. doi:10.3322/caac.21660

Tang, D., Gao, J., Wang, S., Ye, N., Chong, Y., Huang, Y., et al. (2016). Cancer-Associated Fibroblasts Promote Angiogenesis in Gastric Cancer Through Galectin-1 Expression. *Tumor Biol.* 37 (2), 1889–1899. doi:10.1007/s13277-015-3942-9

Thiery, J. P., and Sleeman, J. P. (2006). Complex Networks Orchestrate Epithelial-Mesenchymal Transitions. *Nat. Rev. Mol. Cel Biol.* 7 (2), 131–142. doi:10.1038/nrm1835

Thrift, A. P., and El-Serag, H. B. (2020). Burden of Gastric Cancer. *Clin. Gastroenterol. Hepatol.* 18 (3), 534–542. doi:10.1016/j.cgh.2019.07.045

Tommelein, J., Verset, L., Boterberg, T., Demetter, P., Bracke, M., and De Wever, O. (2015). Cancer-Associated Fibroblasts Connect Metastasis-Promoting Communication in Colorectal Cancer. *Front. Oncol.* 5, 63. doi:10.3389/fonc.2015.00063

Uhlén, M., Fagerberg, L., Hallström, B. M., Lindskog, C., Oksvold, P., Mardinoglu, A., et al. (2015). Tissue-Based Map of the Human Proteome. *Science.* 347 (6220), 1260419. doi:10.1126/science.1260419

Veenstra, V. L., Damhofer, H., Waasdorp, C., Steins, A., Kocher, H. M., Medema, J. P., et al. (2017). Stromal SPOCK1 Supports Invasive Pancreatic Cancer Growth. *Mol. Oncol.* 11 (8), 1050–1064. doi:10.1002/1878-0261.12073

Wagner, G. P., Kin, K., and Lynch, V. J. (2012). Measurement of mRNA Abundance Using RNA-Seq Data: RPKM Measure Is Inconsistent Among Samples. *Theor. Biosci.* 131 (4), 281–285. doi:10.1007/s12064-012-0162-3

Wang, W., Zhang, Y., Liu, M., Wang, Y., Yang, T., Li, D., et al. (2018). TIMP2 Is a Poor Prognostic Factor and Predicts Metastatic Biological Behavior in Gastric Cancer. *Sci. Rep.* 8 (1), 9629. doi:10.1038/s41598-018-27897-x

Wang, Z., Yao, Y.-T., Xu, H., Chen, Y.-B., Gu, M., Cai, Z.-K., et al. (2016). SPOCK1 Promotes Tumor Growth and Metastasis in Human Prostate Cancer. *Drug Des. Devel Ther.* 10, 2311–2321. doi:10.2147/DDDT.S91321

Wu, X., Tao, P., Zhou, Q., Li, J., Yu, Z., Wang, X., et al. (2017). IL-6 Secreted by Cancer-Associated Fibroblasts Promotes Epithelial-Mesenchymal Transition and Metastasis of Gastric Cancer via JAK2/STAT3 Signaling Pathway. *Oncotarget.* 8 (13), 20741–20750. doi:10.18632/oncotarget.15119

Yan, L., Sun, K., Liu, Y., Liang, J., Cai, K., and Gui, J. (2017). MiR-129-5p Influences the Progression of Gastric Cancer Cells Through Interacting With SPOCK1. *Tumour Biol.* 39 (6), 1010428317706916. doi:10.1177/1010428317706916

Yang, W., Soares, J., Greninger, P., Edelman, E. J., Lightfoot, H., Forbes, S., et al. (2013). Genomics of Drug Sensitivity in Cancer (GDSC): a Resource for Therapeutic Biomarker Discovery in Cancer Cells. *Nucleic Acids Res.* 41 (D1), D955–D961. doi:10.1093/nar/gks1111

Yarchoan, M., Hopkins, A., and Jaffee, E. M. (2017). Tumor Mutational Burden and Response Rate to PD-1 Inhibition. *N. Engl. J. Med.* 377 (25), 2500–2501. doi:10.1056/NEJMc1713444

Yeung, T.-L., Leung, C. S., Wong, K.-K., Samimi, G., Thompson, M. S., Liu, J., et al. (2013). TGF-β Modulates Ovarian Cancer Invasion by Upregulating CAF-Derived Versican in the Tumor Microenvironment. *Cancer Res.* 73 (16), 5016–5028. doi:10.1158/0008-5472.CAN-13-0023

Yoon, S.-J., Park, J., Shin, Y., Choi, Y., Park, S. W., Kang, S.-G., et al. (2020). Deconvolution of Diffuse Gastric Cancer and the Suppression of CD34 on the BALB/c Nude Mice Model. *BMC cancer.* 20 (1), 314. doi:10.1186/s12885-020-06814-4

Yorozu, A., Yamamoto, E., Niinuma, T., Tsuyada, A., Maruyama, R., Kitajima, H., et al. (2020). Upregulation of Adipocyte Enhancer-Binding Protein 1 in Endothelial Cells Promotes Tumor Angiogenesis in Colorectal Cancer. *Cancer Sci.* 111 (5), 1631–1644. doi:10.1111/cas.14360

Yoshihara, K., Shahmoradgoli, M., Martínez, E., Vegesna, R., Kim, H., Torres-Garcia, W., et al. (2013). Inferring Tumour Purity and Stromal and Immune Cell Admixture from Expression Data. *Nat. Commun.* 4, 2612. doi:10.1038/ncomms3612

Yu, G., Wang, L.-G., Han, Y., and He, Q.-Y. (2012). ClusterProfiler: an R Package for Comparing Biological Themes Among Gene Clusters. *OMICS: A J. Integr. Biol.* 16 (5), 284–287. doi:10.1089/omi.2011.0118

Zhang, L., Jiang, X., Li, Y., Fan, Q., Li, H., Jin, L., et al. (2020). Clinical Correlation of Wnt2 and COL8A1 With Colon Adenocarcinoma Prognosis. *Front. Oncol.* 10, 1504. doi:10.3389/fonc.2020.01504

Zheng, L., Xu, C., Guan, Z., Su, X., Xu, Z., Cao, J., et al. (2016). Galectin-1 Mediates TGF-β-Induced Transformation From Normal Fibroblasts Into Carcinoma-Associated Fibroblasts and Promotes Tumor Progression in Gastric Cancer. *Am. J. Transl Res.* 8 (4), 1641–1658.

Zhou, J., Song, Y., Gan, W., Liu, L., Chen, G., Chen, Z., et al. (2020). Upregulation of COL8A1 Indicates Poor Prognosis Across Human Cancer Types and Promotes the Proliferation of Gastric Cancer Cells. *Oncol. Lett.* 20 (4), 34. doi:10.3892/ol.2020.11895

Conflict of Interest: The authors declare that the research was conducted in the absence of any commercial or financial relationships that could be construed as a potential conflict of interest.

Publisher's Note: All claims expressed in this article are solely those of the authors and do not necessarily represent those of their affiliated organizations, or those of the publisher, the editors, and the reviewers. Any product that may be evaluated in this article, or claim that may be made by its manufacturer, is not guaranteed or endorsed by the publisher.

frontiers in Molecular Biosciences

ORIGINAL RESEARCH
published: 19 October 2021
doi: 10.3389/fmolb.2021.739978

Clinical Value and Potential Mechanisms of Oxysterol-Binding Protein Like 3 (OSBPL3) in Human Tumors

Na Hao, Yudong Zhou, Yijun Li, Huimin Zhang, Bin Wang, Xiaona Liu, Yu Ren, Jianjun He, Can Zhou and Xiaojiang Tang**

Department of Breast Surgery, First Affiliated Hospital of Xi'an Jiaotong University, Xi'an, China

Cancer remains one of the top culprits causing disease-related deaths. A lack of effective multi-cancer therapeutic targets has limited the prolongation of cancer patients' survival. Therefore, it is important to explore novel oncogenic genes or versatile targets and perform a comprehensive analysis to assess their roles in the process of tumorigenesis. OSBPL3 protein is an intracellular lipid receptor of the oxysterol-binding protein superfamily, which participates in some pathological and physiological processes in tumor progression. However, its clinical roles and potential mechanisms in cancers remain unknown. Thus, we aimed to systematic explore the potential oncogenic roles of OSBPL3 across thirty-three tumors using multiple web-based and publicly available tools, including the Cancer Genome Atlas, Gene Expression Omnibus, Genotype-Tissue Expression, cBioPortal, and Human Protein Atlas database. OSBPL3 is highly expressed in major subtypes of cancers, distinctly associated with the prognosis of tumor patients. We observed X676_splice/V676G alteration in the oxysterol domain and frequent mutations of OSBPL3 involve cell survival in skin cutaneous melanoma. We also first presented that the expression of OSBPL3 was associated with tumor mutational burden (TMB) in nine cancer types. Additionally, OSBPL3 shows an enhanced phosphorylation level at S426, S251, and S273 loci within the pleckstrin homology domain in multiple tumors, such as breast cancer or lung adenocarcinoma. And OSBPL3 expression was associated with active immune cells ($CD8^+$ T cells) and cancer-associated fibroblasts in breast cancer, colon adenocarcinoma, and kidney renal clear cell carcinoma and immune checkpoint genes in more than 30 tumors, but weakly associated with immune suppressive cells (myeloid-derived suppressor cells, T regulatory cells). Moreover, protein processing and mRNA metabolic signaling pathways were involved in the functional mechanisms of OSBPL3. Our study first demonstrated that a novel agent OSBPL3 plays an important role in tumorigenesis from the perspective of publicly available databases and clinical tumor samples in various cancers, which comprehensively provide insights into its biological functions and may be helpful for further investigation.

Keywords: OSBPL3, cancer, prognosis, phosphorylation, immune infiltration

OPEN ACCESS

Edited by:
Na Luo,
Nankai University, China

Reviewed by:
Lingquan Kong,
Chongqing Medical University, China
Lixue Cao,
Guangdong Provincial People's Hospital, China

****Correspondence:***
Can Zhou
zhoucanz2005@126.com
Xiaojiang Tang
jdyfytxj@xjtufh.edu.cn

Specialty section:
This article was submitted to Molecular Diagnostics and Therapeutics, a section of the journal Frontiers in Molecular Biosciences

Received: *12 July 2021*
Accepted: *10 September 2021*
Published: *19 October 2021*

Citation:
Hao N, Zhou Y, Li Y, Zhang H, Wang B, Liu X, Ren Y, He J, Zhou C and Tang X (2021) Clinical Value and Potential Mechanisms of Oxysterol-Binding Protein Like 3 (OSBPL3) in Human Tumors. Front. Mol. Biosci. 8:739978. doi: 10.3389/fmolb.2021.739978

INTRODUCTION

Given the complexity of carcinogenesis, it is important to explore novel oncogenic genes or targets and perform a pan-cancer analysis to assess their roles in the process of tumorigenesis. In recent years, cancer genomes and databases have yielded valuable insights into the etiology of molecular processes and have fueled the promises of pan-cancer analysis, which provides a fully comprehensive understanding of genes with clinical outcomes and potential molecular mechanisms across different types of tumors (Zhang et al., 2019).

OSBPL3 (oxysterol-binding protein like 3) protein encodes a member of the oxysterol-binding protein family, a group of intracellular lipid receptors (Gregorio-King et al., 2001; Lehto et al., 2001). The "full-length" OSBPL3 gene comprises 23 exons and encodes a predicted protein of 887 amino acids with a C-terminal OSBP domain and an N-terminal pleckstrin homology (PH) domain (Collier et al., 2003). Under physiological conditions, OSBPL3 locates in the endoplasmic reticulum and plasma membrane, regulating cell adhesion, the actin cytoskeleton, vesicle transport, and cellular lipid metabolism (Lehto and Olkkonen, 2003; Lehto et al., 2005; Yan et al., 2007; Lehto et al., 2008; D'Souza et al., 2020; Gulyas et al., 2020). So far, there are few studies on OSBPL3 in tumors. Recent transcriptome analyses from the perspective of pathology and clinical pathways have suggested that OSBPL3 is expressed and involved in the development of cancers, including colorectal cancer (Xu et al., 2020; Chen et al., 2021), pancreatic ductal adenocarcinoma (Li et al., 2017), recurrent glioblastoma (Erdem-Eraslan et al., 2016), and metastatic breast cancers (Lefebvre et al., 2016). Furthermore, OSBPL3 is generally considered to be an oncogene factor in colorectal cancer progression, acting through upregulation by HIF1A and activation of the RAS signaling pathway (Jiao et al., 2020). However, there has been little clear evidence about the expression and role of OSBPL3 in tumors, and still, there is no pan-cancer study on the relationship between OSBPL3 and various cancers.

Here, we aim to conduct a comprehensive analysis of OSBPL3 based on the TCGA project and summarize a group of roles of OSBPL3 in pathogenesis, clinical outcomes, and molecular mechanisms with various cancers, including gene expression, survival prognosis, genetic alteration, protein phosphorylation, immune infiltration, and relevant cellular pathways, which provide a better understanding of OSBPL3 in tumorigenesis and will be valuable for further in-depth research.

MATERIALS AND METHODS

Cell Culture and Human Sample Collection

MDA-MB-231 cells were cultured in L15 medium. T-47D, MCF-10A, HeLa, BT549, A549, H446, H460, SW480, HCT116, HepG2, ZR-75-1, SK-BR-3, MDA-MB-488, and MCF-7 cells were cultured in DMEM. All culture media were supplemented with 10% FBS (Hyclone). All cells except MDA-MB-231 were grown at 37°C in 5% CO_2 incubators, and MDA-MB-231 cells were grown at 37°C in 0% CO_2 incubators. All cells were passaged for less than 3 months before renewal from frozen, early-passage stocks. All cells were purchased from the ATCC, and all were tested to ensure that they were mycoplasma negative.

qRT-PCR

Total RNAs were purified with the RNeasy Mini Kit (Qiagen), and cDNA was synthesized with the SuperScript III First-Strand Synthesis SuperMix for qRT-PCR (Thermo Fisher Scientific). The expression levels of OSBPL3 and GAPDH mRNA were quantified with the LightCycler 480 Real-Time PCR System with Universal ProbeLibrary Probe #36 (Roche). The primers were as follows: OSBPL3, 5′-TTGGTGTGTCCCAAAAATTGGT-3′ (forward) and 5′-TCCTGGGTGTAATTCATCTCCC-3′ (reverse), and GAPDH, 5′-TCATCCCTGCCTCTACTG-3′ (forward) and 5′-TGCTTCACCACCTTCTTG-3′ (reverse).

Western Blotting

Western blotting (WB) was performed as described previously (Hao et al., 2020) with the following modifications. The primary antibodies were OSBPL3 (sc-514097, Santa Cruz, United States) at a 1:500 dilution and β-actin (sc-47778, Santa Cruz Biotechnology) at a 1:1,200 dilution. Images were acquired using the Bio-Rad ChemiDoc MP Imaging System (Bio-Rad). All western blots were a representative image of three separate experiments.

Immunohistochemistry and Immunofluorescence

IHC and IF staining was performed as described previously (Hao et al., 2020) with the following modifications. Antigen retrieval for sections of tissue microarrays (TMA PR803b, US Biomax, Inc.) was performed in a pressure cooker. The antibodies was both anti-OSBPL3 (sc-514097, Santa Cruz, United States).

Expression of OSBPL3 in Various Cancers

We searched OSBPL3 on the TIMER2 web (tumor immune estimation resource, version 2) (http://timer.cistrome.org/) with the "Gene_DE" module and obtained the expression pattern of OSBPL3 between tumor and corresponding normal tissues from the TCGA project. For tumors' lack of normal tissues [e.g., GBM (glioblastoma multiforme), LAML (acute myeloid leukemia)], we searched the GEPIA2 web server (Gene Expression Profiling Interactive Analysis, version 2) (http://gepia2.cancerpku.cn/#analysis) with the "Expression analysis-Box Plots" module from the GTEx (Genotype-Tissue Expression) database and added the expression of OSBPL3 with box plots. The related parameters are as follows: p-value cutoff = 0.01, $\log_2$FC (fold change) cutoff = 1, and "matched TCGA normal and GTEx data." We also obtained the expression difference of OSBPL3 in pathological stages (stages I–IV) of different tumors with violin plots via the "Pathological Stage Plot" module of GEPIA2. Then, $\log_2$ [TPM (transcripts per million) + 1] transformation was applied.

We searched the Oncomine database (https://www.oncomine.org/resource/main.html) and obtained the expression difference data of the OSBPL3 gene between tumor and normal tissues by setting the threshold of p-value = 0.001, gene rank = 10%, and fold change = 2.

Survival Prognosis Value of OSBPL3

We obtained the overall and disease-free survival data of OSBPL3 across all types of tumors via the "Survival Map" module of GEPIA2. High (50%) and low (50%) cutoff values were split into high and low expression cohorts. The log-rank test was used in the hypothesis test, and the survival plots were also plotted. We also used the interactive operation interface of the Kaplan–Meier plotter (http://kmplot.com/analysis/) to pool the GEO datasets for a series of meta-analyses of progression-free interval (PFI) and disease-free interval (DFI) survival. The hazard ratios (HRs), 95% confidence intervals (95% CIs), and log-rank *p*-values were computed, and the Kaplan–Meier survival plots were generated. The meta-analysis was statistically mapped by STATA 12.0 software (StataCorp LP, College Station, TX, United States).

Genetic Alteration and Mutation Landscapes of OSBPL3

We queried the genetic alteration characteristics of OSBPL3 and obtained the alteration frequency, mutation site, and type and CNA (copy number alteration) across all TCGA tumors on the cBioPortal web (https://www.cbioportal.org/) with the "TCGA Pan Cancer Atlas Studies" module. The mutation sites of OSBPL3 were plotted with a schematic diagram of the protein and the 3D (three-dimensional) structure with the "Mutations" module. We also generated the data on the overall, disease-free, progression-free, and disease-free survival curves for the different cancer types with or without OSBPL3 genetic alteration by Kaplan–Meier plots via the log-rank *p*-value.

We investigated the correlation between OSBPL3 expression and tumor mutational burden (TMB)/microsatellite instability (MSI) in different tumors from the TCGA project on the web of "http://sangerbox.com/Tool." Spearman's rank correlation test was performed, and the *p*-value and partial correlation (cor) value are shown.

Protein Phosphorylation Analysis

We searched the expression level of the total protein and phosphoprotein of OSBPL3 (NP_055205.2) using the CPTAC dataset. The available datasets of six tumors are shown—BRCA (breast cancer), OV (ovarian cancer), colon cancer, RCC (clear cell), UCEC (uterine corpus endometrial carcinoma), and lung adenocarcinoma.

Immune Infiltration Analysis

We explored the association between OSBPL3 expression and immune infiltrates on the TIMER2 database with the "Immune-Gene" module and analyzed the immune score and stromal score using R software "Estimations" with Spearman's analysis. The immune cells of neutrophils, macrophages, dendritic cells, $CD8^+$ T cells, $CD4^+$ T cells, B cells, myeloid-derived suppressor cells (MDSCs), T regulatory cells (Tregs), and cancer-associated fibroblasts (CAFs) were selected. The algorithms of immune infiltration estimations include TIMER, CIBERSORT, CIBERSORT-ABS, QUANTISEQ, XCELL, MCPCOUNTER, and EPIC. The results were visualized with a heatmap and a scatter plot.

Identification of Differentially Expressed Genes and OSBPL3 Co-Expressed Genes

We obtained the top 50 available experimentally determined OSBPL3-binding proteins via searching the STRING website (https://string-db.org/). The main parameters are organism ("*Homo sapiens*"), minimum required interaction score ["low confidence (0.150)"], meaning of network edges ("evidence"), max. number of interactors to show ("no more than 50 interactors" in the first shell), and active interaction sources ("experiments"). We also obtained the top 100 OSBPL3-correlated targeting genes from GEPIA2 with the "Similar Gene Detection" module and performed a pairwise Pearson correlation analysis of OSBPL3 and selected genes applying the "correlation analysis" module of GEPIA2. The value of TPM was converted with Log_2 for the dot plot, and the *p*-value and the correlation coefficient (R) were labeled. The heatmap of the selected genes used the "Gene_Corr" module of TIMER2, and we conducted an intersection Venn analysis to access the OSBPL3-binding genes using FUNRICH software.

OSBPL3-Related Gene Enrichment and Molecular Mechanism Analysis

Moreover, we performed KEGG (Kyoto Encyclopedia of Genes and Genomes) and GO (Gene Ontology) enrichment analyses. Briefly, we uploaded the gene lists (above-mentioned) to DAVID (the Database for Annotation, Visualization, and Integrated Discovery) with the settings of selected identifier ("OFFICIAL_GENE_SYMBOL") and species ("*Homo sapiens*") and obtained the functional annotation chart. The enriched pathways were finally visualized with the "tidyr," "ggplot2," and "clusterProfiler" R packages. The analysis of GO enrichment including biological process (BP), cellular component (CC), and molecular function (MF) was visualized as cnetplots, using the cnetplot function (circular = F, colorEdge = T, node_label = T).

Statistical Analysis

All the data of gene expression were normalized by log_2 transformation. The comparison of tumor and normal tissues used two sets of *t*-tests; $p < 0.05$ indicates statistical significance. The Kaplan–Meier curve and log-rank test were used for all survival analyses. The correlation analysis between the two variables used Spearman's or Pearson's test. All statistical analyses were processed by R software (version 4.0.2).

RESULTS

Expression Pattern of OSBPL3 in Various Cancers

In this study, we aimed to explore the roles of the human OSBPL3 gene in different cancers. We first explored the gene and protein

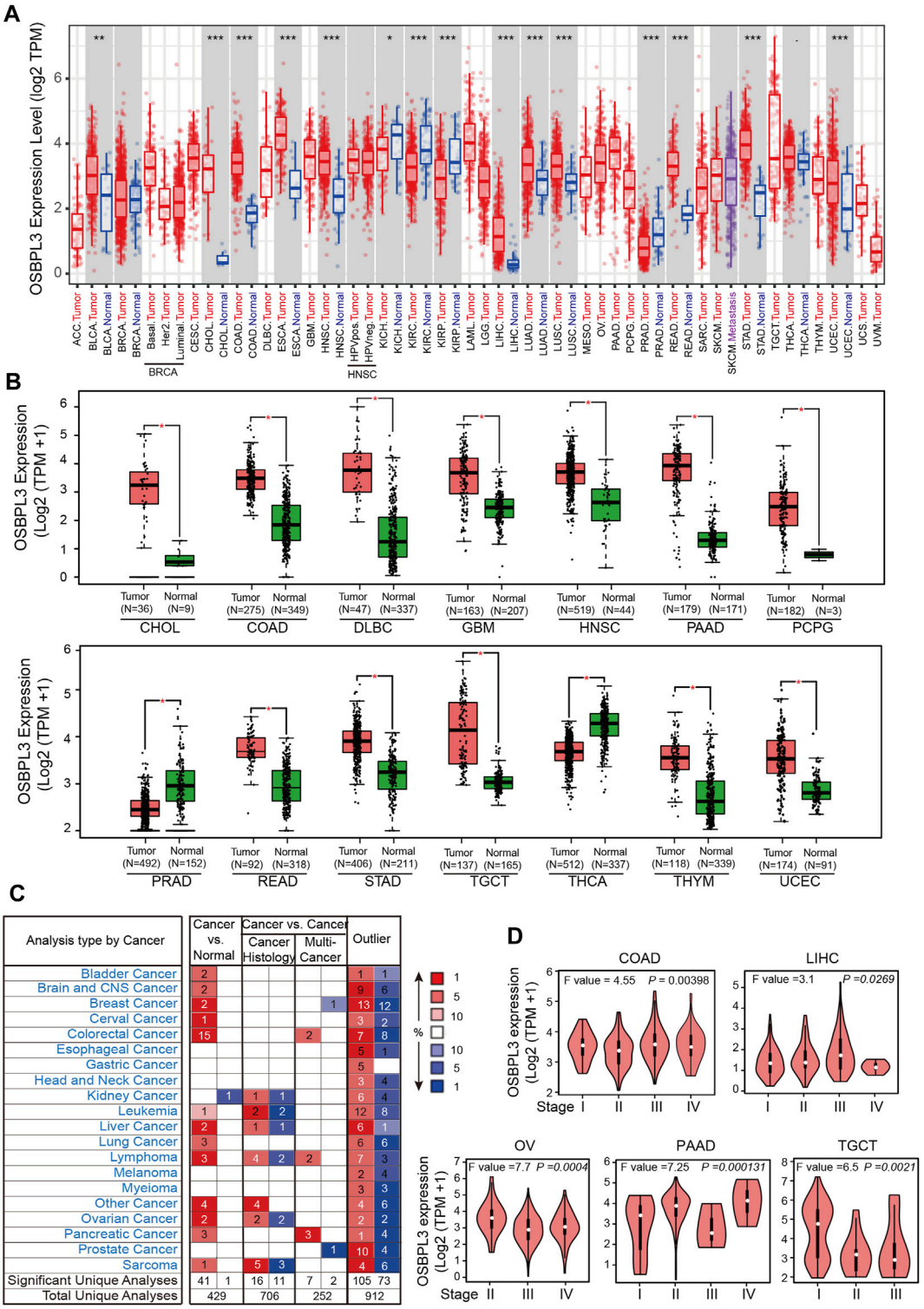

FIGURE 1 | Expression level of the OSBPL3 gene in different tumors and pathological stages. **(A)** Expression status of the OSBPL3 gene across diverse cancers from the TCGA dataset in TIMER. **(B)** Expression of OSBPL3 in the cancers from the TCGA project and the corresponding normal tissues from the GTEx database of CHOL, COAD, DLBC, GBM, HNSC, PAAD, PCPG, PRAD, READ, STAD, TGCT, THCA, THYM, and UCEC. The box plot data were supplied. **(C)** Transcription levels of OSBPL3 in different types of human cancers from Oncomine. The cell number represents the dataset number that meets all of the thresholds (blue: downregulated; red: upregulated). The best gene rank percentile was applied for the analyses within the cell. **(D)** The expression levels of the OSBPL3 gene were analyzed by pathological stages (stages I–IV) of COAD, LIHC, OV, PAAD, and TGCT in the TCGA project. Log_2 (TPM+1) transformation was applied. $^*p < 0.05$; $^{**}p < 0.01$; $^{***}p < 0.001$.

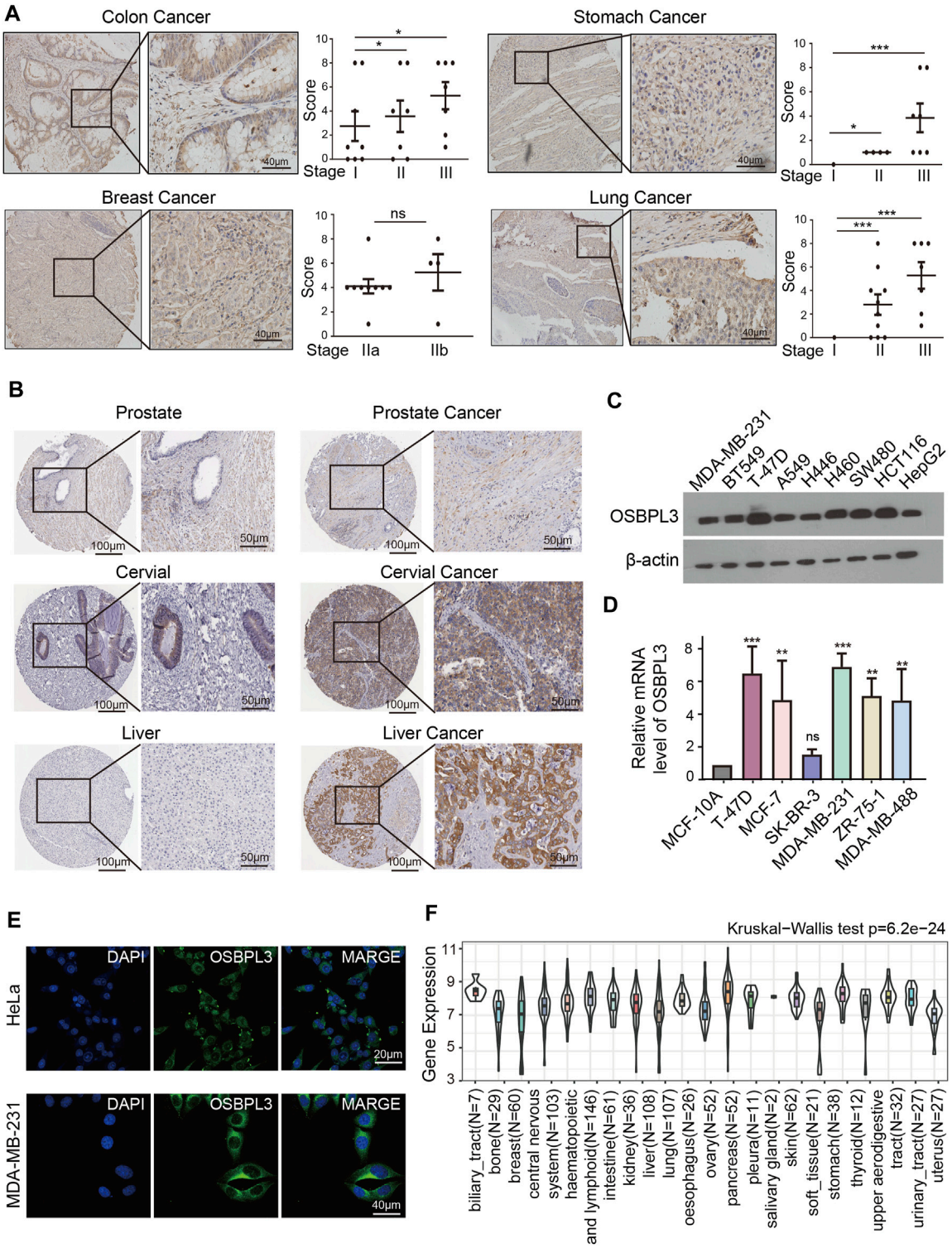

FIGURE 2 | Expression and location of OSBPL3 in a variety of cancer tissues and cells. **(A)** OSBPL3 expression of multi-tissue arrays of colon cancer, stomach cancer, breast cancer, and lung cancer by IHC staining and statistical analysis of the relationship of OSBPL3 expression with tissue status. **(B)** OSBPL3 expression in different tumor tissues of prostate cancer, cervical cancer, liver cancer, and lung cancer by IHC staining from the HPA (Human Protein Atlas) database. **(C)** IF assays for subcellular localization of OSBPL3 in cervical cancer HeLa (up) and breast cancer MDA-MB-231 (down) cell lines (blue: nucleus; green: OSBPL3). **(D)** The protein expression levels of OSBPL3 in nine cancer cell lines (MDA-MB-231, BT549, T47D, A549, H446, H460, SW480, HCT116, and HepG2) were detected by WB. **(E)** The mRNA expression levels of OSBPL3 in six breast cancer cell lines (T-47D, MCF-7, SK-BR-3, MDA-MB-231, MDA-MB-468, and ZR-75-1) and one normal breast ductal epithelial cell line (MCF-10A) were detected by qRT-PCR (down). **(F)** Gene expression in various tumor cells from the CCLE database. $^{*}p < 0.05$; $^{**}p < 0.01$; $^{***}p < 0.001$.

information of OSBPL3. As shown in **Supplementary Figure S1A**, the OSBPL3 gene is located on chr7: 24,827,146-24,949,571 and contains four isoforms, and the OSBPL3 protein structure is relatively conserved among different species (e.g., *H. sapiens*, *P. troglodytes*, *M. mulatta*) and generally consists of the oxysterol-binding protein (Oxysterol_BP) (pfam01237) domain and pleckstrin homology (PH) domain (cl17171) (**Supplementary Figure S1B**). The phylogenetic tree shows the evolutionary relationship of the OSBPL3 protein between different species (**Supplementary Figure S1C**).

To explore the expression pattern of OSBPL3 under physiological conditions, we detected OSBPL3 expression in all types of normal tissues based on the HPA (Human Protein Atlas), GTEx, and FANTOM5 (Functional ANnoTation Of the Mammalian genome 5) datasets (**Supplementary Figure S2A**). OSBPL3 was expressed in all detected tissues (all consensus normalized expression values > 1) and highly expressed in the parathyroid gland followed by the appendix (**Supplementary Figure S2B)** but presented low RNA tissue specificity as well as low RNA cell type specificity in different normal cells (**Supplementary Figure S2C**).

Next, we evaluated the expression status of OSBPL3 across various cancers from the TCGA project. As shown in **Figure 1A**, the expression level of OSBPL3 is significantly higher than the corresponding normal tissues in multiple tumor tissues except breast cancer. We also compared the expression of OSBPL3 between the tumor tissues from TCGA and the normal tissues from the GTEx dataset. **Figure 1B** and **Supplementary Figure S3A** indicate that the expression of OSBPL3 is significantly upregulated in all types of cancers except only kidney renal clear cell carcinoma (KICH). The results of the CPTAC dataset also showed similar results in cancer types of renal, colon, and lung cancers and uterine corpus endometrial carcinoma (**Supplementary Figure S3B**, $p < 0.001$).

Furthermore, we identified the mRNA expression of OSBPL3 across different types of human cancers and the corresponding normal tissues from the Oncomine database. **Figure 1C** shows that OSBPL3 expression was higher in multiple cancer groups, including bladder, brain, breast, cervical, colorectal, liver, lung, ovarian, and pancreatic cancers as well as leukemia and lymphoma. The pooling analysis results of over 40 reports confirmed that OSBPL3 is highly upregulated in different kinds of cancers than in normal tissues—pancreatic cancer, lung cancer, colorectal cancer, liver cancer, and cervical cancer (all $p < 0.05$) (**Supplementary Figures S4A–E**).

To fully appreciate the expression and correlation of OSBPL3 with different cancers, we experimented the expression levels of OSBPL3 in multiple types of cancer tissues (breast, lung, stomach, and colon) using microarrays consisting of 63 biopsies (**Figure 2A**) and three cancer tissues (prostate, cervical, and liver) from the HPA dataset (**Figure 2B**) by IHC staining. The results showed that OSBPL3 was expressed at abnormally high levels in these tumor biopsies. The clinical pathological grade of a tumor cancer closely correlates with malignancy and differentiation, and we found a positive correlation between elevated expression levels of OSBPL3 and high-grade tumors in both the cancer biopsies (breast, lung, stomach, and colon cancers) (**Figure 2A**) and the tumor statistics data from the GEPIA2 database (COAD, LIHC, OV, PAAD, and TGCT) (**Figure 1D**). We also checked the protein (**Figure 2C**) and mRNA expression levels of OSBPL3 (**Figure 2D**) in four cancer cells (breast, lung, colon, and liver) and the protein expression in all types of human cancer cells from the CCLE dataset (**Figure 2F**), and the results showed that OSBPL3 had high expression levels in cancer cell lines. Additionally, the IF assays localized endogenous OSBPL3 to the cytoplasm (**Figure 2E**).

Based on the above-mentioned findings, OSBPL3 is generally upregulated in multiple human cancer tissues, in particular in digestive system carcinoma (e.g., gastrointestinal cancer, colorectal cancer, liver cancer, and pancreatic cancer) and female cancers (e.g., breast cancer, cervical cancer, and ovarian cancer), which may act as an oncogene in most cancer types.

Survival and Prognostic Value of OSBPL3

To determine whether the expression of OSBPL3 is associated with the outcome of patients with different tumors, we performed survival analysis using progression or deaths cases as endpoints. As shown in **Figure 3A**, high expression level of OSBPL3 correlates with poor prognosis of OS (overall survival) for LGG (low-grade glioma), MESO, THYM, and UVM (uveal melanoma) cancers and DFS (disease-free survival) for GBM, LGG, LUAD, and UVM cancers (all $p < 0.05$) (**Figure 4A**). To further evaluate the relationship between OSBPL3 and tumor progression (relapse/metastasis), we confirmed the PFI (**Figure 5A**) and DFI (**Supplementary Figure S5A**), and the data showed highly expressed OSBPL3 was linked to poor PFI and DFI for both LGG and PAAD cancers and poor PFI for LIHC, MESO, PCPG, PRAD, TGCT, and UVM cancers (all $p < 0.05$).

We also performed meta-analysis of the correlation between OSBPL3 expression and prognosis with different cancers using the Kaplan–Meier plotter (**Figures 3B**, **4B**, **5B**, **Supplementary Figure S5B**). The results presented a significant correlation between highly expressed OSBPL3 and poor OS, DFS, PFI, and DFI prognosis for LGG; poor OS, DFS, and PFI for UVM; and poor PFI and DFI for PAAD. In contrast, a low OSBPL3 expression level was associated with poor OS ($P = 0.004$) and DFS ($P = 0.028$) prognosis for TGCT (**Figures 3A**, **4A**).

The above data indicated that OSBPL3 expression is significantly associated with the poor prognosis of patients with LGG, UVM, PAAD, and MESO cancers but differentially associated with other tumors and may act as a detrimental prognostic factor in these tumors, which is worth further exploration.

Genetic Alteration and Mutation Landscapes of OSBPL3

Next, we investigated the genetic alteration status of OSBPL3 in various tumors of the TCGA cohorts. As shown in **Figure 6A**, the highest mutation frequency of OSBPL3 (>6%) appears for patients with uterine corpus endometrial carcinoma and the amplification (an alteration frequency of ~5%) appears for the

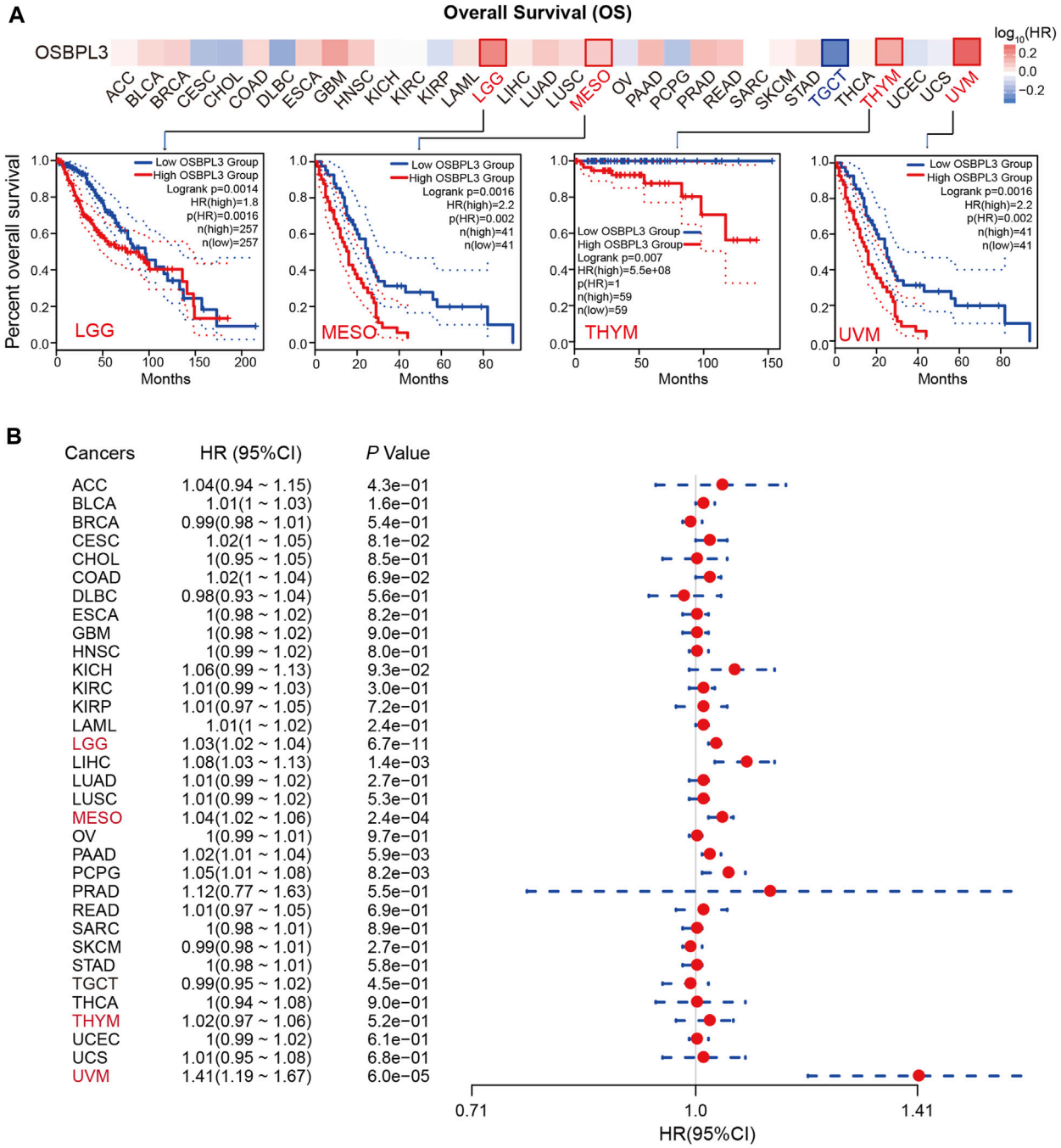

FIGURE 3 | Correlation between OSBPL3 expression and overall survival prognosis of different cancers. **(A)** Overall survival (OS) analyses of OSBPL3 gene expression across different tumors in TCGA via the GEPIA2 dataset. Up: survival map; down: Kaplan–Meier plotter curves. **(B)** A meta-analysis (forest plot) for pooling of a series of univariate overall survival of OSBPL3 expression in different tumors. Hazard ratios (HRs), 95% confidence intervals (95% CIs), and *p*-values are shown.

esophageal adenocarcinoma. **Figure 6B** shows the mutation types, sites, and case numbers of OSBPL3 and the main type of genetic alteration was the missense mutation. And the X676_splice/V676G alteration in the oxysterol domain induces a frame shift mutation of OSBPL3 with the translation from P (Proline) to L (Leucine) at the 673 site of OSBPL3 protein, and **Figure 6C** shows subsequent OSBPL3 protein truncation with the 3D structure. We also explored the potential association between the genetic alteration of OSBPL3 and the clinical survival outcome with different types of cancers. **Figure 6D** indicates that patients with altered OSBPL3 showed poorer prognosis compared with non-alteration in overall survival (P = 1.245e-3) and disease-specific survival (P= 5.047e-3), but not progression-free survival (P = 0.0613) in SKCM (skin cutaneous melanoma).

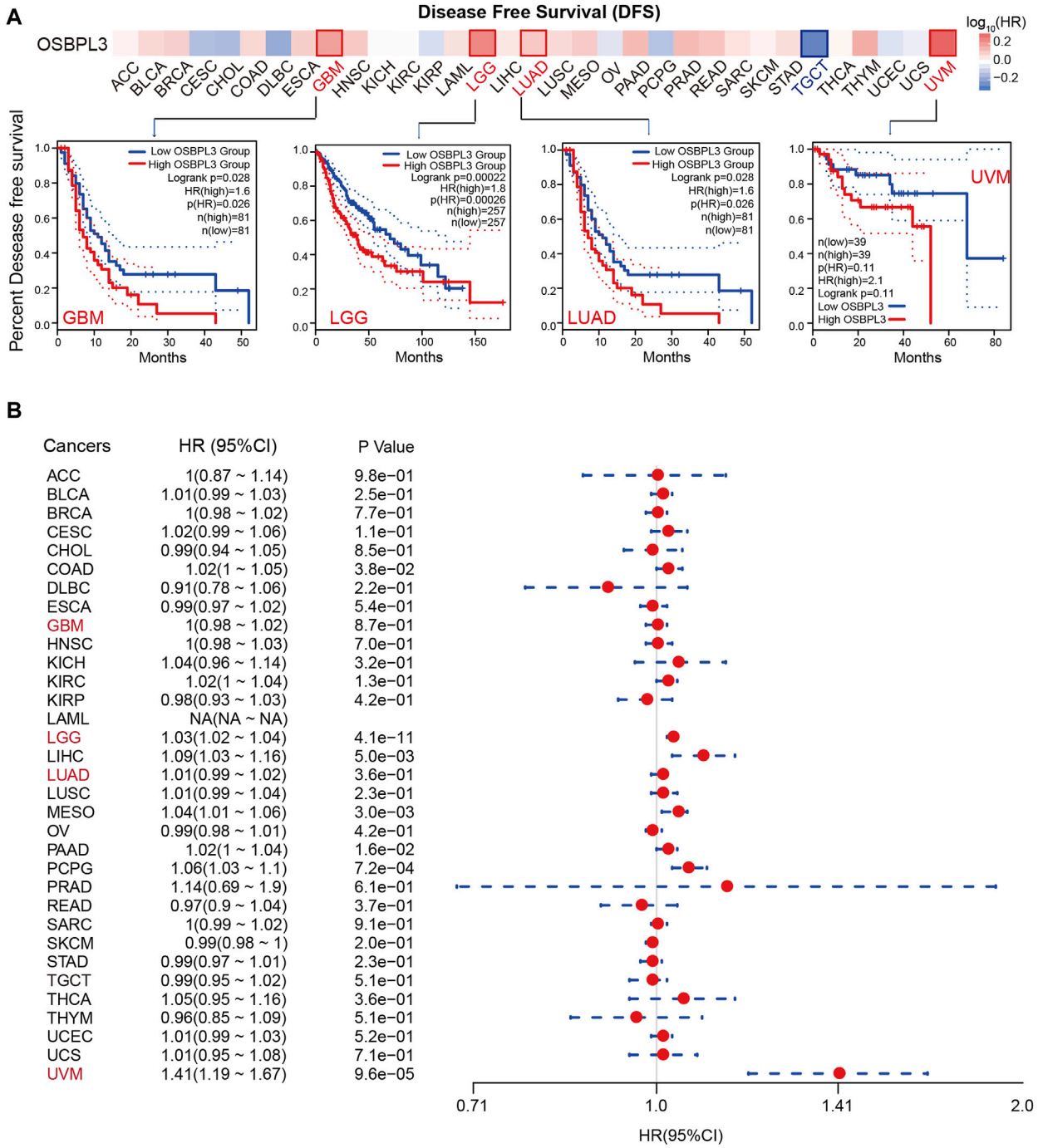

FIGURE 4 | Correlation between OSBPL3 expression and disease-free survival (DFS) prognosis of different cancers. **(A)** Disease-free survival analyses of OSBPL3 gene expression across different tumors in TCGA via the GEPIA2 dataset. Up: survival map; down: Kaplan–Meier plotter curves. **(B)** A meta-analysis (forest plot) for pooling of a series of univariate disease-free survival of OSBPL3 expression in different tumors. Hazard ratios (HRs), 95% confidence intervals (95% CIs), and *p*-values are shown.

We also analyzed the correlation between OSBPL3 expression and tumor mutational burden (TMB)/microsatellite instability (MSI) across diverse tumors from TCGA. **Figures 6E,F** show a positive correlation between high OSBPL3 expression and TMB for DLBC, ESCA, LIHC, LUAD, PRAD, SARC, STAD, THYM, and UVM (all $P = 0.05$) but a positive correlation with MSI only for LUSC ($P = 0.019$), SKCM ($P = 0.042$), and HNSC ($P = 0.0028$). The meta-analysis showed the details (**Supplementary Figures S6A,B**). This result suggested that most of the cancers with high expression of OSBPL3 have more tumor mutation burden and

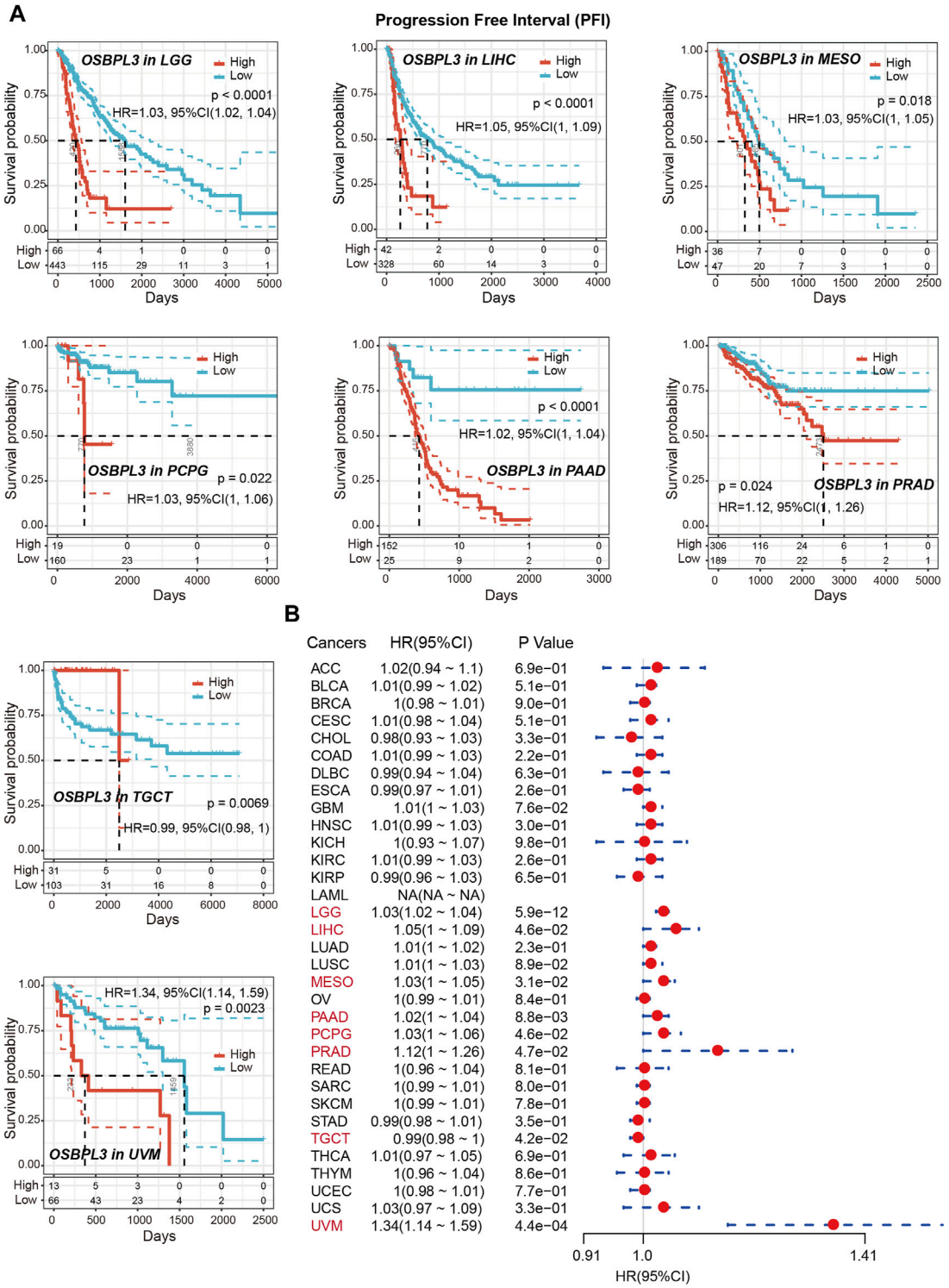

FIGURE 5 | Correlation between OSBPL3 expression and progression-free survival (PFS) prognosis of cancers in TCGA. **(A)** Progression-free survival analyses of OSBPL3 gene expression by Kaplan–Meier curves in LGG, LIHC, MESO, PCPG, PAAD, PRAD, TGCT, and UVM cancers. **(B)** A meta-analysis (forest plot) for pooling of a series of univariate progression-free survival analyses of OSBPL3 expression in different tumors. Hazard ratios (HRs), 95% confidence intervals (95% CIs), and *p*-values are shown.

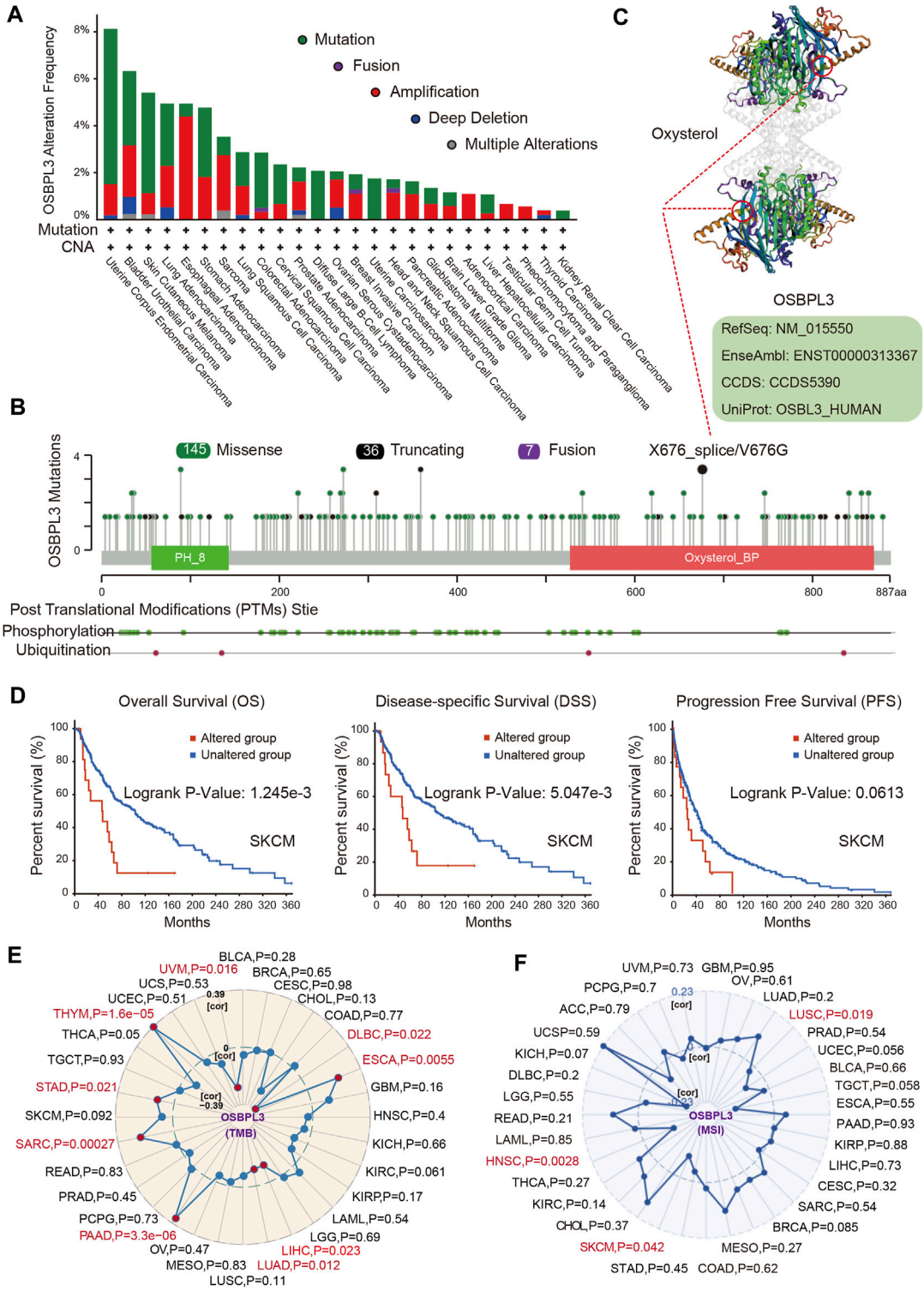

FIGURE 6 | Alteration feature of OSBPL3 and correlation between OSBPL3 expression and tumor mutational burden (TMB)/microsatellite instability (MSI) in different tumors of TCGA on the cBioPortal database. **(A)** Alteration frequency with the mutation type of OSBPL3. **(B)** Alteration with the mutation site of OSBPL3. **(C)** 3D structure of the mutation site of OSBPL3 with the highest alteration frequency (X676_splice/V676G). **(D)** Correlation between the mutation status of OSBPL3 and overall, disease-specific, and progression-free survival of SCM cancer. **(E–F)** Correlation between OSBPL3 expression and TMB **(E)**/MSI **(F)** with different tumors of TCGA. The *p*-value is supplied.

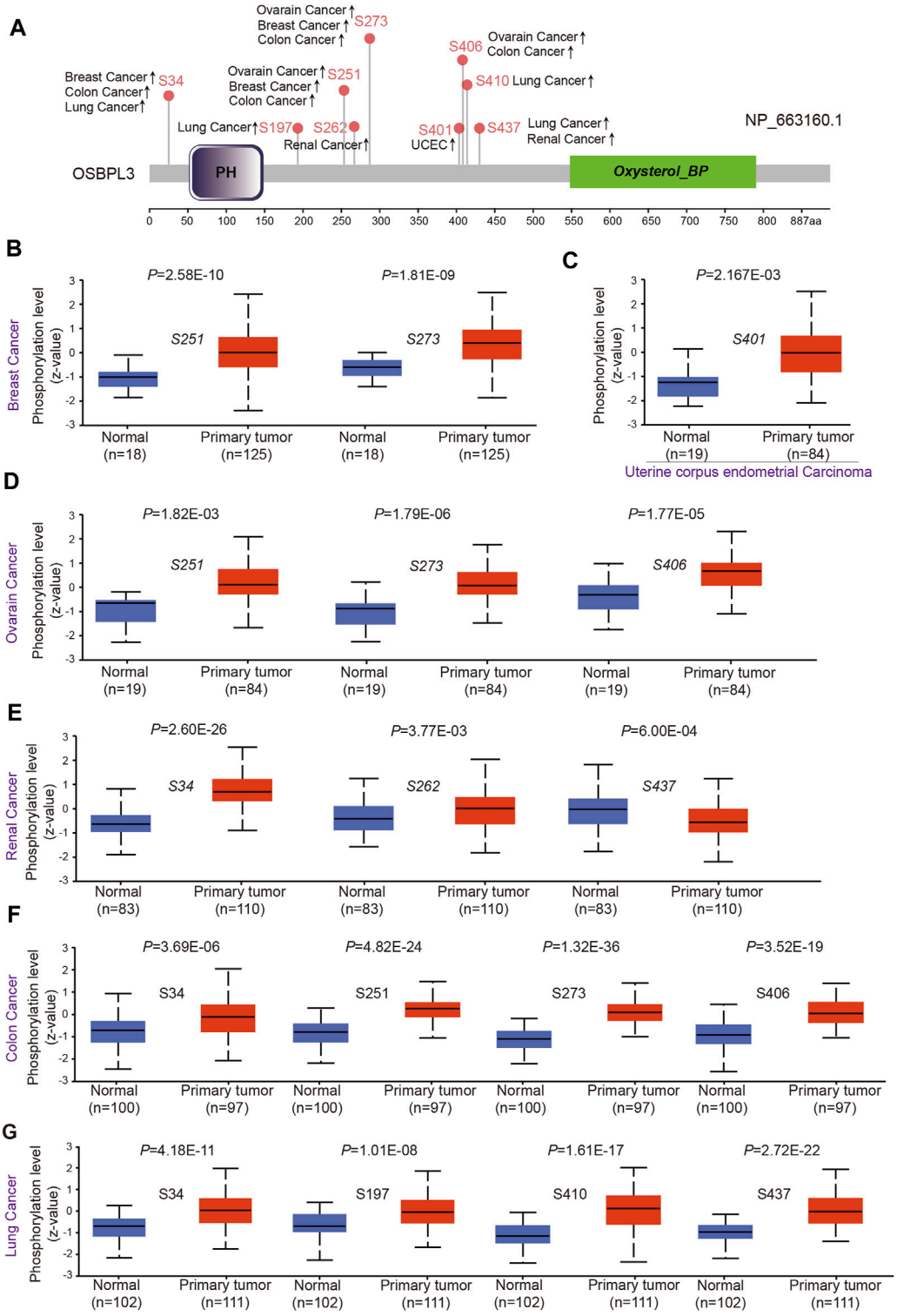

FIGURE 7 | Phosphorylation analysis of OSBPL3 protein in different tumors. **(A)** Expression level of OSBPL3 phosphoprotein sites (NP_663, 160.1, S34, S197, S251, S262, S273, S401, S406, and S437 sites) between primary tumors and corresponding normal tissues via the UALCAN and CPTAC datasets, which are displayed in the schematic diagram with positive results. **(B–G)** Box plots of phosphorylation analysis of OSBPL3 for different cancers, including breast cancer **(B)**, uterine corpus endometrial carcinoma **(C)**, ovarian cancer **(D)**, renal cancer **(E)**, colon cancer **(F)**, and lung cancer **(G)**.

TABLE 1 | Analysis of CPTAC-identified phosphorylation sites of OSBPL3 via the PhosphoNET database.

Site	Sequence	Experimentally confirmed[a]	Hydrophobicity	Phosphorylation site similarity score	Maximum kinase specificity	Sum kinase specificity score	Conservation score
S34	KQGSRQDSWEVVEGL	19,369,195	−1.240	−57.5	534	22,348	7.3
S197	QNLFQTGSNVSFSCG	NA	−0.280	−62.4	385	14,942	9.1
S251	DVLHRTYSAPAINAI	19,369,195	−0.167	−61.0	510	21,466	18.8
S262	INAIQGGSFESPKKE	NA	−0.920	−58.0	310	13,168	4.6
S273	SPKKEKRSHRRWRSR	NA	−3.213	−58.6	420	16,727	9.7
S410	AESLLLDSPAVAKSG	NA	0.220	−51.8	501	20,366	13.6
S437	RALVHQLSNESRLSI	19,369,195	−0.373	−56.6	381	15,792	17.6

[a]*The PMID (PubMed Unique Identifier) information of the publication was provided.*
NA, not available.

less microsatellite instability, which need more sample tests for confirmation and in-depth research.

Protein Phosphorylation Analysis of OSBPL3

To evaluate whether phosphorylation of OSBPL3 has an effect on tumors, we compared the differences in OSBPL3 phosphorylation levels between primary tumor and normal tissues. **Figure 7A** summarizes the OSBPL3 phosphorylation sites, and **Figures 7B–G** analyze the phosphorylation status of OSBPL3 at different sites in different tumors—breast cancer, uterine corpus endometrial carcinoma, ovarian cancer, renal cancer, colon cancer, and lung cancer. The results showed S34, S251, and S273 loci within the PH domain of OSBPL3 represent a higher phosphorylation level in all primary tumor tissues compared with corresponding normal tissues, followed by S406 and S437. We also confirmed the CPTAC-identified phosphorylation of OSBPL3 used the PhosphoNET database and found that OSBPL3 phosphorylation in the cell cycle was experimentally supported by one publication and our previous data (**Table 1**).

This observation merits further molecular and cellular experiments to explore the potential role of phosphorylation of OSBPL3 in tumorigenesis.

Immune Infiltration Analysis

The tumor microenvironment (TME) plays an important role in prognosis and treatment response (Jiang et al., 2020). To evaluate the effect of OSBPL3 expression level on tumor-infiltrating immune and stromal cells—the two main components of the TME closely associated with the initiation, progression, or metastasis of cancer—we performed the ESTIMATE algorithm to calculate the immune scores and stromal scores from different types of tumors (**Supplementary Figures S7–9**). As shown in **Figure 8**, OSBPL3 was significantly associated with infiltrating immune and stromal cells in the top three tumors (BRCA, LGG, PRAD) (all $p < 0.001$).

Based on the characteristics of the immune cell infiltrates in the TME, the tumors were preliminarily divided into "hot" and "cold" tumors (Galon and Bruni, 2019). The "hot" tumors are infiltrated with more immune active cells (neutrophils, macrophages, $CD8^+$ T cells, dendritic cells, $CD4^+$ T cells, Th1), which can produce a better response to immunotherapy drugs; in contrast, the "cold" tumors with less immune cell infiltration and more proportion of immune suppressive cells (myeloid-derived suppressor cells (MDSCs), T regulatory cells (Tregs)) have a weak response to immunotherapy (Lui et al., 2020; Yang et al., 2020; Biffi and Tuveson, 2021). Thus, we explored the relationship between the OSBPL3 expression level and the active immune cells in different cancer types of TCGA. **Figure 9A** shows a statistical positive correlation between OSBPL3 expression and the immune active cells of neutrophils, dendritic cells, and $CD8^+$ T cells in the tumors of PRAD and LIHC. The top three tumors with the strongest correlation between OSBPL3 expression and all the immune infiltration cells are BRAC, COAD, and KIRC (**Figure 9B**) (all $p < 0.001$). Unfortunately, OSBPL3 appears to be weakly correlated with immune suppressive cells of MDSCs and Tregs in multiple tumors, which suggests that patients with high expression of OSBPL3 are more likely to have the "hot" tumors in the TME and might have a better immunotherapeutic response.

Additionally, cancer-associated fibroblasts (CAFs) play a role in regulating the interaction between immune effector cells and cancer cells and are associated with tumor progression and poor prognosis (Desbois and Wang, 2021). Thus, we explored the relationship of OSBPL3 with CAFs, and the results showed a positive correlation between the infiltration level of CAFs and OSBPL3 expression in the tumors of BRCA-luminal A, BRCA-luminal B, LGG, LIHC, MESO, PRAD, TGCT, and THYM (**Figures 10A,B**) while a negative correlation in TGCT.

Immune checkpoint inhibitors (ICIs) have affected the therapeutic landscape for a variety of tumors, but biomarkers associated with ICIS efficacy are still lacking (Bagchi et al., 2021). To analyze the relationship between OSBPL3 and immune checkpoint genes, we extracted and calculated more than 40 common immune checkpoint genes in diverse cancer types of TCGA (**Figure 11**). The results showed over 30 immune checkpoint genes were strongly associated with OSBPL3 expression in UVM, PRAD, and ACC tumors, and then in LIHC, LGG, and BRAC, which are the ones that are positively associated with OSBPL3 prognosis.

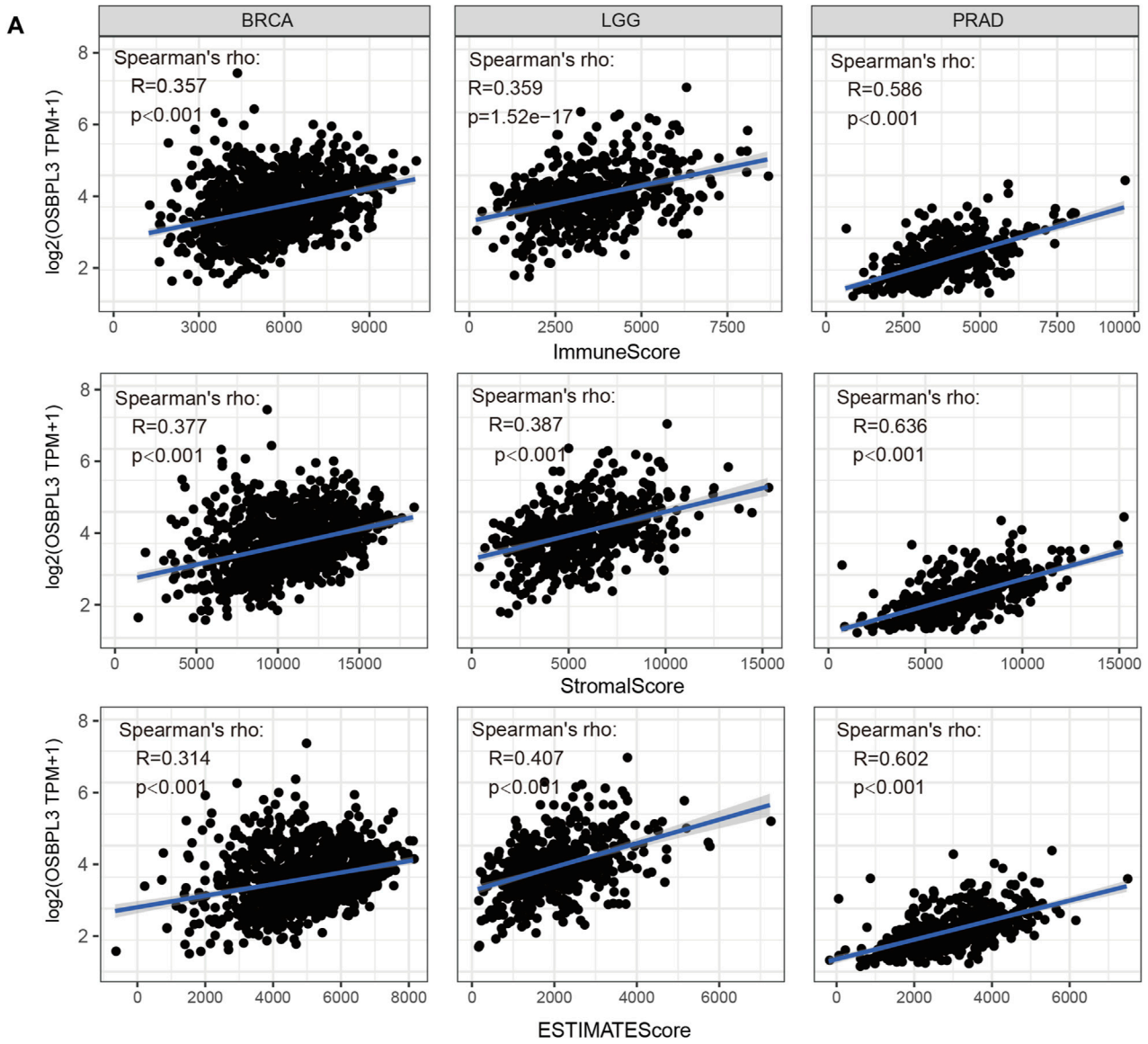

FIGURE 8 | Correlation analysis between OSBPL3 expression and immune infiltration score in different tumors. We estimated the immune cells, stromal cells, and tumor purity in the tumor microenvironment based on the ESTIMATE algorithm for "Est_ImmuneScore," "ESTIMATEScore," and "StromalScore," and we analyzed the relationship between them and the expression level of OSBPL3, respectively, in the top three tumors—breast cancer (BRCA), lung cancer (LGG), and prostate adenocarcinoma (PRAD)—which are most relevant.

These results indicated that tumors with high expression of OSBPL3 are infiltrated with more immune active cells and seem to represent "hot" tumors and more immune checkpoint genes, which may play a potential role in response to the immune microenvironment and may benefit from immune therapeutic interventions.

Enrichment and Molecular Mechanism Analysis of OSBPL3-Related Partners

To further investigate the molecular mechanism and function of the OSBPL3 gene in tumorigenesis, we screened out the OSBPL3-binding proteins and correlated genes by a series of pathway enrichment analyses. **Figure 12A** shows the interaction network of top 20 OSBPL3-binding proteins, and **Figure 12B** shows the top six of the top 100 positively correlated genes with the OSBPL3 expression level—ANKLE2 (R = 0.44), BIRC6, LRIG2, TMEM170A, ZNF490, and C1GLAT1 genes (all $p < 0.001$). Similar results were found in the majority of cancers by a corresponding heatmap (**Figure 12C**). An intersection analysis of the above two groups reached one common member, namely, CRN1 (**Figure 12D**).

Next, we performed KEGG and GO enrichment analyses. The KEGG enrichment analysis of **Figures 12E**, **13A** suggests that

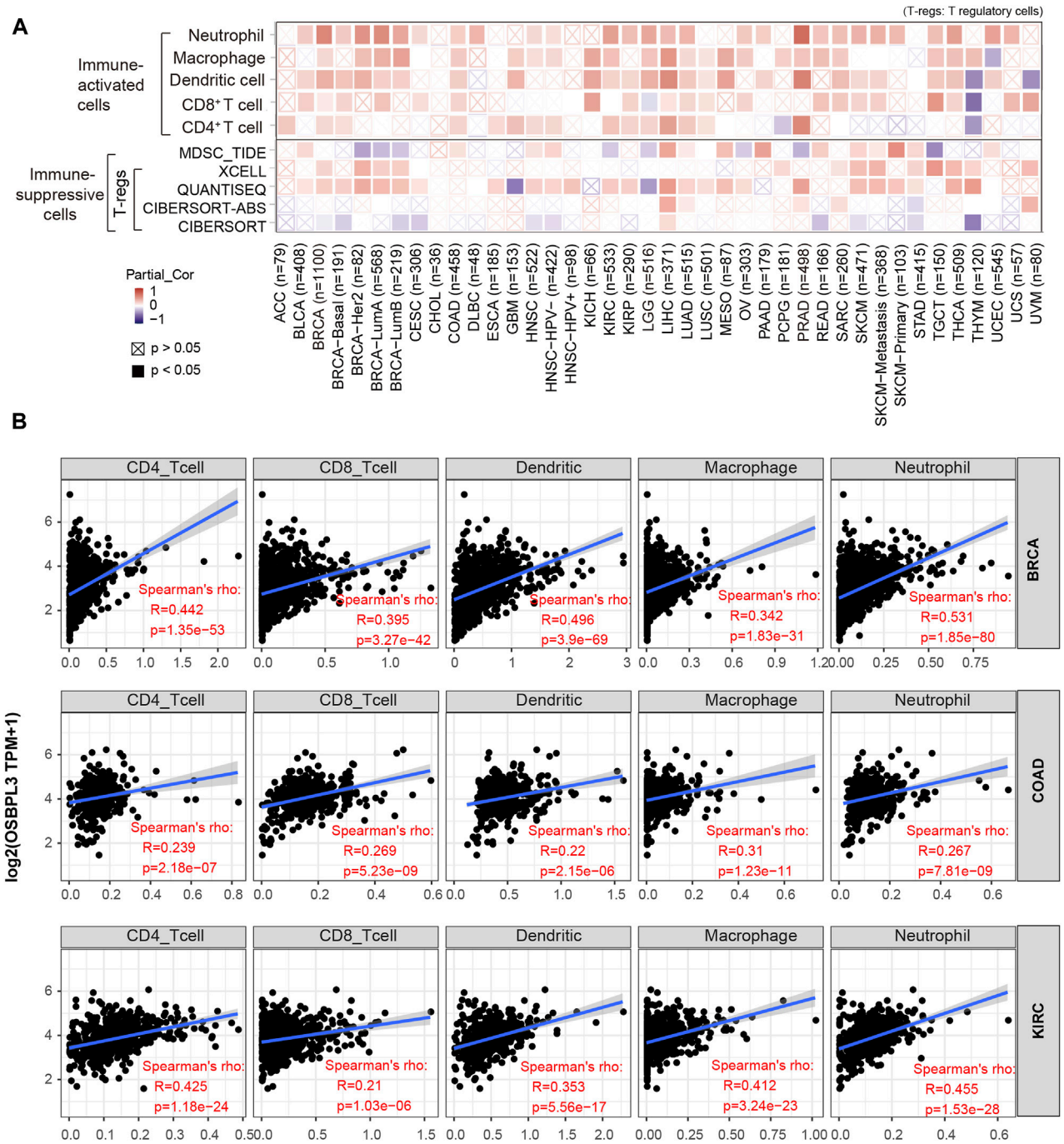

FIGURE 9 | Correlation analysis between OSBPL3 expression and immune cells. **(A)** Spearman correlation analysis heatmap of infiltration level of various immune cells and OSBPL3 gene expression in diverse tumor tissues (horizontal axis: different tumor tissues; vertical axis: different immune scores; different colors represent correlation coefficients; negative values represent negative correlations. The stronger the correlation, the darker the color. The Wilcox test was performed. *$p < 0.05$; **$p < 0.01$; ***$p < 0.001$). **(B)** Correlation between the expression level of OSBPL3 gene and the infiltration level of $CD4^+$ T cells, $CD8^+$ T cells, dendritic cells, macrophages, and neutrophils in breast cancer (BRCA), colon adenocarcinoma (COAD), and kidney renal clear cell carcinoma (KIRC) (Spearman correlation analysis was performed).

"SNARE interactions in vesicular transport," "Endocytosis," "Synaptic vesicle cycle," and "Ribosome biogenesis in eukaryotes" might be involved in the molecular mechanism of OSBPL3 on tumor pathogenesis. The GO enrichment analysis—biological process (BP), molecular function (MF), and cellular component (CC)—further showed that most of the related genes are associated with the pathways or cellular biology of mRNA metabolism, synaptic/endocytic/exocytic

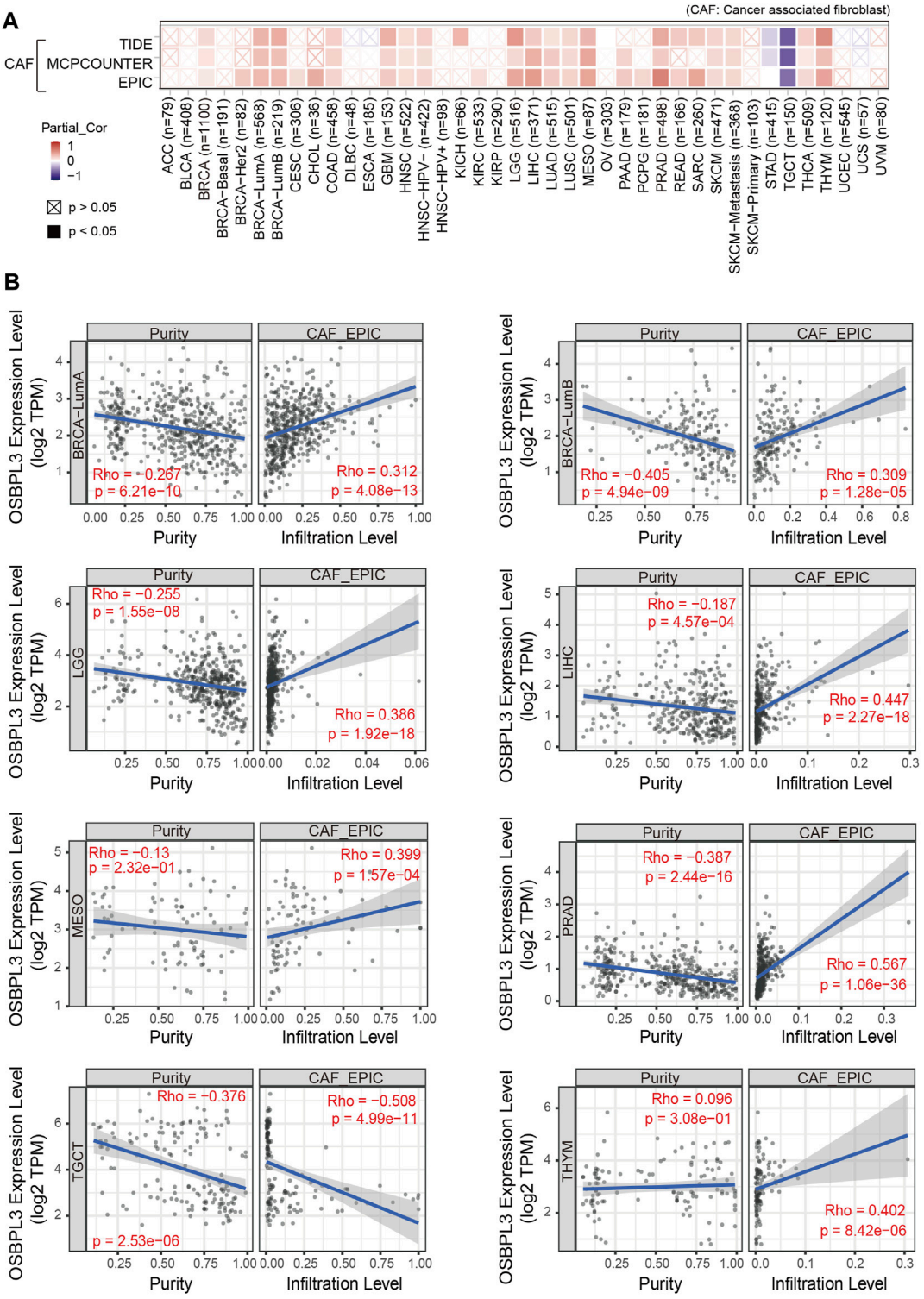

FIGURE 10 | Correlation analysis between OSBPL3 expression and infiltration of cancer-associated fibroblasts (CAFs). **(A)** Heatmaps of infiltration level of OSBPL3 gene expression and CAFs in multiple tumor tissues (horizontal axis: different tumor tissues; vertical axis: different immune scores; different colors represent correlation coefficients. The stronger the correlation, the darker the color. The Wilcox test was performed. $^{*}p < 0.05$; $^{**}p < 0.01$; $^{***}p < 0.001$). **(B)** Correlation between the expression level of OSBPL3 gene and the infiltration level of CAFs in BRCA-luminal A, BRCA-luminal B, LGG, LIHC, MESO, PRAD, TGCT, and THYM (Spearman correlation analysis was performed).

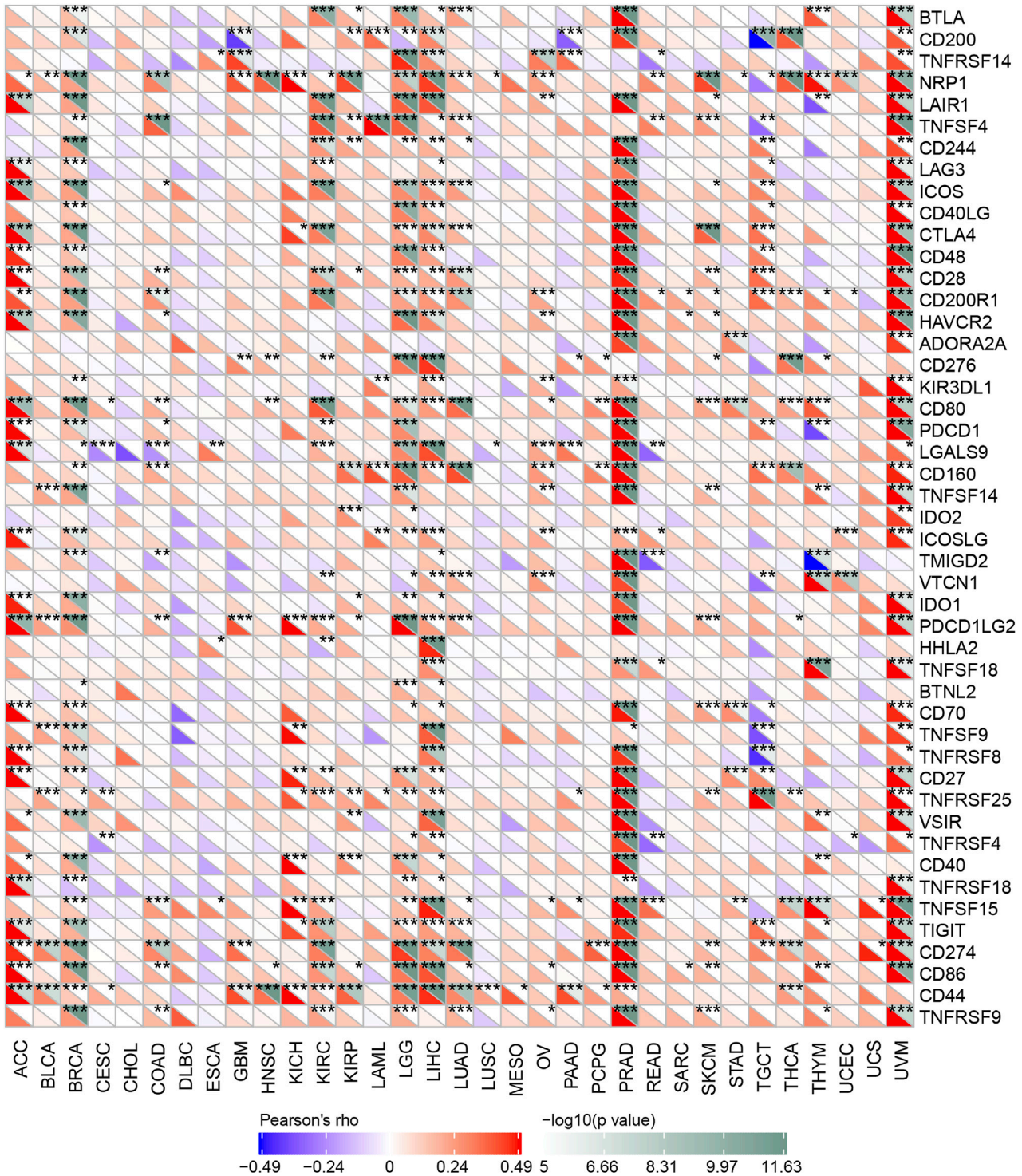

FIGURE 11 | Correlation analysis between OSBPL3 expression and immune checkpoints. Heatmaps of the immune checkpoint–related genes with OSBPL3 expression in different tumor tissues (horizontal axis: different immune checkpoint genes; vertical axis: different tumor tissues. Each box represents the correlation between the expression of the immune checkpoint gene and the OSBPL3 gene in corresponding tumors, and different colors represent changes in correlation coefficients. *$p < 0.05$; **$p < 0.01$; ***$p < 0.001$).

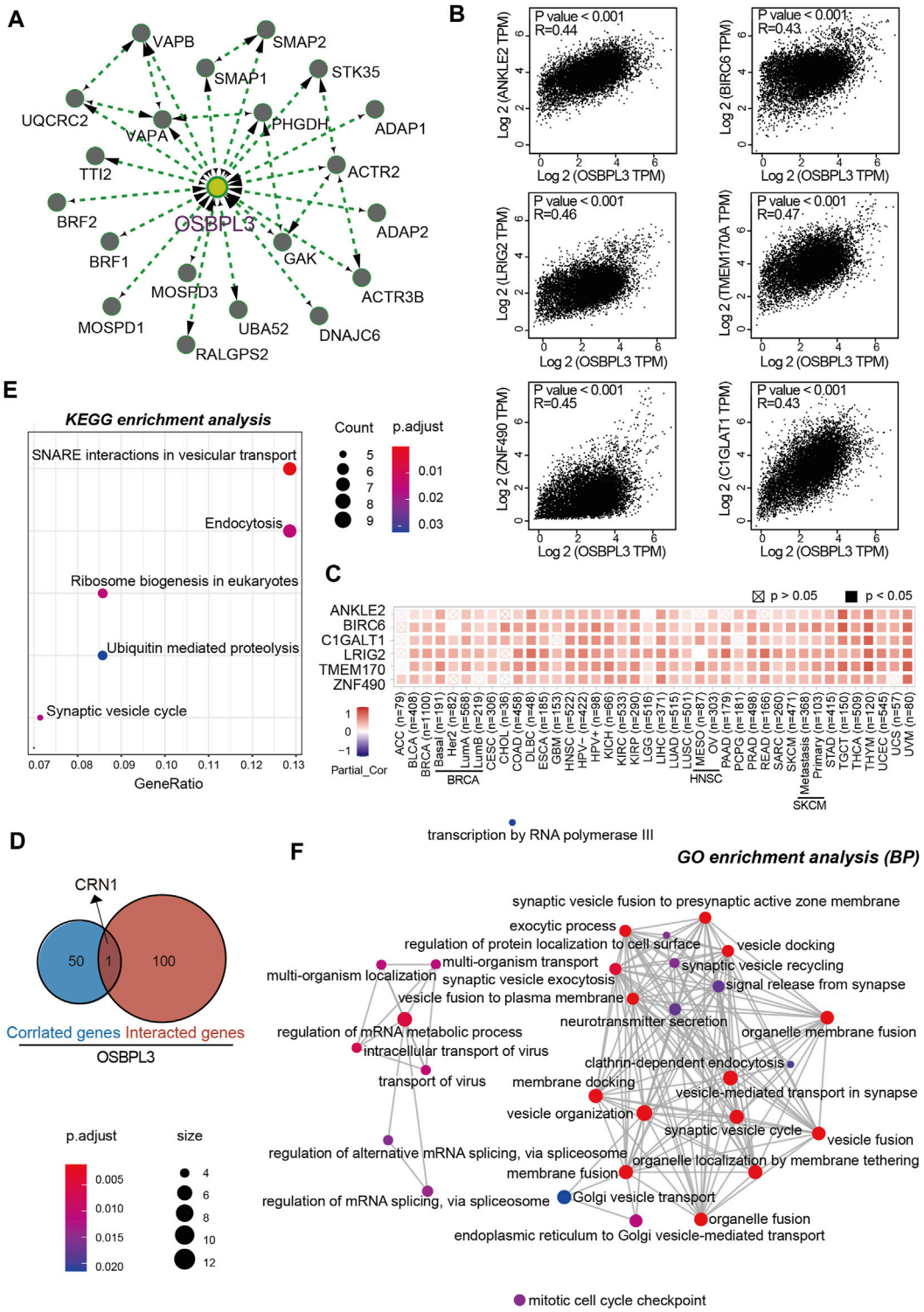

FIGURE 12 | OSBPL3-related gene enrichment analysis. **(A)** The top 20 available experimentally determined OSBPL3-binding proteins using the STRING tool. **(B)** The top 100 OSBPL3-correlated genes in TCGA projects on GEPIA2 and expression correlation between OSBPL3 and top six genes, including ANKLE2, BIRO6, LRIG2, TMEM170A, ZNF490, and C1GLAT1. **(C)** Heatmap of correlation between OSBPL3 and top six genes in different cancer types. **(D)** An intersection analysis of OSBPL3-binding and -correlated genes. **(E–F)** KEGG pathway analysis **(E)** and GO enrichment analysis-biological process (BP) **(F)** of the OSBPL3-binding and -interacted genes were performed.

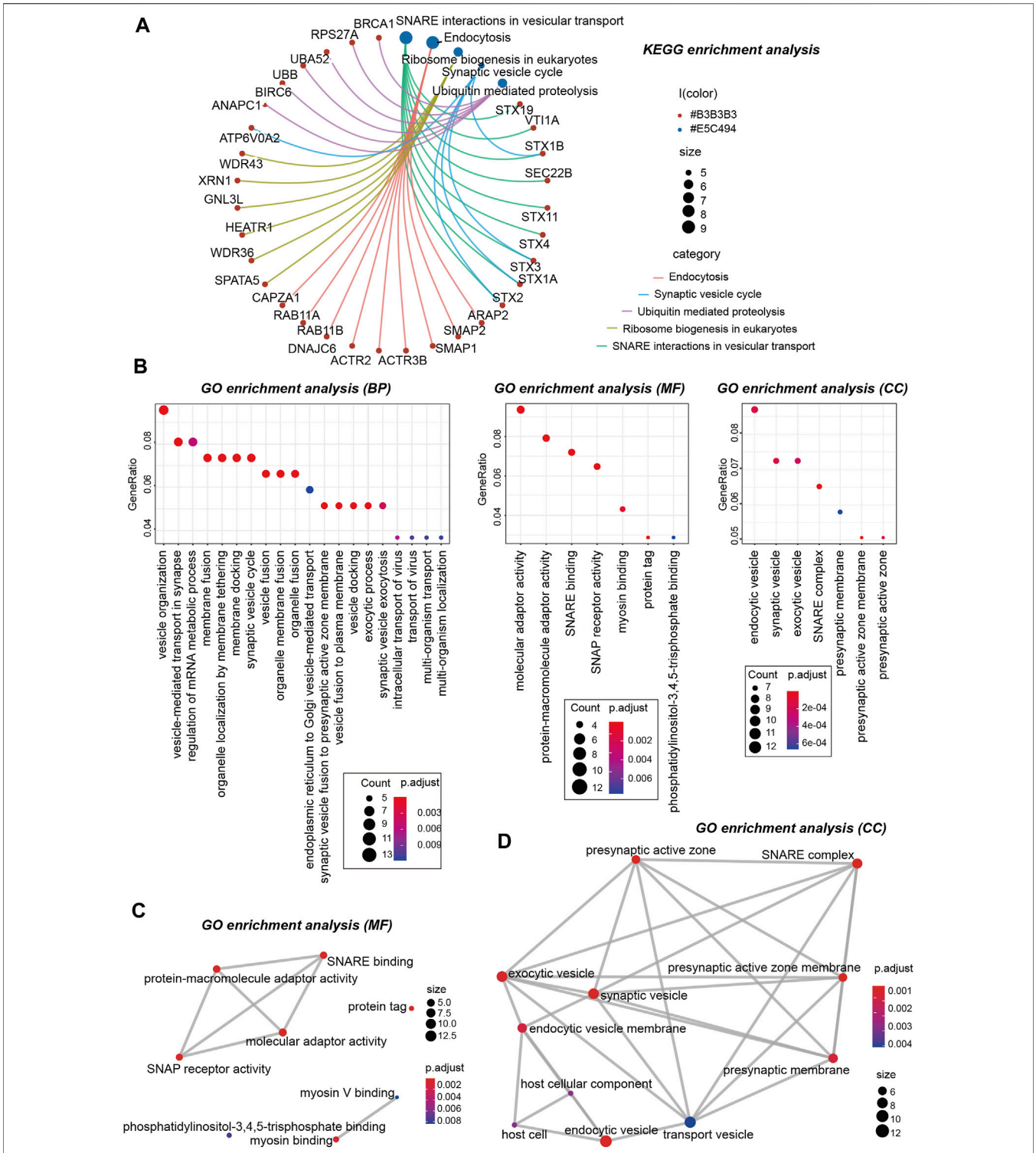

FIGURE 13 | KEGG and GO analyses-biological process (BP)/cellular component (CC)/molecular function (MF) of OSBPL3-related genes in tumors. **(A)** cnetplot for the KEGG analysis. **(B)** Bubble diagram of GO enrichment analysis. **(C–D)** GO enrichment analysis-MF **(C)** and CC **(D)** were performed.

vesicles, SNARE binding, protein molecular adaptor activity, membrane fusion/tethering/docking, and others (**Figures 12F**, **13B–D–D**; **Supplementary Figure S10**).

Taken together, these data suggest the biological processes and molecular mechanism in which OSBPL3 may be involved and further investigations are needed for exploration and confirmation.

DISCUSSION

This is the first systematic pan-cancer analysis, to our knowledge, to comprehensively summarize the molecular features, clinical prognosis, and mechanisms characterizing the presentation of the OSBPL3 gene and its impact on the process of tumorigenesis in a total of 33 different tumors. We show a general high level of OSBPL3 expression in major cancers compared with normal tissues from multiple databases and cancer biopsies. A high abundance of intra-tumoral OSBPL3 cells had prolonged survival that are seen in a significant proportion of cancer patients, and it seems likely that the mutation, phosphorylation, immune infiltration, and cell membrane pathways of OSBPL3 affect the disease forward. On the basis of this analysis and the previous work, it is clear that OSBPL3 plays an important role in the process of tumorigenesis.

Although there are few studies on the expression and role of OSBPL3 in tumors, our study shows that OSBPL3 was highly expressed in multiple human tumors compared with normal tissues from both the detection of the TCGA database and experiments of tissues of tumor patients. Nevertheless, the survival outcome data for OSBPL3 show distinct conclusions for different tumors. In this work, a group of survival analyses by GEPIA2, OncoLnc tools, and Kaplan–Meier plotter indicated a strong prognostic relevance between high level of OSBPL3 expression and poor OS, DFS, PFI, and DFI prognosis for low-grade glioma; poor OS, DFS, and PFI for uveal melanoma; and poor PFI and DFI for prostate adenocarcinoma while better clinical prognosis for testicular germ cell tumor cases. Xu et al. reported that downregulation of OSBPL3 correlates with reduced survival of colon cancer patients with advanced nodal metastasis and grade 3 colon cancer (Xu et al., 2020), but another recent research showed the contrary result that upregulation of OSBPL3 by HIF1A promotes colorectal cancer progression (Jiao et al., 2020). Interestingly, our experimental data showed that the higher the grade of colon cancer, the higher the level of OSBPL3 expression. Thus, the current clinical evidence still cannot support the role of OSBPL3 expression with the clinical outcome in different cancers, and more sample sizes are needed for exploration and confirmation.

In this work, we integrated the alterations of the OSBPL3 gene, including splice, mutations, and its prognosis data. Komor et al. reported that the spliced region of OSBPL3 exon 9 is one of the cancer-specific aberrant splicing biomarkers in colorectal cancer cells (Komor et al., 2017), and we also found the X676_splice/V676G alteration in the oxysterol domain. Additionally, we show that the greater the number of mutations present within an individual patient, the worse the outcome in skin cutaneous melanoma. Lefebvre et al. reported that OSBPL3 was more frequently mutated in metastatic breast cancer—and associated with poor outcomes—as compared to early breast cancer (Lefebvre et al., 2016), and Njeru et al. suggested the mutations of OSBPL3 contribute to carcinogenesis involving the deregulation of various molecular processes such as lipid metabolism, proliferation, and cell survival (Njeru et al., 2020). We also first presented evidence that the tumor with high expression of OSBPL3 had higher TMB, which is one of the important prediction markers of the efficacy of tumor immunotherapy. These data will be helpful for future research on the mechanism and therapeutic application of OSBPL3 in cancers.

Notably, the total protein and phosphorylation of OSBPL3 at the S426, S251, and S273 loci within the pleckstrin homology (PH) domain were both at elevated levels. Lehto et al. reported that the PH domain of OSBLP3 binds the phosphoinositide-3-kinase (PI3K) products by an FFAT motif (EFFDAxE) (Lehto et al., 2005), and Gulyas et al. showed that ORP3 phosphorylation regulates phosphatidylinositol-4-phosphate and Ca (2+) dynamics (Gulyas et al., 2020). More experimental evidence is fully needed to determine how the phosphorylation of OSBPL3 affects the initiation and progress of tumors.

We also first integrated the correlation between OSBPL3 expression and the tumor microenvironment including immune infiltration and stromal cells, immune-related cells, and immune checkpoint inhibitors (ICIs) in a variety of tumors. We found that high expression of OSBPL3 is infiltrated with more immune active cells and seems to represent "hot" tumors and more immune checkpoint genes, which may play a potential role in response to the immune microenvironment and may benefit from immune therapeutic interventions. Although the role and interaction between OSBPL3 and immune infiltration need more in-depth molecular experimental verification, our large sample analysis and prediction of cancer database validation play a positive and hint role. Interestingly, based on the BELOB trial, the expression of OSBPL3 is significantly associated with treatment response of bevacizumab and CCNU chemotherapy in recurrent GBM patients (Taal et al., 2014). In the further, we may be able to predict prognosis by detecting OSBPL3 expression in tumors. And our laboratory is also trying to further explore the application of targeted OSBPL3 therapy.

In addition, the "HomoloGene" and phylogenetic tree indicated the conservation of the OSBPL3 gene structure across diverse species, suggesting that similar mechanisms might exist under normal physiological conditions (Lopez-Guerra et al., 2008; Song et al., 2012; Zhou et al., 2012). Our analysis of the reproductive system tumors agreed with the finding of previous reports (Weber-Boyvat et al., 2015; Darbyson and Ngsee, 2016; Stein et al., 2017; Santos et al., 2018; Xue et al., 2019) but also suggested the existence of specific mechanisms, including synaptic/endocytic/exocytic vesicles, mRNA metabolism, SNARE binding, and protein molecular adaptor activity. Whether OSBPL3 plays a similar role in tumorigenesis through certain molecular mechanisms needs further verification and exploration.

There are still some limitations in our study. First, this work mostly focused on the bioinformatic analysis of the expression and potential molecular mechanisms of OSBPL3 without more experiments to explore the phenotype and function *in vitro* and *in vivo*. Our lab is focusing and trying to clarify the role of OSBPL3 at both cellular and molecular levels in different types of cancers. Second, although the ratio of immune components in the TME is significantly associated with OSBPL3, it was unable to determine whether and how OSBPL3 influences patient survival through immune infiltration. Future experimental studies may provide additional mechanistic insights into immune cell infiltration.

In summary, our studies have demonstrated that OSBPL3 plays an important role in tumorigenesis from the perspective of public databases and clinical tumor samples and is potentially a novel and specific target for cancers, which comprehensively provides insights for further investigation.

CONCLUSION

In conclusion, we first identified a comprehensive analysis of OSBPL3 based on the TCGA project and summarized the molecular features, clinical prognosis, and mechanisms characterizing the presentation of the OSBPL3 gene and its impact on the process of tumorigenesis in a total of 33 different tumors, which provide a comprehensive understanding of OSBPL3 in oncogenesis and will be valuable for further in-depth research.

DATA AVAILABILITY STATEMENT

The original contributions presented in the study are included in the article/**Supplementary Material**, and further inquiries can be directed to the corresponding authors.

AUTHOR CONTRIBUTIONS

NH, CZ, and XT contributed to conception and drafting of the article and critically revised the article. NH, YZ, YL, and HZ contributed to conception, performed the experiments, and analyzed the data. NH, BW, CZ, YR, and XT performed the in silico data exploration, integration, and analysis. All authors contributed to the article and approved the submitted version.

ACKNOWLEDGMENTS

We thank YR, Department of Breast Surgery, First Affiliated Hospital of Xi'an Jiaotong University, Xi'an, China, for the collection of breast cancer tissues and clinicopathologic data from patients with breast cancer. We also thank the financial support from the National Natural Science Foundation of China (NSFC; no. 82003183, to NH).

SUPPLEMENTARY MATERIAL

The Supplementary Material for this article can be found online at: https://www.frontiersin.org/articles/10.3389/fmolb.2021.739978/full#supplementary-material

REFERENCES

Bagchi, S., Yuan, R., and Engleman, E. G. (2021). Immune Checkpoint Inhibitors for the Treatment of Cancer: Clinical Impact and Mechanisms of Response and Resistance. *Annu. Rev. Pathol. Mech. Dis.* 16, 223–249. doi:10.1146/annurev-pathol-042020-042741

Biffi, G., and Tuveson, D. A. (2021). Diversity and Biology of Cancer-Associated Fibroblasts. *Physiol. Rev.* 101 (1), 147–176. doi:10.1152/physrev.00048.2019

Chen, J., Song, Y., Li, M., Zhang, Y., Lin, T., Sun, J., et al. (2021). Comprehensive Analysis of ceRNA Networks Reveals Prognostic lncRNAs Related to Immune Infiltration in Colorectal Cancer. *BMC Cancer* 21 (1), 255. doi:10.1186/s12885-021-07995-2

Collier, F. M., Gregorio-King, C. C., Apostolopoulos, J., Walder, K., and Kirkland, M. A. (2003). ORP3 Splice Variants and Their Expression in Human Tissues and Hematopoietic Cells. *DNA Cel Biol.* 22 (1), 1–9. doi:10.1089/104454903321112442

D'Souza, R. S., Lim, J. Y., Turgut, A., Servage, K., Zhang, J., Orth, K., et al. (2020). Calcium-stimulated Disassembly of Focal Adhesions Mediated by an ORP3/IQSec1 Complex. *Elife* 9. doi:10.7554/eLife.54113

Darbyson, A., and Ngsee, J. K. (2016). Oxysterol-binding Protein ORP3 Rescues the Amyotrophic Lateral Sclerosis-Linked Mutant VAPB Phenotype. *Exp. Cel Res.* 341 (1), 18–31. doi:10.1016/j.yexcr.2016.01.013

Desbois, M., and Wang, Y. (2021). Cancer-associated Fibroblasts: Key Players in Shaping the Tumor Immune Microenvironment. *Immunol. Rev.* 302, 241–258. doi:10.1111/imr.12982

Erdem-Eraslan, L., van den Bent, M. J., Hoogstrate, Y., Naz-Khan, H., Stubbs, A., van der Spek, P., et al. (2016). Identification of Patients with Recurrent Glioblastoma Who May Benefit from Combined Bevacizumab and CCNU Therapy: A Report from the BELOB Trial. *Cancer Res.* 76 (3), 525–534. doi:10.1158/0008-5472.CAN-15-0776

Galon, J., and Bruni, D. (2019). Approaches to Treat Immune Hot, Altered and Cold Tumours with Combination Immunotherapies. *Nat. Rev. Drug Discov.* 18 (3), 197–218. doi:10.1038/s41573-018-0007-y

Gregorio-King, C. C., Collier, G. R., McMillan, J. S., Waugh, C. M., McLeod, J. L., Collier, F. M., et al. (2001). ORP-3, a Human Oxysterol-Binding Protein Gene Differentially Expressed in Hematopoietic Cells. *Blood* 98 (7), 2279–2281. doi:10.1182/blood.v98.7.2279

Gulyás, G., Sohn, M., Kim, Y. J., Várnai, P., and Balla, T. (2020). ORP3 Phosphorylation Regulates Phosphatidylinositol 4-phosphate and Ca2+ Dynamics at PM-ER Contact Sites. *J. Cel Sci* 133 (6). doi:10.1242/jcs.237388

Hao, N., Shen, W., Du, R., Jiang, S., Zhu, J., Chen, Y., et al. (2020). Phosphodiesterase 3A Represents a Therapeutic Target that Drives Stem Cell-like Property and Metastasis in Breast Cancer. *Mol. Cancer Ther.* 19 (3), 868–881. doi:10.1158/1535-7163.MCT-18-1233

Jiang, X., Wang, J., Deng, X., Xiong, F., Zhang, S., Gong, Z., et al. (2020). The Role of Microenvironment in Tumor Angiogenesis. *J. Exp. Clin. Cancer Res.* 39 (1), 204. doi:10.1186/s13046-020-01709-5

Jiao, H.-l., Weng, B.-s., Yan, S.-s., Lin, Z.-m., Wang, S.-y., Chen, X.-p., et al. (2020). Upregulation of OSBPL3 by HIF1A Promotes Colorectal Cancer Progression through Activation of RAS Signaling Pathway. *Cell Death Dis* 11 (7), 571. doi:10.1038/s41419-020-02793-3

Komor, M. A., Pham, T. V., Hiemstra, A. C., Piersma, S. R., Bolijn, A. S., Schelfhorst, T., et al. (2017). Identification of Differentially Expressed Splice Variants by the Proteogenomic Pipeline Splicify. *Mol. Cell Proteomics* 16 (10), 1850–1863. doi:10.1074/mcp.TIR117.000056

Lefebvre, C., Bachelot, T., Filleron, T., Pedrero, M., Campone, M., Soria, J.-C., et al. (2016). Mutational Profile of Metastatic Breast Cancers: A Retrospective Analysis. *Plos Med.* 13 (12).e1002201. doi:10.1371/journal.pmed.1002201

Lehto, M., Hynynen, R., Karjalainen, K., Kuismanen, E., Hyvärinen, K., and Olkkonen, V. M. (2005). Targeting of OSBP-Related Protein 3 (ORP3) to Endoplasmic Reticulum and Plasma Membrane Is Controlled by Multiple Determinants. *Exp. Cel Res.* 310 (2), 445–462. doi:10.1016/j.yexcr.2005.08.003

Lehto, M., Laitinen, S., Chinetti, G., Johansson, M., Ehnholm, C., Staels, B., et al. (2001). The OSBP-Related Protein Family in Humans. *J. Lipid Res.* 42 (8), 1203–1213. doi:10.1016/s0022-2275(20)31570-4

Lehto, M., Mäyränpää, M. I., Pellinen, T., Ihalmo, P., Lehtonen, S., Kovanen, P. T., et al. (2008). The R-Ras Interaction Partner ORP3 Regulates Cell Adhesion. *J. Cel Sci* 121 (Pt 5), 695–705. doi:10.1242/jcs.016964

Lehto, M., and Olkkonen, V. M. (2003). The OSBP-Related Proteins: a Novel Protein Family Involved in Vesicle Transport, Cellular Lipid Metabolism, and Cell Signalling. *Biochim. Biophys. Acta (Bba) - Mol. Cel Biol. Lipids* 1631 (1), 1–11. doi:10.1016/s1388-1981(02)00364-5

Li, H., Wang, X., Fang, Y., Huo, Z., Lu, X., Zhan, X., et al. (2017). Integrated Expression Profiles Analysis Reveals Novel Predictive Biomarker in Pancreatic Ductal Adenocarcinoma. *Oncotarget* 8 (32), 52571–52583. doi:10.18632/oncotarget.16732

Lopez-Guerra, M., Trigueros-Motos, L., Molina-Arcas, M., Villamor, N., Casado, F. J., Montserrat, E., et al. (2008). Identification of TIGAR in the Equilibrative Nucleoside Transporter 2-mediated Response to Fludarabine in Chronic Lymphocytic Leukemia Cells. *Haematologica* 93 (12), 1843–1851. doi:10.3324/haematol.13186

Lui, P. P., Cho, I., and Ali, N. (2020). Tissue Regulatory T Cells. *Immunology* 161 (1), 4–17. doi:10.1111/imm.13208

Njeru, S. N., Kraus, J., Meena, J. K., Lechel, A., Katz, S.-F., Kumar, M., et al. (2020). Aneuploidy-inducing Gene Knockdowns Overlap with Cancer Mutations and Identify Orp3 as a B-Cell Lymphoma Suppressor. *Oncogene* 39 (7), 1445–1465. doi:10.1038/s41388-019-1073-2

Santos, M. F., Rappa, G., Karbanová, J., Kurth, T., Corbeil, D., and Lorico, A. (2018). VAMP-associated Protein-A and Oxysterol-Binding Protein-Related Protein 3 Promote the Entry of Late Endosomes into the Nucleoplasmic Reticulum. *J. Biol. Chem.* 293 (36), 13834–13848. doi:10.1074/jbc.RA118.003725

Song, Y.-B., An, Y. R., Kim, S. J., Park, H.-W., Jung, J.-W., Kyung, J.-S., et al. (2012). Lipid Metabolic Effect of Korean Red Ginseng Extract in Mice Fed on a High-Fat Diet. *J. Sci. Food Agric.* 92 (2), 388–396. doi:10.1002/jsfa.4589

Stein, S., Lemos, V., Xu, P., Demagny, H., Wang, X., Ryu, D., et al. (2017). Impaired SUMOylation of Nuclear Receptor LRH-1 Promotes Nonalcoholic Fatty Liver Disease. *J. Clin. Invest.* 127 (2), 583–592. doi:10.1172/JCI85499

Taal, W., Oosterkamp, H. M., Walenkamp, A. M. E., Dubbink, H. J., Beerepoot, L. V., Hanse, M. C. J., et al. (2014). Single-agent Bevacizumab or Lomustine versus a Combination of Bevacizumab Plus Lomustine in Patients with Recurrent Glioblastoma (BELOB Trial): a Randomised Controlled Phase 2 Trial. *Lancet Oncol.* 15 (9), 943–953. doi:10.1016/S1470-2045(14)70314-6

Weber-Boyvat, M., Kentala, H., Lilja, J., Vihervaara, T., Hanninen, R., Zhou, Y., et al. (2015). OSBP-related Protein 3 (ORP3) Coupling with VAMP-Associated Protein A Regulates R-Ras Activity. *Exp. Cel Res.* 331 (2), 278–291. doi:10.1016/j.yexcr.2014.10.019

Xu, P., Richter, J., Blatz, A., Gärtner, F., Alberts, R., Azoitei, A., et al. (2020). Downregulation of ORP3 Correlates with Reduced Survival of Colon Cancer Patients with Advanced Nodal Metastasis and of Female Patients with Grade 3 Colon Cancer. *Ijms* 21 (16), 5894. doi:10.3390/ijms21165894

Xue, J., Scotti, E., and Stoffel, M. (2019). CDK8 Regulates Insulin Secretion and Mediates Postnatal and Stress-Induced Expression of Neuropeptides in Pancreatic β Cells. *Cel Rep.* 28 (11), 2892–2904. doi:10.1016/j.celrep.2019.08.025

Yan, D., Lehto, M., Rasilainen, L., Metso, J., Ehnholm, C., Ylä-Herttuala, S., et al. (2007). Oxysterol Binding Protein Induces Upregulation of SREBP-1c and Enhances Hepatic Lipogenesis. *Atvb* 27 (5), 1108–1114. doi:10.1161/ATVBAHA.106.138545

Yang, Y., Li, C., Liu, T., Dai, X., and Bazhin, A. V. (2020). Myeloid-Derived Suppressor Cells in Tumors: From Mechanisms to Antigen Specificity and Microenvironmental Regulation. *Front. Immunol.* 11, 1371. doi:10.3389/fimmu.2020.01371

Zhang, Z., Li, H., Jiang, S., Li, R., Li, W., Chen, H., et al. (2019). A Survey and Evaluation of Web-Based Tools/databases for Variant Analysis of TCGA Data. *Brief Bioinform* 20 (4), 1524–1541. doi:10.1093/bib/bby023

Zhou, Y., Robciuc, M. R., Wabitsch, M., Juuti, A., Leivonen, M., Ehnholm, C., et al. (2012). OSBP-related Proteins (ORPs) in Human Adipose Depots and Cultured Adipocytes: Evidence for Impacts on the Adipocyte Phenotype. *PLoS One* 7 (9).e45352 doi:10.1371/journal.pone.0045352

Conflict of Interest: The authors declare that the research was conducted in the absence of any commercial or financial relationships that could be construed as a potential conflict of interest.

Publisher's Note: All claims expressed in this article are solely those of the authors and do not necessarily represent those of their affiliated organizations, or those of the publisher, the editors, and the reviewers. Any product that may be evaluated in this article, or claim that may be made by its manufacturer, is not guaranteed or endorsed by the publisher.

frontiers in Cell and Developmental Biology

ORIGINAL RESEARCH
published: 20 October 2021
doi: 10.3389/fcell.2021.740455

Genome Instability and Long Noncoding RNA Reveal Biomarkers for Immunotherapy and Prognosis and Novel Competing Endogenous RNA Mechanism in Colon Adenocarcinoma

Ziyuan Ren[1,2†], Zhonglin Wang[1,3†], Donghong Gu[4], Hanchen Ma[2], Yan Zhu[5], Menghua Cai[1] and Jianmin Zhang[1*]*

[1] Department of Immunology, CAMS Key Laboratory for T Cell and Cancer Immunotherapy, Institute of Basic Medical Sciences, Chinese Academy of Medical Sciences and School of Basic Medicine, Peking Union Medical College, State Key Laboratory of Medical Molecular Biology, Beijing, China, [2] Cheeloo College of Medicine, Shandong University, Jinan, China, [3] School of Physical Science, University of California, Irvine, Irvine, CA, United States, [4] Weihai Municipal Hospital, Cheeloo College of Medicine, Shandong University, Weihai, China, [5] Department of Translational Molecular Pathology, The University of Texas MD Anderson Cancer Center, Houston, TX, United States

OPEN ACCESS

Edited by:
Na Luo,
Nankai University, China

Reviewed by:
Simin Li,
Southern Medical University, China
Sheik Pran Babu Sardar Pasha,
University of California, Davis, United States

***Correspondence:**
Menghua Cai
menghuacai@ibms.pumc.edu.cn
Jianmin Zhang
jzhang42@163.com

[†] These authors have contributed equally to this work and share first authorship

Specialty section:
This article was submitted to Molecular and Cellular Pathology, a section of the journal Frontiers in Cell and Developmental Biology

Received: 13 July 2021
Accepted: 16 September 2021
Published: 20 October 2021

Citation:
Ren Z, Wang Z, Gu D, Ma H, Zhu Y, Cai M and Zhang J (2021) Genome Instability and Long Noncoding RNA Reveal Biomarkers for Immunotherapy and Prognosis and Novel Competing Endogenous RNA Mechanism in Colon Adenocarcinoma. Front. Cell Dev. Biol. 9:740455. doi: 10.3389/fcell.2021.740455

Background: Long noncoding RNAs (lncRNAs) crucially modulate DNA damage responses/repair in cancer cells. However, the underlying regulatory role of genome integrity and its clinical value in colon adenocarcinoma (COAD) remains unclear. This study links genome instability to lncRNA using computational biology techniques, in attempt to propose novel biomarkers of immunotherapy outcome, and investigated a potential competing endogenous RNA (ceRNA) as a molecular regulatory mechanism.

Methods: TCGA-COAD patients were divided into genome unstable (GU)-like and genome stable (GS)-like clusters *via* hierarchical clustering to predict immunotherapy outcomes. Multivariate Cox model was established to predict the overall survival rate in COAD patients. Additionally, SVM and LASSO algorithms were applied to obtain hub lncRNAs. A novel genome instability-related ceRNA network was predicted with the Starbase 2.0 database. To better understand how these genes fundamentally interact during tumor progression and development, the mutation analysis and single-gene analysis for each gene was performed.

Results: In contrast to those in the GS-like cluster, GU-like-cluster patients demonstrated a higher tumor mutational burden (TMB)/microsatellite instability (MSI), DNA polymerase epsilon (*POLE*) mutation rate, and immune checkpoint expression, all indicate a greater predictive power for response rate for immunotherapy. The novel prognostic signature demonstrated an outstanding predictive performance (AUC $>$ 0.70). The genes in the genome insatiability-related ceRNA network (including four axes: *AL161772.1-has-miR-671-5p* (*hsa-miR-181d-5p*, *has-miR-106a-5p*)-*NINL*,

AL161772.1-has-miR-106a-5p-TNFSF11, *AC124067.4-hsa-miR-92b-3p* (*hsa-miR-589-5p*)-*PHYHIPL*, and *BOLA3-AS1-has-miR-130b-3p-SALL4*) were identified as critical regulators of tumor microenvironment infiltration, cancer stemness, and drug resistance. qPCR was performed to validate the expression patterns of these genes. Furthermore, the MSI-high proportion was greater in patients with mutated type than in those with the wild type according to all four target genes, indicating that these four genes modulate genomic integrity and could serve as novel immunotherapy biomarkers.

Conclusion: We demonstrated that genome instability-related lncRNA is a novel biomarker for immunotherapy outcomes and prognosis. A novel ceRNA network that modulates genomic integrity, including four lncRNA-miRNA-mRNA axes, was proposed.

Keywords: genome instability, lncRNA, ceRNA, immune checkpoint inhibitor, MSI, tumor heterogeneity, colon adenocarcinoma

INTRODUCTION

Colon adenocarcinoma (COAD) is the primary subtype of colorectal cancer, ranking fourth in lethal malignancies worldwide and second across the United States (Brody, 2015). Although the establishment of a series of molecularly targeted therapies has led to a noticeable increase in the survival of COAD patients, chemotherapy is still the standard and irreplaceable treatment, and the 5-year survival rate for Stage IV COAD patients is less than 10% (Ganesh et al., 2019). Thus, there is an urgency to further develop novel treatment regimens (Garrido-Castro et al., 2019).

In recent years, immunotherapy has become an ideal option for advanced COAD with the emergence and rapid development of immune checkpoint inhibitors (ICIs) (Qin et al., 2019; Hu et al., 2020). Considering that patient response rates to nivolumab and pembrolizumab (both PD-1/PD-L1 inhibitors) are diverse and often less than 50%, additional predictive biomarkers need to be identified (Schrock et al., 2019). Genome instability was reported as one of the top 10 promising discoveries for cancer treatment in the twenty-first century and has elicited a corresponding interest (Hanahan and Weinberg, 2011). Recent clinical practice has demonstrated that genome instability is associated with ICI outcomes. Microsatellite instability (MSI) is a critical biomarker for ICIs (Boland and Goel, 2010). In general, *MLH1* promoter hypermethylation or germline mutations in four DNA mismatch repair (dMMR) machinery genes (*MSH6*, *MSH2*, *PMS2*, *MLH1*) lead to MSI (Dudley et al., 2016). PD-1/PD-L1 inhibitors in MSI-high (MSI-H) metastatic colorectal carcinoma have been confirmed to have a favorable cancer-control effect with high progression-free survival (Schrock et al., 2019).

Long noncoding RNAs (lncRNAs) are nonprotein coding RNAs that are longer than 200 nucleotides. They are involved in a series of diverse biological processes, including cell development, differentiation (Fatica and Bozzoni, 2014), the cell cycle response (Hung et al., 2011), and gene imprinting (Kanduri, 2016). Current studies on these molecules have mainly focused on their dysregulation in cancers, which leads to alterations in tumor behavior (Bhan et al., 2017). Therefore, lncRNAs are promising candidates for clinical cancer biomarker exploration (Li Y. et al., 2020; Goyal et al., 2021). A novel role for lncRNAs is modulating DNA damage response pathways, such as the TP53 and ATM/ATR pathways (Su et al., 2018). This study linked genome instability to lncRNA, which was termed genome instability-related lncRNA (GIRlncR), and hypothesized that GIRlncR could serve as a novel immunotherapy biomarker for COAD.

Advances in RNA sequencing (RNA-seq) techniques have largely promoted the functional annotation and progress on the computational characteristics of lncRNAs (Chen et al., 2016). Yin et al. (2021) identified a genome instability-related lncRNA prognostic signature in COAD using computational biological techniques. However, they did not focus enough on the predictive ability of GIRlncR for immunotherapy outcomes. They also did not explore the regulatory mechanisms of lncRNAs (Yin et al., 2021). This study established a patient stratification clustering method for COAD to predict ICI outcomes in these patients. A novel genome instability-related competing endogenous RNA (ceRNA) network (including four axes: *AL161772.1-has-miR-671-5p* (*hsa-miR-181d-5p*, *has-miR-106a-5p*)-*NINL*, *AL161772.1-has-miR-106a-5p-TNFSF11*, *AC124067.4-hsa-miR-92b-3p* (*hsa-miR-589-5p*)-*PHYHIPL*, and *BOLA3-AS1-has-miR-130b-3p-SALL4*) was constructed using machine learning algorithms. Furthermore, the MSI-H proportion was greater in patients with mutated type than in those with the wild type according to all four target genes, indicating that these genes modulate genomic integrity and could serve as novel immunotherapy biomarkers.

MATERIALS AND METHODS

Data Selection and Code Availability

The graphical abstract presents the flow chart and online resources for this study. The original data of RNA-seq (FPKM format), miRNA-seq, corresponding clinical characteristics, including gender, age, overall survival (OS), and stage, and simple nucleotide variation (SNV) were downloaded from the TCGA-COAD project (December 24, 2020). The tumor mutational burden (TMB) and MSI data were retrieved from cBioportal

(Cerami et al., 2012). The clustering method was used to detect and exclude the outlier RNA-seq samples. Eventually, 453 RNA-seq samples were acquired; however, only 446 patients with both matching RNA-seq data and corresponding clinical features were included in this study. All biological and clinical samples in this study are publicly available. The data availability policies of the open-accessed databases were strictly followed. All code utilized in this study can be acquired *via* email 201800413040@mail.sdu.edu.cn with reasonable grounds.

Differential Expression Gene Extraction

The R package "limma" was used to extract differential expression genes (DEGs). All tumor RNA-seq samples were sorted according to their SNV numbers, from largest to smallest. The first 25% and last 25% of samples were named the genome-unstable (GU) group and genome-stable (GS) group. Differentially expressed lncRNAs between the GS and GU groups were considered GIRlncRs. The cutoff value was adjusted a p-Value (adj. p) < 0.05, and $|\log_2$ fold-change$| > 1$. Similarly, genome instability-related mRNA (GIRmR) and miRNA (GIRmiR) were extracted.

Hierarchical Clustering to Establish a Novel Immunotherapy Outcome Predictive Stratification Method

The "sparcl" package was implemented to perform unsupervised hierarchical clustering based on GIRlncRs ($k = 2$). The clusters with higher and lower SNV numbers were named GU-like and GS-like clusters, respectively. We compared the tumor mutational burden (TMB), MSI, expression, and mutation rates of four MMR genes, expression of six immune-related genes, and the mutation rates of *POLE* (a novel biomarker for immunotherapy outcomes (Wang et al., 2019)) between the two clusters. The MMR and immune-related genes included in this study are listed in **Table 1**. Single-sample gene set enrichment analysis (ssGSEA) was used to compare tumor microenvironment (TME) infiltration and functions between the two clusters (**Supplementary Table 1**). Survival analysis using the log-rank test between the GS-like and GU-like clusters was performed to evaluate the prognostic value of clustering. By calculating the Pearson's correlation coefficients, we ranked the relevance of associations between each mRNA and GIRlncR expression. The first 10 ranked mRNAs were considered coexpressed with GIRlncR. Cytoscape, a biological network modifying software, was used to visualize the lncRNA-mRNA coexpression network (Shannon et al., 2003). To explore the potential functions of GIRlncRs, functional gene enrichment analysis based on the Gene Ontology (GO) (Ashburner et al., 2000) and Kyoto Encyclopedia of Genes and Genomes (KEGG) (Kanehisa and Goto, 2000) databases was performed.

Multivariate Cox Regression to Construct a Novel Gene Signature

Multivariate Cox regression is the most widely utilized regression model for analyzing medical survival time and survival status data (Bradburn et al., 2003), and it was used to explore the association with event incidence (surviving/deceased in this study). The hazard ratio (HR) represents the probability of event occurrence under the currently observed feature patterns (gene expression pattern in this study). First, we divided 446 patients equally into the training and test cohorts. Chi-square tests were used to detect selection bias for each feature during patient division. Second, univariate Cox regression analysis of each GIRlncR was used for feature selection. Only statistically significant features ($p < 0.05$) were used for model construction. Third, multivariate Cox regression was performed to construct the genome instability-related lncRNA prognostic signature (GIlncPS) using the training cohort. The constructed model is as follows:

$$\text{Risk\_score} = \Sigma(\text{gene expression} \times \text{coefficient})$$

$$\text{HR} = \exp(\text{coefficient})$$

The model was applied to the test cohort. In both training and test cohorts, patients who had a risk score higher than the median value of the risk score were classified as the high-risk group and vice versa. Survival analysis and receiver operating characteristic (ROC) curves and the area under the curve (AUC) were utilized to evaluate the reliability of the GIlncPS. Moreover, given that *BRAF* is a frequently mutated gene with prognostic value (Sanz-Garcia et al., 2017), we tested whether our signature has better predictive performance than this event. Survival analysis among *BRAF* mutation-type/high-risk, *BRAF* mutation-type/low-risk, *BRAF* wild-type/high-risk, AND *BRAF* wild-type/low-risk groups was performed using the log-rank test. To demonstrate that our signature has a better predictive performance than other lncRNA signatures, we found two proposed lncRNA signatures for COAD, namely, Li's signature (Li Z. et al., 2020) and Jin's signature (Jin et al., 2020). AUC was used to rank the predictive performance of these signatures according to OS at 1, 3, and 5 years for 446 patients. To demonstrate that our signature has prognostic ability independent of general factors, we performed multivariate Cox regression, including clinical features (age, gender stage, T (tumor), M (metastasis), N (lymph node), *KRAS* mutation type, *TP53* mutation type, *BRAF* mutation type, and *POLE* mutation type) and the risk score. The nomogram, including our signature, was plotted for clinical reference, which was evaluated using a calibration curve.

TABLE 1 | The MMR genes and immune-related genes utilized in this study.

MMR genes	Immune-related genes
MSH2	PDCD1 (PD-1)
MSH6	CD274 (PD-L1)
PMS2	PDCD1LG2 (PD-L2)
MLH1	CTLA4
	CD80
	CD86

MMR, mismatch repair.

Analysis of Mutation Profile and Identification of Hub-Long Noncoding RNAs in Genome Stable- and Genome Unstable-Like Clusters

To investigate the relationship between the clusters and risk groups, Sankey plots were constructed. Waterfall plots were generated to explore the diversity of mutation profiles between GS- and GU-like clusters. To extract lncRNAs that had the closest relationship with clustering, LASSO and SVM algorithms were applied. The lncRNAs included in LASSO-screened lncRNAs, SVM-screened lncRNAs, and prognostic signatures were considered hub lncRNAs.

Competing Endogenous RNA Network

The hub-lncRNA and target mRNA interactions were predicted using an online comprehensive RNA database, ENCORI[1] (Li et al., 2014). The overlapping mRNAs in GIRmRs and hub-lncRNA target mRNAs require further research. Only the statistically significant lncRNA-mRNA pairs ($p < 0.05$) in COAD remained for further research. We then retrieved the miRNAs mediating the relationships between the lncRNAs and mRNAs. The retrieved miRNAs that were differentially expressed between the GS and GU groups were retained for ceRNA network construction. **Figure 4G** illustrated the screening process of ceRNA network.

Comprehensive Single-Gene Analysis

It is hypothesized that the genes included in the ceRNA network play a pivotal role in COAD. A comprehensive single-gene analysis was performed. Differential expression analysis was performed between normal and tumor tissues from COAD patients by employing the Mann-Whitney *U* test. Thorsson et al. (2018) identified six immune subtypes across 33 TCGA cancer types (C1–C6) and compared the expression of each gene among these six subtypes using the Kruskal-Wallis test. Spearman correlation analysis was performed to detect the correlation between each gene and TME infiltration, the expression of MMR genes, immune-related genes (**Table 1**), and two previously discovered crucial lncRNAs regulating genome instability (*NOARD* (Munschauer et al., 2018), *GUARDIN* (Hu et al., 2018)). The TME was evaluated by the estimation of stromal and immune cells in malignant tumor tissues using expression data (ESTIMATE) immune data, stromal score (Yoshihara et al., 2013), and cell-type identification by estimating relative subsets of RNA transcripts (CIBERSORT) and specific immune cell types (Newman et al., 2019). Given that genome instability contributes to tumor heterogeneity, which leads to drug resistance (Morel et al., 2017; Dagogo-Jack and Shaw, 2018; Sansregret et al., 2018), we performed cancer stemness and drug sensitivity analysis for these genes. Malta et al. (2018) identified a novel index to evaluate cancer stemness features based on DNA methylation patterns (DNA stemness score (DNAss)) and mRNA expression patterns (RNA stemness score (RNAss)). We calculated the Spearman correlation between each gene and cancer stemness. Drug sensitivity analysis was also performed using an open-access database, specifically National Cancer Institute (NCI)-60. The Kolmogorov-Smirnov test was applied to verify the normality of the included indexes, including TMB/MSI scores, NCI-60 indexes, TME indexes, and cancer stemness indexes (**Supplementary Table 2**). We found that the drug sensitivity index was normally distributed. Therefore, the method of Pearson's correlation to explore the association between gene expression and drug sensitivity is appropriate.

[1] http://starbase.sysu.edu.cn

Expression Pattern Validation by qPCR

Total RNA was isolated from COAD cell lines named Caco-2, Lovo, HCT116, and HT29 using the RNeasy Mini Kit (QIAGEN, Hilden, Germany), according to the manufacturer's instructions. Complementary DNA (cDNA) was produced by RNA using the PrimeScript^{TM} Reverse Transcription Kit (TakaRa, Maebashi, Japan) in an ABI 7500 System (Applied Biosystems, Thermo Fisher Scientific, Waltham, MA, United States). The primers specific for target genes were designed and synthesized by Tianyi Huiyuan Biotech (Beijing, China). The following procedures were performed: activation of enzymes at 50°C for 2 min and then 95°C for 2 min, 45 cycles of denaturation at 95°C for 15 s, annealing at 58°C for 20 s, and extension at 72°C for 30 s. The relative expression levels of the target genes were calculated using the $2^{-\Delta\Delta CT}$ method. Glyceraldehyde 3-phosphate dehydrogenase (GAPDH) was used as the internal control. All qPCR reactions were performed in triplicate. The primers used in this study are listed below.

Genes	Primer sequence (5′–3′)
AC124067.4 (lncRNA)	Forward: ATGAGAGGGTTGGGTGCAAG Reverse: GCCTTTTCCTTGTGGCTGTG
AL161772.1 (lncRNA)	Forward: ATGCCCATGAACAGCCATGA Reverse: GGCTGTTGCTCCTTTCTCCT
BOLA3-AS1 (lncRNA)	Forward: AGTCAGAAGCTCCGAGGCTA Reverse: TTTGCGGACAGTTCTACCCC
SALL4	Forward: TCGATGGCCAACTTCCTTC Reverse: GAGCGGACTCACACTGGAGA
GAPDH	Forward: TGTTCGTCATGGGTGTGAAC Reverse: ATGGCATGGACTGTGGTCAT

Mutation Analysis

Specific somatic mutations drive cancer development (Koch, 2017). Therefore, the mutation analysis of the target mRNAs was applied, including somatic mutations and copy number variation (CNV) analysis. The R package "RCircos" was used to explore the chromosome location and CNV number for each gene. We then explored the alteration rate, type, and site in the COAD datasets and examined the association between the alteration status and gene expression. We calculated the Spearman's correlation TMB and MSI scores and assessed the expression of each gene to explore whether the target mRNAs were directly associated with genome instability. Furthermore, the association between target mRNA alteration status and MSI

status was explored. All mutation analyses were performed using the online database cBioportal.

Statistics

SPSS Statistics (version 26.0; IBM, Armonk, NY, United States) and Microsoft Excel (Microsoft Corporation, Redmond, WA, United States) were used to present the retrieved data and perform the Chi-square test. R language (version 4.0.3) was used to perform machine learning algorithms and correlation analysis (R Core Team, 2013). The Benjamini and Hochberg method was used to adjust the *p*-Value for DEG extraction.

RESULTS

Differential Expression Genes Extraction and Hierarchical Clustering

In total, 123 GIRlncRs were extracted between the GS and GU groups (**Figure 1A**). We constructed a mRNA and GIRlncR coexpression network (**Figure 1B**) to show the top 10 close interactions between each GIRlncR and corresponding mRNAs, indicating that the GIRlncRs regulate genome instability and complex tumor cell biological processes. Functional analysis further illustrated the relationship between GIRlncRs and tumor immunity (**Figures 1C,D**). Almost all GO- and KEGG-enriched pathways involved immune responses, such as antigen processing and T-cell activation. The unsupervised hierarchical clustering based on GIRlncRs was employed to divide COAD patients into two clusters with various genome instability statuses and immune therapy response rates. In total, 453 samples were clustered into GS-like (302 samples) and GU-like groups (151 samples; **Figure 1E**). Surprisingly, the TMB, MSI score, and expression of all immune checkpoint-related genes were higher in the GU-like cluster ($p < 0.05$), whereas expression of the three MMR genes (*MLH1*, *PMS2*, *MSH2*) was lower ($p < 0.05$; **Figures 1F–I**). The mutation rates of all four MMR genes were higher in the GU-like group ($p < 0.05$). The ssGSEA showed that almost all immune cells and immune functions were increased in the GU-like group (**Figures 1J,K**). Furthermore, the mutation rate of the novel immunotherapy response rate biomarker *POLE* was also significantly higher in the GU-like group ($p < 0.05$; **Figure 1L**). These findings strongly suggest that our clustering based on GIRlncRs could predict TME infiltration and ICI response rates in COAD patients. However, as shown in **Figure 1M**, the OS of the two clusters did not differ, indicating that the clustering method could not fulfill the purpose of prognosis.

Multivariate Cox Regression to Construct the Genome Instability-Related LncRNA Prognostic Signature

Since our clustering could not predict OS in COAD patients, we constructed a novel GIlncPS. The basic characteristics of the training and test cohorts are shown in **Supplementary Table 3**. The Chi-square test showed that the division of training and test cohorts was proper without selection bias (all $p > 0.05$). The regression results are shown in **Supplementary Table 4**. An eight-lncRNA GIlncPS was acquired as follows: risk score = 0.239 × *LINC01807* + 0.235 × *AC009237.14* + 0.310 × *LOXL1-AS1* + 0.028 × *AC005392.2* + 0.751 × *AP003555.1* + 0.384 × *BOLA3-AS1* − 0.330 × *PTPRD-AS1* + 0.258 × *AC004009.1*. The high- and low-risk groups were divided according to median risk score. Survival analysis indicated that OS was significantly longer in the low-risk group in the training, test, and entire TCGA cohorts ($p < 0.05$; **Figures 2A–C**). Notably, all the included lncRNAs, except *PRPRD-AS1*, were risk factors for poor prognosis in COAD patients. The heatmap shows that all of these lncRNAs, except *PRPRD-AS1*, were overexpressed in high-risk groups because only *PRPRD-AS1* was a protective factor (**Figures 2D–F**). The AUCs of the ROC in the three cohorts were acceptable for the lncRNA prognostic signature. Only the AUC at 1 year in the test cohort did not reach 0.7 (**Figures 2G–I**). Compared with the prognostic models of Li and Jin, our GIlncPS had the best performance (AUC = 0.735, 0.745, and 0.741, respectively; **Figures 2J–L**). Independent prognostic analysis indicated that old age, advanced stage, and occurrence of metastasis were significantly related to poor prognosis, and a low-risk score was significantly related to good prognosis ($p < 0.05$; **Figures 3A,B**). **Figure 3C** shows the nomogram for clinical use. The calibration curve demonstrated the reliability of the nomogram (**Figure 3D**). We also compared TMB/MSI and TME infiltration and functions between the high- and low-risk groups. However, the results differed from those of hierarchical clustering. As shown in **Supplementary Figures 1A–H**, all ICI outcome predictive biomarkers, except MSI, were not significantly different between the two groups, indicating that our prognostic signature behaved poorly in predicting genome instability, TME infiltration, and ICI response rates for COAD patients. Furthermore, **Supplementary Figure 1I** shows that the mutation rate of *BRAF* was higher in the high-risk group (19% vs. 11%). The prognostic ability of the GIlncPS was better than that of *BRAF* ($p < 0.01$; **Supplementary Figure 1J**). The OS in the high-risk groups was always lower than that in the low-risk groups, regardless of the *BRAF* mutation type. To conclude, we constructed a GIlncPS with strong prognostic ability, but it could not predict the TME infiltration and ICI response rates for COAD patients.

Analysis of Mutation Profile and Identification of Hub-Long Noncoding RNAs in Clusters and Risk Groups

The Sankey plot showed the relationship among the GS-and GU-like clusters, risk groups, and survival status (**Figure 4A**). The results showed no significant difference between the clusters and risk groups, and the death proportion in the high-risk group was higher. The top three genes with the highest mutation frequencies in the GS-like cluster were *APC* (86%), *TNN* (40%), and *TP53* (65%) (**Figure 4B**), whereas those in the GU-like cluster were *APC* (53%), *TTN* (69%), and *TP53* (31%) (**Figure 4C**). In general, the mutation frequency in the GU-like cluster was higher than that in the GS-like group, and the frequencies of multi-hit and frame-shift mutations were much higher. LASSO and SVM

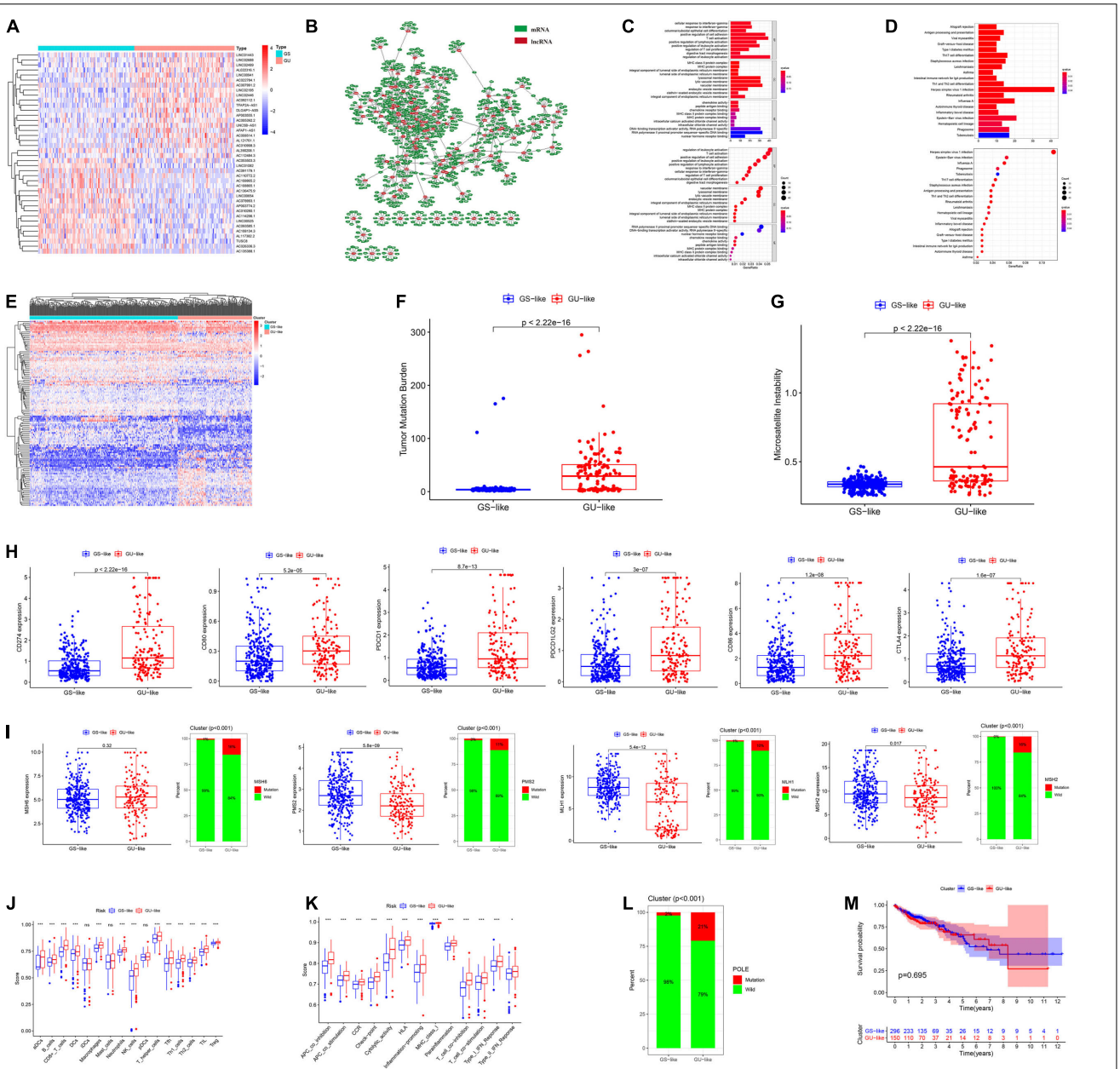

FIGURE 1 | Hierarchical clustering and analysis of the genome stable (GS)-like and genome unstable (GU)-like clusters. **(A)** The heatmap of 123 genome instability-related lncRNAs (GIRlncRs) between the GS and GU groups. **(B)** The coexpression network of the GIRlncRs and top-10 correlated mRNAs for each lncRNAs by Pearson's correlation. The functional enrichment analysis of the coexpressed mRNAs of GIRlncRs based on GO **(C)** and KEGG **(D)**. **(E)** The unsupervised hierarchical clustering based on 123 genome instability-related lncRNAs. The comparison of the tumor mutational burden **(F)**, microsatellite instability **(G)**, expression of six immune checkpoint-related genes (*CD274* (*PD-L1*), *CD80*, *PDCD1* (*PD-1*), *PDCD1LG2*(*PD-L2*), *CD86*, and *CTLA4*) **(H)**, expression and mutation rate of four DNA mismatch repair protein gene (*MLH1*, *MSH2*, *MSH6*, and *PMS2*) **(I)** and mutation rate of *POLE* **(L)** between the two clusters by Mann-Whitney *U* test. The comparison of the immune cell infiltration **(J)** and Immune functions **(K)** of the two clusters by ssGSEA. **(M)** The survival analysis of the two clusters by log-rank test. $^{*}p < 0.05$; $^{***}p < 0.001$; and *ns*, not significant.

algorithms were utilized to extract hub-lncRNAs in GS- and GU-clusters for further investigation. We selected the minimum value of λ, a penalty parameter of 0.1, and the L1 norm of the default (**Figures 4D,E**). Here, 43 lncRNAs were screened using LASSO regression. The average weight of each lncRNA acquired from the 10-fold test SVM algorithm is provided in **Supplementary Table 5**. The cut-off value was set at | 0.28|. The Venn plot of the selection process of hub-lncRNA among SVM, LASSO, and the prognostic signature is presented in **Figure 4F**. In total, 55 hub lncRNAs were identified. The screening process of the lncRNAs, miRNAs, and mRNAs included in the ceRNA network is presented in **Figure 4G**.

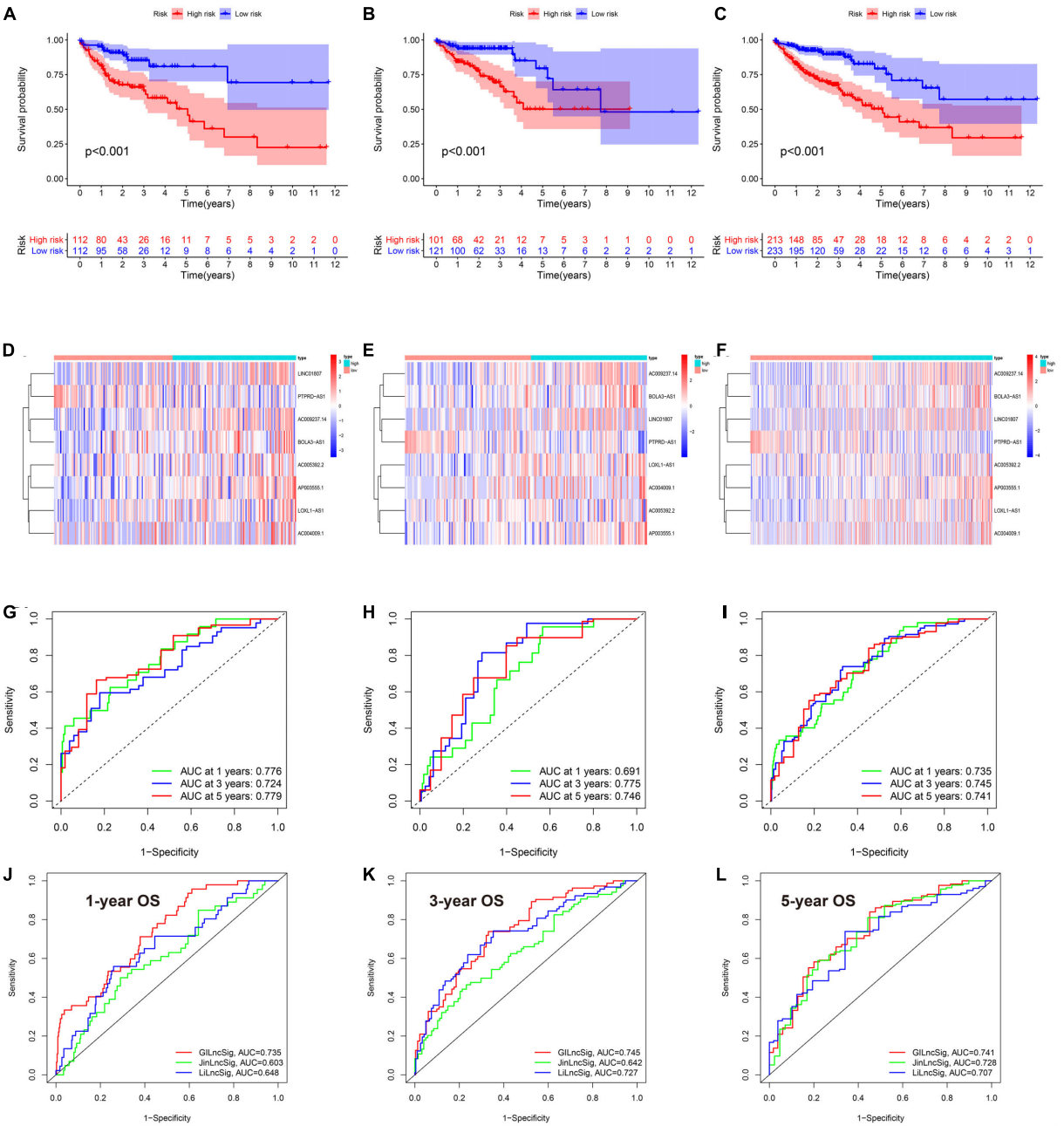

FIGURE 2 | The eigth lncRNA prognostic signature in TCGA cohort. **(A–C)** Survival analysis between the high- and low-risk groups based on overall survival **(D–F)**. Heatmap of the eight lncRNA between high- and low-risk groups **(G–I)**. rROCeceiver operating characteristics curve of the signature model based on OS at 1-3-5-year. AUC, the area under the curve. **(A,D,G)** Training cohort; **(B,E,H)** are test cohort; **(C,F,I)** are TCGA cohort. Model comparison with two previously published lncRNA prognostic signatures by ROC curve based on overall survival in TCGA cohort at 1-**(J)**, 3-**(K)**, 5-**(L)** year.

Genome Instability-Related Competing Endogenous RNA Network and Single-Gene Analysis

The ENCORI database was utilized to predict the interactions between hub lncRNAs and their target mRNAs. The constructed ceRNA network is shown in **Figure 5A** and **Table 2**. Seven lncRNA-miRNA-mRNA pairs were found in the ceRNA network. To comprehensively understand these three lncRNAs (*BOLA3-AS1*, *AC124067.4*, and *AL161772.1*) and four target RNAs (*NINL*, *SALL4*, *TNFSF11*, *PHYHIPL*), we performed differential expression, cancer stemness, immune subtype, TME infiltration, and drug sensitivity analyses.

First, we compared the expression of seven genes between normal and tumor tissues using the Mann-Whitney *U* test in COAD. As shown in **Figures 5B–H**, *AC124067.4*, *AL161772.1*,

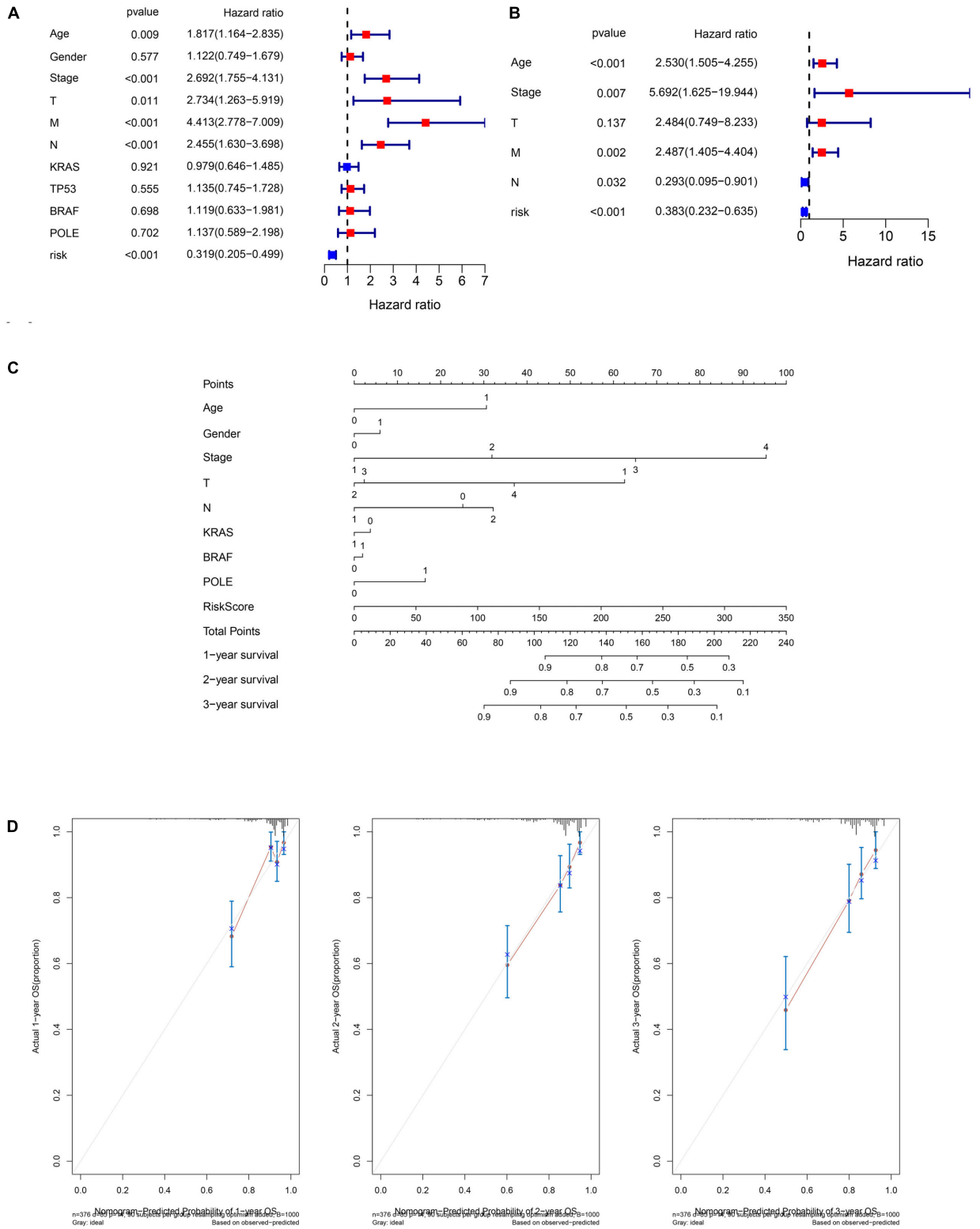

FIGURE 3 | Independent prognostic analysis and nomogram of the 8-lncRNA prognostic signature. **(A)** Univariate Cox regression of the TCGA cohort. **(B)** Multivariate Cox regression of the TCGA cohort based on overall survival. Age (>65 vs. ≤65), gender (male vs. female), stage (III/IV vs. I/II), T (III/IV vs. I/II), M (I vs. 0), N (I/II vs. 0), *KRAS* (mutation vs. wild), *TP53* (mutation vs. wild), *BRAF* (mutation vs. wild), *POLE* (mutation vs. wild), and risk (low-risk vs. high-risk). **(C)** Nomogram of the TCGA cohort based on overall survival (M was not included in the nomogram due to only 20 patients with M1). **(D)** Calibration curve of the TCGA cohort based on overall survival at 1, 2, and 3 years.

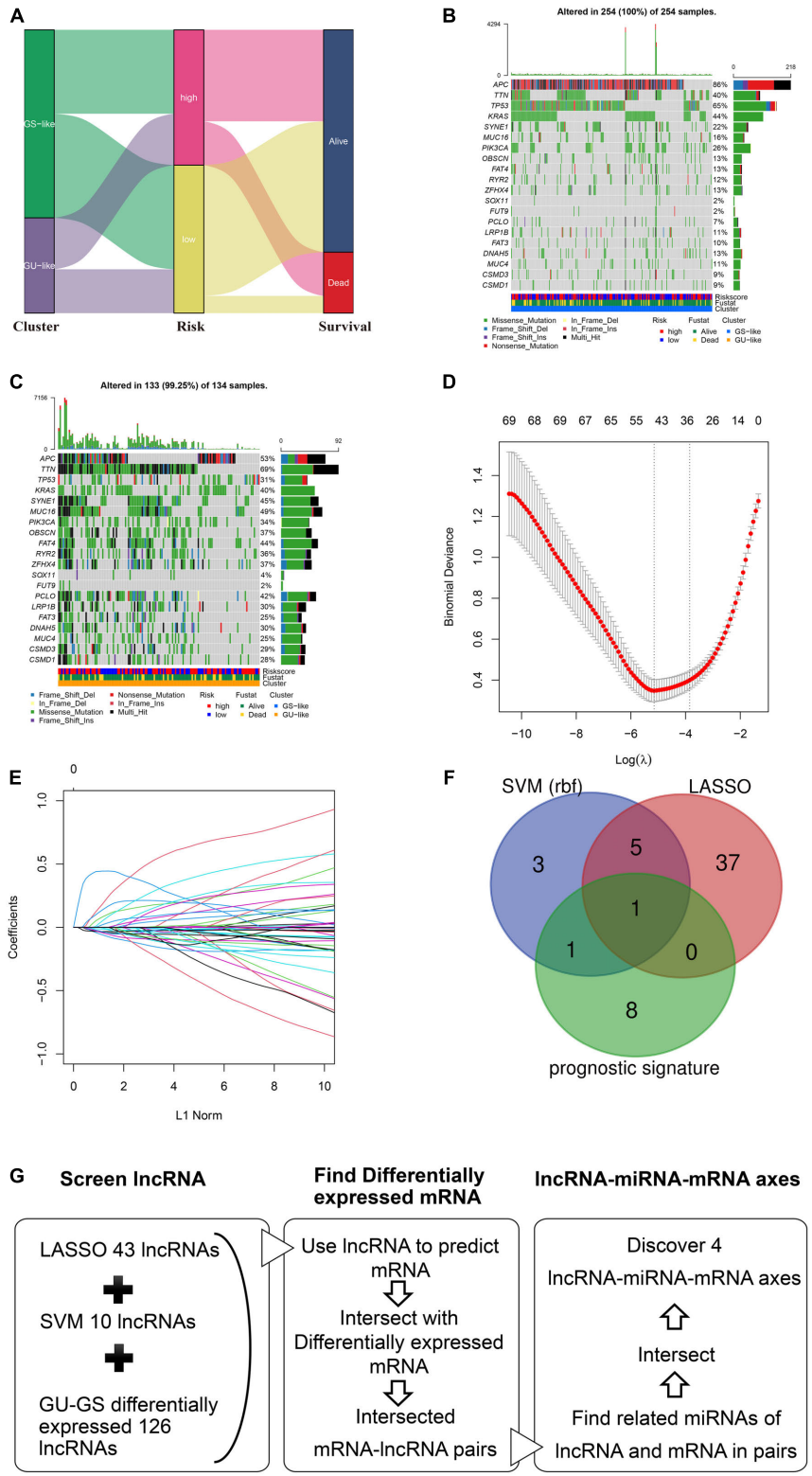

FIGURE 4 | Analysis of mutation profile and identification of hub-lncRNAs in genome stable (GS)- and genome unstable (GU)-like clusters. **(A)** Sankey plot of the relationship among GS- and GU-like clusters, risk groups, and survival status. The mutation profile of GS-like cluster **(B)** and GU-like cluster **(C)**. **(D)** The selection of λ in least absolute shrinkage and selection operator regression. **(E)** The selection of L1 norm in LASSO regression. **(F)** The Venn plot of hub-lncRNA in SVM (support vector machine), LASSO, or prognostic signature. **(G)** Screening process of the lncRNA, miRNA, mRNA included in the ceRNA network.

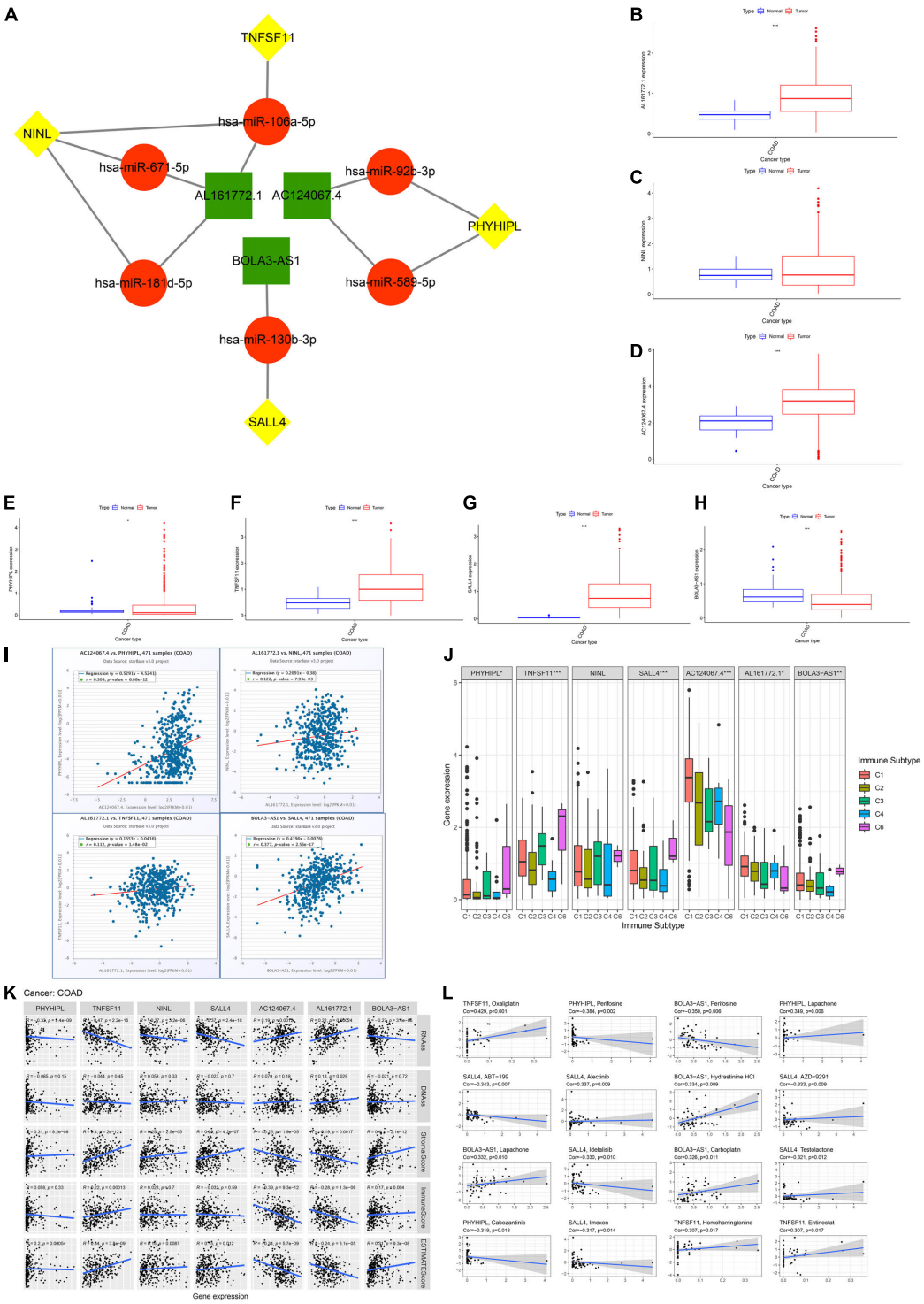

FIGURE 5 | Competing endogenous RNA (ceRNA) network construction and immune, cancer stemness, and drug sensitivity analysis. **(A)** The genome instability-related ceRNA network in colon adenocarcinoma (COAD) based on ENCORI. **(B–H)** The differential expression analysis included three lncRNAs (*BOLA3-AS1*, *AC124067.4*, *AL161772.1*) and four target mRNAs (*NINL*, *SALL4*, *TNFSF11*, *PHYHIPL*) by Mann-Whitney *U* test. **(I)** The correlation between the expression of each lncRNA and its target mRNAs based on ENCORI. **(J)** The association between the seven gene expression and five immune subtypes in COAD. **(K)** The association between the seven-gene expression and cancer stemness based on mRNA expression (ssRNA) and DNA methylation patterns (DNAss); the association between the seven-gene expression and the ESTIMATE immune score, stromal score, and ESTIMATE score. **(L)** The association between the seven-gene expression between drug sensitivity based on the NCI60 database (top 16 ranked by correlation). *$p < 0.05$, ** $p < 0.01$, and ***$p < 0.001$.

TABLE 2 | The genome instability-related competing endogenous RNA network in COAD.

lncRNA	miRNA	mRNA
AL161772.1	hsa-miR-106a-5p	NINL
AL161772.1	hsa-miR-671a-5p	NINL
AL161772.1	hsa-miR-181d-5p	NINL
AL161772.1	hsa-miR-106a-5p	TNFSF11
AC124067.4	hsa-miR-92b-3p	PHYHIPL
AC124067.4	hsa-miR-589-5p	PHYHIPL
BOLA3-AS1	hsa-miR-130b-3p	SALL4

SALL4, and *TNFSF11* were highly expressed in COAD, whereas *BOLA3-AS1* and *PHYHIPL* were expressed at low levels ($p < 0.05$). These results indicate that *AC124067.4*, *AL161772.1*, *SALL4*, and *TNFSF11* might promote COAD development and that *BOLA3-AS1* and *PHYHIPL* might inhibit its development (**Figure 5I**). As expected, the four lncRNA-mRNA expression patterns met the ceRNA criterion, especially *AC124067.4-PHYHIPL* ($r = 0.309$, $p = 6.88e\text{-}12$) and *BOLA3-AS1-SALL4* ($r = 0.377$, $p = 2.56e\text{-}17$). It has been reported that genome instability is closely related to tumor immunity. ANOVA was used to detect whether the expression of the seven genes was significantly related to the immune subtypes in COAD (**Figure 5J**). The results showed that six genes (*BOLA3-AS1*, *AC124067.4*, *AL161772.1*, *SALL4*, *PHYHIPL*, and *TNFSF11*) were significantly associated with the COAD immune subtype ($p < 0.05$), indicating that these seven genes could modulate tumor immune functions at the genetic level. These seven genes were also closely related to genome instability and immune-related genes (**Supplementary Figure 2**). All seven genes were positively related to *MLH1*, *PMS2*, and *NORAD* ($p < 0.01$). In addition, most genes (4/7, 57.1%) were negatively correlated with *PD-L1* (*CD274*; $p < 0.05$). These findings suggest that the high expression of these seven genes contributes to genomic integrity and predicts poor ICI outcomes. Moreover, these seven genes are closely related to COAD TME infiltration and function (**Figure 5K**). Most genes were positively related to stromal cell infiltration (5/7, 71.4%) and immune cell infiltration (4/7, 57.1%) and negatively related to tumor purity (5/7, 71.4%). According to the Spearman's correlation between cancer stemness features and these seven genes, we found that most genes were negatively related to cancer stemness (5/7 (71.4%) for RNAss and 4/7 (57.1%) for DNAss; **Figure 5K**). Finally, drug sensitivity analysis was performed to explore the relationship between the seven genes and drug resistance. The results showed that the expression of these seven genes was positively associated with the sensitivity of drugs regulating DNA replication and synthesis. For example, *TNFSF11* expression was positively associated with sensitivity to oxaliplatin, a common platinum-based antineoplastic drug for colorectal cancer, which is believed to function by blocking the duplication of DNA ($r = 0.429$, $p < 0.001$). Meanwhile, some protein kinase inhibitors, such as perifosine and cobimetinib, were negatively related to these genes. In conclusion, we proposed a novel ceRNA network that modulates genome instability and found that these seven genes are involved in TME infiltration, cancer stemness, and drug resistance.

Expression Pattern Validation by qPCR

To ascertain these potential prognostic biomarkers, three lncRNAs (*AC124067.4*, *AL161772.1*, *BOLA3-AS1*) with significant expression alterations and one mRNA *SALL4* were further performed by qRT-PCR validation. The results showed that *AC124067.4*, *AL161772.1*, and *SALL4* gene levels were significantly increased in COAD cell lines (**Figures 6A–D**) whereas *BOLA3-AS1* (**Figure 6**) was significantly reduced, which was consistent with the above analysis. Taken together, the expressions of *AC124067.4*, *AL161772.1*, and *SALL4* were significantly upregulated, and their expression level was also associated with the OS rate in patients with COAD. These findings indicate the possibility of using the panel as a prognostic biomarker for COAD.

Mutation Analysis

First, we explored the rates of alteration and types with respect to the four target mRNAs. As shown in **Figures 7A–D**, the rates of *NINL*, *PHYHIPL*, *SALL4*, and *TNFSF11* alteration were 5%, 0.8%, 6%, and 2%, respectively. For *NINL* and *SALL4*, somatic mutations and CNVs accounted for almost half of these for each. Regarding *PHYHIPL* alterations, somatic mutations were predominant, whereas CNVs formed the majority of *TNFSF11* alterations. Missense mutations accounted for most somatic mutations among the four gene alterations, and amplification accounted for most CNVs among the *NINL*, *SALL4*, and *TNFSF11* alterations. The alteration sites of each target gene were also explored. Notably, all four gene alteration sites were dispersed across the entire gene, rather than clustering on specific domains, indicating that the four-gene alterations mainly affect mRNA expression but not the coded protein activity (**Figures 7E–H**). Therefore, we investigated whether alterations in the four genes were associated with their expression. As expected, three genes (*NINL*, *SALL4*, and *TNFSF11*) were expressed at low levels for mutated types, and the CNVs of the three genes were positively related to mRNA expression. However, the rate of *PHYHIPL* alterations was only 0.8%, and *PHYHIPL* expression was not related to its alteration type.

Microsatellite instability has become a recognized biomarker for immunotherapy and has been widely used in clinical practice. It is speculated that the seven genes proposed in this study could serve as clinically novel TMB and MSI biomarkers. As shown in **Figures 8A–D**, we explored the association between each gene and TMB/MSI in the pan-cancer database (the abbreviations are provided in **Supplementary Table 6**). Surprisingly, all the expression of all seven genes was negatively related to TMB and MSI scores in COAD ($p < 0.05$), indicating that these seven genes could maintain genomic integrity in COAD, which was particularly apparent for *AC124067.4* (correlation coefficient *R* reached approximately −0.4 for TMB and −0.5 for MSI) and *SALL4* (R reached approximately −0.3 for TMB and −0.35 for MSI; **Figures 8A–D**). Moreover, we compared MSI status between patients with mutated and wild-type disease using cBioPortal. The MSI-H proportions were greater in patients with the mutated type than in those with the wild type according to all four genes (**Figure 8E**). Especially, the MSI-H proportion

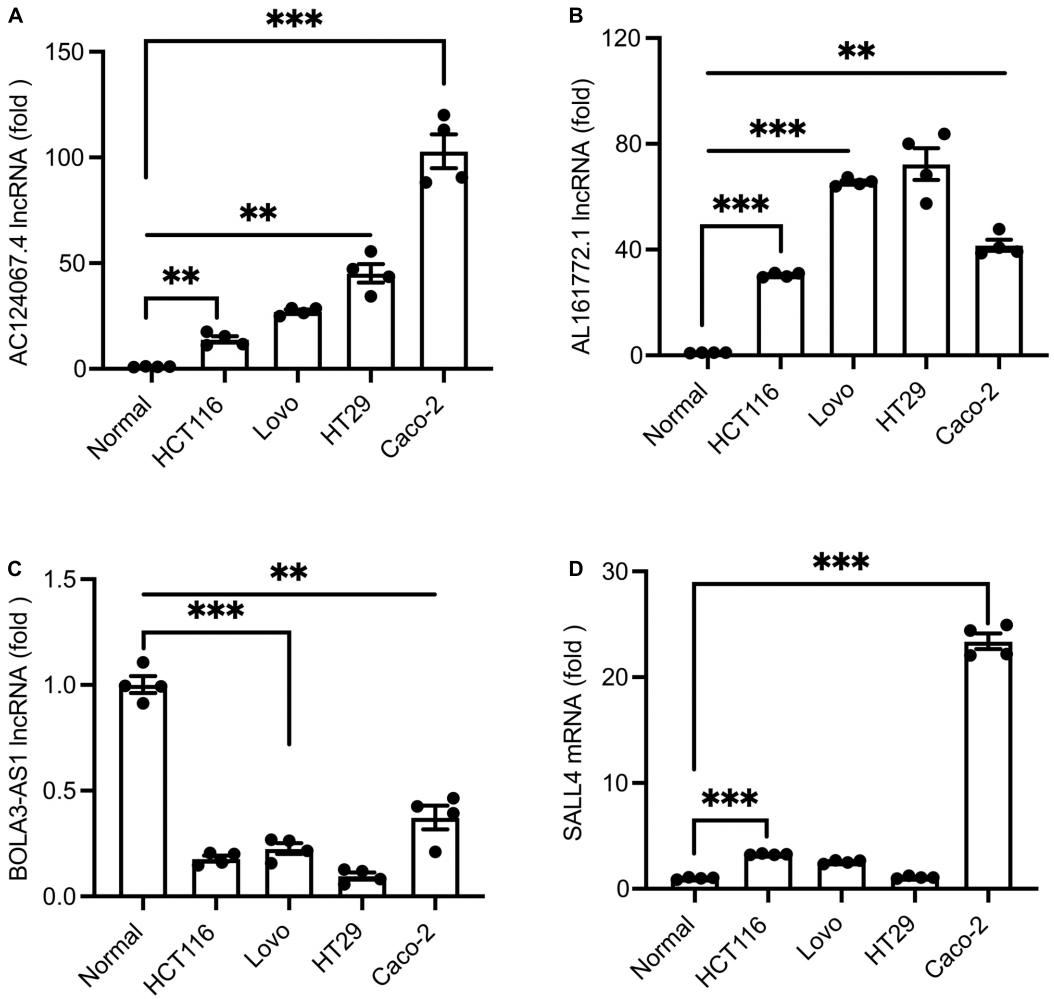

FIGURE 6 | (A–D) qPCR verification of the expression levels of differential lncRNAs in COAD cell lines and normal cells. Values are shown as the mean ± SEM ($n = 4$). ***$p < 0.001$ and **$p < 0.01$ by Student's *t*-test. Normal cells were employed as controls.

reached almost 60% in patients with mutated *SALL4*, whereas only 10% of wild-type patients had MSI-H. We next explored the association between the seven CNVs and the MSI status. As shown in **Figure 8F**, the CNVs of *NINL*, *SALL4*, and *TNFSF11* were fewer in patients with MSI-H COAD. In conclusion, the seven genes proposed in this study were closely related to genome instability in COAD and could serve as novel immunotherapy outcome biomarkers.

DISCUSSION

This study presented primary work comprising a computational bioinformatics analysis to identify the critical genetic/epigenetic biomarkers from the genome instability-related ceRNA network involved in COAD. This study first provided a hierarchical clustering method to stratify patients for immunotherapy and a prognostic signature for clinical reference. Subsequently, genome insatiability-related ceRNA network genes were identified as critical regulators modulating TME infiltration, cancer stemness, and drug resistance. The identification of the lncRNA-miRNA-mRNA axes *AL161772.1-has-miR-671-5p* (*hsa-miR-181d-5p*, *has-miR-106a-5p*)*-NINL*, *AL161772.1-has-miR-106a-5p-TNFSF11*, *AC124067.4-hsa-miR-92b-3p* (*hsa-miR-589-5p*)*-PHYHIPL*, and *BOLA3-AS1-has-miR-130b-3p-SALL4* and the construction of a ceRNA network based on these four axes were the most significant findings of this study and are the main object of this discussion.

Among the four identified lncRNA-miRNA-mRNA signaling axes, *BOLA3-AS1-has-miR-130b-3p-SALL4* was considered the most valuable in modulating the tumorigenesis of COAD. *SALL4* and *BOLA3-AS1* were identified and defined as the most promising biomarkers, not only because of their respective high correlations with the same miRNA, which plays a role as a sponge and an intermediate, but also because of their highly consistent and synergic features. The explicit role of *SALL4* in COAD can be attributed to its pivotal role in cell proliferation, apoptosis, invasive migration, chemoresistance,

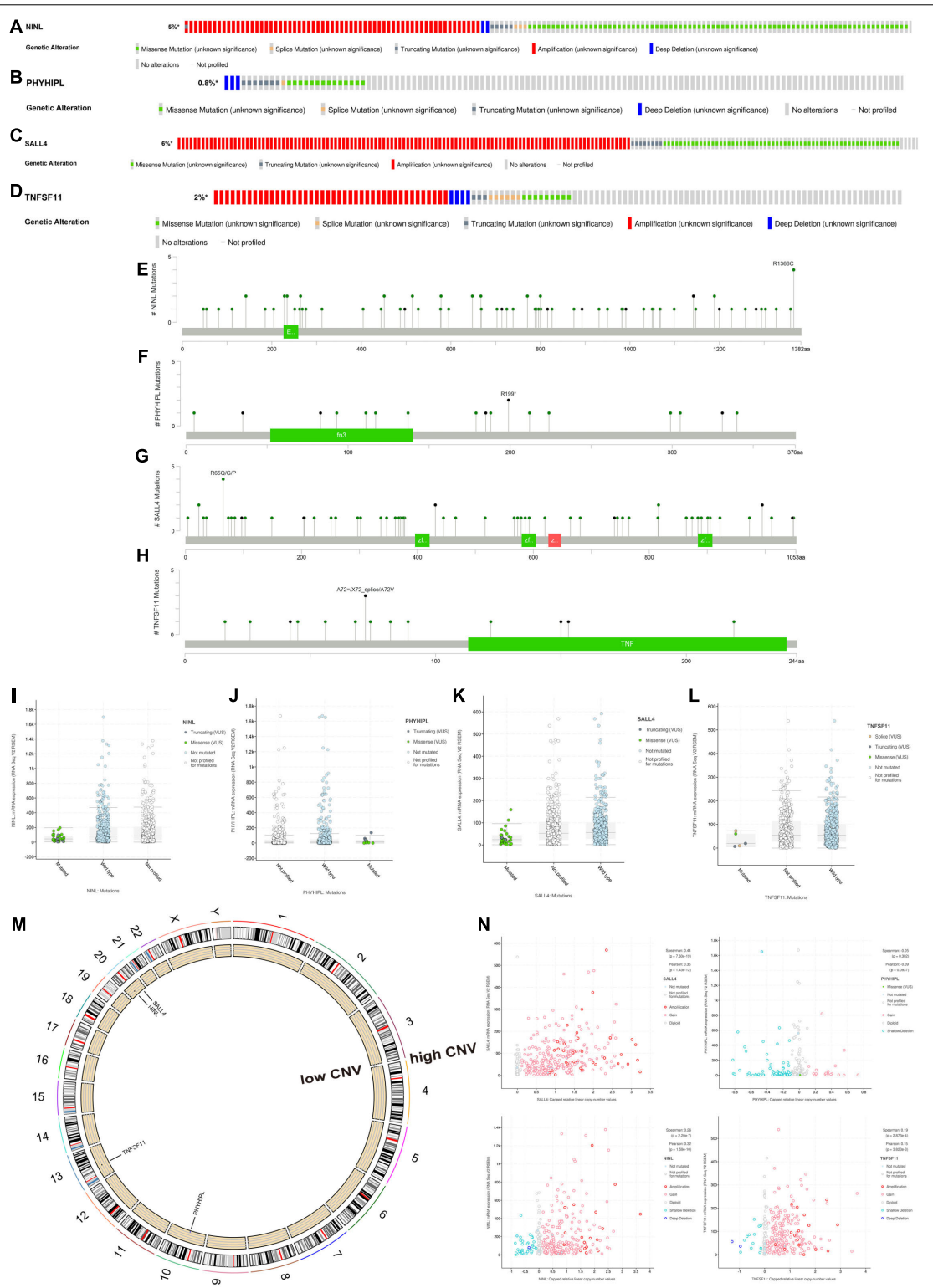

FIGURE 7 | Somatic mutation and copy number variation (CNV) analysis of three lncRNAs (*BOLA3-AS1*, *AC124067.4*, *AL161772.1*) and four target mRNAs (*NINL*, *SALL4*, *TNFSF11*, *PHYHIPL*). The alteration rates and types of *NINL* **(A)**, *PHYHIPL* **(B)**, *SALL4* **(C)**, and *TNFSF11* **(D)**. The alteration sits of each gene on the coding protein domains for *NINL* **(E)**, *PHYHIPL* **(F)**, *SALL4* **(G)**, and *TNFSF11* **(H)**. The comparison of gene expression between wild type and mutated type for *NINL* **(I)**, *PHYHIPL* **(J)**, *SALL4* **(K)**, and *TNFSF11* **(L)**. **(M)** The location on a chromosome and the most common CNV status of the four target mRNAs. **(N)** The association between gene expression and CNV for *NINL*, *PHYHIPL*, *SALL4*, and *TNFSF11*.

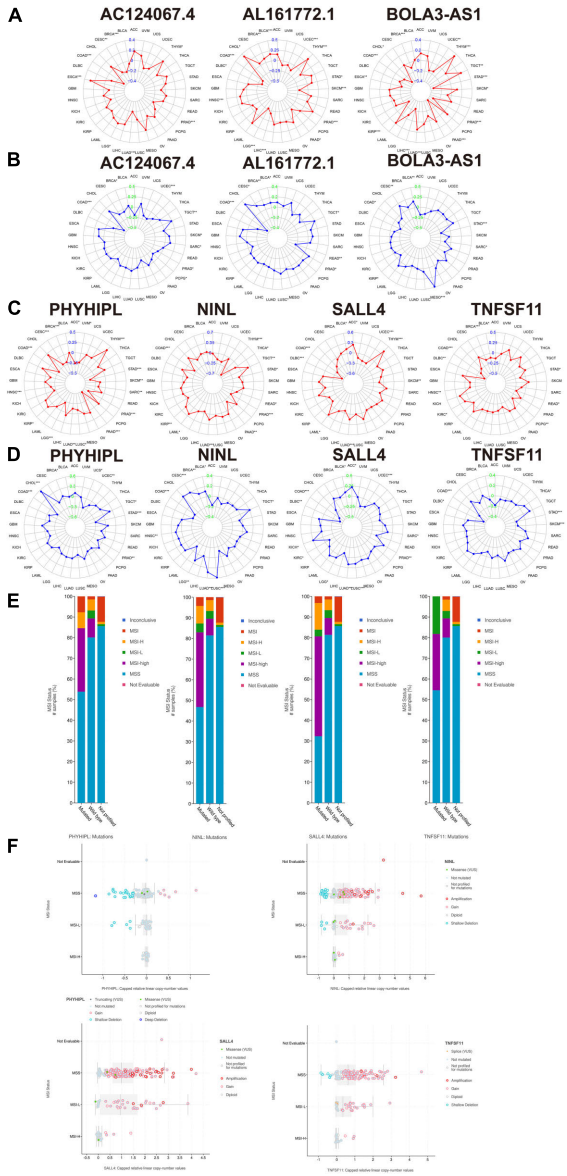

FIGURE 8 | The association between the three lncRNAs (*BOLA3-AS1*, *AC124067.4*, and *AL161772.1*), four target mRNAs (*NINL*, *SALL4*, *TNFSF11*, and *PHYHIPL*), and the tumor mutational burden (TMB), microsatellite instability (MSI) score, and MSI status. **(A)** The association between the three lncRNA expression and the TMB in pan-cancer using Spearman's correlation. **(B)** The association between the three lncRNA expression and the MSI score in pan-cancer. The association between the four target mRNAs and the TMB **(C)** and MSI score **(D)** in pan-cancer. **(E)** The comparison of the MSI status between the wild type and mutated type of the four target mRNAs (adjusted by each gene mutation rate) in COAD based on cBioPortal. **(F)** The association between the MSI status and the copy number variation of the four target mRNAs in COAD based on cBioPortal.

and the maintenance of cancer stem cells (Zhang et al., 2015). First, *SALL4* is highly expressed and positively associated with *BOLA3-AS1* in COAD tumor tissues (**Figure 5I**), suggesting a positive regulation between them. Second, this work provides a novel viewpoint on how *SALL4* interacts with cancer cell stemness, thereby participating in tumor metastasis and progression. This work resulted in an estimate stemness score to contrast and evaluate the degree of stemness associated with genes (**Figure 5K**). *SALL4* and *BOLA3-AS1* both yielded impressive results in the multidimensional grading scale of the stemness score. *SALL4* has long been regarded as an essential modulator in maintaining embryonic stem cell (ESC) self-renewal and pluripotency (Miettinen et al., 2014). Considering that it is largely considered that ESCs and cancer stem cells share similar metabolic states, *SALL4* regulates the activation of several critical signaling pathways in stem cells by upregulating the expression of target genes in the Wnt/β-catenin pathway, and thus, its powerful regulatory role in cancer stemness might be explained in a similar way (Ma et al., 2006; Jang et al., 2015). Third, *SALL4* and *BOLA3-AS1* were associated with significant drug sensitivity (**Figure 5l**). Among the selected panels, filtered based on significance ranking, *SALL4*-related and *BOLA3-AS1*-related drugs accounted for the largest proportion. Through a literature search on PubMed, almost all related drugs are associated with their outstanding function as inhibitors of oxidative phosphorylation (de Witte et al., 2004; Burgeiro et al., 2013; Hammadi et al., 2015). Tan et al. (2019) reported the high-throughput screening of inhibitors of oxidative phosphorylation and *SALL4*, activating the transcription of genes that regulate oxidative phosphorylation to increase oxygen consumption, mitochondrial membrane potential, and ATP generation in cancer cells, which is the most predominant scientific finding on *SALL4*. Oxidative phosphorylation plays a critical role in the repair of DNA damage repair (dMMR). This is associated with the genome instability discussed in this article because dMMR is one of the culprits regulating genome instability. It is important to consider how *SALL4* was selected at first; specifically, it comprises one end of an axis, and at the other end is one of the most core genome instability-related lncRNAs, *BOLA3-AS1*. An entire ceRNA network was constructed on this basis. Therefore, although we still do not know the precise role of *SALL4* in COAD, the mechanism by which it influences genome instability and further promotes tumor progression *via* such a *BOLA3-AS1*-miRNA-*SALL4* axis is very likely to exist and could be explained.

Another important line of evidence when discussing these axes is the pan-cancer TMB/MSI correlation. For the *AL161772.1*-miRNA-*NINL* axes, both *AL161772.1* and *NINL* showed a significantly negative correlation with TMB and MSI in COAD, which indicates a function in maintaining genomic integrity. Similarly, *AL161772.1-has-miR-106a-5p-TNFSF11* and *AC124067.4-hsa-miR-92b-3p*(*hsa-miR-589-5p*)*-PHYHIPL* both reduce the TMB and MSI in COAD, decreasing the risk of alterations and genome instability.

Diverse degrees of mutations were noted for *NINL*, *TNFSF11*, and *PHYHIPL*. *NINL* and *TNFSF11* have relatively high genetic alteration rates, and the type is primarily amplification. The sites of *NINL* alterations were the coding protein domains, which were scattered and concentrated in segments. The main mutation site of *NINL* is on chromosome 22, which is associated with relatively lower CNV, which is the same as that for *SALL4*, but *SALL4* has a higher CNV, and the mutation rate of *PHYHIPL* is not high. The genetic alteration site was also not dense. It is reasonable to speculate that major alterations do not include *PHYHIPL* mutations.

Two major weaknesses of this study should be further improved. One is that even though a novel ceRNA mechanism, regulating certain lncRNA-miRNA-mRNA axes and cancer promotion in COAD, was suggested, whether these genes could play a synergistic role in regulating tumor progression needs to be confirmed. More work also needs to be done to provide more details on how these genes interact with each other at the cellular level, with validation based on a clinical cohort. Another limitation is that the crucial genes screened have been rarely reported and researched previously. Although it is easy to find clues relevant to this topic, it is difficult to find direct support of the importance of these genes in the literature. In fact, this finding underlies the importance of this work, which suggests valuable biomarkers for COAD treatment for further research.

This study constructed a prognostic signature of genome instability-related lncRNA and immunotherapy for clinical reference. It also provided a potential ceRNA mechanism through which lncRNAs play a role via specific lncRNA-miRNA-mRNA axes to participate in the process of cancer development.

DATA AVAILABILITY STATEMENT

The original contributions presented in the study are included in the article/**Supplementary Material**, further inquiries can be directed to the corresponding author/s.

AUTHOR CONTRIBUTIONS

ZR and ZW performed the data analysis and wrote the first draft. DG and HM revised the first and the second drafts. MC and YZ performed the experiments. YZ revised the second draft. JZ designed and supervised the study. All authors contributed to the article and approved the submitted version.

FUNDING

This work was supported by the National Natural Science Foundation of China (82071791 and 31471016), the CAMS Initiative for Innovative Medicine (2016-I2 M-1-008), the National Key Research and Development Program of China (2016YFA0101001), and the CAMS Basic Research Expenses (2018PT31052).

ACKNOWLEDGMENTS

We would like to thank Dr. Jonathan Josephs-Spaulding for his linguistics assistance during the preparation of this manuscript.

SUPPLEMENTARY MATERIAL

The Supplementary Material for this article can be found online at: https://www.frontiersin.org/articles/10.3389/fcell.2021.740455/full#supplementary-material

Supplementary Figure 1 | Genome instability and immune analysis of high- and low-risk groups. **(A)** Association between somatic mutation count and risk score. Comparison of tumor mutational burden **(B)**, microsatellite instability **(C)**, expression and mutation rate of four DNA mismatch repair protein genes (*MLH1*, *MSH2*, *MSH6*, and *PMS2*) **(D)**, and expression of six immune checkpoint-related genes (*CD274* (*PD-L1*), *CD80*, *PDCD1* (*PD-1*), *PDCD1LG2* (*PD-L2*), *CD86*, *CTLA4*) **(E)** between the two groups using the Mann-Whitney *U* test. Comparison of immune cell infiltration **(F)** and immune functions **(G)** of the two groups using single-sample gene set enrichment analysis (ssGSEA). $*p < 0.05$; $**p < 0.01$; and $***p < 0.001$. **(H)** Comparison of the mutation rate of *POLE* between the two groups using the Mann-Whitney *U*-test. **(I)** Comparison of BRAF mutation rates. **(J)** Survival analysis among *BRAF* mutated/high-risk, *BRAF* mutated/low-risk, *BRAF* wild/high-risk, *BRAF* wild/low-risk groups by Kaplan-Meier curve and log-rank test.

Supplementary Figure 2 | Supplemental gene correlation analysis of the three lncRNAs (*BOLA3-AS1*, *AC124067.4*, and *AL161772.1*) and four target mRNAs (*NINL*, *SALL4*, *TNFSF11*, and *PHYHIPL*). **(A)** The association between the expression of seven genes and genome instability and immune-related genes (*PDCD1*, *CD274*, *PDCD1LG2*, *CTLA4*, *CD80*, *CD86*, *MSH2*, *MLH1*, *PMS2*, *MSH6*, *NOARD*, *GUARDIN*) by Spearman's correlation. **(B)** Correlation between the expression of each miRNA and its paired lncRNAs based on ENCORI. **(C)** Correlation between the expression of each miRNA and its paired mRNAs based on ENCORI. $*p < 0.05$; $**p < 0.01$; and $***p < 0.001$.

Supplementary Figure 3 | The association between the three lncRNAs (*BOLA3-AS1*, *AC124067.4*, and *AL161772.1*), four target mRNAs (*NINL*, *SALL4*, *TNFSF11*, *PHYHIPL*), and each specific type of immune cell based on the CIBERSORT database.

REFERENCES

Ashburner, M., Ball, C. A., Blake, J. A., Botstein, D., Butler, H., Cherry, J. M., et al. (2000). Gene ontology: tool for the unification of biology. *Gene Ontol. Consort. Nat. Genet.* 25, 25–29. doi: 10.1038/75556

Bhan, A., Soleimani, M., and Mandal, S. S. (2017). Long noncoding RNA and cancer: a new paradigm. *Cancer Res.* 77, 3965–3981. doi: 10.1158/0008-5472.Can-16-2634

Boland, C. R., and Goel, A. (2010). Microsatellite instability in colorectal cancer. *Gastroenterology* 138, 2073–2087.e3. doi: 10.1053/j.gastro.2009.12.064

Bradburn, M. J., Clark, T. G., Love, S. B., and Altman, D. G. (2003). Survival analysis part II: multivariate data analysis–an introduction to concepts and methods. *Br. J. Cancer* 89, 431–436. doi: 10.1038/sj.bjc.6601119

Brody, H. (2015). Colorectal cancer. *Nature* 521:S1. doi: 10.1038/521S1a

Burgeiro, A., Pereira, C. V., Carvalho, F. S., Pereira, G. C., Mollinedo, F., and Oliveira, P. J. (2013). Edelfosine and perifosine disrupt hepatic mitochondrial oxidative phosphorylation and induce the permeability transition. *Mitochondrion* 13, 25–35. doi: 10.1016/j.mito.2012.11.003

Cerami, E., Gao, J., Dogrusoz, U., Gross, B. E., Sumer, S. O., Aksoy, B. A., et al. (2012). The cBio cancer genomics portal: an open platform for exploring multidimensional cancer genomics data. *Cancer Dis.* 2, 401–404. doi: 10.1158/2159-8290.Cd-12-0095

Chen, J., Shishkin, A. A., Zhu, X., Kadri, S., Maza, I., Guttman, M., et al. (2016). Evolutionary analysis across mammals reveals distinct classes of long non-coding RNAs. *Genome Biol.* 17:19. doi: 10.1186/s13059-016-0880-9

Dagogo-Jack, I., and Shaw, A. T. (2018). Tumour heterogeneity and resistance to cancer therapies. *Nat. Rev. Clin. Oncol.* 15, 81–94. doi: 10.1038/nrclinonc.2017.166

de Witte, N. V., Stoppani, A. O., and Dubin, M. (2004). 2-Phenyl-beta-lapachone can affect mitochondrial function by redox cycling mediated oxidation. *Arch. Biochem. Biophys.* 432, 129–135. doi: 10.1016/j.abb.2004.09.020

Dudley, J. C., Lin, M. T., Le, D. T., and Eshleman, J. R. (2016). Microsatellite instability as a biomarker for PD-1 blockade. *Clin. Cancer Res.* 22, 813–820. doi: 10.1158/1078-0432.Ccr-15-1678

Fatica, A., and Bozzoni, I. (2014). Long non-coding RNAs: new players in cell differentiation and development. *Nat. Rev. Genet.* 15, 7–21.

Ganesh, K., Stadler, Z. K., Cercek, A., Mendelsohn, R. B., Shia, J., Segal, N. H., et al. (2019). Immunotherapy in colorectal cancer: rationale, challenges and potential. *Nat. Rev. Gastroenterol. Hepatol.* 16, 361–375. doi: 10.1038/s41575-019-0126-x

Garrido-Castro, A. C., Lin, N. U., and Polyak, K. (2019). Insights into molecular classifications of triple-negative breast cancer: improving patient selection for treatment. *Cancer Dis.* 9, 176–198. doi: 10.1158/2159-8290.Cd-18-1177

Goyal, B., Yadav, S. R. M., Awasthee, N., Gupta, S., Kunnumakkara, A. B., and Gupta, S. C. (2021). Diagnostic, prognostic, and therapeutic significance of long non-coding RNA MALAT1 in cancer. *Biochim. et Biophy. Acta Rev. Cancer* 1875:188502. doi: 10.1016/j.bbcan.2021.188502

Hammadi, S. A., Almarzooqi, S., Abdul-Kader, H. M., Saraswathiamma, D., and Souid, A. K. (2015). The PI3Kδ inhibitor idelalisib suppresses liver and lung cellular respiration. *Int. J. Physiol. Pathophysiol. Pharmacol.* 7, 115–125.

Hanahan, D., and Weinberg, R. A. (2011). Hallmarks of cancer: the next generation. *Cell* 144, 646–674. doi: 10.1016/j.cell.2011.02.013

Hu, F., Wang, Q., Yang, Z., Zhang, Z., and Liu, X. (2020). Network-based identification of biomarkers for colon adenocarcinoma. *BMC Cancer* 20:668. doi: 10.1186/s12885-020-07157-w

Hu, W. L., Jin, L., Xu, A., Wang, Y. F., Thorne, R. F., Zhang, X. D., et al. (2018). GUARDIN is a p53-responsive long non-coding RNA that is essential for genomic stability. *Nat. Cell. Biol.* 20, 492–502. doi: 10.1038/s41556-018-0066-7

Hung, T., Wang, Y., Lin, M. F., Koegel, A. K., Kotake, Y., Grant, G. D., et al. (2011). Extensive and coordinated transcription of noncoding RNAs within cell-cycle promoters. *Nat. Genet.* 43, 621–629. doi: 10.1038/ng.848

Jang, H., Yang, J., Lee, E., and Cheong, J. H. (2015). Metabolism in embryonic and cancer stemness. *Arch. Pharm. Res.* 38, 381–388. doi: 10.1007/s12272-015-0558-y

Jin, L., Li, C., Liu, T., and Wang, L. (2020). A potential prognostic prediction model of colon adenocarcinoma with recurrence based on prognostic lncRNA signatures. *Hum. Genom.* 14:24. doi: 10.1186/s40246-020-00270-8

Kanduri, C. (2016). Long noncoding RNAs: Lessons from genomic imprinting. *Biochim. et Biophys. Acta (BBA) Gene Regulatory Mech.* 1859, 102–111.

Kanehisa, M., and Goto, S. (2000). KEGG: kyoto encyclopedia of genes and genomes. *Nucleic Acids Res.* 28, 27–30. doi: 10.1093/nar/28.1.27

Koch, L. (2017). The driving force of cancer evolution. *Nat. Rev. Genet.* 18:703. doi: 10.1038/nrg.2017.95

Li, J. H., Liu, S., Zhou, H., Qu, L. H., and Yang, J. H. (2014). starBase v2.0: decoding miRNA-ceRNA, miRNA-ncRNA and protein-RNA interaction networks from large-scale CLIP-Seq data. *Nucleic Acids Res.* 42, D92–D97. doi: 10.1093/nar/gkt1248

Li, Y., Jiang, T., Zhou, W., Li, J., Li, X., Wang, Q., et al. (2020). Pan-cancer characterization of immune-related lncRNAs identifies potential oncogenic biomarkers. *Nat. Commun.* 11:1000. doi: 10.1038/s41467-020-14802-2

Li, Z., Wang, D., and Yin, H. (2020). A seven immune-related lncRNA signature predicts the survival of patients with colon adenocarcinoma. *Am. J. Trans. Res.* 12, 7060–7078. *b-Z

Ma, Y., Cui, W., Yang, J., Qu, J., Di, C., Amin, H. M., et al. (2006). SALL4, a novel oncogene, is constitutively expressed in human acute myeloid leukemia (AML) and induces AML in transgenic mice. *Blood* 108, 2726–2735. doi: 10.1182/blood-2006-02-001594

Malta, T. M., Sokolov, A., Gentles, A. J., Burzykowski, T., Poisson, L., Weinstein, J. N., et al. (2018). Machine learning identifies stemness features associated with oncogenic dedifferentiation. *Cell* 173, 338–354.e15.

Miettinen, M., Wang, Z., McCue, P. A., Sarlomo-Rikala, M., Rys, J., Biernat, W., et al. (2014). SALL4 expression in germ cell and non-germ cell tumors: a systematic immunohistochemical study of 3215 cases. *Am. J. Surg. Pathol.* 38, 410–420. doi: 10.1097/pas.0000000000000116

Morel, A. P., Ginestier, C., Pommier, R. M., Cabaud, O., Ruiz, E., Wicinski, J., et al. (2017). A stemness-related ZEB1-MSRB3 axis governs cellular pliancy and breast cancer genome stability. *Nat. Med.* 23, 568–578. doi: 10.1038/nm.4323

Munschauer, M., Nguyen, C. T., Sirokman, K., Hartigan, C. R., Hogstrom, L., Engreitz, J. M., et al. (2018). The NORAD lncRNA assembles a topoisomerase complex critical for genome stability. *Nature* 561, 132–136. doi: 10.1038/s41586-018-0453-z

Newman, A. M., Steen, C. B., Liu, C. L., Gentles, A. J., Chaudhuri, A. A., Scherer, F., et al. (2019). Determining cell type abundance and expression from bulk tissues with digital cytometry. *Nat. Biotechnol.* 37, 773–782. doi: 10.1038/s41587-019-0114-2

Qin, S., Xu, L., Yi, M., Yu, S., Wu, K., and Luo, S. (2019). Novel immune checkpoint targets: moving beyond PD-1 and CTLA-4. *Mol. Cancer* 18:155. doi: 10.1186/s12943-019-1091-2

R Core Team (2013). R: A Language and Environment for Statistical Computing. Vienna: R Foundation for Statistical Computing.

Sansregret, L., Vanhaesebroeck, B., and Swanton, C. (2018). Determinants and clinical implications of chromosomal instability in cancer. *Nat. Rev. Clin. Oncol.* 15, 139–150. doi: 10.1038/nrclinonc.2017.198

Sanz-Garcia, E., Argiles, G., Elez, E., and Tabernero, J. (2017). BRAF mutant colorectal cancer: prognosis, treatment, and new perspectives. *Ann. Oncol. Off. J. Eur. Soc. Med. Oncol.* 28, 2648–2657. doi: 10.1093/annonc/mdx401

Schrock, A. B., Ouyang, C., Sandhu, J., Sokol, E., Jin, D., Ross, J. S., et al. (2019). Tumor mutational burden is predictive of response to immune checkpoint inhibitors in MSI-high metastatic colorectal cancer. *Ann. Oncol.* 30, 1096–1103. doi: 10.1093/annonc/mdz134

Shannon, P., Markiel, A., Ozier, O., Baliga, N. S., Wang, J. T., Ramage, D., et al. (2003). Cytoscape: a software environment for integrated models of biomolecular interaction networks. *Genome Res.* 13, 2498–2504. doi: 10.1101/gr.1239303

Su, M., Wang, H., Wang, W., Wang, Y., Ouyang, L., Pan, C., et al. (2018). LncRNAs in DNA damage response and repair in cancer cells. *Acta Biochim. et Biophys. Sin.* 50, 433–439. doi: 10.1093/abbs/gmy022

Tan, J. L., Li, F., Yeo, J. Z., Yong, K. J., Bassal, M. A., Ng, G. H., et al. (2019). New high-throughput screening identifies compounds that reduce viability specifically in liver cancer cells that express high levels of SALL4 by inhibiting oxidative phosphorylation. *Gastroenterology* 157, 1615–1629.e17. doi: 10.1053/j.gastro.2019.08.022

Thorsson, V., Gibbs, D. L., Brown, S. D., Wolf, D., Bortone, D. S., Yang, T.-H. O., et al. (2018). The immune landscape of cancer. *Immunity* 48, 812–830.e14.

Wang, F., Zhao, Q., Wang, Y. N., Jin, Y., He, M. M., Liu, Z. X., et al. (2019). Evaluation of POLE and POLD1 mutations as biomarkers for immunotherapy outcomes across multiple cancer types. *JAMA Oncol.* 5, 1504–1506. doi: 10.1001/jamaoncol.2019.2963

Yin, T., Zhao, D., and Yao, S. (2021). Identification of a genome instability-associated LncRNA signature for prognosis prediction in colon cancer. *Front. Genet.* 12:679150. doi: 10.3389/fgene.2021.679150

Yoshihara, K., Shahmoradgoli, M., Martínez, E., Vegesna, R., Kim, H., Torres-Garcia, W., et al. (2013). Inferring tumour purity and stromal and immune cell admixture from expression data. *Nat. Commun.* 4:2612. doi: 10.1038/ncomms3612

Zhang, X., Yuan, X., Zhu, W., Qian, H., and Xu, W. (2015). SALL4: an emerging cancer biomarker and target. *Cancer Lett.* 357, 55–62. doi: 10.1016/j.canlet.2014.11.037

Conflict of Interest: The authors declare that the research was conducted in the absence of any commercial or financial relationships that could be construed as a potential conflict of interest.

Publisher's Note: All claims expressed in this article are solely those of the authors and do not necessarily represent those of their affiliated organizations, or those of the publisher, the editors and the reviewers. Any product that may be evaluated in this article, or claim that may be made by its manufacturer, is not guaranteed or endorsed by the publisher.

frontiers in Cell and Developmental Biology

ORIGINAL RESEARCH
published: 25 October 2021
doi: 10.3389/fcell.2021.723346

TR35 Exerts Anti-tumor Effects by Modulating Mitogen-Activated Protein Kinase and STAT3 Signaling in Lung Cancer Cells

Zhiyong Shi[1†], Yang Gao[1†], Lifeng Feng[1], Wencong Tian[1], Zhihua Dou[2], Chen Liu[2], Jie Liu[1], Yang Xu[1], Yachen Wang[1], Jie Yan[1], Qiang Wu[3], Jing Li[1], Liang Yang[1], Zhaocai Zhang[4], Jie Yang[2*] and Zhi Qi[1*]*

[1] Department of Molecular Pharmacology, School of Medicine, Nankai University, Tianjin, China, [2] Department of Bioengineering, College of Life Science and Technology, Xinjiang University, Ürümqi, China, [3] Key Laboratory of Emergency and Trauma of Ministry of Education, Research Unit of Island Emergency Medicine, School of Tropical Medicine and Laboratory Medicine, Chinese Academy of Medical Sciences (No. 2019RU013), Hainan Medical University, Haikou, China, [4] Department of Critical Care Medicine, Second Affiliated Hospital, Zhejiang University School of Medicine, Hangzhou, China

Cancer is a complex disease extremely dependent on its microenvironment and is highly regulated by a variety of stimuli inside and outside the cell. Evidence suggests that active camel whey fraction (TR35) confer anti-tumor effects in non-small cell lung cancer (NSCLC). However, its exact mechanisms remain elusive. Here, we investigated the mechanisms underlying suppression of NSCLC cell growth and proliferation by TR35. Treatment of A549 and H1299 cells with TR35 suppressed their growth and enhanced apoptosis, as revealed by CCK-8, colony formation and flow cytometric analyses. We find that TR35 suppresses tumor growth in a xenograft nude mouse model without losses in body weight. RNA-seq and KEGG pathway analyses showed that the DEGs were enriched in mitogen-activated protein kinase (MAPK) and Jak-STAT signaling pathways. After test the key factors' activity associated with these pathways by Immunohistochemical (IHC) staining and western blotting, the activation of JNK phosphorylation and inhibition of p38 and STAT3 phosphorylation was observed both in TR35 treated lung cancer cell and tumor tissue. Taken together, these results showed that TR35 play a significant role in the NSCLC progression in the tumor microenvironment via MAPK and Jak-STAT signaling, highlighting TR35 as a potential therapeutic agent against lung cancer.

Keywords: anti-tumor, camel milk, lung cancer, microenvironment, MAPK, STAT3

OPEN ACCESS

Edited by:
Hongming Miao, Army Medical University, China

Reviewed by:
Zhongxiao Wan, Soochow University, China
Xiaolei Zhang, Sun Yat-sen University, China
Lihui Wang, Shenyang Pharmaceutical University, China

***Correspondence:**
Zhaocai Zhang
2313003@zju.edu.cn
Jie Yang
yangjie234@xju.edu.cn
Zhi Qi
qizhi@nankai.edu.cn

† These authors have contributed equally to this work

Specialty section:
This article was submitted to Molecular and Cellular Pathology, a section of the journal Frontiers in Cell and Developmental Biology

Received: *10 June 2021*
Accepted: *05 October 2021*
Published: *25 October 2021*

Citation:
Shi Z, Gao Y, Feng L, Tian W, Dou Z, Liu C, Liu J, Xu Y, Wang Y, Yan J, Wu Q, Li J, Yang L, Zhang Z, Yang J and Qi Z (2021) TR35 Exerts Anti-tumor Effects by Modulating Mitogen-Activated Protein Kinase and STAT3 Signaling in Lung Cancer Cells. Front. Cell Dev. Biol. 9:723346. doi: 10.3389/fcell.2021.723346

INTRODUCTION

Lung cancer is a most common malignancy that is associated with high morbidity and mortality worldwide. Non-small cell lung cancer (NSCLC) accounts for 80–85% of lung cancers (No authors listed, 2020). Although treatment advances have significantly improved lung cancer prognosis, its 5-year survival remains low, at <15% (Miller et al., 2016), underscoring the need for effective preventive and therapeutic strategies against NSCLC.

In recent years, camel milk has been shown to be one of the most important special dairy products. Some dietary ingredients exhibit effectiveness against diabetes (Agrawal et al., 2005), hepatitis (El Miniawy et al., 2014), allergies (Shabo et al., 2005), autism, lactose intolerance (Shabo and Yagil, 2005), as well as cancer (Badawy et al., 2018; Kamal et al., 2018). In the traditional medicine of ethnic minorities in Xinjiang, camel milk has long been applied as an adjuvant anti-cancer treatment, including in lung cancer. Our previous study showed that, TR35, an active component of camel milk have inhibitory effects against esophageal cancer (Yang J. et al., 2019), but its effects against lung cancer are unclear.

The mitogen-activated protein kinase (MAPK) signaling cascade is made up of P38, JNK and ERK, and influences various processes, including cell proliferation, differentiation, apoptosis, and autophagy (Li et al., 2020). Numerous small molecule drugs and natural products inhibit cancer cell proliferation through MAPK signaling activation (Sui et al., 2017), highlighting its potential as an anti-cancer therapeutic target.

Signal transducer and activator of transcription 3 (STAT3) is overexpressed in various cancer types and modulates various cellular processes like proliferation, apoptosis, and differentiation, which makes it an attractive anticancer target (Subramaniam et al., 2013). Persistent STAT3 inhibition suppresses expression of its downstream targets, such as c-Myc, Bcl-XL, blocking cell cycle progression, and promoting apoptosis (Yu et al., 2007; Laudisi et al., 2018). STAT3 signaling is vital in lung cancer treatment (Bousquet Mur et al., 2020).

Here, we find that TR35 inhibits the growth and proliferation of lung cancer cells *in vitro* and *in vivo*. RNA-seq and Kyoto Encyclopedia of Genes and Genomes (KEGG) pathway analyses implied that TR35 may mediate its anti-cancer effects via MAPK and Jak-STAT signaling. Our data indicate that p-JNK, p-p38, and p-STAT3 might be key TR35 targets. Together, our findings highlight TR35 as a potential anti-NSCLC therapeutic factor.

MATERIALS AND METHODS

Materials

TR35 was purified from Xinjiang Bactrian camel milk as previously described (Yang J. et al., 2019), dissolved in RPMI 1640 complete medium, and then filtered to remove bacteria.

Cells Culture

H1299 and A549 (human lung cancer cell lines) were obtained from the Cell Bank of Shanghai. They were cultured in RPMI 1640 medium supplemented with 10% heat-inactivated FBS (BI, China) and 1% penicillin/streptomycin (Gibco, 10378016), in an incubator at 37°C, 5% CO_2.

Cell Cytotoxic Assay

Cell seeding was in a 96-well microplate at a density of 2,000 cells/well. Then, to allow attachment, they were cultured overnight. They were then treated with TR35 at 0, 1, 2, and 4 mg/ml for 24 and 48 h. To evaluate proliferation, 10 μL of CCK-8 (Dojindo, CK04-500) was added and cells incubated for 4 h. Next, absorbance was read at 450 nm after which we calculated the number of living cells per well. Each experiment was repeated at least three times.

Colony Formation Assay

Cell seeding at a density of 500 cells/well was done in six-well plates, in triplicate. Then, they were cultured until visible colonies formed, with media change every 3 days. After 12 days, colonies were fixed in anhydrous methanol for a duration of 15 min, stained using 0.2% crystal violet (Sigma-Aldrich, C0775-25G), and the number of cells determined using a light microscope. The clone formation rate was given by the formula: clone formation rate% $= \frac{\text{number of clones}}{\text{number of inoculated cells}} \times 100$.

Analysis of Cell Cycle and Apoptosis

Cell seeding was done on six-well plate at 1×10^6 cells/well and grown to 70% confluence before treatment with TR35 at 0, 1, 2, and 4 mg/ml for 24 and 48 h. Cell cycle analysis was done using propidium iodide (PI) following manufacturer instructions (cell cycle detection kit, BD, 550825). Apoptosis analysis was done using a Annexin V-FITC Apoptosis Detection Kit I (BD Biosciences, 556547) and Annexin V-APC/PI Apoptosis Kit (Sungene Biotech, AO2001-11A-H) using manufacturer protocol and analyzed by flow cytometry on FACSCalibur (BD Biosciences). The flow cytometry data were analyzed using FlowJo X.

RNA-seq Analysis

Seeding of A549 cells was done at a density of 5×10^6 cells/flask in two 75 cm^2 flasks. Treatment with TR35 (4 mg/ml) for 48 h was done in one flask while the other was used as the untreated (control). Then, a High Pure RNA Isolation Kit (Roche, 11828665001) was used to extract Total RNA. cDNA was synthesized using RNA-Seq Sample Prep Kit (Illumina) as per the manufacturers' instructions. Quality control analysis of the sample library was done on an Agilent 2100 Bioanalyzer and ABI StepOnePlus RT-PCR. The cDNA libraries were sequenced at the Beijing Genomics Institute (BGI, Shenzhen, China) using a HiSeq 2000 platform (Illumina).

Protein Extraction and Western Blot

The procedures of Western blot analysis were as described previously (Tian et al., 2020). Briefly, cells were lysed using RIPA lysis buffer (Santa, sc-24948, Germany). The BCA Protein Assay Kit (Thermo Fisher Scientific, 23227) was used to determine protein concentrations, according to the manufacturer's instructions. Protein samples were resolved by SDS-PAGE and detected by immunoblotting with antibodies against c-Myc (CST, 13987), Bcl-XL (CST, 2764), p-STAT3 (CST, 9145), STAT3 (CST, 9139S), p-JNK (CST, 4668), JNK (CST, 9252T), p-p38 (CST, 4551), and p38 (CST, 8690T). Tubulin was used as the loading control and band intensities evaluated on Image J.

Animals and Treatment

A total of twenty 4-week old BALB/c nude mice (18–22 g) were obtained from the Beijing Vital River Laboratory Animal

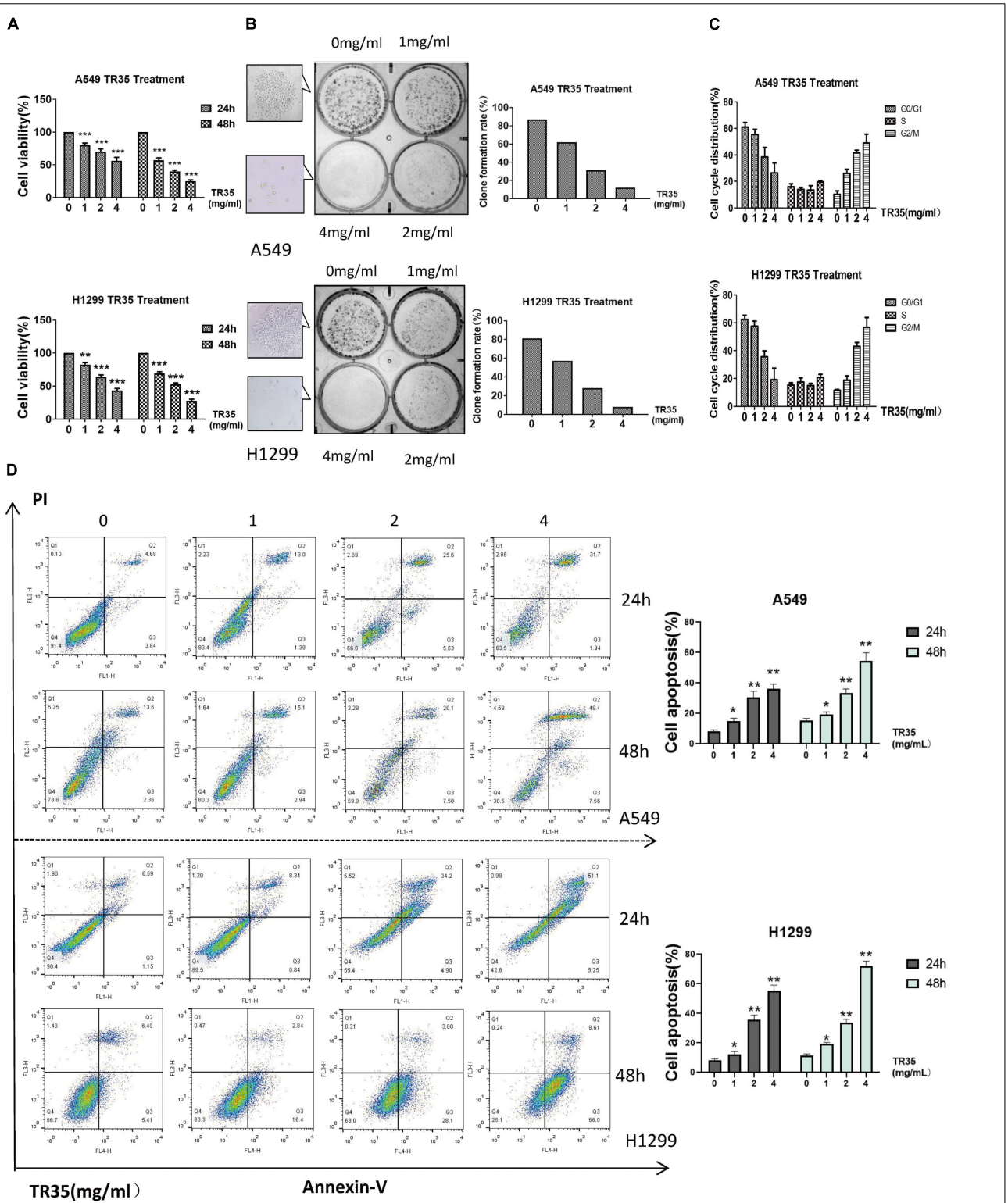

FIGURE 1 | TR35 induced inhibition of A549 and H1299 cell growth. **(A)** CCK-8 assay evaluation of the inhibition of proliferation of A549 and H1299 cells incubated with TR35 at different concentrations and different times. **(B)** Colony-formation of A549 and H1299 cells inhibited by TR35. Cells were exposed to different concentrations of TR35 for 11 days in the colony formation assay. **(C)** TR35-induced G2/M cell cycle arrest. G2/M cell cycle arrest increased in the TR35 treated A549 and H1299 cells. **(D)** Flow cytometry of Annexin V and PI double staining of A549 and H1299 cells treated with TR35 at different concentrations for 24 and 48 h. Columns show the percentages of apoptotic cancer cells incubated with TR35. The data are representative of three independent experiments. Data are expressed as the mean ± SEM of three determinations (*$p < 0.05$, **$p < 0.01$, ***$p < 0.001$ vs. CON).

Technology Co., Ltd. (Beijing, China). The mice were kept in specific pathogen-free (SPF) conditions, at 23 ± 2°C, 12 h light/dark cycles at the animal facility, School of Life Sciences, Nankai University. The mice were randomly split into four groups (five mice each). Two treated groups and two control groups were given TR35 (4 mg/ml, in Milli-Q H_2O) and an equal volume of H_2O, respectively, by oral gavage, twice a day. After 1 week, one treated group and one control group were subcutaneously injected with 2×10^6 A549 cells on the back side by axillary. The other treated and control groups were subcutaneously injected with 2×10^6 H1299 cells on the back side by axillary. The body weights of mice were determined after every 3 days. Thirty days after the appearance of subcutaneous scleroma, the nude mice were sacrificed, after which tumors were harvested and weighed. The tumors were divided into two pieces for western blot and Immunohistochemical (IHC) staining analysis.

Immunohistochemical Staining

The paraformaldehyde fixed tumor tissue were subjected to IHC staining according to standard procedures recommended by CST. Primary antibodies against p-JNK (1:200, CST, 4668), p-p38 (1:150, CST, 4551), p-STAT3 (1:200, CST 9145) diluted in 5% goat serum in 0.1% TBST were incubated with different tissues at 4°C overnight. Second and third antibody labeling was done using the rabbit anti-histochemical kit (Zhongshan Jinqiao, China), according to the manufacturer's instructions. The IHC positive rate was determined using the H-Score method by two independent pathologists at our center.

Statistical Analysis

Statistical testing was divided into three independent experiments, each in triplicate and data were presented as mean ± SEM. The differences between the two groups were analyzed with Student's t test. The significant differences among the three groups or more than three groups were analyzed by single factor analysis of variance (ANOVA) and then compared many times by LSD test (SPSS ver. 17). $P \leq 0.05$ was set as the threshold for statistical significance. $^*p < 0.05$; $^{**}p < 0.005$; $^{***}p < 0.001$.

RESULTS

TR35 Inhibits Lung Cancer Cells Proliferation

To evaluate the effects of TR35 on lung cancer cells, A549 and H1299 cells were administered with TR35 at 1, 2, and 4 mg/ml for 24 and 48 h followed by clonogenic and CCK-8 assays to assess growth and proliferation. This analysis revealed that TR35 suppressed lung cancer cells growth and proliferation in a dose-dependent manner, and these effects were most pronounced using TR35 at 4 mg/ml for 48 h (**Figure 1A**; inhibition rate = 76.4% in A549 and 72.5% in H1299). Examination TR35 long-term effects using clonogenic assays showed that treatment with TR35 for 12 days suppressed the colony-forming capacity of lung cancer cells (**Figure 1B**).

TR35 Induced G2/M Cell Cycle Arrest and Apoptosis

Since treatment with TR35 reduced lung cancer cells viability, we assessed its effects on the cell cycle. Flow cytometry analysis showed that treatment with TR35 enhanced cell numbers in the G2/M phase and inhibited cell numbers in the G0/G1 phase (**Figure 1C**). Suggesting that treatment with TR35 may suppress cell growth by promoting cell cycle arrest. Additionally, treating lung cancer cells with various TR35 concentrations for 48 h significantly increased the number of cells in early or late

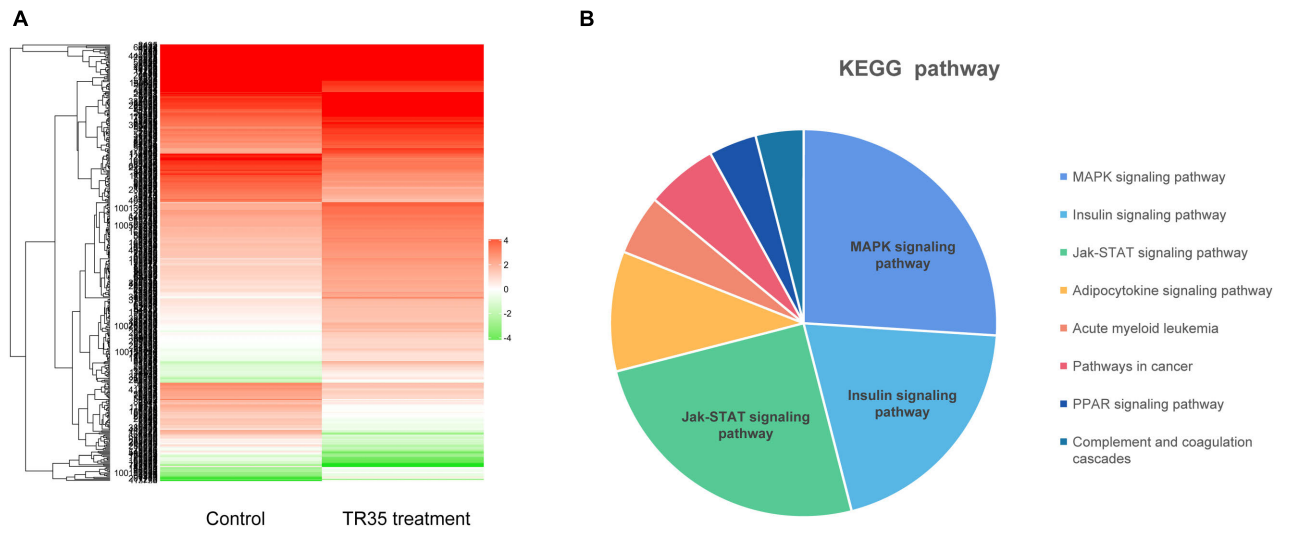

FIGURE 2 | The Heatmap and KEGG pathway enrichment analysis of DEGs in A549 cells after TR35 treatment. **(A)** Heatmap of expression profile for the 433 DEGs. **(B)** KEGG pathway enrichment analysis of DEGs.

apoptosis, while reducing the number of viable cells (**Figure 1D**). Together, these data show that TR35 suppresses lung cancer cell growth by inducing cycle arrest and apoptosis.

RNA-seq

Next, RNA-seq was used to better evaluate the mechanisms driving TR35 effects on lung cancer cell growth and proliferation. To this end, a cDNA library from A549 cells treated with 4 mg/ml TR35 for 48 h and a mock-treated control library were sequenced. A total of 433 differential expression genes (DEGs) were identified (TR35-v-control), including 180 downregulated genes and 253 upregulated genes (twofold as the cut off value). The heatmap used for hierarchical clustering analysis (HCA) exhibited distinct gene expression between control and treated group (**Figure 2A**). KEGG pathway analysis indicated that the DEGs were enriched for eight pathways, especially MAPK and

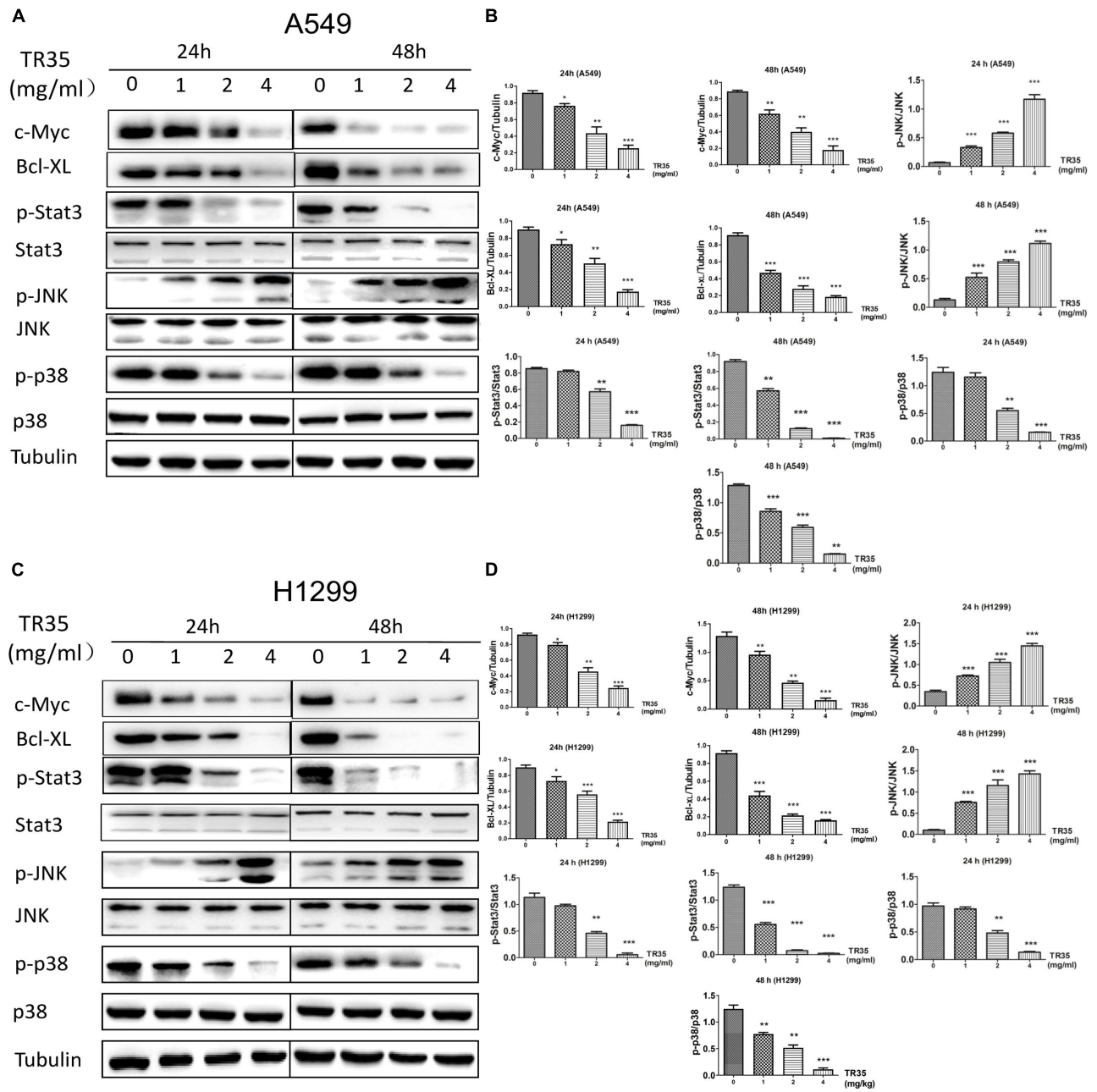

FIGURE 3 | Activation of JNK and reduction of p38 and STAT3 activities by TR35 treatment in H1299 and A549 cells. **(A,C)** A549 and H1299 cells were treated with TR35 (0–4 mg/mL) for 24 and 48 h. STAT3, p38, and JNK steady state and phosphorylated levels were analyzed by western blotting. Tubulin was used as loading controls. **(B,D)** Quantification of the band density was analyzed by ImageJ software. Data are presented as the mean ± SEM, $n = 3$ (*$p < 0.05$, **$p < 0.01$, ***$p < 0.001$ vs. CON).

Jak-STAT signaling pathway, which were significantly different in TR35-treated cells vs. controls as determined by hypergeometric distribution ($p \leq 0.05$, **Figure 2B**).

TR35 Activates JNK and Suppresses STAT3 Signaling in Lung Cancer Cells

Mitogen-activated protein kinase and Jak-STAT signaling are crucial mediators of extracellular stimuli to the nucleus, modulating gene expression and thus, cell proliferation and apoptosis. RNA-seq and KEGG pathway suggested that TR35 affects lung cancer cell proliferation and apoptosis through these pathways. To test this possibility, we used western blotting to evaluate the levels of total and phosphorylated p38, JNK, and STAT3 proteins in A549 and H1299 cells treated with TR35 at 1, 2, and 4 mg/ml for 24 and 48 h. This analysis showed that TR35 dose-dependently enhanced p-JNK level while reducing p-p38 and p-STAT3 levels without significantly affecting total JNK, p38, and STAT3 protein levels. At the same time, the expression level of c-Myc and Bcl-XL, which are downstream molecules of STAT3, was also downregulated (**Figures 3A–D**). These results indicated that TR35 affects lung cancer cell growth, proliferation and apoptosis via MAPK and Jak-STAT signaling.

TR35 Suppresses Non-small Cell Lung Cancer Xenograft Tumor Growth *in vivo*

To evaluate the *in vivo* effects of TR35 on NSCLC cell growth and proliferation, a xenograft mouse model was established through the subcutaneous injection of A549 and H1299 cells into SPF nude mice. Two treated groups and two control groups were treated with TR35 or a corresponding volume of H_2O (mock), respectively. Subcutaneous tumor formation was observed by naked eye in all nude mice 7–10 days after injection. Thirty

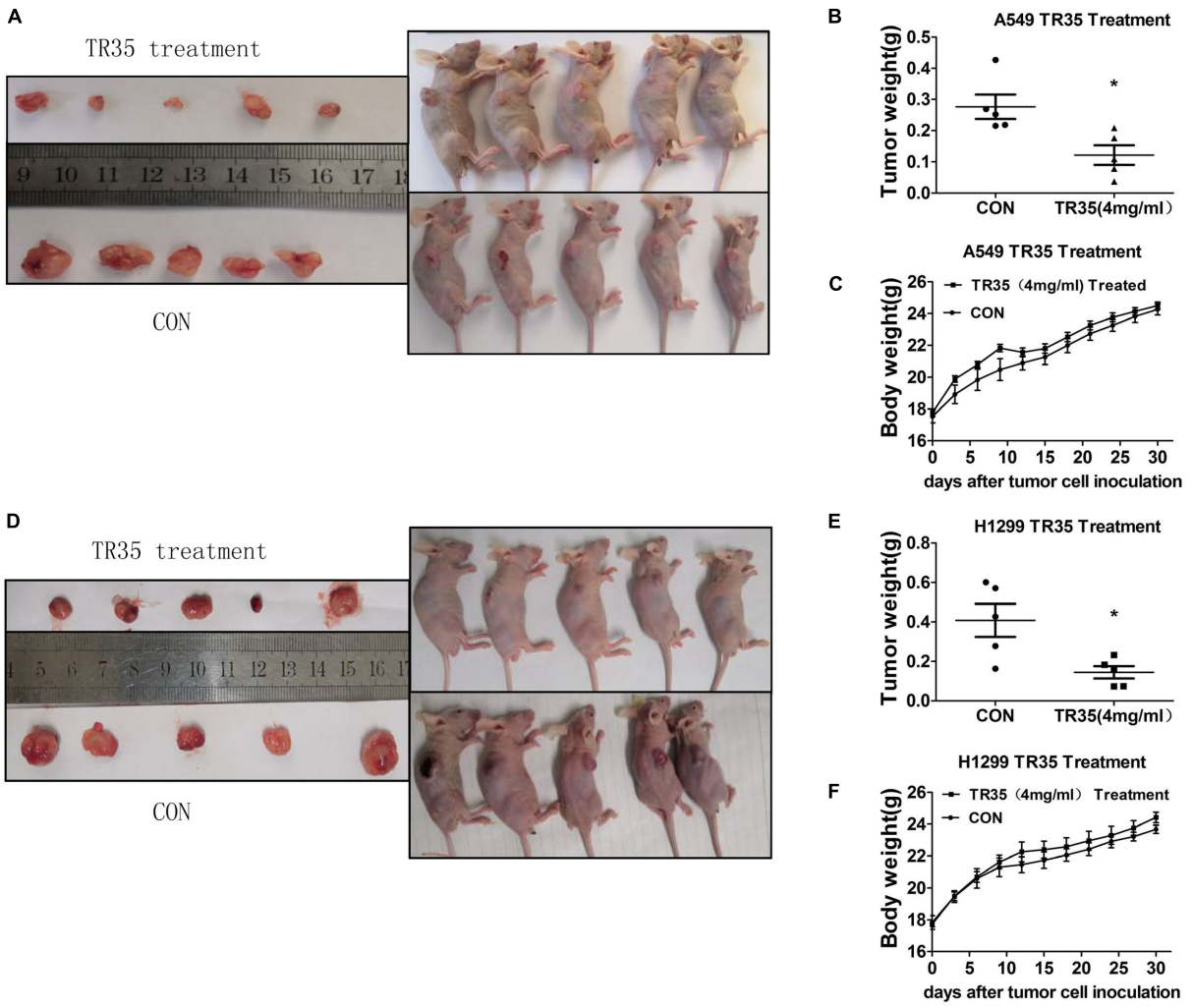

FIGURE 4 | The inhibitory effect of TR35 intragastric feeding on the growth of lung cancer xenograft in nude mice. Equal amounts of A549 and H1299 cells were inoculated under the skin of the back of nude mice. **(A,D)** After TR35 treatment, the animal images of unresectable tumors and tumor images of resected tumors were obtained in animals injected with different cell lines. **(B,E)** The comparison of tumor weights of two groups in animals injected with different cell lines. **(C,F)** Animal weight was recorded once every 3 days in animals injected with different cell lines. Data are presented as the mean ± SEM, $n = 5$ (*$p < 0.05$ vs. CON).

days later, tumors were harvested and their final weights taken to assess TR35 anti-tumor effects *in vivo*. This analysis found that the size and weight of tumors from TR35-treated mice were significantly lower than control tumors. However, mouse weight did not differ significantly between the groups (**Figures 4A–F**).

Immunohistochemical analysis revealed that relative to controls, TR35-treated tumors had significantly higher p-JNK levels and significantly lower levels of p-p38 and p-STAT3 (**Figures 5A,B**). Similar results were obtained by western blotting (**Figure 5C**).

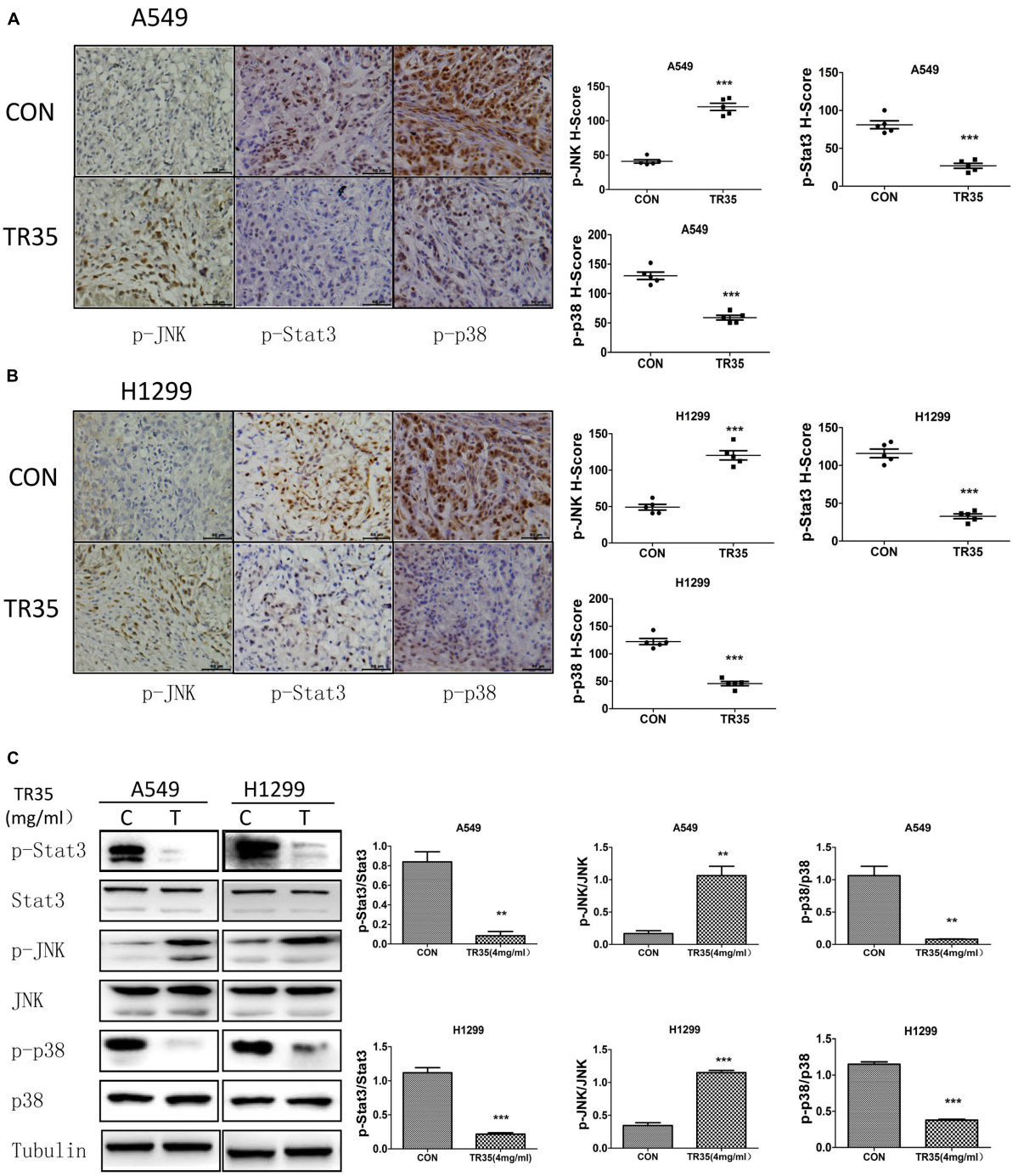

FIGURE 5 | Western blotting and Immunohistochemistry were used to evaluate the effect of TR35 on the expression of p-JNK, p-p38, p-STAT3 protein in dissected tumor tissue. **(A,B)** The expressions of p-JNK, p-p38, and p-STAT3 in dissected tumor samples formed by different cell lines were measured by IHC under a light microscope. Scale bar 50 μm. **(C)** STAT3, p38, and JNK steady state and phosphorylated levels were analyzed in dissected tumor samples formed by different cell lines were measured by western blotting (**$p < 0.01$, ***$p < 0.001$ vs. CON).

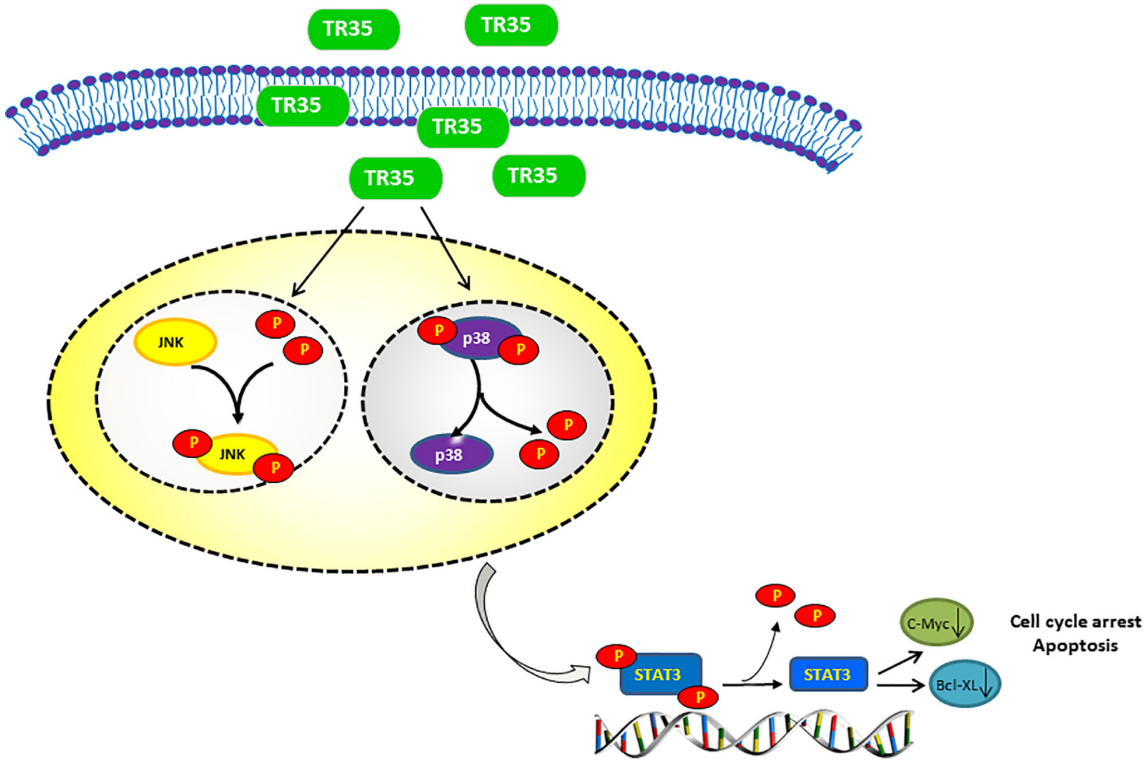

FIGURE 6 | Proposed model of the mechanism underlying the TR35 inhibit NSCLC cell growth and proliferation via MAPK and Jak-STAT signaling pathway. Mechanistically, In TR35 treated NSCLC cells, JNK activation in the JNK-STAT3 signaling axis suppresses STAT3 phosphorylation accompanying the p-p38 downregulation, and thereby suppressing the growth and proliferation of NSCLC cells.

DISCUSSION

Some dietary constituents are known to be chemoprevention and multiple studies have reported dietary adjuvant therapy for cancer, including camel milk. However, few studies have examined molecular mechanisms underlying the anti-tumor effect of camel milk, especially in lung cancer. Here, we show that TR35, an active fraction obtained from Xinjiang Bactrian camel milk, effectively suppresses lung cancer cell growth by inducing apoptosis and G2/M cycle arrest. Mechanistically, we find that TR35 exerts anti-tumor effects by activating p-JNK/MAPK signaling and suppressing STAT3 signaling (including its downstream molecules such as c-Myc and Bcl-XL). However, p-p38 expression was reduced. These observations were suggested by RNA-seq data and confirmed using *in vivo* and *in vitro* assays (**Figure 6**).

Natural compounds are reported to induce apoptosis via MAPK signaling (Park et al., 2017; Chen and Chen, 2018). Apoptosis is influenced by a variety of intracellular proteins and complex signaling pathways. Mounting evidence implicates STAT3 and MAPK signaling in cancer cell proliferation and apoptosis (Zou et al., 2016; Meng et al., 2018). MAPK signaling pathways fall into 3 main classes: ERK, JNK and p38 (Haagenson and Wu, 2010). ERK regulates cancer cell differentiation, proliferation and apoptosis (Zhai et al., 2016). Toxic and environmental stresses activate JNK, which modulates inflammation by controlling cell differentiation, proliferation, survival, as well as migration (Park et al., 2016). Cell-stress induced signaling activates P38 in response to oxidative stress and toxic chemicals (Tsai et al., 2017). STAT3 activation promotes cell proliferation, angiogenesis, multidrug resistance, and suppresses apoptosis (Miao and Zhang, 2015). Our findings show that TR35 activates JNK signaling, while inhibiting p38 and STAT3 signaling. JNK signaling is associated with the development of numerous disorders, including cancers (Johnson and Nakamura, 2007; Weston and Davis, 2007; Wang et al., 2016). STAT3 is constitutively activated in many cancers and may be oncogenic (Kim et al., 2007). Various studies suggest STAT3 expression is elevated in tumors relative to normal tissues and its long-term activation correlates with development of various cancers (Inoue et al., 2007). Elevated STAT3 function is reported to prevent tumor cell apoptosis, while its inhibition suppresses proliferation and induces apoptosis in cancer cells (Thorburn et al., 2008; Tournier, 2013; Tan et al., 2017). This may be due to many proteins downstream of STAT3, which are crucial for tumor cell proliferation and survival were also downregulated in this process, such as c-Myc and Bcl-XL (Yu et al., 2007). JNK has been suggested as an upstream STAT3 kinase (Sun et al., 2014), and its activation in the JNK-STAT3 signaling axis suppresses STAT3 phosphorylation. JNK activation and STAT3 inhibition are reported to induce M1 macrophage polarization in lung cancer, which may have anti-tumor effects (Cui et al., 2020).

These reports are consistent with our data from NSCLC cells and tumor tissues (**Figures 3**, **5**).

Numerous studies have shown that JNK/MAPK and P38/MAPK signaling inactivate STAT3, inducing apoptosis. In this process, p-JNK and p-p38 levels are elevated. However, we observed that TR35 suppressed p-p38 levels in NSCLC cells and tumor tissues. Previous studies have reported the persistent phosphorylation of p38 and STAT3 in NSCLC. The constitutive activation of p38 and STAT3 is related to increase in cell proliferation and metastasis in NSCLC (Greenberg et al., 2002; Dutta et al., 2014; Harada et al., 2014). Greenberg et al. (2002) analyzed tissues from 20 NSCLC cases and found that the activity level of p38 was twice higher than in adjacent tissues, suggesting that p38 modulates malignant growth and transformation of cells. Additionally, Zhou et al. confirmed that reducing p-p38 levels and increasing p-JNK level inhibits cell proliferation (Zhou et al., 2020). These reports are consistent with our findings, indicating that the anti-tumor effects of p-p38 downregulation may occur via other factors, apart from p38-STAT3 signaling axis. However, the specific mechanism is unclear and further research is needed.

Cell cycle homeostasis is important in the maintenance of intracellular stability. However, cell cycle is arrested through various mechanisms, including inhibition of cyclins and expression of CDKs, when cells are damaged (Sarita Rajender et al., 2010; Bonelli et al., 2014; Cheng et al., 2017). Here, flow cytometry revealed that TR35 elevated cell numbers in the G2/M phase and suppressed cell numbers in the G0/G1 phase. Previous studies have showed that the inhibition of STAT3 signaling pathways will lead to tumor-associated G2/M phase arrest. This is because STAT3 can mediate the activity of cyclin B1/CDK protein complex (Shao et al., 2017; Yang L. et al., 2019; Nyiramana et al., 2020).

In summary, we find that TR35 inhibits NSCLC cells growth and proliferation, induces G2/M cell cycle arrest and apoptosis. This suppression process in NSCLC is via MAPK and Jak-STAT signaling. Our data highlight TR35 as a promising candidate for lung cancer therapy.

DATA AVAILABILITY STATEMENT

The datasets presented in this study can be found in online repositories. The names of the repository/repositories and accession number(s) can be found below: European Nucleotide Archive, ERS7253991 and ERS7253992.

ETHICS STATEMENT

The animal study was reviewed and approved by the Institutional Animal Care and Use Committee of Nankai University.

AUTHOR CONTRIBUTIONS

ZS: writing – original draft and investigation. YG: investigation and writing – review and editing. LF: software and writing – review and editing. WT: validation and writing – review and editing. ZD, CL, JLiu, YX, YW, JYan, QW, JLi, and LY: writing – review and editing. ZZ: conceptualization and writing – review and editing. JYang: resources and writing – review and editing. ZQ: writing – original draft and funding acquisition. All authors contributed to the article and approved the submitted version.

FUNDING

This work was supported by the National Natural Science Foundation of China (Nos. 82072187, 81971887, 32071263, 81772252, 31971194, 81801949, 81802091, and 81860339), Key Technology Research and Development Program in Autonomous Region (Grant 2018B01003), Natural Science Foundation of Tianjin (Nos. 20JCYBJC01260, 20JCQNJC01850, 17JCQNJC10700, and 20YDTPJC00250), and Key Laboratory of Emergency and Trauma (Hainan Medical University), Ministry of Education (No. KLET-201906).

REFERENCES

Agrawal, R. P., Beniwal, R., Kochar, D. K., Tuteja, F. C., Ghorui, S. K., Sahani, M. S., et al. (2005). Camel milk as an adjunct to insulin therapy improves long-term glycemic control and reduction in doses of insulin in patients with type-1 diabetes A 1 year randomized controlled trial. *Diabetes Res. Clin. Pract.* 68, 176–177. doi: 10.1016/j.diabres.2004.12.007

Badawy, A. A., El-Magd, M. A., and AlSadrah, S. A. (2018). Therapeutic Effect of Camel Milk and Its Exosomes on MCF7 Cells In Vitro and In Vivo. *Integr. Cancer Ther.* 17, 1235–1246. doi: 10.1177/1534735418786000

Bonelli, P., Tuccillo, F. M., Borrelli, A., Schiattarella, A., and Buonaguro, F. M. (2014). CDK/CCN and CDKI alterations for cancer prognosis and therapeutic predictivity. *Biomed Res. Int.* 2014:361020. doi: 10.1155/2014/361020

Bousquet Mur, E., Bernardo, S., Papon, L., Mancini, M., Fabbrizio, E., Goussard, M., et al. (2020). Notch inhibition overcomes resistance to tyrosine kinase inhibitors in EGFR-driven lung adenocarcinoma. *J. Clin. Invest.* 130, 612–624. doi: 10.1172/jci126896

Chen, X., and Chen, J. (2018). miR-3188 Regulates Cell Proliferation, Apoptosis, and Migration in Breast Cancer by Targeting TUSC5 and Regulating the p38 MAPK Signaling Pathway. *Oncol. Res.* 26, 363–372. doi: 10.3727/096504017X14953948675421

Cheng, C. W., Leong, K. W., Ng, Y. M., Kwong, Y. L., and Tse, E. (2017). The peptidyl-prolyl isomerase PIN1 relieves cyclin-dependent kinase 2 (CDK2) inhibition by the CDK inhibitor p27. *J. Biol. Chem.* 292, 21431–21441. doi: 10.1074/jbc.M117.801373

Cui, L., Yang, G., Ye, J., Yao, Y., Lu, G., Chen, J., et al. (2020). Dioscin elicits anti-tumour immunity by inhibiting macrophage M2 polarization via JNK and STAT3 pathways in lung cancer. *J. Cell. Mol. Med.* 24, 9217–9230. doi: 10.1111/jcmm.15563

Dutta, P., Sabri, N., Li, J., and Li, W. X. (2014). Role of STAT3 in lung cancer. *JAKSTAT* 3:e999503. doi: 10.1080/21623996.2014.999503

El Miniawy, H. M. F., Ahmed, K. A., Tony, M. A., Mansour, S. A., and Salah Khattab, M. M. (2014). Camel milk inhibits murine hepatic carcinogenesis, initiated by diethylnitrosamine and promoted by phenobarbitone. *Int. J. Vet. Sci. Med.* 2, 136–141. doi: 10.1016/j.ijvsm.2014.10.004

Greenberg, A. K., Basu, S., Hu, J., Yie, T. A., Tchou-Wong, K. M., Rom, W. N., et al. (2002). Selective p38 activation in human non-small cell lung cancer. *Am. J. Respir. Cell Mol. Biol.* 26, 558–564. doi: 10.1165/ajrcmb.26.5.4689

Haagenson, K. K., and Wu, G. S. (2010). Mitogen activated protein kinase phosphatases and cancer. *Cancer Biol. Ther.* 9, 337–340. doi: 10.4161/cbt.9.5.11217

Harada, D., Takigawa, N., and Kiura, K. (2014). The Role of STAT3 in Non-Small Cell Lung Cancer. *Cancers* 6, 708–722. doi: 10.3390/cancers6020708

Inoue, J., Gohda, J., Akiyama, T., and Semba, K. (2007). NF-kappaB activation in development and progression of cancer. *Cancer Sci.* 98, 268–274. doi: 10.1111/j.1349-7006.2007.00389.x

Johnson, G. L., and Nakamura, K. (2007). The c-jun kinase/stress-activated pathway: regulation, function and role in human disease. *Biochim. Biophys. Acta* 1773, 1341–1348. doi: 10.1016/j.bbamcr.2006.12.009

Kamal, H., Jafar, S., Mudgil, P., Murali, C., Amin, A., and Maqsood, S. (2018). Inhibitory properties of camel whey protein hydrolysates toward liver cancer cells, dipeptidyl peptidase-IV, and inflammation. *J. Dairy Sci.* 101, 8711–8720. doi: 10.3168/jds.2018-14586

Kim, H. J., Hwang, N. R., and Lee, K. J. (2007). Heat shock responses for understanding diseases of protein denaturation. *Mol. Cells* 23, 123–131.

Laudisi, F., Cherubini, F., Monteleone, G., and Stolfi, C. (2018). STAT3 Interactors as Potential Therapeutic Targets for Cancer Treatment. *Int. J. Mol. Sci.* 19:1787. doi: 10.3390/ijms19061787

Li, Z., Zhang, L., Gao, M., Han, M., Liu, K., Zhang, Z., et al. (2020). Retraction Note: endoplasmic reticulum stress triggers Xanthoangelol-induced protective autophagy via activation of JNK/c-Jun Axis in hepatocellular carcinoma. *J. Exp. Clin. Cancer Res.* 39:164. doi: 10.1186/s13046-020-01668-x

Meng, L. Q., Liu, C., Luo, Y. H., Piao, X. J., Wang, Y., Zhang, Y., et al. (2018). Quinalizarin exerts an anti-tumour effect on lung cancer A549 cells by modulating the Akt, MAPK, STAT3 and p53 signalling pathways. *Mol. Med. Rep.* 17, 2626–2634. doi: 10.3892/mmr.2017.8110

Miao, D., and Zhang, L. (2015). Leptin modulates the expression of catabolic genes in rat nucleus pulposus cells through the mitogen-activated protein kinase and Janus kinase 2/signal transducer and activator of transcription 3 pathways. *Mol. Med. Rep.* 12, 1761–1768. doi: 10.3892/mmr.2015.3646

Miller, K. D., Siegel, R. L., Lin, C. C., Mariotto, A. B., Kramer, J. L., Rowland, J. H., et al. (2016). Cancer treatment and survivorship statistics, 2016. *CA Cancer J. Clin.* 66, 271–289. doi: 10.3322/caac.21349

No authors listed. (2020). Erratum: global cancer statistics 2018: GLOBOCAN estimates of incidence and mortality worldwide for 36 cancers in 185 countries. *CA Cancer J. Clin.* 70:313. doi: 10.3322/caac.21609

Nyiramana, M. M., Cho, S. B., Kim, E. J., Kim, M. J., Ryu, J. H., Nam, H. J., et al. (2020). Sea Hare Hydrolysate-Induced Reduction of Human Non-Small Cell Lung Cancer Cell Growth through Regulation of Macrophage Polarization and Non-Apoptotic Regulated Cell Death Pathways. *Cancers* 12:726. doi: 10.3390/cancers12030726

Park, K. R., Yun, H. M., Quang, T. H., Oh, H., Lee, D. S., Auh, Q. S., et al. (2016). 4-Methoxydalbergione suppresses growth and induces apoptosis in human osteosarcoma cells in vitro and in vivo xenograft model through down-regulation of the JAK2/STAT3 pathway. *Oncotarget* 7, 6960–6971. doi: 10.18632/oncotarget.6873

Park, S. G., Kim, S. H., Kim, K. Y., Yu, S. N., Choi, H. D., Kim, Y. W., et al. (2017). Toyocamycin induces apoptosis via the crosstalk between reactive oxygen species and p38/ERK MAPKs signaling pathway in human prostate cancer PC-3 cells. *Pharmacol. Rep.* 69, 90–96. doi: 10.1016/j.pharep.2016.10.014

Sarita Rajender, P., Ramasree, D., Bhargavi, K., Vasavi, M., and Uma, V. (2010). Selective inhibition of proteins regulating CDK/cyclin complexes: strategy against cancer–a review. *J. Recept. Signal Transduct. Res.* 30, 206–213. doi: 10.3109/10799893.2010.488649

Shabo, Y., Barzel, R., Margoulis, M., and Yagil, R. (2005). Camel milk for food allergies in children. *Isr. Med. Assoc. J.* 7, 796–798.

Shabo, Y., and Yagil, R. (2005). Etiology of autism and camel milk as therapy. *Int. J. Disabil. Hum. Dev.* 4, 67–70. doi: 10.1515/IJDHD.2005.4.2.67

Shao, D., Ma, J., Zhou, C., Zhao, J. N., Li, L. L., Zhao, T. J., et al. (2017). STAT3 down-regulation induces mitochondria-dependent G2/M cell cycle arrest and apoptosis in oesophageal carcinoma cells. *Clin. Exp. Pharmacol. Physiol.* 44, 413–420. doi: 10.1111/1440-1681.12708

Subramaniam, A., Shanmugam, M. K., Perumal, E., Li, F., Nachiyappan, A., Dai, X., et al. (2013). Potential role of signal transducer and activator of transcription (STAT)3 signaling pathway in inflammation, survival, proliferation and invasion of hepatocellular carcinoma. *Biochim. Biophys. Acta* 1835, 46–60. doi: 10.1016/j.bbcan.2012.10.002

Sui, C., Zhuang, C., Sun, D., Yang, L., Zhang, L., and Song, L. (2017). Notch1 regulates the JNK signaling pathway and increases apoptosis in hepatocellular carcinoma. *Oncotarget* 8, 45837–45847. doi: 10.18632/oncotarget.17434

Sun, J., Yu, M., Lu, Y., Thakur, C., Chen, B., Qiu, P., et al. (2014). Carcinogenic metalloid arsenic induces expression of mdig oncogene through JNK and STAT3 activation. *Cancer Lett.* 346, 257–263. doi: 10.1016/j.canlet.2014.01.002

Tan, W., Zhu, S., Cao, J., Zhang, L., Li, W., Liu, K., et al. (2017). Inhibition of MMP-2 Expression Enhances the Antitumor Effect of Sorafenib in Hepatocellular Carcinoma by Suppressing the PI3K/AKT/mTOR Pathway. *Oncol. Res.* 25, 1543–1553. doi: 10.3727/096504017X14886444100783

Thorburn, A., Behbakht, K., and Ford, H. (2008). TRAIL receptor-targeted therapeutics: resistance mechanisms and strategies to avoid them. *Drug Resist. Updat.* 11, 17–24. doi: 10.1016/j.drup.2008.02.001

Tian, W., Yang, L., Liu, Y., He, J., Yang, L., Zhang, Q., et al. (2020). Resveratrol attenuates doxorubicin-induced cardiotoxicity in rats by up-regulation of vascular endothelial growth factor B. *J. Nutr. Biochem.* 79:108132. doi: 10.1016/j.jnutbio.2019.01.018

Tournier, C. (2013). The 2 Faces of JNK Signaling in Cancer. *Genes Cancer* 4, 397–400. doi: 10.1177/1947601913486349

Tsai, W. C., Bai, L. Y., Chen, Y. J., Chu, P. C., Hsu, Y. W., Sargeant, A. M., et al. (2017). OSU-A9 inhibits pancreatic cancer cell lines by modulating p38-JAK-STAT3 signaling. *Oncotarget* 8, 29233–29246. doi: 10.18632/oncotarget.16450

Wang, L., Luo, J. Y., Li, B., Tian, X. Y., Chen, L. J., Huang, Y., et al. (2016). Integrin-YAP/TAZ-JNK cascade mediates atheroprotective effect of unidirectional shear flow. *Nature* 540, 579–582. doi: 10.1038/nature20602

Weston, C. R., and Davis, R. J. (2007). The JNK signal transduction pathway. *Curr. Opin. Cell Biol.* 19, 142–149. doi: 10.1016/j.ceb.2007.02.001

Yang, J., Dou, Z., Peng, X., Wang, H., Shen, T., Liu, J., et al. (2019). Transcriptomics and proteomics analyses of anti-cancer mechanisms of TR35-An active fraction from Xinjiang Bactrian camel milk in esophageal carcinoma cell. *Clin. Nutr.* 38, 2349–2359. doi: 10.1016/j.clnu.2018.10.013

Yang, L., Li, J., Xu, L., Lin, S., Xiang, Y., Dai, X., et al. (2019). Rhein shows potent efficacy against non-small-cell lung cancer through inhibiting the STAT3 pathway. *Cancer Manag. Res.* 11, 1167–1176. doi: 10.2147/CMAR.S171517

Yu, H., Kortylewski, M., and Pardoll, D. (2007). Crosstalk between cancer and immune cells: role of STAT3 in the tumour microenvironment. *Nat. Rev. Immunol.* 7, 41–51.

Zhai, H., Hu, S., Liu, T., Wang, F., Wang, X., Wu, G., et al. (2016). Nitidine chloride inhibits proliferation and induces apoptosis in colorectal cancer cells by suppressing the ERK signaling pathway. *Mol. Med. Rep.* 13, 2536–2542. doi: 10.3892/mmr.2016.4827

Zhou, H., Liu, J., and Chen, Z. (2020). Coronarin D suppresses proliferation, invasion and migration of glioma cells via activating JNK signaling pathway. *Pathol. Res. Pract.* 216:152789. doi: 10.1016/j.prp.2019.152789

Zou, F., Mao, R., Yang, L., Lin, S., Lei, K., Zheng, Y., et al. (2016). Targeted deletion of miR-139-5p activates MAPK, NF-kappaB and STAT3 signaling and promotes intestinal inflammation and colorectal cancer. *FEBS J.* 283, 1438–1452. doi: 10.1111/febs.13678

Conflict of Interest: The authors declare that the research was conducted in the absence of any commercial or financial relationships that could be construed as a potential conflict of interest.

Publisher's Note: All claims expressed in this article are solely those of the authors and do not necessarily represent those of their affiliated organizations, or those of the publisher, the editors and the reviewers. Any product that may be evaluated in this article, or claim that may be made by its manufacturer, is not guaranteed or endorsed by the publisher.

frontiers in Molecular Biosciences

ORIGINAL RESEARCH
published: 01 November 2021
doi: 10.3389/fmolb.2021.714053

Characterization of the Immune Cell Infiltration Landscape of Thyroid Cancer for Improved Immunotherapy

Jing Gong[1†], Bo Jin[2†], Liang Shang[3] and Ning Liu[4]*

[1]Department of Geriatrics, The First Hospital of China Medical University, Shenyang, China, [2]Department of Medical Oncology, Key Laboratory of Anticancer Drugs and Biotherapy of Liaoning Province, Liaoning Province Clinical Research Center for Cancer, The First Hospital of China Medical University, Shenyang, China, [3]Innovative Research Center for Integrated Cancer Omics, The Second Affiliated Hospital of China Medical University, Shenyang, China, [4]Department of Pancreatic and Biliary Surgery, The First Affiliated Hospital of China Medical University, Shenyang, China

Within the endocrine system, thyroid cancer (THCA) is the most typical malignant tumor. Tumor-infiltrating immune cells play vital roles in tumor progression, recurrence, metastasis as well as response to immunotherapy. However, THCA's immune infiltrative landscape is still not clarified. Therefore, we utilized two statistical algorithms to investigate the immune cell infiltration (ICI) landscape of 505 THCA samples and defined three ICI immune subtypes. The ICI scores were calculated using principal-component analysis. Increased tumor mutation burden (TMB) and immune-related signaling pathways were associated to a high ICI score. The high ICI score group indicated a relatively longer overall survival (OS) than the low ICI score group. Most immune checkpoint-related and immune activation-related genes were considerably upregulated in the ICI high group, which indicates stronger immunogenicity and a greater likelihood of benefiting from immunotherapy. In two cohort studies of patients receiving immunotherapy, high-ICI-score group showed notable therapeutic effects and clinical advantages compared to those with lower ICI scores. These results demonstrate that ICI score acts as an effective prognostic indicator and predictor of response to immunotherapy.

Keywords: landscape, thyroid cancer, immunotherapy, infiltration, prediction, prognosis

OPEN ACCESS

Edited by:
Shengtao Zhou,
Sichuan University, China

Reviewed by:
Prabhat Kumar Sharma,
Children's Hospital of Philadelphia, United States
Vikram Srivastava,
Iowa State University, United States

****Correspondence:***
Ning Liu
liuning811103@sina.com

†These authors have contributed equally to this work

Specialty section:
This article was submitted to Molecular Diagnostics and Therapeutics, a section of the journal Frontiers in Molecular Biosciences

Received: *24 May 2021*
Accepted: *22 September 2021*
Published: *01 November 2021*

Citation:
Gong J, Jin B, Shang L and Liu N (2021) Characterization of the Immune Cell Infiltration Landscape of Thyroid Cancer for Improved Immunotherapy. Front. Mol. Biosci. 8:714053. doi: 10.3389/fmolb.2021.714053

INTRODUCTION

The most common malignant tumor of the endocrine system is thyroid cancer (THCA). As tumor detection has advanced, the global incidence of THCA has risen rapidly. Younger people and women are more likely to suffer from it (La Vecchia et al., 2015; Du et al., 2018; Siegel et al., 2020). There are four major pathological subtypes of thyroid cancer: papillary thyroid carcinoma, follicular thyroid carcinoma, medullary thyroid carcinoma, and undifferentiated carcinoma. The prognoses vary greatly (Cabanillas et al., 2016). Traditional treatments including chemotherapy and radiotherapy cannot improve the therapeutic effect of locally advanced or metastatic thyroid cancer, which makes the development of effective treatments crucial.

The tumor microenvironment (TME) of thyroid cancer is rich in immune cells, which indicates that it is an ideal candidate for immunotherapy. And certain immune properties have been shown to affect the prognosis of thyroid cancer (Ferrari et al., 2019). Extensive researches on the immune microenvironment of thyroid cancer have shown that components of an individual's immune system were closely related to the occurrence, invasion, and metastasis as well as the therapeutic response to

TABLE 1 | Clinical information of TCGA-THCA datasets.

		TCGA-THCA
Survial		
OS	status_0	489
	status_1	16
histological_type	Classical.usual	361
	Follicular	99
	Tall.Cell	36
	Others	9
Age		
	Age>60	113
	Age< = 60	392
Gender		
	Female	367
	Male	138
Stage		
	Stage_I	284
	Stage_II	52
	Stage_III	112
	Stage_IV	55
	Stage_un	2
Mstage	M0	286
	M1	8
	MX	210
	M_un	1
Nstage	N0	227
	N1	229
	NX	49
Tstage	T1	142
	T2	165
	T3	174
	T4	22
	TX	2
RT (Radiation therapy)	YES	310
	NO	177
	UN	18
TMT (Targeted molecular therapy)	YES	5
	NO	94
	UN	406

immunotherapy (Xie et al., 2020; Yin et al., 2020). A new clinical experiment showed that tumor immune cell infiltration (ICI) in thyroid cancer is related to sensitivity to immunotherapy and a better prognosis (Na and Choi, 2018). In papillary thyroid carcinoma, tumor-associated macrophages (TAMs) are correlated to lymph node metastasis, increased tumor size, and a diminished survival rate (Kim et al., 2013; Fang et al., 2014). Increased regulatory T cell (Treg) infiltration suggests a positive correlation with disease stage, whereas natural killer (NK) cell infiltration is adversely associated with disease stage (Gogali et al., 2012). Additionally, thyroid cancer cells can produce a variety of cytokines and chemokines, which can promote the tumor progression. Reducing the concentration of cytokines and chemokines in the tumor microenvironment produces therapeutic benefits (Coperchini et al., 2019). An improved understanding of the molecular and immunological properties of the THCA tumor microenvironment can be used to aid immunotherapy.

We collected The Cancer Genome Atlas (TCGA)-THCA datasets, evaluating the immune microenvironment and immune cell infiltration in THCA using two calculation tools, CIBERSORT, and ESTIMATE. According to the TCGA-THCA immunophenoscores (IPSs), we identified the relevant genes to establish an immune cell infiltration (ICI) scoring model and verified it using the TCGA-THCA dataset. In summary, this ICI score system can be an effective prognostic biomarker and predictor for the valuation of THCA immunotherapy response.

METHODS

Obtaining Expression Profile Data and Clinical Data

The overall analysis ideas of this research are shown as follows. First, download THCA expression profile data as well as follow-up clinical evidences based on the TCGA database (https://portal.gdc.cancer.gov/). The RNA sequence data of TCGA-THCA is processed in the following steps: 1) Remove samples which did not include subsequent clinical information; 2) Remove samples with no survival period and survival status; 3) Convert the probe to Gene Symbol; 4) One probe corresponds to several genes, remove the probe; 5) Use the median value for the expression of multiple Gene Symbols. The pre-processed TCGA-THCA data has a total of 505 tumor samples, and the clinical statistics of the samples are shown in **Table 1**.

Tumor Immunophenoscore (IPS Database)

Tumor immunophenoscore (IPS) comes from the website of The Cancer Immunome database (TCIA) (https://tcia.at/patients). It is in view of the characteristics of tumor-infiltrating immune cells, acting as a bridge between immune cell infiltrating subtypes and immune gene subtypes. (Charoentong et al., 2016).

Consensus Clustering Analysis of Immune Cell Infiltration

22 different immune cells infiltration level in THCA (naïve B cells, memory B cells, plasma cells, $CD8^+$ T cells, naïve $CD4^+$ T cells, inactivated and activated memory $CD4^+$ T cells, T follicular helper cells, Tregs, gamma delta T cells, resting and activated NK cells, monocytes, M0, M1, and M2 macrophages, resting and activated dendritic cells, resting and activated mast cells, eosinophils, and neutrophils) was quantified utilizing the CIBERSORT R package, based on the LM22 signature and 1,000 permutations. We use ESTIMATE R package to estimate the degree of immune infiltration and matrix purity scores in each THCA sample. "Pam" method according to Euclid and Ward's linkages was utilized, and executed by "ConsensuClusterPlus package" R package. Unsupervised clustering was performed, and researchers repeated the clustering 1,000 times to ensure the classification's stability.

Differential Expression of Genes Associated With the Tumor IPS

The tumor samples were divided into two groups according to the optimal density gradient threshold of tumor immunophenoscore (IPS) related to survival with the method of R Survminer package.

The differential expression of genes was analyzed between the TCGA-THCA tumor sample with different score groups through specifying the cutoff value 0.05 (adjusted) and | log2 (Fold Change) | >1 using the limma R package. Furthermore, the genes which are positively related to the consistent classification result are called immune genotype-related feature A, and the remaining genes are called for feature B.

Dimension Reduction of Gene Features and Construction of ICI Score

In order to measure the immune cell infiltration in tumors through gene expression, this study constructed a tumor immune cell infiltration score (ICI scores) model based on feature A and feature B gene sets related to immune gene subtypes. First of all, we conduct the Boruta algorithm to reduce dimension of the feature A and B genes. After reduction, ICI score A and B which were defined by ICI feature gene A and B were evaluated by the principal component analysis (PCA). Thirdly we construct an immune cell infiltration score (ICI scores) model, and the calculation formula is as follows (Sotiriou et al., 2006):

$$ICI\_scores = \sum PC1(A) - \sum PC1(B)$$

Collection of Somatic Alteration Data

Mutation data of TCGA-THCA were downloaded from the TCGA (https://www.cancer.gov/tcga/). We used the Survminer R package to calculate the optimal density gradient threshold related to the tumor mutation burden (TMB) and survival and categorized the samples into high and low tumor TMB groups. Implementing the maftool R package, the mutation frequencies of the top 30 driver genes in different immune cell infiltration score (ICI scores) groups were compared.

Acquisition of Immunotherapy Data Sets

To explore the effectiveness of ICI score in predicting the benefit of immunotherapy treatment, we downloaded the expression profile data and clinical materials of the IMvigor210 cohort (http://research-pub.gene.com/IMvigor210CoreBiologies/), the ICI scoring model is used to divide all samples into a high and a low scoring group. Similarly, the GSE78220 data set was downloaded from GEO and analyzed accordingly.

Statistical Analyses

All the statistical comparisons involved in this study and the hypothesis testing of the significance of differences between groups are based on the statistical analysis method of R 3.6.

RESULTS

The Immune Cell Infiltration Landscape

For each sample in the TCGA-THCA dataset, 22 types of immune cell's infiltration statuses (naïve B cells, memory B cells, plasma cells, $CD8^+$ T cells, naïve $CD4^+$ T cells, resting and activated memory $CD4^+$ T cells, T follicular helper cells, Tregs, gamma delta T cells, resting and activated NK cells, monocytes, M0, M1, and M2 macrophages, resting and activated dendritic cells, resting and mast cells, eosinophils, and neutrophils) were recorded (**Supplementary Table S1**). From this, a cluster correlation and cumulative distribution function (CDF) curve were calculated (k = 3) and used for stable Immune Cell Infiltration (ICI) subtype classification (**Figures 1A,B**). Of the three main subtypes, ICI3 had the worst prognosis and a median OS of 937 days, whereas ICI1/2 had a mean OS of 1,017 days (p = 0.0065, **Figure 1C**).

To better clarify the inherent biological causes of the different clinical phenotypes, the TMEs of the three molecular subtypes were compared and visualized using heat maps (**Figure 1D,E**). The ICI3 samples were characterized by high stromal scores, low infiltration of $CD8^+$ T cells, and greater infiltration of static memory $CD4^+$ T cells and active dendritic cells. Subtypes ICI1 and ICI2, which had better prognoses, were characterized by lower stromal scores, greater $CD8^+$ T cell infiltration, lower infiltration of Tregs, inactive memory $CD4^+$ T cells and active dendritic cells.

In addition to analyzing immune cell infiltration, the expression levels of two important immune checkpoints (PD1 and PD-L1) in each ICI subtype were further analyzed. One of the characteristics of the ICI3 subtype was significantly lower PD1/PD-L1 expression, while the ICI2 subtype had higher PD1/PD-L1 expression. To assess the statistical significance of the differences in immune infiltration and PD1/PD-L1 expression among the ICI subtypes, the Kruskal-Wallis test and a hypothesis test were used. As shown in **Figures 1F,G**, the differences in PD1/PD-L1 expression and the infiltration of most immune cell types were statistically significant.

Immune Gene Expression Subtypes

In order to display different biological characteristics of immune phenotype, the tumor immunophenoscores (IPSs) samples in the TCGA-THCA dataset were collected from The Cancer Immunome database (TCIA), as shown in **Supplementary Table S2**. The Survminer R package was used to calculate the optimal density gradient threshold for the IPSs. A high and a low group of IPS with a threshold of seven were presented from TCGA-THCA tumor samples. The survival of high IPS group was much longer than the other group significantly (**Supplementary Figure S1**).

We analyzed differential gene expression (DEG) of different IPS group utilizing the limma R package with the set screening threshold changed ($p < 0.05$ and | log2 (Fold Change) | >1). One thousand two-hundred and ten differentially expressed genes (**Supplementary Table S3**) were identified, of which 1,030 genes were actively expressed in the high IPS group and 180 genes were greatly expressed in the low IPS group. We then performed unsupervised clustering of 1,210 differentially expressed genes related to IPS (IPS_DEGs) with the ConsensuClusterPlus R package. Finally, according to the cluster correlation and CDF curve, the TCGA-THCA tumor samples were divided into four immune gene expression subtypes, IPS_DEGs Clusters 1-4 (**Figures 2A,B**). There were clear

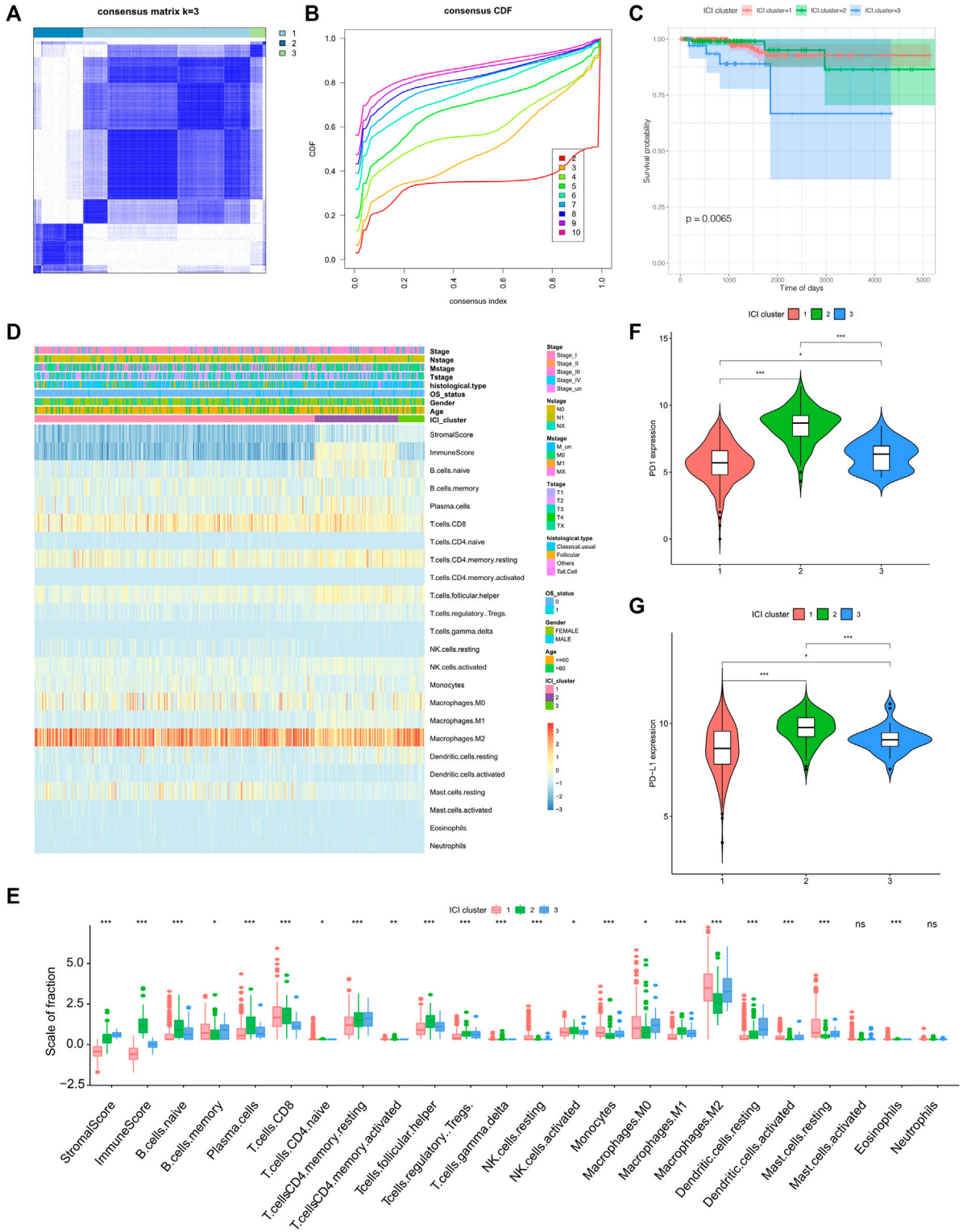

FIGURE 1 | Identification of tumor immune subtypes and characteristics of immune infiltration. **(A)** Clustering result when k = 3; **(B)** CDF curve distribution of consistent clustering; **(C)** Survival curve when K = 3; **(D)** Heat map of immune cell infiltration characteristics; **(E)** Box diagram of differences in immune cell infiltration characteristics among the three ICI subtypes; **(F)** The expression difference of PD1 among the three ICI subtypes; **(G)** the expression difference of PD-L1 among the three ICI subtypes.

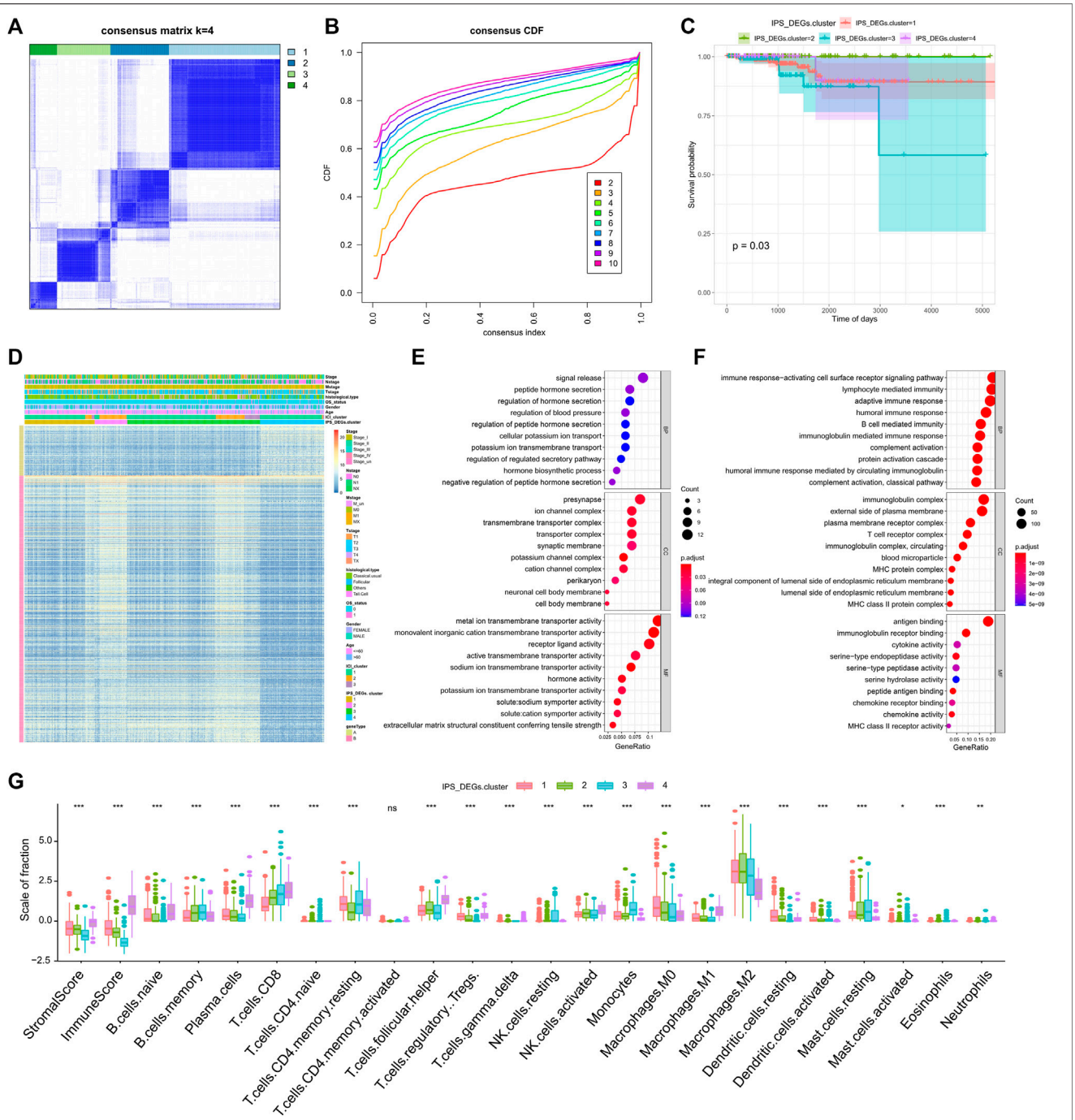

FIGURE 2 | Consistent clustering of differentially expressed genes related to tumor immune antigenicity. **(A)** Clustering results when k = 4; **(B)** CDF curve distribution of consistent clustering; **(C)** Survival curve of molecular subtypes when k = 4; **(D)** Heat map of immune gene subtypes; **(E)** Functional enrichment of immune gene subtype related features A gene; **(F)** Functional enrichment of immune gene subtype related features B gene; **(G)** Differences in infiltration characteristics of immune cells between immune gene subtypes.

differences in survival between the different immune gene expression subtypes (log rank test, p = 0.03, **Figure 2C**). Gene Type A includes 191 gene signatures which had a positive association with immune gene subtypes, while the remaining 1019 IPS_DEGs were represented by Gene Type B (**Supplementary Table S4**)

We revealed the heatmap of gene expression for each ICI subtype, IPS_DEGs Cluster, and Gene Type (**Figure 2D**) and implemented gene ontology (GO) functional enrichment study on Gene Type A and B genes using the clusterProfiler R package. A bubble map was used to display the first 10

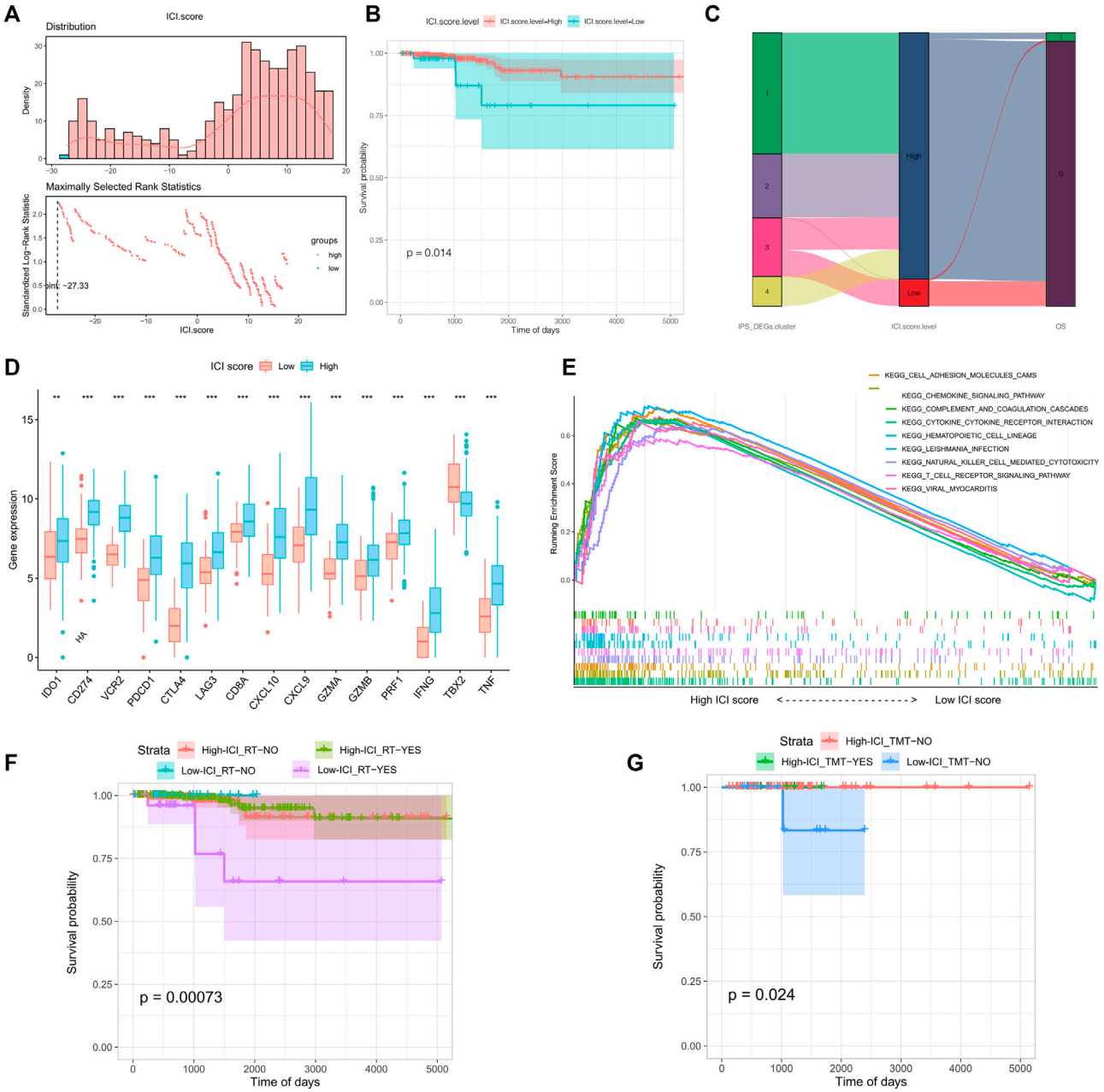

FIGURE 3 | Grouping and model construction of tumor immune cell infiltration scores (ICI scores). **(A)** Distribution **(above)** and the selection of the best density gradient points **(below)** of immune cell infiltration score (ICI scores); **(B)** survival curve between high and low ICI scores; **(C)** Sankey diagram of immune gene subtypes, ICI scores grouping and survival status; **(D)** Differences in immune checkpoints and immune activation gene expression between ICI scores groups; **(E)** Gene set function enrichment of differentially expressed genes between ICI scores groups; **(F)** Survival curve between radiotherapy and ICI scores groups; **(G)** Survival curve received therapy in different ICI scores.

pathways enriched in three groups of different functions (Biological Process, Cellular Component, Molecular Function), as shown in **Figures 2E,F**. Most of the enriched pathways were related to immunobiological processes.

We examined the 22 immune infiltration cells in the four IPS_DEG subtypes and found considerable differences between different subtypes (**Figure 2G**). We also observed great differences in PD1/PD-L1 expression. IPS_DEGs clusters 1, 2, and 4 were related to greater PD1/PD-L1 expression, while IPS_DEGs cluster 3 had the lowest PD1/PD-L1 expression (**Supplementary Figure S2A, B**). This low PD1/PD-L1 expression indicates a lack of sensitivity to immunotherapy, which is related to a poor prognosis. The consistent associations between immune cell infiltration characteristics

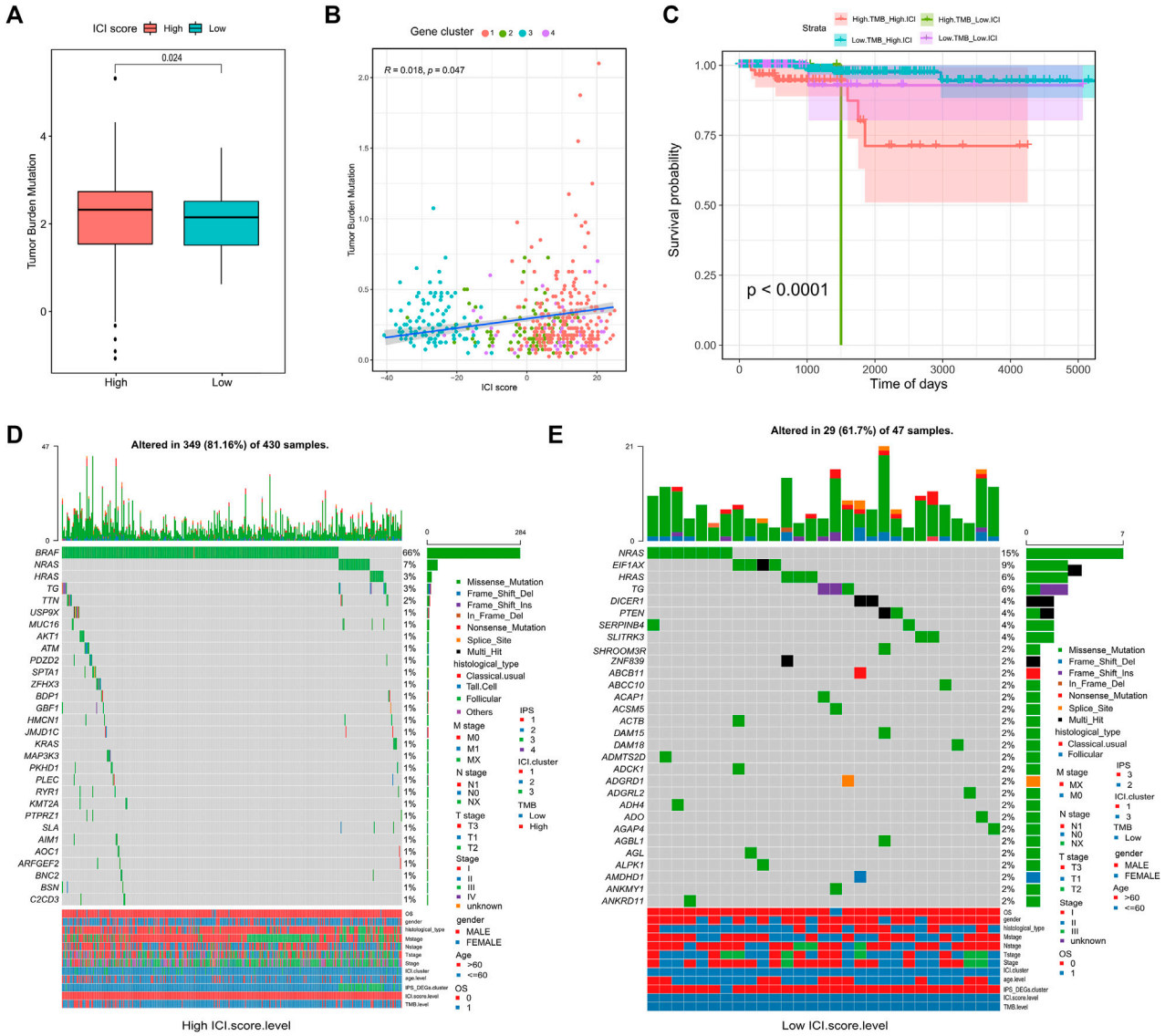

FIGURE 4 | Correlation between ICI scores and Somatic Variants. **(A)** Tumor mutation burden **(TMB)** between high and low ICI scores groups; **(B)** Association between ICI scores and tumor mutation burden **(TMB); (C)** Survival curve between tumor mutation burden **(TMB)** and ICI scores groups; **(D)** waterfall chart of gene mutation distribution in tumors of high ICI scores group; **(E)** waterfall chart of gene mutation distribution in tumors of low ICI scores group.

and the prognosis of different gene expression subtypes indicate that the classification strategy for the immune cell subtype is scientific and reasonable.

ICI Score Construction

To measure the immune cell infiltration in thyroid tumors using differential expression genes, we constructed a tumor immune cell infiltration (ICI) score model based on the type A and type B gene sets associated with immune gene subtypes. The Survminer R package was utilized to calculate the most accurate density gradient threshold related to ICI scores and survival. The cutoff value was -27.33, which divided the TCGA-THCA tumor samples into high and low ICI score groups. The high ICI score group manifested longer OS than the low ICI score group in **Figures 3A,B** ($p = 0.014$). A Sangji diagram was adopted to visualize the relations between the immune gene expression subtypes, ICI score groups, and survival statuses (**Figure 3C**).

Before the prognostic value of ICI score could be assessed for the TCGA-THCA cohort, it was necessary to analyze the immune activity and tolerance conditions within different groups. We chose CD274, CTLA4, HAVCR2, IDO1, LAG3, and PDCD1 as immune checkpoint features, and CD8A, CXCL10, CXCL9, GZMA, GZMB, IFNG, PRF1, TBX2, and TNF as immune activation-related genes (Zhang et al., 2020a). Except for IDO1, TBX2, and TNF, expression of most genes related to immune checkpoints and immune activity was significantly increased in the high ICI score group

(**Figure 3D**). We conducted gene set enrichment analysis (GSEA) to make an in-depth exploration of the biological differences between the two ICI score groups. The top ten enriched pathways were cell adhesion molecules (CAMs), chemokine signaling pathways, complement and coagulation cascades, cytokine receptor interactions, hematopoietic cell lineage, leishmania infection, NK cell mediated cytotoxicity, T cell receptor signaling, and viral myocarditis (**Figure 3E**). We also evaluated the impact of radiotherapy and targeted therapy on the prognosis of each ICI subgroup. The patients of high ICI score group had a better survival compared with the other group no matter what kind of treatment they received (**Figures 3F,G**).

Somatic Variants in Different ICI Groups

A large body of data suggests that the tumor mutation burden (TMB) may forecast the response to immunotherapy. Thus, researching on the relationship between TMB and ICI score to clarify the genetic characteristics is crucial. We first used the Survminer R package to calculate the optimal density gradient threshold for TMB and survival. A score of 0.42 was the threshold that divided the TCGA-THCA tumor samples into two groups: high TMB group and low TMB group. There were significant differences in survival between the two groups, as shown in **Supplementary Figure S3**.

We first conducted a comparison of the TMB in the high and low ICI score groups. According to **Figure 4A**, TMB were significantly higher in the high ICI score group (Wilcoxon test, $p = 0.024$). Further correlation analysis showed a significant positive relationship between ICI score and TMB score (Spearman coefficient: $R = 0.018$, $p = 0.047$; **Figure 4B**). However, the prognosis of patients with high TMB performed worse prognosis compared with low TMB patients, which was conflicted with the prognoses based on ICI scores. Therefore, in the prognostic stratification of THCA, we further analyzed the synergy of TMB and ICI score. According to the TMB, the stratified survival analysis showed that either in the high or low TMB subgroups, the prognosis of patients with the high ICI score were always better than the low ICI score group ($p < 0.05$; **Figure 4C**). This indicates that TMB status does not impede predictive effects of ICI scores. Accordingly, the above-mentioned results demonstrated that the ICI score may be a potential predictor of patient prognosis independent of TMB and that it is an effective predictor of response to immunotherapy.

In addition to overall TMB, the distribution of somatic variation in THCA driver genes between different ICI subgroups was further analyzed. And the 30 drive genes with the most significant change frequencies were compared (**Figures 4D,E**). We analyzed the mutation annotation files from the TCGA-THCA data and found huge variations in the mutation profiles of the high and low ICI subgroups. These findings may provide new insight for studying the tumor ICI composition and understanding mutational mechanisms affecting immune checkpoint inhibitor therapy.

The Value of ICI Scores in Predicting Response to Immunotherapy

Immune checkpoint blockade therapy has emerged to treat cancer by blocking T cell inhibition pathways. To explore the relationship between ICI scores and response to immunotherapy, we analyzed expression profile data and clinical materials from the IMvigor210 cohort. All samples were defined within high and low ICI score groups using the ICI scoring model. Our results showed that in the IMvigor210 cohort, high ICI scores were associated with greater objective response to anti-PD-L1 treatment (Wilcoxon test, $p = 0.036$, **Figure 5A**) and longer survival (log rank test, $p = 0.046$, **Figure 5B**). Patients in the high ICI score group had higher objective responses to anti-PD-L1 treatment than (Wilcoxon test, $p < 0.01$; **Figure 5C**). The GSE78220 cohort in GEO, which received different types of immunotherapies, including cytokines, vaccines, and checkpoint blockers, showed similar findings (Wilcoxon test, $p = 0.017$; **Figure 5D**; log rank test, $p = 0.023$, **Figure 5E**; chi-square test, p0.01, **Figure 5F**). Overall, these findings pointed out that the ICI score may predict response to immunotherapy.

DISCUSSION

Immunotherapy has shown amazing efficacy against a variety of malignant tumors, but for thyroid cancer it is still in exploratory stages. An early clinical trial showed that the PD-1 inhibitor pembrolizumab may be safe and effective in treating PD-L1-positive thyroid cancer. Studies have also shown a positive therapeutic effect of immunotherapy for patients with undifferentiated thyroid cancer (Capdevila et al., 2020; Ma et al., 2020). Combination therapies, including immune checkpoint inhibitors and tyrosine kinase (TK) or serine/threonine protein kinase B-Raf (BRAF) inhibitors, have shown significant potential for the treatment of advanced thyroid cancer (Iyer et al., 2018; Varricchi et al., 2019). Finding predictive indicators for evaluating the efficacy and prognosis of immunotherapy in thyroid cancer has now become a problem that needs to be solved urgently.

We analyzed the ICI of 505 THCA samples and divided the samples into three immune subtypes. Activated $CD8^+$ T lymphocytes are critical for adaptive immune defense and kill cancer cells through a variety of mechanisms; they are generally considered the main cytotoxic lymphocytes exerting anti-tumor effects (Farhood et al., 2019; van der Leun et al., 2020). $CD8^+$ T cell infiltration into the tumor indicates better prognosis (Bai et al., 2017; Ye et al., 2019; E et al., 2018). Tumor-associated dendritic cells (DCs) have functional defects, which can cause cancer immunosuppression (Veglia and Gabrilovich, 2017). In the TME, there are DCs with impaired antigen cross-presentation, and this can lead to changes in the activation and maintenance of anti-tumor immunity and promote tumor progression (Liu and Cao, 2015). In the present study, the ICI3 subtype with poor prognosis was characterized by low $CD8^+$ T cell infiltration, high infiltration of static memory $CD4^+$ T cells and active DCs, and a high stromal score. The ICI1 and ICI2 subtypes, which had good prognoses, were characterized by high

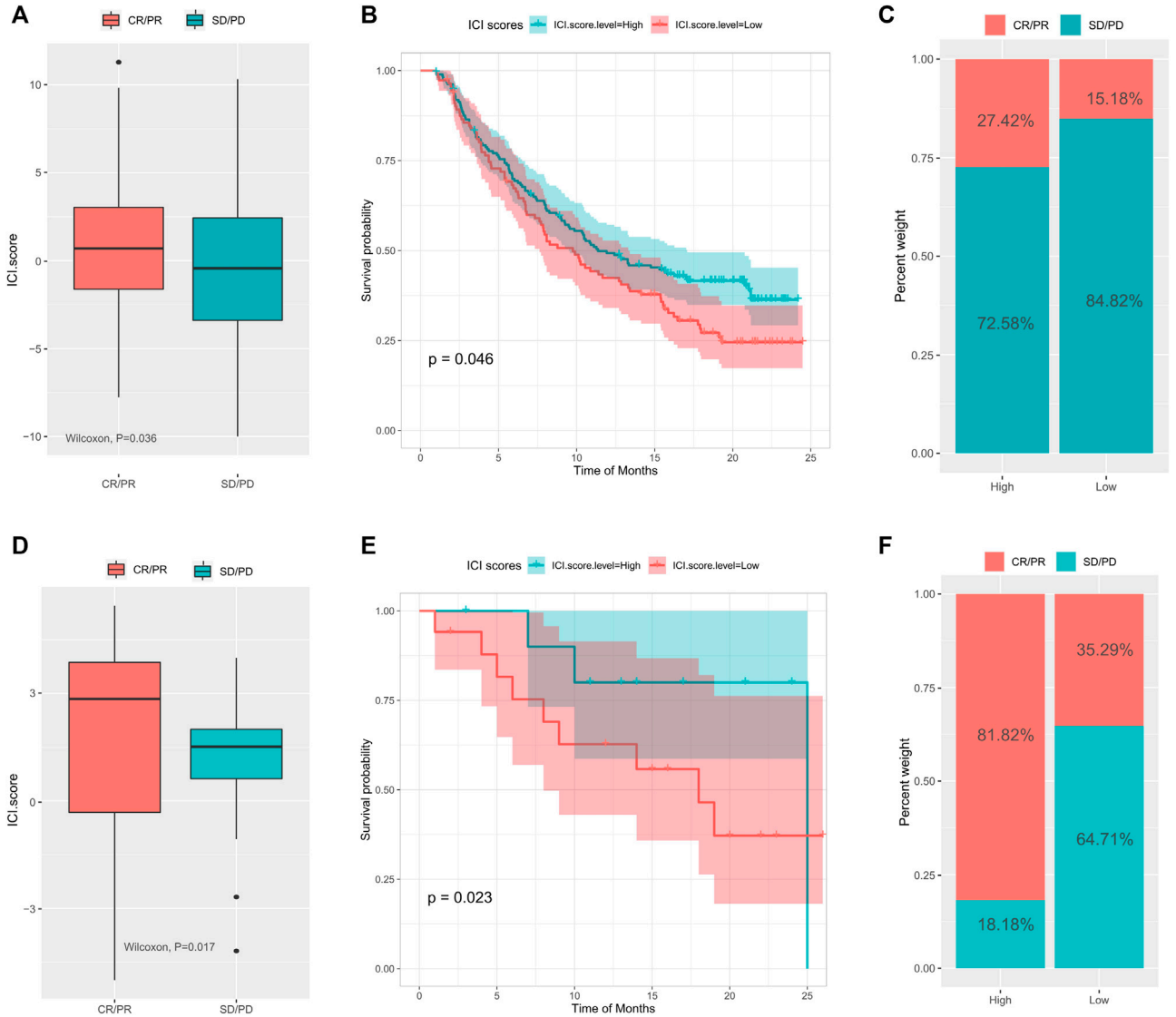

FIGURE 5 | The role of tumor immune cell infiltration scores in the prediction of immunotherapy. **(A)** The difference of ICI scores between different treatment response groups in the IMvigor210 cohort; **(B)** the survival curve between the high and low ICI scores groups in the IMvigor210 cohort; **(C)** the difference of response between different ICI scores in the IMvigor210 cohort; **(D)** Difference of ICI scores between different treatment response groups in the GSE78220 cohort; **(E)** survival curve between different ICI score groups in the GSE78220 cohort; **(F)** difference of proportion of response between different ICI score groups in the GSE78220 cohort.

infiltration of $CD8^+$ T cells, low infiltration of regulatory T cells and activated DCs, and a low stromal score; this was consistent with previous results. Our survival analysis showed a higher OS of the high ICI score group, which is in agreement with previous studies on TME and patient prognosis (Li et al., 2019). We also found that most immune checkpoint-related and immune activation-related genes were upregulated in the high ICI score group, which indicates better immunogenicity and greater benefit from immunotherapy.

The gene set enrichment analysis (GSEA) was applied to study the biological distinctions between the two ICI score subgroups and to obtain the following immune-related pathways: chemokine signaling, cytokine receptor interactions, NK cell-mediated cytotoxicity, and T cell receptor signaling. Chemokines play important immunomodulatory roles by regulating cell proliferation, migration, activation, differentiation, and homing (Nagarsheth et al., 2017). NK cells mediate anti-tumor immunity through cytotoxicity and cytokine secretion (Müller-Hermelink et al., 2008; Gross et al., 2013). The TME of thyroid cancer produces soluble modulators that negatively regulate the maturation, proliferation, and effector functions of NK cells (Melaiu et al., 2020). It has also been shown that TCR signaling shapes the TCR composition of Foxp3+ regulatory T cells (Burchill et al., 2008). Research on cytokine receptor signaling pathways in

thyroid cancer has thus far focused on the role of IL-1 family members (Mantovani et al., 2019).

Previous work has suggested that TMB is a prognostic marker and effective predictor of response towards immunotherapy in many cancers (Marabelle et al., 2020). The correlation between TMB and immune infiltration can be used to further assess the response to immunotherapy for a variety of tumors more effectively, including melanoma, bladder urothelial cancer, head and neck cancer, renal clear cell carcinoma, endometrial cancer, and others. Low TMB is associated with reduced immune infiltration, suggesting a poor prognosis for patients (Zhang et al., 2019; Zhang et al., 2020b; Jiang et al., 2020; Kang et al., 2020; Jiang et al., 2021; Zhou et al., 2021). In this study, ICI scores showed significant differences in survival either in high TMB or low TMB subgroups. Moreover, regardless of the expression in TMB, the prognosis of patients in the high ICI score group is always better than that of the low ICI score group, which shows that the TMB status will not interfere with the prediction based on the ICI score. These findings indicate that ICI score and TMB represent different aspects of tumor immunobiology, and ICI score may be a potential biomarker independent of TMB and effective in predicting response to immunotherapy.

There is prior evidence for gene mutations associated with response or tolerance to immunotherapy. For example, POLE/POLD1 gene mutations are associated with microsatellite instability (MSI), mismatch repair (MMR), and TMB, and CMTM6 is related to PD-L1 expression and regulation of anti-tumor immunity (Burr et al., 2017; Yao et al., 2019). In the present study, there were significant differences in gene mutation profiles between the different ICI score groups; this may provide new insight for studying the ICI composition of thyroid tumors and its relationship to gene mutations.

To further evaluate the value of the ICI score for estimating patient responses to immunotherapy, the IMvigor210, and GSE78220 cohorts of patients receiving immunotherapy were analyzed. As seen from the results, patients of the high ICI score group possessed higher objective responses to anti-PD-L1 therapy and greater overall survival. These results suggested that the ICI score relates to immunotherapy response and is an effective predictor of immunotherapy efficacy. Patients with high ICI scores may benefit more from immunotherapy.

Considering the enriched chemokine signaling pathways in the high ICI score group, the patients may also benefit from chemokine suppression and immune checkpoint blockade therapies. Previous studies have shown that the CXCR1/2 inhibitor Reparixin affects the viability of various thyroid cancer cells (Liotti et al., 2017). A CXCR4 antagonist (AMD3100) has also been shown to have significant anti-tumor effects on BHP10-3 papillary thyroid carcinoma cells *in vivo* and *in vitro* (Jung et al., 2016). Chemokine antagonists are expected to be adjuvant in the thyroid cancer's treatment.

In the present study, we adapted retrospective research and used public databases and bioinformatic approaches to discover potential biomarkers related to the development of THCA and the efficacy of immunotherapy. Due to tumor heterogeneity, future studies should include more clinicopathological characteristics to improve the accuracy of predictions. Further validation of our approach is still needed in a potential large-scale cohort of THCA patients treated immunotherapy.

In summary, we revealed the characteristics of ICI in THCA and established an ICI score which could accurately predict the patient's prognosis and response to immunotherapy. The results exhibited a comprehensive outlook of the internal immune landscape of THCA tumors.

DATA AVAILABILITY STATEMENT

The datasets presented in this study can be found in online repositories. The names of the repository/repositories and accession number(s) can be found in the article/ **Supplementary Material**.

ETHICS STATEMENT

Ethical review and approval was not required for the study on human participants in accordance with the local legislation and institutional requirements. Written informed consent for participation was not required for this study in accordance with the national legislation and the institutional requirements.

AUTHOR CONTRIBUTIONS

BJ designed the article, made important revisions to the paper and provided financial support; JG was responsible for data analysis and wrote the manuscript; LS was responsible for data collection; NL provided financial support and approved the final version of the paper to be published.

FUNDING

This research was supported by National Natural Science Foundation of China (Grant No. 81301767), Science and Technology Plan Project of Liaoning Province (Grant No. 20180551230).

SUPPLEMENTARY MATERIAL

The Supplementary Material for this article can be found online at: https://www.frontiersin.org/articles/10.3389/fmolb.2021.714053/full#supplementary-material

REFERENCES

Bai, M., Zheng, Y., Liu, H., Su, B., Zhan, Y., and He, H. (2017). CXCR5+ CD8+ T Cells Potently Infiltrate Pancreatic Tumors and Present High Functionality. *Exp. Cel Res.* 361 (1), 39–45. doi:10.1016/j.yexcr.2017.09.039

Burchill, M. A., Yang, J., Vang, K. B., Moon, J. J., Chu, H. H., Lio, C.-W. J., et al. (2008). Linked T Cell Receptor and Cytokine Signaling Govern the Development of the Regulatory T Cell Repertoire. *Immunity* 28 (1), 112–121. doi:10.1016/j.immuni.2007.11.022

Burr, M. L., Sparbier, C. E., Chan, Y.-C., Williamson, J. C., Woods, K., Beavis, P. A., et al. (2017). CMTM6 Maintains the Expression of PD-L1 and Regulates Anti-tumour Immunity. *Nature* 549 (7670), 101–105. doi:10.1038/nature23643

Cabanillas, M. E., McFadden, D. G., and Durante, C. (2016). Thyroid Cancer. *The Lancet* 388 (10061), 2783–2795. doi:10.1016/S0140-6736(16)30172-6

Capdevila, J., Wirth, L. J., Ernst, T., Ponce Aix, S., Lin, C.-C., Ramlau, R., et al. (2020). PD-1 Blockade in Anaplastic Thyroid Carcinoma. *Jco* 38 (23), 2620–2627. doi:10.1200/JCO.19.02727

Charoentong, P., Finotello, F., Angelova, M., Mayer, C., Efremova, M., Rieder, D., et al. (2016). Pan-cancer Immunogenomic Analyses Reveal Genotype-Immunophenotype Relationships and Predictors of Response to Checkpoint Blockade. *Cell Rep* 18 (1), 248–262. doi:10.1101/056101

Coperchini, F., Croce, L., Marinò, M., Chiovato, L., and Rotondi, M. (2019). Role of Chemokine Receptors in Thyroid Cancer and Immunotherapy. *Endocr. Relat. Cancer* 26 (8), R465–R478. doi:10.1530/ERC-19-0163

Du, L., Wang, Y., Sun, X., Li, H., Geng, X., Ge, M., et al. (2018). Thyroid Cancer: Trends in Incidence, Mortality and Clinical-Pathological Patterns in Zhejiang Province, Southeast China. *BMC Cancer* 18 (1), 291. doi:10.1186/s12885-018-4081-7

E, J., Kang, Z., Zhu, L., Xing, J., and Yu, E. (2018). CD8+CXCR5+ T Cells in Tumor-Draining Lymph Nodes Are Highly Activated and Predict Better Prognosis in Colorectal Cancer. *Hum. Immunol.* 79 (6), 446–452. doi:10.1016/j.humimm.2018.03.003

Fang, W., Ye, L., Shen, L., Cai, J., Huang, F., Wei, Q., et al. (2014). Tumor-associated Macrophages Promote the Metastatic Potential of Thyroid Papillary Cancer by Releasing CXCL8. *Carcinogenesis* 35 (8), 1780–1787. doi:10.1093/carcin/bgu060

Farhood, B., Najafi, M., and Mortezaee, K. (2019). CD8 + Cytotoxic T Lymphocytes in Cancer Immunotherapy: A Review. *J. Cel Physiol* 234 (6), 8509–8521. doi:10.1002/jcp.27782

Ferrari, S. M., Fallahi, P., Galdiero, M. R., Ruffilli, I, Elia, G., Ragusa, F., et al. (2019). Immune and Inflammatory Cells in Thyroid Cancer Microenvironment. *Ijms* 20 (18), 4413. doi:10.3390/ijms20184413

Gogali, F., Paterakis, G., Rassidakis, G. Z., Kaltsas, G., Liakou, C. I., Gousis, P., et al. (2012). Phenotypical Analysis of Lymphocytes with Suppressive and Regulatory Properties (Tregs) and NK Cells in the Papillary Carcinoma of Thyroid. *J. Clin. Endocrinol. Metab.* 97 (5), 1474–1482. doi:10.1210/jc.2011-1838

Gross, E., Sunwoo, J. B., and Bui, J. D. (2013). Cancer Immunosurveillance and Immunoediting by Natural Killer Cells. *Cancer J.* 19 (6), 483–489. doi:10.1097/PPO.0000000000000005

Iyer, P. C., Dadu, R., Gule-Monroe, M., Busaidy, N. L., Ferrarotto, R., Habra, M. A., et al. (2018). Salvage Pembrolizumab Added to Kinase Inhibitor Therapy for the Treatment of Anaplastic Thyroid Carcinoma. *J. Immunotherapy Cancer* 6 (1), 68. doi:10.1186/s40425-018-0378-y

Jiang, A.-M., Ren, M.-D., Liu, N., Gao, H., Wang, J.-J., Zheng, X.-Q., et al. (2021). Tumor Mutation burden, Immune Cell Infiltration, and Construction of Immune-Related Genes Prognostic Model in Head and Neck Cancer. *Int. J. Med. Sci.* 18 (1), 226–238. doi:10.7150/ijms.51064

Jiang, F., Wu, C., Wang, M., Wei, K., Zhou, G., and Wang, J. (2020). Multi-omics Analysis of Tumor Mutation burden Combined with Immune Infiltrates in Melanoma. *Clinica Chim. Acta.* 511, 306–318. doi:10.1016/j.cca.2020.10.030

Jung, Y. H., Lee, D. Y., Cha, W., Kim, B. H., Sung, M.-W., Kim, K. H., et al. (2016). Antitumor Effect of CXCR4 Antagonist AMD3100 on the Tumorigenic Cell Line of BHP10-3 Papillary Thyroid Cancer Cells. *Head Neck* 38 (10), 1479–1486. doi:10.1002/hed.24461

Kang, K., Xie, F., Mao, J., Bai, Y., and Wang, X. (2020). Significance of Tumor Mutation burden in Immune Infiltration and Prognosis in Cutaneous Melanoma. *Front. Oncol.* 10, 573141. doi:10.3389/fonc.2020.573141

Kim, S., Cho, S. W., Min, H. S., Kim, K. M., Yeom, G. J., Kim, E. Y., et al. (2013). The Expression of Tumor-Associated Macrophages in Papillary Thyroid Carcinoma. *Endocrinol. Metab.* 28 (3), 192. doi:10.3803/enm.2013.28.3.192

La Vecchia, C., Malvezzi, M., Bosetti, C., Garavello, W., Bertuccio, P., Levi, F., et al. (2015). Thyroid Cancer Mortality and Incidence: A Global Overview. *Int. J. Cancer* 136 (9), 2187–2195. doi:10.1002/ijc.29251

Li, B., Cui, Y., Nambiar, D. K., Sunwoo, J. B., and Li, R. (2019). The Immune Subtypes and Landscape of Squamous Cell Carcinoma. *Clin. Cancer Res.* 25 (12), 3528–3537. doi:10.1158/1078-0432.CCR-18-4085

Liotti, F., de Pizzol, M., Allegretti, M., Prevete, N., and Melillo, R. M. (2017). Multiple Anti-tumor Effects of Reparixin on Thyroid Cancer. *Oncotarget* 8 (22), 35946–35961. doi:10.18632/oncotarget.16412

Liu, Y., and Cao, X. (2015). Intratumoral Dendritic Cells in the Anti-tumor Immune Response. *Cell Mol Immunol.* 12 (4), 387–390. doi:10.1038/cmi.2014.130

Ma, M., Lin, B., Wang, M., Liang, X., Su, L., Okose, O., et al. (2020). Immunotherapy in Anaplastic Thyroid Cancer. *Am. J. Transl Res.* 12 (3), 974–988.

Mantovani, A., Dinarello, C. A., Molgora, M., and Garlanda, C. (2019). Interleukin-1 and Related Cytokines in the Regulation of Inflammation and Immunity. *Immunity* 50 (4), 778–795. doi:10.1016/j.immuni.2019.03.012

Marabelle, A., Fakih, M., Lopez, J., Shah, M., Shapira-Frommer, R., Nakagawa, K., et al. (2020). Association of Tumour Mutational burden with Outcomes in Patients with Advanced Solid Tumours Treated with Pembrolizumab: Prospective Biomarker Analysis of the Multicohort, Open-Label, Phase 2 KEYNOTE-158 Study. *Lancet Oncol.* 21 (10), 1353–1365. doi:10.1016/S1470-2045(20)30445-9

Melaiu, O., Lucarini, V., Cifaldi, L., and Fruci, D. (2020). Influence of the Tumor Microenvironment on NK Cell Function in Solid Tumors. *Front. Immunol.* 10, 3038. doi:10.3389/fimmu.2019.03038

Müller-Hermelink, N., Braumüller, H., Pichler, B., Wieder, T., Mailhammer, R., Schaak, K., et al. (2008). TNFR1 Signaling and IFN-γ Signaling Determine whether T Cells Induce Tumor Dormancy or Promote Multistage Carcinogenesis. *Cancer Cell.* 13 (6), 507–518. doi:10.1016/j.ccr.2008.04.001

Na, K. J., and Choi, H. (2018). Immune Landscape of Papillary Thyroid Cancer and Immunotherapeutic Implications. *Endocr. Relat. Cancer* 25 (5), 523–531. doi:10.1530/ERC-17-0532

Nagarsheth, N., Wicha, M. S., and Zou, W. (2017). Chemokines in the Cancer Microenvironment and Their Relevance in Cancer Immunotherapy. *Nat. Rev. Immunol.* 17 (9), 559–572. doi:10.1038/nri.2017.49

Siegel, R. L., Miller, K. D., and Jemal, A. (2020). Cancer Statistics, 2020. *CA A. Cancer J. Clin.* 70 (1), 7–30. doi:10.3322/caac.21590

Sotiriou, C., Wirapati, P., Loi, S., Harris, A., Fox, S., Smeds, J., et al. (2006). Gene Expression Profiling in Breast Cancer: Understanding the Molecular Basis of Histologic Grade to Improve Prognosis. *J. Natl. Cancer Inst.* 98 (4), 262–272. doi:10.1093/jnci/djj052

van der Leun, A. M., Thommen, D. S., and Schumacher, T. N. (2020). CD8+ T Cell States in Human Cancer: Insights from Single-Cell Analysis. *Nat. Rev. Cancer.* 20 (4), 218–232. doi:10.1038/s41568-019-0235-4

Varricchi, G., Loffredo, S., Marone, G., Modestino, L., Fallahi, P., Ferrari, S. M., et al. (2019). The Immune Landscape of Thyroid Cancer in the Context of Immune Checkpoint Inhibition. *Ijms* 20 (16), 3934. doi:10.3390/ijms20163934

Veglia, F., and Gabrilovich, D. I. (2017). Dendritic Cells in Cancer: the Role Revisited. *Curr. Opin. Immunol.* 45, 43–51. doi:10.1016/j.coi.2017.01.002

Xie, Z., Li, X., He, Y., Wu, S., Wang, S., Sun, J., et al. (2020). Immune Cell Confrontation in the Papillary Thyroid Carcinoma Microenvironment. *Front. Endocrinol.* 11, 570604. doi:10.3389/fendo.2020.570604

Yao, J., Gong, Y., Zhao, W., Han, Z., Guo, S., Liu, H., et al. (2019). Comprehensive Analysis of POLE and POLD1 Gene Variations Identifies Cancer Patients Potentially Benefit from Immunotherapy in Chinese Population. *Sci. Rep.* 9 (1), 15767. doi:10.1038/s41598-019-52414-z

Ye, L., Li, Y., Tang, H., Liu, W., Chen, Y., Dai, T., et al. (2019). CD8+CXCR5+T Cells Infiltrating Hepatocellular Carcinomas Are Activated and Predictive of a Better Prognosis. *Aging* 11 (20), 8879–8891. doi:10.18632/aging.102308

Yin, H., Tang, Y., Guo, Y., and Wen, S. (2020). Immune Microenvironment of Thyroid Cancer. *J. Cancer* 11 (16), 4884–4896. doi:10.7150/jca.44506

Zhang, C., Li, Z., Qi, F., Hu, X., and Luo, J. (2019). Exploration of the Relationships between Tumor Mutation burden with Immune Infiltrates in clear Cell Renal Cell Carcinoma. *Ann. Transl. Med.* 7 (22), 648. doi:10.21037/atm.2019.10.84

Zhang, C., Shen, L., Qi, F., Wang, J., and Luo, J. (2020). Multi-omics Analysis of Tumor Mutation burden Combined with Immune Infiltrates in Bladder Urothelial Carcinoma. *J. Cel Physiol.* 235 (4), 3849–3863. doi:10.1002/jcp.29279

Zhang, X., Shi, M., Chen, T., and Zhang, B. (2020). Characterization of the Immune Cell Infiltration Landscape in Head and Neck Squamous Cell Carcinoma to Aid Immunotherapy. *Mol. Ther. - Nucleic Acids.* 22, 298–309. doi:10.1016/j.omtn.2020.08.030

Zhou, H., Chen, L., Lei, Y., Li, T., Li, H., and Cheng, X. (2021). Integrated Analysis of Tumor Mutation burden and Immune Infiltrates in Endometrial Cancer. *Curr. Probl. Cancer.* 45 (2), 100660. doi:10.1016/j.currproblcancer.2020.100660

Conflict of Interest: The authors declare that the research was conducted in the absence of any commercial or financial relationships that could be construed as a potential conflict of interest.

Publisher's Note: All claims expressed in this article are solely those of the authors and do not necessarily represent those of their affiliated organizations, or those of the publisher, the editors and the reviewers. Any product that may be evaluated in this article, or claim that may be made by its manufacturer, is not guaranteed or endorsed by the publisher.

frontiers in Cell and Developmental Biology

REVIEW
published: 02 November 2021
doi: 10.3389/fcell.2021.739392

Ferroptosis-mediated Crosstalk in the Tumor Microenvironment Implicated in Cancer Progression and Therapy

Yini Liu, Chunyan Duan, Rongyang Dai and Yi Zeng**

Department of Biochemistry and Molecular Biology, Southwest Medical University, Luzhou, China

Ferroptosis is a recently recognized form of non-apoptotic regulated cell death and usually driven by iron-dependent lipid peroxidation and has arisen to play a significant role in cancer biology. Distinct from other types of cell death in morphology, genetics, and biochemistry, ferroptosis is characterized by the accumulation of lipid peroxides and lethal reactive oxygen species controlled by integrated oxidant and antioxidant systems. Increasing evidence indicates that a variety of biological processes, including amino acid, iron, lactate, and lipid metabolism, as well as glutathione, phospholipids, NADPH, and coenzyme Q10 biosynthesis, are closely related to ferroptosis sensitivity. Abnormal ferroptotic response may modulate cancer progression by reprogramming the tumor microenvironment (TME). The TME is widely associated with tumor occurrence because it is the carrier of tumor cells, which interacts with surrounding cells through the circulatory and the lymphatic system, thus influencing the development and progression of cancer. Furthermore, the metabolism processes play roles in maintaining the homeostasis and evolution of the TME. Here, this review focuses on the ferroptosis-mediated crosstalk in the TME, as well as discussing the novel therapeutic strategies for cancer treatment.

Keywords: ferroptosis, metabolism, cancer progress, immunity, tumor microenvironment

OPEN ACCESS

Edited by:
Shengtao Zhou,
Sichuan University, China

Reviewed by:
Shenglin Huang,
Fudan University, China
Yin Sun,
University of Rochester, United States
Xianming Mo,
Sichuan University, China

****Correspondence:***
Rongyang Dai
dryrun2502@163.com
Yi Zeng
yizeng@swmu.edu.cn

Specialty section:
This article was submitted to Molecular and Cellular Pathology, a section of the journal Frontiers in Cell and Developmental Biology

Received: *10 July 2021*
Accepted: *18 October 2021*
Published: *02 November 2021*

Citation:
Liu Y, Duan C, Dai R and Zeng Y (2021) Ferroptosis-mediated Crosstalk in the Tumor Microenvironment Implicated in Cancer Progression and Therapy. Front. Cell Dev. Biol. 9:739392. doi: 10.3389/fcell.2021.739392

INTRODUCTION

Iron is the most abundant element, by mass, in the Earth (Frey and Reed, 2012), and it is required in a variety of important biological processes in the human body, such as oxygen transport, DNA biosynthesis, adenosine triphosphate (ATP) synthesis, etc. (Bogdan et al., 2016). However, recent studies have increasingly found that disruption of iron metabolism and attendant overload of iron were closely related to the occurrence and development of tumors (Bogdan et al., 2016; Manz et al., 2016). In addition, the presence of iron, especially divalent iron, greatly accelerates lipid peroxidation of saturated fatty acids (FAs) in humans (Pratt et al., 2011). During the iron-related oxidative phosphorylation process in mitochondria, cells produce reactive oxygen species (ROS) along with the generation of ATP. ROS levels that exceed the antioxidation capacity of cells can lead to an oxidative stress response, which directly or indirectly damages proteins, nucleic acids, lipids, and other large molecular substances (Ray et al., 2012), leading to cell injury or death. This newly discovered iron-dependent form of regulated cell death (RCD) caused by unrestricted lipid peroxidation-mediated membrane damage is defined as ferroptosis (Dixon et al., 2012).

Cell death, which is currently divided into accidental cell death (ACD) and RCD (Galluzzi et al., 2018), is closely linked with oxidative stress and tightly integrated with diverse aspects of biological processes in various organisms. Unlike ACD (an uncontrolled and unavoidable process), RCD can be modulated by pharmacological or genetic interventions based on a series of specific intrinsic cellular

mechanisms and signaling pathways. Recently, RCD has been classified into apoptotic or non-apoptotic forms (ferroptosis (Dixon et al., 2012), necroptosis (Weinlich et al., 2017), pyroptosis (Bergsbaken et al., 2009), and alkaliptosis (Song et al., 2018b; Liu et al., 2020)), with distinct features in terms of the molecular mechanism and the signals transduction as well as disease implications. Ferroptosis, one such newly identified non-apoptotic modality of cell death, is obviously distinct from other types of RCD in cell morphology, biochemistry, and genetics. Morphologically, cells undergoing ferroptosis usually have the typical necrosis-like morphological changes, such as swelling of the cytoplasm organelles and plasma membrane rupture. These features are distinct from traditional apoptotic cells that are characterized by cell plasma membrane blebbing and shrinking, fragmentation and margination of chromatin, generation of apoptotic bodies, and cytoskeleton breakdown. Biochemically, it is becoming clear that ferroptosis is primarily triggered by the massive lipid peroxidation-mediated membrane rupture in an iron-dependent manner and modulated by lipid repair systems involving glutathione (GSH) and phospholipid peroxidase glutathione peroxidase 4 (GPX4) (Yang et al., 2014). Genetically, a few genes involved in lipid metabolism, such as prostaglandin-endoperoxide synthase 2 (PTGS2/COX2) (Yang et al., 2014), Acyl-CoA synthetase long-chain family member 4 (ACSL4) (Yuan et al., 2016b; Doll et al., 2017), as well as genes responsible for antioxidant defense, have been considered as biomarkers of ferroptosis. As a kind of selenoprotein, active GPX4 can covert potentially toxic lipid hydroperoxides (L-OOH) to non-toxic lipid alcohols (L-OH) (Ursini et al., 1982; Friedmann Angeli et al., 2014; Yang et al., 2014), and suppress the activation of arachidonic acid (AA)-metabolizing enzymes (Kagan et al., 2017).

Mounting evidence has shown that a great variety of human diseases related to iron or ROS including cancer have been connected to the malfunctions of ferroptosis (Stockwell et al., 2017; Galluzzi et al., 2018; Fang et al., 2019). Of note, ferroptosis has been reported to play a dual role in tumor promotion and suppression in different models. As previously mentioned, iron is an essential element for cell proliferation and a co-factor for metabolic enzymes. The absorption of iron by cancer cells can promote the occurrence and progression of tumors. Furthermore, ferroptotic cells may contribute to tumor initiation by playing a positive role in inflammation through immunogenicity within the tumor microenvironment (TME). In contrast, the ferroptosis inducers, such as FDA-approved anti-cancer drugs sorafenib, sulfasalazine, and artesunate, have shown a strong ability to kill cancer cells. Meanwhile, ferroptosis could also mediate the tumor suppression activity of interferon γ (IFNγ) released by $CD8^+$ T cells (Stockwell and Jiang, 2019). In particular, cancer cells with malignant mutations that are resistant to common cancer therapies or with a mesenchymal-like phenotype might be vulnerable to ferroptosis (Hangauer et al., 2017; Viswanathan et al., 2017). Therefore, in addition to the effects of oncogenes and tumor suppressors, the TME also plays a critical role in the complex process of ferroptosis in tumor treatment and tumorigenesis.

The TME refers to the complex and diverse multicellular environment in which tumor cells develop. In general, the TME comprises the peripheral blood and lymphatic vessels, immune cells, stromal cells, bone marrow-derived inflammatory cells, extracellular matrix (ECM), and various secreted signaling molecules (Quail and Joyce, 2013). Tumors and TME are often referred to as the relationship between "seed" and "soil," and the TME plays an essential role in tumor growth and progression. Notably, cancer cells can affect the microenvironment by releasing cell signaling molecules to promote tumor angiogenesis and induce immune tolerance, while immune cells in the microenvironment could regulate the growth and development of cancer cells. Emerging evidence has shown that ferroptosis is closely related to cancer progression and therapy. The triggers of ferroptosis, including iron accumulation, lipid peroxidation, and ROS, are generated by a series of environmental and genetic stimuli, such as heat and radiation exposure, metabolism, redox homeostasis, and intercellular interactions, as well as oncogenic and tumor-suppressive signaling (Ryter et al., 2007; Berghe et al., 2014). On the other hand, recent evidence indicated that ferroptotic cancer cells could release signal molecules, including oxidized lipid mediators, eicosanoids, and high mobility group box1 (HMGB1) (Friedmann Angeli et al., 2014; Kagan et al., 2017; Wen et al., 2019), into the ECM to modulate the anti-cancer immunity. These findings suggested the potential roles of TME in regulating ferroptosis, and the ferroptosis of cancer cells could also affect the TME in turn.

Recently, the process and function of ferroptosis and its impact on disease have been better explained. Although ferroptosis plays an important role in maintaining the survival of normal cells and tissues, it is increasingly recognized that some carcinogenic pathways are related to ferroptosis, which makes cancer cells vulnerable to ferroptosis and death (Yu et al., 2017; Wang Y. et al., 2020). Here, we aimed to discuss the emerging regulatory network between ferroptosis and TME in cancer cells and its potential role in cancer treatment.

THE DISCOVERY OF FERROPTOSIS

The early observation of ferroptosis-like cell death can be traced back to the mid-twentieth century, when oxidative stress-induced cell death was detected in neuronal cells and metabolism studies termed "oxytosis" (Tan et al., 2001). In the 1950s and 1960s, Harry Eagle's pioneering work demonstrated a ferroptosis-like cell death that is induced by the lack of the amino acid cysteine (Eagle, 1955), and the endogenous synthesis of cysteine makes cells resistant to this cell death (Coltorti et al., 1956; Eagle et al., 1961). The first identified ferroptosis inducer was caught in the search for new therapeutic drugs targeting RAS mutation, which is often involved in cancer. In 2003, Dolma et al. identified a small chemical compound, erastin, by using synthetic lethal high-throughput screening, which can cause selectively toxic to cancer cells expressing oncogenic RAS, but not wild-type cells in a manner different from traditional apoptosis (Dolma et al., 2003). Subsequently, RAS-selective lethal small molecule (RSL)3

and RSL5, which have the same effect as erastin that leads to a nonapoptotic, MEK-dependent, and iron-dependent oxidative cell death, were discovered in 2008 (Yang and Stockwell, 2008). In 2012, Dixon et al. formally coined this kind of RCD to ferroptosis based on the characteristics that the anti-cancer activity of erastin in RAS-mutated tumors could be completely blocked by the iron chelators and lipophilic antioxidants (instead of the apoptotic inhibitor Z-VAD-FMK) (Dixon et al., 2012). The term "ferroptosis" is a combination of the Greek word "ptosis" for corruption and the Latin word "Ferrum" for iron, indicating the importance of iron in this non-apoptotic form of cell death (Tsoi et al., 2018). Afterward, multiple inducers of ferroptosis, such as sorafenib (Louandre et al., 2013), artemisinins (Eling et al., 2015; Ooko et al., 2015), FIN56 (Liang et al., 2019), and $FINO_2$ (Abrams et al., 2016), were identified to affect the accumulation of lipid peroxidation products and lethal ROS derived from iron metabolism. Although ferroptosis has only been observed in mammalian systems in recent years (Dixon et al., 2012), it is considered to be one of the most widespread and oldest forms of cell death, since ferroptotic-like cell death has also been observed in evolutionary-distant species, such as those belonging to plants, protozoa, and fungi (Distefano et al., 2017; Bogacz and Krauth-Siegel, 2018; Shen et al., 2020). Since the Nomenclature Committee on Cell Death (NCCD) named such RCD type as "ferroptosis", it gradually entered the explosive stage of ferroptosis research, and provided a novel insight into cancer research.

THE REGULATORY MECHANISMS OF FERROPTOSIS

Ferroptosis is a ROS-dependent form of cell death associated with the accumulation of excessive iron and lipid peroxidation, as well as changes in specific genes involved in regulating iron homeostasis and lipid peroxidation metabolism (Yan et al., 2021). Generally, increased free iron and lipid peroxidation are considered to be the two key components that contribute to oxidative damage to the lipid bilayer of the membrane in ferroptosis (Dixon et al., 2012). The process of ferroptosis is regulated by the balance between integrated oxidation and antioxidant systems (Chen et al., 2021).

The Activation Mechanisms of Ferroptosis

Lipid peroxidation is a trigger of ferroptosis and is caused by a complicated process of lipid metabolism. In the process of ferroptosis, polyunsaturated fatty acids (PUFAs), especially AA and adrenic acid (AdA), are sensitive to be oxidized to lipid peroxides by ROS, resulting in damage to the lipid bilayer and thus promoting ferroptosis. ACSL4 and lysophosphatidylcholine acyltransferase 3 (LPCAT3) are required for biosynthesis and modification of PUFAs in cell membranes and act as important drivers of ferroptosis. In the ferroptotic process, ACSL4 catalyzes the ligation of AA and AdA with coenzyme A to form lipid derivatives AA-CoA or AdA-CoA (Yuan et al., 2016b; Doll et al., 2017; Kagan et al., 2017). These products can be re-esterified into membrane phosphatidylethanolamine (PE) by LPCAT3 to produce AA-PE or AdA-PE (Dixon et al., 2015; Doll et al., 2017). However, loss function of ACLS4 could induce a substantial change of long-chain PUFAs tails to short-chain and monounsaturated fatty acids (MUFAs) tails in phospholipids (Kim et al., 2001; Doll et al., 2017). These MUFAs, including exogenously supplemented and endogenously produced stearoyl-CoA desaturase 1 (SCD1), can be converted to acyl-coenzyme A esters, which can bind to the membrane phospholipids, thereby protecting cancer cells from ferroptotic cell death (Chen et al., 2021). Thus, depletion of ACSL4 or LPCAT3 could inhibit ferroptosis by reducing the accumulation of lipid peroxidation substrates in cells.

Moreover, the accumulation of iron can promote the activity of arachidonate lipoxygenases (ALOXs), which are a class of non-heme iron-dependent enzymes, and induce ferroptosis. ALOXs, including ALOXE3, ALOX5, ALOX12, ALOX12B, ALOX15, and ALOX15B, can directly oxygenate PUFAs to generate various hydroperoxy PUFA derivatives, such as lipid hydroperoxides (LOOHs), malondialdehyde (MDA), and 4-hydroxynonenal (4HNE), thus inducing ferroptosis (Kagan et al., 2017). Moreover, ALOXs also play important physiological roles in the immune system by producing pro-inflammatory and anti-inflammatory molecules that directly modulate (neuro) inflammatory processes and the TME (Friedmann Angeli et al., 2019; Proneth and Conrad, 2019). Besides the context-dependent role of ALOXs in ferroptosis, recent findings suggest that the cytochrome P450 oxidoreductase (POR) also plays a role in promoting lipid peroxidation in cancer cells in an ALOX-independent manner (Zou et al., 2020). Prostaglandin-endoperoxide synthase 2 (PTGS2/COX2) is not involved in the oxidation of phospholipids, but can oxidize lysophospholipids. PTGS2 is usually upregulated during ferroptosis and considered as a biomarker, rather than as a driver, of ferroptosis (Yang et al., 2014). However, the inhibitor of PTGS has little effect on the lethality of erastin or RSL3, but PTGS2 may modulate ferroptosis in neural cells after traumatic brain injury (Yang et al., 2014; Yang et al., 2016; Xiao et al., 2019). The specific role of PTGS2 in ferroptosis of cancer cells remains to be elucidated.

The Inhibition Mechanisms of Ferroptosis

The antioxidant enzyme GPX4 can covert GSH into oxidized glutathione (GSSG) and directly reduce toxic phospholipid hydroperoxides (PL-OOH) to nontoxic phospholipid alcohols (PLOH), thus acting as a central repressor of ferroptosis in cancer cells (Yang et al., 2014). Inactivation of GPX4-dependent antioxidant defense leads to the accumulation of the lipid peroxides, which is a trigger of ferroptosis. Selenium and GSH are necessary components for the expression and activity of GPX4 in ferroptosis (Ingold et al., 2018; Ursini and Maiorino, 2020). Selenium can boost the anti-ferroptosis activity of GPX4 by inserting selenocysteine into GPX4 residue at Sec 46 (U46) (Ingold et al., 2018). Meanwhile, selenium-supplementation has been demonstrated to upregulate GPX4 expression by coordinated activation of the transcription factor AP-2 gamma (TFAP2C) and specificity protein 1 (SP1), which protects against ferroptosis-related cerebral hemorrhage (Alim

et al., 2019). The antioxidant GSH is composed of three amino acids, cysteine, glycine, and glutamic acid; cysteine is considered to be the main rate-limiting factor in *de novo* synthesis of GSH. In mammalian cells, cystine (the oxidized form of cysteine) is imported into cells by system Xc^- for subsequent GLC (glutamate-cysteine ligase)-mediated GSH production. As a transporter that facilitates the exchange of cystine and glutamate across the plasma membrane, system Xc^- is a heterodimeric protein complex consists of two subunits: solute carrier family 7 member 11(SLC7A11; also known as xCT) and solute carrier family 3 member 2 (SLC3A2, also known as CD98 or 4F2). The expression of SLC7A11 is promoted by nuclear factor erythroid 2 like 2 (NFE2L2/NRF2) and downregulated by the tumor suppressor genes, such as TP53, BAP1, and BECN1 (Jiang et al., 2015; Song et al., 2018a; Zhang et al., 2018). This dual regulation of SLC7A11 expression and activity creates a fine-tuning mechanism to modulate cell antioxidant capacity and lipid ROS during ferroptosis (Chen et al., 2021). Inhibition system Xc^- (with erastin, sulfasalazine, or sorafenib) or GPX4 (with RSL3, ML162, ML210, FIN56, or FINO2) can produce ROS in the absence of GSH depletion and trigger ferroptosis. Similarly, depletion of SLC7A11 or GPX4 promotes lipoxygenase-mediated lipid peroxidation and leads to ferroptosis in specific cells or organs (Sato et al., 2005; Friedmann Angeli et al., 2014). In addition, the endogenous antioxidant coenzyme Q10 (CoQ10) produced by the mevalonate (MVA) pathway is converted to a reduced form to suppress lipid peroxidation, thereby protecting cells from undergoing ferroptosis in a GPX4-independent manner (Mullen et al., 2016). Tetrahydrobiopterin (BH_4) and ESCRT (endosomal sorting complexes required for transport)-III membrane repair systems also show a context-dependent antioxidant property (independent of the Cysteine/GSH/GPX4 axis) during ferroptosis (Dai et al., 2020c; Kraft et al., 2020). Furthermore, the ferroptosis suppressor protein 1 (FSP1/AIFM2) controls the generation of reduced CoQ10, and can also inhibit ferroptosis in cancer cells by activating the ESCRT-III membrane repair system (Dai et al., 2020d). This indicates that the antioxidant system could prevent ferroptosis through mutual synergy or complementation.

ROLE OF FERROPTOSIS IN CANCERS

As previously mentioned, the earliest chemical inducer of ferroptosis was discovered in screening for novel therapeutic compounds targeting cancers with RAS mutation (Dolma et al., 2003). Subsequent studies have revealed that excessive or defective ferroptosis is tightly implicated in the treatment and tumorigenesis of various tumor types. In general, cancer cells are thought to be more susceptible to ferroptosis due to their active metabolism, high ROS load, and high iron supply demand. The sensitivity of different tumor types to ferroptosis, on the other hand, varies, which may be due to a distinct genetic background or epigenetic modification. In this section, we summarize the role of ferroptosis in various tumors.

Pancreatic Cancer

Pancreatic ductal adenocarcinoma (PDAC) is a one of the deadliest tumors that is resistant to most therapies. In recent years, an increasing number of researchers have investigated the role of ferroptosis in the treatment, initiation, and progression of pancreatic cancer. Daniel et al. found that cytosolic aspartate aminotransaminase (GOT1) inhibition represses mitochondrial metabolism and enhances labile iron availability through autophagy, which accelerates pancreatic cancer cell death by ferroptosis (Kremer et al., 2021). Furthermore, specific and conditional depletion of pancreatic *Slc7a11* could induce pancreatic tumor ferroptosis and inhibit pancreatic tumorigenesis in mice (Badgley et al., 2020). However, ferroptosis may play oncogenic roles in pancreatic cancer in addition to suppressing tumor progression. During *Kras*-driven PDAC in mice, ferroptotic cancer cells promote the release of damage-associated molecular patterns (DAMPs) such as 8-hydroxy-2′-deoxyguanosine (8-OHG) and KRAS-G12D protein, leading to macrophage polarization and subsequent pancreatic tumor growth (Dai et al., 2020a; Dai et al., 2020b). The dual role of ferroptosis in pancreatic cancer needs to be considered when developing new cancer therapeutic approaches based on ferroptosis induction.

Hepatocellular Carcinoma (HCC)

HCC is the most major form of liver cancer diagnoses and deaths (McGlynn et al., 2021). Clinically, sorafenib is one of the six approved systemic therapies for patients with advanced HCC (Llovet et al., 2021), and inducing ferroptosis of cells is an important mechanism in sorafenib treating HCC. In terms of mechanism, sorafenib blocks the import of cysteine by inhibiting SLC7A11, the subunit of cystine/glutamate antiporter system Xc^-, thereby triggering ferroptosis and ultimately killing HCC cells (Louandre et al., 2013). The effect of sorafenib on HCC cells is closely related to ferroptosis process. GSH depletion through cysteine deprivation or cysteinase inhibition can enhance the susceptibility of HCC cells to sorafenib-induced ferroptosis, which provides a new sight in therapeutic combinations for advanced HCC (Li Y. et al., 2021). Moreover, research also reported that iron chelator deferoxamine (DFX) protects HCC cells from the sorafenib-induced ferroptotic cell death (Louandre et al., 2013). The status of retinoblastoma (Rb) protein modulates the tumorigenesis of liver and the response of human liver cancer cells to sorafenib (Mayhew et al., 2007; Louandre et al., 2015). HCC cells with Rb-negative status promote the occurrence of ferroptosis and cell death upon exposure to sorafenib (Louandre et al., 2015).

It has been reported that several proteins, such as NRF2, DAZAP1, metallothionein-1G (MT-1G), Branched-chain amino acid aminotransferase 2 (BCAT2), and CDGSH iron-sulfur domain 1 (CISD1), inhibit ferroptosis in HCC cells through different ways. Sun et al. revealed that activation of the p62-Keap1-NRF2 pathway prevents HCC cells from ferroptosis, and the Ras/Raf/MEK pathway is an important target for ferroptosis in the treatment of HCC (Sun et al., 2016b; Nie et al., 2018). RNA-binding protein DAZAP1 maintains the SLC7A11 mRNA stability to negatively regulate ferroptosis in HCC cells (Wang Q. et al., 2021). MT-1G knockdown increases GSH depletion and lipid peroxidation, thereby enhancing sorafenib-induced ferroptosis (Sun et al., 2016a).

The aminotransferase BCAT2 protects HCC cells from system Xc^- inhibitor-induced ferroptosis by mediating the metabolism of sulfur amino acid (Wang K. et al., 2021). Inhibition of CISD1, an iron-containing outer mitochondrial membrane protein, contributes to erastin-induced ferroptosis in HCC cells (Yuan et al., 2016a). In addition, inhibition of sigma 1 receptor (S1R) by haloperidol also promotes erastin- and sorafenib-induced ferroptosis in HCC cells (Bai et al., 2017).

Breast Cancer

Breast cancer is one of the most common causes of cancer-related death in women (DeSantis et al., 2019). The triple-negative breast cancer (TNBC) is an aggressive breast cancer subtype with poor prognosis, and lacks effective therapeutic target. Notably, TNBC have been shown to more sensitive to ferroptosis than estrogen receptor (ER) positive breast cancer, suggesting that ferroptosis is a promising treatment for TNBC patients. The drug-tolerant persister breast cancer cells acquire a dependency on GPX4, making cells sensitive to ferroptosis triggered by GPX4 inhibition (Hangauer et al., 2017). Sulfasalazine (SAS) can trigger ferroptosis in breast cancer cells by inactivating GPX4 and system Xc^-, especially in cells with low ER expression (Yu et al., 2019). It was observed that the tyrosine kinase inhibitors lapatinib and neratinib induce ferroptosis by increasing the level of iron-dependent ROS in breast cancer cells (Ma et al., 2017; Nagpal et al., 2019). Cystine is one of the most essential amino acids in TNBC. Starvation of cystine reduces the level GSH by directly decreasing synthesis and the GCN2-eIF2α-ATF4-CHAC1 pathway, thereby inducing ferroptosis in TNBC cells (Chen et al., 2017). The anti-diabetic drug metformin reduces the stability of xCT by inhibiting its UFMylation, thus inducing ferroptosis and inhibiting the proliferation of breast cancer cells (Yang et al., 2021). In contrast, MUC1-C, a transmembrane protein, can maintain the GSH level and redox balance by forming a complex with xCT and the CD44 variants (CD44v), which inhibits ferroptosis in breast cancer cells (Ishimoto et al., 2011). Another study found that prominin-2 protects breast cancer cells from ferroptotic cell death by promoting the formation of ferritin-containing multivesicular bodies and exosomes that transport ferritin out of the cell (Brown et al., 2019).

Lung Cancer

Several studies revealed that iron is closely associated with the development of lung cancer, and the disruption of iron homeostasis makes cells more sensitive to ferroptosis (Kuang and Wang, 2019). USP35 is abundant in lung cancer cells and acts as a deubiquitinase to maintain the protein stability of ferroportin, which is a cellular efflux channel for iron (Tang et al., 2021). Depletion of USP35 can promote ferroptotic cell death and sensitivity to cisplatin and paclitaxel chemotherapy in lung cancer cells (Tang et al., 2021). The iron-sulfur cluster biosynthetic enzyme NFS1 is overexpressed in well-differentiated lung adenocarcinomas and protects cells from ferroptosis within high oxygen environment by sustaining the levels of iron-sulfur cofactors (Alvarez et al., 2017). Accumulating evidence showed that system Xc^- is increased in several types of cancers, including lung cancer. As a result, suppression of system Xc^- by either genetic depletion or pharmacological inhibition to trigger ferroptosis becomes a potential therapy target for lung cancer. Recently, Wang et al. reported that the stem cell factor SOX2 increases the resistance of lung cancer cells to ferroptosis by increasing the expression of SLC7A11. Oxidation of SOX2 at Cys265 can inhibit its transcriptional activity and make lung cancer cells with high SOX2 expression more susceptible to ferroptosis. (Wang X. et al., 2021). In addition to the typical GSH-dependent GPX4 pathway, FSP1 acts as a ferroptosis-resistance factor by reducing CoQ10 to inhibits lipid peroxidation in lung cancer cells (Bersuker et al., 2019).

Gastric Cancer

Recently, researchers have shown that the PUFA biosynthesis pathway is critical in the ferroptosis of gastric cancer. Gastric cancer cells with high expression of elongation of very long-chain fatty acid protein 5 (ELOVL5) and fatty acid desaturase 1 (FADS1) are more sensitive to ferroptosis, while cells that highly expressed stearoyl-CoA Desaturase 1 (SCD1) exhibit ferroptosis resistance (Wang C. et al., 2020; Lee et al., 2020). Similarly, inhibition of the GSH-GPX4 antioxidation system, which directly reduces lipid hydroperoxides to nontoxic lipid alcohols, can also induce ferroptosis in gastric cancer. Apatinib, an approved anti-angiogenic agent for advanced gastric cancer therapy, can induce lipid peroxidation by inhibiting the expression of GPX4 in gastric cancer cells, and thus leading to ferroptosis (Zhao et al., 2021). In addition, Sirtuins 6 (SIRT6) is significantly expressed in sorafenib-resistant gastric cancer cells. Depletion of SIRT6 inactivates the Keap1-NRF2 pathway and downregulates GPX4 expression, and enhances the sensitivity of gastric cancer cells to sorafenib-induced ferroptosis (Cai et al., 2021). Cysteine dioxygenase 1 (CDO1), on the other hand, regulates erastin-induced ferroptosis in gastric cancer cells by limiting the synthesis of GSH (Hao et al., 2017). Increasing CDO1 activity can competitively absorb cysteine and oxidize it to its sulfinic acid, thereby reducing cellular GSH levels and promoting ferroptosis.

THE FERROPTOSIS-RELATED METABOLISMS WITHIN THE TUMOR MICROENVIRONMENT

In recent years, it has been widely appreciated that TME is involved in dynamically controlling cancer development and impacting therapeutic outcomes. In solid tumors, the vascular system is incomplete due to the rapid growth of cells, so the oxygen supply in tumor tissue is insufficient, and the TME is characterized by hypoxia (Albini and Sporn, 2007). In this context, solid tumor cells mainly metabolize energy through anaerobic glycolysis, which leads to the accumulation of lactic acid and thus acidification of the microenvironment (Ferreira, 2010). At the same time, the initiation and progression of the tumor itself will also trigger the immune response of the immune system, resulting in the buildup of inflammatory cells in the region, leading to a significant inflammatory response. Mounting

evidence has shown that ferroptosis plays a dual role in cancer promotion and suppression, which is dependent not only on the expression of oncogenes and tumor suppressors but also on the TME. Meanwhile, the release of DAMPs mediated by ferroptosis damage may maintain an inflammatory TME, thereby limiting anti-tumor immunity. However, the specific mechanism of the crosstalk between ferroptotic cancer cells and their microenvironment remains to be clarified. Therefore, it's necessary to elucidate the interaction between ferroptosis and TME, which might provide a novel anti-cancer treatment (Binnewies et al., 2018). Here, we discuss the major metabolism processes that influence ferroptosis within the TME.

Interplay Between Iron Metabolism and Ferroptosis in the TME

Iron is a fundamental element that plays a critical role in a variety of vital biological processes *via* distinct oxidation states (from −2 to +6). In biological systems, iron is primarily restricted to ferrous (Fe^{2+}), ferric (Fe^{3+}), and ferryl (Fe^{4+}) states. Due to its flexible oxidation states, iron is usually employed as an electron transporter in crucial biological reactions, such as DNA synthesis and cellular respiration. As previously mentioned, iron metabolism has been identified as one of the pivotal regulators of ferroptosis. Studies have shown that the excess iron overload could result in ferroptosis by accumulating ROS through the Fenton reaction. In this reaction, hydrogen peroxides react with ferrous iron (Fe^{2+}) to produce hydroxyl radicals and ferric iron (Fe^{3+}) (Winterbourn, 1995). In turn, the generation of Fe^{3+} in the Fenton reaction can be reduced to Fe^{2+} by the superoxide, a by-product of cellular respiration, to undergo further Fenton reaction. This cycle between oxidized and reduced form of iron, known as Haber-Weiss reaction, enables it to produce massive amounts of harmful ROS, which could attack most cellular proteins, lipids, and nucleic acids (Torti et al., 2018). When the GSH-mediated anti-oxidative system is insufficient to eliminate the increasing iron-dependent lipid peroxides, cells were induced into ferroptosis.

Multiple areas of research have found that cancer cells exhibit a distinct iron metabolism from their non-malignant counterparts (Torti and Torti, 2013; Fonseca-Nunes et al., 2014). Cancer cells, especially cancer stem cells, are iron addicted and uptake more iron into cellular to maintain the activity of iron-dependent proteins and enhance tumor growth and metastasis (Ludwig et al., 2015). The intracellular iron metabolism is tightly regulated by iron regulatory proteins (IRP1 and IRP2), which modulate the cellular Fe^{2+} concentrations by regulating iron import, storage, release, and efflux (Andrews and Schmidt, 2007). Of note, cancer cells likely to express different IRPs to promote iron uptake and repress iron export due to the rapid proliferation rate and high metabolic activities that are commonly associated with malignancy. Down-regulation of IRP2 protects cells against ferroptosis, while depletion of FBXL5, an IRP2 negative regulator, sensitizes HT-1080 cells to erastin-induced ferroptosis (Dixon et al., 2012). Moreover, the ferritin heavy subunit (FTH) produced by cancer cells can activate circulating T cells to secret cytokines such as TNF-α and IFNγ, resulting in increased iron retention in macrophages (Meng et al., 2017). Degradation of FTH by lysosomes can accumulate large amounts of iron (Terman and Kurz, 2013). Increasing FTH levels in fibrosarcoma HT1080 cells by inhibiting lysosomal activity or silencing nuclear receptor activator 4 (NCOA4), a cargo receptor that mediates FTH autophagic degradation and iron release, can inhibit ferroptosis (Gao et al., 2016; Hou et al., 2016). Emerging studies, on the other hand, have revealed that iron metabolism in cancer cells is implicated in the complicated nature of tumor-associated macrophages (TAMs) polarization in the TME. In general, the macrophages with high plasticity can be polarized into two forms: the classical M1 (proinflammatory) and the alternative activated M2 (anti-inflammatory) macrophages (Murray, 2017). The M1 macrophages (activated by microbial agents and/or Th1 cytokines) are highly expressed with iron storage protein ferritin and low expressed with iron exporter ferroportin, thus M1 macrophages exhibit iron-accumulating properties (Agoro et al., 2018). However, M2 macrophages (activated by Th2 cytokines IL-4 or IL-13) display the opposite expression profile, with high expression of ferroportin and low expression of ferritin, which enhanced the release of iron and dysregulated iron metabolism in cancer cells (Recalcati et al., 2010). Changes in iron metabolism-related components involving ferritin, ferroportin, and iron levels could stimulate the M1 and M2 polarization (Liang and Ferrara, 2020). Ferroptotic tumor cells induced by excessive iron overload can release 8-OHG, the main product of oxidative DNA damage, to activate the stimulator of interferon genes protein (STING)-mediated DNA sensor pathway in TAMs, which results in TAMs infiltration and M2 polarization, thus enhancing pancreatic carcinogenesis (Dai et al., 2020b).

Emerging evidence shows that innate immune cells in the TME, such as TAMs and neutrophils, play a critical role in the regulation of iron metabolism by controlling iron availability in cancer cells (**Figure 1**). A large amount of iron required for daily iron metabolism was retrieved by macrophages from senescent red blood cells and then returned into the circulation (De Domenico et al., 2008). Therefore, cancer cells are iron consumers, while neutrophils and macrophages are iron providers. Within the TME, TAMs are implicated in cancer cell proliferation, angiogenesis, as well as immunosuppression and therapy resistance (Mantovani et al., 2006; Cassetta and Pollard, 2018). Moreover, TAMs could also increase the release of IRPs, such as the paracrine factor lipocalin 2 (Lcn2), to serve as an iron donor and promote the progression of breast cancer cells (Duan et al., 2018). TAMs can therefore engage in iron metabolism modulation by altering their polarization and interact with cancer cells to influence tumor development. Like macrophages, immune cell neutrophils could also generate iron-related proteins Lcn2 and lactoferrin to affect the iron metabolism in the TME (Cronin et al., 2019). With the stimulation of Lcn2, renal cell carcinoma cells demonstrated resistance to erastin-induced ferroptosis (Meier et al., 2021). In turn, Lcn2 is also involved in promoting the chemotaxis of neutrophils and stimulating M2 polarization to promote tumor progression (Sola et al., 2011; Ye et al., 2016). Hepcidin

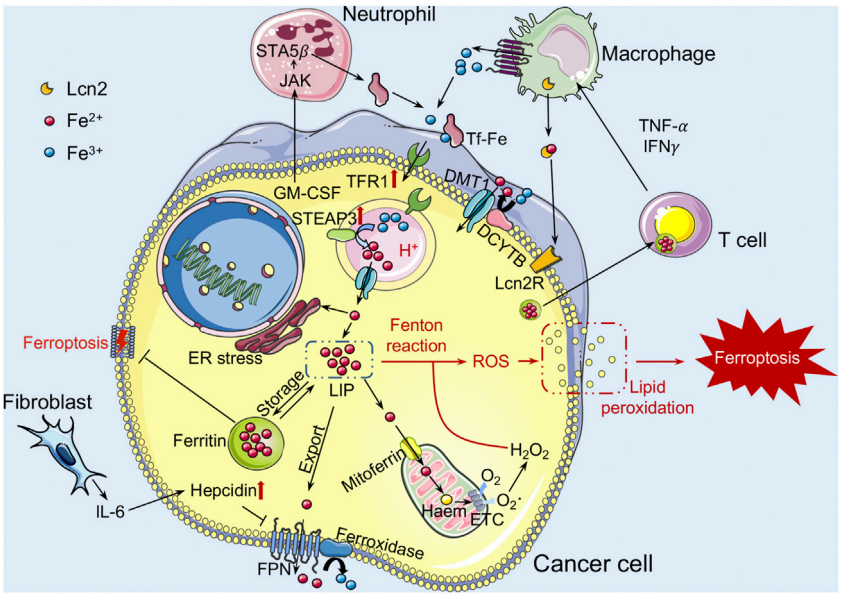

FIGURE 1 | The role of iron metabolism in ferroptosis within the TME. Iron binds to iron-bound transferrin (TF) and enters the cell through endocytosis of transferrin receptor (TFR). Iron is dissociated from the TF-TFR1 complex in the acidified environment of the early endosome, and is transported to the cytoplasm *via* DMT1 after reduced by STEAP3. Next, iron is gathered in the cytoplasm as a labile iron pool (LIP). Iron in the LIP can be stored inside ferritin (Ft) nanocages or transported to the mitochondria to support oxidative respiration. It can also be exported into extracellular to supplement TF-bound iron by ferroxidase binding ferroportin (FPN), which can be blocked by the hepcidin hormone. Increased LIP levels may generate reactive oxygen species (ROS) through Fenton reactions, leading to lipid peroxidation and inducing ferroptosis. TFR1 and STEAP3 proteins tend to be upregulated in cancer cells. In addition, IL-6 produced by CAFs can also increase the production of hepcidin in cancer cells. Cancer cells can also obtain more iron from the M2 macrophages with an iron-releasing phenotype to meet their exuberant metabolic demands. DMT1, divalent metal transport-1; STEAP3, steap3 family member-3; CAFs, cancer-associated fibroblasts; Lcn2, lipocalin 2.

is an iron-regulatory hormone that induces degradation of ferroportin and negatively regulates iron efflux. Proinflammatory cytokines such as tumor necrosis factor (TNF)-α and IFNγ have been shown to induce hepcidin production in macrophages and neutrophils (Sow et al., 2009; Wu et al., 2012; Blanchette-Farra et al., 2018). Meanwhile, it has been demonstrated that interleukin (IL)-6 generated by cancer-associated fibroblasts (CAFs), TAMs, and neutrophils enhances hepcidin expression, thereby boosting the iron concentration in breast cancer cells (Nemeth et al., 2004; Blanchette-Farra et al., 2018). Overall, the crosstalk between tumor-associated innate immunity in the TME and dysregulated iron metabolism in cancer cells is crucial for triggering ferroptosis.

Ferroptosis-related Amino Acid Metabolism Linked to the Tumor Immunity in the TME

Abnormal iron overload in cancer cells promotes the production of ROS *via* the Fenton reaction and hence increases oxidative stress. Accumulating ROS oxidizes the PUFAs to lipid peroxides to induce ferroptosis of cancer cells. Amino acid metabolism is involved in the regulation of ferroptosis (**Figure 2**). To protect from ferroptosis, cancer cells activate their antioxidant capabilities through a variety of mechanisms such as increasing demand for cysteine to synthesize the antioxidant GSH. GSH is a tripeptide composed of cysteine, glutamate, and glycine. Cysteine availability is the main rate-limiting factor in *de novo* biosynthesis of GSH. The system Xc^- functions as a cystine/glutamate antiporter in a sodium-independent manner and consists of SLC7A11 (also known as xCT) and SLC3A2. SLC7A11 is the light chain subunit of system Xc^- with 12 transmembrane domains, and mediates the activity of system Xc^- to specifically transport cystine and glutamate. SLC3A2, the heavy chain component, is a single transmembrane protein that acts as a chaperone protein to regulate the localization and protein stability of SLC7A11 (Nakamura et al., 1999; Shin et al., 2017). In extracellular environment, cysteine is often found in its oxidized form, cystine, and the cystine transported into cells through the system Xc^- will be immediately reduced into cysteine to synthesize GSH. Recently, it has been reported that the limiting of exogenous cystine can promote the ferroptosis of pancreatic cancer cells by enhancing the transaminase enzyme GOT1 inhibition (Kremer et al., 2021). The canonical function of GOT1 is to regulate the malate-aspartate shuttle to generate reduced NADPH, which is used to maintain redox balance and proliferation in PDAC. Inhibition of GOT1 impairs mitochondrial oxidative phosphorylation and iron release in PDAC cells, thereby increasing their susceptibility to ferroptosis. In addition, high extracellular glutamate levels could inhibit system Xc^- function and cause ferroptosis. Increasing SLC7A11 expression induced by anti-VEGF treatment in glioma leads to the accumulation of extracellular glutamate, which subsequently promotes the proliferation and activation of regulatory T cells (Tregs) in glioblastoma (Long et al., 2020). Like the iron-carrier protein transferrin, the extracellular amino acid glutamine has been discovered as an

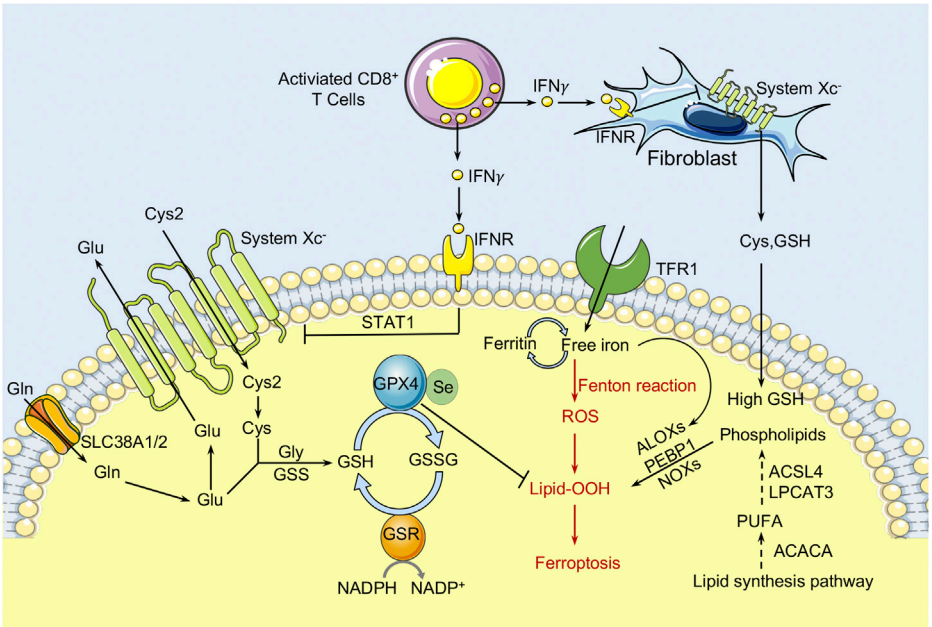

FIGURE 2 | The role of amino acid/glutathione metabolism and lipid metabolism in ferroptosis within the TME. Cystine (Cys2) is transferred into cells by System Xc^- at a ratio of 1:1 and then oxidized to cysteine. GPX4 inhibits the toxicity of lipid peroxides through its enzyme activity and maintains the homeostasis of the membrane lipid bilayer. In the process of ferroptosis, PUFAs are prone to peroxidation, resulting in the destruction of the lipid bilayer and affecting membrane function. The free PUFA and CoA are catalyzed by ACSL4 to form derivatives AA-CoA or AdA-CoA, then they are catalyzed by LPCAT3 to form polyunsaturated fatty acid-containing phospholipids (PUFA-PLs). In addition, the immunotreatment-activated $CD8^+$ T cells can enhance ferroptosis in cancer cells by releasing IFNγ, which activates the JAK1-STAT1 signaling and thereby inhibit the expression of SLC7A11 and SLC3A2. CAFs could protect cancer cells from chemoresistance-induced oxidative stress by releasing cysteine and GSH to nearby ovarian cancer cells. Meanwhile, $CD8^+$ T cells act as a repressor and prevent Cys and GSH release from the CAFs through IFNγ induced SLC7A11 and SLC3A2 downregulation. Cys, cysteine; GPX4, glutathione peroxidase 4; PUFAs, polyunsaturated fatty acids; ACSL4, Acyl-CoA synthetase long-chain family member 4; LPCAT3, lysophosphatidylcholine acyltransferase 3; IFNγ, interferon γ; SLC7A11, solute carrier family 7 member 11; SLC3A2, solute carrier family 3 member 2.

inducer of ferroptotic cell death (Gao et al., 2015). Furthermore, the glutamine-driven intracellular metabolic process glutaminolysis, which is highly active in cancer cells, is required for ferroptosis triggered by starvation of full amino acids or of cystine alone (Gao et al., 2015).

With the ability to import cysteine from and export glutamate into the extracellular environment, SLC7A11 can exert effects on the interplay with cancer cells and TME, which in turn influence tumor growth and response to cancer therapies. SLC7A11 has been regarded as a primary TME-redox state homeostasis regulator and controls the prooxidant levels including $O_2^{\bullet-}$ and H_2O_2 (Chaiswing and Oberley, 2010). It has been reported that CAFs released cysteine and GSH can protect ovarian cancer cells from chemoresistance-induced oxidative stress, leading to resistance to platinum-based chemotherapy. However, IFNγ produced by effector $CD8^+$ T cells downregulates SLC7A11 and SLC3A2 by reducing the release of cysteine and GSH from CAFs, thereby inhibiting cystine uptake in cancer cells, resulting in the induction of tumor lipid peroxidation and ferroptotic cell death (Wang et al., 2016). The role of effector $CD8^+$ T cells in abrogating CAFs-mediated chemoresistance indicates the anti-cancer potential of the interplay between chemotherapy and immunotherapy. Meanwhile, Wang et al. further proved that the combination of cyst(e)inase (an engineered enzyme which depletes extracellular cystine and cysteine) with PD-L1 blockade synergistically inhibit cystine uptake through system Xc^- in tumor cells, resulting in intracellular GSH deficiency and thus inducing potent tumor cell ferroptosis (Wang et al., 2019). In summary, T cells activated by immune checkpoint inhibitor (ICI) therapy can cause amino acid metabolic reprogramming in tumor cells, ultimately contributing to ICI-induced anti-tumor T cell immunity. In addition, ferroptotic cancer cells can release some signals, notably DAMPs and eicosanoids, which increase their immunogenicity to induce tumor-specific immune responses, enhancing the efficacy of ICI therapy (Turubanova et al., 2019; Yu et al., 2020). Of note, SLC7A11 deficiency has no effect on the anti-tumor activity of T cells, but inhibits mouse T cells proliferate *in vitro* (Arensman et al., 2019). Thus, the role of SLC7A11 in immune cells within the TME warrant further investigation. Taken together, the interaction of amino acid metabolism and immune cells within the TME precisely regulates cancer cell ferroptosis and tumor progression.

Lipid Metabolism and Ferroptosis Interact to Regulate Tumor Immunity Microenvironment

Lipid metabolism is tightly linked to the cell sensitivity to ferroptosis (**Figure 2**). Oxidized PUFAs, especially oxidized

AA and AdA, have been shown to drive cells to ferroptosis, but exogenous MUFAs, such as exogenous oleic acid (OA) and palmitoleic acid (POA), can protect cancer cells from ferroptosis (Yang et al., 2016; Kagan et al., 2017; Magtanong et al., 2019). Blood and lymphatic vessels are the main sources of intracellular FAs. Meanwhile, the absorption and release of FAs are strictly regulated by the state of the cells and external stimuli. Cancer cells always display aberrant lipid metabolism, which has been regarded as one of the hallmarks of aberrant cell growth and cancer progression. Elevated *de novo* synthesized lipids and FA oxidation are necessary for cancer cells to produce energy and required for post-translational modification of proteins (Carracedo et al., 2013; Rohrig and Schulze, 2016). The intricate interactions within the TME and adjacent stroma frequently impact the ways how cancer cells utilize lipids. For example, the presence of tumor low oxygen (hypoxia) environment results in the stabilization and activation of hypoxia inducible factors (HIFs), which regulate the transcription of target genes and consequently modulate lipid metabolism (Metallo et al., 2011). Activation of HIF1 in the head and neck tumor cells enhances SIAH2-mediated OGDN2 degradation, resulting in glutamine-derived carbon shunting to FA synthesis (Sun and Denko, 2014). The sterol regulatory element binding proteins (SREBPs), which control cholesterol and FA synthesis and uptake, are upregulated in hypoxic conditions and essential for glioblastoma multiforme cell survival (Lewis et al., 2015). SREBP can control the FA desaturases to introduce the double bonds into newly synthesized FAs and protect cancer cells from lipotoxicity under nutrient stress (Peck and Schulze, 2016). Furthermore, in response to metabolic stress and extracellular acidification, SREBP2 drives acetyl-CoA synthetase 2 (ACSS2) expression enabling the conversion of acetate to acetyl-CoA for lipid synthesis to promote tumor progression (Schug et al., 2015; Kondo et al., 2017). Recently evidence suggests that CAFs may also influence lipid transfer and uptake from the TME by enhancing the expression of FATP1 in breast cancer (Lopes-Coelho et al., 2018). In summary, the TME regulates fatty acid pools in cancer cells, which in turn affects ferroptosis sensitivity.

On the other hand, FAs secreted by cancer cells into the microenvironment could also impact infiltrating immune cell function and phenotype during tumor progression. During the stromal invasion, cancer cells can be impacted by circulating free fatty acids (FFAs) and other lipid molecules, which can substantially affect cell signaling or supply new substrates for cell development. Cancer cell-secreted FAs within the TME may stimulate TAMs to an M2 phenotype, which is marked by an increase in fatty acid oxidation (FAO) (Cook and Hagemann, 2013). The role of FFAs from circulation or within the TME in modulating the $CD8^+$ T cell effector functions depends on context. Within hypoxic environments, Tregs in glioblastoma utilize extracellular FFAs to support the suppression of $CD8^+$ T cells (Miska et al., 2019). Accumulation of lipid within lipid droplets in tumor-associated DCs reduces the antigen presentation, leading to dysfunction of DCs and poor stimulation of T cell responses, thereby modulating anti-tumor immunity (Herber et al., 2010; Ramakrishnan et al., 2014). Several studies demonstrate that exogenous lipids can disrupt the mTORC1-mediated glycolytic increase, which is necessary for the synthesis of granzyme B and IFNγ, leading to a deleterious impact on melanoma natural killer (NK) cell effector functions and their capacity to respond to stimuli, especially in the context of obesity (Michelet et al., 2018). Moreover, when the availability of glucose in the TME is limited, neutrophils and polymorphonuclear myeloid-derived suppressor cells (PMN-MDSCs) can utilize FAO to support ROS production and lead to T cell suppression (Hossain et al., 2015; Rice et al., 2018). Therefore, exogenous lipids within the TME can influence the activity of immune cells to promote tumor progression.

As previously stated, lipid peroxidation is a hallmark of ferroptosis and is tightly linked to the process of lipid metabolism. The interplay between ferroptosis and lipid metabolism is important in anti-tumor immunity modulation. Accumulating evidence has revealed that ferroptotic cancer cells can affect the activity of immune cells by releasing various oxidized lipid metabolites. In ferroptotic cancer cells, AA can be metabolized to different eicosanoids and their derivatives, such as prostaglandin E2 (PGE2), 15-hydroperoxy-eicosatetra-enoyl-phosphatidylethanolamine (15-HpETE-PE), 15-HETE, 12-HETE, and 5-HETE, through the function of various pathways and released into the tumor immune microenvironment (Friedmann Angeli et al., 2019). PGE2 has been identified as an immunosuppressive factor that suppresses the anti-tumor functions of NK cells, conventional type 1 dendritic cells (cDC1s), and cytotoxic T cells to alter the TME and promote colon cancer cell proliferation, migration and invasion (Johnson et al., 2020). The pro-ferroptotic lipid 15-HpETE-PE that released by ferroptotic cancer cells will induces immune cells undergo ferroptosis in the TME (Kapralov et al., 2020). Taken together, lipid metabolic abnormalities of ferroptotic cancer cells can impact infiltrating immune cell function and phenotype in the TME, while TME often affects the way cancer cells utilize lipids. The interaction of lipid metabolism and immune cells within the TME builds a regulatory network for modulating ferroptosis sensitivity of cancer cells.

The Role of Lactate Metabolism in Ferroptosis Within the TME

Lactate is a hydroxycarboxylic acid that is used as a fuel source by the heart, brain, and skeletal muscle under physiological conditions (Gladden, 2004). Based on the "lactate shuttle theory," lactate can transcend compartment barriers and shuttle occur within and among cells, tissues, and organs to deliver oxidative and gluconeogenic substrates as well as in cell signaling (Brooks, 2009; 2018). In 1926, *Otto Warburg* demonstrated that glucose, as a primary energy source, was heavily ingested in several cancer cells, producing an excessive amount of lactate, even in the presence of oxygen (Warburg et al., 1927). Tumor cells and CAFs in the TME are the main sources of lactate production. Due to the accumulation of extracellular lactate, the extracellular pH is ranging between 5.5 and 6.6 (Webb et al., 2011; Justus et al., 2013). It seems that the acidic environment in tumors is associated with the more aggressive

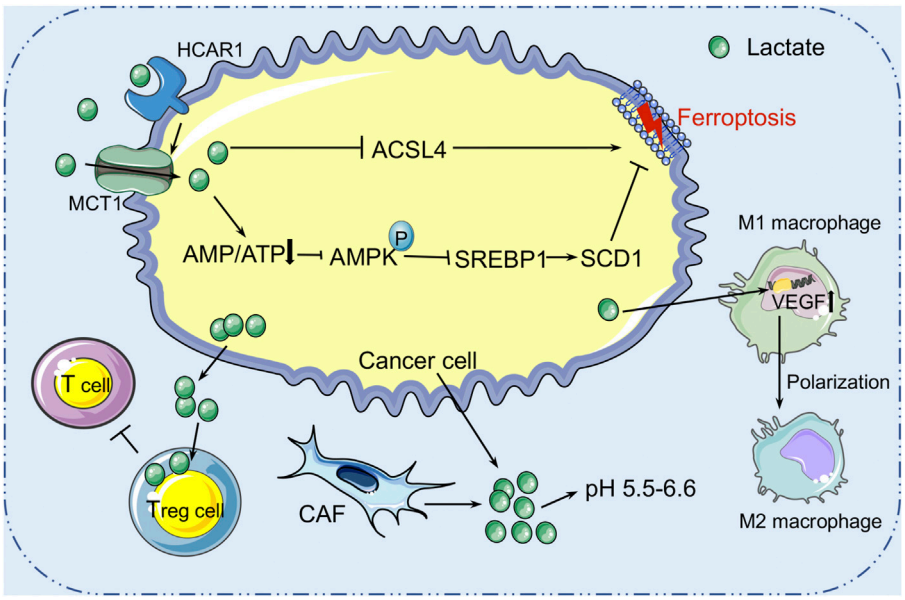

FIGURE 3 | The role of lactate metabolism in ferroptosis within the TME. Lactic acid is mainly derived from tumor cells and cancer-associated fibroblasts (CAFs) in the tumor microenvironment. High concentration of lactic acid forms an acidic environment with pH 5.5–6.6 in the TME. Cancer cells secrete lactic acid to nourish Treg cells to protect the tumor from immune attack. Lactic acid can also induce the formation of mono-unsaturated fatty acids through the HCAR1/MCT1-SREBP1-SCD1 pathway, which contributes to the resistance of liver cancer cells to ferroptosis induced by oxidative stress. HCAR1, hydroxycarboxylic acid receptor 1; MCT1, monocarboxylate transporter-1; SREBP1, sterol regulatory element-binding protein-1; SCD1, stearoyl-CoA desaturase-1.

tumor characteristics such as metastasis, angiogenesis, and therapy resistance (Estrella et al., 2013; Garcia-Canaveras et al., 2019). For instance, lactate induces the expression of transforming growth factor-β2 (TGF-β2), a key regulator of tumor cell invasion, in glioma cells (Baumann et al., 2009). Therefore, increasing evidence reveals that lactate is not only a major energy source (Brooks et al., 1991; Bergman et al., 1999) but also a signaling molecule (Brooks, 2002; Hashimoto et al., 2007; Brooks, 2009) that has many regulatory roles in the TME, and particular relevance to oxidative stress resistance (Tauffenberger et al., 2019; Tasdogan et al., 2020) and lipid biosynthesis (Chen et al., 2016). Pucino et al. reported that the accumulation of extracellular lactate contributes to regulating the production of various lipid substances, including acetyl-CoA and citrate, *via* AMP-activated protein kinase (AMPK) or signal transducer and activator of transcription 3 (STAT3) signaling (Pucino et al., 2019). These finds suggest that lactate may play a role in cancer cell ferroptosis regulation. Recently, Zhao et al. discovered the aberrantly high level of lactate in the HCC extracellular environment could promote ATP production and further deactivate the AMPK signals (Zhao et al., 2020). In addition, it was also confirmed that lactate can induce the formation of MUFAs through the HCAR1/MCT1-SREBP1-SCD1 pathway, which contributes to the resistance of liver cancer cells to ferroptosis induced by oxidative stress (Zhao et al., 2020) (**Figure 3**). Therefore, the role of lactate receptor HCAR1 and transporter MCT1 in the maintenance of redox homeostasis has been found, suggesting that HCAR1 may be a potential therapeutic target for ferroptosis in HCC (Zhao et al., 2020). In addition, lactate in the TME can impair the immune system and promote tumor development by triggering and recruiting immunosuppressive related cells and molecules (de la Cruz-Lopez et al., 2019; Ivashkiv, 2020). It has been reported that Treg cells can use lactate to maintain the strong suppression of effector T cells within the TME (Watson et al., 2021). Tumor cell-derived lactate can polarize TAM into M2 type, activate the expression of VEGF and arginase 1 (ARG1) through the HIF1-α signaling pathway in macrophages, and assist TAM to promote tumor growth (de la Cruz-López et al., 2019; Zhang et al., 2020). Overall, high lactate concentration promotes acidification of the TME and suppresses the immune system, thereby contributing to immune evasion and tumor growth, invasion, and migration. The definitive information regarding the lactate in regulating ferroptosis of cancer cells is limited. Considering the role of lactate in immune suppression, the hypothesis that lactate modulates the sensitivity to ferroptosis through the immune system within the TME deserves consideration in future studies.

FERROPTOSIS-BASED CROSSTALK BETWEEN TUMOR CELLS AND IMMUNE CELLS IN THE TME

Mounting evidence suggests that ferroptosis is tightly linked to tumor suppression and immunity (**Figure 4**). The role of ferroptosis in tumor immunity is determined by the interactions between cancer cells and distinct immune cell subgroups. As all we known, ferroptosis is an iron-dependent form of RCD caused by lipid peroxidation and plays an important role in cancers. Many metabolites, particularly those involved in

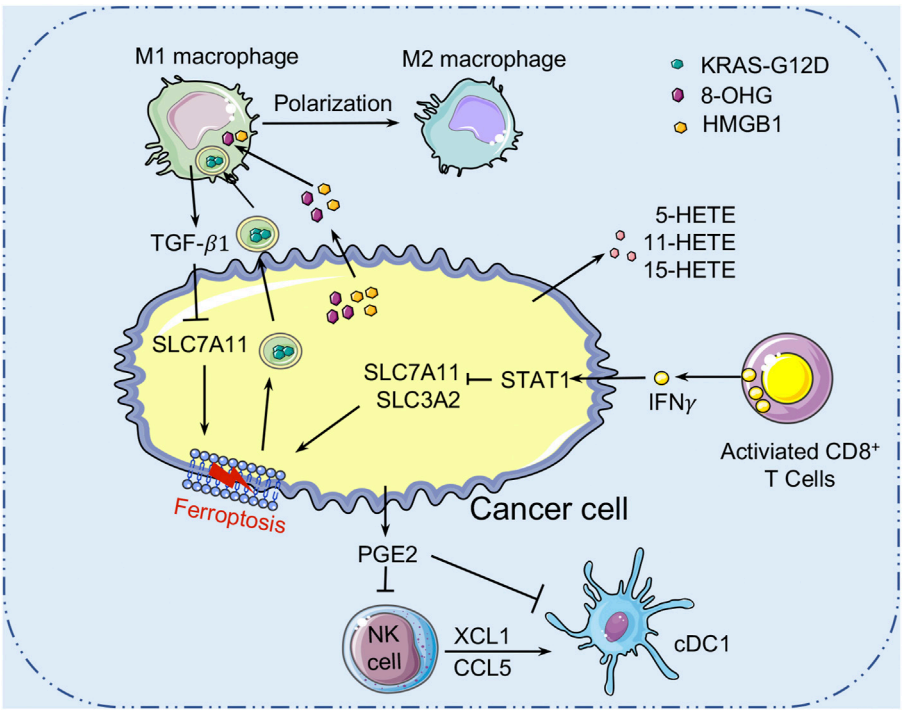

FIGURE 4 | Crosstalk between ferroptosis and tumor immunity. Ferroptotic cancer cells release the KRAS-G12D proteins. Extracellular KRAS-G12D proteins are packaged into exosomes, which are absorbed by macrophages through an AGER-dependent mechanism, thereby inducing macrophages to switch to the M2 phenotype to accelerate cancer development. Ferroptotic cancer cells can also release HMGB1 and 8-OHG to affect the innate immune cells' functions in the TME. In addition, ferroptotic cancer cells released PGE2 can inhibit the infiltration of cDC1s by suppressing the chemokines CCL5 and XCL1 that secreted by NK cells. PGE2 can also downregulate chemokine receptors to block cDC1s directly. Many cell types (such as macrophages) release TGF-β1 to activate SMAD proteins to inhibit the expression of SLC7A11, thereby promoting the ferroptosis of cancer cells. AGER, advanced glycosylation end-product-specific receptor; HMGB1, high mobility group box1; 8-OHG, 8-Hydroxyguanosine; cDC1s, conventional type 1 dendritic cells; PGE2, Prostaglandin E2; TGF-β1, transforming growth factor-β1.

the metabolism of iron, lipids, amino acids and lactate, regulate the complicated ferroptotic response by directly or indirectly regulating iron accumulation or lipid peroxidation in cancer cells. For example, AA and AdA, the metabolites of lipid metabolism, can be esterified by ACSL4 and LPCAT3 into PE, while LOXs may oxidize AA-PE and AdA-PE to AA-PE-OOH and AdA-OOH (e.g., 5-HETE, 11-HETE, and 15-HETE), which leads to membrane rupture and increases membrane permeability, leading to ferroptosis. Recently, several researches have indicated that ferroptotic cancer cells may release a variety signals to activate immune cells (e.g., neutrophils) in the TME (Friedmann Angeli et al., 2019). DAMPs, which are mainly released by dead or dying cells, are thought to be mediators of inflammation and immune responses in various types of RCD. Extracellular DAMPs can recruit and activate effector immune cells by binding to their receptors on various immune cells, such as macrophages and monocytes, aggravating inflammatory responses that support tumor growth (Tang et al., 2012). DAMP release, on the other hand, can also mediate immunogenic cell death, which can enhance anti-tumor immunity (Galluzzi et al., 2017). Ferroptotic cancer cells can release and activate distinct signals including DAMPs (e.g., HMGB1, KRAS-G12D, and 8-OHG) or oxidized lipid mediators (e.g., 4HNE, oxPLs, LTB4, LTC4, LTD4, and PGE2) that may modulate inflammatory and anti-tumor immunity. HMGB1 released by ferroptotic cancer cells is a prototypical DAMP involved in the immunogenicity of cancer cells, and it triggers an inflammatory response in macrophages through binding to advanced glycosylation end-product-specific receptor (AGER/RAGE) (Wen et al., 2019). Interaction of RAGE and HMGB1 leads to the phosphorylation of MAPKs and activation of the NF-κB signaling pathway in macrophages, which stimulates the release of pro-inflammatory cytokines (e.g., TNF-α and IL-1) by macrophages to promote tumor progression (Wen et al., 2019). Meanwhile, the ferroptosis-mediated DAMP release may promote tumor progression by driving the polarization of macrophages in TME. In this context, KRAS-G12D can be released within exosomes by ferroptotic cancer cells and taken up by macrophages through an AGER-dependent mechanism, resulting in the polarization of macrophages to an M2 phenotype and promotion of tumor growth (Dai et al., 2020a). Moreover, it has been reported that the PGE2 released by ferroptotic cancer cells could disrupt the anti-tumor immunity of the innate immune system by targeting NK cells and cDC1s, thereby promoting the progression of colon cancer (Bottcher et al., 2018). However, reports on the roles of these lipid-derived products released by ferroptotic cancer cells are still rare and require further investigation. In conclusion, the DAMPs and lipid

mediators released by cancer cells might form a complicated network that modulates anti-tumor immunity during ferroptosis. At the same time, further research is warranted to figure out the immunomodulatory function of ferroptotic cancer cells in anti-tumor immunity.

Recent studies have found that $CD8^+$ T cells can trigger ferroptosis in cancer cells, indicating that ferroptosis might be modulated by immune cells (**Figure 4**). Mechanistically, $CD8^+$ T cell-derived IFNγ inhibits SLC7A11 expression in cancer cells through activating the transducer and activator of transcription 1 (STAT1), thereby inducing tumor cell ferroptosis and contributes to the anti-tumor efficacy of immunotherapy (Wang et al., 2019). TGF-β1 released by macrophages can promote cancer cells ferroptosis by activation of the SMAD-related signaling to inhibit the expression of SLC7A11 (Kim et al., 2020). In addition, the lymphatic system promotes tumor metastasis by increasing the production of ACSL3-dependent MUFAs that protects melanoma cells from ferroptosis (Chen et al., 2021). Moreover, immune cells in the TME also influence a variety of metabolisms, including the metabolism of iron, lipid, and lactate, to modulate the ferroptosis sensitivity of cancer cells. The interactions between ferroptosis and the immune microenvironment in cancer cells provide a novel way to cancer therapies.

ROLE OF THE TUMOR MICROENVIRONMENT IN FERROPTOSIS-DEPENDENT CANCER THERAPY

Cancer therapies that are widely utilized include surgery, chemotherapy, hormone therapy, radiation therapy, and immunotherapy. The purpose of these strategies is to remove or kill cancer cells. According to recent studies, the complicated role of ferroptosis in tumor therapy and tumorigenesis is influenced not only by the tumor-associated genes, but also by the TME. The novel chemotherapy, immunotherapy, and radiation therapy targeting ferroptosis-related pathways and metabolism have shown promising potential for cancer therapies.

Immunotherapy

Recently, Wang et al. reported that ferroptosis induction-based treatment can be combined with ICIs to enhance the potency of killing cancer cells (Wang et al., 2019). ICIs (e.g., anti-PD-1 and anti-PD-L1 antibodies) can activate cytotoxic T cells to exert anti-tumor immunity, thereby inducing ferroptosis in cancer cells. It has been reported that ICI anti-PD-L1 antibodies can potentiate ferroptosis activators (e.g., erastin and RSL3) induced tumor growth inhibition *in vitro* and *in vivo* (Wang et al., 2019). Specifically, anti-PD-L1 antibodies stimulate $CD8^+$ T cells to release cytokine IFNγ to activate the JAK-STAT1 pathway in cancer cells, thereby reducing the expressions of SLC7A11 and SLC3A2, and ultimately increasing the sensitivity of cancer cells to ferroptosis (Wang et al., 2019). In melanoma patients, an increase in ICIs efficacy is consistently associated with a decrease in SLC3A2 expression (Wang et al., 2019). Furthermore, depletion of STAT1 in tumor cells disrupts the IFNγ-mediated SLC7A11 suppression and reverses RSL3-induced ferroptosis. Notably, STAT1 can be activated by a variety of ligands, which means that other cytokines may have similar effects to that of IFNγ in triggering ferroptosis. Meanwhile, the released DAMPs play a dual role in anti-tumor immunity. As mentioned above, ferroptotic cancer cells release HMGB1 to promote the inflammatory responses of macrophages through binding to AGER (Wen et al., 2019). Therefore, blocking the HMGB1-AGER pathway with small molecules or genetic methods could limit the inflammatory response mediated by ferroptosis (Chen et al., 2021). These DAMPs, oxidized lipid mediators, and cytokines released into the extracellular formed a complex regulatory network between ferroptotic cancer cells and the immune system. As a result, immunotherapy combined with ferroptosis induction is a promising method that synergistically promotes anti-tumor effect.

Radiotherapy

Radiotherapy can directly cause oxidative damage to lipid membrane, leading to the accumulation of toxic lipid peroxidation and triggering ferroptosis in cancer cells. Meanwhile, recent studies suggest that radiotherapy can enhance the anti-tumor effect by synergizing with ferroptosis triggers and immunotherapy. Mechanically, radiotherapy can activate Ataxia-Telangiectasia mutated gene (ATM) to produce IFNγ and synergizes with immunotherapy-activated $CD8^+$ T cells to suppress SLC7A11 expression in cancer cells. In addition, radiotherapy also upregulates ACSL4 expression in cancer cells, thereby increasing lipid peroxidation and inducing ferroptosis (Lei et al., 2020). Li et al. reported that mitochondrial DNA damage can activate the STING1/TMEM173-dependent DNA sensing pathway and lead to ferroptotic cancer cell death (Li C. et al., 2021). Similarly, this or other DNA sensor pathways activated by radiotherapy may similarly enhance the anti-tumor effect of inducing ferroptosis. Thus, the combination of radiotherapy and immunotherapy also increases the sensitivity of cancer cells to ferroptosis, indicating that inducing ferroptosis is a promising anti-cancer strategy.

Chemotherapy

Nanoparticle-based delivery of ferroptosis inducers can precisely and efficiently kill tumor cells with low toxicity by controlling the release of the drug and improving the pharmacokinetic properties of drugs. For example, due to the poor solubility of ferroptosis inducer withaferin A in water, withaferin A can be formulated in the amphiphilic degradable pH-sensitive nanocarrier to improve the convenience of drug delivery and reduce drug toxicity (Hassannia et al., 2018). Furthermore, nanoparticle-based ferroptosis induction is often combined with other treatments to enhance the anti-tumor effect. Chemodynamic therapy (CDT) is one of the ROS-dependent anti-cancer therapies that generate ROS through the iron-mediated Fenton reaction to kill cancer cells efficiently (Tang et al., 2019). Khalaf et al. used the novel tumor-targeted conjugated polymer nanoparticles (CPNPs) to deliver iron to the targeted tumor cells to trigger ferroptosis-

assisted CDT through Fenton reaction that produces ROS (Jasim and Gesquiere, 2019). They conjugated iron-carrying CPNPs with the endothelin 3 (EDN3-CPNP), which specifically targets the melanoma endothelin-B receptor (EDNRB), and showed enhanced melanoma tumor targeting and tumor cell killing effects (Jasim and Gesquiere, 2019). In addition, nanoparticle-based ferroptosis induction can combination with photodynamic therapy (PDT) to markedly enhance the anti-tumor effect of PDT (Zhu et al., 2019). In order to counteract the depressant effect of the hypoxic TME in solid tumors on PDT, researchers constructed a nanoparticle containing the photosensitizer chlorin e6 (Ce6) and the ferroptosis inducer erastin *via* supramolecular interaction (Zhu et al., 2019). The obtained Ce6-erastin nanodrugs by cancer cells subsequently trigger ferroptosis and increases oxygen concentration, thus promoting the PDT anti-tumor efficacy upon light irradiation (Zhu et al., 2019). It has been reported that nanoparticle-based ferroptosis induction can also collaborate with photothermal therapy (PTT) to construct the nanoparticles named SRF@MPDA-SPIO. This nanoparticle is composed of ferroptosis inducer sorafenib (SRF) and super-paramagnetic iron oxide (SPIO) loaded into the mesopores or onto the surface of mesoporous polydopamine (MPDA) NPs through π–π stacking and/or hydrophobic interaction. In this system, the PTT (provide by MPDA NPs under laser emissions) synergizes with ferroptosis (induced by SPIO and SRF) to develop a promising cancer therapy (Guan et al., 2020). For chemotherapy, the ability of nanoparticle-induced ferroptotic cell death is highly dependent on nanoparticle structure and chemical modifications.

CONCLUSIONS AND PERSPECTIVES

Over the last few years, we have gained a better understanding of ferroptosis or ferroptosis-like cell death. In general, the sensitivity of cancer cells to ferroptosis is dependent on the state of cellular metabolisms, such as the metabolisms of lipid, iron, lactate, and amino acid. A variety of reagents, most of which are used in cancer treatment, have recently been found with the ability to modulate the ferroptotic process by directly or indirectly targeting iron metabolism and lipid peroxidation. Although its involvement in tumor treatment is currently unknown, pharmacologically triggering ferroptosis is a promising therapeutic therapy. Of note, hypoxic environment and infiltrating immune cells within the TME influence cancer cells' vulnerability to ferroptosis by altering the metabolism of cancer cells. In turn, molecular factors involved in the metabolic pathways and released by ferroptotic cancer cells can affect infiltrating immune cell function and phenotype and reshape the tumor niche.

In carcinogenesis, these secreted DAMPs within the TME induced by ferroptotic damage exhibit a dual function in tumor growth and inhibition. However, the function and phenotype changes of infiltrating immune cells in response to ferroptosis remain unclear. Therefore, it is necessary to conduct more detailed research on the effect of ferroptosis in the tumor immune microenvironment to provide a new approach for cancer treatment through ferroptosis-induced cell death and anti-tumor immunity. Furthermore, the mechanism of TME in regulating the ferroptotic process (especially the metabolism of lipid, iron, amino acid, and lactate) of cancer cells still needs to be clarified. In summary, a better understanding of the TME in regulating ferroptosis will create a new way to develop novel cancer-eradication therapies.

AUTHOR CONTRIBUTIONS

RD and YZ conceived and supervised the project. YL and YZ wrote the manuscript. YZ, YL, and CD revised the manuscript. All authors contributed to the article and approved the submitted version.

FUNDING

This work was supported by the National Natural Science Foundation of China (grant number 82002993).

ACKNOWLEDGMENTS

Figures were produced using Sevier Medical Art (https://smart.servier.com).

REFERENCES

Abrams, R. P., Carroll, W. L., and Woerpel, K. A. (2016). Five-Membered Ring Peroxide Selectively Initiates Ferroptosis in Cancer Cells. *ACS Chem. Biol.* 11 (5), 1305–1312. doi:10.1021/acschembio.5b00900

Agoro, R., Taleb, M., Quesniaux, V. F. J., and Mura, C. (2018). Cell Iron Status Influences Macrophage Polarization. *PLoS One* 13 (5), e0196921. doi:10.1371/journal.pone.0196921

Albini, A., and Sporn, M. B. (2007). The Tumour Microenvironment as a Target for Chemoprevention. *Nat. Rev. Cancer* 7 (2), 139–147. doi:10.1038/nrc2067

Alim, I., Caulfield, J. T., Chen, Y., Swarup, V., Geschwind, D. H., Ivanova, E., et al. (2019). Selenium Drives a Transcriptional Adaptive Program to Block Ferroptosis and Treat Stroke. *Cell* 177 (5), 1262–1279.e25. doi:10.1016/j.cell.2019.03.032

Alvarez, S. W., Sviderskiy, V. O., Terzi, E. M., Papagiannakopoulos, T., Moreira, A. L., Adams, S., et al. (2017). NFS1 Undergoes Positive Selection in Lung Tumours and Protects Cells from Ferroptosis. *Nature* 551 (7682), 639–643. doi:10.1038/nature24637

Andrews, N. C., and Schmidt, P. J. (2007). Iron Homeostasis. *Annu. Rev. Physiol.* 69, 69–85. doi:10.1146/annurev.physiol.69.031905.164337

Arensman, M. D., Yang, X. S., Leahy, D. M., Toral-Barza, L., Mileski, M., Rosfjord, E. C., et al. (2019). Cystine-Glutamate Antiporter xCT Deficiency Suppresses Tumor Growth While Preserving Antitumor Immunity. *Proc. Natl. Acad. Sci. USA* 116 (19), 9533–9542. doi:10.1073/pnas.1814932116

Badgley, M. A., Kremer, D. M., Maurer, H. C., DelGiorno, K. E., Lee, H.-J., Purohit, V., et al. (2020). Cysteine Depletion Induces Pancreatic Tumor Ferroptosis in Mice. *Science* 368 (6486), 85–89. doi:10.1126/science.aaw9872

Bai, T., Wang, S., Zhao, Y., Zhu, R., Wang, W., and Sun, Y. (2017). Haloperidol, A Sigma Receptor 1 Antagonist, Promotes Ferroptosis in Hepatocellular

Carcinoma Cells. *Biochem. Biophysical Res. Commun.* 491 (4), 919–925. doi:10.1016/j.bbrc.2017.07.136

Baumann, F., Leukel, P., Doerfelt, A., Beier, C. P., Dettmer, K., Oefner, P. J., et al. (2009). Lactate Promotes Glioma Migration by TGF-β2-Dependent Regulation of Matrix Metalloproteinase-2. *Neuro Oncol.* 11 (4), 368–380. doi:10.1215/15228517-2008-106

Berghe, T. V., Linkermann, A., Jouan-Lanhouet, S., Walczak, H., and Vandenabeele, P. (2014). Regulated Necrosis: The Expanding Network of Non-Apoptotic Cell Death Pathways. *Nat. Rev. Mol. Cel Biol* 15 (2), 135–147. doi:10.1038/nrm3737

Bergman, B. C., Wolfel, E. E., Butterfield, G. E., Lopaschuk, G. D., Casazza, G. A., Horning, M. A., et al. (1999). Active Muscle and Whole Body Lactate Kinetics After Endurance Training in Men. *J. Appl. Physiol.* 87 (5), 1684–1696. doi:10.1152/jappl.1999.87.5.1684

Bergsbaken, T., Fink, S. L., and Cookson, B. T. (2009). Pyroptosis: Host Cell Death and Inflammation. *Nat. Rev. Microbiol.* 7 (2), 99–109. doi:10.1038/nrmicro2070

Bersuker, K., Hendricks, J. M., Li, Z., Magtanong, L., Ford, B., Tang, P. H., et al. (2019). The CoQ Oxidoreductase FSP1 Acts Parallel to GPX4 to Inhibit Ferroptosis. *Nature* 575 (7784), 688–692. doi:10.1038/s41586-019-1705-2

Binnewies, M., Roberts, E. W., Kersten, K., Chan, V., Fearon, D. F., Merad, M., et al. (2018). Understanding the Tumor Immune Microenvironment (TIME) for Effective Therapy. *Nat. Med.* 24 (5), 541–550. doi:10.1038/s41591-018-0014-x

Blanchette-Farra, N., Kita, D., Konstorum, A., Tesfay, L., Lemler, D., Hegde, P., et al. (2018). Contribution of Three-Dimensional Architecture and Tumor-Associated Fibroblasts to Hepcidin Regulation in Breast Cancer. *Oncogene* 37 (29), 4013–4032. doi:10.1038/s41388-018-0243-y

Bogacz, M., and Krauth-Siegel, R. L. (2018). Tryparedoxin Peroxidase-Deficiency Commits Trypanosomes to Ferroptosis-Type Cell Death. *Elife* 7, e37503. doi:10.7554/eLife.37503

Bogdan, A. R., Miyazawa, M., Hashimoto, K., and Tsuji, Y. (2016). Regulators of Iron Homeostasis: New Players in Metabolism, Cell Death, and Disease. *Trends Biochem. Sci.* 41 (3), 274–286. doi:10.1016/j.tibs.2015.11.012

Böttcher, J. P., Bonavita, E., Chakravarty, P., Blees, H., Cabeza-Cabrerizo, M., Sammicheli, S., et al. (2018). NK Cells Stimulate Recruitment of cDC1 into the Tumor Microenvironment Promoting Cancer Immune Control. *Cell* 172 (5), 1022–1037.e14. doi:10.1016/j.cell.2018.01.004

Brooks, G. A., Butterfield, G. E., Wolfe, R. R., Groves, B. M., Mazzeo, R. S., Sutton, J. R., et al. (1991). Decreased Reliance on Lactate During Exercise After Acclimatization to 4,300 M. *J. Appl. Physiol.* 71 (1), 333–341. doi:10.1152/jappl.1991.71.1.333

Brooks, G. A. (2002). Lactate Shuttles in Nature. *Biochem. Soc. Trans.* 30 (2), 258–264. doi:10.1042/bst0300258

Brooks, G. A. (2009). Cell-Cell and Intracellular Lactate Shuttles. *J. Physiol.* 587 (Pt 23), 5591–5600. doi:10.1113/jphysiol.2009.178350

Brooks, G. A. (2018). The Science and Translation of Lactate Shuttle Theory. *Cel Metab.* 27 (4), 757–785. doi:10.1016/j.cmet.2018.03.008

Brown, C. W., Amante, J. J., Chhoy, P., Elaimy, A. L., Liu, H., Zhu, L. J., et al. (2019). Prominin2 Drives Ferroptosis Resistance by Stimulating Iron Export. *Develop. Cel* 51 (5), 575–586. doi:10.1016/j.devcel.2019.10.007

Cai, S., Fu, S., Zhang, W., Yuan, X., Cheng, Y., and Fang, J. (2021). SIRT6 Silencing Overcomes Resistance to Sorafenib by Promoting Ferroptosis in Gastric Cancer. *Biochem. Biophysical Res. Commun.* 577, 158–164. doi:10.1016/j.bbrc.2021.08.080

Carracedo, A., Cantley, L. C., and Pandolfi, P. P. (2013). Cancer Metabolism: Fatty Acid Oxidation in the Limelight. *Nat. Rev. Cancer* 13 (4), 227–232. doi:10.1038/nrc3483

Cassetta, L., and Pollard, J. W. (2018). Targeting Macrophages: Therapeutic Approaches in Cancer. *Nat. Rev. Drug Discov.* 17 (12), 887–904. doi:10.1038/nrd.2018.169

Chaiswing, L., and Oberley, T. D. (2010). Extracellular/Microenvironmental Redox State. *Antioxid. Redox Signaling* 13 (4), 449–465. doi:10.1089/ars.2009.3020

Chen, Y.-J., Jr., Mahieu, N. G., Huang, X., Singh, M., Crawford, P. A., Johnson, S. L., et al. (2016). Lactate Metabolism Is Associated with Mammalian Mitochondria. *Nat. Chem. Biol.* 12 (11), 937–943. doi:10.1038/nchembio.2172

Chen, M.-S., Wang, S.-F., Hsu, C.-Y., Yin, P.-H., Yeh, T.-S., Lee, H.-C., et al. (2017). CHAC1 Degradation of Glutathione Enhances Cystine-Starvation-Induced Necroptosis and Ferroptosis in Human Triple Negative Breast Cancer Cells via the GCN2-eIF2α-ATF4 Pathway. *Oncotarget* 8 (70), 114588–114602. doi:10.18632/oncotarget.23055

Chen, X., Kang, R., Kroemer, G., and Tang, D. (2021). Broadening Horizons: The Role of Ferroptosis in Cancer. *Nat. Rev. Clin. Oncol.* 18 (5), 280–296. doi:10.1038/s41571-020-00462-0

Coltorti, M., De Ritis, F., and Giusti, G. (1956). Enzymatic Mechanisms of Transsulfuration in Biology and Clinical Practice. *G Clin. Med.* 37 (3), 285–323.

Cook, J., and Hagemann, T. (2013). Tumour-Associated Macrophages and Cancer. *Curr. Opin. Pharmacol.* 13 (4), 595–601. doi:10.1016/j.coph.2013.05.017

Cronin, S. J. F., Woolf, C. J., Weiss, G., and Penninger, J. M. (2019). The Role of Iron Regulation in Immunometabolism and Immune-Related Disease. *Front. Mol. Biosci.* 6, 116. doi:10.3389/fmolb.2019.00116

Dai, E., Han, L., Liu, J., Xie, Y., Kroemer, G., Klionsky, D. J., et al. (2020a). Autophagy-Dependent Ferroptosis Drives Tumor-Associated Macrophage Polarization via Release and Uptake of Oncogenic KRAS Protein. *Autophagy* 16 (11), 2069–2083. doi:10.1080/15548627.2020.1714209

Dai, E., Han, L., Liu, J., Xie, Y., Zeh, H. J., Kang, R., et al. (2020b). Ferroptotic Damage Promotes Pancreatic Tumorigenesis Through a TMEM173/STING-Dependent DNA Sensor Pathway. *Nat. Commun.* 11 (1), 6339. doi:10.1038/s41467-020-20154-8

Dai, E., Meng, L., Kang, R., Wang, X., and Tang, D. (2020c). ESCRT-III-Dependent Membrane Repair Blocks Ferroptosis. *Biochem. Biophysical Res. Commun.* 522 (2), 415–421. doi:10.1016/j.bbrc.2019.11.110

Dai, E., Zhang, W., Cong, D., Kang, R., Wang, J., and Tang, D. (2020d). AIFM2 Blocks Ferroptosis Independent of Ubiquinol Metabolism. *Biochem. Biophysical Res. Commun.* 523 (4), 966–971. doi:10.1016/j.bbrc.2020.01.066

De Domenico, I., McVey Ward, D., and Kaplan, J. (2008). Regulation of Iron Acquisition and Storage: Consequences for Iron-Linked Disorders. *Nat. Rev. Mol. Cel Biol* 9 (1), 72–81. doi:10.1038/nrm2295

de la Cruz-López, K. G., Castro-Muñoz, L. J., Reyes-Hernández, D. O., García-Carrancá, A., and Manzo-Merino, J. (2019). Lactate in the Regulation of Tumor Microenvironment and Therapeutic Approaches. *Front. Oncol.* 9, 1143. doi:10.3389/fonc.2019.01143

DeSantis, C. E., Ma, J., Gaudet, M. M., Newman, L. A., Miller, K. D., Goding Sauer, A., et al. (2019). Breast Cancer Statistics, 2019. *CA A. Cancer J. Clin.* 69 (6), 438–451. doi:10.3322/caac.21583

Distéfano, A. M., Martin, M. V., Córdoba, J. P., Bellido, A. M., D'Ippólito, S., Colman, S. L., et al. (2017). Heat Stress Induces Ferroptosis-Like Cell Death in Plants. *J. Cel Biol* 216 (2), 463–476. doi:10.1083/jcb.201605110

Dixon, S. J., Lemberg, K. M., Lamprecht, M. R., Skouta, R., Zaitsev, E. M., Gleason, C. E., et al. (2012). Ferroptosis: An Iron-Dependent Form of Nonapoptotic Cell Death. *Cell* 149 (5), 1060–1072. doi:10.1016/j.cell.2012.03.042

Dixon, S. J., Winter, G. E., Musavi, L. S., Lee, E. D., Snijder, B., Rebsamen, M., et al. (2015). Human Haploid Cell Genetics Reveals Roles for Lipid Metabolism Genes in Nonapoptotic Cell Death. *ACS Chem. Biol.* 10 (7), 1604–1609. doi:10.1021/acschembio.5b00245

Doll, S., Proneth, B., Tyurina, Y. Y., Panzilius, E., Kobayashi, S., Ingold, I., et al. (2017). ACSL4 Dictates Ferroptosis Sensitivity by Shaping Cellular Lipid Composition. *Nat. Chem. Biol.* 13 (1), 91–98. doi:10.1038/nchembio.2239

Dolma, S., Lessnick, S. L., Hahn, W. C., and Stockwell, B. R. (2003). Identification of Genotype-Selective Antitumor Agents Using Synthetic Lethal Chemical Screening in Engineered Human Tumor Cells. *Cancer Cell* 3 (3), 285–296. doi:10.1016/s1535-6108(03)00050-3

Duan, X., He, K., Li, J., Cheng, M., Song, H., Liu, J., et al. (2018). Tumor Associated Macrophages Deliver Iron to Tumor Cells via Lcn2. *Int. J. Physiol. Pathophysiol Pharmacol.* 10 (2), 105–114.

Eagle, H., Piez, K. A., and Oyama, V. I. (1961). The Biosynthesis of Cystine in Human Cell Cultures. *J. Biol. Chem.* 236, 1425–1428. doi:10.1016/s0021-9258(18)64190-0

Eagle, H. (1955). Nutrition Needs of Mammalian Cells in Tissue Culture. *Science* 122 (3168), 501–504. doi:10.1126/science.122.3168.501

Eling, N., Reuter, L., Hazin, J., Hamacher-Brady, A., and Brady, N. R. (2015). Identification of Artesunate as a Specific Activator of Ferroptosis in Pancreatic Cancer Cells. *Oncoscience* 2 (5), 517–532. doi:10.18632/oncoscience.160

Estrella, V., Chen, T., Lloyd, M., Wojtkowiak, J., Cornnell, H. H., Ibrahim-Hashim, A., et al. (2013). Acidity Generated by the Tumor Microenvironment Drives Local Invasion. *Cancer Res.* 73 (5), 1524–1535. doi:10.1158/0008-5472.CAN-12-2796

Fang, X., Wang, H., Han, D., Xie, E., Yang, X., Wei, J., et al. (2019). Ferroptosis as a Target for Protection Against Cardiomyopathy. *Proc. Natl. Acad. Sci. USA* 116 (7), 2672–2680. doi:10.1073/pnas.1821022116

Ferreira, L. M. R. (2010). Cancer Metabolism: The Warburg Effect Today. *Exp. Mol. Pathol.* 89 (3), 372–380. doi:10.1016/j.yexmp.2010.08.006

Fonseca-Nunes, A., Jakszyn, P., and Agudo, A. (2014). Iron and Cancer Risk-A Systematic Review and Meta-Analysis of the Epidemiological Evidence. *Cancer Epidemiol. Biomarkers Prev.* 23 (1), 12–31. doi:10.1158/1055-9965.EPI-13-0733

Frey, P. A., and Reed, G. H. (2012). The Ubiquity of Iron. *ACS Chem. Biol.* 7 (9), 1477–1481. doi:10.1021/cb300323q

Friedmann Angeli, J. P., Schneider, M., Proneth, B., Tyurina, Y. Y., Tyurin, V. A., Hammond, V. J., et al. (2014). Inactivation of the Ferroptosis Regulator Gpx4 Triggers Acute Renal Failure in Mice. *Nat. Cel Biol* 16 (12), 1180–1191. doi:10.1038/ncb3064

Friedmann Angeli, J. P., Krysko, D. V., and Conrad, M. (2019). Ferroptosis at the Crossroads of Cancer-Acquired Drug Resistance and Immune Evasion. *Nat. Rev. Cancer* 19 (7), 405–414. doi:10.1038/s41568-019-0149-1

Galluzzi, L., Buqué, A., Kepp, O., Zitvogel, L., and Kroemer, G. (2017). Immunogenic Cell Death in Cancer and Infectious Disease. *Nat. Rev. Immunol.* 17 (2), 97–111. doi:10.1038/nri.2016.107

Galluzzi, L., Vitale, I., Aaronson, S. A., Abrams, J. M., Adam, D., Agostinis, P., et al. (2018). Molecular Mechanisms of Cell Death: Recommendations of the Nomenclature Committee on Cell Death 2018. *Cell Death Differ* 25 (3), 486–541. doi:10.1038/s41418-017-0012-4

Gao, M., Monian, P., Quadri, N., Ramasamy, R., and Jiang, X. (2015). Glutaminolysis and Transferrin Regulate Ferroptosis. *Mol. Cel* 59 (2), 298–308. doi:10.1016/j.molcel.2015.06.011

Gao, M., Monian, P., Pan, Q., Zhang, W., Xiang, J., and Jiang, X. (2016). Ferroptosis Is an Autophagic Cell Death Process. *Cell Res* 26 (9), 1021–1032. doi:10.1038/cr.2016.95

García-Cañaveras, J. C., Chen, L., and Rabinowitz, J. D. (2019). The Tumor Metabolic Microenvironment: Lessons from Lactate. *Cancer Res.* 79 (13), 3155–3162. doi:10.1158/0008-5472.CAN-18-3726

Gladden, L. B. (2004). Lactate Metabolism: A New Paradigm for the Third Millennium. *J. Physiol.* 558 (Pt 1), 5–30. doi:10.1113/jphysiol.2003.058701

Guan, Q., Guo, R., Huang, S., Zhang, F., Liu, J., Wang, Z., et al. (2020). Mesoporous Polydopamine Carrying Sorafenib and SPIO Nanoparticles for MRI-Guided Ferroptosis Cancer Therapy. *J. Controlled Release* 320, 392–403. doi:10.1016/j.jconrel.2020.01.048

Hangauer, M. J., Viswanathan, V. S., Ryan, M. J., Bole, D., Eaton, J. K., Matov, A., et al. (2017). Drug-tolerant Persister Cancer Cells Are Vulnerable to GPX4 Inhibition. *Nature* 551 (7679), 247–250. doi:10.1038/nature24297

Hao, S., Yu, J., He, W., Huang, Q., Zhao, Y., Liang, B., et al. (2017). Cysteine Dioxygenase 1 Mediates Erastin-Induced Ferroptosis in Human Gastric Cancer Cells. *Neoplasia* 19 (12), 1022–1032. doi:10.1016/j.neo.2017.10.005

Hashimoto, T., Hussien, R., Oommen, S., Gohil, K., and Brooks, G. A. (2007). Lactate Sensitive Transcription Factor Network in L6 Cells: Activation of MCT1 and Mitochondrial Biogenesis. *FASEB j.* 21 (10), 2602–2612. doi:10.1096/fj.07-8174com

Hassannia, B., Wiernicki, B., Ingold, I., Qu, F., Van Herck, S., Tyurina, Y. Y., et al. (2018). Nano-Targeted Induction of Dual Ferroptotic Mechanisms Eradicates High-Risk Neuroblastoma. *J. Clin. Invest.* 128 (8), 3341–3355. doi:10.1172/JCI99032

Herber, D. L., Cao, W., Nefedova, Y., Novitskiy, S. V., Nagaraj, S., Tyurin, V. A., et al. (2010). Lipid Accumulation and Dendritic Cell Dysfunction in Cancer. *Nat. Med.* 16 (8), 880–886. doi:10.1038/nm.2172

Hossain, F., Al-Khami, A. A., Wyczechowska, D., Hernandez, C., Zheng, L., Reiss, K., et al. (2015). Inhibition of Fatty Acid Oxidation Modulates Immunosuppressive Functions of Myeloid-Derived Suppressor Cells and Enhances Cancer Therapies. *Cancer Immunol. Res.* 3 (11), 1236–1247. doi:10.1158/2326-6066.CIR-15-0036

Hou, W., Xie, Y., Song, X., Sun, X., Lotze, M. T., Zeh, H. J., 3rd, et al. (2016). Autophagy Promotes Ferroptosis by Degradation of Ferritin. *Autophagy* 12 (8), 1425–1428. doi:10.1080/15548627.2016.1187366

Ingold, I., Berndt, C., Schmitt, S., Doll, S., Poschmann, G., Buday, K., et al. (2018). Selenium Utilization by GPX4 Is Required to Prevent Hydroperoxide-Induced Ferroptosis. *Cell* 172 (3), 409–422. doi:10.1016/j.cell.2017.11.048

Ishimoto, T., Nagano, O., Yae, T., Tamada, M., Motohara, T., Oshima, H., et al. (2011). CD44 Variant Regulates Redox Status in Cancer Cells by Stabilizing the xCT Subunit of System Xc− and Thereby Promotes Tumor Growth. *Cancer Cell* 19 (3), 387–400. doi:10.1016/j.ccr.2011.01.038

Ivashkiv, L. B. (2020). The Hypoxia-Lactate Axis Tempers Inflammation. *Nat. Rev. Immunol.* 20 (2), 85–86. doi:10.1038/s41577-019-0259-8

Jasim, K. A., and Gesquiere, A. J. (2019). Ultrastable and Biofunctionalizable Conjugated Polymer Nanoparticles with Encapsulated Iron for Ferroptosis Assisted Chemodynamic Therapy. *Mol. Pharmaceutics* 16 (12), 4852–4866. doi:10.1021/acs.molpharmaceut.9b00737

Jiang, L., Kon, N., Li, T., Wang, S.-J., Su, T., Hibshoosh, H., et al. (2015). Ferroptosis as a P53-Mediated Activity During Tumour Suppression. *Nature* 520 (7545), 57–62. doi:10.1038/nature14344

Johnson, A. M., Kleczko, E. K., and Nemenoff, R. A. (2020). Eicosanoids in Cancer: New Roles in Immunoregulation. *Front. Pharmacol.* 11, 595498. doi:10.3389/fphar.2020.595498

Justus, C. R., Dong, L., and Yang, L. V. (2013). Acidic Tumor Microenvironment and pH-Sensing G Protein-Coupled Receptors. *Front. Physiol.* 4, 354. doi:10.3389/fphys.2013.00354

Kagan, V. E., Mao, G., Qu, F., Angeli, J. P. F., Doll, S., Croix, C. S., et al. (2017). Oxidized Arachidonic and Adrenic PEs Navigate Cells to Ferroptosis. *Nat. Chem. Biol.* 13 (1), 81–90. doi:10.1038/nchembio.2238

Kapralov, A. A., Yang, Q., Dar, H. H., Tyurina, Y. Y., Anthonymuthu, T. S., Kim, R., et al. (2020). Redox Lipid Reprogramming Commands Susceptibility of Macrophages and Microglia to Ferroptotic Death. *Nat. Chem. Biol.* 16 (3), 278–290. doi:10.1038/s41589-019-0462-8

Kim, J.-H., Lewin, T. M., and Coleman, R. A. (2001). Expression and Characterization of Recombinant Rat Acyl-CoA Synthetases 1, 4, and 5. *J. Biol. Chem.* 276 (27), 24667–24673. doi:10.1074/jbc.M010793200

Kim, D. H., Kim, W. D., Kim, S. K., Moon, D. H., and Lee, S. J. (2020). TGF-β1-mediated Repression of SLC7A11 Drives Vulnerability to GPX4 Inhibition in Hepatocellular Carcinoma Cells. *Cell Death Dis* 11 (5), 406. doi:10.1038/s41419-020-2618-6

Kondo, A., Yamamoto, S., Nakaki, R., Shimamura, T., Hamakubo, T., Sakai, J., et al. (2017). Extracellular Acidic pH Activates the Sterol Regulatory Element-Binding Protein 2 to Promote Tumor Progression. *Cel Rep.* 18 (9), 2228–2242. doi:10.1016/j.celrep.2017.02.006

Kraft, V. A. N., Bezjian, C. T., Pfeiffer, S., Ringelstetter, L., Müller, C., Zandkarimi, F., et al. (2020). GTP Cyclohydrolase 1/Tetrahydrobiopterin Counteract Ferroptosis Through Lipid Remodeling. *ACS Cent. Sci.* 6 (1), 41–53. doi:10.1021/acscentsci.9b01063

Kremer, D. M., Nelson, B. S., Lin, L., Yarosz, E. L., Halbrook, C. J., Kerk, S. A., et al. (2021). GOT1 Inhibition Promotes Pancreatic Cancer Cell Death by Ferroptosis. *Nat. Commun.* 12 (1), 4860. doi:10.1038/s41467-021-24859-2

Kuang, Y., and Wang, Q. (2019). Iron and Lung Cancer. *Cancer Lett.* 464, 56–61. doi:10.1016/j.canlet.2019.08.007

Lee, J.-Y., Nam, M., Son, H. Y., Hyun, K., Jang, S. Y., Kim, J. W., et al. (2020). Polyunsaturated Fatty Acid Biosynthesis Pathway Determines Ferroptosis Sensitivity in Gastric Cancer. *Proc. Natl. Acad. Sci. USA* 117 (51), 32433–32442. doi:10.1073/pnas.2006828117

Lei, G., Zhang, Y., Koppula, P., Liu, X., Zhang, J., Lin, S. H., et al. (2020). The Role of Ferroptosis in Ionizing Radiation-Induced Cell Death and Tumor Suppression. *Cel Res* 30 (2), 146–162. doi:10.1038/s41422-019-0263-3

Lewis, C. A., Brault, C., Peck, B., Bensaad, K., Griffiths, B., Mitter, R., et al. (2015). SREBP Maintains Lipid Biosynthesis and Viability of Cancer Cells under Lipid- and Oxygen-Deprived Conditions and Defines a Gene Signature Associated with Poor Survival in Glioblastoma Multiforme. *Oncogene* 34 (40), 5128–5140. doi:10.1038/onc.2014.439

Li, C., Zhang, Y., Liu, J., Kang, R., Klionsky, D. J., and Tang, D. (2021a). Mitochondrial DNA Stress Triggers Autophagy-Dependent Ferroptotic Death. *Autophagy* 17 (4), 948–960. doi:10.1080/15548627.2020.1739447

Li, Y., Xia, J., Shao, F., Zhou, Y., Yu, J., Wu, H., et al. (2021b). Sorafenib Induces Mitochondrial Dysfunction and Exhibits Synergistic Effect with Cysteine Depletion by Promoting HCC Cells Ferroptosis. *Biochem. Biophysical Res. Commun.* 534, 877–884. doi:10.1016/j.bbrc.2020.10.083

Liang, W., and Ferrara, N. (2020). Iron Metabolism in the Tumor Microenvironment: Contributions of Innate Immune Cells. *Front. Immunol.* 11, 626812. doi:10.3389/fimmu.2020.626812

Liang, C., Zhang, X., Yang, M., and Dong, X. (2019). Recent Progress in Ferroptosis Inducers for Cancer Therapy. *Adv. Mater.* 31 (51), e1904197. doi:10.1002/adma.201904197

Liu, J., Kuang, F., Kang, R., and Tang, D. (2020). Alkaliptosis: A New Weapon for Cancer Therapy. *Cancer Gene Ther.* 27 (5), 267–269. doi:10.1038/s41417-019-0134-6

Llovet, J. M., Kelley, R. K., Villanueva, A., Singal, A. G., Pikarsky, E., Roayaie, S., et al. (2021). Hepatocellular Carcinoma. *Nat. Rev. Dis. Primers* 7 (1), 6. doi:10.1038/s41572-020-00240-3

Long, Y., Tao, H., Karachi, A., Grippin, A. J., Jin, L., Chang, Y., et al. (2020). Dysregulation of Glutamate Transport Enhances Treg Function that Promotes VEGF Blockade Resistance in Glioblastoma. *Cancer Res.* 80 (3), 499–509. doi:10.1158/0008-5472.CAN-19-1577

Lopes-Coelho, F., André, S., Félix, A., and Serpa, J. (2018). Breast Cancer Metabolic Cross-Talk: Fibroblasts Are Hubs and Breast Cancer Cells Are Gatherers of Lipids. *Mol. Cell Endocrinol.* 462 (Pt B), 93–106. doi:10.1016/j.mce.2017.01.031

Louandre, C., Ezzoukhry, Z., Godin, C., Barbare, J.-C., Mazière, J.-C., Chauffert, B., et al. (2013). Iron-Dependent Cell Death of Hepatocellular Carcinoma Cells Exposed to Sorafenib. *Int. J. Cancer* 133 (7), 1732–1742. doi:10.1002/ijc.28159

Louandre, C., Marcq, I., Bouhlal, H., Lachaier, E., Godin, C., Saidak, Z., et al. (2015). The Retinoblastoma (Rb) Protein Regulates Ferroptosis Induced by Sorafenib in Human Hepatocellular Carcinoma Cells. *Cancer Lett.* 356 (2 Pt B), 971–977. doi:10.1016/j.canlet.2014.11.014

Ludwig, H., Evstatiev, R., Kornek, G., Aapro, M., Bauernhofer, T., Buxhofer-Ausch, V., et al. (2015). Iron Metabolism and Iron Supplementation in Cancer Patients. *Wien Klin Wochenschr* 127 (23-24), 907–919. doi:10.1007/s00508-015-0842-3

Ma, S., Dielschneider, R. F., Henson, E. S., Xiao, W., Choquette, T. R., Blankstein, A. R., et al. (2017). Ferroptosis and Autophagy Induced Cell Death Occur Independently After Siramesine and Lapatinib Treatment in Breast Cancer Cells. *PLoS One* 12 (8), e0182921. doi:10.1371/journal.pone.0182921

Magtanong, L., Ko, P.-J., To, M., Cao, J. Y., Forcina, G. C., Tarangelo, A., et al. (2019). Exogenous Monounsaturated Fatty Acids Promote a Ferroptosis-Resistant Cell State. *Cel Chem. Biol.* 26 (3), 420–432. doi:10.1016/j.chembiol.2018.11.016

Mantovani, A., Schioppa, T., Porta, C., Allavena, P., and Sica, A. (2006). Role of Tumor-Associated Macrophages in Tumor Progression and Invasion. *Cancer Metastasis Rev.* 25 (3), 315–322. doi:10.1007/s10555-006-9001-7

Manz, D. H., Blanchette, N. L., Paul, B. T., Torti, F. M., and Torti, S. V. (2016). Iron and Cancer: Recent Insights. *Ann. N.Y. Acad. Sci.* 1368 (1), 149–161. doi:10.1111/nyas.13008

Mayhew, C. N., Carter, S. L., Fox, S. R., Sexton, C. R., Reed, C. A., Srinivasan, S. V., et al. (2007). RB Loss Abrogates Cell Cycle Control and Genome Integrity to Promote Liver Tumorigenesis. *Gastroenterology* 133 (3), 976–984. doi:10.1053/j.gastro.2007.06.025

McGlynn, K. A., Petrick, J. L., and El-Serag, H. B. (2021). Epidemiology of Hepatocellular Carcinoma. *Hepatology* 73 (Suppl. 1), 4–13. doi:10.1002/hep.31288

Meier, J. K., Schnetz, M., Beck, S., Schmid, T., Dominguez, M., Kalinovic, S., et al. (2021). Iron-Bound Lipocalin-2 Protects Renal Cell Carcinoma from Ferroptosis. *Metabolites* 11 (5), 329. doi:10.3390/metabo11050329

Meng, F., Zhen, S., and Song, B. (2017). HBV-specific CD4+ Cytotoxic T Cells in Hepatocellular Carcinoma Are Less Cytolytic Toward Tumor Cells and Suppress CD8+ T Cell-Mediated Antitumor Immunity. *APMIS* 125 (8), 743–751. doi:10.1111/apm.12704

Metallo, C. M., Gameiro, P. A., Bell, E. L., Mattaini, K. R., Yang, J., Hiller, K., et al. (2011). Reductive Glutamine Metabolism by IDH1 Mediates Lipogenesis under Hypoxia. *Nature* 481 (7381), 380–384. doi:10.1038/nature10602

Michelet, X., Dyck, L., Hogan, A., Loftus, R. M., Duquette, D., Wei, K., et al. (2018). Metabolic Reprogramming of Natural Killer Cells in Obesity Limits Antitumor Responses. *Nat. Immunol.* 19 (12), 1330–1340. doi:10.1038/s41590-018-0251-7

Miska, J., Lee-Chang, C., Rashidi, A., Muroski, M. E., Chang, A. L., Lopez-Rosas, A., et al. (2019). HIF-1α Is a Metabolic Switch Between Glycolytic-Driven Migration and Oxidative Phosphorylation-Driven Immunosuppression of Tregs in Glioblastoma. *Cel Rep.* 27 (1), 226–237.e4. doi:10.1016/j.celrep.2019.03.029

Mullen, P. J., Yu, R., Longo, J., Archer, M. C., and Penn, L. Z. (2016). The Interplay Between Cell Signalling and the Mevalonate Pathway in Cancer. *Nat. Rev. Cancer* 16 (11), 718–731. doi:10.1038/nrc.2016.76

Murray, P. J. (2017). Macrophage Polarization. *Annu. Rev. Physiol.* 79, 541–566. doi:10.1146/annurev-physiol-022516-034339

Nagpal, A., Redvers, R. P., Ling, X., Ayton, S., Fuentes, M., Tavancheh, E., et al. (2019). Neoadjuvant Neratinib Promotes Ferroptosis and Inhibits Brain Metastasis in a Novel Syngeneic Model of Spontaneous HER2+ve Breast Cancer Metastasis. *Breast Cancer Res.* 21 (1), 94. doi:10.1186/s13058-019-1177-1

Nakamura, E., Sato, M., Yang, H., Miyagawa, F., Harasaki, M., Tomita, K., et al. (1999). 4F2 (CD98) Heavy Chain Is Associated Covalently with an Amino Acid Transporter and Controls Intracellular Trafficking and Membrane Topology of 4F2 Heterodimer. *J. Biol. Chem.* 274 (5), 3009–3016. doi:10.1074/jbc.274.5.3009

Nemeth, E., Rivera, S., Gabayan, V., Keller, C., Taudorf, S., Pedersen, B. K., et al. (2004). IL-6 Mediates Hypoferremia of Inflammation by Inducing the Synthesis of the Iron Regulatory Hormone Hepcidin. *J. Clin. Invest.* 113 (9), 1271–1276. doi:10.1172/JCI20945

Nie, J., Lin, B., Zhou, M., Wu, L., and Zheng, T. (2018). Role of Ferroptosis in Hepatocellular Carcinoma. *J. Cancer Res. Clin. Oncol.* 144 (12), 2329–2337. doi:10.1007/s00432-018-2740-3

Ooko, E., Saeed, M. E. M., Kadioglu, O., Sarvi, S., Colak, M., Elmasaoudi, K., et al. (2015). Artemisinin Derivatives Induce Iron-dependent Cell Death (Ferroptosis) in Tumor Cells. *Phytomedicine* 22 (11), 1045–1054. doi:10.1016/j.phymed.2015.08.002

Peck, B., and Schulze, A. (2016). Lipid Desaturation - the Next Step in Targeting Lipogenesis in Cancer? *FEBS J.* 283 (15), 2767–2778. doi:10.1111/febs.13681

Pratt, D. A., Tallman, K. A., and Porter, N. A. (2011). Free Radical Oxidation of Polyunsaturated Lipids: New Mechanistic Insights and the Development of Peroxyl Radical Clocks. *Acc. Chem. Res.* 44 (6), 458–467. doi:10.1021/ar200024c

Proneth, B., and Conrad, M. (2019). Ferroptosis and Necroinflammation, a Yet Poorly Explored Link. *Cel Death Differ* 26 (1), 14–24. doi:10.1038/s41418-018-0173-9

Pucino, V., Certo, M., Bulusu, V., Cucchi, D., Goldmann, K., Pontarini, E., et al. (2019). Lactate Buildup at the Site of Chronic Inflammation Promotes Disease by Inducing CD4+ T Cell Metabolic Rewiring. *Cel Metab.* 30 (6), 1055–1074.e8. doi:10.1016/j.cmet.2019.10.004

Quail, D. F., and Joyce, J. A. (2013). Microenvironmental Regulation of Tumor Progression and Metastasis. *Nat. Med.* 19 (11), 1423–1437. doi:10.1038/nm.3394

Ramakrishnan, R., Tyurin, V. A., Veglia, F., Condamine, T., Amoscato, A., Mohammadyani, D., et al. (2014). Oxidized Lipids Block Antigen Cross-Presentation by Dendritic Cells in Cancer. *J. Immunol.* 192 (6), 2920–2931. doi:10.4049/jimmunol.1302801

Ray, P. D., Huang, B.-W., and Tsuji, Y. (2012). Reactive Oxygen Species (ROS) Homeostasis and Redox Regulation in Cellular Signaling. *Cell Signal.* 24 (5), 981–990. doi:10.1016/j.cellsig.2012.01.008

Recalcati, S., Locati, M., Marini, A., Santambrogio, P., Zaninotto, F., De Pizzol, M., et al. (2010). Differential Regulation of Iron Homeostasis During Human Macrophage Polarized Activation. *Eur. J. Immunol.* 40 (3), 824–835. doi:10.1002/eji.200939889

Rice, C. M., Davies, L. C., Subleski, J. J., Maio, N., Gonzalez-Cotto, M., Andrews, C., et al. (2018). Tumour-Elicited Neutrophils Engage Mitochondrial Metabolism to Circumvent Nutrient Limitations and Maintain Immune Suppression. *Nat. Commun.* 9 (1), 5099. doi:10.1038/s41467-018-07505-2

Röhrig, F., and Schulze, A. (2016). The Multifaceted Roles of Fatty Acid Synthesis in Cancer. *Nat. Rev. Cancer* 16 (11), 732–749. doi:10.1038/nrc.2016.89

Ryter, S. W., Kim, H. P., Hoetzel, A., Park, J. W., Nakahira, K., Wang, X., et al. (2007). Mechanisms of Cell Death in Oxidative Stress. *Antioxid. Redox Signaling* 9 (1), 49–89. doi:10.1089/ars.2007.9.49

Sato, H., Shiiya, A., Kimata, M., Maebara, K., Tamba, M., Sakakura, Y., et al. (2005). Redox Imbalance in Cystine/Glutamate Transporter-Deficient Mice. *J. Biol. Chem.* 280 (45), 37423–37429. doi:10.1074/jbc.M506439200

Schug, Z. T., Peck, B., Jones, D. T., Zhang, Q., Grosskurth, S., Alam, I. S., et al. (2015). Acetyl-CoA Synthetase 2 Promotes Acetate Utilization and Maintains Cancer Cell Growth Under Metabolic Stress. *Cancer Cell* 27 (1), 57–71. doi:10.1016/j.ccell.2014.12.002

Shen, Q., Liang, M., Yang, F., Deng, Y. Z., and Naqvi, N. I. (2020). Ferroptosis Contributes to Developmental Cell Death in Rice Blast. *New Phytol.* 227 (6), 1831–1846. doi:10.1111/nph.16636

Shin, C.-S., Mishra, P., Watrous, J. D., Carelli, V., D'Aurelio, M., Jain, M., et al. (2017). The Glutamate/Cystine xCT Antiporter Antagonizes Glutamine Metabolism and Reduces Nutrient Flexibility. *Nat. Commun.* 8, 15074. doi:10.1038/ncomms15074

Sola, A., Weigert, A., Jung, M., Vinuesa, E., Brecht, K., Weis, N., et al. (2011). Sphingosine-1-Phosphate Signalling Induces the Production of Lcn-2 by Macrophages to Promote Kidney Regeneration. *J. Pathol.* 225 (4), 597–608. doi:10.1002/path.2982

Song, X., Zhu, S., Chen, P., Hou, W., Wen, Q., Liu, J., et al. (2018a). AMPK-Mediated BECN1 Phosphorylation Promotes Ferroptosis by Directly Blocking System Xc- Activity. *Curr. Biol.* 28 (15), 2388–2399. doi:10.1016/j.cub.2018.05.094

Song, X., Zhu, S., Xie, Y., Liu, J., Sun, L., Zeng, D., et al. (2018b). JTC801 Induces pH-Dependent Death Specifically in Cancer Cells and Slows Growth of Tumors in Mice. *Gastroenterology* 154 (5), 1480–1493. doi:10.1053/j.gastro.2017.12.004

Sow, F. B., Alvarez, G. R., Gross, R. P., Satoskar, A. R., Schlesinger, L. S., Zwilling, B. S., et al. (2009). Role of STAT1, NF-Kb, and C/EBPβ in the Macrophage Transcriptional Regulation of Hepcidin by Mycobacterial Infection and IFN-γ. *J. Leukoc. Biol.* 86 (5), 1247–1258. doi:10.1189/jlb.1208719

Stockwell, B. R., and Jiang, X. (2019). A Physiological Function for Ferroptosis in Tumor Suppression by the Immune System. *Cel Metab.* 30 (1), 14–15. doi:10.1016/j.cmet.2019.06.012

Stockwell, B. R., Friedmann Angeli, J. P., Bayir, H., Bush, A. I., Conrad, M., Dixon, S. J., et al. (2017). Ferroptosis: A Regulated Cell Death Nexus Linking Metabolism, Redox Biology, and Disease. *Cell* 171 (2), 273–285. doi:10.1016/j.cell.2017.09.021

Sun, R. C., and Denko, N. C. (2014). Hypoxic Regulation of Glutamine Metabolism Through HIF1 and SIAH2 Supports Lipid Synthesis that Is Necessary for Tumor Growth. *Cel Metab.* 19 (2), 285–292. doi:10.1016/j.cmet.2013.11.022

Sun, X., Niu, X., Chen, R., He, W., Chen, D., Kang, R., et al. (2016a). Metallothionein-1G Facilitates Sorafenib Resistance Through Inhibition of Ferroptosis. *Hepatology* 64 (2), 488–500. doi:10.1002/hep.28574

Sun, X., Ou, Z., Chen, R., Niu, X., Chen, D., Kang, R., et al. (2016b). Activation of the P62-Keap1-NRF2 Pathway Protects Against Ferroptosis in Hepatocellular Carcinoma Cells. *Hepatology* 63 (1), 173–184. doi:10.1002/hep.28251

Shirlee Tan, B. S. P., David Schubert, B. S. P., and Pamela Maher, B. S. P. (2001). Oxytosis: A Novel Form of Programmed Cell Death. *Ctmc* 1 (6), 497–506. doi:10.2174/1568026013394741

Tang, D., Kang, R., Coyne, C. B., Zeh, H. J., and Lotze, M. T. (2012). PAMPs and DAMPs: Signal 0s that Spur Autophagy and Immunity. *Immunol. Rev.* 249 (1), 158–175. doi:10.1111/j.1600-065X.2012.01146.x

Tang, Z., Liu, Y., He, M., and Bu, W. (2019). Chemodynamic Therapy: Tumour Microenvironment-Mediated Fenton and Fenton-like Reactions. *Angew. Chem. Int. Ed.* 58 (4), 946–956. doi:10.1002/anie.201805664

Tang, Z., Jiang, W., Mao, M., Zhao, J., Chen, J., and Cheng, N. (2021). Deubiquitinase USP35 Modulates Ferroptosis in Lung Cancer via Targeting Ferroportin. *Clin. Translational Med.* 11 (4), e390. doi:10.1002/ctm2.390

Tasdogan, A., Faubert, B., Ramesh, V., Ubellacker, J. M., Shen, B., Solmonson, A., et al. (2020). Metabolic Heterogeneity Confers Differences in Melanoma Metastatic Potential. *Nature* 577 (7788), 115–120. doi:10.1038/s41586-019-1847-2

Tauffenberger, A., Fiumelli, H., Almustafa, S., and Magistretti, P. J. (2019). Lactate and Pyruvate Promote Oxidative Stress Resistance Through Hormetic ROS Signaling. *Cel Death Dis* 10 (9), 653. doi:10.1038/s41419-019-1877-6

Terman, A., and Kurz, T. (2013). Lysosomal Iron, Iron Chelation, and Cell Death. *Antioxid. Redox Signaling* 18 (8), 888–898. doi:10.1089/ars.2012.4885

Torti, S. V., and Torti, F. M. (2013). Iron and Cancer: More Ore to Be Mined. *Nat. Rev. Cancer* 13 (5), 342–355. doi:10.1038/nrc3495

Torti, S. V., Manz, D. H., Paul, B. T., Blanchette-Farra, N., and Torti, F. M. (2018). Iron and Cancer. *Annu. Rev. Nutr.* 38, 97–125. doi:10.1146/annurev-nutr-082117-051732

Tsoi, J., Robert, L., Paraiso, K., Galvan, C., Sheu, K. M., Lay, J., et al. (2018). Multi-Stage Differentiation Defines Melanoma Subtypes with Differential Vulnerability to Drug-Induced Iron-Dependent Oxidative Stress. *Cancer Cell* 33 (5), 890–904.e5. doi:10.1016/j.ccell.2018.03.017

Turubanova, V. D., Balalaeva, I. V., Mishchenko, T. A., Catanzaro, E., Alzeibak, R., Peskova, N. N., et al. (2019). Immunogenic Cell Death Induced by a New Photodynamic Therapy Based on Photosens and Photodithazine. *J. Immunotherapy Cancer* 7 (1), 350. doi:10.1186/s40425-019-0826-3

Ursini, F., and Maiorino, M. (2020). Lipid Peroxidation and Ferroptosis: The Role of GSH and GPx4. *Free Radic. Biol. Med.* 152, 175–185. doi:10.1016/j.freeradbiomed.2020.02.027

Ursini, F., Maiorino, M., Valente, M., Ferri, L., and Gregolin, C. (1982). Purification from Pig Liver of a Protein Which Protects Liposomes and Biomembranes from Peroxidative Degradation and Exhibits Glutathione Peroxidase Activity on Phosphatidylcholine Hydroperoxides. *Biochim. Biophys. Acta (Bba) - Lipids Lipid Metab.* 710 (2), 197–211. doi:10.1016/0005-2760(82)90150-3

Viswanathan, V. S., Ryan, M. J., Dhruv, H. D., Gill, S., Eichhoff, O. M., Seashore-Ludlow, B., et al. (2017). Dependency of a Therapy-Resistant State of Cancer Cells on a Lipid Peroxidase Pathway. *Nature* 547 (7664), 453–457. doi:10.1038/nature23007

Wang, W., Kryczek, I., Dostál, L., Lin, H., Tan, L., Zhao, L., et al. (2016). Effector T Cells Abrogate Stroma-Mediated Chemoresistance in Ovarian Cancer. *Cell* 165 (5), 1092–1105. doi:10.1016/j.cell.2016.04.009

Wang, W., Green, M., Choi, J. E., Gijón, M., Kennedy, P. D., Johnson, J. K., et al. (2019). CD8+ T Cells Regulate Tumour Ferroptosis During Cancer Immunotherapy. *Nature* 569 (7755), 270–274. doi:10.1038/s41586-019-1170-y

Wang, C., Shi, M., Ji, J., Cai, Q., Zhao, Q., Jiang, J., et al. (2020a). Stearoyl-CoA Desaturase 1 (SCD1) Facilitates the Growth and Anti-ferroptosis of Gastric Cancer Cells and Predicts Poor Prognosis of Gastric Cancer. *Aging* 12 (15), 15374–15391. doi:10.18632/aging.103598

Wang, Y., Wei, Z., Pan, K., Li, J., and Chen, Q. (2020b). The Function and Mechanism of Ferroptosis in Cancer. *Apoptosis* 25, 786–798. doi:10.1007/s10495-020-01638-w

Wang, K., Zhang, Z., Tsai, H.-i., Liu, Y., Gao, J., Wang, M., et al. (2021a). Branched-chain Amino Acid Aminotransferase 2 Regulates Ferroptotic Cell Death in Cancer Cells. *Cel Death Differ* 28 (4), 1222–1236. doi:10.1038/s41418-020-00644-4

Wang, Q., Guo, Y., Wang, W., Liu, B., Yang, G., Xu, Z., et al. (2021b). RNA Binding Protein DAZAP1 Promotes HCC Progression and Regulates Ferroptosis by Interacting with SLC7A11 mRNA. *Exp. Cel Res.* 399 (1), 112453. doi:10.1016/j.yexcr.2020.112453

Wang, X., Chen, Y., Wang, X., Tian, H., Wang, Y., Jin, J., et al. (2021c). Stem Cell Factor SOX2 Confers Ferroptosis Resistance in Lung Cancer via Upregulation of SLC7A11. *Cancer Res.* 81, 5217–5229. doi:10.1158/0008-5472.CAN-21-0567

Warburg, O., Wind, F., and Negelein, E. (1927). The Metabolism of Tumors in the Body. *J. Gen. Physiol.* 8 (6), 519–530. doi:10.1085/jgp.8.6.519

Watson, M. J., Vignali, P. D. A., Mullett, S. J., Overacre-Delgoffe, A. E., Peralta, R. M., Grebinoski, S., et al. (2021). Metabolic Support of Tumour-Infiltrating Regulatory T Cells by Lactic Acid. *Nature* 591 (7851), 645–651. doi:10.1038/s41586-020-03045-2

Webb, B. A., Chimenti, M., Jacobson, M. P., and Barber, D. L. (2011). Dysregulated pH: A Perfect Storm for Cancer Progression. *Nat. Rev. Cancer* 11 (9), 671–677. doi:10.1038/nrc3110

Weinlich, R., Oberst, A., Beere, H. M., and Green, D. R. (2017). Necroptosis in Development, Inflammation and Disease. *Nat. Rev. Mol. Cel Biol* 18 (2), 127–136. doi:10.1038/nrm.2016.149

Wen, Q., Liu, J., Kang, R., Zhou, B., and Tang, D. (2019). The Release and Activity of HMGB1 in Ferroptosis. *Biochem. Biophysical Res. Commun.* 510 (2), 278–283. doi:10.1016/j.bbrc.2019.01.090

Winterbourn, C. C. (1995). Toxicity of Iron and Hydrogen Peroxide: The Fenton Reaction. *Toxicol. Lett.* 82-83, 969–974. doi:10.1016/0378-4274(95)03532-x

Wu, S., Zhang, K., Lv, C., Wang, H., Cheng, B., Jin, Y., et al. (2012). Nuclear Factor-Kb Mediated Lipopolysaccharide-Induced mRNA Expression of Hepcidin in Human Peripheral Blood Leukocytes. *Innate Immun.* 18 (2), 318–324. doi:10.1177/1753425911405087

Xiao, X., Jiang, Y., Liang, W., Wang, Y., Cao, S., Yan, H., et al. (2019). miR-212-5p Attenuates Ferroptotic Neuronal Death After Traumatic Brain Injury by Targeting Ptgs2. *Mol. Brain* 12 (1), 78. doi:10.1186/s13041-019-0501-0

Yan, H.-f., Zou, T., Tuo, Q.-z., Xu, S., Li, H., Belaidi, A. A., et al. (2021). Ferroptosis: Mechanisms and Links with Diseases. *Sig Transduct Target. Ther.* 6 (1), 49. doi:10.1038/s41392-020-00428-9

Yang, W. S., and Stockwell, B. R. (2008). Synthetic Lethal Screening Identifies Compounds Activating Iron-dependent, Nonapoptotic Cell Death in Oncogenic-RAS-Harboring Cancer Cells. *Chem. Biol.* 15 (3), 234–245. doi:10.1016/j.chembiol.2008.02.010

Yang, W. S., SriRamaratnam, R., Welsch, M. E., Shimada, K., Skouta, R., Viswanathan, V. S., et al. (2014). Regulation of Ferroptotic Cancer Cell Death by GPX4. *Cell* 156 (1-2), 317–331. doi:10.1016/j.cell.2013.12.010

Yang, W. S., Kim, K. J., Gaschler, M. M., Patel, M., Shchepinov, M. S., and Stockwell, B. R. (2016). Peroxidation of Polyunsaturated Fatty Acids by Lipoxygenases Drives Ferroptosis. *Proc. Natl. Acad. Sci. USA* 113 (34), E4966–E4975. doi:10.1073/pnas.1603244113

Yang, J., Zhou, Y., Xie, S., Wang, J., Li, Z., Chen, L., et al. (2021). Metformin Induces Ferroptosis by Inhibiting UFMylation of SLC7A11 in Breast Cancer. *J. Exp. Clin. Cancer Res.* 40 (1), 206. doi:10.1186/s13046-021-02012-7

Ye, D., Yang, K., Zang, S., Lin, Z., Chau, H.-T., Wang, Y., et al. (2016). Lipocalin-2 Mediates Non-Alcoholic Steatohepatitis by Promoting Neutrophil-Macrophage Crosstalk via the Induction of CXCR2. *J. Hepatol.* 65 (5), 988–997. doi:10.1016/j.jhep.2016.05.041

Yu, H., Guo, P., Xie, X., Wang, Y., and Chen, G. (2017). Ferroptosis, A New Form of Cell Death, and its Relationships with Tumourous Diseases. *J. Cel. Mol. Med.* 21 (4), 648–657. doi:10.1111/jcmm.13008

Yu, H., Yang, C., Jian, L., Guo, S., Chen, R., Li, K., et al. (2019). Sulfasalazine-Induced Ferroptosis in Breast Cancer Cells is Reduced by the Inhibitory Effect of Estrogen Receptor on the Transferrin Receptor. *Oncol. Rep.* 42 (2), 826–838. doi:10.3892/or.2019.7189

Yu, B., Choi, B., Li, W., and Kim, D.-H. (2020). Magnetic Field Boosted Ferroptosis-Like Cell Death and Responsive MRI Using Hybrid Vesicles for Cancer Immunotherapy. *Nat. Commun.* 11 (1), 3637. doi:10.1038/s41467-020-17380-5

Yuan, H., Li, X., Zhang, X., Kang, R., and Tang, D. (2016a). CISD1 Inhibits Ferroptosis by Protection Against Mitochondrial Lipid Peroxidation. *Biochem. Biophysical Res. Commun.* 478 (2), 838–844. doi:10.1016/j.bbrc.2016.08.034

Yuan, H., Li, X., Zhang, X., Kang, R., and Tang, D. (2016b). Identification of ACSL4 as a Biomarker and Contributor of Ferroptosis. *Biochem. Biophysical Res. Commun.* 478 (3), 1338–1343. doi:10.1016/j.bbrc.2016.08.124

Zhang, Y., Shi, J., Liu, X., Feng, L., Gong, Z., Koppula, P., et al. (2018). BAP1 Links Metabolic Regulation of Ferroptosis to Tumour Suppression. *Nat. Cel Biol* 20 (10), 1181–1192. doi:10.1038/s41556-018-0178-0

Zhang, J., Muri, J., Fitzgerald, G., Gorski, T., Gianni-Barrera, R., Masschelein, E., et al. (2020). Endothelial Lactate Controls Muscle Regeneration from Ischemia by Inducing M2-Like Macrophage Polarization. *Cel Metab.* 31 (6), 1136–1153.e7. doi:10.1016/j.cmet.2020.05.004

Zhao, Y., Li, M., Yao, X., Fei, Y., Lin, Z., Li, Z., et al. (2020). HCAR1/MCT1 Regulates Tumor Ferroptosis Through the Lactate-Mediated AMPK-SCD1 Activity and its Therapeutic Implications. *Cel Rep.* 33 (10), 108487. doi:10.1016/j.celrep.2020.108487

Zhao, L., Peng, Y., He, S., Li, R., Wang, Z., Huang, J., et al. (2021). Apatinib Induced Ferroptosis by Lipid Peroxidation in Gastric Cancer. *Gastric Cancer* 24 (3), 642–654. doi:10.1007/s10120-021-01159-8

Zhu, T., Shi, L., Yu, C., Dong, Y., Qiu, F., Shen, L., et al. (2019). Ferroptosis Promotes Photodynamic Therapy: Supramolecular Photosensitizer-Inducer Nanodrug for Enhanced Cancer Treatment. *Theranostics* 9 (11), 3293–3307. doi:10.7150/thno.32867

Zou, Y., Li, H., Graham, E. T., Deik, A. A., Eaton, J. K., Wang, W., et al. (2020). Cytochrome P450 Oxidoreductase Contributes to Phospholipid Peroxidation in Ferroptosis. *Nat. Chem. Biol.* 16 (3), 302–309. doi:10.1038/s41589-020-0472-6

Conflict of Interest: The authors declare that the research was conducted in the absence of any commercial or financial relationships that could be construed as a potential conflict of interest.

Publisher's Note: All claims expressed in this article are solely those of the authors and do not necessarily represent those of their affiliated organizations, or those of the publisher, the editors and the reviewers. Any product that may be evaluated in this article, or claim that may be made by its manufacturer, is not guaranteed or endorsed by the publisher.

frontiers in Cell and Developmental Biology

ORIGINAL RESEARCH
published: 04 November 2021
doi: 10.3389/fcell.2021.751800

Identification of Key Genes Driving Tumor Associated Macrophage Migration and Polarization Based on Immune Fingerprints of Lung Adenocarcinoma

Jing Wu[1,2,3†], Jiawei Zhou[1,2†], Qian Xu[4], Ruth Foley[4], Jianqiang Guo[1,2], Xin Zhang[1,2], Chang Tian[1,2,3], Min Mu[1,2,3], Yingru Xing[5], Yafeng Liu[1,2], Xueqin Wang[1,2] and Dong Hu[1,2,3*]*

[1] School of Medicine, Anhui University of Science and Technology, Huainan, China, [2] Anhui Province Engineering Laboratory of Occupational Health and Safety, Anhui University of Science and Technology, Huainan, China, [3] Key Laboratory of Industrial Dust Prevention and Control & Occupational Safety and Health of the Ministry of Education, Anhui University of Science and Technology, Huainan, China, [4] The Charles Institute of Dermatology, School of Medicine, University College Dublin, Dublin, Ireland, [5] Affiliated Cancer Hospital, Anhui University of Science and Technology, Huainan, China

The identification of reliable indicators in the tumor microenvironment (TME) is critical for tumor prognosis. Tumor associated macrophages (TAMs) are the major component of non-tumor stromal cells in TME and have increasingly been recognized as a predictive biomarker for lung adenocarcinoma (LUAD) prognosis. Here, we report the development of a prognosis model for LUAD using three immune-related genes (IRGs) detected in The Cancer Genome Atlas (TCGA) which potentially regulate TAMs in TME. In 497 LUAD patients, higher immune scores conferred better overall survival (OS). We identified 93 hub IRGs out of 234 for further prognostic significance. Among them, three IRGs (BTK, Cd1c, and S100P) were proved to be closely correlated to the prognosis of patients with LUAD. Moreover, the immune risk score (IRS) based on the gene expression level of the three IRGs was an independent prognostic factor for OS. Higher IRS predicted lower OS, higher mortality and worse tumor stage. With a good predictive ability [area under the ROC curve (AUC) in TCGA = 0.701, AUC in GEO = 0.722], the IRS contributed to a good risk stratification ability of the nomogram. Immunologically, the three IRGs were related to M1 macrophages and NK cell subsets in TME. Interestingly, by characterizing these immune components *in situ* we found that S100P is a driver for tumor cells to induce TAM migration and M2 polarization in the immunosuppressive tumor niche. We identified the key genes driving TAM migration and transformation and elucidated the immune landscape of LUAD. The data suggest that IRGs from TME have the potential to become indicators for estimating cancer prognosis and guiding individualized treatment.

Keywords: lung adenocarcinoma, tumor infiltrating cells, tumor microenvironment, clinical prognosis, macrophage polarization

OPEN ACCESS

Edited by:
Na Luo,
Nankai University, China

Reviewed by:
Yang Guo,
Hubei University of Medicine, China
Weina Zhang,
National Center of Biomedical Analysis (NCBA), China

***Correspondence:**
Jing Wu
wujing8008l@126.com
Dong Hu
dhu@aust.edu.cn

† These authors have contributed equally to this work

Specialty section:
This article was submitted to Molecular and Cellular Pathology, a section of the journal Frontiers in Cell and Developmental Biology

Received: *02 August 2021*
Accepted: *09 September 2021*
Published: *04 November 2021*

Citation:
Wu J, Zhou J, Xu Q, Foley R, Guo J, Zhang X, Tian C, Mu M, Xing Y, Liu Y, Wang X and Hu D (2021) Identification of Key Genes Driving Tumor Associated Macrophage Migration and Polarization Based on Immune Fingerprints of Lung Adenocarcinoma. Front. Cell Dev. Biol. 9:751800. doi: 10.3389/fcell.2021.751800

INTRODUCTION

Lung adenocarcinoma (LUAD) is one of the leading causes of cancer-related deaths globally due to early metastasis and poor prognosis (Skoulidis et al., 2018). An effective and accurate method for prognosis prediction is urgently needed. Immunosuppressive cells in the tumor microenvironment (TME) facilitate tumor metastasis and tumor stem cell formation, which are closely related to clinically poor prognosis (Li et al., 2019). Recent studies have found that the status of TME was modulated by tumor infiltrating cell (TIC) types and immune-related genes (IRGs), during which the immune cells undergo transformation and dysfunction, particularly the polarization of macrophages towards M2 and suppression of CD8+ T cells and NK cells (Tuo et al., 2020; Zheng et al., 2020). Single cell sequencing is well suited to identify diverse immune cell subsets in TME, however, it costs too much for routine diagnostic and prognostic evaluation of LUAD patients (Guo et al., 2020). Biopsy specimens are not sufficient for high throughput analysis of TIC subsets. Therefore, it is necessary to identify crucial IRGs closely related to immune cell dysfunction for an economically acceptable and reliable prognostic prediction. A network analysis integrating the immune gene signature and cell map is important to illuminate the mechanism of TME development, which could ultimately improve the accuracy of prognosis prediction.

The TME is the cellular environment in which tumors are located. It is composed of immune cells, mesenchymal cells, endothelial cells, inflammatory mediators, cytokines, and extracellular matrix (ECM) (Lim and Ghajar, 2021). Immune cells and stromal cells are two main non-tumor components in TME. Understanding of the cross-talk between them is of great value for the diagnosis and prognosis of tumors (Hill et al., 2020). Apart from promoting tumor growth and progression, immunocompromised TICs are closely related to the poor clinical outcomes of targeted therapy, radiotherapy, and chemotherapy (Koliaraki et al., 2020). Tumor associated macrophages (TAMs) are the major component of tumor-infiltrating immune cells, and usually have a tumor-suppressing M1 phenotype or tumor-promoting M2 phenotype. After being tamed by tumor cells, TAMs were polarized to M2 with a phenotype of IL-10^{high}, IL-12^{low}, arginase-1^{high}, CD206^{high}, CD204^{high}, and MHC-II^{low}. M2 polarization promotes immunosuppressive tumor niche formation and is often associated with poor prognosis for patients, possibly due to the inhibited cytotoxicity of tumor killer cells. However, the mechanism of promoting M2 polarization by cross-talk between tumor cell and TIC remains unclear. The Cancer Genome Atlas (TCGA) and Gene Expression Omnibus (GEO) databases provide abundant data of differentially expressed genes (DEGs) in tumor tissues. Based on these DEGs, we have previously developed a prediction model for LUAD prognosis (Jiawei et al., 2020). However, most of these data come from the whole TME and fail to distinguish the source from tumor cells or immunocytes. To date, only few studies systematically explored the correlation between infiltrating immune cell population and the prognosis of LUAD patients. In view of the important role of tumor-associated immune cells in the TME status and prognosis, it is necessary to identify the key genes which can represent the immune status of TME and predict the prognosis of LUAD patients.

In this study, we identified S100P as a driver gene for tumor cells to recruit and polarize TAMs, a critical TIC subset for immunosuppressive tumor niche formation. We characterized the immune landscape of LUAD in which BTK, Cd1c, and S100P were highlighted as signature genes in both NK and TAM cells. The immune risk score (IRS) based on the three IRGs was identified as an independent predictive factor for LUAD prognosis. These findings may provide potential biomarkers for the diagnosis and prognostic prediction of LUAD, which is of great significance for understanding the mechanism of LUAD at the molecular level.

MATERIALS AND METHODS

Raw Data Download

In this study, the RNA expression profile (GSE31210) data of LUAD was obtained from GEO public database.[1] The selection criteria for the expression profile are as follows: (1) the detected samples are tissues, (2) all tissues are diagnosed as LUAD tissues and normal tissues, (3) the gene expression profile is mRNA, (4) samples collected from the same ethnic group, (5) the probes can be converted into the corresponding gene symbols, and (6) complete information analysis. The array data of GSE31210 includes 226 LUAD tumor tissues, including 20 cases where data on adjacent normal tissues was available. Subsequently, RNA sequencing data sets of 54 normal lung tissue cases and 497 LUAD cases and corresponding clinical data were downloaded from TCGA[2] database.

Estimated Scores of Immune and Stromal Tissues

ESTIMATE algorithm of R code version 3.6.2 was used to estimate the proportion of immune-stromal component in TME of each sample of LUAD in TCGA, exhibited in the form of three kinds of scores: Immune Score, Stromal Score, and ESTIMATE Score, which positively correlated with the ratio of immune component, stromal component and the sum of both, respectively (thus the higher the score, the larger the proportion of the corresponding component in TME).

Survival Analysis

The survival R package was used to analyze the immune/stromal score and the survival rate of patients. A total of 458 tumor samples out of 497 had a detailed survival time record, with time span from 0 to 18.7 years, which were used for survival analysis. The survival curve was plotted by the Kaplan–Meier method with log-rank test; $p < 0.05$ was considered significant.

[1] http://www.ncbi.nlm.nih.gov/geo

[2] https://portal.gdc.Cancer.gov/

Correlation Analysis Between Clinical Stages and Immune/Stromal Score

Clinicopathologic characteristics data corresponding to LUAD samples were downloaded from TCGA. R code was employed for analysis, and the Wilcoxon rank sum test was used to analyze the correlation between immune/stromal score and each clinical characteristic according to the number of clinical stages.

Immune-Differentially Expressed Genes Between High-Score and Low-Score Groups Regarding Immune/Stromal Score

A total of 497 LUAD patients were categorized in high-score or low-score groups compared to the median, regarding immune score, and stromal score. Gene expression differential analysis was performed using the Limma in R software package and DEGs were generated by comparing high-score and low-score samples. Based on the immune genes in ImmPort database, the immune-DEGs in high-score and low-score samples were screened out. Screening condition: $|\log2(FC)| \geq 1, p < 0.05$.

Kyoto Encyclopedia of Genes and Genomes Pathway and Gene Ontology Enrichment Analysis

Through Gene Ontology (GO) enrichment and Kyoto Encyclopedia of Genes and Genomes (KEGG) analysis, the biological functions of these immune-DEGs were comprehensively detected. Cellular component (CC), molecular function (MF), and biological process (BP) were selected in GO enrichment. All analysis used online was based on network of gene set analysis tool (WebGestalt[3]). Both the primary p-value and adjusted p-value (FDR) were less than 0.05, which was statistically significant.

Protein–Protein Interaction Network Construction and Module Screening

The STRING database[4] was used to detect protein–protein interaction (PPI) among all immune-DEGs. Cytoscape 3.6.1 software was used to build and visualize the PPI network. Molecular complex detection (MCODE) plug-in was used to screen out important modules and genes in the PPI network. Both MCODE score and node number greater than 5, and $p < 0.05$, were considered significant differences. Weighted correlation network analysis (WGCNA) was used to sort the modules of co-expressed genes in PPI network.

Establishment of Prognostic Prediction Model

Univariate Cox regression analysis was performed on all key genes in the PPI network by using survival package in R, and candidate immune-DEGs related to prognosis were screened by log-rank test, and then further screened by LASSO regression analysis. Three IRGs were selected based on the correlation with prognosis from the core immune genes in the PPI network for further analysis as described below. Subsequently, based on the important candidate genes from the preliminary screening above, a risk regression model was constructed and the risk score was calculated to evaluate the prognosis of patients. The risk score of each sample was obtained according to the following formula:

$$Risk\ score = \sum_{i=1}^{n} Expi\,\beta i,$$

β, regression coefficient; Exp, gene expression value. To assess the performance of this prognostic model, LUAD patients were divided into low-risk and high-risk groups according to the median risk score. The risk score based on expression of three selected IRGs was named IRS. The difference of overall survival (OS) between the two groups was compared by log-rank test. Then, the prediction ability of the above model was evaluated using the survival ROC (receiver operating characteristic curve) package. In addition, 226 LUAD patient samples from GSE31210 data[5] were acquired as validation samples to verify the predictive value of the prognostic model.

Prognostic Value and Nomogram Construction of Different Clinical Features

The prognostic value of different clinical features of LUAD patients in TCGA and GSE31210 data sets was analyzed through univariate and multivariate Cox regression. ROC curve was used to verify the accuracy of different clinical features as independent prognostic factors in predicting the OS of LUAD patients. Then, the rms R package was utilized to draw a nomogram for predicting 3-year and 5-year OS of patients from the IRS based on expression of three selected IRGs, combined with other clinical features, and performed internal verification in the TCGA samples.

Analysis of Immune Gene Expression and Clinical Characteristics

In order to study the correlation between the expression of three selected IRGs and patient survival and TNM (size of tumor, degree of regional lymph node involvement, and presence of metastasis) stage, we analyzed the expression level of each gene in LUAD tumor and adjacent cancer in the TCGA database, as well as the prognosis correlation, respectively, and used the network data GEPIA to verify the results. At the same time, we also analyzed the correlation between the expression of three genes and the clinical characteristics of LUAD patients.

GSEA of Immune Genes

To study the regulatory mechanisms of three IRGs in LUAD patients, we divided LUAD patients into high-expression and low-expression groups according to the expression levels of three genes, and carried out GSEA.

[3]http://www.WebGestalt.org/

[4]http://www.STRING-db.org/

[5]https://www.ncbi.nlm.nih.gov/geo/query/acc.cgi?acc=GSE31210

The Correlation Between Immune Genes and Tumor Infiltrating Cells

In order to study the correlation between three genes and TICs expression in LUAD patients, the CIBERSORT calculation method was utilized to estimate the TIC abundance distribution in all tumor samples. After quality filtration was performed, only 421 tumor samples with $p < 0.05$ were selected for the following analysis. The correlation between three genes and expression of prognostic immune cells was then analyzed by univariate analysis.

Identification of Immune Genes and Prognosis-Related Tumor Infiltrating Cells in Clinical Specimens

Samples from patients with LUAD were selected to verify the expression of immune genes and prognostic TICs. All formalin-fixed and paraffin-embedded tissue samples were collected to detect the infiltration level of immune genes and prognostic immune cells. A total of 5 μm sections were taken from paraffin-embedded specimens, dewaxed and rehydrated. The tissue sections were then placed in EDTA antigen repair buffer (pH 8.0). After natural cooling, the glass slides were placed in PBS (pH 7.4) and shaken and washed on the decolorizing shaker for three times, each time for 5 min. Samples were incubated for 30 min with serum after hydrogen peroxide sealing. The primary antibody was added after appropriate dilution in PBS, and the slices were incubated at 4°C in a wet box overnight. After washing with PBS (pH 7.4) three times on the decolorizing shaker, the secondary antibody labeled with HRP of the corresponding species was added into the slides to cover tissues, and incubated for 50min at room temperature. The slides were washed in PBS (pH 7.4) for 5 min three times on the decolorizing shaker. When the slices were slightly dried, the CY3-TSA (GB1223, 1:2000; Servicebio) was added into the circle and incubated at room temperature for 10 min. The primary and secondary were removed by microwave treatment, and the second primary antibody and the corresponding HRP-labeled secondary antibody were added successively, then labeled with FITC-TSA (GB1222, 1:1000; Servicebio). Similarly, the slices were labeled by CY5. After DAPI re-staining of the nucleus, the film was sealed and photographed under microscope. All immunofluorescence (IF) sections were analyzed by ImageJ software. Primary antibodies were supplied and diluted as follows: CD68, GB14043, 1:1000; CD163, GB13340, 1:3000; CD16, GB14026, 1:1000; CD56, GB14041, 1:100; S100P, GB14147, 1:200 from Servicebio; BTK, A1576, 1:100 from Abclonal. CD68 and CD163 were used as markers for different types of TAMs, and CD16 and CD56 as NK cell markers. Nine visual fields were randomly selected in each section, and the correlation between immune cell infiltration and gene expression was analyzed by ImageJ.

Primary Macrophage Culture and siRNA Transfection

To study the effect of S100P gene on the growth and polarization of macrophages in TME, we transfected siRNA_S100P into A549 cells for S100P gene knockdown. The siRNA_S100P was chemically synthesized by Gene Pharma Company (Shanghai, China), according to the sequence previously published by Camara et al. (2020), with sequence as follows: forward, 5-color AUGGAUGCCCAGGUGGGACTT-mur3′ and reverse-5′GUCCACCUGGCAUCUCCAUTTMU3′. In addition, the negative control siRNA NC was synthesized with scrambled sequences. A549 cells were transfected with siRNA_S100P and siRNA_NC for 12 h, and then co-cultured with PBMC-M (primary macrophages induced from human peripheral mononuclear cells) and THP-1 cells induced by PMA (180 ng/ml) for 48 h. All macrophages were identified by morphological characteristics and CD68 expression. Macrophage migration was detected by crystal violet staining in transwell incubation. Immunofluorescence (IF) was used to detect the transformation of macrophages to M1 and M2 after co-culture for 48 h. All the slides were analyzed by ImageJ software. The PBMC-M was induced as follows: (1) PBMC were isolated from human peripheral blood by discontinuous density gradient centrifugation on Ficoll-Isopaque. (2) PBMC were added into to 60 mm dishes and cultured in the incubator for 3 h. After the incubation, the supernatant was discarded, cells were washed slowly with PBS twice, and 2.5 ml DMEM was added followed by observation of the cells' condition. (3) The cells were cultured with GM-CSF (100 ng/ml) for 7 days, changing half of the medium daily after the third day. THP-1 was induced by PMA as follows: (1) After THP-1 cells were treated with PMA (180 ng/ml) for 24 h, the cells were induced to differentiate into macrophages. (2) The cells were re-suspended with serum-free RPMI without irritants and PMA. The purity of the induced macrophages was identified by Giemsa staining and CD68 labeling.

RESULTS

The Analysis Process of the Study

The analysis process was shown in **Supplementary Figure 1**. To estimate the proportion of TICs and the content of immune and stromal components in LUAD samples, transcriptome RNA sequence data of 551 patients were obtained from the TCGA database, and then calculated with the CIBERSORT and ESTIMATE algorithms, respectively. The PPI network was constructed, including immune genes differentially expressed between immune and stromal components. Next, three prognostic-related IRGs (BTK, Cd1c, and S100P) were obtained by univariate COX and lasso analysis on the core immune genes in the PPI network. The IRS calculated by the IRGs was used for relationship analysis. Clinical analysis includes survival rate and pathological features, and immunity analysis includes immunocyte populations by CIBERSORT and immune pathways by GSEA.

The Correlation Between Immune and Stromal Score With Prognosis of Lung Adenocarcinoma Patients

To calculate the correlation between the immune and stromal score with the survival rate of LUAD patients, Kaplan–Meier

survival analyses on the immune score, stromal score, and ESTIMATE score were performed, respectively. The data showed that the higher the immune or stromal score, the more immune or stromal components in TME. ESTIMATE score was the sum of immune and stromal score, which represented the combined proportion of these two components in TME. As shown in **Figure 1A**, the proportion of combined components (immune components and stromal components) was positively correlated with OS rate. The immune score was positively correlated with survival rate (**Figure 1B**), while the stromal score was not significantly correlated with OS rate (**Figure 1C**). These data suggest that the immune components in TME could better reflect the prognosis of LUAD patients than all components.

The Correlation Between Score and TNM Stage of LUAD Patients

To determine the relationship between the proportion of immune and stromal components and clinicopathological features, the clinical information of LUAD patients from TCGA database were considered. As shown in **Supplementary Figure 2**, the ESTIMATE score was negatively correlated with TNM stages (**Supplementary Figure 2A**, $p = 0.0055$), T grades (**Supplementary Figure 2B**, $p = 0.0027$), and M grades (**Supplementary Figure 2D**, $p = 0.013$). The immune score was also negatively correlated with TNM stages (**Supplementary Figure 2E**, $p = 0.017$), T grades (**Supplementary Figure 2F**, $p = 0.00069$) and M grades (**Supplementary Figure 2H**, $p = 0.059$) classification. Similarly, the stromal score was negatively correlated with stage (**Supplementary Figure 2I**, $p = 0.0023$), T grades (**Supplementary Figure 2J**, $p = 0.017$), and M grades (**Supplementary Figure 2L**, $p = 0.0041$). These results indicated that the proportion of immune and stromal components was related to the invasion and metastasis of LUAD, although N grades were not correlated to ESTIMATE score (**Supplementary Figure 2C**, $p = 0.47$), immune score (**Supplementary Figure 2G**, $p = 0.58$) and stromal score (**Supplementary Figure 2K**, $p = 0.57$).

The Gene Ontology and Kyoto Encyclopedia of Genes and Genomes Functional Enrichment Analysis of Differentially Expressed Genes Shared by Immune and Stromal Components

To confirm the exact changes related to immune and stromal components in TME, we compared gene expression of 458 tumor samples. A total of 1,426 DEGs from the immune components were achieved, among which 1,167 genes were up-regulated and 259 genes were down-regulated (**Figure 2A**). Similarly, 1,613 DEGs were obtained from stromal components, including 1,413 up-regulated genes and 200 down-regulated genes (**Figure 2B**). Next, we selected DEGs with same trend between the two components, and showed on Venn diagrams that 644 genes were up-regulated (**Figure 2C**), and 97 genes were down-regulated (**Figure 2D**) in both stromal and immune components. These 741 common DEGs were subjected to GO and KEGG enrichment analysis. Almost all the 741 DEGs were related to immune function, such as lymphocyte immunity and humoral immune response (**Figure 2E**), and these genes were enriched in Rap1 signaling pathway, drug metabolism, and cytochrome P450 metabolism (**Figure 2F**). These data suggested that the overall function of DEGs was closely related to immune activity, which means immune genes could be important parts of TME.

The Analysis of Immune Genes and Protein–Protein Interaction Network

To further study the correlation between DEGs and immune function, 1,811 IRGs were taken from the ImmPort database and intersected with DEGs. The Venn diagram displayed a total of 234 immune genes (**Supplementary Figure 3A**). To further identify the key genes in the immune network, we imported these 234 IRGs into the STRING database, and used Cytoscape to visualize the PPI network and construct sub-networks. A total of 93 nodes and 961 edges were identified (**Supplementary Figure 3B**). The nodes represent the key proteins in the PPI network. The more edges a node had, the more important it was as a network hub. So, a total of 93 IRGs were identified from the PPI network. Then the MCODE tool was applied to process the co-expression network, identify possible key modules, and obtain a key module, including 31 nodes and 290 edges (**Supplementary Figure 3C**).

The functions of DEGs in key modules were mainly enriched in the following aspects: leukocyte proliferation, lymphocyte proliferation, monocyte proliferation, immune cell proliferation regulation, and some functions closely related to immunity. Among them, the gene with the largest number of connected nodes in the PPI network was IL-10 (**Supplementary Figure 3D**). To clarify the co-expression relationship between genes, we used WGCNA to analyze the co-expression modules of 234 network key genes and obtained three co-expression enrichment modules (**Supplementary Figure 3E**). In addition, we used WGCNA to analyze the co-expression of 93 network key genes and obtained two modules (**Supplementary Figure 3F**). We found that BTK, Cd1c and S100P belong to the same gene enrichment module, suggesting that three genes were co-expressed.

Identification of Prognosis-Related Genes

To study the prognostic significance of these genes, we performed univariate Cox regression analysis to assess the correlation between the expression levels of 93 IRGs and the survival rate of patients. Twenty-six prognosis-related IRGs were found (**Figure 3A**). Subsequently, to identify the key genes that were important in prognosis, we performed lasso analysis of these 26 prognosis-related IRGs. The resulting top three IRGs were identified as BTK, Cd1c, and S100P, and were found to correlate closely to the prognosis of LUAD patients (**Figures 3B,C**).

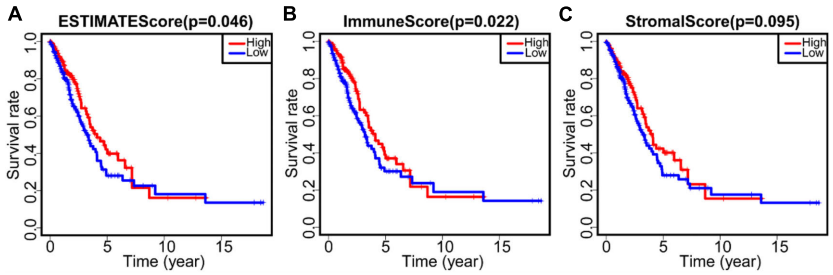

FIGURE 1 | The correlation between score and survival rate of LUAD patients. **(A)** Kaplan–Meier survival curve of ESTIMATE score and survival rate of LUAD patients (p = 0.046). **(B)** Kaplan–Meier survival curve of immune score and survival rate of LUAD patients (p = 0.022). **(C)** Kaplan–Meier survival curve of stromal score and survival rate of LUAD patients (p = 0.095).

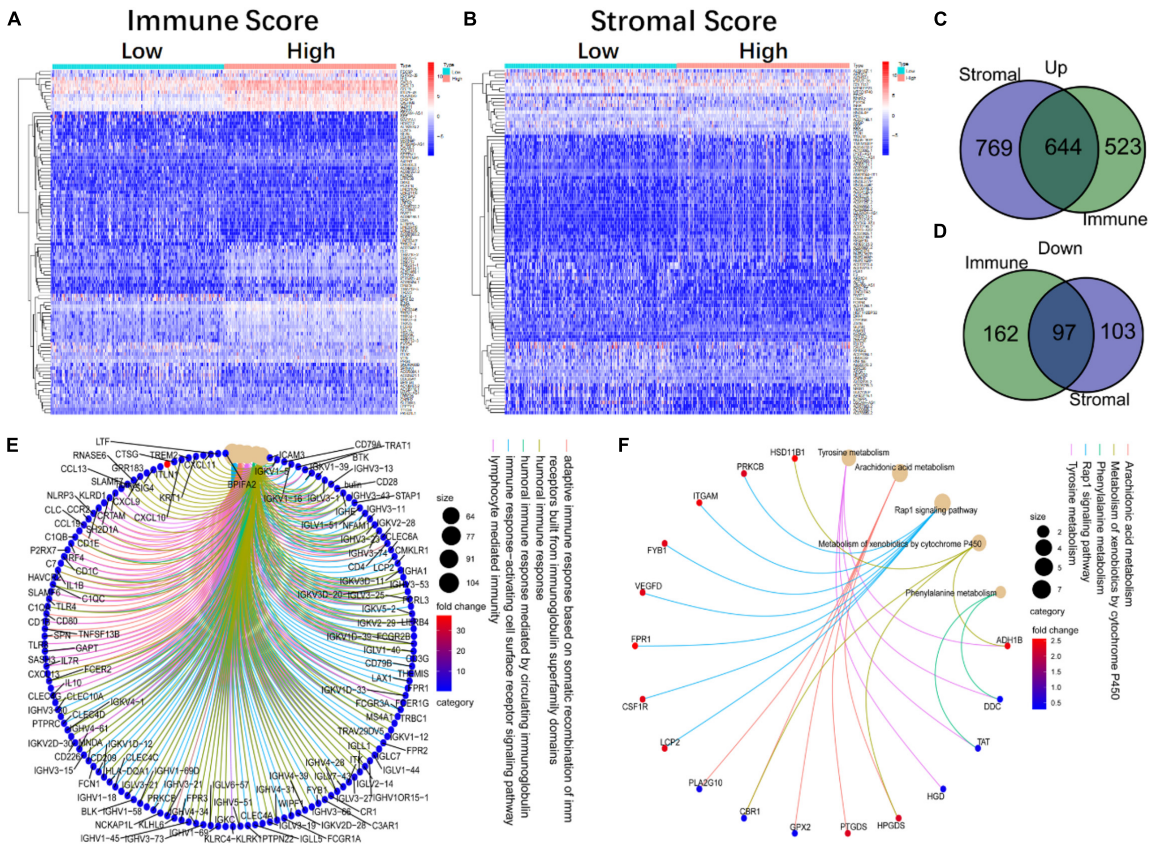

FIGURE 2 | The heatmap, Venn diagram, GO, and KEGG enrichment analysis of DEGs in immune and stromal components. **(A)** The heatmap of DEGs in high and low immune score groups. **(B)** The heatmap of DEGs in the high and low stromal score groups. **(C,D)** The Venn diagram of up-regulated and down-regulated genes co-expressed in immune and stromal component. **(E,F)** The GO and KEGG enrichment analysis of 741 DEGs.

Construction and Analysis of Immune Risk Score Model From Prognosis-Related Genes

To construct a prognostic model, we calculated the IRS based on the three IRGs (**Table 1**). The calculation formula is as follows:

$$\mathrm{IRS} = (-0.15982 \times \mathrm{EXP\_BTK}) + (-0.08222 \times \mathrm{EXP\_Cd1c}) + (0.049485 \times \mathrm{EXP\_S100P}).$$

To evaluate the predictive ability of the model, we divided the 458 LUAD patients from the TCGA into high-risk and low-risk groups for survival analysis based on the median of IRS (median = 0.997). The results showed that compared with the low-risk group, patients in the high-risk group had a poorer survival prognosis (**Figure 4A**). To further evaluate prognostic prediction ability of IRS, ROC analysis related to survival time was carried out. The area under the ROC curve (AUC) of the IRS model was 0.701 (**Figure 4B**), indicating a good

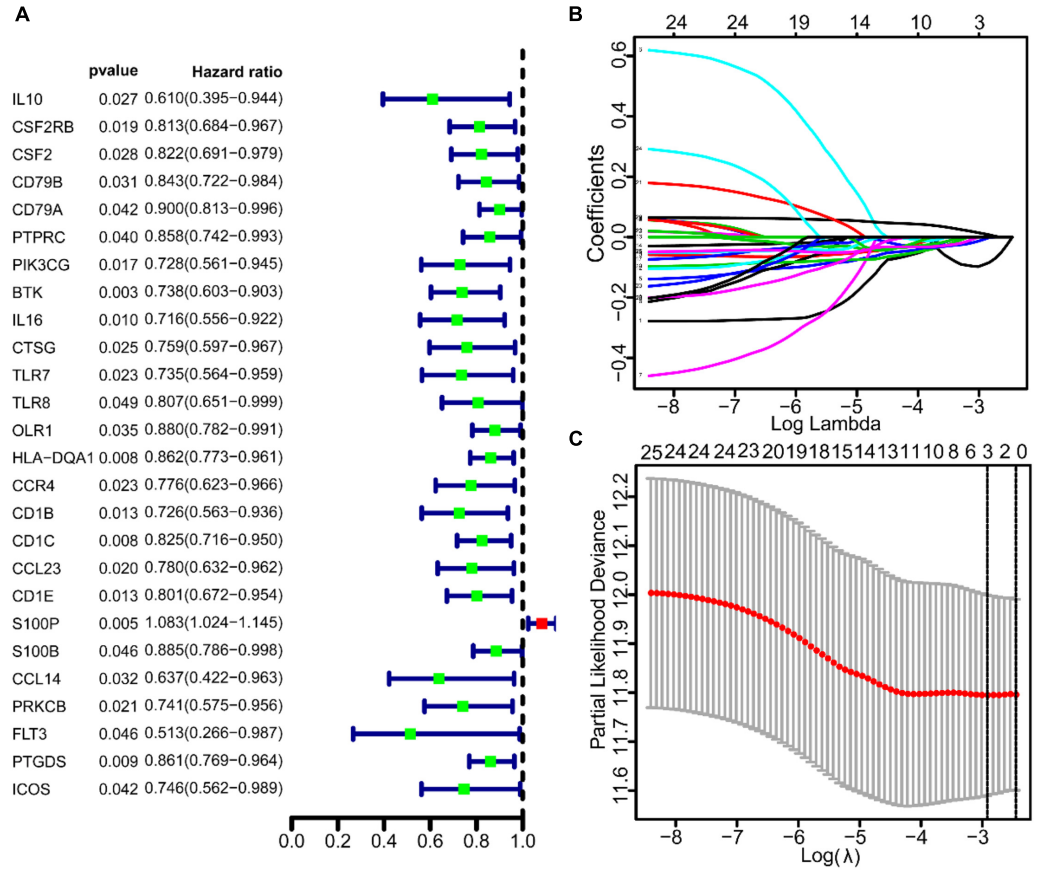

FIGURE 3 | The univariate COX and lasso analysis of immune genes. **(A)** The univariate COX analysis of 93 IRGs. **(B,C)** The lasso analysis of 26 immune genes.

TABLE 1 | Top three prognosis-associated genes identified by lasso regression analysis.

Gene symbol	Coefficient	HR	HR.95L	HR.95H
BTK	−0.159	0.852	0.657	1.105
Cd1c	−0.082	0.921	0.77	1.101
S100P	0.049	1.05	0.989	1.115

performance in prognosis. Meanwhile, IRS was closely related to the expression levels of the three IRGs (**Figure 4C**) and the survival status of patients (**Figure 4D**). In addition, we selected the dataset of LUAD patients from GSE31210 for verification, and we found that IRS could also effectively predict survival rate (**Figures 4E–H**).

The Prognostic Value of Different Clinical Features and the Construction of Nomogram

Currently, the clinical features of tumor patients are commonly used indicators for clinical evaluation of prognosis. Therefore, we used univariate and multivariate Cox regression to analyze the prognostic value of different clinical features of LUAD patients. The results from univariate COX analysis showed that tumor stage, primary tumor, lymph node metastasis and IRS were related to OS of LUAD patients ($p < 0.001$) (**Table 2**) in the TCGA. However, multivariate COX regression analysis results stated that tumor stage, lymph node metastasis (N) and IRS were only independent prognostic factors of OS (**Table 2**).

In the GSE31210 dataset, univariate COX analysis found that stage and IRS were related to OS of LUAD patients ($p < 0.001$), while multivariate COX regression analysis found that stage and IRS were independent prognostic factors related to OS (**Table 3**). Subsequently, ROC curve was plotted to evaluate the reliability of each clinical feature to predict the prognosis of patients in TCGA and GSE31210 (**Figures 5A,B**).The area under the ROC curve of IRS was >0.7, predicting the prognosis of patients. The data indicate that IRS is an independent prognostic factor of OS. To visualize the predictive effect of each independent prognostic factor on OS, rms R package was employed to draw a nomogram of 3 to 5-year OS (**Figure 5C**). To evaluate the reliability of the nomogram, a correction chart was constructed and the 3-year and 5-year survival rate of LUAD patients was calculated by drawing the vertical line between the total point axis and each prognostic axis, showing a good consistency between the predicted result and the observed result (**Figures 5D,E**).

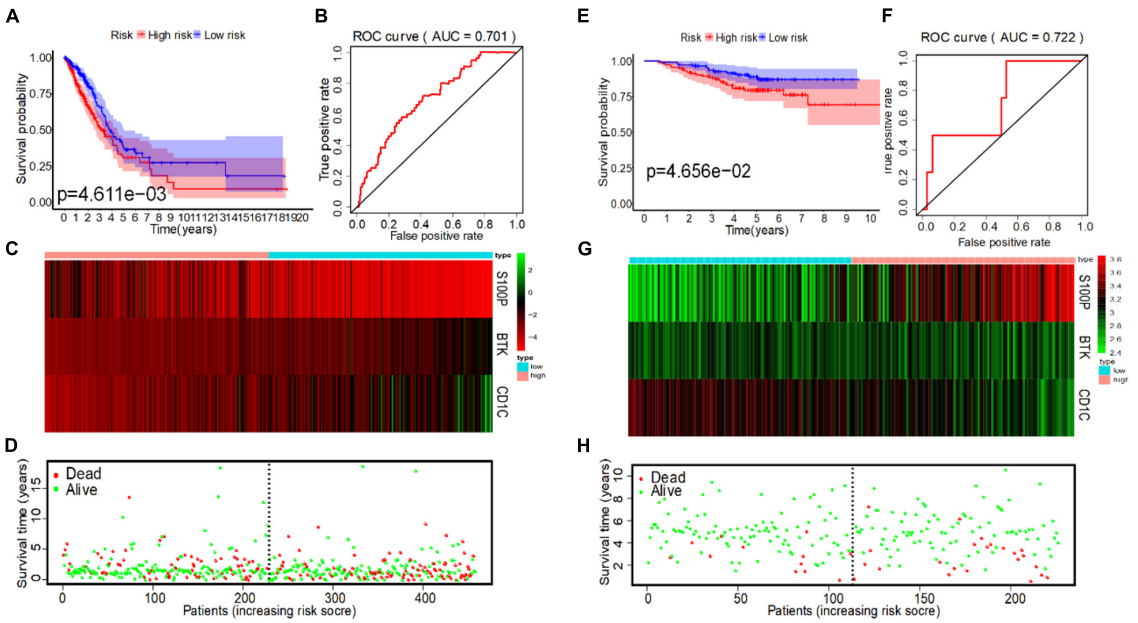

FIGURE 4 | IRS analysis of prognosis models of 3 immune genes in TCGA and GSE31210 datasets. **(A)** The survival curves of low-risk and high-risk group in TCGA. **(B)** The ROC curve for predicting OS of patients based on the IRS to in TCGA. **(C)** The expression heatmap of three immune prognostic genes in the low-risk and high-risk group from TCGA. **(D)** IRS distribution and survival status of patients in the low-risk and high-risk group from TCGA. **(E)** The survival curve of low-risk and high-risk group in GSE31210. **(F)** The ROC curve for predicting OS of patients based on IRS in GSE31210. **(G)** The expression heatmap of three immune prognostic genes in the low-risk and high-risk group from GSE31210. **(H)** IRS distribution and survival status of patients in the low-risk and high-risk group from GSE31210.

TABLE 2 | The prognostic effect of clinical and molecular parameters in TCGA.

Parameter	Univariate analysis			Multivariate analysis		
	HR	95% CI	*p*-Value	HR	95% CI	*p*-Value
Age	1.011	0.994 – 1.028	0.18	1.014	0.997 – 1.031	0.102
Gender	1.07	0.777 – 1.474	0.676	0.82	0.586 – 1.148	0.248
Stage	1.671	1.441 – 1.938	<0.001	1.302	1.027 – 1.652	0.029
T	1.599	1.305 – 1.957	<0.001	1.248	0.999 – 1.599	0.051
N	1.84	1.522 – 2.225	<0.001	1.398	1.071 – 1.825	0.014
IRS	2.512	1.523 – 4.124	<0.001	2.451	1.426 – 4.212	<0.001

TABLE 3 | The prognostic effect of clinical and molecular parameters in GEO.

Parameter	Univariate analysis			Multivariate analysis		
	HR	95% CI	*p*-Value	HR	95% CI	*p*-Value
Age	1.025	0.977 – −1.075	0.306	1.035	0.985 – 1.083	0.181
Gender	1.519	0.780 – 2.955	0.219	1.482	0.572 – 2.366	0.676
Stage	4.232	2.175 – 8.236	<0.001	3.904	1.966 – 7.752	0.001
IRS	1.928	1.107 – 3.357	<0.001	1.484	1.810 – 2.719	<0.001

The Relationship Between the Three Immune-Related Genes and the Survival Time of Lung Adenocarcinoma Patients and TNM Stage

To study the correlation between the expression of the three IRGs and survival rate of patients and TNM stage, we analyzed the expression level of each gene separately. In the TGGA, BTK had low expression in tumor tissues of LUAD patients (**Figures 6A,B**), and patients with high gene expression of BTK had significantly longer survival time (**Figure 6C**). Similarly, Cd1c was expressed at low levels in tumor tissues (**Figures 6D,E**), and LUAD patients with high gene expression of Cd1c survived longer (**Figure 6F**). On the contrary, S100P was highly expressed in tumor tissues

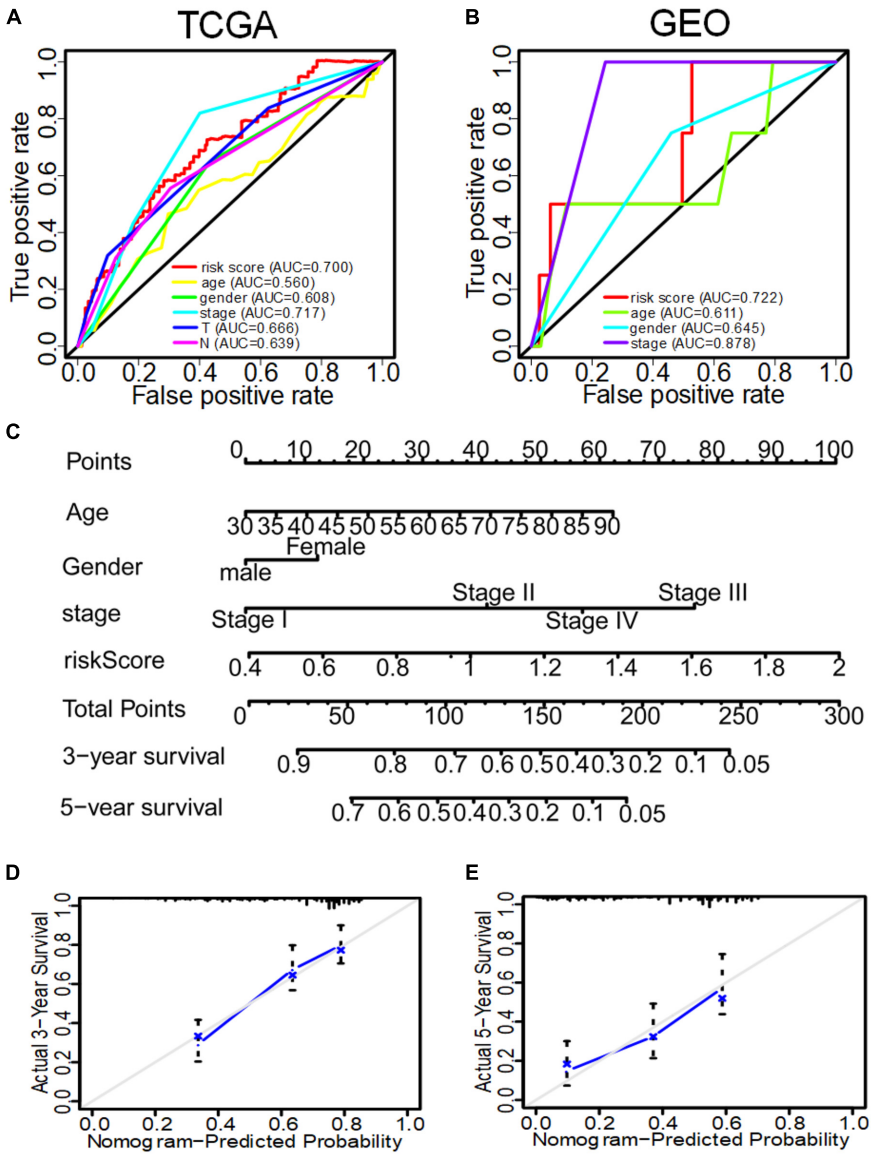

FIGURE 5 | The ROC curve of evaluating the reliability of each clinical feature to predict the prognosis of patients in TCGA and GEO in and the nomogram of 3–5-year OS predicted by the IRS of three immune genes combined with other clinical features. **(A)** The ROC curve of each clinical feature to predict the prognosis of patients in TCGA. **(B)** The ROC curve of each clinical feature to predict the prognosis of patients in GEO. **(C)** The nomogram to predict the 3-year and 5-year OS of patients in TCGA. **(D)** The correction nomogram of predicting the 3-year OS of patients. **(E)** The correction nomogram of predicting the 5-year OS of patients.

(**Figures 6G,H**), and patients with low expression of S100P survived longer (**Figure 6I**).

Further, data in the GEPIA database were verified, and results confirmed the low expression of BTK and Cd1c in LUAD tumor tissues (**Supplementary Figures 4A,C**), and the finding that patients with high expression of BTK or Cd1c survived longer (**Supplementary Figures 4B,D**). S100P showed high expression in tumor tissues (**Supplementary Figure 4E**), but patients with low expression of S100P survived longer (**Supplementary Figure 4F**), which were consistent with the data from TGGA.

Further analysis showed that expression of BTK was negatively correlated with stage (**Supplementary Figure 5A**, p = 0.0071), T (**Supplementary Figure 5B**, p = 0.0018), and M classification (**Supplementary Figure 5D**, p = 0.036) of TNM stage, but there was no significant correlation with N classification (**Supplementary Figure 5C**, p = 0.3). Similarly, the expression of Cd1c was negatively correlated with stage (**Supplementary Figure 5E**, p = 0.005), T (**Supplementary Figure 5F**, p = 0.039), and M (**Supplementary Figure 5H**, p = 0.019) classification of TNM stage, but there was no significant correlation with N classification (**Supplementary Figure 5G**, p = 0.93). It is unexpected that there was no significant correlation between S100P and these clinical features (**Supplementary Figures 5I–L**).

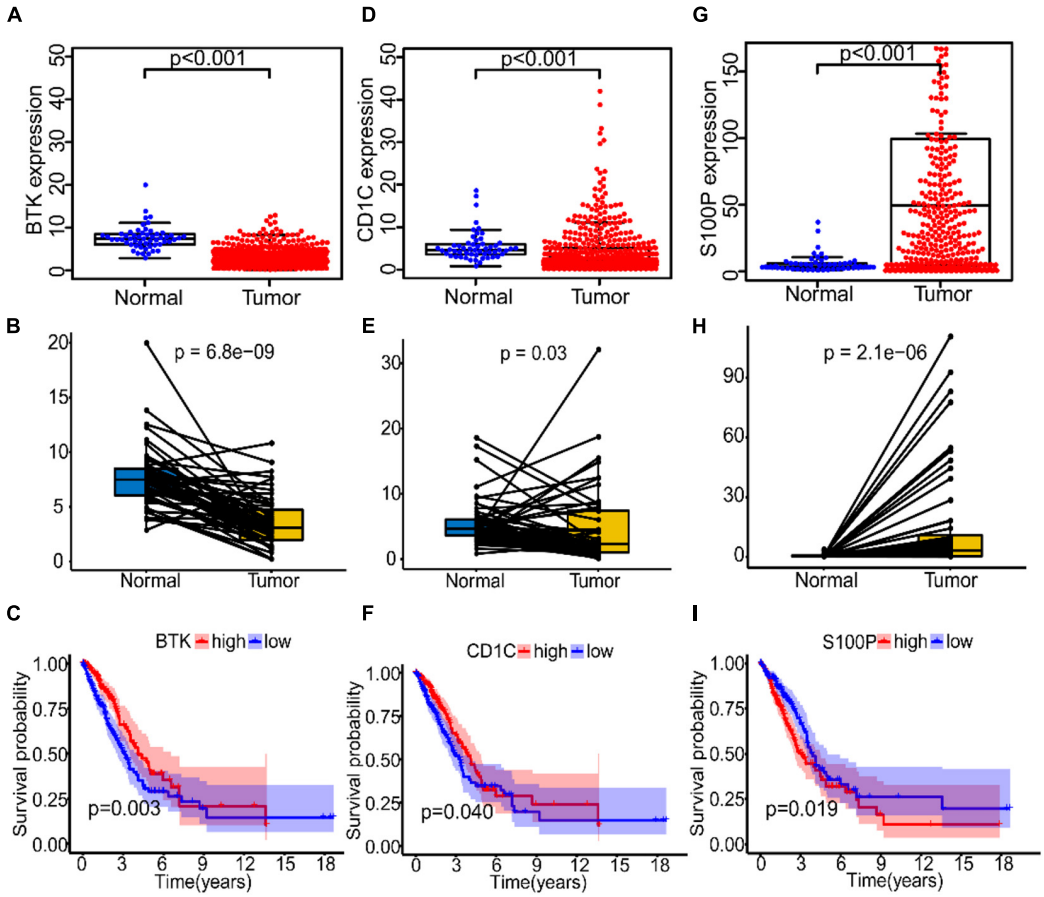

FIGURE 6 | The expression and prognostic analysis of three immune genes in LUAD patients. **(A–C)** The correlation between the expression level of BTK in normal and tumor tissues and prognosis of patients. **(D–F)** The correlation between the expression level of Cd1c in normal and tumor tissues and prognosis of patients. **(G–I)** The correlation between the expression level of S100P in normal and tumor tissues and prognosis of patients.

The Immune-Related Signaling Pathways Involving the Three Immune-Related Genes

To explore the immune-related signaling pathways involved in the three IRGs, we divided LUAD patients into high-expression and low-expression groups based on gene expression, and then GSEA was performed. The function of the high-expression group of BTK was mainly enriched in immune-related activities, such as autoimmunity, cell adhesion, chemotactic cytokines, and T cell receptors signaling pathway (**Supplementary Figure 6A**). The function of the low-expression group of BTK was mainly enriched in amino acid metabolism, base excision repair and some typical tumor pathways produced by proteins (**Supplementary Figure 6B**). The function of the high-expression group of Cd1c was mainly enriched in pathways related to immune function such as autoimmunity, B cell receptor signaling pathway, cell adhesion, cytokine receptor signaling pathway, and T cell receptor signaling pathway (**Supplementary Figure 6C**). The function of the low-expression group of Cd1c was mainly enriched in aminoacyl biosynthesis, cell cycle, P53 signaling pathway and RNA degradation pathway (**Supplementary Figure 6D**). The function of the high-expression group of S100P was mainly enriched in B cell receptor signaling pathway, cell adhesion molecule, cytokine receptor interaction, JAK_STAT_signaling pathway, and T cell receptor signaling pathway (**Supplementary Figure 6E**). The function of the low-expression group of S100P was mainly enriched in amino acid metabolism, base excision repair, cell cycle, sodium citrate cycle, and pathways related to polysaccharide biosynthesis (**Supplementary Figure 6F**). These results suggested that the three immune genes that we identified in this research may be a potential indicator of TME status.

Tumor Infiltrating Cells Expression Profile in Lung Adenocarcinoma

To describe the expression profile of immune cells in the TME, CIBERSORT was taken to analyze the TIC abundance distribution in all tumor samples. We found that there was a significant correlation between the gene expression profiles of at least one kind of immune cell subsets in 421 tumor samples ($p < 0.05$), and these samples were selected to construct the

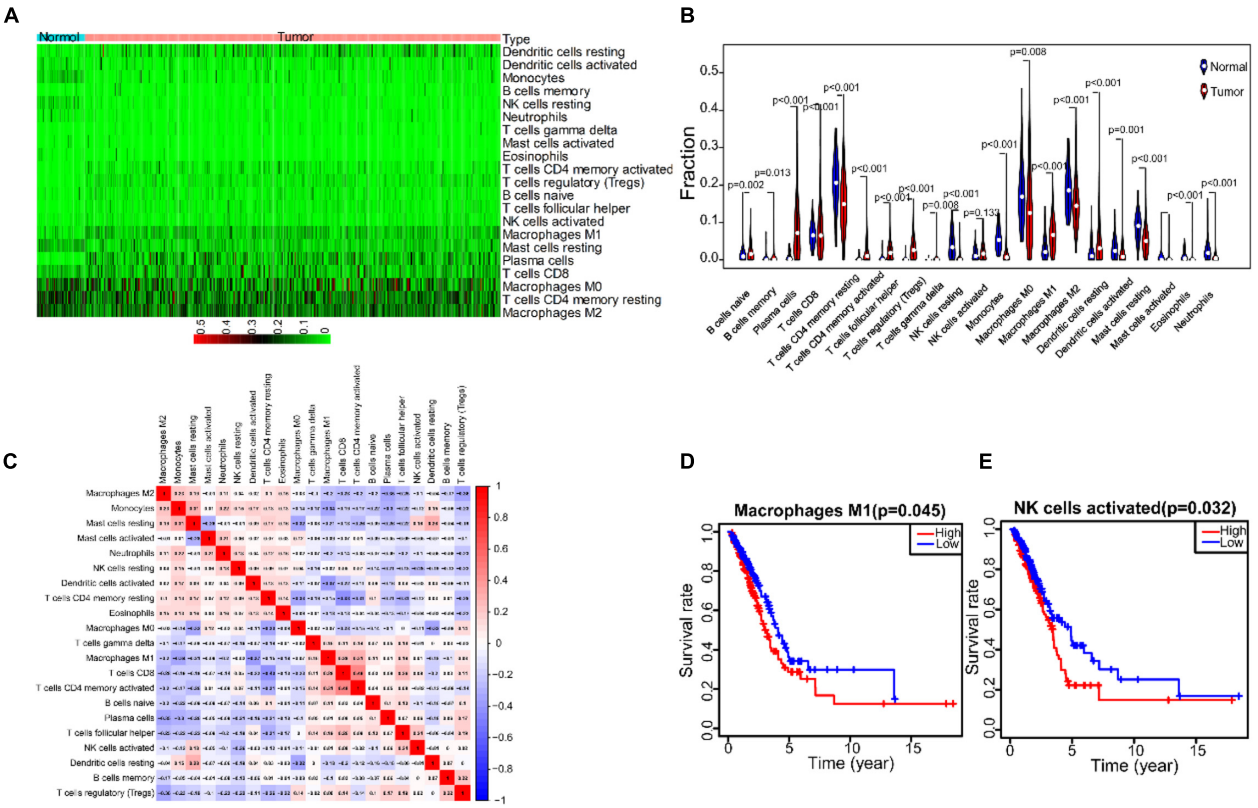

FIGURE 7 | The correlation analysis between TICs expression profile in LUDA tumor tissue and prognostic. **(A)** The expression heatmap of 21 immune cells in LUAD tumor tissue and normal tissue. **(B)** The expression violin diagram of 21 immune cells in LUAD tumor tissue and normal tissue. **(C)** The correlation test of 21 immune cells expression. **(D)** The correlation between M1 macrophages and the prognosis of LUAD patients. **(E)** The correlation between NK cells activated and the prognosis of LUAD patients.

expression profile of 21 immune cells in LUAD (**Figure 7A**). The results of differential and correlation analysis showed that a total of 18 immune cells were differentially expressed. Among them, the cells with the highest amount in tumor tissues are M2 macrophages, M0 macrophages, M1 macrophages, CD4+ resting T cells and resting mast cells, which were all significantly more than those in normal tissue (**Figure 7B**). We also studied the correlation among the five cell subpopulations. M1 macrophages were negatively correlated with activated dendritic cells, monocytes and resting mast cells, and positively correlated with (γδ) T cells. Activated NK cells were negatively correlated with resting NK cells, monocytes and resting CD4 memory cells, and positively correlated with T follicular helper cells and resting mast cells (**Figure 7C**). Prognostic analysis showed that M1 macrophages and activated NK cells were closely related to prognosis of patients, and it was statistically significant (**Figures 7D,E**).

Study of Three Immune-Related Genes and the Expression of Tumor Infiltrating Cells Related to Prognosis

To explore the correlation between the three IRGs and prognostic immune cell subgroups, we analyzed the expression level of each gene and the content of M1 macrophages and NK cell subgroup. The expression of BTK was positively correlated with M1 macrophages (**Figure 8A**, p = 0.031), and negatively correlated with activated NK cells (**Figure 8B**, p = 1.9e-06). Cd1c was negatively correlated with M1 macrophages (**Figure 8C**, p = 4.4e-07) and activated NK cells (**Figure 8D**, p = 0.015). S100P was not significantly correlated with M1 macrophages (**Figure 8E**, p = 0.089), but positively correlated with activated NK cells (**Figure 8F**, p = 0.00077).

Verification of Immune-Related Gene Expression and Tumor Infiltrating Cells *in situ* Related to Prognosis

To verify the accuracy of the results of TCGA and GEO data sets (**Supplementary Figures 4A–C**), we collected clinical samples from three patients with LUAD. The correlation between the expression of S100P and BTK gene in macrophages and NK cells was analyzed by immunofluorescence. It was found that S100P gene expression was localized on cancer cells and higher in tumor than in paracancerous tissues (**Figures 9A,C**). The expression of S100P was positively correlated with M2 macrophages (**Figure 9B**). In tumor tissues, S100P was negatively correlated with M1 macrophages (**Figure 9D**, p = 0.012) and

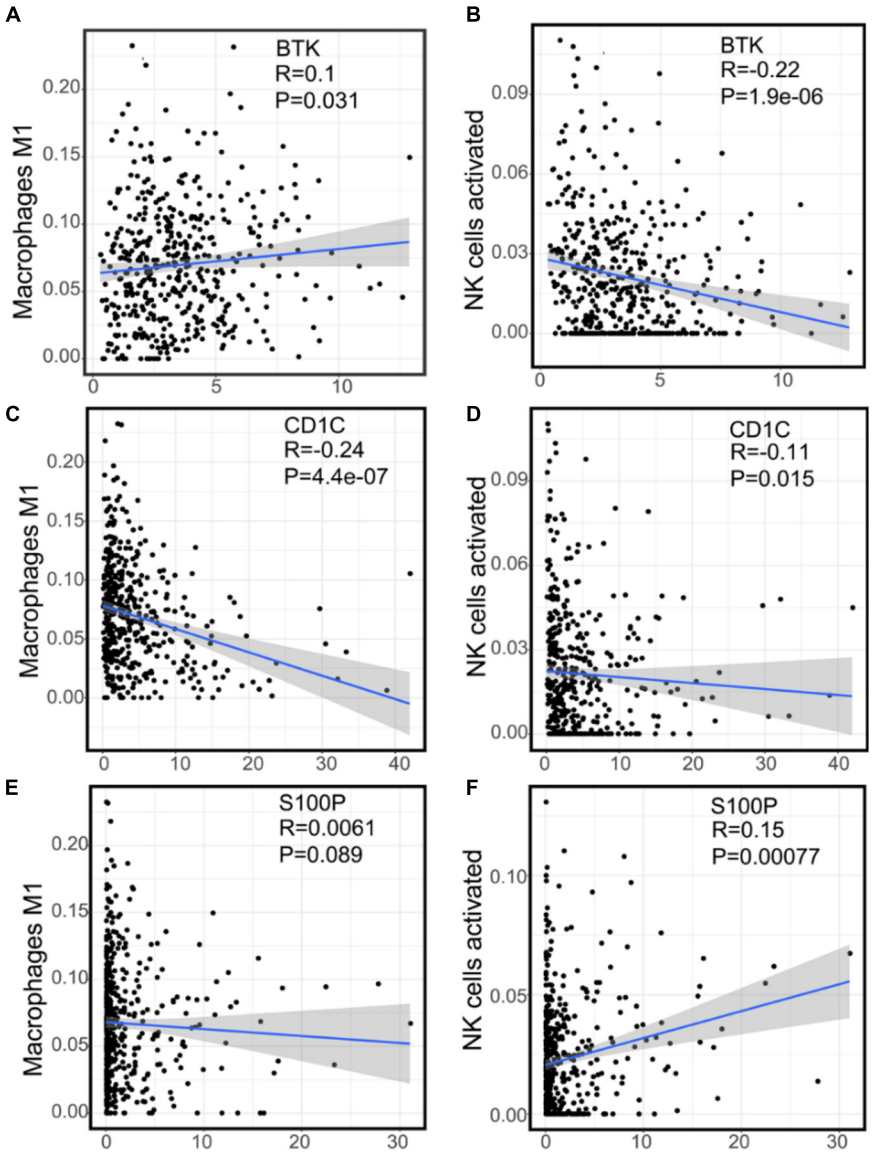

FIGURE 8 | The correlation between the expression of three immune genes and two kinds of prognostic immune cells. **(A)** The correlation scatter plot of the expression of BTK and M1 macrophages. **(B)** The correlation scatter plot of the expression of BTK and NK cells activated. **(C)** The correlation scatter plot of the expression of Cd1c and M1 macrophages. **(D)** The correlation scatter plot of the expression of Cd1c and NK cells activated. **(E)** The correlation scatter plot of the expression of S100P and M1 macrophages. **(F)** The correlation scatter plot of the expression of S100P and NK cells activated.

positively with M2 macrophages (**Figure 9D**, p = 0.033). It can be seen that S100P may be closely related to the transformation of macrophages in the order of number list 9→8→5→2 and 9→6→1→2, and it was found that along with the increase of S100P, the number of M2 macrophages increases (**Figure 9C**). In NK cells, S100P was not localized, but highly expressed in tumor tissues (**Supplementary Figures 7A–D**). There were not correlations between S100P and NK either in paracancerous tissues (**Figure 9E**, p = 0.214) or tumor tissues (**Figure 9F**, p = 0.808). It can be concluded that the expression of S100P is closely related to the infiltration of M2 macrophages.

BTK in paracancerous tissues was significantly higher than that in tumor tissues (**Supplementary Figures 8A–D**), which was consistent with the results in the TCGA and GEO (**Supplementary Figure 4A**). BTK is mainly located on macrophages (**Supplementary Figures 8A–D**), though not related to any types of TAM (**Figures 9G,H**). BTK was not localized on NK cells (**Supplementary Figures 9A–D**). Between NK cells and BTK levels, no correlation was found in paracancerous tissues (**Figure 9I**, p = 0.479), but there was a negative correlation (**Figure 9J**, p = 0.0003) in cancer tissues. These data suggest that lower BTK in tumor tissues is possibly related to the infiltration of NK cells.

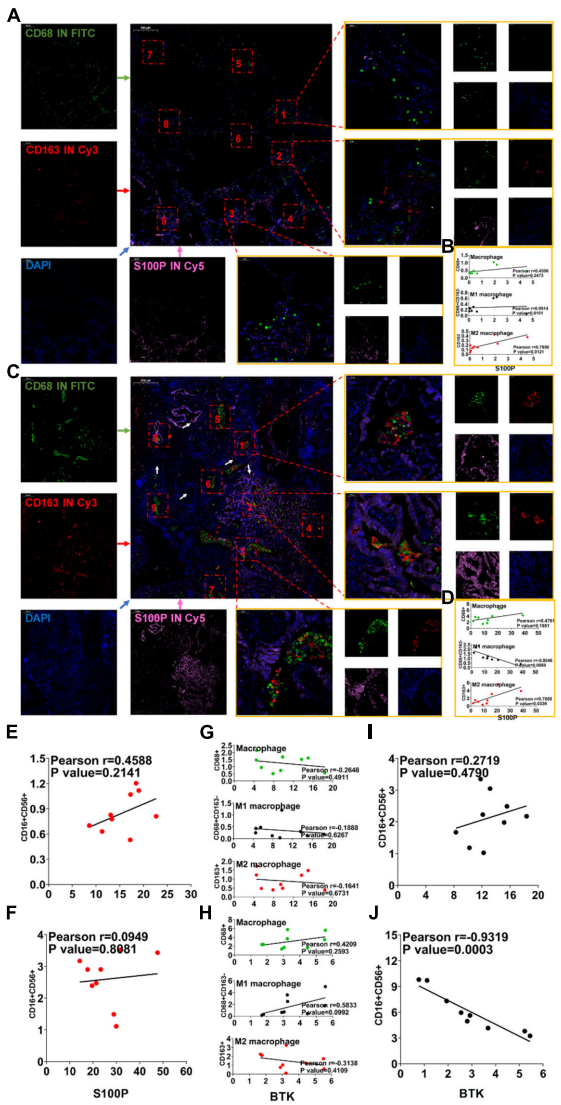

FIGURE 9 | Immunofluorescence verification of IRG expression and TICs related to prognosis. **(A)** Immunofluorescence of S100P and macrophages in paracancerous tissues. **(B)** Correlation map of S100P and macrophage expression in paracancerous tissues. **(C)** Immunofluorescence of S100P and macrophages in cancer tissues. **(D)** Correlation map of S100P and macrophage expression in cancer tissue. **(E)** Correlation map of expression of S100P and NK cells in paracancerous tissues. **(F)** Correlation map of expression of S100P and NK cells in cancer tissues. **(G)** Correlation map of BTK and macrophage expression in paracancerous tissues. **(H)** Correlation map of BTK and macrophage expression in cancer tissue. **(I)** Correlation map of expression of BTK and NK cells in paracancerous tissues. **(J)** Correlation map of expression of BTK and NK cells in cancer tissues.

S100P Suppression Inhibits M2 Macrophages Polarization

The above IF assays *in situ* showed that S100P was closely related to the transformation and migration of TAM in tumor tissue. To further verify the relationship between S100P and macrophage polarization, we designed a loss of function assay by transfecting siRNA_S100P to A549 cells in co-culture with primary or inducible human macrophages (**Figure 10**). Twelve hours after transfection with siRNA_S100P or siRNA_NC, A549 cells were co-cultured with PBMC-M and THP-1 cells induced by PMA (180 ng/ml) for 24 h, respectively. Cell migration was detected by crystal violet staining and transformation of macrophages to M1 or M2 by IF labeling after co-culture for 48 h. We found that cell migration was inhibited by S100P knockdown in both PBMC-M and THP-1 cells in a time-dependent manner (**Figures 10A,B**). Similarly, S100P knockdown inhibited the survival of PBMC-M (**Figure 10C**) and THP-1 (**Figure 10D**). Interestingly, following S100P downregulation, A549 also inhibited the transformation into M2 in primary PBMC-M (**Figure 10C**), while this was not observed in THP-1 cells (**Figure 10D**).

DISCUSSION

The immune status of TME is closely related to the prognosis of LUAD patients. However, the composition of TME is very complex, including highly heterogeneous tumor stromal cells and dozens of infiltrating immune cells, expressing thousands of DEGs. The relationship between these factors is not fully elucidated. Identification of key genes that can represent the immune status of TME could be a promising approach for predicting the prognosis of LUAD. In this study, we identified three key IRGs – BTK, Cd1c and S100P – from the TCGA database for assessing the immune status of TME and predicting the prognosis of LUAD. We found that the three key genes are specifically expressed in different tumor or tumor-associated cells and affect the prognosis and progression of LUAD patients by directly or indirectly regulating tumor-associated immunocytes (**Supplementary Figure 1**).

The gene signature of LUAD can be used to predict the outcome of clinical treatment (Jiawei et al., 2020). However, the cellular origin of this gene signature is unclear, because both stromal cells and immune cells in TME express DEGs (Lambrechts et al., 2018; Camara et al., 2020). We used immune score and stromal score to partially represent the gene signature of stromal cells and immune cells (Li et al., 2020; Zhang et al., 2020). It was found that OS of 497 LUAD patients from TCGA was significantly positively correlated with immune score (**Figure 1**), suggesting that immune status is particularly important for the clinical outcome of LUAD patients (Bi et al., 2020). At the same time, immune score and stromal score were negatively correlated with clinical stages (**Supplementary Figure 2**), suggesting that immune and stromal components in TME may be involved in the development and metastasis of LUAD (Ge et al., 2019; Levayer, 2020). In accordance with this, we found 741 common DEGs in immune and matrix components. GO and KEGG analysis showed that these genes were mainly enriched in immune regulatory pathways (**Figure 2**).

The immune status of TME depends on the characteristic expression of IRGs, which can be used to predict the prognosis of LUAD patients. We found 93 IRGs that are characteristically expressed in LUAD, whose functions are mainly enriched in leukocyte proliferation, lymphocyte proliferation, monocyte

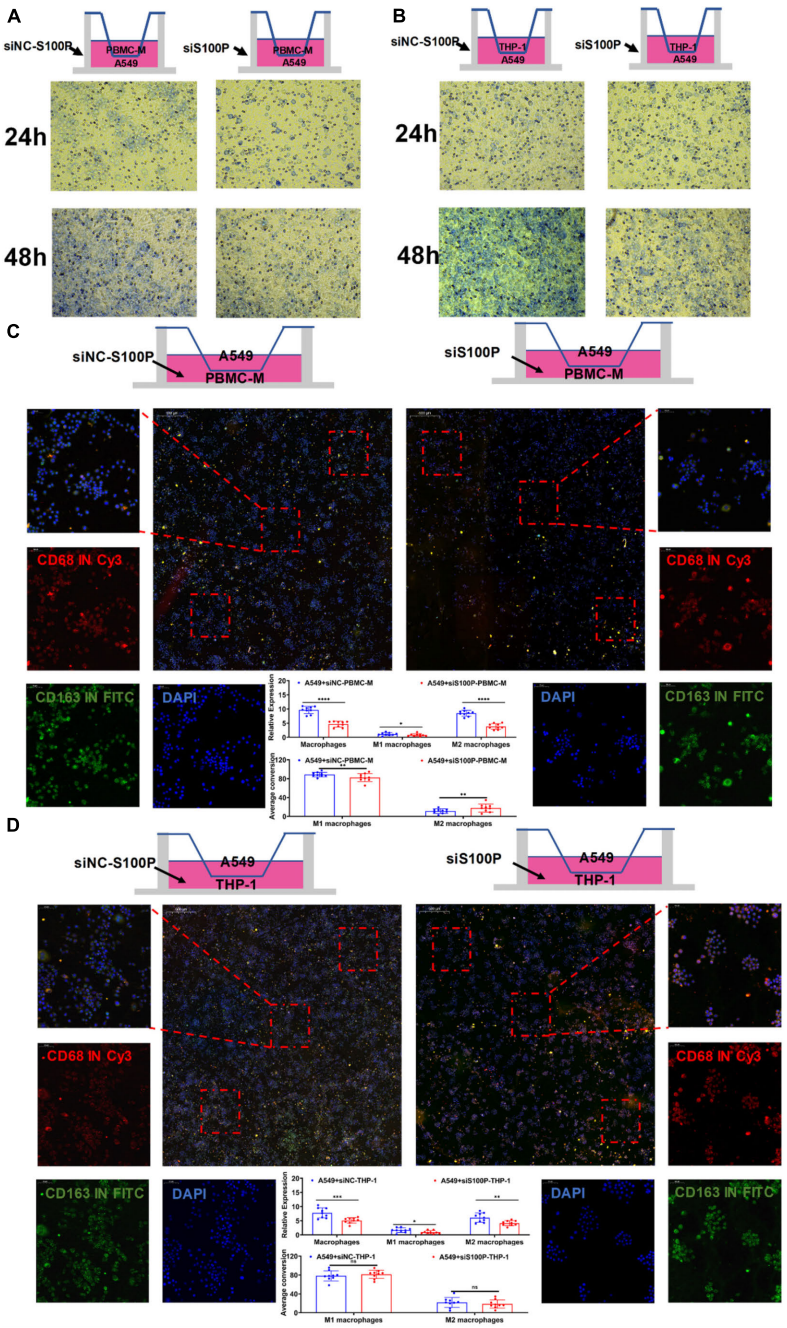

FIGURE 10 | Primary macrophage culture and siRNA transfection. **(A)** Co-culture of PBMC-M after treatment of A549 cells with siNC-S100P and siRNA-S100P. **(B)** Co-culture of THP-1 after treatment of A549 cells with siNC-S100P and siRNA-S100P. **(C)** Effect of A549 cells knocking down S100P on the transformation of PBMC-M cells. **(D)** Effect of A549 cells knocking down S100P on the transformation of THP-1 cells. $^{*}p < 0.05$, $^{**}p < 0.01$, $^{***}p < 0.001$, $^{****}p < 0.0001$.

proliferation, and immune-related activities (**Supplementary Figure 3**). Cox and Lasso analyses showed that 26 IRGs were associated with the prognosis of LUAD patients, of which BTK, Cd1c, and S100P were the most closely related (**Figure 3**). Multivariate regression analysis of data from GEO and TCGA showed that IRS based on these three genes could be an independent predictor for clinical outcome in patients with LUAD (**Table 3**). These results demonstrated the possibility of the development of a specific, sensitive, and cost-effective biomarker assay for the evaluation of immune targeted therapy in patients with LUAD.

We further studied the effects of the three genes on regulating the immune status of TME. We analyzed the abundance of TIC in LUAD tissues and made comparison between LUAD and

normal tissues (**Figure 7**). We found that the cell types and cell amounts in tumor tissues are significantly different from normal tissues. Macrophages and NK cells found in the tumor tissues were significantly correlated with the survival rate of LUAD patients (**Figure 7**).

BTK is a tyrosine kinase, which belongs to the Tec kinase family and plays an important role in the proliferation and differentiation of B cells (Kim, 2019; Good et al., 2021). However, BTK inhibitors have been extended to treat some of the solid tumors, such as non-small cell lung cancer, breast cancer, and pancreatic cancer (Zhang B. et al., 2019; Metzler et al., 2020), suggesting that BTK may affect other immune cells in various TMEs. In accordance with this, TCGA data analysis showed that there was a negative correlation between BTK expression and NK cell abundance (**Figure 8**), confirmed by clinical tissue samples using an *in situ* labeling experiment (**Supplementary Figure 9**). Unexpectedly, the expression profile data showed that the expression of mRNA and protein of BTK was inhibited in LUAD tumor tissue (**Figure 6** and **Supplementary Figure 5**), and the down-regulation of BTK was associated with poor survival, which seemed to contradict the strategy of BTK targeted therapy (Pang et al., 2020; Ramalingam et al., 2020). We speculate that the effect of BTK on the immune status of TME depends on its tissue distribution. Immunofluorescence assays of tissue sections showed that BTK was mainly located in macrophages at the junction of cancer nest and stroma, and negatively correlated with the abundance of NK cells (**Supplementary Figures 9C,D**), suggesting that BTK promotes tumor progression by promoting local immunosuppression. As a specific marker of dendritic cells, Cd1c has the function of regulating antigen presentation of dendritic cells and improving TME (Yuan et al., 2019; Gherardin et al., 2021). We found that both mRNA and protein expression of *Cd1c* were down-regulated in LUAD tumor tissues (**Supplementary Figures 4**, **5**), while the down-regulation of Cd1c was associated with poor survival (**Supplementary Figure 4**). This may be due to the up-regulation of the function of dendritic cells by Cd1c in TME of patients with non-small cell lung cancer (Bol et al., 2019). S100P is highly expressed in a variety of tumor cells and is a biomarker for early diagnosis of tumors. S100P inhibitors have been used in targeted therapy of LUAD (Tan et al., 2019; Kazakov et al., 2020). Consistent with this, we analyzed the TCGA and GEPIA databases and found that S100P was highly expressed in LUAD tumor tissues (**Supplementary Figure 4**), and was significantly negatively correlated with patient survival (**Figure 6**). However, we found that there was no significant correlation between the staging of LUAD patients and the expression of S100P (**Supplementary Figure 5**), suggesting that S100P may indirectly promote the growth and metastasis of LUAD by regulating TME. Tumor-associated M2 macrophages are one of the main cell types that promote the formation of tumor immunosuppressive niches (Zhang J. et al., 2019; Pan et al., 2020). Interestingly, we found that high expression of S100P was restricted to tumor cells, and along the direction adjacent to the cancer nest, S100P positive tumor cells and M2 macrophages significantly increased, while M1 macrophages significantly decreased (**Figure 9**). These results suggest that tumor cells with high expression of S100P may drive the polarization of macrophages in TME toward M2 phenotype (**Figure 9**). Consistent with the results, cell co-culture assays in vitro showed that S100P knockdown in lung cancer cells could inhibit the migration and M2 polarization of primary or cell line-derived macrophages (**Figure 10**). The discovery of an S100P-induced tumor immunosuppressive niche may provide a new understanding for targeted therapy based on S100P (Zhang et al., 2021).

These findings highlight an important scientific issue for elucidating the immune landscape of TME and understanding the crosstalk between tumor cells and immune cells in TME. Clinically, we constructed a prognostic prediction model based on key IRGs regulating immune cell subsets in TME. However, due to the complexity of the LUAD microenvironment, more comprehensive analysis is needed to reveal the essential regulatory mechanisms that coordinate immune cells infiltrated in tumors.

DATA AVAILABILITY STATEMENT

The original contributions presented in the study are included in the article/**Supplementary Material**, further inquiries can be directed to the corresponding author/s.

ETHICS STATEMENT

This study was approved by the Medical Ethics Committee of Anhui University of Science and Technology (No. 20190116).

AUTHOR CONTRIBUTIONS

DH and JW contributed to conception and design, and study supervision. QX, RF, JW, JZ, JG, MM, YL, XW, CT, and DH contributed to development of methodology, performance of assays, analysis and interpretation of data, and writing of the manuscript. RF, YX, and DH contributed to review of the manuscript. All authors contributed to the article and approved the submitted version.

FUNDING

This study was supported by the National Natural Science Foundation of China (No. 81971483) and the Collaborative Innovation Project of Colleges and Universities of Anhui Province (GXXT-2020-058). The funders had no role in the study design, data collection, analysis, and decision to publish or preparation of the manuscript.

SUPPLEMENTARY MATERIAL

The Supplementary Material for this article can be found online at: https://www.frontiersin.org/articles/10.3389/fcell.2021.751800/full#supplementary-material

REFERENCES

Bi, K. W., Wei, X. G., Qin, X. X., and Li, B. (2020). BTK Has potential to be a prognostic factor for lung adenocarcinoma and an indicator for tumor microenvironment remodeling: a study based on TCGA data mining. *Front. Oncol.* 10:424. doi: 10.3389/fonc.2020.00424

Bol, K. F., Schreibelt, G., Rabold, K., Wculek, S. K., Schwarze, J. K., Dzionek, A., et al. (2019). The clinical application of cancer immunotherapy based on naturally circulating dendritic cells. *J. Immunother. Cancer* 7:109. doi: 10.1186/s40425-019-0580-6

Camara, R., Ogbeni, D., Gerstmann, L., Ostovar, M., Hurer, E., Scott, M., et al. (2020). Discovery of novel small molecule inhibitors of S100P with in vitro anti-metastatic effects on pancreatic cancer cells. *Eur. J. Med. Chem.* 203:112621. doi: 10.1016/j.ejmech.2020.112621

Ge, P., Wang, W., Li, L., Zhang, G., Gao, Z., Tang, Z., et al. (2019). Profiles of immune cell infiltration and immune-related genes in the tumor microenvironment of colorectal cancer. *Biomed. Pharmacother.* 118:109228. doi: 10.1016/j.biopha.2019.109228

Gherardin, N. A., Redmond, S. J., McWilliam, H., Almeida, C. F., Gourley, K., Seneviratna, R., et al. (2021). CD36 family members are TCR-independent ligands for CD1 antigen-presenting molecules. *Sci. Immunol.* 6:eabg4176. doi: 10.1126/sciimmunol.abg4176

Good, L., Benner, B., and Carson, W. E. (2021). Bruton's tyrosine kinase: an emerging targeted therapy in myeloid cells within the tumor microenvironment. *Cancer Immunol. Immunother.* 5, 1–13.

Guo, T., Li, W., and Cai, X. (2020). Applications of single-cell omics to dissect tumor microenvironment. *Front. Genet.* 11:548719. doi: 10.3389/fgene.2020.548719

Hill, B. S., Sarnella, A., D'Avino, G., and Zannetti, A. (2020). Recruitment of stromal cells into tumour microenvironment promote the metastatic spread of breast cancer. *Semin. Cancer Biol.* 60, 202–213. doi: 10.1016/j.semcancer.2019.07.028

Jiawei, Z., Min, M., Yingru, X., Xin, Z., Danting, L., Yafeng, L., et al. (2020). Identification of key genes in lung adenocarcinoma and establishment of prognostic mode. *Front. Mol. Biosci.* 7:561456. doi: 10.3389/fmolb.2020.561456

Kazakov, A. S., Mayorov, S. A., Deryusheva, E. I., Avkhacheva, N. V., Denessiouk, K. A., Denesyuk, A. I., et al. (2020). Highly specific interaction of monomeric S100P protein with interferon beta. *Int. J. Biol. Macromol.* 143, 633–639. doi: 10.1016/j.ijbiomac.2019.12.039

Kim, H. O. (2019). Development of BTK inhibitors for the treatment of B-cell malignancies. *Arch. Pharm. Res.* 42, 171–181. doi: 10.1007/s12272-019-01124-1

Koliaraki, V., Henriques, A., Prados, A., and Kollias, G. (2020). Unfolding innate mechanisms in the cancer microenvironment: the emerging role of the mesenchyme. *J. Exp. Med.* 217, e20190457. doi: 10.1084/jem.20190457

Lambrechts, D., Wauters, E., Boeckx, B., Aibar, S., Nittner, D., Burton, O., et al. (2018). Phenotype molding of stromal cells in the lung tumor microenvironment. *Nat. Med.* 24, 1277–1289. doi: 10.1038/s41591-018-0096-5

Levayer, R. (2020). Solid stress, competition for space and cancer: the opposing roles of mechanical cell competition in tumour initiation and growth. *Semin. Cancer Biol.* 63, 69–80. doi: 10.1016/j.semcancer.2019.05.004

Li, T., Fu, J., Zeng, Z., Cohen, D., Li, J., Chen, Q., et al. (2020). TIMER2.0 for analysis of tumor-infiltrating immune cells. *Nucleic Acids Res.* 48, W509–W514. doi: 10.1093/nar/gkaa407

Li, X., Wenes, M., Romero, P., Huang, S. C., Fendt, S. M., and Ho, P. C. (2019). Navigating metabolic pathways to enhance antitumour immunity and immunotherapy. *Nat. Rev. Clin. Oncol.* 16, 425–441. doi: 10.1038/s41571-019-0203-7

Lim, A. R., and Ghajar, C. M. (2021). Thorny ground, rocky soil: tissue-specific mechanisms of tumor dormancy and relapse. *Semin. Cancer Biol.* 2021, S1044-579X(21)00135-8. doi: 10.1016/j.semcancer.2021.05.007

Metzler, J. M., Burla, L., Fink, D., and Imesch, P. (2020). Ibrutinib in gynecological malignancies and breast cancer: a systematic review. *Int. J. Mol. Sci.* 21:4154. doi: 10.3390/ijms21114154

Pan, Y., Yu, Y., Wang, X., and Zhang, T. (2020). Tumor-associated macrophages in tumor immunity. *Front. Immunol.* 11:583084. doi: 10.3389/fimmu.2020.583084

Pang, Z., Chen, X., Wang, Y., Wang, Y., Yan, T., Wan, J., et al. (2020). Comprehensive analyses of the heterogeneity and prognostic significance of tumor-infiltrating immune cells in non-small-cell lung cancer: development and validation of an individualized prognostic model. *Int. Immunopharmacol.* 86:106744. doi: 10.1016/j.intimp.2020.106744

Ramalingam, S. S., Vansteenkiste, J., Planchard, D., Cho, B. C., Gray, J. E., Ohe, Y., et al. (2020). Overall survival with osimertinib in untreated, EGFR-mutated advanced NSCLC. *N. Engl. J. Med.* 382, 41–50. doi: 10.1056/NEJMoa1913662

Skoulidis, F., Goldberg, M. E., Greenawalt, D. M., Hellmann, M. D., Awad, M. M., Gainor, J. F., et al. (2018). STK11/LKB1 mutations and PD-1 inhibitor resistance in KRAS-mutant lung adenocarcinoma. *Cancer Discov.* 8, 822–835.

Tan, B. S., Yang, M. C., Singh, S., Chou, Y. C., Chen, H. Y., Wang, M. Y., et al. (2019). LncRNA NORAD is repressed by the YAP pathway and suppresses lung and breast cancer metastasis by sequestering S100P. *Oncogene* 38, 5612–5626. doi: 10.1038/s41388-019-0812-8

Tuo, Z., Zheng, X., Zong, Y., Li, J., Zou, C., Lv, Y., et al. (2020). HK3 is correlated with immune infiltrates and predicts response to immunotherapy in non-small cell lung cancer. *Clin. Transl. Med.* 10, 319–330. doi: 10.1002/ctm2.6

Yuan, X., Qin, X., Wang, D., Zhang, Z., Tang, X., Gao, X., et al. (2019). Mesenchymal stem cell therapy induces FLT3L and CD1c+ dendritic cells in systemic lupus erythematosus patients. *Nat. Commun.* 10:2498. doi: 10.1038/s41467-019-10491-8

Zhang, B., Wang, L., Zhang, Q., Yan, Y., Jiang, H., Hu, R., et al. (2019). The Ibr-7 derivative of ibrutinib exhibits enhanced cytotoxicity against non-small cell lung cancer cells via targeting of mTORC1/S6 signaling. *Mol. Oncol.* 13, 946–958. doi: 10.1002/1878-0261.12454

Zhang, D., Han, M., Zhou, M., Liu, M., Li, Y., Xu, B., et al. (2021). Down-regulation of S100P induces apoptosis in endometrial epithelial cell during GnRH antagonist protocol. *Reprod. Biol. Endocrinol.* 19:99. doi: 10.1186/s12958-021-00787-0

Zhang, J., Li, H., Wu, Q., Chen, Y., Deng, Y., Yang, Z., et al. (2019). Tumoral NOX4 recruits M2 tumor-associated macrophages via ROS/PI3K signaling-dependent various cytokine production to promote NSCLC growth. *Redox Biol.* 22:101116. doi: 10.1016/j.redox.2019.101116

Zhang, X., Shi, M., Chen, T., and Zhang, B. (2020). Characterization of the immune cell infiltration landscape in head and neck squamous cell carcinoma to aid immunotherapy. *Mol. Ther. Nucleic Acids* 22, 298–309. doi: 10.1016/j.omtn.2020.08.030

Zheng, B. H., Ma, J. Q., Tian, L. Y., Dong, L. Q., Song, G. H., Pan, J. M., et al. (2020). The distribution of immune cells within combined hepatocellular carcinoma and cholangiocarcinoma predicts clinical outcome. *Clin. Transl. Med.* 10, 45–56. doi: 10.1002/ctm2.11

Conflict of Interest: The authors declare that the research was conducted in the absence of any commercial or financial relationships that could be construed as a potential conflict of interest.

Publisher's Note: All claims expressed in this article are solely those of the authors and do not necessarily represent those of their affiliated organizations, or those of the publisher, the editors and the reviewers. Any product that may be evaluated in this article, or claim that may be made by its manufacturer, is not guaranteed or endorsed by the publisher.

frontiers in Molecular Biosciences

ORIGINAL RESEARCH
published: 19 November 2021
doi: 10.3389/fmolb.2021.666623

Prognostic Potential of Secreted Modular Calcium-Binding Protein 1 in Low-Grade Glioma

*Jing Wang, Shu Xia, Jing Zhao, Chen Gong, Qingsong Xi and Wei Sun**

Department of Oncology, Tongji Hospital, Tongji Medical College, Huazhong University of Science and Technology, Wuhan, China

Background: Secreted modular calcium-binding protein 1 (SMOC1) belongs to a family of matricellular proteins; it was involved in embryo development, endothelial cell proliferation, angiogenesis, integrin–matrix interactions, cell adhesion, and regulation of glucose metabolism. Previous studies showed that the expression of SMOC1 was increased in some tumors. However, the prognostic value and the biological function of SMOC1 in tumor remain unclear.

Methods: In this study, we explored the expression profile and prognostic value of SMOC1 in pan-cancers, especially glioma, *via* multiple databases, including Oncomine, Gene Expression Profiling Interactive 2, PrognoScan, Kaplan–Meier plotter, and the Chinese Glioma Genome Atlas database. Furthermore, LinkedOmics was used to identify the genes coexpressed with SMOC1 and to perform Kyoto Encyclopedia of Genes and Genomes pathways and Gene Ontology analysis in low-grade glioma (LGG). Also, the Cancer Single-Cell State Atlas database was used to evaluate the correlation between SMOC1 expression and functional state activities in glioma cells. In addition, the Tumor Immune Estimation Resource and TISIDB databases were used to evaluate the correlations between SMOC1 expression and tumor-infiltrating immune cells in the tumor microenvironment.

Results: Compared with normal brain tissues, the expression of SMOC1 was increased in LGG tissues. The higher expression of SMOC1 was significantly correlated with better survival of LGG patients. Additionally, functional analyses showed that the SMOC1 coexpressed genes were inhibited in processes such as response to type I interferon and interferon-gamma, lymphocyte-mediated immunity, leukocyte migration, adaptive immune response, neutrophil-mediated immunity, T cell activation, and pathways including EMC–receptor interaction, Th17 cell differentiation, and leukocyte *trans*-endothelial migration in LGG. Moreover, the expression of SMOC1 was correlated with stemness, hypoxia, EMT, and metastasis of glioma cells. Additionally, the expression of SMOC1 expression was negatively correlated with levels of infiltrating B cells, $CD8^+$ T cells, $CD4^+$ T cells, macrophages, neutrophils and dendritic cells, and gene markers of most immune cells in LGG.

Conclusion: Our results suggest that SMOC1 could be a potential biomarker to determine prognosis and might play a specific role in the tumor microenvironment of

OPEN ACCESS

Edited by:
Shengtao Zhou,
Sichuan University, China

Reviewed by:
Ajay Dixit,
University of Minnesota Twin Cities, United States
Bingjie Li,
First Affiliated Hospital of Zhengzhou University, China

****Correspondence:***
Wei Sun
sunweitjh@163.com

Specialty section:
This article was submitted to Molecular Diagnostics and Therapeutics, a section of the journal Frontiers in Molecular Biosciences

Received: *10 February 2021*
Accepted: *20 October 2021*
Published: *19 November 2021*

Citation:
Wang J, Xia S, Zhao J, Gong C, Xi Q and Sun W (2021) Prognostic Potential of Secreted Modular Calcium-Binding Protein 1 in Low-Grade Glioma. Front. Mol. Biosci. 8:666623. doi: 10.3389/fmolb.2021.666623

glioma, thereby influencing the development and progression of glioma. These findings provide some new insights for further investigation.

Keywords: SMOC1, low-grade glioma, prognostic value, biological function, tumor microenvironment

INTRODUCTION

For the past century, the classification of tumors has been based largely on the concept that tumors can be classified according to their histological features under a light microscope. Over the past 10 years, studies have clarified the genetic basis of tumorigenesis in various tumors, and such understanding raises the possibility that it may contribute to the further classification of tumors (Louis, 2012). Also, a better understanding and identification of predictive and prognostic biomarkers are needed for individualized treatment and improved survival.

Secreted modular calcium-binding protein 1 (SMOC1) was first isolated in 2002, which encodes a secreted modular glycoprotein (Vannahme et al., 2002). SMOC1 contains a follistatin-like domain, an EF-hand calcium-biding domain, two thyroglobulin-like domains, and a unique domain and is usually localized in the basement membrane of different tissues and also can present in other extracellular matrices (Vannahme et al., 2002). It belongs to a family of matricellular proteins that also include basement membrane-40 (also known as secreted protein acidic and rich in cysteine), as well as SMOC2 (Bornstein and Sage, 2002). SMOC2 was involved in multiple biological processes, including cell cycle progression (Liu et al., 2008), cell attachment (Maier et al., 2008), and tumor development (Su et al., 2016; Huang et al., 2017). Also, in previous studies, the expression of SMOC2 was decreased in gallbladder cancer (Gu et al., 2015) and advanced breast cancer (Fidalgo et al., 2015) but increased in metastatic head and neck squamous cell carcinoma (Hyakusoku et al., 2016). In endometrial carcinoma, SMOC2 was able to inhibit cell proliferation and overcome chemoresistance (Lu et al., 2019). SMOC1 has similar domains to SMOC2, except for its own unique domain (Vannahme et al., 2003). We assume that similar to SMOC2, SMOC1 might also be involved in tumor development. The expression of SMOC1 was increased in some brain tumors, such as oligodendroglioma (Brellier et al., 2011) and astrocytic tumors (Boon et al., 2004). Moreover, SMOC1 was identified as a new cancer-related protein by interacting with tenascin-c, which was an ECM protein and was highly expressed in many human cancers (Brellier et al., 2011). In U87 glioma cells, SMOC1 inhibits the tenascin-c-induced chemo-attractive effect (Brellier et al., 2011). Previous studies indicated that SMOC1 was involved in embryogenesis (Gersdorff et al., 2006), endothelial cell proliferation, angiogenesis (Awwad et al., 2015), integrin–matrix interactions, cell adhesion (Klemencic et al., 2013), and glucose metabolism (Montgomery et al., 2020). However, the role of SMOC1 in tumor genesis and progression is still unclear.

In this study, we aimed to systematically explore the gene expression and evaluate the prognostic values of SMOC1 in different cancers and uncover the potential functions of SMOC1 in specific cancers. The findings explored the prognostic value of SMOC1 in low-grade glioma (LGG) and provided new ideas for exploring the potential mechanism of SMOC1 in glioma development and progression.

METHODS

Oncomine Database Analysis

The expression levels of SMOC1 messenger RNA (mRNA) in different types of tumors were analyzed in the Oncomine database (https://www.oncomine.org) (Rhodes et al., 2007). The threshold was determined according to the following values: gene ranking of top 10%, a p-value of 0.05, and fold change of 2.

Tumor Immune Estimation Resource Analysis

The Tumor Immune Estimation Resource (TIMER, https://cistrome.shinyapps.io/timer/) (Li et al., 2017) was used to explore the expression of SMOC1 in various types of cancers and to evaluate the correlation between SMOC1 expression and the infiltrating level of immune cells, including B cell, $CD8^+$ T cell, $CD4^+$ T cell, macrophage, neutrophil, and dendritic cell. In addition, the correlation between SMOC1 expression and tumor-infiltrating immune cell gene markers was also explored through the correlation modules in the TIMER database. The gene markers were selected according to a previous report (Danaher et al., 2017), the CellMarker database (http://biocc.hrbmu.edu.cn/CellMarker/index.jsp) (Zhang X. et al., 2019), and the website of R&D Systems (https://www.rndsystems.com/cn/resources/cell-markers/immune-cells), which include markers of B cells, $CD8^+$ T cells, T cells, follicular helper T cells (Tfh), T helper cells (Th1, Th2, and Th17), regulatory T cells (Treg), exhausted T cells, monocytes, TAMs, M1 macrophages, M2 macrophages, neutrophils, DCs, natural killer cells (NKs), and Mast cells. $p < 0.05$ was considered as statistically significant.

PrognoScan Database Analysis

The PrognoScan database (http://dna00.bio.kyutech.ac.jp/PrognoScan/index.html) (Mizuno et al., 2009) was used to investigate the association between SMOC1 expression and survival in different types of tumors. To evaluate the prognostic value of SMOC1, the Cox p-value and hazard ratio (HR) with 95% confidence intervals (95% CIs) were calculated and displayed.

Gene Expression Profiling Interactive Two Analysis

The Gene Expression Profiling Interactive 2 (GEPIA2, http://gepia2.cancer-pku.cn/#index) (Tang et al., 2017) was used to analyze the correlations between SMOC1 expression and patient prognosis in various types of tumors, as well as the expression of SMOC1 in LGG and glioblastoma (GBM). Furthermore, the correlations between gene SMOC1 and selected gene markers of tumor-infiltrating immune cells were also established *via* the GEPIA2 database. $p < 0.05$ was considered as statistically significant.

Kaplan–Meier Plotter Analysis

The Kaplan–Meier Plotter (http://kmplot.com/analysis/index.php?p=service&cancer=lung) (Nagy et al., 2018) was used to evaluate the correlations between SMOC1 expression and survival of lung adenocarcinoma (LUAD) patients in lung cancer dataset. The HR with 95% CIs, log-rank *p*-value, and survival curve were calculated and displayed.

Chinese Glioma Genome Atlas Database Analysis

The Chinese Glioma Genome Atlas (CGGA, http://www.cgga.org.cn/) (Yan et al., 2012) was used to analyze the expression of SMOC1 in different grades and subtypes of glioma and to perform survival analysis in specific glioma subtype. The HR with 95% CIs and log-rank *p*-value were calculated.

Cancer Single-Cell State Atlas

The Cancer Single-Cell State Atlas (CancerSEA, http://biocc.hrbmu.edu.cn/CancerSEA/) (Yuan et al., 2019) database was used to evaluate the correlation between SMOC1 expression and functional state of various tumor cells. Significant correlations between gene expression and functional state activities were identified using Spearman's rank correlation test (correlation > 0.3) and Benjamini and Hochberg's false discovery rate (<0.05).

TISIDB

TISIDB (http://cis.hku.hk/TISIDB/) (Ru et al., 2019) was used to verify the association of SMOC1 expression and the abundance of tumor-infiltrating lymphocytes. Spearman's test was performed to measure the correlations between SMOC1 expression and tumor-infiltrating lymphocytes. $p < 0.05$ was considered as statistically significant.

LinkedOmics Database

The LinkedOmics database (http://www.linkedomics.org/login.php) (Vasaikar et al., 2018) was applied to identify SMOC1 coexpressed genes in The Cancer Genome Atlas (TCGA)–LGG cohort. Pearson's correlation coefficients were used to analyze the results and presented in volcano plots and heat maps. Gene set enrichment analysis (GSEA) tool was used to perform Kyoto Encyclopedia of Genes and Genomes (KEGG) pathways and Gene Ontology analysis, enrichment with 500 simulations and a minimum number of three genes.

RESULTS

Expression Levels of Secreted Modular Calcium-Binding Protein 1 in Different Type of Tumors

To preliminarily evaluate the role of SMOC1 in tumor genesis, the expression levels of SMOC1 mRNA in different types of tumors and normal tissue samples were analyzed in the Oncomine database. The expression levels of SMOC1 were higher in the kidney, brain, and central nervous system (CNS) cancers compared with the corresponding normal tissues (**Figure 1A**). Meanwhile, lower expression of SMOC1 was observed in melanoma, breast, colorectal, gastric, prostate, and other cancers. The details of SMOC1 expression in different types of tumors are listed in **Supplementary Table S1**. To further explore the expression of SMOC1 in pan-cancers, we analyzed the RNA-seq data from TCGA using the TIMER database. The differential expression patterns of SMOC1 in tumors and adjacent normal tissues are shown in **Figure 1B**. Obviously, SMOC1 expression was significantly downregulated in bladder urothelial carcinoma, breast invasive carcinoma (BRCA), cholangiocarcinoma, kidney renal clear cell carcinoma, kidney renal papillary cell carcinoma, liver hepatocellular carcinoma, prostate adenocarcinoma, thyroid carcinoma, and uterine corpus endometrial carcinoma, whereas the expression of SMOC1 was increased in kidney chromophobe and LUAD. Due to the lack of adjacent normal tissue, the changes of SMOC1 expression in cancers such as LGG and GBM were unable to show.

Prognostic Value of Secreted Modular Calcium-Binding Protein 1 Expression in Different Type of Cancers

To evaluate the prognostic value of SMOC1 in different types of cancers, we analyzed the correlations between SMOC1 expression and survival of human cancers in different databases. First, we examined the effect of SMOC1 expression on cancer survival in PrognoScan and listed the full results in **Supplementary Table S2**. The expression of SMOC1 was significantly correlated with the survival of six cancer types, including brain glioma, colorectal cancer, eye uveal melanoma, breast cancer, LUAD, and ovarian cancer (**Table 1**). Compared with low SMOC1 expression, high expression level of SMOC1 was correlated with better prognosis in brain glioma [overall survival (OS), HR = 0.55, 95% CIs, 0.4–0.75, Cox *p*-value = 0.0001], breast cancer, and ovarian cancer. However, high expression of SMOC1 was associated with poor prognosis in colorectal cancer and LUAD.

Then, we further evaluated the relationships between SMOC1 expression and prognosis in 33 cancer types from the TCGA project in GEPIA2. The impact of SMOC1 expression on the survival of these 33 cancer types is presented in **Figure 2A** (OS) and **2B** (disease-free survival). Notably, survival of LGG and LUAD were also significantly correlated with SMOC1 expression. Higher expression of SMOC1 was correlated with better survival of LGG (OS, HR = 0.43, *p*-value = 3.3e-06; disease-free survival, HR = 0.58, *p*-value = 0.0005) (**Figure 2C**) but worse survival of LUAD (OS, HR = 1.4, *p*-value = 0.043) (**Figure 2D**). No correlation was observed between SMOC1 expression and the survival probability of GBM (**Supplementary Figure S1A**).

We then used Kaplan–Meier plotter database to further examine the prognostic value of SMOC1 in LUAD. High expression of SMOC1 was correlated with poor prognosis of LUAD (progression-free survival, HR = 1.5, *p*-value = 0.014) but was not related to OS in LUAD (**Supplementary Figure S1B**). The CGGA database was used as an independent database to confirm the prognostic value of SMOC1 in glioma. Consist with GEPIA2 analysis, a significant positive correlation was found

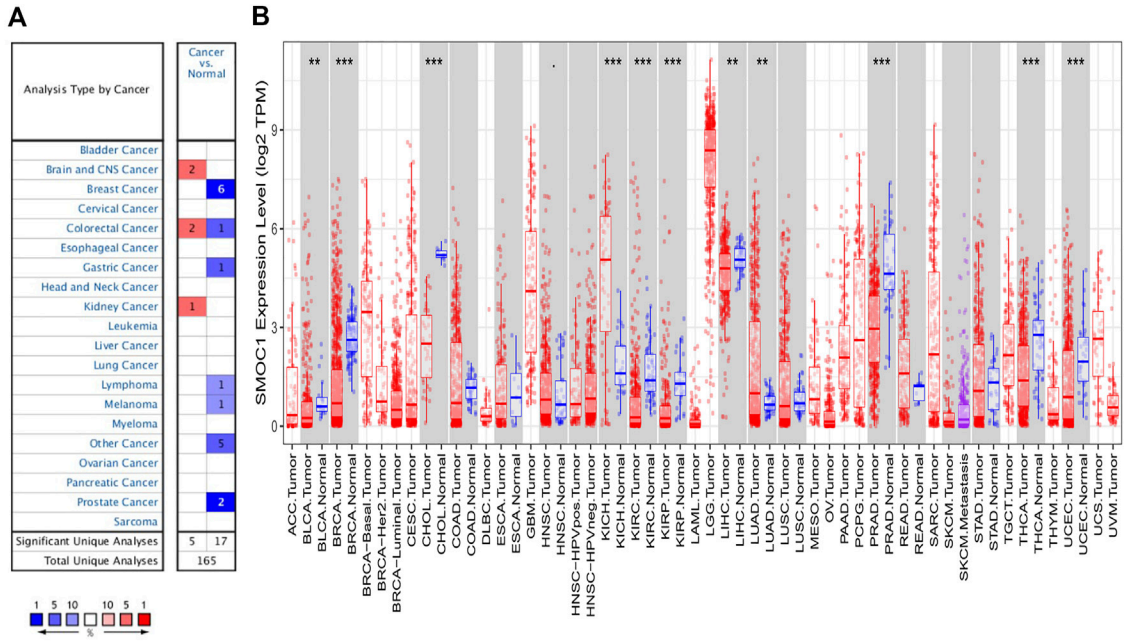

FIGURE 1 | The expression levels of SMOC1 in different type of tumors. **(A)** The expression levels of SMOC1 in different type of tumors and normal tissues in Oncomine database. **(B)** The expression levels of SMOC1 in different type of tumors and adjacent normal tissues in TIMER database. (*p*-value < 0.1; *: *p*-value < 0.05; **: *p*-value < 0.01; ***: *p*-value < 0.001).

TABLE 1 | Prognostic value of SMOC1 in different types of tumors in PrognoScan database.

Dataset	Cancer type	Subtype	Endpoint	Cohort	N	Cox *p*-VALUE	ln (HR)	HR [95% CI-low CI-upp]
GSE4412-GPL97	Brain cancer	Glioma	Overall Survival	UCLA (1996–2003)	74	0.000141867	-0.592464	0.55 [0.41–0.75]
GSE4412-GPL97	Brain cancer	Glioma	Overall Survival	UCLA (1996–2003)	74	0.00106869	-0.281186	0.75 [0.64–0.89]
GSE14333	Colorectal cancer		Disease Free Survival	Melbourne	226	0.00834547	0.263706	1.30 [1.07–1.58]
GSE17537	Colorectal cancer		Overall Survival	VMC	55	0.0143359	1.39887	4.05 [1.32–12.41]
GSE14333	Colorectal cancer		Disease Free Survival	Melbourne	226	0.0147715	0.24837	1.28 [1.05–1.57]
GSE22138	Eye cancer	Uveal melanoma	Distant Metastasis Free Survival	BRCIC	63	0.0151028	-32.3066	0.00 [0.00–0.00]
GSE17536	Colorectal cancer		Disease Free Survival	MCC	145	0.0178348	0.631362	1.88 [1.12–3.17]
GSE9893	Breast cancer		Overall Survival	Montpellier, Bordeaux, Turin (1989–2001)	155	0.0308433	-0.56531	0.57 [0.34–0.95]
GSE17536	Colorectal cancer		Disease Free Survival	MCC	145	0.0374849	0.987085	2.68 [1.06–6.80]
GSE31210	Lung cancer	Adenocarcinoma	Overall Survival	NCCRI	204	0.0377567	0.36064	1.43 [1.02–2.02]
GSE1378	Breast cancer		Relapse Free Survival	MGH (1987–2000)	60	0.038728	0.282083	1.33 [1.01–1.73]
GSE17260	Ovarian cancer		Progression Free Survival	Niigata (1997–2008)	110	0.0400779	-0.513388	0.60 [0.37–0.98]
GSE9195	Breast cancer		Relapse Free Survival	GUYT2	77	0.0423734	1.23944	3.45 [1.04–11.43]

Note: This table only shows those of significant difference (Cox p *< 0.05).*

between SMOC1 expression and better prognosis of all World Health Organization (WHO) grade I ($p < 0.0001$), WHO grade II ($p = 0.024$), and WHO grade III ($p = 0.003$) glioma, but no correlation was observed between the expression of SMOC1 and WHO grade IV glioma ($p = 0.094$) (**Figure 2E**).

Expressions of Secreted Modular Calcium-Binding Protein 1 in Glioma and Lung Adenocarcinoma

The expressions of SMOC1 in glioma (LGG and GBM) and LUAD were further analyzed in the GEPIA2 database. The

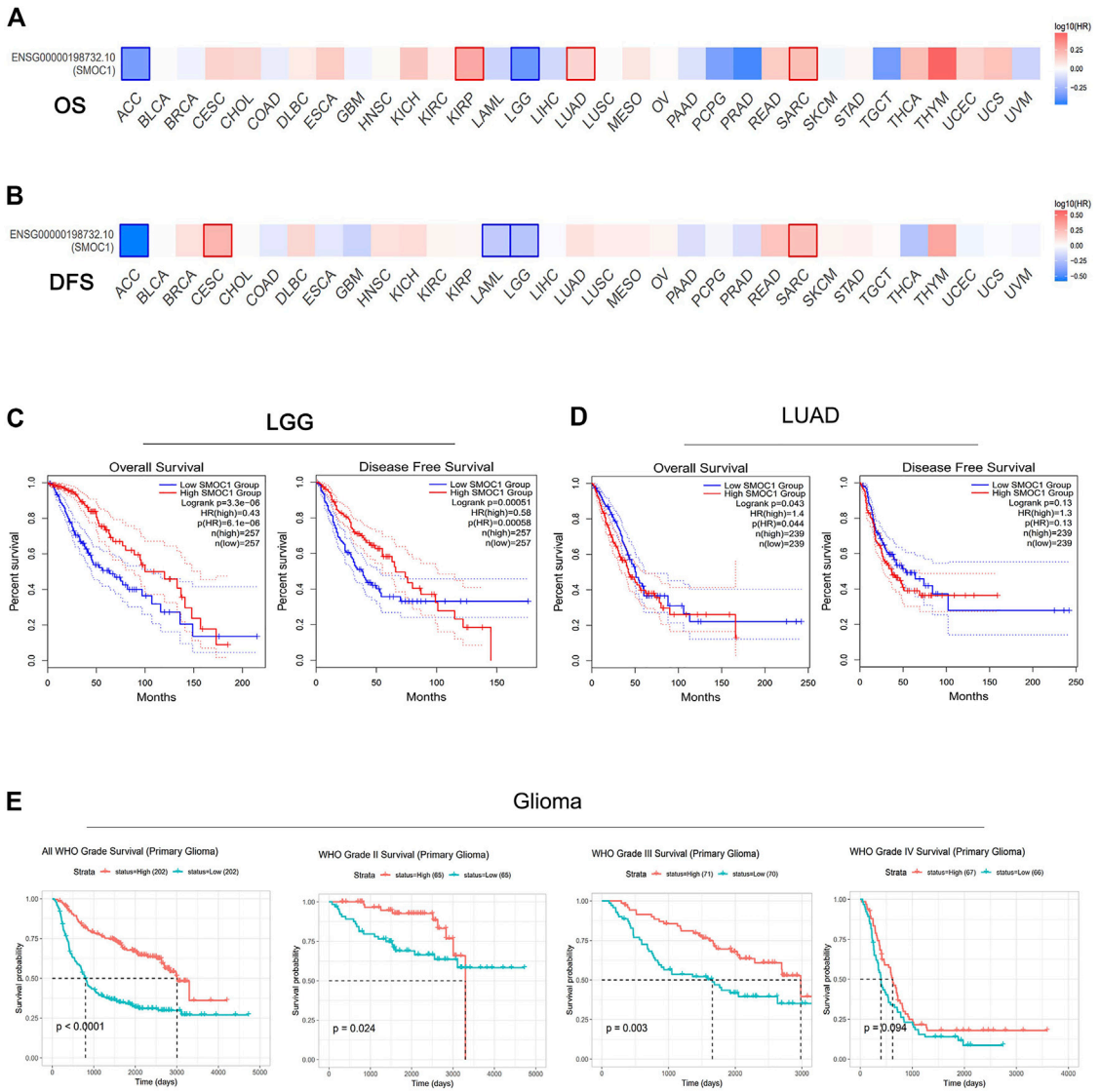

FIGURE 2 | Prognostic value of SMOC1 expression in different type of tumors. **(A,B)** Survival heat map of SMOC1 in 33 TCGA cancer types in GEPIA2. The HRs of SMOC1 were shown in logarithmic scale (log10) in the heat map. The red and blue blocks represent higher and lower risks, respectively. The significant results in prognostic analysis were marked with framed rectangles. OS and DFS survival curves of **(C)** LGG and **(D)** LUAD in GEPIA2. **(E)** Survival probability of primary gliomas (all WHO Grade, WHO Grade II, Grade III and Grade IV) in CGGA database. (HR, hazard ratios; OS, overall survival; DFS, disease free survival).

expression of SMOC1 was significantly increased in tumor samples of LGG (**Figure 3A**). When compared with normal tissues, GBM and LUAD samples showed no marked changes in SMOC1 expression levels (**Figures 3B, C**). Furthermore, we analyzed the expression of SMOC1 in the CGGA database. Compared with WHO grade IV glioma, SOMC1 expression was remarkably increased in WHO grade II and grade III glioma (p = 1.8e-36) (**Figure 3D**). We further studied the relationship between SMOC1 expression and LGG subtypes. Through the CGGA dataset, we explored the relationship between SMOC1 expression and glioma subtypes, including IDH mutant status, 1p19q codeletion status, recurrent status, and patient's age status. We found that the expression of SMOC1 was significantly increased in IDH mutant gliomas (p = 3.1e-69) (**Figure 3E**), 1p19q co-deletion gliomas (p = 5.6e-38) (**Figure 3F**), primary gliomas (p = 0.00074) (**Figure 3G**), and the age< 42 group (p = 5.1e-07) (**Figure 3H**).

Genes Correlated With Secreted Modular Calcium-Binding Protein 1 in Low-Grade Glioma

To explore the potential biological role of SMOC1 in LGG, we used the LinkedOmics database to identify the differentially

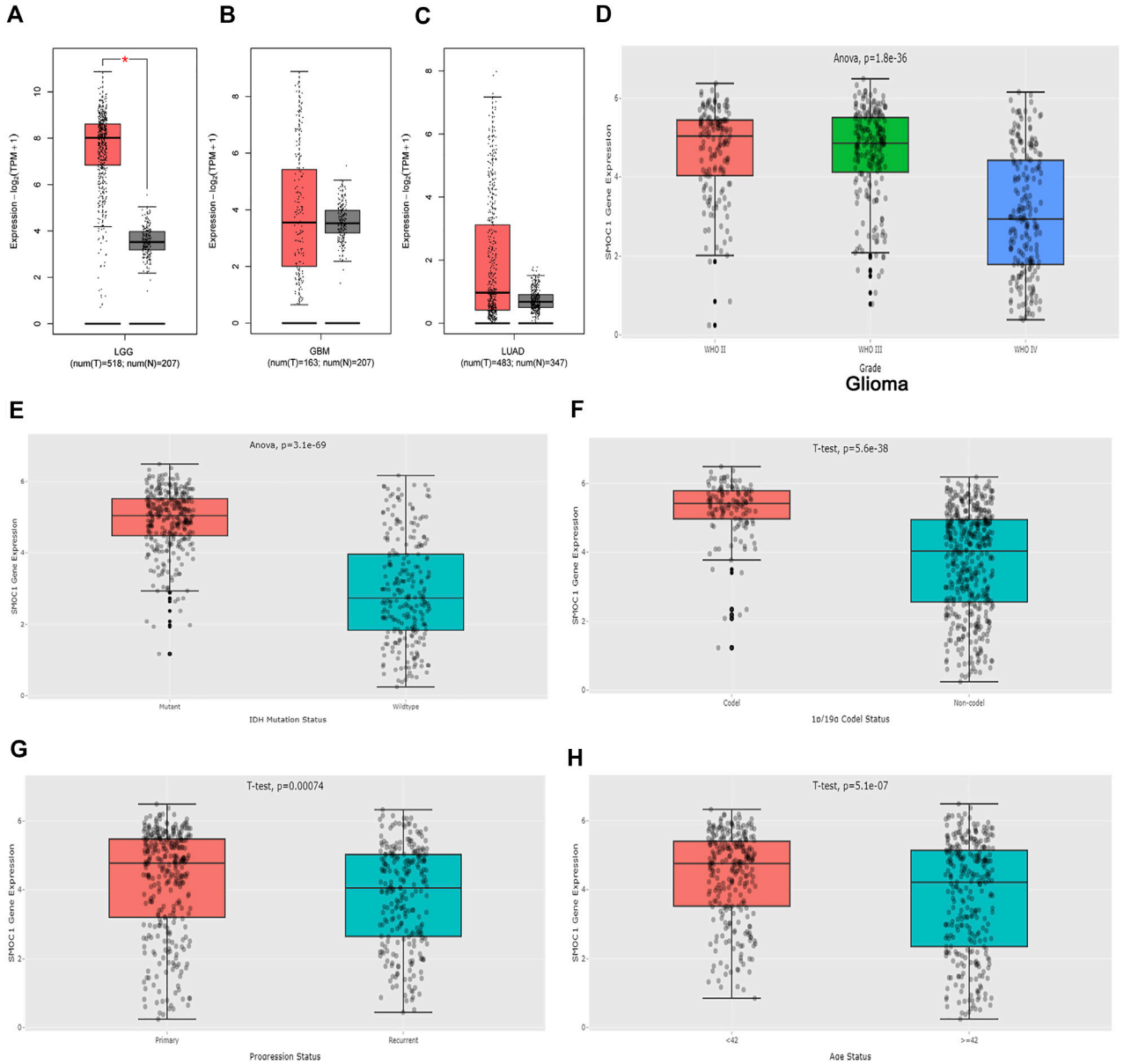

FIGURE 3 | Expression of SMOC1 in Glioma and LUAD. The expression of SMOC1 in LGG **(A)**, GBM **(B)** and LUAD **(C)** analyzed by GEPIA2. Red box: tumor samples from TCGA, grey box: paired normal tissues from TCGA and GTEx. The expression of SMOC1 in different grade **(D)** and subtype **(E–H)** of Glioma analyzed by CGGA.

expressed genes that were correlated with SMOC1. The identified genes that positively (red dots) and negatively (green dots) correlated with SMOC1 are shown in **Figure 4A**. Also, the heat maps present the top 50 positively (**Figure 4B**) and negatively (**Figure 4C**) correlated genes. GSEA tool was used to perform analyses of KEGG pathways and Gene Ontology functional enrichment of the differentially expressed genes. The results showed that the SMOC1 coexpressed genes were enriched for transnational initiation, ribonucleoprotein complex biogenesis, and protein localization, whereas the genes involved in processes such as response to type I interferon and interferon-gamma, lymphocyte-mediated immunity, leukocyte migration, adaptive immune response, neutrophil-mediated immunity, and T cell activation were inhibited in LGG (**Figure 4D**). The KEGG pathway analyses showed that the SMOC1 coexpressed genes were mainly enriched in pathways such as ribosome and spliceosome. The pathways such as EMC–receptor interaction, allograft rejection, graft-*versus*-host disease, Th17 cell differentiation, and leukocyte *trans*-endothelial migration were inhibited in LGG (**Figure 4E**).

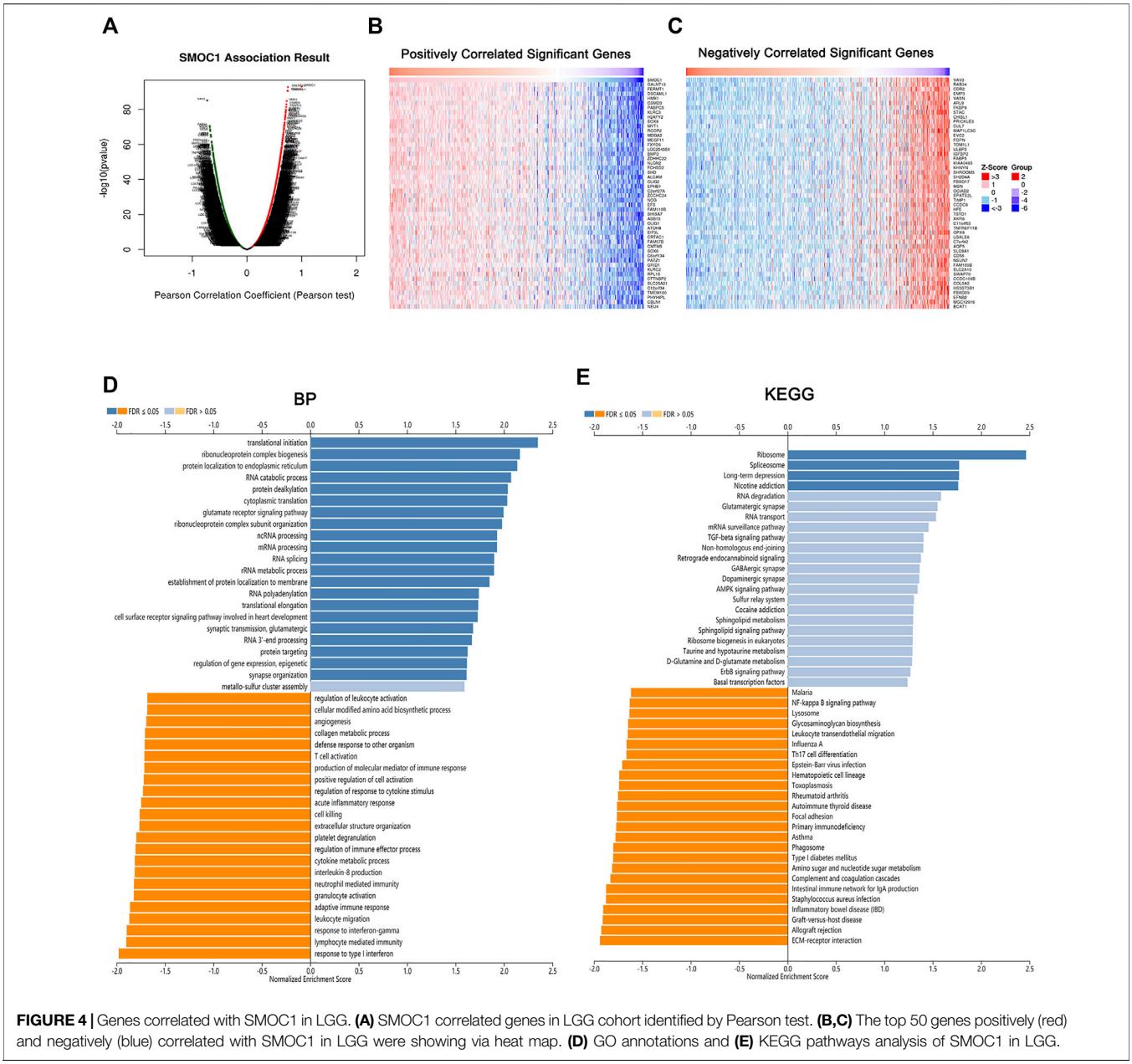

FIGURE 4 | Genes correlated with SMOC1 in LGG. **(A)** SMOC1 correlated genes in LGG cohort identified by Pearson test. **(B,C)** The top 50 genes positively (red) and negatively (blue) correlated with SMOC1 in LGG were showing via heat map. **(D)** GO annotations and **(E)** KEGG pathways analysis of SMOC1 in LGG.

Correlations Between Secreted Modular Calcium-Binding Protein 1 Expression and Functional State Activities in Glioma Cells

To get a better understanding of the underlying mechanisms of SMOC1 in glioma, we analyzed the correlations between SMOC1 expression and functional state activities across various types of tumors in the CancerSEA database. The expression of SMOC1 has been analyzed at the single-cell level of different types of tumors (**Figure 5A**), including CNS/brain tumors (GBM, glioma, aspartate aminotransferase, high-grade glioma, and oligodendroglioma), lung cancer (LUAD and nonsmall cell lung cancer), skin melanoma, renal cell carcinoma, chronic myelogenous leukemia, and BRCA. The expression of SMOC1 was associated with various functional states in different types of glioma cells (**Figure 5A**). In high-grade glioma, SMOC1 was significantly positively correlated with stemness (correlation = 0.42, $p < 0.001$) and negatively associated with hypoxia (correlation = -0.39, $p < 0.001$), EMT (correlation = -0.38, $p < 0.001$), and metastasis (correlation = -0.32, $p < 0.001$) (**Figure 5B**).

Correlations Between Secreted Modular Calcium-Binding Protein 1 Expression and Immune Infiltration in Glioma

The TIMER database was used to investigate the relationship between immune infiltration and SMOC1 expression in glioma.

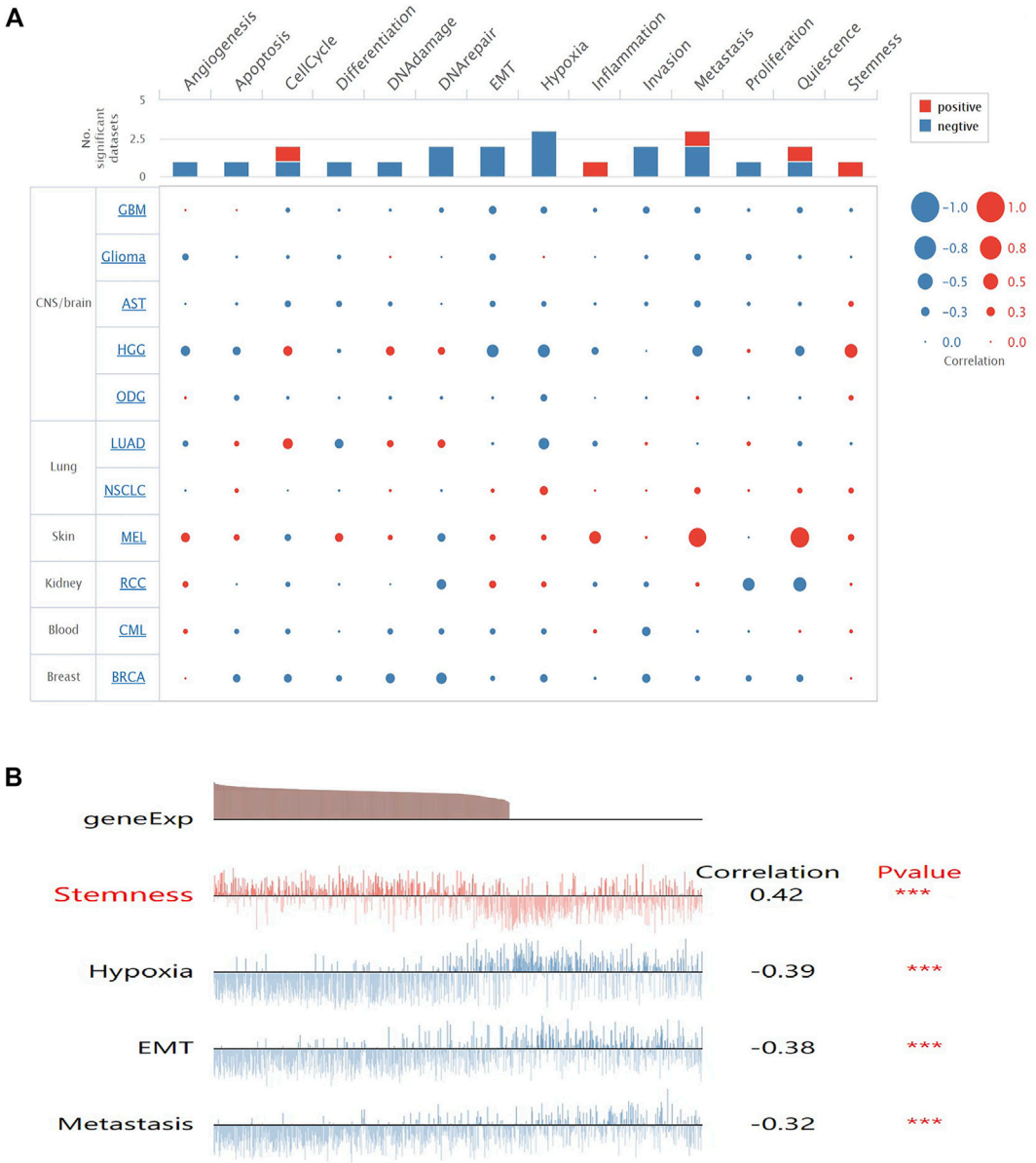

FIGURE 5 | Correlations between SMOC1 expression and functional state activities in glioma cells. **(A)** The relevance of SMOC1 expression and functional state activities in different type of tumors. The size of plots indicates the strength of correlation, red indicates positive correlation, and blue indicates negative correlation, **(B)** Details of correlations between SMOC1 expression and functional state activities in HGG. ***p<0.001.

We found that SMOC1 was positively correlated with tumor purity (cor = 0.347, p = 5.82e-15) in LGG but not in GBM. The expression of SMOC1 was significantly negatively correlated with levels of infiltrating B cells (cor = −0.263, p = 5.13e-09), $CD8^+$ T cells (cor = −0.355, p = 1.31e-15), $CD4^+$ T cells (cor = −0.108, p = 1.81e-02), macrophages (cor = −0.212, p = 3.47e-06), neutrophils (cor = -336, p = 5.69e-14), and dendritic cells (cor = −0.296, p = 4.26e-11) in LGG tumor microenvironment (**Figure 6A**). However, there was no correlation between SMOC1 expression and levels of infiltrating immune cells in GBM, except for $CD4^+$ T cells (cor = 0.221, p = 1.11e-02) (**Figure 6B**). Similar results were also observed in the TISIDB analysis (**Supplementary Figure S2**).

Correlations Between Secreted Modular Calcium-Binding Protein 1 and Gene Markers of Infiltrating Immune Cells in Glioma

To evaluate the more specific link between SMOC1 and tumor immune infiltration, we analyzed the correlations between SMOC1 and markers of various immune cells in LGG using

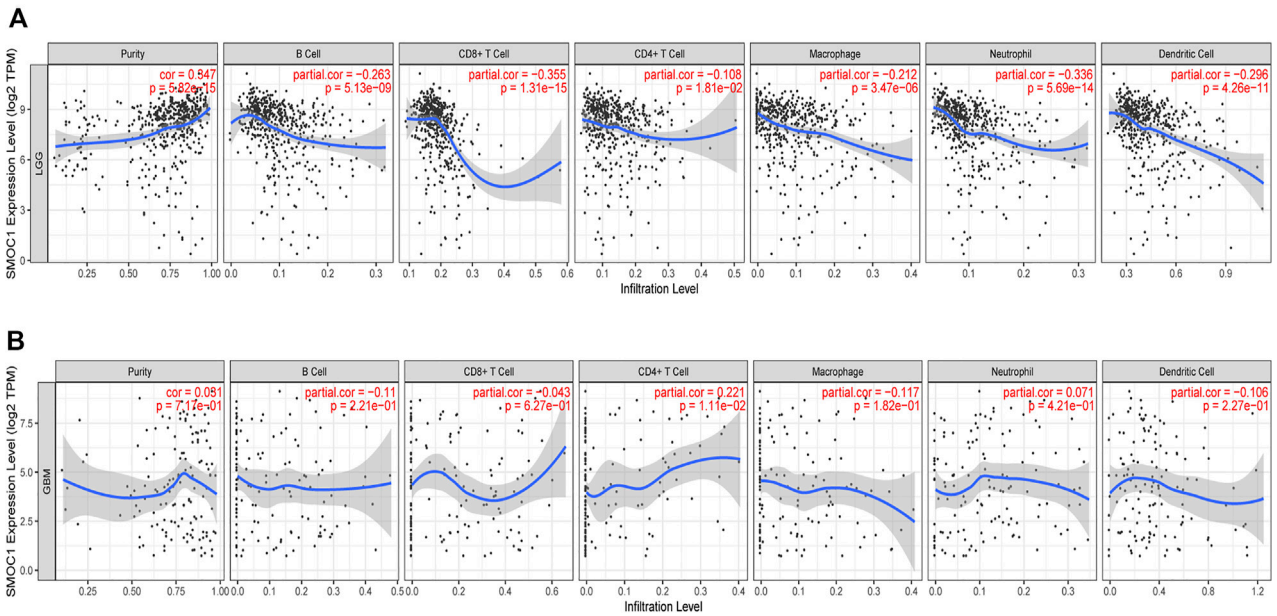

FIGURE 6 | Correlations between SMOC1 expression and immune infiltration in Glioma. The correlation between SMOC1 expression and the immune infiltrations of tumor purity, B cell, CD8+ T cell, CD4+ T cell, Macrophage, Neutrophil, and Dendritic cell in LGG **(A)** and GBM **(B)**.

the TIMER (**Table 2**) and GEPIA2 databases (**Supplementary Table S3**). Also, the correlations in GBM were analyzed as a control. According to previous research, we selected gene markers of different immune cell populations, including B cells, $CD8^+$ T cells, T cells (general), monocytes, TAMs, M1 and M2 macrophages, neutrophils, DCs, NKs, mast cells, and different functional T cells, such as Tfh, Treg, exhausted T cells, Th1, Th2, and Th17. After adjusting for tumor purity, the expression of SMOC1 was significantly negatively correlated with gene markers of most immune cells in LGG, especially gene markers of $CD8^+$ T cells, T cells (general), Th2 cells, dendritic cells, TAMs, and M1 macrophages (**Table 2**). However, there were only six gene markers significantly correlated with SMOC1 expression in GBM. The results from the GEPIA2 database (**Supplementary Table S3**) were similar to those of the TIMER analysis.

DISCUSSION

Gliomas are the most common malignant tumor of the CNS, with a character of aggressive growth, poor outcome of the patient, and high rates of recurrence (Wen and Kesari, 2008). According to the CBTRUS report, glioma represents approximately 25.1% of all primary and 80.8% of malignant tumors in the brain and other CNS tumors diagnosed in the United States in 2013–2017 (Ostrom et al., 2020). Also, the WHO classifies glioma into four grades: WHO grades I, II, III, and IV (Louis et al., 2016). LGG usually refers to gliomas other than WHO grade IV glioma (GBM) and accounts for approximately 10% of all primary brain tumors (Ostrom et al., 2020). The prognosis of gliomas varies widely by WHO classification. Compared with GBM patients, LGG patients usually have an indolent course and longer survival (Forst et al., 2014). However, despite initially growing slow, LGG can transform to GBM with time (Morshed et al., 2019). According to the previous study (Afra et al., 1999), nearly half of the patients with LGG will experience malignant transformation, usually within 5 years. However, the risk factors for the development of LGG are poorly understood at present, and the current understanding of the mechanism underlying the growth and invasion of glioma is limited. The application of IDH mutate-status in 2016 WHO Classification of CNS tumors showed a great significance of molecular diagnosis in glioma (Louis et al., 2016). However, more molecular biomarkers are still needed to be discovered.

SMOC1 was first reported in 2002; we know not much about the biological function of SMOC1. However, its potential importance cannot be ignored because it has been linked with embryogenesis (Gersdorff et al., 2006), osteoblast differentiation (Choi et al., 2010), and some forms of cancer. One *in silico* study analyzed the expression and prognostic data of long noncoding RNAs, microRNAs, and mRNAs in the colon cancer dataset from the TCGA database and identified five mRNAs, including SMOC1, as potential prognostic biomarkers for colon cancer (Huang and Pan, 2019). Besides, another study suggests that the aberrant expression of SMOC1 can inhibit the proliferation and colony formation in colorectal cancer cells, as well as tumor formation *in vivo* (Aoki et al., 2018). This suggests that SMOC1 may act as a tumor suppressor. A recent study has analyzed the methylation data of the glioma project from the TCGA database and identified 10 glioma grade-associated cytosine-phosphate guanine sites, which targeted four genes, including SMOC1 (Weng and Salazar, 2021). Another *in silico* study identified a

TABLE 2 | Correlations between SMOC1 and gene markers of immune cells in LGG and GBM by TIMER.

Immune cell	Gene markers	LGG				GBM			
		None		Purity		None		Purity	
		Cor	*p* -value	Cor	*p* -value	Cor	*p* -value	Cor	*p* -value
B cell	*CD19*	−0.312	***	−0.273	***	0.011	0.892	−0.001	0.988
	CD79A	−0.023	0.596	−0.014	0.757	0.021	0.798	0.027	0.753
$CD8^+$ T cell	CD8A	−0.462	***	-0.378	***	−0.025	0.762	−0.045	0.601
	CD8B	−0.253	***	−0.16	**	−0.009	0.912	−0.008	0.926
T cell (general)	CD3D	0.377	***	−0.32	***	−0.041	0.617	−0.037	0.664
	CD3E	−0.388	***	−0.345	***	−0.097	0.233	−0.109	0.206
	CD2	−0.389	***	−0.356	***	−0.053	0.515	−0.056	0.519
Tfh	*BCL6*	0.319	***	0.283	***	0.111	0.173	0.116	0.176
	IL21	−0.052	0.243	−0.063	0.167	-0.044	0.586	−0.037	0.666
Th1	*TBX21*	−0.165	**	−0.165	**	0.326	***	0.351	***
	STAT4	−0.292	***	−0.244	***	0.059	0.466	0.049	0.572
	STAT1	−0.293	***	−0.298	***	−0.016	0.841	−0.019	0.824
	IFNG	−0.216	***	−0.195	***	0.021	0.799	0.017	0.84
Th2	*STAT6*	−0.483	***	−0.386	***	0.114	0.161	0.189	0.027
	GATA3	−0.331	***	−0.309	***	−0.176	0.03	−0.17	0.047
	STAT5A	−0.348	***	−0.253	***	−0.167	0.039	−0.155	0.07
	IL13	0.015	0.74	0.011	0.803	0.119	0.143	0.1	0.248
Th17	*STAT3*	−0.103	0.019	−0.118	*	−0.133	0.102	−0.133	0.123
	IL17A	0.009	0.834	−0.002	0.958	−0.013	0.87	−0.015	0.862
Treg	FOXP3	0.102	0.02	0.099	0.031	0.002	0.984	0.008	0.923
	CCR8	−0.125	*	−0.13	*	−0.05	0.536	−0.056	0.515
	STAT5B	0.349	***	0.256	***	0.007	0.93	−0.004	0.96
	TGFB1	−0.209	***	−0.125	*	−0.151	0.063	−0.151	0.078
T cell exhaustion	PDCD1	−0.241	***	−0.204	***	0.076	0.349	0.081	0.342
	CTLA4	−0.285	***	−0.244	***	-0.006	0.943	−0.004	0.961
	LAG3	0.054	0.222	0.038	0.412	0.22	*	0.243	*
	HAVCR2	−0.284	***	−0.201	***	0.114	0.162	0.162	0.059
	GZMB	−0.269	***	−0.292	***	−0.135	0.097	−0.113	0.188
Monocyte	*CD86*	−0.253	***	−0.17	**	0.029	0.718	0.062	0.472
	CSF1R	−0.153	**	−0.038	0.411	0.108	0.183	0.14	0.102
TAM	*CD68*	−0.192	***	−0.132	*	0.058	0.472	0.122	0.157
	CCL2	−0.313	***	−0.266	***	−0.195	0.016	−0.196	0.022
	CCL5	−0.385	***	−0.345	***	−0.049	0.548	−0.028	0.745
M1	*NOS2*	−0.16	**	−0.128	*	−0.277	**	−0.277	*
	IRF5	−0.264	***	−0.172	**	0.17	0.035	0.224	*
	PTGS2	−0.245	***	−0.186	***	−0.107	0.186	−0.107	0.212
M2	*CD163*	−0.165	**	−0.164	**	−0.101	0.213	−0.105	0.223
	VSIG4	−0.085	0.054	−0.011	0.816	0.022	0.783	0.043	0.619
	MS4A4A	−0.065	0.138	−0.056	0.221	−0.022	0.782	−0.007	0.934
Neutrophil	*CEACAM8*	0.003	0.953	−0.005	0.917	0.04	0.62	0.06	0.484
	ITGAM	−0.279	***	−0.18	***	0.033	0.683	0.058	0.498
	CCR7	−0.211	***	−0.178	***	0.053	0.519	0.081	0.346
	MPO	−0.303	***	−0.221	***	0.187	0.021	0.204	0.017
DC	*CD1C*	0.093	0.035	−0.064	0.162	−0.068	0.401	−0.065	0.447
	HLA-DPB1	−0.423	***	−0.381	***	−0.03	0.711	−0.002	0.986
	HLA-DQB1	−0.38	***	−0.344	***	−0.1	0.218	−0.102	0.235
	HLA-DRA	−0.424	***	−0.389	***	−0.029	0.723	−0.028	0.749
	HLA-DPA1	−0.403	***	−0.366	***	−0.007	0.93	0.017	0.847
	NRP1	−0.11	0.012	−0.16	**	−0.188	0.02	−0.196	0.022
	ITGAX	−0.219	***	−0.115	0.012	0.137	0.091	0.183	0.033
NK cell	*KIR3DL1*	−0.057	0.194	−0.038	0.409	0.023	0.779	0.034	0.696
	KIR2DL1	−0.072	0.101	−0.087	0.059	0.034	0.674	0.07	0.415
	KIR2DL3	−0.207	***	−0.208	***	0.032	0.698	0.051	0.555
	KIR2DL4	−0.187	***	−0.182	***	0.011	0.896	−0.023	0.793
	KIR3DL2	−0.13	*	−0.128	*	−0.066	0.417	−0.057	0.512
	KIR3DL3	-0.015	0.74	−0.021	0.639	0.105	0.198	0.092	0.287
	KIR2DS4	−0.128	*	−0.095	0.039	−0.039	0.629	−0.029	0.736
Mast cell	*TPSB2*	−0.085	0.054	−0.093	0.042	0.182	0.025	0.191	0.026
	CPA3	−0.121	*	−0.158	**	0.15	0.064	0.144	0.093
	HDC	−0.398	***	−0.386	***	0.134	0.1	0.153	0.074

Note: None, correlation without adjustment; Purity, correlation adjusted by tumor purity; M1, M1 Macrophage; M2, M2 Macrophage; DC, Dendritic cell; NK cell: Natural killer cell; Cor, R value of Spearman's correlation. p-*value significant codes:* *p < *0.01;* **p < *0.001;* ***p < *0.0001.*

seven-gene signature, including SMOC1, which was positively correlated with 5-years OS of glioma patients (Zhang G.-H. et al., 2019). However, the specific relationship between the expression level of SMOC1 and the prognosis of glioma patients has not been evaluated yet.

In this study, we first systematically analyzed the expression level of SMOC1 and its prognostic value in glioma. Compared with levels in normal tissue, the expression of SMOC1 was aberrantly in many cancers; it was reduced in bladder urothelial carcinoma, BRCA, cholangiocarcinoma, kidney renal clear cell carcinoma, kidney renal papillary cell carcinoma, liver hepatocellular carcinoma, prostate adenocarcinoma, thyroid carcinoma, and uterine corpus endometrial carcinoma but increased in kidney chromophobe, LUAD, and LGG. These data suggest that the alterations in SMOC1 expression depend on the type of cancer. Survival analyzes from PrognoScan and GEPIA2 showed that the expression level of SMOC1 was correlated with the prognosis of brain glioma (LGG) and LUAD patients. Therefore, we further analyzed the expression of SMOC1 in glioma and LUAD *via* the GEPIA2 and CGGA databases. The results showed that the expression of SMOC1 was remarkably increased in tumor samples of LGG, whereas there were no significant changes in GBM and LUAD samples, which was consistent with previous studies (Boon et al., 2004; Brellier et al., 2011). In addition, we found that the expression of SMOC1 was significantly increased in subtypes of glioma through the CGGA dataset. Compared with IDH-wild-type, 1p19q non-codeletion, and recurrent subtypes, the expression of SMOC1 was increased in IDH mutant, 1p19q co-deletion, and primary gliomas. In the age < 42 years group, a higher expression level of SMOC1 was also observed. As we know, IDH wild-type, 1p19q non-codeletion, recurrent gliomas, and age > 40 years were poor prognostic factors in LGG (Nabors et al., 2017). These results confirmed the upregulation of SMOC1 expression in LGG and suggested that the expression of SMOC1 increases with the decrease of tumor malignancy. Consistent with the analysis of the TCGA datasets in GEPIA2, the survival analysis of CGGA datasets also showed a significant positive correlation between SMOC1 expression and better prognosis in all WHO grade I, WHO grade II, and WHO grade III gliomas but not in WHO grade IV glioma. These findings further confirmed the prognostic value of SMOC1 in specific types of cancer. Therefore, based on the consistent results of the association between SMOC1 expression and survival of LGG patients, we have reason to believe that SMOC1 can serve as a good prognostic biomarker in LGG. As mentioned before, the expression of SMOC1 was increased in oligodendroglioma (Brellier et al., 2011) and astrocytic tumors (Boon et al., 2004). Also, SMOC1 has even been identified as a new cancer-related protein by interacting with tenascin-c, and it inhibits the tenascin-c induced chemo-attractive effect (Brellier et al., 2011) in U87 glioma cells. However, the function of SMOC1 in glioma is still unclear. Also, it is necessary to focus on its precise effects in this cancer type, as well as the underlying mechanisms.

According to previous studies, the gene SMOC1 encodes a secreted modular glycoprotein (Vannahme et al., 2002). This protein belongs to a family of matricellular proteins, and it was generally expressed on the basement membrane of different tissues in adult animals and also can be present in other extracellular matrices (Vannahme et al., 2002). During mouse development, SMOC1 was expressed in the basement membrane zones of the brain, blood vessels, lung, heart, and many other tissues. This broad distribution suggests that SMOC1 might have multifunctional roles during mouse embryogenesis (Gersdorff et al., 2006). Besides, previous studies have shown that SMOC1 might also involve in angiogenesis. SMOC1 was highly expressed in proliferation endothelial cells, and the expression of SMOC1 was regulated by inflammatory cytokines and nitric oxide (Dreieicher et al., 2009). Another study indicated that SMOC1 acts as a negative feedback regulator of the activin-like kinase 5 signal pathway by binging to endothelin, leading to activation of transforming growth factor-beta signal pathway and activin-like kinase 1, thus promoting endothelial cell proliferation and angiogenesis (Awwad et al., 2015). Moreover, one study reported that SMOC1 might be involved in integrin–matrix interactions and cell adhesion (Klemencic et al., 2013). In addition to its role in matrix remodeling, SMOC1, as a circulating glycoprotein, was identified as a regulator of glucose homeostasis (Montgomery et al., 2020). A recent study identified SMOC1 as a novel thrombin-activating protein, which enhances the action of thrombin *in vivo* and *in vitro* (Delgado Lagos et al., 2021).

In this study, with the GSEA tool of LinkedOmics database, we found that the SMOC1 coexpressed genes were mainly enriched for protein localization and in pathways such as ribosome in LGG, whereas the genes involved in processing such as response to lymphocyte- and neutrophil-mediated immunity, leukocyte migration, adaptive immune response, T cell activation and in pathways such as ECM–receptor interaction, Th17 cell differentiation, and leukocyte *trans*-endothelial migration were inhibited in LGG. In the further analysis in CancerSEA, we found that the expression of SMOC1 was correlated with several important functional states in glioma cells, especially stemness, hypoxia, EMT, and metastasis. These results strongly suggested that SMOC1 might influence various processes in the glioma tumor microenvironment. It is well known that interactions between malignant cells and the extracellular environment are critical for cancer development and progression (Rangarajan and Weinberg, 2003). Additionally, we observed in our analysis that there was a positive correlation between SMOC1 expression and tumor purity in LGG, which suggested that the expression of SMOC1 was more likely from tumor cells, which was consistent with a previous study (Brellier et al., 2011). The expression of SMOC1 was negatively correlated with levels of infiltrating B cells, $CD8^+$ T cells, $CD4^+$ T cells, macrophages, neutrophils, and dendritic cells, as well as gene markers of most immune cells in the LGG tumor microenvironment. Interestingly, there was no significant correlation between SMOC1 expression and tumor purity or most of the infiltrating immune cells in GBM. These results indicate that the expression of SMOC1 was significantly related to immune infiltrating cells in LGG. Together with the functional analysis, our findings strongly suggest that SMOC1 might play an important role in the tumor microenvironment of glioma, thereby influencing glioma development and progression. Further experimental studies are needed to validate our conclusions and explore the specific function of SMCO1 in glioma.

CONCLUSION

In conclusion, our findings in this study suggest that SMOC1 was highly expressed in LGG, and the expression of SMOC1 was positively correlated with the survival of LGG patients. The functional analyses indicate that SMCO1 might play an important role in the glioma microenvironment, thereby influencing the development and progression of glioma. However, the prognostic value of SMOC1 in glioma needs to be validated in clinic samples, and as little was known about the biological function of SMOC1 in tumor genesis and progression, further *in vitro* and *in vivo* investigations are required to clarify the role of SMOC1 in glioma.

DATA AVAILABILITY STATEMENT

The original contributions presented in the study are included in the article/**Supplementary Material**; further inquiries can be directed to the corresponding author.

AUTHOR CONTRIBUTIONS

JW and WS conceived and designed the study. JW and WS wrote and revised the manuscript. SX, CG, JZ, and QX were responsible for the data analysis. All authors contributed to the article and approved the submitted version.

ACKNOWLEDGMENTS

We would like to thank the public databases, including Oncomine, TIMER, GEPIA2, PrognoScan, Kaplan–Meier Plotter, CGGA, TISIDB, CancerSEA, and LinkedOmics, for providing open access.

SUPPLEMENTARY MATERIAL

The Supplementary Material for this article can be found online at: https://www.frontiersin.org/articles/10.3389/fmolb.2021.666623/full#supplementary-material

REFERENCES

Afra, E. Osztie, L. Sipos, D. Vitan, D., Osztie, E., Sipos, L., and Vitanovics, D. (1999). Preoperative History and Postoperative Survival of Supratentorial Low-Grade Astrocytomas. *Br. J. Neurosurg.* 13 (3), 299–305. doi:10.1080/02688699943727

Aoki, H., Yamamoto, E., Takasawa, A., Niinuma, T., Yamano, H.-O., Harada, T., et al. (2018). Epigenetic Silencing of SMOC1 in Traditional Serrated Adenoma and Colorectal Cancer. *Oncotarget* 9 (4), 4707–4721. doi:10.18632/oncotarget.23523

Awwad, K., Hu, J., Shi, L., Mangels, N., Abdel Malik, R., Zippel, N., et al. (2015). Role of Secreted Modular Calcium-Binding Protein 1 (SMOC1) in Transforming Growth Factor β Signalling and Angiogenesis. *Cardiovasc. Res.* 106 (2), 284–294. doi:10.1093/cvr/cvv098

Boon, K., Edwards, J. B., Eberhart, C. G., and Riggins, G. J. (2004). Identification of Astrocytoma Associated Genes Including Cell Surface Markers. *Bmc Cancer* 4, 39. doi:10.1186/1471-2407-4-39

Bornstein, P., and Sage, E. H. (2002). Matricellular Proteins: Extracellular Modulators of Cell Function. *Curr. Opin. Cel Biol.* 14 (5), 608–616. doi:10.1016/s0955-0674(02)00361-7

Brellier, F., Ruggiero, S., Zwolanek, D., Martina, E., Hess, D., Brown-Luedi, M., et al. (2011). SMOC1 Is a Tenascin-C Interacting Protein Over-expressed in Brain Tumors. *Matrix Biol.* 30 (3), 225–233. doi:10.1016/j.matbio.2011.02.001

Choi, Y.-A., Lim, J., Kim, K. M., Acharya, B., Cho, J.-Y., Bae, Y.-C., et al. (2010). Secretome Analysis of Human BMSCs and Identification of SMOC1 as an Important ECM Protein in Osteoblast Differentiation. *J. Proteome Res.* 9 (6), 2946–2956. doi:10.1021/pr901110q

Danaher, P., Warren, S., Dennis, L., D'Amico, L., White, A., Disis, M. L., et al. (2017). Gene Expression Markers of Tumor Infiltrating Leukocytes. *J. Immunotherapy Cancer* 5, 18. doi:10.1186/s40425-017-0215-8

Delgado Lagos, F., Elgheznawy, A., Kyselova, A., Meyer Zu Heringdorf, D., Ratiu, C., Randriamboavonjy, V., et al. (2021). Secreted Modular Calcium-Binding Protein 1 Binds and Activates Thrombin to Account for Platelet Hyperreactivity in Diabetes. *Blood* 137, 1641–1651. doi:10.1182/blood.2020009405

Dreieicher, E., Beck, K.-F., Lazaroski, S., Boosen, M., Tsalastra-Greul, W., Beck, M., et al. (2009). Nitric Oxide Inhibits Glomerular TGF-β SignalingviaSMOC-1. *Jasn* 20 (9), 1963–1974. doi:10.1681/ASN.2008060653

Fidalgo, F., Rodrigues, T. C., Pinilla, M., Silva, A. G., Maciel, M. d. S., Rosenberg, C., et al. (2015). Lymphovascular Invasion and Histologic Grade Are Associated with Specific Genomic Profiles in Invasive Carcinomas of the Breast. *Tumor Biol.* 36 (3), 1835–1848. doi:10.1007/s13277-014-2786-z

Forst, D. A., Nahed, B. V., Loeffler, J. S., and Batchelor, T. T. (2014). Low-Grade Gliomas. *The Oncologist* 19 (4), 403–413. doi:10.1634/theoncologist.2013-0345

Gersdorff, N., Müller, M., Schall, A., and Miosge, N. (2006). Secreted Modular Calcium-Binding Protein-1 Localization during Mouse Embryogenesis. *Histochem. Cel Biol* 126 (6), 705–712. doi:10.1007/s00418-006-0200-7

Gu, X., Li, B., Jiang, M., Fang, M., Ji, J., Wang, A., et al. (2015). RNA Sequencing Reveals Differentially Expressed Genes as Potential Diagnostic and Prognostic Indicators of Gallbladder Carcinoma. *Oncotarget* 6 (24), 20661–20671. doi:10.18632/oncotarget.3861

Huang, Q. R., and Pan, X. B. (2019). Prognostic lncRNAs, miRNAs, and mRNAs Form a Competing Endogenous RNA Network in Colon Cancer. *Front. Oncol.* 9, 712. doi:10.3389/fonc.2019.00712

Huang, X.-Q., Zhou, Z.-Q., Zhang, X.-F., Chen, C.-L., Tang, Y., Zhu, Q., et al. (2017). Overexpression of SMOC2 Attenuates the Tumorigenicity of Hepatocellular Carcinoma Cells and Is Associated with a Positive Postoperative Prognosis in Human Hepatocellular Carcinoma. *J. Cancer* 8 (18), 3812–3827. doi:10.7150/jca.20775

Hyakusoku, H., Sano, D., Takahashi, H., Hatano, T., Isono, Y., Shimada, S., et al. (2016). JunB Promotes Cell Invasion, Migration and Distant Metastasis of Head and Neck Squamous Cell Carcinoma. *J. Exp. Clin. Cancer Res.* 35, 6. doi:10.1186/s13046-016-0284-4

Klemenčič, M., Novinec, M., Maier, S., Hartmann, U., and Lenarčič, B. (2013). The Heparin-Binding Activity of Secreted Modular Calcium-Binding Protein 1 (SMOC-1) Modulates its Cell Adhesion Properties. *PLoS One* 8 (2), e56839. doi:10.1371/journal.pone.0056839

Li, T., Fan, J., Wang, B., Traugh, N., Chen, Q., Liu, J. S., et al. (2017). TIMER: A Web Server for Comprehensive Analysis of Tumor-Infiltrating Immune Cells. *Cancer Res.* 77 (21), e108–e110. doi:10.1158/0008-5472.CAN-17-0307

Liu, P., Lu, J., Cardoso, W. V., and Vaziri, C. (2008). The SPARC-Related Factor SMOC-2 Promotes Growth Factor-Induced Cyclin D1 Expression and DNA Synthesis via Integrin-Linked Kinase. *MBoC* 19 (1), 248–261. doi:10.1091/mbc.e07-05-0510

Louis, D. N., Perry, A., Reifenberger, G., von Deimling, A., Figarella-Branger, D., Cavenee, W. K., et al. (2016). The 2016 World Health Organization Classification of Tumors of the Central Nervous System: a Summary. *Acta Neuropathol.* 131 (6), 803–820. doi:10.1007/s00401-016-1545-1

Louis, D. N. (2012). The Next Step in Brain Tumor Classification: "Let Us Now Praise Famous Men"... or Molecules? *Acta Neuropathol.* 124 (6), 761–762. doi:10.1007/s00401-012-1067-4

Lu, H., Ju, D.-D., Yang, G.-D., Zhu, L.-Y., Yang, X.-M., Li, J., et al. (2019). Targeting Cancer Stem Cell Signature Gene SMOC-2 Overcomes Chemoresistance and Inhibits Cell Proliferation of Endometrial Carcinoma. *EBioMedicine* 40, 276–289. doi:10.1016/j.ebiom.2018.12.044

Maier, S., Paulsson, M., and Hartmann, U. (2008). The Widely Expressed Extracellular Matrix Protein SMOC-2 Promotes Keratinocyte Attachment and Migration. *Exp. Cel Res.* 314 (13), 2477–2487. doi:10.1016/j.yexcr.2008.05.020

Mizuno, H., Kitada, K., Nakai, K., and Sarai, A. (2009). PrognoScan: a New Database for Meta-Analysis of the Prognostic Value of Genes. *BMC Med. Genomics* 2, 18. doi:10.1186/1755-8794-2-18

Montgomery, M. K., Bayliss, J., Devereux, C., Bezawork-Geleta, A., Roberts, D., Huang, C., et al. (2020). SMOC1 Is a Glucose-Responsive Hepatokine and Therapeutic Target for Glycemic Control. *Sci. Transl Med.* 12 (559). doi:10.1126/scitranslmed.aaz8048

Morshed, R. A., Young, J. S., Hervey-Jumper, S. L., and Berger, M. S. (2019). The Management of Low-Grade Gliomas in Adults. *J. Neurosurg. Sci.* 63 (4), 450–457. doi:10.23736/S0390-5616.19.04701-5

Nabors, L. B., Portnow, J., Ammirati, M., Baehring, J., Brem, H., Butowski, N., et al. (2017). NCCN Guidelines Insights: Central Nervous System Cancers, Version 1.2017. *J. Natl. Compr. Canc Netw.* 15 (11), 1331–1345. doi:10.6004/jnccn.2017.0166

Nagy, Á., Lánczky, A., Menyhárt, O., and Győrffy, B. (20182018). Validation of miRNA Prognostic Power in Hepatocellular Carcinoma Using Expression Data of Independent Datasets. *Sci. Rep.* 8, 9227. doi:10.1038/s41598-018-27521-y

Ostrom, Q. T., Patil, N., Cioffi, G., Waite, K., Kruchko, C., and Barnholtz-Sloan, J. S. (2020). CBTRUS Statistical Report: Primary Brain and Other Central Nervous System Tumors Diagnosed in the United States in 2013-2017. *Neuro Oncol.* 22 (12 Suppl. 2), iv1–iv96. doi:10.1093/neuonc/noaa200

Rangarajan, A., and Weinberg, R. A. (2003). Comparative Biology of Mouse versus Human Cells: Modelling Human Cancer in Mice. *Nat. Rev. Cancer* 3 (12), 952–959. doi:10.1038/nrc1235

Rhodes, D. R., Kalyana-Sundaram, S., Mahavisno, V., Varambally, R., Yu, J., Briggs, B. B., et al. (2007). Oncomine 3.0: Genes, Pathways, and Networks in a Collection of 18,000 Cancer Gene Expression Profiles. *Neoplasia* 9 (2), 166–180. doi:10.1593/neo.07112

Ru, B., Wong, C. N., Tong, Y., Zhong, J. Y., Zhong, S. S. W., Wu, W. C., et al. (2019). TISIDB: an Integrated Repository portal for Tumor-Immune System Interactions. *Bioinformatics* 35 (20), 4200–4202. doi:10.1093/bioinformatics/btz210

Su, J.-R., Kuai, J.-H., and Li, Y.-Q. (2016). Smoc2 Potentiates Proliferation of Hepatocellular Carcinoma Cells via Promotion of Cell Cycle Progression. *Wjg* 22 (45), 10053–10063. doi:10.3748/wjg.v22.i45.10053

Tang, Z., Li, C., Kang, B., Gao, G., Li, C., and Zhang, Z. (2017). GEPIA: a Web Server for Cancer and normal Gene Expression Profiling and Interactive Analyses. *Nucleic Acids Res.* 45 (W1), W98–W102. doi:10.1093/nar/gkx247

Vannahme, C., Gösling, S., Paulsson, M., Maurer, P., and Hartmann, U. (2003). Characterization of SMOC-2, a Modular Extracellular Calcium-Binding Protein. *Biochem. J.* 373 (Pt 3), 805–814. doi:10.1042/BJ20030532

Vannahme, C., Smyth, N., Miosge, N., Gösling, S., Frie, C., Paulsson, M., et al. (2002). Characterization of SMOC-1, a Novel Modular Calcium-Binding Protein in Basement Membranes. *J. Biol. Chem.* 277 (41), 37977–37986. doi:10.1074/jbc.M203830200

Vasaikar, S. V., Straub, P., Wang, J., and Zhang, B. (2018). LinkedOmics: Analyzing Multi-Omics Data within and across 32 Cancer Types. *Nucleic Acids Res.* 46 (D1), D956–D963. doi:10.1093/nar/gkx1090

Wen, P. Y., and Kesari, S. (2008). Malignant Gliomas in Adults. *N. Engl. J. Med.* 359 (5), 492–507. doi:10.1056/NEJMra0708126

Weng, J. Y., and Salazar, N. (2021). DNA Methylation Analysis Identifies Patterns in Progressive Glioma Grades to Predict Patient Survival. *Int. J. Mol. Sci.* 22 (3).1020 doi:10.3390/ijms22031020

Yan, W., Zhang, W., You, G., Zhang, J., Han, L., Bao, Z., et al. (2012). Molecular Classification of Gliomas Based on Whole Genome Gene Expression: a Systematic Report of 225 Samples from the Chinese Glioma Cooperative Group. *Neuro Oncol.* 14 (12), 1432–1440. doi:10.1093/neuonc/nos263

Yuan, H., Yan, M., Zhang, G., Liu, W., Deng, C., Liao, G., et al. (2019). CancerSEA: a Cancer Single-Cell State Atlas. *Nucleic Acids Res.* 47 (D1), D900–D908. doi:10.1093/nar/gky939

Zhang, G.-H., Zhong, Q.-Y., Gou, X.-X., Fan, E.-X., Shuai, Y., Wu, M.-N., et al. (2019a). Seven Genes for the Prognostic Prediction in Patients with Glioma. *Clin. Transl Oncol.* 21 (10), 1327–1335. doi:10.1007/s12094-019-02057-3

Zhang, X., Lan, Y., Xu, J., Quan, F., Zhao, E., Deng, C., et al. (2019b). CellMarker: a Manually Curated Resource of Cell Markers in Human and Mouse. *Nucleic Acids Res.* 47 (D1), D721–D728. doi:10.1093/nar/gky900

Conflict of Interest: The authors declare that the research was conducted in the absence of any commercial or financial relationships that could be construed as a potential conflict of interest.

Publisher's Note: All claims expressed in this article are solely those of the authors and do not necessarily represent those of their affiliated organizations or those of the publisher, the editors, and the reviewers. Any product that may be evaluated in this article, or claim that may be made by its manufacturer, is not guaranteed or endorsed by the publisher.

frontiers in Cell and Developmental Biology

ORIGINAL RESEARCH
published: 25 November 2021
doi: 10.3389/fcell.2021.753004

Development of an Oxidative Phosphorylation-Related and Immune Microenvironment Prognostic Signature in Uterine Corpus Endometrial Carcinoma

Jinhui Liu[1†], Tian Chen[1†], Min Yang[2†], Zihang Zhong[2†], Senmiao Ni[2], Sheng Yang[2], Fang Shao[2], Lixin Cai[2], Jianling Bai[2] and Hao Yu[2*]*

[1]Department of Gynecology, The First Affiliated Hospital of Nanjing Medical University, Nanjing, China, [2]Department of Biostatistics, School of Public Heath, Nanjing Medical University, Nanjing, China

OPEN ACCESS

Edited by:
Na Luo,
Nankai University, China

Reviewed by:
Chun Wang,
Thomas Jefferson University, United States
Shizhi Wang,
Southeast University, China
Fangrong Yan,
China Pharmaceutical University, China

***Correspondence:**
Hao Yu
haoyu@njmu.edu.cn
Jianling Bai
baijianling@njmu.edu.cn

[†]These authors have contributed equally to this work

Specialty section:
This article was submitted to Molecular and Cellular Pathology, a section of the journal Frontiers in Cell and Developmental Biology

Received: 04 August 2021
Accepted: 25 October 2021
Published: 25 November 2021

Citation:
Liu J, Chen T, Yang M, Zhong Z, Ni S, Yang S, Shao F, Cai L, Bai J and Yu H (2021) Development of an Oxidative Phosphorylation-Related and Immune Microenvironment Prognostic Signature in Uterine Corpus Endometrial Carcinoma. Front. Cell Dev. Biol. 9:753004. doi: 10.3389/fcell.2021.753004

Background: As the fourth most common malignant tumors in women, uterine corpus endometrial carcinoma (UCEC) requires novel and reliable biomarkers for prognosis prediction to improve the overall survival. Oxidative phosphorylation (OXPHOS) is found to be strongly correlated with the progression of tumor. Here, we aimed to construct an OXPHOS-related and immune microenvironment prognostic signature to stratify UCEC patients for optimization of treatment strategies.

Method: Prognosis-associated OXPHOS-related differentially expressed genes were identified by multivariable Cox regression from TCGA–UCEC cohort. Based on the candidate genes, an OXPHOS-related prognostic signature was constructed by the train set data and verified by the entire set. When integrated with relevant clinical characteristics, a nomogram was also created for clinical application. Through comparison of tumor microenvironment between different risk groups, the underlying mechanism of the model and the inner correlation between immune microenvironment and energy metabolism were further investigated.

Results: An OXPHOS-related signature containing ATP5IF1, COX6B1, FOXP3, and NDUFB11 was constructed and had better predictive ability compared with other recently published signatures in UCEC. Patients with lower risk score showed higher immune cell infiltration, higher ESTIMATE score (p = 2.808E−18), lower tumor purity (p = 2.808E−18), higher immunophenoscores (IPSs) ($p < 0.05$), lower expression of mismatch repair (MMR) proteins ($p < 0.05$), higher microsatellite instability (MSI), lower expression of markers of N6-methyladenosine (m6A) mRNA methylation regulators, higher tumor mutation burden (TMB) (p = 1.278E−9), and more sensitivity to immune checkpoint blockade (ICB) ($p < 0.001$) and chemotherapy drugs, thus, possessing improved prognosis.

Conclusion: An OXPHOS-related and immune microenvironment prognostic signature classifying EC patients into different risk subsets was constructed in our study, which could

be used to predict the prognosis of patients and help to select a specific subset of patients who might benefit from immunotherapy and chemotherapy, thus, improving the overall survival rate of UCEC. These findings may contribute to the discovery of novel and robust biomarkers or target therapy in UCEC and give new insights into the molecular mechanism of tumorigenesis and progression of UCEC.

Keywords: uterine corpus endometrial carcinoma, oxidative phosphorylation, prognosis, tumor microenvironment, immunotherapy

1 INTRODUCTION

Uterine corpus endometrial carcinoma (UCEC) is the fourth most common malignancy among women in the United States, with a trend of increasing morbidity and mortality worldwide (Cancer Genome Atlas Research et al., 2013). According to the GLOBOCAN, there would be an estimated 382,069 (2.1% of the total cancer cases) new cases, with 89,929 (0.9% of total cancer deaths) deaths in 2018 (Bray et al., 2018). Due to the advance in techniques for early diagnosis, the patients diagnosed at an early stage account for approximately 75% of UCEC, and most of the patients in stage I can be nearly cured by surgery, with a 5-years overall survival rate of 47–69%. In comparison, advanced-stage patients (stage III or IV) have a poor prognosis due to high risk for recurrence and limited therapeutic strategies, with a 5-years overall survival rate of 15–17% (Lee et al., 2017). Therefore, attention should be paid to discovering novel and reliable biomarkers for prognosis prediction, which can also work as a sensitive classifier for a specific subset of UCEC patients who will benefit from immunotherapy and have improved survival.

Recently, increasing attention has been paid into the exploration of the relationship between cancer cell metabolic plasticity and migration and metastasis (Mosier et al., 2021). Cancer cells with a more invasive and distal metastasis phenotype are found to be strongly correlated with the upregulated expression of peroxisome proliferator-associated receptor gamma and coactivator 1-alpha, which are hallmarks of active mitochondrial biogenesis and oxidative phosphorylation (OXPHOS) (LeBleu et al., 2014). OXPHOS is supposed to be a potential biomarker of tumor progression (Commander et al., 2020). In addition, emerging evidence shows that OXPHOS inhibition can be a valuable target in cancer treatment (Ashton et al., 2018; Molina et al., 2018; Xu et al., 2020a; Cardenas et al., 2020). OXPHOS provides the required energy for cancer cells to strive, and cancer stem cells with primary or acquired resistance against chemotherapy or tyrosine kinase inhibitors are characterized with markedly enhanced OXPHOS dependency (Sica et al., 2020). Metformin and thiazolidinediones can inhibit the mitochondrial electron transport chain, which provides energy for ovarian cancer growth. Thus, interfering with the process of OXPHOS may be considered as a new target for cancer therapy (Nayak et al., 2018). With the development of molecular medicine and next-generation sequencing technology, OXPHOS has been employed in the cancer risk prediction model in lung adenocarcinoma (Xu et al., 2020b). OXPHOS has also attached great importance to UCEC. As a regulator participating in oxidative phosphorylation and glycolysis, PKM2 can function as a biomarker for malignant and premalignant endometrial lesions, and the presence of $PKM2^{high}$ tumor cells in UCEC tissue also indicates a poor prognosis (Lai et al., 2019). To the best of our knowledge, OXPHOS has not been included in the UCEC prognostic model in previous studies, which deserves to be explored for subgrouping of the patients with distinct prognosis for personal treatment and identifying potential novel therapeutic targets.

Here, we identified prognosis-associated OXPHOS-related differentially expressed genes (DEGs) from TCGA–UCEC cohort (Tomczak et al., 2015). Based on the candidate genes, we constructed an OXPHOS-related prognostic signature model using the train dataset and verified it using the entire dataset. To further investigate the underlying mechanism of the model and its correlation with immune microenvironment and energy metabolism, then between high- and low-risk groups, we compared tumor-infiltrating immune cells (TIICs), ESTIMATE score, tumor purity, immunophenoscores (IPSs), the expression of mismatch repair (MMR) proteins, mRNA expression-based stemness index (mRNAsi), microsatellite instability expression (MSI), the expression of markers of N^6-methyladenosine (m^6A) mRNA methylation regulators, tumor mutation burden (TMB) and the response to immune checkpoint blockade (ICB) and chemotherapy agents, which may provide evidence for clinical application of the signature for immunotherapy and chemotherapy option (**Figure 1**). The findings in this study not only provided a useful predictive model for UCEC but also offered evidence for mutual impacts of OXPHOS, immune microenvironment, and tumor malignant biology.

2 MATERIALS AND METHODS

2.1 Data Collection

The gene expression profiles were collected from TCGA–UCEC database (https://tcga-data.nci.nih.gov/tcga/), which contained 552 tumor and 23 normal tissues. Meanwhile, the corresponding clinical and pathological information was also obtained from TCGA database, including patient age, tumor grade, tumor stage, and histological type of each sample. After removing the samples with unknown survival time, <30 days, and no survival status, we finally integrated the transcriptome and complete clinical data, enrolling a total of 511 patients in this study (**Table 1**).

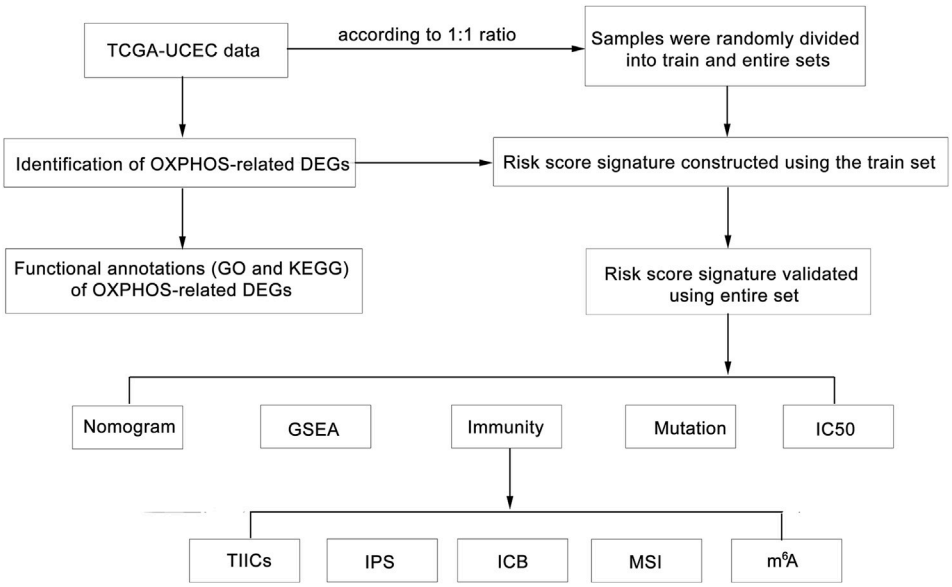

FIGURE 1 | Flow chart of the bioinformatic analyses.

TABLE 1 | Clinical information of the included UCEC patients in TCGA.

Covariates	Type	Total N (Percentage)	Train N (Percentage)
Age	<=60	199 (38.94%)	109 (42.58%)
	>60	312 (61.06%)	147 (57.42%)
Histological type	Endometrial	384 (75.15%)	197 (76.95%)
	Mixed and serous	127 (24.85%)	59 (23.05%)
Grade	G1 and G2	91 (17.81%)	44 (17.19%)
	G3 and G4	420 (82.19%)	212 (82.81%)
Stage	Stage I & Stage II	370 (72.41%)	182 (71.09%)
	Stage III Stage IV	141 (27.59%)	74 (28.91%)

2.2 Oxidative Phosphorylation-Related Survival-Related Differentially Expressed Genes and Functional Annotation

We used the R package *limma* to define the differentially expressed genes among 289 OXPHOS-related genes acquired from the National Center for Biotechnology Information—GENE and the Metabolic Atlas database (Xu et al., 2020b). The genes with $p < 0.05$ and $|\log2 \text{ (fold change)}| > 1$ were regarded as DEGs. We used the *survival* package to show the association between OXPHOS-related DEGs and survival time. We defined the DEGs with p less than 0.05 as survival-related DEGs (sDEGs). To explore the potential biological functions of the OXPHOS-related sDEGs, we implemented the *ClusterProfiler* package of R software for Gene Ontology (GO) term enrichment analysis (Ashburner et al., 2000), which included three categories: biological process (BP), molecular functions (MF), cellular components (CC), as well as the Kyoto Encyclopedia of Genes and Genomes (KEGG) pathway enrichment analysis (Kanehisa and Goto, 2000).

2.3 Construction of an Oxidative Phosphorylation-Related Prognostic Signature

We randomly assigned 256 patients as the train set and took the entire set for validation. First, we utilized the univariate Cox regression in the train set to identify candidate sDEGs with a significant level of $p < 0.05$. Then, we performed the least absolute shrinkage and selection operator (LASSO) Cox regression analysis by the *glmnet* package (Qu et al., 2018). Finally, we employed multivariate Cox proportional hazard regression analysis to construct an OXPHOS-related prognostic signature. The formula for calculating risk score was as follows: risk score = $\sum_{i=1}^{n}$ the expression level of n^{*} the regression coefficient calculated by multivariate Cox proportional hazard regression.

We treated the median of risk score in the train set as the cutoff value to divide the validation data into the high- and low-risk groups and plotted the Kaplan–Meier curves, as well as the ROC curves by *survminer*, *survivalROC* package (Heagerty et al., 2000). To confirm the independence of the signature, a conjoint univariate and multivariate Cox analyses were conducted. In

addition, we compared the subgroup survival analysis in tumor stage (stages I and II, stages III and IV), tumor grade (grades 1 and 2, grades 3 and 4), histological type (endometrial, mixed, and serous), and age (≤60, >60) to further evaluate the value of the signature combined with clinical factors in the survival prediction of UCEC. We used the *rms* package to construct a baseline nomogram for clinical application in UCEC patients (Iasonos et al., 2008).

2.4 RNA Isolation and Quantitative Real-Time PCR

UCEC and normal endometrial tissues were obtained from patients of the First Affiliated Hospital of Nanjing Medical University with the approval of the ethics committee and with informed consent. The clinicopathological parameters are shown in **Supplementary Table S1**. Total RNA was isolated from tissue samples with TRIzol reagent (Thermo Fisher Scientific, Waltham, MA, United States), and the integrity of the extracted RNA was estimated by the Agilent Bioanalyzer 2100 (Agilent Technologies, Santa Clara, CA, United States). RNA was reversely transcribed into cDNA using high-capacity reverse transcription kits (TaKaRa, Shiga, Japan), and quantitative real-time PCR (qRT-PCR) was conducted on Light Cycler 480 (Roche, Switzerland) using SYBR Green PCR Kit (Thermo Fisher Scientific) with the $2^{-\Delta\Delta Ct}$ method, in which GAPDH was the endogenous control. All program procedures of qRT-PCR were performed according to the protocol of the manufacturer. Primer sequences for GAPDH and four OXPHOS-related genes are presented in **Supplementary Table S2**.

2.5 Gene Set Enrichment Analysis and Immunity Analyses

Gene set enrichment analysis (GSEA) was utilized to elucidate the molecular mechanisms of the OXPHOS-related sDEGs. We separated the samples in the entire set into the high- and low-risk groups based on scores calculated by the signature and then compared the enriched BP between the two groups. The value of $p < 0.05$ was regarded as the cutoff criterion (Zhu et al., 2016). Furthermore, we employed the ESTIMATE algorithm by the *ESTIMATE* package to calculate the stromal, immune, and estimate scores of each sample and evaluate the relationship between the OXPHOS-related prognostic signature and immunization (https://bioinformatics.mdanderson.org/public-software/estimate/) (Yoshihara et al., 2013).

2.6 Analysis of Tumor-Infiltrating Immune Cells

We employed CIBERSORT (https://cibersort.stanford.edu/) to explore the immune cell infiltration of each sample based on the RNA-seq data (Newman et al., 2015). To further analyze the association between risk score and tumor-infiltrating immune cells (TIICs), single-sample gene-set enrichment analysis (ssGSEA) was also performed to quantify the immune activity in different risk groups by exploring 29 immune-related genes (He et al., 2018).

2.7 Analysis of Immune Status Between Different Risk Groups

The immunogenicity of tumor is determined by the four dominant components containing immunomodulators, immunosuppressive cells, effector cells as well as MHC molecules. Immunophenoscores (IPSs) (including IPS, IPS-CTLA4, IPS-PD1-PD-L1-PD-L2, IPS-PD1-PD-L1-PD-L2-CTLA4 scores) are calculated based on the representative cell-type gene expression z-scores to evaluate and compare the potential response to immune checkpoint inhibitor between different risk groups (Charoentong et al., 2017). IPS data of each UCEC patient in the entire set was downloaded from The Cancer Immunome Atlas (TCIA) (https://tcia.at/home). Besides, the immunotherapy response could be predicted with high accuracy by an Immune Cell Abundance Identifier (ImmuCellAI) result-based model, which precisely estimates the abundance of 24 immune cell types including 18 T-cell subsets from gene expression data (http://bioinfo.life.hust.edu.cn/ImmuCellAI) (Wang et al., 2020a; Toh et al., 2021). Microsatellite instability (MSI) (Toh et al., 2021) and the expression of markers of N^6-methyladenosine (m^6A) mRNA methylation regulators (Wang et al., 2020a) of each sample were also collected from TCGA, which can predict potential response to immune checkpoint inhibitors (ICIs) and help explain the association between the signature and immunogenicity. Tumor cells sharing more similarities with stem cells represents cancer progression. Malta et al. developed an innovative mRNAsi algorithm to calculate the degree of similarities for UCEC patients in TCGA database (Malta et al., 2018). We also downloaded the mRNAsi information from the research for analyses.

2.8 Analysis of Tumor Mutation Burden

The mutation data collected from TCGA were analyzed by R package maftools (Robinson et al., 2017). The tumor mutation burden (TMB) was calculated by the formula: TMB = (total mutation/total covered bases) * 10^6.

2.9 Potential Chemotherapeutic Response

The response to temsirolimus, roscovitine, AZD6244, PD.0325901, RDEA119, PF.02341066, AKT. inhibitor.VIII, BMS.509744, vinblastine, bryostatin.1, metformin, AZ628, nutlin.3a, bortezomib, bicalutamide, AZD6482, cytarabine, rapamycin, camptothecin, mitomycin. C, S. Trityl.L.cysteine, tipifarnib, parthenolide, sorafenib, and methotrexate, the 25 common chemo drugs, were predicted by the Genomics of Drug Sensitivity in Cancer (GDSC) (https://www.cancerrxgene.org/) to analyze the relationship between the signature and chemotherapeutic response (Yang et al., 2013). We used R package *pRRophetic* to estimate and compare the half-maximal inhibitory concentration (IC50) between different risk groups (Geeleher et al., 2014).

2.10 Statistical Analysis

All statistical analyses were applied by R version 3.6.1 (Package: *limma*, *survival*, *ClusterProfiler*, *glmnet*, *survminer*, *survivalROC*, *rms*, *ESTIMATE, pRRophetic*). Categorical variables were presented by counts and percentages. Continuous variables in normal distribution were analyzed using Student's t-test and presented as mean ± standard deviation, while in abnormal distribution, they were presented as median (range). Multiple groups of continuous variables were analyzed by one-way ANOVA. The hazard ratio and 95% confidence interval were calculated to identify genes associated with overall survival. Unless with special explanation, $p < 0.05$ was considered statistically significant.

3 RESULTS AND DISCUSSION

3.1 Results

3.1.1 Identification of Oxidative Phosphorylation-Related Differentially Expressed Genes

We conducted the differential expression analysis of 289 OXPHOS-related genes between tumor and normal endometrium (Xu et al., 2020b). Sixty-six OXPHOS-related DEGs were identified, including 54 upregulated genes and 12 downregulated genes (**Supplementary Figures S1A,B** and **Supplementary Table S3**). The GO term enrichment analysis presented that they were related to ATP metabolic process ($p < 0.0005$) and purine ribonucleoside triphosphate metabolic process ($p < 0.0005$) in the BP group, mitochondrial inner membrane ($p < 0.0005$), and organelle inner membrane ($p < 0.0005$) in the CC group, oxidoreductase activity, acting on NAD(P)H and electron transfer activity ($p < 0.0005$) in the MF group (**Supplementary Figures S1C**); the KEGG results manifested that they mainly took part in pathways of oxidative phosphorylation ($p < 0.05$), endocannabinoid signaling ($p < 0.05$), and HIF-1 signaling ($p < 0.05$) in cancer (**Supplementary Figures S1D**).

3.1.2 Establishment of Oxidative Phosphorylation-Related Prognostic Signature

Using univariate Cox regression from the train data, we defined seven OXPHOS-related sDEGs, including ATP5IF1, MRPL12, FOXP3, NDUFA13, ATP5F1E, and NDUFB11 (**Supplementary Table S4**). ATP5IF1 and FOXP3 were protective elements of UCEC, while the others were dangerous ones. Then we conducted LASSO Cox regression analysis and multivariate Cox regression analysis (**Supplementary Figures S2A,B**) to construct a reliable OXPHOS-related prognostic signature. Consequently, ATP5IF1, COX6B1, FOXP3, and NDUFB11 were included in the signature as key prognosis-associated ones (**Supplementary Figures S2C**). Furthermore, the results of the expression analyses of the four genes showed that all of them were highly expressed in tumor compared with normal tissue, but only ATP5IF1 and FOXP3 were highly associated with overall survival (OS) of UCEC patients (**Supplementary Figures S3A–F**). The qRT-PCR results of our own samples also demonstrated that the expression level of ATP5IF1 ($p = 0.0311$), COX6B1 ($p = 0.0212$), FOXP3 ($p = 0.1082$), and NDUFB11 ($p = 0.0450$) were significantly higher in UCEC tissues than in normal endometrial tissues (**Supplementary Figures S3G–J**). The formula to calculate the risk score of patients is shown as follows: risk score = (−0.011678 * expression value of ATP5IF1) + (0.0014649 * expression value of COX6B1) + (−0.309569 * expression value of FOXP3) + (0.0029791 * expression value of NDUFB11).

3.1.3 Validation of Prognostic Signature in Uterine Corpus Endometrial Carcinoma

We used the validation data to evaluate the performance of the risk model in survival prediction. Using the preceding equation, we calculated the risk score and divided the samples of the train and entire sets separately into high- and low-risk groups by taking the median risk score in the train set as the cutoff line. The distribution of risk score (**Figure 2A**), survival status of each sample (**Figure 2B**), and the key gene expression profiles in each set (**Figure 2C**) are exhibited in **Figure 2**. By comparison with the low-risk group, Kaplan–Meier survival curves revealed that the OS of the high-risk group was significantly worse (log rank test, $p = 1.35E{-}4$) (**Figure 2D**). Besides, a survival ROC curve analysis was conducted, and the area under the curve (AUC) at 1 year in the train set was 0.748 (**Figure 2E**), which verified the predictive value of the signature, and the AUC value in the entire set also suggested a similar potential for prediction of survival with the above results (**Figure 2E**). The PCA plots indicated that patients in different risk groups tended to distribute differently (**Figure 2F**).

3.1.4 Clinical Utility of the Oxidative Phosphorylation-Related Prognostic Signature

The conjoint univariate and multivariate analyses in both sets confirmed the independence of the OXPHOS-related prognostic signature (**Figure 3**). Integrated with clinical factors, we performed subgroup survival analysis in stages I and II, stages III and IV, grades 1 and 2, grades 3 and 4, endometrial, mixed, and serous, age ≤6 0, age >60, and we found that a higher risk score was related to poorer prognosis in all subgroups (**Supplementary Figures S4A–H**). The correlation between risk core and clinical characteristics is shown in **Supplementary Figures S4I–L** and a heatmap (**Supplementary Figure S5**), indicating that patients with lower stage, lower grade, endometrial histological type, and lower age tended to have a lower risk score. Aimed at creating a feasible method for clinical application, we constructed a nomogram cooperating risk core, patient age, histological type, tumor grade, and tumor stage (**Figure 4A**). By comparing the AUC values at 1, 3, and 5 years plotted by the signature and clinical factors, we discovered that the gene-based signature was superior to others in the OS prediction. What is more, when the gene-based signature was combined with the clinical characteristics, it had better predictive ability than the signature alone (**Figure 4B**). The calibration curves also demonstrated that the results predicted by the nomogram

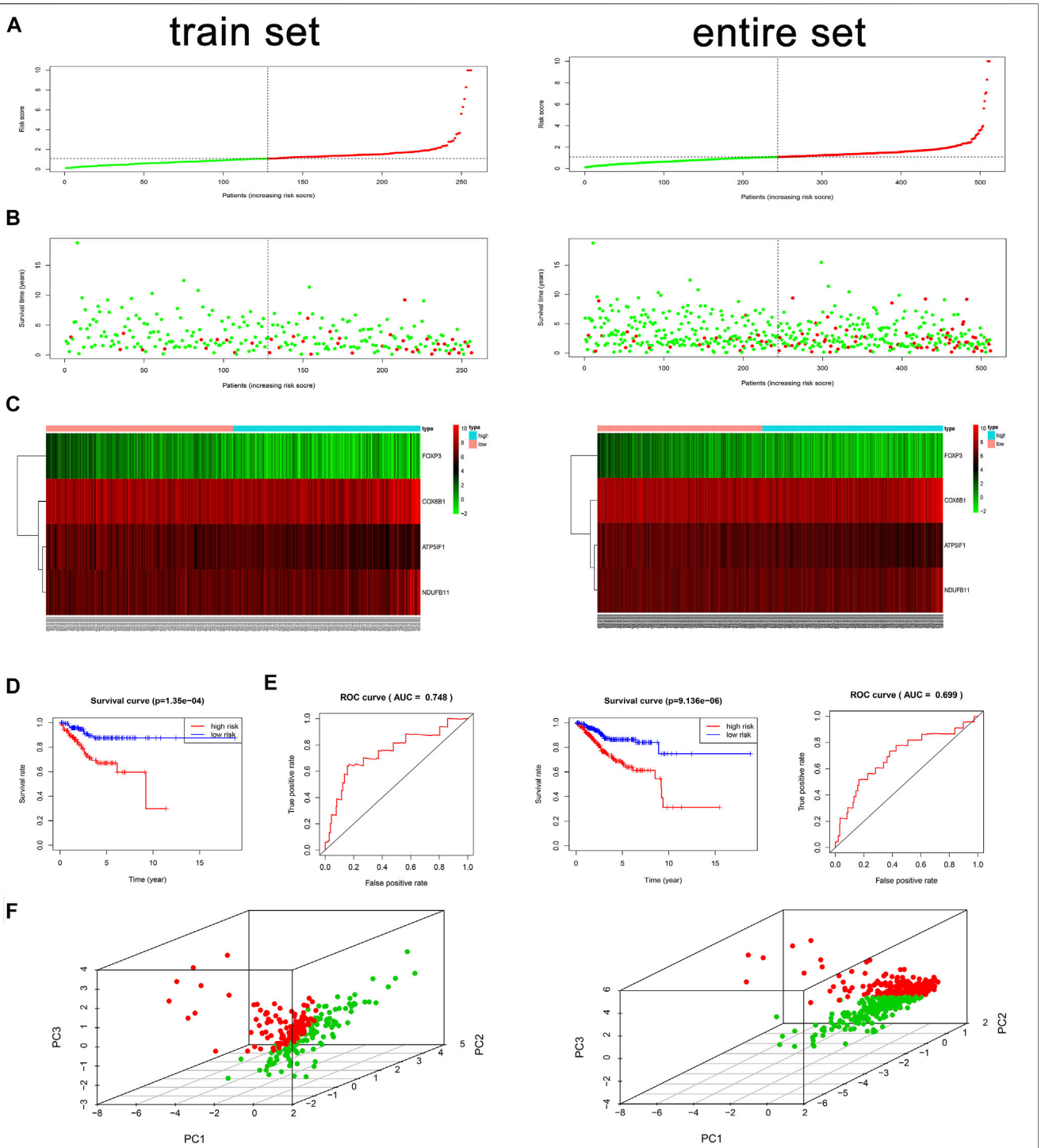

FIGURE 2 | Risk score analysis, time-dependent ROC analysis, Kaplan–Meier analysis, and PCA plots for the validation of the oxidative phosphorylation (OXPHOS)-related prognostic signature in the train and entire sets based on overall survival (OS). **(A)** Rank of risk score and distribution of groups based on the signature. Patients in each group were divided into the high- or low-risk groups. **(B)** Survival status of patients in each group. **(C)** Heatmap of expression profiles of selected four OXPHOS-related prognostic differentially expressed genes (DEGs). **(D)** Kaplan–Meier survival curves analyses of risk score in TCGA cohort. In the train set, in the low-risk group, $N = 128$; in the high-risk group, $N = 128$. In the entire set, in the low-risk group, $N = 244$; in the high-risk group, $N = 267$. **(E)** Survival ROC analysis of risk score in predicting prognoses in the train and entire sets. **(F)** PCA plots of the train and entire sets. In the train set, $N = 256$; in the entire set, $N = 511$.

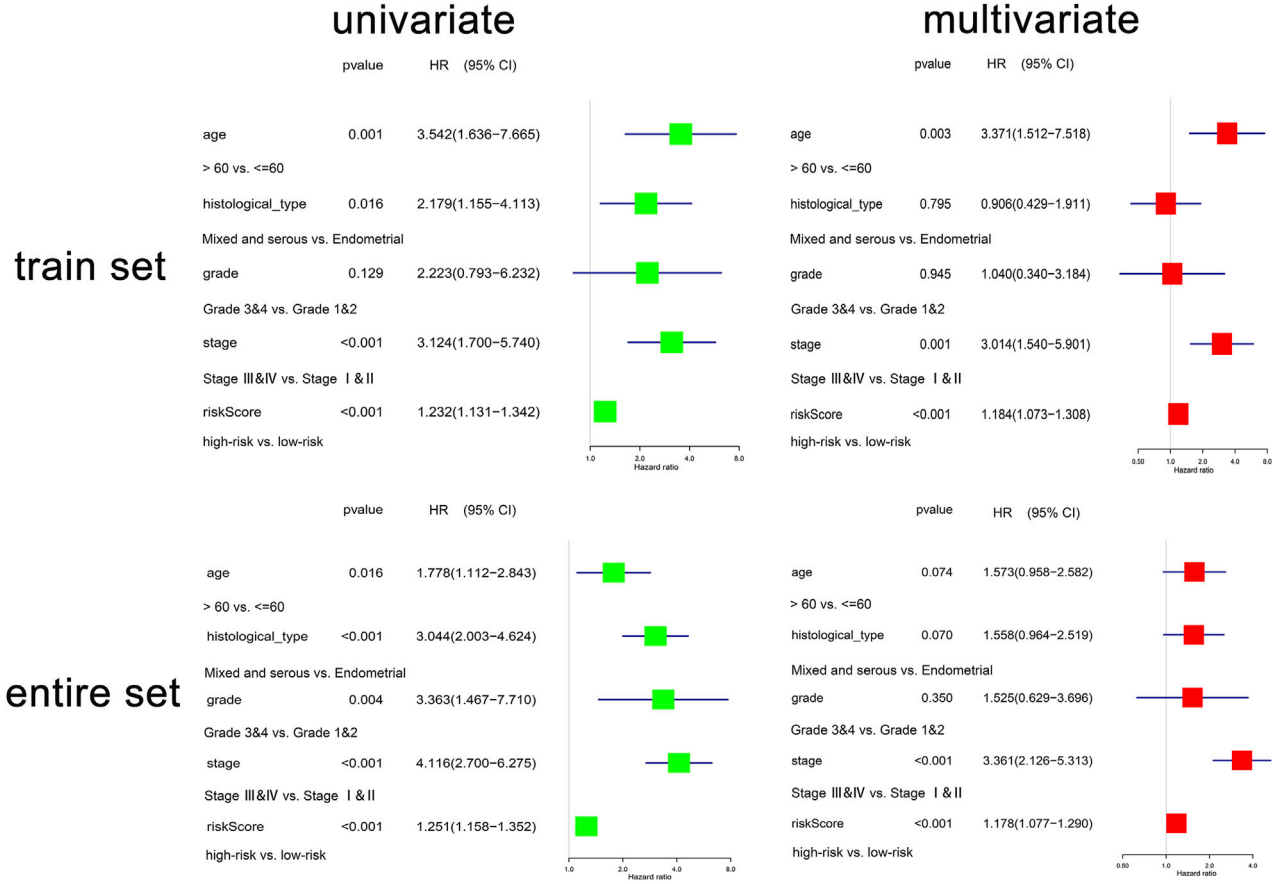

FIGURE 3 | The regression analyses of the independent predictor of uterine corpus endometrial carcinoma (UCEC). In the train set, *N* = 256; in the entire set, *N* = 511.

were in high consistency with actual survival, which suggested that the nomogram had a high clinical value (**Figure 4C**).

3.1.5 Gene Set Enrichment Analyses

To ascertain involved biological processes, we employed GSEA to analyze the transcript message of patients in different risk groups. In the high-risk group, representative KEGG pathways were axon guidance, glycosaminoglycan biosynthesis ghondroitin sulfate, glycosaminoglycan biosynthesis heparan sulfate, RNA polymerase, and tight junction (**Figure 5A**), while in the low-risk group, representative KEGG pathways were cytokine–cytokine receptor interaction, chemokine signaling pathway, and so on (**Figure 5B**). Through comparison, we discovered that in the low-risk group, the representative biological processes were mainly related to immunization. Furthermore, we implemented the ESTIMATE algorithm and found that the higher the risk score, the lower the immune score, the stromal score, and the ESTIMATE score, and the higher the tumor purity (**Figures 5C–F**), which further proved that the signature was significantly related to immunization.

3.1.6 Difference of Tumor-Infiltrating Immune Cells in Different Risk Groups

To further explore the relationship between the OXPHOS-related prognostic signature and immunization, we found the difference of TIICs between different risk groups. M0 macrophages, M2 macrophages, and activated mast cells were significantly elevated in the high-risk group ($p < 0.05$). In contrast, plasma cells, $CD8^+$ T cells, activated memory $CD4^+$ T cells, and regulatory T cells (Tregs) were evidently elevated in the low-risk group ($p < 0.05$) (**Figure 6A**). We analyzed the correlation of risk score and TIICs; as we can see in **Figures 6B,C**, M0 macrophages, M2 macrophages, plasma cells, activated memory $CD4^+$ T cells, $CD8^+$ T cells, gamma delta T cells, and regulatory T cells (Tregs) were the seven most relevant types of immune cells with risk core. There was a significant difference in the enrichment scores of diverse immune cell subpopulations and related functions or pathways with ssGSEA between different risk groups, such as TIL and HLA, which showed coherence with the GO and KEGG analyses results (**Figures 6D,E**).

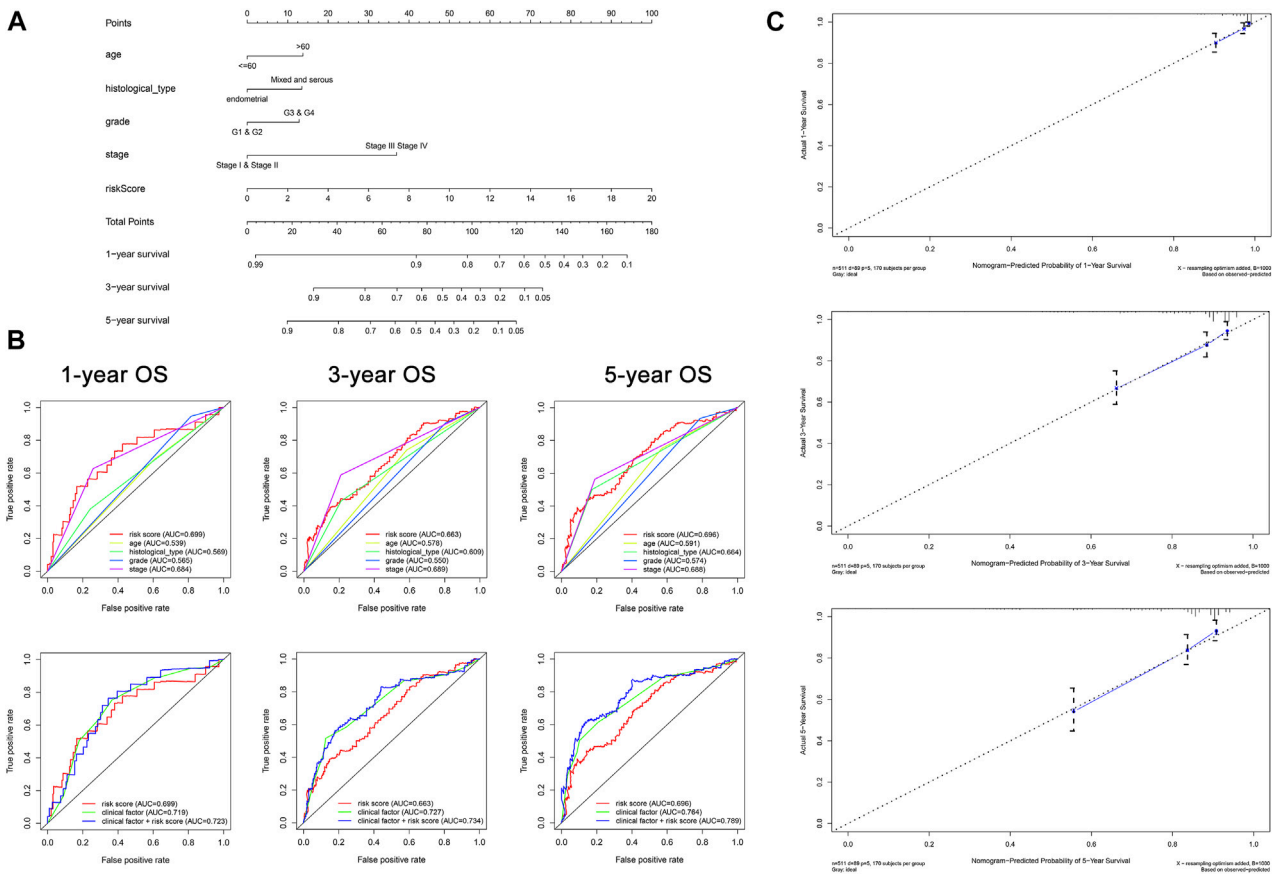

FIGURE 4 | Construction of nomogram for predicting survival of patients with UCEC (*N* = 511). **(A)** The baseline nomogram including five factors: patient age, histological type, tumor grade, tumor stage, and risk score. **(B)** ROC curves of 1-, 3-, and 5-years OS indicated that the gene-based signature had better predictive ability compared with other clinical characteristics. In addition, the nomogram composed of the signature and clinical characteristics showed superior prediction value for the prognosis. **(C)** Calibration plots of 1-, 3-, and 5-years OS suggested that the prognosis predicted by the nomogram was consistent with the actual outcome.

3.1.7 Comparison of Immune Status Between Different Risk Groups

IPS and the expression of immune modulators are able to predict the potential response of the patients to the immune checkpoint inhibitor. The scores of IPS (p = 0.004), IPS-PD1-PD-L1-PD-L2 (p = 1.297E−8), IPS-CTLA4 (7.334E−7), and IPS-PD1-PD-L1-PD-L2-CTLA4 (p = 3.776E−11) in the high-risk group were clearly higher than that in the low-risk group (**Figures 7A–D**). The expression of immune modulators including CD27, CTLA4, ICOS, PD-L2, TIGIT, PD-1, LAG3, TIM-3, CD86, PD-L1, CD70, and CD270 ($p < 0.001$) in the low-risk group was also remarkably higher than in the high-risk group (**Figure 7E**). We further discovered that the genes related to immune checkpoint inhibitor (ICI), including TIGIT, ICOS, CTLA4, CD27, CD58, PD-1, CD86, TIM-3, IDO1, and PD-L1 were negatively related to risk score (**Figures 7F–Q**), which suggested that the patients in the low-risk group promised to respond to immunotherapy.

By comparing the reaction to immune checkpoint blockade (ICB), we found that the percentage of patients with response to ICB in the high-risk group (53.18%, 142/267) was lower than that in the low-risk group (75.41%, 184/244) (**Figure 8A**). The risk scores of the responders were also lower than those of the nonresponders (**Figure 8B**). These results could demonstrate that the OXPHOS-related prognostic signature had the potential to predict the possible effect of ICB in UCEC patients and work as a classifier for therapy selection.

Moreover, we compared the MSI status of different risk groups and found, as shown in **Figures 8C–G**, the expression level of dominant mismatch repair (MMR) proteins, such as MLH1, MSH2, MSH6, PMS2, and EPCAM, in the low-risk group were lower, and risk score was negatively correlated with the MSI expression (**Figure 8I**). The patients in the low-risk group had a lower score of mRNAsi (**Figure 8H**), which can partly explain the poor prognosis in the high-risk group. In addition, significantly decreased gene expression of KIAA1429, FMR1, HINRNPC, ZC3H13, YTHDF1, and YTHDF3, which are key factors of m^{6}A mRNA methylation could be found in **Figure 8J**. These findings all provided evidence for the efficiency of immunotherapy for patients in the low-risk group and helped to elucidate the mechanisms of different outcomes.

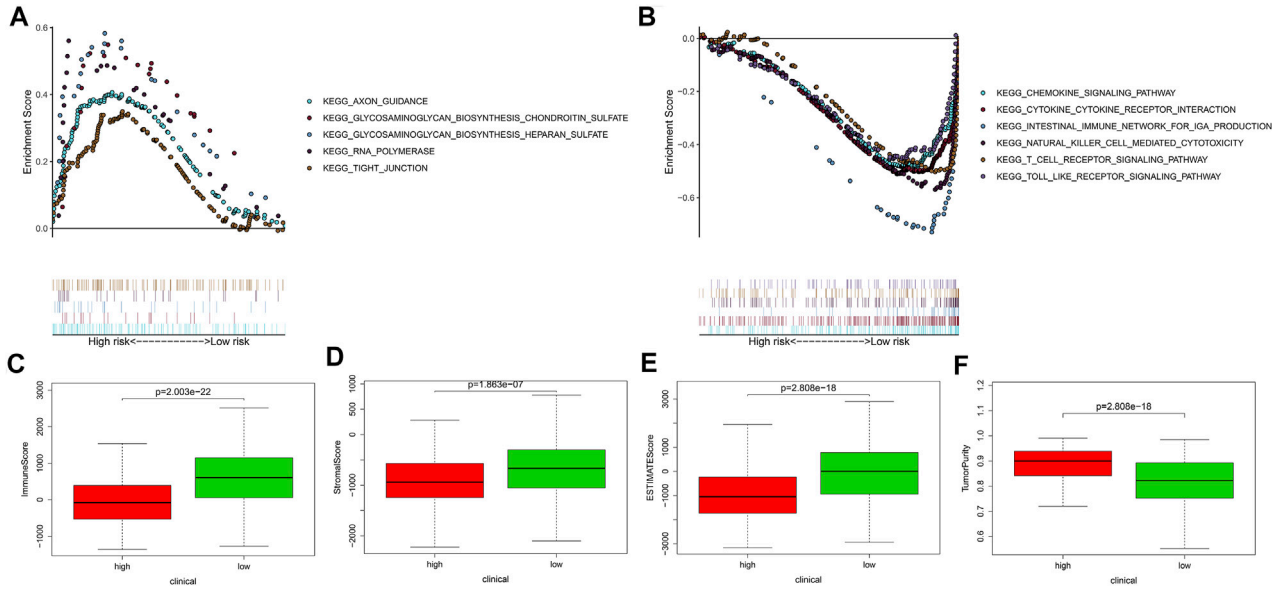

FIGURE 5 | The gene set enrichment analysis, the immune, stromal, and ESTIMATE scores, and the tumor purity of different risk groups. **(A,B)** The gene set enrichment analysis showed the significantly enriched Kyoto Encyclopedia of Genes and Genomes (KEGG) pathways in TCGA. **(C–F)** The AVONA results of the immune, stromal, and ESTIMATE scores and tumor purity in the high- and low-risk groups. Patients in the high-risk group had lower immune score, stromal score, ESTIMATE score, and higher tumor purity. In the high-risk group, *N* = 267; in the low-risk group, *N* = 244.

3.1.8 Relationship Between Tumor Mutational Burden and Risk Score

To further clarify the mechanism of tumorigenesis and development of UCEC patients, we compared the tumor mutational burden (TMB) between different risk groups based on somatic mutation data. We discovered that the low-risk group has remarkably higher TMB than the high-risk group (p = 1.278E−8) (**Figure 9A**). The correlation between risk score and TMB was negative (Cor = −0.269, p = 6.178E−11) (**Figure 9B**). We also found that only the mutation of TP53 was found in the high-risk group, whereas the others were found in the low-risk group (**Figure 9C**). Next, we divided UCEC patients into H-TMB and L-TMB groups based on the median TMB; as shown in **Figure 9D**, the OS of the H-TMB group was better than that of the L-TMB group (log-rank test, $p < 0.001$). Stratified survival analysis was conducted to assess the synergistic effect of these factors, which corroborated that TMB would not influence the effect of the signature in prognosis prediction. Significant survival differences were observed in both TMB-stratified subgroups [log-rank test, H-TMB and high risk score (HH) versus H-TMB and low risk score (HL), $p < 0.001$; L-TMB and high risk score (LH) versus L-TMB and low risk score (LL), $p < 0.001$; **Figure 9E**], which indicated that the signature could function as an independent predictive indicator and effectively evaluate the potential response to immunotherapy. The most frequent somatic mutations in the high-risk group were as follows: PTEN > TP53 > PIK3CA > ARID1A > TTN > PIK3R1 > CTNNB1 > KMT2D > CHD4 > CSMD3 (**Figure 9F**). While the most frequent somatic mutations in the low-risk group followed the order PTEN > ARID1A > PIK3CA > TTN > PIK3R1 > CTCF > MUC16 > ZFHX3 > KMT2D > MUC5B (**Figure 9G**). Other mutation details, including variant classification, mutation type, SNV class, mutation load, and top 10 mutated genes in UCEC between different risk groups, are shown in **Supplementary Figure S6**.

3.1.9 The Chemotherapeutic Response Between Different Risk Groups

The high-risk group had a higher estimated IC50 of temsirolimus, roscovitine, AZD6244, PD.0325901, RDEA119, PF.02341066, AKT. inhibitor.VIII, BMS.509744, vinblastine, bryostatin.1, metformin, AZ628, nutlin.3a, bortezomib, bicalutamide, AZD6482, cytarabine, rapamycin, camptothecin, mitomycin. C, S. Trityl.L.cysteine, tipifarnib, parthenolide, sorafenib, and methotrexate than the low-risk group ($p < 0.0001$), which demonstrated that patients with a low risk score were more sensitive to these drugs (**Figure 10**). Therefore, the OXPHOS-related prognostic signature could also be utilized as a robust and valuable classifier for chemotherapy.

4 DISCUSSION

Though the overall survival state of UCEC patients has improved a lot due to the development of early diagnostic techniques (Braun et al., 2016), there are still 15% of patients with UCEC diagnosed at an advanced stage, thus, suffering from tumor recurrence owing to a limited response to unsuitable therapies (Li and Wan, 2020). Therefore, developing valid and reliable biomarkers for survival prediction and treatment selection to avoid overtreatment in patients who will not relapse and propose

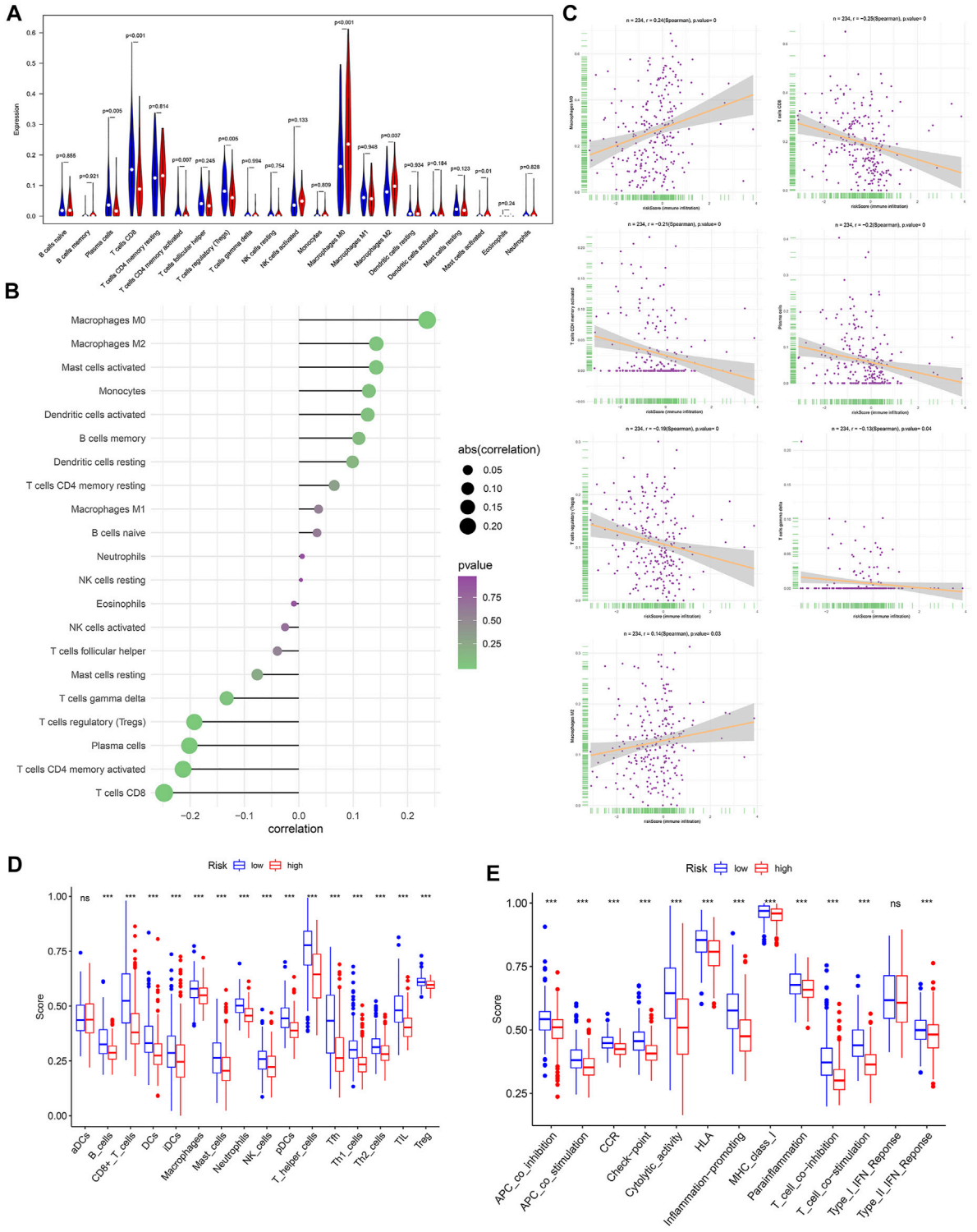

FIGURE 6 | The relationship between risk score and the tumor-infiltrating immune cells (TIICs). **(A)** Comparison of the TIICs between different risk groups. **(B)** The correlation of risk score and TIICs. **(C)** The associations between M0 macrophages, M2 macrophages, plasma cells, activated memory $CD4^+$ T cells, $CD8^+$ T cells, gamma delta T cells, regulatory T cells (Tregs), and risk score. Comparison of the single-sample gene-set enrichment analysis (ssGSEA) scores between different risk groups in TCGA cohort, including the scores of 16 immune cells **(D)** and 13 immune-related functions **(E)** displayed in boxplots. CCR, cytokine–cytokine receptor. Adjusted *p*-values were shown as ns, not significant; $^*p < 0.05$; $^{**}p < 0.01$; $^{***}p < 0.001$. In the high-risk group, $N = 267$; in the low-risk group, $N = 244$.

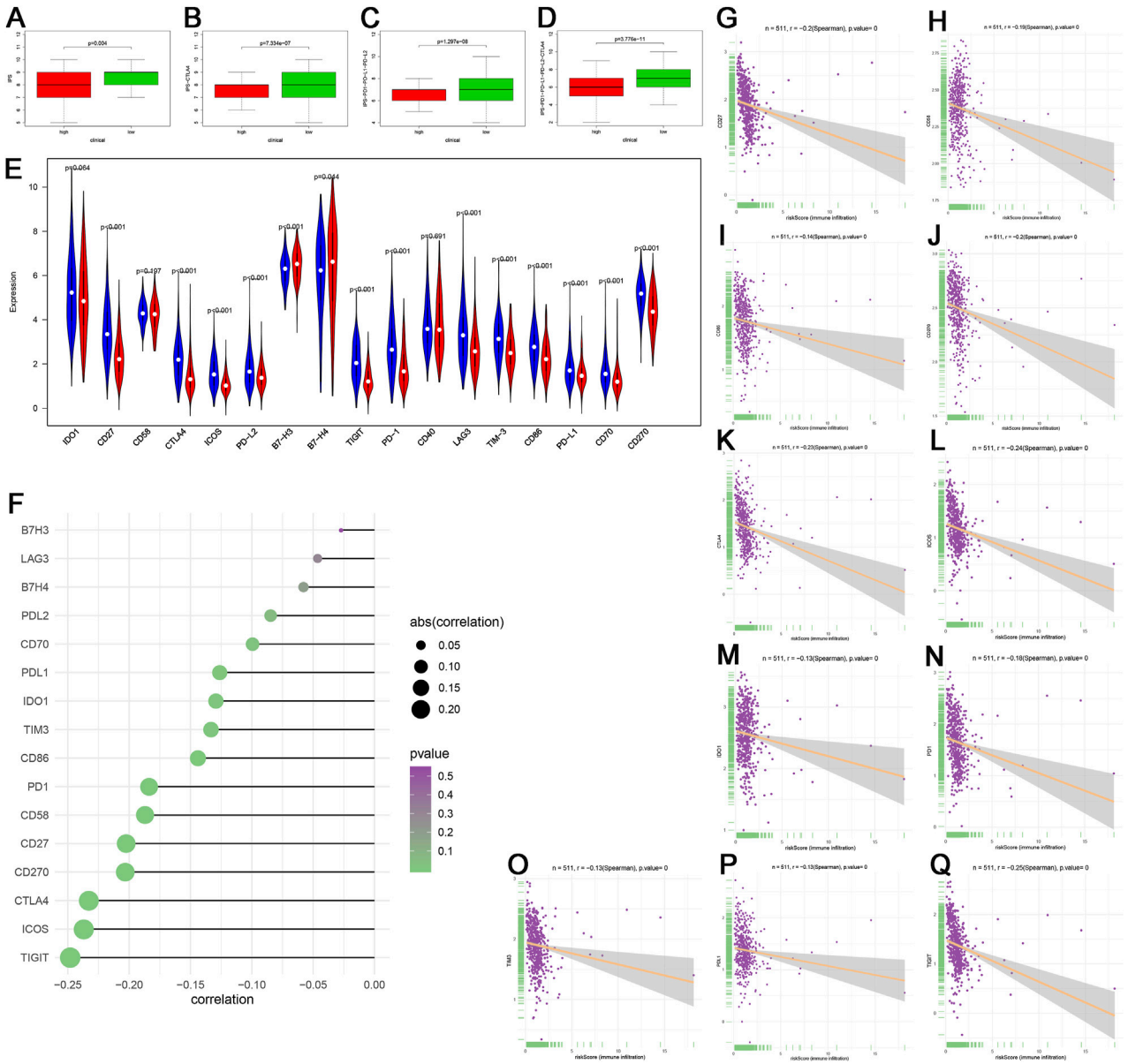

FIGURE 7 | Immunophenoscore (IPS) and gene expression analyses of immune checkpoint. **(A–D)** Patients in the low-risk group had higher scores of IPS, IPS-PD1-PD-L1-PD-L2, IPS-CTLA4, and IPS-PD1-PD-L1-PD-L2-CTLA4 than patients in the high-risk group. **(E)** Comparison of the expression of immune checkpoint between the different risk groups. **(F–Q)** The associations among TIGIT, ICOS, CTLA4, CD27, CD270, CD58, PD-1, CD86, TIM-3, IDO1, PD-L1, and risk score. In the high-risk group, *N* = 267; in the low-risk group, *N* = 244.

individual adjuvant treatment to patients who will recur counts (Lee et al., 2017), and efforts have been put into developing a robust prognostic signature based on DEGs for identification of biologic subsets to guide treatment strategies for UCEC patients, such as a cell cycle-related prognostic signature (Liu et al., 2020a), an autophagy-related prognostic signature (Wang et al., 2020b), and so on. However, there is no consensus on predictive biomarkers for scientifically validated therapy.

In recent years, emerging evidence has proved that OXPHOS could function as a new target in cancer therapy (Ashton et al., 2018). However, OXPHOS has not been involved in developing a prognostic signature for UCEC, thus far, and the potential underlying mechanism and possible clinical application of OXPHOS-related signature in cancer are worth exploring.

Based on the 289 OXPHOS-related gene matrix obtained from the research of Zihao Xu, we used differential expression analysis and identified 66 OXPHOS-related DEGs, including 54 upregulated genes and 12 downregulated genes; most of them have been reported to be associated with cancer. For instance, EPAS1 could enhance the effect of paclitaxel on breast cancer cells by inhibiting growth and promoting apoptosis of MCF-7/TAX cells (Song et al., 2020). Furthermore, functional annotation of

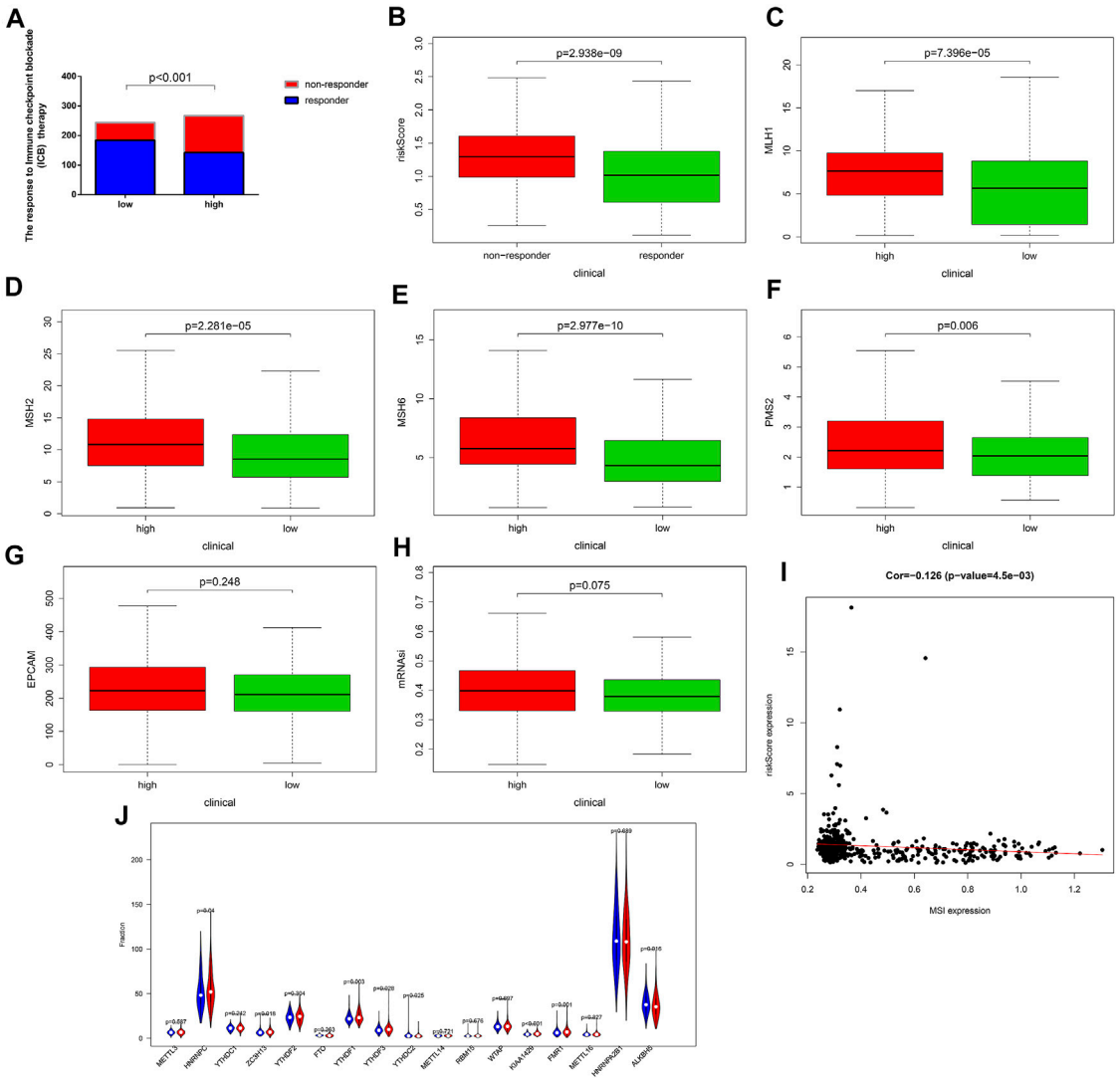

FIGURE 8 | The response to immune checkpoint blockade (ICB) therapy and the microsatellite instability (MSI) status of different risk groups. **(A)** Comparison of the response to immune checkpoint blockade (ICB) therapy between the low- and the high-risk groups. Patients in the low-risk group showed more sensitive response to ICB therapy than those in the high-risk group. **(B–G)** Patients in the low-risk group had lower expression of the dominant mismatch repair (MMR) proteins including MLH1, MSH2, MSH6, PMS2, and EPCAM than patients in the high-risk group. **(H)** The mRNAsi of the low-risk group is lower than that of the high-risk group. **(I)** The correlation between the MSI expression and the risk score. **(J)** The expression of the markers of m^6A mRNA methylation regulators in the high- and low-risk groups. m^6A, N^6-methyladenosine. In the high-risk group, N = 267; in the low-risk group, N = 244.

the OXPHOS-related DEGs also indicated that the candidate genes were significantly related to ATP metabolic process, purine ribonucleoside triphosphate metabolic process, and the essential pathways reported in many cancers (Matsuda et al., 2017; Fallah and Rini, 2019), including retrograde endocannabinoid signaling and HIF-1 signaling pathways.

Then, we randomly selected samples from the entire set in half into the train set and constructed the model based on it. After univariate Cox analysis and LASSO Cox regression analysis, finally, a prognostic model composed of four OXPHOS-related genes (ATP5IF1, COX6B1, FOXP3, and NDUFB11) was built. Except for ATP5IF1, other candidate genes included in the prognostic signature have been proven to play a vital role in cancer development. COX6B1, as one of the core proteins involved in the molecular basis of the below-background radiation stress response, might inhibit the proliferation of laryngeal squamous cell carcinoma cells (Liu et al., 2020b). FOXP3 can activate the Wnt/beta-catenin signaling pathway, thus, inducing epithelial–mesenchymal transition and promoting the progression of non-small cell lung cancer (Yang et al., 2017). In addition, the regulation of the expression of the NDUFB11 gene can regulate the programmed cell death process, so it promises to be a new target for cancer therapy (Panelli et al., 2013).

Furthermore, Kaplan–Meier survival curves in the train and entire set indicated that the patients with high risk score tend to

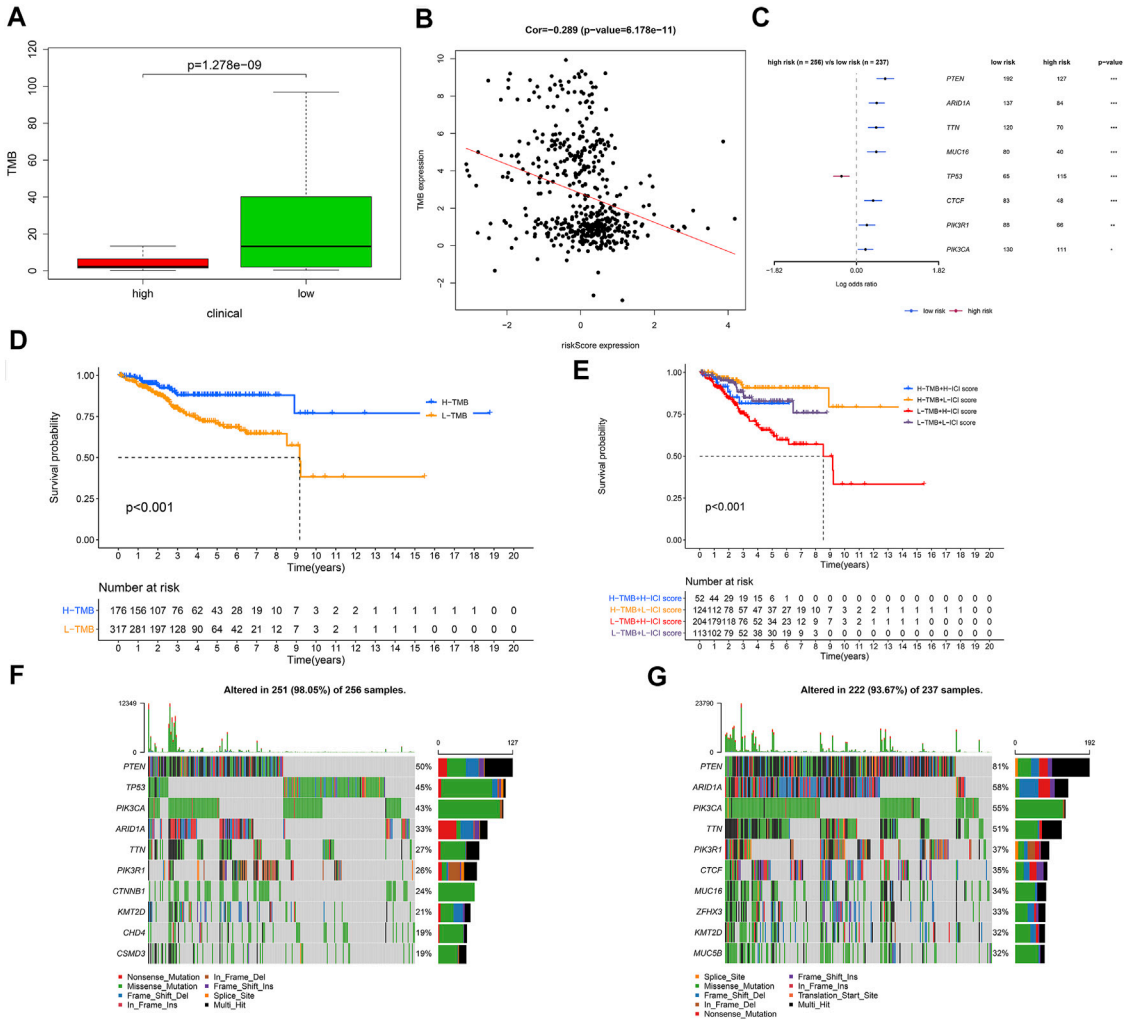

FIGURE 9 | The relationship between risk score and tumor mutational burden (TMB). **(A)** Comparison of TMB between the low- and high-risk groups. **(B)** The correlation between risk score and TMB was negative. **(C)** The regression analyses of the mutated genes. **(D)** Kaplan–Meier curves for the high and low TMB groups of the TCGA–UCEC cohort. Log-rank test, $p < 0.001$. **(E)** Kaplan–Meier curves for patients in the TCGA–UCEC cohort stratified by both TMB and risk score. Log-rank test, $p < 0.001$. **(F)** Oncoplot displaying the somatic landscape of UCEC in the high-risk group. **(G)** Oncoplot displaying the somatic landscape of UCEC in the low-risk group. In the high-risk group, $N = 267$; in the low-risk group, $N = 244$.

have a worse prognosis. Besides, a survival ROC curve analysis demonstrated the predictive value of the OXPHOS-related prognostic signature. In addition, by conjoint univariate and multivariate analyses, the independence of the OXPHOS-related signature for prognosis prediction was verified. By combining the clinical features, we performed subgroup survival analysis in different risk groups and discovered that high risk was related to poor prognosis in all subgroups. Primarily, we observed that the risk score was highly correlated to tumor stage, tumor grade, histological type, and patient age. What is more, multi-ROC curve analyses and the evaluation of the nomogram provided evidence for the potential clinical application of the signature in prognosis prediction.

The results of GSEA indicated that the representative pathways in the low-risk group were mainly related to immunization. What is more, the immune score, stromal score, and ESTIMATE score of the low-risk group were higher, and the tumor purity was lower, which implied that patients with a low risk score appeared to be more immunogenic and might preferentially benefit from immunotherapy. To penetrate the immune mechanism of the signature, we compared TIICs between the two different risk groups and analyzed the relationship between the infiltrating immune cells and risk score. We found that plasma cells, $CD8^+$ T cells, activated memory $CD4^+$ T cells, and regulatory T cells (Tregs) were remarkably elevated in the low-risk group, while M0 macrophages, M2 macrophages, and activated mast cells were significantly elevated in the high-risk group. Immune cell profiles in the tumor microenvironment (TME) of UCEC tissues could be utilized to predict the survival of patients with UCEC (Li and Wan, 2020). Under the influence of environmental stimuli, tumor-associated macrophages (TAMs) can differentiate into

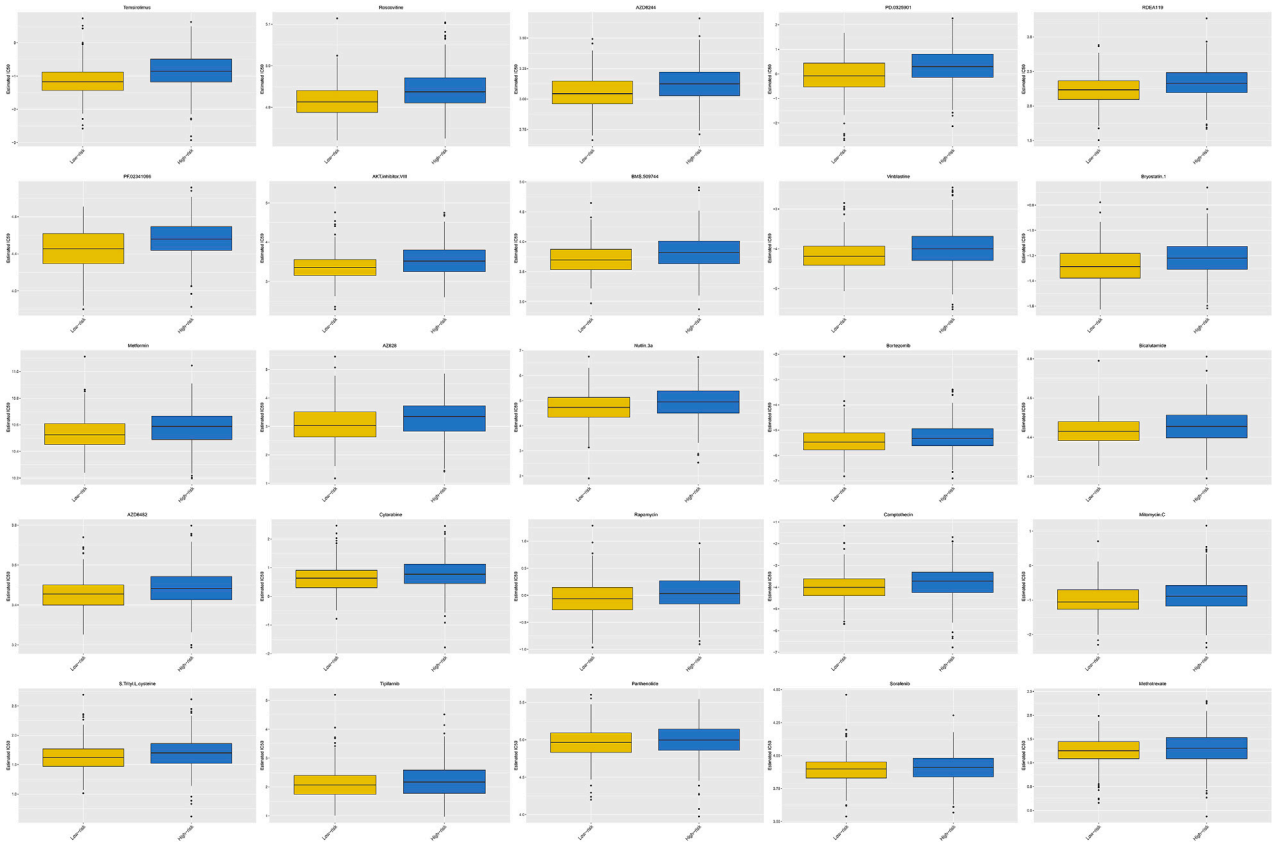

FIGURE 10 | Prediction of the response to common chemotherapy drugs between the low- and high-risk groups. Patients in the high-risk group possessed higher estimated IC50 than patients in the low-risk group. In the high-risk group, *N* = 267; in the low-risk group, *N* = 244.

two types of macrophage with opposite functions, in which M1 macrophages are protective immune cells that can remove pathogens and malignant cells. In contrast, M2 macrophages are dangerous factors, which can promote angiogenesis and the growth of tumor. High M2 macrophage infiltration in most tumor types is correlated with an adverse prognosis (Zhao et al., 2017; Wang et al., 2018), which is consistent with our results. A meta-analysis proved that UCEC patients with a high $CD8^+$ T-cell density had a favorable prognosis (Guo et al., 2020). Increased expression of activated $CD4^+$ memory T cells had been confirmed to be beneficial for prognosis in bladder cancer (Li et al., 2020), and the previous study of our team also provided evidence for the opinion (Liu et al., 2020c). The regulatory T cell (Treg) could suppress the antitumor immune response, thus, becoming a target of immunotherapy (Tanaka and Sakaguchi, 2017; Antomarchi et al., 2019), which is different from our results. However, another study showed that FOXP3 lymphocytic infiltration had no significant impact on the survival state of UCEC patients (Giatromanolaki et al., 2008). Our results suggested that $CD8^+$ T cells, activated memory $CD4^+$ T cells, regulatory T cells (Tregs), M0 macrophages, and M2 macrophages were crucial to the development of UCEC, which had the potential to be targeted for immunotherapies. The immune cell subpopulation enrichment analyses, as well as the ssGSEA-related functions or pathway analyses, showed that the scores of all the items except for aDCs and type I IFN response were higher in the low-risk group, which further proved that UCEC patients with low risk scores appeared to be more immunogenic.

Furthermore, patients with low risk scores had significantly higher scores of IPS, IPS-PD1-PD-L1-PD-L2, IPS-CTLA4, and IPS-PD1-PD-L1-PD-L2-CTLA4; thereby, they tend to respond more sensitively to immune checkpoint inhibitors. The Food and Drug Administration (FDA) has approved a series of monoclonal antibodies (mAbs) targeting PD-1, PD-L1, and CTLA-4 in several malignancy therapies (Arora et al., 2018). Besides, several clinical trials demonstrated the clinical value of anti-PD-1 antibody, pembrolizumab, which can inhibit tumor immune escaping in endometrial cancer. It has been approved as an alternative therapy for patients in the advanced stage (Musacchio et al., 2020). Also, the expression of CD27, CTLA4, ICOS, PD-L2, TIGIT, PD-1, LAG3, TIM-3, CD86, PD-L1, CD70, and CD270 were also remarkably higher in the low-risk group, which deserved to be explored as a new target for immunotherapy. TIGIT could enhance T-cell function by inhibiting PVRIG, so TIGIT-PVRIG pathways play a vital role in human cancers (Whelan et al., 2019). LAG-3 has been identified on various tumor cells, including UCEC, as a critical inducer for the

malignancy progression (Friedman et al., 2020). There is also increasing evidence for TIM-3 as an emerging target for malignancy immunotherapy (Moore et al., 2019). The difference found in the comparison of the response to immune checkpoint blockade (ICB) therapy between different risk groups showed the same trend with the above findings. We also compared the risk score of the patients showing a different response to ICB, and found that the responders tended to possess a low risk score. These results demonstrated that the OXPHOS-related prognostic signature had the potential to be the classifier for a specific subset of UCEC patients, who would have a favorable effect on ICB therapy. Compared with UCEC patients in the advanced stage, patients with primary tumor tend to have more somatic loss of mismatch repair (MMR) protein expression; thus, the loss of MMR should be considered as guidance for immunotherapy (Ta et al., 2018). We compared the MSI status of different risk groups and found that the expression of dominant MMR proteins (MLH1, MSH2, MSH6, PMS2, and EPCAM) and mRNAsi in the low-risk group was downregulated, which illustrated that the patients with low risk score were burdened with high-MSI and showed fewer stemness features associated with oncogenic dedifferentiation. Haoya Xu et al. found that cell stemness can predict patient prognosis and constructed an mRNAsi-related prognostic signature in endometrial cancer (Xu et al., 2021). Accumulating evidence revealed that m^6A mRNA methylation participates in the pathogenesis and progression of cancers through molecular mechanisms, such as inhibiting the antitumor response of $CD8^+$ T cells (Chen et al., 2019; Sun et al., 2019). Patients with a low risk score had decreased gene expression of the m^6A mRNA methylation, thus, showing a favorable response to immunotherapy.

To explore the cause of tumorigenesis, we compared the TMB of each group, and we discovered that the low-risk group had remarkably higher TMB, and the risk score was negatively correlated with TMB. It is reported that patients with high TMB had a more sensitive response to immune checkpoint blockade, such as anti-PD-1 agents (Fancello et al., 2019). A multicohort study demonstrated the value of tissue TMB (tTMB) as a predictive biomarker for response to pembrolizumab monotherapy (Marabelle et al., 2020). In our present study, the most frequent somatic mutations in the low-risk group were PTEN, ARID1A, PIK3CA, TTN, PIK3R1, CTCF, MUC16, ZFHX3, KMT2D, and MUC5B. PTEN functions as a tumor inhibitor by decreasing the activity of phosphoinositide 3-kinase (PI3K) (Bian et al., 2018), and its expression diminished with the progression of UCEC (Xi et al., 2019). It has been proven that ARID1A alterations indicated improved prognosis of tumor patients for compromising MMR and enhancing the infiltration of lymphocytes (Jiang et al., 2020). UCEC patients with high PIK3CA had shorter survival time because PIK3CA could change the tumor immune microenvironment by altering the fraction of tumor-associated neutrophils (Pan et al., 2019). Eighty-five percent of lung squamous cell carcinoma patients with TTN mutant type had missense variations and favorable overall survival (Cheng et al., 2019). In addition, patients in the high TMB group showed better overall survival than in the low TMB group, and the combined Kaplan–Meier analyses proved that risk score was a reliable predictive indicator independent of TMB. Our results were consistent with previous studies, indicating that UCEC patients with low risk score tend to have improved response to immunotherapy and favorable prognosis.

We compared the predicted effectiveness of chemotherapy drugs between different risk groups by using the GDSC dataset. Patients with UCEC in the low-risk group were more sensitive to temsirolimus, roscovitine, AZD6244, PD.0325901, RDEA119, PF.02341066, AKT. inhibitor.VIII, BMS.509744, vinblastine, bryostatin.1, metformin, AZ628, nutlin.3a, bortezomib, bicalutamide, AZD6482, cytarabine, rapamycin, camptothecin, mitomycin. C, S. Trityl.L.cysteine, tipifarnib, parthenolide, sorafenib, and methotrexate, which might be a potential helpful treatment option for UCEC.

These findings indicated that patients with low risk scores possessed higher IPS, higher TMB, and responded more sensitively to ICI and chemotherapy, which partly explained the reason for the improved prognosis of the low-risk patients.

However, there are still some deficiencies with our study. First of all, our data were based entirely on TCGA databases and lacked an external database for validation. Second, our molecular results lack the evidence of the experiments *in vitro* or *in vivo*. Third, these OXPHOS-related prognostic genes are supposed to be further examined by cell function assay for biological function and pathway analyses.

5 CONCLUSION

In conclusion, an OXPHOS-related and immune microenvironment prognostic signature classifying EC patients into different risk subsets was constructed in our study. This model could predict the prognosis of patients and help to select a specific subset of patients who might benefit from immunotherapy and chemotherapy, thus, improving the overall survival rate. These results may also contribute to the identification of novel immune biomarkers or target therapy in UCEC and give a new insight into the tumorigenesis and progression of UCEC.

DATA AVAILABILITY STATEMENT

The datasets presented in this study can be found in online repositories. The names of the repository/repositories and accession number(s) can be found in the article/ **Supplementary Material**.

ETHICS STATEMENT

The studies involving human participants were reviewed and approved by the Nanjing Medical University. The patients/ participants provided their written informed consent to participate in this study. Written informed consent was

obtained from the individual(s) for the publication of any potentially identifiable images or data included in this article.

AUTHOR CONTRIBUTIONS

JB, HY, JL, TC, and ZZ conceived the study and participated in the study design, performance, and manuscript writing. MY, SN, and SY conducted the bioinformatics analysis. LC and FS revised the manuscript. All authors read and approved the final manuscript.

ACKNOWLEDGMENTS

We would like to thank the researchers and study participants for their contributions.

SUPPLEMENTARY MATERIAL

The Supplementary Material for this article can be found online at: https://www.frontiersin.org/articles/10.3389/fcell.2021.753004/full#supplementary-material

Supplementary Figure S1 | Selected OXPHOS-related DEGs from uterine corpus endometrial carcinoma samples. Heatmap **(A)** and volcano plot **(B)** of OXPHOS-related DEGs between UCEC and normal endometrium. Red dots represented up-regulated OXPHOS-related DEGs, green dots represented down-regulated OXPHOS-related DEGs and black dots represented no OXPHOS-related DEGs. Functional annotation of the OXPHOS-related DEGs included Gene ontology analysis **(C)** and Kyoto Encyclopedia of Genes and Genomes pathway analysis **(D)**. **(E)** The PPI network indicated the interactions between OXPHOS-related DEGs.

Supplementary Figure S2 | Construction of a prognostic model based on OXPHOS-related DEGs. **(A,B)** LASSO Cox regression analysis and multivariate Cox regression analysis. **(C)** Forest plots present the multivariate Cox proportional hazards regression analysis of the prognosis-associated OXPHOS-related DEGs.

Supplementary Figure S3 | (A–D) The expression of the four prognostic OXPHOS-related DEGs in tumor (N = 511) and normal tissue (N = 23). **(E,F)** The relationship between ATP5IF1, FOXP3 and the overall survival of UCEC patients. **(G–J)** Expression levels of the four OXPHOS-related DEGs mRNA in clinical tissue samples.

Supplementary Figure S4 | Stratified analysis. **(A–H)** The Kaplan-Meier survival analyses based on the prognostic signature stratified by tumor stage, tumor grade, histological type, patient age in the TCGA-UCEC cohort. **(I–L)** Relationship between the prognostic signature and tumor stage, tumor grade, histological type and age in the TCGA-UCEC cohort.

Supplementary Figure S5 | The heatmap shows the OXPHOS-related prognostic genes expression and clinical characteristics of the TCGA-UCEC cohort.

Supplementary Figure S6 | Variant classification, mutation type, SNV class, mutation load and top 10 mutated genes in UCEC between low **(A)** and high risk groups **(B)**. In the high risk group, N = 267; in the low risk group, N = 244.

REFERENCES

Antomarchi, J., Ambrosetti, D., Cohen, C., Delotte, J., Chevallier, A., Karimdjee-Soilihi, B., et al. (2019). Immunosuppressive Tumor Microenvironment Status and Histological Grading of Endometrial Carcinoma. *Cancer Microenvironment* 12, 169–179. doi:10.1007/s12307-019-00225-1

Arora, E., Masab, M., Mittar, P., Jindal, V., Gupta, S., and Dourado, C. (2018). Role of Immune Checkpoint Inhibitors in Advanced or Recurrent Endometrial Cancer. *Cureus* 10, e2521. doi:10.7759/cureus.2521

Ashburner, M., Ball, C. A., Blake, J. A., Botstein, D., Butler, H., Cherry, J. M., et al. (2000). Gene Ontology: Tool for the Unification of Biology. *Nat. Genet.* 25, 25–29. doi:10.1038/75556

Ashton, T. M., McKenna, W. G., Kunz-Schughart, L. A., and Higgins, G. S. (2018). Oxidative Phosphorylation as an Emerging Target in Cancer Therapy. *Clin. Cancer Res.* 24, 2482–2490. doi:10.1158/1078-0432.ccr-17-3070

Bian, X., Gao, J., Luo, F., Rui, C., Zheng, T., Wang, D., et al. (2018). PTEN Deficiency Sensitizes Endometrioid Endometrial Cancer to Compound PARP-Pi3k Inhibition but Not PARP Inhibition as Monotherapy. *Oncogene* 37, 341–351. doi:10.1038/onc.2017.326

Braun, M. M., Overbeek-Wager, E. A., and Grumbo, R. J. (2016). Diagnosis and Management of Endometrial Cancer. *Am. Fam. Physician* 93, 468–474.

Bray, F., Ferlay, J., Soerjomataram, I., Siegel, R. L., Torre, L. A., and Jemal, A. (2018). Global Cancer Statistics 2018: GLOBOCAN Estimates of Incidence and Mortality Worldwide for 36 Cancers in 185 Countries. *CA: a Cancer J. clinicians* 68, 394–424. doi:10.3322/caac.21492

Cancer Genome Atlas Research, N., Kandoth, C., Schultz, N., Cherniack, A. D., Akbani, R., Liu, Y., et al. (2013). Integrated Genomic Characterization of Endometrial Carcinoma. *Nature* 497, 67–73. doi:10.1038/nature12113

Cardenas, C., Lovy, A., Silva-Pavez, E., Urra, F., Mizzoni, C., Ahumada-Castro, U., et al. (2020). Cancer Cells with Defective Oxidative Phosphorylation Require Endoplasmic Reticulum-To-Mitochondria Ca2+ Transfer for Survival. *Sci. Signal.* 13, eaay1212. doi:10.1126/scisignal.aay1212

Charoentong, P., Finotello, F., Angelova, M., Mayer, C., Efremova, M., Rieder, D., et al. (2017). Pan-cancer Immunogenomic Analyses Reveal Genotype-Immunophenotype Relationships and Predictors of Response to Checkpoint Blockade. *Cel Rep.* 18, 248–262. doi:10.1016/j.celrep.2016.12.019

Chen, X.-Y., Zhang, J., and Zhu, J.-S. (2019). The Role of m6A RNA Methylation in Human Cancer. *Mol. Cancer* 18, 103. doi:10.1186/s12943-019-1033-z

Cheng, X., Yin, H., Fu, J., Chen, C., An, J., Guan, J., et al. (2019). Aggregate Analysis Based on TCGA: TTN Missense Mutation Correlates with Favorable Prognosis in Lung Squamous Cell Carcinoma. *J. Cancer Res. Clin. Oncol.* 145, 1027–1035. doi:10.1007/s00432-019-02861-y

Commander, R., Wei, C., Sharma, A., Mouw, J. K., Burton, L. J., Summerbell, E., et al. (2020). Subpopulation Targeting of Pyruvate Dehydrogenase and GLUT1 Decouples Metabolic Heterogeneity during Collective Cancer Cell Invasion. *Nat. Commun.* 11, 1533. doi:10.1038/s41467-020-15219-7

Fallah, J., and Rini, B. I. (2019). HIF Inhibitors: Status of Current Clinical Development. *Curr. Oncol. Rep.* 21, 6. doi:10.1007/s11912-019-0752-z

Fancello, L., Gandini, S., Pelicci, P. G., and Mazzarella, L. (2019). Tumor Mutational burden Quantification from Targeted Gene Panels: Major Advancements and Challenges. *J. Immunotherapy Cancer* 7, 183. doi:10.1186/s40425-019-0647-4

Friedman, L. A., Ring, K. L., and Mills, A. M. (2020). LAG-3 and GAL-3 in Endometrial Carcinoma. *Int. J. Gynecol. Pathol.* 39, 203–212. doi:10.1097/pgp.0000000000000608

Geeleher, P., Cox, N. J., and Huang, R. (2014). Clinical Drug Response Can Be Predicted Using Baseline Gene Expression Levels and *In Vitro* Drug Sensitivity in Cell Lines. *Genome Biol.* 15, R47. doi:10.1186/gb-2014-15-3-r47

Giatromanolaki, A., Bates, G. J., Koukourakis, M. I., Sivridis, E., Gatter, K. C., Harris, A. L., et al. (2008). The Presence of Tumor-Infiltrating FOXP3+ Lymphocytes Correlates with Intratumoral Angiogenesis in Endometrial Cancer. *Gynecol. Oncol.* 110, 216–221. doi:10.1016/j.ygyno.2008.04.021

Guo, F., Dong, Y., Tan, Q., Kong, J., and Yu, B. (2020). Tissue Infiltrating Immune Cells as Prognostic Biomarkers in Endometrial Cancer: A Meta-Analysis. *Dis. Markers* 2020, 1805764. doi:10.1155/2020/1805764

He, Y., Jiang, Z., Chen, C., and Wang, X. (2018). Classification of Triple-Negative Breast Cancers Based on Immunogenomic Profiling. *J. Exp. Clin. Cancer Res.* 37, 327. doi:10.1186/s13046-018-1002-1

Heagerty, P. J., Lumley, T., and Pepe, M. S. (2000). Time-dependent ROC Curves for Censored Survival Data and a Diagnostic Marker. *Biometrics* 56, 337–344. doi:10.1111/j.0006-341x.2000.00337.x

Iasonos, A., Schrag, D., Raj, G. V., and Panageas, K. S. (2008). How to Build and Interpret a Nomogram for Cancer Prognosis. *J. Clin. Oncol.* 26, 1364–1370. doi:10.1200/jco.2007.12.9791

Jiang, T., Chen, X., Su, C., Ren, S., and Zhou, C. (2020). Pan-cancer Analysis of ARID1A Alterations as Biomarkers for Immunotherapy Outcomes. *J. Cancer* 11, 776–780. doi:10.7150/jca.41296

Kanehisa, M., and Goto, S. (2000). KEGG: Kyoto Encyclopedia of Genes and Genomes. *Nucleic Acids Res.* 28, 27–30. doi:10.1093/nar/28.1.27

Lai, Y. J., Chou, Y. C., Lin, Y. J., Yu, M. H., Ou, Y. C., Chu, P. W., et al. (2019). Pyruvate Kinase M2 Expression: A Potential Metabolic Biomarker to Differentiate Endometrial Precancer and Cancer that Is Associated with Poor Outcomes in Endometrial Carcinoma. *Int. J. Environ. Res. Public Health* 16, 4589. doi:10.3390/ijerph16234589

LeBleu, V. S., O'Connell, J. T., Gonzalez Herrera, K. N., Wikman, H., Pantel, K., Haigis, M. C., et al. (2014). PGC-1α Mediates Mitochondrial Biogenesis and Oxidative Phosphorylation in Cancer Cells to Promote Metastasis. *Nat. Cel Biol* 16, 9921–100315. doi:10.1038/ncb3039

Lee, Y. C., Lheureux, S., and Oza, A. M. (2017). Treatment Strategies for Endometrial Cancer: Current Practice and Perspective. *Curr. Opin. Obstet. Gynecol.* 29, 47–58. doi:10.1097/gco.0000000000000338

Li, B. L., and Wan, X. P. (2020). Prognostic Significance of Immune Landscape in Tumour Microenvironment of Endometrial Cancer. *J. Cel Mol Med* 24, 7767–7777. doi:10.1111/jcmm.15408

Li, W., Zeng, J., Luo, B., Mao, Y., Liang, Y., Zhao, W., et al. (2020). High Expression of Activated CD4+ Memory T Cells and CD8+ T Cells and Low Expression of M0 Macrophage Are Associated with Better Clinical Prognosis in Bladder Cancer Patients. *Xi Bao Yu Fen Zi Mian Yi Xue Za Zhi* 36, 97–103.

Liu, J., Mei, J., Li, S., Wu, Z., and Zhang, Y. (2020a). Establishment of a Novel Cell Cycle-Related Prognostic Signature Predicting Prognosis in Patients with Endometrial Cancer. *Cancer Cel Int* 20, 329. doi:10.1186/s12935-020-01428-z

Liu, J., Ma, T., Gao, M., Liu, Y., Liu, J., Wang, S., et al. (2020b). Proteomic Characterization of Proliferation Inhibition of Well-Differentiated Laryngeal Squamous Cell Carcinoma Cells under Below-Background Radiation in a Deep Underground Environment. *Front. Public Health* 8, 584964. doi:10.3389/fpubh.2020.584964

Liu, J., Chen, X., Jiang, Y., and Cheng, W. (2020c). Development of an Immune Gene Prognostic Classifier for Survival Prediction and Respond to Immunocheckpoint Inhibitor Therapy/chemotherapy in Endometrial Cancer. *Int. immunopharmacology* 86, 106735. doi:10.1016/j.intimp.2020.106735

Malta, T. M., Sokolov, A., Gentles, A. J., Burzykowski, T., Poisson, L., Weinstein, J. N., et al. (2018). Machine Learning Identifies Stemness Features Associated with Oncogenic Dedifferentiation. *Cell* 173, 338–354. doi:10.1016/j.cell.2018.03.034

Marabelle, A., Fakih, M., Lopez, J., Shah, M., Shapira-Frommer, R., Nakagawa, K., et al. (2020). Association of Tumour Mutational burden with Outcomes in Patients with Advanced Solid Tumours Treated with Pembrolizumab: Prospective Biomarker Analysis of the Multicohort, Open-Label, Phase 2 KEYNOTE-158 Study. *Lancet Oncol.* 21, 1353–1365. doi:10.1016/s1470-2045(20)30445-9

Matsuda, F., Toya, Y., and Shimizu, H. (2017). Learning from Quantitative Data to Understand central Carbon Metabolism. *Biotechnol. Adv.* 35, 971–980. doi:10.1016/j.biotechadv.2017.09.006

Molina, J. R., Sun, Y., Protopopova, M., Gera, S., Bandi, M., Bristow, C., et al. (2018). An Inhibitor of Oxidative Phosphorylation Exploits Cancer Vulnerability. *Nat. Med.* 24, 1036–1046. doi:10.1038/s41591-018-0052-4

Moore, M., Ring, K. L., and Mills, A. M. (2019). TIM-3 in Endometrial Carcinomas: an Immunotherapeutic Target Expressed by Mismatch Repair-Deficient and Intact Cancers. *Mod. Pathol.* 32, 1168–1179. doi:10.1038/s41379-019-0251-7

Mosier, J. A., Schwager, S. C., Boyajian, D. A., and Reinhart-King, C. A. (2021). Cancer Cell Metabolic Plasticity in Migration and Metastasis. *Clin. Exp. metastasis* 38 (4), 343–359. doi:10.1007/s10585-021-10102-1

Musacchio, L., Boccia, S. M., Caruso, G., Santangelo, G., Fischetti, M., Tomao, F., et al. (2020). Immune Checkpoint Inhibitors: A Promising Choice for Endometrial Cancer Patients? *J. Clin. Med.* 9, 1721. doi:10.3390/jcm9061721

Nayak, A. P., Kapur, A., Barroilhet, L., and Patankar, M. S. (2018). Oxidative Phosphorylation: A Target for Novel Therapeutic Strategies against Ovarian Cancer. *Cancers (Basel)* 10, 337. doi:10.3390/cancers10090337

Newman, A. M., Liu, C. L., Green, M. R., Gentles, A. J., Feng, W., Xu, Y., et al. (2015). Robust Enumeration of Cell Subsets from Tissue Expression Profiles. *Nat. Methods* 12, 453–457. doi:10.1038/nmeth.3337

Pan, Y., Jia, L. P., Liu, Y., Han, Y., and Deng, Q. (2019). Alteration of Tumor Associated Neutrophils by PIK3CA Expression in Endometrial Carcinoma from TCGA Data. *J. Ovarian Res.* 12, 81. doi:10.1186/s13048-019-0557-6

Panelli, D., Lorusso, F. P., Papa, F., Panelli, P., Stella, A., Caputi, M., et al. (2013). The Mechanism of Alternative Splicing of the X-Linked NDUFB11 Gene of the Respiratory Chain Complex I, Impact of Rotenone Treatment in Neuroblastoma Cells. *Biochim. Biophys. Acta (Bba) - Gene Regul. Mech.* 1829, 211–218. doi:10.1016/j.bbagrm.2012.12.001

Qu, L., Wang, Z.-l., Chen, Q., Li, Y.-m., He, H.-w., Hsieh, J. J., et al. (2018). Prognostic Value of a Long Non-coding RNA Signature in Localized Clear Cell Renal Cell Carcinoma. *Eur. Urol.* 74, 756–763. doi:10.1016/j.eururo.2018.07.032

Robinson, D. R., Wu, Y.-M., Lonigro, R. J., Vats, P., Cobain, E., Everett, J., et al. (2017). Integrative Clinical Genomics of Metastatic Cancer. *Nature* 548, 297–303. doi:10.1038/nature23306

Sica, V., Bravo-San Pedro, J. M., Stoll, G., and Kroemer, G. (2020). Oxidative Phosphorylation as a Potential Therapeutic Target for Cancer Therapy. *Int. J. Cancer* 146, 10–17. doi:10.1002/ijc.32616

Song, Y., Zhang, M., Lu, M. M., Qu, L. Y., Xu, S. G., Li, Y. Z., et al. (2020). EPAS1 Targeting by miR-152-3p in Paclitaxel-Resistant Breast Cancer. *J. Cancer* 11, 5822–5830. doi:10.7150/jca.46898

Sun, T., Wu, R., and Ming, L. (2019). The Role of m6A RNA Methylation in Cancer. *Biomed. Pharmacother.* 112, 108613. doi:10.1016/j.biopha.2019.108613

Ta, R. M., Hecht, J. L., and Lin, D. I. (2018). Discordant Loss of Mismatch Repair Proteins in Advanced Endometrial Endometrioid Carcinoma Compared to Paired Primary Uterine Tumors. *Gynecol. Oncol.* 151, 401–406. doi:10.1016/j.ygyno.2018.10.012

Tanaka, A., and Sakaguchi, S. (2017). Regulatory T Cells in Cancer Immunotherapy. *Cell Res* 27, 109–118. doi:10.1038/cr.2016.151

Toh, J. W. T., Phan, K., Reza, F., Chapuis, P., and Spring, K. J. (2021). Rate of Dissemination and Prognosis in Early and Advanced Stage Colorectal Cancer Based on Microsatellite Instability Status: Systematic Review and Meta-Analysis. *Int. J. colorectal Dis.* 36 (8), 1573–1596. doi:10.1007/s00384-021-03874-1

Tomczak, K., Czerwińska, P., and Wiznerowicz, M. (2015). The Cancer Genome Atlas (TCGA): an Immeasurable Source of Knowledge. *Contemp. Oncol. (Pozn)* 19, A68–A77. doi:10.5114/wo.2014.47136

Wang, N., Liu, W., Zheng, Y., Wang, S., Yang, B., Li, M., et al. (2018). CXCL1 Derived from Tumor-Associated Macrophages Promotes Breast Cancer Metastasis via Activating NF-Kb/sox4 Signaling. *Cell Death Dis* 9, 880. doi:10.1038/s41419-018-0876-3

Wang, T., Kong, S., Tao, M., and Ju, S. (2020a). The Potential Role of RNA N6-Methyladenosine in Cancer Progression. *Mol. Cancer* 19, 88. doi:10.1186/s12943-020-01204-7

Wang, H., Ma, X., Liu, J., Wan, Y., Jiang, Y., Xia, Y., et al. (2020b). Prognostic Value of an Autophagy-Related Gene Expression Signature for Endometrial Cancer Patients. *Cancer Cel Int* 20, 306. doi:10.1186/s12935-020-01413-6

Whelan, S., Ophir, E., Kotturi, M. F., Levy, O., Ganguly, S., Leung, L., et al. (2019). PVRIG and PVRL2 Are Induced in Cancer and Inhibit CD8+ T-Cell Function. *Cancer Immunol. Res.* 7, 257–268. doi:10.1158/2326-6066.cir-18-0442

Xi, Z., Jing, L., Le-Ni, K., Zhu, L., Ze-Wen, D., Hui, Y., et al. (2019). Evaluation of PTEN and CD4+FOXP3+ T Cell Expressions as Diagnostic and Predictive Factors in Endometrial Cancer. *Medicine* 98, e16345. doi:10.1097/md.0000000000016345

Xu, H., Zou, R., Liu, J., and Zhu, L. (2021). A Risk Signature with Nine Stemness Index-Associated Genes for Predicting Survival of Patients with Uterine Corpus Endometrial Carcinoma. *J. Oncol.* 2021, 6653247. doi:10.1155/2021/6653247

Xu, Y., Xue, D., Bankhead, A., 3rd, and Neamati, N. (2020a). Why All the Fuss about Oxidative Phosphorylation (OXPHOS)? *J. Med. Chem.* 63, 14276–14307. doi:10.1021/acs.jmedchem.0c01013

Xu, Z., Wu, Z., Zhang, J., Zhou, R., Ye, L., Yang, P., et al. (2020b). Development and Validation of an Oxidative Phosphorylation-Related Gene Signature in Lung Adenocarcinoma. *Epigenomics* 12, 1333–1348. doi:10.2217/epi-2020-0217

Yang, S., Liu, Y., Li, M.-Y., Ng, C. S. H., Yang, S.-l., Wang, S., et al. (2017). FOXP3 Promotes Tumor Growth and Metastasis by Activating Wnt/β-Catenin

Signaling Pathway and EMT in Non-small Cell Lung Cancer. *Mol. Cancer* 16, 124. doi:10.1186/s12943-017-0700-1

Yang, W., Soares, J., Greninger, P., Edelman, E. J., Lightfoot, H., Forbes, S., et al. (2013). Genomics of Drug Sensitivity in Cancer (GDSC): a Resource for Therapeutic Biomarker Discovery in Cancer Cells. *Nucleic Acids Res.* 41, D955–D961. doi:10.1093/nar/gks1111

Yoshihara, K., Shahmoradgoli, M., Martínez, E., Vegesna, R., Kim, H., Torres-Garcia, W., et al. (2013). Inferring Tumour Purity and Stromal and Immune Cell Admixture from Expression Data. *Nat. Commun.* 4, 2612. doi:10.1038/ncomms3612

Zhao, X., Qu, J., Sun, Y., Wang, J., Liu, X., Wang, F., et al. (2017). Prognostic Significance of Tumor-Associated Macrophages in Breast Cancer: a Meta-Analysis of the Literature. *Oncotarget* 8, 30576–30586. doi:10.18632/oncotarget.15736

Zhu, X., Tian, X., Yu, C., Shen, C., Yan, T., Hong, J., et al. (2016). A Long Non-coding RNA Signature to Improve Prognosis Prediction of Gastric Cancer. *Mol. Cancer* 15, 60. doi:10.1186/s12943-016-0544-0

Conflict of Interest: The authors declare that the research was conducted in the absence of any commercial or financial relationships that could be construed as a potential conflict of interest.

Publisher's Note: All claims expressed in this article are solely those of the authors and do not necessarily represent those of their affiliated organizations, or those of the publisher, the editors and the reviewers. Any product that may be evaluated in this article, or claim that may be made by its manufacturer, is not guaranteed or endorsed by the publisher.

frontiers in Molecular Biosciences

ORIGINAL RESEARCH
published: 02 December 2021
doi: 10.3389/fmolb.2021.714906

Integrative Analysis of MALT1 as a Potential Therapeutic Target for Prostate Cancer and its Immunological Role in Pan-Cancer

Haotian Tan[1†], Yaqi Xie[2†], Xuebao Zhang[3], Shuang Wu[1], Hongwei Zhao[1], Jitao Wu[1], Wenting Wang[4] and Chunhua Lin[1]**

[1]Department of Urology, The Affiliated Yantai Yuhuangding Hospital of Qingdao University, Yantai, China, [2]Department of Urology, The Affiliated Yantai Yuhuangding Hospital of Binzhou Medical University, Yantai, China, [3]Department of Reproductive Medicine, The Affiliated Yantai Yuhuangding Hospital of Qingdao University, Yantai, China, [4]Central Laboratory, Yantai Yuhuangding Hospital, Yantai, China

OPEN ACCESS

Edited by:
Shengtao Zhou,
Sichuan University, China

Reviewed by:
Tabish H. Khan,
University of Virginia, United States
Zhan Wang,
Zhejiang University, China

***Correspondence:**
Wenting Wang
wwting_78@163.com
Chunhua Lin
linchunhua1980@163.com

†These authors have contributed equally to this work and share first authorship

Specialty section:
This article was submitted to Molecular Diagnostics and Therapeutics, a section of the journal Frontiers in Molecular Biosciences

Received: 26 May 2021
Accepted: 15 November 2021
Published: 02 December 2021

Citation:
Tan H, Xie Y, Zhang X, Wu S, Zhao H, Wu J, Wang W and Lin C (2021) Integrative Analysis of MALT1 as a Potential Therapeutic Target for Prostate Cancer and its Immunological Role in Pan-Cancer. Front. Mol. Biosci. 8:714906. doi: 10.3389/fmolb.2021.714906

Background: Mucosa-associated lymphoma antigen 1 (MALT1) is an oncogene in subsets of diffuse large B cell lymphoma (DLBCL) and mucosa-associated lymphoid tissue type (MALT) lymphoma. However, the role of MALT1 across cancers, especially in prostate cancer is still poorly understood.

Methods: Here, we used several public datasets to evaluate MALT1 expression. Then, PCa cell lines and nude mice were used to investigate the cellular functions *in vitro* and *in vivo*. Microarray data were downloaded from The Cancer Genome Atlas and MALT1 was subjected to gene set enrichment analysis (GSEA) and Gene Ontology (GO) analysis to identify the biological functions and relevant pathways. Additionally, the correlations between MALT1 expression and mismatch repair (MMR) gene mutation, immune checkpoint gene expression, tumor mutational burden (TMB), and microsatellite instability (MSI) were investigated by Pearson correlation analysis. Moreover, the correlation between MALT1 expression and tumor immune infiltration was analyzed by the Tumor Immune Evaluation Resource (TIMER) database.

Results: MALT1 overexpression was significantly correlated with MMR gene mutation levels and crucially promoted proliferation and colony genesis while reducing PCa cell apoptosis levels *in vivo* and *in vitro*. MALT1 expression showed strong correlations with immune checkpoint genes, TMB, and MSI in most cancers. The GO analysis indicated that MALT1-coexpressed genes were involved in heterotypic cell-cell adhesion, actin filament-based movement regulation, and action potential regulation. GSEA revealed that MALT1 expression was associated with several signaling pathways, including the NF-κB signaling, Wnt/β-catenin and TGF-β signaling pathways, in PCa. Additionally, MALT1 expression was significantly correlated with the infiltration of immune cells, including B cells, $CD8^+$ T cells, dendritic cells and macrophages, and negatively correlated with $CD4^+$ cell infiltration in PCa.

Conclusion: MALT1 expression is higher in pancancer samples than in normal tissues. MALT1 promoted proliferation and colony genesis while reducing PCa cell apoptosis

levels, and MALT1 suppression could inhibit xenograft tumor establishment in nude mice. Furthermore, MALT1 expression is closely related to the occurrence and development of multiple tumors in multiple ways. Therefore, MALT1 may be an emerging therapeutic target for a variety of cancers especially PCa.

Keywords: prostate cancer, pancancer, Malt1, bioinformatics analysis, therapeutic target

INTRODUCTION

Prostate cancer (PCa), also called prostate adenocarcinoma (PRAD), is the most common malignant cancer apart from lung cancer in males worldwide, and the second leading cause of male cancer-related death in worldwide (Gasnier and Parvizi, 2017; Bray et al., 2018). Most patients with PCa usually receive localized radical prostatectomy, radiation therapy, proton beam therapy, and cryosurgery after diagnosis (Shipley et al., 1995; Donnelly et al., 2010; Hayden et al., 2010). Androgen deprivation therapy (ADT) or castration therapy is considered the first-line therapy for patients with locally advanced cancer or recurrent or metastatic disease (Perlmutter and Lepor, 2007). However, fatal therapy-resistant disease eventually emerges in most PCa patients (Miller et al., 2017; Moreira et al., 2017). Therefore, there is an urgent need for a detailed investigation of the underlying mechanisms of PCa to discover novel molecular targets for gene therapy in order to thereby improve the prognosis of patients with PCa.

Mucosa-associated lymphoma antigen 1 (MALT1), is a paracaspase that belongs to the caspase family of proteases and has arginine-specific cysteine protease activity (Ruland et al., 2003). Together with coactivator-associated arginine methyltransferase 1 (CARMA1, also known as CARD11) and B cell lymphoma 10 (BCL10), MALT1 assembles the CARMA1/Bcl10/MALT1 (CBM) complex that bridges proximal antigen receptor signaling events to the IkB kinase (IKK) complex, causes the degradation of inhibitor of κB (IKK), activates the NF-κB pathway (Turvey et al., 2014). T cell receptor (TCR) stimulation leads to cleavage of Regnase-1 at R111 by Malt1/paracaspase, freeing T cells from Regnase-1-mediated suppression. In addition to its scaffolding role in NF-κB activation, MALT1 acts as a protease to enzymatically cleave and inactivate multiple substrates, including several negative regulators of canonical NF-κB signaling, such as TNFAIP3/A20 (Coornaert et al., 2008; McAllister-Lucas et al., 2011; Afonina et al., 2015). A tumor-promoting role of MALT1 has been found in a subset of diffuse large B cell lymphoma (DLBCL) and MALT lymphoma, indicating MALT1 as an attractive anticancer drug target (Ngo et al., 2006; Hailfinger et al., 2009; Nagel et al., 2012). MALT1 was also recently reported to be aberrantly expressed in solid tumors, including glioblastoma multiforme (Jacobs et al., 2020), especially in PCa(Wang et al., 2016; Ashcraft et al., 2020). However, the role of MALT1 in tumors, especially PCa, has not been extensively investigated.

To this end, this study aimed to explore the effects of downregulation of MALT1 expression on malignant biological behavior of PCa cells both *in vivo* and *in vitro* and to investigate their possible mechanism. Following additional in-depth bioinformatics analysis on the basis of a public database, the function and signaling pathways of MALT1 were elucidated.

MATERIALS AND METHODS

The Expression of MALT1 in Public Databases

We performed a systematic analysis based on the TCGA(Blum et al., 2018) and Genotype-Tissue Expression (GTEx) databases (Lonsdale et al., 2013) to explore the expression levels in various types of cancers. To determine the expression level of MALT1 in different tissues, GTEx tissue expression was downloaded from the GTEx web portal. In addition, gene expression microarray datasets of MALT1 expression in PCa compared to that in normal prostate tissues were retrieved from the National Center for Biotechnology Information (NCBI) (GEO datasets GSE45016, GSE55945, GSE17906, GSE17951, GSE26910 and GSE3325), then use the RMA method for standardization and normalization, and use the combat algorithm to remove batch effects. After merging, there are a total of 237 samples of expression profile data, of which 121 are tumor samples and 116 are normal samples. Box-and-dot plots were generated using ggplot2 package in R. Two-sided Wilcoxon rank-sum test was used for statistical comparison between two groups.

Cell Culture and Cell Transfection

The human prostate cancer cell lines LNCaP and PC-3 were acquired from Cobioer (Nanjing, CN). Both cell lines were grown in Roswell Park Memorial Institute-1640 medium (Thermo Fisher Scientific, NY, United States) with 10% (FBS; Biyuntian Company, Shanghai, CN), and 1% penicillin-streptomycin (Solarbio, Beijing, CN); 37°C and 5% carbon dioxide were the most suitable conditions for cell incubation. Cells were harvested in the logarithmic phase of growth for all experiments.

shRNA for MALT1 (shMALT1, target sequence 5′-CCATTC ACATCCTGGTAAT-3′) and control shRNA (shCtrl, target sequence 5′- TTCTCCGAACGTGTCACGT-3′) were from Genesil Biotechnology (Wuhan, CN). shMALT1 and shCtrl was cloned into a lentiviral vector (PLKO.1-C1). Cell transfection was performed with Lipofectamine 2000 (Invitrogen, Shanghai, CN) following the manufacturer's protocol. Nonspecific shRNA was used as a negative control (NC). LNCaP was transfected with lentiviruses carrying shCtrl and shMALT1 respectively, and so was PC-3. KD cell lines was constructed by LNCaP and PC-3 which were transfected with lentiviruses carrying shMALT1.At 48 h after transfection PCa cells were transduced with lentivirus to knockdown MALT1. The culture medium was changed to normal medium 8–12 h after

infection. Cells were observed 72 h post-infection with fluorescent microscope to ensure a positive infection rate of >70%. The selective silencing of MALT1 was identified by Western blot analysis.

RNA Isolation and Quantitative Real-Time PCR

Total RNA was isolated from LNCap and PC-3 cells transfected with lentiviruses.by using TRIzol reagent (Tiangen Biotech, Beijing, CN) according to the manufacturer's instructions. Reverse transcription was carried out using a reverse transcription kit (Thermo Fisher Scientific, NY, United States) according to the kit instructions. The obtained complementary DNA (cDNA) was applied for later testing. SYBR is a marker used to conduct quantitative reverse transcription PCR (qRT-PCR). The reaction conditions were 50°C for 2 min and 95°C for 10 min, followed by 40 cycles of 95°C for 30 s and 60°C for 30 s. The relative expression levels of genes were calculated using the 2−ΔΔCt method. GAPDH was used as an internal reference. We performed qRT-PCR experiments on a LightCycler®480 II (Roche Life Science, CA, United States), and SYBR Green Master Mix was purchased from Roche.

Western Blot Analysis

Phosphate-buffered saline (PBS) was used to wash the cultured cells, and radioimmunoprecipitation assay (RIPA) buffer was added. Quantification of protein concentration was performed by BCA Protein Assay Kit (Beyotime, Shanghai, CN). Protein isolated from polyacrylamide gel according to the relative molecular mass was transferred to a polyvinylidene difluoride (PVDF) membrane (Millipore, MA, United States).

After 1 h of blocking with 5% blocking solution at room temperature, membranes were incubated at 4°C for 12 h with primary antibodies, and the secondary antibody was then added. Rabbit monoclonal antibody against MALT1 was from Abcam (ab33921, Cambridge, United Kingdom). After each incubation, the membrane was washed five times with PBS with 0.05% Tween-20 (Malinckrodt Baker, NJ, United States) (5 min per wash). Finally, the protein bands were visualized through a chemiluminescence detection system (Pierce, IL, United States).

MTT Cell Viability Assay

Cell viability along with proliferation were measured by MTT assay. Cells were evenly introduced to 96-well plates at 2,000 cells per well and cultured under routine conditions. 10 μL of 5 mg/ml MTT (Sigma-Aldrich, Shanghai, CN) was added to each well at each time-point, followed by a 4-h incubation after which the culture medium was changed with 100 μL DMSO. After 2–5 min of agitation, the microplate reader (Thermo Fisher Scientific, NY, United States) was used to measure the optical densities at 490 nm wavelength (OD490). Growth curves based on OD490.

Colony Formation Assay

LNCap and PC-3 cells infected with lentivirus for 24 h were seeded into six-well plates at a density of 500 cells per well; then cultured for 10–12 days to allow colony formation. Cells were fixed with 10% neutral buffered formalin solution and stained with 0.01% crystal violet solution (Beyotime, Shanghai, CN). The number of colonies was counted after full decolorization with PBS.

Cell Apoptosis Assay

After transfection, LNCap and PC-3 cells were digested with 0.25% trypsin and transferred to a centrifuge tube. After that, samples were washed with D-Hanks buffer at 4°C, washed with 1× binding buffer and then resuspended in 300 μL of 1× binding buffer. Then, 5 μL of Annexin V-APC solution was added to the cells, followed by a 15-min incubation in the dark. Propidium iodide staining solution was added to the suspension, and the cells were analyzed with a flow cytometer to determine the percentage of apoptotic cells.

Migration Assay

Transwell chambers (Corning, United States) were used to assess prostate cancer cell metastasis ability. The upper inserts of 24-well Transwell chambers were added, and 2×10^4 cells were resuspended in 0.1 ml of serum-free medium. Then, 0.6 ml of medium with 30% FBS was added to the lower compartments as a chemoattractant. After 24 h of culture, the cells on the surface of the membrane were gently removed with cotton buds, fixed with 4% paraformaldehyde (Dalian Meilun Biotechnology, Dalian, CN) for 15 min, washed three times with PBS, fixed and stained with 0.1% crystal violet for 30 min. The stained cells were photographed under an inverted fluorescence microscope (magnification ×200; Olympus, TKY, JPN). Five visual fields were observed in each group.

Cell Invasion Analysis

The invasive ability of the cells was detected by the Boyden chamber method. The cells were collected with trypsin and resuspended in 0.1% (W/V) bovine serum albumin in serum-free medium. Then, 200 ml of cell suspension (2×10^5 cells) was inoculated into the upper cavity of the splint, and a polyethylene terephthalate (PET) membrane (pore diameter: 8.0 μm) (SPL Lifesciences, Pocheon, Kr) precoated with matrix gel (BD Biosciences, San Jose, CA) was implanted into the upper cavity of the splint. The bottom hole of the 24-well plate was filled with a cell medium containing 10% (v/v) FBS with or without isoplumbagin. Dimethyl sulfoxide or isoplumbagin were separately added to the superior lumen cell suspension. After 24 h of incubation, the cells migrating to the bottom side of the PET membrane were fixed with 4% paraformaldehyde and stained with crystal violet. Photos of the cells stained under the PET membrane were acquired with the microscope. The number of cells was counted by ImageJ, and the relative invasive ability was calculated by the number of cells per unit area.

Subcutaneous Xenograft

Male nude mice (aged 4–6 weeks) were purchased from Shanghai SLAC Laboratory Animal Co. Ltd. (SH, CN). All 10 male nude mice were divided into a normal control (NC) group and a knockdown (KD) group, with 5 mice in each

group. 1×10^7 LNCaP lentivirus-infected cells carrying shCtrl (NC group) or shPNO1 (KD group) for 7 days were subcutaneously injected into the right arm pit of each mouse. The length (L) and width (W) of tumours were measured from day 7 post-inoculation and every 7 days until day 31 (tumour volume = 3.14/6 × L × W × W). All mice were then killed by injection of an overdose of 2% pentobarbital sodium followed by cervical vertebra dislocation, and tumours were excised and measured for volume and weight.

For tissue morphology evaluation, hematoxylin and eosin staining was performed on sections of the embedded samples. Immunohistochemistry (IHC) staining for MALT1 and Ki-67 was performed on sections from the xenograft tumors.

Correlation Between MALT1 Expression and the Abundance of Immune Infiltrates

In the present study, we downloaded the infiltrating immune cell scores of 33 cancer types from the Tumor Immune Estimation Resource (TIMER) dataset (https://cistrome.shinyapps.io/timer/), which contains 10,897 samples from different cancer types included in the TCGA dataset. Spearman correlation analysis was utilized to investigate the correlation of MALT1 expression and the scores of these immune cells (B cells, $CD4^+$ T cells, $CD8^+$ T cells, neutrophils, macrophages and dendritic cells) in PCa patients. In addition, the correlation between MALT1 expression and immune checkpoint marker levels was evaluated *via* the "correlation" module in PCa.

Correlation Between MALT1 Expression and Mismatch Repair Gene Mutation

Mismatch repair (MMR) genes play a crucial role in the intracellular MMR mechanism (Meiser et al., 2020). The loss of the function of a key gene in this mechanism may lead to DNA replication errors that cannot be repaired, which in turn leads to more somatic mutations. MLH1, MSH2, MSH6, PMS2, and EPCAM are five MMR genes, and their expression level in multiple cancers were obtained from the TCGA database. Correlation between MMR gene expression levels and MALT1 expression levels was analyzed using Spearman's correlation method.

Association Between MALT1 and Tumor Mutation Burden and Microsatellite Instability

TMB is defined as the number of mutations per megabyte of a database, which is used to reflect the number of mutations in tumor cells and is a quantitative biomarker (Krieger et al., 2020). TMB was calculated by the sum of the number of non-silent mutations in the TCGA samples. We downloaded the TMB data of 33 tumors from TCGA. Here, the TMB of each tumor sample was counted separately, and the correlation between MALT1 expression and TMB was summarized using the Spearman rank correlation coefficient by using "ggstatsplot" R package.

MSI is defined as the change in the length of a microsatellite DNA caused by the insertion or deletion of repetitive units in tumor tissue (Bonneville et al., 2017). We analyzed the correlation between the expression of MALT1 and MSI in 33 tumors using the Spearman method. MSI data were obtained from Bonneville et al. regarding pan-cancer MSI. In this study, we calculated the MANTIS scores for most of the tumor samples in the TCGA database by calculating the differences in the distribution of alleles at each microsatellite locus in the tumor-normal tissue paired samples and taking the average as the MSI score value for the tumor-normal tissue paired samples.

Weighted Gene Coexpression Network Analysis Based on the Expression of MALT1

A total of 499 prostate cancer samples were obtained by downloading PCa expression profile data from the TCGA database. According to the median expression of MALT1, patients in TCGA with PCa were divided into the MALT1-high group and the MALT1-low group. The differentially expressed genes were screened between the MALT1-high group and the MALT1-low group (FC > 1.2 or FC < 5/6, $p < 0.05$), and the differentially expressed genes were obtained. Soft power 20 was set for network construction and module detection and the R package WGCNA was used to construct the gene co-expression.

Construction of the Correlation Network and Gene Ontology Enrichment Analysis

GO analysis of the most highly correlated genes (cor >0.4) by using the clusterprofiler and GOplot package in R software V.3.5.2. Then, these correlated genes were used to generate a heatmap using the R package pheatmap after Spearman correlation analysis.

Gene Set Enrichment Analysis

According to the median value of MALT1 expression, the samples were divided into two groups: the MALT1-high group and the MALT1-low group. For GSEA of single gene, the enriched background set was *hallmark: h.all.v7.1.symbols.gmt*. In order to analyze the biological function of MALT1 in prostate cancer, single GSEA was performed by using the ClusterProfiler and org.Hs.eg.db packages. Raw data of PCa were downloaded from TCGA database for the analysis of MALT1 expression between PCa patients and normal prostate tissues.

Statistical Analysis

All experiments were repeated at least three times. The statistical analysis in this project was performed using GraphPad Prism 6.0 (version 6, California, United States). First, the F test was used to check the quality of variances. The data with $F < 0.05$ were subjected to two-tailed Welch's t-test, and those with $F > 0.05$ were subjected to two-tailed Student's t-test. Each group of data is represented by the mean ± SD. The p-value was used to indicate the statistical significance between the groups. When $p < 0.05$, the results were considered statistically significant.

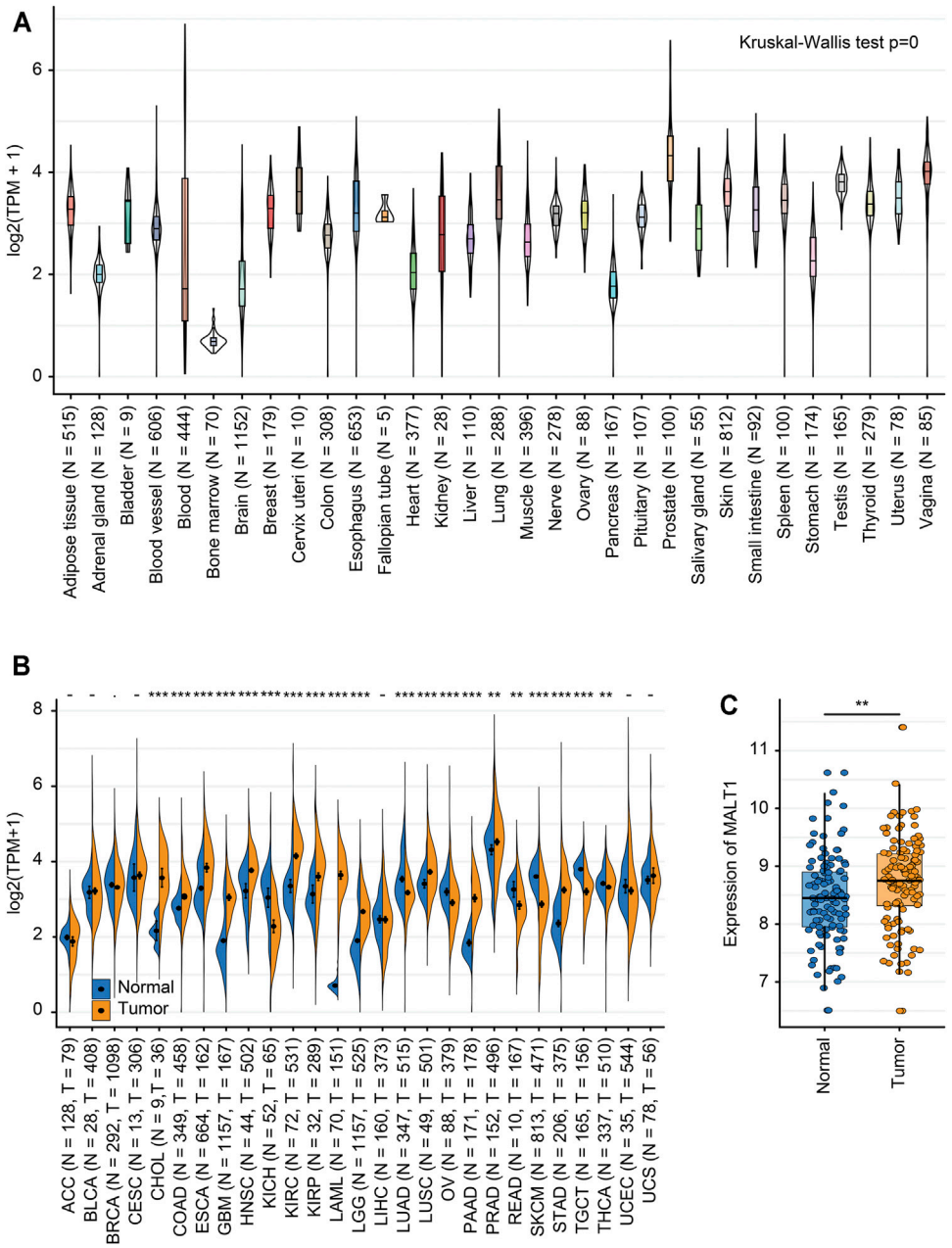

FIGURE 1 | Expression levels of MALT1 in tissues from different origins and tumors. **(A)** Normal mRNA expression levels of MALT1 in different tissues from the GTEx database. **(B)** mRNA expression difference in MALT1 among normal, peritumor and tumor samples, combining data from the TCGA and GTEx databases. **(C)** mRNA expression difference in MALT1 between normal and tumor samples, based on data from the GEO database. * indicates $p < 0.05$, ** indicates $p < 0.01$, *** indicates $p < 0.001$.

RESULTS

The Expression Level of MALT1 in Various Kinds of Tissues

We analyzed the MALT1 expression level in different tissues from the GTEx dataset, and there were significant differences among tissues (**Figure 1A**). Integration analysis of TCGA and GTEx RNA-seq data showed that compared to that in paired normal tissues, MALT1 was overexpressed in PRAD, cholangiocarcinoma (CHOL), colon adenocarcinoma (COAD), esophageal carcinoma (ESCA), glioblastoma multiforme (GBM), lung squamous cell carcinoma (LUSC), pancreatic adenocarcinoma (PAAD), and stomach adenocarcinoma (STAD) and was expressed at lower levels in kidney renal

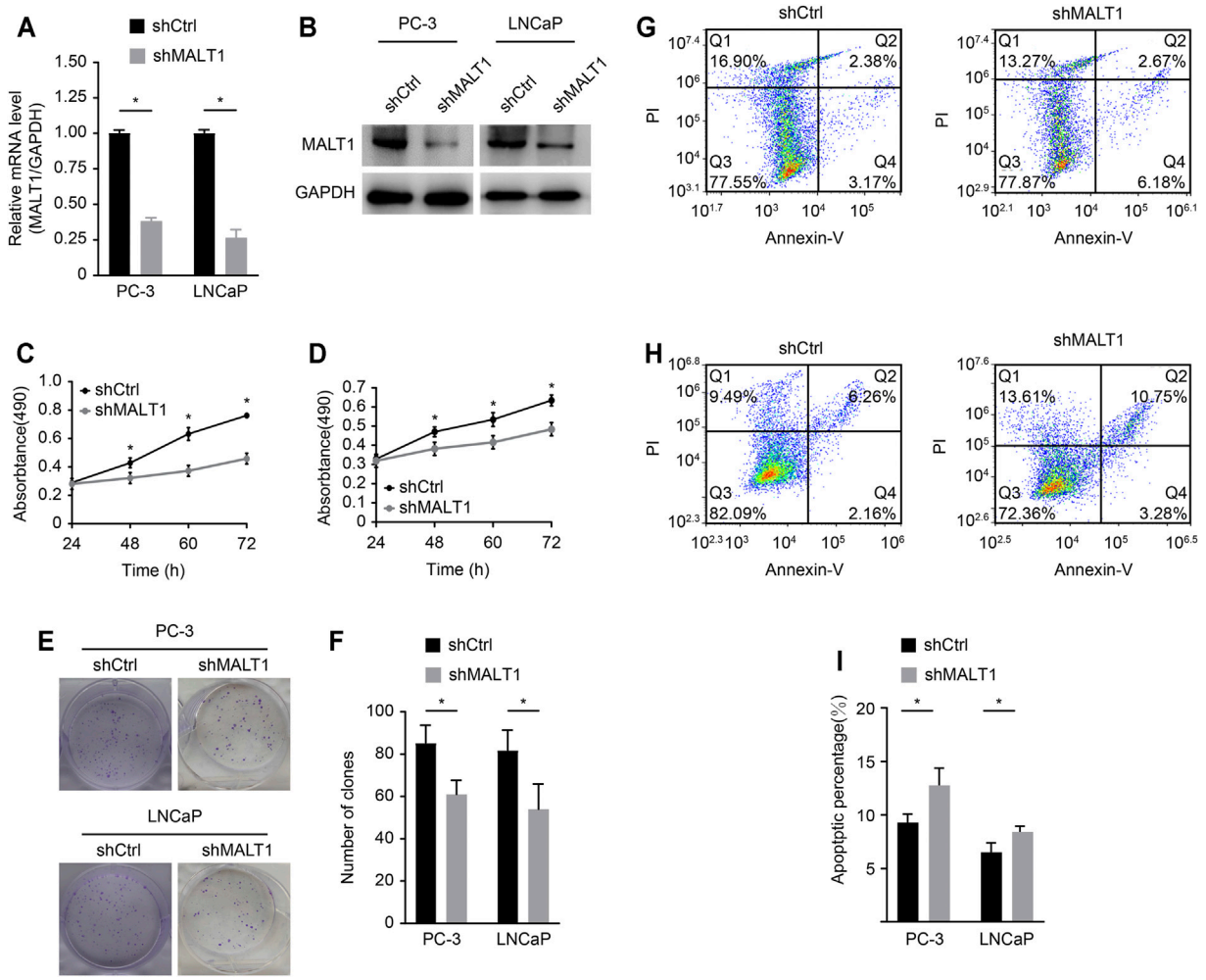

FIGURE 2 | Role of MALT1 in the growth and survival of prostate cancer cells. **(A)** qRT-PCR results showing significantly reduced mRNA expression levels of MALT1 vs GAPDH in MALT1 KD cells. **(B)** Western blot showing reduced MALT1 protein expression in MALT1 KD cells. **(C)** Growth curves of PC-3 cells and **(D)** LNCaP cells measured by MTT assay. **(E, F)** Comparison of colony-forming ability between control and MALT1 KD cells. **(G)** The apoptosis ability of LNCaP cells and **(H)** PC-3 cells was detected by flow cytometry. Cells were divided into four quadrants: Q1: Annexin V-FITC -/PI +, which was representative of mechanical error; Q2: Annexin V-FITC+/PI+, which was representative of late apoptotic or necrotic cells; Q3: Annexin V-FITC -/PI-, which was representative of living cells; and Q4: Annexin V- FITC+/PI-, which was representative of early apoptotic cells. **(I)** Statistic analysis of **(G, H)**.

clear cell carcinoma (KIRC), lung adenocarcinoma (LUAD), ovarian serous cystadenocarcinoma (OV), skin cutaneous melanoma (SKCM), and rectum adenocarcinoma (READ) (**Figure 1B**). Using GEO databases to analyze MALT1 expression in the human PCa sample array also suggested that PCa tissues have significantly higher MALT1 expression than normal tissues ($p < 0.005$) (**Figure 1C**).

Role of MALT1 in the Growth and Survival of PCa Cells

We studied the role of MALT1 in two PCa cell lines, PC-3 and LNCaP. MALT1 expression was then knocked down by MALT1-targeting shRNA (shMALT1) *via* lentivirus, and cells transduced with shCtrl were used as controls. The knockdown (KD) of MALT1 in these cell lines was confirmed by qRT-PCR, which showed 62% ($p < 0.05$) and 73% ($p < 0.05$) reductions in MALT1 mRNA levels in PC-3 and LNCaP cells, respectively (**Figure 2A**), and by Western blot (**Figure 2B**).

The effect of MALT1 KD on the proliferative activity of PC-3 and LNCaP cells was studied using the MTT assay (**Figures 2B,C**). The results showed that compared with that of the control cells (shCtrl), the proliferation of MALT1 KD cells (shMALT1) was significantly attenuated in both cell lines. It was also confirmed that for both cell lines in the KD group, the colony genesis ability was significantly decreased ($p < 0.05$ (keep the same as 0.05); **Figures 2D,E**), while cell apoptosis was significantly activated ($p < 0.05$; **Figures 2F,G**). These results indicated that MALT1 was important for the proliferation and survival of prostate cancer cells.

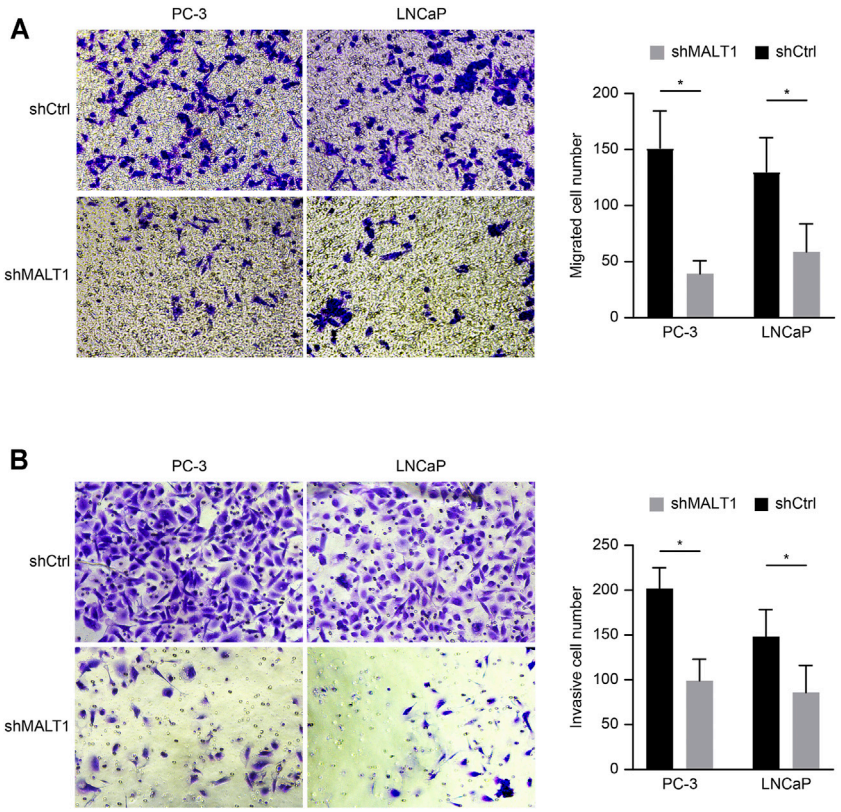

FIGURE 3 | Downregulation of MALT1 inhibited the migration and invasion of PCa cells. PCa cells were treated with a lentiviral vector for 24 h. Then, **(A)** PCa cell migration ability was tested using a Transwell migration assay. **(B)** PCa cell invasion ability was tested using a Transwell invasion assay. Total magnification of all images is 200×. Data are shown as mean ± SD based on at least three independent experiments.

Downregulation of MALT1 Expression Inhibits the Invasion and Migration of PCa Cells

Transwell assay chambers with a Matrigel coating were used to evaluate tumor aggressiveness. The cells observed to degrade the Matrigel and pass through the membrane were counted, and the results revealed that the number of aggressive PC-3 cells was lower in the KD group than in the control group. Similar results were obtained for LNCaP cells ($p < 0.05$; **Figure 3A**). To evaluate whether downregulation of MALT1 expression affects the metastatic ability of PC-3 and LNCaP cells, we performed a Transwell experiment. The results indicated that MALT1 KD significantly reduced cell migration ($p < 0.05$; **Figure 3B**).

All these results demonstrated that after downregulating the expression of MALT1, the invasion and migration ability of tumor cells decreased, and the difference was statistically significant.

Attenuation of Tumor Growth *in vivo* After MALT1 Knocking Down

We established xenograft models to investigate the tumorigenic potential of MALT1 in prostate cancer; 10 male nude mice were subcutaneously inoculated with LNCaP cells expressing shCtrl (NC group) or shMALT1 (KD group), with 5 mice in each group. Tumor size was measured from the seventh day after inoculation (**Figure 4A**), and the mice were sacrificed on the 31st day. Tumor volume and tumor weight in the NC group were 440.93 ± 118.66 mm^3 and 0.225 ± 0.096 g, respectively, which was compared with 90.04 ± 48.52 mm^3 ($p < 0.05$) and 0.056 ± 0.035 g ($p < 0.05$) in the KD group (**Figures 4B,C**). Moreover, IHC analysis revealed that MALT1 and Ki-67 levels were substantially decreased in the KD group (**Figure 4D**). In consistent with *in vitro* results, the volumes and weights of tumors formed by MALT1 KD cells were significantly smaller and lighter tumors than those of tumors formed by control cells *in vivo*.

WGCNA and GO Enrichment Analysis

A total of 1,540 differentially expressed genes were screened between the MALT1-high group and the MALT1-low group (FC > 1.2 or FC < 5/6, $p < 0.05$). The expression profile was constructed for WGCNA and further analysis. WGCNA was performed with soft-thresholding power = 20 and obtained three modules, among which the turquoise module and blue module were significantly correlated with the traits of high and low expression of MALT1, respectively (**Figures 5A–D**).

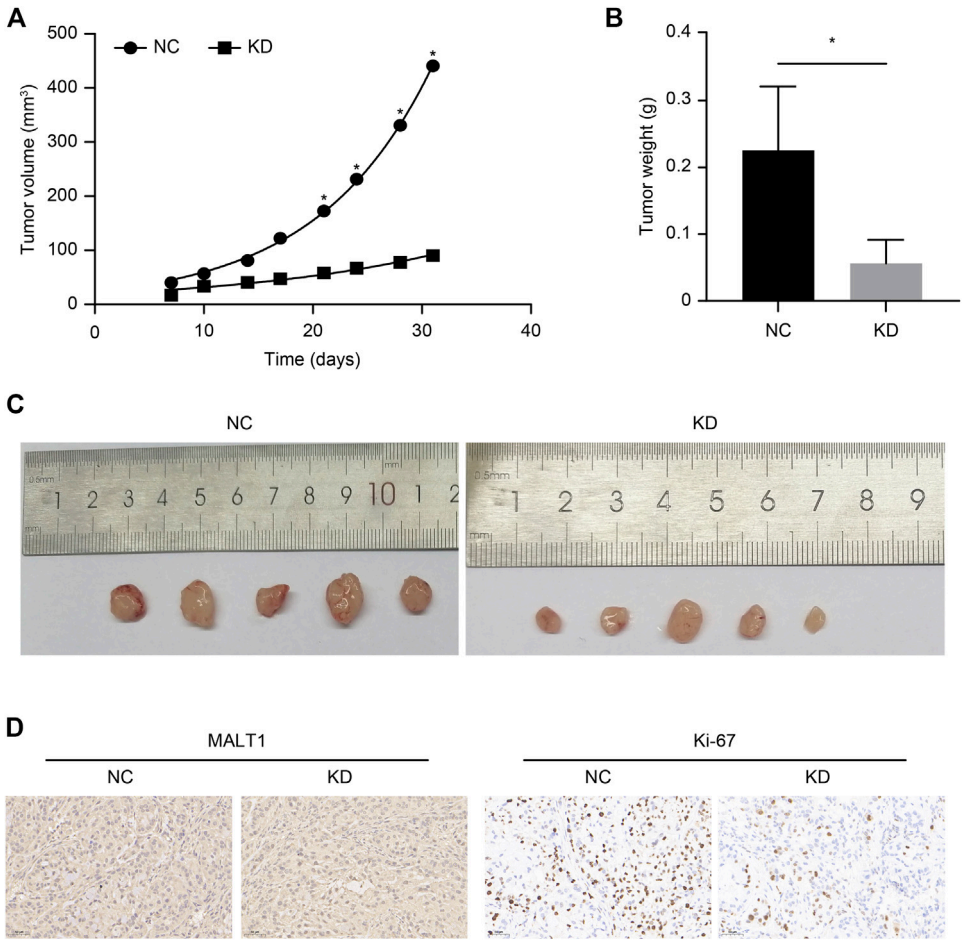

FIGURE 4 | Subcutaneous xenotransplantation of PC-3 human PCa cells in BALB/c nude mice. Comparison of the volume of xenografts between the NC (shCtrl) and KD (shMALT1) groups of mice. **(A)** Comparison of the volume and **(B)** weight of xenografts on day 31 post-inoculation between the NC and KD groups of mice. **(C)** Representative photographs of the tumors. **(D)** IHC analysis showing a decrease in MALT1 and Ki-67 expression.

A total of 86 coexpressed genes were obtained from the genes with a significant positive correlation with MALT1 expression (cor >0.4). A heat map of the coexpressed genes is shown in **Figure 5E**. GO functional enrichment analysis of the 86 coexpressed genes showed that they were related to heterotypic cell-cell adhesion, regulation of actin-based movement, regulation of action potentials and other functions, as shown in **Figure 5F**.

Correlation Between the Expression of MALT1 and Immune Checkpoint Genes

We analyzed the correlation between MALT1 and immune checkpoint genes and found that MALT1 was associated with immune checkpoints in most tumors. In PAAD, breast invasive carcinoma (BRCA), and COAD, MALT1 expression was positively correlated with that of most immune checkpoint genes. In PRAD, expression of ADORA2A and KIR3DL was positively correlated with MALT1 expression, but that of other immune checkpoint genes was not (**Figure 6**).

Correlation Between MALT1 Expression and Tumor Mutational Burden and Mismatch Repair Genes

We compared the immune infiltration levels among tumors with the presence of different somatic copy number alterations for the MALT1 gene by performing a TIMER analysis.

We analyzed the correlation between MALT1 and MMR genes (MLH1, MSH2, MSH6, PMS2, and EPCAM). The results showed that there was a significant positive correlation between MLH1, MSH2, MSH6, and PMS2 and MATL1 in PRAD, liver hepatocellular carcinoma (LIHC), lower grade glioma (LGG), and thyroid carcinoma (THCA) (**Figure 7A**).

The relationship between MALT1 gene expression and TMB was analyzed by the Spearman correlation coefficient. The results

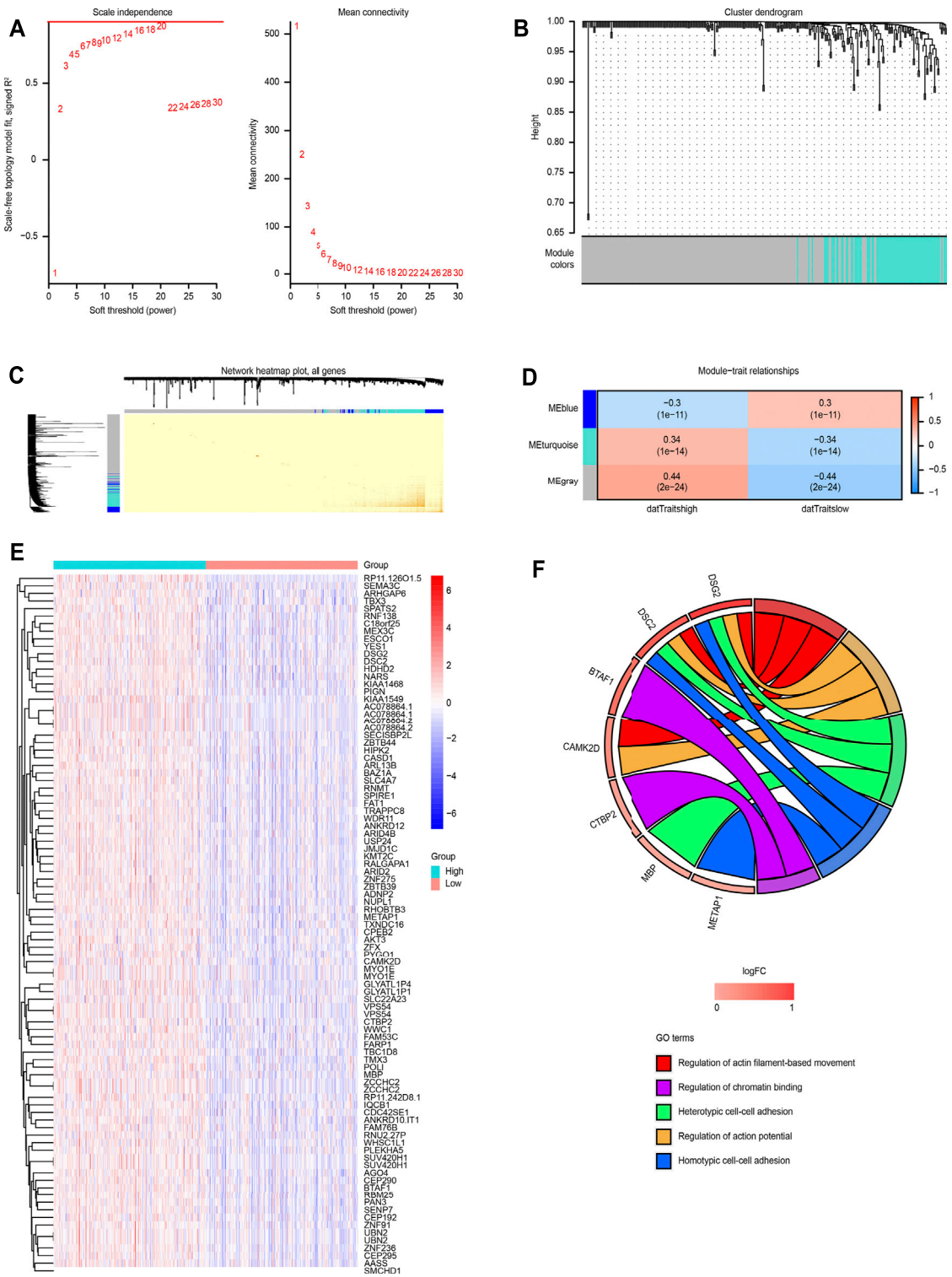

FIGURE 5 | WGCNA based on MALT1 expression and GO analysis. **(A)** Screening out the soft-thresholding power through scale independence and mean connectivity. **(B)** Gene clustering tree (dendrogram) obtained by hierarchical clustering of adjacency-based dissimilarity. **(C)** Visualization of TOM of co-expressed genes in different modules by a heat map. Light colors indicate low overlap and dark red indicates high overlap. The darker color blocks along the diagonal are coexpression modules. **(D)** Module-trait relationship representing the relationship between modules and traits (high gene expression group, low gene expression group). The numbers inside each cell are the coefficient value and P value, and the color of each cell is assigned based on the correlation value of the module; red represents a strong positive correlation, and blue represents a strong negative correlation, The stronger the correlation, the darker is the color. **(E)** Heat map of MALT1 coexpressed genes

(*Continued*)

FIGURE 5 | each row and column represent one specific gene and patient, respectively; **(F)** GOplot representation of the analysis of the gene ontology (GO) items enriched among the coexpressed genes. The left side of the circle displays the gene, and the right side shows the GO item. The assorted colors represent different GO items, and the color of each GO item is annotated below the circle. If the gene belongs to a GO item, there will be a line between the gene and the GO item. The z-score (bottom) shows log2 (gene foldchange).

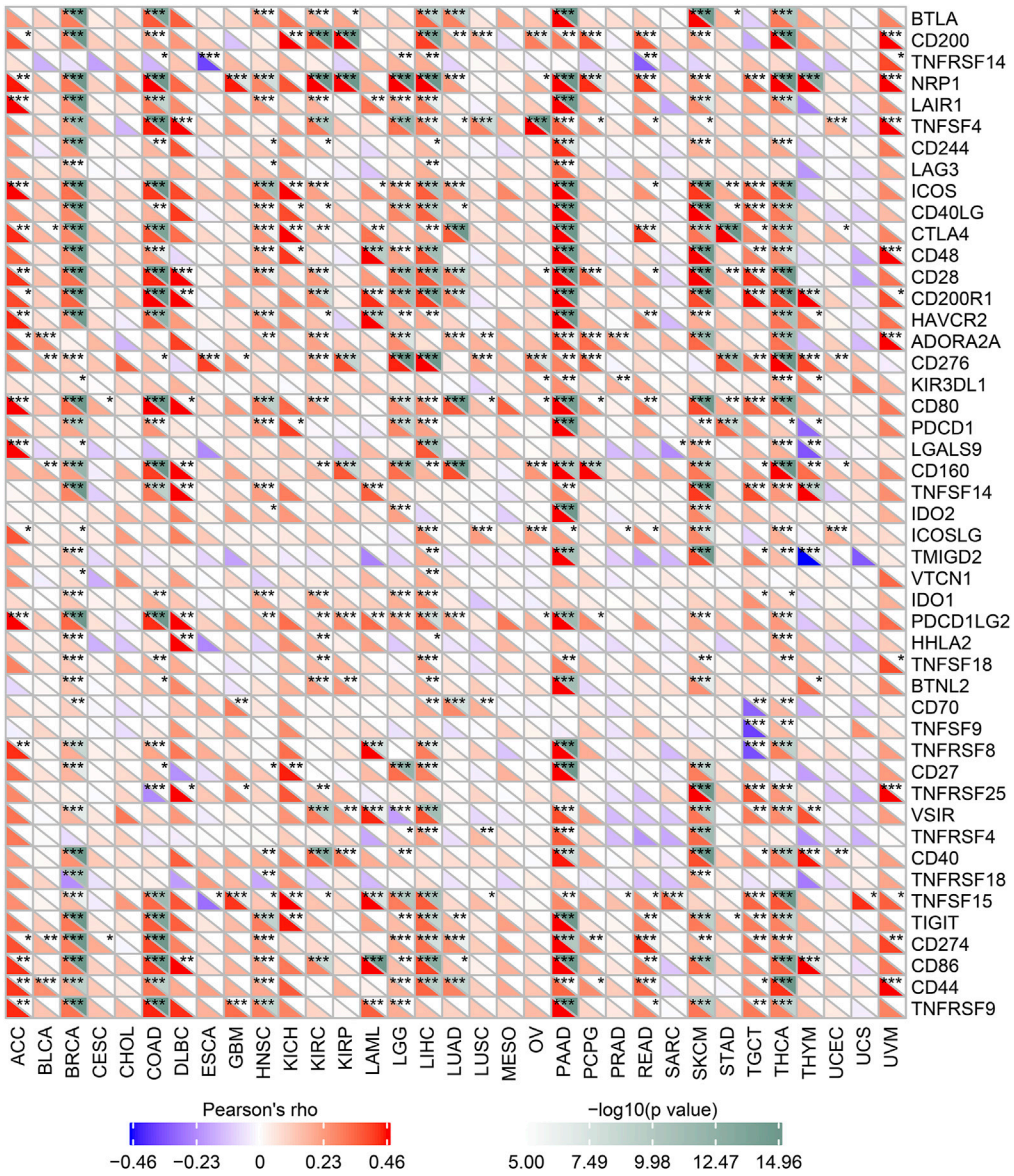

FIGURE 6 | Correlation between MALT1 expression levels and acknowledged immune checkpoint genes expression in multiple tumors from the TCGA database. The correlation between of MALT1 expression level and immune checkpoint gene expression level in pan-cancer. The abscissa lists the cancer names and the ordinate lists the gene names. The lower triangle in each tile indicates coefficients calculated by Pearson's correlation test, and the upper triangle indicates the log10-transformed P-value. *$p < 0.05$, **$p < 0.01$, ***$p < 0.001$.

showed that there was a significant negative correlation between MALT1 expression and TMB in PRAD, THCA, BRCA, CHOL, and ESCA (cor <0, $p < 0.05$) but a significant positive correlation between MALT1 expression and TMB in COAD, LGG, and thymoma (THYM) (cor >0, $p < 0.05$) (**Figure 7B**).

The correlation between gene expression and MSI was also analyzed by the Spearman correlation coefficient. The results showed that there was a significant negative correlation between MSI and MALT1 expression in SKCM, lymphoid neoplasm diffuse large B-cell lymphoma (DLBC), and head and neck

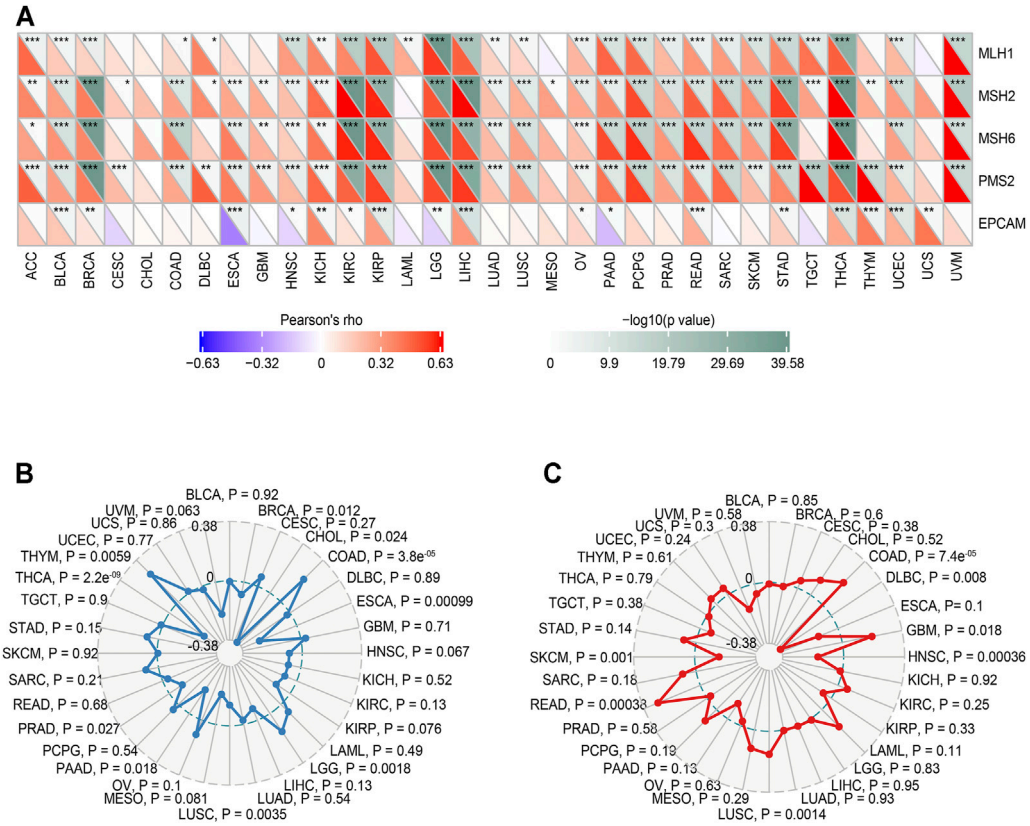

FIGURE 7 | Relationship between MMR defects, TMB, MSI and MALT1 mRNA expression levels in various tumors in the TCGA database. **(A)** Correlation between MALT1 and five significant MMR genes (MLH1, MSH2, MSH6, PMS2, and EPCAM) in 33 types of cancers. The lower triangle in each tile indicates coefficients calculated by Pearson's correlation test, and the upper triangle indicates the log10-transformed P-value. *: $p < 0.05$, **: $p < 0.01$, ***: $p < 0.001$. **(B)** Correlation between TMB and MALT1 expression, the black value is the scale of the correlation coefficient. **(C)** Correlation between MSI and MALT1 expression, the black value is the scale of the correlation coefficient. Spearman correlation test; $p < 0.05$ was considered significant.

squamous cell carcinoma (HNSC), while there was a significant negative correlation between MSI and MALT1 expression in COAD, GBM, LUSC, and READ (**Figure 7C**).

Correlation of MALT1 Expression With Tumor-Infiltrating Immune Cells and GSEA

The correlation between MALT1 expression and tumor-infiltrating immune cells was analyzed by the TIMER database. The results showed that MALT1 expression was positively correlated with the infiltration of B cells, $CD8^+$ cells, macrophages, and dendritic cells and negatively correlated with the infiltration of $CD4^+$ cells. Among them, the correlation with $CD8^+$ cells were the most significant (**Figure 8A**, Cor = 0.306, $p < 0.05$).

Furthermore, the correlation between the change in somatic cell copy number of the MALT1 gene and immune infiltration was analyzed. Copy number variation analysis showed that high amplification of MALT1 was correlated with $CD8^+$ cell infiltration ($p < 0.05$), while deep deletion of MALT1 was associated with $CD4^+$ cell infiltration ($p < 0.05$).

According to the median value of MALT1 expression, the samples were divided into a MALT1-high group and a MALT1-low group. GSEA showed that MALT1 was associated with several tumor-related pathways, including the androgen response, G2M checkpoint, NF-κB signaling pathway, Wnt/β-catenin pathway and TGF-β signaling pathway (**Figures 8C–H**).

DISCUSSION

PCa is a malignant disease that seriously endangers the health of men, and the molecular mechanism of its pathogenesis is very significant. Many studies have attempted to clarify hub genes that have an important impact on the development and metastasis of PCa at the transcriptome level (Varambally et al., 2005; Uhlén et al., 2015).

MALT1 is a well-known immune cell effector protein that manages adaptive immune responses driven by NF-κB (Jaworski et al., 2016). Enhanced expression of MALT1 has been linked to the development of leukemia and lymphoma (Xu et al., 2015; Saba et al., 2017). Therefore, MALT1 has been proposed to be a

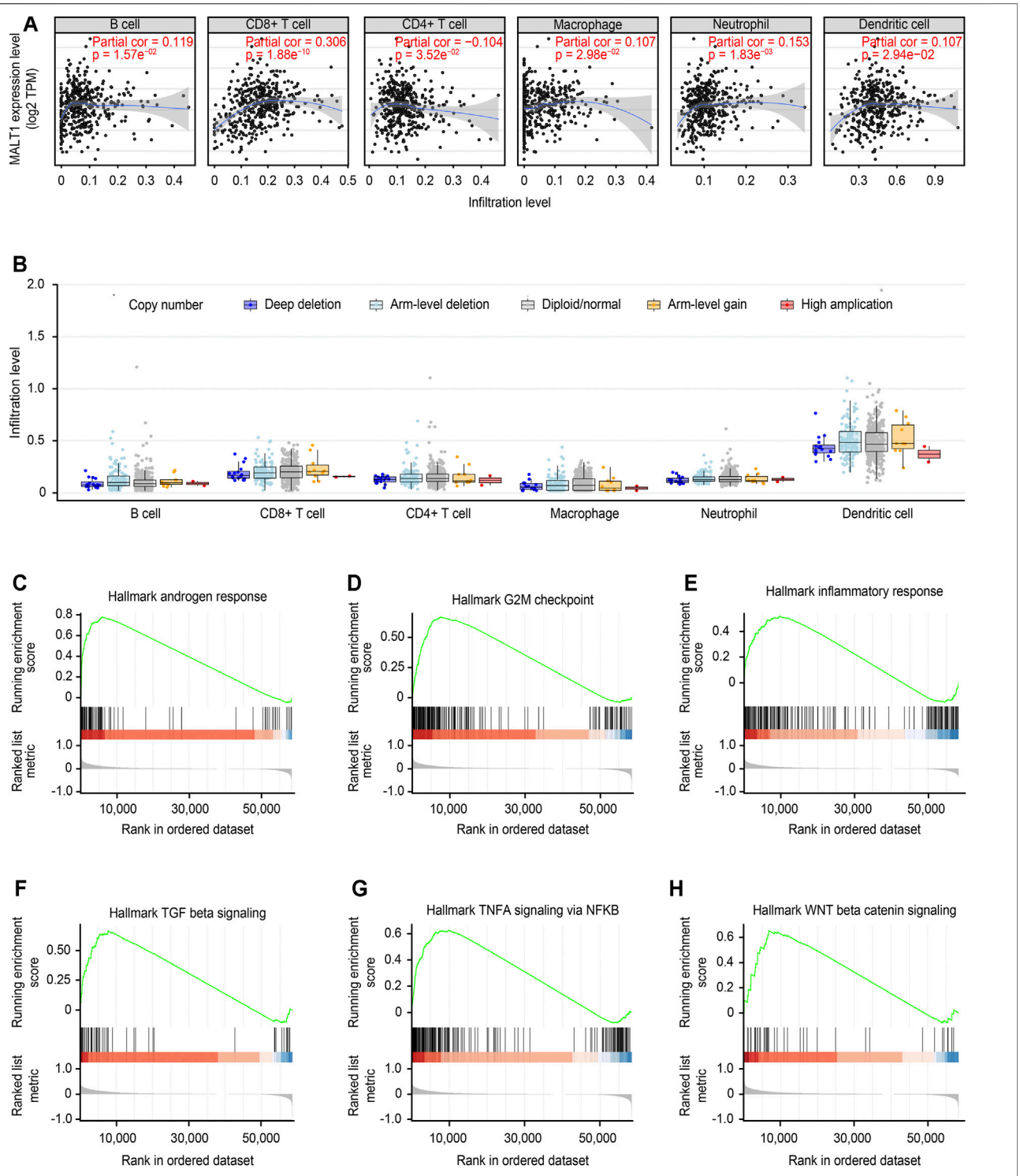

FIGURE 8 | Immune correlation of MALT1 in PCa and GSEA of MALT1. **(A)** T Correlation of MALT1 expression level with immune infiltration level (B cells, $CD4^+$ T cells, $CD8^+$ T cells, neutrophils, macrophages, and dendritic cells) in PCa, as calculated by TIMER with data from the TCGA database. **(B)** Comparison of tumor infiltration levels among tumors with different somatic copy number alterations (SCNAs) for MATL1. SCNAs were defined by GISTIC 2.0, including deep deletion (–2), arm-level deletion (–1), diploid/normal (0), arm-level gain (1), and high amplification (2). Box plots are presented to show the distributions of each immune subset at each copy number status in selected cancer types. The infiltration level for each SCNA category was compared with the normal using a two-sided Wilcoxon rank-sum test; **(C–H)** Gene set enrichment analysis (GSEA) for the expression level of MALT1 and the signal pathways activated were present.

promising therapeutic target for the treatment of lymphomas and autoimmune disorders. MALT1 has been proven to be overexpressed in various solid tumors, and increasing numbers of research studies have confirmed that MALT1 is a key regulator of tumor development (Pan et al., 2016). According to Dai et al, MALT1 gene transcription tripled in pancreatic cancer cells cocultured with mouse dorsal root ganglion (Dai et al., 2007). Liu et al. revealed that MALT1 played an important role in cell proliferation *in vitro* and *in vivo* by inducing G1 phase arrest and confirmed that the activation of NF-κB could be significantly blocked by MALT1 inhibition and further regulates the proliferation and survival of glioblastoma pleomorphic cells (Liu et al., 2020).

According to the GEO, TCGA and GTEx datasets, the expression of MALT1 in PCa tissues was significantly higher than that in normal tissues and paracancerous tissues. Next, bioinformatics analysis of the functions and mechanisms of MALT1 was conducted. GO enrichment analysis with the genes positively related to MALT1 expression and GSEA revealed that MALT1 is related to heterotypic cell-cell adhesion, regulation of actin-based movement, and regulation of action potentials. Recent studies have indicated that the NF-κB pathway can be used as a target for castration-resistant PCa(McCall et al., 2012) and that the Wnt/β-catenin pathway is involved in the proliferation, invasion and metastasis of PCa (Clevers and Nusse, 2012; Zhang and Li, 2020). In addition, through GSEA, MALT1 was found to be associated with several cancer-related signaling pathways that promote cancer processes, including NF-κB pathway and Wnt/β-catenin pathway. All these above results support the protumor role of MALT1 in PCa.

Deregulation of cell proliferation and evasion of apoptosis are two hallmarks of cancer cells. In this study, knocking down MALT1 in PCa cell lines distinctly suppressed cells proliferation, migration, and invasion, and promoted apoptosis *in vitro*. In addition, the results of *in vivo* assays confirmed the tumor-promotive roles of MAL1 in PCa growth. Through the experiments reported here, we confirmed that MALT1 acts as a proto-oncogene and plays an important role in the development of PCa.

The TME has been a recent focus of tumor research. Since the tumor microenvironment was composed of a large number of immune cells, we then examined the association between MALT1 copy number and infiltration level of several immune cells in PCa, such as B cell, $CD4^+$ T cell, $CD8^+$ T cell, macrophage, neutrophil and dendritic cell (DC). The main function of B cell is to produce antibody mediated immune response and $CD4^+$ T cells were reported to be helper T cells that are capable of promoting effective antitumor immune responses. $CD8^+$ T cells mainly refer to cytotoxic T lymphocytes (CTLs), and an increase in $CD8^+$ CTL levels could lead to efficient killing of tumors (Ness et al., 2014). In addition, macrophages can promote or inhibit tumor progression (such as cell proliferation, metastasis and invasion) (Gorchakov et al., 2020). Tumor-associated neutrophil cells (TAN) play an significant role in promoting angiogenesis, and they can affect tumor migration through releasing matrix metalloproteinase 9 (MMP9) (Granot, 2019). DC can activate B cells, NK cells and NK-T cells, induce and maintain tumor immune response (Garofano et al., 2019). In this study, we found that MALT1 expression was significantly correlated with the levels of these 6 types of infiltrating immune cells. Here, we also found that the deep deletion and high amplification of MALT1 significantly decreased the infiltration of $CD8^+$ T cells and $CD4^+$ T cells, respectively. These results indicate that MALT1 may lead to tumorigenesis or inhibit tumor progression by changing the TIL status in PCa. These novel findings constitute substantial progress in identifying the important role of MALT1 in immune infiltration.

The latest research demonstrated that MALT1 is indispensable for the development of regulatory T cells and plays a significant role in immune homeostasis (Gewies et al., 2014; Jaworski et al., 2014). In the current study, the expression of MALT1 was also related to the expression of some specific immune checkpoint genes across multiple tumors. Therefore, we speculated that MALT1 could impact cancer progression and metastasis by regulating the activity of immune checkpoint genes.

We also demonstrated that there is a relationship between MALT1 expression and TMB and MSI in some cancer types and that some tumors show coexpression of MALT1 and major MMR genes. MSI and high TMB (TMB-high) are promising pancancer biomarkers to guide immune checkpoint blockade (ICB) treatment. Previous studies have linked TMB and MSI to drug responses in patients, particularly drugs targeting immune checkpoint inhibitors, such as TGF-β antagonists and PD-1 inhibitors (Overman et al., 2017; Mariathasan et al., 2018; Kwon et al., 2020; Lagos et al., 2020; Shim et al., 2020; Yoshino et al., 2020). Therefore, we suggest that MALT1 expression be used as an additional indicator for the evaluation of immunotherapy in cancer patients after treatment. Interestingly, MSI is now considered an indicator of tumor types in patients with COAD. In addition, COAD patients with high MSI showed better checkpoint inhibitor response and survival in both early and late clinical stages (El Agy et al., 2019; Allan et al., 2020; Dzunic et al., 2020). In our study, both the TMB and MSI of COAD were positively correlated with the expression of MALT1, which supports our claim that MALT1 may be a good indicator of potential drug response (and MSI), as well as in COAD.

CONCLUSION

This is the first time the cellular function of MALT1 in PCa was investigated, and its molecular mechanism was explored through bioinformatics analysis. Our findings confirm that MALT1 participates in promoting proliferation and colony genesis while reducing the level of apoptosis of PCa cells and is also predicted to be associated with migration and metastasis of PCa. Knocking down of MALT1 attenuated the tumorigenesis ability of PCa in mice. This study will add to our understanding of the molecular mechanism of PCa and hopefully provide novel targets for individualized cancer therapy. Furthermore, we identified Correlation of MALT1 expression with immune check points, TBM and MSI in most cancers by bioinformatic analysis. Authors have identified very significant correlation of MALT1 expression with tumor burden and various cancer driven pathways in multiple cancers. However, a limitation of our study is that only 1 cell line was studied *in vivo*. Thus, it is important to

verify our findings in other NSCLC cell lines before reaching a final conclusion.

DATA AVAILABILITY STATEMENT

The original contributions presented in the study are included in the article/Supplementary Material, further inquiries can be directed to the corresponding authors.

ETHICS STATEMENT

The animal study was reviewed and approved by Yantai Yu Huang Ding Hospital's ethical committee.

AUTHOR CONTRIBUTIONS

HT, WW, and CL contributed to the conception and design. HT and YX extracted the data from the databases. HT, YX, SW, and XZ contributed to the data analysis and interpretation. HT, WT, CL, and YX have done the experiments and statistical analysis.

FUNDING

Natural Science Foundation of Shandong Province, Grant/Award Number: ZR2019MH132; Yantai Key Research and Development Project, Grant/Award Number: 2020MSGY079 and 2019MSGY135.

REFERENCES

Afonina, I. S., Elton, L., Carpentier, I., and Beyaert, R. (2015). MALT1 - a Universal Soldier: Multiple Strategies to Ensure NF-Kb Activation and Target Gene Expression. *Febs J.* 282 (17), 3286–3297. doi:10.1111/febs.13325

Allan, R.-E., Luis, R.-P., and Juan, P. (2020). Microsatellite Instability in Costa Rican Patients with Colorectal Adenocarcinoma and its Association with Overall Survival and Response to Fluoropyrimidine-Based Chemotherapy. *Cancer Epidemiol.* 65, 101680. doi:10.1016/j.canep.2020.101680

Ashcraft, K. A., Johnson-Pais, T. L., Troyer, D. A., Hernandez, J., and Leach, R. J. (2020). "A Copy Number Gain on 18q Present in Primary Prostate Tumors Is Associated with Metastatic Outcome," in *Urologic Oncology: Seminars and Original Investigations* (Amsterdam: Elsevier).

Blum, A., Wang, P., and Zenklusen, J. C. (2018). SnapShot: TCGA-Analyzed Tumors. *Cell* 173 (2), 530. doi:10.1016/j.cell.2018.03.059

Bonneville, R., Krook, M. A., Kautto, E. A., Miya, J., Wing, M. R., Chen, H.-Z., et al. (2017). Landscape of Microsatellite Instability across 39 Cancer Types. *JCO Precision Oncol.* 1, 1–15. doi:10.1200/po.17.00073

Bray, F., Ferlay, J., Soerjomataram, I., Siegel, R. L., Torre, L. A., and Jemal, A. (2018). Global Cancer Statistics 2018: GLOBOCAN Estimates of Incidence and Mortality Worldwide for 36 Cancers in 185 Countries. *CA: A Cancer J. Clinicians* 68 (6), 394–424. doi:10.3322/caac.21492

Clevers, H., and Nusse, R. (2012). Wnt/β-Catenin Signaling and Disease. *Cell* 149 (6), 1192–1205. doi:10.1016/j.cell.2012.05.012

Coornaert, B., Baens, M., Heyninck, K., Bekaert, T., Haegman, M., Staal, J., et al. (2008). T Cell Antigen Receptor Stimulation Induces MALT1 Paracaspase-Mediated Cleavage of the NF-Kb Inhibitor A20. *Nat. Immunol.* 9 (3), 263–271. doi:10.1038/ni1561

Dai, H., Li, R., Wheeler, T., Ozen, M., Ittmann, M., Anderson, M., et al. (2007). Enhanced Survival in Perineural Invasion of Pancreatic Cancer: an *In Vitro* Approach. *Hum. Pathol.* 38 (2), 299–307. doi:10.1016/j.humpath.2006.08.002

Donnelly, B. J., Saliken, J. C., Brasher, P. M. A., Ernst, S. D., Rewcastle, J. C., Lau, H., et al. (2010). A Randomized Trial of External Beam Radiotherapy versus Cryoablation in Patients with Localized Prostate Cancer. *Cancer* 116 (2), 323–330. doi:10.1002/cncr.24779

Dzunic, M., Andjelkovic-Apostolovic, M., Vrbic, S., Pejcic, I., Petkovic, I., Cvetanovic, A., et al. (2020). Survival of Patients with Liver Metastases from Colorectal Cancer Treated with Bevacizumab and FOLFOX4. *J. BUON* 25 (1), 212–219.

El Agy, F., Otmani, I. E., Mazti, A., Lahmidani, N., Oussaden, A., El Abkari, M., et al. (2019). Implication of Microsatellite Instability Pathway in Outcome of Colon Cancer in Moroccan Population. *Dis. Markers* 2019, 1–10. doi:10.1155/2019/3210710

Garofano, F., Gonzalez-Carmona, M. A., Skowasch, D., Schmidt-Wolf, R., Abramian, A., Hauser, S., et al. (2019). Clinical Trials with Combination of Cytokine-Induced Killer Cells and Dendritic Cells for Cancer Therapy. *Ijms* 20 (17), 4307. doi:10.3390/ijms20174307

Gasnier, A., and Parvizi, N. (2017). Updates on the Diagnosis and Treatment of Prostate Cancer. *Bjr* 90 (1075), 20170180. doi:10.1259/bjr.20170180

Gewies, A., Gorka, O., Bergmann, H., Pechloff, K., Petermann, F., Jeltsch, K. M., et al. (2014). Uncoupling Malt1 Threshold Function from Paracaspase Activity Results in Destructive Autoimmune Inflammation. *Cell Rep.* 9 (4), 1292–1305. doi:10.1016/j.celrep.2014.10.044

Gorchakov, A. A., Kulemzin, S. V., Kochneva, G. V., and Taranin, A. V. (2020). Challenges and Prospects of Chimeric Antigen Receptor T-Cell Therapy for Metastatic Prostate Cancer. *Eur. Urol.* 77 (3), 299–308. doi:10.1016/j.eururo.2019.08.014

Granot, Z. (2019). Neutrophils as a Therapeutic Target in Cancer. *Front. Immunol.* 10, 1710. doi:10.3389/fimmu.2019.01710

Hailfinger, S., Lenz, G., Ngo, V., Posvitz-Fejfar, A., Rebeaud, F., Guzzardi, M., et al. (2009). Essential Role of MALT1 Protease Activity in Activated B Cell-like Diffuse Large B-Cell Lymphoma. *Proc. Natl. Acad. Sci.* 106 (47), 19946–19951. doi:10.1073/pnas.0907511106

Hayden, A. J., Catton, C., and Pickles, T. (2010). Radiation Therapy in Prostate Cancer: a Risk-Adapted Strategy. *Curr. Oncol.* 17 (Suppl. 2), S18–S24. doi:10.3747/co.v17i0.704

Jacobs, K. A., André-Grégoire, G., Maghe, C., Thys, A., Li, Y., Harford-Wright, E., et al. (2020). Paracaspase MALT1 Regulates Glioma Cell Survival by Controlling Endo-Lysosome Homeostasis. *EMBO J.* 39 (1), e102030. doi:10.15252/embj.2019102030

Jaworski, M., Marsland, B. J., Gehrig, J., Held, W., Favre, S., Luther, S. A., et al. (2014). Malt1 Protease Inactivation Efficiently Dampens Immune Responses but Causes Spontaneous Autoimmunity. *Embo J.* 33 (23), 2765–2781. doi:10.15252/embj.201488987

Jaworski, M., Thome, M., and Sciences, M. L. (2016). The Paracaspase MALT1: Biological Function and Potential for Therapeutic Inhibition. *Cell. Mol. Life Sci.* 73 (3), 459–473. doi:10.1007/s00018-015-2059-z

Krieger, T., Pearson, I., Bell, J., Doherty, J., and Robbins, P. (2020). Targeted Literature Review on Use of Tumor Mutational burden Status and Programmed Cell Death Ligand 1 Expression to Predict Outcomes of Checkpoint Inhibitor Treatment. *Diagn. Pathol.* 15 (1), 6. doi:10.1186/s13000-020-0927-9

Kwon, M., Hong, J. Y., Kim, S. T., Kim, K.-M., and Lee, J. J. P.-R. (2020). Association of Serine/threonine Kinase 11 Mutations and Response to Programmed Cell Death 1 Inhibitors in Metastatic Gastric Cancer. *Res. Pract.* 216, 152947. doi:10.1016/j.prp.2020.152947

Lagos, G. G., Izar, B., and Rizvi, N. A. (2020). Beyond Tumor PD-L1: Emerging Genomic Biomarkers for Checkpoint Inhibitor Immunotherapy. *Am. Soc. Clin. Oncol. Educ. Book* 40, e47–e57. doi:10.1200/edbk_289967

Liu, X., Yue, C., Shi, L., Liu, G., Cao, Q., Shan, Q., et al. (2020). MALT1 Is a Potential Therapeutic Target in Glioblastoma and Plays a Crucial Role in EGFR-induced NF-κB Activation. *J. Cell Mol. Med.* 24, 7550–7562. doi:10.1111/jcmm.15383

Lonsdale, J., Thomas, J., Salvatore, M., Phillips, R., Lo, E., Shad, S., et al. (2013). The Genotype-Tissue Expression (GTEx) Project. *Nat. Genet.* 45 (6), 580–585. doi:10.1038/ng.2653

Mariathasan, S., Turley, S. J., Nickles, D., Castiglioni, A., Yuen, K., Wang, Y., et al. (2018). TGFβ Attenuates Tumour Response to PD-L1 Blockade by Contributing to Exclusion of T Cells. *Nature* 554 (7693), 544–548. doi:10.1038/nature25501

McAllister-Lucas, L. M., Baens, M., and Lucas, P. C. (2011). MALT1 Protease: A New Therapeutic Target in B Lymphoma and beyond? *Clin. Cancer Res.* 17 (21), 6623–6631. doi:10.1158/1078-0432.ccr-11-0467

McCall, P., Bennett, L., Ahmad, I., Mackenzie, L. M., Forbes, I. W. G., Leung, H. Y., et al. (2012). NFκB Signalling Is Upregulated in a Subset of Castrate-Resistant Prostate Cancer Patients and Correlates with Disease Progression. *Br. J. Cancer* 107 (9), 1554–1563. doi:10.1038/bjc.2012.372

Meiser, B., Kaur, R., Kirk, J., Morrow, A., Peate, M., Wong, W., et al. (2020). Evaluation of Implementation of Risk Management Guidelines for Carriers of Pathogenic Variants in Mismatch Repair Genes: a Nationwide Audit of Familial Cancer Clinics. *Fam. Cancer* 19, 1–10. doi:10.1007/s10689-020-00183-4

Miller, E. T., Chamie, K., Kwan, L., Lewis, M. S., Knudsen, B. S., and Garraway, I. P. (2017). Impact of Treatment on Progression to Castration-resistance, Metastases, and Death in Men with Localized High-grade Prostate Cancer. *Cancer Med.* 6 (1), 163–172. doi:10.1002/cam4.981

Moreira, D. M., Howard, L. E., Sourbeer, K. N., Amarasekara, H. S., Chow, L. C., Cockrell, D. C., et al. (2017). Predicting Time from Metastasis to Overall Survival in Castration-Resistant Prostate Cancer: Results from SEARCH. *Clin. Genitourinary Cancer* 15 (1), 60–66. e62. doi:10.1016/j.clgc.2016.08.018

Nagel, D., Spranger, S., Vincendeau, M., Grau, M., Raffegerst, S., Kloo, B., et al. (2012). Pharmacologic Inhibition of MALT1 Protease by Phenothiazines as a Therapeutic Approach for the Treatment of Aggressive ABC-DLBCL. *Cancer Cell* 22 (6), 825–837. doi:10.1016/j.ccr.2012.11.002

Ness, N., Andersen, S., Valkov, A., Nordby, Y., Donnem, T., Al-Saad, S., et al. (2014). Infiltration of CD8+ Lymphocytes Is an Independent Prognostic Factor of Biochemical Failure-free Survival in Prostate Cancer. *Prostate* 74 (14), 1452–1461. doi:10.1002/pros.22862

Ngo, V. N., Davis, R. E., Lamy, L., Yu, X., Zhao, H., Lenz, G., et al. (2006). A Loss-Of-Function RNA Interference Screen for Molecular Targets in Cancer. *Nature* 441 (7089), 106–110. doi:10.1038/nature04687

Overman, M. J., McDermott, R., Leach, J. L., Lonardi, S., Lenz, H.-J., Morse, M. A., et al. (2017). Nivolumab in Patients with Metastatic DNA Mismatch Repair-Deficient or Microsatellite Instability-High Colorectal Cancer (CheckMate 142): an Open-Label, Multicentre, Phase 2 Study. *Lancet Oncol.* 18 (9), 1182–1191. doi:10.1016/s1470-2045(17)30422-9

Pan, D., Zhu, Y., Zhou, Z., Wang, T., You, H., Jiang, C., et al. (2016). The CBM Complex Underwrites NF-Kb Activation to Promote HER2-Associated Tumor Malignancy. *Mol. Cancer Res.* 14 (1), 93–102. doi:10.1158/1541-7786.mcr-15-0229-t

Perlmutter, M. A., and Lepor, H. (2007). Androgen Deprivation Therapy in the Treatment of Advanced Prostate Cancer. *Rev. Urol.* 9, S3–S8.

Ruland, J., Duncan, G. S., Wakeham, A., and Mak, T. W. (2003). Differential Requirement for Malt1 in T and B Cell Antigen Receptor Signaling. *Immunity* 19 (5), 749–758. doi:10.1016/s1074-7613(03)00293-0

Saba, N. S., Wong, D. H., Tanios, G., Iyer, J. R., Lobelle-Rich, P., Dadashian, E. L., et al. (2017). MALT1 Inhibition Is Efficacious in Both Naïve and Ibrutinib-Resistant Chronic Lymphocytic Leukemia. *Cancer Res.* 77 (24), 7038–7048. doi:10.1158/0008-5472.can-17-2485

Shim, J., Kim, H., Cha, H., Kim, S., Kim, T., Anagnostou, V., et al. (2020). HLA-corrected Tumor Mutation burden and Homologous Recombination Deficiency for the Prediction of Response to PD-(L) 1 Blockade in Advanced Non-small–cell Lung Cancer Patients. *Ann. Oncol.* 31, 902–911. doi:10.1016/j.annonc.2020.04.004

Shipley, W. U., Verhey, L. J., Munzenrider, J. E., Suit, H. D., Urie, M. M., McManus, P. L., et al. (1995). Advanced Prostate Cancer: the Results of a Randomized Comparative Trial of High Dose Irradiation Boosting with Conformal Protons Compared with Conventional Dose Irradiation Using Photons Alone. *Int. J. Radiat. Oncology*Biology*Physics* 32 (1), 3–12. doi:10.1016/0360-3016(95)00063-5

Turvey, S. E., Durandy, A., Fischer, A., Fung, S.-Y., Geha, R. S., Gewies, A., et al. (2014). The CARD11-BCL10-MALT1 (CBM) Signalosome Complex: Stepping into the Limelight of Human Primary Immunodeficiency. *J. Allergy Clin. Immunol.* 134 (2), 276–284. doi:10.1016/j.jaci.2014.06.015

Uhlén, M., Fagerberg, L., Hallström, B. M., Lindskog, C., Oksvold, P., Mardinoglu, A., et al. (2015). Proteomics. Tissue-Based Map of the Human Proteome. *Science* 347 (6220), 1260419. doi:10.1126/science.1260419

Varambally, S., Yu, J., Laxman, B., Rhodes, D. R., Mehra, R., Tomlins, S. A., et al. (2005). Integrative Genomic and Proteomic Analysis of Prostate Cancer Reveals Signatures of Metastatic Progression. *Cancer Cell* 8 (5), 393–406. doi:10.1016/j.ccr.2005.10.001

Wang, S., Clarke, P. A. G., Davis, R., Mumuni, S., and Kwabi-Addo, B. (2016). Sex Steroid-Induced DNA Methylation Changes and Inflammation Response in Prostate Cancer. *Cytokine* 86, 110–118. doi:10.1016/j.cyto.2016.07.006

Xu, Y., Hu, J., Wang, X., Xuan, L., Lai, J., Xu, L., et al. (2015). Overexpression of MALT1-A20-NF-Kb in Adult B-Cell Acute Lymphoblastic Leukemia. *Cancer Cell Int* 15 (1), 73. doi:10.1186/s12935-015-0222-0

Yoshino, T., Pentheroudakis, G., Mishima, S., Overman, M., Yeh, K.-H., Baba, E., et al. (2020). JSCO/ESMO/ASCO/JSMO/TOS: International Expert Consensus Recommendations for Tumour-Agnostic Treatments in Patients with Solid Tumours with Microsatellite Instability or NTRK Fusions. *Ann. Oncol.* 31, 861–872. doi:10.1016/j.annonc.2020.03.299

Zhang, Y., and Li, Y. (2020). Long Non-coding RNA NORAD Contributes to the Proliferation, Invasion and EMT Progression of Prostate Cancer via the miR-30a-5p/RAB11A/WNT/β-catenin Pathway. *Cancer Cell Int* 20 (1), 571–614. doi:10.1186/s12935-020-01665-2

Conflict of Interest: The authors declare that the research was conducted in the absence of any commercial or financial relationships that could be construed as a potential conflict of interest.

Publisher's Note: All claims expressed in this article are solely those of the authors and do not necessarily represent those of their affiliated organizations, or those of the publisher, the editors, and the reviewers. Any product that may be evaluated in this article, or claim that may be made by its manufacturer, is not guaranteed or endorsed by the publisher.

frontiers in Cell and Developmental Biology

ORIGINAL RESEARCH
published: 06 December 2021
doi: 10.3389/fcell.2021.697748

CREM Is Correlated With Immune-Suppressive Microenvironment and Predicts Poor Prognosis in Gastric Adenocarcinoma

Kuai Yu[1,2], *Linju Kuang*[1,2], *Tianmei Fu*[1,2], *Congkai Zhang*[1,2], *Yuru Zhou*[1,2], *Chao Zhu*[1,2], *Qian Zhang*[1,2], *Zhanglin Zhang*[1,2]* *and Aiping Le*[1,2]*

[1]*Department of Blood Transfusion, The First Affiliated Hospital of Nanchang University, Nanchang, China,* [2]*Key Laboratory of Jiangxi Province for Transfusion Medicine, The First Affiliated Hospital of Nanchang University, Nanchang, China*

OPEN ACCESS

Edited by:
José Alexandre Ferreira, Portuguese Oncology Institute, Portugal

Reviewed by:
Xian-Yang Li, Zhuhai People's Hospital, China
Hui Zhou, Central South University, China
Shaojun Zhang, Guangdong Provincial People's Hospital, China

***Correspondence:**
Zhanglin Zhang
ndyfy02270@ncu.edu.cn
Aiping Le
Leaiping@126.com

Specialty section:
This article was submitted to Molecular and Cellular Pathology, a section of the journal Frontiers in Cell and Developmental Biology

Received: *20 April 2021*
Accepted: *18 October 2021*
Published: *06 December 2021*

Citation:
Yu K, Kuang L, Fu T, Zhang C, Zhou Y, Zhu C, Zhang Q, Zhang Z and Le A (2021) CREM Is Correlated With Immune-Suppressive Microenvironment and Predicts Poor Prognosis in Gastric Adenocarcinoma. Front. Cell Dev. Biol. 9:697748. doi: 10.3389/fcell.2021.697748

The transcriptional repressor cAMP response element modulator (CREM) has an important role in T-cell development. In this study, we used the integrated Bioinformatics Methods to explore the role of CREM in gastric adenocarcinoma (GAC). Our results showed that high CREM expression was closely related with poorer overall survival in GAC. By GSEA cluster analysis, we found that the high expression of CREM was associated with the cancer-associated pathway in GAC. Moreover, single-cell sequencing data showed that CREM is mainly localized in exhausted $CD8^+$ T cells. Its prognostic value and the potential function lead to T-cell exhaustion in the tumor microenvironment (TME). Similar results were also obtained in glioma and lung cancer. High expression of CREM, correlated with clinical relevance of GAC, was associated with T-cell exhaustion and M2 polarization in GAC. These findings suggest that CREM can be used as a prognostic biomarker in GAC, which might provide a novel direction to explore the pathogenesis of GAC.

Keywords: CREM, exhausted T cell, tumor-associated macrophages, tumor-infiltrating, immunosuppression, gastric cancer tumor microenvironment, prognosis

INTRODUCTION

Gastric adenocarcinoma (GAC), which arises from glandular epithelia of the gastric mucosa, is the most common type of gastric cancer, which is the fourth most common cancer, and the second most common cause of cancer death in the world (Bray et al., 2018). At present, the first-line treatment of advanced GAC is still chemotherapy (Song et al., 2017). Monoclonal antibodies targeting human epidermal growth factor (HER2; trastuzumab) (Zaanan et al., 2018) have been approved by the FDA for first-line treatment of patients with HER2-positive GAC. In addition, Ramucirumab, a vascular endothelial growth factor (VEGF) targeted drug (Yazici et al., 2016), for whom first-line treatment has failed, has also been approved for patients with advanced GAC. Although there are many treatments for GAC, the overall survival rate is only 5–20% in the world.

Immunotherapy is a revolutionary anti-cancer therapy in the past decade. Immune checkpoint inhibitors, which are closely related to the elimination of T-cell exhaustion, have achieved certain results in the treatment of various tumors. The most widely used checkpoint inhibitors are antibodies of cytotoxic T lymphocyte antigen 4 (CTLA-4), programmed cell death protein 1 (PD-1), and its ligand programmed death-ligand 1 (PD-L1) (Fuchs et al., 2014). However, current

immunotherapies, such as anti-CTLA4 (Fuchs et al., 2014; Li et al., 2019), showed poor clinical efficacy in GAC; in addition, anti-PD-1 and anti-PD-L1 showed a partial response in GC. With the dramatic development of next-generation sequencing (NGS) and single-cell sequencing, more and more exhaustion T-cell-related molecules have been identified, such as TIM3, LAG3, TIGIT (Anderson et al., 2016), PD1 (Xing et al., 2018), and LAYN (Zheng et al., 2017). The identification of these molecules is of great significance in predicting the prognosis of cancer prognosis. Because the existing marker is still unable to effectively identify exhaustion T cells, this field requires new biomarkers as prognostic indicators to effectively enhance prognosis and individualized immunotherapy.

The transcriptional repressor cAMP response element modulator (CREM) is inducible by activation of the cAMP signaling pathway with the kinetics of an early response gene (Lamas et al., 1996). The CREM gene encodes both activators and repressors of cAMP-dependent transcription. Previous studies have shown that cyclic AMP-dependent signals are associated with T-cell exhaustion (Maine et al., 2016; Schmetterer et al., 2019). Moreover, CREM contributes to various cellular and molecular abnormalities in T cells, including increased IL-17 and decreased IL-2 expression (Verjans et al., 2013). Previous studies have shown that CREM has important roles in normal T-cell physiology and contributes to aberrant T-cell function in patients with systemic lupus erythematosus (SLE) (Rauen et al., 2011). RNAi targeting of ICER/CREM in responder $CD25^{-}$ $CD4^{+}$ T cells antagonizes Treg-mediated suppression (Bodor et al., 2007). These findings suggest that CREM has multifaceted functional roles in immune microenvironment. However, the underlying functions of CREM in TME is still unclear.

This study aims to delineate the role of CREM, through TCGA GAC public data and TISCH single-cell database. We analyzed the expression of CREM and the correlation with prognosis of GAC patients in the TCGA database. Through KOBAS database and GSEA analysis, we found that the high expression of CREM is closely related to cancer-associated pathways. To investigate the underlying causes, we investigated the correlation of CREM with tumor-infiltrating immune cells in the tumor microenvironment (TME) *via* CIBERSORT. Our report depicted the important role of CREM in GAC, and revealed the relationship between CREM and tumor-infiltrating lymphocytes in GAC. These results suggest that CREM may be a potential clinical prognostic indicator in GAC. In addition, we briefly explored the role of CREM in lung cancer and glioma.

METHODS

Data Download and Processing

The mRNA profiling information is from the TCGA (The Cancer Genome Atlas, https://cancergenome.nih.gov/) database. The download mRNA expression data were alternate with log2, so we restored them to raw FPKM (Fragments Per kilobase per Million) and count value. Besides, we changed FPKM gene expression value to TPM (Transcripts Per Million) expression value. There were 375 GAC patients in mRNA expression data and were listed in descending order by CREM TPM expression value. Finally, we selected the top 98 patients as CREM high expression group (CREM TPM expression value >9) and the last 44 patients as CREM low expression group (CREM TPM expression value <4).

CREM Gene Expression Analysis in Bulk and Single-Cell RNA Sequence Datasets

The CREM expression level was analyzed by the GEPIA2 and TISCH web-based tools. GEPIA2 contained TCGA and GTEx datasets (Tang et al., 2019). TISCH (Tumor Immune Single-cell Hub) provided detailed cell-type annotation and gene expression profile at the single-cell level (Sun et al., 2021). We invested CREM single-cell gene expression level in the GSE134520 (Zhang et al., 2019) GAC dataset and the GSE131928 (Neftel et al., 2019) glioma dataset. T-cell single-cell dataset of non-small cell lung cancer was analyzed in web database (http://lung.cancer-pku.cn) (Guo et al., 2018).

Differentially Expressed Genes About CREM

In this study, we explored differential expression genes between high CREM expression and low CREM expression group in gastric cancer based on the TCGA GAC dataset. We used R package DESeq2 and filtered genes with base Mean >200, $|\log2FoldChange| > 1.5$, p-value < 0.05. Finally, there were 723 up genes and 6,714 down genes.

Functional Enrichment Analysis

In order to analyze the molecular mechanism of CREM in gastric cancer, we used these up genes in CREM high expression group to enrich in the KOBAS database (Xie et al., 2011) with the KEGG signaling pathway. We filtered these KEGG items with corrected p-value < 0.05. Besides, we also analyzed the TCGA GAC dataset with GSEA (gene set enrichment analysis) software (Subramanian et al., 2005) in KEGG pathways.

Immune Cell Infiltration Analysis

We investigated every patient tumor-infiltrating immune cell abundance *via* the web-based tool Tumor Immune Estimation Resource (TIMER) version 2 (Li et al., 2020). We uploaded TCGA GAC TPM mRNA expression matrix in estimation web page and finally downloaded the estimated result. We analyzed the abundance of tumor-infiltrating immune cells with CIBERSORT (Chen et al., 2018). CIBERSORT was a mathematics method for characterizing cell composition of complex tissues including solid tumors *via* their gene expression profiles.

Relationship Between CREM and T-Cell Exhaustion Analysis

In order to analyze the role of CREM in T cell's function, we compared mRNA expression correlation between CREM and T cell's exhausted marker genes in TCGA GAC datasets, such as

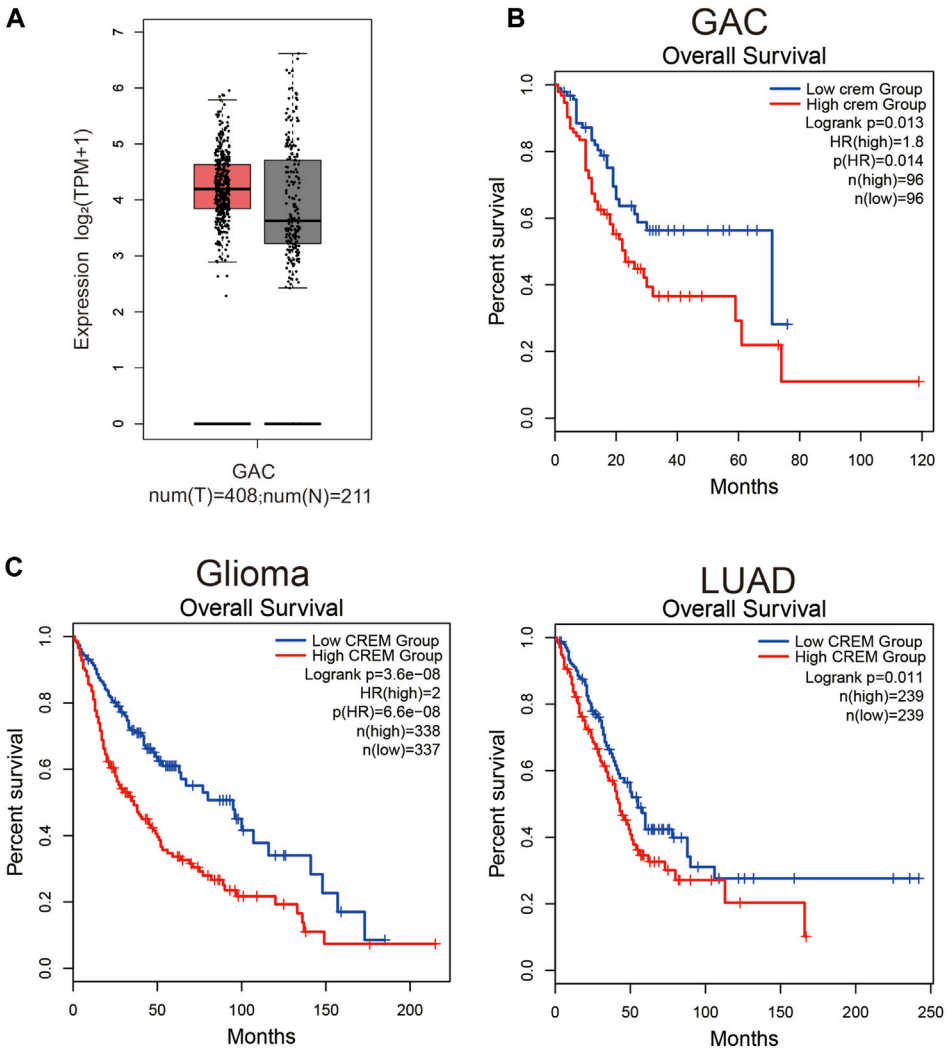

FIGURE 1 | Expression level analysis of CREM in GAC tissues. Kaplan–Meier survival curves comparing the high and low expression of CREM in different types of cancer in GEPIA2. **(A)** CREM expression level between tumor samples and normal samples in GAC. **(B)** Kaplan–Meier survival curves comparing high and low CREM expression groups in the GAC dataset. **(C)** Kaplan–Meier survival curves comparing high and low CREM expression groups in the glioma, LUAD dataset.

HAVCR2, LAYN, TIGIT, PD1, and LAG3. Scatterplots were taken in GEPIA2 database with Spearman correlation coefficient. In addition, we defined T-cell exhausted score as $CD8^+$ T-cell estimated infiltration abundance multiplied by the TPM expression value of T cell's exhausted marker gene in every patient. Compared distribution of exhausted score between high CREM and low CREM groups. $p < 0.05$ was considered statistically significant ($^*p \leq 0.05$, $^{**}p \leq 0.01$, $^{***}p \leq 0.001$, $^{****}p \leq 0.0001$).

Survival Analysis

Overall survival curves were taken by Kaplan–Meier plot of CREM high expression group and CREM low expression group with log rank test, and $p < 0.05$ was considered statistically significant ($^*p \leq 0.05$, $^{**}p \leq 0.01$, $^{***}p \leq 0.001$, $^{****}p \leq 0.0001$). Individual patients who did not have survival information were not considered in survival analysis. Besides, we explored overall survival of glioma and LUAD (lung adenocarcinoma) in the GEPIA2 web database. We chose GBM (glioblastoma) and LGG (brain lower grade glioma) as the glioma dataset; group was cut off by median.

RESULTS

High CREM Expression in GAC Predicts Unfavorable Overall Survival

To reveal the role of CREM in GAC, we investigated whether CREM expression was correlated with prognosis in GAC patients. By exploring CREM mRNA expression level and clinical characteristics of GAC in GEPIA2, the expression of CREM in GAC was higher than that in normal tissues (**Figure 1A**). CREM is highly expressed in tumor tissues and may play an important role in GAC. To better understand the potential function of

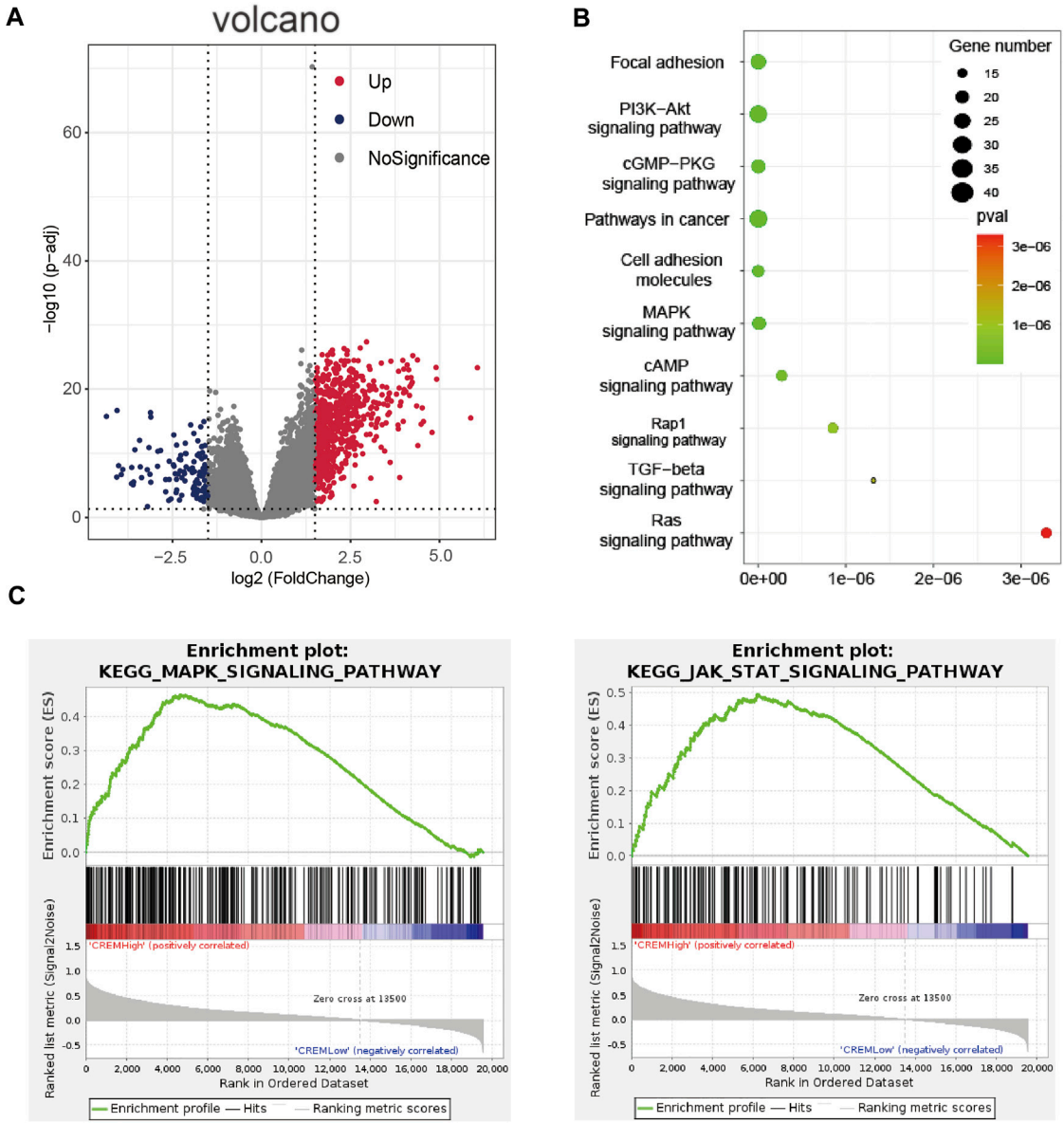

FIGURE 2 | Enrichment analyses of CREM in TCGA GAC (stomach adenocarcinoma). **(A)** Volcano map of different expression genes between high expression CREM group and low expression CREM group. Red represents upregulation of gene expression, purple represents downregulation of gene expression, and gray represents no difference in gene expression. **(B)** Enrichment analysis of CREM different expression up genes in KOBAS database with KEGG pathways. Plot sizes show gene counts enriched in the enrichment of pathway. Color indicates the p-value from low (red) to high level (cyan). **(C)** Enrichment plot from gene set enrichment analysis including enrichment score. The significantly enriched signaling pathways were MAPK and JAK-STAT signaling pathway.

CREM in GAC, we analyzed the relationship between the CREM expression and clinical characteristics of GC patients in the TCGA database. GAC patients with higher CREM expression had shorter overall survival ($p = 0.013$) (**Figure 1B**). These results indicated that CREM was frequently expressed in GAC and could serve as a prognostic biomarker in GAC. Notably, CREM expression significantly impacts prognosis in gliomas and LUAD. LUAD patients and glioma patients with higher CREM expression had shorter overall survival (**Figure 1C**). These results indicated that CREM expression is an independent risk factor and leads to a poor prognosis in GAC patients.

CREM Was Involved in Many Cancer-Associated Signaling Pathways

In order to further verify the role of CREM in GAC, by analyzing TCGA database, we cluster the genes with high and low expression of CREM (**Figure 2A**, **Supplementary Table S1**). These genes with high expression of CREM were clustered

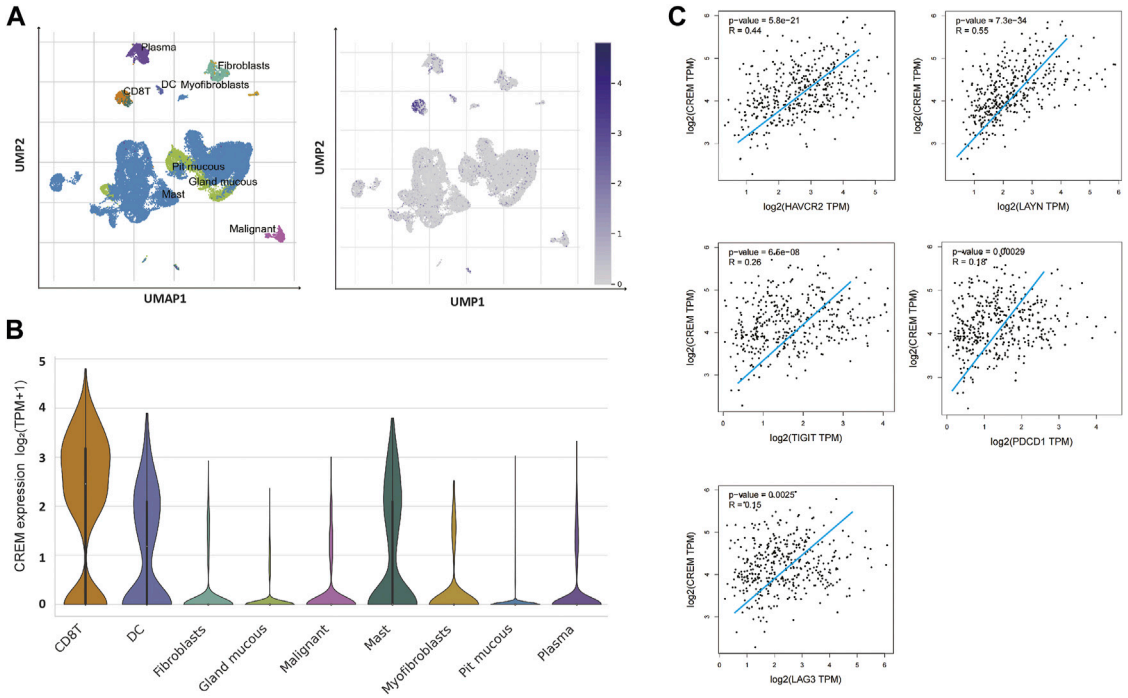

FIGURE 3 | The CREM expression analysis of tumor-infiltrating lymphocytes in GAC. **(A)** UMAP of GAC tumor tissue single-cell dataset, UMAP of GAC single cell dataset showed that high expression of CREM in CD8+ T cells. The depth of blue represents the amount of gene expression. **(B)** Violin plots showing the expression of CREM in various cell types. **(C)** Relationship between CREM expression level and T-cell exhausted marker genes expression level in the TCGA database (gene expression value is log2 TPM).

into the KEGG pathway by the KOBAS database (**Figure 2B**). We found that CREM is associated with a variety of cancer-associated pathways, such as focal adhesion, PI3K-Akt signaling pathway, cGMP-PKG signaling, cell adhesion molecules, MAPK signaling pathway, Rap1 signaling pathway, TGF-beta signaling pathway, and Ras signaling pathway. Notably, we also analyzed KEGG pathway in GSEA software. In the CREM overexpression group, MAPK signaling pathway and JAK-STAT signaling pathway were enriched (**Figure 2C**). MAPK signaling pathway plays a crucial role in the survival and development of tumor cells. The JAK-STAT signaling pathway also plays the external role of tumor and supports tumor survival by regulation of paracrine cytokine signaling. The identity of these tumor-related pathways in CREM high expression group proved that the high expression of CREM in tumor and TME did change the characteristics of tumor, and the high expression of CREM in tumor tissues led to the activation of cancer-associated signaling pathways and poor prognosis.

CREM is Positively Correlated With Exhausted T-Cell Marker Genes in GAC

In order to further explore the potential reasons for the positive correlation between CREM and tumorigenesis and development, we further investigated the correlation between CREM expression with tumor immune microenvironment. T-cell exhaustion is a state of T-cell dysfunction that arises during cancer and chronic inflammation in immune microenvironment. It is defined by poor function and sustained expression of inhibitory receptors. T-cell exhaustion prevents optimal control of infection and tumor progression. Previous studies have confirmed that CREM can affect T-cell function. In our study, we questioned whether the effect of CREM on poor prognosis in cancer was associated with immune-suppressive microenvironment. To investigate the cause of poor prognosis in GAC with high expression of CREM, we further explored CREM mRNA expression profile in the TISCH single-cell database in GC. We found that CREM can be expressed in a variety of cells, such as $CD8^+$ T cells, DC cells, mast cells, myofibroblasts, malignant cells, and fibroblasts. Notably, CREM is highly expressed in $CD8^+$ T cells in TME (**Figures 3A,B**). Furthermore, we speculate that CREM may affect T-cell function in TME. To evaluate whether the high expression of CREM affects the function of T cells in GAC, we compared the gene expression levels of CREM and exhausted T-cell marker genes (TIM3, TIGIT, LAG3, PD1, and LAYN). Our results indicated that CREM was significantly correlated with exhausted T-cell marker genes (**Figure 3D**). In addition, in the high CREM group, the number of estimated exhausted

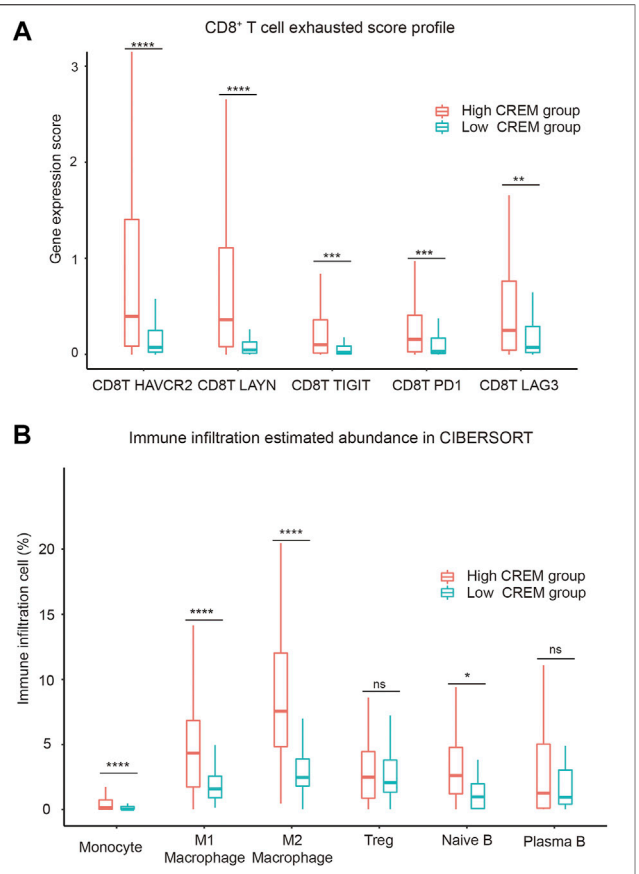

FIGURE 4 | Correlation between CREM expression and immune-suppressive microenvironment. **(A)** $CD8^+$ T-cell exhausted score profile between the high CREM group and low CREM group. **(B)** The immune infiltration estimated abundance in CIBERSORT; the estimated abundance is absolute type in CIBERSORT method.

T cells increased significantly (**Figure 4A**). Overall, these results indicated that CREM is associated with $CD8^+$ T-cell exhaustion in GAC. Notably, we analyzed the role of CREM in lung cancer and glioma. $CD4^+$ CTLA4 and $CD8^+$ LAYN are considered to be part of the T-cell exhaustion population. Single-cell sequencing data showed that CREM is highly expressed in the $CD4^+$ CTLA4 and $CD8^+$ LAYN population in non-small cell lung cancer (**Supplementary Figure S1C**), and CREM is highly expressed in the $CD8^+$ T-cell exhaustion population in glioma (**Supplementary Figure S1B**). These findings suggest that CREM plays a specific role in T-cell exhaustion in GAC and may affect the exhaustion of T cell in lung cancer and glioma.

The Role of CREM Expression on the Abundance of Immune Cell Infiltration

Tumor-infiltrating lymphocytes are an independent predictor of survival in cancer (Stanton and Disis, 2016; Badalamenti et al., 2019). To assess if high CREM expression was correlated with immune infiltration levels in GC, CIBERSORT was used to analyze the infiltration abundance of several immune cells between the high CREM group and low CREM group. Our results showed that the infiltration rates of M1 macrophages and M2 macrophages were significantly higher in the CREM high expression group. Treg cells (regulatory T cells) and plasma B cells had no significant changes. Interestingly, there was more infiltration of M1 and M2 macrophages in the CREM overexpression group, while the infiltration of M2 macrophages was more obvious than that of M1 macrophages or other immune cells (**Figure 4B**). These results indicated that CREM was positively correlated with the M2 polarization of macrophage in GAC. In general, these findings indicated that CREM-mediated immunosuppression may attribute to M2 polarization of TAMs.

DISCUSSION

Most malignant tumors are immunologically silent. In order to grow in an immune-competent host, acquired tumor cells undergo changes that result in immune-resistant phenotypes (Jiang et al., 2020). The high expression of CREM in tumor and TME may be a way for tumors to fight immune cells. CREM is part of the cAMP responsive element modulator family responsible for regulation of gene expression. Our study depicts the relationship between CREM and cancer-associated signaling pathway, and the immune features associated with CREM in the TME of GAC.

Higher CREM expression predicted poor outcome in patients with GAC, glioma, and LUAD. We found different expression genes between high CREM expression and low in the GAC TCGA dataset. The GSEA analysis revealed that the CREM expression level was strongly positively correlated with the KEGG MAPK signaling pathway and the JAK-STAT pathway. These results indicated that the high expression of CREM in tumor tissue led to the activation of the cancer-associated pathway in tumor cells and tumor progression.

Of note, our results revealed that CREM expression is associated with the exhausted T cells and infiltration of immune-suppressive macrophages in GAC, indicating a critical role of CREM in modulating the immune-suppressive microenvironment. The previous study provided evidence that CREM prevents production of IL-2 during chronic viral infection, thereby contributing to T-cell exhaustion (Maine et al., 2016). T-cell exhaustion refers to the loss of effector function of T cells, such as decreased production of IL-2 and IFN-γ, and expression of PD-1, Tim-3, CTLA-4, LAG-3, and other inhibitory receptors. We compared the expression levels of CREM and T-cell inhibitory receptors in GAC and found that CREM expression was positively correlated with the expression of T-cell suppressor molecules. On the other hand, M1 macrophages are associated with anti-tumor properties that efficiently eliminate cancer cells through phagocytosis and cytotoxicity while M2 macrophages promote tissue repair and tumor growth. The increased presence of M1 macrophages denotes lower tumor malignancy, while a higher M2 presence causes increased tumor growth and decreased

survival (Ruffell et al., 2012; Xia et al., 2020). We analyzed and compared the proportion of tumor-infiltrating lymphocytes in GAC between the high CREM group and the low CREM group. Significantly, the results showed that CREM high expression was significantly correlated with M2 polarization of microphage. These results support the notion that the high expression of CREM in tumor-infiltrating T cells leads to the development of immune-suppressive microenvironment, activation of tumor-related pathways, and proliferation and development of tumor cells. These results reveal the potential regulating role of CREM in polarization of tumor-associated macrophages. The above indicated that CREM could serve as an important prognostic risk factor for GAC, and this study may provide a new biomarker for immunotherapy of GAC.

Experimental studies are needed to validate the findings of this study. The experimental validation of the predicted results by different methods should be further confirmed. Lastly, it is not clear whether the immune-suppressive microenvironment would induce CREM expression or *vice versa*, and further research is needed. This study provides preliminary results that CREM is correlated with T-cell exhaustion and M2 polarization of macrophages in GAC.

DATA AVAILABILITY STATEMENT

Publicly available datasets were analyzed in this study. This data can be found here: https://gdc-hub.s3.us-east-1.amazonaws.com/download/TCGA-STAD.htseq_counts.tsv.gz http://lung.cancer-pku.cn.

AUTHOR CONTRIBUTIONS

KY and AL conceived the project and wrote the manuscript. LK, TF, CKZ, YZ, CZ, and QZ participated in data analysis. ZZ participated in discussion and language editing and reviewed the manuscript.

FUNDING

This work was supported by the Natural Science Foundation of China (32100729, 32071223, 81760381, 81760539 and 82160037), the Scientific research and training program for young talents of the First Affiliated Hospital of Nanchang University (YFYPY202017), the special fund project for postgraduate innovation of Jiangxi province in 2021 (YC2021-B057) and the project for postgraduate research interest team of Nanchang University in 2021.

SUPPLEMENTARY MATERIAL

The Supplementary Material for this article can be found online at: https://www.frontiersin.org/articles/10.3389/fcell.2021.697748/full#supplementary-material

Supplementary Figure S1 | The CREM expression analysis of tumor infiltrating lymphocytes in glioma and non-small cell lung cancer in single cell dataset. **(A)** Cluster profile of glioma single cell dataset in glioma GSE131928. **(B)** CREM expression levels of different cell types in glioma single cell dataset. **(C)** CREM expression levels of different T cell populations in the single cell data set of non-small cell lung cancer. **(D)** Cluster profile of T cells in non-small cell lung cancer dataset in web database (http://lung.cancer-pku.cn).

Supplementary Table S1 | Table of differential expression genes.

REFERENCES

Anderson, A. C., Joller, N., and Kuchroo, V. K. (2016). Lag-3, Tim-3, and TIGIT: Co-Inhibitory Receptors with Specialized Functions in Immune Regulation. *Immunity* 44 (5), 989–1004. doi:10.1016/j.immuni.2016.05.001

Badalamenti, G., Fanale, D., Incorvaia, L., Barraco, N., Listì, A., Maragliano, R., et al. (2019). Role of Tumor-Infiltrating Lymphocytes in Patients with Solid Tumors: Can a Drop Dig a Stone? *Cell Immunol.* 343, 103753. doi:10.1016/j.cellimm.2018.01.013

Bodor, J., Fehervari, Z., Diamond, B., and Sakaguchi, S. (2007). ICER/CREM-mediated Transcriptional Attenuation of IL-2 and its Role in Suppression by Regulatory T Cells. *Eur. J. Immunol.* 37 (4), 884–895. doi:10.1002/eji.200636510

Bray, F., Ferlay, J., Soerjomataram, I., Siegel, R. L., Torre, L. A., and Jemal, A. (2018). Global Cancer Statistics 2018: GLOBOCAN Estimates of Incidence and Mortality Worldwide for 36 Cancers in 185 Countries. *CA: A Cancer J. Clin.* 68 (6), 394–424. doi:10.3322/caac.21492

Chen, B., Khodadoust, M. S., Liu, C. L., Newman, A. M., and Alizadeh, A. A. (2018). Profiling Tumor Infiltrating Immune Cells with CIBERSORT. *Methods Mol. Biol.* 1711, 243–259. doi:10.1007/978-1-4939-7493-1_12

Fuchs, C. S., Tomasek, J., Yong, C. J., Dumitru, F., Passalacqua, R., Goswami, C., et al. (2014). Ramucirumab Monotherapy for Previously Treated Advanced Gastric or Gastro-Oesophageal junction Adenocarcinoma (REGARD): an International, Randomised, Multicentre, Placebo-Controlled, Phase 3 Trial. *Lancet* 383 (9911), 31–39. doi:10.1016/s0140-6736(13)61719-5

Guo, X., Zhang, Y., Zheng, L., Zheng, C., Song, J., Zhang, Q., et al. (2018). Global Characterization of T Cells in Non-Small-Cell Lung Cancer by Single-Cell Sequencing. *Nat. Med.* 24 (7), 978–985. doi:10.1038/s41591-018-0045-3

Jiang, L., Wang, Y.-J., Zhao, J., Uehara, M., Hou, Q., Kasinath, V., et al. (2020). Direct Tumor Killing and Immunotherapy through Anti-SerpinB9 Therapy. *Cell* 183 (5), 1219–1233. doi:10.1016/j.cell.2020.10.045

Lamas, M., Monaco, L., Zazopoulos, E., Lalli, E., Tamai, K., Penna, L., et al. (1996). CREM: a Master-Switch in the Transcriptional Response to cAMP. *Philos. Trans. R. Soc. Lond. B Biol. Sci.* 351 (1339), 561–567. doi:10.1098/rstb.1996.0055

Li, B., Chan, H. L., and Chen, P. (2019). Immune Checkpoint Inhibitors: Basics and Challenges. *Curr. Med. Chem.* 26 (17), 3009–3025. doi:10.2174/0929867324666170804143706

Li, T., Fu, J., Zeng, Z., Cohen, D., Li, J., Chen, Q., et al. (2020). TIMER2.0 for Analysis of Tumor-Infiltrating Immune Cells. *Nucleic Acids Res.* 48 (W1), W509–W514. doi:10.1093/nar/gkaa407

Maine, C. J., Teijaro, J. R., Marquardt, K., and Sherman, L. A. (2016). PTPN22 Contributes to Exhaustion of T Lymphocytes during Chronic Viral Infection. *Proc. Natl. Acad. Sci. USA* 113 (46), E7231–E7239. doi:10.1073/pnas.1603738113

Neftel, C., Laffy, J., Filbin, M. G., Hara, T., Shore, M. E., Rahme, G. J., et al. (2019). An Integrative Model of Cellular States, Plasticity, and Genetics for Glioblastoma. *Cell* 178 (4), 835–849. doi:10.1016/j.cell.2019.06.024

Rauen, T., Benedyk, K., Juang, Y.-T., Kerkhoff, C., Kyttaris, V. C., Roth, J., et al. (2011). A Novel Intronic cAMP Response Element Modulator (CREM) Promoter Is Regulated by Activator Protein-1 (AP-1) and Accounts for Altered Activation-Induced CREM Expression in T Cells from Patients with Systemic Lupus Erythematosus. *J. Biol. Chem.* 286 (37), 32366–32372. doi:10.1074/jbc.m111.245811

Ruffell, B., Affara, N. I., and Coussens, L. M. (2012). Differential Macrophage Programming in the Tumor Microenvironment. *Trends Immunol.* 33 (3), 119–126. doi:10.1016/j.it.2011.12.001

Schmetterer, K. G., Goldhahn, K., Ziegler, L. S., Gerner, M. C., Schmidt, R. L. J., Themanns, M., et al. (2019). Overexpression of PDE4A Acts as Checkpoint Inhibitor against cAMP-Mediated Immunosuppression *In Vitro*. *Front. Immunol.* 10, 1790. doi:10.3389/fimmu.2019.01790

Song, Z., Wu, Y., Yang, J., Yang, D., and Fang, X. (2017). Progress in the Treatment of Advanced Gastric Cancer. *Tumour Biol.* 39 (7), 1010428317714626. doi:10.1177/1010428317714626

Stanton, S. E., and Disis, M. L. (2016). Clinical Significance of Tumor-Infiltrating Lymphocytes in Breast Cancer. *J. Immunother. Cancer* 4, 59. doi:10.1186/s40425-016-0165-6

Subramanian, A., Tamayo, P., Mootha, V. K., Mukherjee, S., Ebert, B. L., Gillette, M. A., et al. (2005). Gene Set Enrichment Analysis: a Knowledge-Based Approach for Interpreting Genome-wide Expression Profiles. *Proc. Natl. Acad. Sci.* 102 (43), 15545–15550. doi:10.1073/pnas.0506580102

Sun, D., Wang, J., Han, Y., Dong, X., Ge, J., Zheng, R., et al. (2021). TISCH: a Comprehensive Web Resource Enabling Interactive Single-Cell Transcriptome Visualization of Tumor Microenvironment. *Nucleic Acids Res.* 49 (D1), D1420–D1430. doi:10.1093/nar/gkaa1020

Tang, Z., Kang, B., Li, C., Chen, T., and Zhang, Z. (2019). GEPIA2: an Enhanced Web Server for Large-Scale Expression Profiling and Interactive Analysis. *Nucleic Acids Res.* 47 (W1), W556–W560. doi:10.1093/nar/gkz430

Verjans, E., Ohl, K., Yu, Y., Lippe, R., Schippers, A., Wiener, A., et al. (2013). Overexpression of CREMα in T Cells Aggravates Lipopolysaccharide-Induced Acute Lung Injury. *J. Immunol.* 191 (3), 1316–1323. doi:10.4049/jimmunol.1203147

Xia, Y., Rao, L., Yao, H., Wang, Z., Ning, P., and Chen, X. (2020). Engineering Macrophages for Cancer Immunotherapy and Drug Delivery. *Adv. Mater.* 32 (40), e2002054. doi:10.1002/adma.202002054

Xie, C., Mao, X., Huang, J., Ding, Y., Wu, J., Dong, S., et al. (2011). KOBAS 2.0: a Web Server for Annotation and Identification of Enriched Pathways and Diseases. *Nucleic Acids Res.* 39 (Web Server issue), W316–W322. doi:10.1093/nar/gkr483

Xing, X., Guo, J., Ding, G., Li, B., Dong, B., Feng, Q., et al. (2018). Analysis of PD1, PDL1, PDL2 Expression and T Cells Infiltration in 1014 Gastric Cancer Patients. *Oncoimmunology* 7 (3), e1356144. doi:10.1080/2162402x.2017.1356144

Yazici, O., Sendur, M. A., Ozdemir, N., and Aksoy, S. (2016). Targeted Therapies in Gastric Cancer and Future Perspectives. *Wjg* 22 (2), 471–489. doi:10.3748/wjg.v22.i2.471

Zaanan, A., Bouché, O., Benhaim, L., Buecher, B., Chapelle, N., Dubreuil, O., et al. (2018). Gastric Cancer: French Intergroup Clinical Practice Guidelines for Diagnosis, Treatments and Follow-Up (SNFGE, FFCD, GERCOR, UNICANCER, SFCD, SFED, SFRO). *Dig. Liver Dis.* 50 (8), 768–779. doi:10.1016/j.dld.2018.04.025

Zhang, P., Yang, M., Zhang, Y., Xiao, S., Lai, X., Tan, A., et al. (2019). Dissecting the Single-Cell Transcriptome Network Underlying Gastric Premalignant Lesions and Early Gastric Cancer. *Cel Rep.* 27 (6), 1934–1947. doi:10.1016/j.celrep.2019.04.052

Zheng, C., Zheng, L., Yoo, J.-K., Guo, H., Zhang, Y., Guo, X., et al. (2017). Landscape of Infiltrating T Cells in Liver Cancer Revealed by Single-Cell Sequencing. *Cell* 169 (7), 1342–1356.e16. doi:10.1016/j.cell.2017.05.035

Conflict of Interest: The authors declare that the research was conducted in the absence of any commercial or financial relationships that could be construed as a potential conflict of interest.

Publisher's Note: All claims expressed in this article are solely those of the authors and do not necessarily represent those of their affiliated organizations, or those of the publisher, the editors, and the reviewers. Any product that may be evaluated in this article, or claim that may be made by its manufacturer, is not guaranteed or endorsed by the publisher.

frontiers in Molecular Biosciences

REVIEW
published: 07 December 2021
doi: 10.3389/fmolb.2021.788440

Ikaros Proteins in Tumor: Current Perspectives and New Developments

Ruolan Xia†, *Yuan Cheng*†, *Xuejiao Han*, *Yuquan Wei** *and Xiawei Wei**

Laboratory of Aging Research and Cancer Drug Target, State Key Laboratory of Biotherapy, National Clinical Research Center for Geriatrics, West China Hospital, Sichuan University, Chengdu, China

Ikaros is a zinc finger transcription factor (TF) of the Krüppel family member, which significantly regulates normal lymphopoiesis and tumorigenesis. Ikaros can directly initiate or suppress tumor suppressors or oncogenes, consequently regulating the survival and proliferation of cancer cells. Over recent decades, a series of studies have been devoted to exploring and clarifying the relationship between Ikaros and associated tumors. Therapeutic strategies targeting Ikaros have shown promising therapeutic effects in both pre-clinical and clinical trials. Nevertheless, the increasingly prominent problem of drug resistance targeted to Ikaros and its analog is gradually appearing in our field of vision. This article reviews the role of Ikaros in tumorigenesis, the mechanism of drug resistance, the progress of targeting Ikaros in both pre-clinical and clinical trials, and the potential use of associated therapy in cancer therapy.

Keywords: Ikaros, Aiolos, hematological malignancies, targeted therapy, immunotherapy

OPEN ACCESS

Edited by:
Hongming Miao,
Army Medical University, China

Reviewed by:
Tian Xiaohe,
Anhui University, China
Guihua Wang,
Huazhong University of Science and Technology, China

****Correspondence:***
Yuquan Wei
yuquanwei@scu.edu.cn
Xiawei Wei
xiaweiwei@scu.edu.cn

†These authors have contributed equally to this work

Specialty section:
This article was submitted to Molecular Diagnostics and Therapeutics, a section of the journal Frontiers in Molecular Biosciences

Received: *02 October 2021*
Accepted: *09 November 2021*
Published: *07 December 2021*

Citation:
Xia R, Cheng Y, Han X, Wei Y and Wei X (2021) Ikaros Proteins in Tumor: Current Perspectives and New Developments. Front. Mol. Biosci. 8:788440. doi: 10.3389/fmolb.2021.788440

1 INTRODUCTION

Ikaros is a zinc finger transcription factor (TF) and a member of the Krüppel family, which is called the IKAROS family zinc finger protein family (IKZF) and consists of other TFs named Ikaros, Helios, Aiolos, Eos, and Pegasus. Ikaros is encoded by the IKZF1 gene (Zhao et al., 2020), exerting an essential effect on regulating normal lymphopoiesis and functions as a tumor suppressor (Winandy et al., 1995; Sigvardsson, 2018). It covers four zinc fingers at the N-terminal for binding to DNA by directly combining with the GGGAA core motif *in vitro* and at the A/GGAAA core motif *in vivo*. At the C-terminal of Ikaros, two additional zinc fingers are required to form homo- and hetero-dimerization between isoforms. The mutations in IKZF are associated with recurrent infections, cytopenia (neutropenia, immune thrombocytopenia, and autoimmune hemolytic anemia), autoimmune diseases, and hematological malignancies (Kuehn et al., 2020).

Current knowledge of the Ikaros family suggests that these TFs are primarily concerned with the development of lymphocytes (Heizmann et al., 2018), covering extensive cellular processes like proliferation, differentiation, cell cycle arrest, and apoptosis (Fan and Lu, 2016). Nevertheless, the absence of Ikaros proteins results in a detrimental production of B lymphocytes, T lymphocytes, NK cells, and dendritic cells (Georgopoulos, 2002; Hariri and Hardin, 2020). Germline mutation in IKZF1 has also been reported to be associated with congenital pancytopenia (Goldman et al., 2012).

1.1 Classification and Genome

The Ikaros protein family includes five members named Ikaros, Helios, Aiolos, Eos, and Pegasus. Ikaros, Helios, and Aiolos are principally expressed in some hematopoietic cells and lymphoid cells; notwithstanding, Ikaros is also found in the brain. Eos and Pegasus are widely detected throughout the body, including the brain, liver, skeletal muscle, kidney, and heart (Fan and Lu, 2016) (**Table 1**).

TABLE 1 | Classification of Ikaros family proteins.

Members	Alias	Distribution	Key function	Related diseases
Ikaros	IKZF1	Hematopoietic system	1). exerts function during specific stages of lymphocyte development 2). abnormal expression leads to the occurrence and development of some autoimmune diseases, hematological malignancies, and solid tumors	ITP, PIH, SLE, asthma, type 1 diabetes, IBD, sjogren's syndrome, antiphospholipid syndrome, systemic sclerosis, BCP-ALL, MM, ALL, MCL, CLL, CML, lung cancer, ovarian cancer, HCC, CRC
Helios	IKZF2	Hematopoietic system	1). strengthens and represents fetal Treg differentiation 2). abnormal expression is related to autoimmune diseases, hematological malignancies, and solid tumors 3). associated with specific infection	RA, SLE, type 1 diabetes, IBD, di George syndrome, HT, PD, AML, BCP-ALL, ALL, hypertension, gastric cancer
Aiolos	IKZF3	Hematopoietic system	1). of importance for *trans*-differentiation of innate lymphoid 2). abnormal expression is related to autoimmune diseases, and solid tumors 3). up-regulates cancer stem cell-like properties	Graves' disease, SLE, RA, MCL, MM, CLL, ALL, NCC, lung cancer
Eos	IKZF4	Non-hematopoietic system	1). leads to gene silencing in Tregs 2). selective deletion leads to systemic autoimmunity 3). associated with specific infection	IBD, EAE, type 1 diabetes, T-CLL
Pegasus	IKZF5	Non-hematopoietic system	1). related to megakaryopoiesis	thrombocytopenia

Abbreviation: ITP, immune thrombocytopenia; PIH, presumed autoimmune hepatitis; SLE, systemic lupus erythematosus; IBD, inflammatory bowel disease; BCP-ALL, pediatric B-cell precursor acute lymphoblastic leukemia; MM, multiple myeloma; ALL, acute lymphoblastic leukemia; MCL, mantle cell lymphoma; CLL, chronic lymphocytic leukemia; CML, chronic myelogenous leukemia; HCC, hepatocellular carcinoma; CRC, colorectal cancer; RA, rheumatoid arthritis; HT, Hashimoto thyroiditis; PD, Parkinson disease; NCC, nasopharyngeal carcinoma; EAE, experimental autoimmune encephalomyelitis.

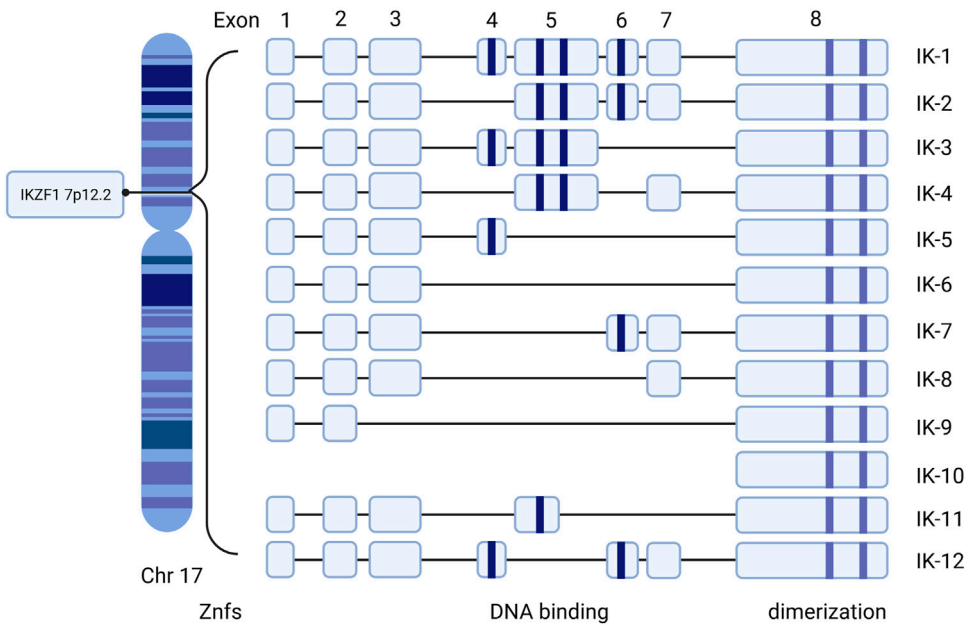

FIGURE 1 | Human Ikaros isoforms produced by IKZF1 transcription. Exons 1–8 refer to the encoding exons. The N-terminal zinc fingers are shown in blue column bars and C-terminal zinc fingers are shown in purple column bars. Znfs: zinc-fingers.

Various IKZF protein TFs emit diverse effects in the maintenance of normal physiological activities or progression of some diseases.

1.1.1 Ikaros

The IKZF1 gene that encodes Ikaros is located on chromosome 7 at 7p12.2 (HGNC, 2021). It consists of 8 exons and codes 519 amino acids. Exon 8 at the C-terminal includes the two domain zinc fingers required to form homo- and hetero-dimerization and four N-terminal DNA-binding zinc fingers for binding to the core motif at DNA (Ruiz et al., 2004; Zhang et al., 2020; Payne, 2011). Different combinations of zinc finger modules influence the capacity of DNA-binding and functional properties (Molnár and Georgopoulos, 1994; Vairy and Tran, 2020). At least 12 isoforms, including Ik1–12, are generated through alternative splicing Ikaros genes encoding a zinc finger protein with eight exons (Molnár and Georgopoulos, 1994; Yamamoto et al., 2005;

Hahm et al., 1994) (**Figure 1**). Among all the isoforms, the largest isoforms are Ik1 or Ik-H, which have four zinc finger domains at the N-terminal and two at the end of the C-terminal (Ronni et al., 2007). In addition, dimerization among Ikaros isoforms either enhances or suppresses its affinity of DNA binding, thus affecting the general Ikaros transcriptional activity through specific mechanisms such as chromatin-remodeling complexes and epigenetic modification (Georgopoulos et al., 1997; McCarty et al., 2003).

Isoforms with at least three DNA binding domains can combine with Ikaros conservative DNA binding sites, while isoforms with less than three DNA binding domains are not able to bind these motifs and remain in the cytoplasm (Hahm et al., 1994). Hence, the functional characteristics and subcellular localization of Ikaros isotypes may be different. Besides, the expression of Ikaros is correlated to the morphology of the nucleus. When cytogenetic outcomes are not available, the morphology of the cuplike nucleus can help to indicate the presence of IKZF1 deletion at a high predictive value (Li et al., 2019). IK6, due to the deficiency of exons 4–7, lacks four N-terminal zinc fingers but retains the C-terminal dimerization domain, which is most closely related to oncogenicity (Vairy and Tran, 2020). The presence of certain isoforms may be associated with the occurrence and prognosis of corresponding clinical diseases. Ik6 and Ik10 are highly related to a poor clinical outcome in B-lineage acute lymphoblastic leukemia (ALL) in children (Moreira et al., 2019). There is a correlation between Ik6 expression and t (4; 11) translocation in patients with leukemia (Ruiz et al., 2004; Zhang et al., 2020).

1.1.2 Helios

Helios, also called IKZF2, is of immediate clinical significance due to the fact that it plays a similar function to Ikaros in regulating the functional property of immune cells and the progression of hematological malignancies. Helios is a marker of stable and inhibitory T regulated cells (Tregs) (Thornton and Shevach, 2019), acting as an essential part to preferentially strengthen the differentiation of fetal Tregs and fine-adjusting of fetal Tregs (Ng et al., 2019). Helios-deficient Tregs show an unstable phenotype in the process of inflammation, characterized by decreased expression of FoxP3 and increased expression of effector cytokines following weakened activation of the STAT5 pathway (Kim et al., 2015).

In addition, the high expression of IKZF2 and low level of interleukin-7 receptor (IL7R) are identifiable transcriptional spectra demonstrated in CD16 $^{+}$ CD8 T cells, which are related to chronic untreated HIV-1 infection (Naluyima et al., 2019). Furthermore, Helios was found to be expressed in acute myeloid leukemia (AML) cells, and its depletion in AML cells resulted in decreased colony formation and slowed down oncogenesis (Park et al., 2019). The elevating Helios levels are related to the capacity of Tregs in malignant pleural effusion due to the downregulation of miR-4772-3p (Yu et al., 2019).

1.1.3 Aiolos

Aiolos, encoded by the IKZF3 gene, is located in 17q11.2~21 and made up of eight exons and seven introns (Hosokawa et al., 1999). The *trans*-differentiation from innate lymphoid cell 3 (ILC3) to ILC1/NK cells is linked with high expression of Aiolos and can be reduced through lenalidomide (Len) targeting Aiolos and Ikaros (Mazzurana et al., 2019). In addition, it is of great importance in the occurrence, metastasis, and prognosis of certain hematological malignancies and solid tumors (Duhamel et al., 2008; Li et al., 2014). Aiolos has been found to be expressed in lung cancer cells ectopically, which instigates cancer metastasis through reducing expression of many adhesion-related genes, spoiling cell-cell or cell-matrix interactions, and promoting anchorage independence (Wang et al., 2019; Li et al., 2014). Moreover, solid tumors are able to mimic the cellular behavior related to lymphocyte transport during immune surveillance through the "identity theft" of hematopoiesis led by the expression of Aiolos (Li et al., 2014). In addition to increasing invasive and migratory ability in lung cancer cells through upregulation of the phosphatidylinositol-3 kinase (PI3K)/AKT/Twist axis induced by Aiolos overexpression, the overexpression of Aiolos also upregulates cancer stem cell-like properties through the same pathway (Hung et al., 2019).

1.1.4 Eos

Eos, a novel transcriptional regulator encoded by the IKZF4 gene, is required for the suppressive function of Treg cells *in vivo* (Gokhale et al., 2019). Eos directly interacts with Foxp3, leading to chromatin modifications, which results in gene silencing in Tregs (Pan et al., 2009). While Tregs of mice with an overall absence of Eos were demonstrated to have completely normal suppressive function both *in vivo* and *in vitro* (Rieder et al., 2015; Gokhale et al., 2019). In peripheral blood mononuclear cells of individuals with HTLV-1 infection, the aberrant expression of Eos may correlate to the pathological progression of HTLV-1-related adult T-cell leukemia/lymphoma and myelopathy/tropical spastic paraparesis (Naito et al., 2019).

1.1.5 Pegasus

Pegasus is a novel transcriptional regulator encoded by IKZF5, with an unclear physiological function of normal hematopoiesis. It was reported that Pegasus was related to megakaryopoiesis and dominant thrombocytopenia in humans (Lentaigne et al., 2019).

1.2 Ikaros Family Proteins and Related Diseases

Ikaros proteins are identified to serve as suppressors in diverse types of lymphoma or leukemia (Heizmann et al., 2018; Chan, 2019), whereas they are overexpressed in other malignancies to maintain cancer cell proliferation and survival, such as in malignant plasma cells, monoclonal gammopathy of undetermined significance, and multiple myeloma (MM) (Cippitelli et al., 2021). Detailed functional analyses showed that Ikaros could excite or suppress oncogenes or tumor suppressors genes; consequently, Ikaros-mediated transcriptional expression of target genes regulates survival and proliferation of cancer cells (Gowda et al., 2017a). Specifically, Ikaros was reported to control human skin fibroblast cell migration negatively by GSK3β-Ikaros-ANXA4 signaling (Wang et al., 2020a).

It is assumed that Ikaros family deficiency may lead to a variety of immune-associated diseases, including immune thrombocytopenia (Sriaroon et al., 2019), presumed autoimmune hepatitis (Groth et al., 2020), systemic lupus erythematosus (SLE) (Cunninghame Graham et al., 2011; Jeng et al., 2019; Chen et al., 2020), rheumatoid arthritis (Yang et al., 2019), asthma (Igartua et al., 2015), type 1 diabetes (Davidson and Diamond, 2001; Swafford et al., 2011; Lempainen et al., 2013; Khamechian et al., 2018), Graves' disease (Li et al., 2018a), Hashimoto thyroiditis (Hu et al., 2019), inflammatory bowel disease (Crohn disease) (Barrett et al., 2008; Eskandarian et al., 2019; Sznurkowska et al., 2020), di George syndrome (Klocperk et al., 2014), antiphospholipid syndrome (Dieudonné et al., 2019), Parkinson disease (Daneshvar Kakhaki et al., 2020), Sjogren's syndrome, and systemic sclerosis (Gorlova et al., 2011).

It also shows that Ikaros can manage myeloid cell proliferation, and somatic Ikaros mutations are related to myeloproliferative disorders (Theocharides et al., 2015). In addition, the occurrence and maintenance of numerous human cancers, such as pediatric B-cell precursor acute lymphoblastic leukemia (BCP-ALL) (Churchman et al., 2018; Stanulla et al., 2018; Tayel et al., 2019), lung cancer (Li et al., 2014; Zhao et al., 2020), breast cancer (Edgren et al., 2011), nasopharyngeal carcinoma (Verhoeven et al., 2019), ovarian (He et al., 2012), liver (Liu et al., 2017), and colorectal cancer (Javierre et al., 2011), are also correlated with the abnormal expression of Ikaros family proteins. Recently, for some solid tumors, it was shown that a higher level of Ikaros is correlated with poor differentiation and advanced stage of ovarian cancer (He et al., 2012), while it functions as an anticancer character in hepatocellular carcinoma through inhibiting CD133 and ANXA4 expression (Liu et al., 2017). Besides, the hypermethylation of Ikaros levels could be considered as a sign of the progression of colorectal cancer (CRC) and inform adequacy of surgical resection about CRC (Javierre et al., 2011; Symonds et al., 2018; Symonds et al., 2020).

For patients with MM, the Ikaros family proteins served as predictors of prognosis for MM patients treated by Len (Kriegsmann et al., 2019; Tachita et al., 2020). However, a correlation between the expression of IKZF1 or IKZF3 and patients' reaction to Len from immunohistochemical analysis remains obscure (Dimopoulos et al., 2019). It is considered that the effect of low IKZF1 or IKZF3 levels on the adverse outcome of Len therapy results in shorter progression-free survival and overall survival (Zhu et al., 2014; Pourabdollah et al., 2016; Dimopoulos et al., 2019).

In ALL, approximately 50% of adult patients possess IKZF1 genetic mutations, including beyond 80% of patients with BCR-ABL1-positive (Ph+) ALL. A total of 15% of IKZF1 genetic alteration can be found in childhood B-cell ALL, covering about 70% of Ph + ALL patients (Mullighan et al., 2007; Mullighan et al., 2008). Patients with ALL have Ikaros mutations with characteristic resistance to treatment (Marke et al., 2016), high relapse rate (Kuiper et al., 2010; Berry et al., 2020), and poor prognosis (Mullighan et al., 2009; Aref et al., 2020). Genetic and functional abnormalities of IKZF1, including deletion of a single Ikaros, were regarded as new prognostic indicators for high-risk leukemia in clinical trials (NCT00993538; NCT03709719, NCT01431664) (Mi et al., 2012; Tang et al., 2019; Granados-Zamora et al., 2020).

In chronic myelogenous leukemia (CML), the deletions in IKZF1 and codeletion of other genes are identified in a chronic phase CML diagnostic sample (Klumb et al., 2019). Moreover, the deficiency or reduction of Ikaros is deemed as a common step and potential diagnostic precursor of progressive myeloid disease in patients with CML (Beer et al., 2015).

Immunomodulatory drugs (IMiDs), consist of thalidomide, Len, pomalidomide, and an analog, target a ubiquitous protein called CRBN to induce the degradation of Ikaros. The efficacy and safety of those drugs have been verified in a wide range of clinical trials, and it is increasingly clear that the efficacy of IMiDs in the treatment of MM (Gao et al., 2020), myelodysplastic syndrome (MDS) with deletion of chromosome 5q (Fenaux et al., 2011), mantle cell lymphoma (MCL) (Ruan et al., 2018) and chronic lymphocytic leukemia (CLL) (Vitale et al., 2016; Zhou et al., 2020) is promising. Despite the development of Ikaros-targeted therapy, the incidence of drug resistance is increasing. Herein, we summarized the molecular characteristic of Ikaros, the mechanism of the Ikaros-associated pathway, and recent anti-Ikaros drug development based on clinical trials in our review.

2 IKAROS FAMILY SIGNALING

Ikaros seems to act both as a transcriptional repressor and as an activator by binding to assorted nuclear factors referred to as epigenetic regulation and chromatin remodeling. If recruiting histone remodeling complexes such as nucleosome remodeling and deacetylase complex (NuRD) *via* direct binding to Mi-2, it will mediate tumor inhibition. If integrating into the ATP-dependent chromatin remodeling complexes SW1/SNF, it will cause gene activation (Dhanyamraju et al., 2020; Payne et al., 2020). Ikaros also directly engages with and recruits distinct histone deacetylase complexes (HDAC1 and HDAC2) to specific promoters of its target genes to modulate gene expression and to exert tumor-suppressive effects (Koipally et al., 1999; Song et al., 2016). Ikaros participates in a NuRD complex with acetyltransferases, methyltransferases, deacetylases, and the chromatin remodeling complex (Oliveira et al., 2019). In addition to the NuRD complex, the positive-transcription elongation factor b and the protein phosphatase 1α (PP1) are required to assist transcription extension of Ikaros target genes and regular differentiation of hematopoietic progenitor cells (Bottardi et al., 2014). In addition, Ikaros manipulates cellular proliferation by means of suppressing the PI3K pathway and genetic expression that promote cell cycle progression (Song et al., 2015).

2.1 Signaling Pathways About Ikaros Family

Studies on signaling pathways about Ikaros have attracted some attention (**Figure 2**). The most fully studied Ikaros-related pathway is the preBCR (B-cell receptor) signal pathway, which

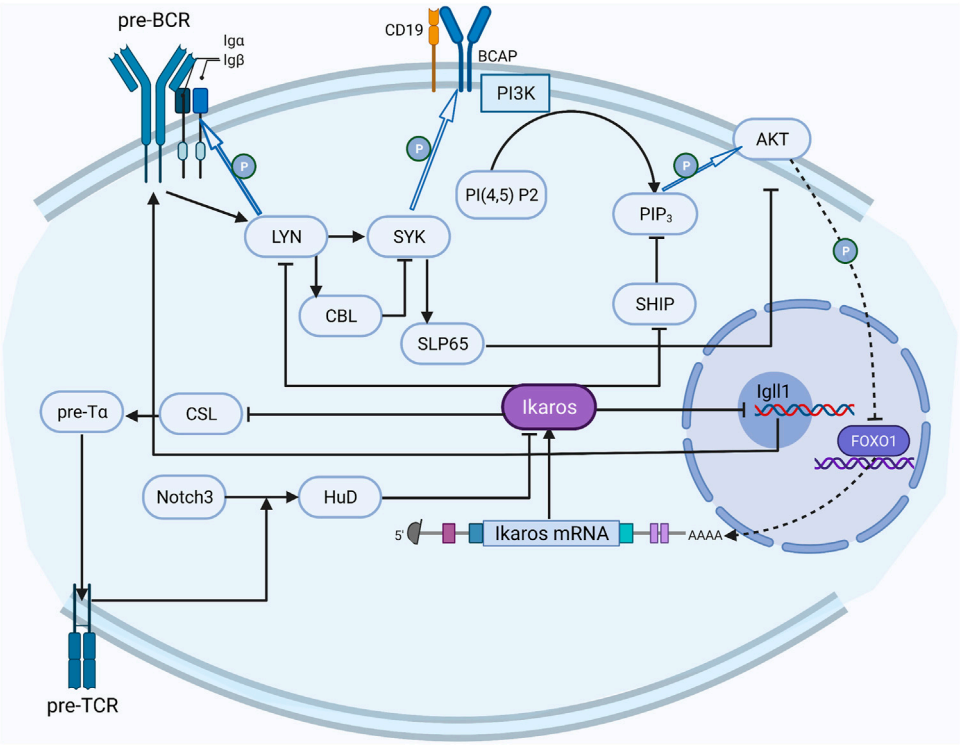

FIGURE 2 | The regulation network of Ikaros. The activated preBCR pathway decreases the activity of Ikaros, Ikaros counteracts this inhibition by repressing LYN and SHIP in the pathway; Notch3 upregulates HuD to convert Ikaros to the dominant negative isoform, and Ikaros counteracts the Notch effect on CSL activation through competing with the CSL DNA binding site in the promoter region.

has formed a distinct picture of the regulatory network (Alkhatib et al., 2012). Reciprocally, the activated preBCR pathway eventually decreased the activity of Ikaros; Ikaros can counteract this effect by suppressing two sites in the pathway (Yasuda et al., 2000; Nera et al., 2006; Nakayama et al., 2009).

The Notch pathway has also been relatively well studied. Notch3 converts the alternative splicing mode of Ikaros to a dominant-negative isoform by upregulating the expression of RNA binding protein HuD (Bellavia et al., 2007). On the contrary, Ikaros counteracts the Notch effect on CSL activation through competing with the CSL DNA binding site in the promoter region and inhibits the expression of the downstream genes, including the components of preTCR (Dumortier et al., 2006).

It was regarded that ERK1/2-mediated ETS1 phosphorylation decreased the ability of ETS1 to increase Ikaros expression (Joshi et al., 2014). And the activated integrin signaling pathway was reported to be restrained by Ikaros as well. Ikaros is affected by several interferon regulatory factors (IRFs), among which IRF4 and IRF8 were considered to induce the expression of Ikaros and its homologous gene Aiolos (Ma et al., 2008); however, another study showed that IRF8 rather than IRF4 triggers the IKZF1 promoter, and IRF5 could inhibit this activation (Fang et al., 2012).

2.2 Activation of Ikaros

Ikaros activities are thought to be regulated by post-translational phosphorylation, small ubiquitin-related modifier (SUMOylation), and ubiquitination (Sridharan and Smale, 2007). Besides, the hypomethylated pattern of CpG island in the IKZF1 promoter region may be the basis of abnormal Ikaros expression patterns associated with malignant tumors (Chen et al., 2019; Rahmani et al., 2019). SUMOylation interferes in the interaction of Ikaros with transcriptional co-repressors SIN3A, SIN3B, Mi-2β, and CtBP and weakens the inhibitory activity of Ikaros (Gómez-del Arco et al., 2005). And the participations of Ikaros in HDAC-dependent and HDAC-independent inhibition are disrupted by Ikaros SUMOylation, but the nuclear localization to pericentromeric heterochromatin is not affected (Gómez-del Arco et al., 2005). Ikaros SUMOylation was discovered to exist in B-ALL cells, whereas it did not show up in normal peripheral blood leukocytes, indicating its potential work in leukemia (Chen et al., 2019). The process of deSUMOylation was actively modulated by SUMO-specific protease Senp1, Axam, and yeast Ulp1 (Ihara et al., 2007). Certainly, Ikaros is ubiquitinated by E3 ligase CRBN7 and degraded by proteasome under the induction of IMiDs, while inhibition of Ikaros ubiquitination is correlated to interact with some TFs like runt-related transcription factor families (RUNXs) (Zhou et al., 2019; Liu et al., 2021). Otherwise, the absence of the E120 enhancer led to an evidential decrease in Ikzf1 mRNA. Nevertheless, the epigenetic pattern and 3D topology of this locus are only slightly impacted, emphasizing the complicacy of the regulatory pattern of the Ikzf1 locus (Alomairi et al., 2020).

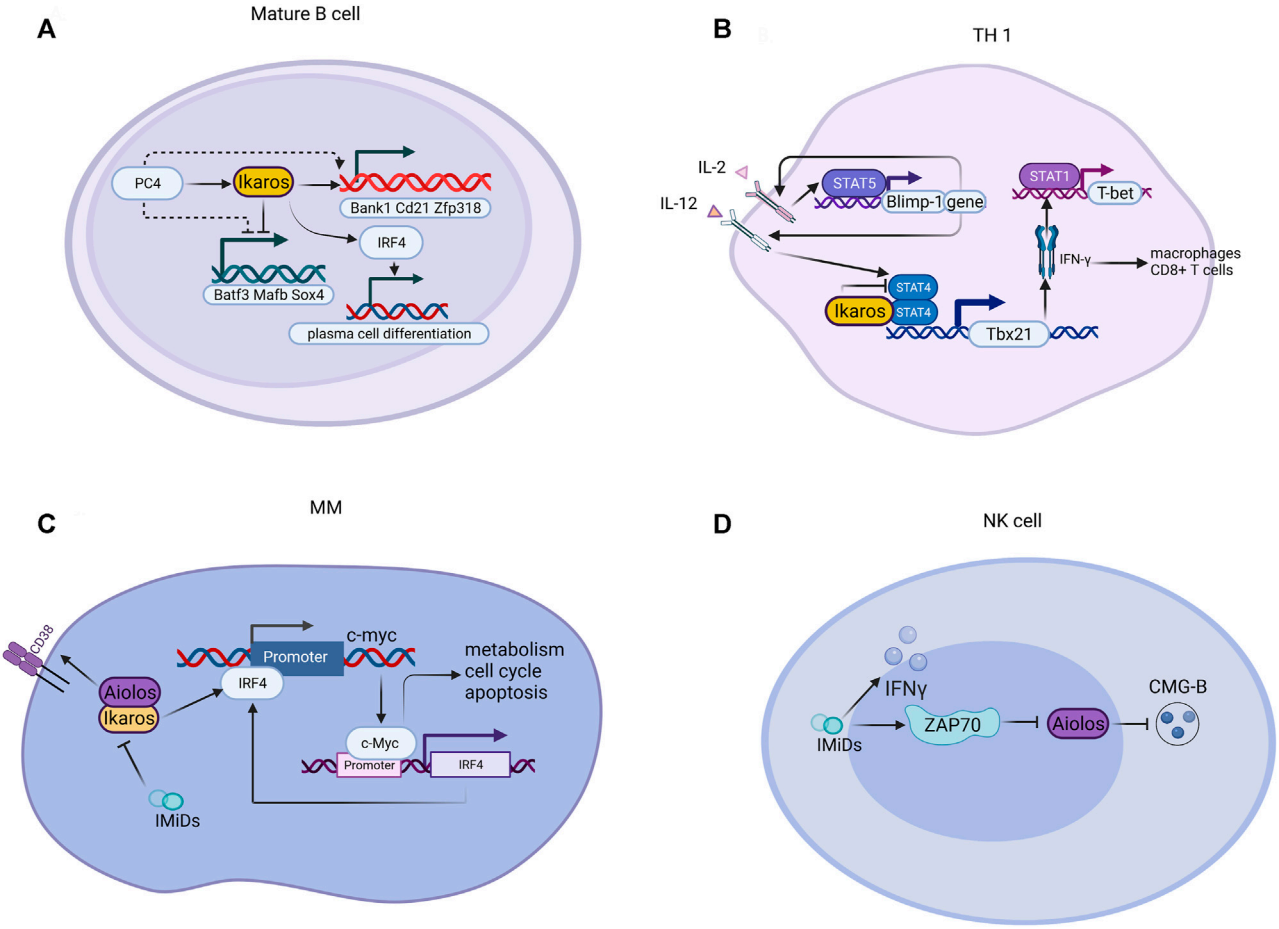

FIGURE 3 | Illustration of genes regulated by Ikaros in tumors. Ikaros is a tumor suppressor gene, controlling the transcription of ma genes related to leukemogenesis.

The effect of carcinogenic casein kinase II (CK2) on the phosphorylation of Ikaros has been widely studied. CK2 is a multipotent serine/threonine kinase, which is overexpressed in various cancers, including leukemia (Cunninghame Graham et al., 2011; Jeng et al., 2019; Chen et al., 2020). Studies have shown that CK2 directly phosphorylates multiple amino acids in the whole Ikaros protein, and hyperphosphorylated Ikaros facilitates self-degradation through the ubiquitin/proteasome pathway (Dovat et al., 2011). The application of phosphomimetic esters and phosphoresistant Ikaros mutants found that the phosphorylation of CK2 phosphate sites seriously decreases the ability of Ikaros to bind to DNA and alters the localization to pericentromeric heterochromatin, resulting in the dysfunction of Ikaros proteins (Gurel et al., 2008). Pharmacological inhibition of CK2 can restore the DNA binding ability and tumor inhibitory activity of Ikaros and cause leukemia cytotoxicity in the high-risk model of xenotransplantation in patients with ALL, highlighting the fact that CK2 inhibitors can be used as potential therapeutic strategies for high-risk pediatric leukemia (Song et al., 2015; Gowda et al., 2017a). Ikaros phosphorylation by CK2 is cell periodicity, indicating that CK2 effects the regulation of Ikaros function during G1/S transition and S phase in human leukemia (Arco et al., 2004; Li et al., 2012). Besides, CK2-mediated phosphorylation of Ikaros was vital to regulate the transcriptionally of the terminal deoxy transferase gene during differentiation of thymocytes (Wang et al., 2014). SYK is able to phosphorylate Ikaros at dissimilar sites, affecting Ikaros' nuclear localization (Uckun et al., 2012).

CK2-mediated phosphorylation is reversed by PP1 to dephosphorylate Ikaros (Popescu et al., 2009; Song et al., 2011). The mutation of the PP1 interaction site of Ikaros or the pharmacological inhibition of PP1 lead to the hyperphosphorylation of Ikaros, which seriously reduces the DNA binding ability of Ikaros, loses the pericentromeric localization of Ikaros, and increases degradation of Ikaros through the ubiquitous protein pathway (Popescu et al., 2009).

2.3 Molecular Mechanisms of Ikaros in Immune Cells

Ikaros has different effects on the growth, reproduction, and differentiation of many kinds of innate or adaptive lymphocytes *in vivo* (**Figure 3**). It has been previously reported that Ikaros is

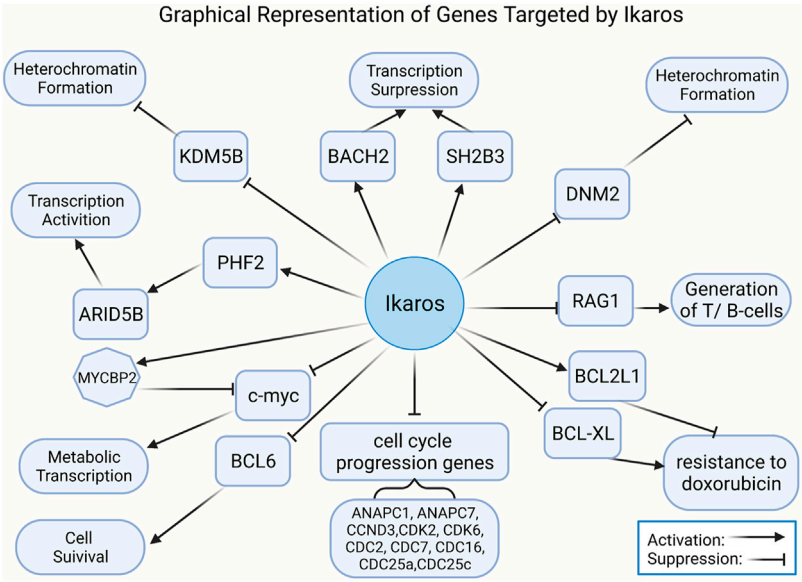

FIGURE 4 | Mechanism of Ikaros family proteins in various cells. **(A)** For mature B cells, PC4 increases and cooperatively assists Ikaros proteins to regulate gene expression; the PC4-IKAROS-IRF4 axis activates genes (e.g., Bank1, Cd21, and Zfp318), represses non-B cell genes (e.g., Batf3, Mafb, and Sox4), and promotes plasma cell differentiation. **(B)** Ikaros suppresses the polarization of Th1 through suppressing transcription mediated by STATA4 and downstream factors. **(C)** IMiDs interfere with disease-promoting activities of c-Myc and IRF4 *via* Aiolos and Ikaros in MM. **(D)** IMiDs bind to ZAP70, downregulate Aiolos, and enhance CMG-B. CMG-B, cytotoxic molecular granzyme B.

vital for the conversion between the large and small pre-B stages (Schwickert et al., 2014). Ikaros also sustains B-cell proliferation and differentiation through initiating kinase-signaling cascades and collaborating with chromatin protein 4 (Ochiai et al., 2020). In addition, the plasma cell mal-differentiation of sub1 deficient B cells can be saved by Ikaros and IRF4 (Ochiai et al., 2020). For innate lymphoid cells, Ikaros, the significant regulator of ILC3 existence and function, represses the transcriptional activity of aryl hydrocarbon receptors in a zinc finger-dependent manner, inhibits ILC3 in a cellular manner, and controls intestinal immune response in steady-state and disease (Li et al., 2016). Ikaros and Aiolos play a critical role in regulating the *trans*-differentiation of ILC3-ILC1/NK cells (Bald et al., 2019).

IKZF1 was demonstrated to regulate embryonic T lymphopoiesis of zebrafish via chemokine receptor 9 and IRF4 (Huang et al., 2019). Members of the IKZF family are also involved in the differentiation and property of single T helper cell subsets, covering TH1, TH2, TH17, T follicular, and Tregs (Powell et al., 2019). The function of Ikaros protein in T cell differentiation has been revealed, whereas contradictory results were obtained in certain mouse models. Research utilizing T cells possessing germline Ikaros gene mutations demonstrated that Ikaros promotes Th17 and Treg cell differentiation and suppresses the polarization of Th1 (Cippitelli et al., 2021). Nevertheless, in a mouse model in which Ikaros conditioned knockout in mature T cells, the deficiency of Ikaros is related to the acquirement of Th1, Th2, Th17 but not Treg cells (Lyon de Ana et al., 2019).

Ikaros supports signal-induced downregulation of recombination-activating gene 1 (RAG1) and RAG2 gene expression in $CD4^{+}$ $CD8^{+}$ positive thymocytes through a non-redundant manner (Naik et al., 2019). Ikaros plays a role in preventing autoimmunity by administering BCR unresponsiveness and repressing TLR signaling transduction (Schwickert et al., 2019). Although lymphocytes need Ikaros to differentiate, the role of the Ikaros protein family in the myeloid cell is not clear (Park et al., 2015). The mouse model has shown that Ikaros participates in the regulation of differentiation of neutrophils by silencing permissible or specific pathways in the ordinary precursors of macrophage-monocyte evolution (Dumortier et al., 2003). Ikaros modulates early phase differentiation of neutrophils but is optional for mature neutrophils (Dumortier et al., 2003).

2.4 Tumorigenesis and Antitumor Effect of Ikaros

Ikaros appears to function as a transcriptional inhibitor and activator by binding to different targets, such as some nuclear factors related to epigenetic regulation (**Figure 4**). Ikaros suppresses target gene transcription by directly binding or recruiting HDAC1 (Ikaros-HDAC1 complex) to induce the formation of inhibitory chromatin: the former way results in the increase of H3K9me3 and the reduction of H3K9ac, while the latter complex can promote the affinity for DNA binding to the promoter of lysine [K]-specific demethylase 5B (KDM5B) by CK2 inhibitors and raise formation of H3K27me3 and reduce H3K9ac (Song et al., 2016; Wang et al., 2016). The CK2-Ikaros axis also exerts beneficial control over Ikaros target gene expression, increasing PHD finger protein 2 (PHF2) expression, which

forms a complex with AT-rich interactive domain-containing protein 5B (ARID5B) to activate the target genes' transcription (Ge et al., 2018a; Ge et al., 2018b). The phosphorylation by CK2 overexpressed in B-ALL depresses Ikaros combining and recruiting HDAC1 to the promoter of BCL2L1, which causes repression of BCL2L1 and increases expression of BCL-XL (Schott et al., 2020). Recent studies have indicated that Ikaros has a negative effect on the development of T cell leukemia *via* globally regulating the enhancer or super-enhancer landscape and pioneering activity (Ding et al., 2019). Ikaros has a critical role in regulating *de novo* enhancer formation, super-enhancers formation, depletion of enhancers, and stimulation of poised enhancers, demonstrating that Ikaros direct modulates the expression of numerous genes than hypothesized formerly (Gowda et al., 2020). Furthermore, miR-26b expression is induced by the differential expression of Ikaros isoforms and transcriptional regulators of miR-26b modulated by PTEN (Yuan et al., 2017). The negative prognosis of IKZF1 deletion in BCP-ALL may be strengthened by the activation of Janus kinase signal transducer and activator of transcription (JAK/STAT) signaling and recede by ERG deletion (Stanulla et al., 2018). The mutual control of Notch1 and Ikaros in DN2 subsets of the thymus in tumor-bearing mice promotes the early stagnation of T cell development at the DN2a stage and its transfer to dendritic cells lineage (Guha et al., 2020). In terms of metabolism, the expression of functional paired box 5(PAX5) and Ikaros induces the powerful upregulation of glucose-6-phosphate dehydrogenase (G6PD). Interestingly, in clinical trials of patients with lymphoma, patients with high expression of G6PD were linked to poor overall prognosis (Xiao et al., 2018).

These variants of IKZF1 were distributed across the whole gene, particularly located to the C-terminal zinc finger dimerization domain, whereas in immunodeficient patients, germline IKZF1 variants are restricted to the N-terminal zinc fingers (Churchman et al., 2018). IKZF1 mutations and deletions have been suggested to contribute to the occurrence and poor prognosis of ALL and AML (Mullighan et al., 2008; Mullighan et al., 2009; de Rooij et al., 2015; Zhang et al., 2020). Deletion of IKZF1 was also demonstrated as an acquired convert at the transformation phase from CML to lymphoid blast crisis or ALL (Li et al., 2018b). The IKZF1 deletions lead to haploinsufficiency, dominant-negative Ikaros forms, or complete loss of expression of Ikaros. The principle of this dominant-negative effect may be that the high level of mutant unbinding DNA isomers with less than three N-terminal sequences occurs through the formation of heterodimers with wild-type isomers, resulting in alteration in DNA binding properties and them becoming repressors (Vairy and Tran, 2020). Mutations at the C-terminal zinc fingers could also cause a deep effect on the transcription of target genes (Vairy and Tran, 2020). Even after a comprehensive analysis of DNA binding sites of Ikaros in murine hematopoietic cells, the molecular mechanism of tumor suppressor effects in leukemia regulated by Ikaros-mediated transcription is still not clear (Song et al., 2015).

Overexpression of Ikaros leads to inhibition of transcription of genes supporting the PI3K pathway and generates transcription of genes, like INPP5D, repressing the PI3K pathway (Song et al., 2015). And AKT phosphorylation decreasing by overexpression of Ikaros in leukemia cells is identical to the effect of treatment with imatinib (Gowda et al., 2017a). Nevertheless, the JAK/STAT pathways and PI3K/AKT pathways were proved to activate with Ik6 expression in ALL (Song et al., 2015; Qu et al., 2019). Ikaros overexpression also directly suppresses the promoter activity of these clinically significant cell cycle progression genes, including ANAPC1, ANAPC7, CCND3, CDK2, CDK6, CDC2, CDC7, CDC16, CDC25a, CDC25c, and CCNE2 (Dhanyamraju et al., 2020). In addition, KDM5B expression is downregulated by Ikaros through recruiting HDAC1 to the KDM5B gene promoter, which causes an inhibitory chromatin condition and transcriptional inhibition consequently (Dhanyamraju et al., 2020). Ikaros upregulates the PHF2 expression through chromatin remodeling, as demonstrated by the appearance of increased H3K4me3 in the promoter of the PHF2 gene (Ge et al., 2016a; Ge et al., 2018a; Maciel et al., 2019). The expression of ARID5B is positively adjusted by Ikaros, and the loss of a single copy of IKZF1 is associated with low ARID5B expression (Ge et al., 2018b). Gain- and loss-of-function experiments of Ikaros in ALL shows that Ikaros inhibits c-myc gene transcription but controls transcription of MYC binding protein 2 positively, which suppresses the activity of myc (Ge et al., 2015). STAT5 regulates the super-enhancer of the myc gene by means of competition for binding to target sites or regulating histone acetylation in an opposing way to Ikaros (Katerndahl et al., 2017). It was revealed that the genes related to the BCR signal pathway and the IKZF family are presumed to be upstream of the MYC/IRF4 axis (Tsukamoto et al., 2020). In patients with trisomy 12 CLL, IRF4 by means of inducing Ikaros mediates the overexpression of CD49d, which was considered to identify those patients treated with ibrutinib with the characteristics of inferior nodal responses and shorter clinical outcomes (Fiorcari et al., 2019).

Moreover, Ikaros was also verified to negatively regulate IL7R expression and promote SH2B adaptor protein 3 (SH2B3) transcription (Ge et al., 2016b). Ikaros represses B-cell lymphoma 6 (BCL6) transcription and initiates basic leucine zipper transcription factor 2 (BACH2) gene transcription, suggested by BCL6 and BACH2 functional experiments (Ge et al., 2017). Some data identified that Ikaros inhibits dynamin 2 in leukemia by directly combining with the promoter and inducing heterochromatin formation (Ge et al., 2016). PAX5, RUNX1, and IKZF1 were found to overlap abundant target genes, and a modality with dominant-negative effective of IKZF1 or ETV6-RUNX1 fusion protein cooperates with the loss of heterozygosity of PAX5 to regulate gene expression (Okuyama et al., 2019). Furthermore, RAG1 is considered as an immediate target of Ikaros (Li et al., 2016; Dimopoulos et al., 2019). IKZF1 was defined as a crucial *trans*-activator of the SLAMF-7 gene, which is mainly expressed in MM cells and deemed as an ideal target for immunotherapy (Kikuchi et al., 2020).

In contrast to the role of IKZF2 as a tumor suppressor gene in hypodiploid B-ALL, it is essential for AML (Park et al., 2019). The deficiency of IKZF2 in AML cells is related to the reduction of colony formation, augment of differentiation and apoptosis,

TABLE 2 | Classification and characteristic of IMiDs.

Description	Mechanism	Indications	Adverse-effect
Thalidomide	1). Anti-angiogenic properties 2). Anti-proliferative effects a). Enhances degradation of Ikaros and Aiolos b). Induces cell cycle arrest	MM, PCDs, erythema; sarcoidosis, CLE, Behçet's disease; GVHD; RA, AS, Still's disease, systemic sclerosis, Sjögren's syndrome, CD, Kaposi's sarcoma, CHF, Waldenström's macroglobulinemia, myelodysplasia, prostate cancer, Renal-cell carcinoma, Glioma, CRC, Melanoma	neuropathy, constipation, sedation, DVT, AIHA, vasculitis
Lenalidomide	1). Anti-angiogenic properties 2). Anti-proliferative effects a). Enhances degradation of Ikaros and Aiolos b). Induces cell cycle arrest c). Cytoskeletal reorganization d). Inhibition of tumor oncogenes, induction of tumor suppressor genes 3). Immunomodulatory a). Increases number of NK cells and NK cell ADCC b). Restores formation of immune synapse c). Suppresses Treg multiplication d). Increases production of IFNγ, IL2 and Th1 cytokine e). Co-stimulation of tyrosine phosphorylation f). Activation of PI3 kinase signaling pathway	MM, FL, MCL, DLBCL, primary CNS/intraocular lymphoma, myelofibrosis, MDS	myelosuppression, skin rash, DVT, interstitial pneumonitis, AIHA, ITP, Evans syndrome, thrombocytopenia, autoimmune thyroiditis, optic neuritis, polymyositis
Pomalidomide	1). Anti-angiogenic properties 2). Anti-proliferative effects i. Enhances degradation of Ikaros and Aiolos ii. Induces cell cycle arrest 3). Immunomodulatory a). Increases number of NK cells and NK cell ADCC b). reverts Th2 cells into Th1 like effector cells c). Suppresses Treg multiplication d). Increases production of IFNγ, IL2 and IL-10 e). Co-stimulation of tyrosine phosphorylation f). Activation of PI3 kinase signaling pathway	MM, AL amyloidosis, MF, Waldenström's macroglobulinemia, sarcoma, lung cancer, HIV	neutropenia, fatigue, asthenia, anemia, constipation, nausea, diarrhea, dyspnea, upper respiratory tract infections, back pain, pyrexia

Abbreviation: IMiDs, immunomodulatory drugs; PCDs, plasma cell diseases; MM, multiple myeloma; CLE, cutaneous lupus erythematosus; GVHD, Graft-versus-host disease; RA, rheumatoid arthritis; AS, Ankylosing spondylitis; CD, Crohn's disease; CHF, congestive heart failure; CRC, colorectal cancer; FL, Follicular lymphoma; MCL, mantle cell lymphoma; DBLCL, Diffuse large B-cell lymphoma; CNS, central nervous system; MDS, myelodysplastic syndrome; MF, myelofibrosis; HIV, human immunodeficiency virus; DVT, deep vein thrombosis; AIHA, autoimmune hemolytic anemia; ITP, idiopathic thrombocytopenic purpura.

defective leukemic stem cells function, and tardive leukemogenesis (Park et al., 2015; Park et al., 2019). One of the main mechanisms may be that IKZF2 determines a self-renewal gene expression procedure called HOXA9 and represses a C/EBP-driven differentiation program. In addition, this forced reduction of Ikzf2 is accompanied by decreasing HOXA9 and BCL2, but not Mll, Myc, or Meis1.

3 TARGETED THERAPY FOR IKAROS

IMiDs, covering thalidomide, Len, and pomalidomide, are clinically approved medicine for the therapy of MM and other malignancies (**Table 2**). Among them, the relatively well-studied diseases are MM and MDS. These drugs lead to selective ubiquitination and proteasomal degradation of Ikaros and Aiolos through recruiting TFs to the $CRL4^{CRBN}$ E3 ubiquitin ligase, representing an original mechanism of therapy through altering the substrate specificity (Lu et al., 2014; Sievers et al., 2018; Zeidner et al., 2020). Different IMiDs target the degradation of distinct sets of TFs. Furthermore, IMiDs have the ability of direct inhibition of tumor cell growth and strong immunostimulatory characteristics, consequently having multiple implications on the presence of different cellular components in the tumor microenvironment (Cippitelli et al., 2021).

3.1 Antitumor Effect of IMiDs in MM

The deletion of Ikaros and Aiolos maintains the occurrence and progress of MM by contributing to downregulate c-Myc and IRF4 (Bjorklund et al., 2015). There is a positive feedback loop between IRF4 and c-Myc; IRF4 combines with the region of c-myc promoter and promotes c-myc expression, while the C-Myc protein transactivates the IRF4 gene directly (Shaffer et al., 2008). The target genes of C-Myc cover genes that regulate cell metabolism (GLUT1), cell cycle (CDKs, cyclins, and E2FTF), and apoptosis (Jovanović et al., 2018). On the side, Krüppel-like factor 2 (KLF2) and B lymphocyte maturation inducing protein-1 (Blimp-1) exert a significant effect on regulating the growth and survival of MM. In the positive feedback loop, IRF4 and KLF2 transactivate and promote the expression of each other and are also upregulated by KDM3A via removing H3K9me marks at promoters (Ohguchi et al., 2016). Therefore, the lessening of each protein induced by IMiDs represses the expression of integrin alpha-4/beta-7, thus affecting the migration and homing of MM cells to bone marrow. In addition, the expression and activity of Blimp-1 decreased by IMiDs through a variety of mechanisms: 1) Blimp-1 is repressed at the transcriptional level as the target gene of IRF4; 2) Aiolos interacts with Blimp-1 and synergistically inhibits apoptosis-related genes; and 3) ubiquitination and proteasome degradation of Blimp-1 can be enhanced directly (Hung et al., 2016). Moreover, the degradation of Ikaros and Aiolos induced by IMiDs can upregulate the surface expression of CD38 in MM cells, preparing for the antibody-dependent cytotoxicity induced by daratumab in NK cells (Fedele et al., 2018).

3.2 Immunomodulatory Activity of IMiDs in MM

IKZF TFs are central to regulate the innate or adaptive immune response in patients with MM. The ILCs consist of lymphoid tissue inducer cells, NK cells, ILC1s, ILC2s, and ILC3s (Vivier et al., 2018; Krabbendam et al., 2021). For NK cells, their activity induced by IMids is due to the fact that T lymphocytes are stimulated to produce IL-2 (Gandhi et al., 2014). Drugs also directly bind to activate kinase ZAP70, downregulate Aiolos, and enhance the expression of cytotoxic molecular granzyme B (Hideshima et al., 2021). Len directly enhances the activity of NK cells by increasing the proportion of synapses that can penetrate IFN-γ vesicles and increasing the production of IFN-γ (Lagrue et al., 2015). Len and pomalidomide increased the MICA expression of NK cell-mediated immune surveillance molecule NKG2D ligand and PVR/CD155 of dNaM-1 ligand on the human MM cell membrane, thus enhancing the sensitivity to the identification and killing of MM cells (Fionda et al., 2015). As for ILCs, it was demonstrated that the activity of ILCs was enhanced by reducing Ikaros and Aiolos protein (Bald et al., 2019). The 2 TFs are significant regulators for the conversion of ILC3 into ILC1/NK cells. Len increased the expression of certain ILC3-related genes (such as rorc, baff, il22, and nrp1) and upregulated the proportion of ILC3 producing IL-22. Concomitantly, a process of transdifferentiation of ILC3 to ILC1 was inhibited by Len with the downregulation of Aiolos and depression of ILC1-associated transcripts (prf1, gzmb, cd244, lef1, and ncr3). After treatment with Len, DC differentiated from peripheral blood and bone marrow monocytes in patients with MM expressed higher standards of cytokines and chemokines (IL-8, TNF, CCL2, and CCL5) and strengthened the function to stimulate the proliferation of allogeneic T cells (Costa et al., 2017).

IMiDs promote specific $CD4^+$ and $CD8^+$ T cell responses in MM, whereas they inhibit the expansion and function of Tregs. T cells with less expression of Ikaros require less TCR to participate in immune cell activation, show greater proliferation response to IL-2, and are less sensitive to inhibitors of TCR and IL-2R signal transduction, suggesting that the lower the expression of Ikaros, the lower the T cell activation threshold (Avitahl et al., 1999). Besides, the loss of IKZFs is the reason for the increase of IFN-γ, IL-21, and IL-2 production by T cells treated with IMiDs (Gandhi et al., 2014; Brissot et al., 2015). In addition, Len also decreased the levels of Ikaros and Aiolos in chimeric antigen receptor (CAR) T-cells, which helped to enhance the ability of CAR T-cells to restore IL-2 gene transcription and facilitate IL-2 secretion against solid cancer cells (Wang et al., 2020b).

4 CLINICAL APPLICATIONS

4.1 Immunomodulatory Drugs

IMiDs, including thalidomide, Len, and pomalidomide, are effective in treating certain hematological malignancies, in combination with steroids, proteasome inhibitors (PIs), or monoclonal antibodies, such as MM (Gao et al., 2020), MDS with deletion of chromosome 5q (Fenaux et al., 2011), MCL (Ruan et al., 2018), and CLL (Vitale et al., 2016). IMiDs exert their antitumor activity directly through different treatment-related effects, such as inhibiting angiogenesis, repressing cancer cell proliferation, and inducing apoptosis (Le Roy et al., 2018). The cellular target of IMiDs is CRBN, a ubiquitous protein that acts as a substrate receptor for Cullin-4-RING E3 ubiquitin ligase complexes, as well as DDB1, ROC1, and CUL4.

4.1.1 Treatment of IMiDs in MM

Different IMiDs have been applied to different conditions. Thalidomide was the first IMiD to be discovered, and its history served as a lesson in the history of drug development (Franks et al., 2004). Len is commonly used in new MM patients, maintenance therapy after transplant, and relapsed/refractory MM (RRMM) patients, while pomalidomide is only applied to RRMM (Zou et al., 2020).

Patients with newly diagnosed MM (NDMM) who were unsuitable for stem cell transplantation are associated with a considerable benefit in progression-free survival (PFS) [lenalidomide-dexamethasone vs. melphalan-prednisone-thalidomide (MPT); HR, 0.72; $p < 0.001$] and overall survival (OS) at the interim analysis and less frequent grade 3 or 4 toxic and adverse events (70 vs. 78%), with continuous lenalidomide-dexamethasone intervention until disease progression compared with MPT (NCT00689936) (Benboubker et al., 2014). For patients with MM after transplantation, maintenance therapy with Len significantly

extended PFS (41 months, vs. 23 months with placebo; HR, 0.50; $p < 0.001$), while differences in OS were not discovered in two cohorts (NCT00430365) (Attal et al., 2012). Identically, Len maintenance significantly improved PFS in patients with NDMM but did not enhance OS in the trial population (ISRCTN49407852) (Jackson et al., 2019). Early intervention with Len in smoldering MM notably decelerates progression to symptomatic MM and the damage of target-organ. The 1-, 2-, and 3-years progression-free survival for the lenalidomide and observation arm was 98 vs. 89%, 93 vs. 76%, and 91 vs. 66%, respectively (NCT01169337) (Lonial et al., 2020). Moreover, in contrast to high-dose dexamethasone, pomalidomide plus low-dose dexamethasone significantly prolonged median PFS (4.0 months, vs. 1.9 months with high-dose dexamethasone; HR, 0.48; CI, 0.39–0.60; $p < 0.0001$), and is considered a new medical strategy for patients with RRMM, despite the fact that the occurrence of grades 3–4 neutropenia were higher (NCT01311687) (Miguel et al., 2013). In another phase III trial, on the basis of BTZ and dexamethasone, pomalidomide was added in the treatment of patients with RRMM to significantly improve PFS (11.20 vs. 7.10 months; HR, 0.61; 95%CI, 0·49–0.77; $p < 0·0001$), with acceptable hemocyte toxicity (NCT01734928) (Richardson et al., 2019). In addition to malignancy, pomalidomide is a well-tolerated and efficient treatment for advanced steroid-refractory chronic graft-versus-host disease (cGVHD), indicating the antifibrotic effects of pomalidomide are related to the increased levels of blood regulatory T cells and IL-2 (NCT01688466) (Curtis et al., 2021).

Subcutaneous BTZ delivery + lenalidomide + dexamethasone (VRD) is a safe and effective therapeutic schedule for induction in NDMM with valuable partial responses (55.6% by cycle 3, 63.8% by cycle 4, 68.3% by cycle 5, and 70.4% after induction) (NCT01916252) (Rosiñol et al., 2019). Furthermore, pretreatment of cells with BTZ, a PI, leads to the accumulation of Ikaros, thus suppressing the efficacy of Len (Shi et al., 2015). Nevertheless, with the therapy of Len combined with BTZ, Ikaros was demonstrated to be degraded by a pathway independent from the autophagy and proteasome pathways, such as activating calpain and caspase to downregulate Ikaros by calcium flux (Ganesan et al., 2020).

Pan-proviral insertion in murine malignancy kinase inhibitors covering SGI1776 and LGH447 presented inspiriting results in patients with RRMM, which was associated with upregulation of CRBN and downregulation of Ikaros and Aiolos (Zheng et al., 2019). Nonselective HDAC inhibitors like A452 induce synergistic cytotoxicity of MM without modifying CRBN expression combined with IMiDs, thus downregulating IKZF1/3, c-Myc, and IRF4 (Won et al., 2019).

4.1.2 Treatment of IMiDs in Leukemia

IMiDs are conventionally used for the therapy of MM, MDS, and B-cell lymphoma; nevertheless, little is realized about the efficacy of IMiDs in AML (Le Roy et al., 2018) (**Table 3**). Len induces degradation of Ikaros, reducing the expression of GPR68 and RCAN1, which upregulates the Ca2+/calpain pro-apoptotic pathway and inhibits the CaN pro-survival pathway, respectively. Hence, cyclosporine, a CaN inhibitor, is able to extend the therapeutic potential of Len to MDS as well as AML without affecting immune function (Dou and Fang, 2020). Compared to azacytidine (AZA) monotherapy, patients with higher-risk MDS treated with AZA in conjunction with Len or Vorinostat achieved an overall response rate (ORR). In stratified analysis, patients with CMML could benefit from AZA plus Len (NCT01522976) (Sekeres et al., 2017). In patients with 5q-deletion-related MDS, Len rendered significant clinical outcomes compared with thalidomide and pomalidomide, which was related to induced degradation of CK1 α (Krönke et al., 2015; Petzold et al., 2016). Len was revealed to be given safely in patients with a relapsed AML/MDS post-allograft combined with AZA without reversing impaired INF-γ/TNF-α production; 7 of 15 (47%) patients ultimately reached a major clinical response after LEN/AZA therapy (ISCRCTN98163167) (Craddock et al., 2019). For patients with AML, the results of the current study illustrated that the addition of Len to standard remission induction chemotherapy (cytarabine + daunorubicin) could not ameliorate the therapeutic effect of elderly patients with AML (NTR2294) (Ossenkoppele et al., 2020).

In a phase I trial, following timed sequential induction therapy (TST), pomalidomide administration in the early stages of lymphocyte recovery has been revealed to be well tolerated in patients with newly diagnosed AML and adverse cytogenetics of MDS with particularly high CR rates (NCT02029950). The exact mechanism of benefit from pomalidomide application after chemotherapy remains obscure. It is of probability that pomalidomide remarkably decreases Aiolos expression in peripheral blood and bone marrow CD4+/CD8+ T cells, strengthens T cell differentiation and proliferation, and promotes cytokine production (Zeidner et al., 2020). Additionally, pomalidomide may be serviceable for the treatment of HTLV-1 and EBV-induced tumors by causing infected cells to become more vulnerable to innate and adaptive host immune responses (Davis et al., 2019).

Lenalidomide has been approved for application with rituximab in patients with relapsed/refractory follicular lymphoma in the United States. Lenalidomide + rituximab was demonstrated to be a safe and effective chemotherapy-free approach that improves upon single-agent rituximab and may become a substitution to chemoimmunotherapy (Flowers et al., 2020). Efficacy results of rituximab plus lenalidomide were similar to rituximab plus chemotherapy and both regimens were followed by rituximab maintenance therapy among patients with untreated follicular lymphoma. In contrast, the two groups presented different safety profiles. A higher percentage of grades 3 or 4 neutropenia appeared in the rituximab + chemotherapy group (32 vs. 50%) (NCT01476787 and NCT01650701) (Morschhauser et al., 2018). PFS of patients with recurrent indolent lymphoma was notably promoted for lenalidomide plus rituximab compared with rituximab plus placebo (HR, 0.46; 95% CI, 0.34–0.62; $p < 0.001$), and the safety profile of the test group was acceptable (NCT01938001) (Leonard et al., 2019). For patients with DLBCL who achieved CR or PR by R-CHOP induction, a randomized phase III trial demonstrated that Len maintenance monotherapy in elderly

TABLE 3 | Ongoing clinical trials of IMiDs in tumors.

NCT number	Phase	Status	Condition	Intervention
Lenalidomide (also known as Revlimid, CC-5013, and CDC-501)				
NCT01996865	III	Active, not recruiting	Non Hodgkin Lymphoma	Lenalidomide + Rituximab
NCT04038411	IV	Recruiting	NK/T Cell Lymphoma	PD-1 Antibody + Chidamide + Lenalidomide + Etoposide
NCT03829371	IV	Recruiting	MM	Velcade + Melphalan + Prednisone + Lenalidomide + Dexamethasone
NCT03901963	III	Recruiting	MM	Daratumumab + Lenalidomide
NCT01938001	III	Active, not recruiting	Lymphoma, Non-Hodgkin	Rituximab + Lenalidomide
NCT02659293	III	Active, not recruiting	MM	Lenalidomide + Carfilzomib + Dexamethasone
NCT04217967	IV	Recruiting	MM	Ixazomib + Lenalidomide
NCT01090089	III	Active, not recruiting	MM	Lenalidomide + Dexamethasone + PBSCT
NCT04490707	III	Recruiting	Acute Myeloid Leukemia in Remission	Azacitidine + Lenalidomide
NCT03952091	III	Recruiting	Relapse/Refractory MM	TJ202 + Lenalidomide + Dexamethasone
NCT04040491	III	Recruiting	Peripheral T-cell Lymphoma	PD-1 blocking antibody + chidamide + Lenalidomide + Gemcitabine
NCT04071457	III	Recruiting	MM	Lenalidomide + Daratumumab
NCT00843882	III	Active, not recruiting	Chronic Myelomonocytic Leukemia	Epoetin Alfa + Lenalidomide
NCT02076009	III	Active, not recruiting	MM	Daratumumab + Lenalidomide + Dexamethasone
NCT02215980	III	Active, not recruiting	MM	Lenalidomide + Dexamethasone
NCT03836014	III	Recruiting	Relapse MM	Daratumumab + Lenalidomide + Dexamethasone
NCT04270409	III	Recruiting	Plasma Cell Myeloma	Isatuximab + Lenalidomide + Dexamethasone
NCT03652064	III	Active, not recruiting	MM	Daratumumab + Bortezomib + Lenalidomide + Dexamethasone
NCT01476787	III	Active, not recruiting	Follicular Lymphoma	Lenalidomide + R-CHOP + CVP + Bendamustine
NCT03729804	III	Recruiting	MM	Carfilzomib + Lenalidomide + Dexamethasone + Bortezomib
NCT01650701	III	Active, not recruiting	Follicular Lymphoma	Lenalidomide + R-CHOP + CVP + Bendamustine
NCT02252172	III	Active, not recruiting	MM	Daratumumab + Lenalidomide + Dexamethasone
NCT01685814	III	Active, not recruiting	Previously Untreated Symptomatic MM	Lenalidomide + Bortezomib + ASCT + allo-HSCT
NCT04824092	III	Recruiting	Diffuse Large B-cell Lymphoma	Tafasitamab + Lenalidomide + Rituximab + Cyclophosphamide + Doxorubicin + Vincristine + Prednisone
NCT01564537	III	Active, not recruiting	Relapsed/Refractory MM	Ixazomib + Lenalidomide + + Dexamethasone
NCT02390869	III	Recruiting	Lymphoma, Follicular	Rituximab + Lenalidomide
NCT04680052	III	Recruiting	Follicular Lymphoma, Marginal Zone Lymphoma	Tafasitamab + Rituximab + Lenalidomide
NCT01208662	III	Active, not recruiting	MM	Lenalidomide + Bortezomib + Dexamethasone + ASCT
NCT01093196	III	Active, not recruiting	MM	Melphalan + Prednisone + Lenalidomide + Cyclophosphamide + Dexamethasone
NCT03937635	III	Recruiting	Smoldering Plasma Cell Myeloma	Daratumumab + Dexamethasone + Lenalidomide
NCT03617731	III	Active, not recruiting	MM	Lenalidomide + Bortezomib Dexamethasone + Isatuximab
NCT04751877	III	Not yet recruiting	MM	Isatuximab + Lenalidomide + Bortezomib + Dexamethasone
NCT03173092	III	Recruiting	MM	Ixazomib + Lenalidomide + Dexamethasone
NCT03710603	III	Active, not recruiting	MM	Daratumumab + Velcade + Lenalidomide + Dexamethasone
NCT03319667	III	Active, not recruiting	Plasma Cell Myeloma	Isatuximab + Bortezomib + Lenalidomide + Dexamethasone + Acetaminophen + Ranitidine + Diphenhydramine
NCT00644228	III	Active, not recruiting	Stage I-III Plasma Cell Myeloma	Bortezomib + Dexamethasone + Lenalidomide
NCT04712097	III	Not yet recruiting	Relapsed/Refractory Follicular Lymphoma	Mosunetuzumab + Lenalidomide + Rituximab + Tociluzumab
NCT02495922	III	Active, not recruiting	MM	Elotuzumab + Lenalidomide + Bortezomib + Dexamethasone

(Continued on following page)

TABLE 3 | (*Continued*) Ongoing clinical trials of IMiDs in tumors.

NCT number	Phase	Status	Condition	Intervention
NCT03948035	III	Recruiting	Newly Diagnosed MM	Elotuzumab + Carfilzomib + Lenalidomide + Dexamethasone + ASCT
NCT01865110	III	Active, not recruiting	Mantle Cell Lymphoma	R-CHOP + R-HAD + Lenalidomide
NCT01850524	III	Active, not recruiting	MM	Ixazomib + Dexamethasone + Lenalidomide
NCT00551928	III	Active, not recruiting	Newly Diagnosed MM	Melphalan + Lenalidomide + Prednisone
NCT03859427	III	Recruiting	Relapsed/Refractory MM	Carfilzomib + Lenalidomide + Dexamethasone
NCT03941860	III	Recruiting	Plasma Cell Myeloma	Ixazomib Citrate + Lenalidomide
NCT04404283	III	Recruiting	Diffuse Large B-cell Lymphoma	Brentuximab vedotin + Rituximab + Lenalidomide
NCT01091831	III	Active, not recruiting	MM	Cyclophosphamide + Lenalidomide + Dexamethasone + Melphalan
NCT03720041	III	Recruiting	MM	Ixazomib + Lenalidomide + Dexamethasone
NCT00602641	III	Active, not recruiting	Plasma Cell Myeloma	Lenalidomide + Melphalan + Prednisone + Thalidomide
NCT01863550	III	Active, not recruiting	Plasma Cell Myeloma	Bortezomib + Carfilzomib + Dexamethasone + Lenalidomide
NCT01335399	III	Active, not recruiting	MM	Lenalidomide + Dexamethasone + Elotuzumab
NCT02285062	III	Active, not recruiting	Lymphoma, Large B-Cell, Diffuse	Lenalidomide + Rituximab + Cyclophosphamide + Doxorubicin + Prednisone + Vincristine
NCT01208766	III	Active, not recruiting	MM	Bortezomib + Melphalan + Prednisone + Lenalidomide + Dexamethasone
NCT04923893	III	Not yet recruiting	MM	Bortezomib + Dexamethasone + Lenalidomide + Cilta-cel + Cyclophosphamide + Fludarabine
NCT00098475	III	Active, not recruiting	DS Stage I-III Plasma Cell Myeloma	Dexamethasone + Lenalidomide + Thalidomide
NCT00114101	III	Active, not recruiting	DS Stage I-III Plasma Cell Myeloma, Refractory Plasma Cell Myeloma, Smoldering Plasma Cell Myeloma	Autologous Hematopoietic Stem Cell Transplantation + Lenalidomide + Melphalan + PBSCT
NCT02544308	III	Active, not recruiting	Plasmacytoma	Lenalidomide + Dexamethasone
NCT02516696	III	Active, not recruiting	MM	Clarithromycin + Lenalidomide + Dexamethasone
NCT04834024	III	Not yet recruiting	Follicular Lymphoma, Marginal Zone Lymphoma	Recombinant Humanized Monoclonal Antibody MIL62 + Lenalinomide
NCT04152577	III	Recruiting	Lymphoma, B-Cell	R-DA-EPOCH + R-CHOP + R-HD MTX
NCT02516423	III	Active, not recruiting	Solitary Osseous Plasmacytoma	Ixazomib + Lenalidomide + Dexamethasone + Zoledronic acid
NCT04483739	III	Recruiting	MM	Carfilzomib + Lenalidomide + Dexamethasone + Isatuximab
NCT02575144	III	Active, not recruiting	MM	Clarithromycin + Lenalidomide + Dexamethasone
NCT04096066	III	Recruiting	MM/New Diagnosis Tumor	Carfilzomib + Lenalidomide + Dexamethasone
NCT01169337	II/III	Active, not recruiting	Light Chain Deposition Disease, Smoldering Plasma Cell Myeloma	Lenalidomide
NCT03151811	III	Active, not recruiting	MM	Melflufen + Pomalidomide + Dexamethasone
NCT04287660	III	Recruiting	MM	Clarithromycin + Lenalidomide + Dexamethasone + CAR T-cells
NCT04566328	III	Recruiting	Plasma Cell Myeloma, RISS Stage I-II Plasma Cell Myeloma	Bortezomib + Daratumumab + Hyaluronidase-fihj + Dexamethasone + Lenalidomide
NCT04224493	III	Recruiting	Relapsed/Refractory Follicular Lymphoma	Tazemetostat + Lenalidomide + Rituximab
NCT03742297	III	Recruiting	Newly Diagnosed MM	Lenalidomide + Carfilzomib + Bortezomib + Daratumumab + Dexamethasone + Prednisone + Melphalan
NCT03829371	III	Recruiting	MM	Velcade + Melphalan + Prednisone + Lenalidomide + Dexamethasone
NCT03934684	III	Recruiting	Relapsed/Refractory MM	Carfilzomib + Dexamethasone + Lenalidomide
NCT03908138	III	Recruiting	MM	Lenalidomide, Bortezomib + Dexamethasone
NCT04181827	III	Recruiting	MM	JNJ-68284528 + Pomalidomide + Bortezomib + Dexamethasone + Daratumumab
NCT03180736	III	Active, not recruiting	MM	Daratumumab + Pomalidomide + Dexamethasone
NCT04989140	III	Not yet recruiting	MM	Ixazomib + Pomalidomide + Dexamethasone

(Continued on following page)

TABLE 3 | (*Continued*) Ongoing clinical trials of IMiDs in tumors.

NCT number	Phase	Status	Condition	Intervention
NCT04934475	III	Not yet recruiting	MM	Isatuximab + ASCT
NCT03428373	II/III	Recruiting	Relapse MM, MM Progression, MM Stage I-III	Lenalidomide + Dexamethasone + Rivaroxaban + Aspirin
NCT04348006	III	Recruiting	Newly Diagnosed MM	Cyclophosphamide + Dexamethasone + Lenalidomide + Bortezomib
NCT03651128	III	Recruiting	MM	bb2121 + Daratumumab + Pomalidomide + Dexamethasone + Bortezomib + Ixazomib + Lenalidomidem Carfilzomib + Elotuzumab
NCT03143049	III	Recruiting	Relapse MM	Pomalidomide + Cyclophosphamide + Dexamethasone
Thalidomide (also kown as 3-phthalimidoglutarimide, CC-5013, and Thalomid)				
NCT02507336	II	Active, not recruiting	Mantle Cell Lymphoma	Thalidomide
NCT03143036	II	Recruiting	Relapse/Refractory Myeloma	Daratumumab + Thalidomide + Dexamethasone
NCT03140943	II	Recruiting	Relapsed/Refractory MM	Carfilzomib + Thalidomide + Dexamethasone
NCT04891744	I/II	Not yet recruiting	MM	Selinexor + Thalidomide + Dexamethasone
NCT04382300	II	Recruiting	Non-small-cell Lung Cancer	Pyrotinib + Thalidomide
NCT03062800	II	Recruiting	Advanced NSCLC	Thalidomide + Pemetrexed + Cisplatin + Carboplatin
NCT03896737	II	Recruiting	MM	Daratumumab + Velcade + Cyclophosphamide + Dexamethasone + Thalidomide
NCT02586038	II	Active, not recruiting	MM	MLN9708 + Dexamethasone + Cyclophosphamide + Thalidomide
NCT03143036	II	Recruiting	Relapse/Refractory Myeloma	Daratumumab + Thalidomide + Dexamethasone
NCT00602641	III	Active, not recruiting	Plasma Cell Myeloma	Lenalidomide + Melphalan + Prednisone + Thalidomide
NCT00098475	III	Active, not recruiting	DS Stage I-III Plasma Cell Myeloma	Dexamethasone + Lenalidomide + Thalidomide
NCT01554852	III	Active, not recruiting	MM	Cyclophosphamide + Lenalidomide + Dexamethasone + Thalidomide + Carfilzomib + Protocol + Vorinostat + Melphalan + ASCT
NCT02085655	III	Recruiting	Extranodal NK-T-Cell Lymphoma	Pegaspargase + Gemcitabine + Oxaliplatin + Methotrexate + Dexamethasone + Thalidomide
NCT02541383	III	Active, not recruiting	MM	Bortezomib + Thalidomide + Dexamethasone + Daratumumab
NCT04941937	II	Not yet recruiting	MM	Selinexor + Thalidomide + Lenalidomide + Pomalidomide + Dexamethasone
NCT02891811	II	Recruiting	MM	Carfilzomib + Thalidomide + Lenalidomide + Dexamethasone
NCT01661400	I	Recruiting	Glioma, Neuroectodermal Tumors, Wilms Tumor, Rhabdomyosarcoma, Sarcoma, Ewing, Osteosarcoma, Retinoblastoma	Metronomic Cyclophosphamide + Thalidomide
NCT03792620	III	Recruiting	MM Stage I	Cyclophosphamide + Thalidomide + Dexamethasone + Daratumumab
NCT00572169	III	Active, not recruiting	MM	Velcade + Thalidomide + Dexamethasone + Adriamycin + Cisplatin + Cyclophosphamide + Etoposide
NCT04352205	II	Recruiting	Plasma Cell Myeloma	Bortezomib + Daratumumab + Dexamethasone + Lenalidomide + Thalidomide
NCT03759093	II/III	Not yet recruiting	MM	Bortezomib + Cyclophosphamide + Dexamethasone + Thalidomide
NCT03562169	III	Recruiting	MM	Ixazomib + Thalidomide + Dexamethasone + Conventional ASCT
NCT03980002	II	Recruiting	Chronic Lymphocytic Leukemia	FCR + Ibrutinib + BR + Thalidomide
NCT00871013	II	Active, not recruiting	Myeloma	Melphalan + Velcade + Thalidomide + Dexamethasone + Cisplatin + Adriamycin + Cyclophosphamide + Etoposide
NCT00869232	II	Active, not recruiting	MM	Velcade + Melphalan + Thalidomide + Dexamethasone + Cisplatin + Adriamycin + Cyclophosphamide + Etoposide
NCT03004287	II	Active, not recruiting	MM	Carfilzomib + Thalidomide + Dexamethasone + Daratumumab + Cisplatin + Adriamycin + Cyclophosphamide + Etoposide + Melphalan + ASCT + Lenalidomide + Bortezomib
NCT01356290	II	Recruiting	Medulloblastoma Recurrent, Ependymoma Recurrent, ATRT Recurrent	Bevacizumab + Thalidomide + Celecoxib + Fenofibric acid + Etoposide + Cyclophosphamide + Cytarabine

(Continued on following page)

TABLE 3 | (*Continued*) Ongoing clinical trials of IMiDs in tumors.

NCT number	Phase	Status	Condition	Intervention
NCT01998971	I	Active, not recruiting	MM	Daratumumab + Velcade + Pomalidomide + Dexamethasone + Melphalan + Prednisone + Thalidomide + Diphenhydramine + Acetaminophen + Carfilzomib + Lenalidomide + Montelukast
Pomalidomide (also known as POMALYST, Actimid, CC-4047)				
NCT04762745	I/II	Not yet recruiting	Relapsed/Refractory MM	Pomalidomide + Bendamustine + Dexamethasone
NCT03257631	II	Active, not recruiting	Medulloblastoma	Pomalidomide
NCT04577755	II	Not yet recruiting	Skin Kaposi Sarcoma	Pomalidomide
NCT03715478	I/II	Recruiting	Relapsed/Refractory MM	Pomalidomide + Dexamethasone
NCT02415153	I	Active, not recruiting	Neurofibromatosis Type 1, Recurrent Childhood Brain Stem Glioma, Recurrent Childhood Visual Pathway Glioma, Recurrent//Refractory Primary Central Nervous System Neoplasm	Pomalidomide
NCT01997840	I/II	Active, not recruiting	MM	ACY-1215 + Pomalidomide + Dexamethasone
NCT02045017	II	Active, not recruiting	MM	Pomalidomide + Dexamethasone
NCT04902443	I	Not yet recruiting	Kaposi Sarcoma, EBV/KSHV-associated Lymphomas	Pomalidomide + Nivolumab
NCT04584307	II	Not yet recruiting	MM	Elotuzumab + Pomalidomide
NCT03798314	I	Active, not recruiting	Recurrent/Refractory Primary Vitreoretinal DLBCL	Nivolumab + Pomalidomide
NCT01734928	III	Active, not recruiting	MM	Pomalidomide + Bortezomib + Dexamethasone
NCT03601806	II	Recruiting	Skin Kaposi Sarcoma	Pomalidomide
NCT02004275	I/II	Active, not recruiting	Relapse MM	Pomalidomide + Ixazomib + Dexamethasone
NCT04176718	II	Recruiting	Relapse/Refractory MM, MM	Daratumumab + Carfilzomib + Pomalidomide + Dexamethasone
NCT01754402	I/II	Active, not recruiting	MM	Bendamustine + Pomalidomide + Dexamethasone
NCT02406222	II	Active, not recruiting	MM	Pomalidomide + Dexamethasone + Cyclophosphamide
NCT03151811	III	Active, not recruiting	MM	Melflufen + Pomalidomide + Dexamethasone
NCT03143985	I	Recruiting	MM	Vactosertib + Pomalidomide
NCT01946477	II	Recruiting	MM	Pomalidomide + Dexamethasone + Daratumumab
NCT03180736	III	Active, not recruiting	MM	Daratumumab + Pomalidomide + Dexamethasone
NCT04850599	II	Not yet recruiting	Recurrent/Refractory Plasma Cell Myeloma	Carfilzomib + Isatuximab + Pomalidomide
NCT04790474	II	Recruiting	Relapse/Refractory MM	Ixazomib + Pomalidomide + Dexamethasone
NCT03030261	II	Recruiting	Relapse MM	Elotuzumab + Pomalidomide + Dexamethasone
NCT04802161	II	Not yet recruiting	Acute Myeloid Leukemia, Chronic Myelomonocytic Leukemia, Myelodysplastic Syndrome	Liposome-encapsulated Daunorubicin-Cytarabine + Pomalidomide
NCT02990338	III	Active, not recruiting	Plasma Cell Myeloma	Isatuximab + Pomalidomide + Dexamethasone
NCT04764942	I/II	Recruiting	Recurrent/Refractory Plasma Cell Myeloma	Carfilzomib + Dexamethasone + Pomalidomide + Selinexor
NCT04094961	I/II	Recruiting	Relapse MM	Ixazomib + Pomalidomide + Dexamethasone
NCT03756896	II	Recruiting	Plasma Cell Myeloma	Carfilzomib + Dexamethasone + Pomalidomide
NCT01166113	I/II	Active, not recruiting	MM	Pomalidomide + Cyclophosphamide + Prednisone
NCT02659930	I	Recruiting	Kaposi Sarcoma	liposomal Doxorubicin + Pomalidomide
NCT04508790	II	Recruiting	Recurrent/Refractory Plasma Cell Myeloma	Dexamethasone + Leflunomide + Pomalidomide
NCT02400242	I	Active, not recruiting	MM	ACY-241 + Pomalidomide + Dexamethasone
NCT03015922	I	Active, not recruiting	MM	Lenalidomide + Pomalidomide + Reolysin
NCT03590652	II	Recruiting	Relapsed/Refractory MM	Ixazomib + Pomalidomide + Dexamethasone + Daratumumab

(Continued on following page)

TABLE 3 | (*Continued*) Ongoing clinical trials of IMiDs in tumors.

NCT number	Phase	Status	Condition	Intervention
NCT04162210	III	Recruiting	MM	Belantamab mafodotin + Pomalidomide + Dexamethasone)
NCT04191616	II	Recruiting	Relapsed/Refractory MM	Carfilzomib + Dexamethasone + Pomalidomide
NCT02542657	I/II	Active, not recruiting	Myeloma	Clarithromycin + Dexamethasone + Ixazomib + Pomalidomide
NCT04883242	II	Recruiting	Recurrent/Refractory Plasma Cell Myeloma	Carfilzomib + Dexamethasone + Isatuximab + Pomalidomide
NCT03143049	III	Recruiting	Relapse MM	Pomalidomide + Cyclophosphamide + Dexamethasone
NCT03683277	II	Not yet recruiting	Relapsed/Refractory MM	Ixazomib + Pomalidomide + Dexamethasone
NCT04843579	II	Not yet recruiting	Myeloma/Refractory MM	Selinexor + Clarithromycin + Pomalidomide + Dexamethasone
NCT01665794	I/II	Recruiting	MM	Pomalidomide + Carfilzomib + Dexamethasone + Daratumumab
NCT04661137	II	Recruiting	MM	Selinexor + Carfilzomib + Pomalidomide + Daratumumab + Dexamethasone
NCT03539744	III	Recruiting	MM	Pomalidomide + Dexamethasone + Venetoclax
NCT04700176	II	Not yet recruiting	MM	Daratumumab + Pomalidomide + All-trans retinoic acid + Dexamethasone
NCT04302324	II	Recruiting	Refractory/Relapse MM	Daratumumab + Clarithromycin + Pomalidomide + Dexamethasone
NCT02547662	II	Active, not recruiting	Plasma Cell Leukemia/Plasma Cell Myeloma/Plasmacytoma	Ixazomib citrate + Pomalidomide
NCT02654132	II	Active, not recruiting	MM	Elotuzumab + Pomalidomide + Dexamethasone
NCT04484623	III	Recruiting	MM	Belantamab mafodotin + Pomalidomide + Dexamethasone + Bortezomib
NCT01745588	II	Active, not recruiting	MM	Pomalidomide + Dexamethasone + Clarithromycin
NCT03202628	II	Active, not recruiting	Recurrent/Refractory Plasma Cell Myeloma	ASCT + Dexamethasone + Ixazomib + Pomalidomide
NCT03287908	I	Recruiting	Relapsed/Refractory MM	AMG 701 + Pomalidomide + Dexamethasone
NCT04124497	II	Recruiting	MM/Deletion 17P Syndrome	Daratumumab + Pomalidomide + Dexamethasone
NCT04667663	I	Not yet recruiting	MM	Daratumumab + Cyclophosphamide + Pomalidomide + Dexamethasone
NCT01575925	I	Active, not recruiting	MM with Renal Impairment	Pomalidomide + Dexamethasone
NCT04989140	IV	Not yet recruiting	MM	Ixazomib + Pomalidomide + Dexamethasone
NCT04835129	II	Not yet recruiting	MM	Isatuximab + Pomalidomide + Elotuzumab + Dexamethasone
NCT03841565	II	Recruiting	Recurrent Plasma Cell Myeloma	Daratumumab + Dexamethasone + Pomalidomide
NCT02185820	I/II	Active, not recruiting	MM	Carfilzomib + Pomalidomide + Dexamethasone
NCT03713294	II	Recruiting	Refractory Plasma Cell Myeloma	Dexamethasone + Elotuzumab + Pomalidomide
NCT04181827	III	Recruiting	MM	JNJ-68284528 + Pomalidomide + Bortezomib + Dexamethasone + Daratumumab
NCT04762745	I/II	Not yet recruiting	Relapsed, Refractory, MM	Pomalidomide + Bendamustine + Dexamethasone
NCT03170882	II	Active, not recruiting	Relapsed/Refractory MM	Ixazomib + Pomalidomide + Dexamethasone
NCT02726581	III	Active, not recruiting	MM	Nivolumab + Elotuzumab + Pomalidomide + Dexamethasone
NCT04287855	II	Active, not recruiting	Relapse/Refractory MM	Isatuximab + Carfilzomib + Pomalidomide + Dexamethasone
NCT02188368	II	Active, not recruiting	MM	Pomalidomide + Steroids + Doxorubicin + Carfilzomib + Bortezomib + Clarithromycin + Cyclophosphamide
NCT02616640	I	Active, not recruiting	MM	Durvalumab + Pomalidomide + Dexamethasone
NCT03104270	II	Active, not recruiting	MM	Elotuzumab + Pomalidomide + Carfilzomib + Dexamethasone
NCT03731832	II	Recruiting	Refractory MM	MLN9708 + Pomalidomide + Dexamethasone + Cyclophosphamide
NCT04941937	II	Not yet recruiting	MM	Selinexor + Thalidomide + Lenalidomide + Pomalidomide + Dexamethasone
NCT02939183	I	Active, not recruiting	Relapsed/Refractory MM	Dexamethasone + Pomalidomide

(Continued on following page)

TABLE 3 | (*Continued*) Ongoing clinical trials of IMiDs in tumors.

NCT number	Phase	Status	Condition	Intervention
NCT03439280	I/II	Active, not recruiting	Relapsed/Refractory/MM	TAK-079 + Pomalidomide + Dexamethasone
NCT04643002	I/II	Recruiting	Plasma Cell Myeloma Refractory	Isatuximab + Dexamethasone + Pomalidomide + SAR439459 + Belantamab mafodotin
NCT03582033	I	Recruiting	MM	SEA-BCMA + Dexamethasone + Pomalidomide
NCT04108195	I	Recruiting	MM	Daratumumab + Talquetamab + Teclistamab + Pomalidomide
NCT04150965	I/II	Recruiting	Relapsed/Refractory MM	Elotuzumab + Pomalidomide + Dexamethasone + Anti-LAG-3 + Anti-TIGIT
NCT04045795	I	Recruiting	MM	Isatuximab + Pomalidomide + Dexamethasone
NCT02963493	II	Active, not recruiting	MM	Melphalan + Dexamethasone
NCT04942067	I/II	Recruiting	MM	APG2575 + Lenalidomide + Pomalidomide + Dexamethasone
NCT02807454	II	Active, not recruiting	MM	Daratumumab + Durvalumab + Pomalidomide + Dexamethasone
NCT03269136	I	Active, not recruiting	MM	PF-06863135 + Dexamethasone + Lenalidomide + Pomalidomide
NCT02343042	I/II	Recruiting	MM	Selinexor + Dexamethasone + Lenalidomide + Pomalidomide + Bortezomib + Daratumumab + Carfilzomib + Ixazomib + Elotuzumab + Clarithromycin + Belantamab Mafodotin
NCT04895410	I	Not yet recruiting	MM	Lemzoparlimab + Dexamethasone + Carfilzomib + Pomalidomide + Daratumumab
NCT04458831	NA	Recruiting	Plasma Cell Myeloma	Isatuximab + Pomalidomide + Dexamethasone + Carfilzomib
NCT04892446	II	Not yet recruiting	MM	Magrolimab + Daratumumab + Pomalidomide + Dexamethasone + Bortezomib
NCT04925193	II	Not yet recruiting	Relapse MM	Selinexor + Pomalidomide + Daratumumab + Carfilzomib + Dexamethasone
NCT04855136	I/II	Recruiting	MM	BB2121 + CC-220 + BMS-986405 + Pomalidomide + Dexamethasone + Bortezomib
NCT03828292	I	Recruiting	MM	Belantamab mafodotin + Bortezomib + Dexamethasone + Pomalidomide
NCT03732703	I/II	Recruiting	Relapsed/Refractory MM	Abemaciclib + Dexamethasone + Ixazomib + Pomalidomide + Enasidenib + Cobimetinib + Erdafitinib + Venetoclax + Daratumumab + Belantamab mafodotin + Selinexor
NCT04722146	I	Recruiting	MM	Teclistamab + Daratumumab + Pomalidomide + Lenalidomide + Bortezomib + Nirogacestat
NCT03984097	I	Active, not recruiting	MM	TAK-079 + Lenalidomide + Dexamethasone + Bortezomib + Pomalidomide
NCT02294357	II	Active, not recruiting	MM	Carfilzomib + Dexamethasone + Prednisone + Methylprednisolone + Lenalidomide + Pomalidomide
NCT03651128	III	Recruiting	MM	bb2121 + Daratumumab + Pomalidomide + Dexamethasone + Bortezomib + Ixazomib + Lenalidomide + Carfilzomib + Elotuzumab
NCT02206425	I/II	Active, not recruiting	MM	Melphalan + Prednisone + Cyclophosphamide + Dexamethasone + Doxorubicin + Lenalidomide + Pomalidomide
NCT01592370	I/II	Active, not recruiting	Non-Hodgkin's Lymphoma, Hodgkin Lymphoma, MM	Nivolumab + Ipilimumab + Daratumumab + Pomalidomide + Dexamethasone
NCT01998971	I	Active, not recruiting	MM	Daratumumab + Velcade + Pomalidomide + Dexamethasone + Melphalan + Prednisone + Thalidomide + Diphenhydramine + Acetaminophen + Carfilzomib + Lenalidomide + Montelukast
NCT02719613	II	Active, not recruiting	MM	Elotuzumab + Dexamethasone + Lenalidomide + Bortezomib + Pomalidomide + Nivolumab
NCT03732703	I/II	Recruiting	Relapsed/Refractory MM	Abemaciclib + Dexamethasone + Ixazomib + Pomalidomide + Enasidenib + Cobimetinib + Erdafitinib + Venetoclax + Daratumumab + Belantamab + Selinexor
NCT03269136	I	Active, not recruiting	MM	PF-06863135 + Dexamethasone + Lenalidomide + Pomalidomide
NCT04150965	I/II	Recruiting	Relapsed/Refractory MM	Elotuzumab + Pomalidomide + Dexamethasone
NCT03143985	I	Recruiting	MM	Vactosertib + Pomalidomide
NCT03257631	II	Active, not recruiting	Central Nervous System Neoplasms	Pomalidomide

(Continued on following page)

TABLE 3 | (*Continued*) Ongoing clinical trials of IMiDs in tumors.

NCT number	Phase	Status	Condition	Intervention
NCT01734928	III	Active, not recruiting	MM	Pomalidomide + Bortezomib + Dexamethasone
NCT01575925	I	Active, not recruiting	MM	Pomalidomide + Dexamethasone
NCT02188368	II	Active, not recruiting	MM	Pomalidomide + Steroids + Doxorubicin + Carfilzomib + Bortezomib + Clarithromycin + Cyclophosphamide

**Lenalidomide has been widely investigated in clinic, therefore only clinical trials in phase III and IV are included.*
Abb: R-CHOP, Rituximab, Cyclophosphamide, Doxorubicin, Vincristine, Prednisone; CVP, Rituximab Cyclophosphamide, Vincristine, Prednisone; ASCT, autologous stem cell transplant; allo-HSCT, allogeneic hematopoietic stem cell transplantation; G-CSF, granulocyte-colony stimulating factor; R-HAD, Rituximab, Cytarabine, Dexamethasone; PBSCT, Peripheral Blood Stem Cell Transplantation; R-HD MTX, Rituximab, Methotrexate; R-DA-EPOCH, Rituximab, Epirubicin, Etoposide, Vincristine, Cyclophosphamide, Prednisone; BR, Rituximab, Bendamustine; VBMCP, Vincristine; BCNU, Cyclophosphamide, Melphalan, Prednisone; VBAD, Vincristine, Adriamycine, Dexamethasone; GDPT, Gemcitabine, Cisplatin,Prednisone, Thalidomide; FCR, Fludarabine, Cyclophosphamide, Rituximab; MM, Multiple myeloma.

patients with DLBCL is safe and effective (mPFS was not reached, vs. 58.9 months with placebo; HR, 0.708; 95% CI, 0.537–0.933; $p = 0.01$) (Thieblemont et al., 2017). Despite inescapable toxicity (63%, vs. 12% in observation group; $p < 0{\cdot}0001$), Len improved PFS in patients with an MCL post-autograft (NCT02354313) (Ladetto et al., 2021).

Long-term IMiDs used continuously, like maintenance treatment for MM, may raise the frequency of uncontrolled immunostimulatory diseases by inducing a chronic inflammatory response, resulting in certain autoimmune diseases covering vasculitis, rashes, optic neuritis, interstitial pneumonitis, Graves' disease, and polymyositis (Montefusco et al., 2014; Brissot et al., 2015; Shao et al., 2017; Phan et al., 2020; Shafi et al., 2020; Cippitelli et al., 2021).

4.2 Treatment of Cereblon-Modulating Agent

CRBN E3 ligase modulating drugs (CELMoDs), such as avadomide (CC-122), iberdomide (CC-220), CC-885, CC-92480, and novel thalidomide analogs, are in current clinical trials as a monotherapy and in combination (NCT01421524; NCT02773030; NCT03374085) (**Table 4**). The CELMoDs have strong antitumor and immunostimulatory capabilities in patients with hematological malignancies (Matyskiela et al., 2016; Matyskiela et al., 2018; Ito and Handa, 2019; Rasco et al., 2019; Gao et al., 2020; Hansen et al., 2020).

CC-122 (avadomide) was combined with $CRL4^{CRBN}$ E3 ligase to conduce the degradation of Ikaros and Aiolos in MM cells and DLBCL cells (Hagner et al., 2015). CC-122 has been applied to a variety of clinical trials for diverse diseases, including non-Hodgkin's lymphoma, MM, HCC, melanoma, and CLL/SLL (Rasco et al., 2019). It was found in research in pre-clinical experiments and a phase I clinical trial that avadomide + obinutuzumab was a tolerable therapeutic regimen for plenty of patients with manageable toxicity. Nevertheless, the predetermined activity threshold was not reached in this trial. There is no denying that cereblon-modulators plus anti-CD20 antibodies should be investigated further as a chemotherapy-free approach for relapsed or refractory non-Hodgkin lymphoma (NCT02417285) (Michot et al., 2020). In another phase I clinical trial, avadomide monotherapy presented manageable toxicity and promising pharmacokinetics in patients with solid tumors, NHL, and multiple myeloma. Of five patients with NHL, one realized CR, and two achieved PR (NCT01421524) (Rasco et al., 2019).

CC-220 (iberdomide) is another analog of thalidomide, which enhances the efficacy to downregulate Ikaros and Aiolos by tightly binding to $CRL4^{CRBN}$ E3 ligase for the treatment of RRMM and SLE (Matyskiela et al., 2018). The peripheral blood mononuclear cells of patients with SLE showed strikingly higher levels of IKZF1 (2.1-fold) and IKZF3 (4.1-fold) mRNA than a healthy person. And iberdomide significantly decreased levels of Ikaros and Aiolos protein in B cells, T cells, and monocytes, supporting its further clinical development for treating SLE (NCT01733875) (Schafer et al., 2018).

In addition to the pharmacologic function of CC-220, CC-885 can also induce $CRL4^{CRBN}$-dependent delegation of translation termination factor GSPT1, which cannot be degraded by neither Len nor pomalidomide, demonstrating the spectrum of the different substrates of CC-885 from pomalidomide and Len (Matyskiela et al., 2016). Hence, CC-885 may have the extra potential for AML therapy. Relevant pre-clinical and clinical trials are ongoing and being analyzed due to their novelty. CC-92480 is another novel protein degrader acting on the refractory/relapsed MM (RRMM) of Len (Hansen et al., 2020).

4.3 Treatment of Proteasome Inhibitors

PIs are a class of important drugs for the treatment of MM and MCL, and are being studied for the treatment of other diseases. BTZ is the first PI to be approved by the Food and Drug Administration (FDA) of the United States. Carfilzomib and ixazomib have been approved successively, and more drugs are in development (Fricker, 2020). The phase III GIMEMA-MMY-3006 trial illuminated the superiority of the BTZ + thalidomide + dexamethasone (VTD) regimen over thalidomide and dexamethasone (TD) in improving CR and prolonging PFS (HR, 0·60; 95% CI, 0·48–0.76; $p < 0{\cdot}0001$) as an induction regimen before and intensification therapy after double autologous hematopoietic stem-cell transplantation (ASCT) for patients with NDMM (NCT01134484) (Cavo et al., 2010; Tacchetti et al., 2020). The randomized phase III trial SWOG S0777 and long-term follow-up of SWOG S0777 revealed a similar pattern that the addition of

TABLE 4 | Clinical trials of CELMoDs in tumors.

Drug	Alias	NCT number	Phase	Conditions	Interventions
CC-122	Avadomide	NCT02509039	1	NHL, Solid Tumors	CC-122
		NCT02859324	1, 2	Unresectable HCC	CC-122, Nivolumab
		NCT02323906	1	HCC	CC-122, Sorafenib
		NCT03834623	2	Advanced Melanoma	CC-122, Nivolumab
		NCT02031419	1	DLBCL, FL	CC-122, CC-223, Rituximab, CC-292
		NCT02417285	1	Relapsed/Refractory DLBCL, iNHL	Obinutuzumab, CC-122
		NCT02406742	1,2	CLL, SLL	CC-122, Ibrutinib, Obinutuzumab
		NCT03283202	1	DLBCL	CC-122, R-CHOP
		NCT01421524	1	NHL, Solid Tumors, MM	CC-122
CC-220	Iberdomide	NCT04882163	1, 2	B-cell Lymphoma	CC-220, Polatuzumab vedotin, Rituximab, Tafasitamab, Gem, DDP, DEX, Bendamustine, Len
		NCT03161483	2	SLE	CC-220, Placebo
		NCT02185040	2	SLE	CC-220, Placebo
		NCT04884035	1	a-BCL	CC-220, R-CHOP, CC-99282
		NCT04464798	1	RR Lymphoma	CC-220, Rituximab, Obinutuzumab
		NCT02773030	1, 2	MM	CC-220, DEX, DARA, BTZ, CFZ
		NCT02192489	2	Skin Sarcoidosis	CC-220, Placebo
		NCT04564703	2	MM	CC-220
		NCT04392037	2	MM	CC-220, cyclophosphamide, DEX
		NCT04855136	1, 2	MM	BB2121, CC-220, BMS-986405, Pom, DEX, BTZ
		NCT03310619	1, 2	NHL, DLBCL, FL	JCAR017, Durvalumab, CC-122, Ibrutinib, CC-220, Relatlimab, Nivolumab, CC-99282
CC-92480	—	NCT03989414	1, 2	MM	CC-92480, BTZ, DEX, DARA, CFZ, Elotuzumab, Isatuximab
		NCT03374085	1, 2	MM	CC-92480, DEX

Abbreviation: NHL, Non-Hodgkin's lymphoma; HCC, hepatocellular carcinoma; DBLCL, Diffuse large B-cell lymphoma; iNHL, indolent NHL; CLL, Chronic lymphocytic leukemia; FL, Follicular lymphoma; MM, multiple myeloma; BCL, B-cell Lymphoma; SLE, systemic lupus erythematosus; RR, Lymphoma, relapsed/refractory lymphoma; R-CHOP (Rituximab, cyclophosphamide, doxorubicin, vincristine, prednisone); DEX, dexamethasone; DARA, daratumumab; BTZ, bortezomib; CFZ, carfilzomib; Len, Lenalidomide; Gem, gemcitabine; DDP, Cisplatin; Pom, Pomalidomide.

BTZ to Len and Dex for induction therapy led to a statistically and clinically meaningful increase in PFS as well as OS (NCT00644228) (Durie et al., 2017; Durie et al., 2020). Another trial demonstrated that the first single-agent ixazomib option in patients with NDMM not undergoing ASCT promoted mPFS (17.4 vs. 9.4 months; HR, 0.659; 95% CI, 0.542–0.801; $p < 0.001$; median follow-up, 21.1 months) without unexpected toxicity (NCT02312258) (Dimopoulos et al., 2020a). For combination therapy of ixazomib, the addition of ixazomib to a Len and Dex regimen was correlated to longer PFS (20.6 vs. 14.7 months in Len and Dex; HR, 0.74; $p = 0.01$) with limited toxic effects (NCT01564537) (Moreau et al., 2016). Besides, in patients with RRMM, carfilzomib in conjunction with Len and Dex (KRd) generated markedly improved mPFS (26.3 months, vs. 17.6 months in the Len and Dex group; HR, 0.69; 95% CI, 0.57–0.83; $p = 0.0001$) at the interim analysis and presented an improving risk-benefit profile (NCT01080391) (Stewart et al., 2015). However, the KRd scheme cannot effectively improve PFS (34·6 months vs. 34·4 months in the Len and Dex group; HR, 1·04; 95% CI, 0.83–1.31; $p = 0·74$) compared with a control group in patients with NDMM, and had more toxicity (NCT01863550) (Kumar et al., 2020).

4.4 Immunotherapy

Immunotherapy is one of the most promising treatments for several cancers. In future clinical trials, early identification of high-risk patients with ALL is essential for the best treatment, and to ensure innovative treatments, such as immunotherapy, are introduced in a timely manner (Stanulla et al., 2018). In some studies about certain solid tumors that lack IKZF1 expression, overexpression of Ikaros leads to increased immune recruitment infiltration and tumor sensitivity to cytotoxic T lymphocyte-associated antigen-4 (CTLA4) and programmed cell death protein 1 (PD1) inhibitors (Chen et al., 2015; Chen et al., 2018). Nevertheless, meaningful MM regression was not achieved by single-drug PD-1 blockade in early clinical studies. Besides, the FDA established that the risks of the pembrolizumab plus pomalidomide and dexamethasone combination outweighed its benefits for patients with RRMM and halted the study (NCT02576977) (Mateos et al., 2019). Equally, the interim analysis results presented that the benefit-risk event of pembrolizumab plus lenalidomide and dexamethasone is adverse for patients with NDMM. Survival and long-term safety follow-up are ongoing (NCT02579863) (Usmani et al., 2019). CAR-T immunotherapy faces many problems in the treatment of solid tumors, and T-cell dysfunction or failure is one of them. Len improved CAR-T function by inducing the degradation of Ikaros and Aiolos, promoting the killing of CD133-CAR-T and increasing the secretion of the cytokine and the proliferation of CD133-CAR-T (Wang et al., 2020b).

4.5 Targeted Therapy

Adding imatinib to the therapy for patients with BCR-ABL1 fusion to strengthen the treatment of IKZF1-del patients can eliminate the adverse effect of IKZF1-del in contemporary ALL treatment (Yeoh et al., 2018). Imatinib, as an intensifying

therapy for childhood B-ALL with IKZF1-del, significantly decreased the risk of recurrence and improved the 5-years OS from 69.6% in MS2003 to 91.6% in MS 2010 (p = 0.007) (NCT0289464) (Yeoh et al., 2018). Besides, ibrutinib also presented enduring single-agent efficacy in patients with relapsed or refractory MCL. A CR rate of 21% and a PR rate of 47% were detected. And the most common adverse events related to treatment were diarrhea, fatigue, and nausea (NCT01236391) (Wang et al., 2013).

DD-03–171 is an optimized Bruton tyrosine kinase (BTK) inhibitor analog, which showed an enhanced anti-proliferation outcome on MCL cells *in vitro* through the degradation of BTK, Ikaros, and Aiolos (Dobrovolsky et al., 2019). Acalabrutinib, a selective second-generation BTK inhibitor, provided superior durable responses and an acceptable toxicity profile in patients with relapsed or refractory MCL. At the median follow-up of 15.2 months, 81% of patients attained an overall response, and 40% of patients achieved a CR. The most common adverse events were headache (38%), diarrhea (31%), fatigue (27%), and myalgia (21%) (NCT02213926) (Wang et al., 2018).

The CK2 inhibitor CX4945 can restore Ikaros function and exert the antileukemia effect *in vitro* or in pre-clinical leukemia models (Gowda et al., 2017b; Borgo et al., 2021). There are also many cancer clinical trials currently running (NCT01199718, NCT00891280, NCT03897036, NCT02128282, NCT03904862, and NCT03571438).

Bromodomain-containing protein 4 (BRD4) is a chromatin-binding protein that was considered to immediately regulate a range of genes involved in the BCR signal pathway, covering Aiolos, B-cell linker, PAX5, and several oncogenes, like MYB. Thalidomide derivatives to various Brd4 small molecule inhibitors through different junctions were used to synthesize $CRL4^{CRBN}$ E3-based PROTAC targeting Brd4. For example, the synthesis of many pre-clinical trials like dBET1, ARV-825, BETd-246, BETd-260, and QCA570. Of course, there are other degradation pathways, such as the $CRL2^{VHL}$ E3-based pathway (Duan et al., 2018). BRD4 inhibitors were suggested to enhance the anti-MCL effect of Len or ibrutinib synergistically. It works even in BTZ-resistant MCL cells (Tsukamoto et al., 2020).

In breast cancer, the application of ginseng polysaccharide was able to suppress MDA-MB-231 cell proliferation by the activation of IKZF1 (Zhou et al., 2020). The anticancer capability of imatinib in Ik6+ and Ph + ALL can be strengthened by plant elements such as Huaier extract (Qu et al., 2019). The use of caffeic acid phenethyl ester analogs in the so-called Achilles heel of myeloma, aimed at the Ikaros/IRF4 axis, showed positive clinical outcomes (Murugesan et al., 2020).

Daratumumab, a monoclonal antibody targeting CD38, has presented substantial efficacy as a monotherapy in heavily pretreated and refractory patients with MM and in conjunction with bortezomib in patients with NDMM as well as with IMiD in patients with RRMM. Overall responses were noted in 29.2% of refractory patients with MM treated with daratumumab monotherapy (NCT01985126) (Lonial et al., 2016; Usmani et al., 2020). In addition, the combined administration may be an ideal backbone for the future research of anti-CD38 monoclonal antibodies in terms of their good safety and oral administration. The addition of daratumumab with Len-Dex induced a high ORR and PFS, markedly decreasing the risk for progression and associated death in patients with RRMM and NDMM who were ineligible for ASCT in contrast to Len-Dex therapy (Dimopoulos et al., 2016). And after 44.3 months of follow-up, triple therapy significantly prolonged PFS in the treated population (44.5 vs. 17.5 months; HR, 0.44; 95% CI, 0.35–0.55; $p < 0.0001$). In terms of adverse profiles, a higher frequency of neutropenia and pneumonia was noticed in the daratumumab group (NCT02076009, NCT02252172) (Facon et al., 2019; Bahlis et al., 2020). Moreover, daratumumab plus Pom-Dex could also reduce the risk of disease progression and improve mPFS (12·4 vs. 6·9 months; HR, 0·63; 95% CI, 0·47–0.85) in patients with RRMM compared to Pom-Dex, and can be considered a new therapeutic strategy (NCT03180736) (Chari et al., 2017; Dimopoulos et al., 2021a). Besides, daratumumab applied with carfilzomib and Dex in patients with RRMM was associated with a promising benefit-risk profile and prolonging PFS (NCT03158688) (Dimopoulos et al., 2020b). In quadruple therapy, induction and remarkable consolidation treatment of daratumumab plus Len, BTZ, and Dex improved response depth and PFS with acceptable safety in patients with transplant-eligible NDMM (NCT02874742, NCT02541383) (Moreau et al., 2019; Voorhees et al., 2020). Isatuximab, another monoclonal antibody targeting CD38, has been evaluated as a monotherapy and combined with Dex in patients with RRMM. The combination of isatuximab and Dex promoted ORR (43.6 vs. 23.9% in the Isa arm) and survival outcomes with no adverse effect on safety (NCT01084252) (Dimopoulos et al., 2021b). On the basis of Pom-Dex, the addition of isatuximab was able to importantly improve PFS in patients with RRMM, particularly for patients who are refractory to Len and a PI (NCT02990338) (Attal et al., 2019).

In phase Ib-III clinical studies, elotuzumab, an immunostimulatory antibody against signaling lymphocytic activation molecule F7 (SLAMF7), achieved a reduction of 30% in the risk of disease progression or death in patients with RRMM combined with Len and Dex (NCT01239797) (Lonial et al., 2015; Dimopoulos et al., 2020c). Particularly among patients with MM who failed after treatment with Len and a PI, the addition of elotuzumab to Pom-Dex tremendously lowered the risk of disease progression or death and prolonged mPFS (10.3 vs. 4.7 months in the control group) versus Pom-Dex alone (NCT02654132) (Dimopoulos et al., 2018). Nevertheless, in the SWOG-1211 trial, elotuzumab combined with BTZ, Len, and Dex did not improve clinical outcomes of patients with NDMM as induction and maintenance treatments (Usmani et al., 2021) (NCT01668719).

4.6 Reversal of Drug Resistance

The majority of newly diagnosed patients respond to therapy of an immunomodulator, and yet most develop resistance to administered therapies eventually. Strategies to surmount resistance have been proposed (Mogollón et al., 2019). In MM,

distinguishing mechanisms of resistance to both Len and Pom are apparent, therefore, tumors with acquired resistance to pomalidomide react to Len and vice versa (Ocio et al., 2015). STAT3 and MEK1/2 inhibitors have been testified to overcome IMiDs resistance effectively in pre-clinical studies (Ocio et al., 2015; Zhu et al., 2019). Enhancing degradation of CRBN has also been proved to be more sensitive to IMiDs (Kim et al., 2020). Protecting IKZFs from degradation through RUNXs inhibition resulted in conquering the resistance of IMiDs in MM (Zhou et al., 2019). In addition, a synthesized HDAC6 selective inhibitor, A452, is a strategy to overcome resistance to IMiDs (He et al., 2020). Furthermore, Cys reinforced the sensitivity of MDS/AML cells to Len without affecting the activation of T cells (He et al., 2020). It has been reported that the addition of cyclophosphamide to an IMiD could enhance the efficacy of IMiDs, prolong PFS and OS, and even save patients with Len-refractory disease, regardless of whether they have pre-accepted ASCT (NCT02244125) (Garderet et al., 2018). In patients with Len-refractory MM, the combination of pomalidomide, cyclophosphamide, and Dex confer a superior ORR and PFS than pomalidomide and Dex (NCT01432600) (Baz et al., 2016). In ALL, treatment with retinoid receptor agonists is able to fortify the sensitivity of IKZF1-aberrant BCR-ABL1 ALL patients to tyrosine kinase inhibitor therapy (Churchman et al., 2015).

5 CONCLUSION

Ikaros and its analogues play an important role in regulating normal lymphopoiesis, immune diseases, and generation of some tumors. In terms of categories, the Ikaros protein family consists of five members named Ikaros, Helios, Aiolos, Eos, and Pegasus. Ikaros acts both as a transcriptional repressor and as an activator by binding to assorted nuclear factors referred to epigenetic regulation and chromatin remodeling in different malignancies. And its own activities are thought to be regulated by post-translational phosphorylation, SUMOylation, and ubiquitination. Studies on signaling pathways about Ikaros have clarified that the preBCR signal pathway, Notch pathway, integrin signaling pathway, and IRFs are related to Ikaros signal transduction. For lymphocytes in healthy subjects, the Ikaros protein family exerts different effects on the growth, reproduction, and differentiation of many kinds of innate or adaptive lymphocytes *in vivo* and prevents autoimmunity by administering BCR unresponsiveness and repressing TLR signaling transduction.

Ikaros appears to function as a transcriptional inhibitor and activator by binding to different nuclear factors related to epigenetic regulation or targeting genes directly. The Ikaros-HDAC1 complex, inducing the formation of inhibitory chromatin, suppresses the transcription of its target genes accordingly. Ikaros has an adverse effect on the development of leukemia *via* globally regulating the enhancer or super-enhancer landscape and pioneer ring activity. Analogically, Ikaros is able to directly act on some target genes, such as those that activate the target genes' transcription, cause transcription suppression, determine cell cycle progression, control cell survival, and develop drug resistance. Ikaros induces the powerful upregulation of G6PD, effecting malignancies through glucose metabolism.

IMiDs lead to selective ubiquitination and proteasomal degradation of Ikaros and Aiolos through recruiting TFs to the $CRL4^{CRBN}$ E3 ubiquitin ligase, achieving the purpose of therapy for MM and other malignancies. Novel thalidomide analogs, are currently in clinical trials as a monotherapy and in combination with other drugs, illustrating that CELMoDs have strong antitumor and immunostimulatory capabilities in patients with hematological malignancies. Even so, developing resistance to administered therapies is a huge obsession. Combination therapy and developing drugs against new targets may be potential treatments. Other treatments, such as protease kinase inhibitors, monoclonal antibodies, and phytochemicals were also applied to patients with IKZF-missing phenotypes, but the efficacy remains to be verified.

AUTHOR CONTRIBUTIONS

YW and XW developed the main direction and offered significant guidance for this manuscript. RX and YC drafted the manuscript. XH illustrated the figures and tables for the manuscript. All authors approved the final manuscript.

FUNDING

This work is supported by the National Natural Science Foundation Regional Innovation and Development (No. U19A2003), the National Major Scientific and Technological Special Project for "Significant New Drugs Development" (No. 2018ZX09733001), the Excellent Youth Foundation of Sichuan Scientific Committee grant in China (No. 2019JDJQ008), and the Development Program of China (No. 2016YFA0201402).

REFERENCES

Alkhatib, A., Werner, M., Hug, E., Herzog, S., Eschbach, C., Faraidun, H., et al. (2012). FoxO1 Induces Ikaros Splicing to Promote Immunoglobulin Gene Recombination. *J. Exp. Med.* 209, 395–406. doi:10.1084/jem.20110216

Alomairi, J., Molitor, A. M., Sadouni, N., Hussain, S., Torres, M., Saadi, W., et al. (2020). Integration of High-Throughput Reporter Assays Identify a Critical Enhancer of the Ikzf1 Gene. *PloS one* 15, e0233191. doi:10.1371/journal.pone.0233191

Arco, P. G.-d., Maki, K., and Georgopoulos, K. (2004). Phosphorylation Controls Ikaros's Ability to Negatively Regulate the G 1 -S Transition. *Mol. Cell Biol* 24, 2797–2807. doi:10.1128/mcb.24.7.2797-2807.2004

Aref, S., Khaled, N., Menshawy, N. E., Sabry, M., and Agder, M. A. (2020). Clinical Value of RAG1 Expression and IKZF1 Deletions in Philadelphia Negative Pediatric B Cell Precursor Acute Lymphoblastic Leukemia. *Pediatr. Hematol. Oncol.* 37, 380–389. doi:10.1080/08880018.2020.1767739

Attal, M., Richardson, P. G., Rajkumar, S. V., San-Miguel, J., Beksac, M., Spicka, I., et al. (2019). Isatuximab Plus Pomalidomide and Low-Dose Dexamethasone versus Pomalidomide and Low-Dose Dexamethasone in Patients with Relapsed and Refractory Multiple Myeloma (ICARIA-MM): a Randomised, Multicentre, Open-Label, Phase 3 Study. *Lancet* 394, 2096–2107. doi:10.1016/S0140-6736(19)32556-5

Attal, M., Lauwers-Cances, V., Marit, G., Caillot, D., Moreau, P., Facon, T., et al. (2012). Lenalidomide Maintenance after Stem-Cell Transplantation for Multiple Myeloma. *N. Engl. J. Med.* 366, 1782–1791. doi:10.1056/nejmoa1114138

Avitahl, N., Winandy, S., Friedrich, C., Jones, B., Ge, Y., and Georgopoulos, K. (1999). Ikaros Sets Thresholds for T Cell Activation and Regulates Chromosome Propagation. *Immunity* 10, 333–343. doi:10.1016/s1074-7613(00)80033-3

Bahlis, N. J., Dimopoulos, M. A., White, D. J., Benboubker, L., Cook, G., Leiba, M., et al. (2020). Daratumumab Plus Lenalidomide and Dexamethasone in Relapsed/refractory Multiple Myeloma: Extended Follow-Up of POLLUX, a Randomized, Open-Label, Phase 3 Study. *Leukemia* 34, 1875–1884. doi:10.1038/s41375-020-0711-6

Bald, T., Wagner, M., Gao, Y., Koyasu, S., and Smyth, M. J. (2019). Hide and Seek: Plasticity of Innate Lymphoid Cells in Cancer. *Semin. Immunol.* 41, 101273. doi:10.1016/j.smim.2019.04.001

Barrett, J. C., Hansoul, S., Hansoul, S., Nicolae, D. L., Cho, J. H., Duerr, R. H., et al. (2008). Genome-wide Association Defines More Than 30 Distinct Susceptibility Loci for Crohn's Disease. *Nat. Genet.* 40, 955–962. doi:10.1038/ng.175

Baz, R. C., Martin, T. G., 3rd, Lin, H.-Y., Zhao, X., Shain, K. H., Cho, H. J., et al. (2016). Randomized Multicenter Phase 2 Study of Pomalidomide, Cyclophosphamide, and Dexamethasone in Relapsed Refractory Myeloma. *Blood* 127, 2561–2568. doi:10.1182/blood-2015-11-682518

Beer, P. A., Knapp, D. J. H. F., Miller, P. H., Kannan, N., Sloma, I., Heel, K., et al. (2015). Disruption of IKAROS Activity in Primitive Chronic-phase CML Cells Mimics Myeloid Disease Progression. *Blood* 125, 504–515. doi:10.1182/blood-2014-06-581173

Bellavia, D., Mecarozzi, M., Campese, A. F., Grazioli, P., Talora, C., Frati, L., et al. (2007). Notch3 and the Notch3-Upregulated RNA-Binding Protein HuD Regulate Ikaros Alternative Splicing. *Embo J.* 26, 1670–1680. doi:10.1038/sj.emboj.7601626

Benboubker, L., Dimopoulos, M. A., Dispenzieri, A., Catalano, J., Belch, A. R., Cavo, M., et al. (2014). Lenalidomide and Dexamethasone in Transplant-Ineligible Patients with Myeloma. *N. Engl. J. Med.* 371, 906–917. doi:10.1056/nejmoa1402551

Berry, N. K., Scott, R. J., Sutton, R., Law, T., Trahair, T. N., Dalla-Pozza, L., et al. (2020). Enrichment of Atypical Hyperdiploidy and IKZF1 Deletions Detected by SNP-Microarray in High-Risk Australian AIEOP-BFM B-Cell Acute Lymphoblastic Leukaemia Cohort. *Cancer Genet.* 242, 8–14. doi:10.1016/j.cancergen.2020.01.051

Bjorklund, C. C., Lu, L., Kang, J., Hagner, P. R., Havens, C. G., Amatangelo, M., et al. (2015). Rate of CRL4CRBN Substrate Ikaros and Aiolos Degradation Underlies Differential Activity of Lenalidomide and Pomalidomide in Multiple Myeloma Cells by Regulation of C-Myc and IRF4. *Blood Cancer J.* 5, e354. doi:10.1038/bcj.2015.66

Borgo, C., D'Amore, C., Sarno, S., Salvi, M., and Ruzzene, M. (2021). Protein Kinase CK2: a Potential Therapeutic Target for Diverse Human Diseases. *Sig Transduct Target. Ther.* 6, 183. doi:10.1038/s41392-021-00567-7

Bottardi, S., Mavoungou, L., Pak, H., Daou, S., Bourgoin, V., Lakehal, Y. A., et al. (2014). The IKAROS Interaction with a Complex Including Chromatin Remodeling and Transcription Elongation Activities Is Required for Hematopoiesis. *Plos Genet.* 10, e1004827. doi:10.1371/journal.pgen.1004827

Brissot, E., Clavert, A., Blin, N., Roland, V., Guillaume, T., Dubruille, V., et al. (2015). Impact of Lenalidomide on Immune Functions in the Setting of Maintenance Therapy for Multiple Myeloma. *Leukemia* 29, 2098–2100. doi:10.1038/leu.2015.64

Cavo, M., Tacchetti, P., Patriarca, F., Petrucci, M. T., Pantani, L., Galli, M., et al. (2010). Bortezomib with Thalidomide Plus Dexamethasone Compared with Thalidomide Plus Dexamethasone as Induction Therapy before, and Consolidation Therapy after, Double Autologous Stem-Cell Transplantation in Newly Diagnosed Multiple Myeloma: a Randomised Phase 3 Study. *The Lancet* 376, 2075–2085. doi:10.1016/s0140-6736(10)61424-9

Chan, S. M. (2019). The Making of a Leukemic Stem Cell: A Novel Role for IKZF2 in AML Stemness and Differentiation. *Cell Stem Cell* 24, 5–6. doi:10.1016/j.stem.2018.12.007

Chari, A., Suvannasankha, A., Fay, J. W., Arnulf, B., Kaufman, J. L., Ifthikharuddin, J. J., et al. (2017). Daratumumab Plus Pomalidomide and Dexamethasone in Relapsed And/or Refractory Multiple Myeloma. *Blood* 130, 974–981. doi:10.1182/blood-2017-05-785246

Chen, J. C., Cerise, J. E., Jabbari, A., Clynes, R., and Christiano, A. M. (2015). Master Regulators of Infiltrate Recruitment in Autoimmune Disease Identified through Network-Based Molecular Deconvolution. *Cell Syst.* 1, 326–337. doi:10.1016/j.cels.2015.11.001

Chen, J. C., Perez-Lorenzo, R., Saenger, Y. M., Drake, C. G., and Christiano, A. M. (2018). IKZF1 Enhances Immune Infiltrate Recruitment in Solid Tumors and Susceptibility to Immunotherapy. *Cell Syst.* 7, 92–103. doi:10.1016/j.cels.2018.05.020

Chen, L., Niu, Q., Huang, Z., Yang, B., Wu, Y., and Zhang, J. (2020). IKZF1 Polymorphisms Are Associated with Susceptibility, Cytokine Levels, and Clinical Features in Systemic Lupus Erythematosus. *Medicine* 99, e22607. doi:10.1097/md.0000000000022607

Chen, Q., Shi, Y., Chen, Y., Ji, T., Li, Y., and Yu, L. (2019). Multiple Functions of Ikaros in Hematological Malignancies, Solid Tumor and Autoimmune Diseases. *Gene* 684, 47–52. doi:10.1016/j.gene.2018.10.045

Churchman, M. L., Low, J., Qu, C., Paietta, E. M., Kasper, L. H., Chang, Y., et al. (2015). Efficacy of Retinoids in IKZF1-Mutated BCR-ABL1 Acute Lymphoblastic Leukemia. *Cancer cell* 28, 343–356. doi:10.1016/j.ccell.2015.07.016

Churchman, M. L., Qian, M., Te Kronnie, G., Zhang, R., Yang, W., Zhang, H., et al. (2018). Germline Genetic IKZF1 Variation and Predisposition to Childhood Acute Lymphoblastic Leukemia. *Cancer Cell* 33, 937–948. e8. doi:10.1016/j.ccell.2018.03.021

Cippitelli, M., Stabile, H., Kosta, A., Petillo, S., Gismondi, A., Santoni, A., et al. (2021). Role of Aiolos and Ikaros in the Antitumor and Immunomodulatory Activity of IMiDs in Multiple Myeloma: Better to Lose Than to Find Them. *Int. J. Mol. Sci.* 22. doi:10.3390/ijms22031103

Costa, F., Vescovini, R., Bolzoni, M., Marchica, V., Storti, P., Toscani, D., et al. (2017). Lenalidomide Increases Human Dendritic Cell Maturation in Multiple Myeloma Patients Targeting Monocyte Differentiation and Modulating Mesenchymal Stromal Cell Inhibitory Properties. *Oncotarget* 8, 53053–53067. doi:10.18632/oncotarget.18085

Craddock, C., Slade, D., De Santo, C., Wheat, R., Ferguson, P., Hodgkinson, A., et al. (2019). Combination Lenalidomide and Azacitidine: A Novel Salvage Therapy in Patients Who Relapse after Allogeneic Stem-Cell Transplantation for Acute Myeloid Leukemia. *Jco* 37, 580–588. doi:10.1200/jco.18.00889

Cunninghame Graham, D. S., Morris, D. L., Bhangale, T. R., Criswell, L. A., Syvänen, A.-C., Rönnblom, L., et al. (2011). Association of NCF2, IKZF1, IRF8, IFIH1, and TYK2 with Systemic Lupus Erythematosus. *Plos Genet.* 7, e1002341. doi:10.1371/journal.pgen.1002341

Curtis, L. M., Ostojic, A., Venzon, D. J., Holtzman, N. G., Pirsl, F., Kuzmina, Z. J., et al. (2021). A Randomized Phase 2 Trial of Pomalidomide in Subjects Failing Prior Therapy for Chronic Graft-Versus-Host Disease. *Blood* 137, 896–907. doi:10.1182/blood.2020006892

Daneshvar Kakhaki, R., Kouchaki, E., Dadgostar, E., Behnam, M., Tamtaji, O. R., Nikoueinejad, H., et al. (2020). The Correlation of Helios and Neuropilin-1 Frequencies with Parkinson Disease Severity. *Clin. Neurol. Neurosurg.* 192, 105833. doi:10.1016/j.clineuro.2020.105833

Davidson, A., and Diamond, B. (2001). Autoimmune Diseases. *N. Engl. J. Med.* 345, 340–350. doi:10.1056/nejm200108023450506

Davis, D. A., Shrestha, P., Aisabor, A. I., Stream, A., Galli, V., Pise-Masison, C. A., et al. (2019). Pomalidomide Increases Immune Surface Marker Expression and Immune Recognition of Oncovirus-Infected Cells. *Oncoimmunology* 8, e1546544. doi:10.1080/2162402x.2018.1546544

de Rooij, J. D. E., Beuling, E., van den Heuvel-Eibrink, M. M., Obulkasim, A., Baruchel, A., Trka, J., et al. (2015). Recurrent Deletions of IKZF1 in Pediatric Acute Myeloid Leukemia. *Haematologica* 100, 1151–1159. doi:10.3324/haematol.2015.124321

Dhanyamraju, P. K., Iyer, S., Smink, G., Bamme, Y., Bhadauria, P., Payne, J. L., et al. (2020). Transcriptional Regulation of Genes by Ikaros Tumor Suppressor in Acute Lymphoblastic Leukemia. *Int. J. Mol. Sci.* 21. doi:10.3390/ijms21041377

Dieudonné, Y., Guffroy, A., Vollmer, O., Carapito, R., and Korganow, A.-S. (2019). IKZF1 Loss-Of-Function Variant Causes Autoimmunity and Severe Familial Antiphospholipid Syndrome. *J. Clin. Immunol.* 39, 353–357. doi:10.1007/s10875-019-00643-2

Dimopoulos, K., Fibiger Munch-Petersen, H., Winther Eskelund, C., Dissing Sjö, L., Ralfkiaer, E., Gimsing, P., et al. (2019). Expression of CRBN, IKZF1, and IKZF3 Does Not Predict Lenalidomide Sensitivity and Mutations in the Cereblon Pathway Are Infrequent in Multiple Myeloma. *Leuk. Lymphoma* 60, 180–188. doi:10.1080/10428194.2018.1466290

Dimopoulos, M. A., Dytfeld, D., Grosicki, S., Moreau, P., Takezako, N., Hori, M., et al. (2018). Elotuzumab Plus Pomalidomide and Dexamethasone for Multiple Myeloma. *N. Engl. J. Med.* 379, 1811–1822. doi:10.1056/nejmoa1805762

Dimopoulos, M. A., Lonial, S., White, D., Moreau, P., Weisel, K., San-Miguel, J., et al. (2020). Elotuzumab, Lenalidomide, and Dexamethasone in RRMM: Final Overall Survival Results from the Phase 3 Randomized ELOQUENT-2 Study. *Blood Cancer J.* 10, 91. doi:10.1038/s41408-020-00357-4

Dimopoulos, M. A., Oriol, A., Nahi, H., San-Miguel, J., Bahlis, N. J., Usmani, S. Z., et al. (2016). Daratumumab, Lenalidomide, and Dexamethasone for Multiple Myeloma. *N. Engl. J. Med.* 375, 1319–1331. doi:10.1056/nejmoa1607751

Dimopoulos, M. A., Špička, I., Quach, H., Oriol, A., Hájek, R., Garg, M., et al. (2020). Ixazomib as Postinduction Maintenance for Patients with Newly Diagnosed Multiple Myeloma Not Undergoing Autologous Stem Cell Transplantation: The Phase III TOURMALINE-MM4 Trial. *Jco* 38, 4030–4041. doi:10.1200/jco.20.02060

Dimopoulos, M. A., Terpos, E., Boccadoro, M., Delimpasi, S., Beksac, M., Katodritou, E., et al. (2021). Daratumumab Plus Pomalidomide and Dexamethasone versus Pomalidomide and Dexamethasone Alone in Previously Treated Multiple Myeloma (APOLLO): an Open-Label, Randomised, Phase 3 Trial. *Lancet Oncol.* 22, 801–812. doi:10.1016/s1470-2045(21)00128-5

Dimopoulos, M., Bringhen, S., Anttila, P., Capra, M., Cavo, M., Cole, C., et al. (2021). Isatuximab as Monotherapy and Combined with Dexamethasone in Patients with Relapsed/refractory Multiple Myeloma. *Blood* 137, 1154–1165. doi:10.1182/blood.2020008209

Dimopoulos, M., Quach, H., Mateos, M.-V., Landgren, O., Leleu, X., Siegel, D., et al. (2020). Carfilzomib, Dexamethasone, and Daratumumab versus Carfilzomib and Dexamethasone for Patients with Relapsed or Refractory Multiple Myeloma (CANDOR): Results from a Randomised, Multicentre, Open-Label, Phase 3 Study. *The Lancet* 396, 186–197. doi:10.1016/s0140-6736(20)30734-0

Ding, Y., Zhang, B., Payne, J. L., Song, C., Ge, Z., Gowda, C., et al. (2019). Ikaros Tumor Suppressor Function Includes Induction of Active Enhancers and Super-enhancers along with Pioneering Activity. *Leukemia* 33, 2720–2731. doi:10.1038/s41375-019-0474-0

Dobrovolsky, D., Wang, E. S., Morrow, S., Leahy, C., Faust, T., Nowak, R. P., et al. (2019). Bruton Tyrosine Kinase Degradation as a Therapeutic Strategy for Cancer. *Blood* 133, 952–961. doi:10.1182/blood-2018-07-862953

Dou, A., and Fang, J. (2020). Cyclosporine Broadens the Therapeutic Potential of Lenalidomide in Myeloid Malignancies. *J. Cell Immunol* 2, 237–244. doi:10.33696/immunology.2.049

Dovat, S., Song, C., Payne, K. J., and Li, Z. (2011). Ikaros, CK2 Kinase, and the Road to Leukemia. *Mol. Cell Biochem* 356, 201–207. doi:10.1007/s11010-011-0964-5

Duan, Y., Guan, Y., Qin, W., Zhai, X., Yu, B., and Liu, H. (2018). Targeting Brd4 for Cancer Therapy: Inhibitors and Degraders. *Med. Chem. Commun.* 9, 1779–1802. doi:10.1039/c8md00198g

Duhamel, M., Arrouss, I., Merle-Béral, H., and Rebollo, A. (2008). The Aiolos Transcription Factor Is Up-Regulated in Chronic Lymphocytic Leukemia. *Blood* 111, 3225–3228. doi:10.1182/blood-2007-09-113191

Dumortier, A., Jeannet, R., Kirstetter, P., Kleinmann, E., Sellars, M., dos Santos, N. R., et al. (2006). Notch Activation Is an Early and Critical Event during T-Cell Leukemogenesis in Ikaros-Deficient Mice. *Mol. Cell Biol* 26, 209–220. doi:10.1128/mcb.26.1.209-220.2006

Dumortier, A., Kirstetter, P., Kastner, P., and Chan, S. (2003). Ikaros Regulates Neutrophil Differentiation. *Blood* 101, 2219–2226. doi:10.1182/blood-2002-05-1336

Durie, B. G. M., Hoering, A., Abidi, M. H., Rajkumar, S. V., Epstein, J., Kahanic, S. P., et al. (2017). Bortezomib with Lenalidomide and Dexamethasone versus Lenalidomide and Dexamethasone Alone in Patients with Newly Diagnosed Myeloma without Intent for Immediate Autologous Stem-Cell Transplant (SWOG S0777): a Randomised, Open-Label, Phase 3 Trial. *The Lancet* 389, 519–527. doi:10.1016/s0140-6736(16)31594-x

Durie, B. G. M., Hoering, A., Sexton, R., Abidi, M. H., Epstein, J., Rajkumar, S. V., et al. (2020). Longer Term Follow-Up of the Randomized Phase III Trial SWOG S0777: Bortezomib, Lenalidomide and Dexamethasone vs. Lenalidomide and Dexamethasone in Patients (Pts) with Previously Untreated Multiple Myeloma without an Intent for Immediate Autologous Stem Cell Transplant (ASCT). *Blood Cancer J.* 10, 53. doi:10.1038/s41408-020-0311-8

Edgren, H., Murumagi, A., Kangaspeska, S., Nicorici, D., Hongisto, V., Kleivi, K., et al. (2011). Identification of Fusion Genes in Breast Cancer by Paired-End RNA-Sequencing. *Genome Biol.* 12, R6. doi:10.1186/gb-2011-12-1-r6

Eskandarian, Z., Fliegauf, M., Bulashevska, A., Proietti, M., Hague, R., Smulski, C. R., et al. (2019). Assessing the Functional Relevance of Variants in the IKAROS Family Zinc Finger Protein 1 (IKZF1) in a Cohort of Patients with Primary Immunodeficiency. *Front. Immunol.* 10, 568. doi:10.3389/fimmu.2019.00568

Facon, T., Kumar, S., Plesner, T., Orlowski, R. Z., Moreau, P., Bahlis, N., et al. (2019). Daratumumab Plus Lenalidomide and Dexamethasone for Untreated Myeloma. *N. Engl. J. Med.* 380, 2104–2115. doi:10.1056/nejmoa1817249

Fan, Y., and Lu, D. (2016). The Ikaros Family of Zinc-finger Proteins. *Acta Pharmaceutica Sinica. B* 6, 513–521. doi:10.1016/j.apsb.2016.06.002

Fang, C.-M., Roy, S., Nielsen, E., Paul, M., Maul, R., Paun, A., et al. (2012). Unique Contribution of IRF-5-Ikaros axis to the B-Cell IgG2a Response. *Genes Immun.* 13, 421–430. doi:10.1038/gene.2012.10

Fedele, P. L., Willis, S. N., Liao, Y., Low, M. S., Rautela, J., Segal, D. H., et al. (2018). IMiDs Prime Myeloma Cells for Daratumumab-Mediated Cytotoxicity through Loss of Ikaros and Aiolos. *Blood* 132, 2166–2178. doi:10.1182/blood-2018-05-850727

Fenaux, P., Giagounidis, A., Selleslag, D., Beyne-Rauzy, O., Mufti, G., Mittelman, M., et al. (2011). A randomized phase 3 study of lenalidomide versus placebo in RBC transfusion-dependent patients with Low-/Intermediate-1-risk myelodysplastic syndromes with del5q. *Blood* 118, 3765–3776. doi:10.1182/blood-2011-01-330126

Fionda, C., Abruzzese, M. P., Zingoni, A., Cecere, F., Vulpis, E., Peruzzi, G., et al. (2015). The IMiDs Targets IKZF-1/3 and IRF4 as Novel Negative Regulators of NK Cell-Activating Ligands Expression in Multiple Myeloma. *Oncotarget* 6, 23609–23630. doi:10.18632/oncotarget.4603

Fiorcari, S., Benatti, S., Zucchetto, A., Zucchini, P., Gattei, V., Luppi, M., et al. (2019). Overexpression of CD49d in Trisomy 12 Chronic Lymphocytic Leukemia Patients Is Mediated by IRF4 through Induction of IKAROS. *Leukemia* 33, 1278–1302. doi:10.1038/s41375-018-0296-5

Flowers, C. R., Leonard, J. P., and Fowler, N. H. (2020). Lenalidomide in Follicular Lymphoma. *Blood* 135, 2133–2136. doi:10.1182/blood.2019001751

Franks, M. E., Macpherson, G. R., and Figg, W. D. (2004). Thalidomide. *The Lancet* 363, 1802–1811. doi:10.1016/s0140-6736(04)16308-3

Fricker, L. D. (2020). Proteasome Inhibitor Drugs. *Annu. Rev. Pharmacol. Toxicol.* 60, 457–476. doi:10.1146/annurev-pharmtox-010919-023603

Gandhi, A. K., Kang, J., Havens, C. G., Conklin, T., Ning, Y., Wu, L., et al. (2014). Immunomodulatory Agents Lenalidomide and Pomalidomide Co-stimulate T Cells by Inducing Degradation of T Cell Repressors I Karos and A Iolos via Modulation of the E 3 Ubiquitin Ligase Complex CRL 4 CRBN. *Br. J. Haematol.* 164, 811–821. doi:10.1111/bjh.12708

Ganesan, S., Palani, H. K., Balasundaram, N., David, S., Devasia, A. J., George, B., et al. (2020). Combination Lenalidomide/Bortezomib Treatment Synergistically Induces Calpain-dependent Ikaros Cleavage and Apoptosis in Myeloma Cells. *Mol. Cancer Res.* 18, 529–536. doi:10.1158/1541-7786.mcr-19-0431

Gao, S., Wang, S., and Song, Y. (2020). Novel Immunomodulatory Drugs and Neo-Substrates. *Biomark Res.* 8, 2. doi:10.1186/s40364-020-0182-y

Garderet, L., Kuhnowski, F., Berge, B., Roussel, M., Escoffre-Barbe, M., Lafon, I., et al. (2018). Pomalidomide, Cyclophosphamide, and Dexamethasone for Relapsed Multiple Myeloma. *Blood* 132, 2555–2563. doi:10.1182/blood-2018-07-863829

Ge, Z., Gu, Y., Han, Q., Sloane, J., Ge, Q., Gao, G., et al. (2018). Plant Homeodomain finger Protein 2 as a Novel IKAROS Target in Acute Lymphoblastic Leukemia. *Epigenomics* 10, 59–69. doi:10.2217/epi-2017-0092

Ge, Z., Gu, Y., Han, Q., Zhao, G., Li, M., Li, J., et al. (2016). Targeting High Dynamin-2 (DNM2) Expression by Restoring Ikaros Function in Acute Lymphoblastic Leukemia.. *Sci Rep.* 6, 38004. doi:10.1038/srep38004

Ge, Z., Gu, Y., Xiao, L., Han, Q., Li, J., Chen, B., et al. (2016). Co-existence of IL7R High and SH2B3 Low Expression Distinguishes a Novel High-Risk Acute Lymphoblastic Leukemia with Ikaros Dysfunction. *Oncotarget* 7, 46014–46027. doi:10.18632/oncotarget.10014

Ge, Z., Gu, Y., Zhao, G., Li, J., Chen, B., Han, Q., et al. (2016). High CRLF2 Expression Associates with IKZF1 Dysfunction in Adult Acute Lymphoblastic Leukemia without CRLF2 Rearrangement. *Oncotarget* 7, 49722–49732. doi:10.18632/oncotarget.10437

Ge, Z., Guo, X., Li, J., Hartman, M., Kawasawa, Y. I., Dovat, S., et al. (2015). Clinical Significance of High C-MYC and Low MYCBP2 Expression and Their Association with Ikaros Dysfunction in Adult Acute Lymphoblastic Leukemia. *Oncotarget* 6, 42300–42311. doi:10.18632/oncotarget.5982

Ge, Z., Han, Q., Gu, Y., Ge, Q., Ma, J., Sloane, J., et al. (2018). Aberrant ARID5B Expression and its Association with Ikaros Dysfunction in Acute Lymphoblastic Leukemia. *Oncogenesis* 7, 84. doi:10.1038/s41389-018-0095-x

Ge, Z., Zhou, X., Gu, Y., Han, Q., Li, J., Chen, B., et al. (2017). Ikaros Regulation of the BCL6/BACH2 axis and its Clinical Relevance in Acute Lymphoblastic Leukemia. *Oncotarget* 8, 8022–8034. doi:10.18632/oncotarget.14038

Georgopoulos, K. (2002). Haematopoietic Cell-Fate Decisions, Chromatin Regulation and Ikaros. *Nat. Rev. Immunol.* 2, 162–174. doi:10.1038/nri747

Georgopoulos, K., Winandy, S., and Avitahl, N. (1997). The Role of the Ikaros Gene in Lymphocyte Development and Homeostasis. *Annu. Rev. Immunol.* 15, 155–176. doi:10.1146/annurev.immunol.15.1.155

Gokhale, A. S., Gangaplara, A., Lopez-Occasio, M., Thornton, A. M., and Shevach, E. M. (2019). Selective Deletion of Eos (Ikzf4) in T-Regulatory Cells Leads to Loss of Suppressive Function and Development of Systemic Autoimmunity. *J. Autoimmun.* 105, 102300. doi:10.1016/j.jaut.2019.06.011

Goldman, F. D., Gurel, Z., Al-Zubeidi, D., Fried, A. J., Icardi, M., Song, C., et al. (2012). Congenital Pancytopenia and Absence of B Lymphocytes in a Neonate with a Mutation in the Ikaros Gene. *Pediatr. Blood Cancer* 58, 591–597. doi:10.1002/pbc.23160

Gómez-del Arco, P., Koipally, J., and Georgopoulos, K. (2005). Ikaros SUMOylation: Switching Out of Repression. *Mol. Cell Biol* 25, 2688–2697. doi:10.1128/MCB.25.7.2688-2697.2005

Gorlova, O., Martin, J.-E., Rueda, B., Koeleman, B. P. C., Ying, J., Teruel, M., et al. (2011). Identification of Novel Genetic Markers Associated with Clinical Phenotypes of Systemic Sclerosis through a Genome-wide Association Strategy. *Plos Genet.* 7, e1002178. doi:10.1371/journal.pgen.1002178

Gowda, C., Sachdev, M., Muthusami, S., Kapadia, M., Petrovic-Dovat, L., Hartman, M., et al. (2017). Casein Kinase II (CK2) as a Therapeutic Target for Hematological Malignancies. *Curr. Pharm. Des.* 23, 95–107. doi:10.2174/1381612822666161006154311

Gowda, C., Soliman, M., Kapadia, M., Ding, Y., Payne, K., and Dovat, S. (2017). Casein Kinase II (CK2), Glycogen Synthase Kinase-3 (GSK-3) and Ikaros Mediated Regulation of Leukemia. *Adv. Biol. Regul.* 65, 16–25. doi:10.1016/j.jbior.2017.06.001

Gowda, C., Song, C., Ding, Y., Iyer, S., Dhanyamraju, P. K., McGrath, M., et al. (2020). Cellular Signaling and Epigenetic Regulation of Gene Expression in Leukemia. *Adv. Biol. Regul.* 75, 100665. doi:10.1016/j.jbior.2019.100665

Granados-Zamora, M., Chaves-Herrera, K., Morera-Araya, E., Granados-Alfaro, P., Valverde-Muñoz, K., Soto-Herrera, G., et al. (2020). IKZF1 Deletions as a Prognostic Factor in Costa Rican Patients with Pediatric B-Cell Acute Lymphoblastic Leukemia. *J. Pediatr. hematology/oncology* 42, e401–e406. doi:10.1097/mph.0000000000001807

Groth, D. J., Lakkaraja, M. M., Ferreira, J. O., Feuille, E. J., Bassetti, J. A., and Kaicker, S. M. (2020). Management of Chronic Immune Thrombocytopenia and Presumed Autoimmune Hepatitis in a Child with IKAROS Haploinsufficiency. *J. Clin. Immunol.* 40, 653–657. doi:10.1007/s10875-020-00781-y

Guha, I., Bhuniya, A., Shukla, D., Patidar, A., Nandi, P., Saha, A., et al. (2020). Tumor Arrests DN2 to DN3 Pro T Cell Transition and Promotes its Conversion to Thymic Dendritic Cells by Reciprocally Regulating Notch1 and Ikaros Signaling. *Front. Immunol.* 11, 898. doi:10.3389/fimmu.2020.00898

Gurel, Z., Ronni, T., Ho, S., Kuchar, J., Payne, K. J., Turk, C. W., et al. (2008). Recruitment of Ikaros to Pericentromeric Heterochromatin Is Regulated by Phosphorylation. *J. Biol. Chem.* 283, 8291–8300. doi:10.1074/jbc.m707906200

Hagner, P. R., Man, H.-W., Fontanillo, C., Wang, M., Couto, S., Breider, M., et al. (2015). CC-122, a Pleiotropic Pathway Modifier, Mimics an Interferon Response and Has Antitumor Activity in DLBCL. *Blood* 126, 779–789. doi:10.1182/blood-2015-02-628669

Hahm, K., Ernst, P., Lo, K., Kim, G. S., Turck, C., and Smale, S. T. (1994). The Lymphoid Transcription Factor LyF-1 Is Encoded by Specific, Alternatively Spliced mRNAs Derived from the Ikaros Gene. *Mol. Cel. Biol.* 14, 7111–7123. doi:10.1128/mcb.14.11.7111

Hansen, J. D., Correa, M., Nagy, M. A., Alexander, M., Plantevin, V., Grant, V., et al. (2020). Discovery of CRBN E3 Ligase Modulator CC-92480 for the Treatment of Relapsed and Refractory Multiple Myeloma. *J. Med. Chem.* 63, 6648–6676. doi:10.1021/acs.jmedchem.9b01928

Hariri, L., and Hardin, C. C. (2020). Covid-19, Angiogenesis, and ARDS Endotypes. *N. Engl. J. Med.* 383, 182–183. doi:10.1056/nejme2018629

He, L.-C., Gao, F.-H., Xu, H.-Z., Zhao, S., Ma, C.-M., Li, J., et al. (2012). Ikaros Inhibits Proliferation and, through Upregulation of Slug, Increases Metastatic Ability of Ovarian Serous Adenocarcinoma Cells. *Oncol. Rep.* 28, 1399–1405. doi:10.3892/or.2012.1946

He, X., Dou, A., Feng, S., Roman-Rivera, A., Hawkins, C., Lawley, L., et al. (2020). Cyclosporine Enhances the Sensitivity to Lenalidomide in MDS/AML *In Vitro*. *Exp. Hematol.* 86, 21–27. doi:10.1016/j.exphem.2020.05.001

Heizmann, B., Kastner, P., and Chan, S. (2018). The Ikaros Family in Lymphocyte Development. *Curr. Opin. Immunol.* 51, 14–23. doi:10.1016/j.coi.2017.11.005

Hgnc (2021). The Resource for Approved Human Gene Nomenclature. www.genenames.org.

Hideshima, T., Ogiya, D., Liu, J., Harada, T., Kurata, K., Bae, J., et al. (2021). Immunomodulatory Drugs Activate NK Cells via Both Zap-70 and Cereblon-dependent Pathways. *Leukemia* 35, 177–188. doi:10.1038/s41375-020-0809-x

Hosokawa, Y., Maeda, Y., Takahashi, E.-i., Suzuki, M., and Seto, M. (1999). Human Aiolos, an Ikaros-Related Zinc finger DNA Binding Protein: cDNA Cloning, Tissue Expression Pattern, and Chromosomal Mapping. *Genomics* 61, 326–329. doi:10.1006/geno.1999.5949

Hu, Y., Zhang, L., Chen, H., Liu, X., Zheng, X., Shi, H., et al. (2019). Analysis of Regulatory T Cell Subsets and Their Expression of Helios and PD-1 in Patients with Hashimoto Thyroiditis. *Int. J. Endocrinol.* 2019, 5368473. doi:10.1155/2019/5368473

Huang, Y., Lu, Y., He, Y., Feng, Z., Zhan, Y., Huang, X., et al. (2019). Ikzf1 Regulates Embryonic T Lymphopoiesis via Ccr9 and Irf4 in Zebrafish. *J. Biol. Chem.* 294, 16152–16163. doi:10.1074/jbc.ra119.009883

Hung, J.-J., Kao, Y.-S., Huang, C.-H., and Hsu, W.-H. (2019). Overexpression of Aiolos Promotes Epithelial-Mesenchymal Transition and Cancer Stem Cell-like Properties in Lung Cancer Cells. *Sci. Rep.* 9, 2991. doi:10.1038/s41598-019-39545-z

Hung, K.-H., Su, S.-T., Chen, C.-Y., Hsu, P.-H., Huang, S.-Y., Wu, W.-J., et al. (2016). Aiolos Collaborates with Blimp-1 to Regulate the Survival of Multiple Myeloma Cells. *Cell Death Differ* 23, 1175–1184. doi:10.1038/cdd.2015.167

Igartua, C., Myers, R. A., Mathias, R. A., Pino-Yanes, M., Eng, C., Graves, P. E., et al. (2015). Ethnic-specific Associations of Rare and Low-Frequency DNA Sequence Variants with Asthma. *Nat. Commun.* 6, 5965. doi:10.1038/ncomms6965

Ihara, M., Koyama, H., Uchimura, Y., Saitoh, H., and Kikuchi, A. (2007). Noncovalent Binding of Small Ubiquitin-Related Modifier (SUMO) Protease to SUMO Is Necessary for Enzymatic Activities and Cell Growth. *J. Biol. Chem.* 282, 16465–16475. doi:10.1074/jbc.m610723200

Ito, T., and Handa, H. (2019). [Cereblon as a Primary Target of IMiDs]. *Rinsho Ketsueki* 60, 1013–1019. doi:10.11406/rinketsu.60.1013

Jackson, G. H., Davies, F. E., Pawlyn, C., Cairns, D. A., Striha, A., Collett, C., et al. (2019). Lenalidomide Maintenance versus Observation for Patients with Newly Diagnosed Multiple Myeloma (Myeloma XI): a Multicentre, Open-Label, Randomised, Phase 3 Trial. *Lancet Oncol.* 20, 57–73. doi:10.1016/s1470-2045(18)30687-9

Javierre, B. M., Rodriguez-Ubreva, J., Al-Shahrour, F., Corominas, M., Graña, O., Ciudad, L., et al. (2011). Long-range Epigenetic Silencing Associates with Deregulation of Ikaros Targets in Colorectal Cancer Cells. *Mol. Cancer Res.* 9, 1139–1151. doi:10.1158/1541-7786.mcr-10-0515

Jeng, M. Y., Mumbach, M. R., Granja, J. M., Satpathy, A. T., Chang, H. Y., and Chang, A. L. S. (2019). Enhancer Connectome Nominates Target Genes of Inherited Risk Variants from Inflammatory Skin Disorders. *J. Invest. Dermatol.* 139, 605–614. doi:10.1016/j.jid.2018.09.011

Joshi, I., Yoshida, T., Jena, N., Qi, X., Zhang, J., Van Etten, R. A., et al. (2014). Loss of Ikaros DNA-Binding Function Confers Integrin-dependent Survival on Pre-B Cells and Progression to Acute Lymphoblastic Leukemia. *Nat. Immunol.* 15, 294–304. doi:10.1038/ni.2821

Jovanović, K. K., Roche-Lestienne, C., Ghobrial, I. M., Facon, T., Quesnel, B., and Manier, S. (2018). Targeting MYC in Multiple Myeloma. *Leukemia* 32, 1295–1306. doi:10.1038/s41375-018-0036-x

Katerndahl, C. D. S., Heltemes-Harris, L. M., Willette, M. J. L., Henzler, C. M., Frietze, S., Yang, R., et al. (2017). Antagonism of B Cell Enhancer Networks by STAT5 Drives Leukemia and Poor Patient Survival. *Nat. Immunol.* 18, 694–704. doi:10.1038/ni.3716

Khamechian, T., Irandoust, B., Mohammadi, H., Nikoueinejad, H., and Akbari, H. (2018). Association of Regulatory T Cells with Diabetes Type-1 and its Renal and Vascular Complications Based on the Expression of Forkhead Box Protein P3 (FoxP3), Helios and Neurophilin-1. *Iran J. Allergy Asthma Immunol.* 17, 151–157.

Kikuchi, J., Hori, M., Iha, H., Toyama-Sorimachi, N., Hagiwara, S., Kuroda, Y., et al. (2020). Soluble SLAMF7 Promotes the Growth of Myeloma Cells via Homophilic Interaction with Surface SLAMF7. *Leukemia* 34, 180–195. doi:10.1038/s41375-019-0525-6

Kim, G. W., Yoo, J., Won, H.-R., Yeon, S.-K., Lee, S. W., Lee, D. H., et al. (2020). A452, HDAC6-Selective Inhibitor Synergistically Enhances the Anticancer Activity of Immunomodulatory Drugs in IMiDs-Resistant Multiple Myeloma. *Leuk. Res.* 95, 106398. doi:10.1016/j.leukres.2020.106398

Kim, H.-J., Barnitz, R. A., Kreslavsky, T., Brown, F. D., Moffett, H., Lemieux, M. E., et al. (2015). Stable Inhibitory Activity of Regulatory T Cells Requires the Transcription Factor Helios. *Science* 350, 334–339. doi:10.1126/science.aad0616

Klocperk, A., Grecová, J., Šišmová, K., Kayserová, J., Froňková, E., and Šedivá, A. (2014). Helios expression in T-regulatory cells in patients with di George Syndrome. *J. Clin. Immunol.* 34, 864–870. doi:10.1007/s10875-014-0071-y

Klumb, C. E., Barbosa, T. d. C., Nestal de Moraes, G., Schramm, M. T., Emerenciano, M., and Maia, R. C. (2019). IKZF1 Deletion and Co-occurrence with Other Aberrations in a Child with Chronic Myeloid Leukemia Progressing to Acute Lymphoblastic Leukemia. *Pediatr. Blood Cancer* 66, e27570. doi:10.1002/pbc.27570

Koipally, J., Renold, A., Kim, J., and Georgopoulos, K. (1999). Repression by Ikaros and Aiolos Is Mediated through Histone Deacetylase Complexes. *EMBO J.* 18, 3090–3100. doi:10.1093/emboj/18.11.3090

Krabbendam, L., Bernink, J. H., and Spits, H. (2021). Innate Lymphoid Cells: from Helper to Killer. *Curr. Opin. Immunol.* 68, 28–33. doi:10.1016/j.coi.2020.08.007

Kriegsmann, K., Baertsch, M.-A., Awwad, M. H. S., Merz, M., Hose, D., Seckinger, A., et al. (2019). Cereblon-binding Proteins Expression Levels Correlate with Hyperdiploidy in Newly Diagnosed Multiple Myeloma Patients. *Blood Cancer J.* 9, 13. doi:10.1038/s41408-019-0174-z

Krönke, J., Fink, E. C., Hollenbach, P. W., MacBeth, K. J., Hurst, S. N., Udeshi, N. D., et al. (2015). Lenalidomide induces ubiquitination and degradation of CK1α in del(5q) MDS. *Nature* 523, 183–188. doi:10.1038/nature14610

Kuehn, H. S., Niemela, J. E., Stoddard, J., Ciullini Mannurita, S., Shahin, T., Goel, S., et al. (2020). *Germline IKAROS Dimerization Haploinsufficiency Causes Hematologic Cytopenias and Malignancies. Blood* 137 (3), 349–363. doi:10.1182/blood.2020007292

Kuiper, R. P., Waanders, E., van der Velden, V. H. J., van Reijmersdal, S. V., Venkatachalam, R., Scheijen, B., et al. (2010). IKZF1 Deletions Predict Relapse in Uniformly Treated Pediatric Precursor B-ALL. *Leukemia* 24, 1258–1264. doi:10.1038/leu.2010.87

Kumar, S. K., Jacobus, S. J., Cohen, A. D., Weiss, M., Callander, N., Singh, A. K., et al. (2020). Carfilzomib or Bortezomib in Combination with Lenalidomide and Dexamethasone for Patients with Newly Diagnosed Multiple Myeloma without Intention for Immediate Autologous Stem-Cell Transplantation (ENDURANCE): a Multicentre, Open-Label, Phase 3, Randomised, Controlled Trial. *Lancet Oncol.* 21, 1317–1330. doi:10.1016/s1470-2045(20)30452-6

Ladetto, M., Cortelazzo, S., Ferrero, S., Evangelista, A., Mian, M., Tavarozzi, R., et al. (2021). Lenalidomide Maintenance after Autologous Haematopoietic Stem-Cell Transplantation in Mantle Cell Lymphoma: Results of a Fondazione Italiana Linfomi (FIL) Multicentre, Randomised, Phase 3 Trial. *Lancet Haematol.* 8, e34–e44. doi:10.1016/s2352-3026(20)30358-6

Lagrue, K., Carisey, A., Morgan, D. J., Chopra, R., and Davis, D. M. (2015). Lenalidomide Augments Actin Remodeling and Lowers NK-Cell Activation Thresholds. *Blood* 126, 50–60. doi:10.1182/blood-2015-01-625004

Le Roy, A., Prébet, T., Castellano, R., Goubard, A., Riccardi, F., Fauriat, C., et al. (2018). Immunomodulatory Drugs Exert Anti-leukemia Effects in Acute Myeloid Leukemia by Direct and Immunostimulatory Activities. *Front. Immunol.* 9, 977. doi:10.3389/fimmu.2018.00977

Lempainen, J., Härkönen, T., Laine, A., Knip, M., and Ilonen, J. (2013). Associations of Polymorphisms in Non-HLA Loci with Autoantibodies at the Diagnosis of Type 1 diabetes:INSandIKZF4associate with Insulin Autoantibodies. *Pediatr. Diabetes* 14, 490–496. doi:10.1111/pedi.12046

Lentaigne, C., Greene, D., Sivapalaratnam, S., Favier, R., Seyres, D., Thys, C., et al. (2019). Germline Mutations in the Transcription Factor IKZF5 Cause Thrombocytopenia. *Blood* 134, 2070–2081. doi:10.1182/blood.2019000782

Leonard, J. P., Trneny, M., Izutsu, K., Fowler, N. H., Hong, X., Zhu, J., et al. (2019). AUGMENT: A Phase III Study of Lenalidomide Plus Rituximab versus Placebo Plus Rituximab in Relapsed or Refractory Indolent Lymphoma. *Jco* 37, 1188–1199. doi:10.1200/jco.19.00010

Li, L., Ding, X., Wang, X., Yao, Q., Shao, X., An, X., et al. (2018). Polymorphisms of IKZF3 Gene and Autoimmune Thyroid Diseases: Associated with Graves' Disease but Not with Hashimoto's Thyroiditis. *Cell Physiol Biochem* 45, 1787–1796. doi:10.1159/000487870

Li, S., Heller, J. J., Bostick, J. W., Lee, A., Schjerven, H., Kastner, P., et al. (2016). Ikaros Inhibits Group 3 Innate Lymphoid Cell Development and Function by Suppressing the Aryl Hydrocarbon Receptor Pathway. *Immunity* 45, 185–197. doi:10.1016/j.immuni.2016.06.027

Li, W., Cooley, L. D., August, K. J., Richardson, A. I., Shao, L., Ahmed, A. A., et al. (2019). Cuplike Nuclear Morphology Is Highly Associated with IKZF1 Deletion in Pediatric Precursor B-Cell ALL. *Blood* 134, 324–329. doi:10.1182/blood.2019000604

Li, X., Xu, Z., Du, W., Zhang, Z., Wei, Y., Wang, H., et al. (2014). Aiolos Promotes anchorage independence by Silencing p66Shc Transcription in Cancer Cells. *Cancer Cell* 25, 575–589. doi:10.1016/j.ccr.2014.03.020

Li, Z., Li, S.-P., Li, R.-Y., Zhu, H., Liu, X., Guo, X.-L., et al. (2018). Leukaemic Alterations of IKZF1 Prime Stemness and Malignancy Programs in Human Lymphocytes. *Cell Death Dis* 9, 526. doi:10.1038/s41419-018-0600-3

Li, Z., Song, C., Ouyang, H., Lai, L., Payne, K. J., and Dovat, S. (2012). Cell Cycle-specific Function of Ikaros in Human Leukemia. *Pediatr. Blood Cancer* 59, 69–76. doi:10.1002/pbc.23406

Liu, M., Jin, J., Ji, Y., Shan, H., Zou, Z., Cao, Y., et al. (2021). *Hsp90/C Terminal Hsc70-Interacting Protein Regulates the Stability of Ikaros in Acute Myeloid Leukemia Cells*. China: Life sciences.

Liu, Y. Y., Ge, C., Tian, H., Jiang, J. Y., Zhao, F. Y., Li, H., et al. (2017). The Transcription Factor Ikaros Inhibits Cell Proliferation by Downregulating ANXA4 Expression in Hepatocellular Carcinoma. *Am. J. Cancer Res.* 7, 1285–1297.

Lonial, S., Dimopoulos, M., Palumbo, A., White, D., Grosicki, S., Spicka, I., et al. (2015). Elotuzumab Therapy for Relapsed or Refractory Multiple Myeloma. *N. Engl. J. Med.* 373, 621–631. doi:10.1056/nejmoa1505654

Lonial, S., Jacobus, S., Fonseca, R., Weiss, M., Kumar, S., Orlowski, R. Z., et al. (2020). Randomized Trial of Lenalidomide versus Observation in Smoldering Multiple Myeloma. *Jco* 38, 1126–1137. doi:10.1200/jco.19.01740

Lonial, S., Weiss, B. M., Usmani, S. Z., Singhal, S., Chari, A., Bahlis, N. J., et al. (2016). Daratumumab Monotherapy in Patients with Treatment-Refractory Multiple Myeloma (SIRIUS): an Open-Label, Randomised, Phase 2 Trial. *The Lancet* 387, 1551–1560. doi:10.1016/s0140-6736(15)01120-4

Lu, G., Middleton, R. E., Sun, H., Naniong, M., Ott, C. J., Mitsiades, C. S., et al. (2014). The Myeloma Drug Lenalidomide Promotes the Cereblon-dependent Destruction of Ikaros Proteins. *Science* 343, 305–309. doi:10.1126/science.1244917

Lyon de Ana, C., Arakcheeva, K., Agnihotri, P., Derosia, N., and Winandy, S. (2019). Lack of Ikaros Deregulates Inflammatory Gene Programs in T Cells. *J.I.* 202, 1112–1123. doi:10.4049/jimmunol.1801270

Ma, S., Pathak, S., Trinh, L., and Lu, R. (2008). Interferon Regulatory Factors 4 and 8 Induce the Expression of Ikaros and Aiolos to Down-Regulate Pre-B-cell Receptor and Promote Cell-Cycle Withdrawal in Pre-B-cell Development. *Blood* 111, 1396–1403. doi:10.1182/blood-2007-08-110106

Maciel, A. L. T., Poubel, C. P., Noronha, E. P., Pombo-de-Oliveira, M. S., Mansur, M. B., and Emerenciano, M. (2019). CRLF2 Expression Associates with ICN1

Stabilization in T-cell Acute Lymphoblastic Leukemia. *Genes Chromosomes Cancer* 58, 396–401. doi:10.1002/gcc.22723

Marke, R., Havinga, J., Cloos, J., Demkes, M., Poelmans, G., Yuniati, L., et al. (2016). Tumor Suppressor IKZF1 Mediates Glucocorticoid Resistance in B-Cell Precursor Acute Lymphoblastic Leukemia. *Leukemia* 30, 1599–1603. doi:10.1038/leu.2015.359

Mateos, M.-V., Blacklock, H., Schjesvold, F., Oriol, A., Simpson, D., George, A., et al. (2019). Pembrolizumab Plus Pomalidomide and Dexamethasone for Patients with Relapsed or Refractory Multiple Myeloma (KEYNOTE-183): a Randomised, Open-Label, Phase 3 Trial. *Lancet Haematol.* 6, e459–e469. doi:10.1016/s2352-3026(19)30110-3

Matyskiela, M. E., Lu, G., Ito, T., Pagarigan, B., Lu, C.-C., Miller, K., et al. (2016). A Novel Cereblon Modulator Recruits GSPT1 to the CRL4CRBN Ubiquitin Ligase. *Nature* 535, 252–257. doi:10.1038/nature18611

Matyskiela, M. E., Zhang, W., Man, H.-W., Muller, G., Khambatta, G., Baculi, F., et al. (2018). A Cereblon Modulator (CC-220) with Improved Degradation of Ikaros and Aiolos. *J. Med. Chem.* 61, 535–542. doi:10.1021/acs.jmedchem.6b01921

Mazzurana, L., Forkel, M., Rao, A., Van Acker, A., Kokkinou, E., Ichiya, T., et al. (2019). Suppression of Aiolos and Ikaros Expression by Lenalidomide Reduces Human ILC3–ILC1/NK Cell Transdifferentiation. *Eur. J. Immunol.* 49, 1344–1355. doi:10.1002/eji.201848075

McCarty, A. S., Kleiger, G., Eisenberg, D., and Smale, S. T. (2003). Selective Dimerization of a C2H2 Zinc finger Subfamily. *Mol. Cel.* 11, 459–470. doi:10.1016/s1097-2765(03)00043-1

Mi, J.-Q., Wang, X., Yao, Y., Lu, H.-J., Jiang, X.-X., Zhou, J.-F., et al. (2012). Newly Diagnosed Acute Lymphoblastic Leukemia in China (II): Prognosis Related to Genetic Abnormalities in a Series of 1091 Cases. *Leukemia* 26, 1507–1516. doi:10.1038/leu.2012.23

Michot, J.-M., Bouabdallah, R., Vitolo, U., Doorduijn, J. K., Salles, G., Chiappella, A., et al. (2020). Avadomide Plus Obinutuzumab in Patients with Relapsed or Refractory B-Cell Non-hodgkin Lymphoma (CC-122-NHL-001): a Multicentre, Dose Escalation and Expansion Phase 1 Study. *Lancet Haematol.* 7, e649–e659. doi:10.1016/s2352-3026(20)30208-8

Miguel, J. S., Weisel, K., Moreau, P., Lacy, M., Song, K., Delforge, M., et al. (2013). Pomalidomide Plus Low-Dose Dexamethasone versus High-Dose Dexamethasone Alone for Patients with Relapsed and Refractory Multiple Myeloma (MM-003): a Randomised, Open-Label, Phase 3 Trial. *Lancet Oncol.* 14, 1055–1066. doi:10.1016/s1470-2045(13)70380-2

Mogollón, P., Díaz-Tejedor, A., Algarín, E. M., Paíno, T., Garayoa, M., and Ocio, E. M. (2019). Biological Background of Resistance to Current Standards of Care in Multiple Myeloma. *Cells* 8, 1. doi:10.3390/cells8111432

Molnár, A., and Georgopoulos, K. (1994). The Ikaros Gene Encodes a Family of Functionally Diverse Zinc finger DNA-Binding Proteins. *Mol. Cel. Biol.* 14, 8292–8303. doi:10.1128/mcb.14.12.8292

Montefusco, V., Galli, M., Spina, F., Stefanoni, P., Mussetti, A., Perrone, G., et al. (2014). Autoimmune Diseases during Treatment with Immunomodulatory Drugs in Multiple Myeloma: Selective Occurrence after Lenalidomide. *Leuk. Lymphoma* 55, 2032–2037. doi:10.3109/10428194.2014.914203

Moreau, P., Attal, M., Hulin, C., Arnulf, B., Belhadj, K., Benboubker, L., et al. (2019). Bortezomib, Thalidomide, and Dexamethasone with or without Daratumumab before and after Autologous Stem-Cell Transplantation for Newly Diagnosed Multiple Myeloma (CASSIOPEIA): a Randomised, Open-Label, Phase 3 Study. *The Lancet* 394, 29–38. doi:10.1016/s0140-6736(19)31240-1

Moreau, P., Masszi, T., Grzasko, N., Bahlis, N. J., Hansson, M., Pour, L., et al. (2016). Oral Ixazomib, Lenalidomide, and Dexamethasone for Multiple Myeloma. *N. Engl. J. Med.* 374, 1621–1634. doi:10.1056/nejmoa1516282

Moreira, L. B. P., Queiróz, R. P., Suazo, V. K., Perna, E., Brandalise, S. R., Yunes, J. A., et al. (2019). Detection by a Simple and Cheaper Methodology of Ik6 and Ik10 Isoforms of the IKZF1 Gene Is Highly Associated with a Poor Prognosis in B-Lineage Paediatric Acute Lymphoblastic Leukaemia. *Br. J. Haematol.* 187, e58–e61. doi:10.1111/bjh.16172

Morschhauser, F., Fowler, N. H., Feugier, P., Bouabdallah, R., Tilly, H., Palomba, M. L., et al. (2018). Rituximab Plus Lenalidomide in Advanced Untreated Follicular Lymphoma. *N. Engl. J. Med.* 379, 934–947. doi:10.1056/nejmoa1805104

Mullighan, C. G., Goorha, S., Radtke, I., Miller, C. B., Coustan-Smith, E., Dalton, J. D., et al. (2007). Genome-wide Analysis of Genetic Alterations in Acute Lymphoblastic Leukaemia. *Nature* 446, 758–764. doi:10.1038/nature05690

Mullighan, C. G., Miller, C. B., Radtke, I., Phillips, L. A., Dalton, J., Ma, J., et al. (2008). BCR-ABL1 Lymphoblastic Leukaemia Is Characterized by the Deletion of Ikaros. *Nature* 453, 110–114. doi:10.1038/nature06866

Mullighan, C. G., Su, X., Zhang, J., Radtke, I., Phillips, L. A. A., Miller, C. B., et al. (2009). Deletion ofIKZF1and Prognosis in Acute Lymphoblastic Leukemia. *N. Engl. J. Med.* 360, 470–480. doi:10.1056/nejmoa0808253

Murugesan, A., Lassalle-Claux, G., Hogan, L., Vaillancourt, E., Selka, A., Luiker, K., et al. (2020). Antimyeloma Potential of Caffeic Acid Phenethyl Ester and its Analogues through Sp1 Mediated Downregulation of IKZF1-IRF4-MYC Axis. *J. Nat. Prod.* 83 (12), 3526–3535. doi:10.1021/acs.jnatprod.0c00350

Naik, A. K., Byrd, A. T., Lucander, A. C. K., and Krangel, M. S. (2019). Hierarchical Assembly and Disassembly of a Transcriptionally Active RAG Locus in CD4+CD8+ Thymocytes. *J. Exp. Med.* 216, 231–243. doi:10.1084/jem.20181402

Naito, T., Ushirogawa, H., Fukushima, T., Tanaka, Y., and Saito, M. (2019). EOS, an Ikaros Family Zinc finger Transcription Factor, Interacts with the HTLV-1 Oncoprotein Tax and Is Downregulated in Peripheral Blood Mononuclear Cells of HTLV-1-Infected Individuals, Irrespective of Clinical Statuses. *Virol. J.* 16, 160. doi:10.1186/s12985-019-1270-1

Nakayama, J., Yamamoto, M., Hayashi, K., Satoh, H., Bundo, K., Kubo, M., et al. (2009). BLNK Suppresses Pre-B-cell Leukemogenesis through Inhibition of JAK3. *Blood* 113, 1483–1492. doi:10.1182/blood-2008-07-166355

Naluyima, P., Lal, K. G., Costanzo, M. C., Kijak, G. H., Gonzalez, V. D., Blom, K., et al. (2019). Terminal Effector CD8 T Cells Defined by an IKZF2+IL-7R- Transcriptional Signature Express FcγRIIIA, Expand in HIV Infection, and Mediate Potent HIV-specific Antibody-dependent Cellular Cytotoxicity. *J. Immunol.* 203, 2210–2221. doi:10.4049/jimmunol.1900422

Nera, K.-P., Alinikula, J., Terho, P., Narvi, E., Törnquist, K., Kurosaki, T., et al. (2006). Ikaros Has a Crucial Role in Regulation of B Cell Receptor Signaling. *Eur. J. Immunol.* 36, 516–525. doi:10.1002/eji.200535418

Ng, M. S. F., Roth, T. L., Mendoza, V. F., Marson, A., and Burt, T. D. (2019). Helios Enhances the Preferential Differentiation of Human Fetal CD4+ Naïve T Cells into Regulatory T Cells. *Sci. Immunol.* 4. doi:10.1126/sciimmunol.aav5947

Ochiai, K., Yamaoka, M., Swaminathan, A., Shima, H., Hiura, H., Matsumoto, M., et al. (2020). Chromatin Protein PC4 Orchestrates B Cell Differentiation by Collaborating with IKAROS and IRF4. *Cell Rep.* 33, 108517. doi:10.1016/j.celrep.2020.108517

Ocio, E. M., Fernández-Lázaro, D., San-Segundo, L., López-Corral, L., Corchete, L. A., Gutiérrez, N. C., et al. (2015). *In Vivo* murine Model of Acquired Resistance in Myeloma Reveals Differential Mechanisms for Lenalidomide and Pomalidomide in Combination with Dexamethasone. *Leukemia* 29, 705–714. doi:10.1038/leu.2014.238

Ohguchi, H., Hideshima, T., Bhasin, M. K., Gorgun, G. T., Santo, L., Cea, M., et al. (2016). The KDM3A-KLF2-IRF4 axis Maintains Myeloma Cell Survival. *Nat. Commun.* 7, 10258. doi:10.1038/ncomms10258

Okuyama, K., Strid, T., Kuruvilla, J., Somasundaram, R., Cristobal, S., Smith, E., et al. (2019). PAX5 Is Part of a Functional Transcription Factor Network Targeted in Lymphoid Leukemia. *Plos Genet.* 15, e1008280. doi:10.1371/journal.pgen.1008280

Oliveira, V. C. d., Lacerda, M. P. d., Moraes, B. B. M., Gomes, C. P., Maricato, J. T., Souza, O. F., et al. (2019). Deregulation of Ikaros Expression in B-1 Cells: New Insights in the Malignant Transformation to Chronic Lymphocytic Leukemia. *J. Leukoc. Biol.* 106, 581–594. doi:10.1002/jlb.ma1118-454r

Ossenkoppele, G. J., Breems, D. A., Stuessi, G., van Norden, Y., Bargetzi, M., Biemond, B. J., et al. (2020). Lenalidomide Added to Standard Intensive Treatment for Older Patients with AML and High-Risk MDS. *Leukemia* 34, 1751–1759. doi:10.1038/s41375-020-0725-0

Pan, F., Yu, H., Dang, E. V., Barbi, J., Pan, X., Grosso, J. F., et al. (2009). Eos Mediates Foxp3-dependent Gene Silencing in CD4 + Regulatory T Cells. *Science* 325, 1142–1146. doi:10.1126/science.1176077

Park, S.-M., Cho, H., Thornton, A. M., Barlowe, T. S., Chou, T., Chhangawala, S., et al. (2019). IKZF2 Drives Leukemia Stem Cell Self-Renewal and Inhibits Myeloid Differentiation. *Cell stem cell* 24, 153–165. e7. doi:10.1016/j.stem.2018.10.016

Park, S.-M., Gönen, M., Vu, L., Minuesa, G., Tivnan, P., Barlowe, T. S., et al. (2015). Musashi2 Sustains the Mixed-Lineage Leukemia-Driven Stem Cell Regulatory Program. *J. Clin. Invest.* 125, 1286–1298. doi:10.1172/jci78440

Payne, J. L., Song, C., Ding, Y., Dhanyamraju, P. K., Bamme, Y., Schramm, J. W., et al. (2020). Regulation of Small GTPase Rab20 by Ikaros in B-Cell Acute Lymphoblastic Leukemia. *Int. J. Mol. Sci.* 21. doi:10.3390/ijms21051718

Payne, M. A. (2011). Zinc finger Structure-Function in Ikaros Marvin A Payne. *Wjbc* 2, 161–166. doi:10.4331/wjbc.v2.i6.161

Petzold, G., Fischer, E. S., and Thomä, N. H. (2016). Structural Basis of Lenalidomide-Induced CK1α Degradation by the CRL4CRBN Ubiquitin Ligase. *Nature* 532, 127–130. doi:10.1038/nature16979

Phan, V., Ito, T., Inaba, M., Azuma, Y., Kibata, K., Inagaki-Katashiba, N., et al. (2020). Immunomodulatory Drugs Suppress Th1-Inducing Ability of Dendritic Cells but Enhance Th2-Mediated Allergic Responses. *Blood Adv.* 4, 3572–3585. doi:10.1182/bloodadvances.2019001410

Popescu, M., Gurel, Z., Ronni, T., Song, C., Hung, K. Y., Payne, K. J., et al. (2009). Ikaros Stability and Pericentromeric Localization Are Regulated by Protein Phosphatase 1. *J. Biol. Chem.* 284, 13869–13880. doi:10.1074/jbc.m900209200

Pourabdollah, M., Bahmanyar, M., Atenafu, E. G., Reece, D., Hou, J., and Chang, H. (2016). High IKZF1/3 Protein Expression Is a Favorable Prognostic Factor for Survival of Relapsed/refractory Multiple Myeloma Patients Treated with Lenalidomide. *J. Hematol. Oncol.* 9, 123. doi:10.1186/s13045-016-0354-2

Powell, M. D., Read, K. A., Sreekumar, B. K., and Oestreich, K. J. (2019). Ikaros Zinc Finger Transcription Factors: Regulators of Cytokine Signaling Pathways and CD4+ T Helper Cell Differentiation. *Front. Immunol.* 10, 1299. doi:10.3389/fimmu.2019.01299

Qu, P., Han, J., Qiu, Y., Yu, H., Hao, J., Jin, R., et al. (2019). Huaier Extract Enhances the Treatment Efficacy of Imatinib in Ik6+ Ph+ Acute Lymphoblastic Leukemia. *Biomed. Pharmacother.* 117, 109071. doi:10.1016/j.biopha.2019.109071

Rahmani, M., Fardi, M., Hagh, M. F., Feizi, A. A. H., Talebi, M., and Solali, S. (2019). An Investigation of Methylation Pattern Changes in the IKZF1 Promoter in Patients with Childhood B-Cell Acute Lymphoblastic Leukemia. *Blood Res.* 54, 144–148. doi:10.5045/br.2019.54.2.144

Rasco, D. W., Papadopoulos, K. P., Pourdehnad, M., Gandhi, A. K., Hagner, P. R., Li, Y., et al. (2019). A First-In-Human Study of Novel Cereblon Modulator Avadomide (CC-122) in Advanced Malignancies. *Clin. Cancer Res.* 25, 90–98. doi:10.1158/1078-0432.ccr-18-1203

Richardson, P. G., Oriol, A., Beksac, M., Liberati, A. M., Galli, M., Schjesvold, F., et al. (2019). Pomalidomide, Bortezomib, and Dexamethasone for Patients with Relapsed or Refractory Multiple Myeloma Previously Treated with Lenalidomide (OPTIMISMM): a Randomised, Open-Label, Phase 3 Trial. *Lancet Oncol.* 20, 781–794. doi:10.1016/S1470-2045(19)30152-4

Rieder, S. A., Metidji, A., Glass, D. D., Thornton, A. M., Ikeda, T., Morgan, B. A., et al. (2015). Eos Is Redundant for Regulatory T Cell Function but Plays an Important Role in IL-2 and Th17 Production by CD4+ Conventional T Cells. *J. Immunol.* 195, 553–563. doi:10.4049/jimmunol.1500627

Ronni, T., Payne, K. J., Ho, S., Bradley, M. N., Dorsam, G., and Dovat, S. (2007). Human Ikaros Function in Activated T Cells Is Regulated by Coordinated Expression of its Largest Isoforms. *J. Biol. Chem.* 282, 2538–2547. doi:10.1074/jbc.m605627200

Rosiñol, L., Oriol, A., Rios, R., Sureda, A., Blanchard, M. J., Hernández, M. T., et al. (2019). Bortezomib, Lenalidomide, and Dexamethasone as Induction Therapy Prior to Autologous Transplant in Multiple Myeloma. *Blood* 134, 1337–1345. doi:10.1182/blood.2019000241

Ruan, J., Martin, P., Christos, P., Cerchietti, L., Tam, W., Shah, B., et al. (2018). Five-year Follow-Up of Lenalidomide Plus Rituximab as Initial Treatment of Mantle Cell Lymphoma. *Blood* 132, 2016–2025. doi:10.1182/blood-2018-07-859769

Ruiz, A., Jiang, J., Kempski, H., and Brady, H. J. M. (2004). Overexpression of the Ikaros 6 Isoform Is Restricted to T(4;11) Acute Lymphoblastic Leukaemia in Children and Infants and Has a Role in B-Cell Survival. *Br. J. Haematol.* 125, 31–37. doi:10.1111/j.1365-2141.2004.04854.x

Schafer, P. H., Ye, Y., Wu, L., Kosek, J., Ringheim, G., Yang, Z., et al. (2018). Cereblon Modulator Iberdomide Induces Degradation of the Transcription Factors Ikaros and Aiolos: Immunomodulation in Healthy Volunteers and Relevance to Systemic Lupus Erythematosus. *Ann. Rheum. Dis.* 77, 1516–1523. doi:10.1136/annrheumdis-2017-212916

Schott, C. A., Ascoli, C., Huang, Y., Perkins, D. L., and Finn, P. W. (2020). Declining Pulmonary Function in Interstitial Lung Disease Linked to Lymphocyte Dysfunction. *Am. J. Respir. Crit. Care Med.* 201, 610–613. doi:10.1164/rccm.201910-1909le

Schwickert, T. A., Tagoh, H., Gültekin, S., Dakic, A., Axelsson, E., Minnich, M., et al. (2014). Stage-specific Control of Early B Cell Development by the Transcription Factor Ikaros. *Nat. Immunol.* 15, 283–293. doi:10.1038/ni.2828

Schwickert, T. A., Tagoh, H., Schindler, K., Fischer, M., Jaritz, M., and Busslinger, M. (2019). Ikaros Prevents Autoimmunity by Controlling Anergy and Toll-like Receptor Signaling in B Cells. *Nat. Immunol.* 20, 1517–1529. doi:10.1038/s41590-019-0490-2

Sekeres, M. A., Othus, M., List, A. F., Odenike, O., Stone, R. M., Gore, S. D., et al. (2017). Randomized Phase II Study of Azacitidine Alone or in Combination with Lenalidomide or with Vorinostat in Higher-Risk Myelodysplastic Syndromes and Chronic Myelomonocytic Leukemia: North American Intergroup Study SWOG S1117. *Jco* 35, 2745–2753. doi:10.1200/jco.2015.66.2510

Shaffer, A. L., Emre, N. C. T., Lamy, L., Ngo, V. N., Wright, G., Xiao, W., et al. (2008). IRF4 Addiction in Multiple Myeloma. *Nature* 454, 226–231. doi:10.1038/nature07064

Shafi, A., Rehman, J. U., Nawaz, A., and Aljohani, N. I. (2020). Lenalidomide-induced Interstitial Pneumonitis. *J. Coll. Physicians Surg. Pak* 30, 1117–1118. doi:10.29271/jcpsp.2020.10.1117

Shao, C., Yang, J., Kong, Y., Cheng, C., Lu, W., Guan, H., et al. (2017). Overexpression of Dominant-Negative Ikaros 6 Isoform Is Associated with Resistance to TKIs in Patients with Philadelphia Chromosome Positive Acute Lymphoblastic Leukemia. *Exp. Ther. Med.* 14, 3874–3879. doi:10.3892/etm.2017.4941

Shi, C. X., Kortüm, K. M., Zhu, Y. X., Jedlowski, P., Bruins, L., Braggio, E., et al. (2015). Proteasome Inhibitors Block Ikaros Degradation by Lenalidomide in Multiple Myeloma. *Haematologica* 100, e315–7. doi:10.3324/haematol.2015.124297

Sievers, Q. L., Petzold, G., Bunker, R. D., Renneville, A., Słabicki, M., Liddicoat, B. J., et al. (2018). Defining the Human C2H2 Zinc finger Degrome Targeted by Thalidomide Analogs through CRBN. *Science* 362, eaat0572. doi:10.1126/science.aat0572

Sigvardsson, M. (2018). Molecular Regulation of Differentiation in Early B-Lymphocyte Development. *Int. J. Mol. Sci.* 19. doi:10.3390/ijms19071928

Song, C., Gowda, C., Pan, X., Ding, Y., Tong, Y., Tan, B.-H., et al. (2015). Targeting Casein Kinase II Restores Ikaros Tumor Suppressor Activity and Demonstrates Therapeutic Efficacy in High-Risk Leukemia. *Blood* 126, 1813–1822. doi:10.1182/blood-2015-06-651505

Song, C., Li, Z., Erbe, A. K., Savic, A., and Dovat, S. (2011). Regulation of Ikaros Function by Casein Kinase 2 and Protein Phosphatase 1. *Wjbc* 2, 126–131. doi:10.4331/wjbc.v2.i6.126

Song, C., Pan, X., Ge, Z., Gowda, C., Ding, Y., Li, H., et al. (2016). Epigenetic Regulation of Gene Expression by Ikaros, HDAC1 and Casein Kinase II in Leukemia. *Leukemia* 30, 1436–1440. doi:10.1038/leu.2015.331

Sriaroon, P., Chang, Y., Ujhazi, B., Csomos, K., Joshi, H. R., Zhou, Q., et al. (2019). Familial Immune Thrombocytopenia Associated with a Novel Variant in IKZF1. *Front. Pediatr.* 7, 139. doi:10.3389/fped.2019.00139

Sridharan, R., and Smale, S. T. (2007). Predominant Interaction of Both Ikaros and Helios with the NuRD Complex in Immature Thymocytes. *J. Biol. Chem.* 282, 30227–30238. doi:10.1074/jbc.m702541200

Stanulla, M., Dagdan, E., Zaliova, M., Möricke, A., Palmi, C., Cazzaniga, G., et al. (2018). IKZF1plus Defines a New Minimal Residual Disease-dependent Very-Poor Prognostic Profile in Pediatric B-Cell Precursor Acute Lymphoblastic Leukemia. *Jco* 36, 1240–1249. doi:10.1200/jco.2017.74.3617

Stewart, A. K., Rajkumar, S. V., Dimopoulos, M. A., Masszi, T., Špička, I., Oriol, A., et al. (2015). Carfilzomib, Lenalidomide, and Dexamethasone for Relapsed Multiple Myeloma. *N. Engl. J. Med.* 372, 142–152. doi:10.1056/nejmoa1411321

Swafford, A. D.-E., Howson, J. M. M., Davison, L. J., Wallace, C., Smyth, D. J., Schuilenburg, H., et al. (2011). An Allele ofIKZF1(Ikaros) Conferring Susceptibility to Childhood Acute Lymphoblastic Leukemia Protects against Type 1 Diabetes. *Diabetes* 60, 1041–1044. doi:10.2337/db10-0446

Symonds, E. L., Pedersen, S. K., Murray, D., Byrne, S. E., Roy, A., Karapetis, C., et al. (2020). Circulating Epigenetic Biomarkers for Detection of Recurrent Colorectal Cancer. *Cancer* 126, 1460–1469. doi:10.1002/cncr.32695

Symonds, E. L., Pedersen, S. K., Murray, D. H., Jedi, M., Byrne, S. E., Rabbitt, P., et al. (2018). Circulating Tumour DNA for Monitoring Colorectal Cancer-A Prospective Cohort Study to Assess Relationship to Tissue Methylation, Cancer Characteristics and Surgical Resection. *Clin. Epigenet* 10, 63. doi:10.1186/s13148-018-0500-5

Sznurkowska, K., Luty, J., Bryl, E., Witkowski, J. M., Hermann-Okoniewska, B., Landowski, P., et al. (2020). Enhancement of Circulating and Intestinal T Regulatory Cells and Their Expression of Helios and Neuropilin-1 in Children with Inflammatory Bowel Disease. *Jir* 13, 995–1005. doi:10.2147/jir.s268484

Tacchetti, P., Pantani, L., Patriarca, F., Petrucci, M. T., Zamagni, E., Dozza, L., et al. (2020). Bortezomib, Thalidomide, and Dexamethasone Followed by Double Autologous Haematopoietic Stem-Cell Transplantation for Newly Diagnosed Multiple Myeloma (GIMEMA-MMY-3006): Long-Term Follow-Up Analysis of a Randomised Phase 3, Open-Label Study. *Lancet Haematol.* 7, e861–e873. doi:10.1016/s2352-3026(20)30323-9

Tachita, T., Kinoshita, S., Ri, M., Aoki, S., Asano, A., Kanamori, T., et al. (2020). Expression, Mutation, and Methylation of Cereblon-pathway Genes at Pre- and post-lenalidomide Treatment in Multiple Myeloma. *Cancer Sci.* 111, 1333–1343. doi:10.1111/cas.14352

Tang, S. H., Lu, Y., Zhang, P. S., Liu, X. H., Du, X. H., Chen, D., et al. (2019). [Ikaros Family Zinc finger 1 Mutation Is a Poor Prognostic Factor for Adult Philadelphia Chromosome Positive Acute Lymphoblastic Leukemia]. *Zhonghua nei ke za zhi* 58, 301–306. doi:10.3760/cma.j.issn.0578-1426.2019.04.012

Tayel, S. I., El-Hefnway, S. M., Abo El-Fotoh, W. M. M., and El-Zayat, R. S. (2019). The Genetic Variants of IKZF1 Gene Linked with the Growing Risk of Childhood Acute Lymphoblastic Leukaemia. *Cmm* 19, 32–39. doi:10.2174/1566524019666190219123900

Theocharides, A. P. A., Dobson, S. M., Laurenti, E., Notta, F., Voisin, V., Cheng, P.-Y., et al. (2015). Dominant-negative Ikaros Cooperates with BCR-ABL1 to Induce Human Acute Myeloid Leukemia in Xenografts. *Leukemia* 29, 177–187. doi:10.1038/leu.2014.150

Thieblemont, C., Tilly, H., Gomes da Silva, M., Casasnovas, R.-O., Fruchart, C., Morschhauser, F., et al. (2017). Lenalidomide Maintenance Compared with Placebo in Responding Elderly Patients with Diffuse Large B-Cell Lymphoma Treated with First-Line Rituximab Plus Cyclophosphamide, Doxorubicin, Vincristine, and Prednisone. *Jco* 35, 2473–2481. doi:10.1200/jco.2017.72.6984

Thornton, A. M., and Shevach, E. M. (2019). Helios: Still behind the Clouds. *Immunology* 158, 161–170. doi:10.1111/imm.13115

Tsukamoto, T., Nakahata, S., Sato, R., Kanai, A., Nakano, M., Chinen, Y., et al. (2020). BRD4-Regulated Molecular Targets in Mantle Cell Lymphoma: Insights into Targeted Therapeutic Approach. *Cancer Genomics Proteomics* 17, 77–89. doi:10.21873/cgp.20169

Uckun, F. M., Ma, H., Zhang, J., Ozer, Z., Dovat, S., Mao, C., et al. (2012). Serine Phosphorylation by SYK Is Critical for Nuclear Localization and Transcription Factor Function of Ikaros. *Proc. Natl. Acad. Sci.* 109, 18072–18077. doi:10.1073/pnas.1209828109

Usmani, S. Z., Hoering, A., Ailawadhi, S., Sexton, R., Lipe, B., Hita, S. F., et al. (2021). Bortezomib, Lenalidomide, and Dexamethasone with or without Elotuzumab in Patients with Untreated, High-Risk Multiple Myeloma (SWOG-1211): Primary Analysis of a Randomised, Phase 2 Trial. *Lancet Haematol.* 8, e45–e54. doi:10.1016/s2352-3026(20)30354-9

Usmani, S. Z., Nahi, H., Plesner, T., Weiss, B. M., Bahlis, N. J., Belch, A., et al. (2020). Daratumumab Monotherapy in Patients with Heavily Pretreated Relapsed or Refractory Multiple Myeloma: Final Results from the Phase 2 GEN501 and SIRIUS Trials. *Lancet Haematol.* 7, e447–e455. doi:10.1016/s2352-3026(20)30081-8

Usmani, S. Z., Schjesvold, F., Oriol, A., Karlin, L., Cavo, M., Rifkin, R. M., et al. (2019). Pembrolizumab Plus Lenalidomide and Dexamethasone for Patients with Treatment-Naive Multiple Myeloma (KEYNOTE-185): a Randomised, Open-Label, Phase 3 Trial. *Lancet Haematol.* 6, e448–e458. doi:10.1016/s2352-3026(19)30109-7

Vairy, S., and Tran, T. H. (2020). IKZF1 Alterations in Acute Lymphoblastic Leukemia: The Good, the Bad and the Ugly. *Blood Rev.* 44, 100677. doi:10.1016/j.blre.2020.100677

Verhoeven, R. J. A., Tong, S., Mok, B. W.-Y., Liu, J., He, S., Zong, J., et al. (2019). Epstein-Barr Virus BART Long Non-coding RNAs Function as Epigenetic Modulators in Nasopharyngeal Carcinoma. *Front. Oncol.* 9, 1120. doi:10.3389/fonc.2019.01120

Vitale, C., Falchi, L., Ten Hacken, E., Gao, H., Shaim, H., Van Roosbroeck, K., et al. (2016). Ofatumumab and Lenalidomide for Patients with Relapsed or Refractory Chronic Lymphocytic Leukemia: Correlation between Responses and Immune Characteristics. *Clin. Cancer Res.* 22, 2359–2367. doi:10.1158/1078-0432.ccr-15-2476

Vivier, E., Artis, D., Colonna, M., Diefenbach, A., Di Santo, J. P., Eberl, G., et al. (2018). Innate Lymphoid Cells: 10 Years on. *Cell* 174, 1054–1066. doi:10.1016/j.cell.2018.07.017

Voorhees, P. M., Kaufman, J. L., Laubach, J., Sborov, D. W., Reeves, B., Rodriguez, C., et al. (2020). Daratumumab, Lenalidomide, Bortezomib, and Dexamethasone for Transplant-Eligible Newly Diagnosed Multiple Myeloma: the GRIFFIN Trial. *Blood* 136, 936–945. doi:10.1182/blood.2020005288

Wang, H., Xu, Z., Du, W., Lin, Z., and Liu, Z. (2019). N160 of Aiolos Determines its DNA-Binding Activity. *Anat. Rec. (Hoboken)* 302, 2014–2019. doi:10.1002/ar.24213

Wang, H., Song, C., Ding, Y., Pan, X., Ge, Z., Tan, B.-H., et al. (2016). Transcriptional Regulation of JARID1B/KDM5B Histone Demethylase by Ikaros, Histone Deacetylase 1 (HDAC1), and Casein Kinase 2 (CK2) in B-Cell Acute Lymphoblastic Leukemia. *J. Biol. Chem.* 291, 4004–4018. doi:10.1074/jbc.m115.679332

Wang, H., Song, C., Gurel, Z., Song, N., Ma, J., Ouyang, H., et al. (2014). Protein Phosphatase 1 (PP1) and Casein Kinase II (CK2) Regulate Ikaros-Mediated Repression ofTdTin Thymocytes and T-Cell Leukemia. *Pediatr. Blood Cancer* 61, 2230–2235. doi:10.1002/pbc.25221

Wang, M. L., Rule, S., Martin, P., Goy, A., Auer, R., Kahl, B. S., et al. (2013). Targeting BTK with Ibrutinib in Relapsed or Refractory Mantle-Cell Lymphoma. *N. Engl. J. Med.* 369, 507–516. doi:10.1056/nejmoa1306220

Wang, M., Rule, S., Zinzani, P. L., Goy, A., Casasnovas, O., Smith, S. D., et al. (2018). Acalabrutinib in Relapsed or Refractory Mantle Cell Lymphoma (ACE-LY-004): a Single-Arm, Multicentre, Phase 2 Trial. *The Lancet* 391, 659–667. doi:10.1016/s0140-6736(17)33108-2

Wang, Y., Zheng, X., Wang, Q., Zheng, M., and Pang, L. (2020). GSK3β-Ikaros-ANXA4 Signaling Inhibits High-Glucose-Induced Fibroblast Migration. *Biochem. biophysical Res. Commun.* 531, 543–551. doi:10.1016/j.bbrc.2020.07.142

Wang, Z., Zhou, G., Risu, N., Fu, J., Zou, Y., Tang, J., et al. (2020). Lenalidomide Enhances CAR-T Cell Activity against Solid Tumor Cells. *Cell Transpl.* 29, 963689720920825. doi:10.1177/0963689720920825

Winandy, S., Wu, P., and Georgopoulos, K. (1995). A Dominant Mutation in the Ikaros Gene Leads to Rapid Development of Leukemia and Lymphoma. *Cell* 83, 289–299. doi:10.1016/0092-8674(95)90170-1

Won, H. R., Lee, D. H., Yeon, S. K., Ryu, H. W., Kim, G. W., and Kwon, S. H. (2019). HDAC6-selective I-nhibitor S-ynergistically E-nhances the A-nticancer A-ctivity of I-mmunomodulatory D-rugs in M-ultiple M-yeloma. *Int. J. Oncol.* 55, 499–512. doi:10.3892/ijo.2019.4828

Xiao, G., Chan, L. N., Klemm, L., Braas, D., Chen, Z., Geng, H., et al. (2018). B-Cell-Specific Diversion of Glucose Carbon Utilization Reveals a Unique Vulnerability in B Cell Malignancies. *Cell* 173, 470–484. e18. doi:10.1016/j.cell.2018.02.048

Yamamoto, E., Ito, T., Abe, A., Sido, F., Ino, K., Itakura, A., et al. (2005). Ikaros Is Expressed in Human Extravillous Trophoblasts and Involved in Their Migration and Invasion. *Mol. Hum. Reprod.* 11, 825–831. doi:10.1093/molehr/gah239

Yang, M., Liu, Y., Mo, B., Xue, Y., Ye, C., Jiang, Y., et al. (2019). Helios but Not CD226, TIGIT and Foxp3 Is a Potential Marker for CD4+ Treg Cells in Patients with Rheumatoid Arthritis. *Cell Physiol Biochem* 52, 1178–1192. doi:10.33594/000000080

Yasuda, T., Maeda, A., Kurosaki, M., Tezuka, T., Hironaka, K., Yamamoto, T., et al. (2000). Cbl Suppresses B Cell Receptor-Mediated Phospholipase C (Plc)-Γ2 Activation by Regulating B Cell Linker Protein-Plc-Γ2 Binding. *J. Exp. Med.* 191, 641–650. doi:10.1084/jem.191.4.641

Yeoh, A. E. J., Lu, Y., Chin, W. H. N., Chiew, E. K. H., Lim, E. H., Li, Z., et al. (2018). Intensifying Treatment of Childhood B-Lymphoblastic Leukemia with IKZF1 Deletion Reduces Relapse and Improves Overall Survival: Results of Malaysia-Singapore ALL 2010 Study. *Jco* 36, 2726–2735. doi:10.1200/jco.2018.78.3050

Yu, W.-Q., Ji, N.-F., Gu, C.-J., Sun, Z.-X., Wang, Z.-X., Chen, Z.-Q., et al. (2019). Downregulation of miR-4772-3p Promotes Enhanced Regulatory T Cell Capacity in Malignant Pleural Effusion by Elevating Helios Levels. *Chin. Med. J.* 132, 2705–2715. doi:10.1097/cm9.0000000000000517

Yuan, T., Yang, Y., Chen, J., Li, W., Li, W., Zhang, Q., et al. (2017). Regulation of PI3K Signaling in T-Cell Acute Lymphoblastic Leukemia: a Novel PTEN/Ikaros/miR-26b Mechanism Reveals a Critical Targetable Role for PIK3CD. *Leukemia* 31, 2355–2364. doi:10.1038/leu.2017.80

Zeidner, J. F., Knaus, H. A., Zeidan, A. M., Blackford, A. L., Montiel-Esparza, R., Hackl, H., et al. (2020). Immunomodulation with Pomalidomide at Early Lymphocyte Recovery after Induction Chemotherapy in Newly Diagnosed AML and High-Risk MDS. *Leukemia* 34, 1563–1576. doi:10.1038/s41375-019-0693-4

Zhang, X., Zhang, X., Li, X., Lv, Y., Zhu, Y., Wang, J., et al. (2020). The Specific Distribution Pattern of IKZF1 Mutation in Acute Myeloid Leukemia. *J. Hematol. Oncol.* 13, 140. doi:10.1186/s13045-020-00972-5

Zhao, W., Chen, T. B., and Wang, H. (2020). Ikaros Is Heterogeneously Expressed in Lung Adenocarcinoma and Is Involved in its Progression. *J. Int. Med. Res.* 48, 300060520945860. doi:10.1177/0300060520945860

Zheng, J., Sha, Y., Roof, L., Foreman, O., Lazarchick, J., Venkta, J. K., et al. (2019). Pan-PIM Kinase Inhibitors Enhance Lenalidomide's Anti-myeloma Activity via Cereblon-Ikzf1/3 cascade. *Cancer Lett.* 440-441, 1–10. doi:10.1016/j.canlet.2018.10.003

Zhou, H., Yan, Y., Zhang, X., Zhao, T., Xu, J., and Han, R. (2020). Ginseng Polysaccharide Inhibits MDA-MB-231 Cell Proliferation by Activating the Inflammatory Response. *Exp. Ther. Med.* 20, 229. doi:10.3892/etm.2020.9359

Zhou, N., Gutierrez-Uzquiza, A., Zheng, X. Y., Chang, R., Vogl, D. T., Garfall, A. L., et al. (2019). RUNX Proteins Desensitize Multiple Myeloma to Lenalidomide via Protecting IKZFs from Degradation. *Leukemia* 33, 2006–2021. doi:10.1038/s41375-019-0403-2

Zhu, Y. X., Braggio, E., Shi, C.-X., Kortuem, K. M., Bruins, L. A., Schmidt, J. E., et al. (2014). Identification of Cereblon-Binding Proteins and Relationship with Response and Survival after IMiDs in Multiple Myeloma. *Blood* 124, 536–545. doi:10.1182/blood-2014-02-557819

Zhu, Y. X., Shi, C.-X., Bruins, L. A., Wang, X., Riggs, D. L., Porter, B., et al. (2019). Identification of Lenalidomide Resistance Pathways in Myeloma and Targeted Resensitization Using Cereblon Replacement, Inhibition of STAT3 or Targeting of IRF4. *Blood Cancer J.* 9, 19. doi:10.1038/s41408-019-0173-0

Zou, J., Jones, R. J., Wang, H., Kuiatse, I., Shirazi, F., Manasanch, E. E., et al. (2020). The Novel Protein Homeostatic Modulator BTX306 Is Active in Myeloma and Overcomes Bortezomib and Lenalidomide Resistance. *J. Mol. Med.* 98, 1161–1173. doi:10.1007/s00109-020-01943-6

Conflict of Interest: The authors declare that the research was conducted in the absence of any commercial or financial relationships that could be construed as a potential conflict of interest.

Publisher's Note: All claims expressed in this article are solely those of the authors and do not necessarily represent those of their affiliated organizations, or those of the publisher, the editors and the reviewers. Any product that may be evaluated in this article, or claim that may be made by its manufacturer, is not guaranteed or endorsed by the publisher.

GLOSSARY

TF transcription factor
IKZF IKAROS family zinc finger
AML acute myeloid leukemia
Len lenalidomide
MM multiple myeloma
BCP-ALL pediatric B-cell precursor acute lymphoblastic leukemia
ALL acute lymphoblastic leukemia
CRBN cereblon
MCL mantle cell lymphoma
IMiDs immunomodulatory drugs
MDS myelodysplastic syndrome
CLL chronic lymphocytic leukemia
NuRD nucleosome remodeling and deacetylase complex
HDAC histone deacetylase complexes
PP1 protein phosphatase 1 protein phosphatase 1α
PI3K phosphatidylinositol-3 kinase
BCR B-cell receptor
TCR T-cell receptor
IRF interferon regulatory factor
SUMOylation small ubiquitin-related modifier
RUNX runt-related transcription factor family
CK2 carcinogenic casein kinase II
ILC innate lymphoid cell
TH T helper cell
Treg T regulated cell
KDM5B lysine [K]-specific demethylase 5B
PHF2 PHD finger protein 2
ARID5B AT-rich interactive domain-containing protein 5B
G6PD glucose-6-phosphate dehydrogenase
JAK-STAT Janus kinase-signal transducer and activator of transcription
IL7R interleukin-7 receptor
BCL6 B-cell lymphoma 6
BACH2 basic leucine zipper transcription factor 2
RAG recombination-activating gene
KLF2 Krüppel-like factor 2
Blimp-1 B lymphocyte maturation inducing protein-1
CAR T-cell chimeric antigen receptor T-cell
CELMoDs CRBN E3 ligase modulating drugs
SLL small lymphocytic lymphoma
RRMM relapsed/refractory multiple myeloma
NDMM newly diagnosed multiple myeloma
BTZ bortezomib
BTK Bruton tyrosine kinase
BRD4 bromodomain-containing protein 4
PAX5 paired box 5

frontiers in Cell and Developmental Biology

REVIEW
published: 20 December 2021
doi: 10.3389/fcell.2021.750084

Current Research Progress of the Role of LncRNA LEF1-AS1 in a Variety of Tumors

Qingyuan Zheng[1,2,3,4], *Xiao Yu*[1,2,3,4], *Menggang Zhang*[1,2,3,4], *Shuijun Zhang*[1,2,3,4], *Wenzhi Guo*[1,2,3,4]* and *Yuting He*[1,2,3,4]*

[1]Department of Hepatobiliary and Pancreatic Surgery, The First Affiliated Hospital of Zhengzhou University, Zhengzhou, China, [2]Key Laboratory of Hepatobiliary and Pancreatic Surgery and Digestive Organ Transplantation of Henan Province, The First Affiliated Hospital of Zhengzhou University, Zhengzhou, China, [3]Open and Key Laboratory of Hepatobiliary and Pancreatic Surgery and Digestive Organ Transplantation at Henan Universities, Zhengzhou, China, [4]Henan Key Laboratory of Digestive Organ Transplantation, Zhengzhou, China

Long non-coding RNAs (lncRNA), as key regulators of cell proliferation and death, are involved in the regulation of various processes in the nucleus and cytoplasm, involving biological developmental processes in the fields of immunology, neurobiology, cancer, and stress. There is great scientific interest in exploring the relationship between lncRNA and tumors. Many researches revealed that lymph enhancer-binding factor 1-antisense RNA 1 (LEF1-AS1), a recently discovered lncRNA, is downregulated in myeloid malignancy, acting mainly as a tumor suppressor, while it is highly expressed and carcinogenic in glioblastoma (GBM), lung cancer, hepatocellular carcinoma (HCC), osteosarcoma, colorectal cancer (CRC), oral squamous cell carcinoma (OSCC), prostatic carcinoma, retinoblastoma, and other malignant tumors. Furthermore, abnormal LEF1-AS1 expression was associated with tumorigenesis, development, survival, and prognosis via the regulation of target genes and signaling pathways. This review summarizes the existing data on the expression, functions, underlying mechanism, relevant signaling pathways, and clinical significance of LEF1-AS1 in cancer. It is concluded that LEF1-AS1 can serve as a novel biomarker for the diagnosis and prognosis of various tumors, thus deserves further attention in the future.

Keywords: long non-coding RNA, LEF1-AS1, cancer biomarker, function, molecular mechanism

OPEN ACCESS

Edited by:
José Alexandre Ferreira, Portuguese Oncology Institute, Portugal

Reviewed by:
Salvatrice Mancuso, Division of Hematology, University of Palermo, Italy
Manal S. Fawzy, Suez Canal University, Egypt

***Correspondence:**
Wenzhi Guo
fccguowz@zzu.edu.cn
Yuting He
fccheyt1@zzu.edu.cn

Specialty section:
This article was submitted to Molecular and Cellular Pathology, a section of the journal Frontiers in Cell and Developmental Biology

Received: *30 July 2021*
Accepted: *06 December 2021*
Published: *20 December 2021*

Citation:
Zheng Q, Yu X, Zhang M, Zhang S, Guo W and He Y (2021) Current Research Progress of the Role of LncRNA LEF1-AS1 in a Variety of Tumors. Front. Cell Dev. Biol. 9:750084. doi: 10.3389/fcell.2021.750084

INTRODUCTION

Cancer is a major global public health problem (Siegel et al., 2020; Li N. et al., 2021; Leyva-González et al., 2021), which has become the leading cause of death in China (Li T. et al., 2020). Recently, the morbidity and mortality of cancer have been clearly on the rise in the country, comprising a significant health burden that it is likely to further increase (Islami et al., 2017). Altered gene expression is a major feature of many cancers, thus it has been extensively studied. RNAs are essential for gene expression (Yin et al., 2017), whether they are protein-encoded RNAs (mRNAs) or non-encoded RNAs involved in the regulation of transcription, such as long noncoding RNAs (lncRNAs) (Goodall and Wickramasinghe, 2021). In recent years, there has been a great deal of research into the role of lncRNAs in malignant tumors (Li G. et al., 2021; Guo et al., 2021; Hou and Peng, 2021; Teng et al., 2021), which proved that lncRNAs are key regulators of cancer-associated pathways and thus are important disease biomarkers (Liu S. J. et al., 2021).

Long-chain non-coding RNAs are a group of RNA molecules, which are over 200 nucleotides long and lack the protein coding function (Silva et al., 2019; Wang P.-S. et al., 2021). They are involved in a series of processes that regulate tumor biology, and play important roles in regulating oncogenes or tumor suppressor genes (Huang et al., 2017). Researchers have reported the abnormal expression of lncRNAs in a variety of cancers, indicating their important role in regulating cancer cell proliferation, chemotherapy resistance, and metastasis. For example, LINC00504 is upregulated and promotes tumor cell proliferation and migration in breast cancer (Hou et al., 2021). LncRNAs are often used as competitive endogenous RNA (ceRNA) to regulate gene expression by specifically sponging the corresponding microRNA to establish a large regulatory system across the transcriptome (Wang X. et al., 2021; Chen et al., 2021). The regulated target genes are widely involved in multiple signaling pathways, most of which are closely related to tumors (Gao et al., 2021).

LEF1 (lymph enhancer-binding factor 1), also known as a nuclear transcription factor, is normally expressed in T cells and pro-B cells (Kühnl et al., 2011). LEF1 antisense RNA 1 (LEF1-AS1) is a recently discovered lncRNA located in the 4q25 chromosome and encoded in the lymphoid enhancer-binding factor 1 (LEF1) locus. LEF1 was shown to be highly expressed in several cancer types, such as ovarian cancer (Zhang and Ruan, 2020), lung cancer (Wang et al., 2019), and liver cancer (Gao et al., 2020), etc., and regulate tumor development and progression. Besides, LEF1 could increase the osteogenic differentiation of dental pulp stem cells through the regulation of miR-24-3p (Wu et al., 2020). LEF1-AS1 can also regulate the proliferation and migration of vascular smooth muscle cells by targeting the miR-544a/PTEN axis (Zhang L. et al., 2019). Moreover, LEF1-AS1 is a conserved transcript of hematopoietic dysfunction. Studies have indicated that it is associated with higher-risk myelodysplastic syndrome (Szikszai et al., 2020).

This review mainly discusses the biological functions of LEF1-AS1 and the related molecular mechanisms in a variety of different tumors, primarily elaborating on clinical and animal models, as well as cell experiments, and focusing on summarizing the clinical significance of LEF1-AS1, its functions in tumors, and the related signaling pathways. Several major pathways associated with LEF1-AS1 are further discussed. This paper intends to provide a reference for finding new and feasible targets for tumor treatment and assist with the search for biomarkers.

STUDIES ON LEF1-AS1 USING CLINICAL PATIENTS, ANIMAL MODELS AND CELL EXPERIMENTS

A large number of studies have reported that LEF1-AS1 is abnormally expressed in various human cancers, essentially manifested as increased expression, which was often associated with the poor prognosis of tumors. In addition, LEF1-AS1 was shown to play a key role in a variety of biological processes, such as proliferation (Xiang et al., 2020), invasion (Wang et al., 2019; Xiang et al., 2020), migration, angiogenesis (Li W. et al., 2020; Dong et al., 2020), and apoptosis. On this basis, we consider the research progress on the role of LEF1-AS1 in tumors from the perspectives of clinical patients, mouse models and cell experiments.

HUMAN STUDIES

Clinical studies have shown that LEF1-AS1 expression is significantly increased in a variety of malignant tumors, and is closely related to tumor size, TNM staging, histological grade, lymph node metastasis, and overall survival (OS). Most of these studies have used adjacent normal tissues as control (**Supplementary Table S1**).

Glioma

Glioma is one of the most prevalent types of primary intracranial carcinoma, which includes astrocytoma, glioblastoma multiform (GBM), oligodendrogliomas, and mixed tumors (Peng et al., 2018; Zhang et al., 2021). In particular, GBM has a high degree of malignancy, rapid clinical course, poor prognosis, and a median survival time of fewer than 1.5 years. Currently, there is no effective targeted therapy for GBM (Osswald et al., 2015). Many studies have shown that abnormal gene expression is pivotal in the development of glioma (Steponaitis et al., 2016), which is accompanied by the increase of abnormal expression of functional lncRNAs. Chen et al. pointed out that the TCGA database and the comparison of cancerous and paracancerous tissues of 40 patients with glioma showed that LEF1-AS1 was significantly upregulated in cancer tissues, and this was significantly associated with the poor survival rate of GBM patients, indicating the potential malignancy roles of LEF1-AS1 in glioma (Cheng Z. et al., 2020). Other studies have also confirmed that LEF1-AS1 was abnormally expressed in GBM, and the 5-year OS period of GBM patients with high LEF1-AS1 expression was significantly shortened ($p < 0.0001$) (Wang et al., 2017).

Lung Cancer

The leading cause of cancer-related deaths is lung cancer worldwide (Thai et al., 2021), which is classified into two major histological types: small cell lung cancer (SCLC) and non-small cell lung cancer (NSCLC) (Tan et al., 2016). LncRNAs were recently identified as the primary regulators of initiation, progression, and therapeutic response in a variety of cancers (Zhang et al., 2013). Many studies have shown that LEF1-AS1 is highly expressed in lung cancer, has oncogenic function, and may be a potential target for research and treatment (Wang et al., 2019; Yang et al., 2019; Xiang et al., 2020).

To investigate the role of LEF1-AS1 in lung cancer, the expression of LEF1-AS1 in lung cancer specimens and normal tissues adjacent to cancer was first detected by qRT-PCR. Wang et al. found that the expression level of LEF1-AS1 in tumor tissues was significantly higher than that in paracancerous tissues. Further studies have proved that the overall survival rate of patients with high LEF1-AS1 expression is much lower than

that of patients with low LEF1-AS1 expression (Wang et al., 2019). Yang and his team also pointed out that the upregulation of LEF1-AS1 in NSCLC tissues affects the prognosis of patients with NSCLC; the group with high LEF1-AS1 was significantly correlated with tumor size ($p = 0.037$) and TNM stage ($p = 0.04$) (Yang et al., 2019).

Hepatocellular Carcinoma

The most common form of liver cancer is HCC, which accounts for approximately 90% of cases (Llovet et al., 2021). According to global cancer statistics, HCC is the fifth most common cancer and the third most common cause of cancer-related deaths (Jiang et al., 2019; Thuluvath et al., 2021). From a strictly oncologic standpoint, liver transplantation is the best treatment for HCC that is confined to the liver. However, this approach is unsuitable for a wide range of HCC patients due to its high cost and limited ligands (Vibert et al., 2020). Therefore, further studies are urgently needed to determine the best therapeutic regimen for HCC. LncRNAs have been recognized as cancer-related biomolecules that contribute to the progression of HCC. A recent study found that LEF1-AS1 has a significantly higher expression in HCC tissues in comparison to adjacent normal tissues. The relationship between lncRNA LEF1-AS1 expression and clinicopathological parameters was analyzed, and the results showed that the expression of lncRNA LEF1-AS1 was significantly correlated with TNM staging, tumor size, and lymph node metastasis. Meanwhile, it had little correlation with age and gender (Dong et al., 2020).

Colorectal Cancer

Increasing evidence suggests that lncRNAs participate in diverse cancers. Among these, LEF1-AS1 was recently recognized as an oncogenic lncRNA in CRC (Chen et al., 2017). Colorectal cancers are some of the most common cancers worldwide, with more than one million new cases diagnosed each year (Siegel et al., 2018). Among them, colon cancer is the third globally most common malignant tumor in men and the second most common malignant tumor in women, with nearly 1.2 million new cases and 600,000 deaths each year (Ku et al., 2012). The morbidity and mortality associated with CRC in China are increasing year by year. The high mortality rate is due to the late diagnosis and rapid metastasis (Siegel et al., 2017a). In order to improve the early diagnosis rate of CRC and reduce its high metastatic rate, it is crucial to screen new biomarkers that can predict the diagnosis and treatment of CRC, and improve its prognosis.

Dysregulated lncRNA spectrum and metastasis-related lncRNA were identified in colorectal cancer through genome-wide analysis, and it was found that LEF1-AS1 expression might be closely linked to the development of colorectal cancer. Successive studies were then performed on LEF1-AS1 and CRC. Shi et al. collected 91 CRC tissue samples and 60 plasma samples to evaluate the expression of LEF1-AS1. The results showed the upregulation of LEF1-AS1 expression. In addition, the expression of LEF1-AS1 in CRC tissues was significantly correlated with the expression of lymph node metastasis and Ki67. Plasma LEF1-AS1 expression was also associated with carcinoembryonic antigen (CEA) levels. Further studies found that the OS and DFS of CRC patients with higher expression levels of LEF1-AS1 were significantly shorter (Shi et al., 2019). Other studies have also supported these findings, and pointed out that high LEF1-AS1 levels are also significantly related to higher histological grades and Dukes stages (Cheng Y. et al., 2020; Sun et al., 2020).

Oral Squamous Cell Carcinoma

OSCC, as one of the most common malignancies that originate in the oral mucosa, is the main component of oral cancer (Siegel et al., 2014; Chai et al., 2020), and presents a very high mortality rate and extremely low survival rate (Huang et al., 2020). Zhang et al. explored the connection between LEF1-AS1 and OSCC (Zhang C. et al., 2019). First, they evaluated the expression of LEF1-AS1 in OSCC tumor tissue and adjacent normal tissues. The results revealed that the expression of LEF1-AS1 was upregulated in OSCC tissues, and this was closely related to poor prognosis. In addition, the expression of LEF1-AS1 was found to be associated with tumor staging. These results suggest that LEF1-AS1 may be a prognostic marker of OSCC.

Ovarian Cancer

One of the most common gynecological tumors causing death in women is ovarian cancer (Yokoi et al., 2018), which often has poor prognosis, and most women are diagnosed at an advanced stage (Menon et al., 2021). The role of lncRNAs in cancer development has received growing attention. Zhang and his team (Zhang and Ruan, 2020) found that LEF1-AS1 was closely related to OC, regulating its occurrence and development. They collected 62 pairs of OC tissues and adjacent non-tumor controls, and found increased levels of LEF1-AS1 in ovarian cancer tissues. In addition, LEF1-AS1 was highly expressed in ovarian cancer tissues with lymph node metastasis and advanced stage, and patients with high LEF1-AS1 expression had low overall survival.

Esophageal Squamous Cell Carcinoma

Esophageal cancer is globally the eighth most common tumor and the sixth leading cause of tumor-related deaths (Siegel et al., 2017b). In China, the main histological type of esophageal cancer is esophageal squamous cell carcinoma (ESCC), which is a type of cancer with poor prognosis and a limited understanding of its molecular etiology (Li B. et al., 2021). Recently, lncRNA LEF1-AS1 has been shown to be dysfunctional in many cancer types. The evaluation of the level and function of LEF1-AS1 in ESCC showed that LEF1-AS1 upregulation was observed in 136 (73.5%) cases of ESCC specimens. LEF1-AS1 expression was associated with clinical stage ($p = 0.008$) and lymph nodes metastasis ($p = 0.009$), and higher LEF1-AS1 expressions were correlated with poor prognosis in ESCC patients. The results of univariate and multivariate analyses to further determine the prognostic impact of LEF1-AS1 expression indicated that LEF1-AS1 can be regarded as an independent poor prognostic factor of ESCC (Zong et al., 2019).

Other Cancers

Certain studies reported a significant overexpression of LEF1-AS1 in osteosarcoma, prostate cancer, and retinoblastoma (Liu

et al., 2019; Li W. et al., 2020; He and Qin, 2020; Lu et al., 2020). He et al. pointed out that high expression of LEF1-AS1 predicted poor prognosis in retinoblastoma. They found that LEF1-AS1 expression levels in retinoblastoma and IIRC D-E patients were remarkably increased compared with IIRC A-C patients. In addition, LEF1-AS1 has been reported to be downregulated in bone marrow-related disorders, while no specific clinical studies have been conducted (Congrains-Castillo et al., 2019; Szikszai et al., 2020).

IN VIVO STUDIES

Increasing evidences have demonstrated the effects of LEF1-AS1 silencing or over-expression in xenograft animal models. In lung cancer, the tumor size of sh-LEF1-AS1 was significantly smaller compared to the control group, and Ki-67 expression was also significantly reduced (Wang et al., 2019). Yang et al. evaluated the *in vivo* metastatic efficacy of LEF1-AS1 in a mouse model, and more metastatic nodules were detected in the mice injected with LEF1-AS1-overexpressed A549 cells group compared with those of the control group, implying that LEF1-AS1 could serve as an oncogenic driver in the pathogenesis of NSCLC (Yang et al., 2019). In colorectal cancer, researchers injected LEF1-AS1 into nude mice and then monitored the growth of tumor xenografts. They found that LEF1-AS1 may be beneficial to tumor growth and lung metastasis *in vivo* (Sun et al., 2020). Qi et al. also confirmed the tumorigenic effect of LEF1-AS1 in colorectal cancer (Qi et al., 2021). In terms of HCC, *in vivo* experiments on tumor-bearing nude mice exhibiting positive WNK1 expression confirmed the interference effect of lncRNA LEF1-AS1 on HCC (Dong et al., 2020). In addition, studies on OSCC (Zhang C. et al., 2019), prostatic carcinoma (Liu et al., 2019; Li W. et al., 2020), ESCC (Zong et al., 2019), glioma (Cheng Z. et al., 2020), and GBM (Wang et al., 2017) indicated that LEF1-AS1 can promote tumor formation *in vivo*.

CELL LINE STUDIES

LncRNAs can function as ceRNAs targeting specific microRNAs and then acting through complex molecular mechanisms. We have already discussed the level of LEF1-AS1 in different kinds of cancer and its clinical-pathological features above, and *in vivo* experiments have further verified the tumorigenic effect of LEF1-AS1. In the following sections, we aim to describe the role and related mechanisms of this lncRNA in different cancer cell lines (**Supplementary Table S2**).

Glioma

Cheng et al. pointed out that the expression level of LEF1-AS1 was markedly elevated in cell lines, which is consistent with the results for glioma tissues. Besides, the knockdown of LEF1-AS1 could inhibit tumor cell proliferation while activating apoptosis in glioma cells *in vitro*. This was primarily achieved through the upregulation of HIGD1A expression by targeting miR-489-3p (Cheng Z. et al., 2020). In GBM, researchers also found that low LEF1-AS1 gene knockout significantly inhibited the growth state of GBM cells and reduced their malignancy (Wang et al., 2017).

Non-Small-Cell Lung Cancer

LEF1-AS1 inhibits cell apoptosis and promotes NSCLC proliferation mainly through two pathways: the miR-221/PTEN axis and the miR-489/SOX4 axis. In NSCLC cells, researchers observed that the overexpression of LEF1-AS1 caused the downregulation of PTEN expression and the upregulation of miR-221 expression. Studies have revealed that miR-221 can directly target PTEN. Therefore, researchers considered that the carcinogenic effect of LEF1-AS1 is mainly realized through the miR-221/PTEN signaling pathway (Xiang et al., 2020), and LEF1-AS1 can also induce EMT progression through the miR-489/SOX4 axis (Yang et al., 2019).

Hepatocellular Carcinoma

Dong et al. demonstrated through a series of cellular experiments that the overexpression of LEF1-AS1 affects the tumor state and is conducive to its proliferation, migration, and invasion. The results of a tube-forming assay showed that LEF1-AS1 also increases angiogenesis in the human umbilical vein endothelial cell (HUVEC). The specific mechanism of LEF1-AS1 promoting HCC may be through the miR-136-5p/WNK1 axis (Dong et al., 2020).

Colorectal Cancer

Many studies have indicated that the lncRNA LEF1-AS1 has a carcinogenic role in the pathogenesis of colorectal cancer (Shi et al., 2019; Cheng Y. et al., 2020; Sun et al., 2020; Qi et al., 2021). Cheng et al. downregulated LEF1-AS1 through si-LEF1-AS1 and found that the growth, migration, invasion, and EMT of CRC cells were decreased, and apoptosis was elevated. They further explored the specific mechanism and established that LEF1-AS1 mainly acts through ceRNA on miR-489 to increase the DIAPH1 level (Cheng Y. et al., 2020). This is consistent with the findings of Qi et al. (2021). In colon cancer, a series of cell experiments was conducted to verify the function of LEF1-AS. The results showed that LEF1-AS1 negatively regulated miR-30-5p and SOX9 was the downstream target of miR-30-5p. Specifically, the overexpression of LEF1-AS1 increased SOX9 expression, and the recovery of SOX9 weakened the effects caused by LEF1-AS1 knockdown on cell migration, invasion, and non-anchoring growth (Sun et al., 2020) (**Figure 1**).

Oral Squamous Cell Carcinoma

LEF1-AS1 was significantly elevated in the OSCC cell line. Functionally, the downregulation of LEF1-AS1 inhibits cell survival, proliferation, and migration, but enhances apoptosis. The cell cycle was also significantly affected. The downregulation of LEF1-AS1 significantly increased the G0/G1 phase arrest ratio, and the cells stayed in this period for longer (Zhang C. et al., 2019).

Other Cancers

In lung cancer (Wang et al., 2019), osteosarcoma (Lu et al., 2020) and retinoblastoma (He and Qin, 2020), it has been

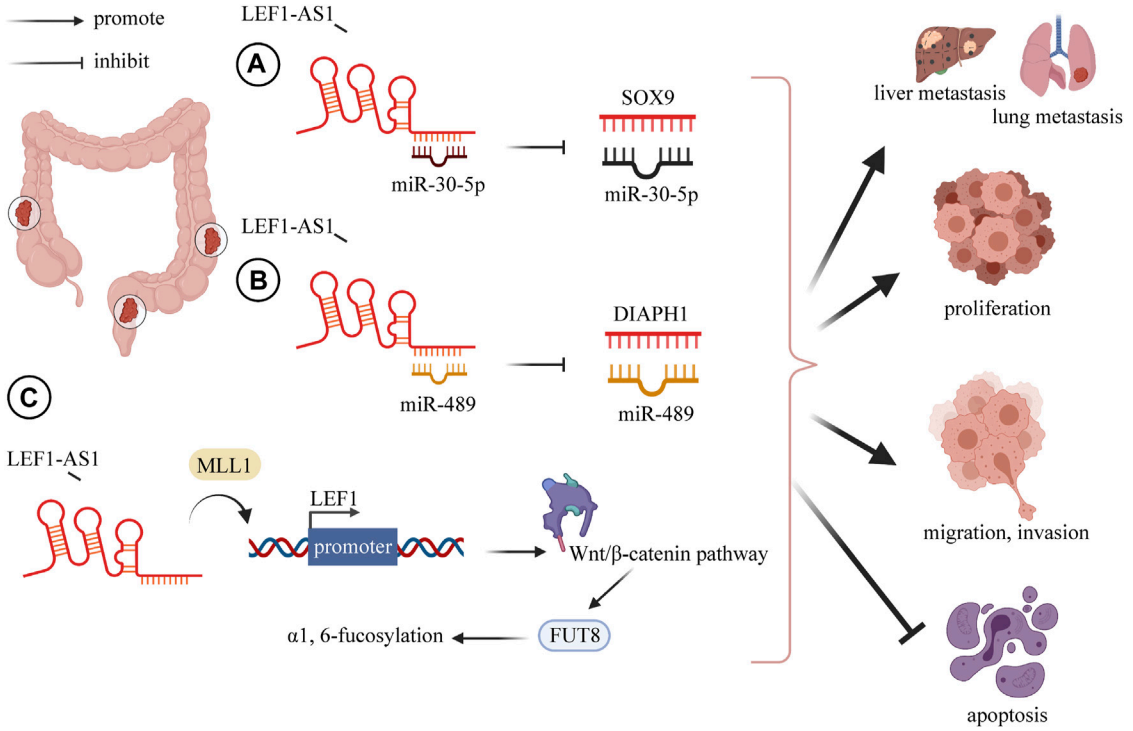

FIGURE 1 | LncRNA LEF1-AS1 plays a carcinogenic role in CRC, overexpression of LEF1-AS1 promotes CRC proliferation, invasion, migration, distant metastasis (liver and lung), and inhibits apoptosis. **(A)** LEF1-AS1 binds to miR-30-5p and mediates the expression of SOX9 by negatively regulating miR-30-5p. **(B)** LEF1-AS1 binds to miR-489 and mediates the expression of DIAPH1 by negatively regulating miR-489. **(C)** LEF1-AS1/LEF1/FUT8 axis mediates colorectal cancer progression by regulating α1, 6-fucosylation via Wnt/β-catenin pathway. Abbreviations: LEF1-AS1, lymph enhancer-binding factor 1-antisense RNA 1; CRC, colorectal cancer; SOX4, SRY-related HMG box transcription factor 4; DIAPH1, diaphanous related formin 1.

reported that LEF1-AS1 is an upregulated oncogene promoting tumor progression. One study on ovarian cancer showed that the downregulation of LEF1-AS1 gene inhibited the proliferation, migration, and invasion of ovarian cancer cells. In terms of mechanism, LEF1-AS1 is the sponge of miR-1285-3p, which exerts its carcinogenic function by suppressing miRNA activity through interaction with miR-1285-3p (Zhang and Ruan, 2020). Moreover, Liu and his colleagues found that the silencing of LEF1-AS1 inhibits the occurrence and development of prostate cancer through blocking LEF1 as a molecular sponge for miR-330-5p (Liu et al., 2019). On the basis of previous studies, Li et al. further demonstrated that LEF1-AS1 promotes the angiogenesis of prostatic carcinoma (Li W. et al., 2020). Although LEF1-AS1 plays a carcinogenic role in most tumors, it has been found to be a cancer suppressor for bone marrow malignancies. It is significantly overexpressed in normal hematopoietic stem cells, but is barely detected in myeloid malignant cells. Cell experiments showed that LEF1-AS1 can inhibit the proliferation of bone marrow malignant tumors, and plays a protective role in the occurrence and development of tumors (Congrains-Castillo et al., 2019). The above findings could provide novel aspects for the diagnosis and targeted therapy of patients with cancer (**Figure 2**).

SIGNALING PATHWAY ASSOCIATED WITH LEF1-AS1

As mentioned above, LEF1-AS1 can be used as a ceRNA sponging miRNAs to downregulate the level of miRNAs, and thus affect the transcription and translation of target genes. Many target genes are widely involved in a variety of signaling pathways, such as the ERK (extracellular regulatory protein kinase) and Akt/mTOR signaling pathway, the Wnt/β-catenin pathway, and the Hippo signaling pathway, which are involved in the process of tumor occurrence and development. In the previous section, this review summarized the molecular mechanisms of LEF1-AS1 in exerting the biological functions in tumors (**Supplementary Table S2**). In the next section, we briefly introduce several signaling pathways involved in LEF1-AS1, so as to provide some ideas for finding tumor therapeutic targets.

ERK and Akt/mTOR Signaling Pathway

The dysfunction of PI3K/AKT/mTOR is common in a variety of human malignancies, including renal cell carcinoma (Ke et al., 2017), lung cancer (Jian et al., 2019), breast cancer (Kanumuri et al., 2020), and HCC (Wu et al., 2018). It functions by targeting genes as a downstream molecule of the PI3K/AKT signal. AKT increases the activation of mTOR by inhibiting the

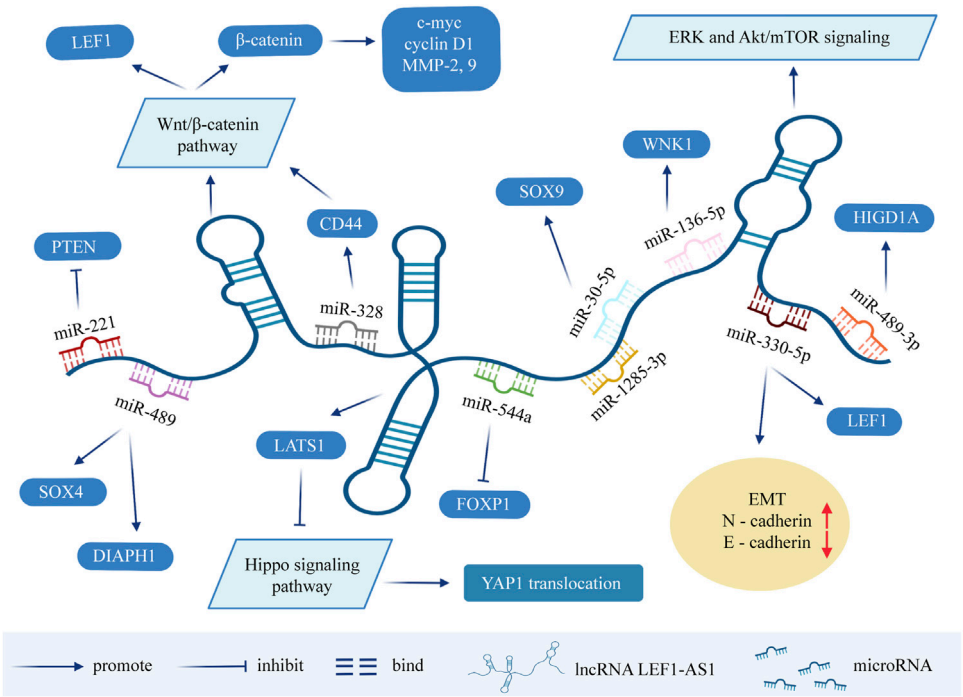

FIGURE 2 | Molecular mechanisms and related signaling pathways of lncRNA LEF1-AS1 in cancers. MicroRNA can cause gene silencing by binding to mRNA, while ceRNA can regulate gene expression by competitively binding to microRNA. LEF1-AS1 can be used as ceRNA, sponge miRNA, thereby affecting the expression of target genes. LEF1-AS1 also participates in signaling pathways such as ERK and Akt/mTOR signaling pathway, Wnt/β-catenin pathway, and Hippo signaling pathway. Abbreviations: LEF1-AS1, lymph enhancer-binding factor 1-antisense RNA 1; ceRNA, competing endogenous RNA; EMT, epithelial-mesenchymal transition.

phosphorylation of the mTOR inhibitor, which is the nodular sclerosis complex (TSC) protein 1/2 (Jin et al., 2019). ERK, an important member of the MAPK family, mainly includes ERK1 and ERK2, is activated by growth factors, and regulates cell proliferation and survival. Most ERK substrate molecules are proteins that regulate the cell cycle. Moreover, the inhibition of ERK activity can downregulate the expression of c-myc and promote apoptosis (Asati et al., 2016; Yue et al., 2019). In conclusion, the Akt/mTOR and ERK pathways play a fundamental role in cancer, and drugs targeting these pathways are expected to provide new options for tumor treatment. Wang et al. (Wang et al., 2017) found that the LEF1-AS1-mediated downregulation of tumor inhibition in GBM cells may be achieved by reducing ERK and Akt/mTOR signaling activities.

Wnt/β-Catenin Pathway

This pathway inhibits the degradation of β-catenin that regulates the transcription of multiple genes, and many of the regulated genes are closely linked to cancer (Moon et al., 2002; Tanaka et al., 2002; Zhou and Liu, 2015). Li and his colleagues pointed out that LEF1-AS1 promotes the metastasis of prostatic carcinoma through the Wnt/β-catenin pathway (Li W. et al., 2020). Similarly, He et al. (He and Qin, 2020) found that silent LEF1-AS1 inhibited the biological function of retinoblastoma cells by inhibiting the expressions of β-catenin and LEF1. The Wnt/β-catenin pathway has also been confirmed to be involved in the occurrence and progression of osteosarcoma (Lu et al., 2020) and colorectal cancer (Qi et al., 2021).

Hippo Signaling Pathway

The pervasively activated Hippo pathway has been recognized to have essential roles in different cancer types (Goyal et al., 2021; Pham et al., 2021), and is involved in cancer initiation and progression, as well as resistance to cancer treatment (Liu Q. et al., 2021). There are many components in the mammalian Hippo pathway, including the kinase cascade, transcriptional co-activation factors YAP, MST1/2 and LATS1/2, and downstream effector (Hong et al., 2016). These core components of the Hippo pathway control the transcriptional processes involved in different functions, such as proliferation, mobility, and differentiation (Ma et al., 2019). In a study on OSCC (Zhang C. et al., 2019), researchers found that LEF1-AS1 directly interacts with LATS1 and affects downstream MOB and YAP1 to inactivate the Hippo signal. It was demonstrated that LEF1-AS1 has a carcinogenic effect in OSCC by inhibiting the Hippo signaling pathway.

CONCLUSION

LncRNAs are involved in the regulation of various biological functions in the nucleus and cytoplasm, involving developmental processes in the fields of immunology, neurobiology, cancer, and

stress, and are also key regulators of cell proliferation and apoptosis. Researches on the role of lncRNAs in cancer are increasingly popular. The occurrence and development of cancer can be mediated by various mechanisms involving lncRNAs, which is mainly through epigenetic regulation, the activation of carcinogenic or tumor suppressor pathways, and so on.

This review mainly discusses the role and research progress of lncRNA LEF1-AS1 in a variety of human tumors. According to the literature, LEF1-AS1 is highly expressed in most tumors, and its expression is reduced in bone marrow malignant tumors. The high expression of LEF1-AS1 is associated with the low survival rate of patients with cancers such as glioma, osteosarcoma, lung cancer, ovarian cancer, colorectal cancer, esophageal squamous cell carcinoma, etc., suggesting that LEF1-AS1 can be used as a biomarker for early detection and prognostic evaluation. In addition, a large number of cell experiments further verified that LEF1-AS1 is involved in cell proliferation, migration, invasion, apoptosis, angiogenesis, and the process of the epithelial cell to mesenchymal transformation. Gao et al. also found that LEF1-AS1, as a miR-10a-5p regulatory factor, enhances the expression of MSI1 in liver cancer cells by activating the AKT signaling pathway, and promotes resistance to chemotherapy. In short, with LEF1-AS1 as a starting point, a series of related applications can be developed with respect to tumor detection, diagnosis, treatment, and prognosis. However, the current research on LEF1-AS1 has certain defects. First of all, there is still a lack of research on LEF1-AS1 in breast cancer, pancreatic cancer, and other tumors. There are very few studies in hematological malignancies. Secondly, more research is still being carried out *in vitro*, lacking clinical correlation. In short, it is worth more in-depth research in the future.

AUTHOR CONTRIBUTIONS

All of the authors worked collaboratively on the work presented here. YH, SZ, and WG designed the experiments and supervised the study. XY and MZ searched the articles and made figures; QZ wrote this manuscript. All authors read and approved the final manuscript.

FUNDING

This work was supported by Leading Talents of Zhongyuan Science and Technology Innovation (214200510027), Henan Provincial Medical Science and Technology Research Plan (SBGJ2018002), Science and Technology Innovation Talents in Henan Universities (19HASTIT003), and Outstanding Foreign Scientist Studio in Henan Province (GZS2020004).

SUPPLEMENTARY MATERIAL

The Supplementary Material for this article can be found online at: https://www.frontiersin.org/articles/10.3389/fcell.2021.750084/full#supplementary-material

REFERENCES

Asati, V., Mahapatra, D. K., and Bharti, S. K. (2016). PI3K/Akt/mTOR and Ras/Raf/MEK/ERK Signaling Pathways Inhibitors as Anticancer Agents: Structural and Pharmacological Perspectives. *Eur. J. Med. Chem.* 109, 314–341. doi:10.1016/j.ejmech.2016.01.012

Chai, A. W. Y., Lim, K. P., and Cheong, S. C. (2020). Translational Genomics and Recent Advances in Oral Squamous Cell Carcinoma. *Semin. Cancer Biol.* 61, 71–83. doi:10.1016/j.semcancer.2019.09.011

Chen, K., Hou, Y., Liao, R., Li, Y., Yang, H., and Gong, J. (2021). LncRNA SNHG6 Promotes G1/S-phase Transition in Hepatocellular Carcinoma by Impairing miR-204-5p-Mediated Inhibition of E2F1. *Oncogene* 40 (18), 3217–3230. doi:10.1038/s41388-021-01671-2

Chen, Y., Yu, X., Xu, Y., and Shen, H. (2017). Identification of Dysregulated lncRNAs Profiling and Metastasis-Associated lncRNAs in Colorectal Cancer by Genome-wide Analysis. *Cancer Med.* 6 (10), 2321–2330. doi:10.1002/cam4.1168

Cheng, Y., Wu, J., Qin, B., Zou, B.-c., Wang, Y.-h., and Li, Y. (2020). CREB1-induced lncRNA LEF1-AS1 Contributes to Colorectal Cancer Progression via the miR-489/DIAPH1 axis. *Biochem. biophysical Res. Commun.* 526 (3), 678–684. doi:10.1016/j.bbrc.2020.03.153

Cheng, Z., Wang, G., Zhu, W., Luo, C., and Guo, Z. (2020). LEF1-AS1 Accelerates Tumorigenesis in Glioma by Sponging miR-489-3p to Enhance HIGD1A. *Cell Death Dis* 11 (8), 690. doi:10.1038/s41419-020-02823-0

Congrains-Castillo, A., Niemann, F. S., Santos Duarte, A. S., and Olalla-Saad, S. T. (2019). LEF1-AS1, Long Non-coding RNA, Inhibits Proliferation in Myeloid Malignancy. *J. Cel Mol Med* 23 (4), 3021–3025. doi:10.1111/jcmm.14152

Dong, H., Jian, P., Yu, M., and Wang, L. (2020). Silencing of Long Noncoding RNA LEF1-AS1 Prevents the Progression of Hepatocellular Carcinoma via the Crosstalk with microRNA-136-5p/WNK1. *J. Cel Physiol* 235 (10), 6548–6562. doi:10.1002/jcp.29503

Gao, J., Dai, C., Yu, X., Yin, X.-B., and Zhou, F. (2020). LncRNA LEF1-AS1 Silencing Diminishes EZH2 Expression to Delay Hepatocellular Carcinoma Development by Impairing CEBPB-Interaction with CDCA7. *Cell Cycle* 19 (8), 870–883. doi:10.1080/15384101.2020.1731052

Gao, J., Dai, C., Yu, X., Yin, X. B., and Zhou, F. (2021). Long Noncoding RNA LEF1-AS1 Acts as a microRNA-10a-5p Regulator to Enhance MSI1 Expression and Promote Chemoresistance in Hepatocellular Carcinoma Cells through Activating AKT Signaling Pathway. *J. Cel Biochem* 122 (1), 86–99. doi:10.1002/jcb.29833

Goodall, G. J., and Wickramasinghe, V. O. (2021). RNA in Cancer. *Nat. Rev. Cancer* 21 (1), 22–36. doi:10.1038/s41568-020-00306-0

Goyal, B., Yadav, S. R. M., Awasthee, N., Gupta, S., Kunnumakkara, A. B., and Gupta, S. C. (2021). Diagnostic, Prognostic, and Therapeutic Significance of Long Non-coding RNA MALAT1 in Cancer. *Biochim. Biophys. Acta (Bba) - Rev. Cancer* 1875 (2), 188502. doi:10.1016/j.bbcan.2021.188502

Guo, R., Zou, B., Liang, Y., Bian, J., Xu, J., Zhou, Q., et al. (2021). LncRNA RCAT1 Promotes Tumor Progression and Metastasis via miR-214-5p/E2F2 axis in Renal Cell Carcinoma. *Cel Death Dis* 12 (7), 689. doi:10.1038/s41419-021-03955-7

He, H., and Qin, M. (2020). Long Non-coding RNA LEF1-AS1 Is Involved in the Progression of Retinoblastoma through Regulating the Wnt/β-catenin Pathway. *Clin. Exp. Pharmacol. Physiol.* 47 (5), 886–891. doi:10.1111/1440-1681.13263

Hong, A. W., Meng, Z., and Guan, K.-L. (2016). The Hippo Pathway in Intestinal Regeneration and Disease. *Nat. Rev. Gastroenterol. Hepatol.* 13 (6), 324–337. doi:10.1038/nrgastro.2016.59

Hou, J., and Peng, W. (2021). LIMITing Tumours with an Immunogenic lncRNA. *Nat. Cel Biol* 23 (5), 443–445. doi:10.1038/s41556-021-00682-1

Hou, T., Ye, L., and Wu, S. (2021). Knockdown of LINC00504 Inhibits the Proliferation and Invasion of Breast Cancer via the Downregulation of miR-140-5p. *Onco Targets Ther.* 14, 3991–4003. doi:10.2147/ott.S294965

Huang, F., Xin, C., Lei, K., Bai, H., Li, J., and Chen, Q. (2020). Noncoding RNAs in Oral Premalignant Disorders and Oral Squamous Cell Carcinoma. *Cell Oncol.* 43 (5), 763–777. doi:10.1007/s13402-020-00521-9

Huang, G.-Q., Ke, Z.-P., Hu, H.-B., and Gu, B. (2017). Co-expression Network Analysis of Long Noncoding RNAs (lncRNAs) and Cancer Genes revealsSFTA1P and CASC2abnormalities in Lung Squamous Cell Carcinoma. *Cancer Biol. Ther.* 18 (2), 115–122. doi:10.1080/15384047.2017.1281494

Islami, F., Chen, W., Yu, X. Q., Lortet-Tieulent, J., Zheng, R., Flanders, W. D., et al. (2017). Cancer Deaths and Cases Attributable to Lifestyle Factors and Infections in China, 2013. *Ann. Oncol.* 28 (10), 2567–2574. doi:10.1093/annonc/mdx342

Jian, M., Yunjia, Z., Zhiying, D., Yanduo, J., and Guocheng, J. (2019). Interleukin 7 Receptor Activates PI3K/Akt/mTOR Signaling Pathway via Downregulation of Beclin-1 in Lung Cancer. *Mol. carcinogenesis* 58 (3), 358–365. doi:10.1002/mc.22933

Jiang, Y., Sun, A., Sun, A., Zhao, Y., Ying, W., Sun, H., et al. (2019). Proteomics Identifies New Therapeutic Targets of Early-Stage Hepatocellular Carcinoma. *Nature* 567 (7747), 257–261. doi:10.1038/s41586-019-0987-8

Jin, J., Guo, Y., Liu, Y., Wang, Z., Yang, X., and Sun, S. (2019). Synergistic Antitumor Effect of BRMS1 and Sorafenib via Inhibition of the PI3K/AKT/mTOR/ERK Signaling Pathway. *Oncol. Rep.* 42 (3), 1183–1193. doi:10.3892/or.2019.7210

Kanumuri, R., Saravanan, R., Pavithra, V., Sundaram, S., Rayala, S. K., and Venkatraman, G. (2020). Current Trends and Opportunities in Targeting P21 Activated kinase-1(PAK1) for Therapeutic Management of Breast Cancers. *Gene* 760, 144991. doi:10.1016/j.gene.2020.144991

Ke, M., Mo, L., Li, W., Zhang, X., Li, F., and Yu, H. (2017). Ubiquitin Ligase SMURF1 Functions as a Prognostic Marker and Promotes Growth and Metastasis of clear Cell Renal Cell Carcinoma. *FEBS open bio* 7 (4), 577–586. doi:10.1002/2211-5463.12204

Ku, G., Tan, I. B., Yau, T., Boku, N., Laohavinij, S., Cheng, A.-L., et al. (2012). Management of colon Cancer: Resource-Stratified Guidelines from the Asian Oncology Summit 2012. *Lancet Oncol.* 13 (11), e470–e481. doi:10.1016/s1470-2045(12)70424-2

Kühnl, A., Gökbuget, N., Kaiser, M., Schlee, C., Stroux, A., Burmeister, T., et al. (2011). Overexpression of LEF1 Predicts Unfavorable Outcome in Adult Patients with B-Precursor Acute Lymphoblastic Leukemia. *Blood* 118 (24), 6362–6367. doi:10.1182/blood-2011-04-350850

Leyva-González, C. A., Salas-Treviño, D., Contreras-Torres, F. F., Loera-Arias, M. d. J., Gómez-Tristán, C. A., Piña-Mendoza, E. I., et al. (2021). Hyaluronate Functionalized Multi-Wall Carbon Nanotubes Loaded with Carboplatin Enhance Cytotoxicity on Human Cancer Cell Lines. *Materials* 14 (13), 3622. doi:10.3390/ma14133622

Li, B., Yu, Y., Jiang, Y., Zhao, L., Li, A., Li, M., et al. (2021). Cloperastine Inhibits Esophageal Squamous Cell Carcinoma Proliferation *In Vivo* and *In Vitro* by Suppressing Mitochondrial Oxidative Phosphorylation. *Cell Death Discov.* 7 (1), 166. doi:10.1038/s41420-021-00509-w

Li, G., Kryczek, I., Nam, J., Li, X., Li, S., Li, J., et al. (2021). LIMIT Is an Immunogenic lncRNA in Cancer Immunity and Immunotherapy. *Nat. Cel Biol* 23 (5), 526–537. doi:10.1038/s41556-021-00672-3

Li, N., Wu, P., Shen, Y., Yang, C., Zhang, L., Chen, Y., et al. (2021). Predictions of Mortality Related to Four Major Cancers in China, 2020 to 2030. *Cancer Commun.* 41 (5), 404–413. doi:10.1002/cac2.12143

Li, T., Yang, C., Wei, Z., Pei, D., and Jiang, G. (2020). Recent Advances of Magnetic Nanomaterials in the Field of Oncology. *Onco Targets Ther.* 13, 4825–4832. doi:10.2147/ott.S243256

Li, W., Yang, G., Yang, D., Li, D., and Sun, Q. (2020). LncRNA LEF1-AS1 Promotes Metastasis of Prostatic Carcinoma via the Wnt/β-Catenin Pathway. *Cancer Cel Int* 20 (1), 543. doi:10.1186/s12935-020-01624-x

Liu, D. C., Song, L. L., Liang, Q., Hao, L., Zhang, Z. G., and Han, C. H. (2019). Long Noncoding RNA LEF1-AS1 Silencing Suppresses the Initiation and Development of Prostate Cancer by Acting as a Molecular Sponge of miR-330-5p via LEF1 Repression. *J. Cel Physiol* 234 (8), 12727–12744. doi:10.1002/jcp.27893

Liu, Q., Liu, X., and Song, G. (2021). The Hippo Pathway: A Master Regulatory Network Important in Cancer. *Cells* 10 (6), 1416. doi:10.3390/cells10061416

Liu, S. J., Dang, H. X., Lim, D. A., Feng, F. Y., and Maher, C. A. (2021). Long Noncoding RNAs in Cancer Metastasis. *Nat. Rev. Cancer* 21 (7), 446–460. doi:10.1038/s41568-021-00353-1

Llovet, J. M., Kelley, R. K., Villanueva, A., Singal, A. G., Pikarsky, E., Roayaie, S., et al. (2021). Hepatocellular Carcinoma. *Nat. Rev. Dis. Primers* 7 (1), 6. doi:10.1038/s41572-020-00240-3

Lu, X., Qiao, L., and Liu, Y. (2020). Long Noncoding RNA LEF1-AS1 Binds with HNRNPL to Boost the Proliferation, Migration, and Invasion in Osteosarcoma by Enhancing the mRNA Stability of LEF1. *J. Cel Biochem* 121 (10), 4064–4073. doi:10.1002/jcb.29579

Ma, S., Meng, Z., Chen, R., and Guan, K.-L. (2019). The Hippo Pathway: Biology and Pathophysiology. *Annu. Rev. Biochem.* 88, 577–604. doi:10.1146/annurev-biochem-013118-111829

Menon, U., Gentry-Maharaj, A., Burnell, M., Singh, N., Ryan, A., Karpinskyj, C., et al. (2021). Ovarian Cancer Population Screening and Mortality after Long-Term Follow-Up in the UK Collaborative Trial of Ovarian Cancer Screening (UKCTOCS): a Randomised Controlled Trial. *The Lancet* 397 (10290), 2182–2193. doi:10.1016/s0140-6736(21)00731-5

Moon, R. T., Bowerman, B., Boutros, M., and Perrimon, N. (2002). The Promise and Perils of Wnt Signaling through β-Catenin. *Science* 296 (5573), 1644–1646. doi:10.1126/science.1071549

Osswald, M., Jung, E., Sahm, F., Solecki, G., Venkataramani, V., Blaes, J., et al. (2015). Brain Tumour Cells Interconnect to a Functional and Resistant Network. *Nature* 528 (7580), 93–98. doi:10.1038/nature16071

Peng, Z., Liu, C., and Wu, M. (2018). New Insights into Long Noncoding RNAs and Their Roles in Glioma. *Mol. Cancer* 17 (1), 61. doi:10.1186/s12943-018-0812-2

Pham, T. H., Hagenbeek, T. J., Lee, H.-J., Li, J., Rose, C. M., Lin, E., et al. (2021). Machine-Learning and Chemicogenomics Approach Defines and Predicts Cross-Talk of Hippo and MAPK Pathways. *Cancer Discov.* 11 (3), 778–793. doi:10.1158/2159-8290.Cd-20-0706

Qi, Y., Shan, Y., Li, S., Huang, Y., Guo, Y., Huang, T., et al. (2021). LncRNA LEF1-AS1/LEF1/FUT8 Axis Mediates Colorectal Cancer Progression by Regulating α1, 6-Fucosylationvia Wnt/β-Catenin Pathway. *Dig. Dis. Sci.* doi:10.1007/s10620-021-07051-w

Shi, Q., He, Y., Zhang, X., Li, J., Cui, G., Zhang, X., et al. (2019). Two Novel Long Noncoding RNAs - RP11-296E3.2 and LEF1-AS1can - Separately Serve as Diagnostic and Prognostic Bio-Markers of Metastasis in Colorectal Cancer. *Med. Sci. Monit.* 25, 7042–7051. doi:10.12659/msm.916314

Siegel, R. L., Miller, K. D., Fedewa, S. A., Ahnen, D. J., Meester, R. G. S., Barzi, A., et al. (2017a). Colorectal Cancer Statistics, 2017. *CA: a Cancer J. clinicians* 67 (3), 177–193. doi:10.3322/caac.21395

Siegel, R. L., Miller, K. D., and Jemal, A. (2017b). Cancer Statistics, 2017. *CA: a Cancer J. clinicians* 67 (1), 7–30. doi:10.3322/caac.21387

Siegel, R. L., Miller, K. D., and Jemal, A. (2018). Cancer Statistics, 2018. *CA: a Cancer J. clinicians* 68 (1), 7–30. doi:10.3322/caac.21442

Siegel, R. L., Miller, K. D., and Jemal, A. (2020). Cancer Statistics, 2020. *CA A. Cancer J. Clin.* 70 (1), 7–30. doi:10.3322/caac.21590

Siegel, R., Ma, J., Zou, Z., and Jemal, A. (2014). Cancer Statistics, 2014. *CA A Cancer J. Clinicians* 64 (1), 9–29. doi:10.3322/caac.21208

Silva, A. M., Moura, S. R., Teixeira, J. H., Barbosa, M. A., Santos, S. G., and Almeida, M. I. (2019). Long Noncoding RNAs: a Missing Link in Osteoporosis. *Bone Res.* 7, 10. doi:10.1038/s41413-019-0048-9

Steponaitis, G., Skiriutė, D., Kazlauskas, A., Golubickaitė, I., Stakaitis, R., Tamašauskas, A., et al. (2016). High CHI3L1 Expression Is Associated with Glioma Patient Survival. *Diagn. Pathol.* 11, 42. doi:10.1186/s13000-016-0492-4

Sun, T., Liu, Z., Zhang, R., Ma, S., Lin, T., Li, Y., et al. (2020). Long Non-coding RNA LEF1-AS1 Promotes Migration, Invasion and Metastasis of Colon Cancer Cells through miR-30-5p/SOX9 Axis. *Onco Targets Ther.* 13, 2957–2972. doi:10.2147/ott.S232839

Szikszai, K., Krejcik, Z., Klema, J., Loudova, N., Hrustincova, A., Belickova, M., et al. (2020). LncRNA Profiling Reveals that the Deregulation of H19, WT1-AS, TCL6, and LEF1-AS1 Is Associated with Higher-Risk Myelodysplastic Syndrome. *Cancers* 12 (10), 2726. doi:10.3390/cancers12102726

Tan, W.-L., Jain, A., Takano, A., Newell, E. W., Iyer, N. G., Lim, W.-T., et al. (2016). Novel Therapeutic Targets on the Horizon for Lung Cancer. *Lancet Oncol.* 17 (8), e347–e362. doi:10.1016/s1470-2045(16)30123-1

Tanaka, K., Kitagawa, Y., and Kadowaki, T. (2002). Drosophila Segment Polarity Gene Product porcupine Stimulates the Posttranslational N-Glycosylation of Wingless in the Endoplasmic Reticulum. *J. Biol. Chem.* 277 (15), 12816–12823. doi:10.1074/jbc.M200187200

Teng, L., Feng, Y. C., Guo, S. T., Wang, P. L., Qi, T. F., Yue, Y. M., et al. (2021). The Pan-Cancer lncRNA PLANE Regulates an Alternative Splicing Program to Promote Cancer Pathogenesis. *Nat. Commun.* 12 (1), 3734. doi:10.1038/s41467-021-24099-4

Thai, A. A., Solomon, B. J., Sequist, L. V., Gainor, J. F., and Heist, R. S. (2021). Lung Cancer. *Lancet.* 398, 535–554. doi:10.1016/s0140-6736(21)00312-3

Thuluvath, P. J., To, C., and Amjad, W. (2021). Role of Locoregional Therapies in Patients with Hepatocellular Cancer Awaiting Liver Transplantation. *Am. J. Gastroenterol.* 116 (1), 57–67. doi:10.14309/ajg.0000000000000999

Vibert, E., Schwartz, M., and Olthoff, K. M. (2020). Advances in Resection and Transplantation for Hepatocellular Carcinoma. *J. Hepatol.* 72 (2), 262–276. doi:10.1016/j.jhep.2019.11.017

Wang, A., Zhao, C., Gao, Y., Duan, G., Yang, Y., Fan, B., et al. (2019). LEF1-AS1 Contributes to Proliferation and Invasion through Regulating miR-544a/FOXP1 axis in Lung Cancer. *Invest. New Drugs* 37 (6), 1127–1134. doi:10.1007/s10637-018-00721-z

Wang, J., Liu, X., Yan, C., Liu, J., Wang, S., Hong, Y., et al. (2017). LEF1-AS1, a Long Non-coding RNA, Promotes Malignancy in Glioblastoma. *Onco Targets Ther.* 10, 4251–4260. doi:10.2147/ott.S130365

Wang, P.-S., Wang, Z., and Yang, C. (2021). Dysregulations of Long Non-coding RNAs – the Emerging "lnc" in Environmental Carcinogenesis. *Semin. Cancer Biol.* 76, 163–172. doi:10.1016/j.semcancer.2021.03.029

Wang, X., Li, X., Lin, F., Sun, H., Lin, Y., Wang, Z., et al. (2021). The Lnc-CTSLP8 Upregulates CTSL1 as a Competitive Endogenous RNA and Promotes Ovarian Cancer Metastasis. *J. Exp. Clin. Cancer Res.* 40 (1), 151. doi:10.1186/s13046-021-01957-z

Wu, T., Dong, X., Yu, D., Shen, Z., Yu, J., and Yan, S. (2018). Natural Product Pectolinarigenin Inhibits Proliferation, Induces Apoptosis, and Causes G2/M Phase Arrest of HCC via PI3K/AKT/mTOR/ERK Signaling Pathway. *Onco Targets Ther.* 11, 8633–8642. doi:10.2147/ott.S186186

Wu, Y., Lian, K., and Sun, C. (2020). LncRNA LEF1-AS1 Promotes Osteogenic Differentiation of Dental Pulp Stem Cells via Sponging miR-24-3p. *Mol. Cel Biochem* 475 (1-2), 161–169. doi:10.1007/s11010-020-03868-7

Xiang, C., Zhang, Y., Zhang, Y., Liu, C., Hou, Y., and Zhang, Y. (2020). lncRNA LEF1-AS1 Promotes Proliferation and Induces Apoptosis of Non-small-cell Lung Cancer Cells by Regulating miR-221/PTEN Signaling. *Cancer Manag. Res.* 12, 3845–3850. doi:10.2147/cmar.S246422

Yang, J., Lin, X., Jiang, W., Wu, J., and Lin, L. (2019). lncRNA LEF1-AS1 Promotes Malignancy in Non-small-cell Lung Cancer by Modulating the miR-489/SOX4 Axis. *DNA Cel. Biol.* 38 (9), 1013–1021. doi:10.1089/dna.2019.4717

Yin, X., Zheng, S.-S., Zhang, L., Xie, X.-Y., Wang, Y., Zhang, B.-H., et al. (2017). Identification of Long Noncoding RNA Expression Profile in Oxaliplatin-Resistant Hepatocellular Carcinoma Cells. *Gene* 596, 53–88. doi:10.1016/j.gene.2016.10.008

Yokoi, A., Matsuzaki, J., Yamamoto, Y., Yoneoka, Y., Takahashi, K., Shimizu, H., et al. (2018). Integrated Extracellular microRNA Profiling for Ovarian Cancer Screening. *Nat. Commun.* 9 (1), 4319. doi:10.1038/s41467-018-06434-4

Yue, S.-J., Zhang, P.-X., Zhu, Y., Li, N.-G., Chen, Y.-Y., Li, J.-J., et al. (2019). A Ferulic Acid Derivative FXS-3 Inhibits Proliferation and Metastasis of Human Lung Cancer A549 Cells via Positive JNK Signaling Pathway and Negative ERK/p38, AKT/mTOR and MEK/ERK Signaling Pathways. *Molecules* 24 (11), 2165. doi:10.3390/molecules24112165

Zhang, C., Bao, C., Zhang, X., Lin, X., Pan, D., and Chen, Y. (2019). Knockdown of lncRNA LEF1-AS1 Inhibited the Progression of Oral Squamous Cell Carcinoma (OSCC) via Hippo Signaling Pathway. *Cancer Biol. Ther.* 20 (9), 1213–1222. doi:10.1080/15384047.2019.1599671

Zhang, L., Zhou, C., Qin, Q., Liu, Z., and Li, P. (2019). LncRNA LEF1-AS1 Regulates the Migration and Proliferation of Vascular Smooth Muscle Cells by Targeting miR-544a/PTEN axis. *J. Cel Biochem* 120 (9), 14670–14678. doi:10.1002/jcb.28728

Zhang, H., Chen, Z., Wang, X., Huang, Z., He, Z., and Chen, Y. (2013). Long Non-coding RNA: a New Player in Cancer. *J. Hematol. Oncol.* 6, 37. doi:10.1186/1756-8722-6-37

Zhang, X.-N., Yang, K.-D., Chen, C., He, Z.-C., Wang, Q.-H., Feng, H., et al. (2021). Pericytes Augment Glioblastoma Cell Resistance to Temozolomide through CCL5-CCR5 Paracrine Signaling. *Cell Res* 31, 1072–1087. doi:10.1038/s41422-021-00528-3

Zhang, Y., and Ruan, F. (2020). LncRNA LEF1-AS1 Promotes Ovarian Cancer Development through Interacting with miR-1285-3p. *Cancer Manag. Res.* 12, 687–694. doi:10.2147/cmar.S227652

Zhou, L., and Liu, Y. (2015). Wnt/β-catenin Signalling and Podocyte Dysfunction in Proteinuric Kidney Disease. *Nat. Rev. Nephrol.* 11 (9), 535–545. doi:10.1038/nrneph.2015.88

Zong, M. Z., Feng, W. T., Du, N., Yu, X. J., and Yu, W. Y. (2019). Upregulation of Long Noncoding RNA LEF1-AS1 Predicts a Poor Prognosis in Patients with Esophageal Squamous Cell Carcinoma. *Eur. Rev. Med. Pharmacol. Sci.* 23 (18), 7929–7934. doi:10.26355/eurrev_201909_19007

Conflict of Interest: The authors declare that the research was conducted in the absence of any commercial or financial relationships that could be construed as a potential conflict of interest.

Publisher's Note: All claims expressed in this article are solely those of the authors and do not necessarily represent those of their affiliated organizations, or those of the publisher, the editors and the reviewers. Any product that may be evaluated in this article, or claim that may be made by its manufacturer, is not guaranteed or endorsed by the publisher.

frontiers in Molecular Biosciences

ORIGINAL RESEARCH
published: 24 December 2021
doi: 10.3389/fmolb.2021.781307

Identification of Novel Tumor Microenvironment-Related Long Noncoding RNAs to Determine the Prognosis and Response to Immunotherapy of Hepatocellular Carcinoma Patients

Shenglan Huang[1,2], *Jian Zhang*[1,2], *Xiaolan Lai*[3], *Lingling Zhuang*[1,2] *and Jianbing Wu*[1,2]*

[1]The Second Affiliated Hospital of Nanchang University, Nanchang, China, [2]Jiangxi Key Laboratory of Clinical and Translational Cancer Research, Nanchang, China, [3]Ningde Municipal Hospital Affiliated to Ningde Normal University, Ningde, China

OPEN ACCESS

Edited by:
José Alexandre Ferreira,
Portuguese Oncology Institute,
Portugal

Reviewed by:
Amy Paschall,
University of Georgia, United States
Thomas John Brett,
Washington University in St. Louis,
United States

***Correspondence:**
Jianbing Wu
Ndefy93008@ncu.edu.cn

Specialty section:
This article was submitted to Molecular Diagnostics and Therapeutics, a section of the journal Frontiers in Molecular Biosciences

Received: 22 September 2021
Accepted: 25 November 2021
Published: 24 December 2021

Citation:
Huang S, Zhang J, Lai X, Zhuang L and Wu J (2021) Identification of Novel Tumor Microenvironment-Related Long Noncoding RNAs to Determine the Prognosis and Response to Immunotherapy of Hepatocellular Carcinoma Patients. Front. Mol. Biosci. 8:781307. doi: 10.3389/fmolb.2021.781307

Introduction: Hepatocellular carcinoma (HCC) is one of the most common malignant tumors with poor prognosis. The tumor microenvironment (TME) plays a vital role in HCC progression. Thus, this research was designed to analyze the correlation between the TME and the prognosis of HCC patients and to construct a TME-related long noncoding RNA (lncRNA) signature to determine HCC patients' prognosis and response to immunotherapy.

Methods: We assessed the stromal–immune–estimate scores within the HCC microenvironment using the ESTIMATE (Estimation of Stromal and Immune Cells in Malignant Tumor Tissues Using Expression Data) algorithm based on The Cancer Genome Atlas database, and their associations with survival and clinicopathological parameters were also analyzed. Thereafter, differentially expressed lncRNAs were filtered out according to the immune and stromal scores. Cox regression analysis was performed to build a TME-related lncRNA risk signature. Kaplan–Meier analysis was used to explore the prognostic value of the risk signature. Furthermore, we explored the biological functions and immune microenvironment features in the high- and low-risk groups. Lastly, we probed the association of the risk model with treatment responses to immune checkpoint inhibitors (ICIs) in HCC.

Results: The stromal, immune, and estimate scores were obtained utilizing the ESTIMATE algorithm for patients with HCC. Kaplan–Meier analysis showed that high scores were

Abbreviations: AIC, Akaike information criterion; AUC, area under the ROC curve; CI, confidence interval; CTLA4, cytotoxic T lymphocyte antigen 4; DElncRNAs, differentially expressed lncRNAs; DEGs, differentially expressed genes; DFS, disease-free survival; EGFR, epidermal growth factor receptor; FDR, false discovery rate; GO, Gene Ontology; GSEA, gene set enrichment analysis; HCC, hepatocellular carcinoma; HR, hazard ratio; ICIs, immune checkpoint inhibitors; IPS, immunophenoscore; LncRNAs, long noncoding RNAs; ORR, objective response rate; OS, overall survival; PD-1, programmed death-1; PD-L1, programmed death-ligand 1; PD-L2, programmed death-ligand 2; PFS, progression-free survival; *R*, Spearman's correlation coefficient; ROC, receiver operating characteristic; ssGSEA, single-sample gene set enrichment analysis; TCGA, The Cancer Genome Atlas; TGF-β, transforming growth factor beta; TILs, tumor-infiltrating lymphocytes; TME, tumor microenvironment

significantly correlated with better prognosis in HCC patients. Six TME-related lncRNAs were screened to construct the prognostic model. The Kaplan–Meier curves suggested that HCC patients with low risk had better prognosis than those with high risk. Receiver operating characteristic (ROC) curve and Cox regression analyses indicated that the risk model could predict HCC survival exactly and independently. Functional enrichment analysis revealed that some tumor- and immune-related pathways were activated in the high-risk group. We also revealed that some immune cells, which were important in enhancing immune responses toward cancer, were significantly increased in the low-risk group. In addition, there was a close correlation between ICIs and the risk signature, which can be used to predict the treatment responses of HCC patients.

Conclusion: We analyzed the influence of the stromal, immune, and estimate scores on the prognosis of HCC patients. A novel TME-related lncRNA risk model was established, which could be effectively applied as an independent prognostic biomarker and predictor of ICIs for HCC patients.

Keywords: hepatocellular carcinoma, tumor microenvironment, lncRNA, prognostic signature, immune checkpoint inhibitors

INTRODUCTION

Liver cancer is a common malignant tumor globally (Yoon et al., 2019). More than 800,000 new individuals are diagnosed with liver cancer annually, and the number of liver cancer-related deaths has reached approximately 780,000. Hepatocellular carcinoma (HCC) is the most common liver cancer, accounting for 75%–85% of all primary liver cancers (Siegel et al., 2018). Currently, potentially curative treatments, such as surgical resection, radiofrequency ablation, and liver transplantation, can be applied to patients with early-stage HCC (Demir et al., 2021; Llovet et al., 2021). However, most HCC patients are diagnosed at an advanced stage, when curative treatments are limited, which results in poor prognosis with a 5-year survival rate of no more than 18% (Jemal et al., 2017; Llovet et al., 2021). Recently, immunotherapy for advanced HCC has become a research hotspot, including immune checkpoint blockade (ICB), adoptive cell therapy, oncolytic viruses, and oncolytic bacteria. Among them, ICBs, represented by programmed death-1 (PD-1), programmed death-ligand 1 (PD-L1), and cytotoxic T lymphocyte antigen 4 (CTLA4) blockades, have provided promising treatment options for HCC (Qin et al., 2019). The clinical studies Checkmate-040 (El-Khoueiry et al., 2017) and Keynote-224 (Zhu et al., 2018) have evaluated the efficacy and safety of anti-PD-1 in advanced HCC, and the results demonstrated that the median survival times of patients on nivolumab and pembrolizumab were 15.6 and 12.9 months, respectively. However, PD-1 and PD-L1 inhibitors were only beneficial in ~20% of HCC patients, and a considerable number of patients did not respond to immunotherapy (Khemlina et al., 2017). Thus, it is of great clinical value to discover novel biomarkers for predicting the survival and clinical response to immunotherapy of HCC patients.

The tumor microenvironment (TME) plays a crucial role in tumorigenesis, progression, immune escape, and therapeutic resistance (Kurebayashi et al., 2018). TME mainly consists of tumor cells, stromal cells, immune cells, and the extracellular matrix (Li et al., 2021). The bidirectional communication between tumor cells and stromal cells or immune cells is critical for maintaining the balance of the TME, which leads to tumor development or suppression (Wu et al., 2021a). Previous studies have demonstrated that monocytes, stimulated by a certain TME, are polarized into the M2 macrophages and secrete anti-inflammatory cytokines such as interleukin-8 (IL-8), interleukin-10 (IL-10), and transforming growth factor beta (TGF-β), which participate in angiogenesis, inflammation, and matrix remodeling, thereby inducing the apoptosis of $CD8^+$ T cells, inhibiting T helper 1 (Th1) immune response, and reshaping the TME to promote tumor growth, invasion, and metastasis (Galdiero et al., 2013; Yu et al., 2018; Ovais et al., 2019). In addition, stromal cell types within the TME also play a vital role in cancer development and metastasis. A study found that targeting tumor-associated stromal cells can reduce the risk of treatment resistance and tumor recurrence (Quail and Joyce, 2013). Therefore, a better understanding of the TME of HCC is essential to identifying new prognostic and therapeutic targets, which will consequently predict the response to and efficacy of immunotherapy.

Long noncoding RNAs (lncRNAs), which account for 80%–90% of all ncRNAs, structurally contain more than 200 nucleotides (nt) in length and play indispensable roles in tumorigenesis and progression (Sanchez Calle et al., 2018). Hence, lncRNAs are widely used as tumor biomarkers to determine early diagnosis, prognosis, and potential therapeutic targets (Fan et al., 2016; Necula et al., 2019; Yuan et al., 2020). Moreover, lncRNAs are key players in regulating the TME by mediating the interactions of immune or stromal cells and cancer cells (Wu et al., 2020). Some pieces of evidence suggest that lncRNAs are involved in the process of cancer immunity, including antigen release, antigen presentation, immune cell priming, T-cell activation, and immune cell migration (Wu

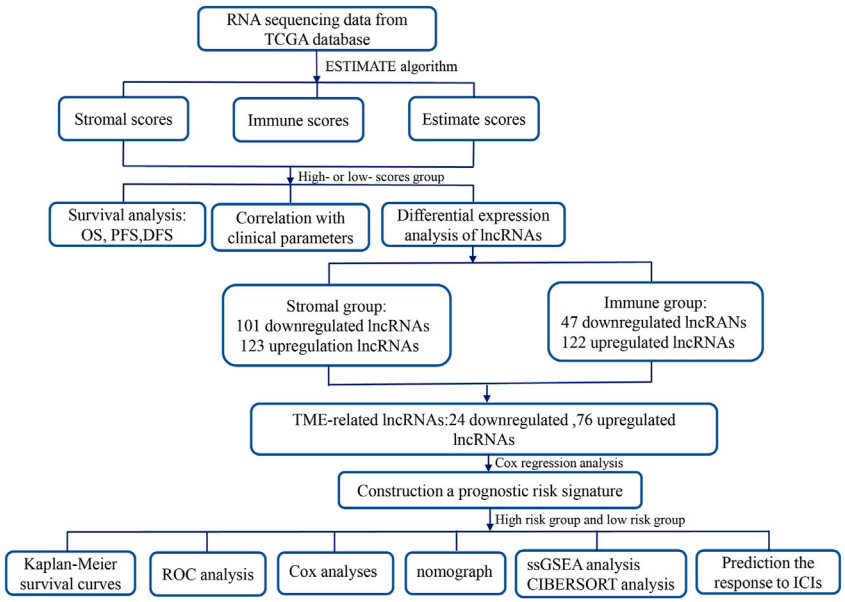

FIGURE 1 | Flowchart of this study. *TME*, tumor microenvironment; *lncRNAs*, long noncoding RNAs; *TCGA*, The Cancer Genome Atlas; *OS*, overall survival; *PFS*, progression-free survival; *DFS*, disease-free survival; *ROC*, receiver operating characteristic; *COX*, univariate and multivariate Cox proportional hazards regression; *GSEA*, gene set enrichment analysis; *GO*, Gene Ontology; *ICIs*, immune checkpoint inhibitors.

et al., 2020). It has been reported that the lncRNA UCA1 promoted the proliferation, migration, and immune escape of cancer cells in gastric cancer, induced PD-L1 expression, and decreased the secretion of IFN-γ by restraining the expression levels of miR-26a/b, miR-193a, and miR-214 (Wang et al., 2019). In HCC, lncRNA epidermal growth factor receptor (EGFR) suppressed cytotoxic T lymphocyte (CTL) activity, stimulated regulatory T cell (Treg) differentiation, and accelerated HCC growth *via* blocking EGFR ubiquitination with c-CBL (Jiang et al., 2017). Wang et al. (2020) have revealed that the lncRNA NNT-AS1 impaired $CD4^+$ T-cell infiltration *via* activation of the TGF-β signaling pathway in HCC. Moreover, several studies have reported the remarkable role of an lncRNA risk model for survival prediction in HCC (Sun et al., 2019; Xu et al., 2021a; Zhou et al., 2021a), as well as including immune-related lncRNAs, which was capable of predicting the survival and therapeutic responses of HCC patients (Zhang et al., 2020; Wang et al., 2021a; Wu et al., 2021b; Xu et al., 2021b; Zhou et al., 2021b). However, the TME-related lncRNA signature for predicting prognosis requires further exploration. Thus, we focused on the TME of HCC as the cut-in point to discover novel prognostic TME-related lncRNA markers and further investigate latent molecular mechanisms.

This study, we first utilized the ESTIMATE (Estimation of Stromal and Immune Cells in Malignant Tumor Tissues Using Expression Data) algorithm to assess the stromal–immune–estimate scores of the HCC microenvironment based on The Cancer Genome Atlas (TCGA) database and analyzed the associations of these scores with survival and clinicopathological parameters. Subsequently, we constructed a novel TME-related lncRNA risk model, which was filtered out by integrating differentially expressed lncRNAs (DElncRNAs) into the TME, and identified its prognostic value in HCC patients. The latent biological mechanisms were investigated *via* functional enrichment analysis. In addition, the relationship between the TME-related lncRNA signatures and specific TME features was investigated in depth. Furthermore, we explored the associations between the signature and ICB-related genes and applied the TME-related lncRNAs to forecast the treatment response of HCC patients to immune checkpoint inhibitors (ICIs). A flowchart of this research design is shown in **Figure 1**.

MATERIALS AND METHODS

Data Acquisition and Processing

The RNA sequencing (RNA-seq) data of 374 tumor samples and 50 normal samples were downloaded from TCGA Genomic Data Commons database (https://portal.gdc.cancer.gov/). The genes were annotated and classified as 14,142 lncRNAs and 19,659 protein-coding genes according to the ENSEMBL database (http://asia.ensembl.org/index. html). LncRNAs with average expression value less than "0.1" were discarded; finally, 3,848 lncRNAs were retained for subsequent differential analysis. Corresponding clinical information were downloaded from the UCSC XENA database (https://xenabrowser.net/), which incorporates gender, age, histological grade, clinical stage, TNM stage, survival status, and survival time [including overall survival (OS), progression-free survival (PFS), and disease-free survival (DFS)]. After excluding patients without follow-up data, the remaining 365 HCC samples with both expression and survival data were included in this study.

Analysis of the Relationship Between Tumor Microenvironment Scores and Prognosis of Hepatocellular Carcinoma Patients

To evaluate the heterogeneity of the TME for each HCC patient, the ESTIMATE algorithm (Yoshihara et al., 2013) was applied to calculate the stromal and immune scores using the "estimate" package in R 4.0.5 software (version 4.0.5; http://www.r-project.org/), which is a specific method that uses the RNA-seq transcriptome profiles of certain genes to quantitatively estimate the scores of stromal and immune cells in the TME. Stromal scores represent the abundance of stromal cells, immune scores display the presence of infiltrating immune cells in the TME, and estimate scores are the sum of the stromal and immune scores. HCC patients were assigned into a low- or a high-stromal/immune/estimate score group according to the best statistical cutoff values, which were calculated using maximally selected rank statistics. Kaplan–Meier survival curves were used to validate the associations between the stromal, immune, and estimate scores and the OS, PFS, and DFS; a p-value <0.05 was considered statistically significant. In addition, we also assessed the association of the stromal, immune, and estimate scores in HCC samples with their clinical features, including sex, age, tumor grade, and clinical stage. The results were analyzed and visualized with the "limma" and "ggpubr" packages in R 4.0.5 software; a p-value <0.05 represented statistical significance.

Screening of DElncRNAs Based on the Stromal and Immune Scores

Firstly, 374 HCC samples from TCGA database were divided into high- and low-stromal/immune score subgroups according to the median scores. Thereafter, differential lncRNAs were screened out between the low- and high-score subgroups *via* the "limma" package in R. Wilcoxon's test was applied to obtain p-values, and the significant DElncRNAs were defined as fold change > $|\pm 1|$ and a false discovery rate (FDR) <0.05. The results were visually displayed in volcano plots and heatmaps *via* the packages "ggplot2" and "pheatmap" in R. The heatmaps display the top 20 lncRNAs according to fold change. Subsequently, a Venn diagram was depicted to intersect DElncRNAs that were upregulated or downregulated in both high stromal and immune score subgroups, and the intersecting lncRNAs were defined as TME-related DElncRNAs and used for further analysis.

Building and Identification of Prognostic Tumor Microenvironment-Related LncRNA Signature for Hepatocellular Carcinoma

To construct a prognostic signature based on the TME-related lncRNAs, we first adopted the univariate Cox regression method to identify lncRNAs related to survival. Thereafter, the multivariate Cox regression method was performed based on the minimum Akaike information criterion (AIC). The prognostic lncRNAs were exhibited with hazard ratio (HR), 95% confidence interval (CI), and p-value. A $p < 0.05$ represented the lncRNAs significantly affecting prognosis, lncRNAs with HR > 1 were considered as unfavorable to prognosis, and those with HR < 1 were deemed as improving prognosis. According to the expression value of each lncRNA and its regression coefficient, the risk score of each HCC patient was calculated as follows:

$$\text{Risk}score = \sum_{i=0}^{n} \exp \times \beta_i$$

where exp is the expressive value of each TME-related lncRNA and β is the regression coefficient of each lncRNA.

Subsequently, HCC patients were classified into high- and low-risk subgroups based on the median risk score. We applied the Kaplan–Meier curve and log-rank test to compare the survival differences in the two subgroups. The R package "survivalROC" was used to draw the receiver operating characteristic (ROC) curve, and the area under the ROC curve (AUC) was calculated to assess the predictive accuracy of the risk model. Moreover, stratification analysis was performed to evaluate the prognostic value of the risk model in different populations based on the following clinical factors: age (≤65 and >65 years), sex (male and female), grade (grades 1–2 and grades 3–4), and clinical stage (stages I–II and stages III–IV). A $p < 0.05$ was deemed as statistically significant for the above analyses.

Thereafter, a Cox proportional hazards model was derived to identify the independent prognostic factors for HCC patients, including the following clinical features: age, sex, grade, stage, and risk score groups. The results were shown as forest plots, and $p < 0.05$ represented statistical difference.

Nomogram Building and Validation

According to the risk scores and conventional clinical prognostic indicators (i.e., pathological grade and stage), we built and plotted a nomogram using the R packages "survival" and "rms" to quantitatively calculate the 1-, 2-, and 3-year survival probabilities of HCC patients. Thereafter, the calibration curves and ROC curves were drawn to assess the predictive survival performance of the nomogram.

Functional Enrichment Analysis

Firstly, gene set enrichment analysis (GSEA) was performed to reveal latent functional enrichment pathways based on the TME-related lncRNA risk signature. We analyzed the gene sets of "c2.cp.kegg.v7.4.symbols.gmt " obtained from MsigDB (http://www.gseamsigdb.org/gsea/msigdb/collections.jsp) using GSEA 4.1.0, and gene set permutations of 1,000 times were conducted to obtain a standardized enrichment score for each analysis. FDR < 0.05 represented significantly enriched pathways. Subsequently, the significant differentially expressed genes (DEGs) were extracted from TCGA sequencing data depending on risk grouping, and statistical significance was defined as FDR < 0.05 and $|\log_2 FC| \geq 1$. Based on the DEGs, we conducted Gene Ontology (GO) analysis to discover the related biological pathways in the risk signature.

Exploring the Correlation of the Tumor Microenvironment–lncRNA Risk Signature With the Tumor Immune Microenvironment

To explore the association of the TME-related lncRNAs with immune cell infiltration in HCC, a range of analytical approaches

were conducted. Firstly, single-sample gene set enrichment analysis (ssGSEA) (Rooney et al., 2015) was conducted using the R packages "gsva" and "GSEABase" to explore the differences in the immune cells between the low- and high-risk groups. Thereafter, we obtained the immune cell infiltration information of the HCC samples from the Tumor Immune Estimation Resource (https://cistrome.shinyapps.io/timer/), and CIBERSORT (https://cibersort.stanford.edu/) was used to calculate the relative proportions of 22 tumor-infiltrating immune cells (TIICs) in each HCC patient. Spearman's correlation analysis was performed to elucidate the correlation of the proportions of TIICs with the risk score. A Spearman's correlation coefficient (R) >1 denotes a positive correlation, and $R < 1$ means a negative correlation; a p-value <0.05 was considered statistically significant.

We further investigated the potential values of the risk signature to predict the treatment responses of HCC patients to ICIs. Previous studies have indicated that the immunophenoscore (IPS) is a good predictor of the response to ICIs, and the expressions of immune checkpoint genes are associated with the response to ICIs (Nishino et al., 2017). Firstly, differential expression analysis of the ICI-related genes was performed in the low- and high-risk groups, and we emphatically discussed the correlation of the risk signature with four key genes of ICIs: *CTLA4*, *PD-1*, *PD-L1*, and *PD-L2* (Nishino et al., 2017). Thereafter, the IPS [four subtypes: IPS-CTLA4(−)/PD-1(−), IPS-CTLA4(−)/PD-1(+), IPS-CTLA4(+)/PD-1(−), and IPS-CTLA4(+)/PD-1(+)] was calculated to predict the treatment response to ICIs of the low- and high-risk groups, which were downloaded from the Cancer Immunome Atlas database (https://tcia.at/home). The Wilcoxon rank-sum test was adopted to compare the IPS between the two risk groups, and a p-value <0.05 was deemed statistically significant.

Statistical Analyses

The R 4.0.5 software was used to conduct statistical analyses. Student's t-test or Wilcoxon's rank-sum test was used to compare the differences between the two groups. Cox regression analysis was performed to build a prognostic model. We applied the Kaplan–Meier method and ROC curve to analyze the survival difference and the predictive ability of the risk signature. Spearman's correlation analysis was performed to reflect the relationship between the proportions of tumor-infiltrating immune cells and risk scores. All statistical tests were two-sided, and statistical significance was set at $p < 0.05$.

RESULTS

The Stromal–Immune–Estimate Scores of the Tumor Microenvironment Were Significantly Associated With the Prognosis of Hepatocellular Carcinoma Patients

The transcriptome and relevant clinical data of HCC patients were downloaded from TCGA and UCSC Xena databases, respectively. The transcriptome data contained 374 tumor and 50 normal tissues, and 377 HCC patients had clinical information. After removing repeated samples and patients without follow-up data, a total of 365 patients were included in the subsequent survival analysis. Thereafter, the stromal, immune, and estimate scores were calculated with the ESTIMATE algorithm (**Supplementary Table S1**). The 365 HCC patients were split into low- and high-score subgroups in line with the best statistical cutoff values, which were −914.61 (ranging from −1,622.33 to 1,180.26) in the stromal groups, 41.48 (ranging from −861.77 to 3,157.28) in the immune groups, and −909.71 (ranging from −2,165.59 to 3,722.93) in the estimate groups. Subsequently, the Kaplan–Meier survival curves were used to analyze the association of the stromal, immune, and estimate scores with OS (**Figures 2A–C**), PFS (**Figures 2D–F**), and DFS (**Figures 2G–I**). The results revealed that HCC patients with high stromal scores showed longer OS ($p = 0.005$), PFS ($p < 0.001$), and DFS ($p < 0.001$) than did patients with low stromal scores (**Figures 2A, D, G**). Significantly better OS ($p = 0.018$), PFS ($p < 0.001$), and DFS ($p < 0.001$) were seen in the high-immune score subgroup compared to the low-immune score subgroup. Similar survival results were observed in the estimate score groups. These results suggest that TME scores are remarkably associated with the prognosis of HCC patients and deserve further investigation.

Furthermore, we investigated whether there was any association between the stromal, immune, and estimate scores and the clinicopathological characteristics of HCC patients. As shown in **Figures 3A–L**, no significant association was observed between the estimate scores and gender (male *vs.* female), age (≥65 *vs.* <65 years), tumor grade (grades 1–2 *vs.* grades 3–4), and clinical stage (stages I–II *vs.* stages III–IV). Moreover, the immune and stromal scores showed no significant differences in the age and sex subgroups. However, we noticed that patients in the late stages (stages III–IV) had lower immune scores than those in stages I–II ($p = 0.031$), and a higher grade (grades 3–4) was associated with lower stromal scores ($p = 0.013$). These results demonstrate that the presence of immune and stromal cells in the TME might play an important role in HCC progression.

Identification of DElncRNAs Based on Low and High Stromal and Immune Scores

To establish a plausible connection between lncRNAs and the TME, hoping to discover novel prognostic predictors for HCC patients, we conducted lncRNA differential expression analysis of the 374 HCC samples from TCGA cohort. Firstly, the patients were partitioned into a low- or a high-score group based on the median values of the stromal and immune scores. DElncRNAs were filtered out between the low- and high-stromal/immune score groups. The results were visualized with volcano plots and heatmap. Moreover, 101 downregulated and 123 upregulated lncRNAs were identified in the high-stromal score group (**Figure 4A** and **Supplementary Table S2**), and 47 downregulated and 122 upregulated lncRNAs were identified in the high-immune score group (**Figure 4B** and **Supplementary Table S3**). Among them, the intersecting lncRNAs that were commonly downregulated or upregulated both in the high-stromal and high-immune score subgroups were

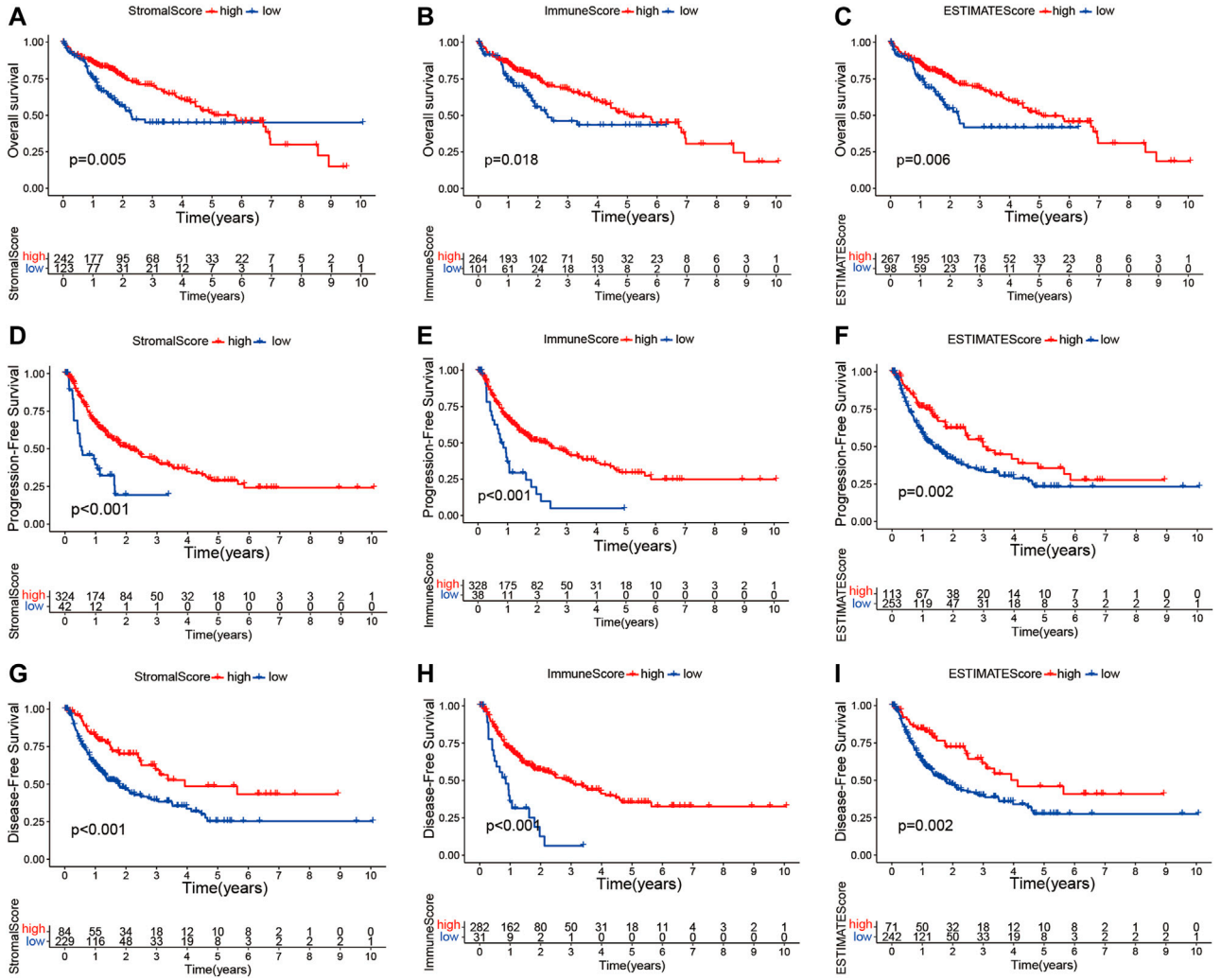

FIGURE 2 | Kaplan–Meier survival curve analysis of the stromal, immune, and estimate scores with the prognosis of HCC patients. **(A–I)** Correlations of the stromal, immune, and estimate scores with overall survival **(A–C)**, progression-free survival **(D–F)**, and disease-free survival **(G–I)**. *HCC*, hepatocellular carcinoma.

considered most likely associated with the TME of HCC. Thus, compared with the low-score groups, 24 downregulated and 76 upregulated lncRNAs were selected as TME-related DElncRNAs, as shown in the Venn diagram (**Figures 4C, D** and **Supplementary Table S4**).

Construction of a Prognostic Risk Signature Using the Tumor Microenvironment-Related DElncRNAs and Exploring Its Prognostic Value

Cox regression analyses were conducted to explore the association between the TME-related DElncRNAs and the prognosis of HCC patients. Firstly, among the 100 TME-related DElncRNAs, 9 lncRNAs were screened out as prognosis-related candidates using univariate Cox regression analysis ($p < 0.05$). These lncRNAs are listed in **Table 1**. Subsequently, multivariate Cox regression analysis was performed to identify the prognostic lncRNA signature with a minimum AIC value (AIC = 1,254), which contained six TME-related lncRNAs (LINC01150, LINC02273, LINC00426, AP002954.1, AC007277.1, and AC008549.1). Among them, LINC02273, AC008549.1, and LINC00426 benefited prognosis, with a HR < 1, whereas LINC01150, AP002954.1, and AC007277.1 were poor prognostic factors with HR > 1 (**Table 2**).

According to the expression values of the six TME-related lncRNAs and the multivariate Cox regression coefficients, the risk score of each patient was calculated basing on the following equation: risk score = (0.947 × LINC01150 expression) + (−0.838 × LINC02273 expression) + (−3.083 × LINC00426 expression) + (1.255 × AP002954.1 expression) + (0.178 × AC007277.1 expression) + (−0.014 × AC008549.1 expression). The 365 HCC patients were divided into two groups according to the median score (median value = 1.119). Kaplan–Meier analysis

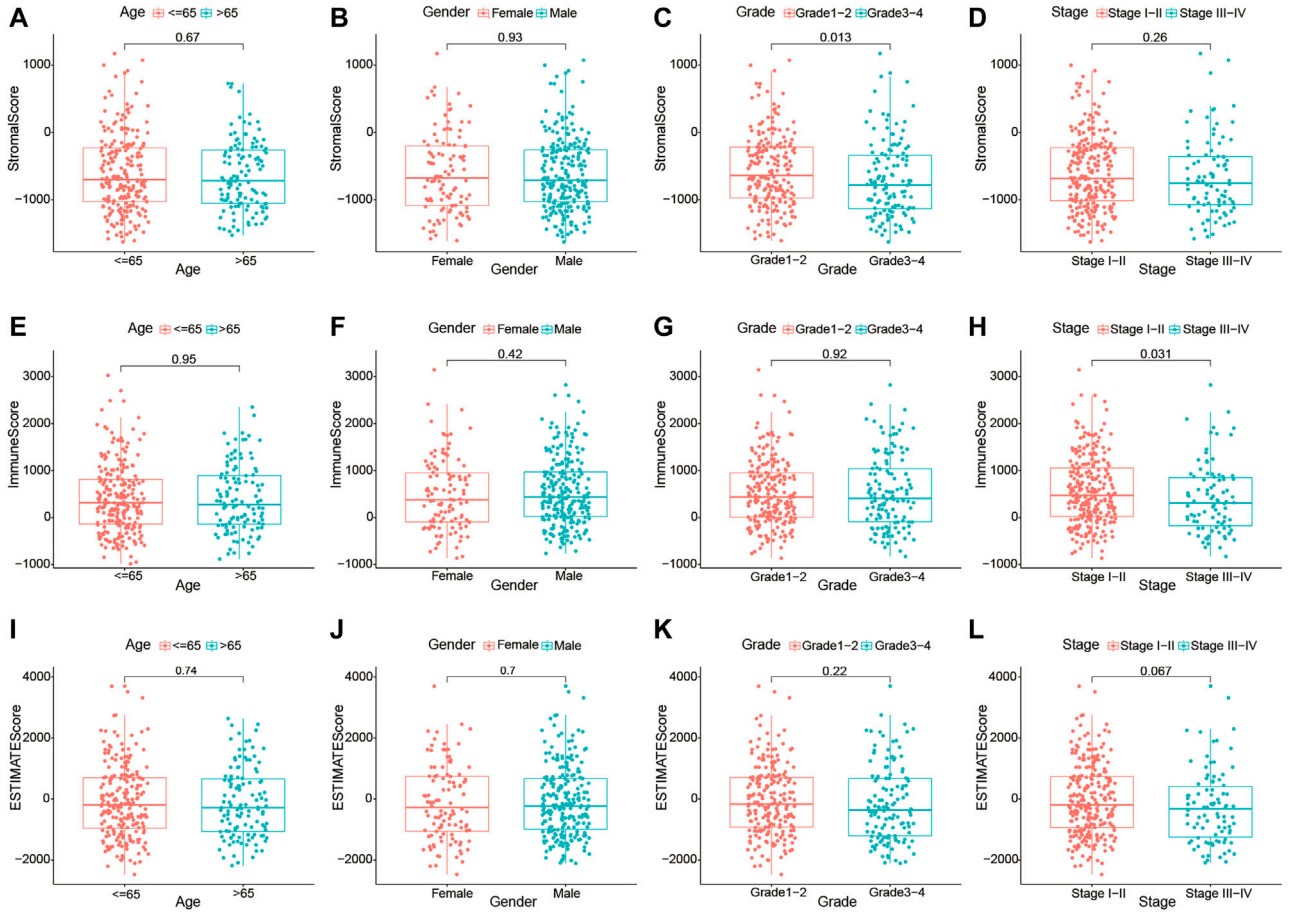

FIGURE 3 | Relationship of the immune, stromal, and estimate scores with the different clinicopathological parameters of hepatocellular carcinoma **(**HCC) patients. **(A–D)** Association of the stromal scores with different age subgroups (≤65 and >65 years), gender subgroups (female and male), grade subgroups (grades I–II and grades III–IV), and stage subgroups (stages I–II and stages III–IV). **(E–H)** Association of the immune scores with different age subgroups (≤65 and >65 years), gender subgroups (female and male), grade subgroups (grades I–II and grades III–IV), and stage subgroups (stages I–II and stages III–IV). **(I–L)** Association of the estimate scores with different age subgroups (≤65 and >65 years), gender subgroups (female and male), grade subgroups (grades I–II and grades III–IV), and stage subgroups (stages I–II and stages III–IV).

suggested that HCC patients with low risk had longer OS than those with high risk ($p = 5.506E{-}06$). The results are shown in **Figure 5A**. The ROC curve demonstrated that the TME-related signature was effective in predicting the OS of HCC patients, with an AUC of 0.707 (**Figure 5B**). The risk score curve and the scatter plot revealed that the risk score was proportional to the number of deaths in HCC patients (**Figures 5C, D**). The heatmap indicted that the expressions of LINC01150, AP002954.1, and AC007277.1 were upregulated in the high-risk group, whereas the other three lncRNAs (LINC02273, LINC00426, and AC008549) were upregulated in the low-risk group (**Figure 5E**). Furthermore, univariate and multivariate Cox proportional hazards regression analyses were performed to explore the independent prognostic factors for OS. The results suggested that the clinical stage and risk score were independent predictors (**Figures 5F, G**). The above results demonstrated that the TME-related lncRNA risk model could act as a prospective independent predictor for the survival of HCC patients.

In addition, stratification analysis was conducted in different subgroups to investigate the prognostic value of the risk signature. Firstly, the HCC patients were categorized into different subgroups based on age (≤65 and >65 years), sex (male and female), grade (grades 1–2 and grades 3–4), clinical stage (stages I–II and stages III–IV), and tumor stage (T1–T2 and T3–T4); then, Kaplan–Meier survival curve analysis was performed in different subgroups. As shown in **Figures 6A–H**, patients of different ages and in different tumor and clinical stages in the low-risk group had longer OS than those in the high-risk group; similar results were obtained in the male and grade 1–2 subgroups. However, there were no significant differences in female and grade 3–4 patients. The association between the risk scores of the TME-related lncRNAs and the clinical features of HCC was assessed, and it was found that the prognostic model was significantly correlated with gender

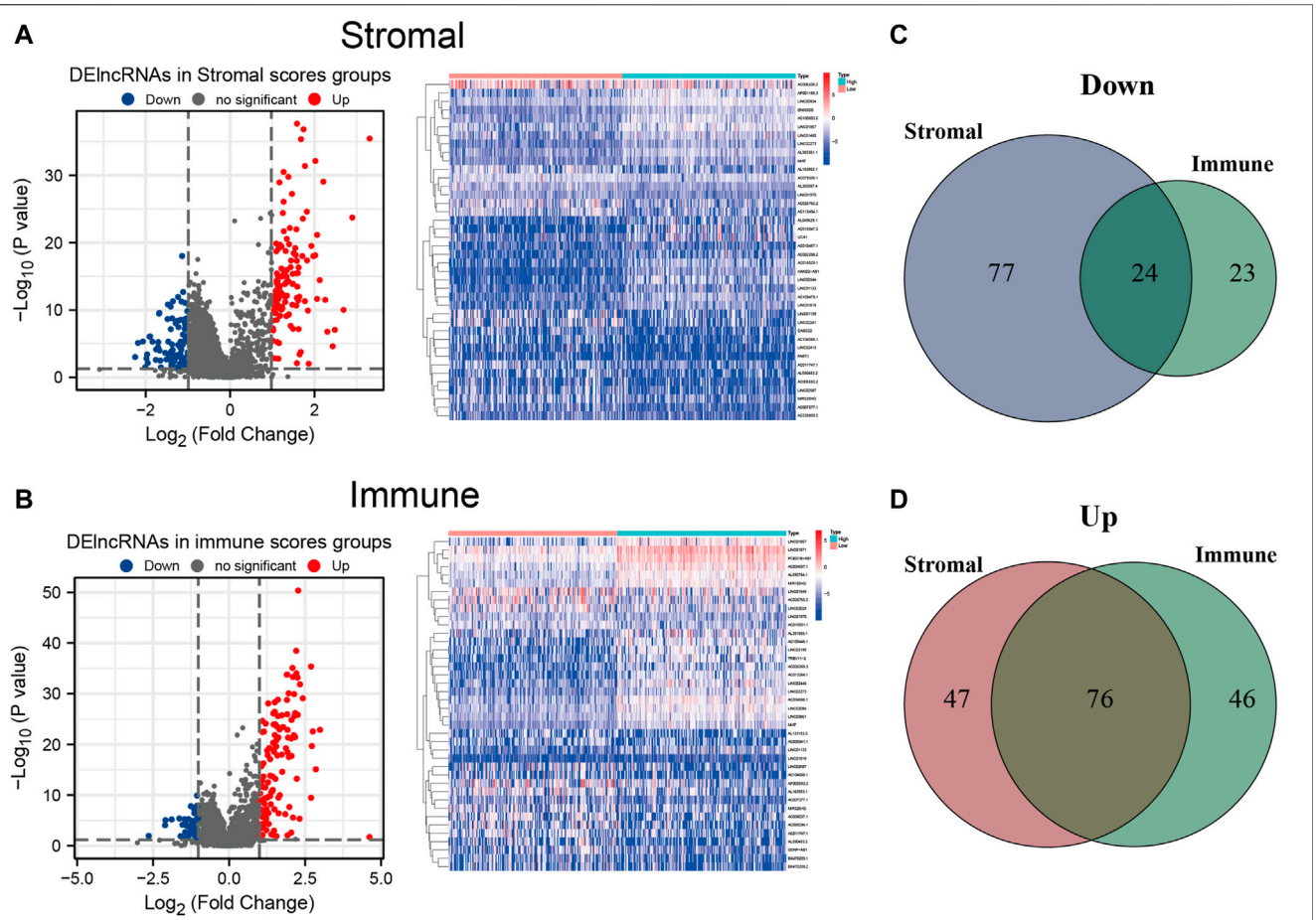

FIGURE 4 | Differentially expressed long noncoding RNAs (DElncRNAs) between the high- and low-stromal/immune score groups. **(A,B)** Volcano plot and heatmap of the DElncRNAs in the high- and low-stromal score groups **(A)** and in the high- and low-immune score groups **(B)**. **(C)** Downregulated lncRNAs both in the high-stromal score and high-immune score groups using a Venn diagram. **(D)** Upregulated lncRNAs both in the stromal score and immune score groups using a Venn diagram.

TABLE 1 | Univariate Cox regression analysis of TME-related lncRNAs

LncRNA	HR	HR.95L	HR.95H	*p*-value
LINC01150	2.279	1.421	3.655	0.0006
LINC02273	0.245	0.062	0.973	0.046
LINC00426	0.187	0.037	0.938	0.042
LINC01094	2.007	1.393	2.891	0.0002
LINC00892	0.246	0.061	0.989	0.048
LINC01871	0.907	0.823	0.999	0.049
AP002954.1	1.583	1.000	2.504	0.05
AC007277.1	1.242	1.009	1.527	0.04
AC008549.1	0.985	0.972	0.998	0.025

TME, *tumor microenvironment;* lncRNA, *long noncoding RNA;* HR, *hazard ratio;* HR.95L, *low 95% confidence interval (CI) of HR;* HR.95H, *high 95%CI of HR*

TABLE 2 | Multivariate Cox regression analysis of TME-related lncRNAs

LncRNA	Coefficient	HR	HR.95L	HR.95H	*p*-value
LINC01150	0.947	2.579	1.524	4.365	0.0004
LINC02273	−1.838	0.159	0.024	1.036	0.054
LINC00426	−3.083	0.046	0.005	0.451	0.008
AP002954.1	1.255	3.507	1.71	7.192	0.0006
AC007277.1	0.179	1.195	0.997	1.433	0.054
AC008549.1	-0.014	0.986	0.974	0.999	0.039

TME, *tumor microenvironment;* lncRNA, *long noncoding RNA;* HR, *hazard ratio;* HR.95L, *low 95% confidence interval (CI) of HR;* HR.95H, *high 95% CI of HR*

($p = 0.048$), tumor stage ($p < 0.001$), and clinical stage ($p = 0.011$), but not with age or tumor grade (**Figures 6I–N**). Collectively, it can be concluded that the risk signature could predict the survival of diverse populations of HCC patients, and the risk score may be associated with HCC progression.

The Nomogram Exact Prediction of the Survival of Hepatocellular Carcinoma Patients

We quantitatively calculated the survival probabilities of HCC patients according to the pathological grade, stage, and risk score by constructing a nomogram. The points for each clinical factor were summed to comprehensive scores.

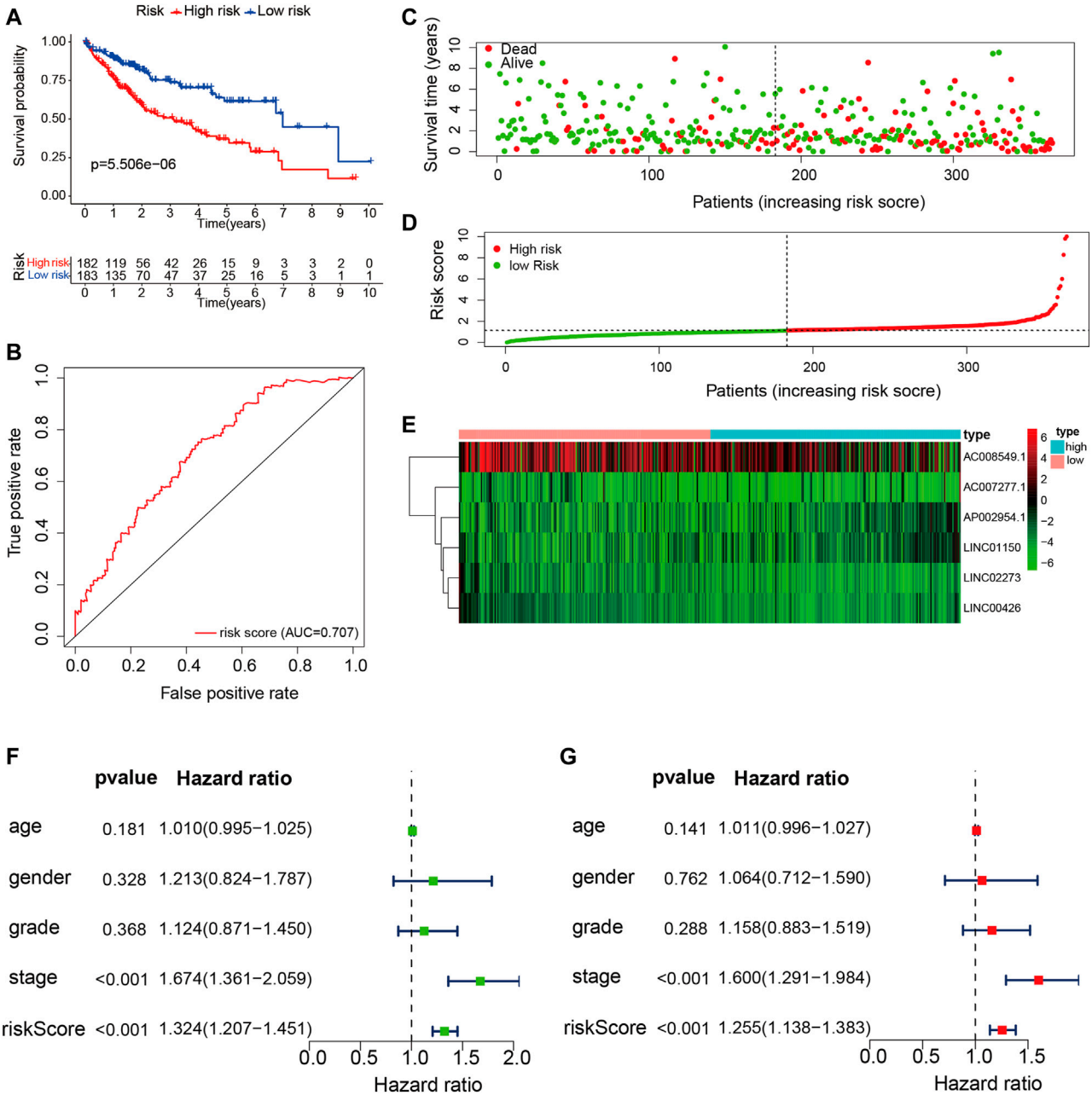

FIGURE 5 | Construction and validation of the tumor microenvironment (TME)-related long noncoding RNA (lncRNA) signature in hepatocellular carcinoma (HCC) samples. **(A)** Kaplan–Meier survival analysis of the high- and low-risk groups. **(B)** Receiver operating characteristic (ROC) curve evaluating the predictive accuracy of the prognostic model. **(C)** Risk score curves based on the risk score of each HCC patient. **(D)** Scatter plots displaying the survival status of each HCC patient. **(E)** Heatmap exhibiting the expression levels of the six TME-related lncRNAs in the high- and low-risk groups. **(F)** Univariate Cox regression analysis of the clinical features and risk scores in HCC samples. **(G)** Multivariate Cox regression analysis of clinical features and risk scores in HCC samples.

The nomogram showed higher total points and worse prognoses (**Figure 7A**). The consistency and accuracy of the nomogram were evaluated using a calibration curve and the ROC curves. The calibration curves showed that the nomogram could precisely predict the probability of OS (**Figures 7B–D**), and ROC analysis indicated that the nomogram achieved better prediction performance than did the other clinical features, with AUCs of 0.720 for 1-year OS, 0.712 for 2-year OS, and 0.740 for 3-year OS, as shown in **Figures 7E–G**. In summary, the nomogram exhibited preferable clinical practicality for predicting the survival probability of HCC patients.

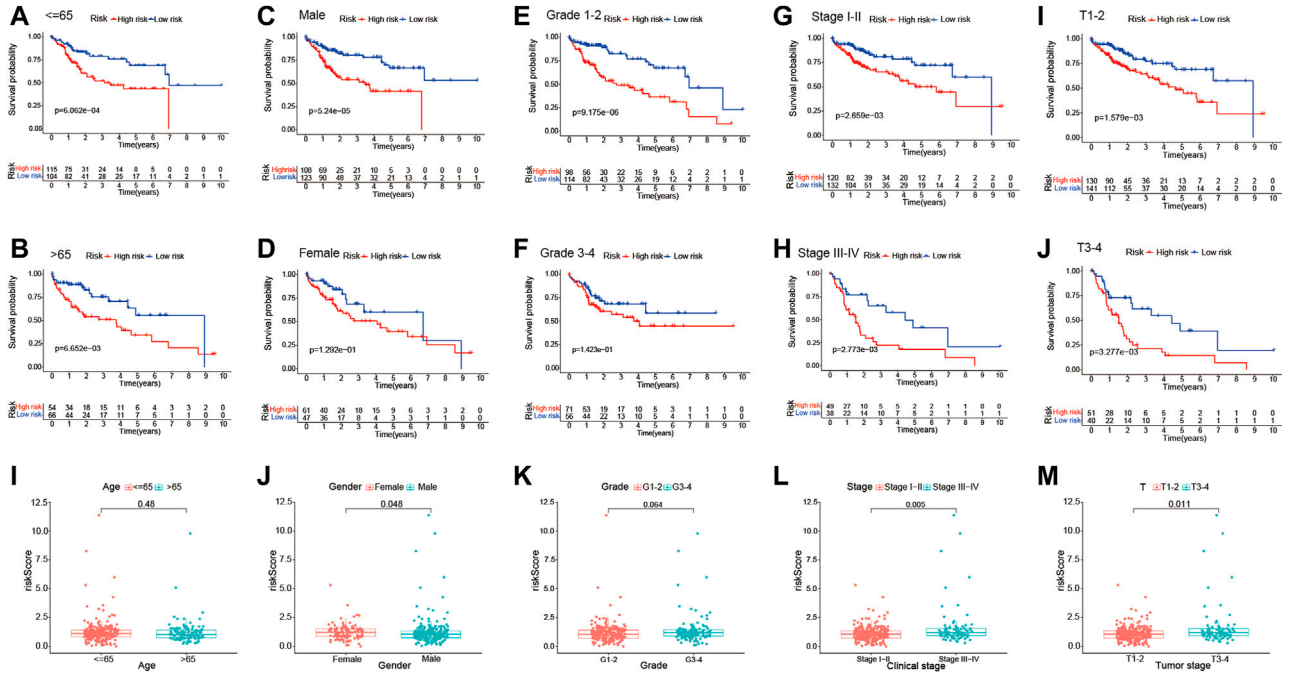

FIGURE 6 | Subgroup analysis of the correlation of clinical features with the risk signature. **(A–J)** Kaplan–Meier survival curve analysis of the risk group with age subgroups (≤65 and >65 years), gender subgroups (female and male), grade subgroups (grades I–II and grades III–IV), and stage subgroups (stages I–II and stages III–IV), and tumor stage subgroups (T1–T2 and T3–T4). **(I–M)** Differential analysis of the risk scores in different subgroups using the Student's *t*-test or Wilcoxon's rank-sum test.

Potential Biological Pathway and Functional Enrichment Analysis Based on the Risk Signature

Firstly, GSEA was performed to probe the latent functional enrichment pathways of the TME-related lncRNAs signature, and the results revealed that tumor-related pathways, including bladder cancer, renal cell carcinoma, DNA replication, cell cycle, ErbB, and Notch signaling pathway, were highly enriched in the high-risk group ($p < 0.05$; **Figure 8A**). To further determine the possible biological pathways associated with the risk signature, DEGs were selected from the high- and low-risk groups based on the criteria $|\log2FC| \geq 1$ and $p < 0.05$. Compared with the low-risk group, a total of 256 DEGs (119 upregulated genes and 136 downregulated genes) were identified in the high-risk group. We then selected DEGs for GO enrichment analysis. The results indicated that certain pathways related to immune response were enriched, such as "humoral immune response," "complement activation," "adaptive immune response," and "B-cell-mediated immunity" (**Figure 8B**). Thus, we can conclude that the prognostic TME-related lncRNA signature might play an important role in reshaping the tumor immune microenvironment, tumorigenesis, and progression of HCC.

The Prognostic Risk Signature Affected Tumor Immune Features and Predicted Treatment Response to Immune Checkpoint Inhibitors

To determine whether the TME-related lncRNA signature influences the infiltration levels of immune cells in HCC, we evaluated the differences in the immune cells between the high- and low-risk groups in HCC patients using ssGSEA and the CIBERSORT algorithm. From the ssGSEA results, we found that the immune cells, including B cells, $CD8^+$ T cells, mast cells, follicular Th cells, Th1 cells, and tumor-infiltrating lymphocytes (TILs), were obviously increased in the low-risk set, and some pathways related to immune function (i.e., immune checkpoint pathway, cytolytic activity, inflammation-promoting, T-cell co-inhibition/stimulation, and INF-II response) were significantly activated in the low-risk group compared with that in the high-risk group ($p < 0.05$; **Figure 9A**). Moreover, the CIBERSORT analysis results suggested that the following immune cell infiltration levels were negatively associated with the risk score: naive B cells ($R = -0.16$, $p = 0.0021$), activated memory $CD4^+$ T cells ($R = -0.2$, $p = 1e{-}04$), $CD8^+$ T cells ($R = -0.23$, $p = 7.1e{-}06$), and γδT cells ($R = -0.16$, $p = 0.003$). On the other hand, a significant positive correlation was observed in the proportions of memory B cells ($R = 0.16$, $p = 0.0021$), M0

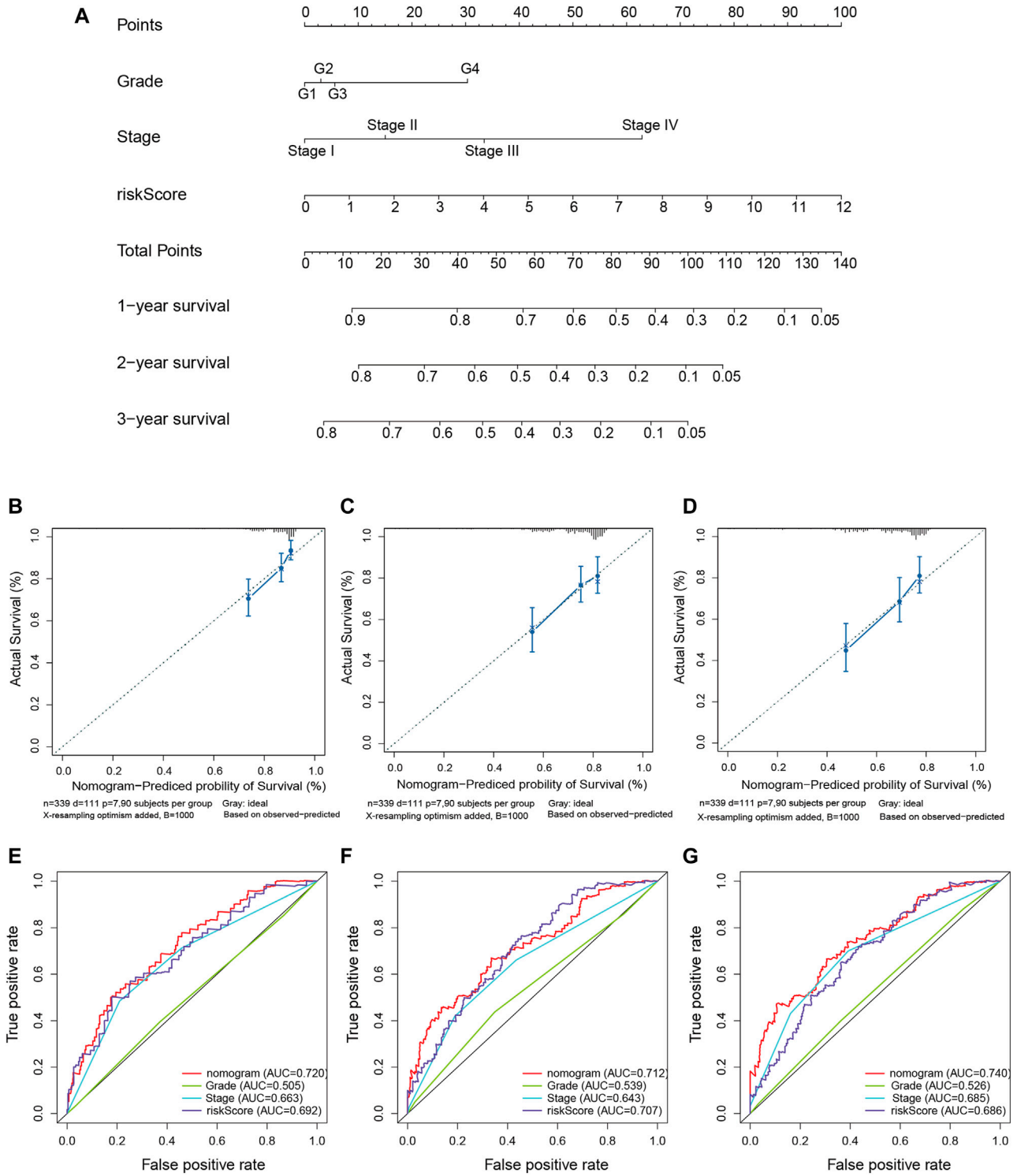

FIGURE 7 | Construction of the predictive nomogram for hepatocellular carcinoma (HCC) patients from The Cancer Genome Atlas (TCGA). **(A)** Nomogram predicting the probability of the 1-, 2-, and 3-year overall survival (OS) of HCC patients. **(B–D)** Calibration curve showing the predictive accuracy of the nomogram. The *Y*-axis represents actual survival, whereas the *X*-axis represents the nomogram-predicted survival. **(E–G)** Receiver operating characteristic (ROC) curve analysis assessing the predictive performance of the nomogram for 1-, 2-, and 3-year OS.

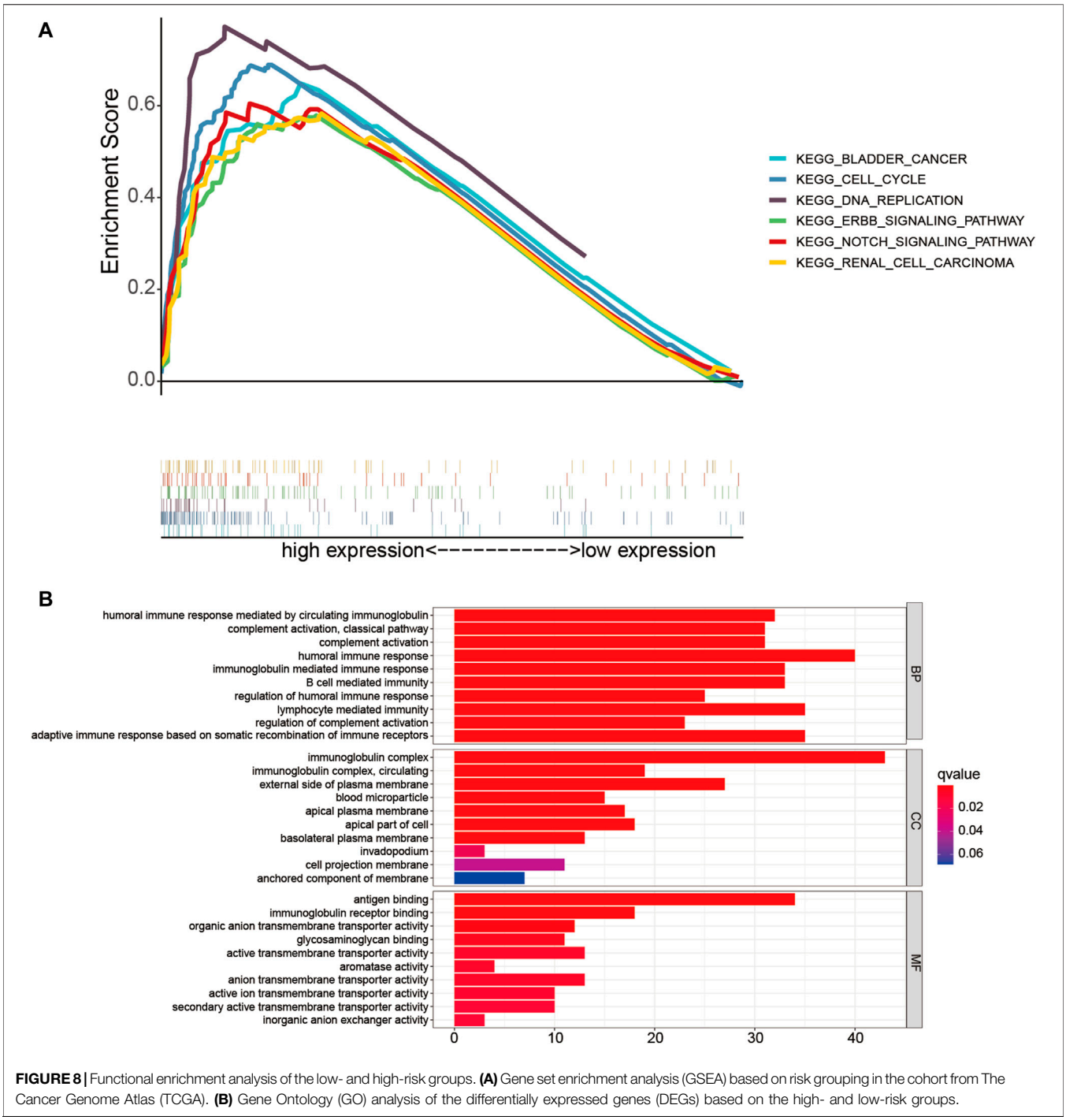

FIGURE 8 | Functional enrichment analysis of the low- and high-risk groups. **(A)** Gene set enrichment analysis (GSEA) based on risk grouping in the cohort from The Cancer Genome Atlas (TCGA). **(B)** Gene Ontology (GO) analysis of the differentially expressed genes (DEGs) based on the high- and low-risk groups.

macrophages ($R = 0.26$, $p = 7.3e{-}07$), and M2 macrophages ($R = 0.17$, $p = 0.0011$) with the risk score (**Table 3** and **Figures 9B–H**). These findings indicate that the signature of six TME-related lncRNAs affected the immune cell infiltration in HCC.

Given the significant differences in the immune checkpoint pathways in the two risk groups, we further investigated whether the risk signature could predict the treatment response to ICIs. We first explored the relationship between the TME-related lncRNAs signature and 46 ICI-related genes and concentrated on the four pivotal ICI-related genes (*PD-1*, *PD-L1*, *PD-L2*, and *CTLA4*). We found significant expression differences in 20 ICI-related genes between the high- and low-risk groups ($p < 0.05$; **Figure 10A**). Among the four key genes, the expression levels of *PD-L2* and *CTLA4* were significantly upregulated in the low-risk group (**Figures 10B–E**), indicating that the risk signature might play a vital role in predicting the treatment response of HCC

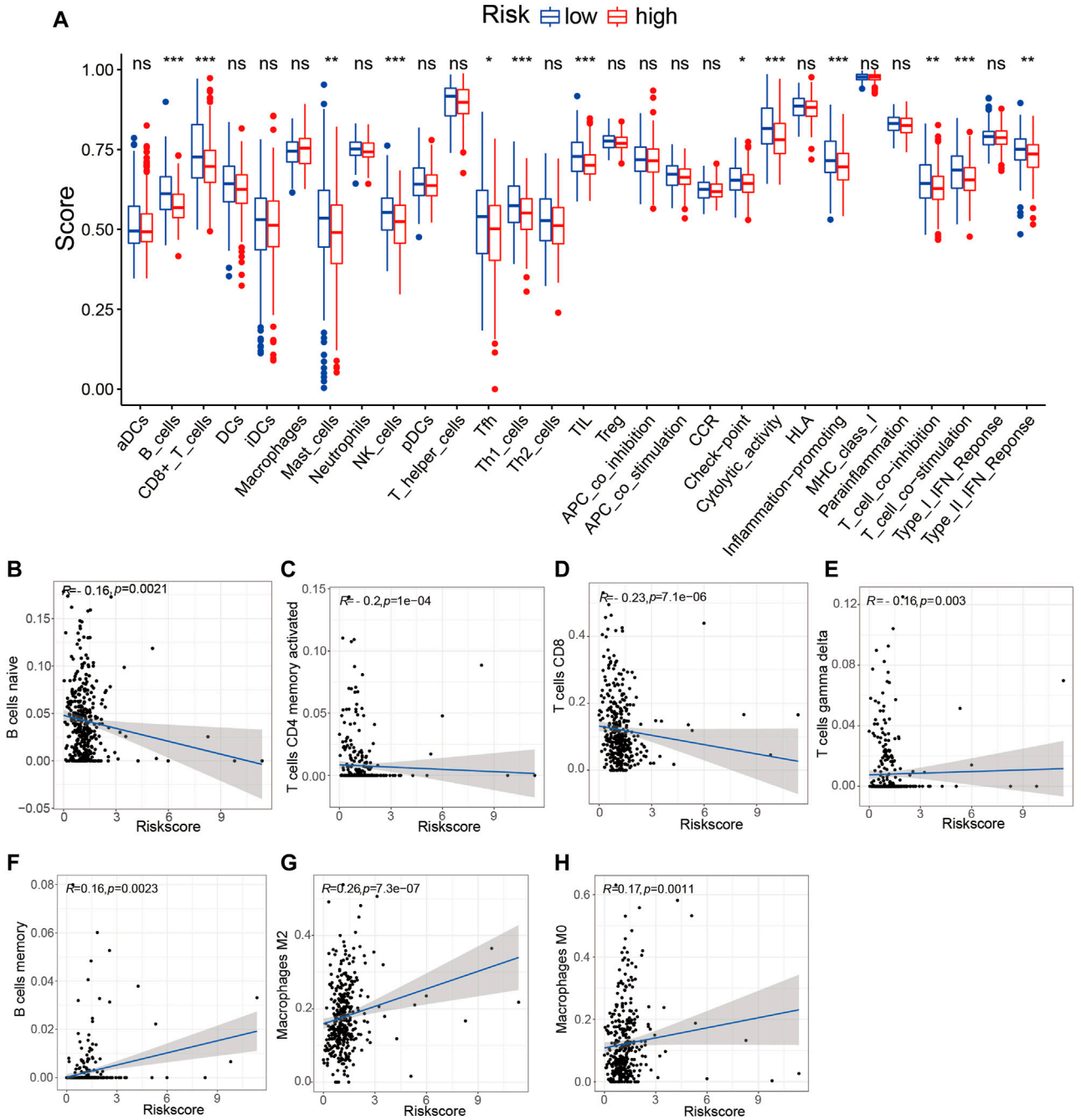

FIGURE 9 | Tumor immune microenvironment state analysis of the tumor microenvironment (TME)-related long noncoding RNA (lncRNA) signature using ssGSEA and the CIBERSORT algorithm. **(A)** Comparison of the immune cell infiltration and immune functions between the low- and high-risk groups. **(B–H)** Correlation analysis between the immune cell infiltration levels and risk scores. *$p < 0.05$; **$p < 0.01$; ***$p < 0.001$. *ssGSEA*, single-sample gene set enrichment analysis.

patients to ICIs. Thus, we further verified the association of the risk signature with the IPS in HCC samples. The results showed that patients in the low-risk group exhibited higher IPS, involving four IPS subtypes [IPS-CTLA4(−)/PD-1(+), IPS-CTLA4(−)/PD-1(+), IPS-CTLA4(+)/PD-1(−), and IPS-CTLA4(+)/PD-1(+)], suggesting that HCC patients with low risk might benefit more from ICI therapy (**Figures 10F–I**).

DISCUSSION

HCC is one of the most prevalent malignancies with high mortality rates, high recurrence rates, and poor prognosis. Increasing evidence suggests that the TME plays a vital role in tumorigenesis and progression (Li et al., 2021). Thus, we focused on the TME of HCC as an entry point to discovering novel

TABLE 3 | Correlation analysis of the 22 immune cell infiltration levels with the risk scores

Immune cells	*R*	*p*-value
Naive B cells	−0.16	0.002095003
Memory B cells	0.16	0.002336936
Plasma cells	−0.1	0.05199941
$CD8^+$ T cells	−0.23	7.15E−06
Naive $CD4^+$ T cells	−0.059	0.263867315
Resting memory CD4 T cells	0.013	0.810632983
Activated memory CD4 T cells	−0.2	0.000102883
Follicular helper T cells	−0.013	0.807812793
Regulatory T cells (Tregs)	−0.055	0.30002029
Gamma delta T cells	−0.16	0.002975049
Resting NK cells	−0.088	0.095016394
Activated NK cells	0.0096	0.855642376
Monocytes	0.061	0.250214059
Macrophages M0	0.17	0.001087181
Macrophages M1	−0.065	0.216904497
Macrophages M2	0.26	7.33E−07
Resting dendritic cells	−0.017	0.743538196
Activated dendritic cells	0.1	0.051715294
Resting mast cells	−0.023	0.666050316
Activated mast cells	0.00092	0.986067845
Eosinophils	−0.037	0.4874298
Neutrophils	0.089	0.09158816

R, *Spearman's rank correlation rho;* NK cells, *natural killer cells.*

prognostic markers. In this study, we found that the stromal, immune, and estimate scores of the TME were significantly positively correlated with longer survival, including OS, PFS, and DFS, in patients with HCC. The TME-related lncRNA risk signature was directly constructed from the DElncRNAs of TME *via* Cox regression analysis. The Kaplan–Meier survival curve analysis manifested that the survival in the high-risk group was worse than that in the low-risk group, and the risk signature could accurately and independently predict the prognosis of HCC patients. In addition, we discovered that the TME-related lncRNA risk signature could significantly affect the infiltration levels of immune cells, and the prognostic risk signature might be able to predict the clinical response of HCC patients to ICIs.

HCC is an inflammation-associated malignancy that comprise numerous immune cell subtypes (i.e., tumor-associated macrophages, tumor-associated neutrophils, and myeloid-derived suppressor cells), forming a complex immune tolerance microenvironment and contributing to the development of HCC (Nishida and Kudo, 2017; Kurebayashi et al., 2018). In recent years, with the wide application of bioinformatics, increasing numbers of research works have applied statistical algorithms to investigate the characteristics of the TME and explore new targets for immunotherapy (Xiang et al., 2021). The study by Li et al. reported that the TME of HCC could be classified into different molecular subtypes based on the immune gene expression profiles, which exhibited different immunogenetic features and survival outcomes (Li et al., 2019a). In this study, the ESTIMATE algorithm was used to explore the correlation of the TME scores (including the stromal, immune, and estimate scores) with survival and clinicopathological parameters in HCC. The results showed that higher TME scores were significantly correlated with longer survival, including OS, PFS, and DFS. Moreover, the immune and stromal scores were inversely correlated with tumor grade and clinical stage. Our results are in accordance with a previous study reporting that the stromal and immune scores were correlated with the 3-year OS of HCC patients (Tian et al., 2020). Therefore, the stromal, immune, and estimate scores might predict the survival of HCC patients and the malignancy of tumors.

According to previous studies, lncRNAs were reported to be indispensable regulators of the TME, ultimately affecting tumor behaviors (Wu et al., 2020; Atianand et al., 2017). For instance, lncRNA-ROR, a stress-responsive lncRNA highly expressed in HCC cells and enriched in extracellular vesicles derived from tumor cells, could induce primary chemoresistance by activating the TGF-β pathway in HCC (Takahashi et al., 2014). Moreover, immune-related lncRNA signatures have been reported as prognostic biomarkers and therapeutic targets in several tumors, including lung adenocarcinoma, bladder cancer, esophageal cancer, gastric cancer, rectal cancer, cervical cancer, and HCC (Chen et al., 2021; Lai et al., 2021; Liu et al., 2021; Nie et al., 2021; Pang et al., 2021; Song et al., 2021; Xing et al., 2021; Ye et al., 2021), indicating that immune-related lncRNAs could effectively be applied to determine the survival, prognosis, and treatment response. However, all these studies focused on excerpting the immune-related lncRNA profiles from the obtained immune-related genes based on co-expression analysis while ignoring the important role of the stromal components in tumor progression; immune-related genes remain inconclusive in different research studies, and there are no uniform criteria for filtering immune-related lncRNAs, which may limit the generalization of the predictive model. Hence, we directly screened DElncRNAs based on the stromal and immune scores to construct a novel prognostic TME-related lncRNA marker, which were considered most likely associated with the TME of HCC. Eventually, we identified six TME-related lncRNAs (LINC01150, LINC02273, LINC00426, AP002954.1, AC007277.1, and AC008549.1) for the construction of a prognostic risk signature. We found that the survival in the low-risk group was better than that in the high-risk group, and the risk score model was reliable for predicting prognosis as an independent indicator of HCC. Stratification analyses revealed that the signature could serve as a prognostic marker for diverse populations of HCC, whether older or younger patients or early- or advanced-stage patients. In addition, the established nomogram based on the risk scores showed better clinical practicality than did the traditional tumor grade or clinical stage system.

Growing evidence highlights the importance of lncRNA in the cancer landscape, such as cell cycle, cell differentiation, DNA repair, epithelial–mesenchymal transition (EMT), and immune regulation (Hu et al., 2018). Some of the lncRNAs in this risk model have already been identified as involved in the malignant phenotypes of HCC or other cancers. For instance, LINC00426 was significantly upregulated in lung adenocarcinoma and played a notable role in accelerating tumor proliferation, invasion, metastasis, and EMT *in vitro* and *in vivo* (Li et al., 2020). LINC00426 may reshape the tumor immune

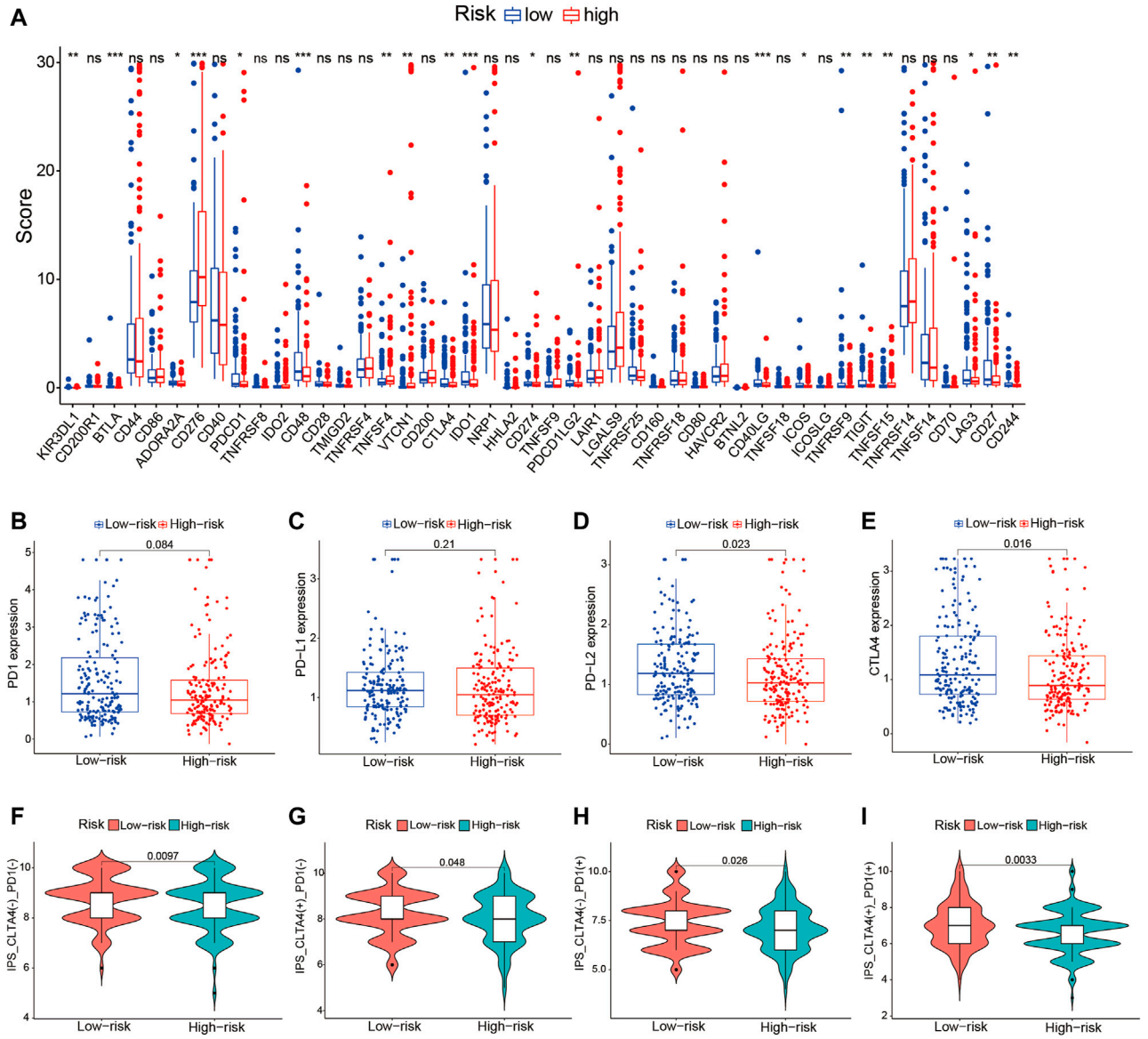

FIGURE 10 | Correlation of the tumor microenvironment (TME)-related long noncoding RNA (lncRNA) signature with ICI-related genes and treatment response to ICIs. **(A)** Comparison of the expression levels of 46 ICI-related genes in the high- and low-risk score groups. **(B–E)** Differences in the expression levels of *PD-1*, *PD-L1*, *PD-L2*, and *CTLA4* between the high- and low-risk groups. **(F–I)** Comparison of the treatment response to ICIs in the two risk score groups. *ICIs*, immune checkpoint inhibitors.

microenvironment, which is positively associated with Th cell differentiation, cytokine signaling pathways, and multiple immune markers, including cytotoxic markers, co-inhibitory and co-stimulatory molecules (i.e., PD1, CTLA4, HAVCR2, TIGIT, FOXP3, and ICOS), and chemokine receptors and ligands (i.e., CXCR3/6, CXCL9/13, CCL4/5/7/19, and CCR7) (Wang et al., 2021b). LINC002273 was reported to be correlated with tumor proliferation, migration, and invasion by epigenetically increasing the AGR2 transcription in breast cancer (Xiu et al., 2019). Nevertheless, the other four prognostic TME-related lncRNAs (LINC01150, AP002954.1, AC007277.1, and AC008549.1) have been rarely reported. Thus, this TME-related lncRNA signature could identify novel biomarkers for further research. In addition, we found that the TME-related lncRNA risk signature was primarily involved in regulating DNA replication, cell cycle, ErbB signaling pathway, Notch signaling pathway, and immunologic function.

In recent years, ICIs have shown survival benefit and have been approved as first- or second-line therapies for HCC (Ntziachristos et al., 2014). Nevertheless, only a minority of patients with HCC can benefit from immune therapy, and less than 30% of patients have an objective response to ICIs. Thus, exploring more accurate biomarkers

to forecast responsiveness to ICI treatment and further screening of the dominant population have become a major challenge in HCC. However, currently, there is no standard and effective biomarker that predicts the treatment response of HCC patients to ICIs (Li et al., 2019b). It was reported that a high PD-L1 expression on tumor cells was associated with better survival, but not predictive of the objective response rate (ORR) (Cho et al., 2009). A high PD-1 expression in tumor was associated with ORR (Cho et al., 2009; Sangro et al., 2020). Recently, pieces of evidence have indicated that some lncRNAs were involved in the regulation of ICI-related genes in the cancer immunity cycle (Tchekneva et al., 2019; Wu et al., 2020). For instance, the lncRNA AFAP1-AS1 has been discovered to regulate PD-1/PD-L1 signaling in the TME of nasopharyngeal carcinoma, and its expression was positively associated with PD-1 (Tang et al., 2017; Tchekneva et al., 2019). Previous studies reported that immune-related lncRNA signatures can predict the treatment response to ICIs, which focused on analyzing the association of lncRNAs and ICB-related key genes (*PD-1*, *PD-L1*, *PD-L2*, and *CTLA4*) (Zhang et al., 2020; Zhou et al., 2021b). In this study, we comprehensively explored the association among 46 immune checkpoint-related genes, IPS, and the TME-related lncRNA signature, with the aim of finding reliable predictors of ICI therapy in HCC. We revealed that 20 out of the 46 ICB-related genes were significantly different between the high- and low-risk groups, and the expression levels of *PD-L2* and *CTLA4* were significantly upregulated in the low-risk group. Furthermore, HCC patients in the low-risk group exhibited higher IPS and tended to have a better response to ICI treatment. These findings indicate that the prognostic TME-related lncRNA signature may be able to predict the clinical outcome of ICI therapy in HCC samples. In addition, increasing evidence has demonstrated that lncRNAs seriously affect immune cell infiltration (Wang et al., 2010). Thus, we analyzed the correlation between the TME-related lncRNA risk signature and specific immune cells or immune pathways. We discovered that some immune cells, which were beneficial for enhancing immune responses toward cancer, were remarkably upregulated in the low-risk group, including B cells, $CD8^+$ T cells, mast cells, follicular Th cells, Th1 cells, and TILs. Moreover, some immune infiltration cells were negatively correlated with the risk score, such as those of naive B cells, activated memory $CD4^+$ T cells, $CD8^+$ T cells, and γδ T cells, which can be understood as, the higher the risk score, the lower the infiltration level of the immune response cells. Conversely, M2 macrophages were significantly positively correlated with the risk score, which contributes to tumor angiogenesis, metastasis, EMT, and immune suppression in HCC (Sierra et al., 2017). The differences in the immune cells between the high- and low-risk groups may partly account for HCC patients in the high-risk group showing worse prognosis than those in the low-risk group.

When comparing this study with previous studies that explored the immune-related biomolecular predictors in HCC, some advantages of our research are identified. Firstly, we focused on identifying novel prognostic lncRNA markers from the perspective of the TME. Secondly, we established a reasonable relationship between lncRNAs and the TME based on the intersecting DElncRNAs of the TME scores and constructed a reliable risk signature, rather than relying on immune-related genes. Finally, we comprehensively explored the association of the TME-related lncRNA signatures with the ICI response of HCC patients according to the ICI-related genes and IPS.

In conclusion, we performed an overall analysis of the association between the TME scores and survival of HCC patients. A novel TME-related prognostic risk signature was established, which could be effectively applied as an independent prognostic biomarker and a predictive factor of ICI therapy for HCC patients.

DATA AVAILABILITY STATEMENT

The original contributions presented in the study are included in the article/**Supplementary Material**. Further inquiries can be directed to the corresponding author.

AUTHOR CONTRIBUTIONS

JW conceived and designed the study. SH and JZ were responsible for the collection and analysis of the research data. SH drafted the manuscript. XL, LZ, and JW critically and carefully revised the manuscript. All authors read and approved the final manuscript.

FUNDING

This research was supported by the National Natural Science Foundation of China (no. 82060435).

ACKNOWLEDGMENTS

We acknowledge and appreciate our colleagues for their valuable efforts and comments on this paper.

SUPPLEMENTARY MATERIAL

The Supplementary Material for this article can be found online at: https://www.frontiersin.org/articles/10.3389/fmolb.2021.781307/full#supplementary-material

REFERENCES

Atianand, M. K., Caffrey, D. R., and Fitzgerald, K. A. (2017). Immunobiology of Long Noncoding RNAs. *Annu. Rev. Immunol.* 35, 177–198. doi:10.1146/annurev-immunol-041015-055459

Chen, Y., Zhang, X., Li, J., and Zhou, M. (2021). Immune-Related Eight-lncRNA Signature for Improving Prognosis Prediction of Lung Adenocarcinoma. *J. Clin. Lab. Anal.* 35, e24018. doi:10.1002/jcla.24018

Cho, O. H., Shin, H. M., Miele, L., Golde, T. E., Fauq, A., Minter, L. M., et al. (2009). Notch Regulates Cytolytic Effector Function in CD8+ T Cells. *J. Immunol.* 182 (6), 3380–3389. doi:10.4049/jimmunol.0802598

Demir, T., Lee, S. S., and Kaseb, A. O. (2021). Systemic Therapy of Liver Cancer. *Adv. Cancer Res.* 149, 257–294. doi:10.1016/bs.acr.2020.12.001

El-Khoueiry, A. B., Sangro, B., Yau, T., Crocenzi, T. S., Kudo, M., Hsu, C., et al. (2017). Nivolumab in Patients with Advanced Hepatocellular Carcinoma (CheckMate 040): An Open-Label, Non-comparative, Phase 1/2 Dose Escalation and Expansion Trial. *Lancet* 389 (10088), 2492–2502. doi:10.1016/s0140-6736(17)31046-2

Fan, Y., Wang, Y.-f., Su, H.-f., Fang, N., Zou, C., Li, W.-f., et al. (2016). RETRACTED ARTICLE: Decreased Expression of the Long Noncoding RNA LINC00261 Indicate Poor Prognosis in Gastric Cancer and Suppress Gastric Cancer Metastasis by Affecting the Epithelial-Mesenchymal Transition. *J. Hematol. Oncol.* 9 (1), 57. doi:10.1186/s13045-016-0288-8

Galdiero, M. R., Bonavita, E., Barajon, I., Garlanda, C., Mantovani, A., and Jaillon, S. (2013). Tumor Associated Macrophages and Neutrophils in Cancer. *Immunobiology* 218 (11), 1402–1410. doi:10.1016/j.imbio.2013.06.003

Hu, X., Sood, A. K., Dang, C. V., and Zhang, L. (2018). The Role of Long Noncoding RNAs in Cancer: the Dark Matter Matters. *Curr. Opin. Genet. Development* 48, 8–15. doi:10.1016/j.gde.2017.10.004

Jemal, A., Ward, E. M., Johnson, C. J., Cronin, K. A., Ma, J., Ryerson, B., et al. (2017). Annual Report to the Nation on the Status of Cancer, 1975-2014, Featuring Survival. *J. Natl. Cancer Inst.* 109 (9), djx030. doi:10.1093/jnci/djx030

Jiang, R., Tang, J., Chen, Y., Deng, L., Ji, J., Xie, Y., et al. (2017). The Long Noncoding RNA Lnc-EGFR Stimulates T-Regulatory Cells Differentiation Thus Promoting Hepatocellular Carcinoma Immune Evasion. *Nat. Commun.* 8, 15129. doi:10.1038/ncomms15129

Khemlina, G., Ikeda, S., and Kurzrock, R. (2017). The Biology of Hepatocellular Carcinoma: Implications for Genomic and Immune Therapies. *Mol. Cancer* 16 (1), 149. doi:10.1186/s12943-017-0712-x

Kurebayashi, Y., Ojima, H., Tsujikawa, H., Kubota, N., Maehara, J., Abe, Y., et al. (2018). Landscape of Immune Microenvironment in Hepatocellular Carcinoma and its Additional Impact on Histological and Molecular Classification. *Hepatology* 68 (3), 1025–1041. doi:10.1002/hep.29904

Lai, C., Wu, Z., Li, Z., Yu, H., Li, K., Tang, Z., et al. (2021). A Robust Signature of Immune-related Long Non-Coding RNA to Predict the Prognosis of Bladder Cancer. *Cancer Med.* 10 (18), 6534–6545. doi:10.1002/cam4.4167

Li, H., Mu, Q., Zhang, G., Shen, Z., Zhang, Y., Bai, J., et al. (2020). Linc00426 Accelerates Lung Adenocarcinoma Progression by Regulating miR-455-5p as a Molecular Sponge. *Cell Death Dis.* 11 (12), 1051. doi:10.1038/s41419-020-03259-2

Li, W., Wang, H., Ma, Z., Zhang, J., Ou-Yang, W., Qi, Y., et al. (2019). Multi-omics Analysis of Microenvironment Characteristics and Immune Escape Mechanisms of Hepatocellular Carcinoma. *Front. Oncol.* 9, 1019. doi:10.3389/fonc.2019.01019

Li, Z., Wu, T., Zheng, B., and Chen, L. (2019). Individualized Precision Treatment: Targeting TAM in HCC. *Cancer Lett.* 458, 86–91. doi:10.1016/j.canlet.2019.05.019

Li, Z., Zhang, X., Liu, C., and Ma, J. (2021). Non-Immune Cell Components in the Gastrointestinal Tumor Microenvironment Influencing Tumor Immunotherapy. *Front. Cell Dev. Biol.* 9, 729941. doi:10.3389/fcell.2021.729941

Liu, Y., Wu, Q., Fan, X., Li, W., Li, X., Zhu, H., et al. (2021). A Novel Prognostic Signature of Immune-Related lncRNA Pairs in Lung Adenocarcinoma. *Sci. Rep.* 11 (1), 16794. doi:10.1038/s41598-021-96236-4

Llovet, J. M., Kelley, R. K., Villanueva, A., Singal, A. G., Pikarsky, E., Roayaie, S., et al. (2021). Hepatocellular Carcinoma. *Nat. Rev. Dis. Primers* 7 (1), 6. doi:10.1038/s41572-020-00240-3

Necula, L., Matei, L., Dragu, D., Neagu, A. I., Mambet, C., Nedeianu, S., et al. (2019). Recent Advances in Gastric Cancer Early Diagnosis. *World J. Gastroenterol.* 25 (17), 2029–2044. doi:10.3748/wjg.v25.i17.2029

Nie, Y., Li, J., Wu, W., Guo, D., Lei, X., Zhang, T., et al. (2021). A Novel Nine-lncRNA Risk Signature Correlates with Immunotherapy in Hepatocellular Carcinoma. *Front. Oncol.* 11, 706915. doi:10.3389/fonc.2021.706915

Nishida, N., and Kudo, M. (2017). Immunological Microenvironment of Hepatocellular Carcinoma and its Clinical Implication. *Oncology* 92 (Suppl. 1), 40–49. doi:10.1159/000451015

Nishino, M., Ramaiya, N. H., Hatabu, H., and Hodi, F. S. (2017). Monitoring Immune-Checkpoint Blockade: Response Evaluation and Biomarker Development. *Nat. Rev. Clin. Oncol.* 14 (11), 655–668. doi:10.1038/nrclinonc.2017.88

Ntziachristos, P., Lim, J. S., Sage, J., and Aifantis, I. (2014). From Fly Wings to Targeted Cancer Therapies: A Centennial for Notch Signaling. *Cancer Cell* 25 (3), 318–334. doi:10.1016/j.ccr.2014.02.018

Ovais, M., Guo, M., and Chen, C. (2019). Tailoring Nanomaterials for Targeting Tumor-Associated Macrophages. *Adv. Mater.* 31 (19), e1808303. doi:10.1002/adma.201808303

Pang, J., Pan, H., Yang, C., Meng, P., Xie, W., Li, J., et al. (2021). Prognostic Value of Immune-Related Multi-lncRNA Signatures Associated with Tumor Microenvironment in Esophageal Cancer. *Front. Genet.* 12, 722601. doi:10.3389/fgene.2021.722601

Qin, S., Xu, L., Yi, M., Yu, S., Wu, K., and Luo, S. (2019). Novel Immune Checkpoint Targets: Moving beyond PD-1 and CTLA-4. *Mol. Cancer* 18 (1), 155. doi:10.1186/s12943-019-1091-2

Quail, D. F., and Joyce, J. A. (2013). Microenvironmental Regulation of Tumor Progression and Metastasis. *Nat. Med.* 19 (11), 1423–1437. doi:10.1038/nm.3394

Rooney, M. S., Shukla, S. A., Wu, C. J., Getz, G., and Hacohen, N. (2015). Molecular and Genetic Properties of Tumors Associated with Local Immune Cytolytic Activity. *Cell* 160 (1-2), 48–61. doi:10.1016/j.cell.2014.12.033

Sanchez Calle, A., Kawamura, Y., Yamamoto, Y., Takeshita, F., and Ochiya, T. (2018). Emerging Roles of Long Non-Coding RNA in Cancer. *Cancer Sci.* 109 (7), 2093–2100. doi:10.1111/cas.13642

Sangro, B., Melero, I., Wadhawan, S., Finn, R. S., Abou-Alfa, G. K., Cheng, A.-L., et al. (2020). Association of Inflammatory Biomarkers with Clinical Outcomes in Nivolumab-Treated Patients with Advanced Hepatocellular Carcinoma. *J. Hepatol.* 73 (6), 1460–1469. doi:10.1016/j.jhep.2020.07.026

Siegel, R. L., Miller, K. D., and Jemal, A. (2018). Cancer Statistics, 2018. *CA Cancer J. Clin.* 68 (1), 7–30. doi:10.3322/caac.21442

Sierra, R. A., Trillo-Tinoco, J., Mohamed, E., Yu, L., Achyut, B. R., Arbab, A., et al. (2017). Anti-Jagged Immunotherapy Inhibits MDSCs and Overcomes Tumor-Induced Tolerance. *Cancer Res.* 77 (20), 5628–5638. doi:10.1158/0008-5472.can-17-0357

Song, S., Liu, S., Wei, Z., Jin, X., Mao, D., He, Y., et al. (2021). Identification of an Immune-Related Long Noncoding RNA Pairs Model to Predict Survival and Immune Features in Gastric Cancer. *Front. Cell Dev. Biol.* 9, 726716. doi:10.3389/fcell.2021.726716

Sun, Y., Zhang, F., Wang, L., Song, X., Jing, J., Zhang, F., et al. (2019). A Five lncRNA Signature for Prognosis Prediction in Hepatocellular Carcinoma. *Mol. Med. Rep.* 19 (6), 5237–5250. doi:10.3892/mmr.2019.10203

Takahashi, K., Yan, I. K., Kogure, T., Haga, H., and Patel, T. (2014). Extracellular Vesicle-Mediated Transfer of Long Non-coding RNA ROR Modulates Chemosensitivity in Human Hepatocellular Cancer. *FEBS Open Bio.* 4, 458–467. doi:10.1016/j.fob.2014.04.007

Tang, Y., He, Y., Shi, L., Yang, L., Wang, J., Lian, Y., et al. (2017). Co-Expression of AFAP1-AS1 and PD-1 Predicts Poor Prognosis in Nasopharyngeal Carcinoma. *Oncotarget* 8 (24), 39001–39011. doi:10.18632/oncotarget.16545

Tchekneva, E. E., Goruganthu, M. U. L., Uzhachenko, R. V., Thomas, P. L., Antonucci, A., Chekneva, I., et al. (2019). Determinant Roles of Dendritic Cell-Expressed Notch Delta-like and Jagged Ligands on Anti-tumor T Cell Immunity. *J. Immunother. Cancer* 7 (1), 95. doi:10.1186/s40425-019-0566-4

Tian, Z., Wang, Z., Chen, Y., Qu, S., Liu, C., Chen, F., et al. (2020). Bioinformatics Analysis of Prognostic Tumor Microenvironment-Related Genes in the Tumor Microenvironment of Hepatocellular Carcinoma. *Med. Sci. Monit.* 26, e922159. doi:10.12659/MSM.922159

Wang, B., Mou, H., Liu, M., Ran, Z., Li, X., Li, J., et al. (2021). Multiomics Characteristics of Neurogenesis-Related Gene Are Dysregulated in Tumor Immune Microenvironment. *NPJ Genom. Med.* 6 (1), 37. doi:10.1038/s41525-021-00202-y

Wang, C.-J., Zhu, C.-C., Xu, J., Wang, M., Zhao, W.-Y., Liu, Q., et al. (2019). The lncRNA UCA1 Promotes Proliferation, Migration, Immune Escape and Inhibits Apoptosis in Gastric Cancer by Sponging Anti-Tumor miRNAs. *Mol. Cancer* 18 (1), 115. doi:10.1186/s12943-019-1032-0

Wang, H., Jiang, W., Wang, H., Wei, Z., Li, H., Yan, H., et al. (2021). Identification of Mutation Landscape and Immune Cell Component for Liver Hepatocellular Carcinoma Highlights Potential Therapeutic Targets and Prognostic Markers. *Front. Genet.* 12, 737965. doi:10.3389/fgene.2021.737965

Wang, Y., Yang, L., Dong, X., Yang, X., Zhang, X., Liu, Z., et al. (2020). Overexpression of NNT-AS1 Activates TGF-β Signaling to Decrease Tumor CD4 Lymphocyte Infiltration in Hepatocellular Carcinoma. *Biomed. Res. Int.* 2020, 8216541. doi:10.1155/2020/8216541

Wang, Y.-C., He, F., Feng, F., Liu, X.-W., Dong, G.-Y., Qin, H.-Y., et al. (2010). Notch Signaling Determines the M1 versus M2 Polarization of Macrophages in Antitumor Immune Responses. *Cancer Res.* 70 (12), 4840–4849. doi:10.1158/0008-5472.can-10-0269

Wu, F., Wei, H., Liu, G., and Zhang, Y. (2021). Bioinformatics Profiling of Five Immune-Related lncRNAs for a Prognostic Model of Hepatocellular Carcinoma. *Front. Oncol.* 11, 667904. doi:10.3389/fonc.2021.667904

Wu, M., Fu, P., Qu, L., Liu, J., and Lin, A. (2020). Long Noncoding RNAs, New Critical Regulators in Cancer Immunity. *Front. Oncol.* 10, 550987. doi:10.3389/fonc.2020.550987

Wu, W., Jia, L., Zhang, Y., Zhao, J., Dong, Y., and Qiang, Y. (2021). Exploration of the Prognostic Signature Reflecting Tumor Microenvironment of Lung Adenocarcinoma Based on Immunologically Relevant Genes. *Bioengineered* 12 (1), 7417–7431. doi:10.1080/21655979.2021.1974779

Xiang, S., Li, J., Shen, J., Zhao, Y., Wu, X., Li, M., et al. (2021). Identification of Prognostic Genes in the Tumor Microenvironment of Hepatocellular Carcinoma. *Front. Immunol.* 12, 653836. doi:10.3389/fimmu.2021.653836

Xing, X.-L., Xing, C., Huang, Z., Yao, Z.-Y., and Liu, Y.-W. (2021). Immune-Related lncRNAs to Construct Novel Signatures and Predict the Prognosis of Rectal Cancer. *Front. Oncol.* 11, 661846. doi:10.3389/fonc.2021.661846

Xiu, B., Chi, Y., Liu, L., Chi, W., Zhang, Q., Chen, J., et al. (2019). LINC02273 Drives Breast Cancer Metastasis by Epigenetically Increasing AGR2 Transcription. *Mol. Cancer* 18 (1), 187. doi:10.1186/s12943-019-1115-y

Xu, Q., Wang, Y., and Huang, W. (2021). Identification of Immune-Related lncRNA Signature for Predicting Immune Checkpoint Blockade and Prognosis in Hepatocellular Carcinoma. *Int. Immunopharmacol.* 92, 107333. doi:10.1016/j.intimp.2020.107333

Xu, Z., Peng, B., Liang, Q., Chen, X., Cai, Y., Zeng, S., et al. (2021). Construction of a Ferroptosis-Related Nine-lncRNA Signature for Predicting Prognosis and Immune Response in Hepatocellular Carcinoma. *Front. Immunol.* 12, 719175. doi:10.3389/fimmu.2021.719175

Ye, J., Chen, X., and Lu, W. (2021). Identification and Experimental Validation of Immune-Associate lncRNAs for Predicting Prognosis in Cervical Cancer. *Onco Targets Ther.* 14, 4721–4734. doi:10.2147/ott.s322998

Yoon, J. S., Sinn, D. H., Lee, J. H., Kim, H. Y., Lee, C. H., Kim, S. W., et al. (2019). Tumor Marker-Based Definition of the Transarterial Chemoembolization-Refractoriness in Intermediate-Stage Hepatocellular Carcinoma: A Multi-Cohort Study. *Cancers* 11 (11). doi:10.3390/cancers11111721

Yoshihara, K., Shahmoradgoli, M., Martínez, E., Vegesna, R., Kim, H., Torres-Garcia, W., et al. (2013). Inferring Tumour Purity and Stromal and Immune Cell Admixture from Expression Data. *Nat. Commun.* 4, 2612. doi:10.1038/ncomms3612

Yu, W., Wang, Y., and Guo, P. (2018). Notch Signaling Pathway Dampens Tumor-Infiltrating CD8+ T Cells Activity in Patients with Colorectal Carcinoma. *Biomed. Pharmacother.* 97, 535–542. doi:10.1016/j.biopha.2017.10.143

Yuan, L., Xu, Z.-Y., Ruan, S.-M., Mo, S., Qin, J.-J., and Cheng, X.-D. (2020). Long Non-coding RNAs towards Precision Medicine in Gastric Cancer: Early Diagnosis, Treatment, and Drug Resistance. *Mol. Cancer* 19 (1), 96. doi:10.1186/s12943-020-01219-0

Zhang, Y., Zhang, L., Xu, Y., Wu, X., Zhou, Y., and Mo, J. (2020). Immune-related Long Noncoding RNA Signature for Predicting Survival and Immune Checkpoint Blockade in Hepatocellular Carcinoma. *J. Cell Physiol.* 235 (12), 9304–9316. doi:10.1002/jcp.29730

Zhou, C., Zhang, H., and Lu, L. (2021). Identification and Validation of Hypoxia-Related lncRNA Signature as a Prognostic Model for Hepatocellular Carcinoma. *Front. Genet.* 12, 744113. doi:10.3389/fgene.2021.744113

Zhou, P., Lu, Y., Zhang, Y., and Wang, L. (2021). Construction of an Immune-Related Six-lncRNA Signature to Predict the Outcomes, Immune Cell Infiltration, and Immunotherapy Response in Patients with Hepatocellular Carcinoma. *Front. Oncol.* 11, 661758. doi:10.3389/fonc.2021.661758

Zhu, A. X., Finn, R. S., Edeline, J., Cattan, S., Ogasawara, S., Palmer, D., et al. (2018). Pembrolizumab in Patients with Advanced Hepatocellular Carcinoma Previously Treated with Sorafenib (KEYNOTE-224): A Non-Randomised, Open-Label Phase 2 Trial. *Lancet Oncol.* 19 (7), 940–952. doi:10.1016/s1470-2045(18)30351-6

Conflict of Interest: The authors declare that the research was conducted in the absence of any commercial or financial relationships that could be construed as a potential conflict of interest.

Publisher's Note: All claims expressed in this article are solely those of the authors and do not necessarily represent those of their affiliated organizations, or those of the publisher, the editors, and the reviewers. Any product that may be evaluated in this article, or claim that may be made by its manufacturer, is not guaranteed or endorsed by the publisher.

frontiers in Molecular Biosciences

ORIGINAL RESEARCH
published: 24 December 2021
doi: 10.3389/fmolb.2021.673918

Immune Signature-Based Risk Stratification and Prediction of Immunotherapy Efficacy for Bladder Urothelial Carcinoma

Fangfang Liang[1†], Yansong Xu[2†], Yi Chen[3], Huage Zhong[3], Zhen Wang[3], Tianwen Nong[1] and Jincai Zhong[1]*

[1]Department of Medical Oncology, Guangxi Medical University First Affiliated Hospital, Nanning, China, [2]Emergency Department, Guangxi Medical University First Affiliated Hospital, Nanning, China, [3]College of Oncology, Guangxi Medical University, Nanning, China

Immune-related genes (IRGs) are closely related to tumor progression and the immune microenvironment. Few studies have investigated the effect of tumor immune microenvironment on the survival and response to immune checkpoint inhibitors of patients with bladder urothelial carcinoma (BLCA). We constructed two IRG-related prognostic signatures based on gene–immune interaction for predicting risk stratification and immunotherapeutic responses. We also verified their predictive ability on internal and overall data sets. Patients with BLCA were divided into high- and low-risk groups. The high-risk group had poor survival, enriched innate immune-related cell subtypes, low tumor mutation burden, and poor response to anti-PD-L1 therapy. Our prognostic signatures can be used as reliable prognostic biomarkers, which may be helpful to screen the people who will benefit from immunotherapy and guide the clinical decision-making of patients with BLCA.

Keywords: bladder urothelial carcinoma, immune-related genes, tumor immune microenvironment, immune checkpoint inhibitor, immunotherapy, prognostic model

OPEN ACCESS

Edited by:
Shengtao Zhou,
Sichuan University, China

Reviewed by:
Sanjay Mishra,
The Ohio State University, United States
Paula Dobosz,
MNM Diagnostics Sp. z o. o., Poland

***Correspondence:**
Jincai Zhong
13907719863@163.com

†These authors have contributed equally to this work and share first authorship

Specialty section:
This article was submitted to Molecular Diagnostics and Therapeutics, a section of the journal Frontiers in Molecular Biosciences

Received: *28 February 2021*
Accepted: *15 November 2021*
Published: *24 December 2021*

Citation:
Liang F, Xu Y, Chen Y, Zhong H, Wang Z, Nong T and Zhong J (2021) Immune Signature-Based Risk Stratification and Prediction of Immunotherapy Efficacy for Bladder Urothelial Carcinoma. Front. Mol. Biosci. 8:673918. doi: 10.3389/fmolb.2021.673918

INTRODUCTION

Bladder cancer is the 10th most common cancer worldwide. In 2017, 474,000 new cases of bladder cancer were diagnosed and 197,000 deaths from the disease were reported worldwide (Fitzmaurice et al., 2019). Bladder urothelial carcinoma (BLCA) accounts for about 80–90% of all pathological types (Felsenstein and Theodorescu, 2018). About 25% of patients have muscle-invasive or metastatic lesions at the time of onset (Kamat et al., 2016). Patients have only 12–15 months of overall survival (OS) after being diagnosed before 2016 because of the lack of substantial progress in

Abbreviations: AUCs, areas under the curve; BLCA, bladder urothelial carcinoma; BP, biological process; CR, complete response; CTLA-4, cytotoxic T lymphocyte antigen 4; CC, cellular component; DEGs, differentially expressed genes; DE-IRGs, differentially expressed immune-related genes; DFS, disease-free survival; DE-TFs, differentially expressed transcription factor-related genes; EGF, epidermal growth factor; GSEA, gene set enrichment analysis; GTEx, Genotype-Tissue Expression; HB-EGF, Heparin-binding EGF; IRGs, immune-related genes; ICIs, immune checkpoint inhibitors; LASSO, least absolute shrinkage and selection operator; MF, molecular function; mUC, metastatic urothelial cancer; PR, partial response; PD, progressive disease; ROC, receiver operating characteristic; SD, stable disease; TMB, tumor mutation burden; TCGA, The Cancer Genome Atlas; TF, transcription factor-related; TILs, Tumor-infiltrating lymphocytes.

BLCA treatment; this finding has been maintained for the past 30 years (Bellmunt et al., 2017; Vlachostergios and Faltas, 2018). However, since 2016, several studies on immune checkpoint inhibitors (ICIs) have changed the treatment paradigm for metastatic urothelial cancer (mUC) and outlined a future therapeutic landscape (Rosenberg et al., 2016; Sharma et al., 2016; Apolo et al., 2017; Powles et al., 2017).

Considering that bladder cancer has high tumor mutation burden (TMB) and many mutations may be antigenic (Felsenstein and Theodorescu, 2018), traditional immunotherapy using *Bacillus* Calmette-Guérin has been successful for the treatment of early diagnosed bladder cancer (Kamat et al., 2015). Compared with previous first-line or second-line chemotherapy for mUC, new immunotherapy is undoubtedly an exciting breakthrough. However, the response rate of PD-1/PD-L1 inhibitors is only 20–24% (Kamat et al., 2015). PD-L1 status cannot highly predict treatment response; in this regard, more accurate predictive biomarkers should be identified to prescreen appropriate patients for immunotherapy and design personalized treatment. Existing immune and inflammatory markers in tumor may be the best biomarkers for evaluating the potential response of ICIs (Felsenstein and Theodorescu, 2018).

Studies have found that bladder cancer, similar to breast cancer, can be divided into different subtypes based on gene expression diversity and histological characteristics; this classification may be conducive to hierarchical management and precise treatment (Groenendijk et al., 2016; The Cancer Genome Atlas Research Network, 2014). Epigenetic regulatory mechanisms, such as DNA methylation, histone modification, and ncRNA expression, change with the development of bladder cancer and therefore may be used as potential biomarkers and therapeutic targets (Dudziec et al., 2011; Schulz and Goering, 2016; Peng et al., 2018). Additionally, differences in the molecular and genetic characteristics of tumor cells (such as gene mutation and copy number alteration) and the tumor microenvironment have a high impact on tumor invasiveness and sensitivity to treatment. The molecular profiles of immune components in the tumor microenvironment have great value as prognostic biomarkers. Immune-related genes (IRGs) can be quantified from a variety of cell types in a sample and have a predictive value for BLCA prognosis; these genes may be suitable biomarkers (Sweis et al., 2016; Li et al., 2020; Xu et al., 2020).

In this study, we downloaded the expression profiles and clinical information of patients from The Cancer Genome Atlas (TCGA)-BLCA cohort, analyzed the resulting differentially expressed genes (DEGs), and intersected the DEGs with the IRG sets downloaded from the ImmPort database (https://www.immport.org/home) to obtain differentially expressed immune-related genes (DE-IRGs). The DE-IRGs associated with prognosis were further analyzed to construct prognostic models. Furthermore, we assessed the differences in the immune cell infiltration, TMB, and response to ICI treatment between the high- and low-risk groups. The robust prognostic model may improve risk stratification and provide a more accurate assessment for the clinical management of BLCA.

MATERIALS AND METHODS

Data Acquisition

The latest RNA-Seq expression profile data and clinical information of patients with BLCA were downloaded from TCGA (https://www.nature.com/articles/ng.2764, 2013), and data were also obtained from the Genotype-Tissue Expression (GTEx, https://www.gtexportal.org/home/) project. The lists of 456 IRGs and 318 transcription factors were derived from the ImmPort database (Sweis et al., 2016; Li et al., 2020; Xu et al., 2020) and Cistrome Cancer database (Mei et al., 2017), respectively, for subsequent analysis. The detailed clinicopathological and sequencing information of patients with advanced urothelial cancer treated with anti-PD-L1 agents (IMvigor210 cohort) were downloaded from the "IMvigor210CoreBiologies" R package (Mariathasan et al., 2018).

DE-IRG Identification

The expression profiles from TCGA and GTEx portal were integrated using the "limma" R package (Ritchie et al., 2015) to calculate the DEGs between BLCA tumor tissues and normal tissues (FDR <0.05 and |log2FC| > 1). All DEGs and IRGS were crossed to obtain 172 DE-IRGs. GO and KEGG pathway enrichment analyses of the DE-IRGs were conducted using the "clusterProfiler" R package (v3.16.1) (Yu et al., 2012).

Construction and Validation of OS and Disease-Free Survival Prognostic Signatures for Bladder Urothelial Carcinoma

Univariate Cox regression analysis was conducted to screen for DE-IRGs that are significantly associated with prognosis ($p < 0.05$). Least absolute shrinkage and selection operator (LASSO) Cox regression model (Tibshirani, 1996; Goeman, 2010) was used to construct an immune-related risk model using the "glmnet" R package as follows (Simon et al., 2011): Risk score = (level of gene a × coefficient a) + (level of gene b × coefficient b) + (level of gene c × coefficient c) + . . . + (level of gene n × coefficient n) (Yang et al., 2019). LASSO regression model is a compression estimation method, which constructs a penalty function to obtain a more refined model. This approach is a common method for biased data estimation with multicollinearity and has the advantage of preserving subset contraction. All samples were substituted into the formula to calculate the risk score value, which was then converted into Z-score using Z-score standardization. The samples with Z > 0 were included the high-risk group, and those with Z < 0 were included into the low-risk group. Kaplan–Meier survival curve analysis, log-rank test, and time-dependent Receiver operating characteristic (ROC) curve analysis were used to evaluate the predictive capability of the immune signatures.

TABLE 1 | The clinical characteristics and chi square test of each subgroup of BLCA patients.

		Patients with OS		X-squared	*p*-value	Patients with DFS		X-squared	*p*-value
		Training group	Testing group			Training group	Testing group		
Total		305	102			295	99		
OS/DFS	status_0	177	52	1.3	0.3	213	59	1.9	0.2
	status_1	128	50			82	40		
Age	Age > 60	223	77	0.12	0.7	216	75	0.13	0.7
	Age <= 60	82	25			79	24		
Gender	Female	75	31	1.1	0.3	72	29	0.69	0.4
	Male	230	71			223	70		
M_stage	M0	148	48	3.5	0.3	145	46	0.86	0.7
	M1	7	4			7	4		
	MX	148	49			141	48		
	unknown	1	2			2	1		
N_stage	N0	186	50	5.4	0.4	181	50	4.2	0.4
	N1	32	14			31	14		
	N2	52	23			49	21		
	N3	6	2			6	2		
	NX	24	12			23	11		
	unknown	5	1			5	1		
T_stage	T0	1	0	4.8	0.2	1	0	3.5	0.2
	T1	3	0			3	0		
	T2	94	15			84	25		
	T3	147	46			138	45		
	T4	36	22			36	20		
	TX	1	0			1	0		
	unknown	23	9			22	9		
Stage	stage_I	2	0	3.4	0.2	2	0	3	0.2
	stage_II	102	28			102	28		
	stage_III	107	32			101	31		
	stage_IV	93	41			89	39		
	stage_no	1	1			1	1		
smoke	smoke_yes	211	74	0.091	0.8	205	72	0.013	0.9
	smoke_NO	83	26			79	26		
	smoke_UN	0	13			11	1		

Functional Enrichment Analysis of Gene Set

The "limma" R package (v3.36.5) (Yang et al., 2019) was used to calculate the differences in gene expression between the high- and low-risk groups. Gene set enrichment analysis (GSEA) (Hänzelmann et al., 2013) was used to analyze the KEGG pathway enrichment for the gene set sorted by log2 fold change value.

Estimation of the Tumor Microenvironment

CIBERSORT is a deconvolution analysis tool based on the principle of linear support vector regression for the expression matrix of human immune cell subtypes, which can infer the constituent ratio of 22 immune cell subtypes in complex tissues (Hänzelmann et al., 2013). The CIBERSORT computational tool (Chen et al., 2018) was used to determine the relative abundance of tumor-infiltrating immune cells.

Evaluation of Tumor Mutation Load

The TCGA database was mined for TMB to analyze and visualize the mutation spectrum by "maftools" in R (Mayakonda et al., 2018). The mutation load score of each sample was calculated to compare the TMB difference between the two groups (calculation formula: $\mathrm{TMB} = \frac{\text{total mutation}}{\text{total covered bases}} \times 10^6$).

Statistical Analysis

R software (v3.5.2) was used for statistical analysis. Differences between variables were analyzed by Chi-square test for categorical and continuous variables. Kaplan–Meier survival curve was constructed to compare survival across groups. ROC curve was used to determine the accuracy of the model. Statistical significance was set as $p < 0.05$.

RESULTS

Clinical Information and Identification of Differentially Expressed Immune-Related Genes

After the RNA-seq data from TCGA-BLCA and GTEx was preprocessed, 407 tumor samples with OS information and 394 tumor samples with DFS information were obtained. The statistical results are shown in **Supplementary Table S1**. The patients with complete prognosis information were divided into training group (OS: $n = 305$, DFS: $n = 295$), testing group (OS: $n = 102$, DFS: $n = 99$), and entire group (OS: $n = 407$, DFS: $n = 394$) according to the ratio, 2:1:3. Chi-square test ($p > 0.1$) showed no

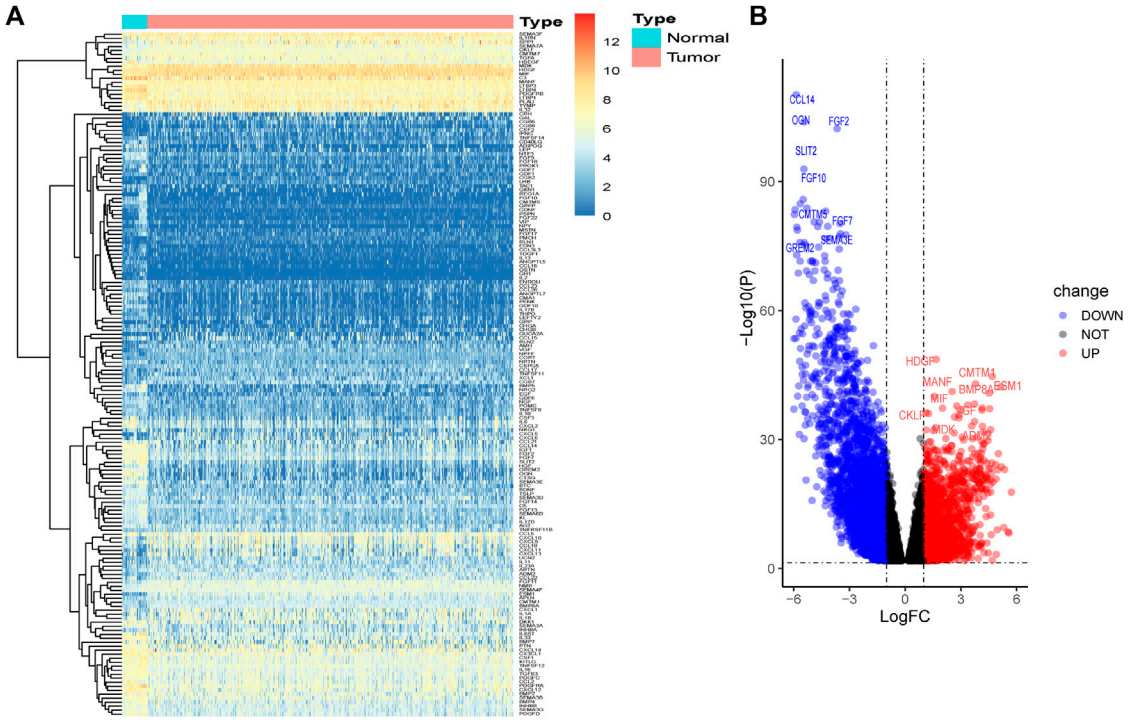

FIGURE 1 | Identification of DE-IRGs between tumors and normal bladder tissues. **(A)** Heatmap of DE-IRGs. **(B)** Volcano plot of DE-IRGs.

difference in the distribution of clinical information between the testing and training groups (**Table 1**).

A total of 1,854 upregulated genes and 3,145 downregulated genes were identified between tumor and normal tissues (**Supplementary Figure S1**). The intersection of the predicted DEGs with the IRGs in BLCA yielded 62 upregulated and 109 downregulated DE-IRGs (**Figure 1**).

Biological Characteristics of Differentially Expressed Immune-Related Genes

Pathway enrichment analysis was performed to interpret the biological function of the DE-IRGs. A total of 195 GO categories were found with an FDR of less than 0.05. The most significant terms are displayed in **Figures 2A–C**. The GO analysis results showed that the enriched biological process (BP) terms were muscle system process and axonogenesis. The enriched cellular component (CC) terms were related to collagen-containing extracellular matrix and synaptic membrane. Among molecular function (MF) terms, channel activity and passive transmembrane transporter activity were dominant. For the KEGG pathway analysis (23 terms, FDR <0.05), the top 20 enriched terms included neuroactive ligand–receptor interaction, calcium signaling pathway, and cAMP signaling pathway (**Figure 2D**). We further studied the relationship between target gene regulation and transcription factors. First, 97 differentially expressed transcription factor-related genes (DE-TFs) were obtained from the intersection of all DE-IRGs and transcription factor-related (TF) genes in BLCA. Univariate Cox proportional hazard regression analysis was conducted using the Coxph function in the "survival" R package, and $p < 0.05$ was selected as the threshold to filter data. Thirty-one OS-related and 27 DFS-related DE-IRGs were screened, and the regulatory network between these genes and DE-TFs (**Supplementary Figure S2**) was constructed using Cytoscape (v3.7.1) software (Cline et al., 2007).

Construction and Verification of Gene Immune Signatures in Bladder Urothelial Carcinoma

The training group was used to identify prognostic immune genes and construct prognostic risk models. The testing and entire groups were used to verify the predictive ability and robustness of the models. First, univariate Cox regression analysis was used to identify the candidate genes that are significantly associated with prognosis ($p < 0.05$). Sixteen genes were screened from 31 OS-related DE-IRGs, and 22 genes were screened from 27 DFS-related DE-IRGs. We then conducted LASSO Cox regression analysis to further compress the genes and found 13 OS-related IRGs and 15 DFS-related IRGs (**Supplementary Figures S3, S4**). Finally, multivariate Cox proportional hazard regression analysis was carried out, and two prediction models were established as follows:

For the 13 OS-IRGs: Risk score = (0.0252 × HGF) + (0.0014 × FGF9) + (0.1379 × INHBB) + (0.0791 × PLAU) + (0.0082 × IL17B) + (−0.0519 × CXCL5) + (0.0775 × SEMA4F) + (0.0446 ×

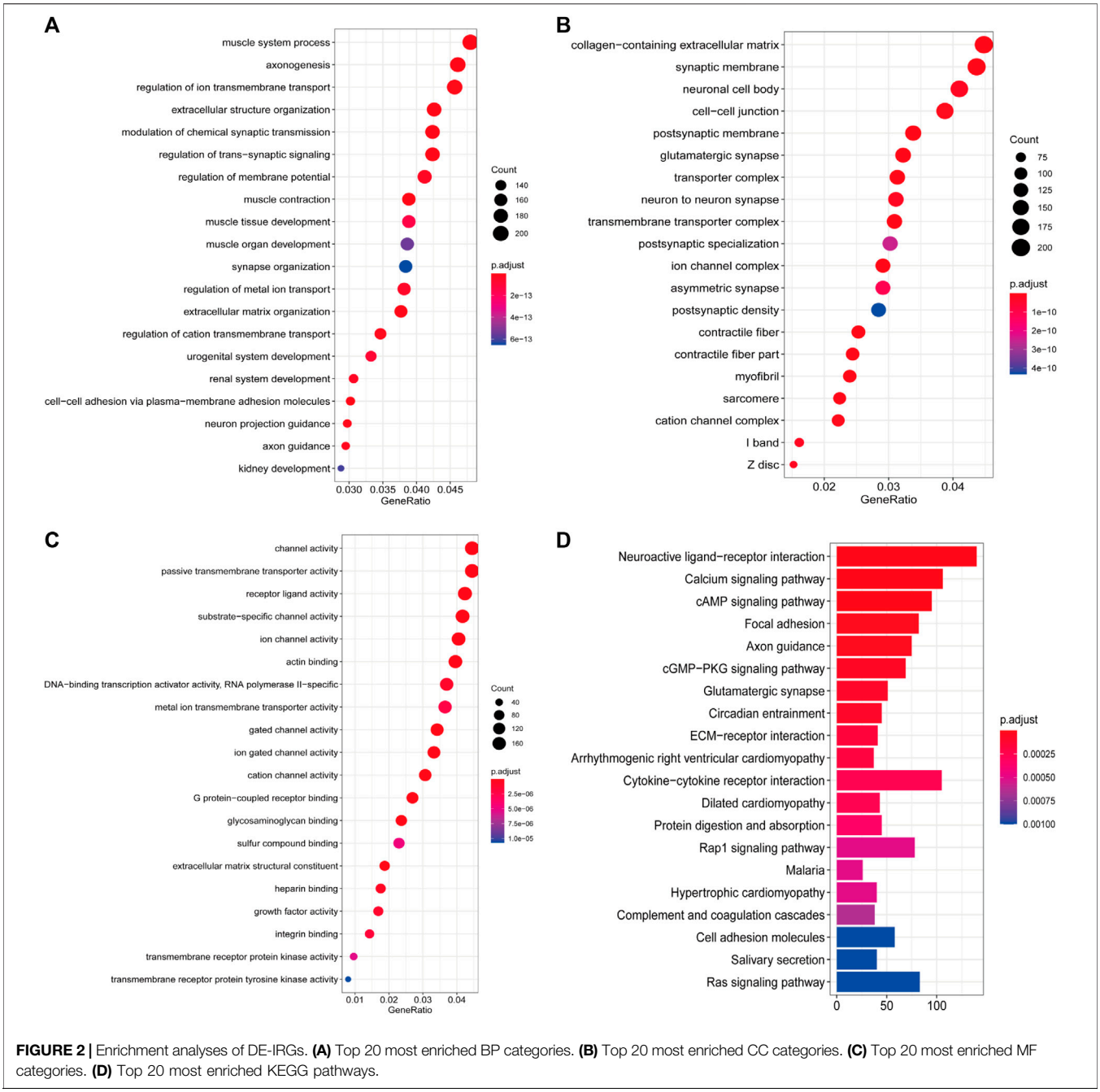

FIGURE 2 | Enrichment analyses of DE-IRGs. **(A)** Top 20 most enriched BP categories. **(B)** Top 20 most enriched CC categories. **(C)** Top 20 most enriched MF categories. **(D)** Top 20 most enriched KEGG pathways.

PDGFRB) + (0.0621 × LTBP1) + (−0.0545 × FGF18) + (−0.1726 × CCL17) + (0.0618 × CGB8) + (0.1069 × CCL26) + (0.0550 × EGF) + (−0.0196 × CXCL1).

For the 15 DFS-IRGs: Risk score = (0.0252 × HGF) + (0.0014 × FGF9) + (0.1379 × INHBB) + (0.0791 × PLAU) + (0.0082 × IL17B) + (−0.0519 × CXCL5) + (0.0775 × SEMA4F) + (0.0446 × PDGFRB) + (0.0621 × LTBP1) + (−0.0545 × FGF18) + (−0.1726 × CCL17) + (0.0618 × CGB8) + (0.1069 × CCL26) + (0.0550 × EGF) + (−0.0196 × CXCL1).

The risk score for each patient was calculated using these formulas. The patients with complete OS/DFS information were divided into the high-risk groups (OS: n = 294, DFS: n = 308) and low-risk groups (OS: n = 113, DFS: n = 86). The ROC analysis results revealed that the three groups had large areas under the curve (AUCs) for 1-, 3-, and 5-years survival (**Figures 3A–C** and Figures 4A–**C**). The risk score distribution maps (**Figures 3D–F** and **Figures 4D–F**) show a remarkable increase in the number of deaths in the high-risk group. This finding indicates that the samples with high-risk scores have a poor OS. In the training group, the Kaplan–Meier curves for OS and DFS consistently showed that patients in the low-risk group exhibited a better prognosis than patients in the high-risk group (**Figure 3G** and

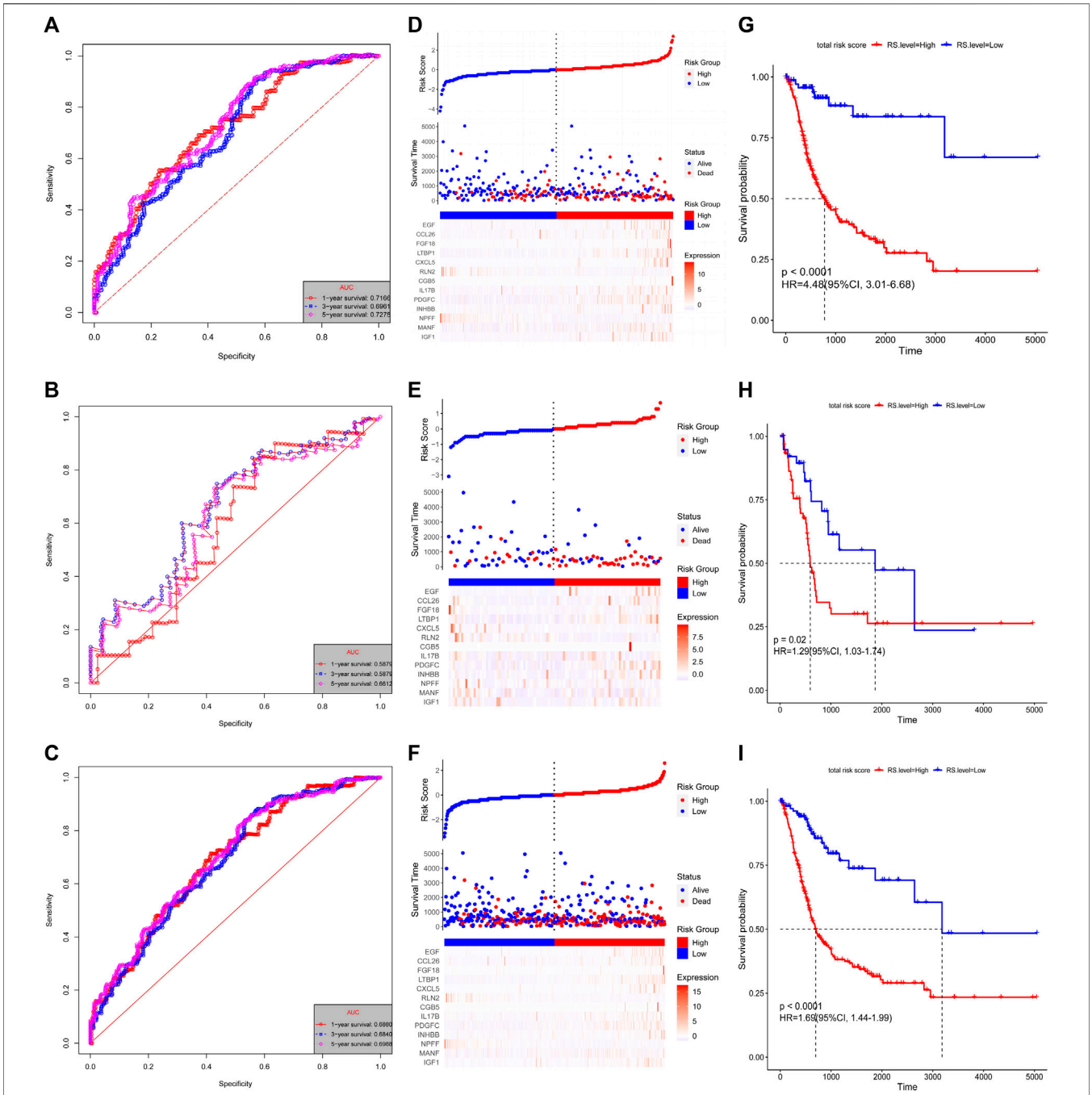

FIGURE 3 | Validation of the 13-IRG signature. Kaplan–Meier estimates of the OS of the training group **(A)**, testing group **(B)**, and entire group **(C)**. Risk score distributions and heatmaps of the mRNA expression of the 13-IRG signature in the training group **(D)**, testing group **(E)**, and entire group **(F)**. Time-dependent ROC analyses of the 13-IRG signature in the training group **(G)**, testing group **(H)**, and entire group **(I)**.

Figure 4G). The results were verified in the testing and entire groups (**Figures 3H,I** and **Figures 4H,I**). The results of the analyses of the three groups were consistent, which suggests the good predictive ability and robustness of the two models. In addition, the 13-IRG signature identified *EGF*, *CCL26*, *FGF18*, *LTBP1*, *CXCL5*, *CGB5*, *IL17B*, *PDGFC*, *INHBB*, *MANF*, and *IGF1* as risk factors, and their high expression was associated with high risk. By contrast, *RLN2* and *NPFF* were protective factors, and their high expression was associated with low risk. For the 15-IRG signature, 14 genes were protective factors (*HGF*, *FGF9*, *INHBB*, *PLAU*, *IL17B*, *CXCL5*, *SEMA4F*, *PDGFRB*, *LTBP1*, *FGF18*, *CGB8*, *CCL26*, *EGF*, and *CXCL1*), and one gene was identified to be a risk factor (*CCL17*).

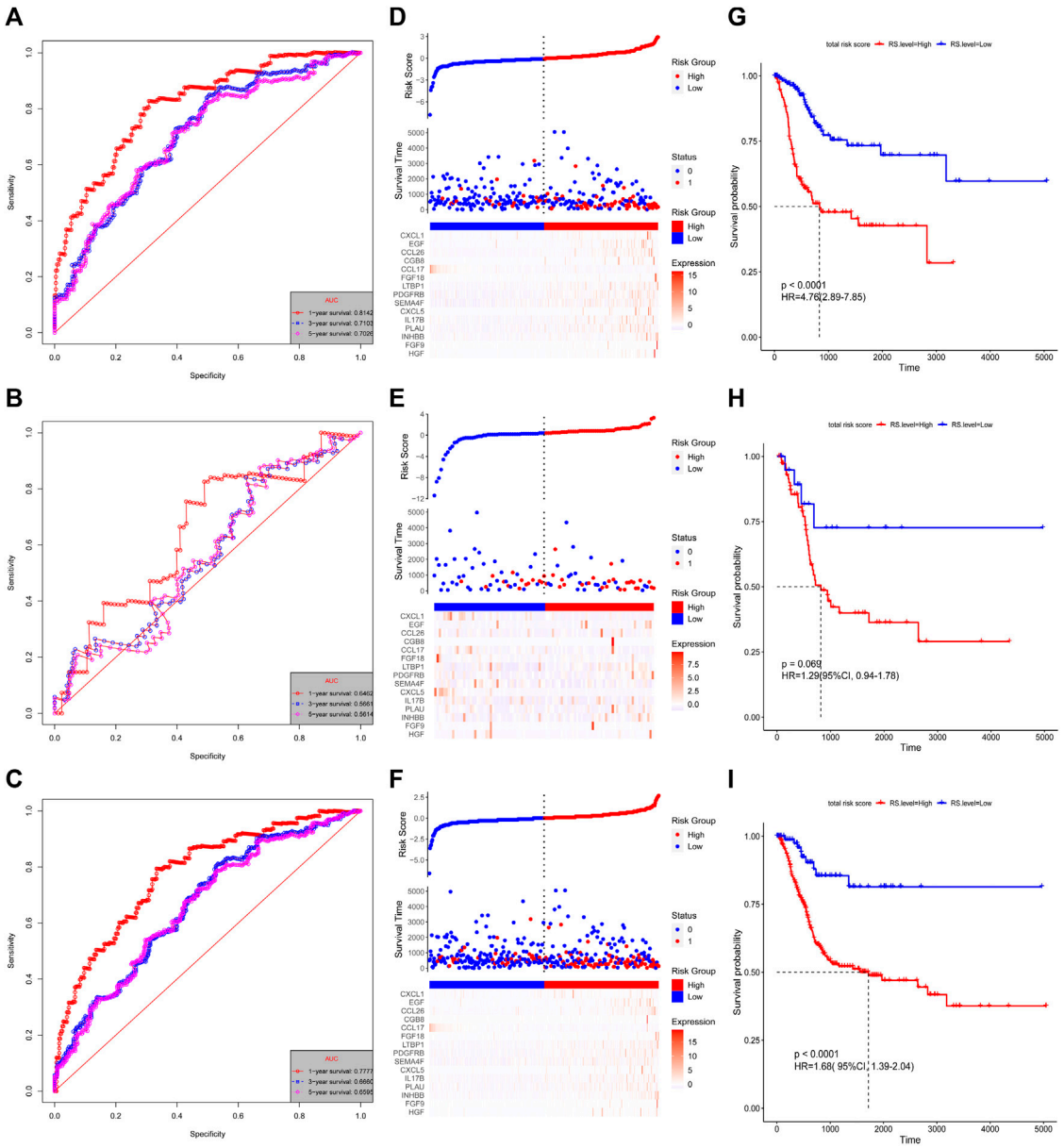

FIGURE 4 | Validation of the 15-IRG signature. Kaplan–Meier estimates of the DFS of the training group **(A)**, testing group **(B)**, and entire group **(C)**. Risk score distributions and heatmaps of the mRNA expression of the 15-IRG signature in the training group **(D)**, testing group **(E)**, and entire group **(F)**. Time-dependent ROC analysis of the 15-IRG signature in the training group **(G)**, testing group **(H)**, and entire group **(I)**.

Potential Biological Functions of Different Genes in High- and Low-Risk Groups

The KEGG pathway-based GSEA of the DEGs between the high- and low-risk groups revealed potential biological importance (the top 10 pathways are shown in **Supplementary Figure S5**). In OS and DFS models, "cell adhesion molecules cams," "chemokine signaling pathway," "cytokine–cytokine receptor interaction," and "JAK–STAT signaling pathway" were enriched in both gene sets. Hence, the key DEGs may be involved in tumor metastasis and immunosuppression.

Prognostic Value of Immune Gene Signatures in Patients With Bladder Urothelial Carcinoma

Univariate and multivariate Cox regression analyses were conducted to systematically analyze the clinical information (including age, gender, T stage, N stage, M Stage, and smoking level) and risk score (high vs. low) of patients with BLCA in the training and entire groups (**Table 2** and **Supplementary Table S2**). The univariate Cox regression analysis showed that a high-risk score was unfavorable for OS and DFS. The multivariate Cox regression analysis showed that

TABLE 2 | Univariate and multivariate Cox analysis in each group of BLCA patients with OS.

Variables	Univariate analysis		*p*-value	Multivariate analysis		*p*-value
	HR	95% CI		HR	95% CI	
training group						
Age (<60 vs. ≥ 60)	1.039	1.020–1.059	0	1.035	1.015–1.055	0
Gender (female vs. male)	0.84	0.571–1.236	0.382	0.889	0.600–1.316	0.557
Tstage (T1/T2 vs. T3/T4)	1.381	1.013–1.882	0.034	0.743	0.515–1.073	0.113
Nstage (N0 vs. N1/N2/N3)	1.378	1.155–1.644	0.001	0.952	0.705–1.286	0.747
Stage (I/II vs. III/IV)	1.693	1.350–2.123	0	1.688	1.117–2.553	0.013
Smoke_level (YES vs. NO)	1.071	0.778–1.473	0.672	1.023	0.741–1.411	0.892
Riskscore (high/low)	4.82	3.246–7.159	0	3.804	2.528–5.724	0
entire group						
Age (<60 vs. ≥ 60)	1.033	1.017–1.049	0	1.031	1.015–1.047	0
Gender (female vs. male)	0.891	0.642–1.236	0.492	1.01	0.713–1.430	0.957
Tstage (T1/T2 vs. T3/T4)	1.487	1.140–1.941	0.002	0.889	0.655–1.207	0.451
Nstage (N0 vs. N1/N2/N3)	1.385	1.196–1.605	0	0.951	0.741–1.221	0.695
Stage (I/II vs. III/IV)	1.683	1.393–2.034	0	1.668	1.193–2.332	0.003
Smoke_level (YES vs. NO)	1.219	0.909–1.634	0.176	1.144	0.849–1.540	0.377
Riskscore (high/low)	1.693	1.438–1.993	0	1.576	1.303–1.906	0

the risk scores of the immune signatures were a remarkable predictor of survival. Therefore, our 13- and 15-IRG signatures had good predictive performance in the clinic.

A prognostic nomogram for OS/DFS with scales for three independent prognostic factors, including age, stage, and risk score, was constructed according to the results of the multivariate analysis. The nomogram displayed that risk score had the greatest impact on the prediction of survival rate (**Figure 5A** and **Supplementary Figure S6A**). This finding further confirmed that the immune signatures could predict prognosis. Calibration plots were used to visualize the predictive performance of the nomograms. **Figure 5B** shows that the calibration plots of 1-, 3-, and 5-years OS nomograms exhibited good performance and accurately estimated mortality. The DFS results are shown in **Supplementary Figure S6B**. The time-dependent ROC curves indicated the accuracy of the nomograms. The AUCs of 1-, 3-, and 5-years OS were 0.70, 0.653, and 0.723, respectively (**Figure 5C**), and the 1-, 3-, and 5-years DFS were 0.698, 0.751, and 0.70, respectively (**Supplementary Figure S6C**). In conclusion, risk score had better predictive ability compared with a single clinical factor. Moreover, the combined model of risk score and clinical factor showed the highest predictive accuracy.

In addition, the relationship between the characteristics of the 13- and 15-IRG signatures and clinicopathological parameters was analyzed. The results suggest that the risk score of patients >60 years, female, with lymph node metastasis and/or distant metastasis, T3/T4, and stage III/IV is substantially increased (**Figure 6**).

Immune Gene Signatures and Tumor Immune Microenvironment

Our study revealed the possible interaction and correlation between these identified IRGs and the tumor immune microenvironment. Differences in immune cell infiltration were found between the high- and low-risk groups of the OS model (**Figure 7**). In the high-risk group, the proportions of naïve B cells, CD4 memory T cells, macrophage M0, macrophage M1, and neutrophils were considerably higher, whereas the abundance of memory B cells and T naïve CD4 cells increased substantially in the low-risk group. In the DFS model, CD4 memory T cells, macrophage M1, neutrophils, and memory B cells showed the same distribution characteristics (**Supplementary Figure S7**). Multiple innate immune-related cell types, including macrophage M0, macrophage M1, and neutrophils, were enriched in the high-risk group, which may indicate adverse clinical outcomes.

Immune Gene Signatures and Tumor Mutation Burden

The frequency of mutation was high in all samples (>90%), and the main type of mutation was missense mutation. The mutation frequency of tumor suppressor gene, *TP53* (tumor protein p53), was the highest in the high-risk group, whereas the mutation frequency of titin was the highest in the low-risk group (**Figures 8A,B**, **Supplementary Figures S8A,B**). The box plot of TMB scores shows that the low-risk group had higher TMB and longer OS than the high-risk group (**Figure 8C**), and the corresponding DFS model analysis did not indicate the same results (**Supplementary Figure S8C**). However, after stratification according to the TMB of the sample, the Kaplan–Meier survival curve demonstrated that the difference between the two groups was statistically significant (**Figure 8D**, **Supplementary Figure S8D**).

Prediction of Anti-PD-L1 Response With the Immune Gene Signatures

The analysis of the real ICI treatment cohort confirmed the predictive value of the immune signatures for checkpoint immunotherapy. We downloaded the gene expression profiles and clinical data of the IMvigor210 cohort. The IMvigor210 study is a single arm, multicenter, phase 2 clinical trial that investigated the clinical activity of PD-L1 blockade with atezolizumab in mUC. A total of 298 pre-treatment tumor samples were used for transcriptome RNA sequencing to evaluate the integrated

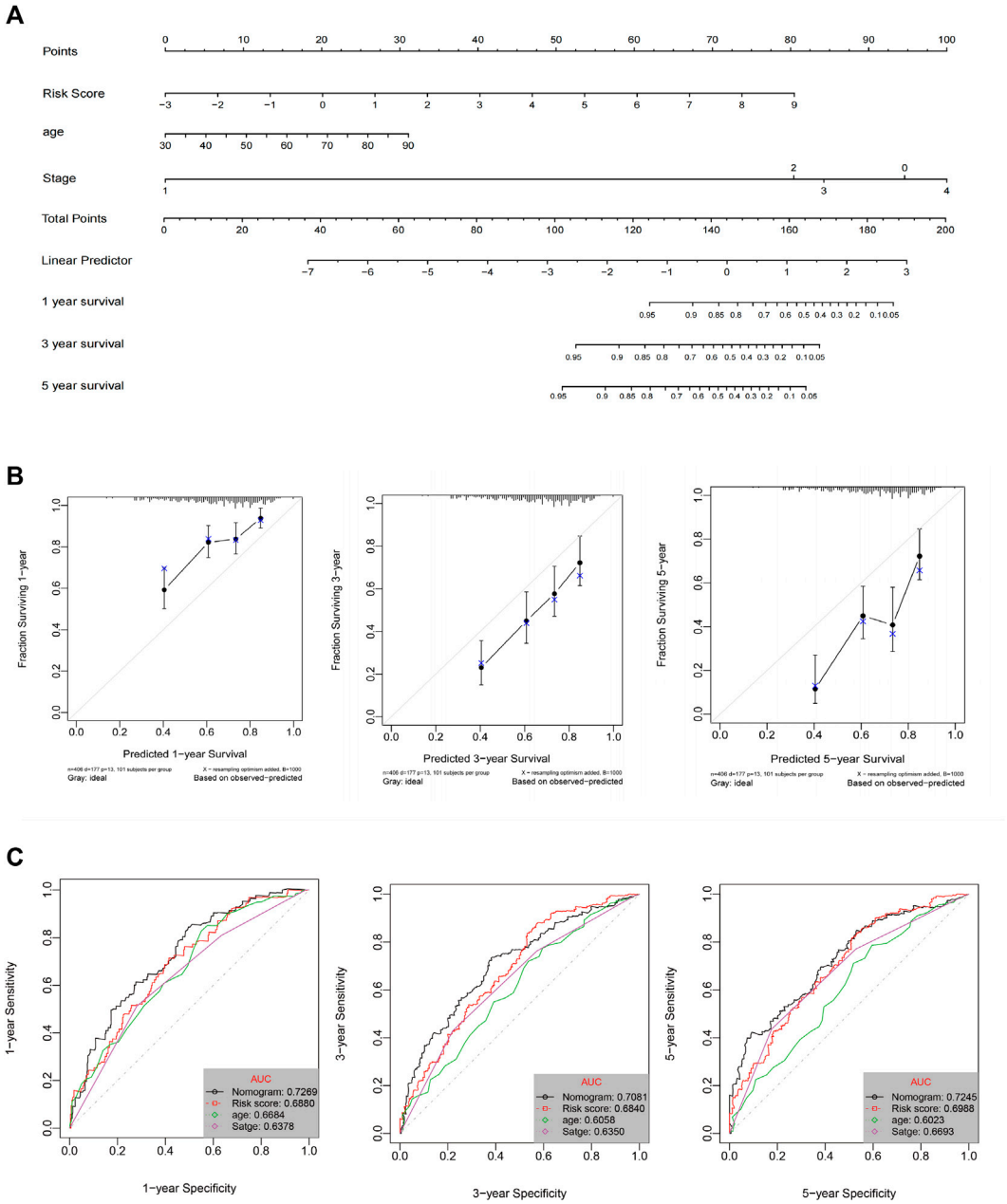

FIGURE 5 | (A) Nomogram prediction of OS probability. **(B)** Calibration plots of the nomogram for 1-, 3-, and 5-years OS prediction. **(C)** Time-dependent ROC curves of 1-, 3-, and 5-years OS.

biomarkers (Cline et al., 2007). Considering the absence of DFS data, we only explored the use of OS-related risk signature in predicting the benefit of anti-PD-L1 therapy for urothelial carcinoma. All samples were divided into high- and low-risk groups by the OS risk model. The risk score of patients with treatment response [complete response (CR) or partial response (PR)] was significantly lower than that of patients without treatment response [stable disease (SD) or progressive disease (PD); Wilcoxon, p = 2.076e-08; **Figure 9A**]. Moreover, the prognosis of the low-risk group was significantly better than that of the high-risk group (p = 0.0083, **Figure 9B**). After evaluating the distribution of CR/PR and SD/PD in the high- and low-risk groups, we found that patients with low-risk scores had better response to ICI treatment than patients with high-risk score (**Figure 9C**).

DISCUSSION

The main aim in this study was to construct a model using IRGs to predict the prognosis of patients BLCA, as well as the clinical benefit of immunotherapy. In addition, we performed GO and

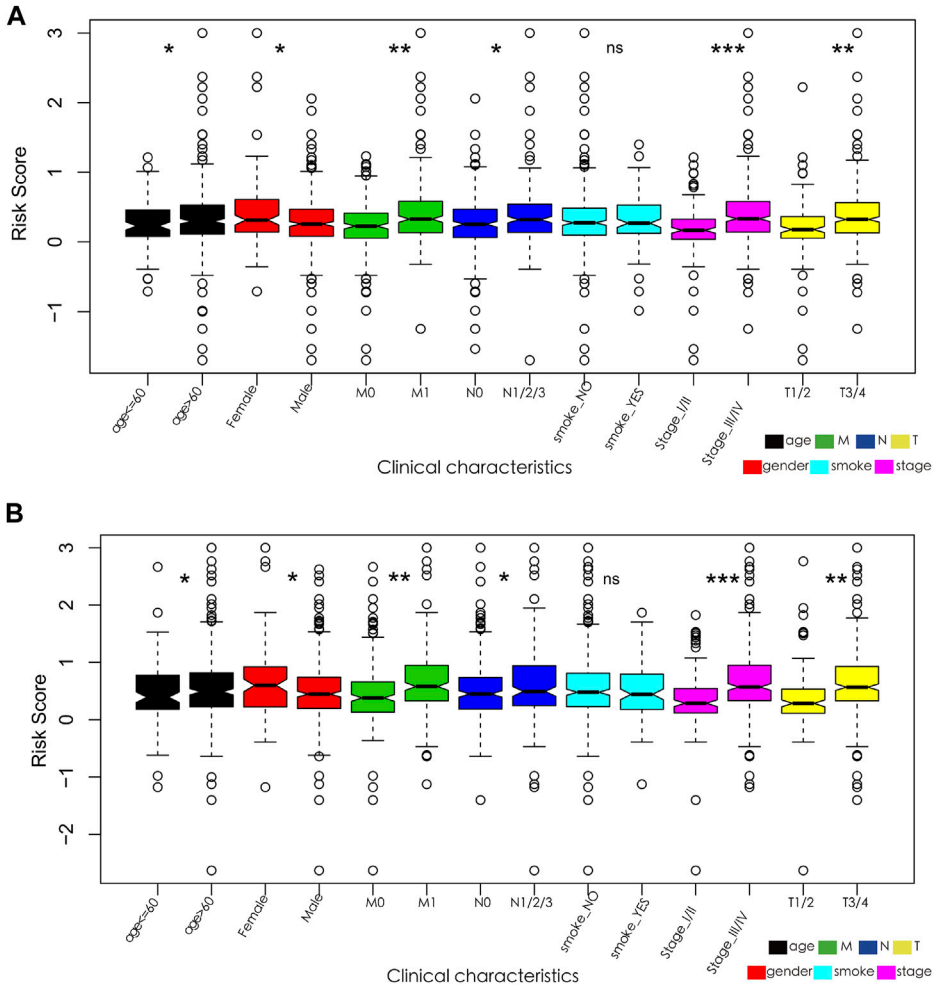

FIGURE 6 | (A) Relationships between the 13-IRG signature and clinicopathological parameters. **(B)** Relationships between the 15-IRG signature and clinicopathological parameters.

KEGG pathway enrichment analyses for the DE-IRGs and further screened the DE-IRGs associated with OS or DFS to construct network interaction relationships with DE-TFs to explore the possible biological mechanisms of DE-IRGs associated with prognosis. We constructed 13- and 15-IRG signatures using the RNA-Seq data of TCGA-BLCA and the immune-related gene set from the ImmPort database, respectively. The univariate Cox regression analysis showed that the risk scores of the immune signatures were an independent predictor of survival. We next constructed a prognostic nomogram of OS/DFS using three variables (age, stage, and risk score), which showed good discrimination and prediction ability. Besides, we also found that the low-risk score group had better response to ICI therapy than the high-risk score group, and the two groups showed differences in immune cell infiltration and TMB.

Previous studies indicated that IRGs are involved in shaping the immune landscape and influence the prognosis and response to immunotherapies of patients with tumor (Liu et al., 2020; Yi et al., 2021). In the present study, the IRGs identified were related to the progression of malignant tumors, and some of them can regulate the occurrence and development of cancer by simultaneously regulating the state of the tumor immune microenvironment and the malignant biological characteristics of tumor cells. Yeh et al. (2015) found that fibroblast ERα increased the expression of CCL cytokines and IL-6 in the tumor microenvironment and promoted bladder cancer invasion. CXCL5 upregulates the expression of MMP2/MMP9 by activating PI3K/AKT signal to promote the migration and invasion of bladder cancer cells (Gao et al., 2015). In addition, CXCL5 is involved in changing the tumor microenvironment of bladder cancer. The interaction between endothelial cells and bladder cancer cells potentiates the recruitment of vascular endothelial cells through the CXCL1/CXCL5/CXCL8–CXCR2 pathway, which leads to tumor progression (Gao et al., 2015). Furthermore, research had found that *Salmonella* local immune stimulation considerably enhanced the expression of complement component 5a, CXCL2, CXCL5, CCL5, and CCL8; thus, it recruits specific CD8 T cells and promotes bladder cancer

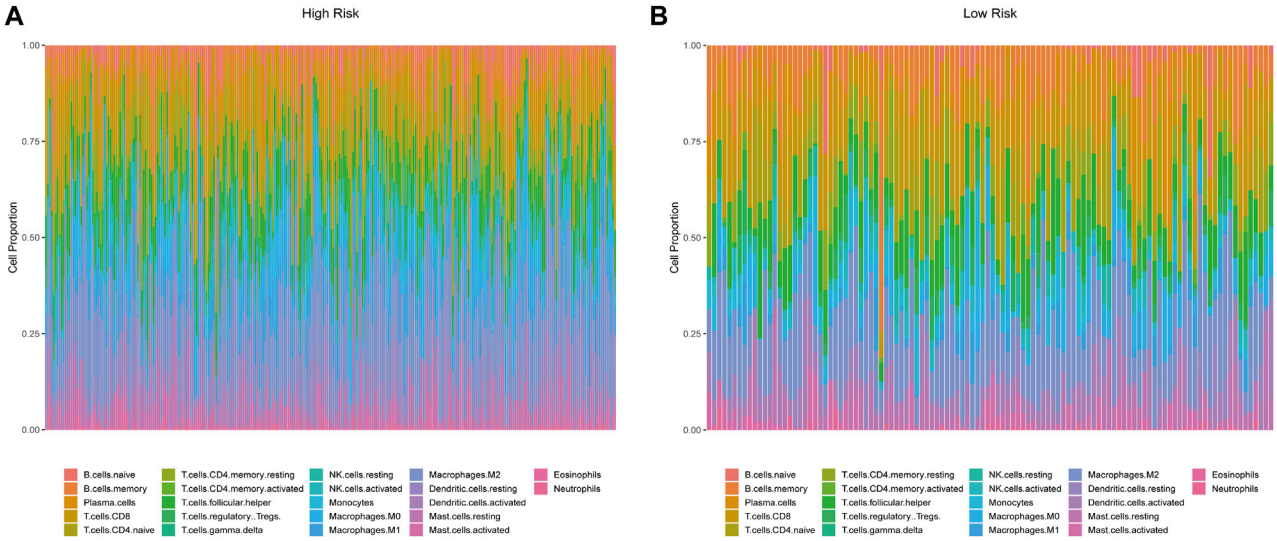

FIGURE 7 | Characterization of immune cell infiltrate in high-risk **(A)** and low-risk groups **(B)** based on the 13-IRG signature.

progression (Domingos-Pereira et al., 2015). Similarly, based on the principle of gene–immune interaction, CXCL5 plays an important role in the progression of colon cancer, gastric cancer, liver cancer, and other tumors by recruiting or activating neutrophils. A large number of studies have reported that the abnormal expression of epidermal growth factor (EGF) and its receptor is involved in the invasion and metastasis of a variety of tumors (Ma et al., 2012; Perera and Bardeesy, 2012; Tomas et al., 2014; Chen et al., 2021), such as bladder cancer, gastric cancer, liver cancer, breast cancer, and melanoma. Heparin-binding EGF-like growth factor (HB-EGF) accumulates in the nucleus of invasive bladder transitional cell carcinoma, which can promote the autocrine cycle of cells, lead to the proliferation of cancer cells, and protect cancer cells from apoptosis (Kim et al., 2005). Moreover, as a powerful tumor growth and angiogenesis inducer, HB-EGF promotes the migration of bladder cancer cells by inducing MMP-9 and MMP-3 expression and activity (Ongusaha et al., 2004). Therefore, a prognosis model constructed using these genes would have relatively sufficient basis, and our follow-up study confirmed this hypothesis.

Considering that studying the biological mechanism and function of gene sets involved in specific pathways is an effective method for cancer research (Ge et al., 2018; Liu et al., 2018), we conducted a functional enrichment analysis of the identified DE-IRGs in BLCA tumor tissues. The KEGG analysis indicated that DEGs in the high- and low-risk groups were enriched in immune-related pathways, such as "cell adhesion molecules," "chemokine signaling pathway," "cytokine–cytokine receptor interaction," "JAK–STAT signaling pathway," "leukocyte transendothelial migration," and "natural killer cell-mediated cytotoxicity." The results may indicate that related pathways are involved in the shaping of the immune landscape. These results provide new insights into the potential biological mechanism and function of IRGs.

Based on the principle of gene–immune interaction, we designed OS and DFS immune signatures to predict the prognosis and response to ICI of patients with BLCA. According to the univariate and multivariate Cox regression analyses, the risk scores of the immune signatures were an independent prognostic indicator of OS/DFS for patients with BLCA; that is, patients with low immune signature scores have a better prognosis. The nomogram and ROC analyses further verified the prediction performance of the IRG signatures. Risk score was also remarkably correlated with sex, age, and TNM stage; that is, patients with worse clinicopathological characteristics had higher risk scores. Through comprehensive analysis, we demonstrated that the IRG signatures might be a suitable guide for clinicians in conducting the risk stratification of patients with BLCA and could help to adopt appropriate treatment modes.

Tumor cells escape from immune surveillance by suppressing the effect of T cells through the immune checkpoint, which leads to a decrease in tumor surveillance and tumor recognition and the occurrence of immune escape (Gervois et al., 1996). Two key immune checkpoint receptors, namely, cytotoxic T lymphocyte antigen 4 (CTLA-4) and PD-1, have been widely used in emerging immunotherapy. The accurate mode of action and the determination of predictive markers are key research topics because of the minority of patients who appear to benefit from immunotherapy. Several biomarkers have been developed at the genome, transcriptome, and immunogenome levels (Havel et al., 2019). The expression of PD-L1 in tumor cells is a biomarker for predicting response to anti-PD-1 or anti-PD-L1 therapy, but data remain insufficient. Patients who tested negative for PD-L1 can still achieve an objective remission rate of 11–20% (Mahoney and Atkins, 2014; Rui et al., 2019). Tumor-infiltrating lymphocytes (TILs) (Mahoney and Atkins, 2014; Rui et al., 2019), TMB (Yarchoan et al., 2017; Wang et al., 2020), and microsatellite instability (Pećina-Šlaus et al., 2020) are related to therapeutic response to

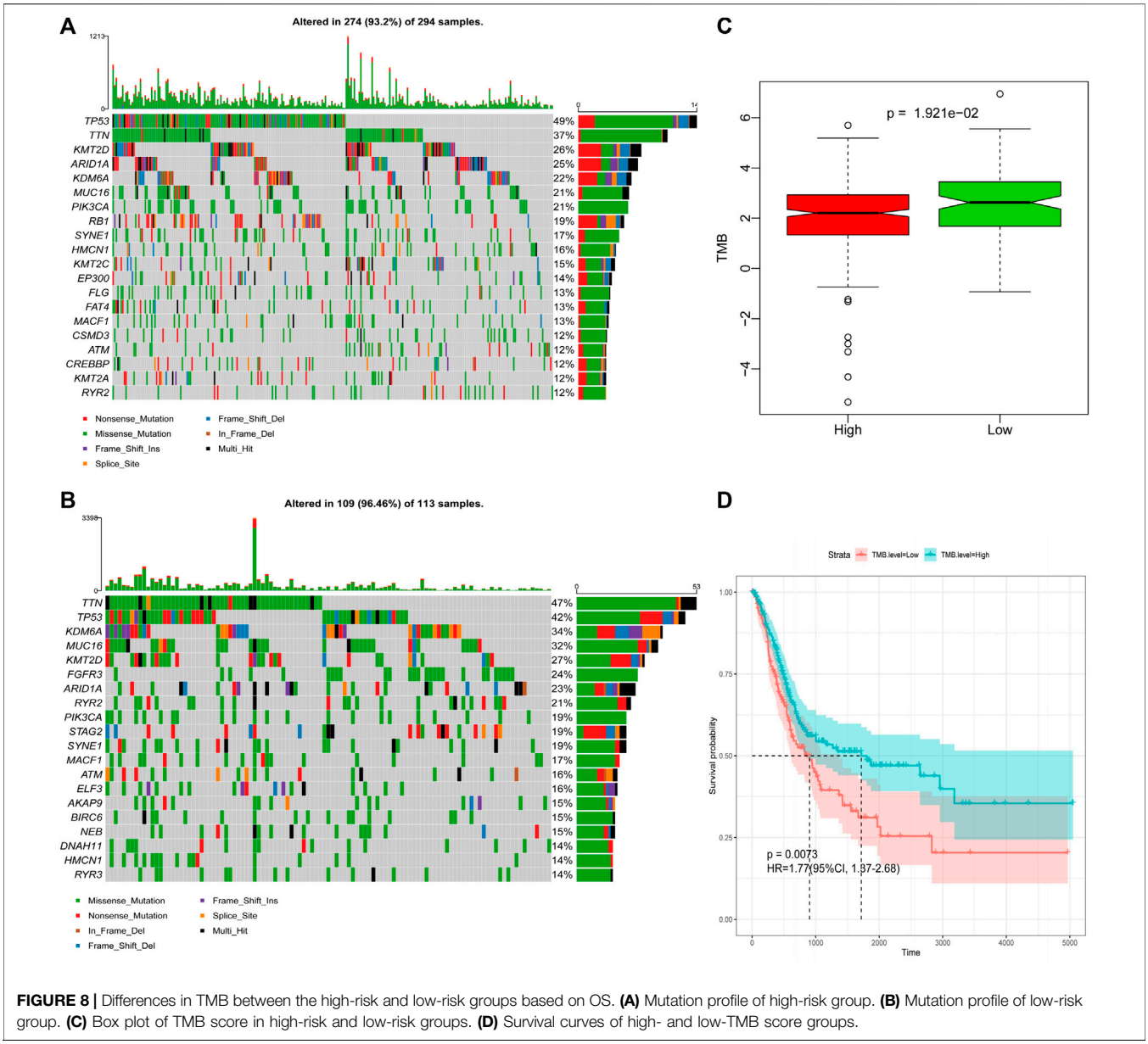

FIGURE 8 | Differences in TMB between the high-risk and low-risk groups based on OS. **(A)** Mutation profile of high-risk group. **(B)** Mutation profile of low-risk group. **(C)** Box plot of TMB score in high-risk and low-risk groups. **(D)** Survival curves of high- and low-TMB score groups.

ICI treatment. Our study found that the IRG signatures were associated with immune cell infiltration and TMB, and their predictive effects were verified in the immunotherapy cohort.

The enrichment of TIL subsets associated with adaptive immunity decreased with tumor progression, whereas that associated with innate immunity increased (Charoentong et al., 2017). Using our analytical strategy, we found a similar evolving nature in infiltrating immune cell components during tumor progression; that is, TIL subpopulations related to innate immunity, such as macrophage M0, macrophage M1, neutrophils, and resting dendritic cells, were enriched in the high-risk group, whereas TILs related to adaptive immunity, such as memory B cells, naive CD4 T cells, and gamma delta T cells (Tγδ), were enriched in the low-risk group. Therefore, we speculate that the 13- and 15-IRG sets for model construction may change the biological behavior and therapeutic response of tumor cells by changing the tumor microenvironment. The predictive role of TMB in ICI treatment has been confirmed in many clinical studies (Davoli et al., 2017). Tumor cells with high TMB can produce more tumor-specific antigens and thus can be easily recognized and killed by immune cells (Kakoti et al., 2020). In our OS model, the TMB of the low-risk group was higher and the prognosis of the high-TMB group was remarkably better after the samples were grouped according to TMB. This finding suggests that a low-risk score predicts a good response rate to PD-1 inhibition and satisfactory clinical outcomes.

The IMvigor210 cohort study confirmed the above results. Compared with the PD-1 treatment nonresponse group, the risk score of the response group was considerably lower, and the low-risk group had a higher response to anti-PD-1 treatment and better prognosis. These data further supported that the IRG signatures may serve as a biomarker to predict the prognosis of patients with BLCA and their response to immunotherapy.

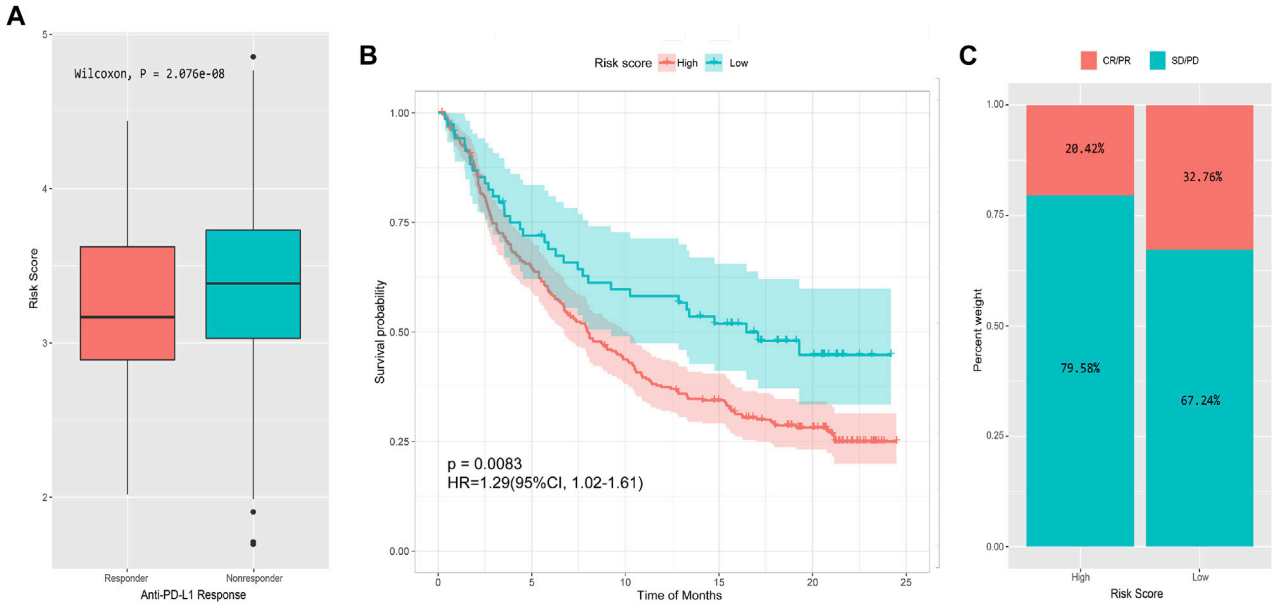

FIGURE 9 | Performance of the 13-IRG signature in predicting response to anti-PD-L1 therapy in the IMvigor210 cohort. **(A)** Box plot of risk score and objective response to immunotherapy. **(B)** Survival curve of high- and low-risk groups. **(C)** Immunotherapy response rates of high- and low-risk groups.

This study has some limitations. First, the 13- and 15-IRG signatures only used a series of immune genes, which are nonspecific to the specific immune microenvironment of patients with urothelial carcinoma. Second, the factors influencing tumor progression and immunotherapy are very complex, and the influence of immune genes may only be a part of them. Third, basic experiments and studies with larger sample sizes are needed to verify these associations. Despite these limitations, our analysis showed that the 13- and 15-IRG signatures can effectively predict the prognosis and response to ICI of patients with BLCA.

In summary, the 13- and 15-IRG signatures may be helpful to determine the prognosis of patients with BLCA and stratify those who will benefit from checkpoint blockade immunotherapy. This finding may contribute to cancer immunotherapy and promote the development of precise immune oncology.

DATA AVAILABILITY STATEMENT

The datasets presented in this study can be found in online repositories. The names of the repository/repositories and accession number(s) can be found in the article/ **Supplementary Material**.

ETHICS STATEMENT

The studies involving human participants were reviewed and approved by the Ethics and Human Subject Committee of Guangxi Medical University Cancer Hospital. Written informed consent for participation was not required for this study in accordance with the national legislation and the institutional requirements.

AUTHOR CONTRIBUTIONS

FL and YX designed the study. FL and HZ carried out the data analysis. FL and YC interpreted the entire results and drafted the manuscript. YX, ZW, and TN helped carry out the data analysis. JZ reviewed the manuscript. All authors read and approved the final manuscript.

FUNDING

This study was funded by Guangxi Medical University First Affiliated Hospital.

ACKNOWLEDGMENTS

We sincerely acknowledge all the online databases for the availability of the data.

SUPPLEMENTARY MATERIAL

The Supplementary Material for this article can be found online at: https://www.frontiersin.org/articles/10.3389/fmolb.2021.673918/full#supplementary-material

REFERENCES

Apolo, A. B., Infante, J. R., Balmanoukian, A., Patel, M. R., Wang, D., Kelly, K., et al. (2017). Avelumab, an Anti-programmed Death-Ligand 1 Antibody, in Patients with Refractory Metastatic Urothelial Carcinoma: Results from a Multicenter, Phase Ib Study. *J. Clin. Oncol.* 35, 2117–2124. doi:10.1200/JCO.2016.71.6795

Balar, A. V., Castellano, D., O'Donnell, P. H., Grivas, P., Vuky, J., Powles, T., et al. (2017a). First-line Pembrolizumab in Cisplatin-Ineligible Patients with Locally Advanced and Unresectable or Metastatic Urothelial Cancer (KEYNOTE-052): A Multicentre, Single-Arm. *Lancet Oncol.* (18), 1483–1492. doi:10.1016/s1470-2045(17)30616-2

Balar, A. V., Galsky, M. D., Rosenberg, J. E., Powles, T., Petrylak, D. P., Bellmunt, J., et al. (2017b). Atezolizumab as First-Line Treatment in Cisplatin-Ineligible Patients with Locally Advanced and Metastatic Urothelial Carcinoma: A Single-Arm. *multicentre* (389), 67–76. doi:10.1016/s0140-6736(16)32455-2

Bellmunt, J., de Wit, R., Vaughn, D. J., Fradet, Y., Lee, J.-L., Fong, L., et al. (2017). Pembrolizumab as Second-Line Therapy for Advanced Urothelial Carcinoma. *N. Engl. J. Med.* 376, 1015–1026. doi:10.1056/nejmoa1613683

Bellmunt, J., and Nadal, R. (2018). Changes in Expectations for Metastatic Urothelial Carcinoma. *Nat. Rev. Clin. Oncol.* 15 (2), 73–74. doi:10.1038/nrclinonc.2017.184

Bhattacharya, S., Andorf, S., Gomes, L., Dunn, P., Schaefer, H., Pontius, J., et al. (2014). ImmPort: Disseminating Data to the Public for the Future of Immunology. *Immunol. Res.* 58 (2-3), 234–239. doi:10.1007/s12026-014-8516-1

Charoentong, P., Finotello, F., Angelova, M., Mayer, C., Efremova, M., Rieder, D., et al. (2017). Pan-cancer Immunogenomic Analyses Reveal Genotype-Immunophenotype Relationships and Predictors of Response to Checkpoint Blockade. *Cel Rep.* 18 (1), 248–262. doi:10.1016/j.celrep.2016.12.019

Chen, B., Khodadoust, M. S., Liu, C. L., Newman, A. M., and Alizadeh, A. A. (2018). Profiling Tumor Infiltrating Immune Cells with CIBERSORT. *Methods Mol. Biol. (Clifton, N.J.).* 1711, 243–259. doi:10.1007/978-1-4939-7493-1_12

Chen, Y., Qian, B., Sun, X., Kang, Z., Huang, Z., Ding, Z., et al. (2021). Sox9/INHBB axis-mediated Crosstalk between the Hepatoma and Hepatic Stellate Cells Promotes the Metastasis of Hepatocellular Carcinoma. *Cancer Lett.* 499, 243–254. doi:10.1016/j.canlet.2020.11.025

Cline, M. S., Smoot, M., Cerami, E., Kuchinsky, A., Landys, N., Workman, C., et al. (2007). Integration of Biological Networks and Gene Expression Data Using Cytoscape. *Nat. Protoc.* 2 (10), 2366–2382. doi:10.1038/nprot.2007.324

Davoli, T., Uno, H., Wooten, E. C., and Elledge, S. J. (2017). Tumor Aneuploidy Correlates with Markers of Immune Evasion and with Reduced Response to Immunotherapy. *Science* 355 (6322). doi:10.1126/science.aaf8399

Domingos-Pereira, S., Hojeij, R., Reggi, E., Derré, L., Chevalier, M. F., Romero, P., et al. (2015). LocalSalmonellaimmunostimulation Recruits Vaccine-specific CD8 T Cells and Increases Regression of Bladder Tumor. *Oncoimmunology* 4 (7), e1016697. doi:10.1080/2162402x.2015.1016697

Dudziec, E., Goepel, J. R., and Catto, J. W. (2011). Global Epigenetic Profiling in Bladder Cancer. *Epigenomics* 3 (1), 35–45. doi:10.2217/epi.10.71

Felsenstein, K. M., and Theodorescu, D. (2018). Precision Medicine for Urothelial Bladder Cancer: Update on Tumour Genomics and Immunotherapy. *Nat. Rev. Urol.* 15 (2), 92–111. doi:10.1038/nrurol.2017.179

Fitzmaurice, C., Fitzmaurice, C., Abate, D., Abbasi, N., Abbastabar, H., Abd-Allah, F., et al. (2019). Global, Regional, and National Cancer Incidence, Mortality, Years of Life Lost, Years Lived with Disability, and Disability-Adjusted Life-Years for 29 Cancer Groups, 1990 to 2017: A Systematic Analysis for the Global burden of Disease Study. *JAMA Oncol.* 5 (12), 1749–1768. doi:10.1001/jamaoncol.2019.2996

Gao, Y., Guan, Z., Chen, J., Xie, H., Yang, Z., Fan, J., et al. (2015). CXCL5/CXCR2 axis Promotes Bladder Cancer Cell Migration and Invasion by Activating PI3K/AKT-Induced Upregulation of MMP2/MMP9. *Int. J. Oncol.* 47 (2), 690–700. doi:10.3892/ijo.2015.3041

Ge, Z., Leighton, J. S., Wang, Y., Peng, X., Chen, Z., Chen, H., et al. (2018). Integrated Genomic Analysis of the Ubiquitin Pathway across Cancer Types. *Cell Rep* 23 (1), 213–e3. doi:10.1016/j.celrep.2018.03.047

Gervois, N., Guilloux, Y., Diez, E., and Jotereau, F. (1996). Suboptimal Activation of Melanoma Infiltrating Lymphocytes (TIL) Due to Low Avidity of TCR/MHC-tumor Peptide Interactions. *J. Exp. Med.* 183 (5), 2403–2407. doi:10.1084/jem.183.5.2403

Goeman, J. J. (2010). *L1 Penalized Estimation in the Cox Proportional Hazards Model. Biom J.* 52, 70–84. doi:10.1084/jem.183.5.2403

Groenendijk, F. H., de Jong, J., Fransen van de Putte, E. E., Michaut, M., Schlicker, A., Peters, D., et al. (2016). ERBB2 Mutations Characterize a Subgroup of Muscle-Invasive Bladder Cancers with Excellent Response to Neoadjuvant Chemotherapy. *Eur. Urol.* 69 (3), 384–388. doi:10.1016/j.eururo.2015.01.014

Gros, A., Parkhurst, M. R., Tran, E., Pasetto, A., Robbins, P. F., Ilyas, S., et al. (2016). Prospective Identification of Neoantigen-specific Lymphocytes in the Peripheral Blood of Melanoma Patients. *Nat. Med.* 22 (4), 433–438. doi:10.1038/nm.4051

Hänzelmann, S., Castelo, R., and Guinney, J. (2013). GSVA: Gene Set Variation Analysis for Microarray and RNA-Seq Data. *BMC Bioinformatics* 14, 7. doi:10.1186/1471-2105-14-7

Havel, J. J., Chowell, D., and Chan, T. A. (2019). The Evolving Landscape of Biomarkers for Checkpoint Inhibitor Immunotherapy. *Nat. Rev. Cancer* 19 (3), 133–150. doi:10.1038/s41568-019-0116-x

Huang, Z., Zhang, M., Chen, G., Wang, W., Zhang, P., Yue, Y., et al. (2019). Bladder Cancer Cells Interact with Vascular Endothelial Cells Triggering EGFR Signals to Promote Tumor Progression. *Int. J. Oncol.* 54 (5), 1555–1566. doi:10.3892/ijo.2019.4729

Kakoti, S., Sato, H., Laskar, S., Yasuhara, T., and Shibata, A. (2020). DNA Repair and Signaling in Immune-Related Cancer Therapy. *Front. Mol. Biosci.* 7, 205. doi:10.3389/fmolb.2020.00205

Kamat, A. M., Flaig, T. W., Grossman, H. B., Konety, B., Lamm, D., O'Donnell, M. A., et al. (2015). *Expert Consensus Document: Consensus Statement on Best Practice Management Regarding the Use of Intravesical Immunotherapy with BCG for Bladder Cancer*. London, England: Reprinted, 225–235. doi:10.1038/nrurol.2015.58

Kamat, A. M., Hahn, N. M., Efstathiou, J. A., Lerner, S. P., Malmström, P.-U., Choi, W., et al. (2016). Bladder Cancer. *The Lancet* 388 (10061), 2796–2810. doi:10.1016/S0140-6736(16)30512-8

Kim, J., Adam, R. M., and Freeman, M. R. (2005). Trafficking of Nuclear Heparin-Binding Epidermal Growth Factor-like Growth Factor into an Epidermal Growth Factor Receptor-dependent Autocrine Loop in Response to Oxidative Stress. *Cancer Res.* 65 (18), 8242–8249. doi:10.1158/0008-5472.can-05-0942

Li, J., Lou, Y., Li, S., Sheng, F., Liu, S., Du, E., et al. (2020). Identification and Immunocorrelation of Prognosis-Related Genes Associated with Development of Muscle-Invasive Bladder Cancer. *Front. Mol. Biosci.* 7, 598599. doi:10.3389/fmolb.2020.598599

Li, X., Wang, M., Gong, T., Lei, X., Hu, T., Tian, M., et al. (2020). A S100A14-Ccl2/cxcl5 Signaling axis Drives Breast Cancer Metastasis. *Theranostics* 10 (13), 5687–5703. doi:10.7150/thno.42087

Lin, Y., Cheng, L., Liu, Y., Wang, Y., Wang, Q., Wang, H. L., et al. (2021). Intestinal Epithelium-Derived BATF3 Promotes Colitis-Associated colon Cancer through Facilitating CXCL5-Mediated Neutrophils Recruitment. *Mucosal Immunol.* 14 (1), 187–198. doi:10.1038/s41385-020-0297-3

Liu, C.-J., Hu, F.-F., Xia, M.-X., Han, L., Zhang, Q., and Guo, A.-Y. (2018). GSCALite: A Web Server for Gene Set Cancer Analysis. *Bioinformatics (Oxford, England)* 34 (21), 3771–3772. doi:10.1093/bioinformatics/bty411

Liu, J., Meng, H., Nie, S., Sun, Y., Jiang, P., Li, S., et al. (2020). Identification of a Prognostic Signature of Epithelial Ovarian Cancer Based on Tumor Immune Microenvironment Exploration. *Genomics* 112 (6), 4827–4841. doi:10.1016/j.ygeno.2020.08.027

Ma, L., Lan, F., Zheng, Z., Xie, F., Wang, L., Liu, W., et al. (2012). Epidermal Growth Factor (EGF) and Interleukin (IL)-1β Synergistically Promote ERK1/2-Mediated Invasive Breast Ductal Cancer Cell Migration and Invasion. *Mol. Cancer* 11, 79. doi:10.1186/1476-4598-11-79

Mahoney, K. M., and Atkins, M. B. (2014). Prognostic and Predictive Markers for the New Immunotherapies. *Oncology (Williston Park)* 28 Suppl 3 (Suppl. 3), 39–48.

Mao, Z., Zhang, J., Shi, Y., Li, W., Shi, H., Ji, R., et al. (2020). CXCL5 Promotes Gastric Cancer Metastasis by Inducing Epithelial-Mesenchymal Transition and Activating Neutrophils. *Oncogenesis* 9 (7), 63. doi:10.1038/s41389-020-00249-z

Mariathasan, S., Turley, S. J., Nickles, D., Castiglioni, A., Yuen, K., Wang, Y., et al. (2018). TGFβ Attenuates Tumour Response to PD-L1 Blockade by

Contributing to Exclusion of T Cells. *Nature* 554 (7693), 544–548. doi:10.1038/nature25501

Mayakonda, A., Lin, D.-C., Assenov, Y., Plass, C., and Koeffler, H. P. (2018). Maftools: Efficient and Comprehensive Analysis of Somatic Variants in Cancer. *Genome Res.* 28 (11), 1747–1756. doi:10.1101/gr.239244.118

Mei, S., Meyer, C. A., Zheng, R., Qin, Q., Wu, Q., Jiang, P., et al. (2017). Cistrome Cancer: A Web Resource for Integrative Gene Regulation Modeling in Cancer. *Cancer Res.* 77 (21), e19–e22. doi:10.1158/0008-5472.CAN-17-0327

Network, T. C. G. A. (2014). Comprehensive Molecular Characterization of Urothelial Bladder Carcinoma. *Nature* 507 (7492), 315–322. doi:10.1038/nature12965

Newman, A. M., Liu, C. L., Green, M. R., Gentles, A. J., Feng, W., Xu, Y., et al. (2015). Robust Enumeration of Cell Subsets from Tissue Expression Profiles. *Nat. Methods* 12 (5), 453–457. doi:10.1038/nmeth.3337

Ongusaha, P. P., Kwak, J. C., Zwible, A. J., Macip, S., Higashiyama, S., Taniguchi, N., et al. (2004). HB-EGF Is a Potent Inducer of Tumor Growth and Angiogenesis. *Cancer Res.* 64 (15), 5283–5290. doi:10.1158/0008-5472.can-04-0925

Pećina-Šlaus, N., Kafka, A., Salamon, I., and Bukovac, A. (2020). Mismatch Repair Pathway, Genome Stability and Cancer. *Front. Mol. Biosci.* 7, 122. doi:10.3389/fmolb.2020.00122

Peng, D., Ge, G., Xu, Z., Ma, Q., Shi, Y., Zhou, Y., et al. (2018). Diagnostic and Prognostic Biomarkers of Common Urological Cancers Based on Aberrant DNA Methylation. *Epigenomics* 10 (9), 1189–1199. doi:10.2217/epi-2018-0017

Perera, R. M., and Bardeesy, N. (2012). *Ready, Set, GoThe EGF Receptor at the Pancreatic Cancer Starting Line*, 281–282. doi:10.1016/j.ccr.2012.08.019

Petrylak, D. P., de Wit, R., Chi, K. N., Drakaki, A., Sternberg, C. N., Nishiyama, H., et al. (2020). *Ramucirumab Plus Docetaxel versus Placebo Plus Docetaxel in Patients with Locally Advanced or Metastatic Urothelial Carcinoma after Platinum-Based Therapy (RANGE): Overall Survival and Updated Results of a Randomised, Double-Blind*, 105–120. (Reprinted.

Powles, T., O'Donnell, P. H., Massard, C., Arkenau, H.-T., Friedlander, T. W., Hoimes, C. J., et al. (2017). Efficacy and Safety of Durvalumab in Locally Advanced or Metastatic Urothelial Carcinoma. *JAMA Oncol.* 3, e172411. doi:10.1001/jamaoncol.2017.2411

Ritchie, M. E., Phipson, B., Wu, D., Hu, Y., Law, C. W., Shi, W., et al. (2015). Limma powers Differential Expression Analyses for RNA-Sequencing and Microarray Studies. *Nucleic Acids Res.* 43 (7), e47. doi:10.1093/nar/gkv007

Rosenberg, J. E., Hoffman-Censits, J., Powles, T., van der Heijden, M. S., Balar, A. V., Necchi, A., et al. (2016). *Atezolizumab in Patients with Locally Advanced and Metastatic Urothelial Carcinoma Who Have Progressed Following Treatment with Platinum-Based Chemotherapy: A Single-ArmMulticentre, Phase 2 Trial*, 1909–1920. (Reprinted. doi:10.1016/s0140-6736(16)00561-4

Rui, X., Gu, T.-T., Pan, H.-F., and Zhang, H.-Z. (2019). Evaluation of PD-L1 Biomarker for Immune Checkpoint Inhibitor (PD-1/pd-L1 Inhibitors) Treatments for Urothelial Carcinoma Patients: A Meta-Analysis. *Int. Immunopharmacology* 67, 378–385. doi:10.1016/j.intimp.2018.12.018

Schulz, W. A., and Goering, W. (2016). DNA Methylation in Urothelial Carcinoma. *Epigenomics* 8 (10), 1415–1428. doi:10.2217/epi-2016-0064

Sharma, P., Callahan, M. K., Bono, P., Kim, J., Spiliopoulou, P., Calvo, E., et al. (2016). *Nivolumab Monotherapy in Recurrent Metastatic Urothelial Carcinoma (CheckMate 032): A Multicentre, Open-Label, Two-Stage, Multi-Arm, Phase 1/2 Trial*, 1590–1598. doi:10.1016/s1470-2045(16)30496-x

Simon, N., Friedman, J., Hastie, T., and Tibshirani, R. (2011). Regularization Paths for Cox's Proportional Hazards Model via Coordinate Descent. *J. Stat. Softw.* 39 (5), 1–13. doi:10.18637/jss.v039.i05

Sweis, R. F., Spranger, S., Bao, R., Paner, G. P., Stadler, W. M., Steinberg, G., et al. (2016). Molecular Drivers of the Non-T-cell-inflamed Tumor Microenvironment in Urothelial Bladder Cancer. *Cancer Immunol. Res.* 4 (7), 563–568. doi:10.1158/2326-6066.CIR-15-0274

Tibshirani, R. (1996). Regression Shrinkage and Selection via the Laaso. J. R. Stat. Soc. *Ser. B (Methodological)* 58 (No. 1), 267–288. doi:10.1111/j.2517-6161.1996.tb02080.x

Tomas, A., Futter, C. E., and Eden, E. R. (2014). EGF Receptor Trafficking: Consequences for Signaling and Cancer. *Trends Cel Biol.* 24 (1), 26–34. doi:10.1016/j.tcb.2013.11.002

Tumeh, P. C., Harview, C. L., Yearley, J. H., Shintaku, I. P., Taylor, E. J. M., Robert, L., et al. (2014). PD-1 Blockade Induces Responses by Inhibiting Adaptive Immune Resistance. *Nature* 515, 568–571. doi:10.1038/nature13954

Vlachostergios, P. J., and Faltas, B. M. (2018). Treatment Resistance in Urothelial Carcinoma: An Evolutionary Perspective. *Nat. Rev. Clin. Oncol.* 15 (8), 495–509. doi:10.1038/s41571-018-0026-y

Wang, Y., Chen, L., Ju, L., Xiao, Y., and Wang, X. (2020). Tumor Mutational burden Related Classifier Is Predictive of Response to PD-L1 Blockade in Locally Advanced and Metastatic Urothelial Carcinoma. *Int. Immunopharmacology* 87, 106818. doi:10.1016/j.intimp.2020.106818

Xia, J., Xu, X., Huang, P., He, M., and Wang, X. (2015). The Potential of CXCL5 as a Target for Liver Cancer - what Do We Know So Far. *Expert Opin. Ther. Targets* 19, 141–146. doi:10.1517/14728222.2014.993317

Xu, N., Ke, Z.-B., Lin, X.-D., Chen, Y.-H., Wu, Y.-P., Chen, Y., et al. (2020). Development and Validation of a Molecular Prognostic index of Bladder Cancer Based on Immunogenomic Landscape Analysis. *Cancer Cel Int* 20, 302. doi:10.1186/s12935-020-01343-3

Yang, S., Wu, Y., Deng, Y., Zhou, L., Yang, P., Zheng, Y., et al. (2019). Identification of a Prognostic Immune Signature for Cervical Cancer to Predict Survival and Response to Immune Checkpoint Inhibitors. *Oncoimmunology* 8 (12), e1659094. doi:10.1080/2162402X.2019.1659094

Yarchoan, M., Hopkins, A., and Jaffee, E. M. (2017). Tumor Mutational Burden and Response Rate to PD-1 Inhibition. *N. Engl. J. Med.* 377, 2500–2501. doi:10.1056/nejmc1713444

Yeh, C. R., Hsu, I., Song, W., Chang, H., Miyamoto, H., Xiao, G. Q., et al. (2015). Fibroblast ERα Promotes Bladder Cancer Invasion via Increasing the CCL1 and IL-6 Signals in the Tumor Microenvironment. *Am. J. Cancer Res.* 5 (3), 1146–1157.

Yi, M., Li, A., Zhou, L., Chu, Q., Luo, S., and Wu, K. (2021). Immune Signature-Based Risk Stratification and Prediction of Immune Checkpoint Inhibitor's Efficacy for Lung Adenocarcinoma. *Cancer Immunol. Immunother.* 70 (6), 1705–1719. doi:10.1007/s00262-020-02817-z

Yu, G., Wang, L.-G., Han, Y., and He, Q.-Y. (2012). ClusterProfiler: An R Package for Comparing Biological Themes Among Gene Clusters. *OMICS: A J. Integr. Biol.* 16 (5), 284–287. doi:10.1089/omi.2011.0118

Conflict of Interest: The authors declare that the research was conducted in the absence of any commercial or financial relationships that could be construed as a potential conflict of interest.

Publisher's Note: All claims expressed in this article are solely those of the authors and do not necessarily represent those of their affiliated organizations, or those of the publisher, the editors and the reviewers. Any product that may be evaluated in this article, or claim that may be made by its manufacturer, is not guaranteed or endorsed by the publisher.

frontiers in Cell and Developmental Biology

ORIGINAL RESEARCH
published: 10 January 2022
doi: 10.3389/fcell.2021.782529

Comprehensive Characterization of Tumor Purity and Its Clinical Implications in Gastric Cancer

*Shenghan Lou[1], Jian Zhang[2], Xin Yin[1], Yao Zhang[1], Tianyi Fang[1], Yimin Wang[1] and Yingwei Xue[1]**

[1]Department of Gastroenterological Surgery, Harbin Medical University Cancer Hospital, Harbin, China, [2]Department of Thoracic Surgery, Harbin Medical University Cancer Hospital, Harbin, China

Solid tumour tissues are composed of tumour and non-tumour cells, such as stromal cells and immune cells. These non-tumour cells constitute an essential part of the tumour microenvironment (TME), which decrease the tumour purity and play an important role in carcinogenesis, malignancy progression, treatment resistance and prognostic assessment. However, the implications of various purity levels in gastric cancer (GC) remain largely unknown. In the present study, we used an in-silico approach to infer the tumour purity of 2,259 GC samples obtained from our hospital and 12 public datasets based on the transcriptomic data. We systematically evaluated the association of tumour purity with clinical outcomes, biological features, TME characteristics and treatment response in GC. We found that tumour purity might be a patient-specific intrinsic characteristic of GC. Low tumour purity was independently correlated with shorter survival time and faster recurrence and significantly associated with mesenchymal, invasive and metastatic phenotypes. Integrating GC purity into a clinical prognostic nomogram significantly improved predictive validity and reliability. In addition, low tumour purity was strongly associated with immune and stromal cell functions. Fibroblasts, endothelial cells and monocytes were markedly enriched in low-purity tumours, serving as robust indicators of a poor prognosis. Moreover, patients with low GC purity may not benefit more from adjuvant chemotherapy. Our findings highlight that tumour purity confers important clinical, biological, microenvironmental and treatment implications for patients with GC. Therefore, a comprehensive evaluation of tumour purity in individual tumours can provide more insights into the molecular mechanisms of GC, facilitate precise classification and clinical prediction and help to develop more effective individualised treatment strategies.

Keywords: tumor purity, gastric cancer, prognosis, tumor microenvironment, chemotherapy resistance

OPEN ACCESS

Edited by:
José Alexandre Ferreira, Portuguese Oncology Institute, Portugal

Reviewed by:
Youliang Wang, Beijing Institute of Technology, China
Changyu He, Shanghai Jiao Tong University, China

****Correspondence:***
Yingwei Xue
xueyingwei@hrbmu.edu.cn

Specialty section:
This article was submitted to Molecular and Cellular Pathology, a section of the journal Frontiers in Cell and Developmental Biology

Received: *24 September 2021*
Accepted: *20 December 2021*
Published: *10 January 2022*

Citation:
Lou S, Zhang J, Yin X, Zhang Y, Fang T, Wang Y and Xue Y (2022) Comprehensive Characterization of Tumor Purity and Its Clinical Implications in Gastric Cancer. Front. Cell Dev. Biol. 9:782529. doi: 10.3389/fcell.2021.782529

1 INTRODUCTION

Gastric cancer (GC) is the fifth most prevalent cancer and the third most frequent cause of cancer-related deaths worldwide (Bray et al., 2018), with almost 1,000,000 new cases and 800,000 deaths each year (Torre et al., 2015; Bray et al., 2018). Owing to a lack of symptoms in the early stage, most patients with GC are usually diagnosed at an advanced stage (Dai et al., 2019). Treatment options for patients at an advanced stage are limited, resulting in a relatively low 5-year survival rate (<20%)

(Katai et al., 2018). GC is a heterogeneous disease (Han et al., 2015), and different histopathological and molecular classification systems have been reported for its diagnosis (Serra et al., 2019). However, despite the widespread clinical use of histopathological classification (such as Lauren classification), the currently available histopathological systems remain insufficient to guide precise treatment for individual patients (Dicken et al., 2005). To date, the tumour–node–metastasis (TNM) staging system is considered the gold-standard method to predict prognosis and guide treatment decisions for patients with GC (Sasako et al., 2010). However, the high heterogeneity of GC leads to different outcomes among patients with the same TNM stage receiving the same treatments (Tang et al., 2020), suggesting that clinical prediction and treatment outcomes are unsatisfactory.

Solid tumour tissue comprises cellular components originating from various cancerous and noncancerous tissues, including immune, stromal, endothelial and epithelial cells (Joyce and Pollard, 2009). Such these noncancerous cells form an important part of the tumour microenvironment (TME) and interact with each other and tumour cells to sustain tumour growth and survival (Aran et al., 2015). GC tissues contain abundant GC-associated noncancerous cells within their microenvironments. With the increased understanding of the diversity and complexity of the TME of GC, these noncancerous cells, represented by stromal and immune cells, have been found to play an important role in carcinogenesis, malignancy progression and treatment resistance (Junttila and de Sauvage, 2013; Zeng et al., 2019; Zhang et al., 2020). However, the currently available classification systems merely consider the noncancerous factors present within GC tissues, and there is limited knowledge regarding the characteristics of GC cells under various purity levels.

Tumour purity, defined as the proportion of cancer cells in the tumour tissue, can be estimated by expert pathologists who review tumour sections or based on computational methods (Haider et al., 2020). However, pathological assessment may be inconsistent because of human error and bias (Smits et al., 2014). More importantly, tumour sections reviewed by pathologists may not always represent the tumour region that is subject to molecular profiling (Haider et al., 2020). However, estimation of tumour purity using alternative in-silico techniques can circumvent these problems. The continuously accumulating transcriptomic and genomic data provide an ideal resource for examining the multi-omic features underlying tumour purity in different cases. Integration of multiple independent studies is considered a better approach to enhancing the reliability of results, thus enabling us to identify the common core features of diseases (Ricketts et al., 2018).

Therefore, in the present study, we systematically evaluated the role of tumour purity in GC by integrating the clinical and multi-omic data of 2,259 GC samples obtained from our hospital, Gene Expression Omnibus (GEO) and The Cancer Genome Atlas (TCGA). We analysed the association of GC purity with clinical outcomes, functional characterisation and TME. In addition, we found that GC purity could predict the response of patients to chemotherapy. These findings provide novel insights into developing individualised treatment strategies for GC, which can help to improve prognostic risk stratification and facilitate treatment decision-making for patients with GC.

2 MATERIALS AND METHODS

2.1 Gastric Cancer Dataset Source

Demographic information, clinical data and tissue samples were obtained from 214 patients with GC who had undergone gastrectomy as the primary treatment between 2016 and 2019 at the Harbin Medical University (HMU) Cancer Hospital. These data were used to construct the HMU-GC cohort. All samples were collected after written informed consent was obtained from the patients. This study was approved by the Institutional Review Board of the HMU Cancer Hospital. RNA isolation, library construction and mRNA sequencing were performed by Novogene (Beijing, China). The data were deposited in the GEO repository (GSE184336).

We systematically searched for publicly available GC gene expression datasets in GEO and TCGA databases. Datasets missing the follow-up data were excluded. In addition, to enhance the robustness of downstream analyses, samples with survival time less than 3 months were excluded (Joung and Merkow, 2021; Resio et al., 2021). A total of 12 public treatment-naive GC cohorts (GSE62254/ACRG, GSE15459, GSE57303, GSE34942, GSE38749, GSE15456, GSE84437, GSE26901, GSE26899, GSE13861, GSE26253 and TCGA-STAD) were selected for further analysis. In addition, four GC cell datasets, namely, Cancer Cell Line Encyclopedia (CCLE), GSE22183, GSE15455 and GSE146361, were included as references.

2.2 Data Preprocessing

To process microarray data, the raw CEL files obtained from Affymetrix were processed using the robust multichip average (RMA) algorithm for background correction and normalisation using the affy package (Irizarry et al., 2003; Gautier et al., 2004). The raw data from Illumina were processed using the limma package (Ritchie et al., 2015). For microarray datasets without raw data, the normalised matrix files were directly downloaded.

For high-throughput sequencing data obtained from the HMU-GC and TCGA-STAD datasets, raw read count values were converted to transcripts per kilobase million (TPM) values, which are more similar to those generated from microarrays and are comparable between samples (Wagner et al., 2012). Batch effects from non-biological technical biases among different datasets were corrected using the ComBat algorithm in the sva package (Leek et al., 2012).

The gene expression profile at the probe level (or Ensembl ID level) was converted to the official gene symbol level using the biomaRt package (Durinck et al., 2005). When multiple probes (or Ensembl IDs) were mapped to the same gene symbol, the probe (or Ensembl ID) with the largest mean expression values across samples was selected.

2.3 Identification of GC Purity and a Purity-Related Co-expression Network

Tumour purity was calculated using the ESTIMATE algorithm (Yoshihara et al., 2013). In addition, GC tissues in the TCGA-STAD cohort were reviewed to infer GC purity based on visual evaluation of the whole-slide images of haematoxylin and eosin

(H&E) staining. Two pathologists independently confirmed the results of histological purity.

Weighted correlation network analysis (WGCNA) was performed using the WGCNA package to screen for purity-related gene modules (Langfelder and Horvath, 2008). A scale-free topology fitting index (R^2) of 0.85 was set as the threshold to construct a signed weighted gene co-expression network. The minimum co-expression module size was set as 30, and the minimum cut height for module merging was set as 0.25. A biweight midcorrelation coefficient (R) > 0.4 and p-value < 0.05 were set as thresholds to screen for gene modules significantly associated with GC purity.

2.4 Association of GC Purity With Clinical, Molecular and Prognostic Features

Nearest template prediction (NTP) analysis was performed to classify samples based on the known clinical and molecular features (Hoshida, 2010). Univariate and multivariate Cox regression analyses were performed to calculate the hazard ratio (HR) and 95% confidence interval (CI). The Kaplan–Meier survival analysis with log-rank test was used to compare the survival rates of patients in different subgroups. Differences in prognosis between the high- and low-purity subgroups were compared using the restricted mean survival time (RMST) analysis (Kim et al., 2017). In addition, subgroup analyses were performed to examine the association between GC purity and other clinical characteristics.

Furthermore, GC purity was integrated with other independent prognostic factors to generate a composite prognostic nomogram for model visualisation and evaluation of clinical applications. The predictive value of the nomogram was compared with that of the TNM staging system in terms of concordance index (C-index). The performance of the composite model was evaluated based on calibration curves, time-dependent receiver operating characteristic (ROC) analysis, and decision curve analysis (DCA) (Vickers and Elkin, 2006).

2.5 Functional and Pathway Enrichment Analyses

Gene annotation enrichment analysis was performed using the clusterProfiler package (Yu et al., 2012). Gene set enrichment analysis (GSEA) was performed to screen for biological processes related to GC purity (Subramanian et al., 2005), and gene set variation analysis (GSVA) was performed to quantify the pathway enrichment scores using the GSVA package (Hänzelmann et al., 2013) and screen for significantly enriched pathways in each cluster. The well-defined 'Hallmark gene sets' were selected to quantify the pathway activity (Liberzon et al., 2015).

2.6 Estimation of Infiltrating Cells in the GC Microenvironment

To quantify the infiltration level of stromal and immune cells in each GC sample, we calculated the stromal and immune scores using the ESTIMATE algorithm (Yoshihara et al., 2013). Based on the guidelines of transcriptome-based cell-type quantification methods (Sturm et al., 2019), we used the MCPcounter and xCell algorithms to quantify specific immune and stromal cells in the GC samples (Becht et al., 2016; Aran et al., 2017). Based on the whole-slide images of H&E staining obtained from the TCGA-STAD cohort, we further used the convolutional neural network, a supervised deep-learning approach, to identify the proportion of tumour-infiltrating lymphocytes (TILs) in digitised H&E-stained tissue specimens (Saltz et al., 2018).

2.7 Estimation of the Potential Response to Chemotherapy

Seven common chemotherapeutic agents (5-fluorouracil, cisplatin, oxaliplatin, capecitabine, paclitaxel, docetaxel and irinotecan), which are approved for GC treatment, were selected to predict the chemotherapeutic response. Based on two public drug sensitivity databases, namely, CTRP (Basu et al., 2013) and PRISM (Corsello et al., 2020), the chemotherapeutic response was predicted via the pRRophetic package using ridge regression to estimate the area under the curve (AUC) value of each sample (Geeleher et al., 2014). Lower AUC values indicated increased sensitivity to treatment. The prediction accuracy was evaluated *via* 10-fold cross-validation based on each training set. Default values were selected for all parameters, including the combat algorithm for removing batch effects and the mean value for summarising duplicate gene expression.

2.8 Statistical Analyses

Differences between groups for continuous variables were evaluated using the Kolmogorov–Smirnov, Mann–Whitney or Kruskal–Wallis tests. The two-sided Pearson's chi-squared or Fisher exact test was used to analyse the categorical data. The association between continuous variables was tested using Spearman correlation analysis. Restricted cubic splines were used to test potential non-linear associations. All statistical analyses were conducted using the R software, and p-values were two-sided. A p-value < 0.05 was considered statistically significant. The Benjamini–Hochberg method was used to control the false discovery rate (FDR) for multiple hypothesis testing.

3 RESULTS

3.1 Tumour Purity Is an Intrinsic Property of GC

More than 40 GC cell lines involving 215 cell samples were analysed as references (**Supplementary Table S1**). A high degree of purity, i.e. median purity of 0.999 (inter-quartile range [IQR], 0.996–1), was observed in GC cell lines. Furthermore, no significant difference was found between the microarray and RNA-seq datasets (Kolmogorov–Smirnov test, p = 0.789), which verified the validity and robustness of the ESTIMATE algorithm.

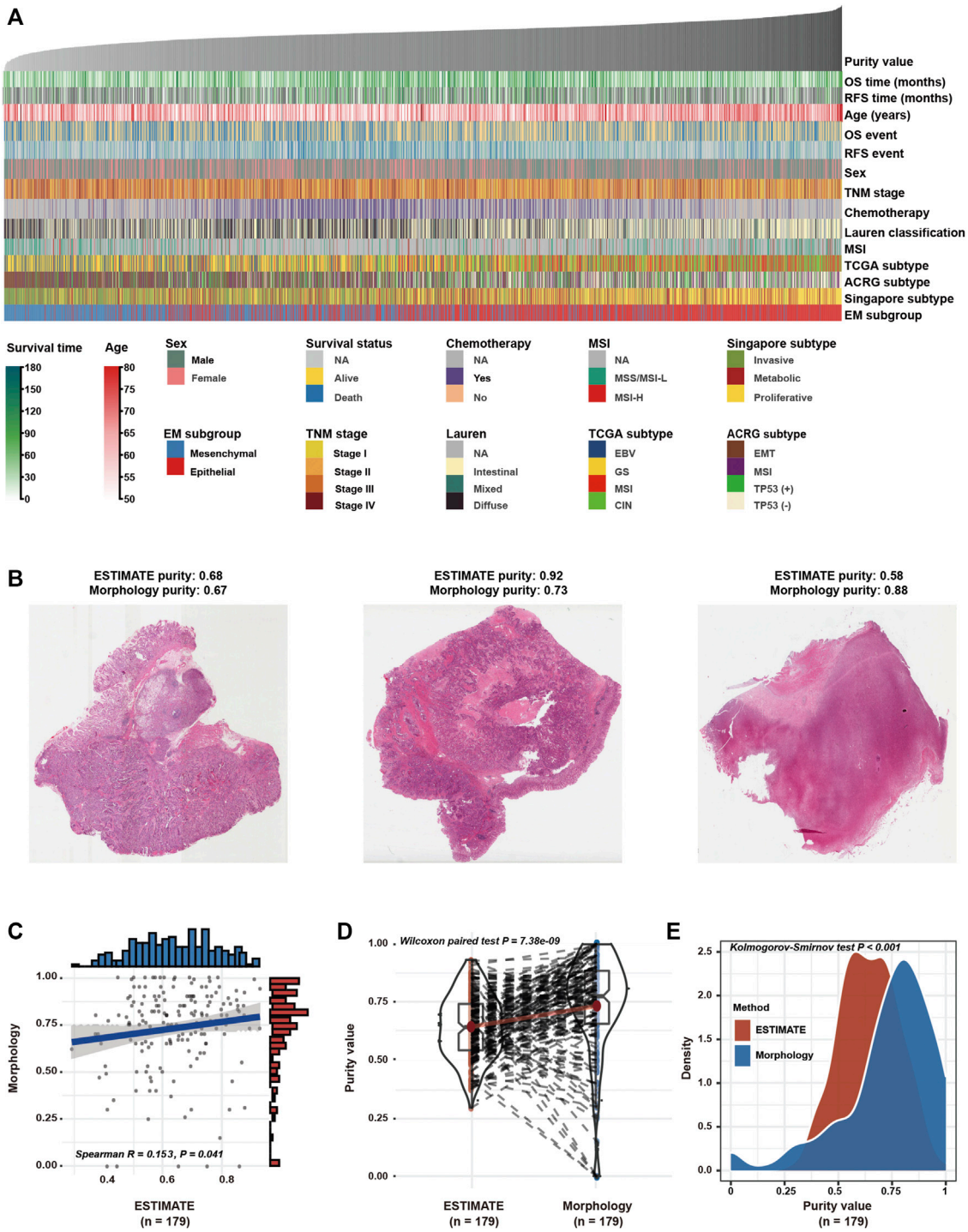

FIGURE 1 | Tumour purity is an intrinsic property of gastric cancer (GC). **(A)** The landscape of clinicopathological and molecular characteristics associated with GC purity. **(B)** Representative slides of GC tissues. **(C)** Spearman correlation analysis of GC purity based on morphological assessment and the ESTIMATE method. **(D)** Distribution of GC purity evaluated based on morphological assessment and the ESTIMATE method. The upper and lower ends of the boxes represent the inter-quartile range of values. The lines in the boxes represent the median value. The whisker edges are the last data points within 1.5 of the inter-quartile range. The horizontal width of the violin represents the data density. **(E)** Density distribution of GC purity estimated based on morphological assessment and the ESTIMATE method.

In the GC meta-dataset (**Supplementary Figure S1A**), a total of 2,599 GC tissues from 13 cohorts were initially selected. After excluding samples with survival time less than 3 months (Joung and Merkow, 2021; Resio et al., 2021), 2,259 samples were retained for further analyses. As demonstrated in **Figure 1A**, GC samples were arranged in order of increasing purity, and a

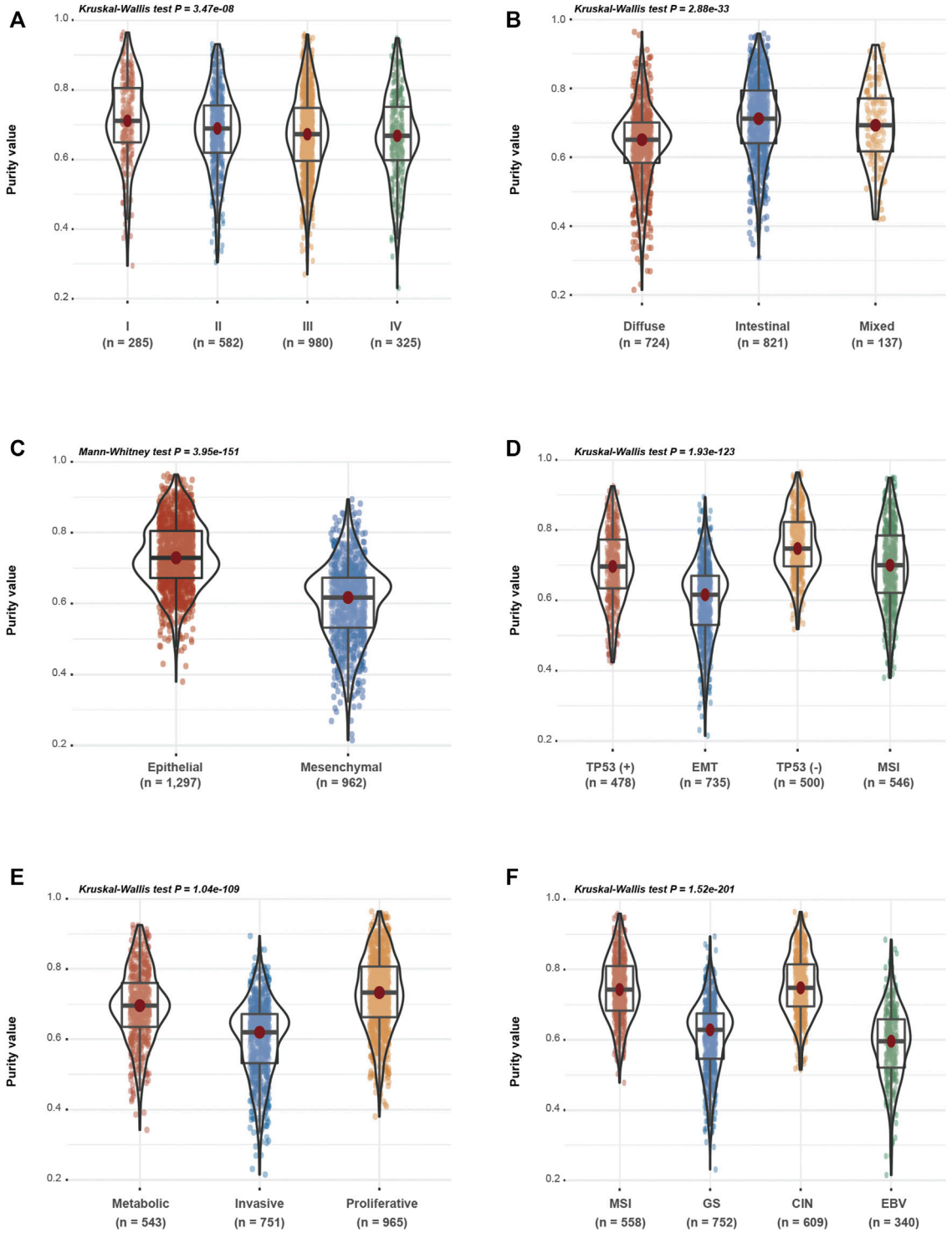

FIGURE 2 | Gastric cancer (GC) purity is characterised by specific clinicopathological and molecular features. **(A–F)** Distribution of GC purity in terms of **(A)** TNM stage, **(B)** Lauren classification, **(C)** EM (epithelial and mesenchymal) subtype, **(D)** ACRG subtype, **(E)** Singapore subtype and **(F)** TCGA subtype. The upper and lower ends of the boxes represent the inter-quartile range of values. The lines in the boxes represent the median value. The whisker edges are the last data points within 1.5 of the inter-quartile range. The horizontal width of the violin represents the data density.

wide range (0.215–0.964) of purity was observed among the 2,259 samples, with a median purity of 0.681 (IQR, 0.608–0.759). In addition, the morphological features of GC cells were assessed in 179 patients in the TCGA cohort (**Figure 1B**; **Supplementary Table S2**). Consistent with the findings of the previous study (Aran et al., 2015), GC purity evaluated based on the ESTIMATE algorithm was significantly correlated with morphology (**Figure 1C**). However, significant differences were observed between the two evaluation methods (**Figures 1D,E**), which suggested that morphology evaluation can only provide a qualitative estimation of GC purity.

Furthermore, we investigated different samples from the same patient to determine their consistency. In the GSE14209 dataset, 22 patients were analysed twice (pre- and post-chemotherapy). We observed high concordance between the pre- and post-chemotherapy samples (**Supplementary Figure S1B**). The results suggest that tumour purity levels among patients with cancer are robust and consistent, implying that tumour purity may be an intrinsic property of GC.

3.2 GC Purity Is Characterised by Specific Clinicopathological and Molecular Features

Based on the speculation that tumour purity is an intrinsic property of GC, we assessed the association between GC purity and clinical and molecular features. We found a negative correlation between GC purity and age at diagnosis (Spearman R = 0.122; $p < 0.001$; **Supplementary Figure S1C**). According to the TNM staging system and histopathological features, GC samples were classified into the corresponding clinicopathological and molecular features. A consistent decrease in GC purity was observed as the TNM stages advanced (**Figure 2A**). Based on the Lauren classification, intestinal-type GC had the highest purity level, whereas diffuse-type GC was accompanied had the lowest purity level (**Figure 2B**). These results suggest that low tumour purity is closely associated with the malignant progression of GC.

Based on clinical features, low-purity GC samples were more likely to belong to the mesenchymal subtype, whereas high-purity GC samples were enriched in the epithelial subtype (**Figure 2C**). Based on the other three molecular classifications, namely, the ACRG (**Figure 2D**), Singapore (**Figure 2E**) and TCGA (**Figure 2F**) classification systems, decreased tumour purity levels were associated with epithelial–mesenchymal transition (EMT) and invasive or genomically stable (GS) molecular subtypes, which were usually correlated with the invasion and metastasis of GC. These findings indicate that GC purity is closely related to specific clinicopathological and molecular features.

3.3 GC Purity Confers Different Survival and Recurrence Outcomes

We found that low purity was significantly related to the malignant phenotype. To further evaluate the prognostic value of GC purity in combination with other clinical variables, we performed univariate and multivariate Cox proportional hazard regression analyses based on combined clinicopathologic variables in the GC meta-dataset cohort. In addition to chemotherapy history and TNM stage, which is a well-known prognostic factor, GC purity was identified as a significant predictor of overall survival (OS) and recurrence-free survival (RFS) based on the univariate analysis (**Table 1**).

Although the Epstein–Barr virus (EBV) subtype is characterised by lower purity scores (**Figure 2F**), it is associated with a good prognosis (Sohn et al., 2017). Therefore, the relationship between GC purity and prognosis may not necessarily be linear. We used restricted cubic splines to assess the possible non-linear association between GC purity and prognosis. However, a non-linear relationship (a U-shaped curve) was observed between GC purity and OS (**Figure 3A**) and RFS (**Figure 3B**).

Furthermore, patients with GC were stratified into two (high or low purity) and three (high, moderate or low purity) subgroups using the optimal cut-off values determined using the X-tile software (Camp et al., 2004). In both subgroup analyses, the OS (**Figures 3C,D**) and RFS (**Figures 3E,F**) rates were lower in patients with low purity scores than in patients with high purity scores. The RMST difference also determined a benefit of high purity, and the benefit seemed to increase over time (**Table 2**). For example, the RMST differences between the two groups were 2 months for OS and 4 months for RFS after 5 years of follow-up, which increased to 7 months for OS and 12 months for RFS after 10 years. These results suggested that low GC purity was associated with a shorter survival time and faster recurrence.

When all relevant clinical variables were included in the multivariate Cox regression analysis, GC purity was identified as a significant prognostic factor (**Table 1**). Subgroup analyses were further performed to assess the association between GC purity and other prognostic factors. No significant association was observed between GC purity and both OS and RFS (**Table 3**), indicating that GC purity retained its prognostic relevance even after classic clinicopathological prognostic features were considered.

Furthermore, we integrated these independent factors (tumour purity, TNM stage and chemotherapy history) to establish a prognostic nomogram for predicting the OS of patients with GC (**Supplemenatry Figure S2A**). The calibration plot revealed an optimal agreement between nomogram prediction and actual observation at different time points (**Figure 3G**). Moreover, we compared the OS prediction power between the nomogram and clinical model. The C-index of the nomogram was significantly higher than that of the clinical model for predicting OS (**Figure 3H**). In addition, the time-dependent ROC curve confirmed that the nomogram exhibited better performance in predicting the prognosis of GC (**Figure 3I**).

Lastly, DCA curves were used to assess the clinical usefulness and net benefit of these two models. The composite nomogram demonstrated a larger net benefit than that exhibited by the clinical model within most of the threshold probabilities (**Figure 3J**). Similar results were also found for RFS (**Supplemenatry Figure S2B**; **Figures 3K–N**). These results indicated that integrating GC purity into a prognostic model can significantly improve its predictive power. In addition, the nomogram exhibited better clinical utility for predicting

TABLE 1 | Univariate and multivariate cox analyses for tumor purity in gastric cancer.

	Overall survival						Recurrence-free survival					
	Univariate			Multivariate			Univariate			Multivariate		
	Samples	HR (95%CI)	*p* value	Samples	HR (95%CI)	*p* value	Samples	HR (95%CI)	*p* value	Samples	HR (95%CI)	*p* value
Age												
Increasing years	2254	1.014 (1.009, 1.019)	<**0.001**	772	1.002 (0.991, 1.012)	0.765	1155	1.003 (0.995, 1.011)	0.499			
Gender												
Female	764	Reference					400	Reference				
Male	1495	1.052 (0.922, 1.200)	0.449				757	1.045 (0.858, 1.273)	0.66			
Chemotherapy												
No	131	Reference		112	Reference		104	Reference		103	Reference	
Yes	732	0.497 (0.364, 0.678)	<**0.001**	660	0.337 (0.239, 0.475)	<**0.001**	556	0.290 (0.209, 0.403)	<**0.001**	556	0.243 (0.174, 0.338)	<**0.001**
Lauren classification												
Intestinal	821	Reference		328	Reference		541	Reference				
Mixed	137	1.521 (1.174, 1.970)	**0.001**	60	1.218 (0.780, 1.903)	0.386	60	1.505 (0.984, 2.303)	0.06			
Diffuse	724	1.152 (0.991, 1.340)	0.065	384	1.007 (0.773, 1.311)	0.962	505	1.128 (0.928, 1.370)	0.227			
TNM stage												
Stage I	285	Reference		129	Reference		193	Reference		125	Reference	
Stage II	582	1.579 (1.142, 2.182)	**0.006**	222	1.328 (0.806, 2.188)	0.266	375	1.303 (0.882, 1.924)	0.183	202	1.411 (0.886, 2.247)	0.147
Stage III	980	3.407 (2.527, 4.593)	<**0.001**	289	3.209 (2.035, 5.061)	<**0.001**	382	2.630 (1.819, 3.802)	<**0.001**	206	3.273 (2.120, 5.051)	<**0.001**
Stage IV	325	7.363 (5.378, 10.079)	<**0.001**	132	5.768 (3.599, 9.244)	<**0.001**	201	5.464 (3.752, 7.956)	<**0.001**	125	4.454 (2.862, 6.932)	<**0.001**
Tumor purity												
Increasing values	2259	0.455 (0.269, 0.771)	**0.003**	772	0.120 (0.025, 0.570)	**0.007**	1157	0.372 (0.158, 0.874)	**0.023**	659	0.129 (0.025, 0.663)	**0.014**

CI, confidence interval; HR, hazard ratio. The bold values mean that the results were statistical significance.

prognosis, emphasising the requirement of considering GC purity in clinical practice.

3.4 Biological Insights Into GC Purity

Given that tumour purity is closely related to the clinicopathological, molecular and prognostic features, we used RNA expression profiles to examine the underlying biological processes associated with GC purity. We performed principal components analysis (PCA) to identify the transcriptomic features related to GC purity and found a strong association between mRNA expression profiles and GC purity (**Figure 4A**), implying that distinct biological phenotypes are attributed to varied GC cell percentages.

Furthermore, we performed GSEA to assess the biological features associated with GC purity. The results suggested that samples with different GC purity exhibited distinct biological processes (**Figure 4B**). Consistent with the clinical and molecular features, low tumour purity was significantly related to pathways associated with invasion and metastasis and multiple immune-related pathways. However, high purity was considerably associated with metabolism and proliferation-related pathways.

Subsequently, we used WGCNA to obtain purity-related modules. We constructed a cluster dendrogram according to the soft threshold power (**Supplemenatry Figure S3A**) and identified 11 colour modules (**Supplemenatry Figure S3B**). Among the identified modules, four were highly associated ($|R| > 0.4$) with tumour purity (**Figure 4C**; **Supplemenatry Table S3**). In addition, gene significance significantly correlated with module membership in each module (**Supplemenatry Figure S3C**), suggesting that genes in these modules might play an essential role associated with GC purity.

Furthermore, module enrichment analyses were performed to explore the biological features of purity-related modules (**Figure 4D**). Consistent with the results of GSEA, genes in the

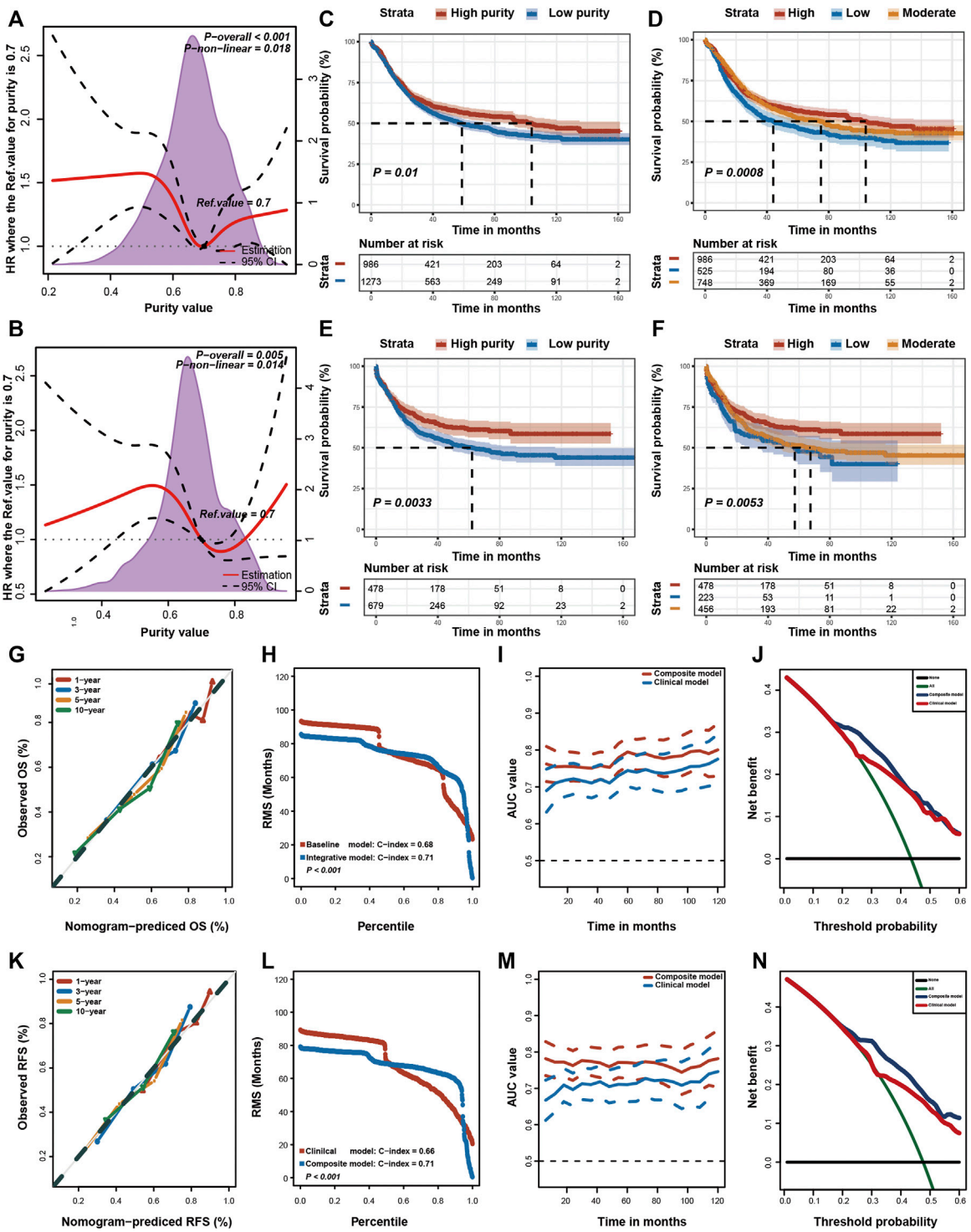

FIGURE 3 | Prognostic value of tumour purity in gastric cancer. **(A,B)** Association of tumour purity and **(A)** overall survival (OS) and **(B)** recurrence-free survival (RFS) estimated using restricted cubic splines. **(C–F)** Kaplan–Meier curves for **(C,D)** OS and **(E,F)** RFS among different subgroups. *p*-values were obtained using the log-rank test. The + symbols in the panels indicate censored data. **(G,K)** Calibration plots of the nomogram for the predicted **(G)** OS and **(K)** RFS at 1, 3, 5, and 10 years. **(H,L)** Restricted mean survival (RMS) time curves for **(H)** OS and **(L)** RFS. **(I,M)** Time-dependent ROC curves for **(I)** OS and **(M)** RFS. **(J,N)** Decision curve analysis for the prediction of **(J)** OS and **(N)** RFS using the nomogram. HR, hazard ratio.

TABLE 2 | Restricted mean survival time (RMST) differences in different time points.

Overall survival										
Time point	**High purity (*n* = 986)**			**Low purity (*n* = 1273)**			**RMST difference[a]**			
	RMST	**95% CI**		**RMST**	**95% CI**		**Effect size**	**95% CI**		***p* value**
12 months	11.096	10.938	11.253	11.009	10.862	11.156	0.087	−0.128	0.303	0.428
36 months	28.054	27.294	28.813	27.509	26.841	28.176	0.545	−0.466	1.557	0.291
60 months	42.216	40.742	43.689	40.361	39.091	41.632	1.855	−0.091	3.8	0.062
84 months	55.412	53.179	57.644	51.701	49.797	53.606	3.71	0.776	6.645	**0.013**
120 months	73.604	70.179	77.03	67.03	64.118	69.942	6.574	2.078	11.071	**0.004**
160 months[b]	91.961	86.98	96.942	83.132	78.979	87.285	8.829	2.344	15.314	**0.008**
Recurrence free survival										
Time point	**High purity (*n* = 478)**			**Low purity (*n* = 679)**			**RMST difference[a]**			
	RMST	**95% CI**		**RMST**	**95% CI**		**Effect size**	**95% CI**		***p* value**
12 months	10.408	10.088	10.728	10.355	10.084	10.625	0.054	−0.365	0.472	0.802
36 months	27.384	26.131	28.637	25.688	24.633	26.744	1.695	0.057	3.333	**0.043**
60 months	42.541	40.22	44.862	38.472	36.529	40.416	4.069	1.042	7.096	**0.008**
84 months	57.137	53.67	60.604	50.045	47.174	52.916	7.092	2.591	11.594	**0.002**
120 months	78.252	72.882	83.621	66.409	62.032	70.787	11.842	4.914	18.77	**0.001**
150 months[b]	95.8	88.686	102.915	79.602	73.837	85.367	16.198	7.041	25.355	**0.001**

RMST, restricted mean survival time. The bold values mean that the results were statistical significance.

[a]*RMST difference = $RMST_{high\ purity}$–$RMST_{low,\ purity}$.*

[b]*Final follow-up time point.*

TABLE 3 | Subgroup analysis for tumor purity in gastric cancer.

	Overall survival			**Recurrence free survival**		
	Samples	**HR (95%CI)**	***p* value for interaction**	**Samples**	**HR (95%CI)**	***p* value for interaction**
Gender						
Female	764	**0.013 (0.001, 0.286)**	0.2	400	**0.001 (0.0001, 0.024)**	0.003
Male	1495	0.214 (0.035, 1.300)		757	0.590 (0.081, 4.288)	
Age						
<65	1461	**0.063 (0.009, 0.447)**	0.589	797	0.065 (0.008, 0.506)	0.4716
>65	793	0.274 (0.021, 3.627)		358	0.147 (0.009, 2.353)	
Chemotherapy						
No	131	0.201 (0.018, 2.301)	0.681	104	0.074 (0.006, 0.970)	0.7392
Yes	732	**0.100 (0.014, 0.706)**		556	0.148 (0.017, 1.320)	
Lauren type						
Intestinal	821	0.135 (0.018, 1.040)	0.849	541	0.062 (0.007, 0.522)	0.1588
Mixed	137	1.238 (0.012, 130.179)		60	42.089 (0.045, 39,734.047)	
Diffuse	724	0.140 (0.009, 2.252)		505	0.302 (0.014, 6.298)	
TNM stage						
Stage I	285	0.355 (0.009, 13.991)	0.076	193	0.017 (0.0004, 0.800)	0.3875
Stage II	582	0.002 (0.00003, 0.072)		375	0.004 (0.0001, 0.186)	
Stage III	980	0.572 (0.057, 5.730)		382	0.245 (0.013, 4.500)	
Stage IV	325	0.115 (0.005, 2.812)		201	0.291 (0.015, 5.804)	

HR, hazard ratio; CI, confidence interval. The bold values mean that the results were statistical significance.

red module were enriched in pathways associated with metabolic activation (**Supplemenatry Table S4**). Genes in the blue module were significantly enriched in proliferation-specific pathways (**Supplemenatry Table S5**). In addition, genes in the turquoise (**Supplemenatry Table S6**) and yellow (**Supplemenatry Table S7**) modules were prominently related to stromal and immune activation pathways, respectively.

Eventually, we analysed proteomic data generated using reverse-phase protein arrays in the TCGA cohort (**Figure 4E**). Consistent with the clinical and gene expression data, α-catenin, E-cadherin and other crucial epithelial adhesion proteins in epithelial cells were positively correlated with tumour purity. Low tumour purity was associated with high expression of MYH11, RICTOR and CAV1, which are markers for mesenchymal lineage or EMT. In addition, low GC purity was associated with increased expression of numerous stromal- and immune-associated proteins. High GC purity was, however, associated with increased expression of multiple proliferation- and metabolism-associated proteins.

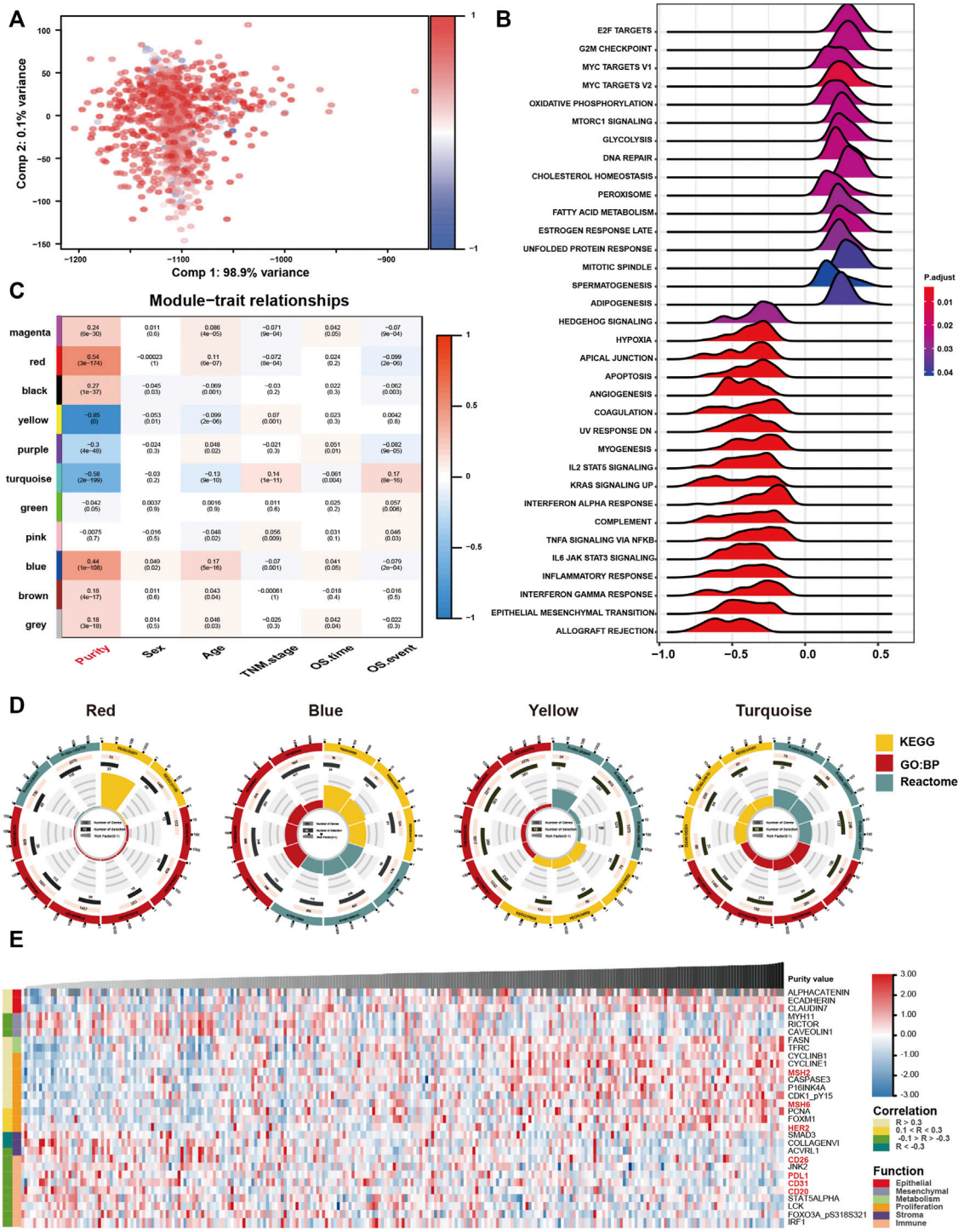

FIGURE 4 | Biological features of tumour purity in gastric cancer. **(A)** Principal component analysis score plot for the gene expression profile underlying different purity levels. **(B)** Gene set enrichment analysis associated with purity levels. **(C)** Trait and module relationship analysis. Each row corresponds to a module eigengene and each column to a trait. The top number represents the biweight midcorrelation coefficient of each cell, and the corresponding *p*-values are mentioned in brackets. **(D)** Representative results of functional enrichment analysis for the yellow, blue, red and turquoise modules. **(E)** Heatmap of the reverse-phase protein arrays demonstrating purity-associated protein production. The coefficient was evaluated via Spearman correlation analysis.

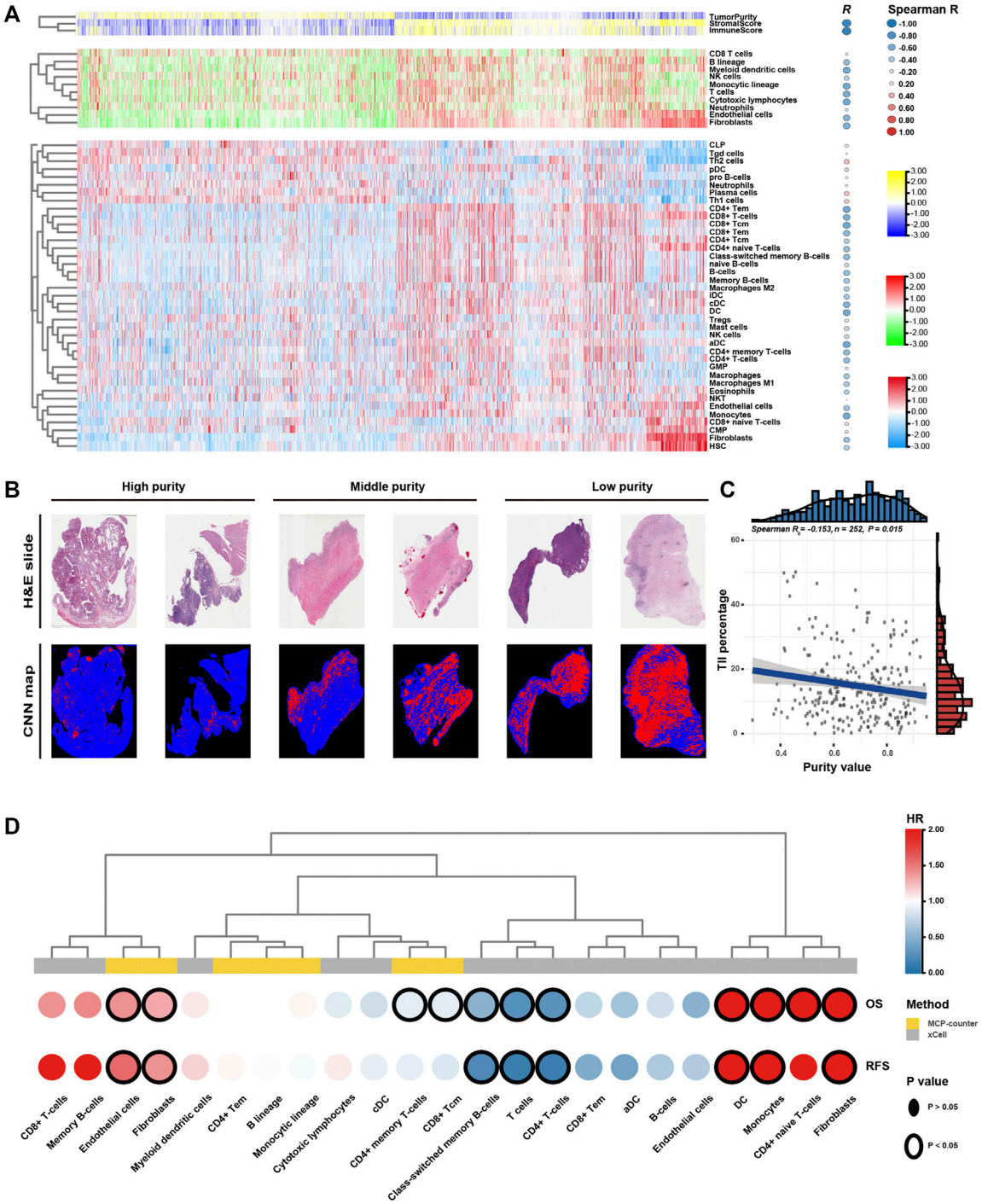

FIGURE 5 | Tumour microenvironment features of tumour purity in gastric cancer (GC). **(A)** Heatmap of the infiltration level of stromal and immune cells among the purity-based subtypes. **(B)** Representative slides (top) and tumour-infiltrating lymphocyte (TIL) maps (bottom) of GC tissues with different purity values. The red colour represents a positive TIL patch, the blue colour represents a tissue region with no TIL patch and the black colour represents no tissue. **(C)** The Spearman correlation between TILs and purity value. **(D)** Heatmap of survival analysis of purity-related stromal and immune cells for overall survival (OS) and recurrence-free survival (RFS). CNN, convolutional neural network; H&E, haematoxylin and eosin; OS, overall survival; RFS, recurrence-free survival; HR, hazard ratio.

3.5 GC Purity is Associated With Infiltration of Distinct Stromal and Immune Cells

Low GC purity was markedly associated with stromal and immune activation pathways (**Figure 4**). Therefore, we further examined the relationship between TME features and GC purity to characterise TME heterogeneity. Both stromal and immune scores, representing the overall infiltration of stromal and immune cells, respectively, in tumour tissues, were inversely correlated with GC purity (**Figure 5A**), suggesting that TME with decreased tumour purity had a significantly increased infiltration of stromal and immune cells. In addition, TILs were confirmed to be negatively correlated with GC purity (**Figures 5B,C**) (Saltz et al., 2018).

Furthermore, we used the MCPcounter algorithm to evaluate the relative abundance of infiltrating stromal and immune cell subpopulations against GC purity (**Figure 5A**). T cells, cytotoxic lymphocytes, B lineage, myeloid dendritic cells, monocytic lineage, fibroblasts and endothelial cells exhibited a consistently negative correlation ($R < -0.4$) with GC purity. We further characterised TME heterogeneity using the xCell algorithm, which can evaluate as many as 39 different immuno-oncology cell types (**Figure 5A**). Similar to the previous result, fibroblasts, endothelial cells, myeloid dendritic cells and several T and B cell types were found to be negatively correlated with GC purity ($R < -0.4$). Although numerous immune cell types ($CD8^+$ naive T cells, Th_1 cells and Th_2 cells) were positively associated with GC purity, the correlation was relatively weak.

Lastly, we attempted to assess the prognostic implications of these purity-related stromal and immune cells in GC (**Figure 5D**). Survival analyses revealed that fibroblasts and endothelial cells were consistently associated with worse OS and RFS. However, T cells, particularly memory T cells, were consistently associated with better OS and RFS. The results of the xCell algorithm revealed that monocytes might correlate with worse OS and RFS. Therefore, T cells, fibroblasts, endothelial cells and monocytes can be a cluster of nontumour cells contributing to TME and specific clinical outcomes for patients with GC with varying purity levels.

3.6 GC Purity is Strongly Correlated With Chemotherapy Response

Chemotherapy is the mainstay of treatment for patients with advanced GC. However, chemotherapy resistance is the primary cause of treatment failure. Given that distinct clinical, biological and microenvironmental features are associated with GC purity, we further investigated the relationship between GC purity and chemotherapy response to promote individualised treatment decisions. The analysis was performed in a subset of patients in the meta-data cohort with data on chemotherapy ($n = 863$). Of the 863 patients, 732 received adjuvant chemotherapy. We found that GC purity could serve as an independent predictor for adjuvant chemotherapy benefit (**Table 4**). Patients with GC with a high purity level who received adjuvant chemotherapy had a significant OS benefit (HR, 0.101; 95% CI, 0.014–0.719; $p = 0.022$).

Furthermore, we determined whether varied purity levels were associated with differences in clinical benefit from adjuvant chemotherapy. Among patients who received adjuvant chemotherapy ($n = 732$), we found significant OS differences among three subgroups (**Figures 6A,B**). Adjuvant chemotherapy was associated with significantly increased OS and RFS rates in patients with GC in the high- and middle-purity subgroups (**Figures 6C,D**). However, no benefit from adjuvant chemotherapy was observed among patients with GC in the low-purity subset (**Figure 6E**).

Eventually, we assessed the value of GC purity in facilitating individualised chemotherapy regimens. We performed ridge regression to predict the drug susceptibility results for each sample (**Figure 6F**) using the CTRP and PRISM-derived drug response data. Spearman correlation analysis between the AUC value and GC purity was used to select agents with a significant correlation coefficient (**Figure 6G**). In addition, a differential analysis among the three subtypes was conducted to identify agents with lower estimated AUC values in each subgroup (**Figures 6H,I**). These analyses yielded two CTRP-derived compounds (fluorouracil and paclitaxel) and four PRISM-derived compounds (fluorouracil, capecitabine, cisplatin, and oxaliplatin). These compounds had lower estimated AUC values in the high-purity subgroup and a negative correlation with GC purity, suggesting that chemotherapy resistance to these five agents was observed in patients with GC with low tumour purity.

4 DISCUSSION

GC tissues have a diverse mixture of tumour and nontumour cells within their microenvironment. Tumour purity has been recognised as a potential prognostic factor for GC (Aurello et al., 2017; Zhou et al., 2017; Ahn et al., 2018; Kemi et al., 2018). However, the purity level in previous studies was estimated by pathologists through visual evaluation, which could be affected by the sensitivity of histopathological characteristics, interobserver bias and variability in accuracy (Cohen et al., 2012; Smits et al., 2014). Moreover, because GC is a highly heterogeneous disease, analyses based on one or a few datasets inevitably lead to the neglect of tumour heterogeneity, a non-negligible factor for cancer biology and treatment (McGranahan et al., 2016). Therefore, previous single-centre studies with relatively small sample size limited the significance of their results. More importantly, previous studies failed to assess features other than clinical outcomes owing to the lack of different omic data.

Instead of the routine pathology-based estimation, we used the ESTIMATE algorithm, a computational method, in this study owing to its compatibility with RNA-seq and microarray transcriptome profiles, thus resulting in a more objective and accurate assessment (Aran et al., 2015). The extremely high tumour purity in various GC cell lines further suggested that the ESTIMATE algorithm has excellent robustness in calculating

TABLE 4 | Univariate and multivariate cox analyses for tumor purity in patients who received adjuvant chemotherapy.

	Univariate			Multivariate		
	Samples	**HR (95%CI)**	***p* value**	**Samples**	**HR (95%CI)**	***p* value**
Age						
Increasing years	732	1.006 (0.996, 1.017)	0.22			
Gender						
Female	250	Reference				
Male	482	0.929 (0.731, 1.180)	0.545			
Lauren classification						
Intestinal	248	Reference	Reference	248	Reference	Reference
Mixed	46	1.783 (1.092, 2.911)	**0.021**	46	1.662 (1.013, 2.728)	**0.044**
Diffuse	366	1.253 (0.957, 1.640)	0.101	366	1.088 (0.827, 1.432)	0.548
TNM stage						
Stage I	84	Reference	Reference	79	Reference	Reference
Stage II	220	3.027 (1.443, 6.351)	**0.003**	204	2.681 (1.272, 5.653)	**0.01**
Stage III	294	7.258 (3.555, 14.819)	**<0.001**	263	6.581 (3.213, 13.480)	**<0.001**
Stage IV	134	14.248 (6.913, 29.369)	**<0.001**	114	11.932 (5.747, 24.777)	**<0.001**
Tumor purity						
Increasing values	732	0.066 (0.013, 0.343)	**0.001**	660	0.101 (0.014, 0.719)	**0.022**

HR, hazard ratio; CI, confidence interval. The bold values mean that the results were statistical significance.

tumour purity in GC. In the present study, we integrated 2,259 GC cases from 13 different cohorts into a meta-data cohort and systematically investigated the role of GC purity. Owing to the benefits of the meta-data cohort with large sample size, tumour heterogeneity could be fully considered, which enhanced the reliability of our results and enabled us to reveal common key features of GC purity (Ricketts et al., 2018). We found that GC tissues from the same patient had a high concordance of purity level. Moreover, GC purity was strongly associated with clinical, biological and microenvironmental features. These findings suggest that tumour purity may be a patient-specific intrinsic characteristic of GC (Aran et al., 2015). Therefore, false interpretations owing to varied purity levels may negatively affect our understanding of GC biology and our ability to select the optimal treatment strategy.

For clinical features, consistent with the results of previous studies (Aurello et al., 2017; Zhou et al., 2017; Ahn et al., 2018; Kemi et al., 2018), low tumour purity was more likely to be found in the malignant phenotype and was associated with poor prognosis outcomes (OS and RFS). In addition, low tumour purity was strongly associated with mesenchymal, invasive and EMT phenotypes. Previous studies have suggested that malignant GC cells can recruit abundant surrounding cells within the TME and subjugate them to create a protective shield against immune attack (Silver et al., 2016). However, GC cells with limited invasive and metastatic features tend to form a solid bulk with less nontumour cell infiltration (Zhang et al., 2017). Therefore, the strong relationship between GC purity and clinicopathological and molecular factors may be partially attributed to their role in maintaining the balance between tumour and nontumour cells (Ying et al., 2011). Low tumour purity and correlated cellular heterogeneity may be responsible for the aggressive phenotype and poor prognosis of GC. Therefore, GC purity provides novel insights into estimating malignant phenotypes, thus explaining why most therapeutic strategies aimed purely against GC cells do not have an ideal outcome.

Furthermore, we determined that tumour purity is a robust independent prognostic indicator for GC. GC purity retained its prognostic relevance even after the classic clinicopathological prognostic factors were considered. These findings highlight the pivotal role of nontumour cells in the prediction of prognosis. Therefore, we integrated GC purity with other independent indicators to develop a prognostic nomogram. Compared with the TNM staging system, the nomogram showed superior validity and reliability in predicting survival time (OS and RFS), which further emphasised the requirement of considering GC purity in clinical management, especially for prognostic prediction.

Concerning biological features, distinct functional processes were the primary differential phenotype that resulted from varied GC purity levels. High tumour purity was associated with metabolism- and proliferation-related pathways. However, low tumour purity was associated with stromal- and immune-related pathways. For example, the IL6–JAK–STAT3 pathway, which is involved in the proliferation, survival, invasiveness and metastasis of tumour cells and suppresses the antitumour immune response in TME (Johnson, 2018), had high pathway activity in the low-purity group. The IL2–STAT5 signalling pathway, which is important for maintaining the development and function of regulatory T cells (Jones et al., 2020), was activated in the low-purity group. These results may explain the malignant phenotype and unfavourable prognosis of low-purity tumours.

Concerning the microenvironmental features, consistent with the finding that low GC purity was markedly associated with stromal and immune activation pathways, we found that tumour purity had a close relationship with the characteristics of cell infiltration in TME. Endothelial cells and fibroblasts were markedly enriched in low-purity tumours. Survival analyses revealed that the proportion of endothelial cells and fibroblasts

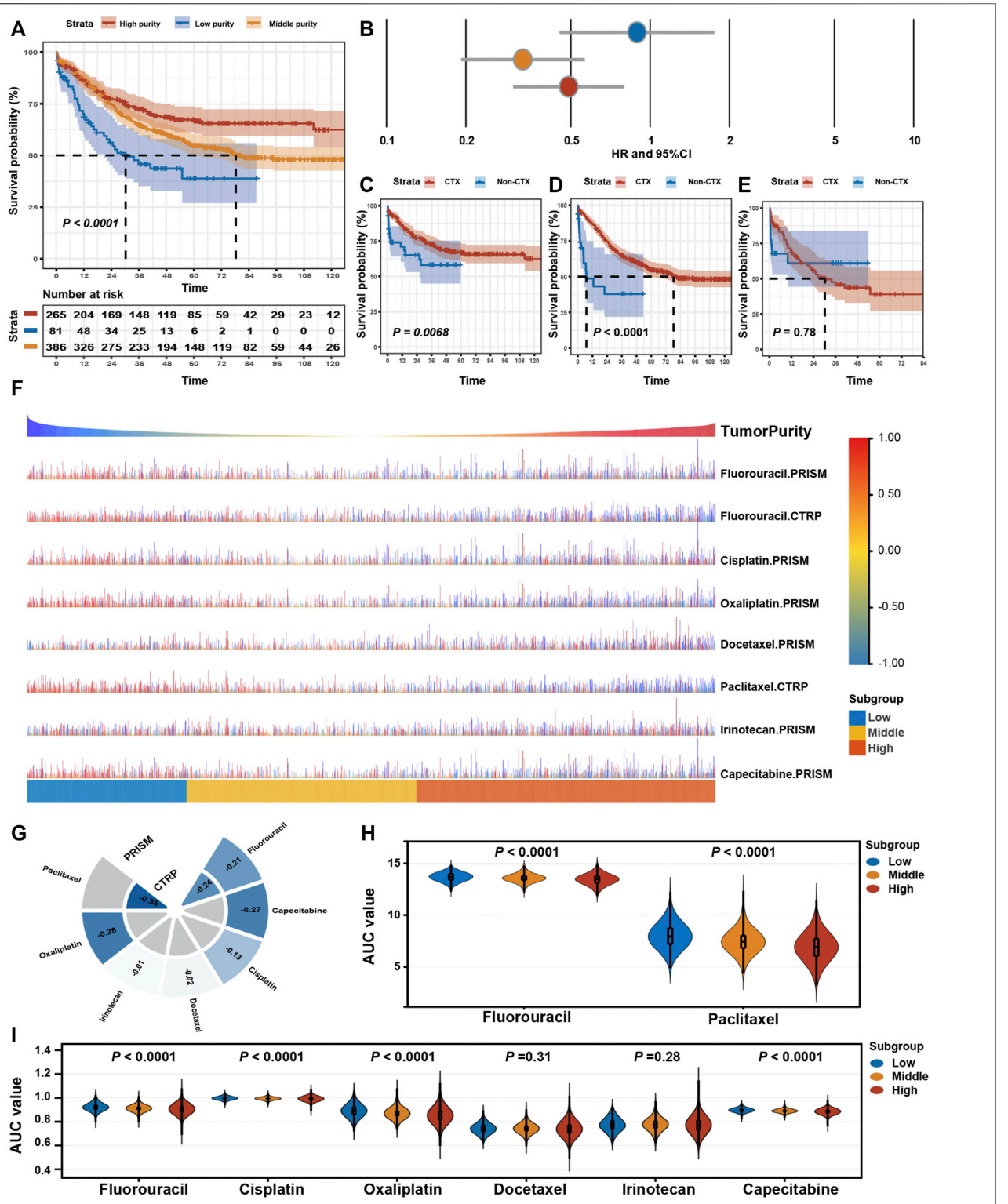

FIGURE 6 | Drug response features of tumour purity for chemotherapy of gastric cancer. **(A)** Kaplan–Meier curves for overall survival (OS) among different purity subgroups of patients who received adjuvant chemotherapy. *p*-values were obtained using the log-rank test. The + symbols in the panels indicate censored data. **(B)** Subgroup analyses for adjuvant chemotherapy using the Cox proportional hazards regression model. The lines represent the 95% confidence intervals of the hazard ratios. **(C–E)** Kaplan–Meier curves for OS among patients who received adjuvant chemotherapy (CTX) and those who did not (non-CTX) in the **(C)** high-purity, **(D)** middle-purity and **(E)** low-purity subgroups. *p*-values were obtained using the log-rank test. The + symbols in the panels indicate censored data. **(F)** The predicted area under the curve (AUC) value of chemotherapeutic drugs for each patient. **(G)** The Spearman correlation coefficient between tumour purity and AUC values. **(H,I)** Differences in the predicted AUC value for chemotherapeutic drugs based on the **(H)** CTRP and **(I)** PRISM databases among the three subgroups. The upper and lower ends of the boxes represent the inter-quartile range of values. The horizontal width of the violin represents the data density. *p*-values were obtained via the Kruskal–Wallis test. CTX, adjuvant chemotherapy; non-adjuvant chemotherapy, non-CTX.

presented negative prognostic value, partially explaining the unfavourable prognosis in the low-purity group. However, not all immune cells were substantially enriched in tissues with low GC purity. The number of antitumour cells, represented by $CD8^+$ T cells and NK cells, may not increase in low-purity tumours, suggesting that these antitumour immune cells cannot infiltrate the established protective shield around GC cells (Zhang et al., 2020).

Eventually, we assessed the potential therapeutic effects of tumour purity in GC. The clinical data suggest that high GC purity can serve as an independent predictor for adjuvant chemotherapy benefits. Compared with those in the low-purity subgroup, patients in the high- and middle-purity subgroups could benefit more from adjuvant chemotherapy. Consistently, the drug response analysis revealed that the high tumour purity was positively correlated with chemotherapy sensitivity, suggesting that patients with high purity values are more sensitive to chemotherapy. Significant activation of proliferation- and metabolism-related pathways in high-purity tumours may induce considerable sensitivity to paclitaxel and fluorouracil. The low sensitivity of low-purity tumours to adjuvant chemotherapy is consistent with our observation that low-purity tumours contain abundant fibroblasts, which are associated with chemotherapy resistance (Yu et al., 2017). Low-purity tumours are also characterised by significant activation of the EMT signalling pathway. EMT has been reported to confer resistance to chemotherapy (Sale et al., 2019). Signalling pathways that regulate EMT, such as TGF-β and hedgehog pathways, are activated in low-purity tumours and correlated with chemotherapy resistance (Chen et al., 2021).

One of the main advantages of this study was the use of meta-data cohorts with large sample size and systematic analysis of tumour purity in multidimensional profiles. Our findings highlight the critical role of tumour purity in GC biology and clinical management. However, the present study had several limitations, such as the retrospective nature of clinical data. This study focussed on analysing the association of clinical and molecular factors with the whole microenvironment (tumour purity) without referring to specific cell types. Therefore, further in-depth studies should be conducted to interpret the effects of specific cell types on TME and assess their relationship with GC cells.

In conclusion, this study highlights that GC purity is closely associated with clinical, biological, TME and drug-response features. Therefore, ideal clinical management of GC should focus on not only the properties of tumour cells but also non-tumour components. A comprehensive evaluation of tumour purity in individual patients with GC can help to elucidate the complex role of the GC microenvironment and provide novel insights into individualised treatment regimens.

DATA AVAILABILITY STATEMENT

The datasets presented in this study can be found in online repositories. The names of the repository/repositories and accession number(s) can be found in the article/ **Supplementary Material**.

ETHICS STATEMENT

The studies involving human participants were reviewed and approved by the Harbin Medical University Cancer Hospital Institutional Review Board. The patients/participants provided their written informed consent to participate in this study.

AUTHOR CONTRIBUTIONS

YX and SL designed this work. SL, JZ, and YZ integrated and analyzed the data. SL, and JZ wrote this manuscript. SL, JZ, XY, YZ, TF, and YW edited and revised the manuscript. All authors approved this manuscript.

FUNDING

This study was supported by funding from the Project Nn10 of Harbin Medical University Cancer Hospital (Grant Number: Nn102017-03).

SUPPLEMENTARY MATERIAL

The Supplementary Material for this article can be found online at: https://www.frontiersin.org/articles/10.3389/fcell.2021.782529/full#supplementary-material

Supplementary Figure 1 | Tumour purity in gastric cancer (GC) cells and tissues. **(A)** Principal component analysis (PCA) score plot for the expression profile of the 13 datasets before (left) and after (right) batch effect removal. **(B)** Spearman correlation analysis of purity value before and after chemotherapy. **(C)** Spearman correlation between purity value and age.

Supplementary Figure 2 | Prognostic nomogram based on tumour purity and clinical factors for gastric cancer. **(A)** Prognostic nomogram for overall survival (OS). **(B)** Prognostic nomogram for recurrence-free survival (RFS).

Supplementary Figure 3 | Weighted correlation network analysis (WGCNA) for tumour purity. **(A)** Evaluation of soft-thresholding power. **(B)** Hierarchical dendrogram of the co-expression modules identified using WGCNA. **(C)** The biweight midcorrelation correlation between module membership and gene significance for the yellow, blue, red and turquoise modules.

REFERENCES

Ahn, B., Chae, Y.-S., Kim, C. H., Lee, Y., Lee, J. H., and Kim, J. Y. (2018). Tumor Microenvironmental Factors Have Prognostic Significances in Advanced Gastric Cancer. *Apmis* 126, 814–821. doi:10.1111/apm.12889

Aran, D., Hu, Z., and Butte, A. J. (2017). xCell: Digitally Portraying the Tissue Cellular Heterogeneity Landscape. *Genome Biol.* 18, 220. doi:10.1186/s13059-017-1349-1

Aran, D., Sirota, M., and Butte, A. J. (2015). Systematic Pan-Cancer Analysis of Tumour Purity. *Nat. Commun.* 6, 8971. doi:10.1038/ncomms9971

Aurello, P., Berardi, G., Giulitti, D., Palumbo, A., Tierno, S. M., Nigri, G., et al. (2017). Tumor-Stroma Ratio Is an Independent Predictor for Overall Survival and Disease Free Survival in Gastric Cancer Patients. *The Surgeon* 15, 329–335. doi:10.1016/j.surge.2017.05.007

Basu, A., Bodycombe, N. E., Cheah, J. H., Price, E. V., Liu, K., Schaefer, G. I., et al. (2013). An Interactive Resource to Identify Cancer Genetic and Lineage

Dependencies Targeted by Small Molecules. *Cell* 154, 1151–1161. doi:10.1016/j.cell.2013.08.003

Becht, E., Giraldo, N. A., Lacroix, L., Buttard, B., Elarouci, N., Petitprez, F., et al. (2016). Estimating the Population Abundance of Tissue-Infiltrating Immune and Stromal Cell Populations Using Gene Expression. *Genome Biol.* 17, 218. doi:10.1186/s13059-016-1070-5

Bray, F., Ferlay, J., Soerjomataram, I., Siegel, R. L., Torre, L. A., and Jemal, A. (2018). Global Cancer Statistics 2018: GLOBOCAN Estimates of Incidence and Mortality Worldwide for 36 Cancers in 185 Countries. *CA: a Cancer J. clinicians* 68, 394–424. doi:10.3322/caac.21492

Camp, R. L., Dolled-Filhart, M., and Rimm, D. L. (2004). X-tile: A New Bio-Informatics Tool For Biomarker Assessm Ent And Outcome-Based Cut-Point Optimization. *Clin. Cancer Res.* 10, 7252–7259. doi:10.1158/1078-0432.CCR-04-0713

Chen, H., Yao, J., Bao, R., Dong, Y., Zhang, T., Du, Y., et al. (2021). Cross-talk of Four Types of RNA Modification Writers Defines Tumor Microenvironment and Pharmacogenomic Landscape in Colorectal Cancer. *Mol. Cancer* 20, 29. doi:10.1186/s12943-021-01322-w

Cohen, D. A., Dabbs, D. J., Cooper, K. L., Amin, M., Jones, T. E., Jones, M. W., et al. (2012). Interobserver Agreement Among Pathologists for Semiquantitative Hormone Receptor Scoring in Breast Carcinoma. *Am. J. Clin. Pathol.* 138, 796–802. doi:10.1309/AJCP6DKRND5CKVDD

Corsello, S. M., Nagari, R. T., Spangler, R. D., Rossen, J., Kocak, M., Bryan, J. G., et al. (2020). Discovering the Anticancer Potential of Non-oncology Drugs by Systematic Viability Profiling. *Nat. Cancer* 1, 235–248. doi:10.1038/s43018-019-0018-6

Dai, H., Chen, H., Xu, J., Zhou, J., Shan, Z., Yang, H., et al. (2019). The Ubiquitin Ligase CHIP Modulates Cellular Behaviors of Gastric Cancer Cells by Regulating TRAF2. *Cancer Cel Int* 19, 132. doi:10.1186/s12935-019-0832-z

Dicken, B. J., Bigam, D. L., Cass, C., Mackey, J. R., Joy, A. A., and Hamilton, S. M. (2005). Gastric Adenocarcinoma: Review And Considerations For Future Directions. *Ann. Surg.* 241, 27–39. doi:10.1097/01.sla.0000149300.28588.23

Durinck, S., Moreau, Y., Kasprzyk, A., Davis, S., De Moor, B., Brazma, A., et al. (2005). BioMart and Bioconductor: a Powerful Link between Biological Databases and Microarray Data Analysis. *Bioinformatics* 21, 3439–3440. doi:10.1093/bioinformatics/bti525

Gautier, L., Cope, L., Bolstad, B. M., and Irizarry, R. A. (2004). affy--analysis of Affymetrix GeneChip Data at the Probe Level. *Bioinformatics* 20, 307–315. doi:10.1093/bioinformatics/btg405

Geeleher, P., Cox, N., and Huang, R. S. (2014). pRRophetic: an R Package for Prediction of Clinical Chemotherapeutic Response from Tumor Gene Expression Levels. *PloS one* 9, e107468. doi:10.1371/journal.pone.0107468

Haider, S., Tyekucheva, S., Prandi, D., Fox, N. S., Ahn, J., Xu, A. W., et al. (2020). Systematic Assessment of Tumor Purity and its Clinical Implications. *JCO Precis. Oncol* 4, 995–1005. doi:10.1200/PO.20.00016

Han, T.-S., Hur, K., Xu, G., Choi, B., Okugawa, Y., Toiyama, Y., et al. (2015). MicroRNA-29c Mediates Initiation of Gastric Carcinogenesis by Directly Targeting ITGB1. *Gut* 64, 203–214. doi:10.1136/gutjnl-2013-306640

Hänzelmann, S., Castelo, R., and Guinney, J. (2013). GSVA: Gene Set Variation Analysis for Microarray and RNA-Seq Data. *BMC bioinformatics* 14, 7. doi:10.1186/1471-2105-14-7

Hoshida, Y. (2010). Nearest Template Prediction: a Single-Sample-Based Flexible Class Prediction with Confidence Assessment. *PloS one* 5, e15543. doi:10.1371/journal.pone.0015543

Irizarry, R. A., Bolstad, B. M., Collin, F., Cope, L. M., Hobbs, B., and Speed, T. P. (2003). Summaries of Affymetrix GeneChip Probe Level Data. *Nucleic Acids Res.* 31, e15. doi:10.1093/nar/gng015

Johnson, D. E., O'Keefe, R. A., and Grandis, J. R. (2018). O', Keefe, R. A., and Grandis, J. RTargeting the IL-6/JAK/STAT3 Signalling axis in Cancer. *Nat. Rev. Clin. Oncol.* 15, 234–248. doi:10.1038/nrclinonc.2018.8

Jones, D. M., Read, K. A., and Oestreich, K. J. (2020). Dynamic Roles for IL-2-STAT5 Signaling in Effector and Regulatory CD4+ T Cell Populations. *J.I.* 205, 1721–1730. doi:10.4049/jimmunol.2000612

Joung, R. H.-S., and Merkow, R. P. (2021). Is it Time to Abandon 30-Day Mortality as a Quality Measure? *Ann. Surg. Oncol.* 28, 1263–1264. doi:10.1245/s10434-020-09262-3

Joyce, J. A., and Pollard, J. W. (2009). Microenvironmental Regulation of Metastasis. *Nat. Rev. Cancer* 9, 239–252. doi:10.1038/nrc2618

Junttila, M. R., and de Sauvage, F. J. (2013). Influence of Tumour Microenvironment Heterogeneity on Therapeutic Response. *Nature* 501, 346–354. doi:10.1038/nature12626

Katai, H., Ishikawa, T., Ishikawa, T., Akazawa, K., Isobe, Y., Miyashiro, I., et al. (2018). Five-year Survival Analysis of Surgically Resected Gastric Cancer Cases in Japan: a Retrospective Analysis of More Than 100,000 Patients from the Nationwide Registry of the Japanese Gastric Cancer Association (2001-2007). *Gastric Cancer* 21, 144–154. doi:10.1007/s10120-017-0716-7

Kemi, N., Eskuri, M., Herva, A., Leppänen, J., Huhta, H., Helminen, O., et al. (2018). Tumour-stroma Ratio and Prognosis in Gastric Adenocarcinoma. *Br. J. Cancer* 119, 435–439. doi:10.1038/s41416-018-0202-y

Kim, D. H., Uno, H., and Wei, L.-J. (2017). Restricted Mean Survival Time as a Measure to Interpret Clinical Trial Results. *JAMA Cardiol.* 2, 1179–1180. doi:10.1001/jamacardio.2017.2922

Langfelder, P., and Horvath, S. (2008). WGCNA: an R Package for Weighted Correlation Network Analysis. *BMC bioinformatics* 9, 559. doi:10.1186/1471-2105-9-559

Leek, J. T., Johnson, W. E., Parker, H. S., Jaffe, A. E., and Storey, J. D. (2012). The Sva Package for Removing Batch Effects and Other Unwanted Variation in High-Throughput Experiments. *Bioinformatics* 28, 882–883. doi:10.1093/bioinformatics/bts034

Liberzon, A., Birger, C., Thorvaldsdóttir, H., Ghandi, M., Mesirov, J. P., and Tamayo, P. (2015). The Molecular Signatures Database Hallmark Gene Set Collection. *Cel Syst.* 1, 417–425. doi:10.1016/j.cels.2015.12.004

McGranahan, N., Furness, A. J. S., Rosenthal, R., Ramskov, S., Lyngaa, R., Saini, S. K., et al. (2016). Clonal Neoantigens Elicit T Cell Immunoreactivity and Sensitivity to Immune Checkpoint Blockade. *Science* 351, 1463–1469. doi:10.1126/science.aaf1490

Resio, B. J., Gonsalves, L., Canavan, M., Mueller, L., Phillips, C., Sathe, T., et al. (2021). Where the Other Half Dies: Analysis of Mortalities Occurring More Than 30 Days after Complex Cancer Surgery. *Ann. Surg. Oncol.* 28, 1278–1286. doi:10.1245/s10434-020-09080-7

Ricketts, C. J., De Cubas, A. A., Smith, C. C., Lang, M., Reznik, E., Bowlby, R., et al. (2018). The Cancer Genome Atlas Comprehensive Molecular Characterization of Renal Cell Carcinoma. *Cell Rep* 23, 3698. doi:10.1016/j.celrep.2018.06.032

Ritchie, M. E., Phipson, B., Wu, D., Hu, Y., Law, C. W., Shi, W., et al. (2015). Limma powers Differential Expression Analyses for RNA-Sequencing and Microarray Studies. *Nucleic Acids Res.* 43, e47. doi:10.1093/nar/gkv007

Sale, M. J., Balmanno, K., Saxena, J., Ozono, E., Wojdyla, K., McIntyre, R. E., et al. (2019). MEK1/2 Inhibitor Withdrawal Reverses Acquired Resistance Driven by BRAFV600E Amplification whereas KRASG13D Amplification Promotes EMT-Chemoresistance. *Nat. Commun.* 10, 2030. doi:10.1038/s41467-019-09438-w

Saltz, J., Gupta, R., Hou, L., Kurc, T., Singh, P., Nguyen, V., et al. (2018). Spatial Organization and Molecular Correlation of Tumor-Infiltrating Lymphocytes Using Deep Learning on Pathology Images. *Cel Rep* 23, 181. doi:10.1016/j.celrep.2018.03.086

Sasako, M., Inoue, M., Lin, J.-T., Khor, C., Yang, H.-K., and Ohtsu, A. (2010). Gastric Cancer Working Group Report. *Jpn. J. Clin. Oncol.* 40 (40 Suppl. l), i28–i37. doi:10.1093/jjco/hyq124

Serra, O., Galán, M., Ginesta, M. M., Calvo, M., Sala, N., and Salazar, R. (2019). Comparison and Applicability of Molecular Classifications for Gastric Cancer. *Cancer Treat. Rev.* 77, 29–34. doi:10.1016/j.ctrv.2019.05.005

Silver, D. J., Sinyuk, M., Vogelbaum, M. A., Ahluwalia, M. S., and Lathia, J. D. (2016). The Intersection of Cancer, Cancer Stem Cells, and the Immune System: Therapeutic Opportunities. *Neuro Oncol.* 18, 153–159. doi:10.1093/neuonc/nov157

Smits, A. J. J., Kummer, J. A., de Bruin, P. C., van den Tweel, J. G., Seldenrijk, K. A., Willems, S. M., et al. (2014). The Estimation of Tumor Cell Percentage for Molecular Testing by Pathologists Is Not Accurate. *Mod. Pathol.* 27, 168–174. doi:10.1038/modpathol.2013.134

Sohn, B. H., Hwang, J. E., Jang, H. J., Lee, H. S., Oh, S. C., Shim, J. J., et al. (2017). Clinical Significance of Four Molecular Subtypes of Gastric Cancer Identified by the Cancer Genome Atlas Project. *Clin. Cancer Res. : official J. Am. Assoc. Cancer Res.* 23, 4441–4449. doi:10.1158/1078-0432.CCR-16-2211

Sturm, G., Finotello, F., Petitprez, F., Zhang, J. D., Baumbach, J., Fridman, W. H., et al. (2019). Comprehensive Evaluation of Transcriptome-Based Cell-type Quantification Methods for Immuno-Oncology. *Bioinformatics* 35, i436–i445. doi:10.1093/bioinformatics/btz363

Subramanian, A., Tamayo, P., Mootha, V. K., Mukherjee, S., Ebert, B. L., Gillette, M. A., et al. (2005). Gene Set Enrichment Analysis: a Knowledge-Based Approach for Interpreting Genome-wide Expression Profiles. *Proc. Natl. Acad. Sci.* 102, 15545–15550. doi:10.1073/pnas.0506580102

Tang, S., Lin, L., Cheng, J., Zhao, J., Xuan, Q., Shao, J., et al. (2020). The Prognostic Value of Preoperative Fibrinogen-To-Prealbumin Ratio and a Novel FFC Score in Patients with Resectable Gastric Cancer. *BMC cancer* 20, 382. doi:10.1186/s12885-020-06866-6

Torre, L. A., Bray, F., Siegel, R. L., Ferlay, J., Lortet-Tieulent, J., and Jemal, A. (2015). Global Cancer Statistics, 2012. *CA: a Cancer J. clinicians* 65, 87–108. doi:10.3322/caac.21262

Vickers, A. J., and Elkin, E. B. (2006). Decision Curve Analysis: a Novel Method for Evaluating Prediction Models. *Med. Decis. Making* 26, 565–574. doi:10.1177/0272989X06295361

Wagner, G. P., Kin, K., and Lynch, V. J. (2012). Measurement of mRNA Abundance Using RNA-Seq Data: RPKM Measure Is Inconsistent Among Samples. *Theor. Biosci.* 131, 281–285. doi:10.1007/s12064-012-0162-3

Ying, H., Elpek, K. G., Vinjamoori, A., Zimmerman, S. M., Chu, G. C., Yan, H., et al. (2011). PTEN Is a Major Tumor Suppressor in Pancreatic Ductal Adenocarcinoma and Regulates an NF-Kb-Cytokine Network. *Cancer Discov.* 1, 158–169. doi:10.1158/2159-8290.CD-11-0031

Yoshihara, K., Shahmoradgoli, M., Martínez, E., Vegesna, R., Kim, H., Torres-Garcia, W., et al. (2013). Inferring Tumour Purity and Stromal and Immune Cell Admixture from Expression Data. *Nat. Commun.* 4, 2612. doi:10.1038/ncomms3612

Yu, G., Wang, L.-G., Han, Y., and He, Q.-Y. (2012). clusterProfiler: an R Package for Comparing Biological Themes Among Gene Clusters. *OMICS: A J. Integr. Biol.* 16, 284–287. doi:10.1089/omi.2011.0118

Yu, T., Yang, G., Hou, Y., Tang, X., Wu, C., Wu, X.-a., et al. (2017). Cytoplasmic GPER Translocation in Cancer-Associated Fibroblasts Mediates cAMP/PKA/CREB/glycolytic axis to Confer Tumor Cells with Multidrug Resistance. *Oncogene* 36, 2131–2145. doi:10.1038/onc.2016.370

Zeng, D., Li, M., Zhou, R., Zhang, J., Sun, H., Shi, M., et al. (2019). Tumor Microenvironment Characterization in Gastric Cancer Identifies Prognostic and Immunotherapeutically Relevant Gene Signatures. *Cancer Immunol. Res.* 7, 737–750. doi:10.1158/2326-6066.CIR-18-0436

Zhang, B., Wu, Q., Li, B., Wang, D., Wang, L., and Zhou, Y. L. (2020). m6A Regulator-Mediated Methylation Modification Patterns and Tumor Microenvironment Infiltration Characterization in Gastric Cancer. *Mol. Cancer* 19, 53. doi:10.1186/s12943-020-01170-0

Zhang, C., Cheng, W., Ren, X., Wang, Z., Liu, X., Li, G., et al. (2017). Tumor Purity as an Underlying Key Factor in Glioma. *Clin. Cancer Res.* 23, 6279–6291. doi:10.1158/1078-0432.CCR-16-2598

Zhou, Z.-H., Ji, C.-D., Zhu, J., Xiao, H.-L., Zhao, H.-B., Cui, Y.-H., et al. (2017). The Prognostic Value and Pathobiological Significance of Glasgow Microenvironment Score in Gastric Cancer. *J. Cancer Res. Clin. Oncol.* 143, 883–894. doi:10.1007/s00432-017-2346-1

Conflict of Interest: The authors declare that the research was conducted in the absence of any commercial or financial relationships that could be construed as a potential conflict of interest.

Publisher's Note: All claims expressed in this article are solely those of the authors and do not necessarily represent those of their affiliated organizations, or those of the publisher, the editors and the reviewers. Any product that may be evaluated in this article, or claim that may be made by its manufacturer, is not guaranteed or endorsed by the publisher.

frontiers in Molecular Biosciences

ORIGINAL RESEARCH
published: 18 January 2022
doi: 10.3389/fmolb.2021.762729

Lung Adenocarcinoma Cells Promote Self-Migration and Self-Invasion by Activating Neutrophils to Upregulate Notch3 Expression of Cancer Cells

Weidong Peng[1,2†], Youjing Sheng[1,2†], Han Xiao[1†], Yuanzi Ye[1], Louis Boafo Kwantwi[2], Lanqing Cheng[3], Yuanchong Wang[4], Jiegou Xu[5] and Qiang Wu[1,2]**

[1]Department of Pathology, The First Affiliated Hospital of Anhui Medical University, Hefei, China, [2]Department of Pathology, School of Basic Medical Science, Anhui Medical University, Hefei, China, [3]Department of Pathology, The Second Affiliated Hospital of Anhui Medical University, Hefei, China, [4]Department of Neonatology, Anhui Provincial Children's Hospital, Hefei, China, [5]Department of Immunology, School of Basic Medical Science, Anhui Medical University, Hefei, China

OPEN ACCESS

Edited by:
Shengtao Zhou,
Sichuan University, China

Reviewed by:
Lichun Sun,
Harbin Medical University, China
Peicheng Li,
The First Affiliated Hospital of Soochow University, China

***Correspondence:**
Qiang Wu
wuqiang@ahmu.edu.cn
Jiegou Xu
xujiegou@ahmu.edu.cn

[†]These authors have contributed equally to this work and share first authorship

Specialty section:
This article was submitted to Molecular Diagnostics and Therapeutics, a section of the journal Frontiers in Molecular Biosciences

Received: 22 August 2021
Accepted: 14 December 2021
Published: 18 January 2022

Citation:
Peng W, Sheng Y, Xiao H, Ye Y, Kwantwi LB, Cheng L, Wang Y, Xu J and Wu Q (2022) Lung Adenocarcinoma Cells Promote Self-Migration and Self-Invasion by Activating Neutrophils to Upregulate Notch3 Expression of Cancer Cells. Front. Mol. Biosci. 8:762729. doi: 10.3389/fmolb.2021.762729

Background: Invasion and migration of cancer cells play a key role in lung cancer progression and metastasis. Tumor-associated neutrophils (TANs) are related to poor prognosis in many types of cancer. However, the role of TANs in lung cancer is controversial. In this study, we investigated the effect of TANs on the invasion and migration of lung adenocarcinoma.

Methods: Immunohistochemistry was performed to detect the density of infiltrating TANs and the expression of Notch3 in 100 lung adenocarcinoma tissues. Flow cytometry was used to observe the viability of neutrophils, which were isolated from healthy peripheral blood and then exposed to the supernatant of cultured lung adenocarcinoma cell lines. After treating with tumor-associated neutrophils culture supernatant, NeuCS (supernatant of cultured neutrophils), tumor cells culture supernatant, Medium (serum-free medium), respectively, the migration and invasion of the lung cancer cells before and after transfected by si-Notch3 were detected by transwell assay and wound healing assay. Kaplan-Meier plotter (http://kmplot.com/analysis/index.php?p) was used to analyze the prognostic role of the density of TANs on lung adenocarcinoma and TIMER ((http://cistrome.dfci.harvard.edu/TIMER/) was used to detect the expression of Notch3 on lung adenocarcinoma.

Results: The infiltration of TANs was observed in the parenchyma and stroma of the lung adenocarcinoma, the density of TANs was positively related to the TNM stage and negatively related to the differentiation and prognosis. Notch3 expression of cancer cells was negatively related to the tumor differentiation and prognosis. Compared to quiescent neutrophils, the viability of TCCS-activated neutrophils was enhanced. Both migration and invasion of A549 and PC9 cells were significantly promoted by TANs, while after knocking down Notch3, the migration and invasion of the cancer cells were not affected by TANs. Bioinformatics analysis showed that the density of TANs and the expression of Notch3 were related to the poor prognosis.

Conclusion: The results indicated that lung adenocarcinoma cells promote self-invasion and self-migration by activating neutrophils to upregulate the Notch3 expression of cancer cells. The density of infiltrating TANs may be a novel marker for the poor prognosis of lung adenocarcinoma. Targeting TANs might be a potential therapeutic strategy for lung cancer treatment.

Keywords: lung adenocarcinoma, Notch3, migration, invasion, tumor-associated neutrophils

INTRODUCTION

Lung cancer continues to be the most commonly diagnosed cancer type and the leading cause of cancer-related death worldwide (Bade and Dela, 2020). Although the overall survival has improved with surgical advances, the 5-years survival rate is still less than 17% (Hirsch et al., 2017). This poor prognostic outcome is primarily attributed to recurrence and metastasis existing in postoperative (Yan et al., 2017). Therefore, exploring further possible prognostic and predictive biomarkers and a potential therapeutic strategy for lung cancer treatment is necessary.

Current evidence has indicated that cross-talk between tumor cells and immune cells creates a unique microenvironment that promotes tumor cell growth, invasion, and metastasis (Zhou et al., 2016). As the most abundant immune cells in the microenvironment, Neutrophils respond to various inflammatory and cancerous signals. Emerging evidence has suggested that tumor-associated neutrophils (TANs) are involved in the malignant progression of several cancer types (Masucci et al., 2019). The infiltration of neutrophils in tumors has been associated with a poor prognosis. In renal cell carcinoma, the infiltration of neutrophils has been shown to correlate with short recurrence-free survival (RFS) and overall survival (OS) in patients (Jensen et al., 2009). Wang et al. have indicated that increased intratumoral neutrophils independently predict poor prognostic outcomes in esophageal carcinoma (Wang et al., 2014). However, the role of TANs in lung cancer has been a controversial issue. Carus et al. reported the density of CD66b + neutrophils has no significant correlation with RFS or OS in non-small cell lung cancer (Carus et al., 2013), While Rakaee et al. noted that the density of CD66b + TANs to be an independent negative prognostic factor in patients with lung adenocarcinoma (Rakaee et al., 2016). These contradictory observations highlight the diversity of TANs and a pressing need to further evaluate their roles and underlying mechanisms in lung cancer.

Notch signaling is crucial for cell fate and normal embryonic development (Liang et al., 2019). However, recent evidence showed that the Notch family plays a vital role in malignancies (Garcia and Kandel, 2012). Among the four receptors (Notch1-4) in the Notch family, accumulated evidence has shown the overexpression of Notch3 to be associated with recurrence and metastasis in some cancer types (Kim et al., 2017; Tang et al., 2019)). In lung cancer, Notch3 has been reported to be associated with poor prognosis (Ye et al., 2013). In gastric cancer, the expression of Notch3 is correlated with the infiltration of immune cells, including $CD8^+$ T cells, Tregs, and M2 macrophages (Cui et al., 2020). According to Yan et al., Notch3 expression is closely related to the infiltration of M2 macrophage in melanoma tissues (Yan et al., 2021). Although the aforementioned evidence suggests an interaction between Notch3 and immune cells, how Notch3 interacts with immune cells, particularly TANs in lung cancer, remained unexplored.

In this study, we investigated the prognostic role of CD66b + TANs in lung adenocarcinoma tissues and found a correlation between the density of TANs and the expression of Notch3. We further investigated the activation of neutrophils by supernatant of cultured lung adenocarcinoma cells and the effect of these TANs on the migration and invasion of lung cancer cells via the Notch3 pathway.

MATERIALS AND METHODS

Patients and Specimens

Formalin-fixed-paraffin-embedded (FFPE) tissue specimens were obtained from 100 lung adenocarcinoma patients who underwent surgical operation from 2014 to 2017 at the First Affiliated Hospital of Anhui Medical University. Patients included in this study had not received any preoperative adjuvant therapy. All specimens and protocols used in this study were approved by the Ethics Committee of Anhui Medical University (No. 2021H004). The protocols used to be under the ethical standards of the Biomedical Ethics Committee of Anhui Medical University Committee and the 1964 Helsinki Declaration.

Immunohistochemistry

FFPE samples sliced into 4 μm sections were deparaffinized in xylene and graded alcohol, followed by hydration. Antigen retrieval was performed in a pressure cooker containing 0.01 M sodium citrate buffer (pH 6.0) for 10 min. Tissue sections were incubated with either anti-CD66b (Cat.No.555723, BD Pharmingen) or anti-Notch3 (Cat.No.5276S, Cell Signaling Technology) overnight at 4°C. After blocking by endogenous peroxidase for 30 min, samples were incubated with the HRP-labeled sheep anti-mouse/rabbit IgG polymer (Cat.No.PV-6000, ZSGB-BIO) for 20 min at room temperature. Finally, 3,3′-Diaminobenzidine

(DAB) was used as chromogen, and the sections were counterstained with hematoxylin.

Scoring Stained Sections

The density of CD66b + neutrophils infiltrating in tumor parenchyma was evaluated as previously reported (Wang et al., 2019). Briefly, CD66b + neutrophils were counted under ten random microscopic high power fields (×40 objective lenses). According to the median value of all samples, CD66b + neutrophils were divided into high-density and low-density groups. Notch3 immunostaining intensity was graded on 0–3 scales: 0, absence of staining; 1, weak staining; 2, moderate staining; 3, strong staining. Notch3 positive cancer cells were similarly scored on a scale of 0–4 as follows: 0, 0–5% positive tumor cells; 1, 6–25% positive tumor cells; 2, 26–50% positive tumor cells; 3, 51–75% positive tumor cells; 4, >75% tumor cells. The IHC scores (0–12) were obtained by multiplying the staining intensity by the percentage scores; the score <4 was negative, ≥4 was positive.

Isolation and Culture of Neutrophils

Blood obtained from healthy adults was centrifuged at 250 g for 15–20 min. After discarding the plasma, normal saline was added. The diluted blood was carefully added onto a Ficoll solution and centrifuged at 450 g for 25 min. After discarding the supernatant, RBC lysing buffer was added twice each for 10 min. After centrifuging at 1500 rpm and discarding the supernatant, the cells were washed twice with PBS, and the cells were resuspended in a serum-free medium.

Preparation of Tumor Cells Culture Supernatant and NeuCS and Tumor-Associated Neutrophils Culture Supernatant

TCCS (tumor cells culture supernatant) was obtained from the supernatant of A549 and PC-9 lung cancer cells cultured for 48 h in a serum-free medium. NeuCS (Neutrophils culture supernatant) was obtained from the supernatant of neutrophils cultured in the serum-free medium for 10 h. TANCS (tumor-associated neutrophils culture supernatant) was obtained from the supernatant of neutrophils stimulated by TCCS for 10 h.

Flowcytometry

The viability of TANs and neutrophils was determined by Annexin-V/PI apoptosis detection kits (Biobest). The data were analyzed by FlowJo (Version. 7.6.1).

Migration and Invasion Assay

Migration and invasion were performed in an 8 μm 24-well culture insert (Corning Company). For invasion assay, Matrigel (BD Company) diluted with the serum-free medium was precoated in the chambers and solidified for 30 min at 37°C. Lung cancer cells were added to the upper chamber, whereas TANCS, NeuCS, TCCS, and medium were added to the lower chamber, respectively. The cancer cells were cultured for 7 and 12 h for migration and invasion assay, respectively. *Cancer* cells attached to the underside of the chambers were fixed and stained. Quantification was performed by evaluating the mean number of cells in five microscopic fields per chamber.

Wound Healing Assay

The cells were seeded in a 6-well plate at 3.6 × 105 cells per well and were cultured overnight. After the next day, 75 pmol si-Notch3 or negative control was transfected by using Lipofectamine3000. The transfected cells and untransfected cells were cultured in opti-mem. After 6 h, each group of cells was treated with TANCS, NeuCS, TCCS, and medium, respectively. At the same time, the cells were grown to confluence and wounded by dragging a 0.2-ml pipette tip through the monolayer. The extent of cell migration was observed. The rate of wound closure was expressed as a percentage of the initial scraped gap.

Real-Time Polymerase Chain Reaction

RNA was extracted from A549 and PC9 cells using TRIzol reagent (ThermoFisher Scientific), and cDNA was made by reverse transcription with (Evo M-MLV RT Master Mix) according to the manufacturer's instructions. qRT-PCR was performed using (SYBR® Green Pro Taq HS Premix) in 20 μL reactions. Primers were designed using Primer3 software and purchased from Sangon Biotech: GAPDH (Sangon Biotech, B662104-0001), Notch3 Fw 5′-GCTACACTGGACCTCGCT GT-3′, Notch3 Rv 5′-AGACCCCACCGTTGACACAG-3'. Reactions were carried out in LightCycler® 96 Application Software (Roche). The cycling program used was 95°C for 30 s, followed by 40 cycles of 95°C for 5 s, 60°C for 30 s. Data were analyzed using GAPDH as a reference gene.

Western Blotting

Proteins extracted using RIPA buffer were loaded onto SDS–polyacrylamide gels and then transferred to PVDF membranes. Membranes were blocked with 5% nonfat milk in TBS-T for 1 h at room temperature. Membranes were incubated overnight at 4°C with the following primary antibodies: NOTCH3 (Cat.No. 5276S, CellSignaling Technology) and GAPDH (Cat.No. abs132004, Absin). After incubating the membranes with peroxidase-conjugated secondary antibodies (Cat.No. ZB-2301, ZSGB-BIO) for 2 h, the reaction was visualized by an enhanced chemiluminescence assay.

Bioinformatics Analysis

The Kaplan–Meier plotter ofers a means of readily exploring the impact of a wide array of genes on patient survival in 21 diferent types of cancer, with large sample sizes for the lung adenocarcionma (n = 865) cohorts. We therefore used this database to explore the association between Notch3 expression and outcome in patients with lung cancers (http://kmplot. com/analysis/).

TIMER (https://cistrome.shinyapps.io/timer/) is a database designed for the analysis of immune cell infltrates in multiple cancers. This database employs pathological examination-validated statistical methodology to estimate infltration by

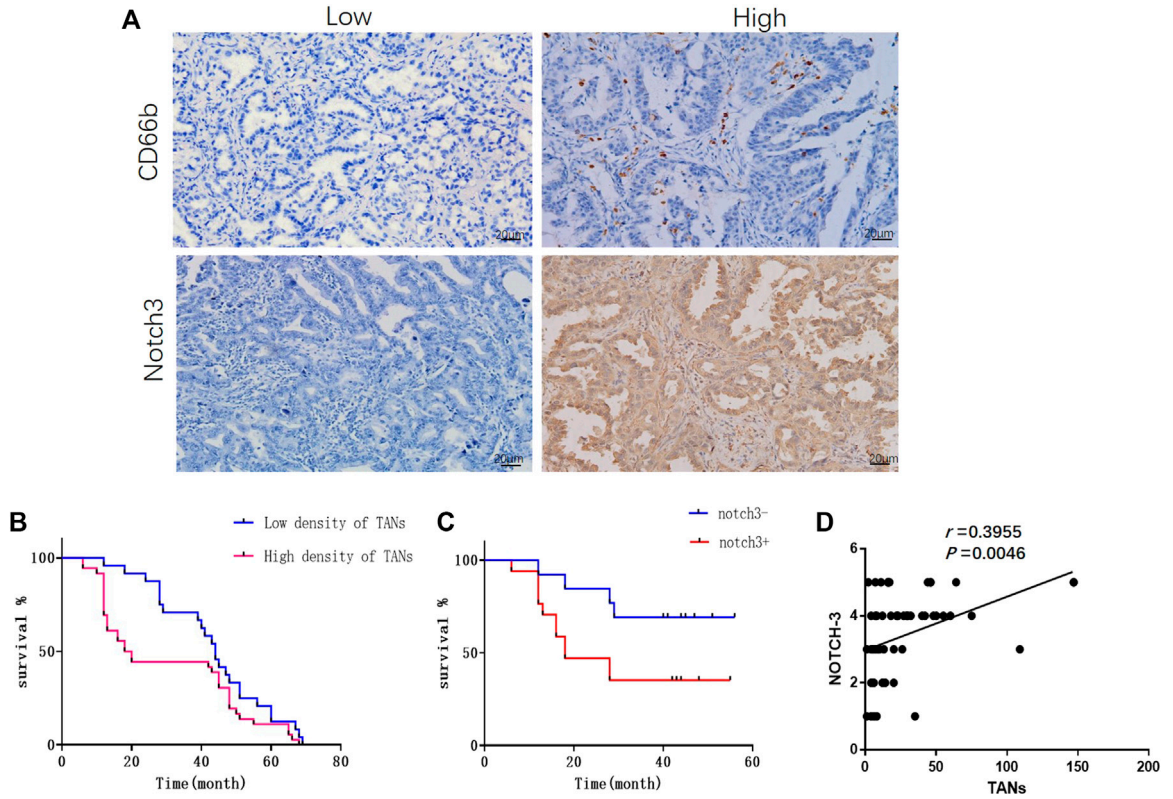

FIGURE 1 | The infiltration of TANs and the expression of Notch3 in lung adenocarcinoma were associated with poor prognosis. **(A)** Representative images for immunohistochemical staining of CD66b and Notch3 in lung adenocarcinoma. **(B)** Survival analysis showed that the density of TANs was negatively correlated with disease-free survival (DFS). **(C)** Survival analysis showed that the expression of Notch3 was negatively correlated to DFS. **(D)** The correlation between the density of TANs and the expression of Notch3 in lung adenocarcinoma.

neutrophils, macrophages, dendritic cells, B cells and CD4+/CD8+ T cells into tumors. We therefore explore the efect of neutrophils infltration on the survival rate of lung adenocarcinoma patients (n = 496).

Statistics

All experiments were carried out three times. The data were expressed as a mean ± standard deviation (SD). Comparison between groups was analyzed by chi-square test. Kaplan-meier was used for survival analysis and p-value < 0.05 was considered statistically significant.

RESULTS

The Infiltrating of TANs and the Expression of Notch3 in Lung Adenocarcinoma

TANs were observed in both parenchyma and stroma of lung adenocarcinoma (**Figure 1A**). Only those infiltrating in tumor parenchyma were counted. The density of TANs infiltrating in solid and micropapillary adenocarcinoma was significantly higher than that in lepidic adenocarcinoma. The density of TANs showed a positive correlation to the TNM stage but correlated negatively to tumor differentiation (p < 0.05, **Supplementary Table S1**). Survival analysis showed that the density of TANs was negatively associated with disease-free survival (DFS) (p < 0.05, **Figure 1B**).

Notch3 was mainly expressed in the cytoplasm of cancer cells as detected by immunohistochemistry (**Figure 1A**), and the expression of Notch3 in solid adenocarcinoma was significantly higher than that in lepidic adenocarcinoma. The expression of Notch3 was negatively correlated to tumor differentiation (p < 0.05), but showed no significant correlation with gender, age, tumor size, TNM stage, or lymph node metastasis (**Supplementary Table S1**). Survival analysis showed that the expression of Notch3 was negatively correlated to DFS (p < 0.05, **Figure 1C**). In lung adenocarcinoma tissues, the infiltration of TANS was positively correlated with the expression of Notch3 (p < 0.05, **Figure 1D**).

Neutrophils Were Activated to TANs by Supernatant of Cultured Lung Adenocarcinoma Cell Lines

The purity of neutrophils isolated from peripheral blood of healthy adults is 94.0% (**Figure 2A**). The supernatant of cultured A549 and PC-9 lung adenocarcinoma cell lines was used to stimulate

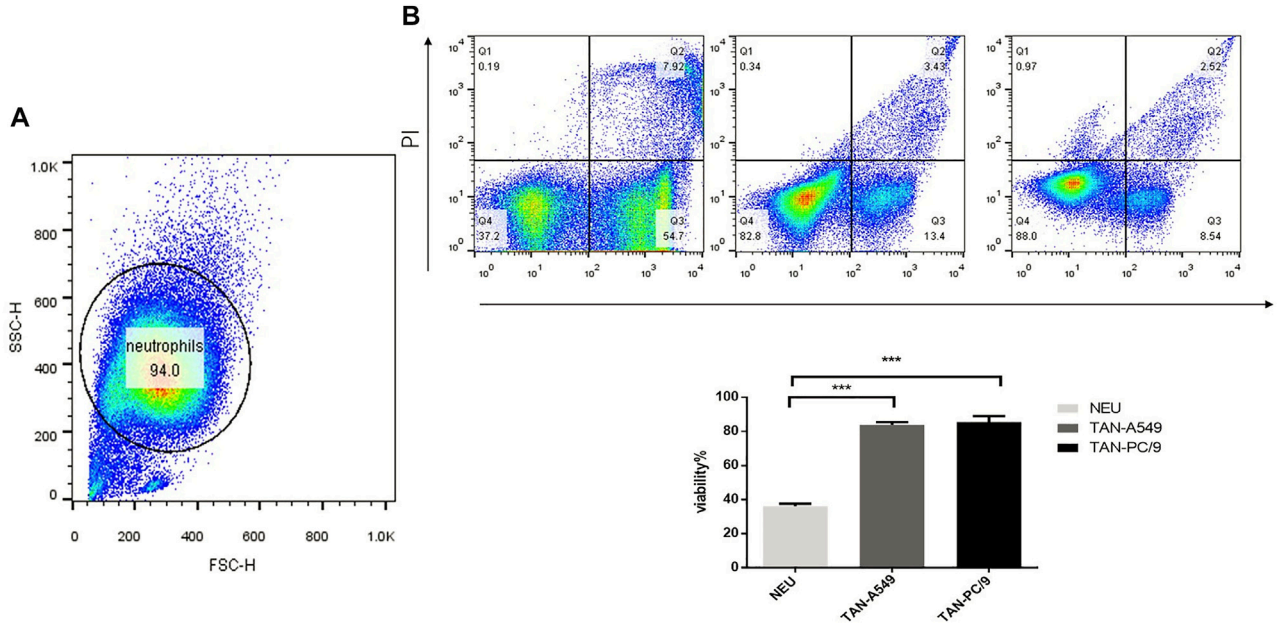

FIGURE 2 | Supernatant of cultured lung adenocarcinoma cells prolonged the lifespan of neutrophils. **(A)** The purity of neutrophils was analyzed by flow cytometry. **(B)** The viability of neutrophils, neutrophils treated with the supernatant of cultured lung adenocarcinoma cells PC-9 and A549 respectively, was verified using flow cytometry.

neutrophils isolated from the peripheral blood of healthy adults for 10 h respectively. Compared with unstimulated neutrophils, a significant increase was observed in the lifespan of neutrophils treated with supernatant of cultured PC-9 (87.3% v. s 38.5%) and A549 (82.0% v. s.38.5%) cell lines (**Figure 2B**).

The Migration and Invasiveness of Lung Adenocarcinoma Cells Were Promoted by TANs via Notch3

Transwell assays were performed to investigate the effect of TANs on migration and invasiveness of lung adenocarcinoma cells. Compared with lung adenocarcinoma cells that were stimulated by medium, NeuCS, TCCS, the migration and invasion of lung adenocarcinoma cells stimulated by TANCS were significantly higher (**Figures 3A,B**). The same result was observed on the wound healing assay (**Supplementary Figure S1**).

Notch3 has been widely reported to be associated with cancer development. Therefore, whether Notch3 is involved in the migration and invasion of lung adenocarcinoma cells was explored. Our results showed a significant increase in the expression of Notch3 in lung adenocarcinoma cells treated with TANCS than that treated with medium, NeuCS, and TCCS respectively (**Figures 3C,D**). However, after knocking down of Notch3, the migration and invasion of lung adenocarcinoma cells stimulated with TANCS were not enhanced (**Figures 3E–J** and **Supplementary Figure S2**). The results suggested that TANs promoted the migration and invasion of lung adenocarcinoma cells via Notch3.

Bioinformatics Analysis Showed That TANs and Notch3 Were Associated With Poor Prognosis

The results from the Kaplan-Meier plotter showed that the expression of Notch3 correlated negatively with OS (overall survival), FPS (first-progression, survival), and PPS (post-progression survival) of patients (**Figure 4A**). From the TIMER (http://cistrome.dfci.harvard \.edu/TIMER/, **Figure 4B**) analysis, the infiltration of TANs was found to correlate negatively to the OS of patients. Our findings indicated that both TANs and Notch3 were associated with poor prognostic outcomes in patients.

DISCUSSION

Neutrophils, the most abundant immune cells in peripheral blood (Hidalgo et al., 2019), act as the body's first line of defense against infection and respond to diverse inflammatory cues, including cancer (Shaul and Fridlender, 2019). Recently, the neutrophil-to-lymphocyte ratio in peripheral blood (pNLR) has been used as a significant prognostic factor for survival in many cancer types, including gastric cancer, melanoma, and lung cancer (Capone et al., 2018; Zhang et al., 2018; Sebastian et al., 2020). Although several studies have indicated that pNLR is associated with poor prognosis of cancer patients, the detection of pNLR can be influenced by various factors, including infection, medication, invasive surgery (Mouchemore et al., 2018).

In recent years, neutrophils infiltrated into tumors have gained attention as suitable biomarkers due to their ability to

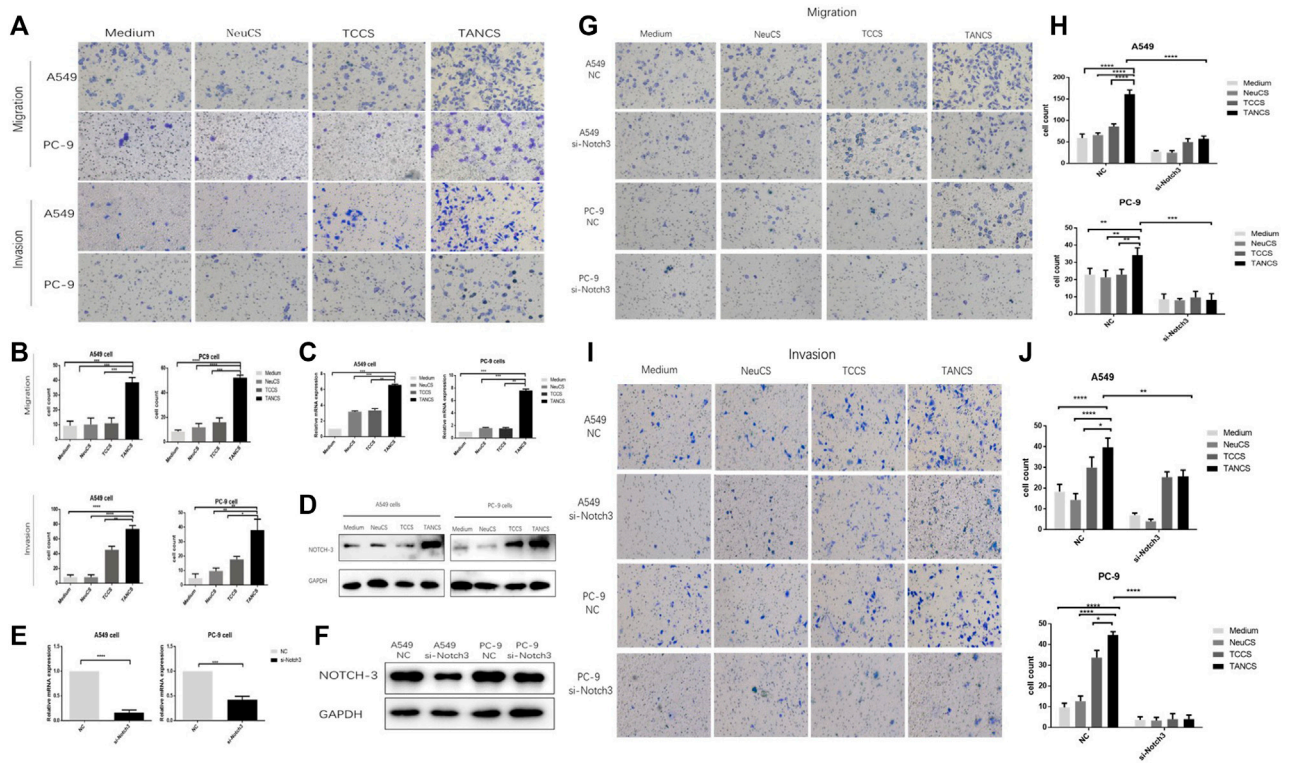

FIGURE 3 | TANs promoted the migration and invasion of lung adenocarcinoma cells via Notch3. **(A,B)** A549 and PC-9 cells were stimulated with Medium, NeuCS, TCCS, and TANCS, respectively, then the migration and invasion of cells were observed. The expression of Notch3 in A549 and PC-9 cells stimulated with Medium, NeuCS, TCCS, and TANCS, respectively was detected by PCR assay **(C)** and Western blot assay **(D)**. The knockdown effect of specific siRNA (si-Notch3) in A549 and PC-9 cells was verified at both the mRNA **(E)**, by qRT-PCR) and protein levels **(F)**, by western blot). **(G–J)** A549-NC, A549-si-Notch3, PC9-NC, and PC9-si-Notch3 cells were stimulated by Medium, NeuCS, TCCS, TANCS, respectively, then the migration **(G–H)** and invasion **(I-J)** of the cells were observed.

predict the progression of several cancer types. In gastric cancer, TANs are negatively correlated to the DFS of patients (Cong et al., 2020). In pancreatic neuroendocrine tumors, TANs have been shown to correlate negatively to the PFS and OS of patients (Zhang et al., 2020). Herein, we found the high density of TANs to be associated with poor prognostic outcomes in both immunohistochemical and Bioinformatics analysis. Our *in vitro* experiments revealed the abilities of TANs to promote the migration and invasion of A549 and PC-9 cells, which is consistent with the results found in other studies (Cong et al., 2020). Taken together, our findings suggest that the infiltration of TANs in lung adenocarcinoma can be further evaluated to predict the metastasis of tumor cells.

Several mechanisms regulating the effect of TANs on the metastasis of tumor cells have been reported. In gastric cancer, TANs promoted the migration and invasion of tumor cells by secreting IL-17a (Li et al., 2019). In colon cancer, TANs promoted the metastasis of tumor cells through the CCL15-CCR2 axis (Yamamoto et al., 2017). In our previous study, breast cancer cells induced neutrophil extracellular traps (NETs) by secreting IL-8, and these NETs promoted the migration of tumor cells (Cai et al., 2020). However, the tumor-promoting mechanisms of TANs with particular emphasis on lung cancer cell behavior are unclear.

According to numerous reports, notch-3 is associated with the development of cancer, including lung cancer (Aburjania et al., 2018). Ye and her co-workers discovered that Notch3 was associated with lymph node metastasis and poor prognosis (Ye et al., 2013). Therefore, we speculated that if TANs promoted the migration and invasion of lung cancer via Notch3. To verify this, we detected the expression of Notch3 in lung cancer by immunohistochemical staining and analyzed its correlation with TANs. We found Notch3 to be associated with poor prognosis and correlated positively with the infiltration of TANs. Results from our *in vitro* experiments demonstrated that TANs increased the expression of Notch3 in lung cancer cells. We further noted inhibition of the migration and invasion of lung cancer cells mediated by TANs after the knockdown of Notch3. Our findings suggest an interaction between Notch3 and neutrophils in the lung cancer tumor microenvironment. This is consistent with the results of Yang et al., who found TANs to promote the progression of ovarian cancer cells via the Notch3 pathway (Yang et al., 2020).

Collectively, our study indicated that lung adenocarcinoma cells promote self-invasion and self-migration

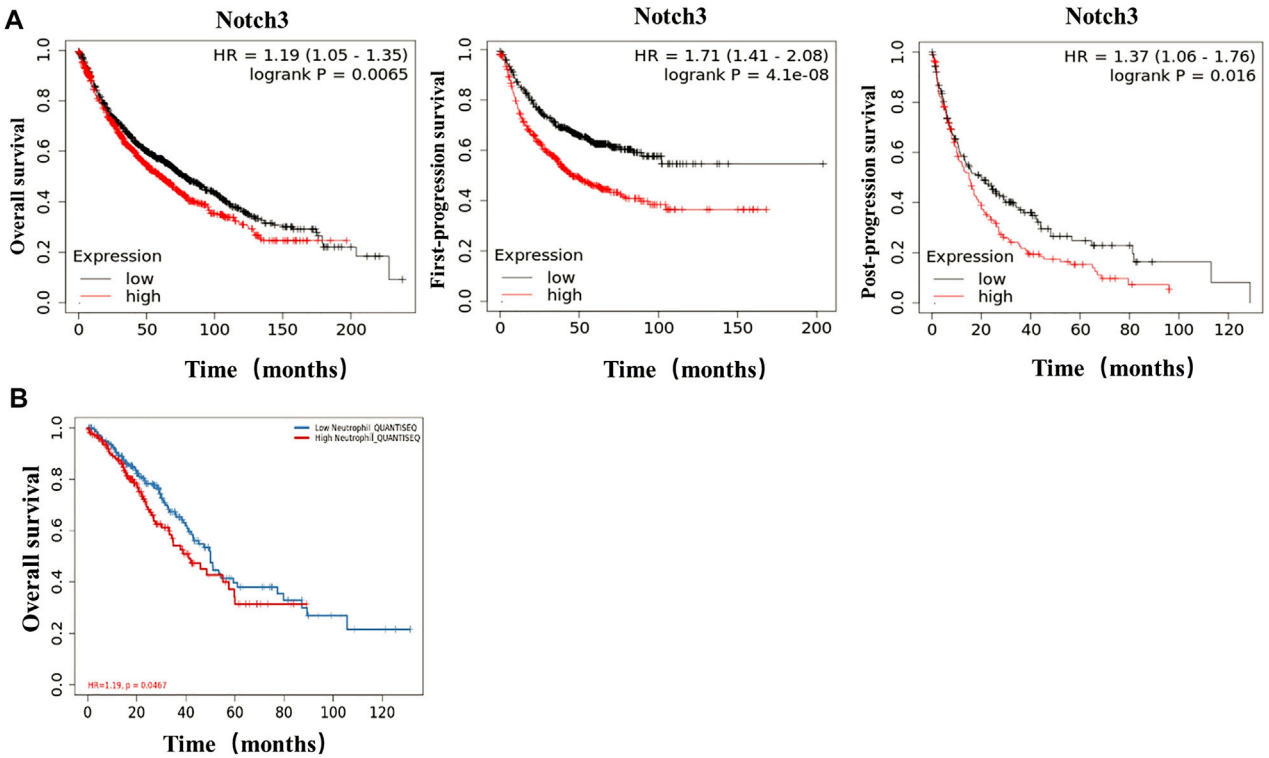

FIGURE 4 | In lung adenocarcinoma, TANs and Notch3 correlate with poor prognosis. **(A)** The correlation of Notch3 and OS, FPS, PPS in lung adenocarcinoma was analyzed by Bioinformatics data. **(B)** The correlation of TANs and OS in lung adenocarcinoma was analyzed by Bioinformatics data.

by activating neutrophils to upregulate the Notch3 expression of cancer cells. Our study has given new insights into the pathogenesis of lung cancer. Targeting TANs with Notch3 could be a new diagnostic and therapeutic strategy for treating lung cancer.

DATA AVAILABILITY STATEMENT

The raw data supporting the conclusions of this article will be made available by the authors, without undue reservation.

ETHICS STATEMENT

The studies involving human participants were reviewed and approved by Ethics Committee of Anhui Medical University (No. 2021H004). The patients/participants provided their written informed consent to participate in this study.

AUTHOR CONTRIBUTIONS

QW, JX, and WP designed the experiments; WP performed the experiments and YS offered help. WP contributed to certain key experiments. WP prepared the figures; YS, HX, YY, LC, YW were involved in specific experiments; QW, WP, and LK wrote the manuscript; QW funded the work and provided overall research supervision.

FUNDING

We acknowledge the funding support from The Academic and Technological Leaders and Reservoirs Foundation of Anhui Province for the 2019 academic year. We also acknowledge the support offered by the Center for Scientific Research of Anhui Medical University.

ACKNOWLEDGMENTS

Thank JX and his research group for providing A549 and PC9 cell lines from the Department of Immunology, Anhui Medical University. Thanks to Meijuan Zheng from the laboratory of the First Affiliated Hospital of Anhui Medical University for her help in flow cytometry.

SUPPLEMENTARY MATERIAL

The Supplementary Material for this article can be found online at: https://www.frontiersin.org/articles/10.3389/fmolb.2021.762729/full#supplementary-material

REFERENCES

Aburjania, Z., Jang, S., Whitt, J., Jaskula-Stzul, R., Chen, H., and Rose, J. B. (2018). The Role ofNotch3in Cancer. *Oncol.* 23, 900–911. doi:10.1634/theoncologist.2017-0677

Bade, B. C., and Dela Cruz, C. S. (2020). Lung Cancer 2020. *Clin. Chest Med.* 41, 1–24. doi:10.1016/j.ccm.2019.10.001

Cai, Z., Zhang, M., Boafo Kwantwi, L., Bi, X., Zhang, C., Cheng, Z., et al. (2020). Breast Cancer Cells Promote Self-Migration by Secreting Interleukin 8 to Induce NET Formation. *Gene* 754, 144902. doi:10.1016/j.gene.2020.144902

Capone, M., Giannarelli, D., Mallardo, D., Madonna, G., Festino, L., Grimaldi, A. M., et al. (2018). Baseline Neutrophil-To-Lymphocyte Ratio (NLR) and Derived NLR Could Predict Overall Survival in Patients with Advanced Melanoma Treated with Nivolumab. *J. Immunotherapy Cancer* 6, 74. doi:10.1186/s40425-018-0383-1

Carus, A., Ladekarl, M., Hager, H., Pilegaard, H., Nielsen, P. S., and Donskov, F. (2013). Tumor-associated Neutrophils and Macrophages in Non-small Cell Lung Cancer: No Immediate Impact on Patient Outcome. *Lung Cancer* 81, 130–137. doi:10.1016/j.lungcan.2013.03.003

Cong, X., Zhang, Y., Zhu, Z., Li, S., Yin, X., Zhai, Z., et al. (2020). CD66b + Neutrophils and α-SMA + Fibroblasts Predict Clinical Outcomes and Benefits from Postoperative Chemotherapy in Gastric Adenocarcinoma. *Cancer Med.* 9, 2761–2773. doi:10.1002/cam4.2939

Cui, Y., Li, Q., Li, W., Wang, Y., Lv, F., Shi, X., et al. (2020). NOTCH3 Is a Prognostic Factor and Is Correlated with Immune Tolerance in Gastric Cancer. *Front. Oncol.* 10, 574937. doi:10.3389/fonc.2020.574937

Garcia, A., and Kandel, J. J. (2012). Notch: a Key Regulator of Tumor Angiogenesis and Metastasis. *Histol. Histopathol* 27, 151–156. doi:10.14670/HH-27.151

Hidalgo, A., Chilvers, E. R., Summers, C., and Koenderman, L. (2019). The Neutrophil Life Cycle. *Trends Immunol.* 40, 584–597. doi:10.1016/j.it.2019.04.013

Hirsch, F. R., Scagliotti, G. V., Mulshine, J. L., Kwon, R., Curran, W. J., Wu, Y.-L., et al. (2017). Lung Cancer: Current Therapies and New Targeted Treatments. *The Lancet* 389, 299–311. doi:10.1016/s0140-6736(16)30958-8

Jensen, H. K., Donskov, F., Marcussen, N., Nordsmark, M., Lundbeck, F., and von der Maase, H. (2009). Presence of Intratumoral Neutrophils Is an Independent Prognostic Factor in Localized Renal Cell Carcinoma. *Jco* 27, 4709–4717. doi:10.1200/jco.2008.18.9498

Kim, M. J., Kim, A.-R., Jeong, J.-Y., Kim, K.-i., Kim, T.-H., Lee, C., et al. (2017). Correlation of ALDH1 and Notch3 Expression: Clinical Implication in Ovarian Carcinomas. *J. Cancer* 8, 3331–3342. doi:10.7150/jca.18955

Li, S., Cong, X., Gao, H., Lan, X., Li, Z., Wang, W., et al. (2019). Tumor-associated Neutrophils Induce EMT by IL-17a to Promote Migration and Invasion in Gastric Cancer Cells. *J. Exp. Clin. Cancer Res.* 38, 6. doi:10.1186/s13046-018-1003-0

Liang, S.-j., Li, X.-g., and Wang, X.-q. (2019). Notch Signaling in Mammalian Intestinal Stem Cells: Determining Cell Fate and Maintaining Homeostasis. *Cscr* 14, 583–590. doi:10.2174/1574888x14666190429143734

Masucci, M. T., Minopoli, M., and Carriero, M. V. (2019). Tumor Associated Neutrophils. Their Role in Tumorigenesis, Metastasis, Prognosis and Therapy. *Front. Oncol.* 9, 1146. doi:10.3389/fonc.2019.01146

Mouchemore, K. A., Anderson, R. L., and Hamilton, J. A. (2018). Neutrophils, G-CSF and Their Contribution to Breast Cancer Metastasis. *Febs J.* 285, 665–679. doi:10.1111/febs.14206

Rakaee, M., Busund, L.-T., Paulsen, E.-E., Richardsen, E., Al-Saad, S., Andersen, S., et al. (2016). Prognostic Effect of Intratumoral Neutrophils across Histological Subtypes of Non-small Cell Lung Cancer. *Oncotarget* 7, 72184–72196. doi:10.18632/oncotarget.12360

Sebastian, N. T., Raj, R., Prasad, R., Barney, C., Brownstein, J., Grecula, J., et al. (2020). Association of Pre- and Posttreatment Neutrophil-Lymphocyte Ratio with Recurrence and Mortality in Locally Advanced Non-small Cell Lung Cancer. *Front. Oncol.* 10, 598873. doi:10.3389/fonc.2020.598873

Shaul, M. E., and Fridlender, Z. G. (2019). Tumour-associated Neutrophils in Patients with Cancer. *Nat. Rev. Clin. Oncol.* 16, 601–620. doi:10.1038/s41571-019-0222-4

Tang, X., Cao, Y., Peng, D., Zhao, G., Zeng, Y., Gao, Z., et al. (2019). Overexpression of Notch3 Is Associated with Metastasis and Poor Prognosis in Osteosarcoma Patients. *Cmar* Vol. 11, 547–559. doi:10.2147/cmar.s185495

Wang, J., Jia, Y., Wang, N., Zhang, X., Tan, B., Zhang, G., et al. (2014). The Clinical Significance of Tumor-Infiltrating Neutrophils and Neutrophil-To-Cd8+ Lymphocyte Ratio in Patients with Resectable Esophageal Squamous Cell Carcinoma. *J. Transl Med.* 12, 7. doi:10.1186/1479-5876-12-7

Wang, Y., Chen, J., Yang, L., Li, J., Wu, W., Huang, M., et al. (2019). Tumor-Contacted Neutrophils Promote Metastasis by a CD90-TIMP-1 Juxtacrine-Paracrine Loop. *Clin. Cancer Res.* 25, 1957–1969. doi:10.1158/1078-0432.ccr-18-2544

Yamamoto, T., Kawada, K., Itatani, Y., Inamoto, S., Okamura, R., Iwamoto, M., et al. (2017). Loss of SMAD4 Promotes Lung Metastasis of Colorectal Cancer by Accumulation of CCR1+ Tumor-Associated Neutrophils through CCL15-CCR1 Axis. *Clin. Cancer Res.* 23, 833–844. doi:10.1158/1078-0432.ccr-16-0520

Yan, K., Wang, Y., Lu, Y., and Yan, Z. (2021). Coexpressed Genes that Promote the Infiltration of M2 Macrophages in Melanoma Can Evaluate the Prognosis and Immunotherapy Outcome. *J. Immunol. Res.* 2021, 6664791. doi:10.1155/2021/6664791

Yan, X., Jiao, S.-C., Zhang, G.-Q., Guan, Y., and Wang, J.-L. (2017). Tumor-associated Immune Factors Are Associated with Recurrence and Metastasis in Non-small Cell Lung Cancer. *Cancer Gene Ther.* 24, 57–63. doi:10.1038/cgt.2016.40

Yang, M., Zhang, G., Wang, Y., He, M., Xu, Q., Lu, J., et al. (2020). Tumour-associated Neutrophils Orchestrate Intratumoural IL-8-driven Immune Evasion through Jagged2 Activation in Ovarian Cancer. *Br. J. Cancer* 123, 1404–1416. doi:10.1038/s41416-020-1026-0

Ye, Y.-z., Zhang, Z.-h., Fan, X.-y., Xu, X.-l., Chen, M.-l., Chang, B.-w., et al. (2013). Notch3 Overexpression Associates with Poor Prognosis in Human Non-small-cell Lung Cancer. *Med. Oncol.* 30, 595. doi:10.1007/s12032-013-0595-7

Zhang, W. H., Wang, W. Q., Gao, H. L., Xu, S. S., Li, S., Li, T. J., et al. (2020). Tumor-Infiltrating Neutrophils Predict Poor Survival of Non-functional Pancreatic Neuroendocrine Tumor. *J. Clin. Endocrinol. Metab.* 105, 196. doi:10.1210/clinem/dgaa196

Zhang, Y., Lu, J. J., Du, Y. P., Feng, C. X., Wang, L. Q., and Chen, M. B. (2018). Prognostic Value of Neutrophil-To-Lymphocyte Ratio and Platelet-To-Lymphocyte Ratio in Gastric Cancer. *Medicine (Baltimore)* 97, e0144. doi:10.1097/MD.0000000000010144

Zhou, S.-L., Zhou, Z.-J., Hu, Z.-Q., Huang, X.-W., Wang, Z., Chen, E.-B., et al. (2016). Tumor-Associated Neutrophils Recruit Macrophages and T-Regulatory Cells to Promote Progression of Hepatocellular Carcinoma and Resistance to Sorafenib. *Gastroenterology* 150, 1646–1658. doi:10.1053/j.gastro.2016.02.040

Conflict of Interest: The authors declare that the research was conducted in the absence of any commercial or financial relationships that could be construed as a potential conflict of interest.

frontiers in Molecular Biosciences

ORIGINAL RESEARCH
published: 24 January 2022
doi: 10.3389/fmolb.2022.786864

Immune Response on Optimal Timing and Fractionation Dose for Hypofractionated Radiotherapy in Non–Small-Cell Lung Cancer

*Xianlan Zhao[1†], Jixi Li[1†], Linpeng Zheng[1†], Qiao Yang[2], Xu Chen[1], Xiewan Chen[3], Yongxin Yu[1], Feng Li[1], Jianxiong Cui[1] and Jianguo Sun[1]**

[1]Cancer Institute, Xinqiao Hospital, Army Medical University, Chongqing, China, [2]Department of Ultrasound, The 941st Hospital of the PLA Joint Logistic Support Force, Xining, China, [3]Department of Basic Medicine, Army Medical University, Chongqing, China

OPEN ACCESS

Edited by:
Na Luo,
Nankai University, China

Reviewed by:
Honglin Jin,
Huazhong University of Science and Technology, China
Jun Wang,
The First Affiliated Hospital of Shandong First Medical University and Shandong Provincial Qianfoshan Hospital, China
Bicheng Zhang,
Wuhan University, China

***Correspondence:**
Jianguo Sun
sunjg09@aliyun.com

†These authors have contributed equally to this work

Specialty section:
This article was submitted to Molecular Diagnostics and Therapeutics, a section of the journal Frontiers in Molecular Biosciences

Received: 30 September 2021
Accepted: 04 January 2022
Published: 24 January 2022

Citation:
Zhao X, Li J, Zheng L, Yang Q, Chen X, Chen X, Yu Y, Li F, Cui J and Sun J (2022) Immune Response on Optimal Timing and Fractionation Dose for Hypofractionated Radiotherapy in Non–Small-Cell Lung Cancer. Front. Mol. Biosci. 9:786864. doi: 10.3389/fmolb.2022.786864

Background: The intervention timing of immune checkpoint inhibitors (ICIs) and radiotherapy fractionations are critical factors in clinical efficacy. This study aims to explore dynamic changes of the tumor immune microenvironment (TIME) after hypofractionated radiotherapy (HFRT) at different timepoints and fractionation doses in non–small-cell lung cancer (NSCLC).

Methods: In the implanted mouse model, the experimental groups received HFRT 3.7 Gy × 4 F, 4.6 Gy × 3 F, 6.2 Gy × 2 F, and 10 Gy × 1 F, respectively, with the same biological equivalent dose (BED) of 20Gy. Tumor volume and survival time were compared with those of the control group. Flow cytometry was performed to detect immune cells and their PD-1/PD-L1 expressions using tail-tip blood at different timepoints and tumor tissues at 48 h after radiotherapy. In NSCLC patients, immune cells, PD-1/PD-L1, and cytokines were detected in peripheral blood for 4 consecutive days after different fractionation radiotherapy with the same BED of 40Gy.

Results: Tumor volumes were significantly reduced in all experimental groups compared with the control group, and the survival time in 6.2 Gy × 2 F ($p < 0.05$) was significantly prolonged. In tail-tip blood of mice, $CD8^+$ T counts increased from 48 h to 3 weeks in 4.6 Gy × 3 F and 6.2 Gy × 2 F, and $CD8^+$ PD-1 shortly increased from 48 h to 2 weeks in 6.2 Gy × 2 F and 10 Gy × 1 F ($p < 0.05$). Dentritic cells (DCs) were recruited from 2 to 3 weeks ($p < 0.01$). As for NSCLC patients, $CD8^+$ T counts and PD-1 expression increased from 24 h in 6.2 Gy × 4 F, and $CD8^+$ T counts increased at 96 h in 10 Gy × 2 F ($p < 0.05$) in peripheral blood. DC cells were tentatively recruited at 48 h and enhanced PD-L1 expression from 24 h in both 6.2 Gy × 4 F and 10 Gy × 2 F ($p < 0.05$). Besides, serum IL-10 increased from 24 h in 6.2 Gy × 4 F ($p < 0.05$). Conversely, serum IL-4 decreased at 24 and 96 h in 10 Gy × 2 F ($p < 0.05$).

Conclusion: HFRT induces the increase in $CD8^+$ T cells and positive immune cytokine response in specific periods and fractionation doses. It was the optimal time window from 48 h to 2 weeks for the immune response, especially in 6.2 Gy fractionation. The best

immune response was 96 h later in 10 Gy fractionation, delivering twice instead of a single dose. During this time window, the intervention of immunotherapy may achieve a better effect.

Keywords: lung cancer, immune checkpoint inhibitor, hypofractionated radiotherapy, tumor immune microenvironment, dynamic changes

INTRODUCTION

Studies have shown that radiotherapy, especially stereotactic body radiation therapy (SBRT) or hypofractionated radiotherapy (HFRT), can cause DNA damage, which leads to tumor cell death, induces release of pro-inflammatory factors, and enhances tumor immune stimulation cells and cytokines to remodel the tumor immune microenvironment (TIME) (Formenti and Demaria, 2013; Demaria et al., 2015). More importantly, radiotherapy can also promote immune cell infiltration and transform "cold" tumors into "hot" tumors, a status suitable to immune checkpoint inhibitors (ICIs) (Ostrand-Rosenberg and Sinha, 2009). Therefore, the combination of radiotherapy and ICI therapy has gained more and more attention and is considered a promising treatment for cancer (Formenti et al., 2018; Chicas-Sett et al., 2019). Dewan et al. (Dewan et al., 2009) found that the combination of HFRT and ICI therapy could induce an abscopal effect in a mouse model of breast cancer. Besides, Verbrugge et al. (Verbrugge et al., 2012) verified that ICI therapy enhanced the curative capacity of radiotherapy in established breast malignancy.

ICI treatment was given at different timepoints after radiotherapy in many studies; therefore the optimal time window remains elusive (Dovedi et al., 2015; Schapira et al., 2018). The PACIFIC study showed that interventional immunotherapy within 14 days after radiotherapy had the longer progression-free survival (PFS) and overall survival (OS) in patients with locally advanced NSCLC (Antonia et al., 2018). The KEYNOTE-001 study found that radiotherapy followed by immunotherapy had better PFS (4.4 months vs. 2.1 months) and OS (10.7 months vs. 5.3 months) in patients with advanced NSCLC (Shaverdian et al., 2017). The Pembro-RT study verified that pembrolizumab within 1 week after SBRT doubled the objective response rate (ORR), and prolonged PFS (6.6 months vs. 1.9 months) and OS (15.9 months vs. 7.6 months) in patients with advanced NSCLC (Theelen et al., 2019). Bauml's study revealed that pembrolizumab in 4–12 weeks after local ablations had a PFS of 19.1 months in patients with metastatic NSCLC, tripling the previous PFS of 6.6 months (Aggarwal et al., 2019). However, Wegner (Wegner et al., 2019) showed that immunotherapy at least 3 weeks after radiotherapy would exhibit longer OS in a retrospective study. Therefore, to explore the right timing for ICI therapy intervention after radiotherapy has great significance in clinical treatment.

What is more, different fractionations also have different effects on TIME. Lugade (Lugade et al., 2008) found that a single 15 Gy was more effective than 3 Gy × 5 F in activating DC cells in lymph nodes in the B16 melanoma model. However, Schaue (Schaue et al., 2012) found that the 7.5 Gy × 2 F was better than a single dose of 15 Gy in inducing T cell initiation in another melanoma model. An appropriate fractionation could enhance an immunoreactive effect, but an extra high dose would cause damage to lymphocyte subsets and produce an immunosuppressive effect and immune dysfunction (Zitvogel and Kroemer, 2015). A single high-dose radiotherapy could cause damage and collapse of the tumor vasculature, which was not conducive to the infiltration of T cells into the tumor (Timke et al., 2008). It would cause radioresistance of tumor cells due to hypoxia caused by destruction of the vascular system (Barker et al., 2015). Radiation produces two-way immune effects like the "seesaw," including positive and negative responses. The appropriate fractionation could push the immune effects into the positive response. Previous studies have shown that HFRT or SBRT was more capable of mobilizing local and systemic immune responses than conventional fractionation (Schaue and Mcbride, 2015). Since there are many choices in clinical practice, it is a conundrum as to which fractionation is appropriate and optimal.

As the intervention timepoints of ICI therapy after radiotherapy and the fractionations are various and controversial in previous studies, this study aimed at exploring the dynamic changes of TIME at different timepoints and fractionation doses of HFRT in NSCLC and providing an experimental basis for the optimal intervention timing and fractionation dose for the combination of radiotherapy and ICI therapy.

MATERIALS AND METHODS

Radiation of Lung Cancer Implanted Mouse Model

Mice and Cell Line

A total of 60 C57BL/6 male mice (6–8 weeks old) were purchased from the animal center of our hospital (No. SYXK 2012-0011). All protocols were approved by the Laboratory Animal Welfare and Ethics Committee of Army Medical University (Chongqing, China). Lewis lung carcinoma (LLC) cells were maintained in DMEM culture medium (Gibco, United States) supplemented with 10% fetal bovine serum (HyClone, United States), 100 U/ml penicillin, and 100 μg/ml streptomycin.

Lewis Cell Inoculation Into Mouse

1×10^6 Lewis cells were inoculated subcutaneously to the right leg of the mice. Tumor size was measured using a vernier caliper every 3 days. Tumor volume was calculated as follows: tumor volume (mm^3) = (long axis) × (short axis) $^2/2$.

Irradiation Plans

25 mice were selected with a tumor volume of about 100 mm^3 and randomly divided into the control group and 4 experimental

groups with 5 mice in each group. Experimental groups were anesthetized and given radiotherapy 3.7 Gy × 4 F, 4.6 Gy × 3 F, 6.2 Gy × 2 F, and 10 Gy × 1 F, respectively, using 6MV X-ray with a radiation field of 10 cm × 10 cm. The selection of radiotherapy dose in mice was consistent with a previous study (Mathieu et al., 2021), in which a single dose of 10 Gy induced immune response and even abscopal effects. The four fractionations had the same biological equivalent dose (BED, 20Gy) with the calculation formula BED = nd [1 + d/(α/β)]. Radiotherapy plans were designed using a Varian eclipse treatment planning system (TPS, version 13.5) with the spare of the area of lymph nodes and delivered by the Varian Trilogy Accelerator. The source skin distance (SSD) was 100 cm, the irradiation was at a depth of 0.5 cm, and the dosage rate was 400 MU/min.

Tail-tip blood samples were collected at different timepoints, 1 day before radiotherapy as the baseline and 24 h, 48 h, 96 h, 1 week, 2 weeks, and 3 weeks after finishing radiotherapy. The survival time was observed every 3 days with the following endpoints and given euthanasia: tumor dimension reaching 20 mm, tumor with ulceration, necrosis or infection, and morbility or disability. Another experiment of 20 implanted mice with 4 in each group received the same irradiation, and tumor tissues were collected at 48 h after finishing radiotherapy.

Clinical Practice

All patients were diagnosed with unresectable stage IV NSCLC by histology or cytology according to the eighth edition of the American Joint Committee on Cancer (AJCC) Union. Other inclusion criteria included 18–75 years old, ECOG performance status 0~1, and measurable or evaluable lesions. The exclusion criteria included inadequate cardiac, pulmonary, renal, and hepatic functions and blood count/chemistry tests, uncontrolled malignant pleural/pericardial effusions, and previous radiotherapy at the same lesions. We designed the radiotherapy plan based on the NCCN guideline for the lesions. Four plans (3.7 Gy × 8 F, 4.6 Gy × 6 F, 6.2 Gy × 4 F, and 10 Gy × 2 F) with the same BED of 40 Gy were conducted using 6MV X-ray with at least 5 patients in each group. Peripheral blood samples were collected within 1 week before radiotherapy as the baseline and 24, 48, 72, and 96 h after radiotherapy. In clinical practice, BED 40Gy is a better palliative radiotherapy dose than BED 20Gy by NCCN guideline recommendation to relieve symptoms of local lesions. Actually, some patients boost the dose after continuous 4-day blood sample collection to reach the clinical requirement. To better protect the immune system, peripheral draining lymph nodes in mice or patients were not delineated and irradiated as the targets. This study was registered in the Clinical Trials Register (NCT03073902, https://clinicaltrials.gov/). All patients have signed written informed consent forms.

Tumor Sample Preparation

We collected tumor tissues from implanted mice by cervical dislocation at 48 h after irradiation. Tumor-infiltrating lymphocytes (TILs) were processed by using a gentle Macs dissociator and a murine tumor dissociation kit. Lymphocytes from mice and patients' anti-freezing blood were obtained with mouse and human peripheral blood lymphocyte isolation fluid (LTS10771, TBD, China). The serum of the NSCLC patient was collected after centrifuging for 10 min at 1,000 rpm.

Flow Cytometry

The single cell suspension of mouse or human samples was centrifuged at 2500 rpm for 3 min, mixed with CD4 (#100408), CD8 (#100712), Ly-6G/Ly-6C (Gr-1) (# 108412), CD11b (#101208), CD11c (#117306), CD25 (#101908), CD127 (# 135012), CD274 (PD-L1) (#124314), CD279 (PD-1) (#109110) anti-mouse (BD Biosciences, United States) or CD4 (#560650), CD8 (#563256), CD279 (#561787) (R&D system, United States), CD11b (#101228), CD11c (#301624), CD19 (# 302226), CD25 (#302609), CD33 (#303436), CD45 (#304029), HLA-DR (#307616) (Biolegend, Germany), CD274 (#2338640), and CD127 (# 2071281) (Invitrogen, United States) anti-human antibody of immune cells, respectively, after removing the supernatant and then stained at 4°C for 30 min. Dead cells were identified using a LIVE/Dead (LD) immobile dye kit (#1968231, Invitrogen, United States). Data was acquired by multi-parameter flow cytometry (BD Biosciences, United States), and the results were analyzed using FlowJo10.0. Based on the PD1/PD-L1 signaling pathway in tumor immunology (Jiang et al., 2015), we detected the counts of $CD4^+$ T cells, $CD8^+$ T cells, DC, Treg, and MDSC, the PD-1 expression in circulating immune cells including $CD4^+$ T, $CD8^+$ T, and Treg cells, and the PD-L1 expression in circulating immune cells including DC and MDSC cells at different timepoints after radiotherapy.

Serum Cytokine Assay

The serum was centrifuged at 10,000 rpm for 10 min, and then we diluted the supernatant in 1:2 ratio as sample. Human High Sensitivity Cytokine Premixed Kit A (FCSTM09-08, RandD system, United States) was used to incubate the samples, antibody, and Streptavidin-PE for 3 h, 1 h, and 30 min, respectively. Then serum IL-2, IL-4, IL-5, IL-10, IL-12p, GM-CSF, IFN-γ, and TNF-α were detected using a Luminex 200 system (Luminex Corporation, Austin, TX, United States). What is more, the mixture of standard, blank, and diluted samples was incubated at room temperature for 2 h. Then detection antibody, Streptavidin-HRP, and TMB Subsrate Solution were added and incubated for 1 h, 45 min, and 30 min, respectively. TGF-β1 (#227437–039) and CXCL16 (#309072121) were detected using an ELISA kit (Invitrogen/Thermo Fisher Scientific, United States).

Statistical Analysis

The experimental data were input and analyzed using SPSS (version 26.0). The survival rate of mice was analyzed by Kaplan–Meier. Continuous variables including tumor growth volumes, counts of immune cells, PD-1/PD-L1 expressions, and cytokine levels were analyzed by one-way ANOVA. All statistical tests were two-sided, and $p < 0.05$ was considered as statistically significant.

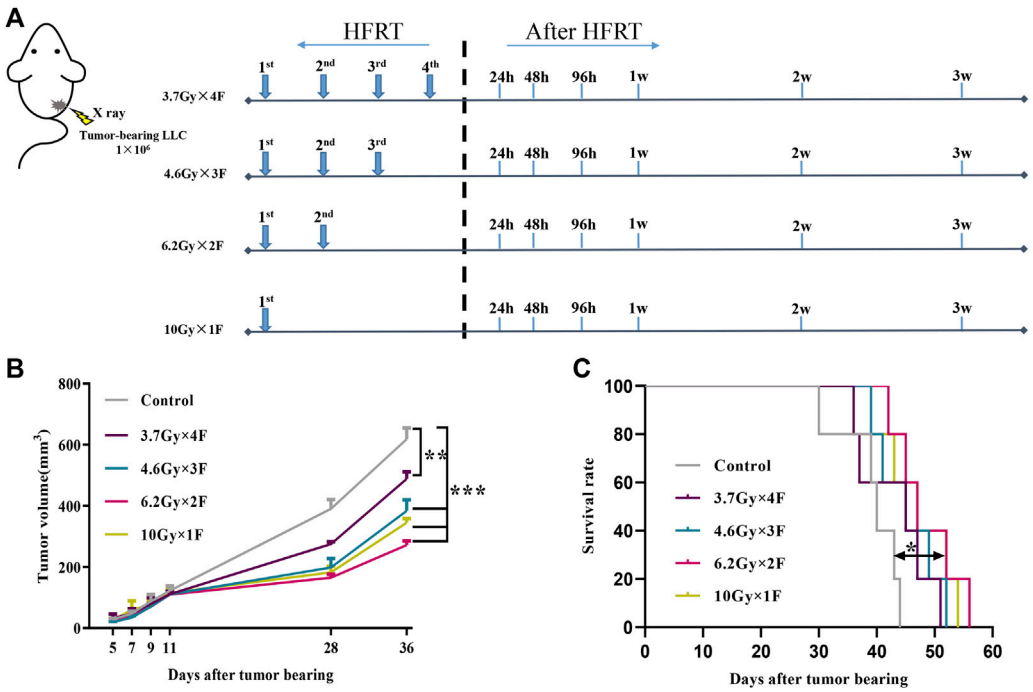

FIGURE 1 | Study design, tumor growth, and survival curves. **(A)** Study design. LLC cells were implanted subcutaneously into the right leg of C57BL/6 mouse on day 0. The mouse received 3.7 Gy × 4 F, 4.6 Gy × 3 F, 6.2 Gy × 2 F, and 10 Gy × 1F radiotherapy. Then collected tail-tip blood samples at different timepoints after radiotherapy. **(B)** Growth curve of tumor in mouse. The tumor volume was significantly reduced in different fractionation radiotherapies. **(C)** Survival curve of mouse. The survival time of 6.2 Gy × 2 F fractionation was significantly prolonged. $^{*}p < 0.05$, $^{**}p < 0.01$, $^{***}p < 0.001$, compared with the control group.

RESULTS

Tumor Growth and Survival in Lewis Lung Carcinoma Implanted Mouse

We observed the tumor volume and survival time of implanted mice after radiotherapy. Tumors occurred at about day 5 after implanting. Mice were irradiated when tumor volume reached about 100 mm^3. We collected tail-tip blood at the following timepoints: 1 day before radiotherapy and 24 h, 48 h, 96 h, 1 week, 2 weeks, and 3 weeks after radiotherapy (**Figure 1A**). Tumor growth was significantly delayed in all experimental groups compared with the control group ($p < 0.01$, **Figure 1B**). Among them, the minimum volume was in the 6.2 Gy × 2 F group ($p < 0.001$, **Figure 1B**). As for the survival time, there was a significant improvement in the 6.2 Gy × 2 F group compared with the control ($p < 0.05$, **Figure 1C**).

Dynamic Changes of Immune Cells in Peripheral Blood in Implanted Mice

An increase in the counts of $CD4^+$ T cells was identified from 24 h to 1 week after radiotherapy in the 3.7 Gy × 4 F group, but not in other groups (**Figure 2A**). There was an increase in $CD8^+$ T cells from 48 h to 3 weeks after radiotherapy in 4.6 Gy × 3 F and 6.2 Gy × 2 F ($p < 0.05$), but not in 3.7 Gy × 4 F and 10 Gy × 1F (**Figures 2A,B**). DC counts began to increase from 2 to 3 weeks after radiotherapy in most groups ($p < 0.01$, **Figures 2A,C**). Treg began to rise at 48 h after radiotherapy in 3.7 Gy × 4 F and returned to baseline at about 3 weeks (**Figure 2A**). MDSC counts increased from week 2 to week 3 after radiotherapy in all groups (**Figure 2A**). In the period of 48 h to 2 weeks, the ratio of $CD4^+$/Treg and $CD8^+$/Treg were 1.41 (0.93–2.51) and 1.62 (1.20–2.73) in 6.2 Gy × 2 F, respectively.

Expression of PD-1/PD-L1 of Circulating Immune Cells in Implanted Mice

$CD4^+$ PD-1 and $CD8^+$ PD-1 shortly increased from 48 h to 2 weeks after radiotherapy in the 6.2 Gy × 2 F and 10 Gy × 1 F groups ($p < 0.05$, **Figures 3A,B**). DC PD-L1 gradually decreased from 48 h to 3 weeks after radiotherapy in all experimental groups ($p < 0.001$, **Figures 3A,C**). Treg PD-1 and MDSC PD-L1 also gradually decreased in most groups (**Figure 3A**).

Tumor Immune Microenvironment Changes of Tumor Tissues in Mice

The counts of $CD4^+$ T cells, $CD8^+$ T cells, and Treg decreased at 48 h after radiotherapy in all experimental groups and had an increased proportion of DC and MDSC in tumor tissues ($p < 0.05$, **Figure 4A**). Both $CD8^+$ PD-1 and DC PD-L1 in tumors were

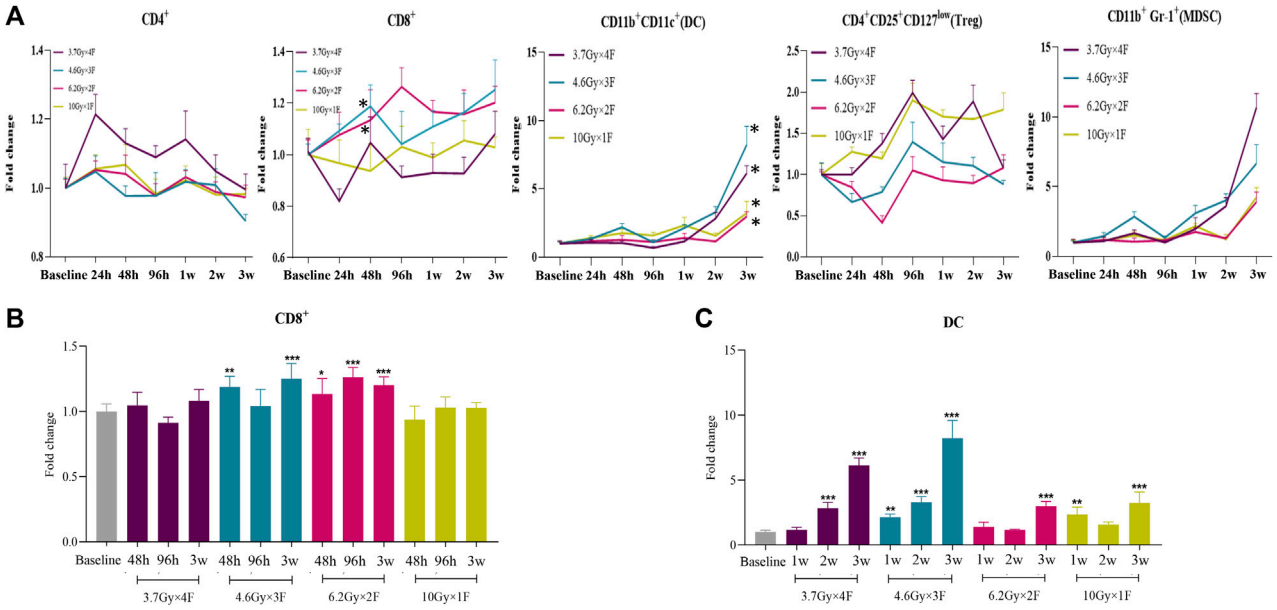

FIGURE 2 | Dynamic changes of immune cell counts in LLC implanted mouse peripheral blood after radiotherapy. **(A)** Trends of $CD4^+$ T cells, $CD8^+$ T cells, DC, Treg, and MDSC after 4 different fractionation radiotherapies. * The dose in which trend was significant and the time at which difference began. **(B)** Changes of $CD8^+$ T cells at 48 h, 96 h, and 3w after radiotherapy, respectively. **(C)** Changes of DC at 1, 2, and 3w after radiotherapy. $^*p < 0.05$,$^{**}p < 0.01$, $^{***}p < 0.001$, compared with baseline.

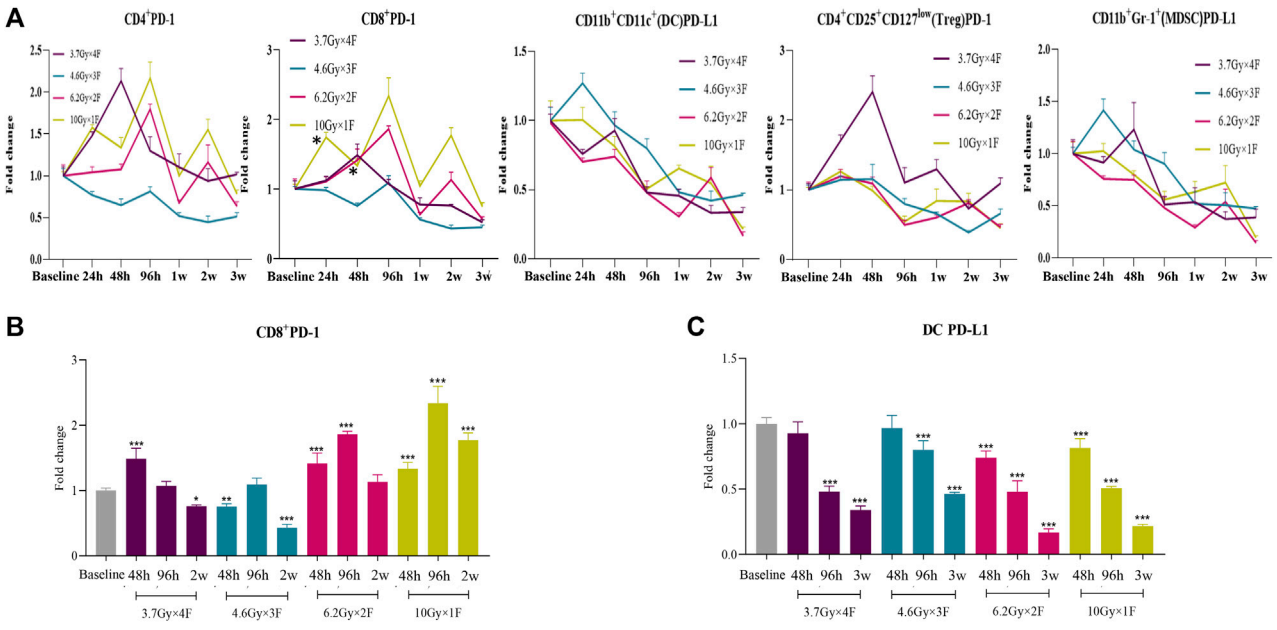

FIGURE 3 | Dynamic trends of PD-1 and PD-L1 expression after radiotherapy in LLC implanted mouse peripheral blood. **(A)** Trends of $CD4^+$ PD-1, $CD8^+$ PD-1, DC PD-L1, Treg PD-1, and MDSC PD-L1 after 4 different fractionation radiotherapies. * The dose in which trend was significant and the time at which difference began. **(B)** Discrepancy of $CD8^+$ PD-1 at 48 h, 96 h, and 2w after radiotherapy, respectively. **(C)** Discrepancy of DC PD-L1 at 48 h, 96 h, and 3w after radiotherapy. $^*p < 0.05$,$^{**}p < 0.01$, $^{***}p < 0.001$, compared with baseline.

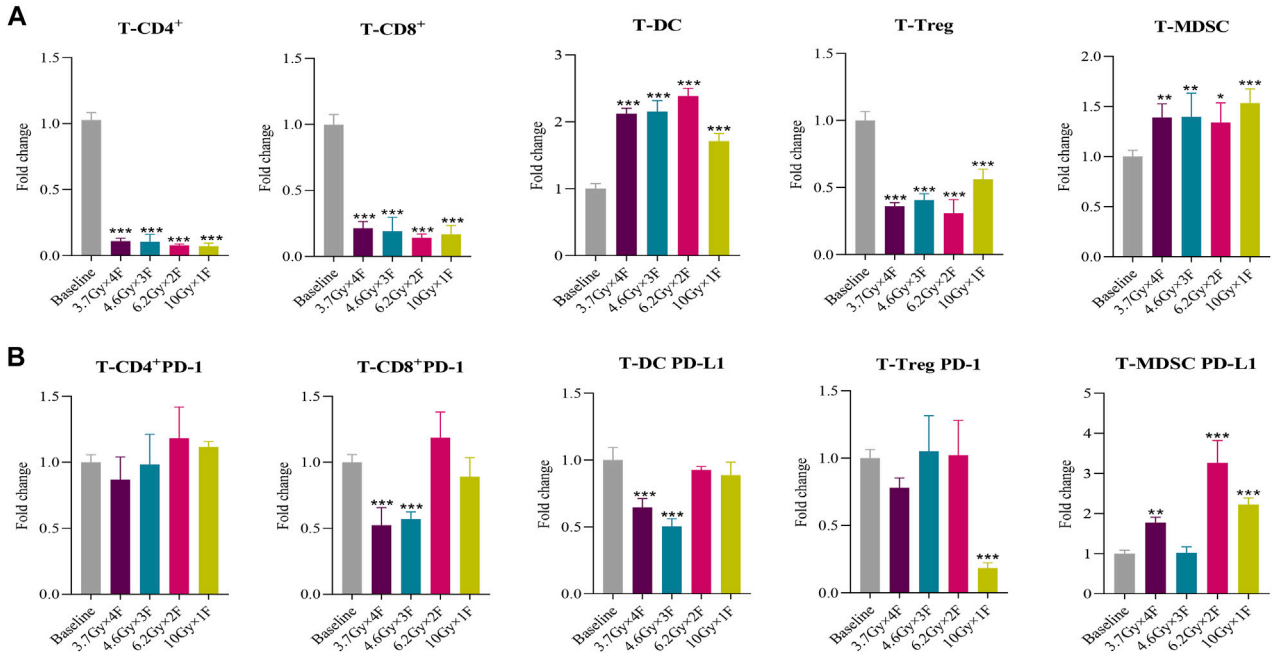

FIGURE 4 | Immune cells and PD-1/PD-L1 changes of tumor tissues in mouse at 48 h after 4 different fractionation radiotherapies. **(A)** Changes of different immune cells at 48 h after radiotherapy in mouse tumor tissues. **(B)** Changes of PD-1 and PD-L1 expression at 48 h after radiotherapy in mouse tumor tissues. $^{*}p < 0.05$,$^{**}p < 0.01$, $^{***}p < 0.001$, compared with baseline.

downregulated in the 3.7 Gy × 4 F and 4.6 Gy × 3 F groups ($p < 0.001$, **Figure 4B**). Treg PD-1 decreased at 10 Gy × 1 F, and MDSC PD-L1 was increased except for the 4.6 Gy × 3 F group ($p < 0.01$, **Figure 4B**). The ratio of $CD8^+$ T cells in tumor tissues and peripheral blood was 0.13 (0.10–0.16), and the $CD8^+$ PD-1 was 1.03 (0.91–1.17).

Dynamic Changes of Immune Cells in Human Peripheral Blood

A total of 22 NSCLC patients were recruited from Nov. 1st, 2020 to Aug. 31st, 2021. The clinical characteristics in different groups were collected (**Table 1**). The bOR (best overall response) rates of patients with immunotherapy and those without immunotherapy were 53.33 and 42.86%. The mPFS and mOS were 5.59 months (0.92–14.30+) and 6.58 months (1.02–14.30+) in patients with immunotherapy, and mPFS and mOS have not reached (NR) in patients without immunotherapy up to the time of follow-up. $CD8^+$ T cells increased from 24 h and maintained a high level to 96 h in 6.2 Gy × 4 F ($p < 0.05$, **Figures 5A,B**). $CD8^+$ T cells also increased in 10 Gy × 2 F at a later timepoint of 96 h ($p < 0.01$, **Figures 5A,B**). There was an increase in DC cells at 48 h after radiotherapy in 6.2 Gy × 4 F and 10 Gy × 2 F ($p < 0.001$, **Figures 5A,C**). We did not find dramatic changes in $CD4^+$ T cells, Treg, and MDSC in peripheral blood between pre and post-radiotherapy (**Figure 5A**). From 24 to 96 h, the ratio of $CD4^+$/Treg and $CD8^+$/Treg were, respectively, 1.09 (0.96–1.17) and 1.43 (1.33–1.50) in 6.2 Gy × 4 F.

Expression of PD-1/PD-L1 of Circulating Immune Cells in Patients

There were significant increases in $CD8^+$ PD-1 from 24 to 96 h after radiotherapy in 6.2 Gy × 4 F, from 48 h in 3.7 Gy × 8 F, and at 96 h in 4.6 Gy × 6 F, respectively ($p < 0.05$, **Figures 6A,B**). DC PD-L1 significantly increased from 24 to 96 h in 6.2 Gy × 4 F and 10 Gy × 2 F except for the timepoint of 48 h ($p < 0.05$, **Figures 6A,C**). There were no obvious changes in $CD4^+$ PD-1 and Treg PD-1 between pre and post-radiotherapy at most timepoints of the experimental groups. MDSC PD-L1 increased at 96 h in all experimental groups (**Figure 6A**).

Detection of Cytokines in Serum of Patients

There was a significant increase in IL-10 from 24 to 96 h after radiotherapy in 6.2 Gy × 4 F ($p < 0.05$) and an increase in IL-2 and IL-5 in 4.6 Gy × 6 F ($p < 0.05$, **Figure 7A**). On the contrary, there was a significant decrease in TGF-β1 at different timepoints in 3.7 Gy × 8 F, 4.6 Gy × 6 F, and 6.2 Gy × 4 F ($p < 0.05$) and a decrease in IL-4 at 24 and 96 h in 10 Gy × 2 F ($p < 0.05$, **Figure 7A**). There were no obvious changes in IL-12p, GM-CSF, IFN-γ, TNF-α, and CXCL16 between pre and post-radiotherapy in all the groups (**Figure 7B**).

DISCUSSION

Radiotherapy can achieve a synergistic effect with immunotherapy by recruiting T cells to the irradiated tumor

TABLE 1 | Demographics and clinical characteristics in different fractionations of NSCLC patients.

Variables	Total (N = 22)	3.7Gy*8F (n = 5)	4.6Gy*6F (n = 6)	6.2Gy*4F (n = 6)	10Gy*2F (n = 5)
Age	—	—	—	—	—
< 65	12	2	5	3	2
≥65	10	3	1	3	3
Sex	—	—	—	—	—
Male	14	4	2	4	4
Female	8	1	4	2	1
Smoking	—	—	—	—	—
Yes	14	4	3	4	3
No	8	1	3	2	2
Pathology	—	—	—	—	—
ADC	14	2	4	5	3
SCC	8	3	2	1	2
T stage	—	—	—	—	—
T1	1	0	0	1	0
T2	4	1	0	1	2
T3	4	2	2	0	0
T4	13	2	4	4	3
N stage	—	—	—	—	—
N0	1	0	0	0	1
N1	1	0	1	0	0
N2	6	1	0	4	1
N3	14	4	5	2	3
M stage	—	—	—	—	—
M0	0	0	0	0	0
M1	22	5	6	6	5
Concurrent chemotherapy	—	—	—	—	—
Yes	6	2	1	2	1
No	16	3	5	4	4
Concurrent immunotherapy	—	—	—	—	—
Yes	15	3	4	4	4
Pembrolizumab	3	2	0	0	1
Nivolumab	1	1	0	0	0
Atezolizumab	1	0	1	0	0
Tislelizumab	2	0	1	1	0
Toripalimab	4	0	1	1	2
Camrelizumab	3	0	0	2	1
Sintilimab	1	0	1	0	0
No	7	2	2	2	1
Target gene mutation	—	—	—	—	—
Yes	7	0	2	3	2
EGFR	4	0	1	1	2
ALK	1	0	1	0	0
KRAS	1	0	0	1	0
BRAF	1	0	0	1	0
No	15	5	4	3	3

ADC, adenocarcinoma; SCC, squamous cell carcinoma.

area and increasing the vulnerability of tumor cells to T cells (Galluzzi et al., 2017). Nevertheless, how to determine the optimal combination strategy of radiotherapy and immunotherapy remains an unsolved problem in clinical practice.

As regarded, timing between radiotherapy and immunotherapy as well as the fractionations are important considerations. Studies have shown that the timing of radiotherapy combined with ICIs depends on different types of tumors and ICIs (Young et al., 2016; Lesueur et al., 2018). Therefore, there is controversy about the optimal timepoints of ICIs and radiotherapy. Most studies have revealed that the comprehensive immune effect is positive and $CD8^+$ T cells play a vital role in HFRT and SBRT (Reits et al., 2006; Lee et al., 2009). $CD8^+$ T cells residing in tumors are mainly a group of high proliferation capability and exhausted function, which cannot effectively kill tumor cells (Li et al., 2019; Sanmamed et al., 2021). After HFRT, $CD8^+$ T cells in peripheral blood migrate to tumors, kill tumor cells, and further activate DCs, thereby turning "cold" tumors into "hot" tumors. The effect of PD-1 inhibitors depends on the intratumoral infiltration of $CD8^+$ T cells derived from peripheral blood (Huang et al., 2017; Yost et al., 2019). In this study, we found that immune cells, especially $CD8^+$ T cells, in mice tumor tissues and peripheral blood showed a time-dependent dynamic change after radiotherapy. $CD8^+$ T counts increased from 48 h to 3 weeks in 4.6 Gy × 3 F and 6.2 Gy × 2 F, and $CD8^+$ PD-1 shortly increased from 48 h to 2 weeks in 6.2 Gy ×

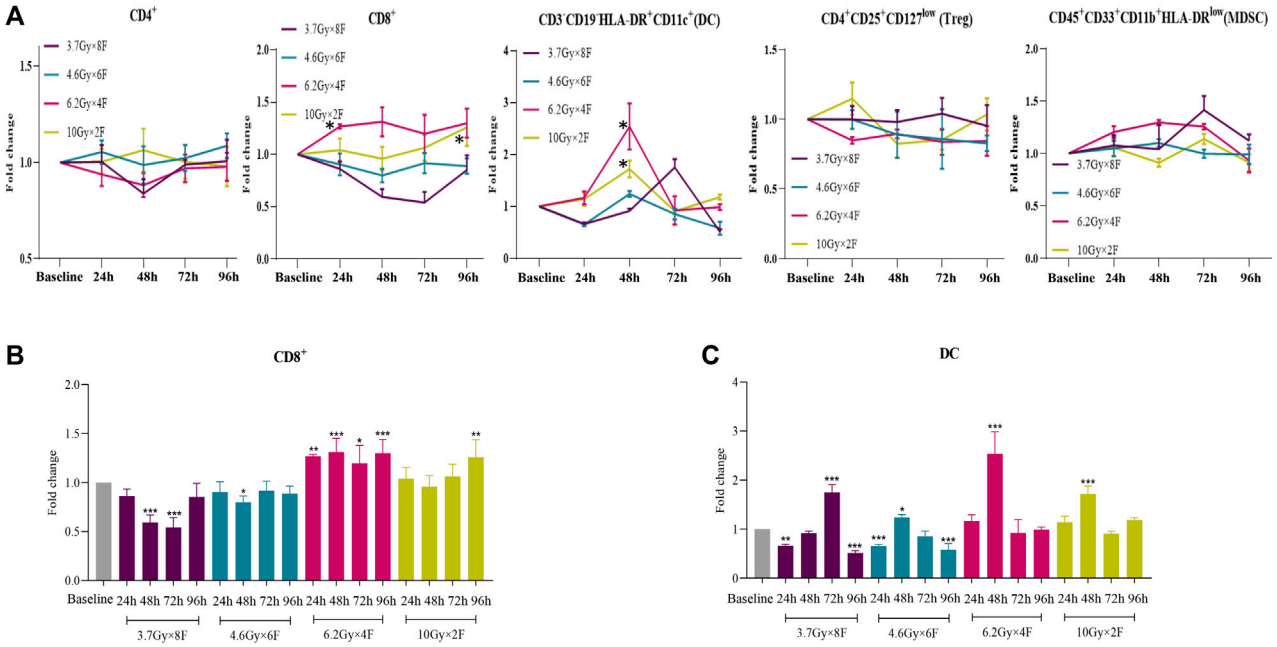

FIGURE 5 | Dynamic changes of different immune cells after radiotherapy in peripheral blood of NSCLC patients. **(A)** Trends of $CD4^+$ T cells, $CD8^+$ T cells, DC, Treg, and MDSC after 4 different fractionation radiotherapies. * The dose in which trend was significant and the time at which difference began. **(B)** Changes of $CD8^+$ T cells at different timepoints after radiotherapy, respectively. **(C)** Changes of DC at different timepoints after radiotherapy.*$p < 0.05$,**$p < 0.01$, ***$p < 0.001$, compared with baseline.

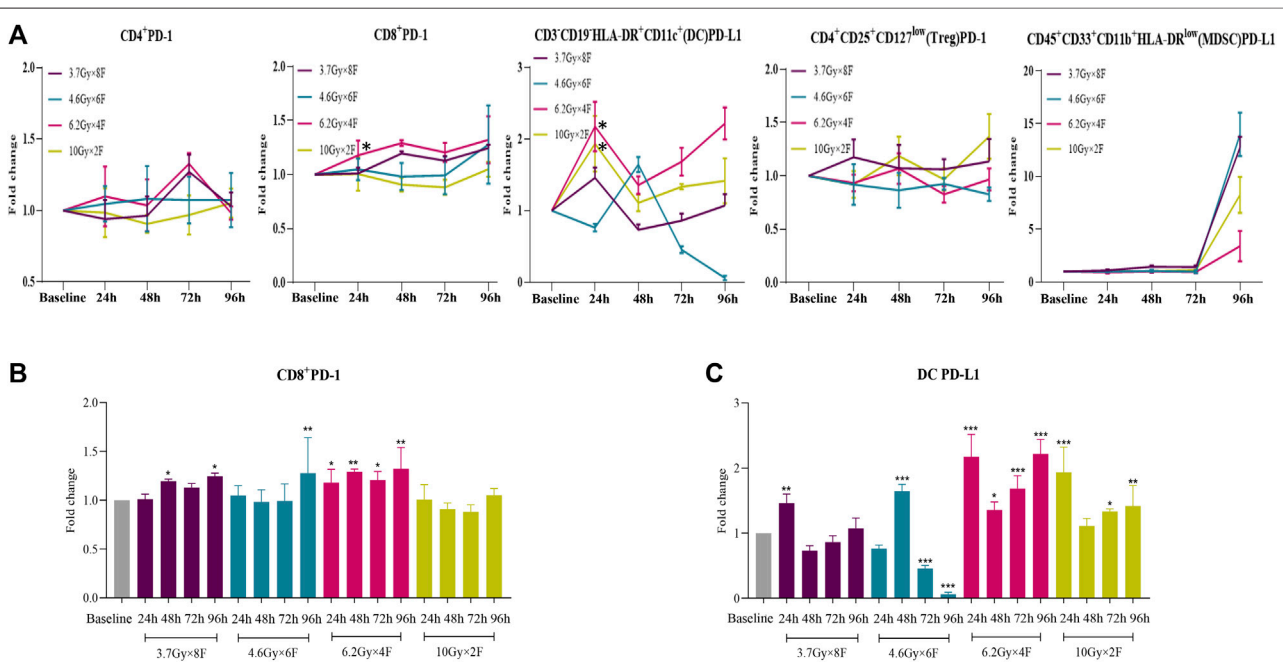

FIGURE 6 | Dynamic changes of PD-1 and PD-L1 expression after radiotherapy in peripheral blood of NSCLC patients. **(A)** Trends of $CD4^+$ PD-1, $CD8^+$ PD-1, DC PD-L1, Treg PD-1, and MDSC PD-L1 after 4 different fractionation radiotherapies. * The dose in which trend was significant and the time at which difference began. **(B)** Discrepancy of $CD8^+$ PD-1 at different timepoints after radiotherapy, respectively. **(C)** Discrepancy of DC PD-L1 at different timepoints after radiotherapy.*$p < 0.05$,**$p < 0.01$, ***$p < 0.001$, compared with baseline.

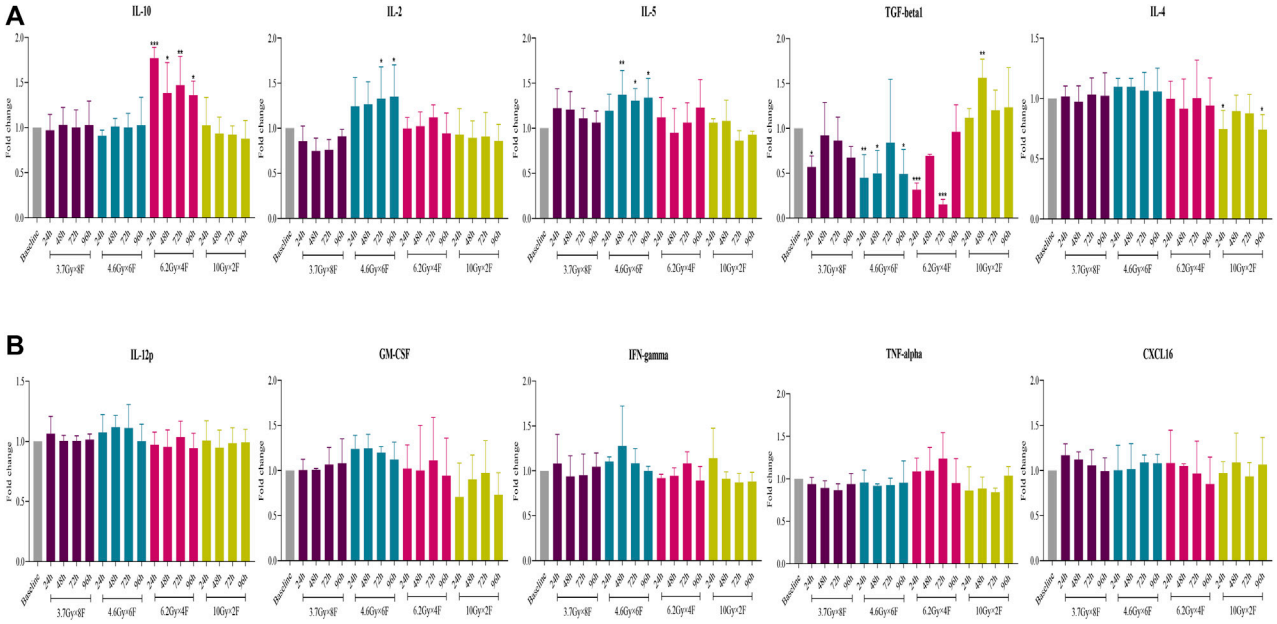

FIGURE 7 | Changes of cytokine expression after radiotherapy in peripheral blood of NSCLC patients. **(A)** Expression of IL-10, IL-2, IL-5, TGF-β1, and IL-4 had different changes after 4 fractionation radiotherapies. **(B)** No significant change on IL-12p, GM-CSF, IFN-γ, TNF-α, and CXCL16 between pre and post-radiotherapy. $^{*}p < 0.05$, $^{**}p < 0.01$, $^{***}p < 0.001$, compared with baseline.

2 F and 10 Gy × 1 F. These results indicate that 48 h after HFRT may be a critical timepoint for immune response. Then we selected the timepoint of 48 h to verify in mouse tumor tissue and found that $CD8^+$ T cells were not increased yet, indicating that the immune system has been activated in blood within 48 h after radiotherapy, earlier than in tumor tissue, which was consistent with the research by Matsumura (Matsumura et al., 2008). Besides, in peripheral blood of NSCLC patients, $CD8^+$ T cells and $CD8^+$ PD-1 were increased significantly from 24 to 96 h after radiotherapy. Furthermore, DC cells began to be significantly increased and continued to rise until 3 weeks in mice, and there was a similar trend in NSCLC patients before 96 h. DC PD-L1 showed a high level from 24 to 96 h in patients. On the other hand, MDSCs, which were regarded as suppressors of the immune cell response, increased from 2 weeks and continued to rise until 3 weeks in mouse peripheral blood. Besides, we also compared the ratio of $CD4^+$/Treg and $CD8^+$/Treg, respectively. All the ratios were consistent with the cell counts.

Collectively, the rule of changes in our study suggests that intratumoral infiltrating T cells being induced after local radiotherapy may be derived from the mobilization and chemotaxis of the systemic immune system. We speculate that $CD8^+$ T cells are mobilized fully in the peripheral blood from 48 h to 2 weeks after radiotherapy, preferentially recruited and activated into tumor tissue; in that period, the efficacy of radiotherapy will be enhanced when combined with ICIs. This result is consistent with the PACIFIC study in which the timing of intervention ICIs is within 14 days. Most studies have shown that early interventional immunotherapy after radiotherapy has better efficacy (Shaverdian et al., 2017; Aggarwal et al., 2019; Theelen et al., 2019), and only a retrospective study reported at the 2019 ASCO meeting showed that immunotherapy given at 3 weeks after SBRT has better OS (Wegner et al., 2019). Using evidence-based medicine, the subgroup analysis of randomized controlled studies is more reliable than that of retrospective analysis. Therefore, it is possible that a shorter interval of immunotherapy after radiotherapy leads to better effect. However, due to the high single dose of SBRT or HFRT, synchronization immunotherapy or premature use of ICIs after radiotherapy may cause an increase in side effects. Our results are generally consistent with previous research, but differ slightly in the specific timepoints. We speculate that the difference may be due to race, number of cases, type of ICIs, and fractionation dose. In future, the optimal timepoints for combining radiotherapy with immunotherapy need further study.

When radiotherapy is combined with ICIs, the fractionation dose is another key factor for optimal outcome. Dewan et al. (Dewan et al., 2009) used the TSA breast cancer cell model and the MCA38 colorectal cancer model and found that when combined with CLTA-4 inhibitors, 8 Gy × 3F was significantly better than 6 Gy × 5 F or 12 Gy × 1 F regardless of local tumor control or abscopal immune response, suggesting that different fractionations also have different effects on the cancer therapy when combined with ICIs. In this study, the tumor volume was significantly reduced after radiotherapy with 4 different fractionations of the same BED. Moreover, the longer survival time appeared after radiotherapy of 6.2 Gy × 2 F. A clinical trial in the United Kingdom demonstrated the similar results that different fractionation doses with similar BED could cause different efficacy and prognosis of tumors (The et al., 2008). On the other hand, we found that $CD8^+$ T cells were significantly increased in 6.2 Gy × 2 F, along with $CD8^+$ PD-1 being increased

in 6.2 Gy × 2 F fractionation in the peripheral blood of mice. In peripheral blood of NSCLC patients, $CD8^+$ T cells and $CD8^+$ PD-1 maintained a high level in 6.2 Gy × 4 F, and $CD8^+$ T cells also increased in 10 Gy × 2 F. Besides, DC cells began to be significantly increased after radiotherapy in all fractionations in mice. In peripheral blood of NSCLC patients, we discovered that DC cells significantly increased and hit a small peak in 6.2 Gy × 4 F and 10 Gy × 2 F and then gradually returned to the baseline level, being accompanied by a high expression of DC PD-L1 in 6.2 Gy × 4 F and 10 Gy × 2 F.

Chen et al. (Welsh et al., 2020a) conducted a phase I/II randomized clinical trial comparing the efficacy of paprizumab alone versus combination with conventional fractionated radiotherapy (45Gy/15F) or SBRT (50Gy/4F) in the treatment of advanced NSCLC. The mPFS of the paprizumab + SBRT group was significantly better than that of the paprizumab + conventionally fractionated radiotherapy group (9.1 months vs. 5.1 months). In addition, Baas et al. (Welsh et al., 2020b) analyzed pembro-RT and MDACC studies and found that the combination of pabulizumab with ablative radiotherapy (24Gy/3F and 50Gy/4F) had a better ORR than non-ablative radiotherapy (45Gy/15F) and the pabulizumab alone group. Therefore, in terms of fractionation dose, studies tend to support SBRT or HFRT combined with immunotherapy, which can enhance the antitumor effect more than conventional fractionated radiotherapy. Here, we demonstrate that 6.2 and 10 Gy would be better doses of HFRT, which will produce an optimal immunoactivated status from 48 h after radiotherapy and the immune synergistic effect may be maximized when combined with ICIs. At these doses, both numbers and PD-1 expression of positive immune cells increase in TIME, which will be beneficial for ICIs in NSCLC. There is a reminder that the best timing of immune intervention could be 96 h later under 10 Gy fractionation, especially in two but not single doses.

Due to the limit of tail vein blood in each mouse, we detected the immune cells in tumor tissues instead of cytokines. Likewise, we detected cytokines in NSCLC patients instead of immune cells in tumor tissues. Interleukin-10 (IL-10) was discovered as an anti-inflammatory factor. However, increasing evidence revealed IL-10 can induce antitumor effects in an immune-dependent manner, which indicates that it also plays a bidirectional role in immune regulation of tumors (Sato et al., 2011). Studies have demonstrated that effector T cells were the main source of IL-10, and IL-10 can promote $CD8^+$ T cell responses by binding to IL-10 receptor (Fujii et al., 2001; Wilke et al., 2011). Besides, Qiao (Qiao et al., 2019) generated a Cetuximab-based IL-10 fusion protein (CmAb-(IL10)2) and found that it could prevent $CD8^+$ tumor-infiltrating lymphocyte apoptosis, further revealing that IL-10 could potentiate $CD8^+$ T cell-mediated antitumor immunity. In this study, IL-10 was increased significantly from 24 to 96 h, when the number of $CD8^+$ T cells and $CD8^+$ PD-1 expression were also increased after 6.2G×4F radiotherapy in human peripheral blood. The result revealed that HFRT can induce $CD8^+$ T cells to produce IL-10, which enhances the proliferation, differentiation, activity, and function of $CD8^+$ T cells, especially in 6.2 Gy. In the TGF family, TGF-β1 is the most widely distributed in the immune system, and with the development of tumors, it can continuously promote the invasion, metastasis, and deterioration. Marie confirmed that TGF-β1 mainly plays a role in Tregs induction by regulating Foxp3 positive expression in Tregs (Marie et al., 2005). Furthermore, convincing evidence has verified that IL-4 directly acts on $CD8^+$ T cells, reduces or even eliminates its cytotoxicity, and promotes the infiltration of Treg into tumors, thus establishing the immunosuppressive state and promoting tumor growth by avoiding the recognition of the immune system (Wynn, 2003). Here, we found that TGF-β1 decreased significantly in 3.7 Gy × 8 F, 4.6 Gy × 6 F, and 6.2 Gy × 4 F and that IL-4 decreased in 10 Gy × 2 F after radiotherapy, revealing that HFRT also achieves antitumor immunity by reducing TGF-β1 and IL-4, thus contributing to regulating Tregs and $CD8^+$ T cell function in TIME. Besides, IL-2 and IL-5, which are regarded as positive immune regulators, are also found to increase significantly in 4.6 Gy × 6 F. Therefore, we find different cytokines change in different fractionations and speculate that the immune effect of different fractionation radiotherapies may be related to different target cytokines and induce an immune activation state after HFRT.

In the part of clinical data, we provided the bOR, mPFS, and mOS. However, there are many impact factors in this clinical practice, such as the baseline of patients, the number of treatment lines, and the different duration of immunotherapy. We do not think the efficacy and survival for the patients with or without immunotherapy are important results. Moreover, most of the clinical cases who received immunotherapy were not in the time window of 48 h to 2 weeks because we did not have any conclusion before this work.

To the best of our knowledge, this study is the first to prove the positive comprehensive immune effect on the timing and fractionation dose of HFRT. $CD8^+$ T cells are the most important indicator of TIME, so we took $CD8^+$ T cells as the main effector cells to judge the immune response. $CD8^+$ T increased after HFRT both in peripheral blood of NSCLC patients and mouse models, revealing that HFRT can induce a positive immune response which may be beneficial for ICIs. Comprehensively considering the results of $CD8^+$ T cells, DC cells, and cytokines, 3.7 and 4.6Gy are not recommended as the preferred fractionations compared with 6.2 and 10Gy. However, this is just our preliminary result. We are designing another animal experiment and prospective study based on our current findings and carry out clinical trials with larger samples for verification in the future.

In spite of the major strength of validating the changes of TIME after HFRT in both animal and human experiments, this study still has several limitations. First, taking into account clinical treatment efficacy, we adopted different fractionation doses between mouse and human. Second, we only choose LLC cells to establish the implanted mice model because it is not suitable to use xenografts derived from human cancer cells in immunodeficient mice to explore the immune microenvironment. Third, there were some other combination treatments during radiotherapy in different groups in patients. Finally, we did not perform cell isolation

to detect cytokine secretion in tumor tissue and cell killing experiments *in vitro*.

CONCLUSION

In summary, HFRT induces the increase in $CD8^+$ T cells and positive immune cytokine response in specific periods and fractionation doses. It was the optimal time window from 48 h to 2 weeks for immune response, especially in 6.2 Gy fractionation. The best immune response was 96 h later in 10 Gy fractionation, delivered twice instead of a single dose. During this time window, the intervention of immunotherapy may achieve a better effect. Future work should include exploration of the relationship between radiotherapy and TIME deeply.

DATA AVAILABILITY STATEMENT

The original contributions presented in the study are included in the article/Supplementary Material; further inquiries can be directed to the corresponding author.

ETHICS STATEMENT

This study was registered in the Clinical Trials Register (NCT03073902, https://clinicaltrials.gov/). The patients/participants provided their written informed consent to participate in this study. A total of 60 C57BL/6 male mice (6–8 weeks old) were obtained from the animal center of our hospital (No. SYXK 2012–0011). All animal procedures were performed with the approval of the Laboratory Animal Welfare and Ethics Committee of Army Medical University (Chongqing, China).

AUTHOR CONTRIBUTIONS

XZ, JL, and LZ carried out the experiments. XZ, JL, and YY analyzed the data. QY, XC, and XC conceived and designed the experiments. JL, FL, and JC drafted the manuscript. All authors have read and approved the final manuscript.

FUNDING

This study was supported by the National Natural Science Foundation of China (grant numbers: 81602688, 81773245, 82172670, and 81972858), the Chongqing Innovation Leading Talents Program (cstccxljrc201910), and the Cultivation Program for Clinical Research Talents of Army Medical University in 2018 (2018XLC1010).

ACKNOWLEDGMENTS

The authors thank all the patients for providing their samples and clinical data.

REFERENCES

Aggarwal, C., Thompson, J. C., Black, T. A., Katz, S. I., Fan, R., Yee, S. S., et al. (2019). Clinical Implications of Plasma-Based Genotyping With the Delivery of Personalized Therapy in Metastatic Non-Small Cell Lung Cancer. *JAMA Oncol.* 5 (2), 173–180. doi:10.1001/jamaoncol.2018.4305

Antonia, S. J., Villegas, A., Daniel, D., Vicente, D., Murakami, S., Hui, R., et al. (2018). Overall Survival With Durvalumab after Chemoradiotherapy in Stage III NSCLC. *N. Engl. J. Med.* 379 (24), 2342–2350. doi:10.1016/j.jtho.2018.08.010

Barker, H. E., Paget, J. T. E., Khan, A. A., and Harrington, K. J. (2015). The Tumour Microenvironment after Radiotherapy: Mechanisms of Resistance and Recurrence. *Nat. Rev. Cancer* 15 (7), 409–425. doi:10.1038/nrc3958

Chicas-Sett, R., Morales-Orue, I., Castilla-Martinez, J., Zafra-Martin, J., Kannemann, A., Blanco, J., et al. (2019). Stereotactic Ablative Radiotherapy Combined with Immune Checkpoint Inhibitors Reboots the Immune Response Assisted by Immunotherapy in Metastatic Lung Cancer: A Systematic Review. *Int J Mol Sci* 20 (9), 2173. doi:10.3390/ijms20092173

Demaria, S., Golden, E. B., and Formenti, S. C. (2015). Role of Local Radiation Therapy in Cancer Immunotherapy. *JAMA Oncol.* 1, 1325–1332. doi:10.1001/jamaoncol.2015.2756

Dewan, M. Z., Galloway, A. E., Kawashima, N., Dewyngaert, J. K., Babb, J. S., Formenti, S. C., et al. (2009). Fractionated but Not Single-Dose Radiotherapy Induces an Immune-Mediated Abscopal Effect when Combined with Anti-CTLA-4 Antibody. *Clin. Cancer Res.* 15, 5379–5388. doi:10.1158/1078-0432.CCR-09-0265

Dovedi, S. J., Illidge, T. M., Grazyna, L. B., Conor, M., Sherrie, J., Eleanor, C., et al. (2015). The Antitumor Immune Response Generated by Fractionated Radiation Therapy May Be Limited by Tumor Cell Adaptive Resistance and Can Be Circumvented by PD-L1 Blockade. *Oncoimmunology* 4 (7), e1016709. doi:10.1080/2162402X.2015.1016709

Formenti, S. C., and Demaria, S. (2013). Combining Radiotherapy and Cancer Immunotherapy: a Paradigm Shift. *J. Natl. Cancer Inst.* 105, 256–265. doi:10.1093/jnci/djs629

Formenti, S. C., Rudqvist, N.-P., Golden, E., Cooper, B., Wennerberg, E., Lhuillier, C., et al. (2018). Radiotherapy Induces Responses of Lung Cancer to CTLA-4 Blockade. *Nat. Med.* 24, 1845–1851. doi:10.1038/s41591-018-0232-2

Fujii, S.-i., Shimizu, K., Shimizu, T., and Lotze, M. T. (2001). Interleukin-10 Promotes the Maintenance of Antitumor CD8+ T-Cell Effector Function *In Situ*. *Blood* 98 (7), 2143–2151. doi:10.1182/blood.V98.7.2143

Galluzzi, L., Buque, A., Kepp, O., Zitvogel, L., and Kroemer, G. (2017). Immunogenic Cell Death in Cancer and Infectious Disease. *Nat. Rev. Immunol.* 17 (2), 97–e1792. doi:10.1038/nri.2016.107

Huang, A. C., Postow, M. A., Orlowski, R. J., Mick, R., Bengsch, B., Manne, S., et al. (2017). T-cell Invigoration to Tumour burden Ratio Associated with Anti-PD-1 Response. *Nature* 545 (7652), 60–65. doi:10.1038/nature22079

Jiang, Y., Li, Y., and Zhu, B. (2015). T-cell Exhaustion in the Tumor Microenvironment. *Cell Death Dis* 6 (6), e1792. doi:10.1038/cddis.2015.162

Lee, Y., Auh, S. L., Wang, Y., Burnette, B., Wang, Y., Meng, Y., et al. (2009). Therapeutic Effects of Ablative Radiation on Local Tumor Require CD8+ T Cells: Changing Strategies for Cancer Treatment. *Blood* 114 (3), 589–595. doi:10.1182/blood-2009-02-206870

Lesueur, P., Escande, A., Thariat, J., Vauléon, E., Monnet, I., Cortot, A., et al. (2018). Safety of Combined PD-1 Pathway Inhibition and Radiation Therapy for Non-small-cell Lung Cancer: A Multicentric Retrospective Study from the GFPC. *Cancer Med.* 7 (11), 5505–5513. doi:10.1002/cam4.1825

Li, H., van der Leun, A. M., Yofe, I., Lubling, Y., Gelbard-Solodkin, D., van Akkooi, A. C. J., et al. (2019). Dysfunctional CD8 T Cells Form a Proliferative,

Dynamically Regulated Compartment within Human Melanoma. *Cell* 176 (4), 775–789. doi:10.1016/j.cell.2018.11.043

Lugade, A. A., Sorensen, E. W., Gerber, S. A., Moran, J. P., Frelinger, J. G., and Lord, E. M. (2008). Radiation-Induced IFN-γ Production within the Tumor Microenvironment Influences Antitumor Immunity Radiation-Induced IFN-Gamma Production within the Tumor Microenvironment Influences Antitumor Immunity. *J. Immunol.* 180 (5), 3132–3139. doi:10.4049/jimmunol.180.5.3132

Marie, J. C., Letterio, J. J., Gavin, M., and Rudensky, A. Y. (2005). TGF-β1 Maintains Suppressor Function and Foxp3 Expression in CD4+CD25+ Regulatory T Cells. *J. Exp. Med.* 201 (7), 1061–1067. doi:10.1084/jem.20042276

Mathieu, M., Nepali, P. R., Budhu, S., Powell, S. N., Humm, J., Deasy, J. O., et al. (2021). Activation of Sting in Response to Partial-Tumor Radiation Exposure. *Oral Scientific Session Abstr.* 111 (3), S69. doi:10.1016/j.ijrobp.2021.07.171

Matsumura, S., Wang, B., Kawashima, N., Braunstein, S., Badura, M., Cameron, T. O., et al. (2008). Radiation-induced CXCL16 Release by Breast Cancer Cells Attracts Effector T Cells. *J. Immunol.* 181 (5), 3099–3107. doi:10.4049/jimmunol.181.5.3099

Ostrand-Rosenberg, S., and Sinha, P. (2009). Myeloid-derived Suppressor Cells: Linking Inflammation and Cancer. *J. Immunol.* 182 (8), 4499–4506. doi:10.4049/jimmunol.0802740

Qiao, J., Liu, Z., Dong, C., Luan, Y., Zhang, A., Moore, C., et al. (2019). Targeting Tumors with IL-10 Prevents Dendritic Cell-Mediated CD8+ T Cell Apoptosis. *Cancer Cell* 35, 901–915. doi:10.1016/j.ccell.2019.05.005

Reits, E. A., Hodge, J. W., Herberts, C. A., Groothuis, T. A., Chakraborty, M., Neefjes, K., et al. (2006). Radiation Modulates the Peptide Repertoire, Enhances MHC Class I Expression, and Induces Successful Antitumor Immunotherapy. *J. Exp. Med.* 203 (5), 1259–1271. doi:10.1084/jem.20052494

Sanmamed, M. F., Nie, X., Desai, S. S., Villaroel-Espindola, F., Badri, T., Zhao, D., et al. (2021). A Burned-Out CD8+ T-Cell Subset Expands in the Tumor Microenvironment and Curbs Cancer Immunotherapy. *Cancer Discov.* 11, 1700–1715. doi:10.1158/2159-8290.CD-20-0962

Sato, T., Terai, M., Tamura, Y., Alexeev, V., Mastrangelo, M. J., and Selvan, S. R. (2011). Interleukin 10 in the Tumor Microenvironment: a Target for Anticancer Immunotherapy. *Immunol. Res.* 51 (2/3), 170–182. doi:10.1007/s12026-011-8262-6

Schapira, E., Hubbeling, H., Yeap, B. Y., Mehan, W. A., Shaw, A. T., Oh, K., et al. (2018). Improved Overall Survival and Locoregional Disease Control with Concurrent PD-1 Pathway Inhibitors and Stereotactic Radiosurgery for Lung Cancer Patients with Brain Metastases. *Int. J. Radiat. Oncology*Biology*Physics* 101 (3), 624–629. doi:10.1016/j.ijrobp.2018.02.175

Schaue, D., and Mcbride, W. H. (2015). Opportunities and Challenges of Radiotherapy for Treating Cancer. *Nat. Rev. Clin. Oncol.* 12 (9), 527–540. doi:10.1038/nrclinonc.2015.120

Schaue, D., Ratikan, J. A., Iwamoto, K. S., and Mcbride, W. H. (2012). Maximizing Tumor Immunity with Fractionated Radiation. *Int. J. Radiat. Oncology*Biology*Physics* 83 (4), 1306–1310. doi:10.1016/j.ijrobp.2011.09.049

Shaverdian, N., Lisberg, A. E., Bornazyan, K., Veruttipong, D., Goldman, J. W., Formenti, S. C., et al. (2017). Previous Radiotherapy and the Clinical Activity and Toxicity of Pembrolizumab in the Treatment of Non-small-cell Lung Cancer: A Secondary Analysis of the KEYNOTE-001 Phase 1 Trial. *Lancet Oncol.* 18 (7), 895–903. doi:10.1016/S1470-2045(17)30380-7

The, S. T. G., Bentzen, S. M., Agrawal, R. K., Aird, E. G., Barrett, J. M., Barrett-Lee, P. J., et al. (2008). The UK Standardisation of Breast Radiotherapy (START) Trial A of Radiotherapy Hypofractionation for Treatment of Early Breast Cancer: a Randomised Trial. *Lancet Oncol.* 9 (4), 331–341. doi:10.1016/s1470-2045(08)70077-9

Theelen, W. S. M. E., Peulen, H. M. U., Lalezari, F., van der Noort, V., de Vries, J. F., Aerts, J. G. J. V., et al. (2019). Effect of Pembrolizumab after Stereotactic Body Radiotherapy vs Pembrolizumab Alone on Tumor Response in Patients With Advanced Non-Small Cell Lung Cancer. *JAMA Oncol.* 5 (9), 1276–1282. doi:10.1001/jamaoncol.2019.1478

Timke, C., Zieher, H., Roth, A., Hauser, K., Lipson, K. E., Weber, K. J., et al. (2008). Combination of Vascular Endothelial Growth Factor Receptor/platelet-Derived Growth Factor Receptor Inhibition Markedly Improves Radiation Tumor Therapy. *Clin. Cancer Res.* 14, 2210–2219. doi:10.1158/1078-0432.CCR-07-1893

Verbrugge, I., Hagekyriakou, J., Sharp, L. L., Galli, M., West, A., Mclaughlin, N. M., et al. (2012). Radiotherapy Increases the Permissiveness of Established Mammary Tumors to Rejection by Immunomodulatory Antibodies. *Cancer Res.* 72, 3163–3174. doi:10.1158/0008-5472.CAN-12-0210

Wegner, R. E., Abel, S., Hasan, S., White, R., Finley, G. G., Monga, D., et al. (2019). Time from Stereotactic Body Radiotherapy to Immunotherapy as a Predictor for Outcome in Metastatic Non Small Cell Lung Cancer. *Jco* 37 (15), 9024. doi:10.1200/JCO.2019.37.15_suppl.9024

Welsh, J., Menon, H., Chen, D., Verma, V., Tang, C., Altan, M., et al. (2020). Pembrolizumab with or without Radiation Therapy for Metastatic Non-small Cell Lung Cancer: a Randomized Phase I/II Trial. *J. Immunother. Cancer* 8 (2), e001001. doi:10.1136/jitc-2020-001001

Welsh, J. W., Chen, D., Baas, P., Chang, J. Y., Verma, V., Comeaux, N., et al. (2020). Radiotherapy to Augment Pembrolizumab Responses and Outcomes in Metastatic Non-small Cell Lung Cancer: Pooled Analysis of Two Randomized Trials. *Jco* 38, 9548. doi:10.1200/jco.2020.38.15_suppl.9548

Wilke, C. M., Wei, S., Wang, L., Kryczek, I., Kao, J., and Zou, W. (2011). Dual Biological Effects of the Cytokines Interleukin-10 and Interferon-γ. *Cancer Immunol. Immunother.* 60 (11), 1529–1541. doi:10.1007/s00262-011-1104-5

Wynn, T. A. (2003). IL-13 Effector Functions. *Annu. Rev. Immunol.* 21 (21), 425–456. doi:10.1146/annurev.immunol.21.120601.141142

Yost, K. E., Satpathy, A. T., Wells, D. K., Qi, Y., Wang, C., Kageyama, R., et al. (2019). Clonal Replacement of Tumor-specific T Cells Following PD-1 Blockade. *Nat. Med.* 25 (8), 1251–1259. doi:10.1038/s41591-019-0522-3

Young, K. H., Baird, J. R., Savage, T., Cottam, B., Friedman, D., Bambina, S., et al. (2016). Optimizing Timing of Immunotherapy Improves Control of Tumors by Hypofractionated Radiation Therapy. *Plos One* 11 (6), e0157164. doi:10.1371/journal.pone.0157164

Zitvogel, L., and Kroemer, G. (2015). Subversion of Anticancer Immunosurveillance by Radiotherapy. *Nat. Immunol.* 16 (10), 1005–1007. doi:10.1038/ni.3236

Conflict of Interest: The authors declare that the research was conducted in the absence of any commercial or financial relationships that could be construed as a potential conflict of interest.

Publisher's Note: All claims expressed in this article are solely those of the authors and do not necessarily represent those of their affiliated organizations, or those of the publisher, the editors, and the reviewers. Any product that may be evaluated in this article, or claim that may be made by its manufacturer, is not guaranteed or endorsed by the publisher.

frontiers in Molecular Biosciences

ORIGINAL RESEARCH
published: 23 February 2022
doi: 10.3389/fmolb.2022.780200

Metformin Combining PD-1 Inhibitor Enhanced Anti-Tumor Efficacy in *STK11* Mutant Lung Cancer Through AXIN-1-Dependent Inhibition of STING Ubiquitination

Zhiguo Wang[1†], Conghua Lu[1†], Kejun Zhang[2†], Caiyu Lin[1], Fang Wu[3], Xiaolin Tang[1], Di Wu[1], Yuanyao Dou[1], Rui Han[1], Yubo Wang[1], Chao Hou[1], Qin Ouyang[4], Mingxia Feng[1], Yong He[1]* and Li Li[1]**

[1]Department of Respiratory Disease, Daping Hospital, Third Military Medical University (Army Medical University), Chongqing, China, [2]Department of Outpatients, Daping Hospital, Third Military Medical University (Army Medical University), Chongqing, China, [3]Department of Oncology, Hunan Key Laboratory of Tumor Models and Individualized Medicine, Hunan Key Laboratory of Early Diagnosis and Precision Therapy in Lung Cancer, The Second Xiangya Hospital, Central South University, Changsha, China, [4]School of Pharmacy, Third Military Medical University (Army Medical University), Chongqing, China

OPEN ACCESS

Edited by:
Na Luo,
Nankai University, China

Reviewed by:
Zhenyu Ding,
Sichuan University, China
Yong Zhang,
Central South University, China
Wenya Li,
The First Affiliated Hospital of China Medical University, China

***Correspondence:**
Mingxia Feng
fmx19810306@tmmu.edu.cn
Yong He
heyong@tmmu.edu.cn
Li Li
dpyyhxlili@tmmu.edu.cn

[†]These authors have contributed equally to this work

Specialty section:
This article was submitted to Molecular Diagnostics and Therapeutics, a section of the journal Frontiers in Molecular Biosciences

Received: 20 September 2021
Accepted: 04 February 2022
Published: 23 February 2022

Citation:
Wang Z, Lu C, Zhang K, Lin C, Wu F, Tang X, Wu D, Dou Y, Han R, Wang Y, Hou C, Ouyang Q, Feng M, He Y and Li L (2022) Metformin Combining PD-1 Inhibitor Enhanced Anti-Tumor Efficacy in STK11 Mutant Lung Cancer Through AXIN-1-Dependent Inhibition of STING Ubiquitination. Front. Mol. Biosci. 9:780200. doi: 10.3389/fmolb.2022.780200

Background: Non-small-cell lung cancer (NSCLC) with *STK11* mutation showed primary resistance to immune checkpoint inhibitors (ICIs). The glucose-lowering drug metformin exerted anti-cancer effect and enhanced efficacy of chemotherapy in NSCLC with *KRAS/STK11* co-mutation, yet it is unknown whether metformin may enhance ICI efficacy in *STK11* mutant NSCLC.

Methods: We studied the impact of metformin on ICI efficacy in *STK11* mutant NSCLC *in vitro* and *in vivo* using colony formation assay, cell viability assay, Ki67 staining, ELISA, CRISPR/Cas9-mediated knockout, and animal experiments.

Results: Through colony formation assay, Ki67 incorporation assay, and CCK-8 assay, we found that metformin significantly enhanced the killing of H460 cells and A549 cells by T cells. In NOD-SCID xenografts, metformin in combination with PD-1 inhibitor pembrolizumab effectively decreased tumor growth and increased infiltration of $CD8^+$ T cells. Metformin enhanced stabilization of STING and activation of its downstream signaling pathway. siRNA-mediated knockdown of *STING* abolished the effect of metformin on T cell-mediated killing of tumor cells. Next, we found that CRISPR/Cas9-mediated knockout of the scaffold protein AXIN-1 abolished the effect of metformin on T cell-mediated killing and STING stabilization. Immunoprecipitation and confocal macroscopy revealed that metformin enhanced the interaction and colocalization between AXIN-1 and STING. Protein-protein interaction modeling indicated that AXIN-1 may directly bind to STING at its K150 site. Next, we found that metformin decreased K48-linked ubiquitination of STING and inhibited the interaction of E3-ligand RNF5 and STING. Moreover, in *AXIN-1*$^{-/-}$ H460 cells, metformin failed to alter the interaction of RNF5 and STING.

Conclusion: Metformin combining PD-1 inhibitor enhanced anti-tumor efficacy in *STK11* mutant lung cancer through inhibition of RNF5-mediated K48-linked ubiquitination of STING, which was dependent on AXIN-1.

Keywords: metformin, lung cancer, STING, AXIN-1, immunotherapy, *STK11*

INTRODUCTION

Lung cancer is the leading cause of cancer-related deaths worldwide, despite the mortality has fallen continuously due to improved treatment (Siegel et al., 2021). Immune checkpoint inhibitors (ICIs), including PD-1/PD-L1 inhibitors, have produced remarkably durable responses in advanced non-small-cell lung cancer (NSCLC) (Qu et al., 2021). However, only a minority of patients achieve durable benefit from ICIs and the landscape of primary resistance to PD-1 blockade is largely unknown. Mutation of *STK11* (Liver Kinase B1-LKB1), a tumor suppressor gene which encodes an evolutionary conserved serine/threonine kinase (Sanchez-Cespedes et al., 2002), has been suggested to be a potential driver of primary resistance to PD-1 blockade (Jure-Kunkel et al., 2018; Skoulidis et al., 2018). Mechanistically, *STK11* mutation leads to LKB1 loss, which then results in the suppression of stimulator of interferon genes (STING) (Kitajima et al., 2019), whose activation is critical for anti-cancer immune response (Su et al., 2019; Zhu et al., 2019). Therefore, activation of STING in *STK11* mutant cancer is a promising approach to convert an immune-resistant, noninflamed tumor into an immune-sensitive, inflamed tumor.

Mounting evidence has suggested that the anti-diabetes drug metformin exerted anti-cancer effect in various cancer types, including lung, prostate, and colon (Kirtonia et al., 2021). Previous studies have found that *STK11* mutation can lead to increased sensitivity of cells to metformin or other inhibitors of mitochondrial respiration by restraining their ability to upregulate glucose uptake and glycolysis (Shackelford et al., 2013; Parker et al., 2017). Indeed, metformin enhanced cisplatin-induced apoptosis in *KRAS/STK11* co-mutated NSCLC (Moro et al., 2018). More recently, metformin can induce STING expression in pancreatic cancer and activate the STING/IRF3/IFN-β pathway by inhibiting AKT signaling in pancreatic ductal adenocarcinoma (Ren et al., 2020). However, it is unknown whether metformin may enhance the efficacy of immunotherapy in *STK11* mutant lung cancer. Therefore, we aim to study whether metformin can enhance T cell-mediated killing of *STK11* mutant lung cancer and the underlying mechanisms.

MATERIALS AND METHODS

Cell Culture and Reagents

The human lung cancer cell lines H460, A549, and 293T cell were purchased from the American Type Culture Collection (ATCC). Human peripheral blood mononuclear cells (PBMC) and human peripheral blood T cells were both from SAILYBIO (Shanghai, China). Cells were cultured in RPMI-1640 (Hyclone) supplemented with 10% fetal bovine serum (FBS, Gibco) and 1% penicillin/streptomycin at 37°C in a humidified 5% CO_2 atmosphere. Metformin and MG132 were from Selleck (TX, United States), and pembrolizumab were from MSD (NJ, United States). Antibodies against STING, TBK1, p-TBK1, IRF3, p-IRF3, CD8 and β-tubulin were purchased from Cell Signaling Technology (MA, United States), and those against RNF5, RNF26, TRIM32, and TRIM56 were from Abcam (Cambridge, United Kingdom), and anti-Flag tag and anti-His tag were from Bioss (Beijing, China).

Generation of Activated T Cells

Activated T cells were acquired as previously reported (Li et al., 2016). Briefly, human peripheral blood T cells were cultured in ImmunoCult-XF T cell expansion medium with ImmunoCult Human CD3/CD28/CD2 T cell activator (both from STEMCELL Technologies, Vancouver, CA, United States) and IL-2 (10 ng/ml; PeproTech, NJ, United States) for 1 week according to the manufacturer's protocol. All experiments were performed in DMEM/F12 medium with anti-CD3 antibody (100 ng/ml; eBioscience, Thermo Scientific, MA, United States) and IL-2 (10 ng/ml).

Colony Formation Assay

Cancer cells were incubated with activated T cells for 48 h with or without metformin. The ratios between cancer cells and activated T cells were set as 1:1. T cells and cell debris were removed by PBS wash, and cancer cells were left to grow for 2 weeks and then the colonies were subjected to crystal violet staining.

Cell Viability Assay

Cell viability was determined by cell counting kit-8 (CCK8; MedChemExpress, NJ, United States) according to the operation manual. Briefly, cells were seeded in a 96-well plate at a density of 3×10^3 per well and cultured overnight. On the next day the medium was refreshed with the indicated doses of drug-containing medium and cultured for another 48 h. Then the medium was refreshed and absorbances were measured at 450 nm on a Sunrise R microplate reader (Thermo Fisher Scientific, Germany).

Ki67 Staining

Cell proliferation was assessed by the Ki67 incorporation assay with a Ki67 labeling and detection kit (Boster, Wuhan, China). Briefly, cells were seeded in six-well plates (3×10^5) and treated as indicated for 48 h. Then cells were fixed and incubated overnight with Ki67 (1:200 dilution). Cells were counterstained with 4′, 6-diamidino-2-phenylindole (DAPI) for 15 min and observed under a fluorescence microscope.

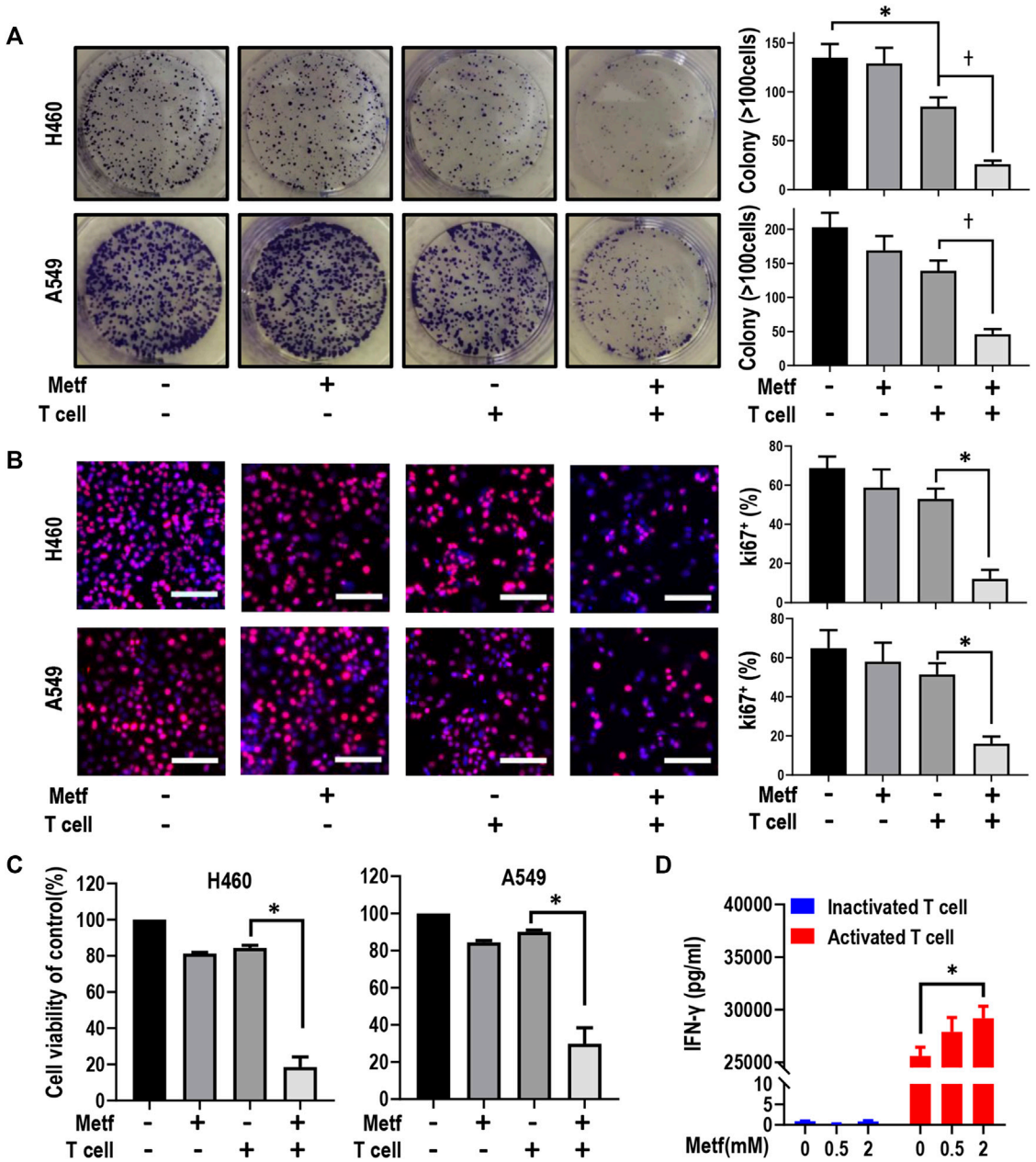

FIGURE 1 | Metformin enhanced T cell-mediated killing of lung cancer H460 and A549 cells. **(A)**, H460 cells and A549 cells were co-cultured with activated T cells (cancer cells to T cells ratio, 1:1) for 48 h with or without metformin (0.5 mM). Cell colonies were visualized by crystal violet staining. *$p < 0.05$; †$p < 0.01$. **(B)**, Ki67 incorporation assay on H460 cells and A549 cells treated as indicated. Activated T cells (1:1 ratio to cancer cells) or metformin (0.5 mM) were added to the culture medium for 48 h. Cells were then counterstained with DAPI. Data represent mean ± SEM. *$p < 0.01$. Scale bars: 100 μm. **(C)**, Cell viability CCK-8 assay for cells treated with metformin (0.5 mM), or activated T cells (1:1 ratio to cancer cells), or the combination. Data are shown as mean ± SEM of triplicate determinations. *$p < 0.01$. **(D)**, ELISA analysis of the protein expression level of IFN-γ in inactivated or activated T cells with the treatment with metformin (0 mM, 0.5 mM, or 2 mM, respectively) for 24 h. Data presented as the mean ± SEM of three independent experiments. *$p < 0.05$.

Enzyme-Linked Immunosorbent Assay

IFN-γ levels were measured by ELISA assay (Solarbio, Beijing, China). Briefly, the conditioned medium from human peripheral blood T cells of different groups was collected and assayed according to the manufacturer's instructions. Values represent the average of three replicates from at least three independent experiments.

siRNA Transfection

Small interfering RNAs (siRNAs) were synthesized by RiboBio Co., Ltd. (Guangzhou, China). For the evaluation of efficacy, H460 cells cultured in 6-well plates were transfected with either 100 pmol siRNA (sequences: CTGGCATGGTCATATTACA; ACAGCAACAGCATCTATGA; GGATTCGAACTTACAATC

A) or negative control siRNA (siNC) using Lipofectamine RNAiMAX (Thermo Fisher Scientific, MA, United States), following the manufacturer's instructions. At 72 h post-transfection, knockdown efficiency was determined by examining endogenous protein expression by Western blot.

Establishment of PBMCs-CDX Mouse Model (Cell-Derived Xenograft)

Animal experiments were approved by the ethics committee on animal experimentation of the Army Medical University. To establish PBMCs-CDX mouse model (Lin et al., 2018), H460 cells (5×10^5) were injected into the hind flanks of 6-8-week-old female NOD-SCID BALB/c mice. The mice were subjected to tumor growth monitoring, and tumor volumes were calculated from caliper measurements using the following formula: (length × width^2)/2. When tumors reached 80–100 mm^3 in volume, 5×10^6 human PBMCs were intravenously transplanted. PD-1 inhibitor (Pembrolizumab, 25 mg/kg) was injected every 3 days intraperitoneally. Metformin (1 mg/ml) was dissolved in drinking water and given to mice orally. Tumor growth was monitored every 3 days. Cohorts were sacrificed when control mice tumors reached 15 mm in any direction measured. The levels of serum Aspartate aminotransferase (AST), Alanine aminotransferase (ALT), Urea and Creatinine were analyzed using the Beckman Coulter AU5821 auto-Chemistry System (CA, United States). Tumors were harvested, fixed with 4% paraformaldehyde, and embedded in paraffin. The infiltration of $CD8^+$ T cells were stained with immunohistochemistry (IHC) and the expression of STING was determined by immunofluorescence staining according to the manufacturers' instructions.

CRISPR/Cas9-Mediated Knockout of *AXIN-1* and Construction of AXIN1 Expression

To generate *AXIN-1*$^{-/-}$ cell lines, CRISPR/Cas9 gene editing technology was utilized as reported (Moser et al., 2021) Two independent sgRNAs targeting *AXIN-1* were designed using the online tool from Zhang lab (http://crispr.mit.edu; sg *AXIN-1* -1: TTCTGAGGGAGTCTTCCGGG; sg *AXIN-1* -2: GGATCCGTA AGCAGCACCGC). The sgRNAs were incorporated into the plentiCRISPR v2-Blast (Plasmid #83480, Addgene) construct to generate lentivirus. After transfection, single-cell isolation, and expansion, *AXIN-1*$^{-/-}$ and control cell lines were obtained and confirmed using both genome sequencing and Western blot analysis. To generate cell lines overexpressing AXIN1, the human *AXIN-1* cDNA sequence (Genebank accession number: NM_003502) was searched for suitable target sequences. LentiCRISPRv2-AXIN1-2 was designed and generated by Sino Biological (Suzhou, China). The transfection efficiency was determined by examining endogenous protein expression by Western blot.

Western Blot and Immunoprecipitation

Western blot was performed as previously described (Li et al., 2019a). Briefly, cells were harvested from 6-well plates after washing with PBS and lysed for 30 min at 4°C in RIPA lysis buffer (Sigma-Aldrich, France) added with 1% protease and phosphatase inhibitors. The quantitative analysis of protein was determined by the BCA protein assay kit after centrifugation at 12,000 *g* for 20 min at 4°C. Equal amounts of protein were loaded to SDS-PAGE gels and then transferred to polyvinylidene difluoride (PVDF) membranes (Millipore, German), which were then blocked with 5% non-fat milk in TBST for at least 1 h at room temperature and incubated with primary antibodies overnight at 4°C. Then the membranes were washed with TBST, and incubated with horseradish peroxidase-conjugated goat anti-rabbit or anti-mouse IgG (Cell Signaling Technology, USA) for 1 h. After that, the membranes were imaged with ChemiDoc Touch System (Bio-Rad, USA).

The immunoprecipitation experiment was performed according to the manufacturer's instructions. Cell lysates were incubated with respective antibodies (1:50) overnight, followed by adding the protein A/G beads and incubated overnight at 4°C. Then, the immunoprecipitates were washed 3 times and levels of total proteins were analyzed by western blot as described.

IP-Mediated Endogenous Ubiquitination Assay

To detect STING ubiquitination, H460 or 293T cells were transfected with plasmids containing His-Ubi and Flag-STING (SinoBiological, Beijing, China) according to the manufacturer's instructions. Cells were cultured with metformin for 36 h and further incubated with MG132 (20 μM, Selleck) for another 12 h and then lysed. The cell lysates were then boiled for 10 min after adding 1% SDS and diluted to 0.1% SDS with lysis buffer. Protein concentrations of the extracts were measured, and equal amounts of extracts were used for immunoprecipitation of target protein.

Homology Modeling of AXIN-1 and STING and Protein-Protein Docking Prediction

Due to the full-length structure of AXIN-1 and STING was not available, a homology model was generated. The amino acid sequence was downloaded from Uniprot protein database (https://www.uniprot.org/uniprot/O15169; https://www.uniprot.org/uniprot/Q86WV6). Homology modeling of Axin-1 and Sting was constructed through I-TASSER server (Yang and Zhang, 2015). Parameters for modeling were set as default values. The docking study was performed using Hex 8.0.0 software (Li et al., 2019b). The binding interactions were generated using PyMOL. Parameters for docking were set as default values.

Statistical Analysis

All data are expressed as mean ± SEM and the statistical analysis was performed by GraphPad Prism 8 for Windows, GraphPad Software, San Diego, CA, United States, www.graphpad.com. Differences between two groups were analyzed by Student's t test. A p value <0.05 was considered statistically significant.

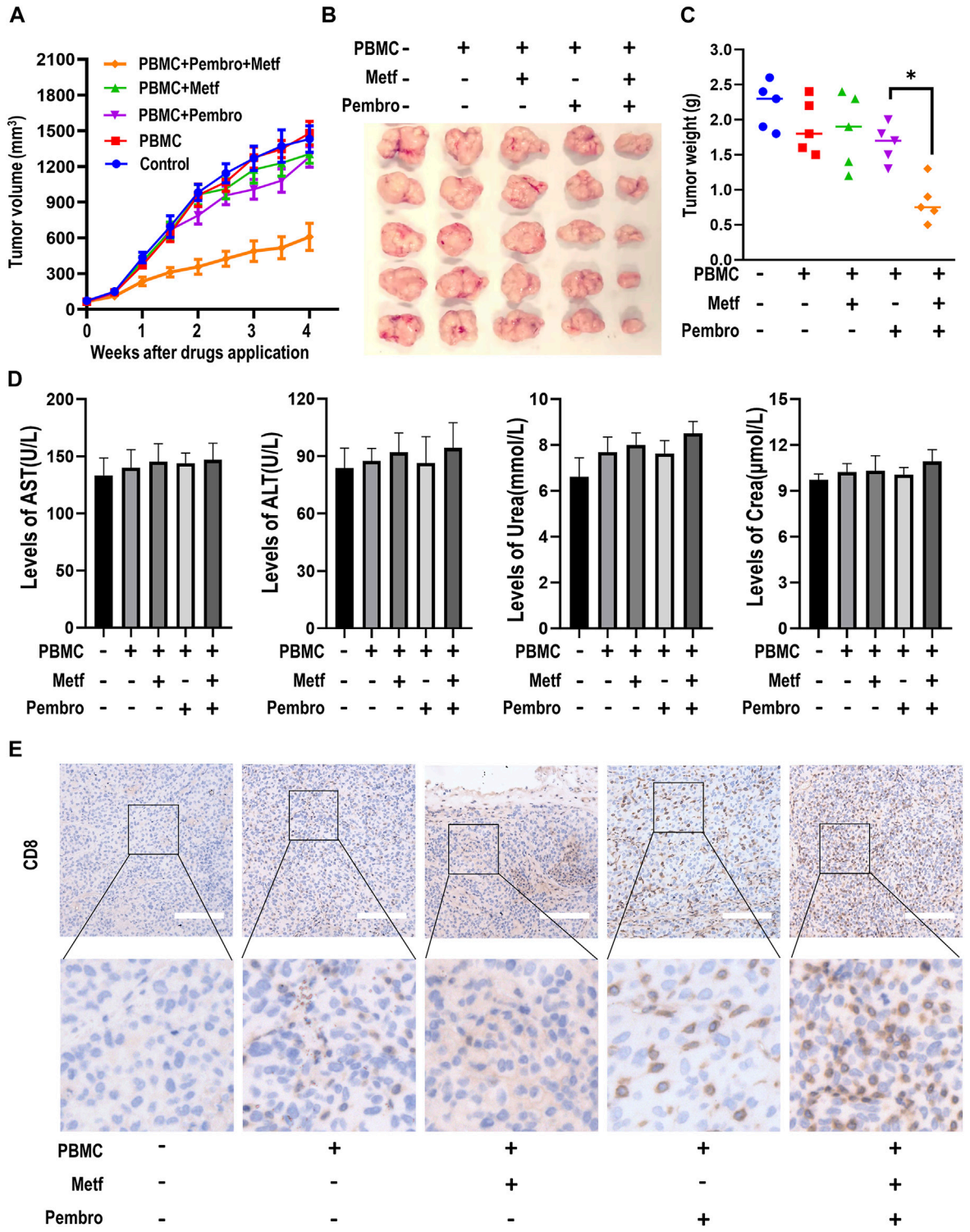

FIGURE 2 | Metformin enhanced the efficacy of PD-1 inhibitor in PBMCs-CDX mouse model. **(A)**, Tumor growth curve of H460-derived xenograft mouse models treated as indicated. Tumor volume was shown as mean ± SEM ($n = 5$). *, $p < 0.01$ compared with the pembrolizumab group. **(B)**, Macroscopic appearance of tumors after drug application for 4 weeks **(C)**, Tumor weight (g) of each mouse was shown. *, $p < 0.01$. **(D)**, The levels of serum AST, ALT, Urea and Creatinine in mice serum were presented as mean ± SEM ($n = 5$). **(E)**, Immunohistochemistry analysis of CD8 in tumor sections from different groups. Representative images were shown. Scale bars: 200 μm. AST, Aspartate aminotransferase; ALT, Alanine aminotransferase; Crea, Creatinine.

RESULTS

Metformin Enhanced T Cell-Mediated killing of *STK11* Mutant Lung Cancer Cells *In Vitro*

We first asked whether metformin can enhance T-cell mediated killing of lung cancer cells with *STK11* mutation. Colony formation assay was performed in H460 cells and A549 cells. As shown in **Figure 1A** and **Supplementary Figure S1**, activated T cells (1:1 ratio to cancer cells) or metformin (0.5 mM) alone showed little effect on colony formation of both cell lines, while the combination significantly decreased cancer cell growth. Conversely, inactivated T cells alone or in combination with metformin had little effect on tumor cell proliferation (**Supplementary Figure S2**). Next, the Ki67 incorporation assay and CCK-8 assay was applied to measure cell proliferation. Similarly, activated T cells or metformin alone failed to inhibit cell proliferation, while the combination significantly decreased the percentage of Ki67-positive cells (**Figure 1B**) and decreased cell viability (**Figure 1C**). As previously reported, the tumor cell killing by cytotoxic T cells was in large part mediated by the pro-apoptotic effects of IFN-γ (Mezzadra et al., 2019). We then performed ELISA assay and found that metformin treatment in inactivated T cells had little effect on interferon (IFN)-γ secretion, while it increased the release of IFN-γ in activated T cells in a dose-dependent manner (**Figure 1D**). Taken together, these results suggest that metformin enhanced T cell-mediated killing of *STK11* mutant lung cancer cells *in vitro*.

Metformin Enhanced the Anti-Tumor Efficacy With PD-1 Inhibitor *In Vitro* and *In Vivo*

We next asked whether metformin can enhance the anti-tumor efficacy with PD-1 inhibitor. We performed Ki67 incorporation assay *in vitro*. As shown in **Supplementary Figure S3**, in the presence of activated T cells, addition of pembrolizumab showed little effect on cancer cell growth, while addition of metformin further decreased the proliferation of both H460 cells and A549 cells. More importantly, the combination of metformin with pembrolizumab significantly decreased the percentage of Ki67-positive cells to a much greater extent, which indicates that metformin enhanced anti-tumor efficacy with PD-1 inhibitor *in vitro*.

We next examined the effects of combination of metformin and PD-1 inhibitor on tumor growth in a PBMCs-CDX mouse model. Intravenous injection of PBMCs alone had little effect on tumor growth. PBMCs plus metformin or pembrolizumab also did not inhibit the growth of tumors. In contrast, the combination of pembrolizumab and metformin resulted in a significant reduction of tumor volume (**Figures 2A,B**). Next, the tumor weight of each group was calculated and mapped in a scatter plot, which confirmed that tumors from the combination group had the lowest weight (**Figure 2C**). Meanwhile, there is no significant difference of mice body weight, or the level of AST, ALT, urea, and creatinine among groups (**Figure 2D**; **Supplementary Figure S4**). We next investigated the infiltration of $CD8^+$ T cells in tumor microenvironment among groups by IHC. Metformin or pembrolizumab alone led to a slight increase of $CD8^+$ T cell numbers, while the combination resulted in a remarkable $CD8^+$ T cell infiltration (**Figure 2E**; **Supplementary Figure S5**). Taken together, these findings indicate that combined treatment of metformin and PD-1 inhibitor can suppress tumor growth and promote T-cell infiltration *in vivo*.

Metformin Enhanced T Cell-Mediated Killing Through Stabilization of STING

Previously, inactivation of STING was suggested to be responsible for resistance to immunotherapy in *STK11* mutant cells (Kitajima et al., 2019). We then asked whether activation of STING signaling was involved in enhanced T cell-mediated killing of cancer cells by metformin. Western blot analysis and immunofluorescence staining of tumor tissues from PBMCs-CDX mouse model described earlier showed increased expression of STING in the combination group (**Figures 3A,B**). Next, we determined whether metformin affects STING degradation in order to clarify the mechanism by which metformin modulates STING levels. In the presence of the protein synthesis inhibitor cycloheximide (CHX), metformin substantially slowed the degradation of STING in comparison with control (**Figure 3C**), suggesting that STING is stabilized in metformin-treated H460 cells. Previously, cGAS-STING-TBK1 signaling pathway was reported to play a crucial role in the anti-tumor immunity (Ding et al., 2020; Ren et al., 2020). Then, western blot results showed that expression of STING and downstream p-TBK1 and p-IRF3 were all increased by metformin treatment (**Figure 3D**), which suggests that metformin can activate STING signaling pathway.

We then asked whether STING activation was required for metformin-enhanced T cell-mediated killing of cancer cells. After small interfering (si) RNA-mediated knockdown of *STING*, metformin failed to increase STING expression in H460 cells (**Figures 3E,F**). Moreover, in siNC group, metformin together with activated T cells significantly decreased colony numbers and sizes of tumor cells, while the knockdown of *STING* abolished this effect (**Figure 3G**; **Supplementary Figure S6A**). Similarly, the combination of metformin and activated T cells decreased cell viability and inhibited cell proliferation in siNC group, yet this effect was abrogated after knockdown of *STING* (**Figures 3H,I**; **Supplementary Figure S6B**). Overall, these findings suggested that enhancement of T cell-mediated killing of cancer cells by metformin is affected by expression of STING.

AXIN-1 Was Required for Metformin to Stabilize STING

It has been reported that the scaffold protein AXIN-1, which tether LKB1 to AMPK, plays an essential role in lysosome-dependent activation of AMPK and lifespan extension effect by metformin (Chen et al., 2017). However, it is unknown whether AXIN-1 is required for metformin to stabilize STING. Therefore, we generated AXIN-1-deficient H460 cells by CRISPR/Cas9 (*AXIN-1*$^{-/-}$ cells, **Figure 4A**). In control *AXIN-*

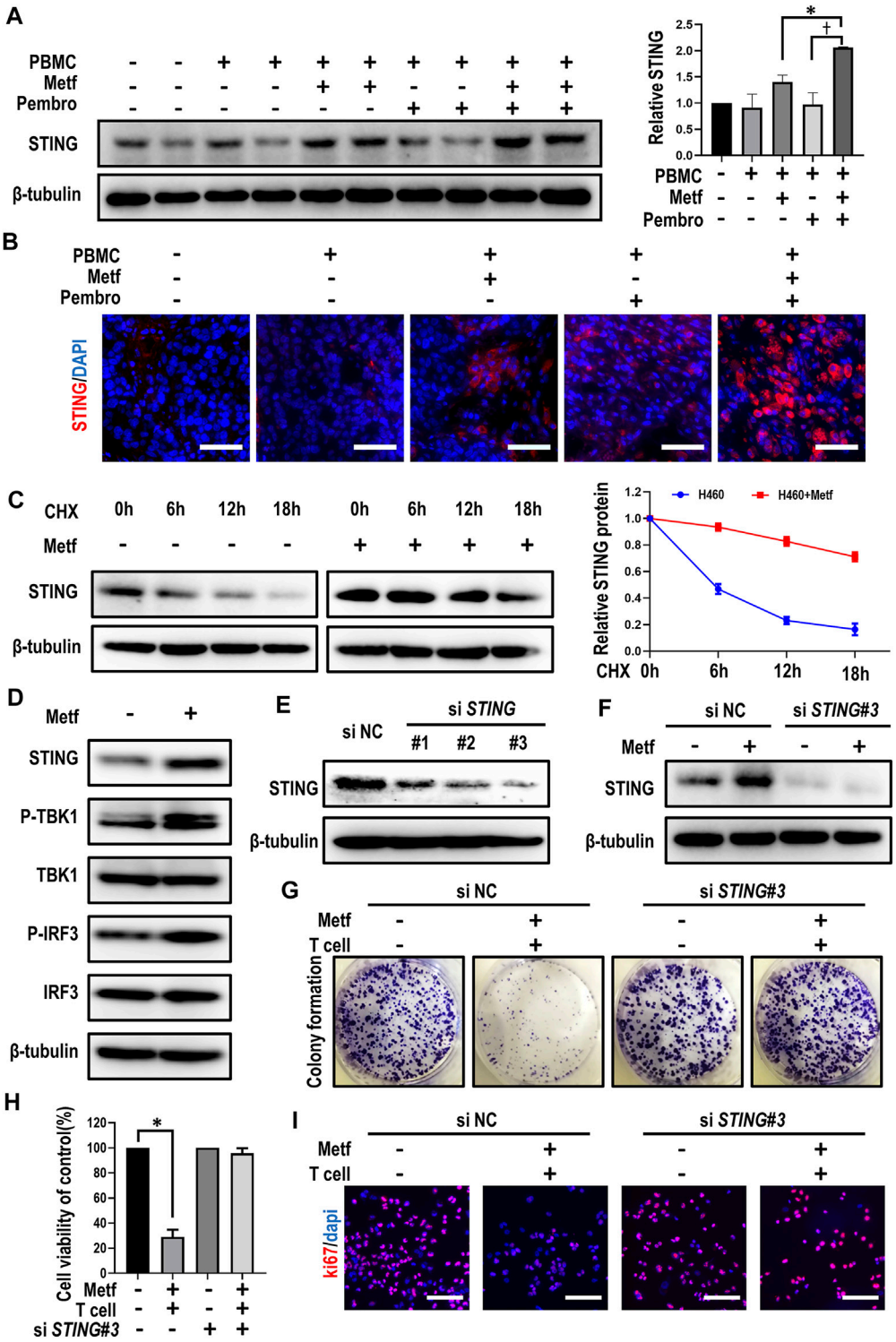

FIGURE 3 | Metformin enhanced T cell-mediated killing through stabilization of STING. **(A)**, Western blot analysis of STING from tumor sections of each group and expression levels were presented. *$p < 0.05$; †$p < 0.01$. **(B)**, Immunofluorescence staining of STING from tumor sections of different groups as indicated. Scale bars: 30 μm. **(C)**, H460 cells were treated with 10 μM CHX at indicated intervals in the presence of metformin or not, and the level of STING was quantified using ImageJ software. **(D)**, Western blot analysis of indicated proteins in H460 cells with metformin treatment. **(E)**, Western blot showing the expression levels of STING in H460 cells after transfection with control or *STING* siRNAs, respectively. **(F)**, Western blot analysis of STING expression under metformin treatment after siRNA-mediated knockdown of STING. **(G)**, H460 cells transfected with control or *STING* siRNAs were co-cultured with activated T cells (cancer cells to T cells ratio, 1:1) for 48 h with or without metformin and then subjected to crystal violet staining. **(H)**, Cell viability CCK-8 assay for cells treated as indicated. Data are shown as mean ± SEM of triplicate determinations. *$p < 0.01$. **(I)**, Ki67 incorporation assay on H460 cells treated as indicated. Cells were counterstained with DAPI.

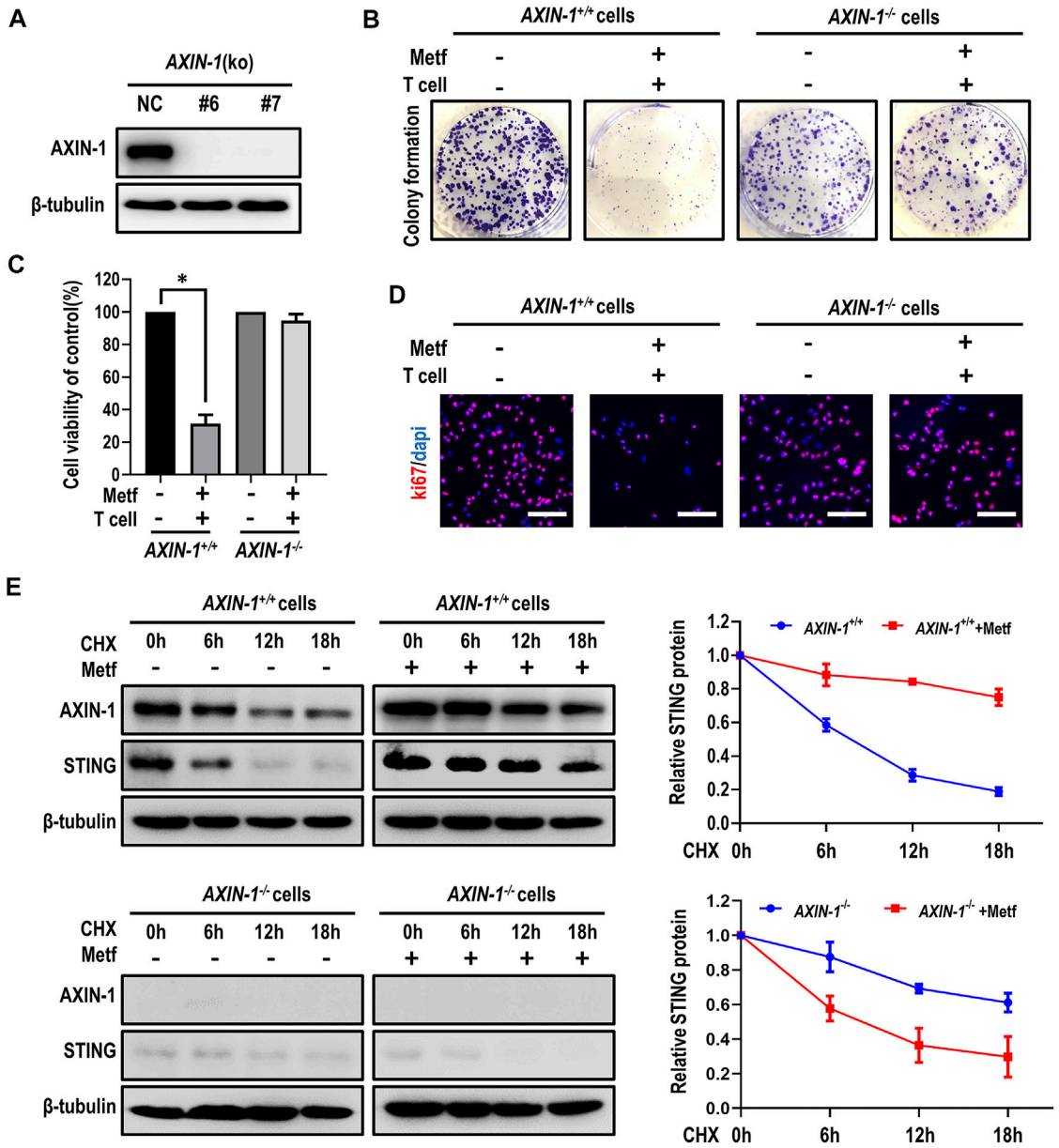

FIGURE 4 | AXIN-1 was required for metformin to stabilize STING. **(A)**, Cell lysates from AXIN-1 knockout clones of H460 cells by CRISPR/CAS9 (KO-6 and KO-7) were subjected to western blot. **(B)**, *AXIN-1*$^{+/+}$cells and *AXIN-1*$^{-/-}$ cells co-cultured with activated T cells (cancer cells to T cells ratio, 1:1) for 48 h with or without metformin were subjected to crystal violet staining. **(C)**, Cell viability CCK-8 assay for *AXIN-1*$^{+/+}$cells and *AXIN-1*$^{-/-}$ cells treated as indicated. Data are shown as mean ± SEM. *$p < 0.01$. **(D)**, Ki67 incorporation assay on *AXIN-1*$^{+/+}$cells and *AXIN-1*$^{-/-}$ cells treated as indicated. Cells were counterstained with DAPI. **(E)**, *AXIN-1*$^{+/+}$cells and *AXIN-1*$^{-/-}$ cells were treated with 10 μM CHX at indicated intervals in the presence of metformin or not. The intensity of STING protein was quantified using ImageJ software.

$1^{+/+}$ H460 cells, metformin together with activated T cells decreased colony formation of cancer cells. However, in *AXIN-1*$^{-/-}$ cells, this combination had little effect in inhibiting growth of cancer cells (**Figure 4B**; **Supplementary Figure S7A**). Similarly, metformin in combination with activated T cells decreased cell viability and inhibited cell proliferation in *AXIN-1*$^{+/+}$ H460 cells, while this effect was abrogated in *AXIN-1*$^{-/-}$ cells (**Figures 4C,D**; **Supplementary Figure S7B**). These results indicated specific involvement of AXIN-1 in metformin-enhanced T cell-mediated cancer cell killing. Next, we investigated the contribution of AXIN-1 to stabilization of STING by metformin. Compared to *AXIN-1*$^{+/+}$, *AXIN-1*$^{-/-}$ cells showed decreased STING expression. Moreover, metformin failed to increase STING expression, or to slow down the degradation of STING in *AXIN-1*$^{-/-}$ cells (**Figure 4E**). To further confirm the role of AXIN-1 in regulation of STING

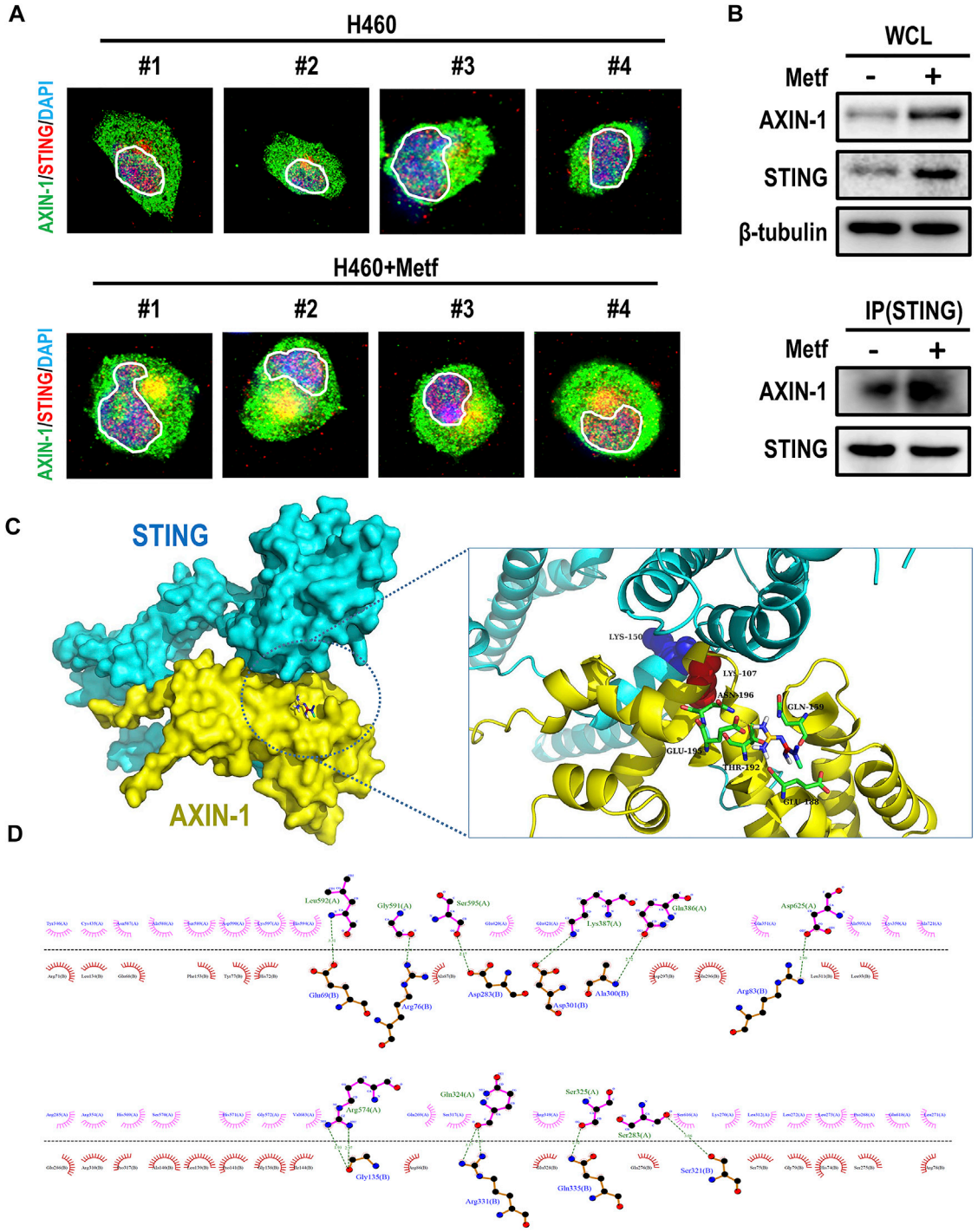

FIGURE 5 | Metformin enhanced the co-localization and binding of AXIN-1 and STING. **(A)**, Representative immunofluorescence images for AXIN-1 and STING of H460 cells following metformin treatment. Yellow signals indicated co-localization. **(B)**, Cell lysates from H460 cells with metformin treatment were immunoprecipitated with an anti-STING antibody and then immunoblotted with anti-AXIN-1 antibody. **(C)**, Protein-protein docking prediction between AXIN-1 and STING. **(D)**, The 2D visualization and interactions between AXIN-1 and STING. The hydrogen bonds and the hydrophobic interactions were shown in green-dashed lines and red arcs, respectively.

stability, we constructed *AXIN-1*$^{-/-}$ + AXIN1 cells with ectopic expression of AXIN-1 (**Supplementary Figure S8A**). Although metformin combining activated T cells failed to decrease cell viability and inhibit cell proliferation in *AXIN-1*$^{-/-}$ cells, this effect was rescued in *AXIN-1*$^{-/-}$ + AXIN1 cells (**Supplementary Figures S8B, C**). Furthermore, metformin increased STING

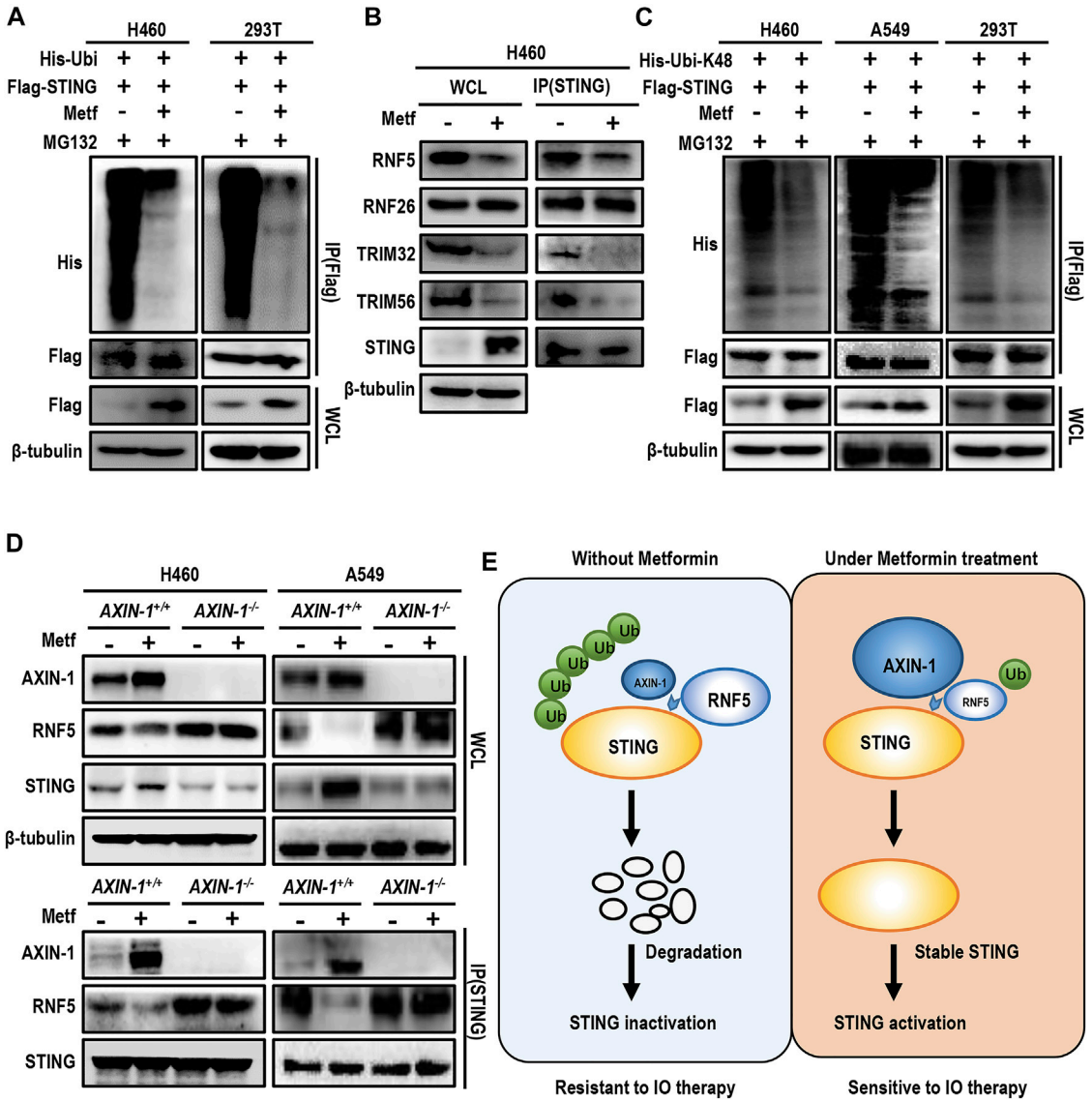

FIGURE 6 | AXIN-1 promotes stabilization of STING via competitive inhibition of RNF5-mediated K48-linked ubiquitination of STING. **(A)**, H460 cells and HEK293T cells were transiently transfected with the indicated plasmids with MG132 for 12 h. Immunoprecipitation analysis of exogenous STING ubiquitination with the indicated antibodies. **(B)**, Cell lysates from indicated groups were immunoprecipitated with an anti-STING antibody and then immunoblotted with the indicated antibodies. **(C)**, Cells were transfected with the indicated plasmids and then immunoprecipitation analysis of K48-linked ubiquitination of exogenous STING was performed. **(D)**, Cell lysates from *AXIN-1*$^{+/+}$ cells or *AXIN-1*$^{-/-}$ cells with different treatments were immunoprecipitated with an anti-STING antibody and then immunoblotted with RNF5. **(E)**, Working model for the mechanism of STING activation by metformin.

expression and slowed down its degradation in *AXIN-1*$^{-/-}$ + AXIN1 cells (**Supplementary Figure S8D**). Taken together, *AXIN-1* is required for metformin to stabilize STING and enhance T cell-mediated killing of cancer cells.

Metformin Enhanced the Co-localization and Binding of AXIN-1 and STING

To elucidate the mechanism how AXIN-1 stabilizes STING under metformin treatment, we then studied whether AXIN-1 directly interacted with STING. To this end, we performed immunofluorescence staining of AXIN-1 and STING in H460 cells with or without metformin treatment. Compared to the control group, metformin treatment led to obvious co-localization of AXIN-1 and STING (**Figure 5A**, yellow signal). We then confirmed this finding using immunoprecipitation. As shown in **Figure 5B**, the binding of AXIN-1 and STING was significantly enhanced under metformin treatment. Next, a protein-protein docking prediction was performed to predict the binding models of AXIN-1 and STING. The docking

results suggest that AXIN-1 could bind with STING, and the key amino acid residue Lys150 (K150) in STING was occupied by the loops of the Lys 107 (K107) in AXIN-1 (**Figure 5C**). On the other hand, the small molecule metformin docks in a pocket of AXIN-1 near the K107 site, which is composed of GLU-195, ASN-196, GLN-159, THR-192, and GLU-188 amino acid residues. Among them, metformin forms hydrogen bonds with GLU-195 and interacts with other amino acid residues (**Figure 5C**). The interface analysis suggested that interaction between AXIN-1 and STING was maintained by hydrogen bonds and hydrophobic interactions (**Figure 5D**). Taken together, these results suggest that metformin enhanced the binding of AXIN-1 and STING at K150 site.

AXIN-1 Promotes Sabilization of STING *via* Competitive Inhibition of RNF5-Mediated K48-Linked Ubiquitination of STING

STING is reported to be extensively modified by post-translational modification (Chiang and Gack, 2017). For example, ubiquitination of STING at K150 site dynamically regulates the activity of STING. We then asked whether metformin affects ubiquitination of STING. In both H460 cells and 293T cells, metformin treatment significantly decreased STING ubiquitination in the presence of MG132 (**Figure 6A**). Ubiquitination of STING at K150 site is regulated by several E3 ubiquitin ligases. For example, RNF5 modifies STING at K150 with K48-linked polyubiquitin and promotes STING degradation (Chiang and Gack, 2017). On the contrary, RNF26 catalyzes K11-linked polyubiquitination of STING at K150, and competes with RNF5 to ubiquitinate STING (Fenech et al., 2020). Besides, the E3 ubiquitin ligases TRIM32 and TRIM56 also target STING at K150 for K63-linked ubiquitination, and facilitates the recruitment of TBK1 to STING for STING activation (Yang et al., 2018; Bodda et al., 2020). We then performed immunoprecipitation assay to detect the binding of STING with different E3 ubiquitin ligases under metformin treatment. Results showed that metformin decreased the binding of STING with RNF5, TRIM32, and TRIM56, while had little effect in binding with RNF26 (**Figure 6B**). Thus, we speculated that metformin decreased STING degradation through inhibition of RNF5-mediated K48-linked ubiquitination. As expected, metformin treatment decreased K48-linked ubiquitination of STING in H460 cells, A549 cells and 293T cells (**Figure 6C**).

Since AXIN-1 was predicted to bind with STING at K150, we then asked whether AXIN-1 affected the binding of RNF5 and STING. As shown in **Figure 6D**, metformin significantly enhanced the binding of AXIN-1 and STING, while decreased the binding of STING and RNF5 in both H460 and A549 cell lines. On the contrary, in *AXIN-1*$^{-/-}$ cells, the binding of RNF5 with STING was significantly increased, and metformin treatment failed to decrease the binding of RNF5 with STING. Thus, these results suggest that AXIN-1 competitively inhibited RNF5-STING binding, thus decreasing RNF5-mediated K48-linked ubiquitination of STING (**Figure 6E**).

DISCUSSION

In the current study, we reported that metformin enhanced T cell-mediated killing and PD-1 inhibitor efficacy in *STK11* mutant lung cancer. AXIN-1 was required for metformin to stabilize STING via enhanced binding at K150 site and a competitive inhibition of RNF5-mediated K48-linked ubiquitination of STING. Thus, our study indicated that metformin in combination with PD-1 inhibitor may be a potential therapeutic approach for *STK11* mutant lung cancer.

The current study provided a new approach, the combination of metformin and PD-1 inhibitor, to treat *STK11* mutant lung cancer. *STK11* mutation is associated with dismal prognosis in NSCLC. Most *STK11* missense mutations negatively impact upon the LKB1 protein activity (Benci et al., 2016), which then lead to alterations of cancer-associated metabolism, lung cancer initiation, differentiation, local progression and metastatic dissemination (Faubert et al., 2014; Murray et al., 2019). In a large-scale, real-world, retrospective study involving 2407 advanced NSCLC patients, those with *STK11* mutation (13.6% of the whole population) had worse PFS and OS, regardless of treatment types (either chemotherapy or immunotherapy) or treatment lines (either first- or second-line settings) (Shire et al., 2020). Besides, *STK11* mutation was identified as a major driver of primary resistance to PD-1/PD-L1 blockade in NSCLC (Skoulidis et al., 2018). In a retrospective analysis, advanced non-squamous NSCLC patients with *STK11* mutation did not achieve clinical benefit from pembrolizumab plus chemotherapy (Skoulidis et al., 2019). Currently, very few therapeutic interventions have been developed to specifically treat *STK11* mutant tumors. In the current study, we found that metformin enhanced T cell-mediated killing of lung cancer cells *in vitro* through colony formation assay, cell viability CCK-8 assay and Ki67 incorporation assay. Moreover, we found that metformin in combination with PD-1 inhibitor enhanced anti-tumor efficacy *in vitro* and *in vivo*. In the future, *in vivo* rescue experiments are needed to demonstrate whether metformin can enhance the efficacy of PD-1 inhibitor. Previously, metformin has also been shown to induce immune cell infiltration in tumors, and promote antitumor $CD8^+$ T cell immune responses (Cha et al., 2018). These reports, together with our findings, suggest that metformin has the promising potential to overcome the primary resistance to ICIs in *STK11* mutant lung cancer.

Although metformin has been identified as a potentially efficacious antitumor agent, results from clinical studies are not always satisfactory. We previously reported that in EGFR mutant NSCLC without diabetes, metformin in combination with gefitinib resulted in non-significantly worse outcomes but increased the risks of diarrhea (Li et al., 2019c). Recently, in a randomized trial involving unresected locally advanced NSCLC without diabetes, the addition of metformin to chemoradiotherapy was associated with worse treatment efficacy and increased toxic effects compared with chemoradiotherapy alone (Tsakiridis et al., 2021). In another randomized phase II study, addition of metformin to chemotherapy provided no survival benefit in unselected

NSCLC patients, while it significantly improved the survival of the selected squamous cell carcinoma patients with high FDG uptake (Lee et al., 2021). These studies indicate that only specific NSCLC subgroups may benefit from adding metformin to standard therapy. Careful patient selection on biomarker expression will be essential to select suitable population who may benefit from metformin. Recent studies found that *STK11* mutation exposed cancer cells to metabolic crisis and apoptosis, and sensitized those cells to the antidiabetic compounds (Shackelford et al., 2013), which lower intracellular ATP levels by inhibiting mitochondrial oxidative phosphorylation. Metformin could prevent acquired resistance to cisplatin in *STK11* mutant lung cancer through reducing the number of tumor-initiating cells (Moro et al., 2018). These results, together with findings from the current study, suggest that *STK11* mutant lung cancer may be the potential population that can benefit from adjuvant metformin. Currently, a phase II study is being conducted to exploit metformin and fasting-mimicking diet to improve the efficacy of chemotherapy in advanced *STK11* mutant lung adenocarcinoma (Vernieri et al., 2019).

There is a compelling need to understand the resistance mechanism to PD-1 inhibitors in *STK11* mutant NSCLC, so as to envisage effective therapeutic interventions. *STK11* mutation was associated with a specific "cold" tumor immune microenvironment (TIME), characterized by production of pro-inflammatory cytokines, decrease in tumor-infiltrating $CD8^+$ lymphocytes and low PD-L1 expression on tumor cells (Koyama et al., 2016). Recent studies suggest that STING may play an important role in "cold" to "hot" transformation of TIME (Della Corte and Byers, 2019). STING is a signaling molecule that controls the transcription of many host defense genes, including pro-inflammatory cytokines and chemokines, and type I IFNs (Ishikawa and Barber, 2008; Ishikawa et al., 2009). Activation of STING pathway promotes the trafficking and infiltration of T cells to tumors, and is required for the recognition and killing of cancer cells by T cells (Zhu et al., 2019). Ectopic expression of STING in *STK11* mutant cells engages IRF3 and STAT1 signaling, leading to the release of the immune inflammatory cytokines IFNβ, CXCL10, CCL5, GM-CSF, CCL3, and IL1α, and suppression of IL6 (Kitajima et al., 2019). In the current study, we found that metformin can enhance STING stabilization and activation *in vitro*, and increased STING expression *in vivo* in PBMCs-CDX model. Moreover, STING was required for metformin to enhance T cell-mediated killing of cancer cells. In a previous report, metformin was also reported to activate STING/IRF3/IFN-β pathway and promote T cells infiltration, through inhibition of AKT phosphorylation (Ren et al., 2020). Taken together, these results suggest that metformin enhances PD-1 inhibitor efficacy in *STK11* mutant NSCLC through activation of STING.

Preclinically and clinically, STING agonists have been investigated for cancer immunotherapy. Cyclic dinucleotides (CDNs), or CDN derivatives are a representative class of STING agonists that can elicit immune responses. MK-1454, a synthetic CDN which binds directly to STING, showed a safe tolerability profile and encouraging efficacy together with pembrolizumab in a phase I trial (NCT03010176) (Harrington et al., 2018). However, natural CDNs are hydrophilic, with negative charges and are susceptible to enzymatic degradation, and requires intratumor injection, leading to low bioavailability in target tissues and challenges in clinical practice in patients whose tumors are not easily accessible, such as lung cancer (Su et al., 2019). Recently, it was reported that an intravenous STING agonist, which was made up of two linked amidobenzimidazole compounds, showed strong antitumor activity in a colon cancer model (Ramanjulu et al., 2018). The current study found that metformin may be potentially applied as an activator of STING to activate STING and its downstream pathway, thus enhancing anti-cancer immune responses. Given a satisfactory safety profile, metformin holds the potential to be applied in combination with ICIs to activate STING and enhance anti-cancer immune response.

In search of mechanism how metformin activates STING signaling, we found that AXIN-1 was required for stabilization of STING by metformin. AXIN-1 is a scaffold protein which serves as a platform for functioning of multiple proteins. Previously, it was reported that AMPK activation by metformin was dependent on the formation of the v-ATPase-Ragulator-AXIN/LKB1-AMPK complex (Zhang et al., 2016; Chen et al., 2017). In the current study, we found that AXIN-1 was required for metformin to enhance T cell-mediated killing of cancer cells. Also, knockout of AXIN-1 abolished the effect of metformin to stabilize STING. As previously reported, AXIN-1 was required for the degradation complex of β-catenin, and served as a negative regulator of Wnt/β-catenin signaling (Jackson et al., 2020). In the current study, we found that in *STK11* mutant lung cancer without LKB1 expression, AXIN-1 served as a platform for binding with STING, which was enhanced by metformin treatment. The binding of AXIN-1 with STING reduced RNF5-mediated K48-linked ubiquitination of STING. Therefore, AXIN-1-based STING stabilization was required for metformin to activate STING pathway and enhance immunotherapy efficacy in *STK11* mutant lung cancer.

In conclusion, the current study demonstrated that metformin overcomes primary resistance to PD-1 inhibitor in *STK11* mutant lung cancer. Future clinical studies are required to further investigate the clinical benefits of metformin combined with PD-1 inhibitors in *STK11* mutant lung cancer.

DATA AVAILABILITY STATEMENT

The original contributions presented in the study are included in the article/**Supplementary Material**, further inquiries can be directed to the corresponding authors.

ETHICS STATEMENT

The animal study was reviewed and approved by the Ethics Committee on animal experimentation of the Army Medical University.

AUTHOR CONTRIBUTIONS

Concept and design: LL, YH, MF, and FW. Acquisition, analysis, or interpretation of data: ZW, CHL, KZ, CYL, XT, DW, YD, RH, YW, CH, and QO. Drafting of the manuscript: ZW, CHL, and LL. Critical revision of the manuscript for important intellectual content: ZW, CHL, KZ, CYL, FW, XT, DW, YD, RH, YW, CH, QO, MF, YH, and LL All authors. Obtained funding: LL, YH, and MF. Supervision: YH.

FUNDING

This work was supported by National Natural Science Foundation of China (81672287, 81902352, 81972189), Guangdong Association of Clinical Trials (GACT)/Chinese Thoracic Oncology Group (CTONG) and Guangdong Provincial Key Lab of Translational Medicine in Lung Cancer (2017B030314120), Daping Hospital of Army Medical University (2019CXJSB004, 2019CXLCB011) and a Science Foundation for Outstanding Young People of the Army Medical University (To LL). The funders of the current study had no role in study design, data collection and analysis, decision to publish, or preparation of the manuscript.

SUPPLEMENTARY MATERIAL

The Supplementary Material for this article can be found online at: https://www.frontiersin.org/articles/10.3389/fmolb.2022.780200/full#supplementary-material

REFERENCES

Benci, J. L., Xu, B., Qiu, Y., Wu, T. J., Dada, H., Twyman-Saint Victor, C., et al. (2016). Tumor Interferon Signaling Regulates a Multigenic Resistance Program to Immune Checkpoint Blockade. *Cell.* 167 (6), 1540–1554 e1512. doi:10.1016/j.cell.2016.11.022

Bodda, C., Reinert, L. S., Fruhwürth, S., Richardo, T., Sun, C., Zhang, B. C., et al. (2020). HSV1 VP1-2 Deubiquitinates STING to Block Type I Interferon Expression and Promote Brain Infection. *J. Exp. Med.* 217 (7), 217. doi:10.1084/jem.20191422

Cha, J.-H., Yang, W.-H., Xia, W., Wei, Y., Chan, L.-C., Lim, S.-O., et al. (2018). Metformin Promotes Antitumor Immunity via Endoplasmic-Reticulum-Associated Degradation of PD-L1. *Mol. Cel* 71 (4), 606–620 e607. doi:10.1016/j.molcel.2018.07.030

Chen, J., Ou, Y., Li, Y., Hu, S., Shao, L. W., and Liu, Y. (2017). Metformin Extends *C. elegans* Lifespan through Lysosomal Pathway. *Elife.* 6, 6. doi:10.7554/eLife.31268

Chiang, C., and Gack, M. U. (2017). Post-translational Control of Intracellular Pathogen Sensing Pathways. *Trends Immunol.* 38 (1), 39–52. doi:10.1016/j.it.2016.10.008

Della Corte, C. M., and Byers, L. A. (2019). Evading the STING: LKB1 Loss Leads to STING Silencing and Immune Escape in KRAS-Mutant Lung Cancers. *Cancer Discov.* 9 (1), 16–18. doi:10.1158/2159-8290.cd-18-1286

Ding, C., Song, Z., Shen, A., Chen, T., and Zhang, A. (2020). Small Molecules Targeting the Innate Immune cGAS–STING–TBK1 Signaling Pathway. *Acta Pharmaceutica Sinica B* 10 (12), 2272–2298. doi:10.1016/j.apsb.2020.03.001

Faubert, B., Vincent, E. E., Griss, T., Samborska, B., Izreig, S., Svensson, R. U., et al. (2014). Loss of the Tumor Suppressor LKB1 Promotes Metabolic Reprogramming of Cancer Cells via HIF-1. *Proc. Natl. Acad. Sci.* 111 (7), 2554–2559. doi:10.1073/pnas.1312570111

Fenech, E. J., Lari, F., Charles, P. D., Fischer, R., Laétitia-Thézénas, M., Bagola, K., et al. (2020). Interaction Mapping of Endoplasmic Reticulum Ubiquitin Ligases Identifies Modulators of Innate Immune Signalling. *Elife.* 9, 9. doi:10.7554/eLife.57306

Harrington, K. J., Brody, J., Ingham, M., Strauss, J., Cemerski, S., Wang, S., et al. (2018). Preliminary Results of the First-In-Human (FIH) Study of MK-1454, an Agonist of Stimulator of Interferon Genes (STING), as Monotherapy or in Combination with Pembrolizumab (Pembro) in Patients with Advanced Solid Tumors or Lymphomas. *Ann. Oncol.* 29, 712. doi:10.1093/annonc/mdy424.015

Ishikawa, H., and Barber, G. N. (2008). STING Is an Endoplasmic Reticulum Adaptor that Facilitates Innate Immune Signalling. *Nature* 455 (7213), 674–678. doi:10.1038/nature07317

Ishikawa, H., Ma, Z., and Barber, G. N. (2009). STING Regulates Intracellular DNA-Mediated, Type I Interferon-dependent Innate Immunity. *Nature* 461 (7265), 788–792. doi:10.1038/nature08476

Jackson, D. N., Alula, K. M., Delgado-Deida, Y., Tabti, R., Turner, K., Wang, X., et al. (2020). The Synthetic Small Molecule FL3 Combats Intestinal Tumorigenesis via Axin1-Mediated Inhibition of Wnt/β-Catenin Signaling. *Cancer Res.* 80 (17), 3519–3529. doi:10.1158/0008-5472.can-20-0216

Jure-Kunkel, M., Wu, S., Xiao, F., Abdullah, S. E., Gao, G., Englert, J. M., et al. (2018). Somatic STK11/LKB1 Mutations to Confer Resistance to Immune Checkpoint Inhibitors as Monotherapy or in Combination in Advanced NSCLC. *Jco* 36 (15_Suppl. l), 3028. doi:10.1200/jco.2018.36.15_suppl.3028

Kirtonia, A., Gala, K., Fernandes, S. G., Pandya, G., Pandey, A. K., Sethi, G., et al. (2021). Repurposing of Drugs: An Attractive Pharmacological Strategy for Cancer Therapeutics. *Semin. Cancer Biol.* 68, 258–278. doi:10.1016/j.semcancer.2020.04.006

Kitajima, S., Ivanova, E., Guo, S., Yoshida, R., Campisi, M., Sundararaman, S. K., et al. (2019). Suppression of STING Associated with LKB1 Loss in KRAS-Driven Lung Cancer. *Cancer Discov.* 9 (1), 34–45. doi:10.1158/2159-8290.cd-18-0689

Koyama, S., Akbay, E. A., Li, Y. Y., Aref, A. R., Skoulidis, F., Herter-Sprie, G. S., et al. (2016). STK11/LKB1 Deficiency Promotes Neutrophil Recruitment and Proinflammatory Cytokine Production to Suppress T-Cell Activity in the Lung Tumor Microenvironment. *Cancer Res.* 76 (5), 999–1008. doi:10.1158/0008-5472.can-15-1439

Lee, Y., Joo, J., Lee, Y. J., Lee, E. K., Park, S., Kim, T.-S., et al. (2021). Randomized Phase II Study of Platinum-Based Chemotherapy Plus Controlled Diet with or without Metformin in Patients with Advanced Non-small Cell Lung Cancer. *Lung Cancer.* 151, 8–15. doi:10.1016/j.lungcan.2020.11.011

Li, C.-W., Lim, S.-O., Xia, W., Lee, H.-H., Chan, L.-C., Kuo, C.-W., et al. (2016). Glycosylation and Stabilization of Programmed Death Ligand-1 Suppresses T-Cell Activity. *Nat. Commun.* 7, 12632. doi:10.1038/ncomms12632

Li, L., Jiang, L., Wang, Y., Zhao, Y., Zhang, X.-J., Wu, G., et al. (2019). Combination of Metformin and Gefitinib as First-Line Therapy for Nondiabetic Advanced NSCLC Patients with EGFR Mutations: A Randomized, Double-Blind Phase II Trial. *Clin. Cancer Res.* 25 (23), 6967–6975. doi:10.1158/1078-0432.ccr-19-0437

Li, L., Wang, Y., Jiao, L., Lin, C., Lu, C., Zhang, K., et al. (2019). Protective Autophagy Decreases Osimertinib Cytotoxicity through Regulation of Stem Cell-like Properties in Lung Cancer. *Cancer Lett.* 452, 191–202. doi:10.1016/j.canlet.2019.03.027

Li, P., Xu, Y., Zhang, Q., Li, Y., Jia, W., Wang, X., et al. (2019). Evaluating the Role of RAD52 and its Interactors as Novel Potential Molecular Targets for Hepatocellular Carcinoma. *Cancer Cel Int.* 19, 279. doi:10.1186/s12935-019-0996-6

Lin, S., Huang, G., Cheng, L., Li, Z., Xiao, Y., Deng, Q., et al. (2018). Establishment of Peripheral Blood Mononuclear Cell-Derived Humanized Lung Cancer Mouse Models for Studying Efficacy of PD-L1/pd-1 Targeted Immunotherapy. *MAbs.* 10 (8), 1301–1311. doi:10.1080/19420862.2018.1518948

Mezzadra, R., de Bruijn, M., Jae, L. T., Gomez-Eerland, R., Duursma, A., Scheeren, F. A., et al. (2019). SLFN11 Can Sensitize Tumor Cells towards IFN-γ-Mediated T Cell Killing. *PLoS One.* 14 (2), e0212053. doi:10.1371/journal.pone.0212053

Moro, M., Caiola, E., Ganzinelli, M., Zulato, E., Rulli, E., Marabese, M., et al. (2018). Metformin Enhances Cisplatin-Induced Apoptosis and Prevents Resistance to Cisplatin in Co-mutated KRAS/LKB1 NSCLC. *J. Thorac. Oncol.* 13 (11), 1692–1704. doi:10.1016/j.jtho.2018.07.102

Moser, B., Hochreiter, B., Basílio, J., Gleitsmann, V., Panhuber, A., Pardo-Garcia, A., et al. (2021). The Inflammatory Kinase IKKα Phosphorylates and Stabilizes C-Myc and Enhances its Activity. *Mol. Cancer* 20 (1), 16. doi:10.1186/s12943-021-01308-8

Murray, C. W., Brady, J. J., Tsai, M. K., Li, C., Winters, I. P., Tang, R., et al. (2019). An LKB1-SIK Axis Suppresses Lung Tumor Growth and Controls Differentiation. *Cancer Discov.* 9 (11), 1590–1605. doi:10.1158/2159-8290.cd-18-1237

Parker, S. J., Svensson, R. U., Divakaruni, A. S., Lefebvre, A. E., Murphy, A. N., Shaw, R. J., et al. (2017). LKB1 Promotes Metabolic Flexibility in Response to Energy Stress. *Metab. Eng.* 43 (Pt B), 208–217. doi:10.1016/j.ymben.2016.12.010

Qu, J., Mei, Q., Liu, L., Cheng, T., Wang, P., Chen, L., et al. (2021). The Progress and challenge of Anti-PD-1/pd-L1 Immunotherapy in Treating Non-small Cell Lung Cancer. *Ther. Adv. Med. Oncol.* 13, 1758835921992968. doi:10.1177/1758835921992968

Ramanjulu, J. M., Pesiridis, G. S., Yang, J., Concha, N., Singhaus, R., Zhang, S. Y., et al. (2018). Design of Amidobenzimidazole STING Receptor Agonists with Systemic Activity. *Nature* 564 (7736), 439–443. doi:10.1038/s41586-018-0705-y

Ren, D., Qin, G., Zhao, J., Sun, Y., Zhang, B., Li, D., et al. (2020). Metformin Activates the STING/IRF3/IFN-β Pathway by Inhibiting AKT Phosphorylation in Pancreatic Cancer. *Am. J. Cancer Res.* 10 (9), 2851–2864.

Sanchez-Cespedes, M., Parrella, P., Esteller, M., Nomoto, S., Trink, B., Engles, J. M., et al. (2002). Inactivation of LKB1/STK11 Is a Common Event in Adenocarcinomas of the Lung. *Cancer Res.* 62 (13), 3659–3662.

Shackelford, D. B., Abt, E., Gerken, L., Vasquez, D. S., Seki, A., Leblanc, M., et al. (2013). LKB1 Inactivation Dictates Therapeutic Response of Non-small Cell Lung Cancer to the Metabolism Drug Phenformin. *Cancer Cell.* 23 (2), 143–158. doi:10.1016/j.ccr.2012.12.008

Shire, N. J., Klein, A. B., Golozar, A., Collins, J. M., Fraeman, K. H., Nordstrom, B. L., et al. (2020). STK11 (LKB1) Mutations in Metastatic NSCLC: Prognostic Value in the Real World. *PLoS One.* 15 (9), e0238358. doi:10.1371/journal.pone.0238358

Siegel, R. L., Miller, K. D., Fuchs, H. E., and Jemal, A. (2021). Cancer Statistics, 2021. *CA A. Cancer J. Clin.* 71 (1), 7–33. doi:10.3322/caac.21654

Skoulidis, F., Arbour, K. C., Hellmann, M. D., Patil, P. D., Marmarelis, M. E., Awad, M. M., et al. (2019). Association of STK11/LKB1 Genomic Alterations with Lack of Benefit from the Addition of Pembrolizumab to Platinum Doublet Chemotherapy in Non-squamous Non-small Cell Lung Cancer. *J. Clin. Oncol.* (15), 37. doi:10.1200/jco.2019.37.15_suppl.102

Skoulidis, F., Goldberg, M. E., Greenawalt, D. M., Hellmann, M. D., Awad, M. M., Gainor, J. F., et al. (2018). STK11/LKB1 Mutations and PD-1 Inhibitor Resistance in KRAS-Mutant Lung Adenocarcinoma. *Cancer Discov.* 8 (7), 822–835. doi:10.1158/2159-8290.cd-18-0099

Su, T., Zhang, Y., Valerie, K., Wang, X.-Y., Lin, S., and Zhu, G. (2019). STING Activation in Cancer Immunotherapy. *Theranostics.* 9 (25), 7759–7771. doi:10.7150/thno.37574

Tsakiridis, T., Pond, G. R., Wright, J., Ellis, P. M., Ahmed, N., Abdulkarim, B., et al. (2021). Metformin in Combination with Chemoradiotherapy in Locally Advanced Non-small Cell Lung Cancer: The OCOG-ALMERA Randomized Clinical Trial. *JAMA Oncol.*

Vernieri, C., Signorelli, D., Galli, G., Ganzinelli, M., Moro, M., Fabbri, A., et al. (2019). Exploiting FAsting-Mimicking Diet and MEtformin to Improve the Efficacy of Platinum-Pemetrexed Chemotherapy in Advanced LKB1-Inactivated Lung Adenocarcinoma: The FAME Trial. *Clin. Lung Cancer* 20 (3), e413–e417. doi:10.1016/j.cllc.2018.12.011

Yang, J., and Zhang, Y. (2015). I-TASSER Server: New Development for Protein Structure and Function Predictions. *Nucleic Acids Res.* 43 (W1), W174–W181. doi:10.1093/nar/gkv342

Yang, L., Wang, L., Ketkar, H., Ma, J., Yang, G., Cui, S., et al. (2018). UBXN3B Positively Regulates STING-Mediated Antiviral Immune Responses. *Nat. Commun.* 9 (1), 2329. doi:10.1038/s41467-018-04759-8

Zhang, C.-S., Li, M., Ma, T., Zong, Y., Cui, J., Feng, J.-W., et al. (2016). Metformin Activates AMPK through the Lysosomal Pathway. *Cel Metab.* 24 (4), 521–522. doi:10.1016/j.cmet.2016.09.003

Zhu, Y., An, X., Zhang, X., Qiao, Y., Zheng, T., and Li, X. (2019). STING: a Master Regulator in the Cancer-Immunity Cycle. *Mol. Cancer* 18 (1), 152. doi:10.1186/s12943-019-1087-y

Conflict of Interest: The authors declare that the research was conducted in the absence of any commercial or financial relationships that could be construed as a potential conflict of interest.

The reviewer YZ declared a shared affiliation, with no collaboration, with one of the authors, FW, to the handling editor at the time of the review.

Publisher's Note: All claims expressed in this article are solely those of the authors and do not necessarily represent those of their affiliated organizations, or those of the publisher, the editors and the reviewers. Any product that may be evaluated in this article, or claim that may be made by its manufacturer, is not guaranteed or endorsed by the publisher.

frontiers in Molecular Biosciences

REVIEW
published: 15 March 2022
doi: 10.3389/fmolb.2022.723846

CXCL8 in Tumor Biology and Its Implications for Clinical Translation

Xingyu Xiong[1]†, Xinyang Liao[1†], Shi Qiu[1,2†], Hang Xu[1], Shiyu Zhang[1], Sheng Wang[1], Jianzhong Ai[1] and Lu Yang[1]**

[1]Department of Urology, National Clinical Research Center for Geriatrics, Institute of Urology, West China Hospital of Sichuan University, Chengdu, China, [2]Center of Biomedical Big Data, West China Hospital, Sichuan University, Chengdu, China, [3]Department of Endocrinology and Metabolism, West China Hospital of Sichuan University, Chengdu, China

The chemokine CXCL8 has been found to play an important role in tumor progression in recent years. CXCL8 activates multiple intracellular signaling pathways by binding to its receptors (CXCR1/2), and plays dual pro-tumorigenic roles in the tumor microenvironment (TME) including directly promoting tumor survival and affecting components of TME to indirectly facilitate tumor progression, which include facilitating tumor cell proliferation and epithelial-to-mesenchymal transition (EMT), pro-angiogenesis, and inhibit anti-tumor immunity. More recently, clinical trials indicate that CXCL8 can act as an independently predictive biomarker in patients receiving immune checkpoint inhibitions (ICIs) therapy. Preclinical studies also suggest that combined CXCL8 blockade and ICIs therapy can enhance the anti-tumor efficacy, and several clinical trials are being conducted to evaluate this therapy modality.

Keywords: CXCL8, tumor microenvironment, tumor progression, tumor immune suppression, immunotherapy

OPEN ACCESS

Edited by:
José Alexandre Ferreira, Portuguese Oncology Institute, Portugal

Reviewed by:
Liwei Lang, Augusta University, United States
Song Yao, Tongji University, China

****Correspondence:***
Jianzhong Ai
ajz6363@126.com
Lu Yang
wycleflue@163.com

†These authors have contributed equally to this work

Specialty section:
This article was submitted to Molecular Diagnostics and Therapeutics, a section of the journal Frontiers in Molecular Biosciences

Received: *11 June 2021*
Accepted: *21 February 2022*
Published: *15 March 2022*

Citation:
Xiong X, Liao X, Qiu S, Xu H, Zhang S, Wang S, Ai J and Yang L (2022) CXCL8 in Tumor Biology and Its Implications for Clinical Translation. Front. Mol. Biosci. 9:723846. doi: 10.3389/fmolb.2022.723846

INTRODUCTION

The chemokine CXCL8, also known as interleukin-8 (IL-8), is initially known as a cytokine expressed by epithelial cells and macrophages for neutrophil recruitment to areas of inflammation, infection, or injury (Horn et al., 2020a). The biological effects of CXCL8 are mediated through its binding to two cell-surface G-protein-coupled receptors: CXCR1 and CXCR2, which are generally expressed on monocytes, granulocytes, and endothelial cells (Waugh and Wilson, 2008; Liu et al., 2016). Furthermore, CXCL8 monomer binds CXCR1 with high affinity, however, both monomer and dimer show similar affinities to CXCR2 (Helen et al., 2017).

Although CXCL8 has been originally described as a proinflammatory chemokine, in the context of cancer, CXCL8 is produced by multiple cell types in the tumor microenvironment (TME), including the infiltrating immune cells, stromal cells, and the tumour cells (Waugh and Wilson, 2008; Alfaro et al., 2017). Additionally, the mechanism of CXCL8-CXCR1/2 pathway in tumourigenesis, tumour progression and immune suppression in TME has been explored extensively. Recent investigations demonstrate several novel mechanisms of the crosstalk between CXCL8 and components in TME to facilitate tumor progression, even forming positive feedback loops. Immune checkpoint inhibitions (ICIs) have become the cornerstone of immunotherapy in many types of cancers. Emerging trials underline the crucial roles of CXCL8 in ICIs therapy.

In this review, we summarized the current understanding of CXCL8 signaling cascades and recently developed mechanisms of facilitating tumor survival, invasion, and immune suppression. Additionally, we discussed the CXCL8 as a biomarker of ICIs therapy and the role of anti-CXCL8 as a combination agent in immunotherapy.

STRUCTURE AND SECRETION OF CXCL8

CXCL8 is initially translated as a protein with 99 amino acids, which is subsequently processed into two active isoforms: 1) 72 amino acids in monocytes and macrophages; 2) 77 amino acids in non-immune cells (Waugh and Wilson, 2008). According to the position of the first two cysteine residues on the N-terminus, chemokines can be divided into four highly conserved subtypes: CXC (the two cysteines nearest the N-termini are separated by a another single amino acid), CC (the first two cysteines nearest the N-termini are adjacent), C (only one cysteine near its N-terminus) and CX3C (with three amino acids between the first two cysteines at the N-terminal) (Rollins, 1997; Balkwill, 2004). Further, the family of CXC chemokines can be divided into to ELR- and ELR + groups based on the absence or presence of the tripeptide Glu-Leu-Arg (the ELR motif) which precedes the cysteine on the N-terminus (Baggiolini et al., 1997). CXCL8 is one of the ELR + CXC chemokines (Baldwin et al., 1991).

The gene encoding CXCL8 is located on 4q13-q21 (Modi et al., 1990). There are four common polymorphisms in the CXCL8 gene: rs4073(-251 A/T), rs2227532(-845T/C), rs2227307(+396 G/T) and rs2227306(+781 C/T) (Mukaida et al., 1989; Yao et al., 2019). Previously studies indicated that the single nucleotide polymorphism (SNPs) of CXCL8 gene were significantly associated with increased risk or progression of non small cell lung cancer, gastric cancer, differentiated thyroid cancer and ovarian cancer, especially CXCL8-251 A/T (Rafrafi et al., 2013; Koensgen et al., 2015; Kilic et al., 2016; Boonyanugomol et al., 2019). One of the most remarkable characteristics of CXCL8 is the variation of its expression levels. Normally, CXCL8 is undetectable in noninduced cells (Hoffmann et al., 2002). Mechanismly, in these unstimulated cells, the promoter of CXCL8 gene is repressed by three events: firstly, NF-κB-repressing factor (NRF) binds to the negative regulatory element (NRE) which overlaps the NF-κB binding site (Nourbakhsh et al., 2001); secondly, octamer-1 (OCT-1) binds to the complementary strand of the CXCL8 gene promoter in the opposite direction of the C/EBP site (Wu et al., 1997); and thirdly, deacetylation of the histone protein by histone deacetylase 1 (HDAC-1) (Ashburner et al., 2001). However, its expression is rapidly induced by various stimuli including cytokines such as IL-1 or TNFα, viral products or bacterials, other environmental stresses and transcription factors (including activator protein-1 (AP-1) and NF-κB) (Hoffmann et al., 2002; Helen et al., 2017). Remarkably, these stimuli cause a 5–100 folds increasing in CXCL8 expression(Hoffmann et al., 2002; Helen et al., 2017). Maximal CXCL8 expression and secretion is generated at least by a combination of three different mechanisms: 1) derepression of CXCL8 gene promoter; 2) transcriptional activation of CXCL8 gene by NF-κB and JNK pathways; 3) stabilization of CXCL8 mRNA by the p38 mitogen-activated protein kinase (MAPK) pathway (Hoffmann et al., 2002; Helen et al., 2017). The stability of the CXCL8 mRNA also plays an impact role on the secretion of CXCL8. In terms of mechanism, dual specificity mitogen-activated protein kinase kinase 6 (MKK6) by selectively activating p38 MAPK to activates MAP kinase-activated protein kinase 2 (MK2) which helps the stability of the CXCL8 mRNA (Helen et al., 2017; Hoffmann, et al., 2002). Additionally, in intestinal epithelial cells, carnosine could inhibit the translation of CXCL8 mRNA by phosphorylation of eIF4E (Son et al., 2008). Post-translational modification (PTM) of chemokines is an important mechanism of fine-tuning chemokine secretion, activation and selection of receptor (Vanheule et al., 2018). N-terminal shortening always associated with significantly increasing biological activity and receptor affinity of CXCL8. Numerous studies indicate that N-terminal truncation of CXCL8 (2 to 9–77) by CD13, CD26, MMP and so on (Van den Steen et al., 2003; Mortier et al., 2011; Vanheule et al., 2018). On the other side, citrullination of CXCL8 by peptidylarginine deiminase (PAD) could impair the effect of CXCL8 (Proost et al., 2008; Loos et al., 2009).

RECEPTORS OF CXCL8: CXCR1 AND CXCR2

The receptors that bind to CXCL8 are two G protein coupled receptors (GPCR): CXCR1 and CXCR2 (**Figure 1**). The two receptors that are both the ELR + CXC receptors sharing 78% sequence homology between each other (Holmes et al., 1991; Murphy and Tiffany, 1991). CXCR1 and CXCR2 show different affinity to the different complexes of CXCL8. Both monomer and dimer forms of CXCL8 show similar affinity to CXCR2, however, only CXCL8 monomer functions as a potent CXCR1 agonist (Nasser et al., 2009; Das et al., 2010; Berkamp et al., 2017).

Upon CXCL8 binding, the following stable complexes will be formed: CXCL8(monomer)-CXCR1/2-G protein and CXCL8(dimer)-CXCR2-G protein (Park et al., 2012; Liu et al., 2020), which induce a conformational change of CXCR1/2 and facilitate the initiation of activation. Then, CXCR1/2 dissociate with the heterotrimeric G protein and then release the βγ subunites from the α subunite, which promotes the activation of several downstream signaling cascades (Waugh and Wilson, 2008; Liu et al., 2016). Similar to most GPCR, CXCR1/2 can also become phosphorylated, desensitized, and internalized upon binding to CXCL8. Despite evidenced that CXCR1/2 display similar downstream pathways, there remain marked differences between CXCR1 and CXCR2 in activation and signaling cascades. CXCR2 internalization occurs more rapidly and at lower ligand concentrations than CXCR1, and CXCR2 is also recycled back to the surface at a much slower rate than CXCR1 (Alfaro et al., 2017; Helen et al., 2017), which might be one possible mechanism that CXCR1 not CXCR2 can activate PLD (Stillie et al., 2009; Raghuwanshi et al., 2012; Cheng et al., 2019).

Signaling Pathways of CXCL8-CXCR1/2 Axis

Upon CXCL8 binding, CXCR1/2 can active multiple G-protein-mediated signalling cascades (**Figure 2**). Phosphatidylinositol-3 kinase (PI3K)/Akt is one of the

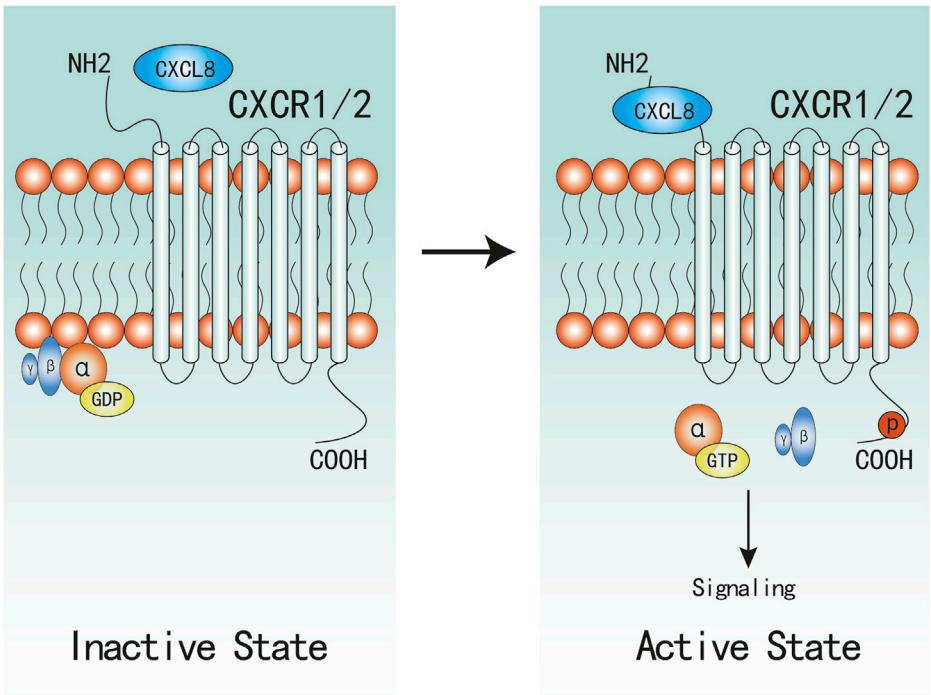

FIGURE 1 | Active and Inactive Structures of CXCR1/2 Complex. CXCR1/2 is in complex with Gαβγ in inactive state. When CXCL8 binds to the N-terminal of CXCR1/2, α-GDP changes into α-GTP, and dissociates with βγ subunites, which would subsequently active associated signaling.

principal downstream signal of CXCL8, which plays vital roles in modulating tumor motility, angiogenesis, and survival (Wilson et al., 2006; Waugh and Wilson, 2008). In androgen-independent prostate cancer, CXCL8 can also increase the expression of Akt (MacManus et al., 2007). PI3K can also act as an intermediate in coulping CXCR1/2 to MAPK and focal adhesion kinase (FAK)-Src signaling cascades (Knall et al., 1996; Waugh and Wilson, 2008). Phosphorylation of CXCR1/2 can also lead to two MyD88-dependent MAPK pathway: Erk-MAPK and p38 MAPK (Knall et al., 1997; Zhang et al., 2017; Cheng et al., 2019). Further, the Erk-MAPK cascades can be activated in indirect ways. Transactivation of epidermal growth factor receptor (EGFR) has been shown to occur in response to ligands of various GPCRs (Daub et al., 1996). The binding of CXCL8 to CXCR2 has been demonstrated to transactivate the EGFR resulting in Ras-GTPase activation, and subsequently actives the Erk-MAPK signaling cascades (Venkatakrishnan et al., 2000; Luppi et al., 2007). Activation of phospholipase C (PLC) by CXCL8 has been characterized in neutrophils and multiple cancer cells (Waugh and Wilson, 2008). The activated protein kinase C (PKC) can phosphorylate many cytoskeletal proteins that trigger dynamic alternations, facilitate cell adhesion and migration (Larsson, 2006; Quann et al., 2011). PKC can be classified into three categories (Larsson, 2006), and CXCL8 can active all the three categories of PKC mediated by PLC (Waugh and Wilson, 2008; Alassaf and Mueller, 2020). As a result of promoting these upstream signaling pathways, including PI3K/Akt, MAPK, and PLC/PKC, the activation of numerous transcription factors would be induced, one of which was nuclear factor-κB (NF-κB) (Waugh and Wilson, 2008; Gales, et al., 2013). Besides, activation of NF-κB is also one of the main mechanism to promote CXCL8 expression and secretion (Hoffmann, et al., 2002; Gales, et al., 2013; Helen, et al., 2017). Therefore, there exist a positive feedback between CXCL8 secretion and NF-κB activation, which has also been well described in a previous review (Gales, et al., 2013). Additionally, Numerous studies have confirmed that CXCL8 can induce the phosphorylation of protein tyrosine kinases, including FAK and Src kinases (Waugh and Wilson, 2008; Liu et al., 2016; Ju et al., 2017; Mohamed et al., 2020). Activation of FAK and Src kinases has been uncovered to promote cell proliferation, invasion, survival, and motility (Sulzmaier et al., 2014; Roskoski, 2015). In endothelial cells, it has revealed that CXCL8 can induce vascular endothelial growth factor receptor-2 (VEGFR2) phosphorylation mediated by the activation of Src kinases (Petreaca et al., 2007). CXCL8 can also promote dynamic and time-dependent induction of Rho-GTPases family in prostate cancer and endothelial cells (Schraufstatter et al., 2001; Waugh and Wilson, 2008; Yan et al., 2016). Recently, increased studies evidence that CXCL8 can induce the activation of Janus kinases and signal transducer and activator of transcription protein 3 (JAK/STAT3) signaling in both cancer and immune cells (Fu et al., 2015; Guo et al., 2017; Wu et al., 2019; Hu et al., 2020). Wu et al. demonstrated that CXCL8 could impair the function of NK cells by promoting STAT3 (Wu et al., 2019).

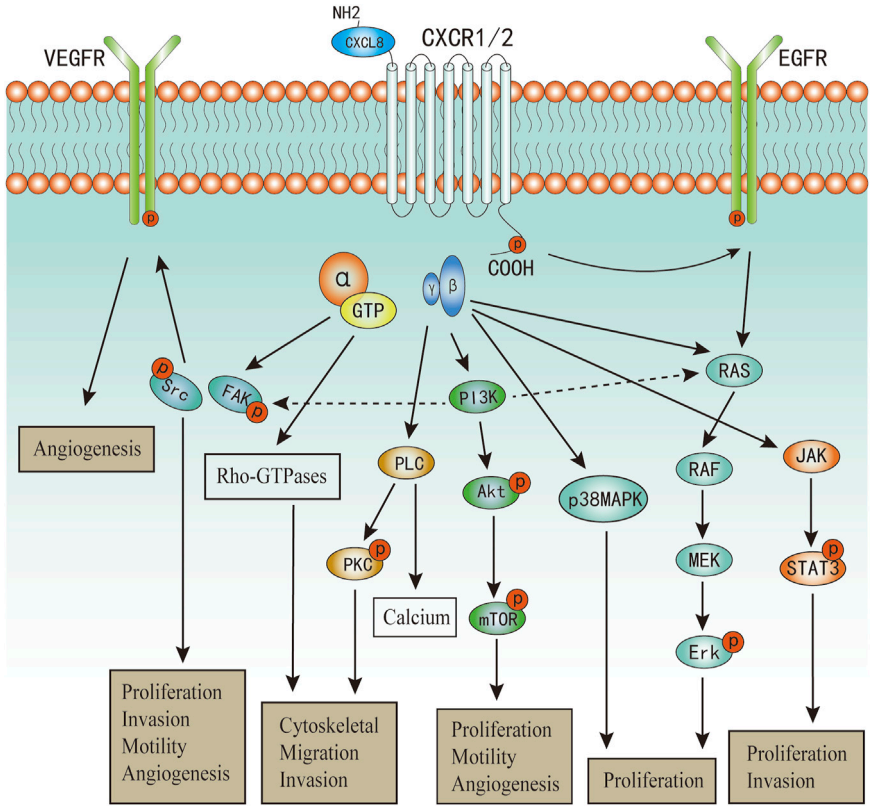

FIGURE 2 | The major signaling pathways of CXCL8 in cancers.

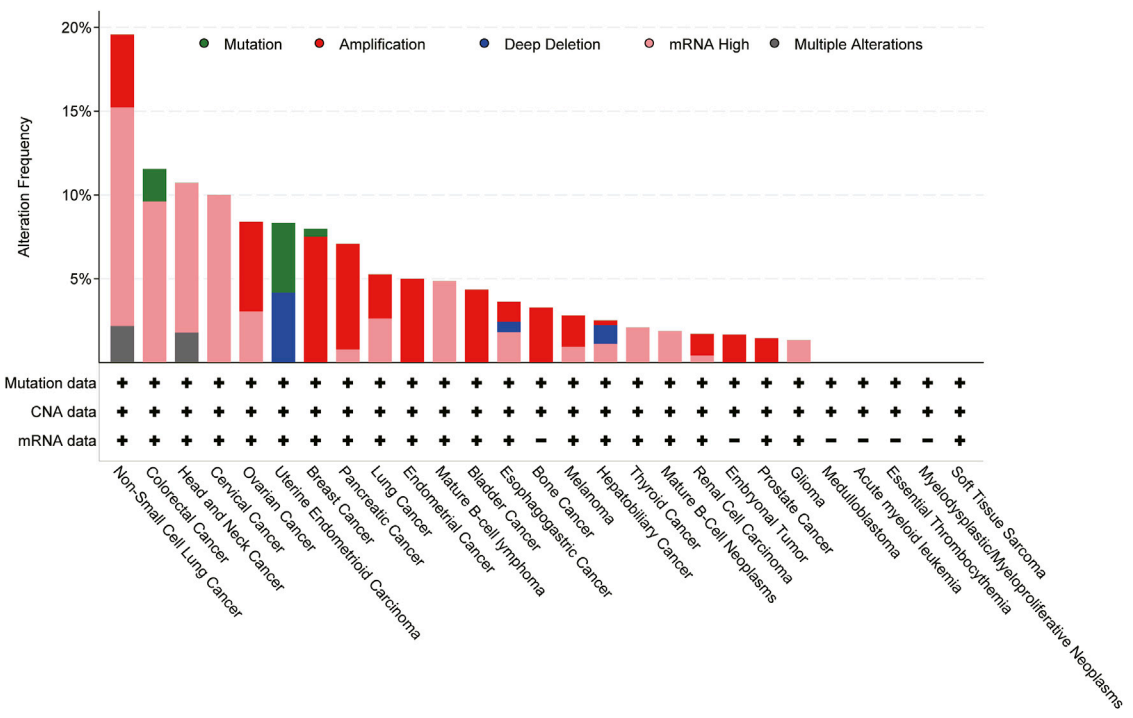

FIGURE 3 | Genomic alterations of CXCL8 cross 27 cancer types; TCGA pan-cancer cohort from cBioPortal for Cancer Genomics were used for this analysis.

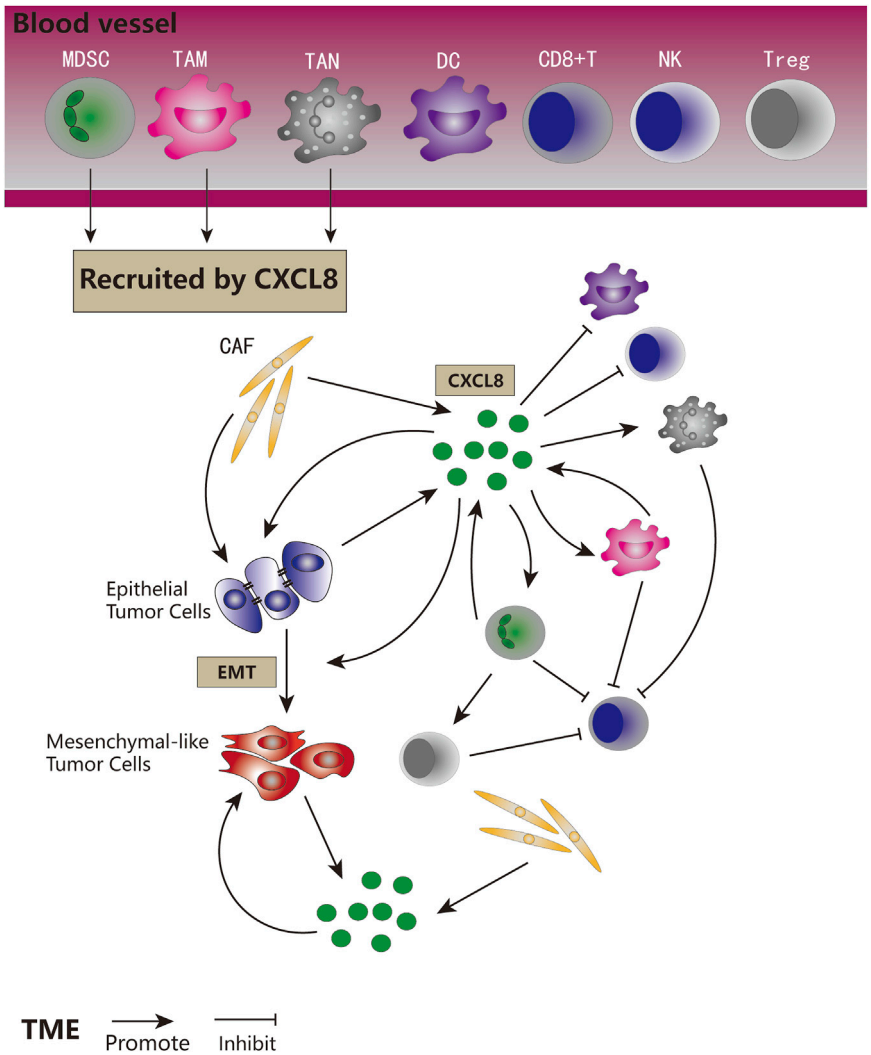

FIGURE 4 | The role of CXCL8 signaling in tumor biology. CXCL8 recruited MDSCs, TAMs, and TANs to the TME. CXCL8 could be secreted by tumor cells, CAFs, MDSCs, and TAMs. CXCL8 could promote tumor cells proliferation and EMT, directly and indirectly. CXCL8 could facilitate the accumulation of pro-tumorigenic immune cells and tumor immune suppression, and inhibit anti-tumor immune cells in direct and indirect ways.

Roles of CXCL8 in Tumor Biology

Expression of CXCL8 is significantly higher in numerous types of cancers (**Figure 3**), and many studies have evidenced that serum level of CXCL8 in patients with cancer can act as a prognostic marker (Cheng et al., 2019; Fousek et al., 2021). CXCL8 can promote tumor proliferation, survival, invasion, angiogenesis, tumor stemness and suppress anti-tumor immunity in direct and indirect manner (**Figure 4**) (**Table 1**). Growing evidence indicates that CXCL8 can directly contribute to the development of resistance to chemotherapy, molecularly targeted therapy, and immune checkpoint inhibition (ICI) therapy (Alfaro et al., 2017; Fousek et al., 2021). Therefore, CXCL8 has already been described as a pro-tumorigenic chemokine by impacting cancer cells and modifying TME to promote tumor progression and metastasis.

Promoting Tumor Cells Proliferation and Survival by Novel Mechanisms

Many studies have proved that CXCL8 can promote cell proliferation and inhibit apoptosis in multiple cancers, including breast cancer, prostate cancer, lung cancer, colon cancer and so on (Liu et al., 2016). CXCL8 can mediate cancer cell proliferation both in autocrine and paracrine manner. Previous review has demonstrated that CXCL8 could be secreted by tumor cells and subsequently promote themselves growth and/or inhibit apoptosis (Liu et al., 2016). Some recent researches again proved this

TABLE 1 | The role of CXCL8 in common cancers. CSCs=Cancer Stem Cells

Cancer type	Function
Breast Cancer	Proliferation, Invasion and Migration, Angiogenesis, CSCs, Tumor Immune Suppression
Prostate Cancer	Proliferation, Invasion and Migration, Angiogenesis, CSCs, Tumor Immune Suppression
Lung Cancer	Proliferation, Angiogenesis, CSCs, Tumor Immune Suppression
Colon Cancer	Proliferation, Invasion and Migration, Angiogenesis, CSCs
Head and Neck Squamous Cell Carcinoma	Proliferation, Invasion and Migration
Osteosarcoma	Invasion and Migration
Glioma	Invasion and Migration, CSCs
Clear Cell Renal Cell Carcinoma	CSCs
Bladder Cancer	CSCs
Esophageal Carcinoma	CSCs
Hepatocellular Carcinoma	CSCs
Melanoma	Proliferation, Invasion and Migration, Angiogenesis, Tumor Immune Suppression
Ovarian Cancer	Proliferation, Invasion and Migration, Angiogenesis, Tumor Immune Suppression
Diffuse Large B-Cell Lymphoma	Tumor Immune Suppression
Pancreatic Cancer	Proliferation, Invasion and Migration, Angiogenesis, Tumor Immune Suppression
Gastric Cancer	Proliferation, Invasion and Migration, Angiogenesis, Tumor Immune Suppression

mechanism (Guo et al., 2017; Cui et al., 2018; Jia et al., 2018; Kumar et al., 2019).

Recently, increased evidence highlighted several novel mechanisms. As metabolism reprogramming has already become a hallmark of cancer, Xu et al. illustrate that CXCL8 could mediate enhancement of aerobic glycolysis in colorectal cancer (CRC) cells and reduce intracellular reactive oxygen species (ROS) levels, which subsequently promote CRC cell proliferation and invasion (Xu et al., 2017). We have also shown that CXCL8 can reduce the level of intracellular ROS by inhibiting the function of GSK-3β to suppress prostate cancer cell apoptosis (Sun L. et al., 2019). Components of TME play a vital role in progression and metastasis of cancer and can induce an upregulated cytokines and chemokines, such as CXCL8. Two studies conducted in CRC and pancreatic ductal adenocarcinoma indicated that mesenchymal stem cells (MSCs) and cancer-associated fibroblasts (CAFs) could promote cancer cells secreting CXCL8, then enhancing the ability of proliferation and invasion (Wang et al., 2015; Awaji et al., 2019). Furthermore, Yang et al. have demonstrated that there exists a positive feedback between CRC and neutrophil extracellular traps (NETs) mediated by CXCL8 (Yang L. et al., 2020). In addition to malignant cells, cells in TME can also secret CXCL8 and promote cancer cell proliferation, which can be supported by a recent study that suggested that CAFs in TME can release CXCL8 to increase the proliferation ability of gallbladder cancer cells (Chen et al., 2020).

Promoting Tumor Cells Invasion and Migration by Novel Mechanisms

One of the main mechanisms used by tumor cells to obtain invasiveness and motility is the epithelial-to-mesenchymal transition (EMT). Present studies have proved that CXCL8 is essential for tumor cells to acquire and maintain this aggressive phenotype (Long et al., 2016; Fousek et al., 2021). As displayed above, components of TME can secret or promote cancer cells to secret CXCL8 which can also subsequently mediate the EMT of tumor cells. Further, there also exists an autocrine positive feedback loop between EMT and CXCL8 (David et al., 2016; Long et al., 2016). Many published researches indicate the important role of EMT in tumor resistance to chemotherapy, molecularly targeted therapy, and immune checkpoint inhibition (ICI) therapy (Horn et al., 2020b). Additionally, there are many excellent reviews about other mechanisms of CXCL8 in tumor therapy resistance (Alfaro et al., 2017; Cheng et al., 2019; Horn et al., 2020a; Fousek et al., 2021).

Emerging investigations have highlighted several novel mechanisms that are associated with the role of CXCL8 in cancer cell invasion and migration, including tumor heterogeneity, formation of feedback loop, and interacting with TME. Tumor heterogeneity is a vital feature of cancers, and cell sub-populations may interact with others to facilitate tumor progression (Meacham and Morrison, 2013). In the context of CRC, both hypoxic and fusobacterium nucleatum infected cancer cells can secret CXCL8 which subsequently contribute to the EMT of normoxic and noninfected cancer cells (Casasanta et al., 2020; Mi et al., 2020). Maynard et al. also demonstrate that only part of prostate cancer cells express CXCL8 in prostate cancer tissue microarrays, and high level of CXCL8 is associated with a more aggressive disease (Maynard et al., 2020). Pro-tumor feedback loops mediated by CXCL8 has been observed in multiple types of cancers. Xu et al. reported an intracellular feedback loop between CXCL8 and PTEN in HNSCC (Xu et al., 2020). Similarly, PTEN loss can also selectively upregulate the CXCL8 signaling in prostate cancer cells (Maxwell et al., 2013). Effects of CXCL8 on tumor cells could also influence the TME or be influenced by the components of TME. MSCs and NET can also form a positive pro-tumor feedback loop with osteosarcoma and glioma cells *via* CXCL8, respectively (Kawano et al., 2018; Zha et al., 2020). Previous reviews and many recent studies have illustrated that multiple cell types in TME can directly secret CXCL8, or regulate the expression of CXCL8 in cancer cells, or be regulated by

CXCL8 derived from cancer cells to promote tumor invasion and migration (Zheng et al., 2018; Cheng et al., 2019; Nie et al., 2019; Fousek et al., 2021).

Promoting Tumorogenic Angiogenesis

Angiogenesis has been recognized as a hallmark of cancer, which is necessary for tumor survival and disseminating to a new location (Hanahan and Weinberg, 2011). Effect of CXCL8 on tumor angiogenesis has been widely investigated, and CXCL8 has already be defined as a pro-angiogenesis chemokine (Liu et al., 2016; Cheng et al., 2019; Fousek et al., 2021; Ueda et al., 2022). Human vascular endothelial cells constitutively express CXCR2 (Cheng et al., 2019). Upon cancer cells and some types of stroma cells secreting CXCL8 in TME, endothelial cells begin to express and secret matrix metalloproteinases (MMPs) to break down the extracellular matrix (ECM), then, resulting in angiogenesis (Li et al., 2003). In addition, CXCL8 can also induce recruitment of endothelial cells which participate directly in vascularization (Strieter et al., 1995). Intriguingly, there is also a crosstalk between CXCL8 and VEGFR2 in angiogenesis (Petreaca et al., 2007). In this context, a loop in endothelial cells have been discovered, which is that CXCL8 can increase the secretion of VEGF-A and induce the expression of VEGFR2 in endothelial cells (Martin et al., 2009; Alfaro et al., 2017).

Promoting Development of Cancer Stem Cells

A plethora of literature indicates that CXCL8 is involved in the maintenance of cancer stem cells (CSCs) which is always associated with tumor development and progression, treatment resistance and used to explain heterogeneity in solid tumors (Raza et al., 2022). Generally, the CXCL8-CXCR1/2 axis plays impact roles on formation, development or invasion of CSCs in colon cancer (Luo et al., 2018; Fisher et al., 2019; Kim et al., 2021), breast cancer (Choi et al., 2009), glioblastoma (Zhou et al., 2014; McCoy et al., 2019), clear cell renal cell carcinoma (ccRCC) (Corrò et al., 2019), pancreatic cancer (Chen et al., 2014), hepatocellular carcinoma (HCC) (Kahraman et al., 2019), lung cancer (Shimizu and Tanaka, 2019), bladder cancer (Zhou et al., 2021) and esophageal carcinoma (Huang et al., 2017). Furthermore, CXCL8 has also been found to promote the interaction between CSCs and mesenchymal stem cells (MSCs) to further enlarging the population of CSCs in colon cancer (Ma et al., 2020; Ma et al., 2021). Given the crucial role of CXCL8 in CSCs, targeting CXCL8-CXCR1/2 axis as a component of combination therapy has also been explored. Pre-clinical studies demonstrate that combining CXCR1/2 inhibitors with the human epidermal growth factor receptor 2 (HER2)-targeted therapies has potential as an effective treatment strategy to repress CSCs activity in breast cancer (Singh et al., 2013). In HCC, after inhibiting CXCR1/2 by Reparixin or knockdown CXCL8, CSCs features of HCC were reduced, and sensitivity to Sorafenib increased significantly (Kahraman et al., 2019).

Inhibiting Anti-Tumor Immunity

CXCL8 also has potent ability on modulating immune cell chemotaxis and functions. CXCL8 derived from tumor can act in a paracrine manner to change the composition of immune infiltration in TME, resulting the accumulation of pro-tumorigenic immune cells and tumor immune suppression (Alfaro et al., 2017; Horn et al., 2020b). Published reports collectively suggest that CXCL8 can recruit tumor-associated macrophages (TAMs), myeloid derived suppressor cells (MDSCs), and neutrophils to the TME, resulting in dampening the anti-tumor immune response of cytotoxic immune cells. Correspondingly, it can also attenuate the anti-tumor activity of dendritic cells (DCs) and NK cells (Alfaro et al., 2017; Fousek et al., 2021).

Neutrophils make up a sizeable part of immune cells in TME, so-called tumor-associated neutrophils (TANs), which can be divided into antitumor N1 and pro-tumor N2 phenotypes (Fridlender et al., 2009). Further, the N2 TANs promote tumor progression by activating tumor angiogenesis, suppressing the function of anti-tumor T cells, and recruiting T regulatory cells (Tregs) (Rodriguez et al., 2004; Nozawa et al., 2006; Mishalian et al., 2014; David et al., 2016). Unfortunately, there are no groups directly investigating the relationship between CXCL8 and N2 phenotype. Several recent reports preliminary demonstrate the effect of CXCL8 on TANs. In ovarian cancer, CXCL8 can recruit TANs in TME and induce the expression of Jagged2 (JAG2) in TANs which subsequently inhibit the activity of CD8(+) T cells (Yang M. et al., 2020). Additionally, TANs in the TME of diffuse large B-cell lymphoma (DLBCL) can also increase the secretion of april mediated by CXCL8, and promote DLBCL progression (Manfroi et al., 2017).

MDSCs are known as a heterogeneous population of immature immunosuppressive cells, which derive from myeloid progenitor cells, accumulate in the circulation and the TME of most cancer patients (Gabrilovich and Nagaraj, 2009; David et al., 2016). Generally, MDSCs can be divided into two subtypes: granulocytic ($CD33^+$ CD11b + HLA-DR-/low $CD15^+$, PMN-MDSC) or monocytic (CD33 + CD11b + HLA-DR-/low $CD14^+$, M-MDSC) (Poschke and Kiessling, 2012). In TME, MDSCs have been shown to act as a driver of immune suppression by inactivating T cell receptors, starving T cell, inhibiting T cell proliferation, recruiting CAFs, and inducing Tregs (David et al., 2016; Horn et al., 2020a). Increasing investigations evidence the role of CXCL8 in attracting and enhancing the function of MDSCs which then attenuate the activation of CD8(+) T cell (Asfaha et al., 2013; Katoh et al., 2013; Dominguez et al., 2017; Najjar et al., 2017; Li et al., 2018). Interestingly, CXCL8 can recruit the both subtypes of MDSCs to TME, but they play different functions (Alfaro et al., 2016). The M-MDSCs can directly suppress the activity of T cells, however, the PMN-MDSC subset only induce the formation of NETs which might facilitate tumor cell migration. Further, a recent report indicates a novel subtype of MDSCs that attract by CXCL8 in human gastric cancer (Mao et al., 2018). After attracting CD45(+)CD33(low)CD11b(dim) MDSCs to TME, CXCL8 will promote this novel subset MDSCs expressing arginase I that contributes to CD8(+) T cell suppression via PI3K/Akt signaling.

Supportively, in prostate cancer and melanoma, the increasing level of circulating MDSCs are evidenced to be associated poor clinical outcomes and high plasma CXCL8 concentration (Chi et al., 2014; Tobin et al., 2019).

Tumor-associated macrophages (TAMs) are present in all stages of tumors and exert a dual effectiveness on tumor progression (Noy and Pollard, 2014; Mantovani et al., 2017). Similar to TANs, TAMs have been divided into two subsets: antitumor M1-like and tumor-promoting M2-like phenotype (Noy and Pollard, 2014). Numerous studies have concentrated on the role of TAMs on CXCL8, which have indicated that TAMs can express or induce tumor cell secreting CXCL8 to contribute to tumor progression (Chen et al., 2003; Chen et al., 2018; Zheng et al., 2018). Emerging reports uncover that CXCL8 also have vital roles in recruiting and directing the polarization of TAMs. The findings of Zhang and colleagues suggest that the CXCL8-CXCR2 axis can promote trafficking of CXCR2(+) CD68(+) macrophages to pancreatic cancer TME, and the recruitment TAMs can inhibit the efficacy of PD1 blockade (Zhang et al., 2020). Further investigation performed in gastric cancer indicates that TAMs can induce themselves increasing the expression of PD-L1 and decrease CD8(+) T cells infiltration by secreting CXCL8 (Lin et al., 2019). Meanwhile, CXCL8 also plays a role in inducing a shift in TAMs toward the M2 phenotype (Krawczyk et al., 2017; Ning et al., 2018).

DCs and NK cells play important roles in adaptive and innate anti-tumor immune response, respectively. Previous studies suggest that CXCL8 derived from tumor cells can disorients DCs migration without impairing the stimulation of T-cell (Feijoó et al., 2005; Alfaro et al., 2011; Li et al., 2021). A recent investigations indicates that tumor cells can secret CXCL8 to impair the functions of NK cells via STAT3 signaling (Wu et al., 2019).

CXCL8 in Immune Checkpoint Therapy

Many excellent reviews demonstrate the role of CXCL8-CXCR1/2 axis in target therapy, chemotherapy and the prognostic role of plasma level of CXCL8 in cancer (Liu et al., 2016; Alfaro et al., 2017; Cheng et al., 2019; Fousek et al., 2021). Here, we highlight current preclinical and clinical studies correlating CXCL8 to immunotherapy. Immune checkpoint inhibitions (ICIs) has become the cornerstone of immunotherapy in many types of cancers (Ribas and Wolchok, 2018; Bakouny and Choueiri, 2020). However, not all cancer patients have a good response to ICIs, and early determining the clear group which is sensitive or resistant to ICIs can improve clinical outcomes. Recent evidences suggest that CXCL8 plays an important role in response quality on ICIs.

A small retrospective trial suggests that increasing level of serum CXCL8 can predict resistant to anti-PD-1 treatment in non-small-cell lung cancer (NSCLC) patients (Sanmamed et al., 2017). To further investigating the role of CXCL8 in predicting response of patients treated with ICIs, two recent trials with large sample size have been performed to evaluate the correlation between plasma CXCL8 and cancer progression (Schalper et al., 2020; Yuen et al., 2020). Schalper et al., using a large cohort with 1,344 patients, show that high baseline plasma CXCL8 level is associated with poor clinical outcomes in participants with advanced melanoma, NSCLC, and renal-cell carcinoma (RCC) treated with nivolumab or ipilimumab, everolimus or docetaxel, which indicate that serum CXCL8 level is an unfavorable factor in tumor immunobiology and can act as an independently predictive biomarker in patients receiving ICIs (Schalper et al., 2020). Another multiple randomized trials with 1,445 patients in metastatic urothelial carcinoma (mUC) and mRCC confirms this finding (Yuen et al., 2020). Both trials further suggest that greater CXCL8 expression in tumor is associated with higher plasma CXCL8 level, an immunosuppressive myeloid-enriched TME, and T cell suppression (Schalper et al., 2020; Yuen et al., 2020). Additionally, Yuen and colleagues also further stratify patients using plasma CXCL8 level and T cell effector signature score. Patients with high T cell effector signature score and low plasma CXCL8 level can derive best benefit from ICIs (Yuen et al., 2020).

Emerging studies suggest that combination of targeting CXCL8-CXCR1/2 axis and ICIs can provide further benefit in anti-tumor efficacy. In the context of breast and lung cancer, combined SX-682, an bioavailable small-molecule inhibitor of CXCR1 and CXCR2, and anti-PD-1/PD-L1 can achieve best tumor control in murine model (Sun Y. et al., 2019; Horn et al., 2020b). Interestingly, both studies indicate that inhibition of CXCR1/2 eventually results in reducing infiltration with PMN-MDSCs which play a vital role in T cell suppression. Zhang et al. discover that treated with interferon gamma (IFN-γ) can suppress a variety of pancreatic cancer derived CXCL8 and tumor-derived CXCL8 deficiency inhibit the trafficking of M2 TAM (Zhang et al., 2020). Further, combined IFN-γ and anti-PD-1 treatment enhance the anti-tumor efficacy. As for directly targeting CXCL8, in triple-negative breast cancer (TNBC), HuMax-IL8, a fully human monoclonal antibody that inhibits CXCL8, can significantly reduce the infiltration of PMN-MDSCs to TME and enhance the efficacy of immunotherapy (Dominguez et al., 2017).

Bilusic et al. conduct a phase I clinical trial including 15 patients with metastatic or unresectable solid tumors treated with HuMax-IL8 (Bilusic et al., 2019). The results of this trial indicate that HuMax-IL8 is safe and well-tolerated. This trial could be a basic evidence for further evaluating the combination of CXCL8 blockade and other immunotherapies. In addition, several ongoing studies have been designed to evaluate the safety and efficacy of combined HuMax-IL8 and immunotherapy in cancer patients (**Table 2**).

Future Directions

Expression of CXCL8 is significantly higher in numerous types of cancers, and high expression of CXCL8 is significantly associated with shorter median overall survival in many kinds of cancers based on TCGA database (**Table 3**). The findings of numerous researches involving preclinical *in vitro* and *in vivo* models illustrate that combination of targeting CXCL8-CXCR1/2 axis and ICIs can provide further benefit in anti-tumor efficacy. In addition, clinical trials demonstrate that CXCL8 plays an important role in response quality on ICIs. Furthermore, activation of CXCL8-CXCR1/2 axis and its downstream

TABLE 2 | Clinical Studies of combination of ICI agents and CXCL8 blockade. A = active; R = recruiting.

Checkpoint agent	CXCL8 blockade	Cancer type	Sample size	Clinical trial number	Status
Nivolumab	HuMax-IL8	Advanced Cancers	320	NCT03400332	A
Nivolumab	HuMax-IL8	Hepatocellular Carcinoma	74	NCT04050462	R
Nivolumab	HuMax-IL8	Hormone-Sensitive Prostate Cancer	60	NCT03689699	R

TABLE 3 | The correlation between CXCL8 expression and cancer survival in TCGA cohorts. HR, hazard ratio; CI, confidence interval; OS, overall survival; NA, not analysis.

Cancer type	HR(95%CI)	Median OS (Months)	
		Low expression cohort	High expression cohort
Cervical squamous cell carcinoma	2.97 (1.78, 4.94)	68.40	25.77
Esophageal Adenocarcinoma	2.76 (1.40, 5.54)	46.73	9.07
Head-neck squamous cell carcinoma	1.54 (1.15, 2.07)	58.27	33.27
Kidney renal clear cell carcinoma	1.89 (1.37, 2.61)	55.23	31.53
Kidney renal papillary cell carcinoma	2.44 (1.03, 5.77)	NA	NA
Liver hepatocellular carcinoma	2.40 (1.60, 3.59)	104.17	45.73
Lung adenocarcinoma	1.58 (1.09, 2.29)	59.27	42.93
Lung squamous cell carcinoma	1.38 (1.05, 1.81)	63.73	38.47
Pancreatic ductal adenocarcinoma	2.10 (1.23, 3.58)	72.73	19.73
Sarcoma	1.66 (1.09, 2.50)	89.80	54.97
Stomach adenocarcinoma	1.49 (1.06, 2.10)	43.13	22.50
Thyroid carcinoma	3.29 (1.18, 9.17)	NA	NA

signaling pathways play important roles in tumor survival and invasion, and suppress antitumor immune responses in the TME. Therefore, therapies targeting this axis are likely to benefit patients with cancer by inhibiting tumor growth and stimulating antitumor immunity. Clinical trials are ongoing to prove this.

As metabolism reprogramming has already become a hallmark of cancer, the relationship between CXCL8 and tumor metabolism reprogramming is not widely explored. How CXCL8 influences tumor metabolism and subsequently facilitate cancer proliferation needing further investigation. In addition, present studies demonstrated that part of CRC cells could secreted CXCL8 which contributed to the EMT of the remaining cells not secreting CXCL8. However, the mechanism of this phenomenon is not clear. Further exploration is needed to determine if other types of cancer exist similar phenomenon. As mentioned, CXCL8 can recruit TANs in TME. Unfortunately, there are no groups directly investigating the relationship between CXCL8 and N2 phenotype. Meanwhile, CXCL8 also plays a role in inducing a shift in TAMs toward the M2 phenotype. However, the mechanism is unclear.

CONCLUSION

The Chemokine CXCL8 is well accepted to play a crucial role in tumor survival, invasion, and TME angiogenesis, immune suppression via several types of intracellular signaling pathway. To date, many novel mechanisms to mediate the above tumor biology by CXCL8 have been highlighted. More and more evidences indicate that CXCL8 should be considered as a pro-tumor factor with dual roles: directly promoting tumor survival and affecting components of TME to indirectly facilitate tumor progression. Further, CXCL8 can also act as an important predictor of the clinical outcomes for ICIs. As cancer therapy advances, some emerging clinical trials are ongoing to explore the efficacy and safety of combining anti-CXCL8 and ICIs therapy.

AUTHOR CONTRIBUTIONS

LY and JA were responsible for the conception and design of the study. XX and SQ did the articles' search. XX, XL, SZ, and SQ were responsible for the acquisition of relevant information. XX, HX, SZ, and SW wrote the first draft of the manuscript. SW, SZ, JA, and LY interpreted the relevant information and wrote the final version. All authors critically revised the Article for important intellectual content and approved the final version. LY and AJZ obtained public funding.

FUNDING

This work was supported by Sichuan International Science and technology innovation cooperation/Hong Kong, Macao and Taiwan Science and technology innovation cooperation project (2021YFH0172); the National key research and development program of China (Grant No. 2017YFC0908003); National Natural Science Foundation of China (Grant No.81974099,

81974098); Post-doctoral Science Research Foundation of Sichuan University (2020SCU12041); National Clinical Research Center for Geriatrics, West China Hospital, Sichuan University (Z2018C01); Technology Innovation Research and Development Project, Chengdu Science and Technology Bureau (2019-YF05-00296-SN). project (2021YFH0172).

REFERENCES

Alassaf, E., and Mueller, A. (2020). The Role of PKC in CXCL8 and CXCL10 Directed Prostate, Breast and Leukemic Cancer Cell Migration. *Eur. J. Pharmacol.* 886, 173453. doi:10.1016/j.ejphar.2020.173453

Alfaro, C., Sanmamed, M. F., Rodríguez-Ruiz, M. E., Teijeira, Á., Oñate, C., González, Á., et al. (2017). Interleukin-8 in Cancer Pathogenesis, Treatment and Follow-Up. *Cancer Treat. Rev.* 60, 24–31. doi:10.1016/j.ctrv.2017.08.004

Alfaro, C., Suárez, N., Martínez-Forero, I., Palazón, A., Rouzaut, A., Solano, S., et al. (2011). Carcinoma-derived Interleukin-8 Disorients Dendritic Cell Migration without Impairing T-Cell Stimulation. *PLoS One* 6, e17922. doi:10.1371/journal.pone.0017922

Alfaro, C., Teijeira, A., Oñate, C., Pérez, G., Sanmamed, M. F., Andueza, M. P., et al. (2016). Tumor-Produced Interleukin-8 Attracts Human Myeloid-Derived Suppressor Cells and Elicits Extrusion of Neutrophil Extracellular Traps (NETs). *Clin. Cancer Res.* 22, 3924–3936. doi:10.1158/1078-0432.CCR-15-2463

Asfaha, S., Dubeykovskiy, A. N., Tomita, H., Yang, X., Stokes, S., Shibata, W., et al. (2013). Mice that Express Human Interleukin-8 Have Increased Mobilization of Immature Myeloid Cells, Which Exacerbates Inflammation and Accelerates colon Carcinogenesis. *Gastroenterology* 144, 155–166. doi:10.1053/j.gastro.2012.09.057

Ashburner, B. P., Westerheide, S. D., and Baldwin, A. S. (2001). The P65 (RelA) Subunit of NF-Kb Interacts with the Histone Deacetylase (HDAC) Corepressors HDAC1 and HDAC2 to Negatively Regulate Gene Expression. *Mol. Cel Biol* 21, 7065–7077. doi:10.1128/MCB.21.20.7065-7077.2001

Awaji, M., Futakuchi, M., Heavican, T., Iqbal, J., and Singh, R. K. (2019). Cancer-Associated Fibroblasts Enhance Survival and Progression of the Aggressive Pancreatic Tumor via FGF-2 and CXCL8. *Cancer Microenvironment* 12, 37–46. doi:10.1007/s12307-019-00223-3

Baggiolini, M., Dewald, B., and Moser, B. (1997). Human Chemokines: an Update. *Annu. Rev. Immunol.* 15, 675–705. doi:10.1146/annurev.immunol.15.1.675

Bakouny, Z., and Choueiri, T. K. (2020). IL-8 and Cancer Prognosis on Immunotherapy. *Nat. Med.* 26, 650–651. doi:10.1038/s41591-020-0873-9

Baldwin, E. T., Weber, I. T., St Charles, R., Xuan, J. C., Appella, E., Yamada, M., et al. (1991). Crystal Structure of Interleukin 8: Symbiosis of NMR and Crystallography. *Proc. Natl. Acad. Sci.* 88, 502–506. doi:10.1073/pnas.88.2.502

Balkwill, F. (2004). Cancer and the Chemokine Network. *Nat. Rev. Cancer* 4, 540–550. doi:10.1038/nrc1388

Berkamp, S., Park, S. H., De Angelis, A. A., Marassi, F. M., and Opella, S. J. (2017). Structure of Monomeric Interleukin-8 and its Interactions with the N-Terminal Binding Site-I of CXCR1 by Solution NMR Spectroscopy. *J. Biomol. NMR* 69, 111–121. doi:10.1007/s10858-017-0128-3

Bilusic, M., Heery, C. R., Collins, J. M., Donahue, R. N., Palena, C., Madan, R. A., et al. (2019). Phase I Trial of HuMax-IL8 (BMS-986253), an anti-IL-8 Monoclonal Antibody, in Patients with Metastatic or Unresectable Solid Tumors. *J. Immunotherapy Cancer* 7, 240. doi:10.1186/s40425-019-0706-x

Boonyanugomol, W., Rukseree, K., Kongkasame, W., Palittapongarnpim, P., Baik, S.-C., and Manwong, M. (2019). Genetic Polymorphisms of CXCL8 (−251) Are Associated with the Susceptibility of *Helicobacter pylori* Infection Increased the Risk of Inflammation and Gastric Cancer in Thai Gastroduodenal Patients. *Ijaai* 18, 393–401. doi:10.18502/ijaai.v18i4.1417

Casasanta, M. A., Yoo, C. C., Udayasuryan, B., Sanders, B. E., Umaña, A., Zhang, Y., et al. (2020). Fusobacterium Nucleatum Host-Cell Binding and Invasion Induces IL-8 and CXCL1 Secretion that Drives Colorectal Cancer Cell Migration. *Sci. Signal.* 13. doi:10.1126/scisignal.aba9157

Chen, C., Zhang, R., Ma, L., Li, Q., Zhao, Y. L., Zhang, G. J., et al. (2020). Neuropilin-1 Is Up-regulated by Cancer-associated Fibroblast-secreted IL-8 and Associated with Cell Proliferation of Gallbladder Cancer. *J. Cel. Mol. Med.* 24, 12608–12618. doi:10.1111/jcmm.15825

Chen, J. J., Yao, P. L., Yuan, A., Hong, T. M., Shun, C. T., Kuo, M. L., et al. (2003). Up-regulation of Tumor Interleukin-8 Expression by Infiltrating Macrophages: its Correlation with Tumor Angiogenesis and Patient Survival in Non-small Cell Lung Cancer. *Clin. Cancer Res.* 9, 729–737.

Chen, L., Fan, J., Chen, H., Meng, Z., Chen, Z., Wang, P., et al. (2014). The IL-8/CXCR1 axis Is Associated with Cancer Stem Cell-like Properties and Correlates with Clinical Prognosis in Human Pancreatic Cancer Cases. *Sci. Rep.* 4, 5911. doi:10.1038/srep05911

Chen, S.-j., Lian, G.-d., Li, J.-j., Zhang, Q.-b., Zeng, L.-j., Yang, K.-g., et al. (2018). Tumor-driven like Macrophages Induced by Conditioned media from Pancreatic Ductal Adenocarcinoma Promote Tumor Metastasis via Secreting IL-8. *Cancer Med.* 7, 5679–5690. doi:10.1002/cam4.1824

Cheng, Y., Ma, X.-l., Wei, Y.-q., and Wei, X.-W. (2019). Potential Roles and Targeted Therapy of the CXCLs/CXCR2 axis in Cancer and Inflammatory Diseases. *Biochim. Biophys. Acta (Bba) - Rev. Cancer* 1871, 289–312. doi:10.1016/j.bbcan.2019.01.005

Chi, N., Tan, Z., Ma, K., Bao, L., and Yun, Z. (2014). Increased Circulating Myeloid-Derived Suppressor Cells Correlate with Cancer Stages, Interleukin-8 and -6 in Prostate Cancer. *Int. J. Clin. Exp. Med.* 7, 3181–3192.

Choi, H. S., Kim, J.-H., Kim, S.-L., and Lee, D.-S. (2009). Disruption of the NF-κB/IL-8 Signaling Axis by Sulconazole Inhibits Human Breast Cancer Stem Cell Formation. *Cells* 8, 1007. doi:10.3390/cells8091007

Corrò, C., Healy, M. E., Engler, S., Bodenmiller, B., Li, Z., Schraml, P., et al. (2019). IL-8 and CXCR1 Expression Is Associated with Cancer Stem Cell-like Properties of clear Cell Renal Cancer. *J. Pathol.* 248, 377–389. doi:10.1002/path.5267

Cui, Z. Y., Jo, E., Jang, H. J., Hwang, I.-H., Lee, K.-B., Yoo, H.-S., et al. (2018). Modified Ginseng Extract Induces Apoptosis in HepG2 Cancer Cells by Blocking the CXCL8-Mediated Akt/Nuclear Factor-Kb Signaling Pathway. *Am. J. Chin. Med.* 46, 1645–1662. doi:10.1142/S0192415X18500842

Das, S. T., Rajagopalan, L., Guerrero-Plata, A., Sai, J., Richmond, A., Garofalo, R. P., et al. (2010). Monomeric and Dimeric CXCL8 Are Both Essential for *In Vivo* Neutrophil Recruitment. *PLoS One* 5, e11754. doi:10.1371/journal.pone.0011754

Daub, H., Ulrich Weiss, F., Wallasch, C., and Ullrich, A. (1996). Role of Transactivation of the EGF Receptor in Signalling by G-Protein-Coupled Receptors. *Nature* 379, 557–560. doi:10.1038/379557a0

David, J., Dominguez, C., Hamilton, D., and Palena, C. (2016). The IL-8/IL-8R Axis: A Double Agent in Tumor Immune Resistance. *Vaccines* 4, 22. doi:10.3390/vaccines4030022

Dominguez, C., McCampbell, K. K., David, J. M., and Palena, C. (2017). Neutralization of IL-8 Decreases Tumor PMN-MDSCs and Reduces Mesenchymalization of Claudin-Low Triple-Negative Breast Cancer. *JCI Insight* 2. doi:10.1172/jci.insight.94296

Feijoó, E., Alfaro, C., Mazzolini, G., Serra, P., Peñuelas, I., Arina, A., et al. (2005). Dendritic Cells Delivered inside Human Carcinomas Are Sequestered by Interleukin-8. *Int. J. Cancer* 116, 275–281. doi:10.1002/ijc.21046

Fisher, R. C., Bellamkonda, K., Alex Molina, L., Xiang, S., Liska, D., Sarvestani, S. K., et al. (2019). Disrupting Inflammation-Associated CXCL8-CXCR1 Signaling Inhibits Tumorigenicity Initiated by Sporadic- and Colitis-Colon Cancer Stem Cells. *Neoplasia* 21, 269–281. doi:10.1016/j.neo.2018.12.007

Fousek, K., Horn, L. A., and Palena, C. (2021). Interleukin-8: A Chemokine at the Intersection of Cancer Plasticity, Angiogenesis, and Immune Suppression. *Pharmacol. Ther.* 219, 107692. doi:10.1016/j.pharmthera.2020.107692

Fridlender, Z. G., Sun, J., Kim, S., Kapoor, V., Cheng, G., Ling, L., et al. (2009). Polarization of Tumor-Associated Neutrophil Phenotype by TGF-β: "N1" versus "N2" TAN. *Cancer Cell* 16, 183–194. doi:10.1016/j.ccr.2009.06.017

Fu, X.-T., Dai, Z., Song, K., Zhang, Z.-J., Zhou, Z.-J., Zhou, S.-L., et al. (2015). Macrophage-secreted IL-8 Induces Epithelial-Mesenchymal Transition in Hepatocellular Carcinoma Cells by Activating the JAK2/STAT3/Snail Pathway. *Int. J. Oncol.* 46, 587–596. doi:10.3892/ijo.2014.2761

Gabrilovich, D. I., and Nagaraj, S. (2009). Myeloid-derived Suppressor Cells as Regulators of the Immune System. *Nat. Rev. Immunol.* 9, 162–174. doi:10.1038/nri2506

Guo, Y., Zang, Y., Lv, L., Cai, F., Qian, T., Zhang, G., et al. (2017). IL-8 Promotes Proliferation and Inhibition of Apoptosis via STAT3/AKT/NF-κB Pathway in Prostate Cancer. *Mol. Med. Rep.* 16, 9035–9042. doi:10.3892/mmr.2017.7747

Ha, H., Debnath, B., and Neamati, N. (2017). Role of the CXCL8-Cxcr1/2 Axis in Cancer and Inflammatory Diseases. *Theranostics* 7, 1543–1588. doi:10.7150/thno.15625

Hanahan, D., and Weinberg, R. A. (2011). Hallmarks of Cancer: the Next Generation. *Cell* 144, 646–674. doi:10.1016/j.cell.2011.02.013

Hoffmann, E., Dittrich-Breiholz, O., Holtmann, H., and Kracht, M. (2002). Multiple Control of Interleukin-8 Gene Expression. *J. Leukoc. Biol.* 72, 847–855. doi:10.1189/jlb.72.5.847

Holmes, W. E., Lee, J., Kuang, W.-J., Rice, G. C., and Wood, W. I. (1991). Structure and Functional Expression of a Human Interleukin-8 Receptor. *Science* 253, 1278–1280. doi:10.1126/science.1840701

Horn, L. A., Fousek, K., and Palena, C. (2020a). Tumor Plasticity and Resistance to Immunotherapy. *Trends Cancer* 6, 432–441. doi:10.1016/j.trecan.2020.02.001

Horn, L. A., Riskin, J., Hempel, H. A., Fousek, K., Lind, H., Hamilton, D. H., et al. (2020b). Simultaneous Inhibition of CXCR1/2, TGF-β, and PD-L1 Remodels the Tumor and its Microenvironment to Drive Antitumor Immunity. *J. Immunother. Cancer* 8, e000326. doi:10.1136/jitc-2019-000326

Hu, X., Yuan, L., and Ma, T. (2020). Mechanisms of JAK-STAT S-ignaling P-athway M-ediated by CXCL8 G-ene S-ilencing on E-pithelial-mesenchymal T-ransition of H-uman C-utaneous M-elanoma C-ells. *Oncol. Lett.* 20, 1973–1981. doi:10.3892/ol.2020.11706

Huang, L., Lian, J., Chen, X., Qin, G., Zheng, Y., and Zhang, Y. (2017). WASH Overexpression Enhances Cancer Stem Cell Properties and Correlates with Poor Prognosis of Esophageal Carcinoma. *Cancer Sci.* 108 (12), 2358–2365. doi:10.1111/cas.13400

Jia, L., Li, F., Shao, M., Zhang, W., Zhang, C., Zhao, X., et al. (2018). IL-8 Is Upregulated in Cervical Cancer Tissues and Is Associated with the Proliferation and Migration of HeLa Cervical Cancer Cells. *Oncol. Lett.* 15, 1350–1356. doi:10.3892/ol.2020.11706

Ju, L., Zhou, Z., Jiang, B., Lou, Y., and Guo, X. (2017). Autocrine VEGF and IL-8 Promote Migration via Src/Vav2/Rac1/PAK1 Signaling in Human Umbilical Vein Endothelial Cells. *Cell Physiol Biochem* 41, 1346–1359. doi:10.1159/000465389

Kahraman, D. C., Kahraman, T., and Cetin Atalay, R. (2019). Targeting PI3K/Akt/mTOR Pathway Identifies Differential Expression and Functional Role of IL-8 in Liver Cancer Stem Cell Enrichment. *Mol. Cancer Ther.* 18, 0004–2157. doi:10.1158/1535-7163.MCT-19-0004

Katoh, H., Wang, D., Daikoku, T., Sun, H., Dey, S. K., and Dubois, R. N. (2013). CXCR2-expressing Myeloid-Derived Suppressor Cells Are Essential to Promote Colitis-Associated Tumorigenesis. *Cancer Cell* 24, 631–644. doi:10.1016/j.ccr.2013.10.009

Kawano, M., Tanaka, K., Itonaga, I., Iwasaki, T., and Tsumura, H. (2018). Interaction between Human Osteosarcoma and Mesenchymal Stem Cells via an Interleukin-8 Signaling Loop in the Tumor Microenvironment. *Cell Commun Signal* 16, 13. doi:10.1186/s12964-018-0225-2

Kilic, I., Guldiken, S., Sipahi, T., Palabiyik, O., Akker, M., Celik, O., et al. (2016). Investigation of VEGF and IL-8 Gene Polymorphisms in Patients with Differentiated Thyroid Cancer. *Clin. Lab.* 62, 2319–2325. doi:10.7754/Clin.Lab.2016.160403

Kim, B., Seo, Y., Kwon, J. H., Shin, Y., Kim, S., Park, S. J., et al. (2021). IL-6 and IL-8, Secreted by Myofibroblasts in the Tumor Microenvironment, Activate HES1 to Expand the Cancer Stem Cell Population in Early Colorectal Tumor. *Mol. Carcinogenesis* 60, 188–200. doi:10.1002/mc.23283

Knall, C., Worthen, G. S., and Johnson, G. L. (1997). Interleukin 8-stimulated Phosphatidylinositol-3-Kinase Activity Regulates the Migration of Human Neutrophils Independent of Extracellular Signal-Regulated Kinase and P38 Mitogen-Activated Protein Kinases. *Proc. Natl. Acad. Sci.* 94, 3052–3057. doi:10.1073/pnas.94.7.3052

Knall, C., Young, S., Nick, J. A., Buhl, A. M., Worthen, G. S., and Johnson, G. L. (1996). Interleukin-8 Regulation of the Ras/Raf/mitogen-Activated Protein Kinase Pathway in Human Neutrophils. *J. Biol. Chem.* 271, 2832–2838. doi:10.1074/jbc.271.5.2832

Koensgen, D., Bruennert, D., Ungureanu, S., Sofroni, D., Braicu, E. I., Sehouli, J., et al. (2015). Polymorphism of the IL-8 Gene and the Risk of Ovarian Cancer. *Cytokine* 71, 334–338. doi:10.1016/j.cyto.2014.07.254

Krawczyk, K. M., Nilsson, H., Allaoui, R., Lindgren, D., Arvidsson, M., Leandersson, K., et al. (2017). Papillary Renal Cell Carcinoma-Derived Chemerin, IL-8, and CXCL16 Promote Monocyte Recruitment and Differentiation into Foam-Cell Macrophages. *Lab. Invest.* 97, 1296–1305. doi:10.1038/labinvest.2017.78

Kumar, S., O'Malley, J., Chaudhary, A. K., Inigo, J. R., Yadav, N., Kumar, R., et al. (2019). Hsp60 and IL-8 axis Promotes Apoptosis Resistance in Cancer. *Br. J. Cancer* 121, 934–943. doi:10.1038/s41416-019-0617-0

Larsson, C. (2006). Protein Kinase C and the Regulation of the Actin Cytoskeleton. *Cell Signal.* 18, 276–284. doi:10.1016/j.cellsig.2005.07.010

Li, A., Dubey, S., Varney, M. L., Dave, B. J., and Singh, R. K. (2003). IL-8 Directly Enhanced Endothelial Cell Survival, Proliferation, and Matrix Metalloproteinases Production and Regulated Angiogenesis. *J. Immunol.* 170, 3369–3376. doi:10.4049/jimmunol.170.6.3369

Li, E., Yang, X., Du, Y., Wang, G., Chan, D. W., Wu, D., et al. (2021). CXCL8 Associated Dendritic Cell Activation Marker Expression and Recruitment as Indicators of Favorable Outcomes in Colorectal Cancer. *Front. Immunol.* 12, 667177. doi:10.3389/fimmu.2021.667177

Li, P., Chen, X., Qin, G., Yue, D., Zhang, Z., Ping, Y., et al. (2018). Maelstrom Directs Myeloid-Derived Suppressor Cells to Promote Esophageal Squamous Cell Carcinoma Progression via Activation of the Akt1/RelA/IL8 Signaling Pathway. *Cancer Immunol. Res.* 6, 1246–1259. doi:10.1158/2326-6066.CIR-17-0415

Lin, C., He, H., Liu, H., Li, R., Chen, Y., Qi, Y., et al. (2019). Tumour-associated Macrophages-Derived CXCL8 Determines Immune Evasion through Autonomous PD-L1 Expression in Gastric Cancer. *Gut* 68, 1764–1773. doi:10.1136/gutjnl-2018-316324

Liu, K., Wu, L., Yuan, S., Wu, M., Xu, Y., Sun, Q., et al. (2020). Structural Basis of CXC Chemokine Receptor 2 Activation and Signalling. *Nature* 585, 135–140. doi:10.1038/s41586-020-2492-5

Liu, Q., Li, A., Tian, Y., Wu, J. D., Liu, Y., Li, T., et al. (2016). The CXCL8-Cxcr1/2 Pathways in Cancer. *Cytokine Growth Factor. Rev.* 31, 61–71. doi:10.1016/j.cytogfr.2016.08.002

Long, X., Ye, Y., Zhang, L., Liu, P., Yu, W., Wei, F., et al. (2016). IL-8, a Novel Messenger to Cross-Link Inflammation and Tumor EMT via Autocrine and Paracrine Pathways (Review). *Int. J. Oncol.* 48, 5–12. doi:10.3892/ijo.2015.3234

Loos, T., Opdenakker, G., Van Damme, J., and Proost, P. (2009). Citrullination of CXCL8 Increases This Chemokine's Ability to Mobilize Neutrophils into the Blood Circulation. *Haematologica* 94, 1346–1353. doi:10.3324/haematol.2009.006973

Luo, C.-W., Hsiao, I.-L., Wang, J.-Y., Wu, C.-C., Hung, W.-C., Lin, Y.-H., et al. (2018). Cell Motility Facilitated by Mono(2-Ethylhexyl) Phthalate via Activation of the AKT–β-Catenin-IL-8 Axis in Colorectal Cancer. *J. Agric. Food Chem.* 66, 9635–9644. doi:10.1021/acs.jafc.8b03558

Luppi, F., Longo, A. M., de Boer, W. I., Rabe, K. F., and Hiemstra, P. S. (2007). Interleukin-8 Stimulates Cell Proliferation in Non-small Cell Lung Cancer through Epidermal Growth Factor Receptor Transactivation. *Lung Cancer* 56, 25–33. doi:10.1016/j.lungcan.2006.11.014

Ma, X., Chen, J., Liu, J., Xu, B., Liang, X., Yang, X., et al. (2021). IL-8/CXCR2 Mediates Tropism of Human Bone Marrow-derived Mesenchymal Stem Cells toward CD133 +/CD44 + Colon Cancer Stem Cells. *J. Cel Physiol* 236, 3114–3128. doi:10.1002/jcp.30080

Ma, X., Liu, J., Yang, X., Fang, K., Zheng, P., Liang, X., et al. (2020). Mesenchymal Stem Cells Maintain the Stemness of colon Cancer Stem Cells via Interleukin-8/mitogen-Activated Protein Kinase Signaling Pathway. *Exp. Biol. Med. (Maywood)* 245, 562–575. doi:10.1177/1535370220910690

MacManus, C. F., Pettigrew, J., Seaton, A., Wilson, C., Maxwell, P. J., Berlingeri, S., et al. (2007). Interleukin-8 Signaling Promotes Translational Regulation of Cyclin D in Androgen-independent Prostate Cancer Cells. *Mol. Cancer Res.* 5, 737–748. doi:10.1158/1541-7786.MCR-07-0032

Manfroi, B., McKee, T., Mayol, J. F., Tabruyn, S., Moret, S., Villiers, C., et al. (2017). CXCL-8/IL8 Produced by Diffuse Large B-Cell Lymphomas Recruits Neutrophils Expressing a Proliferation-Inducing Ligand APRIL. *Cancer Res.* 77, 1097–1107. doi:10.1158/0008-5472.CAN-16-0786

Mantovani, A., Marchesi, F., Malesci, A., Laghi, L., and Allavena, P. (2017). Tumour-associated Macrophages as Treatment Targets in Oncology. *Nat. Rev. Clin. Oncol.* 14, 399–416. doi:10.1038/nrclinonc.2016.217

Mao, F.-y., Zhao, Y.-l., Lv, Y.-p., Teng, Y.-s., Kong, H., Liu, Y.-g., et al. (2018). CD45+CD33lowCD11bdim Myeloid-Derived Suppressor Cells Suppress CD8+ T Cell Activity via the IL-6/IL-8-arginase I axis in Human Gastric Cancer. *Cell Death Dis* 9, 763. doi:10.1038/s41419-018-0803-7

Martin, D., Galisteo, R., and Gutkind, J. S. (2009). CXCL8/IL8 Stimulates Vascular Endothelial Growth Factor (VEGF) Expression and the Autocrine Activation of VEGFR2 in Endothelial Cells by Activating NFκB through the CBM (Carma3/Bcl10/Malt1) Complex. *J. Biol. Chem.* 284, 6038–6042. doi:10.1074/jbc.C800207200

Maxwell, P. J., Coulter, J., Walker, S. M., McKechnie, M., Neisen, J., McCabe, N., et al. (2013). Potentiation of Inflammatory CXCL8 Signalling Sustains Cell Survival in PTEN-Deficient Prostate Carcinoma. *Eur. Urol.* 64, 177–188. doi:10.1016/j.eururo.2012.08.032

Maynard, J. P., Ertunc, O., Kulac, I., Baena-Del Valle, J. A., De Marzo, A. M., and Sfanos, K. S. (2020). IL8 Expression Is Associated with Prostate Cancer Aggressiveness and Androgen Receptor Loss in Primary and Metastatic Prostate Cancer. *Mol. Cancer Res.* 18, 153–165. doi:10.1158/1541-7786.MCR-19-0595

McCoy, M. G., Nyanyo, D., Hung, C. K., Goerger, J. P., R. Zipfel, W., Williams, R. M., et al. (2019). Endothelial Cells Promote 3D Invasion of GBM by IL-8-dependent Induction of Cancer Stem Cell Properties. *Sci. Rep.* 9, 9069. doi:10.1038/s41598-019-45535-y

Meacham, C. E., and Morrison, S. J. (2013). Tumour Heterogeneity and Cancer Cell Plasticity. *Nature* 501, 328–337. doi:10.1038/nature12624

Mi, Y., Mu, L., Huang, K., Hu, Y., Yan, C., Zhao, H., et al. (2020). Hypoxic Colorectal Cancer Cells Promote Metastasis of Normoxic Cancer Cells Depending on IL-8/p65 Signaling Pathway. *Cel Death Dis* 11, 610. doi:10.1038/s41419-020-02797-z

Mishalian, I., Bayuh, R., Eruslanov, E., Michaeli, J., Levy, L., Zolotarov, L., et al. (2014). Neutrophils Recruit Regulatory T-Cells into Tumorsviasecretion of CCL17-A New Mechanism of Impaired Antitumor Immunity. *Int. J. Cancer* 135, 1178–1186. doi:10.1002/ijc.28770

Modi, W., Dean, M., Seuanez, H., Mukaida, N., Matsushima, K., and O'Brien, S. (1990). Monocyte-derived Neutrophil Chemotactic Factor (MDNCF/IL-8) Resides in a Gene Cluster along with Several Other Members of the Platelet Factor 4 Gene Superfamily. *Hum. Genet.* 84, 185–187. doi:10.1007/BF00208938

Mohamed, H. T., El-Ghonaimy, E. A., El-Shinawi, M., Hosney, M., Götte, M., Woodward, W. A., et al. (2020). IL-8 and MCP-1/CCL2 Regulate Proteolytic Activity in Triple Negative Inflammatory Breast Cancer a Mechanism that Might Be Modulated by Src and Erk1/2. *Toxicol. Appl. Pharmacol.* 401, 115092. doi:10.1016/j.taap.2020.115092

Mortier, A., Berghmans, N., Ronsse, I., Grauwen, K., Stegen, S., Van Damme, J., et al. (2011). Biological Activity of CXCL8 Forms Generated by Alternative Cleavage of the Signal Peptide or by Aminopeptidase-Mediated Truncation. *PLoS One* 6, e23913. doi:10.1371/journal.pone.0023913

Mukaida, N., Shiroo, M., and Matsushima, K. (1989). Genomic Structure of the Human Monocyte-Derived Neutrophil Chemotactic Factor IL-8. *J. Immunol.* 143, 1366–1371.

Murphy, P. M., and Tiffany, H. L. (1991). Cloning of Complementary DNA Encoding a Functional Human Interleukin-8 Receptor. *Science* 253, 1280–1283. doi:10.1126/science.1891716

Najjar, Y. G., Rayman, P., Jia, X., Pavicic, P. G., Jr, Rini, B. I., Tannenbaum, C., et al. (2017). Myeloid-Derived Suppressor Cell Subset Accumulation in Renal Cell Carcinoma Parenchyma Is Associated with Intratumoral Expression of IL1β, IL8, CXCL5, and Mip-1α. *Clin. Cancer Res.* 23, 2346–2355. doi:10.1158/1078-0432.CCR-15-1823

Nasser, M. W., Raghuwanshi, S. K., Grant, D. J., Jala, V. R., Rajarathnam, K., and Richardson, R. M. (2009). Differential Activation and Regulation of CXCR1 and CXCR2 by CXCL8 Monomer and Dimer. *J. Immunol.* 183, 3425–3432. doi:10.4049/jimmunol.0900305

Nie, M., Yang, L., Bi, X., Wang, Y., Sun, P., Yang, H., et al. (2019). Neutrophil Extracellular Traps Induced by IL8 Promote Diffuse Large B-Cell Lymphoma Progression via the TLR9 Signaling. *Clin. Cancer Res.* 25, 1867–1879. doi:10.1158/1078-0432.CCR-18-1226

Ning, Y., Cui, Y., Li, X., Cao, X., Chen, A., Xu, C., et al. (2018). Co-culture of Ovarian Cancer Stem-like Cells with Macrophages Induced SKOV3 Cells Stemness via IL-8/STAT3 Signaling. *Biomed. Pharmacother.* 103, 262–271. doi:10.1016/j.biopha.2018.04.022

Nourbakhsh, M., Kälble, S., Dörrie, A., Hauser, H., Resch, K., and Kracht, M. (2001). The NF-Kb Repressing Factor Is Involved in Basal Repression and Interleukin (IL)-1-induced Activation of IL-8 Transcription by Binding to a Conserved NF-Kb-Flanking Sequence Element. *J. Biol. Chem.* 276, 4501–4508. doi:10.1074/jbc.M007532200

Noy, R., and Pollard, J. W. (2014). Tumor-associated Macrophages: from Mechanisms to Therapy. *Immunity* 41, 49–61. doi:10.1016/j.immuni.2014.06.010

Nozawa, H., Chiu, C., and Hanahan, D. (2006). Infiltrating Neutrophils Mediate the Initial Angiogenic Switch in a Mouse Model of Multistage Carcinogenesis. *Proc. Natl. Acad. Sci.* 103, 12493–12498. doi:10.1073/pnas.0601807103

Park, S. H., Das, B. B., Casagrande, F., Tian, Y., Nothnagel, H. J., Chu, M., et al. (2012). Structure of the Chemokine Receptor CXCR1 in Phospholipid Bilayers. *Nature* 491, 779–783. doi:10.1038/nature11580

Petreaca, M. L., Yao, M., Liu, Y., Defea, K., and Martins-Green, M. (2007). Transactivation of Vascular Endothelial Growth Factor Receptor-2 by Interleukin-8 (IL-8/CXCL8) Is Required for IL-8/CXCL8-induced Endothelial Permeability. *MBoC* 18, 5014–5023. doi:10.1091/mbc.e07-01-0004

Poschke, I., and Kiessling, R. (2012). On the Armament and Appearances of Human Myeloid-Derived Suppressor Cells. *Clin. Immunol.* 144, 250–268. doi:10.1016/j.clim.2012.06.003

Proost, P., Loos, T., Mortier, A., Schutyser, E., Gouwy, M., Noppen, S., et al. (2008). Citrullination of CXCL8 by Peptidylarginine Deiminase Alters Receptor Usage, Prevents Proteolysis, and Dampens Tissue Inflammation. *J. Exp. Med.* 205, 2085–2097. doi:10.1084/jem.20080305

Quann, E. J., Liu, X., Altan-Bonnet, G., and Huse, M. (2011). A cascade of Protein Kinase C Isozymes Promotes Cytoskeletal Polarization in T Cells. *Nat. Immunol.* 12, 647–654. doi:10.1038/ni.2033

Rafrafi, A., Chahed, B., Kaabachi, S., Kaabachi, W., Maalmi, H., Hamzaoui, K., et al. (2013). Association of IL-8 Gene Polymorphisms with Non Small Cell Lung Cancer in Tunisia: A Case Control Study. *Hum. Immunol.* 74, 1368–1374. doi:10.1016/j.humimm.2013.06.033

Raghuwanshi, S. K., Su, Y., Singh, V., Haynes, K., Richmond, A., and Richardson, R. M. (2012). The Chemokine Receptors CXCR1 and CXCR2 Couple to Distinct G Protein-Coupled Receptor Kinases to Mediate and Regulate Leukocyte Functions. *J.I.* 189, 2824–2832. doi:10.4049/jimmunol.1201114

Raza, S., Rajak, S., Tewari, A., Gupta, P., Chattopadhyay, N., Sinha, R. A., et al. (2022). Multifaceted Role of Chemokines in Solid Tumors: From Biology to Therapy. *Semin. Cancer Biol.* S1044-579X, 00304–00307. doi:10.1016/j.semcancer.2021.12.011

Ribas, A., and Wolchok, J. D. (2018). Cancer Immunotherapy Using Checkpoint Blockade. *Science* 359, 1350–1355. doi:10.1126/science.aar4060

Rodriguez, P. C., Quiceno, D. G., Zabaleta, J., Ortiz, B., Zea, A. H., Piazuelo, M. B., et al. (2004). Arginase I Production in the Tumor Microenvironment by Mature Myeloid Cells Inhibits T-Cell Receptor Expression and Antigen-specific T-Cell Responses. *Cancer Res.* 64, 5839–5849. doi:10.1158/0008-5472.CAN-04-0465

Rollins, B. J. (1997). Chemokines. *Blood* 90, 909–928. doi:10.1182/blood.V90.3.909

Roskoski, R. (2015). Src Protein-Tyrosine Kinase Structure, Mechanism, and Small Molecule Inhibitors. *Pharmacol. Res.* 94, 9–25. doi:10.1016/j.phrs.2015.01.003

Sanmamed, M. F., Perez-Gracia, J. L., Schalper, K. A., Fusco, J. P., Gonzalez, A., Rodriguez-Ruiz, M. E., et al. (2017). Changes in Serum Interleukin-8 (IL-8) Levels Reflect and Predict Response to Anti-PD-1 Treatment in Melanoma and Non-small-cell Lung Cancer Patients. *Ann. Oncol.* 28, 1988–1995. doi:10.1093/annonc/mdx190

Schalper, K. A., Carleton, M., Zhou, M., Chen, T., Feng, Y., Huang, S.-P., et al. (2020). Elevated Serum Interleukin-8 Is Associated with Enhanced Intratumor Neutrophils and Reduced Clinical Benefit of Immune-Checkpoint Inhibitors. *Nat. Med.* 26, 688–692. doi:10.1038/s41591-020-0856-x

Schraufstatter, I. U., Chung, J., and Burger, M. (2001). IL-8 Activates Endothelial Cell CXCR1 and CXCR2 through Rho and Rac Signaling Pathways. *Am. J. Physiology-Lung Cell Mol. Physiol.* 280, L1094–L1103. doi:10.1152/ajplung.2001.280.6.L1094

Shimizu, M., and Tanaka, N. (2019). IL-8-induced O-GlcNAc Modification via GLUT3 and GFAT Regulates Cancer Stem Cell-like Properties in colon and Lung Cancer Cells. *Oncogene* 38, 1520–1533. doi:10.1038/s41388-018-0533-4

Singh, J. K., Farnie, G., Bundred, N. J., Simões, B. M., Shergill, A., Landberg, G., et al. (2013). Targeting CXCR1/2 Significantly Reduces Breast Cancer Stem Cell Activity and Increases the Efficacy of Inhibiting HER2 via HER2-dependent

and -independent Mechanisms. *Clin. Cancer Res.* 19, 643–656. doi:10.1158/1078-0432.CCR-12-1063

Son, D. O., Satsu, H., Kiso, Y., Totsuka, M., and Shimizu, M. (2008). Inhibitory Effect of Carnosine on Interleukin-8 Production in Intestinal Epithelial Cells through Translational Regulation. *Cytokine* 42, 265–276. doi:10.1016/j.cyto.2008.02.011

Stillie, R., Farooq, S. M., Gordon, J. R., and Stadnyk, A. W. (2009). The Functional Significance behind Expressing Two IL-8 Receptor Types on PMN. *J. Leukoc. Biol.* 86, 529–543. doi:10.1189/jlb.0208125

Strieter, R. M., Polverini, P. J., Kunkel, S. L., Arenberg, D. A., Burdick, M. D., Kasper, J., et al. (1995). The Functional Role of the ELR Motif in CXC Chemokine-Mediated Angiogenesis. *J. Biol. Chem.* 270, 27348–27357. doi:10.1074/jbc.270.45.27348

Sulzmaier, F. J., Jean, C., and Schlaepfer, D. D. (2014). FAK in Cancer: Mechanistic Findings and Clinical Applications. *Nat. Rev. Cancer* 14, 598–610. doi:10.1038/nrc3792

Sun, L., Clavijo, P. E., Robbins, Y., Patel, P., Friedman, J., Greene, S., et al. (2019a). Inhibiting Myeloid-Derived Suppressor Cell Trafficking Enhances T Cell Immunotherapy. *JCI Insight* 4. doi:10.1172/jci.insight.126853

Sun, Y., Ai, J. Z., Jin, X., Liu, L. R., Lin, T. H., Xu, H., et al. (2019b). IL-8 Protects Prostate Cancer Cells from GSK-3β-induced Oxidative Stress by Activating the mTOR Signaling Pathway. *Prostate* 79, 1180–1190. doi:10.1002/pros.23836

Tobin, R. P., Jordan, K. R., Kapoor, P., Spongberg, E., Davis, D., Vorwald, V. M., et al. (2019). IL-6 and IL-8 Are Linked with Myeloid-Derived Suppressor Cell Accumulation and Correlate with Poor Clinical Outcomes in Melanoma Patients. *Front. Oncol.* 9, 1223. doi:10.3389/fonc.2019.01223

Ueda, G., Matsuo, Y., Murase, H., Aoyama, Y., Kato, T., Omi, K., et al. (2022). 10Z-Hymenialdisine I-nhibits A-ngiogenesis by S-uppressing NF-κB A-ctivation in P-ancreatic C-ancer C-ell L-ines. *Oncol. Rep.* 47, 48. doi:10.3892/or.2022.8259

Van den Steen, P. E., Wuyts, A., Husson, S. J., Proost, P., Van Damme, J., and Opdenakker, G. (2003). Gelatinase B/MMP-9 and Neutrophil collagenase/MMP-8 Process the Chemokines Human GCP-2/CXCL6, ENA-78/CXCL5 and Mouse GCP-2/LIX and Modulate Their Physiological Activities. *Eur. J. Biochem.* 270, 3739–3749. doi:10.1046/j.1432-1033.2003.03760.x

Vanheule, V., Metzemaekers, M., Janssens, R., Struyf, S., and Proost, P. (2018). How post-translational Modifications Influence the Biological Activity of Chemokines. *Cytokine* 109, 29–51. doi:10.1016/j.cyto.2018.02.026

Venkatakrishnan, G., Salgia, R., and Groopman, J. E. (2000). Chemokine Receptors CXCR-1/2 Activate Mitogen-Activated Protein Kinase via the Epidermal Growth Factor Receptor in Ovarian Cancer Cells. *J. Biol. Chem.* 275, 6868–6875. doi:10.1074/jbc.275.10.6868

Wang, J., Wang, Y., Wang, S., Cai, J., Shi, J., Sui, X., et al. (2015). Bone Marrow-Derived Mesenchymal Stem Cell-Secreted IL-8 Promotes the Angiogenesis and Growth of Colorectal Cancer. *Oncotarget* 6, 42825–42837. doi:10.18632/oncotarget.5739

Waugh, D. J. J., and Wilson, C. (2008). The Interleukin-8 Pathway in Cancer. *Clin. Cancer Res.* 14, 6735–6741. doi:10.1158/1078-0432.CCR-07-4843

Wilson, C., Seaton, A., and Maxwell, P. J. (2006). CXCR2/NF-kB/BCL-2-survivin Signalling Pathway Promotes Resistance to Oxaliplatin in Metastatic Prostate Cancer Cells. Proceedings of 99th AACR Annual Meeting. Washington (DC).

Wu, G. D., Lai, E. J., Huang, N., and Wen, X. (1997). Oct-1 and CCAAT/Enhancer-binding Protein (C/EBP) Bind to Overlapping Elements within the Interleukin-8 Promoter. *J. Biol. Chem.* 272, 2396–2403. doi:10.1074/jbc.272.4.2396

Wu, J., Gao, F.-x., Wang, C., Qin, M., Han, F., Xu, T., et al. (2019). IL-6 and IL-8 Secreted by Tumour Cells Impair the Function of NK Cells via the STAT3 Pathway in Oesophageal Squamous Cell Carcinoma. *J. Exp. Clin. Cancer Res.* 38, 321. doi:10.1186/s13046-019-1310-0

Xu, H., Zeng, Y., Liu, L., Gao, Q., Jin, S., Lan, Q., et al. (2017). PRL-3 Improves Colorectal Cancer Cell Proliferation and Invasion through IL-8 Mediated Glycolysis Metabolism. *Int. J. Oncol.* 51, 1271–1279. doi:10.3892/ijo.2017.4090

Xu, Q., Ma, H., Chang, H., Feng, Z., Zhang, C., and Yang, X. (2020). The Interaction of Interleukin-8 and PTEN Inactivation Promotes the Malignant Progression of Head and Neck Squamous Cell Carcinoma via the STAT3 Pathway. *Cel Death Dis* 11, 405. doi:10.1038/s41419-020-2627-5

Yan, Z., Liu, J., Xie, L., Liu, X., Zeng, Y., and Yang, X. (2016). Role of Heparan Sulfate in Mediating CXCL8-Induced Endothelial Cell Migration. *PeerJ* 4, e1669. doi:10.1038/s41419-020-2627-510.7717/peerj.1669

Yang, L., Liu, L., Zhang, R., Hong, J., Wang, Y., Wang, J., et al. (2020a). IL-8 Mediates a Positive Loop Connecting Increased Neutrophil Extracellular Traps (NETs) and Colorectal Cancer Liver Metastasis. *J. Cancer* 11, 4384–4396. doi:10.7150/jca.44215

Yang, M., Zhang, G., Wang, Y., He, M., Xu, Q., Lu, J., et al. (2020b). Tumour-associated Neutrophils Orchestrate Intratumoural IL-8-driven Immune Evasion through Jagged2 Activation in Ovarian Cancer. *Br. J. Cancer* 123, 1404–1416. doi:10.1038/s41416-020-1026-0

Yao, W., Sun, Y., Sun, Y., Chen, P., Meng, Z., Xiao, M., et al. (2019). A Preliminary Report of the Relationship between Gene Polymorphism of IL-8 and its Receptors and Systemic Inflammatory Response Syndrome Caused by Wasp Stings. *DNA Cel Biol.* 38, 1512–1518. doi:10.1089/dna.2019.4855

Yuen, K. C., Liu, L.-F., Gupta, V., Madireddi, S., Keerthivasan, S., Li, C., et al. (2020). High Systemic and Tumor-Associated IL-8 Correlates with Reduced Clinical Benefit of PD-L1 Blockade. *Nat. Med.* 26, 693–698. doi:10.1038/s41591-020-0860-1

Zha, C., Meng, X., Li, L., Mi, S., Qian, D., Li, Z., et al. (2020). Neutrophil Extracellular Traps Mediate the Crosstalk between Glioma Progression and the Tumor Microenvironment via the HMGB1/RAGE/IL-8 axis. *Cancer Biol. Med.* 17, 154–168. doi:10.20892/j.issn.2095-3941.2019.0353

Zhang, H., Ye, Y.-L., Li, M.-X., Ye, S.-B., Huang, W.-R., Cai, T.-T., et al. (2017). CXCL2/MIF-CXCR2 Signaling Promotes the Recruitment of Myeloid-Derived Suppressor Cells and Is Correlated with Prognosis in Bladder Cancer. *Oncogene* 36, 2095–2104. doi:10.1038/onc.2016.367

Zhang, M., Huang, L., Ding, G., Huang, H., Cao, G., Sun, X., et al. (2020). Interferon Gamma Inhibits CXCL8-CXCR2 axis Mediated Tumor-Associated Macrophages Tumor Trafficking and Enhances Anti-PD1 Efficacy in Pancreatic Cancer. *J. Immunother. Cancer* 8, e000308. doi:10.1136/jitc-2019-000308

Zheng, T., Ma, G., Tang, M., Li, Z., and Xu, R. (2018). IL-8 Secreted from M2 Macrophages Promoted Prostate Tumorigenesis via STAT3/MALAT1 Pathway. *Ijms* 20, 98. doi:10.3390/ijms20010098

Zhou, J., Yi, L., Ouyang, Q., Xu, L., Cui, H., and Xu, M. (2014). Neurotensin Signaling Regulates Stem-like Traits of Glioblastoma Stem Cells through Activation of IL-8/CXCR1/STAT3 Pathway. *Cell Signal.* 26, 2896–2902. doi:10.1016/j.cellsig.2014.08.027

Zhou, Q., Jin, P., Liu, J., Li, S., Liu, W., and Xi, S. (2021). HER2 Overexpression Triggers the IL-8 to Promote Arsenic-Induced EMT and Stem Cell-like Phenotypes in Human Bladder Epithelial Cells. *Ecotoxicology Environ. Saf.* 208, 111693. doi:10.1016/j.ecoenv.2020.111693

Conflict of Interest: The authors declare that the research was conducted in the absence of any commercial or financial relationships that could be construed as a potential conflict of interest.

Publisher's Note: All claims expressed in this article are solely those of the authors and do not necessarily represent those of their affiliated organizations, or those of the publisher, the editors and the reviewers. Any product that may be evaluated in this article, or claim that may be made by its manufacturer, is not guaranteed or endorsed by the publisher.

Frontiers in
Molecular Biosciences

Explores biological processes in living organisms on a molecular scale

Focuses on the molecular mechanisms underpinning and regulating biological processes in organisms across all branches of life.

Discover the latest Research Topics

See more →

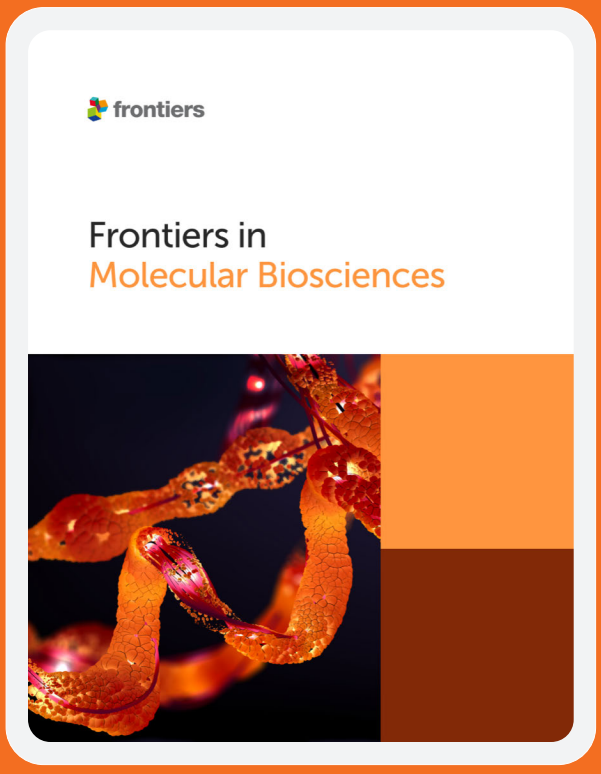

Frontiers

Avenue du Tribunal-Fédéral 34
1005 Lausanne, Switzerland
frontiersin.org

Contact us

+41 (0)21 510 17 00
frontiersin.org/about/contact